




ECR 2018 DIVERSE & UNITED

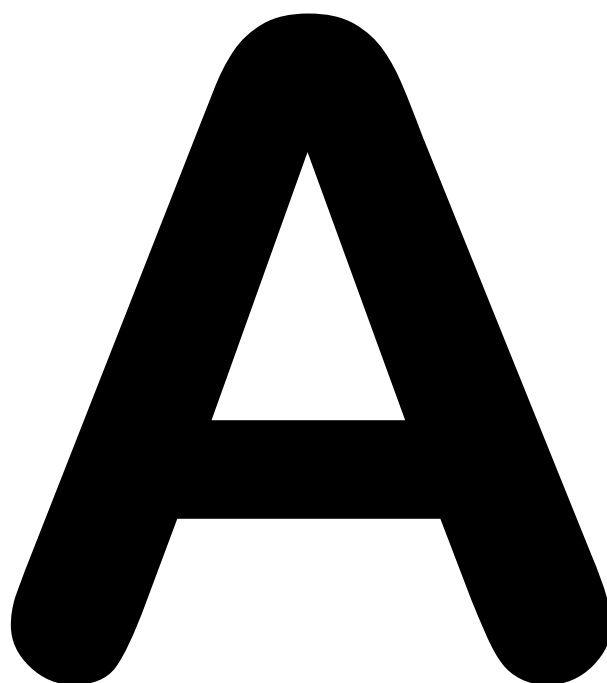
BOOK OF ABSTRACTS



CONTENTS

Postgraduate Educational Programme (A)	S2-187
Scientific Sessions (SS), My Thesis in 3 Minutes (MY), Clinical Trials in Radiology (CT) (B)	S188-537
Scientific and Educational Exhibits ©	S538
Satellite Symposia (D)	S539-548
Author's Index (E)	S549-608
List of Authors & Co-Authors (F)	S609-639
List of Moderators (G)	S640-642





Postgraduate Educational Programme

EFOMP Workshop (EF)
ESR/EFRS meets Sessions (EM)
European Excellence in Education (E³)
Headline Sessions
Joint Sessions
Mini Courses (MC)
Multidisciplinary Sessions (MS)
New Horizons Sessions (NH)
Professional Challenges Sessions (PC)
Pros & Cons Session (PS)
Refresher Courses (RC)
Special Focus Sessions (SF)
State of the Art Symposia (SA)

Wednesday, February 28.....	3
Thursday, March 1	36
Friday, March 2.....	75
Saturday, March 3.....	117
Sunday, March 4	168

Wednesday, February 28

08:30 - 10:00

Room A

E³ - ECR Academies: Interactive Teaching Sessions for Young (and not so Young) Radiologists

E³ 121

Emergency radiology I

A-001 08:30

A. Acute aortic syndrome

H. [Alkadhi](mailto:hatem.alkadhi@usz.ch); Zurich/CH (hatem.alkadhi@usz.ch)

Computed tomography (CT) imaging - often preceded by conventional radiography - represents the major imaging modality for the diagnosis of acute aortic syndromes. This lecture will review the various underlying diseases of acute aortic syndrome, demonstrate typical imaging features enabling the diagnosis and discuss management options depending on the type, extent, and location of the disease. Clinical examples will be shown.

Learning Objectives:

1. To understand the different types of acute aortic syndrome.
2. To learn about imaging findings and management options.

A-002 09:15

B. Abdominal trauma

R. [Basilico](mailto:rbasilic@unich.it); Chieti/IT (rbasilic@unich.it)

Abdominal traumas can be classified into two categories: penetrating and blunt traumas. Abdominal injuries are more often observed in the setting of polytrauma; in fact, they are present in about 10% of patients admitted to level 1 trauma. However, only 11% of patients with abdominal trauma require laparotomy when a correct imaging-guide approach is performed. In fact, because the management of trauma patients mainly depends on the mechanism and severity of the trauma, it is crucial to choose the correct imaging modality and/or technique when evaluating a trauma patient on the basis of these two parameters. For example, an ultrasound examination, possibly integrated by contrast-enhanced ultrasonography, may be adequate to image a minor blunt abdominal trauma. This modality, however, is not appropriate when evaluating a severe blunt or penetrating abdominal trauma or even a polytrauma patient with a minor mechanism of injury. Multidetector CT is actually the modality of choice for evaluating severe trauma patients, accompanied by an appropriate CT protocol to image these patients so as to avoid missed injuries and to correctly detect abdominal solid organ injuries, mesenteric and intestinal injuries and abdominal vascular traumatic lesions. Moreover, due to the fact that during the past decades there has been a major change from operative to increasingly conservative management of abdominal traumatic injuries, even in patients with higher grades of injuries or those with older age, imaging features together with hemodynamic considerations play an essential role in the treatment choice: surgery, conservative management, and endovascular treatment.

Learning Objectives:

1. To identify the signs of trauma.
2. To provide an indication of their clinical significance.

08:30 - 10:00

Room B

GI Tract

RC 101

GI bleeding: how to solve the problem?

A-003 08:30

Chairperson's introduction

S. [Wirth](mailto:stefan.wirth@med.uni-muenchen.de); Munich/DE (stefan.wirth@med.uni-muenchen.de)

Sometimes, things may become more difficult and easier at the same time. On one hand advances in imaging allow for very precise and also fast diagnoses in a continuous increasing number of cases. Consequently, even the bleeding of the GI-tract comes even more into radiological play. On the other hand, radiologists have to be more and more aware of clinical entities, pathological patterns, and interdisciplinary networks to quickly and precisely provide our clinical partners with the information they need. Besides that, more and more cases can be managed by minimal-invasive interventional procedures, i.e., by radiologists themselves.

Session Objectives:

1. To define acute, overt and occult GI bleeding.
2. To learn about different imaging modalities that can be utilised in the work-up of GI bleeding.
3. To define the role of the interventional radiologist in the management of the GI bleeding.

A-004 08:35

A. Acute GI bleeding

G.H. [Mostbeck](mailto:gerhard.mostbeck@wienkav.at); Vienna/AT (gerhard.mostbeck@wienkav.at)

Acute gastrointestinal (GI) bleeding is a common medical problem associated with high morbidity and mortality. The clinical presentation of acute GI bleeding varies with the location of the bleeding site, the cause, the amount of blood loss, and the presence of comorbidities. Anatomically, the ligament of Treitz is the border between upper (mouth to Treitz) and lower (Treitz to anus) GI bleeding. However, it is not always possible to differentiate between upper and lower GI bleeding clinically, despite the fact that clinical presentation is different, as is the etiology. In decreasing order, erosions and ulcer, variceal bleeding, Mallory-Weiss tears, vascular lesions, and neoplasms are responsible for upper GI bleeding. In contrast, lower GI bleeding occurs in the elder population, with diverticular disease, angiodysplasia, neoplasms, colitis and benign anorectal lesions being the major etiologies. The main diagnostic objective is the identification of the etiology and site of bleeding. Endoscopy is the initial diagnostic step in upper GI bleeding, but limited in lower GI bleeding due to difficulties in colonic cleansing in an emergency situation. Accordingly, CT is the imaging method of choice [technique: no positive oral contrast, high dose /iodine content/flow of contrast material (e.g., 100-150 ml, 350 mg/ml, 4-6 ml/sec), plain, arterial and parenchymal phases, dual-energy CT with iodine maps if available, multiplanar reformation, high anatomic resolution]. We search for high-attenuation (> 80HU) luminal or wall lesions not seen on unenhanced CT data. Detection rates vary, and an amount of bleeding > 0.35-0.5 ml/min is required. As bleeding might be intermittent, CT should be performed when active bleeding is present.

Learning Objectives:

1. To learn about the common causes of the acute upper and lower GI bleeding.
2. To understand the rationale for different investigative pathways depending on the likely site of bleeding.
3. To appreciate how best to optimise imaging protocols to identify the site and cause of bleeding, and assist with treatment planning.

A-005 08:58

B. Occult and overt GI bleeding: the role of radiology

J. [Brito](mailto:jmbrito@gmail.com); Portimão/PT (jmbrito@gmail.com)

The term obscure gastrointestinal bleeding (OGIB) was traditionally used to include patients with gastrointestinal bleeding who underwent normal upper and lower endoscopic examinations in addition to a small bowel series that did not reveal a source of bleeding. This definition was a sign of the difficulties experienced in small bowel exploration in the past. Given to recent advances in small bowel investigative methods, including endoscopic (video capsule endoscopy, deep enteroscopy) and radiological (CT and MR enterography, CT angiography) techniques, the cause of bleeding is no longer obscure and can now be reached in majority of the patients. For this reason, the term OGIB has been reclassified as "small bowel bleeding", which corresponds to ~5-10% of all patients presenting with gastrointestinal bleeding. "OGIB" is now reserved for patients in whom a source of bleeding cannot be identified anywhere in the gastrointestinal tract after a comprehensive investigation. Small bowel bleeding can be overt, if patient presents with melena or hematochezia, or occult for patients presenting with iron-deficiency anaemia. Causes of small bowel bleeding are varied and the likelihood to be due to a vascular, inflammatory or mass lesion is related to the patient's age. Algorithms for investigation of suspected small bowel bleeding include endoscopic and radiological methods, frequently with a complementary role, indicating that an adequate interaction is required among the elements of a multidisciplinary team.

Learning Objectives:

1. To learn about the differences between obscure, occult and overt GI bleeding, and the most common causes of each.
2. To understand when imaging is indicated which tests to perform, and the most important diagnoses to look for.
3. To appreciate the interaction between endoscopic and radiologic investigations in managing patients with obscure GI bleeding.

A-006 09:21

C. When is the interventional radiologist needed?

D.K. [Tsetis](mailto:tsetis@med.uoc.gr); Iraklion, Crete/GR (tsetis@med.uoc.gr)

Acute significant gastrointestinal bleeding is generally defined as a bleeding requiring transfusion of at least 4 units of blood within 24 hours or showing signs of hemodynamic instability (hypotension, tachycardia, signs of hypovolemic shock). Most cases are resolved endoscopically, pharmacologically, or by correction of coagulation parameters. Due to its minimally invasive nature, the endovascular solution is currently in most cases, after the previous methods fail, considered the method of choice. The most often used access to undergo embolisation is percutaneous access via common femoral or brachial artery. After reaching the appropriate visceral artery with a diagnostic 4 or 5F catheter, and verification of the source of bleeding, microcatheters are introduced coaxially. The most commonly used embolic materials are microcoils, PVA microspheres and gelatin foam. In the case of more massive bleeding, using of tissue glue (Histoacryl, etc.) may be considered. Upper gastrointestinal tract is characterised by a rich network of collateral supply with lower risk of ischemia. In the risk of rebleeding via collaterals, it is necessary to perform embolisation proximally and distally from the site of bleeding (so-called sandwich method). In the lower gastrointestinal tract, and in particular in the colon, due to the higher portion of terminal branches, ischemia risk is higher and embolisation should be as selective as possible.

Learning Objectives:

1. To learn about the role of interventional radiology in the management of acute and chronic GI bleeding.
2. To learn about the variety of techniques available to the interventional radiologist to evaluate obscure GI bleeding and control acute GI bleeding.
3. To understand when interventional radiology is clearly indicated, when it should be considered, and when it should be avoided if possible.

09:44

Panel discussion: Guidelines for management of GI bleeding and real life: why are they different?

08:30 - 10:00

Room C

Chest

RC 104

When and how to use perfusion imaging in pulmonary vascular and airway disease?

Moderator:

C.J. Herold; Vienna/AT

A-007 08:30

A. CT

M. [Rémy-Jardin](mailto:martine.remy@chru-lille.fr); Lille/FR (martine.remy@chru-lille.fr)

Since the introduction of dual-energy CT (DECT) in clinical practice, great interest has been directed toward analysis of the distribution of iodine in the most distal parts of the pulmonary circulation, often referred to as perfusion imaging. Initially only available with dual-source CT, dual-energy CT has become accessible to single-source CT, with the introduction of rapid kV switching and more recently, dual-layer (sandwich) detectors. Regardless of the difference in the technological approach, perfusion images are generated from the same data set as that used for morphological evaluation, offering the possibility of a simultaneous approach of structure and function in respiratory patients. This combined information provided with CT is a major advantage over scintigraphy and MRI, not only in the field of primary disorders of the pulmonary circulation, like acute pulmonary embolism, but also in the context of bronchopulmonary diseases where perfusion alterations can be interpreted with precise knowledge of the underlying morphologic changes. More recently, this complementarity has also been extended in the field of chronic thromboembolic disease and pulmonary hypertension while a growing interest is reported in oncologic indications. The purpose of this presentation is to make radiologists familiar with the use of CT lung perfusion in clinical practice.

Learning Objectives:

1. To learn about the creation of CT perfusion images.
2. To understand the complementarity between morphological and functional information.
3. To learn the various causes of perfusion defects.

Author Disclosure:

M. Rémy-Jardin: Research/Grant Support; Research grant support from Siemens Healthcare.

A-008 09:00

B. MRI

M.O. [Wielpütz](mailto:wielpuetz@uni-heidelberg.de); Heidelberg/DE (wielpuetz@uni-heidelberg.de)

Among functional lung magnetic resonance imaging (MRI) techniques, dynamic contrast-enhanced (4D) perfusion MRI is probably the most robust and widely used method that has entered the clinical arena of routine patient management. Because it delivers temporally resolved datasets, perfusion parameters such as time-to-peak or pulmonary blood flow may be directly quantified by dedicated post-processing. In pulmonary vascular disease it may help to identify arterio-venous-malformations, pulmonary shunts or anomalous venous return. In combination with contrast-enhanced and non-contrast enhanced lung MR angiography, 4D perfusion MRI is now considered an alternative for computed tomography angiography for pulmonary embolism. In case of airways disease such as cystic fibrosis or chronic obstructive pulmonary disease, 4D perfusion imaging exploits the physiological mechanism of hypoxic pulmonary vasoconstriction. This effects a downregulation of perfusion to functional lung units with reduced ventilation, i.e. airway obstruction. Thus, 4D perfusion MRI can directly visualize functional lung impairment associated with airways disease, even when small airways are affected that cannot be otherwise captured with structural imaging. The lecture will summarise technical aspects of performing 4D perfusion imaging with clinical MRI scanners, discuss the most important routine indications including implementation into routine workflow, and discuss most relevant imaging findings in vascular and airways disease. Further, future developments and non-contrast-dependent techniques will be reviewed.

Learning Objectives:

1. To become familiar with the technical aspects of MRI perfusion.
2. To learn key imaging features.
3. To discuss the most relevant clinical indications.

Author Disclosure:

M.O. Wielpütz: Advisory Board; Boehringer Ingelheim. Investigator; Boehringer Ingelheim, Vertex.

A-009 09:30

C. Nuclear medicine and hybrid imaging

E.J.R. [van Beek](mailto:edwin-vanbeek@ed.ac.uk); Edinburgh/UK (edwin-vanbeek@ed.ac.uk)

Initial management of pulmonary vascular and lung diseases has consisted of lung scintigraphy, enabling the study of both lung perfusion and ventilation. The advent of CT and CTPA has replaced many of the acute indications. Nevertheless, there remains an important role for the use of both lung scintigraphy and the combined use of new hybrid systems (SPECT/CT) to study these disease and facilitate in their management. This presentation will evaluate the historical and current state-of-the-art capabilities of lung scintigraphy to study lung perfusion and ventilation. It will also evaluate the potential best applications in the current diagnostic management, as well as demonstrate some of the pitfalls of this technology.

Learning Objectives:

1. To learn about the specificities of perfusion scintigraphy.
2. To understand the advantages of hybrid imaging.
3. To appreciate potential pitfalls of nuclear medicine techniques.

Author Disclosure:

E.J.R. van Beek: Advisory Board; Aidence BV. Equipment Support Recipient; Siemens Healthineers. Founder; QCTIS Ltd. Owner; QCTIS Ltd.

08:30 - 10:00

Room O

Paediatric

RC 112

Paediatric musculoskeletal imaging

Moderator:

A.C. Offiah; Sheffield/UK

A-010 08:30

A. How to distinguish normal variants from pathology on musculoskeletal MRI in children

D. [Avenarius](mailto:Derk.Avenarius@unn.no); Tromsø/NO (Derk.Avenarius@unn.no)

Normal variations of development of the skeleton are well documented when it comes to radiographs; with the introduction of MRI there are many more features to consider that are often less known. Normal variations are common and these can simulate disease. It is important for radiologist to be aware of this and an overview of cases will be presented. Protocols for MRI imaging in paediatric MSK imaging will be discussed.

Postgraduate Educational Programme

Learning Objectives:

1. To discuss MRI protocols for MSK-imaging in children.
2. To give an overview of normal development and variations in MR anatomy and signal patterns.
3. To provide an understanding of features indicative of pathology.

A-011 09:00

B. MRI of the temporomandibular joints: findings that can mimic arthritis

T. [von Kalle](mailto:vonkalle@klinikum-stuttgart.de); Stuttgart/DE (t.vonkalle@klinikum-stuttgart.de)

Arthritis of the temporomandibular joint (TMJ) is common in children and adolescents with juvenile idiopathic arthritis (JIA). Early treatment is warranted to prevent severe growth disturbances and joint deformities. As TMJ arthritis is often clinically silent, MRI with contrast-enhancement has been considered to be the most reliable method to assess signs of inflammation. To reliably guide therapeutic decisions and monitor outcomes, it would be of utmost importance to clearly define the MR characteristics of a normal TMJ as a basis for the assessment of minor pathologies. However, similar to other small joints in children, we are just beginning to understand its developmental, physiological and anatomical characteristics as well as its reaction to inflammatory diseases and their treatment. Recent studies on normal TMJ in children have revealed age dependent changes in shape and angulation of the mandibular condyle as well as typical time-intensity curves of contrast-enhancement in the soft joint tissue and the condyle. To date, the differentiation between normal synovial findings and mild signs of synovitis remains challenging. This lecture presents typical MR images of normal and inflamed TMJs in children and adolescents, including age dependent anatomical variations. It discusses the available data on possible cut-offs between normality and pathology, the impact of the temporal dynamics of contrast-enhancement, and presents findings that can mimic arthritis. It summarizes the minimum requirements of image quality and spatial resolution, the best image orientation, as well as the advantages of fat suppression and subtraction analysis in contrast-enhanced imaging.

Learning Objectives:

1. To discuss MRI protocols for imaging of the temporomandibular joints (TMJ).
2. To give an overview of MR imaging finding in arthritis of the TMJ.
3. To highlight the major differential diagnoses of TMJ arthritis and its MR imaging characteristics.

A-012 09:30

C. Skeletal trauma in children

I. [Barber](mailto:ibarber@hsjbcn.org); Esplugues de Llobregat/ES (ibarber@hsjbcn.org)

Musculoskeletal injuries are common in children. They account for 15-20% of admissions to the ED. Children have an immature skeleton with unique biomechanical features and a stronger, thicker and richly vascularized periosteum. Paediatric fractures may present with unique patterns including plastic deformation, buckled fractures, and greenstick fractures. Fractures in children include the ones involving the physis (epiphysiolysis) and we will review their classification and prognosis after treatment. We will review these injuries making special remarks on the imaging techniques used for their correct diagnosis and treatment planning.

Learning Objectives:

1. To become familiar with the types of injuries seen in children.
2. To understand the basic mechanisms.
3. To learn about the diagnostic imaging approach.

08:30 - 10:00

Room N

Head and Neck

RC 108

Differential diagnoses you don't want to miss

Moderator:

M.R. Eriksen; Stavanger/NO

A-013 08:30

A. Differential diagnoses of orbital masses

V. [Chong](mailto:vincent_chong@nuhs.edu.sg); Singapore/SG (vincent_chong@nuhs.edu.sg)

The approach to orbital mass analysis follows two basic rules. The first rule emphasizes the general fact that diseases arise from pre-existing tissues or structures unique to different spaces in the orbit. The second rule highlights exceptions to the general rule. For example, metastatic or other systemic diseases may involve the orbit, while trans-spatial pathological processes such as infiltrative lesions may affect multiple compartments simultaneously or

metachronously. The orbit can be divided (by the muscle cone) into an intra-conal and an extra-conal compartment. Structures in the intra-conal compartment include the optic nerve/sheath complex and the surrounding fibro-fatty tissues, small vessels and small nerve branches. The contents of the extra-conal space include the lacrimal gland, cranial nerves (V1 and V2) and the periosteum of the orbit. Hence, knowledge of the applied anatomy of the orbit with a working knowledge of commonly seen diseases is a prerequisite for generating lists of differential diagnoses. The analysis of orbital masses should always be carried out in the clinical context of the patient. Tentative as well as definitive diagnosis can often be made with reference to the clinical information. For example, a lesion with unusual morphology or location can be tentatively diagnosed as metastatic disease in the presence of a history of malignancy elsewhere. In conclusion, the integration of knowledge of orbital anatomy, pathology and clinical information provides the basis of sound radiological differential diagnoses for further patient management.

Learning Objectives:

1. To become familiar with the anatomy of the orbit.
2. To learn which imaging technique to use.
3. To understand the typical imaging appearance of orbital masses.

A-014 09:00

B. Differential diagnoses of the jaw masses

C. [Czerny](mailto:christian.czerny@meduniwien.ac.at); Vienna/AT (christian.czerny@meduniwien.ac.at)

Cystic and tumorous pathologies of the jaws can be imaged with cone-beam CT, CT and MRI. These pathologies include, e.g. in most cases inflammation or tumours. PET-CT or PET-MR may also be used. CT may be used without or with the i.v. application of iodinated contrast material dependent on the pathology. The images can be documented in soft-tissue- and/or bone-window-level setting. Imaging planes are usually axial, coronal or sagittal depending on the pathology. MRI has the advantage of higher soft tissue contrast and the possibility of using different sequences. Depending on the pathology, e.g. fat-suppressed T2-weighted, diffusion-weighted, T1-weighted sequences before and after the i.v. use of gadolinium and T1-weighted contrast-enhanced sequences with fat suppression are used. The imaging planes may be axial, coronal or sagittal. In this refresher course, the normal anatomy of the jaw, variants mimicking osteolytic or osteoblastic lesions, and cystic and tumorous pathologies of the jaws will be shown, and the imaging characteristics will be explained.

Learning Objectives:

1. To become familiar with the anatomy of the jaw.
2. To learn which imaging technique to use.
3. To understand the typical imaging appearance of jaw lesions.

A-015 09:30

C. Differential diagnoses of soft tissue masses

D. [Farina](mailto:nappaje@yahoo.it); Brescia/IT (nappaje@yahoo.it)

Soft tissue masses of the supra and infrahyoid neck are a rather heterogeneous group of tumours, classified by WHO in nine categories, based on their histologic differentiation: adipocytic, fibroblastic or myofibroblastic, fibrohistiocytic, smooth muscle, skeletal muscle, vascular, pericytic, and chondro-osseous tumours, and tumours of uncertain differentiation. Based on their clinical behavior and history such tumours may be described as benign, malignant or intermediate, the latter further subclassified as locally invasive or metastasising at distant sites. US is generally the first imaging step in infrahyoid neck lesions; MDCT or MRI are mandatory in suprahyoid masses, but are also needed to better define the deep extent and anatomic relationships of infrahyoid tumours. In many cases, imaging findings are overlapping and insufficient for tumour characterisation; nonetheless, some specific clues may orient the differential diagnosis. Site of origin of the lesion is probably the first brick in the wall; therefore, knowledge of the space-based neck anatomy is essential prerequisite. Patient's age, size and number of lesions, presence and pattern of calcifications are useful additional details. Some specific density or signal intensity patterns may cut the list of differentials, whereas the potential role of the additional information provided by DWI-MRI or dual-energy CT is far from being fully elucidated. However, it is clearly assumed that imaging diagnosis does not replace pathologic assessment, which in a significant number of cases can be accurately obtained with FNA.

Learning Objectives:

1. To become familiar with the anatomy.
2. To learn which imaging technique to use.
3. To understand the typical imaging appearance of soft tissue masses.

08:30 - 10:00

Room E1

Special Focus Session

SF 1

Hepatocellular carcinoma: diagnosis, staging and current guidelines

A-016 08:30

Chairperson's introduction

G. [Branca](#); Palermo/IT (gbranca@yahoo.com)

Hepatocellular carcinoma (HCC) is the second leading cause of cancer death worldwide. In this session, the rationale behind the need for screening for HCC will be discussed, and the geographic differences in screening programs will be highlighted. The benefits of using LI-RADS terminology, interpretation, and reporting for both clinical care and research will be presented. Typical and atypical appearance of HCC will be shown, along with common mimickers and useful tips of differentiation of focal hepatic nodules in cirrhotic liver. Finally, the speakers will be exposed to challenging cases in the form of unknown, will share their reasoning with each other, and engage in discussions with the chairperson and the audience.

Session Objectives:

1. To become familiar with the international guidelines for HCC screening.
2. To understand why a standardised report facilitates patient management.
3. To learn about the key concepts of diagnosis of typical and atypical HCC with CT and MRI.

Author Disclosure:

G. [Branca](#): Speaker; Bayer, Guerbet.

A-017 08:35

Screening for HCC, American, Asian and European guidelines: why are they different?

V. [Vilgrain](#); Clichy/FR (valerie.vilgrain@aphp.fr)

Hepatocellular carcinoma (HCC) is the most common type of liver cancer, accounting for 80-90% of all cases of liver cancer. It is the fifth most common cancer and the third leading cause of cancer-related deaths around the world. As HCC occurs in 90% of the cases in patients with chronic liver disease, screening is indicated in those patients having compensated cirrhosis. Several guidelines have been implemented to help the practitioner to manage the patients during the screening, when a nodule is detected and to decide the optimal treatment in patients with HCC. Among the HCC guidelines which are the most used: AASLD, EASL, Japanese, Korean, and Asia-Pacific ones, there are common features. All agree : (i) on the noninvasive diagnosis of HCC using contrast-enhanced CT or MR imaging with two hallmarks: hypervascularisation on arterial-phase and wash-out on portal and/or delayed phase in lesions larger than one centimeter; (ii) on the role of liver biopsy when diagnosis cannot be achieved with imaging. Yet they differ in many other issues: stratification according to lesion size, first-line imaging modality, role of hepatobiliary MR contrast agents, and role of contrast-enhanced ultrasound. These differences are explained by the different prevalence of HCC worldwide and the different goals of diagnostic performance (high specificity or high sensitivity).

Learning Objectives:

1. To be aware of the different guidelines in HCC screening.
2. To know the most striking differences.
3. To understand the consequences in patient management.

A-018 08:58

Diagnosis of HCC, LI-RADS 2017: why we need it?

C.B. [Sirlin](#); San Diego, CA/US (csirlin@ucsd.edu)

LI-RADS is a comprehensive system for imaging HCC in adults with cirrhosis or other risk factors for HCC. It provides standardized terminology with precise definitions and illustrations for screening and surveillance using US, diagnosis and staging using CT, MRI, and CEUS, and treatment response assessment using CT and MRI. It addresses the entire spectrum of lesions and pseudo lesions encountered in the cirrhotic liver as well as the full range of malignant neoplasms associated with chronic liver disease. This lecture will review LI-RADS terminology, interpretation, and reporting and explain why standardization is needed for clinical care, research, and education.

Learning Objectives:

1. To understand the need for standardised terminology, interpretation, and reporting for clinical care.
2. To understand the need for standardised terminology, interpretation, and

reporting for research.

3. To become familiar with LI-RADS terminology, interpretation, and reporting.

Author Disclosure:

C.B. [Sirlin](#): Advisory Board; Bayer. Grant Recipient; Bayer, GE, Siemens, Philips, ACR.

A-019 09:21

Atypical appearance of HCC and mimics: how to solve the challenging cases

J.M. [Lee](#); Seoul/KR (jmsh@snu.ac.kr)

Hepatocellular carcinoma (HCC) poses a burden on global health. As HCC typically has a poor prognosis with a 5-year survival rate of only 28.6%, it is of paramount importance to achieve the earliest possible diagnosis of HCC and to recommend the most up-to-date optimal treatment strategy in order to increase the survival rate of patients who develop this disease. HCC is commonly diagnosed using dynamic CT and/or dynamic MRI without histological confirmation, on the basis of a characteristic arterial enhancement and portal venous or delayed phase washout. Indeed, the noninvasive diagnosis of HCC in high-risk patients by typical imaging findings alone is widely adopted in major practice guidelines for HCC. HCC usually presents with typical imaging characteristics but at times can present with a wide spectrum of atypical appearances. Familiarity with unusual presentations and their imaging findings is critical to ensuring prompt, accurate diagnosis and treatment. Moreover, while imaging techniques have markedly improved in detecting small liver lesions, they often detect incidental benign liver lesions and non-hepatocellular malignancy that can be misdiagnosed as HCC. The common mimickers of HCC in the cirrhotic liver include nontumorous arterioportal shunts, rapidly enhancing hemangiomas, intrahepatic mass-forming type cholangiocarcinoma (CC), angiomyolipomas, focal inflammatory liver lesions and focal nodular hyperplasia-like nodules. Among them, it is important to recognize the suggestive imaging findings for intrahepatic CC as the management of CC is largely different from that of HCC. Recognition of the typical imaging findings of common HCC mimickers can reduce false-positive HCC diagnosis.

Learning Objectives:

1. To demonstrate imaging spectrum of hepatocellular carcinoma including typical and atypical appearance.
2. To illustrate common mimickers of hepatocellular carcinoma in cirrhotic liver.
3. To provide useful tips of differentiation of focal hepatic nodules in cirrhotic liver.

Author Disclosure:

J.M. [Lee](#): Grant Recipient; Bayer, Guerbet, Philips, Samsung Medison, GE Healthcare, Starmed, RF medical, Acuzen, Toshiba. Research/Grant Support; Siemens, GE Healthcare, Philips, Samsung Medison, Toshiba. Speaker; Bayer, GE Healthcare, Siemens, Philips, Samsung Medison, Guerbet.

09:44

Panel discussion: At the plateau of the learning curve: how do experts reason?

Postgraduate Educational Programme

08:30 - 10:00

Room E2

Neuro

RC 111

The degenerative cervical spine

Moderator:

A. Cianfoni; Lugano/CH

A-020 08:30

A. Degenerative uncovertebral and facet disease

J. Van Goethem; Antwerp/BE (johan.vangoethem@uantwerpen.be)

Neck pain is a common problem with many possible causes. The facet joint and the uncovertebral joint are frequently involved in degenerative cervical spine disease. It is important to learn how to differentiate normal and asymptomatic changes that occur with age from abnormal findings that are causing neck and/or arm pain. I will demonstrate the use of plain film, CT, SPECT, and MRI in diagnosing an offending uncovertebral or facet joint. Many of these offending joints can be targeted specifically, leading to easy and fast pain reduction in many patients with aspecific neck pain.

Learning Objectives:

1. To learn about the physiological and pathophysiological degeneration of the cervical spine.
2. To understand the role of imaging in the diagnosis and clinical decision making in the degenerative cervical spine.
3. To appreciate the clinical relevance of imaging findings in the degenerative cervical spine.

A-021 09:00

B. Cervical spinal stenosis and cervical spondylotic myelopathy

A.S. Gersing; Munich/DE (alexandra.gersing@ucsf.edu)

Degenerative changes of the cervical spine occur during the aging process or are caused by segmental mechanical overload. Among the degenerative processes leading to spinal stenosis are marginal osteophytes of the vertebral bodies and joints, intervertebral disc degeneration with herniation and hypertrophy of the ligaments. CT, CT-myelography, and MR imaging are essential in assessing the extent and severity of spinal canal stenosis, especially with a view to guiding conservative or surgical treatment. Next to the assessment of the osseous and soft tissue structures of the vertebral column as well as spinal canal stenoses, T2-weighted MRI imaging is crucial for the assessment of signal changes within the myelon. The differentiation between signs of an acute myelopathy and myelomalacia, caused by an irreversible damage of the spinal cord, is essential to select the appropriate treatment option. Moreover, patients present with a broad spectrum of clinical symptoms ranging from neck pain to spastic paraparesis; therefore, it is crucial to put imaging findings in context with clinical symptoms to assess the potential benefit of different conservative and surgical treatment options.

Learning Objectives:

1. To learn about the pathophysiology and imaging findings in spinal stenosis and cervical spondylotic myelopathy.
2. To understand the relation between imaging findings and clinical presentation.
3. To appreciate the importance of imaging findings and the clinical presentation with respect to possible treatment options.

A-022 09:30

C. The postoperative cervical spine

I. Herrera; Madrid/ES (isabel.herherrer@gmail.com)

Cervical spine surgery is common, so it is important for radiologists to know what the normal imaging findings are to avoid pitfalls. This is not easy as there are substantial imaging overlaps between normal early postoperative findings and surgical complications. Because there are a vast variety of surgical approaches and hardware that can be applied to the spine, it is a challenge for the radiologists to know their anatomical implications and possible complications. The use of a particular imaging technique is dictated by multiple factors including the underlying pathology, surgical approach, device or instrumentation used, and suspected complications. The postoperative imaging should be able to assess progression of osseous fusion, confirm correct positioning and integrity of instrumentation, and detect suspected complications such as new disease or disease progression. Radiographs are most commonly used for assessment of fusion. CT is the modality of choice for the evaluation of graft position, hardware, bone integrity, and fractures. It also provides imaging of bone detail to accurately assess the degree of osseous fusion. MRI is the best option for evaluation of endplates, paraspinous soft

tissues, epidural spaces, and intrathecal structures, making it useful for detecting and monitoring infection or postoperative collections.

Learning Objectives:

1. To learn about the imaging findings and pitfalls of postoperative cervical spine imaging.
2. To understand the heterogeneity of imaging findings and their clinical relevance.
3. To appreciate the importance of standardised imaging, interpretation and reporting of postoperative imaging findings in the cervical spine.

08:30 - 10:00

Room F1

E³ - Rising Stars Programme: Basic Session

BS 1

Head and neck: inflammation, tumour or something else?

Moderator:

B. Verbist; Leiden/NL

A-023 08:30

Sinuses

R. Maroldi; Brescia/IT

"no abstract submitted"

Learning Objectives:

1. To discuss current imaging techniques for evaluation of normal anatomy.
2. To describe common imaging manifestations of inflammatory diseases.
3. To review tumour and tumour-like lesions.

A-024 08:53

Thyroid and parathyroid

H. Imhof; Vienna/AT

The thyroid gland consists of two lobes which are interconnected by the isthmus. The gland is directly attached to the larynx and trachea. The standard view is axial, visualising the main overlying (strap) muscles, the great vessels and lymphnodes and the oesophagus, as well. The main congenital abnormalities are thyroglossal duct cyst, lingual thyroid gland and aberrant thyroid tissue. Diagnosis of the thyroid masses/nodules is done by sonography using the TI-RADS classification and colour-doppler, lesion size suspicion grade, and fine needle aspiration biopsy (FNAB) reaching an accuracy of 94%. Very important is to differentiate malignancy (papillary / follicular / anaplastic / medullary carcinoma) and inflammatory changes (Hashimoto and DeQuervain thyroiditis). Standard imaging procedures for the parathyroid glands are sonography and Sesta-MIBI-SPECT reaching an accuracy of 97%. In unclear cases 4D-CT and/or MRI + contrast may be used additionally.

Learning Objectives:

1. To discuss current imaging techniques for evaluation of normal anatomy.
2. To describe common imaging manifestations of inflammatory diseases.
3. To identify and describe the imaging appearance of malignant pathologies.

A-025 09:15

Salivary glands

S.J. Golding; Oxford/UK (stephen.golding@nds.ox.ac.uk)

This presentation offers a clinically orientated approach to imaging salivary gland disease in which the alignment between findings and further management is defined. Salivary imaging has been changed dramatically by the development of cross-sectional imaging. Ultrasound, CT and MRI have consigned radiographs and sialograms to a subsidiary role. Scintigraphy offers the best measure of global salivary gland function, but currently is not widely used in practice. Today investigation is closely related to the underlying pathology of salivary disorders and to provide reliable guide to surgical or medical treatment. Masses are well detected by cross-sectional imaging, which provides accurate guidance on appropriate approaches for surgical management. Differential diagnosis cannot always be achieved, but this is rarely a clinical problem because biopsy or resection are usually indicated. Sialography remains a reliable method of showing calculi and ductal changes in sialadenitis, but cross-sectional techniques, especially ultrasound and MRI, have advantages in inflammatory disease and complete sensitivity in detecting ductal disease may not be necessary in practice because patients may be treated symptomatically. A strong case can be made for using MRI as a sole investigation as this has been shown to be sensitive to both surgical and medical conditions. On this basis, the radiologist may be well placed to offer a primary referral service with triage, directing clinical management of patients or

Wednesday

further referral on the basis of findings on MRI. Salivary interventional techniques have more recently extended the role of the radiologist.

Learning Objectives:

1. To discuss current imaging techniques for evaluation of normal anatomy.
2. To describe common imaging manifestations of inflammatory diseases.
3. To identify and describe the imaging appearance of malignant pathologies.

A-026 09:38

Lymph nodes

S.S. Özbek; Izmir/TR (sureyya.ozbek@ege.edu.tr)

In case of a visible or palpated neck mass, lymph node enlargement is routinely included in the differential diagnosis list. Medical imaging can be effectively used to distinguish other causes of cervical swelling, as well as characterizing enlarged lymph nodes. Although commonly used as a criterion, nodal size is not reliable in characterization. Imaging parameters including internal structure, vascularity pattern, degree of enhancement, and perinodal tissue changes may shed light on the etiology of any lymphadenopathy, which may be reactive hyperplasia, infection, inflammation or neoplastic infiltration. Characteristically, reactive hyperplastic lymph nodes have well-defined borders, reniform shape and central fatty hilum contiguous with adjacent cervical fat tissue. In children, and in most of the adult cases with a low risk of malignancy, ultrasound is the first choice of imaging modality owing to its radiation-free nature, and due to practical reasons. However, when further characterization of nodal abnormality or evaluation of sonographically inaccessible anatomic locations is required, use of other cross-sectional techniques, like CT and MRI are mandatory. They provide not only more detailed information including anatomic localization, size, number, internal structure, and enhancement characteristics of lymph nodes, but also important data about perinodal soft tissue and other associated pathologic processes in the region. Although the choice of imaging modalities to be used in the evaluation of cervical lymph nodes changes according to the means, experience, and preferences of institutions, the role of medical imaging remains pivotal and decisive in this common indication.

Learning Objectives:

1. To discuss current imaging techniques for evaluation of normal anatomy.
2. To describe the imaging features of infectious and inflammatory disorders.
3. To describe the imaging appearance of neoplastic disorders.

Author Disclosure:

S.S. Özbek: Other; Advisory Panelist -Siemens Healthineers Ultrasound Radiology.

08:30 - 10:00

Room F2

E³ - ECR Master Class (Oncologic Imaging)

E³ 126

Novelties in oncologic imaging

Moderator:

C.J. Zech; Basle/CH

A-027 08:30

A. Imaging and response assessment of immune-related therapies

P. Brader; Graz/AT (peter.brader@diagnostikum-graz.at)

The immune system is capable of preventing the development of tumour diseases and stimulation of cytotoxic T-lymphocytes can repress existing tumours. A new class of antibody-based medication, the immune checkpoint inhibitors, influences the activation of T-lymphocytes. Immune checkpoint inhibitors are active against a number of tumours. In some cases, such as malignant melanoma and non-small cell lung cancer, the response rates are impressive and exceed those achieved with conventional chemotherapies. Modern immunotherapies in oncology show tumour response patterns differing from conventional chemotherapies including initial pseudo-progression which can occur in up to 10% of cases depending on the immunomodulating drug and tumour entity. Response Evaluation Criteria in Solid Tumours (RECIST 1.1) represent the currently most used response criteria for conventional chemotherapy of solid tumours. However, atypical response patterns of immunotherapies are not correctly classified using RECIST 1.1 so that the effectiveness is also incorrectly interpreted. To correctly interpret these atypical response patterns, special Immune-Related Response Criteria in Solid Tumours (iRECIST) have been published. iRECIST was developed only for usage in trials testing modern immunotherapeutics. In contrast to RECIST 1.1, according to iRECIST an initially unconfirmed progressive disease (iUPD) requires confirmation (iCPD) in clinically stable patients by subsequent control imaging after 4-8 weeks. New lesions are separately assessed within iRECIST.

Learning Objectives:

1. To understand the basic principle of immune related therapies.
2. To learn how tumour morphology and functional parameters change with therapy.
3. To appreciate the existing evidence for immune therapy follow-up strategies.

A-028 09:00

B. Radiomics: the role of imaging

S. Rizzo; Milan/IT (stefania.rizzo@ieo.it)

Radiomics is an emerging translational field of research, aiming to extract data from clinical images, containing information that may reflect the underlying pathophysiology of tumoural tissue. The extracted information may be associated with clinical data, and can be used to assess prognosis and to support clinical decision. Specific softwares allow the extraction of radiomic features, representative of the entire tumors or defined subvolumes within tumors, from digital images (CT, MR, PET), and convert them into mineable high dimensional data for hypothesis generation, testing, or both. The steps necessary for a radiomic approach to digital radiological examinations include: acquisition of the images; identification of volumes of interest that may contain prognostic value; segmentation of volumes; extraction of radiomic features from the volume; clustering of the features; creation of a database; inclusion of the extracted data to develop models to predict outcomes, possibly in combination with demographic, clinical, comorbidity, or genomic data. Imaging is used in routine practice for oncological patients worldwide, at many stages of diagnosis and treatment. In the current era of targeted therapies, radiomics guarantees a nearly limitless supply of imaging biomarkers over time during and after therapy, to quantify and monitor phenotypic changes many times during treatment. The power of a predictive classifier model is dependent on the amount of data; hence, it is desirable that the radiomic studies will consider sharing of data between different centers, with the creation of databases including radiomics data and covariates, such as genomic profiles, histology, serum markers, patient histories, and biomarkers.

Learning Objectives:

1. To learn about the concept of radiomics and individualised medicine.
2. To learn how radiomics can be extracted from standard clinical examinations.
3. To appreciate the consequences of radiomics for radiologists in the future.

A-029 09:30

C. Imaging-guided liver interventions in oncology

B. Gebauer; Berlin/DE (bernhard.gebauer@charite.de)

Oncologic liver interventions play an important role in patients management, specially in HCC, colorectal cancer, and neuroendocrine tumors. Percutaneous, ablative techniques (thermal ablation (RFA, MWA, brachytherapy) and transarterial techniques (TACE, TAE, RE/SIRT) are available. Precise pre-interventional imaging is essential to select the correct patients for these techniques. In transarterial liver interventions enhanced intraprocedural imaging with ultrasound and cone-beam-CT increased technical opportunities for patients treatment and widened the opportunities for interventional oncology.

Learning Objectives:

1. To learn about new established treatment options in interventional oncology.
2. To understand the role of pre- and post-treatment imaging in increasing clinical outcome.
3. To appreciate potential future application of interventional oncology.

Author Disclosure:

B. Gebauer: Speaker; BARD, SIRTEx Medical, St. Jude Medical, COOK, AngioDynamics, Pharmcept, Roche, Merck, 3M, Siemens, Philips, IPSEN, Bayer, Pfizer. Other; ICON Bioscience, PAREXEL, BAYER.

Postgraduate Educational Programme

08:30 - 10:00

Room D

Musculoskeletal

RC 110

MRI of articular cartilage and bone: areas of imaging confusion and practical solutions

Moderator:

O. Papakonstantinou; Athens/GR

A-030 08:30

A. Bone oedema syndromes and avascular necrosis

B. [Vande Berg](mailto:bruno.vandenberg@uclouvain.be); Brussels/BE (bruno.vandenberg@uclouvain.be)

Bone marrow edema is a pattern of marrow alteration frequently observed at MRI. It is defined by the presence of an ill-delimited area of moderate and homogeneous decrease in signal intensity on SE T1 images that converts to high signal intensity on fat-saturated proton density or T2-weighted images. It is non-specific and may be associated with almost any abnormal marrow, bone or joint conditions. Epiphyseal bone marrow edema can be associated with self-limited spontaneously resolvable conditions (overuse, stress insufficiency fractures, transient osteoporosis), or with evolutive disorders including chondropathy or spontaneous osteonecrosis. The main task of the radiologist is to assess the cause for bone marrow edema and to highlight imaging features that contribute to a specific diagnosis and subsequently a prognosis (resolutive versus non-resolutive). The current lecture aims at emphasizing imaging features indicative of bone marrow edema to avoid confusion with systemic osteonecrosis. We will also highlight imaging features of prognostic significance that enable the clinician to tailor the treatment to the patient's condition.

Learning Objectives:

1. To understand the aetiologies of bone marrow oedema syndromes.
2. To learn about the imaging characteristics of avascular necrosis of bone.

A-031 09:00

B. Osteochondral injury, subchondral fractures and traumatic bone oedema: what is important and how do I describe it

F.W. [Roemer](mailto:frank.roemer@uk-erlangen.de); Erlangen/DE (frank.roemer@uk-erlangen.de)

Bone marrow contusions are frequently identified at magnetic resonance imaging after an injury to the musculoskeletal system. These osseous injuries may result from a direct blow to the bone, from compressive forces of adjacent bones impacting one another, or from traction forces that occur during an avulsion injury. Commonly these injuries resolve without long term sequelae. However, they may also involve the cartilaginous surface with or without an associated fracture line defining these as osteochondral injuries, which may have a different prognostic relevance. Subchondral fractures have been implicated in the genesis of some well-known destructive articular conditions whose cause was previously undetermined, such as rapidly progressive osteoarthritis of the hip or spontaneous osteonecrosis of the knee. Subchondral fractures may ultimately lead to bone collapse, secondary osteonecrosis, and severe articular damage. It should be suspected in the appropriate clinical setting, as in early stages it is usually indistinct on initial plain radiographs and magnetic resonance imaging is required for a definitive diagnosis. The fracture line usually appears as a band of low signal intensity in the subchondral bone plate, adjacent to the articular surface, most often surrounded by bone marrow edema. As these injuries may be occult on radiographs, the differentiation of bone contusions from osteochondral injuries or subchondral fractures is possible only with MRI including fat-suppressed and non-fat suppressed sequences. While purely subchondral lesion may have a good prognosis if diagnosed early, disruption of the articular surface may lead to early degenerative alterations including focal cartilage loss and other features of osteoarthritis.

Learning Objectives:

1. To understand the pathomechanisms of osteochondral injury and subchondral fractures.
2. To learn about the imaging techniques and prognostic values.

Author Disclosure:

F.W. Roemer: Shareholder; Boston Imaging Core Lab (BICL), LLC.

A-032 09:30

C. Rheumatoid arthritis

I. [Sudoł-Szopińska](mailto:sudolszopinska@gmail.com); Warsaw/PL (sudolszopinska@gmail.com)

Rheumatoid arthritis is the most common inflammatory rheumatic disease. The pathogenesis of RA is subject to ongoing discussion. The traditional concept of inflammatory pannus, in which fibroblast-like synoviocytes provoke cartilage and bone destruction through direct invasion and indirect triggering of catabolic cascades has been termed the outside-in hypothesis. There is also evidence supporting the inside-out hypothesis, in which joint inflammation and destruction originates from the bone marrow. Next to synovium and subchondral bone, another tissue involved in cartilage and bone damage in RA is extra- or intraarticular fat tissue which produces ca. 50 adipo(cyto)kines which may be involved in degradation of all components of the connective tissue, including cartilage. Finally, the hyaline cartilage autoantigens, activated by cartilage damage, may activate and maintain synovitis and lead to joint damage. In everyday practice, the clinical relevance of synovitis and bone marrow inflammation in terms of their role as an erosions precursors is known and ultrasound and MRI are used to detect synovitis, BME, inflammatory cysts, hyaline cartilage loss, and bone erosions. Less in known about inflammatory and destructive potential of intra- and extraarticular fat tissue which may also be evaluated in US and MRI. And only research centers use quantitative MR applications to cartilage to show glucosaminoglycans loss possibly preceding visible cartilage damage. In this presentation pathomechanisms that result in articular cartilage and bone damage in RA will be presented, including the clinical relevance of synovitis and BME in terms of their role as an erosion precursors, as well as the role of imaging techniques to detect early cartilage damage and bone erosions.

Learning Objectives:

1. To understand the pathomechanisms that result in articular cartilage and bone damage in rheumatoid arthritis, including the clinical relevance of synovitis and BME in terms of their role as an erosion precursor.
2. To learn about the role of imaging techniques to detect early cartilage damage and bone erosions.

08:30 - 10:00

Room G

Physics in Medical Imaging

RC 113

Single-dual-multi-energy CT

A-033 08:30

Chairperson's introduction

A. [Torresin](mailto:alberto.torresin@unimi.it); Milan/IT (alberto.torresin@unimi.it)

CT dual energy publications have heavily increased in the last years. The trend seems to be continuing since PubMed has found, from Jan 2015 until Nov 2017, around 1000 peer review abstracts. Publications on phantom simulation (for algorithm verification) and patient's study regarding the most important area of diagnostic have been published sourcing from CT imaging and Hybrid Imaging (PET CT for examples). Bone and high density tissue evaluation are one of the most important application with high density artifact reduction, materials analysis based on attenuation spectra observed, tumor analysis and no contrast imaging application. A lot of technological solutions have been introduced during the last years, but the technique has not yet seen widespread implementation in routine protocols. During the course, the basic principle of dual energy and some new trend of spectral imaging will be introduced both technologically and clinically. To compare image quality and radiation dose of single-energy CT and dual energy, it is very important to quantify the patient risk with the introduction of these new technologies. Quantitative evaluation studies (retrospective and prospective) will be more and more important. During the refresh-course, the basic principle of patient dose in spectral imaging will be presented and attention is paid to the quantitative method of image analysis.

Session Objectives:

1. To learn about the basics of dual-energy CT (DECT).
2. To understand today's photon counting detector technology.
3. To learn how DECT is applied in clinical practice.

A-034 08:35

A. Basics of dual- and multi-energy CT

K. [Perisinakis](mailto:Kostas.Perisinakis@med.uoc.gr); Iraklion/GR (Kostas.Perisinakis@med.uoc.gr)

Dual energy CT (DECT) refers to the use of two CT beams of different photon energy spectrum to collect two separate sets of projection data and provide two corresponding image datasets of the same anatomical body region to

Wednesday

Postgraduate Educational Programme

exploit spectral information regarding attenuation ability of tissues for diagnostic purposes. Despite conceived during '70s soon after the first clinical CT, the clinical endorsement and widespread application of DECT was initiated with the advent of dual-source CT systems in 2006. Providing the potential to improve CT image quality through artifact suppression and extracting valuable information regarding tissue composition and function, DECT is the new exciting field for the radiology community and the main driving force for CT technology evolution over the last decade. Currently, all CT vendors put considerable efforts in developing CT systems capable of performing DECT studies, while novel clinical applications of DECT are continuously introduced. However, comprehension of the basic physics of DECT and familiarisation with the advanced technological features of modern DECT scanners is prerequisite to fully exploit the advantages of DECT imaging.

Learning Objectives:

1. To learn about the underlying physics and today's technology.
2. To see potential advantages compared to single-energy CT.
3. To appreciate the rationale behind clinical applications.

A-035 08:58

B. Photon counting detectors in diagnostic CT

A. Altman; Haifa/IL (ami.altman@philips.com)

Recent years' advances in room-temperature semi-conductors, especially CZT and CdTe, have enabled the transformation from energy-integrated (EI) detectors to photon-counting (PC) detectors in diagnostic CT, enhancing significantly its clinical benefits. The higher signal per x-ray photon (X10) and the short rise time of ~10 nanoseconds enable spectral analysis of each counted photon, use of adjustable multi-energy bins, K-edge imaging, and increased CNR through different energy weightings, while reducing the dose significantly. The continuous sensitivity of a pixelated sensor and the elimination of electronic noise through a threshold above it enable using much smaller detection pixels than in a conventional EI CT and contribute to further lowering of the dose. Consequently, spatial resolution is improved compared to EI CT (> 20 lp/cm). Reduction of the detection pixel size is essential also for lowering photon rates per pixel to avoid pile-up effects. However, charge sharing and K α escapes of Te and Cd cause severe distortions to the recorded x-ray spectrum. A forward model of the detector response is used to address it and restore spectral capability, using a projection domain material decomposition. It will be shown that this can be accomplished as long as the peak-to-tail ratio is not too large, namely, detection pixel of about 0.5 mm. HW and SW methods of pile-up corrections will be shown too. Phantom and pre-clinical verifications on the PHILIPS Spectral Photon-Counting CT (SPCCT) in Lyon demonstrate the capability of such a system achieving spectral results superior to dual-energy CT, and the advantage of dual-contrast injection in a single scan.

Learning Objectives:

1. To learn about the underlying physics and technological solutions.
2. To understand the potential advantages compared to dual-energy CT.
3. To appreciate how mature today's photon counting technology is.

Author Disclosure:

A. Altman: Employee; PHILIPS Healthcare.

A-036 09:21

C. Clinical need of multi-energy CT

S.T. Schindera; Aarau/CH (sschindera@aol.com)

During the last decade, dual-energy CT has gained increasing attention in clinical routine due to improved diagnostic performance from the quantitative analysis of different tissue composition. Various clinical indications for a dual-energy CT scan will be reviewed with a focus on the added value. Potential future opportunities of dual-energy CT, which still are viewed as research tools, will be also discussed.

Learning Objectives:

1. To learn about medical applications and potential benefits.
2. To understand which single-energy applications could be replaced by dual-energy applications, and why.
3. To learn which additional multi-energy CT applications could be developed.

09:44

Panel discussion: Are there sufficient benefits of this technique?

08:30 - 10:00

Room K

Radiographers

RC 114

Forensic imaging

A-037 08:30

Chairpersons' introduction (part 1)

J. McNulty; Dublin/IE (jonathan.mcnulty@ucd.ie)

Radiographers play an essential role in the provision of high quality forensic imaging services. This is recognised in many countries and forensic imaging has been recognised by the European federation of radiographer societies (EFRS) as one of nine specialist areas of advanced practice for radiographers. While the concept of optimisation is at the heart of the profession, there remains room for improvement in further advancing optimisation for forensic applications. As with all specialist areas, or areas of advanced practice, appropriate education and training, and continuous professional development are fundamental. Through international organisations such as the international society for forensic radiology and imaging (ISFRI) and the international association of forensic radiographers (IAFR), together with national organisations and groups, forensic imaging continues to move in the right direction.

Session Objectives:

1. To provide insights into the role of imaging, and radiographers, in forensic imaging and mass fatality incidents.
2. To appreciate the key aspects of a quality forensic imaging service.
3. To understand the challenges associated with forensic imaging.

A-038 08:30

Chairpersons' introduction (part 2)

R.R. van Rijn; Amsterdam/NL (r.r.vanrijn@amc.uva.nl)

Forensic radiology and imaging is a relatively new field within the realm of forensic science and medicine. This introduction provides a short overview of the scientific challenges facing the forensic radiological technician radiologist.

Session Objectives:

1. To provide insights into the role of imaging, and radiographers, in forensic imaging and mass fatality incidents.
2. To appreciate the key aspects of a quality forensic imaging service.
3. To understand the challenges associated with forensic imaging.

Author Disclosure:

R.R. van Rijn: Author; Author books published by Thieme and Springer.

A-039 08:35

A. Disaster victim identification

J. Kroll; Maastricht/NL (j.kroll@mumc.nl)

Forensic radiology, mainly as a tool for forensic odontology, has long been an essential discipline in the post-mortem identification of human remains. Because forensic radiology is a rapidly developing field due to the fast technical developments of CT scanners, the possible applications are increasing. A whole body CT contains a wealth of identification information that can be used in an identification process. This presentation will highlight the contribution of forensic radiology within a DVI process, discussing its applications, equipment, advantages and positioning within a DVI-process. It will also discuss future developments, opportunities and challenges which futures DVI processes will face.

Learning Objectives:

1. To appreciate the role of forensic radiology in a disaster victim identification process.
2. To learn about the methods using forensic radiology in a disaster victim identification process.
3. To discuss added value of forensic radiology in a disaster victim identification process.

A-040 08:58

B. The role of CT angiography in forensic imaging

A. Dominguez; Lausanne/CH (Alexandre.DOMINGUEZ@hesav.ch)

Multiphase post-mortem CT angiography (MPMCTA) has been set up almost ten years ago at the University Center of Legal Medicine of Lausanne-Geneva, Switzerland (CURML). A research project allowed the creation of the Virtangio® device: a specific injection system for post-mortem angiography. Nowadays, this setting is regularly used as almost a third of the autopsies

Postgraduate Educational Programme

benefit of this technique at the CURML. The indication to perform the MPMCTA is the suspicion of vascular lesions due to natural or traumatic origin, such as traffic accidents, homicides (stab wounds, ballistic), medical malpractice (especially in a post-surgery context), or unexpected adults death. This procedure allows examining vascular anatomy: analyses of the vascular lumen with potential stenosis or dilatation; analyse of the vascular walls with potential dissections or ruptures; characterization of the nature of an arterial and/or venous leakage. It also permits to obtain morphological information of the organs parenchyma. At the CURML, the MPMCTA is fully executed by the forensic radiographer. He is in charge of preparing the body, collecting samples before the angiography, denudating the arterial and venous vessels for the injections and proceeding the CT-scan acquisition. The duration of this technique lasting about 30 minutes won't disturb the investigation work flow. The MPMCTA is then interpreted by a team involving forensic pathologist and a radiologist. Limitations and pitfalls of this technique should be known to identify artefacts and pitfalls.

Learning Objectives:

1. To learn about the development of multiphase post-mortem CT angiography (MPMCTA).
2. To appreciate the benefits and limitations of MPMCTA examinations.
3. To understand the role of the radiographer in the MPMCTA.

A-041 09:21

C. The importance of the radiographer's role in forensic imaging

A.L. Brookes; London/UK (amyleebrookes@outlook.com)

Forensic imaging is an ever-expanding sub-speciality of both radiology and forensic medicine. The overall role of forensic imaging is to obtain evidence and answer legal questions associated with either living or deceased individuals. Forensic imaging can be utilised in a variety of cases including suspected physical abuse, medical negligence, drug trafficking and mass fatalities incidents. In forensic pathology, forensic imaging has established a role in the assessment of identification and establishment of cause of death, particularly in cases of severely decomposed or burnt remains. The role of radiographers within forensic imaging contrasts significantly with that of the routine clinical environment. Those individuals involved in forensic imaging must understand and be aware of the medico-legal features and professional guidelines that impact their practice.

Learning Objectives:

1. To appreciate the role of the radiographer in forensic imaging.
2. To learn about the importance of continuity of evidence and record keeping.
3. To discuss the various situations a radiographer can be exposed to during forensic imaging.

09:44

Panel discussion: Developing a service/getting involved in forensic imaging

08:30 - 10:00

Room M 1

Vascular

RC 115

Peripheral vascular malformations: what every radiologist should know

A-042 08:30

Chairperson's introduction

J.A. Reekers; Amsterdam/NL (j.a.reekers@amc.uva.nl)

Vascular malformations are rare and therefore the diagnosis is often unknown to a general radiologist. It is important to differentiate a congenital vascular malformation from an infantile hemangioma. Congenital vascular malformations have a specific anamnesis, which is often the major clue to the final diagnosis. There are 3 main types of congenital vascular malformations. Arterial (high flow with direct fistula), venous (low flow) and lymphatic. There are some related vascular tumours like capillary malformation and port-wine stains. There are several syndromes in relation to vascular malformations. The most known is Klippel-Trenaunay-Weber syndrome. For a general radiologists it is important to recognise a vascular malformation. Treatment and further work-up diagnosis should only be undertaken in centres of expertise. Only malformations that give complaints like pain, bleeding or cosmetic issues should be treated. Both embolisation (for high flow) and local sclerotherapy (for low flow) are used to treat vascular malformations.

Session Objectives:

1. To review classification and description.
2. To identify the role of imaging modalities.
3. To understand the role of interventional radiologist in management and treatment.

A-043 08:35

A. The diagnostic assessment

M. Köcher; Olomouc/CZ (martin.kocher@seznam.cz)

Vascular malformations are categorised into the low-flow malformations and high-flow malformations. From imaging methods is expected to distinguish between the low-flow lesions and high-flow lesions, localisation, volume and range of lesion and relationship to the surrounding tissues and organs. Color doppler ultrasonography (DUS) can offer good differentiation between high-flow and low-flow lesions. Magnetic resonance (MR) offers good differentiation between high-flow and low-flow lesions also, and moreover good evaluation of volume and extent of lesion, good interpretation of anatomical relationship to the surrounding tissues and organs. On DUS the low-flow malformations are demonstrated as hypoechogenic or heterogeneous lesions with minimal flow inside, flow during augmentation and normal arterial flow volumes and normal high arterial resistance flow. The high-flow malformations are heterogeneous lesions with tortuous feeding arteries, high velocity and low-resistance flow in feeding arteries, multiple arteriovenous shunts and pulsatile flow in draining veins. On MR the low-flow malformations typically have low signal intensity in T1 weighted images in abnormal vascular structures and high signal intensity in T2 weighted images, whereas the high-flow lesions usually demonstrate a signal voids in abnormal vascular structures on most sequences. At follow-up DUS demonstrates thrombosis and fibrosis of the low-flow lesion. In the high-flow lesion the waveform will be normalised and the resistive indexes and the flow volumes will become normalised as well. MR demonstrates thrombosis and fibrosis of low-flow malformation by the loss of high signal in T2 weighted images and loss of signal voids in high-flow lesions.

Learning Objectives:

1. To learn about classification and terminology.
2. To understand the role of US, CT and MRA in diagnostic assessment.
3. To learn the optimal imaging algorithm for diagnosis and follow-up.

A-044 08:58

B. Percutaneous or endovascular treatment: when and how?

B. Peynircioglu; Ankara/TR (borapeynir@gmail.com)

Vascular anomalies, are divided in two different categories which carry different prognosis and management: "Vascular tumors" and "Vascular malformations" (VM). Their precise identification is crucial and involves a good knowledge of the biological classification published by Mulliken and Glowacki and that has recently been updated by the International Society for the Study of Vascular Anomalies (ISSVA). Vascular malformations are always congenital and grow with the child. They can involve type of vessels solely or combined with others. A rheologic differentiation between low and high flow malformations is essential to characterise the seriousness of the lesion. Interventional radiology (IR) plays major role in both curative and palliative treatments of these VM. Once understanding the nature and high/low flow characteristics of VM, transcatheter/endovascular (transarterial or transvenous) or direct percutaneous puncture under imaging guidance are the 2 main techniques for treating these lesions. Depending on the type, nature, location and surroundings of the VM, one should decide the best strategy for treatment. Another key point is to decide whether to use embolisation or sclerotherapy. Again, the type, location of the VM is vital and the patient based decision is to be made carefully by a multidisciplinary team. Operator's experience is of most importance in determining all of the above variables, together with the local circumstances. There are many different types of embolic and sclerotherapy agents available around the world.

Learning Objectives:

1. To recognise the indications and the real need for treatment.
2. To learn about technical approach and how to plan the intervention.
3. To understand possible limitations and the final result prediction.

A-045 09:21

C. Paediatric vascular malformations: diagnosis and treatment

A. Barnacle; London/UK (Alex.Barnacle@gosh.nhs.uk)

Haemangiomas are by far the most common type of vascular anomaly that present in childhood. Haemangiomas are benign vascular tumours; several subtypes exist. Infantile haemangiomas are the commonest subtype and the vast majority of these require no intervention at all, because they involute spontaneously over the first few years of childhood. These well defined vascular masses have a highly characteristic growth pattern and typical

imaging features. They can be distinguished from the rarer congenital haemangiomas by their clinical presentation. Rarer benign childhood vascular tumours include kaposiform haemangioendotheliomas (KHEs) and tufted angiomas, both of which are associated with thrombocytopaenia and have characteristic imaging features to distinguish them from haemangiomas. Unlike vascular tumours, vascular malformations are present from birth and grow slowly in childhood. Lymphatic malformations (LMs) tend to present earlier and are encountered much more commonly in children than adults. Macrocystic LMs consist of thin-walled cysts containing lymph or clot and microcystic lesions appear more solid. Ultrasound is often sufficient to make a diagnosis but MRI may be required to determine the extent of deep-seated lesions. Small lesions may not require treatment; larger lesions are usually treated with percutaneous image-guided sclerotherapy, though surgery has an important adjunctive role in debulking larger lesions. Finally, some children present with complex overgrowth, often of just one limb, which is associated with a vascular malformation. These patients require expert input from a multidisciplinary team and imaging is key.

Learning Objectives:

1. To understand the specifics of vascular malformations in children.
2. To recognise when to observe and when to intervene.
3. To learn about interventional techniques used and results of treatment.

09:44

Panel discussion: How could we improve diagnosis and optimise the results of our interventions?

08:30 - 10:00

Room M 2

Computer Applications

RC 105

Everything you need to know about 3D post-processing

A-046 08:30

Chairperson's introduction

E. Sorantin; Graz/AT (erich.sorantin@medunigraz.at)

Progress in imaging technology equipment enables scanning patients in high geometrical and temporal resolution as well as in multidimensional space (e.g. 4D). The amount of resulting data cannot be read any more in 2D as done in the last millennium. Furthermore, advances in computational power enable the use of sophisticated processing algorithms in real time. Thus reading in 2D, as done in the previous millennium, will be gradually replaced by volumetric reading as well as extracting diagnostic information from parametric images. Moreover, for personalized medicine, radiology has to deliver more detailed information, especially to measure tumour volumes or characterize contrast uptake on perfusion imaging. To get familiar with those now really emerging techniques, three well-known speakers will cover essential subtopics and provide a road map on how to migrate from the reading style in the last millennium to that in the current millennium.

Session Objectives:

1. To learn about the state of the art in 3D post-processing.
2. To understand how 3D post-processing can most optimally be used in daily clinical practice.
3. To appreciate how automated 3D post-processing and quantification will lead to increased use of 3D visualisations for diagnostics and therapy planning, over 2D viewing.

Author Disclosure:

E. Sorantin: Advisory Board; ESPR Representative at WHO. Author; Scientific papers and book contributions. Consultant; Ulrich Medical Inc. Germany.

A-047 08:35

A. 3D post-processing in 2018

A. Alberich-Bayarri; Valencia/ES (alberich_ang@gva.es)

One of the most important developments in radiological interpretation is the need for the incorporation of advanced tools to assist the specialist in the study evaluation. Automated segmentation of structures based on convolutional neural networks (CNN) in the frame of deep learning would allow to significantly increase the efficiency of the study evaluation by the radiologist. Although the detailed segmentation of organs is still intricate in the field of abdomen and modalities like MR, current technology allows for the automated detection of the organs' location and identification of most of the tissue using bounding boxes. These applications may be used today in clinics for the

automated assessment of tissue properties. A clear example is the automated detection and identification of vertebrae centroids, which allows for the acceleration of the radiologist reading process in spine CT examinations while it also allows for the automated calculation of trabecular bone quality properties in each identified vertebrae, therefore providing a high value to perform osteoporosis population studies without the need for a user interaction. These algorithms have been recently labelled as zero-click solutions and will provide a paradigm shift in 3D post-processing for radiologists, having the results of the 3D assessment already generated in their PACS even before starting review of the study.

Learning Objectives:

1. To learn about recent advances in 3D post-processing techniques.
2. To understand how these techniques can be used in clinical practice now.
3. To learn new tips and tricks to use in your daily practice.

Author Disclosure:

A. Alberich-Bayarri: CEO; QUIBIM SL. Founder; QUIBIM SL.

A-048 08:58

B. Making better use of your 3D package: tips and tricks

P.M.A. van Ooijen; Groningen/NL (p.m.a.van.ooijen@umcg.nl)

Advanced visualization, simulation and planning software is increasingly used in clinical practice providing a shift from 2D to 3D visualization, processing and interpretation. With this ongoing trend the radiological profession should not only focus on the diagnosis to be made, but also on the utilization of our imaging data in patient simulation, planning, and treatment. Current functionality moves in this direction with providing extensive possibilities for support of surgical interventions and treatment planning in 3D including the advent of Virtual and Augmented Reality. With this 3D is also moving into the operating theater. Although these new possibilities are interesting and exciting one should be very aware of the pitfalls that come with 3D visualization and processing of data. This not only includes the technical but also the procedural pitfalls where image acquisition optimal for diagnosis is not always optimized for the intended use by the referring physician. To adequately use the new techniques and to provide optimal support from radiology to the referring physicians training is required and dedicated staff should be involved in this process.

Learning Objectives:

1. To learn about the functionality of state-of-the-art 3D packages.
2. To understand the pitfalls in use of 3D post-processing.
3. To appreciate the need for training in 3D post-processing techniques.

A-049 09:21

C. Interpretation of 3D processing results: from image to volume reading

T. Frauenfelder; Zurich/CH (thomas.frauenfelder@usz.ch)

The widespread introduction of multidetector computed tomography (MDCT) has revolutionized the field of computed tomography (CT). This revolution can be attributed to three primary properties of MDCT: its ability to produce a vast quantity of volumetric data in a reduced amount of time, the high resolution, and the ability to create isotropic voxel data and, consequently, reliable multiplanar and three-dimensional (3D) reconstructions. Diagnostic approaches that rely solely on axial reconstructions of MDCT data are often insufficient for formulating an accurate diagnosis or for documentation of clinical cases. Specialized 3D reconstruction techniques permit the visualization of anatomical details, which would be difficult to evaluate using axial reconstructions alone. Such details may require the use of oblique or curved reconstructions, or more complex methods, such as maximum intensity projection (MIP), minimum intensity projection (MinIP), surface-shaded volume rendering (SS-VRT), and virtual endoscopy. For example, small pulmonary nodules can only be rapidly and reliably identified through the use of MIP Slab slices. The current trend is to merge the routine diagnostic console and 3D reconstruction workstation. The integration of 3D reconstruction utilities into the standard bi-dimensional diagnostic software has increased the number of operations possible on each exam data, greatly increasing the perceived complexity of CT diagnosis. Although many of us believe that the use of 3D reconstructions greatly increases total exam evaluation time, there are reports show how using 3D reconstruction techniques for examining volumetric data are effective and also improve the speed of interpretation, recognition, and description of specific clinical conditions. Many of these reconstruction techniques are of particular importance for the analysis of subspecialty exams, as for example the 3D depiction and quantification of lung emphysema.

Learning Objectives:

1. To learn about different developments in creating 3D anatomical and functional models for diagnostic and therapy planning purposes.
2. To understand the pros and cons of such technologies.
3. To appreciate that automated 3D image analysis will lead to new ways in which diagnosis and therapy planning will be performed.

Author Disclosure:

T. Fraunfelder: Other; Bayer.

09:44

Panel discussion: Will we still look at 2D images in 10 years' time?
Image interpretation of 3D results: from image reading to volume reading.

08:30 - 10:00

Room M 3

Interventional Radiology

RC 109

Portal hypertension and interventional radiology (IR)

A-050 08:30

Chairperson's introduction

A. Msida/MT (adrianmizzi@yahoo.co.uk)

Portal hypertension is characterized by high pressure in the hepatic portal venous circulation. Clinically significant portal hypertension is diagnosed when the hepatic venous pressure gradient (HVPG) exceeds 10 mmHg. It may be caused by hepatic, pre-hepatic or post-hepatic aetiologies. Diagnostic radiology plays a crucial role in establishing the aetiology, identifying complications and in planning management. Interventional radiology (IR) plays a major role in both the diagnostic and therapeutic management of portal hypertension. HVPG measurement is a minimally invasive IR technique that establishes the diagnosis of portal hypertension. Different therapeutic IR procedures may be used in different clinical scenarios and have replaced more invasive open surgical techniques. The hepatobiliary radiologist is a key player in the multidisciplinary team caring for patients with portal hypertension. The imaging findings of portal hypertension and the different IR procedures used in this condition will be discussed during this session. Emphasis will be made on the practical aspects of interventional radiology procedures, including transjugular intrahepatic portosystemic shunt (TIPS), variceal embolization, splenic artery embolization and balloon-occluded retrograde transvenous obliteration (BRTO) - including their indications, methodology, complications, and clinical outcomes.

Session Objectives:

1. To appreciate the role of multidisciplinary treatment of portal hypertension.
2. To learn about imaging and intervention in portal hypertension.
3. To discuss outcomes of interventions in portal hypertension.

A-051 08:35

A. Imaging of portal hypertension

I. Bargellini; Pisa/IT (irenebargellini@hotmail.com)

Portal hypertension (PH) represents a fearful complication of several diseases (most frequently liver cirrhosis), associated with high morbidity and mortality. Definitive diagnosis of PH is based on the measurement of hepatic venous pressure gradient (HVPG). PH is diagnosed by measuring a HVPG higher than 5 mmHg, it is considered clinically significant when HVPG is higher than 10 mmHg and severe when HVPG is above 12 mmHg. A direct relation has been demonstrated between HVPG and risk of variceal bleeding, hepatic decompensation and liver related mortality, and HVPG has become a surrogate endpoint in the assessment of treatment response and reduction of risk of liver-related mortality. However, HVPG measurement is invasive, is not routinely available and it is reliably standardized only in expert centers. Thus, non-invasive methods, such as elastography, are under investigation, in the attempt to diagnose and grade PH, and to predict presence, extent and risk of variceal bleeding. Non-invasive imaging, such as ultrasound (US), computed tomography (CT) and magnetic resonance imaging (MR) may enable diagnosis of PH through the identification of complications (such as varices, splenomegaly, ascites). The anatomic information provided by these imaging modalities becomes essential to identify the causes of PH and when treatment planning is required (such as in patients indicated for TIPS or candidate for liver transplantation). Imaging plays a crucial role also to assess response to treatment and post-treatment complications.

Learning Objectives:

1. To appreciate imaging features of portal hypertension.
2. To discuss the appropriate choice and timing of imaging technique in investigation of portal hypertension and its complications.
3. To learn about relevant findings that influence therapy choice in portal hypertension.

Author Disclosure:

I. Bargellini: Advisory Board; Bayer Spa. Speaker; GE Healthcare, BTG, Sirtex Medical.

A-052 08:58

B. Embolisation of varices and splenic artery in portal hypertension

I.E. Keussen; Lund/SE (inger.keussen@med.lu.se)

Portal hypertension is most common secondary to liver cirrhosis, however it can also be caused by portal/splenic vein thrombosis or occlusion. A bleeding secondary to portal hypertension, usually originates from esophageal or gastric varices, other sites may be duodenal, stomal or rectal varices. A bleeding from esophageal varices is primarily most often treated endoscopically with sclerotherapy or rubber banding. Gastric varices are less prevalent, but more difficult to treat endoscopically. If medical and endoscopic treatment methods fail, interventional treatment is the next option, which includes embolisation of varices, TIPS, BRTO and partial splenic arterial embolisation. Embolisation of varices may be performed by percutaneous or transjugular-transhepatic approach, but transsplenic route or direct puncture of the stomal varices are also reported. A BRTO may be applied in patients with a splenorenal shunt and secondary gastric varices. Partial splenic embolisation may decrease inflow of blood to the portal vein and secondary decrease the portal hypertension. In most cases a combination of different techniques is necessary to achieve good results.

Learning Objectives:

1. To discuss the rationale for embolisation.
2. To learn about the selection of technique and choice of material.
3. To understand outcomes from embolisation techniques.

A-053 09:21

C. Transjugular intrahepatic portosystemic shunt (TIPS): critical appraisal of techniques and guidelines for treatment

A. Krajina; Hradec Králové/CZ (antonin.krajina@fnhk.cz)

TIPS is a minimally invasive method of creating a portosystemic shunt for decompression of portal hypertension (PH). A side-to-side shunt of determined diameter is created to shunt blood flow from the portal vein (PV) to hepatic vein or inferior vena cava above the liver using transjugular approach, long needle, balloon angioplasty, and stent-graft. The most often indication for TIPS is cirrhotic ascites, which is sometimes combined with severe hydrothorax. However, TIPS is used in those patients who are intolerant of repeated large-volume paracentesis. TIPS has been used as a rescue treatment in rare cases of endoscopically uncontrollable variceal bleeding, especially from gastric fundal varices. Emergent TIPS (in 72 hours) performed in patients with severe PH and high risk of early rebleeding, has been proved to have better bleeding control and survival in 1 year. Partial or complete PV thrombosis does not change usual technique of TIPS. TIPS is technically difficult in chronic extrahepatic PV obstruction, in children, and in patients with massive hepatic veins thrombosis (Budd-Chiari Syndrome - BCS). The absence of hepatic veins and distorted anatomy due to the caudate lobe hypertrophy requires sometimes direct transcaval approach to the PV in patients with BCS. Moreover, these patients must be anticoagulated life long due to underlying hypercoagulopathy. TIPS demonstrated good control of ascites and reversal of liver failure in large series of patients with BCS. All patients with TIPS must be followed regularly in specialized multidisciplinary center, and the surveillance of TIPS function is mandatory.

Learning Objectives:

1. To discuss the selection of patients for TIPS.
2. To learn about the techniques for TIPS formation.
3. To discuss outcomes of TIPS and role of imaging surveillance.

09:44

Panel discussion: Appropriate selection of patients for IR including the role of balloon-occluded retrograde transvenous obliteration (BRTO) for gastric varices

08:30 - 10:00

Room M 4

E³ - ECR Academies: Chest Imaging

E³ 118

Lung cancer in the era of molecular oncology and immune therapy

A-054 08:30

Chairperson's introduction

H. Prosch; Vienna/AT (helmut.prosch@meduniwien.ac.at)

Lung cancer is the most common cause of cancer-related death in Western countries. In the last several years, a number of new drugs have revolutionized systemic therapy in lung cancer. These new therapies can be divided into two major groups, the targeted therapies and the immunotherapies. Targeted therapies, such as EGFR tyrosine kinase inhibitors, or ALK inhibitors, are a class of drugs that specifically target a well-defined molecular pathway. They have been shown to be more effective than classic chemotherapies in patients who harbor the specific mutation and are associated with fewer toxicities. As these drugs target molecules with a specific mutation, patients who harbor this specific mutation need to be identified. In addition to bronchoscopy, image-guided biopsies are the main modality for obtaining tissue for molecular analysis. Imaging may have a potential role in identifying tumors that harbor a specific mutation, and thus, in guiding further pathologic and genetic work-up. Immunotherapy, however, targets immunological pathways to induce an immunological response against tumors. Immunotherapy has been shown to be a very effective treatment in a subset of patients with non-small cell cancer. Imaging plays a major role in the follow-up evaluation of patients undergoing immunotherapy, as immune reactions must be differentiated from disease progression.

A-055 08:35

A. Lung adenocarcinomas with EGFR mutations

M. Lederlin; Rennes/FR (Mathieu.LEDERLIN@chu-rennes.fr)

Adenocarcinoma is the most prevalent type of lung cancer, showing a large spectrum of genetics, histologic subtype, CT appearance, clinical behavior and prognosis. Activating mutations of EGFR are found in 30%-50% of lung adenocarcinomas in East Asian patients and approximately 15% in Caucasian patients. EGFR mutation status is correlated with nonsmoking status, female sex, lepidic subtype, and high response rate to EGFR tyrosine kinase inhibitors (TKI). Some CT findings have shown to be associated with EGFR mutation such as nonsolid or mixed ground-glass opacity, air bronchogram, smaller and peripheral tumors, and pleural retraction. Furthermore, non-smoking patients presenting with diffuse miliary metastatic disease at diagnosis may be diagnosed with adenocarcinoma harboring EGFR mutation and may show dramatic response to EGFR-TKI. The most common resistance mechanism to EGFR-TKI is the T790M mutation, against which new irreversible TKIs have been found to be clinically effective, thus increasing demand for rebiopsy in progressive NSCLC to analyze mutational status. Rebiopsies are feasible and informative in most of patients with acceptable rates of complications. Furthermore, continued EGFR-TKI therapy may be indicated beyond RECIST progression, because these tumors grow slowly and some tumor cells remain sensitive to EGFR-TKI. Radiologists should also be aware of the risk of class-effect toxicity of EGFR-TKI, in particular pneumonitis with an incidence rate of 4-5% in the Japanese population. Finally, European radiologists should keep in mind that a majority of studies dealing with EGFR mutations in adenocarcinomas arise from Asian countries with results that might not be transposable to Caucasian populations.

Learning Objectives:

1. To be aware of the importance of detecting EGFR mutation.
2. To learn about demographic and CT features suggestive of EGFR mutation.
3. To learn about the various initial and follow-up CT features.

A-056 09:03

B. ALK-rearranged lung adenocarcinomas

M. Silva; Parma/IT (mariosilvamed@gmail.com)

The 2-7% of non-small cell lung cancers (NSCLC) harbor the rearrangement of anaplastic lymphoma kinase (ALK) - an oncogene related to a tyrosine kinase pathway - notably in adenocarcinoma histology and in non-smokers (about 60% of all ALK-rearranged NSCLC). Target therapy by tyrosine kinase inhibitors (TKI) is clinically available for ALK-positive advanced NSCLC and improves progression-free survival (PFS) compared with previous reference chemotherapy. Hence, testing for mutations is paramount for optimal planning of medical treatment of advanced NSCLC. In the face of a better disease

control by TKI, however, it happens that ALK-positive tumors are prone to driver mutation with resistance to first-line TKI, in the first months of therapy. In clinical practice, diagnostic imaging, notably computed tomography (CT), has high yield in the management of patients under target therapy. The CT evidence of disease progression, either local or systemic (note: brain metastases are relatively common because first-line TKIs have low trespassing coefficient through emato-encephalic barrier) is paramount for timely adaptation of therapy. Rapid radiologic progression demands prompt TKI swap towards second-line (e.g., ceritinib, brigatinib, or alectinib) or third-line target therapy (e.g., lorlatinib) or otherwise. Re-biopsy is suggested to pitch the optimal second (or further) line therapy by continuous molecular testing. In clinical trials, again, diagnostic imaging has high yield in the assessment of target therapies, namely for definition of PFS. Adverse events occur in a minority of patients under TKI (1% incidence of lung toxicity). Therapy discontinuation is usually sufficient to reduce toxic effects, with only 3-6% of cases lingering after therapy withdrawal.

Learning Objectives:

1. To learn about clinicopathologic features characterising ALK-rearrangement.
2. To understand the impact of ALK rearrangement on the prognosis of non-small cell lung cancer.
3. To see some illustrative cases.

A-057 09:31

C. PD-L1 positive lung tumours

O.L. Sedlacek; Heidelberg/DE (sedlacek@web.de)

Immune checkpoint inhibitors (ICI) are effective in the treatment of many cancers, blocking immunosuppressive pathways; they play an increasing role in the first-line treatment of lung-cancers. This is particularly true when there is evidence for a significant pretreatment tumor lymphocytic infiltration and/or tumors exhibit a positive staining for PD-L1. As ICIs work through a different mode of action there is good reason to use therapy response criteria other than RECIST. In contrast to cytotoxic agents anti-tumour response in immunotherapy may take longer and in the initial phase the response to immune therapies can manifest in a morphologic "progressive disease", therefore, called "pseudoprogression". In this situation a early discontinuation of the treatment would not be appropriate, unless PD is confirmed. "Clinically insignificant" PD may even include the detection of new lesions ("unconfirmed progression") that may not lead immediately to a discontinuation of the oncologic regimen and has to be reevaluated. As ICIs act through a different mechanism than cytotoxic agents or tyrosine inhibitors, deblocking the immune system a broad spectrum of auto immune diseases can be triggered. Imaging characteristics of frequent and serious immune-related adverse events (irAEs) will be discussed.

Learning Objectives:

1. To know about the impact of PD-L1 positivity.
2. To know how to evaluate the tumour response after immunotherapeutics.
3. To be aware of the imaging features of immune therapy complications.

08:30 - 10:00

Room M 5

Molecular Imaging

RC 106

Merging the best: hybrid imaging

Moderator:

G. Antoch; Düsseldorf/DE

A-058 08:30

A. Hybrid imaging with SPECT/CT

A. Scarsbrook; Leeds/UK (a.scarsbrook@nhs.net)

Latest generation SPECT/CT cameras incorporate multi-detector CT and state-of-the-art gamma camera technology in tandem. These scanners improve the efficacy of a wide variety of nuclear medicine tests by providing more accurate localisation of lesions, exclusion of potentially misleading physiological uptake, characterisation of equivocal or indeterminate activity and detection of additional lesions. In addition, they offer the potential for a more efficient "one-stop-shop" imaging approach. Iterative reconstruction algorithms and faster processing power facilitate radiation dose reduction and increased image resolution. The clinical utility of SPECT/CT is diverse and a cross-spectrum of applications in musculoskeletal, oncological, cardiovascular, endocrine, hepatobiliary and GI tract imaging will be presented.

Learning Objectives:

1. To learn the basic principles of hybrid SPECT/CT imaging.
2. To understand what complementary information can be given by SPECT/CT.
3. To learn about clinical applications of SPECT/CT.

Postgraduate Educational Programme

A-059 09:00

B. Hybrid imaging with MR/PET

F.M.A. [Kiessling](mailto:kiessling@ukaachen.de); Aachen/DE (kiessling@ukaachen.de)

In this talk an overview on the technological state of the art in PET-MRI as well as an outlook on emerging new technologies will be provided. Concerning the latter in particular new PET-insert solutions will be highlighted that are tailored to specific medical applications and body parts. Besides this, there will be a brief overview on new detector setups providing higher sensitivity and spatial resolution as well as on the methods to improve absorption correction and quantification. In the final part of the talk the focus will be set on the medical applications of PET-MRI. In this context, it will be discussed, which applications inevitably demand for PET-MRI hybrid imaging. Thus, with this talk I will try to convince the audience of the high development potential and clinical value of PET-MRI and its future role in patient management.

Learning Objectives:

1. To learn the basic principles of hybrid MR/PET imaging.
2. To understand what new information can be given by MR/PET.
3. To learn about emerging clinical applications of MR/PET.

A-060 09:30

C. Hyperpolarised MRI

F.A. [Gallagher](mailto:fag1000@cam.ac.uk); Cambridge/UK (fag1000@cam.ac.uk)

There is increasing evidence to support a role for metabolism in many diseases; for example, deregulation of cellular energetics is now considered to be one of the key hallmarks of cancer. There are a number of imaging methods that have been used to probe this metabolism: the most widely available is 18F-fluorodeoxyglucose (FDG), an analogue of glucose, used in PET. Hyperpolarised carbon-13 MRI (13C-MRI) is an emerging molecular imaging technique for studying cellular metabolism, particularly in the fields of oncology and cardiology. This method allows non-invasive measurements of tissue metabolism in real-time. To date, the most promising probe used in conjunction with hyperpolarised MRI has been 13C-labelled pyruvate: pyruvate is metabolised into lactate in normal tissue in the absence of oxygen, but in tumours this occurs very rapidly even in the presence of oxygen. Results from many animal models have shown that there is a reduction in the metabolism of pyruvate to lactate following successful treatment with chemotherapy. In the heart, pyruvate is also metabolised to carbon dioxide in addition to lactate and this balance between anaerobic and aerobic metabolism alters in many disease states. There are now a small number of sites performing human hyperpolarised carbon-13 MRI imaging. This talk will discuss the progress that has been made in this field within the areas of oncology and cardiology and potential clinical applications.

Learning Objectives:

1. To learn the basic principles of hyperpolarisation.
2. To understand what new information can be given by hyperpolarised MRI.
3. To learn about oncological and non-oncological applications of hyperpolarised MRI.

Author Disclosure:

F.A. [Gallagher](mailto:fag1000@cam.ac.uk): Research/Grant Support; GE Healthcare, GSK.

10:30 - 12:00

Room A

E³ - ECR Academies: Interactive Teaching Sessions for Young (and not so Young) Radiologists

E³ 221

Musculoskeletal radiology: inflammation

A-061 10:30

A. Inflammatory and infections in the soft tissues

S. [Martin](mailto:silvia.m.martin@gmail.com); Palma de Mallorca/ES (silvia.m.martin@gmail.com)

The diagnosis of infections is based on the presence of clinical symptoms like erythema, swelling, and pain. Also the diagnosis is based on the presence of clinical signs such as fever, tachycardia, shock, and hypotension and laboratory test such as leukocytosis, C protein reactive and Erythrocyte sedimentation rate. However, the clinical symptoms and signs of infection may not be specific, especially in the early stages of the disease. In these cases, imaging tests play a fundamental role in the early diagnosis of infections and in the differential diagnosis. The most important radiological findings for inflammatory and infections soft tissue are: (1) intramuscular fluid collections; (2) soft tissue air; (3) fascial fluid collections; and (4) muscle edema. Potential causes of these radiological findings are diverse, including, infectious, autoimmune, inflammatory, neoplastic, neurologic, traumatic and iatrogenic conditions. Some of these conditions require prompt medical or surgical

management, whereas others do not benefit from medical intervention. Necrotizing fasciitis is a rare, life-threatening soft-tissue infection and a medical and surgical emergency that radiologist must know. The presence of gas within the necrotized fascia is characteristic, but may be lacking. The main finding is thickening of the deep fascia due to fluid accumulation and reactive hyperemia. All these findings may be seen in other different conditions. The ability to accurately diagnose these conditions is therefore necessary, and biopsy may be required to establish the correct diagnosis. Clues to the correct diagnosis and whether biopsy is necessary or appropriate are often present on the images techniques, especially when they are correlated with clinical features.

Learning Objectives:

1. To learn the key signs for differential diagnosis.
2. To learn about imaging findings and management options.

A-062 11:15

B. Arthropathies

U. [Aydingoz](mailto:uaydingo@hacettepe.edu.tr); Ankara/TR (uaydingo@hacettepe.edu.tr)

Arthritis is a common problem involving the joints in the axial and/or appendicular skeleton across all age groups. Imaging plays a key role in the diagnosis and management of arthropathies, which are generally divided into degenerative, inflammatory, and metabolic categories. Digital radiography is the main imaging tool for joint diseases. Magnetic resonance imaging (MRI), computed tomography and ultrasonography are also used along with digital radiographs in the initial diagnosis and follow-up of joint diseases. The multiplicity and distribution of the involved joints, the pattern of joint space narrowing, and periarticular bone and soft tissue changes are important considerations for radiological diagnosis. The involvement of a single joint with inflammatory arthritis requires the exclusion of infection, whereas c involvement with degenerative arthritis may be due to an identifiable remote trauma. Septic arthritis does not have a pathognomonic radiological finding and, in the presence of clinical suspicion for infection, imaging should not delay joint fluid aspiration for microbiological investigation. This interactive session will cover the radiographic clues of arthropathies and the use of cross-sectional imaging methods, especially MRI, for suggesting the likely diagnosis. Some conditions, such as rotator cuff arthropathy and degenerative disease of the medial compartment of the knee secondary to medial meniscus posterior root avulsion, that have typical MRI findings shedding light on the pathophysiology of arthropathies will also be addressed.

Learning Objectives:

1. To explain the key points in the differential diagnosis of common arthropathies.
2. To describe the imaging findings of common arthropathies as they relate to pathophysiology.

10:30 - 12:00

Room F1

E³ - Rising Stars Programme: Basic Sessions

BS 2

Gastrointestinal: 'the gut'

Moderator:

B. [Marincek](mailto:marincek@kch.ch); Kilchberg/CH

A-063 10:30

Oesophagus

S. [Romano](mailto:stefromano@libero.it); Naples/IT (stefromano@libero.it)

In this presentation focused on the first segment of the alimentary tract, current imaging techniques for evaluation of normal anatomy will be considered and described. From conventional radiography to modern hybrid imaging, essential information regarding the methods will be included. The second part of the lecture will describe the imaging features in most common benign pathologies, to give the attending useful informations for the daily clinical practise. Elective and Emergency conditions for the evaluation of the oesophagus will be considered. Finally, a pictorial guided review of the imaging features of malignant pathologies will be done.

Learning Objectives:

1. To discuss current imaging techniques for evaluation of normal anatomy.
2. To describe the imaging features in most common benign pathologies.
3. To review and illustrate the imaging features of malignant pathologies.

Wednesday

A

B

C

D

E

F

G

S16

A-064 10:53

Stomach

M. Laniado; Dresden/DE (michael.laniado@uniklinikum-dresden.de)

Today, the stomach is well accessible for endoscopic evaluation. Therefore, double-contrast barium studies of the stomach have almost completely disappeared from the armamentarium of imaging studies in radiology. However, abdominal computed tomography (CT) - not so much magnetic resonance imaging (MRI) - has become the number one procedure in many scenarios if ultrasonography fails to provide a conclusive diagnosis. As the stomach is always imaged when abdominal CT is performed knowledge of normal anatomy, incidental findings, and the most often benign and malignant gastric pathologies is mandatory. Depending on the clinical request, imaging techniques are slightly different. If the main focus is on a lesion of the stomach, maximum wall distention should be achieved by oral administration of up to 2 L of water shortly before the study and i.v. administration of a hypotonic agent. In addition, i.v. administration of iodinated contrast material is mandatory. The presentation will cover normal anatomy of the stomach including locoregional lymph nodes. Examples of common and uncommon gastric lesions (e.g., carcinoma, lymphoma, GIST, NET, metastases, ulcer, portal gastropathy, pneumatosis, ischemia, pseudocysts) will be shown and discussed. Also examples of postoperative anatomy and potential complications will be part of the presentation.

Learning Objectives:

1. To discuss current imaging techniques for evaluation of normal anatomy.
2. To describe the imaging features in most common benign pathologies.
3. To review and illustrate the imaging features of malignant pathologies.

A-065 11:15

Small bowel

N. Papanikolaou; Lisbon/PT

(nickolas.papanikolaou@research.fchampalimaud.org)

Magnetic resonance imaging (MRI) provides excellent soft-tissue contrast without radiation exposure and three-dimensional imaging capabilities, which are important when studying the small intestine. Various sequences and contrast agents have been proposed for MRI examination of the small bowel. The development of high performance gradient systems improved the performance of ultra fast sequences and allowed comfortable breath-hold acquisition times. For a more detailed evaluation of small bowel diseases, MRI examination should be performed in conjunction with duodenal intubation and administration of a suitable contrast agent, i.e., iso-osmotic water solution (PEG) for homogeneous lumen opacification and adequate distention. A comprehensive MR enteroclysis imaging protocol should comprise single shot turbo spin echo (SSTSE), diffusion weighted imaging, true FISP, HASTE and fat suppressed T1 FLASH sequences. SSTSE is utilized for monitoring the infusion process and performing MR fluoroscopy while true FISP and HASTE, classified as sequential ultra fast techniques insensitive to motion, are mainly used for anatomic demonstration and detection of the pathology. T1 FLASH sequences after intravenous gadolinium injection may aid tissue characterization. For the assessment of Crohn's disease activity other alternative techniques may be used including perfusion and calculation of the magnetization transfer ratio of the bowel wall. These techniques may be useful for differentiating edematous or inflammatory bowel thickening from fibrotic thickening, but a more extensive evaluation is required to determine the clinical utility of these methods.

Learning Objectives:

1. To discuss current imaging techniques for evaluation of normal anatomy.
2. To describe the imaging features in most common benign pathologies.
3. To review and illustrate the imaging features of malignant pathologies.

Author Disclosure:

N. Papanikolaou: Advisory Board; Advantis. CEO; MRIcons.

A-066 11:38

Colon

R.G.H. Beets-Tan; Amsterdam/NL (r.beetstan@nki.nl)

Ultrasound, CT and MRI has a role in the workup of diseases of the large bowel. Transabdominal US is accurate to detect appendicitis. Contrast enhanced CT identifies the causes of bowel obstruction and dilatation. CT shows postoperative complications such as leakage of surgical anastomosis, internal herniation, bowel strangulations, and bowel ischemia. Inflammation of the bowel, diverticulitis, epiploic appendagitis are well detected on CT. While endorectal US and MRI have been widely adopted in the staging work up of rectal tumors, the role of imaging in Colon cancer is limited to preoperatively roadmap the extent of the tumor into surrounding structures and to identify distant disease. Nevertheless this role may increase in the near future. This lecture will deal with various diseases of the colon and its imaging features and highlights future direction in imaging of colon cancer.

Learning Objectives:

1. To discuss current imaging techniques for evaluation of normal anatomy.
2. To describe the imaging features in most common benign pathologies.
3. To review and illustrate the imaging features of malignant pathologies.

10:30 - 12:00

Room M 4

E³ - ECR Academies: Chest Imaging

E³ 218

CT of vascular pulmonary diseases

A-067 10:30

Chairperson's introduction

J.D. Dodd; Dublin/IE

Pulmonary vascular disease includes a wide spectrum of disease entities, many of which have overlapping clinical and imaging features. CT of the pulmonary vasculature has become an integral part of the investigation of such entities. In this session we are going to evaluate three distinct disease sub-categories of pulmonary vascular disease: pulmonary arterial hypertension, pulmonary vasculitis and Rendu-Osler disease. The first talk will cover pulmonary hypertension, the current clinical classification of pulmonary vasculitis, CT signs suggestive of the diagnosis, and CT signs that help discriminate between different causes. The comprehensive nature of CTPA in evaluating the mediastinum, vasculature and lung parenchyma will be shown. The second talk covering pulmonary vasculitis will emphasise the importance of combining CT signs with the clinical features and laboratory results since vasculitis may mimic other disorders and sometimes the clinical features are the major clue. CT findings in granulomatosis with polyangiitis and eosinophilic granulomatosis with polyangiitis will be shown, particularly emphasising the imaging differences between the two entities. The imaging findings of pulmonary hemorrhage will also be shown alongside the commonest causes. Finally the association between interstitial lung disease and the ANCA associated vasculitis will be discussed. The third talk covering Rendu-Osler disease will show the typical imaging features of this disease with a particular emphasis on those imaging aspects that determine outcome and treatment strategies. The talk will also cover contemporary aspects of endovascular treatment modalities and their complications.

A-068 10:35

A. CT imaging of pulmonary hypertension

N.J. Screaton; Cambridge/UK (Nicholas.Screaton@papworth.nhs.uk)

Pulmonary hypertension (PH) typically presents insidiously with non-specific symptoms and is usually progressive with poor outcome independent of aetiology. CT plays a vital role both in suggesting the possibility of pulmonary hypertension, whether initially clinically suspected or not, and in identifying a specific cause of pulmonary hypertension. The causes of pulmonary hypertension can be broadly divided into those affecting primarily the small vessels, PH secondary to left heart disease or chronic lung disease / hypoxia (the most common causes), chronic thromboembolic PH, and multifactorial causes. CT is widely available, inexpensive, and permits comprehensive assessment of the heart, pulmonary vasculature and lung parenchyma. CT signs such as dilatation of the proximal pulmonary arteries and right heart chambers can be considered as generic features associated with PH of any cause. Signs of a specific cause may lie in the mediastinum (left heart disease, shunt, oesophageal varices, oesophageal dilatation), vasculature (signs of CTEPH, tumour, large vessel vasculitis, fibrosing mediastinitis) or lungs (parenchymal lung disease, mosaic perfusion in CTEPH, signs of a small vessel vasculopathy). CTEPH is a not uncommon sequela of previous acute embolism. If the distribution is proximal it is potentially cured by surgical pulmonary endarterectomy or by balloon pulmonary angioplasty. Imaging in general and CT in particular play fundamental roles in both identification of CTEPH, its differentiation from acute PE, and in characterising its distribution. Imaging signs in CTEPH can be subtle and systematic evaluation of a CTPA is essential.

Learning Objectives:

1. To learn about the CT signs of pulmonary hypertension (PHT).
2. To become familiar with the current classification of PHT.
3. To be aware of the imaging features suggesting a thromboembolic origin.

Postgraduate Educational Programme

A-069 11:03

B. Evaluating the pulmonary vasculitis

E. Castañer; Sabadell/ES (ecastaner@tauli.cat)

We will emphasize the importance of combine CT signs with the clinical features and laboratory results as vasculitis may mimic other disorders and sometimes the clinical features rate the clue. We will describe the findings in granulomatosis with polyangiitis (GPA) and eosinophilic granulomatosis with polyangiitis, highlighting the differences. Diffuse alveolar hemorrhage (DAH) is one of the manifestations of primary pulmonary vasculitis, among other entities (idiopathic alveolar hemorrhage, collagen vascular diseases, drug reactions, anticoagulation disorders). GPA and microscopic polyangiitis are the most common causes of DAH. Radiologic signs of DAH are nonspecific and variable, but must be considered in patients with otherwise unexplained alveolar infiltrates, particularly when seen with new onset renal insufficiency or a connective tissue disease. Finally we will mention the association between interstitial lung disease and ANCA associated vasculitis.

Learning Objectives:

1. To learn the common imaging features of granulomatosis with polyangiitis (GPA).
2. To learn how to differentiate between GPA and eosinophilic granulomatosis with polyangiitis (Churg-Strauss).
3. To learn about the imaging features and differential diagnosis of pulmonary haemorrhage.

A-070 11:31

C. Rendu-Osler disease

S.D. Qanadli; Lausanne/CH (Salah.Qanadli@chuv.ch)

Rendu Osler disease (ROD) is an autosomal dominant genetic disorders characterized by the presence of telangiectasias and/or arteriovenous malformations. Pulmonary arteriovenous malformations (PAVM) are observed in up to 80% in ROD patients and it is believed that up to 30% of ROD patients will develop PAVM. During the last decade CT became the standard of reference in assessing pulmonary and associated subphrenic anomalies in patients with ROD. This lecture will focus on current protocols and recommendations for CT depending on the objective of the examination (screening, diagnostic or follow-up). Typically, PAVM is a well circumscribed rounded lesion that is connected to an afferent feeding artery and an enlarged efferent vein. PAVMs can be focal, multiple or diffuse. Imaging features as well as a comprehensive classification is provided. In asymptomatic patients, the risk of complications was reported to be high in PAVMs with an afferent artery diameter of 3 mm or more. The role of CT is then not only crucial in diagnosis, but also in therapeutic decision making process even if the 3 mm threshold concept in matter of debate and controversies. Principles of endovascular management of PVAM are reviewed. The transarterial access is the most common procedure. The modern approach includes the use of coils and/or plugs. CT flow up studies aim diagnosis of early complications, PAVM reperfusion detection, surveillance of small PAVMs, and diagnosis of new PAVMs.

Learning Objectives:

1. To become familiar with the CT manifestations of this disease.
2. To identify imaging features determining outcome and treatment strategies.
3. To learn about endovascular treatment modalities and complications.

12:30 - 13:30

Room C

E³ - The Beauty of Basic Knowledge: Cardiovascular and Interventional Radiology

E³ 24A

No time to lose: aortic dissection - revisited

Moderator:

M. Krokidis; Cambridge/UK

A-077 12:30

Acute diagnosis and imaging in aortic dissection

R. Iezzi; Rome/IT (roberto.iezzi.md@gmail.com)

Aortic dissection is the most common acute emergency condition of the aorta, often resulting in the death of the patient. The overall outcome is determined by the type and extent of dissection and the presence of associated complications; therefore, evaluation of the entire aorta, branch vessels, and iliac and proximal femoral arteries is recommended to aid in treatment planning. Early diagnosis and treatment are essential for improving the

prognosis. Patients may present with the classic history of acute onset of tearing central chest pain that radiates to the back. Stanford type A dissection involves the ascending thoracic aorta, and the dissection flap may extend into the descending aorta. Type A dissections account for 60%-70% of cases, requiring urgent surgical intervention to prevent extension into the aortic root, pericardium, or coronary arteries. If untreated, type A dissections are associated with a mortality rate of over 50% within 48 hours. Stanford type B dissection involves the descending thoracic aorta distal to the left subclavian artery and accounts for 30%-40% of cases. Management takes the form of medical treatment of hypertension, unless there are complications due to extension of the dissection. CT imaging of the aorta is fast and widely available, which are the important features in making an accurate diagnosis quickly in unstable patients. Multidetector CT allows imaging of the entire aorta with rapid acquisition and data reconstruction to provide prompt and accurate diagnosis and to help identify relevant complications that may have an impact on treatment and management.

Learning Objectives:

1. To learn about definition and classification of aortic dissections and subtypes.
2. To understand the importance of accurate diagnosis for appropriate treatment planning.
3. To appreciate the need for acute diagnosis and treatment indication.

A-078 13:00

Endovascular treatment in aortic dissection

J.P. Schäfer; Kiel/DE

Acute aortic dissection represents a life-threatening condition, which must be diagnosed immediately. CTA is considered the imaging modality of choice, offering all relevant information on the pathoanatomy with highest spatial resolution. Stanford classification is used to distinguish between type A- and B-dissections, whereas the left subclavian artery represents the border in between the two types. Actually, surgical repair is the method of choice and indicated in type A dissection, and endovascular repair is the method of choice in type B-dissection, if indicated. Type B dissection may be uncomplicated or complicated. For uncomplicated type B, best medical treatment is the method of choice, and it is defined by no further symptoms, relief of symptoms and absence of additional dissection associated findings. For complicated type B, endovascular repair including a variety of interventions is the method of choice, and it is defined by mesenteric, renal, peripheral and spinal malperfusion, progressive dissection, aneurysm forming, uncontrollable hypertension, rupture, progressive periaortic and pleural haemorrhage, severe hypotension and shock. Regarding symptom onset and imaging based diagnosis, type B-dissection is classified as acute (<2 weeks), subacute (2-8 weeks), and chronic (>8 weeks). Endovascular repair usually includes prosthesis placement in the descending aorta, in order to seal the proximal entry tear. This excludes the perfusion of the false lumen along the covered aortic segment and restores the blood flow into the true lumen, maintaining and improving the visceral and peripheral perfusion. Additionally, target visceral artery stenting, membrane fenestrating or embolising may be indicated. Protocolled CTA follow-up is mandatory.

Learning Objectives:

1. To learn about endovascular treatment possibilities for aortic dissections.
2. To understand the role of radiology in modern treatment of aortic dissections.
3. To appreciate the need to combine the radiological information with the clinical situation.

12:30 - 13:30

Room D

E³ - The Beauty of Basic Knowledge: A Survival Guide to Musculoskeletal Imaging

E³ 25A

Degenerative disorders

Moderator:

V.N. Cassar-Pullicino; Oswestry/UK

A-079 12:30

Degenerative disorders

A. Cotten; Lille/FR (anne.cotten@chru-lille.fr)

Osteoarthritis is the most common joint disease worldwide. It is a major source of pain, disability, and socioeconomic cost. The epidemiology of the disorder is complex and multifactorial, with genetic, biological, and biomechanical components. Conventional X-ray is the standard diagnostic method to confirm the clinical diagnosis, to evaluate the degree of severity of osteoarthritis and to look for predisposing conditions. CT can be performed for the assessment of

bone stock, anatomic conditions and bone deformation. MRI can be used to confirm early forms and to clarify possible damage and/or wear and tear, which cannot be seen on X-rays. Finally, intraarticular administration of contrast will be performed in selected cases, when a precise assessment of the cartilage or fibrocartilage is required. This lecture will focus on the role of imaging in clinical practice, the typical and atypical imaging features of OA, the radiological features which should not be read as OA, and the main predisposing factors that have to be known and searched.

Learning Objectives:

1. To appreciate the musculoskeletal imaging manifestations of degenerative disorders.
2. To understand the underlying pathomechanisms involved in these imaging abnormalities.
3. To appreciate the strengths and weaknesses of imaging modalities in assessing these disorders.

14:00 - 15:30

Room F1

E³ - Rising Stars Programme: Basic Sessions

BS 3

Neurologic emergencies

Moderator:

N. Chidambaranathan; Chennai/IN

A-080 14:00

Brain injury

J. Walecki; Warsaw/PL

Head injuries are one of the most frequent causes of death and disability. The following presentation will discuss the indications for imaging in patients with traumatic brain injury (TBI), review the role of X-ray examination, computed tomography (CT) and magnetic resonance imaging (MRI) in the management of TBI. CT still remains the method of choice in brain injury diagnosis and allows rapid assessment of the extent and type of brain pathology which ensures us which patients require urgent surgical intervention. There are many CT structural modalities such as MPR, volume rendering and CT angiography important in particular cases of traumatic patients. In addition to above, author will also discuss TBI diagnosis in MRI applications which are newly applied to clinical practice like TDI, fMRI and analyse potential applications of these imaging modalities. Using a complex variety of MR sequences, we can provide data concerning both structural and pathophysiological derangements. Future developments with such imaging techniques could improve understanding of the pathophysiology of brain injury and provide data that improve management and prediction of functional outcome. In this presentation all type of brain injury and its imaging features will be presented. Goals and objectives - to understand the mechanisms of traumatic brain injury - to learn about CT and MR imaging findings in different traumatic lesions of the brain - to be familiar with advantages and disadvantages of different imaging techniques in traumatic brain injury

Learning Objectives:

1. To review mechanisms of brain injury.
2. To present current imaging techniques for evaluation of brain injury.
3. To illustrate different types of traumatic intracranial lesions.

A-081 14:30

Subarachnoid haemorrhage

C. Calli; Izmir/TR (cem.calli@gmail.com)

Subarachnoid hemorrhage (SAH) is a very common and life-threatening disease. It occurs most commonly secondary to trauma and intracranial vascular abnormalities. The early diagnosis is very important and imaging modalities have an important role. Non-contrast CT (NCCT) should be the first choice for imaging. It can provide the visualisation of hyperdense blood products in the cisterns and sulci. In cases of negative NCCT scan, MRI may be a choice, especially in patients in the subacute phase using FLAIR and SWI sequences. However, every case with non-traumatic SAH should be examined with digital subtraction angiography (DSA) in order to exclude a vascular abnormality, particularly aneurysm. In this lecture both common and uncommon causes of SAH will be discussed and a multi-modality approach to the diagnosis will be reviewed.

Learning Objectives:

1. To review the most common pathologies leading to SAH.
2. To present current imaging techniques for evaluation of SAH.
3. To describe the radiological findings of SAH.

A-082 15:00

Ischaemic stroke

Z. Merhemic; Sarajevo/BA (merhemic.zulejha@gmail.com)

CT is primary imaging modality in patients with acute stroke. The early signs of brain infarction on non contrast CT are insular ribbon sign reflect cytotoxic edema and relates to specificity of of arterial anatomy. Disappearing basal ganglia sign is caused by MCA occlusion proximally to lenticulostriate artery. Early mass effect includes narrowing of Sylvian fissure or loss of cortical sulci. Hyperdense artery sign represent stasis of flow due to arterial thrombus and correlates positively with angiographic finding of occlusion. CTA is essential for evaluation of intra- and extracranial vessels and intravascular thrombi. Conventional MRI finding in acute stroke are hyperintense zones on T2 and FLAIR, mass effect, sulcal effacement, loss of arterial flow voids, and abnormal blooming and parenchymal black dots due to the hemorrhage on T2*GE and SWI. DWI with ADC maps is most sensitive for detection of hyperacute stroke at first 6 hours. In ischemic stroke, reduction of perfusion occurs, typically in an affected vascular territory. Regions with hypoperfusion are shown as decreased CBF, decreased CBV, prolonged MTT, and prolonged measures of contrast transit such as TTP, Tmax or DT. Since these parametric changes are detectable minutes after stroke onset, they are of great use for early diagnosis of ischemic stroke and to differentiate ischemic penumbra from infarct core. There are two perfusion approaches with good application in acute stroke, MR perfusion and CT perfusion. Compared the two methods, CT perfusion (CTP) has the advantage of rapidity and wide accessibility in emergency room together with CTA which may be used to guide thrombolytic treatment and may guide predictions of functional outcome and hemorrhagic complications.

Learning Objectives:

1. To become familiar with the most common aetiologies of stroke.
2. To present current imaging techniques for evaluation of stroke.
3. To recognise the imaging signs of stroke.

14:00 - 15:30

Room M 4

E³ - ECR Academies: Chest Imaging

E³ 318

MR imaging of the lungs

A-083 14:00

Chairperson's introduction

E.J.R. van Beek; Edinburgh/UK (edwin-vanbeek@ed.ac.uk)

MRI of the lungs is increasingly used for a variety of reasons. In some diseases, it can be used as an escape from harmful radiation, such as in young or pregnant patients with suspected pulmonary embolism. This is being extended by short, focused protocols as a first line test in some centres. In other diseases, it is the "go to" modality; for instance, in patients with superior sulcus tumours or where difficult anatomical structures need to be evaluated before treatment decisions can be made. Lastly, airway imaging and evaluation of dynamics of breathing can be assessed using novel methods. This session will go into detail for the three areas described.

Author Disclosure:

E.J.R. van Beek: Advisory Board; Aidence BV. Equipment Support Recipient; Siemens Healthineers. Founder; QCTIS Ltd. Owner; QCTIS Ltd.

A-084 14:05

A. Diagnosing pulmonary embolism

B. Ghaye; Brussels/BE (benoit.ghaye@uclouvain.be)

Twenty-five% of patients suspected of PE may present with contraindication to iodinated CM which indicates a potential role for MR. Recent MR technical refinements have been substantial in this field with faster sequences, larger coverage, lung perfusion imaging and high-resolution pulmonary MR angiography (MRA). Basic sequences for PE include unenhanced SSFP and 3D GRE pulmonary MRA. Technically inadequate examinations are reported in 25-30%, mainly due to poor vascular opacification and artifacts. MR direct signs of acute PE are similar to those of CT, including partially occluding endoluminal filling defects and complete arterial obstruction showing a meniscus termination outlining the clot. Reported sensitivity and specificity of MRA in large series were around 80% and 95-100%, respectively. Sensitivity decreases from central to lobar level (close to 100%), segmental level (70-90%) and subsegmental level (30%). Unenhanced MRA has 82% sensitivity and 90% specificity in the 50% interpretable examinations, showing a similar decrease of sensitivity from proximal to distal level. Perfusion also showed 75% sensitivity and 90% specificity in the 50% interpretable examinations. Similar to CT, MR can provide alternative diagnoses or ancillary findings

altering the management of the patient. A comprehensive assessment of the venous thromboembolic disease may be achieved by the addition of a MR venous phase without further injection of Gadolinium CM. The sensitivity of the combined test may however be increased at the expense of a higher rate of technically inadequate examinations. It is expected that newer 3D MR angiography sequences will increase yield in the field of venous thromboembolism.

Learning Objectives:

1. To learn about the various MR sequences for pulmonary arteries imaging.
2. To become familiar with the MR signs of pulmonary embolism.
3. To understand the current limitations of MR for PE diagnosis.

A-085 14:33

B. Evaluating lung neoplasms

J. [Dinkel](#); [Munich/DE](#)

The purpose of this presentation is to review the currently available MR techniques useful in thoracic oncology and to provide an overview of present and emerging clinical applications of oncologic thoracic MRI. Although many studies have advocated a valuable role for thoracic MRI, it has currently limited clinical utilization with the exception of cardiovascular imaging. However, new technical developments and MRI sequences have continuously improved the quality and broadened the clinical indications for thoracic MRI, especially in thoracic oncology. Furthermore, due to its high soft tissue contrast and the lack of radiation exposure, MRI allows for repeated measurements of the lung structures and, therefore, appears to be appropriate for functional investigation of lung.

Learning Objectives:

1. To review the role of MR for assessing the T status.
2. To learn about MR diffusion sequence performance for N staging.
3. To review the persisting limitations.

A-086 15:01

C. Evaluating the airways

G. [Dournes](#); [Bordeaux/FR](#) (gael.dournes@chu-bordeaux.fr)

Due technical difficulties related to motions and susceptibility artifacts, MR imaging has long been considered out of the scope of routine application in the field of imaging of airways, except in a few expert centers. However, recent improve and simplification in MR acquisition techniques have enabled MRI to reach high resolution imaging for morphological evaluation of both large and small airways. In addition, acute and chronic airway diseases are largely misunderstood by far, so that the ability of MRI to combine both morphology and functional information in a single radiation-free examination will eventually make MRI a modality of choice for better understanding, improving patient care and long term follow up requiring iterative examinations. Finally, recent advances in treatment are also prone to make radiologist reconsider the role and place of imaging in chronic diseases (cystic fibrosis, idiopathic pulmonary fibrosis, etc) to assess sensitively and specifically response to treatment.

Learning Objectives:

1. To review the role of MR for evaluating the large and small airways.
2. To learn about the current state-of-the-art MR sequences.
3. To learn about the current role of MR in cystic fibrosis.

14:00 - 15:30

Room M 5

E³ - ECR Academies: Update on Hepatobiliary Imaging

E³ 320

Diffuse liver disease

A-087 14:00

Chairperson's introduction

C. [Triantopoulou](#); [Athens/GR](#) (ctriantopoulou@gmail.com)

The session is focused on the different aspects of diffuse liver disease. An update in non-invasive imaging will be offered in detail, pointing mainly to fat, iron, and fibrosis deposition and the accuracy of quantitative methods in disease grading and severity assessment. Non-alcoholic fatty liver disease is the most common cause of chronic liver disease in Western countries. US, CT and MRI are used to evaluate the disease, to assess severity, and quantify the amount of fat deposition. Despite advances in imaging techniques accurate measurements are still challenging, and new evolving methods are applied on US and MRI. MRI remains the gold standard and the method of choice, answering the clinically important questions. Congenital diffuse liver diseases comprise some rather uncommon conditions, while iron overload is related to a variety of congenital and hereditary conditions. Differential diagnosis is of

outmost importance for patients' management. MRI is the method of choice to evaluate and quantify iron overload provided that specific imaging protocols are used and the standardized techniques together with validated acquisitions are applied. Diagnosis and staging of liver fibrosis is one of the most challenging aspects of non-invasive imaging. Current application of US and MRI are nowadays able to provide accurate measurements based on US and MRI elasticity tools. "Virtual biopsy" refers to the possibility of imaging techniques to depict, map and measure fibrosis minimizing the need for liver biopsies in chronic diffuse liver diseases. MR allows an accurate determination of steatosis, iron overload and fibrosis, even if they coexist.

A-088 14:05

A. Assessment and quantification of fat in NAFLD

M. [Ronot](#); [Clichy/FR](#) (maxime.ronot@bjn.aphp.fr)

The diagnosis of steatosis in patients with NAFLD is historically based on histological examination of a tissue specimen obtained by liver biopsy. However, liver biopsy has well-known limitations (invasiveness and sampling variability) and cannot be proposed for all patients, especially given the high prevalence of NAFLD worldwide. Several imaging techniques can be used for the non-invasive diagnosis and quantification of steatosis. Ultrasonography and computed tomography are useful for the detection of marked steatosis, but of limited use for precise quantification of mild to moderate fat deposition. MR proton spectroscopy (MRS) is the most accurate technique, but it is not feasible in routine use and is time consuming. Chemical shift sequences offer now an accurate alternative and have been shown to be very well correlated to MRS and liver biopsy. As a consequence, they are progressively accepted as a reference technique for detection and quantification of hepatic fat deposition. Recently, novel parameters, such as the controlled attenuation parameter (CAP), or the speed of sound estimation have been proposed and offer promising results. As for liver fibrosis, the diagnostic strategy should rely on the combination of several non-invasive techniques.

Learning Objectives:

1. To be familiar with the pathogenesis of NAFLD.
2. To recognise current non-invasive imaging methods used to evaluate hepatic steatosis.
3. To realise the clinical applications, diagnostic accuracy and limitations of each method.

A-089 14:33

B. Congenital diffuse liver diseases and iron overload

M.M. [França](#); [Porto/PT](#) (mariamanuela.franca@gmail.com)

Congenital and inherited hepatic diseases, like congenital hepatic fibrosis, Wilson disease or hereditary hemochromatosis, are rare diffuse liver diseases that may progress to cirrhosis. Liver imaging, particularly magnetic resonance (MR) imaging, provides important information on diffuse parenchymal abnormalities, but may also reveal focal liver lesions. Iron overload is found in hereditary hemochromatosis, but also in transfusional hemosiderosis and iron loading anemias, and chronic liver diseases. Quantification of liver iron concentration by MR imaging is crucial for the diagnosis and treatment monitoring of iron overload diseases. MR quantification of liver iron can be performed with signal intensity ratio (SIR) methods or relaxometry techniques. Both R2 and R2* values are increasingly being used for quantification of liver iron concentration, but they must be performed with validated acquisition and analysis protocols. Hereditary hemochromatosis will be presented as an example of a clinical scenario, to emphasize the relevance of MR for detection and quantification of liver iron deposits and its role in patients' management and treatment monitoring.

Learning Objectives:

1. To recognise specific imaging findings in patients with congenital hepatic diseases such as Wilson's disease and congenital hepatic fibrosis.
2. To be able to determine iron content in liver by MRI.
3. To be able to differentiate common focal lesions found in storage disease of the liver.

A-090 15:01

C. Diagnosis and staging of liver fibrosis

L. [Martí-Bonmatí](#); [Valencia/ES](#) (marti_lui@gva.es)

Chronic liver disease is a major public health problem with an increasing prevalence and an emergence clinical interest. Fat, inflammation and iron deposits induce an oxidative stress on the liver with synergistic effects in the progression of fibrosis and cirrhosis. In this sense, it is well known that around 7% of the adult population without known liver disease have liver fibrosis, mostly associated with NAFLD. The up-till-now gold standard biopsy is limited by sample size ($\approx 1/50.000$); sample quality; sampling variability errors (30-40%); inter- and intraobserver variability (>30%); morbidity (1%); and not being

feasible for follow-up and research studies. Therefore, radiologists need to understand the hallmarks and therapeutic implications of liver fibrosis. However, correlation with pathology is troublesome, unless digital pathological quantitation is achieved. In this way, radiologists need to depict, map and measure fibrosis in chronic liver disorders to initiate treatment and evaluate response. The fat-suppressed T2w, STIR, and equilibrium phase DCE T1w images show fine hyperintense reticular septa. These changes are late in the course of disease. Although diagnostic accuracy by texture analysis might be earlier (skewness, GLGM categories). T1p MR imaging is also able to detect early liver fibrosis as correlates with collagen content. Elasticity can be measured with US and MR elastography. IVIM elasticity measures can be also incorporated into the imaging armamentarium. All this radiomic and imaging biomarkers features have different reproducibility and accuracy, but can be excellent tools for the non-invasive diagnosis, follow-up, and treatment evaluation metrics in liver fibrosis.

Learning Objectives:

1. To be able to understand the clinical relevance of detection, characterisation and grading of liver fibrosis.
2. To recognise the imaging techniques that have an emerging role in non-invasive assessment of liver fibrosis.
3. To be able to detect portal hypertension.

16:00 - 17:30

Room B

Abdominal Viscera

RC 401

Imaging of the complicated postoperative abdomen

A-095 16:00

Chairperson's introduction

C.J. Zech; Basle/CH (christoph.zech@usb.ch)

Imaging of the postoperative abdomen is a crucial part in the evaluation of postoperative complications and will lead the clinician in the decision for treatment of postoperative complications with either re-laparotomy, interventional-radiology treatment or conservative/medical treatment. Knowledge of the performed surgical techniques and procedures, the normal imaging appearance postoperative and typical findings of frequent complications are inevitable to successfully treat patients with complications. A good interaction between the surgeon and the abdominal radiologist is needed. Nowadays, radiology should be able to diagnose most complications and minimise the number of mere diagnostic laparoscopies to evaluate a complicated postoperative clinical course.

Session Objectives:

1. To learn about the most common indications for abdominal surgery.
2. To understand the normal imaging findings in postoperative abdomen.
3. To describe and identify the most common postoperative complications.

Author Disclosure:

C.J. Zech: Speaker; Bayer HealthCare.

A-096 16:05

A. Liver

C. Ayuso; Barcelona/ES (cayuso@clinic.ub.es)

Liver resection is proven to achieve long term survival in selected patients with primary or secondary focal liver lesions. Advances in surgical techniques including robotic liver surgeries, systemic adjuvant chemotherapy and postoperative intensive care improved the outcome of liver resection. Adequate liver remnant is crucial to guarantee the correct liver function after radical potentially curative liver resection. In borderline cases, portal vein embolisation (PVE), or associating liver partition and portal vein ligation for staged hepatectomy (ALPPS) has been proposed before surgery to increase the liver remnant. Preoperative volumetric analysis of the liver based on imaging plays an essential role in the preoperative work-up previous to liver resection. Also the knowledge of the vascular hepatic anatomy and possible variants of the biliary system are also key aspects to avoid postoperative complications. Imaging tools based on multidetector computed tomography (MDCT) and magnetic resonance (MR) influencing preoperative decisions and surgical approaches will be discussed. The role of different imaging techniques as plain ultrasonography (US), contrast enhanced ultrasound (CEUS), MDCT and MR for the detection and management of hepatic complications after liver resection or transplantation (infectious, vascular, biliar, parenchymatous (liver rejection) will be analysed.

Learning Objectives:

1. To learn about indications for liver interventions and different surgical approaches to focal liver lesions.
2. To understand the role for the different imaging techniques (US, CEUS, CT and MRI) in assessing different types of complications.
3. To appreciate the spectrum of parenchymal, biliary and vascular complications occurring after liver resection or transplantation.

A-097 16:28

B. Pancreas

R.M. Gore; Evanston, IL/US (rgore@uchicago.edu)

Both benign and malignant pancreatic disease carry significant morbidity and mortality. Because of the fastidious nature of the pancreas and its local and regional anatomy, treatment of these disorders also carries significant morbidity. Indeed, perioperative morbidity of pancreaticoduodenectomy is approximately 30-40%. Due to the diversity of pathology, detection, and characterisation of postoperative complications can be challenging. Familiarity with the normal imaging appearances of the spectrum of surgical procedures and their complications is vital. In this presentation the common pancreatic surgical procedures performed for tumour resection (i.e., the Whipple's operation, enucleation, central and distal pancreatectomy, spleen preserving distal pancreatectomy) and chronic pancreatitis (i.e., Puestow procedure, Beger procedure, Frey procedure) and their normal postoperative appearances are discussed. The common postsurgical complications including pancreatic fistulas and leaks, abscess formation, haemorrhage, and delayed gastric emptying are then described in detail.

Learning Objectives:

1. To learn about the various surgical approaches for acute and chronic pancreatitis, benign and malignant pancreatic neoplasms.
2. To understand profound impact that the partial and complete pancreatectomy have on the adjacent abdominal organs.
3. To appreciate the common postoperative complications of pancreatic surgery.

A-098 16:51

C. Bowel

D.J.M. Tolan; Leeds/UK (djmtolan@doctors.org.uk)

Post operative assessment of the luminal GI tract is very complex and relies heavily on CT. It presents a major challenge for interpretation and detection of abnormalities in the context of a very broad range of normal post operative appearances. In judging whether the imaging appearances are normal or not it is essential to consider the time that has elapsed since the operation and the complexity of the procedure that was performed, since a straight forward procedure or one performed laparoscopically with carbon dioxide insufflation should have very little residual fluid or gas, compared with a complex open surgical procedure. Anastomotic leak is the most important complication to detect, and in this regard positive luminal contrast is the most sensitive for evaluation and this can be administered orally or rectally depending on the position of the anastomosis. An 8% concentration of 300mg/ml concentration non ionic contrast is used by the author. Other complications such as abscess can be detected by CT but this must be differentiated from haemostatic surgical material which is left in situ deliberately.

Learning Objectives:

1. To learn about the most common types of major oesophago-gastric, small bowel and colorectal surgical procedures and the expected postoperative anatomy and imaging findings.
2. To understand how to optimise imaging protocols to maximise the opportunity to detect postoperative complications after enteric surgery.
3. To appreciate and identify early and late complications after bowel surgery.

17:14

Panel discussion: Tips and tricks for my routine clinical practice

Postgraduate Educational Programme

16:00 - 17:30

Room C

Chest

RC 404

CT - patterns in chest radiology: back to basics and beyond

A-099 16:00

Chairperson's introduction

M.A. Mazzei; Siena/IT (mmazzei@sirm.org)

Today the majority of diagnosis in chest radiology is accomplished by high-resolution computerised tomography (HRCT) and advanced HRCT imaging interpretation which have improved a lot the accuracy in diagnosing diffuse lung diseases, such as interstitial pneumonia, thus avoiding the need for a surgical biopsy in many patients. All this can be possible because of the anatomical distribution of the lesions often suggests the diagnosis in pulmonary diseases, owing to the close relationship between HRCT pattern and some diseases and also because of the exact depiction of pulmonary anatomy at HRCT imaging. For this reason the knowledge of anatomy in reading CT is essential for radiologists: recognising the anatomical distribution of lesions or a typical pattern at HRCT imaging is the key to a successfully correct diagnosis.

Session Objectives:

1. To emphasise the importance of anatomy in reading CT.
2. To appreciate the necessity of defining patterns to improve CT diagnoses.

A-100 16:05

A. Secondary pulmonary lobule anatomy: essential to tackle with the nodular pattern

T. Frauenfelder; Zurich/CH (thomas.frauenfelder@usz.ch)

The goal of this lecture is to provide information about the anatomy of the lung and to provide a structured approach to nodular pattern. High-resolution CT gives detailed morphologic information about lung structures. This allows distinguishing findings by their typical predominance in certain anatomical compartments. The secondary pulmonary lobule is the functional unit of the lung and is the key to HRCT terminology. The anatomy of secondary lobule, therefore, plays a key role. Based on the distribution of nodular lesions in relation to the bronchial, vascular and lymphatic structure of the secondary lobule the number of possible pathologies can be narrowed down. For example, centrilobular predominance of nodules is a frequent sign of bronchiolitis. Perilymphatic predominance in the periphery of the lobules is associated with sarcoidosis or lymphangitic spread of cancer. Random distribution of nodules is interpreted as a sign of haematogenic spread of disease. Therefore, a subtle interpretation can contribute substantially to clinical decision making. Nevertheless, these signs may not always replace biopsy and histologic workup. Sometimes it can be difficult to determine the pattern of lung nodules within the secondary pulmonary lobule. By following a consistent approach it will minimise the difficulty in interpretation. During this lecture, a stepwise algorithm for differentiating nodular pattern will be provided that allows a pragmatic approach for a successful reading of HRCT.

Learning Objectives:

1. To become confident in recognising the anatomical compartments of the lung.
2. To describe typical nodular imaging patterns of lung disease using appropriate terminology.

Author Disclosure:

T. Frauenfelder: Other; Bayer.

A-101 16:28

B. Linear and reticular pattern

F. Molinari; Lille/FR (francescomolinari.dr@gmail.com)

The reticular pattern is one of the imaging findings that may suggest the presence of a diffuse parenchymal lung disease at HRCT. Reticulations are typically formed by a collection of innumerable small linear opacities that by summation produce an appearance resembling a "net". Lines may vary from smooth to nodular and irregular. The resulting "net" may alter the normal HRCT appearance of the lung and become suspected for an underlying lung disease. Chest radiologists typically use a structured approach to interpret this finding and eventually to propose a diagnosis. The radiologic approach consists in identifying the dominant types of lines, in establishing what portion of the lung interstitium is predominantly involved, and in correctly classifying the type of reticulation (namely inter-lobular, peri-lobular, intra-lobular). When all the radiologic features are correctly interpreted, the radiologist can differentiate

reticulations that represent an acute disease from those that indicate a chronic inflammatory or fibrotic change in the lung. In addition, by integrating clinical and laboratory data, it is possible to significantly narrow the final differential diagnosis.

Learning Objectives:

1. To recognise and interpret typical reticular imaging patterns.
2. To differentiate acute and chronic diseases which cause septal patterns.

A-102 16:51

C. Ground glass opacities (GGO) and consolidation

J. Vogel-Claussen; Hannover/DE (vogel-claussen.jens@mh-hannover.de)

Ground glass opacity (GGO) is a nonspecific finding on computed tomography (CT) scans of the chest that indicates a partial filling of air spaces in the lungs by exudate or transudate, as well as interstitial thickening or partial collapse of lung alveoli. The term derives from the similarity in appearance of the small objects to small chips of glass that are a by-product of glass grinding. The differential diagnosis of the many causes of GGO includes pulmonary oedema, infections (including cytomegalovirus and *Pneumocystis jirovecii* pneumonia), various noninfectious interstitial lung diseases (such as hypersensitivity pneumonitis, Hamman-Rich syndrome), diffuse alveolar haemorrhage, and cryptogenic organising pneumonia. Thus, clinical correlation and disease dynamics are important to narrow down the differential diagnosis. The aim of this refresher course is to distinguish ground glass opacities from consolidations on chest CT and give practical instructions for daily clinical routine.

Learning Objectives:

1. To appreciate different conditions which cause GGO pattern and consolidation.
2. To learn how to interpret GGO and consolidation in different clinical settings.

Author Disclosure:

J. Vogel-Claussen: Advisory Board; Bayer. Board Member; IWPF. Consultant; Novartis, Boehringer Ingelheim. Grant Recipient; Siemens.

17:14

Panel discussion: Is it always easy to detect a pattern? Tips for success

16:00 - 17:30

Room X

Joint Session of the ESR Working Group on Ultrasound with EFSUMB

WG/EFSUMB 1

Elastography of superficial structures: where are we now?

Moderators:

M. Claudon; Vandoeuvre-les-Nancy/FR
P.S. Sidhu; London/UK

A-103 16:00

Thyroid US elastography: indications and limitations

V. Cantisani; Rome/IT (vito.cantisani@uniroma1.it)

Thyroid gland examination by palpation is a basic method in the assessment of thyroid nodules as firm and anelastic lesions should be suspected being of malignant nature. On the other hand, US, despite its high sensitivity for the detection of thyroid lesion, has limited accuracy to differentiate benign and malignant lesions. Indeed, to date, FNAC is still considered the gold standard for optimal characterisation of thyroid lesions, but still in 15% to 25% of cases FNAC findings can be suspicious and in 5% to 15% of cases inconclusive. Elastography is a new imaging modality where elastic tissue parameters related to the structural organisation of normal and pathological tissues are imaged. The relationship of tissue elasticity and hardness to Cy follows the basic principle that to be palpable, the object must be harder than the surrounding tissue. The evaluation of stiffness can be qualitative with a color coding system or semiquantitatively by means of strain ratio or ECI or quantitatively (sp-SWE or 2D-SWE). Elastography has showed good diagnostic values both with qualitative and quantitative modalities. However, to date, still some issues may be answered. The main features, the diagnostic accuracy and the main recognised limitations of the different elastographic techniques, suggesting how we can improve accuracy, and reduce interobserver variability will be presented. Personal experience and review of the literature will be provided.

Learning Objectives:

1. To learn about updated status on thyroid nodule evaluation by using TIRADS and US-elastography.

Wednesday

2. To provide tips and tricks, guidelines established indications and limitation of thyroid US-elastography.

Author Disclosure:

V. Cantisani: Speaker; bracco, samsung, toshiba.

A-104 16:20

Elastography of the breast: when should we assess tumour stiffness?

J. [Carlsen](#); Copenhagen/DK (jonathan.carlsen@gmail.com)

Elastography is an adjunct to B-mode imaging in breast tumour evaluation and has been included in the latest BIRADS atlas of 2013. Both quantitative and qualitative elastography methods can be used to assess breast tumour stiffness, which correlates with the risk of malignancy. Elastography is easily performed, and is implemented in most new ultrasound systems, but depending on the elastography method used, different diagnostic cut-offs or visual scoring systems are used. As a stand-alone examination elastography is inferior to B-mode imaging, but in combination with B-mode imaging, elastography may be used to determine whether or not to perform biopsies or do follow-up examinations in low-suspicion tumours. Different ways of combining the two diagnostic methods have been proposed, and the diagnostic algorithms will vary depending on the clinical practice and setting used. It is therefore important, to understand the different elastography methods, their pitfalls and limitations.

Learning Objectives:

1. To learn how to perform elastography of the breast with different US techniques.
2. To learn when breast elastography is a useful adjunct to the standard breast ultrasound examination.
3. To understand the potentials and limitations of breast elastography.

A-105 16:40

Is there any value in tendon and nerve assessment?

A. [Klauser](#); Innsbruck/AT

The Achilles tendon has been the most studied musculoskeletal structure with strain and shear wave elastography (SWT). Alterations in strain elastograms of asymptomatic Achilles tendons mainly occur in the mid-portion, they do not always correspond to changes on conventional US. This has been correlated with histology, where the sensitivity of strain elastography was better than B-mode US in Achilles tendons, flexor and extensor tendon insertions of the elbow for the detection of tendinotic changes. SWT confirmed and quantified softening within the Achilles tendon in patients and in lateral epicondylitis significantly lower strain ratios in the common extensor tendon origins in terms of tendon softening can be observed. For peripheral nerves strain elastography has shown, that the diagnostic accuracy of ultrasonographic assessment can be improved. Furthermore the stiffness of the intracarpal tunnel contents in untreated CTS patients is higher than that of healthy volunteers but decreases after corticosteroid injection. Shear-wave elastography provides a further exciting tool for examining nerve biomechanics; however, longitudinal studies are needed to elucidate clinical relevance before they can be adopted into routine clinical practice. To summarize, elastography can be used as a supplementary tool to conventional US scanning to increase the diagnostic confidence in diagnosing tendinopathies.

Learning Objectives:

1. To learn about the value of sonoelastography in musculoskeletal disorders.
2. To understand the impact of sonoelastography in tendon and nerves.
3. To appreciate the meaning of sonoelastographic findings in tendon and nerve disorders.
4. To become familiar with sonoelastographic techniques used in tendons and nerves.

A-106 17:00

Scrotal elastography: hype or real?

M. [Bertolotto](#); Trieste/IT (bertolotto@units.it)

The testis is readily palpable, allowing a direct examination of masses. Hard lesions at palpation are considered likely malignant, until proved differently. Compared to palpation elastography provides a more objective evaluation of tissue consistency, but the information provided is basically the same. As a consequence, benign pathologies that are hard at palpation will display increased consistency at elastography as well. On contrary, malignant tumours may display soft areas, or appear globally soft. Correlation with histologic features helps explain these discrepancies, and changes in time of elastographic appearance of evolving lesions. Use of elastography in evaluation of diffuse testicular pathologies affecting endocrine function and spermatogenesis is undergoing investigation in an attempt to find new clinically useful independent parameters. A quantitative evaluation of testicular stiffness is feasible using shear-wave modes. In preliminary experience, the elasticity

pattern of the testis seems to be related to the volume and function. Elastography, in particular, seems promising to differentiate azoospermia from different causes. The clinical impact of these findings in the current practice is, however, questionable and technical optimization is necessary.

Learning Objectives:

1. To learn about how to perform elastography of the testis with the different US equipment.
2. To become familiar with the appearance of normal testis at strain and at shear wave elastography.
3. To understand the potential and limitation of elastographic modes in imaging scrotal pathologies.

17:20

Discussion

16:00 - 17:30

Room O

Paediatric

RC 412

Vascular and interventional radiology in children

Moderator:

E. Alexopoulou; Athens/GR

A-107 16:00

A. Common IR procedures in children: state-of-the-art

A. [Barnacle](#); London/UK (Alex.Barnacle@gosh.nhs.uk)

Interventional radiology (IR) procedures are now a vital part of paediatric care for most complex diseases, providing reliable intravenous access and feeding tube support during intensive therapy such as chemotherapy and delivering innovative minimally invasive therapies for other conditions to avoid surgery. Central venous access in children can be technically challenging, but is quicker and less invasive than open surgical techniques and there is evidence to suggest that the central veins are preserved for longer, which is key in children with chronic disease. Looking beyond central venous access, paediatric IR delivers therapies such as sclerotherapy for vascular malformations, percutaneous nephrolithotomy (PCNL) for renal stone extraction, oesophageal dilatations to manage oesophageal structures and biopsy to safely and accurately stage childhood tumours.

Learning Objectives:

1. To learn about the most common causes for image-guided intervention in children.
2. To understand how the practical and technical approach to intervention in a child differs from that in adults.
3. To appreciate tips, tricks and pitfalls in the paediatric intervention.

A-108 16:30

B. Vascular malformations: diagnosis and interventions

N.N.

Learning Objectives:

1. To learn about the classification of paediatric vascular malformations.
2. To understand the diagnostic work-up and the indications for percutaneous treatment of paediatric vascular malformations.
3. To appreciate the treatment options for different vascular malformations.

A-109 17:00

C. Percutaneous treatment of osteoid osteoma

D. [Filippiadis](#); Athens/GR (dfilippiadis@yahoo.gr)

Percutaneous treatment of osteoid osteoma. Osteoid osteoma is a benign inflammatory bone tumor encompassing 2-3% of all bone tumors and 10% of benign bone tumors; it is most common in males < 25 years of age with patients typically complaining of pain that worsens at night and is promptly relieved by salicylates. The tumor was first reported by Jaffe in 1953; osteoid osteoma is composed of the nidus which is bone at various maturity stages surrounded by highly vascular connective tissue stroma. Depending on the location and axial imaging findings, osteoid osteoma can be classified into subperiosteal, intracortical, endosteal or intramedullary, and intra-articular with the latter being the least common type and refers to lesions located within or near a joint. In the literature there are scarce studies with limited patient number reporting disappearance of the pain post conservative therapy even if the imaging findings remain with no change; however, the long term use of

Postgraduate Educational Programme

NSAIDs can result in potential complications and additionally there is a chance of muscular atrophy and bone deformity in ages <5 years. The application of radiofrequency ablation (RFA) was introduced in clinical practice by Rosenthal in 1992 performing a percutaneous approach for the treatment of osteoid osteoma. Nowadays thermal ablation of osteoid osteoma constitutes a first line therapy. Numerous studies upon all ablation techniques, others with lesser and others with higher numbers of patients report high pain reduction rates (up to 96%) and low recurrence rates (~7% at 2 years). Comparing percutaneous ablation to the traditional surgical techniques for osteoid osteoma (wide excision removing a bone block, marginal resection of the entire nidus, curettage or high speed burr techniques) favors percutaneous approach in terms of minimum trauma, minimum functional restriction and significantly lower cost.

Learning Objectives:

1. To learn about the treatment options for osteoid osteomas.
2. To understand the techniques for percutaneous treatment of osteoid osteoma: preparations, procedure and follow-up.
3. To appreciate advantages and potential complications in percutaneous treatment of osteoid osteoma in children.

16:00 - 17:30

Room N

Head and Neck

RC 408

Pathways for tumour spread

Moderator:

J. Huyskens; Antwerp/BE

A-110 16:00

A. Pathways for oral cavity and oropharynx tumour spread

A. Borges; Lisbon/PT (borgalexandra@gmail.com)

90% of oral cavity and oropharyngeal malignancies originate from the epithelial lining and spread superficially along the mucosa and deeply into the submucosa, adjacent muscles, bone, and along cranial nerves. As local tumour staging is based on size, depth of invasion and involvement of adjacent structures, imaging is crucial in this regard. There are 8 tumour subsites in the oral cavity each with different patterns of spread and different implications on management. Those with direct impact on surgical management are the midline raphe, extrinsic tongue muscles, bone and oropharyngeal spread. Tumours of the retromolar trigone disseminate in a complex pattern as they lay in the crossroad between the oral cavity, masticator space and oropharynx. Patients tend to present in late stages, often with trismus. Whereas tumours of the superior alveolar ridge can invade the maxilla and spread along the superior alveolar nerves and V2, tumours of the inferior alveolar ridge can invade the mandible, the inferior alveolar nerve and spread along V3. Invasion of the neurovascular tongue bundle prone tumours to spread along the lingual or hypoglossal nerves. There are 4 different oropharyngeal subsites. The palatine tonsil has the highest association with lymph node metastases. Local spread is through the palatoglossus muscle and transgression of the constrictor muscles and pterygomandibular raphe lead to tumour extent into the retromolar trigone and pterygoid plates. Tongue base tumours can spread anteriorly to the tongue root and floor of the mouth and posteriorly into the supraglottic larynx. Palatal tumours spread inferiorly into the palatine fossa, laterally into the parapharyngeal space and are prone to perineural spread along the greater and lesser palatine nerves.

Learning Objectives:

1. To become familiar with the anatomy of the oral cavity and oropharynx.
2. To learn which imaging technique to use.
3. To understand the typical local and remote spread of oral cavity and oropharynx tumours.

A-111 16:30

B. Pathways for nasopharyngeal tumour spread including perineural spread

M. Lell; Nuremberg/DE

The nasopharynx is the uppermost portion of the pharynx, extending from the skull base to the soft palate. Its main connections are the nasal cavity anteriorly and the oropharynx inferiorly. The nasopharynx is best imaged by MRI to detect the primary tumour, lymph node metastases as well as intracranial and bone invasion and perineural tumour spread (PNS). Nasopharyngeal cancer (NPC) frequently arises in the fossa of Rosenmuller, invades or displaces the parapharyngeal fat laterally and can cause obstruction of the Eustachian tube, leading to fluid retention in the tympanon and mastoid cells. Often subtle and therefore more difficult to detect than direct invasion is PNS. PNS most commonly occurs in a contiguous retrograde fashion from the

primary tumour toward the intracranial compartment. PNS in NPC most commonly involves branches of the trigeminal and facial nerves. These 2 nerves are responsible for most of the sensory and motor innervation of the face. The trigeminal nerve provides sensory information from the face and motor innervation to the muscles of mastication. Understanding the CN anatomy is critical in identifying PNS.

Learning Objectives:

1. To become familiar with the anatomy of the nasopharynx.
2. To learn which imaging technique to use.
3. To understand the typical local and remote spread of nasopharyngeal tumours, including perineural spread.

A-112 17:00

C. Pathway for laryngeal and hypopharyngeal tumour spread

R. Kohler; Sion/CH (romain.kohler@hopitalvs.ch)

Squamous cell carcinoma is by far the most frequent malignant neoplasm of the larynx and hypopharynx and imaging plays a critical role in its diagnosis and management as only its superficial part is accessible to endoscopic evaluation. The larynx and hypopharynx are both divided into three subsites (supraglottis, glottis, subglottis and piriform sinus, retro cricoarytenoid region and posterior wall, respectively). Other important landmarks are the cartilages (especially the thyroid and cricoid cartilages) and the paraglottic and preepiglottic spaces. After a short overview of the imaging techniques, we will discuss in detail the most important pathways of tumour dissemination of supraglottic, glottic, subglottic, piriform sinus, retro cricoarytenoid, and posterior wall cancer. Endolaryngeal dissemination is from one anatomical structure to another in the same subsite, from one subsite to another, to the prepiglottic/paraglottic spaces or to the cartilages. Extralaryngeal dissemination means extension through the cartilages or laryngeal membranes into the soft parts of the neck. Criteria for cartilage invasion, dissemination to lymph nodes and distant metastases will also be discussed. The description of all invaded structures is of greatest importance for the planification of surgery or radiation therapy as invasion of some specific structures upstages the tumour. Finally, two non-epithelial malignancies with particular appearance and neoplastic extension are presented: lymphoma and chondrosarcoma.

Learning Objectives:

1. To become familiar with the anatomy of the larynx and hypopharynx.
2. To learn which imaging technique to use.
3. To understand the typical local and remote spread of laryngeal and hypopharyngeal tumours.

16:00 - 17:30

Room L 8

Joint Session of the ESR and ESMRMB

ESR/ESMRMB 1

Exploring the microscopic from macroscopic: the strengths of multiparametric MRI

Moderators:

D. Sappey-Marini; Lyon/FR

T. Leiner; Utrecht/NL

A-113 16:00

C. Modelling brain multicompartement microscopic diffusion

C. Poupon; Gif-sur-Yvette/FR (cyril.poupon@cea.fr)

Diffusion-weighted magnetic resonance imaging (dMRI), sensitised to the diffusive motion of water along the direction of an applied magnetic field gradient, has become a well established technique to non-invasively probe the cellular organisation of tissues, providing access, for instance, to the human brain structural connectivity in vivo. Because the contrast of results from restrictions of water molecule trajectories by cell membranes populating the tissue, it also embeds key information about the tissue at cellular scales than can be deciphered using advanced models. Such models rely on the use of several compartments corresponding to the numerous cell populations composing the tissue that can be modeled using analytical equations involving the key characteristics of the various populations, like their volume fraction or statistics of cell dimensions (eg axon diameter, size of neuron bodies, ...). The presentation will address the various models proposed in the literature to characterise brain white matter microstructure, including CHARMED, AxCaliber, ActiveAx, and how they are about to revolutionise the in vivo mapping of the human brain cytoarchitecture. The NODDI model also able to characterise the dendrite arborisation within the cortical ribbon will be presented too, as well as the Intra-Voxel-Incoherent-Motion model providing

Postgraduate Educational Programme

insights about the microvascular compartment irrigating the brain parenchyma. Case studies will be presented during the whole presentation to illustrate the strengths and weaknesses of these novel tools that progressively turns diffusion MRI into a virtual microscope able to perform virtual biopsies in vivo.

Learning Objectives:

1. To learn about the basic principles of diffusion MRI used to turn MRI into a virtual microscope.
2. To understand the potential of diffusion MR microscopy to map in vivo the organisations of brain tissues at cellular scales.
3. To appreciate the potential of brain microstructure maps to provide more specific imaging biomarkers of brain disorders.

A-114 16:30

How quantitative MRI reveals brain microstructure

C. [Granziera](#); *Basle/CH (cristina.granziera@usb.ch)*

This lecture will first introduce the difference between quantitative and conventional MRI, underlying the advantages and disadvantages of both. Then, we will focus on the biological and pathological significance of quantitative and semi-quantitative MRI contrasts (q/sqMRI) such as T1, T2, T2* relaxometry, magnetization transfer imaging, quantitative susceptibility mapping, and diffusion MRI. In the second part of the lecture, several examples will be presented related to studies where multiple q/sq MRI metrics were applied to answer specific pathophysiological or clinical questions in patients affected by neurological diseases (i.e., multiple sclerosis, stroke, migraine and neurodegenerative diseases). Through these exemplary studies, we will present the advantages and disadvantages of q/sqMRI in clinical research and the potential perspectives for clinical routine applications. As well as, we will illustrate the potential gain derived by the combination of multiple q/sqMRI contrasts in comparison to single contrasts approaches. Finally, on-going developments will be presented in the field of quantitative MRI, especially regarding fast and robust qMRI acquisition schemes, multi-parametric qMRI protocols as well as personalized ways of quantifying brain damage and repair using multiple q/sq MRI metrics.

Learning Objectives:

1. To learn about the biological and pathological significance of quantitative and semi-quantitative MRI contrasts (q/sqMRI).
2. To understand the on-going methodological developments in the field of q/sqMRI.
3. To appreciate the potential perspectives of multiple q/sqMRI contrasts for clinical routine applications.

Author Disclosure:

C. Granziera: Patent Holder; Patent #16171060.3-1501 (07-29-2016): "Apparatus and method for visualizing tissue macro- and microstructure for pathology evaluation in magnetic resonance imaging". Other: Ongoing scientific collaborations with the ACIT Siemens-Radiology team in Lausanne (CH).

A-115 17:00

MRI of cardiac muscle microstructure

M. [Froeling](#); *Utrecht/NL (M.froeling@umcutrecht.nl)*

Investigating microstructural changes in the heart using DWI is mostly done using the DTI model. However, other models are being explored, e.g. IVIM and DKI. DWI of the can be challenging due to its low T2 relaxation time of only 30 to 50 ms. DWI imaging is typically done using a spin echo - echo planar imaging sequence (SE-EPI). The diffusion of water in the heart is fast ($MD \approx 1.6$ to 1.8 mm²/s) and the diffusion anisotropy is low ($FA \approx 0.20$ to 0.4). DWI of the beating heart is challenging due to that the heart is always moving. Measuring the microscopic motion of water in the presence of macroscopic motion needs a different diffusion sequence design. To overcome this two different approaches are possible: (1) using a stimulated echo acquisition (STEAM) which applies the diffusion weighting over two consecutive heartbeats and (2) Designing the diffusion weighting wave form to become insensitive for macroscopic motion. Diffusion tensor imaging in the heart is of great interest since it allows to, next to diffusion parameters, obtain detailed information about the cardiac myocardial architecture. Myocytes are aligned in a left-handed helix in the epicardium, to circumferential in the mid wall, to a right handed-helix in the endocardium. The heart muscle fibers are arranged in a laminar structure, called sheetlets. Changes of myocardial architecture over the cardiac cycle during development and in pathology have been studied and can potentially give new insights in cardiac function and disease and monitor of cardiac therapy.

Learning Objectives:

1. To learn about the state-of-the-art quantitative diffusion MRI acquisition strategies to investigate cardiac and skeletal muscle.
2. To understand the limitations of such methods and confounding factors, such as noise, inflammation, fat and other artefacts.
3. To appreciate the potential perspectives in a clinical setting.

16:00 - 17:30

Room E1

Breast

RC 402

Screening for breast cancer

A-116 16:00

Chairperson's introduction

F.J. [Gilbert](#); *Cambridge/UK (fjg28@cam.ac.uk)*

In 2003 the European Council recommended implementation of screening according to best practice guidelines and that mammography is offered every two years to women between the ages of 50-70 years. Apart from the three yearly programme in the UK all countries offer two yearly mammography or digital breast tomosynthesis (DBT). Nine countries start at age 40 or 45 years with 18 at age 50 years. Three countries stop at 64 years, with the majority at stopping at age 69 years although 3 countries continue until age 74 years. Uptake varies between 37-85% with Latvia and Poland having the lowest uptakes and Finland, Ireland and Holland having the highest acceptance rates. Some countries offer supplemental screening with ultrasound to women with increased breast density. It is known that high breast density increases the likelihood of developing breast cancer by twofold in the over 50 year age group and that increased breast density increases the chance of a cancer being missed or not being detected until the tumour is of a larger size. Digital breast tomosynthesis has been shown to have increased cancer detection together with reduced recall rates. Some countries have adopted this technology while others are conducting large randomised controlled trials to establish the impact, costs and benefits of this more complex examination. It is important to ascertain that when changing an established population screening programme this will result in a survival benefit and not merely increase over diagnosis.

Session Objectives:

1. To learn about mammography screening and how it should be monitored.
2. To understand the value of supplementary techniques and how it should be used in practice.
3. To recognise that tomosynthesis presents significant advantages and disadvantages when used in a screening setting.

Author Disclosure:

F.J. Gilbert: Equipment Support Recipient; GE Healthcare. Grant Recipient; GE Healthcare. Research/Grant Support; Hologic.

A-117 16:05

A. Screening with mammography only

R.M. [Pijnappel](#); *Utrecht/NL (r.m.pijnappel@umcutrecht.nl)*

Screening with mammography has proven to save lives. The reduction in mortality is substantial. In Netherlands, woman who attend all biannual offered screening rounds from 50-75 years reduce their change of dying from breast cancer before the age of 80 with 50%. The basis for this positive effect from screening with mammography only is training and auditing. The shift from analogue form to digital between 2005-2010 has improved these results and showed that more high risk tumors were detected by mammography. The cost effectiveness of screening with mammography only is acceptable. The drawbacks of screening with mammography only, i.e., false positive and overdiagnosis will be discussed. So far, no other modality has proven to save lives and no information is available regarding the aggressiveness of the breast cancers detected by other modalities like ultrasound MRI and tomosynthesis. The positive predictive value of ultrasound is substantially lower and quality control (operator dependent) is difficult. Tomosynthesis is very promising, but at this moment there is very little information regarding detection in subsequent rounds and interval cancers. For these reasons screening with mammography only still is the gold standard for population based screening with an average risk.

Learning Objectives:

1. To learn about benefits and limitations of mammography screening.
2. To become familiar with common findings, recall rates and assessment outcomes.
3. To appreciate errors.

A-118 16:30

B. Screening with mammography and ultrasound

T.H. [Helbich](#); *Vienna/AT (Thomas.Helbich@meduniwien.ac.at)*

The sensitivity and specificity of mammography are limited in highly fibroglandular /dense breasts. Digital mammography provides increased sensitivity in young women and those with moderately dense breasts, and digital three-dimensional mammography (tomosynthesis) promises further

Postgraduate Educational Programme

improvement. For women with the densest breasts, however, radiography is unlikely to be the optimum solution. MRI, although not affected by breast density, is expensive and access is often limited. Ultrasonography is attractive for breast cancer screening because, likewise, it is not impaired by breast density, and it avoids the use of ionizing radiation and the need for breast compression. Nevertheless, enthusiasm for the use of ultrasonography has been limited because its specificity has been much lower than that of mammography, but technical developments have given rise to sharper, more informative images. These improvements foster the use of ultrasound particular in those women with higher breast density. Different trials have been performed and promising results have been reported. This talk will focus on benefits, harms, and cost-effectiveness of supplemental ultrasonography screening for women with dense breasts.

Learning Objectives:

1. To learn about the added value of US in screening and its indication.
2. To become familiar with the common level of evidence.
3. To appreciate its role in clinical practice.

A-119 16:55

C. Screening with tomosynthesis

U. Bick; Berlin/DE (Ulrich.Bick@charite.de)

By eliminating ambiguity from superposition of normal breast parenchymal structures, digital breast tomosynthesis (DBT) holds the potential to improve cancer detection rates while at the same time reducing call-backs related to false-positive findings. The magnitude of these two effects will depend on the clinical setting. In European population-based screening programs, where recall rates are kept low, DBT will primarily increase detection rates. On the other hand, in screening practices with high recall rates such as North America, the main effect of DBT will be to lower recall rates by improving specificity. In screening, the advantages of DBT must be weighed against the potential disadvantages of DBT such as higher costs (higher equipment and image storage costs, longer reading times) and possible increases in radiation exposure, especially if DBT is used as an adjunct to 2D mammography. However, synthetic 2D views reconstructed from the DBT dataset can be used to replace 2D mammography in screening. Although depiction of subtle microcalcifications may be slightly inferior on synthetic 2D views, studies have shown no significant difference in terms of detection rates or recall frequency between 2D mammography and synthetic 2D views. Despite the very promising data from the available first DBT screening trials, which all showed a significant increase in detection rates with DBT, further studies are needed before DBT can replace 2D mammography in population-based screening programs. The key question still unanswered up to now is whether the additional cancers found by DBT are in the majority clinically relevant and contribute to a reduction in advanced-stage interval cancers.

Learning Objectives:

1. To learn about the role of tomosynthesis in the screening setting.
2. To become familiar with the different protocols.
3. To appreciate potential advantages of tomosynthesis in screening.

Author Disclosure:

U. Bick: Patent Holder; Hologic, Inc.

17:20

Panel discussion: What is the best modality approach to screen for breast cancer?

16:00 - 17:30

Room E2

Professional Challenges Session

PC 4

Mass casualties

A-120 16:00

Chairperson's introduction

M. Scaglione; Castel Volturno/IT

Recent mass casualty incidents have raised many problems in the western world, requiring a wide revision of many aspects of the civil life, ranging from the public order to medical facilities. More specifically, this "new" emergency needs planning, governance, education and specifically, a new team work mentality. In this Session, not only the strength and limits of imaging in massive attacks from Paris to Brussels, Thai tsunami and migrant victims drowned in the Mediterranean sea will be discussed, but also the need for a plan and areas of improvements will be illustrated. Finally, the new roles and challenges for the radiologists in A&E will be pointed out.

Session Objectives:

1. To understand about the need of a new plan for emergency hospitals.
2. To become familiar with the range of imaging findings related to MCI.
3. To learn about new roles and challenges for radiologists in Europe.

A-121 16:05

Mass casualty incidents: the London framework for planning

S. Vaidya; London/UK (Sujit.Vaidya@bartshhealth.nhs.uk)

Mass casualty events challenge and have a capacity to rapidly overwhelm healthcare systems. Over recent years, we have felt the need to have an organized response to major events, to effect better patient care and flow. Collaboration, co-operation, and meticulous planning eventually helps save lives and limbs. This talk will outline some of the guiding principles of this collaboration. There is a need for the imaging department to adapt to the altered demands in such situations. Our experiences, successes and inefficiencies will be shared with a view to understand the challenges.

Learning Objectives:

1. To understand the objectives of the plan.
2. To appreciate the role of imaging in mass casualty.
3. To provide an overview of the major incident planning in London.

A-122 16:23

Lesson learned from the Paris attacks

P.A. Grenier; Paris/FR (philippe.grenier@aphp.fr)

Following the multiple mass casualty terrorist attacks on November 13th, 2015 in Paris, several measures have been taken in France to improve our medical capacity to face the unexpected. French Military Medical Service was asked to transfer their expertise into the civilian setting, favouring the concept of prehospital damage control to the civilian prehospital phase. A teaching of civilian surgeons, anesthesiologists, and emergency physicians by their military colleagues about damage control resuscitation and surgery, triage and care "under fire" was organized at national and regional levels. An online course is now accessible on demand. Dedicated teaching for all medical students and dedicated course in trauma management during residency have been implemented. Mobilization of the other regions seems to be essential to activate rapidly distant additional means and to identify quickly additional preserved resources, according to a medical strategy coordinated by experience health care professionals. Hospital trauma teams have improved their ability to triage between absolute and relative emergencies. Some multidisciplinary simulation exercises particularly focused on triage were performed. Identification of the victims was clearly a deficiency during the Paris and Nice attacks particularly those left dead on scene. Priority is given to identification process with the collection of primary identifiers combined with external examinations of deceased victims. During and after the attacks, a large number of individuals required psychological care. It requires a large mobilization of psychiatrists and psychologists able to cope with acute stress and to take on a continuous flow of patients over weeks or months.

Learning Objectives:

1. To learn from the terrorist attacks in Paris and Nice.
2. To understand the planning for pre-hospital damage control, medical strategy for quick mobilisation of resources, training and multidisciplinary simulation exercises, and post-trauma psychological care.
3. To appreciate the role of imaging in case of massive attack.

A-123 16:41

Postmortem imaging of migrant victims drowned in the Mediterranean Sea

G. Lo Re; Palermo/IT (giuseppe.lore12@gmail.com)

Europe is involved in a large-scale migratory flow coming from Africa and Middle East, and Italy is often the first step towards European countries for migrants. This high number of people may determine some issues related to public security, financial aspects, and ethical issues. In the last years, and until now, we have assisted to numerous shipwrecks in the Sicilian Sea, and sometimes we had the opportunity to study, with radiological images, the dead corps recovered at sea. For example, in 2016, a large number of corpses, more than 150, were studied using a multislice CT scanner; the bodies came from a shipwreck of an overcrowded boat drowned off the Libyan coasts in April 2015. Other corpses were recovered at sea, and in particular near Trapani we recovered two child corpses drowned during transshipment operations. Radiology in these cases could be essential in helping forensic pathologists and police activities, speeding up and making more secure identification of people and diagnosis of eventual pathological events. Study of number, type, congruency, calluses, fractures and anthropometric measurements of bones, teeth, growth-cartilages and of internal/external genitals helped to identify sea victims. Furthermore, study of foreign objects

Postgraduate Educational Programme

was useful for bodies identification and for a better knowledge of the travel conditions of migrants. Radiology has a pivotal role in mass disasters, especially in migrant victims, and can help in determining age of people died and alive.

Learning Objectives:

1. To describe typical findings and pitfalls of virtopsy in mass casualty emergency.
2. To understand the strength and limits of forensic radiological examination.
3. To become familiar with postmortem imaging.

A-124 16:59

High-end CT imaging in forensic medicine: experience after recent Brussels terror attacks

W. [Develter](mailto:wim.develter@uzleuven.be); Leuven/BE (wim.develter@uzleuven.be)

The importance of radiology in the evolution of the ID-process. Experiences from former mass disasters revealed an evolution in the identification process. Digitalisation boosted logistics and the ongoing technical revolution made of radiology an indispensable versatile instrument. Radiology that was used for individual diagnostics is now applied for screening - triage and diverse documentation (identification, legal inquiry and reconciliation).

Learning Objectives:

1. To illustrate MC findings from the Thai Tsunami over the MH-17 to the Brussel attacks.
2. To become familiar with the imaging findings related to unidentified people and its medico-legal related issues.
3. To understand the importance of imaging in the reconciliation process with the relatives of the victims.

17:17

Panel discussion: How to be prepared accordingly?

16:00 - 17:30

Room F1

E³ - Rising Stars Programme: Basic Sessions

BS 4

Thoracic emergencies

Moderator:

K. Malagari; Athens/GR

A-125 16:00

Acute aortic syndrome

T. [Jargiello](mailto:tojarg@interia.pl); Lublin/PL (tojarg@interia.pl)

Acute aortic syndrome (AAS) describes symptoms relevant to severe chest or back pain caused by several aortic pathologies which can be potentially life threatening. The most common aetiology, compromises the majority of AAS is aortic dissection. Other causes of AAS with similar presentation include intramural haematoma, penetrating aortic ulcer (atherosclerotic), aneurysm formation (rupture, enlargement), and traumatic transection (pseudoaneurysm). Imaging plays a vital role in diagnosing AAS. The role of the plain chest radiograph is nowadays historic. Echocardiography (plain or transoesophageal) is an effective portable tool, but does not visualise the whole thoracic aorta. It may only suggest a certain AAS aetiology. Contrast enhanced CT is now considered as the diagnostic method of choice. It provides accurate aortic assessment as well as detailed evaluation of other thoracic structures. CT permits 3D reconstructions, essential for intervention planning and it is widely available. Its sensitivity for aortic disorders reaches 100%. MRI is another imaging modality to diagnose AAS. Although it provides greater anatomical detail than CT, it is seriously limited. The limitation involve procedure time, lesser availability, and the expense.

Learning Objectives:

1. To become familiar with the most common aetiologies of acute aortic diseases.
2. To present current imaging techniques for evaluation of acute aortic diseases.
3. To demonstrate the most important imaging findings.

A-126 16:30

Pulmonary embolism

C. [Loewe](mailto:christian.loewe@meduniwien.ac.at); Vienna/AT (christian.loewe@meduniwien.ac.at)

Pulmonary embolism (PE) represent a daily clinical challenge at the emergency department: out of the patients admitted to an emergency room because of the very unspecific clinical symptom of chest pain and/or dyspnea,

the early identification of patients with an high clinical likelihood for PE is a difficult task. The D-Dimer test is very sensitive, but unspecific for pulmonary embolism, and using this test without clinical assessment, a high number of false positive patients will result. On the other hand, PE is potentially life threatening; and early and safe diagnosis of this relevant disease is important to improve patient's outcome. CT angiography of the pulmonary arteries has been established as the first method of choice to accurately detect PE with an high PPV and NPV. This presentation will provide an overview about the diagnostic challenges in the chest pain unit will explain the need for accurate clinical assessment to select the right patient for the appropriate diagnostic test. Furthermore, the risks due to overdiagnosis or false-positive diagnosis will be exemplified. In the second part, this presentation will focus on the radiological view on this picture by explaining an optimized imaging technique and possible pitfalls and problems. Challenging situations in the daily clinical practice will be discussed by addressing the role of imaging in suspected PE in pregnancy and in the oncologic patients. Finally typical findings in acute and chronic pulmonary embolism will be reviewed.

Learning Objectives:

1. To review the most common pathologies leading to pulmonary embolism.
2. To present current imaging techniques for evaluation of pulmonary embolism.
3. To become familiar with the typical findings in acute and chronic pulmonary embolism.

Author Disclosure:

C. Loewe: Speaker; GE Healthcare, Bracco, Siemens.

A-127 17:00

Acute coronary syndrome

R.M.M. [Hinzpeter](mailto:Ricarda.Hinzpeter@usz.ch); Zurich/CH (Ricarda.Hinzpeter@usz.ch)

Normal anatomic conditions of the coronary arteries consists of two main coronary arteries, a left coronary artery and a right coronary artery arising from the coronary sinuses in the proximal ascending aorta immediately distal of the aortic valve. The right coronary artery descends in the right atrioventricular groove to the inferior surface of the heart, continuing as the posterior descending artery representing a right dominant circulation. After a short common stem the left coronary artery bifurcates into the left anterior descending, coursing in the anterior interventricular groove and the left circumflex artery coursing in the left atrioventricular groove. After the initial work-up of acute coronary syndrome in the emergency department, including laboratory values and ECG changes, coronary CT angiography (CCTA) as a non-invasive examination plays an important role besides invasive techniques. Especially in patients with low to intermediate risk CCTA is a quick and reliable method for ruling out coronary artery disease with a very high negative predictive value in the absence of coronary artery calcifications. Besides the detection of significant coronary artery stenosis, the presence, amount and composition of non-calcified plaques and the degree of coronary remodelling is substantial. In addition, information about structural changes of the myocardium and myocardial perfusion can be obtained by CCTA.

Learning Objectives:

1. To become familiar with segmental coronary anatomy.
2. To present different techniques for assessment of acute coronary syndrome.
3. To become familiar with the typical findings of acute coronary syndrome.

16:00 - 17:30

Room F2

Multidisciplinary Session

MS 4

The heart team: coronary imaging and treatment

A-128 16:00

Chairperson's introduction

E. [Mershina](mailto:elena_mershina@mail.ru); Moscow/RU (elena_mershina@mail.ru)

Due to the rapid technological progress of non-invasive methods of cardiac visualisation frequent updates on the clinical indications to perform coronary CT angiography (cCTA) and cardiac magnetic resonance (CMR) are required. The role of each method including invasive coronary angiography in diagnostic algorithm in the patients with different degree of coronary artery disease (CAD) probability will be underlined. Various challenges still exist in acquiring high-quality imaging in cardiac CT, such as artifacts due to calcification and metallic densities, motion, noise and poor contrast enhancement. Nevertheless cCTA is the first-line diagnostic tool for low-to-intermediate risk CAD patients. On the other hand an invasive angiography supported by FFR is the method of choice for the patients with high probability of CAD. CMR myocardial perfusion imaging produces accurate information on the presence of myocardial

Postgraduate Educational Programme

ischemia. As a means of guiding the initial management of patients with stable angina and an intermediate-to-high risk of CAD, noninvasive CMR perfusion imaging is comparable to a strategy with invasive angiography supported by FFR. The implementation of different methods for coronary imaging will be illustrated by clinical examples.

Session Objectives:

1. To recognise the possibilities of modern coronary imaging modalities.
2. To explain possible discrepancies in the results of different diagnostic investigations and clinical picture.
3. To understand how to translate the results of coronary imaging into clinical practice.

A-129 16:05

Non-invasive cardiac imaging

V.E. [Sinityn](mailto:vsini@mail.ru); Moscow/RU (vsini@mail.ru)

Major indications for cardiac CT angiography are imaging of coronary arteries in suspected coronary artery disease, visualization of pulmonary veins and planning of endovascular surgical procedures (such as TAVI). Modern types of CT scanners open up the opportunity to reach significant improvements of image quality of coronary arteries and heart structures even in "difficult" patients and to get high quality diagnostic images with very low radiation exposure and less volume of contrast media. The contemporary standard of coronary CTA (CCTA) is prospective-gated or high pitch wide detector or dual source acquisition with iterative image reconstruction. There are some new technologies for assessment of coronary or myocardial blood flow with the help of CCTA such as perfusion CT, CT-FFR, dual-energy CT. Major indications for cardiac MR (CMR) are cardiomyopathies, myocarditis or coronary artery disease (imaging of scars and perfusion). Selection of cardiac MR protocols is dependent on the main indication for examination. Cine-MR, black-blood sequences, perfusion and late gadolinium enhancement modules together with blood flow analysis are the most used ones. Today the tissue characterization modules (T1, T2 mapping) have become the essential part of CMR protocols. Recent changes in cardiological paradigms about approaches to diagnosis, treatment, and assessment of prognosis in patients with coronary artery disease (CAD) together with the technical development of CCTA and CMR and accumulation of scientific data proving the high diagnostic value of both imaging modalities have shown their high value in assessment of prognosis and selection of the optimal therapy.

Learning Objectives:

1. To get knowledge about modern technology and protocols used in coronary/cardiac CT and MRI in coronary artery disease (CAD).
2. To learn about scientific evidence (including results of major clinical trials) supporting use of these technologies in CAD.
3. To be aware about new developments in non-invasive cardiac imaging including studies of coronary flow, myocardial perfusion and hybrid imaging.
4. To understand the role of co-operation between radiologists and cardiologists in non-invasive cardiac imaging for benefit of CAD patients.

A-130 16:25

Interventional treatment/percutaneous

A. [Osiev](mailto:osiev_ag@mail.ru); Moscow/RU (osiev_ag@mail.ru)

The strategy of diagnosis of coronary artery disease (CAD) was changed since non-invasive multi-detector computed tomography (MDCT) had been introduced into the common clinical practice. However, in case of high coronary calcium score the invasive coronary angiography remains the "Gold standard" in CAD diagnostics. Randomised clinical studies demonstrated that primary PCI significantly improve the outcomes in pts with ACS especially presenting with STEMI, but influence of PCI on long-term prognosis in pts with stable CAD is still unclear. Today the most controversial issues are the management of the Left Main CAD and strategy selection of myocardial revascularisation in pts with multivessel disease (MVD). According to recent research data in these cases, we shouldn't make a decision if not to consider SYNTAX Score and SYNTAX score II. As well, the questions of chronic total occlusion revascularisation remain unresolved and require meticulous preliminary non-invasive assessment of myocardial viability. The innovative methods of visualisation are helpful in decision-making in the presence of complex cases. Fractional flow reserve (FFR) measurement provides important information about lesion severity especially in the presence of MVD. Indications for stenting and result assessment can be evaluated by intravascular ultrasound imaging (IVUS) and optical coherent tomography (OCT). MDCT allows the physicians to verify the anatomical features of culprit lesion and key criteria of strategy definition and prediction of procedure success.

Learning Objectives:

1. To learn about the current indications for diagnostic coronary catheterisation and transluminal interventions.
2. To know about the latest innovations in percutaneous coronary revascularisation technique.
3. To understand difficulties in assessment of stenosis and occlusions during coronary interventions.
4. To be aware how combined analysis of coronary CTA and invasive coronary angiography could help in planning of interventional treatment of coronary lesions.

A-131 16:45

The role of coronary imaging in the coronary artery bypass and valve surgery

K. [Mershin](mailto:mershin@moscow.ru); Moscow/RU

Learning Objectives:

1. To learn about surgeon's opinion and the possibilities of different methods of coronary imaging.
2. To understand which coronary imaging modality should be the best in complicated cases.
3. To be aware of CT coronary angiography benefits in the redo procedures.

A-132 17:05

Multidisciplinary case presentation and discussion

Y. [Ashikhmin](mailto:ashikhmin@gmail.com); Moscow/RU (ya.ashikhmin@gmail.com)

At present time, non-invasive cardiac imaging tools intensively penetrate clinical guidelines. Nevertheless, use of modern imaging devices capabilities by majority of cardiologists are still scanty. On the other hand, some physicians have many footless expectations about potential of conventional scanners. The rational diagnostics pathways in typical clinical situations and difficult diagnostic cases will be highlighted within multidisciplinary discussion. An important place will be given to the discussion of implementation of the current guidelines in the real world clinical practice, mentioning the areas of uncertainty and discrepancies in the guidelines as well as evidence-based personalized diagnostic strategies. Furthermore, attention will be paid to cardiovascular prophylaxis, in particular, the usefulness of the coronary calcium scoring will be highlighted. It will be explained how to switch clinicians from invasive procedures to cardiac MRI and CT when it is the best bet. At last, the future of imaging technologies will be discussed, including the present transition from the technology-driven model to the unmet clinical need-driven progress in imagine tools.

Learning Objectives:

1. To outline the rational diagnostics pathways in typical situations: following the guidelines.
2. To learn how to manage the difficult diagnostic cases: beyond the guidelines.
3. To explain how to switch clinicians from invasive procedures to cardiac MRI and CT when it is the best bet.
4. To discuss the future in imaging technologies translation: from the technology-driven to the unmet clinical need-driven progress in imagine tools.

16:00 - 17:30

Room D

Musculoskeletal

RC 410

Bone, joint and soft tissue infection

Moderator:

T. Kaya; Eskisehir/TR

A-133 16:00

A. Osteomyelitis

K. [Verstraete](mailto:ghent.be); Ghent/BE (koenraad.verstraete@ugent.be)

Osteomyelitis (OM) is an infection of the bone, and can present clinically in an acute, subacute or chronic form. Acute OM affects mostly children, just like subacute OM which predominantly presents as a Brodie's abscess. Chronic OM is more prevalent in adults (vascular insufficiency, diabetes mellitus). Routes of contamination are hematogenous (predominantly in children), spread from a contiguous source (cutaneous, dental), or direct implantation (bites, open fractures, postoperative). One to 2 weeks after onset, when >50 % of trabecular bone is destroyed, radiography can detect OM as ill-defined radiolucencies; later findings include extensive osteolysis, periosteal reaction, sequestra, involucrum, sinus (cloaca) through the cortex, and permeative bone destruction, which may resemble a malignant bone tumor. Bone scintigraphy is

highly sensitive for OM and within 48 hours a focus of increased activity in the affected bone can be seen. Specificity is low however, as tumors, trauma, and neuropathic osteoarthropathy can result in hot spots. CT has a limited role in acute OM, but is useful to evaluate complex findings in chronic OM (e.g., sequestra). MRI is the modality of choice to detect acute OM in an early stage: it is highly sensitive and specific demonstrating bone marrow edema, periosteal reaction, soft-tissue edema, abscess formation and sequestra. Gadolinium administration demonstrates enhancement of granulation tissue in the abscess wall, along sinus tracts and around sequestra. Special manifestations are Garré's sclerosing OM, tuberculous OM, diabetic foot (may resemble neuropathic osteoarthropathy), spondylodiscitis, CRMO (chronic recurrent multifocal OM) and SAPHO.

Learning Objectives:

1. To understand the pathophysiology and disease spectrum of osteomyelitis.
2. To learn about the basic imaging criteria for diagnosis of acute and chronic osteomyelitis in children and adults.

A-134 16:30

B. Septic arthritis

M. Zanetti; Zurich/CH (marco.zanetti@hirslanden.ch)

Septic arthritis is often a clinical diagnosis based on physical examination and prompt arthrocentesis. Sampling at arthrocentesis can usually be achieved with needle aspiration imaging guided, such as fluoroscopy, ultrasound, MRI, or CT. Plain radiography and ultrasound have been suggested to be the preferred initial imaging method. If further imaging is required, MRI is the most accurate technique. FDG-PET is also used less commonly. Staphylococcus aureus infection is most commonly seen in acute bacterial arthritis in adults and in children older than 2 years. Most septic joints develop hematogenously. Rarely, acute septic arthritis may also occur as a result of joint aspiration or local corticosteroid joint injection. In addition, bacterial arthritis may arise secondary to trauma even without an obvious break in the skin. Bacterial arthritis, in association with arthroplasties is commonly seen in our areas. In infants, small capillaries cross the epiphyseal growth plate and permit extension of infection into the epiphysis and joint space. In children older than 1 year, osteomyelitis infection presumably starts in the metaphyseal sinusoidal veins and is usually contained by the growth plate. The joint is spared unless the metaphysis is intracapsular. In adults, the growth plate has resorbed and the infection may again extend to the joint spaces. Based on these considerations the basic imaging criteria for diagnosis of septic arthritis in adults will be shown.

Learning Objectives:

1. To understand the pathophysiology and disease spectrum of septic arthritis.
2. To learn about the basic imaging criteria for diagnosis of septic arthritis in children and adults.

A-135 17:00

C. Pyomyositis and other soft tissue infections

D.J. Wilson; Oxford/UK (davidwilson.stlukes@btconnect.com)

Soft tissue infection can range from a minor wound infection through cellulitis to pyomyositis and necrotising fasciitis. At one end of the spectrum the treatment may be limited to anti-sepsis and oral antibiotics whilst at the other many months of intravenous antibiotics and radical surgery may be necessary. Severe infection may be rapidly fatal. Imaging plays a crucial role in the detection of the extent of infection, the detection of abscesses and the planning of surgical procedures. It is also very useful in determining response to therapy. Ultrasound and MRI are the principal techniques. The strength of ultrasound has its rapid availability and discrimination of free fluid from oedematous solid tissue. It is also critically helpful in detecting foreign material which could be a source and irritant causing persisting infection. MRI gives us a much better overview showing bone involvement and extent of tissue damage or destruction. There is a role for both techniques and their often complementary. The first and perhaps most important lesson is to recognise the risk of infection. This is particularly true for patients who are immunosuppressed or diabetic. The symptoms may be relatively minor and these immune compromised individuals should be a low threshold for performing imaging investigations. Imaging may be used to guide aspiration of cavities and biopsy of tissue to identify organisms. On rare occasions the primary treatment of abscesses may be via sump drainage catheter is placed using ultrasound guidance. Normally these patients are treated with surgery to include excision of necrotic tissue, but there are occasions when patients are unfit for anaesthetic and ultrasound guided techniques assist.

Learning Objectives:

1. To understand the pathophysiology and disease spectrum of pyomyositis and other soft-tissue infections.
2. To learn about the basic imaging criteria for diagnosis of these conditions.

16:00 - 17:30

Room G

Special Focus Session

SF 4

Gadolinium deposition: is it harmful?

A-136 16:00

Chairperson's introduction

P.M. Parizel; Antwerp/BE (paul.parizel@uantwerpen.be)

Since the initial introduction of gadolinium-based contrast agents (GBCAs) in the late 1980's, this class of products has historically been considered safe and well tolerated. In a landmark article published in 2014, authors from Japan demonstrated that gadolinium is deposited in the brain, as evidenced by T1-shortening in the dentate nucleus, globus pallidus, and pulvinar of patients who had received repeated administrations of gadodiamide and/or gadopentetate dimeglumine. Subsequently, many other investigators have confirmed the finding that gadolinium deposition occurs, even in patients with normal renal function. In the brain, residual gadolinium is mostly discovered in the endothelial walls, although small quantities apparently cross the blood-brain barrier and accumulate within the neuronal interstitium. Moreover, we now know that residual gadolinium is not only deposited in certain brain regions, but also in tissues such as liver, skin and bone. Today, although gadolinium accumulation in tissues is well documented, there is very limited clinical information regarding the potential risks and mechanisms of toxicity. In this special focus session, 3 of the world leading experts on this topic will explore WHERE gadolinium is deposited in the brain, HOW it gets there, what are the RISKS and COMPLICATIONS of possible gadolinium toxicity, WHICH AGENTS are associated with greater amounts of gadolinium deposition, and WHAT are the recommendations of the European Medicines Agency (EMA). The special focus session will conclude with a discussion about the future strategy to be adopted by the radiological community regarding GBCAs.

Session Objectives:

1. To review the evidence of intracranial gadolinium deposits after intravenous administration of gadolinium-based contrast agents (GBCAs).
2. To summarise current theories about why, how, and where gadolinium is deposited in the brain and other tissues.
3. To assess the clinical relevance of this finding for daily radiological practice.

Author Disclosure:

P.M. Parizel: Advisory Board; Bracco. Research/Grant Support; Bayer, Bracco, General Electric. Speaker; Bracco.

A-137 16:05

Gadolinium deposition in the brain: from preclinical studies to clinical implications

R.J. McDonald; Rochester, MN/US

"no abstract submitted"

Learning Objectives:

1. To understand how gadolinium is deposited in the brain (chemistry and pathophysiology).
2. To demonstrate where gadolinium is deposited in the brain (and other tissues) (neuropathology).
3. To assess the potential clinical implications of gadolinium deposition in the human body.

A-138 16:30

Assessing tissue integrity in the presence of gadolinium deposition in the brain

C. Olchow; Wroclaw/PL (cyprian.olchow@gmail.com)

A growing evidence of the accumulation of small amounts of gadolinium in the cerebellum structures after repeated administrations of selected gadolinium-based contrast agents (GBCAs) dictates the search for sensitive markers of brain tissue damage. Sodium (^{23}Na) MRI can detect possible tissue abnormalities. It enables measuring intracellular sodium concentration, which is considered a useful marker of tissue viability and has been proved to be elevated in many brain disorders. In patients with multiple sclerosis, elevated sodium levels were detected in contrast-enhancing lesions to much greater extent than in non-enhancing T1 hypointense lesions. These findings may be linked to the increase in the blood-brain barrier permeability and signs of edema. Multiple sclerosis patients often present with signal hyperintensity within the dentate nucleus and globus pallidus as a possible result of multiple applications of GBCAs. However, the total sodium concentration within the hyperintense dentate nucleus of MS patients did not significantly differ from that of the dentate nucleus of MS patients without increased signal intensity and healthy controls. Gadolinium deposits have been detected in tissues from

Postgraduate Educational Programme

autopsy samples of patients who had been exposed to GBCAs; however, until today, there has been no evidence of the direct harmful effect of GBCAs on brain tissues. One of the possible reasons is the lack of precise diagnostic methods and, the other, the lack of the knowledge of the type of damage resulting on using improper diagnostic methods. The hypotheses about the possible mechanism and signs of damage will be discussed.

Learning Objectives:

1. To detect possible tissue abnormalities with sodium (^{23}Na) MRI in the brain of MS patients.
2. To measure total sodium concentrations in the brains of patients exposed to repeated gadolinium administrations.
3. To predict possible harmful effects of gadolinium deposition in the brain in view of the presence or absence of tissue abnormalities.

Author Disclosure:

C. Olchowik: Advisory Board; none. Author; none. Board Member; none. CEO; none. Consultant; none. Employee; none. Equipment Support Recipient; none. Founder; none. Grant Recipient; none. Investigator; none. Owner; none. Patent Holder; none. Research/Grant Support; none. Shareholder; none. Speaker; none. Other; none.

A-139 16:55

Clinical recommendations in consideration of the EMA's pharmacovigilance and risk assessment committee recommendation for suspension of linear agents

V. [Runge](mailto:val.runge@mac.com); *Berne/CH*

After a two year long consideration of the latest issue (gadolinium deposition in the brain and body), including many meetings, rounds of questions from the EMA to industry with responses, and two ad hoc expert group meetings, the pharmacovigilance and risk assessment committee (PRAC) concluded its assessment of the gadolinium based agents and, on March 10, 2017, recommended the following regulatory action (further confirmed by the PRAC on July 7, 2017): suspension of the marketing authorization for body imaging of 4 linear GBCAs (gadodiamide - omniscan, gadoversetamide - optimark, gadopentetate dimeglumine - magnevist, and gadobenate dimeglumine - multiHance), which would leave—of the linear agents—only gadoxetic acid (primovist) and gadobenate dimeglumine on the market (for liver scans only) and a formulation of gadopentetic acid for joint injections. Approval for the macrocyclic agents was left unchanged; this recommendation was confirmed by the committee for medicinal products for human use of the EMA on July 21. The final stage of review is the adoption by the European Commission of a decision, applicable and legally binding, for all European Union Member States.

Learning Objectives:

1. To review the in vivo distribution, possible dechelation, and subsequent deposition of gadolinium.
2. To clarify this phenomenon and to stratify gadolinium-based contrast agents on this basis.
3. To provide clinical recommendations to radiologists on how to deal with gadolinium deposition in the brain and body.

Author Disclosure:

V. Runge: Grant Recipient; Bayer, Bracco, Guerbet, Siemens. Speaker; Bayer, Guerbet, Siemens.

17:20

Panel discussion: Strategies for the future

16:00 - 17:30

Room K

Radiographers

RC 414

Maximising outputs from research

A-140 16:00

Chairpersons' introduction (part 1)

F. [Zarb](mailto:zarb@um.edu.mt); *Msidra/MT*

The radiography profession has gone through numerous developments over the past decades. It is also important that we acknowledge these developments and the educational requirements to fulfill the developing roles of the radiographer. The radiography profession has been required to use and also generate quality research on which to develop evidence-based practice. The presenters of this session are active researchers within the field of radiography and we will be benefitting from their knowledge and experience of radiographic research.

Session Objectives:

1. To appreciate the importance of study design in enhancing research outcomes.
2. To become familiar with the benefits of collaboration in designing and disseminating research.
3. To understand current funding opportunities and strategies for success.

A-141 16:03

Chairpersons' introduction (part 2)

M. [Raissaki](mailto:raissaki@traklion.gr); *Iraklion/GR*

The cornerstone of academic medicine has always been balanced on the concepts of teaching, research and clinical practice. The same concepts are interacting with each other in academic radiography. In the era of innovation and advancing technology, imaging biomarkers, evidence-based medicine and ALARA, radiographers have the opportunity to perceive research on a local, National and International level, as their opportunity to make a visible difference as health specialists, to better appreciate and understand aspects of their craft, to reduce dose and improve or maintain image quality in all imaging modalities. Radiographers can and should be aware of the role of research in optimization of clinical practice. Familiarization and a positive and attitude towards research are important for implementing the paradigm shift from the traditional model of practice to evidence-based practice. Research is a learning process both on an undergraduate and on a postgraduate level. Research can only be mastered through team work, careful design, trial and error, dedication, and appropriate funding. Collaboration among institutions can lead to enormous benefits for local, National, and International evidence and guidelines.

Session Objectives:

1. To appreciate the importance of study design in enhancing research outcomes.
2. To become familiar with the benefits of collaboration in designing and disseminating research.
3. To understand current funding opportunities and strategies for success.

A-142 16:05

A. Designing robust research projects

L.A. [Rainford](mailto:louise.rainford@ucd.ie); *Dublin/IE*

The presenter will provide the audience with a detailed discussion of the key steps required to be fulfilled in the design of research projects. The principles discussed will bear relevance to a range of research project types from local studies to research activity involving international collaborators. The information provided will be based on the presenter's personal experience and from referenced literature. The presentation will outline details of support mechanisms available to radiography researchers active or those interested in becoming research active. The scope of information will range from local academic institutions support, professional society support, national and international research agencies and European groups, in particular the European Federation of Radiography Societies (EFRS). The importance of understanding how careful project design is critical to a research project success and core considerations in the design process will be provided to the audience. Matters such as appropriate supervisory teams, understanding roles, maintenance of progress, meeting deadlines, appropriate ethical oversight, preparing for unforeseen issues, ensuring novel and innovative approaches, ensuring standards are maintained, and positive student development. Considerations required if planning multi-site studies either within one jurisdiction or internationally will be included in the presentation.

Learning Objectives:

1. To learn about the research design process.
2. To understand the mechanisms available to support the successful design of research studies in radiography.
3. To appreciate the importance of careful research design for successful projects.

A-143 16:28

B. Collaborating across Europe

G. [Paulo](mailto:graciano@estescoimbra.pt); *Coimbra/PT*

Radiography profession is evolving in an exponential way, driven mostly by the technological development and the new models of delivering care to the patient. It's because these two main drivers that is essential to promote research, as a tool to develop the radiographer profession field of knowledge. Radiographers, as the guardians of the profession, have the obligation to improve the knowledge basis of professional work through research, which is only accepted and adopted by the peers, if published: "It doesn't exist if it isn't written down". The number of publications in one year is higher than all the publications until 1970, and this has a tremendous impact on our daily life. According to the European Research Area, Europe must increase the

Postgraduate Educational Programme

efficiency and effectiveness of its public research system. This requires more cooperation so that the brightest minds work together to make greater impact on grand challenges. We have to bear in mind that research paradigm has changed. Changes came from a lonely scientist closed in his laboratory to a whole worldwide network of knowledge (as the common maxim states: "it's not what you know, it's who you know."), reason why networking and integrating a multidisciplinary approach into research is essential, not only to avoid unnecessary duplication of research and infrastructure investment, but also to create knowledge and increase the visibility of radiographers in the patient clinical pathway.

Learning Objectives:

1. To learn about the importance of networking to promote research activities.
2. To understand the potential of research collaborations in a multinational approach.
3. To be aware about the importance of research in developing the professions' field of knowledge.

A-144 16:51

C. Winning research grants

C. Malamateniou; London/UK (christina.malamateniou@kcl.ac.uk)

Research in healthcare professions allied to Medicine has been traditionally seen as the "difficult to achieve", "challenging" and often "an additional, different to clinical practice" task, that was demanding more time from an already overloaded clinical schedule of the healthcare practitioners. Recent work has shown that research can increase quality of practice, improve patient outcomes and job satisfaction and make the service more efficient. Radiography research capacity and quality building has been identified as one of the key areas for development under the 2016-2021 Research strategy agenda of the Society and College of Radiographers. Research capacity building involves enhancing research awareness, facilitating research involvement but also and most importantly ensuring high quality research leadership. There are many different methods one can employ to achieve these outcomes, but in order to cement a research leadership role for Radiography, one needs to consider how to increase the research income and how to succeed in Research grant applications. There is not sadly a cookbook on how this can be achieved and it is recognised that one needs to travel through rough waters and often learn from constructive feedback and through failure, in order to become better in successful grant writing. This talk is about the challenges in securing grant funding in Radiography in the UK, some tips to help people increase their chances of securing a grant as well as to present the currently available research funding opportunities for radiographers.

Learning Objectives:

1. To learn about potential research funders for radiographers.
2. To understand challenges and opportunities in research grant applications.
3. To appreciate strategies for successful research bids.

17:14

Panel discussion: How to avoid strategic mistakes in research?

16:00 - 17:30

Room M 1

EuroSafe Imaging Session

EU 1

Euratom Basic Safety Standards Directive: a comprehensive approach for radiation protection

Moderator:

G. Frija; Paris/FR

A-145 16:00

Chairperson's introduction

S. Ebdon-Jackson; Didcot/UK (steve.ebdon-jackson@phe.gov.uk)

EC Directive 2013/59/Euratom lays down basic safety standards for protection against the dangers arising from exposure to ionising radiation. Previously, such directives have addressed occupational and public exposure and a separate directive considered medical exposures (EC Directive 97/43/Euratom). In contrast, this latest "Basic Safety Standards Directive" includes medical exposures and therefore, provides a comprehensive EC approach to radiation protection for radiology and other activities in medicine that utilise ionising radiation. For occupational exposure, new dose limits are introduced for the lens of the eye. For medical exposures, the directive extends requirements for justification, at generic and individual levels, and optimisation and gives greater detail regarding equipment and the role of the medical

physics expert. It includes new requirements for non-medical imaging using medical radiological equipment and accidental and unintended medical exposures.

Session Objectives:

1. To become familiar with the new Basic Safety Standards Directive (Council Directive 2013/59/EURATOM).
2. To learn about the most important changes compared to the previous directive.
3. To understand the implications of the new directive for medical imaging.

A-146 16:05

The technical approach: achievements and future of dose reduction

W.A. Kalender; Erlangen/DE (willi.kalender@imp.uni-erlangen.de)

The introduction of spiral-CT in the 1990s followed by the development of multi-slice detector technology led to substantial increases in CT performance and in its use. In consequence, the cumulative patient exposure also increased. Fortunately, new efforts of developing intelligent dose reduction approaches, meanwhile helped reducing patient dose significantly. These comprise the following innovative approaches: Tube current modulation (TCM), automated exposure control (AEC), application-dependent optimal choice of X-ray spectra, elimination of z-overscanning effects, dose-efficient iterative image reconstruction, advanced detector technology. They all have in common that dose will be reduced, but not combined with compromising image quality, i.e., not by reducing the mAs product. The underlying principles and the resulting reduction of dose will be explained. The total effect has actually been very successful during the last two decades allowing for a reduction by a factor of 10 or higher and for sub-mSv CT imaging in many CT-applications.

Learning Objectives:

1. To learn about the technical perspective from the BSS.
2. To become familiar with dose reduction.
3. To become familiar with the achievements and future of dose reduction.

Author Disclosure:

W.A. Kalender: Consultant; Bayer Schering AG, Advanced Breast-CT GmbH. Shareholder; Advanced Breast-CT GmbH.

A-147 16:17

The clinical approach: the gap to be closed

G. Frija; Paris/FR (guy.frija@aphp.fr)

Several aspects of optimisation and justification are clearly relating to a clinical task and this will be introduced. The talk will focus for example on optimisation driven by the clinical indication and patient characteristics, and the report, which should include dose metrics. Examples will be taken for illustrating the importance of considering an integration of radiation protection into the clinical work, and thus increasing healthcare professionals' awareness.

Learning Objectives:

1. To learn about the clinical perspective.
2. To become familiar with the concept of clinical DRLs.
3. To understand the need for DRLs based on clinical indications.

A-148 16:29

The clinical audit: the missing link

E.J. Adam; London/UK (drjaneadam@gmail.com)

Translating legislation into routine practice can be challenging. European legislation deadlines relating to radiation protection are looming. Regulatory agencies across Europe may take different approaches to assessing compliance, but there is no need to wait. Self audit within departments is easy to carry out, and will mean that departments will have evidence to show that they have high standards of safe practice in line with the legislation. The ESR audit system makes it straightforward to start, and bridges the gap between regulation and routine practice. It should be a continuous, multidisciplinary process which is professionally led and aims to improve the performance rather than be a pass or fail assessment. Ultimately, it can expand to cover all areas of practice and all parts of the patient journey.

Learning Objectives:

1. To understand what clinical audit is.
2. To learn how to implement clinical audit in practice.
3. To become familiar with the ESR audit pack.

A-149 16:41

The regulatory approach

S. Ebdon-Jackson; Didcot/UK (steve.ebdon-jackson@phe.gov.uk)

EC Directive 2013/59/Euratom is intended to provide basic safety standards for protection against the dangers arising from exposure to ionising radiation.

Member States are expected to transpose the Directive into national law. The Directive requires member states to have in place a competent authority which will undertake a range of activities including regulatory control through a graded approach, which includes notification, registration and licensing. Justification of new types or classes of practices provides a particular challenge for medical exposures and member states will be required to put in place meaningful and responsive processes. The principle of justification is extended to individual justification and the justification process will be subject to scrutiny. Member states are required to have in place inspection programmes that may be proactive. In addition, new requirements relating to accidental and unintended medical exposures mean reactive inspection processes must be available. The heads of the European Radiation protection Competent Authorities (HERCA) working group on medical applications has undertaken a range of activities to enhance common understanding of Directive requirements, including Multi-Stakeholder Meetings and Workshops which have informed position papers and statements on a range of topics included within 2013/59/Euratom. Regulators and professionals have the common goal of ensuring safe practice and common understanding of regulatory approaches and good medical practice will enable increased safety for patients, workers and the public.

Learning Objectives:

1. To understand the regulator's perspective on the BSS.
2. To learn about the regulator's role and tasks.
3. To become familiar with inspection.

A-150 16:53

The European Commission's perspective and update on the transposition in the European Member States

G. Simeonov; Luxembourg/LU (georgi.simeonov@ec.europa.eu)

The "Basic Safety Standards" (BSS) Directive 2013/59/Euratom was published in 2014 and has to be implemented in the EU Member States by 6 February 2018. The BSS Directive updates and consolidates previous pieces of European legislation and introduces some important changes, including in relation to protection of patients. The European Commission is empowered to monitor the implementation of the European BSS in the Member States and take corrective action, wherever necessary. The Commission implements also a series of 'soft measures' to support the implementation of the BSS Directive into practice, with recent examples on paediatric DRLs, MPE qualification framework and education and training of medical professionals. The main focus in the next years will be on ensuring full implementation of the BSS Directive. One specific area, where the Commission will focus further efforts, is the development and use of DRLs, where a European survey on clinically-specified DRLs has been recently launched.

Learning Objectives:

1. To learn about the Euratom Basic Safety Standards Directive.
2. To understand the European Commission's perspective.
3. To understand how the European Commission ensures implementation of the BSS Directive.

A-151 17:05

The industry's perspective and work needed to comply with the Basic Safety Standards

N. Denjoy; Brussels/BE (denjoy@cocir.org)

The medical technology sector in Europe represented by COCIR is highly technological and innovative, with around 28 billion € total turnover and 7-8% of annual revenues invested in research and development. COCIR Companies are working already to implement the new requirements, in particular article 60 and 78. Nonetheless companies have a few concerns in particular regarding a non-harmonized transposition with different requirements at national and local level regarding important topics such as justification and information on equipment. Manufacturers provide to undertakings manuals and accompanying documentation when selling a medical device, containing all the information required for safe use. The additional requirements on information in the BSS Directive, e.g., article 78, may end requiring a duplication of documentation, adding a significant burden on manufacturers and on undertakings as well.

Learning Objectives:

1. To learn about industry's perspective on the BSS.
2. To understand the work needed to comply with the BSS.
3. To identify regulatory hurdles for industry.

17:17

Panel discussion: Is the Basic Safety Standards Directive a step forward for patients, clinical professionals and regulators?

G. Frija¹, S. Ebdon-Jackson², W.A. Kalender³, E.J. Adam⁴, N. Denjoy⁵, G. Simeonov⁶; ¹Paris/FR, ²Didcot/UK, ³Erlangen/DE, ⁴London/UK, ⁵Brussels/BE, ⁶Luxembourg/LU

16:00 - 17:30

Room M 2

E³ - ECR Master Class (Paediatric)

E³ 426

Juvenile idiopathic arthritis (JIA)

Moderator:

K. Rosendahl; Bergen/NO

A-152 16:00

A. Conventional radiography, still a helpful method?

S.C. Sheldermine; London/UK

Juvenile idiopathic arthritis (JIA) is a chronic, rheumatic illness that is associated with a high risk of long-term physical disabilities. Radiography can help identify changes related to JIA, which are primarily those of chronic, destructive changes seen in late disease, but it can also provide indirect information on soft tissue inflammation (such as peri-articular increased soft tissue density or the presence of a joint effusion). In the initial assessment of a child with joint pain, radiography is also useful to rule out other differential diagnoses such as neoplasms, posttraumatic changes and developmental defects. In this lecture, we will focus on the typical findings of joint inflammation and destruction seen in a variety of commonly affected joints and review the literature regarding the specificity and sensitivity of such radiographic signs. We will also touch upon common pitfalls and how such features may overlap with normal findings of a skeletal maturation. We conclude by reviewing the benefits and drawbacks of using radiography as a follow-up imaging tool and how this modality compares with other radiology techniques for JIA imaging.

Learning Objectives:

1. To learn about the features of joint inflammation on plain radiographs.
2. To understand the role of this technique in the diagnosis and follow-up of children with JIA.
3. To appreciate the strengths and limitations of conventional radiography compared to other modalities in JIA.

A-153 16:30

B. Ultrasound for detecting and grading of inflammation in JIA

L. Tanturri De Horatio; Rome/IT (laura.tanturri@opbg.net)

Musculoskeletal ultrasound (MSUS) is an attractive imaging technique in children; particularly, it is a useful tool for joint assessment and guidance of steroid injection therapy in JIA. The method is radiation free without any need for sedation and allows for a dynamic evaluation of several joints per session including assessment of the vasculature with Doppler. Moreover, the new high-resolution probes provide exquisite image quality. Caution should be taken when translating adult musculoskeletal sonographic findings to the paediatric joints, as age-related variations in thickness of cartilage and appearances of ossification centres can mimic pathology. Moreover in children it may be challenging to distinguish between synovial hypertrophy and the adjacent cartilage or joint fluid because all these structures may have a similar, hypoechoic appearance. Furthermore, the interpretation of intra-articular Doppler signals as a marker for synovitis is difficult due to physiologically enhanced blood flow which should not be misinterpreted as pathology. Over the past decades a great deal of effort has been done by the Outcome Measures in Rheumatology Clinical Trials (OMERACT) Ultrasound Task Forces to provide a definition of the normal age-dependent sonographic anatomy and to standardise an approach to MSUS scanning in children. The results from these studies provide the basis to develop definitions for pathology and to support the standardised use of MSUS in paediatric rheumatology. However, at present, very few studies have addressed the repeatability/reproducibility of MSUS finding. Moreover, validated definitions and scoring systems for ultrasound pathology in children with JIA are lacking.

Learning Objectives:

1. To learn about normal features vs pathology on ultrasound of joints in children.
2. To understand the role of ultrasound in diagnosing and grading of joint inflammation.
3. To appreciate the research-based evidence of ultrasound.

A-154 17:00

C. MRI and role of contrast in the assessment of synovitis

L.-S. Ordning Müller; Oslo/NO (lilsofie.ording@googlemail.com)

MRI scanning is the current gold standard modality for imaging synovitis and tenosynovitis in patients with Juvenile idiopathic arthritis. Enhancement of the synovium after gadolinium injection is traditionally regarded as mandatory in the assessment of synovitis, both for diagnosis and grading, and to distinguish

Postgraduate Educational Programme

between active and inactive disease. There have been huge advances in medical treatment of JIA over the last two decades and disease remission is now the ultimate goal for all patients. This increases the role of imaging to detect early signs of disease or relapse and to monitor subtle response to treatment. Several research groups work on establishing scoring systems to create objective imaging measures for disease activity in JIA. However it is challenging to reliably differentiate between normal synovial enhancement and inflammation and to grading contrast enhancement in early disease. Timing of imaging post contrast injection has shown to play an important role in the assessment and grading of synovitis and dynamic contrast-assessment might be a better method to improve quantification of synovitis. Focus on potential harmful effects of Gd-injection forces us to search for alternative methods in synovitis imaging. The diffusion weighted imaging (DWI)-derived apparent diffusion coefficient (ADC) seems to be higher in active JIA and may serve as a non-invasive imaging biomarker for JIA in the future. In this lecture current knowledge on the role of contrast in synovitis assessment, challenges in standardisation of imaging, and potential alternative methods for detection and grading of synovitis in JIA will be presented.

Learning Objectives:

1. To learn about the definition of synovitis on MRI.
2. To understand the appearances of synovitis and potential pitfalls on MRI.
3. To appreciate new techniques that may replace contrast-enhanced MRI in the assessment of synovitis.

16:00 - 17:30

Room M 3

Molecular Imaging

RC 406

Molecular imaging in oncology

A-155 16:00

Chairperson's introduction

K. Nikolaou; Tübingen/DE (Konstantin.Nikolaou@med.uni-tuebingen.de)

Radiology is playing a central role in the set-up of multidisciplinary cancer centers and in the comprehensive work-up of oncologic patients, integrating an ever increasing amount of qualitative and quantitative diagnostic information. Still, radiology is facing significant challenges, as "precision medicine" develops and matures. Integrating functional and molecular information in a quantitative fashion and adding complementary multimodality information is crucial. In detail, molecular imaging is regarded as the direct or indirect noninvasive monitoring and recording of the spatial and temporal distribution of *in vivo* molecular, genetic, and/or cellular processes for biochemical, biological, diagnostic, or therapeutic applications. Molecular and functional image information that indicate the presence of malignancy can be acquired using an abundance of modalities, including optical, ultrasonic, radiologic, radionuclide, and magnetic resonance techniques. In this session, multimodality imaging of oncologic processes will be reviewed with respect to their physical basics and imaging characteristics, including attributes of hypoxia, proliferation, and metabolism. Also, the role of prognostic, predictive and therapy response oncologic imaging biomarkers will be discussed and current and future clinical applications in oncologic diagnosis will be reviewed.

Session Objectives:

1. To understand the basics of molecular imaging.
2. To appreciate the unmet needs of oncological imaging.
3. To learn the role of molecular imaging in oncology.

A-156 16:05

A. Imaging of hypoxia

V.J. Goh; London/UK (vicky.goh@kcl.ac.uk)

Tumour hypoxia is present in up to 60% of locally advanced solid tumours. Tumour hypoxia is a significant challenge to successful therapy, contributing to treatment resistance and a poor prognosis. Intra-tumoural hypoxia may be assessed by molecular markers including hypoxia inducible factor 1 (HIF-1) and carbonic anhydrase isoenzyme IX (CA-IX). However, hypoxia is a dynamic process and alters depending on perfusion and oxygenation status. Noninvasive imaging of intra-tumoural hypoxia provides an opportunity to better stratify patients to improve local control. Tumour hypoxia may be assessed *in vivo* by direct and indirect imaging techniques. Positron emission tomography (PET) imaging targets hypoxic cells with tracers including 18F fluoromisonidazole (18F-MISO), 18F-fluoroazomycin arabinofuranoside (18FFAZA) and 64Cu-diacetyl-bis(N4-methylthiosemicarbazone (64Cu-ATSM). Hypoxia imaging may also be undertaken by magnetic resonance imaging (MRI) with techniques such as blood oxygenation level-dependent (BOLD) MRI and oxygen enhanced MRI measuring R2* and R1 changes, respectively. This

lecture will review the biological basis and fundamentals of hypoxia imaging and potential clinical applications including radiotherapy.

Learning Objectives:

1. To review the fundamentals of hypoxia imaging.
2. To review the advantages and disadvantages of hypoxia imaging and its relation to perfusion.
3. To learn about hypoxia imaging in radiation treatment.

Author Disclosure:

V.J. Goh; Research/Grant Support; Siemens Healthineers. Speaker; Bayer, Siemens Healthineers.

A-157 16:23

B. Imaging of proliferation

A. Kjaer; Copenhagen/DK (akjaer@sund.ku.dk)

Uncontrolled proliferation is a hallmark of cancer and may be imaged both at the DNA level with 18F-FLT and at the protein level through amino acid PET tracers, e.g., 18F-FET. The value of proliferation imaging with PET in oncology will be reviewed with particular focus on use for tumor delineation, prognostication and therapy monitoring. Additionally, the relative value compared to that of 18F-FDG for the same applications will critically be discussed.

Learning Objectives:

1. To understand basic principles of proliferation imaging.
2. To become familiar with imaging of proliferation.
3. To learn about difficulties in liver proliferation imaging.

A-158 16:41

C. Imaging of metabolism

C. Nanni; Bologna/IT (cristina.nanni@aosp.bo.it)

18F-FDG PET/CT is an imaging technique that is aimed to evaluate glucose metabolism of tissues and organs. PET/CT scanners consist of a combination of a PET scanner and a CT scanner providing both morphological and functional images that can be fused to accurately localize any pathological finding. The procedure is standard and includes several steps. Patients are not allowed to consume any food or sugar for at least 6 h prior to the start of the PET study. Injection should be fully intravenous. Optimal uptake time is 60 min. In general, for a 3D system and 3 MBq/Kg of FDG, 2 min/bed position is enough, leading to an average overall acquisition time of 14 minutes. Low dose CT (120 kV, 80 mA) is necessary both for attenuation correction and for image interpretation. Once reconstructed, images must be interpreted on a dedicated workstation. SUV max based on body weight is the standard semi-quantitative index. FDG PET/CT was proved to be accurate for several malignancies for the definition of TNM at staging and in the suspect of relapse. Furthermore, changing in SUV max are related to the response to systemic therapies, both during and after treatment. This parameter is considered a non invasive surrogate for therapy assessment. Some particular kinds of malignant tumors are not detectable at FDG PET. In particular mucinous ca, transitional cell cancers, clear cell cancers, indolent HCC and some adenocarcinomas fail to significantly concentrate FDG. Low accuracy can also be found in some particular areas of the body where FDG is physiologically concentrated such the brain and the urinary tract.

Learning Objectives:

1. To learn the clinical indications for FDG imaging.
2. To become familiar with imaging protocol.
3. To learn about difficulties in FDG imaging.

A-159 16:59

D. Biomarker imaging with MR

M.E. Mayerhöfer; Vienna/AT (marinus.mayerhoefer@meduniwien.ac.at)

Originally regarded as a purely morphological imaging technique with excellent soft-tissue contrast, MRI today is recognised as a technique that can also provide functional biomarkers through different approaches. For treatment response assessment, diffusion-weighted imaging (DWI), which indirectly provides information on cell density in tumours, is already well-established, and for some tumors (e.g., lymphoma), it has even been proposed as a radiation-free alternative to [18F]FDG-PET for staging and treatment response assessment. Nevertheless, limitations for DWI include artefacts and standardisation of apparent diffusion coefficients between different DWI pulse sequences, and between MR scanners of different vendors. Perfusion-weighted imaging (PWI) is another technique that is increasingly being used in the response evaluation of hypervascular tumours, such as hepatocellular carcinoma. In the body, PWI is most commonly performed on the basis of dynamic contrast-enhanced sequences, with k-trans, a measure of capillary permeability, being the best-known parameter. Alternatively, PWI may be performed using arterial spin labeling, without contrast media. MR

Postgraduate Educational Programme

spectroscopy (MRS), which today is most frequently based on protons, is another technique that can be used to assess biomarkers in the form of metabolites, such as lactate and choline. While several studies reported encouraging data, for instance, in breast cancer and prostate cancer, limitations such as, long acquisition times and difficulties in terms of standardisation and quantification have prevented MRS from being introduced into routine clinical imaging. Cutting-edge techniques, such as chemical exchange saturation transfer (CEST) imaging, may overcome the limitations of MRS.

Learning Objectives:

1. To learn the clinical indications for biomarker imaging.
2. To become familiar with quantification.
3. To learn about difficulties in quantification.

17:17

Panel discussion: The pros and cons of molecular imaging in oncology

16:00 - 17:30

Room M 4

E³ - ECR Academies: Chest Imaging

E³ 418

Cavitary and cystic diseases of the lung

A-160 16:00

Chairperson's introduction

N. [Howarth](mailto:Howarth@grangettes.ch); *Chêne-Bougeries/CH (nigel.howarth@grangettes.ch)*

The session will provide an overview of cavitary and cystic diseases of the lung. Diagnostic criteria for cavitary lesions and cysts will be explained and the differential diagnosis will be explored in a variety of clinical situations. The pathogenesis of different forms of cavitary and cystic lesions will be explained. Key CT features will be reviewed. Attendees will learn a practical and logical approach for CT interpretation based on clinical setting, of value in everyday work.

A-161 16:05

A. Cavitary lung lesions

A.P. [Parkar](mailto:apparkar@gmail.com); *Bergen/NO (apparkar@gmail.com)*

A cavity is defined as "a gas-filled space, seen as a lucency or low-attenuation area, within pulmonary consolidation, a mass, or a nodule". The wall thickness may vary considerably. There is a continuous transition from cavities to cysts. Cysts are usually thin walled (i.e., < 2 mm). A wall thickness < 7 mm is highly specific for benign disease, a thickness >24 mm is highly specific for malignant disease. However, this is not absolute, as thin-walled carcinomas do exist. An additional indicator for malignancy is the lack of perilesional centrilobular nodules around a cavity. The cavity content is unhelpful in differentiating benign and malignant lesions. Wall rim enhancement on contrast-enhanced CT is common in abscesses. A connecting pulmonary artery may be seen in smaller metastases, but not in larger ones, as the larger nodules tend to compress the vessels, so no feeding artery does not always imply benign nodules. The acute onset of symptoms is sometimes helpful to distinguish malignant and non-malignant disease. Hemoptysis is not a useful symptom to differentiate between benign and malignant cavities. Benign diseases may also cause fatigue and weight loss similar to malignancies. Acute onset of fever is usually helpful to distinguish benign disorders from malignant, but a pulmonary cancer may cause a super-infection secondary to the tumor. However, the combination of symptoms, laboratory results, past clinical history, and imaging findings leads to recognition of the correct diagnosis. This presentation will guide you through the most commonly encountered cavitary lung in adults.

Learning Objectives:

1. To review the diagnostic criteria and differentials of cavitary lung lesions.
2. To learn about the most common causes.
3. To learn about an algorithmic approach to narrow the differential diagnosis.

A-162 16:33

B. Langerhans cell histiocytosis (LCH)

A. [Devaraj](mailto:Devaraj@london.uk); *London/UK*

This presentation will review the characteristic and atypical CT appearances of Langerhans. The challenges in establishing a confirmed diagnosis in atypical cases will be reviewed as well as a discussion of the differential diagnoses when faced with cystic lung disease. The role of CT beyond diagnosis will be highlighted, including a review of complications and outcomes of the disease.

Learning Objectives:

1. To understand the pathophysiology of LCH.
2. To review key features on CT.
3. To learn about the various stages of the disease.

A-163 17:01

C. Lymphangioleiomyomatosis

A. [Oikonomou](mailto:anastasia.oikonomou@sunnybrook.ca); *Toronto, ON/CA (anastasia.oikonomou@sunnybrook.ca)*

Lymphangioleiomyomatosis (LAM) is a rare cystic lung disease caused by infiltration of the lung with smooth muscle cells. It occurs in patients with tuberous sclerosis complex (TSC-LAM) and in a "sporadic" form in patients without tuberous sclerosis (S-LAM). S-LAM is seen exclusively in women of reproductive age while TSC-LAM may also be seen in men. Parenchymal lesions in LAM mainly include cysts, which are thin-walled, well-defined, rounded, usually small in size up to 2 cm and may reach large numbers. They have no zonal lung predominance. Nodules are extremely rare in S-LAM and are more commonly seen in TSC-LAM. They may either be solid or ground-glass and usually tiny. They represent multifocal micronodular pneumocyte hyperplasia. Pleural manifestations include chylothorax and pneumothorax. Chylous pericardial effusions may be seen. Recent guidelines for the diagnosis of LAM from the European Respiratory Society LAM task force classify LAM as definite, probable and possible. LAM is differentiated by other cystic lung diseases such as Langerhans histiocytosis (PLCH), Birt-Hogg-Dube (BHD), lymphocytic interstitial pneumonia (LIP) and amyloidosis. In PLCH the cysts have a bizarre shape, are variable in number and are upper and middle lobe predominant. In LIP the cysts are round and variable in size but usually small and random in distribution surrounded by ground glass opacity. In BHD the cysts are elliptical in shape and have a subpleural, lower zone predominance adjacent to vessels. In amyloid the cysts are variable in size but usually large and diffusely distributed. Nodules are seen in PLCH and amyloid.

Learning Objectives:

1. To learn about the current concepts on pathogenesis.
2. To review the typical and atypical CT features.
3. To learn about the tuberous sclerosis complex.

16:00 - 17:30

Room M 5

E³ - ECR Academies: Update on Hepatobiliary Imaging

E³ 420

Advanced MR techniques and imaging biomarkers

A-164 16:00

Chairperson's introduction

D.-M. [Koh](mailto:dowmu.koh@icr.ac.uk); *Sutton/UK (dowmu.koh@icr.ac.uk)*

Advanced MR imaging is being applied to the hepatobiliary system to improve disease diagnosis and patient management. These include diffusion-weighted MRI, MR and US elastography, as well as liver selective contrast media. These techniques enhance the diagnostic potential of MR imaging for focal and liver diseases, and have impacted on imaging pathways and patient management. This session will demonstrate the application of these techniques for patient care.

A-165 16:05

A. Diffusion-weighted imaging

N. [Papanikolaou](mailto:papanikolaou@research.fchampalimaud.org); *Lisbon/PT*

(nickolas.papanikolaou@research.fchampalimaud.org)

Diffusion-weighted MR imaging (DWI), based on the thermally driven random motion of water molecules (otherwise called Brownian motion) has been increasingly applied in the evaluation of a wide variety of oncological diseases not only in the brain, but in the body during recent years. Promising results for improved detection and treatment evaluation, in terms of prediction and early response assessment, have been reported. DWI is probing water mobility propelled by thermal energy, and since water molecules are interacting with cellular membranes or other structures, DWI has the potential to provide us with information regarding the cellular architecture in a non-invasive manner. The apparent diffusion coefficient (ADC) is a property of tissue that reflects local water mobility. In the presence of pathology, ADC, has been correlated with important histologic properties, including the tumor proliferation index, tumor grade, the presence of necrosis, and tumor cell apoptosis. The model that is used to calculate the ADC value is based on a mono-exponential function that generally works well. However, in the presence of increased

vascularity, there is a second component that is called microperfusion and needs to be taken into consideration. In that case the use of a bi-exponential function where ADC is decomposed into D and D*, the true diffusion coefficient and the microperfusion coefficient is providing more accurate modeling of diffusion signals. In the presence of increased tissue heterogeneity a non-Gaussian diffusion model should be considered to take into account the interactions between water molecules and local tissue architecture components.

Learning Objectives:

1. To recognise the general principles of liver DW MRI.
2. To be familiar with the clinical applications of DW imaging in diffuse and focal liver diseases.
3. To be aware of the evolving developments in liver DW imaging.

Author Disclosure:

N. Papanikolaou: Advisory Board; Advantis. Founder; MRIcons.

A-166 16:33

B. MR and US elastography

D.J. Lomas; Cambridge/UK

Elastography is the measurement of tissue stiffness which is routinely assessed by subjective clinical palpation. Non-invasive in vivo imaging methods for quantitative elastography have been developed over the last few decades using ultrasound and MRI. These involve vibrating the tissue of interest and measuring the speed of the generated acoustic waves as they pass through the tissue. Essentially waves travel faster in stiffer tissues. This information, with some important assumptions, can be used to estimate absolute tissue stiffness. Multiple ultrasound methods are available which use different wave generation techniques, frequencies and which vary by the volume of tissue sampled and their ability to image simultaneously. Two MRI based methods have been developed both using relatively similar techniques for wave generation and image processing. MRI methods report liver stiffness using the "Shear" modulus, whereas US methods use "Elastic" or "Young's" Modulus (typically 3X larger). The MRI methods are probably more accurate for the detection of early and moderate liver fibrosis and sample larger volumes than the US methods, but are more expensive and less widely available. Both approaches have the potential to replace some liver biopsies in clinical practice and have particular screening value in diagnosing the "normal" liver when patients are referred with mild liver function test abnormalities. All these elastography methods are now being applied directly to clinical outcome studies, rather than just comparison studies with liver biopsy and other fibrosis measures, and these may demonstrate additional clinical prognostic and therapeutic applications for the management of liver disease.

Learning Objectives:

1. To recognise the clinical applications and diagnostic performance of MR and US elastography.
2. To be able to compare both techniques.
3. To be familiar with the factors confounding the accuracy of elastography.

A-167 17:01

C. MR contrast agents in liver imaging

M. Karcaaltincaba; Ankara/TR (musturayk@yahoo.com)

Contrast choice for liver MR imaging is important for correct diagnosis. Extracellular contrast agents should be preferred for diagnosis of hemangioma. Dynamic contrast-enhanced imaging phases are early and late arterial, portal venous, equilibrium phases. These phases can demonstrate perfusion characteristics of common liver lesions. Hepatocyte specific agents should be preferred for differentiation of focal nodular hyperplasia (FNH) from hepatic adenoma and preoperative planning for metastatic colorectal cancer. Recent evidence suggests use of Gd-EOB-DTPA for diagnosis of early HCC. A hypervascular lesion appearing as focal hyperintensity on hepatobiliary phase images is consistent with FNH in patients without risk factor for HCC and cancer. Oxaliplatin (mostly used for colorectal cancer) can induce focal nodular hyperplasia like lesions. Gd-EOB-DTPA may also be helpful in the assessment of liver function in patients with steatohepatitis, fibrosis and segmental dysfunction.

Learning Objectives:

1. To understand the dynamic contrast-enhanced imaging and liver perfusion.
2. To recognise the role of hepatocyte specific contrast agents in liver function and lesion characterisation.
3. To learn the weaknesses of extracellular and hepatospecific contrast agents.

Author Disclosure:

M. Karcaaltincaba: Speaker; Bayer, GE Healthcare, Philips Healthcare, Pfizer.

Thursday, March 1

Postgraduate Educational Programme

08:30 - 10:00

Room A

E³ - ECR Academies: Interactive Teaching Sessions for Young (and not so Young) Radiologists

E³ 521

Imaging of the skull base

A-168 08:30

A. Non-tumoural pathology of the temporal bone

B. [Ozgen Mocan](mailto:burce@hacettepe.edu.tr); Ankara/TR (burce@hacettepe.edu.tr)

The temporal bone has a complex anatomy, but the pathologies involving the temporal bone structures are somewhat limited with specific and diagnostic imaging findings. During this lecture, the most common non-tumoural causes of conductive and sensorineural hearing loss will be reviewed in an interactive manner with emphasis on the clinical and imaging findings that are helpful for the differential diagnosis.

Learning Objectives:

1. To learn the most common inflammatory lesions of the temporal bone.
2. To become familiar with the most common malformations and non-tumoural pathologies.

A-169 09:15

B. Tumours of the skull base

T. [Beale](mailto:timothy.beale@uclh.nhs.uk); London/UK (timothy.beale@uclh.nhs.uk)

The lecture will describe a classification system for tumours of the skull base that will aid in the differential diagnosis. Using clinical cases the imaging features of the common skull base tumours will be highlighted. The important review areas for the individual tumours will be discussed including those features that may alter the clinical management and help in the differential diagnosis. The common pitfalls and non-neoplastic differential diagnosis will be highlighted and an imaging technique for assessing the skull base will be discussed.

Learning Objectives:

1. To become familiar with the imaging technique of the skull base.
2. To identify imaging criteria for improved differential diagnosis.

08:30 - 10:00

Room B

New Horizons Session

NH 5

The machines are coming: how will they change our future?

A-170 08:30

Chairperson's introduction

H.-U. [Kauczor](mailto:Hans-Ulrich.Kauczor@med.uni-heidelberg.de); Heidelberg/DE (Hans-Ulrich.Kauczor@med.uni-heidelberg.de)

Novel developments in computer science and performance have prepared the ground for the implementation of so-called artificial intelligence algorithms and have computers learn "deeply" from the analysis of big data. This session will provide an introduction into machine based learning algorithms touching reflecting opportunities, but also limitations. Obviously, quantitative image analysis will be a promising field for machine learning and the integration of the "machines" in the workflow of radiology will lead to major challenges to generate benefits for patients, the health care system and their economics as well as our profession. Done properly, machines will help us to cope with the ever increasing volume of imaging exams and scans, increase quality and safety, while radiologists will generate the value from imaging and the added value provided by the machines to strengthen our role as physicians.

Session Objectives:

1. To understand the basics of machine learning.
2. To appreciate the opportunities to improve quality in radiology.
3. To redefine the professional role of the radiologist.

Author Disclosure:

H.-U. Kauczor: Research/Grant Support; Siemens, Bayer. Speaker; Siemens, Boehringer Ingelheim, GSK, Novartis, Astra Zeneca, Philips, Bracco.

A-171 08:35

Deep learning: current performance

B. [van Ginneken](mailto:bram.vanginneken@radboudumc.nl); Nijmegen/NL (bram.vanginneken@radboudumc.nl)

The application of deep learning to medical image analysis has resulted in much-improved performance for many algorithms. There is early evidence that for many specific, narrowly defined detection and interpretation tasks, computers perform on par with or even better than radiologists. A requirement is that these deep learning algorithms are trained on a sufficiently large amount of high-quality annotated data. Larger multi-center validation studies are still needed to demonstrate that these algorithms work correctly on the variety of real-world data, obtained with different scanners and protocols. In this talk, I will showcase several examples of high-performing deep learning algorithms and argue that the radiological community should play a more active role in (1) identifying which tasks should be automated; (2) evaluating and validating automated systems in a fair and comparative manner; (3) collecting the high-quality annotated training and evaluation data; (4) clearly defining the role of human readers together with automated systems.

Learning Objectives:

1. To learn about the principles of machine learning.
2. To appreciate the current performance of deep learning in radiology and beyond.
3. To learn about the limitations due to the complexity of radiology.

Author Disclosure:

B. van Ginneken: Founder; Thirona. Owner; Thirona. Research/Grant Support; MeVis Medical Solutions, Delft Imaging Systems. Shareholder; Thirona.

A-172 08:58

Artificial intelligence applications in radiology

J.B. [Seo](mailto:seojb@amc.seoul.kr); Seoul/US (seojb@amc.seoul.kr)

The recent advances in artificial intelligence, particularly deep learning algorithm, have shown performances superior to those of human in image recognition of non-medical fields. Accordingly, many researchers and companies have tried to apply artificial intelligence in radiology. Artificial intelligence can be applied in various aspects of medical imaging such as noise reduction, artefact reduction, lesion segmentation, detection, classification, and differential diagnosis. Early studies have shown promising results in several applications such as detecting nodule or tuberculosis on chest radiograph. Furthermore, this technique can be applied in finding similar cases from the database, predicting disease outcome and so on. In this talk, general concept of artificial intelligence and early results of various applications of artificial intelligence in medical image will be introduced.

Learning Objectives:

1. To become familiar with first clinical applications.
2. To consolidate knowledge about the integration in the clinical workflow.
3. To appreciate the future roadmap and its impact on training of young radiologists.

Author Disclosure:

J.B. Seo: Shareholder; Coreline Soft Co. Speaker; Siemens / Guerbet.

A-173 09:21

Big data for deep learning

C.L. [Schlett](mailto:christopher.schlett@med.uni-heidelberg.de); Heidelberg/DE (christopher.schlett@med.uni-heidelberg.de)

Deep learning is currently an extremely active research area and has the potential to be the biggest game changer in medical imaging since the advent of digital imaging. It requires massive amount of training dataset with accurate annotation; however, annotation of medical images is particularly difficult and resource consuming as compared to other examples outside of medicine. Potentially induced error and bias due to imperfect annotation and/or inconsistency increase further the needed sample size. Several sources of medical images can be considered. While clinically acquired data are broadly available, they are often not interlinked with other data and face the issue of a high variability. A potentially more suitable source for big data could be large, population-based cohort studies such as the Rotterdam Study, the UK BioBank or the German National Cohort, since they have a high level of data quality and consistency regarding imaging, and they further frequently linked with clinical outcomes and annotations. However, deep learning in medical imaging remains a great challenge, not only because of the necessity for big data.

Learning Objectives:

1. To become familiar with the opportunities of big data analysis.
2. To understand that quality of big data is pivotal.
3. To learn how to generate "evidence" from big data analysis in radiology.

Thursday

Postgraduate Educational Programme

09:44

Panel discussion: Machines in radiology: do we still need the radiologist?

08:30 - 10:00

Room C

Breast

RC 502

New mammography: tomosynthesis and future techniques

A-174 08:30

Chairperson's introduction

E.M. [Fallenberg](#); Berlin/DE (eva.fallenberg@charite.de)

Early detection of breast cancer through X-ray mammography (MG) has been shown to reduce mortality; however, the method is limited by a decreased sensitivity and specificity particularly in young patients and women with radiographically dense breasts due to tissue overlying and masking tumours or architectural distortions. The introduction of full field digital mammography gave the possibility to develop further technical methods, to overcome these limitations. Some of these are tomosynthesis, contrast enhanced mammography and contrast enhanced tomosynthesis as well as most recently also breast CT. In this talk will be presented the background of 2D-mammography, tomosynthesis and contrast enhanced mammography techniques and breast CT. Potential advantages and disadvantages will be indicated and a sample of clinical cases will be presented to illustrate how the different techniques contribute to the detection of lesions.

Session Objectives:

1. To learn about 2D mammography and digital breast tomosynthesis.
2. To recognise the advantages and disadvantages of tomosynthesis compared to 2D mammography.
3. To look into the future and hear about the potential of new breast imaging techniques in lesion assessment.

Author Disclosure:

E.M. Fallenberg: Board Member; EUSOBI. Research/Grant Support; GE Healthcare, Guerbet. Speaker; GE Healthcare, Bayer Healthcare, Gurbet.

A-175 08:35

A. Should we abandon 2D mammography?

S. [Zackrisson](#); Malmö/SE (sophia.zackrisson@med.lu.se)

Full-field digital mammography (FFDM), also called 2D mammography, with flat panel detectors has been broadly used in clinical routine for about a decade. Even if there has been advances in the technical development of the digital detectors, the detectors are not the main limiting factor in breast cancer detection; the challenge is the anatomical noise, i.e., dense breast tissue. FFDM is a two-dimensional modality and inherent in that is that dense breast tissue may cause overprojection and hide or simulate the presence of a tumour on these images even if several views are acquired. Digital breast tomosynthesis, DBT is a 3D mammography technique that, to a large extent, can suppress the confounding effect of the overlapping tissue. DBT is a strong competitor to 2D mammography both for screening and clinical examinations. This presentation will cover 2D mammography in terms of technical background and optimisation of image quality. Furthermore, it will discuss the advantages and disadvantages of 2D mammography compared to DBT and evaluate if there are situations where 2D mammography still could be the preferred method if DBT is transitioned into screening and clinical practice.

Learning Objectives:

1. To understand the technique of 2D mammography and what the limits could be.
2. To learn if there are ways to improve image quality of 2D mammography.
3. To understand when 2D mammography is better than DBT.

Author Disclosure:

S. Zackrisson: Speaker; Speaker's fees and travel support from Siemens Healthineers.

A-176 09:00

B. Clinical validation of tomosynthesis and results in the last 10 years: where do we stand?

P. [Skaane](#); Oslo/NO (per.skaane@outlook.com)

Digital breast tomosynthesis (DBT), an advanced mammographic technique, has the potential to improve two inherent limitations of conventional mammography, FFDM: poor sensitivity in women with dense breasts (caused

by superimposed parenchyma, "masking effect") and low specificity (caused by parenchyma simulating a mass, "pseudotumor"). In diagnostic setting, DBT can replace conventional supplemental views for evaluation of indeterminate noncalcified lesions, "downgrade" some indeterminate (BI-RADS 3) lesions, and "upgrade" other equivocal masses indicating the need for biopsy. Thus, fewer lesions need to have follow-up. Evaluation of extent and multifocality of cancer is better demonstrated at DBT, and consequently preoperative cancer staging is improved. All the retrospective US screening studies comparing FFDM versus FFDM+DBT have shown a significantly lower recall rate for DBT, and most studies also an increased cancer detection rate. Lack of significant increase in cancer detection in other US studies might have been caused by study design and lack of power. The four prospective European trials comparing FFDM vs. FFDM+DBT in screening published so far have all demonstrated a significantly higher cancer detection rates for DBT, but variable recall rates. Challenges regarding implementation of DBT in screening include number of projections, reading time, and women with very dense breasts (BI-RADS d). The radiation dose problem is solved by synthetic 2D images. Studies on cost-effectiveness, harm-benefit analyses, overdiagnosis, and subsequent interval cancer rates and potential reduction of advanced stage cancers would be of importance. Overall, DBT has clearly shown a higher accuracy than FFDM in diagnostic as well as screening settings.

Learning Objectives:

1. To become familiar with the technique of DBT.
2. To understand the results of DBT in the screening and diagnostics settings.
3. To know the evolution of tomosynthesis in screening organisation.

Author Disclosure:

P. Skaane: Equipment Support Recipient; Tomosynthesis equipment for the Oslo Tomosynthesis Screening Trial was provided by Hologic..

A-177 09:25

C. The future of mammography: my predictions

E. [Giannotti](#); Nottingham/UK (Elisabetta.Giannotti@nuh.nhs.uk)

Breast screening aims to diagnose breast cancer at the earliest opportunity, maximize treatment success and reduce breast cancer-related mortality. Mammography is the mainstay of screening but it is less sensitive for some women, particularly those with dense breasts. Supplemental imaging leads to the detection of additional cancers, but this approach increases unnecessary recalls and healthcare costs and screening tools by definition should be feasible and affordable. In the future, tailored screening based on different (personal) risk factors is expected to replace the current standard (one size fits all) mammography screening programs, in order to reduce the potential harm and costs of screening and increase cancer detection. To achieve this it is crucial to develop more accurate risk assessment models that can be easily adopted in routine clinical practice. Innovative diagnostic techniques (such as digital mammography, quantitative breast density analysis, texture analysis and deep learning) could have a crucial role not only in the early diagnosis, but also being an active part of the risk assessment for developing breast cancer. Lately new digital techniques have been implemented, for example, digital breast tomosynthesis and contrast enhanced spectral mammography, improving mammographic sensitivity and offering new opportunities that will assist in the risk stratification of the patient. In order to increase cancer detection rate and reduce breast cancer related mortality we have the potential to improve mammographic sensitivity and utilization, and use these techniques not only for diagnosis but for stratifying breast cancer risk in order to tailor breast cancer screening for "individual women".

Learning Objectives:

1. To understand the role of mammography in analysing and characterising breast lesions.
2. To become familiar with new developments in digital mammography such as contrast mammography, tomosynthesis and 3D contrast mammography.
3. To learn about the new potential of combining mammography with molecular imaging, optical imaging and texture analysis.

09:50

Panel discussion: Mammography and/or tomosynthesis: where will we stand in 10 years?

Thursday

Postgraduate Educational Programme

08:30 - 10:00

Room Z

Joint Session of the ESR and UEMS

ESR/UEMS 1

ESR and UEMS: a united European voice

A-178/A-179 08:30

Chairpersons' introduction

L. Bonomo¹, M. Adriaensen²; ¹Rome/IT, ²Heerlen/NL
(lorenzo.bonomo@unicatt.it)¹, (miraude@gmail.com)²

The UEMS - European Union of Medical Specialists is the oldest European medical organisation representing the interests of more than 50 different medical specialities and involving more than 1.6 million of healthcare professionals. The ESR - European Society of Radiology is the world's biggest radiological society, encompassing 67.500 members from 155 different countries. It was founded in 2005 by merging the European Congress of Radiology and the European Association of Radiology, aiming at establishing a single, powerful and unified voice for European radiologists. Through the section of radiology of the UEMS, UEMS and ESR share the same ambitious objective of promoting the highest quality of care and medical practice in radiology, by serving the needs of patients and general public, harmonizing radiological training and defending free movement and professional interests of European radiologists. This Joint session will focus on the concept and importance of advocacy at the level of the European Union, with specific emphasis on clinical audit in radiology and the impact of the European BSS Directive. With regard to the harmonisation of radiological training, the history and the future of the assessment programme of European training centers will be discussed. Finally, particular attention will be dedicated to the working methodologies of EACCME (European Accreditation Council for Continuing Medical Education) and ACI (Accreditation Council in Imaging) in the framework of CME - Continuing Medical Education and CPD - Continuing Professional Development programmes.

Session Objectives:

1. To describe the role of the UEMS within the EU.
2. To understand the difference between ESR and UEMS.
3. To understand the importance of cooperation between ESR and UEMS.

Author Disclosure:

M. Adriaensen: Other; Board Member; UEMS SECTION of RADIOLOGY; member, Standards Committee of the European Board of Radiology; member, EBR-UEMS ETAP 2.0 working group.

A-180 08:35

Differences and similarities between ESR and UEMS (part 1)

P.M. Parizel; Antwerp/BE

The UEMS and the ESR share a common ideal of serving the healthcare needs of the general public through the support of science, teaching and research and improving the quality of service. However, UEMS and ESR have a different structure: whereas the UEMS is the representative organisation of the National Associations of Medical Specialists in the European Union and its associated countries, the ESR is foremost a society of individual members. The UEMS was founded in 1958 and it is the oldest European medical organisation. With a current membership of 39 National Member Associations, it comprises 43 different Specialist Sections and Boards, 14 Multidisciplinary Joint Committees and over 20 Divisions, involving more than 1.6 million healthcare professionals. As the representative organisation of National Medical Associations (NMAs) in the EU and its associated countries, the UEMS sets standards for high quality healthcare practice, which are transmitted to authorities and institutions of the EU and the NMAs, stimulating and encouraging them to implement its recommendations. With more than 75,500 members from 157 different countries, the ESR, an apolitical, non-profit-organisation, is the world's biggest radiological society. Founded in 2005 by merging the European Congress of Radiology (ECR) and the European Association of Radiology (EAR), the ESR aims to offer a single, powerful and unified voice for European radiologists, thus providing a single house of radiology in Europe. In this session, the speakers will highlight the intense and positive collaboration between ESR and UEMS.

Learning Objectives:

1. To understand the structure of the UEMS and ESR.
2. To understand the differences between ESR and UEMS.
3. To understand the importance of UEMS/ESR political involvement in EU affairs.

A-181 08:40

Differences and similarities between ESR and UEMS (part 2)

B. Maillet; Brussels/BE (bernie.mail@skynet.be)

European legislation has three levels, from the highest level to the lowest level the Regulation, the Directive to the Recommendation. The strongest, the Regulation has immediate effect at National level while the Directive has to be transposed into National legislation and here derogations can be included while Recommendations are not really binding. The European Commission drafts those pieces of legislation that have to be then approved both by the European Parliament and by the European Council of Ministers jointly. This is the so-called EU institutional triangle. And the lobbying can be organised, first, at the level of the Drafting of the legislation, contacting the European Commission and trying to explain why we as Medical Specialists have some positions on some issues but also by contacting the individual Members of the European Parliament. There are some MEP's who are physicians and so they are the first "target" of our Lobbying activity at the European Parliament. As both the ESR as well as the UEMS Section of Radiology as an integral part of the UEMS have both as aim the defense of Radiology and the Radiologists for the benefit of better diagnosis for the European citizen and patient, they should lobby together in order to avoid duplication and be much more efficient. In the recent past such a common action has proven to be effective with for instance the derogation for MRI in field of the European Directive on Magnetic Fields.

Learning Objectives:

1. To understand the structure of the UEMS and ESR.
2. To understand the differences between ESR and UEMS.
3. To understand the importance of UEMS/ESR political involvement in EU affairs.

A-182 08:45

The European Perspective (part 1): advocacy at the EU Level (part 1)

V.E. Sinitzyn; Moscow/RU

Advocacy in medicine and radiology could be defined as a coordinated combination of problem identification, solution creation, strategy development, and actions taken by all participants in order to achieve the positive changes. Today the European radiological community has been facing a serious problem: the role of our specialty in modern healthcare is undervalued. This situation urgently needs to be corrected with help of large-scale advocacy campaign organised both by UEMS and ESR. Through advocacy, rights and needs of radiologists could be expressed and represented. So far radiologists and national radiological societies have the insufficient political influence to change a view of EU, national governments and health authorities on the new role of radiologists in the value-based system of healthcare. UEMS has contacts with the Authorities and Institutions of the EU, representing multiple organisations of the National Associations of Medical Specialists in the EU. From another side, ESR has vast professional expertise in all fields of radiology, including training of radiologists, setting of standards and guidelines, organisation of quality control, patient safety, information management and value-based imaging. Advocacy and political lobbying of European radiology from multiple combined actions from UEMS and ESR will stimulate and encourage EU and national authorities to implement recommendations from both professional organisations. Digital technologies and social media make such advocacy campaign more visible and effective. Advocacy campaign supporting European radiologists will result also in recognition of UEMS and ESR as trusted and effective organisations providing added value to the healthcare system of EU.

Learning Objectives:

1. To understand the concept of advocacy.
2. To understand the importance of advocacy in the EU.
3. To learn how the advocacy can improve the role of UEMS and the ESR in Europe.

A-183 08:50

The European Perspective (part 1): advocacy at the EU Level (part 2)

B. Maillet; Brussels/BE (bernie.mail@skynet.be)

The Union Européenne des Médecins Spécialistes is an umbrella organisation representing the Professional Medical Associations of the European Union and even broader, the European Area. The members are the National Medical Associations (NMA) representing medical specialists in the different Member States (MS) and was created by the NMA's of the six countries that created the European Economic Community (EEC, as was the name of the EU at that time) by the signing of the Rome Treaty in 1957 so the UEMS is the largest and oldest European Medical Organization (EMO) and will celebrate in 2018 its 60th anniversary. Aside the NMA's the UEMS also has 43 specialist Sections one of those being the UEMS Section of Radiology. The aims and objectives of the UEMS are the highest level of training of medical specialists and works also on the harmonisation of CME-CPD in Europe through the European

Thursday

Postgraduate Educational Programme

Council for CME (EACCME) that has an agreement on mutual recognition of Credits with the American Medical Association (AMA) and with the Royal College of Physicians and Surgeons of Canada (RCPSC) as well as harmonisation of training through European Examinations and the Council for European Specialist Medical Assessment (CESMA) that is part of the UEMS European Council for Accreditation of Medical Specialist Qualification (ECAMSQ).

Learning Objectives:

1. To understand the concept of advocacy.
2. To understand the importance of advocacy in the EU.
3. To learn how the advocacy can improve the role of UEMS and the ESR in Europe.

A-184 08:55

The European Perspective (part 2): clinical audit and its implementation in view of the European BSS Directive

B.E. Kelly; Belfast/UK

In 2018, Euratom Directive 2013/59 will come into effect. This will mandate the regular use of clinical audit as a tool for measuring, among other parameters, patient safety and radiation protection. In 2017, the audit subcommittee produced a booklet (Esperanto) designed to guide the user through the principles of clinical audit. A pilot study, performed during the summer of 2017, tested the efficacy of the templates within the booklet. The results of this indicated that respondents found the algorithm straightforward, the templates navigable and the subjects audited, relevant.

Learning Objectives:

1. To understand the definition of clinical audit.
2. To learn about the existence and the legal consequences of the current European directive addressing clinical audit in radiology.
3. To hear about best practices with regard to the implementation of clinical audit in radiology

A-185 09:05

ETAP 2.0 (part 1): history of ETAP

H. Aronen; Turku/FI (hannu.aronen@utu.fi)

The European Training Assessment Programme (ETAP) is a subcommittee of the education committee of the European Society of Radiology (ESR). It was established in 2001 as a joint initiative between the EAR (European Association of Radiology) and the UEMS (European Union of Medical Specialists). It has been funded equally by the ESR and the UEMS. ETAP is one of the oldest collaboration forms between ESR and UEMS radiology section. The aims of ETAP are to improve and harmonise the standards of radiology training in Europe, provide institutions that offer postgraduate radiology education with objective assessment of their training programmes by external assessors nominated by ESR and UEMS and develop assessment systems and guidelines for use by postgraduate education authorities at the national level. The program has been voluntary, and visits have been made on requests from the individual training centers. ETAP has also developed a self assessment tool for training centres. ETAP programmes encourage self regulation of the specialist training in radiology, further increasing the autonomy of European radiologists. The recommendations in the guidelines are compatible with the European Training Curriculum for Radiology and modern international educational references. ETAP has offered an objective method based on external systematic evaluation and self assessment to develop radiological specialist programs in Europe. It is necessary that we radiologists evaluate our specialist training ourselves.

Learning Objectives:

1. To understand the importance of ETAP in the past years.
2. To know about the structure of ETAP.
3. To learn about facts and figures of ETAP.

A-186 09:15

ETAP 2.0 (part 2): modernisation of ETAP

L. Oleaga Zúñiga; Barcelona/ES (lauraoleaga@gmail.com)

The European Training Assessment Programme (ETAP) was established in 2001 as a joint initiative of the European Society of Radiology (ESR) with the UEMS (European Union of Medical Specialists) radiology section. The aims of the programme were to improve and harmonise the standards of radiology training in Europe based on the ESR European Training Curriculum for Radiology (ETC) and provide institutions that offer postgraduate radiology education with an objective assessment of their training programmes by external assessors nominated by the ESR. The main limitation of the programme was the limited availability due to the necessity to displace advisors. This constraint made the program inefficient since it could not reach a large number of institutions. Another limitation was the lack of official

certification. The new ETAP 2.0 configuration changes from onsite assessment to virtual assessment. The assessment programme is divided into 4 phases: 1st phase: application and completion of the documents. 2nd phase video report of the facilities of the centre. 3rd phase online interviews in a structured manner with the trainees, tutors and head of the department. 4th phase certification by the accreditation council in Imaging (ACI). There are three levels of certification: basic, intermediate and excellence, based on the score reached by the centre after the evaluation of the three phases. A report with recommendations for improvement is sent to the centre that has to report back within the established time frame as it was done in the prior ETAP programme. It is foreseen a reaccreditation every 5 years.

Learning Objectives:

1. To understand the limits of ETAP 1.0.
2. To learn about the new configuration of ETAP.
3. To learn about the "starring system".

A-187 09:25

CME/CPD in Europe (part 1): EACCME 2.0

P. Ricci; Rome/IT (paolo.ricci@uniroma1.it)

The European Accreditation Council for Continuing Medical Education (EACCME) has been created by the European Union of Medical Specialists (UEMS) in 1999 and started operating in January 2000 with the aim of encouraging high standards in development, delivery, and harmonisation of Continuing Medical Education (CME) through the international accreditation of CME events, and the establishment of a system for the international acceptance of CME credits (ECMEC). EACCME can validate and grant the official number of ECMEC after professional evaluation has been performed by a CME National Accreditation Authority or UEMS Specialty Board. To facilitate the transfer of credits and allow the free movement of healthcare professionals within Europe, 1 ECMEC equates to 1 hour of CME, with a maximum of 6 ECMECs for a day and 3 ECMECs for half a day. Beyond European member states, mutual recognition agreements have been signed with the American Medical Association and the Royal College of Physicians and Surgeons of Canada, thus enhancing the international status of EACCME. To comply with the growing scopes of CPD-Continuing Professional Development, broader than CME, EACCME currently recognises the review and publication of scientific and educational material, e-learning by teaching and the participation in UEMS examinations as an examiner. As of January 2017, EACCME 2.0 version has become applicable, resulting in a new interactive platform for providers and users, a faster and more efficient accreditation process and in the recognition of e-learning materials (e-platform, e-library, apps).

Learning Objectives:

1. To learn about the European Accreditation Council for Continuing Medical Education (EACCME®).
2. To know about the existence of European CME and CPD credits.
3. To learn about the new EACCME 2.0.

Author Disclosure:

P. Ricci: Other; ACI, Scientific Director; UEMS Section of Radiology, President; UEMS EEC, Member.

A-188 09:30

CME/CPD in Europe (part 2): the Accreditation Council in Imaging

P. Ricci; Rome/IT (paolo.ricci@uniroma1.it)

Educational events sent to UEMS/EACCME for European Accreditation have to be evaluated by two distinct structures: the National Accreditation Authority of the country where the activity is to take place, and the related UEMS Section or European Specialty Accreditation Board (ESAB). Based on the mutual agreement between the Accreditation Authorities, the Sections and ESABs, the process is recognised throughout Europe and the different specialties of the UEMS. Recent steps have been taken by the EACCME in order to harmonise the whole system in Europe independently from the specialty or the country where the activity has taken place. The Section of Radiology keeps the role of back-up reviewer for those countries not yet enlisted in EACCME accreditation agreements. In 2015, the Section started a fruitful cooperation with the Accreditation Council in Imaging (ACI), the body established by the European Board of Radiology - an initiative of the European Society of Radiology - in Barcelona to reach homogenisation of radiology education across Europe. Following an amended agreement in 2016, representatives of the Section hold the chair of Scientific Director on alternate basis and sit permanently in ACI Policy and Reviewing Committees, each guided by a chairperson. The necessary adaptation of ACI Terms & Conditions to the revised criteria for the accreditation of Live Educational Events (LEE) and of E-learning materials (ELM) has been recently conducted November 2016 - January 2017. ACI team is offering constructive feedback on the successful implementation of the EACCME 2.0 online platform.

Learning Objectives:

1. To learn about the ESABs under the EACCME umbrella.

Postgraduate Educational Programme

2. To learn about the structure of the Accreditation Council in Imaging (ACI).
3. To understand the importance of cooperation with and recognition by the EACCME®.

Author Disclosure:

P. Ricci: Other; ACI, Scientific Director; UEMS Section of Radiology, President; UEMS EEC, Member.

A-189 09:35

CME/CPD in Europe (part 3): the many ways to gain European CME/CPD credits

M.A. [Lucic](mailto:milos.a.lucic@gmail.com); *Sremska Kamenica/RS (milos.a.lucic@gmail.com)*

Recognising the tendency of continuing-medical-education (CME) shift from voluntary to mandatory within Europe, the European Union of Medical Specialists (UEMS) and its European Accreditation Council for CME (EACCME®) introduced European Continuing Medical Education Credits® (ECMECs), as CME "tokens" reflecting objectively the CME activity that facilitates the exchange of CME credits between European countries and comparable systems outside Europe. Considering CME as educational activities which serve to maintain, develop or increase the knowledge, skills, professional performance and relationships that physician/radiologist uses to provide services for patients or profession, ECMECs are awarded for both live educational events, and e-learning materials, but from recently also for continuing professional development (CPD), defined as the educative means of updating, developing and enhancing how physicians apply the knowledge, skills and attitudes required in their working lives (Basle Declaration, 2001). As CPD incorporates and goes beyond CME, EACCME 2.0, adopted in 2016, enabled EACCME® recognition of the several CPD/CME activities that include reviewing and/or publishing scientific and educational material, learning by teaching, and examining in UEMS exams, including EDiR exam. Being aware that CME/CPD systems in Europe differ between countries, the Accreditation Council in Imaging (ACI) has recently conducted two surveys, addressed to ESR Institutional Member Societies and individual ESR members, which provided valuable information on differences in accreditation systems in European countries, but also reflected several important standpoints, including the recognition of ECMECs as universal European CME "tokens", and unification of CME/CPD systems within Europe, which shall be acknowledged as the "voice of European radiologists" in future considerations.

Learning Objectives:

1. To know about the existence of European CME Credit (ECMEC®).
2. To learn about the concept of CPD.
3. To learn about the importance of credits in different European countries.

Author Disclosure:

M.A. Lucic: Board Member; EBR ACI Policy Committee Chairman. Consultant; Affidea Serbia. Research/Grant Support; Secretariat for Higher Education and Scientific Research of AP Vojvodina; Research Grant Nr. 142-451-2487/2016.

09:45

Questions

08:30 - 10:00

Room O

Paediatric

RC 512

Imaging in abdominal emergencies: an (evidence-based) update

Moderator:

C.E. de Lange; Oslo/NO

A-190 08:30

A. The acute abdomen in neonates

S. [Stafrace](mailto:samstafrace@yahoo.com); *Doha/QA (samstafrace@yahoo.com)*

Common causes of neonatal abdominal emergencies are reviewed focusing on congenital intestinal obstruction, malrotation and necrotising enterocolitis (NEC). Radiologists play a pivotal part in the management of neonates with suspected obstruction and are often asked for an opinion on the presence or not of obstruction, the level of obstruction and the cause. The standard choice of radiological modalities includes plain film, ultrasound (US) and fluoroscopy. Neonatal intestinal obstruction is classified as upper/high versus low obstruction done through presenting symptoms and plain film appearances. High obstruction presents with vomiting or increased aspirates. Main differential diagnoses include congenital obstructions of the duodenum/jejunum and malrotation. High obstruction often leads to surgical exploration with some

radiographic patterns being diagnostic enough to recommend surgery including the 'double bubble' and 'triple bubble' signs. Bilious vomiting and/or the start of symptoms in the immediate postnatal period increases the clinical suspicion for malrotation. In such cases an urgent upper GI study is indicated. Operators should be comfortable with the fluoroscopic technique, normal duodenal landmarks and with the less common duodenal anatomical variants. Low obstruction presents with distention, vomiting and failure to pass meconium. Multiple dilated loops are seen on radiography. Differential diagnoses include Hirschsprung disease (HD), small left colon, meconium ileus and atresias. Outside HD (when rectal biopsy is diagnostic), suspected low obstruction warrants a contrast enema; providing high diagnostic specificity. NEC is the leading gastrointestinal emergency of the premature neonate. Imaging mainly involves plain films and ultrasound; guided by the clinical course of the neonate.

Learning Objectives:

1. To learn about typical neonatal abdominal emergencies.
2. To understand the choice of modalities in acute abdomen in neonates.
3. To appreciate typical findings and 'red flag' features.

A-191 09:00

B. The acute abdomen in young children

A.D. [Calder](mailto:Alistair.Calder@gosh.nhs.uk); *London/UK (Alistair.Calder@gosh.nhs.uk)*

Common causes of the acute abdomen in children beyond the neonatal period are reviewed, with a focus on three conditions with major roles for imaging: hypertrophic pyloric stenosis, intussusception, and acute appendicitis. The evidence base underlying the roles imaging plays is evaluated for each condition.

The role of ultrasound in pyloric stenosis is well established and is generally highly sensitive and specific. Pyloric length and muscle thickness parameters remain robust measures for correct diagnosis, but may need to be adjusted for age and size. Additional signs which may be useful, such as pyloric shape and colour doppler findings are discussed. Surgical management remains the mainstay of treatment, despite evidence of effectiveness of medical therapy in some children. The role of ultrasound in the diagnosis of intussusception is similarly well supported and is highly accurate even in relatively inexperienced hands. Radiologists also typically play the leading role in initial attempts to reduce intussusception, and are mostly successful. Various techniques for reduction are available, each with their own advocates and evidence base. Acute appendicitis is the most common abdominal emergency requiring surgery. Pre-operative imaging diagnosis is now the norm. Ultrasound is recommended as the primary imaging tool in children, but can lack sensitivity and in most centres, equivocal sonography is followed by cross sectional imaging. CT has a strong evidence base for accurate diagnosis of appendicitis, but confers significant radiation burden. Low dose protocol CT and MRI offer alternatives with potentially similar levels of accuracy. Differential diagnoses for appendicitis including adnexal torsion and mesenteric adenitis are briefly explored.

Learning Objectives:

1. To learn about the causes of acute abdominal pain in children.
2. To understand the choice of imaging techniques and their limitations.
3. To appreciate typical radiological features of abdominal emergencies.

A-192 09:30

C. Polytrauma: differences between adult and paediatric protocols

M. Raissaki; *Iraklion/GR*

Trauma is still the most frequent cause of mortality and disability in childhood and adolescence. Emergency physicians have to thoroughly assess injured children following high-energy trauma. Traumatized children differ from adults: haemodynamically stable children may be actively bleeding. Conversely, children have smaller caliber vessels, stronger vasoconstriction, stronger solid organ capsules; bleedings may stop spontaneously, organ rupture is more difficult and delayed rupture rare. This is why children are imaged aggressively although few will undergo surgery or trans-arterial embolisation. Imaging is mandatory for diagnosis and management especially during the primary survey. Its goal is to exclude life-threatening injuries, identify children that may rapidly deteriorate because of clinically silent active bleeding, increase the surgeon's confidence level by clarifying injuries that need to be treated and ultimately determine short and long-term management. Radiographs and ultrasonography play a basic role in haemodynamically unstable patients. Contrast-enhanced ultrasound is an emerging diagnostic tool in low-energy trauma and in suspected isolated abdominal injuries. In stabilized patients CT scanning has been considered a sensitive, specific, and accurate test for identification and grading of multi-organ injuries. Due to children' increased radiosensitivity, CT scans should be indicated based on appropriate early clinical evaluation of the closely monitored child and assessment of risk factors for CNS, chest, MSK and abdominal injuries. ALARA includes avoiding non-contrast scans, avoiding multiple phases and applying age/weight-dependent

Thursday

Postgraduate Educational Programme

exposure parameters and radiation-saving reconstruction algorithms. CT should not be performed for follow-up unless there is clinical deterioration. Objective documentation of injuries is extremely important in suspected child abuse.

Learning Objectives:

1. To learn how paediatric trauma differs from adult trauma.
2. To understand how examination techniques and protocols must be tailored accordingly.
3. To appreciate the importance of multidisciplinary team collaboration in planning and conducting radiological investigations in a trauma setting.

08:30 - 10:00

Room N

Cardiac

RC 503

From diagnosis to prognosis: how does cardiac imaging affect patient outcome?

Moderator:

U. Reiter; Graz/AT

A-193 08:30

A. In myocarditis

M. [Francone](mailto:marco.francone@uniroma1.it); Rome/IT (marco.francone@uniroma1.it)

Natural history of acute and chronic myocarditis is often unpredictable being independent on the clinical onset of disease and even poorly correlated with more traditional clinical predictors like end-diastolic volume or ejection fraction. In most cases, patients typically improve within weeks to months, but an unfavourable clinical evolution may be observed in a minority of individuals consisting with the development of chronic ventricular dysfunction progressing leading to transplantation or death in 25% of cases. CMR has emerged as a central prognostic indicator in inflammatory cardiomyopathies, mainly because of its ability to detect tissue fibrosis in vivo. This has been demonstrated with a growing and consistent scientific evidence, derived from late enhancement imaging and more recently from native T1 mapping and ECV. Present lecture will aim to illustrate of CMR capabilities as prognostic indicator in acute and chronic myocarditis, providing an overview of most important published studies and ongoing clinical trials. Particular emphasis will given to the importance of T1 and T2 mapping techniques, being a new standard of reference for CMR diagnosis and patient's prognostic stratification.

Learning Objectives:

1. To learn about the link between clinical presentation and imaging signs.
2. To understand the current state-of-the-art MRI method for the diagnosis of myocarditis.
3. To learn how MRI could be used to assess prognosis in myocarditis.

A-194 09:00

B. In non-ischaeamic cardiomyopathy

A. [Jacquier](mailto:alexis.jacquier@ap-hm.fr); Marseille/FR (alexis.jacquier@ap-hm.fr)

Non-ischaeamic cardiomyopathy is one of the major indications of cardiac MR worldwide. MRI is now included in all European guidelines for diagnosis and prognosis assessment in cardiomyopathy. During that talk we will focus on dilated cardiomyopathy, hypertrophic cardiomyopathy and arrhythmogenic right ventricular dysplasia. MRI is a potent tool to assess phenotype of the myocardium and characterise tissue in both patients and proband. New sequences or post treatment tools could be helpful to better characterise myocardial tissue such as parametric maps and feature tracking.

Learning Objectives:

1. To recognise the tell-tale signs of early ARVC, HCM and dilated cardiomyopathy that affect progression or prognosis.
2. To understand what should be measured and reported.
3. To appreciate the role of MRI in early diagnosis and prognosis assessment in these cardiomyopathies.

Author Disclosure:

A. **Jacquier**: Research/Grant Support; Guerbet.

A-195 09:30

C. In coronary artery disease

R. [Salgado](mailto:rodrigo.salgado@uza.be); Antwerp/BE (rodrigo.salgado@uza.be)

Non-invasive imaging of the coronary arteries using CT has in the past decade reached worldwide clinical implementation. This is the consequence of both technical advances of CT imaging, as well as the validation of this technique in multiple clinical trials and randomised studies. One of the main strengths of

non-invasive coronary artery imaging is the ability to exclude obstructive disease, as such eliminating the need for further invasive examinations. Furthermore, the quantification of coronary calcium provides a quantitative measure of the degree of arteriosclerosis, further helping in the risk stratification of patients. During this lecture, we will review the scientific evidence regarding the use CT-angiography of the coronary arteries in different populations, their impact on actual clinical management and their significance for mid- and long-term prognosis. Additionally, new technologies aimed at improving triage for further testing in patients with intermediate stenosis (including CT-derived fractional flow reserve) and their potential role will be discussed. Finally, a structured reporting scheme will be provided to streamline the communication of findings to referring physicians.

Learning Objectives:

1. To understand which patients will benefit from anatomic assessment or functional assessment of the coronary arteries.
2. To learn about how to report on anatomic and functional assessment of coronary arteries.
3. To appreciate the role of non-invasive imaging in prognosis assessment.

08:30 - 10:00

Studio 2018

State of the Art Symposium

SA 5a

Whole-body MRI: ready for prime time?

A-196 08:30

Chairperson's introduction

F.E. [Lecouvet](mailto:frederic.lecouvet@uclouvain.be); Brussels/BE (frederic.lecouvet@uclouvain.be)

WB-MRI is now a commonly applied modality for bone screening for "osteophilic" metastatic cancers, lymphomas, and multiple myeloma and can also assess visceral and nodal involvement. WB-MRI's applications have been expanded to other fields, mainly in rheumatology; it has shown promise for diagnosis and evaluation of treatment response of spondyloarthropathies, and many muscle, bone, neurological, and vascular disorders. The diversity of indications is reflected by the segmentation of this session: the different medical fields where WB-MRI contributes to improvement in patient care will be addressed by expert speakers from varied geographical origins who will share their respective experience. They will illustrate imaging findings, provide technical recommendations, and describe the place of the technique amongst others in modern management of diseases.

Session Objectives:

1. To become aware of the feasibility of whole-body MRI.
2. To learn about its roles: detect, monitor and provide prognostic information.
3. To understand the anatomic targets: bone and beyond.
4. To become familiar with current developments in the technique and their implementation.

A-197 08:35

The case of metastatic bone disease

A.R. [Padhani](mailto:anwar.padhani@talk21.com); London/UK (anwar.padhani@talk21.com)

WB-MRI will replace current, ineffective & indirect methods of malignant disease detection in the bone marrow with applications in myeloma, breast, and prostate cancer. Multiple imaging standards are published including the MET-RADS system which will be summarised. WB-MRI has the potential to alter diagnostic thinking when assessing bone response: by adding new categories that positively assess the success of therapies in bone disease (NOT just absence of progression). It is unclear whether this will allow patients to live better for longer?. WB-MRI can help deliver the promise of high precision medicine for patients with metastatic bone disease.

Learning Objectives:

1. To understand the clinical rationale for the use of whole-body MRI when evaluating metastatic disease.
2. To learn about the use of METRADS data acquisition and response assessment guidelines.
3. To become aware of the potential benefits of whole-body tumour load quantification.
4. To review examples of clinical pathway benefits, including precision medicine approaches.

Author Disclosure:

A.R. **Padhani**: Speaker; Siemens Healthineers, Janssen, Sanofi.

A-198 08:55

The case of multiple myeloma

L.-A. Mouloupoulos; Athens/GR (lmouloup@med.uoa.gr)

WBMRI is more sensitive than WBXR and WBCT for the early detection of bone marrow involvement in multiple myeloma and it performs better than PET-CT in the diagnosis of small lesions or diffuse bone marrow infiltration. In the updated (2014) international myeloma working group (IMWG) criteria for the definition of myeloma, MRI is considered a biomarker of malignancy, with the presence of more than one focal lesion on MRI establishing the diagnosis of symptomatic disease. When MRI of the spine and pelvis is performed, an approximately 10% false negative rate may be observed because of focal lesions located exclusively in the appendicular skeleton. WBMRI, on the other hand, provides a means of bone marrow tumour burden assessment and at the same time identifies possible extraskelatal locations of myeloma. Bone marrow patterns of involvement and tumour burden on WBMRI have also emerged as important tools for prognosis. Regarding assessment of response to therapy, even though PET-CT is currently the preferred modality for optimal definition of a complete response to treatment in patients with myeloma, ADC values extracted from DWI images, have been shown to change early after treatment, suggesting a possible role for WBDWI in the evaluation and prediction of successful therapy. In the era of novel therapies for multiple myeloma, the role of a non-ionizing imaging modality like WBMRI for the search of minimal residual disease in the bone marrow and extraskelatal sites of disease at the same time, is appealing and warrants further investigation.

Learning Objectives:

1. To become aware of the value of whole-body MRI in myeloma.
2. To learn about its roles: detect, monitor and provide prognostic information.
3. To understand current imaging protocols.

A-199 09:10

The case of lymphoma

M.E. Mayerhoefer; Vienna/AT (marius.mayerhoefer@meduniwien.ac.at)

Lymphomas are a heterogeneous group of hematological malignancies that can be roughly divided into Hodgkin (HL) and non-Hodgkin (NHL) lymphomas, and account for about 5% of all cases of cancer. The NHL group is characterized by a high level of heterogeneity between the different subtypes, not only with regard to their histological features, but also with regard to growth rates and clinical course/prognosis, as well as treatment options. Nevertheless, the majority of lymphomas show a high cell density, which makes them an attractive target for diffusion-weighted imaging (DWI), because of the associated compression of extracellular space. Even though [18F]FDG-PET/CT is generally regarded as the technique of choice for imaging of lymphomas (and in particular, for assessment of treatment response), there are several justifications for the use of whole-body DWI in lymphoma patients. For instance, the fact that some lymphoma subtypes (such as HL) are common in children and adolescents makes DWI attractive due to its lack of exposure to ionizing radiation, which is relevant because these patients may require life-long follow-up. In addition, slowly growing NHL subtypes such as MALT lymphoma frequently show low, or no, FDG uptake, whereas they still show the diffusion restriction pattern on DWI, due to their high cell density. Finally, access to MRI, and thus, also to DWI, is far easier than to [18F]FDG-PET/CT due to the relative abundance of MR scanners, which may decrease waiting intervals and lead to earlier treatment initiation. Nevertheless, while several studies have shown that whole-body DWI is only slightly to moderately inferior to [18F]FDG-PET/CT, DWI is still limited with regard to the evaluation of small lymph nodes, the assessment of diffuse bone marrow involvement, and, mainly due to motion artifacts, for lesion assessment in the lower neck and the mediastinum.

Learning Objectives:

1. To become aware of the role of whole-body MRI for imaging lymphoma subtypes.
2. To learn about its roles: detect, monitor and provide prognostic information.
3. To understand the current limitations of whole-body DWI.

A-200 09:25

Beyond oncology: rheumatology and more

S. [Weckbach](mailto>Weckbach); Heidelberg/DE (sabine.weckbach@med.uni-heidelberg.de)

The high soft tissue contrast and anatomical resolution of whole body MRI (WBMRI) in combination with an excellent sensitivity and specificity for the musculoskeletal system offer many advantages in the diagnostic process of rheumatological and neuromuscular disorders. Disease specific adaption of different protocol modules allow the replacement of multiple separate exams by one whole-body MRI (WB-MRI) examination so that WB-MRI is capable of a combined visualisation of the spine and all relevant joints, the vessel system and potentially affected organs such as the brain, the kidneys or the heart in only one exam. It is able to directly and simultaneously show (even subtle)

active and chronic inflammation including synovial, cartilaginous and bony changes. It is very well suited for the visualisation of enthesitis and arthritis in central and peripheral joints at one examination. Moreover, WB-MRI allows the early detection of bone marrow changes and muscle pathologies. Therefore, it holds the potential to estimate the total disease load and disease activity of different rheumatological and neuromuscular disorders as well as follow-up patients under therapy. Due to the exact localization of inflammatory processes present at multiple sites and visualisation of typical disease pattern, it enables us to distinguish between a variety of rheumatological and neuromuscular disorders.

Learning Objectives:

1. To become aware of the protocols and diagnostic value of whole-body MRI in rheumatological and neuromuscular disorders.
2. To understand the role of whole-body MRI screening for multi-site inflammation in one single examination.
3. To learn about its role in differential diagnosis quantification of disease burden and assessment of therapeutic response.

09:45

Panel discussion: Whole-body MRI: when, how and why should you do it?

08:30 - 10:00

Room L 8

Joint Session of the ESR and ESHI

When to use hybrid imaging

Moderators:

K. Riklund; Umea/SE

T. Beyer; Vienna/AT

A-201 08:30

Imaging prostate cancer: MRI or PSMA-PET/CT?

L. Schimmöller; Düsseldorf/DE (lars.schimmoller@med.uni-duesseldorf.de)

The multiparametric magnetic resonance imaging (mp-MRI) of the prostate and also imaging with prostate-specific membrane antigen (PSMA-PET) are innovative methods that significantly improved the diagnostic of prostate cancer. A remarkable change in clinical routine has been the increasing role of MRI in prostate cancer detection. Mp-MRI examinations (with T2, DWI, and DCE-Images) are already part of international guidelines in secondary diagnostics (after previous negative systematic TRUS-GB) and also in active surveillance. But in primary diagnostic, staging, and recurrence MRI have got a qualification and validly, too. In its updated guidelines 2017 the German Society of Radiology notably insists on the importance of mp-MRI and MRI-guided biopsy for prostate cancer diagnosis. The main significance of the MRI is the detection of clinical relevant prostate cancers with its additional functional sequences, but nationwide coverage of qualitative mp-MRI examinations and qualitative standardized reporting are two of the most important challenges. PSMA-PET is the most promising imaging tool primary for prostate cancer recurrence and may be currently used for detection in unclear cases with high suspicion of prostate cancer, but especially costs and availability are limiting this promising diagnostic tool. PSMA-PET shows good results already in patients with low PSA-values regardless of previous applied therapy. As a consequence logically a combination of PSMA-PET and MRI might be very nice, but PSMA-PET/MRI is rarely available and its clinical benefit remains to be demonstrated. Furthermore, with MRI and PSMA a lot of new individual therapeutic opportunities are given.

Learning Objectives:

1. To learn about indications of MRI and PSMA-PET in prostate cancer.
2. To appreciate differences in indications for initial diagnosis and PSA-recurrence.

A-202 09:00

Differentiating radiation necrosis from tumour recurrence: do we need hybrid imaging?

E.-M.B. Larsson; Uppsala/SE (elna-marie.larsson@radiol.uu.se)

Magnetic resonance imaging (MRI) without and with intravenous contrast agent injection is the primary imaging method for the evaluation of treatment effects on brain tumours, such as gliomas and metastases. However, the method has difficulties to differentiate tumour progression from reactive, treatment-related changes after surgery, radiotherapy, chemotherapy or immunotherapy. The additional use of positron emission tomography (PET), MR perfusion or proton MR spectroscopy (MRS) may improve the diagnostic specificity. 18F-FDG-PET is widely used for body imaging, but suboptimal for this purpose due to the high glucose uptake in normal brain tissue. Radiolabelled amino acid tracers, such as 11C-MET with short half-life or 18F-FET with longer half-life, show a high tumour-to-background contrast. Amino

acids accumulate in recurrent tumour, but not in reactive or reparative processes after treatment. MR perfusion with evaluation of relative cerebral blood volume (rCBV) is also helpful, since high rCBV usually indicates tumour recurrence. MRS shows the relative concentrations of different metabolites and increase of choline (Cho) supports the suspicion of recurrent malignant tumour with cell proliferation. However, the areas of increased PET uptake and increased rCBV and/or high Cho do not always coincide, which makes the interpretation difficult. In addition, a combination of recurrent tumour and reactive changes is often present. Since each of the PET and MR techniques mentioned above has limitations, hybrid PET/MR combining the information from uptake of radiolabelled amino acids, measurement of rCBV and also of Cho, may provide improved diagnostic accuracy.

Learning Objectives:

1. To learn about different radiopharmaceuticals available for differentiation of tumour from radiation necrosis.
2. To understand typical hybrid imaging findings in radiation necrosis and tumour recurrence.

Author Disclosure:

E.-M.B. Larsson: Research/Grant Support; Bayer Pharma AG, Berlin, Germany. Speaker; Bayer Pharma AG, Berlin, Germany.

A-203 09:30

What can we expect as future targets for new radiopharmaceuticals?

G. Cook; London/UK

There are now few hallmarks of cancer that we cannot exploit with imaging. In particular, there are several PET and SPECT probes that can measure abnormal metabolic processes (e.g., 18F-FDG, 99mTc-sestamibi), proliferation (e.g., 18F-FLT, 18F/11C-choline), receptor overexpression (e.g., 68Ga-dotatate, 68Ga-PSMA, apoptosis (e.g., 18F-ML10), hypoxia (e.g., 18F-MISO, 64/62Cu-ATSM) and angiogenesis (e.g., 89Zr-bevacizumab, 18F-RGD) amongst others. Whilst some of these tracers are useful for diagnosis and phenotyping, many are of interest for predicting early treatment response, especially in the setting of targeted biologic therapies where an early reduction in tumour volume is not expected and where morphologic CT and MRI are therefore limited. Of particular current interest is the evaluation of response to immunotherapies that may cause pseudoprogression, caused by immunocellular infiltration before subsequent tumour shrinkage. In this situation early pseudoprogression may also be seen with 18F-FDG PET and hence the interest in more specific tracers such as 89Zr-PDL1 antibody. Whilst PET and SPECT probes are invaluable in reporting on underlying biological tumour characteristics, both CT and MRI provide valuable supportive information in hybrid imaging scanners allowing anatomical reference as well as some functional measurements, e.g., cellularity with DWI and perfusion with DCE MRI / pCT. The ultimate goal of predicting which patients will respond to which treatment, or at least to determine non-response as soon as possible, is not fully achieved in the clinic with imaging as yet but some areas are now contributing to clinical practice, e.g., 18F-FDG PET/CT to guide treatment escalation / de-escalation in lymphoma.

Learning Objectives:

1. To become familiar with future targets in oncological hybrid imaging.
2. To learn how hybrid imaging can support the oncologist in diagnosis and therapy response assessment.

Author Disclosure:

G. Cook: Research/Grant Support; Siemens, GEHC, Alliance Medical, Theragnostics.

08:30 - 10:00

Room E1

Pros & Cons Session

PS 527

Do we need dynamic contrast enhancement (DCE) in prostate mpMRI?

A-204/A-205 08:30

Chairpersons' introduction

H.-P. Schlemmer¹, J.J. Fütterer²; ¹Heidelberg/DE, ²Nijmegen/NL (h.schlemmer@dkfz.de)¹ (jürgen.futterer@radboudumc.nl)²

Multiparametric MR imaging (mpMRI) is increasingly important for individualized decision making in prostate cancer patients. A large number of clinical studies have demonstrated that the combination of morphologic and functional MR parameters are advantageous for detection and localization of significant cancer, for biopsy guidance, for local staging and for active surveillance. Various MR-guided or TRUS/MR image fusion biopsy technologies are already used in clinical practice for transrectal or a

transperineal targeted +/- systematic biopsy. High-quality mpMRI including standardized image acquisition and image interpretation is crucial and recommendations according to PI-RADS are meanwhile widely accepted. But there is still controversial discussion about the optimal state-of-the-art mpMRI protocol. While meanwhile several studies have shown compelling evidence that diffusion-weighted MRI (DWI) is fundamental for prostate cancer detection and characterization, the clinical value of dynamic contrast-enhanced MRI (DCE) is still under debate. Different views were brought forward weighting increased examination time and costs against the clinical benefit. This session will point out the controversial discussion to balance pros and cons.

Session Objectives:

1. To understand the clinical significance of mpMRI for detection and local-regional staging of prostate cancer.
2. To learn about the potential and limits of DCE MRI.
3. To understand the controversial discussion about the added value of DCE as part of mpMRI in clinical routine.

A-206 08:35

A. Yes we do!

G.M. Villeirs; Ghent/BE

Like many other cancers, prostate cancers can release angiogenic factors that cause growth of existing blood vessels and de novo angiogenesis. As these new vessels are loosely organized, with varying sizes, leaky endothelium and arteriovenous shunts, their permeability is higher than in normal vessels. Dynamic contrast-enhanced (DCE) MRI exploits this difference using a series of rapid T1-gradient-echo sequences (every ≤ 10 seconds over ≥ 2 minutes) after a 2-3cc/sec bolus administration of 0.1 mmol/kg of gadolinium contrast agent. Tumor foci show earlier, faster and more intense enhancement due to increased influx of contrast in an expanded vascular space and increased extravasation to the extravascular space, followed by marked washout due to increased backflow to the vascular compartment. These temporal tissue enhancement changes can be evaluated qualitatively (visual analysis of enhancing areas), semi-quantitatively (evaluation of enhancement curve types), or quantitatively. The latter is based on pharmacokinetic modelling techniques that calculate parameters such as Ktrans (leakage to the extravascular space), kep backflow to the blood vessels, and ve (size of the extracellular extravascular space). DCE can be used to detect prostate cancer in the peripheral zone (less in the transition zone due to false positive enhancement in benign prostatic hyperplasia), especially in case of doubt on DWI or poor DWI quality in multiparametric MRI. It also improves the staging accuracy, especially in less-experienced users. Most importantly, it is the best technique to assess the location and extent of recurrent disease, both after radical prostatectomy, external beam radiotherapy or focal therapy.

Learning Objectives:

1. To understand how DCE enables improved cancer detection by revealing microvasculature and perfusion.
2. To become familiar with quantitative analysis of signal intensity-time curves after intravenous contrast agent administration in order to reveal cancer specific perfusion-related parameters.
3. To appreciate the diagnostic potential of DCE to detect significant prostate cancer.

A-207 09:00

B. No we don't!

H. Hricak; New York, NY/US

T1-weighted imaging (T1WI) and T2-weighted imaging (T2WI), joined recently by DWI, have become the mainstay of prostate evaluation by mpMRI. The question is whether, in our clinical protocols, we also need to include dynamic contrast-enhanced MRI (DCE-MRI) and/or proton MR spectroscopic imaging (MRSI). DCE-MRI improves assessment of tumor aggressiveness, but its value in tumor detection remains controversial. Based on studies from the last 5 years, in the setting of cancer detection, the combination of DCE-MRI+T2WI has similar or lower accuracy and is significantly less specific than the combination of DWI+T2WI; adding DCE-MRI to DWI+T2WI significantly increased sensitivity, but it also significantly lowered specificity. A recent study of 542 men with elevated PSA levels found that for tumor detection, T2WI+DWI had accuracy comparable to that of T2WI+DWI+DCE-MRI, with diagnosis of clinically significant cancer being the endpoint. Overall, the literature suggests DCE-MRI adds limited or no value in most scenarios. While MRSI can improve tumor characterization, its routine application is not recommended because of long scan times, operator dependence and limited spatial resolution. Therefore, if we are to advocate the inclusion of mpMRI in a prostate cancer screening algorithm, we should recommend a streamlined protocol of T1W+T2WI+DWI, as it provides higher accuracy, reduced scan times, greater patient comfort and safety, and is less costly than protocols also incorporating DCE-MRI or MRSI. However, use of DCE-MRI should be recommended in

Postgraduate Educational Programme

searching for recurrence after treatment, in situations where artifacts degrade the quality of DWI, or in patients on experimental medical therapy protocols.

Learning Objectives:

1. To become familiar with the diagnostic potential of mpMRI including T2w, advanced DWI and MRSI.
2. To understand the diagnostic potential non-contrast-enhanced mpMRI to detect significant prostate cancer.
3. To appreciate the benefits of a shortened mpMRI protocol by omitting DCE.

Author Disclosure:

H. Hricak: Board Member; Ion Beam Application (IBA).

09:25

Discussion

08:30 - 10:00

Room E2

State of the Art Symposium

SA 5b

Current guidelines and diagnostic criteria in multiple sclerosis (MS)

A-208 08:30

Chairperson's introduction

A. **Rovira-Cañellas;** Barcelona/ES (alex.rovira@idi.gencat.cat)

In the last few years, techniques and clinical implementation of MR imaging of multiple sclerosis (MS) have markedly evolved based on the relative large amount of new published data from clinical trials and observational studies, which assessed the value of this tool in the early and accurate diagnosis of MS. However, the role of MR imaging in MS goes far beyond the diagnostic process and differential diagnosis. MR imaging can also provide useful prognostic information in terms of long term disability prediction. Moreover, with the introduction of the new generation of immunomodulating /immunosuppressive drugs for the treatment of MS, MR imaging also plays an important role in treatment monitoring. This includes the prediction of treatment response, the assessment of treatment efficacy and treatment safety. In this state of the art symposium, the speakers will present up to date on the diagnostic criteria of MS, and on the value of MR imaging for monitoring and predicting treatment response and in the detection of treatment related adverse effects. All these information should help radiologists in the standardization and optimization of the use of MR imaging in the management of MS in clinical practice.

Session Objectives:

1. To appreciate the importance of an accurate diagnosis of MS.
2. To learn about the value of diagnostic criteria for MS.
3. To understand the relevance of MRI for monitoring and predicting treatment response.
4. To become familiar with treatment-related adverse effects.

Author Disclosure:

A. Rovira-Cañellas: Advisory Board; Novartis, Biogen, Sanofi-Genzyme. Speaker; Novartis, Stendhal America, Biogen, Bracco, Bayer, Sanofi-Genzyme, TEVA.

A-209 08:40

Update on new clinical diagnostic criteria

C. **Enzinger;** Graz/AT (chris.enzinger@medunigraz.at)

In the diagnostic process applied to people suspected to have multiple sclerosis (MS), MRI of the brain and spinal cord has become an indispensable tool to objectively demonstrate lesions disseminated in time and space, which are considered as a hallmark of the disease. MRI has been formally integrated in the diagnostic criteria first in 2001 by an international panel and - based on accumulating scientific evidence - revisions of these criteria have been provided in 2005, 2010 and, most recently, in 2017. The presentation will briefly review the scientific data underlying the evolution of the current diagnostic criteria, highlight the chances (e.g., rapid diagnosis) and implications (e.g., establishing early therapy) linked with their use, and raise awareness of the challenges (overdiagnosis) and pitfalls (misdiagnosis) potentially associated with the application of the new diagnostic criteria.

Learning Objectives:

1. To understand the scientific data underlying the evolution of the current diagnostic criteria.
2. To recognise chances and implications linked with the use of the new diagnostic criteria.

3. To become aware of the challenges implicated with the application of the new diagnostic criteria.

Author Disclosure:

C. Enzinger: Advisory Board; Bayer Schering, Biogen, Merck Serono, Novartis, Roche and Teva Pharmaceutical Industries Ltd./sanofi-aventis. Board Member; MAGNIMS; IMSCOGSMS; OHBM Alpine Chapter. Consultant; Bayer Schering, Biogen, Merck Serono, Novartis, Roche and Teva Pharmaceutical Industries Ltd./sanofi-aventis. Research/Grant Support; Unrestricted research support from Merck Serono, Biogen, and Teva Pharmaceutical Industries Ltd./sanofi-aventis. Speaker; Funding for travel and speaker honoraria from Biogen, Bayer Schering, Merck Serono, Novartis, Shire, Genzyme and Teva Pharmaceutical Industries Ltd./sanofi-aventis.

A-210 09:00

MRI for MS monitoring: the use of guidelines in clinical practice

M.P. **Wattjes;** Hannover/DE (m.wattjes@vumc.nl)

Magnetic resonance imaging (MRI) plays an important role in the diagnosis of multiple sclerosis and has been incorporated into the McDonald diagnostic criteria for MS. The role of MRI in MS disease monitoring, particularly for MS treatment monitoring purposes, has been less clear defined. The need for standardization in terms of MR acquisition, scan intervals and image interpretation in MS pharmacovigilance is further stressed by the increasing numbers of MS therapeutics in the postmarketing setting. Therefore, MRI in MS pharmacovigilance is becoming increasingly important. The main goals of the use of MRI for this purpose are treatment efficacy monitoring, prediction of treatment response, and safety monitoring. Recent guidelines provided by the MAGNIMS collaboration (www.magnims.eu) and the consortium of MS centers (CMSC) provide some guidance how to implement MRI in the setting of MS pharmacovigilance. The standardized implementation of these guidelines in clinical practice will be of great help for (neuro)radiologists, neurologists, and patients.

Learning Objectives:

1. To understand the importance of standardisation in terms of image acquisition and scan intervals in MS monitoring.
2. To learn about the most relevant and possible future MRI outcome measures for MS treatment monitoring purposes.
3. To appreciate the potential role of MRI in predicting MS treatment response.

Author Disclosure:

M.P. Wattjes: Board Member; European Radiology, Neuroradiology, Journal of Neuroimaging, Frontiers in Neurology. Consultant; Biogen, IXICO, Roche. Speaker; Biogen, Sanofi-Genzyme, Novartis, Roche, Springer.

A-211 09:20

MRI in monitoring treatment complications

J. **Hodel;** Créteil/FR (jerome.hodel@gmail.com)

Several immunosuppressive therapies are available in MS patients with a risk of progressive multifocal leukoencephalopathy (PML). MRI is crucial for the follow-up of treated patients because recognition of PML before the onset of clinical symptoms has important implications for patient care. The diagnosis of presymptomatic PML remains highly challenging due to the coexistence of MS lesions and the various imaging patterns observed at the early stages of disease. Recognition of the most predictive imaging features and comparison with previous MRI data may facilitate the detection of presymptomatic PML. Hyperintensity on diffusion-weighted images, punctate lesions and involvement of U fibers are highly predictive features. Brain magnetic susceptibility changes may be explained by the increased iron deposition and could also constitute a useful tool for the diagnosis of PML. Such imaging findings may be the first imaging feature of PML at the presymptomatic stage. A dedicated MRI protocol including optimized diffusion and high-resolution MR sequences may potentially improve the sensitivity of MRI for the diagnosis of presymptomatic PML.

Learning Objectives:

1. To learn about the most important treatment-related adverse events and their incidence.
2. To learn about the imaging pattern of these adverse events.
3. To become familiar with the algorithms used to monitor these side events and the central role of imaging in them.

09:40

Panel discussion: Do we need MRI to monitor and predict treatment response in MS?

Thursday

Postgraduate Educational Programme

08:30 - 10:00

Room F1

E³ - Rising Stars Programme: Basic Sessions

BS 5

Musculoskeletal: bones and soft tissues

Moderator:

D.P. Patkar; Mumbai/IN

A-212 08:30

Bone marrow diseases

K. Verstraete; Ghent/BE (koenraad.verstraete@ugent.be)

Bone marrow consists of trabecular bone, a stroma of connective tissue, haematopoietic cells (red marrow) and fat (yellow marrow). Distribution of red and yellow marrow is age dependent, with gradual conversion of red to yellow marrow in the limbs during childhood, and patchy heterogeneity in the spine in the elderly patient. There are many causes of reconversion from yellow to red bone marrow, like smoking, long distance running, obesity, anemia, erythropoietin, etc. Depletion may occur in aplastic anaemia and after radiation therapy. Gelatinous transformation is seen in anorexia nervosa, cachexia, and HIV. Bone infarction and avascular necrosis are well delineated areas of dead bone marrow. The value of different imaging techniques, including plain radiography, dual-energy CT, bone scintigraphy, PET and the most sensitive technique, MRI (conventional T1, T2, fat suppression techniques, in-phase, out-phase and diffusion imaging), will be explained. The imaging characteristics of many diseases will be reviewed (diffuse bone marrow replacement in hematologic diseases, multiple myeloma, metastases; treatment related changes of bone marrow, primary bone tumours, and multiple causes of bone marrow oedema, like bone contusion, stress fracture, insufficiency fracture, Modic changes, spondylodiscitis, osteomyelitis, abscess, arthritis and specific bone tumours).

Learning Objectives:

1. To describe the typical features of normal bone marrow.
2. To determine origin of bone marrow changes.
3. To present the imaging characteristics of a bone marrow disease of the different types.

A-213 09:00

Soft tissue tumours

V.N. Cassar-Pullicino; Oswestry/UK (Victor.Pullicino@rjah.nhs.uk)

All imaging modalities can play a role in the diagnosis and management of soft tissue tumours and pseudotumours with a variable contributory performance to both sensitivity and specificity. MRI steals the show with an unparalleled role in soft tissue assessment ranging from detection, localisation, characterisation, identifying multiple lesions, other syndrome stigmata, probability of benignity/malignancy, local staging and recurrence identification. Sonography does have a supporting role especially in initial assessment of the likelihood of cystic/benign/abnormal malignant Colour Doppler flow patterns. This presentation aims to provide a distillation of the knowledge regarding soft tissue tumour imaging which can be applied in practice using a stepwise analytical approach. Despite an overwhelming spectrum of potential histological diagnosis, the radiologist needs to remember that eight benign and six malignant lesions account for 80% of all soft tissue tumours.

Learning Objectives:

1. To determine the origin of a soft tissue tumour (e.g. fat, neural, vascular, etc.).
2. To present current imaging techniques for evaluation of soft tissue tumours.
3. To discuss the imaging findings which are important for the diagnosis of soft tissue tumours.

A-214 09:30

Bone tumours

J.L. Bloem; Leiden/NL (j.l.bloem@lumc.nl)

Bone sarcomas are rare (0.2% of all neoplasms, annual incidence in Europe is 0.8 per 100.000 population), in contrast to benign bone tumors and the so-called tumor-like lesions. The incidence of these benign entities is relatively high, but not known exactly as these are often asymptomatic. The WHO (version 2013) classified benign and malignant bone tumors in 13 main categories; chondrogenic, osteogenic, fibrogenic, fibrohistiocytic, hematopoietic, osteoclastic giant cell rich, notochordal, vascular, myogenic, lipogenic, undefined neoplastic nature, and miscellaneous tumors. Each category is further subdivided into 1-14 tumor types. Imaging plays an important role in diagnosis, monitoring therapy, staging, and detecting recurrent disease. Diagnosis is mainly based on conventional radiography

using morphologic appearance in combination with location, and age. Advanced imaging techniques are used for local staging (MR), detection of metastases (chest CT), monitoring therapy (MR, ultra-sound, PET-CT), detecting recurrence (MR, ultra-sound, PET-CT). Typical imaging features based on the WHO classification system will be presented with focus on conventional radiography, common tumors, and relevance.

Learning Objectives:

1. To review the classification of bone tumours.
2. To present current imaging techniques for evaluation of bone tumours.
3. To describe the typical features of common bone tumours.

08:30 - 10:00

Room F2

Oncologic Imaging

RC 516

Functional imaging in oncology beyond morphology: where are we now?

A-215 08:30

Chairperson's introduction: What are the problems of morphologic evaluation

C.D. Becker; Geneva/CH

Morphologic criteria such as size, number or attenuation of solid tumour lesions may be used to assess partial or complete treatment response in certain clinical situations. However, certain tumours in certain organs cannot be reliably assessed without additional biomarkers such as perfusion or diffusion or metabolic activity that can be provided by CT, MRI or PET. This is especially true in the case of immunotherapy or in situ tumour ablation by radio- frequency or chemo-embolisation, where inactivated tumour tissue may remain in place. The most recent advances in the field of functional imaging biomarkers (also called "radiomics") include mathematical analysis of image data (texture analysis) and other quantitative parameters that may correspond with histopathologic and even genotypic features. The goal is to develop image-based predictive models for tumour treatment in specific neoplasms. This course will discuss the most important imaging biomarkers beyond morphology.

Session Objectives:

1. To briefly address the limitations of mere morphological imaging modalities.
2. To introduce the basics of the concept of functional imaging in oncology.
3. To learn about current status of these techniques in daily clinical practice.

A-216 08:35

A. Functional MRI techniques

V.J. Goh; London/UK (vicky.goh@kcl.ac.uk)

It is recognised that cancer is a biologically heterogeneous disease. Thus, a 'one size fits all' management approach may not bring about the best outcome for the individual patient. Oncologic therapies have evolved substantially over the last two decades providing cancer patients with a greater opportunity for a cure. This personalised approach has also required a paradigm shift in oncologic imaging to capture this biological heterogeneity and improve patient triage. MRI provides a unique opportunity to combine high contrast and spatial resolution imaging of tumour morphology with physiological imaging of water diffusion, vascularisation and oxygenation status. At initial diagnosis and staging this may allow tumours to be phenotyped better and during therapy for tumours to be assessed more comprehensively, particularly where therapy is cytostatic and will not result in significant size change. In this lecture the different functional imaging techniques that can be applied in clinical practice will be discussed and evidence for practice highlighted. The potential of integrated PET/MRI will also be considered.

Learning Objectives:

1. To learn about the different functional MR techniques (diffusion, perfusion).
2. To understand the basic principle behind each technique.
3. To appreciate the clinical usefulness of these techniques in daily clinical practice.

Author Disclosure:

V.J. Goh: Research/Grant Support; Siemens Healthineers. Speaker; Bayer, Siemens Healthineers.

A-217 08:58

B. CT perfusion techniques

H. Schöllnast; Graz/AT (helmut.schoellnast@medunigraz.at)

CT-perfusion imaging is a functional imaging tool which enables qualitative and quantitative evaluation of tumor perfusion and, therefore, assessment of tumor-

Thursday

related angiogenesis. Clinical applications for CT-perfusion imaging have mainly evolved to include lesion characterization, prediction of prognosis, prediction of response to therapy and assessment of response to local or systemic therapies. Perfusion values have shown significant differences when comparing normal tissue with tumors and between benign and malignant lesions, although there is overlap between benign and malignant lesions. The degree of tumor perfusion is potentially associated with tumor aggressiveness as tumor-related angiogenesis determines the ability of tumors to metastasize and, therefore, affects prognosis. On the other hand, hypoxia within the tumor reflected by restricted perfusion limits the effect of chemotherapy and radiotherapy, potentially allowing for prediction of response. Both, conventional chemotherapy and targeted therapies such as angiogenesis inhibitors may affect tumor vascularization. In contrast to conventional chemotherapy, which mainly shows a cytotoxic effect on the tumor, angiogenesis inhibitors show rather a cytostatic effect. Traditional tumor size-based response criteria may underestimate the response to angiogenesis inhibitors in the early course of treatment due to stable tumor size despite effective therapy. In contrary, CT-perfusion imaging allows detection of decrease in tumor perfusion which precedes decrease in size. Use of different models for perfusion calculation such as compartmental model and deconvolution model, use of different CT-perfusion protocols including contrast media injection protocols and inter- and intraobserver variability when using perfusion software limit use of CT-perfusion imaging in clinical routine.

Learning Objectives:

1. To learn about current approaches for CR perfusion techniques.
2. To understand the basic principle behind each technique.
3. To discuss radiation exposure generated by CT perfusion techniques.
4. To appreciate the clinical usefulness of these techniques in daily clinical practice.

A-218 09:21

C. Assessment by molecular imaging

J. Grimm; New York, NY/US (grimmj@mskcc.org)

Molecular imaging describes imaging and measurements of biological processes at the cellular and molecular level. In a clinical setting this entails predominantly PET imaging, measuring increased glycolytic activity. However, other radiotracers allow for detecting different and predominantly structural or even functional entities, e.g., the imaging of PSMA in prostate cancer to detect primary or recurrent disease; or the imaging with amino acids, reflecting increased amino acid metabolism in brain tumors. However, existing tracers can also be used to explore new signatures, such as in the case of positron lymphography using 18F-FDG to characterize sentinel lymph nodes. Lastly, optical imaging of radiotracers has been achieved and utilized both preclinically and clinically in novel applications. While most of clinical functional and molecular imaging is achieved in the area of nuclear medicine, there are other emerging areas: Intraoperative optical imaging is using available as well as new targeted fluorescent agents, aiding the surgeon visually during surgery to sentinel lymph nodes, remaining tumors and defining the surgical margin. Optoacoustic imaging, where novel scanners are listening to the light absorption in the body from either intrinsic targets or extrinsic specific contrast agents, have reached the clinical realm and have been used to detect specific cancers. Metabolic imaging has enjoyed a new boost beyond nuclear imaging in the form of hyperpolarized MR imaging, enabling interrogating metabolic key pathways to detect and characterize cancers in new ways. All this has been supported by the development of new and specific agents, interrogating disease signatures.

Learning Objectives:

1. To learn about the different concepts in molecular imaging.
2. To see and understand how molecular imaging might be integrated into patient care.
3. To appreciate clinical examples where molecular imaging is already established.

Author Disclosure:

J. Grimm: Board Member; Society of Molecular Imaging. Research/Grant Support; NCI (Clinical Cerenkov Imaging).

09:44

Panel discussion: Where are we using functional evaluations in clinical practice?

08:30 - 10:00

Room D

Special Focus Session

SF 5

Cystic pancreatic lesions: how to differentiate, how to manage?

A-219 08:30

Chairperson's introduction

C. Matos; Lisbon/PT (celso.matos@fundacaochampalimaud.pt)

Increased use of cross-sectional imaging has led to increased detection of pancreatic cysts. Although the most commonly used management guidelines assume knowledge of a specific cyst type, many of detected pancreatic cysts are indeterminate. During this multidisciplinary session we will focus on the clinical significance of small and large pancreatic cysts, we will review how to improve diagnostic accuracy and we will underline shared decision making for successful management.

Session Objectives:

1. To understand how imaging helps make the differential diagnosis of cystic lesions of the pancreas.
2. To address key questions that should be answered when diagnosing an incidental pancreatic cystic lesion.
3. To discuss how to improve patient management through multidisciplinary interaction.

A-220 08:35

Diagnostic accuracy of non-invasive imaging modalities for characterising cystic pancreatic lesions

N. Kartalis; Stockholm/SE (nikolaos.kartalis@me.com)

Pancreatic cystic lesions are increasingly diagnosed due to the widespread use of imaging studies (i.e., US, CT and MRI) in the evaluation of abdominal pathologies and to the aging population. They encompass a variety of entities with different biological behavior, ranging from benign lesions such as pseudocysts and serous cystic adenomas (SCA) to premalignant and malignant lesions, such as intraductal papillary mucinous neoplasms (IPMN), mucinous cystic neoplasms (MCN), cystic neuroendocrine tumours and cystic adenocarcinomas. Imaging plays a pivotal role in accurate diagnosis and appropriate management of patients with cystic pancreatic lesions. In this talk, we will analyze the specific imaging features of pancreatic cystic lesions on US, EUS, CT, and MRI. Furthermore, we will discuss the accuracy of cross-sectional imaging in the diagnosis of cystic pancreatic lesions and, finally, comment on the added value of contrast-enhanced US and EUS in the characterisation of cystic pancreatic lesions.

Learning Objectives:

1. To become familiar with the specific imaging features of pancreatic cystic lesions on US, EUS, CT, and MRI.
2. To learn about the accuracy of cross-sectional imaging in the diagnosis of cystic pancreatic lesions.
3. To understand the added value of contrast-enhanced US and EUS in characterising cystic pancreatic lesions.

A-221 08:58

The evolving role of pathology: can we improve patient stratification?

P. Demetter; Brussels/BE (Pieter.Demetter@erasme.ulb.ac.be)

Distinguishing between the various types of cystic pancreatic lesions has important prognostic and therapeutic implications. The sensitivity of cytology varies depending on the expertise of the endoscopist and the pathologist. Diagnostic accuracy can increase up to 80-90% if cytology is complemented with measurements of CEA, amylase levels and mucin staining. Although cyst fluid analysis is a tool in preoperative diagnosis, final diagnosis is often obtained only after histopathological analysis. Molecular markers in the cyst fluid are being increasingly studied in recent years. The four most common cystic pancreatic tumours bear tumour-specific genetic alterations, such as GNAS mutations in intraductal papillary mucinous neoplasms, β -catenin mutations in solid pseudopapillary neoplasms and VHL mutations or loss of heterozygosity in serous cystadenoma. Molecular tests of the aspirated cystic fluid seem particularly useful for detecting the accumulation of genetic mutations associated with lesion progression from early dysplasia to carcinoma. DNA-based biomarkers have made the most progress and are offered clinically, but prospective data are lacking and how DNA testing should be integrated into pancreatic cyst evaluation is unclear. In addition to the analysis of DNA, there are promising approaches in distinguishing benign and premalignant/malignant cystic tumours by evaluating miRNA profiles. At

Postgraduate Educational Programme

present, however, molecular analyses cannot replace more conventional tests, but should be used in parallel with them and clinical findings.

Learning Objectives:

1. To understand the carcinogenic pathway in pancreatic cystic lesions.
2. To become familiar with the most frequent molecular alterations seen in pancreatic cystic lesions.
3. To learn how the integration of cytohistomorphology, cyst fluid biochemistry and molecular testing helps better stratify patients before therapy.

A-222 09:21

When not to operate and when to operate an incidental cystic pancreatic lesion

M. [Del Chiaro](mailto:marco.del.chiaro@ki.se); Stockholm/SE (marco.del.chiaro@ki.se)

Pancreatic cystic neoplasms (PCNs) are a very common group of diseases with a prevalence of 20-30% in the general population. It is today well known that some of these lesions (SCN) are benign. In contrast, others, can progress from adenoma to cancer (i.e. IPMN or MCN). In front of a so different biological behaviour, the differential diagnosis of these lesions still remains a major clinical problem. The accuracy in pre-operative diagnosis, independently by the diagnostic modality used, remain low and not superior to 70% even in high specialized centers. IPMNs are the most common cystic neoplasms of the pancreas (50%). Considering the high prevalence of these lesions and the low incidence of pancreatic cancer, it is quite logical to understand that only the minority of these lesions will progress to cancer. At the moment, no biomarkers are available to discriminate the grade of dysplasia and surgery is recommended according mostly with radiological signs. When the IPMNs are involving the main pancreatic duct, the risk of malignancy is extremely higher. MPD dilatation over 5-6 mm represents probably the optimal cut-off for resection. More complicated is the management of IPMNs involving the branch ducts (BD-IPMN). The large majority of these patients can be managed conservatively through a radiological follow-up. Considering however the risk of progression, the surveillance of these patients can't be discontinued until the patient is potentially fit for surgery. Traditionally MCNs should be always removed. No surgery is required for SCNs, excluding cases of symptomatic lesions or unclear diagnosis.

Learning Objectives:

1. To become familiar with surgical options for the management of pancreatic cystic lesions.
2. To understand how information obtained by imaging impact surgical management.
3. To learn how to avoid unnecessary surgery in patients with benign pancreatic cystic lesions.

09:44

Panel discussion: Are current management recommendations appropriate?

08:30 - 10:00

Room K

Radiographers

RC 514

Successful paediatric imaging

A-223 08:30

Chairpersons' introduction: Paediatrics: more than just 'small adults' (part 1)

V. [Syrgiamiotis](mailto:syrgiamiotis@gmail.com); Athens/GR (syrgiamiotisvasillis@gmail.com)

From paediatricians usually one listens the very common phrase "children are not just small adults". It is for sure idea for the calculation of drug doses and the assessment of physiological parameters, the definition of child medicine in such defensive, negative and exclusionary terms deals with some inherent dangers and misconceptions as well. In the last decades it is a common phrase used in radiology as well. Both children and adults belong to the human race. Progress in medicine more often can be applied to and be of benefit to all and the transition from childhood to adulthood should be one of continuity rather than migration. Indeed we recognise that children, including the embryo, fetus, infant and all life stages until the completion of adolescence, are often at a different and increased risk from environmental hazards from that of adults. Children often have different, and sometimes unique, exposures to environmental hazards from those of adults. Due to their dynamic developmental physiology children are often subjected to higher exposures to pollutants found in air, water, food and radiation. These exposures may be handled quite differently by an immature set of systems to the way they are dealt with in adults. Children have a longer life expectancy. Therefore, they

have longer to manifest a disease with a long latency period, and longer to live with toxic damage. Finally, children are politically powerless; they are defenceless. With no political standing of their own, they must rely on adults to protect them.

Session Objectives:

1. To appreciate strategies for successful imaging of uncooperative children and those with disabilities.
2. To review current guidelines on imaging in suspected non-accidental injury.
3. To demonstrate potential techniques to avoid sedation during paediatric MRI.

A-224 08:33

Chairpersons' introduction: Paediatrics: more than just 'small adults' (part 2)

N. [Mitreska](mailto:mitreska_nadica@hotmail.com); Skopje/MK (mitreska_nadica@hotmail.com)

Paediatric radiology is a unique subspecialty of diagnostic radiology. Radiological findings as well as diagnoses are frequently different in infants and children from adults and knowledge and expertise are important for evaluation of the images. The child and its parents need special care and diagnostic methods must be appropriate selected. Mental development, position and structure of organs, increased susceptibility to radiation are different from adults. Reduction of radiation dose and radiation protection in radiographic examination of children is critical. In paediatric imaging risk-benefit dialogue obtain risk control and maximizing the benefit. Radiographers working with paediatric patients always are facing unique problems, so they must develop competence in knowledge, understanding and skills in paediatric imaging. Exposure is reduced by appropriate selection of study, using non-ionizing examination whenever possible, shielding the gonads and other organs. Radiographer have to capture the attention of the child to keep it still, response to verbal direction, use immobilization devices, understand the role of the family and other modalities for optimization of exposure. For good image quality paediatric protocols should be used to prevent repeat examinations and sedation or general anesthesia is usually require for MRI in children under 7 years of age. Radiologist, paediatric radiologist and radiographers must create team work, partnership and close cooperation.

Session Objectives:

1. To appreciate strategies for successful imaging of uncooperative children and those with disabilities.
2. To review current guidelines on imaging in suspected non-accidental injury.
3. To demonstrate potential techniques to avoid sedation during paediatric MRI.

A-225 08:35

A. Imaging the uncooperative child and children with disabilities

C. [Simcock](mailto:clare.simcock@gosh.nhs.uk); London/UK (clare.simcock@gosh.nhs.uk)

Paediatric radiography and imaging requires modification of techniques by the radiographer or imaging technologist to ensure that optimal radiographs are produced. Following textbook methods, is simply not always possible in children and for successful outcomes, adaptation of practice is necessary. When faced with imaging children with learning disabilities and challenging behaviours, the task can appear daunting. There is limited literature available to assist the radiographer to meet the needs of children with disabilities. Over 40% of children attending our institution have complex needs and it is important that we learn strategies that both benefit the patient and result in a successful examination across all modalities. Therefore, reasonable adjustments should be made, whilst imaging this cohort of patients which will ensure that the radiographers actions do not have a negative impact on future visits to the imaging department for the patient.

Learning Objectives:

1. To learn about behaviours and disabilities that can present a challenge to successful imaging.
2. To understand practical techniques and strategies during projection radiography examinations.
3. To appreciate practical advice for imaging in specialist modality areas such as CT, MRI and US.

A-226 08:58

B. Suspected non-accidental injury: best practice and advice

B.R. [Mussmann](mailto:bo.mussmann@rsyd.dk); Odense/DK (bo.mussmann@rsyd.dk)

Sub optimal imaging in suspected non-accidental injury (NAI) has major consequences for the child and family. The procedures must work properly each time and the images must be of superior quality to point out the abusers and withdraw the suspicion when no abuse has taken place. Furthermore, performing NAI imaging is a specialist task and special attention should be

paid to radiation dose, image quality, and number of projections. The talk will focus on current guidelines and legal issues in NAI imaging.

Learning Objectives:

1. To appreciate non-accidental injury imaging as a highly specialised procedure.
2. To understand the image quality requirements in non-accidental injury imaging.
3. To be aware of the legal aspects of performing non-accidental injury imaging.

A-227 09:21

C. Reducing the need for sedation and anaesthesia in MRI: the role of play therapy and other techniques

J. Gårdling; Lund/SE (jenny.gardling@med.lu.se)

When a child undergo MRI the unfamiliar environment, meeting new healthcare professionals and the need to keep still might imply anxiety, fear and/or stress. Depending on the child's age or inability to comply, sedation or general anaesthesia may be required, which implies risks and additional anxiety and discomfort for the children and their parents. Previous research have shown that children needs to have their parents close, play and feel joy, participate in care and have good relation with the healthcare professionals. Furthermore, children needs to know what to expect as this enables them to handle the situation better with increased coping and compliance, and with decreased anxiety. Age-appropriate information and preparation procedures have shown an impact on the child's anxiety and their ability to comply during different procedures. It have also shown to decrease the need for general anaesthesia. Since children learn and understand situations differently depending on age and cognitive development combining different information and preparation procedures might be considered as an advantage.

Learning Objectives:

1. To review the current use of sedation and anaesthesia in paediatric MRI.
2. To understand how play therapy and other techniques can be used to prepare patients for imaging.
3. To become familiar with practical skills and techniques that might reduce sedation rates in paediatric MRI.

09:44

Panel discussion: How to avoid mistakes and to learn from working with paediatrics?

08:30 - 10:00

Room M 1

Joint Session of the ESR and EFOMP

ESR/EFOMP

CT screening: benefits, doses and associated risks

Moderators:

J. Damilakis; Iraklion/GR
D. Tack; Baudour/BE

A-228 08:30

Dose and risk assessment

M. Brambilla; Novara/IT (marco.brambilla@maggioreosp.novara.it)

The radiation output of a CT system can be measured in a consistent and robust fashion through CT dose indexes (CTDI_w for axial scans and CTDI_{vol} for spiral scans). The CTDI tells precisely how the machine was operated, and it can be used, in conjunction with information regarding patient size and the scanned anatomy by mean of the dose length product (DLP), to estimate patient dose. The CTDI and DLP values are not, however, patient dose estimates. Similarly, the use of effective dose and the application of the nominal coefficient of risk, averaged over sex, several populations and all ages to calculate the cancer risk is in principle inappropriate. Estimates of individual patient risk, and epidemiologic studies assessing potential late effects, must use patient size-specific organ dose estimates in conjunction with the BEIR VII model. The BEIR VII committee has derived risk models for cancer mortality. The models consider the cancer site, sex, age at the exposure and attained age. Risks models have been developed for leukaemia, solid cancers in some organs and for all solid cancers combined. The cancer risks are non-zero only after a latency period (5 years for solid cancer and 2 years for leukaemia). For practical purposes, at typical dose levels encountered in X-ray diagnostics, risk of exposure-induced death (REID) and lifetime attributable risks (LAR) can be interpreted to present the excess radiation-induced cancer risk and their

numerical values are close enough to be interpreted identical considering the uncertainties involved in the models.

Learning Objectives:

1. To learn about the correct methodology to assess the stochastic risk associated with radiation exposure.
2. To understand the differences between exposure indexes (CTDI, DLP, etc.), organ doses, effective doses and risk.
3. To appreciate the risks associated with CT screening.

A-229 08:50

Quantitative benefit-risk analysis

J. Damilakis; Iraklion/GR (damilaki@med.uoc.gr)

CT is an important tool for screening such as lung cancer screening and colorectal cancer screening in high-risk patients. Can screening reduce mortality? Are radiation doses and radiogenic risks associated with the above screening methods an important disadvantage for their acceptance as a mass screening tool? Studies have found that screening with low-dose CT could reduce lung cancer mortality by 20% in comparison with chest radiography. Decision for CT screening should be based on careful consideration and discussion between patient and health care provider. Low dose CT screening for lung cancer has its risks. Thus, individuals screened with low dose CT have a high rate of false positive results that may lead to unnecessary follow-up invasive testing for example bronchoscopy or biopsy. Another point of concern is radiation dose from low dose CT. Patient dose from a low-dose chest CT examination is about 1.5 mSv. Little information exists in the literature regarding the risk for radiation-induced cancer following low dose CT for lung cancer screening. Studies are needed to determine absorbed doses to the primarily irradiated radiosensitive organs of female and male patients subjected to low-dose CT screening for lung cancer on modern multi-slice CT scanners and assess the potential risk of radiation-induced cancer for a typical patient cohort subjected to screening. CT colonography (CTC) has been used as a method to screen for colorectal tumours as well as for large colorectal polyps mainly because of its accuracy, less-invasiveness in comparison with colonoscopy and potential for detection of extra-colonic abnormalities. Effective dose from CTC ranges from about 3 mSv to about 9 mSv. A single low-dose CTC would result in about a 0.01% lifetime cancer risk, i.e., 1 in 10000 for a typical patient cohort.

Learning Objectives:

1. To learn about medical benefits of CT screening and how they can be expressed quantitatively.
2. To compare the benefits of CT screening with potential radiogenic risks.
3. To learn the limitations of benefit-risk analyses.

A-230 09:10

Breast CT

W.A. Kalender; Erlangen/DE (willi.kalender@imp.uni-erlangen.de)

Efforts of improving the early detection of breast cancer are a necessity further on. Breast screening programs are being criticized frequently because of their cancer detection rates considered as too low. X-ray computed tomography (CT) has been proposed and evaluated multiple times as a potential alternative method for breast imaging. All efforts shown so far suboptimal because of their limited spatial resolution and high patient dose when compared to mammography. In consequence, we developed a new concept for breast CT (BCT) aiming at both high isotropic spatial resolution of about 100 μ m and average glandular dose levels of 5 mGy or below. For this we chose single photon-counting technology, not available in CT so far, combined with spiral scanning. The complete scanner concept was evaluated by simulations and measurements; the results for dose and technical image quality parameters were confirmed. For comparison purposes, lumpectomies and mastectomies were imaged with digital mammography, breast tomosynthesis and BCT; these tests also confirmed expectations. The direct-conversion photon-counting detector technology showed revealed BCT's unprecedented performance. It provided the highest quality in imaging microcalcifications in specimens; combined with contrast medium injection as in standard clinical CT use, it outperformed the other modalities. Conclusion: CT scanners dedicated to breast imaging with photon-counting detectors and spiral scan capability can provide superior, unprecedented performance.

Learning Objectives:

1. To learn about early efforts at CT imaging of the breast.
2. To note image quality requirements for improving breast cancer diagnosis.
3. To understand the importance of advanced detector technology for the low-dose high-resolution breast CT.

Author Disclosure:

W.A. Kalender: Consultant; Bayer Pharma AG, Advanced Breast-CT GmbH. Shareholder; Advanced Breast-CT GmbH.

Postgraduate Educational Programme

A-231 09:30

How to communicate

G. Paulo; Coimbra/PT (graciano@estescoimbra.pt)

Medical imaging departments present an excellent test environment to study interventions to enhance patient satisfaction as: (a) the imaging environment is highly complex and workflow and time schedule constraints are extensive; (b) there is a wide spectrum of patients referred from multiple clinical specialties whose conditions vary in acuity, ranging from outpatients undergoing routine examinations to critically ill patients undergoing emergency imaging studies. Research indicate that training radiologists and radiographers to make simple modifications in their language and behavior, during patient, care can significantly impact patient satisfaction which can impact quality-of-care. We need to incorporate into our daily practice the fact that the 21st century patients have higher expectations and are becoming more demanding, as they are progressively being part of the process and therefore have access to information, allowing them to make better informed choices. Imaging departments should adopt communication strategies and policies in the new digital environment, explaining the procedure in an understandable manner, adapted to patient social and economic characteristics, with the objective to give the patient the adequate information for him/her to be able to make a proper decision. Radiographers usually are the ones that contact with patients and are the only professionals who might notice duplicate or inappropriate examinations before they occur and the ones to be asked about the risk. Therefore, its crucial to develop guidelines with clearly defined roles and responsibilities on how to communicate risks in a harmonized way, to avoid patient misinterpretation in their imaging clinical pathway.

Learning Objectives:

1. To become familiar with the principals of patient communication strategies.
2. To be aware of patients' needs and fragilities at the point of care.
3. To understand the patients' fears and perceptions about risk.

09:50

Discussion

08:30 - 10:00

Room M 2

E³ - ECR Master Class (Musculoskeletal)

E³ 526a

State-of-the-art imaging of postoperative joints

Moderator:

M.F. Reiser; Munich/DE

A-232 08:30

A. Postoperative shoulder

C.W.A. Pfirrmann; Zurich/CH

Imaging of the postoperative shoulder is challenging because of various surgical techniques, distorted anatomy and the presence of artifacts because of metallic implants. The most commonly performed surgical procedures include rotator cuff reconstruction, instability surgery, and joint replacements. The radiologists should have knowledge of these techniques. In this presentation these surgical techniques, the normal imaging findings after these procedures and the abnormal findings as well as imaging strategies will be discussed.

Learning Objectives:

1. To become familiar with the most frequently used surgical techniques for glenohumeral instability, subacromial decompression, rotator cuff repair, and arthroplasty and their imaging appearance.
2. To learn about potential postoperative complications.

A-233 09:00

B. Postoperative knee

E.H.G. Oei; Rotterdam/NL (e.oei@erasmusmc.nl)

In this masterclass we will review the indications for the most commonly performed surgical techniques in the field of meniscal repair, knee ligament reconstruction, and knee cartilage repair, followed by a brief explanation of the surgical procedure. We will also highlight recent advances in joint preserving procedures around the knee. Of each discussed technique, the normal postoperative appearance on imaging will be presented, with an emphasis on MR imaging. This is followed by a discussion on the assessment of potential complications. Among the discussed topics will be complications after ACL reconstruction (tunnel positions, graft rerupture, impingement, arthrofibrosis,

cyclops lesions), assessment of meniscus re-tear after surgical repair and assessment of the success after cartilage repair procedures.

Learning Objectives:

1. To become familiar with the most frequently used surgical techniques for meniscal repair, ligament reconstruction and cartilage repair techniques.
2. To learn about potential postoperative complications.

A-234 09:30

C. Postoperative ankle and foot

M.J. Ereno Ealo; Galdacano/ES (mjeren@gmail.com)

Foot and ankle traumatic pathologies are frequent conditions, and sometimes cause big deformities. Our objectives are to focus on all aspects of diagnosis, treatment and subsequent management of these injuries. The most current and innovative techniques of internal fixation and their applications will be showed. Identifying problems and complications and also talking about reconstructive surgery of the lower extremity is important. Very different injuries and cases are detailed: surgical management and complications of high-energy distal tibial and pilon fractures, other fractures like calcaneus, talus, lisfranc, toe and forefoot fractures and stress fractures. Other conditions like Achilles pathology, bunions, diabetic (Charcot) foot, Morton's neuroma, hammer toe, tarsal coalition, and adult acquired flatfoot are also shown. Patients with arthroplasty, arthrodesis, triple fusion, ankle replacement should be recognised

Learning Objectives:

1. To become familiar with the most frequently used surgical techniques for osteosynthesis, instability, tendon repair and arthroplasty and their imaging appearance.
2. To learn about potential postoperative complications.

08:30 - 10:00

Room M 3

Interventional Radiology

RC 509

Musculoskeletal interventions: what every radiologist should know

Moderator:

A. Gangi; Strasbourg/FR

A-235 08:30

A. Musculoskeletal ablation and embolisation

A. Basile; Catania/IT (basile.antonello73@gmail.com)

During the past decade we have seen an increasing role of interventional radiology (IR) in the treatment of musculoskeletal both benign and malign lesions with palliative or curative goal. A common indication for treatment is the presence of localized pain, furthermore in some situation the disease progression can lead to pathologic fracture, with or without mechanical instability. Most frequent malign lesions are spinal and bone metastases. Percutaneous tumor ablation is performed under imaging guidance and generating cytotoxic temperatures that cause tumor necrosis. Ablation may be considered for example for symptomatic spinal metastases, with tumor control indication, for uncomplicated painful spinal metastases and stable pathological vertebral compression fracture. Ablation can be also performed in association to radiation therapy with a better control of local tumor; also vertebral augmentation can be performed as fracture prophylaxis at the same time as ablation through the same percutaneous access cannula. There are many instruments employed for the treatment of the bone lesions: ablation (thermal ablation with radiofrequency, microwaves MW, laser ablation and magnetic-resonance-guided focused ultrasound surgery MRgFUS and cryoablation), osteoplasty and vascular procedures. Another indication for percutaneous ablation are painful benign tumours such as osteoid osteoma, osteoblastoma, chondroblastoma, osteochondroma, giant cell tumour, aneurysmal bone cyst, eosinophilic granuloma, vertebral haemangioma and fibrous dysplasia; all these lesions can be treated either via ablation and/or embolisation. Embolisation can be also performed in the preoperative management of bone metastases to reduce perioperative blood loss. Physicians involved in the care of patients with oncological musculoskeletal disease should be familiar with these treatments and refer patients appropriately based on best available evidence. This is challenging, but necessary because of the increasing diagnosis of this kind of lesions and the major role that the IR will assume in the future in this field.

Postgraduate Educational Programme

Learning Objectives:

1. To appreciate the indications for ablations and embolisation.
2. To learn about different techniques and combination of them.
3. To discuss the results and literature data of interventional radiology procedures.

A-236 09:00

B. Vertebral augmentation and discectomy techniques: can we challenge surgery?

D. Filippiadis; Athens/GR (dfilippiadis@yahoo.gr)

Vertebral augmentation and discectomy techniques: can we challenge surgery? Vertebral augmentation techniques include standard vertebroplasty or vertebral augmentation on terms of balloon kyphoplasty or percutaneous implant insertion combined to PMMA injection. Indications include osteoporotic, traumatic, pathologic, and cancer-related fractures as well as benign (eg symptomatic atypical aggressive hemangiomas) or malignant (e.g., metastatic) lesions. Under proper patient selection these techniques provide pain relief and functional improvement along with spine alignment height restoration and endplate reduction. Additionally, kyphotic angle restoration or maintenance seems to prevent future vertebral fracture in the adjacent levels and improved sagittal balance. Studies in the literature report that load distribution in patients with vertebral fractures post vertebroplasty returns to values of normal population. Variety in the morphology, location, and etiology of vertebral fractures demands a tailored patient centered approach. Percutaneous technique for intervertebral disc herniation and discogenic pain can be either decompression or biomaterial implantation techniques. The former can be classified into mechanical (discectomy), thermal (RF, laser, coblation, IDET) or chemical (Discogel, ozone) methods whilst the later include hydrogel, PRP and stem cell therapies. Decompression techniques are indicated for small- to medium-sized symptomatic contained hernias. Percutaneous techniques are performed as outpatient, low cost procedures and are governed by good patient compliance, high success (75-85%) and low complication rates (<1-2%). In case of treatment failure, percutaneous techniques can be repeated without interfering with surgery at a later stage. Percutaneous vertebral augmentation and discectomy techniques compared to surgical approaches are favored in terms of reduced blood loss and operating time, shorter hospital stay, fewer complications, and less postoperative pain.

Learning Objectives:

1. To appreciate the rationale for the using of interventional radiology procedures.
2. To learn about different techniques and treatment strategy.
3. To discuss results and literature data in comparison with other treatments.

A-237 09:30

C. Bone biopsy and pain treatment using cone-beam CT (CBCT)

L. Tselikas; Villejuif/FR (lambros.tselikas@gustaveroussy.fr)

Oncology has dramatically changed the last decade, and new therapies have been proven to be effective in metastatic cancer patients. But bone tumours remain difficult to treat, and interventional radiology plays a key role in their management. Both biopsy, ablation and consolidation techniques are feasible and effective with a very good safety profile. Cone beam CT is the guidance method of choice because of its versatility, and comfort of use. Guiding softwares are mandatory to improve technical results and take full advantage of this technology. Future developments including combined guiding systems based on optic or electromagnetic needle position estimation and dose reduction solutions.

Learning Objectives:

1. To appreciate the high imaging quality and guidance accuracy using CBCT for biopsy and pain treatment.
2. To learn about the advantages of CBCT-guided interventions, reconstruction algorithms, image enhancement and dose reduction.
3. To discuss about techniques, limitations of CBCT and future applications.

08:30 - 10:00

Room M 4

E³ - ECR Master Class (Vascular)

E³ 526b

TEVAR/EVAR: where we are and where we are going

Moderator:

F. Fanelli; Rome/IT

A-238 08:30

A. TEVAR

H. Rousseau; Toulouse/FR (rousseau.h@chu-toulouse.fr)

Thoracic endovascular aneurysm repair (TEVAR) has proven to be a safe and effective therapy. In the last 2 decades, TEVAR has been established as first-line treatment for most descending thoracic aortic pathology due to reductions in perioperative morbidity and mortality compared to open surgical repair. Improvements in materials, reduction in delivery sheath size, improved conformability, tapered grafts, and a wider range of sizes have improved TEVAR applicability and outcomes over this initial decade of widespread use, for traumatic aortic transection, aneurysms, as well as acute and chronic type B aortic dissection. Looking into the future, industry and physicians are working together to improve thoracic stent-graft design (branched and fenestrated stent-grafts, chimney technique) to further improve safety, effectiveness, and applicability to a wider range of patients and aortic pathologies. Treatment of the ascending aorta remains less established, but is expected to evolve as technology allows integration of ascending, and arch devices. Hybrid ORs combining optimal imaging with the ideal environment to perform complex open and endovascular operations are available, allowing several features such as CTA fusion, CB-CT, and low-dose protocols to reduce the radiation exposure to a patient and an operator. This presentation will review the indications, technical aspects and results of endovascular TAA repairs. We also examine the advantages and limitations of new stent graft treatment of the arch and our experience in technological innovation in performing these complex procedures.

Learning Objectives:

1. To understand the evidence supporting endovascular therapy vs surgery.
2. To learn what is new for aortic arch disease.
3. To learn the impact of technological innovation in planning and performing the procedure.

A-239 09:00

B. EVAR

E. Broutzou; Athens/GR (ebrountz@med.uoa.gr)

To understand the evidence supporting endovascular therapy vs surgery EVAR is the method of choice because three principal, randomised controlled trials have shown better 30-day mortality for EVAR compared to open surgery. However, the mortality benefit was lost (catch-up of mortality) after 2 to 5 years. The main cause of aneurysm-related mortality in the EVAR group was secondary aortic sac rupture, caused by late device failures. Careful patient selection, diligent adherence to instructions for use and meticulous life long imaging follow up are mandatory for a successful EVAR. Thoracoabdominal aneurysms are rare and various. Open surgery carries a mortality rate of 2-12% depending on the aneurysm type. Endovascular treatment includes the use of fenestrated and branched devices with high technical success rates and significant improvement in perioperative mortality. Additional strategies such as hybrid techniques and parallel grafts (chimneys and snorkels) are also successful. Standard EVAR requires bilateral or unilateral surgical exposure of the common femoral artery. Complications specific for this surgical procedure include hematoma (5%), seroma (10%), and femoral nerve damage. Following the introduction of the new low profile devices and the development of the suture mediated closure devices EVAR can be performed without the need of surgical cut down. Recent studies have shown that percutaneous EVAR is possible with 96-100% technical success rates, with complication rates less than 2%.

Learning Objectives:

1. To understand the evidence supporting endovascular therapy vs surgery.
2. To learn what is new for thoracoabdominal aortic disease and iliac axis.
3. To learn when and how to perform a percutaneous approach.

Thursday

A-240 09:30

C. Post-EVG complication

R. Uberoi; Oxford/UK (Raman.Uberoi@ouh.nhs.uk)

Abdominal endovascular repair (EVAR) and thoracic endovascular aortic repair (TEVAR) have become an accepted alternative to surgery for the treatment of aortic pathologies, particularly aneurysm disease and dissections. Lifelong surveillance is obligatory following EVAR and TEVAR to monitor the aortic morphology and detect associated complications. The main imaging techniques used in evaluating TEVAR follow up are computed tomography angiography (CTA), magnetic resonance angiography (MRA) and catheter angiography in assessing the technical success, outcome and complications, which may necessitate re-intervention. In the abdominal aorta ultrasound (duplex) including contrast enhanced ultrasound (CEUS) with plain X-ray may also be used as alternative imaging modalities. Of these, computed tomography angiography offers a fast, accessible and sensitive imaging modality and is established as the default surveillance tool. Long term common complications include thrombosis, limb kinking and occlusion, aneurysm sac leak which may result in persistent pressurisation of the sac called endoleaks type I-V. Device migration, and device failure can contribute to endoleaks and need to be closely monitored. Type I and III endoleaks need urgent treatment usually with placement of a proximal or distal cuff and or relining of the graft. However not all type II endoleaks need treatment, but where there is continued sac expansion or aneurysm development this will require embolization of feeding vessels. Type IV is less common with the newer devices and usually resolve over a period of weeks and months. Type V endoleaks also may require relining of the whole device or conversion to an open procedure.

Learning Objectives:

1. To learn about individualised post-EVG surveillance programme.
2. To learn which are the most common complications.
3. To understand how to select and perform the optimal treatment.
4. To understand the role of contrast-enhanced US (CEUS).

Author Disclosure:

R. Uberoi: Advisory Board; merit. Grant Recipient; Gore and Bolton. Speaker; Spectranetics.

Learning Objectives:

1. To understand the CT and MR imaging protocols to identify HCC in cirrhotic liver.
2. To be familiar with LI-RADS .
3. To review the role of each modality in detecting, staging and follow-up of HCC.

Author Disclosure:

G. Brancatelli: Speaker; Bayer.

A-243 09:03

B. Early HCC and well-differentiated HCC

C. Avuso; Barcelona/ES (cayuso@clinic.ub.es)

Non invasive criteria for the diagnosis HCC ≥ 10 mm in patients with liver cirrhosis are based on the development of neoangiogenesis and on the progressive reduction of portal supply within the tumour, leading to the characteristic arterial wash-in and portal wash-out pattern detected on dynamic CT/ MR studies performed with extracellular contrast agents (CA). Imaging criteria have a sensitivity of 60% and a specificity close to 100% for the diagnosis of small HCC. When RM is obtained with gadoxetic acid, the arterial and early portal phases demonstrate also the typical wash-in/wash-out pattern of HCC. In the transitional and hepatobiliary phases, another key imaging is found, the hyposignal intensity of close to 90% of HCCs compared to the surrounding liver parenchyma, based on the progressive reduction/absence of the expression of organic anion transporting polypeptides (OATPs) during the hepatocarcinogenesis process. LI-RADS can be applied on CT, on MR independently of the CA used, and also on contrast enhanced ultrasound. The sensitivity, specificity and interobserved concordance of the standardised imaging interpretation do not have strong prospective data available. Early diagnosis is the only way to improve the outcome of patients with HCC. Up to now, the active work-up for the diagnosis of HCC is recommended for new liver lesion ≥ 10 mm detected in the context of surveillance programmes. A confident imaging diagnosis of HCC in smaller lesions is limited and treatment of such a tiny possible pre-malignant but not confirmed HCC lesions is not recommended to avoid overdiagnosis and overtreatment.

Learning Objectives:

1. To review key imaging criteria of HCC in a cirrhotic liver.
2. To be able to differentiate HCC from other lesions in a cirrhotic liver.
3. To reflect the role of early diagnosis of HCC in the management of the patient.

A-244 09:31

C. Mimickers and pitfalls

D. Akata; Ankara/TR (dakata@hacettepe.edu.tr)

HCC can develop in non-cirrhotic liver and even without identifiable risk factors. In this setting it is more likely to manifest as a symptomatic dominant lobulated mass. Non-invasive diagnostic criteria such as, arterial enhancement and subsequent "washout" during portal venous or equilibrium phases on both CT and MR are present in more than 90% of cases. The imaging findings of HCC are the same in both cirrhotic or non-cirrhotic liver. However, focal liver lesions mimicking HCC in non-cirrhotic liver are different than the ones in cirrhotic liver. This presentation describes the typical and atypical imaging features of common hypervascular lesions such as hemangiomas, focal nodular hyperplasia, metastasis, cholangiocarcinoma and fat containing liver lesions such as angiomyolipoma and adenomas. It outlines a general approach to distinguishing between benign and malignant hepatic lesions. The role, pearls, and pitfalls of the hepatobiliary specific contrast agents as well as diffusion weighted imaging in the detection and characterization of the lesions will be discussed in detail.

Learning Objectives:

1. To review a diagnostic algorithm to detect HCC mimics in non-cirrhotic liver.
2. To review the imaging characteristics of a wide spectrum of potential pitfalls.
3. To understand the potential role of extracellular and hepatobiliary contrast agents as the problem solvers.

08:30 - 10:00

Room M 5

E³ - ECR Academies: Update on Hepatobiliary Imaging

E³ 520

Imaging of HCC

A-241 08:30

Chairperson's introduction

A. Palkó; Szeged/HU (palkoand@gmail.com)

Imaging of hepatocellular carcinoma is one of the important tasks of abdominal radiology. Early detection and accurate characterisation of this disease is challenging, especially in cases of advanced cirrhosis, nevertheless of utmost importance since it allows for conducting timely and effective treatment which may be curative or palliative, depending on the overall condition of the patient. Speakers of this session introduce the state of the art CT and MRI examination techniques, the typical morphological characteristics of HCC, the objective criteria for establishing the diagnosis and the difficulties of differential diagnosis.

A-242 08:35

A. CT or MRI for diagnosis and follow-up?

G. Brancatelli; Palermo/IT (gbranca@yahoo.com)

Multiphase CT and MRI allow non-invasive diagnosis of hepatocellular carcinoma in cirrhotic patients. Moreover, they are able to stage the tumour burden to choose the most appropriate treatment for each patient. Furthermore, they have a role in the follow-up of; (1) indeterminate nodules such as LI-RADS 3 and (2) treated HCC nodules to confirm the effectiveness of treatment or to detect residual tumour or recurrence. LI-RADS is a classification system that allows; (1) predicting with CT and MR the likelihood that a lesion is HCC in patients with chronic liver disease or cirrhosis and (2) standardising terminology among different centers.

Postgraduate Educational Programme

10:30 - 12:00

Room A

E³ - ECR Academies: Interactive Teaching Sessions for Young (and not so Young) Radiologists

E³ 621

Basic breast imaging

A-245 10:30

A. Calcifications in mammography

C.S. [Balleyguier](mailto:Balleyguier@med.uni-heidelberg.de); [Villejuif/FR \(Corinne.BALLEYGUIER@gustaveroussy.fr\)](mailto:Corinne.BALLEYGUIER@gustaveroussy.fr)

Breast calcifications are common findings detectable on mammography. Breast calcifications are most likely benign; nevertheless irregular microcalcifications cluster may be the only imaging findings suggesting a ductal carcinoma in situ (DCIS). Analysis of microcalcifications on mammography remains on magnification views; size, density, number, pleomorphism and distribution within the breast have to be carefully analysed to differentiate benign and suspicious microcalcifications clusters. Benign calcifications are categorised as BI-RADS 2 and are more likely round, regular, with a calcified rim, tea-cup or egg-shell shape. Suspicious microcalcifications may be amorphous, irregular, with a linear or segmental distribution. When a microcalcifications cluster is categorised as BI-RADS 4, a stereotactic biopsy should be performed. Ultrasound may be performed first to detect non-calcified mass. Vacuum assisted stereotactic biopsy with at least 6 11 Gauge samples must be performed. New technologies such as BLES biopsy, associating biopsy and radiofrequency can be performed to remove entirely the cluster. In this topic, biopsy techniques and diagnostic strategies to diagnose microcalcifications will be presented on a basis of clinical cases.

Learning Objectives:

1. To become familiar with different types of calcifications.
2. To learn the differential diagnosis of different calcifications.
3. To learn the different tools to biopsy calcification clusters.

A-246 11:15

B. Asymmetry and architectural distortion

L.J. [Pina Insausti](mailto:Pina.Insausti@unav.es); [\(ljpina@unav.es\)](mailto:Pamplona/ES (ljpina@unav.es))

Asymmetries and architectural distortions: Asymmetries are unilateral deposits of fibroglandular tissue not conforming to the definition of a mass. Four types of asymmetries can be considered: (1) Asymmetry as an area of fibroglandular tissue visible on only one mammographic projection, mostly caused by superimposition of normal breast tissue. (2) Focal asymmetry visible on two projections, hence a real finding rather than superposition. (3) Global asymmetry consisting of an asymmetry over at least one quarter of the breast and is usually a normal variant. (4) Developing asymmetry new, larger and more conspicuous than on a previous examination. After the detection of one of the previous asymmetries, it is mandatory to compare with previous mammograms, if available. Palpation and additional techniques can be used to study the lesion, such as spot compressions, tomosynthesis, US and in some cases MRI. A biopsy is needed if malignancy cannot be excluded. The term architectural distortion is used when the normal architecture is distorted with no definite mass visible. This includes thin straight lines or speculations radiating from a point, and focal retraction, distortion or straightening at the edges of the parenchyma. Architectural distortion can also be seen as an associated feature. Tomosynthesis is a very sensitive technique to detect architectural distortions. Surgery, radial scar and carcinoma are the most common causes of distortions. A biopsy is mandatory if a surgical scar is excluded. The management of radial scars needs further work-up after a core needle biopsy: both surgery or vacuum-assisted biopsy can be used.

Learning Objectives:

1. To understand the concept of asymmetry and architectural distortion.
2. To become familiar with the respective imaging features.
3. To learn about the diagnostic approach using all breast imaging modalities.

Author Disclosure:

L.J. Pina Insausti: Speaker; Speaker in session organized by SIEMENS.

10:30 - 12:00

Room X

EuroSafe Imaging Session

EU 2

Strategies for dose reduction in computed tomography: from technical concepts to clinical practice

Moderator:

R.W.R. Loose; Nuremberg/DE

A-247 10:30

Chairperson's introduction

W. [Stiller](mailto:Stiller@med.uni-heidelberg.de); [Heidelberg/DE \(wolfram.stiller@med.uni-heidelberg.de\)](mailto:wolfram.stiller@med.uni-heidelberg.de)

In the field of computed tomography (CT) technical improvements have constantly extended the range of clinical applications and made new radiodiagnostic indications accessible. As CT examinations always involve the exposure of patients to ionizing radiation, dose reduction is an imperative when applying CT in clinical practice and approaches for reducing the dose associated with CT are required. To this end, different strategies for dose reduction in CT have been developed, spanning technical approaches as well as specific examination techniques applied in clinical practice. To date, several technical possibilities such as automated tube current modulation and voltage selection as well as dynamic beam collimation are available for reducing the dose associated with CT examinations. Of late, methods for iterative image reconstruction in CT enable noise suppression in image data, which may be exploited for enabling further dose reduction. While all scanner technology currently available should be exploited for reducing the radiation exposure of CT examinations in general, this is especially important in pediatric CT imaging. Careful selection and individual adaptation of the CT protocol parameters to each specific diagnostic task have the potential to enable systematic dose reduction, e.g., for pediatric and chest CT examinations. While dose reduction is imperative in CT, excessive reductions will result in a loss of diagnostic image quality. In clinical routine, dose reduction of CT examinations therefore is limited by the image quality requirements inherent to each specific diagnostic task that have to be fulfilled for ensuring confident diagnosis.

Session Objectives:

1. To raise awareness of different strategies for dose reduction in computed tomography.
2. To learn about and understand technical concepts facilitating dose reduction in CT.
3. To become familiar with methods for dose reduction in CT applied in clinical practice.

A-248 10:35

Systems for dose reduction in CT: more than automated exposure control

M. [Prokop](mailto:Prokop@isg.umcn.nl); Nijmegen/NL

"no abstract submitted"

Learning Objectives:

1. To learn about the technical possibilities available for reducing the dose associated with CT examinations.
2. To become familiar with the functionality of technical systems for dose reduction in CT.
3. To understand the potential and limitations of these dose reduction systems.

A-249 10:51

Iterative image reconstruction for dose reduction in CT: technical background and concepts for clinical practice

P.B. [Noel](mailto:Noel@tum.de); [Munich/DE \(peter.noel@tum.de\)](mailto:peter.noel@tum.de)

After introduction in the 1970s, computed tomography has developed to be a major tool in day-to-day clinical routine. A rapid growth in CT examinations can be attributed to its wide availability, speed, and diagnostic benefits. In the same time, public health concerns have arisen with respect to patient and population radiation dose. Industrial and academic CT development teams have, therefore, worked on strategies to reduced radiation exposure from CT, for example, with concepts like: tube-current modulation, over-beam reduction, or organ-specific dose reduction. Over the last decade one promising development is the paradigm of advanced reconstruction algorithms. The idea of this software solution is to reduce image noise and improve image quality. Image noise as well as image quality are directly linked to the radiation exposure, and thus the reduction of noise via iterative reconstruction allows a reduction in dose. This presentation will give insight into the different flavors of

Thursday

Postgraduate Educational Programme

reconstruction algorithms, including hybrid-, model-based, and full statistical iterative algorithms. Furthermore, we will discuss its clinical translation and the challenges associated with its introduction into the clinical routine. Additionally, the talk will provide an outlook of potential solutions to further reduce CT radiation dose.

Learning Objectives:

1. To learn about current methods for the iterative image reconstruction in CT.
2. To raise awareness about the potential of the iterative image reconstruction for enabling dose reduction in CT.
3. To understand technical limitations of the iterative image reconstruction in view of image quality at very low doses.

Author Disclosure:

P.B. Noël: Equipment Support Recipient; Philips Healthcare. Research/Grant Support; Philips Healthcare. Speaker; Philips Healthcare.

A-250 11:07

Dose reduction strategies in paediatric CT

E. Castellano; London/UK (ely.castellano@rmh.nhs.uk)

The benchmarking of paediatric CT imaging practice at non-specialist centres is likely to show that there is scope for radiation dose reduction because general radiologists are not as accustomed to noisy images of small patients as their paediatric counterparts. Dose reduction endeavours should first focus on reducing local diagnostic reference levels (DRLs) below national or European ones, then on adopting specialist centre DRLs as performance targets and moving towards them in small steps to permit the radiologists to adapt to the image quality. The outcome will be an imaging practice better aligned with that of specialist paediatric centres. Scan protocols may need to be developed along the way for specific clinical indications and weight categories. The slice thickness set for the reporting image set strongly influences the radiation dose and must be appropriate for the diagnostic task. Particular attention must be given to the choice of tube voltage: lowering the kV from 120 kV to 100 kV for body imaging will permit the tube current to modulate with patient size; 80 kV is feasible for contrast-enhanced studies of the thorax, resulting in increased conspicuity of iodine-perfused vessels and tissues. Decreasing the tube voltage will also reduce patient dose if the tube current modulation settings are reviewed alongside. Iterative reconstruction can be used to improve the appearance of lower-dose images. Good radiographic practice must be promoted at all times: careful centering of the patient, effective immobilisation and correct positioning of the arms are essential.

Learning Objectives:

1. To become familiar with dose reduction strategies employed in paediatric CT.
2. To understand how scanner technology can be used for reducing dose of paediatric CT examinations.
3. To raise awareness of the importance of dose reduction in paediatric CT examinations.

A-251 11:23

Adapting protocols towards dose reduction in chest CT

D. Tack; Baudour/BE (denis.tack@skynet.be)

Once a new CT device is installed, it is the responsibility of users to check all parameters to fit with the ALARA principle. This is made in a team approach. Objectives for dose delivery should not be based on DRLs, but rather on P25 of national surveys or on best-published practices in agreement with their equipment. Default protocols include standard CT, low or ultra-low-dose CT (ULD-CT) and CT pulmonary angiography (CTPA). Submillisievert routine CT scanning in standard-sized patients is feasible (DLP < 70 mGy.cm) in routine as standard acquisitions. DLP of ULD-CT could be lower than 15 mGy.cm. CTPA can be obtained at DLP lower than 100 mGy.cm in standard patients. Subjective image quality should be assessed by radiologists on a five-point scale (1=non-diagnostic; 5=excellent). An optimised dose would have a score approximating 3.5, whereas a ULD CT would have a score of 2.5. Inter-observer variability in assessing image quality is often observed. Training and consensus readings for choosing the final acceptable IQ are mandatory. Adjustments of automatic exposure control and tube potential selection for optimising the dose are vendor-specific, and include pitfalls that will be detailed. Specific technical settings available on some CT devices can also be utilised such as volumetric sequential scanning, Sn filtering, and high-pitch acquisitions.

Learning Objectives:

1. To become familiar with strategies for dose reduction applied in chest CT.
2. To learn about the adaptation of acquisition protocol parameters for reducing dose of chest CT examinations.
3. To raise awareness of the potential for dose reduction in chest CT in clinical routine.

A-252 11:39

Dose reduction and image quality: when low is too low

S.T. Schindera; Aarau/CH (sschindera@aol.com)

Dose reduction in CT, according to the ALARA principle is very well known but at the same time also very challenging. Depending of the clinical task, different magnitudes exist to reduce the dose (e.g., detection of hepatic metastasis vs. renal stone detection). Many radiologists are still afraid of losing the diagnostic accuracy while reducing the dose. The key question is, how low can we go while preserving the diagnostic accuracy. To date, various possibilities (e.g., phantom studies, studies with virtual added noise) exist of evaluating the possibility of dose reduction in CT. In the future, task specific model observer will play an increasing role in the dose optimization process in CT.

Learning Objectives:

1. To learn about the implications of dose reduction on the image quality of CT examinations.
2. To become familiar with examples of excessive dose reduction from clinical practice.
3. To understand that dose reduction potential in CT is limited by the image quality requirements inherent to each specific diagnostic task.

10:30 - 12:00

Room F1

E³ - Rising Stars Programme: Joint Sessions with ESOR

ESR/ESOR 1

Radiologic anatomy: lower extremities

Moderator:

U. Aydingoz; Ankara/TR

A-253 10:30

Hip

A.H. Karantanas; Iraklion/GR (akarantanas@gmail.com)

The painful hip is a common clinical problem in all age groups. Magnetic resonance imaging (MRI) is an invaluable tool to assess the hip joint because of its ability to directly visualize bone marrow, cartilage and soft tissues in multiple planes. MR arthrography (MRA) using intra-articular contrast material is the standard method for imaging labral lesions and cartilage degeneration and trauma. Understanding normal hip anatomy and common variants is important, in order to accurately detect and localize areas of pathology and to prevent misinterpreting normal structures as diseased. Plain radiographs should always be available when reporting MRI because basic measurements allow assessment of underlying deformities which might explain the clinical and MRI findings. The most important to know are: joint space width (JSW), CE angle, VCA angle, alpha angle and acetabular retroversion. Among the disorders causing hip pain, osteoarthritis (OA) is the most common one. Age is a risk factor strongly correlated with OA. Early OA is related to CAM type femoroacetabular impingement, developmental dysplasia and previous trauma, inflammation or infection. The diagnosis of OA is based on a combination of radiographic findings and characteristic symptoms. The progression of OA traditionally has been measured using radiographic JSW. Weight-bearing radiographs centered on the hip are the most reproducible and reliable ones. The sequence of degeneration includes the following radiographic findings: joint space narrowing, osteophyte formation, subchondral sclerosis, and cyst formation. In cases that radiographs show minor changes and high clinical suspicion of early disease, OA can be confirmed with MRI and/or MRA.

Learning Objectives:

1. To identify intra- and extra-articular anatomy on MRI.
2. To learn what we see and what we miss on radiographs.
3. To understand osteoarthritis and learn its key features on imaging.

A-254 11:00

Knee

M. Klontzas; London/UK (miklontzas@gmail.com)

Knee pain is one of the most prevalent musculoskeletal symptoms which is increasing together with the steady increase in life expectancy and the prevalence of obesity. MRI is the imaging modality of choice for the evaluation of knee disorders, offering a comprehensive evaluation of the bone marrow, the soft tissues and the articular cartilage. As an imaging modality it combines high sensitivity and specificity aiding the investigation and differential diagnosis of pathology such as cruciate ligament and meniscal tears, which cannot be visualized with plain radiographs. This lecture will provide the outlines of the normal cross-sectional anatomy of the knee with a special focus on MRI. An outline of pathology missed or identified on plain films will be provided before focusing on more detail in MR imaging anatomy which is extremely important

for the evaluation of knee pathology and the differential diagnosis between anatomical variations and clinically relevant knee lesions. Finally, an outline of meniscal lesion evaluation with the use of MRI will be providing since they are one of the most commonly injured knee structures. The combination of imaging with data provided from the clinical examination and medical history can lead to the correct diagnosis and this is why the knowledge on the normal anatomy as well as variants can lead to the successful diagnosis and the avoidance of unnecessary diagnostic arthroscopic procedures.

Learning Objectives:

1. To identify intra- and extra-articular anatomy on MRI.
2. To learn what we see and what we miss on radiographs.
3. To understand and learn the key features of meniscal injury.

A-255 11:30

Ankle

F. [Smithuis](#); Amsterdam/NL

"no abstract submitted"

Learning Objectives:

1. To identify intra- and extra-articular anatomy on MRI.
2. To learn what we see and what we miss on radiographs.
3. To understand and learn key features of ankle sprain.

10:30 - 12:00

Room M 4

E³ - ECR Academies: Chest Imaging

E³ 618

The heart between the lungs

A-256 10:30

Chairperson's introduction

J.E. [Wildberger](#); Maastricht/NL (j.wildberger@mumc.nl)

Modern high end CT scanners with faster scan acquisition times allow for routine assessment of cardiac pathologies, even on a standard chest CT. Relevant information regarding the heart can be retrieved, incidental cardiac findings will play a major role for patient management in the future. Plain CT allows for fat distribution as well as for coronary calcium analysis. On contrast-enhanced scans, coronary arteries and myocardial changes can be assessed. During this session, three esteemed speakers will present an overview on the diagnostics and the clinical impact of various cardiac pathologies on standard thoracic CT scans.

A-257 10:35

A. Cardiomyopathies

D.J. [Murphy](#); London/UK (murphy.84@gmail.com)

Cardiomyopathies are a heterogeneous, important group of diseases with significant morbidity and mortality. They can be broadly classified into five major subtypes based on morphology (hypertrophic, dilated, restrictive, arrhythmogenic and unclassified). Diagnosis is based on a composite of clinical history and examination, laboratory and genetic testing, electrocardiography and cardiac imaging. Despite advances in medical therapy, overall prognosis remains poor, and early diagnosis is important. Echocardiography is the first-line imaging test for the evaluation of cardiac structure and function, with cardiac magnetic resonance imaging (CMR) the gold standard. Computerised tomography (CT) has a growing role in this area. ECG-gated cardiac CT is a well-established test for coronary artery imaging, but it also allows an excellent opportunity to assess for structural cardiac abnormalities characteristic of an underlying cardiomyopathy, such as septal hypertrophy in asymmetric hypertrophic cardiomyopathy, or left ventricular dilatation in dilated cardiomyopathy; the CT features of the common cardiomyopathies will be reviewed with comparison to CMR, along with a revision of normal cardiac chamber anatomy. The improved temporal resolution of modern CT scanners has reduced the deleterious effect of cardiac motion artefact on routine non-ECG gated chest CT, allowing an opportunity for the detection of cardiac structural abnormalities. Standard non-ECG gated chest CT has a reported sensitivity of 68% in the detection of cardiomyopathies and the most reliable imaging features of cardiomyopathies on standard chest CT will also be reviewed.

Learning Objectives:

1. To review the normal anatomy on standard chest CT.
2. To learn about the CT signs of various cardiomyopathies.
3. To learn about CT performance for the diagnosis of cardiomyopathy.

A-258 11:03

B. Coronary artery disease

M. [Williams](#); Edinburgh/UK (michelle.williams@ed.ac.uk)

The heart and coronary arteries can be identified on imaging performed specifically to assess the heart and also on imaging of the chest performed for other reasons. Normal imaging coronary artery anatomy will be reviewed. Coronary artery calcification (CAC) is a marker of atherosclerotic plaque burden. CAC identified on electrocardiogram gated computed tomography (CT) is associated with an increased risk of cardiovascular morbidity and mortality. Randomised controlled trials have shown that management guided by CT coronary angiography can improve outcomes for patients with suspected coronary artery disease. CAC can also be identified on non-gated CT performed for other reasons. Calcium scoring or ordinal assessment of CAC on non-gated CT correlate with results from gated imaging. CAC on non-gated CT is associated with increased mortality in a variety of diseases, including patients with respiratory diseases. Evidence of previous myocardial infarction can also be identified on non-gated CT with features including mural thinning, fatty infiltration, and complications such as aneurysms.

Learning Objectives:

1. To review the normal coronary artery anatomy.
2. To learn about calcium scoring on non-gated CT.
3. To learn about the CT signs of healed myocardial infarction.

A-259 11:31

C. Fat and calcium in the heart

F. [Pontana](#); Lille/FR (francois.pontana@chru-lille.fr)

Population ageing and other risk factors are not only associated with calcification of coronary arteries but are also likely to induce changes in the cardiac structure. These changes can be evaluated by CT and MR. Calcifications of the cardiac valves may be a sign of valvulopathy. Aortic valve calcium scoring by CT is useful to estimate aortic stenosis severity when echocardiography is not feasible or not conclusive. Physiological age-related fat deposits within the myocardium or the atrial septum are frequent and must not be misreported as pathological. Benign or more rarely malignant cardiac tumors may present fatty component. More recently epicardial adipose tissue seems to be a new cardiac risk factor quantifiable by imaging.

Learning Objectives:

1. To learn about physiologic changes.
2. To review the main causes of fat and calcium.
3. To learn how to differentiate pathologic from physiologic images.

10:30 - 12:00

Room M 5

E³ - ECR Academies: Update on Hepatobiliary Imaging

E³ 620

Characterisation of focal liver lesions

A-260 10:30

Chairperson's introduction

C. [Stoupis](#); Männedorf/CH (c.stoupis@spitalmaennedorf.ch)

One of the most important focus of current liver imaging techniques is the potential to characterize liver lesions, facilitating the final diagnosis and avoiding unnecessary biopsies. Upon detection of a focal liver lesion on a routine imaging study, the question of characterization arises and may times the differentiation between a benign and a malignant lesion can be challenging. In this session, the important role of current imaging techniques will be discussed, reviewing typical imaging appearances of liver lesions, targeting to their underlying pathology; the differential diagnosis of hypervascular lesions, fat containing or fibrotic lesions, will be discussed, to provide helpful information to approach to correct diagnosis.

A-261 10:35

A. Hypervascular lesions

R. [Manfredi](#); Rome/IT (riccardo.manfredi@unicatt.it)

Liver parenchyma is fed by both the hepatic artery and portal vein; classical hepatocellular carcinoma (HCC) is usually fed by the hepatic artery only. Therefore, imaging of hepatic blood flow, including arterial and portal venous flow, is important for diagnosing liver tumours. Dynamic computed tomography (CT) and magnetic resonance imaging (MRI), have been developed to evaluate hepatic blood flow. In particular, dynamic CT or MRI are essential for diagnosis and characterisation of liver tumours. Moreover, MRI with tissue-

Postgraduate Educational Programme

specific MR contrast media and enhanced ultrasonography with real-time high-spatial-resolution imaging are clinically available. Hypervascular liver tumours may be both benign and malignant being important to avoid unnecessary interventions for benign lesions. There are many types of benign liver tumours that may have typical and atypical imaging features, therefore, describe an approach to distinguishing between benign and malignant hepatic lesions may help in clinical practice. Dynamic imaging is helpful in diagnosing hypervascular pseudotumors, such as focal nodular hyperplasia, and nodular lesions associated with alcohol-induced hepatitis, from hepatocellular carcinoma. There are also some hypervascular malignant tumours, such as cholangiocarcinoma, cholangiocellular carcinoma, mixed type tumours, and metastatic liver tumours, which also required differentiation from HCC. Imaging information enables us to deliver precise diagnoses, but some benign tumours are still difficult to differentiate from malignant lesions. In such cases, patients require invasive examinations, such as biopsy.

Learning Objectives:

1. To understand the imaging techniques to characterise focal liver lesions.
2. To get familiar with the typical and atypical imaging features of hypervascular lesions including haemangioma, focal nodular hyperplasia and liver cell adenomas.
3. To be able to differentiate benign hypervascular lesions from malignant ones.

A-262 11:03

B. Fat-containing lesions

O. Benjaminov; Petach Tikva/IL

"no abstract submitted"

Learning Objectives:

1. To list the wide spectrum of fat-containing lesions of the liver.
2. To be able to identify the imaging features of fat-containing liver lesions.
3. To describe the patterns of fatty change within hepatic neoplasms, in order to use them for differential diagnosis.

A-263 11:31

C. Fibrotic lesions

V. Vilgrain; Clichy/FR (valerie.vilgrain@aphp.fr)

Fibrotic lesions of the liver are defined by tumours that have a fibrous stroma. The most common fibrotic tumours are represented by liver metastases in particular of colorectal origin and intrahepatic cholangiocarcinoma. Less common fibrotic tumours are fibrolamellar carcinoma, epithelioid haemangiopericytoma, and solitary fibrous tumours. On contrast-enhanced CT or MR imaging, the fibrotic tumours share common findings such as delayed and persistent enhancement, and capsular retraction. Venous involvement when present is usually not endoluminal invasion, but encasement. On MR imaging during hepatobiliary phase, central enhancement may be seen. This lecture will review these imaging features and highlight the one enabling specific diagnosis.

Learning Objectives:

1. To be aware of the imaging techniques and contrast enhancement patterns of the fibrotic lesions.
2. To get familiar with the spectrum of fibrotic lesions in the liver and their imaging features.
3. To be able to differentiate benign from the malignant conditions.

12:15 - 12:45

Room A

Headline Session

HL 1

Wilhelm Conrad Röntgen Honorary Lecture

Presiding:

B. Hamm; Berlin/DE

A-273 12:15

Value-based radiology: the future is now!

M. Dewey; Berlin/DE (marc.dewey@charite.de)

"no abstract available"

Learning Objectives:

1. To get to know why the time for value-based radiology is now.
2. To appreciate the potential of value-based radiology in the clinical care process.
3. To understand the challenges in implementing value-based radiology.

12:30 - 13:30

Room C

E³ - The Beauty of Basic Knowledge: Cardiovascular and Interventional Radiology

E³ 24B

Every step counts: imaging and treatment of peripheral arterial disease

Moderator:

C. Loewe; Vienna/AT

A-278 12:30

State-of-the-art: non-invasive imaging of peripheral arteries

T. Leiner; Utrecht/NL (t.leiner@umcutrecht.nl)

The diagnosis of peripheral arterial disease is made on the basis of the typical history and an abnormal ankle/brachial index (ABI). It is important to understand that imaging is only indicated when an invasive intervention is contemplated. Both CTA and MRA are highly reliable methods for depicting vascular anatomy prior to peripheral arterial intervention. Multiple meta-analyses have reported high sensitivity and specificity for the detection of angiographically significant peripheral arterial disease. In my presentation I will discuss imaging protocols and strategies to optimise both techniques in daily clinical practice.

Learning Objectives:

1. To learn about state-of-the-art technique of peripheral MRA and CTA.
2. To understand the indications for non-invasive peripheral imaging.
3. To appreciate the importance of radiological diagnosis for treatment decision making in pAOD.

Author Disclosure:

T. Leiner: Research/Grant Support; Philips Healthcare; Bayer Healthcare. Speaker; Philips Healthcare; Bayer Healthcare.

A-279 13:00

Endovascular treatment in peripheral arterial disease

M. Das; Duisburg/DE (Marco.Das@helios-kliniken.de)

Endovascular therapies are important treatment options in patients with peripheral artery disease. Following regular treatment options like medical therapy and exercise training endovascular therapies have become the first choice in most clinical stages of the disease. While endovascular treatment used to be applied only in limited disease (TASC A/B), endovascular therapies nowadays are often seen as first choice option in almost all stages (TASC C/D). This is mainly due to the successful evolution of experience of interventional radiologists as well as new developments in endovascular material. Percutaneous transluminal angioplasty (PTA) with plain balloons is usually the first method of choice, while balloons loaded with anti-proliferative drugs such as paclitaxel [drug eluting balloons (DEB)] are often used in restenosis. Stents are commonly used as second option or as first choice in complex lesions. Evidence has to be found when to use drug eluting stents. Stentgrafts are often used in difficult situation when acute bleeding is involved, while scaffolds are often used in long lesions in areas with a lot of movement, in which regular stents would easily be compressed or kinked. This presentation will give an overview about different endovascular techniques including indications when to use which material and provide current evidence.

Learning Objectives:

1. To learn about different possible access routes in endovascular treatment in pAOD.
2. To understand the meaning of different acronyms and terms used in pAOD treatment including PTA, DEB, stents, stentgrafts, scaffolds.
3. To appreciate the value of interventional radiology for the treatment of pAOD.

Thursday

Postgraduate Educational Programme

12:30 - 13:30

Room D

E³ - The Beauty of Basic Knowledge: A Survival Guide to Musculoskeletal Imaging

E³ 25B

Chronic trauma: spectrum of bone response

Moderator:

V.N. Cassar-Pullicino; Oswestry/UK

A-280 12:30

Chronic trauma: spectrum of bone response

A.H. Karantanas; Iraklion/GR (akarantanas@gmail.com)

Bones are able to develop adaptive mechanisms which are sensitive to their mechanical environment. Thus, bone is constantly remodeled, throughout life, by the coordinated action of bone-resorbing osteoclasts and bone-forming osteoblasts. This remodeling process serves to prevent and heal fatigue-related microinjuries due to overloading. The balance between the amount of bone resorption and formation determines whether the process of bone remodeling leads to a net loss or gain of bone mass. Chronic trauma may be applied on normal or weakened bone and on the mature or immature skeleton. The imaging findings of the resulting painful syndromes cover a wide spectrum. Chronic overload ranges from a stress reaction to a stress fracture. The former is occult and the latter rarely obvious on radiographs. Fatigue injuries result from stress on normal bone and insufficiency injuries from stress on weakened bones. Both pathomechanisms may coexist in certain groups of adults. In the immature skeleton, the repetitive injury may cause in addition osteochondritis dissecans, osteochondral lesions, physiolyis, and chronic apophysitis. Abnormal loading matched with various parameters may result in periprosthetic fractures. Bisphosphonates may induce suppression on the bone turnover, particularly in the jaw and proximal femur, resulting in osteonecrosis and insufficiency fractures. Plain films remain the first imaging modality for exploring a pain response in chronic trauma. However, very often, plain films are normal. MRI is able not only to show even subtle findings, responsible for the clinical syndrome, but also to grade lesions and matched with known risk factors to guide the treatment.

Learning Objectives:

1. To become familiar with the pathomechanisms that can affect the axial and peripheral skeleton in chronic trauma.
2. To understand the radiological manifestation of these pathological mechanisms.
3. To appreciate how to best use imaging modalities in diagnosing occult and overt injury and monitoring the response to treatment.

12:30 - 13:30

Sky High Stage

Special Focus Session

SF 6

Artificial intelligence: a strategic view

A-979 12:30

Chairperson's introduction

E. Neri; Pisa/IT

A-980 12:35

Keynote lecture

E.L. Siegel; Baltimore, MD/US

A variety of difficult challenges in statistics can be solved best with the creation of a "machine" which can provide a simulation or model to discern patterns in a dataset and make predictions. The rapid adoption of "Deep Learning" in Diagnostic Imaging has resulted in the development of algorithms for detection, diagnosis, and quantification of medical images at an ever accelerating pace. Major successes in the application of "Deep Learning/AI" in speech recognition, self-driving cars, translation and strategic games such as Chess, Go, and Poker have resulted in major financial investments and bold and controversial predictions by "experts" about the rapidity of general adoption in Radiology and other medical imaging specialties such as pathology, dermatology, and ophthalmology. However, tremendous challenges exist in the implementation of machine learning. The current state of the art would require thousands of algorithms and many millions of imaging studies to replace more than a tiny fraction of the tasks of a diagnostic radiology and would require

hundreds of thousands or millions of hours of "expert" time to tag these. Although algorithm development times have been drastically reduced, the time and effort required for testing, verification, and validation of these algorithms in clinical practice has not decreased. Regulatory bottlenecks and medico-legal issues and constraints will need change substantially for widespread adoption within the next several years or decades. Finally, Deep Learning may actually have its greatest initial success in solving non-image related challenges such as image quality, workflow efficiency, improved communication and patient safety.

Learning Objectives:

1. Describe the relationship between artificial relationship, machine learning and deep learning.
2. List the challenges associated with the adoption of a general AI programme that could interpret studies in a manner similar to a radiologist.
3. Explain the reason for the recent excitement about "AI" in diagnostic imaging when the technology has been around for many years.
4. List applications that are not related to image pixel interpretation that can benefit imaging departments that use machine learning.

A-981 12:45

Image computing in radiology

P. Suetens; Leuven/BE

The 1970s was the decade that "computed imaging" radically changed the field of radiology. Today "image computing" has become sufficiently mature to have a similar influence on this discipline. In this talk the principles and history of image computing will be shortly summarized and its potential will be illustrated on clinical examples of computer-assisted detection, screening, quantitative measurements, evidence-based diagnosis, early outcome prediction of therapy, and imaging biomarkers. Exploiting this new technology is a logical evolution in the context of value-based health care and should therefore not be postponed or neglected. Instead, it should be considered as an opportunity and embraced by radiologists as an indispensable tool for quality assurance.

Learning Objectives:

1. To become familiar with the principles and history of image computing (automated image analysis, artificial intelligence (AI), artificial neural networks (ANN), deep learning).
2. To learn about the opportunities of image computing in radiology.
3. To have a realistic view of the current and future role and impact of image computing to radiology.

Author Disclosure:

P. Suetens: Founder; icometrix. Shareholder; icometrix.

A-982 13:00

Deep learning: basic principles

M. de Bruijine; Rotterdam/NL (marleen.debruijine@erasmusmc.nl)

With deep learning techniques computers can now solve some image interpretation tasks as good as - or even better than - human experts. This lecture explains the basic principles of deep learning and its application in radiology, discusses technical requirements, and presents examples of successful application of deep learning techniques in radiology.

Learning Objectives:

1. To become familiar with the basic principles behind deep learning.
2. To understand the requirements and limitations of deep learning.
3. To learn about successful applications of deep learning in radiology.

Author Disclosure:

M. de Bruijine: Grant Recipient; NWO, DFF, Vertex. Patent Holder; US8126240, US7561727, US7844090, US8811724, US7463758. Research/Grant Support; Quantib, Cosmonio.

A-983 13:15

Machine learning for analysing medical images

B. Glocker; London/UK

Due to an ever-increasing complexity, large volume of data and high economic pressure the interpretation of medical images pushes human abilities to the limit. Machine learning has emerged as a key technology to address some of the major challenges in medical imaging. In particular, machine learning-based algorithms can be employed to accurately extract quantitative measures such as volumes of anatomical and pathological structures from 3D medical scans, a task that is very difficult to achieve by a human expert. Additionally, ML has potential to discover new patterns of disease, identify abnormalities and extract clinically useful information from high-dimensional, multi-modal imaging data which otherwise would remain hidden. This presentation will provide an overview of the recent successes and challenges of today's machine learning approaches when applied to the automatic analysis of brain, cardiac and whole-body imaging. Particular focus is put on the interaction between

Thursday

Postgraduate Educational Programme

computational and clinical disciplines and we argue for the need of an even closer collaboration between these disciplines and the importance for a common language and understanding of the demands of successful employment of machine learning in clinical practice.

Learning Objectives:

1. To learn how machine learning can help to analyse medical images.
2. To appreciate the need for close cross-discipline collaboration.
3. To understand what are the key ingredients for successful use of today's machine learning technology.

Author Disclosure:

B. Glocker: Advisory Board; Definiens. Consultant; Kheiron Medical Technologies. Grant Recipient; Research Councils UK, European Research Council.

14:00 - 15:30

Room A

E³ - ECR Academies: Interactive Teaching Sessions for Young (and not so Young) Radiologists

E³ 721

Gastrointestinal radiology

A-281 14:00

A. Inflammatory bowel disease

J. Rimola; Barcelona/ES (jrimola@clinic.ub.es)

Cross-sectional imaging has an established role in evaluating patients with Crohn's disease (CD) providing additional information to clinical and endoscopic assessment, which is crucial for therapeutic decision-making algorithms. Imaging findings are highly predictive of tissue inflammation and can be used in clinical practice in evaluating disease activity and identifying both stricturing and penetrating complications. Recent evidence demonstrates that cross-sectional imaging is useful for the assessment of therapeutic response and monitoring the course of the disease. The latter represents a clear advantage over endoscopy providing a more global assessment of treatment efficacy including luminal activity and disease-related complications (i.e., stenosis and fistula). The overall cross-sectional imaging techniques characteristics and benefits have driven a rapid increase in their use for CD imaging as part as routine practice in many institutions.

Learning Objectives:

1. To review the spectrum of imaging findings in inflammatory bowel disease, mainly in Crohn's disease.
2. To learn about the management options.

Author Disclosure:

J. Rimola: Advisory Board; Gilead, TiGenix. Consultant; Robarts Clinical Research. Investigator; Abbvie. Speaker; Takeda, BMS.

A-282 14:45

B. Rectal cancer staging: key findings

G. Brown; Sutton/UK (gina.brown@rmh.nhs.uk)

Report [#rectalcancer](https://profginabrown.com/reporting-proformas/) using the reporting proforma <https://profginabrown.com/reporting-proformas/> and use a proper high resolution MRI scan technique <https://profginabrown.com/wp-content/uploads/2017/04/mri-techniques-for-rectal-cancer.pptx> The mrCRM is defined as involved if the distance of tumour or EMVI or extranodal tumour deposits to mesorectal fascia is 1mm or less. Lymph nodes do not cause positive CRM but EMVI and Extranodal Vascular Tumour Deposits cause pCRM and are a risk for local recurrence. Identifying patients who require surgery beyond TME <https://profginabrown.com/wp-content/uploads/2017/04/beyond-tme-why-the-need-for-pelvic-exenteration1.pptx> MRI defined mucinous tumours have a poor prognosis <http://www.ejancer.com/article/S0959-8049%2813%2901101-5/pdf> Stage low rectal cancers using the MERCURY 2 staging system to ensure appropriate selection for Low Anterior resection vs intersphincteric APE vs ELAPE vs Beyond TME MRI assessment of depth of tumour spread gives the most accurate prognostic information. MRI assessment of extramural venous invasion identifies more patients at risk of recurrent disease than current pathology staging of lymph nodes or venous invasion. <https://profginabrown.com/wp-content/uploads/2017/04/mri-detection-of-emvi-in-rectal-cancer.pptx> TRG1-2 represents a population of patients highly likely to have no viable tumour in the long term and hence suitable for MRI monitoring and avoiding surgery in the TRIGGER trial. No need to biopsy. <https://profginabrown.com/trigger/> Early rectal cancer staging and rectal preservation can be optimised, recurrences after TEM avoided by better staging <https://www.ncbi.nlm.nih.gov/pmc/articles/PMC4891388/>.

Learning Objectives:

1. To understand the imaging technique.
2. To identify the key imaging findings.

Author Disclosure:

G. Brown: Advisory Board; EISAI Ltd. Grant Recipient; NIHR BRC Royal Marsden, NIHR BRC Senior Investigator Award, Pelican Cancer Foundation.

14:00 - 15:30

Room M 3

ESOR Session

Trends in quality education in radiology

Moderators:

B. Brkljačić; Zagreb/HR
N. Gourtsoyiannis; Athens/GR

A-283 14:00

Introduction

B. Brkljačić; Zagreb/HR (boris@brkljacic.com)

The European School of Radiology (ESOR) is an institution, fulfilling the mission of the European Society of Radiology (ESR) in the field of education. One of its main goals is to assist in harmonising radiological education in Europe. With its wide range of activities, ESOR additionally aims to raise standards in the field of scientific radiology, extend and coordinate teaching resources worldwide and help young radiologists achieve the knowledge and skills to fulfil tomorrow's requirements.

A-284 14:05

ESOR in action 2018

N. Gourtsoyiannis; Athens/GR

A-285 14:15

The beauty of face-to-face teaching

Y. Menu; Paris/FR (yves.menu@sat.aphp.fr)

Today, many ways of teaching are available. In addition to press and books, video recorded sessions and webinars play an increasing role in teaching. Advantages are many: the offer endlessly increases, access is obtained via personal equipment, distances are deleted, availability is defined by the trainee who selects recorded sessions. Face to face teaching has none of these advantages, but nevertheless remains necessary for three main reasons; (1) It is the only manner for the trainer to sample in real time the exact level of the trainees and to calibrate his teaching objectives, (2) It is the only way to install full and appropriate interactivity, and (3) communication between the teacher and the trainees goes through much more tunnels than scientific knowledge, including non-verbal communication. All of these cannot be transmitted electronically until now.

A-286 14:30

Flipped classroom: paradigm shift with pathologists

V. Vilgrain; Clichy/FR (valerie.vilgrain@aphp.fr)

Flipped classroom is an instructional strategy and a type of blended learning that reverses the traditional learning environment. Residency education in radiology is individual and mostly based on image interpretation with faculty and conference teaching. Education is completed by reading textbooks and online material. Interaction with clinicians is also very important for residents and senior radiologists. Yet radiology is close to pathology and radio-pathologic correlations give many insights to radiology. The purpose of this lecture is to show that interaction with pathologists is very helpful for the two medical specialties. Examples will be provided showing that both contribute to a better understanding of the diseases and increase the diagnostic performance.

A-287 14:45

Integration of big data in radiological education

L. Martí-Bonmati; Valencia/ES (marti_lui@gva.es)

Big data are challenging the way radiology is being performed and taught. In a big learning data world, rethinking our data sources and adopting a strategic approach to presenting data is crucial. Most efforts with big data and radiology relate to the discovery on new diagnostic pathways and opportunities to better diagnose and treat diseases. Access to data can help residents and radiologists define their learning goals and strategies. Medical imaging big data analysis and the use of biobanks' data recently emerged for advancing on the

Postgraduate Educational Programme

study of rare diseases, the identification of early surrogate biomarkers and the development of population studies. These new aspects will change the way radiological science is being taught, as better information on new radiomic biomarkers on early disease diagnosis, disease phenotyping, disease grading, targeting therapies, and evaluation of disease response to treatment will develop. Big data results' analysis will help radiology providing new model of cooperative science to share knowledge within the scientific community; to increase production of scientific researcher contribution from radiology; to improve healthcare through image quality and radiation dose, technical and protocol comparisons and follow-up assessment of clinical guidelines; to improve the therapeutic process through the translation of research findings into clinical trials with guided imaging, assessment of imaging biomarkers endpoints, and early assessment of treatment response; to improve epidemiological knowledge of the population through the introduction of quantitative diagnostic tests markers; and to create knowledge databases from representative cases, semantic, and semiotic advanced searches.

15:00

Awards

14:00 - 15:30

Room M 4

E³ - ECR Academies: State-of-the-Art and Advanced MR Imaging of the Musculoskeletal system

E³ 719 Shoulder

A-288 14:00

Chairperson's introduction

A. [Karantanas](mailto:akarantanas@gmail.com); *Iraklion/GR* (akarantanas@gmail.com)

Shoulder pain is a common clinical problem. A painful syndrome may result from previous trauma, chronic degeneration or rupture of tendons with or without impingement, internal derangement of the glenohumeral joint and failure of a previous operation. Imaging methods include plain X-rays, ultrasonography, MR imaging and rarely CT. Each modality has its own and distinct role depending on the clinical indication. Current indications, as well as advantages and limitations of one or more imaging methods for evaluating patients with shoulder pain, will be discussed in the following 3 lectures on common and uncommon disorders.

A-289 14:05

A. Post-traumatic

K.-F. [Kreitner](mailto:Karl-Friedrich.Kreitner@unimedizin-mainz.de); *Mainz/DE* (Karl-Friedrich.Kreitner@unimedizin-mainz.de)

The most common sequelae of shoulder trauma comprise fractures of the humeral head, glenohumeral instabilities, SLAP lesions and traumatic ruptures of the rotator cuff. Conventional radiography with use of the so-called trauma series consisting of true ap, true lateral and axial views of the affected shoulder is useful in documentation of dislocations, fractures and fracture dislocations of the shoulder, their direction, the result after reduction as well as in first assessment of humeral head fractures. CT is mandatory in complex humeral head fractures for planning of the operative procedure. In instability, it delineates humeral impression fractures and defects of the bony glenoid, and thus allows for assessment of on-track and off-track lesions. Direct MR-arthrography is the imaging modality of choice especially in younger patients with glenohumeral instability and SLAP lesions due to its superior resolution of soft tissue structures. Furthermore, it enables differentiation of atraumatic and microinstabilities of the shoulder, especially when using sequences obtained in abduction and external rotation of the shoulder (ABER position). In the acute phase after shoulder trauma, unenhanced MR imaging may be sufficient due to an existing joint effusion. Precise planning of sequences are the basis for assessment of bony defects of the glenoid and humeral head, and thus MR is also capable for assessment of on-track/off-track lesions in shoulder instability. Direct CT arthrography may be an alternative for assessment of patients with glenohumeral instability and SLAP lesions when MR imaging is not available or when there contraindications for its use.

Learning Objectives:

1. To identify the most common post-traumatic entities.
2. To know the role of MR imaging, and MR arthrography (direct/indirect) and how to optimise MR protocols.
3. To differentiate post-traumatic changes from typical reasons for chronic pain.

A-290 14:33

B. Chronic pain

P. [Omoumi](mailto:patrick.omoumi@chuv.ch); *Lausanne/CH* (patrick.omoumi@chuv.ch)

Chronic shoulder pain, defined as shoulder pain persisting over six months, is frequent, representing about 15% of all musculoskeletal complaints. In the work-up of chronic shoulder pain, conventional radiography is the first diagnostic modality to perform. Radiographs can reveal a wide range of common shoulder pathology that can be source of pain, including glenohumeral or acromioclavicular osteoarthritis, calcific tendinitis, indirect signs of large rotator cuff tendon tears, as well as sequelae of previous trauma. MRI is the diagnostic modality of choice to further clarify the cause of the pain. MRI has high diagnostic performance for rotator cuff tears, tendinitis, and subacromial bursitis. The diagnosis of adhesive capsulitis is made clinically, but signs of capsulitis have been described at MRI, which mostly serves at ruling out other diagnoses in case of atypical presentation. In case of chronic instability, MR arthrography should be preferred because of its higher performance in detecting labra-ligamento-cartilaginous lesions. Findings of shoulder pathology at MRI are not necessarily related to symptoms, however. For instance, as many as 50% of asymptomatic patients over 60 years old have partial or full-thickness rotator cuff tears.

Learning Objectives:

1. To identify the most common entities leading to chronic shoulder pain.
2. To know the role of MR imaging and MR interventions in the shoulder.
3. To differentiate entities leading to chronic pain from post-traumatic changes.

A-291 15:01

C. Postoperative

S. [Waldt](mailto:simone.waldt@tum.de); *Munich/DE* (simone.waldt@tum.de)

Scope of this course is to discuss technical requirements and strategies concerning the interpretation of MR examinations in the postoperative setting. The quality of MR images of the shoulder obtained after surgery can be significantly impaired by susceptibility artifacts due to metallic implants and metal shavings from use of surgical instruments. The use of artefact reduction techniques, which will be summarized in this presentation, is a prerequisite for a sufficient diagnostic accuracy. Basic knowledge concerning different surgical techniques, their common complications and sources of failure are necessary to interpret MR examinations. This talk gives an overview on the most commonly performed surgical procedures that are used for treatment of shoulder instability, impingement syndromes, and rotator cuff lesions. Criteria that may be used to differentiate between normal and abnormal postoperative findings will be discussed in detail, because findings that indicate pathology in non-operated patients are often less significant and unreliable in the postoperative situation.

Learning Objectives:

1. To identify the most common postoperative changes.
2. To know the role of MR imaging and MR arthrography (direct/indirect) and how to optimise MR protocols for the postoperative patient.
3. To understand the typical appearances and complications following rotator cuff repair.

14:00 - 15:30

Room M 5

E³ - ECR Academies: Update on Hepatobiliary Imaging

E³ 720

Personalised medicine in liver tumours

A-292 14:00

Chairperson's introduction

B.J. [Op De Beeck](mailto:bart.op.de.beeck@uza.be); *Antwerp/BE* (bart.op.de.beeck@uza.be)

Metastatic disease to the liver is one of the most common problems encountered in patients with cancer. However, not all focal liver lesions in oncologic patients are metastases. Although the true prevalence of metastatic disease is unknown, some individuals who die of malignancy will have liver metastases at autopsy. Autopsy series also reveal the presence of benign hepatic lesions in up to 52% of the general population. Imaging protocols and findings to differentiate benign lesions from metastases will be presented. Management of malignant liver lesions depends on the tumour stage, liver function reserve, and patient performance status, and requires a multidisciplinary approach for optimal treatment. Treatment options and strategies for liver tumours will be discussed including indications of ablation techniques and intra-arterial embolisation techniques and their outcome. Radiologists must become familiar with the different methods of assessing tumour response. Size criteria, including the WHO criteria and RECIST, have

Thursday

Postgraduate Educational Programme

served for years as methods to standardise outcomes of therapy. New evolving methods of treatment including antiangiogenic and locoregional therapy do not always cause a decrease in size. Therefore, assessment of necrosis will need to be incorporated into size-related criteria. Finally, the imaging findings of cancer therapy-induced toxicities and their adverse effects will be discussed.

A-293 14:05

A. Focal liver lesions in oncology patient

F. [Caseiro Alves](mailto:CaseiroAlves@coimbra.pt); Coimbra/PT (caseiroalves@gmail.com)

Currently, the widespread use of volumetric cross-sectional imaging methods, has led to an increased fortuitous detection of focal liver lesions in all groups especially in the oncologic context of extra-hepatic cancer patients. Since imaging techniques can now provide high spatial resolution small nodules are easily depicted posing the problem of the characterization of the so-called incidental liver lesions. The vast majority correspond to cysts, hemangiomas, benign hepatocyte-specific-cellular tumors and pseudo lesions such as focal fatty infiltration, and focal fatty sparing. Additionally, intra-hepatic vascular shunting and vascular variants can be an important source of false positives for malignancy in the oncologic setting. A particular sub-set to nodules relates to multicentric regenerative nodules, closely linked to sinusoidal obstruction syndrome observed after chemotherapy. The scope of this lecture is to provide guidance regarding the imaging aspects that may assist to the differentiation of metastases. Emphasis will be put on a multimodality approach generally using MR as a problem solver to this important issue in current oncological practice.

Learning Objectives:

1. To be aware of the most common incidental liver lesions in patients with extrahepatic cancer.
2. To understand the imaging protocols and findings to differentiate benign lesions from metastases.
3. To be familiar with the strategies for optimising patient management of these incidental hepatic lesions.

A-294 14:33

B. Treatment options and strategies for liver tumours

T.K. [Helmberger](mailto:Helmberger@klinikum-muenchen.de); Munich/DE (Thomas.Helmberger@klinikum-muenchen.de)

Primary and secondary hepatic malignancies are a common clinical issue. Considering the general oncological (isolated hepatic tumor load; prognostic benefit), and technical (size, number, location of hepatic metastases; expected hepatic functional reserve) framework surgical resection is usually considered to be the method of therapeutic choice. However, in clinical reality only 15-30 % of patients with liver malignancies may qualify for resection. In consequence, the majority of patients need other or at least modified therapeutic pathways including adjuvant or neoadjuvant chemotherapy and more and more image guided local ablative therapies. Interventional oncology (IO) provides mainly three image-guided local and loco regional cytoreductive therapeutic approaches: (1) percutaneous thermal-ablation (mainly radiofrequency and microwave ablation) with current techniques 3 cm tumors can safely be coagulated achieving 5-year survival rates of up to 50% comparable to surgical results, (2) transarterial chemo-ablation for larger, multifocal, or diffuse HCC is established and is currently getting adopted in metastatic disease. While classic (Lipiodol) TACE is worldwide still well accepted in HCC transarterial chemo-embolization with drug eluting beads (DEB-TACE) is gaining promising results with comparable response rates to classic TACE in HCC and to systemic chemotherapy in metastases, and (3) transarterial radio-embolization (TARE, SIRT) could prove its efficacy in HCC patients not suitable for TACE and in chemorefractory patients improving hepatic progression free survival. Minimal-invasive, image-guided therapies are suitable in a large number of cases and getting implemented increasingly in multimodality treatment regimens according to interdisciplinary consensus of oncologists, interventional radiologists, and surgeons.

Learning Objectives:

1. To understand the main options of tumour treatment and to be able to discuss the appropriate method for treatment given the results of imaging.
2. To recognise the indications of ablation techniques and their outcome.
3. To know when intra-arterial embolisation techniques are needed and what their outcome is.

Author Disclosure:

T.K. [Helmberger](mailto:Helmberger@klinikum-muenchen.de): Consultant; Boston Scientific.

A-295 15:01

C. Assessment of response to treatment

V.J. [Goh](mailto:goh@kcl.ac.uk); London/UK (vicky.goh@kcl.ac.uk)

Imaging is essential to the management of cancer patients. Better assessment of disease burden, prognostication, treatment triage, and treatment response is required to improve patient outcome. For patients with liver tumours

undergoing systemic or locoregional therapy, imaging provides an objective method for assessing response/non-response to therapy, allowing patients to transition to alternative therapies when therapy is ineffective. Imaging also enables therapy related adverse effects to be depicted and treated. The strengths and limitations of the different imaging modalities including CT, MRI, PET/CT, and PET/MRI will be discussed for systemic and locoregional therapies of liver tumour. The different response criteria will also be highlighted and future directions discussed.

Learning Objectives:

1. To appreciate the value of different imaging techniques and the criteria for assessment of tumour response to systemic therapy.
2. To become familiar with post-treatment imaging after intra-arterial therapies and ablation techniques.
3. To be aware of imaging findings of cancer therapy-induced toxicities and adverse effects.

Author Disclosure:

V.J. [Goh](mailto:goh@kcl.ac.uk): Research/Grant Support; Siemens Healthineers. Speaker; Bayer, Siemens Healthineers.

16:00 - 17:30

Room A

E³ - ECR Academies: Interactive Teaching Sessions for Young (and not so Young) Radiologists

E³ 821

Dementia and movement disorders

A-302 16:00

A. MR contribution to diagnosis and differential diagnosis in dementia

M. [Sasiadek](mailto:Sasiadek@umed.wroc.pl); Wroclaw/PL (marek.sasiadek@umed.wroc.pl)

Imaging methods play an increasing role in diagnosing, differentiating, prognosing and follow-up of dementia. The most important imaging methods are: CT, MR, SPECT, and PET. Among them MR, including MR spectroscopy (MRS), perfusion MR (PWI), diffusion tensor imaging (DTI) and functional MRI (fMRI), appears to be the most valuable modality. Plain MR might provide important contribution to the diagnostics of dementia. The distribution of the brain atrophy indicates the specific dementia disease, e.g., hippocampal atrophy is highly suggestive of Alzheimer disease and frontotemporal atrophy of frontotemporal dementia. There are also specific MR patterns of progressive supranuclear palsy (mesencephalic atrophy) or multiple system atrophy (cerebellar/brainstem or putaminal atrophies). Vascular dementia changes (e.g., small vessel disease, CADASIL, amyloid angiopathy) could be reliably diagnosed with MR, including MR angiography and susceptibility weighted sequences. There are also typical MR patterns of many other diseases, which may be accompanied by dementia, e.g., normal pressure hydrocephalus, multiple sclerosis, Wilson disease, Fahr disease, Creutzfeldt-Jakob disease, etc. Advanced MR techniques provide further contribution to diagnosing dementia by adding quantitative data. MRS could reveal increase of myoinositol level in degenerative diseases or of choline in multiple sclerosis. PWI shows decrease of perfusion in vascular dementia, but also in Alzheimer disease. DTI detects decrease of fractional anisotropy in white matter tracts affected by degenerative, ischaemic or inflammatory process. fMRI provides assessment of the impaired cognitive functions in dementia disorders. MR, due to the advantages described above, should be a part of routine diagnostic protocol in patients with dementia.

Learning Objectives:

1. To become familiar with imaging in different types of dementia.
2. To learn the imaging criteria for differentiation.

A-303 16:45

B. Imaging in Parkinsonism and other extrapyramidal disorders

T. [Stosic-Opincal](mailto:Stosic-Opincal@stosic.tanja@yahoo.com); Belgrade/RS (stosic.tanja@yahoo.com)

Extrapyramidal disorders can be classified as pathologies that affect basal ganglia (*caudate, putamen, and globus pallidus*), subthalamic nucleus and structures that are functionally connected with them (substantia nigra). On histological level affected tissues exhibit high level of deposits of paramagnetic ions (presumably iron and copper) and loss of neural tissue. This is manifested in loss of volume of brain structures and dysfunction of specific neural tracts. Parkinsonism refers to any condition that causes a combination of the movement abnormalities such as tremors, slow movement, impaired speech or muscle stiffness. Beside idiopathic Parkinson's disease, a several conditions fulfill definition, such as progressive supranuclear palsy, multisystem atrophy, and corticobasal degeneration. Role of imaging techniques is assessment of structural and physiological changes caused by EPD. Magnetic resonance imaging is primary choice since it provides morphological, structural, and physiological insight in changes caused by extrapyramidal disorders. Positron

Postgraduate Educational Programme

emission tomography gives additional information about physiological changes using neurotransmitters labeled with positron emitters. Computerised tomography has limited possibilities which are restricted to assessment of morphological changes.

Learning Objectives:

1. To become familiar with the different imaging modalities.
2. To learn the imaging criteria.

16:00 - 17:30

Room C

Chest

RC 804

Chronic obstructive pulmonary disease (COPD)

A-304 16:00

Chairperson's introduction

K. [Irlon](#); Manchester/UK (klaus.irlon@mft.nhs.uk)

"Chronic Obstructive Pulmonary Disease (COPD) is a common, preventable and treatable disease that is characterized by persistent respiratory symptoms and airflow limitation that is due to airway and/or alveolar abnormalities usually caused by significant exposure to noxious particles or gases". "The clinical diagnosis of COPD requires the presence of a post-bronchodilator FEV1/FVC < 0.70 to be established." Both sentences above are from the 2017 Global Initiative for Chronic Obstructive Lung Disease (GOLD) Report. They probably represent the biggest challenge to the imaging diagnosis and phenotyping of COPD patients. The GOLD statements above imply that COPD cannot be diagnosed without persistent respiratory symptoms and a post-bronchodilator FEV1/FVC < 0.70: as if a persistent airflow limitation due to airway and/or alveolar abnormalities without the two criteria would not be COPD. One of the key methodological problems in quantitative CT for the assessment of COPD is that the selection of patients is tied up to the above criteria, where correlations with pulmonary function tests are taken as the references for the diagnostic capability of CT or MRI. To learn how to avoid the progression of emphysema and/or chronic airway disease to a symptomatic phase when the FEV1/FVC reaches the critical level (< 0.70) for a COPD diagnosis, the medical community should first accept that a significant extent of the anatomical changes that lead to various degrees of chronic airflow limitation (i.e. COPD) will be present much before the current threshold set as a diagnostic criteria of COPD is met.

Session Objectives:

1. To describe the current challenges of COPD phenotyping.
2. To learn how to personalise management in COPD.
3. To understand the methodological problems at the stages of selection of patients.

A-305 16:05

A. CT phenotyping and visual assessment

P.A. [Grenier](#); Paris/FR (philippe.grenier@aphp.fr)

COPD is a slowly progressive obstructive airway disorder resulting from an exaggerated inflammatory response to cigarette smoking and air pollution that ultimately destroys lung parenchyma and induces irreversible reduction in caliber and number of small airways. Both phenomena [emphysema and small airway disease (SAD)] are responsible for airflow limitation. Because often SAD precedes lung destruction, patients having equal impairment of lung function may present different morphologic appearances on CT scans. Although quantitative CT is useful for identifying and sequentially evaluating the extent of emphysematous lung destruction, changes in airway walls, and expiratory air trapping, visual assessment of CT scans is important to describe patterns of altered lung structures in COPD. Emphysema is classified as centrilobular (subclassified as trace, mild, moderate, confluent, and advanced destructive emphysema), panlobular and paraseptal (subclassified as mild or substantial). Airway disease is commonly found with all forms of emphysema but also commonly occurs in the absence of emphysema as a predominant expression of COPD. The CT features of bronchial disease include thickening of the walls of segmental and subsegmental airways. CT features of SAD include peripheral centrilobular micronodular opacities (inflammatory SAD) and gas trapping on expiratory CT (obstructive SAD). Associated features may be seen on large airway disease (tracheobronchomalacia, saber sheath trachea, tracheobronchial outpouching/diverticula). Interstitial lung abnormalities include patchy ground glass abnormality and/or mid subpleural reticular abnormality. Other associated features include pulmonary arterial enlargement suggesting pulmonary hypertension, and bronchiectasis

Learning Objectives:

1. To learn about imaging-based phenotypes.
2. To understand the strengths and limitations of visual assessment.
3. To review the phenotypes and comorbidities approachable by CT.

A-306 16:28

B. Quantitative imaging biomarkers

J.B. [Seo](#); Seoul/KR (seojb@amc.seoul.kr)

With excellent spatial and contrast resolution, CT can be used as an important tool to evaluate quantitative imaging biomarkers of COPD. The extent of low attenuation area and bronchial wall thickening at segmental and distal level on volumetric CT scan acquired at suspended inspiration state are commonly used as useful markers for evaluating the severity of emphysema and airway wall inflammation, respectively. The clinical values of these two imaging biomarkers are as follows: (1) Many studies have proved that the extent of emphysema and bronchial wall thickening are independently related with the degree of airflow limitation, (2) The extent of emphysema is correlated with other clinical parameters such as osteoporosis, exercise capacity, respiratory symptoms, and most importantly with BODE index, (3) Both parameters may be useful in subgrouping/phenotyping of patients, prediction of treatment response, disease progression, and exacerbation. The extent of air trapping can be assessed by quantitative volumetric expiratory CT or by comparing the density changes on matched inspiratory/expiratory CT. Other potential imaging biomarkers on CT include peripheral vascular changes, size and shape distribution of emphysema holes, and so on. Despite these advances, several important challenges remain before these quantitative imaging biomarkers can be used in clinical practice. In patient side, variation in inspiratory and expiratory lung volumes is most important issue, which has a major influence on lung attenuation values. Technically, variation in measured CT attenuation across scanner manufacturers and models, differing reconstruction kernels, and varying methods of automatic exposure control should be considered.

Learning Objectives:

1. To learn about the COPD biomarkers that may be helpful for managing COPD patients.
2. To understand the potential role for quantitative imaging in identifying imaging phenotypes.
3. To appreciate the recent development of quantitative imaging methods.

Author Disclosure:

J.B. Seo: Shareholder; Coreline Soft Co. Speaker; Siemens / Guerbet.

A-307 16:51

C. Is there a role for MRI?

B.J. [Jobst](#); Heidelberg/DE

Today, computed tomography (CT) is the imaging modality of choice for the assessment of pulmonary diseases, but it requires ionizing radiation. Unfortunately, magnetic resonance imaging (MRI) of the lung is complicated by low proton density and high magnetic susceptibility of the alveolar structures, decreasing the MR-signal obtained from the lungs. Hence, the depiction of the pulmonary morphology is hampered by low contrast and spatial resolution. Besides, respiratory and cardiac motion artifacts have impact on image quality. In the recent years, novel MRI techniques based on parallel imaging and advanced gating techniques have been developed and implemented in routine MRI protocols, which lead to improved depiction of pulmonary structures. Innovative MRI techniques such as ultra-short echo time acquisitions (UTE) further improve the structural characterization of airways and parenchyma. Although MRI is still inferior to CT concerning the depiction of subtle morphological features, MRI offers a broad spectrum of functional acquisitions, especially for perfusion, ventilation, and respiratory mechanics. Lacking ionizing radiation, MRI can be repeated as often as necessary and represents a powerful instrument for longitudinal observations. In this context, MRI provides quantitative and semi-quantitative biomarkers which may be helpful in the evaluation of the course of lung disease as well as monitoring of the therapeutic response.

Learning Objectives:

1. To learn about the morpho-functional pulmonary measurements achievable with MRI.
2. To review the various methodological approaches.
3. To appreciate current and forthcoming developments.

17:14

Panel discussion: How is imaging currently used in COPD patient management?

Thursday

16:00 - 17:30

Room O

Special Focus Session

SF 8a

CT examination of pregnant patients: a dilemma for the radiologist and the mother

A-308 16:00

Chairperson's introduction

V. Gershan; Skopje/MK (vesna.gershan@pmf.ukim.mk)

CT examinations of pregnant patient when the fetus is within the primary beam are challenging for radiologist and mother, as well. Two main scenarios in CT examination of pregnant patient are possible. The first one is so called inadvertent exposure, while patient is scanned and pregnancy is still unknown. The second one is when there are strong CT indications due to non-obstetrical emergencies like as appendicitis, renal colic, ovarian torsion, hemorrhagic ovarian cysts, trauma, and pulmonary embolism. Explanation of benefits vs. risks to mother could be challenging and it is good practice to obtain informed consent before proceeding with the examination. If CT examination is duly justified, then an acquisition protocol that ensures diagnostic image quality at lowest possible dose should be applied. There are several dose reduction techniques like is decreasing of kV, mA, limit the field of view, increasing of pitch, using of iterative reconstruction techniques, etc. There are several models for assessment of fetal dose, like is MC simulated whole-body or individual organ doses, patient-specific voxel-based computational phantoms or dose assessment using of dose conversion factor and exposure parameters. Delivered dose to the fetus from a single diagnostic abdominal CT is highly unlikely to exceed the estimated threshold dose of 100 mGy for induction of malformations. Estimated radiation risk depends on the dose, gestational age and applied risk model, and for example, for 50 mGy dose it can be 1 in 909 to 1 in 334. All these aspects will be addressed under the current session topics.

Session Objectives:

1. To give an overview of radiation risk associated with the CT examination of pregnant patients.
2. To learn how to optimise CT imaging of pregnant patients.
3. To suggest actions for dose management of pregnant patients in CT.

A-309 16:05

Radiation risks vs clinical benefits

M. Prokop; Nijmegen/NL

"no abstract submitted"

Learning Objectives:

1. To give an overview of radiation risks of pregnant patients during CT examinations.
2. To learn about the choice of the modality.
3. To learn how to manage risk in the CT examination of pregnant patients.

A-310 16:23

How to reduce radiation dose and keep CT diagnostics

M. Kortensniemi; Helsinki/FI (mika.kortensniemi@hus.fi)

A developing fetus has an increased sensitivity to ionizing radiation exposure. Therefore, dose monitoring and optimisation of CT exposures of an expecting mother is important. The typical clinical indications related to CT scans during pregnancy include pulmonary embolism, appendicitis, and trauma. In these situations, the fetus can be fully or partially in the primary CT scan range or in its immediate vicinity. In pulmonary embolism scans, increased distance of the fetus from the scan range serves as a practical tool for fetal dose optimisation. Modern CT scanners have several technical tools for dose reduction. Those tools include automatic tube current modulation, automatic tube voltage selection, dynamic z-collimation and iterative reconstruction algorithms. When used together in a proper way, they may provide tens of percentages of dose reduction for the mother and the fetus, depending of the clinical indication and individual patient characteristics. The actual purpose is not to use as little radiation as possible but to achieve a maximum benefit-to-risk ratio for the patient (mother and fetus). Adequate image quality for reliable diagnosis must always be reached. Otherwise the dose is unnecessary, however, small it could be.

Learning Objectives:

1. To give an overview of optimisation methods and techniques in CT.
2. To describe the method of choice in particular cases.
3. To learn about examples for different clinical requests.

A-311 16:41

Dosimetry methods available

J. Damilakis; Iraklion/GR (damilaki@med.uoc.gr)

Several methods for the estimation of conceptus dose from CT examination have been developed during the last years. Twenty four patient models selected to represent a range of gestational ages were created using image data from a group of pregnant patients who had previously undergone abdominal and pelvic CT examination (Radiology 2008, 249, 220-227). The authors provide an equation for the estimation of conceptus dose. A methodology has been created for the accurate estimation of conceptus dose from CT examinations performed on pregnant patients during the first weeks of gestation (Radiology 2010, 257, 483-489). This period of early pregnancy is particularly important because the conceptus is considered to be sensitive to radiation in the period of organogenesis. A two-variable equation provided a relationship among normalised conceptus dose, body perimeter and skin-to-conceptus-distance. A general-purpose Monte Carlo simulation code and mathematical phantoms simulating pregnancy during all trimesters of gestation were used to provide normalised dose data for conceptus dose estimation from any CT examination performed in the trunk of the pregnant patient (Medical Physics 2010, 37, 6411-6420). CoDE (conceptus dose estimation) online software tool allows; (a) calculation of conceptus radiation dose and associated risk from X-ray examinations performed on the expectant mother and (b) anticipation of conceptus dose for the pregnant employee who participates in fluoroscopically-guided interventional procedures. CoDE is available free of charge.

Learning Objectives:

1. To provide information about the available conceptus dosimetry methods in CT.
2. To understand the accuracy and limitations of the dosimetry methods.
3. To learn how to estimate radiation dose in pregnant patients during CT examinations.

A-312 16:59

Dose and risk communication to doctors and patients

P. Gilligan; Dublin/IE (PGilligan@materprivate.ie)

Pregnant patients are recognised as a high risk and sensitive group in radiation protection. There may be perceived conflict between the benefit of the required treatment of the mother and the risk to the foetus. Patient focussed care requires open disclosure of any risks. The implications of these risks must be well understood by the patient. Radiation risks in the foetus can be complex, dependent on the modality, procedure type, radiation dose, and stage of pregnancy. The communication of appropriate risks to the mother particularly in an emergent context can be challenging. Experience has shown that preparation of accurate and well contextualised information assists the patient and their care providers to make appropriate health care decisions. The environment, context, timing delivery of such information is also important. Patients are reassured when good radiation protection culture is evident. The use of methods to identify possible pregnancy and minimise the risks in early pregnancy have proved divisive and have led to divergent practices and opinions even among experts. Inadvertent exposure in pregnancy occurs in most hospitals on an occasional basis. Follow up with such patients, particularly after systems failures, requires a tailored approach. This talk examines the possible risks from diagnostic procedures during pregnancy and the contexts and environments in which such information is delivered. It looks at both pre planned foetal exposures and inadvertent exposures. The multidisciplinary approach involving radiology is essential in providing accurate and relevant information on which medical decisions can be based.

Learning Objectives:

1. To provide information about the latest scientific knowledge about conceptus risk.
2. To learn how to manage incidents and accidents involving pregnant patients in CT.
3. To learn how to communicate to doctors and patients about dose and risk.

17:17

Panel discussion: CT during pregnancy: what are the suggested actions for patient dose management?

16:00 - 17:30

Room N

Head and Neck

RC 808

Pitfalls in interpretation of head and neck disease

Moderator:

S. Robinson; Vienna/AT

A-313 16:00

A. Anatomical variants without clinical consequence

F.A. Pameijer; Utrecht/NL (f.a.pameijer@umcutrecht.nl)

Variant: "Something that is slightly different." Imaging methods can provide an extraordinary amount of useful data to specialists treating head and neck (cancer) patients. It is crucial that these data are used to full advantage of individual patients. The most important factor in this process is mutual cooperation between the physicians in charge of patient care and the diagnostic imaging specialist. Anatomical variants in the head and neck are frequently encountered and may result in interpretation problems for the radiologist: usually, anatomical variants are without clinical consequence. However, normal variants may simulate disease. If not recognised, normal variants (or pseudolesions) may lead to unnecessary interventions. The presentation aims to familiarise general radiologists, who have an interest in head and neck imaging, with common anatomical variants encountered on head and neck CT and MR studies. Many examples from daily practice will be discussed.

Learning Objectives:

1. To gain insight into the great variability of head and neck anatomy.
2. To be able to recognise pseudo lesions.

A-314 16:30

B. Anatomical variants posing surgical risks

D. Farina; Brescia/IT (nappaja@yahoo.it)

Several anatomic variants may pose a threat during surgery. A large part is found in the sinonasal region, basically due to the widespread use of endoscopy which, inherently, provides the operator with narrow accesses and limited exposure of submucosal anatomic structures. Onodi cell is probably the most feared anatomic threat, because if not correctly indicated by the radiologist and identified by the surgeon, it generates a high risk of disastrous intracranial penetration. Similarly, bone dehiscence of the lamina papyracea of the ethmoid increases the risk of iatrogenic damage, mainly of intrinsic ocular muscles. The inferior alveolar nerve is at high risk of surgical damage during molar teeth extraction, particularly when the curved apices of roots embrace the inferior wall of the nerve canal. In the neck the main threats are related to anomalous course of major vessels: not infrequently the common and/or internal carotid artery display a medialized course reaching the lateral aspect of the pharyngeal wall or even protruding in the retropharyngeal space towards the midline. Simultaneous medial deviation of the arteries on both sides is referred to as kissing (common or internal) carotids. The risk in these eveniences are mainly related to the possible effects of a deep biopsy performed by an unaware surgeon. At the cervico mediastinal junction, vascular rings may embrace the trachea or the oesophagus and, consequently, pose a threat during intubation or tracheostomy.

Learning Objectives:

1. To learn about structures at risk during functional endoscopic sinus surgery (FESS).
2. To become familiar with vascular variants in the head and neck.
3. To appreciate surgical anatomical landmarks in the head and neck.

A-315 17:00

C. Distinct head and neck disease or systemic disease?

M.G. Mack; Munich/DE (m.mack@radiologie-muenchen.de)

Head and neck manifestations of systemic disease is characterized by a multitude of maladies that have manifestations in the head and neck. This lecture relates commonly encountered head and neck symptoms and signs to an array of diseases and disorders that should be considered in the differential diagnosis. During this lecture, systemic disorders with head and neck manifestation (e.g., Sjögren's syndrome, Adamantiades-Bechet's disease, granulomatous disease like Wegener's granulomatosis), infectious disease (e.g., tuberculosis fungal rhinosinusitis and HIV related disease), malignant disease (e.g., lymphoma, myeloproliferative disorders and leukemia, malignant melanoma, histiocytosis, sickle cell anaemia, and rhabdomyosarcoma) or other

systemic disorders (e.g., Paget's disease of bone and fibrous dysplasia) will be presented.

Learning Objectives:

1. To recognise head and neck manifestations of systemic disease.
2. To categorise lesions into different pathologic entities.

16:00 - 17:30

Studio 2018

Genitourinary

RC 807

Imaging of the prostate

Moderator:

P. Puech; Lille/FR

A-316 16:00

A. MRI diagnosis of prostate cancer

A.R. Padhani; London/UK (anwar.padhani@talk21.com)

The PI-RADS v2 analysis system for mpMRI detection of prostate cancer was developed by expert opinion, using the observed performance and utilization of the PI-RADS v1 system. Test performance of PI-RADS v2 in research and clinical practice has been shown to an improvement over v1, maintaining high accuracy compared to systematic TRUS biopsies for prostate cancer diagnosis. PI-RADS v2 fails to detect all cancers, but does detect the majority of tumors capable of causing patient harms; test performance is dependent on the definition used to identify clinically significant disease. Good performance can be attained in practice provided that the quality of the diagnostic process can be assured (including MRI scanner, PI-RADS compliant imaging protocol, biopsy procedures, image interpretation, reporting, and communication), backed up by the robust training of radiologists and urologists working jointly within multidisciplinary teams. This talk summarises the accuracy, strengths, and weakness PI-RADS v2, discusses potential pathway implications and outlines opportunities for improvements and future developments.

Learning Objectives:

1. To become familiar with the different components of mpMRI of the prostate (T2, DWI and DCE).
2. To discuss the role of PI-RADS version 2 in the diagnosis of clinically significant prostate cancer.
3. To understand the correct indications and guidelines on the use of mpMRI.

Author Disclosure:

A.R. Padhani: Speaker; Siemens Healthineers, Janssen, Sanofi.

A-317 16:30

B. MRI staging of prostate cancer

G.M. Villeirs; Ghent/BE

Staging involves the correct assessment of the local tumour situation (T), involvement of lymph nodes (N) and of distant metastases (M). According to the European Association of Urology (EAU) Guidelines, assessment of lymph nodes is only useful in patients with a PSA >10, Gleason score >7, >cT2b. Imaging can be performed using the well known size criteria (round node >8mm, short axis of oval node >10mm) on CT or MRI, but this approach clearly lacks both sensitivity and specificity. Diffusion-weighted MRI incorporating morphologic features, MR-lymphangiography using ultra-small particles of iron oxide (USPIO), and nuclear medicine techniques such as choline- and PSMA-PET/CT offer higher sensitivity and specificity, but cannot (yet) replace the current gold standard (pelvic lymphadenectomy). The search for distant metastases (T) primarily involves skeletal assessment in patients at increased risk (PSA >20, Gleason >8, cT3-cT4). The current gold standard is the bone scan, but whole body MRI and new PET tracers seem to be on track to replace the bone scan as gold standard. In the absence of N+ or M+ disease, MRI can be used to assess the local status (T). High-resolution T2-weighted images are used to assess potential extracapsular extension or seminal vesicle invasion. Although this is a recommended approach according to the EAU guidelines, the accuracy of such T-staging is currently still quite variable. However, standardization of scanning techniques for staging and standardization of diagnostic criteria may solve this problem.

Learning Objectives:

1. To understand the current role of prostate MRI.
2. To learn how to optimise imaging and reporting.
3. To illustrate the staging approach.

Postgraduate Educational Programme

A-318 17:00

C. Imaging of PSA recurrence

H.-P. Schlemmer; Heidelberg/DE (h.schlemmer@dkfz.de)

Ca. 40% of prostate carcinoma patients develop biochemical recurrence after radical prostatectomy and radiotherapy, which are nevertheless in accordance to current guidelines first-line treatment options for patients with organ-confined prostate cancer. In the situation of PSA recurrence, early detection and precise localization of cancer is essential for individualized treatment decision making and for prognosis assessment. Early detection of local recurrence after radical prostatectomy is particular challenging as salvage radiotherapy is feasible with curative intention only in case of very low PSA serum levels. Conventional TRUS has limited sensitivity and specificity for detection of local recurrence. Multiparametric MRI (mpMRI) has been shown to be superior for detection of local recurrence, although early detection of small cancer foci is also significantly limited. Concerning early detection of lymphatic cancer spreading CT and MRI are significantly limited. Highest sensitivity for cancer detection is achieved by PET, although it is important to note that the accuracy significantly depends on the used radiotracer. In clinical routine most frequently C-11 or F-18 choline and Ga-68 or F-18 PSMA PET/CT is performed. PET/MR imaging provides additional advantages by combining the highest sensitivity of PET with superior anatomical referencing as well as soft tissue and bone marrow assessment by MR. This lecture will provide an overview about the currently available imaging methods for detection of recurrence in case of PSA relapse. Their clinical relevance will be discussed against the background of the potential therapy options.

Learning Objectives:

1. To understand the clinical need and indications for imaging in patients with PSA recurrence.
2. To discuss the optimal imaging modalities for detection of local recurrence.
3. To illustrate the potential of whole-body MRI and new radiotracers for detection of distant recurrence.

16:00 - 17:30

Room L 8

EIBIR Session

EIBIR Research Session: European imaging researchers united in diversity

A-319 16:00

Chairperson's introduction

G.P. Krestin; Rotterdam/NL

The European Institute for Biomedical Imaging Research (EIBIR) is an organization aiming to coordinate research in, and innovation of, biomedical imaging technologies within Europe and support the dissemination of knowledge with the ultimate goal of improving prevention, detection, diagnosis, and treatment of disease. EIBIR promotes networking activities within Europe and ensures the pooling of resources among members to promote a culture of cooperation between them. EIBIR also generates publicity concerning new opportunities for access, provide dissemination of knowledge, and training courses for potential users. In the competitive landscape of European funding, EIBIR has enabled numerous consortia to successfully apply and perform large collaborative research projects. Recently within the Horizon 2020 framework EIBIR is supporting a number of innovative ventures related to cancer research. The expertise that the office has built up over the past years did not only provide a competitive edge in obtaining funding, but will also guarantee the dissemination of the promising results of these projects. This session should provide information on how the EIBIR services can help the researchers in their endeavors and give an overview of three successfully running projects aiming to have an impact in cancer diagnostics and therapy.

Session Objectives:

1. To learn about major EU-funded research projects related to cancer imaging in which EIBIR is a partner.
2. To appreciate the impact these projects will have on cancer diagnosis and care.
3. To understand the role of the European Institute for Biomedical Imaging Research (EIBIR) in such projects.

A-320 16:10

Laser and Ultrasound Co-analyser for Thyroid Nodules (LUCA) Project: latest results

U. Weigel; Barcelona/ES (udo.weigel@hemophotonics.com)

Near-infrared diffuse optics is receiving increasing interest in cancer diagnostics for its capability to measure unique and complementary parameters based on hemodynamics (microvascular blood flow, blood oxygen

saturation and blood volume), tissue structure (cell density, size) as well as water and other chromophore concentrations in combination with established imaging technologies in a non-invasive, relatively fast and safe procedure. After description of the background physics, the basics of the technology, and different approaches for probe development, a particular focus will be given to hybrid technologies that combine diffuse correlation spectroscopy (DCS) and diffuse optical time resolved spectroscopy (TRS) for biomedical applications. Finally, I will introduce and report the present status of LUCA (<http://www.luca-project.eu>), a European project, aiming at development and validation of a combined ultrasound-optical prototype for thyroid cancer diagnostics.

Learning Objectives:

1. To learn about the application of diffuse optics to human tissue.
2. To understand the technology of LUCA.
3. To learn about the project's status and its initial results.

Author Disclosure:

U. Weigel: CEO; HemoPhotonics S.L.. Founder; HemoPhotonics S.L.. Shareholder; HemoPhotonics S.L..

A-321 16:30

Testing hybrid MR/PET (HYPMED) device for enhanced breast diagnosis in a multicentre clinical trial

T.H. Helbich; Vienna/AT (Thomas.Helbich@meduniwien.ac.at)

With a consortium of ten partners from across Europe, including major universities, research institutes, SMEs and major industry corporations, the HYPMED project brings together a wide range of expertise. In this project "Digital Hybrid Breast PET/MRI for Enhanced Diagnosis of Breast Cancer (HYPMED)", we aim to develop a hybrid system combining MRI and PET that facilitates earlier diagnosis of breast cancer and personalized therapy control. To achieve this, we are designing and testing a combined PET-radiofrequency (RF) insert that can be connected to a conventional clinical MR scanner, transforming the device into a high-resolution PET/MRI hybrid system. This PET-RF insert can be used to identify even the smallest breast cancer foci and better characterize the cancer, as well as its response to therapy. Another key benefit of this technology for patients is that the radiation dose of the new technology will, unlike other PET-MRI examinations, be comparable to the low dose of a regular digital mammogram. Apart from merely diagnosing the presence or absence of breast cancer, HYPMED will improve the non-invasive biological classification of breast cancers, in other words it will improve the assessment of its aggressiveness, therefore facilitate better selection of appropriate treatments. In a bench to bedside approach HYPMED includes several work packages spanning the spectrum from designing to clinical testing.

Learning Objectives:

1. To learn about a multicentre clinical trial of the project's hybrid MR/PET insert.
2. To understand how the trial will validate the project's ground-breaking MR/PET technology.
3. To appreciate the complexity of undertaking such a multicentre clinical trial at European level.

Author Disclosure:

T.H. Helbich: Board Member; EUSOBI, ESHMIMT. Grant Recipient; EU grant. Research/Grant Support; Siemens, Hologic.

A-322 16:50

Smart Optical and Ultrasound Diagnostics of Breast Cancer (SOLUS) Project: aims and objectives

P. Taroni; Milan/IT (paola.taroni@polimi.it)

Due to the high false-positive risk of mammography, there is an unmet clinical need for higher specificity in breast cancer imaging following screening. Photonics and ultrasound-based imaging are both non-invasive and have, to some extent, been proven effective in characterising breast lesions, discriminating malignant from benign ones. However, up to now, no individual technique proved to be adequate in replacing conventional methods. The EU-funded research project SOLUS will develop innovative photonic components, combining photonics with ultrasound techniques, and clinically validate the resulting multi-modal approach in breast cancer patients. To meet the clinical need, SOLUS develops novel pulsed laser sources and high dynamic range single-photon detectors, providing unprecedented sensitivity and depth penetration, making diffuse optical tomography feasible in real clinical settings. For the first time, this approach will allow; (1) a comprehensive quantitative characterisation of breast tissue, including composition (water, lipid, collagen content) and functional blood parameters as provided by diffuse optical tomography; (2) morphological information from B-mode ultrasound imaging; and (3) mechanical parameters (stiffness) from shear wave elastography. Subsequent multi-parametric data analysis, using new reconstruction algorithms, allows high specificity in the discrimination between borderline malignant and benign breast lesions. SOLUS is a trans-disciplinary, 48-month

Postgraduate Educational Programme

project that brings together 9 partners (industry, academia and hospitals) from 5 countries.

Learning Objectives:

1. To understand how the system developed by the project will combine optical methods with ultrasound.
2. To appreciate how the technology developed by the project will improve the ability to differentiate between benign and malignant lesions.

A-323 17:10

EIBIR's role in imaging research projects

P. Zolda; Vienna/AT (pamela.zolda@myesr.org)

Due to shrinking national research budgets, European researchers more frequently apply for EU funding sources. However, navigating through the rules and regulations of large EU projects while simultaneously carrying out innovative research with partners from across Europe can be challenging. Thus, multidisciplinary and multinational consortia require professional project management to ensure the successful accomplishment of their project goals. The European Institute for Biomedical Imaging Research, EIBIR, is a non-profit organisation founded by the European Society of Radiology and supports researchers and industry partners in the coordination of biomedical imaging research throughout Europe and beyond. EIBIR offers expert advice, professional project management and coordination, dissemination and exploitation services for dedicated international collaborative research projects. The EIBIR services also include advice on funding opportunities, identifying consortium partners and proposal writing support by a team of experienced writers with knowledge of the European Commission's requirements. Partners also benefit from EIBIR's established, extensive network for dissemination. Through the large and diverse landscape of network members, shareholder organisations, industry partners and media contacts the conducted research is be widely and rapidly communicated. EIBIR is currently partner and/or coordinator of seven projects that are funded under Horizon 2020, the biggest EU Research and innovation programme. The offered support relieves researchers of the administrative burden, allowing them to focus on the scientific aspects and thereby ensuring the best possible outcome for the project.

Learning Objectives:

1. To learn about EIBIR and its services for researchers.
2. To understand project management and dissemination activities of European projects.
3. To appreciate how EIBIR can support your research project.

16:00 - 17:30

Room E1

Special Focus Session

SF 8b

My three top tips for breast imaging

A-324 16:00

Chairperson's introduction

M.H. Fuchsjaeger; Graz/AT (michael.fuchsjaeger@medunigraz.at)

This session will provide practical information on the fundamental tips and tricks of the most renowned European breast radiologists for everyday clinical practice with a focus on a tertiary setting. All relevant topics from screening with tomosynthesis and automated ultrasound to image-guided interventional techniques as well as post-therapy evaluation will be addressed. Attendees will be able to learn and experience the most important aspects for successfully performing and avoiding common pitfalls at diagnostic and interventional breast examinations.

Session Objectives:

1. To appreciate fundamental tips and tricks of the most renowned European breast radiologists for clinical practice.
2. To acknowledge the single most important aspects for successfully performing breast examinations.
3. To learn how to avoid common pitfalls in breast radiology.

A-325 16:05

Screening with tomosynthesis

S. Zackrisson; Malmö/SE (sophia.zackrisson@med.lu.se)

It is well known that digital mammography (DM) has limitations in detecting breast cancers, especially in women with dense breasts. Studies show that up to 30% of the cancers in screening may not be detectable with DM, mainly due to the overlapping tissue effect, i.e., dense breast tissue or the so-called anatomical noise obscuring the tumor on the two-dimensional images. Digital

breast tomosynthesis (DBT) is an emerging pseudo 3D technique in breast imaging based on the acquisition of low-dose projections over a limited arc, reconstructed into a volume of generally up to 50 images of the breast. This reduces the overlapping tissue effect and hence tumors may be more easily detected with DBT. The published population based European screening trials with DBT (alone or in combination with DM or synthetic DM) show incremental breast cancer detection attributed to DBT in the range of 2.2 to 2.7 cancers per 1000 screens. In other settings, mainly in the US, retrospective studies with the combination of DBT and DM has been conducted with large reductions in recall rates as the main effect. In this presentation, the use of DBT in screening will be presented and discussed in terms of screening performance measures and what needs to be further investigated before DBT can fully implemented in routine screening.

Learning Objectives:

1. To understand why tomosynthesis is better than mammography for breast cancer screening.
2. To appreciate the current scientific evidence of tomosynthesis in screening.
3. To acknowledge what further steps are needed before implementation in screening.

Author Disclosure:

S. Zackrisson: Speaker; Speaker's fees and travel support from Siemens Healthineers.

A-326 16:11

Automated breast ultrasound

R.M. Mann; Nijmegen/NL (r.mann@rad.umcn.nl)

ABUS is a relatively novel automated ultrasound technique that enables volume scanning of large portions of the breast. In fact the entire breast can usually be imaged in 3 to 5 volumes. The standardised approach for image acquisition enables remote interpretation and therefore, the reporting radiologist is no longer required to obtain the images him/herself. As such specific artefacts such as non-black cysts and wandering shadows (due to a suboptimal angle of the transducer to the coopers ligaments) need to be understood as these cannot be prevented. A further advantage of ABUS is the possibility to perform multilane reconstructions of the image volume. Particularly the coronal reconstruction is useful. Not only because it reduces the amount of images to be evaluated substantially, but also because in the coronal plane often a retraction pattern becomes evident around malignant lesions. Therefore, it improves diagnostic accuracy. ABUS has been developed as a screening tool and seems to have most benefit as a supplemental screening tool in women with dense breasts on mammography. It also improves ultrasound staging of breast cancers as the extent of especially multifocal and diffuse lesions are easier grasped than with single ultrasound shots. A further possibility is the evaluation of lesions treated with me-adjuvant chemotherapy, however, data for this indication are limited.

Learning Objectives:

1. To recognise artefacts that are specific to ABUS.
2. To appreciate the value of multiplanar reconstruction and the coronal spiculation pattern.
3. To gain insight into possible indications for ABUS.

Author Disclosure:

R.M. Mann: Advisory Board; Screenpoint Medical, Transonic imaging. Grant Recipient; Siemens Healthineers, Bayer Healthcare, Medtronic, Elwood, Identification Solutions inc., Seno Medical, Micirima.

A-327 16:17

Complex cystic and solid lesions

P. Kapetas; Vienna/AT (panagiotis.kapetas@meduniwien.ac.at)

Cysts are the most usual breast pathology and up to one third of all women between 30 and 50 years of age are diagnosed with them. According to the BI-RADS® lexicon, cystic breast lesions are classified into simple cysts, complicated cysts and complex cystic and solid lesions. Simple cysts are anechoic fluid collections with an imperceptible wall and constitute the biggest part of cystic breast lesions. Complicated cysts also have an imperceptible wall, but present either with homogeneous hypoechoic content due to the presence of debris or with fluid-fluid levels. Complex cystic and solid lesions represent either a cystic lesion with a thick (>0.5mm) wall or thick septations or a lesion with a combination of cystic and solid components. Several complementary sonographic techniques can aid in the correct identification of the cyst type. These include compound and harmonic imaging, elastography, Doppler, and contrast enhanced ultrasound. A complex cystic and solid lesion represents a BI-RADS® 4 or 5 finding and merits histopathological work-up with a percutaneous, ultrasound-guided biopsy. In cases of cystic lesions with thick walls or thick septations or of predominantly cystic lesions with a small solid component a 9-10G vacuum assisted biopsy system should be used, to ensure proper sampling and reduce the risk of a false negative result. A post-

biopsy marker needs to be introduced after the intervention if the residual mass is difficult to identify.

Learning Objectives:

1. To understand the difference between complex cystic and solid lesions from other cystic lesions of the breast.
2. To become familiar with complementary sonographic techniques for the accurate characterisation of cystic breast lesions.
3. To be able to properly manage complex cystic and solid lesions of the breast.

16:23

Questions and discussion

A-328 16:29

Imaging the axilla

F. Kilburn-Toppin; Cambridge/UK (fleur.kilburn-toppin@addenbrookes.nhs.uk)

Evaluation of regional lymph node status is important for staging, treatment planning, and prognosis in breast cancer patients. Pre-operative axillary ultrasound and ultrasound-guided biopsy are routinely used to detect nodal metastases, allowing patients to proceed directly to axillary lymph node dissection thereby avoiding sentinel lymph node biopsy. However, following recent clinical trials and with improvement in systemic and radiation therapies, the role of staging sonography has been questioned. In this lecture, the current role of axillary staging will be reviewed and the future for nodal staging in the advent of evolving surgical management of the axilla and a trend towards less aggressive surgery will be considered.

Learning Objectives:

1. To understand the clinical role of axillary staging.
2. To learn imaging features of abnormal lymph nodes and criteria for biopsy.
3. To understand the importance of discriminating minimal vs advanced nodal disease.

A-329 16:35

Contrast-enhanced spectral mammography

E.M. Fallenberg; Berlin/DE (eva.fallenberg@charite.de)

In this talk the technical principles and possible artefacts will be addressed. In a couple of example cases the image appearance depending on lesion size and 2D images will be explained. The value of CEMM in comparison to mammography MRI and ultrasound will be demonstrated.

Learning Objectives:

1. To understand the technical principles of contrast-enhanced spectral mammography.
2. To understand the added value of information provided by contrast-enhanced spectral mammography.
3. To become familiar with the information provided by contrast-enhanced spectral mammography and breast MRI regarding lesion morphology and enhancement.

Author Disclosure:

E.M. Fallenberg: Board Member; EUSOBI. Research/Grant Support; GE Healthcare, Guerbet, Siemens Healthcare. Speaker; GE Healthcare, Guerbet, Bayer Healthcare.

A-330 16:41

Stereotactic-guided biopsy

E.J. Cornford; Cheltenham/UK (eleonor.cornford@nhs.net)

Stereotactic guided breast biopsy has become increasingly sophisticated over the past 15 years due mainly to improvements in equipment. It was initially used to biopsy mammographic abnormalities not visible on ultrasound, but indications have expanded to include diagnostic excision of histopathologically indeterminate lesions. Although the underlying principle is the same, the technique varies in terms of needle biopsy device, equipment type, and patient positioning. More recently the introduction of tomosynthesis guided biopsy has facilitated even faster biopsy times. Post procedure placement of marker clips is important to confirm accurate biopsy and to facilitate subsequent removal of the mammographic abnormality should prove this necessary.

Learning Objectives:

1. To understand the indications for stereotactic-guided breast biopsy.
2. To learn about the technical aspects of stereotactic biopsy.
3. To understand the importance of marker clip placement post-biopsy.

16:47

Questions and discussion

A-331 16:53

US-guided biopsy

A. Athanasiou; Athens/GR (aathanasiou@mitera.gr)

Ultrasound-guided percutaneous biopsies are nowadays widely used in clinical practice. They include FNA (Fine Needle Aspiration, with 19-21 gauge needles), core-biopsy (14-gauge or rarely 16-gauge automated or semi-automated systems) and vacuum-assisted biopsy (11-gauge to 8-gauge systems). They are minimally invasive, well tolerated, rapid and cost-effective. They can provide histological diagnosis in a safe and accurate way, comparable to open surgical biopsies. According to the international guidelines, pre-operative diagnosis should preferably be ensured by imaging-guided procedures; open surgical biopsies should be exceptional and performed only when percutaneous procedures are not feasible. BI-RADS 4 and 5 lesions as well as abnormal lymph nodes represent the main indications for performing US-guide biopsies. Simple or complicated cysts are subject to FNA when symptomatic or when it is not clear if the lesion is indeed a complicated cyst and not a solid nodule. Contraindications include allergies, anti-coagulant medications or inability to correctly visualize the target lesion. Post-biopsy markers are helpful and should be used, notably in case of small, difficult to visualize lesions or in case of complex-cystic lesions. Technique should be rigorous and optimized to ensure result accuracy. Radiologic-pathologic correlation is mandatory and all discordant cases should be discussed in MDT.

Learning Objectives:

1. To understand current indications, contraindications and possible complications of US-guided biopsy.
2. To be familiar with different available biopsy systems and know which one to choose according to the clinical setting.
3. To learn the most important technical tips for performing a US-guided biopsy successfully.

A-332 16:59

MRI-guided biopsy

G. Eşen; Istanbul/TR (gulesenicten@gmail.com)

MRI frequently detects suspicious lesions that cannot be demonstrated on other imaging modalities and need to undergo MRI-guided biopsy. Before an MRI-guided biopsy is scheduled, we have to make sure that the lesion is real and not a benign hormonal change; and then to check again with a second-look US. If it is not detectable on US, the patient can be scheduled, preferably during the second week of the menstrual cycle. On the day of the biopsy, patient has to be informed that it is possible to cancel biopsy, because the lesion is no longer detected on MRI. During biopsy, patient has to be informed that she will be coming in and out of the magnet, and she should not move. The sequences that are needed for a biopsy session should be prepared in advance, and employed in a standard fashion. MRI-guided biopsy is a team work and if everybody involved know what to do, it can be performed efficiently and rapidly, before the contrast washes out. CAD or a biopsy software would be very helpful in MRI-guided biopsies. Vacuum-assisted biopsy is the procedure of choice, because it is fast and accurate. It is possible to achieve more tissue from the suspicious region, if the lesion-needle relation is determined from the image and more samples are collected from that location. A marker should be placed at the biopsy site in each case and radiological-pathological correlation should always be performed.

Learning Objectives:

1. To understand the importance of pre-biopsy preparation including patient information.
2. To be familiar how to relate lesion and needle positions.
3. To appreciate tricks for targeting lesions in complicated locations (superficial, deep, retroareolar).

A-333 17:05

Treatment response and therapy monitoring

C. Van Ongeval; Leuven/BE (chantal.vanongeval@uz.kuleuven.ac.be)

Neoadjuvant therapy is increasingly been used in the treatment of breast cancer. For the monitoring of treatment (chemotherapy or hormonal therapy) response, an adequate staging of the breast cancer is needed: marking invasion or skin thickening, size of the index tumour, description of multifocal or multicentric disease, presence of bilateral breast cancer, and evaluation of nodal status (level 1, 2, 3). Besides mammography, ultrasound and biopsy procedures, magnetic resonance imaging (MRI) can be added to come to the correct staging. During the neoadjuvant treatment, a radiological investigation (ultrasound) is performed after 3 to 4 cycles of therapy or earlier in case of a tumour growth is suspected (non-responder). In the latter case, MRI will be added to the radiological investigation. After the last cycle of treatment, a new staging of the tumour is necessary to decide the optimal surgical treatment, i.e., mastectomy, breast conserving therapy and/or lymphadenectomy or

sentinel node resection. The imaging characteristics of tumour response or tumour growth during therapy will be discussed.

Learning Objectives:

1. To learn what is important in the reporting of the treatment response.
2. To understand the accuracy of mammography, ultrasound and magnetic resonance in the monitoring of therapy.

A-334 17:11

Post-therapy evaluation

J. Camps Herrero; Valencia/ES (juliacamps@gmail.com)

To understand the changes that occur in the breast after treatment, one must know the different phases of fat necrosis and their translation in mammographic, ultrasound or MRI images. In reporting the findings, it is important to focus on the ones that have the greatest clinical value for the requesting physician. It will also be very important to know how to diagnose recurrence and, most of all, how to proceed when mammography or ultrasound are equivocal.

Learning Objectives:

1. To understand and learn the different phases of fat necrosis and its imaging correlates in all modalities.
2. To know what to report in patients with breast implants and oncological reconstructions.
3. To learn the different appearances of breast cancer recurrence.

Author Disclosure:

J. Camps Herrero: Consultant; Bayer, Bard. Speaker; Bayer.

17:17

Questions and discussion

16:00 - 17:30

Room E2

Neuro

RC 811

State-of-the-art paediatric neuroradiology

A-335 16:00

Chairperson's introduction

C. Amarnath; Chennai/IN (amarrd02@yahoo.co.in)

This session highlights concepts of myelination and its maturation, role of imaging in diagnosing leukodystrophies. The topics focusses on wide spectrum of developmental disorders entity and importance of our role in diagnosis and add points on some relevant genetic or predisposing factors in pediatric CNS tumours. This session review the structural MRI findings in myelination disorders, paediatric CNS tumours, with an emphasis on posterior fossa tumours. The session emphasizes the contribution of advanced MRI techniques in pediatric neuroradiology. This lecture list the spectrum of applications and indications for imaging in paediatric neuroradiology. Spectators will be able to understand the relevance to apply the appropriate image acquisition protocols of disease in the field and appreciate the clinical relevance of imaging for the diagnostic process of neurological disorders in infants and children.

Session Objectives:

1. To learn the spectrum of applications and indications for imaging in paediatric neuroradiology.
2. To understand the relevance to apply the appropriate image acquisition protocols of disease in the field.
3. To appreciate the clinical relevance of imaging for the diagnostic process of neurological disorders in infants and children.

A-336 16:05

A. Imaging myelin maturation disorders

N. Wolf; Amsterdam/NL (n.wolf@vumc.nl)

Hypomyelinating leukodystrophies are frequent and have to fulfill both criteria of significant and permanent myelin deficit. Hypomyelination can be diagnosed by MRI. Care should be taken that, in children younger than 12 months of age, two MRIs at least 6 months apart are needed to make the diagnosis, in order to differentiate hypomyelination from the more frequent finding of delayed myelination. Severe atrophy in young children usually indicates a primary grey matter disorder with secondary myelin deficit and comes with its own differential diagnosis. MRI findings in hypomyelination consist of diffuse white matter signal hyperintensity on T2-weighted images and, depending on the amount of myelin deposited, hypo-, iso- or hyperintensity on T1-weighted

images. Additional features may be cerebellar atrophy, signal and volume changes of deep grey matter structures and signal changes of the pyramidal tracts. These findings, when present, help differentiating the diverse hypomyelinating conditions. Some entities (e.g., 4H syndrome, H-ABC, HBSL, HCC, Salla disease, Pelizaeus-Merzbacher like disease...) can be easily diagnosed by MRI pattern recognition. This allows direct confirmation of the diagnosis by sequencing of the appropriate gene(s). Other hypomyelinating disorders do not come with extra features, necessitating a different genetic approach.

Learning Objectives:

1. To learn about normal and pathological patterns of myelination.
2. To understand the role of imaging with respect to narrowing the differential diagnosis and supporting the clinical diagnosis.
3. To appreciate the importance of pattern recognition for the diagnosis of myelination disorders in children.

A-337 16:28

B. Imaging of developmental disorders

B. Ertl-Wagner; Munich/DE (Birgit.Ertl-Wagner@med.uni-muenchen.de)

To understand congenital abnormalities of the brain, it is important to be familiar with the embryologic development. Neuronal proliferation, migration and cortical organization are important steps in the development of the cortex. Group I disorders of cortical development are disorders of neuronal and/or glial apoptosis or proliferation. Among these are congenital microcephalies (I.A), congenital megalencephalies (I.B), and diffuse or focal cortical dysgenesis or dysplasia (I.C). Microlissencephaly is characterised by a reduced gyration and microcephaly. Hemimegalencephaly is a hamartomatous overgrowth of one cerebral hemisphere or parts thereof. Group II disorders are disorders of neuronal migration. Among these are periventricular (subependymal) heterotopia (II.A), lissencephalies (II.B), focal subcortical heterotopia (II.C), or disorders of terminal migration, e.g. cobblestone lissencephalies (II.D). Heterotopia are defined as areas of grey matter in an ectopic location; they are isointense to cortex. Group III disorders are disorders of postmigrational development. Among these are polymicrogyria with schizencephaly (III.A), polymicrogyria without clefts or calcifications (III.B), focal cortical dysplasia (III.C), or postmigrational microcephaly. In schizencephaly, there is a cleft that extends from the ependymal to the cortical surface and that is lined by dysplastic grey matter. In polymicrogyria, there are too many too small gyri and sulci. Agenesis and dysgenesis of the corpus callosum are common disorders with a wide clinical spectrum. They may be associated with other congenital abnormalities. Important infratentorial congenital abnormalities include Chiari malformations, cystic abnormalities of the posterior fossa/the Dandy Walker spectrum, molar tooth malformations/Joubert syndrome and dysplastic cerebellar gangliocytoma/Lhermitte-Duclos syndrome.

Learning Objectives:

1. To learn about the spectrum of developmental disorders of the brain.
2. To understand the key imaging features that lead to the correct diagnosis.
3. To appreciate the importance of making a correct imaging diagnosis.

A-338 16:51

C. Imaging in paediatric neuro-oncology

E. Vázquez; Barcelona/ES (evazquez@vhebron.net)

Central nervous system tumours are the most common group of solid tumours in the paediatric age and the main cause of death from solid tumours in childhood. The clinical onset commonly includes signs and symptoms related to increased intracranial pressure, gait disorders, or cranial nerve deficits. Magnetic resonance (MR) imaging has an important role in characterizing these lesions, planning surgery, and follow-up. Advanced MR techniques, especially diffusion, help to predict the histological type and degree of malignancy, and facilitate the diagnosis of recurrence during follow-up. Identification of taurine within the tumour on spectroscopy is typical of medulloblastoma. Perfusion imaging, including dynamic susceptibility of contrast perfusion and arterial spin-labelling perfusion are particularly useful in differentiating recurrence versus radiation necrosis. Specifically referring to cerebellar tumours, they may be associated with diverse inherited cancer syndromes such as neurofibromatosis type 1 (pilocytic astrocytoma), Von Hippel Lindau syndrome (hemangioblastoma), Cowden syndrome (gangliocytoma), Li-Fraumeni syndrome (astrocytoma, medulloblastoma) and Gorlin and Turcot syndromes (medulloblastoma). In the differential diagnosis, conditions that can mimic neoplasms should be included, such as infections (e.g., rhombencephalitis), autoimmune processes (e.g., acute disseminated encephalomyelitis and multiple sclerosis), and radionecrosis. Proper recognition of these entities can help to prevent unnecessary surgery. Of note, certain previous histological classifications, such as that of medulloblastoma, are being replaced by new classifications based on genetic characteristics, which enable better prediction of tumour aggressiveness and help to guide

Postgraduate Educational Programme

therapy according to the specific tumour type. Current research focuses not only on prolonging survival, but also on improving long-term quality-of-life.

Learning Objectives:

1. To learn about the spectrum of neuro-oncological diseases in children.
2. To understand the role of imaging beyond the diagnostic process.
3. To appreciate the increasing clinical relevance of advanced imaging techniques in paediatric neuro-oncology.

17:14

Panel discussion: Ask the expert: what is relevant for my own daily clinical practice?

16:00 - 17:30

Room F1

E³ - Rising Stars Programme: Joint Sessions with ESOR

ESR/ESOR 2

Radiologic anatomy: abdomen

Moderator:

S. Gourtsoyianni; Athens/GR

A-339 16:00

Liver

G. Brancatelli; Palermo/IT (gbranca@yahoo.com)

The liver is the largest organ in the human body. The penetration and branching of the hepatic artery, portal vein, and hepatic veins allow dividing the organ into the eight traditional segments of the Couinaud scheme. Knowledge of vascular and segmental anatomy is important to correctly locate the site of disease and to perform increasingly demanding and challenging liver resection and transplantation. Anatomy of the liver can be altered by congenital variants, diseases causing hepatic dysmorphism and after surgery.

Learning Objectives:

1. To locate and identify, using cross sectional medical imaging, superficial and internal structures of common liver anatomy.
2. To learn and understand how the vasculature defines the eight Couinaud segments.
3. To explain how common pathological conditions affect the structure of the liver.

Author Disclosure:

G. Brancatelli: Speaker; Bayer.

A-340 16:30

Biliary tree

O. Benjaminov; Petach Tikva/IL

"no abstract submitted"

Learning Objectives:

1. To discuss current imaging techniques for evaluation of normal biliary anatomy.
2. To learn and understand possible anatomical variants that may occur.
3. To explain how common pathological conditions affect the bile ducts.

A-341 17:00

Pancreas

M. Dioguardi Burgio; Clichy/FR (marco_dioguardi@hotmail.it)

The pancreas is a retroperitoneal gland, which is anatomically divided in 4 portions: head, neck, body and tail. Main anatomical relationships of the head are duodenal loop, the porta hepatis and the superior mesenteric vessels. Body and tail anatomical relationships include left kidney and adrenal gland, posterior gastric wall and lesser sac, splenic hilum, celiac region, and duodenojejunal junction. Main pancreatic duct (Wirsung) drains into the major papilla most of the pancreatic secretions. A common biliopancreatic tract may be present. An accessory duct (Santorini) is usually present draining the anterior part of the pancreatic head in the minor papilla. Pancreatic gland is the results of the fusion of two buds. During the seventh gestational week the ventral bud rotate around the duodenum and it locates inferiorly and posteriorly to the dorsal bud. The fusion of the two buds leads to anastomosis of the ductal systems. Anomalies of this fusion process are at the base of the wide spectrum of anatomical variants which pancreatic parenchyma and ductal system may present. Most common anatomical variants include pancreas divisum, ansa pancreatica and annular pancreas. Knowledge of normal CT and MR appearance of the pancreas is crucial to recognize anatomical variants as well as to identify pancreatic anomalies. The use of both techniques is often

necessary for an exhaustive evaluation of the pancreatic gland and to reach a proper diagnosis.

Learning Objectives:

1. To review and illustrate the imaging features of normal pancreatic anatomy.
2. To review the possible congenital variants and anomalies of the pancreas and pancreatic duct.
3. To explain how common pathological conditions affect the pancreas.

16:00 - 17:30

Room F2

Oncologic Imaging

RC 816

Monitoring response: the essential guide for all radiologists

A-342 16:00

Chairperson's introduction

P. Brader; Graz/AT (peter@brader.md)

Imaging-based therapy monitoring is essential to visualise and quantify the effect of cancer therapy. Therefore, criteria-based reporting methods were established to ensure standardised and reproducible results for response evaluation of oncologic patients. Response Evaluation Criteria in Solid Tumors (RECIST) as the most widely accepted morphologic, size-based evaluation system is based on imaging assessment of change in tumor burden, to determine if the tumor has shrunk or grown. However they only evaluate the size of the lesion, not its viability, proliferative rate or physiologic state. In recent years a broad range of novel molecular cancer therapeutics were introduced into clinical use. These new therapy regimes demonstrated significant effects on tumor angiogenesis and tumor metabolism, but often only subtle effects on tumor morphology. Established methods of monitoring cytotoxic tumor therapies, such as RECIST have been shown to be not sufficiently sensitive for monitoring the therapeutic effects of molecular anti-cancer agents to allow for a timely differentiation of responders from non-responders because such treatments are less likely to result in tumor shrinkage. The complementary acquisition of morphological, functional and molecular information using advanced imaging methods such as diffusion weighted imaging or perfusion imaging as well as hybrid imaging techniques (PET/CT, PET/MRI) allows for a higher sensitivity and specificity in the timely differentiation of responders from non-responders. The tremendous development in oncology and technical innovations in imaging present a particular challenge for radiology.

Session Objectives:

1. To understand the correlation of functional imaging evaluation with the pathophysiological effect of treatment on oncological pathology.
2. To understand the necessity of functional imaging for an accurate (early) evaluation of the therapy regimen on the response (or non-response) of oncological disease.
3. To learn about the added value of functional imaging for evaluating treatment (e.g. anti-angiogenic treatment).
4. To learn about the technical principles of functional imaging in correlation with the impact of the therapy on tumour cells and neo-vasculature.

A-343 16:05

A. RECIST made easy

A.G. Rockall; London/UK (a.rockall@imperial.ac.uk)

A significant part of modern day cancer imaging involves the assessment of change in the extent of tumour in the context of a clinical trial or research study. The reporting requirements for these imaging studies are documented in the research protocol. A standardized response assessment is important to be able to collate data between different centres, as well as to evaluate published data from different studies. Response evaluation criteria in solid tumours (RECIST) were developed and published in 2000. RECIST criteria have been widely adopted for the evaluation of treatment response in the clinical trial setting. A revised version, RECIST 1.1 was subsequently published in 2009, to address several problems that had been encountered with RECIST 1.0. New studies frequently use RECIST 1.1 but in some cases, new studies will still use RECIST 1.0 to allow direct comparison with a previous similar study. In this lecture, the key features of RECIST will be presented with worked examples. Selection of appropriate target lesions will be illustrated. Frequently asked questions will be addressed and the criteria for response will be illustrated.

Learning Objectives:

1. To learn about the basic idea of RECIST.
2. To understand how to use RECIST in daily clinical practice.
3. To become familiar with the detailed rules of RECIST.

Thursday

A-344 16:28

B. PERCIST: PET response criteria

C.C. [Cyran](mailto:clemens.cyran@med.uni-muenchen.de); Munich/DE (clemens.cyran@med.uni-muenchen.de)

With the implementation of novel oncologic strategies and prolonged survival of cancer patients, early and longitudinal monitoring of therapy response to treatment in individual patients has become a key request to imaging. Known limitations of morphological size-based criteria (e.g., RECIST) for the monitoring of tumor response led to the investigation of additional functional and molecular imaging techniques to allow for a reliable and timely distinction of responders and non-responders, particularly under novel molecular cancer therapies. Particularly hybrid imaging techniques, such as PET/CT or PET/MRI, demonstrated significantly improved diagnostic accuracy for the evaluation of treatment response in different tumor entities under a variety of treatments with a reported change-in-intended management of up to 35% in oncologic indications compared to conventional imaging alone. To allow for a standardized evaluation of therapy response, criteria-based reporting of target and non-target lesions has been established to classify therapy response into different categories ranging from complete response to progressive disease and has found broad application particularly within clinical studies. Similar to the size-based RECIST (response criteria in solid tumors) criteria, PERCIST (PET response criteria in solid tumor) criteria were developed to provide a systematic, standardized approach for the criteria-based evaluation of metabolic tumor response to therapy using ¹⁸F-FDG PET. Studies evaluating PERCIST criteria suggest, that the inclusion of standardized metabolic criteria may allow for an increased sensitivity, specificity and diagnostic accuracy in the evaluation of therapy response compared to morphological imaging criteria alone.

Learning Objectives:

1. To learn about the basic principles of PERCIST.
2. To understand how to use PERCIST for structured quantitative research and clinical reporting.
3. To appreciate the advantages of PERCIST over mere morphological methods.

Author Disclosure:

C.C. Cyran: Research/Grant Support; Novartis AG, iThera. Speaker; Siemens Healthineers.

A-345 16:51

C. Assessment of response using functional MR and CT imaging: the essentials

L.S. [Fournier](mailto:laure.fournier@aphp.fr); Paris/FR (laure.fournier@aphp.fr)

Key issues in oncology include patient selection based on pre-treatment tumour characteristics, and assessment of tumour response in the absence of actual shrinkage. There is accumulating evidence that functional imaging using advanced techniques such as dynamic contrast enhanced imaging (MRI, CT or ultrasound), diffusion weighted-MRI, magnetic resonance spectroscopy, and positron emission tomography-CT using various labelled radioactive tracers has the potential to address these challenges. New approaches quantifying heterogeneity such as texture and radiomics are also emerging. Functional imaging allows quantifying physiological or molecular processes, yielding information not accessible to morphological imaging. In preclinical animal studies, they may give insight into biological mechanisms of efficacy and help select best candidate drugs. In human studies, early phase studies can use functional imaging to indicate early likelihood of response to a specific therapy, and guide the optimal biological dose and drug schedule. Though a very large number of studies have been performed using functional imaging, very few are used to make clinical decisions. Among the challenges facing functional imaging for the past years are standardisation of acquisition and image processing, as well as validation of clinical utility.

Learning Objectives:

1. To learn about the portfolio of functional imaging response methods in CT and MRI.
2. To understand the current clinical value of each technique.
3. To appreciate potential advantages compared to PERCIST.

Author Disclosure:

L.S. Fournier: Advisory Board; Keosys. Grant Recipient; Novartis, Invectys. Research/Grant Support; Philips, Arian Pharma, Evolucare. Speaker; Novartis, Pfizer, Merck, Sanofi.

17:14

Panel discussion: When and how will functional imaging overcome morphological assessment?

16:00 - 17:30

Room D

Musculoskeletal

RC 810

Musculoskeletal ultrasound in the management of sports injuries

Moderator:

M. Reijniers; Leiden/NL

A-346 16:00

A. Ultrasound of ankle injuries: technique and diagnosis

A. [Martinoli](mailto:carlo.martinoli@libero.it); Genoa/IT (carlo.martinoli@libero.it)

In sports medicine, the role of ultrasound (US) has become increasingly important in the assessment of ligaments, tendons, joints, and other soft-tissue injuries about the ankle. Being many structures to be examined, the US examination should be focused on clinical findings in an attempt to save time and increase the efficacy of the study. In the area around the lateral malleolus, that is the most frequently involved in inversion trauma, ligaments and tendons can be injured individually or in association. US can assess the status of the anterior talofibular and calcaneofibular ligaments with effective results by means of static and dynamic scans. Some tarsal ligaments, such as the dorsal calcaneocuboid, the superior talonavicular and the bifurcate, can be also evaluated. In high sprains, US can provide evaluation of the anterior inferior tibiotalar ligament, including the Bassett fascicle. US can give demonstration of peroneal tendon instability based on tendon displacement relative to the malleolar groove and is able to recognise retinacular/periosteal tears. Dynamic scanning can help to detect cases of intermittent subluxation that often go unnoticed at MR imaging. Some predisposing conditions of peroneal tendon instability (e.g. convex retromalleolar groove, peroneus quartus, low myotendinous junction of the peroneus brevis) may also be identified. Longitudinal splits of the peroneus brevis often occur in athletes. US can depict early changes with weakening and thinning of the central part of the tendon. In more advanced lesions, a complete cleft with formation of two distinct hemi-tendons, irregularities of the tendon substance and tenosynovitis is observed.

Learning Objectives:

1. To become familiar with ultrasound findings seen in ankle instability.
2. To learn about the ultrasound patterns of tendon abnormalities.

A-347 16:30

B. Ultrasound of the hip and knee: what is it good for and what are its limitations?

A. [Klauser](mailto:innsbruck@at); Innsbruck/AT

The hip and knee are anatomically and biomechanically complex joints, often causing diagnostic uncertainty for clinicians, therefore, most often MRI is requested. But does US have any value in knee and hip sport injuries? In cases of intraarticular pathology US can accurately detect effusion and synovitis, paralabral and meniscal cysts, however, further imaging assessment as by MRI (arthrography) is necessary. Extraarticular pathologies like tendinopathy, enthesopathy, tendon strains, different types of bursitis (trochanteric, iliopsoas, iliopsoas, prepatellar, infrapatellar, semimembranosus ...), muscle strains and ruptures, and collateral knee ligament injuries can be assessed and graded by US. US is also great in delineation of various neuropathies. The major advantage of US is the possibility of dynamic evaluation, for example, in the assessment of iliopsoas abnormalities, including snapping iliopsoas tendon and iliotibial band friction syndrome. In terms of sport injury management, ultrasound guided punctures and injections are highly appreciated by patients and clinicians as well and also the ability for therapeutic short terms follow-up is of great importance to better understand point of sport return in the athletes.

Learning Objectives:

1. To become familiar with examination technique and typical findings of ultrasound of the hip and knee.
2. To understand the limitations of ultrasound of the hip and knee.

A-348 17:00

C. Ultrasound-guided intervention in the athlete: indications and techniques

H. [Guerini](mailto:guerini@paris.fr); Paris/FR

Diagnostic and interventional ultrasound is a rapidly evolving field in sports medicine. The use of ultrasound has increased exponentially during the past decade. Ultrasound-guided procedure is performed for joint and tendon sheath

Postgraduate Educational Programme

injections with PRP or steroid drugs. We will discuss of the the indications, technical considerations about interventional ultrasound in sports medicine.

Learning Objectives:

1. To become familiar with the indications for ultrasound-guided interventions in the athlete.
2. To learn about the different injection techniques.

16:00 - 17:30

Room G

Special Focus Session

SF 8c

The ten-minute abdominal MRI: make the dream come true!

A-349 16:00

Chairperson's introduction

N. Papanikolaou; Lisbon/PT

(nickolas.papanikolaou@research.fchampalimaud.org)

Abdominal MRI images are sensitive to a variety of artifacts related to respiratory, cardiac and peristaltic motion, the presence of air in the gastrointestinal tract and chemical shift due to abdominal fat. One factor that enhances respiration-related artifacts is the level of patient collaboration and compliance either to breath-hold commands, or the capability of the patient to achieve a steady respiratory pattern during image acquisition. Technical advances related to a further reduction of scan times have been applied for abdominal imaging purposes, including parallel imaging algorithms, alternative ways to fill k-space, radial scanning and compressed sensing. Apart from improving the patient experience due to shorter examination times, these techniques may result in enhancing the problematic image quality of abdominal MRI exams by minimizing the level of artifacts. Additionally, new diagnostic information related to the amount of angiogenesis can be obtained by novel perfusion sequences that can simultaneously provide very high temporal resolution and adequate in-plane resolution and anatomical coverage maintaining acceptable image quality. Innovative RF coil designs, taking into consideration the patient body habits are also improving the acquired MR signal, that can be exploited by further increasing spatial resolution.

Session Objectives:

1. To become familiar with technical challenges of MRI examinations in the abdomen.
2. To review current MR examination protocols of the abdominal organs.
3. To discuss future developments.

Author Disclosure:

N. Papanikolaou: Advisory Board; Advantis Medical Imaging. Owner; MRIcons LTD.

A-350 16:05

Liver

T.C. Lauenstein; Essen/DE (thomas.lauenstein@evk-duesseldorf.de)

MRI has vast potential to non-invasively diagnose and characterize focal liver lesions as well as diffuse liver disease. Due to the large extent of different sequence types, various information about pathological changes can be obtained. Hence, it is sometimes difficult to shorten MRI protocols and to withdraw certain MRI sequences without losing relevant information. Furthermore, MRI of the upper abdomen can be challenging. Motion and breathing artifacts can considerably impede a reliable diagnostic workup. In addition, it can be difficult to acquire MR images during the correct contrast phases after i.v. gadolinium injection. Hence, it is crucial to choose and apply the right contrast delay. Strategies to overcome limitations and to handle the outlines challenges will be proposed in this lecture. A comprehensive and abbreviated examination protocol for liver MRI will be presented with a special focus on diffusion weighted imaging and liver specific contrast agents. Eventually, clinical cases and pitfalls will be discussed.

Learning Objectives:

1. To briefly review MRI challenges in the liver.
2. To review techniques and methods to optimise image quality.
3. To compare comprehensive and abbreviated protocol strategies.

A-351 16:28

Pancreas

N. Kartalis; Stockholm/SE (nikolaos.kartalis@me.com)

Magnetic resonance imaging/magnetic resonance cholangiopancreatography (MRI/MRCP) is increasingly used for the evaluation of patients with pancreatic

diseases, such as pancreatic cystic neoplasms (PCN), pancreatic cancer and pancreatitis as well as for screening purposes, such as in individuals at increased risk of developing pancreatic malignancy (i.e. family history of pancreatic cancer, genetic factors, etc.). Particularly for the surveillance of patients with PCNs, MRI is the suggested imaging modality according to various existing clinical practice guidelines due to its exquisite contrast resolution, high sensitivity for the detection of lesion communication with the pancreatic ductal system and lack of ionizing radiation. However, MRI/MRCP protocols are time-consuming, costly and, in the case of serial follow-up examinations, the repeated use of gadolinium-based contrast agents raises potentially safety concerns. In this presentation, we will discuss various strategies for the development of abbreviated protocols useful in everyday clinical practice.

Learning Objectives:

1. To briefly review MRI challenges in the pancreas.
2. To review techniques and methods to optimise image quality.
3. To compare comprehensive and abbreviated protocol strategies.

A-352 16:51

Ovaries

E. Sala; Cambridge/UK (evis.sala@gmail.com)

Magnetic resonance imaging (MRI) is recommended as a second line investigation for characterisation of complex adnexal masses indeterminate on US. MRI gives superb contrast resolution and involves non-ionizing radiation. Typical protocols include both T1 and T2 weighted sequences, with imaging acquisition performed in 3 planes. Coronal FSE T2WI is very helpful in evaluating complex adnexal lesions. Adnexal lesions can be characterised by their specific signal characteristics on T1WI and T2WI. Simple fluid has homogeneous low signal on T1WI and high signal intensity on T2WI. Fat and haemorrhage have high signal intensity on T1WI. Fat suppression (FS) on T1W sequences is utilised to differentiate these entities. If the adnexal lesion demonstrates low or intermediate signal intensity on T1WI and low signal intensity on T2WI, these characteristics suggest fibrotic and/or smooth muscle components. Such lesions include pedunculated leiomyoma, fibroma, fibrothecoma, cystadenofibroma and Brenner tumours. Multi-phase contrast enhanced (CE) MRI after administration of intravenous gadolinium is very useful for characterisation of adnexal masses. Solid components will demonstrate enhancement, enabling the distinction between debris or retracting clot in the cyst wall from papillary projections. Subtraction images are essential to evaluate enhancing nodules within a background of hyperintense T1W lesion. Gadolinium also improves detection of peritoneal and omental implants in case of ovarian carcinoma. Dynamic-CE (DCE)-MRI are not yet routinely performed in evaluation of adnexal masses. Diffusion-weighted imaging (DWI) is very useful for visualisation of peritoneal implants.

Learning Objectives:

1. To briefly review MRI challenges of the adnexa.
2. To review techniques and methods to optimise image quality.
3. To compare comprehensive and abbreviated protocol strategies.

17:14

Panel discussion: MRI technological advances: impact on radiologist routine

16:00 - 17:30

Room K

Radiographers

RC 814

Contrast media in imaging

Moderators:

M.-F. Bellin; Le Kremlin-Bicêtre/FR

L. Popovic; Belgrade/RS

A-353 16:00

A. Contrast-enhanced ultrasound: principles and applications

G. Johnson; Manchester/UK (gerry.johnson@tgh.nhs.uk)

The use of contrast enhanced media in medical imaging is well established allowing greater visualisation and characterisation of disease processes. Ultrasound imaging has been relatively late in creating a specific contrast agent, but many contrast agents or micro bubbles exist and are being used routinely in clinical practice to aid better diagnoses in a non invasive manner. Microbubbles are the scientific basis for all current developments in ultrasound contrast media. The principal characteristic is their backscatter effect, simply put when gas filled microbubbles are present in a region of interest, a higher proportion of the ultrasound beam is backscattered and

therefore a stronger return echo is received at the transducer. The clinical use of contrast media was first used in cardiac imaging in the 1968 by Gramiak and Shah (Invest Radiol 3:356-366), their early work found the microbubble technology to be "rough and ready", microbubbles were very large and size distribution was poorly defined. It was not until the mid 1980's that methods were developed to produce smaller more stable microbubbles by means of sonication, although the use of this media was limited as they were unable to survive passage through the lungs after i.v. injection. Since then there have been numerous developments in generating stable and reliable ultrasound contrast agents. This presentation will review their basic physical principles, try to elaborate on the technical requirements required to perform it, and learn about various clinical indications and applications of CEUS.

Learning Objectives:

1. To review the basic physical principles of contrast-enhanced ultrasound.
2. To understand the technical requirements to perform it.
3. To learn about the various clinical indications and applications of contrast-enhanced ultrasound.

A-354 16:30

B. Radiotracers in PET/RNI

P. [Laverman](mailto:Laverman@radboudumc.nl); Nijmegen/NL (Peter.Laverman@radboudumc.nl)

Different types of radiopharmaceuticals for both PET and SPECT imaging are used for various indications. In this session we will focus on recent developments in the field of radiopharmaceuticals. A brief overview of current radiotracers for PET and SPECT will be given and - in more general - the development and production of these tracers as well as their in vivo behaviour will be discussed. The biodistribution and uptake mechanism of a radiotracer will be exemplified by radiolabeled PSMA-ligands for imaging of prostate cancer. The use of these radio tracers have become very popular over the last few years and are now an important tool in PET and SPECT imaging. Differences in these prostate cancer imaging tracers will be explained and their various applications will be discussed.

Learning Objectives:

1. To learn about current radiotracers in use in PET/RNI.
2. To understand the mechanism of distribution and uptake of various radiotracers.
3. To appreciate the most appropriate clinical indications and applications of PET/RNI radiotracers.

A-355 17:00

C. How safe really are gadolinium agents?

A. [Cradock](mailto:cradock@ucd.ie); Dublin/IE (andrea.cradock@ucd.ie)

Gadolinium based contrast agents (GdBCA's) have been used in MRI to aid diagnosis since the 1980's. The gadolinium ion (Gd+3), a heavy metal ion, is toxic to within the body and is chelated to prevent deposition of the gadolinium ion in tissues. The stability of the chemical bonding between Gd+3 influences the tendency for release of free Gd+3 over time. Macrocyclic agents tend to have a higher stability than linear agents. Ionic agents tend to have a higher stability than non-ionic agents. However, in 2006 the first reports of the association between nephrogenic systemic fibrosis (NSF) and GdBCAs were described. NSF can progress to a debilitating disease and is potentially fatal. It is thought that patients with severe renal insufficiency are more at risk than patients with normal renal function. The advent of these reports introduced restrictions for the administration of GdBCAs to patients with impaired renal function in clinical departments. In recent times, there have been reports of accumulation of gadolinium within the brain tissues of patients with normal renal function.

Learning Objectives:

1. To be aware of the differences between macrocyclic and linear gadolinium-based contrast agents.
2. To review current advice regarding the use of gadolinium on patients with renal impairment.
3. To become familiar with our current understanding of gadolinium deposition in the body.

16:00 - 17:30

Room M 1

Vascular

RC 815

Post-treatment evaluation: what every radiologist should know

A-356 16:00

Chairperson's introduction

P. [Haage](mailto:haage@helios-kliniken.de); Wuppertal/DE (patrick.haage@helios-kliniken.de)

Appropriate post-treatment evaluation after any intervention is key for a good outcome and superior long term success rates. Accordingly it is necessary to supervise the outcomes, define follow-up strategies and to identify potential complications and possibly prepare for re-intervention. In this refresher course, pathways and most common complications after thoracic aortic interventions, abdominal aorta surgical, and endovascular repair and endovascular peripheral arterial disease treatment will be presented including imaging specifics, i.e., normal and pathological appearances and indications for re-intervention. Ample information on the selection of modality (ultrasonography, CT, MRI), the typical time interval between follow-up examinations plus specific suggestions including items to cover in a structured report will be given.

Session Objectives:

1. To briefly introduce the distinctive role of proper post-treatment evaluation after intervention.
2. To control the results and to know possible complications in order to be prepared for re-intervention.

A-357 16:05

A. Thoracic aorta

T. [Leiner](mailto:leiner@umcutrecht.nl); Utrecht/NL (t.leiner@umcutrecht.nl)

The aorta plays a central role in connecting the heart to various end organs. Pathological changes in the aorta have a retrograde effect on the heart, as well as affecting perfusion of end-organs. In my presentation I will discuss CT and MR imaging protocols optimised for imaging the post-operative aorta and the typical appearance of various post-operative conditions. Topics covered will include choice of modality, acquisition strategies as well as practical tips on how to report important findings. Theoretical considerations will be illustrated with case material from clinical practice.

Learning Objectives:

1. To learn about the most common complications after thoracic aortic interventions.
2. To understand imaging specifics after thoracic aortic interventions.
3. To know indications for re-intervention.

Author Disclosure:

T. **Leiner**: Research/Grant Support; Philips Healthcare; Bayer Healthcare. Speaker; Philips Healthcare; Bayer Healthcare.

A-358 16:28

B. Abdominal aorta

C. [Loewe](mailto:loewe@meduniwien.ac.at); Vienna/AT (christian.loewe@meduniwien.ac.at)

The endovascular treatment (EVAR) has become a well established treatment option for aortic diseases. In contrary to patients after surgical repair, patients after EVAR require lifetime follow up imaging since the chronic and progressive character of atherosclerosis can cause progression of aortic dilatation leading to movement of the prosthesis or insufficient aneurysm exclusion with time. Additionally, persistent perfusion of the aneurysm sac (endoleaks) can occur even years after stentgraft placement. Finally, the life expectancy of the materials used for endovascular treatment might be limited. CT angiography was established as the first method of choice for follow up after abdominal aortic repair. The advantages of CT angiography are manifold and include optimal comparability with the pre-treatment examination (usually done by means of CT angiography), high resolution, direct visualisation of the device itself and the possibility of multiphase acquisition to detect even slow flow endoleaks. As it is true for all treatment-follow up examinations knowledge about primary procedure and typical post-therapeutic findings as well as about most common complications is a prerequisite in patient care after abdominal aortic repair. Device migration, device fracture and/or persistent sac perfusion - in most of the cases related to each other - are the most common procedure related complications. In this presentation, different therapeutic means for abdominal aortic disease will be presented as well as the typical, normal findings after treatment. Furthermore, most common complications will be introduced and discussed based on clinical examples. Finally, possible follow up strategy depending on disease and procedure should be proposed.

Postgraduate Educational Programme

Learning Objectives:

1. To learn about the most common complications after abdominal aortic interventions.
2. To understand imaging specifics after thoracic aortic interventions.
3. To know indications for re-intervention.

Author Disclosure:

C. Loewe: Speaker; GE Healthcare, Bracco, Siemens.

A-359 16:51

C. Peripheral arterial disease

M. Anzidei; Rome/IT (michele.anzidei@gmail.com)

CT and MR angiography (CTA and MRA) substantially changed the diagnostic approach in planning and follow-up of treatment for peripheral arterial disease (PAD), enabling early identification of treatment failure or treatment-related complications after endovascular and surgical procedures. Doppler ultrasound is the first line imaging modality during follow-up after treatment, but CTA and MRA enable more detailed and panoramic imaging that is extremely valuable in the assessment of treatment outcome. The aim of this presentation is to review the imaging findings in the most common complications after endovascular treatment for PAD, to discuss the best imaging modality in the various clinical scenarios and to explain when and how to re-intervene on the basis of imaging findings.

Learning Objectives:

1. To learn about the most common complications after PAD endovascular repair.
2. To understand what imaging technique is preferred (any diagnostic).
3. To explain when to re-intervene and how to prepare for it.

17:14

Panel discussion: How to optimise post-treatment imaging: getting proper diagnosis without performing too many examinations

16:00 - 17:30

Room M 2

Computer Applications

RC 805

Daily use of mobile devices in radiology

A-360 16:00

Chairperson's introduction

O. Ratib; Geneva/CH

Mobile devices such as tablets and high-resolution smartphones are becoming widely available providing convenient mobile solutions for physicians and healthcare providers to access imaging data. This is particularly attractive in medicine where "nomad" physicians who need to be able access relevant patient data and images anywhere-anytime in their daily practice where they are rarely a single location. While they may not always be adequate for routine diagnostic tasks they provide a convenient mobile solution for on-call and remote consultations. There are different types of software architecture that can be implemented for such tasks. Two major different design are: (1) online web-based applications where the device serves as a "thin-client" to display images rendered and manipulated on a remote computer and (2) local applications that reside on the mobile device and can run independently after images have been downloaded on the device. The first solution requires the user to be constantly connected to the network, while the second solution can continue to function after disconnecting from the network. Most vendors are starting to provide web access to their imaging solutions that can be accessed from mobile devices. Web access can however be slow and dependent on reliable access to wireless network.

Session Objectives:

1. To give an overview of tools available on mobile devices for education and exam reporting.
2. To underline the impact of mobile devices in routine clinical activity.
3. To learn about the legislative backbone and potential drawbacks of mobile technology.

A-361 16:05

A. What did mobile devices change in radiology education?

E. Kotter; Freiburg/DE (elmar.kotter@uniklinik-freiburg.de)

E-learning has been used in radiology for more than 30 years. The lecture will give an introduction to and an overview of e-learning systems for radiology with emphasis on e-learning on mobile devices. Advantages and limitations of

mobile e-learning will be discussed. An outlook to future development of e-learning will be given.

Learning Objectives:

1. To give an overview of tools available for e-learning.
2. To explore the potential impact of e-learning in the daily radiological practice.
3. To explore future developments and limits of e-learning.

A-362 16:28

B. Is it appropriate to read a study on a smartphone or a tablet?

N.H. Strickland; London/UK (nicola.strickland@nhs.net)

The portability of tablets and smartphones make them suitable for accessing and displaying digital radiological imaging studies particularly in on call or remote settings, in wards or clinics and in the emergency setting. The purpose of this display can be for primary diagnosis or for review. The portable device must be fit for purpose. The small screen size and limited display resolution of smartphones limits their appropriateness for primary diagnosis. However studies have shown equivalent diagnostic accuracy of tablets compared with DICOM-calibrated PACS workstation displays. It is now technically possible to satisfy the requirements for viewing large multi-image studies on mobile devices: processor and network speeds are fast enough to receive images quickly from a PACS; screen resolutions and DICOM conformance can display images with appropriate fidelity; memory and graphics processor capacities can allow image viewing and manipulation similar to that on a PACS workstation; and hospital information technology departments can institute appropriate management to ensure functional stability of mobile devices and security of the patient data displayed on them. Simultaneous comparative viewing of multiple studies is inevitably suboptimal on portable devices due to their limited screen real estate. Radiologists should consider exploiting mobile devices to raise their profile as clinical doctors, for example, using them to interact in person with their clinical colleagues on ward rounds and in outpatient departments, and with patients to explain their imaging to them.

Learning Objectives:

1. To give an overview of available DICOM viewers and software for reporting imaging studies.
2. To discuss technical requirements of mobile devices for use in imaging interpretation.
3. To provide insight on future developments of imaging viewing technology.

A-363 16:51

C. Security and ethical issues of mobile device technology

E.R. Ranschaert; Mol/BE (ranschaert@telenet.be)

Medical specialists and radiologists are using mobile devices to share and exchange medical information and images with other health care professionals. Usually they need the advice regarding a diagnosis or treatment, sometimes in an acute setting. Popular messaging services such as whatsapp are often used for such purpose. Transmission of patient data with mobile devices and messaging services, however, does have several ethical and legal limitations, mostly related to the security and privacy of patients. Some questions need to be answered: is this type of communication unsafe and/or illegal, and if yes, why? Are there any regulations and/or guidelines available? Are there any secure solutions available? In this refresher course these issues will be discussed in more detail.

Learning Objectives:

1. To provide an overview of technical solutions for patients' image and data mobility.
2. To provide a risk assessment analysis (data loss, privacy, etc.) of mobile technology.
3. To give an overview of European legislation in relation to patient image and data mobility.

17:14

Panel discussion: Can mobile technology supplement stationary technology in radiology?

Discussion will address main controversies of the use of mobile technology in a clinical environment such as image quality, data mobility, safety and legal issues, etc.

Postgraduate Educational Programme

16:00 - 17:30

Room M 3

Interventional Radiology

RC 809

Percutaneous interventional procedures: a practical guide

A-364 16:00

Chairperson's introduction

R. Iezzi; Rome/IT (roberto.iezzi.md@gmail.com)

Percutaneous imaging-guided interventions are making an increasing contribution to the treatment of patients with many non-vascular conditions. Minimally invasive techniques enable effective treatment that is followed by rapid recovery, with a low morbidity and mortality rate. However, the effectiveness of such methods of treatment is enhanced by an accurate preprocedural planning, an adequate selection of image guidance technique, as well as an optimal intra/periprocedural sedation. In detail, analgesia and sedation before, during, and after interventional procedures allow a safe, comfortable, and technically successful procedure to be performed. This session will explore different imaging-guided methods to define advantages, disadvantages, as well as tips and tricks for successful percutaneous intervention.

Session Objectives:

1. To appreciate the importance of pre-procedure planning and selection of image guidance technique.
2. To learn about intra-procedure patient analgesia and adjunctive techniques for access to sites for intervention.
3. To discuss tips and tricks for successful percutaneous intervention.

A-365 16:05

A. How to safely perform US-guided procedures

D. Akinçi; Ankara/TR (akincid@hotmail.com)

Ultrasound (US) guidance is a frequent modality of choice in percutaneous biopsy, drainage, and ablation procedures, because it enables continuous real-time visualization, is radiation-free, has a lower cost, is better for angled access. In most of the abdominal organ biopsies (e.g., liver, kidney, pancreas, and spleen) and drainage of fluid collections, local ablation of liver tumors, drainage of pleural collections, biopsy of peripheral pleural based thoracic lesions, US guidance is utilized. Endocavitary approaches can be used safely in pelvic biopsy and drainage procedures with transvaginal or transrectal US guidance. Fusion techniques combine US images with CT or MRI images, enabling targeted US guided procedures for lesions that are difficult to see on US.

Learning Objectives:

1. To learn about patient positioning for US-guided percutaneous and endocavitary approaches to sites in the body.
2. To learn about real time guidance advantages of US-guided intervention.
3. To explain image fusion techniques for US-guided intervention.

A-366 16:28

B. How to safely perform CT-guided procedures

R. García Marcos; Valencia/ES (raulgamar@hotmail.com)

Percutaneous computed tomography (CT) guided is a minimally invasive approach for interventional procedures. Although is a procedure with few complications precise planning and knowledge of the indications, technique and material. CT-guided interventions may be divided into diagnostic (biopsies) and therapeutic interventions (drainages, thermal ablation, vertebroplasty, etc.). The main problems of access to lesions depend on the situation due to poor imagery, mobility and distance. Therefore, we are obliged to know and identify the structures along the established route. Different techniques of CT exist. Multidetector CT is commonly used for guiding percutaneous biopsy and catheter drainage of fluid collections. CT fluoroscopy has the potential to improve the efficacy of CT-guided interventions and to reduce the procedure time. C-arm cone-beam CT (CBCT) is a real-time needle guidance technique that can be used to visualise the needle trajectory from skin to target lesions. The aim of this study is to present the types and advantages of the CT-guided interventions, the patient positioning and adjunctive techniques for access to sites for intervention.

Learning Objectives:

1. To learn about patient positioning for CT-guided percutaneous approaches to sites in the body.
2. To learn the types of CT guidance and advantages of CT-guided intervention.
3. To learn about adjunctive techniques for access to sites for intervention.

A-367 16:51

C. Post-procedure follow-up and complication management

M. Seidensticker; Munich/DE (max.seidensticker@med.uni-muenchen.de)

Biopsy procedures bare - although commonly at a low rate - potentially life threatening risks. To know about potential complications and proper patient monitoring is the key to identify the complications and to react accordingly. The lecture will give informations about common and uncommon complications after biopsy procedures and help will be given to identify the patient at risk and how to avoid/reduce specific complications. Further on, management of complications will be addressed. Of note, not all complications are avoidable, but proper patient management helps to reduce associated morbidity and mortality.

Learning Objectives:

1. To appreciate the potential for complications in common biopsy procedures.
2. To learn about management of post-procedure complications.
3. To discuss the role of quality improvement.

Author Disclosure:

M. Seidensticker: Advisory Board; BAYER. Grant Recipient; SIRTEX Medical, BAYER. Speaker; Cook, Bayer, Sirtex.

17:14

Panel discussion: Tips and tricks for choosing your first cases.

Controversial case-based review of approaches to difficult lesions

16:00 - 17:30

Room M 4

E³ - ECR Academies: State-of-the-Art and Advanced MR Imaging of the Musculoskeletal system

E³ 819

Lower extremity

A-368 16:00

Chairperson's introduction

C.W.A. Pfirrmann; Zurich/CH

A-369 16:05

A. Hip and pubic symphysis

S.J. Eustace; Dublin/IE (eustacesj@gmail.com)

This presentation will review common causes of groin pain arising from the hip and from the symphysis pubis. In relation to hip pain the talk will focus on the role of the acetabular labrum in maintaining hip stability in normality, dysplasia and in patients with forms of impingement. The talk will outline appearances on non contrast MR studies and following arthrographic evaluation. The presentation will then review common pathologies in the symphysis pubis that can contribute to the development of groin pain contrasting symptoms and appearances of micro tearing of the adductor longus attachment (superior cleft sign) with appearances of micro tearing at the short adductor attachment (secondary cleft sign) with appearances of primary osteitis pubis.

Learning Objectives:

1. To identify the most common post-traumatic entities.
2. To identify the most common entities leading to chronic pain.
3. To know the role of MR imaging and MR arthrography (direct/indirect) and how to optimise imaging protocols for the hip.

A-370 16:43

B. Post-traumatic ankle

M.-A. Weber; Rostock/DE

MRI is excellent for depicting normal ankle anatomy and it can elegantly demonstrate ligamentous injuries of the ankle and associated conditions after ankle sprain. In 85% of all ligament ruptures, the lateral ligament complex is affected and the anterior talofibular ligament is the most often ruptured ligament followed by the calcaneofibular ligament. Additionally, dedicated MRI protocols can delineate the cartilage, as well as the appearance of acute and chronic osteochondral lesions of the talus. Recent advances in MRI include 3D

Thursday

isotropic ankle joint imaging. Subchondral microfractures, osteochondral fractures and solely chondral fractures are different manifestations of impaction injuries, the two last-mentioned affect the articular surface. Since osteochondral lesions of the talus may eventually result in post-traumatic osteoarthritis, recognition of early cartilage damage and associated lesions may help determining the proper treatment of the patient to delay or prevent progression to osteoarthritis. Additionally, osteochondral injuries can often explain persisting symptoms. MRI, where necessary complemented by CT-arthrography, has become a decisive tool in diagnosing and characterizing cartilage lesions of the ankle. In case of disrupted cartilage layers and fluid around undetached fragments as well as in case of a dislodged fragment operative treatment may be indicated after consideration of the patient's general clinical condition. The interventional procedures, which have been developed for the repair of such lesions, essentially include abrasion, microfracture, autologous osteochondral transplantation, allograft transplantation, and (matrix-associated) autologous chondrocyte implantation. MRI enables the non-invasive assessment of the repair tissue, the success of implantation, and the state of cartilage maturation.

Learning Objectives:

1. To identify the most common post-traumatic entities.
2. To know the role of MR imaging and MR arthrography (direct/indirect) and how to optimise imaging protocols for the ankle.
3. To differentiate post-traumatic changes from typical reasons for chronic pain.

A-371 17:06

C. Chronic ankle pain

J. [Teh](#); Oxford/UK (jamesteh1@googlemail.com)

This lecture will focus on the causes of chronic ankle pain, other than osteochondral and ligamentous injuries. The topics covered will include: (1) Tendinopathy: The spectrum of tendinopathy in the ankle ranges from tendinosis through to complete ruptures. There are specific abnormalities that occur in relation to the tibialis posterior tendinopathy such as spring ligament disruption and pes planus. On the lateral aspect of the ankle splits of the peroneus brevis, the painful os peroneum syndrome (POPS) and peroneal dislocation are discussed. (2) Plantar fascia: The plantar fascia is prone overuse injury resulting in plantar fasciitis. Acute disruption may also occur. Baxter's neuropathy is discussed. (3) Masses: For many soft tissue masses the position of the lesion is often useful for narrowing the differential. For some benign soft tissue masses (e.g., Morton's neuroma, lipomas, hemangiomas, cysts, abscesses), the MRI findings may be sufficient to clinch a diagnosis. In some cases further imaging and biopsy may be required. (4) Diabetic foot: Certain features may help us differentiate between the infected diabetic foot from Charcot arthropathy. The key to diagnosing infection is the presence of soft tissue ulceration contiguous to the bone abnormality. Ulceration in the foot tends to occur in weight bearing areas such as at the heel, the ball of the foot and around the toes. Charcot arthropathy is characterized by destruction, disorganization, increased density and debris.

Learning Objectives:

1. To identify the most common entities leading to chronic pain.
2. To know the role of MR imaging and MR arthrography (direct/indirect).
3. To differentiate entities leading to chronic pain from post-traumatic changes.

16:00 - 17:30

Room M 5

E³ - ECR Academies: Update on Hepatobiliary Imaging

E³ 820

Liver and bile duct pathologies

A-372 16:00

Chairperson's introduction

M. [Zins](#); Paris/FR (mzins@hpsj.fr)

In this liver and bile duct session we will review, through interactive case presentations, challenging cases of liver abscesses, acute cholangitis, intra, and extrahepatic cholangiocarcinoma as well as benign and malignant conditions of the Gallbladder. The main differentials will be discussed and many tips in assessing accurate diagnosis in liver and bile ducts diseases will be presented.

A-373 16:05

A. Inflammatory and infectious disease

A. [Arora](#); Worthing/UK (Ankur.Arora@wshst.nhs.uk)

Infective and inflammatory disorders of the hepatobiliary system are routinely encountered in a radiologist's day to day practice and one ought to be aware of

their common and uncommon clinico-radiological manifestations. Imaging undoubtedly plays a crucial role in their timely detection and characterisation and guiding appropriate clinical management. A broad spectrum of infective/inflammatory disorders can affect the hepatobiliary system which for simplicity can be broadly classified into disorders affecting the liver, gallbladder, and the biliary tree, although often these structures are concomitantly involved. We shall appraise the common imaging appearances of different liver infections (bacterial, viral, parasitic, and fungal) on multimodal imaging and discuss relevant differential diagnoses. Whilst in most instances US and CT are sufficient to diagnose and characterise hepatic infections MRI may be resorted to as a problem solving tool for, e.g., to exclude necrotic liver tumours. We shall also review the key imaging manifestation of biliary and gallbladder inflammation/infections with a view to familiarise ourselves with pertinent diagnostic pointers on cross-sectional imaging.

Learning Objectives:

1. To recognise and describe the radiological appearance of the inflammatory-infectious processes that may involve the liver.
2. To describe the imaging findings in inflammatory-infectious processes that may involve bile ducts.
3. To assess the role of different imaging modalities in the detection, characterisation, and management of patients with inflammatory-infectious hepatobiliary disease.

A-374 16:43

B. Cholangiocarcinoma: diagnosing and staging

C. [Matos](#); Lisbon/PT (celso.matos@fundacaochampalimaud.pt)

The goals of imaging in patients with suspected or known cholangiocarcinoma (CCA) are multiple: (a) to show the size and the location of a primary lesion and assess the longitudinal and radial extent of bile duct involvement; (b) to enable the characterization of a biliary stenosis; (c) to show involvement of the hepatic artery main and lobar branches and of the portal vein main and lobar branches for the purpose of surgical planning; (d) to depict the presence and extent of liver invasion and of lobar atrophy or hypertrophy, and (e) to enable the detection of regional lymph nodes and metastases. The lecture will address the complementary role of non-invasive and invasive imaging modalities to achieve those goals and will illustrate imaging characteristics that may indicate a specific diagnosis and may help predict prognosis.

Learning Objectives:

1. To be familiar with the multimodality imaging techniques and protocols.
2. To be aware of the imaging findings of different types of cholangiocarcinoma in diagnosing and staging.
3. To be able to recognise recurrent and metastatic disease in the follow-up.

A-375 17:06

C. Gallbladder pathologies

R. [Maksimović](#); Belgrade/RS (ruzica.maksimovic@med.bg.ac.rs)

Imaging of gallbladder is including variety of diagnostic imaging modalities such as ultrasonography (US), multidetector computed tomography (MDCT), magnetic resonance imaging (MRI), positron emission tomography (PET), and scintigraphy. Wide variety of diagnostic armamentarium provides accuracy of noninvasive imaging of benign and malignant gallbladder conditions, and thus improves laparoscopic surgery as well as endoscopic and radiologic interventional techniques. US has been the first imaging modality for evaluating gallbladder disease, due to its high sensitivity and specificity for evaluating not only morphology, but also for functional evaluation of the gallbladder. MDCT is valuable diagnostic procedure in differential diagnosis, and for preoperative assessment of different conditions, including the tumour and its sagging, as well as to evaluate therapy response MR is taking place in gall bladder imaging preferentially in patients with limited assessment by US. It allows assessment of anatomic and physiologic features of not only a gallbladder but also biliary tract in preinterventional and postoperative setting. Furthermore, respiratory-triggered three-dimensional MR cholangiopancreatography (3D-MRCP) is a promising new toll for better visualisation of gall bladder lumen, bile duct, and pancreatic duct. The utility of 18F-fluorodeoxyglucose positron emission tomography-computed tomography (18FDG PET-CT) is to provide optimal pre-treatment staging of patients and to tailor subsequent treatment. Cholescintigraphy is the use of radiotracers to assess the anatomy and function of the biliary system, and liver indirectly. Currently this is most commonly performed with Tc99m-IDA analogues, for evaluation of different conditions including biliary atresia where it could be a problem solving tool.

Learning Objectives:

1. To understand the multimodality approach to gallbladder diseases.
2. To be able to identify gallbladder cancer.
3. To be able to differentiate benign conditions from the malignant ones.

Friday, March 2

Postgraduate Educational Programme

08:30 - 10:00

Room A

E³ - ECR Academies: Interactive Teaching Sessions for Young (and not so Young) Radiologists

E³ 921

Emergency radiology II

A-379 08:30

A. Urinary system trauma

V. [Logager](mailto:Logager@regionh.dk); Copenhagen/DK (vibeke.loegager@regionh.dk)

According to the American Association of Surgeons in Trauma (AAST), approximately, 10% of all trauma admissions have kidney injuries. Blunt traumas can be graded in a 5-point Renal Injury Scale. On the basis of the patient's clinical findings an imaging algorithm is set. In general, patients that are normotensive with microscopic hematuria have less than 0.2% risk of serious kidney damage and imaging is unnecessary, whereas patients with either: (A) gross hematuria, (B) microscopic haematuria and blood pressure less than 90 mmHg or occasionally, (C) microscopic haematuria will require imaging. Contrast-enhanced CT is the way to go. Imaging should be in 3 phases (cortico-medullary, delayed 3-5 min and late phase (more than 10 min). Image reading should be by multiplane approach. Most of the findings do not require surgical intervention. But the rest do. On the basis of case presentations, findings will be analysed, discussed and correlated to the patient's clinical status and treatment possibilities, including where and which signs to look for. Which modality could be used to solve the diagnostic problem when the clinical picture does not fit with the radiological picture. Relevant questions will be asked during this session for the participants to vote and the results will be discussed.

Learning Objectives:

1. To identify the signs of trauma.
2. To outline the clinical impact of these findings.

A-380 09:15

B. Non-traumatic urinary tract emergencies

G. [Masselli](mailto:Masselli@libero.it); Rome/IT (gabrielemasselli@libero.it)

Urinary tract (UT) obstruction secondary to urolithiasis is the most common urologic emergency in patients presenting with abdominal pain. Serious complications of acute obstruction include ureteral rupture, pyelonephrosis or abscesses. Radiologists need to define the extent of obstruction, its likely duration and whether an intervention is required, aware that ultrasound (US) is usually normal in case of acute onset. In such cases computerised tomography (CT) is the gold standard diagnostic tool. UT infection (UTI) is another common emergency and it may vary in severity, from ureteral to focal renal infection, emphysematous pyelonephritis or pyonephrosis. UTI diagnosis is usually clinical, but in case of uncertainty CT provides early diagnosis, outlining the extent and severity of the disease. Magnetic resonance diffusion-weighted imaging (DWI) is of particular value when differentiating pyonephrosis from simple hydronephrosis. DWI of the kidneys is highly sensitive for the detection of focal or diffuse infections, reason why is gaining more and more popularity. T2-weighted (static fluid) urography is performed in pregnant women to outline the ureters in their entirety. A challenge of MR urography is the differentiation between physiologic hydronephrosis and pathologic obstruction. Vascular UT emergencies include renal infarcts (commonly of thromboembolic origin), renal vein thrombosis (typical of hypercoagulable states and neoplastic patients), and spontaneous hemorrhage (due to angiomyolipoma rupture). These are among the most common non-traumatic UT emergencies and it is fundamental for every radiologist to be fully confident in their diagnosis. The role of each imaging modality will be interactively discussed in the different clinical scenarios.

Learning Objectives:

1. To understand the imaging technique.
2. To become familiar with the differential diagnosis.

08:30 - 10:00

Room B

Abdominal Viscera

RC 901

Imaging of benign liver lesions: still difficult?

A-381 08:30

Chairperson's introduction

L. [Marti-Bonmati](mailto:Marti-Bonmati@gva.es); Valencia/ES (marti_lui@gva.es)

Benign liver tumours are a heterogeneous group of lesions with different cellular origins and clinical relevance. In this session there will be an interesting discussion on the difficulties and imaging strategies to properly diagnose liver cysts, haemangiomas, FNH and adenomas. These benign lesions are frequently found incidentally during imaging exams performed for unrelated reasons. Most often they do have a benign course, but management difficulties might arise. Radiologists have to recognize the best radiological approaches in terms of modalities and the use of contrast media, the pearls and pitfalls commonly related to these lesions, the main radiological features and diagnostic criteria, and the epidemiological data, pathology, pathophysiology, and their natural progression. Radiological reports should also include recommendations for their management.

Session Objectives:

1. To understand the role of different imaging techniques in characterisation of focal liver lesions.
2. To be aware of malignant lesions which may mimic benign liver conditions.
3. To underline current guidelines for characterisation of equivocal liver lesions.

A-382 08:35

A. Hepatic cysts: always simple?

I. [Santiago](mailto:Santiago@fundacoachampalimaud.pt); Lisboa/PT (ines.santiago@fundacoachampalimaud.pt)

The differential diagnosis of cystic liver lesions is as broad as their clinical significance, which ranges from benign to malignant and/or potentially lethal conditions. These lesions include foregut and ductal plate malformations, infectious diseases, primary and secondary neoplasms and traumatic/iatrogenic fluid collections. The number of lesions, morphology, fluid content characteristics, presence/absence of septae and/or solid components are the key imaging features for the diagnostic approach and different imaging modalities pose different advantages and disadvantages for their characterisation. Given imaging characteristics may overlap between distinct conditions, patient history and laboratory data should be integrated to allow a more definitive diagnosis.

Learning Objectives:

1. To learn about different types of cystic lesions in the liver including giant biliary hamartomas or foregut cysts.
2. To understand diagnostic approach to differentiate simple and complex cysts/cystic lesions.
3. To appreciate advantages and limitations of imaging for differentiating simple cyst from other cystic lesions.

A-383 08:58

B. Liver haemangiomas and mimickers

P.R. [Ros](mailto:Ros@UHhospitals.org); Cleveland, OH/US (Pablo.Ros@UHhospitals.org)

Hemangioma is the most common benign tumor-like condition in the liver, with a prevalence up to 20% of the general population. Unfortunately its demographics (predominance in women, post-menopausal and without geographic distribution) is similar to that of other primary benign and malignant neoplasms and secondary malignancies. On the other hand, and fortunately, is one of the most successful focal liver lesions to be characterized by imaging. Particularly if a contrast agent is used. Hemangiomas have a (1) distinct morphology, (2) enhancement pattern and (3) signal characteristics by MRI scans. These 3 parameters allow the characterization of hemangiomas in almost all cases. This ease of characterization obviates in almost all cases the use of percutaneous biopsy. Image guided percutaneous biopsy particularly in superficial hemangiomas and using a true cut needle can have serious complications. Hemangiomas can have an atypical imaging appearance since they may contain cystic change, calcification, sclerosis and large central scars, particularly when giant (more than 10cm in size). There is overlap with some other focal lesions that mimic the imaging findings of hemangioma by all imaging modalities: (1) epithelioid hemangioendothelioma (2) angiosarcoma, (3) other vascular sarcomas and (4) treated breast cancer metastasis, which can present with a pseudohemangioma pattern. We offer throughout the presentation imaging/pathologic correlation approach to support the typical and

Friday

atypical ultrasound, CT and MRI appearance of hemangioma and its major mimickers.

Learning Objectives:

1. To learn about typical imaging findings of liver haemangioma.
2. To understand the atypical imaging findings of liver haemangiomas.
3. To appreciate the role of multiparametric and liver-specific contrast MRI in differentiation between haemangiomas and malignant lesions mimicking haemangiomas.

A-384 09:21

C. FNH or adenoma?

A. Ba-Ssalamah; Vienna/AT (ahmed.ba-ssalamah@meduniwien.ac.at)

FNH and HCA are liver lesions of hepatocellular origin. Whereas FNH commonly occurs, HCA is very rare. Distinguishing FNH from HCA is of great importance clinically, as FNH is considered a benign lesion and needs no further management. In contrast, HCA, according to its subtype, can be considered a borderline tumor due to the risk of hemorrhage, growth, and even malignant transformation, and requires individualized management. The genotype/phenotype classification of HCA is an evolving issue and there is now a recent HCA molecular classification by which to stratify patients according to the risk of complications. On imaging, HCA is no longer a distinct entity and imaging features reflect the tumor subtypes. Contrast-enhanced MRI is much more accurate because of its ability to visualize the textural composition of the HCA. However, even after the administration of MRI hepatobiliary contrast agents, a small proportion of HCA subtypes still show either inhomogeneous uptake or inhomogeneous washout in the hepatobiliary phase (HBP); therefore, it is difficult to differentiate these subtypes from FNH on the basis of imaging presentation alone. This may pose a diagnostic dilemma as both FNH and HCA tend to occur in women of child-bearing age. Clinical presentation and risk factors, male gender, patient age, presence of storage disease, obesity, metabolic syndrome or inflammatory syndrome, hepatitis, alcohol abuse and tumour over 5 cms, as well as significant growth have been identified as factors associated with an HCA subtype of higher malignant potential. In difficult cases histological analysis remains the gold standard.

Learning Objectives:

1. To learn the imaging features associated with FNH and adenoma on contrast-enhanced CT and MRI.
2. To understand how the imaging characteristics are related to the underlying pathological findings.
3. To appreciate the optimal use of liver-specific contrast media for distinguishing between FNH and adenoma, and current classification and pathological characteristics and its impact on the management.

Author Disclosure:

A. **Ba-Ssalamah**: Consultant; Bayer. Speaker; Bayer.

09:44

Panel discussion: What imaging strategy for my routine clinical practice?

08:30 - 10:00

Room C

New Horizons Session

NH 9

Immunotherapy: a revolution in cancer care?

A-385 08:30

Chairperson's introduction: What the radiologist needs to know

V.J. Goh; London/UK

Evasion of the immune system plays an important role in the development and progression of cancers. Cancer immunotherapies are a promising class of agents that re-engage the immune system in its fight against cancer cells. Strategies range from activating innate/adaptive immune effector mechanisms to neutralising inhibitory/suppressive mechanisms. For example, treatment with interleukin 2 (IL-2) or interferon- α (IFN α) stimulate effector immune cells; conversely antibodies against immune-checkpoint molecules, e.g., cytotoxic T lymphocyte-associated protein 4 (CTLA4)-targeted antibodies and programmed cell death 1 (PD1)-targeted antibodies neutralise immune suppressor mechanisms. Immunotherapies have been shown to be effective in a number of advanced cancers including melanoma, renal cancer, and non-

small cell lung cancer. As immunotherapies generate anti-tumour effects by enhancing tumour-specific T cell responses rather than the direct cell killing, response assessment may be challenging. Response may take longer to be detectable by imaging and standard methods, such as response evaluation criteria in solid tumours (RECIST) may be misleading. In this session the role of imaging will be explored and future directions considered.

Session Objectives:

1. To be familiar with the concept of immunotherapy.
2. To be aware of the current imaging methods for assessing immunotherapies.
3. To learn about new methods in development for assessing immunotherapies.

Author Disclosure:

V.J. **Goh**: Research/Grant Support; Siemens Healthineers. Speaker; Bayer, Siemens Healthineers.

A-386 08:40

CT: looks bigger, but it's better

C. Dromain; Lausanne/CH (Clarisse.Dromain@chuv.ch)

A wide range of cancer immunotherapy approaches have been developed including non-specific immune-stimulant such as cytokines (Interferon, IL2), cancer vaccines (peptide or dendritic cell-based vaccines), adoptive T-cell therapy (TILs, CAR, TRC) and immune checkpoint inhibitors (anti CTLA-4, anti PD1 and anti PDL1). The most commonly used and intensively studied are the immune checkpoint inhibitors (ICIs). Their mechanism of action signifies a true shift in oncology where instead of targeting the tumor cells, ICIs target the immune system to break the cancer tolerance and stimulate the anti-tumor immune response. These new drugs have, since 2011, received marketing authorisation for melanoma, lung, bladder, renal, and head and neck cancer with remarkable and long-lasting treatment response. The novel mechanism of action of these drugs, with immune and T-cell activation, lead to unusual patterns of response with presence of flare phenomenon or pseudo-progression more pronounced and more frequent than previously described responses. Pseudo-progression, that has been described in about 3-10% of patients treated using ICIs, corresponds to increase of tumor burden and/or appearance of new lesions due to infiltration of the tumor by activated T cells before the disease responds to treatment. To overcome the limitation of RECIST criteria to assess this specific changes in tumour burden, new criteria so-called irRC and then irRECIST were proposed. The major modification involved the inclusion of the measurements of new target lesions into disease assessments and the need of a 4-week CT re-assessment to confirm progression. More recently (2017) a consensus guideline iRECIST was developed by the RECIST working group.

Learning Objectives:

1. To be aware of the different types of immunotherapies and to understand their mode of action.
2. To understand the limitations of RECIST and be aware of immune response criteria.
3. To understand the limitations of CT for assessment of immunotherapies.

A-387 09:03

The MR armoury in follow-up

D.-M. Koh; Sutton/UK (dowmu.koh@icr.ac.uk)

Drugs that modulate the body immune responses are being utilised to treat a range of cancers, including malignant melanoma, non-small cell lung cancer, hepatocellular and bladder carcinomas. In patients receiving immunotherapies, CT is still the most widely used imaging technique for assessing tumour response to treatment and to identify drug related side-effects. However, anatomical MR imaging can also be effectively applied to evaluate tumour regression with treatment using size measurement criteria (e.g., iRECIST). Like CT, increase in tumour size may be observed on MRI in pseudo-progression, which can confound response assessment. Nonetheless, the superior soft tissue contrast of MRI helps to depict subtle disease (e.g., intracranial) and specific complications (e.g., hypophysitis) that are difficult to visualise on CT. There is great interest in applying quantitative MR imaging, including whole body MRI techniques, to study functional changes in tumour cellularity (diffusion-weighted MRI), vascularity (contrast-enhanced MRI) and macromolecules (magnetisation transfer). These are areas of on-going research. Whole body MRI can provide information about inter-tumoural heterogeneity, thus allowing insights into tumour evolution and differential response to treatment. Active research in molecular probes is being undertaken to develop PET imaging tracers that can identify and predict treatment response, which can be explored alongside multi-parametric MRI measurements on a MRI/PET hybrid system as imaging biomarkers.

Learning Objectives:

1. To be aware of the advantages and limitations of MRI for assessment of immunotherapies.
2. To describe the potential role of whole-body MRI and quantitative MRI techniques in follow-up.
3. To consider the potential of integrated MRI/PET for the assessment of immunotherapies.

A-388 09:26

Systemic and immunologic effects of image-guided interventions in oncology

S.N. Goldberg; Jerusalem/IL (sgoldber@bidmc.harvard.edu)

Although interventional oncologists have traditionally assumed that our local therapies including tumor ablation and chemoembolization have minimal systemic effects, there is increasing compelling animal evidence to back up anecdotal clinical reports suggesting that these therapies can stimulate distant effects and can potentially have more widespread effects than just eliminating a focal tumor. On the positive side, several studies have reported that tumor ablation can, under poorly defined "favorable" conditions, induce systemic immunologic "abscopal" effects that induce distant tumor regression. Thus, several groups are pioneering combining interventional oncologic procedures with immunotherapies with the express goal of stimulating immune anti-cancer responses. Simultaneously and by contrast, we and others have demonstrated that radiofrequency and other therapies can in some cases also cause increased cancerous effects by inducing tumor initiation and progression in non-ablated areas. For liver ablation, this has been linked to an increased inflammatory response including cellular recruitment of neutrophils, macrophages, and activated myofibroblasts to the peri-ablated zone and several pro-tumorigenic cytokines such as IL-6 and HGF that increase following ablation. Thus, in all likelihood, there is a balance between pro-oncogenic and pro-immunogenic effects that differs from patient to patient. Thus, our ultimate goal - achievable only through additional mechanistic study - should be to alter the post-ablation milieu to prevent any untoward tumorigenic effects while simultaneously promoting desired abscopal effects.

Learning Objectives:

1. To be aware of abscopal effects with immunotherapy.
2. To describe how focal therapies can be combined with immunotherapies.
3. To be aware of the challenges of focal treatments for systemic effects.

Author Disclosure:

S.N. Goldberg: Consultant; Angiodynamics, XACT Robotics, and Cosman Instruments. Research/Grant Support; Angiodynamics, XACT Robotics.

09:49

Panel discussion: How should radiology improve imaging to support this revolutionary care?

08:30 - 10:00

Room O

Paediatric

RC 912

Dose reduction: tips and tricks

Moderator:

C. Granata; Genoa/IT

A-389 08:30

A. Dose reduction in paediatric CT

D. Aadnevik; Bergen/NO (daniel.aadnevik@helse-bergen.no)

Computed tomography (CT) is an invaluable tool in diagnostics and the use of CT has rapidly increased since the 1970s. Ionising radiation can damage human tissues, and is associated with an increased risk of cancer. The effect is of particular concern in children as they have a higher radiosensitivity and longer life expectancy. Modern CT scanners have a high level of automation regarding acquisition parameters which may leave the imaging professionals insecure whether the radiation dose is appropriate for the diagnostic task at hand. Studies have shown that in some cases adult protocols are directly implemented in paediatric imaging, resulting in unnecessary high doses. As radiation professionals, it is our duty to keep the radiation dose as low as reasonably achievable (ALARA). It is important to have a basic understanding of how technical factors influence image quality and how to properly balance the output parameters of the scanner in accordance with the ALARA-principle. A review of how the basic imaging parameters like tube-current (mA) and tube voltage (kV) affect image quality and patient dose will be given. The use of technique charts and size-specific dose estimates (SSDE) as a tool to ensure appropriate dose levels and consistent image quality for children will be explained. Examples from local

optimization studies will also be shown, and a brief review of some vendor-specific solutions for dose reduction will be given.

Learning Objectives:

1. To explain the factors that affect patient radiation exposure from CT exams.
2. To discuss the importance of dose reduction in paediatric CT.
3. To give an overview of CT dose-reduction strategies and techniques.

A-390 09:00

B. Diagnostic reference levels in paediatric imaging: international recommendations

R. Seuri; Helsinki/FI (raija.seuri@hus.fi)

The small number of paediatric patients is a challenge to the optimization of imaging protocols. Optimization of parameters and image quality for children of all sizes requires both time and expertise, which might not be easy to find in daily practice. Diagnostic reference levels (DRLs) are a tool to help the optimization process. DRLs are used by collecting patient dose values and comparing the median value to the reference level. In this comparison dose should always be considered together with the indication of imaging and image quality. Diagnostic reference levels were introduced already in 1990s, but only recently have the challenges of paediatric imaging got more attention in the international recommendations. The huge variation of sizes of paediatric patients has usually been tackled by establishing DRLs for different age-groups. Now both ICRP and EC recommend the use of weight for grouping of paediatric patients. Instead of different groups, also a continuous DRL-curve can be used. Detailed advice for the use of DRLs in practice is included in the recent international publications. The international guidelines also provide recommended dose metrics for each modality to be used in DRL comparison. By European recommendation the National DRLs should be based on collection of doses from representative institutions in the country, not phantom measurements. The European DRLs offer a guidance level for optimization in those countries which have not yet established their National DRLs. The most recent European guidelines including the paediatric DRLs were published by the EC in 2017.

Learning Objectives:

1. To discuss the need for establishing diagnostic reference levels (DRLs) in paediatric diagnostic imaging.
2. To give an overview of DRL values for typical paediatric examinations.
3. To understand the way of implementation and use of DRLs in dose reduction and protocol optimisation.

A-391 09:30

C. The impact of dose management systems

L.A. Rainford; Dublin/IE (louise.rainford@ucd.ie)

It is mandated by European directive that the establishment and use of DRLs is fulfilled by all member states. Existing levels of dose information varies across imaging sub-specialities, as evidenced by the recent European PiDRL project. Specific challenges continue to confound paediatric dose data collections, including: reduced frequency of examinations compared to adults, patient age/weight/size variations, procedural variability and varied data survey methodologies. Increasing numbers of dose tracking software packages, including those providing web-based dose data collection, tracking and analytics are available. These systems although varied in scope of content offer services, including: dose documentation; dose reference levels setting; performance benchmarking; imaging protocol management; and outlier identification. An overview of products and their management of big data will be provided. Furthermore the current clinical reality that substantial amounts of both unstructured and structured dose data is routinely being captured, with the employment of varied mechanisms of data recording, will be evidenced. Why this information is potentially not being used optimally will be discussed, as will communication matters relevant to dose management products. Practical issues relevant to clinical data required for dose and imaging protocol evaluation will be incorporated based on feedback from a number of European sites. Finally the role of dose management systems in the review of population dose data and protocol optimisation will be discussed and the potential barriers to the successful completion of multi-centre surveys will be considered.

Learning Objectives:

1. To discuss the importance of dose monitoring in paediatric imaging.
2. To have an overview of the features and functions of dose-monitoring systems.
3. To understand the role of dose-monitoring systems in the evaluation of population dose and protocol optimisation.

08:30 - 10:00

Room N

Cardiac

RC 903

Novel ways to characterise myocardial tissue: T1 and T2 mapping

Moderator:

L.P. Lawler; Dublin/IE

A-392 08:30

A. T1 mapping: technical considerations

M.R. Makowski; Berlin/DE (marcus.makowski@charite.de)

This lecture will introduce the physical principles of T1 mapping for the characterisation of the left ventricular myocardium. Different MR sequence types for the acquisition of T1 mapping will be discussed. The technical challenges of T1 mapping will be highlighted and strategies to overcome these challenges will be introduced. The evaluation of datasets derived from T1 mapping will be discussed. The clinical relevance of T1 mapping techniques in the context the different myocardial diseases will be highlighted.

Learning Objectives:

1. To learn about the principles of T1 mapping.
2. To learn about specific issues of T1 mapping.
3. To learn how to do and assess T1 mapping.

A-393 09:00

B. T2 mapping: technical considerations

C. Tessa; Lido di Camaiore/IT (ctessa@sirm.org)

Cardiac T2-mapping is a technique that allows to measure myocardial T2 relaxation time. To this purpose, T2-prepared steady-state free-precession sequences, turbo-spin-echo or gradient-spin-echo sequences with a minimum of 3 source images can be employed. T2 mapping sequences can be acquired both in breath-hold or during free breathing, utilizing respiratory navigators. Cardiac motion is normally avoided by acquiring for a short duration at end diastole, but it is also possible to obtain the maps in systole. Motion correction algorithms are usually applied to source images to compensate for image-to-image displacement. T2 maps are often acquired on a short-axis view at basal and mid-ventricular level. At apical levels, long-axis views should be preferred to avoid partial-volume effects. T2 maps can be analyzed both visually and quantitatively, by means of ROIs or automatic thresholds. Small ROIs (<20 pixels) should be avoided. The reproducibility of T2 mapping sequences is very good. However T2 relaxation time is very sensitive to cofactors and it is therefore, necessary to generate reference values specific for each site, technique and imaging setting. In clinical report, the local reference ranges (mean \pm 2 standard deviations of the normal data) should be quoted. Additionally, phantom-based periodic control of the CMR system is recommended. Until recently, T2 mapping sequences have not been commercially available, and therefore, current recommendations rely mainly on single-center studies. Nevertheless, there is now growing evidence on the clinical value of T2 mapping, that is expected to become part of a routine cardiac MR examination.

Learning Objectives:

1. To learn about the principles of T2 mapping.
2. To learn about specific issues of T2 mapping.
3. To learn how to do and assess T2 mapping.

A-394 09:30

C. Clinical use of T1 and T2 mapping

J. Bremerich; Basle/CH (jens.bremerich@usb.ch)

Comprehensive tissue characterisation is a unique feature of cardiac MRI. Today, a variety of quantification sequences are available as clinical tools. This paper shall illustrate clinical applications of T1- and T2-mapping techniques. Late Gadolinium enhanced MRI (LGE-MRI) opened the door to scar imaging, today even more refined techniques such as T1- and T2-mapping have matured to clinical tools. The combination of pre- and postcontrast T1-mapping might even be used to calculate extracellular volume (ECV), when hematocrit is measured from blood samples. Contrast enhanced T1-mapping enables assessment of structural changes such as in mild inflammation. ECV enables detection and quantification of fibrosis such as in treatment with cardiotoxic medication or infiltrative diseases such as amyloidosis. It should be emphasized, however, that normal T1-values may vary among sequences and magnets. This explains the requirement to establish normal values for every hardware and sequence system. Moreover, T1-times at 3 Tesla are typically longer than at 1.5 Tesla. T2-mapping helps to identify tissue edema as an

unspecific imaging marker of myocardial injury. Moreover, T2*-mapping is used to measure iron overload of the heart in hemosiderosis or haematologic diseases. Detailed myocardial tissue characterization with T1- and T2-mapping has matured to a robust clinical tool and adds value to cardiac MRI.

Learning Objectives:

1. To learn about the main fields of application for T1-T2 mapping.
2. To learn the specific parameters useful for the clinical implementation of T1-T2 mapping.
3. To understand the incremental value of T1-T2 mapping over current methodologies.

08:30 - 10:00

Studio 2018

Special Focus Session

SF 9a

Focal treatment of prostate cancer

A-395 08:30

Chairperson's introduction

H.-P. Schlemmer; Heidelberg/DE (h.schlemmer@dkfz.de)

PSA-screening has led to a higher detection rate of localized, early stage prostate cancer. In this situation whole gland treatment by radical prostatectomy could bear the risk of overtreatment with side effects that may significantly reduce quality of life. To reduce the treatment-related toxicity, alternative therapy options causing less damage of prostate tissue and adjacent structures are increasingly considered. Hemiablation and focal ablation therapies are delivered with intention to cure and are on principle achievable for patients with localised PCa. But a lot of open questions still exist concerning e.g. eligibility criteria of patients, preinterventional diagnostic workup, type of ablation therapy, need for additional treatment, etc. This session will provide the current knowledge about opportunities and challenges of focal therapy of prostate cancer. The role of imaging for diagnosis and image-guided interventions by high-intensity ultrasound (HIFU) and irreversible electroporation (IRE) will be discussed in detail.

Session Objectives:

1. To recognise the demand for minimal invasive therapy of prostate cancer.
2. To understand the technologies as well as the pros and cons of focal therapies.
3. To be aware of the value of multiparametric MRI for planning and guidance of focal therapy.

A-396 08:35

Focal treatment of prostate cancer: opportunities, challenges and indications

R. Sanchez-Salas; Paris/FR (rafael.sanchez-salas@imm.fr)

Focal therapy (FT) has emerged as an alternative to whole-gland radical treatments with the objective to reduce treatment-related toxicity by sparing prostatic tissue. The FT approach stands on the concept of identifying and treating de index lesion. Selection criteria, optimal treatment modalities and follow-up strategies remain divergent across published series. A recent consensus from field-experts brings guidance to focal treatment strategies in PCa while standardizing the selection criteria and follow-up schemes. Efforts are being made to improve diagnostic tools to optimize patient selection. Multiparametric MRI represents the cornerstone imaging tool for guided diagnostic, treatment and follow-up of these patients. With further development of image-guided diagnostics and deployment of transperineal prostate mapping (TTMB) and MRI-ultrasound fusion biopsies, the histological accuracy at diagnosis has increased with optimal risk definitions and patient selection. Post-ablation surveillance protocols entail monitoring residual post-ablated and preserved tissue. It should be noted that while serum prostate-specific antigen (PSA) kinetics is considered a reliable tool for following patients after local whole-gland treatment, its role after focal therapy is yet to be defined and the thresholds for defining success and failure have not been defined. Key energy sources delivering FT for PCa include cryotherapy, high-intensity focused ultrasound (HIFU), irreversible electroporation (IRE), photodynamic therapy (PDT) and focused laser ablation. In the future, the natural history of non-index lesions in the post ablation setting needs to be addressed. Combined immunological or hormonal interventions could be considered to further improved cancer control of FT.

Learning Objectives:

1. To learn the conceptual possibilities and limitations of focal therapy for prostate cancer.
2. To understand indications and patient selection criteria.
3. To know achievable cure rates, possible causes for failure and treatment-related toxicity.

Author Disclosure:

R. Sanchez-Salas: Consultant; EDAP-TMS. Speaker; EDAP-TMS.

A-397 08:52

Imaging of prostate cancer: how accurately can prostate cancer be localised?

C. Allen; London/UK (clare.allen@uclh.nhs.uk)

Successful focal treatment of prostate cancer requires accurate anatomical localisation which can only be provided by Mp MR. Exclusion of disease in the rest of the prostate is also essential. Mp MRI technique is well established and documented in Pirads vs2. However despite this scan quality remains variable. The assessment of quality will be discussed along with the current status of tumour detection within the gland. The size, position and concordance of the MR target with histological target will be discussed. Critical to the success of focal ablation is the communication of a well defined target. The various techniques available to deliver this are discussed along with contouring techniques.

Learning Objectives:

1. To know the examination protocol and the required quality standard of multiparametric MRI.
2. To recognise opportunities and limits of prostate MRI for cancer localisation and delineation.
3. To learn about standardised reporting necessary for precise communication with urologists.

A-398 09:09

Image-guided focal treatment using high-intensity ultrasound (HIFU)

S. Crouzet; Lyon/FR

"no abstract submitted"

Learning Objectives:

1. To understand the technology of image-guided high-intensity focused ultrasound (HIFU).
2. To recognise the value of MRI for treatment planning and guidance.
3. To learn about indications, achievable therapeutic results and side effects.

A-399 09:26

Image-guided focal treatment using irreversible electroporation (IRE)

F. Collettini; Berlin/DE (federico.collettini@charite.de)

In recent years, focal therapy of prostate cancer has gained great interest from both health care professionals and patients. Irreversible electroporation (IRE) has emerged as a promising technique for tumor ablation and is currently one of the most intensively studied technologies. IRE refers to the generation of permanent, nanoscale pores in the cell membrane by ultra-short, high voltage impulses, resulting in cell death. Features that make this technique particularly attractive comprise its negligible thermal effect on tissue and the lack of connective tissue destruction distinctive of thermal ablative techniques. Available data from clinical studies indicate IRE as a safe and feasible technique for treatment of selected patients suffering from localized prostate cancer, with limited genitourinary toxicity and promising short-term oncological results. Herein we will review the rationale, as well as the preclinical and clinical data supporting the use of IRE for the treatment of prostate cancer. Furthermore, we will discuss the importance of patient's selection and pretreatment workup with emphasis on the value of magnetic resonance imaging (MRI) for treatment planning.

Learning Objectives:

1. To understand the technology of irreversible electroporation (IRE).
2. To recognise the value of MRI for treatment planning and guidance.
3. To learn about indications, achievable therapeutic results and side effects.

Author Disclosure:

F. Collettini: Advisory Board; Guerbet. Grant Recipient; Berlin Institute of Health (BIH), German-Israeli Foundation for Scientific Research (GIF). Research/Grant Support; Boston Scientific, PharmaCept, Guerbet. Speaker; PharmaCept, Bayer Helathcare, Siemens, Abbott.

09:43

Panel discussion: Can focal therapy already be recommended to prostate cancer patients?

08:30 - 10:00

Room L 8

ESR Research Committee Session

How to foster clinical research in imaging departments

Moderator:

O. Clément; Paris/FR

A-400 08:30

Results of the ESR Survey on European Research

O. Clément; Paris/FR (olivier.clement@aphp.fr)

A survey about the imaging research was launched by the European Society of Radiology in October 2017. There were questions about: (1) preclinical imaging research and small animal imaging platforms. (2) clinical research with the radiologist as a provider of imaging for the clinician. (3) imaging research performed by the radiologist. The results of the survey will be presented, future actions for the development of research in radiology will be discussed.

Learning Objectives:

1. To learn about the results the European survey on research.
2. To understand how preclinical and clinical research in radiology is organised in Europe.
3. To appreciate the differences between countries.

A-401 08:50

An overview of the roles of radiographers in research

J. McNulty; Dublin/IE (jonathan.mculty@ucd.ie)

Research and evidence-based practice (EBP) underpin modern health care and can lead to enhanced patient safety, improved patient outcomes, and efficiencies in service delivery. The contribution of radiographers, academic and clinical, to this evidence through undertaking quality research, on any scale, and subsequent dissemination is essential and will also serve to raise the profile and standing of radiography beyond our profession. Radiographers are much more than facilitators, or data providers, in medical imaging research and some of the leading radiography researchers in the world can be found in Europe. These individuals lead large research groups, successfully compete for national and international research funding, collaborate beyond their profession, and publish in high-impact peer-review journals. In 2016, the European Federation of Radiographer Societies (EFRS) published a Statement on Radiography Research in Europe which clearly sets out the EFRS position on encouraging, supporting and developing high-quality radiographer-led research to strengthen the knowledge base underpinning our profession. This statement, together with the 2015 Statement on Evidence-Based Practice in the Undergraduate Curriculum and the European Qualifications Framework (EQF) Level 6 (bachelors) and Level 7 (masters) Benchmarking documents for radiographers, clearly sets out the importance of a clear research focus on educational programmes. Radiographers can add value at all stages of the research process and for medical imaging research to have a true impact, and to benefit our patients it must be inclusive and multidisciplinary and span the academic-clinical divide.

Learning Objectives:

1. To learn about radiographer roles in research studies.
2. To explore the current status of research education and training for radiographers across Europe.
3. To appreciate the added value radiographers can bring to imaging research.

A-402 09:10

How to structure a research management unit in an imaging department

S. Mallard; Bordeaux/FR (Sabine.mallard@chu-bordeaux.fr)

To structure imaging platforms in our hospitals is a necessity to meet the current criteria of quality insurance in clinical research. Strengthening optimisation and harmonisation of organisations and practices in our imaging departments will increase their attractiveness to pharmaceutical and industrial companies and will provide better chances of success in research calls. Management of such a research unit requires conciliating perspectives of business management, administrative rationalisation and scientific interests. The purpose of this presentation is to report the experience of implementing a research unit in the imaging department of the University Hospital of Bordeaux since 2011.

Learning Objectives:

1. To learn about the role of a specific imaging research unit in an imaging department.
2. To understand how to structure a research unit in an imaging department.
3. To appreciate the results in terms of quality and performance.

A-403 09:30

Implementing quality imaging in multicentre trials

Y. Liu; Brussels/BE (yan.liu@eortc.be)

Imaging is a key component of clinical cancer research and essentially used for trial eligibility confirmation and response assessment in most cases. Nevertheless, difficulties associated with integrating imaging biomarkers into trials have often been ignored, especially for sites that are not familiar with imaging biomarker driven studies. The principles of imaging quality assurance and quality control (QA/QC) are therefore critical to be embedded in infrastructure to guarantee therapeutic progress, taking into account inherent challenges in the complexity of imaging technologies, standardisation of image acquisition across multivendor platforms, and various post-processing options available with advanced software. Ignorance of these pitfalls has a direct negative impact on the quality of the imaging read-out, even leading to trial failure. The imaging modality by which QA is applied varies substantially within and across the disciplines. The imaging quality requirements should be adapted to the role of imaging, disease types, feasibility, and potential variability of imaging readout, additionally with full operational support through the entire conduct of the trial. In this regard, a risk-based framework is practical and recommendations for trials driven by imaging biomarkers will be introduced in this presentation, including identification of risks at trial initiation to better allocate resources and prioritise key tasks.

Learning Objectives:

1. To learn about the role of imaging in clinical trials.
2. To understand the importance of imaging standardisation in multicentre trials.
3. To appreciate the implementation of quality imaging based on risk assessment.

09:50

Panel discussion: How to structure imaging departments for clinical research?

08:30 - 10:00

Room E1

Breast

RC 902

Minimally-invasive local treatment of breast cancer: the time is now

A-404 08:30

Chairperson's introduction

A. Athanasiou; Athens/GR (aathanasiou@mitera.gr)

Breast cancer management has been evolving toward minimally invasive approaches. Image-guided percutaneous biopsy techniques can provide accurate histologic diagnosis thus replacing open surgical biopsies in more than 90% of cases. Breast conservation therapy has become the treatment standard for early-stage breast cancer. Sentinel lymph node biopsy has replaced routine axillary lymph node dissection in selected cases. Is treating early breast cancer without surgery the next challenge? For liver metastases, treatment by means of ablative techniques has widely replaced surgery. Is there any place for minimally invasive treatment of early breast cancer? During this course three main procedures will be presented, and current possible indications, advantages and disadvantages will be analyzed. These procedures include radiofrequency ablation, high intensity focused ultrasound ablation, and cryotherapy ablation. They may offer effective tumor management in selected cases (small < 2cm tumors, elderly patients) and provide treatment options that are psychologically and cosmetically more acceptable than traditional surgery. By means of excessive local heating or freezing under imaging guidance, these procedures can cause cell death and tumor destruction. Surgical excision remains the standard local treatment of breast cancer. However, these procedures may represent an interesting alternative of successful treatment in selected cases. Large prospective trials should evaluate the efficacy, cost-effectiveness, cosmetic results and long-term outcome of minimally invasive, imaging-guided local treatments compared with traditional open surgery approach.

Session Objectives:

1. To learn about HIFU, radiofrequency ablation and cryotherapy that challenge traditional surgical excision in the management of breast cancer.
2. To become familiar with role of imaging in using these new technologies.
3. To understand the potential advantages and disadvantages for each of these techniques.

A-405 08:35

A. High-intensity focused ultrasound (HIFU) therapy

F. Pediconi; Rome/IT (federica.pediconi@uniroma1.it)

Surgical treatment of breast cancer has changed overtime, evolving from radical mastectomy to more conservative approaches. This has been possible thanks to technical advantages in the field of diagnostic imaging that allowed early diagnosis of breast cancers with very small dimensions. Mini-invasive technologies (radiofrequency ablation, cryoablation, etc.) can preserve the original breast volume avoiding glandular resections and surgical scars and ensuring at the same time complete tumor ablation. Ablation with high-intensity focused ultrasound (HIFU) is based on the use of an extra-corporeal ultrasound transducer that selectively destroys target tissue avoiding thermal damages to surrounding structures. The technique can be performed under ultrasound or magnetic resonance (MR) guidance. MR guidance offers several advantages that improve safety and efficacy of the procedure: a visualization of the planned US beam during each phase of the procedure, a real-time monitoring of the progressive temperature increase within the target tissue and surrounding tissues, an accurate treatment planning, an evaluation of the treatment efficacy thanks to the use of intravenous gadolinium-based contrast agent. HIFU ablation of breast cancer is a new and promising technique that deserves large interest in the field of clinical research in order of its potential application in the clinical practice.

Learning Objectives:

1. To learn about the basics of HIFU therapy.
2. To become familiar with the different types of imaging guidance.
3. To appreciate its role in treating benign and malignant lesions.

A-406 09:00

B. Radiofrequency ablation therapy

B. Brkličić; Zagreb/HR (boris@brkljacic.com)

Radiofrequency ablation (RFA) is a promising, but quite rarely used minimally invasive modality to treat small breast cancer in patients in whom general anaesthesia is contraindicated or who refuse surgery. In most studies, cancers were surgically excised shortly after RFA. In very few studies, RFA was used as the only treatment modality, instead of surgery. The procedure is most conveniently performed under ultrasound guidance, in local analgesia, which allows constant contact with the patient during the procedure. Precise preprocedural imaging is crucial, and should include contrast-enhanced MRI in addition to mammography and ultrasound. Preprocedural core biopsy is mandatory, with the precise assessment of the tumour type, grade, and immunohistochemical features. Typical US findings of hyperechogenicity of ablated mass are noted during the procedure. Postprocedural mammographic and MRI findings are characteristic and will be presented. The complete ablation can be achieved in small T1-2 N0 M0 breast cancers that present as masses of maximum 2-3 cm in diameter, with the sufficient distance from the skin and pectoral muscle to avoid the thermal lesion of these tissues. In larger lesions only partial ablation may be achieved. Only solitary, unicentric, invasive ductal cancers, preferably ER/PR positive should be treated. Invasive lobular cancers should not be treated with RFA. Our results will be presented in a small group of patients who were treated with RFA, and who refused surgery, had contraindication to general anaesthesia and opted for RFA. The technique, preprocedural, intraprocedural and postprocedural imaging findings, as well as long-term result will be presented.

Learning Objectives:

1. To learn about how radiofrequency works.
2. To become familiar with its use in clinical practice.
3. To appreciate the advantages and disadvantages.

A-407 09:25

C. Cryotherapy

M.H. Fuchsjaeger; Graz/AT (michael.fuchsjaeger@medunigraz.at)

Cryotherapy is a new, minimal-invasive image-guided treatment option for breast tumours. A specific 12-17G probe is applied into the tumour. Argon gas making use of the Joule-Thomson effect cools down the needle tip to minus 187 degrees centigrade. An ice ball covering lesion and an adequate safety margin is formed. Coagulative necrosis of the tumour cells after two freezing cycles is the result. Cryoablation for breast tumours can be performed under US, CT or MR guidance. Several studies showed an overall success rate of more than 90%. Indications for cryotherapy are small tumours, contraindications to general anaesthesia or increased risk of complications, support of standard therapies and palliative approach. Cryotherapy can be performed under local anaesthesia on out-patient basis with a potential better cosmetic outcome than standard surgical therapies. Minimal-invasive therapies ask for a paradigm-shift as the eradicated tumour is left in situ and resection with clear margins will not be proven histopathologically, but functionally by MR imaging. It is important to emphasize that radiology is not aiming to take over

therapy of breast cancer patients but to help with innovative, less invasive treatment options as a member of a multidisciplinary team. Close cooperation with our clinical partners (surgery, gynaecology, oncology, radiation therapy, etc.) is the key to success and avoidance of turf battles. The goal for the future should be minimal-invasive ablation therapy for breast cancer as a valid therapeutic option.

Learning Objectives:

1. To learn about cryotherapy technique.
2. To become familiar with its use in clinical practice.
3. To appreciate its role in treating benign and malignant lesions.

09:50

Panel discussion: How can we overcome resistance of clinical partner specialities to refer eligible women to radiology?

08:30 - 10:00

Room E2

Neuro

RC 911

Cerebrovascular disease

Moderator:

J.-F. Meder; Paris/FR

A-408 08:30

A. Vascular distribution territories: arterial and venous

T. Engelhorn; Erlangen/DE (Tobias.Engelhorn@uk-erlangen.de)

After a short overview on the vascular anatomy of the brain with a focus on vascular distribution territories, the main focus of this talk is to present neurovascular pathologies closely associated with arterial and venous vascular distribution territories. One focus is also put on the acute stroke and subsequent patient selection for interventional stroke therapy. Another aim is to provide a better understanding of pathophysiology of different neurovascular diseases in an interactive matter. In addition, advantages and limitations of CTA, flat-panel CTA and MRA compared to conventional angiography are presented.

Learning Objectives:

1. To become familiar with the vascular anatomy of the brain.
2. To understand the advantages and limitations of CTA and MRA.
3. To recognise the different imaging patterns in stroke and their prognostic value.

A-409 09:00

B. Arterial dissection and vasculitis

L. van den Hauwe; Antwerp/BE (lucvdhauwe@mac.com)

Cerebrovascular disease may arise from diverse vessel wall pathologies such as atherosclerosis, dissection, and vasculitis. Careful evaluation of the supra-aortic vessels from the aortic arch through the intracerebral vessels is mandatory in all stroke patients, especially in young stroke patients as the second most common cause of stroke in the young is cervicocerebral arterial dissection accounting for 10-25% of ischemic strokes. Reversible cerebral vasoconstriction syndrome (RCVS) and CNS vasculitis are two distinct disease entities with overlapping presenting symptoms. Conventional vascular imaging techniques such as DSA, MRA, and CTA fail to distinguish both entities, as a result of shared nonspecific luminal findings. More recently, there is a growing interest in high-resolution MRI vessel wall imaging that allows direct characterization of the vessel wall abnormalities. Distinct spatial characteristics of arterial wall thickening and wall enhancement have been described. Moreover, differences in the temporal evolution exist with a long period of stable persisting arterial wall findings for CNS vasculitis compared with a shorter period of resolution of vessel wall abnormalities for RCVS. Also these techniques can help to differentiate vasculitis from other causes of vasculopathy, such as atherosclerosis.

Learning Objectives:

1. To learn how to image dissections of the neck vessels and intracranial arteries.
2. To learn about the imaging features of cerebral vasculitis and how to differentiate it from reversible cerebral vasoconstriction syndrome.
3. To become familiar with the most important causes of secondary vasculitis, including infectious causes such as TB and HIV.

Author Disclosure:

L. van den Hauwe: Consultant; icometrix, Leuven/BE.

A-410 09:30

C. Cerebral perfusion studies in cerebrovascular disease: techniques, indications and applications

H.R. Jäger; London/UK

"no abstract submitted"

Learning Objectives:

1. To understand how advanced imaging can help select patients for treatment of acute ischaemic stroke.
2. To show the importance of collateral flow in ischaemic patients.
3. To discuss the current evidence-based medicine (EBM) for treatment of patients with acute ischaemic stroke.

08:30 - 10:00

Room F1

E³ - Rising Stars Programme: Basic Sessions

BS 6

Image-guided therapies in oncology

Moderator:

V. Bérczi; Budapest/HU

A-411 08:30

Kidney

O. Akhan; Ankara/TR (oakhan@hacettepe.edu.tr)

Renal Cell Carcinoma (RCC) is the most common malignant renal tumour seen for an estimated 2% to 3% of all malignancies in the United States. The incidence of renal tumours has reached a plateau in the developed countries in recent period it is still an increasing problem in the developing countries. However the incidence of the incidentally detected renal masses has increased in the last decade. Therefore, the management of RCC has greatly changed in this period from radical nephrectomy to nephron-sparing treatment options such as partial nephrectomy or local ablative therapies carried out with RFA, Microwave or Cryoablation. Although the guideline of the American Urological Association suggests partial nephrectomy as a standard treatment option for T1 renal masses, local ablative approach with RFA, Microwave or Cryoablation are getting to be more applied for the treatment. Relative contraindications for the ablative procedures include proximity to the central collecting system, bowel or adrenal glands. These limitations are overcome by the fluid injection along the margin of the targeted lesion by displacing these anatomical structures. The main indications for Renal Artery Embolisation (RAE) include preoperative embolisation before nephrectomy, angiographic treatment of angiomyolipoma, an adjunctive treatment for RCC ablation and for palliation of advanced-stage RCC. RAE is also indicated to reduce blood loss before resection of metastatic RCC.

Learning Objectives:

1. To have a basic knowledge about indications and limitations of interventional radiology procedures in renal malignancies.
2. To have a basic knowledge about embolisation of renal tumours.
3. To become familiar with ablation of renal tumours.

A-412 08:53

Lungs

M. Bezzi; Rome/IT (mario.bezzi@uniroma1.it)

Percutaneous needle biopsy has been a mainstay of oncologic diagnosis for more than three decades, since the advent of CT and ultrasound. Percutaneous needle biopsy has become the standard of care in the diagnosis of most lung tumors and is also used to diagnose non cancerous conditions, such as infection. The technique is also beneficial in the staging of patients with cancer, particularly when another treatment method may be more appropriate than surgical resection. Advantages of percutaneous biopsy over surgical excisional biopsy include time and cost savings and reduction in morbidity. Aim of this presentation is to discuss the practical aspects of lung biopsy, needle selection, and guidance techniques and to show how to approach difficult lesions and avoid complications. About 70% of patients with lung cancer are not surgical candidates, either due to advanced disease or comorbidities. Thermal ablation is a minimally invasive treatment that is commonly used in this group of patients, with promising results. Currently, the most widely used ablation techniques in the treatment of lung malignancies are radiofrequency ablation (RFA), microwave ablation, and cryoablation. This presentation reviews the application of thermal ablation in the thorax, including patient selection, basics of procedure technique, imaging follow-up, and treatment results.

Postgraduate Educational Programme

Learning Objectives:

1. To have a basic knowledge about indications and limitations of interventional radiology procedures in lung malignancies.
2. To have a basic knowledge about image-guided biopsy.
3. To become familiar with ablation of lung cancer.

A-413 09:15

Bones

A. Gangji; Strasbourg/FR (gangji@unistra.fr)

Different image-guided percutaneous techniques can be used for treatment of musculoskeletal tumours. The management of patients with bone tumours requires consideration of: histology of the tumour with differentiation of benign and malignant tumours, careful clinical evaluation of the patient's general condition, understanding of the disease process, appreciation of the degree of bone destruction (biomechanics and consolidation), thorough working knowledge of available treatment options, multidisciplinary decision-making, and precision of the treatment goal: curative or palliative. Curative ablation can be applied for the treatment of specific benign or in selected cases of malignant localized bone tumours. Curative treatment: the therapeutic goal is to ablate the tumour completely and definitively. Pain palliation therapy of primary and secondary bone tumours can be achieved with safe, fast, effective, and tolerable percutaneous methods. Palliative treatment: the therapeutic goal is not complete ablation of the tumour, but pain palliation. Ablation (chemical, thermal, mechanical), and consolidation (cementoplasty, screw fixation...), embolisation techniques can be used separately or in combination.

Learning Objectives:

1. To have a basic knowledge about indications and limitations of interventional radiology procedures in bone malignancies.
2. To understand the basic concepts of embolisation of bone tumours.
3. To have a basic knowledge about bone tumours ablation.

Author Disclosure:

A. Gangji: Other; proctoring Galil medical.

A-414 09:38

Liver

J.I. Bilbao; Pamplona/ES (jibilbao@unav.es)

The liver has a dual vascular supply with seventy five percent of the blood comes from the portal vein and the rest from the hepatic artery. Small (< 1mm) tumors are initially nourished by portal branches; however, when they start growing they deliver pro-angiogenic agents which may create an arterial network that ensures its vascularization. Thus, liver tumors are almost exclusively vascularized by the hepatic artery and can be safely treated by an endovascular approach. The angiographic appearance of a liver tumor depends on the amount of the arterio-capillary network and hypervascular tumors are easily detected and more adequate for receiving endovascular treatments. One therapeutic possibility is to occlude the vascular network and close the afferent vessels ("embolization") provoking ischemia that will lead to necrosis. However, since the tumor send continuous pro-angiogenic signals, if there is a decrease in the blood supply, the ischemic effect will trigger an increase in angiogenesis. For abolishing such effect it is possible to add chemotherapeutic agents ("chemoembolization"), together with the occluding particles, with the aim of obtaining a more complete antineoplastic effect. A different approach consists in the use of small particles just as carriers, with no occluding effect, that will place an anticancer agent intratumourly. When the agent is a radioisotope the procedure is called "radioembolization", a form of brachytherapy. By using a percutaneous access, some tumors (<3cm) can be punctured with probes through which energy (heat radiofrequency/microwaves or cold cryotherapy) is delivered which will lead to tumoural necrosis ("ablation").

Learning Objectives:

1. To understand the basic concepts of chemoembolisation in liver malignancies.
2. To understand the basic concepts of radioembolisation in liver malignancies.
3. To have a basic knowledge about liver tumours ablation.

Author Disclosure:

J.I. Bilbao: Advisory Board; sirtex medical, Terumo.

08:30 - 10:00

Room D

Musculoskeletal

RC 910

Imaging the hip and thigh

Moderator:

M. Klontzas; London/UK

A-415 08:30

A. Femoroacetabular impingement: what is it, how do I image it and does it matter?

R. Sutter; Zurich/CH

The last decade has seen a constant rise in the number of patients diagnosed and treated for femoroacetabular impingement (FAI). However, there are ongoing controversies about the accuracy of measurements for assessing FAI and an associated overdiagnosis of FAI. This refresher course covers the pathophysiology of FAI, the classic osseous hallmarks, and the characteristic damage to the articular cartilage and labrum. It gives an overview of state-of-the-art FAI imaging with different radiological modalities, including the use of traction at MR arthrography, and addresses possible pitfalls when evaluating the hip joint. Additional anatomical factors are described that contribute to the development of FAI, such as abnormal femoral antetorsion and acetabular version. And finally, the relevance of the different parts of the diagnostic algorithm for evaluating FAI are discussed.

Learning Objectives:

1. To understand the mechanism of femoroacetabular impingement.
2. To learn about the imaging findings in patients with femoroacetabular impingement.

A-416 09:00

B. Groin pain in the athlete: what causes it and what does imaging contribute?

P. Robinson; Leeds/UK (philip.robinson10@nhs.net)

Groin pain in the athlete is a complex process with different researchers focusing on the symphysis pubis joint, the adductor longus enthesis, pubic subchondral stress fractures, lower abdominal muscle abnormalities as well as inguinal muscular and aponeurotic tears. There is also confusion over terminology with, for example, osteitis pubis and sportsman's hernia encompassing many different potential conditions for different clinicians. In reality there is a lot of crossover with many or all of the above regions thought to be involved by chronic shearing forces acting through the symphysis pubis and surrounding soft tissues. This lecture will review: (1) Biomechanics and functional anatomy of the anterior pelvis in relation to athletes especially kicking sports. (2) Theories and nomenclature for the pathogenesis of chronic groin pain in athletes. (3) Imaging findings in symptomatic and asymptomatic athletes focussing on the use of MR imaging. (4) The interpretation of these findings and what research shows they relate to in terms of diagnosis, prognosis and decision making for treatment.

Learning Objectives:

1. To understand the anatomy of the groin region.
2. To learn about the imaging findings in athletes with groin pain.

A-417 09:30

C. Muscle injury of the hip and thigh

M.-A. Weber; Rostock/DE (marc-andre.weber@med.uni-rostock.de)

This lecture will focus on MRI for the assessment of muscle injuries at the hip and thigh using fluid sensitive sequences. Muscle injuries include a large variety of imaging patterns from occasionally subtle changes in muscle strain to complete muscle tears. Exercise-related chronic changes such as delayed onset muscle soreness, compartment syndrome, and muscle hernias, as well as complications of muscle injuries such as myositis ossificans may be encountered. The MRI appearance of a muscle contusion may be similar to a muscle strain/tear. Mild post exercise oedema can persist for some time and can mimic a low grade muscle strain injury. 35% of all soccer injuries are muscle injuries and they are the most frequent cause for missing a game. The myotendinous junction is the weakest link in the muscle-tendon-bone chain. The widely used grading system for muscle injuries divides muscle injuries in four grades (grade 0: normal MRI, i.e., functional injury of the muscle, grade 1: oedema, grade 2: partial rupture, grade 3: complete tear). However, this grading system is only a rough estimate, because grade 2 injuries comprise a wide range from tiny fibre discontinuities to subtotal muscle ruptures. Measures of the longitudinal length as well as the percentage and volume of the muscle injury in MRI have some predictive value with respect to time to return to sports

Postgraduate Educational Programme

activities. Moreover, injury to the intramuscular component of the tendon has prognostic significance. A complete tear (grade 3) may require surgery.

Learning Objectives:

1. To understand the imaging patterns of muscle injury at the hip and thigh.
2. To learn about grading and prognostic values of muscle injuries.

08:30 - 10:00

Room G

EFOMP Workshop: Radiation dose management systems and repositories: the present and the future

EF 1

Dose management systems and repositories: part A

Moderator:

A. Trianni; Udine/IT

A-418 08:30

Chairperson's introduction

J. [Damilakis](mailto:damilaki@med.uoc.gr); Iraklion/GR (damilaki@med.uoc.gr)

Dose management systems collect dose data from imaging systems that can be displayed in a variety of formats for analysis and benchmarking. Reviewing practices helps identify areas for improvement. They also play an important role in the establishment of local dose reference levels. Dose repositories are central places directly accessible to users in which an aggregation of dose data is kept in an organised way for benchmarking, research, dose optimisation, and patient dose reduction. However, there are challenges in developing these systems. Their creation is an expensive process, there are technological difficulties, security and legal issues and issues related to coding systems. Coding is required in different steps across the imaging workflow, i.e., for ordering and performing of imaging procedures, reporting of findings and for quality processes such as radiation exposure measurement and reporting. The degree of variability in procedure names is a considerable challenge. A tool is needed to help facilities map names of procedures, clinical symptoms, anatomical locations, findings, etc. to the closest matching of a standardised catalogue.

Session Objectives:

1. To become familiar with the main features of dose management systems and repositories.
2. To discuss the services provided by these systems.
3. To understand how dose management systems can optimise medical imaging.

A-419 08:35

The 'EuroSafe Imaging' campaign's point of view

G. [Frija](mailto:guy.frija@aphp.fr); Paris/FR (guy.frija@aphp.fr)

"no abstract submitted"

Learning Objectives:

1. To become familiar with the EuroSafe Imaging campaign's point of view regarding dose management systems and repositories.
2. To understand why collaboration among radiologists, medical physicists and radiographers is needed for the optimum use of these systems.
3. To learn the impact of dose management systems and repositories in the clinical practice.

A-420 09:05

Strategies for dose management for achieving optimised imaging

J.N. [Vassileva](mailto:j.n.vassileva@gmail.com); Vienna/AT (j.n.vassileva@gmail.com)

International standards and guidelines express the need for medical facilities to monitor patient radiation doses for the imaging procedures they perform. The monitoring process includes several steps: recording of relevant patient exposure and dose-related data at the facility and their collection and analysis. The amount of information and the method of recording and collecting depend on the purpose, modality, and model. Collected data from different patients, modalities, and units are combined and processed to perform relevant dose analysis, which might include statistics, trending, tracking, or comparisons. This can be done at local, regional, national, or international level. Data quality evaluations should be conducted at all steps. Analysis of collected data may be at the level of group of patients, or at the level of individual patients. Analysis at the level of group includes setting typical doses and diagnostic reference levels, procedural optimisation, monitoring operations and trends in the clinical practice, and tracking over time. Samples based on specific examination, patient group, or acquisition conditions should be well defined. Availability of a

good coding system of examination and protocol nomenclature is crucial. Tracking of exposure history of individuals requires patient identification. It is useful to avoid performing redundant radiological examination and optimise the overall patient care. A dose data management infrastructure may deploy an integrated electronic system, the interface and functionalities of which depend on the intentional user groups. Ideally, it should be integrated with the general patient information systems. If properly implemented, the patient exposure data management contributes to the improvement of radiation protection and patient care.

Learning Objectives:

1. To learn about the main features of a system for collection and analysis of dosimetric data.
2. To become familiar with different analytical uses of collected dose data.
3. To understand how patient exposure data management fits into the framework of continuous optimisation of medical imaging.

A-421 09:35

The benefits of dose management systems in view of the new Euratom Directive

V. [Tsapaki](mailto:virginia@otenet.gr); Athens/GR (virginia@otenet.gr)

The New Council Directive 2013/59/Euratom lays down basic safety standards for protection against the dangers arising from exposure to ionising radiation, repealing relevant previous directives. It forms a solid pillar for radiation protection in Europe and aims to enhance it according to the state of science and technology. Dose management systems are sophisticated software with friendly interface, that provide a structured way to monitor all data included in the digital Imaging and communication in medicine (DICOM) header of digital X-ray machines or data recorded in the picture archiving and communication system (PACS) of the hospital. They can facilitate in defining diagnostic reference levels, in identifying unusual high patient radiation dose, in detecting incidents and/or accidents in all imaging X-ray modalities of the radiology department. The presentation will go through the articles of the directive and show possible ways that these systems can help to comply with the directive.

Learning Objectives:

1. To understand how the dose management tools can help in implementation of the new European Directive.
2. To become familiar with the different capabilities of the dose management tools and their connection with the European Directive.
3. To identify the possible limitations of dose management tools in relation with the European Directive.

08:30 - 10:00

Room K

Special Focus Session

SF 9b

Radiographers in preclinical imaging research

A-422 08:30

Chairpersons' introduction (part 1)

C. [Buissink](mailto:c.buissink@pl.hanze.nl); Groningen/NL (c.buissink@pl.hanze.nl)

The role of radiographers in preclinical imaging research - that's the question? There are several methods and opinions to give answers on this question. To formulate your own opinion you need background information. Get familiar with the preclinical imaging research objectives and constraints and the impact of the radiographers in this process.

Session Objectives:

1. To learn more about the techniques devoted to preclinical imaging research.
2. To become familiar with the preclinical image research objectives and constraints.
3. To appreciate the impact of radiographers in preclinical imaging research.

A-423 08:33

Chairpersons' introduction (part 2)

N. [Grenier](mailto:nicolas.grenier@chu-bordeaux.fr); Bordeaux/FR (nicolas.grenier@chu-bordeaux.fr)

Involvement of radiographers in preclinical imaging remains limited because most centres are driven by researchers. Radiographers' skills covering technical, anatomical and clinical fields could be highly beneficial to these research centres. On the other hand, involvement of radiographers in new preclinical molecular and quantitative imaging methods, which are highly growing fields, could be highly beneficial for their own professional development and to clinical structures when returning to clinical imaging. This

Postgraduate Educational Programme

session will develop these win-win issues as well as, several fields of quantitative imaging using MRI and nuclear medicine.

Session Objectives:

1. To learn more about the techniques devoted to preclinical imaging research.
2. To become familiar with the preclinical image research objectives and constraints.
3. To appreciate the impact of radiographers in preclinical imaging research.

Author Disclosure:

N. Grenier: Advisory Board; Supersonic Imagine, Aix-en-Provence, France.

A-424 08:35

Radiographers in preclinical research: challenges and chances

J.-P. [Dillenseger](mailto:jdillenseger@ipdil.me.com); Strasbourg/FR ([ipdil@me.com](mailto:jdillenseger@ipdil.me.com))

Small animals imaging is a growing field which is appearing as an essential step filling the gap between preclinical and clinical research domains; at the University Hospital of Strasbourg, a preclinical imaging unit has been identified since 2011. This unit is located in the middle of the clinical imaging department. Its philosophy is to apply translational imaging research with the same modalities that can be found in a clinical imaging department (e.g., SPECT, CT and clinical field MRI), but it also aimed at working with a similar organisation. We believe that the best way to achieve this goal is to recruit a radiographer in such preclinical department. The place of radiographers in such a preclinical laboratory seems evident for us to benefit from their clinical experience, practical skills as well as general and deep knowledge in medical imaging. All the tasks performed are in accordance with the new French decree (decree 2016-1672 - Dec. 5, 2016); preparation of the subject before any imaging act (e.g., care and registration). - Radiation safety procedures implementation (e.g., dosimetry management, laboratory contamination controls, management of radioactive waste products) - Quality controls - Preparation and administration of contrast agents and radioactive tracers - Imaging devices operation (positioning, parameters setting, post-processing and data management) - Research and training (e.g., close relationship with researchers, physicians and engineers; radiographers trainees). Our experience demonstrates that the integration of a radiographer in a preclinical imaging department is an added value to scientific projects and provides a fluent organisation. Radiographer collaboration with a research team improves and facilitates sequence of procedures and consequently increases the throughput. We believe that preclinical imaging will offers new opportunities for radiographers in the future.

Learning Objectives:

1. To learn about the importance of translational imaging research.
2. To understand the contribution radiographers can play in preclinical research.
3. To appreciate essential skills and knowledge required in preclinical imaging.

A-425 08:53

Preclinical evaluation of PET tracers

M. [Zeilinger](mailto:markus.zeilinger@thwn.ac.at); Wiener Neustadt/AT (markus.zeilinger@thwn.ac.at)

Molecular imaging, especially the field of PET, becomes a vital and versatile modality for modern medicine, as well as for applied medicinal research. Common indications belong to diagnosis, differential diagnosis, therapy control, prevention of diseases and research of pathophysiological processes. The potential of molecular imaging and their capabilities strongly depends on the presently developed and established imaging probes. Hence the evaluation and development of new selective radiopharmaceuticals would be an indispensable part to increase the scope of application for molecular imaging. The key factor in the evaluation of potential PET radiotracers is the selection of substances with high affinity, selectivity and low unspecific binding. Thus, several preclinical procedures, such as biodistribution experiments, ex-vivo and in-vitro autoradiography, metabolic stability testing, cell binding studies, μ PET-experiments, and the appropriate data post-processing, as well as biomedical imaging quantification procedures are necessary.

Learning Objectives:

1. To understand the connection between molecular imaging and the drug discovery process.
2. To become familiar with quantitative molecular imaging approaches.
3. To review technical and biomedical limitations and future perspectives.

A-426 09:11

SPECT/CT

S. [Heskamp](mailto:Heskamp@radboudumc.nl); Nijmegen/NL (Sandra.Heskamp@radboudumc.nl)

MicroSPECT/CT imaging can provide important information regarding the biology of tumours and other disease processes. It can be used to measure the expression of tumour-associated antigens, for example, to develop a novel biomarker for targeted therapies. Furthermore, theranostic agents can be

developed which combine the potential of diagnosis and radionuclide therapy. For example, ^{111}In -PSMA targeting molecules have been used to image prostate cancer xenografts and to calculate the maximum tolerable dose before kidney toxicity would occur during ^{177}Lu -PSMA-targeted radionuclide therapy. Finally, microSPECT/CT imaging can be used to monitor therapy induced changes in the tumour microenvironment, such as the expression of growth factors, tumour vasculature, and the presence of immune cells.

Learning Objectives:

1. To understand the basic principles of preclinical SPECT/CT and the differences with clinical SPECT/CT.
2. To become familiar with the practical aspects which are relevant for preclinical SPECT/CT.
3. To appreciate how preclinical SPECT/CT can help to answer basic oncological research questions.

A-427 09:29

Small animal imaging studies

F. Pichler, M. [Zeilinger](mailto:zeilinger@wiener-neustadt.at); Wiener Neustadt/AT

Several topics like species differences, technical limitations, anaesthesia, and physiological constraints have to be taken into account for small animal imaging studies. Considering that mice are approximately 20 times smaller and 1500 times lighter compared to humans certain challenges occur. Furthermore, nuclear medicine positron emission tomography (PET) systems for humans are around 5 times larger in diameter compared to preclinical μ PET-systems. Besides that, injected activities are increased in small animals to compensate for the lack of sensitivity in preclinical systems. In this regard, also the substance volume that can be administered is a limiting factor, especially when several substances like the radiotracer, inhibitors and possibly contrast media have to be applied. Anaesthesia effects are another source of error which have to be considered on an individual basis. For instance, intraperitoneal administered ketamine/xylocaine leads to increased FDG uptake in peripheral regions while inhaled isoflurane decreases FDG uptake in the brain. The origin of these effects is not yet fully understood. The choice of anaesthesia can also influence the final positioning in the field of view of the scanner. This means that with injection anaesthesia a free positioning is possible whereas with gas anaesthesia the inhalation mask limits the final position. Lastly, all experiments have to be planned in compliance with the 3R principle (replacement, reduction, and refinement), which has to be considered for all decisions.

Learning Objectives:

1. To understand work-related challenges in preclinical small animal imaging.
2. To consider limitations in the quantification of preclinical μ PET data.
3. To appreciate the radiographers role in a preclinical environment in contrast to clinical work.

09:47

Panel discussion: Is there a role for radiographers in preclinical imaging research?

08:30 - 10:00

Room M 1

Professional Challenges Session

PC 9

How can radiologists expand their role in peripheral vascular intervention?

A-428 08:30

Chairperson's introduction

R. [Iezzi](mailto:roberto.iezzi.md@gmail.com); Rome/IT (roberto.iezzi.md@gmail.com)

Peripheral arterial disease (PAD) continues to grow in global prevalence, consuming an increasing amount of resources in the health care system. Overall rates of intervention for PAD have been rising steadily in recent years. Changing demographics, evolution of technologies, and an expanding database of outcomes studies are primary forces influencing clinical decision making in PAD. The management of PAD is multidisciplinary, involving primary care physicians and vascular specialists with varying expertise in diagnostic and treatment modalities. This approach has the greatest chance of providing optimal care for the patients and ensuring ongoing surveillance of the patient's overall health, ultimately resulting in better quality of life and increased longevity. Furthermore, it has been recognized that clinical management of patients undergoing interventional radiological procedures is an essential component of a successful, contemporary interventional radiology practice, with several well-respected interventional radiologists emphasizing the importance of direct patient management. To effectively participate in patient

Postgraduate Educational Programme

management, interventionalists require a clinical knowhow as well as an infrastructure within their practice to support these services. All these clinical as well as radiological aspects need to be integrated and implemented in dedicated vascular intervention training programmes. Main goals of these programs should be to provide IR fellows with an organized, comprehensive, supervised, full-time educational experience including the ability to provide consultation and case selection, perform the full array of vascular and interventional procedures, identify and manage potential complications, provide appropriate peri-procedure care, and assist in long-term management integrated with the clinical management of referring physicians.

Session Objectives:

1. To focus on the needs for and challenges in organising a multidisciplinary team.
2. To understand the role of clinical as well as radiological evaluation for outpatients consultation and post-procedure visits.
3. To understand how to implement vascular intervention training programmes.

A-429 08:35

How to improve your clinical knowledge

C.W. Kopp; Vienna/AT (christoph.kopp@meduniwien.ac.at)

For decision-making within the vascular board, it is important to understand not only the anatomy and potential revascularisation strategies, but also to respect the patient's clinical status, age and frailty, renal impairment, as well as cardiovascular and bleeding risk to impact on both symptom relief and prognosis in PAD patients, regarding wound healing and limb salvage. Cutting edge studies have recently changed our understanding of how to implement the best medical treatment for the underlying disease of atherosclerosis and atherothrombosis. This talk will focus on major cardiovascular risk factors and their respective best medical treatment, ranging from goals of antihypertensive and lipid-lowering treatment and vascular protection from new antidiabetics to strategic changes in the treatment of atherothrombosis, including the current recommendation of NOACs and antiplatelet therapy in PAD. Finally, caveats of age such as frailty, renal impairment and the safe use of contrast media will be covered.

Learning Objectives:

1. To become familiar with clinical diagnosis and classification of arterial occlusive disease.
2. To understand the disease states being treated and their clinical management.
3. To learn about intraprocedural and postprocedural medical treatment.

A-430 08:53

How to improve your diagnostic skills

T. Leiner; Utrecht/NL (t.leiner@umcutrecht.nl)

Non-invasive vascular imaging is now considered a cornerstone of the pre-interventional workup of patients with peripheral arterial disease. Although imaging is not needed to establish the diagnosis, imaging provides a roadmap for endovascular intervention and it can outline surgical therapeutic options. In my lecture I will discuss the strengths and limitations as well as the practical implementation of the most commonly used non-invasive imaging tools to assess peripheral arterial disease.

Learning Objectives:

1. To understand the crucial role of US in the diagnostic assessment and patient recruitment.
2. To learn when is needed to perform a MRA, CTA, or DSA examination.
3. To learn the optimal imaging algorithm for diagnosis and follow-up.

Author Disclosure:

T. Leiner: Research/Grant Support; Philips Healthcare; Bayer Healthcare. Speaker; Philips Healthcare; Bayer Healthcare.

A-431 09:11

How to improve your relationship with the vascular surgeon

C. Ferrer; Rome/IT

"no abstract submitted"

Learning Objectives:

1. To understand the challenges of open surgical treatments.
2. To learn about hybrid (surgical and endovascular) treatments.
3. To learn about outcomes of open surgical procedures.

A-432 09:29

How to improve your technical/procedural skills

K. Katsanos; Patras/GR (katsanos@med.upatras.gr)

Percutaneous endovascular interventions have evolved to the mainstay treatment of peripheral arterial disease manifesting as short distance claudication or critical limb ischemia (CLI). Several new technologies, such as biomimetic metal stents, drug-eluting stents, covered stents, and drug-coated balloons, have emerged to address the Achilles heel of neointimal hyperplasia and restenosis, and thereby improve long-term patency outcomes. Novel techniques of arterial access and recanalisation, like the pedal or transradial approach, the pedal-loop techniques, and complex rendezvous strategies may help save legs in cases of advanced CLI with severe anatomical complexity. Transcatheter atherectomy may achieve atherosclerotic plaque clearance by means of directional plaque excision or rotational plaque removal or laser plaque ablation. Debulking atherectomy may allow for a more uniform angioplasty result at lower pressures with consequently less vessel barotrauma, improved luminal gain and potential combination with drug-coated balloons without permanent stent implants. Newer functional imaging modalities such as perfusion angiography and near infrared spectroscopy to monitor deep tissue oxygen levels will be part of multimodality peripheral interventions of the future.

Learning Objectives:

1. To understand how to perform an accurate treatment planning.
2. To learn how to select the right endovascular treatment for the right patient.
3. To understand the challenges and future prospective of endovascular devices and treatments.

09:47

Panel discussion: Are we ready to be more of a clinician rather than an operator?

08:30 - 10:00

Room M 2

E³ - ECR Master Class (Head and Neck)

E³ 926

Distant metastases of head and neck cancer

A-433 08:30

Chairperson's introduction

P.-Y. Marcy; Ollioules/FR (brozpy@gmail.com)

We aim to understand the impact of distant metastases diagnosis in head and neck treatment. Imaging modalities are important in diagnosis and treatment planning, post-treatment assessment, and residual mass (DCE MR), local failure (early intra-treatment DW MR), and locoregional and distant metastases recurrence/second primary/complication assessment. They provide anatomical images, but also functional-based MRI/ PET: molecular/metabolic/physiological information. Cost-effectiveness studies are mandatory to evaluate the impact of imaging on the QoL and overall survival in head and neck cancer patients.

Session Objective:

1. To understand impact of the distant metastases in the head and neck treatment.

A-434 08:35

A. Incidence and prognosis of synchronous cancer or distant metastases from head and neck tumours

A.D. King; Hong Kong/CN (king2015@cuhk.edu.hk)

Distant metastases: The advance in treatment of head & neck carcinoma (HNC) has improved locoregional control and so distant metastases (DM) are emerging as a major determinant of survival. Therefore, a more active approach is being taken to detect and manage distant site disease, including the use of a new generation of immunotherapy agents. Most DM do not manifest until after initial treatment, prognosis tends to be poor with patients succumbing to disease within a year. However, prognosis is dependent on many factors which include histology, site and number of DM. Notably some patients survive long term and there is a subgroup of patients with oligometastases who have potentially curable disease. In this presentation, incidence, risk factors, sites, prognosis, and management will be discussed according to the main histological groups of carcinoma that arise in the aerodigestive tract including squamous cell carcinoma (SCC), thyroid and salivary glands. Second primary tumours: Head & neck cancer has one of the highest associations with a second primary tumour (SPT). Risk factors for SCC

include smoking and high alcohol intake, and so these patients are also at risk of SPTs in other sites of the head & neck, lungs and oesophagus. Less commonly SPTs arise in the colon, pancreas and bladder. SPTs are usually metachronous, with synchronous tumours being diagnosed in only ~ 4% of patients. SPTs are a leading cause of death in patients with early stage SCC, but those SPTs detected early are potentially curable.

Learning Objectives:

1. To become familiar with the incidence of the synchronous tumours in the head and neck population.
2. To become familiar with the incidence of the distant metastases in the patients with newly diagnosed head and neck cancer.
3. To understand the consequences in a prognosis.

A-435 08:58

B. Is morphologic imaging enough to stage patients with head and neck tumours before therapy?

S. Rohde; Dortmund/DE (stefan.rohde@klinikumdo.de)

The lecture will focus on the importance of morphologic imaging in the management of patients with head and neck malignancies. Imaging features of local and distant tumour recurrence will be presented, and the potential and limitations of morphologic imaging modalities including diffusion and perfusion techniques will be discussed.

Learning Objectives:

1. To review current guidelines and clinical practice.
2. To understand the advantages and disadvantages of the conventional imaging modalities.
3. To appreciate cost-effectiveness of different imaging modalities.

A-436 09:21

C. Is functional imaging necessary to detect distant metastases in head and neck cancers?

R. Maroldi; Brescia/IT

"no abstract submitted"

Learning Objectives:

1. To learn about functional imaging (DWI, DECT, PET) in head and neck cancer patients.
2. To understand the advantages and disadvantages of the functional imaging modalities.
3. To review the advanced imaging for detection of distant metastases of head and neck cancer.

09:44

Panel discussion: Where and how to search for distant metastases in head and neck cancer

08:30 - 10:00

Room M 3

ESR Working Group on Ultrasound

WG 2

Tips and tricks for abdominal ultrasound

A-437 08:30

Chairpersons' introduction (part 1)

M. Claudon; Vandoeuvre-les-Nancy/FR (m.claudon@chu-nancy.fr)

The evaluation of normal and abnormal abdomen is one of the major clinical indications for sonography. Flow imaging, including Doppler techniques and contrast-enhanced ultrasound (CEUS), are now commonly used for the liver and more and more often for the spleen, pancreas and intestine. Elastography of the liver has slowly arisen as a current modality in many institutions. The ability to fuse CT, MRI, or PET-CT/MRI with real-time ultrasound has further increased the interest of ultrasound as a second- or third-level diagnostic modality as well as for interventional purpose. Radiologists, especially juniors, should be confident in using these modalities and be aware of the many tips and tricks they offer.

Session Objectives:

1. To learn about actual indications and applications of ultrasound Doppler imaging, CEUS, elastography and ultrasound fusion imaging.
2. To show better parameter settings for optimal technical results illustrating tips and tricks for technical and clinical successful examinations.
3. To become familiar with the new ultrasound imaging techniques and applications.

Author Disclosure:

M. Claudon: Speaker; Philips Ultrasound.

A-438 08:35

Chairpersons' introduction (part 2)

V. Valek; Brno/CZ (vlvaleb@med.muni.cz)

Ultrasound is a non-invasive accessible and versatile diagnostic technique that uses high frequency ultrasound waves to outline organs of the human body without ionising radiation in real time and with the capacity to visualise several planes. The high diagnostic yield of the technique has made it a routine method in daily medical practice. CEUS has the ability to characterise parenchymal organ lesions and has been proven superior to colour and power Doppler ultrasound in the detection of tumour vascularity. Ultrasound Tissue Doppler imaging (US-TDI) has been used to diagnose regional wall motion (WM) abnormalities in coronary artery disease and other indications. The recent development of ultrasound elastography techniques allows a non-invasive method of estimating organ structure. Transient elastography (TE) is a non-imaging elastographic technique, while point shear wave (p-SWE) and 2D-SWE combine imaging with elastography. The evidence at this time suggests that p-SWE is as accurate but more reliable than TE, while 2D-SWE is more accurate than TE. Fusion imaging combines the advantages of ultrasound and CT/MRI while avoiding their disadvantages. It is often achieved by using an external electromagnetic field system with a position sensor mounted on an ultrasound transducer. This allows tracking of transducer movements and matching ultrasound and CT/MRI image datasets, the real-time ultrasound image moves with the CT/MRI image. Once the two images match well, the target lesion on ultrasound image can be located according to the CT/MRI image. It is important to become familiar with these new ultrasound imaging techniques and their applications.

Session Objectives:

1. To learn about actual indications and applications of ultrasound Doppler imaging, CEUS, elastography and ultrasound fusion imaging.
2. To show better parameter settings for optimal technical results illustrating tips and tricks for technical and clinical successful examinations.
3. To become familiar with the new ultrasound imaging techniques and applications.

A-439 08:40

Doppler imaging

F. Calliada; Pavia/IT (fabrizio.calliada@gmail.com)

Doppler is surely not a new imaging technique, but an adequate knowledge of the basic physics and of the scanner tuning is essential to avoid errors and misunderstanding. The first part the presentation will cover the principal sources of error that should be avoided during a Doppler examination and the major tuning tricks needed for an optimal and successful examination. In the second part, we will try to become familiar with new Doppler imaging techniques dedicated both to very low velocity microvascular flow and to high velocity complex flow representation.

Learning Objectives:

1. To learn about actual indications and applications of Doppler imaging.
2. To show better parameter settings for optimal technical results.
3. To illustrate tips and tricks for technical and clinical successful examinations.
4. To become familiar with the new Doppler imaging techniques and applications.

Author Disclosure:

F. Calliada: Speaker; Toshiba, Mindray, Hitachi.

A-440 09:00

CEUS

M. D'Onofrio; Verona/IT (mirko.donofrio@univr.it)

Contrast-enhanced ultrasonography (CEUS) is a safe and accurate imaging method to evaluate the vascularity of abdominal organs. CEUS improve the ultrasound characterization of tumoural masses. CEUS should be performed when possible immediately after the US detection of indeterminate mass in abdominal organs. CEUS is accurate in the characterization of neoplastic lesions such as liver metastases and pancreatic ductal adenocarcinoma. The use of CEUS in studying focal liver and pancreatic lesions found at US, especially in the same session of ultrasound examination, is therefore recommended to promote faster diagnosis. In particular, liver metastases detection could be improved by the use of contrast-enhanced ultrasound with respect to basal examination. The actual indications and applications of CEUS are presented in official published guidelines. Every CEUS examination should be performed with the better parameter settings for optimal technical results.

Postgraduate Educational Programme

Learning Objectives:

1. To learn about actual indications and applications of CEUS.
2. To show better parameter settings for optimal technical results.
3. To illustrate tips and tricks for technical and clinical successful examinations.
4. To become familiar with the new CEUS techniques and applications.

Author Disclosure:

M. D'Onofrio: Advisory Board; Siemens, BRACCO. Consultant; Bracco, Siemens. Speaker; Bracco, Siemens.

A-441 09:20

Elastography

D.A. [Clevert](mailto:Dirk.Clevert@med.uni-muenchen.de); Munich/DE (Dirk.Clevert@med.uni-muenchen.de)

Elastography has become a standard-of-care supplementary ultrasound imaging modality in modern radiological diagnostic in recent years and is an ideal tool for the detection and characterization of tissue properties. With different elastography techniques, it is possible to quantitatively as well as qualitatively assess tissue properties. In daily clinical routine, elastography is mostly used in oncological imaging as well as in the quantification of liver stiffness for the evaluation of liver fibrosis and cirrhosis. The benefits of elastography are the cost-effectiveness of the method, being a non-invasive imaging modality and the easy application of the technique. This course describes the most common applications of ultrasound elastography in daily clinical routine.

Learning Objectives:

1. To learn about actual indications and applications of elastography.
2. To show better parameter settings for optimal technical results.
3. To illustrate tips and tricks for technical and clinical successful examinations.
4. To become familiar with the new elastography techniques and applications.

Author Disclosure:

D.A. Clevert: Advisory Board; Siemens, Samsung, Philips, Bracco. Speaker; Siemens, Samsung, Philips, Bracco.

A-442 09:40

Fusion imaging

C. [Ewertsen](mailto:caroline.ewertsen@dadnet.dk); Copenhagen OE/DK (caroline.ewertsen@dadnet.dk)

Image fusion software is available on most high-end ultrasound systems and several publications for different clinical applications are available. Ultrasound images can be fused with images from CT, MRI or PET/CT, which enables the user to target biopsies or verify the nature of inconspicuous lesions. In order to fuse the images a co-registration or alignment must be made. This can be done manually, by choosing common points or planes in the different datasets, or automatically by the system by recognition of pixel intensities in the images. This applies for some systems, but not for all modalities. The theory behind these different co-registration methods will be covered as well as their accuracy. Furthermore examples of clinical applications will be demonstrated. The technique is more time consuming than conventional B-mode ultrasound but time spent decreases with increasing user experience. Depending on the body size of the patient and the organ of interest patient positioning should be identical to when the previously recorded data set was recorded, but this is not mandatory. However, for liver applications accuracy of the co-registration may improve if this is taken into account. Also identical in- or expiration may improve the accuracy. Real time image fusion enables real-time assessment of lesions in several anatomical regions.

Learning Objectives:

1. To learn about actual indications and applications of fusion imaging.
2. To show better parameter settings for optimal technical results.
3. To illustrate tips and tricks for technical and clinical successful examinations.
4. To become familiar with the new fusion imaging techniques and applications.

08:30 - 10:00

Room M 4

E³ - ECR Academies: State-of-the-Art and Advanced MR Imaging of the Musculoskeletal system

E³ 919

Upper extremity

A-443 08:30

Chairperson's introduction

M.C. [De Jonge](mailto:mdjonge@zuwehofpoort.nl); Amsterdam/NL (mdjonge@zuwehofpoort.nl)

DISI and VISI are descriptions of the position of the lunate bone on plain radiographs. They are not diagnoses as such but a reflection of underlying pathology. It is important to realise that this description is made on standard plain radiographs and not on cross sectional imaging. The X-rays have to be made in the correct way for ulnar and radial deviation of the hand will result in a different position of the lunate and therefore false-positive DISI and VISI descriptions. Calling DISI and VISI inappropriately will lead to additional imaging to look for the cause of the 'abnormal' lunate position. It is important to realise this so that patients will not undergo unnecessary imaging. The concepts of DISI and VISI will be discussed together with its implications.

A-444 08:35

A. Elbow

A.J. [Grainger](mailto:andrewgrainger@nhs.net); Leeds/UK (andrewgrainger@nhs.net)

The elbow is subject to both acute and chronic trauma, including ligamentous, osteochondral and tendon injury. MRI is well suited to demonstrate these injuries, but due to the complex anatomy of the elbow joint, optimisation of the imaging is required in terms of plane of section, sequence employed and the decision of whether to use intravenous or intraarticular contrast medium. The talk will address acute injury, looking at mechanisms and appearances of ligamentous, tendon and osteochondral injury at the elbow. The anatomy of these structures will be discussed along with imaging optimisation. Patterns of injury will be highlighted. Causes of chronic elbow pain will also be discussed and the relevant appearances on MRI will be illustrated. Patterns of impingement at the elbow will be shown and the relationship between chronic repetitive injury and pain will be reviewed. Important nerves pass by the elbow and the movement of the elbow and muscular structures around the elbow can lead to entrapment of nerves - another cause of chronic pain. Common patterns of nerve entrapment will also be discussed.

Learning Objectives:

1. To identify the most common post-traumatic entities.
2. To identify the most common entities leading to chronic pain.
3. To know the role of MR imaging and MR arthrography (direct/indirect) and how to optimise imaging protocols for the elbow.

A-445 09:17

B. Wrist

M. [Shahabpour](mailto:maryam.shahabpour@uzbrussel.be), M. De Maeseneer; Brussels/BE (maryam.shahabpour@uzbrussel.be)

The wrist is highly vulnerable to injuries with significant long-term consequences if diagnosis is delayed. When initial radiographs are negative in presence of strong clinical suspicion, further imaging is appropriate including CT and MRI. MRI can accurately show scaphoid fractures or other unsuspected fractures of distal radius or carpus as well as soft-tissue injuries. CT is recommended preoperatively for displaced fractures where surgery is performed to avoid complications. It helps evaluate intra-articular fractures and detect fractures of the hook of hamate, subluxations of distal radioulnar joint, and fractures-dislocations of metacarpal bases. MRI of hand and wrist requires high spatial resolution. The patient is placed in supine position with the hand along the body using a dedicated phased-array wrist coil or in prone position with the arm overhead. Imaging protocols include 2mm coronal PDFS and T1 (or PD), sagittal PD and T2, axial PD and PDFS for analysis of ligaments and tendons. Using MR arthrography (with double or triple compartment injection), 2mm thick coronal T1FS and PDFS or 0.5mm 3D PDFS and 3D DESS sequences followed by multiplanar reconstructions are performed for the detection of ulnar attachments TFCC tears and lesions of extrinsic and intrinsic ligaments, especially in (sub)acute trauma to determine if the patient requires surgery. In chronic phase, indirect MR arthrography is obtained after addition of intravenous contrast prior to the examination to assess ligaments and cartilage despite the presence of scarring. For nonunion, SNAC, avascular necrosis and SLAC lesions, images are obtained before and after intravenous contrast administration.

Postgraduate Educational Programme

Learning Objectives:

1. To identify the most common post-traumatic entities.
2. To identify the most common entities leading to chronic pain.
3. To know the role of MR imaging and MR arthrography (direct/indirect) and how to optimise imaging protocols for the wrist.

08:30 - 10:00

Room M 5

E³ - ECR Academies: Chest Imaging

E³ 918

Updates on lung cancer management

A-446 08:30

Chairperson's introduction

A.R. [Larici](mailto:annarita.larici@unicatt.it); Rome/IT (annarita.larici@unicatt.it)

Several studies on lung cancer screening have been performed by low dose computed tomography (LDCT) in the last decades. Among these, only the US National Lung Screening Trial demonstrated a benefit for the annual LDCT (a 20% reduction of lung cancer mortality). So far, a major concern in all published studies has been the high rate of false positive results leading to an increase risk of overdiagnosis whose effects are still not completely known. Lung cancer may present as nodule or mass. Mass has a high likelihood of being malignant while the majority of lung nodules remains indeterminate at CT scans. The most reliable method to characterise lung nodules is to follow them over time with CT. In the recently published guidelines for managing solid and subsolid nodules by the Fleischner society, the most relevant change is the reduction of CT examinations performed during the follow-up period. Once a lung lesion is characterised as malignant, the further step is staging the disease. The 8TH edition of the TNM classification introduced relevant changes regarding the descriptors T (from 1 to 5 cm every centimeter counts; T3 if greater than 5 cm; T4 if greater than 7 cm) and M by introducing the category M1b and M1c to indicate, respectively, one (oligometastatic disease) and more than one extrathoracic lesion. Several limitations still remains, as the classification of lymphangitic carcinomatosis and the evaluation of multiple lung lesions. Certainties and controversies of each proposed topic will be argued in this session.

A-447 08:35

A. Lung cancer screening

M.A. [Heuvelmans](mailto:m.a.heuvelmans@umcg.nl); Groningen/NL (m.a.heuvelmans@umcg.nl)

After the largest randomised-controlled lung cancer screening trial, the National Lung Screening Trial (NLST), published a 20% decrease in lung cancer specific mortality in heavy (ex)-smokers screened by annual low-dose chest CT compared to annual chest radiography, lung cancer screening has been implemented in clinical practice in the United States. Although in Europe the results of the second largest trial, the Dutch-Belgian randomized-controlled lung cancer screening trial (NELSON trial) are still awaited, planning for implementation of low dose CT screening in high risk individuals is recommended by the EU position statement expert group, since lung cancer screening can save lives.

Learning Objectives:

1. To review the results of the large randomised trials.
2. To learn about the lung cancer screening modalities.
3. To understand the overdiagnosis risk.

A-448 09:03

B. Lung nodule management

A.A. [Bankier](mailto:bankier@bwh.harvard.edu); Boston, MA/US

This presentation will discuss the background, novel elements, and clinical implications of two recently published guidelines on the management and the measurement of pulmonary nodules. Participants will learn about the required framework for the application of the guidelines, and their potential and limitations. The intention of the guidelines, i.e., a more standardised and rationale approach to the management of pulmonary nodules will be highlighted.

Learning Objectives:

1. To review the current guidelines for solid nodule management.
2. To learn about the subsolid nodule management guidelines.
3. To review the role of computer-aided tools.

A-449 09:31

C. Lung cancer staging

G. [Aviram](mailto:aviramgalit@hotmail.com); Tel Aviv/IL (aviramgalit@hotmail.com)

Lung cancer continues to be the leading cause of cancer-related mortality worldwide. Accurate staging is fundamental for estimating prognosis, selecting treatment, and conducting and reporting clinical trials internationally. The International Association for the Study of Lung Cancer (IASLC) has recently published the eighth edition of the tumour, node, and metastasis (TNM-8) staging system used for lung cancer. This revised classification is based on significant differences in patient survival identified on analysis of a new large international database. Key changes include: further modifications to the T descriptors based on 1 cm increments in tumour size; grouping of tumours resulting in partial or complete lung atelectasis/pneumonitis, and those involving a main bronchus regardless of distance from the carina, and reassignment of diaphragmatic invasion. In addition, specific new coding for adenocarcinoma in situ and minimally invasive adenocarcinoma was incorporated as well as their recommended measurements method. The clinical N descriptors used are unchanged from the 7th edition; however, the description of the number of pathological lymph node stations involved, has been added. Further subdivision of metastatic disease into distinct descriptors based on the number of extrathoracic metastases and involved organs were also added. As a result of the new modifications, several new stage groups have been developed, and others have shifted. Although TNM-8 represents more advanced understanding of tumour behavior and patient management, several limitations, controversies and unaddressed issues persist.

Learning Objectives:

1. To learn about the eighth edition of the TNM classification.
2. To review the main differences with the 2009 edition.
3. To review the persisting limitations.

Author Disclosure:

G. Aviram: Other; My institution received a research grant from Philips Health Care.

10:30 - 12:00

Room B

ESR meets Switzerland

EM 1

Radiology and Swiss chocolate: a sweet combination

Presiding:

B. Hamm; Berlin/DE

D. Weishaupt; Zurich/CH

A-450 10:30

Introduction: What Swiss radiology and Swiss chocolate have in common

D. [Weishaupt](mailto:dominik.weishaupt@triemli.zuerich.ch); Zurich/CH (dominik.weishaupt@triemli.zuerich.ch)

The Swiss Society of Radiology, with more than 100 years of history and about 1,000 members, is a professional medical society dedicated to promoting radiology in Switzerland. The aims of the society - among others - are: to assure high-quality postgraduate training in radiology by maintaining the radiology residency training curriculum as well as conducting the Swiss board examinations in radiology, to support education in radiology by organising the Swiss Congress of Radiology, offer activities dealing with quality assurance, patient safety and radiation protection, improve patient care and the health of the population through medical imaging, support the professional and economic interests of our members, and serve as a responsible counterpart to the Swiss Health authorities and other official bodies. The aim of providing high quality radiology and the pursuit of excellence are important characteristics of radiology in Switzerland. These characteristics link Swiss radiology with Swiss chocolate, which is considered to be one of the highest quality products manufactured in our country. Within this session, three educational presentations by three renowned Swiss radiologists will underline the broad spectrum of cutting edge radiology performed in the country. In addition, you will learn about the secret of production and refinement of high-quality chocolate made in Switzerland. A representative of a leading family owned Swiss chocolate manufacturer will present the fascinating chocolate production process and illustrate how high quality chocolate is handmade and how innovative chocolate products are designed for the future.

Session Objectives:

1. To become familiar with the status of radiology in Switzerland.
2. To learn how Swiss Society of Radiology supports radiology in Switzerland.
3. To discuss the link between Swiss radiology and top-quality innovative Swiss chocolate culture.

Postgraduate Educational Programme

A-451 10:35

Truffle No. 1: MR-diffusion of the urogenital tract: where it really helps
H.C. Thoeny; Berne/CH (harriet.thoeny@insel.ch)

After its initial application in the brain diffusion-weighted MRI (DWI) is now part of most MR exams in the abdomen. In the urogenital tract DWI is particularly helpful because it can be applied without contrast medium administration which is a major advantage in patients with renal impairment. For daily clinical routine image analysis of DWI is performed qualitatively based on visual assessment of the high b-value images and the corresponding ADC map. However, image interpretation of DWI has always to be performed in combination with morphological images to avoid misinterpretation, e.g., a tumour, an abscess and a haematoma have the same findings on DWI but can be differentiated in combination with anatomical sequences. The ADC value, the quantitative parameter of DWI can further provide more detailed information of the underlying tissue. DWI in the urogenital tract can be applied for detection, characterisation and monitoring of various pathologies. DWI helps to detect pyelonephritis in adults and children without contrast medium administration and typically normal findings on morphology. It is also routinely applied to detect significant prostate cancer and provides even information on tumour aggressiveness when the ADC value is taken into account. The differentiation between cystic renal cell carcinoma and an abscess is also possible based on DWI and even the differentiation of renal cell carcinoma subtypes is possible in many cases based on the underlying ADC-value. Several applications and examples showing the usefulness of this technique in the urogenital tract will be discussed and explained.

Learning Objectives:

1. To learn how DWI can be integrated in the acquisitions protocols and whether it precludes the need for other sequences.
2. To learn if DWI can provide useful information for tissue characterisation.
3. To understand the clinical circumstances in which DWI is most helpful.

Author Disclosure:

H.C. Thoeny: Advisory Board; Guerbet SA.
Swiss chocolate culture.

A-452 10:55

Interlude 1: From cocoa bean to chocolate creations
A. Trümpler; Ennenda/CH

A-453 11:05

Truffle No. 2: hip preservation surgery: a fast evolving field also for imaging
C.W.A. Pfirrmann; Zurich/CH

Joint-preserving surgery of the hip is one of the most important fields of innovation in orthopedics and sports medicine. Before the era of hip replacement hip osteotomies were popular to treat osteoarthritis of the hip. Hip osteotomies lost a lot of their importance with the introduction of the total hip arthroplasty which is considered one of the most successful surgical procedures. With the scientific work of Reinhold Ganz and his team at the University of Bern in Switzerland joint-preserving surgery of the hip has regained importance and has become one of the fastest evolving fields in the last two decades. The goal of joint-preserving hip surgery is to prevent osteoarthritis in the hip before degeneration becomes evident. Studies on the detailed anatomy of the blood supply of the femoral head were the scientific bases to develop a new approach for open surgical dislocation of the hip without the risk of avascular necrosis. This gave new insights in hip biomechanics and the development of the new concept of femoroacetabular impingement (FAI). FAI has been identified as the leading cause of the premature osteoarthritis of the hip. Imaging of the hip has become increasingly important to assess morphology of the hip joint as well as the structural damages mainly to the cartilage and the labrum.

Learning Objectives:

1. To learn about the history and recent advances in hip preservation surgery.
2. To understand the biomechanics of the abnormal hip and how to integrate biomechanical aspects in the imaging protocol and image interpretation.
3. To know imaging pitfalls and asymptomatic findings.

A-454 11:25

Interlude 2: From cocoa bean to chocolate creations
A. Trümpler; Ennenda/CH

A-455 11:35

Truffle No. 3: multiparametric imaging in head and neck oncology
M. Becker; Geneva/CH (minerva.becker@hcuge.ch)

Contrast enhanced CT and MRI with diffusion-weighted imaging (DWI) are routinely used for the assessment of submucosal tumour spread in head and neck carcinoma, to stage nodal disease, to monitor treatment response and to detect recurrent disease. PET/CT is widely used to stage nodal disease, to detect distant metastases and synchronous tumours, to identify unknown primary tumours in patients with metastatic neck nodes, to assess treatment response and prognosis after chemo radiotherapy and for radiotherapy planning. Recent data regarding the complementarity of multiparametric information derived from hybrid MR/PET systems in clinical settings holds promise because it can combine morphologic, functional and molecular information and helps to avoid diagnostic pitfalls. This lecture focuses on clinical applications of multiparametric imaging in head and neck cancer. Current evidence about the complementarity of CT, MRI, DWI, perfusion and PET is discussed with particular emphasis on the added value of multiparametric information and quantification. The variable appearance of functional phenomena mimicking disease as well as diagnostic pitfalls and how they can be avoided are discussed. Current research trends regarding texture analysis are addressed. Emphasis will be put on ongoing developments in head and neck oncology.

Learning Objectives:

1. To understand the complementary role of morphologic, functional and metabolic imaging techniques in head and neck oncology.
2. To review the role of diffusion and perfusion imaging for the diagnosis and follow-up of head and neck cancers.
3. To discuss diagnostic pitfalls and how they can be avoided with multiparametric imaging.

Author Disclosure:

M. Becker: Grant Recipient; Swiss National Science Foundation SNSF grant No 320030_173091/1 Multiparametric and quantitative imaging in head and neck squamous cell carcinoma.

11:55

Panel discussion: The way of maintaining and improving quality of Swiss radiology

10:30 - 12:00

Room G

EFOMP Workshop: Radiation dose management systems and repositories: the present and the future

EF 2

Dose management systems and repositories: part B

Moderator:

M. Mahesh; Baltimore, MD/US

A-456 10:30

Chairperson's introduction

M. Brambilla; Novara/IT (marco.brambilla@maggioreosp.novara.it)

The purposes of this session are to provide an overview of imaging and dose repositories, to explain the possibilities and limitations of current implementations and standards, to illustrate the technical challenges faced by already established dose index registries, such as the ACR dose index registry, and to emphasize the role that such systems could have in boosting researches on radiation protection. This session will introduce the IHE REM profile as one of the potential benchmark standard, explaining its limitations in the field of radioprotection and how this standard could be complemented by other technologies to cover present and future needs in the domain of radioprotection and biomedical research. An overview of the services provided by imaging and dose repositories will be provided illustrating how these services could be used in the field of radioprotection and biomedical research. The issues of security, data protection, privacy and other legal issues associated with the implementation of such repositories will be discussed. Finally, an existing and well established example of dose repository systems, such as the ACR dose index registry, will be introduced and illustrated in its past technical development and in its future perspectives.

Session Objectives:

1. To provide an overview of imaging and dose repositories.
2. To understand the main strengths and limitations of these systems.
3. To understand why dose management systems and repositories are capable of supporting research.

Postgraduate Educational Programme

A-457 10:35

Organisation of dose management systems and repositories for radiation protection and biomedical research: possibilities and limitations of current implementations and standards

B. Gibaud; Rennes/FR (bernard.gibaud@univ-rennes1.fr)

Radiation protection and related biomedical research require that dosimetric information can be estimated and shared. To meet this objective, the integrating HealthCare Enterprise initiative developed an integration profile called radiation exposure monitoring (REM). This profile "facilitates the collection and distribution of information about estimated patient radiation exposure resulting from imaging procedures". This profile specifies the roles of the various actors involved, namely: 'Imaging modality', that creates and transmits the dose information; the 'Image Manager/Image Archive' that may store and manage dose objects; the dose information consumer (e.g., implemented in a RIS or a reporting workstation) that may query/retrieve and analyze such dose objects; the 'Dose Information Reporter' that may submit dose information to national or regional repositories implementing a 'Dose register' actor. The presentation will introduce this integration profile and present in detail the DICOM objects and services involved in the previous transactions. The presentation will highlight the possibilities and the limitations of this profile, especially regarding the DICOM encoding of the dose reports. It will also introduce other complementary technology, based on the semantic web technologies, that allow complementing these standards, in a way that is compatible with the needs of biomedical research.

Learning Objectives:

1. To introduce the IHE REM profile.
2. To discuss its relevance and limitations regarding radiation protection needs.
3. To introduce other technology that may complement IHE REM to cover future needs of both radiation protection and biomedical research.

A-458 11:05

Imaging and dose repositories: tools to boost radiation protection and research?

E. Neri; Pisa/IT (emanuele.neri@med.unipi.it)

The dose monitoring tools allows a precise internal audit of the dose behaviour in the radiological department, tracking the general dosimetric trend, that mainly depend on the adopted imaging protocols. Such imaging protocols are frequently designed by an anatomical orientation with few concern about the specific clinical context in which the exam is performed. In parallel the attention of dose reference levels (DRL) is oriented to the anatomical segments, and not the clinical context.

Learning Objectives:

1. To provide the rationale of imaging and dose repositories.
2. To describe the services provided by imaging and dose repositories.
3. To understand the security, legal and other issues associated with the implementation of imaging and dose repositories.

Author Disclosure:

E. Neri: Advisory Board; QUIBIM.

A-459 11:35

The ACR dose index registry: setting a benchmark

M. Mahesh; Baltimore, MD/US (mmahesh@jhmi.edu)

Radiation dose information is essential towards establishing standards, reviewing and optimising protocols, to develop safe imaging practices. In this regard, Dose Index Registry (DIR) is one of the registry with in National Radiology Data Registries (NRDR) hosted by the American College of Radiology (ACR). Launched in 2011, the ACR-DIR is a tool for quality improvement enabling facilities to review dose indices and optimise protocols. The goal of ACR-DIR is to assist in establishing national and regional benchmarks and practice patterns and to develop patient size specific diagnostic reference levels (DRLs). As of now, ACR-DIR is primarily collects CT dose data, however, it has plans to expand registry for interventional fluoroscopy, computed and digital radiology, and nuclear medicine. The presentation will discuss what is DIR and how it works, the type of CT dose data collected and reported. Presentation will also discuss how certain sites are using feedback from DIR reports to plan, implement, and measure the success of CT dose reduction program. Technical implementation issues a site needs to address upon signing with the registry will be discussed. Finally, the presentation will discuss how DIR data were used to establish US national dose levels for the most common adult CT examinations based on patient size.

Learning Objectives:

1. To give an overview of the ACR dose index registry.
2. To understand issues related to technical implementation of the registry.
3. To learn about the new prospects of the ACR dose index registry.

10:30 - 12:00

Room M 2

PIER @ ECR Session

PI 1

Establishing competence in radiology

Moderators:

J. McNulty; Dublin/IE
P. Valdés Solís; Marbella/ES

A-460 10:30

Achieving homogeneity in radiology education: linking content to competence through the European training curriculum

L. Oleaga Zufiria; Barcelona/ES (lauraoleaga@gmail.com)

There is a great heterogeneity in the training programmes across Europe. The curriculum defines the process of training and the competences needed to ensure trainees provide a high-quality service after the completion of the training programme. The European Training Curriculum (ETC) represents a guide to standardised education and harmonise skills and competences among radiologists in Europe. Assessment of the competences acquired during the training period is not harmonised and there is not a standardised method applicable to all European countries. A common e-Portfolio with the individual record of each year trainee's progress, based on the European Training Curriculum (ETC) could be a useful tool to standardise education. A final examination to assess clinical competence is not mandatory in all countries. The European Diploma in Radiology (EDIR) represents a valuable certificate to standardise and facilitate the accreditation of radiologists across the EU borders. Education is evolving; new technologies and innovative approaches are integrated into the radiology field. e-Learning online activities, simulator programmes and artificial intelligence are getting incorporated into the clinical work and training. Trainees must embrace and participate in value-adding activities in radiology using guidelines and appropriateness criteria to lead imaging decisions to provide high-value care. Communication skills in radiology including the interaction between radiologists, radiographers, referring physicians, and patients constitute important aspects of radiology education; failure of communication can result in negative results. They have to be trained in communication and conflict management. Learning these skills is critical for their future.

Learning Objectives:

1. To discuss the impact of major inhomogeneities on European radiology.
2. To describe the European training curriculum's role in achieving homogeneity and the importance of linking content to competence.
3. To evaluate the current status and what must happen next in radiology education.

A-461/A-462 10:45

Establishing competence in radiology: a UK perspective

C. Rubin¹, W. Ramsden², ¹Southampton/UK, ²Leeds/UK
(caroline.rubin@uhs.nhs.uk), (william.ramsden1@nhs.net)²

Radiology training in the UK is undertaken in quality assured training programmes, over 5 years for clinical radiology, 6 years for subspeciality training in interventional radiology and aspires to produce proficient radiologists. National systems of assessing competence in the UK are divided into summative formal examinations and formative workplace based assessments (WPBAs). Allied to these are local evaluations of performance in specific techniques such as acute ultrasound and CT. Formal examination material is rigorously tested for validity and reliability, and the Royal College of Radiologists (RCR) sets national standards. Although examinations address knowledge and some elements of competence, they are weaker in assessing performance. Passing examinations does not invariably equate to trainees performing satisfactorily in the workplace. Although WPBAs occur in clinical departments and addresses trainees' performance of day-to-day tasks, they are only used formatively as mandated by national guidance. The RCR is improving standardisation, with particular emphasis upon the oral (viva) component of the final FRCR examination, to ensure similar material is seen by all candidates and it is blueprinted to the curriculum. WPBAs are being revised to remove most scoring, allowing greater use of free text comment to help trainees' development. The RCR curricula are being rewritten, and specific assessments mapped to individual areas. This ensures that the evaluation of competence covers all subjects, both generic and radiology specific. National roll-out and training of assessors and examiners are particularly important factors in ensuring the success of this work.

Friday

Postgraduate Educational Programme

Learning Objectives:

1. To explore the current UK structures for establishing competence in radiology.
2. To discuss the challenges and opportunities arising from these systems.
3. To consider the key steps to facilitate the successful implementation of a competence system in radiology.

A-463 11:00

The value of the European Diploma

P.C. [Maly Sundgren](mailto:Maly.Sundgren@med.lu.se); Lund/SE (Pia.Sundgren@med.lu.se)

The number of young colleagues in Europe that sit for the European Diploma in Radiology (EDiR) is constantly increasing and the number of examinations performed per year is now 8 with a potential to further increase in the coming years. In some countries the EDiR is part of the educational program for radiology residents. In some countries the Diploma has been discussed to, in part, replace national examination. The curriculum level I and II for residents in training is the ground for the EDiR while level III is considered subspecialisation and is therefore, not covered in questions and cases at the current form of EDiR. By establishing the EDiR and increase the number of participants sitting the exam reinforces the homogenization of the radiology education and training in Europe which is favourable for the residents regardless of country and may in the future open the European market or young radiologist to seek work outside their own country - a more flexible market.

Learning Objectives:

1. To demonstrate the value of the European diploma in overcoming issues relating to competence.
2. To discuss the areas of competence which are currently outside the scope of the European diploma.
3. To propose a route through which the European diploma could form part of a European radiology competence structure.

Author Disclosure:

P.C. Maly Sundgren: Board Member; chair written evaluation committee, member of the EDiR Scientific Board, member in the ESR Research committee.

A-464 11:15

Obstacles to establishing competence in radiology

P. [Valdés Solís](mailto:Valdés Solís; Marbella/ES (pabvalsol@gmail.com)); Marbella/ES (pabvalsol@gmail.com)

A competence focused professional system in Radiology is important to improve quality and safety. The Spanish Society of Radiology, aware of this, began a strategy to develop an advanced system of measuring competence in radiology. We had the first experience in interventional radiology and after creating a working group and defining the model, a book including the competence elements was successfully published. However, when trying to adapt the model in other radiology subspecialities, the experience was everything but successful: we realized that Spanish radiologist did not believe in the necessity of going through an exam of their performance and competence. Now we are facing a new chance to give life to the project, because the Spanish National Medical Association will ask their members to apply for a professional validation which, though not compulsory, will probably be the standard. The Spanish Medical Association has asked SERAM to define the minimum required to radiologist to get the professional validation, so just minimal changes in the competence model will be needed. Our experience was useful to redesign the way of facing complex projects as this. First of all, you have to face the possibility of rejection. Many radiologists in Spain are civil servants, and won't get many advantages when passing a competence evaluation exam, and personal recruitment is not designed taking into account professional competence in many cases. Knowing this, we are now facing a new project that we hope will be successful in a few years.

Learning Objectives:

1. To show the difficulties that, as a Society, the Spanish Society of Radiology has faced in order to establish a national system of competences.
2. To explain why radiologists are reluctant to join competence programmes, especially those that are not proposed by their own health authorities.
3. To discuss the strategies that should be kept in mind before beginning a national competence programme in order to get radiologists compliance and participation.

A-465 11:30

How to manage the incompetent professional?

J.K. [Bell](mailto:Bell; Manchester/UK (Jon.Bell@christie.nhs.uk)); Manchester/UK (Jon.Bell@christie.nhs.uk)

Radiologists must achieve and maintain a certain level of competence to be safe and effective. However, the definition of competence is challenging and may differ between countries. European accreditation continues to develop to define standards of practice in order to ensure that Radiologists perform to an

acceptable level. There are multiple factors that influence performance in the work place and these need to be addressed to ensure a healthy working environment. Early signs that a Radiologist is experiencing professional and/or personal difficulties should be identified and addressed within a supportive management structure. Here we explore clinical competence, optimisation of the working environment, identification of colleagues in difficulty and the development of a supportive management structure.

Learning Objectives:

1. To define competence and how to identify radiologists in difficulty.
2. To assess factors that lead to poor performance and what can be done to promote well-being.
3. To outline processes for helping incompetent radiologists and managing those that cannot be helped.

11:45

Panel discussion: Overcoming heterogeneity in radiology competence across Europe: a dream or reality?

10:30 - 12:00

Room M 4

E³ - ECR Academies: State-of-the-Art and Advanced MR Imaging of the Musculoskeletal system

E³ 1019

Knee

A-466 10:30

Chairperson's introduction

J. [Kramer](mailto:Kramer; Linz/AT (kramer@ctmri.at)); Linz/AT (kramer@ctmri.at)

In this session acute posttraumatic as well as chronic disorders leading to pain/complaints in the knee region are focussed on. Further more postoperative changes including postop. complications are debated. To some extent technical considerations for imaging of the cartilage and to avoid artifacts are mentioned. At the beginning of the session some cases are demonstrated and the final diagnosis is shown after the end of the 3 lectures.

A-467 10:35

A. Post-traumatic

A.P. [Parkar](mailto:Parkar; Bergen/NO (apparkar@gmail.com)); Bergen/NO (apparkar@gmail.com)

Knee trauma with injury of the menisci, ligaments, cartilage and bone, all contribute to the development of osteoarthritis. Acute/traumatic meniscal ruptures run obliquely or vertically and affect the articular surface (either femoral or tibial). Degenerative ruptures run horizontally and do not affect the articular surfaces. Long standing chronic ruptures thin out the meniscus and lead to lateral extrusion. Complex ruptures with displaced fragments, be it medially/anteriorly/posteriorly, need to be treated swiftly as they cause knee locking. Considering isolated injury to the lateral knee stabilisers, a total rupture is important to recognise, as this requires surgical reconstruction, while partial ruptures are treated conservatively. Chronic injuries may be recognised by healed bony avulsion (like Segond or Pellegrini Stieda). MRI findings of ruptured ACL with direct and indirect signs is well established. Awareness of the reporting "not to be missed" concomitant injuries (posterolateral corner, anterolateral ligament, meniscal root avulsions) is on the rise. Chronic post-traumatic ACL may develop mucoid degeneration or ganglion cysts within the ligament. The acute PCL injury is recognised when fibres are disrupted, or with high signal and when thickened >8mm. An indirect sign is posterior sagging of the medial tibia. It is important to know that intact PCL fibres does not exclude a chronic PCL injury, as MRI has very low sensitivity and indirect signs may be the only clue. Patella luxations may occur due to underlying dysplasia or severe trauma. The acute findings are femoral/patellar bone edemas, rupture of the medial retinaculum, and cartilage damage.

Learning Objectives:

1. To identify the most common post-traumatic entities.
2. To know the role of MR imaging and MR arthrography (direct/indirect).
3. To differentiate post-traumatic changes from typical reasons for chronic pain.

A-468 11:03

B. Chronic pain

P. [Van Dyck](mailto:Van Dyck; Antwerp/BE (pieter.van.dyck@uza.be)); Antwerp/BE (pieter.van.dyck@uza.be)

Many conditions can cause or contribute to chronic knee pain, including trauma, degenerative disease, infections, connective tissue disorders, metabolic disorders, and tumors. Imaging continues to play an important role in

Postgraduate Educational Programme

the assessment of these entities to select an appropriate treatment. This presentation will give an overview of the most common entities leading to chronic knee pain and discuss the basic and advanced imaging methods for evaluating the knee joint with particular emphasis on MR imaging techniques (including 2D and 3D turbo-spin-echo, 3D gradient-echo, 3D ultrashort echo-time and quantitative mapping techniques). Degenerative osteoarthritis (OA) is the most common form of chronic knee arthritis. It is currently diagnosed using clinical and radiographic findings. However, in recent years, MRI has increasingly been used to study OA. The diagnostic utility of MRI for diagnosis of OA in a clinical setting will be discussed. Chronic anterolateral rotatory laxity, typically occurring after injury of the anterior cruciate ligament (ACL) or ACL surgery, is a major cause of degenerative OA. A brief update will be provided on the anatomy of the anterolateral knee complex (including the superficial and deep fibers of the iliotibial tract and the anterolateral ligament) and how to assess it on MR images. Finally, clinical case series will illustrate how to differentiate entities leading to chronic pain from post-traumatic changes.

Learning Objectives:

1. To identify the most common entities leading to chronic pain.
2. To know the role of MR imaging in evaluating cartilage (including new techniques).
3. To differentiate entities leading to chronic pain from post-traumatic changes.

A-469 11:31

C. Postoperative

P.M. [Jungmann](#); Zurich/CH

Surgical techniques and MR imaging techniques are undergoing continuous developments and optimization. At the knee, frequently a standard MR imaging protocol is sufficient to account for most clinical queries; however, cases in which dedicated protocols and sequences, intravenous contrast administration or intraarticular contrast administration (arthrography) are required will be demonstrated as well. Current orthopedic surgical techniques with respect to ligament, meniscus and cartilage reconstruction at the knee will be explained to allow the radiologist to provide specific information to the demanding orthopedic surgeon. Knowledge of the techniques is crucial to fulfill the expectations and requirements of the clinicians. This part of the knee session discusses normal and pathological postoperative findings on MR imaging of the knee during postoperative follow-up after several knee surgeries, such as ligament reconstruction (ACL, PCL, MPFL), meniscectomy and meniscus repair and after different cartilage repair techniques. Typical and severe complications will be pointed out using clinical examples. Particularly, also novel metal artifact reduction sequences (MARS) will be explained using examples of knee prostheses and other implants. Not only technical background knowledge, but also typical postoperative findings at the knee will be discussed, that may be depicted using these new sequences. The session aims to provide clinically important knowledge on MR techniques and postoperative findings at the knee to the interested MSK- or non-MSK radiologist.

Learning Objectives:

1. To identify the most common postoperative changes.
2. To know the role of MR imaging and how to optimise protocols for postoperative imaging including the use of MR arthrography.
3. To understand the different techniques of ligament reconstruction and meniscal repair and their complications.

13:00 - 13:30

Room A

Headline Session

HL 2

Marie Curie Honorary Lecture

Presiding:

B. Hamm; Berlin/DE

A-486 13:00

Hybrid imaging: the story so far and what to expect next

K. [Riklund](#); Umea/SE (katrine.riklund@umu.se)

Hybrid imaging, the combination of structural and functional or molecular imaging started with visual and software fusion and has developed into new scanners with hardware fusion of PET or SPECT together with CT or MRI. During the session I will take you on an amazing tour behind the scenes in secret chamber; the human body, visualised in structures and biochemistry, and molecular medicine. I will present a fascinating story of the development of something really astonishing on one hand and on the other hand something you cannot be without in daily imaging work.

Learning Objectives:

1. To learn about the development of hybrid imaging.
2. To understand the principles for molecular imaging exemplified in PET/CT and MR/PET.
3. To appreciate the combination of molecular and functional imaging.
4. To become familiar with a few clinical areas with high potential in hybrid imaging.

Author Disclosure:

K. Riklund: Advisory Board; scientific advisory board Swedish Drug authority. Speaker; GE, Paris meeting 2016, Nordic Conf in Radiology 2017 Iceland.

12:30 - 13:30

Room C

E³ - The Beauty of Basic Knowledge: Cardiovascular and Interventional Radiology

E³ 24C

Open and closed: the role of radiology in treatment of valvular heart disease

Moderator:

M. Gardarsdottir; Reykjavik/IS

A-483 12:30

How to approach valvular heart disease using MRI

A. [Redheuil](#); Paris/FR (alban.redheuil@gmail.com)

Magnetic Resonance Imaging (MRI) has recently evolved as a comprehensive modality to provide a reference non-invasive assessment study of cardiac remodeling and dysfunction related to valvular disease, but also to quantify valvular dysfunction - either stenotic or regurgitant valvular lesions - using 2D and 4D phase contrast-based flow imaging. Furthermore, comprehensive vascular assessment such as of the thoracic aorta or pulmonary arterial tree is feasible within a single exam. If MRI is established for the assessment of complex congenital valvular and heart disease it may also be very helpful in case of incomplete or non-diagnostic echocardiography to evaluate valvular disease mechanism, anatomy and quantify disease severity in the more common valvular heart disease settings. Finally, new myocardial mapping tools may provide an insight into myocardial tissue changes including diffuse fibrosis that may be at play in valvular heart disease and precede heart failure. A review of the aforementioned issues and potential value of MRI in valvular heart disease will be provided in this lecture.

Learning Objectives:

1. To learn about the MR techniques available for functional assessment in valvular heart disease.
2. To understand possibilities and limitations of cardiac MR in valvular heart disease.
3. To appreciate the advantages of cardiac MR in valvular heart disease.

A-484 13:00

What to measure prior to transcatheter aortic valve implantation (TAVI)

R. [Salgado](#); Antwerp/BE (rodrigo.salgado@uza.be)

Aortic valve stenosis is the most common valvular heart disease in the Western World. When symptomatic, aortic valve stenosis is a debilitating disease with a dismal short-term prognosis invariably leading to heart failure and death. Elective surgical valve replacement is traditionally considered the standard of care for symptomatic aortic valve stenosis. However, several studies have identified various subgroups of patients who have a significant elevated risk for operative complications and death. Accordingly, not every patient is suitable for surgery. Recent developments in transcatheter-based therapies have provided an alternative therapeutic strategy for the non-surgical patient population, replacing the native aortic valve by a bioprosthetic valve brought in place using a non-surgical endovascular or trans-apical pathway. This procedure has been named transcatheter aortic valve replacement or implantation (TAVR, TAVI), or also percutaneous aortic valve replacement (PAVR). Nevertheless, several anatomic and technical criteria have to be fulfilled to safeguard procedural eligibility and success. Therefore, there is a crucial role for non-invasive imaging in both patient selection and subsequent matching to a specific transcatheter valve size, to ensure accurate prosthesis deployment and minimize peri- and post-procedural complications. In this lecture, the relevant anatomy will be reviewed, emphasising anatomic pitfalls, their implications for correct reporting of imaging-derived measurements, and highlighting important differences between imaging modalities. Furthermore, the evolving role of CT-imaging and the role of the radiologist in the triage of patients will be discussed, reviewing current viewpoints in both patient and proper device size selection and the pre-procedural evaluation of the possible access routes.

Postgraduate Educational Programme

Learning Objectives:

1. To learn about prerequisites prior to TAVI.
2. To understand the importance of accurate measurements for TAVI planning.
3. To appreciate the need for communication with implanting physicians.

12:30 - 13:30

Room D

E³ - The Beauty of Basic Knowledge: A Survival Guide to Musculoskeletal Imaging

E³ 25C

Bone tumours

Moderator:

V.N. Cassar-Pullicino; Oswestry/UK

A-485 12:30

Bone tumours

K. Wörtler; Munich/DE (klaus.woertler@tum.de)

The diagnosis of a bone tumour is based on clinical findings, the age of the patient, the location of the lesion, its radiologic appearance, and if imaging does not allow for a specific diagnosis, its histopathologic features. Radiography remains the initial imaging modality for evaluation of the localisation of the lesion with respect to the longitudinal and axial planes of the involved bone, for the depiction of matrix mineralisation, and for estimation of biologic activity by analysing the patterns of bone destruction and periosteal response. CT is typically used to obtain "radiographic" information in regions of complex skeletal anatomy such as the skull, spine, pelvis and shoulder girdle. MR imaging is best suited to determine the local extent of a bone tumour (local staging), but can also be helpful to narrow the differential diagnosis in specific lesions such as cysts and cartilage-forming tumours. With a clear emphasis on conventional radiography, this course will review the basic imaging features of the most common benign and malignant bone tumours. Important radiographic findings, such as bone destruction patterns, types of periosteal reactions and matrix mineralisation, will be explained step by step in correlation with histopathology as well as advanced imaging techniques.

Learning Objectives:

1. To become familiar with the imaging features of benign and malignant bone tumours.
2. To appreciate their imaging characteristic hallmarks on plain film radiography.
3. To learn how best to use imaging modalities in differential diagnosis.

12:30 - 13:30

Sky High Stage

Special Focus Session

SF 10

Artificial intelligence (AI) applications

A-990 12:30

Chairperson's introduction

A. Brady; Cork/IE (adrianbrady@me.com)

As artificial intelligence increases its penetration into all aspects of life, radiology will change in the future. Radiology reports will become more standardised in format and language, and will become rich sources of information for teaching, research and machine learning, feeding back into a loop of continuing improvement of technological tools. This session will explore how these processes will operate, how radiology report data will be mined and utilised in the future, and what issues this will highlight in terms of data ownership and protection.

Session Objectives:

1. To explain the likely future development of structured reporting.
2. To highlight the opportunities which will arise from availability of radiological data in formats which can be searched and used as imaging biobanks.
3. To discuss the data protection issues which arise from these developments.

A-991 12:35

Imaging biobanks

B. Gibaud; Rennes/FR (bernard.gibaud@univ-rennes1.fr)

Significant progress in computer-aided or even automated image interpretation are expected in the near future. Machine learning and assessment of the performances of these new tools will require large quantities of annotated image data. The development of imaging biobanks should be able to provide

such data. The presentation will summarise the challenges of gathering large sets of image data, either from past clinical research studies, or from large cohorts and population studies. Particular emphasis will be put on the definition of consensual ontological models to guarantee a good standardisation of semantics borne by image annotations. Indeed, the latter must cover a wide scope from general characteristics of the clinical cases (e.g. known pathology, patient sex and age) up to quantitative image biomarkers derived from the images. The issue of relating image data to other biological data (e.g. genetic / genomic) will be underlined, justifying a strategy of designing information models for imaging biobanks that are consistent with those used in biobanking (e.g. BBMRI-ERIC).

Learning Objectives:

1. To discuss the role that the imaging biobanks can play in providing the data necessary for machine learning and for the assessment of the performances of diagnostic tools.
2. To understand the role ontologies play in the standardisation of image annotations in imaging biobanks.
3. To understand the need to collaborate with the domain of (specimen) biobanking.

A-992 12:50

Big data and structured reporting

D. Pinto dos Santos; Cologne/DE

There has been a tremendous increase in interest towards artificial intelligence and machine learning applications in radiology. In order for such systems and algorithms to perform sufficiently well, large amounts of training data are required. These data need to be either standardised and of adequate quality or available in large enough amounts, that enough relevant information can be extracted. However, in current clinical and radiological IT ecosystems access to relevant pieces of information is difficult. This is mostly due to the fact, that a large portion of information is handled as a collection of narrative texts and interoperability is still lacking. This lecture will give an overview on how structured reporting can help to facilitate research in artificial intelligence and in the context of big data. Potential approaches to implementing structured reporting will be discussed, focusing also on interoperability and standardisation.

Learning Objectives:

1. To discuss the data requirements for artificial intelligence and big data.
2. To understand how structured reporting can facilitate research in machine learning.
3. To become familiar with informatics standards, relevant to structured reporting.

A-993 13:05

Data control in the era of AI: man or machine?

P.M.A. van Ooijen; Groningen/NL (p.m.a.van.ooijen@umcg.nl)

Recent years has shown an explosive growth in the use of Artificial Intelligence (AI) and Deep Learning not in the least for medical applications. These new technological developments have started a whole new discussion on privacy of data processed by these computerised systems. Especially those applications in health care demand a high level of patient privacy and patient data security. The actual ownership of medical data is also part of this discussion where we can have different situations with original, de-identified, anonymised and processed data. Questions like what data is still personal data for an individual patient or participant in a clinical trial and who actually owns the data that is produced with self-learning computer systems. This educational course will discuss these issues with respect to ownership, intellectual property and the different aspects that are involved in this when moving towards the era of AI.

Learning Objectives:

1. To understand the current and future role of data.
2. To understand the issues surrounding data control and ownership.
3. To discuss the role of AI in the future of radiology.

Author Disclosure:

P.M.A. van Ooijen: Advisory Board; MedicalPHIT. Board Member; EuSoMII.

13:20

Discussion

Friday

14:00 - 15:30

Room K

EFRS meets Switzerland and Portugal

EM 4

EFRS meets Switzerland and Portugal

Presiding:

J. McNulty; Dublin/IE
M. Mordasini; Berne/CH
J. Santos; Coimbra/PT

Moderators:

J. McNulty; Dublin/IE
I. Gremion; Lausanne/CH
J. Santos; Coimbra/PT

A-493 14:00

Introduction

J. McNulty; Dublin/IE (jonathan.mculty@ucd.ie)

Introduced for the first time for ECR 2013, the 'EFRS meets' sessions follow the tradition of the 'ESR meets' sessions and give the European Federation of Radiographer Societies (EFRS) the opportunity to highlight the contribution of one of their member societies to the profession of radiography each year. Having met Spain (2013), Russia (2014), Germany (2015), Sweden (2016), and Belgium (2017), all of which were the home countries of the congress presidents in the respective years, the EFRS will meet both Portugal and Switzerland, which are two of the 'ESR meets' countries for 2018. Both the Portuguese society, Associação Portuguesa dos Técnicos de Radiologia, Radioterapia e Medicina Nuclear (ATARP), and the Swiss society, Schweizerische Vereinigung der Fachleute für Medizinisch Technische Radiologie (SVMTRA) were founding members of the EFRS in 2008. We also now count five Portuguese and two Swiss educational institutions among the affiliate members that make up our Educational Wing. Portuguese and Swiss radiographers alike come from strong organisational and educational backgrounds; they contribute to radiography research and continue to contribute to the activities of the EFRS.

Session Objective:

1. The introductions will give a very short overview of the aim and history of the Meets sessions (EFRS president) and the characteristics of Portugal and Switzerland (association presidents).

A-494 14:05

Introduction: Across Switzerland

M. Mordasini; Berne/CH (michela.mordasini@insel.ch)

Although not member of the European Union, Switzerland is closely integrated with the EU by bilateral sectoral agreements, known as Bilateral one and Bilateral two. By these contracts, free movement of persons between Switzerland and EU (and vice versa) is warranted and certifications and diplomas in the field of medicine, esp. also in the field of radiological technicians are recognised on both sides as long as the training has been similar to the equivalent Swiss qualification, which means, that the content and duration of training must be comparable. With respect to the four Swiss-national languages the bilateral exchange of technicians comes to pass mainly between Ticino and Italy, Bern/Basle/Zürich with Germany and Austria and Lausanne/Geneva with France, whereas the official language of Romance is used in the small southeastern Swiss canton Grisons mostly alongside with German, French or Italian. The radiographer qualification in Switzerland is based on a 3 or 4 year training in an advanced technical college and covers special courses in Diagnostic Radiology, Radio-Oncology and Nuclear Medicine. Most of the radiographers, working in one of about 630 radiological institutes (including radio-oncology and nuclear medicine) of swiss hospitals or in one of about 150 private radiological practices have been trained in a university of applied medical science or a college of higher education in Switzerland, which train and certify about 125 technicians each year. This is not enough, thus about one third of the 3,496 technicians, working in Switzerland at the moment have been trained abroad.

Learning Objective:

1. The introductions will give a very short overview of the aim and history of the Meets sessions (EFRS president) and the characteristics of Portugal and Switzerland (association presidents).

A-495 14:10

Introduction: Across Portugal

J. Santos; Coimbra/PT (presidente@atarp.pt)

Portugal is a European Union country with the 10 millions of habitants. The total land area is 91,590 Km² with 850 Km of splendid beaches bathed by the Atlantic Ocean. Per year Portugal has around 3000 hours of sun however 66.3% of the population is urban. The number of medical imaging equipment's is higher than the Organisation for Economic Co-operation and Development (OECD) recommendations. Structurally the supervisory authorities in the area of ionising radiation for medical exposures in Portugal are Regional Health Administrations, the Nuclear Technological Institute and the Health Authorities. The Portuguese health system is divided in five Regional Health Administrations (ARS). These government agencies ensure the efficiency of health care and manage the human and technical resources. They are responsible for the enforcement of the provisions of the Portuguese law regarding the facilities to radiology practice. Portugal has three dedicated Paediatric Hospitals and three further sites with specialised paediatric services, which have a 24 hour service, a large proportion of paediatric medical imaging examinations are performed in adult hospitals. The National Health Service (Serviço Nacional de Saúde) meets Portuguese healthcare needs. The majority of health care institutions are public but the number of private institutions had increased on the last decades.

Learning Objective:

1. The introductions will give a very short overview of the aim and history of the Meets sessions (EFRS president) and the characteristics of Portugal and Switzerland (association presidents).

A-496 14:15

Radiographers in Switzerland: challenges and chances

Y. Jaermann; Vevey/CH (yves.jaermann@hopitalrivierachablais.ch)

Our profession is relatively new in Switzerland. It remains largely unknown by the general population as well as by other health professionals. The current political and economical context obliges us to explore ways in which to defend the position of our profession in the health community. While certain professions seek to take over important areas of established radiography skills, an update of our training system is absolutely indispensable. At the same time, it is vital for us to develop new areas of activity that will allow the profession to acquire the recognition that it deserves.

Learning Objectives:

1. To understand the curriculum of the Swiss radiographers' education and CPD.
2. To acknowledge the competition with other professions and the need for new skills and activities.
3. To evaluate the next steps to professional independence.

A-497 14:30

The Portuguese NHS: the structural pillar that strengthens Portuguese democracy

G. Paulo; Coimbra/PT (graciano@estescoimbra.pt)

Over four decades Portugal has been governed under a dictatorship system, leading our country into one of less developed in Europe, specially in the education and health system. On the 25th of April of 1974 a military-led coup put an end to the 40 years of dictatorship, through what is called the "revolução dos cravos", named to the fact that from one day to another, and without a civil war or any kind of deaths, Portuguese went to bed in a dictatorship regime and woke up in a Democracy. One of the main pillars on which the Portuguese democracy has been raised is the SNS (Serviço Nacional de Saúde): Portuguese NHS. The SNS guarantees equal rights and equal access to all Portuguese, independently of age, gender, race, religion, with no social or economic discrimination. Due to the qualitative and civilisational improvement raised from the creation of the Portuguese SNS, Portugal, in the last 38 years, has passed from one of the countries with the worse health indicators to one of the top 10 WHO ranking. The quality of the education of radiographers and radiologists is highly recognised, honouring the Portuguese Nobel prize in Medicine, Egas Moniz (1949), that aside from several achievements in the field of neurosurgery was the pioneer of the cerebral angiography. Medical imaging in Portugal had an important role in the national program against the incidence and prevalence of tuberculosis. Portugal was also one of the first European countries to successfully implement a national mammography screening program.

Learning Objectives:

1. To learn about the development of the Portuguese NHS.
2. To understand the impact of the Portuguese NHS in the social development.
3. To learn about the role of radiology in improving the Portuguese health indicators.

A-498 14:45

(Helv)ethic: from a project to a new culture

F. Riondel; Geneva/CH (francois.riondel@hcuge.ch)

At the University Hospital of Geneva, the radiographers collectively produced a document to improve the recognition of their profession within their institution. A reflexion spanning several years with the aim of clarifying their autonomy and responsibilities, and written as an ethical code, presented as a charter. Different elements of this charter reflect themes that are debated in the french speaking part of Switzerland or elsewhere in the country. It covers the development of a radiographer's expertise and recognition of the necessity for access to continuous professional education, centered around the patients needs. New ways of positioning the radiographer in the inter-professional partnership, increasing their autonomy and their independence for certain medicotechnical acts.

Learning Objectives:

1. To learn about a team building philosophy able to promote our profession and build new career opportunities.
2. To understand the central role of radiographers within the growth and promotion of the professional environment and within the profession itself.
3. To acknowledge the importance of patient care and human relationships in radiography.

A-499 15:00

MRI, the image modality for the future: hybrid, diagnostic and therapeutic

V. Silva; Porto/PT (vitorsoft@gmail.com)

Magnetic resonance (MR) is a medical imaging modality in permanent evolution. Nowadays, MR is becoming a hybrid technique, functioning for diagnostic and therapeutic considering the superb soft tissue contrast. Dedicated hybrid positron emission tomography (PET) combined with MR - PET/MR have been recently introduced and these equipments have the potential to combine the molecular and functional information of PET with MR excellent soft tissue contrast, perceiving better the localization of pathologies. PET/MR offers opportunities for more efficient, accurate and safe diagnoses. MR can be used to therapeutic methods when combined to a hybrid linear accelerator (linac). MR will provide optimal soft tissue contrast for image guidance in multiple sites in human body providing diagnostic quality images during treatment delivery, and, consequently, permitting very accurate image guided adaptive radiotherapy. Associated to these new paradigms on MR hybrid imaging, the knowledge of MR safety issues and considerations are fundamental for better practices. Knowing how a MR scanner works and its inherent physics is vital. For its functioning, MR has three different types of electromagnetic fields: (i) a static magnetic field; (ii) time varying gradient fields; and (iii) radiofrequency fields. These have different risks and hazards. The MR potential for improving the health care provided to patients is proved by the combination with other diagnostic and therapeutic imaging modalities.

Learning Objectives:

1. To recognise MRI as an image modality with great clinical potential for diagnosis.
2. To learn about MRI/PET opportunities, challenges and new directions in clinical practice.
3. To understand the MRI potential to improve radiotherapy planning and treatment.
4. To be aware of MRI safety considerations and risks to promote best practices.

15:15

Panel discussion

14:00 - 15:30

Room M 1

EuroSafe Imaging Session

EU 3

Clinical diagnostic reference levels for x-ray medical imaging

A-500/A-501 14:00

Chairpersons' introduction and update on the project on clinical DRLs for x-ray medical imaging

J. Damilakis¹, G. Frija²,¹Iraklion/GR, ²Paris/FR (damilaki@med.uoc.gr)¹, (guy.frija@aphp.fr)²

Different image quality is needed for different clinical indications of the same anatomical area. Kidney stone evaluation, for instance, can be performed

using lower radiation doses than those used in evaluation of appendicitis because detection of high-contrast structures is affected less by high image noise than low contrast structures. Clinical indications dictate the main parameters that affect patient dose from CT such as scanning length, collimation and number of phases. The EC launched the 'European study on clinical diagnostic reference levels for X-ray medical imaging' (EUCLID) project to provide up-to-date clinical DRLs. The main objectives of the project are to: (a) conduct a European survey to collect data needed for the establishment of DRLs for the most important, from the radiation protection perspective, X-ray imaging tasks in Europe; and (b) specify up-to-date DRLs for these clinical tasks. This introductory presentation will provide a brief update on EUCLID project.

Session Objectives:

1. To understand the general concept of diagnostic reference levels (DRLs), in particular clinical DRLs and the project on clinical DRLs for x-ray medical imaging.
2. To learn about the current status of DRLs in paediatric imaging.
3. To become familiar with the concept of local DRLs.

A-502 14:05

The concept of diagnostic reference levels (DRLs)

E. Vaño; Madrid/ES (eliseov@med.ucm.es)

Diagnostic reference Levels (DRLs) were introduced by the International Commission on Radiological Protection (ICRP) as a tool to help optimise medical imaging in diagnostic and interventional procedures. ICRP has published a new set of recommendations on DRLs (ICRP Publication 135; 2017). Several issues have been updated: definitions of the terms used in previous guidance, determination of the DRLs values (including multimodality procedures), the appropriate interval for re-evaluating these values, appropriate use of DRLs in clinical practice and application of the DRL concept to newer imaging technologies. Weight bands are recommended for establishing paediatric DRLs. Concerning medical imaging tasks, the DRL values should be tied to defined clinical and technical requirements. The assessment of clinical image quality or the proper diagnostic information when multiple images are used should be performed as part of the optimisation process. ICRP has also included recommendations on establishing regional (for several countries) DRL values that can be based on either a representative sample of health facilities or on national DRL values. Regional DRL values may provide guidance on how to optimise the protection of neighbouring countries with no DRL surveys of their own. When relatively few national DRL values exist for the countries within a region, regional DRL values may be derived through a consensus of the region's competent authorities. ICRP suggested that the problem to combine large and small countries could be dealt with by weighting national DRL values according to the population of each participating country.

Learning Objectives:

1. To understand the concept of DRLs in general.
2. To learn about the International Commission on Radiological Protection's (ICRP) work and perspective.

A-503 14:20

The concept of clinical diagnostic reference levels (DRLs)

G. Frija; Paris/FR (guy.frija@aphp.fr)

Diagnostic reference levels (DRLs) are an important tool for optimisation. They are usually established for specific anatomical locations, although some countries established also DRLs based on clinical indications. This talk will highlight the advantages of this latter approach, and will briefly introduce the EUCLID project (European Study on Clinical DRLs), a European Commission tender project aimed at establishing DRLs on clinical indications.

Learning Objectives:

1. To become familiar with the concept of clinical DRLs.
2. To learn about the EUCLID project.
3. To learn about practical implications and advantages of clinical DRLs.

A-504 14:30

An update on current European diagnostic reference levels (DRLs) in adult imaging

J. Damilakis; Iraklion/GR (damilaki@med.uoc.gr)

The clinical indication is the main determinant of patient radiation dose. Therefore, DRLs should be specified for a given clinical indication. The 'European study on clinical diagnostic reference levels for X-ray medical imaging' (EUCLID) project aims to specify up-to-date DRLs for the most important, from the radiation protection perspective, X-ray imaging tasks in Europe. A comprehensive review has been carried out to identify the status of existing clinical DRLs for CT, interventional radiology and radiography in

Postgraduate Educational Programme

Europe and beyond by analysing recent studies, standards and publications. Information about existing clinical DRLs has also been collected from national competent authorities and other organisations involved in the project. A few national radiation protection authorities, only, have defined a limited number of DRLs for different clinical indications, so far. Although a large number of studies on doses from X-ray imaging are available, there is very limited information about clinical-indication specific DRLs.

Learning Objectives:

1. To learn about methodological requirements for establishing DRLs.
2. To learn about the current status of DRLs in adult imaging in Europe and beyond.
3. To understand why clinical DRLs are needed in adult imaging.

A-505 14:45

An update on current paediatric diagnostic reference levels (DRLs)

C. [Granata](#); *Genoa/IT (cgranata@sirm.org)*

Particular attention should be paid to using diagnostic reference levels (DRLs) in paediatric radiology, as children are at higher risk compared to adults of being affected by the detrimental effects of radiations in some organs and body areas. However, only a few European countries have established paediatric DRLs, mostly for a limited set of examinations. The existing DRLs are often derived from old European Commission (EC) recommendations or from surveys conducted in other countries with inconsistent methodology and rarely updated. Furthermore, DRLs are still largely based on age and not on size, which can be very different among children of the same age. Recently, an EC project on new European guidelines for DRLs in paediatric imaging (PiDRL) was assigned to a consortium directed by ESR with the involvement of ESPR, EFRS, EFOMP, and STUK. This project resulted in a series of recommendations concerning the appropriate methods to establish new paediatric DRLs. These recommendations define what is intended for local, national, and European paediatric DRLs, the set of examinations for which paediatric DRLs should be established, patient subdivision into groups, dosimetric parameters to be considered, and instructions on how to make good use of paediatric DRLs.

Learning Objectives:

1. To become familiar with paediatric DRLs.
2. To learn about the European Guidelines on DRLs for Paediatric Imaging (PiDRL).
3. To learn about recent work undertaken by the ESR to establish paediatric DRLs.

A-506 15:00

The concept of local diagnostic reference levels (DRLs)

N. [Saltybaeva](#); *Zurich/CH (Natalia.Saltybaeva@usz.ch)*

Diagnostic reference levels (DRLs) are an important dose optimization tool endorsed by many professional and regulatory organizations. National DRLs (NDRLs) are commonly set by the local health authority at the third quartile values (75%) of the dose distribution determined for representative examinations conducted across different healthcare facilities. Besides NDRLs, local DRLs (LDRLs) can be also established for a single center or group of healthcare facilities and used as a baseline for quality control and dose optimization. The invited speaker will give an overview of how LDRL should be defined; which dose tracking tools can be used for this purpose and how the DRLs can be adjusted to the specific needs of the individual healthcare facility.

Learning Objectives:

1. To become familiar with the concept of local diagnostic reference levels (LDRLs).
2. To understand the key factors affecting LDRLs.
3. To learn how the LDRLs can be established and used for dose optimisation; what action should be taken if LDRLs are exceeded.

15:15

Panel discussion

J. [Damilakis](#)¹, G. [Frija](#)², E. [Vaño](#)³, J.N. [Vassileva](#)⁴, M. [del Rosario Perez](#)⁵;

¹Iraklion/GR, ²Paris/FR, ³Madrid/ES, ⁴Sofia/BG, ⁵Geneva/CH

14:00 - 15:30

Room M 2

PIER @ ECR Session

PI 2

Radiology will survive, but will the radiologist still be there?

Moderators:

P. Leander; Malmö/SE
S. Morozov; Moscow/RU

A-507 14:00

The landscape in radiology is changing: the radiologists need to adapt

P. [Leander](#); *Malmö/SE (peter.leander@med.lu.se)*

Diagnostic imaging is of great importance and will become even more so with addition of new techniques. In the western world, annual growth-rates of imaging are around 10%. Not only the number of examinations increase also are the studies more complex requiring highly specific reports and more quantitative measurements. To respond to the growing demands radiologists try to run faster, but may have reached the limit of capacity when working in a traditional way. If other strategies not are implemented the increasing workload cannot be handled and requests from clinical colleagues may be turned down. In many countries, workload is handled partly by external reading from teleradiology companies. However, teleradiology is also controversial as it shifts radiology from being an interactive specialty to a commodity that can be ordered and delivered as a common laboratory service. In radiology, traditionally examinations have been performed by technicians and presented to a radiologist for reading. Throughout development of new potent modalities as CT, MRI and PET-CT and filmless departments using RIS and PACS that has not changed. Do we now stand in front of a big paradigm shift? Now the radiologist may become a conductor of several systems performing reading, i.e., machine learning, artificial intelligence (AI), reading radiographers and teleradiology. The technical development may give more opportunities in radiology than ever for giving the radiologist help with the right tasks in the right time.

Learning Objectives:

1. To understand the worldwide trends in workload change.
2. To appreciate the development of teleradiology and commoditisation of the radiology.
3. To become familiar with the role of information technologies in radiology.

Author Disclosure:

P. [Leander](#): Board Member; Spago Nanomedical MRI contrast media research company, Lument, contrast media research in the area of oral CT contrast.

A-508 14:23

Big-data, artificial intelligence, machine learning, deep learning etc.: what radiologists should know

K.J. [Dreyer](#); *Boston, MA/US (kdreyer@partners.org)*

As computers outperform humans at complex cognitive tasks, disruptive innovation will increasingly remap the familiar with waves of creative destruction. And in healthcare, nowhere is this more apparent or imminent than at the crossroads of Radiology and the emerging field of Clinical Data Science. As leaders in our field, we must shepherd the innovations of cognitive computing by defining its role within diagnostic imaging, while first and foremost ensuring the continued safety of our patients. If we are dismissive, defensive or self-motivated - industry, payers and provider entities will innovate around us achieving different forms of disruption, optimised to serve their own needs. To maintain our leadership position, as we enter the era of machine learning, it is essential that we serve our patients by directly managing the use of clinical data science towards the improvement of care—a position which will only strengthen our relevance in the care process as well as in future federal, commercial and accountable care discussions. In this session, we will explore the state of clinical data science in medical imaging and its potential to improve the quality and relevance of radiology as well as the lives of our patients.

Learning Objectives:

1. To learn the basic principles of artificial intelligence.
2. To appreciate the current and future applications of artificial intelligence in radiology.
3. To become familiar with available tools of artificial intelligence in clinical and research radiology.

Postgraduate Educational Programme

A-509 14:45

How to cope with the new IT developments: the developer's perspective
S. Tolle; Galway/IE (Steven.Tolle1@ibm.com)

It is humanly impossible for radiologists these days to keep up with the sheer volume of medical images generated and the huge reporting workloads, complicated by shrinking radiologist workforce in Europe. Thus, radiology departments and radiologists need to embrace technology that helps make things more efficient and improve their job satisfaction. Through advanced image analysis, machine and deep learning as well as a robust knowledge base, AI can revolutionise healthcare. The power AI can quickly sort abnormal from normal, compare sequential datasets to show changes, detect abnormalities, speed up reporting, and increase capacity. Ultimately, AI in radiology can bring greater confidence in diagnostic decisions, improved workflows, optimised reporting times and better connect people, medical images as well as unstructured and structured data.

Learning Objectives:

1. To understand the market trends of IT and AI in healthcare.
2. To appreciate the clinical needs for IT, AI, machine learning and big-data analysis tools.
3. To understand the current business models and future trends of IT/AI products in healthcare.

Author Disclosure:

S. Tolle: Employee; IBM Watson Health.

A-510 15:08

The value of the radiologist in the evolving digital environment: challenges for leadership
C.D. Becker; Geneva/CH

The radiologic profession is at the forefront of digitisation in medicine, and had to adapt continuously to many disruptive changes over the past few decades. Today, images and image processing tools are no longer owned by radiologists but readily accessible for all authorised physicians. Patients may have direct access to medical information via digital platforms and may wish to participate in diagnostic and therapeutic decisions and procedures that are based on radiologic images. The diagnostic radiologist must be able to act as an imaging consultant, with expert knowledge dedicated to a subspecialty area. Although there is a general trend towards a value-based health system, the radiologist's role as guarantor of the quality chain of medical imaging is often underestimated or even taken for granted. Recent advances in data science such as machine-learning algorithms for automated image interpretation, quantitative image processing tools for mathematical texture analysis in the context of advanced oncology, and automated data extraction by means of big data processing tools are on the horizon, heralding new disruptive changes for the radiologic profession. The leadership challenges in radiology for the next decade include the questions how these new tools can best be harnessed and how the clinical relevance of the radiologist can be ensured in this rapidly changing digital environment.

Learning Objectives:

1. To review the impact of the digital environment on the radiologist's role.
2. To examine strategies to ensure the clinical relevance of the imaging specialist in the future.
3. To discuss the challenges for leadership in radiology.

14:00 - 15:30

Room M 4

E³ - ECR Academies: State-of-the-Art and Advanced MR Imaging of the Musculoskeletal system

E³ 1119

Small joints

A-511 14:00

Chairperson's introduction

M. Zanetti; Zurich/CH (marco.zanetti@hirslanden.ch)

This state of the art course will address how MR imaging can be improved in the assessment of the small joints in the fingers, forefoot, midfoot, temporomandibular joint, and in the pubic symphysis. Optimized MR protocols will be suggested. Based on the challenges to assess the anatomical structures in the small joints the use of contrast media may be considered by some radiologists, but the general use is debated. Thus, this use of contrast media in small joints will be specifically discussed.

A-512 14:05

A. Fingers

E. Llopis; Valencia/ES (evallopis@gmail.com)

The purpose of this educational lecture is to become familiar with imaging of the fingers. We will review the anatomy based on a compartmental approach: flexor, extensor, supportive structures, and bones. We will list the most common ligament and tendon traumatic injuries, and the more frequent tumors where imaging can be specific and the role of the different modalities. To finalize we will give a structured report.

Learning Objectives:

1. To identify the most common post-traumatic entities.
2. To identify the most common entities leading to chronic pain.
3. To know the role of MR imaging and how to optimise protocols with and without contrast administration.

A-513 14:26

B. Forefoot and midfoot

N. Mamisch-Saupe; Zurich/CH (nsaupe@hotmail.com)

Many disorders produce pain in the forefoot and the metatarsal region. Sometimes it is difficult to establish a diagnosis only on the clinical findings. MRI with its excellent soft tissue contrast and multiplanar imaging capability can often reveal a specific diagnosis. MRI allows a specific diagnosis based on the localization, signal intensity characteristics as well as morphologic features of the lesion. Commonly present disorders include trauma related lesions such as stress fractures or stress reactions of the bone as well as sesamoiditis or Freiberg fracture. Traumatic soft tissue lesions include plantar plate tears which occurs more often in women with increased weight bearing load and hyperextension forces involving the lesser metatarsal joints compared to the turf toe involving the greater metatarsal joint after hyperextension arm more commonly in men. There are additionally many non-neoplastic soft tissue masses to differentiate such as Morton neuroma, ganglia, bursitis or pseudobursae leading to chronic pain. Additionally, other chronic diseases such as gout and rheumatoid arthritis often affect the metatarsal joints. An additional value of contrast-enhanced MRI over standard MRI and STIR sequences exists in imaging mid- and forefoot. There is a slightly more added value for soft tissue lesions compared to bony lesions. Especially in detection of lesser metatarsophalangeal joint plantar plate tears a substantial portion of the lesions becoming only visible or after the administration of gadolinium or leading to change the diagnosis in many cases.

Learning Objectives:

1. To identify the most common post-traumatic entities.
2. To identify the most common entities leading to chronic pain.
3. To know the role of MR imaging and how to optimise protocols with and without contrast administration.

A-514 14:47

C. Temporomandibular joint

G. Andreisek; Münsterlingen/CH (gustav@andreisek.de)

The temporomandibular joint (TMJ) is one of the small joint of the body which usually gets only little attention by radiologists. It is also often covered clinically by dentists. Unfortunately, the interaction between dentists and radiologists is usually limited and as such there is also little knowledge among radiologists regarding TMJ disorders. However, the incidence of TMJ joint disorders is fairly high with subsequent problems for the patients. They typically complain about pain or tenderness in the face, jaw joint area, neck and shoulders, and in or around the ear when chewing, speaking, or opening the mouth wide. Patients also describe jaws that get "stuck" or "lock" in the open- or closed-mouth position, clicking, popping, or grating sounds in the jaw joint when opening or closing the mouth or chew. Patients may also develop toothaches, headaches, neck aches, dizziness, earaches, hearing problems, upper shoulder pain, and ringing in the ears (tinnitus). In my lecture, I will review the normal anatomy of the TMJ as well as normal appearance on MR imaging. In addition, comments on a proper imaging protocol which fulfil both the needs for sufficient image quality, but also time-and-cost efficient. Results from own research on ultra-high field MR imaging of the TMJ will also be presented. Finally, typical acute and chronic TMJ disorders will be discussed.

Learning Objectives:

1. To identify the most common post-traumatic entities.
2. To identify the most common entities leading to chronic pain.
3. To know the role of MR imaging and how to optimise protocols with and without contrast administration.

Postgraduate Educational Programme

A-515 15:08

D. Pubic symphysis

P. [Robinson](#); Leeds/UK (philip.robinson10@nhs.net)

This lecture will describe the anatomy and function of the symphysis pubis and surrounding soft tissues and how this can vary between the sexes and during pregnancy. Proposed mechanisms of injury will be presented. Primary stresses during athletic activity are thought to be shearing in nature while in pregnancy distraction predominates. Post-partum 'osteitis pubis' is thought to be due to residual instability, but rarely requires surgical intervention. Athletic pubalgia has a more controversial aetiology, but more consistent MRI findings involving and surrounding the symphysis pubis. However, in both areas imaging abnormalities can exist in asymptomatic patients and therefore, clinical context and correlation is vital.

Learning Objectives:

1. To identify the most common post-traumatic entities.
2. To identify the most common entities leading to chronic pain.
3. To know the role of MR imaging and how to optimise protocols with and without contrast administration.

Author Disclosure:

P. [Robinson](#): Advisory Board; European PGA. Board Member; seminars in musculoskeletal radiology.

16:00 - 17:30

Room A

E³ - ECR Academies: Interactive Teaching Sessions for Young (and not so Young) Radiologists

E³ 1221

Imaging of the chest

A-516 16:00

A. Fibrosing lung diseases

F. [Molinari](#); Lille/FR (francescomolinari.dr@gmail.com)

The diagnostic approach to patients with fibrosing interstitial lung disease (FILD) is often complicated even when clinical history and physical findings are correctly assessed at presentation. In fact, many disorders of known and unknown etiology may result in lung fibrosis and have overlapping clinical and radiographic features. Surgical lung biopsy is a viable tool for establishing the diagnosis. However, the procedure is associated to morbidity and mortality risks. HRCT remains the most important noninvasive modality for the diagnosis and management of patients with FILD. HRCT findings such as parenchymal reticulation, ground-glass attenuation, traction bronchiectasis and bronchiolectasis, architectural distortion, and honeycombing indicate the presence of FILD. Honeycombing also indicates that lung fibrosis is irreversible and potentially progressive. To differentiate the most commonly encountered FILDs, current guidelines recommend to consider the presence of subpleural and basilar reticulation associated with honeycombing, altogether as the "UIP pattern". In the absence of known causes of lung fibrosis, a "definite" UIP is consistent with a diagnosis of idiopathic pulmonary fibrosis and does not require lung biopsy. The forms of FILD that manifest at HRCT as "possible" UIP and for which an alternative diagnosis of NSIP exists require lung biopsy. Finally, if the FILD manifests with HRCT findings that are inconsistent with UIP, the potential diagnosis of chronic HP is considered and lung biopsy is usually not indicated. This clinical-HRCT interpretative algorithm facilitates the assessment of HRCT scans that show the presence of lung fibrosis and provides guidance in the management of patients with FILD.

Learning Objectives:

1. To become familiar with the differential diagnosis.
2. To identify the key imaging findings.

A-517 16:45

B. Pleural disease

C. [Beigelman](#); Lausanne/CH

Diffuse or focal pleural disorders are commonly encountered in routine practice, including pleural effusions, pleural thickenings, calcified or not, pneumothoraces or masses. Differential diagnosis must be known. In particular, focal pleural thickening (PT) may be related to typical pleural plaques, but also to normal structures, previous tuberculosis, pleural metastasis, silicosis, or other rarer conditions. Furthermore, postero-basal PT in supine examination may be reversible on prone position. Any atypical shape, location or change of a PT should suggest a pleural metastasis in a context of malignancy. In all cases, a careful analysis of other CT findings, previous imaging studies and clinical history are determinant for the final diagnosis. Parenchymal bands or rounded atelectasis are helpful for the diagnosis of

benign diffuse pleural thickening. Features suggestive of malignancy include circumferential pleural thickening, nodular pleural thickening, parietal pleural thickening greater than 1 cm, and mediastinal pleural involvement. Atypical aspects such as pleural effusion even without plaque and pleural irregularity may be observed in mesothelioma, and slight changes in the mediastinal or interlobar pleura should be considered as suspicious of this diagnosis. Mistakes may be related to the difficult recognition of features such as in case of pneumothorax in supine position or to atypical features such as loculated effusions or atypical presentations of malignant pleural involvement, that may lead to a delayed diagnosis.

Learning Objectives:

1. To identify the key imaging findings.
2. To become familiar with the differential diagnosis.

16:00 - 17:30

Room B

Special Focus Session

SF 12a

My three top tips for abdominal imaging

A-518 16:00

Chairperson's introduction

D.J.M. [Tolan](#); Leeds/UK (djmtolan@doctors.org.uk)

A rapid review of the key areas for professional learning and development will be provided from a group of expert radiologists for a full range of gastrointestinal conditions. This will provide opportunities for both the general radiologists and specialists to improve the services they offer patients and clinicians dealing with abdominal diseases.

Session Objectives:

1. To learn how to avoid common mistakes in abdominal radiology.
2. To understand how to get over an area of difficulty through the clinical expertise of selected abdominal radiologists.

A-519 16:05

Postoperative abdomen

D.J.M. [Tolan](#); Leeds/UK (djmtolan@doctors.org.uk)

Anastomotic leaks on CT are heralded by a number of signs including increasing free gas and free fluid in the abdomen, localised fluid around the anastomosis and in particular the extravasation of positive contrast from the bowel lumen. This is recommended for routine use in the post operative evaluation of patients wherever possible. Surgeons utilise haemostatic agents in the intraoperative management of bleeding. These can cause confusion in imaging interpretation and can mimic an abscess. Radiologists should have a heightened awareness of this appearance and discuss such cases with the surgical team for clarification. Similarly retention of surgical swabs remains a substantial cause of morbidity for patients in the post operative period. Such swabs are readily identifiable by a radiolucent marker and in such cases the surgical team needs immediate notification to allow a return to theatre for swab retrieval.

Learning Objectives:

1. To learn how to optimise detection of anastomotic leaks on CT using radiological signs and positive luminal contrast.
2. To recognise material in the abdomen surgeons may leave deliberately.
3. To recognise material in the abdomen surgeons may leave by accident.

A-520 16:11

Appendicitis

J.B.C.M. [Puylaert](#); The Hague/NL (dr.jbcmputylaert@wxs.nl)

Abdominal ultrasound plays a pivotal role in the imaging workup of patients with suspected appendicitis. It should be the primary modality, and only in case of a negative or inconclusive examination should it be followed by CT or MR. The specific advantages of US over CT are: US has an image definition in the close range which is much higher than that of CT. US is more interactive than CT. The patient's history as well as the painful area or palpable mass can directly be correlated with the US findings. US is real time and shows peristalsis, pulsations and blood flow. US also shows the effects of respiration, Valsalva manoeuvre, gravity and compression with the probe, allowing to assess whether the appendix or other organs such as the bowel and gallbladder are soft or rigid. US allows immediate US-guided puncture of intraperitoneal fluid and drainage of pus. US in appendicitis should be performed with graded compression. Compression is necessary to displace or compress bowel to eliminate the disturbing influence of bowel gas and to approach the pathological structure closely. This allows the use of a high-

frequency transducer with a better image quality. The final US report should be integrated with the clinical findings, laboratory data, CT-scan and possible other radiological examinations. It is clear that the US examination, as described here, should not be performed by a technician or by a clinician, but by an experienced (abdominal) radiologist.

Learning Objectives:

1. To learn that US has a pivotal and unique role in appendicitis and should be done prior to CT.
2. To learn that US in acute abdomen allows the radiologist to get closer to the patient than CT and MRI.
3. To learn that US should be performed by abdominal radiologists, and not by clinicians or technicians.

A-521 16:17

Bile duct stones

J.A. Guthrie; Leeds/UK (Ashley.Guthrie@nhs.net)

The first investigations in patients with suspected gallstone disease, especially if stones within the common bile duct (CBD) are suspected, are US and liver function tests (LFTs). On the basis of this, the risk of CBD stones can be estimated and the decision whether or not to perform the next test, MRCP, can be made. In the presence of stones in the gallbladder, the risk increases with a CBD of > 8 mm and increasing abnormal LFTs. My preference is for 2D T2 sequences without fat saturation in two planes. Breath-hold when possible is preferred in the interests of time, but can be gated in those that struggle. HASTE/SS-FSE/FSE-ADA/FASE is the first set of sequences, followed by FISP/GRASS/FFE/SARGE if a diagnosis is not made as stones vary in their conspicuity between the sequences. The examination can be terminated as soon as a positive diagnosis is made. T1-weighted images occasionally help.

Learning Objectives:

1. To learn that in patients with a high index of clinical suspicion of bile duct stone, MRCP should be employed early.
2. To know that 2D HASTE/SS-FSE/FSE-ADA/FASE without fat saturation in two planes (oblique coronal and axial) will establish a diagnosis in most cases and are the "work horse" sequences in most patients.
3. To understand that FISP/GRASS/FFE/SARGE (which can be gated) are a useful adjunct especially in those patients that have difficulty holding their breath.

Author Disclosure:

J.A. Guthrie: Speaker; Bayer Healthcare, Siemens AG. Other; Attended a symposium organised and at the expense of Bayer Healthcare.

16:23

Questions and discussion

A-522 16:29

Dilated pancreatic duct

R. Manfredi; Rome/IT (riccardo.manfredi@unicatt.it)

The prognosis of pancreatic adenocarcinoma is very poor, and little improvement has been reported in the past several decades. Only a low percentage of patients in whom pancreatic cancer is detected at an early stage without local infiltration have the potential for long-term survival after surgical resection. The earliest possible diagnosis may be the most effective way to improve the prognosis. Dilatation of the main pancreatic duct may represent a secondary sign of pancreatic adenocarcinoma. Therefore, the diagnosis of dilated main pancreatic duct may be a predictive sign of pancreatic adenocarcinoma; therefore, careful follow-up in people with such signs and eventually prompt treatment have been recommended. Pancreatic endocrine neoplasms are relatively rare, with an incidence rate of approximately five cases per one million person-years. Some pancreatic endocrine neoplasms release hormones into the blood stream that cause clinical syndromes, whereas others are non-syndromic and present as a mass lesion. At diagnostic imaging, pancreatic endocrine neoplasms typically produce hyperenhanced well-demarcated lesions that are best seen on arterial phase images. Pancreatic endocrine neoplasms may be responsible for pancreatic duct stenosis, even when they are small in size (<2 cm) and be responsible for marked dilatation of the main pancreatic duct and/or marked atrophy of the upstream pancreas. Intraductal papillary mucinous neoplasm (IPMN) originates from the ductal epithelium and overproduce mucin which is responsible for the dilatation of the main pancreatic duct and/or the side branches. Diagnostic imaging is helpful in the diagnosis and follow-up of these patients.

Learning Objectives:

1. To learn how to diagnose and manage adenocarcinoma of the pancreas mimickers: autoimmune pancreatitis and paraduodenal pancreatitis.
2. To appraise how to manage incidental cystic lesions of the pancreas.
3. To learn how to diagnose and manage neuroendocrine neoplasms of the pancreas.

A-523 16:35

Liver biopsy

V. Vilgrain; Clichy/FR (valerie.vilgrain@aphp.fr)

Liver biopsy is the most common invasive procedure of the liver. Indications of biopsy in diffuse liver diseases have declined due to improvements in noninvasive assessment of fibrosis and steatosis. On the contrary, biopsy of liver tumours is still indicated mostly for diagnostic purpose and to a lesser extent for assessing the prognosis or the prediction of tumour response. Three keys are important. First, check the indication. There are very few contraindications (mostly related to coagulation disorders) and the most important is to ensure that there is a good indication for liver biopsy. Second, use ultrasound guidance, which is faster, easier and more accurate than CT. It allows real-time control. Third, if a primary tumour liver is considered, always perform a biopsy in the adjacent liver. This will help the pathologist in the diagnosis.

Learning Objectives:

1. To understand the risk/benefit of liver biopsy.
2. To know the absolute contraindications.
3. To be aware of the most important technical tricks.

A-524 16:41

Bowel ischaemia

M. Zins; Paris/FR (mzins@hpsj.fr)

Acute mesenteric ischaemia (AMI) is defined by inadequate blood supply through the mesenteric vessels resulting in intestine injury and carries a high mortality rate. A combination of two phenomena is needed to generate AMI: vascular insufficiency and intestinal injury. The diagnosis of AMI should be made as soon as possible, since early stages of ischaemia are reversible if properly treated. The three main messages for the radiologist are: 1) CT angiography (CTA) should use a triple-phase protocol (unenhanced, arterial and portal venous phase), 2) assessment of bowel wall abnormalities at CTA (decreased enhancement, increased attenuation on pre-contrast phase, wall thickening, wall thinning) is a major step in the interpretation of CT scans and 3) always carefully check the mesenteric vessels (for thrombus, embolism, dissection) in patients with acute abdominal pain of unknown origin.

Learning Objectives:

1. To understand the limited value of isolated mesenteric pneumatosis.
2. To learn about the added value of unenhanced scan.
3. To understand the crucial role of vascular assessment at CT angiography.

16:47

Questions and discussion

A-525 16:53

Colon polyp

F. lafrate; Rome/IT (francoiafrate@gmail.com)

"no abstract submitted"

Learning Objectives:

1. To quickly review different morphological aspects and "weapons" in the hand of radiologist to detect colonic polyps with CT colonography with small focus on correct preparation and the use of CAD.
2. To define large, small and intermediate polyp size and to review polyp pathology including the risk of cancer and high-grade dysplasia moreover in small and intermediate polyps.
3. To summarise the current debate with regard to intermediate polyps (conservative management vs polypectomy) and the rationale for non-reporting of diminutive polyps.

A-526 16:59

Acute pancreatitis

W. Schima; Vienna/AT (wolfgang.schima@khgh.at)

For diagnosis of acute pancreatitis, at least two of the three following criteria, (1) abdominal pain consistent with pancreatitis, (2) increase (≥ 3 -fold) in serum amylase or lipase levels and (3) imaging findings of acute pancreatitis, have to be fulfilled. According to the Revised Atlanta Classification, the disease is categorized as interstitial oedematous or necrotizing pancreatitis. Development of necrosis may take some time, so that CT imaging should be performed not earlier than 2-3 days after clinical onset. Imaging too early may lead to underestimation of disease severity. Necrotizing pancreatitis presents with either combined pancreatic and peripancreatic necrosis (most common) or with pancreatic necrosis or with peripancreatic necrosis alone. Acute necrotic collections (ANC) in the early phase may evolve into walled-off necrosis (WON) in the late stage (≥ 4 weeks). A WON containing chunks of digested fat and

parenchyma must not be confused with a pseudocyst containing enzymatic fluid (requiring different therapy). They may appear similarly hypodense at CT, but US or MRI will show the predominantly solid nature of a WON. Secondary infection of necrotizing pancreatitis usually occurs in the 3rd week after onset or later. Diagnosis of infection is difficult based on imaging alone. Infection is more likely if collections have broad contact with bowel. Gas within a collection is not a sensitive sign, but quite specific. In case of infection, percutaneous aspiration is sought, followed by drainage in positive cases. However, necrotic collections with large proportions of debris require a more aggressive approach for clearance.

Learning Objectives:

1. To learn about the proper timing of imaging studies in acute pancreatitis.
2. To learn about the imaging manifestations of necrotising pancreatitis.
3. To understand the different nature of fluid collections with regard to further therapy.

A-527 17:05

Crohn's disease

J. Rimola; Barcelona/ES (jrimola@clinic.ub.es)

My three top tips for Crohn's disease. In this session we are going to highlight the MUSTs in the assessment of Crohn's disease using cross-sectional imaging techniques: (1) What to look for first: thickness and enhancement, and T2 sequences. (2) What to look after: complications- all sequences. (3) Not forget to look at: other sequences, and areas other than the bowel.

Learning Objectives:

1. To learn about useful signs indicating active Crohn's disease.
2. To understand the changes which occur after treatment of intestinal inflammation.
3. To become familiar with complications related to Crohn's disease.

Author Disclosure:

J. Rimola: Advisory Board; TiGenix, Gilead. Consultant; Takeda, Roberts Clinical Reserach. Research/Grant Support; Abbvie. Speaker; BMS, Takeda.

A-528 17:11

Liver metastases follow-up

Y. Menu; Paris/FR (yves.menu@sat.aphp.fr)

Follow-up of liver metastases relies mostly on imaging. The need for standardisation was initially prompted by clinical trials. Several systems, from WHO to RECIST, have been proposed, allowing better intra- and interobserver reproducibility and guiding treatment strategy. However, the need for follow-up might be different according to clinical situations, like neo-adjuvant, palliative or adjuvant therapy. The standard might also be adapted to the type of drug, cytotoxic, targeted or immune therapies. Therefore, the radiologist needs to be aware of the clinical situation and learn to identify the drug, to perform a personalised evaluation.

Learning Objectives:

1. To learn how to quickly identify three most common systemic treatments of liver metastases (cytotoxic, targeted and immune), and to understand why knowledge of the regimen is essential for the radiological report.
2. To understand the rationale of international standards for the evaluation of response to treatment, and how to build accordingly a useful report.
3. To appraise the respective objectives of neoadjuvant and palliative chemotherapy, and to be able to explain the specific endpoints for each clinical situation.

17:17

Questions and discussion

16:00 - 17:30

Room C

Chest

RC 1204 Pneumonia

A-529 16:00

Chairperson's introduction

I.E. Tyurin; Moscow/RU (igortyurin@gmail.com)

Pneumonia is a major health-care and economic problem because of high morbidity and mortality rate, and due to direct and indirect costs of its management. The most common cause is community-acquired pneumonia, caused by common bacteria like *S. pneumoniae* as well as different viral agents. Tuberculosis is one of the most important respiratory infections in developing countries and in immune-compromised patients with AIDS everywhere. Tuberculosis pneumonia can easily mimic bacterial CAP and other pulmonary infections. Viral and mycotic infections represent a common course of febrile neutropaenia in immune-compromised patients under aggressive therapy. In most of all these patients, a diagnosis is made on the basis of a combination of clinical, radiographic, and laboratory findings. High-resolution CT is usually performed in patients with nonspecific clinical and radiologic findings and in patients with progression of disease despite therapy. A large number of acute and chronic infectious and noninfectious diseases may also result in parenchymal lung disease in both immune-competent and immune-compromised patients. Thin-section CT is also performed in patients with noninfectious causes of acute parenchymal lung disease such as organizing pneumonia, acute interstitial pneumonia, hypersensitivity pneumonitis, acute eosinophilic pneumonia, and pulmonary haemorrhage. These diseases often have clinical and functional features similar to one another, but obviously requiring different treatment. Therefore, the differential diagnosis of these entities is important in daily clinical practice.

Session Objectives:

1. To review the role of imaging in infectious lung diseases.
2. To understand the key role of multidisciplinary approach to diagnosis of lung infections.

A-530 16:05

A. Community-acquired pneumonia

I. Hartmann; Rotterdam/NL (i.j.c.hartmann@gmail.com)

Community-acquired pneumonia (CAP) refers to pneumonia acquired outside of hospitals or extended-care facilities and is one of the most common infectious diseases. CAP is an important cause of mortality and morbidity worldwide. According to the IDSA/ATS/AAFP guidelines, a chest radiograph is required for the routine evaluation of patients with suspected CAP to exclude conditions that mimic CAP (e.g. acute bronchitis) and to confirm the presence of an infiltrate compatible with the presentation of CAP. Although chest radiography findings usually do not allow identifying the causative organism, they may be helpful in narrowing down the differential diagnosis, prognosis, and detection of associated conditions. Serial chest radiography can be performed to observe the progression of CAP. CT scanning is increasingly used in clinical practice. Performing CT should be considered if any of the abnormalities at presentation or at follow-up are not consistent with the diagnosis of pneumonia, or if concomitant disease is suspected such as an underlying bronchogenic carcinoma, for the confirmation of pleural effusion and for the detection of pulmonary complications. The aim of the presentation is to provide an overview of the imaging findings of the most common aetiological organisms in patients with CAP. In addition, imaging findings that may help in the differentiation between pneumonia and other common non-infectious causes of abnormal chest radiographs in patients with suspected CAP will be discussed.

Learning Objectives:

1. To appreciate the role of imaging in the management of community-acquired pneumonia.
2. To consolidate knowledge of how to discriminate from noninfectious diseases.

A-531 16:28

B. Tuberculosis

E. Castañer; Sabadell/ES (ecastaner@tauli.cat)

Pulmonary tuberculosis (TB) remains a common worldwide infection that produces high mortality and morbidity, especially in developing countries. In 2013, an estimated 9.0 million (360 000 of whom were HIV-positive) people developed TB and 1.5 million died from the disease. Chest radiographs play a

Postgraduate Educational Programme

major role in the screening, diagnosis, and response to treatment of patients with TB. However, the radiographs may be normal or show only mild or nonspecific findings in patients with active disease. We will review the chest radiographs findings of TB, which vary widely in the function of several host factors, age, prior exposure to TB, and underlying immune status. CT is useful in detecting TB incidentally, in resolving cases with inconclusive findings on chest radiographs, and in assessing disease activity. Cavities, centrilobular nodules, and tree-in-bud appearance are the most common CT findings of active pulmonary tuberculosis. We will discuss the classic, and some not-so-classic, signs that should suggest the diagnosis of TB.

Learning Objectives:

1. To appreciate typical and atypical tuberculosis manifestations on imaging.
2. To differentiate between acute and chronic tuberculosis infection.

A-532 16:51

C. Fungal pneumonia in immunocompromised hosts

C.P. Heussel; Heidelberg/DE (heussel@uni-heidelberg.de)

The radiological characterisation of infiltrates gives a first and rapid hint to differentiate between different types of infectious (e.g. typical bacterial, atypical bacterial, fungal) and non-infectious aetiologies. Follow-up investigations need careful interpretation according to disease, recovery, concomitant treatment and eventually vessel arrosion requiring contrast-enhanced angio-CT. Due to a high incidence of fungal infiltrates in immunocompromised hosts, interpretation of the follow-up of an infiltrate must use further parameters besides the lesion size.

Learning Objectives:

1. To learn the patterns of fungal lung infection depending on the type of immune depression.
2. To become familiar with CT signs suggesting angioinvasive fungal infection.

Author Disclosure:

C.P. Heussel: Consultant; Schering-Plough, Pfizer, Basilea, Boehringer Ingelheim, Novartis, Roche, Astellas, Gilead, MSD, Lilly, Intermune, Fresenius. Employee; Head of Diagnostic and Interv Radiology with Nuclear Medicine, Thoraxklinik Heidelberg, Member of the German Center for Lung Research. Patent Holder; Method and Device For Representing the Microstructure of the Lungs. IPC8 Class: AA61B5055FI, PAN: 20080208038, Inventors: W Schreiber, U Wolf, AW Scholz, CP Heussel. Research/Grant Support; Siemens, Pfizer, MeVis, Boehringer Ingelheim, German Center for Lung Research. Speaker; Gilead, Essex, Schering-Plough, AstraZeneca, Lilly, Roche, MSD, Pfizer, Bracco, MEDA Pharma, Intermune, Chiesi, Siemens, Covidien, Pierre Fabre, Boehringer Ingelheim, Grifols, Novartis, Basilea, Bayer. Other; Stock ownership in medical industry: GSK, Comitee membership: Chest working group of the German Roentgen society; National guidelines: bronchial carcinoma, mesothelioma, COPD, screening for bronchial carcinoma, CT and MR imaging of the chest., Comitee membership: Consultant of ECIL-3, ECCMID, EORTC/MSG: Guideline for diagnosis of infections in immunocompromised hosts, Comitee membership: Founding member of the working team in infections in immunocompromised hosts of the German society of Hematology/Oncology: Guideline for diagnosis of infections in immunocompromised, Comitee membership: Faculty member of European Society of Thoracic Radiology (ESTI), European Respiratory Society (ERS), and member in EIBALL (European Imaging Biomarkers Alliance) Editor of „Medizin.

17:14

Panel discussion: What is the role of radiologists in the diagnosis and management of lung infections?

16:00 - 17:30

Room X

E³ - ECR Master Class (Abdominal Viscera)

E³ 1226

Dual-energy CT of the abdomen: the time is now

Moderator:

P. Vock; Berne/CH

A-533 16:00

A. Basic principles and different approaches

L.S. Guimaraes; Toronto, ON/CA (luis.s.guimaraes@gmail.com)

Dual-energy CT (DECT) refers to the use of CT data from two different energy spectra to differentiating and classifying tissue composition, in addition to displaying anatomy and pathology. DECT data can be obtained using various

hardware solutions (dual-source, fast kilovolt peak-switching, 2-rotation fast kV-mA switch, dual-layer detector and split filter). An explanation on how each of these solutions works, as well as the advantages and disadvantages of each, will be presented. Abdominal DECT has as main advantages the ability to identify/quantify certain materials (iodine, calcium, urate, etc.), as well as to increase the possibility of performing low kV imaging in a wider range of patients, which in turn is associated with an increased conspicuity of enhancing structures and lesions. The background and reasons for each of these advantages will be reviewed. Several challenges remain for full implementation of Dual Energy CT in routine clinical abdominal practices. These challenges, including absence of standardised post-processing (which may be time-consuming), lack of well-defined advantageous routine applications and limitations in terms of patient size/radiation dose will be discussed.

Learning Objectives:

1. To learn about the types of dual-energy scanners and principles of dual-energy CT.
2. To understand issues of radiation dose and image quality in comparison with single-energy CT.
3. To appreciate the possible advantages of this technology with its many post-processing applications.

Author Disclosure:

L.S. Guimaraes: Research/Grant Support; Institutional Research Grant from Toshiba Medical Systems.

A-534 16:30

B. Applications for genitourinary system

H. Ringl; Vienna/AT (helmut.ringl@meduniwien.ac.at)

Dual energy CT is increasingly becoming an important diagnostic tool for the non-invasive assessment of the genitourinary system, with a wide range of applications and several advantages over conventional single-energy CT, as detailed below: (1) The use of dual-energy CT with optimised split-bolus protocols enables considerable dose savings by eliminating two scan phases. However, using virtual non-contrast images, this protocol provides the same information as an unenhanced, an arterial, a venous, and a urographic phase; (2) Virtual non-contrast images and iodine maps enable better characterisation of renal cysts with dense content, which often pose a diagnostic dilemma in single-energy CT, and which might require MRI or CT follow-up examinations; (3) The reconstruction of low kV mono-energetic images results in a higher iodine contrast, and, therefore, in better lesion conspicuity in the kidneys and the bladder wall; (4) Dual-energy CT enables the quantification of iodine-uptake, and may, therefore, be used for therapy monitoring of cancer of the urinary tract; and (5) The material decomposition algorithms of dual-energy CT are able to discriminate urate from non-urate stones in the case of nephrolithiasis in the clinical routine, making this method a game-changer in therapy.

Learning Objectives:

1. To learn about the role of dual-energy CT in the genitourinary system.
2. To understand the value of determination of renal stone composition with dual-energy CT.
3. To appreciate the ability of dual-energy CT to exactly quantify the iodine uptake in renal lesions.

Author Disclosure:

H. Ringl: Research/Grant Support; Siemens.

A-535 17:00

C. Applications for abdominal organs

M. Karcaaltincaba; Ankara/TR (musturayk@yahoo.com)

Dual-energy CT (DECT) is increasingly used for abdominal applications. DECT can be performed by dual-source CT, fast kVp switching and dual-layer detector CT. The major advantage of DECT is availability of virtual non-contrast (water) images in every patient. Spectral CT images can allow the diagnosis of a low amount of fat (normally invisible on CT) within lesions similar to in-out of phase T1-weighted MR images. DECT can allow diagnosis of calcification or haemorrhage within lesions encountered during routine abdominal CT. Low kV images obtained by DECT are more sensitive to hepatic and pancreas hypervascular lesions compared to standard kV images. DECT can also be helpful in differentiation of colonic polyp/mass from stool detected during routine abdominal CT. In the future, all CT scanners will be most likely produced with DECT capability.

Learning Objectives:

1. To learn about the current applications of dual-energy CT in evaluating the abdominal viscera.
2. To understand the role of dual-energy CT for characterisation of incidental lesions discovered during routine abdominal CT.
3. To appreciate how dual-energy CT increases sensitivity for detecting both hypervascular and hypovascular liver and pancreatic lesions.

Postgraduate Educational Programme

Author Disclosure:

M. Karcaaltincaba: Speaker; Bayer, GE Healthcare, Philips Healthcare, Pfizer.

16:00 - 17:30

Room O

Special Focus Session

SF 12b

Imaging of the brain in preterm infants

A-536 16:00

Chairperson's introduction

P.C. [Maly Sundgren](mailto:Maly.Sundgren@med.lu.se); Lund/SE (Pia.Sundgren@med.lu.se)

In this session, focus will be on ultrasound and MR and their role in investigating the brain in preterms, and the use of these techniques for clinical outcome prediction and measures as well as for diagnostic decision-making.

Session Objectives:

1. To learn about different imaging techniques to study the preterm brain.
2. To understand the clinical importance of assessing the preterm brain.
3. To become familiar with novel imaging techniques and their clinical value.

A-537 16:05

The role of cerebral ultrasound

M.I. [Argyropoulou](mailto:Argyropoulou@cc.uoi.gr); Ioannina/GR (Ioannina@cc.uoi.gr)

Ultrasound (US) represents the imaging modality with which to start the evaluation of the neonatal brain in premature babies. A state-of-the-art technique should be applied using appropriate transducers (linear and sectorial) and different acoustic windows such as the anterior, the posterior and the mastoid fontanelle. Familiarisation with the normal US appearance of the brain as a function of gestational age is important to detect brain abnormalities. In very premature babies peri-occipital hyperechogenicity may represent a normal appearance and should be differentiated from periventricular leukomalacia. Increased echogenicity of the basal ganglia is a normal finding and should be differentiated from severe hypoxia lesions. Colour Doppler should be used and offers important additional information not only on blood flow, but also on the presence of subarachnoid haemorrhage. In the context of intraventricular haemorrhage, the disappearance of the normal flow at the level of the terminal vein represents a sign of pending venous infarct. Alternating red and blue colour signals at the level of the aqueduct of Sylvius represent an early finding of the presence of blood into the CSF spaces. The delta resistivity index (RI) evaluated at the anterior cerebral artery is calculated from the RI before and after compression of the anterior fontanelle and is very useful for treatment decision of post-haemorrhagic hydrocephalus.

Learning Objectives:

1. To learn about the technique and typical findings of cerebral ultrasound in preterm infants.
2. To understand indications for cranial ultrasound in neonates.
3. To discuss potential adverse effects and added value of US Doppler.

A-538 16:30

The role of cerebral MRI: morphology and beyond

F.M. [Triulzi](mailto:Triulzi@policlinico.mi.it); Milan/IT (Fabio.triulzi@policlinico.mi.it)

Preterm birth with subsequent brain injury is an increasing public health concern. Advances in neonatal intensive care have significantly improved survival rates among very-low-birth-weight infants, but survivors are still at considerable risk of developing cognitive, behavioural, neurosensory, and motor disabilities. The most common preterm brain injury patterns are white matter (WM) injury; germinal matrix-intraventricular haemorrhage and its correlates periventricular haemorrhagic venous infarction and post-haemorrhagic ventricular dilation. Diffuse non-cystic types of WM injury, the so-called "punctate" WM lesions, are the most frequent lesions seen on MRI and the leading cause of disturbed brain growth. Although MR imaging is superior to cranial sonography in detecting diffuse WM injury, conventional MR studies fail to exactly predict outcome. Advanced MR imaging acquisition sequences and post-processing techniques, such as DTI, volumetric MR imaging measurements, and proton MR spectroscopy may contribute to a better understanding of subtle microstructural, volumetric and metabolic abnormalities in preterm newborns, allowing a more precise prognosis at term-equivalent age. Early MR imaging, though of great interest to obtain very precocious biomarkers and enabling an early counselling to the parents, has still too many limitations to be considered a standard of care.

Learning Objectives:

1. To learn about protocol and typical findings in premature babies.
2. To understand indications and timing for MR exams in preterm infants.
3. To discuss the prognostic value of performing advanced MR techniques.

A-539 16:55

US screening in preterm infants: prognostic value from a clinical point of view

J.-P. [Schenk](mailto:jens-peter.schenk@med.uni-heidelberg.de); Heidelberg/DE (jens-peter.schenk@med.uni-heidelberg.de)

Preterm (born before 37 weeks of gestational age) and especially very premature infants (gestational age 32 weeks and less) have a great risk for intraventricular haemorrhage (IVH) and periventricular leukomalacia (PVL). Because of the possibility of a poorer neurodevelopmental outcome, the detection of IVH, PVL and subsequent hydrocephalus is mandatory. Due to the possibility of an examination inside the incubator with a high resolution, transfontanelar ultrasound is the method of choice for routine examination and follow-up studies. Typical ultrasound findings and pathology will be presented in context to follow-up findings, especially the posthaemorrhagic hydrocephalus and postschaemic cystic PVL. Therefore, the rationale of a US screening will be discussed and the in-Heidelberg-used screening scheme will be presented. US findings of blockage of cerebrospinal fluid pathways and obliterative arachnoiditis will be demonstrated. In context to the literature, the advantages of US screening will be discussed and in case studies the extended imaging with MRI will be demonstrated to see the limitations of US examinations and screening. The evaluation of periventricular echogenicity in PVL typically presents the difficulty of differential diagnosis in single US and demonstrates the necessity of repeated examinations in a screening system. Imaging at multiple time points improves the detection of cystic PVL. US findings in anomalies and tumours complete the range of differential diagnosis.

Learning Objectives:

1. To learn about the rationale for routine follow-up of the premature brain.
2. To understand the clinical impact of US findings in preterm infants.
3. To discuss the prognostic value of routine ultrasound screening of preterm infants.

17:15

Panel discussion: Can we afford the extensive screening programmes proposed today?

16:00 - 17:30

Room N

Special Focus Session

SF 12c

Head and neck emergencies

A-540 16:00

Chairperson's introduction

R. [Kohler](mailto:romain.kohler@hopitalvs.ch); Sion/CH (romain.kohler@hopitalvs.ch)

In this session, traumatic, infectious and inflammatory as well as vascular emergencies of the head and neck will be discussed. In the head and neck, multiple anatomical structures are confined in a small area in which run the airway and major vessels. Moreover, the neck is connected with the brain and thorax. These anatomical factors and the diversity of pathologies explain why emergencies may rapidly lead to potential major complications and disabilities or may even be lethal especially when the diagnosis is wrong or delayed. Besides the medical history, clinical examination and biological tests, imaging therefore plays a crucial role as many pathological processes may extend to adjacent structures, deeper structures or even outside of the head and neck area. Fractures of orbits, temporal bone, face or larynx may for example lead to compromise of the airway or meningitis. All structures of the head and neck may contract infection that can propagate to the surrounding spaces or even outside the head and neck. More rarely, patients present with bleeding which can be secondary to trauma, tumour or vascular malformation. Computed tomography and echography are the first techniques used in the emergency setting. MRI is rarely the first-line technique and is only reserved for selected patients with protected airway that are medically stable. Finally, angiography is reserved nowadays only for endovascular treatments. During this session, participants will become familiar with the most frequent emergencies of the head and neck and learn which imaging technique should be used for a given indication.

Session Objectives:

1. To become familiar with most emergencies of the head and neck in clinical routine.
2. To understand which imaging technique to use for a given indication.

A-541 16:05

What is broken?

E. [Loney](mailto:elizabeth_loney@hotmail.co.uk); *Darlington/UK (elizabeth_loney@hotmail.co.uk)*

Radiological assessment is critical in the management of skull base and facial trauma. CT is the preferred imaging technique, combining detailed visualization of bony and soft tissue injuries with the ability to perform 3D reconstructions and aid surgical planning. The scope of this presentation is broad and therefore we will concentrate on producing useful reports by differentiating Le Fort injuries from naso-orbitoethmoid and zygomaticomaxillary fracture patterns. We will consider orbital and temporal bone injuries and briefly touch upon laryngeal trauma, which in itself could account for a whole session. If attendees feel more comfortable reporting a facial trauma scan by the end of the presentation than they did at the start, our aims will have been achieved!

Learning Objectives:

1. To know which imaging techniques to use in case of trauma.
2. To become familiar with base of skull fracture (including temporal bone and orbit).
3. To learn about maxillofacial fractures.
4. To get acquainted with the traumatic lesions of the larynx.

A-542 16:28

It is red and swollen ...

M. [Becker](mailto:minerva.becker@hcuge.ch); *Geneva/CH (minerva.becker@hcuge.ch)*

Computed tomography (CT), magnetic resonance imaging (MRI) and occasionally ultrasonography (US), play a major role for the correct diagnosis of a variety of infectious head and neck conditions seen in the emergency situation. The purpose of this lecture is to familiarise the radiologist with the most common types of infectious emergencies in the head and neck. A systematic review will include key radiologic features of these potentially life-threatening conditions. The following entities are discussed: otomastoiditis, complicated sinusitis and sialadenitis, suppurative lymphadenitis, paratonsillar, retropharyngeal, parapharyngeal and other neck abscesses, cellulitis, myositis, necrotising fasciitis, osteomyelitis, thrombophlebitis and septic deep venous thrombosis. Associated complications affecting the mediastinum and lung, meninges and brain will be discussed with emphasis on the early detection of lesions. Typical spread patterns of infection within the neck will be summarised. The detection of foreign bodies as a cause of secondary infection, as well as pitfalls and limitations of individual imaging techniques will also be addressed. Major emphasis will be put on what is the most appropriate imaging modality in which clinical situation, how should imaging be performed in an optimal fashion and how to report the findings in a structured and comprehensive way.

Learning Objectives:

1. To learn which imaging techniques to use in the case of an infection and inflammation in the emergency setting.
2. To become familiar with the infections of the base of skull.
3. To understand the diversity of infection patterns of soft tissues.
4. To appreciate the pathologies of the salivary glands that may present in the emergency setting.

A-543 16:51

It is bleeding ...

D.-A. [Varoquaux](mailto:arthur@varoquaux.com); *Marseille/FR (arthur@varoquaux.com)*

Arterial embolisation is the preferred treatment for refractory epistaxes and for certain hemorrhages of the ENT area. When carried out by trained radiologists, it proves to be an efficient method that presents little risk of complications. Hemorrhages of the ENT area are of different nature and etiology. Their approach should be considered according to specific clinical context. The treatment of hemorrhages of venous origin does not fall under the competence of interventional radiology; endovascular or percutaneous embolization treatment of vascular malformations will not be treated in this article. According to circumstances, several types of arterial hemorrhages of the ENT sphere can be distinguished: (1) Hsemorrhages of nasal origin (epistaxes). They can be essential or symptomatic (2) Life threatening ENT haemorrhages in oncology, pre- or postoperative by hemostasis disorders or secondary bleeding specifically after a laryngectomy or a tonsillectomy devascularisation of hypervascular tumours (paragangliomas and nasopharyngeal fibromas) by preoperative embolisation. (3) Carotid blow out, linked to the presence of a progressive tumour, or post-radiation, or traumatic. In some cases, these haemorrhages are cataclysmic and require extreme emergency care. In all cases, close collaboration with the ENT surgery department, the presence of an anaesthetist, and at least a sedation are determining factors in the improvement of care and therefore in the success of the embolisation. Every patient and/or family is to be given true, clear and appropriate information

Learning Objectives:

1. To learn about the vascular blunt and penetrating traumatic injuries.
2. To appreciate the role of the interventional radiologist in the treatment of epistaxis and tumours (juvenile angiofibroma and squamous cell carcinoma) in the emergency setting.
3. To have notions of vascular malformations and their complications.
4. To acquire basic notions of endovascular treatments.

17:14

Panel discussion: Is the radiologist an essential component of the emergency team

16:00 - 17:30

Studio 2018

Genitourinary

RC 1207

MRI for gynaecologic imaging: how I do it

A-544 16:00

Chairperson's introduction

B. [Ahuja](mailto:drbahuja@gmail.com); *Agra/IN (drbahuja@gmail.com)*

Ultrasound is the imaging modality of choice for the female pelvis. It is widely available and is relatively inexpensive. However, there are some shortcomings with this modality, such as limited field of view, obscuration of pelvic organs by bowel gases, inherent limitations due to patient size and dependence on operator skills. With its high contrast resolution, ability to provide good tissue characterisation and its multiplanar capabilities, MRI is increasingly used to evaluate pelvic pathology. Standard MRI protocol includes coronal single shot fast spin echo (FSE), sagittal T2W FSE fat suppressed sequences, axial T2W FSE sequence, axial in phase and opposed phase T1W gradient recall echo and axial diffusion weighted sequence using a dedicated pelvic phased array coil. GRE imaging is done to detect haemorrhagic foci in case of deep infiltrative pelvic endometriosis. Diffusion weighted imaging play a pivotal role in detection & staging of gynaecological malignancies and to see the response of therapy. Fat suppressed T1W sequences following intravenous administration of 10 ml of gadolinium contrast are routinely obtained. For pelvic floor imaging, dynamic 2D GRE imaging may be performed with and without the valsalva manoeuvre.

Session Objectives:

1. To learn how to optimise MRI of the female pelvis.
2. To understand the diagnostic benefit of integration of advanced techniques.

A-545 16:05

A. Basics of patient preparation and T2W-imaging

N.M. [deSouza](mailto:nandita.desouza@icr.ac.uk); *Sutton/UK (nandita.desouza@icr.ac.uk)*

T2-W MR imaging provides exquisite soft tissue contrast for evaluation of pelvic pathology. Maximising contrast and spatial resolution is fundamental to achieving a high diagnostic accuracy. Adequate signal-to-noise ratio with sufficient T2-weighting requires appropriate consideration of available hardware and software. Patient-related factors that result in image degradation can be reduced by careful patient preparation. Motion from bowel peristalsis may be controlled with antiperistaltic agents (Buscopan [hyoscine butylbromide] 20mg or glucagon 1mg); intramuscular administration is crucial as intravenous delivery produces a short period of antiperistalsis insufficient to last through the scanning period. Bladder filling during the scan also can substantially degrade image quality, and therefore an empty bladder at the outset is essential. To minimise diuresis during scanning, caffeine-containing drinks should be avoided and fluid intake limited for 4 hours prior to scanning. Images dedicated to the uterus should be acquired along the long and short axis of the organ, with as small a field of view as feasible without compromising signal-to-noise ratio. For large field-of-view images, T2-W scans in true orthogonal planes to the B0 field are preferred. The sagittal plane is best for visualising the uterus, while the transverse plane is ideal for assessing parametria, adnexae and pelvic sidewall. For the ovaries, the coronal plane may be helpful. 3D acquisitions provide high spatial resolution with the flexibility of multiplanar reconstruction. High-quality T2-W images in orthogonal planes are usually sufficient for detecting, characterising and staging pelvic malignancy, monitoring treatment response and assessing disease recurrence in a range of gynaecological pathologies.

Learning Objectives:

1. To understand the value of patient preparation.
2. To learn how to optimise and tailor protocols in female pelvic imaging.
3. To understand the role of T2WI, and how and when to use 3D techniques.

A-546 16:28

B. Contrast agents

R.A. [Kubik-Huch](mailto:rahel.kubik@ksb.ch); *Baden/CH (rahel.kubik@ksb.ch)*

Gadolinium-based contrast material is not usually necessary for evaluating benign uterine disease, but is recommended in fibroid evaluation. Gadolinium-enhanced sequences are performed for staging endometrial carcinoma, being useful in the assessment of the depth of myometrial tumour invasion. The optimal tumour/myometrial contrast timing was reported between 90 and 150 seconds. Thus, the utility of dynamic acquisition has been debated. Contrast-enhanced imaging will not be routinely performed in cervical carcinoma, but can be valuable in selected cases. It is recommended in the MR assessment of sonographically indeterminate adnexal masses and mandatory for staging ovarian carcinoma. Dynamic contrast-enhanced MRI may provide quantitative information about tumour perfusion, being useful for monitoring the therapeutic effects and predicting the therapeutic outcome. MR angiography should be performed in patients scheduled for fibroid embolisation or in suspected pelvic congestion syndrome. Gadolinium-based contrast agents will cross the placenta and enter the foetal bloodstream. The agents are excreted into the amniotic fluid and will not be removed effectively from the foetal environment. Contrast agents should be avoided in the pregnant patient. Only a small amount of gadolinium is excreted into the breast milk and absorbed by the infant, without any adverse effects being reported. Therefore, breast feeding can be continued, but it might be the preference of the mother to discard the breast milk in the 24 hours after contrast medium. If contrast agents need to be administered in these patients, linear gadolinium chelates should be avoided.

Learning Objectives:

1. To become familiar with the safety considerations and guidelines for the use of gadolinium with a special focus on imaging pregnant and lactating patients.
2. To learn why, how and when to use IV contrast-enhanced imaging in MRI of the female pelvis.
3. To understand different gadolinium T1W techniques and their clinical value in routine imaging, as well as to become familiar with quantification techniques.

A-547 16:51

C. Diffusion and ADC

R. [Forstner](mailto:r.forstner@salk.at); *Salzburg/AT (r.forstner@salk.at)*

Diffusion-weighted Imaging (DWI) has become a powerful imaging technique in the female pelvis providing functional information. It improves tissue characterisation and facilitates lesion depiction. This is based on visualisation of differences of random motion of water molecules within tissues, changes of tissue cellularity, and altered cell membranes. DWI is typically assessed in conjunction with findings obtained by conventional MR imaging sequences. Although several *b* values may be used, at least two *b* values (low <100 and high $\geq 800\text{-}1000\text{mm}^2/\text{sec}$) will provide visual information as well as quantitative analysis, the apparent diffusion coefficient (ADC). DWI has emerged as an available complementary sequence in staging gynaecological cancers, in differentiation of benign from malignant masses, and in imaging recurrent disease. DWI has also been linked to lesion aggressiveness and emerges as an imaging biomarker for tumour response. In pregnancy or in impaired renal function, DWI serves also as an alternative to i.v. contrast media. The main clinical applications include assessment of depth of myometrial invasion in endometrial cancer and identification of local tumour extent in small size or in diffusely growing cervical or endometrial cancers difficult to depict on T2WI. It also aids in characterisation of adnexal masses and facilitates identification of metastatic spread in advanced gynaecologic cancers, particularly to the peritoneum or to lymph nodes. The added value of DWI in various applications in clinical practice will be highlighted and the pitfalls will be demonstrated.

Learning Objectives:

1. To understand the technical principles of DWI.
2. To learn how to optimise and integrate DWI in pelvic imaging.
3. To illustrate the added diagnostic value of DWI in female pelvic imaging.

17:14

Panel discussion: Multiparametric MRI of the female pelvis: should it replace tailored protocols?

16:00 - 17:30

Room L 8

E³ - Rising Stars Programme: EFRS Radiographers' Basic Session

BR 1

Radiography research: a how to guide

A-548 16:00

Chairperson's introduction: Why is radiography research important

M. [Hardy](mailto:M.L.Hardy1@bradford.ac.uk); *Bradford/UK (M.L.Hardy1@bradford.ac.uk)*

Increasing the capacity, volume and quality of radiography research is essential to professional credibility and standing. Research forms the foundation upon which evidence-based decisions are made and enables clinical practice and service delivery innovation. As a result, it is imperative that we are all comfortable with the research processes and understand the sometimes confusing language and terminology adopted, to ensure that our practice is relevant and research informed. This starts with being clear about what research is and the ethical dilemmas that need to be tackled in designing competent and achievable research programmes. A further building block is developing the skills of criticality, understanding the limitations of a piece of work and, importantly, the gaps in the evidence base that need to be plugged to ensure a coherent knowledge base. Finally, it is important to appreciate the responsibility of researchers to disseminate their findings to ensure they are adopted in practice and the necessary skills required to construct high-quality scientific abstracts for conference presentations and posters. This session has some exciting speakers who will guide, inform and inspire you to take forward your research aspirations, whether as a research user or as a future research leader, and I look forward to facilitating this session to enhance your learning.

Session Objectives:

1. To become familiar with common ethical issues arising in radiography research.
2. To understand the value of critical appraisal when reading research publications.
3. To identify good practices for constructing quality scientific abstracts and posters.

Author Disclosure:

M. Hardy: Board Member; British Institute of Radiology. Employee; University of Bradford. Grant Recipient; National Institute of Health Research.

A-549 16:05

How to avoid ethical issues

B.T. [Andersson](mailto:bodil-t.andersson@med.lu.se); *Lund/SE (bodil-t.andersson@med.lu.se)*

Good research practices. Consent from a research ethics committee. Ethical principles: respect, autonomy, non-maleficence, beneficence, justice. Fundamental principles of research integrity: reliability, honesty, respect, accountability. Research environment: research procedures, documentation, data protection and archiving information to participants about the value and confidentiality. The right to integrity. The right to decline participation. The right to withdraw from the study. Informed consent. Ensuring confidentiality. Risks-causing harm, violation or suffering to the participant.

Learning Objectives:

1. To understand the importance of ethics in medical research and the role of research ethics committees.
2. To become familiar with common ethical pitfalls in research design.
3. To appreciate strategies for avoiding ethical problems in research.

A-550 16:23

How to critically appraise a research article

B. [Kraus](mailto:barbara.kraus@fh-campuswien.ac.at); *Vienna/AT (barbara.kraus@fh-campuswien.ac.at)*

To appreciate the role of literature reviews in the research process, students first of all have to find reading strategies for scientific text and particularly for non-native speakers to read an English scientific text. Different methods of reading, e.g. the shopping centre strategy or SQ3R technique (Survey, Question, Read, Recite, Review), are useful for guiding through research articles. Reading the title and abstract of an article is the first selection step with "the quick review", followed by the process of "the detailed review" to get an assessment about not just the quality of the study design, but also the quality and applicability of the results. The aim is to find strengths and weaknesses in each section of a research report and it is necessary to identify the research method (quantitative/qualitative), the methodology with all pros and cons and to screen the questions using the PICO (population, intervention, comparison and outcome) system. Was the study design appropriate to address the research question? How precise are the results and are they

Postgraduate Educational Programme

appropriately presented? Also, the relevant expertise of the author(s) should be clear. Another important point is to figure out clearly in the discussion or conclusion about any conflicts of interest and any acknowledgement of limitations. The presence of an ethics committee approval must also be declared. Finally, knowledge of and the proper use of guidelines/checklists and scoring systems are important key factors that help in the critical appraisal of research work.

Learning Objectives:

1. To appreciate the role of the literature review in the research process.
2. To identify strengths and weaknesses in each section of a research report.
3. To critically appraise the overall value of a research report.

A-551 16:41

How to write a good scientific abstract

R. Decoster; Brussels/BE

Writing an abstract is the art of delicately luring your reader into exploring your research. The abstract, 250 words of carefully selected text, consists of a web built from ideas and findings that pinpoint why someone should spend time on your article or talk. During this presentation, I will dissect an abstract to illustrate the universal backbone of each abstract. We will explore how different science branches put other accents in their carefully woven bait. While reading between the lines of some examples, we will steal like an artist in the search for success.

Learning Objectives:

1. To understand general qualities of good scientific abstracts.
2. To be aware of typical formats of scientific abstracts.
3. To consider tips for success.

A-552 16:59

How to produce a high-quality scientific or educational poster

L.A. Rainford; Dublin/IE (louise.rainford@ucd.ie)

This presentation will firstly discuss the many types of posters and the key matters a prospective presenter must consider in relation to the variation in poster submission processes across national and international conferences. The importance of reading the poster submission guidelines will be highlighted. Suggestions will be proffered with respect to the poster design under a number of key headings. The material covered will include: choosing the correct title, institutional identification, author affiliations and ordering of affiliations, designing sections of the poster to facilitate the reader with an opportunity to logically progress through the material provided in the poster and the importance of clear, scientific language, accurate grammar, spell checks and appropriate labelling of images and figures. The use of appropriate scientific language will be discussed and examples of good practice supplied. Accurate formatting cannot be overstressed and the presentation will include examples of potentially avoidable poster errors. The overall recommendations and design suggestions incorporated in this presentation are aimed at supporting radiographers in achieving high-quality scientific poster submissions, and the content will be appropriate for both radiography students and radiographers.

Learning Objectives:

1. To become familiar with poster formats and layouts.
2. To consider good practices in poster design.
3. To appreciate important considerations when designing a poster.

17:17

Panel discussion: Ask the experts

16:00 - 17:30

Room E1

Breast

RC 1202

MRI for early detection, staging and management of breast cancer

A-553 16:00

Chairperson's introduction

J. Camps Herrero; Valencia/ES (juliacamps@gmail.com)

This Masterclass will tackle three issues that are currently at the forefront of the breast MRI debate: imaging biomarkers, preoperative staging and the so-called "overdiagnosis". Breast MRI should have already passed the phase of diagnostic validation and must now head towards the definition of imaging biomarkers that are capable of sampling the whole cancer in its entire

heterogeneity as well as allowing serial measures in response evaluation. Imaging biomarkers must be solid, reproducible and standardised. This lecture will define common imaging biomarkers in the clinical setting as well as set the path for their further development in the future. Preoperative breast MRI is still being questioned as a valid indication and the MIPA study has been designed to answer the questions raised by published evidence on the contrary (excess mastectomies, no significant difference in mastectomy rates, etc) tainted by methodological biases which will be highlighted during this session. The number of high-risk (B3) lesions has increased after the use of breast MRI, being considered traditionally false-positive diagnoses, when in fact they have underlying prognostic implications. This lecture outlines these implications and lets us see breast MRI under a different light, when pathology correlates are considered.

Session Objectives:

1. To understand the contribution of MRI to preoperative staging and the context within it should be recommended.
2. To learn about the different MRI biomarkers and in which clinical setting they are of value.
3. To recognise the steps required to move to abbreviated MRI for high-risk screening.

Author Disclosure:

J. Camps Herrero: Consultant; Bayer, Bard. Speaker; Bayer.

A-554 16:05

A. Preoperative staging with MRI: did the MIPA trial solve all issues?

F. Sardanelli; San Donato Milanese/IT (f.sardanelli@grupposandonato.it)

Preoperative breast MRI is a highly debated modality. New evidence has been emerging from the MIPA study, an ongoing prospective observational multicentre study, enrolling two concurrent groups with a newly diagnosed first breast cancer, not candidate to neoadjuvant therapy, receiving or non-receiving MRI before surgery. Up to October 2017, over 6,000 patients were recruited. The data from 2,425 patients were as follows: 1,201 (49.5%) with MRI and 1,224 (50.5%) without. Of these 1,224 MRIs, 210 (17%) were performed for screening (4%) and for diagnostic purposes (13%). Of 1,014 preoperative MRIs, 595 (59%) were ordered by radiologists alone and 321 (32%) by surgeons alone; radiologists and surgeons were involved in the request in 68 and 40% of cases, respectively. Mastectomy rate planned at mammography/ultrasound was 185/1201 (15.4%) in the non-MRI-group and 245/1224 (20.0%) in the MRI-group ($p < 0.001$). In the MRI group, 21 additional mastectomies (1.7%) were planned after MRI, while 25 patients planned to have mastectomy shifted to conservative surgery (CS). Of the 1,004 patients planned for CS before MRI, MRI did not indicate a change in performing surgery in 733 (73%), while it prompted a wider CS in 143 (12.5%) and a less extensive CS in 128 (12.7%). Mastectomy rate was 192/1201 (16%) in the non-MRI-group and 257/1224 (21%) in the MRI-group ($p < 0.001$). Per-patient reoperation rates for close/positive margins were 135/1009 (13.4%) and 80/967 (8%), respectively ($p < 0.001$). Most mastectomies were already planned at mammography/ultrasound, using MRI as a confirmation tool. This patient selection also contributed in determining a lower reoperation rate in women undergoing MRI. Conversely, CS was modified by MRI according to disease extent, balancing increased and decreased tissue removal.

Learning Objectives:

1. To learn about the evidence for and against the use of MRI in preoperative staging.
2. To understand the background, design and early results of the MIPA trial.
3. To be able to explain the role of preoperative MRI during multidisciplinary tumour board meetings.

Author Disclosure:

F. Sardanelli: Advisory Board; Bracco, General Electric. Research/Grant Support; Bracco, Bayer, Real Imaging.

A-555 16:28

B. MR imaging biomarkers for the clinical setting

E.A. Morris; New York, NY/US (morrise@msskcc.org)

Background parenchymal enhancement is related to vascular flow and it has been proposed that this may represent an imaging biomarker of the underlying proliferation of fibroglandular tissue. Investigations have shown that there is an extremely strong association between BPE and risk of breast cancer, at least as strong as the association between mammographic density and breast cancer. It has been observed that background parenchymal enhancement is also affected by treatment changes and hormonal manipulation. Radiation therapy to the breast causes marked reduction in background parenchymal enhancement. MRI can further stratify women at high risk for developing breast cancer on the basis of background parenchymal enhancement. Rim enhancement MRI phenotypic features can predict the aggressiveness of breast cancer. For example, we know that spiculation on MRI is associated with a lower histologic grade and lower ki67 expression and is more commonly

seen in ER+ cancer. Rim enhancement has been shown to be associated with cancers that are higher in grade and ER-. Rim enhancement is associated with a worse distant metastatic survival. It has been shown that triple negative tumours without rim enhancement are associated with tumour-infiltrating lymphocytes. High TIL levels are associated with pCR, following NAC and improved survival in TNBC. Peritumoural oedema is caused by increased vascular permeability and release of cytokines. It is seen in <10% of breast cancer and is associated with early distant metastases (<2.5 y). In TNBC peritumoural oedema was a significant independent predictor of worse recurrence-free survival.

Learning Objectives:

1. To learn about the different biomarkers that are available and the evidence for using them in patients with breast cancer.
2. To understand in which clinical settings biomarkers might be of value.
3. To appreciate the newer techniques that are being developed and tested clinically.

Author Disclosure:

E.A. Morris: Advisory Board; Delpjinus, Hologic, GE, Avon. Research/Grant Support; GRAIL, Hologic, Komen.

A-556 16:51

C. Screening with abbreviated protocols

C.K. Kuhl; [Aachen/DE \(ckuhl@ukaachen.de\)](mailto:ckuhl@ukaachen.de)

Early diagnosis improves survival of women with breast cancer. Mammographic screening improves early diagnosis of breast cancer. Yet, there appears to be room for improvement. The major shortcomings of mammographic screening are overdiagnosis of prognostically unimportant cancer, as well as underdiagnosis of cancers that are indeed relevant. Failure to detect biologically relevant breast cancer with mammographic screening is driven by host-related factors, i.e. breast tissue density, but also tumour-related factors: Biologically relevant cancers may exhibit imaging features that renders them indistinguishable from normal or benign breast tissue on mammography. These cancers will then progress to become the advanced-stage interval cancers observed in women undergoing mammographic screening. Since breast cancer continues to represent a major cause of cancer death in women, the search for improved breast cancer screening method continues. Abbreviated breast MRI has been proposed for this purpose because it will greatly reduce the cost associated with this method, due to a greatly reduced magnet time (down to 3 minutes), but especially also due to a greatly abridged image interpretation time, i.e. radiologist reading time. This lecture will review the current evidence and present the EA1141 trial designed to investigate the utility of abbreviated breast MRI for screening average-risk women with dense breast tissue.

Learning Objectives:

1. To learn about the evidence for abbreviated MRI and the comparison with standard protocols.
2. To understand the different protocols for abbreviated MRI and the merits of each sequence used.
3. To appreciate the advantages and limitations for abbreviated MRI.

17:14

Panel discussion: Why are some recommendations not adopted and how can we change practice?

16:00 - 17:30

Room E2

Neuro

RC 1211

Inflammatory and infectious CNS pathology

A-557 16:00

Chairperson's introduction

E.T. Tali; [Ankara/TR \(turgut.tali@gmail.com\)](mailto:Ankara/TR (turgut.tali@gmail.com))

Clinical presentation and imaging features of infectious and noninfectious inflammatory diseases of the spinal cord are variable and usually nonspecific. Differentiating these conditions from the other spinal cord lesions (neoplasms, degenerative disorders, etc.) is still challenging. For both groups, early and accurate diagnosis is important because of the different treatment protocols as well as to decrease neurologic complications. Spinal cord infections are clinically important because of the high rates of morbidity and even mortality. The symptoms are usually nonspecific, which can delay the diagnosis. A combination of clinical history, neurologic examination, laboratory data, spinal

fluid analysis, serological studies, and imaging findings are the main tools for making a correct diagnosis. Spinal inflammatory diseases can be caused by autoimmune, granulomatous, and idiopathic conditions. Demyelinating diseases (multiple sclerosis (MS) and neuromyelitis optica (NMO)) are the most common inflammatory conditions. Transverse myelitis, acute disseminated encephalomyelitis (ADEM) and Guillain-Barré syndrome (GBS) should be thought as differential diagnoses. Demyelinating lesions may also be seen in autoimmune diseases such as sarcoidosis, systemic lupus erythematosus and Sjögren's syndrome. Vascular malformations, arachnoiditis, and even neoplastic diseases may also produce inflammation. For the radiologist, it is crucial to be aware of different imaging features of spinal infections and inflammatory diseases. Comprehensive evaluation of the imaging features associated with the clinical presentation, laboratory data, spinal fluid analysis, and serological studies helps to make the final diagnosis.

Session Objectives:

1. To understand the role of imaging in the diagnosis and monitoring of inflammatory and infectious diseases of the central nervous system.
2. To learn basic principles of the use of imaging in neuroinfection and neuroinflammation.
3. To appreciate the added value of imaging in addition to the clinical findings and laboratory tests including CSF analysis.

A-558 16:05

A. Autoimmune encephalitis

P. [@Demaerel; Leuven/BE \(philippe.demaerel@uzleuven.be\)](mailto:Demaerel; Leuven/BE (philippe.demaerel@uzleuven.be))

Autoimmune encephalitis (AE) is emerging as a more common cause of encephalopathy than previously thought. AE is a difficult clinical diagnosis and occurs both in adults and in children. The presence of antibodies (Ab) in the CSF confirms the diagnosis, but the results can take several weeks to obtain and negative results do not exclude AE. Therefore, MR imaging plays an important role in these patients, who often present with nonspecific neurological symptoms. Subacute encephalopathy, new adult-onset seizures or psychiatric symptoms should raise the suspicion of a possible AE. AE consists of a large number of Ab-related diseases. They are usually divided into three groups: (1) Ab to cell-surface antigens, (2) Ab to intracellular synaptic proteins and (3) Ab to intracellular antigens. The imaging-related findings will be reviewed in this course. The most common imaging finding consists of uni- or bilateral FLAIR hypersignal in the hippocampus, amygdala and/or parahippocampal area. It is important to emphasize that these signal changes can be very subtle. Extratemporal lesions in the cerebral cortex, the grey nuclei, the cerebellum and the brainstem have been reported too and can support the clinical suspicion of AE. But Brain MR can also remain normal and FDG-PET is certainly recommended in these patients. MR imaging is also used to exclude or confirm other autoimmune diseases, e.g. MS, neuromyelitis optica, ADEM and lupus. Finally, MR imaging is helpful to exclude other diseases that can have a similar clinical presentation, e.g. lymphoma, carcinomatous meningitis and Wernicke encephalopathy.

Learning Objectives:

1. To learn about the imaging pattern of autoimmune encephalitis.
2. To understand the limited role of conventional MRI and the need for advanced imaging techniques in the diagnostic process and for follow-up purposes.
3. To appreciate the role of imaging in a multidisciplinary and multimodality approach.

A-559 16:28

B. Infectious encephalitis

K.D. [@Kurz; Stavanger/NO \(kurk@sus.no\)](mailto:Kurz; Stavanger/NO (kurk@sus.no))

Encephalitis is a potentially fatal disease occurring at any age. The most common types of encephalitis are caused by viral infections, with herpes simplex virus (HSV) encephalitis the most known type. It is critical to make a rapid and correct diagnosis to tailor the treatment with the goal of better outcome of the disease. MRI is a powerful tool for the fast detection of typical imaging patterns in CNS caused by viral infections and helps to grade the severity of the disease, especially by using diffusion weighted imaging. In this refresher course, we would like to summarize the current understanding of MRI findings of viral encephalitis, especially related to HSV, varicella zoster, rabies, influenza viruses and haemorrhagic encephalitis. We also discuss the typical CNS complications of the infections. In addition, we would also like to discuss the imaging features of subacute cerebral infections such as Rasmussen encephalitis, HIV, progressive multifocal leukoencephalopathy (PML), and Creutzfeldt-Jakobs disease.

Learning Objectives:

1. To learn about the correct choice of imaging modalities and image acquisition parameters for the detection and monitoring of infectious diseases of the central nervous system.
2. To understand the benefits and challenges of image pattern recognition for

Postgraduate Educational Programme

diagnostic purposes.

3. To appreciate the heterogeneity of the disease spectrum and challenges to interpret imaging findings in the context of the clinical presentation and possible comorbidities.

A-560 16:51

C. Inflammatory and infectious myelitis

M.M. [Thurnher](mailto:majda.thurnher@meduniwien.ac.at); Vienna/AT (majda.thurnher@meduniwien.ac.at)

Transverse myelitis (TM) is an "umbrella term" used to describe inflammatory disorder of the spinal cord that can be idiopathic or associated with central nervous system (CNS) autoimmune inflammatory diseases, connective tissue autoimmune diseases, or post-infectious neurological syndromes. Myelitis can present either as monophasic or recurrent disease. The most common monophasic diseases causing TM are idiopathic transverse myelitis and acute disseminated encephalomyelitis (ADEM), whereas recurrent disorders include multiple sclerosis (MS), neuromyelitis optica spectrum disorder (NMOSD), vasculitis (Behcet disease, SLE, Sjögren syndrome) and neurosarcoidosis. The recent discovery of multiple novel neural-specific autoantibodies accompanying autoimmune and demyelinating disease has improved the current understanding and classifications. This lecture will provide an overview of radiological, clinical, serological, and prognostic differences of inflammatory and infectious spinal cord diseases.

Learning Objectives:

1. To learn about the spectrum of infectious diseases of the spinal cord level and their most characteristic imaging features.
2. To understand the difficulties in image acquisition and image interpretation.
3. To appreciate the clinical relevance of early diagnosis and therapeutic intervention.

17:14

Panel discussion: Ask the expert: Is imaging the key diagnostic modality for an early and specific diagnosis of infectious diseases, leading to a better functional outcome?

16:00 - 17:30

Room F1

E³ - Rising Stars Programme: Joint Sessions with ESOR

ESR/ESOR 3

Radiologic anatomy: neuro

Moderator:

M.A. Lucic; Sremska Kamenica/RS

A-561 16:00

Cortical anatomy and primary functional areas

T.A. [Yousry](mailto:youstry@ucl.ac.uk); London/UK

The anatomy of the brain is often perceived as being complicated. Especially the cortex is seen as an irregular arrangement of variable structures, which are difficult to differentiate and to identify. We will review the overall subdivision of the brain into lobes and describe their boundaries and their major gyri and sulci. We will then describe the location of specific functions. (1) Primary sensorimotor cortex: Motor is located in the precentral gyrus, sensory in the postcentral gyrus around the central sulcus (CS), hence the importance of always correctly identifying the CS. We will present 4 interlocked methods to identify the CS in the axial plane a) Knob, b) lateral axial, c) medial axial, d) gyral/cortical thickness and 3 to identify it in the sagittal plane a) lateral sagittal, b) hook, c) medial sagittal. (2) Primary auditory cortex (A1): Centred at the postero-medial part of Heschl's gyrus (HG), we will present simple landmarks in each of the 3 planes: a) axial: adhaesio interthalamica, b) sagittal: omega/heart shape of HG, c) coronal: omega shape of HG. (3) Primary visual cortex (V1): Centred on the calcarine sulcus, we will discuss the characteristic shape that allows the identification of this structure in all 3 planes. At the end of this lecture, you will know the subdivision of the cortex; the methods and landmarks necessary to identify the primary sensorimotor, speech, auditory, and visual areas.

Learning Objectives:

1. To understand the basic concepts of cortical subdivision.
2. To be able to identify critical cortical structures.
3. To learn to localise primary functional areas.

A-562 16:30

Vascular distribution territories: arterial and venous

T. [Engelhorn](mailto:Tobias.Engelhorn@uk-erlangen.de); Erlangen/DE (Tobias.Engelhorn@uk-erlangen.de)

After a short overview on the vascular anatomy of the brain with a focus on vascular distribution territories, the main focus of this talk is to present neurovascular pathologies closely associated with arterial and venous vascular distribution territories. One focus is also put on acute stroke and subsequent patient selection for interventional stroke therapy. Another aim is to provide a better understanding of the pathophysiology of different neurovascular diseases in an interactive matter. In addition, the advantages and limitations of CTA, flat-panel CTA and MRA compared to conventional angiography are presented.

Learning Objectives:

1. To become familiar with a comprehensive vascular anatomy of the brain.
2. To recognise patterns of various pathologies attributed to vascular distribution territories.
3. To recognise the different imaging patterns in stroke and their prognostic value.

A-563 17:00

The basal ganglia of the brain revisited

D. [Zlatareva](mailto:dorazlat@yahoo.com); Sofia/BG (dorazlat@yahoo.com)

The term "basal ganglia" refers to caudate nucleus, putamen, globus pallidus, substantia nigra and subthalamic nucleus. They are paired symmetric structures located in the telencephalon, diencephalon and mesencephalon. The lenticular nucleus includes putamen and globus pallidus. Together with caudate nucleus, these structures are named corpus striatum. Being part of the extrapyramidal system, the basal ganglia have wide connections not only with each other, but also with the midbrain, thalamus and cerebral cortex. The striatum is the main recipient of afferents from the entire cerebral cortex and thalamus. The information is then processed and integrated with other inputs and transmitted to the globus pallidus internal segment and the substantia nigra pars reticulata. Those are major output structures of the basal ganglia and make GABAergic, inhibitory connections on their targets. According to current concepts in the motor regions of the basal ganglia, there is a motor homunculus similar to that in the primary motor cortex. The basal ganglia and thalami have five functional divisions that are sensorimotor, supplementary motor, premotor, association and limbic territories. Very complex functional cortical-basal-ganglial-thalamocortical circuits enable the execution of automatic and semi-automatic motor programmes, modulation of muscle tone and the harmonisation of movement. If one or more of these regulatory circuits are disrupted, the result will be either a net removal of inhibition, leading to excessive movement like tremor or dystonia, or a net decrease in motor activation causing impaired movement (e.g. rigidity, akinesia).

Learning Objectives:

1. To recall the basal ganglia nuclei and their topography.
2. To identify the classic functional organisation of the basal ganglia and its current concepts.
3. To elucidate the pathophysiology of various movement disorders.

16:00 - 17:30

Room F2

Oncologic Imaging

RC 1216

Cancer screening

A-564 16:00

Chairperson's introduction: Screening for cancer: lessons learned and future challenges

S. [Törnberg](mailto:Sven.Tornberg@ki.se); Stockholm/SE (Sven.Tornberg@ki.se)

Cancer is a lethal disease. The purpose of screening is to find cancer in an early, still curable, phase. Population based screening is a strategy aiming to, in a systematic and organised way, find early cancers in a population at risk, related to sex, age, or risk behaviour. The benefit (of not dying) can't, for obvious reasons, be experienced by the individual person, only a confirmation of not having a cancer (which is not the purpose of screening). Harms of screening are unnecessary exposure to radiation, worry, false negative and false positive results, and over-diagnosis leading to unnecessary and invasive treatment. The balance between harms and benefit needs to be evaluated before recommending population based screening. EU recommends screening for breast cancer, colorectal cancer and cervix cancer. EU has also published guidelines on how to ensure the quality of the entire screening process by using indicators as surrogate measures. If participation rate, cancer detection

Friday

A

B

C

D

E

F

G

S108

rate, interval cancer rate, and stage distribution is equal to the levels experienced in the RTC's, it reflects a similar effect. EU has defined acceptable levels of performance. Individual data needs to be recorded in order to measure the quality and the effect of the screening. EU's 2nd screening report (2017) compared the extent, and the quality of the recommended cancer screening programs between the EU member states. During the session, the above mentioned aspects will be discussed for, lung-, colorectal-, and breast cancer, all three being leading causes of cancer deaths in Europe.

Session Objectives:

1. To understand the basic idea behind cancer screening protocols.
2. To learn about potential harms and benefits of screening protocols.
3. To explain why epidemiological data are so important for successful screening programmes.

A-565 16:05

A. Lung cancer screening: the evidence

H.-U. [Kauczor](#); Heidelberg/DE

Lung cancer is the most common and most fatal cancer in Europe and worldwide, with a 5-year survival of only 13%. The by far most important risk factor for lung cancer is cigarette smoking. In 2011, the results of the largest randomized controlled screening trial (NLST) using low-dose CT (LDCT), performed in the USA showed a significant 20% reduction of lung cancer mortality in elderly (55-74 years) and heavy smokers (> 30 packyears), but has not been replicated by any other trial so far. Although lung cancer screening (LCS) using LDCT was established in the USA in 2015, the introduction of such screening programmes in Europe remains controversial. For a successful LCS programme using LDCT the pretest probability has to be high, while the numbers of false-positive screens and overdiagnosis are low. Thus, a risk model and dedicated nodule management algorithms must be strictly followed. The radiation exposure from LDCT should be < 1 mSv if not obese. The whole workup of positive screens requires strict SOPs at experienced high-throughput centres with clinical audits established. A smoking cessation programme should be a mandatory component of LCS. Furthermore, LCS in the future should tackle the "Big Three" killers associated with cigarette smoking, i.e. lung cancer, COPD and cardiovascular diseases, at the same time. Cost-benefit analyses should be performed on a national basis. All data from comprehensive LCS programmes should be stored in a central registry and undergo independent review to confirm the quality and benefits of LCS for high-risk smokers.

Learning Objectives:

1. To learn about risk populations for lung cancer screening.
2. To understand the benefits and potential drawbacks of a lung cancer screening programme.
3. To appreciate the already existing clinical evidence for lung cancer screening programmes.

A-566 16:28

B. Colorectal cancer screening: what is the radiologist's role?

S. [Halligan](#); London/UK

The speaker will describe the role of the radiologist in colorectal cancer screening. There will be an emphasis on effective and efficient population-based screening, and on the high-level evidence base for this. Examples of current population screening programmes will be given, and the way in which radiological techniques intergrate with these will be described.

Learning Objectives:

1. To learn about already existing clinical screening tools for CLC.
2. To understand the concept of radiological screening tools for CLC.
3. To appreciate the benefit and clinical applications for new imaging-based screening tools.

Author Disclosure:

S. Halligan: Research/Grant Support; Holder of multiple competitive peer-reviewed research grants.

A-567 16:51

C. Breast cancer: to screen or not to screen

P. [Skaane](#); Oslo/NO (per.skaane@outlook.com)

Screening includes "non-programme screening" (opportunistic) and "organised", with higher degree of management, target groups, defined intervals, and specified management procedures. Organised screening is "population based" when women in the target group are individually identified and personally invited, and all steps adequately coordinated. European Guidelines recommend biannual screening for women 50-69 years old. Full-field digital mammography, the "gold standard" for screening women at average risk, has inherent limitations including low specificity and low sensitivity in women with dense breasts. Supplementary annual MRI in addition

to mammography is offered for high-risk women with lifetime risk over 20% and BRCA mutation carriers. Supplementary ultrasound is in general not recommended when MRI is carried out. To maximise the benefits while minimising the harms, there has been much focus on moving from "one-size-fit-all" to personalised screening. Due to economical and practical reasons, reduced screening for women with fatty breast has occasionally been suggested. However, caution is necessary since it is problematic to identify subgroups of women with nondense breasts with less frequent screening. The costs and availability prevent implementation of many new modalities with high accuracy in high-volume screening, including molecular breast imaging (MBI), contrast-enhanced spectral mammography (CESM), and dedicated breast CT. The most promising new technique for population-based screening is digital breast tomosynthesis (DBT). The main challenges of DBT include longer reading time and overdiagnosis. The problem of radiation dose using mammography plus DBT is solved by synthetic 2D images. DBT has reduced sensitivity in women with very dense breasts. However, cost-effectiveness studies on DBT screening programmes should be carried out.

Learning Objectives:

1. To learn about the existing mammography screening programmes.
2. To understand the potential add-on of MR for breast cancer screening (e.g. MR).
3. To balance harm/cost against benefit for new screening programmes.

Author Disclosure:

P. Skaane: Equipment Support Recipient; Tomosynthesis equipment for the Oslo Tomosynthesis Screening Trial was provided by Hologic.

17:14

Panel discussion: Cancer screening: a success story?

16:00 - 17:30

Room D

Musculoskeletal

RC 1210

Shoulder MRI: mastering technique and making my report relevant

A-568 16:00

Chairperson's introduction

I. [Boric](#); Zabok/HR (igor.boric1@zg.t-com.hr)

For a successful MRI of the shoulder, certain conditions should be met. It is necessary to perform the examination in a standardised manner using generally accepted protocols. The applied protocols should be geared towards providing a response to a clear clinical question. Knowledge of the advantages and disadvantages of MRI techniques is the guiding node in choosing the optimal technique: specific protocol, normal positioning or ABER position of the patient, native or contrast-enhanced MR, standard MR examination or MR arthrography. Understanding of normal shoulder anatomy: rotator cuff muscle, other shoulder muscles and its tendons, labrum and ligaments, shoulder bursas, bones and articular cartilage, neurovascular bundles as well as normal variants is crucial for a quality finding interpretation and to make the report relevant. In the case of postoperative shoulder evaluation, knowledge of the applied surgical techniques and the expected anatomical changes is necessary. The analysis of shoulder changes should take into consideration the specificity of each patient: age, gender, occupation, existence of previous injuries and shoulder diseases, and degree of sport activity. Information on the mechanism of injury is helpful in assessing the site and extent of lesions. To improve the quality and reliability of shoulder MRI evaluation, feedback from the clinician and the patient is extremely useful. An experienced MSK radiologist is crucial for a good and reliable MRI of the shoulder.

Session Objectives:

1. To understand the level of expertise that patients expect for adequate performance and reading of shoulder MRI.
2. To gain insight into differentiating normal age-related changes from clinical relevant MR features.

A-569 16:05

A. The normal MRI: techniques and anatomy

E. [Llopis](#); Valencia/ES (evallopis@gmail.com)

MRI is the primary diagnostic imaging modality when of the shoulder joints is suspected. For an accurate evaluation, it is essential to know the normal anatomy and the complex biomechanics with a wide range of motions and variants, to avoid misdiagnosis and to understand which ones are clinically relevant. We will divide shoulder anatomy into static and dynamic structures:

Postgraduate Educational Programme

the bone structures, labrum and ligament as static structures, and rotator cuff muscles as dynamic ones.

Learning Objectives:

1. To become familiar with MRI techniques for imaging the shoulder.
2. To understand normal MRI shoulder anatomy, and normal variants seen.

A-570 16:28

B. Rotator cuff tears: what are they and what do they look like?

K.-F. [Kreitner](mailto:Kreitner@unimedizin-mainz.de); Mainz/DE (Karl-Friedrich.Kreitner@unimedizin-mainz.de)

Rotator cuff (RC) disease is common and maybe a significant cause of shoulder pain. The tendons of the rotator muscles are highly organised structures with five distinct histologic layers. Over the last decade, the rotator cable has received increasing attention, as it acts as a supporting limb of the cuff. The cable is adjacent to the crescent zone of the RC and can be seen on most MR imaging studies. Pathologically, tendinosis/tendinopathy can be differentiated from partial- and full-thickness tears of the cuff. Whereas tears at the rotator crescent are often due to ischaemia and degeneration, tears of the footprint have obtained increased attention as they affect younger patients and have implications on the appropriate operative procedure. Partial-thickness tears can be described as articular, bursal or intrasubstance partial tears and should be further characterised with regard to the degree of tendon involvement. Full-thickness tears allow communication between the glenohumeral joint and the subacromial-subdeltoid bursa and can be pinhole in size or involve an entire tendon. It is further of utmost importance to assess atrophy or fatty infiltration in case of an RC tear, as these findings influence the therapy and outcome of the affected patients. Tears of the subscapularis tendon typically begin in the cranial part of the tendon and are often associated with lesions of the long biceps tendon and the rotator interval. "Novel lesions" of the RC most commonly affect the infraspinatus tendon at the musculotendinous junction and represent a delamination that may be missed at arthroscopy.

Learning Objectives:

1. To become familiar with the anatomical basis of rotator cuff tears.
2. To learn about the MRI findings of rotator cuff pathology.

A-571 16:51

C. Patterns of instability: what does the MRI show?

A.J. [Grainger](mailto:Grainger@nhs.net); Leeds/UK (andrewgrainger@nhs.net)

Two patterns of injury are seen in patients dislocating their shoulder. Younger patients will tend to disrupt the labroligamentous complex, whereas the older population tends to disrupt the integrity of the rotator cuff. In this latter group, tears of supraspinatus are seen along with tears of subscapularis and avulsion fractures of the greater tuberosity. Rotator cuff disruption forms the subject of other talks and so will not be discussed further here. Anterior dislocation leading to avulsion of the anteroinferior labral ligamentous complex from the glenoid is termed the Bankart lesion, or bony Bankart if accompanied by a fracture. Avulsion occurs due to the pull of the anterior band of the inferior glenohumeral ligament (AIGHL) at its attachment to the anteroinferior labrum. The AIGHL is the primary restraint to movement when the arm is abducted and externally rotated. Avulsion of the labrum is well shown on MR arthrography and a number of variants exist which will be discussed. Posterior dislocation will produce a reverse pattern of shoulder injury which will also be discussed.

Learning Objectives:

1. To become familiar with patterns of abnormality seen in shoulder instability.
2. To learn about the MRI findings of shoulder instability.

17:14

Panel discussion: How are the indications for MR arthrography of the shoulder changing?

16:00 - 17:30

Room G

New Horizons Session

NH 12

Radiomics: what is it and how can we use it?

A-572 16:00

Chairperson's introduction

O. [Clément](mailto:olivier.clement@aphp.fr); Paris/FR (olivier.clement@aphp.fr)

The term "Radiomics" has emerged a few years ago and is attracting a lot of attention as a tool to extract quantitative information out of the images. Several softwares are on the market that provide a large amount of quantitative features from medical images using data-characterisation algorithms. These features, termed radiomic features, have the potential to uncover disease characteristics that fail to be appreciated by the naked eye. The goal of the New Horizon session is to review the concepts behind the name and appreciate the potential clinical applications in radiology.

Session Objectives:

1. To understand what radiomics is.
2. To appreciate the clinical potential of radiomics in radiology.
3. To address the professional challenges of radiomics.

A-573 16:03

Radiomics: what is it and how does it work?

L.S. [Fournier](mailto:laure.fournier@aphp.fr); Paris/FR (laure.fournier@aphp.fr)

Radiomics is a new 'data-driven' approach for extracting large sets of complex descriptors from routine (or not) clinical images, based on the assumption that there is a relationship between the imaging features of tumours and their underlying gene expression patterns and biology. The radiomics process aims to establish links between the imaging phenotype and genotypic and phenotypic characteristics of a tumour governed by its molecular substratum. Advanced methods of image processing are applied to images to extract a large number of descriptors, such as texture analysis from histograms, co-occurrence matrices, and fractal analysis. This large set of data can be analysed using bioinformatics and biostatistics methods into clusters defining metadata sets describing combinations of imaging features, or imaging 'profiles'. Finally, these data can be correlated to gene expression profiles, often called radiogenomics, or to outcomes, such as treatment response or survival.

Learning Objectives:

1. To learn about new methods of image analysis derived from 'omics' methods.
2. To understand processing of big data derived from images.
3. To become familiar with new vocabulary such as radiomics, radiogenomics, clusters, heat map, etc.

Author Disclosure:

L.S. [Fournier](mailto:Fournier@aphp.fr): Advisory Board; Keosys. Grant Recipient; Invectys. Research/Grant Support; Philips, Ariana Pharma, Evolucare.

A-574 16:21

Radiomics: technical validation

R. [Leijenaar](mailto:leijenaar@maastro.nl); Maastricht/NL (ralph.leijenaar@maastro.nl)

Radiomics is increasingly more important in cancer research; the high-throughput mining of quantitative image features from standard-of-care medical imaging that enables data to be extracted and applied within clinical decision support systems to improve diagnostic, prognostic, and predictive accuracy. The field of radiomics is emerging rapidly. However, this field lacks standardized evaluation of both the scientific integrity and the clinical significance of the numerous published radiomics investigations resulting from this growth. With the prospect of multicentre clinical applications, it has become clear that variation in, for example, software implementations, feature nomenclature, mathematical definitions and methodology, makes reproducibility and validation of studies in radiomics a major challenge. For radiomics to mature as a discipline, there is a clear need for rigorous evaluation criteria, reporting guidelines and tools to facilitate standardization, interoperability and advancement of the field.

Learning Objectives:

1. To learn about the robustness and reproducibility of radiomics features.
2. To understand the differences and similarities between radiomics software.
3. To understand that quality of big data is the key.

Friday

Postgraduate Educational Programme

Author Disclosure:

R. Leijenaar: Employee; Health Innovation Ventures / OncoRadiomics. Founder; co-founder of OncoRadiomics. Shareholder; OncoRadiomics.

A-575 16:39

Radiomics: biological correlation

E. Sala; Cambridge/UK (evis.sala@gmail.com)

Tumour heterogeneity in cancers has been observed at the histologic and genetic levels, and increased levels of intra-tumour genetic heterogeneity have been reported to be associated with adverse clinical outcomes. In oncologic imaging, phenotypic heterogeneity between and within tumours of a given patient is readily apparent and various imaging features are routinely described subjectively in radiology reports. However, recently, imaging research has focused increasingly on the newly emergent field of radiomics, which involves a high-throughput process in which a large number of shape, edge and texture metrics are extracted and quantified objectively and in a reproducible form. These quantitative metrics can provide important insights into tumour phenotype as well as the interaction of the tumour with its microenvironment, referred to as "habitat imaging". In the effort to delineate the biological and clinical implications of these new quantitative metrics, radiomic metrics obtained from MRI including diffusion-weighted and dynamic-contrast-enhanced MRI sequences, computed tomography and FDG-PET/CT have been further correlated with genomics data, a process intrinsic to the field known as radiogenomics. Radiogenomics and outcome data can be meaningfully mined with the goal of developing robust biomarkers that may potentially aid cancer diagnosis, improve assessment of treatment response and better predict patient outcome.

Learning Objectives:

1. To understand how radiomics features relate to the underlying biology.
2. To learn what information radiomics can give on tumour heterogeneity.
3. To become familiar with potential added value of radiomics in predicting treatment response and outcome.

A-576 16:57

Radiomics: clinical challenges

T. Penzkofer; Berlin/DE (tobias.penzkofer@charite.de)

Radiomics, either as feature classifiers or in the form of machine intelligence, is poised to play an increasing role in clinical imaging. It offers ample potential to extend the current practice of oncological and non-oncological imaging: currently around the corner are automatic anatomy annotation, next-generation CAD systems, lesion tracking and tumour heterogeneity analysis. More complex systems with an integrated understanding of a wider range of pathologies seem markedly further down the road. Before radiomics can be implemented and used to enrich our well-tested and robustly working workflows, a number of prerequisites need to be met: it is important to understand who wants and accepts semiautomated and/or fully automated decision-making systems in radiology. Patients, insurance companies and health-care providers are important stakeholders and might or might not be drivers of the implementation of radiomics. Additionally, current laws governing regulation of medical devices are drafted with monolithic, invariable products in mind. This could be impracticable for continuously self-improving machine learning systems. Lastly, quality control measures will certainly play an important role in tackling these issues, including the liability in case of "algorithmic malpractice". It seems reasonable to assume, that future generations of radiologists, instead of being replaced, will have a wider range of quantitative information at their disposal. Knowledge in data science to better understand, maintain and extend the systems will be a prime skill, just as technological understanding of imaging is part of every radiological curriculum.

Learning Objectives:

1. To understand the potential role in oncological and non-oncological clinical settings.
2. To define prerequisites for the integration into clinical workflows, including: patient acceptance, legal challenges and quality control.
3. To appreciate the future roadmap and its impact on training of young radiologists.

Author Disclosure:

T. Penzkofer: Employee; Charité University Hospital, Berlin, Germany. Grant Recipient; Berlin Institute of Health, Berlin, Germany.

17:15

Panel discussion: Radiomics, the new holy grail in radiology?

16:00 - 17:30

Room K

Special Focus Session

SF 12d

Radiographers' challenge: informing patients about radiation risk

Moderator:

J.N. Vassileva; Vienna/AT

A-577 16:00

Chairperson's introduction: The European BSS (Basic Safety Standards) Directive and current legal requirements

S. Geers-van Gemeren; Utrecht/NL (s.geers@nvmb.nl)

It is necessary that patients understand the risks of radiation associated with medical imaging examinations. Few studies have been conducted to assess patient knowledge of and attitudes towards radiation and only some have focused on the general population. Additionally, these studies showed that although computed tomography (CT) is estimated to be responsible for more than 70% of the collective radiation dose received by patients, most of them lack information about the reasons behind the medical imaging examination prescribed (the benefits) and the associated radiation dose (the risks). There are new requirements in the BSS for informing patients, recording patient doses, and recording, reporting and follow-up of accidental and unintended exposures. The patient or their representative is provided with adequate information relating to the benefits and risks associated with the radiation dose from the medical exposure. Similar information as well as relevant guidance shall be given to carers and comforters. A collaborative approach between referrers, radiologists, medical physicist and radiographers is suggested to help explain these risks to patients. Challenges for all professionals involved, especially for radiographers. Radiographers are the interface between the patient and the technology.

Session Objectives:

1. To learn about the requirements within the BSS Directive for the different healthcare professionals in informing patients.
2. To learn about the important role of radiographers in informing patients.
3. To understand patients' need related to the information about radiation risk.

A-578 16:05

So whose role is it? What different professionals can and should do

G. Paulo; Coimbra/PT (graciano@estesc Coimbra.pt)

Teamwork is needed wherever multiple individuals with multiple skills are required to work interdependently to achieve a favourable outcome. This means that teamwork is absolutely critical in the management of patients, since health care is a complex activity, which needs many different types of professionals, with different knowledge, skills and competences and with specific roles. One individual working alone cannot achieve the target of taking care of a patient, and from the concept defined in 1926 by Francis Peabody that "the secret of the care of a patient is caring for the patient" we have moved nowadays to: "the real secret of the care of a patient is teamwork". An increasing volume of medical imaging procedures combined with a demand for more rapid access to diagnostic services is putting high pressure on radiographers, who, by being the final point of contact for the patient, have the responsibility of providing the best and correct procedure to the patient. Departments should adopt communication strategies to explain the procedure in an understandable manner, adapted to patient social and economic characteristics, giving adequate information for him/her to be able to make a proper decision. Radiographers are, according to the BSS Directive, responsible for the practical aspects of medical imaging procedures, defined as: "means the physical conduct of a medical exposure and any supporting aspects, including handling and use of medical radiological equipment, the assessment of technical and physical parameters (including radiation doses), calibration and maintenance of equipment, preparation and administration of radio-pharmaceuticals, and image processing".

Learning Objectives:

1. To understand the importance of teamwork to improve communication skills when informing about radiation risk.
2. To learn about the importance of the radiographers' role in the healthcare setting.
3. To become familiar with the European Basic Safety Standards challenges for the different health professionals involved in patient clinical pathway.

Friday

Postgraduate Educational Programme

A-579 16:30

What do patients want to hear and need to be told?

J. Portelli; Msida/MT (jonathan.portelli@um.edu.mt)

Recent years have seen an ever-growing movement towards the importance for health-care delivery to be more patient centred, particularly since this has been associated with improved outcomes and quality of care. In effect, the drive towards patient-centred care should compel health professionals to invest more time and consideration to reflect upon and amend their practices, as necessary, so as to ensure that they are always providing care that is respectful of, and responsive to the needs, values and preferences of each individual patient, their families and/or representatives. In the context of medical imaging and radiotherapy, a patient-centred care approach therefore necessitates that radiographers are not only knowledgeable about how to identify the different information, emotional and social needs of each individual patient, but also need to be able to have and master the necessary skills to satisfy such needs in a manner that is meaningful and valuable to each patient. In this regard, this lecture will seek to outline and discuss possible information and communication needs of different patient groups attending medical imaging examinations. Additionally, this lecture will seek to highlight the different expectations, perceptions and concerns patients may have when attending a medical imaging examination and how such factors need to be considered holistically so as to further enhance patients' experiences in medical imaging and radiotherapy departments.

Learning Objectives:

1. To learn about the information and communication needs of patients attending for a medical imaging examination.
2. To appreciate that patients may have different expectations, perceptions and concerns when attending for a medical imaging examination.

A-580 16:55

How to effectively communicate radiation risks

L.R. O'Hara; Dublin/IE (lohara@mater.ie)

The quantification of patient dose and communication of associated risk is now a legislatively mandated function of radiology departments. The practical delivery of this essential service is sometimes lacking in clinical practice. This talk aims to suggest simple steps all diagnostic departments can use to quantify, interpret and communicate diagnostic doses and associated risks to patients.

Learning Objectives:

1. To understand dose metrics.
2. To appreciate the difference between diagnostic dose metrics and effective dose.
3. To understand the concept of "lifetime risks" associated with specific effective doses.
4. To become familiar with relating specific procedure dose to understandable concepts such as equivalent periods of environmental radiation.

17:20

Panel discussion: Speaking a common language: how best to work together to inform patients

16:00 - 17:30

Room M 1

ESHI Session

Non-oncological hybrid imaging: case-based

Moderators:

O. Ratib; Geneva/CH
K. Riklund; Umea/SE

A-581 16:00

Cardiac hybrid imaging indications: case-based

C. Rischpler; Munich/DE (christoph.rischpler@tum.de)

Molecular imaging modalities such as positron emission tomography (PET) and single photon emission computed tomography (SPECT) are usually combined with morphological imaging techniques such as computed tomography (CT) or magnetic resonance imaging (MRI). These hybrid cardiac imaging approaches allow the beneficial combination of radioactive, molecular imaging probes with the detailed assessment of cardiac function and anatomy. As a consequence, hybrid cardiac imaging plays an increasing role in the work up in various clinical scenarios. Possible indications include the workup of coronary artery disease (perfusion and viability), inflammatory diseases and cardiac tumours. This case-based talk discusses the application of hybrid imaging in various cardiac diseases with a special focus on hybrid PET/MRI.

Learning Objectives:

1. To learn about indications of hybrid imaging in cardiology.
2. To appreciate cardiac indications of different hybrid imaging modalities.

A-582 16:30

Non-oncological intracranial indications for hybrid imaging: case-based

A. Drzezga; Cologne/DE

"no abstract submitted"

Learning Objectives:

1. To understand non-oncological indications of hybrid imaging in the brain.
2. To become familiar with non-oncological radiopharmaceuticals for brain imaging.

A-583 17:00

Hybrid imaging in inflammation: case-based

A. Signore; Rome/IT (alberto.signore@uniroma1.it)

In the field of infection, early diagnosis of infection extent and severity is crucial. In some cases the location of the infection is also unknown. The use of hybrid imaging modalities, such as SPECT/CT, PET/CT and PET/MRI has enormously increased the possibility to identify and quantify the severity and extent of an occult infection. The main role is to be attributes to the choice of radiopharmaceutical, followed by the possibility to visualise the anatomy of patient by CT or MRI. In this presentation I will show several example about how to correctly apply different radiopharmaceuticals and what can be the added value of CT and/or MRI in the diagnostic approach. Cases of osteomyelitis, diabetic foot, spondylodiscitis and vascular graft infections will be presented.

Learning Objectives:

1. To learn about indications of hybrid imaging in inflammatory diseases.
2. To appreciate hybrid imaging for therapy response assessment in inflammatory diseases.

16:00 - 17:30

Room M 2

PIER @ ECR Session

PI 3

Value-based radiology

Moderators:

P. Mildenberger; Mainz/DE
G. McGinty; New York, NY/US

A-584 16:00

Basic concepts of value-based radiology: US perspective

J.A. Brink; Boston, MA/US

The value of radiology care may be defined from both the patient's and provider's perspective, including their views about quality and cost. Both perspectives demand image-derived information that is simple to understand, precise and actionable. Traditional quality metrics are informed well by these attributes, providing better pathways to health, risk mitigation and disease avoidance. Non-traditional quality metrics centre on patient experience, care coordination, and integration in care teams with clinical imaging pathways. Both traditional and non-traditional quality systems enable meaningful participation in new health-care delivery systems including accountable care and population health models. Cost models must consider both tangible and intangible costs, from both the patient's and provider's perspective. Tangible patient costs include out-of-pocket expenses as well as lost wages. Tangible provider costs include variable and fixed direct costs as well as indirect costs and overhead. Measuring costs can be particularly challenging, as top-down approaches may be overly simple while bottom-up approaches may be time consuming and difficult to maintain.

Learning Objectives:

1. To understand basic concepts of value-based radiology.
2. To be informed of the current state of value-based radiology in the US.
3. To explain professional implications of value-based radiology.

A-585 16:20

Basic concepts of value-based radiology: European perspective

L. Donoso; Barcelona/ES (ldonoso@clinic.uib.es)

Value-based health care (VBH) is a concept that was primarily developed to address the challenges resulting from the ever-increasing demand on health-care systems coupled with financial constraints. These trends also affect the

Friday

radiology profession, and the ESR established a working group on value-based imaging (VBI WG) in response to these developments and to shape them. The ESR's concept paper on value-based radiology (VBR) sets out the ESR's approach to this topic. At the conceptual level, the ESR argues that the diagnostic process should be included in the VBH framework, which focuses on outcomes but starting only at the point of treatment. However, an accurate and timely diagnosis is the first outcome that matters to patients. In this context, VBR should be a concept not only by and for radiologists, and the ESR plans to engage in this debate with the wider medical community. The focus on outcomes and value also requires organisational changes. The organisation of health-care delivery should be centred on the patient, and the structure must functionally follow the multidisciplinary management of medical conditions. In this new setting, radiologists need to demonstrate the value they provide to referrers, treating physicians, administrators and patients. The ESR proposes different metrics that can help change the perception of radiology from a volume-based cost to a value-driven asset. The metrics focus on five key aspects for a high-quality diagnosis: appropriateness of requests, radiation protection measures, quality of the radiology report, relationship between radiologists and patients, and education, research and innovation.

Learning Objectives:

1. To discuss possible concepts of value-based radiology in the European environment.
2. To discuss possible strategies leading from volume-based to value-based radiology in Europe.
3. To explain implications of value-based radiology on quality.

A-586 16:40

New metrics are required for value-based radiology

G. [McGinty](#); *New York, NY/US* (geraldinemcginty@gmail.com)

This session will provide participants with an understanding of how quality and resource use metrics are currently developed and implemented in the US, both for radiology and the health-care system in general. I will discuss how data are collected and submitted around these metrics and give an overview of the ways in which metrics are used by payers, both governmental and private, in the US health-care system. I will also explore the degree to which existing metrics have succeeded or failed in shaping value-based imaging care as well as the costs associated with demonstrating and reporting compliance.

Learning Objectives:

1. To understand the limitations of current metrics.
2. To understand how to effectively develop metrics around value-based radiology.
3. To understand the connection between metrics and payment.

17:00

Panel discussion: A European - US debate on the value of "value-based radiology"

J.A. [Brink](#)¹, L. [Donoso](#)², G. [McGinty](#)³, L.E. [Derchi](#)⁴, E.J. [Adam](#)⁵;
¹*Boston, MA/US*, ²*Barcelona/ES*, ³*New York, NY/US*, ⁴*Genoa/IT*, ⁵*London/UK*

16:00 - 17:30

Room M 3

Interventional Radiology

RC 1209

Pulmonary embolism: a joint challenge for diagnostic and interventional radiology!

A-587 16:00

Chairperson's introduction

A.G. [Ryan](#); *Waterford City/IE* (jackoriain@yahoo.ca)

Venous thrombo-embolism (VTE) is an enormous health-care issue, resulting in more deaths in Western Europe than AIDS, breast cancer, road traffic accidents, and prostate cancer, all combined. This session focuses on the state of the art in the diagnosis and management of pulmonary embolus (PE). All radiologists need to know how to diagnose and interpret the findings in this important condition, and Dr. Ghaye will describe in detail the optimal clinical and imaging algorithm to diagnose and stratify the condition, and its imaging follow-up. Dr. Uberoi will expand on the risk stratification and optimal management strategies based on current evidence. Once the diagnosis has been established, interventional radiologists have a major role in its treatment via aggressive catheter-based therapy and Dr. Spiliopoulos will discuss the interventional techniques, outcomes and evidence supporting their use in the treatment of massive and sub-massive pulmonary emboli.

Session Objectives:

1. To appreciate the value of imaging in therapy planning and follow-up.
2. To learn about patient selection and evidence in catheter directed therapies for PE.
3. To learn about recent and ongoing trials in the endovascular treatment of PE.

A-588 16:05

A. Imaging algorithm for pulmonary embolism

B. [Ghaye](#); *Brussels/BE* (benoit.ghaye@uclouvain.be)

The diagnosis of pulmonary embolism (PE) is difficult, since the clinical signs and symptoms are non-specific. Unstable patients usually undergo thrombolysis following demonstration of right ventricular (RV) dysfunction at echocardiography. Diagnostic algorithm strategies in stable patients have been developed to limit the number of patients requiring an imaging test. The first step includes the assessment of the clinical probability of PE and D-dimers testing. Patients with either a high clinical probability or a positive D-dimers test should undergo further imaging test. Incompliance to such diagnostic algorithms has been demonstrated to increase the rate of PE recurrence and the rate of false-positive CT pulmonary angiographies. In patients not at high risk of mortality (i.e. without clinical findings such as cardiogenic shock or persistent arterial hypotension), signs of RV dysfunction (at echocardiography or CT pulmonary angiography) are used together with clinical prognostic scores, such as the PESI, and cardiac biomarker dosage to discriminate patients with intermediate or low risk. This is usually performed by measuring the ratio between the diameters of RV and the left ventricle (RV/LV). More recent and potentially more powerful predictor CT findings have been reported, including among others RV/LV surface and volume ratios, the severity of "perfusion" defect and cardiac function parameters as calculated from ECG-gated acquisition. Evidence concerning the follow-up of unselected patients after treatment is still limited in literature. Short-term follow-up after systemic thrombolysis or endovascular treatment has been performed using various techniques, including RV/LV dimensions, pulmonary arterial obstruction scores or pulmonary perfusion comparison.

Learning Objectives:

1. To learn how clinical findings influence the selection of the imaging strategy in PE.
2. To learn about the follow-up after treatment.
3. To learn how imaging may predict the outcome of the patient.

A-589 16:28

B. What is new in the recently published guidelines for pulmonary embolism treatment?

R. [Uberoi](#); *Oxford/UK* (Raman.Uberoi@ouh.nhs.uk)

PE is a major cause of mortality, morbidity, and hospitalization in Europe. 317 000 deaths related to VTE were reported in six countries of the European Union (with a total population of 454.4 million) in 2004. 34% presented with sudden fatal PE and 59% postmortem. Only 7% who died early were correctly diagnosed with PE before death. Following diagnosis, patients should undergo risk stratification using a scoring system such as the pulmonary embolism severity index and patients stratified into high-, intermediate- and low-risk groups based on the clinical status of the patient, i.e. shock, hypotension, signs of RV dysfunction and cardiac biomarkers. Patients with scores of PESI of III-IV will have a 30-day mortality of 24.5%. High-risk and intermediate high-risk patients should undergo consideration for rapid primary pharmacologic treatment or surgery and, where available, interventional treatment to rapidly clear thrombus. Acute right ventricular dysfunction is a critical determinant of the outcome, and persistent arterial hypotension and cardiogenic shock carry a high risk of early death. Primary reperfusion treatment, particularly systemic thrombolysis, is currently the treatment of choice. This can result in the early reduction of pulmonary resistance and improvement in RV function. The maximum benefit is in the first few days, ideally within 48 hours with 90% of patients showing improvement, with no benefit at one week. Low-risk patients, i.e. with PESI scores I-II or sPESI 0, should be considered for early discharge and outpatient treatment with anticoagulation.

Learning Objectives:

1. To learn about the recently published guidelines for PE treatment in stable patients.
2. To learn about the recently published guidelines for PE treatment in unstable patients.
3. To learn about recent therapeutic algorithms in PE treatment.

Author Disclosure:

R. Uberoi: Grant Recipient; Gore and Bolton. Speaker; Spectranetics.

A-590 16:51

C. Updates on the endovascular treatment of massive and submassive pulmonary embolism

S.C. [Spiliopoulos](mailto:Spiliopoulos@med.uoa.gr); Athens/GR (stavspiliop@med.uoa.gr)

Minimal invasive percutaneous endovascular treatment of massive and submassive pulmonary embolism (PE) offers the benefit of low-risk, more aggressive management than systemic anticoagulation and has been correlated with reduced morbidity and mortality rates. Traditional endovascular methods include thrombus dissolution using standard pigtail catheters or balloons, presenting reasonable technical success rates of approximately 86%. Local low-dose catheter-directed thrombolysis combined with thrombectomy (e.g. pharmacomechanical thrombolysis) seems to improve outcomes, without increasing the risk of bleeding. The rationale of recent and ongoing trials is based on the fact that systemic thrombolysis, although more effective than anticoagulation alone, increases by 5-fold the risk of major bleeding and 10-fold that of haemorrhagic stroke, while it is contraindicated in many patients mainly due to recent surgery or intracranial haemorrhage. On the other hand, the majority of evidence for catheter-based interventions is based on few single-centre case series and prospective trials. Over the past few years, several prospective, multi-centre, randomised trials and large registries have investigated novel pharmacological and pharmacomechanical thrombectomy techniques, such as ultrasound-accelerated thrombolysis, providing a high level of evidence regarding the safety and efficacy of endovascular treatment options in acute PE. Nonetheless, studies comparing various endovascular modalities versus systemic fibrinolysis are missing, while additional large-scale, well-designed randomised trials are required to improve the level of evidence of currently available interventional radiology techniques. In this lecture, the outcomes of all available and ongoing clinical data will be presented and future developments will be discussed.

Learning Objectives:

1. To learn about the rationale of recent and ongoing trials.
2. To learn about the level of evidence for interventional radiology techniques in PE treatment.
3. To learn about clinical results and possible further developments.

17:14

Panel discussion: Appropriate diagnosis and risk stratification in the management of acute massive and acute submassive pulmonary embolism

16:00 - 17:30

Room M 4

Pros & Cons Session

PS 1227

Gadolinium: image wisely

Moderators:

P.M. Parizel; Antwerp/BE
A. Rovira-Cañellas; Barcelona/ES

A-591 16:00

A. Intracranial gadolinium deposition: update and perspectives

H.A. [Rowley](mailto:Rowley@uwhealth.org); Madison, WI/US (hrowley@uwhealth.org)

Trace quantities of gadolinium are retained in the brain and other body tissues after intravenous administration of all gadolinium-based contrast agents (GBCAs), even in patients with normal renal function. This phenomenon has been known since pre-clinical studies, but only recently 'rediscovered' when Kanda et al. reported intrinsic T1 hyperintense signal in the dentate and globus pallidus on brain MRI in patients who had received multiple doses of certain linear agents. Subsequent autopsy studies have shown that gadolinium is primarily retained in or near the endothelial walls of these deep grey nuclei. Routine histopathology shows no evidence for gliosis or neuronal injury, even when there is clear-cut visible signal hyperintensity on MRI. Clinical series and population-based studies have not verified any neurologic deficits related to this phenomenon. Certain linear agents (e.g. gadodiamide, gadopentate) show the greatest visible signal changes on MRI, while the high relaxivity linear agent (gadobenate) shows a lower likelihood at similar exposure, perhaps accentuated when there is concomitant radiation or chemotherapy. Macrocyclic agents show lower propensity for visible changes on T1-weighted images, but deposition in brain and other tissues (e.g. bone, spleen, liver) is confirmed for these agents when using techniques such as MR relaxometry and direct tissue assays. Body tissues show about 10- to 100-fold higher concentrations than in brain, in some instances higher for macrocyclic than linear agents. While the EU has largely banned linear agents, the USA and most other countries have suggested new GBCA label warnings, and all agree that more research is needed.

Learning Objectives:

1. To evaluate intracranial gadolinium deposition with direct assessment of gadolinium accumulation in neuronal tissues of patients previously exposed to multiple doses of intravenous gadolinium.
2. To explore the relationship between intracranial gadolinium deposition, the type of contrast agent and renal function.

Author Disclosure:

H.A. Rowley: Consultant; GE Healthcare, Bracco, Bayer, Guerbet, Gore.

A-592 16:20

B. Do we need gadolinium in imaging MS? Pros and cons (part 1)

C. [Lukas](mailto:carsten.lukas@ruhr-uni-bochum.de); Bochum/DE (carsten.lukas@ruhr-uni-bochum.de)

Magnetic resonance imaging (MRI) plays a key role in the diagnostic setup and follow-up of patients with multiple sclerosis (MS). The high sensitivity of the MRI enables the detection of focal inflammatory disease involvement in vivo, contributing substantially to an early diagnosis of MS. The intravenous administration of gadolinium-based contrast agents (GBCAs) in the diagnostic workup provides important information for fulfilling the concept of widely accepted and established diagnosis criteria. Subclinical MRI activity, e.g. detected by enhancing MS lesions, can substitute for a clinical relapse, allowing the diagnosis of MS from one single MRI after the first relapse. Furthermore, regular brain MRI scans play an essential role in monitoring disease progression in treated MS patients. Currently available treatment approaches differ in respect to efficacy and associated risks, stressing the importance of paraclinical tools to individualize the choice of disease-modifying therapy and closely monitor treatment efficacy and drug safety. MR imaging exhibits a higher sensitivity to inflammatory disease activity than clinical relapses alone and provides valuable information for guiding escalating immunotherapy. Furthermore, its ability to detect early signs of side effects such as progressive multifocal leucoencephalopathy (PML) makes it an indispensable tool to closely monitor patients at risk. Although gadolinium-enhanced MRI can increase the confidence of disease activity in the follow-up setting in MS patients, referring clinicians and radiologists should be aware of certain limitations and consider limiting the amount of serial GBCA administration to dedicated situations to reduce the number of unnecessary enhanced MRI scans.

Learning Objectives:

1. To review the role of Gd-enhanced follow-up MRI for management of patients with multiple sclerosis.
2. To explore alternative imaging techniques for assessment of disease progression in order to avoid gadolinium deposition.

Author Disclosure:

C. Lukas: Advisory Board; MerckSerono, Novartis, Sanofi Genzyme, TEVA. Board Member; Review Editor: Applied Neuroimaging (Frontiers in Neurology). Research/Grant Support; Bayer Schering, MerckSerono, TEVA, German Federal Ministry for Education and Research (BMBF). Speaker; Daiichi Sankyo, Bayer Vital / Schering, Biogen, Novartis, Sanofi Genzyme, TEVA. Other; Endowed professorship supported by the Novartis Foundation.

A-593 16:35

B. Do we need gadolinium in imaging MS? Pros and cons (part 2)

W. [Van Hecke](mailto:wim.vanhecke@icomatrix.com); Antwerp/BE (wim.vanhecke@icomatrix.com)

Gadolinium (Gd)-based contrast agents have been used for many years for the diagnosis and follow-up of patients with multiple sclerosis (MS). Post-Gd T1-weighted scans provide the unique ability to assess lesion activity and inflammation through the breakdown of the blood-brain barrier. Gd-enhancing lesions therefore are part of the standard diagnostic criteria in MS. Recently, there have been findings that there might be some Gd retention in the brain for some agents. This has led to a discussion on the use of frequent Gd injections and comments and recommendations by different bodies (CMSC, FDA, etc.). This is especially relevant for patients with MS, as they typically undergo an annual MRI scan for therapeutic monitoring. In addition to the possible Gd retention in the brain, and the unknown impact on the patient's well-being, the clinical need of the use of Gd for follow-up scans can be questioned, as it is known that Gd-enhancing lesions only show this Gd enhancement for a few weeks. Furthermore, some alternative quantitative measures of MS disease activity based on non-contrast MRI scans have been emerging.

Learning Objectives:

1. To review the role of Gd-enhanced follow-up MRI for management of patients with multiple sclerosis.
2. To explore alternative imaging techniques for assessment of disease progression in order to avoid gadolinium deposition.

Author Disclosure:

W. Van Hecke: Board Member; icomatrix. CEO; icomatrix. Founder; icomatrix. Shareholder; icomatrix.

A-594/A-595 16:50

C. Do we need gadolinium in imaging vestibular schwannomas? Pros and cons

B. [Verbist](#)¹, F.B. [Pizzini](#)²; ¹Leiden/NL, ²Verona/IT
(b.m.verbist@lumc.nl), (francescabenedettapizzini@gmail.com)²

Vestibular schwannoma (VS) is a benign nerve sheath tumour that may occur in the cerebellopontine angle cistern, internal acoustic meatus and in the inner ear. Patients will present with unilateral sensorineural hearing loss (SNHL), tinnitus, balance problems and - when tumours become large - cranial nerve palsy of the trigeminal and/or facial nerve. According to the most recent American College of Radiology (ACR) Appropriateness Guidelines, magnetic resonance imaging (MRI) of the head and internal auditory canals with and without contrast is the most appropriate imaging modality in patients with SNHL to evaluate for a possible VS. However, since the 1990s several studies have been conducted to compare the diagnostic accuracy of non-contrast-enhanced sequences with post-contrast MRI, mainly for reasons of cost-effectiveness, but more recently also inspired by concerns about the safety of MR contrast agent. The use of contrast-enhanced MRI during observation of a known VS or surveillance after surgical or radiotherapy treatment has also been questioned. In this lecture, the controversies on the use of gadolinium for the diagnosis of a VS will be discussed based on current literature and clinical experience. The aim of the follow-up studies is to evaluate growth (during a wait and scan policy and after irradiation) or to pick up recurrent disease early (after surgical removal). A literature review of possible follow-up strategies and the results of an own patient review will be presented.

Learning Objectives:

1. To determine whether Gd-enhanced MRI offers advantages in the initial diagnosis and follow-up of patients with (suspected) vestibular schwannoma.
2. To assess the diagnostic accuracy of high-resolution T2-weighted scans as an alternative to Gd-enhanced T1-weighted scans.

Author Disclosure:

B. Verbist: Research/Grant Support; Nucleus, Advanced Bionics. Speaker; Bayer.

17:10

Discussion on the pros and con

16:00 - 17:30

Room M 5

Special Focus Session

SF 12e

Memorable cases in cardiovascular imaging: how to avoid common mistakes

A-596 16:00

Chairperson's introduction

K. [Nikolaou](#); [Tübingen/DE](#) (Konstantin.Nikolaou@med.uni-tuebingen.de)

In this session special and memorable cardiovascular cases will be presented and discussed by experts in cardiovascular imaging. Cardiac imaging modalities covered and discussed will comprise cardiac MRI and cardiac CT imaging, and the potential role of multimodality diagnoses, incorporating information from several examination techniques. Clinical entities will include inflammatory, congenital and ischemic heart disease.

Session Objectives:

1. To learn how to avoid common mistakes in cardiac imaging.
2. To understand how to systematically review complex cardiac cases.
3. To appreciate the importance of clinical context and clinical knowledge for solving differential diagnoses in cardiac imaging.

A-597 16:06

Coronary fistula mimicking a cystic paracardial tumour

C. [Loewe](#); [Vienna/AT](#) (christian.loewe@meduniwien.ac.at)

Coronary fistulas represent a rare type of coronary anomalies. They are classified as abnormal coronary drainage (coronary anomaly group C). Coronary fistulas show a broad variation in the abnormal anatomical areas they could drain into including the atria, the superior vena cava, the pulmonary arteries and many more. The changes in haemodynamics could lead to volume overload, and huge coronary fistulas might even cause heart failure due to this volume overload if they are not treated on time. Additionally, the feeding vessel (=coronary artery) can dilate significantly as well, whereas the distal part of the feeding coronary artery might become hypoplastic due to steal effect, which can cause signs of ischaemic heart diseases and severe problems during

surgical repair of the fistula. However, most of the coronary fistulas remain asymptomatic for a long period of time and are diagnosed usually by chance. In such a situation, the diagnosis can be challenging since the coronary fistula can mimic other diseases, and non-invasive diagnosis had been difficult in the past. With the introduction of non-invasive coronary CT angiography, the diagnosis of coronary fistula has become easy and straightforward, since this technique can provide a detailed anatomical overview. In case treatment is indicated, coronary CT angiography is able to provide all information for treatment planning as well. In the presentation, a memorable case will be presented that was initially diagnosed as cystic paracardial tumour, but finally confirmed as aneurysmatic coronary fistula.

Learning Objectives:

1. To learn how to avoid the most common pitfalls in image interpretation of the coronary arteries.
2. To understand how to systematically review (complex) coronary artery anatomy/disease.
3. To appreciate the importance of clinical context for solving differential diagnoses in coronary imaging.

Author Disclosure:

C. Loewe: Speaker; GE Healthcare, Bracco, Siemens.

A-598 16:20

Right ventricular myocarditis diagnosed with CMR: the great imitator

M. [Francone](#); [Rome/IT](#) (marco.francone@uniroma1.it)

Isolated right ventricular (RV) involvement in acute myocarditis is an uncommon event, sharing overlapped clinical and morphological manifestations with arrhythmogenic right ventricular dysplasia (ARVC). The common features associated with both affections may be the presence of RV regional wall motion abnormalities and volumetric enlargement, impaired ejection fraction and late gadolinium enhancement of the free wall. The condition has shown to be misdiagnosed with cardiac magnetic resonance in approximately 50% of cases with relevant clinical implications on patient's prognosis and therapeutic management, posing a possible source of misdiagnosis in clinical practice.

Learning Objectives:

1. To learn how to avoid the most common pitfalls in image interpretation of myocarditis and inflammatory heart diseases.
2. To understand how to systematically review (complex) inflammatory myocardial cases.
3. To appreciate the importance of clinical context for solving differential diagnoses in myocardial imaging.

A-599 16:34

Congenital elastic band of the aortic valve: a "multimodality" diagnosis

K. [Pagonidis](#); [Iraklion/GR](#) (kpagonidis@yahoo.de)

Aortic stenosis due to supralvalvular membrane (elastic band) usually presents in children. It may be associated with fusion of the left coronary leaflet and the supralvalvular membrane, causing obstruction of the left coronary ostium and resulting in myocardial ischaemia. Despite the immobilization of the left coronary leaflet, these patients present in childhood with aortic stenosis, with or without accompanying myocardial ischaemia. The case is about an adult patient with supralvalvular aortic membrane presenting with turbulent flow due to fusion of the left coronary leaflet with the supralvalvular membrane and left ventricular hypertrophy with mild obstruction in the LVOT and apical aneurysm.

Learning Objectives:

1. To learn how to avoid the most common pitfalls in image interpretation of the valves.
2. To understand how to systematically review (complex) valvular cases.
3. To appreciate the importance of clinical context for solving differential diagnoses in valvular imaging.

A-600 16:48

Dyspnea with an abnormal right ventricle: role of MR imaging

A. [Jacquier](#); [Marseille/FR](#) (alexis.jacquier@ap-hm.fr)

MRI is an accurate and reproducible method to assess right ventricular function and characterise phenotype. Specific protocol and methods are used to estimate the RV function, volume, segmental abnormality and late enhancement. Learning curve for right ventricular assessment is longer than for the left side. MRI is increasingly playing a central role in diagnosis, prognosis and patient management. MR with its ability to assess cine, flow and late enhancement represents the first line exam to assess right ventricular pathologies. Pulmonary hypertension, arrhythmogenic RV dysplasia, tricuspid regurgitation, congenital abnormalities are the main disease that could affect the right ventricle but more rare disease could be encountered.

Learning Objectives:

1. To learn how to avoid most common pitfalls in image interpretation of the right ventricle.
2. To understand how to systematically review right heart function and morphology.
3. To appreciate the importance of clinical context for solving differential diagnoses in the right heart.

Author Disclosure:

A. Jacquier: Research/Grant Support; Guerbet.

A-601 17:02

Misleading CMR LGE artefact in cardiomyopathies

M. Gutberlet; Leipzig/DE

"no abstract submitted"

Learning Objectives:

1. To learn how to avoid the most common pitfalls in image interpretation of LGE images.
2. To understand how to systematically review (complex) LGE datasets.
3. To appreciate the importance of clinical context for solving differential diagnoses in myocardial and LGE imaging.

A-602 17:16

Hypertrabeculation vs non-compaction of the left ventricle: treat or don't touch?

K. Gruszczynska; Katowice/PL (kgruszczynska@poczta.onet.pl)

Left ventricular non-compaction (LVNC) according to ESC classification belongs to unclassified cardiomyopathies. It is defined by the two-layer structure of the myocardium with thin compacted subepicardial and thick non-compacted subendocardial layer with deep recesses and thick trabecula. Two forms of LVNC have been reported: non-familial-isolated and familial-inherited. LVNC was thought to develop due to the arrest of coalescence of foetal myocardial trabeculae in utero, and was linked to different genetic findings. However, hypertrabeculation can also occur in adult life. Clinically, LVNC has been linked to LV failure and increased risk of thromboembolic events. Radiological diagnostic criteria have defined LVNC as the index of NC/C layer >2.3 in LA EDD images or trabecular mass $>20\%$ of total LV mass in ED. According to recent publications, these criteria could be fulfilled by a substantial percentage of the asymptomatic population. Moreover, LV hypertrabeculation was not of higher clinical prognostic value than EF, LV volume or myocardial fibrosis. So, the question that arises is: what is the clinical value of excessive LV trabeculation visible on MRI and CT, both in patients with reduced and preserved cardiac function, as the common mistakes in diagnosis can have tremendous impact on the patient's life.

Learning Objectives:

1. To learn how to avoid most common pitfalls in image interpretation of left ventricular function and morphology.
2. To understand how to systematically review the causes of reduced cardiac function.
3. To appreciate the importance of clinical context for solving differential diagnoses of the left ventricle.

Saturday, March 3

Postgraduate Educational Programme

08:30 - 10:00

Room A

E³ - ECR Academies: Interactive Teaching Sessions for Young (and not so Young) Radiologists

E³ 1321

Oncologic imaging

A-603 08:30

A. Lung cancer: key signs in the new TNM

A.R. [Larici](mailto:annarita.larici@unicatt.it); Rome/IT (annarita.larici@unicatt.it)

Lung cancer is a leading cause of cancer-related mortality worldwide. A correct staging is the prerequisite for an adequate management of patients with lung cancer. Recently, the 8th edition of the TNM classification introduced relevant changes to the descriptors T and M. Regarding T, it has been demonstrated by survival analyses that from 1 to 5 cm of diameter every centimetre counts, and that larger tumours are best aligned with either T3 (tumour size of more than 5 to 7 cm) or T4 (tumour size of more than 7 cm). This finding further confirms the common intuition that the larger the tumour, the worse is the prognosis. Regarding M, the category of extrathoracic lesions has been distinguished in M1b and M1c to indicate, respectively, one (oligometastatic disease) and more than one lesion. In this context, it is advisable that radiologists report the number of lesions if only one organ is involved and the number of organs if many are involved. This approach has a relevant clinical impact because oligometastatic disease nowadays is managed and treated differently with respect to an extensive M stage disease. Several limitations still remain, such as classification of a tumour adjacent to the chest wall, mediastinum and diaphragm, as well as the categorization of lymphangitic carcinomatosis as an independent descriptor and the evaluation of multiple lung lesions. Certainties and controversies on the topic will be argued in this session, taking into account that cancer staging should be always considered a multidisciplinary process.

Learning Objectives:

1. To learn about the new staging system for lung cancer.
2. To highlight the differences in the meaning of CT findings between the new system and the previous one.

Author Disclosure:

A.R. Larici: Consultant; MSD, Boehringer Ingelheim, Roche.

A-604 09:15

B. Incidental findings in oncologic patients

M.-P. [Revel](mailto:marie-pierre.revel@aahp.fr); Paris/FR (marie-pierre.revel@aahp.fr)

Incidentalomas are frequently found during CT follow-up of oncologic patients. Unsuspected pulmonary embolism (UPE) prevalence is reported to be as high as 5%. Symptoms, which had been erroneously attributed to cancer, are often retrospectively found. UPE more often involves distal arteries. The recurrence rate is the same as for suspected PE, around 20%. Up to 30% of UPEs are not initially reported. Incidental pulmonary nodules are very frequently found in oncologic patients. At the initial staging, it is of major importance to distinguish between lung metastasis and other cause of lung nodule. The nature of the primary malignancy must be taken into account, and a histologic assessment might be required if there are implications on treatment. Adrenal masses are also frequently found. An attenuation below 10 UH on unenhanced CT is the best criterion for benign adenoma. If not, 40% relative washout on CT or 20% drop of signal on out-of-phase MR sequences suggests a benign lesion. In case of increased FDG uptake on PET-CT, percutaneous biopsy might be performed after having excluded pheochromocytoma by a dosage of catecholamine metabolites.

Learning Objectives:

1. To recognise the importance of different incidental findings in patients with cancer.
2. To learn how to manage patients with incidental findings.

08:30 - 10:00

Room B

GI Tract

RC 1301

Difficult challenges in imaging the acute abdomen

Moderator:

S.K. Puri; New Delhi/IN

A-605 08:30

A. Perforation of the GI tract

V. [Maniatis](mailto:vmaniatis67@gmail.com); Aabenraa/DK (vmaniatis67@gmail.com)

Perforation of the GI tract represents an emergency and life-threatening condition. The causes of perforation may be traumatic (endoscopy, blunt trauma, ingested foreign body), inflammatory (peptic ulcer disease, diverticulitis, appendicitis, Crohn's disease or other enteritis), bowel schema or neoplasms. Clinical diagnosis may be difficult and patients may be first radiologically evaluated with plain radiographs or ultrasound, but with limited information in cases of perforation. CT scanning is by far the imaging method of choice in these patients. CT findings of GI tract perforation can be direct or indirect. Direct findings include free air or/and oral contrast either intra- or retroperitoneal. Indirect findings comprise inflammatory mass surrounding an appendicolith or a radiopaque foreign body. Non-specific findings include bowel wall thickening, mesenteric infiltration, interloop free fluid and abnormal bowel wall enhancement. With the use of both direct and indirect findings, the sensitivity of CT in diagnosing GI tract perforation is up to 92%. False-positive results usually occur in post-operative patients, where free air as a result of previous operation can be misdiagnosed as a sign of anastomotic leak or iatrogenic bowel trauma. CT is also able to depict the site of perforation with an overall accuracy between 82 and 90% and the cause of perforation in up to 67% of cases. It is well documented that CT plays a crucial role in the assessment of patients with GI tract perforation, by offering fast and accurate essential information to the clinicians and enabling the most correct therapeutic choice.

Learning Objectives:

1. To learn about the main causes and clinical symptoms of GI tract perforation.
2. To become familiar with the imaging methods used to detect GI tract perforation and with relevant diagnostic algorithms.
3. To appreciate the important imaging appearances indicative of GI tract perforation. What should radiologists not miss?

A-606 09:00

B. Bowel obstruction

A.J.B.S. [Madureira](mailto:ajbmadureira@gmail.com); Porto/PT (ajbmadureira@gmail.com)

Bowel obstruction is responsible for a considerable number of surgical admissions for acute abdominal pain in the emergency department. It has a high morbidity and mortality if left untreated. The diagnosis can be suggested by plain abdominal films, but CT, and particularly contrast-enhanced CT, plays a crucial role in the diagnosis and management of these patients. Not only can CT confirm the diagnosis, but it can also grade the severity of the obstruction, locate it, and provide the aetiology. A dedicated technique is necessary and multiplayer reconstructions in the coronal and sagittal planes are mandatory. The causes of small bowel obstruction can be divided into intrinsic (inflammatory diseases, neoplasia), extrinsic (adhesions, hernias), and intraluminal (gallstones, bezoars). The three most frequent causes of large bowel obstruction are neoplasm, volvulus, and diverticulitis. The imaging findings vary according to the cause, and some are very specific. CT can provide a quick diagnosis and allow an early and optimal management of these patients, contributing to better patient care and improved survival.

Learning Objectives:

1. To learn about the different types and causes of bowel obstruction.
2. To become familiar with relevant imaging signs in both small and large bowel obstruction including complications.
3. To appreciate the most widely used imaging approach for detection and evaluation of bowel obstruction.

A-607 09:30

C. Acute biliary conditions

C.D. [Becker](mailto:Geneva/CH); Geneva/CH

Acute cholangitis is a serious condition which occurs most commonly in the context of bile duct obstruction due to stone disease or strictures. Unless diagnosed and treated correctly, acute cholangitis may lead to liver abscess

Saturday

formation, septicaemia and multiorgan failure. The role of noninvasive imaging is to determine the presence of obstruction of the biliary tree., as well as its level and its cause. Although ultrasonography or computed tomography are most commonly used in the emergency situation, magnetic resonance imaging offers the most detailed diagnostic results, especially with regard to the cause of obstruction. Depending on the level and the cause of bile duct obstruction, decompression of the biliary tree may be done by means of minimally invasive interventional techniques via the endoscopic- retrograde or the percutaneous - transhepatic approach. Acute gallbladder disease is most often associated with calculus disease and obstruction of the cystic duct. Depending on the clinical situation, a diagnostic workup may be required to exclude the simultaneous presence of bile duct stones.

Learning Objectives:

1. To learn about the most common pathologies leading to acute biliary conditions.
2. To become familiar with the relevant multimodality imaging appearances in this group of patients.
3. To appreciate the role of interventional radiology in the management of these conditions.

08:30 - 10:00

Room C

Special Focus Session

SF 13a

Chest imaging of cystic fibrosis: from infants to adults

A-608 08:30

Chairperson's introduction

M.O. [Wielpütz](mailto:wielpuetz@uni-heidelberg.de); Heidelberg/DE (wielpuetz@uni-heidelberg.de)

Chronic progressive lung disease in cystic fibrosis (CF) is the major life-limiting factor of this autosomal-recessive genetic disorder. CF newborn screening programmes in Western countries allow for an early diagnosis even before pulmonary symptoms occur. Imaging provides detailed information on the regional distribution of CF lung disease. Chest x-ray (CXR), computed tomography (CT) and, most recently, magnetic resonance imaging (MRI) are now available as routine modalities, each with individual strengths and drawbacks, which need to be considered when choosing the optimal modality adapted to the clinical situation of the CF patient. At the same time, novel treatment strategies with CFTR modulators have revolutionized treatment in CF, starting early to prevent irreversible lung damage. Thus, radiologists are now faced with an increasing demand for imaging to monitor the course of CF lung disease from birth to adult ages. The hallmarks of the CF lung are bronchiectasis as one early sign of lung damage, airway wall thickening, consolidations and atelectasis, as well as emphysema in advanced stages of lung disease. Mucus plugging as well as air trapping and perfusion impairment are linked to basic pathophysiology and potentially reversible under therapy. Bronchiectatic destruction of lung lobes, dilatation of bronchial arteries and pulmonary haemorrhage are sequelae, which may require invasive treatment and lung transplantation. This session aims at teaching the most important imaging findings in CF lung disease and how these are depicted by chest x-ray, CT and MRI.

Session Objectives:

1. To learn about the imaging appearance of cystic fibrosis lung disease.
2. To appreciate the advantages and drawbacks of available imaging modalities.
3. To appreciate the role of repeated surveillance imaging in cystic fibrosis.
4. To understand the current developments in cystic fibrosis lung imaging.

Author Disclosure:

M.O. [Wielpütz](mailto:wielpuetz@uni-heidelberg.de): Advisory Board; Boehringer Ingelheim.

A-609 08:35

X-ray: is there still a value in CF?

C. [Owens](mailto:owensc@gosh.nhs.uk); London/UK (owensc@gosh.nhs.uk)

The so-called "cutting edge" imaging research in cystic fibrosis suggests the use of computed tomography-generated measurements of bronchial wall thickness and airway tapering, sometimes using spirometer-guided CT or hyperpolarised gas MRI measures of regional ventilation, and even computed fluid dynamics based on individual patient airway geometry. But what is the real evidence base for this being reliable, reproducible, scientifically specific and robust? How does this really influence the patients' management and well-being? What of the humble chest radiograph? What other imaging modality provides relatively non-invasive, robust, repeatable diagnostic images in patients ranging from the neonate to a 40-year-old, and even post-lung

transplantation? In the presence of good clinical examination and detailed pulmonary function tests, for annual follow up, or in the presence of acute clinical deterioration, there is no need to provide a potentially "oversensitive" view of the anatomy. Subtle (possible transient/ reversible) mucos plugging and airway thickening may be overread. Clearly if the patient is on an expensive drug trial, CT is more sensitive, but what do we know about how reliable (or reversible) the CT images are in reflecting the patients' real clinical status. The future of advanced airways imaging is extremely bright, but it is not yet time to put the simple chest radiograph to bed.

Learning Objectives:

1. To learn about the typical imaging appearance of cystic fibrosis on radiography.
2. To become familiar with semi-quantitative scoring methods.
3. To appreciate radiography's role in imaging of the cystic fibrosis lung.

A-610 08:55

CT: information content vs dose?

P. [Ciet](mailto:ciet@erasmusmc.nl); Rotterdam/NL (p.ciet@erasmusmc.nl)

Computed tomography (CT) remains the cornerstone of pediatric thoracic imaging. This holds true also for Cystic Fibrosis (CF) lung disease. Chest-CT has proved to be more sensitive than chest radiographs (CR) and lung function to detect disease progression in patients with CF. Chest-CT enables high-quality and diagnostic images both in non-collaborative and collaborative children. In non-collaborative children, fast acquisition CT protocols can be used to avoid sedation or anesthesia without compromising image quality. Specific CF-CT findings can be assessed with CT to monitor CF lung disease progression. The ability to recognize these findings on CT and to summarize them in a radiology report is important for the management of the CF patient. Nonetheless, the main limitation of Chest-CT remains radiation exposure, which always conveys a risk of developing cancer related to its stochastic nature. However, dose reduction measures have been introduced to minimize this risk and nowadays chest-CT can be performed at the same radiation dose of a CR. Further radiation dose reduction might be achieved through Chest-CT protocol standardization across vendors, which is still lacking. Finally, chest-CT has enabled to shift from qualitative to quantitative radiology. Newly developed imaging analysis techniques allows today to extract numbers from CT images that can be used to assess treatment's efficacy or to determine patient's prognosis. This presentation will be a summary of the state of the art of CT imaging in CF lung disease, with description of the CT technique, CF-CT imaging findings, semi-quantitative and quantitative scoring methods, and clinical examples.

Learning Objectives:

1. To learn about the typical imaging appearance of cystic fibrosis on CT.
2. To become familiar with semi-quantitative scoring and quantitative CT.
3. To appreciate CT's role in imaging of the cystic fibrosis lung.

Author Disclosure:

P. [Ciet](mailto:ciet@erasmusmc.nl): Consultant; Vertex Pharmaceutical.

A-611 09:20

MRI: value of routine MRI?

F. [Doellinger](mailto:doellinger@charite.de); Berlin/DE (felix.doellinger@charite.de)

Substantial technical improvements during the last fifteen years have provided a basis for the routine use of chest MRI in the assessment of lung disease in cystic fibrosis. Typical pulmonary disease manifestations, such as bronchial wall thickening, bronchiectasis, and mucus plugging are easily assessable, as they come along with an increase of protons, thereby giving signals. The disadvantages of MRI compared to CT, which is the faster technique and still offers better spatial resolution, are overwhelmed by the fact that MRI is a radiation-free modality and by the possibility of perfusion imaging, which can give important additional information. Morphofunctional MRI scores allow for a reproducible quantification and surveillance of lung changes. Successful response to antibiotic drugs in patients with infectious exacerbations goes along with a decrease of MRI scores. Recent studies have shown that MRI scores can even be helpful in the detection of cystic fibrosis in asymptomatic infants.

Learning Objectives:

1. To learn about the typical imaging appearance of cystic fibrosis on MRI.
2. To become familiar with semi-quantitative scoring and quantitative MRI.
3. To appreciate MRI's role in imaging of the cystic fibrosis lung.

09:50

Panel discussion: X-ray, CT or MRI, or a combination?

To appreciate the different strengths and weaknesses of each modality.

Postgraduate Educational Programme

08:30 - 10:00

Room Z

Joint Session of the ESR and the BBMRI-ERIC (Biobanking and BioMolecular resources Research Infrastructure - European Research Infrastructure Consortium)

Linking imaging biobanks to -omics: the role of BBMRI and ESR

Moderators:

A. Van der Lugt; Rotterdam/NL
E. Steinfelder; Graz/AT

A-612 08:30

Introduction to BBMRI biobanking and biomolecular resources research infrastructure

E. Steinfelder; Graz/AT (erik.steinfelder@bbmri-eric.eu)

The way biobanks see it, researchers have no alternative than to connect and partner up with them when looking for high-quality samples and associated data. In other words, researchers cannot go find a better alternative because there is none. The researchers themselves, however, are often convinced that there are many alternatives to biobanks, which is mainly due to the fact that sample collections hosted by biobanks lack visibility, findability and accessibility, or simply because researchers have a strong desire to have their own collections of specific material. To bridge this gap between biobanks, the research community and the different stakeholders, BBMRI-ERIC's focus will be on building and strengthening value-added sustainable biobanking. The set of services offered by BBMRI-ERIC to support the various stakeholders will be continuously developed and improved. Quality Management will continue to expand its self-assessment survey, launch a quality grade and develop a concept paper for an audit programme. The Common Service IT will focus on improving and supporting the Directory, the Negotiator, the Connector and BIBBOX. The Common Service ELSI will centre its efforts around a number of services and support, including optimising the recently launched help desk, adapting the ethics check and drafting the code of conduct.

Learning Objectives:

1. To learn about biobanking and BBMRI.
2. To understand the diversity of human disease, biological samples and corresponding data.
3. To appreciate the benefits provided by biobanks for personalised medicine.

A-613 08:40

Secondary use of existing data: ethical issues, sharing and data protection

M.T. Mayrhofer; Graz/AT (michaela.th.mayrhofer@bbmri-eric.eu)

In the context of research, the secondary use of data refers to the processing of already existing medical data for a purpose different from the originally intended and for which it was initially collected. Secondary use of data is a common practice in medical research and poses ethical, legal and organisational challenges, among others. To seemingly simplify secondary use, is often recommended or even required to anonymise the data. Leaving aside the fact that anonymisation is a challenged concept in the era of big data, it can (a) deprive research projects from producing meaningful results, (b) to share incidental findings with research participants and (c) deny research participants their right to withdraw. Despite European and international efforts on harmonising practices of re-use of data, substantial differences remain across countries due to legal frameworks and cultural sensibilities. Moreover, appropriate safeguards (e.g., k-anonymity) are only as successful as constantly improved and lived as part of organisational culture. This presentation provides an overview of the challenges of secondary use of data (especially with regard to data sharing and data protection), how our concepts of privacy are challenged by scientific progress and discusses potential solutions (e.g. the Code of Conduct for Health Research initiative).

Learning Objectives:

1. To understand the rationale for patient rights the Code of Conduct for responsible use of human biomaterial and data.
2. To consolidate knowledge about the implementation of anonymization and pseudonymisation.
3. To learn about the sharing data and the General Data Protection Regulation.

A-614 09:00

Types of biobanks in the BBMRI network

P. Holub; Graz/AT (petr.holub@bbmri-eric.eu)

BBMRI-ERIC is a pan-European research infrastructure facilitating access to quality-defined biobanking and biomolecular resources. As such, it comprises heterogeneous partner biobanks ranging from clinical biobanks, disease-

specific biobanks, population biobanks or rare diseases biobanks. Recently as a part of the collaboration with ESR, BBMRI-ERIC is being extended to improve findability of imaging biobanks, too. This presentation provides an overview of types of existing biobanks and biological material and data collected. Ability to assess quality of the biological material and data, i.e., ability to assess fitness for given research purpose and method, has become a paramount and resulted in increasing deployment of quality procedures inside the biobanks. Different present and upcoming quality standards will be discussed, namely CEN and ISO standards, including current standardisation work on provenance information management. The presentation will also cover basic principles of access procedure as implemented by BBMRI-ERIC and showcase how they are practically implemented in a distributed heterogeneous research infrastructure.

Learning Objectives:

1. To learn about the aims of BBMRI and the existing biobanks.
2. To understand how to offer and obtain easy access to samples, data and images.
3. To learn about quality assurance in biobanks.

Author Disclosure:

P. Holub: Employee; BBMRI-ERIC. Founder; Comprinato Systems. Shareholder; Comprinato Systems.

A-615 09:20

Radiomics: enhancing the value of images by standardised feature extraction

S. Trattnig; Vienna/AT (siegfried.trattnig@meduniwien.ac.at)

The need to improve cancer survival rates continuously motivates scientists to uncover the genetic and molecular composition of tumours and use this information to develop more effective cancer therapies. Since tumours differ in their biological makeup, treatments can now often be tailored towards individual patients, in a strategy termed 'personalised medicine'. Radiomics uses computer algorithms to process the data collected by different imaging techniques and is becoming increasingly popular in cancer imaging research. One of its key characteristics is that radiomics recognises that digital medical images are not only pictures, they are also complex data. Radiomic analyses, extracts and measures an array of "features" that describe the image texture and distributions of individual voxel values, the units that make up a 3D image, within a tumour. Features can be descriptive terms derived from radiology reports or mathematical quantities. Feature extraction requires several complex steps in a defined pipeline: defining the regions of interest and segmenting three-dimensional images, extracting features and converting images into "mineable" data. Finally, data from imaging techniques, and from biofluids and tumour tissue, are combined into models to predict patient prognosis or benefit from a specific therapy. One of the main benefits is that medical imaging data acquired in routine health care can be used in a new way to inform clinicians about the biology of a tumour and provide potential prognostic or predictive information. However, several challenges need to be overcome before radiomics, such as statistical problems, standardisation of terminology and PACS integration.

Learning Objectives:

1. To learn how image features can be extracted.
2. To discuss how radiomics can be integrated in "omics" analysis.
3. To explore the potential of radiomics analysis in care.

A-616 09:40

Integrating an imaging biobank in a BBMRI biobank

B. Gibaud; Rennes/FR (bernard.gibaud@univ-rennes1.fr)

Biomedical research related to the development of personalised medicine requires more and more imaging data. Moreover, clinical decision in personalised medicine involves more and more the use of both biological biomarkers and imaging biomarkers, derived from image data through image processing. Besides, the ultimate validation of results in medical image processing often requires a histopathologic diagnosis, which needs to access and analyse the corresponding specimen. In this context, researchers need infrastructure and services to search, locate, and retrieve the bioresources they need for their research (e.g. images, biospecimen, histopathologic diagnosis, genomic data). Such service is being implemented by the BBMRI-ERIC infrastructure which coordinates the sharing of biospecimen throughout Europe. Such infrastructure does not exist for imaging biobanks yet. The presentation will introduce the basic requirements for clinical imaging biobanks. It will analyse the main differences between biobanks and imaging biobanks. Specifically, it will underline the commonalities and differences between image collections and biospecimen collections. It will provide an introduction to the Minimum Information About Biobank data Sharing (MIABIS) model, and to its ontological version OMIABIS. The presentation will discuss how MIABIS/OMIABIS can be extended to facilitate image description and sharing,

Saturday

Postgraduate Educational Programme

in a way that enables native interoperability between biobanks and imaging biobanks data infrastructure.

Learning Objectives:

1. To understand the requirements for a clinical imaging bank.
2. To learn about the intra-operability of clinical image biobank and other data repositories.
3. To consolidate knowledge about "Minimum Information About Biobanking Sharing" (MIABIS) 2.0.

08:30 - 10:00

Room O

E³ - ECR Master Class (Cardiac)

E³ 1326a

Cardiac MRI: from sequence to bedside

A-617 08:30

Chairperson's introduction

L. Natale; Rome/IT (luigi.natale@unicatt.it)

In this session, three main topics will be addressed by speakers: flow, metabolism and myocardial deformation. Flow imaging has been recently enriched by 4D techniques, that demonstrated to be promising either for diagnosis or for prognosis. Metabolic assessment of cardiac diseases has been relegated to research field for a long time, due to time consuming techniques, costs and relatively low clinical impact. However recent advances in metabolic assessment of some cardiomyopathies seems to be promising. Finally, myocardial deformation evaluation and strains calculation are actually hot topics, due to introduction of a new approach, i.e. feature tracking, that allows qualitative and quantitative approach to myocardial function. Differently from tagging techniques, feature tracking is applied on cine-MR data sets, without any additional time and is more robust.

Session Objectives:

1. To understand the current clinical challenge for cardiac MRI in flow, metabolism and myocardial deformation.
2. To understand how the process evolves from method development to clinical application for flow, metabolism and myocardial deformation.

A-618 08:35

A. 4D flow imaging: how and when can it help?

A.A. Azarine; Paris.FR

"no abstract submitted"

Learning Objectives:

1. To learn about technical requirements to perform 4D flow imaging.
2. To understand what the strength and limitations of 4D flow are compared to 2D flow assessment.
3. To learn about potential clinical applications of 4D flow imaging.

A-619 09:00

B. Spectroscopy: implications of myocardial metabolism?

H.J. Lamb; Leiden/NL (h.j.lamb@lumc.nl)

Recently, the concept of the 'metabolic syndrome' was introduced, which is a constellation of risk factors of metabolic origin that are accompanied by increased risk for cardiovascular disease and type 2 diabetes. The two major underlying risk factors for the metabolic syndrome are obesity and insulin resistance. Metabolic imaging and total body fat distribution may be used to determine if obese subjects are at an increased risk for developing type 2 diabetes. In this situation, more intensive lifestyle intervention can be advised and monitored. MR techniques, including MR spectroscopy, offer unique possibilities for monitoring the effects of new dietary strategies. Whole-body imaging may also allow one to study the interaction between different organs. For example, initial results show that high liver triglyceride content in type 2 diabetes is associated with decreased myocardial perfusion, glucose uptake and high-energy phosphate metabolism, in conjunction with impaired whole-body insulin sensitivity. Multi-organ imaging in a single patient opens interesting possibilities to study the interaction between key organs involved in the metabolic syndrome, such as liver, pancreas, kidney and heart, in relation to vascular morphology and function. In summary, metabolic MR imaging, including MR spectroscopy and total body fat distribution, may be used in the future for risk assessment and personalized medicine in patients with the metabolic syndrome. Furthermore, multi-organ MR imaging and spectroscopy are promising for evaluation of the interaction between different organs in metabolic syndrome.

Learning Objectives:

1. To learn about technical requirements and how to perform proton spectroscopy and multinuclear spectroscopy.
2. To understand what has been learned from cardiac spectroscopy.
3. To learn about potential clinical applications of spectroscopy.

A-620 09:25

C. Feature tracking: what to conclude from strain and torsion?

J. Lotz; Göttingen/DE (Joachim.Lotz@med.uni-goettingen.de)

Quantification of wall motion has ever been an unresolved issue in cardiac imaging. Tagging techniques have been employed by MR-imaging in different field strengths and sequence designs to define myocardial features that can be tracked by specific software. However most of these techniques fell short of adequately defining diastolic myocardial wall motion. Diastolic dysfunction however has emerged as a key element in the detection of early stage myocardial disease. Myocardial feature tracking based on SSFP-sequence images has evolved as a reasonably reliable alternative to the classical myocardial tagging techniques in MRI. Similar developments have enriched echocardiography imaging for myocardial characterisation. Myocardial strain and torsion represent quantitative parameters that allow an in depth characterisation of myocardial wall motion. Quantitative myocardial dyssynchrony is a secondary parameter based on the strain and torsion values of left and/or right ventricle. There are numerous reports on the clinical benefit of these parameters for early diagnosis of diastolic heart failure and monitoring therapeutic interventions in cardiomyopathies. They may be helpful in defining the success of electrophysiological interventions in cardiac arrhythmias. This talk gives a comprehensive overview on the status and clinical usability of quantitative myocardial strain and torsion.

Learning Objectives:

1. To learn about a new MRI method to assess myocardial deformation.
2. To understand the strength of MRI feature tracking compared to other methods.
3. To learn about potential clinical applications of feature tracking.

09:50

Panel discussion: Is it time to include these MRI techniques in routine practice?

08:30 - 10:00

Room N

Head and Neck

RC 1308

Post-treatment imaging of the head and neck

A-621 08:30

Chairperson's introduction

H.B. Eggesbø; Oslo/NO (h.b.eggesbo@medisin.uio.no)

Head and neck cancer in the Western countries accounts for 3-4% of all cancers. The worldwide incidence is estimated to be 500,000, and in Europe 250,000. There are three times as many men as women that are affected. Squamous cell carcinoma constitutes more than 80% of the cancer. At the time of the diagnosis, one-third is in stage I/II, and two-thirds are in stage III/IV. The recurrence rates for stage I/II are relatively low, with 5-year-survival of 70-90%. Therefore, the risk of a secondary primary cancer after radiation therapy (RT) may be higher than the risk of recurrence. For stage III/IV, the local recurrence rates vary from 25 to 80%, and metastases from 10 to 30%, and the 5-year-survival is 10-55%. For stage I/II, the treatment options are surgery and/or RT, while for stage III/IV chemo- and RT are the main options. Common for all treatments are major alterations to the tissue that challenge the post-treatment imaging interpretation, independent of the modality. This session will focus on the expected changes after RT and surgery, including the most frequent surgical procedures, and when and how to perform post-treatment imaging, to depict early cancer recurrence.

Session Objectives:

1. To become familiar with different ways of treatment.
2. To understand post-surgical and post-RT complications.
3. To know how to follow-up patients in order to depict early recurrence.

Saturday

A-622 08:35

A. Normal findings after radiotherapy

R. Hermans; Leuven/BE (Robert.Hermans@uzleuven.be)

After radiotherapy, imaging may be used to monitor tumour response and to detect recurrent or persistent disease before it becomes clinically evident. Early tumour recurrence may be difficult to distinguish from treatment-induced tissue changes. Therefore, the expected imaging changes after radiotherapy of a head and neck cancer should be well known. These tissue changes depend on the radiation dose, the irradiated volume, and the time elapsed since treatment. Reticulation of fat layers, retropharyngeal space oedema, postirradiation sialadenitis, lymphatic tissue atrophy, and thickening of the pharyngeal and laryngeal structures may be seen. These expected tissue changes often appear symmetrical, unless asymmetric radiation portals were used. However, at the site of a bulky tumour, scar tissue may cause an asymmetric appearance also after successful treatment. Therefore, obtaining a baseline CT or MR study after therapy for a neoplasm with a high risk for recurrence is recommended, best 3-6 months post-treatment. By comparing subsequent studies with this baseline study, tumour recurrences or treatment complications can be detected with more confidence. Some recommend PET-CT as the initial baseline study, as this technique has a high negative predictive value; the positive predictive value is lower, as therapy-induced inflammatory changes may cause false-positive results. Tissue necrosis is a rare complication of radiotherapy in the head and neck region, usually appearing late after treatment. Both soft tissue, cartilage and bone necrosis may be encountered; differentiation from tumour recurrence at an early stage may be difficult. Other long-term complications may occur, such as development of a secondary tumour.

Learning Objectives:

1. To get acquainted with changes in tissues during and after radiotherapy.
2. To understand expected changes after radiotherapy in CT and MR imaging.
3. To recognise treatment complications from expected tissue changes after radiotherapy.

A-623 08:58

B. Normal findings after surgery

A. Trojanowska; Lublin/PL (agnieszka30@yahoo.com)

Nowadays, the management of head and neck cancer involves multidisciplinary evaluation and treatment, which usually includes surgery, radiation therapy and chemotherapy. The various approaches to surgical resection and tissue reconstruction, the types of neck dissection, different radiation therapy techniques and the addition of concurrent and neoadjuvant chemotherapy regimens may complicate imaging findings. Differentiating post-treatment changes from tumour recurrence with the use of different imaging modalities is challenging because of the presence of altered anatomy secondary to resection, flap reconstructions, oedema, inflammation and the presence of scar tissue. Therefore, it is essential to be familiar with normal findings after surgery and radiotherapy, to distinguish these characteristics from tumour recurrence and treatment-related complications.

Learning Objectives:

1. To get acquainted with most frequent surgical procedures in head and neck.
2. To understand how to evaluate post-surgical patients.
3. To learn how to assess microvascular flaps.

A-624 09:21

C. Treatment monitoring for early detection of recurrence

A.D. King; Hong Kong/CN (king2015@cuhk.edu.hk)

Head and neck tumour recurrence occurs in ~ 15-50% (depending on the initial stage at diagnosis) of patients with squamous cell carcinoma treated by chemoradiotherapy. The majority of recurrences occur in-field and are detected either on the post-treatment assessment or within 2-3 years of follow-up. The role of MR and CT imaging is not only to identify early recurrence amenable to curative salvage surgery, but also to avoid unnecessary biopsy or surgery. Reported size criteria for recurrence include ≥ 1 cm primary focal mass and ≥ 1 cm nodal short axis, or for nodes $< 75\%$ - 90% size reduction. However, size criteria have limitations, notably in HPV+ disease which is associated with large sterile post-treatment nodes. Extracapsular tumour spread and persistent necrosis are also inaccurate signs of persistent nodal disease. The main advantages of MRI over CT are the T2-weighted and diffusion-weighted images (DWI). Tumour recurrence has similar signal intensity to the pre-treatment tumour, T2 intermediate signal intensity and restricted diffusion (b-1000 high + ADC map low signal intensity), compared to inflammation (high signal intensity) or mature scar tissue (low signal intensity) on the T2 images and ADC maps. Contrast enhancement tends to be moderate in recurrence and between that of mature scar tissue (mild/absent) and granulation tissue/inflammation (marked), but there is overlap on the conventional T1W post-contrast images. DWI is also complementary to FDG-PET, helping to

reduce the FDG-PET false-positive results for recurrence caused by inflammation. False-negative findings arise from microscopic disease such as that found at tumour margins or in pre-treatment occult nodal metastases, and also from small/infiltrating tumours mixed with benign post-treatment change. False-positive findings arise from post-treatment changes, especially granulation tissue/inflammation, sterile component of necrotic node (ADC map low signal intensity) and complications such as radionecrosis, radiation-induced tumours and granulomatous polyps.

Learning Objectives:

1. To get acquainted with problem of recurrence in imaging studies.
2. To understand how to estimate signs of recurrence on CT and MRI.
3. To learn about false positive and false negative findings.

09:44

Panel discussion: What are the challenges in differentiating post-treatment changes from tumour recurrence?

08:30 - 10:00

Studio 2018

Genitourinary

RC 1307

Management of incidental findings in the genitourinary tract

Moderator:

R.H. Oyen; Leuven/BE

A-625 08:30

A. Adrenals

L.E. Derchi; Genoa/IT (derchi@unige.it)

Adrenal gland abnormalities are unexpectedly identified in 5%-8% of abdominal imaging studies. Most of them are benign and source of little or no concern; others are potentially fatal. Clinical and imaging criteria make differentiation between benign and malignant lesions possible in most cases. When there is no history of malignancy, adrenal lesions are almost always non-malignant (usually an adenoma). On the contrary, in patients with a history of malignancy, up to 50% are malignant and mostly metastatic. Imaging criteria based on macroscopic appearance of these lesions can easily identify those containing mature fat (myelolipomas), the hyperdense haematomas and the fluid-filled cysts. However, when lesions have non-specific appearance, it is necessary to analyse their structure with lipid-sensitive techniques (density measurement on unenhanced CT; chemical shift evaluation at MR), using perfusion/washout imaging after contrast injection, or with metabolic imaging during PET and CT/PET studies. This presentation will discuss how to behave when an unexpected adrenal lesion is encountered and how to perform its diagnostic workup.

Learning Objectives:

1. To understand the definition of incidental findings in adrenal pathology.
2. To learn about the imaging characteristics of common adrenal incidental masses.
3. To become familiar with the algorithm approach and evidence-based recommendations for management of adrenal incidentalomas.

A-626 09:00

B. Kidneys

H.C. Thoeny; Berne/CH (harriet.thoeny@insel.ch)

Cystic and small solid renal masses are frequently detected as incidental renal lesions with increasing incidence in the elderly population. Therefore, renal cell carcinomas are also increasingly detected as incidental findings on imaging. Nephron-sparing surgery has been the method of choice for the treatment of small solid renal masses. However, a large percentage of these solid renal lesions are benign and most of the incidentally detected malignant renal tumours such as renal cell carcinomas (RCCs) are smaller, with lower stage and are less aggressive than symptomatic RCCs. In addition, a correlation with size of the solid lesion and growth rate has been described ranging from 0.13-0.31 cm per year. Therefore, active surveillance is now a more frequently applied approach to deal with these incidentally detected small solid renal lesions (<3-4cm). Whereas in solid enhancing lesions < 1 cm in diameter, active surveillance is the treatment of choice at any age, in larger lesions, management mainly depends on clinical factors including the age and the performance state of the patient. The role of the radiologist is to exclude benign lesions such as Bosniak I and II cysts and angiomyolipomas as well as non-neoplastic conditions mimicking a tumour (infection, infarct, vascular anomalies and aneurysms). In patients with small solid renal lesions stratified

Postgraduate Educational Programme

for active surveillance, close follow-up with note of the growth rate has to be performed in order not to miss the time point of delayed treatment in case of a fast growth rate or clinical progression.

Learning Objectives:

1. To understand the definition of incidental findings in renal pathology.
2. To learn about the imaging characteristics of common renal incidental masses, namely cystic.
3. To become familiar with the algorithm approach and evidence-based recommendations for management of renal incidentalomas.

Author Disclosure:

H.C. Thoeny: Advisory Board; Guerbet SA.

A-627 09:30

C. Adnexa

C.S. [Balleyguier](mailto:Balleyguier@gustaveroussy.fr); Villejuif/FR (Corinne.BALLEYGUIER@gustaveroussy.fr)

Incidental adnexal lesions are non symptomatic lesions diagnosed on ultrasound, CT or MRI performed for an unrelated reason. They have increased in frequency with increased use of cross-sectional imaging. The majority are benign, even in patients with known malignancy or postmenopausal women. However it is important to reliably differentiate malignant from benign lesions to avoid delays in treating ovarian cancer and prevent unnecessary interventions in benign lesions. To try to characterise these findings, age, menopausal status, previous medical and family history and tumour marker such as CA 125 have to be known. Further management will depend on whether the lesion is clearly benign or malignant, or indeterminate. Specific diagnoses have to be suggested in case of fatty content (teratoma, lipoid cell tumour, etc), calcified content (ovarian leiomyoma, teratoma, Brenner struma, etc), and in extra-gynecological origin (lipoleiomyoma, pelvic teratoma, liposarcoma, etc). Diagnostic algorithms in cystic and solid incidentaloma will be presented in this session, including differential diagnoses. A specific focus will be made on diagnostic strategy in post-menopausal cystic ovarian lesions. Treatment strategy will also be described.

Learning Objectives:

1. To understand the definition of incidental findings in adnexal pathology.
2. To learn about the imaging characteristics of common adnexal incidental masses.
3. To become familiar with the algorithm approach and evidence-based recommendations for management of adnexal incidentalomas.

08:30 - 10:00

Room L 8

E³ - Rising Stars Programme: EFRS Radiographers' Basic Session

BR 2

Radiation protection from A to Z

A-628 08:30

Chairperson's introduction: The radiographers' role in radiation protection

D. [Catania](mailto:cataniadiago@hotmail.com); Milan/IT (cataniadiago@hotmail.com)

This EuroSafe Imaging session will incorporate four important aspects of radiation protection for consideration by the audience. The session will be opened by an update on radiographers' responsibilities with regard to the EU Basic Safety Standards Directive. This is critically important information that all professionals with radiation safety responsibilities in clinical practice should be aware of. The session will progress to include discussion of justification for radiographic examinations, which is an important aspect of all radiographers' daily work practice. As the technology used by radiographers advances, so must our knowledge of how to best use the technology. It is essential that radiographers remain up to date with respect to optimisation techniques in radiography practice. The third presentation in this session will provide the audience with important updates. The focus will be on conventional radiography which remains a core activity in all radiology departments. The final presentation will discuss the radiographers' role in benefit-risk communication. Once more, this professional matter is of high importance to all radiography professionals. The variety of core radiography matters, as included in this EuroSafe session, offers updates to our continuing professional development and are aimed at supporting our professional practice.

Session Objectives:

1. To understand radiographers' current legal responsibilities regarding radiation protection.
2. To consider the role radiographers play in application of the justification principle.

3. To review recent optimisation techniques for projection radiography.
4. To appreciate how radiographers can best communicate risk-benefit information to patients.

Author Disclosure:

D. Catania: Board Member; EFRS, European Federation of Radiographer Societies. Founder; AITRI, Italian Association of Interventional Radiographers.

A-629 08:35

The Basic Safety Standards Directive: all you need to know

S.J. [Foley](mailto:foley@ucd.ie); Dublin/IE (shane.foley@ucd.ie)

The European Commission issued its most recent radiation protection Directive in December 2013 which will repeal five other Directives (including 97/43/Euratom) and must be transposed by all Member States of the EU by February 2018. Therefore, this presentation is timely in coinciding with the European-wide adoption of the new Directive, which takes into account new recommendations from the ICRP in light of new scientific evidence and is hoped to strengthen the culture of radiation safety throughout Europe. While the Directive remains faithful to and maintains the already well-accepted pillars of radiation protection - justification, optimization and dose limitation - these are further strengthened in this Directive. Further new requirements under the Directive will also be discussed, including obligations related to recording dose information and communicating benefit/risk to patients. Additional responsibilities have also been designated to a number of professionals which will impact the work of both radiographers and radiologists alike; so, all imaging staff need to be aware of its implications. This will ensure that the true ethos of the Directive will be effectively implemented into routine clinical practice.

Learning Objectives:

1. To familiarise attendees with the European BSS Directive (2013/59).
2. To discuss the additional responsibilities of radiographers and radiologists under the Directive.
3. To consider how the BSS Directive can improve the culture of radiation safety in clinical practice.

A-630 08:53

The importance of justification

D. [Katsifarakis](mailto:dikatsifarakis@gmail.com); Athens/GR (dikatsifarakis@gmail.com)

Justification derives from the safety culture. It is a crucial procedure in diagnostic radiology, considered as one of the cornerstones of radiation protection. We currently carry out practices of justification appropriate to an era of examinations with minimal radiation dose. The majority of radiological examinations are performed by radiographers. They greet the patient and receive the medical referral simultaneously. Hence, radiographers can easily detect an inappropriate examination, particularly those arising from systems' inconsistencies. Also, according to their education-professional culture and expertise, they can recognize whether the prescribed examination will satisfy the diagnostic requirements. Radiographers bear the responsibility of delivering doses of ionizing radiation to patients and during research applications. Therefore, they must have the authority to exercise their judgement in accepting a referral for medical exposure. This must include an adjusting technique to minimize the exposure to patients, staff and the public whilst optimizing a diagnostic or therapeutic outcome. Radiographers must engage in effective gatekeeping and clinical audits by: reinforcing knowledge and communication skills to facilitate the 3As of justification (awareness, appropriateness, audit), complying with referral guidelines and employing clinical decision support systems. The ISRR promotes the scope of practice of a team approach to authorization and justification as safe and best practice for diagnostic imaging services.

Learning Objectives:

1. To appreciate the key role of justification within radiation protection.
2. To be familiar with the role radiographers can play in justification.
3. To consider initiatives for improving adherence to the principle of justification.

A-631 09:11

The latest optimisation techniques in conventional radiography

P.H. [Hogg](mailto:Hogg@salford.ac.uk); Salford/UK (P.Hogg@salford.ac.uk)

In the clinical routine, demand for medical imaging continues to grow and conventional radiography, comprising DR and CR technologies, enjoys significant utility. Given the moral and legal requirements to minimise radiation dose to patients, optimisation techniques must be used. Methodologically speaking, these techniques must evolve constantly because of technological and philosophical advances. Overall, optimisation seeks to reduce dose without compromising pathology detection/characterisation. Optimisation techniques need robust estimates of patient dose and pathology detection/characterisation performance to determine which interventions are

fruitful. With relevance to conventional radiography, this review will address important philosophical and practical optimisation issues. One philosophical issue will consider the merits and limitations of pathology detection/characterisation in contrast to assessing image quality; it is worth remembering that the latter is often used as a 'proxy' for the former. Following on from this, a critical review of visual and physical image quality measures will be presented. Consideration will also be given to different measures of radiation dose, from 'simple to make', but relatively unhelpful in optimisation (e.g. DAP), to 'complex to make', but potentially more helpful (e.g. effective risk and effective dose). A proposal will be offered on why dose reference levels are of limited value in the absence of pathology detection/characterisation or even image quality data. Finally, I will offer some practical suggestions on what steps might be taken to reduce dose in the clinical setting while maintaining image quality levels fit for pathology detection/characterisation.

Learning Objectives:

1. To discuss the limitations of image quality as a parameter for use in optimising dose in medical imaging examinations.
2. To discuss a range of visual and physical techniques that can be used to assess medical image quality.
3. To discuss a range of practical measures which might be implemented to minimise radiation dose whilst maintaining a level of image quality that is fit for purpose.

A-632 09:29

The radiographers' role in benefit-risk communication

J. Portelli; Msida/MT (jonathan.portelli@um.edu.mt)

By February 2018, each EU Member State is required to transpose Council Directive 2013/59/EURATOM into national legislation, thereby laying down revised basic safety standards for the protection against dangers arising from exposure to ionising radiation. Amongst the changes noted in these revised regulations, apart from the responsibilities relating to the justification and optimisation of each medical radiation exposure, referrers and/or practitioners will now be legally obliged to provide each patient with adequate information relating to the benefits and risks associated with the radiation dose to be received from a proposed medical imaging procedure. While many referrers and practitioners may already be fulfilling this 'new' responsibility in their daily practice, the decision to have such a responsibility well defined within the regulations can be interpreted as a way to oblige more health professionals to realise their duty in delivering patient-centred care and to duly respect each patient's right to information. In this regard, this lecture will seek to highlight the importance of radiographers having a sound understanding of radiation-related concepts, particularly those relating to the benefits and risks of medical imaging procedures they perform. Furthermore, the need for radiographers to develop and have effective communication skills will also be highlighted, since these are necessary to allow them to convey adequate benefit-risk information in accordance to the needs and preferences of different patient groups and their families, as well as to other health professionals that may be involved in the patient's care.

Learning Objectives:

1. To understand new legislative requirements under the BSS Directive.
2. To be aware of the key role radiographers play in benefit-risk communication.
3. To understand key principles for appropriate benefit-risk communication.

09:47

Panel discussion: Teamwork in radiation protection

08:30 - 10:00

Room E1

Breast

RC 1302

Rethinking ductal carcinoma in situ (DCIS)

Moderator:

C. Van Ongeval; Leuven/BE

A-633 08:30

A. New radiologic-pathologic knowledge on DCIS

A. Frigerio; Turin/IT (alfonso.frigerio@gmail.com)

A modern rethinking of ductal carcinoma in situ must take off from the awareness of the utter inadequacy of the terminology currently in use. Already in 1976, Jensen, Rice and Wellings remarked that "ductal carcinoma in situ of the human breast is of lobular (acinar) origin". While the latest (2012) WHO Classification decided to omit the name 'ductal' from the definition of the most common type of invasive breast carcinoma, it still fails to recognize the

inconsistency of this descriptor for its intra-epithelial counterpart. It is time to move to a new inter-disciplinary approach where a mutually respectful interaction between radiologists and pathologists should take full advantage of new imaging techniques and new pathologic methods to achieve better characterization of the different types of breast lesions and their clinicobiological potential. A new classification and terminology based on the site of tumour origin (acinar vs ductal), as best displayed by diagnostic imaging paired with modern pathologic techniques as large-format histologic sections, should open the way to a better understanding of the lesion biology, eventually improving treatment planning decisions. This lecture will include a discussion of: different subtypes of in situ lesions; neoductogenesis as an important feature that should be recognized and reported; the potential of mammographic tumour features as synergistic prognostic factors alongside classical pathological and modern molecular patterns. Overcoming long-lasting barriers to effective communication would be the prerequisite to a new professional setting where all specialists involved mutually enhance the benefits of their clinical knowledge.

Learning Objectives:

1. To learn about different types of DCIS.
2. To become familiar with risk of developing cancer.
3. To appreciate radiologic-pathologic correlations.

A-634 09:00

B. Diagnosing DCIS

S. Schradling; Aachen/DE (sschradling@ukaachen.de)

The presentation gives an overview over the current role and recent data of dynamic contrast-enhanced (DCE) breast MRI for diagnosis ductal carcinoma in situ (DCIS). Special attention is paid on the description and illustration of typical imaging features as well as pitfalls and difficult differential diagnosis of DCIS at MRI. In addition, the impact of DCE MRI on DCIS treatment and recent discussion on overdiagnosis and overtreatment of DCIS are discussed.

Learning Objectives:

1. To understand the evidence on MRI for evaluating DCIS.
2. To become familiar with different imaging appearances of DCIS.
3. To appreciate the value added of MRI for diagnosis.

A-635 09:30

C. Reducing overtreatment of DCIS

M.G. Wallis; Cambridge/UK (matthew.wallis@addenbrookes.nhs.uk)

Breast screening has led to an inexorable rise in the number of women living with a diagnosis of DCIS predominantly but not exclusively as a result of the detection of microcalcification. It is clear from long-term follow-up that conventional treatment fails the 15 to 20% who develop invasive disease, a few of whom then die from breast cancer. There is a larger group that never progresses within their life time which means we have either cured them or overtreated them. Traditional pathology and genetics suggest that there is a low-risk group that either never progress or if they do develop 'low-risk' invasive disease. I will describe the three international randomised controlled trials: LORIS (The Low Risk DCIS trial), LORD (Low Risk DCIS), COMET (Comparison of Operative versus Medical Endocrine Therapy for Low Risk DCIS) and LORETTA a single-arm confirmatory study of endocrine treatment only. I will describe PRECISION that aims to identify markers for progression from retrospective data sets and then prospectively validated these on the three randomised trials. Using LORIS, I will discuss how we have attempted to resolve the hurdles of setting up a 'no treatment trial' and talk about some of the lessons learnt from successfully steering LORIS from feasibility to full trial. Anecdotally, patient views have been more entrenched than those of surgeons and to my surprise the radiology second opinion service set up to reduce the risks of 'active monitoring' up by annual VAB has not been overwhelmed.

Learning Objectives:

1. To learn about the risk of overdiagnosis and overtreatment.
2. To become familiar with the risk of avoiding surgery.
3. To appreciate the level of evidence required to change future practice.

Postgraduate Educational Programme

08:30 - 10:00

Room E2

Neuro

RC 1311

Altered mental state

A-636 08:30

Chairperson's introduction

M.A. [van Buchem](#); *Leiden/NL*

Session Objectives:

1. To learn about the complex spectrum disease entities presenting with cognitive decline.
2. To understand the role of standardised imaging and reporting in the context of diagnosis and monitoring of patients with neurocognitive disorders.
3. To appreciate importance of multimodal imaging approaches in the diagnosis of neurocognitive disorders.

A-637 08:35

A. Patterns of referrals

N.N.

Learning Objectives:

1. To learn about the broad spectrum of clinical presentation of cognitive decline.
2. To understand the role of imaging in the context of the clinical presentation and other biomarkers (e.g. CSF) in the diagnosis of cognitive impairment.
3. To appreciate the heterogeneity of primary and secondary pathologies presenting to the memory clinic.

A-638 08:58

B. Imaging in altered mental state

A.J. [Bastos-Leite](#); *Porto/PT* (ajbastosleite@gmail.com)

The most common causes of altered mental state (AMS) encompass neurological and psychiatric conditions, as well as pharmacological, toxic, infectious, metabolic, or even traumatic disorders. Neuroimaging became a very relevant tool for the diagnosis of AMS, especially for the diagnosis of dementia (major neurocognitive disorder), a clinical syndrome, rather than a single nosological entity, characterised by deficits in one or more cognitive domains, and the most serious consequence of pathological brain ageing. Over the past decades, the role of neuroimaging has revolutionised the diagnosis of neurocognitive disorders by positively predicting the diagnosis rather than just excluding disorders that may mimic dementia. This change has been possible both by visually assessing the extent, pattern and severity of brain volume loss and cerebrovascular pathology, as well as by increasingly using computer-aided techniques, potentially advantageous at the very early stages of pathology progression. Functional neuroimaging techniques, such as arterial spin labelling, represent added value in this setting as well. In addition, cerebrospinal fluid biomarkers (Beta-amyloid- and tau-mediated injury markers) also support the clinical diagnosis of Alzheimer's disease. The challenge, however, persists in other mental conditions, such as psychiatric disorders. A key example here is schizophrenia, in which there are subtle—microscopic—abnormalities involving functional brain networks. This precludes the diagnosis by means of visual inspection, and currently limits the usefulness of neuroimaging. Nevertheless, novel techniques and methods for the assessment of effective (i.e., directed) brain connectivity seem to provide a very promising lead.

Learning Objectives:

1. To learn about the role of imaging in the diagnosis of neurocognitive diseases: from the exclusionary approach to the inclusionary approach.
2. To understand the challenges to diagnose neurocognitive disease in a very early stage using imaging.
3. To appreciate the complexity of differential diagnosis of neuroimaging in cognitively affected individuals and the crucial need for other biomarkers to support the clinical diagnosis.

A-639 09:21

C. MRI in the diagnosis of Alzheimer's disease

A. [Krainik](#); *Grenoble/FR* (akrainik@chu-grenoble.fr)

As the most common cause of neurodegenerative dementia, Alzheimer's disease (AD) is a diagnosis and therapeutic challenge. In clinical practice, diagnosis remains probabilistic without pathological proofs, relying on clinical and neuropsychological examinations, CSF biomarkers, and brain imaging. Multidisciplinary collaborations and recent technical advances deliver now

more accurate and relevant information, to better diagnose AD. Indeed, imaging data provide evidence to step forward and to refine AD diagnosis, based on homogeneous imaging subgroups of patients, despite similar clinical and biological profiles. Additionally, advanced MR techniques investigate new tools to demonstrate supplementary abnormalities, that could be used in clinical practice and suggest new paths for therapeutic research. Imaging of dementia is now far from ruling out neurosurgical aetiologies, only. Clear and reproducible cerebral images allow quantitative assessment to estimate severity, to discuss differential diagnoses, and to monitor evolution. We, radiologists, have to carefully analyse our images to provide the most probable diagnosis and to maximise the value of our work. The present lecture gives you tips and tricks for your daily practice.

Learning Objectives:

1. To learn about the imaging features and possible comorbidities of Alzheimer's dementia.
2. To understand the complexity of differential diagnosis.
3. To appreciate the crucial and so far unmet medical need to use quantitative MRI techniques in the diagnosis of Alzheimer's disease.

09:44

Panel discussion: Ask the expert: How can I standardise my image reading and reporting in order to support the clinical process in cognitively impaired patients?

08:30 - 10:00

Room F1

E³ - European Diploma Prep Session

E³ 1323

Cardiac and vascular

A-640 08:30

Chairperson's introduction

R. [Vliegenthart](#); *Groningen/NL* (r.vliegenthart@umcg.nl)

This European Diploma Prep session covers essential knowledge regarding radiological techniques in cardiovascular imaging, cardiovascular anatomy and highlights of cardiovascular pathology. Radiologists have an increasingly important role in the evaluation of cardiac and vascular diseases, due to the fact that CT/MRI can provide a diagnosis in a non-invasive, more detailed, more reproducible and/or more tissue-specific way than other modalities. In this session, a general basis is provided regarding the technique of cardiovascular imaging with CT and MRI, anatomical depiction in CT/MRI, and the main disorders of the myocardium, pericardium, valves and aorta.

Session Objectives:

1. To understand the basic principles and techniques of cardiovascular imaging including CT and MRI of the heart and great vessels.
2. To become familiar with the imaging presentations of disorders of the endocardium, the pericardium and the cardiac valves.
3. To understand the MR imaging presentation of disorders of the myocardium.

A-641 08:36

A. Cardiovascular imaging: the basics

M. [Gutberlet](#); *Leipzig/DE*

"no abstract submitted"

Learning Objectives:

1. To understand the anatomy, normal variants and abnormalities of the heart and great vessels.
2. To describe the technical aspects and methodology of cardiac and vascular CT.
3. To describe the technical aspects and methodology of cardiac and vascular MRI.

A-642 09:04

B. Cardiovascular imaging: valves, endocardium and aorta

C. [Loewe](#); *Vienna/AT* (christian.loewe@meduniwien.ac.at)

The new possibilities provided by means of non-invasive cardiac imaging moved the heart back into the interest of radiology, and radiologists play an increasing role even in the management of patients suffering from non-coronary cardiac diseases. Despite the outstanding role of echocardiography in the diagnosis and follow-up of valvular diseases in clinical routine, cardiac MR plays an important and CT an increasing role in the management of patients suffering from valvular diseases. The most common and most important valvular diseases including aortic regurgitation and stenosis will be introduced.

Saturday

The role of imaging for diagnosis, treatment decision-making and treatment planning will be discussed as well. After valvular repair, CT evolved as the method of choice to assess possible infectious complications providing exact information about local and systemic manifestations of endocarditis. The importance of early diagnosis and treatment of endocarditis will be clarified and the value of modern imaging will be underlined. In the third part of the presentation insight into the role of CT angiography in the diagnosis and management of acute and chronic aortic diseases will be provided, focusing on aortic dissection and aneurysm. Within this presentation, a short overview about the most important diseases of valves, endocardium and aorta will be provided while defining the most important questions to be answered by imaging. Based on this, current and possible future role of CT and MR in these fields will be explained and basic tips for optimised imaging will be provided.

Learning Objectives:

1. To recognise the imaging presentation of the different forms of valvular disease.
2. To understand the causes and imaging presentations of endocarditis.
3. To describe the diagnostic evaluation and imaging presentation of common diseases of the great vessels, including aortic dissection and aneurysms.

Author Disclosure:

C. Loewe: Speaker; GE Healthcare, Bracco, Siemens.

A-643 09:32

C. Cardiovascular imaging: myocardium and pericardium

J. Bogaert; Leuven/BE (Jan.Bogaert@uz.kuleuven.ac.be)

Cardiovascular magnetic resonance (CMR) provides substantial, often unique, information in the evaluation of myocardial and pericardial diseases. This talk summarizes how CMR can be used to comprehensively study the pericardium and myocardium including tissue characterization, deep phenotyping, assessment of myocardial strain, and ventricular function, as well as the interaction between the pathologic pericardium and the remainder of the heart. The aim is to make the audience familiar with current use of CMR in daily clinical practice to assess this group of cardiac patients.

Learning Objectives:

1. To describe the diagnostic evaluation and imaging presentation of ischaemic heart disease.
2. To understand the diagnostic evaluation and imaging presentation of myocarditis.
3. To become familiar with the causes and imaging presentations of pericardial effusion.

08:30 - 10:00

Room F2

Emergency Imaging

RC 1317

Imaging of 'foreign bodies'

A-644 08:30

Chairperson's introduction

M. Pezzullo; Brussels/BE (martina.pezzullo@erasme.ulb.ac.be)

The presentation starts with an introduction of myself. Foreign bodies could be introduced in human body cavities voluntarily or accidentally. All the medical devices usually belong to the first category and to be familiar with their names, use and radiographic appearance is mandatory to recognise proper positioning and prevent displacement or migration. Accidental introduction of foreign bodies usually happens due to ingestion of food particles or small objects, especially in early childhood or in mentally impaired subjects. These objects can cause gastrointestinal tract complications due to impact or perforation, and a high level of suspicion is required to look for subtle signs as the presence of a foreign body is often unexpected.

Session Objectives:

1. To be familiar with names and image characteristics of commonly used surgical, and orthopaedic devices and materials.
2. To learn their proper positioning and early signs of postoperative complications.
3. To understand the imaging pathway in management of ingested foreign bodies.

A-645 08:35

A. Surgical and orthopaedic devices: are they really properly positioned?

E. Dick; London/UK (elizabeth.dick@imperial.nhs.uk)

This session will address the common surgical and orthopaedic devices that we encounter in everyday radiology practice. What do the clinicians consider to be optimal placement of each device? How can we assess if positioning is suboptimal? What kind of language should we use to describe devices? It will cover: (1) Lines and tubes: how to evaluate whether endotracheal tube and chest and abdominal drains are correctly placed, including: assessing the position of ETT beyond the vocal cords and satisfactory inflation of the ETT balloon. (2) Surgicel (surgical packing used in damage control surgery): how to evaluate the post-operative trauma abdomen even with Surgicel in place. (3) Neurosurgical devices: cervical and thoraco-lumbar spinal fixation: principles of stabilisation, how to evaluate whether correctly positioned, what language to use, complications including epidural haematoma and collections. (4) Orthopaedic devices: rib and pelvic fixation devices: how to assess the stability and considerations of neurovascular compromise.

Learning Objectives:

1. To become familiar with different types of commonly used surgical, neurosurgical and orthopaedic devices in clinical practice.
2. To understand how to evaluate their proper positioning.
3. To be familiar with imaging signs of incorrect implementation of neurosurgical and orthopaedic devices.

A-646 09:00

B. Foreign bodies in the gastrointestinal tract: the role of radiographs, US and CT

J.B.C.M. Puylaert; The Hague/NL (dr.jbcmputylaert@wxs.nl)

Did I swallow that?!: US and CT of sharp foreign bodies penetrating stomach and bowel. Accidental ingestion of sharp foreign bodies is a potentially life-threatening event with a reported mortality of 18%. If a sharp foreign body gets stuck in the oesophagus, the patient usually will notice its presence and seek medical help rapidly. However, when it reaches the stomach or bowel and penetrates the wall there, the ensuing symptoms are atypical and treacherous and serious delay may ensue. Perforating foreign bodies in the stomach and bowel are increasingly recognised by the use of US and spiral CT with multiplanar reconstructions and may be of great help in guiding minimal invasive treatment. The most frequently encountered penetrating sharp foreign bodies are chicken bones, fish bones and wooden sticks such as toothpicks. Most patients do not recall having swallowed such an object. Some patients wear denture plates rendering their palatum insensitive and the phenomenon is reported to be more frequent in mentally retarded patients. However, the majority of our patients were otherwise healthy. Over two-thirds have a history of a previous operation with kinking of bowel loops caused by adhesions, which locally inhibit the foreign body to "take the corner". Once a sharp object penetrates the wall of the stomach or bowel, the omentum and mesentery will try to wall-off the ensuing perforation. Often an abscess develops in the peritoneal cavity, in the liver or in the abdominal wall. Eventually, significant migration of the object may be the result. If the sharp foreign body is beyond reach of the endoscope, patients usually undergo laparotomy for removal of the foreign body and drainage of the abscess. This presentation will emphasise the role of US and CT in the diagnosis and in the minimal invasive treatment of these sharp foreign bodies.

Learning Objectives:

1. To be familiar with characteristics of commonly ingested abdominal foreign bodies.
2. To understand which imaging modalities are best suited for detection of foreign bodies in different clinical scenarios.
3. To recognise the first signs of early complications resulting from ingested abdominal foreign bodies.

A-647 09:25

C. Body packing: what to know about imaging and when should we suspect early complications?

M.K. Scherr; Munich/DE (michael.scherr@bgu-murnau.de)

Body packers, pushers and stuffers incorporate a variable amount of packs containing illicit drugs such as heroin and cocaine by ingestion or insertion vaginally or rectally. Every pack usually contains a lethal dose of narcotic. Due to increased luggage controls and body checks at customs and airports, this practice has a steady increase. Radiologists and emergency departments get confronted with body packers in two different ways. There is the forensic indication when suspects are presented by the authorities or the more familiar medical indication in cases of bowel obstruction or mainly severe intoxication. In both scenarios, the radiologist should know the legal issues and be prepared to perform the adequate examination and proper image interpretation to detect the body packs with a high degree of certainty. Already occurred or potential

complications like complete obstruction, package rupture or leakage have to be clinically and radiologically perceived. The diagnostic limitation of applied conventional x-ray is already known and increasingly replaced by (dose-reduced) computer tomography with its very high sensitivity. In some cases, already the CT scout view gives the clue. It is crucial to know about the CT presentation of packages depending on the manufacturing process and ingredients, where liquid packs become a diagnostic challenge. Attempts have been made to analyse body pack drug content by CT density or dual-energy appearance for further treatment planning. The treatment options are conservative under surveillance, laparotomy and intensive care with or without targeted antidote administration.

Learning Objectives:

1. To be familiar with the phenomenon of drug smuggling by body packing and its medical/legal issues.
2. To learn about imaging modalities and their limitations in case of body packing and variants.
3. To recognise potential or manifested complications in body packing.

09:50

Panel discussion: Common language with clinicians: how to report 'foreign bodies' presence

08:30 - 10:00

Room D

Special Focus Session

SF 13b

Paediatric MRI: can we make gadolinium superfluous?

A-648 08:30

Chairperson's introduction

M. [Alison](#); Paris/FR

Session Objectives:

1. To learn about the risk of gadolinium injection in paediatric patient.
2. To learn about the alternative sequences to study vessels or perfusion.
3. To appreciate the indication of intravenous gadolinium in common paediatric diseases.

A-649 08:35

Safety issues of intravenous gadolinium in children

F.E. [Avni](#); Lille/FR (favni@skynet.be)

A latest report (2017) estimates the adverse drug reaction (AdR) rate between 0.05 and 0.5%. AdR tends to be more frequent with linear GBCA. AdR is mostly mild to moderate and includes nausea, vomiting and urticaria. At approved doses, there is no evidence of renal toxicity even in neonates. 23 cases of nephrogenic systemic fibrosis (NSF) have been reported up to 2012 in children. All (most) cases were related to linear GBCA. No case has been reported in recent years. In the last 3 years, several studies have reported evidence of gadolinium deposits after repeated injections in various tissues, especially in the brain and bones. Most cases are related to the injection of linear GBCA. The rate of AdR and tissue deposits seems influenced by the thermodynamic and kinetics stability of GBCA. This rate is further influenced by pre-existing renal impairment or immaturity. All these data have generated a precautionary approach: (1) The necessity of injection should be evaluated case by case. (2) Exceeding the doses advised or repeating examinations with injections should be avoided, especially in patients with renal impairment. (3) Injecting GBCA in neonates or patients with significant renal impairment should be avoided. (4) Many hospitals should shift from linear to macrocyclic GBCA. (5) The EMA recommends withdrawing the acceptance of linear GBCA. Still, the need to test renal function previous to GBCA injection is presently not confirmed. (6) It is recommended to keep a record of cumulative contrast dose. (7) In general, it is advised to follow adults' recommendations.

Learning Objectives:

1. To learn about the existing literature on potential side effects of intravenous contrast in children.
2. To understand how underlying conditions may influence the risk for side effects.
3. To discuss the implications of the new knowledge for clinical practice in paediatric radiology.

A-650 08:53

The role of intravenous gadolinium in paediatric oncology

P.D. [Humphries](#); London/UK (humphriespaul@gmail.com)

Imaging plays a central role in the diagnostic pathway for children with cancer, being used to investigate clinically apparent lesions, screen children with cancer predisposition syndromes, stage known cancers and monitor treatment response. Magnetic resonance imaging has become a mainstay in the imaging of children with cancer, not only for CNS malignancies, but also for body tumours, owing to a move away from anatomical imaging using ionizing radiation. Intravenous MR contrast agent administration is frequently used as part of MR imaging protocols in paediatric oncology. With respect to body tumour imaging, there is a paucity of literature or systematic investigation of the diagnostic benefit of this, with practice being driven largely by expert opinion. Lesion characterization, anatomical boundary definition and relationships to vascular structures may all benefit from contrast administration, and dynamic-enhanced MR may be used to assess the effects of anti-angiogenic agents. Increasing utility of high-resolution unenhanced MR sequences and diffusion-weighted imaging enable MR protocols to be optimized such that IV contrast administration can be reduced. Additionally, other imaging modalities such as CE-US now provide a broader repertoire of imaging modalities to assess the vascular enhancement characteristics of lesions.

Learning Objectives:

1. To learn about the existing literature on the usefulness of intravenous MRI contrast in paediatric oncology.
2. To understand how protocols can be optimised to avoid the use of intravenous gadolinium in the diagnosis and follow-up of children with cancer.
3. To discuss how non-enhanced MRI sequences could replace gadolinium-enhanced sequences.

Author Disclosure:

P.D. Humphries: Research/Grant Support; Great Ormond Street Hospital Charity.

A-651 09:11

Assessment of musculoskeletal disorders: when is intravenous gadolinium necessary?

M. [Maas](#); Amsterdam/NL (m.maas@amc.nl)

Intravenous use of gadolinium in MSK is mostly seen in the diagnosis of oncology, infection and inflammation. It aids in detecting and characterising pathology, enhances depicting subtle areas of residual disease, and might make a contribution in assessing the response to therapy. Also, dynamic biomarkers might be beneficial and can be added to protocols. For some pathologies, gadolinium is described to be essential to delineate the diseased tissue (i.e. the synovial membrane in juvenile idiopathic arthritis); however for other diseases, this need might not be so prudent. Indications will be discussed during the lecture and will be illustrated with MR images. Novel techniques that might replace intravenous gadolinium-enhanced sequences should at least be equal in defining the presence or absence of pathology. In this lecture, special focus will be given to DWI as a non-contrast alternative: what is the rationale behind using DWI? What are the possible applications of imaging the synovial membrane using DWI? can DWI be used in bone tumour assessment? Literature regarding non-contrast MRI of synovitis, including DWI and inversion recovery techniques, will be addressed and images of our experience as well as images of other authors in the field will be shared.

Learning Objectives:

1. To discuss what are the indications of gadolinium injection in musculoskeletal disorders.
2. To understand how novel techniques may replace intravenous gadolinium-enhanced sequences for some indication (i.e. depiction of synovitis or ischaemia).
3. To discuss current knowledge and future potential of non-enhanced MRI techniques in detecting and grading of synovitis.

A-652 09:29

Brain imaging: when is intravenous gadolinium necessary?

K. [Karli Oguz](#); Ankara/TR (karlioguz@yahoo.com)

Since their first availability for clinical use, Gd-based MR contrast agents have been widely applied in neuroimaging. Apart from nephrogenic systemic fibrosis, there has been an increasing concern about Gd retention in the brain and its possible, yet unravelled, clinical effects among the physicians, patients and parents. Since we have an obligation not to harm paediatric patients, we have to review our contrast material usage policy carefully, present our indications strictly and fully take over the responsibility. By doing so, we should consider using techniques that do not necessitate administration of contrast material (such as arterial spin labelling-ASL instead of T2*EPI perfusion studies, non-contrast-enhanced angiography techniques) or supplementing

routine non-enhanced MRI sequences with other techniques to get more information on focal lesions such as diffusion-weighted imaging, ASL, SWI and MR spectroscopy. Cutting-edge imaging techniques including chemical exchange saturation transfer glucose imaging and magnetic particle imaging that do not need Gd injection will also be mentioned very briefly in this session. The indications such as infections, tumours and vascular diseases will be reviewed and contrast material use, especially on demyelinating and degenerative diseases, will be discussed.

Learning Objectives:

1. To learn about the indications of intravenous gadolinium for brain imaging.
2. To understand the role of non-enhanced sequences for brain vascular imaging.
3. To understand the role of non-enhanced sequences for brain perfusion imaging.

09:47

Panel discussion: How can we reduce our use of intravenous gadolinium in children?

08:30 - 10:00

Room G

Physics in Medical Imaging

RC 1313

Motion artefacts and their management in medical imaging

A-653 08:30

Chairperson's introduction

T. [Beyer](#); Vienna/AT

Session Objectives:

1. To learn about the origins of motion management in medical imaging.
2. To understand motion-related artefacts in medical imaging.
3. To learn about solutions and work-arounds.

A-654 08:35

A. Managing motion in CT: conventional approaches and motion compensating techniques

M. [Kachelrieß](#); Heidelberg/DE (marc.kachelriess@dkfz.de)

Diagnostic CT provides highly quantitative images with very high spatial resolution (0.3 mm isotropic) for complete anatomical areas in scan times as short as about 1 s. CT further routinely achieves an unprecedented temporal resolution of 63 ms, which is one-quarter of the rotation time, for complete anatomical regions. In many cases, this is sufficient to freeze patient motion. For quickly moving organs, even 63 ms may introduce motion blurring. Given the spatial resolution of 0.3 mm, objects moving at a speed of about 4 mm/s or faster will introduce blurring. Velocities of up to 70 mm/s occur in the heart. Typical methods to manage cardiac motion are prospectively or retrospectively gated single breath-hold scans. Recently, new algorithms that have the ability to compensate for the motion during image reconstruction are being developed: they have the potential to significantly increase the temporal resolution or to improve the dose usage. For lung imaging, the intrinsic temporal resolution of CT is sufficient. However, when 4D images are required, as it is the case for radiation therapy planning, the problem arises of how to generate moving images with a CT that freezes motion. The solution is to use respiratory gated scans with a very low pitch value. These methods, however, suffer from artefacts and high patient dose. Although dedicated motion compensation techniques for 4D CT could remove the artefacts and decrease the dose, the manufacturers provide no implementations. The lecture discusses the methods in use and those that are currently being developed.

Learning Objectives:

1. To learn about conventional techniques for motion compensation in CT.
2. To learn about new methods for motion compensation in CT.
3. To contrast the available and up-and-coming motion compensation methods in CT.

A-655 08:58

B. Managing motion in cone-beam CT (CBCT): conventional approaches and motion compensating techniques

P. [Paysan](#); Baden-Dättwil/CH (Pascal.Paysan@varian.com)

Motion management and motion-induced image artefacts in cone-beam CT (CBCT) imaging differ from CT due to inherent technical limitations of CBCT systems. While CT vendors have the possibility of increasing rotation speed to acquire complete slices within one motion state (e.g. breathing phase), the rotation speed is limited on CBCT systems. The major limiting factors are the readout frequency of a flat panel detector and the design-dependent absence of a slip ring (e.g. on C-Arm systems). Understanding the technical differences between CBCT and CT explains the different visual appearance of image artefacts and how motion management can be addressed on CBCT systems. One can distinguish two strategies that are to either reduce (freeze) the motion or in case of periodic motion to collect data from subsequent phases. Methods for motion reduction (immobilization) are fixations such as head frames, bite blocks, abdominal compression and breath-hold acquisitions, and also corrective methods for e.g. rigid (global and local) motion often applied on head scans. Periodic motion can be dependent on the use case, either handled by applying e.g. (prospective) gated CBCT or can be time-resolved reconstructed (4D CBCT). Time-resolved 4D CBCT reconstruction implies optimized acquisition parameters as well as the different algorithms to obtain the 4D reconstruction. Recent research explores new 4D reconstruction techniques such as HDTV or motion-compensated reconstruction that show very promising results in terms of image quality and dose usage. Knowing the technical differences of CBCT over CT helps to understand patient motion-induced image artefacts and the variety of technical solutions to reduce or resolve this motion.

Learning Objectives:

1. To learn about conventional techniques for motion compensation in CBCT.
2. To learn about new methods for motion compensation in CBCT.
3. To contrast the available and up-and-coming motion compensation methods in CBCT.

Author Disclosure:

P. Paysan: Employee; I am Varian Medical Systems employee.

A-656 09:21

C. Motion compensation in MR and PET imaging

C. [Kolbitsch](#); Berlin/DE (christoph.kolbitsch@ptb.de)

MRI provides images with excellent soft tissue contrast and a wide range of diagnostic parameters. Physiological organ motion (e.g. breathing, heartbeat or swallowing) can strongly impair image quality and hence diagnostic accuracy. Advances in MR hardware, plus novel image acquisition and reconstruction approaches, have strongly decreased MR scan times. Nevertheless, still up to 20% of MR scans experience severe motion artefacts and require repeated data acquisition. A wide range of techniques to minimise motion artefacts has been developed for different MR applications. In clinical practice, this is commonly motion prevention (e.g. asking a patient to hold their breath) and motion gating (i.e. restricting data acquisition to a certain motion state). More advanced motion correction approaches measure displacement of organs due to physiological motion and utilise this information to reduce motion artefacts during image reconstruction. PET images are affected by motion in two ways. Movement of organs can lead to blurring of the imaged structures and impair detectability, particularly of small features. In addition, motion can lead to a mismatch between attenuation correction maps and PET image data, resulting in severe errors in PET quantification. The recent introduction of simultaneous PET-MR now offers us the possibility to improve PET image quality and accuracy by utilising MR-based motion information. In addition, PET and MR data can also be combined to improve motion estimation and motion correction.

Learning Objectives:

1. To learn about motion measurement and compensation in MR.
2. To understand how patient motion affects PET images.
3. To learn about how MR data can be used to motion-compensate PET images, in MR/PET.

09:44

Panel discussion: How to optimise motion management in different imaging modalities?

Postgraduate Educational Programme

08:30 - 10:00

Room K

Professional Challenges Session

PC 13

Closing the gap between education and clinical practice for radiographers

A-657 08:30

Chairpersons' introduction (part 1)

K.G. [Vikestad](mailto:karivi@hioa.no); Oslo/NO (karivi@hioa.no)

This session, professional changes, focuses on the gap between education and clinical practice in radiography. At the end of the session, we will discuss the challenges and aim to come up with suggestions to reduce this gap. Three speakers are invited; they will present their perspective on the topic to open the minds of the audience and provide some new thoughts. The speakers are: Anne Bjørnstad, Norway; Eric Wolker Van Der Weij, the Netherlands; and Louise Rainford, Ireland. The speakers represent both the clinical and educational field of radiography. Anne will present how the clinical field views the competence level of the newly graduated radiographers when they start working at Oslo University Hospital and what kinds of competence are important for the clinical field right now. She will also provide some reflections on whether or not specialisation should be part of the bachelor's degree. Eric will give a presentation about a new method for preparing students for clinical practice. They have started using this method at his university, and he will share his thoughts and experiences in using this method. The title of the presentation by Louise is "Tools for success - academic and clinical practice working together". Her focus will be on how to emphasize variation of combined education and training, how to explore collaboration between hospitals and universities, and finally how undergraduate research can enhance academic/clinical relationships.

Session Objectives:

1. To understand the need for updated methods of training radiographers in the context of modern technology.
2. To discuss existing differences and controversies in the education system and teaching methods.
3. To explore possible ways of collaboration between academic institutions and hospitals for optimal education.

A-658 08:33

Chairpersons' introduction (part 2)

M. [Raissaki](mailto:mraissaki@yahoo.gr); Iraklion/GR (mraissaki@yahoo.gr)

Competence refers to what a health specialist is capable of doing in his/her daily clinical practice. To achieve competence, a health specialist in a radiology department should acquire sufficient knowledge of various aspects of anatomy, physiology, physics, radiography and medicine. Performance refers to what a health specialist actually does. Performance is associated with much more than knowledge including ethics, interpersonal relationships, clinical skills, empathy for patients and ability to perform diagnostic tests as safely and efficiently as possible. Living in the era of evidence-based medicine, personalized medicine and ALARA has enhanced the role of the radiographer into a highly-skilled health specialist coping with multiple tasks in demanding environments. Academic activity composes a triangle formed by research, teaching and clinical practice. Teaching is considered one of the most challenging and endangered aspects of academic activities because of continuous changes in the methods of education, technology and patient management. Excellence in performance is the ultimate goal of education throughout pre- and postgraduate teaching programmes, and the possibility of new learning platforms might prove useful in the effort to close the gap between education and clinical practice for radiographers.

Session Objectives:

1. To understand the need for updated methods of training radiographers in the context of modern technology.
2. To discuss existing differences and controversies in the education system and teaching methods.
3. To explore possible ways of collaboration between academic institutions and hospitals for optimal education.

A-659 08:35

Education vs clinical practice

A. [Bjørnstad](mailto:Anne.Bjornstad@oslo-universitetssykehus.no); Oslo/NO (Anne.Bjornstad@oslo-universitetssykehus.no)

Newly qualified diagnostic radiographers' knowledge, skills and competencies do not comply with the expectations and demands of the health care sector in Norway. Continual developments in technology and the changing role of the

radiographer create a need for restructuring of radiography education. To ensure that newly qualified diagnostic radiographers meet the expectations of the clinical site, the Learning outcomes of radiography education should be reevaluated. The level of clinical competencies diagnostic radiographers are expected to have achieved on completion of their education should be revised. This process cannot be initiated without a closer evaluation of the employer's role and responsibility. The employer should consider how the training of both students and newly qualified radiographers is organized. The evaluation of the required competencies of a clinical diagnostic radiographer should be an ongoing and dynamic process. To ensure satisfactory quality of both the academic studies and the clinical training, the collaboration between the educational institutions and clinical placement locations should be improved. Also, the competence of the clinical practice supervisors should be strengthened. Technological advances and the increasing complexity of radiographic procedures demand a continuous increase in competencies beyond the bachelor education. This raises the question; should the bachelor degree include specialization in specific areas within the field of diagnostic radiography or should this remain as a mandatory part of continuing professional development.

Learning Objectives:

1. To understand the different perspectives of theoretical education and practical training of radiographers.
2. To appreciate means of rapid acquisition of clinical skills during education.
3. To discuss the possibility and potential of sub-specialisation during education.

A-660 08:58

How can new teaching methods be implemented?

E. [Wolters van der Weij](mailto:e.m.wolters.van.der.weij@pl.hanze.nl); Groningen/NL (e.m.wolters.van.der.weij@pl.hanze.nl)

Serious Gaming! Didactics is the scientific discipline that deals with the question of how teachers can train knowledge, practical skills and attitude to students. Thirty years ago, education was more teacher controlled which is often associated with passive learning. Currently, activating or self-directed learning are the didactic methods which place the student more in a central position. Self-directed learning is a process in which the student himself takes the initiative for the learning process: the student plans, tests, evaluates and reflects with or without the help of others. Recent scientific literature indicates that contemporary or present-day young people (the so-called network generation) learn in a different way. Authenticity, multitasking, interactivity and gaming are some key concepts. Education does not have to be entirely different, but could be better adapted to this generation of students by new forms of education like serious gaming. The department of Medical Imaging and Radiation Therapy (MIRT) of the Hanze University of Applied Science has started implementing serious gaming in their educational programme in 2015. How and to what extent can serious gaming be used in the Dutch education system for radiographers as a new didactic instrument whose implementation may lead to improvement, or complement or replace current traditional approaches and methods?

Learning Objectives:

1. To understand the different pedagogical methods available for the education of radiographers.
2. To discuss the advantages and disadvantages of expert lectures for education.
3. To demonstrate how EBP can be integrated into the training curriculum.

A-661 09:21

Tools for success: academic and clinical practice working together

L.A. [Rainford](mailto:louise.rainford@ucd.ie); Dublin/IE (louise.rainford@ucd.ie)

This presentation will address the three learning outcomes listed; the principal focus of the talk will be on undergraduate radiography education. An overview will be provided on how education and clinical training of radiography students vary across academic institutions, both within Europe and also internationally, and the implications of these variations upon the profession. The presenter will explore potential best practice models for collaboration between clinical centres and universities in the delivery of radiography training. Reflection upon day-to-day considerations required to run local and national training programmes will be included. Practical difficulties will be discussed and possible mechanisms for enhance into radiography training proffered. A discussion of how undergraduate research activity could possibly support and enhance academic /clinical relationships will be offered to the audience to stimulate further conversation. Reference will be made to initiatives currently employed across a number of training programmes with the permission of the academic institutions.

Learning Objectives:

1. To emphasise variation of combined education and training among different academic institutions.
2. To explore collaboration between hospitals and universities for the

preparation of radiographers.

3. To discuss how undergraduate research can enhance academic/clinical relationships.

09:44

Panel discussion: What is the motivation for change?

08:30 - 10:00

Room M 1

Vascular

RC 1315

US and vascular disease: a perfect match

A-662 08:30

Chairperson's introduction

T. Jarczyk; Lublin/PL (tojarg@interia.pl)

Ultrasound is widely used in the diagnosis of vascular diseases. The technique is unique, as it provides not only imaging of vascular structures morphology but also haemodynamic information (Doppler technique). Its availability, safety and ability to examine real-time blood flow changes makes it very useful in a wide range of vascular pathology investigations. Among the disadvantages, high dependence on operator's personal skills and used equipment are the most important. Additional technical drawback, coming from limitations of ultrasound penetration in tissues (i.e. bones or gas) is also a negative casus. That is why the right placing of ultrasound in a diagnostic algorithm is so important. US examination usually goes first to make initial diagnosis of vascular pathology and to give the information of which modality should be the next. In some cases when US study excludes suspected vascular disorder, the diagnostic process may be stopped. A similar situation arises with vascular evaluation after treatment. US examination is a routine procedure after majority of open surgery or endovascular operations. Its outcome determines further diagnosis.

Session Objectives:

1. To review advantages and disadvantages of US.
2. To identify the role of imaging modalities in vascular disease.
3. To understand the role of US in post-treatment follow-up.

A-663 08:35

A. Abdominal aorta

D.A. Clevert; Munich/DE (Dirk.Clevert@med.uni-muenchen.de)

Abnormalities of the abdominal aorta and the visceral vessels may represent a diagnostic challenge in patients with acute or chronic clinical symptoms. In addition to the primary diagnosis in colour-coded duplex ultrasound, contrast-enhanced ultrasound (CEUS) with low mechanical index (low MI) is a new promising method in the diagnosis and follow-up of pathological aortic lesions. Colour code duplex ultrasound and CEUS with SonoVue® allows a more rapid and noninvasive diagnosis, especially in critical patients because of its bedside availability. This course describes the visceral vessels and focuses on the aetiology and the meaning of abdominal aortic pathologies. These pathologic findings were compared with colour-coded duplex ultrasound, CEUS and multi-slice computed tomography angiography (MS-CTA).

Learning Objectives:

1. To learn how to perform the examination and its role in diagnostic assessment.
2. To learn about US findings in AAA treatment planning and post-treatment evaluation.
3. To appreciate the role of CEUS and technological innovations in routine practice.

Author Disclosure:

D.A. Clevert: Advisory Board: Siemens, Samsung, Philips, Bracco. Speaker: Siemens, Samsung, Philips, Bracco.

A-664 08:58

B. Upper and lower limb: arterial district

B. Brkljačić; Zagreb/HR (boris@brkljacic.com)

B-mode ultrasound enables evaluation of arterial anatomy and of the vessel wall, detects early atherosclerotic changes, and allows detection of stenosis and occlusions, but tends to overestimate the degree of stenosis and should not be used for stenosis grading. Colour duplex Doppler ultrasound (CDUS) enables fast visualization of the vessel to be examined. It demonstrates haemodynamic changes, including velocity increase. Underestimation of disease is likely if only colour is used and the precise assessment of haemodynamic disturbances is impossible without a spectral analysis. In

general, CDUS has a high diagnostic accuracy, it is cheap and widely available, and there is no exposure to ionizing radiation and no contrast media injection. However, the examination is time consuming and requires high operator dependence. The thorough understanding of haemodynamics and physics is needed for adequate interpretation of Doppler findings. The factors influencing spectral morphology will be discussed in the lecture and the different types of spectra presented. Waveform changes will be presented in stenosis and occlusion. The typical findings of pseudoaneurysms and arteriovenous fistulas will be presented. Findings in acute occlusion and collateral flow will be discussed, both for native arteries and bypass grafts. The role of ultrasound in endovascular recanalizations will be discussed, both in planning and performing of the procedure and in the follow-up. Several clinical examples will be presented.

Learning Objectives:

1. To understand how to perform the examination and its role in diagnostic assessment.
2. To understand US findings for diagnosis and follow-up.
3. To underline tips and tricks to start your activity.

A-665 09:21

C. Upper and lower limb: venous district

H. Hoppe; Berne/CH (hanno.hoppe@web.de)

Duplex ultrasound is the initial imaging modality of choice evaluating upper and lower extremity veins. For upper extremity veins, most frequent indications are evaluation for thrombosis and vessel patency, pre- and postoperative mapping of arteriovenous fistula or graft, and venous access procedures. For lower extremity veins, duplex ultrasound is an adequate modality diagnosing venous valvular incompetence. Usually, this study is performed with the patient in an upright position and in addition manual compression manoeuvres are used to initiate reflux. Previously, cutoff values for reflux have been defined. Routinely, perforating veins are identified and the flow direction during compression is recorded. Duplex ultrasound is utilized to examine the extremity veins for venous outflow obstruction including chronic changes in deep or superficial veins post-venous thrombosis. However, additional imaging studies such as magnetic resonance imaging or computed tomography venography are increasingly used for reliable noninvasive identification of post-thrombotic changes and venous outflow obstruction and for treatment planning. In general, anatomic variations in superficial and deep veins are quite frequent and should be identified. Reporting should rely on a proper classification of venous disease including current anatomic description.

Learning Objectives:

1. To understand how to perform the examination and its role in diagnostic assessment.
2. To understand US findings for diagnosis and follow-up.
3. To underline tips and tricks to start your activity.

09:44

Panel discussion: When do we need additional imaging and which modality is best suited for the scenario?

08:30 - 10:00

Room M 2

E3 - ECR Master Class (Neuro)

E³ 1326b

Stroke: emergent large vessel occlusion (ELVO)

Moderator:

M. Pavia; Brescia/IT

A-666 08:30

A. Selecting ELVO patients for endovascular therapy

T. van der Zijden; Antwerp/BE (thijsvanderzijden@hotmail.com)

Endovascular treatment of large vessel occlusions in acute ischaemic stroke has proven to be effective. In an effort to achieve the best clinical outcome, and optimal cost-effectiveness as well, potential candidates for recanalization procedures should be triaged correctly. Besides a proper clinical workup, an adequate neuroradiological workup should be performed. On the one hand, selection of patients with a potential target for endovascular treatment (large vessel occlusion) should be done. On the other hand, exclusion of patients, who are not eligible for recanalization therapy, should be done as well. Imaging should not only be focused on exclusion of haemorrhage and/or stroke mimickers and on structural imaging of craniocervical arteries, but also give an idea about the extent of potential salvageable brain at risk versus already

infarcted brain. During the last years, in addition to plain CT and CT angiography of the brain, CT perfusion techniques and multiphase CT angiography have increasingly been used. Implementing these more advanced imaging tools in addition to basic neuroradiological workup enables theoretically a better prediction of clinical outcome after a potential recanalization procedure in a given patient, using qualitative and quantitative perfusion-based cutoffs and assessment of collateral vessel status. Advanced imaging techniques can also be used in the setting, immediately or early after recanalization, in an attempt to predict potential complications and/or clinical outcome.

Learning Objectives:

1. To learn about the correct indication/patient for endovascular therapy.
2. To understand the importance of clinical and neuroradiological work-up prior to the intervention.
3. To appreciate clinical relevance in terms of outcome measures applying state of the endovascular treatment for the right patient.

A-667 09:00

B. Advanced thrombectomy techniques

O. Jansen; Kiel/DE

Neurothrombectomy has been shown to be the primary choice of treatment in acute stroke-patients with large intracranial vessel occlusion. While the great randomised trials were performed mostly with the use of stent-retrievers or aspiration devices alone more recent papers have shown better recanalisation results in experimental and/or clinical studies. These so called advanced thrombectomy techniques mostly combine retrieval and aspiration techniques to result in fewer recanalisation maneuvers, shorter recanalisation time and less fragmentation of the embolus. While the choice of the best recanalisation technique is important for the recanalisation result periprocedural techniques (anaesthesia, stenting, medication) also show an important impact on clinical outcome. Additional endovascular or medical treatment is also requested in more rare stroke cause like underlying intracranial arterial stenosis or acute dissection of the extra- or intracranial arteries. Recent studies and secondary analysis have also shown that dedicated patient selection with advanced stroke imaging is less important in patients with short time window (<8hrs) but may extend the individual treatment window up to 24hrs.

Learning Objectives:

1. To learn about the spectrum of new and upcoming thrombectomy techniques.
2. To understand the importance of applying correct technique in individual patients.
3. To appreciate the increasing role of thrombectomy in ischaemic stroke therapy.

Author Disclosure:

O. Jansen: Consultant; Rapid Medical. Speaker; Stryker, Medtronic.

A-668 09:30

C. Is endovascular thrombectomy and medical therapy better than medical therapy alone?

S. Bisdas; London/UK (s.bisdas@ucl.ac.uk)

A tipping point has been reached in acute stroke management from evidence provided in recent clinical trials studying the efficacy of thrombectomy in ischaemic stroke. Almost the entire literature has studied anterior proximal occlusion, some studies have performed sub-analyses to clarify if the site of the clot can be used as outcome predictor. The evidence on the endovascular thrombectomy seems still heterogenous in method and underpowered for secondary outcomes. Interestingly, endovascular thrombectomy treatment is advocated in elderly patients whom will have a higher number of comorbidities. Notably, the majority of studies looking at the recanalisation rate in patients who had prior IV thrombolysis against those who had direct thrombectomy revealed that thrombectomy was more likely to successfully recanalise if IV thrombolysis had been administered first. Currently, some of the large 2015 trials and subsequent trials patients have often received a thrombolysis infusion whilst the thrombectomy is being undertaken. In patients with tandem occlusions, any endovascular treatment offered could be the best available treatment since IV thrombolysis has showed no significant benefit. Recent results have shown excellent long term outcomes, with no evidence of delayed complications or restenosis. Additionally, the quality of life score measured between the endovascular treatment and conventional therapy group showed a significant difference in favour of the treatment arm. This advocates the appropriate use of mechanical thrombectomy; however, the specific details about best clinical practise in these patients have yet to be answered.

Learning Objectives:

1. To learn about the current data and medical evidence of the available therapies.
2. To understand the role of individualised therapy concepts.

3. To appreciate the importance of interdisciplinary approach for ischaemic stroke therapy.

Author Disclosure:

S. Bisdas: Advisory Board; Image Analysis Group, Olea Medical, GE Healthcare. Consultant; Diagnose me. Founder; Society of Advanced Neuroimaging. Grant Recipient; NIHR BRC UK. Research/Grant Support; Olea Medical.

08:30 - 10:00

Room M 3

Special Focus Session

SF 13c

Drug elution or drug illusion in vascular disease

A-669 08:30

Chairperson's introduction

R.W. Günther; Berlin/DE

Advances of coronary artery recanalization have essentially influenced the treatment of peripheral artery disease (PAD). Following coronary PTA (1977) and bare metal stents (1988), the concept of local drug delivery was realized using drug-eluting stents (DES) in 2001 and drug-coated balloons (DCB) in 2006. The drugs used for local delivery were the cytotoxic paclitaxel and the immunosuppressive agent sirolimus and its derivatives, which prevent or inhibit vascular restenosis due to suppression of cell proliferation. The pharmacokinetics after different drug applications varies and the mechanism of cellular inhibition differs. In the treatment of PAD, we saw the stepwise development from exclusive mechanical techniques to additional local drug delivery using DCB, DES or bare metal stents combined with DCB before or after stent placement. Also, debulking procedures like percutaneous atherectomy plus DEB have been described. Apart from peripheral artery disease, the problem of restenosis can be approached by DEB also in other areas such as renal arteries, haemodialysis fistulas and transjugular intrahepatic porto-systemic shunts (TIPS). The basic aspects of drug release, biological reaction, clinical evidence and practical consequences in different vascular areas will be presented in this session, which is dedicated to a critical appraisal by showing the clinical evidence of current data as well as the pros and cons.

Session Objectives:

1. To learn more about drug elution and biological reaction.
2. To show the pros and cons of drug elution devices in coronaries, infrainguinal arteries and haemodialysis fistulas.
3. To critically analyse the published data and summarise the current evidence and indications regarding treatment.

A-670 08:35

Drug-eluting balloons and stents, technology and biological interaction: lessons learned from the coronaries

F. Kleber; Berlin/DE (post@fkleber.de)

Dilatation of arterial vessels leads to an increase in luminal and overall vessel dimensions, only partly counteracted by elastic recoil and dissection. Unfortunately, this effect is often short-lived since healing leads to vessel shrinkage. Stents, especially drug-eluting stents, can overcome recoil and shrinkage, but induce intimal hyperplasia, which in turn leads to late luminal loss. Also, late stent malapposition has been found in a sizeable number of treated segments promoting vessel thrombosis. Foreign body reaction and a persisting small thrombosis rate lead to a 5-year target lesion failure (TLF) rate of 13 to 26%. Stents with thinner struts seem to have better long-term results. To avoid such high TLF rates, drug-coated balloons (DCBs) were developed and clinically used to treat in-stent restenosis as well as de novo lesions. It could be shown experimentally and clinically that the most often used drug paclitaxel can induce late luminal gain, which after stenting is a untoward side effect, but without stenting helps to achieve good long-term results. Therefore even in small coronary arteries treated with DCBs, the target lesions revascularisation rate is very low (2.5%) and thrombosis is almost absent on dual antiplatelet therapy. However, excipients for drug-eluting balloons are different and have different efficacy. New drugs are in a late developmental stage and compete with paclitaxel. Future trials will shed light on which excipients and which drugs show the best results. However, even now, in many situations, DCBs are equal or even superior to stents in not jeopardizing the further course by foreign body reaction to the implants and thrombosis.

Learning Objectives:

1. To learn about the individual components of drug-coated balloon catheters and their importance.

2. To summarise key messages from non-clinical studies with coronary balloons and stents.
3. To gain an overview of the key lessons from randomised clinical trials in coronary.

Author Disclosure:

F. Kleber: Advisory Board; Corvia Massachusetts. Consultant; BBraun Germany, Ancora Heart California, Corvia Massachusetts.

A-671 08:50

Drug-eluting balloons and stents in femoropopliteal and crural lesions: pro

F. Fanelli; Rome/IT (fabrizio.fanelli@uniroma1.it)

Drug-eluting stents-DES and drug-eluting balloons-DEB represent "two sides of the same coin" for the ability to deliver locally anti-proliferative drugs. The main goal of drug is to inhibit the neo-intimal reaction. DES and DCB have been evaluated in different studies, both showing a significant increase in primary patency (PP) rate when compared to standard devices. Three randomised trials, using different DCBs, were performed to compare DCB vs. angioplasty (PTA) in de-novo femoro-popliteal lesions. PP at 1-year ranged between 73.5% and 89.0%; the 4-year data of In.Pact SFA trial showed a PP of 69.5% (DCB) vs. 45.1% (PTA) $p < 0.001$, and freedom from clinically-driven target lesion revascularisation (CD-TLR) of 76.8% (DCB) vs. 70.4% (PTA) $p = 0.039$. Many other studies have been performed in different setting such as diabetic patients, in-stent restenosis, long lesions, chronic total occlusions and all of them showed always a better outcome using DCB. The efficacy of DES, in the femoro-popliteal region, was confirmed by the Zilver-PTX trial where PP after 5-year is 64.9% compared to a low 19% for PTA. This study showed also a superior PP when provisional DES was compared to provisional bare metal stent (BMS): 72.4% vs 53.0% respectively. These superior results have been also supported from several other studies. In the infrapopliteal region DCB has not yet demonstrated their superiority in comparison to the standard PTA, but several randomised controlled trials (RCT) are ongoing. DES showed their efficacy in several studies with a PP at 1 year comprised between 75% and 86%.

Learning Objectives:

1. To learn about the difference between the various drug-eluting platforms and medication.
2. To understand the difference between technical success, patency and clinical outcome in patients treated with endovascular technologies.
3. To understand the advantages of drug-eluting balloons and stents in femoropopliteal and crural lesions.
4. To learn which patients and which lesions derive the most benefit from their use.

Author Disclosure:

F. Fanelli: Speaker; Medtronic, Cook, WL Gore & Associates, Spectranetics.

A-672 09:10

Drug-eluting balloons and stents in femoropopliteal and crural lesions: contra

J.A. Reekers; Amsterdam/NL (j.a.reekers@amc.uva.nl)

Restenosis after balloon angioplasty or stenting has been a major drawback of angioplasty. Depending on the vessel area and length of the lesion, restenosis due to intimal hyperplasia is 20%-60% in the first 12 months. Inhibition of intimal proliferation with local drug administration, either with a drug-eluting stent or a drug-releasing balloon, looks like a promising solution to this problem. Paclitaxel and sirolimus have both been shown to be able to inhibit local intimal proliferation and thereby to prevent or reduce local intimal hyperplasia after angioplasty. Drug elution therefore seems, and is also marketed accordingly, the way forward. Unfortunately, there has been no study to show the clinical benefit of local drug elution. Prevention of intimal hyperplasia is a pseudo end point. The real end points are: improvement of walking distance in a patient with intermittent claudication or prevention of amputation in a patient with critical limb ischaemia. Until this has been proven in a prospective randomised trial, drug elution is still an illusion.

Learning Objectives:

1. To understand the limitations of drug-eluting balloons and stents in femoropopliteal and crural lesions.
2. To be familiar with potential complications from their use.
3. To become familiar with a critical review of the current literature and to understand how marketing of new endovascular technologies works.

A-673 09:30

Effect of drug-eluting balloons and stents in haemodialysis access lesions: where is the evidence?

K. Katsanos; Patras/GR (katsanos@med.upatras.gr)

Creation of hemodialysis access in the form of either an autologous arteriovenous fistula or prosthetic arteriovenous graft is one of the commonest vascular procedures and serves as the "lifeline" for dialysis patients. Percutaneous techniques are widely practised for salvage of failing native or synthetic arteriovenous shunts. Nonetheless, balloon angioplasty is frequently associated with recurrent, aggressive, vessel restenosis and early failure. The pathobiology of arteriovenous stenoses is completely different from arterial atherosclerosis, and is typically characterised by aggressive venous neointimal hyperplasia associated with adventitial myofibroblast proliferation and striking fibrosis on the background of repeated endothelial injury, altered hemodynamic shear stress, systemic uremia and oxidative stress. Cutting or high pressure balloons, covered stents or stent-grafts, and paclitaxel-coated balloons have been extensively tested and investigated with the aim to improve immediate anatomical and long-term clinical results. There is high quality of randomised evidence that placement of covered stents for the treatment of draining vein stenosis may prolong the patency of failing synthetic arteriovenous grafts. There is also evidence from mostly proof-of-concept pilot studies that paclitaxel-coated balloons may inhibit restenosis and improve mid-term patency of failing arteriovenous fistulas and grafts when applied in combination with adequate mechanical dilatation of the underlying stenosis. The results of different clinical studies for each device category will be reviewed and a good practice algorithm for percutaneous salvage of failing arteriovenous shunts will be proposed based on anatomical and procedural parameters.

Learning Objectives:

1. To understand the pathophysiology of restenosis and mode of failure of haemodialysis circuits.
2. To analyse amassed clinical evidence about drug-coated balloons and stents in haemodialysis fistulas.
3. To learn about the limitations of current drug-coated balloon technologies.

Author Disclosure:

K. Katsanos: Consultant; MEDTRONIC. Speaker; BOSTON SCIENTIFIC.

09:45

Panel discussion: Scientific evidence and consequences for daily practice

08:30 - 10:00

Room M 4

E³ - ECR Academies: Tips and Tricks in Pancreatic and GI Tract Imaging

E³ 1322

New challenges of pancreatitis

A-674 08:30

Chairperson's introduction

G. Zamboni; Verona/IT (gzamboni@hotmail.com)

The 2012 Revised Atlanta Classification categorizes acute pancreatitis as interstitial oedematous or necrotizing, introducing a uniform terminology for describing its imaging features and fluid collections. Collections are defined based on their timing (early phase <4 weeks from onset; late phase ≥4 weeks). Interstitial pancreatitis may present with acute pancreatic fluid collections in the early phase, which can later either resolve or evolve into pseudocysts. Necrotizing pancreatitis presents with necrosis (pancreatic, peripancreatic, or combined pancreatic and peripancreatic); the acute necrotic collections may later evolve into walled-off necrosis. Autoimmune pancreatitis (AIP) is increasingly recognized, accounting for ≤6% of cases of chronic pancreatitis. Type 1 AIP, more common, is a systemic IgG4-associated disease with elevated IgG4-positive cells in the serum, pancreas, and other organ. Type 2 AIP involves primarily the pancreas, without IgG4-positive cells. On MR, the affected pancreas appears enlarged, either focally or diffusely, hypointense on T1 and hyperintense on T2, with a hypointense capsule-like rim. MPD shows diffuse or focal stenosis. The parenchyma has reduced and delayed enhancement. Pancreatic cystic lesions include neoplastic and non-neoplastic cysts. A combination of imaging findings and demographic, clinical and laboratory data is necessary for a correct diagnosis. MR has higher diagnostic accuracy than CT in lesion identification, characterization and differentiation between benign and malignant lesions. Findings useful for characterization include lesion site, cystic pattern, presence of septa, wall thickness, calcifications and their morphology, mural nodules, communication with the ductal system and dilation of the MPD. Several international guidelines address their diagnosis and management.

A-675 08:35

A. Understanding the Atlanta 2012 classification of acute pancreatitis W. Schima; Vienna/AT (wolfgang.schima@khgh.at)

According to the Revised Atlanta Classification of 2012, acute pancreatitis is categorized as interstitial oedematous or necrotizing pancreatitis. In interstitial oedematous pancreatitis, approximately 50% of patients develop acute peripancreatic fluid collections early (< 4 weeks from onset). In the late phase (≥ 4 weeks), these either resolve or evolve into pseudocysts, which are hypodense on CT and hyperintense on T2w MRI. Treatment of pseudocysts is only indicated in symptomatic patients or if complications (gastric outlet obstruction, cholestasis or haemorrhage) develop. Necrotizing pancreatitis may present either with combined pancreatic and peripancreatic (most common) or with pancreatic necrosis or with peripancreatic necrosis alone. Acute necrotic collections may evolve into walled-off necrosis (WON) in the late stage. A WON containing digested fat and parenchyma must not be confused with a pseudocyst. They are similar on CT, but US/MRI reveals the predominantly solid nature of WON. Secondary infection of necrotizing pancreatitis results in high mortality. Imaging diagnosis of infection is difficult. Gas within a collection is specific, but not sensitive. If feasible, CT-guided abscess drainage is recommended. Necrotic collections with debris require a more aggressive approach. In general, MDCT for diagnosis of pancreatitis should be performed no less than 2-3 days from clinical onset, because development of necrosis may take some time. In case of suspected biliary pancreatitis, early MRCP guides further treatment (endoscopic stone removal). The Revised Atlanta Classification system introduced a uniform terminology for imaging features of pancreatitis. Contrast-enhanced CT is the primary tool of diagnostic imaging and image-guided therapy. MRCP characterizes fluid collections and delineates ductal abnormalities.

Learning Objectives:

1. To be aware of the new terminology for the evaluation of acute pancreatitis.
2. To learn about how to report imaging findings.
3. To understand the relationship between imaging findings and prognosis.

A-676 09:03

B. Autoimmune pancreatitis and its relatives G. Morana; Treviso/IT

"no abstract submitted"

Learning Objectives:

1. To understand the various forms of autoimmune pancreatitis, especially cases that are associated with extra pancreatic disease.
2. To learn about the usual and unusual appearance of autoimmune pancreatitis.
3. To understand the principles of the follow-up.

A-677 09:31

C. Tough clinical cases of cystic pancreatic lesions M.A. Ball; Sutton/UK (mantoniettaball@icr.ac.uk)

Pancreatic cystic lesions (PCL) include epithelial and non-epithelial neoplasm and non-neoplastic cysts and are classified as benign, potentially malignant and malignant, according to WHO. Imaging has a key role in detection and characterization; however, the final diagnosis is provided by the integration of imaging findings with demographic, clinical and laboratory data, including cystic fluid analysis obtained by EUS. MR has higher diagnostic accuracy than CT for detection and characterization. At imaging, several findings, such as the localization, the cystic pattern (unilocular, multilocular), the presence of septa, wall thickness, calcifications (central or peripheral, thin or thick), mural nodules, communication with the pancreatic ducts and the concomitant dilatation of the main pancreatic duct (MPD) may allow the differential diagnosis between PCLs and may also be suggestive of malignancy. However, lesions smaller than 3 cm may lack specific morphological features. Neoplastic cysts such as serous cystadenoma (most common with benign behaviour) followed by mucinous cystic and intraductal papillary mucinous neoplasms (potentially malignant or malignant neoplasm) must be differentiated from non-neoplastic cysts such as pancreatitis-associated pseudocysts (most common) to provide the most adequate treatment and to avoid unnecessary surgery. For the mucinous neoplasm, imaging findings highly suggestive of malignancy are: for branch-duct IPMN, mural nodules and dilatation of the MPD; for main duct-IPMN, MPD larger than 1cm, mural nodules and symptoms; for mucinous cystic neoplasm, large lesion (>4cm), mural nodules, mass-forming lesions and peripheral calcifications. Guidelines (Fukuoka Guidelines 2012, European Guidelines 2013 and American Gastroenterology Association Guidelines 2015) are available to assist in decision-making.

Learning Objectives:

1. To understand how to report a cystic pancreatic lesion, including recommendation for imaging strategy.
2. To become familiar with the most common cystic neoplasms of the pancreas.
3. To learn how to differentiate neoplasms and inflammatory cystic lesions of the pancreas.

08:30 - 10:00

Room M 5

Transatlantic Course of ESR and RSNA (Radiological Society of North America): Sports Imaging

TC 1328

Upper extremity sports injuries

Moderators:

L.W. Bancroft; Orlando, FL/US
A.J. Grainger; Leeds/UK

A-678 08:30

A. Shoulder injuries in the throwing athlete

L. Steinbach; San Francisco, CA/US (lynn.steinbach@ucsf.edu)

Overhead throwing athletes develop significant abnormalities as a result of acquired adaptations to the extremes of motion in the dominant shoulder. These abnormalities may eventually result in an inability to throw with the same velocity, the so-called "dead arm" syndrome. These abnormalities involve tendons, ligaments, labrum, muscles, nerves, vessels, and bones. This presentation will review the biomechanics of throwing forces as they relate to the shoulder. The MR imaging characteristics of the resultant abnormalities in the labroligamentous structures and the rotator cuff will also be highlighted. This will be followed by a brief discussion of pathologic and normal developmental changes in the shoulders of skeletally immature throwing athletes. As a prototype, the throwing motion in baseball occurs over a period of approximately 2 seconds and is divided into six stages: wind up, cocking, early and late acceleration, deceleration, and follow through. The late cocking, acceleration, and deceleration phases produce the greatest stress on the glenohumeral joint structures. As with other throwing sports, the superior labrum and rotator cuff are often affected by these extreme forces.

Learning Objectives:

1. To understand the biomechanics of throwing forces as they relate to the shoulder.
2. To become familiar with rotator cuff and labroligamentous injury patterns caused by overhead sports.
3. To appreciate pathologic and normal developmental changes in skeletally immature throwing athletes.

A-679 09:00

B. Soft tissue wrist injury in the athlete

C.W.A. Pfirrmann; Zurich/CH

Wrist injuries account for 5 % of sports injuries. In the young athlete, fractures are the most common injuries. The hand and wrist are the most common sites for fracture in the young athlete. Physeal injuries are typical overuse injuries in gymnasts. Chronic stress reactions with widening of the growth plate are seen in the distal radial and less common in the ulnar growth plate. Injuries to the TFCC in the athlete occur in acute trauma and with overuse. TFCC injuries are an important cause for ulnar-sided wrist pain. The differential diagnosis includes ulnar styloid impaction syndrome, ulnar impingement syndrome and tenosynovitis of the extensor carpi ulnaris tendon. Injury to the interosseous ligaments may lead to carpal instability. Chronic injury of the intrinsic or extrinsic ligaments of the wrist may cause ganglion cyst formation.

Learning Objectives:

1. To learn about the patterns of injury seen at the wrist in athletes.
2. To understand the advantages and disadvantages of different modalities for imaging the athlete's wrist.
3. To recognise the imaging appearances of cartilage and ligamentous injury at the wrist.

A-680/A-681 09:30

C. Interactive case discussion

L. Steinbach¹, C.W.A. Pfirrmann²; ¹San Francisco, CA/US, ²Zurich/CH
(lynn.steinbach@ucsf.edu)¹, (christian.pfirrmann@balgrist.ch)²

This session will show cases related to upper extremity sports injuries of the shoulder.

Learning Objectives:

1. To appreciate common patterns of athletic injury in the shoulder and wrist.
2. To become familiar with the techniques available and imaging appearances of shoulder and wrist athletic injury.
3. To consolidate the knowledge gained from the session with interactive cases of upper limb athletic injury.

10:30 - 12:00

Room A

E³ - ECR Academies: Interactive Teaching Sessions for Young (and not so Young) Radiologists

E³ 1421

Brain tumours

A-682 10:30

A. Paediatric brain tumours

M.I. Argyropoulou; Ioannina/GR (margyrop@cc.uoi.gr)

Primary brain tumours in childhood are the second most common malignancy after leukaemia. The presenting symptoms depend on age with macrocephaly and failure to thrive in infants, and headache, morning vomiting, diplopia, ataxia motor and sensory deficits, seizures and endocrinological symptoms in older children. Brain tumours may be of glial origin (astrocytomas, ependymomas), neuronal or neuroglial (gangliogliomas, gangliocytomas, DNET), embryonal (PNET, ATRT) and from germ cells (germinomas, teratomas). Tumours arising in the sellar and parasellar region (craniopharyngiomas, hypothalamic hamartomas and pituitary adenomas) may also occur. Neurinomas and meningiomas are rare in children arising mainly in the context of neurofibromatosis type II. Secondary brain tumours arise mainly from CSF seeding, while haematogenous metastases are rare. MRI is the modality of choice for the diagnostic workup of brain tumours. Imaging protocols may include T2W, T1W plain and contrast-enhanced images, diffusion tensor imaging, dynamic susceptibility-weighted contrast-enhanced perfusion imaging (DSC), functional MRI (fMRI) and MR spectroscopy (MRS). Brain tumours may be heterogeneous with cystic and solid components. The latter appears with low signal on T1W and high signal on T2W images. A low signal intensity on T2W images, associated with restricted diffusion and increased perfusion indexes on DSC, may be suggestive of a more aggressive tumour. Increased choline and lactate and decreased N-acetyl aspartate in MRS are also suggestive of malignant tumours. Tractography and f-MRI are useful for preoperative evaluation to assess major white matter tracts and eloquent areas of the brain related with the tumour.

Learning Objectives:

1. To become familiar with different paediatric brain tumours.
2. To learn the imaging criteria for differentiation.

A-683 11:15

B. Adult brain tumours

P.C. Maly Sundgren; Lund/SE (Pia.Sundgren@med.lu.se)

Glioblastomas are the most common malignant neoplasms and together with metastatic tumours comprise half of all malignant tumours in the adult population. The latest WHO classification is from 2016 and several changes have occurred with respect to the classification of brain tumours. The grading of tumours presumes biological behaviour or phenotype of a lesion and is of high importance clinically by guiding therapy selection: adjuvant radiation, chemotherapy, or surgical or palliative treatment of brain tumours. MRI is considered the standard modality for the diagnosis and prognosis of brain tumours, based primarily on gadolinium (Gd) enhancement. However, this concept has become more and more challenging due to the fact that not all high-grade gliomas demonstrate Gd enhancement, while low-grade tumours might enhance in up to 30% of the cases. This lecture will review the more common primary and secondary brain tumours in adults and their imaging characteristics on CT and MRI. The use of advanced imaging for diagnosis and treatment follow-up will be discussed.

Learning Objectives:

1. To become familiar with the different types of brain tumours.
2. To learn the imaging criteria for differentiation.

Author Disclosure:

P.C. Maly Sundgren: Investigator; I conduct research on advanced MR applications on brain tumors and brain metastasis. Research/Grant Support; I have grants from Swedish Research Council, Swedish Cancer Foundation and regional Research Funds for Advanced MR imaging techniques in brain tumors and treatment effects. Speaker; I speak at international meeting on advanced imaging brain tumor treatment effects.

10:30 - 12:00

Room B

ESR meets Portugal

EM 2

Discovering Portuguese radiology: past, present, future

Presiding:

F. Caseiro Alves; Coimbra/PT
B. Hamm; Berlin/DE

A-684 10:30

Introduction: SPRMN President address

F. Caseiro Alves; Coimbra/PT (caseiroalves@gmail.com)

A brief presentation of the past and present history of Portuguese Radiology will be made on behalf of SPRMN. Relevant contributions to angiography will be highlighted as well as a brief overview of the Portuguese Society and its main activities. The future will be presented by the three chosen young lecturers on topics of their research domain.

Session Objectives:

1. To revisit the major Portuguese contribution for radiological sciences.
2. To provide a selection of present and future clinical research on imaging.
3. To explain and display the musical heritage through the Portuguese guitar.

A-685 10:35

Imaging biomarkers for diffuse liver disease

M.M. Franca; Porto/PT (mariamauela.franca@gmail.com)

Fat, iron deposits and fibrosis can be found in different diffuse liver diseases. Because liver biopsy has several limitations, MR imaging biomarkers have been developed for fat and iron quantification, and to stage liver fibrosis. Quantification of proton density fat fraction (PDFF) can be accurately performed with multi-echo chemical shift-encoded (MECSE) gradient echo MR sequences, corrected for T1 relaxation, T2* decay effect, noise and fat spectral complexity. Quantification of liver iron content is needed to detect and stage iron overload, and also to monitor iron-reducing treatments. Iron MR quantification may be performed with R2/R2* relaxometry techniques. Simultaneously, quantification of hepatic fat (PDFF) and iron (R2*) can be achieved with MECSE sequences, which are advantageous in diffuse liver diseases, as fat and iron frequently coexist in the liver parenchyma. MR elastography can detect and stage significant or advanced fibrosis and cirrhosis, with high accuracy, in different diffuse liver diseases. All of these MR imaging biomarkers are increasingly being used for the non-invasive assessment of hepatic steatosis, siderosis and fibrosis for evaluating and monitoring diffuse liver diseases.

Learning Objectives:

1. To understand the need for non-invasive imaging biomarkers to accurately detect and quantify hepatic steatosis, iron overload and fibrosis, in different diffuse liver diseases.
2. To review the different MR imaging techniques to evaluate and to quantify imaging biomarkers of liver steatosis, iron overload and fibrosis.
3. To discuss the role and clinical relevance of MR imaging biomarkers for the evaluation of diffuse liver diseases, in different clinical scenarios.

A-686 10:55

Prostate artery embolisation (PAE) for benign prostate obstruction (BPO): the paradigm shift

T. Bilhim; Lisbon/PT (tiagobilhim@hotmail.com)

Prostate artery embolisation (PAE) has been proven to be safe and effective to relieve lower urinary tract symptoms (LUTS) related to benign prostate obstruction (BPO). Knowledge of the anatomy of the prostate arteries (PAs) is cornerstone to PAE. Pre-procedural CT-angiography (CTA) and intra-procedural cone-beam CT (CBCT) have been proven to be reliable tools to study the PAs. Identification of the PAs is generally performed under fluoroscopy. Developing alternatives are the use of fusion imaging with the pre-procedural CTA images, overlay with the intra-procedural CBCT images and

Postgraduate Educational Programme

the use of vessel-tracking software that automatically identifies the PAs. Up to 25% of patients may have clinical failure after PAE. Most of these patients are nonresponders, with a minority being relapsers. Thus, it is very important to define the predictors of clinical outcome to help exclude those patients less likely to respond to PAE. Predictors of better clinical outcome that have been identified include: younger age; lower baseline LUTS severity; patients under acute urinary retention; and adenomatous-dominant BPO. Bilateral PAE has been proven to be better than unilateral PAE. MR-detected ischaemia after PAE, PSA values 24 hours after PAE, prostate volume reduction and clinical outcome have been shown to be correlated. Prognostic quantification with perfusion imaging of the prostate, developing catheters and embolic agents/sizes are some of the future directions in the investigative field of PAE on the path to inclusion in the guidelines for the management of patients with symptomatic BPO.

Learning Objectives:

1. To learn about the anatomy of male pelvic arteries relevant for selective embolisation of the prostate.
2. To understand what imaging modalities can be used for guidance inside the pelvis to find the prostate arteries.
3. To become familiar with clinical outcome and predictors of treatment response after prostate artery embolisation.

Author Disclosure:

T. Bilhim: Advisory Board; Merit Medical.

A-687 11:15

Cardiac CT from anatomy to functional information: comprehensive CAD evaluation

H. Marques; Lisbon/PT (h919741379@gmail.com)

Coronary CTA has been a fast growing imaging technique to assess the coronary arteries non-invasively. Recently, some guidelines consider it to be the first-line test in patients with non-acute chest pain of possible cardiac origin, regardless of the pre-test probability of CAD. Intense research preceded and accompanied its evolution, from a rule-out test to an all-in-one coronary disease assessment with prognostic validation. We will follow this route and the scientific evidence behind it: from stenosis to plaque presence, segment involvement and plaque characteristics; transluminal gradient, "first-pass" perfusion CT and dual-energy "perfusion" CT; virtual fraction flow reserve (FFR);- evaluation of myocardial viability with CT. Finally, we will focus on artificial intelligence and machine learning techniques applied in this context and how they will be disruptive.

Learning Objectives:

1. To learn and understand the different anatomic information regarding CAD derived from coronary CTA and its prognostic relevance.
2. To review different cardiac CT techniques to access functional relevance from anatomic stenosis and its clinical evidence.
3. To integrate cardiac CT derived data for a comprehensive CAD evaluation.

Author Disclosure:

H. Marques: Employee; Cleerly Inc.

A-688 11:35

The soul of Portugal: Facts and sounds of the Portuguese guitar

F. Caseiro Alves, B. Costa, R. Silva, N. Botelho; Coimbra/PT (caseiroalves@gmail.com)

A historical perspective of the Portuguese guitar will be presented focusing on its construction and structure. Emphasis will be put on the differences between the Lisbon Guitar and the Coimbra Guitar concerning sound and purposes. The explanation will be accompanied by a live performance where players will try to show the audience the major sound differences. The session will end with a live performance of an instrumental theme for each of the two types of guitars. We hope to offer an educative and enjoyable moment of musical détente.

10:30 - 12:00

Room O

RTF - Radiology Trainees Forum

TF 1

Highlighted Lectures

Moderators:

Z. Snoj; Ljubljana/SI
T.G. Teneva; Varna/BG

A-689 10:30

Routine cartilage evaluation and novel approaches

V. Salapura; Ljubljana/SI (salapura@siol.net)

The mechanical properties of cartilage provide repetitive frictionless movements across joint surfaces. Cartilage is constituted of chondrocytes and extracellular matrix (ECM) mainly composed of water (65-80%), collagen (15-20%) and negatively charged proteoglycans (PG) (3-10%). The cartilage's four layers (superficial, transitional, deep and calcified) differ in the shape and orientation of the chondrocytes and the distribution of collagen. The biochemical changes of the damaged cartilage include the reduction of proteoglycans concentration, the elevation of water content, and degradation of matrix macromolecules. Magnetic resonance (MR) imaging is considered to be the best noninvasive method for evaluation of cartilage morphology and its biochemical changes. Routinely used techniques for morphological evaluation are two-dimensional turbo-spin-echo sequences with fat suppression (PDW, T2W), and traditional (FLASH, DESS) or novel (SSFP) 3D gradient-echo sequences. 3D TSE sequences have been recently developed for 3T scanners (SPACE) with capability of contrast properties similar to 2D TSE, allowing better tissue contrast. New MR imaging techniques for detection of ECM have been developed. The delayed gadolinium-enhanced MR imaging of cartilage (dGEMRIC) and Na23 MR imaging use similar principles with Na+ ions attraction to the negative glycosaminoglycans chains. The T1ρ time constant displays a relationship between motion-restricted water molecules and the macromolecular environment and is most sensitive to the changes of PG content. T2 mapping reflects proton movements in the tissue and is affected by the density of collagen fibres and free water content. In healthy articular cartilage, an increase in T2 values from deep to superficial cartilage layers can be observed and therefore zonal evaluation is important in T2 analysis.

Learning Objectives:

1. To learn about normal cartilage morphology and structure.
2. To understand the principles of cartilage imaging.
3. To learn about standard imaging techniques of cartilage.
4. To investigate novel approaches to cartilage imaging.

A-690 11:00

Non-occlusive mesenteric ischaemia: CT diagnosis and signs of reperfusion

M. Mazzei; Siena/IT (mmazzei@sirm.org)

Non-occlusive mesenteric ischaemia (NOMI) is an abdominal emergency that accounts for 20-30% of all intestinal ischaemic events and is the most lethal form of acute mesenteric ischaemia (AMI) (58-70%) because of the delayed diagnosis related to the non-specific symptoms and signs at imaging. Among various mesenteric ischaemia presentations, the early phase of NOMI is not easy to diagnose via CT, because it can reveal a different appearance at imaging dependent on the time in which the CT examination is performed and on the presence of reperfusion, meaning the re-establishment of normal mesenteric blood supply after an ischaemic event is more frequent than in an occlusive ischaemic condition. However, the event of reperfusion could be further worsened if the initial damage was caused by ischaemia, when it occurs in an advanced condition of ischaemia. This entity is known as ischaemia/reperfusion injury and in many cases can progress into shock, multiple organ failure and death. Drawing a distinction between NOMI with or without reperfusion, is necessary to ensure correct treatment (medical or surgical). The analysis of not only vessel features, but also of mesenteric, bowel and peritoneal CT findings propose a potentially useful method to distinguish NOMI with reperfusion (absent or present) and, in addition, any possible prognostic value. Therefore, the introduction of CT in the decision tree of NOMI treatment may bring the benefit of a prompt diagnosis and subsequent early and efficient initiation of therapy in the emergency setting, which may improve the mortality rate.

Learning Objectives:

1. To investigate imaging/pathological and experimental model correlation in NOMI with and without reperfusion.
2. To gain awareness about the CT findings of NOMI with and without a reperfusion event.

Saturday

Postgraduate Educational Programme

3. To learn where to look for reperfusion signs.
4. To understand the potential clinical impact of imaging in treatment planning.

A-691 11:30

Imaging of paediatric gastrointestinal emergencies

D. [Baleva](mailto:dilianabaleva@yahoo.com); *Mistelbach/AT (dilianabaleva@yahoo.com)*

In the newborn and infant age groups, the gastrointestinal pathology manifests often as an emergency condition, which requires a prompt and correct diagnosis to be made. In choosing the most appropriate imaging modality, the higher radiation sensitivity of the paediatric patients, the inability of voluntary follow-of commands and the sparse abdominal fat tissue must be taken into consideration. Thus, ultrasound and conventional x-ray modalities are the main imaging tools to solve paediatric gastrointestinal emergencies. The imaging findings of the most common gastrointestinal emergency entities in the young paediatric patient are presented: necrotising enterocolitis, congenital diaphragmatic hernia, malrotation and volvulus, proximal and distal congenital GI obstructions, intussusception, and hypertrophic pyloric stenosis. Special attention has been paid to the specific clinical hallmarks and age predilection of each entity.

Learning Objectives:

1. To discuss the relevant imaging approach and modalities in the setting of acute gastrointestinal pathology.
2. To review the imaging findings in the most common and important emergencies of the paediatric GIT.
3. To specially emphasise upon the typical clinical setting of the different entities.

10:30 - 12:00

Room L 8

ESR Patient Advisory Group (ESR-PAG)

PA 1

Patient-doctor relationship and interdisciplinary communication in the radiology department

A-692/A-693 10:30

Chairpersons' introduction

N. [Bedlington](mailto:michael.fuchsjaeger@medunigraz.at)¹, M.H. [Fuchsjaeger](mailto:michael.fuchsjaeger@medunigraz.at)²; ¹Vienna/AT, ²Graz/AT
(michael.fuchsjaeger@medunigraz.at)

This session will offer insights not only into the patient-radiographer-radiologist relationship in general, but specifically into communication between patients and health-care professionals (radiographers and radiologists) in the radiology department. The impact of good as well as bad communication on patient journey and well-being will be reported. Effective communication strategies required to avoid miscommunication and misunderstandings will be discussed. The radiology report which is another centre piece of communication between the patient and radiologist should express and generate confidence, be consistent and avoid confusion. Specific focus will be laid on information overload, which might be equally detrimental to a safe feeling as no information at all, as well as on timely information, which is so critical in radiology.

Session Objectives:

1. To understand the patient-doctor relationship and influencing factors, as well as how to improve the relationship.
2. To learn basic principles of communication between the patient and the radiologist or radiographer, as well as the impacts of good and bad communication.

A-694 10:40

A radiologist's point of view

D.-G. [Carrié](mailto:dominiuecarrie@wanadoo.fr); *Toulouse/FR (dominiuecarrie@wanadoo.fr)*

Only in the practice of a few of our specialities (ultrasound, interventional...) does the radiologist enter de facto into a direct relationship expressly with the patient. In other domains (CT, MR), patients are informed (or not) about their imaging by the doctor who prescribed, our secretaries, information searched on the internet, informed consent forms, or even technicians-nurses during their stay in the imaging unit. In each European country, the situations are of course very disparate, but in most cases the patient cannot see the radiologist if the latter decides that it is necessary to consult with the patient (to request some elements necessary to an interpretation, or to announce a diagnosis that seems necessary, or if he has the time). Our patients endure this existing situation. Practical solutions can and must be proposed to facilitate and

improve patient-radiologist communication (for example, systematically offer each patient as much access as possible to the radiologist who will take care of his case, physically organise the imaging department: consultation room located between interpretation offices and waiting rooms, better understand patient expectations by implementing satisfaction questionnaires). Our businesses, increasingly technical and standardised, should not distance us from the very foundation of medicine: helping our patients better understand their disease to better accept treatments that modern medicine is likely to offer them. Radiologists are part of this chain of communication, and it is in their interest to not remain indifferent and to retain their visibility to their patients.

Learning Objectives:

1. To understand the patient-doctor relationship from a radiologist's view.
2. To learn about effective communication and how to avoid miscommunication and misunderstanding.
3. To understand the impact of good communication strategies for the patient's journey.

A-695 10:55

A radiographer's point of view

B.T. [Andersson](mailto:Bodil-T.Andersson@med.lu.se); *Lund/SE (Bodil-T.Andersson@med.lu.se)*

Communication is a vital part of the encounter between the radiologist and the patient. Patients require physical and psychological support when undergoing a radiographic examination or a complex radiological intervention. The rapid growth of technical and scientific knowledge has changed not only the environment but also the requirements on competence for all professionals and the health care system as whole. High technology has transformed the physical appearance of the diagnostic radiology department and influenced its social structure. Along with caring for the patient, technology has affected radiologists' as well as radiographers' everyday life in that it allows less human control in the organisation. When a patient attends the hospital to undergo a radiographic examination or intervention, he/she expects the encounter to involve humane and dignified care, irrespective of how difficult the circumstances may be. Provision of information concerning the examination/intervention is central, as well as communication to ensure that the information provided is accurate and complete and the patient has understood. Communication helps the patient to stay involved and participate in the examination/intervention, and detailed information about what is going to happen next can be of great value to patients experiencing fear and panic. It is important to have an understanding of other professions working inside and outside a diagnostic radiology department to offer a person-centred care and climate, to increase patient safety, including effective communication.

Learning Objectives:

1. To understand the patient-doctor relationship from a radiographer's view.
2. To learn about effective communication and how to avoid miscommunication and misunderstanding.
3. To understand the impact of good communication strategies for the patient's journey.

A-696 11:10

Patients' point of view (part 1)

J. [Birch](mailto:judy_b@dsl.pipex.com); *Poole/UK (judy_b@dsl.pipex.com)*

This presentation will look at: examples of discussion with the radiologist, as well as the lack of it, and the implications from the patients' perspective. Avoiding assumptions: what information is helpful and in what form - verbal or written? The procedure itself, the report, the follow-up.

Learning Objectives:

1. To understand the patient-doctor relationship from patients' view.
2. To learn about effective communication and useful information for patients.
3. To learn that an overload of information is equally detrimental to a safe feeling as no information.

A-697 11:20

Patients' point of view (part 2)

D. [Walsh](mailto:executivedirector@efna.net); *Dublin/IE (executivedirector@efna.net)*

This presentation will explore the perspective of the neurology patient in terms of what is perceived as useful information and the challenges in communicating this effectively. It will also look at how the radiology department and the patients it serves, can work together to ensure that these barriers are overcome. This will encompass a discussion on the theory of good doctor-patient communication, but also consideration of the structures of health service delivery which may create an environment in which effective communication cannot take place.

Learning Objectives:

1. To understand the patient-doctor relationship from patients' view.
2. To learn about effective communication and useful information for patients.

Postgraduate Educational Programme

3. To learn that an overload of information is equally detrimental to a safe feeling as no information.

Author Disclosure:

D. Walsh: Advisory Board; Pfizer Patient Centricity Board. Grant Recipient; The European Federation of Neurological Associations, who I represent as Executive Director, is a patient organisation which is funded by unrestricted grants from a consortia of industry partners..

A-698 11:30

The radiologist as a patient

R. [Stern Padovan](mailto:Stern.Padovan@zagreb.hr); Zagreb/HR (rpstern@mef.hr)

I was working the whole career as academic radiologist and I was for almost 20 years chair of the large academic radiology department. My principal field of work was abdominal and urogenital radiology and I was not directly involved in breast imaging. Shortly after retirement, I was diagnosed with breast cancer and had to undergo complete surgical and oncologic treatment. Imaging is part of diagnosis and follow-up. Suddenly, I have seen the medical system from the side of the patient and understood more than before the importance of communication between patients and physicians. Radiologists often lack communication skills which render them invisible to patients. In the case of breast cancer patients, radiologists are the first among doctors who should very carefully communicate with patients, inform them of all relevant facts and further steps and demonstrate compassion. Doctors and radiologists require the same as patients from other doctors as non-professional patients. Actually, doctors know much more and should be informed in detail, and with great care. Being aware of the clinical course and potential complications of my disease, which eventually occurred, I was even more vulnerable and needed complete information and an even more tailored approach by all managing physicians. Radiologists need to communicate with patients much more and the importance of that cannot be overemphasized. I strongly believe that radiologists should receive training in this area which is largely neglected.

Learning Objectives:

1. To understand the patient-doctor relationship from patients' view.
2. To learn about effective communication and useful information for patients.
3. To learn that an overload of information is equally detrimental to a safe feeling as no information.

11:40

Panel discussion: How can we improve communication in the department and avoid misunderstanding?

10:30 - 12:00

Room F1

E³ - European Diploma Prep Session

E³ 1423

Head and neck

A-699 10:30

Chairperson's introduction

M.G. [Mack](mailto:Mack@radiologie-muenchen.de); Munich/DE (m.mack@radiologie-muenchen.de)

During this session, the participants will learn the most common variants and pathologies of the temporal bone, the skull base, the nose, the paranasal sinuses and the nasopharynx as well as the oral cavity, the oro- and hypopharynx and the larynx. Normal anatomy, variants, inflammatory disease as well as benign and malignant tumours will be presented.

Session Objectives:

1. To become familiar with the anatomy and imaging presentation of the most common disorders of the temporal bone and skull base.
2. To understand the imaging presentation of common inflammatory and neoplastic disorders of the nose, paranasal sinuses and nasopharynx.
3. To describe the typical imaging features of the most common neoplastic disorders of the oral cavity, oropharynx, hypopharynx and larynx.

A-700 10:36

A. Temporal bone and skull base

A. [Trojanowska](mailto:Trojanowska@yaho.com); Lublin/PL (agnieszka30@yahoo.com)

During the lecture we will first discuss the complex anatomy of the temporal bone with special regards to conductive and sensorineural hearing loss. Next, we will go through most common causes of conductive hearing loss, with emphasis on middle ear tumours including cholesteatoma, and chronic inflammation. Afterwards we will focus on sensorineural hearing loss, including acquired inner ear pathology and developmental anomalies. During second part of this lecture we will go through most important tumours of anterior,

middle and posterior skull base. We will discuss the features of different malignancies on CT and MRI images, focusing on providing an informative report for the clinician

Learning Objectives:

1. To differentiate the anatomy, normal variants and congenital disorders of the temporal bone.
2. To understand the causes and imaging features of hearing and vestibular disorders.
3. To describe the imaging presentation of the most common tumours of the skull base.

A-701 11:04

B. Nose, paranasal sinuses and nasopharynx

C. [Czerny](mailto:Czerny@meduniwien.ac.at); Vienna/AT (christian.czerny@meduniwien.ac.at)

Radiological imaging of the nose, paranasal sinuses and the nasopharynx is applied in patients with inflammatory or suspected benign or malignant tumours. The knowledge of the normal anatomy and its variants is necessary to understand the pathways of inflammatory and tumorous pathologies and to establish the correct diagnosis. Multidetector-spiral-CT (MDCT) and MRI are the methods of choice for radiological imaging. Additionally, positron emission-computed tomography (PET-CT) is an extremely valuable imaging tool in patients with malignant disease. It is a combination of MDCT and PET. A contrast-enhanced CT is performed - in most cases for staging covering the whole body - and a PET scan after the intravenous application of a tracer (in most cases, fluorodeoxyglucose). Malignant tissues take up the tracer and with the CT-scan the pathology can be exactly anatomically localised. In recent times, positron emission-magnetic resonance tomography (PET-MR) has been introduced. The normal anatomy and its variants as well as the importance of close neighbouring anatomical structures, which can be involved in inflammatory and tumorous disease, will be described. Pathology consists of inflammation and tumours. Inflammation can be differentiated into acute and chronic. Tumours can be either benign or malignant. It is important to describe the exact localisation and extension of the different pathologies. Imaging characteristics and involvement of the surrounding structures may help to differentiate between benign and malignant disease. Uptake of contrast material and tracer - especially when using PET-CT or PET-MR - may well differentiate benign from malignant disease and additionally enable a whole-body scanning with the exact radiological staging.

Learning Objectives:

1. To describe the anatomy and normal variants of the nose, paranasal sinuses and nasopharynx.
2. To differentiate the imaging features of acute and chronic inflammatory changes of the nose and paranasal sinuses.
3. To understand the imaging features of benign and malignant tumours of the nose, paranasal sinuses and nasopharynx.

A-702 11:32

C. Oral cavity, oro- and hypopharynx and larynx

M. [Becker](mailto:Becker@hcuge.ch); Geneva/CH (minerva.becker@hcuge.ch)

The purpose of this lecture is to review common pathologic conditions of the oral cavity, oropharynx, hypopharynx and larynx, to describe the key anatomic structures relevant to tumour spread and to discuss the clinical implications of CT and MRI in the pre-therapeutic work-up of neoplastic lesions, in particular squamous cell carcinoma of the head and neck. A systematic review will include key radiologic features and characteristic patterns of submucosal tumour spread and implications of cross-sectional imaging for staging and treatment. The lecture will also review the characteristic aspect of less common tumours and tumour-like conditions affecting this area. Typical radiologic features will be discussed with an emphasis on potential pitfalls and on how to avoid them. Imaging aspects of Human papilloma Virus (HPV) positive and HPV- negative squamous cell cancers will be addressed and the impact of the new TNM classification on radiologic reporting will be discussed. Emphasis will be put on what the clinician needs to know and how to report the findings in a systematic way.

Learning Objectives:

1. To describe the normal imaging anatomy of the oral cavity, oropharynx, hypopharynx and larynx.
2. To understand the imaging features of tumours of the oral cavity and oropharynx.
3. To describe the imaging features of tumours of the hypopharynx.
4. To understand the imaging features of tumours of the larynx.

Saturday

10:30 - 12:00

Room M 4

E³ - ECR Academies: Tips and Tricks in Pancreatic and GI Tract Imaging

E³ 1422

Pancreatic tumours

A-703 10:30

Chairperson's introduction

R. Pozzi-Mucelli; Verona/IT (roberto.pozzimucelli@univr.it)

Pancreatic tumours represent a major challenge to the radiologist, in detection, characterisation and staging. Imaging techniques perform well in the diagnosis of typical forms of ductal adenocarcinoma. However, a multimodality imaging approach is essential in equivocal and difficult cases. A variety of imaging studies, including CT, endoscopic ultrasound (EUS), MRI and positron emission tomography with 18F-fluorodeoxyglucose (FDG PET), have important roles in the diagnosis, staging and follow-up of pancreatic tumours. Primary epithelial neoplasms of the pancreas arise either from the exocrine parenchymal tissue or endocrine islet cells. The differential diagnosis among these different tumours is essential, since these tumours require different therapeutic approaches. Although a great improvement has been achieved in the diagnosis of pancreatic diseases by modern imaging modalities, a number of challenging lesions are still difficult to be characterised. This occurs with neoplastic and inflammatory diseases, which, in a limited number of cases, may present with similar imaging features that can be misdiagnosed and subjected to unnecessary surgical treatment. To make a correct differential diagnosis, clinical, morphological and structural (i.e. density and signal intensity) findings have to be evaluated at the same time. The value of the integration of imaging modalities to reach the correct diagnosis will also be discussed in this course.

A-704 10:35

A. Staging adenocarcinoma

N. Kartalis; Stockholm/SE (nikolaos.kartalis@me.com)

Pancreatic cancer is a disease with very dismal prognosis. The 5-year survival is around 5% and has been stable over the last decades. The only potential curative treatment is surgical resection combined with adjuvant and/or neoadjuvant medical therapy. However, at diagnosis less than 20% of patients have a resectable tumour, while the rest have tumours that are locally advanced and/or have distant metastases. In order to improve survival, there is a need to increase the number of patients that undergo surgery. However, for the surgical removal to be meaningful, the goal is to achieve complete macroscopic and microscopic removal of tumour (R0-resection). For the identification of patients who will benefit from surgery, the so-called "resectability status" was developed. It is based on the presence and extent of tumour contact with the major peripancreatic vessels such as portomesenteric axis (PV/SMV), hepatic artery, celiac artery and superior mesenteric artery. Depending on the degree of the circumferential tumour-vessel contact the tumours are classified in one of the three categories: resectable, borderline resectable and unresectable. The criteria of the various existing classification systems will be discussed and their differences outlined. Furthermore, the role of CT, MRI and PET-CT in the evaluation of these patients will be analysed and, finally, important aspects of the post-operative imaging follow-up will be presented.

Learning Objectives:

1. To understand the rationale behind local staging of pancreatic adenocarcinoma.
2. To learn about the respective role of CT, MRI and PET/CT.
3. To become familiar with the principle of postoperative follow-up.

A-705 11:03

B. Neuroendocrine tumours

R. Manfredi; Rome/IT (riccardo.manfredi@unicatt.it)

Neuroendocrine tumours account for 1.2%-1.5% of all gastrointestinal neoplasms, with an incidence of 1.6-2.0 new cases per 100,000 persons per year. The majority of neuroendocrine tumours occur sporadically; that is, they are non-familial. However, they sometimes occur as part of complex familial endocrine cancer syndromes such as type 1 multiple endocrine neoplasia (MEN 1) and neurofibromatosis type 1. Immunohistochemical staining has played an important role in the diagnosis of neuroendocrine tumours. The neuroendocrine cells of the diffuse neuroendocrine system are characterized by the expression of certain marker proteins, such as chromogranin, synaptophysin, and neuron-specific enolase (NSE). Clinically, neuroendocrine

tumours of the pancreas are classified into functioning and non-functioning tumours, according to the symptoms. Non-functioning, hormonally silent, neuroendocrine tumours (NF-NET) represent 68-80% of all NETs, and are diagnosed because of the mass effect exerted by the tumour. Abdominal pain is the most frequent presenting symptom (35-78%), followed by weight loss (20-35%), anorexia and nausea (45%), palpable mass (7-40%), and jaundice (17-50%). According to the 2010 WHO classification, neuroendocrine neoplasms are classified according to the percentage of Ki67, a protein index of cell replication, on the pathologic specimen. There are three categories: G1, Ki-67 index $\leq 2\%$; G2, Ki-67 index between 3% and 20%; G3, with Ki-67 index $>20\%$. At diagnostic imaging, neuroendocrine neoplasms are hypervascular compared to the adjacent pancreas in 74% of the cases. Hyper- or isovascularity represents the most suggestive feature of neuroendocrine neoplasms that are helpful in the differential diagnosis with adenocarcinoma.

Learning Objectives:

1. To understand the basics of histological classification of neuroendocrine tumours.
2. To learn about the natural history of these tumours.
3. To become familiar with the usual appearance and imaging specificities of neuroendocrine tumours.

A-706 11:31

C. Tough clinical cases

T.C. Lauenstein; Essen/DE (thomas.lauenstein@evk-duesseldorf.de)

The ability to non-invasively diagnose and characterise pancreatic tumours has vast therapeutic implications. However, there are several aspects that may impede a reliable characterisation of a pancreatic lesion. While some pancreatic tumours exhibit typical imaging findings, there is often an overlap of imaging findings between different lesions, e.g. pseudotumours due to chronic pancreatitis and adenocarcinoma of the pancreas. We often face the same dilemma as far as cystic pancreatic lesions are concerned, since some cystic tumours have a potential for malignant transformation including IPMN or mucinous cystadenomas. Furthermore, there is a large variety of diagnostic tools available for the assessment of pancreatic disease, including ultrasonography, endosonography, CT, MRI and PET. It is important to understand the strengths and weaknesses of these diagnostic modalities, particularly in equivocal cases of pancreatic lesions. Eventually, biopsy samples are often needed either to establish a diagnosis or to allow for a more profound histopathological analysis of tumour tissue. Several challenging cases of pancreatic tumours will be presented in this lecture. Differential diagnoses will be discussed and a diagnostic algorithm for each case will be proposed.

Learning Objectives:

1. To be able to define diagnostic probabilities when facing an unknown case of solid mass in the pancreas.
2. To understand the role of multimodality approach, including endosonography and biopsy.

10:30 - 12:00

Room M 5

Transatlantic Course of ESR and RSNA (Radiological Society of North America): Sports Imaging

TC 1428

Lower extremity sports injuries

Moderators:

L.W. Bancroft; Orlando, FL/US

A.J. Grainger; Leeds/UK

A-707 10:30

A. Sports-related injuries of the knee: what does the orthopaedic surgeon need to know?

T.T. Miller; New York, NY/US (millertt@hss.edu)

MRI has become the workhorse of musculoskeletal imaging, and in most practices the knee is the most commonly imaged joint. We will review examples of cruciate ligament and meniscal injuries (with attention to diagnostic pitfalls and post operative appearances), patterns of injury, osteochondral injuries and repair, and periarticular tendinous and ligamentous injuries. We will also discuss features of these injuries that help the surgeon decide whether to operate.

Learning Objectives:

1. To learn about what to include in knee MRI dictation templates.
2. To understand the most common sports-related injury patterns in the knee.
3. To appreciate which specific orthopedic indications should prompt additional information in the dictation.

Postgraduate Educational Programme

A-708 11:00

B. Multimodality imaging of foot and ankle injuries in the athlete

A.J. Grainger; Leeds/UK (andrewgrainger@nhs.net)

Ankle injuries are common in many sports, and the complicated anatomy of the ankle joint can be challenging to the reporting radiologist. The ankle joint itself is a synovial hinge joint, but important movement for ankle function also occurs at the joints of the hind and midfoot which are also susceptible to injury. In addition to conventional radiographs, CT, MRI and ultrasound all have important roles to play in the diagnosis of foot and ankle injuries in the athlete. The ligamentous and tendon structures about the ankle are generally superficial in nature and readily amenable to assessment with ultrasound, where assessment can be enhanced due to the dynamic capabilities of the technique. While MRI also demonstrates these structures, it has advantages for assessing deeper joint structures such as the chondral surfaces and bones. The complex 3D anatomy of the foot and ankle means that conventional radiographs can struggle to demonstrate bone injury which means CT also has an important role to play. This lecture will focus on the use of these imaging modalities for the assessment of acute and chronic ligamentous and tendon injury. Emphasis will be put on the mechanisms of injury and how they determine the resultant patterns of injury and the imaging appearances.

Learning Objectives:

1. To appreciate the different and often contributory roles that imaging modalities have in the foot and ankle.
2. To recognise the most common ligamentous and tendon injuries in the ankle.
3. To understand how common patterns of injury relate to the mechanisms involved.

A-709/A-710 11:30

C. Interactive case discussion

T.T. Miller¹, A.J. Grainger²; ¹New York, NY/US, ²Leeds/UK (millerth@hss.edu)¹, (andrewgrainger@nhs.net)²

Several cases of knee MRI will be shown, demonstrating examples of various abnormalities such as internal derangement (cruciate ligament and meniscal injuries), osteochondral injuries, abnormalities of the extensor mechanism, collateral ligamentous injuries, and patterns of injury. These cases will be examples of what the orthopedic surgeon wants to know.

Learning Objectives:

1. To appreciate common patterns of athletic injury in the knee.
2. To become familiar with the techniques available and imaging appearances of knee, foot and ankle athletic injury.
3. To consolidate the knowledge gained from the session with interactive cases of lower limb athletic injury.

12:15 - 12:45

Room A

Headline Session

HL 3

Josef Lissner Honorary Lecture

Presiding:

B. Hamm; Berlin/DE

A-714 12:15

Human papilloma virus and head and neck cancer: the new face of malignancy

A. Trojanowska; Lublin/PL (agnieszka30@yahoo.com)

Head and neck cancer is a commonly encountered pathology. Oropharyngeal location of the disease is increasing rapidly, affecting young people and its relation with oropharyngeal infection by oncogenic type-16 human papillomavirus (HPV) has been proven. The clinical and biologic profile of HPV-positive patients is distinct from any other head and neck squamous cell cancer patients, however, it is not possible to differentiate the HPV status based on imaging studies. HPV-positive patients have a tendency towards early lymph nodes metastasis, more frequent distant metastatic disease and much better response to non-surgical treatment, comparing to HPV-negative ones. Detection of intratumoral oncogenic HPV DNA seems to be mandatory now, since it determines prognosis in terms of long-term survival and locoregional control. A policy of vaccination for both girls and boys may be the key answer to a growing number of this particular cancer

Learning Objectives:

1. To describe the behavior of human papilloma virus.
2. To understand the specific biology and imaging features of HPV - positive cancer of the head and neck.
3. To become familiar with effective diagnostic imaging procedures, treatment and follow-up of these tumour.

12:30 - 13:30

Room C

E³ - The Beauty of Basic Knowledge: Cardiovascular and Interventional Radiology

E³ 24D

CT of the heart made easy

Moderator:

C. Loewe; Vienna/AT

A-718 12:30

Cardiovascular risk estimation made easy: CA-scoring

R. Vliegenthart; Groningen/NL (r.vliegenthart@umcg.nl)

Evaluation of the extent of atherosclerotic plaque may improve cardiovascular risk stratification in primary prevention. Among the non-invasive measures of atherosclerosis, focus has turned to assessment of coronary calcification by non-contrast-enhanced computed tomography (CT). The calcium score increases with age, and is generally higher for men than for women. The calcium score is divided into 4 categories: 0 (none), 1-99 (mild), 100-399 (moderate), and at least 400 (severe coronary calcification). Another commonly used approach is to calculate an age- and gender-matched percentile. The calcium score is predictive of coronary events in men and women, and in younger and older populations. The relative risks for increasing calcium scores are much higher than those reported for cardiovascular risk factors or other measures of atherosclerosis. Additionally, the absence of coronary calcification indicates a very low risk of cardiovascular disease. According to latest guidelines, calcium scoring should be considered in asymptomatic individuals at intermediate risk based on risk factors. In this group, calcium scoring leads to more appropriate risk classification, into the low- or high-risk group. There is increasing interest in a zero calcium score in patients with chest pain. The presence of >50% coronary stenosis and coronary events was found to be very unlikely in case of a zero calcium score, in both acute and non-acute patients. It seems likely that calcium scoring will play a role in the diagnostic algorithm of patients with chest pain in the future, especially to exclude coronary artery disease.

Learning Objectives:

1. To learn about importance of risk estimation in coronary artery disease.
2. To understand the principle of CA-scoring quantification.
3. To appreciate the value of "zero calcium" as well as of "high calcium".

Author Disclosure:

R. Vliegenthart: Research/Grant Support; Institutional grant Siemens.

A-719 13:00

Non-invasive coronary (CT) angiography made easy

F. Bamberg; Tübingen/DE (fabian.bamberg@uni-tuebingen.de)

Cardiac CT angiography has undergone a tremendous development over the last two decades and is diffusing into current medical practice substantially. On the one hand, this can be attributed to emerging scientific evidence demonstrating the incremental value of implementing cardiac CT angiography in diagnostic strategies; on the other hand, the technique itself has become very robust and broadly applicable. Still, performing a cardiac CT angiography requires some basic understanding of the underlying technical principles, physiological circumstances, and the coronary anatomy. The presentation will review available protocols and techniques and provide a straightforward approach to cardiac CTA acquisitions. Practical tips and tricks as well as limitations of the technique will be covered.

Learning Objectives:

1. To learn about optimised examination technique of non-invasive coronary CT angiography.
2. To understand the need for structured approach to coronary CT angiography.
3. To appreciate clinical value of non-invasive coronary CT angiography.

Author Disclosure:

F. Bamberg: Research/Grant Support; Siemens Healthineers, Bayer Healthcare. Speaker; Siemens Healthineers, Bayer Healthcare.

Saturday

12:30 - 13:30

Room D

E³ - The Beauty of Basic Knowledge: A Survival Guide to Musculoskeletal Imaging

E³ 25D

Acute trauma: patterns in the peripheral skeleton

Moderator:

V.N. Cassar-Pullicino; Oswestry/UK

A-720 12:30

Acute trauma: patterns in the peripheral skeleton

J. Teh; Oxford/UK (jamesteh1@googlemail.com)

A systematic approach to analyse trauma imaging of the peripheral skeleton is presented. Typically, imaging begins with x-rays. A stepwise approach may reveal subtle abnormalities that should prompt further action. For example, the presence of a second fracture on x-ray suggests an ACL injury and thus should lead to an MRI scan. It should be recognized that in trauma, certain injuries cannot occur in isolation; therefore, a dislocated radial head on elbow x-ray should prompt imaging of the whole forearm, as Monteggia fracture-dislocation may be present. Understanding the mechanisms of injury allows the radiologist to predict the patterns of injury. So if bone bruising is present on MRI in the lateral femoral condyle and medial patella, a lateral patellar dislocation should be suspected and a specific search for an injury of the medial retinaculum should be made. Conversely, recognizing classic patterns of injury can allow the mechanism of injury to be deduced. This lecture will focus on the classical patterns of acute trauma in the peripheral skeleton.

Learning Objectives:

1. To become familiar with the imaging manifestations of common important injuries in the upper and lower limb.
2. To understand the underlying mechanism that result in combination of injuries.
3. To learn how to best employ imaging modalities in their diagnosis.

12:30 - 13:45

Room M 1

New Horizons Session

NH 14

The new horizon for radiology

A-721/A-722 12:30

Chairpersons' introduction

L. Donoso¹, B. Hamm²; ¹Barcelona/ES, ²Berlin/DE

Session Objectives:

1. To become familiar with the challenge and opportunities of artificial intelligence.
2. To become familiar with the Department of Diagnostics of the future.
3. To learn from experts how to organise integrated diagnostics.
4. To learn about integrated diagnostics from the European and American experience.

A-723 12:35

What will the radiologist's job look like in 2025?

W. Kim; Los Angeles, CA/US (woojinrad@gmail.com)

Today, plenty of fear, hope, and hype encompass the use of artificial intelligence (AI) in radiology. Many AI experts have predicted the demise of radiology by having AI replace radiologists in the near future. These predictions have impacted the career choices of medical students, caused worries for the radiology trainees, and brought concerns to many practising radiologists. However, much of these so-called expert opinions are based on a very simplified view of what we do as radiologists. Furthermore, when it comes to AI in radiology, with media attention and many startups focused on using AI to identify findings within medical images, it is easy for us in the radiology profession to have "tunnel vision" about AI in our field. It is important to widen our view to see the many other ways AI can benefit medical imaging. In 2014, there was a Journal of the American College of Radiology article on something called the "imaging value chain" that described various processes within radiology from ordering to reporting and communication. This value chain illustrates various areas where AI can augment and improve radiology. Throughout history, radiologists have adapted to technological innovations and

made adjustments to integrate them into our workflow. AI will soon become an integral part of our lives and our profession. As we learn to integrate AI into radiology, we must have a wider view to take full advantage of this emerging technology and maximise our role in patient care.

Learning Objectives:

1. To appreciate why some radiologists fear artificial intelligence (AI).
2. To learn about the role AI can play beyond interpretation of images.
3. To learn about how AI can augment radiologists and what we can do to maximise its positive potential.

Author Disclosure:

W. Kim: Employee; Nuance Communications.

A-724 12:50

Transforming the integrated diagnosis (ID) opportunity into the Diagnostic Institute (DI) innovative change management

P. Ros; Cleveland, OH/US (Pablo.Ros@UHhospitals.org)

In recent years, voices have been calling for tighter integration between radiology, pathology, and genomics. This multidisciplinary convergence is captured by the term Integrated Diagnostics (ID). Now is the right time for a move toward ID, based on current technology advances. One major change is that anatomic pathology is transforming from an analogue (slide and microscope) approach to a digital workflow at a rapid pace, thanks to whole slide imaging scanners and pathology picture archiving and communication systems (PACS) for large scale, clinical use. With digital pathology, the cross-disciplinary IT tools greatly expand. Moreover, there is the strong trend for quantification of image contents to enable large-scale computational analysis. We discuss three pillars for an effective ID practice. The first pillar standardizes the pathways through diagnostics that can be quite complex. In our design of an ID practice, the diagnosticians would take on a larger responsibility and would directly decide on follow-up studies when the next step in the pathway is clear. The second pillar is facilitated joint radiology -genomics decision-making. The third pillar is dependent on the service level provided and perceived by the customers—the referring clinicians, patients, and, ultimately, society. This is essential to ensure the ultimate success of radiology, pathology and genomics. The opportunities described sum up a strong call for focusing on ID as one of the key forefronts of health-care development forming diagnostic institutes.

Learning Objectives:

1. To learn the concept of integrated diagnosis (ID) combining the practices of radiology, pathology and genomics into an innovative diagnostic tool.
2. To understand how the computational resolution provides the technology basis for the cross-disciplinary implementation of ID.
3. To share the early experience of first Diagnostic Institute established in a large Academic Health System in the US in 2017.

A-725 13:05

Medical imaging and clinical laboratories: a fruitful liaison

J.E. Wildberger; Maastricht/NL (j.wildberger@mumc.nl)

Setting up a global diagnostic chain offers new opportunities to optimise patient logistics and to become more (cost-)effective. As a first step, all diagnostic departments in our center were clustered into the "division of medical imaging and clinical laboratories" in 2011. In December 2016, the departments of radiology and nuclear medicine were fused. Based on lean principles (operational excellence), a framework of breakthrough objectives has been established. Achievements are shared and updated on a regular basis. From a radiological perspective, the next step to be taken is the implementation of a uniform reporting platform for imaging and pathology. In parallel, all diagnostic laboratory information systems are to be homogenised and clustered. This set-up forms the basis for a deep integration of underlying logistics, shared infrastructure, as well as for optimisation of current management information and reporting. By doing so, bioinformatics can be further developed, not only for the clinics but also in the scientific setting. Standardisation throughout the entire diagnostic chain will guarantee high quality data sets for new insights on a larger scale. Sharing this information openly and cross-disciplinary will help to further optimise patient care.

Learning Objectives:

1. To understand why we should cluster the entire diagnostic chain.
2. To learn how "unity in diversity" can be achieved in a clinical setting.
3. To become familiar with the opportunities of this approach for bioinformatics, data sciences and artificial intelligence.

Author Disclosure:

J.E. Wildberger: Research/Grant Support; (Institutional) AGFA, Bayer, GE, Philips, Siemens. Speaker; Bayer, Siemens.

Postgraduate Educational Programme

14:00 - 15:30

Room A

E³ - ECR Academies: Interactive Teaching Sessions for Young (and not so Young) Radiologists

E³ 1521

Paediatric radiology for the general radiologist

A-731 14:00

A. Fractures in children

K.J. [Johnson](mailto:karl.johnson@bch.nhs.uk); Birmingham/UK

Traumatic injury and fracturing are some of the commonest reasons why children present to hospital and undergo radiological investigation. The anatomy and physiology of the growing skeleton is different from that of adults and, as a consequence, some of the fractures and injuries are unique to children. This presentation will demonstrate the various types of incomplete fracture which occur within the more plastic skeleton of the child. It will detail the different types of Salter-Harris fractures which can occur across the unfused growth plate. The differences in relative strength of bone and ligamental attachments which are seen in children and the consequences of the different types of injuries which can occur will be illustrated. The importance of recognising the normal variants of growth from pathological change will also be highlighted. The importance of understanding the child's development and mobility and how this correlates with the injury patterns seen in normal childhood will be discussed along with an understanding of the injury patterns and fracture types which occur from inflicted physical injury.

Learning Objectives:

1. To become familiar with different traumatic fracture types.
2. To identify possible criteria for child abuse.

A-732 14:45

B. Typical MRI applications in paediatric musculoskeletal imaging

K. [Rosendahl](mailto:karen.rosendahl@helse-bergen.no); Bergen/NO

Magnetic resonance imaging (MRI) has become exceedingly important in the diagnosis and follow-up of MSK disease, allowing for targeted therapy. MRI uses non-ionising radiation, has a high soft-tissue resolution and discrimination and may provide both morphological and functional information. Correct interpretation depends on extensive knowledge of physical properties and normal appearances of the imaged tissue and of the pathophysiological disease processes. Imaging of the paediatric skeleton represents a particular challenge as normal appearances change over time, thus mimicking diseases such as juvenile idiopathic arthritis (JIA), osteomyelitis, malignancies and traumatic changes. All the aforementioned diseases represent typical MRI applications in paediatric MSK imaging. During this lecture, I will discuss imaging strategies, findings and differentials.

Learning Objectives:

1. To learn indications of paediatric MRI.
2. To become familiar with MR imaging findings in children.

14:00 - 15:30

Room B

Professional Challenges Session

PC 15

Artificial intelligence and big data in medical imaging

A-733 14:00

Chairperson's introduction

W.J. [Niessen](mailto:w.niessen@erasmusmc.nl); Rotterdam/NL

The analysis of big data with artificial intelligence techniques will have an enormous impact on disease prevention, cure and care, and by 2030 it will have dramatically changed the landscape of the health-care system. This session will show examples of possible large benefits of big data analytics in health care from the imaging perspective. Specifically, in this introduction I will provide examples to show that the use of AI and big data should be embraced, as it has a large potential to realizing the potential of precision medicine and precision health, both in dementia and oncology.

Session Objectives:

1. To learn about the disruptive role that big data and artificial intelligence can play in medical imaging.
2. To appreciate that these technologies are key to realise the full potential of precision medicine.
3. To appreciate where the big challenges and opportunities are.

Author Disclosure:

W.J. Niessen: Advisory Board; I am Scientific Advisor to Quantib BV. Founder; I am co-founder of Quantib BV. Owner; I have shares in Quantib BV.

A-734 14:15

IT infrastructure, data sharing methods and data analysis aspects

A. [Alberich-Bayarri](mailto:alberich_ang@gva.es); Valencia/ES

Quantitative image analysis solutions and artificial intelligence (AI)-based methods usually find interoperability issues when trying to transfer information with hospital information systems (HIS) and electronic health records (HER). Appropriate quantitative data management would allow for a better understanding of the tissue and organ alterations in the disease and their relationship with patient characteristics and associated clinical or lab data. The image reading process is today in constant improvement, from traditional image reading by the naked eye and free text reporting of the findings, towards the inclusion of new technologies in the loop such as AI computer-aided detection and diagnosis (CAD), imaging biomarker extraction and structured reporting. To cover all clinical needs using AI solutions, quantitative imaging and structured reporting, a technological framework was engineered. The platform is modular and allows the installation both in local and cloud environments. The solution also includes a built-in anonymization module and allows for the incorporation of AI and image processing plug-ins. After the analysis of the images through the different pipelines, a quantitative structured report is generated, which can be integrated with hospital information systems. The platform allows for the mining of quantitative data extracted from patients, a functionality which is not available nowadays in PACS systems and workstations.

Learning Objectives:

1. To understand the importance of creating IT infrastructures for the management of quantitative medical image analysis solutions, both for research and clinical applications.
2. To become familiar with the main storage and computational requirements for high performance infrastructures.
3. To learn about how to move from research to clinical application in the field of quantitative imaging and biomarkers.

Author Disclosure:

A. Alberich-Bayarri: CEO; QUIBIM SL. Founder; QUIBIM SL.

A-735 14:40

Machine learning in the biomedical domain: challenges and opportunities

M. [de Bruijne](mailto:marleen.debruijne@erasmusmc.nl); Rotterdam/NL

This lecture introduces the current state-of-the-art techniques in machine learning in medical imaging, highlights the potential of these techniques for computer-aided diagnosis and quantitative imaging biomarkers, addresses challenges related to variations in scan protocols and a requirement of annotated data for model training, and presents examples of successful applications of machine learning in radiology.

Learning Objectives:

1. To learn about machine learning concepts used for diagnosis, prognosis, and quantitative analysis of medical imaging data.
2. To understand the challenges to introduce these techniques in clinical practice.
3. To appreciate the potential of machine learning in radiology.

Author Disclosure:

M. de Bruijne: Grant Recipient; Danish Council for Independent Research (DFR), Innovative Medical Devices Initiative (IMDI) of The Netherlands Organisation for Health Research and Development, Netherlands Organization for Scientific Research (NWO), Vertex, Astra Zeneca. Patent Holder; US8811724, US7844090, US8126240, US7561727, US7463758. Research/Grant Support; Quantib, COSMONIO Imaging BV.

A-736 15:05

How will AI change radiology

K.J. [Dreyer](mailto:dreyer@bostonma.us); Boston, MA/US

"no abstract submitted"

Learning Objectives:

1. To learn about the current big data and AI initiatives.
2. To discuss the current stage and future of AI in radiology.
3. To discuss the role of the radiologist/radiology department in the AI era.

Saturday

Postgraduate Educational Programme

14:00 - 15:30

Room C

E³ - ECR Master Class (Chest)

E³ 1526a

Patterns of pulmonary toxicity

Moderator:

J.E. Roos; Lucerne/CH

A-737 14:00

A. Drug-induced lung disease

C.M. Schaefer-Prokop; Amersfoort/NL (cornelia.schaeferprokop@gmail.com)

Drug-induced lung disease is an underreported cause of acute and chronic lung disease. It affects up to 10% of patients receiving chemotherapy for hematological and solid organ malignancies. Two mechanisms are differentiated: lung injury due to direct toxic injury and due to hypersensitivity reactions. Numerous CT patterns are seen in the context of drug induced lung disease ranging from diffuse alveolar damage (DAD) to all forms of acute and chronic interstitial pneumonia but also includes nodules, pleural effusion and airways reactions. The presentation will illustrate the most frequent CT patterns to be encountered in drug induced lung injury and provide keys how to differentiate them from other lung pathology such as infection, edema or underlying malignancy. Drugs, known for potential lung injury will be discussed, including new immunotherapeutic drugs. Further on, case-based discussion of typical clinical scenarios will provide you with practical tools for analysis.

Learning Objectives:

1. To learn about the various CT patterns of lung injury.
2. To understand the role of imaging in their recognition.
3. To discuss differential diagnoses.

A-738 14:30

B. Smoking-related lung disease

S.R. Desai; London/UK (s.desai@rbht.nhs.uk)

It is generally accepted that, in addition to the well known consequences of COPD and lung cancer, smoking may cause interstitial lung disease (ILD). The hypothesis that tobacco smoke can cause ILD - and, specifically, pulmonary fibrosis - dates back to the 1960s. The histopathological and radiological features of interstitial lung disease caused by smoking are variable and frequently overlapping, the latter prompting the introduction of the generic term 'smoking-related interstitial lung disease'. The list of interstitial lung disease, in which smoking is believed to have an aetiological role, includes Langerhans' cell histiocytosis, respiratory bronchiolitis/respiratory bronchiolitis-interstitial lung disease and desquamative interstitial pneumonia. There is also evidence which indicates that smoking may be associated with other patterns of pulmonary fibrosis (e.g. nonspecific interstitial pneumonia and smoking-related interstitial fibrosis). In the present session the pathology and imaging of the ILD known to be caused by smoking; the typical appearances and the diagnostic challenges will be discussed.

Learning Objectives:

1. To learn about the classification of smoking-related lung diseases.
2. To understand the most common CT patterns.
3. To highlight newly recognised entities.

Author Disclosure:

S.R. Desai; Board Member; Deputy Editor, European Radiology.

A-739 15:00

C. Inhalation lung injury beyond smoking

J.A. Verschakelen; Leuven/BE (johnny.verschakelen@uz.kuleuven.ac.be)

Non-smoking-related inhalation lung injury is usually secondary to chronic or repetitive occupational or environmental exposures, but may also result from inhalation of smoke or of chemical products of combustion, a condition that is mostly associated with significant morbidity and mortality. Every year new agents causing pulmonary injury are described, and although many are isolated cases others prove to be clustered or repetitive events with more or less specific imaging features. The clinical and radiological presentation of inhalational lung injury depends, on one hand, on the chronicity of inhalation, the amount and phase of the inhaled agent and its toxicity to the lung and, on the other, on the reaction of the lung to this injury. This presentation will focus on the CT features seen after non-smoking-related lung injury caused by direct chemical toxicity to the bronchial tree and lungs and by chronic or repetitive inhalation of particulates and organic dusts. Attention will also be given to the inflammatory syndrome seen in hypersensitivity pneumonitis.

Learning Objectives:

1. To learn about the various causes of environmental lung diseases.
2. To understand the changes related to acute lung injury.
3. To describe the long-term sequelae of inhalation lung injury.

14:00 - 15:30

Room O

Special Focus Session

SF 15a

Hybrid imaging in oncology

A-740 14:00

Chairperson's introduction

M.E. Mayerhöfer; Vienna/AT (marius.mayerhoefer@meduniwien.ac.at)

Hybrid imaging has revolutionized the field of oncologic imaging within the last decade. [18F]FDG-PET/CT in particular is now an integral part of the management guidelines for different tumours (e.g. lymphoma), with a particular emphasis on treatment response assessment. Despite the success of [18F]FDG in oncologic imaging, there is a clear trend towards development and clinical application of novel, tumour-specific PET tracers, such as [68Ga]PSMA for prostate cancer. Since PET/CT is only of limited value for local staging of the primary tumour in several malignancies (e.g., rectal cancer and gynaecological cancers), hybrid MR/PET scanners were developed and are presently being compared to PET/CT in an increasing number of studies. Furthermore, the MR component of MR/PET offers additional functional and even quantitative information, derived from techniques such as diffusion-weighted imaging (DWI) and dynamic contrast-enhanced imaging. The combination of PET- and MRI-based parameters may not only improve non-invasive, image-based characterization of tumours (including assessment of tumour heterogeneity), but may also enable better assessment of response to novel types of immunotherapies that have recently become available. Because of this multi-parametric approach, hybrid imaging has the potential to contribute significantly to the success of precision medicine.

Session Objectives:

1. To identify key clinical applications for hybrid imaging in oncology.
2. To compare PET/CT and MR/PET for tumour detection, staging and restaging.
3. To discuss the use of established and novel radiotracers and functional MR sequences for tumour characterisation and treatment response assessment.

A-741 14:05

Role of hybrid imaging in thoracic malignancies

G. Cook; London/UK (Gary.Cook@kcl.ac.uk)

18F-FDG PET/CT is now established in the management of solitary pulmonary nodules and the staging of lung cancer and mesothelioma when there is curative intent. Whilst 18F-FDG PET/CT is of undoubted clinical value, there are circumstances when the sensitivity or specificity is limited and therefore efforts have been made to evaluate new radiopharmaceuticals to improve characterisation, treatment stratification and treatment monitoring. These include 18F-FLT for cellular proliferation, 18F-MISO (and other compounds) for measuring tumour hypoxia, and angiogenesis-targeting radiopharmaceuticals and 68Ga-DOTA-peptides for detection of neuroendocrine tumours. As well as the development of new tracers to evaluate underlying biological characteristics of thoracic malignancy, there is growing interest in the extraction of additional parameters from PET and CT that describe heterogeneity within an image or in a radiomics approach to better characterise lung cancers and improve the predictive and prognostic ability.

Learning Objectives:

1. To become familiar with the PET tracers used in thoracic malignancies.
2. To learn the interpretation of PET/CT in lung cancer, mesothelioma, and neuroendocrine tumours of the lungs.
3. To discuss the possible benefits of tumour heterogeneity assessment on hybrid imaging.

A-742 14:23

Prostate cancer: the "killer application" for MR/PET?

M.R. Makowski; Berlin/DE (marcus.makowski@charite.de)

In this lecture, we will give an overview of the potential of MR/PET in the context of prostate cancer. The different available MR/PET acquisition protocols will be introduced. The evaluation and interpretation of datasets acquired during MR/PET acquisitions will be discussed. We will highlight the strengths and weaknesses of MR/PET for the evaluation of patients with prostate cancer and give an outlook regarding the potential of this technique.

Saturday

Postgraduate Educational Programme

Learning Objectives:

1. To learn pelvic MR/PET acquisition protocols, normal anatomy, and pitfalls.
2. To become familiar with interpretation of MR/PET in the settings of prostate cancer.
3. To understand strengths and weaknesses of MR/PET applied to prostate cancer.

A-743 14:41

MR/PET of breast tumours

K. [Pinker-Domenig](mailto:pinkerdomenig@mskcc.org); Vienna/AT (pinkerdk@mskcc.org)

Cancer development is characterised by several biological capabilities or so-called hallmarks, which comprise sustaining proliferative signalling, evading growth suppressors, resisting cell death, enabling replicative immortality, inducing angiogenesis, and activating invasion and metastasis. With medicine entering the genomic era, personalised approaches towards treatment, which require a deeper understanding of the hallmarks of cancer, are being explored and ultimately will be implemented in patient care. To match advanced therapeutic strategies in the era of personalised medicine, diagnostic tests must be equally multilayered and complex to identify the relevant underlying processes of cancer development and progression. In this context, multiparametric magnetic resonance imaging (MRI) and positron emission tomography/MRI (PET/MRI), which, in addition to morphologic changes, can simultaneously assess a multitude of functional cancer-related processes, have emerged as exceptionally powerful, versatile, and precise imaging techniques. Multiparametric functional imaging of the breast aims to simultaneously quantify and visualise multiple functional processes at the cellular and molecular levels to further elucidate the development and progression of breast cancer and the response to treatment. There is evidence that multiparametric functional imaging, using different MRI and PET parameters, provides detailed information about the hallmarks of cancer and, thus, improves the diagnostic accuracy and assessment of response to neoadjuvant therapy. Multiparametric functional MRI provides a variety of techniques to assess functional tumour characteristics such as diffusion-weighted imaging, dynamic contrast-enhanced imaging and multi-nuclei magnetic resonance spectroscopic imaging. PET/(MRI) detects and quantifies radiolabelled tracer substances, which allows the measurement of specific functional characteristics of breast cancer such as increased glucose uptake, tumour hypoxia or hormonal receptor expression. This talk aims to summarize the current and emerging applications of PET/MRI in breast tumours.

Learning Objectives:

1. To understand the principle of multimodality multiparametric functional imaging of breast tumours with MR/PET.
2. To identify the potential and challenges of multiparametric breast MR/PET using different quantitative functional parameters.
3. To realise the potential of novel tracers for personalised medicine.

A-744 14:59

MR/PET of pelvic cancers

P.R. [Ros](mailto:Pablo.Ros@UHhospitals.org); Cleveland, OH/US (Pablo.Ros@UHhospitals.org)

PET/MRI raises the hope of providing a comprehensive TNM staging of pelvic malignancies in one single imaging examination. Combining the high diagnostic accuracy from PET with the excellent soft tissue contrast of MR enables accurate assessment of primary tumours and nodal metastases. In our experience, FDG-PET/MR is distinctly helpful in (a) advanced pelvic cancers for staging and treatment planning, (b) in a post-treatment setting of recurrence and (c) in equivocal cases where other methods failed to determine the exact origin and extent of the neoplastic disease. PET/MRI can characterize therapeutic fibrosis and tissue scarring after therapy, which significantly improves the detection of recurrent diseases. FDG-PET/MR plays an important role in ovarian cancer for all stages of disease: (1) the use of DWI in MRI is helpful in detecting small peritoneal deposits, which escape detection on FDG-PET; (2) MRI facilitates the distinction of FDG-avid peritoneal and serosal implants from physiological bowel uptake, and (3) MRI can improve lesion detection and localisation. Another benefit PET/MR provides is a specific GTV (gross tumour volume) which is critical to the treatment of cervical cancer patients. The use of PET/MR for prostatic cancer evaluation with Ga-68 PSMA is the newest application in pelvic malignancies. Several Ga-68-labelled ligands of prostate-specific membrane antigen (PSMA) have recently been developed with promising results. Ga-68 PSMA offers a higher tumour-to-tissue contrast compared to FDG, resulting in an accurate evaluation of the prostate gland, highly sensitive loco-regional staging as well as visualising distant metastases.

Learning Objectives:

1. To learn pelvic MR/PET acquisition protocols, normal anatomy, and pitfalls.
2. To become familiar with interpretation of MR/PET in the settings of pelvic cancers.

3. To understand strengths and weaknesses of MR/PET applied to pelvic cancers.

15:17

Panel discussion: Does the multiparametric approach have a clinical benefit?

14:00 - 15:30

Room N

Cardiac

RC 1503

What a radiologist needs to know about imaging of myocardial viability

A-745 14:00

Chairperson's introduction

C. [Peebles](mailto:Charles.Peebles@suht.swest.nhs.uk); Southampton/UK (Charles.Peebles@suht.swest.nhs.uk)

The concept of myocardial viability is central to the investigation and management of ischaemic heart disease (IHD). Viable myocardium is defined as 'dysfunctional myocardium that maintains the potential to return to normal function' e.g. it is alive and not dead. Dysfunctional, but viable myocardium is the end result of ischaemic myocardial injury that can either be acute (stunning) or chronic (hibernating). In the former, a single acute ischaemic injury causes temporary dysfunction that will recover after restoration of myocardial blood flow, but there may be a delay of weeks or months for this to occur. Hibernation is the end result of chronic or repetitive ischaemia causing downregulation of myocyte metabolism and function, which will again recover following revascularisation. Accurate identification of viable myocardium is critical, as revascularisation of non-viable myocardium confers the risks of revascularisation without the benefits of functional recovery. Conversely, failing to revascularise viable myocardium that is ischaemic may place the patient at increased risk. The two general approaches to identifying viable myocardium are functional improvement of a regional wall motion abnormality during low dose stress or identification of myocardial scar that involves less than the full thickness of a myocardial segment. The first approach is adopted by stress echo and dobutamine stress CMR. The second approach requires the use of extracellular contrast agent and is usually performed by CMR with late gadolinium enhancement or CT with iodinated contrast and delayed imaging. This session will compare the standard techniques for viability imaging and discuss their pros and cons.

Session Objectives:

1. To understand what viability means.
2. To understand current state-of-the-art knowledge about the principle of viability.
3. To understand shortcomings of echo and SPECT compared to other techniques.

A-746 14:05

A. MRI

J. [Bogaert](mailto:Jan.Bogaert@uz.kuleuven.ac.be); Leuven/BE (Jan.Bogaert@uz.kuleuven.ac.be)

Ischaemic heart failure is probably the most challenging issue in cardiology today, posing an enormous medical and financial burden on our society. Conceptually, it represents a maladaptive cardiac remodelling due to acute and/or chronic coronary artery disease (CAD) with varying degrees of left ventricular (LV) dilatation and dysfunction. Though therapeutic options have improved overall survival over the years, mortality rates remain high and in daily practice cardiologists not infrequently face the therapeutic dilemma whether a revascularization procedure will lead to symptomatic and prognostic benefit for the patient. Simple, straightforward guidelines are lacking because of the complexity of the disease. Moreover, the issue of viability imaging grounded on observational, and retrospective studies has recently been challenged by the publication of prospective, randomized trials (e.g. STICH and PARR trial) showing no benefit of revascularization or of pre-procedural viability assessment in those patients. These contradictory findings have obliged us to enquire whether viability imaging still is relevant and what is needed to make it more appropriate.

Learning Objectives:

1. To learn about how MR should be performed to assess viability.
2. To understand the strength and weaknesses of MR compared to other techniques.
3. To learn how to report MRI for viability assessment.

Saturday

A-747 14:28

B. Hybrid imaging
O. [Ratib](#); Geneva/CH

Hybrid imaging combining molecular imaging (PET or SPECT) with anatomical and functional imaging (CT and MRI) offers a scope of new clinical applications. Traditional myocardial perfusion scans (SPECT) combined with advanced CT of coronary arteries anatomy and calcium scoring allows a better assessment of the degree of coronary disease and the risk of future events and objective determination of the appropriateness of therapeutic interventions. The development of new radiotracers for PET imaging of myocardial perfusion and viability opens new perspective for more objective evaluation of the efficacy of new treatments. The emergence of hybrid PET-MR imaging offer new perspectives for cardiac imaging. Functional MR allow identifying areas of decreased myocardial perfusion and tissue viability. PET provides more quantitative data on true tissue perfusion and metabolism and quantitative myocardial flow and coronary flow reserve. The combination of both modalities, improve the accuracy and reproducibility of diagnostic procedures. But the true potential of hybrid PET-MR may reside in applications beyond coronary artery disease. It is shown that the combination of both modalities help better characterise atherosclerotic plaques and identify plaques with high risks of rupture. Development of new tracers will allow evaluating myocardial remodeling and assessment of stem cell therapy in myocardial infarction. It will also provide new means for evaluating alterations in cardiac innervation and angiogenesis and even in assessment of reporter gene technologies.

Learning Objectives:

1. To learn about how hybrid imaging should be performed to assess viability.
2. To understand the strength and weaknesses of hybrid imaging compared to other techniques.
3. To understand how hybrid imaging could be developed in clinical practice.

A-748 14:51

C. CT
F. [Bamberg](#); Tübingen/DE (fabian.bamberg@uni-tuebingen.de)

Given its high relevance, substantial research efforts have been focused on the development of different cardiac CT methods to obtain information on myocardial viability. Despite a relatively low level of scientific evidence, these approaches are currently initially entering the clinical arena. Analogous to the presence of late gadolinium enhancement on MRI, viability imaging using cardiac CT may be limited to the detection of delayed iodinated contrast enhancement on delayed CT acquisitions. However, from a clinical perspective CT myocardia imaging protocols are generally combined with myocardial perfusion imaging at rest and stress. In general, such a protocol includes as a first step perfusion imaging followed by a second step that includes a low-radiation scan for the detection of DCE. Of note, perfusion imaging by CT can be conducted as a "single-shot" acquisition with or without dual energy or as a dynamic acquisition during rest or stress conditions. The talk will provide an overview of available approaches and protocols, highlight limitation, and review current level of evidence related to the role of CT for assessment of myocardial viability.

Learning Objectives:

1. To learn about the potential of CT to assess viability.
2. To understand the strength and weaknesses of CT imaging compared to other techniques.
3. To understand how to report CT for viability assessment.

Author Disclosure:

F. Bamberg: Research/Grant Support; Siemens Healthineers, Bayer Healthcare. Speaker; Siemens Healthineers, Bayer Healthcare.

15:18

Panel discussion: What imaging test in which patient?

14:00 - 15:30

Studio 2018

E³ - ECR Master Class (Genitourinary)

E³ 1526b

Update on functional genitourinary MRI

Moderator:

M. Studniarek; Gdansk/PL

A-749 14:00

A. Kidney
N. [Grenier](#); Bordeaux/FR (nicolas.grenier@chu-bordeaux.fr)

Renal physiology is complex with two compartments functioning under highly different conditions. The cortex is highly perfused with a high level of oxygen, whereas the medulla shows a poor perfusion level and works under hypoxic conditions. Water movements are multiple along the nephrons to maintain normal homeostasis. Glomerular filtration rate is a major marker of renal function, but its measurement is complex to be obtained in clinics. All these parameters can be approached using functional MRI with DCE, DWI, and BOLD. However, validation of these tools and their impact on patient management still requires further prospective studies. Some of these techniques may reflect changes within the extracellular matrix of renal tissue during the process of renal scarring.

Learning Objectives:

1. To learn about the renal physiology and the pharmacokinetics of contrast agents.
2. To understand the clinical and imaging features of renal disorders.
3. To appreciate the incremental value of functional imaging in differential diagnosis.

Author Disclosure:

N. Grenier: Advisory Board; Supersonic Imagine, Aix-en-Provence, France.

A-750 14:30

B. Prostate
G.M. [Villiers](#); Ghent/BE

Multiparametric magnetic resonance imaging (mpMRI) of the prostate combines T2-weighted MRI (T2w) with functional techniques such as diffusion-weighted MRI (DWI) as a marker of cellular density, and dynamic contrast-enhanced MRI (DCE) to assess neoangiogenesis. The minimal technical requirements for these techniques have been described in the Prostate Imaging, Reporting and Data System (PI-RADS) by the American College of Radiology and the European Society of Urogenital Radiology. T2w MRI detects prostate cancer as low signal-intensity (SI) areas in the peripheral zone (PZ) or transition zone (TZ). It provides sensitivity up to 85% for overall prostate cancer detection, but lacks specificity. DWI primarily detects higher-grade prostate cancers as areas of restricted diffusion (high SI on high b-value images; low SI on ADC maps) and improves the overall specificity. DCE detects cancers because of their early and rapid enhancement after contrast administration, but is useful for the PZ only, due to false-positive enhancement of benign prostatic hyperplasia in the TZ. Reporting of mpMRI has been standardized using the PI-RADS 5-point assessment scale, estimating the likelihood of clinically significant prostate cancer. Prostate biopsies directed to mpMRI-detected lesions have shown to be able to decrease the overall number of prostate biopsies, to increase detection of clinically significant prostate cancer and to decrease overdiagnosis of clinically insignificant prostate cancer. mpMRI-guided biopsies are currently recommended in the setting of rebiopsy after a previously negative biopsy, but evidence has been accumulating showing that mpMRI-guided biopsies are equally useful in biopsy-naïve men.

Learning Objectives:

1. To understand the clinical and imaging features of prostatic disorders.
2. To appreciate the incremental value of functional imaging in differential diagnosis.
3. To become familiar with MRI-guided prostate biopsies.

A-751 15:00

C. Uterus
E. [Sala](#); Cambridge/UK (evis.sala@gmail.com)

The standard MRI uterus protocol includes axial SE T1WI with a large FOV to evaluate the entire pelvis and upper abdomen for lymphadenopathy as well as bone marrow changes and high-resolution FSE T2WI in the sagittal, axial and coronal planes. Other extra planes and imaging sequences are specific and designed to answer a specific clinical question. Functional MRI sequences such as DCE-MRI and DW-MRI are now part of routine protocols. DCE-MRI is very useful for assessment of the depth of myometrial invasion in endometrial

cancer. DW-MRI is now part of routine MRI protocol for evaluation of uterine malignancies. It should be performed at two or more b-values, which include one or more low b-values (50-100 s/mm²), since perfusion contribution to diffusion is then eliminated, and a very high b-value (750-1000 s/mm²). Both breath-hold and non-breath-hold DW sequences can be used. However, the type of DW sequence differs among manufacturers and the radiologist should be familiar with the strengths and limitations of their own scanners. A combination of DWI with conventional MRI sequences improves lesion detection and the radiologist confidence in imaging interpretation. DW-MRI can be useful for accurately determining the depth of myometrial invasion in endometrial cancer. In addition, ADC values are inversely related to the cellularity of tumours which may be useful for distinguishing between benign and malignant tissues and for monitoring tumour response to treatment in cervical cancer.

Learning Objectives:

1. To understand the clinical and imaging features of uterine disorders.
2. To appreciate the incremental value of functional imaging in differential diagnosis.
3. To learn about the imaging features of the treated uterus.

14:00 - 15:30

Room E1

Special Focus Session

SF 15b

Contrast-enhanced spectral mammography

A-752 14:00

Chairperson's introduction

A. Athanasiou; Athens/GR (athanasiou@mitera.gr)

Mammography is the only imaging modality that has been shown to reduce mortality from breast cancer. Despite technical advances in full-field digital mammography, it is still not a perfect screening tool, especially in women with dense breasts. Contrast-enhanced spectral mammography has emerged several years ago and has been shown to be superior to FFDM for cancer detection. It can depict lesion neovascularity in an analogous manner to breast MRI. The dual-energy technique consists of acquisition of low- and high-energy images after intravenous iodine contrast agent administration in both CC and MLO views. The total acquisition time is about 5 min. Extra radiation dose depends on breast thickness, but still it is acceptable and inferior to the recommended mammographic dose. Recent studies comparing MG, CESM and MRI confirm better lesion detection with CESM and MRI compared to MG alone, both in the screening and diagnostic setting. Further possible indications include pre-operative local staging in case of multifocality/multicentricity, evaluation of response to NACT and possible correlation of enhancement pattern with intrinsic tumour biology/molecular subtype. CESM can be considered as an alternative to MRI in case of contraindications to MRI (limited availability, cost issues, claustrophobia, gadolinium allergic reactions, etc.). Further studies will define the future role of this promising technique.

Session Objectives:

1. To understand the technical principles of contrast-enhanced spectral mammography.
2. To be familiar with the current indications in clinical practice and current published data on overall performance of contrast-enhanced spectral mammography.
3. To appreciate future perspectives in screening and diagnostics setting.

A-753 14:05

Technique and comparative approaches

M.B.I. Lobbes; Maastricht/NL (marc.lobbes@mumc.nl)

Contrast-enhanced spectral mammography (CESM) or contrast-enhanced dual-energy mammography (CEDM) is a novel mammographic technique which is superior to full-field digital mammography (FFDM) and matches the performance of breast MRI, not only in terms of breast cancer detection but also in the assessment of disease extent. In a typical CESM exam, an iodine-based contrast agent is administered intravenously two minutes prior to image acquisition. In general, an iodine contrast concentration higher than 300 mg/mL is used, with a dose of 1.5 mL/kg body weight. Preferably, an automated injector should be used with a flow rate of 3 mL/s. Next, the patient is positioned in the mammography unit like a regular FFDM exam, with image acquisition consisting of two views per breast: mediolateral oblique and craniocaudal. The exam consists of a low-energy image, which is similar to FFDM. However, the CESM exam also acquires a high-energy image to enable visualization of the iodine uptake. This image is not for diagnostic purposes,

but is used to post-process a recombined image, which shows areas of contrast captation. On a PACS workstation, only the low-energy and recombined images are displayed. The principles behind CESM are similar to those used in breast MRI. Hence, several studies have compared the diagnostic performance of these two. These have shown that CESM has a similar or sometimes even better diagnostic performance than CESM. CESM exams tend to have less false-positive findings than breast MRI and are generally better tolerated by patients that underwent both exams.

Learning Objectives:

1. To understand the technical considerations of contrast-enhanced spectral mammography.
2. To be familiar with the pitfalls and limitations of the technique.
3. To have an overview of different comparative approaches.

A-754 14:30

Evidence for efficacy and implementation

E.M. Fallenberg; Berlin/DE (eva.fallenberg@charite.de)

X-ray mammography (MG) has been the gold standard for detection of breast cancer so far. However, the method is limited due to a reduced contrast difference between breast tumours and surrounding breast tissue, especially in dense breasts. In postoperative surveillance exams, scar tissue can compromise the detection of local recurrence due to postoperative architectural distortions mimicking or masking tumour growth. Also in ultrasound, it can be difficult to differentiate scar tissue, postoperative changes or local recurrence. To overcome the limits of mammography and ultrasound, especially in these conditions, dynamic contrast-enhanced breast MRI is very useful, but is limited in availability and reimbursement. The introduction of full-field digital mammography has presented the possibility of developing further technical methods, which are less expensive and widely available. One of these is contrast-enhanced spectral mammography (CESM). CESM is able to increase sensitivity without decreasing specificity, due to higher contrast and better lesion delineation than mammography alone. In this talk, I will present the clinical performance results of CESM versus mammography and ultrasound. I will show the additional value of CESM in screening assessment. The potential of this technique in imaging the response to neoadjuvant chemotherapy will be elaborated. The role in the detection of recurrence during follow-up examinations after breast-conserving therapy will be addressed as well. The potential advantages and disadvantages will be indicated and a sample of clinical cases will be presented to illustrate how CESM contributes to the detection of lesions and how it can be used in daily clinical workflow.

Learning Objectives:

1. To understand current indications for clinical implementation.
2. To appreciate the added value of information provided by contrast-enhanced spectral mammography as a problem-solving tool in every day diagnostic dilemmas.
3. To become familiar with the results of published studies on overall performance of contrast-enhanced spectral mammography comparing to digital mammography.

Author Disclosure:

E.M. Fallenberg; Board Member; EUSOBI. Research/Grant Support; Siemens Healthcare, Guerbet, GE Healthcare. Speaker; GE Healthcare, Guerbet, Bayer Healthcare.

A-755 14:55

Finding the killer cancers? Can it replace MRI?

C. Dromain; Lausanne/CH (Clarisse.Dromain@chuv.ch)

Contrast-enhanced digital mammography is a relatively recently introduced imaging technique that uses an intravascular contrast agent to identify breast cancer on the basis of iodine signal enhancement from tumour angiogenesis. CESM is generally used in the diagnostic setting with clinical indications similar to breast MRI. However, while both CESM and MRI are based on the analysis of washing and washout of breast lesions, there are several technical differences potentially influencing the clinical performance and image interpretation. These major differences include 2D vs 3D images, contrast and temporal resolution, type and quantity of contrast agent, acquisition under compression vs free of compression, positioning, additional value of LE image and limited kinetic analysis for CESM interpretation. If MRI remains the most sensitive method for breast cancer detection, published data comparing CESM and MRI have shown a similar rate of primary tumour detection and size measurement. The largest prospective multicentre study conducted in 178 patients found the overall sensitivity of MRI to be better than that of CESM (76% vs 72%, p < 0.05), but the overall specificity of CESM was better than that of MRI (94% vs 88%, p < 0.001). The difference in sensitivity in favor of MRI was explained by a better sensitivity for additional lesion detection (39% for CESM vs 49% for MRI), while the sensitivity for index lesion detection was identical (95% for CESM versus 94% for MRI). Based on published data including one meta-analysis, CESM can be considered as an alternative to

Postgraduate Educational Programme

MRI, in particular in the case of contraindications to MRI as well as difficulty in MRI availability.

Learning Objectives:

1. To understand the association between enhancing pattern information provided by contrast-enhanced spectral mammography and tumour biology.
2. To appreciate the comparison of information provided by contrast-enhanced spectral mammography and breast MRI regarding lesion morphology and enhancement.
3. To become familiar with published data comparing sensitivity and positive predictive value of the two techniques.

Author Disclosure:

C. Dromain: Research/Grant Support; GE Health Care.

15:20

Panel discussion: Is contrast-enhanced spectral mammography the "mammography of the future"? Can it provide relevant morphological and functional information in everyday practice in a simpler manner? Can it replace breast MRI?

14:00 - 15:30

Room E2

Special Focus Session

SF 15c

My three top tips for neuroimaging

A-756 14:00

Chairperson's introduction

J. Van Goethem; Antwerp/BE (johan.vangoethem@uantwerpen.be)

Despite the vast amount of knowledge that is available in books, at courses and online, sometimes radiologists still miss basic and practical information for use in their daily practice. This session will provide easy-to-understand, easy-to-learn and easy-to-remember tips on neuro-imaging. Each speaker will provide his or her top three tips in their field of expertise. The information will be presented in short 6-minute lectures focusing on these tips.

Session Objectives:

1. To learn practical tips and tricks usable in daily neuroimaging practice.
2. To avoid common pitfalls in neuroimaging.
3. To learn how to tackle common diagnostic problems in neuroimaging.

A-757 14:05

Leukodystrophies

B. Ertl-Wagner; Munich/DE (Birgit.Ertl-Wagner@med.uni-muenchen.de)

Leukodystrophies of the brain can be difficult to diagnose. It is important to be familiar with the different imaging patterns of metabolic disorders and with the typical clinical presentations. Crucial clinical information needs to include the age at presentation, the gender, the family history and the type and evolution of symptoms. Symptoms may be progressive or occur in crisis-like deteriorations. When interpreting images of patients suspected of suffering from a leukodystrophy always remember these three tips: (1) Know as much as possible about the clinical symptoms, the onset and time course of the symptoms and associated abnormalities. (2) Look for "gradients" in the images, e.g. anterior to posterior, inner to outer gradients of the white matter abnormalities. (3) Look for imaging patterns, such as zones, tigroid patterns or areas of abnormal enhancement.

Learning Objectives:

1. To learn about imaging protocols for the diagnostic evaluation of leukodystrophies.
2. To become familiar with typical imaging patterns of the most common leukodystrophies.
3. To gather an understanding of typical pitfalls in imaging leukodystrophies.

A-758 14:11

Hydrocephalus

S. Kumar; Singapore/SG (sumeet.kumar@singhealth.com.sg)

Hydrocephalus is a disorder of CSF hydrodynamics resulting in dilatation of the ventricular system. Imaging plays an important role in establishing the presence of hydrocephalus and distinguishing communicating hydrocephalus from non-communicating or obstructive hydrocephalus. The cause of hydrocephalus and complications arising from it can often be revealed by imaging. In this lecture, radiological signs of early hydrocephalus and review areas in a patient with hydrocephalus will be discussed. Imaging features distinguishing normal pressure hydrocephalus from age-related atrophy will be

explored and the characteristics of DESH pattern of normal pressure hydrocephalus will be explained.

Learning Objectives:

1. To learn to distinguish communicating from non-communicating hydrocephalus.
2. To identify the DESH pattern of chronic communicating hydrocephalus.
3. To discern ventricular dilatation due to atrophy from chronic communicating hydrocephalus.

A-759 14:17

Acute ischaemic stroke

P.M. Parizel; Antwerp/BE (paul.parizel@uantwerpen.be)

Stroke is now a potentially curable disease, if discovered early enough. Imaging can help to establish an early diagnosis. Radiologists should be familiar with the patient history and understand the neurological signs and symptoms; this information tells us WHERE to look and WHAT to look for. My "top tips" are focused on CT (still the mainstay for detecting acute stroke in most hospitals) and are: (1) Use narrow window-width (high contrast) CT review settings to increase detection of subtle stroke signs on CT. Many radiologists find it difficult to assess the stroke volume and extent on CT. Other tools, such as the ASPECTS score, can also improve sensitivity and specificity, especially for less experienced readers, but narrow window width settings are the first step. (2) Look for the hyperdense vessel sign, which refers to focal increased density in the vessel and reflects the presence of thromboembolic material within the lumen. It is most commonly observed in the middle cerebral artery, and less frequently in other cerebral vessels, e.g. basilar artery tip. (3) Perform CT angiography to look for blocked vessels, in order to decide if the patient is a good candidate for referral to the angiography suite for clot extraction. (4) Perform CT perfusion, to assess potentially viable brain tissue, the so called penumbra. This is the brain tissue at risk, surrounding the infarct core. On CT the penumbra is the area surrounding the core infarct with delayed arrival of contrast and prolonged MTT, and with preserved CBV (reflecting auto-regulation).

Learning Objectives:

1. To learn how to recognise acute infarct on NECT.
2. To know when to use advanced imaging in acute stroke.
3. To learn the indications for thrombectomy depending on NECT findings.

A-760 14:23

Low back pain

M. Muto; Naples/IT (mutomar2@gmail.com)

Clinical finding must correlate always with imaging finding before any type of minimal invasive or surgical procedure. This is a mandatory rule to avoid overtreatment and the development of post-treatment complications that are difficult to solve. Low back pain can be related to soft tissue abnormality, DDD or neoplastic lesion, and for this reason an appropriate diagnostic approach is necessary to exclude or include patients in the treatment. The use of multimodality imaging in evaluating low back pain is very important not only in the case of degenerative spine disease, but also in patients with clinical and imaging findings suspicious of primary or secondary spine neoplasm. Integration of MR with CT can have added value in understanding the pain source and excluding neoplasm or clarifying the type of neoplasm. In this case, never forget Nuclear Medicine study for a complete oncologic balance. Once you have excluded or confirmed the presence of a diffuse or solitary oncologic disease, it is possible to decide about a mini-invasive treatment or surgical treatment. The absence of neurological deficit leads to a mini-invasive approach to disk disease with multiple treatment options.

Learning Objectives:

1. To learn how to match clinical and imaging findings.
2. To understand how to use multimodality imaging in evaluating low back pain.
3. To learn the possibilities of percutaneous treatments in low back pain.

14:29

Questions and discussion

A-761 14:37

Movement disorders

T.A. Youssry; London/UK (t.youssry@ucl.ac.uk)

Disease or degeneration of the basal ganglia, cerebral cortex and sometimes the thalamus give rise to disorders of movements (MD) known as dyskinesias (Greek: difficult movement), which can be differentiated into hypokinetic and hyperkinetic syndromes. We will concentrate on the hypokinetic syndromes, which include Idiopathic Parkinson's disease (IPD), atypical PD (APD): multiple system atrophy (MSA), progressive supranuclear palsy (PSP) and cortico basal

Postgraduate Educational Programme

degeneration (CBD). These movement disorders (MD) are often difficult to diagnose and to treat. Up to now the diagnosis is based on clinical criteria. However, despite the fact that imaging plays an increasing role in establishing and confirming the diagnosis of MD, many radiologists are not familiar with the role of the various imaging techniques, in establishing the diagnosis, monitoring disease progression and furthering our understanding of the pathophysiology of MD. We will present on the most salient imaging signs that will allow the diagnosis of these disorders.

Learning Objectives:

1. To be able to categorise movement disorders.
2. To know the value of MRI in movement disorders.
3. To learn how to differentiate different entities causing movement disorders.

A-762 14:43

Dementia

S. [Haller](mailto:Haller@affidea.ch); Carouge/CH (Sven.Haller@affidea.ch)

"no abstract submitted"

Learning Objectives:

1. To understand how ASL might improve confidence of diagnosing dementia, notably at early stages.
2. To understand how SWI might contribute to the diagnosis of dementia with Lewy bodies.
3. To understand that in many cases dementia has mixed degenerative and vascular pathology.

A-763 14:49

Multiple sclerosis

A. [Rovira-Cañellas](mailto:rovira@idi.gencat.cat); Barcelona/ES (alex.rovira@idi.gencat.cat)

In the last few years, techniques and clinical implementation of MR imaging of multiple sclerosis (MS) have markedly evolved based on the relatively large amount of new published data from clinical trials and observational studies, which assessed the value of this tool in the diagnosis and for monitoring and predicting treatment response of this disease. The aim of this presentation is to provide few tips for the clinical implementation of brain and spinal cord MR imaging in the diagnostic and monitoring process of patients with MS, based on an extensive review of recent literature and personal experience. These tips, which include the recommended brain and spinal cord MRI protocol, some key radiological features that help in the accurate diagnosis of this disease, and the role of MR imaging for monitoring and predicting treatment response, should help neuroradiologists in the optimization of the use of MR imaging in MS in clinical practice.

Learning Objectives:

1. To know the recommended brain and spinal cord MRI protocol in multiple sclerosis.
2. To be familiar with the typical radiological features of multiple sclerosis.
3. To learn how to use MRI for monitoring and predicting treatment response in multiple sclerosis.

Author Disclosure:

A. Rovira-Cañellas: Advisory Board; Biogen, Novartis, Sanofi-Genzyme. Speaker; Biogen, Novartis, Roche, Stendhal, Teva.

14:55

Questions and discussion

A-764 15:01

Non-enhancing brain tumours

M. [Smits](mailto:smits@erasmusmc.nl); Rotterdam/NL (marion.smits@erasmusmc.nl)

A non-enhancing adult brain tumour is commonly a low-grade glioma, but 30% of non-enhancing lesions prove to be anaplastic on histopathology. Moreover, the current molecular data suggest that 20% of the histologically low-grade tumours carry in fact the glioblastoma-like genotype (7+/10- TERT mutated) with a dismal clinical course similar to glioblastoma. Given this prognostic heterogeneity, the question is even whether tumour grade may retain its clinical relevance. Clearly, in patients with non-enhancing tumours mimicking relatively benign low-grade glioma, but with a molecular profile indicating clinical behaviour and prognosis of glioblastoma, any delay in initiating treatment will be detrimental. At the same time, the policy in patients with non-enhancing tumours is controversial. A watch and wait policy is advocated by many physicians, while others recommend immediate surgery. Surgery, however, carries a risk for peri-operative morbidity in patients that are generally clinically asymptomatic, apart from usually well-controlled seizures. An early recognition of specifically patients with glioblastoma-like non-enhancing glioma by - advanced - MR imaging and analysis will greatly improve and allow for personalised treatment decisions.

Learning Objectives:

1. To learn the differential diagnosis of non-enhancing brain tumours.
2. To learn the added value of advanced imaging techniques in non-enhancing brain tumours.
3. To learn the most important pitfalls in assessing non-enhancing brain tumours.

Author Disclosure:

M. Smits: Consultant; independent reviewer for Parexel Ltd.

A-765 15:07

Ring-enhancing brain lesions

M.M. [Thurnher](mailto:thurnher@meduniwien.ac.at); Vienna/AT (majda.thurnher@meduniwien.ac.at)

When ring-like enhancing brain lesion is detected, the following questions arise: a) differentiation between an abscess and a neoplasm, b) bacterial or fungal origin, c) tuberculous lesion, d) parasitic infection, and finally e) demyelinating lesion? Diagnosis will be made using multiparametric MR imaging including conventional and advanced MR techniques (DWI, SWI, MR perfusion). This lecture will teach you how to create a quick road map and how to interpret MR imaging findings on different MR techniques to make a specific diagnosis of a ring-like enhancing brain lesion.

Learning Objectives:

1. To know the top differential diagnosis of ring-enhancing lesions.
2. To recognise less common pathology giving rise to ring-enhancing lesions.
3. To understand the value of advanced imaging in ring-enhancing lesions.

A-766 15:13

Assessment of tumour response/progression

P.C. [Maly Sundgren](mailto:Maly.Sundgren@med.lu.se); Lund/SE (Pia.Sundgren@med.lu.se)

Clinical information about primary diagnosis, treatment in the form of surgery, chemotherapy and radiotherapy and the time between the treatment and the present images are crucial for the correct differentiation between response and progression. Images alone can be misleading. In addition to the conventional MR sequences pre- and post-contrast administration, additional sequences like diffusion-weighted imaging and perfusion-weighted imaging can be valuable to differentiate between response and progression as well as these sequences can help especially to detect progressive disease before the lesion demonstrates contrast enhancement. All imaging shall be analysed together with the clinical information and previous MR examinations.

Learning Objectives:

1. To understand the importance of appropriate clinical information to be able to comment on response or progression.
2. To understand the indications for diffusion and perfusion imaging in assessing response or progression.
3. To be able to discuss the value of advanced imaging in the assessment of response or tumour progression.

Author Disclosure:

P.C. Maly Sundgren: Investigator; I do research on the use of advanced imaging in brain tumor treatment effects. Research/Grant Support; I have funding from Swedish Research Council, Cancer Foundation and regional funding for advanced MRI in monitoring brain tumor treatment, treatment effects and tumor grading.

15:19

Questions and discussion

14:00 - 15:30

Room F1

E³ - European Diploma Prep Session

E³ 1523

Gynaecological and obstetrics

A-767 14:00

Chairperson's introduction

K. [Kinkel](mailto:kinkel@grangettes.ch); Chêne-Bougeries/CH (karen.kinkel@grangettes.ch)

Imaging of the uterus and the adnexa uses primarily subsequent transabdominal AND transvaginal ultrasound with colour Doppler capabilities to determine the myometrial, endometrial or adnexal origin of gynaecological symptoms. According to the complexity or the size of the anomaly, magnetic resonance imaging is the first problem-solving imaging tool with excellent soft tissue capabilities. This session will increase the participants' knowledge in learning adequate patient preparation, the appropriate imaging protocol for frequent clinical questions and important diagnostic features and rules for the

Postgraduate Educational Programme

most common gynaecological problems. Computed tomography of the abdomen and pelvis is usually indicated in emergency situations when a gynaecological versus urinary or bowel origin of the symptom is unclear. The indications, techniques and imaging findings of foetal imaging will be presented.

Session Objectives:

1. To understand the imaging presentation of the most common benign and malignant disorders of the uterus.
2. To become familiar with inflammatory and neoplastic disorders of the adnexa.
3. To understand the principles of foetal images and the imaging presentation of the most common foetal disorders.

Author Disclosure:

K. Kinkel: Consultant; for Bayer in MRI of the uterus. Speaker; Philips symposium on Breast Ultrasound.

A-768 14:06

A. Imaging of the uterus

R.A. [Kubik-Huch](mailto:rahel.kubik@ksb.ch); *Baden/CH (rahel.kubik@ksb.ch)*

In this lecture, the current approach to uterine imaging and the advantages and limits of the various imaging modalities will be discussed. Ultrasound, usually using the high-resolution transvaginal approach, is the imaging modality of choice for the uterus. It is widely available and relatively inexpensive. Shortcomings with this imaging test are the limited field of view, obscuration of pelvic organs by the presence of bowel gas, inherent limitations dependent, and its dependence on the experience of the operator. The role of hysterosalpingography has become very limited in recent years. CT has an inferior soft tissue contrast compared to MRI and the disadvantage of ionising irradiation; its role is thus mainly limited to the emergency setting as well as oncologic staging of disease. With its high-contrast resolution, its ability to provide good tissue characterisation, and its multiplanar imaging capabilities, MRI is increasingly used to evaluate pathologies of the uterus. In this lecture, indications and contraindications of MRI will be reviewed. Patient's preparation for pelvic MRI and the imaging sequences, tailored to the specific clinical questions, will be discussed. The audience will learn about the normal zonal anatomy of the uterus, congenital anomalies as well as variations of the uterus during the menstrual cycle and in the postmenopausal phase. The spectrum of normal and pathologic findings and the most important benign and malignant pathologies of the uterus will be reviewed and the role of MRI for staging cervical and endometrial cancer will be discussed.

Learning Objectives:

1. To comprehend the imaging anatomy of the uterus and its changes throughout life and during pregnancy.
2. To understand typical imaging features and the local imaging-based staging of cervical cancer.
3. To become familiar with the typical imaging features of benign disorders of the uterus, especially uterine leiomyomas, adenomyosis and endometriosis.

A-769 14:34

B. Disorders of the adnexa

T.M. [Cunha](mailto:tmargarida@gmail.com), M. Horta; *Lisbon/PT (tmargarida@gmail.com)*

Adnexal disorders are commonly identified in radiologists' daily practice, mostly after minor pelvic complaints or incidentally. The majority of disorders correspond to benign ovarian lesions of no concern, but the clinical impact in predicting malignancy is crucial for proper patient management. Ultrasonography (US) remains the first-line imaging technique to investigate adnexal disorders, with about two-thirds being correctly characterized using transvaginal US with colour Doppler. Magnetic resonance imaging (MRI) is a second-line technique, with higher accuracy than US, and particularly helpful in the assessment of complex and sonographically indeterminate adnexal masses. An algorithmic MRI approach using basic and problem-solving sequences allows to differentiate benign from malignant tumours, and to ensure a specific diagnosis in the majority of adnexal masses. Solid tissues with intermediate T2 signal, diffusion restriction and time intensity curve type 3 on dynamic contrast-enhanced MRI, as well as peritoneal implants, are important predictors of malignancy. In the emergency setting of acute or subacute pelvic pain of women of reproductive age, inflammatory disorders of the upper gynaecologic tract should be considered. Computed tomography (CT) is often performed to assess gynaecologic disorders and to exclude gastrointestinal and urologic diseases. Tubo-ovarian inflammatory diseases often cause complex cystic masses and simulate malignant adnexal tumours. Bilateral involvement, tubular adnexal masses, perilesional infiltration and endometrial thickening in the appropriate clinical and laboratory context favours pelvic inflammatory disorders.

Learning Objectives:

1. To describe the imaging features of benign tumours of the ovaries.
2. To understand the diagnostic evaluation and imaging features of malignant tumours of the ovaries.
3. To explain the imaging features of inflammatory disorders of the Fallopian tubes.

A-770 15:02

C. Fundamentals of foetal imaging

D. [Prayer](mailto:vienna@at); *Vienna/AT*

Foetal MRI can be done at 1.5T or at 3T. Body or cardiac coils are used and ultrafast sequences are applied, the duration of which does not exceed 20-30 seconds on average. The emphasis of foetal MRI lies on providing information that cannot be received by ultrasound which is still the mainstay of prenatal imaging diagnosis. Cerebral malformations involving cortical development and/or infratentorial regions are among the most frequent indications for foetal MRI, as information on these structures may alter the prognosis of gross malformations considerably and thus change the further management of these pregnancies. Acquired pathologies of the brain comprise infection and/or haemorrhage. The high sensitivity of MRI to visualize parenchymal damage and blood breakdown products allows to give accurate information on such processes. In the foetal body, MRI is used in many centres for the assessment of lung development in a variety of pathologies such as, for instance, congenital diaphragmatic hernia, other lung malformations, or premature rupture of membranes which may also be associated with impaired lung development. Complex malformations including more than one organ system can be classified, establishing a respective prognosis and sometimes allowing a conclusion on a genetic background. Prerequisites of performing foetal MRI successfully is a wide knowledge on prenatal cerebral and extracerebral development and deviations thereof. In addition, a training at a foetal MRI centre might be useful to learn the methodical details and troubleshooting, as foetal MRI differs from other MRI methods.

Learning Objectives:

1. To describe the methodology and technical principles of foetal MR imaging.
2. To understand the imaging presentation of common pathologies of the foetal central nervous system.
3. To understand the imaging presentation of common pathologies of the foetal body.

14:00 - 15:30

Room F2

Joint Session of the ESR and EU Commission

ESR/EU

eHealth in radiology: policies, practices, pitfalls, potential

A-771 14:00

Chairperson's introduction

K. [Riklund](mailto:katrine.riklund@umu.se); *Umea/SE (katrine.riklund@umu.se)*

eHealth is a priority topic in which the ESR is actively engaged, having been a member of the European Commission's eHealth Stakeholder Group since 2012. A white paper on teleradiology has been published on insight into imaging and an online survey was conducted in 2012. Recently, HIMSS Europe and the ESR launched the Digital Imaging Adoption Model (DIAM) as a benchmarking programme to guide the adoption of IT supported processes in radiology departments. So, radiology is heavily involved in eHealth and at the session we will learn a lot more of policies, practices, pitfalls, and potential.

Session Objectives:

1. To learn about the ESR's eHealth policy positions, initiatives and tools.
2. To understand the European Union's eHealth policies.
3. To understand the complementarity of and tensions between eHealth policy and practice.
4. To learn about the present status and future outlook for eHealth in radiology from the policy makers' and practitioners' perspectives.

Author Disclosure:

K. Riklund: Board Member; Swedish Drug Authority. Speaker; GE, Paris meeting 2016, Nordic Conf in Radiology 2017 Iceland.

Postgraduate Educational Programme

A-772 14:05

ESR eHealth SC and eHealth policy positions

E. [Neri](mailto:emanuele.neri@med.unipi.it); Pisa/IT (emanuele.neri@med.unipi.it)

The ESR eHealth and Informatics is a subcommittee of the ESR Quality and Safety Committee. The main activities of the subcommittee have been focused on the following: (A) Development of the ESR-RSNA joint Structured reporting initiative. The initiative is ruled by a memorandum of understanding signed in 2015 between RSNA and ESR aimed at promoting the development of structured reports available on the radreport.org website of RSNA. The initiative led to the creation of a Template Library Advisory Board Panel, an editorial board that revises and validates the SR Templates. The eHealth subcommittee produced a ESR position paper on Structure reporting that is under publication in Insight Into Imaging. (B) Impact of the Data Protection Regulation on the Radiology profession. In 2016 the EU delivered the General Data Protection Regulation (GDPR), that provides rules on how to protect the citizens data in the digital era. The eHealth subcommittee has produced a ESR position paper on "What the radiology should know about the GDPR", recently published in Insight Into Imaging. (C) Proper Use of Mobile Devices in Radiology. In the digital single market mobile devices (smartphone, tablets, PCs) are used by multiple physicians as a tool for helping their clinical practice. In radiology mobile devices are used as DICOM user, as eLearning tool, for social media access to improve communication. All these aspects are discussed in the ESR Position paper on the "Use of mobile devices in radiology" under publication in Insight Into Imaging.

Learning Objectives:

1. To learn about the ESR eHealth SC activities.
2. To understand the role of eHealth tools within radiology.
3. To learn about the ESR policy positions on eHealth issues.

Author Disclosure:

E. Neri: Advisory Board; QUIBIM.

A-773 14:20

EU Strategy for Digital Transformation of Health and Care

T. [Piha](mailto:Piha@brussels.eu); Brussels/EU

"no abstract submitted"

Learning Objectives:

1. To learn about the EU's eHealth policies.
2. To understand the EU Digital Single Market Strategy.
3. To understand how EU policies impact radiology.

A-774 14:35

Member States Joint Action on eHealth

C.M. [Auer](mailto:Auer@vienna.at); Vienna/AT

"no abstract submitted"

Learning Objectives:

1. To learn about the EU Member States Joint Action on eHealth.
2. To understand the links between European Commission and Member State eHealth activities.

A-775 14:45

ESR eHealth tools

B. [Brkljacic](mailto:Brkljacic@zagreb.hr); Zagreb/HR (boris@brkljacic.com)

The adoption of eHealth systems has already revolutionised radiologists' daily routine and, with big data and artificial intelligence, the next revolution appears to be just around the corner. The ESR supports its members caught up in these developments by providing a variety of eHealth tools and materials. CDS: In cooperation with the American College of Radiology and National Decision Support Company, the ESR has developed the clinical decision support system, ESR iGuide. Using the ESR's referral guidelines based on the ACR Appropriateness Criteria, ESR iGuide can be integrated into CPOE systems to provide actionable, evidence-based guidance to help referrers select the most appropriate imaging test at the point of patient care. CDS referrals for the first time enable statistical analysis of incoming requests for radiology departments, and these data can be used to improve performance or be linked with other data sets like dose data or structured reports to understand the correlations between the interrelated tasks in the imaging value chain. The ESR has been working in cooperation with the Radiological Society of North America (RSNA) on a joint structured reporting initiative. The first step in this cooperation is the creation of structured reporting templates for a template library to cover clinical scenarios suitable for structured reporting. To facilitate the adoption of these templates in practice, the ESR is exploring cooperation with PACS and voice recognition systems. In addition, the ESR's eHealth and Informatics Subcommittee is publishing a paper on structured reporting in radiology, setting out the ESR's conceptual approach.

Learning Objectives:

1. To learn about the ESR's clinical decision support initiative ESR iGuide.
2. To learn about the ESR-RSNA cooperation regarding structured reporting.
3. To understand how the ESR views the use of eHealth tools in clinical practice.

A-776 14:55

ESR-HIMSS Digital Imaging Adoption Model

J. [Studzinski](mailto:studzinski@himss.org); Leipzig/DE (studzinski@himss.org)

The Digital Imaging Adoption Model (DIAM) has been jointly developed by ESR and HIMSS Europe to provide clinical and managerial users of medical imaging technology with a tool to assess the maturity of their Imaging-IT investments and implementations. The model is designed to identify potential gaps in infrastructure and workflow, to monitor technological progress, to enable benchmarking with peer organisations and to provide a roadmap for strategic and operational planning as well as investment decisions. The DIAM, launched in 2016 at ECR, can be used by hospitals with imaging departments or external imaging centres collaborating with hospitals across the globe. The DIAM associates participating organisations with one of 8 stages. Stage 0 indicates a low level of imaging IT maturity and Stage 7 represents advanced maturity. Participants of the session will learn how the DIAM can be used, which organisations have been assessed so far and what benefits they have received from participation. An outlook about future developments will also be provided.

Learning Objectives:

1. To understand the concept of the Digital Imaging Adoption Model (DIAM).
2. To learn about the benefits in participating in the DIAM.
3. To learn about the DIAM stages, survey and certification.

Author Disclosure:

J. Studzinski: Employee; HIMSS Europe GmbH.

A-777 15:05

Patient perspective on EU eHealth policies

N. [Bedlington](mailto:Bedlington@vienna.at); Vienna/AT

"no abstract submitted"

Learning Objectives:

1. To learn about the ESR-PAG view of eHealth policy in the EU.
2. To understand how patients can benefit from eHealth tools.
3. To learn about concerns about the adoption of eHealth from the patient's view.

15:15

Panel discussion: The role of medical societies in implementing EU eHealth policy

14:00 - 15:30

Room D

Emergency Imaging

RC 1517

The latest update in imaging of polytrauma patients

A-778 14:00

Chairperson's introduction: The role of proper imaging and management in patients after severe trauma

M. [Stajgis](mailto:Stajgis@poznan.pl); Poznan/PL (stajgis@gmail.com)

The rationale of emergency procedures in severe trauma patients is based on the time factor and adequate selection of patients and proper imaging modalities. The "Golden Hour" concept describes the need for as-fast-as-possible management of these patients very well. The present-day diagnostic workup of polytrauma patients is mostly based on whole body CT (WBCT); however, this method is thought to be overused in some clinical scenarios. Therefore, we should look very carefully again at advantages and limitations of still evolving all modern diagnostic modalities such as ultrasound, CT and MR. All three lectures in this session are dedicated to effective imaging of polytrauma patients, management priorities in different clinical situations and suggested practical approach.

Session Objectives:

1. To understand the role of early and fast diagnostic imaging in patients after severe trauma.
2. To recognise the basic statistics in management of polytrauma patients

Postgraduate Educational Programme

which have impact on practical approach regarding selection of proper diagnostic modalities and imaging findings.
3. To be aware of the position and responsibilities of a radiologist in "decision-making team".

A-779 14:05

A. Ultrasound: when, why and by whom?

P.-A. [Poletti](#); Geneva/CH

"no abstract submitted"

Learning Objectives:

1. To become familiar with the role of modern ultrasound in polytrauma patients.
2. To comprehend the rationale of using FAST protocol in selected patients.
3. To know the advantages and limitations of ultrasound imaging in emergency setting.

A-780 14:31

B. CT: is it always whole body?

F.H. [Berger](#); Toronto, ON/CA (fhberger@gmail.com)

In the Western world, polytrauma is the major cause of mortality in people under 45 years of age. Furthermore, it is a major contributor to loss of quality of life and ability to work. The setting of polytrauma is almost always chaotic, not a favourable environment to come to timely diagnosis and treatment. To decrease morbidity and mortality, time is everything. It is our job as radiologists to contribute to the trauma team and help facilitate timely diagnosis - and in many cases, also timely treatment by interventional radiology. To reach the best treatment strategy for the patient as quickly and accurately as safely possible is the goal. In this update on imaging of polytrauma patients, I will focus on the role of CT to achieve this goal. With the progress in CT scanner development, different protocol options arise. Which CT protocols are being used and what factors do they depend upon? In addition, there has been a widespread increase in the use of whole-body CT internationally: is this a good thing or should we be more selective? What is the current evidence to select patients for targeted CT examinations in polytrauma? A lot of these questions have not been definitively resolved. This lecture aims to provide an update of the current insights into the use of CT for trauma care, with the goal of choosing wisely on how to investigate the polytrauma patient in a timely and meaningful fashion.

Learning Objectives:

1. To be familiar with currently worldwide accepted protocols in polytrauma CT imaging.
2. To know clinical conditions requiring whole-body CT.
3. To comprehend the selection of trauma patients for targeted CT examinations.

A-781 14:57

C. Where is the proper place for MRI?

K. [Katulska](#); Poznan/PL (katarzyna_katulska@op.pl)

A multimodality of imaging should be involved in the diagnosis and management of severely injured multi-trauma patients. The current role of magnetic resonance imaging (MRI) of the spinal cord and brain injuries is confident. MRI examination is the imaging method of choice in the assessment of lesion morphology, extent and severity of trauma. In case of neurological symptom not completely explained in CT findings, an MRI must be performed. Among all post-traumatic intracranial pathologies, the diagnosis of diffuse axial injury remains more complex. In fact, about 30% of negative CTs are already positive on MRI. MRI is a powerful diagnostic tool that can detect signs of injury such as minute bleeding (microhaemorrhage), small areas of bruising (contusion) or scarring (gliosis), which are invisible to the CT scan. Newer, specialized types of MRI can assess brain structure at an even finer level or measure brain function to detect alterations in brain structure and function due to traumatic spinal cord and brain injury (SCI, TBI). The protocol for routine MRI of patients with TBI and SCI, which consists of SE and GRE sequences, is proposed. MRI techniques such as SWI, DWI and DTI are discussed, as a new standard protocol. In the acute setting, MRI can determine the presence and extent of injury and guide surgical planning and minimally invasive interventions. Neuroimaging also can be important in the chronic therapy of injury, identifying chronic sequel, determining prognosis, and guiding rehabilitation.

Learning Objectives:

1. To learn which patients are the best candidates for post-traumatic MRI.
2. To be familiar with standard and short MRI examination protocols.
3. To understand the impact of MR findings on further management of polytrauma patients.

15:23

Panel discussion: Summarising comprehensive guidelines, how to quality post-traumatic patients for the proper imaging modality

14:00 - 15:30

Room G

Physics in Medical Imaging

RC 1513

Dose reduction and image quality implications of iterative image reconstruction in CT

A-782 14:00

Chairperson's introduction

K.N. [Bolstad](#); Bergen/NO (kirsten.bolstad@helse-bergen.no)

Ever since the development of the first CT, the quest has been to get as much information as possible in as short amount of time as possible. In the early days of CT, the reconstruction time per image was limited by computer power and effective reconstruction algorithms. The filtered back projection algorithms (FBP) were a compromise between reconstruction speed and image noise. Iterative reconstruction algorithms (IR) takes into account a mathematical assumption of the CT system, which results in less image noise but with a longer reconstruction time compared to FBP. Today, with more powerful and faster computers, IR has become a part of the daily routine. The noise reduction can either be used to improve image quality at the same dose or maintain similar image quality at a lower dose, typically 25-40% dose reduction compared to FBP. Recently, more advanced model-based iterative reconstruction algorithms have become commercially available with a reconstruction time suitable for the clinical routine. These algorithms take into account a mathematical model of the entire system, from the focal spot size and x-ray spectrum to the detector system, resulting in a nearly "noise-free" image. The dose-saving potential for these newer algorithms is up to 80-90% compared to FBP. However, the application of IR does not come without a cost. Even though the image noise is reduced, the appearance of the image may change. Each vendor's IR has a different appearance and a different dose-saving potential. Radiologists need time to get used to the new appearance.

Session Objectives:

1. To learn about the origins of dose reduction using iterative image reconstruction in CT.
2. To understand dose reduction using iterative image reconstruction in CT.
3. To learn about solutions and workarounds.

A-783 14:05

A. Basics of iterative image reconstruction in CT

M. [Kortesniemi](#); Helsinki/Finland (mika.kortesniemi@hus.fi)

Computed tomography image reconstruction is a mathematical process where the raw data projections (sinogram data) acquired during rotational CT scan exposure are transformed into volumetric (3D) image data. As such, reconstruction is an inverse problem, with no direct analytical solution. Traditional algorithms (filtered back-projection) approximate the true acquisition method and are prone to artefacts and noise. Iterative reconstruction methods approach the final solution gradually in steps and may take quantum statistics, physical properties and limitations of image acquisition more faithfully into account. Thus, a more accurate and correct outcome may be achieved. However, more detailed modelling of the actual CT acquisition system, physics, optics and object also increases the calculation time and related CPU requirements. Especially, the forward projection phase (calculation of simulated raw data) on each iteration step is computationally intensive. More optimised reconstruction techniques with clinically acceptable reconstruction times are under active research. As the main diagnostic benefit, higher image quality in terms of lower noise and artefacts can be achieved by using iterative methods, and/or a lower radiation dose. However, users should be aware that current iterative reconstructions potentially alter the image texture in different clinically relevant contrast and detail levels. Therefore, sufficient clinical image quality should be verified when applying iterative techniques on new exam indications and protocol optimization.

Learning Objectives:

1. To learn about the basic aspects of iterative reconstruction.
2. To learn about potential dose reduction via iterative reconstruction.
3. To compare iterative reconstruction with other techniques.

Saturday

A-784 14:28

B. Iterative image reconstruction in clinical practice (dos and don'ts)

H. Alkadhi; Zurich/CH (hatem.alkadhi@usz.ch)

The broad use of computed tomography (CT) is paralleled by concerns regarding its potential risks. In the past years, these concerns have led to the development of a set of strategies for optimising and lowering the radiation dose of CT. Of these techniques, iterative reconstruction algorithms represent a powerful tool, because they allow lowering the dose at a constant noise level and image quality. However, caution must be taken when iterative reconstruction algorithms are being used, and radiation dose can be lowered only to a level where information in the CT images are not lost. This presentation reviews the clinical challenges of using iterative reconstruction techniques in CT imaging, with a focus on low radiation dose examinations. The different iterative reconstruction techniques are discussed, along with their benefits and potential pitfalls.

Learning Objectives:

1. To understand the radiologist's requirements for image reconstruction.
2. To learn about current best practice in image reconstruction for clinical CT.
3. To learn about the potential benefits and pitfalls of using iterative reconstruction in clinical CT.

A-785 14:51

C. Image quality assessment of iterative reconstruction: pitfalls and future directions

E. Samei; Durham, NC/US (samei@duke.edu)

Enabled by increased computational power of recent years and motivated by a desire to reduce CT radiation dose, iterative reconstruction methods have become a staple component of modern CT technology. While these methods offer a renewed opportunity to optimise dose and image quality, they also necessitate a renewed approach towards image quality in CT. Many metrics that have traditionally been deployed to characterise and optimise CT performance, no longer directly apply to CT images that are iteratively reconstructed. The first-order metrics of contrast, resolution, and noise need to be extended to second- and third-order metrology of task transfer function (TTF), noise power spectrum (NPS), detectability and estimability indices, and noise heterogeneity. New methods have been developed to measure these new metrics and integrate them in the optimisation process. This presentation offers a description of the traditional and new CT image quality metrology, outlines the new methods of their assessment, and highlights their utility for improved patient care.

Learning Objectives:

1. To learn about basic image quality metrics employed in CT.
2. To understand why image quality assessment is difficult with iterative reconstruction.
3. To learn about up-and-coming methods for image quality assessment.

Author Disclosure:

E. Samei: Advisory Board; medInt Holdings, LLC. Grant Recipient; Siemens, GE.

15:14

Panel discussion: How low can we go?

14:00 - 15:30

Room K

EFRS Workshop

EFRS WS

Making the most of social media

A-786 14:00

Chairperson's introduction: Social media in healthcare

J. McNulty; Dublin/IE (jonathan.mculty@ucd.ie)

This is an essential session for any ECR attendees who are active on social media. Each year, the European Federation of Radiographer Societies (EFRS) delivers a workshop session as part of the main ECR programme with this year's session focusing on the pervasive topic of social media. Facebook, Twitter and LinkedIn, which will all be referenced in this session, have a combined total of two billion active users worldwide. Social media offer all health professionals with new opportunities and new challenges. If used appropriately, social media can: enhance peer to peer communication and communication with patients and the public; provide educational and continuous professional development (CPD) opportunities; allow professional societies to more effectively engage with their membership; enhance the reach and engagement at international congresses; and facilitate better patient

engagement with imaging services. For any health professionals using social media, they must be aware of the boundaries between personal use and professional use, consider confidentiality and data protection, and respect best practice guidelines on the appropriate use of social media. For professional societies and professional regulators, there is a growing need to implement clear policies on appropriate and professional use of social media.

Session Objectives:

1. To consider the wide range of use of social media in healthcare, healthcare education, and research.
2. To highlight the importance of all health professionals being aware of best practice in professional social media use.

A-787 14:05

Enhancing communication and collaboration through social media

M.J. Díaz Candamio; Ferrol/ES (mjdcandamio@gmail.com)

Social media (SoMe) that changed our way of getting information and communicating is also an incredibly powerful professional networking tool. Nevertheless, health-care professionals are using SoMe to a lesser extent than specialists from other sectors, probably because it is a highly regulated field, in which data privacy is crucial, with many perceived risks and potential threats. Radiology is among the health-care fields with lesser presence in SoMe. This situation correlates with the fact that radiology professionals perform our work "in the dark", with little recognition on the part of patients. SoMe can end with this unawareness of our work. The SoMe-mediated social interactions allow many kinds of professional collaboration, including not only sharing information and experiences but also discussion on procedures or diagnosis. Personal branding of doctors, practices or institutions as well as academic publishing promotion are other well-known uses of SoMe publishing. We can utilize SoMe in radiology to disseminate knowledge, which is crucial at a time when patient-centred medicine is practised, in which patients participate in diagnostic and imaging-guided procedure decision-making. This collaborative networking is global, with fewer language barriers. Nevertheless, the use of English makes universal sharing of content easier. SoMe networks have also potential risks, including not only false information but even false identities. If you still do not use SoMe for professional purposes in radiology, you should be aware of the risks, but exploit their advantages as soon as possible. Keep in mind about being authentic and professional as well as respecting patient's data confidentiality.

Learning Objectives:

1. To explore how social media allows us to enhance communication and collaboration between colleagues and patients.
2. To consider the importance of establishing clear guidance on the use of social media for radiologists and radiographers.
3. To gain some top tips on the dos and don'ts of professional social media use.

A-788 14:20

#MedRadJClub: a Twitter journal club

N.H. Woznitza; London/UK (nicholas.woznitza@nhs.net)

Social media are increasingly being used by health-care professionals, including radiographers. #MedRadJclub, a Twitter-based monthly radiographer journal club was first held in March 2016. Use of the digital space removes barriers to traditional journal club participation, such as geographical boundaries, and connects radiographers across the globe. An hour-long chat, centred on a key paper chosen from the literature, acts as a forum for radiographers to discuss research, share best practice and access continuing professional development (CPD). Over 1,000 radiographers have participated in the chats, with the website accessed from 101 countries. The impact of #MedRadJclub includes accessible CPD, research collaborations and a bi-annual conference on advanced radiographer practice.

Learning Objectives:

1. To understand how Twitter can be used as an alternative to face to face journal clubs.
2. To learn how #MedRadJclub works, what it offers over conventional journals clubs, and why radiographers should participate.
3. To appreciate the impact of #MedRadJclub.

A-789 14:35

The value of social media to professional societies

E. Alfayate Sáez¹, M.A. de la Cámara Egea², N.I. Vega de Andrea³,
¹Madrid/ES, ²Jaen/ES, ³Girona/ES (ealfayate@fundacioncien.es)

The aim of this paper is to understand the importance of a digital society and the type of knowledge that can be transferred within a digital environment. Online presence that lacks activity is not synonym of success. Activity is what drives information so that it can be conveyed and create a bigger impact in

Postgraduate Educational Programme

digital communities. Use requirements: integrating information related to the entity and other new content or links, and to moderate the interaction of followers in their comments. Digital marketing (content marketing): variables of engagement (encouraging conversation and commitment to the community). Effective use of popular digital channels: Facebook, LinkedIn, YouTube and Twitter. In the recruitment of key users in a WhatsApp group, the conversation has been standardised to: a) improve digital competencies, b) pinpoint interest in digital content, and c) create useful conversations for the profession. Identifying focus in each channel: the informative content (news from the corporate Web or other resources) has been adapted to each type of social network. Twitter: corporate information (digital framework), diverse subjects. Facebook: corporate information, resources for professionals. LinkedIn: corporate information, resources for professionals. YouTube: video reports of events that are useful to focus more attention on the congressional activity of the entity. External relationship: SEGRA joins health conversations that are not related to radiology. Twitter: identifying hashtags related to health. Facebook: share content and foster conversations. Value for followers and following groups: news about technology, information related to events, moderating conversations throughout the social networks, proposals of innovative topics, and to find out what the communities' needs are.

A-790/A-791 14:50

Social media at ECR

S. Lee, K. Friedrich; Vienna/AT, (simon.lee@myesr.org), (konrad.friedrich@myesr.org)

Social media such as Facebook, Twitter and Instagram are frequently a part of participants' experiences at medical meetings, with users' activity ranging from casual photos of their breakfast, to in-depth discussion of scientific content. For meeting organisers, engaging with social media users and encouraging interaction can be of benefit to both the event and its participants. By maintaining an active presence on social media, the organiser gives meeting attendees an easy point of contact and a reliable source of information, while also being able to monitor and contribute to conversations surrounding the event. The European Society of Radiology (ESR) has used social media to connect with attendees of its annual meeting, the European Congress of Radiology (ECR), for a number of years and has explored ways to stimulate the use of those platforms. Many ECR attendees use Facebook and Instagram to share their experience of the congress (and the ESR is active on both platforms), but it is Twitter that has been the most interesting platform for the ESR with regard to the ECR in recent years, especially in terms of feedback and discussion of programme content. A steady rise in participation on Twitter reached another new high at ECR 2017, with an increase in ECR hashtag usage, both in terms of the number of users and the volume of activity. This presentation will look at how and why the ESR uses social media in relation to its annual meeting and why Twitter is currently our primary focus.

Learning Objectives:

1. To learn how social media can be used effectively to enhance engagement in a congress.
2. To explore the scale and impact of social media at ECR 2017.
3. To consider what more social media can add to ECR.

A-792 15:05

Improving patient engagement through social media

L. Robinson; Salford/UK (l.robinson@salford.ac.uk)

The presentation will take a case study approach by presenting one particular example of social media in imaging: the Word of Mouth Mammogram e-Network (WoMMeN) developed for UK breast screening clients. Following a description of WoMMeN, evaluative data from the WoMMeN project will be presented to determine whether social media can lead to improved patient engagement. The definition of 'engagement' here takes on a broad perspective. It will consider not only engagement in the screening programme (i.e. attending for the examination), but also engagement in service quality improvements. Finally, the lens will be focused more narrowly to explore the impact on individual women. This will take the form of illustrative examples, online interactions taken directly from our WoMMeN social media hub and associated Facebook page.

Learning Objectives:

1. To explore how social media can be used to improve patient engagement with imaging services.
2. To learn about social media use in the Word of Mouth Mammogram e-Network (WoMMeN).
3. To appreciate the impact of online interactions with patients.

15:20

Panel discussion: Making better use of social media: what should we consider?

14:00 - 15:30

Room M 4

E³ - ECR Academies: Tips and Tricks in Pancreatic and GI Tract Imaging

E³ 1522

The anal canal: does MRI make it easy?

A-793 14:00

Chairperson's introduction

S. Halligan; London/UK

As chair of this session, I will introduce the topic of anal MRI, its clinical relevance, and how this will be addressed by the speakers. An interactive case presentation illustrating the topic will also be presented.

A-794 14:05

A. MRI of the anal canal: from normal anatomy to local tumour staging

C. Hoefel; Reims/FR

Although a rare disease, anal cancer is increasingly being diagnosed in patients with risk factors, mainly anal infection with the human papilloma virus. Magnetic resonance imaging (MRI) with external phased-array coils is recommended as the imaging modality of choice to grade anal cancers and to evaluate the response assessment after chemoradiotherapy, with a high contrast and good anatomic resolution on the anal canal. MRI provides a performance evaluation of size, extent and signal characteristics of the anal tumour before and after treatment, as well as lymph node involvement and extensions to the adjacent organs. MRI is also particularly helpful in the assessment of complications after treatment and in diagnosis of disease recurrence. We will propose an MRI protocol for imaging of the anal canal, explain the MR anatomy of the anal canal and review possibilities of MRI in the evaluation of tumour in both the pre- and posttreatment context.

Learning Objectives:

1. To learn the relevant sequences for MRI of the anal canal.
2. To understand the anatomy as demonstrated by MRI.
3. To become familiar with the staging of primary tumour, before and after treatment.

A-795 14:33

B. Fistulae-in-ano: detect, stage, classify

D.J.M. Tolan; Leeds/UK (djmtolan@doctors.org.uk)

MRI is a critical tool for the evaluation of fistulae-in-ano and in particular for the surgical management of complex or recurrent cryptoglandular perianal sepsis and in patients with fistula from Crohn's disease who can be treated medically or surgically. The MRI sequence selection can target water/oedema (STIR or fat saturated T2) or contrast enhancement (post contrast fat saturated T1). Correct orientation of MR scan planes to the axis of the anal canal is critical to allow correct assessment of fistula anatomy for surgical planning, and Park's Classification is the most commonly accepted by surgeons and should be used by radiologists. Reports should follow a uniform structure including the Park's classification type of the fistula, the location of internal opening, course of the fistula, position of the external opening and number and position of extensions/secondary tracks.

Learning Objectives:

1. To learn about the relevant MRI sequences in patients suspected of fistulae-in-ano.
2. To understand the most common classification of fistulae.
3. To become familiar with the questions asked by the clinician before treatment.

A-796 15:01

C. My tough cases

F. Maccioni; Rome/IT (francesca.maccioni@uniroma1.it)

Perianal disease (PD) has a low prevalence in the overall population, approximately of 0,01%. It develops more frequently in Crohn's disease (CD) and in haematological malignancies (HM). Usually, perianal CD develops in association with lesions of the small and large bowel, in 23% to 38% of CD patients, including children. In CD, the fistulous tracts are much more complex than that in the fistulas of cryptoglandular origin, and are usually associated with ramifications and abscess. They are considered as some of the most disabling complications of Crohn's disease (CD), especially in children and young adults. Perianal disease is, in fact, frequently associated with aggressive intestinal or colorectal disease. The association of anal fistulas with rectal

Saturday

disease represents a negative prognostic factor due to the higher risk of radical proctectomy and definitive ileostomy. Early diagnosis and prompt clinical management are fundamental for a positive outcome. High-resolution MRI is the gold standard for the first diagnosis and staging of perianal fistulas. MRI results are crucial in the therapeutic planning, addressing the patients towards pharmacological or surgical treatment. MRI also plays a primary role in the assessment of fistula healing after medical or surgical treatment. Perianal fistulas, unfortunately, tend to recur in more than 30% of cases, despite pharmacological and surgical treatments.

Learning Objectives:

1. To learn from clinical experience the unusual presentation of diseases of the anal canal.
2. To understand how to report on MRI after treatment.

14:00 - 15:30

Room M 5

Transatlantic Course of ESR and RSNA (Radiological Society of North America): Sports Imaging

TC 1528

Musculoskeletal interventional procedures

Moderators:

L.W. Bancroft; Orlando, FL/US
A.J. Grainger; Leeds/UK

A-797 14:00

A. Diagnostic and therapeutic injections in the athlete: pearls and pitfalls

P. Peetrons; Brussels/BE (ppeeetrons@his-izz.be)

Before any treatment of tendons and ligaments with any ultrasound-guided technique, a correct diagnosis must be achieved. One of the main pitfalls is to treat incorrectly diagnosed lesions. This is unfortunately too often the case. Patients sometimes come for therapy with a wrong diagnosis or a non-imaged documented diagnosis. Some examples are the so-called pes anserine bursitis, the so-called trochanteric bursitis, an underestimated rotator cuff tear which appears to be a full-thickness instead of a partial thickness tear, and a Haglund deformity considered as an Achilles tendinopathy. The examples are numerous. A second pitfall is the use of a treatment which is non-adapted to the pathology. Using steroids to cure the degenerative changes within a tendon may lead to a short-time improvement, but not to a longtime healing of the lesion. Depending on the scheduled and importance of sports activity, the choice of the treatment can be different. Tendon needling and PRP injections are the major actual treatments for long-term regeneration of collagen fibres within tendons and ligaments. But they need time and rest. A good post-therapy rehabilitation must be followed by the sportsman. The quality and quantity of the plasma and the platelets are also of very big importance. In tendons, in athletes, the plasma must be as poorly cellular as possible, and the centrifugation of the blood must give 1.5 to 2.5 the native amount of platelets. It has been shown that a too heavy concentration may have adverse effects on regeneration.

Learning Objectives:

1. To become familiar with the most common requests and indications for sports-related injections.
2. To learn about technical considerations for performing MSK injections.
3. To understand reasons to delay injections or avoid certain injectables.

Author Disclosure:

P. Peetrons: Investigator; GE for evaluation of an Ultrasound Unit.

A-798 14:30

B. Injectables, percutaneous tendon fenestration and tenotomy: clinical outcomes and current evidence

J. Jacobson; Ann Arbor, MI/US (jjacobsn@umich.edu)

For joint abnormalities and tendinopathy, there exists many percutaneous treatment options. Anaesthetic agents are used, often combined with corticosteroids, to inject joints and bursae for diagnostic and therapeutic purposes. With regard to anaesthetic agents, all are cytotoxic to chondrocytes and synovial cells to some degree. Corticosteroids may be used to decrease inflammation within a synovial space. The use of corticosteroid to treat tendinopathy is counterintuitive, as inflammation is not present, injection into tendon causes tenocyte death, and the analgesic effect of corticosteroids is short lived, and therefore the underlying tendon pathology is not treated. A number of ultrasound-guided tendon treatments can be used for tendinopathy. One treatment is percutaneous tendon fenestration or tenotomy. With this procedure, a needle is passed through the abnormal tendon segment repeatedly to break up the degenerative process, induce bleeding and inflammation, and initiate the healing of the abnormal tendon. Other procedures include the injection of autologous whole blood during the

fenestration process, as well as the injection of platelet-rich plasma during fenestration. With this latter technique, the autologous whole blood is centrifuged to concentrate the platelets for injection. All three of these percutaneous tendon treatments have been shown to be effective, although it is controversial which technique is best. The cost of each procedure should also be considered. There exists newer and more controversial percutaneous tendon treatment, such as injection of mesenchymal stem cells, human amniotic membrane, and deer antler velvet. These procedures are largely considered experimental until research studies demonstrate their safety and efficacy.

Learning Objectives:

1. To be aware of the indications and benefits of available injectables used to treat sports-related injuries.
2. To learn about technical considerations for performing tendon fenestration and tenotomy.
3. To become familiar with the current evidence on results of MSK procedures in the literature.

Author Disclosure:

J. Jacobson: Advisory Board; GE, Philips. Author; Elsevier. Consultant; Bioclinica.

A-799 15:00

C. Interactive case discussion (part 1)

P. Peetrons; Brussels/BE (ppeeetrons@his-izz.be)

Interactive discussions on cases will be performed with the audience. The indication of percutaneous treatment of tendons and muscles will be emphasized, compared with indications of steroid injections. The importance of a correct diagnosis, prior to any interventional technique, will be stressed out.

Learning Objectives:

1. To learn the targeted approach to injecting joints, ligaments, tendons and tendon sheaths.
2. To appreciate pitfalls to avoid in MSK procedures for treatment of sports-related injuries.
3. To understand evidence-based data on various MSK procedures in order to give patients realistic expectations after treatment.

Author Disclosure:

P. Peetrons: Investigator; GE for evaluation of an Ultrasound Unit platform.

A-800 15:15

C. Interactive case discussion (part 2)

J. Jacobson; Ann Arbor, MI/US (jjacobsn@umich.edu)

The purpose of the interactive case discussions is to emphasize the teaching points made in the prior lecture reviewing injectables, percutaneous fenestration, and tenotomy. One topic to be addressed will be the imaging findings and potential treatment algorithm for greater trochanteric pain syndrome. In this clinical scenario, a true distended and inflamed bursa is not common and the primary pathology relates to gluteal tendinopathy. Before pursuing an interventional procedure, conservative management such as proper eccentric physical therapy should be exhausted. The next consideration could be injection of corticosteroid in the subgluteus maximus (or trochanteric bursa) for the primary purpose of providing temporary pain relief so that the patient can tolerate eccentric physical therapy. The corticosteroid injection is not used as an anti-inflammatory agent as true inflammation is not present, and the pain relief is typically short lived. If the patient again fails eccentric physical therapy, then the patient may be offered percutaneous fenestration, autologous whole blood injection, or platelet-rich plasma injection. While all three have been shown to be effective, it is still unclear which treatment is best. The dramatic differences in cost should be a consideration when selecting the tendon treatment.

Learning Objectives:

1. To learn the targeted approach to injecting joints, ligaments, tendons and tendon sheaths.
2. To appreciate pitfalls to avoid in MSK procedures for treatment of sports-related injuries.
3. To understand evidence-based data on various MSK procedures in order to give patients realistic expectations after treatment.

Author Disclosure:

J. Jacobson: Advisory Board; GE, Philips. Consultant; Bioclinica. Other; Elsevier: Book Royalties.

16:00 - 17:30

Room A

E³ - ECR Academies: Interactive Teaching Sessions for Young (and not so Young) Radiologists

E³ 1621

Errare humanum est

A-805 16:00

A. Errors in chest radiograph

J. Cáceres; Barcelona/ES (josecac@gmail.com)

Errors in diagnostic imaging are not uncommon and the radiologist is responsible for most of them. In this presentation, I intend to analyse the most common causes of errors in chest imaging and how to avoid them. Perceptual errors are the most common ones, accounting for up to 50% of errors committed by radiologists. For a variety of reasons, in this type of error the radiologist does not see the abnormality, which may be obvious or subtle. Some search findings are missed because we do not search for additional abnormalities after the first one is found. Perceptual errors can be avoided if we get into the habit of using checklists.

Learning Objectives:

1. To learn to recognise ambiguous signs in plain films.
2. To learn to avoid the most common pitfalls in reading plain chest films.

A-806 16:45

B. Errors in CT of the chest

J. Vilar; Valencia/ES (vilarsamper@gmail.com)

Observer errors in Chest radiographs and chest CT: The aetiology of error in radiology is multi-factorial. In this presentation, I will concentrate on errors attributed to the radiologist. Not seeing a lesion (perceptual error) and not recognizing a pathology (interpretative error) are by far the most common causes. In a study of 500 cases, perceptual errors accounted for 80% and 20% were interpretative errors. Perceptual errors occur in CT, as in chest radiographs, despite the fact that CT is a tomographic technique. These errors may be related to technical factors such as noise, resolution, and use of adequate technical protocols including the use and timing of contrast media. Vigilance errors are those due to an insufficient time (reading too fast), satisfaction of search (interrupting vigilance), or inadequate clinical information (ignoring suspicion of pathology). Erroneous interpretation of the findings may be related to ignorance and inadequate information. The radiologist could avoid these errors by applying simple rules such as using checklists, taking enough time to read the studies, comparing with previous examinations, and using the clinical data. In this interactive presentation of cases, I will analyze some common causes of errors in chest CT and offer simple clues to avoid them.

Learning Objectives:

1. To learn to interpret ambiguous chest CT signs.
2. To learn to avoid the most common pitfalls in reading chest CT images.

16:00 - 17:30

Room B

Abdominal Viscera

RC 1601

Tumour response assessment in abdominal imaging

Moderator:

S.M. Erturk; Istanbul/TR

A-807 16:00

A. Colorectal liver metastases

S.K. Venkatesh; Rochester, MN/US (venkatesh.sudhakar@mayo.edu)

Metastatic liver disease occurs in 30-50% of colorectal cancer patients. Neoadjuvant chemotherapy (NAC) is the treatment of choice for colorectal liver metastases (CRLM). Local control with percutaneous ablation methods and surgical resection in those who show response to NAC have evolved as treatment options in patients with CRLM only. Accurate definition of number, distribution, site and response of CRLM is critical information defining anatomic resectability. It is therefore important to assess the response of CRLM to chemotherapy and ablation methods for assistance in guidance to further management. Standard methods (RECIST) use size criteria to assess decrease in size as response; however, there are pitfalls to these methods.

Viability of CRLM can also be assessed with dynamic contrast-enhanced MRI (DCE-MRI), diffusion weighted imaging (DWI), and positron emission tomography (PET) after NAC. The chemotherapy also causes liver toxicity including sinusoidal obstruction syndrome and fatty change that affect the assessment of response of CRLM and define resectability. This presentation will review the response of CRLM to treatment, methods of response assessment, and limitations and advantages of these methods in the management.

Learning Objectives:

1. To learn about different methods to assess the tumour response in the colorectal metastases.
2. To understand usefulness and limitation of techniques and the role of different contrast media.
3. To appreciate variable response pattern of colorectal liver metastases.

A-808 16:30

B. Rectal carcinoma

M.J. Lahaye; Amsterdam/NL (MJ.Lahaye@gmail.com)

MRI is the modality of choice for rectal cancer (re)staging. The high soft-tissue contrast of MRI can accurately assess the extramural tumour spread and relation to surrounding structures after chemoradiation. This lecture will have practical approach in determining the role of MRI in the restaging of rectal cancer. The relevant anatomy, MRI techniques, rationale for neoadjuvant treatment, and post-chemoradiation therapy imaging (including detection of patients with a complete response) will be discussed with special attention to how to apply recent advances in knowledge to daily clinical practice.

Learning Objectives:

1. To learn about the rationale for neoadjuvant treatment in rectal cancer and the impact on subsequent surgery.
2. To understand why imaging is needed to assess response to neoadjuvant therapy, what to look for when judging response, and where the challenges lie.
3. To appreciate when surgery can be deferred or avoided and how best to follow-up these patients.

A-809 17:00

C. Pancreatic adenocarcinoma

M. Zins; Paris/FR (mzins@hpsj.fr)

Patients with pancreatic ductal adenocarcinoma (PDA) must be selected for first-line surgery based on the likelihood of achieving complete curative resection with negative margins (R0). In doubtful cases and when the risk of incomplete resection (R1 or R2) is high, neoadjuvant chemoradiotherapy should be given. Neoadjuvant therapy can convert tumours classified as locally advanced by initial imaging studies to resectable tumours. However, the imaging study evaluation of the response to neoadjuvant therapy is extremely complex. Thus, the diagnostic performance of imaging studies is not sufficient to ensure the accurate selection of patients in whom negative-margin resection is likely to be achieved. More specifically, standard criteria for predicting vascular invasion, based on the amount of tumour-vessel contact, are not valid after neoadjuvant therapy. The high risk of underestimating the histological response warrants surgery in all patients without indisputable evidence of disease progression after chemo(radio)therapy. Patients with even partial decreases in tumour size and/or tumour-vessel contact are particularly good candidates for surgery. The role for functional imaging techniques can be expected to increase in the next few years.

Learning Objectives:

1. To understand the rationale for neoadjuvant treatment in pancreatic adenocarcinoma.
2. To learn the limitations of CT in assessing treatment response.
3. To learn how to accurately select patients for curative-intent surgery after neoadjuvant therapy.

16:00 - 17:30

Room N

Cardiac

RC 1603

Coronary CT angiography: how to start practice, perform and evaluate the exam?

Moderator:

M. Hrabak Paar; Zagreb/HR

A-810 16:00

A. Beautiful cases from clinical practice: coronary arteries

S. Feger; Berlin/DE (sarah.feger@charite.de)

Coronary computed tomography angiography (CTA) is a non-invasive diagnostic test with high diagnostic accuracy in detecting coronary artery disease (CAD). Due to its very high negative predictive value, it is especially suitable for ruling out CAD in patients with low to intermediate pretest probability. For stable chest pain patients in this pretest probability range, the current European guidelines already recommend the use of CTA. Additionally, in patients with unstable chest pain and a low CAD probability, CTA can be considered to detect relevant differential diagnoses. An important advantage of CTA compared with invasive coronary angiography is the possibility to perform a differentiated plaque analysis including the detection of high-risk plaque features besides the stenosis quantification. Different acquisition techniques are applied in clinical practice. Initially, retrospective ECG-gated CTA was routinely used. While this approach is very robust, especially for high or irregular heart rates, radiation exposure is relatively high. Prospective axial scanning reduces radiation exposure, since data acquisition is only performed in predefined ranges within the RR interval with the tube current entirely being turned off outside the acquisition window. Further approaches to reduce radiation exposure are the adjustment of scanning parameters, ECG-gated tube current modulation (adjusted to the heart rate and variability), automatic tube potential selection and, recently, the introduction of iterative reconstructions.

Learning Objectives:

1. To learn about cardiac CT acquisition techniques, pitfalls, and dose-reduction strategies.
2. To summarise current indications and clinical applications of CT coronary angiography.
3. To review the diagnostic performance of CT for the diagnosis of coronary artery disease.
4. To learn how to make a structured report of the coronary CT angiography.

A-811 16:35

B. Staff training and technical requirements

S. Harden; Southampton/UK (stephen.harden@uhs.nhs.uk)

Imaging the coronary arteries with CT is an increasingly frequent CT examination being performed in radiology departments in Europe and across the world. It is unusual as a diagnostic CT technique in that it is a procedure, involving careful pre-scan drug administration and fine attention to detail such that good image quality is obtained at a reasonable radiation dose to the patient. As such, this requires a team approach, with every member of the team performing a crucial function to ensure the safety of the patient and a successful procedure. Staff training is important and this is required for new staff, but also for experienced staff where practice review and optimisation meetings allow ongoing service improvement. Given that the drugs administered change cardiac physiology, staff must be trained in basic life support techniques and there must be a process for calling for urgent clinical backup even though these situations are rare. As this technique becomes more widely used and available, we are seeing an increasing role for CTCA in acute chest pain imaging and the team approach to patient care is as important if not more important in the acute or emergency setting.

Learning Objectives:

1. To become familiar with technical prerequisites and post-processing tools for coronary CT angiography.
2. To discuss a necessary team setup and training modules for radiologists and technical staff.
3. To evaluate the role of coronary CT angiography and requirements for the radiological team in routine imaging and in emergencies.

A-812 16:55

C. Beautiful cases from clinical practice: stents and bypasses

G. Bastarrika; Pamplona/ES (bastarrika@unav.es)

Advances in cardiac CT and development of new multidetector computed tomography (MDCT) scanners have allowed accurate and robust non-invasive assessment of coronary artery revascularization procedures. This requires development of detailed CT acquisition protocols with specific reconstruction parameters and the appropriate use of different post-processing techniques. From the clinical perspective, radiologists need to become familiar with diverse types of grafts as well as with typical CT findings after coronary artery bypass grafts (CABG) surgery and stent placement. In this lecture, the value of coronary CT angiography after coronary intervention will be underlined by defining MDCT acquisition protocols designed to evaluate coronary artery revascularization procedures. Further, the surgical aspects of CABG, postoperative graft anatomy, and interpretation of pitfalls when evaluating CABG and stent patency will be discussed.

Learning Objectives:

1. To emphasise the value of coronary CT angiography after coronary interventions.
2. To outline CT acquisition protocols and contrast administration strategies to evaluate coronary stents and coronary artery bypass grafts (CABG) in individuals undergoing coronary revascularisation.
3. To describe usefulness and limitations of different post-processing techniques in assessing stent and CABG patency.

16:00 - 17:30

Studio 2018

Special Focus Session

SF 16

Placental imaging: how, when and why?

A-813 16:00

Chairperson's introduction

M. Weston; Leeds/UK (michael.weston2@nhs.net)

The high rates of caesarean delivery and the later ages that women are choosing to have their children are leading to an increase in the incidence of placental problems. Both placenta praevia and abnormal placental attachment disorders are commoner the greater the number of prior uterine surgical interventions and the older an expectant mother is. Radiologists are finding new roles in helping their obstetric colleagues manage these complications. Magnetic resonance imaging and interventional procedures are developing apace. These three presentations will give us an up-to-date insight into their application.

Session Objectives:

1. To understand the new imaging modalities available to assess the placenta.
2. To recognise the signs of abnormal placentation.
3. To learn about new interventional techniques in the management of postpartum haemorrhage.

A-814 16:05

Modern MRI of the placenta

N. Siauve; Colombes/FR (nathalie.siauve@aphp.fr)

Recent developments in magnetic resonance imaging (MRI) offer new perspectives for placental imaging, using fMRI tools to explore vascularisation, oxygenation and metabolism. Diffusion weighting imaging (DWI) and intra-voxel incoherent motion (IVIM) MRI study the movement of water molecules within tissues and provide information about vascularisation and tissular structure. Quantitative parameters are available: the apparent diffusion coefficient (ADC), the perfusion fraction (f), the pseudo-diffusion coefficient (D*) and the diffusion coefficient (D). Blood oxygen level-dependent (BOLD) MRI uses the hemoglobin (Hb) as an endogenous contrast agent. The oxygen saturation of Hb modifies its magnetic properties, and modifications of T2* can be depicted when two different statuses of oxygenation are compared. Arterial spin labelling (ASL) MRI relies on magnetically labelled water to quantify the blood flow (F). Dynamic contrast-enhanced MRI (DCE-MRI) is best able to quantify perfusion and permeability. The enhancement of the organ of interest after intravenous injection of a gadolinium-based contrast agent is compared to the enhancement of the arterial input function, using compartmental model. However, the use of gadolinium-based contrast agents during pregnancy is still limited to situations when the benefits outweigh the potential risks. Modern imaging of the placenta will integrate fMRI techniques in the follow-up of pregnancy as numerous biomarkers will become available. The objectives of such modern imaging will be to improve the detection of placental insufficiency

Postgraduate Educational Programme

and the management of high-risk fetuses. A platform dedicated to human foeto-placental research (LUMIERE) will be created soon and will allow further research in this area.

Learning Objectives:

1. To describe how the vascularisation and the oxygenation of the placenta can be explored, using functional MRI.
2. To list and explain the different parameters of each functional MRI technique that is available.
3. To give an overview of the potential applications in normal and pathologic pregnancies.

A-815 16:30

Placental abnormalities, timing of imaging, methods and diagnosis

G. [Masselli](#); Rome/IT (gabrielemasselli@libero.it)

Placental abnormalities have a profound impact on morbidity and mortality of both mother and foetus, underlining the importance of an early diagnosis. The placenta may show pathologies in terms of size, adherence, cord insertion, cord location and bleeding, and in few cases may also develop trophoblastic and non-trophoblastic tumours. Placental adhesive disorders (PADs) are characterized by different levels of uterine myometrial invasion that relate to different levels of severity and risk of blood loss upon delivery. PADs seem to parallel the increase in C-section rate and maternal age, and can be easily diagnosed by ultrasound (US); magnetic resonance imaging (MRI) is likewise performed either for delivery planning or equivocal cases. Another cause of third trimester bleeding is placenta abruptio, defined as premature separation of the placenta that complicates 1% of pregnancies; US has a sensitivity as low as 25% and, when negative, MRI is usually diagnostic. Systematic assessment of the placenta by US is the standard imaging examination during pregnancy. MRI is used for equivocal cases or when further placental characterization is required in view of its multiplanarity, its improved tissue contrast and lack of radiation. We will discuss which imaging modalities are used to study the placenta, which sequences and planes better delineate this organ, and which are the circumstances that require their use, particularly with regard to PADs. The advantages of MRI in the diagnosis and management of patients affected by these pathologies will be thoroughly discussed along with the most common pitfalls.

Learning Objectives:

1. To learn about the likelihood and causes of abnormal placental attachment.
2. To understand the role of US and MR in making the diagnosis.
3. To appreciate the imaging signs and pitfalls.

A-816 16:55

Abnormally invasive placenta: vascular anatomy and interventional radiology approaches to management

C. [Hammond](#); Leeds/UK (christopherhammond@nhs.net)

Abnormal placentation is increasing in incidence. It now occurs in about 1 in 500 deliveries in the West. It encompasses a range of pathological entities from superficial adherence of placental villi to the myometrium (accreta) to penetration through the uterine wall and invasion into surrounding organs (percreta). It is associated with massive haemorrhage at delivery in some women, though the risks of this are difficult to prospectively determine with any certainty, even in women with typical imaging features of abnormal placentation. The classical approach to management of abnormal placentation has been caesarian hysterectomy, though a number of uterus-conserving surgical techniques have been developed. The interventional radiological [IR] techniques of balloon occlusion (of various arteries) and embolisation (with various agents, and in various vascular territories) have been undertaken to either augment or replace open surgery. Evaluation of these techniques is complicated by a heterogeneity of approaches between studies and the difficulty of accurately assessing haemorrhage risk beforehand. This talk will discuss the vascular anatomy of the gravid uterus and its relevance to both IR and surgical approaches to the management of actual or potential massive obstetric haemorrhage in the presence of abnormal placentation. The evidence in support of these techniques will be examined including evidence of safety and outcome. The logistical and infrastructural requirements for a truly multidisciplinary approach to the management of abnormal placentation will be reviewed and then finally the pre-procedural imaging information needed by the surgeon or IR will be highlighted.

Learning Objectives:

1. To discuss the arterial supply to the uterus and its importance in haemorrhage control in abnormal placentation
2. To discuss the options for haemorrhage control and evidence to support each approach
3. To examine the logistics and infrastructure required to provide an obstetric haemorrhage service

Author Disclosure:

C. Hammond: Advisory Board; NICE GDC AAA. Author; Papers on haemorrhage control in massive obstetric haemorrhage.

17:20

Panel discussion: Is MR scan now a prerequisite for the modern management of placental problems?

16:00 - 17:30

Room L 8

ESR Patient Advisory Group (ESR-PAG)

PA 2

Big data: implications for medical imaging and the need for data protection and cyber security

A-817/A-818 16:00

Chairpersons' introduction

N. [Bedington](#)¹, L.E. [Derchi](#)²; ¹Vienna/AT, ²Genoa/IT (derchi@unige.it)²

This session will see different presenters discuss about "big data" in radiology, each from his/her perspective. This is a difficult but important topic which will have great impact on our discipline (and on the whole healthcare sector). The session will specifically address the need for data protection. It is in fact quite important to understand the topic of protection of "sensible" data and of cyber security. Then, hopefully, it will provide a platform to share opinions and decisions on a topic which is getting more and more important in the whole healthcare sector and, specifically, in the imaging field.

Session Objectives:

1. To understand the importance of big data in medical imaging and related implications for patients, radiologists, and radiographers.
2. To understand the need for data protection and cyber security to combat the vulnerability of healthcare.
3. To learn practical examples.

A-819 16:10

Implications of protection of medical imaging data: a European perspective

C.D. [Becker](#); Geneva/CH

The new general data protection regulation of the European Union will be effective in May 2018. Processing and communication of health data including images will require explicit consent by the data subject and all patients must have access to their personal data. Key elements of the new regulation also include the right to obtain rectification of his/her personal data; the right of the data subject to transfer personal data to another service provider ("data portability"); or the right of the data subject to be informed when his/her data have been hacked. The new GDPR implies that all organisations processing personal data must be able to prove that they comply with the rules. It also proposes a European Data Protection Board and requires institutions which process certain types or volumes of data to have a designated data protection officer (DPO) who is in contact with the national data protection authorities. There is an obvious need to find a reasonable balance between protection of individual health data and data use in the interest of public health and research projects by means of "big data" analysis. Anonymisation and pseudonymisation of digital data are indispensable tools in this context. Codes of conduct may be created by specific groups of users to define exceptions such as big data analysis or biobanks for scientific purposes. Specific rules may also be defined by national law.

Learning Objectives:

1. To understand the impact of the new data protection regulation for processing and sharing of imaging data.
2. To understand the need to find a balance between protection of individual health data and data use in the interest of public health and research projects including "big data".
3. To discuss safeguards for data processing in the context of research and public health projects, including "big data".

A-820 16:25

Cyber security in radiology

J. [Sosna](#); Jerusalem/IL (jacobs@hadassah.org.il)

The increase in the number of imaging studies worldwide and especially in Europe necessitates the need to secure the integrity of the data. Although many organizations have cyber security programmes, many others have not

yet acknowledged the seriousness of the threat. Security breaches occur when hackers enter the Internet Protocol (IP) address of medical equipment and data centres that appears to be at risk. Hackers can use the device as an entry point to access the rest of the facility's network. The hacker could cause the imaging equipment to malfunction or block access to PACS and RIS. This can be potentially life threatening, such as in a case of increasing radiation in a CT scanner for instance or limiting access to patient studies when necessary. Radiologists need to be familiar with such treats and help integrate cyber security into the workplace culture. The threats and possible solutions will be presented and discussed.

Learning Objectives:

1. To understand what cyber security is and its implications for radiology.
2. To learn a practical example from Israel and lessons learnt.

Author Disclosure:

J. Sosna: Advisory Board; Persimio. Consultant; Xact.

A-821 16:40

Importance of data protection from a patient's view

E. [Briers](#); Hasselt/BE (erikbriers@telenet.be)

Not all patients are equal, and not all diseases are equal. Some patients have illnesses that can be interpreted as benign, such as a common cold. For others, the disease is serious and even life threatening. Very often patients with serious diseases face long disease journeys with multiple visits to doctors, hospitals and even treatments. During this journey, data are generated in every step, simple and complex data, but all pertaining to the patient. This information, these data, describes the fate of the patient: what has happened, is happening and what will happen to this patient. Patients do not like this to be read or seen by everybody. If this information is made available to an insurer, the patient, after having been pronounced cured, may not be eligible for insurance coverage. If the patient looks for a new employment, the information on his or her misfortune with the disease may make him unappealing to an employer. But, during the journey and even after the journey, the medical records contain important data that may speed up future diagnosis, make new symptoms understood quickly and help implement correct treatments faster. All those from the multi-professional team then need access to the complete data. They need to be bound by their professional ethics not to abuse this information. In clinical trials, sharing data is from the patient's perspective included in the concept and for patients sharing real-world data that could improve future applications of treatment is so far an unfulfilled dream.

Learning Objectives:

1. To understand the importance of data sharing and protection of patient data.
2. To learn implications of misuse of patient data.
3. To understand the necessity of data sharing to improve the patient journey through her/his disease.

A-822 16:55

Experiences from the US

J.A. [Brink](#); Boston, MA/US

Data security in health care is governed in the United States by the Health Insurance Portability and Accountability Act (HIPAA) of 1996. The HIPAA privacy rule established standards to secure the personal/protected health information (PHI) and medical records of US citizens. It applies to all health-care providers who interact with individual patient's health records and includes all relevant electronic communications and transactions. Moreover, it applies to all relevant health-care institutions, insurance companies, and affiliated institutions that have access to protected health information. PHI refers generally to information that may identify individuals and the care they receive through medical history details, imaging and laboratory results, insurance information and other demographic information.

Learning Objectives:

1. To discuss the status of data protection and cyber security in the US.
2. To learn a practical example of data misuse, implications and lessons learnt.

17:10

Panel discussion: What is the future direction of data protection and cyber security in medical imaging?

16:00 - 17:30

Room E1

ESR Working Group on Ultrasound

WG 1

Ultrasound-guided interventional procedures: new techniques and applications

Moderators:

P.L. Pereira; Heilbronn/DE
D.A. Clevert; Munich/DE

A-823 16:00

Liver

E. [Leen](#); London/UK (edward.leen@imperial.ac.uk)

The real-time nature of US combined with its low cost and higher availability remains the modality of first choice for needle guidance for biopsy, drainage and ablation in the liver. Needle guiding device is recommended for deeply located lesions, especially for less experienced users. The biopsy technique used is dependent on the examiner's skills and the accessibility of the target. Image fusion with CT or MR and navigation systems may be helpful for ultrasound guidance in lesions difficult to visualize on ultrasound with or without contrast agents (CEUS). Local ablative procedures play a key role in the management of patients with malignancies such as hepatocellular carcinoma (HCC) or metastases. US and CEUS play an important role before, during and after ablation procedures. CEUS enables (a) the assessment of the lesions to be treated by ablation (number, size, degree and homogeneity of lesion enhancement, presence of feeding vessels, to define the eligibility for treatment and the best ablation strategy), (b) the depiction of previously undetectable lesions with the support of fusion imaging, enabling needle/probe guidance to occult lesions and (c) the detection of viable tumour persistence following locoregional treatment.

Learning Objectives:

1. To learn about new results and application of ultrasound in guided interventional procedures: liver malignancy biopsy, primary liver malignancy ablation, secondary liver malignancy ablation.
2. To understand consolidated and new indications to ultrasound-guided interventional procedures: PEI, RFA, MWA, IRE.
3. To appreciate accuracy of ultrasound-guided interventional procedures from consolidated to new applications: analysis of data from personal experiences and literature series comparison and discussion.
4. To become familiar with the new techniques of ultrasound guidance and with the new diagnostic and therapeutic indications for ultrasound-guided interventional procedures: CEUS imaging, fusion imaging, elastosonographic imaging for liver malignancy biopsy and treatment, MWA, IRE, combination treatment.

A-824 16:20

Pancreas

M. [D'Onofrio](#); Verona/IT (mirko.donofrio@univr.it)

Percutaneous interventional diagnostic and therapeutic procedures under ultrasound guidance are largely employed in pancreatic diseases. Diagnostic procedures include cytologic and/or histologic sampling with fine needles or coarse needles to sample pathologic tissue or fluids/collections for biochemical, cytologic and microbiologic examinations. Therapeutic procedures include the drainage of fluid collections by needle or catheter and nowadays the ablation procedures. The advantage of ultrasound guidance is strictly linked to the real-time aspect of the examination. Nowadays to amplify the view of the image, a method employing CT or MR fusion imaging can be used. New results and applications of ultrasound-guided interventional procedures such as pancreatic malignancy biopsy or primary pancreatic malignancy ablation have been increasingly reported, moving from consolidated to new indications to ultrasound-guided interventional procedures. The accuracy of ultrasound using new techniques such as CEUS and fusion for guiding interventional procedures has improved as reported in literature.

Learning Objectives:

1. To learn about new results and application of ultrasound-guided interventional procedures: pancreatic malignancy FNA and biopsy, primary pancreatic malignancy ablation.
2. To understand consolidated and new indications to ultrasound-guided interventional procedures: FNA and biopsy, RFA.
3. To appreciate accuracy of ultrasound-guided interventional procedures from consolidated to new applications: analysis of data from personal experiences and literature series comparison and discussion.
4. To become familiar with the new techniques of ultrasound guidance and with

the new diagnostic and therapeutic indications for ultrasound-guided interventional procedures: CEUS imaging, fusion imaging, elastosonographic imaging for pancreatic malignancy biopsy and treatment, RFA, MWA, IRE, combination treatment.

Author Disclosure:

M. D'Onofrio: Advisory Board; Siemens, bRACCO. Consultant; Bracco, Siemens. Speaker; Bracco, Siemens.

A-825 16:40

Kidney

J.-M. **Correas**; Paris/FR (jean-michel.correas@aphp.fr)

Ultrasound-guided interventional procedures are playing an increasing role for both diagnosis of diffuse and focal diseases and therapeutic applications. When the target lesion can be identified using US imaging, it is the modality of choice due to the ability to visualize real-time needles, catheter and electrodes. New techniques such as contrast-enhanced ultrasound, shear-wave elastography and fusion imaging are further improving the capabilities of US-guided procedures. However, adequate training remains mandatory, particularly in the case of difficult procedures.

Learning Objectives:

1. To learn about new results and application of ultrasound-guided interventional procedures: renal malignancy FNA and biopsy, primary renal malignancy ablation.
2. To understand consolidated and new indications to ultrasound-guided interventional procedures: FNA and biopsy, RFA.
3. To appreciate accuracy of ultrasound-guided interventional procedures from consolidated to new applications: analysis of data from personal experiences and literature series comparison and discussion.
4. To become familiar with the new techniques of ultrasound guidance and with the new diagnostic and therapeutic indications for ultrasound-guided interventional procedures: CEUS imaging, fusion imaging, elastosonographic imaging for renal malignancy biopsy and treatment, RFA, radioablation, MWA, combination treatment.

Author Disclosure:

J.-M. Correas: Advisory Board; Philips US. Equipment Support Recipient; Toshiba MS (Aplio i900), SuperSonic Imagine (AixPlorer). Speaker; Toshiba MS, SuperSonic Imagine, Philips US, Bracco, Guerbet.

A-826 17:00

Thyroid

G. **Mauri**; Milan/IT (vanni.mauri@gmail.com)

Ultrasound-guided interventional procedures in thyroid disease have shown great expansion and are more and more widely applied in the clinical practice in a larger spectrum of applications. On the one hand, ultrasound-guided fine needle aspiration has become the standard practice for diagnosing the nature of thyroid nodules, which are increasingly detected in the population. On the other hand, the development of dedicated technique such as laser ablation or radiofrequency ablation with specific devices has expanded the role of interventional ultrasound in the treatment of both benign and malignant thyroid disease. Ultrasound-guided ablation has achieved a more important role in the everyday treatment of benign nodules (even hyperfunctioning ones), representing a minimally invasive, safe and effective treatment strategy. Moreover, the application of thermal ablations to malignant disease, both primary and recurrent, seems to represent a promising strategy in order to reduce the invasiveness of surgical treatment in such difficult anatomical region. In this presentation, consolidated and new applications of interventional procedures in the thyroid will be presented and discussed, with particular focus on new application of thermal ablations in the setting of both benign and malignant disease.

Learning Objectives:

1. To learn about new results and application of ultrasound-guided interventional procedures: thyroid malignancy FNA, thyroid nodule ablation.
2. To understand consolidated and new indications to ultrasound-guided interventional procedures: FNA, RFA.
3. To appreciate accuracy of ultrasound-guided interventional procedures from consolidated to new applications: analysis of data from personal experiences and literature series comparison and discussion.
4. To become familiar with the new techniques of ultrasound guidance and with the new diagnostic and therapeutic indications for ultrasound-guided interventional procedures: CEUS imaging, fusion imaging, elastosonographic imaging for thyroid malignancy FNA.

Author Disclosure:

G. Mauri: Consultant; Elesta SrL.

16:00 - 17:30

Room E2

Multidisciplinary Session

MS 16

Psychoradiology: a blend of molecular, functional and structural imaging with a taste of psychology

A-827 16:00

Chairperson's introduction

B. **Ertl-Wagner**; Munich/DE (Birgit.Ertl-Wagner@med.uni-muenchen.de)

Psychoradiology is a field of radiology that investigates the brain and mind both in health and disease. It usually applies various methods including structural and volumetric magnetic resonance (MR) imaging, functional MR imaging, MR spectroscopy and diffusion tensor imaging (DTI). A combination of methods increases the soundness of the results. Psychoradiology can help to both unravel the physiological processes of the mind and to understand pathological alterations that lead to disease. In recent years brain stimulation techniques have been gaining increasing attention for the treatment of various psychiatric disorders. Psychoradiology may become an important tool to guide the target of the intervention and to understand the changes in the brain's networks associated with this treatment.

Session Objectives:

1. To become familiar with the interdisciplinary aspects of psychoradiology.
2. To learn about the methodological principles of structural, functional and molecular imaging of the brain.
3. To understand the pathophysiological concepts underlying psychiatric disorders.

A-828 16:05

A psychiatrist's view on neuroimaging

F. **Padberg**; Munich/DE (frank.padberg@med.lmu.de)

During the last three decades, psychiatrists have developed a comprehensive view on brain functions, which underly symptoms and syndroms of psychiatric disorders. Different avenues from genetic and molecular research, neurophysiology, and multimodal neuroimaging have contributed to this development. More recently, parallel to the introduction of the Diagnostic Manual DSM-5, the National Institute of Mental Health (NIMH) has challenged the diagnostic categories by introducing Research Domain Criteria (RDoC) as a new matrix for cognitive and behavioral domains forming human experience and behavior. These domains can be addressed from cellular to system levels. Neuroimaging represents a key technology for the investigation of these domains and will play a pivotal role in psychiatric research (Bhugra et al. 2017). This lecture will outline these issues and give examples of the diagnostic value of neuroimaging, research on pathophysiology and mechanisms of therapeutic action (example: brain stimulation; Padberg et al. 2017), and finally prediction of individual outcome as well as monitoring progress of disease. References: Bhugra D, Tasman A, Pathare S, et al. The WPA-Lancet Psychiatry Commission on the Future of Psychiatry. *Lancet Psychiatry*. 2017; 4:775-818. Padberg F, Brem AK, Palm U, et al. Discovering the individual brain: brain stimulation in psychiatry: Editorial I to the supplement from the 2nd European conference on brain stimulation in psychiatry. *Eur Arch Psychiatry Clin Neurosci*. 2017; Nov 20. doi: 10.1007/s00406-017-0853-3.

Learning Objectives:

1. To understand the important role of imaging in the diagnostic evaluation of psychiatric patients.
2. To become familiar with important imaging patterns that may be encountered in patients with psychiatric disorders.
3. To understand future trends in neuroimaging of patients with psychiatric disorders.

Author Disclosure:

F. Padberg: Equipment Support Recipient; neuroCare Group Munich, Germany; Mag&More GmbH Munich, Germany; Brainsway Inc. Jerusalem, Israel. Speaker; neuroCare Group Munich, Germany, Mag&More GmbH Munich, Germany.

A-829 16:23

Advanced imaging techniques: their role in neuropsychiatric disorders

S. **Stöcklein**; Munich/DE (sophia.stoecklein@med.lmu.de)

Structural MR imaging in neuropsychiatric disorders includes volumetric techniques, such as whole-brain voxel-based morphometry and automated segmentation of brain structures, as well as assessment of tissue

characteristics such as myelin content. With the advent of advanced data mining and machine learning techniques, the results of these approaches can be combined to detect disease-specific patterns, as singular volumetric measures might lack specificity. For example, hippocampal volume is not only reduced in Alzheimer's disease, but also in depression and schizophrenia. Ultrahigh field MRI will further facilitate the detection of disease-specific changes, e.g. in the hippocampal subfields in schizophrenia. Functional MRI in neuropsychiatric disorders largely relies on resting-state paradigms, as they are easily implementable and less dependent on patient cooperation and command of language than task-based paradigms. Many fMRI studies have investigated differences between patient and control groups and have provided valuable insight into alterations of functional brain connections and networks in neuropsychiatric diseases. However, applications in the individual patient are still sparse. Technical advances such as individualized functional networks, reliability correction, and also optimized scan length and the collection of large healthy reference populations are currently paving the way towards applications of fMRI as an individualized imaging marker for neuropsychiatric disorders. Molecular imaging techniques such as PET/SPECT and MR spectroscopy have provided insight into alterations in neurotransmission and metabolism in neuropsychiatric disorders. Recently, molecular imaging of neuroinflammatory markers such as microglia activation has increasingly attracted interest, due to increasing evidence suggesting a role for inflammation in the pathogenesis of neuropsychiatric disorders.

Learning Objectives:

1. To become familiar with the principles and practice of using structural and volumetric methods in patients with neuropsychiatric disorders.
2. To understand methods and applications of task-based and resting-state functional MR imaging techniques in neuropsychiatric patients.
3. To learn about the role of spectroscopy and molecular imaging in patients with neuropsychiatric disorders.

A-830 16:41

Can images predict psychiatric diagnosis and treatment response?

N. Koutsouleris; Munich/DE

"no abstract submitted"

Learning Objectives:

1. To become familiar with the principles of imaging-based prediction methods.
2. To understand the role of neuroimaging in predicting neuropsychiatric diagnoses.
3. To learn about imaging-based methods to predict treatment response in psychiatry.

A-831 16:59

Neuroimaging and neuromodulation: where are we heading

D. Keeser; Munich/DE (daniel.keeser@med.lmu.de)

Non-invasive transcranial brain stimulation (NIBS) methods (e.g. transcranial direct current stimulation - tDCS, repetitive transcranial magnetic stimulation - rTMS and others) provide a unique in vivo intervention for probing the functional role of regions and hubs in human neural systems that play a role in the pathophysiology of psychiatric disorders. Recent research has shown that the individual human brain functional MRI connectivity (fcMRI) shows distinct patterns of within- and between-subject variability. Anatomically targeted analyses of NIBS in neuropsychiatric patients and healthy subjects have generated promising results. Even combining several neuroimaging methods (resting state fcMRI, task-based fMRI, magnetic resonance spectroscopy (MRS)) may be useful to detect classifiers that can reliably predict NIBS effects. These neuroimaging methods allow individual brain properties as well as the evaluation of state dependency. By combining neuroimaging and NIBS (term: imaging stimulation), new functional models are expected to be developed and compared in different states of health and pathology, e.g. during the course of psychiatric disorders from preclinical stages to relapsing-remitting or chronic disorders.

Learning Objectives:

1. To understand the principles of neuromodulation.
2. To become familiar with methods of imaging-based neuromodulation.
3. To become familiar with future prospects of neuroimaging and neuromodulation.

17:17

Interdisciplinary case discussion

16:00 - 17:30

Room F1

E³ - European Diploma Prep Session

E³ 1623

Urogenital

A-832 16:00

Chairperson's introduction

R.H. Oyen; Leuven/BE (Raymond.Oyen@uzleuven.be)

We aim to become familiar with the imaging presentation of common neoplastic and infectious disorders of the kidneys, describe the typical imaging features of calculus and neoplastic disorders of the ureter and bladder and understand the imaging presentation of benign and malignant disorders of the prostate. Cross-sectional imaging (ultrasound, CT, MRI) has become the key modality for the evaluation of the adrenals, kidneys, upper urinary tract and bladder in symptomatic patients. In addition, because of the increased use of imaging, abnormalities and disease processes of the urogenital tract are seen more frequently in patients not referred for symptoms related to the urogenital tract. Such findings can be relevant or not relevant and include anatomical variants and inflammatory processes; both may erroneously be interpreted as neoplastic lesions (pseudotumours) and benign and malignant tumours. It is important to become familiar with some typical imaging features of common neoplastic disorders of the kidney and urinary tract, of urolithiasis and of inflammatory processes to enable accurate reporting, provide a diagnosis or at least a list of suitable differential diagnoses, and suggest appropriate further studies (imaging, biopsy,) to eventually refine the diagnosis. The aim is to select patients in whom therapy is indicated from those where therapy has to be avoided. MRI now is the key modality for the detection of prostate cancer and the staging of known prostatic cancer. However other prostatic disease processes, including inflammation, benign hyperplasia and cancer may occur simultaneously to a variable extent, thus complicating the reading and interpretation of MRI. In this respect, structured reporting MRI studies based on the PI-RADS system contributes to standardized reporting and communication with referring physicians.

Session Objectives:

1. To become familiar with the imaging presentation of common neoplastic and infectious disorders of the kidneys.
2. To describe the typical imaging features of calculous and neoplastic disorders of the ureter and bladder.
3. To understand the imaging presentation of benign and malignant disorders of the prostate.

A-833 16:06

A. Renal and adrenal imaging

N. Grenier; Bordeaux/FR (nicolas.grenier@chu-bordeaux.fr)

Kidneys and adrenals are retroperitoneal organs contained within a perirenal space. Variants of adrenals involve essentially their shape, whereas many variants involve kidneys including ectopia, fusion, dystopia and duplication. Renal masses are frequent. Most are simple cysts. Cystic masses must be classified according to Bosniak classification to guide management. Conversely, most of the solid masses are malignant, but diagnosis of benign angiomyolipoma can be confirmed by imaging only. Adrenal masses are usually solid, and most of them are benign with typical imaging features based on evaluation of their lipid content and perfusion level. The role of imaging in parenchymal disease remains limited, except for infections, acute or chronic.

Learning Objectives:

1. To describe the normal imaging anatomy and variants of the kidney and adrenal.
2. To understand the imaging features of benign and malignant tumours of the kidneys.
3. To describe imaging features of benign and malignant tumours of the adrenal glands.
4. To explain the imaging features of infectious disorders of the kidneys.

Author Disclosure:

N. Grenier: Advisory Board; Supersonic Imagine, Aix-en-Provence, France.

A-834 16:34

B. Imaging of the ureter and bladder

M.N. Özmen; Ankara/TR (mozmen@hacettepe.edu.tr)

Imaging has a very important role in evaluating the urinary tract. Over the past years, computed tomographic urography (CTU) has become the main imaging modality for this purpose in various clinical settings. Dose reduction techniques have also enabled us to obtain CTUs with very low radiation doses. Several

anomalies of the ureter may be seen, including duplication, muscular dysfunction or abnormal termination. An intraluminal disease process in the ureter might cause obstruction. Ureteral stone is by far the most frequent with high attenuation values on unenhanced CT. Dual-energy CT may contribute to the prediction of the chemical composition of the stone. A filling defect seen on CTU usually raises the suspicion of urothelial neoplasm. Other entities such as clot, metastasis, and tuberculosis might also obstruct the ureter and must be considered in the differential diagnosis of selected patients. The prevalence of urothelial neoplasms is high in elderly patients with a history of smoking, analgesic use or occupational exposure to chemical carcinogens. Urothelial cancer has to be considered as a 'systemic' disease, with often multiple, synchronous or metachronous lesions. CTU not only depicts the neoplastic lesion, but also enables the examination of the entire urothelium during staging or follow-up. Several treatment options are available and imaging plays an important role for tailoring this treatment. In case of haematuria, where CTU is the main diagnostic tool for upper urinary tract evaluation, cystoscopy is the primary diagnostic tool for screening for bladder neoplasms. CTU is indicated for the evaluation of upper urinary tract and staging purposes.

Learning Objectives:

1. To explain the imaging anatomy and variants of the ureter and bladder.
2. To understand the diagnostic evaluation and imaging features of calculi of the ureter and bladder.
3. To describe the imaging features of benign and malignant tumours of the ureter and bladder.

A-835 17:02

C. Prostate imaging

H.C. [Thoeny](mailto:harriet.thoeny@insel.ch); Berne/CH (harriet.thoeny@insel.ch)

Prostate imaging is increasingly performed using multiparametric MRI (mpMRI) to detect and stage significant prostate cancer as well as for active surveillance in patients with a known cancer. The requirements to perform correct mpMRI including high-resolution T2w, diffusion-weighted MRI (DW-MRI) and dynamic contrast-enhanced MRI (DCE-MRI) are specified in PIRADS vs 2 (Prostate Imaging and Reporting Data System). The aim of prostate imaging is to detect a significant cancer defined as a tumour with a volume ≥ 0.5 cc or a Gleason score of ≥ 7 and/or extraprostatic extension. PIRADS version 2 uses a 5-point scale based on the likelihood that a combination of mpMRI findings on T2w, DW-MRI and DCE-MRI correlates with the presence or absence of clinically significant prostate cancer for each lesion in the prostate gland. PIRADS 1 or 2 means that clinically significant cancer is unlikely to be present, PIRADS 3 is intermediate/equivocal and PIRADS 4 and 5 indicate a high likelihood of significant prostate cancer (PIRADS 4: size < 1.5cm, PIRADS 5: size < 1.5 cm). Most of the prostate cancers are located in the peripheral zone, where DW-MRI is the dominant sequence to make the correct diagnosis. In the transition zone, T2w is the dominant sequence. In this presentation, typical findings will be discussed and also benign diseases such as prostatitis and benign prostatic hyperplasia will be demonstrated as potential differential diagnoses.

Learning Objectives:

1. To explain the PIRADS system in prostate imaging.
2. To describe the imaging features of benign prostatic hypertrophy.
3. To understand the imaging features of prostate cancer.
4. To describe the imaging features of inflammatory changes of the prostate.

Author Disclosure:

H.C. [Thoeny](mailto:harriet.thoeny@insel.ch): Advisory Board; Guerbet SA.

16:00 - 17:30

Room F2

Emergency Imaging

RC 1617

Why do I miss fractures in emergency?

A-836 16:00

Chairperson's introduction

S. [Wirth](mailto:stefan.wirth@med.uni-muenchen.de); Munich/DE (stefan.wirth@med.uni-muenchen.de)

Sometimes, things may become more difficult and easier at the same time. On one hand, advances in imaging allow for very precise and also fast diagnoses in a continuously increasing number of cases. On the other hand, radiologists have to be more and more aware of clinical entities, pathological patterns, and interdisciplinary networks to quickly and precisely provide our clinical partners with the information they need. Although these changes are apparent, overlooked fractures remain a big and also common challenge. Aiming to reduce the typical potential problems like arthrosis and pain, this should also take into account social dimensions like medical costs and patient's ability to work. Which way we should go: More and better education and training? More clinical integration? More lowest-dose CT instead of radiographs? More quality

assurance and management? The three lectures will develop answers to these questions and will also provide high educational value with a focus on differences between children and adults, as well as on likelihood and complexity of related other injuries.

Session Objectives:

1. To learn the typical constellations and findings of missed fractures.
2. To understand the potential complications resulting from missing fractures.
3. To appreciate direct and indirect fracture signs with different imaging modalities.

A-837 16:05

A. Missed fractures in children

A.C. [Offiah](mailto:amaka.offiah@nhs.net); Sheffield/UK (amaka.offiah@nhs.net)

Fractures in children may be missed in the Emergency Department for several reasons. Firstly, a normal variant may be misdiagnosed as a fracture (or vice versa). Secondly, normal physiological absence of ossification of the epiphyseal centres makes assessment of alignment difficult. Finally, some fractures are themselves subtle. This lecture will predominantly focus on radiographs, but use cross-sectional imaging to highlight specific points. Particular fractures to be covered are accidental (as opposed to inflicted) and include skull, vertebral, clavicular, elbow, scaphoid, pelvic (including avulsion injuries and slipped capital femoral epiphysis) and tibial fractures.

Learning Objectives:

1. To become familiar with the common fractures in childhood.
2. To understand the choice of the best-suited imaging modality.
3. To learn about atypical imaging findings in different clinical scenarios.

Author Disclosure:

A.C. [Offiah](mailto:amaka.offiah@nhs.net): Advisory Board; Alexion, BioMarin. Consultant; Alexion, BioMarin. Grant Recipient; Alexion. Research/Grant Support; Alexion. Speaker; Alexion, BioMarin, InfoMed.

A-838 16:30

B. Missed fractures in adults

A. [Pinto](mailto:antopin1968@libero.it); Naples/IT (antopin1968@libero.it)

Falls are the most common cause of injuries among adult patients: advanced age substantially increases the likelihood of hospitalization after a fall. The most commonly fractured bones in adults are: (1) the hip, femur, pelvis, and vertebrae; (2) the humerus, forearm, and hand; (3) the leg and ankle bones. Radiography remains the initial modality to detect or exclude the presence of a fracture. The main cause of diagnostic error in the Emergency Department is the failure to correctly interpret radiographs: the majority of the diagnoses missed on radiography are fractures. Some of the fractures are subtle; however, the majority are obvious, which suggests inadequate training and/or poor technique in radiological interpretation. In other situations, the fractures are observed but misinterpreted as normal variants or old injuries. Misinterpretation of fractures may determine a delayed treatment and poor outcome for patients treated in the Emergency Department. It is also one of the most frequent factors leading to medical legal claims. With a high clinical index of suspicion, further evaluation with additional imaging is typically required, particularly if the results of this imaging will affect clinical management. Radiologists should more completely understand the limitations of radiography in the diagnosis of subtle fractures and can best indicate the need for more advanced imaging, such as CT, for a correct diagnosis in an appropriate time frame. Key elements to reduce errors in the diagnosis of fractures on plain radiographs are knowledge, experience, and correct application of the imaging protocols.

Learning Objectives:

1. To become familiar with the most common fractures in adult patients.
2. To understand which additional data will influence the choice of the correct imaging modality.
3. To learn about atypical imaging findings in adult patients after trauma.

A-839 16:55

C. Missed musculoskeletal injuries in whole-body MDCT examinations

T. [Ruder](mailto:Thomas.Ruder@northlandhb.org.nz); Whangarei/NZ (Thomas.Ruder@northlandhb.org.nz)

Whole-body CT has become the first-line modality in the imaging workup of patients with multiple injury trauma in many hospitals across the world. Accurate and rapid reporting of whole-body CT in trauma patients is critical for patient management. However, reading huge stacks of images under time pressure while being frequently interrupted presents great challenges to radiologists and carries the risk of missed injuries. The aim of this presentation is to provide an overview of common musculoskeletal injuries in multiple injury trauma patients, provide insight into the causes of missed injuries, highlight the effect of missed injuries on patient care, offer strategies to reduce sources of errors, and suggest a systematic approach to reading trauma CT. The first part

of the lecture covers frequently encountered musculoskeletal injuries and their relationship to distinct trauma mechanisms. The second part addresses the reasons for blindness and bias in diagnostic radiology. The third part focuses on a step-by-step approach for reporting whole-body CT in multiple injury trauma patients.

Learning Objectives:

1. To become familiar with the most common musculoskeletal injuries in patients after polytrauma.
2. To understand the clinical impact of missed subtle injuries on clinical outcome of the trauma victims.
3. To be familiar with less typical imaging findings in musculoskeletal injuries.

17:20

Panel discussion: How to reduce the rate of missed fractures most effectively and efficiently

16:00 - 17:30

Room D

Musculoskeletal

RC 1610

The radiological investigation of musculoskeletal tumours

A-840 16:00

Chairperson's introduction

F.M.H.M. [Vanhoenacker](mailto:vanhoenacker@telenet.be); Antwerp/BE (filip.vanhoenacker@telenet.be)

Plain films are the initial imaging modality in the detection and characterization of bone tumours, as they accurately depict matrix, cortical permeation or disruption and periosteal reaction. However, the sensitivity of this technique for the detection of small lesions is limited. CT can be used for characterization in anatomically complex areas, such as the spine, pelvis and skull. The CT appearance is similar to radiography. Due to radiation restraints, CT is not recommended in children or for evaluation of the appendicular skeleton in adults. Conventional MRI may be of additional help in narrowing the differential diagnosis of bone tumours. Soft tissue tumours based on imaging remains even more limited and histology is usually required for a definitive diagnosis. Ultrasound is mostly nonspecific, but may be used for superficially located cystic ST. On MRI, analysis of multiple parameters (shape, presence of signal voids, fluid-fluid levels, SI, intratumoural necrosis, multiplicity, pattern/degree of enhancement) yields the best results. The highest confidence is reached in benign lesions such as lipomas, vascular lesions, benign neural tumours, periarthral cysts, haematomas, PVNS, GCTTS, and abscesses. The major role of MRI consists of local tumour staging and therapy monitoring. The European Society of MusculoSkeletal Radiology (ESSR) has published guidelines for the detection, characterization, and referral pathway of musculoskeletal tumours based on conventional imaging. The specific aim of this session is to discuss the role of recent advances in ultrasound technology, advanced CT and MR techniques, and hybrid imaging in imaging evaluation of musculoskeletal tumours.

Session Objectives:

1. To learn how to differentiate tumours from other non-tumoural pathologies.
2. To understand the value of imaging modalities in this field.
3. To appreciate how to determine resectability and extension of the tumour.

A-841 16:05

A. Radiographs and ultrasound

L.M. [Sconfienza](mailto:io@lucascconfienza.it); Milan/IT (io@lucascconfienza.it)

Besides advanced techniques, such as computed tomography and magnetic resonance imaging which are important in the workup of musculoskeletal tumours, plain films and ultrasound still play a crucial role. Plain films still represent the cornerstone in the evaluation of bone tumours, as they allow detecting the presence of a bone lesion and giving important information about characterization of the lesion such as the presence and type of periosteal reaction, the pattern of bone destruction, the lytic or sclerotic appearance of the lesion, the presence of soft tissue involvement or of associated findings such as pathological fractures. However, plain films have limitations in particularly complex anatomical locations (e.g. spine and pelvis) and in the evaluation of soft tissue tumours not involving the bone. Ultrasound has limitations in the evaluation of bone tumours, as the ultrasound beam can only minimally cross the bony cortex. However, ultrasound may detect the presence of a periosteal reaction in early stages and may be used to assess the involvement of surrounding soft tissues and neurovascular bundles by bone tumours. On the other hand, ultrasound is accurate in the detection and

evaluation of soft tissue tumours, being able to correctly evaluate the size and the relationship of the mass with the surrounding structures. The use of supplementary tools, such as power Doppler, contrast-enhanced ultrasound, and elastography has been proved to be useful in increasing the diagnostic performance of ultrasound in certain conditions. However, ultrasound may be limited by low contrast resolution, small field of view, and deep lesions.

Learning Objectives:

1. To learn about the value of radiography and US in the diagnostic work-up of MSK tumours.
2. To be familiar with the most recent advances and trends in the development of US technology, including contrast-enhanced US and elastography.

Author Disclosure:

L.M. Sconfienza: Other; Travel grants from Bracco Imaging Srl, Esaote, and Abiogen.

A-842 16:28

B. MRI and whole-body MRI

S.L.J. James; Birmingham/UK (stevenjames@nhs.net)

MR imaging is the modality of choice for local staging of musculoskeletal tumours. When dealing with primary bone tumours, MRI enables both the intra- and extraosseous extent of the lesion to be delineated so that limb salvage surgery can be considered. Soft tissue tumours can be assessed relative to the compartmental anatomy and involvement of adjacent neurovascular structures. Once again, this facilitates potential curative excision to be planned. A routine MR protocol will be presented for primary bone and soft tissue musculoskeletal tumours. Additional advanced sequences will be discussed including chemical shift imaging, diffusion-weighted imaging, MR spectroscopy and post-contrast imaging. Current evidence for the use of these advanced imaging sequences will be reviewed. The role of whole-body MRI in staging of musculoskeletal tumours will be discussed including current evidence for its use in primary musculoskeletal tumours. This talk will not, however, discuss the use of MRI or whole-body MRI in the assessment, staging or follow-up of multiple myelomas or metastatic disease.

Learning Objectives:

1. To learn how to perform an advanced clinical MR protocol for MSK tumours.
2. To explore the potential of new MR techniques.
3. To learn the impact of MR imaging and whole-body techniques in MSK tumour imaging.

A-843 16:51

C. CT and hybrid imaging

T. Bauerle; Erlangen/DE (tobias.bauerle@uk-erlangen.de)

For imaging of musculoskeletal tumours, CT as well as the hybrid techniques PET/CT and PET/MRI offer a broad spectrum of methods for diagnosis, staging and follow-up. On the morphologic level, bone destruction ranging from osteolytic to blastic lesions and adjacent soft tissue tumours, e.g. in Ewing sarcoma or lytic bone metastases, are captured by CT. Beyond morphology, PET radiopharmaceuticals including [18F]-fluorodeoxyglucose ([18F]-FDG) or [18F]-sodium fluoride ([18F]-NaF) report on tumour and bone metabolism, respectively. Whereas the soft tissue tumours of rhabdomyosarcoma or bone marrow involvement in multiple myelomas is assessed by [18F]-FDG, osteoblastic activity is captured using [18F]-NaF, for example in sclerotic metastases. Due to the excellent sensitivity of PET, information on the molecular level is available when administering tumour-specific radiotracers such as the [68Ga]- or [18F]-labelled prostate-specific membrane antigen (PSMA) ligands for prostate cancer bone metastases. In conclusion, this lecture will summarize the use of CT and hybrid imaging techniques PET/CT and PET/MRI in primary and secondary musculoskeletal tumours. Current state-of-the-art techniques on the morphologic, metabolic and molecular level will be given as well as an outlook on future developments, particularly in hybrid imaging.

Learning Objectives:

1. To learn about the role of CT and hybrid imaging in the evaluation of MSK tumours.
2. To understand how hybrid imaging allows the intrinsic combination of functional and anatomical image information.
3. To be aware of the future developments of novel PET tracers and integrated PET/CT and MRI/PET in MSK tumours.

Author Disclosure:

T. Bauerle: Research/Grant Support; Bayer Healthcare. Speaker; Bracco, Boehringer Ingelheim.

17:14

Panel discussion: Guidelines for and the role of imaging techniques in the management of musculoskeletal tumours

16:00 - 17:30

Room G

Physics in Medical Imaging

RC 1613

Demystifying MRI: things you always wanted to know

Moderator:

I. Seimenis; Alexandropolis/GR

A-844 16:00

A. Basic MR: the building blocks of pulse sequences

D.G. Norris; Nijmegen/NL (david.norris@fcdonders.ru.nl)

To understand how NMR signals are produced, it is important to realise that the hydrogen nucleus has a magnetic moment which causes it to precess when placed in a static magnetic field. I shall explain how the presence of multiple nuclei gives rise to a bulk magnetisation, and how the orientation of the magnetisation vector can be manipulated by the application of radiofrequency pulses. Using the example of a bicycle dynamo, I will show how rotating transverse magnetisation gives rise to a measurable signal. Following excitation, the longitudinal magnetisation recovers (spin-lattice, or T1 relaxation) and the transverse magnetisation loses phase coherence (spin-spin, or T2 relaxation). I shall explain the physical basis for these processes and the use of inversion-recovery sequences to obtain T1 contrast, and spin-echo sequences to obtain T2 contrast. Finally, I shall show some modern examples of quantitative measurements of T1 and T2.

Learning Objectives:

1. To learn about how NMR signals are produced.
2. To understand the basic concepts of relaxation.
3. To learn about the operation of inversion-recovery and spin-echo pulse sequences.

Author Disclosure:

D.G. Norris: Advisory Board; fMRIB, Oxford.

A-845 16:30

B. MR imaging basic concepts: how to turn signals into images

D.J. Lurie; Aberdeen/UK (d.lurie@abdn.ac.uk)

To generate images in MRI, NMR signals must be "labelled" with their location. Three techniques of spatial encoding are employed, all of which use the magnetic field gradient. By sending electrical current (hundreds of amperes) through a gradient coil, a magnetic field is produced, whose strength varies linearly with position inside the scanner bore. In frequency encoding, the NMR signal is recorded while a field gradient is applied. Since the magnetic field varies with position along the gradient direction (e.g. X), the NMR resonant frequency (Larmor frequency) is a function of position, so the detected signal contains a range of frequencies; analysing the frequency content generates a one-dimensional projection of the water distribution within the patient. A method called phase encoding is employed in the second in-plane dimension (e.g. Y); here, the gradient is pulsed on and off prior to measurement of the signal, affecting the phase of the NMR signal as a function of position. Finally, the slice itself is defined using selective excitation, in which the radiofrequency pulse used for NMR excitation is specially shaped and applied in the presence of a field gradient perpendicular to the slice plane (e.g. along Z). To generate data for an image of NxN pixels, the pulse sequence is usually applied N times, varying the phase-encode gradient amplitude with each repetition. A two-dimensional Fourier transform of the raw data matrix yields the MR image, which can be encoded with NMR parameter (T1, T2, diffusion, etc.) information to assist in diagnosis.

Learning Objectives:

1. To learn how magnetic field gradients encode spatial information.
2. To understand the main ways in which field gradients are used.
3. To appreciate the basic concepts of data collection and image reconstruction in MRI.

Author Disclosure:

D.J. Lurie: Research/Grant Support; GE Healthcare.

A-846 17:00

C. Practical MRI: a toolkit of standard MR pulse sequences

G. Hagberg; Tübingen/DE (gisela.hagberg@tuebingen.mpg.de)

The MR sequence is the essential tool to measure MR properties in tissues, increase contrast between these and quantify relevant data. Besides furnishing the desired tissue-derived MR signal, the sequence must allow spatial encoding to take place as efficiently as possible to enable patient compliance, and high-quality MRI at the same time. Starting with a brief introduction

regarding MR tissue properties and spatial encoding in k-space, I will describe the fundamental MR toolkit, based on single echo spin-echo (SE) and gradient-echo (GE) and show how these are extended to different multiple-echo regimes. I will describe the basic image contrast and how imaging parameters, repetition time, TR; echo time, TE; flip angle, FA; inversion delay, diffusion gradients, etc., influence contrast. The possibility to further enhance imaging by adequate spin-preparation, inversion or magnetization transfer pulses, etc., will also be discussed. Imaging speed can be achieved while remaining in the single echo regime by faster RF pulsing giving valuable information linked with magnetic susceptibility as in the GE-based FLASH method, based on spoiling of unwanted echoes. Another possibility is to use subsequent (spin) echoes to read out different k-space lines, without the cost of greater saturation that comes with shorter TRs, as in the SE-based method RARE. An alternative possibility that further extends available image contrast is to retain the full magnetization in GE-based sequences and acquire images in the different steady-state free-precession regimes. The latter techniques have gained momentum through the advent of magnetic fingerprinting and are a fundamental part of the standard MRI toolkit.

Learning Objectives:

1. To learn about common types of MR pulse sequence.
2. To understand the difference between gradient-echo and spin-echo.
3. To appreciate the factors influencing choice of pulse sequence.

16:00 - 17:30

Room K

Radiographers

RC 1614

Optimising computed tomography

A-847 16:00

Chairpersons' introduction (part 1)

U. Nikupaavo; Helsinki/FI

Computed tomography (CT) is an essential diagnostic tool in many indications. New indications for CT imaging and technical development of the CT systems have increased the number of elective and emergency CT examinations. This has led to an increase in the collective radiation dose. The base of radiation safety in CT is a good referral practice. Justified CT examination includes adequate information of the patient, so that proper indication-based protocol can be used for the best diagnostic result and patient care. The goal of CT optimization is to minimize radiation exposure while maintaining diagnostic image quality. Technical methods for this purpose include the use of automatic exposure control (AEC) (i.e. automatic tube current modulation), bowtie filters, lower tube voltage (kVp) settings, adaptive section collimation, partial scanning, and iterative reconstruction methods. Correct preparation and positioning of the patient and optimized contrast agent protocols have great impact on the resulting radiation dose and image quality. Multiprofessional team work is essential to achieve justified and optimized CT examinations. Traditionally, the radiologist is in charge of adequate image quality level and the physicist coordinates the dose management and quality control. The radiographer has responsibilities in the following areas: daily workflow, preparation of patient, operation of scanner, use of contrast agent, and CT optimization, in general.

Session Objectives:

1. To review the importance of availability and appropriate CT techniques for the diagnosis and treatment of stroke patients.
2. To appreciate practical measures to optimise both, radiation dose and image quality in CT.
3. To understand how intravenous contrast agent delivery can best be optimised in CT to maximise diagnostic capability.

A-848 16:03

Chairpersons' introduction (part 2)

I. Lupescu; Bucharest/RO (ilupescu@gmail.com)

Worldwide, stroke is the second most common cause of mortality and the third most common cause of disability. In most centres, in the hyperacute phase, multimodal computed tomography (CT) evaluation is preferred, because of its availability and rapid scan times, containing three techniques: a noncontrast CT for detecting intracranial haemorrhage, a CT perfusion and a CT angiography, allowing the assessment of the site of vascular occlusion, infarct core, salvageable brain tissue and degree of collateral circulation. CT is widely used to obtain high-quality diagnostic images, with an increase of patient's irradiation. The effective dose for CT examinations can significantly increase, in situations when more CT phases are required. Due to the high CT radiation doses, it is necessary to track patient dose data and CT protocol scanning parameters, and also to apply the system's optimisation and dose reduction

techniques. The dose from the CT examinations can be reduced by controlling certain scanning parameters and optimizing the scanning protocols, delivering the minimum dose required to ensure the proper diagnosis. Current CTs offer reducing dose technologies, such as iterative reconstruction or automatic exposure control. With multidetector CT, intravenous contrast material administration and CT protocols have become challenging and complex. The clinical utility of contrast medium administration and CT scan timing is to achieve diagnostically adequate contrast enhancement in a specific organ using the lowest radiation exposure and the lowest dose of a non-ionic iodinated contrast media injected at the lowest rate in correlation with the renal and cardiovascular function of each patient.

Session Objectives:

1. To review the importance of availability and appropriate CT techniques for the diagnosis and treatment of stroke patients.
2. To appreciate practical measures to optimise both, radiation dose and image quality in CT.
3. To understand how intravenous contrast agent delivery can best be optimised in CT to maximise diagnostic capability.

A-849 16:05

A. Optimising access to CT in stroke

G. Ioannidis; Larissa/GR (*i.giorgio@yahoo.gr*)

Purpose: Computed tomography is the method of choice for the diagnosis of ischaemic stroke. Early diagnosis is of great importance for early treatment. The purpose of this speech is to review the "Golden Hour" of stroke diagnosis and therapy. How useful the cooperation of all the specialities involved will be noted, so that the patient with suspected stroke will arrive on time at the computed tomography department. It is also necessary to indicate the usefulness of CT in relation to the corresponding methods in magnetic tomography (DWI). Finally, the importance of the image of CT in the achievement of thrombolysis is noted. Material and Methods: Protocols that are applied for ischaemic stroke imaging as well as methods for the patient's protection against radiation are mentioned. Modification of all these in the last few years, comparison of the protocols between CT and MRI, estimation of time from the first symptoms up to the initiation of thrombolysis and the usefulness of image analysis are reviewed. Conclusion: The optimizing access to CT is very important for the immediate treatment of ischaemic stroke. The radiographer has a leading role in this process. Therefore, he should be perfectly aware of the subject to provide the maximum care for the immediate indication of the problem so as to achieve early treatment.

Learning Objectives:

1. To review the golden hour of stroke diagnosis and therapy.
2. To understand strategies for providing timely access to CT for patients with suspected stroke.
3. To appreciate challenges involved in providing timely access to CT and the need for multidisciplinary collaboration.
4. To become familiar with optimal CT protocols for diagnosis and therapy of stroke.

A-850 16:28

B. Optimising radiation dose and image quality

R. Booi; Rotterdam/NL (*r.booi@erasmusmc.nl*)

The number of computed tomography (CT) scans performed worldwide is increasing, which makes radiation dose optimisation of the utmost importance. Thereby, continuous technical improvements have been impressive; accordingly increasing the number of adjustable scan acquisition and reconstruction parameters. Overall, these developments led to improved image quality while reducing radiation dose. However, many parameters are interrelated and part of automated algorithms, making them less easy to adjust individually and more difficult to understand. Consequently, optimisation can be a challenge, e.g. patient positioning may seem to be a minor action; however, it is not. Patient positioning affects the patient's shape on a localiser radiograph, directly affecting dose modulation settings, as well as the efficacy of a bowtie filter. Therefore, a consolidate knowledge of CT scan parameters and their effects on radiation dose and image quality is needed to optimise CT exams.

Learning Objectives:

1. To enhance our understanding of the challenge of balancing image quality and dose reduction.
2. To review the options available to users for image quality and dose optimisation.
3. To consolidate knowledge to effectively use scan parameters and innovative technologies to optimise CT protocols.
4. To learn how to improve patient positioning and its effect on radiation dose.

Author Disclosure:

R. Booi; Other; Research collaboration, Siemens Healthineers.

A-851 16:51

C. Optimising contrast delivery with MDCT

A. Svensson; Stockholm/SE (*anders.svensson@karolinska.se*)

The administration of intravenous contrast media (CM) is essential for detecting lesions at most computed tomography (CT) examinations. There are several physiological factors that affect the CM-enhancement, where body size (defined by body weight and body height) and cardiac output are the most important factors. Also, technical factors have great influence on CM-enhancement, e.g. x-ray tube potential (kVp), injection rate and iodine dose. Traditionally, the same amount of CM has been given to all patients. However, the volume of distribution, i.e. plasma and extravascular interstitial space into which the CM is diluted is related to the body size and, therefore, a more individualised dosage of CM is nowadays regarded to be "state-of-the-art". The goal is to achieve a more uniform CM-enhancement independent of body size. This will also reduce the amount of CM given to smaller patients, i.e. reducing the risk of side effects associated with overdosing of CM. When reducing kVp at CT, CM will attenuate a greater number of x-ray photons. Approximately, 50% higher image contrast can thereby be achieved from the same amount of CM when reducing the x-ray tube potential from 120 kVp to 80 or 70 kVp. Vice versa, CM dose can be halved if the tube potential is lowered to down to 70 kVp from 120 kVp.

Learning Objectives:

1. To review injection and patient related factors that affect intravenous contrast medium (IV CM) enhancement during computer tomography (CT).
2. To understand the effect of different tube potential settings and its impact on IV CM enhancement during CT.
3. To gain knowledge about different aspects of individualised IV CM dosage.
4. To appreciate practical "tips and tricks" for successful CT angiography examinations.

17:14

Panel discussion: How to create an optimisation team in CT?

16:00 - 17:30

Room M 1

ESR Audit and Standards Session

Audit across Europe: directive and perspective

A-852/A-853 16:00

Chairpersons' introduction

A. Brady¹, D.C. Howlett²; ¹Cork/IE, ²Eastbourne/UK (*adrianbrady@me.com*)¹, (*david.howlett@nhs.net*)²

Under the EU 2013/59 Directive, Clinical Audit will be a required activity for all radiology departments within the EU from February 2018. Many departments already engage in this activity, but for some this will be a new venture. The ESR Audit & Standards Subcommittee has developed a package of suggested audits, with guidance for their completion, to assist with this new requirement. This package (The Esperanto Audit Project) was piloted among Eurosafe Imaging Star departments in late 2017 and will be made available widely following this pilot. During this session, the principles of Clinical Audit will be explained. The distinction between audit and external inspection will be explored and the complementarity of the two will be discussed. The Esperanto Audit Project pilot will be outlined and the initial results presented. Finally, an industry perspective on audit and quality improvement from a commercial perspective will be presented, with reference to change management.

Session Objectives:

1. To understand the principles of Clinical Audit (CA).
2. To appreciate the distinction between CA and external inspection.

A-854 16:05

The Esperanto Audit Project: results from the pilot project and roll out

B.E. Kelly; Belfast/UK

In 2018, Euratom Directive 2013/59 will come into effect. This will mandate the regular use of Clinical Audit as a tool for measuring, among other parameters, patient safety and radiation protection. In 2017, the Audit subcommittee produced a booklet (Esperanto) designed to guide the user through the principles of clinical audit. A pilot study, performed during the summer of 2017, tested the efficacy of the templates within the booklet. The results of this indicated that respondents found the algorithm straightforward, the templates navigable and the subjects audited relevant.

Postgraduate Educational Programme

Learning Objectives:

1. To learn about the nature of the pilot project.
2. To understand the pilot's significance with regard to the EU 2013/59 Directive.
3. To appreciate the necessity of Clinical Audit.

A-855 16:25

Engaging in the Pilot: The Eurosafe Imaging Star Perspective

G. Paulo; Coimbra/PT (graciano@estescoimbra.pt)

EuroSafe Imaging focuses on promoting appropriateness in medical imaging, maintaining doses within diagnostic reference levels, and emphasising the importance of using up-to-date equipment to develop a patient safety culture in medical imaging. The EuroSafe Imaging Call for Action number 2 focuses on developing and promoting a clinical audit tool for imaging to increase the quality of patient care and improve justification. Clinical audit is a systematic examination or review of medical radiological procedures. It seeks to improve the quality and the outcome of patient care through structured review whereby radiological practices, procedures, and results are examined against agreed standards for good medical radiological procedures. Clinical Audit is required under the Euratom Basic Safety Standards Directive and therefore mandatory in the EU. The ESR Audit Tool aids departments in carrying out audit in a more comprehensive manner and thereby complying with the directive by assuring the protection of their patients. Participating in the pilot project gave us the opportunity to engage better with the clinical audit process concept, mainly by focusing on the specificity of radiology departments, using a comprehensive library of templates. A very positive aspect of taking part in this ESR pilot was the fact that for the first time, a multidisciplinary team has been created, involving radiologists, radiographers, medical physicists, students and academic staff. This strategy revealed important aspects, namely, that integrating audit concepts into the clinical placements of radiography students will contribute to an easy adaptation and understanding to the audit philosophy.

Learning Objectives:

1. To learn about participation in the pilot project.
2. To understand the audit template.
3. To appreciate the advantage of performing Clinical Audit.

A-856 16:45

Quality improvement and change management: Audit in industry

S. Lee; Amsterdam/NL (steven.lee_1@philips.com)

Clinical-audit might be likened to the process of 'continuous improvement' of quality in industry. The latter focuses on improving performance for competitiveness by raising the quality (as perceived by the customer) and reducing the cost of products and services, while the former focuses on improving the quality of patient care by ensuring that clinical practice is delivered in line with defined standards. Both face the challenges of engaging people, developing supportive cultures and using systematic methods for sustaining the improvement process. While industry has deployed quality improvement practices extensively over many decades, the practice of clinical audit in many health-care organisations is by comparison relatively immature. The talk considers the evolution of different industrial management practices and paradigms concerned with quality improvement from the middle of the last century. During that time, the growing emphasis on the people dimension of improvement and change is highlighted, as is the significance of using an agreed, common and structured process (e.g. PDSA, DMAIC) for effecting quality improvement. The central importance of quality improvement for achieving competitiveness in an industrial setting is described, as are the major 'trends' deployed in realising such improvement. Potential areas of symbiosis between clinical-audit and management paradigms (Lean, Six Sigma, etc.) are proposed, particularly Lean principles, people change management and alignment of structured quality improvement processes. Working to align the intrinsic motivation of people with the practice of audit and quality improvement, by highlighting the benefits offered to customers (patients), is emphasised as key to securing staff engagement.

Learning Objectives:

1. To learn about the genesis of audit.
2. To understand the importance of audit in industry.
3. To appreciate the symbiosis between audit and management paradigms.

Author Disclosure:

S. Lee: Employee; Employee of Philips.

A-857 17:05

HERCA and Audit: Inspection vs Clinical Audit. What's the difference?

S. Ebdon-Jackson; Didcot/UK (steve.ebdon-jackson@phe.gov.uk)

EC Directive 2013/59/Euratom is intended to provide basic safety standards for protection against the dangers arising from exposure to ionising radiation. Member States are expected to transpose the Directive into national law. The Directive includes provisions for inspections to be carried out by the competent authority. In addition, within Chapter VII on Medical Exposures, there is a requirement that Member States ensure that clinical audits are carried out in accordance with national procedures, recognising that clinical audit extends beyond the scope of radiation protection and is normally carried out under professional initiatives and not under regulatory frameworks. While there may be some overlap between the information gathered as part of these separate approaches, the aims and conduct of regulatory inspections and clinical audit are different. These differences and the potential for these processes to be complementary are discussed.

Learning Objectives:

1. To learn about the duality of the process.
2. To understand the role of the inspector.
3. To appreciate the differences between Inspection and Clinical Audit.

17:25

Panel discussion: Does Audit make the patient journey safer?

16:00 - 17:30

Room M 2

E³ - ECR Master Class (Interventional Radiology)

E³ 1626a

Interventional radiology in the venous system: vessel and eye opening

Moderator:

C. Binkert; Winterthur/CH

A-858 16:00

A. Varicose vein

L. Oguzkurt; Istanbul/TR (loguzkurt@yahoo.com)

Varicose vein of the leg is a very common disease. Saphenous vein insufficiency is the cause in almost 95% of cases. Varicosities are not a sole cosmetic problem, as it may induce symptoms such as pain, fatigue, heaviness and night cramps which may influence the quality of life of people. Saphenous vein insufficiency is also part of chronic venous insufficiency causing leg swelling, skin changes and rarely venous ulcers. Surgery with saphenous vein stripping and high ligation was the primary treatment for years, but endovenous ablation methods are now the first-line treatment. There are several options for endovenous treatment of the saphenous vein insufficiency, such as laser, radiofrequency and steam (thermal) ablations or mechanicochemical, foam or glue (nonthermal) ablations. All these methods proved to be very effective and safe to treat truncal vein ablation. Ultrasound-guided foam sclerotherapy is not very effective for truncal vein ablation as recurrence rates are high. However, it is very effective for ablation of secondary or residual varicosities. Ambulatory phlebectomy or sclerotherapy for the secondary varicosities can be performed concomitantly or as a staged procedure and the former is preferred in most centres. Complications of truncal vein ablation include pain, bruising, tenderness, and phlebitis over the treated vein which are usually mild and self-limited. Deep vein thrombosis, pulmonary embolisms are extremely rare, but reported as case reports. Technical and short-/long-term clinical outcomes of endovenous ablation of the saphenous veins are very good with improvement of both cosmetic problems and clinical complaints.

Learning Objectives:

1. To learn about clinical and imaging assessment.
2. To understand the role of thermal and non-thermal devices.
3. To review the role of foam sclerotherapy and mini-phlebectomy for ancillary therapies.

A-859 16:30

B. Lower limb acute deep vein thrombosis

J. Kettenbach; St. Pölten/AT (joachim.kettenbach@stpoelten.lknoe.at)

Deep vein thrombosis (DVT) is common and, if left untreated, can lead to life-threatening conditions. Drug anticoagulation as a standard therapy primarily prevents progression of thrombosis and life-threatening pulmonary embolism. Long-term consequences with high morbidity, such as the post-thrombotic syndrome, cannot be prevented by anticoagulation. Systemic thrombolysis is

no longer indicated because of the high rate of major bleeding complications, whereas surgical thrombectomy is increasingly being replaced by endovascular procedures. Open surgical thrombectomy may be suitable only in selected patients who are candidates for anticoagulation, but in whom thrombolytic therapy is contraindicated (2C). In patients with iliofemoral DVT, catheter-assisted procedures, in addition to anticoagulation, are very well suited to rapidly revascularize extensive thrombosis. Combining local thrombolysis and thrombectomy as a pharmaco-mechanical thrombectomy (PMT) may be considered over catheter-directed pharmacologic thrombolysis (CDT) alone if expertise and resources are available. There is increasing evidence that this preserves venous valve function, reduces longer-term venous hypertension, and lowers the incidence of postthrombotic syndrome (PTS). Pharmaco-mechanical thrombectomy also reduces the required thrombolytic dose and allows single-session intervention. Residual stenoses or venous obstructions are treated by balloon dilatation and stent implantation. In the long term, the severity of a after iliofemoral thrombosis can be significantly reduced. Solitary minor deep calf vein thrombosis can be safely treated with compression stockings and anticoagulation without the need for urgent intervention such as CDT or mechanical thrombectomy, given the associated low morbidity and mortality.

Learning Objectives:

1. To understand the evidence supporting endovascular therapy.
2. To learn about clinical and imaging assessment.
3. To review what is new in terms of techniques and devices.

A-860 17:00

C. Lower limb chronic deep vein occlusion

R. de Graaf; Maastricht/NL (r.de.graaf@mumc.nl)

Chronic deep venous obstruction is a relatively prevalent condition caused by either or a combination of two factors: post-thrombotic vein damage or extraluminal venous compression. Post-thrombotic syndrome (PTS) develops in up to 50% of patients in the months or years following a deep venous thrombosis (DVT). Non-thrombotic iliac vein lesions (NIVL) are usually caused by an overriding artery (e.g. May-Thurner), alternatively by any two pelvic structures wedging the iliac vein. Both conditions impede venous outflow of the lower extremity and are linked to symptoms associated with chronic venous disease. Endovascular treatment has been shown to achieve high technical and clinical success. Overall, stents to treat NIVL show higher patency rates than those implanted for post-thrombotic lesions. The variation in patency rates might be dependent on multiple aspects, e.g. diagnostic sensitivity, anticoagulation regimens, stents characteristics and venous inflow impairment. Stent design might pose a very important variable in long-term patency. With increasing awareness and knowledge of deep venous interventions, new devices will be introduced which may improve technical success and support clinical outcome. The nearest challenge will be to identify a common approach in deep venous treatment by appraisal of the current data, moving towards international guidelines.

Learning Objectives:

1. To understand the evidence supporting endovascular therapy.
2. To learn about clinical and imaging assessment.
3. To review what is new in terms of techniques and devices.

Author Disclosure:

R. de Graaf: Consultant; Vesper Medical; Optimed GmbH, Cook Medical, Volcano/Philips, Boston Scientific, Bard.

16:00 - 17:30

Room M 3

E³ - ECR Master Class (Molecular Imaging)

E³ 1626b

Quantitative imaging in oncology

A-861 16:00

Chairperson's introduction

J. O'Connor; Manchester/UK (james.o'connor@manchester.ac.uk)

Tumours are biologically heterogeneous and this is considered to have prognostic significance and may also influence response to therapy. For many decades, diagnostic imaging has been used to provide 3D morphological assessments of the spatial variation in tumours and quantify overall tumour complexity. More recently, there has also been considerable interest in using functional imaging techniques derived from CT, MRI, ultrasound and nuclear medicine techniques to quantify the spatial variation in tumour pathophysiology. In this ECR Masterclass, we will discuss the image analysis methods currently used to quantify spatial heterogeneity within tumours. We will consider how and when analysis of intratumour heterogeneity can provide benefit over more simple biomarkers such as tumour size and average

function. We will consider how imaging biomarkers of heterogeneity are best integrated with genomic and pathology biomarkers into multi-scalar assessments of heterogeneity. The Masterclass will also identify the challenges for imaging tumour heterogeneity that must be addressed before such biomarkers become integrated into guiding patient care.

Session Objectives:

1. To understand the impact of tumour heterogeneity on diagnosis and treatment.
2. To learn the basics of quantitative imaging of heterogeneity.
3. To approach the future impact of quantitative imaging of heterogeneity.

A-862 16:05

A. Intra- and interindividual tumour heterogeneity and the impact for cancer diagnostics

M. Eisenblätter; Münster/DE (eisenblaetter@uni-muenster.de)

Malignant tumours are biologically complex systems with spatially variable gene expression patterns, consecutively variable biochemistry, histopathology and macroscopically variable structure. In the tumour microenvironment, genetic variability of tumour cells meets external stressors and the host immune system. The result is a regional heterogeneity of stromal architecture, biological activity and expression of e.g. chemokines and growth factors. Consecutively, the development of tumour vasculature, nutrient supply, cell growth and death etc. exhibit significant, regional variation. This variation occurs within a single tumour lesion, between primary tumour and metastasis and of course and pronounced between tumour lesions - even of the same tumour type - in different individuals. Generally, a high degree of heterogeneity is associated with poor prognosis and is at the same time increasingly relevant for therapy selection and monitoring, due to ever more specific therapy approaches. Various imaging approaches basically allow for visualisation of spatial heterogeneity in tumours. However, recorded and documented information is often limited to lesion size and macroscopic heterogeneity. In this context, relevant information, silently acquired even during clinical standard examinations, is ignored and dismissed unused. A rigorous analysis of all radiologic imaging data can help discovering this hidden information and provide additive information on tumour biology, relevant for tumour therapy. This talk is intended as an overview of the different levels of tumour heterogeneity, experimental and established imaging approaches to assess tumour heterogeneity and the possibility to provide adequate biomarkers for state of the art tumour therapy by integrated image data analysis.

Learning Objectives:

1. To learn about tumour heterogeneity.
2. To review current strategies to explore biological heterogeneity.
3. To understand how this heterogeneity impacts diagnosis and treatment.

A-863 16:23

B. Quantitative image biomarkers for targeted tumour therapies

R. García Figueiras; Santiago de Compostela/ES
(roberto.garcia.figueiras@sergas.es)

Clinical imaging systems are a significant source of non-invasive imaging biomarkers (IBMs) that may reflect important biological properties of cancers. IBMs can provide quantitative information on tumour hallmarks and can be used to evaluate tumour heterogeneity. They may also help us to understand the mechanism of action of therapies and their effects on the tumour microenvironment, offering objective measures of change in response to a therapy. This presentation will explain the biologic basis for a number of commonly available IBMs obtainable clinically. Besides this, we will illustrate how quantification of IBMs is undertaken and provide the validation of such measurements. Finally, the role of IBMs for the assessment of therapy response will be reviewed.

Learning Objectives:

1. To learn how heterogeneity can be quantified from images.
2. To understand how the main types of heterogeneity features.
3. To review limits and pitfalls of features extraction.

A-864 16:41

C. Requirements for quantitative data extraction and analysis

H.K. Hahn; Bremen/DE

We will focus on the question how to extract valuable quantitative information from in-vivo imaging data, ultimately leading to clinically relevant imaging biomarkers and phenotypes. We enter the topic by discussing the influence of image quality and resolution on the accuracy and precision of the derived measurements. In addition to signal-to-noise and partial volume effects, which always affect image based quantification, image non-uniformity plays a role in particular for MRI. A review of the concept of Radiomics will highlight the potentials of integrated diagnostics. Radiomics relates imaging based quantitative phenotyping to genomics, laboratory medicine, and risk scores

Postgraduate Educational Programme

etc., and ultimately to therapy outcomes and further clinically relevant parameters. Recently, tremendous advances in machine intelligence were demonstrated and successfully applied to medical imaging problems. Deep learning and convolutional neural networks will play an important role in next generations of automated imaging biomarker extraction and big data analysis systems. We will provide a few examples of what is already feasible today and also describe additional technological components required for successful clinical implementation, such as precise anatomical coregistration of multimodal and longitudinal medical images. For instance, the localised assessment of disease progress over time will be greatly facilitated by a combination of prior-to-current image registration and pattern quantification. Not least, we will discuss the requirements regarding infrastructure for the validation and interactive exploration of evolving imaging biomarkers.

Learning Objectives:

1. To learn how to optimise acquisition of images for quantitative imaging.
2. To understand image processing which may impact quantification.
3. To become familiar with the concepts behind quantification.

A-865 16:59

D. Imaging heterogeneity and genomic variability in ovarian cancer

E. Sala; Cambridge/UK (evis.sala@gmail.com)

Cancer is caused by genetic (DNA) and epigenetic alterations and frequently arises as a clonal growth from a founder cell. The subclonal heterogeneity provides the basis for inter-metastatic heterogeneity which is of utmost clinical importance. New tumour sampling techniques and circulating tumour DNA methods may allow for more comprehensive evaluation of clonal composition. As both primary tumours and metastatic lesions are spatially and temporally heterogeneous, they would require multiple biopsies to extract and analyse small portions of tumour tissue, which still does not allow for a complete characterisation of the tumour genomic landscape. Therefore, imaging has great potential for a comprehensive evaluation of the entire tumour burden in ovarian cancer, as it is noninvasive and is already often repeated during treatment in routine practice, in contrast to genomics or proteomics, which are still challenging to implement into clinical routine. While initial retrospective studies linking phenotype with genotype in ovarian cancer have shown high prognostic power, they do not provide any spatial information as quantitative imaging features are generated and averaged over the entire tumour, assuming that tumours are heterogeneous but well mixed. This approach ignores spatial heterogeneity readily apparent on imaging. Indeed, recent genomics work has highlighted the presence of intratumour variation in gene mutation and expression. However, little effort if any has been put into integrating imaging, histopathology and genomics and thus there is a clear need for well-designed prospective studies focused on meaningful integration of phenotype and genotype rather than genomics in isolation.

Learning Objectives:

1. To learn about an application of imaging tumour heterogeneity.
2. To understand how imaging heterogeneity may relate to biological heterogeneity.
3. To become familiar with new imaging concepts such as imaging phenotypes and signatures.

17:17

Panel discussion: What can we quantify and why is it essential?

16:00 - 17:30

Room M 4

E³ - ECR Academies: Tips and Tricks in Pancreatic and GI Tract Imaging

E³ 1622

Peritoneum and mesentery

A-866 16:00

Chairperson's introduction

A. Ba-Ssalamah; Vienna/AT (ahmed.ba-ssalamah@meduniwien.ac.at)

The abdominal cavity is subdivided into the peritoneal cavity, lined by the parietal peritoneum, and the extraperitoneal space. The visceral peritoneum covers the intraperitoneal organs and part of the pelvic organs. The parietal and visceral layers of the peritoneum are in sliding contact, the potential space between them called the peritoneal cavity which is part of the embryologic abdominal cavity or primitive coelomic duct. A thorough understanding of peritoneal anatomy is fundamental in determining the cause and recognising the extent of peritoneal involvement, as well as in decision-making about the appropriate therapeutic approach, whether surgery, conservative treatment, or interventional radiology. On imaging, signs of peritoneal involvement include

fluid collections or solid tumors along the ligaments, mesenteries, and/or within the potential spaces of the peritoneal cavity. The spectrum of disorders include inflammatory, infectious, and neoplastic diseases, as well as trauma. Radiologist, by taking into account the patient's age, gender, symptoms and risk factors, in addition to the key features, including location, textural composition of the lesions either cystic or solid and number of lesions come up with a list of differential diagnoses. Reports should include measurements, pertinent negatives and any other relevant findings that influence patient management.

A-867 16:05

A. Understanding primary tumours

C. Dromain; Lausanne/CH (Clarisse.Dromain@chuv.ch)

Primary tumours arising in the peritoneum and the mesentery are rare. Most imaging findings of primary peritoneal and mesenteric tumours are nonspecific and very similar to those of peritoneal metastases associating soft-tissue masses and ascites. However, several key findings can be helpful for the diagnosis and proper management of these patients. Key points to consider are the clinical context (sex, age, risk factor such as asbestosis exposure, absence of history of cancer, FAP ...), the location of the peritoneal implant (mesentery vs peritoneum cavity meso and fold), tissular composition of the lesions (cystic vs solid, vascularisation), and number of lesions (isolated vs multiples). The most common primary mesenteric tumours are cystic tumours, such as lymphangiomas and mesothelial cysts, and tissular lesions including desmoid tumours (often associated with FAP), GIST, NET (with high fibrous content and retraction), primary mesenteric lymphomas, Castleman tumours (highly vascularized) and mesenchymal benign and malignant tumours. The most common primary peritoneal tumours are mesotheliomas, desmoplastic round cell tumours (young male), primary papillary serous carcinomas (PPSC; mimicking metastases from ovarian cancer), peritoneal lymphomatosis, and leiomyomatosis. Imaging features of mesothelioma depend on the histological type. Multicystic mesothelioma has a very typical multiloculated cystic appearance with thin septations easily diagnosed on MRI. Benign papillary mesothelioma and malignant epithelioid mesothelioma (linked to asbestosis exposure) have very similar pattern mimicking peritoneal metastases. Sarcomatoid and biphasic mesotheliomas are predominantly solid and localized with large masses and no ascites. Differential diagnoses include peritoneal metastases, pseudomyxoma peritonei (PMP), splenosis, tuberculosis, actinomycosis, and peritoneal endometriosis.

Learning Objectives:

1. To become familiar with the spectrum of tumours of the mesentery and peritoneum.
2. To understand how imaging helps in narrowing the differential of mesenteric and peritoneal masses.
3. To learn the role of percutaneous or surgical biopsy.

A-868 16:33

B. Peritoneal carcinomatosis

P.K. Prassopoulos; Alexandroupolis/GR (pprasopo@med.duth.gr)

Intraperitoneal dissemination of primary GI and gynaecological primary tumours - the so-called peritoneal carcinomatosis - is a common process in the evolution of these malignancies and has a significant impact on therapeutic decisions. The location of implants in peritoneal carcinomatosis is governed mostly by peritoneal fluid circulation and by anatomic pathways formed by peritoneal reflections, namely ligaments, mesenteries and omenta. The most common sites where the peritoneal fluid may be temporarily arrested - facilitating implantation of cancer cells - include cul-de-sac, distal small bowel mesentery, right paracolic gutter, posterior sub-hepatic space, greater omentum and subphrenic spaces. The role of imaging is to disclose the presence and extent of the disease - that is fundamental in candidates for cytoreductive surgery - to monitor response to treatment and to reveal recurrences. MDCT with thin collimation and i.v. contrast material supplemented by multiplanar reconstructions remains the primary imaging modality for the investigation of peritoneal carcinomatosis, assessment of disease distribution and routine post-treatment evaluation. Ascites, contrast-enhanced smooth, nodular, or plaque-like peritoneal thickening, peritoneal nodules, plaques or masses, rounded, ill-defined soft-tissue or cystic mesenteric masses, mesenteric fixation with increased attenuation values and thickening, irregular soft-tissue permeation of omental fat or confluent solid omental masses are the most frequent MDCT findings of peritoneal carcinomatosis. MRI-DWI can alternatively be used. Post-gadolinium-enhanced 3d FLASH sequence with fat saturation is advantageous in cases of diffused layered type of peritoneal/mesenteric involvement. PET/CT and DW-MRI have specific indications in post-treatment imaging evaluation.

Postgraduate Educational Programme

Learning Objectives:

1. To become familiar with the usual origin and spread of peritoneal carcinomatosis.
2. To learn about the role of CT, MRI and PET for the detection and staging of peritoneal carcinomatosis.
3. To understand how imaging helps the clinician for the evaluation of response to treatment.

A-869 17:01

C. From misty mesentery to mesenteritis

G.A. [Krombach](mailto:gabriele.krombach@uniklinikum-giessen.de); Giessen/DE (gabriele.krombach@uniklinikum-giessen.de)

The mesentery can be affected by a variety of entities ranging from spread of diseases occurring in adjacent organs, such as necrosis in pancreatitis or oedema following thrombosis of the portal or superior mesenteric vein to benign or malignant diseases directly arising within the mesentery. Sclerosing mesenteritis is an autoimmune disease initiated by an allergic reaction to long-term exposure of allergens regularly contained in food or constantly present in the proximity of the patient. IgG4-antigenes are formed against such antigens and mesenteritis is a sequel of cross reaction of the IgG4-antigenes to proteins contained in the connective tissue of the mesentery. Mesenteritis usually is biphasic with a first active phase, marked by cellular infiltration with plasma cells and lymphocytes and oedema, and a chronic phase with the hallmark of almost acellular storiform fibrosis triggered by the cytokines TNF- α and IL-2 and -4 released by granulocytes. In imaging, in all modalities the mesentery appears "misty", while the tissue immediately surrounding the mesenteric vessels is spared from the change, called fat-ring sign. The area of the increased density (or altered signal intensity in MRI) in almost all cases and phases is sharply surrounded by a pseudocapsule. Contrast enhancement and T2 signal intensity vary with the disease phase. The mesenteric lymph nodes are often enlarged, which can render differentiation from lymphoma challenging in some patients. Symptoms may range from not present to abdominal pain, fever, weight loss to severe complications, including stenosis of the mesenteric vessels and ischaemia of the bowel, ileus or perforation.

Learning Objectives:

1. To become familiar with the differential between incidental mesenteric abnormalities, tumour infiltration and true mesenteritis.
2. To understand how mesenteritis can be associated with other organs lesions in case of systemic disease.
3. To learn which imaging (CT, MRI, PET) is relevant for the detection and follow-up of inflammatory diseases.

16:00 - 17:30

Room M 5

Transatlantic Course of ESR and RSNA (Radiological Society of North America): Sports Imaging

TC 1628

Postoperative imaging of sports injuries

Moderators:

L.W. Bancroft; Orlando, FL/US
A.J. Grainger; Leeds/UK

A-870 16:00

A. Postoperative shoulder MRI after instability surgery

L.W. [Bancroft](mailto:laura.bancroft.md@flhosp.org); Orlando, FL/US (laura.bancroft.md@flhosp.org)

Purpose: To become familiar with the expected and abnormal MR imaging findings after labral repair, capsular shift/capsulorrhaphy, remplissage and Latarjet/Bristow procedures. Methods and Materials: MR imaging will be used to demonstrate the various normal and abnormal imaging appearances after shoulder instability surgery. Results/Conclusion: Labral re-tear will be evident as contrast or joint fluid extension into linear or complex tear cleft, absent/truncated/fragmented labrum, or labral displacement from anatomic location. Capsular shift results in smaller capacity joint and sometimes irregular capsular nodularity. Complications of capsulorrhaphy include capsular tears and subluxation of humeral head. Postoperative MR imaging can evaluate healing after combined remplissage and Bankart repair for moderate size, engaging Hill-Sachs lesions. Latarjet and Bristow procedures may be performed in patients with recurrent dislocations and glenoid deficiency. Incorporated bone will yield non-anatomic glenoid configuration, and complications include non-union, fatty degeneration of subscapularis muscle, and osteoarthritis.

Learning Objectives:

1. To become familiar with the expected and abnormal MR imaging findings after labral repair.
2. To learn about the postoperative imaging features after capsular shift/capsulorrhaphy.

3. To appreciate normal imaging and complications after remplissage and Latarjet/Bristow procedures.

Author Disclosure:

L.W. Bancroft: Author; Lippincott - Book Royalties.

A-871 16:30

B. ACL reconstruction and cartilage repair

C. [Weidekamm](mailto:weidekamm@icloud.com); Vienna/AT (weidekamm@icloud.com)

The aim of ACL reconstruction is to stabilize the knee and prevent chondral and meniscal injuries, which are the sequelae of anteroposterior translation and are associated with early osteoarthritis. The idea of the double-bundle ACL graft was to restore normal joint kinematics by anatomic reconstruction of the anteromedial and the posterolateral bundle of the original ACL. This was expected to improve clinical outcomes and restore anterior and rotational knee stability. The single-bundle technique, however, causes less osseous defects and is still a popular technique. Complications, such as ACL graft failure, impingement, cyclops lesion, arthrofibrosis, and patellar inferior syndrome, are discussed. The second part of this presentation will illustrate cartilage repair techniques and imaging findings. The radiologist must be familiar with the different cartilage repair procedures and characteristics in cartilage imaging to evaluate long-term progression or failure. Abnormal postoperative findings include hypertrophic filling, incomplete integration of the transplant into the surrounding cartilage, or subchondral defects, osteophytes, cysts, and persistent bone marrow oedema and joint effusion.

Learning Objectives:

1. To review the common and uncommon ACL reconstruction techniques.
2. To appreciate the expected and abnormal MR imaging findings after ACL reconstruction.
3. To understand common cartilage repair techniques, and corresponding normal and abnormal postoperative MRIs.

A-872 17:00

C. Interactive case discussion (part 1)

L.W. [Bancroft](mailto:laura.bancroft.md@flhosp.org); Orlando, FL/US

To engage in interactive case discussions with the expected and abnormal MR imaging findings after labral repair, capsular shift/capsulorrhaphy, remplissage and Latarjet/Bristow procedures. An interactive case discussion will be used to demonstrate the various normal and abnormal imaging appearances after shoulder instability surgery. Labral re-tear will be evident as contrast or joint fluid extension into linear or complex tear cleft, absent/truncated/fragmented labrum, or labral displacement from anatomic location. Capsular shift results in smaller capacity joint and sometimes irregular capsular nodularity. Complications of capsulorrhaphy include capsular tears and subluxation of humeral head. Postoperative MR imaging can evaluate healing after combined remplissage and Bankart repair for moderate size, engaging Hill-Sachs lesions. Latarjet and Bristow procedures may be performed in patients with recurrent dislocations and glenoid deficiency. Incorporated bone will yield non-anatomic glenoid configuration, and complications include non-union, fatty degeneration of subscapularis muscle, and osteoarthritis.

Learning Objectives:

1. To learn how to differentiate normal and failed labral repairs with MRI.
2. To become familiar with the diagnostic features of failed ACL reconstructions.
3. To understand the imaging features of intact and failed cartilage repair.

Author Disclosure:

L.W. Bancroft: Other; Lippincott - Book Royalties.

A-873 17:15

C. Interactive case discussion (part 2)

C. [Weidekamm](mailto:weidekamm@icloud.com); Vienna/AT

Postoperative imaging after ACL or cartilage repair is indicated in patients with ongoing pain/instability or repetitive injury. Radiography remains the initial imaging modality; however, further assessment with CT or MRI is recommended. With a clear emphasis on MRI, we will review normal postoperative findings and complications after ACL reconstructions and cartilage repair. The case discussion will cover the most significant pathologies and pitfalls, and normal postoperative findings will be illustrated.

Learning Objectives:

1. To learn how to differentiate normal and failed labral repairs with MRI.
2. To become familiar with the diagnostic features of failed ACL reconstructions.
3. To understand the imaging features of intact and failed cartilage repair.

Sunday, March 4

08:30 - 10:00

Room A

E³ - ECR Academies: Interactive Teaching Sessions for Young (and not so Young) Radiologists

E³ 1721

Cardiac imaging

A-874 08:30

A. Grown-ups with congenital heart disease

A.M. [Taylor](#); London/UK

This session will describe how MRI and CT can be used to image adults with congenital heart disease. The common conditions that occur in childhood will be described (acyanotic and cyanotic heart disease) and what operations they undergo that will be important for imaging them when they become adults. Finally, those CHDs that may be diagnosed in adulthood will be described.

Learning Objectives:

1. To be familiar with the clinical and radiologic presentations of these patients.
2. To learn about imaging findings and management options.

A-875 09:15

B. Imaging cardiac valves

R. [Salgado](#); Antwerp/BE (rodrigo.salgado@uza.be)

Valvular heart disease forms an important part of the workload in every cardiology practice. While echocardiography remains a cornerstone in the assessment and follow-up of valvular heart disease, an important role is reserved for MR and CT imaging, although in different contexts. MR, with its ability to investigate the valvular morphology as well as the haemodynamic consequences on the cardiac chambers, forms an important complementary tool to the echocardiographic findings. It provides a reproducible quantification of transvalvular flow and has in recent years gained further importance in tissue characterisation with the introduction of T1/T2 mapping techniques for the detection and distribution of fibrosis. CT has recently gained a prominent place in the non-invasive investigation of the aortic root before transcatheter aortic valve replacement and is also becoming a primary imaging modality in emerging mitral valve interventions. Furthermore, its role in the evaluation of prosthetic heart valves is currently the subject of intense investigation, providing valuable additional information not easily acquired through other imaging methods. During this lecture, the different advantages and limitations of valvular imaging with CT and MR will be discussed, and practical recommendations for clinical practice will be given.

Learning Objectives:

1. To understand the impact of imaging.
2. To know the limitations and potential pitfalls of CT and MR techniques.
3. To learn about the imaging technique.

08:30 - 10:00

Room B

Abdominal Viscera

RC 1701

Abdominal MRI: from standard to advanced protocols

A-876 08:30

Chairperson's introduction

F. [Caseiro Alves](#); Coimbra/PT (caseiroalves@gmail.com)

Abdominal MR imaging is a continuously evolving technique where researchers, vendors and clinical users get together to push it to the next level of medical practice. Recent advances in the MR field include the development of dedicated DWI sequences, increased spatial resolution and functional imaging capabilities, to name a few. Therefore, there is a clear-cut need to use and take advantage of the most recent and best suited protocols. In this session, we will deal with three important common clinical situations: a) suspected pancreatic cancer where MR appears not only as a problem-solving tool, but also as a competitive diagnostic modality compared with MDCT, ranging from DWI to high-resolution MRCP and time-resolved dynamic imaging; b) inflammatory bowel disease, which, as a chronic relapsing disease, is one of the cases where MR may contribute to drive patient management, exquisitely monitoring the inflammatory activity of the disease; and c) MRI of pelvic floor disorders that consists in the use of high-resolution morphological data together with functional information under straining conditions. Its

diagnostic power and contribution to patient management is well acknowledged today, but protocol optimisation and proper quantification assume vital importance. To enhance the educational value of this session, an illustrative clinical case for each clinical problem will be presented exploring the benefits and/or MR limits.

Session Objectives:

1. To learn the importance of MR protocolling for different abdominal conditions.
2. To become familiar with both dedicated and advanced MR imaging.
3. To learn through a case-based approach its impact on report quality.

A-877 08:35

A. Suspected pancreatic tumour

R. [Manfredi](#); Rome/IT (riccardo.manfredi@unicatt.it)

Pancreatic cancer is the fourth leading cause of cancer-related death. Surgical resection is the sole curative treatment option; however, only 15%-20% are resectable at the time of diagnosis. Furthermore, the prognoses for patients with pancreatic cancer remain poor. Although the 5-year survival rate is up to 20% after complete resection, it is further improved to more than 75% in patients with a diagnosis of stage 1 disease. Computed tomography (CT) remains the initial imaging modality of choice for pancreatic solid neoplasms, because recent improvements in multidetector CT technology, including improved temporal and spatial resolution, have facilitated more precise timing of multiphasic imaging and increased the accuracy of CT for the detection and staging of pancreatic adenocarcinoma. Recently, magnetic resonance (MR) imaging has acquired a role in the early diagnosis of adenocarcinoma, because of diffusion-weighted (DW) MR imaging. By means of DW imaging, MRI is able to depict changes in water mobility caused by interactions with cell membranes, macromolecules, and alterations to the tissue environment, and thus provides a tissue contrast that is different from that on conventional T1- and T2-weighted images. DW imaging plays a role in oncology for tumour detection, in general. DW imaging allows detection of pancreatic adenocarcinomas with high sensitivity and specificity, because it appears hyperintense compared with the rest of the gland. DW-MR imaging is also useful in finding small functioning neuroendocrine neoplasms, responsible for a clinical syndrome, but difficult to diagnose because of their small size.

Learning Objectives:

1. To learn about the role of MRI in the assessment of a patient with suspected pancreatic tumour.
2. To become familiar with the optimal MRI protocols including the role of DWI and secretin in this group of patients.
3. To appreciate the advantages and limitations of MRI in comparison with other imaging techniques.

A-878 08:58

B. Inflammatory bowel disease

S.A. [Taylor](#); London/UK (csytaylor@yahoo.co.uk)

Magnetic resonance enterography (MRE) is increasingly used, particularly for Crohn's disease assessment. It has an evolving role not only in grading inflammation and detecting complications, but also for monitoring the course of the disease. The diagnostic accuracy of MRE is heavily influenced by the technical quality of the examination. Patient preparation, bowel distension, sequence selection and scan technique must all be optimised to produce high-quality examinations. This presentation will review the recommendations of the recent ESGAR consensus statement on MRI small bowel imaging and will address commonly encountered problems that can arise before and during scan acquisition. The utility of novel sequences such as DWI and motility will also be discussed.

Learning Objectives:

1. To learn about the role of MRI in patients with IBD.
2. To become familiar with the optimal MRI protocols including bowel distension in this group of patients.
3. To appreciate the role of functional imaging techniques for assessment of IBD.

Author Disclosure:

S.A. Taylor: Consultant; Robarts.

A-879 09:21

C. Pelvic floor disorder

D. [Weishaupt](#); Zurich/CH (dominik.weishaupt@triemli.zuerich.ch)

Imaging of the female pelvic floor is of rising interest due to an ageing population, harbouring an increasing incidence of pelvic floor disorders (PFD), and the rising need for comprehensive diagnosis and treatment. Magnetic resonance imaging (MRI) of the female pelvic floor combines high-resolution imaging with an excellent soft tissue contrast and provides the possibility to

assess noninvasively and objectively a spectrum of possible disorders affecting the pelvic floor in one examination. There is general agreement that MRI of the pelvic floor should include static and dynamic MR images, whereas dynamic means imaging under maximum stress to the pelvic floor and MR defecography. Static MR images visualize pelvic floor anatomy and defects of the supporting structures, while dynamic MR images visualize pelvic organ mobility, pelvic floor weakness, pelvic organ prolapse (POP) and associated compartment defects. In this lecture, a standardized approach regarding indications, patient preparation, sequence acquisition, interpretation and reporting of MRI for diagnosis and grading of PFD is presented. Due to the different views of the clinical specialists involved in the treatment of PFD, adapting the MRI reporting scheme according to the speciality of the referring physician is discussed. Finally, the limitations of the technique are addressed.

Learning Objectives:

1. To learn about the clinical relevance of MRI in the management of patients with pelvic floor disorders.
2. To become familiar with the optimal patient preparation and MRI protocols in this group of patients.
3. To appreciate the advantages of MRI relative to other imaging modalities including conventional defecography.

09:44

Panel discussion: How to create an efficient MR protocol in abdominal diseases

08:30 - 10:00

Room C

Chest

RC 1704

Thoracic manifestations of systemic disease

Moderator:

A. Chodorowska; Wrocław/PL

A-880 08:30

A. Systemic sclerosis

N. Sverzellati; Parma/IT (nicolasve@tiscali.it)

Systemic sclerosis (SSc) is variably associated with pulmonary involvement, which is a paramount prognostic factor. Interstitial fibrosis and pulmonary vessel abnormalities are the two elementary lung wounds in SSc and can occur independently of each other. Chest radiograph has low sensitivity in the assessment of early interstitial lung disease (ILD) associated with SSc. Oesophageal dilation can be the only apparent finding. High-resolution computed tomography (HRCT) is pivotal in baseline staging. HRCT findings of SSc-ILD include confluent ground-glass opacities, traction bronchiectasis/bronchiolectasis, fine reticulation, and honeycombing. The HRCT pattern of non-specific interstitial pneumonia (NSIP) is common, actually reflecting more than 75% frequency of histologic NSIP. The combination of HRCT and pulmonary function tests (PFTs) has been proposed for prognostication of SSc. ILD extent <10% has lower risk compared to >30%, with minor influence from PFTs. On the other hand, PFTs can further stratify prognosis among subjects with ILD extent 10-30%. Quantitative CT methods are being developed to measure the ILD extent. SSc patients are at increased risk of lung cancer. Its surgical treatment is mostly prevented by extensive ILD. Pulmonary hypertension (PH) can occur independently of ILD, reflected by isolated reduction of DLCO at PFTs. In particular, PH is more common in limited cutaneous systemic sclerosis, also known under the acronym CREST syndrome.

Learning Objectives:

1. To learn about the typical radiological appearances.
2. To be aware of the clinical relevance of scoring.
3. To know how vascular complications affect patient prognosis.

A-881 09:00

B. Granulomatosis and polyangiitis

S. Bayraktaroglu; Izmir/TR (selenb2000@gmail.com)

Granulomatosis with polyangiitis (GPA), formerly known as Wegener's granulomatosis, is a chronic granulomatous necrotising vasculitis of small- and medium-sized vessels. The classical clinical triad of the disease consists of upper and lower airway involvement and glomerulonephritis. The upper respiratory tract is affected in almost all patients. The majority of patients with GPA will also have pulmonary (90%) and renal (80%) involvement. The most common radiologic findings in thoracic involvement are nodules, mass lesions

and areas of consolidation. Cavitation within these lesions may be seen due to the necrotic nature of the disease. Airway involvement is characterised by circumferential tracheal wall thickening. Areas of consolidation, cavity nodules and mass lesions represent active inflammatory disease, whereas areas of bronchiectasis and septal-nonseptal lines more often represent chronic fibrotic changes. The radiologist must be familiar with the common thoracic radiologic manifestations of the disease.

Learning Objectives:

1. To learn about the radiological appearances of small-vessels vasculitis.
2. To learn how clinical and radiological features help in differential diagnosis.
3. To appreciate the actual role of imaging in assessing disease activity.

A-882 09:30

C. Early manifestations in children and young adults

M.P. García-Peña; Barcelona/ES (plgarciapeña@gmail.com)

Lung disease is common in children with systemic diseases, and the radiographic appearance of early-stage pulmonary changes is often subtle. Computed tomography (CT) has higher sensitivity and specificity than radiography. High-resolution computed tomography (HRCT) is the imaging technique of choice for assessing lung involvement in these patients. Even with reduction in the peak voltage and tube charge to minimize the exposure of paediatric patient to radiation, CT performed with a meticulous acquisition technique can provide detailed information. The uses of CT in evaluating systemic disease are to detect lung abnormalities, characterize the findings, assess the extent of disease, and help establish the differential diagnosis. CT also is used for follow-up evaluations, monitor the effects of treatment, and for guidance of lung biopsy when that is required. High-resolution CT may depict lung lesions in children with no clinical respiratory symptoms and normal findings at lung function testing, facilitating early identification of lesions and allowing early treatment that can benefit the course of the disease. This lecture reviews the findings on high-resolution CT of the chest in children with suspected systemic diseases, with emphasis on connective tissue diseases (juvenile rheumatoid arthritis, dermatomyositis, systemic sclerosis, systemic lupus erythematosus, and mixed connective tissue disease), vasculitis, primary and acquired immunodeficiencies, immotile cilia syndrome, cystic fibrosis, and Langerhans cell histiocytosis.

Learning Objectives:

1. To learn about the radiological manifestations in children.
2. To review the most adapted scanning protocols.
3. To appreciate the role of imaging to monitor the effects of treatment.

08:30 - 10:00

Room X

Joint Session of the ESR and ESTRO

New imaging approaches for radiotherapy

A-883/A-884 08:30

Chairpersons' introduction

V. Valentini¹, M.H. Fuchsjaeger²; ¹Rome/IT, ²Graz/AT (michael.fuchsjaeger@medunigraz.at)²

This session focuses on the importance of imaging for radiation oncology. Specific emphasis will be laid not only on current cooperation but also on potential future opportunities for radiology and radiation oncology collaboration. Furthermore, the latest imaging as well as radiotherapy technologies will be discussed. The understanding of these technologies, ultrasound, dual-energy CT, MR-LINAC and MR-PET only forms the basis for clinical applications and successful therapy. A panel discussion on how radiation oncology and radiology as technological innovation leaders will be able to take advantage of each other in the near and distant future will complete this session.

Session Objectives:

1. To understand the increasing importance of imaging in radiation oncology techniques.
2. To learn about the cooperation opportunities between radiologists and radiation oncologists.
3. To become familiar with the most modern radiotherapy technologies.

A-885 08:35

Dual-energy CT: what are the benefits for radiotherapy?

P. Wohlfahrt¹, C. Richter¹, C. Möhler², S. Greilich²; ¹Dresden/DE, ²Heidelberg/DE (patrick.wohlfahrt@oncoray.de)

For about a decade, dual-energy CT (DECT) has been clinically available, mainly for radiology applications. In contrast, in the field of radiotherapy DECT has gained relevant interest over the last few years and here clinical use is still far away from being standard. In this lecture benefits of DECT for radiotherapy applications will be discussed. The focus will be on application for treatment

Postgraduate Educational Programme

planning in proton therapy, namely the individual prediction of tissue stopping power relative to water (SPR) as an alternative to the standard approach using a generic look-up table (HLUT). The manifold information gathered by two CT scans with different X-ray spectra allow for a patient-specific and direct calculation of relative electron density and SPR. This enables the consideration of intra- and inter-patient variabilities in CT-based SPR prediction and ultimately a more accurate range prediction. The talk will cover the validation of the SPR prediction accuracy in realistic ground-truth scenarios, the investigation of clinically relevant differences between the DECT-based and the standard HLUT-based SPR prediction in clinical patient data as well as the status of its clinical implementation. Furthermore, additional applications in radiotherapy, e.g. for photon treatment planning, delineating and material differentiating will be briefly discussed.

Learning Objectives:

1. To learn about technical aspects of dual-energy CT acquisition.
2. To understand the strengths and limitations of the dual-energy CT applications in oncology.
3. To appreciate the benefits relative to the use of dual-energy CT in the radiotherapy workflow.

A-886 08:55

Ultrasound imaging in radiotherapy: "old" technology with new applications in RT?

E. Harris; Sutton/UK (Emma.Harris@icr.ac.uk)

Medical ultrasound was first introduced in the 1940's and has become a powerful diagnostic tool throughout the world. Its real-time, soft-tissue imaging capability and non-ionizing nature have contributed to its ubiquitous use in disease diagnosis and image guidance in interventional and surgical procedures. Ultrasound guidance of radiotherapy is a relatively new field with the first commercial systems becoming available in the late 1990's. Despite possessing clear benefits for imaging a variety of tumour sites, challenges associated with implementing ultrasound in the radiotherapy clinic initially impeded its widespread adoption. The influence of effective training on interobserver variation and operator performance was an early barrier. Contemporary ultrasound image guidance techniques have done much to overcome these problems and modern systems are used clinically for interfraction motion estimation in prostate and breast and for intrafraction prostate motion monitoring. Other promising clinical applications under investigation include interfraction motion estimation in liver, pancreas and kidney, and augmentation of cone beam CT data for the purpose of adaptive radiotherapy of the prostate and gynecological cancer. This talk will give an overview of the clinical use of ultrasound in radiotherapy, discuss the advantages and limitations of ultrasound and present future perspectives for ultrasound guided radiotherapy technology and practice. Finally, some exciting new applications of ultrasound functional imaging for monitoring of tumour response to radiotherapy will be introduced.

Learning Objectives:

1. To learn about ultrasound applications in radiotherapy.
2. To understand the clinical advantage of using ultrasound based techniques.
3. To appreciate the modern perspectives of this technique.

A-887 09:15

MR-LINAC technological advances and potential usability in clinical setting

O. Jäkel; Heidelberg/DE (o.jaekel@dkfz-heidelberg.de)

Radiotherapy has reached a point, where dose highly precise dose delivery is achieved with various techniques. The next big gain can only be made, when dose adaption is achieved not only in 3 dimensions as for static targets, but can also be maintained in 4 dimensions, i.e. including temporal changes in the patient. Image guided radiotherapy, based mainly on X-ray cone beam CT imaging, up to now has mostly been used to improve daily setup accuracy and to a lesser extent enabled modest adaption for inter-fractional changes. MRI, however, being non-invasive and yielding excellent soft tissue contrast, is an optimal tool for continuous monitoring of tumor motion during delivery and for allowing intra-fractional adaption of treatment plans. The idea to integrate a linear accelerator into an MRI was put forward by the Utrecht group already in 2000. Due to the technical complexity, it took until 2017 to realize a clinical prototype. First patients were treated in 2017 and a commercial product by Elekta is expected to be released in 2018. Also in 2017, first patients were treated with another commercial system by Viewray, using a 0.35T split bore Magnet and a 4MV linac. The latter was modified from the MR-Cobalt unit, which is available since 2014. The availability of commercial hybrid systems will now enable investigations of the clinical potential of these hybrid systems in different tumor sites. In parallel the systems will be continuously developed further, in order to exploit their full clinical potential.

Learning Objectives:

1. To learn about the technological advances of MRI-LINAC technology.
2. To understand the physical principles of hybrid treatment units.
3. To appreciate the clinical advantages of the use of this technology.

A-888 09:35

Multiparametric MR-PET for differentiation of residual disease vs treatment-induced inflammatory changes

M. Becker; Geneva/CH (minerva.becker@hcuge.ch)

The purpose of this lecture is to provide a simplified, systematic approach on how to detect tumour recurrence on MR-PET examinations of patients treated for head and neck squamous cell carcinoma. First, the relevant imaging findings of post-therapeutic expected tissue alterations with a special focus on their temporal relationship are discussed. Then a brief discussion of common complications affecting the soft tissues, vasculature and bony structures will follow. A systematic review will include key MRI, diffusion-weighted imaging (DWI) and PET features of osteoradionecrosis, soft tissue necrosis, neck fibrosis and scar tissue mimicking tumour recurrence. Typical radiologic findings of tumour recurrence will be discussed with an emphasis on the early detection of lesions, their appearance on MR-PET with DWI and the added value and complementarity of multiparametric information extracted from hybrid imaging techniques. The potential pitfalls of post-therapeutic image interpretation and how to avoid them taking into consideration multiparametric data will be addressed. Results of combined MR-PET evaluations for the correct staging of recurrent tumours will be presented. Major emphasis will be put recently published research results and on quantitative information that can be easily extracted in clinical routine. Pitfalls of image interpretation will be addressed and how to avoid them.

Learning Objectives:

1. To learn about hybrid imaging based tissue characterisation techniques.
2. To understand the challenges of hybrid imaging use after oncologic treatments.
3. To appreciate the performance of hybrid MR-PET techniques in differential diagnosis.

Author Disclosure:

M. Becker: Grant Recipient; SNSF 320030_173091.

09:55

Panel discussion: Will radiation oncology and radiology be able to take advantage of each other's technological innovation?

08:30 - 10:00

Room O

Paediatric

RC 1712

Understanding paediatric neuroradiology

Moderator:

E. Vázquez; Barcelona/ES

A-889 08:30

A. Imaging of the premature brain

S.M. Aukland; Bergen/NO (stein.magnus.aukland@helse-bergen.no)

Imaging is essential in detecting and monitoring brain injury in premature newborns. Cerebral ultrasonography (CUS) is still the modality of choice in an emergency setting, but magnetic resonance imaging (MRI) is a complementary modality. The classical findings include haemorrhage and white matter disease (WMD)/periventricular leukomalacia (PVL). The haemorrhages are usually part of the germinal matrix haemorrhage-intraventricular haemorrhage continuum (GM-IVH). Small sub-ependymal haemorrhage and small IVH usually disappear in a few weeks, but larger haemorrhages carry a high risk of causing hydrocephalus and/or periventricular venous haemorrhagic infarctions, which demands close follow-up. CUS is an excellent tool in detecting GMH-IVH and cystic WMD, but MRI is more sensitive in detecting non-cystic WMD and cerebellar pathology. MRI is also superior to CUS in detecting hypoglycaemic parenchymal injury. GMH-IVH and cystic-WMD are associated with major disabilities, and the subtle WM and cerebellar lesions seem to be associated with behavioural and attention difficulties later in life. MRI at term-equivalent age (TEA) is now a routine examination in some institutions, but the value of this screening must be evaluated by long-term follow-up studies. In short-term studies of extremely preterm, abnormalities detected on late CUS and near-term MRI are associated with the outcome and TEA may be the best time point for scanning. Several studies have compared the value of serial CUS and near-term MRI without strong conclusions. Conventional MRI at TEA probably

Postgraduate Educational Programme

gives additional prognostic information, and advanced MRI is promising but its role is still unclear.

Learning Objectives:

1. To discuss the roles of US, (CT) and MRI in preterm imaging.
2. To give an overview of the different imaging findings in the preterm brain related to age.
3. To discuss the prognostic role preterm brain imaging.

A-890 09:00

B. Abusive head trauma: the role of CT and MRI

R. Van Riijn; Amsterdam/NL (r.r.vanriijn@amc.uva.nl)

Abusive head trauma (AHT), defined by the American Academy of Pediatrics as an inflicted injury to the head and its contents including those injuries caused by both shaking and blunt impact, is one of the most severe forms of child abuse. Imaging plays an important role in establishing the diagnosis and potential outcome of AHT. In this session, the most common neuroradiological findings, with their evidence base, in AHT are presented. In short, the differential diagnosis and the limitations of CT and MRI will be discussed, as well as the imaging strategy as proposed in the newly published guideline 'The radiological investigation of suspected physical abuse in children' of the Royal College of Radiology and the Society and College of Radiographers.

Learning Objectives:

1. To discuss the role of CT and MRI in imaging of abusive head trauma (AHT).
2. To give an overview of common CT and MRI findings in AHT.
3. To understand the strengths and limitations of CT and MRI in imaging AHT.

A-891 09:30

C. Imaging in hypoxic-ischaemic injury and hypothermia: an update

F.M. Triulzi; Milan/IT (Fabio.triulzi@policlinico.mi.it)

Hypoxic-ischemic encephalopathy (HIE) is the major recognized perinatal cause of neurological morbidity both in premature and full-term newborns. The incidence of HIE ranges from 1 to 8 per 1000 live births in developed countries, it accounts for approximately 15%-20% of neonatal mortality in full-term neonates. Immediately after an acute HIE episode, proton MR spectroscopy is often the most useful modality due to the increase of lactate, while diffusion-weighted imaging (DWI) may be falsely negative in this time frame. However, pseudonormalization of lactate levels, which occurs approximately 24 hours after birth, may confound interpretation of early MR imaging spectra. Cerebral blood flow increases after 24-28 hours in brain areas subsequently exhibiting injury, whether or not hypothermia is administered. Consequently, it has been suggested to combine a perfusion study using arterial spin labelling technique to increase the prognostic value in the acute phase of HIE. After approximately 24 hours of age, even DWI becomes a sensitive technique, due to the presence of cytotoxic oedema and it remains positive for approximately 1-5 days, after which it may pseudonormalize; at this point, T1- and T2-weighted MR images may be most useful to depict brain damage. Due to the reduction in the extent of brain injury on conventional T1- and T2-weighted MRI, it is mandatory to account for hyperthermic treatments when evaluating MR images during the acute phase.

Learning Objectives:

1. To discuss the role of US, (CT) and MRI in hypoxic-ischaemic injury (including advanced MR techniques).
2. To give an overview of common imaging findings in hypoxic-ischaemic injury (HIE).
3. To understand the importance of timing and prognostic value of imaging in HIE.

08:30 - 10:00

Room N

Special Focus Session

SF 17a

New treatments for musculoskeletal tumours

A-892 08:30

Chairperson's introduction: What is changing?

J.L. Bloem; Leiden/NL (j.l.bloem@lumc.nl)

Biologic tumour behaviour and patient compliance should be primary considerations in treating patients with musculoskeletal sarcoma. Diagnostic tests in combination with systemic and focal therapy are used to reach curative or palliative goals. The progress made in diagnostic tests, treatment strategies, and understanding biologic behaviour of tumours increases options to serve

our patients, but also increases therapy-related morbidity, diagnostic tests-related anxiety, and costs. The current challenge is to use our diagnostic and therapeutic means not only to increase survival chances, but also to preserve the quality of remaining life, while involving the patient's opinion in decision-making. The change of ingredients for this balancing act is explored in this introduction.

Session Objectives:

1. To understand the demand for new treatment concepts.
2. To understand how multimodality imaging can influence therapeutic balancing between tumour control and quality of life.

A-893 08:35

New treatment paradigms in orthopaedic oncology

M.A.J. van de Sande; Leiden/NL (majvandesande@lumc.nl)

Knowing if the sarcoma will return remains the basic patient paradigm in cancer treatment and follow-up, but going from if to when it returns seems to be the next step in follow-up optimisation and stress reduction. All prediction models for sarcoma available at present are applicable only at the time of baseline, such as the time of diagnosis or surgery. However, updated patient information during the follow-up as well as changing covariate effects over time may change the prognosis of a patient, which is not accounted for in these models. The concept of dynamic prediction allows to include updated information; on disease status, patient characteristics and imaging results during follow-up. This information can be used to provide better individualised treatment and follow-up options that depend on the dynamic assessment of a patient's prognosis. The findings of time-varying effects as well as the importance of time-dependent covariates such as LR and DM found in our multicentre analysis confirm the inadequacy of the baseline models for predictions later on in follow-up. A model designed for dynamic prediction, which updates survival probabilities, is needed and it is provided in this work. To this end, an APP (PERSARC) was developed to assist in shared decision-making in clinic. Following up on this, we analysed the timing of LR and DM during FU. We concluded that in patients with localised STS after curative surgery, the rates of LR and DM are highly non-constant over time and are strongly modified by tumour characteristics. These findings contradict a "one-size-fits-all" aftercare policy, but rather support the concept of a time- and risk-adapted strategy for personalised post-surgical follow-up.

Learning Objectives:

1. To understand the impact of treatment choices on survival chances and quality of life.
2. To learn about the influence of imaging, patient and disease characteristics on developing new treatment options.

Author Disclosure:

M.A.J. van de Sande: Grant Recipient; National Cancer Fund.

A-894 08:58

Multimodality imaging in treating and monitoring bone sarcoma

M.-A. Weber; Rostock/DE (marc-andre.weber@med.uni-rostock.de)

The histopathologic response to chemotherapy and radiation therapy is an important prognostic indicator of disease-free survival after the treatment of musculoskeletal sarcomas. Several studies report that therapy response assessment may rely on functional PET data. Moreover, a decrease in tracer uptake indicates early response to neoadjuvant chemotherapy. However, to plan surgical resection of the tumour, the surgeon needs reliable information on tumour size and extent of infiltration to the adjacent structures. MRI is the best additional imaging modality for local staging, as it allows for accurate assessment of the extent of the disease and the effect of the tumour on the surrounding structures including the joint, neurovascular structures, muscle compartments and skin. MRI also gives details of the extent of the compartmental involvement to help complete excision of the tumour. Additional MRI techniques such as diffusion-weighted imaging (DWI), MR spectroscopy (MRS), and dynamic contrast-enhanced (DCE) MR imaging are not routinely used for bone tumour assessment. The potential of DWI to reveal tumour cellularity, MRS to noninvasively assess metabolic aberrations, and DCE to assess treatment response in which traditional size-based assessment criteria may underestimate efficacy has been reported. The role of FDG- or NaF-PET/CT and PET/MRI in the initial diagnostic workup of bone tumours is still not established. There is an overlap in the maximum standard uptake value between benign and malignant tumours. Therefore, PET/CT does not yet have a role in the initial differentiation of benign from malignant bone tumours, but may aid in problem-solving in suspected local recurrence.

Learning Objectives:

1. To learn how to use multimodality imaging in personalised treatment planning aimed at survival and preserving quality of life.
2. To learn how to use multimodality imaging in monitoring response to neoadjuvant therapy.

A-895 09:21

Multimodality imaging in treatment and surveillance of soft tissue sarcoma

C. [Messiou](mailto:Christina.Messiou@rmh.nhs.uk); London/UK (Christina.Messiou@rmh.nhs.uk)

Limb-sparing surgery is potentially curative for primary non-metastatic extremity soft tissue sarcomas. The addition of radiotherapy results in higher local control rates. MRI is standard imaging before and after radiotherapy and is critical for surveillance of often complex post-treatment appearances. However, histopathologic changes that occur after radiotherapy confound dimension-based assessments of response. Except for myxoid liposarcoma, significant dimensional radiologic responses are rare. Dimension-based assessments have been shown to have no correlation with outcome or histopathologic response, and alternative assessments are needed. Current consensus from the EORTC-STBSG suggests that the addition of functional diffusion-weighted MRI to standard anatomic and postcontrast MRI greatly facilitates interpretation because the combination of reduced enhancement and increasing apparent diffusion coefficient (ADC) may increase confidence for response. After radiotherapy, new enhancement alone should be interpreted with caution, because this may be a result of vascular disruption rather than histologic response. Machine learning is likely to play a crucial role in allowing us to fully exploit the quantitative capabilities for use in routine, research and adaptive treatment regimens. Alternative methods of assessment are poorly understood; however, a small study of 18F FDG PET/CT in high-grade sarcomas has shown promise. CT is the mainstay of surveillance and response assessment for metastatic disease. However, methods of response assessment are evolving beyond dimension-based (RECIST 1.1) measurements. Furthermore, patients with the best radiological responses often have the worst outcomes, as this reflects high tumour grade. This highlights the need for appreciating the significance of imaging responses with regard to outcome.

Learning Objectives:

1. To learn how to use multimodality imaging in personalised treatment planning aimed at survival and preserving quality of life.
2. To learn how to use multimodality imaging in surveillance strategies.

09:44

Panel discussion: Increasing quality of life in sarcoma patients without decreasing survival. What is needed from an imaging perspective to allow and support this?

08:30 - 10:00

Studio 2018

Genitourinary

RC 1707

Imaging strategies in renal tumours

A-896 08:30

Chairperson's introduction

C. [Nicolau](mailto:nicolau@clinic.ub.es); Barcelona/ES (nicolau@clinic.ub.es)

The detection of incidental renal masses has increased due to a large number of imaging studies being performed for different clinical indications. The characterization and differentiation between benign and malignant renal lesions is essential for their management. The objectives of this session are to become familiar with the indications and optimal protocols of the current and emerging renal imaging modalities as well as to describe the evidence regarding renal mass characterization and learn about the capabilities of renal imaging to stage renal tumours.

Session Objectives:

1. To become familiar with current and emerging renal imaging modalities.
2. To learn about the capabilities of renal imaging in diagnosis and staging of renal tumours.

A-897 08:35

A. Imaging methods, CT and MRI: the best out of two

M.A. [Cova](mailto:cova@gnbts.units.it); Trieste/IT (cova@gnbts.units.it)

CT is currently the imaging modality of choice for the evaluation of renal masses. The advantages of CT are its widespread availability, high speed of acquisition, high spatial resolution and isotropic imaging. MRI can be a powerful problem-solving tool in clinical practice for characterisation of renal masses, especially for characterisation of lesions with indeterminate enhancement at CT and of lesions in which a small amount of fat is suspected. Like CT, MRI provides excellent anatomic information on the evaluation of renal lesions. Moreover, unlike CT, advanced MRI techniques can provide

information about tissue structure and function without exposure to ionising radiation and without using iodinated contrast. The disadvantage of MRI compared to CT is the longer examination time. Optimal MDCT protocol for renal masses includes a noncontrast phase followed by postcontrast acquisitions with corticomedullary, nephrographic and delayed phases of enhancement at approximately 40 seconds, 90 seconds and 7 minutes after contrast injection. The nephrographic phase is acquired for assessing the presence of a renal lesion and its enhancement, and is therefore sufficient for detection and characterisation of renal lesions. Corticomedullary and urographic phases are often performed to provide additional information for presurgical planning. Optimal MRI protocol for renal mass evaluation includes TSE T2-weighted imaging, TSE T1-weighted imaging with and without fat suppression, T1-weighted opposed-phase imaging (with in-phase and out-of-phase sequences) for the detection of microscopic fat, DWI, fat-suppressed 3D T1-weighted gradient-echo acquisition before and after administration of intravenous gadolinium contrast in corticomedullary, nephrographic and urographic phases, and subtraction imaging.

Learning Objectives:

1. To become familiar with the optimal CT and MRI protocols for renal imaging.
2. To understand the best choice of CT or MRI according to the clinical need.
3. To illustrate the advantages and disadvantages of CT and MRI.

A-898 08:58

B. Differential diagnosis of renal masses

N. [Grenier](mailto:nicolas.grenier@chu-bordeaux.fr); Bordeaux/FR (nicolas.grenier@chu-bordeaux.fr)

Imaging is the main source of detection of renal masses. Differentiation between complex cystic and solid masses is not always straightforward and may require several contrast-enhanced methods, and DCE-MRI and CEUS are more sensitive for that purpose. Considering cystic masses, Bosniak classification is required. Considering solid masses, characterization of fat-rich angiomyolipomas is based on plain CT, but fat-poor AMLs can be distinguished from carcinomas by multiparametric MRI only. Multiparametric MRI includes chemical shift gradient echo (GRE) sequences, signal intensity on T2-weighted images, DCE sequences, diffusion-weighted sequences and late contrast-enhanced images. Using different combinations of two or several parameters, now makes it possible to clearly distinguish some renal tumours such as fat-poor AMLs, papillary carcinomas and clear cell carcinomas, the latter being difficult to separate from oncocytoma when a central scar is absent. A larger validation of all these combinations is still necessary to define those having a clinical significance for routine practice. Percutaneous biopsy remains mandatory before such a validation, as soon as pathological result is supposed to have an impact on tumour management.

Learning Objectives:

1. To learn about the histologic spectrum of renal tumours.
2. To understand the capabilities of imaging for renal tumour characterisation.
3. To become familiar with functional techniques applied to characterise renal tumours.

Author Disclosure:

N. Grenier: Advisory Board; Supersonic Imagination, Aix-en-Provence, France.

A-899 09:21

C. Staging and organ-preserving strategies

P. [Asbach](mailto:patrick.asbach@charite.de); Berlin/DE (patrick.asbach@charite.de)

Accurate CT- or MRI-based staging of the two most common malignant neoplasms involving the kidneys, renal cell carcinoma (RCC) and transitional cell carcinoma (TCC) is an important prerequisite for surgical decision-making, especially in the early stages of the disease. The TNM staging system is particularly different between RCC and TCC regarding the T-stage. Tumour size and invasion of the perirenal fat are important criteria for local staging of RCC, whereas invasion of the muscular layer of the renal collecting system and invasion into the renal parenchyma are important criteria for staging TCC, the latter being more complex based on imaging as compared to RCC. Different organ-preserving strategies are evolving, especially for treatment of RCC (e.g. local excision versus partial nephrectomy). Also, important additional information such as detailed vascular anatomy is needed by the surgeon, which has impact on the respective preoperative imaging protocol.

Learning Objectives:

1. To understand the TNM-staging system for renal tumours.
2. To become familiar with optimal staging protocols and imaging findings in staging of renal tumours.
3. To learn about actual organ-preserving strategies.

09:44

Panel discussion: How to implement an optimal renal imaging protocol?

08:30 - 10:00

Room L 8

Special Focus Session

SF 17b

Abdominal emergencies: friends and enemies

A-900 08:30

Chairperson's introduction

I. Arkhipova; Moscow/RU (iarkhipova77@mail.ru)

Non-traumatic emergencies as well as traumatic ones in the abdomen require immediate medical care; however, the absence of a clear reason like trauma or a variety of clinical features may often lead to a life-threatening delay of the correct diagnosis or of a misdiagnosis. Prompt and qualified imaging with either "friendly" or "enemy" pitfalls is a fundamental and crucial part in the evaluation of different diseases and conditions, which are to be discussed in the five (5) lectures with clinical case presentations. The goal of this session is to review current imaging strategies, controversies and reports, corresponding to requests of clinicians in the evaluation of common and uncommon acute non-traumatic abdominal emergencies.

Session Objectives:

1. To learn about the main radiological features of life-threatening non-traumatic emergencies in abdomen.
2. To become familiar with the most frequent requests and expectations of surgeons.
3. To be familiar with interpretation of cases in emergency imaging.
4. To find out possible points that could be useful in daily radiological practice in emergency department.
5. To discuss and understand diagnostic strategy for high-quality and faster diagnosis at the end of the session.

A-901 08:35

Abdominal vascular emergencies: no time to lose

V.E. Sinityn; Moscow/RU (vsini@mail.ru)

Acute abdominal vascular emergencies could be traumatic or non-traumatic according to their aetiology. Risks of rapid blood loss with development of hypovolemic shock and critical organ ischaemia dictate the need for rapid and accurate diagnostic assessment. These emergencies could be a result of arterial or venous pathology. Major types of vessel injuries are ruptures accompanied by active haemorrhage, lacerations or dissections, thrombotic or mechanical occlusions with following organ ischaemia, and the formation of pseudoaneurysms and fistulae. CT is a most used diagnostic technique in such cases. It has several advantages over abdominal US. CT is quick, covers large anatomical areas, is widely available, and its results are not dependent on patient's preparation. MRI or hybrid imaging is not routinely used in such cases. The preferable technique is biphasic CT. In cases of acute vascular emergencies, CT is comparable to catheter angiography. CT can show the direct signs of vessel injury, intraluminal thrombi or extravascular blood and clots, and ischaemia of critical organs (e.g. mesenteric ischaemia). Modern systems can be used to see so-called "blush" - a sign of acute extravasation of contrast material. It helps to locate the site of continuing acute bleeding. Potential pitfalls in CTA interpretation (missed acute bleeding or thrombosis) could be related to the low rate of bleeding, stopped bleeding, dilution of blood by fluid, and missed signs of organ ischaemia. The use of abdominal MDCT in cases of vascular emergencies helps to define and plan the best treatment strategy (endoscopic intervention, angiographic embolization, surgery, or active surveillance).

Learning Objectives:

1. To learn about types and aetiology of non-traumatic abdominal vascular emergencies.
2. To be familiar with the appropriate imaging protocols.
3. To know about CT findings in various acute life-threatening abdominal vascular diseases.
4. To understand modern approach to diagnostic work-up and reporting in vascular emergencies.

A-902 08:50

When to call the interventional radiologist and when to call the surgeon?

K.K. Pyra; Lublin/PL (k.pyra@poczta.fm)

Vascular abdominal emergencies are not common but, when present, may be catastrophic, with significant morbidity and, frequently, mortality. The physical examination may not reveal clear abnormalities, making the diagnosis more difficult. Due to wide MDCT technology availability, the first-line assessment of

vascular abdominal emergencies is CTA. The findings of various types of vessel injury include laceration, rupture with active haemorrhage, occlusion and, for arteries formation of aneurysm, pseudoaneurysm, dissection or fistula. Most of them are life-threatening emergencies, since they may cause a heavy hypovolemic shock and/or severe organ ischaemia and therefore prompt diagnosis and treatment are required. Due to the rapidly growing field of endovascular treatment, interventional radiology is increasingly used as a first-line treatment. This presentation focuses on differences in clinical and radiological presentations of vascular emergencies, usual and unusual emergencies, endovascular methods of treatment and what is most important in choosing appropriate treatment strategy: endovascular or open surgery.

Learning Objectives:

1. To learn about differences in clinical and radiological presentations of vascular emergencies.
2. To demonstrate examples of usual and unusual emergencies of the abdominal vessels.
3. To become familiar with the endovascular methods of treatment.
4. To learn how to choose appropriate treatment strategy.

A-903 09:02

Closed loop obstruction: a challenging diagnosis

M. Zins; Paris/FR (mzins@hpsj.fr)

Closed-loop small bowel obstruction (CL-SBO) is a form of mechanical intestinal obstruction in which a segment of bowel is occluded at two contiguous points. Adhesive bands and internal and external hernias are the main causes of CL-SBO. CL-SBO is the most common cause of strangulation with a rate of intestinal ischaemia ranging from 43 to 84 %. Computed tomography (CT) remains actually the best modality to detect ischaemia in small bowel obstructions (SBO) with reported sensitivities ranging from 73% to 100% and specificities from 61% to 100%. In patients with CL-SBO and absence of other CT signs of ischaemia, non-surgical management is successful in 25% of the cases. Increased unenhanced bowel wall attenuation is the only CT finding significantly associated with bowel necrosis in patients with adhesive bands or internal hernias CL-SBO. When present, this sign could help to differentiate reversible partial mural bowel ischaemia from irreversible transmural bowel infarction.

Learning Objectives:

1. To be able to differentiate simple mechanical small-bowel obstruction from closed loop obstruction (CLO) at CT.
2. To learn about atypical presentation of CLO at CT.
3. To become familiar with the most specific CT signs of ischaemia complication CLO.
4. To learn new insights in clinical outcome of CLO related to adhesive bands.

A-904 09:17

Expected and unexpected emergencies of abdominal viscera: radiology before surgery?

C. Stoupis; Mannedorf/CH (c.stoupis@spitalmaannedorf.ch)

Evaluation of acute abdominal conditions is sometimes difficult. Various factors can obscure the underlying cause, delaying the correct diagnosis with subsequent adverse patient outcome. Imaging is one of the most important diagnostic tools in acute abdomen and many times radiological examinations are done prior to use of other diagnostic tools. This presentation will demonstrate the examples of usual and unusual entities of the upper abdominal organs that are seen as emergency conditions (imaging on demand, not planned) and require timely intervention to limit morbidity and mortality. Examples of life-threatening bleeding conditions of the liver and spleen, examples of immediate treatment requiring infectious diseases of the liver, cases of inflammatory processes of the pancreas and unexpected lesions of the adrenals will be shown. The relation of the organ pathology and the clinical presentation will be discussed, as a potential guide or even indication of danger, to proceed with the correct radiological diagnosis; expected vs surprising radiological findings (treat the patient, not the image). Appropriate imaging techniques will be discussed, with specific emphasis on CT, as a most valued tool, demonstrating the advances of imaging in the evaluation of emergency pathologies. A short overview of interventional techniques will be discussed as well, as an alternative to surgical procedures to treat effectively patients with high morbidity, without open or laparoscopic surgery.

Learning Objectives:

1. To demonstrate examples of usual and unusual emergencies of the upper abdominal organs (liver, pancreas, spleen, adrenal).
2. To learn about differences in clinical and radiological presentations of those entities.
3. To learn about imaging strategies (time, cost, efficiency, protocols).
4. To learn about the potential of interventional radiological procedures as treatment choice.

Postgraduate Educational Programme

A-905 09:32

Life teaches us case by case

M.-L. Riibak; Tallinn/EE (mlriibak@gmail.com)

With a speedy workflow, as is very often necessary at the department of emergency radiology, or on the night shift, it might be quite easy to overlook some important pathologies. Acquiring some useful habits such as measuring densities or comparing and paying attention to 'hints' we see during radiological studies could guide us to serious conditions not noticed initially. Good clinical and laboratory information are often necessary to come to the right conclusion.

Learning Objectives:

1. To recognise the signs of pathology in non-traumatic acute abdomen.
2. To recognise common finding "as friends" in not so common "unfriendly" situations and vice versa.
3. To become familiar with what the clinician might be interested to know besides the diagnosis.

09:44

Panel discussion: Every imaging sign could matter!

08:30 - 10:00

Room E1

E³ - ECR Master Class (Breast)

E³ 1726a

The high-risk patient enigma

Moderator:

F. Kilburn-Toppin; Cambridge/UK

A-906 08:30

A. Lesions with an elevated risk for breast cancer

G. Forrai; Budapest/HU (forrai.gabor@t-online.hu)

The histological, clinical presentation, together with the mammography and US appearance of the high-risk lesions, would be demonstrated. They have very different probability figures of developing cancer, and this would be detailed for each type of lesion. The concept and the global problem of the management of these lesions will be explained, together with the conflict of over/underdiagnosis/treatment.

Learning Objectives:

1. To learn about different types of high-risk lesions.
2. To become familiar with the risk of developing a cancer.
3. To appreciate the different imaging modalities for diagnosis.

A-907 09:00

B. Value of breast MRI. Rate of underestimation and impact on treatment decision: is breast MRI increasing the number of high-risk lesions?

R.M. Mann; Nijmegen/NL (r.mann@rad.umcn.nl)

The evaluation of high-risk lesions on biopsy with MRI is commonly performed. One of the major ideas is to ascertain that there is not more disease present than seen with other techniques. As many high-risk lesions are in fact accidental findings on needle biopsy, the absence of enhancement within the breast reduces the likelihood of more extensive disease. Nevertheless, the underestimation rate with MRI is dependent on the type of high-risk lesion initially found and is still substantial for lesions like atypical ductal hyperplasia and lobular neoplasia. Moreover, several high-risk lesions may in fact enhance strongly in breast MRI, but are not upgraded at subsequent pathological assessment. In this lecture, MRI features of common and less common high-risk lesions will be discussed. In general, MRI cannot preclude the need for extensive tissue sampling, but it may be used for guiding of the biopsy and may obviate complete surgical excision.

Learning Objectives:

1. To learn about the evidence on MRI for evaluating high-risk lesions.
2. To become familiar with various imaging appearances of high-risk lesions.
3. To appreciate the added value for diagnosis and treatment decision.

Author Disclosure:

R.M. Mann: Advisory Board; Screenpoint Medical, Transonic imaging. Grant Recipient; Siemens Healthineers, Bayer Healthcare, Medtronic, Elswood, Identification solutions inc., Seno medical, Micrima.

A-908 09:30

C. Can surgery be avoided?

S.J. Vinnicombe; Dundee/UK (s.vinnicombe@dundee.ac.uk)

Within the UK National Health Service Breast Screening Programme (NHSBSP), a median of 7% of screen-detected lesions subjected to needle core biopsy are categorised as B3, of uncertain malignant potential. These lesions comprise a diverse group of pathological entities, with or without epithelial atypia, mostly manifest as mammographic microcalcification. B3 lesions tend to be heterogeneous (such that the area sampled by needle core biopsy may not be representative) and are associated with a variable rate of upgrade to malignancy, either in situ or invasive, at surgical excision biopsy, which has been the treatment of choice until recently. However, the approach to B3 lesions is changing. With increasing concerns about overdiagnosis (and subsequent overtreatment) in breast screening and the widespread availability of large-bore needle biopsy devices, minimally invasive modes of treatment are increasingly used for these lesions. Various techniques are available, including large-bore vacuum-assisted devices where the lesion is removed in a piecemeal fashion, and devices which remove the lesion in its entirety with a single pass. These approaches to management of B3 lesions are cost-effective and well tolerated, but oncological safety must be the key consideration. In this respect, the literature is challenging to synthesise, since there is wide variability in the rates of surgical excision in differing series and it seems likely that B3 lesions that are surgically excised differ from those treated non-operatively, introducing a source of bias. Nonetheless, many countries are gradually adopting minimally invasive approaches and some consensus has been achieved.

Learning Objectives:

1. To learn about the different non-invasive modalities to excise high-risk lesions.
2. To become familiar with the risk of avoiding surgery.
3. To appreciate the standard protocols in different countries.

08:30 - 10:00

Room E2

Neuro

RC 1711

Diffuse low-grade gliomas: new things you should know

Moderator:

F.W. Cartes-Zumelzu; Innsbruck/AT

A-909 08:30

A. Molecular basis for classification, treatment and predicting outcome in low-grade gliomas

V.C. Keil; Bonn/DE (Vera.Keil@ukbonn.de)

Low-grade gliomas (LGG) are glial tumours with a high degree of diversity on a histological and genetic level. The status of 1p/19q and IDH1/2 genes among others has indeed become the tumour type defining criterion in the 2016 WHO classification of CNS tumours and has impact on therapy choice. Genetic status and protein expression, such as of the oncometabolite 2-HG, are also the key to understand why some LGG de-differentiate to high-grade lesions or show growth, while other lesions remain stable over decades. Quantitative MRI, MRS and PET techniques form the rapidly expanding field of "molecular imaging". Molecular imaging promises to provide the neuroradiologist with non-invasive tools to predict the genetic and histological status of gliomas. Potential applications range from pre-operative assessment of intra-tumoural heterogeneity for biopsy targeting to follow-up and therapy monitoring. However, the greatest challenge lies in the shortage of direct molecular imaging techniques (currently 2-HG MRS is the only one) and the establishment of reliable radiological substitute biomarkers with the ability to predict patient prognosis. Molecular imaging is not yet at a point where unequivocal scientific results rendered watertight imaging biomarkers to rely on in LGG assessment. There are conflicts about the additive value of multiple imaging techniques, the reproducibility of results and also feasibility in clinical practice. In this session we will try to get an overview of the most widely used techniques molecular imaging and their current benefits and limitations for a non-invasive LGG assessment in contrast to standard, non-quantitative MRI.

Learning Objectives:

1. To learn about the role of imaging in the context of histopathology regarding the prediction of outcome.
2. To understand the role of conventional and quantitative beyond diagnosis.
3. To appreciate the translational approach of diagnosis and monitoring of glial tumour based on the histopathological background.

Sunday

A-910 09:00

B. Imaging patterns suggestive of different (molecular) subtypes of low-grade gliomas

M. [Smits](mailto:marion.smits@erasmusmc.nl); Rotterdam/NL (marion.smits@erasmusmc.nl)

Primary brain tumours are histopathologically subtyped into World Health Organisation (WHO) grades I to IV, according to - increasing - degrees of malignancy. These grades provide prognostic information and guidance on management, such as radiotherapy and chemotherapy after surgery. Despite the confirmed value of the WHO grading system, a multitude of studies and prospective interventional trials indicate that tumours with identical morphological criteria, i.e. of the same WHO grade, can have highly different outcomes. To personalise brain tumour management, we need additional diagnostic markers that can differentiate tumours beyond the current morphological WHO grading system. Molecular markers can distinguish subtypes of tumours within the same morphological type and WHO grade, and are therefore of great interest for personalised medicine. Recent genomic-wide studies have resulted in a far more comprehensive understanding of the genomic alterations in gliomas, and the suggestions of a new molecularly based classification. MR imaging phenotypes can serve as non-invasive surrogates for tumour genotypes and as such provide important information on diagnosis, prognosis, and, eventually, personalised treatment. The newly emerged field of RadioGenomics links specific MR imaging phenotypes with gene expression profiles. In this presentation, I will discuss the three best known tumoural genotypes with prognostic and - potential - therapeutic consequences: 1. isocitrate dehydrogenase (IDH) mutation, 2. 1p19q deletion, and 3. methyl guanine methyltransferase (MGMT) promoter methylation. I will give an overview of the known and potential MR imaging features of these genotypes and their value and validity in a clinical context.

Learning Objectives:

1. To learn about whether there is a change of pattern recognition based on conventional and quantitative imaging approaches.
2. To understand the heterogeneity of low-grade gliomas based on histopathology and imaging.
3. To appreciate the perspectives and challenges of diagnostic imaging in phenotyping low-grade gliomas.

Author Disclosure:

M. Smits: Consultant; independent reviewer for Parexel Ltd.

A-911 09:30

C. Advanced imaging in low-grade gliomas

N. [Bulakbasi](mailto:bulakbasi@kyrenia.edu.tr); Mersin/TR (nail.bulakbasi@kyrenia.edu.tr)

Due to the 2016 update of WHO classification, low-grade gliomas (LGGs) are typically IDH mutant, diffusely infiltrating, and slow growing having moderately increased cellularity, generally without mitosis, necrosis and microvascular proliferation. Some Class II and a significant number of Class III series support the addition of diffusion and perfusion-weighted MR imaging and MR spectroscopy (MRS) in the assessment of suspected LGGs. LGGs have lower cellularity (ADC), angiogenesis (rCBV), capillary permeability (K_{trans}), and mitotic activity (Cho/Cr ratio) than those of high-grade gliomas (HGGs). IDH mutation can be indirectly assessed by the identification of 2-hydroxyglutarate in MRS with spectral editing. A gradual decrease in minimum ADC values, increase in Cho/Cr ratio and maximum rCBV values, and the emergence of lactate and free lipid at MRS over time are consistent with tumour progression. Quantitative assessment of peritumoural area, indicating the infiltrative nature of the tumour, also helps in the differential diagnosis of LGGs from solitary metastases and CNS lymphomas. Functional MRI combined with MR tractography is widely used for presurgical planning to demonstrate the spatial relationship between eloquent brain regions and the tumour. Small tumour diameters, artefacts due to bone or air interfaces, vascular structures, haemorrhagic, cystic/necrotic and calcific changes in tumoural area can cause critical distortions in quantifying parameters. So, the selection of a proper ROI avoiding these kinds of areas is critical to obtain proper quantified results. The quantitative multiparametric MR imaging of LGGs can either improve the diagnostic accuracy of their differential diagnosis or assess their prognosis.

Learning Objectives:

1. To learn about the spectrum and diagnostic value of the available advanced imaging techniques in neuro-oncology.
2. To understand the added value and possible pitfalls using quantitative MRI techniques in addition to conventional MRI.
3. To appreciate the importance of standardisation of advanced MR image acquisition in the clinical practice of neuro-oncology.

08:30 - 10:00

Room F1

State of the Art Symposium

SA 17

Interventional treatment of stroke: a game changer

A-912 08:30

Chairperson's introduction

P. [Vilela](mailto:ferrovilela@sapo.pt); Almada/PT (ferrovilela@sapo.pt)

During the last years acute ischemic stroke (AIS) treatment has been revolutionised with the introduction of endovascular treatment - thrombectomy (ET). Several randomised controlled trials have clearly shown the clinical benefits of this treatment and, recent studies have broadening the inclusion criteria, specially concerning the therapeutic time window. Imaging has a central role in the acute ischemic stroke management. Diagnostic neuroradiology is essential to make the correct diagnosis of AIS and to select the appropriate candidates for ET. Imaging provides all the information needed for patient selection, excluding stroke mimics, depicting the vessel occlusion and defining the potential salvage brain tissue: evaluating the collateral arterial circulation status, the extent of irreversible lesion (core) and/or the extension of potentially reversible ischemia (penumbra). Interventional neuroradiology has achieved tremendous clinical results with the fast and high recanalization rates, but further improvements are expected. There are still some technical aspects to be improved, such as the tandem lesions, distal occlusions and anaesthesiology protocol, which will be discussed in this session. In parallel, several organisational processes, from local department/hospital to regional/national organisation, must be optimised, in order to fasten the patient access to the correct stroke center and increase the number of patients treated. The radiology/neuroradiology departments' organisation and professionals are critical for the implementation of AIS national health strategies.

Session Objectives:

1. To review the current imaging techniques and the individualised patient imaging assessment for acute ischaemic stroke.
2. To overview the current endovascular indications and techniques for acute ischaemic stroke.
3. To discuss the current endovascular treatment challenges, such as tandem lesions, distal occlusions and treatment beyond the six-hour time window.

A-913 08:35

Stroke, endovascular treatment: current approaches

T. [van der Zijden](mailto:thijsvanderzijden@hotmail.com); Antwerp/BE (thijsvanderzijden@hotmail.com)

Endovascular thrombectomy has clearly demonstrated its benefit for primary treatment of patients with acute ischaemic stroke from large vessel occlusion. During the past years, mechanical thrombectomy was mostly done by the use of stent retrievers. But, due to ongoing technical developments and experiences on the job, other techniques, such as thrombus aspiration and mixed techniques, has emerged as effective treatment tools as well. Although today very fast procedure times with impressive recanalization rates can be achieved using these techniques, it is still of utmost importance to select the correct patients for endovascular treatment to avoid futile recanalization and to prevent additional harm to ischaemic stroke patients. Besides the proper indication setting, optimal clinical circumstances during and after the procedure should be pursued as well. In this lecture, current insights into the indication setting, different endovascular techniques, choices in supportive care during an endovascular procedure and post-thrombectomy medical care will be discussed and illustrated.

Learning Objectives:

1. To review the current indications for endovascular treatment in acute ischaemic stroke.
2. To overview the endovascular treatment techniques for acute ischaemic stroke: stent retriever and aspiration.
3. To discuss the different options of anaesthesia type, blood pressure control, and post-thrombectomy medical treatment.

A-914 08:58

Stroke, endovascular treatment: tandem lesions and acute phase stenting

W. [van Zwam](mailto:van.Zwam); Maastricht/NL (w.van.zwam@mumc.nl)

In 20 - 30% of patients with acute ischemic stroke due to a large vessel occlusion of the anterior circulation, who are eligible for endovascular treatment, a concomitant ipsilateral cervical internal carotid artery stenosis or (pseud)occlusion is present. These so-called tandem lesions are known to be relatively refractory to intravenous rTPA administration and clinical outcome is therefore poor if not treated endovascularly. Recent studies have shown a large treatment benefit of endovascular treatment in these patients, comparable with the treatment effect in patients who have an intracranial occlusion without cervical carotid pathology. In current guidelines thrombectomy of the intracranial occlusion is therefore recommended for patients with these tandem lesions. However, no clear guidelines for the management of the extracranial carotid pathology exist, because no evidence for the optimal management is yet present. Several options like carotid stenting in the acute phase, before or after thrombectomy, PTA only followed by delayed stenting or delayed carotid endarterectomy are available. Furthermore, different carotid pathologies like dissections and atherosclerotic lesions obviate a uniform treatment recommendation. Various extracranial carotid artery pathologies, different treatment options and available evidence from published studies will be presented and discussed in this presentation.

Learning Objectives:

1. To review the literature data regarding the incidence, natural history and treatment of tandem lesions.
2. To overview the endovascular treatment techniques for the treatment of acute ischaemic stroke: stent retriever vs aspiration, and current indications for endovascular treatment in acute ischaemic stroke.
3. To discuss the potential indications for stenting in the setting of acute ischaemic stroke and tandem lesions.

Author Disclosure:

W. van Zwam: Grant Recipient; Brain Council, the Netherlands. Speaker; Cerenovus, Stryker.

A-915 09:21

Stroke, endovascular treatment: beyond proximal occlusion and six-hour time window

J. [Macho](mailto:jmmacho@clinic.ub.es); Barcelona/ES (jmmacho@clinic.ub.es)

Most of the guidelines recommend endovascular recanalization in patients with acute ischaemic stroke due to large vessel occlusions up until 6 hours after symptom onset. Metaanalysis of pooled individual patient data from 1287 patients in MR CLEAN, ESCAPE, REVASCAT, EXTEND and SWIFTPRIME trials suggests that the benefit of thrombectomy rapidly decays over time and may no longer exist beyond 7.3 hours from stroke onset. The just published DAWN Trial has evaluated late and unwitnessed stroke patients. Eligible patients, with clinical and imaging mismatch (defined by age, core, and NIHSS), who receive mechanical thrombectomy have better outcomes, compared to standard medical therapy. This treatment effect is the highest out of any stroke trials to date and suggests that the presence of clinical-core mismatch is a critical predictor of treatment effect independent of time to presentation. Metaanalysis of randomized trials favoured endovascular treatment across all sites of occlusions with better endovascular treatment effect in patients with thrombi in ICA and proximal M1 MCA segments than in those with thrombi in distal M1 MCA or M2 segments because proximal thrombi are larger in volume, less likely to recanalize with intravenous alteplase and more easily reached by endovascular thrombectomy. The question of benefit with more distally located occlusions in the M2 middle cerebral artery segment is only partially addressed, because randomized trials had very few patients with more distally located occlusions in the M2 middle cerebral artery segment and do not have enough power to fully confirm benefit or harm in these patients.

Learning Objectives:

1. To review the literature data regarding the incidence, natural history and treatment of distal arterial occlusions.
2. To review the literature data regarding the incidence, natural history and treatment of wake-up strokes and arterial ischaemic strokes beyond the six-hour time window.
3. To discuss the potential indications for endovascular treatment beyond the proximal arterial occlusion and beyond the six-hour time window.

Author Disclosure:

J. Macho: Consultant; stryker neurovascular and Medtronic. Speaker; stryker neurovascular.

09:44

Panel discussion: Stroke, endovascular treatment: new horizon

08:30 - 10:00

Room F2

Oncologic Imaging

RC 1716

A multidisciplinary approach to prostate cancer: can we make a difference?

A-916 08:30

Chairperson's introduction

A. [Baur](mailto:alexander.baur@charite.de); Berlin/DE (alexander.baur@charite.de)

Technical advancements and the introduction of guidelines for magnetic resonance imaging (MRI) of the prostate as well as the numerous promising study results have laid the foundation for a widespread application of this imaging technique in patients with suspected or confirmed prostate cancer. Radiological expertise in prostate MRI and standardized image interpretation is crucial to maximize the beneficial impact of imaging. Today, radiologists often work in a multidisciplinary team with urologists and radiation oncologists. To do so proficiently, they have to be familiar with the diagnostic algorithms for prostate cancer. Radiologists should also be aware of available treatment options including surgery, radiotherapy, local ablative and hormonal treatment as well as of the option to put patients under active surveillance. Finally, it is important to be aware of what kind of information urologists and radiation oncologists require to provide optimal treatment for each patient. All of these requirements will be addressed and discussed in this multidisciplinary course with experts from the fields of radiology, urology, and radiation oncology.

Session Objectives:

1. To understand the pathophysiological properties of prostate cancer and its impact on diffusion-weighted imaging and dynamic contrast-enhanced MRI.
2. To understand the necessity of functional MRI (compared with mere morphological MRI) in the assessment of prostate cancer.
3. To learn about PIRADS classification system.
4. To learn about the role of MRI in selecting patient-tailored therapy.
5. To learn about the option of active surveillance vs immediate treatment.

Author Disclosure:

A. Baur: Research/Grant Support; Bayer Pharma. Speaker; Bayer Pharma.

A-917 08:35

A. The urologist: evidence-based clinical decision making

N. [Mottet](mailto:nicolas.mottet@chu-st-etienne.fr); St. Etienne/FR (nicolas.mottet@chu-st-etienne.fr)

Prostate cancer is the third most common cause of cancer death in men. While systematic screening is not promoted, an individual early diagnosis is the standard of care. Based on risk factors (such as family history), PSA and DRE, the pathology obtained after sonography-guided biopsies is the only diagnostic possibility. A systematic pre-biopsy mpMRI is not yet the standard of care, and ongoing RCT are urgently awaited. A quality control of this mpMRI is a major prerequisite and potential limiting factor so far. However, a systematic mpMRI is the standard of care before rebiopsying. This increases the biopsy reliability using a combination of 12 systematic, plus targeted courses. The treatment policy is based on individual life expectancy, patient's wishes and staging. The classical risk categories (known as d'Amico's classification) are more and more challenged by information from image results. Apart from biopsy results (number of positive cores, Gleason score) and DRE, the local staging (T stage) is based on MRI. Its sensitivity is mild (intraprostatic localisation, microscopic extracapsular extension), but its specificity is acceptable and it is a must in intermediate-/high-risk situations. It is also mandatory before considering active surveillance. N staging is poorly done, even with the PET. As for M staging, PSMA represents the future, although its added value regarding improved outcome remains unclear. For M staging, bone scan should be replaced by a whole-body MRI. However for mCRPC progression characterisation, bone and CT scan remain the standard, as no consensus definition of progression with MRI exists yet.

Learning Objectives:

1. To understand how a diagnosis is established by PSA evaluation and biopsy.
2. To learn about different treatment options: surgery, radiotherapy, local ablative and hormonal treatment; as well as active surveillance.
3. To learn how imaging impacts treatment selection.
4. To understand what the urologist needs to know from the radiologist.

Postgraduate Educational Programme

A-918 08:58

B. The radiologist: evidence-based use of multiparametric MRI

H.-P. Schlemmer; Heidelberg/DE (h.schlemmer@dkfz.de)

Early detection of prostate cancer with biologic characterization and staging is of fundamental importance for individualized decision-making. Localized, early-stage prostate cancer has been more frequently detected since the introduction of PSA screening. Active surveillance and less aggressive focal therapy options are accordingly emerging to reduce the side effects that may significantly reduce the quality of life. But delayed and unprecise diagnosis as well as overtreatment is still feared, because prostate cancer is characterized by multifocality with considerable variations of cancer aggressiveness. Meanwhile, a body of evidence from clinical studies is available proving that multiparametric MR imaging (mpMRI) is beneficial for the detection and localization of cancer suspicious lesions, for biopsy guidance to finally diagnose or rule out significant cancer as well as for T-staging. Different transrectal or transperineal TRUS/MR image fusion biopsy methods with targeted +/- random biopsies have been developed. During active surveillance, the combination of morphologic and functional MR parameters yields important objective and reproducible biomarkers for monitoring temporal changes of cancer size and aggressiveness. Accordingly, mpMRI is of increasing importance for individualized decision-making in prostate cancer patients. However, the assurance of high-quality imaging is still challenging. The PI-RADS recommendations have proven very helpful concerning this issue. This lecture will provide detailed knowledge of the evidence-based use of "state-of-the-art" mpMRI in clinical routine. It will demonstrate how the method can be integrated in the urological context of diagnosis and treatment to improve the complex management of prostate cancer patients.

Learning Objectives:

1. To learn how to perform and interpret multiparametric MRI.
2. To become familiar with the PI-RADS classification system.
3. To become familiar with the role of imaging for patient stratification and treatment planning.

A-919 09:21

C. The radiation oncologist

D. Georg; Vienna/AT (dietmar.georg@meduniwien.ac.at)

Various treatment techniques are successfully used for treating prostate cancer (PCa) with irradiation, with an increasing tendency of using higher doses per treatment session. In conventional radiation therapy the tumour volume is irradiated with a homogeneous dose. Widespread clinical practice relies on treatment planning based on computed tomography (CT), often combined with MRI. However, recent technology developments and achievements made during the last decade enable to focus the high dose irradiation very precisely on the tumour, while sparing of the surrounding normal tissue. Improved precision of treatment planning and delivery warrant equally precise tumour definition, moreover new treatment concepts are stimulated by the advancements in imaging to visualise and quantify biological, physiological and pathological processes. Positron emission tomography (PET), perfusion computed tomography (CT) and especially multiparametric magnetic resonance imaging (mp-MRI) are continuously explored for lesion characterisation, target definition, and response assessment during and after radiotherapy of PCa. To elucidate tumor biology and to identify subvolumes of more aggressive behavior, which are often radiotherapy resistant, mp-MRI is more frequently used in clinical studies. The concept of inhomogeneous tumour irradiation according to its biological behavior, called dose painting, is motivated by selective dose escalation based on biological tumour characteristics. This approach may lead not only to higher local control but also to better sparing of normal surrounding tissue. With the clinical implementation of dose painting, improvements in the therapeutic outcome can be expected. Due to the existing technical challenges, extensive collaboration between radiation oncologists, radiologists, medical physicists and radiation biologists is needed.

Learning Objectives:

1. To learn the rationale and scientific basis for focal therapies for prostate cancer.
2. To learn how focal therapies are performed in prostate cancer.
3. To learn through personal experience and from literature how multiparametric MRI can guide focal therapies of the prostate.

09:44

Panel discussion: Prostate cancer: evidence-based multidisciplinary approach to imaging and treatment

08:30 - 10:00

Room D

Musculoskeletal

RC 1710

MR imaging of the knee

Moderator:

M. Tzalonikou; Athens/GR

A-920 08:30

A. Cruciate ligaments: what to know and do

A. Alcalá-Galiano; Madrid/ES (aalcalagaliano@gmail.com)

Cruciate ligaments play a key role in knee kinematics and stability. Cruciate-deficient knees are predisposed to early osteoarthritis due to chronic instability. ACL is the most commonly injured major ligament of the knee. PCL lesions are far less common, but more frequently associated with multiligamentous injuries. MRI is the study of choice to evaluate acutely and chronically injured cruciate ligaments, associated injuries and for postoperative imaging following ligament reconstruction. Understanding the variations of their anatomy (double bundle configuration and insertion sites) is key to performing a tailored anatomic reconstruction. Accurate description and grading of cruciate tears and associated injuries is essential for preoperative planning of ligament reconstruction. The primary and secondary signs and indirect imaging findings of acute and chronic ligament injury will be reviewed. Atypical findings and imaging pitfalls will also be discussed. ACL reconstruction is one of the most common orthopaedic procedures, whilst PCL reconstruction is on the rise. Knowledge of ligament reconstruction techniques allows differentiation of normal postoperative findings from complications, which may be related to graft placement, the graft itself or to the donor site. Any standard knee MRI protocol must ensure adequate detection of both soft tissue and bony injury, including the cruciate ligaments. However, protocols may be tailored for specific needs, including oblique acquisitions, 3D or metal artefact reduction sequences to better demonstrate the anatomy and facilitate detection of small tears.

Learning Objectives:

1. To review the normal anatomy and MR imaging appearances of ACL and PCL and discuss pitfalls.
2. To learn about the imaging appearances of ACL and PCL pathology and discuss imaging sequences and protocols.

A-921 09:00

B. Meniscal tears: obvious and subtle

P. Omoumi; Lausanne/CH (patrick.omoumi@chuv.ch)

This lecture will review the basic aspects of MRI of meniscal pathology, including some elementary technical and anatomical considerations, as well as the description of the basic semiology of meniscal tears and their classification. The common pitfalls and errors that need to be avoided will be presented. MRI is the modality of choice for the diagnosis of meniscal pathology as well as treatment planning. A certain number of technical considerations need to be understood by the radiologist. The standard sequence to image the meniscus is intermediate-weighted fast spin-echo sequences, in 2D or 3D. Certain acquisitions may influence the diagnosis of meniscal tears, including the choice of the echo time. Meniscal tears can manifest either as morphological changes or intrameniscal signal changes, with specific diagnostic criteria that will be reviewed. An appropriate terminology, based on standard arthroscopic classification, needs to be used by the radiologist to properly communicate the description of the tear to the referring surgeon. Secondary signs of meniscal tears, including parameniscal cyst and meniscal extrusion, should be used to increase the diagnostic performance for the detection of meniscal tears. Common pitfalls include anatomical variants (i.e. intermeniscal meniscal and meniscofemoral ligaments, discoid meniscus), as well as other causes for false positive findings such as meniscal flounce, chondrocalcinosis and meniscal ossicles. Knowledge of common mistakes and patterns of injury helps avoid unnecessary mistakes and improve diagnostic accuracy.

Learning Objectives:

1. To review the anatomy of the menisci and the classification of meniscal tear.
2. To familiarise with unusual imaging appearances of meniscal tears and discuss potential pitfalls.

Sunday

A-922 09:30

C. Looking around the corners: posteromedial and posterolateral
U. [Aydingoz](#); Ankara/TR (uydingo@hacettepe.edu.tr)

Despite their contribution to the stability of the knee and their association with multiple ligamentous injuries of this largest joint in the human body, posterolateral and posteromedial corners of the knee are hidden from plain sight in the daily practice of reporting magnetic resonance imaging (MRI). Posterolateral corner (PLC) injuries of the knee are rare, but important conditions because of their association with the much more common anterior cruciate ligament (ACL) and other ligamentous or meniscal injury. If PLC injury is not identified and appropriately addressed, knee instability may persist, ACL reconstruction surgery may fail, and osteoarthritis may ensue. Although the anatomy of PLC is complex, its three main stabilizers that are targets for surgical reconstruction or repair in the presence of high-grade injury are identifiable: the lateral collateral ligament, the popliteus tendon, and the popliteofibular ligament. Avulsion fractures of the fibular head, where some components of the PLC attach, have a characteristic appearance on radiographs (the so-called "arcuate sign") and must alert the radiologist to inspect the entire PLC on MRI for injury. Injuries to the posteromedial corner (PMC) of the knee are also associated with ACL, as well as the posterior cruciate ligament (PCL), tears. Major components of the PMC are the semimembranosus tendon (and its expansions), the oblique popliteal ligament, the posterior oblique ligament, the posteromedial joint capsule, and posterior horn of the medial meniscus. Unrecognized injury to PMC may result in the failure of the ACL or PCL reconstruction surgery with sustained anteromedial rotational instability.

Learning Objectives:

1. To review the relevant anatomical structures of both posteromedial and posterolateral corners.
2. To discuss imaging signs of pathology affecting the aforementioned areas.

08:30 - 10:00

Room G

Physics in Medical Imaging

RC 1713

Patient-specific dosimetry

A-923 08:30

Chairperson's introduction

E. [Samara](#); Sion/CH (elina.samara@hopitalvs.ch)

The use of ionizing radiation in medical imaging offers substantial benefits for the diagnosis and treatment of numerous medical conditions in children and adults. However, exposure to ionizing radiation may be associated with harmful risks. Justification and optimization as principles of radiation protection make radiation dosimetry fundamental. Physicians need to know the levels of exposure and hence the risks from imaging examinations that they have to justify, and operators of x-ray equipment need to determine whether their techniques are optimized. Special cases such as examinations of children and pregnant patients or screening examinations require specific organ dose estimations. Moreover, to prevent tissue reactions, patient skin dose needs to be estimated during radiological interventional procedures. Patient characteristics, such as age, sex and size, should be taken into consideration for specific patient dose assessments. Each modality (radiography, fluoroscopy, mammography, computed tomography, etc.) has its own specificities and demands different methods to calculate the dose. Modern imaging modalities usually display conventional dosimetry metrics, such as dose-area product, incident air-kerma or computed tomography dose index that do not represent individual patient dose. Thus, numerous sophisticated concepts and methods have been proposed to estimate patient radiation dose that include either physical measurements with dosimeters and anthropomorphic phantoms or computational measurements using Monte Carlo simulations. All these methods progressively allow more accurate estimations of individual patient doses.

Session Objectives:

1. To understand the needs for personalised dosimetry.
2. To learn about existing and new methodologies used for patient dosimetry.
3. To understand the challenges for the implementation of patient-specific dosimetry.

A-924 08:35

A. Breast imaging dosimetry

I. [Sechopoulos](#); Nijmegen/NL (ioannis.sechopoulos@radboudumc.nl)

Mammographic dosimetry is a subject of intense interest due to the use of this imaging modality for population-based screening. Although this topic has been studied for the last four decades, advances in the mammography systems, introduction of new imaging modalities such as breast tomosynthesis, and new insights into breast anatomy have resulted in the need for continued development of breast dosimetry methods and models. During this talk, the current method and model for breast dosimetry in mammography and tomosynthesis will be reviewed and its capabilities and limitations discussed. The concept of patient-specific breast dosimetry and its potential applications will be introduced. Finally, the upcoming new developments in the field of breast dosimetry will be presented.

Learning Objectives:

1. To understand the current method to estimate organ dose in mammography and its limitations.
2. To understand breast dosimetry in emerging modalities.
3. To learn about upcoming approaches in breast dosimetry.

Author Disclosure:

I. Sechopoulos: Advisory Board; Fischer Medical Imaging. Research/Grant Support; Siemens Healthcare, Toshiba Medical Systems. Speaker; Siemens Healthcare.

A-925 08:58

B. Patient dosimetry in CT and CBCT

S. [Edyvean](#); London/UK (sue.edyvean@phe.gov.uk)

Conventional CT is a complex imaging device which can utilise narrow or wide beams, helical scanning, varying tube current, varying kV, and operating with various and dynamic collimations - all of which can affect patient dose. Different technology is used in cone beam CT, or flat panel CT, and this term usually refers to cross-sectional imaging with digital x-ray systems used in dental, digital radiography or radiotherapy. Many of the challenges are similar for both conventional CT and cone beam CT; however, there is generally more information available for the former. When considering patient-specific dosimetry, the technology, scan settings and the patient all need to be considered. As with other modalities, the scope to directly measure doses using physical dosimeters is limited. Therefore, doses need to be estimated using regular-shaped, or anthropomorphic, phantoms, or calculated using mathematical modelling techniques. The appropriate application, and the limitations, of standard dose indices (such as the computed tomography dose index, the size-specific dose index), together with their associated methodologies and phantoms, will be addressed. Monte Carlo calculations from modelled scanner and patient characteristics give more precise organ dose information, and there are a number of applied software packages developed to utilise these data. The advantages and limitations of these will be discussed.

Learning Objectives:

1. To understand what is estimated.
2. To learn how to measure it.

Author Disclosure:

S. Edyvean: Speaker; Refresher course.

A-926 09:21

C. Patient dose in fluoroscopy and interventional

A. [Trianni](#); Udine/IT (annalisa.trianni@asuiud.sanita.fvg.it)

Interventional radiology contributes to significant proportion of the collective dose of the population from medical exposures. Moreover, when complex procedures are performed or procedures are repeated for the same patient, high-radiation dose levels can occur because procedures often require long fluoroscopy times and require high-quality images. For all of these reasons, dosimetric evaluations in interventional radiology are demanding. During this talk, patient dosimetry methods currently used in interventional radiology for different purposes (risk evaluation, optimisation and quality assurance) will be reviewed, together with relevant published dosimetric data. In particular, since radiation-induced skin damage might be a complication of interventional procedures, the talk will review available real-time patient skin dosimetry methods and their possible use.

Learning Objectives:

1. To review the fundamental patient dosimetry quantities.
2. To learn about calculation of patient dose for interventional procedures.
3. To learn about real time patient dose monitoring strategies.

09:44

Panel discussion: The future of patient-specific dosimetry

Postgraduate Educational Programme

08:30 - 10:00

Room K

E³ - Rising Stars Programme: EFRS Radiographers' Basic Sessions

BR 3

Planning your career

A-927 08:30

Chairperson's introduction: What employers are looking for from new graduates

S. Huber; Munich/DE (susanne.huber@med.uni-muenchen.de)

What employers are looking for from new graduates? It is obvious that new graduates are expected to have passed the exam with at least good success. They should be interested, motivated and open-minded for their new working life. Additionally the graduate should show a character, which can be trusted to take care for patients and to be responsible for the own work, especially with regard to radiation protection. If the graduate should be from abroad, the language skills must be sufficient to fulfill the work requirements. Unfortunately many European countries are suffering from a shortage of radiographers. While trying to solve this problem, often radiographers are hired from abroad, which in consequence may lead to an even higher shortage in those countries. Fortunately and thanks to the mostly very good educational curricula there are still applicants with the above mentioned qualities available, but in total not enough applicants in comparison to the job vacancies. This session is about to show graduates ways to meet the expectations of their future employers. E.g. how they can prepare their personal presentation in designing their CV and to avoid mistakes while doing so. To make them aware of the importance of CPD (Continuous professional development), which eventually will lead to more competence and future carrier. The graduates will also have the opportunity to learn about the experiences of working as a radiographer in another country.

Session Objectives:

1. To understand how best to prepare your professional profile using various platforms.
2. To appreciate the potential for radiographers to work in various jurisdictions.
3. To consider the utility of professional development planning in achieving your professional goals.

Author Disclosure:

S. Huber: Author; Susanne Huber. Speaker; Susanne Huber.

A-928 08:35

The dos and don'ts of preparing your curriculum vitae

E. Kelly; Galway/IE (eileenma.kelly@hse.ie)

A curriculum vitae (CV) is the first impression made by a potential employee to an employer. The presentation of one's CV can influence the employer to read it or not. Therefore, a well-presented, succinct CV that is tailored to the job is essential. Many graduates consider themselves at a disadvantage when applying for positions as they lack experience, and consequently make attempts to compensate for the lack of experience by unnecessary information when constructing their CV. Many employers will research the background and experience of potential employees through social media sites such as LinkedIn, ResearchGate and EFRS RRN. Such sites can be a valuable promotional and networking tool for professionals and can lead to unexpected career opportunities. This presentation will consider how to design a CV that will grab the immediate attention of an employer. Common mistakes in design and content of a CV and how to avoid them will also be discussed.

Learning Objectives:

1. To understand qualities of a well-designed curriculum vitae.
2. To become familiar with common mistakes to avoid when preparing your CV.
3. To be aware of the potential of social media platforms such as LinkedIn, ResearchGate, EFRS RRN for your professional profile.

A-929 08:58

Radiography: your passport to travel

R. Caroco; London/UK (caroco.rita@gmail.com)

At the present moment, there are several countries that have radiographer shortages and therefore, welcome overseas professionals. These are mostly European countries, that can benefit from the freedom of movement under the EU law. The recognition of professional qualifications, particularly within Europe makes it highly encouraging to work abroad. Countries like Portugal have been affected by the economic and financial crisis, which combined with irresponsible coordination between education training and job opportunities, reflects very limited career prospects for radiographers. This led and continues

to cause a rise in emigration for newly qualified/experienced radiographers to countries where shortages are high. The aim of this presentation is to talk about my personal experience as a radiographer trained in Portugal and working in the UK. It will list the requirements and formalities to register as a radiographer, the job seeking process, the barriers and benefits I encounter(ed). It will also give an overview of the differences in radiography career and opportunities, between these two countries.

Learning Objectives:

1. To be aware of the potential to use your radiography qualification in various jurisdictions.
2. To consider barriers to practicing as a radiographer abroad.
3. To appreciate the potential for charitable/voluntary work in developing countries.

A-930 09:21

Planning your professional development

A. Wareing; Aberdeen/UK (a.wareing@rgu.ac.uk)

This session will support radiographers and students in planning their professional development. There is a critical need for health-care professionals to remain professionally updated regarding continuous changes to the evidence base and technological advancements, particularly in radiography, to facilitate closure of any gaps between 'actual practice' and 'best practice'. Health services across Europe are under increasing stress and a principal factor going forwards will be managing increasing demands on health-care staff whilst supporting enhancement of the knowledge, skills and competency base. A recent body of work completed with individuals in the EFRS network has concluded that the primary feature of CPD activity should be the resulting impact - to patients, the service, the profession and the individual; with all stakeholders working in partnership. CPD activity must be flexible/multi-modal to support the changing growth/dynamic workforce. All stakeholders should utilise available communication and technology resources and make efforts to improve collaboration between the management, regulators and educators. Acknowledgement of barriers is required and actions must be taken to reduce these over time; financial burden remains a concern, whilst increasing literature has identified work pressure and lack of time as the main challenges for radiographers. An applied approach to these findings will be discussed in this session with an emphasis on realistic practices that delegates can realise and share in their own clinical environments.

Learning Objectives:

1. To understand the importance of professional development planning for radiographers in maintaining, developing and improving radiographer competencies.
2. To be aware of the essential role of CPD and further education for radiographers.
3. To appreciate how best to prepare for promotion opportunities.

09:44

Panel discussion: My best career advice

08:30 - 10:00

Room M 1

ESR Publications Committee Session

How to write a scientific paper and how to get it published

Moderators:

R.G.H. Beets-Tan; Amsterdam/NL

F. Sardanelli; San Donato Milanese/IT

A-931 08:30

The study design and the structure of an original article

F. Sardanelli; San Donato Milanese/IT (f.sardanelli@grupposandonato.it)

"Original articles" (ORs), also named "original researches", are the most important category of articles published in medical scientific journals (MSJs): they provide new results. Apart from methodologic papers (which explain methods to be applied in ORs), all the remaining categories of articles refer to ORs as a basis. Particular types of ORs are the "technical notes" (presenting new techniques mostly applied to few cases) and "systematic reviews with/without meta-analysis", evaluating all the previous literature on a topic and providing, when possible, new "secondary" evidence by pooling data from published ORs. In short, ORs are the "core" of MSJs. The typical structure an original article (also reflected in the abstract) is composed of four sections: 1. Background/Introduction (WHY the authors made that work and study aim[s]); 2. Methods (HOW the work was done: study design and other related issues such as study population and sample size, imaging/interventional methods, readings, reference standard, statistics, etc.); 3. Results (WHAT the authors

found); 4. Discussion (interpretation of results, comparison with previous works, study limitations, conclusions). Failures in internal/external validity of an OR are determined by biases (systematic distortions) that can affect the study. The validity of a study is in its Methods. However, the most important part of Methods is the study design, sometimes poorly described in radiological papers: prospective/retrospective; transversal (cross-sectional) or longitudinal (cohort); randomized/non-randomized; patients selection; reading blindness; quality and application of the reference standard. Notably, errors in study design cannot be solved after study termination. Study design is more important than statistics.

Learning Objectives:

1. To understand that the core of an original article is the study design.
2. To understand the structure of an original article and the logics of the blocks of the abstract and of the body text.
3. To learn how systematic reviews and meta-analyses are a particular case of original articles.
4. To learn how to avoid the typical errors that candidate a manuscript for rejection.

A-932 08:50

The review process in radiology

Y. Menu; Paris/FR (yves.menu@sat.aphp.fr)

In single-blind peer reviews, the reviewer is aware of the author's name and institution, while authors ignore the name of the reviewer. In double-blind peer review, both reviewer and authors are anonymous. Obviously, double blind theoretically eliminates the bias of being more prompt to accept papers from renowned authors and/or institutions. Conversely, the reviewer feels safer to express criticism, avoiding potential professional conflicts. However, double blinding may fail. Commonly, manuscripts are prepared immediately after the study had been presented in a major meeting. For very focused research, the number of potential reviewers is somehow limited. However, in most cases double blind is successful in occulting authors' and reviewers' identity. Several studies have compared these two methods and the conclusions are still unclear. Some studies found that double blind ensured higher quality, while others did not find any difference. Some have even questioned the need for peer review. European Radiology has decided to go for double-blind review, as sources of manuscripts are extremely diverse, while reviewers are from a wide range of countries on all continents, therefore diminishing the risk of blinding failure.

Learning Objectives:

1. To know the variety of the review processes in radiological journals.
2. To be aware of pros and cons of the double blinded review.
3. To know how the Editor handles your manuscript.
4. To learn how to answer to reviewers' criticisms.

A-933 09:10

The review process in other clinical journals

R. Madoff; Minneapolis, MN/US (madoff@umn.edu)

Scientific publication is more than the road to academic advancement; it is an opportunity to contribute to your field and to share your work with others who share your interests and expertise. This session will review the principles of manuscript preparation and submission with an eye towards optimizing the chances of acceptance and publication. The practical aspects of how manuscripts are managed on the journal side, peer review, and the editorial process will be emphasized, as will various pitfalls to be avoided. In addition, the opportunities to publish in journals based on related, but non-radiologic, disciplines will be discussed. The goal of this session is to provide practical advice that will be of interest to those early in their publication career as well as to more experienced authors.

Learning Objectives:

1. To know the variety of the review processes in clinical journals.
2. To be aware of pros and cons of single-blinded or unblinded review.
3. To know how the Editor handles your manuscript.
4. To learn how to answer to reviewers' criticisms.

A-934 09:30

Important papers other than original articles

L. Martí-Bonmatí; Valencia/ES (Luis.Marti@uv.es)

Science is crucial for the advance of a discipline, but so is critically reviewing and commenting on hot topics. These are highly cited papers that require expertise on the topic and discipline in writing. Review papers focus either on educational aspects of imaging, with a pearls and pitfalls approach (Pictorial Reviews) or as a critical overview on emerging techniques or state-of-the-art topics with an up-to-date and innovational approach (Critical Reviews). Both Pictorial and Critical Reviews might serve the radiological community to have

access to the best evidence-based knowledge and to foresee the impact of new approaches within the health-care cycle. Position papers include both imaging guidelines on patient's management aspects and consensus statements on imaging-related topics. These papers define the experts' or social representatives' opinions. Reviewing and critiquing the literature requires the ability to juggle multiple tasks. The authors have to find and critically evaluate relevant material while synthesizing the disperse information with the skills of providing new ideas from already known facts. The EQUATOR Network and the PRISMA Statement for the reporting of systematic reviews will help in some of these items. As general rules, the authors have to define the scope of the article, imposing a well-defined structure on the mess that might be the scientific literature.

Learning Objectives:

1. To know the variety of the review processes in clinical journals.
2. To be aware of pros and cons of single-blinded or unblinded review.
3. To know how the Editor handles your manuscript.
4. To learn how to answer to reviewers' criticisms.

09:50

Discussion

08:30 - 10:00

Room M 4

Multidisciplinary Session

MS 17

The polytrauma patient

A-935 08:30

Chairperson's introduction

M. Brink; Nijmegen/NL (M.Brink@rad.umcn.nl)

Severe trauma is one of the leading causes of death and disability in the world. The outcome of trauma patients improves if the trauma team collaborates closely and systematically. In this case-based and interactive session, surgeons and radiologists will discuss the multidisciplinary approach to the polytrauma patient.

Session Objectives:

1. To understand how radiologist can be an active member of the trauma team.
2. To learn how to communicate effectively in the trauma setting.
3. To learn how to optimise logistics and to tailor computed tomography (CT) imaging for an ideal setting of trauma CT acquisition.
4. To understand current controversies and recent developments in diagnosing injuries in the polytrauma patient.
5. To be updated on strengths and weaknesses of current resources and guidelines on polytrauma trauma imaging.

Author Disclosure:

M. Brink: Research/Grant Support; Toshiba Medical Systems.

A-936 08:33

Guidelines and game changers: the radiologist's perspective

M. Brink; Nijmegen/NL (M.Brink@rad.umcn.nl)

The outcome of trauma patients improves if the trauma team collaborates closely and systematically. As a radiologist, you therefore have to be prepared to be an active member of the trauma team. This introduction will discuss the three most important issues that radiologists should address prior to image evaluation of the polytrauma patient. Which imaging modalities are justified? Which modalities should better not be used? And how should you tailor your CT protocol?

Learning Objectives:

1. To be updated on current, most relevant guidelines on trauma imaging.
2. To discuss the most relevant CT parameters that can be tailored in the setting of polytrauma.

Author Disclosure:

M. Brink: Research/Grant Support; Toshiba Medical Systems.

A-937 08:40

The primary survey: talking ABC

J. Peters; Nijmegen/NL (Joost.Peters@radboudumc.nl)

The trauma surgeon's perspective: In the care of the trauma patient, time is of essence and prompt focussed action is frequently needed. The most life-threatening conditions should be diagnosed and addressed first: "Treat first, what kills first". These interventions are prioritised using the simple guidelines of the Advanced Trauma Life Support Course (ATLS), using the first letters of

the alphabet. This method provides a solid framework and common language for all involved in the care of the trauma patient. Radiologists are an essential link in the chain of trauma care. Even more, the role of the radiologist has changed in the last years with the widespread use of focussed ultrasound in trauma and low-threshold CT scanners available in the emergency department. As an active trauma team member, the radiologist needs to be aware of the phases in the trauma survey and should provide the proper input needed for decision-making. The radiological diagnostics need to be in sync with the trauma screening using "ABCDE". To obtain optimal communication and consequently good results, the fundamental guidelines of ATLS must be familiar to all involved in the primary trauma care in the emergency department; including the radiologist. A team briefing prior to patient arrival is very helpful in creating team awareness and a common-team approach.

Learning Objectives:

1. To learn how to communicate effectively within the trauma team according to ATLS principles.
2. To understand which traumatic diagnoses can be game changers during the primary survey.
3. To discuss radiology in the trauma room: how to optimise logistics in the acute setting.

A-938 08:55

The secondary survey: from head to toe

M. [Holla](#); Nijmegen/NL (Micha.Holla@radboudumc.nl)

According to the ATLS, after the assessment of vital functions of a trauma patient, the secondary survey is performed. In patients with Injury Severity Scores (ISS) <16, the treating surgeon often prefers high-quality imaging of the extremities. However, in patients with severe injuries of multiple organs (ISS>16), a quick imaging procedure is needed. Fast CT scanograms and single-direction radiographs can be sufficient to perform damage control orthopaedics. High-resolution imaging of extremities must not delay the treatment of life-threatening injuries. Quick clearance of the spine can reduce the time of unnecessary spinal immobilization and its negative side effects. After the secondary survey, effective communication of a resume of all injuries highly assists in planning further treatment. A fixed order, reporting on different anatomical regions (from brain, face, neck, spine, thorax, abdomen, pelvis, right arm, left arm, right leg, left leg), can increase the speed and accuracy of this communication to all participating disciplines. This session focuses on how to effectively communicate the radiological findings to the orthopaedic surgeon and which pitfalls should be avoided.

Learning Objectives:

1. To get to know how orthopaedic surgeons approach polytrauma extremity trauma.
2. To understand how to report secondary survey findings to the surgeon.
3. To learn from diagnostic pitfalls in orthopaedic injuries and how to avoid them.

A-939 09:15

The neuroradiologist's perspective

F.J.A. [Meijer](#); Nijmegen/NL (Anton.Meijer@radboudumc.nl)

Evaluation of vital functions (ABC) precedes neurological evaluation (D) in the management of trauma patients, which is also applicable to the diagnostic imaging strategy. Nevertheless, adequate and fast neurological evaluation is essential to initiate early treatment when indicated, to reduce morbidity and mortality. Every radiologist on call should therefore be skilled in the evaluation of TBI in the acute stage as part of the polytrauma patient and not consider TBI as an area reserved for specialized neuroradiologists. In this lecture, diagnostic imaging in head trauma will be discussed focused on the imaging strategy and the clinical relevance of imaging findings. Initial diagnostic imaging in the acute stage of traumatic brain injury (TBI) mainly concerns non-contrast CT. The clinical relevance for differentiating primary from secondary TBI will be emphasized. Furthermore, the role of head and neck CTA and the added value of brain MR imaging will be discussed. Finally, tips and tricks for choosing an appropriate CT angiography and MRI scanning protocol will be provided.

Learning Objectives:

1. To learn a structured approach for image interpretation of head trauma.
2. To learn about the clinical relevance of imaging findings in head trauma.
3. To give the updated on current knowledge and imaging guidelines, with emphasis on blunt cerebrovascular injuries.

09:35

Multidisciplinary case presentation and discussion

08:30 - 10:00

Room M 5

E³ - ECR Master Class (Emergency Imaging)

E³ 1726b

Emergencies following tumour therapy

A-940 08:30

Chairperson's introduction: The role of imaging in the early detection of complications in oncologic treated patients

D.R. [Kool](#); Amsterdam/NL (dignakool@gmail.com)

Oncology patients can present with life-threatening conditions. Those conditions may be caused by local expansion and complications of the primary tumour or metastases, as for example haemorrhage, vena cava superior syndrome or spinal cord compression. Furthermore, complications can also be caused indirectly by the malignancy, as for instance thromboembolic disease or paraneoplastic metabolic or neurological symptoms. Life-threatening complications can also be the unwanted consequence of tumour therapy. Surgery, radiotherapy, interventional radiology (IR) procedures, chemotherapy and immunotherapy, each, have their own set of potential complications that can present in the emergency setting. Haematologic and metabolic complications are mainly diagnosed with clinical and laboratory findings. For other complications, diagnostic imaging is essential for making the correct diagnosis and imaging will influence treatment. Complications of surgery, radiotherapy and IR procedures will mostly be in the vicinity of the treated area. Adverse effects of systemic therapies, chemotherapy and immunotherapy can occur at remote sites. Complications of oncological treatment can be life threatening. However, when treated on time, they often are reversible. Recognizing the imaging findings of complications of tumour therapy timely and accurately is of the utmost importance. Immunotherapy is a more recent treatment and the adverse effects of immunotherapy differ from the more familiar complications of the other tumour therapies. Immunotherapy is increasingly used and the radiologist will encounter these complications more frequently. In this session, neurological complications and complications in the chest and abdomen will be discussed and their imaging findings demonstrated.

Session Objectives:

1. To learn about different approaches in tumour therapy.
2. To understand the radiological appearance of complications.
3. To appreciate the role of different imaging modalities in further management of patients.

A-941 08:35

A. Neuro

C. [Calli](#); Izmir/TR (cem.calli@gmail.com)

Post-treatment neurooncological emergencies are usually underdiagnosed by imaging methods although the clinical presentation of these conditions are obvious in many cases. The aim of this presentation is to create awareness for Radiologists who are dealing with follow-up of neurooncology patients. Neurooncology patients may suffer emergency situations secondary to either surgery, or chemotherapy, or radiotherapy. These emergency conditions mostly need the confirmation of imaging techniques to fulfill the diagnosis. Thus the radiologists should be familiar of the imaging findings of these emergency situations, which will lead the Neurooncologists to decide whether to continue the therapy or not, plus to decide further treatment options for these conditions.

Learning Objectives:

1. To be familiar with different strategies in CNS tumour therapy.
2. To understand the most common imaging findings in emergent clinical scenarios.
3. To learn how to recognise life-threatening complications.

A-942 09:00

B. Chest

H. [Prosch](#); Vienna/AT (helmut.prosch@meduniwien.ac.at)

Lung cancer is the most common cause of cancer-related death in Western countries. Treatment of lung cancer is based on three pillars: surgery; radiation therapy; and systemic therapy. Imaging plays a major role in treatment decisions, response evaluation, and last, but not least, also in assessing adverse events following therapy. After surgery, acute (early) complications include pulmonary oedema (hydrostatic, permeability), atelectasis, hemothorax, acute infections, and bronchopleural fistulas. Acute complications after radiation therapy include mainly early radiation pneumonitis and infections. Following systemic therapy, in addition to infections, non-infectious

Postgraduate Educational Programme

pneumonitis and sarcoid-like reactions are important complications that must be considered when investigating a patient who presents with acute symptoms.

Learning Objectives:

1. To be familiar with modern approach to malignant chest tumour therapy.
2. To learn how to differentiate clinically important complications.
3. To understand how to look for the early signs of severe and urgent conditions.

Author Disclosure:

H. Prosch: Advisory Board; Boehringer Ingelheim, Roche, MSD. Speaker; Boehringer Ingelheim, Roche, MSD, BMS.

A-943 09:25

C. Abdomen

R. Basilico; *Chieti/IT (rbasilico@unich.it)*

Despite many improvements in perioperative, post-ionising radiation therapy or pharmacological morbidity in abdominal tumour treatments, acute complications after tumour therapies in the abdomen are still common. A number of different therapies, including surgery, by means of laparoscopic approach or minimally invasive robotic surgery, radiotherapy, chemotherapy and immunotherapy, may be effectively used to treat abdominal tumours. However, these kinds of treatments are not devoid of complications and, last, abdominal emergencies may occur after therapies used for extra-abdominal tumours. Cross-sectional imaging and particularly CT play a crucial role in the diagnosis and management of the most common abdominal emergencies after tumour therapies. The main complications following abdominal, urologic or gynaecologic surgery include peritonitis, abscesses, haemorrhage, small bowel obstruction and anastomotic leaks. Specific complications following hepatobiliary surgery include bile leakage and bile duct injuries: US and MRI with magnetic resonance cholangiopancreatography (MRCP) sequencers are the preferred modalities for assessment of the postoperative biliary tract. Less common postoperative emergencies are vascular complications such as pseudoaneurysms. Small bowel obstruction caused by radiation enteritis represents one of the most frequent abdominal complications after radiotherapy of prostate and rectal cancer, whereas a less known disease such as pneumatosis cystoides intestinalis may be associated with systemic chemotherapy. Due to the increasing use of immunotherapy for different types of tumours, new inflammatory and immune-related adverse events occur also in the abdomen and need to be managed by a multidisciplinary approach.

Learning Objectives:

1. To learn about different techniques used in abdominal tumours therapy.
2. To be familiar with possible complications.
3. To understand the effectiveness of imaging modalities in evaluation of emergent complications.

09:50

Panel discussion: What is the impact of complications findings on the further management of oncologic patients?

10:30 - 12:00

Room A

E³ - ECR Academies: Interactive Teaching Sessions for Young (and not so Young) Radiologists

E³ 1821

Advances in musculoskeletal techniques: whole-body MR

A-944 10:30

A. Oncologic application

F.E. Lecouvet; *Brussels/BE (frederic.lecouvet@uclouvain.be)*

This interactive session will illustrate the wide range of indications of whole-body MRI in oncology, the protocols and technical requirements, the contribution of anatomic and functional diffusion sequences and their respective strengths and pitfalls. Latest technical refinements and efforts to decrease examination duration and tailor sequences to the targeted disease will be presented. Simple and more complex cases will highlight how the technique extends the exploration of the body beyond the musculoskeletal system to lymph nodes and visceral metastases screening. Specific cases will show how WB-MRI has become a modality of choice for detecting bone metastases from many cancers and bone marrow involvement by multiple myeloma or lymphoma. The comparison will be provided with bone scintigraphy, CT and PET by the time of lesion detection and for assessment of the response to treatment.

Learning Objectives:

1. To become familiar with the technical aspects of whole-body MR.
2. To learn the role of whole-body MR in the management of oncologic patients.

A-945 11:15

B. Non-oncologic applications

M. Faruch; *Toulouse/FR (mariefaruch@hotmail.com)*

Thanks to improvement in technique for shortening of examination duration, whole-body MR imaging can now be feasible for use in routine clinical practice in numerous skeletal and neuromuscular disorders as seronegative rheumatologic disease, multifocal ischaemic lesions, multifocal eosinophilic granulomas and inflammatory myopathies. Whole-body MR could be helpful for early diagnosis, evaluation of the extent and activity of the disease, and evaluation of therapeutic response. Current MRI protocols usually include anatomic sequences as T1-weighted and water-sensitive sequences as STIR, but could also provide functional DWI sequences.

Learning Objectives:

1. To become familiar with the indications for whole-body MR in non-oncologic patients.
2. To learn the role of whole-body MR in the management of non-oncologic musculoskeletal disorders.

10:30 - 12:00

Room B

ESR meets China

EM 3

A glance of China through images

Presiding:

B. Hamm; Berlin/DE
Z.Y. Jin; Beijing/CN

A-946 10:30

Introduction

Z.Y. Jin; *Beijing/CN (jin_zhengyu@163.com)*

The Chinese radiological system is continuously innovating. Fifteen years previously, radiologists were writing reports with pens and watching stacks of films from the light box in a dark room. Patients came to the technician with handwritten prescriptions and registration information. Now, we have jumped into a new era. The workflow is greatly facilitated by automatic machine-facilitated workflow processes. Patients receive digital imaging. Radiologists sit in front of a computer and view images from picture archiving and communication system (PACS). Quantitative radiology and precision radiology have become the pursuit of us in our clinical practice. Data show that CT machine possession per million population in China increased from 5.5 in 2007 to 8.6 in 2010, although still low compared to the developed countries. Health-care PACS informational process market survey in 2015 showed that about 50% general public hospitals and 33% community hospitals have PACS. To improve the radiological service in China, multiple factors should be taken care of, not only the equipment, but also the education of radiologists/technicians, the facilitation and optimization of workflow, and the appropriateness and efficiency of patient care. With more than 13.8 billion population and varied economical situation in China, we are still facing great challenges. It is our goal to improve the quality of medical service, especially in rural areas. We will also encourage private health centres, imaging centres and Web-based consulting services in addition to established public health centres. We would like to stretch our arms towards globalization and welcome international communication and collaboration.

Session Objectives:

1. To give an overview of the current situation and trend of radiology in the mainland of China.
2. To show a few examples of the diversity of clinical radiological researches in China.
3. To introduce the special focuses of Chinese radiological society.

10:39

Interlude 1: Experience of Chinese traditional music

A-947 10:42

Multiparametric analysis in imaging liver disease

F.-H. Yan; Shanghai/CN (ruijin665727@qq.com)

China has a serious chronic liver disease burden, especially HBV/HCV-related cirrhosis and hepatocellular carcinoma (HCC). According to the population-based cancer registration data of Chinese National Central Cancer Registry, HCC is the third most common cancer and the second most cause of cancer-related deaths. Over 80% of HCC cases develop in cirrhotic liver by a process of multistep hepatocarcinogenesis, from regenerative nodule (RN), to dysplastic nodule (DN), and finally to overt HCC. Multiparametric imaging plays an important role for HCC surveillance, characterization with benign cirrhosis-associated nodules and noninvasively diagnostic algorithm in these extremely high-risk patients. To date, the diagnosis of HCC is mainly based on its haemodynamic hallmarks, i.e. arterial hyperenhancement followed by venous/delayed washout on multiphase CT and MRI. It forms the foundation of current Western and Eastern HCC practice guidelines. Ancillary features, especially the presence of restricted diffusion on diffusion-weighted imaging (DWI), are preferred for early detection of HCC and to increase diagnostic confidence. MR imaging with hepatocyte-specific contrast agents has shown great promise in identifying high-grade DN and early HCC prior to neo-arterialization and progression to overt HCC. It is gradually changing the standard of diagnosis of HCC and may well be endorsed in future guidelines. Additionally, quantitative imaging techniques, including dual-energy CT, US- or MRI-based elastography, have demonstrated increasing roles for the evaluation of diffuse liver disease such as liver fibrosis, siderosis and nonalcoholic steatohepatitis.

Learning Objectives:

1. To give an introduction to the imaging features of common liver diseases in China.
2. To understand the advantages of multiparametric analysis of liver imaging.
3. To show some interesting cases.
4. To discuss the clinical application of multiparametric analysis in abdominal pathologies.

A-948 10:57

Multimodality imaging for insulinoma detection

H.-D. Xu; Beijing/CN (bjdanna95@163.com)

Insulinomas are the most common hyper-functioning pancreatic endocrine tumours. Clinically, patients with insulinomas are characterized by hypoglycaemic symptoms caused by insulin overproduction. Insulinomas are generally benign and curable with surgery. Recurrence after resection is rare. Multiple lesions can be seen in patients with multiple endocrine neoplasia (MEN) syndrome. For patients with clinically suspected insulinomas, determining the location and number of tumours accurately with imaging workup allows for less invasive surgeries. Historically, detection of insulinomas by cross-sectional imaging has been difficult. Nowadays, a greater sensitivity for insulinoma detection has been reported with state-of-the-art CT and MR scanners. Routine dual-phase enhanced CT has relatively low sensitivity for insulinoma detection because of the presence of isoattenuating tumours, which account for around 25% of all tumours. Volume perfusion CT (VPCT) of the pancreas reveals increased blood flow of the tumour, as most 'isoattenuating tumours' show transient hyperenhancement, which may not be captured by traditional scanning protocols. Intra-individual comparative study shows that VPCT and mp-MR had similar high accuracy in insulinoma detection, and both were significantly more accurate than biphasic CECT. The intrinsic superior soft-tissue contrast with MRI helps to identify the tumour more easily without using contrast agents. Since insulinomas are quite small, the improved signal to noise of 3T MR compared to 1.5T and the introduction of high-resolution DWI are key factors for the improved diagnostic performance compared to the earlier reports.

Learning Objectives:

1. To give a review of "insulinoma imaging" in the past.
2. To understand the advantages of perfusion CT, multiparametric MR and PET/CT with special tracers.
3. To discuss the potential clinical workflow and decision tree for imaging patients with suspected insulinomas and other functional pancreatic endocrine tumours.

A-949 11:12

Interventive therapy for hepatocellular carcinoma: Chinese experiences

X.-G. Li; Beijing/CN (xglee88@126.com)

In China, due to the high prevalence of HBV infection, the incidence rate of hepatocellular carcinoma is still very high. According to the 2017 Chinese cancer statistics report, HCC ranks 3rd and 6th in the incidence of cancer of men and women in urban areas, and it ranks 3rd in the mortality rate. The features of Chinese HCC patients include background of liver cirrhosis,

relatively late stage, large tumor size and high rate of portal vein thrombus. Less than 20% of patients are candidates for liver resection or transplantation, so interventional treatment plays an important role in the management of HCC. Y90 microspheres are not available in the Mainland of China, so TARE is not routinely performed except for those in Hong Kong or Taiwan. In recent several years, DEB-TACE is accepted as an alternative for cTACE in selected patients. Thermal ablation including RFA, MWA and cryoablation is usually performed in combination with TACE. For lesions located at high-risk sites, PEI or 125I seed implantation is a good option and has achieved satisfactory results. Portal vein recanalization with 125I seed loading stent or endovascular RFA is attempted in some tertiary centres.

Learning Objectives:

1. To learn the epidemiology and special features of hepatocellular carcinoma in China.
2. To review the various interventional procedures and compare their efficacies in treating patients with hepatocellular carcinoma.
3. To understand the indications and clinical applications of interventional procedures to treat hepatocellular carcinoma.

11:27

Interlude 2: Experience of Chinese tea culture

A-950 11:30

Application of artificial intelligence in prostate imaging

X.-Y. Wang; Beijing/CN (cjr.wangxiaoying@vip.163.com)

A prostate mpMRI-CAD system has been developed. It can be used for identification of clinically significant prostate cancer with high prediction efficacy. It was validated by a multicentre clinical trial. After integrating the CAD system into the diagnostic process as a second reader, the performance of less experienced readers can be significantly improved.

Learning Objectives:

1. To learn about the basics and feasibility of applications of artificial intelligence.
2. To understand the clinical value of applying artificial intelligence in detection, prognosis and treatment evaluation of prostate cancer.
3. To learn the technique and clinical application of artificial intelligence in abdominal pelvic imaging.

A-951 11:45

Radiomics nomogram to predict lymph node metastasis in colorectal cancer

Z. Liu; Guangzhou/CN (zyluu@163.com)

To develop and validate a radiomics nomogram for preoperative predicting of lymph node (LN) metastasis in colorectal cancer (CRC). The prediction model was developed in a primary cohort consisting of 326 clinicopathologically confirmed CRC patients from January 2007 to April 2010. Radiomics features were extracted from portal venous-phase computed tomography (CT) of CRC. Lasso regression model was used for data dimension reduction, feature selection and radiomics signature building. Then, multivariable logistic regression analysis was used to develop the predicting model, with radiomics signature, CT-reported LN status and independent clinicopathological risk factors incorporated, which was presented with a radiomics nomogram. The performance of the nomogram was assessed with respect to its calibration, discrimination and clinical usefulness. Internal validation was assessed. An independent validation cohort contained 200 consecutive patients from May 2010 to December 2011. The radiomics signature consisting of 24 selected features was significantly associated with LN status ($p < 0.0001$ for both the primary and validation cohorts). The predictors contained in the individualized prediction nomogram included the radiomics signature, CT-reported LN status and carcinoembryonic antigen (CEA) level. The addition of histological grade into the nomogram failed to show incremental prognostic value. The model showed good discrimination with a C-index of 0.736 (0.759 and 0.766 through internal validation), as well as a good calibration. Application of the nomogram in the validation cohort still gave good discrimination (C index=0.778 [95%CI: 0.769-0.787]) and good calibration. Decision curve analysis demonstrated that the radiomics nomogram had clinical usefulness. This study presents a radiomics nomogram incorporating the radiomics signature, CT-reported LN status and clinical risk factors, which can be conveniently used to facilitate the preoperative individualized prediction of LN metastasis in CRC.

Learning Objectives:

1. To learn about the basics of radiomics and feasibility of clinical applications.
2. To understand the clinical value of radiomics nomogram in predicting lymph node metastasis in colorectal cancer.
3. To learn the potential applications of radiomics in various oncological studies.

Postgraduate Educational Programme

10:30 - 12:00

Room F1

E³ - European Diploma Prep Session

E³ 1823 Paediatric

A-952 10:30

Chairperson's introduction
V. Donoghue; Dublin/IE

The aim of this session is to outline the imaging findings seen in congenital and acquired conditions encountered in the brain, chest and abdomen in the paediatric and adolescent population. With improvements in ultrasound and MR imaging techniques, many congenital abnormalities have now been detected antenatally. However, imaging after birth is usually requested to confirm the diagnosis and it may also provide additional information to the clinician. Acquired disorders such as small bowel volvulus and intussusception are true clinical emergencies requiring urgent treatment. Therefore, detailed knowledge of the imaging features in these conditions is mandatory. In children with respiratory distress, the chest radiograph is often invaluable in suggesting a diagnosis. CT, however, is frequently required and knowledge of good technique using the appropriate CT dose is required to get the most information possible. In children with tumours, recognition of detailed imaging findings is important in aiding the correct tumour grading and therefore in guiding appropriate therapy.

Session Objectives:

1. To understand the imaging features of the most common congenital and neoplastic disorders of the brain in children and adolescents.
2. To describe the imaging presentations of the most common disorders of the lung and mediastinum in the paediatric age group.
3. To become familiar with the imaging features of important acute disorders of the abdomen in children and adolescents.

A-953 10:36

A. Paediatric neuro imaging
M.I. Argyropoulou; Ioannina/GR (margyrop@cc.uoi.gr)

Age-related changes depending on neuronal migration, gyration and myelination have been described in the paediatric brain. These changes are responsible for the different imaging patterns as the paediatric brain matures. Conventional MR sequences along with diffusion tensor imaging (DTI) and functional MRI (f-MRI) offer important information regarding the structural and functional maturation of the brain. Congenital malformations of the brain can be assessed with conventional sequences, but DTI using ADC, FA maps and tractography and f-MRI offer valuable structural and functional information and help in the detection of additional malformations. The incidence and localization of different brain tumours depend on the age. Conventional MRI offers useful information, but further evaluation with DTI, susceptibility contrast-enhanced perfusion imaging, spectroscopy and f-MRI is very important in the diagnostic workup and before the application of any therapeutic scheme. A number of brain tumours may metastasize through CSF and additional imaging of the spinal canal to look for seeding metastases is necessary. MRI is the modality of choice for imaging the paediatric brain; nevertheless, in neonates and infants, brain ultrasound with colour Doppler should be the first imaging approach. Brain ultrasound offers valuable information provided that a state-of-the-art technique is applied.

Learning Objectives:

1. To describe the normal development of the brain.
2. To explain the most common congenital disorders of the brain.
3. To understand the most common brain tumours in children and adolescents.

A-954 11:04

B. Paediatric chest imaging
C. Owens; London/UK (owensc@gosh.nhs.uk)

Normal pulmonary and cardiovascular development will be reviewed leading on to a comprehensive overview of congenital disorders of the lung and mediastinum and their imaging features. This will include bronchopulmonary sequestration, congenital pulmonary adenomatoid malformations and thoracic duplication cysts along with an overview of congenital cardiac disorders. The role of imaging in neonatal respiratory distress syndrome will be reviewed along with a discussion of when and how to use CT in particular cases. Lastly, paediatric thoracic neoplastic disease will be comprehensively reviewed.

Learning Objectives:

1. To describe the normal development of the lung and mediastinum.
2. To explain imaging features of congenital disorders of the lung and mediastinum.
3. To understand the imaging manifestations of respiratory distress and bronchopulmonary dysplasia in infants.
4. To describe the most common tumours of the chest in children.

A-955 11:32

C. Paediatric abdominal imaging
S.G.F. Robben; Maastricht/NL (s.robben@mumc.nl)

Paediatric abdominal diseases are highly age dependent. Newborn infants may have congenital diseases as Hirschsprung's disease or meconium ileus or may develop necrotising enterocolitis, incarcerated inguinal herniation and midgut volvulus. Infants and preschool children have intussusceptions, urinary tract infections and (rare) haemolytic uraemic syndrome. Children and adolescents have appendicitis, genito-urinary infections, ovarian torsion and Henoch Schonlein purpura. Abdominal neoplasms can occur at any age, even at birth. Considering radiation dose in children and the excess value of ultrasonography (US) in small individuals, US plays an important role as initial diagnostic modality in paediatric abdominal emergencies. Sensitivity and specificity for US in diagnosing intussusception, midgut volvulus, urinary tract abnormalities and appendicitis is over 90%. Conventional abdominal radiographs or fluoroscopy are valuable in Hirschsprung's disease, meconium ileus, malrotation and necrotising enterocolitis. I consider CT as an additional technique when the initial techniques (US and conventional radiography) are inconclusive. MRI is seldom indicated in paediatric patients with abdominal emergencies because of motion artefacts in anxious children and sometimes limited MR capacity. However, in children with abdominal neoplasms it is the modality of choice.

Learning Objectives:

1. To understand the imaging features of congenital disorders of the abdomen.
2. To describe the diagnostic evaluation and imaging presentation of appendicitis in children.
3. To describe the diagnostic evaluation and imaging presentation of volvulus and intussusception in children.
4. To understand the imaging presentation of the most common oncologic

12:30 - 13:30

Room C

E³ - The Beauty of Basic Knowledge: Cardiovascular and Interventional Radiology

E³ 24E

The heart of the matter: imaging the myocardium

Moderator:
T. Yalynska; Kiev/UA

A-959 12:30

MR in ischaemic cardiomyopathies
F. Cademartiri; Monastier di Treviso/IT (filippocademartiri@gmail.com)

Ischaemic cardiomyopathy is the leading cause of morbidity and mortality in the western world. Over the years, several improvements in terms of knowledge, diagnostic capabilities and treatment options have been developed in such a way that today we are in a constant update of our technologies and treatments. Cardiovascular Magnetic Resonance (CMR) is by far the most flexible and complete imaging modality that can be applied to the evaluation of ischaemic cardiomyopathies. It can provide anatomy, function, flow, ischemia and tissue characterisation. CMR is considered the reference standard for the assessment of inducible ischemia and myocardial viability. Modern MR equipment can deliver a huge amount of information that require wide technical and clinical knowledge to be handled correctly. Especially the newer approaches with quantitative tissue mapping that are being introduced in the clinical field. With the advancement of technology also 3T CMR have become mainstream and able to add some value in certain specific fields. With the rapid growth of Cardiac Computed Tomography as the elective non invasive anatomical tool for the assessment of the coronary arteries CMR becomes the best tool to complete a Cardiovascular Imaging Section (or viceversa).

Sunday

Postgraduate Educational Programme

Learning Objectives:

1. To learn about the MR derived imaging biomarkers in ischaemic cardiomyopathy.
2. To understand the value of cardiac MR to indicate and guide revascularisation in ischaemic cardiomyopathy.
3. To appreciate the potential of cardiac MR to predict the outcome of revascularisation.

A-960 13:00

MR in non-ischaemic cardiomyopathies

C. [Peebles](mailto:Charles.Peebles@suht.swest.nhs.uk); Southampton/UK (Charles.Peebles@suht.swest.nhs.uk)

Non-ischaemic cardiomyopathies are a heterogeneous group of inherited and acquired diseases affecting myocardial function. Cardiac MR is unsurpassed in its ability to quantify myocardial function, identify the pattern and extent of myocardial scar, and assess myocardial oedema and diffuse fibrosis. Established techniques such as late gadolinium enhancement are critical to establishing a diagnosis, particularly in differentiation from ischaemic cardiomyopathy. Newer techniques such as tissue mapping are still finding their role in clinical practice, but seem to be promising tools for both diagnosis and prognosis of cardiomyopathies. This lecture will use predominantly case-based discussion to understand the established and evolving imaging biomarkers for non-ischaemic cardiomyopathy and how these are applied in clinical practice. The focus will be on establishing an accurate diagnosis in the major non-ischaemic cardiomyopathies, whilst highlighting areas of diagnostic challenge and uncertainty. The potential of CMR to provide prognostic information and the associated evidence base will also be explored.

Learning Objectives:

1. To learn about the MR derived imaging biomarkers in non-ischaemic cardiomyopathies.
2. To understand the role of cardiac MR in primary and secondary cardiomyopathies.
3. To appreciate the discriminatory power of cardiac MR in cardiomyopathies.

12:30 - 13:30

Room D

E³ - The Beauty of Basic Knowledge: A Survival Guide to Musculoskeletal Imaging

E³ 25E

Infective/inflammatory disorders

Moderator:

V.N. Cassar-Pullicino; Oswestry/UK

A-961 12:30

Infective/inflammatory disorders

F.M.H.M. [Vanhoenacker](mailto:filip.vanhoenacker@telenet.be); Antwerp/BE (filip.vanhoenacker@telenet.be)

Osteomyelitis is divided into acute, subacute and chronic osteomyelitis. Pathophysiological factors that determines imaging are patient's age, route of contamination, virulence of the causative micro-organism and the immune status of the patient. In haematogenous spread, the site and extent of the infection depends primarily on the vascularisation. The metaphysis is the common site for haematogenous osteomyelitis in children over 18 months, due to stasis of slow-flowing blood. In infants and adults, the presence of transphyseal vessels may cause spread of the infection to the epiphysis. Imaging plays a pivotal role in confirming the diagnosis of musculoskeletal infection, determining the disease extent and guiding early treatment. Plain radiography is not very sensitive for early diagnosis. Ultrasound is a reliable tool to detect subperiosteal spread in children, but its use in adults is restricted to evaluation of soft tissue infection and for aspiration of infected joints. In adults, MRI is the preferred modality, although CT may detect sequestrum formation in chronic osteomyelitis. SpA consists of a spectrum of chronic inflammatory disorders that are distinct from RA. Ultrasound is useful for grading of synovitis and early detection of erosions of peripheral joints in RA. SpA has a predilection for the axial skeleton. MRI is the preferred technique for early diagnosis and detection of active inflammatory lesions by demonstrating bone marrow oedema at the sacro-iliac joints. Two or more areas of BME or one focus of BME on at least two consecutive 3-mm slices is needed to reliably diagnose axial SpA.

Learning Objectives:

1. To learn about the pathomechanisms involved in inflammatory and infectious disorders.
2. To understand the imaging appearances and their differential diagnosis in the acute, sub-acute and chronic phases of infection.
3. To become familiar with the spectrum of imaging features of inflammatory disorders in the axial and peripheral skeleton.

14:00 - 15:30

Room A

E³ - ECR Academies: Interactive Teaching Sessions for Young (and not so Young) Radiologists

E³ 1921

Imaging of abdominal tumours

A-967 14:00

A. Liver tumours

T. [Denecke](mailto:tim.denecke@charite.de); Berlin/DE (tim.denecke@charite.de)

Besides the top three malignant (HCC, CCC, metastases) and the top three benign liver tumours (haemangioma, FNH, adenoma), there is a large variety of rare entities and subtypes, which can be demanding regarding their imaging diagnostics. In this session, a number of cases will be presented to illustrate the typical and also some challenging findings of focal liver lesions, which the radiologist should know, always keeping in view the potentially severe consequences of the radiologist's judgement for patient management.

Learning Objectives:

1. To become familiar with the differential diagnosis.
2. To identify the key imaging findings.

Author Disclosure:

T. [Denecke](mailto:tim.denecke@charite.de): Grant Recipient; Siemens. Speaker; Siemens, Bayer, Toshiba.

A-968 14:45

B. Pancreatic tumours

C. [Matos](mailto:celso.matos@fundacaochampalimaud.pt); Lisbon/PT (celso.matos@fundacaochampalimaud.pt)

Differential diagnosis and management decisions of pancreatic tumours are based on a mixture of clinical and laboratory information and imaging findings involving multiple modalities. The lecture will familiarize the delegates with the main challenges and future trends in the diagnosis of pancreas tumours, differential diagnosis with pancreas inflammation, and in identifying features that may help to select surgical candidates.

Learning Objectives:

1. To become familiar with the differential diagnosis.
2. To identify the key imaging findings.

14:00 - 15:30

Room F1

E³ - European Diploma Prep Session

E³ 1923

Interventional

A-970 14:00

Chairperson's introduction

T. [Struffert](mailto:Struffert@Erlangen.DE); Erlangen/DE

"no abstract submitted"

Session Objectives:

1. To understand the principles and techniques of angiography and image-guided interventions.
2. To become familiar with the different methods of hepatobiliary interventions.
3. To describe the most common vascular interventions.

A-971 14:06

A. Basic principles of angiography and image-guided interventions

T.K. [Helmberger](mailto:Thomas.Helmberger@klinikum-muenchen.de); Munich/DE (Thomas.Helmberger@klinikum-muenchen.de)

Basic knowledge of the indications and contraindications, patient preparation, typical interventional techniques, outcome and complications in vascular and non-vascular interventions is essential for every radiologist. Knowledge of the typical arterial and venous anatomy and potential variants is of ample importance both from a diagnostic perspective and with respect to planning optimal access routes, puncture site/technique, and pathways for transvascular and percutaneous procedures. These procedures include (1) a broad spectrum of transvascular interventional techniques such as vascular recanalization (e.g. balloon and stent angioplasty), occlusion (e.g. bleeding, vascular malformations), and perfusion (e.g. trans-arterial oncological interventions) in a wide variety of diseases; and also (2) basic percutaneous diagnostic (i.e. biopsy, fluid evacuation) and therapeutic procedures (i.e. drainage of e.g. abscess, haemorrhage). The understanding of the comprehensive options and benefits of these interventional techniques, together with the proper use of

image guidance makes the radiologist a valuable companion to almost all clinical specialities in solving diagnostic and therapeutic tasks.

Learning Objectives:

1. To describe the normal anatomy and normal variants of the arterial and venous vascular system.
2. To understand diagnostic and interventional angiographic techniques.
3. To explain basic percutaneous image-guided techniques including abscess drainage and biopsy taking.

Author Disclosure:

T.K. Helmberger: Consultant; Boston Scientific.

A-972 14:34

B. Image-guided interventions in oncology

J.I. Bilbao; Pamplona/ES (jjbilbao@unav.es)

Interventional oncology (IO) is an established pillar in the management of oncologic patients. Endovascular access allows (almost) any kind of therapies. By using devices it is possible to permeabilize, occlude, obtain material, infuse chemotherapy, administer brachytherapy, implant devices or genes, among others. IO within the multidisciplinary management could offer curative procedures such as percutaneous or endovascular ablations using physical or pharmacological methods; thus, radiologists are in the front line of patients' care which carries clinical responsibilities. IO is crucial in the downstaging/bridging towards a curative treatment such as surgery; these adjunctive procedures, are fundamental in allowing patients to be cured and should be actively promoted by radiologists. IO procedures can participate in the palliation of symptoms, offering to bring them within the established treatment protocols; as happens with any bleeding related directly with the tumour or indirectly with its treatment. IO offer other procedures essential to cancer care, but not considered primarily therapeutic such as venous access. Liver's almost exclusive characteristic of having a dual vascularisation offers performing aggressive treatments targeting the tumour while preserving the healthy parenchyma. Particularly in the case of hepatocellular carcinoma, chemoembolization (particles with chemotherapy) and radioembolization (particles with a radioisotope) are included in the therapeutic protocol for this devastating disease. Non-vascular procedures, such as percutaneous ablation, have proved their efficacy, with improvement in overall survival in a certain group of liver tumours and are basic in the management of a wide range of lung and renal tumours.

Learning Objectives:

1. To describe the basic technical and methodological principles of imaging-guided interventions in oncological disorders.
2. To understand the principles of and indications for vascular interventions in cancer, e.g. transarterial (chemo)embolisation techniques of the liver.
3. To become familiar with the principles of and indications for percutaneous image-guided interventions in oncological disorders including thermal ablation techniques.

Author Disclosure:

J.I. Bilbao: Advisory Board; Sirtex Medical, Terumo.

A-973 15:02

C. Vascular interventions

J.A. Reekers; Amsterdam/NL (j.a.reekers@amc.uva.nl)

In the exam preparation talk, a variety of different vascular techniques will be discussed. Endovascular treatment options of atherosclerotic diseases will be explained, and common angioplasty procedures, such as renal, iliac and femoral angioplasties, understood. The indications and techniques for arterial stenting procedures will be described, and techniques of arterial embolisation and coiling explained. All techniques will be illustrated with related patient cases.

Learning Objectives:

1. To explain endovascular treatment options of atherosclerotic diseases.
2. To understand common angioplasty procedures, such as renal, iliac and femoral angioplasties.
3. To describe indications and techniques for arterial stenting procedures.
4. To explain techniques of arterial embolisation and coiling.

B

Scientific Sessions (SS) My Thesis in 3 Minutes (MY) Clinical Trials in Radiology (CT)

Presentation numbers are prefixed
by the letter B.

Sessions and abstracts are listed
by days.

The Clinical Trials in Radiology sessions are listed at
the end of section B. (page 535)

Wednesday, February 28.....	189
Thursday, March 1	273
Friday, March 2.....	356
Saturday, March 3.....	397
Sunday, March 4	456

Wednesday, February 28

10:30 - 12:00

Room B

Abdominal Viscera

SS 201a

Multiparametric liver imaging

Moderators:

A. Filippone; Chieti/IT
S. Ichikawa; Chuo-shi, Yamanashi/JP

K-01 10:30

Keynote lecture

D. Regge; Turin/IT

B-0001 10:39

Long-term follow-up magnetic resonance elastography after novel direct antiviral therapy in chronic hepatitis C virus induced liver fibrosis

S.R. [Marticorena Garcia](#), J. Guo, H. Tzschätzsch, C.E. Althoff, M. Dürr, F. Halleck, B. Hamm, T. Fischer, I. Sack; Berlin/DE
(stephan.marticorena-garcia@charite.de)

Purpose: Chronic hepatitis C virus (HCV) infection predisposes to liver fibrosis. The purpose of this study is to non-invasively monitor elastic properties of the liver and kidney transplants (KTX) using multifrequency magnetic resonance elastography (MRE) after direct antiviral therapy.

Methods and Materials: In this prospective and longitudinal study 13 patients with chronic HCV infection and biopsy proven liver fibrosis were treated with direct-acting antivirals (Daclatasvir/Sofosbuvir). Shear wave speed (SWS) of liver and KTX was measured by multifrequency MRE at baseline (before therapy) and during a follow-up period after therapy at 3, 6 and 15 months. The results were compared to a healthy control group (CTR, n=7). Laboratory results were obtained at each time point.

Results: Mean time point to reach undetectable viral RNA was 22±13 days and remained stable during the entire follow-up period in all responders to treatment. Compared to baseline (1.67±0.33 m/s), analysis of repeated measurements showed a significant decrease in liver SWS at 6 months (1.56±0.27 m/s; p<0.01), being stable at 15 months (1.55±0.26 m/s; p<0.05). Viral relapse occurred in one subject and liver SWS remained unchanged after treatment, despite of serological marker response. No changes of renal stiffness were observed in KTX.

Conclusion: Direct antiviral therapy is associated with an early decrease of liver stiffness and being stable until 1 year after the end of treatment. MRE could be used as biomarker for non-invasive therapy monitoring based on liver stiffness which is a potential early predictor of the treatment response.

Author Disclosures:

B. Hamm: Grant Recipient; Siemens.

B-0002 10:47

Repeatability and reproducibility of multiparametric magnetic resonance imaging of the liver

H.R. [Wilman](#)^{1,2}, V. [Bachitar](#)¹, J. [Jacobs](#)¹, R. [Newbould](#)², M. [Gyngell](#)¹, C.J. [Kelly](#)¹, M.D. [Kelly](#)¹, R. [Banerjee](#)¹; ¹Oxford/UK, ²London/UK
(henry.wilman@perspectum-diagnostics.com)

Purpose: LiverMultiScan™ (LMS) is a multiparametric MRI-based technology for quantitative analysis of hepatic fat, T2*, and iron corrected T1 (cT1). Here we test the robustness of LMS-derived metrics by systematically examining reproducibility of measurements across different MRI scanner manufacturers, models, software versions and field strengths.

Methods and Materials: cT1, T2* and Proton Density Fat Fraction (PDFF) maps were acquired from 61 participants on combinations of three Siemens and two Philips scanners at both 1.5T and 3T. Participants were scanned on at least two different scanner models and field strengths in pseudorandomised order with up to 1 week between scans and two acquisition repeats on each scanner. Standardisation of T1 maps across scanners were based on phantom-derived mappings from 90 acquisitions.

Results: Bland-Altman analysis of the T1 phantom measurements showed a clear reduction in bias (from -20ms to -4.7ms), tightening of the 95% Limits of Agreement (LoA: from -59.2ms - 19ms, to -25.3ms - 15.9ms) and reduction in mean coefficient of variation (CoV: 2.5% to 1.0%) after standardisation. Following T1-standardisation, cT1 in participants demonstrated high reproducibility (CoV, 3.3%, bias, 6.5 ms, 95% LoA of -76.3 ms to 89.2 ms). Both T2* and PDFF measurements also showed excellent reproducibility at both field strengths and across different scanners models.

Conclusion: We demonstrate that following T1 standardization, cT1 is reproducible across scanner manufacturer, model, software version and field strength. Combined with the excellent reproducibility of T2* and PDFF, LMS represents a robust and reliable non-invasive tool for the characterisation of liver tissue.

Author Disclosures:

H.R. [Wilman](#): Shareholder; Perspectum Diagnostics Ltd. V. [Bachitar](#): Employee; Perspectum Diagnostics Ltd. J. [Jacobs](#): Employee; Perspectum Diagnostics Ltd.. Shareholder; Perspectum Diagnostics Ltd. R. [Newbould](#): Employee; Perspectum Diagnostics Ltd. M. [Gyngell](#): Employee; Perspectum Diagnostics Ltd.. Shareholder; Perspectum Diagnostics Ltd. C.J. [Kelly](#): Employee; Perspectum Diagnostics Ltd.. Shareholder; Perspectum Diagnostics Ltd. M.D. [Kelly](#): Employee; Perspectum Diagnostics Ltd.. Shareholder; Perspectum Diagnostics Ltd. R. [Banerjee](#): Board Member; Perspectum Diagnostics Ltd.. CEO; Perspectum Diagnostics Ltd.. Shareholder; Perspectum Diagnostics Ltd..

B-0003 10:55

Molecular features, histological parameters and enhancement measurements in NASH patients using gadoteric acid-enhanced MR imaging

D.S. [Feier](#)^{1,2}, N. [Bastati-Huber](#)², A. [Beer](#)², R.M. [Fragner](#)², H. [Einspieler](#)², A. [Ba-Ssalamah](#)²; ¹Cluj-Napoca/RO, ²Vienna/AT (diana.feier@gmail.com)

Purpose: To assess the relationship of organic anion transporting polypeptide (OATP1B1/3) expression with histological parameters and relative enhancement ratio in patients with nonalcoholic fatty liver disease (NAFLD), defined according to the steatosis activity and fibrosis (SAF) scoring system, which is based on the semi quantitative scoring of steatosis activity and liver fibrosis.

Methods and Materials: The local institutional review committee approved this study and waived written informed consent. This was a retrospective study of gadoteric acid-enhanced 3-T MR imaging performed in 52 patients with NAFLD, mean age (SD) 50.46 (16.52) years. The MR images were analyzed by using the relative enhancement (RLE) (the ratio of signal intensities of the liver parenchyma before and 20 minutes after intravenous administration of gadoteric acid). Univariate and multiple regression analyses were applied to identify variables associated with OATP1B1/3 expression.

Results: OATP1B1/3 expression correlated with RLE (r=0.49, p=0.0002), the degree of liver fibrosis (r=-0.27, p=0.04) but not with steatosis (r = -0.16, p=0.23), ballooning (r=-0.22, p=0.1) or inflammation (r=-0.07, p=0.57). According to multivariate analysis both RLE and liver fibrosis are independent predictors of OATP1B1/3 expression (coefficient of determination R²=0.32, p=0.01).

Conclusion: The degree of OATP1B1/3 expression correlated statistically with gadoteric acid relative enhancement and the degree of liver fibrosis in patients with NAFLD.

B-0004 11:03

Application of T1rho in evaluating liver fibrosis and correlation with liver function

Q. [Yang](#), T. Yu, J. Huang, Y. Su, J. Li, B. Liang; Guangzhou/CN
(yangqih2@mail.sysu.edu.cn)

Purpose: To verify the value of T1rho in evaluating liver fibrosis, find out the diagnosis threshold of T1rho and correlation coefficient between T1rho value and laboratory test results.

Methods and Materials: The study was approved by the local Institutional Review Board and informed consent was obtained from all participants. Patients suspected liver fibrosis were enrolled. Clinical data including laboratory test results were collected within 7 days before or after MRI scan for patients. All patients underwent MR scan including T1rho. Pathology results, laboratory test results were compared with T1rho and correlation test were done among them.

Results: 77 patients were enrolled and T1rho values for F0~F4 were 40.36±4.40ms, 41.99±1.63ms, 44.24±4.40ms, 47.16±2.66ms and 47.87±4.73ms. One-way ANOVA showed statistical difference among T1rho values of F0~F4 groups (P<0.001) and among T1rho values of Child A~C groups in liver cirrhosis(F4) patients. Area below ROC curve of T1rho diagnosing liver fibrosis severer than F2 was 0.87. When 42.86ms was chosen as diagnosis threshold, sensitivity was 0.91 and specificity was 0.76. Among all laboratory tests, PT, PT-INR, Bile acids, TBIL, DBIL, IBIL and APRI were positively correlated with both T1rho and fibrosis stages, while T-CHO, ALB and A/G were negatively correlated with both T1rho and fibrosis stage.

Conclusion: T1rho could be used in early diagnosis of liver fibrosis, in differential diagnosis of mild liver fibrosis and liver cirrhosis. Correlation between laboratory test results and T1rho may be caused by liver dysfunction due to liver fibrosis.

B-0005 11:11

Quantitative evaluation of liver function using coefficient of variation value and contrast enhancement index (CEI) on gadoxetic acid-enhanced MR imaging in preoperative evaluation

S.W. Kim, H. Ryu, Y.R. Kim, Y.H. Lee, K.-H. Yoon; *Iksan/KR*

Purpose: The aim of this study was to evaluate whether coefficient of variation value and contrast enhancement index of gadoxetic acid-enhanced MR imaging can be used for preoperative evaluation of liver function and diagnosis of cirrhosis.

Methods and Materials: From July 2011 to January 2017, we included 22 patients who underwent various hepatic resections due to hepatic tumours. Gadoxetic acid-enhanced 3T MR imaging was performed before hepatic resection within 2 weeks. Heterogeneity and degree of liver parenchymal enhancement on MR imaging were analysed by measuring coefficient of variation (CV) value and contrast enhancement index (CEI). Relationship between these parameters and laboratory findings for liver function such as indocyanine green (ICG) R15 test and prothrombin time (INR) were evaluated.

Results: Among the 22 patients included in our study, 13 patients were proven presence of liver cirrhosis and 9 patients were proven absence of liver cirrhosis on histopathologic examination. CV value was linearly correlated with ICG R15 test ($p=0.018$) and PT INR ($p=0.015$). Also CV value was significantly higher in cirrhosis group than normal liver parenchyma group (3.9 ± 0.73 vs 6.18 ± 2.03 , $p=0.004$). On the contrary, CEI was not correlated with laboratory findings ($p=0.143$, $p=0.816$) and was not significantly different between pathologic proven cirrhosis and normal liver parenchymal group (1.68 ± 0.24 vs 1.74 ± 0.29 , $p=0.616$).

Conclusion: CV value on gadoxetic acid-enhanced MR imaging showed well correlated with laboratory tests for liver function and presence of cirrhosis. So, quantitative evaluation of liver function using CV value on MR imaging can be used in preoperative evaluation for hepatic surgery.

B-0006 11:19

Liver volumetry: a useful tool to predict functional improvement after antiviral treatment in cirrhotic chronic hepatitis C patients

T. Di Maira, A. Torregrosa Andres, V. Navarro Aguilar, D. Sánchez Mateos, V. Fornes, M. Berenguer Haym; *Valencia/ES (asunsuso@gmail.com)*

Purpose: To assess if liver volume measured by CT-MR is a predictor of liver function in patients with sustained viral response (SVR).

Methods and Materials: Consecutive cirrhotic HVC patients assessed for liver transplantation and treated with antivirals between September 2014-September 2015 who achieved SVR were included. Pre-treatment liver volume adjusted by Body Surface Area (BSA) were calculated from CT-MR studies acquired within 360 days of the start of treatment. The liver delineation was performed by two radiologists. Two different semiautomatic software were used for volumetric quantification (one for CT and one for MR). Liver function was assessed by Child-Turcotte-Pugh and MELD scores collected at baseline, 12, 24, 52 weeks and at the end of the follow-up period. Multivariate mixed regression model was used to identify baseline factors associated with improvement of liver function overtime. Follow-up period was up to December 2016.

Results: 42 patients were included, median age 58.6 years (Q1-Q3: 52.7-68.8); MELD 14 (11-17); Child-Turcotte-Pugh 9 (8-10); Liver volume 1400.9 mL ($1183.2-1601.4$); BSA 1.8 m² (1.7-2).

MELD scores at baseline and at last control were 14 (11-17) and 10 (8-12), respectively ($p<0.001$); Child-Turcotte-Pugh scores were 9 (8-10) and 6 (5-7), respectively ($p<0.001$).

In the multivariate mixed regression model, higher liver volume adjusted by BSA was associated with an improvement of MELD and Child-Turcotte-Pugh over time 95% CI (-12.14, -0.97), $p=0.028$ and 95% CI (-4.67, -0.65), $p=0.014$, respectively.

Conclusion: Liver volume adjusted by BSA is a non-invasive radiological tool that can predict functional improvement in cirrhotic patients undergoing antiviral treatment.

Author Disclosures:

T. Di Maira: Grant Recipient; Rio Hortega Research Grant n.15/00133, supported by Instituto Carlos III.

B-0007 11:27

Gd-EOB-DTPA-enhanced MRI T1 relaxometry as an imaging-based liver function test compared with ¹³C-methacetin LiMAX test

D. Theilig¹, P. Raabe¹, L. Lüdemann², J. Pratschke³, B. Hamm¹, T. Denecke¹, D. Geisel¹; ¹Berlin/DE, ²Essen/DE (dorothea.theilig@charite.de)

Purpose: To compare gadolinium ethoxybenzyl diethylenetriaminepentaacetic acid (Gd-EOB-DTPA)-enhanced magnetic resonance imaging (MRI) as an imaging-based liver function test with the ¹³C-methacetin LiMAX (maximum liver function capacity) test.

Methods and Materials: Fifty-three patients who underwent both Gd-EOB-DTPA-enhanced MRI T1 relaxometry before and 20 min after intravenous (IV) Gd-EOB-DTPA administration at our institution as well as a ¹³C-methacetin LiMAX test within 30 days of the MRI examination were retrospectively analysed. In these patients, T1 relaxation times of liver parenchyma, total liver volume and hepatic tumour volume were determined. Patients' laboratory parameters including bilirubin were retrieved from routine laboratory tests. Pearson correlations, multiple linear regression analysis, and receiver-operating characteristic (ROC) curve analysis were performed with indices derived from T1 relaxometry, liver volumetry, and laboratory parameters to identify the best predictor of global liver function as determined by the LiMAX test.

Results: Relaxometry-derived indices, i.e. T1 reduction rate (T1 RR), T1 RR x total liver volume (TLV), T1 RR x functional liver volume (FLV), and T1 relaxation time 20 minutes after IV Gd-EOB administration (T1 post) showed a statistically significant correlation with LiMAX and a statistically significant discriminatory capacity between patients with LiMAX of $>$ and $<$ 315 μ g/kg/h. Of the indices investigated, T1 RR showed the best discriminatory capacity and proved to be the only statistically significant parameter in multiple linear regression analysis.

Conclusion: The T1 reduction rate (T1 RR) of the liver on Gd-EOB-DTPA-enhanced MRI allows prediction of liver function as determined by the LiMAX test.

Author Disclosures:

D. Theilig: Author; Dr. Theilig is participant in the Charité Junior Clinical Scientist Program funded by Charité - Universitätsmedizin Berlin and the Berlin Institute of Health. B. Hamm: Author; Prof. Hamm has received travel support and honoraria from Bayer AG. T. Denecke: Author; Dr. Denecke has received travel support and honoraria from Bayer AG. D. Geisel: Author; Dr. Geisel has received travel support and honoraria from Bayer AG.

B-0008 11:35

Comparison of two liver specific contrast agents in patients with different degrees of liver cirrhosis

C. Khouri Chalouhi¹, F. Vernuccio², B. Tuscano¹, P. Duca¹, G. Brancatelli², A. Vanzulli¹; ¹Milan/IT, ²Palermo/IT

Purpose: Compare the performance of gadobenate dimeglumine (Gd-BOPTA) and gadoxetic acid (Gd-EOB-DTPA) in giving an useful hepatobiliary phase (HBP) in cirrhotic patients with different degrees of liver dysfunction expressed by Model-of-End-Stage-Liver-Disease (MELD) score.

Methods and Materials: We reviewed a total of 258 liver MRI of 258 cirrhotic patients: 131 Gd-BOPTA-enhanced MRI (BOPTA-group) and 127 Gd-EOB-DTPA-enhanced MRI (EOB-group). For each MRI we calculated the contrast enhancement index (CEI) of liver parenchyma. We correlated the MELD score and the CEI in both the groups (multiple linear regression analysis). We made a qualitative analysis of HBP as adequate/inadequate for both the groups and we investigated the difference between the two contrast agents adjusting for MELD score (logistic regression analysis).

Results: In both the groups there was significant reverse correlation between MELD score and the CEI ($r=-0.013$). At the same MELD score value the CEI in EOB-group is increased by 0.23 ($p<0.001$) more than the BOPTA-group. Regarding the qualitative analysis at the same value of MELD score the mean odds ratio to have an adequate HBP was 3.64 ($p<0.001$) in the EOB-group compared to BOPTA-group, the adequacy of HBP is increasing in favour of Gd-EOB-DTPA at the increase of MELD score ($\exp(b)\text{interaction}=1.233$; $p=0.011$).

Conclusion: The HBP is negatively affected by the severity of cirrhosis for both the contrast agents. At the same MELD score value parenchymal enhancement in HBP is higher for Gd-EOB-DTPA. In cirrhotic patients the use of Gd-EOB-DTPA is preferable to have an adequate HBP, especially in patients with advanced disease.

B-0009 11:43

Correlation between Gd-EOB-DTPA-enhanced MRI and T1rho in patients with and without liver cirrhosis

J.D. Stief¹, L. Lüdemann², T. Denecke¹, B. Hamm¹, D. Geisel¹; ¹Berlin/DE, ²Essen/DE (jonas.stief@gmail.com)

Purpose: The aim of this study is to find out whether there is a correlation between the functional parameter of the relative enhancement (RE) using Gd-EOB-DTPA-enhanced MRI and the fibrosis parameter using T1rho-mapping. In addition, it will be investigated which of the parameters is better able to distinguish between liver cirrhosis and the healthy liver.

Methods and Materials: A retrospective analysis was performed in patients ($n=124$) who received both Gd-EOB-DTPA-enhanced MRI and the T1rho-sequence. MRI was performed at 1.5 Tesla. RE was calculated for the entire liver. A T1rho-sequence with acquisition of 6 spin lock times (TSLs: 0, 10, 30, 40, 60 msec) and spin-lock frequency of 500 Hz was applied. T1rho-maps were created. T1rho value was calculated on two different levels with 3 ROIs each.

Results: There was a significant correlation between RE and T1rho time ($p=0.013$). The correlation coefficient according to Pearson was $R = -0.22$. In the ROC analysis for differentiation between liver cirrhosis and normal liver, an AUC for RE of 0.755 and an AUC for T1rho of 0.717 were found. The cut-off value for RE is 0.645 and for T1rho 50.29 (sensitivity 74.0% and specificity 74.3%, respectively, 74.0% and 67.6%).

Conclusion: The MRI liver fibrosis parameter T1rho and the MRI liver function parameter RE of Gd-EOB-DTPA show a weak but significant correlation. Both parameters are able to distinguish between cirrhosis and normal liver parenchyma.

Author Disclosures:

T. Denecke: Speaker; Speaker fee from Bayer AG and Siemens AG.

B. Hamm: Investigator; Elbit Imaging Ltd. Research/Grant Support; Electric Company, Toshiba Medical Services Corporation, Koninklijke Philips NV, Siemens AG, General Electric Company, Elbit Imaging Ltd, Bayer AG, Guerbet SA, Bracco Group, Braun Melsungen, KRAUTH medi. Shareholder; Toshiba Medical Services Corporation. Speaker; Speaker fee from Bayer AG and Siemens AG. **D. Geisel:** Speaker; Speaker fee from Bayer AG and Siemens AG.

B-0010 11:51

Perfusion quantification and hepatic function with Gd-EOB-DTPA: hepatic fibrosis and hepatocellular transport

S. Schmidt Kobbe¹, J.-L. Daire², A. Sciarra¹, B. Leporq³, B. Van Beers², C. Sempoux¹, C. Pastor⁴, ¹Lausanne/CH, ²Clichy/FR, ³Villeurbanne/FR, ⁴Geneva/CH (sabine.schmidt@chuv.ch)

Purpose: To evaluate the hepatocellular expression of the biliary transporters responsible for the uptake of hepatospecific contrast medium Gd-EOB-DTPA in patients with different stages of liver fibrosis undergoing dynamic gadoxetate-enhanced MRI.

Methods and Materials: We prospectively included 50 patients with suspected chronic liver disease that underwent dynamic gadoxetate-enhanced MRI and liver biopsy. After pharmacokinetic modelling we extracted the following MR-parameters: arterial and portal perfusion, Gd-EOB-DTPA hepatocytic uptake rate, biliary efflux, sinusoidal back flux (ml/min/100g for all), and the extracellular volume (%). Histologically, two pathologists classified fibrosis according to METAVIR and assessed the collagen proportionate area (CPA) with automated imaging analysis. The expression of the biliary transporters OATP2/8, MRP2 and MRP3 was investigated by immunohistochemistry and semiquantitatively scored according to the distribution within the lobule.

Results: The final cohort included 42 patients (32 men) with different stages of fibrosis ($F0=5/F1=8/F2=11/F3=10/F4=8$). Pharmacokinetic modelling was able to distinguish the different stages of fibrosis and correlated with CPA ($p<0.01$). At MRI, increasing fibrosis was associated with a progressive change from portal to arterial perfusion, a decrease in hepatocytic Gd-EOB-DTPA uptake rate, biliary efflux, sinusoidal back flux, and increased extracellular volume ($p<0.05$). At immunohistochemistry, increasing fibrosis was associated with more diffuse expression of OATP2/8 and MRP3 to the whole lobule and progressively irregular MRP2 expression ($p<0.05$).

Conclusion: At advanced stages of liver fibrosis, the decrease in Gd-EOB-DTPA hepatocytic uptake could reflect either lower interstitial bioavailability of the contrast agent or altered transporter functions. The modified immunohistochemical expression of the transporters could mean adaptive response to progressive intracellular cholestasis.

Author Disclosures:

S. Schmidt: Grant Recipient; Bayer Schering, Switzerland.

10:30 - 12:00

Room C

Abdominal Viscera

SS 201b

Innovations in pancreatic imaging

Moderators:

E. Kondratyev; Moscow/RU

D. Tamandl; Vienna/AT

K-02 10:30

Keynote lecture

M. D'Onofrio; Verona/IT

B-0011 10:39

Optimisation of MRI screening in hereditary pancreatic adenocarcinoma

B. Boekestijn, M. Wasser; Leiden/NL (B.Boekestijn@lumc.nl)

Purpose: In CDKN2A/p16-mutation carriers with a 15-20% lifetime risk of developing pancreatic ductal adenocarcinoma (PDAC), annual surveillance using MRI has shown to successfully detect PDAC in an early stage, resulting in increased resectability and survival. In a retrospective study we assessed the value of different MRI-techniques in early detection of PDAC.

Methods and Materials: The MRI protocol consisted of axial and coronal T2 TSE, T1 dynamic contrast enhanced GRE with fat suppression and combined 2D/3D MRCP. In 2012 T1-weighted turbo field echo (TFE) was added to the protocol, followed by DWI in 2015. Three readers independently analysed the different MRI sequences of subjects with a proven PDAC for presence and location of the tumours.

Results: Since 2000, 18 pancreatic cancers were found in 205 screened subjects (9%). In 4 cases a tumour was detected at the first MRI. In 14 patients previous examinations were available for comparison. In 9 of these patients pancreatic abnormalities were retrospectively visible on previous examinations. T1 TFE was positive in 12 out of 13 cases when the sequence was available, DWI was positive in 6 of 8, T1 DCE in 18 of 22 and T2 in 15 of 22. In two patients a lesion was detected only on T1 TFE by all readers and not on other sequences.

Conclusion: Annual MRI surveillance in asymptomatic individuals at high risk of developing PDAC results in detection of tumours in a potentially resectable stage. T1 TFE especially seems to be a promising sequence for detection of pancreatic lesions.

B-0012 10:47

CT volumetry of the pancreas: gland size in a normal population and its relation to age, gender and body composition

J. Frøkjær, J. Kipp, E. Mark, A. Drewes, S. Olesen; Aalborg/DK (jebf@rn.dk)

Purpose: The pancreas volume is affected by different diseases, such as chronic pancreatitis, and is also known to be related to age and gender. To distinguish between normal and pathological pancreas volume, the aims were to establish a normal reference material of pancreatic size based on CT, and to explore the influence of age, gender and body composition.

Methods and Materials: 240 trauma patients, 20 in each gender and decade (20-80 years) group, were evaluated. 221 CT scans without pancreatic pathology were analysed: semiautomatic Hounsfield unit based segmentation of pancreas volume, 7 different two-point pancreatic measurements, and a calculated volume (formula with 6 two-point measurements). Body composition with cross-sectional area (CSA) of visceral and subcutaneous fat at L4 level, and body size as L1 vertebral dimensions (height, width, depth) were measured.

Results: Segmented pancreas volume was higher for men ($84.1 \pm 22.6 \text{ cm}^3$) than for women ($72.4 \pm 19.7 \text{ cm}^3$, $P<0.001$), with correlation to both the calculated volume ($r=0.73$, $P<0.001$) and all the two-point measurements (two best: transverse-head: $r=0.50$, $P<0.001$; AP-head: $r=0.48$, $P<0.001$). In a multivariate regression model only age, L1 width and CSA of visceral fat (all $P<0.001$) were explaining the volume, whereas gender was without influence ($P=0.42$).

Conclusion: A gender- and age-specific normal reference material of pancreas volume was established. Several two-point measurement-based parameters are well correlated to pancreas volume. Pancreas volume decrease with age, but body size and visceral fat, which could be the true explanation behind the gender difference, should be taken into consideration when evaluating pancreas volume.

B-0013 10:55

Quantitative MRI of the pancreas: a feasibility study

N. Vietti Violi¹, T. Hilbert¹, J. Bastiaansen¹, J.-B. Ledoux¹, A. Stemmer², A. Stemmer², R. Meuli¹, T. Kober¹, S. Schmidt Kobbe¹, ¹Lausanne/CH, ²Erlangen/DE (sabine.schmidt@chuv.ch)

Purpose: To show the feasibility of quantitative T2 assessment in the pancreas.

Methods and Materials: T2 mapping of the pancreas was performed using an accelerated multi-echo-spin-echo prototype sequence with respiratory trigger on 10 healthy volunteers. The experiment was repeated with repositioning to study intra-subject variability. Quantitative maps were reconstructed by employing a combination of generalised auto-calibrating partially parallel acquisition (GRAPPA) and model-based accelerated relaxometry by iterative non-linear inversion (MARTINI), dubbed "GRAPPATINI". Two radiologists independently delineated 3 regions of interest inside the head, body and tail of pancreas in each acquisition to measure mean T2 and standard deviation (SD). Inter- and intra-subject comparisons were conducted to estimate the range of normal pancreatic T2 values. Robustness of the method was assessed by evaluating the variation between scan and rescan measurements. In addition, T2 values of each liver lobe were measured to compare the obtained T2 value to existing literature.

Results: The respiratory-triggered accelerated T2-mapping GRAPPATINI sequence was successfully performed on all subjects with a mean acquisition time of 2:48±0:43min. T2 values were similar across all subjects (inter-subject) with low SD (head: 52.8±2.8ms, body: 52.8±4.9ms, tail: 55±3.3ms). An intra-subject comparison showed low variability between the different acquisitions (SD<3.7ms). The measured hepatic T2 values (right lobe: 50.6±4.1ms, left lobe: 50.4±4.1ms) showed good agreement with reported in the literature (51±5.4ms).

Conclusion: The feasibility of free-breathing quantitative T2 measurements with GRAPPATINI at 3T in moving abdominal organs was demonstrated in the example of the pancreas. Furthermore, the obtained T2 values of healthy volunteers exhibited good reproducibility and showed low SD between healthy subjects.

Author Disclosures:

A. Stemmer: Employee; Siemens Healthcare GmbH. T. Kober: Employee; Siemens Healthcare GmbH.

B-0014 11:03

Is MRCP necessary to diagnose pancreas divisum?

N. Bogveradze^{1,2}, P. Mayer², M. Klaus², K. Lashkhi¹, H.-U. Kauczor², T.F. Weber², ¹Tbilisi/GE, ²Heidelberg/DE (bogveradze.nino@gmail.com)

Purpose: To compare the performance of magnetic resonance cholangiopancreatography (MRCP) with non-MRCP T2-weighted magnetic resonance imaging (MRI) sequences for diagnosis of pancreas divisum (PD).

Methods and Materials: Retrospective study of 342 consecutive patients with abdominal MRI including MRCP. MRCP was a coronal respiration navigated T2-weighted sequence with 1.6mm slice thickness. Non-MRCP T2-weighted sequences were (1) a coronal inversion recovery sequence (TIRM) with 6mm slice thickness and (2) a transverse single shot turbo spin echo sequence (HASTE) with 4mm slice thickness. For MRCP, TIRM, and HASTE, presence of PD and assessment of image evaluability were determined in a randomized fashion. A consensus read by two radiologists using MRCP, non-MRCP T2-weighted sequences, and other available imaging served as reference standard for diagnosis of PD. Statistical analysis included performance analysis of MRCP, TIRM, and HASTE and testing for non-inferiority of non-MRCP T2-weighted sequences compared with MRCP.

Results: 33 of 342 patients (9.7%) were diagnosed with PD in the reference standard read. Sensitivity/specificity of MRCP for detecting PD was 81.2%/69.7% (p<0.001). Sensitivity/specificity of TIRM and HASTE was 92.5%/93.9% and 98.1%/97.0%, respectively (p<0.001 each). Grouped sensitivity/specificity of non-MRCP T2-weighted sequences was 99.8%/91.0%. Non-MRCP T2-weighted sequences were non-inferior to MRCP alone for diagnosis of PD. 20.2%, 7.3%, and 2.3% of MRCP, TIRM, and HASTE, respectively, were not evaluable due to motion artifacts or insufficient duct depiction.

Conclusion: Non-MRCP T2-weighted MRI sequences have high performance for diagnosis of PD and are non-inferior to MRCP alone. MRCP may not be necessary for diagnosis of PD.

B-0015 11:11

Predicting the relapse of acute pancreatitis based on radiomics signature of contrast-enhanced computed tomography

Y. Chen, X. Zhang; Nanchong/CN (shaohy.cy@gmail.com)

Purpose: To predict the relapse of acute pancreatitis (AP) by analysing first-time AP based on radiomics signature of contrast-enhanced computed tomography (CECT).

Methods and Materials: The radiomics signature was modeled by a primary cohort consisting of 271 first-time AP patients from January 2010 to June 2015, among whom 124 patients endured recurrent attacks afterwards. Clinical data were gathered from medical records of three tertiary referral centers. The performance of radiomics signature was assessed by an independent cohort containing 118 first-time AP patients including 57 recurrent patients. We adopted resampling as the preprocessing method before 740 radiomic features were extracted from CECT. Repeatability of the radiomic features was evaluated by test-retest reliability. The radiomics signature was performed by logistic regression after dimensionality reduction and feature selection by lasso regression. Decision curve was used to evaluate the performance of radiomics signature, clinical risk factors and the combination of the both.

Results: There were 23 radiomic features remaining after test-retest reliability and lasso regression. The accuracy of radiomics signature to predict the relapse of AP was 83.0%. The AUC of radiomics signature of the validation group was remarkably higher than clinical risk factors (0.909 vs. 0.688, p < 0.001). Decision curve showed the performance of radiomics signature was better than clinical risk factors, and was similar to the combination of both.

Conclusion: Radiomics signature based on CECT performed well to predict the relapse of AP. As a quantitative method, radiomics shows a promising future for recurrent patients to potential precaution.

B-0016 11:19

Use of CT texture analysis as a predictive biomarker of response to neoadjuvant FOLFIRINOX chemotherapy and chemORT in pancreatic ductal adenocarcinoma

K.S. Burk, M. Patino, R. Canellas, M.J. Patel, D.V. Sahani; Boston, MA/US (ksburk@partners.org)

Purpose: To investigate the role of CT texture analysis (CTTA) in assessing histologic response of pancreatic ductal adenocarcinoma (PDAC) to neoadjuvant FOLFIRINOX (folinic acid, 5-FU, irinotecan, oxaliplatin) chemotherapy +/- radiation.

Methods and Materials: In this IRB-approved retrospective study, 39 patients with PDAC treated with neoadjuvant FOLFIRINOX chemotherapy +/- radiation (neoadj) were identified. Post-neoadj CT exams were analysed using the CTTA TexRAD Ltd software. Unfiltered and filtered images were evaluated and heterogeneity was quantified using histogram-based texture parameters: mean, standard deviation (SD), mean positive pixels (MPP), skewness, kurtosis, and entropy. Histologic response was collected from surgical resection pathology reports: response = CAP grade 0-1, no response = CAP grade 2-3. Logistic regression analysis was used to assess for correlation between CTTA features and histologic response.

Results: 17 patients (average age 61.9 yrs) achieved histologic response after neoadjuvant treatment, while 22 (average age 59.4 yrs) did not. Analysis of unfiltered images showed that mean (1.05, p=0.035) and MPP (1.052, p=0.039) correlated with histologic response to treatment. Analysis using five spatial scale filters (SSF) showed a significant correlation between entropy and histologic response, which persisted across all filters: SSF2 7.84, p=0.042; SSF3 8.19, p=0.035; SSF4 8.82, p=0.037; SSF5 9.40, p=0.035; SSF6 8.45, p=0.034. There was no correlation between histologic response and mean, SD, MPP, skewness, or kurtosis using any of the filters.

Conclusion: CTTA, particularly entropy, can be used as a predictive biomarker in PDAC to differentiate patients who achieved histologic response to neoadjuvant FOLFIRINOX chemo +/- radiation from those who did not.

B-0017 11:27

Intravoxel incoherent motion diffusion-weighted MR imaging of solid pancreatic masses: reproducibility and usefulness for characterisation

R. De Robertis¹, N. Cardobi¹, P. Martini Tinazzi¹, R. Grimm², A. Stemmer², M. Zanirato³, G. Tortora⁴, M. D'Onofrio⁴, ¹Peschiera del Garda/IT, ²Erlangen/DE, ³Milan/IT, ⁴Verona/IT (riccardo.derobertis@hotmail.it)

Purpose: To evaluate measurement reproducibility and diagnostic potential of apparent diffusion coefficient (ADC) and intravoxel incoherent motion (IVIM)-derived parameters of solid pancreatic masses including ductal adenocarcinoma (PDAC), neuroendocrine neoplasm (panNEN), mass-forming pancreatitis (MFP), and normal pancreas.

Methods and Materials: 48 patients with pathologically confirmed pancreatic tumours (31 PDACs, 17 panNENs), 4 patients with mass-forming pancreatitis (MFP), and 30 subjects with a normal pancreas were included in this study. All patients underwent 1.5-T MR imaging, including IVIM diffusion-weighted imaging with 11 b values (from 0 to 800 sec/mm²). ADC, true diffusion (D), pseudodiffusion (D*), and perfusion fraction (f) were calculated by placing regions of interest (ROIs) within each lesion and normal pancreas. Intraobserver reliability of the measurements was assessed using the intraclass correlation coefficient (ICC). Kruskal-Wallis H test with pairwise comparisons using Dunn's procedure with a Bonferroni adjustment was used for comparison. The diagnostic performance was evaluated using receiver operating characteristic (ROC) analysis.

Results: Intraobserver agreement was excellent (ICC= .996, .991, .995, .993, and .981 for ROI size, ADC, f, D and D*, respectively). D* and f values of PDACs were significantly lower than those of normal pancreas and panNENs ($P < .05$). For differentiation of PDACs from panNENs, perfusion-related parameters (f and D*) had the highest AUC (.981 and .829) in ROC analysis. No significant differences were found between ADC- and IVIM-derived parameters of MFP and PDACs.

Conclusion: The measurement of ADC- and IVIM-related parameters has excellent reproducibility. Perfusion-related parameters could be helpful in distinguishing PDACs from panNENs.

Author Disclosures:

R. Grimm: Employee; Siemens Healthcare. **A. Stemmer:** Employee; Siemens Healthcare. **M. Zanirato:** Employee; Siemens Healthcare.

B-0018 11:35

MRI follow-up of IPMN: can we limit the use of gadolinium administration?

L. Bertuzzo, G. Zamboni, R. Pozzi Mucelli; Verona/IT

Purpose: To assess the feasibility of using a non-Gadolinium enhanced MRI protocol to follow-up patients with intraductal papillary mucinous neoplasia (IPMN).

Methods and Materials: In this retrospective study, we evaluated 138 patients (48M, 90F, average age 64.5 years) with an initial diagnosis of IPMN without malignant features (128 branch-duct IPMN, 10 combined IPMN) who underwent at least two consecutive MRI/MRCP with Gadolinium in our centre (average follow-up 12.04 months). For each patient one reader evaluated, in separate sessions, in the non-contrast and post-contrast scans: cyst size, walls/septa thickening, mural nodules, dilation of the main pancreatic duct (MPD) and contrast enhancement.

Results: We detected 376 cysts with a mean size of 10.9mm (5-29mm). Patients had a median of 2 cysts each (range 1-20; mean 2.7). The MPD was dilated in 22 patients, with a mean caliber of 4.9mm (4-9mm). At the first examination available, in the non-contrast scans 356 (94.7%) lesions did not show suspicious signs. We detected walls/septa thickening in 4 cysts and endoluminal defects in 16: 15 were classified as debris in relation to their dependent position, 1 as mural nodule. After contrast administration, none of these showed enhancement. At the next follow-up MRI, in the non-contrast scans 360 (95.7%) lesions did not show any changes, 11 (3%) showed a slight increase in size and 5 (1.3%) showed signs of progression. This was confirmed in the post-contrast scans.

Conclusion: At follow-up, non-contrast MRI would have been enough to exclude signs of malignancy in 96.4% patients (98.7% cysts).

B-0019 11:43

Multiparametric PET/MR imaging biomarkers are associated with overall survival in patients with pancreatic cancer

B.-B. Chen, T.T. Shih, Y.-W. Tien, M.-C. Chang, M.-F. Cheng; Taipei/TW (bangbin@gmail.com)

Purpose: To correlate the overall survival (OS) with the imaging biomarkers of dynamic contrast-enhanced magnetic resonance imaging (DCE-MRI), diffusion-weighted imaging (DWI), magnetic resonance spectroscopy, and glucose metabolic activity derived from integrated positron emission tomography (PET)/MRI in patients with pancreatic cancer.

Methods and Materials: This prospective study was approved by the institutional review board and informed consent was obtained from all participants. Sixty-three consecutive patients (mean age, 62.7±12 y; men/women, 40/23) with pancreatic cancer underwent PET/MRI before treatment. The imaging biomarkers were comprised of DCE-MRI parameters (peak, IAUC₆₀, K^{trans}, K_{ep}, V_e), the minimal apparent diffusion coefficient (ADC_{min}), choline level, standard uptake values, metabolic tumour volume, and total lesion glycolysis (TLG) of the tumours. The relationships between these imaging biomarkers with OS were evaluated with the Kaplan-Meier and Cox proportional hazard models.

Results: Seventeen (27%) patients received curative surgery, with the median follow-up duration being 638 days. Univariate analysis showed that patients at a low TNM stage (≤ 3 , $P=0.041$), high peak ($P=0.006$), high ADC_{min} ($P=0.002$) and low TLG ($P=0.01$) had better OS. Moreover, high TLG/peak ratio was associated with poor OS ($P=0.016$). Multivariate analysis indicated that ADC_{min} ($P=0.011$) and TLG/peak ratio ($P=0.006$) were independent predictors of OS after adjustment for age, gender, tumour size, and TNM stage. The TLG/peak ratio was an independent predictor of OS in a subgroup of patient who did not receive curative surgery ($P=0.013$).

Conclusion: The flow-metabolism mismatch reflected by the TLG/peak ratio may better predict OS than other imaging biomarkers from PET/MRI in pancreatic cancer patients.

B-0020 11:51

Tumour heterogeneity of pancreas head cancer assessed by CT texture analysis: association with survival outcomes after curative resection

G. Yun¹, Y. Kim², Y. Lee¹; ¹Seongnam-si/KR, ²Gyeonggi-do/KR (gabinyun@gmail.com)

Purpose: To evaluate the association of texture features of CT images with survival outcomes in patients with pancreas head cancer.

Methods and Materials: From January 2006 to December 2014, 88 patients with pancreas head cancer who underwent preoperative CT and curative resection were included. CT texture features (average, standard deviation, kurtosis, skewness, angular second moment, contrast, correlation and entropy) were obtained without filtration and with various filter values (fine, medium and coarse). After dichotomizing patients into recurrent and non-recurrent groups, clinical, pathological and texture features were compared. Based on the optimal cutoff values from ROC analysis, univariate Kaplan-Meier method and multivariate Cox regression analysis were used for the prediction of disease-free survival (DFS).

Results: The presence of nodal metastasis, texture features of average, contrast, correlation, and standard deviation without filtration and with fine and medium filter values, and average, contrast with coarse filter value showed the significant difference between recurrent (n=70, 79.5%) and non-recurrent group (n=18, 20.5%). In Kaplan Meier analysis, average in all filter values, contrast, correlation, and standard deviation without filtration and with fine and medium filter values showed poorer DFS. In Cox regression analysis, lower average values with homogeneous texture features (lower standard deviation and contrast, and higher correlation) were associated with poorer DFS.

Conclusion: In conclusion, CT texture features of lower average and standard deviation values are associated with poorer outcome after curative resection in pancreas head cancer. Texture features from pre-operative CT may serve as an independent prognostic marker in such patients.

10:30 - 12:00

Room X

Vascular

SS 215

The large vessels of the chest

Moderators:

P.M. Kitrou; Patras/GR
M. Prokop; Nijmegen/NL

B-0021 10:30

Contrast volume reduction for aortic CT angiography using a volume calculator and a spiral flow device: a prospective randomised study

D. Raymakers, W. Coudyzer, S.A. Cornelissen, G. Maleux; Leuven/BE (dominic.raymakers@uzleuven.be)

Purpose: To assess a method for reducing iodised contrast volume in aortic computed tomography angiography (CTA) using a contrast volume calculator and a spiral flow device.

Methods and Materials: Sixty patients undergoing aortic CTA were randomly assigned to four groups. Group 1 received a patient-specific calculated contrast volume based on weight, length and heart rate; group 2 a 20% dilution; and groups 3 and 4 a 50% dilution of the calculated volumes. A spiral flow device was used to mix contrast agent and saline. The first three groups were scanned on a Siemens Somatom Flash and group 4 on a Somatom Force with improved tube voltage modulation. Aortic contrast density was measured and image quality was evaluated using visual grading analysis (VGA).

Results: Mean contrast volumes for groups 1 to 4 were, respectively, 93, 78, 52 and 44 ml. The mean tube voltage was 27% lower in group 4 compared to the other groups ($P < 0.0001$). Contrast densities between groups 1, 2 and 4 were not significantly different ($P > 0.05$). The mean density in group 3 was 42% lower than that in group 1 ($P < 0.001$) and 31% lower than in group 2 ($P < 0.01$). The mean density in group 4 was 52% higher than that in group 3 ($P < 0.001$). The VGA score for group 3 was significantly lower than that for the other groups.

Conclusion: Low patient tailored contrast volumes can yield good image quality in aortic CTA using scan protocols combining contrast dilution up to 50%, a spiral flow device and reduced tube voltage.

B-0022 10:38

Non-contrast MR angiography for aortic monitoring in Marfan patients after aortic root surgery

S. Veldhoen¹, C. Behzadi², A. Lenz², F. Henes², M. Rybczynsky², Y. von Kodolitsch², T.A. Bley¹, G. Adam², P. Bannas², ¹Würzburg/DE, ²Hamburg/DE (veldhoen_s@ukw.de)

Purpose: Contrast-enhanced magnetic resonance angiography (CE-MRA) is the established imaging modality for patients with Marfan syndrome (MFS) requiring annual imaging before and after aortic root replacement. Contrast-free MRA techniques have not been evaluated in the postoperative setup. Purpose of the study was to assess the feasibility of non-contrast steady-state free precession (SSFP) MR imaging for aortic monitoring of postoperative MFS patients.

Methods and Materials: Sixty-four adult patients after aortic root replacement were included. Fourteen patients (22%) had a residual aortic dissection after surgical treatment of type A dissection. SSFP imaging and CE-MRA were performed at 1.5 Tesla. Two radiologists evaluated the images regarding image quality, artefacts and aortic pathologies. Readers measured aortic diameters at defined levels. Statistics included observer agreement for image scoring and diameter measurements and ROC analyses for comparison of diagnostic performance of SSFP and CE-MRA.

Results: Both readers observed no significant differences in image quality for both techniques (all $p > .05$). No significant differences were found regarding the frequency of image artefacts (all $p > .05$). Sensitivity and specificity for detection of aortic dissections was 100% for both readers and techniques. Compared to SSFP imaging, CE-MRA resulted in higher diameters (mean bias, 0.9 mm; $p < .05$). The inter-observer biases of diameter measurements were not significantly different (all $p > .05$), except for the distal graft anastomosis ($p = .001$). Using both techniques, the readers correctly identified a graft suture dehiscence with aneurysm requiring surgery.

Conclusion: Unenhanced SSFP MR imaging allows for riskless aortic monitoring with high diagnostic accuracy in MFS patients after aortic root surgery.

B-0023 10:46

Two novel methods for an objective quantification of iliac artery tortuosity derived from CT-angiography datasets in patients prior to transcatheter aortic valve implantation (TAVI)

F. Braun, T. Hadlich, H. Ruhnke, B. Jehs, C. Thilo, C. Scheurig-Muenkler, T.J. Kroencke, F. Schwarz; Augsburg/DE (franziska.braun@klinikum-augsburg.de)

Purpose: To develop parameters for an objective quantification of iliac-artery-tortuosity on the basis of CT-angiography datasets.

Methods and Materials: 150 patients who had undergone wide-range CT-angiography prior to TAVI were included. In a joint reading-session, a cardiologist and interventional radiologist used Volume-Rendering-Technique-Reconstructions to assign a semiquantitative grade for iliac-artery-tortuosity on a 4-point Likert-scale for each side.

As a precise measure for tortuosity ('Tortuosity-Ratio'=TR), the length of the iliac arteries was measured on Curved-Planar-Reformations for each side and related to the straight distance between the start- and end-point of CPR-segmentations.

A second parameter ('Simplified-Tortuosity-Ratio'=STR) was derived from axial reconstructions only by calculating the ratio between the average distance of the aortic bifurcation and femoral artery from a plane tangential to the iliac spine and the shortest distance of the iliac artery from this plane for each side. ANOVA statistics were applied to test for differences in TR and STR in the four tortuosity-grade subgroups.

Results: The four semiquantitative tortuosity grades were assigned in 42, 174, 48 and 36 vessels ($n=300$). Differences in TR and STR between the four subgroups were highly significant with TR's of 1.08 ± 0.02 , 1.17 ± 0.06 , 1.34 ± 0.09 and 1.49 ± 0.16 and STR's of 1.27 ± 0.08 , 1.33 ± 0.09 , 1.46 ± 0.1 and 1.54 ± 0.13 , respectively, for grade 1-4, all $p < 0.01$. However, TR had significantly higher predictive value for tortuosity grade than STR.

Conclusion: We describe two novel parameters for an objective quantification of iliac-artery-tortuosity which can easily be derived from CT-angiography datasets. We demonstrate high validity of these parameters in comparison with a semiquantitative evaluation by experienced interventionalists.

B-0024 10:54

Image quality and radiation dose sparing of CT angiography for TAVI planning with low-kV, low contrast medium volume and model-based iterative reconstruction compared to standard CTA

L. Riva¹, D. Ippolito¹, C. Talei Franzesi¹, A. de Vito¹, C. Maino¹, C. Cangioti¹, A. Santalco¹, S. Sironi²; ¹Monza/IT, ²Bergamo/IT (lr-doc@hotmail.com)

Purpose: To evaluate image quality and radiation dose exposure of low-kV setting and low contrast medium volume (CM) CTA protocol in patients candidates for TAVI, in comparison with standard CTA protocol.

Methods and Materials: Eighty-nine patients, candidates for TAVI, were prospectively enrolled and examined with 256-MDCT (iCT elite, Philips): 46 patients (study-group) were evaluated using 80kV retrospective ECG-gated protocol, with tube-current modulation and 60mL of CM volume (350mgI/mL); while 43 patients (control-group) underwent a standard CTA retrospective ECG-gated protocol (120kV; automated tube-current modulation; 100mL of CM). Subjective image quality was evaluated using a 4-point-scale (4-excellent, 1-low). Vascular enhancement (HU), SNR and CNR were assessed in each patient with multiple regions of interest (ROIs) in lumen of aorta and iliac-femoral axis at different levels (using the infra-scapular and psoas muscles for CNR). The radiation dose exposure of both groups, in terms of CTDIvol and DLP, was calculated and all data were compared and statistically analysed.

Results: In low-kV protocol significantly higher ($p < 0.01$) mean intravascular attenuation values were achieved in all the measurements compared to the standard protocol (aortic root 367.4HU vs 314HU; external-iliac arteries 390.2HU vs 289HU). Mean DLP of study-group was significantly lower ($524.5 \pm 243.8 \text{ mGy} \cdot \text{cm}$) than in control-group ($2044 \pm 130 \text{ mGy} \cdot \text{cm}$), with an overall radiation dose reduction of about 74.3%, while no significant differences were observed in the image quality evaluation in both groups.

Conclusion: Low-kV with low-CM volume and IMR reconstruction CTA protocol allows to correctly perform TAVI-planning study offering high quality images and significant radiation dose exposure reduction (49%), as compared to standard CTA protocol.

B-0025 11:02

Variability of MRI-derived aortic diameters in Marfan patients: comparison of inner vs outer vessel wall measurements

J.M. Weinrich, M. Avanesov, F. Henes, A. Lenz, G. Adam, P. Bannas; Hamburg/DE (m.avanesov@uke.de)

Purpose: To compare the reliability and validity of inner-inner and outer-outer-edge measurements derived from non-contrast steady-state free precession (SSFP) MRI in Marfan patients.

Methods and Materials: ECG-gated 2D-SSFP at 1.5 T were retrospectively evaluated in 40 patients with Marfan syndrome. Two readers rated the delineation of both inner and outer vessel walls on a three-point Likert scale (excellent-poor) at the sinuses of Valsalva, sinotubular junction, ascending aorta, aortic arch and descending aorta. Both readers independently measured aortic diameters by assessing both inner-inner and outer-outer edge measurements at all levels. Aortic root diameters acquired by echocardiography served as reference. Results were compared using Wilcoxon test, f test, t test, and Bland-Altman analysis.

Results: Image quality and vessel wall delineation was significantly better at all levels for inner vessels walls than for outer vessels walls (all $p < 0.001$). Inter- and intraobserver variances of aortic measurements were significantly smaller for inner-inner measurements at the sinuses of Valsalva, sinotubular junction and ascending aorta (all $p < 0.03$). Echocardiographic measurements at the level of sinus of Valsalva were not significantly different from MRI-derived inner-inner measurements (median and interquartile range: 37 [34-40 vs. 36(32-38) mm; $p = 0.14$], but significantly smaller when compared to MRI-derived outer-outer measurements [43(40-46) vs. 36(32-38) mm; $p < 0.001$].

Conclusion: Non-contrast SSFP results in sharper delineation of inner vessel walls compared to outer vessel walls. Inner vessels wall measurements of the aortic root are more reliable and valid than outer vessel wall measurements. Therefore, we propose to monitor aortic root dimensions in Marfan patients using of inner-inner edge measurements in ECG-gated non-contrast MRI.

B-0026 11:10

Aortomitral calcification is an independent predictor of mortality in TAVR patients

M.J. Willemink, E. Maret, K.J. Moneghetti, J.B. Kim, F. Haddad, Y. Kobayashi, K. Higashigaito, W. Fearon, D. Fleischmann; Stanford, CA/US (m.j.willemink@gmail.com)

Purpose: Aortic valve calcification predicts mortality in patients with aortic stenosis; however, it is just one manifestation of left-sided valvular and annular calcification, which has been associated with systemic atherosclerosis, inflammation and cardiovascular events. We sought to evaluate whether the volume of aortomitral calcifications (AMC) as quantified by CT is an

independent predictor of mortality in patients undergoing transcatheter aortic valve replacement (TAVR).

Methods and Materials: 317 consecutive patients undergoing TAVR between October 2013 and March 2016 were included. All patients underwent pre-procedural CT angiography. AMC-volume was quantified on non-contrast thin-section CT images using commercially available software. Patients were followed for all-cause mortality. Baseline characteristics were evaluated with Mann-Whitney U and Chi-square tests. A multivariable prediction model was derived using Cox proportional hazards regression analysis.

Results: Median follow-up time of 317 patients was 367 (interquartiles 178-678) days. In total 63/317 (19.9%) patients died. AMC volume ($P<0.001$) and the clinically used STS score ($P=0.001$) were significantly different between survivors ($N=254$) and non-survivors ($N=63$). Age and gender showed no significant predictive value in the Cox analyses ($P=0.159$ and 0.163 , respectively), whereas AMC volume (HR 1.06 (1.01-1.10) per cm^3 , $P=0.019$) and STS score >8 (HR 1.89 (1.06-3.37), $P=0.032$) were independently associated with mortality after 18 months. Area under the curve 18 months after TAVR was similar ($P=0.910$) for AMC volume (AUC=0.638 [95%CI 0.575-0.684]) compared to STS score (AUC=0.631 [95%CI 0.582-0.691]).

Conclusion: AMC volume measured by CT is independently associated with mortality in TAVR patients and may, therefore, improve risk stratification after TAVR.

Author Disclosures:

M.J. Willemink: Grant Recipient; Niels Stensen Fellowship. Speaker; Philips Healthcare.

B-0027 11:18

Magnetic resonance assessment of thrombus remodeling after endovascular sealing of abdominal aortic aneurysms using the Nellix endosystem

N. Galea, M. Francone, S. Coco, G. Mancuso, O. Martinelli, C. Belli, I. Carbone, B. Gossetti, C. Catalano; *Rome/IT (nicogale2000@yahoo.it)*

Purpose: Novel endovascular aortic sealing (EVAS) technique with the Nellix endosystem is a valid option for the treatment of infrarenal abdominal aortic aneurysms (AAAs). The positive pressure exerted by the endobags in aneurysmal sac reduces endoleak rate and compacts the thrombus, however the impact on sac remodeling is still unclear. Our aim was to elucidate the changes in aneurysmal sac in patients treated by EVAS for AAAs in terms of morphology and thrombus characteristics using MRI.

Methods and Materials: We consecutively enrolled 10 patients EVAS candidates for AAA. All patients underwent MRI before, 1-week and 1-year after treatment. Specific morphological features of AAA (diameter, proximal neck length, AAA sectional areas, sac volume, endoleak presence and lumen volume) and thrombus characteristics (thrombus volume and maximal thickness, T1 and T2 signal) were determined and compared preprocedural and at follow-up.

Results: No early or late endoleaks were observed in all patients after EVAS. A significant reduction of sac and thrombus volume was observed (mean value: 44.5mL Vs 40.9mL and 7.5mL Vs 3.5mL, respectively, $p:0.01-0.23$), as well as AAA diameter and thrombus thickness did not change significantly at 1-year follow-up after EVAS (48.5mm vs 47.3mm, 12.4 vs 11.3mm, respectively, $p > .05$ for both). Analysis of thrombus MR signal showed a reduction of T1 and T2 values (mean difference: -45% and -30%, respectively, $p:0.01-0.03$) at the 1 year follow-up, likely reflecting tissue organizing and fibrous replacement phenomena.

Conclusion: Filling the endobags inside the aneurysmal sac leads to the progressive reduction of thrombus volume and lowering of T1/T2 values, probably due to thrombus organization and squeezing of fluid content into collateral vessels. EVAS could be associated to an acceleration of thrombus remodeling after AAAs treatment

B-0028 11:26

4D flow analysis of abnormal haemodynamics within saccular aneurysm in contrast to fusiform aneurysm in abdominal aorta

M. Sugiyama¹, Y. Takehara², M. Alley³, N. Unno¹, K. Katahashi¹, T. Wakayama⁴, A. Nozaki⁴, S. Naganawa², H. Sakahara¹; ¹Hamamatsu/JP, ²Nagoya/JP, ³Stanford, CA/US, ⁴Hino/JP (m-sugi@hama-med.ac.jp)

Purpose: Most vascular surgeons believe that saccular aortic aneurysms have more ominous natural history than fusiform aneurysm. Majorities of physiological evidences indicate that the decline of wall shear stress (WSS) produces an expression of pro-atherogenic genes. The purpose of our study is to characterise the abnormal flow dynamics within the saccular aneurysm of the abdominal aorta as compared to the fusiform aneurysm.

Methods and Materials: Ten patients with saccular, thirteen patients with fusiform abdominal aneurysm underwent 3D cine PC MR imaging (4DFlow) covering whole abdominal aorta. The MR imagings were conducted on a 1.5T or a 3.0T MR scanner with torso-array coil. Time resolved contrast-enhanced 3D MR angiography was performed for determination of aortic boundary. The acquired data was post-processed with flow analysis software (flova II, R'Tech, Japan). Streamlines of the abdominal aorta were depicted for streamline

analysis. The peak systolic and diastolic WSS within saccular and fusiform aneurysm was calculated and compared using Mann-Whitney's U-test.

Results: The peak systolic WSS of saccular aneurysm was significantly lower than that of fusiform aneurysm ($p=0.013$). The streamline showed vortex flow within the saccular aneurysm which is isolated from the mainstream of the aorta. This trend was not observed within the fusiform aneurysm. The separated turbulent flow within the saccular aneurysm may be the reason for even lower WSS.

Conclusion: The separated vortex flow within the saccular aneurysm and consequent low WSS of its wall may be reflecting the continuing risk of atherogenic changes of the saccular aortic aneurysm compared to fusiform aneurysm.

Author Disclosures:

T. Wakayama: Employee; GE Healthcare Japan. **A. Nozaki:** Employee; GE Healthcare Japan.

B-0029 11:34

Fully automated segmentation of ascending aorta on phase-contrast cardiac MR images: application in healthy and aneurysmatic patients

M. Codari¹, M. Scarabello², F. Secchi¹, C. Sforza², G. Baselli², F. Sardanelli¹; ¹San Donato Milanese/IT, ²Milan/IT (marina.codari@grupposandonato.it)

Purpose: To develop a fully automated method for segmenting the ascending aorta lumen on 2D+t phase-contrast magnetic resonance (MR) images.

Methods and Materials: We randomly selected, out of a large population dataset, 25 subjects with negative cardiac MR and 9 subjects with diagnosed ascending aorta aneurysm. All exams were performed from September 2008 to October 2013. The local Ethics Committee approved this retrospective study. The ascending aorta was automatically identified on all cardiac cycle phases using a priori knowledge on aortic geometry. The frame maximising the area, eccentricity, and solidity parameters was chosen for unsupervised initialisation. Aortic segmentation was then performed on each frame using active contouring without edges techniques. For each frame the aortic lumen was segmented using the previously segmented frame as initialisation mask. The manual segmentation performed by a highly experienced operator was used as a reference standard. Dice similarity coefficient (DSC), Bland-Altman analysis and Pearson's correlation coefficient were used as performance metrics.

Results: Bland-Altman analysis on healthy subjects showed a bias of -6.68 mm^2 , a coefficient of repeatability of 91.22 mm^2 , an average measurement of 581.40 mm^2 , and a corresponding reproducibility of 85%; on aneurysmatic patients, -3.09 mm^2 , 159.64 mm^2 , 1741.42 mm^2 , and 91%, respectively. High correlation coefficients as well as DSC values (mean \pm standard deviation) were recorded in both healthy ($R=0.98$; 94.6 \pm 2.1%) and aneurysmatic ($R=0.99$; 96.4 \pm 1.9%) dataset.

Conclusion: A fully automated and robust method for ascending aorta segmentation on both healthy and pathological phase-contrast MR images was developed. Further studies on larger samples are warranted.

B-0030 11:42

MR angiography in small animals using hyperpolarised water

S. Fischer¹, R. Maeder¹, V. Denysenkov¹, M. Terekhov², S. Zangos¹, T. Priser¹, T.J. Vogl¹; ¹Frankfurt a. Main/DE, ²Würzburg/DE (sebastian.fischer@kgu.de)

Purpose: Gadolinium based contrast agents are associated with the risk of allergic reactions, systemic nephrogenic fibrosis and potential remnants in the brain. Purpose is to examine dynamic nuclear polarisation (DNP) as an alternative method for MR angiography.

Methods and Materials: Liquid-state Overhauser DNP achieves hyperpolarisation by microwave irradiation of electron spins in TEMPOL radicals, which are coupled with the nuclear spins of water molecules. Our setup comprises a 42GHz microwave source and an 1.5T in-bore polariser, equipped with a multimode resonator. Continuously hyperpolarised water was administered with 1.2ml/min into the aorta of five C57BL/6 mice via catheterisation (0.15mm ID) of iliac vessels. The aorta and its branches were visualised with GRE-sequences (TR 110s, TE 3.8s, FoV 78x58x2mm, Matrix 256x192px) and intravascular DNP signal intensities, SNR and CNR values were measured and compared to its native values.

Results: Hyperpolarised water features high T1 signal enhancements in MR imaging and a short relaxation time. Maximum intravascular signal intensities were increased 4.3-fold from 231 \pm 47 to 994 \pm 194. Thus better SNR and CNR values were measured for hyperpolarised vessels with an SNR increased 5.3-fold from 24 \pm 2 to 126 \pm 62 and CNR increased 26.3-fold from 3 \pm 2 to 79 \pm 49.

Conclusion: The strong enhancement and its high CNR made a visualisation of the aorta and its branches possible in mice - even using a standard clinical 1.5T scanner. Thus hyperpolarised water might be a promising future alternative to Gadolinium based contrast agents in MR angiographies without risking the potential adverse effects or intracorporeal remnants of Gadolinium based contrast agents.

Author Disclosures:

S. Fischer: Grant Recipient; Deutsche Forschungsgemeinschaft. **S. Zangos:**

Grant Recipient; Deutsche Forschungsgemeinschaft. **T. Prisner:** Grant Recipient; Deutsche Forschungsgemeinschaft. **T.J. Vogl:** Grant Recipient; Deutsche Forschungsgemeinschaft.

B-0031 11:50

Low-dose CT angiography for thoracic aorta: optimal combination between 80kV and last generation iterative reconstruction algorithm levels

A.D. Annoni, A. Formenti, D. Andreini, M. Guglielmo, G. Muscogiuri, G. Pontone, E. Consiglio, E. Conte, M. Pepi; Milan/IT (andrea.annoni@cfrm.it)

Purpose: To evaluate feasibility and optimization of a low dose CT protocol for thoracic aorta by investigating the best combination of last generation iterative algorithm level and use of 80 kV in comparison with 50% level suggested for standard 100 kV protocols.

Methods and Materials: We enrolled 60 pts scheduled for thoracic aorta CT angiography (48 men) with BMI up to 37 kg/m² (mean 26.3±4.9 kg/m²). All CT examinations were performed with axial ECG-gated acquisition with new generation wide array CT scanner using 80kV, mA modulated on patient's BMI and 50 ml of contrast agent. Aortic values, noise, signal to noise and contrast noise - ratios were evaluated at different aortic locations for FBP images and for images reconstructed at different percentages of adaptive statistical iterative reconstruction algorithm - V (ASIR V) (20%, 40%, 50%, 60%, 80%, 100%). All exams were evaluated for subjective image quality by two independent readers.

Results: No exams were classified as not diagnostic. Overall mean aortic attenuation for all aortic segments was over 600 HU. The best balance between image quality (subjective and objective) and ASIR-V level was found at 60% in the overall population and at 80% in a subgroup of patients with BMI≥30 kg/m². The K coefficient for interobserver agreement was 0.87. Mean effective dose was 0.98±0.26 mSv.

Conclusion: Scanning protocol for CTA of the thoracic aorta using wide detector coverage, 80 kV and ASIR-V allow good balance between dose reduction and image quality also in patients with high BMI.

Author Disclosures:

A.D. Annoni: Speaker; GE healthcare. D. Andreini: Speaker; GE healthcare. G. Pontone: Board Member; ESCR, SCCT. Speaker; GE healthcare, MEDTRONIC, BRACCO.

10:30 - 12:00

Room Z

Interventional Radiology

SS 209

Gastrointestinal interventions

Moderators:

D. Penha; Lisbon/PT
J. Tacke; Passau/DE

B-0032 10:30

Percutaneous treatment of postoperative benign hepaticojunostomy strictures: temporary placement of covered metallic stents versus balloon dilation

G. Yun, C. Yoon, N. Seong, J. Byeon, H. Lee, Y. Kim; Seongnam/KR (gabinyun@gmail.com)

Purpose: To compare percutaneous temporary placement of covered metallic stent with balloon dilatation for the treatment of postoperative benign hepaticojunostomy strictures.

Methods and Materials: From November 2004 to August 2017, 56 patients with postoperative benign hepaticojunostomy strictures underwent percutaneous transhepatic treatments. A covered stent designed for spontaneous migration after temporary indwelling was placed in 23 patients (stent group). Balloon dilation was performed in multiple sessions to achieve <30% residual stricture in 33 patients (balloon group). The technical success, complications, the indwelling duration of percutaneous transhepatic biliary drainage (PTBD), and patency rates were compared between the two groups.

Results: The technical success was achieved in all patients of stent group and 96.8% (32/33) of balloon group after 1-6 sessions of dilation. There was no major complication in both groups. All covered stents spontaneously migrated into jejunum and passed out through the anus 2-12 months after placement (median 5 months). The indwelling duration of PTBD was shorter in stent group (median 9 vs 33 days; $p=0.01$). Recurrent strictures requiring re-intervention occurred more frequently in balloon group (51.5% vs 8.7%; $p=0.01$). The 1- and 2-year primary patency rates were 95.0% and 89.1% in stent group and 74.2% and 49.8% in balloon group, respectively ($p=0.032$).

Conclusion: In patients with postoperative benign hepaticojunostomy stricture, percutaneous temporary placement of a covered stent provides longer patency and shorter PTBD indwelling compared with balloon dilatation.

A covered stent designed for temporary placement seems to be a feasible strategy to prevent stent-related complications in postoperative benign biliary strictures.

B-0033 10:38

Preliminary experience of TIPS creation using the new controlled expansion e-PTFE covered stent

R. Miraglia, L. Maruzzelli, I. Petridis, G. Marrone, A. Luca; Palermo/IT (gmarrone@ismett.edu)

Purpose: To prospectively evaluate short-term outcome of TIPS creation using the new controlled-expansion e-PTFE covered stent (CES), in adult patients with portal hypertension complications.

Methods and Materials: Between 7/2016 and 9/2017, 45 consecutive patients received TIPS using CES. 38/45 patients have a follow up longer than 3 months and represent our study group. Clinical data were obtained at baseline, 4 and 12 weeks after the TIPS.

Results: TIPS indications were: refractory ascites (n=29), variceal bleeding (n=5), other (n=4). Mean age 60.5 yrs (±10.38), mean follow-up 4.0 months (±3.18). 16 patients had partial/subtotal portal vein thrombosis. In 37 patients TIPS was dilated to 8 mm of diameter with a significant reduction of the portocaval pressure gradient (PPG) (≤ 10 mmHg). In 1 patient, not reaching the haemodynamic target, the stent was dilated to 10 mm of diameter during the same session. Mean PPG pre-TIPS was 16.05 mmHg (±4.82), post-TIPS was 6.61 mmHg (±2.79). Grade I-II encephalopathy was registered in 10 patients (26%). Portal vein thrombosis partially/completely resolved in 13/16 patients. No recurrence of bleeding episodes were registered. Disappearance of ascites was observed in 22 cases (75.86%). In 2 patients with ascites persistence the stent was dilated to 10 mm in a further procedure. 4 patients died because of septic episodes (not related to TIPS, 2 to 7 months after TIPS).

Conclusion: CES for TIPS creation can be safely used in patients with severe portal hypertension and seems to be associated with a good short-term outcome.

B-0034 10:46

Outcomes of transjugular intrahepatic portosystemic shunt using 12-mm-diameter stent for portal hypertension with refractory ascites

A.M.K. Abdel Aal^{1,2}, K. Mahmoud¹, S. Kim¹, B. Heeke¹, S. Moawad¹, M. Massoud¹, S. Saddekni¹, N. A. Aboueldahab¹, A. Gunn¹; ¹Birmingham, AL/US, ²Cairo/EG (akamel@uabmc.edu)

Purpose: The objective of this study is to evaluate the efficacy, complications and survival outcomes of transjugular intrahepatic portosystemic shunt (TIPS) creation performed using a 12-mm-diameter stents (Viatorr, Gore) in patients with refractory ascites.

Methods and Materials: We retrospectively reviewed the medical records of 187 patients who underwent TIPS from January 2004 to January 2017, using 12-mm Viatorr stents for refractory ascites. Patients' demographics, comorbidities, need for paracentesis, model for end-stage liver disease (MELD) score, and incidence or worsening of hepatic encephalopathy (HE). Survival outcomes were also calculated.

Results: The study included 115 (61.5%) males with a mean age of 57.1 years (SD=9.2 years). The mean Charlson comorbidity index was 3.9 (SD= 1.1). The mean portosystemic gradient significantly decreased from 15.79 to 4.98 after TIPS ($p<0.0001$). Ascites was resolved at 3, 6 and 12 months after TIPS in 59.5%, 69.8% and 81.7% of the patients, respectively. Freedom from paracentesis was seen in 93.3% of the patients at 12 months after TIPS. Mean MELD score increased significantly after TIPS from 13.2 to 16.9 ($p<0.0001$). HE was seen in 6.5% and 38.2% before and 3 months after TIPS, respectively, with 17.5% of the patients medically uncontrolled. The overall survival at 3, 6, 12 and 60 months was 79.2%, 73.5%, 66.3% and 46.5%, respectively.

Conclusion: The 12-mm-diameter Viatorr stent used for TIPS in patients with refractory ascites appears more efficacious and without increased complication rate compared to published literature on the 8- and 10-mm-diameter similar stents.

B-0035 10:54

Non-invasive pressure monitoring after transjugular intrahepatic portosystemic shunt implantation with integrated sensors

C. Spink¹, B. John¹, D. Schröder¹, W. Krautschneider¹, R. Fischbach², M. Braunschweig², J.-H. Buhk¹, G. Adam¹, A. Koops¹; ¹Hamburg/DE, ²Dresden/DE (c.spink@uke.de)

Purpose: In vitro and ex vivo testing of a novel stent-graft with integrated pressure sensors capable of wireless digital data transmission for non-invasive pressure monitoring after TIPS.

Methods and Materials: Ten stent-grafts for TIPS-implantation (100x10 mm) were designed including integrated pressure sensors at both ends within layers of polytetrafluorethylen (PTFE). Digital data conversion was performed by integrated microcontrollers within the PTFE-membrane providing energy and data transfer by inductive coupling. The stent-grafts were placed in a silicone

liver phantom and in four explanted porcine livers via 16F applicators for intraluminal air pressure measurement.

Results: First in vitro and ex vivo testing demonstrated a capable TIPS stent-graft design with integrated sensors in a stable PTFE-covering after crimping and application into a liver phantom and the explanted porcine livers. In both setups measurements were simultaneously taken from both sensors with an accuracy of ± 1.2 mmHg up to a distance of 10.2 ± 0.9 cm in a liver phantom and a distance of 8.3 ± 0.5 cm in the porcine livers. The minimum power input for successful data transfer had to be increased from 10 ± 1 W in the liver phantom and to 18 ± 2 W in the porcine livers. There was no significant difference in intraluminal air pressure measured at both setups ($p=0.46$).

Conclusion: First in vitro and ex vivo results demonstrate a successful approach for non-invasive pressure monitoring after TIPS implantation using integrated sensors. Further in vivo tests are scheduled before the potential implementation into a product.

B-0036 11:02

Risk factors of survival after TIPS using ePTFE covered stentgrafts in refractory ascites

M. Pitton, M. Moddemann, T. Zimmermann, S. Schotten, P. Galle, C. Düber; Mainz/DE (michael.pitton@unimedizin-mainz.de)

Purpose: To analyse the risk factors of overall survival TIPS with ePTFE-stentgrafts in patients with liver cirrhosis and refractory ascites.

Methods and Materials: 213 patients with liver cirrhosis and refractory ascites (129 male, 84 female) were treated with ePTFE covered TIPS. Patients with portal vein thrombosis, acute and subacute bleeding with need for treatment, and Budd-Chiari-syndrome were excluded from analysis. Overall survival was analysed depending on 1. the baseline clinical characteristics before TIPS (age, sex, etiology of cirrhosis, additional diagnoses, former history of variceal bleeding, former endoscopic ligation (EBL), Child-Pugh-stage, number of paracentesis needed, history of SBP or hepatic encephalopathy (HE), hemodialysis, INR, Bilirubin, Albumin, Creatinin), 2. procedural complications during TIPS, and 3. hemodynamic outcome (portosystemic pressure gradient, PSG) after TIPS, and hemodialysis within 4 weeks after TIPS.

Results: Overall survival was 49.4 ± 4.7 months. Technical success was 100%, with 97.2% primary success rate. 3d-mortality was 0.9%, 30d-mortality 8.0%. The reintervention rate was 26.8% (25.8% dilatation/re canalisation, 8.9% TIPS reduction during follow-up). Significant risk factors for survival were age > 70y, male gender, etiology (hepatitis vs. alcoholic), additional diagnosis (cardiac diseases and others), creatinin, bilirubin > 2mg/dl, Child-C-stage, and need for hemodialysis within 4 weeks after TIPS. Prior history of bleeding, EBL, SBP, HE, and hemodialysis before TIPS were not significant. Procedural complications, and PSG after TIPS, was also not statistically significant.

Conclusion: Survival after TIPS depends on clinical baseline characteristics. Beside clinical measures of liver function and etiology of liver disease, independent co-factors like additional diagnoses and personal characteristics should be realised.

B-0037 11:10

VesOpen procedure: the new percutaneous image-guided treatment option of HCC-induced portal vein thrombosis

M. Mizandari^{1,1}, T. Azrumelashvili¹, N. Habib²; ¹Tbilisi/GE, ²London/UK (mgmizandari@gmail.com)

Purpose: The novel technique of PV malignant thrombus recanalisation is presented.

Methods and Materials: 18 patients underwent percutaneous endoport RF treatment attempt. PV tributary is accessed under US guidance; manipulation by 5 Fr diameter guiding catheter is used to conduct the guidewire across the blocked segment and portography is performed. 15 Watts power was applied for 2 minutes using bipolar endoluminal RF device (Habib™ EndoHPB, EMcision Ltd., London, UK), placed in PV-blocked segment according the guidewire. The number of RF application sessions depends on tumour thrombus extent as shown on portography. After RF application, self-expanding 14-mm-diameter vascular stent is positioned and PV patency restoration is documented by final portography. Procedure is completed by procedure track RF ablation and/or coil embolisation.

Results: The procedure was completed in 13 (72.2%) cases; in 3 (16.7%) cases we could not conduct the wire across the thrombus; in 2 (1.1%) cases we failed to conduct the RF device and procedure was completed by stenting. Portal vein obstructed segment showed the restored blood flow in all completed cases as documented by postprocedure portography, follow-up Doppler and CT studies; this resulted in liver function improvement in 8 (61.5%) of procedure technical success cases. Recanalised PV patency varied from 3 weeks to 22 months; in 4 cases patients underwent successful TACE procedure after PV recanalisation.

Conclusion: PV thrombus percutaneous recanalisation by endoport RFA with subsequent stenting is an effective technique and should be suggested as a possible treatment option for HCC patients with PVT.

B-0038 11:18

Percutaneous treatment of biliary lithiasis: personal experience

S. Zanardi, A. Cappelli, C. Mosconi, M. Renzulli, F. Modestino, R. Golfieri; Bologna/IT (sara.zanardi10@gmail.com)

Purpose: to determine the efficacy of percutaneous procedures to remove intrahepatic bile duct stones and to treat underlying biliary strictures (BSs).

Methods and Materials: we retrospectively analysed the outcome of 91 patients with intrahepatic lithiasis percutaneously treated. Patients were divided into two groups: Group A (n= 50) and Group B (n= 41), without or with intrahepatic stenosis respectively. We also divided patients according to the etiology of the lithiasis. Stones removal was facilitated with an occlusion balloon after sphincteroplasty and mechanical fragmentation.

Results: 1-year-primary patency was 76% and 51.2% [Group A and B respectively ($p= 0.014$)]; 2-year-primary patency was 72% and 39.1 [Group A and B respectively ($p= 0.001$)]. Secondary patency was 84% (Group A) and 63.4% (Group B) ($p= 0.025$). We found a statistically significant difference in the outcome of patients with or without intrahepatic stenosis and a significantly lower success rate in patients with chronic diseases [Caroli's disease and primary sclerosing cholangitis (PSC)]. Patients with post-operative anastomotic strictures tend to recur in the 21.9% at 1 year and 28.1% at 2 years.

Conclusion: percutaneous anterograde biliary stones removal and stenosis treatment resulted effective procedures with an high success rate and low complications. The procedure is a technically feasible approach when endoscopic stones removal failed. The presence of stenosis or underlying chronic diseases affect the clinical and the radiological outcome.

B-0039 11:26

Parenchymal blood volume (PBV) measurement using C-arm-Dyna-CT as a prognostic marker for the response of HCC after repetitive transarterial chemoembolisation (TACE)

T.J. Vogl, K. Graef, L. Alizadeh, R. Hammerstingl, N.-E. Nour Eldin; Frankfurt a. Main/DE (t.vogl@em.uni-frankfurt.de)

Purpose: To evaluate the prognostic value of intraprocedural parenchymal blood volume (PBV) parameters using C-arm-CT for the response in hepatocellular carcinoma (HCC) after transarterial chemoembolization (TACE).

Methods and Materials: 80 patients with HCC underwent at least 2 sessions of TACE. On average the patients had four PBV measurements in 4-6-week intervals. C-arm-CT scan was created with a rotation speed of 2cm. The images were post-processed and reconstructed at a workstation to build a PBV map. Then they were overlapped with MRI to measure tumour diameter and PBV.

Results: Results demonstrate significant correlations between PBV alteration and downsizing of HCC nodules. Initial blood volume of patients was $x=111.39$ ml/1000ml (SD=66.88) with an average size of HCC lesions of 54.24mm. After first TACE, blood volume decreased on average to 69.84ml/1000ml (SD=47.29) and lesions were reduced to 49.14 mm in diameter. After repeated TACE average blood volume decreased to 73.03ml/1000ml (SD=47.82) showing a significant reduction of the lesion to 48.85cm in diameter documented in MRI. In the course of the study a considerable reduction in volume (-34.44%) and diameter (-9.94%) was documented. In patients with initial PBV > 100ml/1000ml lesions decreased 10.27% in size and 52.78% in blood volume, in patients with a PBV of 50-100ml/1000ml lesions decreased 6.88% in size and increased 5.70% in blood volume, in patients with < 50ml/1000ml lesions decreased 8.48% in size and increased 57.54% in blood volume.

Conclusion: PBV measurements can determine TACE effectiveness as patients with high initial PBV respond better to TACE regarding diameter and volume reduction.

B-0040 11:34

Image-guided percutaneous drainage of pancreatic duct: what for and how

M. Mizandari^{1,1}, T. Azrumelashvili¹, N. Habib²; ¹Tbilisi/GE, ²London/UK (mgmizandari@gmail.com)

Purpose: To present the percutaneous image-guided pancreatic duct (PD) drainage.

Methods and Materials: 45 patients underwent PD percutaneous image-guided drainage. In 44 of them, the indication was PD obstruction-related clinical symptoms (pancreatic irritation, recently revealed diabetes); in one case of pancreatic fistula non-dilated PD was drained. PD drainage was performed under combined image guidance - US and fluoroscopy (23) or CT and fluoroscopy (22 cases). After US or CT-guided PD puncture using 22 to 18G needles, drainage catheter was placed under the real-time fluoroscopy guidance over the wire.

Results: Drainage was successful in all cases including the case of non-dilated PD in post-biopsy pancreatic fistula. Clinical improvement was documented, pancreatic fluid discharge varied between 300 and 900 ml/day.

Five patients with recent onset of diabetes showed a dramatic improvement in glycaemic control.

Conclusion: The percutaneous PD drainage appears to be a safe and effective procedure and should be considered in patients with obstructed PD, especially in cases of failed endoscopic retrograde cannulation or where impracticable.

B-0041 11:42

Fluoroscopy-guided percutaneous interventions via pancreatic duct percutaneous drainage track for diagnosis and treatment: feasibility and technique

M. Mizandari¹, T. Azrumelashvili¹, N. Habib², ¹Tbilisi/GE, ²London/UK (mgmizandari@gmail.com)

Purpose: To present the percutaneous procedures, which might be performed after pancreatic duct (PD) percutaneous drainage.

Methods and Materials: 21 patients underwent percutaneous image-guided procedures using PD drainage track; among them - endoluminal RFA with subsequent stenting - 9, balloon-assisted percutaneous descending litholapaxy (BAPDL) - 6, endoluminal biopsy - 3, balloon dilatation - 2, stenting - 1. The obligatory first step of all procedures was the wire conduction into the duodenum performed using 5 Fr diameter advantage catheter. RFA was performed by 5 Fr diameter novel bipolar RF device (15 watts of energy applied for 2 minutes), positioned in the strictured segment over the wire; BAPDL was performed applying the pushing-down efforts by partially inflated balloon after papilla dilatation. Endoluminal biopsy was performed by endobiliary forceps biopsy set. Balloon dilatation and stenting was performed using conventional technique.

Results: In 18 (85.7%) of 21 cases the procedures were completed, achieving either PD patency restoration or adequate tissue sample obtaining; in 3 (14.3%) cases (all pancreatic head cancers) the procedure completion was impossible due to failure of guidewire conduction across the strictured segment of PD. All patients tolerated the procedure well, there was no 30-day or hospital mortality; no technique-specific complications were observed.

Conclusion: Percutaneous fluoroscopy-guided percutaneous diagnostic and treatment procedures via pancreatic duct percutaneous drainage track are safe and effective; this procedure should be routinely suggested as treatment options for selected patients.

B-0042 11:50

Interstitial transpedal MR lymphangiography in pre-interventional work-up for lymphatic interventions in patients with chylous effusions

C.C. Pieper, H. Schild; Bonn/DE (Claus.Christian.Pieper@ukb.uni-bonn.de)

Purpose: To evaluate the clinical usefulness of transpedal MR lymphangiography (tMRL) for pre-interventional work-up for lymphatic interventions in patients with chylous effusions.

Methods and Materials: tMRL was performed in 25 patients (m/f: 13/12, mean age 54 years) with chylous effusions scheduled for lymphatic intervention. Indications were: traumatic/iatrogenic chylothorax n=6, non-traumatic chylothorax n=8, traumatic/iatrogenic chyle ascites n=3, non-traumatic chyle ascites n=3, combined chylothorax/chyle ascites n=5. Patients underwent tMRL at 1.5T with T1-weighted imaging after pedal/interdigital injection of gadolinium contrast-medium under local anaesthesia. Contrast-enhanced images were evaluated regarding depiction of leakage, a possible access site for lymph-vessel-embolisation and anatomical variations.

Results: Contrast injection was well tolerated in all patients without complications. Sedation was necessary in one case. In 20/25 patients enhancing central lymphatics were detectable (cause of failure: restlessness despite sedation n=1, lymphoma with lymphoedema n=1, technical reasons n=3). Leakage was identified in 13/20 patients. In 5 patients with chyle ascites, contrast medium leaked intraabdominally and did not reach the cisterna chyli. In the remaining 15 patients (thoracic/cervical pathologies) a possible access site for thoracic-duct embolisation was identified in 14/15 patients (cisterna chyli in 12/15, thoracic-duct (TD) in 14/15). 8/14 patients had a single TD and 6/14 a duplicated TD. In one patient, the TD terminated in the right venous angle. Overall 20/25 tMRL exams provided useful information to guide interventions.

Conclusion: Transpedal MR lymphangiography is a new and valuable diagnostic tool in patients with chylous effusions scheduled for lymphatic interventions, providing information on the anatomy of central lymphatics. The leakage site, however, cannot be identified in all cases.

10:30 - 12:00

Room O

Chest

SS 204

COPD and infiltrative lung diseases

Moderators:

P.A. Grenier; Paris/FR
C. Romei; Pisa/IT

B-0043 10:30

Inspiratory/expiratory xenon-enhanced area-detector CT (ADCT): capability for pulmonary functional loss and clinical stage evaluations in smokers

Y. Ohno¹, Y. Fujisawa², Y. Kishida¹, S. Seki¹, N. Sugihara², T. Yoshikawa¹; ¹Kobe/JP, ²Otawara/JP (yosirad@kobe-u.ac.jp)

Purpose: To evaluate the capability of inspiratory/expiratory xenon (Xe)-enhanced area-detector CT (ADCT) for pulmonary functional loss and clinical stage evaluations in smokers.

Methods and Materials: Forty consecutive smokers prospectively underwent inspiratory/expiratory xenon-enhanced ADCT as well as pulmonary function tests. Then, all smokers were classified by GOLD classification-based pulmonary function test results. Each CT data were transferred to our proprietary software to generate Xe wash-in (WI), wash-in/wash-out (=WI/WO) ratio and ventilation (=WI-WO/WI) ratio maps between inspiratory/expiratory CT scans. According to the previous study, each pixel within the lung was divided into three lesion groups as follows: normal lung, functional small airway disease (FSAD) and emphysema. To determine regional ventilation differences, each Xe ventilation index was compared between three groups by Tukey's HSD test. To evaluate the capability for pulmonary function loss assessment, step-wise regression analyses were performed among all Xe ventilation indexes and pulmonary function test results such as %FEV₁ and FEV₁/FVC%. Finally, discrimination analysis was performed to determine the concordance capability for GOLD stage classification was also determined.

Results: WI and ventilation ratio had significant difference among three lesion groups (p<0.05) and WI/WO ratio of emphysema had significant difference with that of others (p<0.05). %FEV₁ (r²=0.71, p<0.05) and FEV₁/FVC% (r²=0.71, p<0.05) were significantly affected by ventilation ratio as 1st step and WI as 2nd step. With all Xe ventilation indexes, the concordance capability for GOLD classification was determined as 85.0 (32/40)%.

Conclusion: Inspiratory/expiratory xenon-enhanced ADCT was useful for pulmonary functional loss and clinical stage evaluations in smokers.

Author Disclosures:

Y. Ohno: Research/Grant Support; Toshiba Medical Systems Corporation.
Y. Fujisawa: Employee; Toshiba Medical Systems Corporation. S. Seki: Research/Grant Support; Toshiba Medical Systems Corporation. N. Sugihara: Employee; Toshiba Medical Systems Corporation. T. Yoshikawa: Research/Grant Support; Toshiba Medical Systems Corporation.

B-0044 10:38

A meta-analysis of a UIP pattern on CT: is surgical lung biopsy necessary in patients with a possible UIP pattern?

H. Kim, S.H. Yoon, H. Hong, S. Hahn, J.M. Goo; Seoul/KR (heekyung0363@gmail.com)

Purpose: With the recent introduction of anti-fibrotic agents for idiopathic pulmonary fibrosis (IPF) treatment, accurate diagnosis of IPF has become more important. According to the ATS/ERS/JRS/ALAT statement in 2011, surgical lung biopsy is required to make a diagnosis of IPF for patients with a possible usual interstitial pneumonia (UIP) pattern on HRCT, while not required for those with UIP pattern. We performed a meta-analysis of whether the surgical lung biopsy is essential for IPF diagnosis with the possible UIP pattern.

Methods and Materials: We performed literature searches of the MEDLINE and EMBASE databases and included studies which conducted a radiologic-pathologic evaluation of IPF according to the 2011 guidelines. Outcomes were pooled using a random-effects model.

Results: Twelve studies were included. Pooled proportions of IPF were 99% (95%CI, 93% to 100%; I²=51.7%) for a UIP pattern and 94% (95%CI, 87% to 99%; I²=82.9%) for a possible UIP pattern. The proportion of IPF for an inconsistent UIP pattern was substantially heterogeneous ranging from 0% to 100% (median, 49%). Pooled percentage difference in proportions of IPF between UIP and possible UIP patterns was -1% (95%CI, -4% to 1 %; I²=0.0%). Proportions of IPF in possible and inconsistent UIP patterns were correlated with the prevalence of IPF (Spearman correlation coefficient, 0.605[95%CI, 0.055-0.860] for possible UIP; 0.769 [95%CI, 0.319-0.928] for inconsistent UIP).

Conclusion: Proportions of IPF diagnosis when biopsied were comparable between UIP and possible UIP pattern, indicating that IPF diagnosis can be made with a possible UIP pattern without biopsy as a UIP pattern.

B-0045 10:46

Follow-up of idiopathic pulmonary fibrosis: computed tomography vs functional metrics

G. Milanese^{1,2}, M. Silva¹, V. Seletti¹, C. Galeone², B. Bartholmai³, S. Palmucci⁴, S. Piciucchi⁵, R. Karwoski³, N. Sverzellati¹; ¹Parma/IT, ²Milan/IT, ³Rochester, MN/US, ⁴Catania/IT, ⁵Forlì/IT (gianluca.milanese@studenti.unipr.it)

Purpose: To test the prognostic value of HRCT with either visual or quantitative analysis in both short-term and long-term follow-up of idiopathic pulmonary fibrosis (IPF), and to compare it with pulmonary function test (PFT).

Methods and Materials: Consecutive patients with a multidisciplinary diagnosis of IPF were retrospectively selected from two referral hospitals. Selection criteria included: availability of baseline, 8-12 months, and 18-30 months volumetric HRCT (hereafter HRCT0, HRCT1, HRCT2, respectively); absence of exacerbation within the defined follow-up period. Visual score was performed by two radiologists for the total extent of interstitial lung disease (ILD) and its individual patterns; nominal category of longitudinal disease behavior was defined as follows: improvement, stability, or progression. Quantitative analysis included global histogram descriptors of lung density (mean density, skewness, kurtosis) and textural analysis (CALIPER). Prognostic value of both visual and quantitative measures and their deltas were evaluated by adjusted stepwise multivariate analysis, at HRCT0, HRCT1, and HRCT2. The reference standard for pulmonary function trend was defined by decline in forced vital capacity (FVC), as per official guidelines.

Results: Fifty-eight consecutive patients were followed for 43.8 months. At HRCT1, either a relative increase in ILD extent greater than 20% with CALIPER or visual categorical assessment of disease behavior improved the prognostic value of FVC decline >10% (HR 38.8; 95%CI:6.82-232.2). Likewise, combining either PVRV changes or visual categorical assessment of disease behavior at HRCT2 increased the prognostic value of the HRCT0-HRCT2 FVC trend (HR 10.96; 95%CI:2.31-51.99).

Conclusion: HRCT changes by visual or textural analysis can be added with benefit to the current spirometric reference standard to improve prediction of mortality in IPF. Annual combined HRCT-functional changes showed the greatest prognostic value.

Author Disclosures:

M. Silva: Grant Recipient; ESTI 2016 Experienced Chest Radiology Researchers Grant.

B-0046 10:54

Chest HRCT findings in adult patients with different subtypes of humoral primary immunodeficiencies and correlation with lung function test results

L. Cereser, F. Greco, E. Zanelli, P. D'Angelo, M. De Carli, C. Zuiani, R. Girometti; Udine/IT (elisazanelli@hotmail.it)

Purpose: To assess HRCT findings in different subtypes of patients with humoral primary immunodeficiencies (h-PIDs), and whether they predict pulmonary function test (PFT) results.

Methods and Materials: We retrospectively identified fifty-two consecutive adult patients with h-PIDs who performed HRCT (64-row multidetector equipment) and PFT at the time of diagnosis. On a per-patient basis, one experienced radiologist recorded airway (bronchiectasis, airway wall thickening, mucus plugging, tree-in-bud and air-trapping) and parenchymal-Interstitial abnormalities (consolidations, ground-glass opacities, septal thickening/linear opacities, parenchymal nodules and bullae/cysts) on HRCT. We used the chi-square test to compare the prevalence of each of the above abnormalities between different subtypes of h-PIDs included in the study. On the overall population, we also performed logistic regression analysis to assess whether HRCT findings predicted either obstructive or restrictive PFT results (absent-to-mild vs moderate-to-severe).

Results: Patients showed common variable immunodeficiency (CVID) in 38/52 cases, and CVID-like condition in 14/52 cases (11 IgG subclass deficiencies + 3 selective IgA deficiencies), respectively. We observed no significant difference in the prevalence of airway or parenchymal-Interstitial HRCT abnormalities between CVID and CVID-like patients ($p > 0.05$), with bronchial wall thickening being the most frequent finding in both groups (71%). On multivariate analysis, tree-in-bud and septal thickening-linear opacities were found as independent predictors ($p < 0.05$) of significant obstructive defect (OR, 18.75%) and restrictive defect (OR, 13.95%), respectively.

Conclusion: There was no significant difference in HRCT findings between h-PIDs subtypes. Tree-in-bud and septal thickening-linear opacities were found to be predictors of higher risk of ventilatory obstructive and restrictive defects on PFT, respectively.

B-0047 11:02

Effect of different radiation doses and reconstruction kernels of HRCT on texture analysis-based artificial neural network classification of patients with systemic sclerosis

G. Milanese^{1,2}, M. Mannil², K. Martini², B. Maurel², H. Alkadhi², T. Frauenfelder²; ¹Parma/IT, ²Zurich/CH (gianluca.milanese@studenti.unipr.it)

Purpose: Texture analysis (TA) uses quantitative, statistical metrics to evaluate image characteristics reflecting microstructural changes. We used TA in high-resolution Computed Tomography (HRCT) with different radiation dose (RD) and reconstruction kernels (RK) to discriminate between Systemic Sclerosis (SSc) patients and non-SSc controls by use of an artificial neural network (ANN).

Methods and Materials: Eighty-five HRCT with different RD (36 low-dose, LDCT and 49 standard dose, SDCT) were retrospectively selected. Each CT was reconstructed with filtered-back projection - FBP - and iterative - SAFIRE 3 and 5 - algorithms. Sixty-one individuals were SSc patients. 304 TA metrics were extracted at six levels through manually-drawn regions of interest. Each metric was averaged between the six levels and acted as input in an ANN with backpropagation (MultilayerPerceptron) for classification of SSc and non-SSc patients. Results were compared regarding correctly/incorrectly classified instances and Receiver-Operating Characteristics - Area under the curve (ROC-AUC). Results were compared between CT with different RK, independently from RD, and between CT with different RK and RD.

Results: The highest discriminatory power for TA-based diagnosis was on FBP-CT: the ANN correctly classified patients in the 84.9% of cases (ROC-AUC=0.904). For CT with different RD, the highest discriminatory power for TA-based diagnosis was for LDCT, and among RK, for FBP-CT. With FBP-LDCT, the ANN correctly classified patients in the 93.8% of cases (ROC-AUC=0.981).

Conclusion: TA metrics extracted from six LDCT images reconstructed with FBP show the highest discriminatory power for the TA-based diagnosis of SSc patients.

B-0048 11:10

Description of interstitial findings in patients with diverse severity of telomere shortening

H. Jofré, L. Planas, P. Luburich, A. Conejero, M. Molina; Barcelona/ES (hector.jofre.g@gmail.com)

Purpose: It is known that telomere shortening (TS) is a poor predictor factor for pulmonary fibrosis. This disorder presents in a majority of patients with familial pulmonary fibrosis (FPF) and in 30% of patients with idiopathic pulmonary fibrosis (IPF). A description of radiological findings and the pattern of progression are performed in patients with TS.

Methods and Materials: Descriptive retrospective study including 50 patients with TS. Telomere length was calculated through quantitative polymerase chain reaction and Z-score (mean length +/- SD) for age matched healthy controls, obtained from DNA of mouth epithelial cells. Thoracic CT of included patients were analysed. The radiological findings and their pattern of progression were characterised by comparing subgroups of different severity of TS ($p < 1\%$, $p < 10\%$ and $p < 25\%$).

Results: 90% of patients with TS had interstitial fibrosing changes in thoracic CT. 84% of patients in the subgroup $p < 1\%$ were <60 years old at diagnosis CT, while in the less severe TS subgroups ($p < 10\%$ and $p < 25\%$), 78% of patients were >60 years old at diagnosis CT. The UIP pattern was seen in 7% of patients in the subgroup $p < 1\%$, in 46% $p < 10\%$ and 52% $p < 25\%$. Inconsistent UIP pattern was seen in 84% of patients in the subgroup $p < 1\%$, 20% in $p < 10\%$ and 11% in $p < 25\%$. 77% of patients showed progression, with an average of 1.3 years in the $p < 1\%$ subgroup, 3.8 years in $p < 10\%$ and 3.6 in $p < 25\%$.

Conclusion: Patients with severe telomere shortening ($p < 1\%$) presents earlier and heterogeneous changes at thoracic CT, with faster progression.

B-0049 11:18

Correlation between pulmonary function tests and HRCT indexes in idiopathic pulmonary fibrosis (IPF) patients

S. Palmucci¹, S.E. Torrisi¹, D. Falsaperla¹, A. Torcitto¹, A. Basile¹, R. Rosso¹, A. Stefano², G. Russo², C. Vancheri¹; ¹Catania/IT, ²Cefalù/IT (spalmucci@sirm.org)

Purpose: The aim of this study is to investigate the correlation between pulmonary function tests (FVC and DLCO) and HRCT quantification indexes in a cohort of patients with idiopathic pulmonary fibrosis (IPF).

Methods and Materials: The analysis was carried out on 39 IPF patients having at least two HRCT (baseline and follow-up) and two spirometry tests available - collected no more than 3 months from HRCT evaluation. The extent of fibrotic disease was quantified on HRCT examinations calculating Kurtosis, High attenuation area (HAA) and fibrotic area (FA) indexes. Pearson's

correlation coefficient was performed to assess the strength of association between pulmonary function tests and HRCT indexes.

Results: Considering baseline HRCT and pulmonary function tests, Pearson correlation analysis revealed moderate correlations between Kurtosis and FVC ($r=0.58$ with $p=0.0001$), Kurtosis and DLCO ($r=0.52$ with $p=0.0005$), HAA and FVC ($r=-0.56$ with $p=0.0001$), HAA and DLCO ($r=-0.48$ with $p=0.0017$), FA and FVC ($r=-0.56$ with $p=0.0002$), and FA and DLCO ($r=-0.49$ with $p=0.0013$). On follow-up, analysing HRCT and pulmonary function tests, Kurtosis and FVC showed a positive strong correlation ($r=0.62$ with $p<0.0001$), whereas Kurtosis and DLCO maintained a moderate positive correlation ($r=0.55$ with $p=0.0002$); negative correlations were found for HAA and FVC ($r=-0.62$ with $p<0.0001$), HAA and DLCO ($r=-0.50$ with $p=0.0011$), FA and FVC ($r=-0.57$ with $p=0.0001$) and FA and DLCO ($r=-0.45$ with $p=0.0039$).

Conclusion: HRCT quantification indexes showed a moderate or good strength of association with pulmonary function tests; therefore, these indexes may be useful for radiologists in the monitoring of IPF disease.

B-0050 11:26

Performance of a software prototype for ILD patterns recognition: how does it compare to chest radiologists?

J. Cohen¹, S. Ritter¹, P. Hirt¹, J. Ghelifi², E. Reymond¹, G.R. Ferretti¹;
¹Grenoble/FR, ²Meylan/FR (jcohen@chu-grenoble.fr)

Purpose: To evaluate the performance of a deep-learning software prototype in the recognition of various patterns of interstitial lung diseases (ILDs) compared to 2 chest radiologists.

Methods and Materials: This retrospective study included 20 consecutive patients diagnosed with ILDs. 2 Radiologists retrospectively reviewed each CT and defined region of interests on 5 predefined slices for each of the following patterns: honeycombing, intralobular reticulation, traction bronchiectasis, ground-glass, consolidation and healthy lung. The scans were subsequently processed by a locally designed deep-learning software which analyzed each patch of 16x16 voxels in the designed slices and attributed for each a predominant pattern. We then compared the results of the 2 radiologists and radiologist 1 and 2 versus software.

Results: Among the 20 included patients, the following diagnosis was proposed after multidisciplinary concertation: IPF (n=9), NSIP (n=2), Churg Strauss ILD (n=1), lymphangitic interstitial pneumonia (n=1), antisynthetase syndrome (n=1), amiodarone-induced ILD (n=1), undetermined (n=5). When comparing radiologist 1 versus software, values of sensitivity/specificity/PPV/NPV were 28/97/19/98%, 30/93/25/94%, 14/96/1/100%, 46/85/26/93%, 32/99/13/100%, 52/90/95/34% for honeycombing, intralobular reticulation, traction bronchiectasis, ground-glass, consolidation and healthy lung, respectively. For radiologist 2 versus software, those values were of 24/97/21/98%, 18/93/22/91%, 16/96/7/99%, 39/87/46/84%, 39/99/23/99% and 59/81/84/54% for the same patterns. Comparatively, when comparing radiologists 2 versus 1, values were of 77/98/33/96%, 35/91/24/94%, 42/98/5/100%, 67/84/33/96%, 61/99/41/100%, and 75/88/96/50%.

Conclusion: At this early stage of development, although sensitivity of detection of ILD patterns by the software remained lower than chest radiologists, its specificity was high for most pathologic patterns with very high NPVs.

B-0051 11:34

Computed tomography in primary ciliary dyskinesia: typical imaging findings in the cohort of adult patients with bronchiectasis

S. Dettmer, F. Ringshausen, J. Vogel-Claussen, J. Fuge, A. Faschkami, H.-O. Shin, T. Welte, F. Wacker, J. Rademacher; Hannover/DE (dettmer.sabine@mh-hannover.de)

Purpose: Aim of this study was to evaluate specific features of Primary Ciliary Dyskinesia in computed tomography in the cohort of bronchiectasis to facilitate diagnosis.

Methods and Materials: 121 CT in patients with bronchiectasis were scored for involvement, type, and lobar distribution of bronchiectasis, bronchial dilatation, and bronchial wall thickening. Further-on, associated findings like tree in bud, mucus plugging, consolidations, ground glass opacities, interlobular thickening, intralobular lines, situs inversus, emphysema, and atelectasis were registered. Patients with PCD (n=46) were compared to patients with other underlying diseases (n=75).

Results: In patients with PCD, the extent and severity of bronchiectasis were significantly lower in the upper lobes ($p<0.001$ - $p=0.011$). The lobar distribution was significantly different (<0.001) with predominance in the middle and lower lobes in patients with PCD. Significantly more common in patients with PCD were mucous plugging ($p=0.001$), tree in bud ($p<0.001$), atelectasis ($p=0.009$), and history of resection of a middle or lower lobe ($p=0.047$); less common were emphysematous ($p=0.003$) and fibrotic ($p<0.001$) changes. A situs inversus (Kartagener's Syndrome) was only seen in patients with PCD (17%, $p<0.001$).

Conclusion: Typical imaging features in PCD are a predominance of bronchiectasis in the middle and lower lobes, severe tree in bud pattern, mucous plugging and atelectasis. These findings may help practitioners to identify patients with bronchiectasis in which further work-up for PCD is warranted.

B-0052 11:42

CT quantitative and semi-quantitative thoracic and extra-thoracic biomarkers in COPD patients: how reliably can they predict patients' outcomes?

J. Cohen, G. Ferretti, M. Benmerad, S. Bailly, C. Ozcelik, E. Reymond, A. Jankowski, S. Bayat, J.-L. Pepin; Grenoble/FR (jcohen@chu-grenoble.fr)

Purpose: To evaluate the performance of CT biomarkers for predicting 5-year survival, number of pulmonary infections, hospitalisations and cardiovascular events in COPD patients.

Methods and Materials: This retrospective preliminary study included 30 COPD patients from a prospective cohort, with at least one unenhanced chest CT-scan. A chest radiologist retrospectively assessed the following parameters: inspiration %LAA-950, expiration %LAA-856, pre-pectoral subcutaneous adipose tissue (PSAT), anterior mediastinal fat surface, epicardial fat surface, mean liver attenuation, mean liver/spleen attenuation ratio (LSAR), coronary calcifications using Weston score, presence of bronchiectasis and bronchial thickenings, density of vertebral bodies in T4,7,10. PSAT, anterior mediastinal and epicardial fat were subsequently normalised by the patients' body surface area. These parameters were then compared using univariate analyses with the 5-year survival, number of hospitalisations, pulmonary infections and cardiovascular events.

Results: Median follow up time for the investigated outcomes was 7 years (interquartile range (IQR)=3 years). Median patient age was 65 (IQR=11 years). Mortality was significantly higher in patients who had a higher mean liver attenuation ($p=0.02$) and a lower mean vertebral density in T4-7-10 ($p=0.01$). Patients with more lung infections had a significantly lower PSAT area ($p=0.02$), mean attenuation in T4-7-10 ($p=0.001$) and a higher LSAR ($p=0.001$). A higher number of hospitalisations was associated with a lower PSAT area ($p=0.02$), a higher LSAR ratio ($p=0.01$) and %LAA-950 ($p=0.01$).

Conclusion: Simple CT-biomarkers show the potential to predict the 5-year survival, the risk of intercurrent infections and hospitalisations and in COPD patients. Further analyses, particularly multivariable, are needed to confirm these results.

B-0053 11:50

Solid indeterminate pulmonary nodules less than 300 mm³: application of the British Thoracic Society guidelines in clinical practice

S. Pezzotti, A. Borghesi, G. Nocivelli, A. Scrimieri, R. Maroldi; Brescia/IT (stefy.pezzotti@gmail.com)

Purpose: To evaluate the performance of the British Thoracic Society (BTS) recommendations for the management of solid indeterminate pulmonary nodules (SIPNs) <300 mm³.

Methods and Materials: During a 7-year period we retrospectively reviewed the chest CT of 672 consecutive patients with one or more SIPNs. The study sample was selected according to the following inclusion criteria: solitary SIPN; volume <300 mm³; 2 or more CT scans performed with the same scanner and acquisition/reconstruction protocol; thin-section 1-mm images in DICOM format; histologic diagnosis or follow-up >2 years. Patients with previous oncology history were excluded. Applying such criteria a total of 29 patients with 29 SIPNs were enrolled. For each SIPN, the volume and doubling time (DT) were calculated using a semiautomatic software throughout the follow-up period. For each SIPN, we retrospectively applied the BTS guidelines and this management was compared to what was actually done.

Results: A significant volumetric increase (more than 20% with DT <600 days) has been observed in 6/29 SIPNs. In these SIPNs a histologic diagnosis of malignancy was obtained. Applying the BTS recommendations all 6 malignant nodules would have been identified. None of the SIPNs with volume <300 mm³ and DT >600 days showed a significant growth during the follow-up period. The application of the BTS guidelines would have led to a reduction in CT examinations (1.5 CT scan for patients).

Conclusion: The application of BTS guidelines has proven to be effective in the management of SIPNs <300 mm³ with a significant reduction of radiation dose.

10:30 - 12:00

Room N

Genitourinary

SS 207

Urinary tract tumours

Moderators:

M. D'Anastasi; Munich/DE
S. Hanna; Cairo/EG

B-0054 10:30

Contrast-enhanced ultrasound in evaluation of renal masses: a preliminary experience

M. Altamash, S.B. Grover, S. Suman, A. Katyan, A. Kumar, A.K. Mandal;
New Delhi/IN (md.altamash20@gmail.com)

Purpose: Although grey scale ultrasound (US) and colour doppler are fairly efficient in evaluation of renal masses, characterizing complex renal masses remains a limitation. CECT is associated with significant risk for patients with hyperthyroidism, impaired renal function and allergic reactions because of iodinated contrast agents. Our study was therefore, aimed to evaluate the role of contrast-enhanced ultrasound in characterization of renal masses and to correlate it with contrast-enhanced CT and histopathology.

Methods and Materials: Twenty three patients with clinically or sonographically detected renal masses were included in this IRB approved study. Renal masses were evaluated using gray scale ultrasound and contrast-enhanced ultrasound for location, morphology and enhancement pattern. The mass lesions were categorized in benign and malignant varieties. The criteria for malignant mass lesion on contrast-enhanced ultrasound were centripetal enhancement along-with early contrast wash-in and wash out. Results were compared with contrast-enhanced computed tomography scan and histopathology.

Results: Using histopathology as gold standard, the sensitivity and specificity of contrast enhanced ultrasound in characterization of benign and malignant masses were found to be 95% and 88% respectively.

Conclusion: Currently, renal lesions are characterized by contrast-enhanced computed tomography (CECT). Our study showed that contrast-enhanced ultrasound has almost similar sensitivity and specificity to that of CECT in characterization of renal masses. Thus, contrast-enhanced ultrasound can be used as noninvasive procedure for characterization of renal masses and should be further exploited for its role in characterization of renal masses.

B-0055 10:38

Value of contrast enhanced ultrasound in evaluation of cystic renal lesions compared to computed tomography and magnetic resonance imaging

M.H. Lerchbaumer¹, J. Rübenthaler², F.J. Putz³, T. Slowinski¹, D.A. Clevert², E.-M. Jung³, T. Fischer¹; ¹Berlin/DE, ²Munich/DE, ³Regensburg/DE (markus.lerchbaumer@charite.de)

Purpose: To assess the value of contrast-enhanced ultrasound (CEUS) in the evaluation of cystic renal lesions using the Bosniak classification compared with computed tomography (CT), magnetic resonance imaging (MRI) and histopathologic findings (HP).

Methods and Materials: We performed a multicentre, retrospective analysis of 340 CEUS examinations in high volume ultrasound centres in Germany. Bosniak classification of cystic renal lesions is compared to further diagnostic up imaging (CT or MRI) and HP.

Results: Median age was 64 years (IQR: 56-72) and 69 % were male patients. CEUS showed an overall moderate correlation when compared to CT and MRI ($r^2=0.55$; 95% CI 0.40-0.67, $p<0.001$). Lesions classified by CEUS were significantly higher correlated with CT than MRI with a correlation coefficient of 0.92 (95% CI 0.91-0.98, $p<0.001$) and 0.42 (95% CI 0.23-0.59, $p<0.001$), respectively. Most frequent misclassified renal lesions in CEUS compared to MRI were Bosniak IIF ($n=14/28$) and Bosniak III cysts ($n=11/21$). Of 252 lesions which were classified as Bosniak IV in CEUS and therefore identified as suspect for an active malignancy 84.1% ($n=212$) were identified as renal cell carcinoma through histopathologic examination (Sensitivity 99%, Specificity 0%, PPV 84%, NPV 0%).

Conclusion: Renal lesions classified by CEUS using the Bosniak classification have a high correlation when compared to current gold standard CT. MRI seems to downgrade especially Bosniak IIF and III lesions compared to CEUS. CEUS showed excellent sensitivity in detection of malignancy compared to histopathological report.

B-0056 10:46

Contrast-enhanced ultrasonography (CEUS) and time/intensity curves for the active surveillance of small renal masses

E. Bertelli, S. Agostini, G. Addeo, S. Verna, F. Parretti, C. Raspanti, A. Minervini, A. Mari, V. Miele; Florence/IT (elena.bertelli3@gmail.com)

Purpose: To assess the prognostic efficacy of contrast-enhanced ultrasonography (CEUS) and time/intensity (T/IS) curves for the active surveillance of small renal masses (SRM).

Methods and Materials: We performed CEUS in 288 patients to evaluate 312 renal lesions. All the lesions were confirmed by Contrast-enhanced CT or Contrast-enhanced MR. 66 patients were operated (group A), 246 (group B) are nowadays at least in a 3 years follow up. We performed a quantitative evaluation of the lesions enhancement (QE) by T/IS curves. We identify 4 type of curves: I "quick wash in (WI) and wash out (WO)", II "quick WI and slow WO", III "WI and WO synchronous to the surrounding parenchyma" IV "slow WI and WO".

Results: In the group A we performed the QE in 56 cases, 3 patients were not evaluated by time/intensity curves and 7 had cystic lesions; in the group B we performed the QE in 85 cases, 139 patients have cystic lesions and 22 were not evaluated. Patients with type I curves (16) had aggressive lesions in 96% of cases, patients with type II (40) in 57%, patients with type IV (49) in 18%; no aggressive lesions showed a type III pattern. The limits of our study are the small number of cases and the duration of follow up.

Conclusion: CEUS is a safe, cost-effective procedure, suitable for patients with impaired renal function. T/IS curves are a useful tools for active surveillance because they could provide information about the aggressiveness of renal lesions.

B-0057 10:54

Contrast-enhanced ultrasound (CEUS) as a new technique to characterise suspected malignancies in renal transplants in comparison to standard imaging modalities

K. Mueller-Peltzer, J. Rübenthaler, D.A. Clevert; Munich/DE (katharina.muellerpeltzer@med.uni-muenchen.de)

Purpose: Renal transplant patients have a higher risk for malignancies of the renal transplant. In most cases suspected renal malignancies will be detected during the regular ultrasound follow-up and will require cross-sectional imaging to rule out a malignant aetiology. But it is well known that contrast agents for cross-sectional imaging are critical in patients with limited renal function. Therefore, this study aims to compare the sensitivity and specificity of contrast-enhanced ultrasound (CEUS) and gold standard imaging in characterizing suspected renal transplant malignancies in renal transplant patients.

Methods and Materials: A total of 22 renal transplant patients with a suspected renal transplant malignancy with at least one CEUS and at least one cross-sectional imaging study performed between 2005 and 2017 were included. Patient ages ranged from 28.2 years to 74.6 (mean age 55.7 years; SD \pm 13.0 years). CEUS of 22 patients was correlated with a standard imaging modality, CT (15 out of 22) or MRI (7 out of 22), serving as gold standard.

Results: All 22 lesions of the renal transplants described in CT or MRI could be detected using CEUS. CEUS showed a sensitivity of 100%, a specificity of 94.4%, a positive predictive value (PPV) of 80%, and a negative predictive value (NPV) of 100%.

Conclusion: CEUS is an eligible method to help characterizing suspected renal malignancies in renal transplant patients compared to the well-established imaging modalities CT and MRI. As an imaging modality with no nephrotoxic effects CEUS can be used repeatedly even in patients with limited renal function.

B-0058 11:02

Percutaneous cryoablation for renal cell carcinoma using US-guided targeting and CT-guided ice-ball monitoring: procedure time, radiation dose and mid-term outcomes

D. Kim, S. Park; Seoul/KR (kdk7118@yuhs.ac)

Purpose: To assess procedure time, radiation dose and mid-term outcomes of percutaneous cryoablation (PCA) for renal cell carcinoma (RCC) using US-guided targeting and CT-guided ice-ball monitoring.

Methods and Materials: A consecutive series of 39 patients (mean age, 60.6 \pm 15.3 years) who underwent PCA for biopsy-proven RCC were included. The mass targeting was performed with US guidance and a radiographic ice-ball was monitored with CT. The procedure time was defined by the interval of image acquisition between the first US and last CT images. The effective radiation dose of CT examination during PCA was recorded. The follow-up was conducted with contrast-enhanced CT or MRI (mean follow-up time, 10.1 \pm 7.0 months; range, 1-23 months). The local tumour progression was defined by the presence of focal enhancing areas at the ablation zone (CT, 20 or greater

Hounsfield unit, MRI, presence of focal enhancement on subtraction contrast-enhanced image).

Results: The mean procedure time was 110.3±22.8 minutes (range, 79-183 minutes). The mean effective radiation dose in association with PCA was 13.7±5.2 mSV (range, 8.0-28.6 mSV). The local tumour progression occurred in a single patient (2.6%, 1/39). The local tumour progression-free survival rate was 95.7%.

Conclusion: PCA using US-guided targeting and CT-guided ice-ball monitoring may allow acceptable tumour control for RCC, as reducing radiation dose.

B-0059 11:10

Is multiparametric MRI useful for differentiating oncocytomas from chromophobe renal cell carcinomas

C. Galmiche; Bordeaux/FR (chloe.g1412@gmail.com)

Purpose: The purpose of this study was to retrospectively evaluate the diagnostic accuracy of multiparametric MRI to differentiate oncocytoma from chromophobe renal cell carcinoma.

Methods and Materials: In this retrospective study, 26 histologically confirmed oncocytomas and 16 chromophobe RCCs that underwent full MRI examination were identified in 42 patients (25 men and 17 women) over a 6-year period. Demographic data were recorded. Double-echo chemical-shift, dynamic contrast-enhanced T1- and T2-weighted images, and apparent diffusion coefficient maps were reviewed independently by two radiologists blinded to pathologic results. Signal-intensity index (SII), tumor-to-spleen signal-intensity ratio, ADC ratio, three wash-in indexes, and two washout indexes were calculated and compared using univariate and ROC analyses. Sensitivity and specificity analyses were performed to calculate diagnostic accuracy.

Results: All carcinomas and nine oncocytomas were resected; the remaining 17 oncocytomas were biopsied. Patient age (for oncocytomas: mean, 68.2 years; range, 43-84 years; for RCCs: mean, 60.8 years; range, 20-79 years) and tumor size (for oncocytomas: mean, 35.5 mm; range, 12-98 mm; for RCCs: mean, 37.2 mm; range, 9-101 mm) did not differ significantly across groups ($p = 0.132$ and 0.265 , respectively). Good interobserver agreement was observed for all measurements but four. Oncocytomas presented significantly higher ADC ($p = 0.002$) and faster enhancement ($p = 0.007-0.012$) but lower SII ($p = 0.03$) than carcinomas. This combination provided sensitivity of 92.3% (24/26), specificity of 93.8% (15/16), and accuracy of 92.9% (39/42) for the detection of oncocytomas.

Conclusion: Multiparametric MRI helps to accurately differentiate oncocytomas from chromophobe RCCs with high sensitivity and specificity.

B-0060 11:18

CT texture analysis in clear cell renal cell carcinoma: a radiogenomics prospective

S. Badia¹, D. Bellini¹, C. Marigliano², M. Rengo¹, M. Osimani¹, S. Picchia¹, V. Petrozza¹, A. Laghi¹; ¹Latina/IT, ²Milan/IT (stefano.badia@gmail.com)

Purpose: The aim of this study was to investigate whether quantitative parameters obtained from CT texture analysis (CTTA) correlate with expression of miRNA in clear cell renal cell carcinoma (ccRCC).

Methods and Materials: In a retrospective single-centre study, multiphase CT examination (with arterial, portal and urographic phases) was performed on 64 patients with ccRCC (28 women and 36 men; mean age 65 years ± 6). Measures of heterogeneity were obtained in post-processing by placing a ROI on the entire tumour and CTTA parameters such as entropy, kurtosis, skewness, mean, mean of positive pixels and SD of pixel distribution histogram were measured using multiple filter settings. Quantitative data were correlated with miRNAs obtained from histopathological analysis (miR-21-5p, miR-210-3p, miR-185-5p, miR-221-3p, miR-145-5p). Both evaluations (miRNAs and CTTA) were done on normal corticomedullary and tumour tissue for comparison. Analysis of variance with linear multiple regression model methods were obtained with SPSS statistic software. For all comparisons, statistical significance was assumed $p < 0.05$.

Results: The expression of miR-21-5p, miR-210-3p and miR-221-3p resulted up-regulated in tumour samples. Among all miRNAs, normal tissue entropy was not related to miR-21-5p ($R^2 = 0.06$), while a trend of positive correlation was found with tumour tissues ($R^2 = 0.27$). Excluding some patients with extreme over-expression of miR-21-5 (10%), excellent relation of entropy in tumour with miR21-5p was found ($R^2 = 0.64$; $p < 0.05$).

Conclusion: Entropy and miRNA 21-5p show positive correlation in ccRCC; in addition CTTA features, in particular, mean and entropy show a statistically significant increase in ccRCC as compared with normal tissue.

B-0061 11:26

Assessing venous thrombus in renal cell carcinoma: preliminary results for non-contrast enhanced magnetic-resonance 3D-SSFP

L. Adams, B. Ralla, G. Engel, G. Diederichs, J. Busch, F. Fuller, B. Hamm, M.R. Makowski; Berlin/DE

Purpose: To test the potential of non-contrast-enhanced cardiac- and respiratory-motion-corrected three-dimensional-steady-state-free-precession (3D-SSFP) MR imaging for the assessment of inferior vena cava (IVC) thrombus in patients with renal cell carcinoma (RCC), compared to standard contrast enhanced MRI.

Methods and Materials: 14 patients with RCC and suspected IVC thrombus, who received a contrast-enhanced abdominal MRI and 3D-SSFP at 1.5T as a standard preoperative work-up procedure between June 2015 and September 2017, could be included in this retrospective study. Contrast-to-noise-ratios (CNR), image quality and diagnostic performance of 3D-SSFP and standard MRI were compared. Additionally, in vivo- findings were validated against intraoperative results and histopathological examinations.

Results: Both 3D-SSFP and contrast-enhanced MRI correctly identified the extent and approximate volume of all IVC thrombi, confirmed by surgery and histopathology. 3D-SSFP reached a significantly higher CNR in the supra- and infrarenal IVC compared to morphologic imaging (T2-HASTE), the unenhanced, the portal venous, nephrogenic and delayed phase. 3D-SSFP showed a significantly higher CNR in the infrarenal IVC (mean CNR of 8.61 ± 3.90 vs. 3.84 ± 1.54 in the delayed phase, $p = 0.005$) and a slightly higher CNR in the suprarenal IVC (mean CNR of 8.66 ± 3.76 vs. 5.00 ± 6.31 in the late arterial phase, $p = 0.055$). The thrombus delineation score for 3D-SSFP (4.38 ± 0.76) was higher compared to standard MRI (3.76 ± 0.71 , $p = 0.016$).

Conclusion: This preliminary study indicates that cardiac- and respiratory-motion-corrected 3D-SSFP can achieve an accurate delineation of IVC thrombus in RCC patients without the need for contrast administration. 3D-SSFP may thus offer a valid alternative for patients with contraindications to gadolinium-based contrast agents.

Author Disclosures:

L. Adams: Grant Recipient; LA is participant in the BIH Charité - Junior Clinician Scientist Program funded by the Charité - Universitaetsmedizin Berlin and the Berlin Institute of Health. **B. Ralla:** Grant Recipient; BR is participant in the BIH Charité - Junior Clinician Scientist Program funded by the Charité - Universitaetsmedizin Berlin and the Berlin Institute of Health. **J. Busch:** Grant Recipient; JB is participant in the BIH - Twinning Grant Program funded by the Charité - Universitaetsmedizin Berlin and the Berlin Institute of Health.

M.R. Makowski: Grant Recipient; MRM is grateful for the financial support from the Deutsche Forschungsgemeinschaft (DFG, 5943/31/41/91)..

B-0062 11:34

Can we diagnose T1 stage UB (urinary bladder) cancer from T2 stage with an inchworm/stalk sign on 3T-MRI?

D. Kim, B. Kang, Y. Ko; Seoul/KR (kangbc@ewha.ac.kr)

Purpose: To evaluate diagnostic performance of an inchworm sign/ stalk sign on MRI for T1 stage UB cancer.

Methods and Materials: Among 261 consecutive UB cancer patients underwent radical cystectomy with neobladder. We described the tumorous high signal intensity curve on DWI as an 'inchworm sign' and the fibrovascular stalk on T2WI as a 'stalk sign'. If the inchworm sign(DWI) or stalk sign(T2WI) was shown, it was grouped as T1 staging. If not shown, it was grouped as over T2 staging. If there was hydronephrosis associated with UB tumour, even having that signs, it was grouped as over T2 staging. We compared the preoperative MR T-stage and postoperative pathological T-stage in all enrolled patients. We evaluated the diagnostic significance an inchworm sign (DWI) and a stalk sign (T2WI) statistically by χ^2 -Test and McNemar test/Fisher's exact test.

Results: For diagnosing T1 stage UB cancer, the "inchworm sign(DWI)" and the "stalk sign(T2WI)" showed high specificity (94%, 95%), high positive predictive value (81%, 77%), and high accuracy (80%, 76%). And we found their diagnostic accuracy to increase (86%, 79%) with hydronephrosis. So, even inchworm sign or stalk sign were seen, with associated hydronephrosis, we can preoperatively indicate over T1 staging urinary bladder cancer with more higher prediction.

Conclusion: We can easily diagnose T1 UB cancer from T2 by detecting an inchworm sign(DWI), or a stalk sign(T2WI) on MRI. If there is associated with hydronephrosis, suggesting UVJ muscle layer invasion by UB cancer, its diagnostic value could be increased.

B-0063 11:42

Investigation of intravoxel incoherent motion diffusion-weighted imaging for assessing bladder cancer invasiveness

F. Wang, G. Wu, W. Chen; Shanghai/CN

Purpose: To investigate whether intravoxel incoherent motion (IVIM) diffusion-weighted imaging (DWI) could differentiate non-muscle-invasive bladder cancer (NMIBC) from muscle-invasive bladder cancer (MIBC) and to assess whether there were correlations between IVIM parameters and the Ki-67 labelling index (LI).

Methods and Materials: Thirty-six patients diagnosed with bladder cancer confirmed by histopathological findings underwent magnetic resonance imaging including DWI with 8 b-values ranging from 0 to 1000 s/mm² before transurethral resection (TUR). Molecular diffusion coefficient (D), perfusion-related diffusion coefficient (D*), perfusion fraction (f), and apparent diffusion coefficient (ADC) were calculated by bi-exponential and mono-exponential model fits, respectively. Comparisons were made between the MIBC and NMIBC group. Differences in these values were analysed by comparing the areas under the receiver operating characteristic curves (AUC). The correlations between these parameters and Ki-67 LI were also analysed.

Results: ADC and D values were significantly lower in patients with MIBC compared to those suffering NMIBC (p<0.01). The AUC of D value (0.894) was significantly (p<0.05) larger than those of ADC value (0.786). The sensitivities and specificities of D and ADC values were 95% and 87.5% and 80% and 68.7%, respectively. In addition, there was a negative correlation between D value and Ki-67 LI (r=-0.785, p<0.01).

Conclusion: D value obtained from IVIM could provide better performance than conventional DWI in distinguishing NMIBC from MIBC and serve as an imaging biomarker reflecting the invasive and proliferative potential of bladder cancer.

Author Disclosures:

F. Wang: Speaker; Fang Wang.

B-0064 11:50

Prediction of treatment response after immunotherapy in metastatic or recurrent urothelial carcinoma: potential imaging biomarker using CT texture analysis-a preliminary study

K. Park; Seoul/KR (kyejin629@gmail.com)

Purpose: To evaluate the relationship between tumour heterogeneity assessed by computed tomography (CT) texture analysis and treatment response after immunotherapy in patients with metastatic or recurrent urothelial carcinoma.

Methods and Materials: From January and April 2017, ten consecutive patients who had recurrent/metastatic urothelial carcinoma and underwent immunotherapy (Durvalumab, pembrolizumab or atezolizumab) were retrospectively evaluated. Texture analysis of all metastatic lesions (42 lesions) were performed with CT imaging for immunotherapy planning using in-house software. Histogram-based uniformity, entropy and kurtosis as well as 11 run-length matrix (RLM) and 25 gray level co-occurrence matrix (GLCM) features were obtained with manual delineation of a region of interest on metastatic lesion. Determination of responder and non-responder was done with clinicoradiologic follow-up after at least two consecutive CT reviews. The statistical analysis was done using Mann-Whitney U test.

Results: Six patients were classified as responder and four as non-responder. There was statistically significant difference of all three histogram-based features, seven RLM and ten GLCM features between responder and non-responder (p<0.05). Higher kurtosis (1.25 vs. 0.13, p=0.01) lower entropy (6.80 vs. 7.09, p=0.006), and higher uniformity (0.011 vs. 0.008, p=0.010) were observed in responder group.

Conclusion: In patients with recurrent or metastatic urothelial carcinoma, non-responders appeared to be more heterogeneous on CT texture analysis (higher entropy and lower uniformity) than responders. This preliminary result may be useful to predict treatment response after immunotherapy prospectively.

10:30 - 12:00

Room L 8

Head and Neck

SS 208

Advanced MRI techniques in head and neck imaging

Moderators:

G.C.T.E. Garcia; Villejuif/FR

L. Oleaga Zufiria; Barcelona/ES

B-0065 10:30

The value of readout-segmented diffusion-weighted imaging in the evaluation of parotid gland tumours

Z. Zhang, J. Cheng; Zhengzhou/CN (yinierzhang@sina.com)

Purpose: The purpose was to investigate the role of readout-segmented echoplanar imaging using parallel imaging and a two-dimensional navigator-based reacquisition (RESOLVE) in differentiating various types of common parotid gland tumours.

Methods and Materials: Sixty-five patients with parotid gland tumours confirmed by pathology received preoperative conventional MRI and RESOLVE DWI (b-values of 0 and 1000 s/mm²). The apparent diffusion coefficient (ADC) values of the lesions were calculated and the receiver operating characteristic curves was drawn to obtain the cut-off value for differentiating benign and malignant parotid gland tumours.

Results: The mean ADC value of pleomorphic adenomas were significantly higher than that of all other examined subtypes. ADC values of warthin tumours were significantly lower than pleomorphic adenoma (p=0.000), basal cell adenoma (p=0.000) and malignant tumours (p=0.001). ADC cut-off values were 1.22x10⁻³mm²/s between pleomorphic adenomas and malignant tumours and 0.90x10⁻³mm²/s between Warthin tumours and malignant tumours; using 0.90x10⁻³mm²/s≤ADC values<1.22x10⁻³mm²/s to make a diagnosis of malignant tumour, the sensitivity, specificity, and accuracy were 93.8%, 81.4%, 84.7%, respectively.

Conclusion: RESOLVE has high accuracy in differing benign and malignant lesions of the parotid gland by producing high-resolution DWI.

B-0066 10:38

Sensorineural hearing loss in vestibular schwannoma relies on the presence of utricular hydrops, as diagnosed with heavily weighted T2 sequences

M. Eliezer¹, G. Poillon², A. Gillibert², C. Maquet², J. Horion², E. Gerardin², A. Trintignac², N. Magne², A. Attye³, ¹Paris/FR, ²Rouen/FR, ³Meylan/FR (mheliezer@gmail.com)

Purpose: Due to the increased protein concentration in the perilymph liquid, FIESTA-C has recently been proposed to assess endolymphatic spaces without administration of contrast media in patients with vestibular schwannoma. The aim of this study was to assess whether vestibular endolymphatic space dilatation, as evaluated with 3D-FIESTA-C sequences, is related to the degree of hearing loss in patients with schwannoma.

Methods and Materials: In this retrospective study (IRB E2017-23), we performed 3D-FIESTA-C sequences in 32 patients with schwannoma, as diagnosed on the basis of typical image findings. Two radiologists independently checked the visualization and evaluated the volume of the utricle and saccule. Pearson and Spearman tests were used to explore the correlation between the volume of the tumor, the volume of the vestibular endolymphatic space and the degree of hearing loss - as evaluated with the levels of pure-tone average (PTA) and speech recognition threshold (SRT).

Results: The endolymphatic space can be evaluated in 72% (23 out of 32 patients) of patients with schwannoma on non-contrast 3D-FIESTA-C sequences. The mean saccular, utricular and tumor volume were 3.17 mm³, 14.55 mm³ and 1.74 cm³ respectively. There was a significant correlation between the volume of the utricle and the degree of hearing loss as evaluated with the levels of PTA (p=0.015) and SRT (p=0.004). There was no significant correlation between the saccular and tumour volumes and the degree of hearing loss.

Conclusion: The volume of the utricle in schwannoma patients is related to the degree of hearing loss.

Wednesday

B-0067 10:46

Imaging of facial neuritis using T2-weighted gradient-echo fast imaging employing steady-state acquisition after gadolinium injection

A. Venkatasamy, A. Al Najdi, M. Abu Eid, A. Charpiot, C. Debry, F. Veillon; Strasbourg/FR (aina.vnkt@gmail.com)

Purpose: MRI is the modality of choice for the imaging of facial neuritis. Previously, gadolinium-enhanced T1WI of the petrous bone was thought to be the most informative sequence in the evaluation of facial neuritis. The goal of this study is to evaluate the value of gadolinium-enhanced T2WI steady-state free precession sequences for the diagnosis of facial neuritis.

Methods and Materials: We performed an MRI of the petrous bones in 38 patients with unilateral peripheral facial palsy, using T2WI steady-state-free precession sequences and T1WI after intravenous gadolinium injection, and compared these to 60 normal patients (control group) imaged with the same MRI protocol and to 32 healthy volunteers (volunteers control group) imaged by T2WI steady-state free precession sequence without gadolinium injection.

Results: All patients presenting with a facial neuritis presented with a pathological enhancement of the facial nerve on the pathological side on T2W steady-state free-precession sequences (FIESTA-C and CISS) acquired after gadolinium injection. 94.7% of patients presented with a strong enhancement (Grade 2), which had a specificity of 100%, a sensitivity 94.7% and an accuracy of 97.9%. T1WI sequences following IV gadolinium injection were positive in 79% of the patients with facial neuritis and enhancement was also observed in the control group.

Conclusion: Enhancement of the facial nerve canal on T2WI steady-state free precession sequences (FIESTA-C) is a sensitive and specific sign of homolateral facial neuritis and is superior to T1WI images for the positive imaging diagnosis of facial neuritis.

B-0068 10:54

D-prep magnetic resonance imaging for the visualisation of the facial nerve

P. Bos¹, B. Jaspere¹, A.J.M. Balm¹, L.C. ter Beek¹, F.W. van Leeuwen², M.W.M. van den Brekel¹, R.G.H. Beets-Tan¹, T. Buckle²; ¹Amsterdam/NL, ²Leiden/NL (pa.bos@nki.nl)

Purpose: Facial nerve damage can be a serious complication of parotid surgery. Pre- or peroperative localization of the facial nerve may help the surgeon to avoid this complication. Diffusion-prepared MRI (D-prep MRI) is a novel technique designed to specifically visualize nerve structures. This study evaluates the ability and extent D-prep MRI to detect the Facial nerve.

Methods and Materials: D-prep MRI was performed in 24 patients (13 male/11 female, mean age 60 ± 11 years) that underwent a MRI for (suspected) head and neck cancer between December 2016 and August 2017. The visibility, length and thickness of the different branches of the Facial nerve were assessed by one neuro/head and neck radiologist based on the course of the nerve.

Results: Two patients were excluded because of poor MRI quality. For the remaining 22 patients the main trunk (from the mastoid foramen to the bifurcation of zygomaticofacial and oromandibular branches) was visible in 15 patients (length between 4 and 26 mm, median thickness: 1.3 mm), the posterior auricular nerve in 4 patients (6-11 mm; 0.9 mm), the zygomaticofacial branch in 6 patients (2-12 mm; 1.1 mm), the oromandibular branch in 6 patients (1-23 mm; 1.0 mm) and temporal in 1 patient (6 mm; 1.6 mm). In 7 patients the Facial nerve could not be identified.

Conclusion: The facial nerve can be identified and its course delineated with D-prep MRI in most cases. Further optimization of this sequence will hopefully result in more detailed visualization and delineation of Facial nerve branches.

B-0069 11:02

Is gadolinium really necessary for intralabyrinthine schwannomas MRI examination?

A. Venkatasamy, A. Karol, T. Huynh, A. Charpiot, C. Debry, F. Veillon; Strasbourg/FR (aina.vnkt@gmail.com)

Purpose: Our aim was to confirm the usefulness of T2-weighted (T2W) gradient-echo sequence for detection and topographic diagnosis of intralabyrinthine schwannomas (ILS) compared to T1W contrast-enhanced sequence as gold standard to evaluate the necessity of intravenous gadolinium injection in ILS imaging.

Methods and Materials: 30 patients with ILS were retrospectively enrolled and compared to a control group of 30 patients with no inner ear pathology. All patients underwent a T2W gradient-echo steady-state free precession (SSFP) acquisition at 3T, which was visually analysed by two radiologists and compared to contrast-enhanced T1W sequence. A quantitative analysis was also performed, with the measurement of the tumour and inner ear signal on T2W images and the measurement of the tumour length in cochlear schwannomas.

Results: T2W FIESTA-C sequence correctly diagnosed ILS with a sensitivity (Se) of 95% and a specificity (Sp) of 100%, with matching results for their topographic evaluation (Se 92%, Sp 98%) compared to the gold standard. The error rate was only 2.5%, with excellent interobserver agreement. The tumour signal on T2W images was significantly lower than the normal bright signal of the normal inner ear fluids (mean signal ratio = 0.42 vs 0.98).

Conclusion: The positive and topographic diagnostic accuracy of T2W FIESTA-C sequence was excellent compared to the T1W contrast-enhanced sequence, even though the latter remains easier and faster to analyse for an untrained radiologist. The performances of T2W gradient-echo sequence at 3T renders it sufficient for the imaging of ILS, especially for follow-up imaging.

B-0070 11:10

Is post-contrast MRI imaging necessary in the investigation of cholesteatoma recurrence when non-echo planar diffusion-weighted imaging is available? A diagnostic accuracy study

R. Kavanagh, A. Carroll, Y.M. Purcell, A.E. Smyth, S.G. Khoo, G. McNeill, D.E. Malone, R.P. Killeen; Dublin/IE (richkavanagh@rcsi.ie)

Purpose: The diagnosis of recurrent cholesteatoma is important in order to avoid the associated complications. This has traditionally been done through second-look surgery and more recently with contrast-enhanced MRI. Non-echo planar (EP) diffusion-weighted imaging (DWI) has been shown to be useful in the diagnosis of cholesteatoma. The aim of this study is to assess the diagnostic accuracy of a shortened imaging protocol for cholesteatoma recurrence, without the use of gadolinium, compared to our standard contrast enhanced protocol, used as the gold standard.

Methods and Materials: This is a retrospective study of 100 consecutive MRIs performed for suspected cholesteatoma recurrence in a single institution from Jan 2012 to May 2016. Our standard MRI protocol includes T2, PROPELLER DWI and pre and post-contrast T1-weighted sequences of the temporal bone. Using the standard protocol as the gold standard we assessed the sensitivity and specificity of a shortened protocol, which did not include the post-contrast sequence, for the detection of cholesteatoma recurrence.

Results: Using the standard protocol, including post-contrast imaging, as the gold-standard, the sensitivity and specificity of the shortened protocol is 100% and 95.3%, respectively. The accuracy of the shortened protocol is 98%. The calculated positive predictive value is 96.6% and the negative predictive value is 100%. Using McNemar's Test, no statistical difference was found between the two diagnostic tests (p=0.16).

Conclusion: MRI imaging in patients with suspected cholesteatoma recurrence can be performed using a shortened protocol without the need for further contrast-enhanced sequences.

B-0071 11:18

Role of magnetic resonance neurography [MRN] for the diagnosis of peripheral trigeminal nerve injuries in patients with prior molar tooth extraction

R.A.K. Dessouky^{1,2}, Y. Xi², J.R. Zuniga², A. Chhabra²; ¹Zagazig/EG, ²Dallas, TX/US (rihamdessouky@gmail.com)

Purpose: Evaluate the role of magnetic resonance neurography [MRN] for the diagnosis of peripheral trigeminal nerve [PTN] injuries in patients with prior molar tooth extraction.

Methods and Materials: In this retrospective study, nerve caliber, T2 signal intensity ratio [T2SIR] and contrast to noise ratios [CNR] were recorded by two observers for bilateral PTN branches, the inferior alveolar [IAN] and lingual nerve [LN]. Subject demographics and correlation of the MRN findings with Sunderland classification of nerve injury and intraoperative findings of surgical patients were obtained.

Results: Among 42 subjects, mean ± SD age for cases and controls was 35.8 ± 10.2 and 43.2 ± 11.5. Male to female ratios were 1:1.4 and 1:5, respectively. Cases had significantly larger differences in nerve thickness, T2SIR and CNR than controls for IAN and LN [p values = 0.01 & 0.0001, 0.012 & 0.005 and 0.01 & 0.01, respectively]. ROC analysis showed significant association among differences in nerve thickness, T2SIR and CNR and nerve injury [AUC = 0.83-0.84 for IAN and 0.77-0.78 for LN]. Interobserver agreement was good for IAN [ICC = 0.70 - 0.79] and good to excellent for LN [ICC = 0.75 - 0.85]. MRN correlations with NST and surgical classifications were moderate to good. Kappa of 0.60 and 0.77 and Pearson's correlation coefficients of 0.68 and 0.81 were observed for differences in nerve thickness.

Conclusion: MRN can be reliably used in diagnosis of PTN injuries related to molar tooth extractions with good to excellent correlation of imaging with clinical findings and surgical results.

Author Disclosures:

J.R. Zuniga: Consultant; AxoGen Inc., Merz USA., Daiichi Sankyo.

A. Chhabra: Consultant; ICON Medical, unrelated to this presentation. Other; Book Royalties; Jaypee, Wolters, unrelated to presentation.

B-0073 11:26

DKI can early differentiate radio-insensitive human nasopharyngeal carcinoma xenograft in nude mice

X. Zheng, Y.Y. Chen, Y. Xiao, D. Zheng; Fuzhou/CN

Purpose: To explore the feasibility of DKI sequence in early differentiating radio-insensitivity of nasopharyngeal carcinoma xenografts in nude mice.

Methods and Materials: Seventy-two nude mice were implanted with CNE-1 (low radiosensitivity) and CNE-2 (high radiosensitivity) nasopharyngeal carcinoma cells, and the xenografts were obtained. Then, the mice were underwent fraction irradiation separately. Nude mice of each cell line were randomly divided into non-irradiated group (G0), 10Gy group (G1), 20Gy group (G2), 30Gy group (G3) and 3 and 5 days after the whole dose irradiation group (G4, G5). DKI sequence was performed on each group. Volumes, parameters D and K were measured by two experienced radiologists double blindly. Student's t test and receiver operating characteristic (ROC) curve analyses were included in our study. Significant level α was chosen as 0.05.

Results: The difference of volumes' shrink rate between CNE-1 and 2 were first found in G2, with the shrink rate of 5.954% and 27.716% ($p=0.032$). D value decreased first (D_{G1} , $p=0.001$) and then increased, K value increased first (K_{G1} , $p=0.001$) and then decreased after irradiation in CNE-2, but not in CNE-1 xenografts ($p>0.05$). The AUC of D_{G1} and K_{G1} were 0.875 and 0.917, with sensitivity of 0.667 and 0.833, specificity of 1.000 and 1.000, respectively, in the cutoff values $1.27 \times 10^{-3} \text{mm}^2/\text{s}$ of parameter D and 0.88 of parameter K.

Conclusion: Both D and K can early (before volumes changed) distinguish radio-insensitive NPC xenografts from others. D_{G1} and K_{G1} may be the most useful parameters.

B-0074 11:34

Application of dynamic contrast-enhanced MRI and diffusion-weighted imaging in differentiating nasopharyngeal carcinoma and nasopharyngeal lymphoma

C. Song, C. Jingliang; Zhengzhou/CN (songchengru@126.com)

Purpose: To evaluate the utility of DCE-MRI and DWI in the differentiation of nasopharyngeal carcinoma (NPC) and nasopharyngeal lymphoma (NPL).

Methods and Materials: 42 NPC patients and 27 NPL patients were recruited and underwent conventional MRI and DCE-MRI. The MR signals, time signal-intensity curves (TIC) types, time to peak (TTP), enhancement peak (EP), maximum contrast enhancement ratio (MCEr), mean ADC value, and relative ADC value of all the subjects were calculated and analyzed, thereafter, inter-group comparison was performed. The threshold values of ADC and rADC for differentiating NPC from NPL were determined using a ROC analysis.

Results: For NPC group, 32 cases (76.19%) demonstrated obvious heterogeneous enhancement. The mean TTP, EP, MCEr and WR were 48.29s, 1475.38, 136.89% and 16.81, respectively. For NPL group, 24 cases (88.89%) demonstrated obvious homogeneous enhancement. The mean TTP, EP, MCEr and WR were 63.21s, 1161.82, 113.47% and 7.39, respectively. The ADC and rADC value were $842.34 \times 10^{-6} \text{mm}^2/\text{s}$ and 0.74 in NPC, whereas $652.15 \times 10^{-6} \text{mm}^2/\text{s}$ and 0.56 in NPL. The differences of above parameters between NPC and NPL were statistically significant ($P<0.05$). The TTP of NPC was lower than that of NPL, whereas the opposite for the remaining parameters. The best differentiate threshold value of ADC and rADC were $736.5 \times 10^{-6} \text{mm}^2/\text{s}$, $634.0 \times 10^{-6} \text{mm}^2/\text{s}$, respectively. While the AUC, sensitivity, specificity and Youden index of ADC and rADC were 0.943, 0.909, 0.852, 0.761, and 0.951, 0.955, 0.852, 0.77, respectively. rADC value was slightly superior to ADC value in differentiation.

Conclusion: DCE-MRI and DWI are effective in differentiating NPC from NPL.

B-0075 11:42

Shape-based and quantitative MRI radiomic features in the assessment of non-metastatic nasopharyngeal carcinoma

R. Du, P.-L. Khong, H. Yuan, D.L. Kwong, V.H. Lee, V. Vardhanabathi; Hong Kong/HK (du94@hku.hk)

Purpose: To investigate the association between MRI radiomic features and progression-free survival (PFS) of patients with nasopharyngeal carcinoma (NPC) after treatment.

Methods and Materials: A cohort of 100 patients with histologically confirmed NPC that underwent standard treatment was retrospectively obtained. A total of 102 radiomic features were extracted from contrast-enhanced T1-weighted (CE-T1W) scans acquired at diagnosis. Univariate and multivariate analysis was conducted to assess the association between radiomic features and PFS. Mann-Whitney U test and log-rank test of Kaplan-Meier estimate was conducted for univariate analysis. Minimum redundancy and maximum relevance feature selection was used to select the most optimum subset of features for multivariate analysis. Logistic regression and support vector machine were trained with the selected features and validated using 5x8 repeated k-fold cross validation. The performance of the models was assessed by receiver operator characteristic analysis.

Results: Both univariate and multivariate analysis has identified the shape feature tumour sphericity to be significantly associated with 3-year PFS (Mann-Whitney U test: $p < 0.0001$; log rank: $p < 0.0001$; logistic regression: $\text{AUC}=0.765$; SVM: $\text{AUC}=0.799$). No significant separation in PFS was seen with clinical staging. No increase in performance was found with multivariate models.

Conclusion: There is a significant association between MRI radiomic features and PFS of NPC patients after standard treatment. Tumour sphericity has been identified to be most correlated to 3-year PFS. Radiomic models could potentially offer a non-invasive method of predicting treatment outcomes.

10:30 - 12:00

Room E1

Breast

SS 202a

Digital breast tomosynthesis (DBT)

Moderators:

N.N.

S. Zackrisson; Malmö/SE

K-03 10:30

Keynote lecture

G. Forrai; Budapest/HU

B-0076 10:39

Digital breast tomosynthesis vs digital mammography: early performance measures in a population-based screening programme

T. Hovda¹, A.S. Holen², H. Bjørndal¹, S. Sebuodegård², S. Hofvind²; ¹Drammen/NO, ²Oslo/NO (tone.hovda@vestreviken.no)

Purpose: Screening with digital breast tomosynthesis (DBT) in combination with digital mammography (DM) has demonstrated a higher rate of recalls and screen-detected breast cancer compared with DM alone. We aimed at comparing results of early performance measures when screening with synthetic mammography (SM) and DBT vs DM alone in BreastScreen Norway.

Methods and Materials: The study group consisted of 37,185 women screened with SM+DBT at the screening unit in Oslo, 2014-2015. Data on DM were acquired from two comparable screening units (Vestfold and Vestre Viken) in the same period ($n=61,743$), comprising the control group. We calculated recall rates and cancer detection rates and performed descriptive analyses comparing the two groups. Two-proportion Z-tests were used to test for statistical significance ($p<0.05$).

Results: The recall rate due to abnormal mammographic findings was 3.4% (1253/37,185) and 3.3% (2038/61,743), $p=0.56$, for SM+DBT and DM, respectively. The rate of screen-detected breast cancer was 9.4 per 1000 screened with SM+DBT and 6.1 per 1000 screened with DM ($p<0.01$). Both the rates of screen-detected ductal carcinoma in situ and invasive breast cancer were statistically significantly higher for SM+DBT compared with DM ($p<0.01$ for both).

Conclusion: The rate of screen-detected breast cancer was about 50% higher for women screened with SM+DBT compared with women screened with DM. This represents one of the largest increases in breast cancer detection between SM+DBT vs DM reported in the literature. Further studies are needed to investigate the benefits and potential harms by detecting additional cancers with DBT.

B-0077 10:47

Digital breast tomosynthesis (DBT) as a primary screening test in a population-based screening programme: interim results of the Trento DBT pilot study

D. Bernardi¹, M. Gentilini¹, M. De Nisi¹, M. Pellegrini¹, C. Fantò¹, M. Valentini¹, V. Sabatino¹, N. Houssami²; ¹Trento/IT, ²Sydney/AU (dnbernardi@gmail.com)

Purpose: To report interim results of a pilot screening study implementing DBT (instead of standard mammography, MX) for all women who prospectively attended an invitation to screening, and to compare screen-detection measures with those obtained two years earlier for a historical cohort screened with MX alone

Methods and Materials: From January to December 2015, according to a study protocol approved by local health authorities, a prospective cohort of 24,060 women presenting for screening had DBT screening. Synthetic 2D images were reconstructed and read in integration with DBT. Cancer detection rate (CDR), recall rate (RR) and positive predictive value for recall (PPV) were calculated, and compared with those measured for a historical cohort of 20,815 women screened with MX, by calculating the rate ratio (rr). Results were then analysed for prevalent and incident screens

Results: CDR per 1000 screens for DBT-screened and MX-screened cohorts were 9.68 versus 5.77, respectively (rr 1.68, 95% CI 1.35-2.09). Recall rates

were 2.76% for DBT and 3.42% for MX (rr 0.81, 95% CI 0.73-0.9). DBT implementation increased the PPV for recall from 16.71 to 35.09 (rr 2.10, 95% CI 1.68-2.62). The results have been confirmed both for prevalent and incident examinations, although the reduction of RR and the increase of PPV have been superior in the prevalent

Conclusion: Population-based implementation of DBT screening was associated with increase in cancer detection, reduction in recall with significantly increase PPV for recall. Our results indicate that DBT screening improves screening-detection metrics however further research needs to assess health benefits

B-0078 10:55

A prospective study on sensitivity and reading time of different reading strategies with DBT + synthetic 2D in breast cancer screening

F. Caumo¹, G. Romanucci², M. Zorzi¹, S. Brunelli²; ¹Padua/IT, ²Verona/IT (francesca.caumo@iov.veneto.it)

Purpose: To compare detection rates (DR) and reading time (RT) of five reading strategies within the DBT+synthetic2D-based mammographic screening program of Verona (Italy).

Methods and Materials: From April 2015 to March 2017, 34,071 50-69-year-old asymptomatic women were screened for breast cancer with DBT+synthetic2D. We compared the sensitivity for invasive cancer (IC) and ductal carcinoma in situ (DCIS) and RT of five reading strategies: (1) double reading, (2) single reading, (3) double reading of synthetic2D plus mediolateral oblique (MLO) or (4) craniocaudal (CC) DBT view, and (5) double reading of synthetic2D plus DBT for suspicious findings (BIRADS 3). We report the relative sensitivities (RS) vs strategy (1) with 95% confidence intervals (95%CI).

Results: Strategy (1) detected 315 cancers (271 IC, 44 DCIS; DR 9.26%); mean RT 180 seconds. Strategy (2) detected 276 cancers (238 IC, 38 DCIS; DR 8.11%). RS 0.88 (95%CI 0.70-1.10, p=0.25); mean RT 90 seconds. Strategy (3) detected 307 cancers (264 IC, 43 DCIS; DR 9.02%). RS 0.97 (95%CI 0.78-1.22, p=0.82); RT 102 seconds. Strategy (4) detected 309 cancers (266 IC, 43 DCIS; DR 9.03%). RS 0.98 (95%CI 0.78-1.23, p=0.86); RT 102 seconds. Strategy (5) detected 245 cancers (213 IC, 32 DCIS; DR 7.49%). RS 0.78 (95%CI 0.61-0.98, p=0.03); RT 66 seconds.

Conclusion: Compared with double reading synthetic2D+DBT, double reading of synthetic2D plus a single DBT view reduces RT by 43% without affecting sensitivity for cancer. DBT+synthetic2D single reading is affected by a clinically (although not statistically) significant loss in sensitivity.

B-0079 11:03

Synthetic 2D mammography can replace digital mammography as an adjunct to digital breast tomosynthesis: experience with a wide angle DBT system

P. Clauser¹, P.A.T. Baltzer¹, P. Kapetas¹, R.A. Woitek¹, M. Weber¹, F. Leone², M. Bernathova¹, T.H. Helbich¹; ¹Vienna/AT, ²Milan/IT (paola.clauser@meduniwien.ac.at)

Purpose: To evaluate the diagnostic performance of synthetic mammography (SM) with wide-angle-digital-breast-tomosynthesis (WA-DBT) compared to digital mammography (DM) alone and with WA-DBT using one view (1v, medio-lateral oblique) and two-view (2v) protocols.

Methods and Materials: Included in this retrospective, IRB-approved, study were 205 patients with 179 lesions (89 malignant, 90 benign) who underwent bilateral 2v DM and WA-DBT at our institution. Standard of reference was histology and/or one year stability. Four blinded readers randomly evaluated images according to BIRADS using five protocols: 2vDM alone; 2vDM with 2vWA-DBT; 2vSM with 2vWA-DBT; 1vDM with 1vWA-DBT and 1vSM with 1vWA-DBT. Lesion detection, sensitivity, specificity, and accuracy were calculated and compared using multivariate analysis. Readers' confidence and image quality were evaluated.

Results: Average detection rate was 75.4% for 2vDM, 80.2% for 2vDM with WA-DBT, 78.5% for 2vSM with WA-DBT, 77.4% 1vDM with WA-DBT, and 75.0% 1vSM with WA-DBT. 2vDM with 2vWA-DBT achieved a higher detection compared to 2vDM alone (P=0.004). No significant differences in detection were found between 2vDM with WA-DBT and 2vSM with WA-DBT (P>0.110). Detection was higher when two-views were available, for both SM and DM (P<0.034). Sensitivity and accuracy were lower with DM alone compared to all other reading protocols (P<0.001). Readers' confidence and image quality were good to very good for all protocols.

Conclusion: WA-DBT combined with DM or SM increases lesion detection, sensitivity and accuracy without reducing specificity, with no differences between SM or DM. Two-view protocols allow a higher detection rate than 1-view protocols using DM or SM.

Author Disclosures:

T.H. Helbich: Grant Recipient; The current study (PI T.H.H.) was supported by Siemens Healthineers, Erlangen, Germany.

B-0081 11:11

Microcalcifications in breast tomosynthesis including synthesised mammography, multiple angulated reconstructions and standard stack reconstructions

C. Neubauer, J. Neubauer, M. Windfuhr-Blum, M. Langer; Freiburg/DE (claudia.neubauer@uniklinik-freiburg.de)

Purpose: Our aim was to compare ratings on depiction, diagnostic accuracy and lesion characterisation of conventional synthesized mammography (SM), multiple angulated mammography reconstructions (INSIGHT3D) and standard stack reconstructions in digital breast tomosynthesis (DBT) for microcalcifications.

Methods and Materials: In our retrospective study we included patients with microcalcifications, who had received a DBT and histology over a period of four months and the same number of normal cases without microcalcifications. Patient's data were deidentified and the images randomised and independently analysed by 3 radiologists regarding the depiction, distribution, morphology and BI-RADS score of microcalcifications in SM, INSIGHT3D and standard stack reconstructions. In addition, the reading time was measured. Friedman and post hoc Nemenyi tests, Cochran's Q and post hoc Wilcoxon sign tests, Fleiss' kappa and receiver operating characteristics were used for statistical analysis.

Results: We included 41 histopathologically proven and 41 normal cases. Depiction of microcalcifications was rated best in stack reconstructions and better in INSIGHT3D than in SM (P<0.001). Reading time was lower in both SM and INSIGHT3D compared to stack reconstructions (P<0.001). Diagnostic accuracy and inter-rater correlation were comparable for all analyses.

Conclusion: Although depiction of microcalcifications was best in stack reconstructions, INSIGHT3D depicts microcalcifications better than SM while maintaining a lower reading time compared to stack reconstructions. Our preliminary assessment suggests INSIGHT3D as a potential successor to SM.

B-0082 11:19

Breast screening with synthetic 2D and digital breast tomosynthesis (DBT): is it really more expensive?

F. Caumo¹, G. Romanucci¹, M. Zorzi², S. Brunelli¹; ¹Verona/IT, ²Padua/IT (francesca.caumo@aulss9.veneto.it)

Purpose: To compare the costs of a breast screening program with synthetic2D + DBT versus full-field digital mammography (FFDM).

Methods and Materials: costs of an organized screening program in Verona using FFDM are known. The same analysis was retrospectively carried out for two consecutive years of breast screening using FFDM (and synthetic2D + DBT only on second level assessment) from 1st April 2014 to 31 march 2015 and synthetic2D + DBT from 1st April 2015 to 31 march 2016. The cost of the entire screening process for single screened woman was calculated by adding: the cost of technology (mammograms, ecotomographs, workstations, PACS space); the cost of staff (radiographers, radiologists, nurses, secretarial staff); the cost of material for invasive assessment.

Results: the cost of the screening program with FFDM (14374 screened women with 76 cancers detected; DR 5.29 per 1,000 screens) was 53.8 euros for single screened woman. The cost of the screening program with FFDM (DBT performed only on second level assessment; 14423 screened women with 78 cancers detected; DR 5.41 per 1,000 screens) was 66.8 euros for single screened woman. The cost of the screening program with synthetic 2D + DBT (16666 screened women with 155 cancers detected; DR 9.30 per 1,000 screens) was 64.2 euros for single screened woman.

Conclusion: the implementation of an organized DBT breast screening has a minimal additional cost compared to FFDM-organized screening, especially if additional cancers are found.

B-0083 11:27

Comparing two visualisation protocols for tomosynthesis in screening: specificity and sensitivity of slabs vs planes plus slabs

V. Iotti, P. Giorgi Rossi, S. Ravaioli, A. Nitrosi, M. Bertolini, E. Bacchini, R. Vacondio, M. Pescarolo, P. Pattacini; Reggio Emilia/IT (valentina.iotti@ausr.it)

Purpose: Tomosynthesis (DBT) showed to be more sensitive than digital mammography (DM), but it needs longer reading time, limiting its introduction as primary screening test. Simplified visualisation protocols have been designed. We compared accuracy of a simplified protocol with slab only vs. a standard protocol of slab plus planes, both integrated with synthetic 2D.

Methods and Materials: All DBTs were acquired in RETomo trial experimental arm. The first set, to estimate specificity, included 894 randomly selected DBT (including 12 cancers), and was read by two radiologists(CAM-RV). The second set included 273 screening DBTs enriched with 24 cancers, 8 of which present in the first set; it was read by one of the first radiologists and another radiologist(RV-SR); 28 cancers with 64 independent readings were used to estimate sensitivity. DBTs were read by both radiologists with both protocols

separated by 3 months wash out. The order of protocol reading was randomly assigned 1:1. Only women that were positive at the screening reading were assessed, to date follow up data for negatives are still not available.

Results: Sensitivity was 82.8% (53/64, 95% confidence interval (95%CI) 71.3-91.1) and 90.6% (95%CI 80.7-96.5) with simplified and standard protocol, respectively ($p=0.19$). In the random screening setting specificity was 97.9% (1727/1764, 95%CI 97.1-98.5) and 96.3% (95%CI 95.3-97.1)($p0.005$). Inter-reader agreement was 0.70 and 0.57 with simplified and standard protocol, respectively. Median reading time decreased by 20%.

Conclusion: A simplified protocol without the presentation of planes, increased DBT specificity and reproducibility, but may have a negative impact on sensitivity.

B-0084 11:35

Overview of early clinical implementation of digital breast tomosynthesis: a single-centre experience
S. Soq, K. Rahmat; Kuala Lumpur/MY (suetwoonsoo@gmail.com)

Purpose: To evaluate the impact of performance of mammographic study before and after the introduction of digital breast tomosynthesis (DBT) into the clinical practice in University of Malaya Medical Centre (UMMC).

Methods and Materials: A retrospective study was conducted on patients who underwent breast biopsy in UMMC from October 2013 to February 2015. The biopsy rate, cancer detection rate, sensitivity and positive predictive values (PPV) were calculated and compared between the groups. Analysis was done using SPSS version 22.0 and a p-value <0.05 was considered as statistical significant different.

Results: The patients were divided into two groups: Full Field Digital Mammography (FFDM) (n = 1250) and FFDM + DBT (n = 2174). Histopathological examination results were the gold standard of the study. The combination of FFDM and DBT resulted in significant reduction of biopsy rate from 57.5% to 37.0% ($p = 0.03$). The cancer detection rates were statistically significant different between FFDM and FFDM + DBT groups from 30.1% to 44.5% ($p<0.03$). The sensitivity and positive predictive value (PPV) were 90% and 36% for FFDM group; and 92% and 38% for FFDM + DBT group, respectively.

Conclusion: The combination of FFDM and DBT significantly reduced biopsy rate and increased the cancer detection rate compared to FFDM alone. The sensitivity and PPV were also increased from 90% to 92% and 36% to 38%, respectively, indicating that incorporation of DBT in mammographic examinations increased the number of true positive cases. A larger cohort study is needed to validate these findings.

B-0085 11:43

Breast screening 2D-mammography or breast tomosynthesis: comparison in terms of cancer detection and recalls
F. Fernandez Valverde, S. Romero Martin, J.L. Raya Povedano, J.E. Gordillo Arnaud; Cordoba/ES (sasaromero@hotmail.com)

Purpose: To evaluate tomosynthesis compared with 2D-mammography in terms of cancer detection and recalls in a screening program. To assess positive predictive value (PPV) of recalls.

Methods and Materials: Prospective study included women (age 50-69) who participated in the breast screening program between January 2015 and December 2016. Three digital mammographs and one tomosynthesis were available, being women appointed for different devices randomly. Blind and independent double reading was the standard practice and five radiologists participated. The study was approved by a regional ethics committee. The comparisons between qualitative variables were performed using the Chi-squared test and p value of less than 0.05 was considered statistically significant.

Results: 39851 women participated. 2180 women were recalled (5.5%) and 214 cancers were detected (5.3/1000 screens). 23783 women were appointed for digital mammographs and 16068 women for tomosynthesis. 1471 recalls occurred with digital mammographs (6.2%) compared with 709 recalls with tomosynthesis (4.4%). It meant a significant decreased of 29% (95%IC: 7.8%-66.2%, $p<0.001$). 122 cancers were detected with digital mammographs (5.1/1000 screens), compared with 92 cancers with tomosynthesis (5.7/1000 screens), showing an increase in cancers detection of 10.5% (95%IC: 1.3%-51.5%, $p=0.425$). PPV of recalls was 8.3% with digital mammographs (122 cancers/1471 recalls) and 13.0% with tomosynthesis (92 cancers/709 recalls), which showed an increase of 36.2% (95%IC: 16.1%-62.4%, $p=0.001$).

Conclusion: The use of tomosynthesis in a breast screening program results in an increase in cancer detection rate and significant decreases in recall rate. Tomosynthesis has also shown a significant increase in PPV recalls.

10:30 - 12:00

Room E2

Neuro

SS 211

Brain tumour: advanced imaging techniques

Moderators:

N.N.

M.M. Thurnher; Vienna/AT

B-0086 10:30

Noncontrast ASL-perfusion in pre-surgical glioma diagnostics
A. Batalov, N. Zakharova, I. Pronin, E. Pogobekyan; Moscow/RU (batalov89@gmail.com)

Purpose: To study the tumor blood flow (TBF) in the supratentorial brain gliomas by ASL-perfusion in comparison with the histopathological characteristics of the tumors.

Methods and Materials: The study group included 126 patients with primary supratentorial gliomas of varying degrees of malignancy. Of them, 35 low-grade gliomas (I-II grade WHO) and 91 high-grade gliomas (41-III grade WHO, 50 - IV grade WHO). 64 female and 62 male aged from 12 and 75 (median-44, interquartile range 30-54). Patients were examined on a 3.0 T MR-tomograph. The pseudo-continuous ASL (pcASL) technique was used to determine tumor blood flow. Post-processing of data was carried out in the ReadyView (GE) program. Tumor blood flow was normalized regarding intact white matter of the semiovalicular center of the contralateral hemisphere was performed. All diagnoses were confirmed histopathologically.

Results: Mean tumor blood flow in the group of low-grade gliomas was 28.85 ± 14.99 ml/100 g/min. Normalized TBF was 1.52 ± 0.77 . In the group of high-grade gliomas, the tumor blood flow was 152.75 ± 92.82 ml/100 g/min. Normalized TBF was 8.09 ± 5.24 . The sensitivity and the specificity of this technique in the differential diagnosis of low-grade and high-grade gliomas was 88.6% and 91.2%, accordingly, AUC 0.958. Cutoff-51 ml/100 g/min or 2.3 (normal blood flow).

Conclusion: ASL-perfusion is a reliable quantitative technique that allows estimating blood flow in gliomas. ASL can be used in differential diagnosis of low-grade and high-grade gliomas at the pre-operative stage. This technique has a high sensitivity (88.6%) and specificity (91.2%).

B-0087 10:38

Building an apparent diffusion coefficient radiomics to yield high diagnostic performance in identifying atypical primary CNS lymphoma mimicking glioblastoma

M. Kim, J. Park, H. Kim; Seoul/KR (manzae.kim@gmail.com)

Purpose: To test the technical feasibility, diagnostic performance, and generalizability of a radiomics model utilizing apparent diffusion coefficient (ADC) for identifying atypical primary central nervous lymphoma (PCNSL) mimicking glioblastoma.

Methods and Materials: This retrospective study was approved by our institutional review board. We used a training set of 112 patients (70 glioblastomas, 42 PCNSLs) and extracted 1618 radiomic features (17 first order, 7 volume and shape, 162 texture, and 1432 wavelet) from their ADC maps and contrast-enhanced T1-weighted images (CE-T1WI). Different combinations of 12 feature selection and 8 classification methods were optimized using 10-fold cross-validation. The model was validated internally and externally, in a set of 42 patients (21 glioblastomas, 21 PCNSLs) and 42 patients (28 glioblastomas, 14 PCNSLs) with atypical PCNSL and compared to the histogram parameters of cerebral blood volume (90% cutoff, CBV90) and ADC (10% cutoff, ADC10) using the area under the ROC curve (AUC).

Results: The ADC radiomics model was optimized with the combination of recursive feature elimination and a random forest classifier (mean AUC= 0.983, stability 2.52%). In internal validation, the ADC model (AUC = 0.984) showed similar performance with CE-T1WI radiomics (AUC = 0.968) and was better than CBV90 (AUC= 0.905) or ADC10 (AUC= 0.787) in atypical PCNSL diagnosis. The ADC radiomics model showed robustness (AUC = 0.944) in external validation.

Conclusion: The ADC radiomics model had good generalizability and yields a better diagnostic performance than single-parameter measurements in identifying atypical PCNSL mimicking glioblastoma.

B-0088 10:46

Wavelet-based reconstructions of dynamic susceptibility MR perfusion: a new method to visualize hypervascular brain tumours

T. Huber, L. Rotkopf, W.G. Kunz, S. Bette, B. Wiestler, J. Gempt, C. Zimmer, W.H. Sommer, K. Thierfelder; *Munich/DE (h-thomas@gmx.de)*

Purpose: Wavelet-based reconstructions of dynamic perfusion datasets offer an innovative and elegant way of vascular visualization. This novel technique has shown benefits in dynamic CT-perfusion datasets, but it has not been applied to MRI yet. The aim of this study was to demonstrate if wavelet-based reconstructions can be transferred to dynamic MR-perfusion datasets (wavelet-MRP) to visualize hypervascular tumours, like glioblastoma.

Methods and Materials: Consecutive preoperative 3T dynamic susceptibility MR perfusion datasets of 46 subjects with glioblastoma (mean age: 63±13.1 years, 18f) were included in this IRB-approved feasibility study. Wavelet-MRP was calculated after initial motion correction using the wavelet transform (Paul wavelet, order 1) of each voxel time course. Five different aspects of image quality were each rated on a 5-point Likert scale and compared to cerebral blood volume (CBV) maps. Quantitative analysis included Weber-contrast and signal-to-noise ratio. Wilcoxon signed-rank test was applied.

Results: Generation of wavelet-MRP was successful in 46/46 subjects (mean time 2.45±12 min). Wavelet-MRP achieved higher scores in all qualitative ratings: tumour depiction (4.02 vs 2.33), contrast enhancement (3.93 vs 2.23), central necrosis (3.86 vs 2.40), morphologic correlation (3.87 vs 2.24), and overall impression (4.00 vs 2.41), all $p < .0001$. Quantitative image analysis showed a higher Weber-contrast (8.08 ± 5.14 vs 2.58 ± 8.43 ; $p < .0001$) and a higher signal-to-noise ratio (3.66 ± 1.67 vs 1.80 ± 8.87 ; $p < .0001$) for wavelet-MRP.

Conclusion: Our study demonstrates the feasibility of wavelet reconstructions in MR perfusion datasets. This method allows a fast and reproducible evaluation of MR-perfusion data and generates maps with a clearer tumour depiction compared to standard CBV maps.

Author Disclosures:

T. Huber: Consultant; Smart Reporting GmbH (not related). **L. Rotkopf:** Consultant; Smart Reporting GmbH (not related). **J. Gempt:** Consultant; Brainlab AG (not related). **C. Zimmer:** Advisory Board; Philips, Bayer Schering, Clinical Neuroradiology (not related). Research/Grant Support; Biogen Idec, Quintiles, MSD Sharp & Dome, Boehringer Ingelheim, Inventive Health Clinical UK Ltd., Advance Cor, Brainsgate, Pfizer, Bayer-Schering, Novartis, Roche, Servier, Penumbra, WCT GmbH, WCT GmbH, Syngis, SSS International Clinical Research, PPD Germany GmbH, Worldwide Clinical Trials Ltd., Phenox, Covidien, Actelion, Medivation, Medtronic, Harrison Clinical Research, Concentric, Pharmtrace, Reverse Medical Corp., Premier Research Germany Ltd., Surpass Medical Ltd. and GlaxoSmithKline (all not related). Speaker; Philips, Bayer Schering (not related). **W.H. Sommer:** Founder; Smart Reporting GmbH, Planerio GmbH.

B-0089 10:54

Differentiation of glioblastoma multiforme and single brain metastasis by the distribution pattern of intratumoural susceptibility sign derived from susceptibility-weighted imaging

H. Kang, S. Jang; *Seoul/KR (knroo@hanmail.net)*

Purpose: The aim of this study is to determine whether the distribution pattern of intratumoural susceptibility sign (ITSS) derived from susceptibility-weighted imaging (SWI) could differentiate glioblastoma multiforme (GBM) and single brain metastasis.

Methods and Materials: 58 intracranial brain neoplasm patients (55 male and 3 female, age 69.8 ± 8.2 years (mean \pm SD), 42 brain metastases and 16 with GBM) were enrolled in this study. These patients underwent examinations that included SWI in addition to conventional magnetic resonance (MR) sequences on a 3T. Two radiologists investigated the distribution patterns of ITSS of the tumours and applied an ITSS grading system based on the degree of the ITSS. Then, we compared the grade of the visibility of ITSS in the central portion of tumours; the inner three-quarter area of tumour volume (CITSS) and in the tumour capsular area; the outside one-quarter area of tumour volume (PITSS) on SWI.

Results: Wilcoxon rank sum test showed that the grades of the CITSS in GBM were statistically higher than brain metastasis ($p < 0.0001$) and the PITSS in GBM was statistically lower than brain metastasis ($p < 0.0001$).

Conclusion: Our findings suggest that there were different characteristics of ITSS between GBM and brain metastasis on SWI due to the profound difference in histologic feature of capillary between the two tumour types. The CITSS within the GBM represents the complex immature neovascularity and blood leakage, and PITSS in the metastasis represents the mechanical disruption of the BBB, lack capillaries and prominent feeding or draining vessels.

B-0090 11:02

In vivo assessment of tumour heterogeneity in WHO 2016 glioma grades using diffusion kurtosis imaging

J.-M. Hempel, J. Schittenhelm, C. Brendle, M. Skardelly, B. Bender, G. Tabatabai, S. Castaneda Vega, U. Ernemann, U. Klose; *Tübingen/DE (johann-martin.hempel@uni-tuebingen.de)*

Purpose: To assess the diagnostic performance of normalized and non-normalized diffusion kurtosis imaging (DKI) metrics extracted from different tumour volume data for grading glioma according to the integrated approach of the revised 2016 WHO classification.

Methods and Materials: Sixty patients with histopathologically confirmed glioma were retrospectively assessed between 01/2013 and 08/2016 from a prospective trial approved by the local institutional review board. Mean kurtosis (MK) and mean diffusivity (MD) metrics from DKI were assessed by two blinded physicians from four different volumes of interest (VOI): whole solid tumour including (VOI_{tu-ed}) and excluding peritumoural oedema (VOI_{tu}), infiltrative zone (VOI_{ed}), and single slice of solid tumour core (VOI_{slice}). Intra-class correlation coefficient (ICC) was calculated to assess inter-rater agreement. One-way ANOVA was used to compare MK between 2016 CNS WHO tumour grades. Friedman's test compared MK and MD of each VOI. Spearman's correlation coefficient was used to correlate MK with 2016 CNS WHO tumour grades. ROC analysis was performed on MK for significant results.

Results: The MK assessment showed excellent inter-rater agreement for each VOI (ICC, 0.906-0.955). MK was significantly lower in IDH^{mutant} astrocytoma (0.40 ± 0.07) than in 1p/19q-confirmed oligodendroglioma (0.54 ± 0.10 , $p = 0.001$) or IDH^{wild-type} glioblastoma (0.68 ± 0.13 , $p < 0.001$). MK and 2016 WHO tumour grades were strongly and positively correlated (VOI_{tu-ed}, $r = 0.684$; VOI_{tu}, $r = 0.734$; VOI_{ed}, $r = 0.625$; VOI_{slice}, $r = 0.698$; $p < 0.001$).

Conclusion: Non-normalized MK values obtained from VOI_{tu} and VOI_{slice} showed the best reproducibility and highest diagnostic performance for stratifying glioma according to the integrated approach of the recent 2016 WHO classification.

Author Disclosures:

J. Schittenhelm: Grant Recipient; Else Übelmesser Foundation (30.19845).

B-0091 11:10

Lipid mapping for grading of gliomas

P. Seow, N. Ramli, A.T. Hernowo, V. Narayanan, J.H. Wong; *Kuala Lumpur/MY (norlisahramli@gmail.com)*

Purpose: To evaluate the potential of lipid map generated from magnetic resonance imaging (MRI) chemical shift gradient echo in-and opposed-phase (IOP) sequence for characterisation lipid landscape and as a tool in grading of gliomas.

Methods and Materials: Forty histologically proven glioma patients underwent a standard MRI tumour protocol with the addition of IOP sequence. The subregions of tumour (solid enhancing, solid non-enhancing, cystic and tumour core) were delineated using snake model (ITK-snap) with reference to structural MRI images (T1, T2, FLAIR, ADC & DWI). The lipid maps were computed based on signal loss ratio (SLR) obtained from IOP imaging. The mean SLR values of the subregions were obtained from the lipid maps after post-processing of the MRI images using SPM12.

Results: The mean SLR of solid non-enhancing portion of tumour (mean SLR_{II} = 0.047, mean SLR_{III} = 0.061, mean SLR_{IV} = 0.079, & $p = 0.003$) and tumour core (mean SLR_{II} = 0.057, mean SLR_{III} = 0.059, mean SLR_{IV} = 0.073, & $p = 0.013$) demonstrated statistically significant differences between the WHO grades (grades II, III & IV). The classification probabilities for solid non-enhancing (grade II ($S_{II} = 0.77$), grade III ($S_{III} = 0.25$) and grade IV ($S_{IV} = 0.67$)) and tumour core (grade II ($S_{II} = 0.60$), grade III ($S_{III} = 0.38$) and grade IV ($S_{IV} = 0.59$)) were higher than the other tumour subregions. Moderate positive correlations were seen between WHO grades with mean SLR on lipid map of solid non-enhancing ($= 0.579$, $p < 0.001$) and tumour core ($= 0.461$, $p = 0.003$).

Conclusion: Lipid quantification via lipid mapping provides useful information on lipid landscape in tumour heterogeneity characterisation of glioma.

B-0092 11:18

Arterial spin labelling and diffusion tensor magnetic resonance imaging-derived metrics for differentiation of post-treatment brain tumour recurrence from tissue necrosis

M. Talaat¹, A. Abdel Razek², L. Elserougy², G. Gaballa²; ¹Kafr Elsheikh/EG, ²Mansoura/EG (dr_MonaTalaat@hotmail.com)

Purpose: Differentiating post-treatment brain tumour recurrence from tissue necrosis using arterial spin labelling (ASL) perfusion and diffusion tensor imaging (DTI)-derived metrics in the enhancing and oedema regions.

Methods and Materials: The study was done on 42 treated brain tumour patients with post-treatment enhancing lesions on MRI. Conventional MRI, ASL, and DTI imaging were done. Tumour blood flow (TBF), fractional anisotropy (FA), and mean diffusivity (MD) were measured at the enhancing

and oedema regions and the values were recorded for each case. Lesions were categorised as recurrence or necrosis by histopathology.

Results: Comparing recurrence to necrosis, there was high significant differences in TBF measured in the enhancing and oedema regions (both $P < 0.001$), accuracy (92.5%, 90%), sensitivity (93.8%, 81.2%), and specificity (91.7%, 95.8%), respectively. FA values revealed significant differences ($P < 0.001$, $P < 0.04$), accuracy (80%, 67.6%), sensitivity (81.2%, 68.8%), and specificity (79.2%, 66.7%), respectively. MD values revealed significant difference (both $p < 0.001$), accuracy (92.5%, 80%), sensitivity (93.8%, 81.2%), and specificity (91.7%, 79.2%), respectively. Combined ASL and DTI metrics of the enhanced lesion revealed AUC of 0.98, accuracy of 95%, sensitivity of 93.8%, and specificity of 95.8%. Combined ASL and DTI metrics values in the peri-lesion oedema revealed AUC of 0.97, accuracy of 92.5%, sensitivity of 93.8%, and specificity of 91.7%.

Conclusion: ASL and DTI metrics in enhancing and oedema regions are valuable non-invasive tools in differentiating post-treatment recurrent brain tumour from tissue necrosis using individual and combined metrics.

B-0093 11:26

Histogram analysis of diffusion kurtosis imaging estimates for in vivo assessment of 2016 WHO glioma grades

J.-M. Hempel, J. Schittenhelm, C. Brendle, B. Bender, M. Skardelly, G. Tabatabai, S. Castaneda Vega, U. Ernemann, U. Klose; *Tübingen/DE (johann-martin.hempel@uni-tuebingen.de)*

Purpose: To assess the diagnostic performance of histogram analysis of diffusion kurtosis imaging (DKI) maps for in vivo assessment of the 2016 World Health Organization Classification of Tumours of the Central Nervous System (2016 CNS WHO) integrated glioma grades.

Methods and Materials: Seventy-seven patients with histopathologically confirmed glioma who provided written informed consent were retrospectively assessed between 01/2014 and 03/2017 from a prospective trial approved by the local institutional review board. Ten histogram parameters of mean kurtosis (MK) and mean diffusivity (MD) metrics from DKI were independently assessed by two blinded physicians from a volume of interest around the entire solid tumour. One-way ANOVA was used to compare MK and MD histogram parameter values between 2016 CNS WHO-based tumour grades. Receiver operating characteristic analysis was performed on MK and MD histogram parameters for significant results.

Results: The 25th, 50th, 75th, and 90th percentiles of MK and average MK showed significant differences between IDH1/2_{wild-type} gliomas, IDH1/2_{mutated} gliomas, and oligodendrogliomas with chromosome 1p/19q loss of heterozygosity and IDH1/2_{mutation} ($p < 0.001$). The 50th, 75th, and 90th percentiles showed a slightly higher diagnostic performance (area under the curve (AUC) range; 0.868-0.991) than average MK (AUC range; 0.855-0.988) in classifying glioma according to the integrated approach of 2016 CNS WHO.

Conclusion: Histogram analysis of DKI can stratify gliomas according to the integrated approach of 2016 CNS WHO. The 50th (median), 75th, and the 90th percentiles showed the highest diagnostic performance. However, the average MK is also robust and feasible in routine clinical practice.

Author Disclosures:

J. Schittenhelm: Grant Recipient; Else Übelmesser Foundation (30.19845).

B-0094 11:34

Differentiating primary CNS lymphomas from glioblastomas and inflammatory demyelinating pseudotumour using relative minimum apparent diffusion coefficients

J. Wen; *Shanghai/CN (wen123jianbo@163.com)*

Purpose: Our purpose was to evaluate the diagnostic performance of diffusion-weighted imaging (DWI), the relative ADCmin (rADCmin) in differentiating primary central nervous system lymphomas (PCNSL) from glioblastomas (GBM) and inflammatory demyelinating pseudotumours (IDP).

Methods and Materials: MRI images were reviewed retrospectively in 82 patients including 39 PCNSLs, 35 GBMs, and 8 IDPs. Regions of interest (ROI) were drawn around the tumour on contrast-enhanced images, these images were transferred onto coregistered ADC maps to obtain the minimum ADC (ADCmin) and the normalized ADCmin ratios (rADCmin) were calculated using the formula $rADCmin = ADCmin \text{ of the lesion} / ADCmin \text{ of the normal white matter}$. The rADCmin values were compared between PCNSLs, GBMs and IDPs using the ANOVA test. ROC curves were constructed to evaluate the diagnostic performance of rADCmin values and to determine the optimum thresholds. Simple logistic regression was analysed to evaluate the relationship between ADCs and tumour cellularity.

Results: The rADCmin value was significantly lower in PCNSLs (0.675±0.113) than GBMs (0.765±0.059) and IDPs (0.834±0.067) (PCNSL vs GBM, $p < 0.001$; PCNSL vs IDP, $p < 0.001$). rADCmin was a significant assessor for differentiating PCNSLs from non-PCNSLs ($p < 0.001$). The optimal cut-off value was 0.722 (sensitivity: 74.5%; specificity: 74.1%; AUC: 0.803) on ROC analysis. A stronger negative correlation ($r = -0.755$, $p = 0.000$) was obtained between the cytoplasm and rADCmin.

Conclusion: rADCmin value is helpful in differentiating PCNSL from GBM and IDP. Thus, ADC values may provide a useful supplement to the information obtained from conventional contrast-enhanced MR imaging, and assist in future treatment planning.

B-0095 11:42

Percentage signal recovery (PSR) calculated from dynamic susceptibility contrast perfusion MRI: accuracy in differentiating various enhancing intracranial mass lesions

J.P. Sharma, T. Singh, K. Singh, I. Mohapatra, M. Singh; *Gurgaon/IN (doc.sharmajai24@gmail.com)*

Purpose: To determine whether percentage signal recovery (PSR) derived from dynamic susceptibility-weighted contrast (DSC)-enhanced perfusion MR imaging is accurate in differentiating various enhancing intracranial mass lesions like GBM, metastasis, lymphoma and tuberculoma.

Methods and Materials: This prospective study included 65 patients who underwent DSC perfusion MRI. T2* mean signal intensity recovery curves were drawn to calculate minimum, maximum, mean and relative PSR (rPSR). Accuracy of these parameters was assessed using ROC curves, one-way ANOVA, Student's t test and Chi-square test.

Results: Minimum, maximum, mean, rPSR were much higher in lymphoma (149.6, 216.6, 198.2, $2.16 \pm SD$) as compared to GBM (65.0, 86.7, 78.2, 0.91), tuberculoma (85.5, 122.3, 131.5, 1.54) and metastasis (52.9, 74.3, 63.9, 0.75). Mean curve in all cases of lymphoma crossed above the baseline. ROC curves of minimum, maximum, mean, rPSR for differentiating lymphoma from others (GBM, tuberculoma, metastasis) yield high AUC values of 0.987, 0.988, 0.963 and 0.961, respectively ($p < 0.0001$) and sensitivity of 100%, specificity of 93.0%, 96.5%, 94.7% and 94.7% with optimum cut-off of 108, 147.5, 136.0 and 1.55, respectively. ROC curves of minimum, maximum, mean, rPSR for differentiating metastasis from others (GBM, lymphoma, tuberculoma) yield AUC values of 0.800, 0.803, 0.804, 0.839, respectively, with $p < 0.001$. Similar ROC curves for differentiating tuberculoma from GBM, lymphoma and metastasis yield AUC values of 0.627, 0.722, 0.748 and 0.744 with $p < 0.05$ for mean PSR and rPSR.

Conclusion: PSR is a practical and simplified perfusion MRI parameter which is effective in differentiating lymphoma and metastasis from other enhancing lesions with high sensitivity and specificity.

B-0096 11:50

qMRI using relaxometry detects non-visible peritumoural contrast enhancement in malignant gliomas

I. Blystad^{1,1}, J.B. Warntjes^{1,1}, O. Smedby^{2,1}, P. Lundberg^{1,1}, E.-M.B. Larsson^{3,1}, A. Tisell^{1,1}, ¹Linköping/SE, ²Huddinge/SE, ³Uppsala/SE (ida.blystad@regionostergotland.se)

Purpose: Malignant gliomas are diffusely growing, infiltrative tumours. This study was performed to investigate if there is non-visible contrast enhancement in the peritumoural area of malignant gliomas using relaxometry with synthetic magnetic resonance imaging (syMRI).

Methods and Materials: 25 patients with a radiological appearance of malignant glioma were included. The quantitative MR-sequence (MAGIC), measuring longitudinal relaxation (R_1), transverse relaxation (R_2) and proton density (PD), was added to the standard MRI protocol before surgery. Diagnosis was confirmed by histopathology. Five patients were excluded, three due to another diagnosis and two due to motion during MR examination. In 20 patients, synthetic MR images were created from the quantitative scan. Manual regions of interest (ROIs) outlined the visibly contrast-enhancing border of the tumours and the peritumoural area in conventional and synthetic images. Contrast enhancement was quantified by subtraction of native images from post-Gd-images, creating T1- and R_1 -difference maps, where the ROIs were used to analyse the tissue of interest. Peritumoural T1- and R_1 -differences were normalized to the normal appearing white matter in the contralateral hemisphere. A one-sided T test was performed on the peritumoural- and the NAWM-ROIs.

Results: The malignant gliomas have heterogeneous relaxometry values. After normalization to normal appearing white matter, the quantitative R_1 -difference maps showed significant, non-visible contrast enhancement in the peritumoural area ($p < 0.001$), whereas conventional spin echo images did not.

Conclusion: Relaxometry detects non-visible contrast enhancement in the peritumoural area of malignant gliomas. This could represent infiltrative tumour growth.

Author Disclosures:

J.B. Warntjes: Employee; Part-time employed by Synthetic MR AB.

10:30 - 12:00

Room F2

Breast

SS 202b

Challenging topics in breast imaging

Moderators:

A. Frigerio; Turin/IT
J. Tanner; Cambridge/UK

B-0097 10:30

Vascular calcification on mammography and coronary artery disease identified by computed tomography

S.L. [McLenachan](#), M. Williams, F. Camilleri, D.E. Newby; *Edinburgh/UK*
(suzannemclenachan@gmail.com)

Purpose: This sub-study of the SCOT-HEART randomised controlled trial of computed tomography coronary angiography (CTCA) in patients with suspected stable angina aimed to assess the prevalence of breast arterial calcification (BAC) and associations with cardiovascular risk factors, coronary artery calcification, coronary artery disease on CTCA and subsequent outcomes.

Methods and Materials: 405 female participants underwent CTCA and subsequent mammography. Mammograms were assessed for the presence of BAC.

Results: BAC was identified in 92 (23%) patients who were slightly older (62.9±6.6 versus 58.6±8.0 years; $p<0.001$), had higher cardiovascular risk scores (19.0±17 versus 16.7±10.5; $p=0.018$) and were more likely to be non-smokers (73% versus 51%; $p<0.001$). Age and non-smoking status were the only independent risk factors for BAC. Coronary artery calcification was present in 57 (62%) patients with BAC (relative risk 1.26 (95% confidence intervals 1.04-1.53, $p=0.02$). In patients with BAC, non-obstructive coronary artery disease was identified in 38 (14%) and obstructive coronary artery disease in 19 (21%). Patients with BAC were more likely to have obstructive coronary artery disease (relative risk 1.66 (95% confidence intervals 1.01-2.73; $p=0.046$), but this had poor discrimination (AUC 0.560, $p=0.149$) and was not independent of age or cardiovascular risk factors. Fatal or non-fatal myocardial infarction at 3 years occurred in one patient with BAC (1.1%) and three without BAC (1.0%, $p=0.649$).

Conclusion: BAC occurs in one-fifth of the patients referred for assessment of suspected coronary artery disease, but is not associated with traditional cardiovascular risk factors and is a poor discriminator for obstructive coronary artery disease.

Author Disclosures:

D.E. Newby: Speaker; Toshiba Medical Systems.

B-0098 10:38

Should breast artery calcifications be graded?

Ç.M. [Altay](#)¹, E. Düsünceli Atman², C. Uzun², M.F. Arslan²; ¹*Karabük/TR*, ²*Ankara/TR* (cetinmurataltay@gmail.com)

Purpose: The aim of this study was to determine the relationship between the severity of mammographically detected breast arterial calcifications (BACs) and severity of coronary artery calcium (CAC) score on ECG gating coronary artery computed tomography angiography (CA-CTA).

Methods and Materials: Between July 2011- September 2016, 112 women (age 40-72 years, mean 55.3±8.8) who underwent both mammography and ECG gating CA-CTA were reviewed to determine BACs and CAC score, retrospectively. The exclusion criteria were determined a. malignant microcalcification on mammography, b. previous breast surgery, c. chest radiotherapy, d. chemotherapy for any reason, e. coronary bypass and stenting. BACs on mammography and CAC score on CA-CTA were identified with radiological consensus. BACs were graded in three groups, grade 1: no calcification, grade 2: dot like calcifications and grade 3: linear calcifications on any artery. The computer software was utilized to calculating CAC score.

Results: The rate of patients with left BACs was 15.2% (n:17) and right BACs was 15.2% (n:17). Patients with BACs were older than patients without BACs ($p<0.001$). The presence of right or left BACs predicted with 47.2% sensitivity and 96.1% specificity in patients with CAC ≥1. Positive correlation was detected between BACs severity grading and CAC score ($p<0.001$). CAC score was higher in patients with high BACs grade.

Conclusion: BACs are an indicator of presence of CAC. The relationship between BACs and CAC was evaluated from a different point of view in the general literature. BACs grading is an indicator of severity of CAC score.

B-0099 10:46

Breast arterial calcification on screening mammography can predict significant coronary artery disease in women

B.S. [Kelly](#), E. Heffernan, S. McNally; *Dublin/IE* (brendanskelly@me.com)

Purpose: Breast arterial calcification (BAC) on digital mammography has been associated with an increased risk of coronary artery disease (CAD). We aimed to investigate the association of BAC with findings on coronary computed tomography angiography (CCTA) within a symptomatic cohort of women from the national breast screening programme (BreastCheck).

Methods and Materials: Data of symptomatic women (chest pain) aged between 50 and 65 years who underwent a CCTA and who also had a screening mammography between 2014 and 2015 were recorded. BAC and CAD-RADS™: Coronary Artery Disease-Reporting and Data System were scored by separate blinded specialist radiologists. Cardiac risk factors were recorded. Patients' cardiac follow-up (with exercise stress test, percutaneous coronary intervention or echocardiography) and cardio-protective medications were also documented.

Results: 219 eligible women underwent a CCTA. Of these, 104 patients also underwent digital mammography. Using standard linear regression, BAC was identified as the only significant predictor of CAD-RADS ≥3 disease. Using binomial logistic regression, BAC remained independently associated with CAD-RADS ≥3 ($p=0.023$). A significantly higher proportion of patients with BAC >1 were on cardio-protective medications ($p=0.041$) and had medications initiated or changed, or had further cardiac investigation ($p=0.037$ and $p=0.019$, respectively) than those with no BAC, after a mean follow-up of 20.6 (range 15-27) months.

Conclusion: BAC diagnosed on 2 yearly screening mammography predicts CAD-RADS ≥3 disease in symptomatic patients.

B-0100 10:54

Comparing computer-aided diagnosis (CAD) system with manual method for detecting breast arterial calcification (BAC)

A.N. [Kamble](#), M. Popli; *New Delhi/IN* (akshaykumar.kamble92@gmail.com)

Purpose: Cardiovascular disease pathogenesis starts from vessel changes due to chronic conditions like diabetes and hypertension. Breast arterial calcification (BAC) provides the unique opportunity to screen women for these vascular changes, but unfortunately, they are often ignored in the final report.

Methods and Materials: 299 women were screened with mammography. BAC was evaluated first by manual method followed by CAD method to prevent bias from CAD results. Grading of BAC was done from grade 1 to grade 3. The manual method of detecting BAC, after being confirmed by two readers, was taken as gold standard. 299 women were screened with mammography. Manual method of detecting BAC, after being confirmed by two readers, was taken as gold standard.

Results: There was the statistically significant difference between BAC detected by CAD method and manual method (chi-squared 116.4, $p<0.0001$). Sensitivity of detecting BAC by CAD method was only 56.10%, though it had good specificity 97.67%. Area under curve (AUC) was 0.77, positive predictive value being only 78.83%. CAD detected grade 2 and 3 calcifications with more accuracy than grade 1 calcifications ($p<0.0001$).

Conclusion: CAD has still a long way to go before it could match the sensitivity of manual method of BAC detection. Even though specificity of CAD is good, it cannot replace manual method for detection of breast arterial calcifications.

B-0101 11:02

Do we diagnose it better? - new BI-RADS classification for microcalcifications

J. [Vucetic](#), M. Ortega Millán, J. Rivera Mata, J. Palao Errando, C. Barber Hueso, R. Garcia Garcia; *Valencia/ES* (vucetic_jelena@yahoo.com)

Purpose: To analyze all microcalcification biopsies performed after the publication of new edition of BI-RADS and compare it to our previous approach.

Methods and Materials: A retrospective review was performed for all microcalcification biopsies carried on in our center between June 2013 and May 2017. The cutpoint for two groups was the implementation of the new BI-RADS classification (May 2015), where low suspicion microcalcifications previously classified as BI-RADS 3 (no biopsy), passed to BI-RADS 4a (biopsy). Histology results were reviewed. Fisher's exact test was performed and p-values less than 0.05 were considered statistically significant.

Results: There were 19,086 mammograms performed in the cited period. A total of 269 patients with diagnosed microcalcifications were biopsied. In the period previous to the cut-point there were 86 biopsies and 23 cancers were detected (26.74%). After the new BI-RADS recommendations were implemented in our screening units, we experienced over two fold increase in biopsies performed, 183 biopsies, yet only 37 cancers diagnosed (20.22%). This increase in cancer diagnosis was not significant, $p=0.271$. The increase in

diagnosis of carcinoma in situ (CIS) was also not significant (21 vs 34, $p=0.259$).

Conclusion: Change in management of microcalcifications led to increase in number of biopsies performed as well as cancers diagnosed, especially CIS, although this increase is not significant in our series. It is yet to be seen if diagnosing more CIS reduces the rate of finding infiltrative cancers in years to come.

B-0102 11:10

Incidental breast lesions on chest computed tomography: prevalence, clinical significance, and differential features for referral

Y. Choi, C.H. Park, G. Hye Mi, T.H. Kim, E. Son; *Seoul/KR*

Purpose: With increasing use of chest CT, incidental breast lesions are increasingly being encountered. It is important that clinicians be familiar with CT characteristics of breast lesions. The aims of this study were to evaluate the CT features of incidental breast lesions on chest CT and to suggest useful criteria for referral to specialist breast units.

Methods and Materials: Between May 2009 and April 2014, 12268 chest CT reports containing the keyword "breast" were reviewed retrospectively. Patients with known breast disease or who had undergone non-enhanced CT examination were excluded. Patients who were referred to specialist breast units and then underwent pathological confirmation or follow-up over a 1-year period were included. Finally, 86 patients were enrolled. Two chest radiologists evaluated lesion characteristics, including size, location, shape, margins, and enhancement ratio. The correlations between the CT features and breast pathologies were evaluated, and overall diagnostic accuracy of CT features in various combinations was assessed to diagnose breast cancer.

Results: Overall, the malignancy rate of incidental breast masses on chest CT was 16.3%. Among the CT features, irregular shape, non-circumscribed margin, and enhancement ratio > 1 were significantly different between malignant and benign lesions. The combination of non-circumscribed margin and high contrast enhancement had the highest accuracy (97.7%).

Conclusion: Reliable CT features for incidental malignant breast masses are irregular shape, non-circumscribed margin, and high contrast enhancement. The combination of non-circumscribed margin and high contrast enhancement could help distinguish incidental malignant breast lesions on chest CT and indicate referral to specialized breast units.

B-0103 11:18

Breast MRI: internal thoracic artery lymph node assessment in patients with invasive breast carcinoma

M. Nadrljanski, Z. Milosevic; *Belgrade/RS (dr.m.nadrljanski@gmail.com)*

Purpose: To assess MRI features of physiological and metastatic internal thoracic artery (ITA) lymph nodes (LNs).

Methods and Materials: Thirty-four patients with T2 category histologically confirmed invasive breast carcinoma ($n_1=18$ physiological LNs; $n_2=16$ metastatic LNs), were assessed with DCE-MRI (1.5T) and DWI-ADC (b 0, 1000) for the morpho-functional features of LNs: short axis, long axis, short-to-long axis ratio, DWI-ADC and positive enhancement integral (PEI) values.

Results: Difference in morphologic features (short axis, long axis) between physiologic and metastatic LNs was considered highly statistically significant (short axis: 7.68 ± 0.87 mm vs. 4.50 ± 0.86 mm, $p<0.0001$; 13.0 ± 1.75 mm vs. 8.62 ± 1.61 mm, $p<0.0001$). The same applied for DWI-ADC value (0.58 ± 0.06 vs. 0.80 ± 0.05 , $p<0.0001$). However, the difference in the short-to-long axis ratio and PEI values between the two subgroups was not considered highly statistically significant (0.59 ± 0.08 vs. 0.53 ± 0.09 mm, $p=0.002$; 636.97 ± 74.50 vs. 530.44 ± 68.85 , $p=0.002$). No significant correlation was detected in the subgroup of metastatic LNs between the selected morphologic and functional parameters.

Conclusion: Morphologic LN features like short and long axis, and DWI-ADC values may contribute to better discrimination between physiological and metastatic ITA LNs in patients with invasive breast carcinoma.

B-0104 11:26

Comparison of invasive lobular and invasive ductal carcinomas of the breast using 3T DCE-MRI

T. Torheim, R. Woitek, A.J. Patterson, R. Bedair, I.A. Mendichovszky, C. Caldas, F. Markowitz, F.J. Gilbert; *Cambridge/UK (Turid.Torheim@cruk.cam.ac.uk)*

Purpose: To compare the dynamic contrast-enhanced (DCE) magnetic resonance imaging (MRI) characteristics of invasive lobular carcinomas (ILC) and invasive ductal carcinomas (IDC) of the breast.

Methods and Materials: In this prospective study, 48 patients with biopsy-proven IDC ($n = 30$, mean age 59 years, range 32 - 83) or ILC ($n = 18$, mean age 58 years, range 38 - 81) underwent 3T DCE-MRI prior to surgery. Following motion correction, pharmacokinetic maps (K^{trans} , v_e , k_{ep}) were calculated using the standard Tofts model with T1 mapping and B1 inhomogeneity correction. Distribution measures of mean, median, skewness

and kurtosis for each parameter within the lesions were calculated and compared between the two subtypes using Wilcoxon's signed-rank test.

Results: The k_{ep} parameter was most sensitive to differentiate between IDC and ILC, showing significant differences in all distributional measures (p values < 0.05). ILC had lower k_{ep} values, with a more skewed parameter distribution compared to IDC cases. Apart from K^{trans} being skewed towards lower values in ILC (p value 0.04), there were no significant differences between the two subtypes regarding v_e and K^{trans} .

Conclusion: Our results show that the k_{ep} parameter, which is representative of contrast agent washout, is more sensitive to the difference between ILC and IDC than the more commonly reported K^{trans} and v_e parameters. This highlights a difference in uptake curve shape between these two subtypes of breast cancer.

B-0105 11:34

Role of diffusion-weighted MRI (DWI) and intravoxel incoherent motion (IVIM) in monitoring treatment response to neoadjuvant chemotherapy in locally advanced breast cancer

M.F.A. Kamis¹, K. Rahmat¹, M.T. Ramli Hamid²; ¹Kuala Lumpur/MY, ²Selangor/MY (fandi_mohd@yahoo.com)

Purpose: This study is to investigate diffusion weighted MRI (DWI) and changes in IVIM parameters [Random diffusion(D) and functional fraction(f)] of invasive breast carcinoma in patients undergoing neoadjuvant chemotherapy (NACT). We also aim to evaluate baseline MRI imaging phenotypes of breast carcinoma versus normal breast tissue (using ADC and IVIM parameters).

Methods and Materials: A prospective study involving women with invasive breast carcinoma ($n= 15$) between the age of 29 to 66 years (mean age=43.4) who are planned for 6 cycles of NACT. DCE MRI were performed at 3 different intervals (Pre-NACT, post-first and third cycles of NACT). DWI data of the target lesions were obtained using ROI measurements. The IVIM parameters (from multiple b-values) were calculated.

Results: Mean ADC values for malignant breast lesion is (0.74×10^{-3} mm²/s) compared to normal breast tissue (1.90×10^{-3} mm²/s). Following the three cycles of NACT, quantitative findings showed increase in mean ADC values (1.29×10^{-3} mm²/s). IVIM parameters showed increase in D-value and reduction of f-value which reflects reduce in microcapillaries density post NACT.

Conclusion: DWI is useful to characterize breast tumour cellularity. ADC values showed significant increase as early as the first cycle of NACT. IVIM parameters provides noninvasive indicator to microperfusion properties of malignant breast lesion, thus may be used as alternatives to monitor the response to NACT for patients with contraindication to gadolinium. These tools are expected to enhance the role of MRI in monitoring treatment response of cancerous lesions in the breast.

B-0106 11:42

The diagnostic performance of automated breast ultrasound (ABUS) compared with handheld ultrasound (HHUS)

M. Yoshida¹, K. Enokido², T. Nishiyama¹; ¹Tokyo/JP, ²Kanagawa/JP (ymiwa2000@gmail.com)

Purpose: For women with dense breasts, the combination of mammographic and ultrasound screening was reported to detect more invasive cancers. However, handheld ultrasound (HHUS) has also some limitations, such as operator dependent and insufficient reproducibility. Automated breast ultrasound (ABUS) which acquires 3-D volume images of whole breast can potentially overcome these limitations of HHUS. The aim of this study was to evaluate the diagnostic performance of ABUS compared to HHUS in terms of the detection and characterization of breast lesions.

Methods and Materials: From January 2016 to May 2017, 390 breasts of 195 women (Median age 43) examined by both HHUS and ABUS: using Invenia ABUS (GE Healthcare Inc.) scanner. Of them, 135 women concurrently underwent mammography. The images were interpreted by more than two physicians who has sufficient experience of breast ultrasound.

Results: BI-RADS assessment categories in ABUS coincided with those in HHUS of 92% (357/390 breasts). Twenty-three lesions, which were diagnosed as cancers, were all classified as BI-RADS 4/5 both in ABUS and in HHUS. Three cancers of them were undetectable by mammography. In 7 cases where the lesions were classified as BI-RADS 4 in ABUS but as BI-RADS 1 in HHUS, those were considered as image artifacts. In most cases with disagreements between ABUS and HHUS, there were mismatches of BI-RADS 2 and BI-RADS 3.

Conclusion: The capability of ABUS for detection and characterization of breast lesions was nearly equivalent to HHUS. It can be further improved by learning more about image artifacts peculiar to ABUS.

B-0107 11:50

Primary tumour location predicts the site of local relapse after nipple-areola complex (NAC)-sparing mastectomy

L. Vassallo¹, N. Tomasi Cont¹, V. Doronzio¹, R. Panzone¹, D. Regge², L. Martincich¹; ¹Candiolo/IT, ²Candiolo-Torino/IT (lorenzo.vassallo1987@libero.it)

Purpose: To evaluate if primary tumour location can predict the site of local relapse after nipple-areola complex (NAC)-sparing mastectomy.

Methods and Materials: 518 consecutive women submitted to NAC-sparing mastectomy in the period between 2010 and 2015 were enrolled in the study. All the patients underwent pre-surgical breast MRI (1.5T magnet) following the recommended technical requirements and intraoperative assessment of NAC status. Subsequently, subjects underwent routine clinical and imaging follow-up. For each local recurrence identified, location and imaging and biological characteristics were evaluated.

Results: Fourteen subcutaneous local relapses (2,7%) occurred over a mean follow-up of 33 months. Mean time to recurrence was 38 months. In all the cases, relapse was observed in patients with highly proliferative primary tumour. Recurrences were identified by clinical examination in eight cases, MRI in five and ultrasound in one. A comparison of clinical-pathological characteristics revealed that primary tumours and local recurrences were located in the same breast quadrant in most of the patients (12/14; 85,7%). No local relapses occurred in women who received radiotherapy. A single case of NAC recurrence developed as a Paget's disease in patient without sub-areolar and proximal nipple duct involvement at mastectomy. MRI findings of local recurrences were represented by small mass lesion with regular margin and rapid early homogeneous enhancement. All of them were located in the same breast quadrant of the primary tumour.

Conclusion: Our study shows that local recurrences after NAC-sparing mastectomy almost invariably develop in the same quadrant where the primary tumour was located.

10:30 - 12:00

Room D

Musculoskeletal

SS 210

Musculoskeletal tumour imaging

Moderators:

R. Arkun; Izmir/TR
B. Henninger; Innsbruck/AT

B-0108 10:30

The performances of radiographic criteria for bone malignancy when applied to computed tomography and magnetic resonance imaging

T. Onal¹, G.O. Afacan¹, G. Akansel², A.S. Arslan², Y. Anik², N. Inan¹, B. Muezzinoglu², F. Corapcioglu²; ¹Istanbul/TR, ²Kocaeli/TR (tugayonalx@gmail.com)

Purpose: The conventional radiological features to differentiate benign from malignant bone lesions were originally described using radiography (XR). When evaluating sectional imaging studies such as MRI and CT one may tend to apply these principles to identify malignant bone lesions. The aim of this study is to evaluate the performances of these radiographic features for detecting malignancy when applied to CT and MRI.

Methods and Materials: Thirty-nine patients with histopathological proof of a high-grade bone malignancy and preoperative imaging data obtained at least with two different modalities were included in the study. Four radiologists reviewed the images and scored the lesions for the distinctness of margins, presence and type of periosteal reaction, matrix mineralisation, and presence of soft tissue mass. The average score for each modality was then tested for accuracy with regard to the histopathology.

Results: When lesion margins were considered, XR was the best modality to detect a high-grade malignancy. MRI, especially post-contrast T1-weighted sequence was the least helpful in this regard. There was no significant difference between CT and XR, nor between CT and MRI. When the periosteal reaction was considered, XR was the best modality to detect the malignant type periosteal reaction. In this regard, MRI and CT were misleading either by not detecting or under-grading periosteal reaction.

Conclusion: Conventional imaging criteria for bone malignancy can be misleading when applied to MRI, or CT. When cross-sectional imaging features contradict with those from XR, the latter should be the guide for clinical management.

B-0109 10:38

Can quantitative diffusion weighted imaging segregate malignant from benign bone lesions? A 3-T MRI feasibility study

A.A.A. Doweidar¹, M.R. Nouh², A.M. Khalil¹, K. Dashti¹; ¹Kuwait/KW, ²Alexandria/EG (ahmeddoweidar1@yahoo.com)

Purpose: The study aims to probe the potential of apparent diffusion coefficient (ADC) in differentiating malignant from benign bone tumours and tumour-like lesions on magnetic resonance imaging (MRI) using multiple b values.

Methods and Materials: We included 50 patients (26 males and 24 females) with 56 primary or secondary malignant bone tumours, benign bone tumours or tumour-like lesions in this study. The diagnosis of all lesions was histopathologically confirmed. The MRI studies were conducted using a 3-T scanner. MRI protocol included diffusion weighted (DW) images using multiple b values. ADC maps were derived from DW-MR imaging data and analysed by two radiologists who were blind to the histopathological results. The mean ADC values were obtained for statistical analyses.

Results: The histopathological results revealed that 39/56 (69.6%) lesions were malignant, 11/56 (19.6%) were benign tumours, 3/56 (5.4%) were tumour-like solid, and 3/56 (5.4%) were tumour-like cystic lesions. The mean ADC values were significantly different in the malignant tumours ($[0.92 \pm 0.35] \times 10^{-3} \text{ mm}^2/\text{s}$) versus benign tumours ($[1.25 \pm 0.37] \times 10^{-3} \text{ mm}^2/\text{s}$) ($p < 0.009$), tumour-like solid lesions ($[1.24 \pm 0.11] \times 10^{-3} \text{ mm}^2/\text{s}$) ($p < 0.026$) and all non-malignant lesions ($[1.36 \pm 0.46] \times 10^{-3} \text{ mm}^2/\text{s}$) ($p < 0.001$). Applying a mean ADC cutoff value of $\leq 1.185 \times 10^{-3} \text{ mm}^2/\text{s}$ for detecting malignancy resulted in a sensitivity of 87.2%, a specificity of 64.7%, and an accuracy of 81.5% (95% confidence interval [CI] 70.1%-93%). The inter-rater reliability was nearly perfect (ICC = 0.969; 95% CI = 0.947-0.982).

Conclusion: Although there was some overlap, DWI proved highly useful in differentiating malignant from benign tumours and tumour-like bony lesions.

B-0110 10:46

mDixon is superior to frequency-selective fat suppression in musculoskeletal tumour imaging

W. Huijgen^{1,2}, C.S. van Rijswijk¹, J.L. Bloem¹; ¹Leiden/NL, ²Den Haag/NL

Purpose: The modified Dixon technique (mDixon) allows reduction of acquisition times relative to conventional Dixon, while reducing sensitivity to B0-inhomogeneity and maintaining the advantages of FSE frequency selective fat saturation techniques. The purpose was to determine the value of mDixon relative to conventional FSE (FSE) in musculoskeletal tumour imaging.

Methods and Materials: In a HIPAA-compliant prospective study, 265 patients who required a musculoskeletal tumour MR scan were included. mDixon and FSE sequences with similar acquisition times were compared in fluid sensitive (T2) and non-fat Gd (Gd) images. Two radiologists, blinded to protocols, scored 9 parameters (5-point scale, paired samples t test) including fat suppression homogeneity, motion artefacts, and overall preference.

Results: Overall, reviewers preferred mDixon in 20% (T2) and 27% (Gd) of cases, preferred FSE in 17% (T2) and 10% (Gd) and had no preference in 63% (T2) and 63% (Gd). The mean score for fat suppression homogeneity in mDixon was superior to FSE by 0.56 points in T2 and 0.65 points in Gd ($p < 0.01$). Highest differences in scores in favour of mDixon were found in cases with susceptibility and magnet inhomogeneity problems. In only 2 cases with motion artefacts FSE performed considerably better.

Conclusion: mDixon showed similar image quality to FSE images, without time penalty, but was superior to FSE when susceptibility artefacts were present. Thus, replacing FSE by mDixon water reconstructions in T2 and Gd-enhanced MSK tumour imaging yields superior image quality without disadvantages. The advantage of Dixon to reconstruct multiple water-fat balanced images was not evaluated.

B-0111 10:54

Feasibility study of intra-voxel incoherent motion MR imaging for the differentiation of benign and malignant soft tissue tumours

Y. Li, C. Ren, J. Cheng; Zhengzhou/CN

Purpose: The purpose is to investigate the application of IVIM and furtherly evaluate the ability of IVIM parameters to differentiate benign and malignant soft tissue tumours.

Methods and Materials: Thirty-five patients with tissue tumours (diagnosed according to biopsy) were included in this study. 21 for benign tumours and 14 for malignancies. All the patients were scanned by IVIM sequence based on a 3T MR scanner. The IVIM scanning was performed with 10 b-values. All the above parameters were measured by drawing ROIs within the periphery of the lesions (P_D, P_Dstar, P_f short for periphery D, periphery Dstar, periphery f) and the center of the lesions (C_D, C_Dstar, C_f short for center D, center Dstar, center f). And the all the parameters were compared by using Mann-Whitney U test with SPSS software (version 16.0). And ROC analysis was performed to assess the sensitivity and specificity of every parameter. The

parameters which showed a significant difference were selected and combined as the feature vectors for the classification by using SVM classifier.

Results: The results revealed that P_D and C_D value is significantly different (P < 0.05). The ROC analysis results showed the ability of the above parameters to differentiate lesions. The AUCs (area under the curve) of P_D and C_D are 0.776 and 0.752 respectively. And the SVM classifier showed a high classification accuracy (82.73%), sensitivity (87%) and specificity (76.45%) for differentiating malignant from the benign lesions.

Conclusion: The IVIM related parameters of tissue diffusivity (D) increases diagnostic confidence of soft tissue tumours.

B-0112 11:02

An artificial intelligence approach for the automatic diagnosis of lipoma and liposarcoma: a pilot radiomics study

L. Malinauskaitė, J. Hofmeister, S. Burgermeister, S. Martin, X. Montet, S. Boudabbous; *Geneva/CH (sana.boudabbous@hcuge.ch)*

Purpose: To assess the contribution of MRI-based radiomics in the automatic diagnosis of lipoma and liposarcoma using artificial intelligence (AI).

Methods and Materials: Lipoma (n=20) and liposarcoma (n=17) were retrospectively identified on histopathological analyses of percutaneous or surgical resection specimen, and their respective pre-operative MRI images were retrieved from our institutional PACS. Two senior radiologists manually segmented these lesions on Spin Echo T1-weighted images. An open-source python library was then used to extract a large number of radiomics features (n=123063) from each lesion. Benign (i.e. lipoma) and malignant (i.e. liposarcoma) discrimination based on radiomics data was achieved through features selection, dimension reduction (using principal component analysis) and classification (using a support vector machine classifier). A *Leave-One-Out Cross-Validation* approach was used to estimate the prediction error of our model due to the medium sample-size.

Results: Our approach achieved an overall classification accuracy of 83,8% in identifying lipoma (versus liposarcoma), with a sensitivity of 100%, specificity of 64,7%, positive predicting value of 76,9% and negative predictive value of 100%.

Conclusion: Our radiomics-based method for classification of lipomatous soft tissue tumor yielded promising results, notably with very high accuracy in identifying benign lesions.

B-0113 11:10

Tumour load in patients with multiple myeloma: β_2 -microglobulin levels vs low-dose whole-body CT

V. Pfahler, M. D'Anastasi, H. Duerr, J. Ricke, A. Baur-Melnyk; *Munich/DE (vanessa.pfahler@med.uni-muenchen.de)*

Purpose: Beta-2-microglobulin is a serum marker of tumour burden in multiple myeloma (MM). Our aim was to correlate serum β_2 -microglobulin levels in patients with MM to tumour mass determined by low-dose whole-body CT.

Methods and Materials: 54 patients with newly diagnosed, untreated MM who underwent low-dose whole-body CT at our department between 2003 and 2014 were included retrospectively. The low-dose whole-body CT scans were assessed by two musculoskeletal radiologists in consensus for focal lesions. The Durie and Salmon PLUS staging System was used for staging patients in stage I-III. β_2 -microglobulin was also subdivided into stage I-III (stage I: < 3,5 mg/L; stage II: 3,5-5,5 mg/L; stage III: > 5,5 mg/L) according to R-ISS.

Results: Using the Durie and Salmon PLUS staging system criteria for image evaluation we were able to identify stage I (low grade) MM in 19 patients, stage II (intermediate) MM in nine patients and stage III (high grade) MM in 26 patients. As expected most patients with stage I disease had normal β_2 -microglobulin levels. However eight of nine patients with stage II MM and 16 of 26 patients with stage III MM had normal β_2 -microglobulin levels. Thus, 24 of 35 patients (68,6%) had 5 or more focal lesions and false-negative β_2 -microglobulin levels.

Conclusion: β_2 -microglobulin may not indicate the full extension of bony disease in a significant subset of myeloma patients.

B-0114 11:18

MRgFUS treatment for painful bone metastases, analysis of non-responders: are there imaging features associated with poor clinical response?

S. Guerri¹, D. Mercatelli¹, C. Gasperini¹, M. Aparisi Gomez², E. Rimondi¹, U. Albisinni¹, A. Napoli³, G. Battista¹, A. Bazzocchi¹; *Bologna/IT, ²Valencia/ES, ³Rome/IT (guerri.sara@gmail.com)*

Purpose: Magnetic resonance guided focused ultrasound (MRgFUS) proved to be effective and safe in the treatment of painful bone metastases. However, a few patients experience poor response. The purpose of this study was to evaluate the existence of imaging features at pre-operative examination predictive of poor outcome.

Methods and Materials: We retrospectively reviewed 19 non-responders (patients with no improvement in VAS score, or pain increase after treatment;

group-A: 20 lesions) and compared them to 20 responders (group-B: 25 lesions), out of more than 150 treatments performed at our Institute. The following quantitative imaging features were analysed: size and type of the lesion (osteolytic/non-osteolytic), extent of anterior/posterior cortex destruction (graded 0-5 on pre-treatment-CT), soft-tissue involvement, pretreatment bone and soft-tissue oedema (graded 0-3 on T2-fat-sat sequences), post-treatment bone oedema, degree of vascularisation, minimum/maximum distance of the skin from the lesion, skin and subcutaneous tissue thickness and the presence of vessels/nerves/synovial structures in the proximity of the lesion. The Chi-Square statistic was used to test frequencies in the two groups. This work has been supported by the "Programma di ricerca Regione-Università, Regione Emilia-Romagna, bando Giovani Ricercatori "Alessandro Liberati" 2013 to AB "Magnetic Resonance guided High Intensity Focused Ultrasound treatment of bone metastases: pain palliation, and local tumor control?".

Results: 55% and 75% of lesions in the group-A showed a bone oedema and a soft tissue oedema, respectively, ≥ 2 (vs. 16% and 32% in the group-B); 70% of lesions in the group-A showed an extent of posterior cortical destruction ≥ 3 (vs. 36% in the group-B).

Conclusion: Larger pre-treatment bone and soft tissue oedema areas and greater posterior cortex destruction are associated with poor outcome in terms of VAS reduction after MRgFUS.

B-0115 11:26

Percutaneous image-guided cryoablation of musculoskeletal metastases to the chest wall: a single-centre experience

C. Lord, L. King; *Southampton/UK*

Purpose: A single-centre experience describing the efficacy and safety of percutaneous image-guided cryoablation for local tumour control in the treatment of musculoskeletal metastases to the chest wall.

Methods and Materials: A retrospective review of consecutive patients treated from October 2011 to October 2017 for the indication of oligometastatic cancer to the chest wall was performed. 9 lesions were treated in 9 patients during the time period. The mean age of the cohort was 67 years (range 56-78), 44% female (4/9) and 56% male (5/9). Serial follow-up imaging was assessed for local tumour control against RECIST 1.1 and MDA criteria.

Results: The 9 lesions (5 renal, 1 lung, 1 colon, 1 breast, 1 ocular melanoma) were followed up for a mean of 1 year 3 months (range 3-35 months). Of the patients with available follow up, local tumour control rates were 89% (8/9) at 3 months and 85% (6/7) at 6 months and 83% at (5/6) at 12 months. 3 patients who had stable disease at 6 month follow up had not yet been imaged beyond 12 months. 3 of the patients who had follow up beyond 20 months showed long term local control. Procedural complication rates were low with 1 patient sustaining a haemothorax requiring drainage without long term sequelae.

Conclusion: Percutaneous image guided cryoablation is a safe and effective treatment for oligometastatic disease to the chest wall and in certain patients can provide long-term disease control.

B-0116 11:34

Radiological changes of giant cell tumour of bone in treatment with Denosumab

S. Bonilla, J. Llauger Rossello, C. Nuñez Peralta, S. Valverde Lavirgen, J. Palmer Sancho; *Barcelona/ES (santibonilla22@gmail.com)*

Purpose: To describe the clinical and radiological progressive changes on giant cell tumour of bone (GCT) on patients in treatment with Denosumab.

Methods and Materials: Retrospective study of 20 patients with GCT confirmed histopathologically with an unresectable tumour, post surgical recurrence or disseminated tumour. The follow up was made with MRI and CT. We analysed the treatment response and the radiological changes of tumoural size, the enhancement, tumoural matrix changes, tumoural margin and the changes of signal in the different MRI sequences.

Results: None of the patients in our study demonstrated a progression of the basal disease and the 55% showed a partial response with the treatment. The radiological changes were diverse but the most important and frequent were the decrease of the tumour size, tumoural enhancement, the changes on the tumoural matrix like peripheral sclerosis and central necrosis and/or justification. The radiological features were confirmed histopathologically. A clinical improvement observed in all the patients was most frequently the pain improvement. Only one patient showed a complication with osteonecrosis of the jaw due to the treatment.

Conclusion: The most important radiological changes were the decrease on tumoural size, tumoural enhancement and the changes on tumoural matrix in patients with partial response. None of all the patients showed a progression of the basal disease and more than a half showed a partial response. The treatment with Denosumab on GCT seems to be useful in the clinical and radiological response on a specific group of patients.

B-0117 11:42

MRI characteristics of 26 onychomatricomas

L. Lassalle¹, S. Eminian², A. Buisson¹, E. Pessis³, R. Campagna¹, N.E. Regnard¹, W. Khaled¹, L. Moya¹, J.L. Drape¹; ¹Paris/FR, ²Clarens/CH, ³Saint Denis/FR (louis.lassalle@gmail.com)

Purpose: Onychomatricomas are rare benign fibroépithélial tumours of the nail matrix. We describe the MRI characteristics of onychomatricomas, and identify subgroups with different imaging features.

Methods and Materials: MRI studies of 26 fingers or toes with histopathologically proven onychomatricomas were retrospectively reviewed by two MSK-radiologists. MRI protocol included T1w, T2w and gadolinium-enhanced T1w sequences. MRI characteristics were noted (size, T1 and T2 signal, enhancement, topography, morphology).

Results: 26 MRI were reviewed: 19 (73.1%) fingers and 7 (26.9%) toes. 18 patients (69.2%) were females, and mean patient age was 52.8yrs (range: 31-76). All tumours presented a proximal head in the matrix cul-de-sac (mean diameter 5.9mm) and distal filamentous expansions included inside the nail plate. The proximal head showed a hyposignal in T1w (69.2%) and T2w sequences (69.2%), and enhancement was present in 55.6%. Lesions had a "hairy" pattern (regular filamentous expansions) in 9 cases and a "cryptic" pattern (irregular filamentous expansions) in 17 cases. "Central" (n = 17) and "lateral" (n = 9) subgroups showed significant differences in location (p = 0.01), in T2 signal (p = 0.03) and height (p = 0.01) of the proximal component, in demarcation with the surrounding dermis (p = 0.02), in the deformity of the nail matrix ("glove finger" invagination) (p = 0.0006), and in the length of the filamentous extensions (p = 0.01).

Conclusion: MRI findings of onychomatricomas are specific and allow differentiating two subgroups according to the "central" or "lateral" location in relation to the nail matrix.

B-0118 11:50

Follow-up of incidental cartilaginous tumours in the knee of middle-aged women

S. Breda, B.A. De Vries, G. Bessems, D. Schiphof, J. Heeringa, G.P. Krestin, M.W. Vernooij, S.M. Bierma-Zeinstra, E. Oei; Rotterdam/NL (s.breda@erasmusmc.nl)

Purpose: Enchondromas are benign cartilaginous tumours frequently found incidentally on MRI of the knee and should be differentiated from low-grade chondrosarcoma. Information on natural course is essential to help clinical decision making regarding need to follow-up. We provide follow-up data of incidental cartilaginous tumours on knee MRI in the large population-based Rotterdam Study.

Methods and Materials: 891 females aged 45-60 (mean 55) years underwent non-contrast bilateral knee MRI (1.5T) at baseline. 700 (79%) participants were re-scanned at 5 years follow-up. We analysed growth by comparing the largest dimension (of three directions) between baseline and follow-up. Measurements were obtained independently by two trained researchers. Lesions >1 cm and/or those with endosteal scalloping or cortical disruption were referred for dynamic contrast-enhanced MRI (DCE-MRI).

Results: In 1782 MR scans, we identified 54 incidental cartilaginous tumours in 46 patients at baseline (5.2%), of which 16 were referred (32.6%). In the absence of malignant features on DCE-MRI, none of referred lesions were treated. Mean follow-up duration was 4.6 years (SD 0.6, range 4-6). Mean largest dimensions were 12.1 mm at baseline (range 4.1-40.6) and 12.5 mm (4.1-44.1) after follow-up for observer 1 and 12.1 mm (4.4-41.3) and 12.8 mm (4.1-44.1) for observer 2, with an intraclass correlation coefficient of 0.99 between both observers for all lesions.

Conclusion: In middle-aged women, incidental cartilaginous tumours are present on 5.2% of knee MRI scans, and show only minor progression after 5 years. No features of low-grade chondrosarcoma were found on additional DCE-MRI of referred lesions.

10:30 - 12:00

Room G

Physics in Medical Imaging

SS 213

Optimisation in clinical radiology practice

Moderators:

E. Samara; Sion/CH
W. Stiller; Heidelberg/DE

B-0119 10:30

Teaching radiation safety intuitively with a head-mounted display

N. Loy Rodas¹, P. Ghimire², M. de Mathelin¹, A. Gangi¹, N. Paddy¹; ¹Strasbourg/FR, ²Dijon/FR (nloyrodas@unistra.fr)

Purpose: A considerable amount of unnecessary exposure and risk underestimation results from a lack of awareness and poor knowledge of the behavior of ionizing radiation during x-ray guided procedures. While current radiation safety training is usually based on courses, lectures and presentations of theoretical aspects, we propose to use a head-mounted display (HMD) to teach intuitively about radiation behavior.

Methods and Materials: A virtual interventional room (C-arm, table, clinicians, and patient) is displayed through an HMD (Microsoft's HoloLens). The user interacts with the scene to set the C-arm angulation and imaging parameters. Virtual color-coded radiation safety information corresponding to the current scene configuration is overlaid in the user's view. The displayed radiation-related data is accurately pre-computed with Monte Carlo simulations.

Results: Through an HMD, the trainee can visualize patient and clinicians' models colored according to their ongoing exposure levels or the 3D propagation of scattered radiation for the current scene configuration. First feedback from users has been promising since the system provides an engaging, game-like and risk-free learning environment. Additionally, it provides an immediate feedback to maximize learning about the effects that altering simultaneously interacting parameters can have on radiation exposure.

Conclusion: Reducing medical radiation exposure requires to increase staff's awareness and knowledge about radiation. We propose to make radiation safety training more intuitive and engaging with HMDs. The trainee can visualize the effect of different C-arm configurations on the patient/staff dose and on the scattered radiation diffusion. This allows to learn the best safety practices intuitively, safely and anywhere.

B-0120 10:38

National audit on the appropriateness of CT and MRI examinations in Luxembourg

A. Bouëté¹, A. Karoussou-Schreiner¹, H. Ducou Le Pointe², M. Grieten³, E. de Kerviler², L. Rausin⁴, J.-C. Bouëté⁵, P. Majerus¹; ¹Luxembourg/LU, ²Paris/FR, ³Genk/BE, ⁴Liège/BE, ⁵Montreal, QC/CA (aurelien.bouette@ms.etat.lu)

Purpose: In Luxembourg, the frequency of CT and MRI examinations per inhabitant is among the highest in Europe. A national audit was conducted to evaluate the appropriateness of CT and MRI examinations according to the national referral guidelines for medical imaging.

Methods and Materials: 388 CT and 330 MRI requests forms corresponding to already-performed examinations were provided by all radiology departments in Luxembourg. Four external radiologists analysed the clinical elements for justification present in each request. They consensually assessed the appropriateness of each requested examination with regard to the national referral guidelines and their clinical experience.

Results: The appropriateness rate was higher for MRI requests than for CT requests (79% vs 61%; p < 0.001). For CT, the appropriateness rates were better when the requests concerned paediatric rather than adult patients (82% vs 68%; p < 0.001), when the requests concerned head (79%) and chest (81%) areas rather than spinal (28%), extremity (51%) and abdominal-pelvic (60%) areas (p < 0.001), and when the requests were referred by medical specialists rather than by general practitioners (70% vs 37%; p < 0.001). The appropriateness rates also varied significantly depending on the radiology department for both CT requests ([46%-86%]; p < 0.001) and MRI requests ([57%-92%]; p = 0.001).

Conclusion: A high proportion of CT and MRI examinations requested were found to be inappropriate. Inappropriate requests of CT examinations could potentially lead to unnecessary patient exposures, but the results observed for paediatric imaging requests and for two radiology departments suggest prolonged efforts could improve the justification of imaging in Luxembourg.

B-0121 10:46

Combination of environment recognition sensors and conventional x-ray settings

A. Corbi Bellot¹, F. Albiol¹, A. Albiol²; ¹Paterna/ES, ²Valencia/ES
(alberto.corbi@ific.uv.es)

Purpose: Combination of radiographic information (generated in ordinary x-ray settings) with the patient's volume and/or visible markers to derive 3D anatomical information and density images. These images highlight soft tissues or bony regions, separately.

Methods and Materials: We measure and track the patient's volume/location with scene recognition sensors. This allows the derivation of 3D information from pairs of radiographs generated at different patient positions. Also, using the same tracking equipment, we can derive the traversed lengths (through ray-casting) within the patient's skin isosurface. These lengths are pixel-wise associated to the original radiograph and used to derive densitometric data. To obtain all this information, both the x-ray tube and the tracking sensors have to be optically registered and the captured geometry needs to be translated to the point-of-view of the x-ray system.

Results: Resolution of anatomical lengths with millimetric precision. Besides, the obtention of density-based images that can be used to enhance soft tissues or bone structures, alongside. In the first type, the dynamic range is shrunk, improving the visibility of high gradient areas, extending contrast manipulations, and correcting underexposed X-ray images. This images also contain more information, according to modern pattern recognition algorithms and the concept of mutual information. In the bone-enhancement type, a single radiograph emphasises the skeletal structure just like a DEXA setup (impact in dose reduction).

Conclusion: The interplay of affordable contour assessment and motion detection equipment with plain x-ray settings can be used to add valuable information to plain radiographs: 3D real positions/lengths and density-based images.

Author Disclosures:

A. Corbi Bellot: Patent Holder; IST Storage (Valencia). Research/Grant Support; CPI-15-170, CPAN-13TR01, TSI1001012013019. Other; Hospital La Fe (Valencia).

B-0122 10:54

Radiation dose optimisation in intraoperative computed tomography of the brain

R. Forbrig, M. Patzig, C.G. Trumm, R. Stahl, F. Dorn; Munich/DE
(robert.forbrig@gmx.de)

Purpose: Intraoperative computed tomography (CT) with stereotactic head frames is an integral part of navigated neurosurgery. CT scanners must offer both a maximal diagnostic accuracy with reduced metal artefacts and a reasonable radiation dose. We report on our experience.

Methods and Materials: 200 patients (84 female, mean age 63) received an intraoperative contrast-enhanced CT of the brain on a 128 slice CT scanner (SIEMENS SOMATOM Definition AS+). For metal artefact reduction, the same iterative reconstruction algorithm (ASIR) was used in each patient. Regarding dose optimization, in 100 patients the CT protocol comprised automated tube current (CARE Dose4D) and voltage (CARE kV) modulation, in 100 patients fixed parameters (300 mAs, 120 kV). Radiation doses and image quality of both groups were compared.

Results: In the automated modulation group, tube current ranged between 475 and 1065 mAs (mean, 658 mAs), and tube voltage between 100 and 140 kV (mean, 118 kV). Mean dose length product (DLP) was 1524 mGy*cm (range, 692-2140 mGy*cm), mean CTDI_{vol} 89 mGy (range, 43-135 mGy), and mean effective dose 2.90 mSv (range, 1.31-4.01 mSv). In the group with fixed parameters, mean values of DLP, CTDI_{vol}, and effective dose were 753 mGy*cm (range, 683-896 mGy*cm), 43 mGy (range, 42-43 mGy), and 1.43 mSv (range, 1.30-1.70 mSv). All parameters were significantly lower in the latter group (p<0.01, each). Image quality was sufficient in both groups.

Conclusion: In stereotactic brain CT, automated dose modulation results in an unnecessary boost of radiation dose and should therefore be replaced by a low-dose protocol.

B-0123 11:02

Overranging dose reduction by dynamic collimators: evidence from clinical practice

N. Saltybaeva, H. Alkadhi; Zurich/CH (Natalia.Saltybaeva@usz.ch)

Purpose: Evaluation of dynamic collimators used in spiral CT has been performed so far only on cylindrical phantoms with a limited scan length. The purpose of this study was to assess the efficacy of dynamic collimators in daily clinical routine.

Methods and Materials: The overranging dose was assessed for 1690 CT examinations performed on a third-generation dual-source CT scanner (Somatom Force, Siemens Healthineers, Germany). The data for three

standard clinical protocols (abdomen, chest and heart) with pitch values of 0.6, 1.2 and 3.2, respectively, were collected by dose tracking software (qmDose, Qaelum, Belgium). The overranging length was defined as the difference between the actual scan length and length of the reconstructed volume. The exposed range was calculated as the ratio of reported DLP to the CTDI_{vol}. The collimator efficiency for each of the exams was defined as percentage of overranging dose in terms of DLP which was blocked by the dynamic collimator relative to the total dose of the CT scan.

Results: The number of overranging rotations was inversely proportional to the pitch factor, while the absolute overranging length increases with the increase of pitch from 30 mm for abdomen CT to 50 mm for heart examinations. We found a strong correlation between relative dose reduction and pitch factor (p<0.005). The average efficiency of dynamic collimators was 6%, 11% and 20% for spiral CT examinations with pitch values of 0.6, 1.2 and 3.2, respectively.

Conclusion: In spiral CT, the dynamic collimator is highly efficient for radiation dose reduction, especially in high pitch scan modes.

B-0124 11:10

Evaluating the effect of image truncation in the calculation of water equivalent diameter

A. Dedulle^{1,2}, P. Moussalli^{1,2}, J. Jacobs¹, N. Fytoussi¹; ¹Leuven/BE, ²Lodz/PL
(an.dedulle@qaelum.com)

Purpose: To evaluate the necessity of correcting the Water Equivalent Diameter (WED) that is calculated from truncated axial images.

Methods and Materials: A set of 191 non-truncated chest CT examinations were analyzed and the WED was calculated using the dose management system DOSE by Qaelum (Leuven, Belgium). The middle axial image of each case was manually truncated symmetrically and non-symmetrically at different Truncation Percentages (TP) up to 50%. The TP (ratio of patient border touching image edges to the total patient border) and the truncated WED (WED_{trunc}) were automatically calculated. Correction factors proposed in the literature were applied on WED_{trunc} resulting in WED_{corr}. Percentage difference (D_{trunc}) between the initial WED and WED_{trunc} and percentage difference (D_{corr}) between WED and WED_{corr} were evaluated.

Results: The application of correction factors worked well, especially for symmetrical truncation with TP of 30-50%, where the correction factor improved the WED calculation to a D_{corr} of -0.4% ± 3.7% while D_{trunc} was -6.7% ± 3.1%. For TP up to 20%, the error due to truncation was small (0.6% ± 0.6%), thus the gain from correction is small but nevertheless significant (p<0.0001). In non-symmetrical truncation, the curve fit was significantly different (p<0.0001) than the symmetrical one. When TP increases, the curves deviate more from each other.

Conclusion: A small symmetrical truncation underestimates the WED only by a small percentage. For truncation up to 50%, WED needs to be corrected to reduce the error in the calculation. In non-symmetrical truncation, results deviate more, especially for increased truncation percentages.

Author Disclosures:

A. Dedulle: Research/Grant Support; PhD project supported by the Flanders Innovation & Entrepreneurship agency [grant number HBC.2016.0233]. The research is conducted in cooperation with Qaelum and the University of Leuven. J. Jacobs: Board Member; Qaelum. CEO; Qaelum. Founder; Co-founder of Qaelum. Shareholder; Qaelum. N. Fytoussi: Employee; Qaelum.

B-0125 11:18

Impact of patient size and radiation dose on spectral accuracy in spectral detector CT: a phantom study

S. van Hedent, C. Tatsuoka, S. Carr, B. Eck, R. Kessner, N. Grosse Hokamp, P. Ros, D.W. Jordan; Cleveland, OH/US (svhedent@vub.ac.be)

Purpose: Iodine quantification (IQ) and Virtual Non-Contrast (VNC) images produced by Spectral Detector CT (SDCT) can be used for various clinical applications. We investigate the performance of SDCT in different phantom sizes and varying radiation doses, including a low-dose pediatric setting.

Methods and Materials: Three phantom sizes (simulating a 10-year old child, an average and a large sized adult) were scanned with iodine solution inserts with concentrations ranging 0-32 mg/ml, using the SDCT. Each phantom size was scanned with CTDI_{vol} 2-15 mGy. The smallest phantom underwent additional scans with CTDI_{vol} 0.9-1.8 mGy. All scans were repeated 5 times. We determined the accuracy and precision of VNC attenuation and IQ, by comparison to the known iodine concentrations.

Results: For scans from 2-15 mGy, mean VNC attenuation and IQ error in the iodine inserts in the small, medium and large phantom were +1.15 HU ± 3.19, -1.18 HU ± 14.92, +2.59 HU ± 23.58; and +0.12 mg/cc ± 0.41, -0.88 mg/cc ± 0.88 and -1.81 mg/cc ± 1.76 respectively. Scans with CTDI_{vol} 0.9-1.8 mGy in the small phantom showed very limited, but statistically significant lower VNC attenuation precision and IQ accuracy (-0.4778 HU ± 5.265 and -0.333 mg/cc ± 0.454 respectively) compared to higher dose scans in the same phantom size.

Conclusion: Performance of iodine quantification and subtraction in SDCT is largely dose independent, with the primary factor being patient size. Low dose pediatric scan protocols do not clinically impact IQ or VNC attenuation values.

B-0126 11:26

Validation of a task based automatic dose rate control (ADRC) method for interventional cardiology and radiology x-ray systems

M. Dehairs, N. Marshall; *Leuven/BE (michiel.dehairs@uzleuven.be)*

Purpose: To propose and validate an ADRC control method for specific tasks and requested image quality levels in interventional cardiology and radiology.

Methods and Materials: The new ADRC sets exposure parameters that maximize a figure of merit (FOM) for a specified object material, object velocity and image quality level. To achieve this, three quantities must be accurately predicted: reference air kerma (K_{ref}), detector dose and SDNR. The predicted values were empirically verified on a Siemens Artis Q interventional cardiology system as a function of field size and phantom thickness and a wide range of exposure parameters. SDNR was measured using an iron insert centered in the phantom and afterwards multiplied by MTF based correction factors for focal spot and motion blurring to give $SDNR(u)$: the FOM was $SDNR^2(u)/K_{ref}$. The optimized ADRC settings were then applied and $SDNR(u)$ was measured versus phantom thickness to examine whether the ADRC held image quality at the requested level. Measurements were repeated for tantalum, bismuth, platinum and gadolinium inserts.

Results: Average differences of measured data from the predicted values were $5\pm4\%$, $5\pm4\%$ and $13\pm7\%$, for reference air kerma, detector dose and SDNR respectively. Compared to conventional ADRC methods, the new approach increased the FOM (i.e. efficiency) and held $SDNR(u)$ constant to within $3\pm3\%$ and $5\pm4\%$ for the different materials, for fluoroscopy and acquisition respectively.

Conclusion: Measurements in this study validated the calculations required to design a FOM based ADRC enabling optimized task-specific control of x-ray parameters and leading to potential increases in imaging efficiency.

Author Disclosures:

M. Dehairs: Research/Grant Support; Siemens.

B-0127 11:34

Model observer techniques and an innovative statistical method for detectability evaluation in digital angiography: comparison with a 2AFC experiment

R. Villa, N. Paruccini, C. Spadavecchia, A. Baglivi, R. Corso, A. Crespi; *Monza/IT (raffaale.vill@gmail.com)*

Purpose: Interventional radiology procedures are characterised by high dose level for patients and physicians; thus dose management and protocols optimisation are mandatory. We evaluate the feasibility of different less time consuming approaches for protocol optimisation in interventional radiology.

Methods and Materials: CDRAD Phantom has been acquired with a Flat Panel Angiography equipment. Different protocols have been considered: three fluoroscopy modes and cine-coronary angiography. 3 different insert dimensions (1.3, 2, 3.2 mm of diameter) have been selected to characterise low contrast detectability. A 2AFC experiment has been performed by two observers with "Recommended Display Frame Rate". Furthermore, Low Contrast Detectability has been evaluated with a statistical method using uniform images. This analysis has been performed using an average of 3, 6, 12 images of different runs was calculated, considering 200 ms as the time of noise integration by human eye-brain system. Two different Model Observers has been considered: Non-PreWhitening Eye filter (NPWE) with spatio-temporal contrast sensitivity function and Channelized Hotelling Observer (CHO) with spatio-temporal Gabor filters.

Results: Analysis with both Model Observers and 2AFC experiments suffered from the general low quality of the protocols considered. Nevertheless, a good agreement (within 20%) can be found considering the effects of internal eye noise. Results with the Statistical Method show different degree of accordance related to insert dimension; thus, a single correction factor can be used to obtain an agreement within 30% for every protocols considered.

Conclusion: Every methods show both advantages and disadvantages. Nevertheless, numerical approaches are useful in protocol optimisation involving cine images.

B-0128 11:42

Low-dose protocol in prostatic artery embolisation (PAE): dose assessment

F. Rottoli, C. De Mattia, M. Sutto, P.E. Colombo, A. Rampoldi, A. Torresin; *Milan/IT (frottoli26@gmail.com)*

Purpose: To implement a low dose angiographic protocol for guidance of prostatic artery embolization (PAE) and analyse it in terms of dose, compared with a standard protocol.

Methods and Materials: In our institution, the PAE angiographic procedure showed high Kerma Area Product (KAP) compared to other interventional protocols, associated with high risk of skin lesions. After a retrospective analysis of the exposure values (KAP, entrance dose, Peak Skin Dose (PSD)) using RDIM NEXO[DOSE]@ (Bracco, Italy), for 84 patients, a new protocol was introduced with low entrance detector acquisition dose. In this protocol, images are taken at 2 frames per second (fps) (previously 3) with an additional X-ray filtration of 1mmAl+0.1mmCu (previously no filtration) in acquisition mode; in fluoroscopy, frame rate is reduced from 15 to 7.5 fps.

Before introducing the low-dose protocol into clinical practice, it was analysed in terms of entrance dose on a 20cm PMMA phantom. Image quality was assessed quantitatively as low contrast detectability, using a home-made phantom. After optimisation, patient dose was monitored using KAP, entrance dose and PSD.

Results: Protocol optimisation provides a 60% reduction of KAP (from 686 to 276 $Gycm^2$), 49% of entrance dose (from 3829 to 1904 mGy), 50% of PSD (from 3.2 to 1.6 Gy), without any relevant loss of image quality as determined on the phantom.

Conclusion: Optimisation of the PAE procedure led to a significant reduction of patient dose and without relevant degradation of image quality. This was the result of a multidisciplinary team work (physicians, technicians and medical physicists).

B-0129 11:50

Standardisation and optimisation of MRI examination protocols

E. Karavasilis¹, A. Karatopis¹, P. Szatmari², R. Illing², N. Papanikolaou²; ¹Nicosia/CY, ²Budapest/HU (peter.szatmari@affidea.com)

Purpose: To present a methodology for standardising and optimising heterogeneous MRI systems improving quality and patient experience.

Methods and Materials: The MRI protocol standardisation project was applied in 5 European countries in 33 MRI sites. A total number of 74 standardised protocols were developed in consensus between 6 experienced radiologists. More than 1500 pulse sequences were included in the standardised protocols and optimised in 8 MRI systems from 3 different MRI vendors by a group of 3 MR application consultants. 8 standardisation workshops were organised with a mean duration of 3 hours and 14 min, where all radiologists by consensus decided which sequences should be included on each different protocol dividing them into four categories. The optimisation part was conducted by a combination of site visits of the MR application consultants and remote access to a protocol exchange platform that was developed to easily transfer optimised protocols to those sites where no site visit was performed. The duration of the whole project was 14 months.

Results: The average examination time reduction after optimisation was up to 42.2% for Philips MRI scanners, 17.1% for Siemens scanners and 22.3% for GE scanners. Image quality of the optimised protocols was graded equal or superior to the old protocols in all cases.

Conclusion: Protocol standardisation although a challenging process is necessary to achieve workflow optimisation and, therefore, improve quality of services. A lot of effort needs to be invested and different stakeholders need to be actively involved for such a project to succeed.

Author Disclosures:

E. Karavasilis: Consultant; MRICONS. A. Karatopis: Consultant; MRICONS. P. Szatmari: Employee; Affidea. R. Illing: Board Member; Affidea. N. Papanikolaou: Consultant; Affidea. Owner; MRICONS.

10:30 - 12:00

Room K

Radiographers

SS 214

Optimising mammography

Moderators:

M. Marolt Music; Ljubljana/SI
D. O'Leary; Newcastle/UK

B-0130 10:30

Mammography performance and quality assurance practice among five European countries

A. Henner¹, N. Richli Meystre², C. Sá dos Reis³, B. Ström⁴, J. Pires Jorge², T. Kukkes⁵, E. Metsälä⁶; ¹Oulu/FI, ²Lausanne/CH, ³Perth/AU, ⁴Bergen/NO, ⁵Tartu/EE, ⁶Helsinki/FI (anja.henner@oamk.fi)

Purpose: The purpose of this study was to identify variability in mammography practice focused on approach to select exposure parameters, breast compression, quality control procedures, image quality assessment and guidelines in use in five European countries.

Methods and Materials: This study was cross sectional survey based on an online questionnaire addressed to clinical radiographers in five European countries. Questions were mostly closed-ended with the possibility to add comments. The answers were dichotomous, multiple choice or with a five point Likert Scale. The data collected was analysed and redundant data was disregarded. Statistical data analysis was performed using the software packages SPSS (version 21, IBM) by using descriptive methods, Chi square and independent samples t-test.

Results: Computed Mammography (CR) was used by 10% of the participant institutions and Full Field Digital Mammography (FFDM) by 89%. Recommendations on exposure parameter selection were based mainly on National (23%), EUREF (9%), ACR (7%), local (5%) and IAEA guidelines (4%). The main techniques selected by radiographers were use of automatic exposure control, molybdenum/rhodium (Mo/Rh) as target/filter combination, compression force from 8 kg to 11 kg and standard mediolateral oblique (MLO) projection angle of 45 degrees. Technical quality control was implemented in 99% of the departments involved in this study.

Conclusion: Practice in mammography varies considering the participant institutions. That reveals the need of further studies to identify if the cause is due to the population characteristics or if it is due to the use of different guidelines.

B-0131 10:38

Validation of applied pressures after clinical introduction of pressure-standardised compression mammography

D.d. Boer, L.A. Dam-Vervloet, M.F. Boomsma, J. van Dalen, L. Poot; Zwolle/NL (d.den.boer@isala.nl)

Purpose: Validation of the compression pressure of a pressure-standardized compression mammography (PSCM) system, which aims to reduce discomfort and pain by applying the same force per unit of area to every breast, independent of breast size.

Methods and Materials: We retrospectively studied mammograms of 50 patients acquired with the conventional force-standardized compression mammography (FSCM) technique and intra-individually compared them to mammograms acquired on checkup visits with PSCM technique. Patients received one craniocaudal (CC) and one mediolateral oblique (MLO) compression for both breasts. The contact area between breast and compression paddle enabled the calculation of compression pressures.

Results: A total of 193 FSCM and 193 PSCM images were analysed. The mean compression pressure decreased significantly from 16.6 ± 6.8 to 12.8 ± 3.4 kPa, while also drastically reducing the relative standard deviation of the compression pressure with PSCM. The applied compression pressure is depends very slightly on breast contact area; however, this was likely to be clinically irrelevant. Furthermore, the relative number of compressions of more than 20 kPa reduced significantly from 22.8% to 1.6%, benefiting patients with smaller breasts.

Conclusion: The introduction of the PSCM system led to a nearly constant applied compression pressure for different contact areas and a significant reduction in compression pressures. Especially for higher pressures, which are generally applied to smaller breasts and are generally associated with discomfort and pain. This suggests that using PSCM can reduce patient discomfort and pain during mammographic compression and provide a more constant image quality, which could potentially improve diagnostics.

B-0132 10:46

Breast compression between women imaged using digital mammography and breast tomosynthesis in a population-based breast cancer screening programme

G.G. Waade¹, Å.S. Holen¹, B. Hanestad², S. Sebuodegaard¹, N. Moshina¹, K. Pedersen¹, S. Hofvind¹; ¹Oslo/NO, ²Bergen/NO (Gunvor-Gipling.Wade@hioa.no)

Purpose: Digital breast tomosynthesis (DBT) leads to longer image recording time. We compared breast compression when screening with digital mammography (DM) or DBT.

Methods and Materials: The study included information about 16,832 women participating in the Bergen Tomosynthesis Trial, as a part of BreastScreen Norway, January 2016 to April 2017. We compared mean values of applied compression force (N) and pressure (kPa), for DM and DBT, by view (craniocaudal, CC, and mediolateral-oblique, MLO). Two-sample t tests were used to test statistical significance.

Results: Half the women were screened with DM (n=8354) and the other half with DBT (n=8478). Mean compression force was statistically significantly higher for DM compared to DBT (CC: 108.6N vs 102.7N; MLO: 122.4N vs 120.8N, p<0.01). Mean compression pressure was statistically significantly higher for DM compared to DBT for CC view (13.9kPa vs 13.0kPa, p<0.01). There was no difference in compression pressure between the screening techniques for MLO view (DM and DBT: 9.7kPa, p=0.55).

Conclusion: Radiographers applied less compression when performing screening with DBT compared to DM. However, the observed differences in breast compression between the screening techniques were negligible. Further research is needed to investigate the clinical implications of these findings.

B-0133 10:54

Breast compression and experience of pain: comparing two compression paddles

S. Hofvind, N. Moshina, G.G. Waade, S. Sebuodegård; Oslo/NO (solveig.hofvind@kretftregisteret.no)

Purpose: Women's experience of pain during screening mammography may be related to breast compression and result in non-attendance of the next screening examination. We aimed to compare the pain experienced among women screened using an ordinary flexible paddle and women screened using a fixed paddle, standardizing compression pressure to 10 kilopascal (kPa).

Methods and Materials: Data on experienced pain, compression force (newton, N) and pressure, and related factors (age, breast volume, contact breast area, pain in shoulders and/or neck prior to mammography), were collected via a questionnaire from 1,444 women screened using fixed (n=950) or flexible (n=494) paddle, May-June 2017. Experienced pain was evaluated using a scale from 0 to 10 and presented as no/mild (<3.5) and moderate/severe (≥3.5). We used logistic regression to estimate the odds ratio (OR) with 95% confidence interval (95%CI) for moderate/severe pain associated with type of compression paddle, adjusting for compression force or pressure and related factors.

Results: No difference in experienced pain was observed for women screened using the flexible paddle compared to the study paddle (OR 1.15; 95%CI 0.89-1.49 for compression force; and OR 1.25; 95%CI 0.94-1.65 for compression pressure). Pain in shoulders and/or neck prior to mammography coupled with increasing compression force or pressure during mammography was associated with moderate/severe pain during mammography.

Conclusion: The ordinary flexible paddle and the fixed paddle standardizing compression pressure perform similarly with respect to pain experienced during mammography. Future research on comparing the performance of the paddles should explore the association between breast compression and image quality.

B-0134 11:02

The influence of breast compression on re-attendance in a population-based screening programme

S. Sebuodegård, N. Moshina, G.G. Waade, S. Hofvind; Oslo/NO (solveig.hofvind@kretftregisteret.no)

Purpose: A high attendance rate in organized breast cancer screening programs is a prerequisite to achieve a reduction in breast cancer mortality. We aimed to investigate whether breast compression at prior screening was associated with re-attendance among subsequently screened women in BreastScreen Norway.

Methods and Materials: Information about re-attendance were available for 77,674 women aged 52-69 with at least two prior screening exams, 2007-2013. Data on compression force (kg) and pressure (kPa) were available from automated density assessment software. Two-sample unpaired t-tests were used to identify differences in re-attendance. Logistic regression was used to estimate the odds of re-attendance, adjusting for age, county of residence, prior false positive result, breast volume, breast density, and year of screening.

Results: Overall, 71,241 (91.7%) women re-attended. For compression force, re-attendance was highest for women who received <11.3 kg (92.0%) and lowest for women who received >13.3kg (91.5%) ($p=0.082$). For compression pressure, re-attendance was highest for those who received 11.3-14.3 kPa (92.5%) and lowest for <9 kPa (90.7%) ($p<0.001$). The adjusted odds of re-attendance did not differ statistically significantly by compression force. The odds for re-attendance was 33% higher for women who received pressure ≥ 9 kPa relative to <9 kPa (95% CI: 23%-42%).

Conclusion: Compression force did not show any statistically significant influence on re-attendance, while compression pressure ≥ 9 kPa was associated with a higher odds. Future research focusing on compression variables, experienced pain and image quality is needed to understand this issue.

B-0135 11:10

Impact of contralateral breast shielding on the risk of developing radiation-induced cancer from full field digital mammography (FFDM) screening

R.M.K.M. Ali^{1,2}, A. England², C.E. Mercer², A.K. Tootell², P.H. Hogg²; ¹Najaf/IQ, ²Manchester/UK (p.hogg@salford.ac.uk)

Purpose: To investigate the impact of contralateral breast shielding on the risk of developing radiation-induced cancer from 4-view FFDM screening.

Methods and Materials: A breast phantom and adult ATOM dosimetry phantom were used to measure organ dose on 4 FFDM machines using cranio-caudal and medio-lateral oblique projections for each breast. A lead rubber shield was used to protect the contralateral breast. Organ dose, effective dose and effective risk were calculated; for effective risk estimations, the impact of the shield was considered for all known screening programmes worldwide.

Results: The shield can reduce the contralateral breast dose by more than 95%. For each FFDM machine the figures in μGy were (35.20 reduced to 1.93), (41.40 reduced to 0.01), (22.85 reduced to 1.24) and (22.76 reduced to 1.66). A small reduction was identified in sternum bone marrow dose due to the use of contralateral breast shield. The contralateral breast shield can significantly reduce the total effective risk of worldwide screening programme ($p<0.05$). However, the reduction percent in total effective risk is different for the 4 FFDM machines, ranging between 0.95% and 1.44% with minor differences amongst different worldwide screening programmes.

Conclusion: This novel work demonstrates the value of a contralateral breast shield. More research is required to determine whether such a shield has clinical utility.

B-0136 11:18

Outpointing breasts and hallux valgus: correlation and implications in mammography quality

S. Pacifici, D. Giudice; Rome/IT (s_pacifici@virgilio.it)

Purpose: In mammography, the position of the woman and her feet is critical for positioning the breast correctly and, consequently, regarding quality criteria such as the nipple in profile, the PNL perpendicular to the pectoral muscle edge on MLO view and on the breast midline on CC view. These criteria are hard to meet when non-standard breast shapes are in evidence, such as those which are outpointing. In these cases, positioning could require feet intra-rotation. From our working experience, we have observed a consistent co-existence of outpointing breasts and hallux valgus. For this reason, we began to investigate the correlation.

Methods and Materials: 54 women with at least one outpointing breast were selected and asked about the existence of a hallux valgus condition, assigning a 0-2 value to the variables and analysing the data by concordance tests.

Results: The results showed a 99.7% of concordance which called for a PubMed search to find out any scientific evidence in Western medicine, with negative results. In change, in osteopathy and traditional Chinese medicine concepts, we found links between the big toe and the breast-related muscles explained by the biomechanics of the muscle chains and some energy meridians.

Conclusion: The study seems to offer sufficient data to confirm a correlation, the knowledge of which can facilitate the positioning of outpointing breasts, respecting the quality criteria and thus avoiding technical errors which could influence recalls and repeats, comparative evaluations with previous mammograms and congruence between the PNLs. However, a clinical study with postural evaluation and activation points is required.

B-0137 11:26

Learner's perception, knowledge and behavior assessment within a breast imaging eLearning course for radiographers

I.C. Moreira, S.R. Ventura, I. Ramos, P.P. Rodrigues; Porto/PT (icm@ess.ipp.pt)

Purpose: ELearning has been revealed to be a useful tool to specific training and continuing education within health professionals, namely by radiographers.

This education method needs continuous evaluation in order to validate its effectiveness. One method for this evaluation is Kirkpatrick's framework which consists of four categories: learner perception, knowledge, behavior, and impact on organization. Our aim was to assess an eLearning course on breast imaging for radiographers according to the first three categories.

Methods and Materials: An asynchronous eLearning system was developed for radiographers in order to promote a better knowledge about breast imaging, namely mammography technique and interpretation. The contents of this eLearning course were based on the guidelines proposed by the European Society of Breast Cancer Specialists (EUSOMA). Learner satisfaction was assessed through a questionnaire. Knowledge gain was assessed by using pre- and post-testing. After 6 months finishing the course, learners were contacted through a questionnaire in order to give feedback whether behaviour changed in their profession. Statistical analysis is under progress.

Results: Two editions of the course were performed, totalling 64 learners. In general, learners reported being very satisfied with the experience (above 90%), improved their knowledge, and also changed some attitudes and behaviours (such as communication, positioning, image analysis and processing) within their work routine. These and other results are still being thoroughly analysed.

Conclusion: This course represents an important contribution for the improvement of radiographers' performance in mammography clinical setting, enhancing continuous education models in health professions.

B-0138 11:34

The customised training for radiographers and its importance for image quality improvement and an accurate diagnosis of breast cancer

T.B. Silva, E.C. Mauad, S. Sabino; Barretos/BR (tbuosi@gmail.com)

Purpose: To evaluate the impact of a customized training for radiographers on clinical quality of mammography.

Methods and Materials: Radiographers selected for 80 hours training course submitted 15 days before the course starts a portfolio containing 50 examinations conducted by them for review. Through the evaluation of 18 mammographic positioning quality items stipulated by the European Guidelines it is produced a customized practice-oriented training, based on their most frequent positioning failures. Students in these classes were grouped according to their failures and a personalized training program was established for each one of the students, which spends 80% of their time in hands-on training. Subsequently, we evaluate each exam performed by the students during the course and items in "non-conformity" were counted. The data pre and post-course were tabulated and the performance of the training was assessed.

Results: Since 2012 it was trained 396 radiographers from Brazil. The mean of failures reported per exam was 3.7 at the beginning of the course (portfolio analysis) and 1.1 at the end. The average rate of decrease of failures per exam was 68% ($p=0.001$). The most common positioning-related failures reported were absence of the pectoral muscle at cranio-caudal incidence (89%) and pectoral muscle to nipple level (49.1%) and non-visualization of infra-mammary angle (43.9%) at Medio-lateral oblique.

Conclusion: The trained professionals become able to perform mammography with higher diagnostic quality, reversing the current national framework, where the majority of mammograms performed have errors that make it difficult to provide an accurate diagnosis.

B-0139 11:42

Dose analytics over large DICOM datasets: a case study in mammography and a quest for meta data quality

M. Rodrigues dos Santos, N. Rocha, A. Silva; Aveiro/PT (mrs@ua.pt)

Purpose: The DICOM metadata of the mammographic studies, can contribute to a better knowledge of the exposure to which a population is exposed. The objective of this work was to identify the extent to which the quality of the DICOM metadata stored may contribute to the characterization of the exposure and dose used to perform mammography studies.

Methods and Materials: The studies carried out during the first 12 months of equipment activity were analyzed. The work was carried out in 5 phases: Indexing and extraction of DICOM metadata from PACS archive, image IOD characterization (e.g. Patient Age, Organ Dose), data quality analysis and sample normalization, population and exposure characterization.

Results: An initial sample of 1569 images from 379 studies of 351 patients was obtained. After the normalization process in which 8.55% of patients, 9.76% of the studies and 16.54% of the images were excluded, a final sample consisted of 1302 images, 342 studies performed on 321 patients was obtained. It was possible to characterize the population as well as ESAK ($CC = 7.85 \pm 4.48$ mGy and $MLO = 8.86 \pm 4.96$ mGy) and AGD ($CC = 1.67 \pm 0.73$ mGy and $MLO = 2.37 \pm 0.14$ mGy) as well as the mean compression force and mean breast thickness per age group

Conclusion: It is possible to characterize the exposure to which the population is subject in mammography studies based on the data stored in the PACS file. However, it is pertinent to consider the quality of the stored metadata.

B-0140 11:50

Tomosynthesis-guided vacuum-assisted breast biopsy: a survey of the patient's experience

R. Gullien, A. Haakull, T. Nyborg, B. Sollid, M. Stensvoll, S.M. Ali, J.-G. Andersen; *Oslo/NO (uxraul@ous-hf.no)*

Purpose: To evaluate and measure the patient experience and satisfaction following tomosynthesis-guided breast biopsy.

Methods and Materials: The survey study period was February 3rd-December 21st, 2016. 90 patients were scheduled for tomosynthesis-guided breast biopsy. Of these, 23 patients did not participate in the survey due to cancelled examination, language barriers or they refused. The remaining 67 patients were asked to fill out two questionnaires: part one immediately after the procedure and part two at home two weeks after the examination. Of the 67 participants, 56 participants answered both questionnaires, 11 participants did not answer part two despite reminders. All participants underwent standard procedure for local anaesthesia immediately before the procedure.

Results: 84% (56/67) of the participants answered both surveys. Results part one: 24% (16/67) were much or very much anxious before the examination; 58% (39/67) were a little anxious; 18% (12/67) were not. 69% (46/67) felt the examination uncomfortable; 22% (15/67) did not; 9% neutral. 45% (30/67) felt the examination painful; 42% (28/67) did not; 13% (9/67) neutral. Results from part two: 39% (22/56) no pain five days after; 61% (34/56) had pain or some pain; none had severe pain. 9% (5/56) contacted healthcare (pain, bleeding, infection, discolouration), 91% did not need. 96% (54/56) answered "yes" they received adequate information before, during and after the procedure, 4% (2/56) answered "no". 73% (41/56) was very satisfied with the overall experience of how they were taken care of; 25% (14/56) were satisfied; 2% (1/56) was not satisfied.

Conclusion: Most patients were anxious before examination. They got adequate information, were satisfied and felt they were very well taken care of during the examination.

10:30 - 12:00

Room M 1

Cardiac

SS 203

All about TAVI: pre- and post-procedural assessment

Moderators:

C. Herzog; *Munich/DE*
N.N.

K-04

Keynote lecture

M. Gardarsdottir; *Reykjavik/IS*

B-0141 10:39

Paradoxical low-flow, low-gradient severe aortic stenosis: cardiac magnetic resonance (CMR) evaluation

S. Pradella, C. Vignoli, M. Acquafresca, F. Grossi, I. Fusi, V. Miele; *Florence/IT (pradella3@yahoo.it)*

Purpose: Paradoxical low-flow, low-gradient (LFLG) severe aortic stenosis (AS) despite preserved left ventricular ejection fraction (LVEF) is one of the most challenging entities in valvular heart disease. The outcome is not clear. Aortic valve replacement (AVR) may be indicated in these patients.

Methods and Materials: A year (2016) patient's whit LFLG were assessed by clinical data and 2D-3D echocardiography. CMR imaging was performed on a 1.5 T in LFLG AS patient's. The LV outflow tract (OT) minimal and maximal diameters, to calculate the ellipticity index, and area were measured. LV volumes, stroke volume (SV), and LVEF was calculated on short axis cine images. The aortic valve area (AVA) was measured by direct planimetry of the maximal opening of the aortic valve. Late gadolinium enhancement (LGE) was evaluated to exclude focal replacement fibrosis, and T1 mapping for assessing of diffuse patterns of interstitial fibrosis presence (not in all patients).

Results: 72 patients with severe AS, 13 (18%) paradoxical LFLG, mean age: 78.3±9.5 years; male 4-30%, BMI 24.5±2.6, NYHA 1.8-0.6 BNP 487.8±299.0. The ellipticity index was 1.21±0.3. 48% patients were re-classified as moderate AS with CMR. No LGE was found. T1 values were higher than normal.

Conclusion: Assessment of AS severity can be complex because standard resting echocardiography may not reflect the true severity of stenosis. There may be errors and inaccuracies in the calculation of AVA by the continuity equation, which could erroneously suggest the paradoxical phenotype. Information from CMR may be complementary to provides an accurate diagnosis.

B-0142 10:47

The role of topography of valve calcification in degenerative aortic stenosis: a new marker in CT evaluation

J.A.B. Araújo-Filho¹, A. de Santis¹, C.H. Nomura¹, F. Tarasoutchi¹, M.C. Vieira¹, M. Katz¹, J. Brown², E.R. Edelman³, P.A. Lemos¹; ¹São Paulo/BR, ²Cambridge, MA/US, ³Boston, MA/US (ariaaraujocg@hotmail.com)

Purpose: The relationship between calcium location and the severity of aortic valve stenosis (AS) remains poorly understood. The present study aimed at evaluating whether the location of calcium influences the functional severity of AS.

Methods and Materials: Prospective, single-arm study including 97 patients with diagnosed moderate or severe AS. Aortic valve calcium score was calculated from no-contrast multidetector computed tomography (MDCT). "Low-contrast-dose" MDCT images were acquired for segmentation of the cardiac anatomy, with the attenuation at the aortic valve zone used to quantify its calcium content.

Results: The calcium score was higher among patients with severe AS compared to patients without severe AS (3131±1828 Agatston units [AU] vs. 1302±846 AU respectively; p<0.001). Patients with severe AS had significantly higher attenuations at the center of the valve than at its periphery (507.4±181.7 Hounsfield units [HU] vs. 449.8±114.5 HU; p=0.001). Conversely, patients without severe AS had lower attenuation at the center than at the periphery of the valve (308.7±92.9 HU vs. 347.6±84.2 HU; p<0.001). The center/periphery attenuation ratio was significantly higher for patients with severe AS than for those without severe disease (1.14±0.32 vs. 0.89±0.13; p<0.001), and remained significantly associated with the presence of severe AS even after adjusting for the underlying degree of valve calcification.

Conclusion: The severity of degenerative aortic valve stenosis appears to result not only from the degree of calcification but also from the localization of the calcific deposits within the valve.

B-0143 10:55

Dynamic morphological changes of the aortic annulus in patients with bicuspid aortic valves

S. Boccalini, L.R. Bons, A.T. van den Hoven, G.P. Krestin, A.E. van den Bosch, J. Roos-Hesselink, R.P. Budde; *Rotterdam/NL*

Purpose: Bicuspid aortic valve (BAV) consists of a malformation of the aortic valve. Transcatheter aortic valve implantation is increasingly practiced to treat the associated precocious valvular dysfunction. Precise pre-interventional measurements of the annulus are fundamental to avoid potentially lethal complications. However, in the general population the annulus has an elliptic shape that undergoes shape changes during the cardiac cycle. The aim of our study was to investigate dynamic changes of the annulus in BAV patients.

Methods and Materials: BAV patients who underwent an ECG-gated CTA of the aorta between January 2015-March 2016 were included. The annulus plane was manually identified on reconstructions obtained at 5% intervals of the cardiac cycle. Based on semi-automatically defined contours, maximum and minimum diameter, area, perimeter and asymmetry ratio (maximum diameter/minimum diameter) were calculated. Paired samples Student's t test was used to assess differences.

Results: In 55 BAV patients (age: 38.4±13.3 years; 58% males) 38 had BAV type 1, 10 type 0 and 7 type 2. Minimum diameter, perimeter and area were significantly higher in systole than in diastole (relative changes: 14%, 6%, 17% respectively), while maximum diameter was significantly higher in diastole (all p<0.001). The asymmetry ratio was >1 in all phases, indicating an elliptic shape, with more pronounced flattening in diastole (p<0.001). When examined separately, the different BAV types showed analogous dynamic changes.

Conclusion: The annulus of BAV patients undergoes significant changes in shape during the cardiac cycle with a wider area in systole and a more elliptic conformation in diastole, affecting pre-interventional measurements.

Author Disclosures:

L.R. Bons: Research/Grant Support; Dutch Heart Foundation; Contract grant number: 2013T093. **A.T. van den Hoven:** Research/Grant Support; Dutch Heart Foundation; Contract grant number: 2013T093. **A.E. van den Bosch:** Research/Grant Support; Dutch Heart Foundation; Contract grant number: 2013T093. **J. Roos-Hesselink:** Research/Grant Support; Dutch Heart Foundation; Contract grant number: 2013T093.

B-0144 11:03

Does the heart cycle fase of cardiac-MSCT influence the measurement of the aortic root in patients undergoing TAVI placement?

A. Drago, V. Alberotanza, C. Massarelli, L. Mappa, M. Carbone, M. de Ceglie, E. Ventrella, A.A. Stabile lanora, A. Scardapane; *Bari/IT (angelicadrage07@gmail.com)*

Purpose: To assess the differences between systolic and diastolic dimensions of the aortic root in patients undergoing MSCT before TAVI placement.

Methods and Materials: Coronary-CT examinations of 70 patients, 29 females and 41 males with an average age of 66.2 years were evaluated. Modulated ECG-gated cardiac CTA was performed after the injection of 60-80 ml of iodinate contrast at a flow rate between 4 and 5 ml / sec. Systolic (20% of RR interval) and diastolic (75% RR interval) images were obtained and aortic annulus was measured just below the insertion of the valve leaflets after true axial cuts were obtained aligning the three perpendicular imaging planes. Distances of the coronary ostia were also measured. The differences between systolic and diastolic measure were compared using the T-Test.

Results: The mean diastolic and systolic size of the aortic annulus were respectively 22.28 mm and 22.5 mm in short axis and 27.25 mm and 27.8 mm in long axis. The distance of the right coronary artery from the aortic valve had a mean diastolic value of 14.37 mm and a mean systolic value of 14.15 mm; The distance of the left coronary artery from the aortic valve had a mean diastolic value of 14.21 mm and a mean systolic value of 14.4 mm. No statistically significant differences ($p > 0.05$) were found among these measures.

Conclusion: There was no statistically significant difference between systolic and diastolic measurements, so we believe that measurement should be performed during the best phase of each patient's heart cycle.

B-0145 11:11

Angio-CT: key for landing zone reconstruction in TAVI

D. Araujo Martins, R. Ruiz Salmeron, A. Rivera, C. Caparros Escudero, L. Cueto Álvarez, F. Mateo Carballo; *Sevilla/ES* (danielamromeo@gmail.com)

Purpose: AngioCT has become gold standard for planning TAVI. AngioCT evaluation of aortic annulus is key to define the prosthesis to be implanted. However, anatomical characteristics of TAVI landing zone, the portion between the left ventricle outflow tract and the aortic root receiving prosthesis deployment, have not been fully described. Aim: To describe the anatomical characteristics of the landing zone evaluated by angioCT, and to generate a 3D model to support TAVI procedure strategy.

Methods and Materials: In 83 consecutive patients (56 females) undergoing TAVI, angioCT study of landing zone analysed the values of area (mm²) and eccentricity (1 - (Minor Diameter / Major Diameter)) in 5 cut-off points separated by 5mm: lower cut-point located below the aortic ring, next on the aortic annulus, and the remaining three cut-points above, at the aortic root. With those data, SolidWork graphics software generated a 3D geometric model.

Results: Landing zone showed, at each cut-point, inverse relationship between area and eccentricity: ascending from the left ventricular outflow tract towards the aorta, area increased and eccentricity decreased significantly ($p < 0.001$). We found significant differences between male and female gender regarding the dimensions and degree of eccentricity of the landing zone: men showed larger area and a lower eccentricity ($p < 0.001$). For each patient, SolidWork was able to generate and print a 3D landing zone model.

Conclusion: AngioCT allows an accurate description of the landing zone anatomy of TAVI procedures, and its 3D printing model is an attractive tool for the success of the intervention.

B-0146 11:19

One-stop high definition 64-row CT coronary angiography in patients with severe aortic stenosis candidate to transcatheter aortic valve implantation (TAVI): a pilot feasibility study

L. Faggioni, M. Gabelloni, M. Bianchi, G. Costa, M. De Carlo, A.S. Petronio, D. Caramella; *Pisa/IT* (lfaggioni@sirm.org)

Purpose: To assess the diagnostic performance of high definition 64-row CT coronary angiography (CTCA) integrated in a one-stop-shop CT protocol for TAVI planning.

Methods and Materials: A retrospectively ECG-gated CTCA examination was performed in 57 nonobese patients with severe aortic stenosis as part of a comprehensive CT protocol for TAVI planning. All studies were carried out on a high definition 64-row CT scanner using 100kV tube voltage and an iterative reconstruction algorithm. Patients with inconclusive or positive CTCA findings (defined as presence of stenosis >50% of the left main artery and/or proximal or mid left anterior descending, circumflex, or right coronary arteries) underwent invasive coronary angiography (ICA) prior to TAVI, whereas in a subset of patients with negative CTCA findings (7/30, 23.3%) ICA had previously been performed before CTCA. Per-patient sensitivity, specificity, positive and negative predictive value of CTCA compared to ICA as gold standard were calculated. The association between image quality (graded visually as good, adequate or nondiagnostic), coronary calcium score (CCS) and heart rate (HR) was also evaluated.

Results: A total of 47/57 CTCA examinations (82.5%) were of diagnostic quality. Sensitivity, specificity, positive and negative predictive value of CTCA were 100%, 87.5%, 90.9% and 100%, respectively. Image quality was inversely correlated with CCS and HR ($p < 0.05$), and in particular, adequate or good image quality was associated with $CCS < 350$ and $HR < 74$ bpm.

Conclusion: One-stop CTCA allows accurate detection of critical coronary artery stenoses and can play a role as a gatekeeper to ICA in selected patients candidate to TAVI.

B-0147 11:27

Comparison of aortic annulus dimensions by multimodal measurement before transcatheter aortic valve replacement

R. Qi; *Hangzhou/CN* (tsirea@163.com)

Purpose: We sought to compare 3 methods of measurements of the aortic root in patients of severe aortic stenosis (AS), transthoracic echocardiography (TTE), transesophageal echocardiography (TEE), and multislice computed tomography (MSCT), and to evaluate their potential clinical impact on transcatheter aortic valve implantation (TAVI) strategy.

Methods and Materials: Aortic root dimensions were measured using TTE, TEE, and MSCT in 138 consecutive patients with severe AS referred for TAVI in our institution. The differences among measurements of aortic annulus diameter were compared. The accuracy of the multimodal measurements before TAVI was evaluated with postoperative follow-up.

Results: Mean aortic annulus diameter was 23.37 ± 2.22 mm using TTE and 23.52 ± 1.70 mm using TEE ($p = 0.12$) and correlation between TTE and TEE was excellent ($r = 0.87$). The mean of long- and short-axis diameters according to MSCT multiplanar reconstruction did not differ from the diameter derived from cross-sectional area ($p = 0.08$). However, the diameter derived from circumference was larger than the others, and the difference is 0.43 ± 0.62 mm, 0.51 ± 0.62 mm ($p < 0.01$, respectively). Measurements of the aortic annulus diameter by MSCT were larger than the measurement by TTE and TEE significantly ($p < 0.01$). Implantation was successful in all, but 3 patients with worse than moderate paravalvular leakage and 1 patient with valve-in-valve implantation because of prosthetic valve restenosis.

Conclusion: In patients referred for TAVI, measurements of the aortic root using TTE or TEE were smaller than measurements by MSCT. In the absence of a gold standard, a strategy based on comprehensive consideration would provide good clinical results.

B-0148 11:35

Comparison of cardiovascular magnetic resonance imaging and computed tomography to guide transcatheter aortic valve replacement: a pilot study

A. Mayr, C. Kranewitter, G. Klug, C. Kremser, G. Feuchtner, W. Jaschke, B. Metzler; *Innsbruck/AT* (a.mayr@i-med.ac.at)

Purpose: To compare a comprehensive cardiovascular magnetic resonance (CMR) imaging protocol with contrast-enhanced computed tomography angiography (CTA) for guidance in TAVR evaluation.

Methods and Materials: Non-contrast three-dimensional (3D) "whole heart" CMR imaging for aortic annulus sizing and measurements of coronary ostia heights, contrast-enhanced CMR angiography (MRA) for evaluation of transfemoral routes as well as aortiliofemoral-CTA were performed in 16 patients referred for evaluation of TAVR.

Results: Aortic annulus measurements by CMR and CTA showed a very strong correlation ($r = 0.956$, $p < 0.0001$; effective annulus area for CMR 430 ± 74 vs. 428 ± 78 mm² for CTA, $p = 0.629$). Regarding decision for valve size there was an excellent agreement between CMR and CTA. Moreover, vessel luminal diameters and angulations of aortiliofemoral access as measured by MRA and CTA showed overall very strong correlations ($r = 0.819$ to 0.996 , all $p < 0.001$), the agreement of minimal vessel diameter between the two modalities revealed a bias of 0.02 mm (upper and lower limit of agreement: 1.02 mm and -0.98 mm).

Conclusion: In patients referred for TAVR, CMR measurements of aortic annulus and minimal aortiliofemoral diameters showed good to excellent agreement. Decisions based on CMR measurements regarding prosthesis sizing and transfemoral access would not have modified TAVR-strategy as compared to a CTA-based choice.

B-0149 11:43

Value of left ventricular fibrosis volume as a parameter for long-term survival after TAVI

A.S. Sträter, A. Huber, J. Nadjiri, M. Rasper, M.T. Berndt, E.J. Rummeny, J. Rieber; *Munich/DE* (alexandra.straeter@gmail.com)

Purpose: Patients with severe aortic stenosis develop left ventricular hypertrophy and reduced left ventricular function. Insufficient vascularisation of hypertrophic myocardium may cause development of left ventricular fibrosis. Transcatheter aortic valve implantation (TAVI) is an upcoming procedure to reduce workload and improve left ventricular function. Long-term survival shows huge inter-individual difference. NYHA class 30 days after TAVI has shown to be a strong and independent parameter for long-term survival. This study assesses the value of left ventricular fibrosis volume as a predictive parameter for clinical outcome.

Methods and Materials: The study enrolled 35 consecutive patients for TAVI. The mean characteristics were 81 ± 7 years, NYHA Class 3.2 ± 1.4 , EF $48 \pm 9.3\%$. In each patient pre-interventional contrast-enhanced cardiac MRI was performed in a Philips Ingenia 3T. Left ventricular fibrosis volume was

quantified. Functional recovery was assessed using NYHA class 30 days after the procedure.

Results: NYHA class after TAVI was reduced significantly (1.7 ± 1.3 ; $p < 0.001$). 22 (63%) patients revealed 2 class reduction whereas 12 (34%) patients showed reduction of 1 class and 1 patient remained (this patient had good pre-interventional function: EF 74%). Left ventricular fibrosis volume was inversely related to the reduction of NYHA class (left ventricular fibrosis volume 720.75 ± 43 [NYHA reduction ≥ 2 grades] vs 1501.6 ± 74 [NYHA reduction < 2 grade]; $p < 0.05$).

Conclusion: The left ventricular fibrosis volume shows a strong correlation to the reduction of NYHA class 30 days after successful TAVI implantation. Thus, the quantification of left ventricular volume might possibly be used as a prognostic parameter for long-term survival in TAVI patients.

B-0150 11:51

Left ventricular reverse remodeling after transcatheter aortic valve implantation as assessed by CT angiography

B. Szilveszter, D. Oren, M. Kolossvary, M. Vecsey-Nagy, J. Karady, F. Suhai, A. Apor, B. Merkely, P. Maurovich-Horvat; *Budapest/HU*

Purpose: Transcatheter aortic valve implantation (TAVI) has rapidly emerged as a safe and effective treatment option for high risk patients with severe aortic stenosis. CT imaging provides accurate assessment of left ventricular (LV) dimensions. Therefore, we aimed to assess the impact of TAVI procedure on LV remodeling as assessed by CT angiography.

Methods and Materials: We performed retrospectively gated CT angiography for the planning and follow-up of TAVI procedure in 48 patients. We measured LV mass on serial CT images using a dedicated semi-automated software. Epicardial and endocardial contours were manually adjusted. Pre- and post-procedural left ventricular mass and volumes were compared using Wilcoxon signed rank test. Multivariate linear regression analysis was used to establish independent factors related to LV reverse remodeling.

Results: Mean age was 77.1 ± 15.1 years, 58.3% were male. We found significant reduction in LV mass after TAVI procedure: 166.3 [139.2 - 225.5] grams for pre- and 128.2 [106.2 - 151.6] grams for post-TAVI, respectively, $p < 0.001$. Mean change in LV mass was 48.9 ± 31.4 grams. On multivariate analysis, baseline LV mass is independently associated with LV reverse remodeling ($\beta = 0.63$, $p < 0.001$) above traditional risk factors, age, gender and BMI.

Conclusion: Significant regression of LV mass was observed in almost all cases after TAVI procedure that is presumably associated with the reverse remodeling of the left ventricular structure. In line with previous data larger baseline LV mass was associated with more pronounced remodeling.

10:30 - 12:00

Room M 2

Paediatric

SS 212

Neuro imaging in paediatrics

Moderators:

S.M. Aukland; Bergen/NO

N.N.

B-0151 10:30

Apparent diffusion coefficient (ADC) and its correlation with gestational age (GA) in normal developing foetal brain: preliminary results of a prenatal MRI study

A. Antonelli, S. Capuani, M. Guerreri, S. Bernardo, R. Petrillo, V. Vinci, L. Manganaro, C. Catalano; *Rome/IT (amanda.antonelli@hotmail.it)*

Purpose: To provide a normal comparison base of ADC values in the developing non-pathological foetal brain parenchyma, investigating the potential of ADC as a function of gestational age (GA).

Methods and Materials: Diffusion-weighted imaging (DWI) was performed in 35 pregnancies (GA range: 19-38 weeks) at 1.5T (Siemens Avanto, Erlangen, Germany). A DW-Spin Echo EPI with TR/TE=4000/79; bandwidth=1628 Hz/px; matrix=192x192; FOV 379mm2 was obtained. Eight regions of interest (ROIs) were manually placed in the frontal white matter (FWM), occipital WM (OWM), thalamus (THAL), caudate (CD), basal ganglia (BG) cerebellum (CH), pons and lateral ventricle cerebral spinal fluid (CSF). ADC values of each ROI were measured and mean values for second and third trimester of gestation were obtained. One-way ANOVA was used to calculate the differences between the mean values and Pearson analysis with Bonferroni correction was used to evaluate the linear correlation between ADC values and GA.

Results: ADC values of CH and pons show significant negative correlations with GA ($R = -0.87$, -0.80 , respectively, all $p < 0.0001$); a positive correlation was found between ADC and GA in FWM ($R = 0.56$, $p < 0.01$). In FWM, the ADC increases in parallel to GA during the second trimester; conversely, ADC

decreases with the increasing of GA in the third trimester. ADC mean values of CH, Pons, FWM and BG are significantly different between second and third trimester.

Conclusion: ADC parameters reflect the physiological microstructural changes of myelination, occurring during foetal brain maturation; these ADC results may be useful in the assessment of suspected fetal CNS abnormalities.

B-0152 10:38

A pain in the neck: imaging of the paediatric cervical spine (c-spine) in isolated neck trauma

M. McGill, A. Paterson; *Belfast/UK*

Purpose: To the authors' knowledge there are currently no internationally recognised guidelines which consider the radiological management of focal cervical spine tenderness (FCST) following isolated paediatric c-spine trauma. Our aim was to develop regional guidelines for imaging children with FCST.

Methods and Materials: A retrospective review of 1,000 children (<14yrs) presenting to both tertiary and district general hospitals between 2011 and 16, with isolated c-spine trauma was undertaken to establish current practice with respect to imaging. Guidelines were developed utilising best evidence-based practice in consultation with paediatric spinal and orthopaedic surgeons.

Results: All children evaluated had plain radiograph(s), 39% underwent c-spine CT and 2% c-spine MRI for persistent focal tenderness. Regional differences in local guidelines and practice were identified. Retrospective application of the proposed regional guidelines did not result in the 'miss' of clinically significant c-spine injuries within this study population and would have resulted in a 22% reduction in utilisation of CT and a 45% increase in the utilisation of MRI.

Conclusion: It is possible to decrease the number of CT c-spine exams undertaken in children with FCST. Proposed imaging guidelines are presented for discussion: initially, analgesia is prescribed and consideration of cervical collar placement undertaken by the assessing team. C-spine plain films are obtained and if abnormal, or inadequate, CT is discussed with the radiology team. If pain persists and plain films are normal, referral to the orthopaedic team is undertaken, and a c-spine MRI is organised within 72 hours. Children with focal neurology are all referred for MRI.

B-0153 10:46

Diffusion kurtosis imaging (DKI) can efficiently differentiate low- and high-grade gliomas in paediatric patients

I.P. Voicu, A. Napolitano, L. Lattavo, C. Carducci, M.C. Rossi Espagnet, A. Mastronuzzi, P. Toma, G.S. Colafati; *Rome/IT (paul.voicu@hotmail.it)*

Purpose: To investigate whether diffusion kurtosis imaging (DKI) can be helpful in differentiating low- and high-grade gliomas (LGG and HGG respectively) in paediatric patients.

Methods and Materials: After obtaining informed consent, thirty-two consecutive children (median age 8.5 years, 17 M) affected by histologically confirmed brain gliomas were prospectively studied on a 3T magnet with a 32-channel head coil. Conventional sequences and DKI sequences (30 directions, 3 b values: 0, 1000, 2000) acquired with the simultaneous multislice (SMS) technique were obtained. Mean kurtosis (MK), axial kurtosis (AK), radial kurtosis (RK) and fractional anisotropy (FA) values were calculated and the corresponding maps were obtained. The enhancing and nonenhancing tumour volumes (VOIs) were segmented semiautomatically. Mean and highest 20 percentile (H20%) DKI values in tumour VOIs were calculated for each metric. Differences among DKI values in the enhancing and nonenhancing VOIs of low and high-grade gliomas (LGG and HGG respectively) were assessed with an independent sample t test.

Results: After excluding three patients for motion artefacts, the scans of twenty-nine children (20 LGG and 9 HGG) were analysed. Significantly different mean RK, H20% RK and mean MK values were found in the enhancing tumour VOI between LGG and HGG ($p < 0.029$, $p < 0.015$ and $p < 0.05$ respectively).

Conclusion: DKI can be helpful in differentiating low and high-grade gliomas in paediatric patients.

B-0159 10:54

Grading of hemispheric gliomas in pediatric patients by using Diffusion Kurtosis MR imaging

I.P. Voicu, A. Napolitano, L. Lattavo, C. Carducci, M.C. Rossi Espagnet, A. Mastronuzzi, P. Toma, G. Colafati; *Rome/IT (paul.voicu@hotmail.it)*

Purpose: To investigate whether diffusion kurtosis imaging (DKI) can help differentiate low- and high-grade hemispheric gliomas (hLGG and hHGG respectively) in paediatric patients.

Methods and Materials: After obtaining informed consent, eighteen consecutive children (median age 9.6 years, 9 males) affected by histologically confirmed hemispheric gliomas were prospectively studied on a 3T magnet with a 32-channel head coil. Conventional sequences and DKI sequences (30 directions, 3 b values: 0, 1000, 2000) acquired with simultaneous multislice

technique (SMS) were obtained. Mean kurtosis (MK), axial kurtosis (AK), radial kurtosis (RK) and fractional anisotropy (FA) values were calculated and the corresponding maps were obtained. The enhancing and nonenhancing tumour volumes (VOIs) were segmented semiautomatically. Mean and highest 20 percentile (H20%) DKI values in tumour VOIs were calculated for each metric. Differences among DKI values in the enhancing and nonenhancing VOIs of low and high-grade hemispheric gliomas (hLGG and hHGG respectively) were assessed with an independent sample t test.

Results: After excluding one patient for motion artifacts, the scans of seventeen children (12 LGG and 5 HGG) were analysed. Significantly different mean RK, H20%RK, mean MK and H20% MK values were found in the enhancing tumour VOI between hLGG and hHGG ($p < 0.003$, $p < 0.007$, $p < 0.004$ and $p < 0.001$ respectively). No significant differences in DKI values were found between nonenhancing tumour VOIs in hLGG and hHGG.

Conclusion: DKI can help differentiate low and high-grade hemispheric gliomas in paediatric patients.

B-0157 11:02

Diffusion kurtosis imaging (DKI) can help differentiate low- and high-grade brainstem gliomas in pediatric patients: a pilot study

I. Voicu, A. Napolitano, L. Lattavo, M. Rossi Espagnet, C. Carducci, A. Mastronuzzi, P. Toma, G. Colafati; *Rome/IT (paul.voicu@hotmail.it)*

Purpose: To investigate whether diffusion kurtosis imaging (DKI) can help differentiate low- and high-grade brainstem gliomas (bLGG and bHGG respectively) in paediatric patients.

Methods and Materials: After obtaining informed consent, fourteen consecutive children (median age 7.4 years, 8 males) affected by histologically confirmed brainstem gliomas were prospectively studied on a 3T magnet with a 32-channel head coil. Conventional sequences and DKI sequences (30 directions, 3 b values: 0, 1000, 2000) acquired with simultaneous multislice technique (SMS) were obtained. Mean kurtosis (MK), axial kurtosis (AK), radial kurtosis (RK) and fractional anisotropy (FA) values were calculated and the corresponding maps were obtained. The enhancing and nonenhancing tumor volumes (VOIs) were segmented semiautomatically. Mean and highest 20 percentile (H20%) DKI values in tumor VOIs were calculated for each metric. Differences among DKI values in the enhancing and nonenhancing VOIs of low and high-grade brainstem gliomas (bLGG and bHGG respectively) were assessed with an independent sample t test.

Results: After excluding two patients for motion artifacts, the scans of twelve children (8 LGG and 4 HGG) were analyzed. Significantly different H20% FA, mean MK, H20% MK, mean AK and H20% AK values were found in the nonenhancing tumor VOI between LGG and HGG ($p < 0.05$, $p < 0.008$, $p < 0.007$, $p < 0.045$ and $p < 0.001$ respectively). No significant differences in DKI values were found between enhancing tumor VOIs in bLGG and bHGG.

Conclusion: DKI can help differentiate low and high-grade brainstem gliomas in paediatric patients.

B-0154 11:10

High predictive value of MRI imaging in mitochondrial disease

I. De Beaurepaire, D. Grevent, R. Levy, V. Dangouloff-Ros, A. Munnich, A. Rötig, N. Boddaert; *Paris/FR (isaure.debeaurepaire@orange.fr)*

Purpose: Because the mitochondrial respiratory chain is ubiquitous, its deficiency can theoretically give rise to any symptom in any organ or tissue at any age with any mode of inheritance, owing to the twofold genetic origin of respiratory enzyme machinery, i.e. nuclear and mitochondrial. Yet, not all respiratory enzyme deficiencies are primary. Indeed, secondary deficiency is frequently observed, leading to a number of false conclusions and inappropriate investigations in clinical practice.

Methods and Materials: Starting from a large series of 189 patients at risk of respiratory chain deficiency, for whom both brain MRIs and disease-causing mutations were available, we retrospectively studied the predictive value of brain MRI imaging and its ability to discriminate between two groups: primary deficiency of the mitochondrial respiratory chain machinery ($n=152$) and phenocopies ($n=37$).

Results: Although no anomaly was specific, detection of i) brainstem hyperintensity with basal ganglia involvement ($p \leq 0.001$) and ii) lactate peak with either brainstem or basal ganglia hyper-intensity were highly suggestive of primary respiratory chain deficiency ($p \leq 0.01$). Fourteen items had a positive predictive value $> 95\%$ and biallelic *SLC19A3* mutations represented the main differential diagnosis. Non-significant differences between the two groups were found for cortical/subcortical atrophy, leukoencephalopathy, and involvement of caudate nuclei and corpus callosum.

Conclusion: Based on these results and owing to invasiveness of skeletal muscle biopsies and cost of high-throughput DNA sequencing, we suggest giving consideration to brain MRI imaging as a strong predictive marker and the first investigation to be performed in patients at risk of respiratory chain deficiency.

B-0155 11:18

SMI ultrasound of the neonatal brain: comparison with MRI (1.5 T) in a clinical case series

A. Hojreh, G. Kasprian, K.A. Göral, K. Klebermass-Schrehof, K. Vergesslich Rothschild, M. Weber, J.M. Patsch; *Vienna/AT (azadeh.hojreh@meduniwien.ac.at)*

Purpose: Superb microvascular imaging (SMI) is a novel ultrasound application capable of depicting micro-vasculature. Previously, we have reported feasibility and features of brain SMI in healthy neonates. The purpose of this study was to compare SMI ultrasound and MRI in a clinical case series.

Methods and Materials: Following ethical approval and written informed consent, we performed transcranial ultrasound in thirteen neonates with suspected brain pathologies. Routine examinations were performed and documented according to national standards. SMI ultrasound was performed using linear (18MHz and 14MHz) and curved array transducers (4mHz). Superficial and deep scans were acquired in the coronal and parasagittal plane, using the left and right superior frontal gyrus as anatomical landmarks. All subjects underwent 1.5 T MRI. Regarding visibility of microvessels, T2-weighted turbo-spin-echo sequences and susceptibility-weighted sequences were compared with SMI ultrasound.

Results: In all cases ($n=13/100\%$), cortical and medullary were visible on SMI ultrasound and invisible on MRI. In 23 % of cases (3/13), intraparenchymal striatal microvessels were visible on SMI, but invisible on MRI (100%). In a case with mitochondrial disease, medullary micro-vessels were pathologically elongated/tortuous, which was confirmed by histology. Post-ischemic cortical hyperperfusion was detected in an area of cortical infarction/diffusion restriction. SMI detected tortuous subarachnoid vessels in a case of osteogenesis imperfecta, which could be confirmed by MRI.

Conclusion: SMI ultrasound opens a new diagnostic window in the assessment of vascular pathologies of the neonatal brain. Abnormalities of cortical, medullary, and striatal micro-vessels that are invisible on 1.5T MRI can be readily detected.

B-0156 11:26

Simultaneous decrease of aspartate and NAA levels in the brain after severe TBI: ¹H MRS study

P.E. Menshchikov, M. Ublinskiy, A. Manzhurtsev, T. Akhadov, N. Semenova; *Moscow/RU (peeterem@gmail.com)*

Purpose: N-acetylaspartate (NAA) is a neuronal marker in the brain. Severe TBI is associated with decrease of NAA level. Disturbances in the NAA synthesis from aspartate (Asp) may be the reason of NAA decrease. Thus, the main objective of this study was to estimate simultaneously cerebral Asp and NAA levels in vivo using proton magnetic resonance spectroscopy (¹H MRS).

Methods and Materials: Eight children (mean age: 14±2 years) were examined with quantitative ¹H MRS after closed severe head injury (5-6 months after TBI). Control group consisted of 11 healthy children (mean age: 15±1 years) without history of any TBIs. MRS protocol included MEGA PRESS (aspartate and pure glutamate signals) and conventional PRESS spectra with TE=115 ms. Voxels in size of 25x25x30 mm were located in the frontal lobe. All investigations were performed on Philips 3.0T Achieva TX MRI scanner.

Results: NAA/tCr as well as Asp/tCr ratios were significantly reduced ($P < .001$) in patients by 34% and 44%, respectively. Cho/tCr was significantly increased (by 36%) in patients. GLX and pure glutamate levels were unchanged.

Conclusion: This study for the first time revealed simultaneously reduced cerebral Asp and NAA levels. This result can be a significant confirmation of NAA synthesis disturbances after TBI. Further investigations on Asp/NAA balance in the acute severe TBI will certainly help in understanding of biochemical changes in injured brain.

B-0158 11:34

Assessment of a 33-point software programme for the identification of vertebral fractures in children

F. Alqahtani, F. Messina, A.C. Offiah; *Sheffield/UK (ffmalqahtani1@sheffield.ac.uk)*

Purpose: To measure observer reliability and diagnostic accuracy in children, of a semi-automated programme using a 33-point technique (Avert™) developed for vertebral fracture (VF) diagnosis in adults, which records percentage loss of vertebral body height and to compare Avert with previous results of a 6-point technique (SpineAnalyzer™).

Methods and Materials: Lateral spine radiographs (RA) and dual-energy lateral vertebral assessment (VFA) images of 50 children were analysed using two different programmes (SpineAnalyzer™ and Avert™; 50 RA analysed with SpineAnalyzer (Group 1), 50 RA analysed with Avert (Group 2) 50 VFA analysed with Avert (Group 3). Diagnostic accuracy (sensitivity, specificity) was calculated by comparing with a previously established consensus arrived at by three experienced paediatric radiologists, using a simplified algorithm based

qualitative scoring system. Levels of agreement were calculated using Cohen's kappa.

Results: Overall sensitivity of Groups 1, 2 and 3 was 26%, 37% and 35% and specificity was 98%, 94% and 92% respectively. Fair agreement was found between different modalities/different software; between Groups 2 and 3 kappa 0.29 (95% CI, 0.06 - 0.53), between Groups 1 and 3 kappa 0.35 (95% CI, 0.12 - 0.59). Moderate agreement was noted between identical modalities; Groups 1 and 2 kappa 0.55 (95% CI, 0.28 - 0.82).

Conclusion: The 33-point technique has slightly higher accuracy for the representation of vertebral morphometry in children when compared to the 6-point technique. However, neither Avert nor SpineAnalyzer are satisfactorily reliable for VF diagnosis in children. Therefore, training of either or both software programmes on paediatric images is required.

B-0160 11:42

Systematic approach to the congenital abnormalities of the posterior fossa: a tertiary paediatric referral hospital experience in last five years (2012-2016)

J. Smiechowicz¹, M. Rebollo Polo², M. Gómez Chiari³, J. Muchart Lopez³, C. Fons Estupiña²; ¹Girona/ES, ²Esplugues de Llobregat/ES, ³Barcelona/ES (jareksmie@wp.pl)

Purpose: Congenital abnormalities of the posterior fossa present a wide spectrum of radiological features including normal anatomic variations and severe malformations. MRI permits systematic evaluation of cerebellum and its pathology and employment of the biometric parameters.

Methods and Materials: We reviewed MRI scans of the group of 351 newborns (age: 1-28 days) performed in the tertiary referral hospital in years 2012-2016. 1.5T Signa Excite GE MRI T1 T1 FLAIR, PDT2, DWI, T2, T2* y T1 3D-SPGR. We have taken measurements of cerebellum transversal diameter, craniocaudal and anteroposterior diameter of the vermis, tegmento-vermian angle and analysed the cerebellar fissures. Moreover, the presence of the supratentorial pathology was also recorded.

Results: The range of the tegmento-vermian angle in a group of control is 3 - 14.5 degrees, meanwhile, a significant number of patients with malformation present an angle value higher than 15 degrees. In addition, the differences of the values of cerebellum craniocaudal diameter of the vermis between both groups has drawn our attention. Abnormalities of posterior fossa such as arachnoid cyst, Blake cyst, cerebellar dysplasia, rhombencephalosynapsis, Chudley-McCullough syndrome, Joubert syndrome, Dandy-Walker malformation, pontocerebellar hypoplasia or congenital muscular dystrophy with cerebellar affection were analysed. Anatomic variations such as mega cisterna magna was also recorded.

Conclusion: The systematic revision of the posterior fossa structures increases the sensibility in diagnosing possible congenital malformations. These abnormalities can be classified in order to criteria based in biometric parameters which facilitate suggesting differential diagnosis, genetic disorder orientation and prognostic factors of neurological outcomes.

B-0161 11:50

Dentate and basal ganglia T1-hyperintensity in pediatric patients who had received both linear and macrocyclic Gadolinium-based MRI contrast agents; evidence of a "carry-over" effect

P. Gulino¹, A. Bianchi¹, A. Scionti², S. Diciotti³, E. Bartolini¹, P. Papadopoulos¹, C. Defilippi¹, M. Mascalchi¹; ¹Florence/IT, ²Pisa/IT, ³Bologna/IT (pietrogulino@yahoo.it)

Purpose: The capability of macrocyclic Gadolinium-Based Contrast Agents (GBCAs) to determine hyperintensity of dentate nucleus and basal ganglia in pre-contrast T1-weighted images (T1wH) is controversial. Our study intend to demonstrate the "carry over" effect.

Methods and Materials: Two radiologists visually assessed in consensus sagittal T1-weighted SE or TSE images of 140 index-MRI examinations in pediatric patients with at least one prior contrast-enhanced (CE)-MRI and of 123 control-MRI examinations in pediatric patients without prior CE-MRI.

Results: T1wH was identified in 9 (4 "definite" and 5 "faint": 6.4%) of 140 index-MRI and in none of 123 control-MRI (p=0.004). All of them belonged to the group of 86 patients who had received both linear (gadopentetate dimeglumine) and macrocyclic (gadoterate meglumine) GBCAs, whereas none of the 54 patients who had received only the macrocyclic GBCA showed T1wH (p=0.01). Age, number of prior CE-MRI and the cumulative dose of GBCAs were significantly (p<0.01) higher in patients with T1wH as compared to patients without. Region-of-interest (ROI) analysis showed a progressive increase of pallidal/middle cerebellar peduncle (MCP) signal intensity (SI) ratio in the 4 patients with "definite" T1wH and of dentate/MCP SI ratio in 3.

Conclusion: Dentate and basal ganglia T1wH occurs in pediatric patients after CE-MRI with both linear and macrocyclic GBCAs in line with a "carry over" effect.

10:30 - 12:00

Room M 3

Oncologic Imaging

SS 216

Colorectal cancer revisited

Moderators:

A. Lebovici; Cluj-Napoca/RO
N.N.

B-0162 10:30

MRI texture analysis of rectal cancer with mono- and multivariate analysis using machine learning artificial intelligence

R. Ferrari¹, C. Voena¹, C. Mancini¹, M. Zerunian², F. Rivosecchi², V. Marè¹, R. Paramatti¹, R. Faccini¹, A. Laghi²; ¹Rome/IT, ²Latina/IT (ferrariccardo@gmail.com)

Purpose: To perform texture analysis (TA) of first and second order of T2 weighted images of the entire volume of rectal cancer acquired pre, intermediate and after the treatment. To perform mono and multivariate analysis of texture parameters using AI by means of machine learning.

Methods and Materials: 55 patients. T2 weighted images were analysed using TA: first order (gray-level histogram) in 2D and 3D dimensions, mean, standard deviation, skewness and kurtosis. Local entropy. The grey level co-occurrence matrix (horizontal direction, 1 pixel displacement). The homogeneity, the energy, the contrast and the dissimilarity. Time evolution of these parameters has been studied between the different time-control. The most effective parameters have been combined in a multivariate analysis with the use of the machine learning algorithms.

Results: The most significant parameters are: the ratio of the minimum of the local entropy computed after and before the treatment and some of the parameters extracted from the gray-level co-occurrence matrix computed in the slice where the tumour has maximum area. We also found that the area of the tumour before the treatment, is quite sensitive and it has been included in the multivariate analysis. A cut on the output of the random forest classifier can be placed to separate CR and PR+NR with the performances summarised in the ROC curve.

Conclusion: The use of a automatic multivariate analysis algorithm for analysing values of TA of T2 weighted images in patient with rectal tumour, using 2D and 3D segmentation of the tumour could differentiate Complete responder patients and partial responder/non responder patients to Radiotherapy and chemotherapy.

B-0163 10:38

Radiomic features from pretreatment MRI are associated with prognosis in rectal cancer patients: preliminary findings

S. Yiquan, T.T. Tong, Y.J. Gu; Shanghai/CN (12211230032@fudan.edu.cn)

Purpose: Our goal was to investigate the correlation between histopathology and diffusion parameters by utilizing the most repeatable strategy for ROI- and slice-based diffusion parameters in rectal cancer.

Methods and Materials: Sixty-six patients underwent DKI-MR. Two readers independently measured the parameters using three slice protocols including single slice, three slices and whole tumour slice (WTS), combined with one of two ROIs, including outline and round ROI. Kruskal-Wallis, a paired sample t test, interclass correlation coefficient (ICC), Bland and Altman, Student's t tests, and receiver operating characteristic curves were used for statistical analysis.

Results: There were no significant differences among three slice protocols with regard to diffusion parameters (p > 0.05). The ADC and D derived from outline ROI were higher than those from round ROI (p < 0.05), while the opposite trend was apparent for K (p < 0.05). The WTS-outline ROI method resulted in the most excellent intra- and interobserver ICC. Utilizing the WTS-outline ROI, the AUC for assessment of well-differentiated tumours is greater by K (0.871), compared to ADC (0.809), and AUC for T2 is 0.768 by K.

Conclusion: The most repeatable strategy was the WTS-outline ROI method. In addition to ADC, K correlated with histopathology utilizing the WTS-outline ROI.

B-0164 10:46

Performance of texture analysis in predicting tumoural response to neoadjuvant chemoradiotherapy in rectal cancer patients studied with 3T MR

M. Zerunian, D.M. Bellini, D. Caruso, D. De Santis, T. Biondi, A. Laghi; Latina/IT (marta.zerunian@gmail.com)

Purpose: To determine the performance of texture analysis (TA) in predicting tumoural response in colon rectal cancer (CRC).

Methods and Materials: 40 consecutive CRC patients were prospectively enrolled and underwent 3T MRI before, during and after chemoradiotherapy (CRT). A region of interest was manually drawn around the tumour on axial oblique T2 images and analysed using first order statistical texture parameters (Skewness, Kurtosis, Entropy and mean value of positive pixels (MPP)). Receiver operating characteristic (ROC) curve analysis was performed to assess the diagnostic yield of TA parameters to predict complete response (CR).

Results: Thirteen patients showed histological CR, Twenty-two patients partial response (PR) and five patients were non-responders (NRs). Entropy, Kurtosis and MPP showed significant differences before and after CRT in CR's; PR/NR Entropy and Skewness showed significant differences before and after CRT ($p < 0.05$). Absolute changes among different texture parameters in CR and PR/NR patients before and after CRT showed significant differences in Entropy, Kurtosis and MPP (0.31 ± 0.35 , in CR, -0.02 ± 1.28 in PR/NR, ($p = 0.04$); 1.87 ± 2.19 , in CR, -0.06 ± 3.78 in PR/NR ($p = 0.0005$); 107.91 ± 274.40 , in CR, -28.33 ± 202.91 in PR/NR, ($p = 0.004$), respectively). Kurtosis, evaluated on pre-treatment images, showed significant results in predicting CR ($p = 0.04$; optimal cutoff value ≥ 6.68 , Se 76.92% and Sp 38.46%).

Conclusion: TA from T2 images potentially play an important role as imaging biomarkers of tumoural response to neoadjuvant-CRT in CRC. Kurtosis is accurate in predicting complete responders.

B-0165 10:54

Evaluation of diagnostic accuracy of diffusion weighted (DW) MRI in mesorectal lymph node staging of rectal carcinoma (ReNoRis)

C.G. Monaco¹, G. Parker², R. Little², Y. Watson², S. Cheung², J. O'Connor², A.V. Marchiano¹, D. Scaramuzza¹; ¹Milan/IT, ²Manchester/UK (cristianmonaco87@gmail.com)

Purpose: To assess the pre-operative DW MRI accuracy in detecting mesorectal lymph-node metastasis.

Methods and Materials: 34 patients prospectively enrolled April 2012-May 2014 with newly diagnosed, histologically proven, rectal cancer. T4 and mucinous tumors were excluded. 1.5T MRI Avanto, Siemens, Erlangen, Germany was used with the sequences protocol: pelvis T1 (5mm), T2 sagittal and coronal (3mm), T1 and T2 perpendicular to the rectum (3mm), DWI echo-planar (5mm, b-values 0, 400, 800 mm²/s²), T1 gradient-echo dynamic contrast-enhanced (5mm), T1 VIBE (1mm) and TSE (3mm) post contrast. ADC was evaluated from DWI with ROI's on tumours and mesorectal lymph-nodes. All patients underwent total mesorectal excision within 1 week after MRI, without neoadjuvant-therapy. Surgical specimens were cut at 5mm thickness, TNM classified. The pathologist and the radiologist identified the lymph-nodes location. For predicting mesorectal nodal metastasis we assessed these characteristics using Wilcoxon and Fisher's tests: T stage; lymph-node size, margins, internal homogeneity and location with respect to the upper tumoral border, lymph-node ADC and node to primary tumour (N/T) ADC ratio.

Results: TNM staging: 1 T1, 3 T2, 30 T3 tumours, and 22 N0, 6 N1, 6 N2. Only irregular lymph-node margins ($p = 0.002$), lymph-nodes located at least 1cm above the upper tumoral border ($p = 0.0004$) and N/T ADC ratio ($p = 0.0007$) were significantly associated with metastasis.

Conclusion: Similar cellularity between primary tumour and lymph-nodes is significantly associated to the presence of mesorectum lymph node metastasis, as irregular lymph-node margins. The lymph-node location/distance from tumoral margin is possibly related to the anatomic drainage of rectal tumours.

B-0166 11:02

Prognostic value of bodycomposition parameters assessed at the preoperative CT in patients with colorectal carcinoma

M. Martinelli, M. Chincarini, G. Zamboni, C. Fabris, C. Conti, C. Pedrazzani, R. Pozzi Mucelli; Verona/IT (marco.chincarini@gmail.com)

Purpose: To assess the effects of Body Composition Parameters (BCPs), measured on the preoperative CT in patients with colorectal cancer (CRC), on overall survival and surgical complications.

Methods and Materials: We reviewed the preoperative CTs of 288 patients who were resected for CRC, and measured the BCPs on the L3-L4 transverse sections using a free software (ImageJ, National Institutes of Health, USA). Total Fat Area (TFA), Subcutaneous Fat Area (SFA), Visceral Fat Area (VFA), Retroperitoneal Fat Area (RFA) and Total Muscle Area (erector spinae + psoas + abdominal wall muscles), were measured. The Skeletal Muscle Index (SMI = TMA/height²) was calculated to assess for sarcopenia. The clinical features assessed included gender, age, BMI, tumor location, TNM stage, overall survival and surgical complications. Kaplan-Meier curves for survival were calculated. Chi-square was used to assess the association of the parameters with complications.

Results: 194/288 patients (67.4%) were sarcopenic. 3-year survival and 5-year survival were significantly lower for sarcopenic patients than for the non-sarcopenic (83.2% vs 93.7%, and 78.2% vs 90.1%, respectively; $p = 0.03$). No significant difference was observed regarding surgical complications. BMI and

fat measures did not appear to influence patient survival or surgical complications.

Conclusion: Sarcopenia appears to be significantly associated with a lower overall survival. Amount of visceral, subcutaneous or total fat and obesity did not show any significant correlation with patient prognosis. Assessment of sarcopenia can provide additional prognostic information from the preoperative CT.

B-0167 11:10

Pelvic MRI after induction chemotherapy and before long-course chemoradiation therapy: what are the imaging findings?

I. Blazic, N.M. Campbell, A. Knezevic, M. Gonen, P. Lynn, M. Weiser, J. Garcia-Aguilar, L. Saltz, M.J. Gollub; New York, NY/US (ivanablazic@yahoo.com)

Purpose: To assess the ability of MRI after FOLFOX-based induction chemotherapy (ICT) to predict rectal cancer response to total neoadjuvant treatment (TNT).

Methods and Materials: In this IRB-approved retrospective study, pre- and post-ICT tumour T2 volume and relative T2 signal intensity (rT2SI; tumour/obturator internus muscle) were assessed in 63 patients with 65 tumours by two readers. Node size, signal intensity and border characteristics were recorded. Correlations were made between the reference standard of histopathologic percent tumour response in the primary tumour with tumour volume change, rT2SI and baseline and post-ICT lymph node characteristics.

Results: Post-ICT MRI was obtained within 30 days of completion of ICT. 9/63 (14.3%) patients had a complete response after TNT. Change in T2 volume was not associated with TNT response. Change in rT2SI showed no correlation with TNT response. There was a significant negative correlation between baseline and post-ICT node size and TNT response ($r = -0.25$, $p = 0.05$; $r = -0.35$, $p = 0.005$, readers 1 and 2, respectively). Both baseline and post-induction median node size were significantly smaller in complete responders and 95% responders ($p = 0.03$, 0.001; readers 1, 2, respectively). Median change in largest baseline node size and decrease in post-ICT node signal heterogeneity were associated with 100% tumour response ($p = 0.04$).

Conclusion: In this cohort of patients receiving post-ICT MRI, tumour volume and signal intensity did not correlate with TNT response. Lymph node sizes decreased after ICT and were significantly associated with complete response to TNT. This potentially useful prognostic information will require validation in a prospective study.

B-0168 11:18

Tumour volume vs RECIST criteria in re-staging rectal cancer

E. Guidi, C. Giaconi, C. Arena, E. Neri; Pisa/IT (radiagnostica3.aoup@gmail.com)

Purpose: To compare MRI tumour volume regression grade vs RECIST criteria in the re-staging of rectal cancer.

Methods and Materials: Thirty-three patients with locally advanced rectal cancer (T3-T4 stage or any N+) underwent MRI for staging and re-staging. MRI acquisition was performed on 1.5T and 3T scanners, with a protocol compliant with the ESGAR guidelines. MR tumour volume was calculated by a semi-automatic tool. All patients underwent neo-adijuvant chemo-radiotherapy, followed by total mesorectal excision. Each rectal specimen, analysed by the pathologist, was classified on the basis of the Dworak tumour regression grade.

Results: In 24/33 patients a complete downstaging from T3 to T-T2 was obtained. Among these 7 patients showed a tumour volume reduction grade > 80%. A statistically significant correlation between tumour regression grade and volume reduction was observed (Spearman rank = 0.3626, $p = 0.0189$). According to the RECIST criteria 19/33 (57.6%) patients had partial response and only 3 had complete response.

Conclusion: Tumour volume reduction grade showed the best correlation with pathological grading and should be considered as one indicator/biomarker of response to chemo-radiotherapy in restaging locally advanced rectal cancer.

B-0169 11:26

MRI of rectal cancer response to therapy: comparison of T2, DWI and ADC between 3T and 1.5T

M. Zerunian, D. Caruso, D.M. Bellini, D. De Santis, F. Rivosecchi, A. Laghi; Latina/IT (marta.zerunian@gmail.com)

Purpose: To compare signal intensity (SI) on T2, DWI and ADC maps between 3T and 1.5T MRI of rectal cancer pre, during and post-neoadjuvant-chemoradiotherapy (CRT).

Methods and Materials: Twenty-two consecutive rectal cancer patients were prospectively analyzed on both 3T and 1.5T MRI. All patients underwent to dedicated axial-oblique T2, DWI and ADC performed pre, during and post-CRT. Two expert radiologists selected in agreement the best qualitative single slice where the tumor was detectable for all three chosen sequences of each examination, for a total of 396 slices. Another radiologist, blinded for

histological results, drawn a region of interest of the tumor on the selected slice and registered the corresponding SI of T2, DWI and ADC.

Results: Significant differences were observed for DWI on 3T compared to 1.5T for pre-CRT (324.37±172.21 vs. 70.72±20.83), during CRT (199.86±128.08 vs. 52.59±17.16) and post-CRT (135.53±68.03 vs. 43.17±14.47), and for T2 values between 3T and 1.5T for pre-CRT (599.57±144.83 vs. 339.57±117.87), during CRT (527.24±178.92 vs. 344.76±119.89) and post-CRT (526.19±136.30 vs. 318.91±99.77) (all p<0.05), whereas no significant differences were reported for ADC values between 3T and 1.5 T for pre-CRT (0.85±0.21 vs. 0.83±0.19), during CRT (1.11±0.25 vs. 1.18±0.33) and post-CRT (1.24±0.36 vs. 1.27±0.35) (all p>0.05). A progressive decreasing trend for DWI and T2 was observed during the three controls, while an increasing trend was noticed for ADC in the three examinations, for both fields strength.

Conclusion: DWI and T2 values were significantly higher on 3T than 1.5T while no significant differences were observed on ADC pre, during and post-CRT.

B-0170 11:34

Correlations between the iodine concentrations from dual-energy computed tomography and molecular markers Ki-67 and HIF-1α in rectal cancer: a preliminary study

S. Fan, X. Li, Z. Ye; Tianjin/CN (303533681@qq.com)

Purpose: To investigate whether dual-energy computed tomography (CT) with iodine quantification is correlated with molecular markers Ki-67 and hypoxia-inducible factor 1α (HIF-1α) in rectal cancer (RC).

Methods and Materials: Eighty patients (43 males and 37 females) diagnosed with rectal cancer got pelvic contrast-enhanced CT scan with dual-energy computed tomography before any anticancer treatment. The normalized iodine concentration (NIC) values and CT values at each energy level (40-140 keV) from the virtual monochromatic image of the primary lesions were analysed. The postoperative specimens of all 80 patients underwent Ki-67 and HIF-1α immunohistochemistry staining. By SPSS17.0 software package, we analysed the correlations of NIC values and CT values at each energy level (40-140 keV) with Ki-67 and HIF-1α expression. The receiver operating characteristic (ROC) curves of these dual-energy computed tomography parameters were calculated and the diagnostic value were assessed.

Results: There was a weak positive correlation between NIC values and carcinoembryonic antigen level (r=0.246, P=0.028) in RC. Both the value and the level of Ki-67 expression were correlated positively with the NIC values (r=0.344, P=0.002 and r=0.248, P=0.026). HIF-1α expression was correlated positively with the NIC values of the RC (r=0.598, P<0.001). The best threshold value of NIC values in diagnosing the expression of HIF-1α was 0.5839. The sensitivity was 78%; specificity, 87%; PPV, 86%; NPV, 79%; accuracy, 83%.

Conclusion: The NIC values on dual-energy computed tomography may be used as a measurement of hypoxia in RC and determining the ability of tumour invasion noninvasively.

B-0171 11:42

Utility of CT histogram parameters in discriminating between metastasis and non metastases among colorectal cancer patients with pulmonary lesions

S. Wang, T. Tong, T. Hu, W. Peng, J. Wang, L. Huang; Shanghai/CN (shengpingwang2007@126.com)

Purpose: To determine whether whole-lesion histogram parameters of pulmonary nodules based on computed tomography (CT) images can distinguish between lung metastasis (LMs) and non metastases (NMs) in patients with colorectal cancer (CRC).

Methods and Materials: From January 2012 to December 2014, 276 CRC patients with pulmonary lesions were divided into two groups: LM group and NM group which were confirmed by pathology. Whole-tumour texture analysis was performed on CT images, and histogram parameters were derived from the pixel distribution histogram. Potential predictive parameters to differentiate LM from NM were identified by univariate regression analysis and subsequently tested in multivariable logistic regression analysis.

Results: Of 276 nodules, pathologic analysis confirmed 171 LMs, 105 NMs (13 PLCs and 92 benign lesions). Kurtosis and sphere value were significantly higher (0.73 versus -0.79, P<0.0001; 1.59 versus 0.65, P<0.0001, respectively) while skewness was significantly lower (-1.03 versus 0.13, P<0.0001) in LM group compared to the group. Multivariate analysis revealed that smaller sphere value (adjusted odds ratio, 0.092) and higher kurtosis (adjusted odds ratio, 3.319) are significant differentiators of LM from NM (P < .001). With mean attenuation, the standard deviation of attenuation, volume, kurtosis, and sphere value, the logistic regression model showed excellent accuracy (area under the curve, 0.91) in the differentiation of LM from NM.

Conclusion: In patients with CRC, higher kurtosis and sphere value are significant differentiators of LM from NM, and LM can be accurately differentiated from NM by using CT histogram analysis.

B-0172 11:50

Staging of colon cancer, best technique/modality, a PhD thesis

E. Nerad^{1,2}, M.J. Lahaye², R.G.H. Beets-Tan²; ¹Worcester/UK, ²Amsterdam/NL (nerad19@hotmail.com)

Purpose: Paradigm shift in the treatment for colon cancer is on the horizon with neo-adjuvant therapy possibly becoming available for operable colon cancer patients (FOXTROT study). Staging will become crucial; the focus of this thesis is to determine what technique/modality has the highest accuracy.

Methods and Materials: Two meta-analyses, computed tomography (CT) and CT colonography (CTC) and an original study using magnetic resonance imaging (MRI) to determine the accuracy in the detection of tumour invasion through the bowel wall and nodal involvement of colon cancer were performed.

Results: The sensitivity, specificity for detection of tumour invasion beyond the bowel wall were 90% (95%CI: 83-95%); 69% (95%CI: 62-75%) for CT, 90% (95% CI: 88-92%); 87% (95% CI: 83-90%) for CTC; 91% (76-98%); 84% (60-96%) for MRI respectively. For nodal involvement the estimates were 71% (95%CI: 59-81%); 67% (95%CI: 46-83%) for CT, 84% (95% CI: 80-88%); 66% (95% CI: 59-72%) for CTC, 91% (76-98%); 84% (60-96%) for MRI respectively.

Conclusion: It appears regular CTC and MRI have a better accuracy in the local staging of colon cancer compared with regular CT techniques.

10:30 - 12:00

Room M 5

Imaging Informatics

SS 205

Process improvement and patient communication

Moderators:

M. Fatehi; Tehran/IR
A. Trianni; Udine/IT

B-0173 10:30

Early treatment for PE diagnosed on CTPA: does electronic critical report labelling make a difference?

S.L. Dluzewski, N. Patel, S.R. Tincey, S. Hare; London/UK (sophia_tincey@hotmail.com)

Purpose: Recent guidance for reporting radiologists emphasises the importance of highlighting studies with significant or abnormal findings to requesting clinicians. Pulmonary embolism (PE) represents a significant cause of morbidity and mortality in the hospital setting. The aim of this study was to assess whether electronic critical report labelling has an impact on the rapidity of initiating anticoagulation treatment for PE diagnosed on CTPA.

Methods and Materials: A retrospective observational study was conducted with regard to CTPA studies performed between August 2015 and May 2016 at a District General Hospital, in the UK. All CTPA studies that identified PE were identified. These reports were grouped into those critically labelled and those that were not. Time to therapeutic anticoagulation was compared between the labelled and unlabelled groups.

Results: 410 CTPAs were performed, 85 of which were positive for PE. 8 out of 85 of these were highlighted as critical (9.4%). Patients with critical report labelling were anticoagulated significantly more quickly than those that were not (p=0.0249, u=24). Pre-scan clinical suspicion, pulmonary embolism severity, ward location, time of day and staffing levels were not statistically significant.

Conclusion: This research forms the first UK study in standard clinical practice that provides evidence that labelling reports as critical is associated with significantly shorter delay to treatment.

B-0174 10:38

Appropriateness and pattern of imaging modality choice amongst radiologists from different countries

V. Pozdniakova¹, J. Froehlich², A. Gutzeit³; ¹Stavanger/NO, ²Zurich/CH, ³Lucerne/CH (v.a.pozdnyakova@gmail.com)

Purpose: Appropriate use of medical imaging is a key to the effective diagnostic decision making. Heterogeneity of existing radiological standards yields a big number of improper examinations and leads to unnecessary radiation exposure and high health care costs. In this study we investigated an agreement between radiologists from different countries on imaging modality choice and an appropriateness of selected procedures.

Methods and Materials: A web-based questionnaire with 15 clinical cases was sent to radiologists from 11 European and 3 non-European countries. Responders had to choose the most relevant imaging modality for the suggested clinical situation. Responses appropriateness was ranked according to American College of Radiology (ACR) Appropriateness Criteria from 1 to 9.

The agreement between responders was analyzed using graphical statistics made in R software program. Descriptive statistics were realized in SPSS.

Results: There were significant discrepancies in ACR scores amongst 183 responders who completed the survey. The questions with the worst agreement were related to imaging in blunt abdominal trauma, stroke, physical child abuse and microscopic hematuria. The best agreement was achieved on imaging of lung nodules, cervical spine injury, pylorostenosis and deep vein thrombosis. 56% (n=1247) of responses were ranked as usually appropriate, 13% (n=684) as may be appropriate and 31% (n=295) as not appropriate.

Conclusion: There is a low agreement between radiologists from different countries on preferred imaging modality. It emphasizes a need for an active development and implementation of common radiological guidelines.

B-0175 10:46

Preliminary analysis of a computer tool to avoid repetition of radiological tests

P. Fraga Rivas¹, L. Garcia del Salto¹, J. de Miguel Criado², F. Aguilera del Hoyo¹, C. Benito Vicente¹, A. Marco Sanz¹; ¹Madrid/ES, ²Coslada/ES (fragarivas@gmail.com)

Purpose: To submit a computer tool implanted in the electronic medical history of the notification of repetition of the request of radiological test to analyse the results obtained in the first 10 months after its implantation.

Methods and Materials: In November 2016, this tool was established in the electronic history of our hospital. When a physician requests a radiological test, which was already requested in the previous 180 days, the tool generates a test repetition warning alert. The faculty decides if he continues with the creation of that request, or if he considers that this test should not be repeated.

Results: In these 10 months there have been 8646 notices of repeated radiological request, representing 6.5% of the total of 131593 requests generated. In 3197 notices (36.9%) the physician decided not to request the test again (1273 cases of ultrasound scan, followed by 1109 cases of simple x-ray) and in 5449 (63.02%) he made a new request (3572 were simple radiographs, and 801 cases of ultrasound. 78.2% of simple RX corresponded to trauma).

Conclusion: A large number of unnecessary tests are consequences of ignorance that the patient has a previous and recent one. The tool has proven useful since it has managed to avoid a large number of unnecessary repetitions. The simple x-ray and the traumatology service are the scenes of the greatest number of repetitions of the test. Ultrasonography has been the modality in which more repetitions have been avoided.

B-0176 10:54

Making the best of clinical radiology: a single-institution review of imaging referral appropriateness including cumulative monetary and dose estimates for inappropriate scans

J. Ryan, A. Hollywood, A. Stirling, L. O' Hora, M. Glynn, A. Brady, A. Dolan, L. Lawler, F. Bolster; Dublin/IE (jamesryannchd@gmail.com)

Purpose: There has been a dramatic year on year increase in imaging requests at our academic institution. The iRefer guidelines are produced by the Royal College of Radiologists (RCR) in the UK and are designed to prevent inappropriate imaging and radiation exposure. These guidelines have been available to general practitioners and hospital physicians in Ireland since June 2015. We performed a large retrospective review of radiographs performed in 2015 and 2017 to determine the proportion of inappropriate referrals before and after guideline availability.

Methods and Materials: 1173 radiographs were reviewed. A validated RCR audit template was used for data collection. Emergency department, in-patient and general practitioner referrals were reviewed. Cost and cumulative effective dose estimates were calculated.

Results: The inappropriate abdominal radiograph referral rate was 37% in January 2015 and 47% in January 2017. The inappropriate spinal radiograph referral rate was 48% in 2015 and 39% in 2017. The predicted cost of inappropriate abdominal and spinal radiographs for 2017 was 12,720 euros, the predicted cumulative dose was 927mSv. Paranasal sinus and nasal bone radiographs are considered inappropriate. Over the past 4 years, 573 such scans were performed with an estimated cost of 2,868 euros and a cumulative dose of 8.6 mSv.

Conclusion: Despite the availability of the iRefer guidelines there remains a significant proportion of inappropriate imaging requests. The cost of these scans is significant, as are dose estimates. Interventions are needed to decrease inappropriate referrals. Clinical decision support software may help achieve this.

B-0177 11:02

Metformin and intravenous contrast medium: a systematic review of international radiological societal guidelines

A. Weir¹, B.S. Kelly¹, A. Liew², P. McCarthy²; ¹Dublin 4/IE, ²Galway/IE (arlene weir88@gmail.com)

Purpose: A systematic review was performed to assess the current international radiological societal guidelines on metformin and the risk of lactic acidosis in patients receiving IV contrast media. The quality of supporting evidence was also assessed.

Methods and Materials: Evidence-based guidelines created by established international radiological societies were searched using search terms relating to metformin, contrast media and lactic acidosis in PubMed, Cochrane Library, Embase and Google Scholar databases. Two reviewers assessed the quality of the guidelines using the AGREE collaboration instrument and relevant supporting evidence.

Results: Five international radiological societal guidelines met the inclusion criteria. All guidelines have low scores on many criteria assessed using the AGREE collaboration instrument. Four of the five guidelines had revised their recommendations recently, despite the absence of high-quality evidence. All guidelines, except that of the Royal College of Radiologists, had lowered their threshold for withholding metformin. Despite a lack of agreement between the guidelines in regard to the exact threshold to stop metformin, an improvement in clarity and consistency was noted in relation to the type of renal function assessment, duration for withholding metformin and timing of renal function re-assessment. The data used to support these recently revised guidelines was derived from observational studies alone.

Conclusion: This systematic review showed a significant change in current recommendations for metformin use and IV contrast media, with specific focus on lower renal thresholds for withholding metformin, despite absence of high-quality evidence. Furthermore, there are substantial inconsistencies in the recommendations from various international guidelines.

B-0178 11:10

Study of the current situation of patient information in the example of a CT scan: what are improvement options?

D. Kildal¹, S. Schmidt¹, M. Beer¹, O. Schöffski², T. Blasenbrey¹; ¹Ulm/DE, ²Nürnberg/DE

Purpose: The yearly number of CT shows a steady increase in Germany. Patient information is a significant part of radiologists' daily work. Additionally, in 14% of the legal issues patients complain are focused on the information given by the doctor before the radiological examination. That shows the special importance of correct information and documentation prior to the CT examinations. This study explores the quality, patient satisfaction, doctor satisfaction and spent efforts.

Methods and Materials: 1438 questionnaires from 4 hospitals with different care levels were analysed. Additionally, 512 patients and 106 physicians throughout Germany were asked regarding quality, satisfaction, spent efforts and opportunities for improvement with regard to the patient knowledge concerning CT examination and the acceptance of a computer-assisted information.

Results: Up to 40% of the patients declared that they received no radiological information by a physician. Patients and physicians rate current situation only as "moderately content". 22% of the patients wish extended information. 85.3% of the doctors said that medical information is heavily impacting their daily workflow. Patient information given by radiologists was better than those given by non-radiologist doctors. Finally, the quality of the patient information seems to depend on the size of the staff.

Conclusion: The study shows, that patient information for radiological services is time consuming and currently not very effective. New media (like video-based information and computer-assisted methods) might be promising to set new quality standards and to reduce needed efforts for medical staff.

B-0179 11:18

Patient-adapted communication between radiologist and patient: should radiologists rethink their patient care?

A. Gutzeit; Lucerne/CH (agutzeit2000@gmail.com)

Purpose: The aim of this study was to investigate how patients' perception changes when the radiologist communicates the findings after an examination.

Methods and Materials: After a routine MRT patient group 1 (101 patients) was given the opportunity to discuss the findings with the radiologist. Patient group 2 (101 patients) left the radiological institute without any personal communication. By means of a questionnaire both groups could be compared in terms of stress level, emotional attachment to the institute, and the feeling of competence regarding the radiologist.

Results: 77 % of all patients were concerned about the findings without any difference between the two groups (p>0.05). Significant more patients in group 1 (81%) appreciated that a discussion of these findings represents a good

radiological consultation service in comparison to group 2 (14%)($p<0.005$). Patients in group 1 had a significantly higher binding rate and wanted to be examined in department with communication only ($p<0.05$)(93.1% group, 1/75% group 2). After the interview significantly more patients in group 1 considered the radiology department as being a competent department than in group 2 without a discussion ($p < 0.001$).

Conclusion: Communication and reporting between radiologists and patients after an examination leads to a much better perception of patient well-being, feeling of competence and binding factor between patient and radiologist.

B-0180 11:26

Significant quality improvement of results and patient satisfaction in medical information for radiological examinations applying video information techniques

D. Kildal¹, S. Schmidt¹, M. Beer¹, O. Schöffski², T. Blasenbrey¹, ¹Ulm/DE, ²Nürnberg/DE

Purpose: Correct medical information for radiological examinations is very important and simultaneously expensive and time consuming. Additionally, 14% of legal issues are associated with an incorrect medical-information process. Legal requirements and wishes of patient representatives increase steadily, on the other side, yearly CT examinations in Germany strongly increase. Actually German doctors spend on average 17.7 years only for the CT information procedures. Despite this time effort, patients and physicians are only moderately satisfied with the current situation. This study explores the acceptance of patients and doctors regarding the implementation of using information videos and computer-assisted anamnesis methods for the patient information.

Methods and Materials: 512 patients and 106 doctors throughout Germany were asked regarding the current situation, satisfaction and acceptance of technical innovation. Another survey relating an information video was conducted for validation. It was analysed how many risks and side effects were remembered by the patients depending on the method information was given.

Results: Patients and doctors showed a great acceptance for technical innovation. The second survey (information video) showed a significant rise in all test areas. Patients could better remember the radiation risk, side effects of contrast agents or risk in general after video-based information. The satisfaction after the video information was significantly higher than after a conventional given medical information.

Conclusion: The video-information is future oriented. Patients could be enlightened with higher quality and more satisfactory medical learnings. It is to be expected that the medical-information conversation will be more well prepared, more focused and at least shorter - the last point is also important for cost savings.

B-0181 11:34

Radiologists as co-author in case reports containing radiological images: does their presence influence quality?

E. Luyckx¹, J.M.L. Bosmans^{2,1}, B. Broeckx³, S. Ceysens¹, P.M. Parizel¹, A. Snoeckx¹, ¹Antwerp/BE, ²Ghent/BE, ³Merelbeke/BE (elisaluyckx1@gmail.com)

Purpose: Imaging plays a crucial role in many diagnostic processes. It is, therefore, not surprising that medical case reports often include radiological images. Cui honorem, honorem deberi ("honour to whom honour is due") seems straightforward, but such is not always the case where it concerns including radiologists as co-authors. Clinical specialists often see radiologists as 'image providers', not as clinical colleagues. The purpose of our study was to investigate how often radiologists are mentioned as co-authors in case reports containing radiological images, and to assess if their involvement influences quality.

Methods and Materials: We searched PubMed using "Case report" as search term. Criteria for inclusion were: publication in a non-radiological journal and availability of full text in English. We included 400 case reports, 218 of which contained medical images. The images and figure legends of these 218 case reports were scored by two radiologists and a nuclear medicine physician in consensus, using a self-defined scoring system.

Results: In 21% (45/218) of case reports a radiologist was included as a co-author. In 79% (173/218) of case reports there was no radiologist as co-author. In 7 of those, a radiologist was mentioned in the acknowledgements. The median quality score in case reports with and without a radiologist as co-author was 74% and 51%, respectively; this difference was statistically significant ($p<0.05$).

Conclusion: In a minority of non-radiological case reports containing radiological images, a radiologist was listed as co-author. The participation of a radiologist as co-author did, however, have a significant impact on quality.

B-0182 11:42

Remote radiological audit: a regional quality assurance system

E. Guseva, S. Morozov, D.V. Burenchev, I. Trofimenko, N. Ledikhova, T. Rostovtseva; Moscow/RU (e.guseva@npcmr.ru)

Purpose: To evaluate the effectiveness of electronic quality assurance system in radiology departments.

Methods and Materials: Currently, 75 outpatient clinics are connected to the Unified Radiological Information Service (URIS). The service comprises 130 CT and MRI units, 422 radiologists, and 321 technicians. In 2016, we developed remote quality assurance system and discrepancy detection module (DDM). The software is designed to review studies, provide feedback and accumulate "big data". We have compared the number of discrepancies before and after DDM implementation (4473 anonymized CT and MRI studies). $P<0.05$ was considered statistically significant.

Results: We observed a decrease in significant and non-significant discrepancies from $6.4\pm 2.9\%$ (64) to $2.8\pm 0.8\%$ (104) and from $19.6\pm 3.0\%$ (197) to $9.5\pm 0.7\%$ (352). The number of reports without any discrepancies increased from $51.7\pm 2.9\%$ (520) to $69.1\pm 0.7\%$ (2560). The number of general remarks (terminology, scan protocol) remained roughly the same, $22.4\pm 3.0\%$ (226) vs $18.6\pm 1.59\%$ (691). We have conducted 2622 consultations. Clinics received daily updates and 804 monthly reports. Radiologists with high discrepancy rates were personally notified. 67 training courses and 89 webinars were conducted with 1955 and 10244 participants.

Conclusion: Regional remote quality assurance system improved department effectiveness. In 12 months, the number of discrepancies decreased by more than a half.

B-0183 11:50

Affidea imaging metrics platform: a comprehensive dashboard providing key performance indicators for optimisation of image quality and throughput

N. Papanikolaou¹, G. Papaioannou², A. Iliopoulos², P. Szatmari¹, R. Illing¹; ¹Budapest/HU, ²Nicosia/CY (rowland.illing@affidea.com)

Purpose: To present a web-based imaging analytics platform that can calculate several metrics, the so-called key performance indicators (KPIs) to assess both quality of MRI exams and patient throughput.

Methods and Materials: The Affidea imaging metrics is a web-based system comprised of agents and a central server communicating with the agents to collect, process, quantify and present metrics on an interactive dashboard. Agents were installed in 14 MRI departments in 3 European countries. 18 MRI scanners were connected to the agents through local network and all MRI examinations were sent to the agents through setting an auto-transfer dicom service in the background of the MR scanners. Agents extracted metadata from the dicom headers of each image and transmitted them through secure FTP to a central server. Meta data were compared with a reference database and compliance to standardised protocols was calculated. In addition, deviation was defined as the percentage of sequences not included in the standardised protocols. Other KPIs including number of exams, voxel size, examination time and waste time were also quantified.

Results: All KPIs were presented as info tablets including the name of the KPI, the average value over a user-defined time interval, its percent change comparing to a user-defined time interval in the past. In addition, each KPI was presented on a chart for different countries, sites, MRI models and types of exams.

Conclusion: A comprehensive web-based platform monitoring the performance of MRI scanners by means of several KPIs is presented.

Author Disclosures:

N. Papanikolaou: Owner; MRIcons. **G. Papaioannou:** Consultant; MRIcons. **A. Iliopoulos:** Consultant; MRIcons. **P. Szatmari:** Employee; Affidea.

14:00 - 15:30

Room B

Abdominal Viscera

SS 301a

Detection and staging of HCC

Moderators:

T. Denecke; Berlin/DE

G. D'Ippolito; São Paulo/BR

B-0190 14:00

Differences in liver imaging reporting and data system categorisation between MRI with hepatobiliary-specific vs primary-extracellular agents

V. Bura¹, H. Nguyen², S. Lee², T. Tirkes³, C. Lall²; ¹Cluj-Napoca/RO, ²Orange, CA/US, ³Indianapolis, IN/US (viad.t.bura@gmail.com)

Purpose: The purpose was to assess whether liver lesions are categorised differently using Liver Imaging Reporting and Data System (LI-RADS), in chronic-hepatitis patients at risk for hepatocellular carcinoma (HCC), when undergoing liver-MRI with two different contrast agents: primary-extracellular (ECa) versus hepatobiliary-specific (HBa).

Methods and Materials: We retrospectively selected patients, provided they underwent liver-MRI with both agents within a three-month time interval. The cases were reviewed by two radiologists. The images were downloaded and anonymised, for blinding the radiologists to patient demographics/agents used and further remove any implicit bias. Multiple enhancement and wash-out characteristics, as well as capsule visualisation, were studied throughout arterial, venous and equilibrium MRI-phases. A final category was assigned using LI-RADS-v2014-guidelines.

Results: We reviewed 22 patients, and a total of 36 lesions. For 44% of the lesions, the ECa-MRI upgraded LI-RADS by one or even two categories (5 lesions), based on better wash-out visualisation and/or the presence of a partial/full capsule. Arterial enhancement was assessed as more robust with ECa-MRI in 42% cases. Seven lesions not seen with HBa-MRI were LI-RADS 3 (5/7) or 4 (2/7) category on ECa-MRI.

Conclusion: Although performed on a small number of patients, the present study reveals superiority of EC-agents in a more precise LIRADS categorisation of liver lesions for patients at risk for HCC. There is an improvement in the visualisation of arterial-enhancement, venous wash-out and capsule with an EC-agent. Pertinent negative of the study was the smaller number of patients which showed better characterisation and LI-RADS with the HB-agent MRI (5%).

B-0191 14:08

Prospective evaluation of dynamic MR with gadoteric acid for the non-invasive diagnosis of HCC in newly detected nodules smaller than two centimetres on US in cirrhotic patients

C. Ayuso, A. Darnell, J. Rimola, Á. García-Criado, R. Vilana Puig, A. Forner, J. Bruix; Barcelona/ES (cayuso@clinic.cat)

Purpose: To evaluate the diagnostic accuracy of gadoteric acid-enhanced MR (GA-MR) for non-invasive hepatocellular carcinoma (HCC) diagnosis in nodules ≤ 2 cm detected by US screening programme.

Methods and Materials: Cirrhotic patients with newly detected solitary nodules ≤ 2 cm by screening US were included. Extracellular contrast-MR (EC-MR) and GA-MR were performed in less than 1 month. Final diagnosis was based on the EASL/AASLD guidelines criteria (specific vascular profile on EC-MR or biopsy). Blind, double reading was performed in all GA-MR studies. The criterion for HCC diagnosis using GA was arterial contrast uptake and washout in the portal phase or hypointensity in the hepatobiliary phase (HBp).

Results: 62 consecutive cirrhotic patients Child-Pugh A (53) or B (9) were included. Final diagnosis was: 41 (66.1%) HCC, 2 intrahepatic cholangiocarcinoma (ICC), 1 colo-rectal cancer metastasis, and 18 benign lesions. Benign lesions were followed up during a median of 23 months to discard malignancy. The EC-MR diagnosed 26 out of 41 HCC nodules (sensitivity 63.4%, CI95%: 46.9-77.9). Sensitivity and specificity for GA-MR were 56.1% (CI95%: 39.7-71.5) and 90.5% (CI95%: 69.8-98.8), respectively, with a PPV of 92 (CI95%: 74-99) and NPV of 51.4 (CI95%: 34.4-68.1). False positives were observed in the two ICC. In GA-MR, wash-in was present in 82.9% and portal wash-out in 42%. Low signal intensity in the 20 minutes HBp was observed in 63.4% of HCC nodules, whereas the remaining 15 HCCs were iso- or hyperintense.

Conclusion: GA-MR is not superior than EC-MR for non-invasive diagnosis of HCC in nodules ≤ 2 cm in cirrhotic patients.

Author Disclosures:

C. Ayuso: Research/Grant Support; Bayer. J. Bruix: Advisory Board; Bayer.

B-0192 14:16

Diagnostic accuracy of LR-M criteria for differentiating combined hepatocellular cholangiocarcinoma on gadoxetate-enhanced MRI

H. Lee, C. An, M.-J. Kim; Seoul/KR (ittrue9hsii@yuhs.ac)

Purpose: To determine the diagnostic accuracy of LR-M criteria of LI-RADS version 2017 for differentiating combined hepatocellular cholangiocarcinoma (cHCC-CC) on gadoxetate-enhanced MRI.

Methods and Materials: Preoperative gadoxetate-enhanced MRI of 33 cHCC-CC and 66 hepatocellular carcinoma (HCC) were reviewed by two radiologists, who assessed the presence of nine imaging features favoring other malignancy (LR-M features) and 10 favoring HCC. The sensitivity and specificity of LR-M features for differentiating cHCC-CC from HCC were calculated from consensus opinions.

Results: At least one LR-M feature was seen in 31 (93.9%) of 33 cHCC-CC and 34 (51.5%) of 66 HCC. The sensitivity and specificity for the diagnosis of cHCC-CC using any of LR-M features were 93.9% and 48.5%. Among the LR-M features, the rim arterial phase hyperenhancement (APHE), progressive concentric enhancement, peripheral washout, adjacent biliary obstruction, mixed pattern, and infiltrative margin were significantly more common in cHCC-CC ($p < 0.05$). Three or more LR-M features were seen in 18 (54.5%) cHCC-CC, while two or less were seen in 62 (93.9%) of HCCs. For lesions ≥ 2 cm or larger, the presence of all three major features of HCC including non-rim APHE, washout, and distinct rim showed sensitivity of 46.7% and specificity of 100% for the diagnosis of HCC, regardless of LR-M features.

Conclusion: Current LR-M criteria showed high sensitivity and moderate specificity for the diagnosis of cHCC-CC. Presence of all three major HCC features including distinct rim showed moderate sensitivity and perfect specificity for the diagnosis of HCC for tumours of ≥ 2 cm or larger.

B-0193 14:24

An imaging and clinical scoring system to predict early mortality in spontaneous ruptured hepatocellular carcinoma treated with transarterial embolisation

K.H. Lee, M.L.D. Tse, A.K.C. Cheng, H.Y.F. Wong, M.L. Yu, Y.L. Li, P.Y.C. Chien, Y.C. Ho, F. Chu; Hong Kong/HK (viclkh88@gmail.com)

Purpose: Spontaneous ruptured hepatocellular carcinoma (rHCC) is an emergency associated with significant mortality, and treatment includes transarterial embolisation (TAE). We aim to develop a scoring system using a combination of clinical and imaging parameters to predict 30-day mortality.

Methods and Materials: Retrospective review was performed of all patients with rHCC who underwent abdominal computed tomography (CT) and subsequent TAE between January 2007 and December 2016. CT features were reviewed by two radiologists blinded to patient outcome. Clinical parameters included serum bilirubin, albumin, INR and scores of individual measures according to Child-Pugh score. Independent risk factors for 30-day mortality after TAE were identified using multivariate binary logistic regression, for development of a scoring system.

Results: 98 patients with mean age 65.1 years were included. 30-day mortality rate was 40.8%. Bilobar distribution ($p < 0.001$), maximum tumour size ($p = 0.03$), bilirubin score ($p = 0.01$) and albumin score ($p = 0.02$) were independently associated with 30-day mortality. A 12-point score, based on 1-3 points for each of the four factors, was derived to predict 30-day mortality, and yielded area under receiver operating characteristic curve of 0.905 (95%CI: 0.843, 0.964). A score ≥ 7 was associated with 30-day mortality with sensitivity 100% and specificity 60%; a score ≥ 10 showed sensitivity 55% and specificity 92%. This stratified patients into low-, intermediate- and high-risk groups, with 0%, 45% and 92% 30-day mortality, respectively.

Conclusion: Clinical and imaging parameters can be combined into a scoring system to accurately predict 30-day mortality after TAE in rHCC patients. This may help identify and counsel high-risk patients.

B-0194 14:32

Can gadoteric acid-enhanced MRI predict that a solitary HCC (cT1) is pT1 or pT2?

I.C. Chou, Y.-T. Kuo, I.H.W. Lao, P.-L. Hsieh, Y.-Y. Su, C.-W. Mak, D.-P. Sun, M.-J. Sheu, H.-T. Kuo; Tainan/TW (yichenchou@hotmail.com)

Purpose: To determine which imaging findings can predict pathology T2 stage of a single hepatocellular carcinoma (HCC, cT1) on gadoteric acid-enhanced MRI.

Methods and Materials: Pre-operative gadoteric acid-enhanced MRI were reviewed in a retrospective cohort of patients with solitary HCC. The reference standard of tumour staging was surgical pathology. Univariate and multivariate analyses were performed to identify predictors of microvascular invasion or satellite nodules in patients with HCC. Diagnostic performance of different MR findings was investigated.

Results: There were 39 (34.2%; 39 of 114) pathologically staged T2 HCCs (either with microvascular invasion, satellite nodules or combination of both).

75 HCCs (65.8%; 75 of 114) were staged T1. Large tumour size ($\geq 2.3\text{cm}$) had higher risk of pT2. In multivariate analysis, two MR findings, i.e. corona enhancement (odds ratio: 2.67; 95% CI: 1.101-6.480), and peritumoural hypointensity on hepatobiliary phase (odds ratio: 2.203; 95% CI: 0.961-5.049), were associated with high risk of pT2 HCCs. Positive likelihood ratio was 6.25 (95% CI: 1.788-21.845) and sensitivity to diagnose pT2 HCC on EOB MRI was 86.2% when a HCC was met with two or three of these MR findings. On the other hand, small tumour size and hypointense rim on hepatobiliary phase were 'protective' findings. When small HCCs were with hypointense rim and without aggressive findings, most of them were pT1 lesions (specificity was 100%).

Conclusion: There are 'protective' and 'aggressive' imaging findings of solitary HCCs on MRI. When combining size and imaging findings, gadoxetic acid-enhanced MRI could predict solitary HCC (cT1) as pT1 or pT2.

B-0195 14:40

Liver imaging reporting and data system (LI-RADS) version 2017 with gadoxetic acid-enhanced MRI: utility of ancillary features in diagnosis of hepatocellular carcinoma

H. Chang, H. Park, Y. Kim, M. Yu, S. Jung, H. Jeon; *Seoul/KR (20150113@kuh.ac.kr)*

Purpose: To investigate the utility of ancillary features of liver imaging reporting and data system (LI-RADS) version 2017 using gadoxetic acid-enhanced MRI in the diagnosis of hepatocellular carcinoma (HCC).

Methods and Materials: Our institutional review board approved this retrospective study and informed consent requirement was waived. Between August 2008 and May 2017, 154 high-risk patients with 180 pathologically confirmed HCC nodules who underwent gadoxetic acid-enhanced MRI were included. Two radiologists retrospectively assigned a LI-RADS category for all pathologically proven HCC observations in consensus, before and after considering ancillary features on MRI. For the cases in which category change was observed, ancillary features that caused category upgrade or downgrade were assessed.

Results: Based on major HCC features without considering ancillary features, 13.3% (24/180), 21.7% (39/180), and 65% (117/180) of nodules were categorized as LR-3, LR-4, and LR-5, respectively. After considering ancillary features, 11.1% (20/180) of nodules underwent category change, with all nodules upgraded from LR-3 to LR-4. No cases were downgraded after considering ancillary features. Mild-moderate T2 hyperintensity and hepatobiliary phase hypointensity were the most frequently found ancillary features in nodules with upgraded category (60%, n=12), followed by the restricted diffusion (50%, n=10).

Conclusion: In the diagnosis of HCC on gadoxetic acid-enhanced MRI using LI-RADS version 2017, ancillary features increased the confidence of HCC diagnosis in approximately 10% of the cases. The presence of mild-moderate T2 hyperintensity, hepatobiliary phase hypointensity, or restricted diffusion were found to be useful ancillary features favouring HCC in nodules with intermediate probability for HCC (LR-3).

B-0196 14:48

Liver vein infiltration in patients with hepatocellular carcinoma: impact on survival

S. Schotten, F.-I. Meyer, A. Mähringer-Kunz, A. Weinmann, C. Düber, R. Kloeckner; *Mainz/DE (sebastian.schotten@gmail.com)*

Purpose: Portal vein tumour thrombosis (PVTT) significantly impairs the prognosis of patients with hepatocellular carcinoma (HCC) and classifies them as advanced stage (BCLC-C). However, the relevance of liver vein infiltration (LVI) remains unclear. The aim of this study is to compare the prognosis of patients with different forms of macrovascular infiltration as this might influence the choice of treatment.

Methods and Materials: 1378 HCC patients were extracted from the clinical registry of our tertiary referral centre treated between 01/2005 and 01/2017. Macrovascular infiltration was diagnosed by re-evaluation of all available CT or MRI studies by two experienced radiologists in consensus reading. Overall survival (OS) was calculated from the date of initial diagnosis for all subgroups (no infiltration, PVTT, and LVI). In case of macrovascular infiltration, OS was additionally calculated from the date of its first appearance.

Results: 1341 patients could finally be included. 807 patients had no infiltration, 491 showed PVTT, and 43 an isolated LVI. OS from initial diagnosis was 37.29, 6.53, and 16.03 months, respectively ($p < 0.001$). The OS calculated from the first appearance of macrovascular invasion was 4.9 months for PVTT and 7.33 month for isolated LVI ($p = 0.018$).

Conclusion: Isolated LVI showed significantly better survival compared to patients with PVTT. This renders the question if patients with isolated LVI should be classified and treated like patients with portal vein infiltration (BCLC-C, mainly systemic therapy), or if a local approach is justified in selected patients.

B-0197 14:56

Diagnostic efficacy of conventional gadolinium-enhanced MRI in the detection of recurrent hepatocellular carcinoma: intra-individual comparison with gadoxetic acid-enhanced MRI

J.-H. Yim, Y. Kim; *Seoul/KR (jh111.yim@samsung.com)*

Purpose: To compare the efficacy of extracellular contrast media (ECCM) MRI to gadoxetic acid-enhanced MRI for detection of recurrent hepatocellular carcinoma (HCC) in patients previously treated.

Methods and Materials: One hundred and sixty patients who were suspected of having tumour recurrence after multiple treatments for HCCs (surgery, transarterial chemoembolization, and radiofrequency ablation) underwent ECCM MRI and gadoxetic acid-enhanced MRI with 10- to 30-day interval. A total of 105 liver lesions were diagnosed as HCC recurrence. The ECCM MRI and the gadoxetic acid-enhanced MRI were retrospectively analysed by two observers for detection of HCCs using receiver operating characteristic analysis. The diagnostic accuracy and sensitivity were calculated.

Results: For both observers, the ECCM set showed superior sensitivity and accuracy than the gadoxetic acid set ($p < 0.005$, both). In addition, observer 2 represented higher negative predictive value with the ECCM set (52.3%) than the gadoxetic set (33.3%) ($p = 0.031$). Pooled data for two observers also showed higher sensitivity, accuracy, and negative predictive value with the ECCM set (90%, 90.9%, and 51.1%, respectively) than the gadoxetic set (77.6%, 79.7%, and 31.8%, respectively) ($p < 0.003$). We achieved excellent degree of interobserver agreement for both MRIs ($k = 0.804$ and 0.891).

Conclusion: In detection of recurrent HCC in patients with history of multiple treatments, conventional ECCM MRI showed superior diagnostic efficacy in sensitivity, accuracy, and negative predictive value than gadoxetic acid-enhanced MRI.

B-0198 15:04

Differentiation between hepatocellular carcinoma showing uptake of gadoxetic acid and focal nodular hyperplasia

A. Kitao¹, O. Matsui¹, N. Yoneda¹, R. Kita², K. Kozaka¹, S. Kobayashi¹, T. Minami¹, W. Koda¹, T. Gabata¹; ¹Kanazawa/JP, ²Osaka/JP

Purpose: To clarify the imaging differentiation points between hepatocellular carcinoma (HCC) showing uptake of gadoxetic acid enhanced MRI and focal nodular hyperplasia (FNH)/FNH like nodule.

Methods and Materials: We enrolled the pathologically diagnosed 49 HCC with hypointense area constituting more than two thirds of the nodule on hepatobiliary phase and 15 FNH/FNH like nodule, and compared findings of dynamic CT and gadoxetic acid enhanced MRI between them using Mann-Whitney test, Chi square test and univariate logistic regression analysis

Results: The enhancement pattern of dynamic CT was significantly different between HCC and FNH ($P < 0.0001$): arterial enhancement/washout pattern (89.8% vs 13.3%) and arterial enhancement/no-washout pattern (4.1% vs 86.7%), respectively. Enhancement ratio on arterial phase of dynamic CT was higher in FNH than in HCC ($P < 0.0001$). The frequency of corona like enhancement on portal to equilibrium phase (83.7% vs 13.3%, $P < 0.0001$) and arterial phase enhancement of adjacent hepatic vein (6.5% vs 46.7%, $P = 0.001$) were significantly different between HCC and FNH. Apparent diffusion coefficient (ADC) value was lower in HCC than in FNH ($P = 0.002$). The signal distribution on hepatobiliary phase were significantly different between HCC and FNH ($P = 0.0002$): homogenous hyperintensity (59.2% vs 73.3%), hyperintensity mixed with hypointensity (26.5% vs 0%), hyperintensity with peripheral hypointensity (14.3% vs 0%) and hyperintensity with central hypointensity (0% vs 26.7%).

Conclusion: For the differentiation between HCC with uptake of gadoxetic acid and FNH/FNH like nodule, presence of washout on dynamic CT, corona enhancement, ADC value, distribution of signal intensity on hepatobiliary phase would be important.

B-0199 15:12

T2 mapping and diffusion-weighted imaging of hepatocellular carcinoma: prediction of tumour histological grades

L. Cao, B. Song; *Chengdu/CN (clk2089@icloud.com)*

Purpose: To investigate and compare the diagnostic performance of T2 relaxation time value and apparent diffusion coefficient (ADC) for non-invasive preoperative prediction of the histological grade of hepatocellular carcinoma (HCC).

Methods and Materials: The study consisted of 30 patients with surgically resected HCCs who underwent preoperative MRI exams including DWI and T2 mapping which was acquired using T2-prepared TrueFISP sequence. T2 values and ADC were measured and averaged over ROIs placed in HCC solid regions on T2 mapping and ADC map, respectively. ANOVA was used to evaluate the statistical difference of the mean T2 value and ADC among three histological grades, and the diagnostic performance of T2 value and ADC was

also evaluated and compared using receiver operating characteristic-based positive test. The sensitivity, specificity, and accuracy were calculated.

Results: The mean T2 values of poorly differentiated (Edmondson grade III and IV), moderately differentiated (Edmondson grade II) and well-differentiated HCC (Edmondson grade I) were (38.4±2.40) ms, (44.4±3.0) ms and (49.6±3.9) ms, respectively, and there were differences in statistical meaning among them. The sensitivity, specificity, and accuracy, when an ADC of 0.972 or higher was considered as an indicator of well-differentiated tumours, were 73.1%, 72.9%, and 0.729, respectively, while when T2 = 41.85ms, the sensitivity, specificity, and accuracy were 81.3%, 68.4%, and 0.706. Using both methods, the AUC was elevated to 89.6%.

Conclusion: Higher tumour T2 in combination with higher ADC is a potential biomarker in the prediction of histological grades before treatment.

B-0200 15:20

Prediction of pathological differentiation for hepatocellular carcinoma: preoperative Gd-EOB-DTPA-enhanced MRI and histopathological correlation

K. Huang; Guiyang/CN

Purpose: Our aim of the study is to investigate the feasibility of prediction for pathological differentiation of hepatocellular carcinoma (HCC) using preoperative Gd-EOB-DTPA enhanced magnetic resonance imaging (MRI).

Methods and Materials: 91 patients with solitary HCC who underwent preoperative Gd-EOB-DTPA enhanced MRI were prospectively analyzed. Features including tumor size, signal homogeneity, tumor capsule, tumor margin, intratumoral vessels, peritumor enhancement in mid-arterial phase, peritumor hypointensity during hepatobiliary phase, apparent diffusion coefficient (ADC), T1 relaxation times and the reduction rate between pre- and post-contrast enhancement images were assessed. HCC pathological differentiation in excision specimens were evaluated using Edmanson criteria. Correlation between these MRI features and HCC pathological differentiation were analyzed by chi-square test and multivariate logistic regression so as to establish a prediction model. Receiver operating characteristic (ROC) curve was used to assess the predictive effectiveness for the model.

Results: Univariate analysis showed that tumor margin (p=0.007), intratumoral vessels (p=0.041), peritumoral low signal (p=0.017), maximum tumor diameter (p=0.014) significantly correlated with pathological differentiation. Those HCC lesions with the greater size, the more irregular margin, presence of intratumoral vessels and peritumoral low signal indicated high degree pathological differentiation. There was no relationship between venous thrombosis, tumor signal, tumor capsule, peritumoral enhancement, ADC value, T1 reduction ratio and pathological differentiation. Multivariate logistic regression analysis demonstrated that the maximum tumor diameter (p=0.007, OR=1.0019, 95% CI: 1.005~1.032) was an independent risk factor of HCC with poor differentiation.

Conclusion: Gd-EOB-DTPA contrast-enhanced MRI could noninvasively predict pathological differentiation of HCC before surgery.

14:00 - 15:30

Room C

Abdominal Viscera

SS 301b

Modern imaging techniques of the liver

Moderators:

A. Agostini; Ancona/IT

G.H. Mostbeck; Vienna/AT

B-0201 14:00

Evaluation of hepatic warm ischaemia-reperfusion injury and intervention effect of Lipo-PGE1 in rabbit models: 3.0T BOLD MRI study

Q. Ji^{1,2}, Z.-Q. Chu², J.Y. Li²; ¹Nanjing/CN, ²Tianjin/CN (jiqianq@aliyun.com)

Purpose: To investigate the diagnostic value of blood oxygen level-dependent (BOLD) MRI in the grade of hepatic warm ischaemia-reperfusion injury, and to evaluate the intervention effect of liposome-carried prostaglandins E1 (Lipo-PGE1) in rabbit models.

Methods and Materials: Seventy rabbits were randomly divided into sham-operation group, three test groups and three corresponding intervention groups (n=10 for each group) according to different hepatic warm ischaemia time. BOLD MRI was performed on a 3.0 T MR scanner with 9 TE (2.57 to 24.25 ms). Rabbits were sacrificed for biochemical and histomorphological analysis. In vivo R2* values of hepatic parenchyma were compared between different groups and matched with biochemical parameters.

Results: R2* values had excellent interobserver agreement with ICC of 0.805. There were significant differences of R2* values between all of groups, between sham-operation group and test groups, between sham-operation

group and intervention groups, between test groups and corresponding intervention groups (P<0.05). With the prolonged of warm ischaemia time, R2* values showed a gradual increasing tendency; after the intervention of Lipo-PGE1, the reduction of R2* values was increasingly obvious. R2* values corresponded well with biochemical parameters (r>0.5, P<0.05).

Conclusion: BOLD MRI is a non-invasive and valuable technique in assessing the pathophysiologic changes of hepatic WIRI and relieved degree of Lipo-PGE1 in a rabbit model.

B-0202 14:08

Ultrasonic adaptive sound speed estimation for the diagnosis and quantification of hepatic steatosis

M. Dioguardi Burgio¹, M. Imbault², M. Ronot¹, A. Faccinotto¹, B. Van Beers¹, P.E. Rautou¹, L. Castera¹, M. Tanter², V. Vilgrain¹; ¹Clichy/FR, ²Paris/FR (marco_dioguardi@hotmail.it)

Purpose: to evaluate the ability of a new ultrasound (US) method based on Sound Speed Estimation (SSE) in detection, quantification, and grading of hepatic steatosis using magnetic resonance (MR) proton density fat fraction (PDFF) as reference standard and to calculate one US fat index based on the patient's SSE.

Methods and Materials: we consecutively included N=50 patients as study cohort and further N=50 as validation cohort who underwent both SSE and abdominal MR. Hepatic steatosis was classified according to MR-PDFF cutoffs as: S0 ≤6.5%, S1 from 6.5 to 16.5%, S2 from 16.5 to 22% and S3 ≥ 22%. Receiver operating curve analysis was performed to evaluate the diagnostic performance of SSE in diagnosis of steatosis. Based on the optimal data fit derived from our study, we proposed a correspondence between the MR-PDFF and an US fat index. Coefficient of determination R² was used to evaluate fit quality, and was considered as robust when R2 >0.6.

Results: study and validation cohort presented mean SSE value of 1.570±0.026 and 1.568±0.023 mm/μs for S0 and 1.521±0.031 and 1.514±0.019 mm/μs for S1-S3 (p<0.01) patients respectively. SSE threshold of ≤1.537 mm/μs had 80% sensitivity and 85.7% specificity in diagnosis of steatosis in the study cohort. Robust correspondence between MR-PDFF and the US fat index was found both for the study cohort (R2= 0.73) and the validation cohort (R²= 0.76).

Conclusion: SSE can be used to detect, quantify and grade liver steatosis and to calculate an US fat index.

B-0203 14:16

Performance of a 2D-SWE method for predicting different stages of liver fibrosis, using transient elastography as the reference method

I. Sporea, F.B. Bende, A.S. Popescu, R. Sirlu, M. Danila, S. Nistorescu, R. Fofiu, V. Baldea; Timisoara/RO (isporea@umft.ro)

Purpose: To evaluate the performance of 2D shear-wave elastography from General Electric(2D-SWE-GE), implemented on the LOGIQ S8 system, for the noninvasive assessment of liver fibrosis and to identify liver stiffness(LS) cut-off values for predicting different stages of fibrosis using Transient Elastography(TE) as reference.

Methods and Materials: We included 179 consecutive subjects with or without chronic hepatopathies in whom LS was evaluated in the same session by 2 elastographic techniques: TE(FibroScan, EchoSens) and 2D-SWE-GE(LOGIQ S8, GE Healthcare). Reliable LS measurements were defined for TE as the median value of 10 measurements with a success rate of ≥60% and an interquartile range/median ratio(IQR/M)<0.30 and for 2D-SWE-GE as the median value of 10 measurements acquired in a homogenous area and an IQR/M<0.30. To discriminate between TE fibrosis stages we used the following cut-offs: F2-7; F3-9.5 and F4-12 kPa.

Results: Reliable LS measurements were obtained in 97.2% subjects by 2D-SWE-GE, and 98.3% by TE(p=0.72). 171 subjects were included in the final analysis. Based on TE cut-off values we divided our cohort into four groups: F<2: 51(29.8%); F=2: 40(23.4%); F=3: 31(18.1%); F=4: 49(26.7%). A good positive correlation was found between the LS values obtained by the 2 methods: r=0.72, p<0.0001. The best 2D-SWE-GE cut-off value for F≥2 was 6.9 kPa(AUC 0.93, Sensitivity 85.8, Specificity 90.2), for F≥3 it was 8.2 kPa(AUC 0.93, Sensitivity 87.5, Specificity 86.8) and for F=4 it was 9.3 kPa(AUC 0.91, Sensitivity 85.7, Specificity 81.2).

Conclusion: The best 2D-SWE-GE(S8) cut-off values for predicting F≥2,F≥3 and F=4 were 6.9, 8.2 and 9.3 kPa.

Author Disclosures:

I. Sporea: Consultant; General Electric, Philips. Speaker; Siemens, Philips, General Electric.

B-0204 14:24

Associations between liver fat, visceral fat and microalbuminuria in the general population

I. Dekkers, A. de Vries, A. de Roos, T. Rabelink, F.D. Rosendaal, H.J. Lamb, R. de Mutsert; *Leiden/NL (I.A.Dekkers@lumc.nl)*

Purpose: Abdominal obesity is an established risk factor for metabolic disorders. Our objective was to investigate the relative contributions of visceral adipose tissue (VAT) and hepatic triglyceride content (HTGC) to microalbuminuria in a middle-aged population.

Methods and Materials: In this cross-sectional analysis, VAT was assessed by magnetic resonance imaging, and HTGC by proton spectroscopy. Microalbuminuria was defined as urinary albumin-creatinine ratio $\geq 2.5/3.5$ mg/mmol in men/women. With logistic regression we calculated odds ratios (OR) of microalbuminuria, adjusted for age, sex, ethnicity, education, smoking, alcohol consumption, total body fat, hormonal status in women, and stratified by sex and the patatin-like phospholipase domain-containing (PNPLA3) gene.

Results: Of the 2,023 participants 53% were women, 39% carried a PNPLA3-risk allele, 29% had fatty liver (HTGC $>5.56\%$), and 2% microalbuminuria. In adjusted models, VAT was associated with a two-fold increased risk of microalbuminuria (per SD=55.4 cm², OR: 2.16, 95% CI: 1.29, 3.62). Per SD HTGC (7.9%) the OR of microalbuminuria was 1.34 (95% CI: 1.02, 1.77). In joint models, the OR of microalbuminuria per SD VAT was 2.02 (1.18, 3.47), and per SD HTGC it was 1.20 (0.85, 1.70). Associations of VAT, but not HTGC, were stronger in women and in non-carriers of the PNPLA3-risk allele.

Conclusion: Both liver fat and visceral fat were associated with microalbuminuria. In joint models VAT was more strongly associated with microalbuminuria than HTGC fat and may, therefore, be more important in the development of microalbuminuria. Prospective analyses need to study associations of VAT, fatty liver and the development of chronic kidney disease.

B-0205 14:32

Use of 2D shear-wave elastography in predicting different stages of liver fibrosis according to METAVIR scoring system: a histopathological correlation study

M. Aksakal, S. Ozhan Oktar, G. Esendagli Yilmaz, S. Özenirler, M. Cindoruk, K. Hizel, F.N. Baran Aksakal, C. Yucel; *Ankara/TR (mehmetaksakalmd@gmail.com)*

Purpose: In this study, we investigated accuracy of 2D shear-wave elastography (2D SWE) in detecting liver fibrosis by using histopathological analysis as the reference method.

Methods and Materials: Our single-center prospective study included 53 consecutive adult patients who had liver biopsy within 14 months of elastographic examination. A real time SD SWE evaluation was performed using LOGIQ E9 system (GE Medical Systems, Wisconsin, USA). The median of 10 valid liver stiffness measurements in kPa for each patient were obtained and were compared with the METAVIR scores obtained from the liver biopsy, using Kendall's rank correlation test. The diagnostic performance of real time 2D SWE was assessed and cut-off values were set by ROC curve analysis.

Results: A significant correlation was found between liver stiffness kPa values and degree of liver fibrosis (Kendall's tau=0.53, p=0.0001). AUROCs were 0.97 (95% confidence interval:0.93-1; SD: 0.02) (p= 0.0001) and 0.98 (95% confidence interval:0.95-1, SD: 0.14) (p= 0.0001) when comparing F0-1 versus F2-3-4 and F0-1-2 versus F 3-4, respectively. When we compare F0-1 versus F2-3-4 and F0-1-2 versus F 3-4 groups, optimal cut-off values were determined as 6.5 kPa (sensitivity:%100, specificity %84) and 8.8 kPa (sensitivity:%83, specificity %92), respectively.

Conclusion: Our findings suggest that 2D-SWE can be used for the assessment of liver fibrosis, especially in identifying patients with no or minimum/mild fibrosis and those with severe fibrosis. Studies on larger groups of biopsied patients are required in order to establish the most appropriate cut-off values for each particular stage of liver fibrosis.

B-0206 14:40

Preliminary exploration of the application of super microvascular imaging in focal liver lesions

H. Meng-Na, T.-A. Jiang; *Hangzhou/CN (monahe@163.com)*

Purpose: To explore the ability of super microvascular imaging (SMI) to differentiate diagnose focal liver lesions.

Methods and Materials: 31 FLLs consisted of haemangioma (HE) (n = 17), hepatocellular carcinoma (HCC) (n = 5), metastatic lesions (n = 5), primary hepatic lymphoma (n = 1), focal nodular hyperplasia (FNH) (n = 2) and adenoma (n = 1). 9 lesions were pathologically diagnosed and 22 lesions were radiological confirmed. All patients had been done SMI. The patients were divided into subgroups based on the diagnostic results to analyse the SMI manifestations. We also compared the SMI manifestations between the most common FLLs of HCCs, metastatic lesions and HES.

Results: The HEs were described as three SMI subgroups: diffuse dot-like type (n = 6); strip rim type (n = 8); nodular rim type (n = 3), the size of the three groups were obviously different (P=0.00,<0.05); The HCCs were described as two subgroup: diffuse honeycomb type (n = 2); non-specific type (n = 3). Four of the metastatic lesions were like strip rim type of HE; the other one shared the same type of thick rim type with lymphoma. The FNH was described as spoke-wheel type and the adenoma was diffuse honeycomb type. The SMI types were significantly different between HCCs and metastatic lesions with HEs (P=0.048, <0.05).

Conclusion: SMI technology made the evaluation of micro-vascular of focal liver lesions possible without any enhanced agents. SMI had the potential to add useful information to differential diagnosis between HCCs and metastatic lesions with HES.

B-0207 14:48

Intraoperative shear wave elastography for assessment and staging of liver fibrosis and cirrhosis during open liver tumour surgery in correlation with histopathology: first results

N. Platz Batista da Silva, L.P. Beyer, M. Hornung, S. Brunner, H.J. Schlitt, P. Wiggermann, E.-M. Jung; *Regensburg/DE (natascha.platz-batista-da-silva@klinik.uni-regensburg.de)*

Purpose: Evaluation of feasibility of intraoperative shear wave elastography (SWE) for quantitative assessment and staging of liver fibrosis/cirrhosis during liver tumour surgery in correlation with histopathology after partial liver resection.

Methods and Materials: Retrospective analysis of intraoperative ultrasound (IOUS) data of 103 patients was performed who underwent liver tumour surgery between 08/2015-07/2017. IOUS was performed by one experienced examiner using multifrequency linear/T-shaped probes from 6-9MHz on the freely mobilized liver. SWE images of parenchyma were stored for assessment of shear wave speed (SWS,m/s) and stiffness (kPa). Five ROIs were placed each to measure SWS/stiffness out of which a mean value was calculated. Findings were correlated to histopathology after partial liver resection. For histopathological staging of liver fibrosis/cirrhosis Ishak score (F0-F6) was used. Statistical analysis was performed using ROC analysis.

Results: 103 patients (M:66, F:37) aged 29-87 years (mean 60y, sd±11.8) were included. Postoperative histopathology showed no fibrosis in 52, F1-4 fibrosis in 30, (in)complete cirrhosis (F5-6) in 21 cases. Patients without fibrosis showed a mean of 2.69m/s(1.5-3.8m/s)/19.9kPa(4.6-45.9kPa). In patients with fibrosis (F1-F4) mean was 2.85m/s(1.8-3.96m/s)/ 26.91kPa(3.7-53.1kPa). Patients with cirrhosis presented a mean of 3m/s(1.8-4.3m/s)/29.03kPa(11.7-66.7kPa). By ROC analysis a cut-off of 2.46m/s/20.4kPa was calculated for diagnosis of relevant fibrosis/cirrhosis ($\geq F3$). Sensitivity_{SWS} was 94%, specificity 54.3%, accuracy 67%, NPV95%, PPV49.2% (AUC 0.745,95%CI:0.6482-0.8419). Sensitivity_{stiffness} was 94%, specificity 57.4%, accuracy 69.3%, NPV95.1%, PPV51.7% (AUC 0.7643,95%CI:0.6706-0.8579).

Conclusion: Intraoperative SWE enables staging of liver fibrosis/cirrhosis during liver surgery. Stiffness measurements were superior to SWS. Thereby surgical extent could be adapted individually to prevent postoperative hepatic insufficiency.

B-0208 14:56

Intraoperative CEUS for localisation and characterisation of liver lesions during open liver tumour surgery: a single centre's 7 years experience

N. Platz Batista da Silva, M. Hornung, S. Brunner, C. Hackl, H.J. Schlitt, C. Stroszczynski, E.-M. Jung; *Regensburg/DE (natascha.platz-batista-da-silva@klinik.uni-regensburg.de)*

Purpose: To evaluate the accuracy of intraoperative contrast-enhanced ultrasound (IoCEUS) for localization, characterization and differentiation of focal liver lesions (FLL) during liver tumor surgery in correlation with postoperative histopathological results.

Methods and Materials: A retrospective analysis of IoCEUS of 166 patients with 202 liver lesions was performed who underwent liver tumor surgery between 10/2010-07/2017. IoCEUS was conducted by one experienced examiner on the freely mobilized liver using multifrequency linear/T-shaped probes (6-9 MHz) after i.v.-application of 2.4-10 ml sulphurhexafluoride microbubbles. FLL were characterized dynamically during arterial (15-45s), portal venous (45-90s) and late venous phase (2-5min). An irregular hypervascularization during arterial phase and/or increasing wash out from portal venous to late phase were considered signs of malignancy. Findings of IoCEUS were correlated to postoperative histopathological findings after partial liver resection or biopsy. Statistical analysis was performed using cross-tables, chi-square- and fisher's exact test with p<0.05 as level of significance.

Results: IoCEUS data of 166 patients with 202 FLL (m:104, f:62) aged between 2-81 years (mean 60.5y, sd±12.2y) were retrospectively analyzed. FLLs' size ranged from 0.1-8.88cm (mean 2.51cm, sd±1.44cm). Postoperative histopathology showed 183 malignant and 19 benign FLL. IoCEUS could correctly characterize 180/183 malignant and 15/19 benign FLL. Four benign lesions were mistaken for malignant by IoCEUS, 3 malignant lesions for

benign. Sensitivity was 98.4%, specificity 79%, accuracy 96.5%, PPV 97.8%, NPV 83.3% ($p < 0.0001$).

Conclusion: Intraoperative CEUS is a highly valuable tool for localization and characterization of preoperatively known or unknown FLL during open liver surgery and should be used routinely.

B-0209 15:04

How safe are percutaneous liver biopsy procedures? Complication rate and seeding risk in an oncological setting

K.N. De Paepe¹, L. Bonne², E. Raimondi³, N. Fotiadis¹, D.-M. Koh¹, N. Starling¹, I. Chau¹, G. Brown⁴, D. Cunningham¹; ¹London/UK, ²Leuven/BE, ³Ferrara/IT, ⁴Sutton/UK (katjadepaep@gmail.com)

Purpose: Percutaneous biopsy of liver metastases is common practice in the setting of oncological clinical trials, where it serves as a relatively non-invasive method to obtain sufficient tissue for genetic analyses. Complications can occur, including seeding of the tumour along the biopsy track; however, literature on the incidence of seeding is scarce. The aim of this study was to evaluate the technique's safety.

Methods and Materials: Patients with ultrasound or CT-guided liver biopsy between 2012 and 2016 were included. Medical records were reviewed retrospectively for post-biopsy complications and all follow-up imaging was reassessed for the presence of seeding, defined as tumoural deposits in the biopsy needle track.

Results: In 550 patients (282 women, 268 men; mean age of 61y), 782 biopsies were performed, 43.9% (343/782) for trials and 56.1% (439/782) for diagnostic purposes. 93.7% (733/782) were diagnostic, revealing malignancy in 96.9% (710/733). Patients had 1 (n=387) to 7 (n=1) biopsies; a co-axial system was used in 70.6% (552/782) and multiple passes in 29.4% (230/782). Complication rate was 8.8% (69/782), namely pain (4.7%) and vasovagal reaction (2.3%). Less frequent severe complications were bleeding (1.0%), sepsis/fever (1.1%), pulmonary embolism (0.3%) and pneumothorax (0.4%). Seeding rate was 1.1% (8/782) [2/44 melanoma, 1/9 GIST, 1/39 cholangiocarcinoma, 1/248 colorectal, 1/14 oesophagus, 1/97 breast, 1/31 prostate], mean seeding time was 208 days, mean post-biopsy survival time was 495 days and 349 days in the seeding and non-seeding groups, respectively.

Conclusion: Percutaneous liver biopsy is an effective and safe method for tissue collection, with a minimal risk of seeding.

B-0210 15:12

Role of interventional radiology in the scope of liver transplantation

M. Pitton, F. Becker, S. Schotten, R. Kloeckner, T. Zimmermann, J. Mittler, P.R. Galle, G. Otto, C. Düber; Mainz/DE (michael.pitton@unimedizin-mainz.de)

Purpose: To analyse the role of interventional radiology (IR) in the complex scenario of liver transplantation (LTx).

Methods and Materials: Patients with history of liver transplantation (LTx) were analysed for number and type of interventional procedures in the scope of liver transplantation. The institutional data base was searched for all interventional procedures during the time on waiting list, in the perioperative phase, and during follow-up after LTx. All interventional procedures were categorised in image-guided punctures (e.g. biopsies, drainages), local tumour treatment (e.g. ablations, TACE, SIRT), biliary interventions (e.g. in ischaemic or ischaemic type biliary lesions [IBL/ITBL]), vascular interventions (portal, venous, arterial recanalisation or embolisation), TIPS, and others. The numbers and time point during the patient's course were analysed.

Results: 815 patients who received liver transplantation between 1996 and 2016 were included. 24.4% of patients had no interventions at all. 44.7% of patients received interventions during time on the waiting-list (in 20.4% ≤ 3 procedures per patient, in 24.3% > 3 procedures per patient, e.g. TACE etc). 23 patients (2.8%) received procedures within the perioperative phase (≤ 3 days after LTx). During 30d-Follow-up, a total of 60% of patients received some IR-procedures: 56.4% ≤ 3 per patient (28.7% only one per patient). However, 3.6% of patients received > 3 procedures per patient (range 4-8).

Conclusion: Interventional procedures are an integral part in the scenario of liver transplantation and cover the whole scope of IR, particularly TIPS and local tumour treatment before LTx, peri-/postoperative vascular issues, as well as biliary interventions in IBL/ITBL during follow-up.

B-0211 15:20

Transient elastography (TE), shear wave elastography (SWE) and magnetic resonance elastography (MRE) for fibrosis assessment in chronic viral hepatitis: preliminary data

L. Cevasco, S. Perugin Bernardi, L. Bacigalupo, F. Paparo, M. De Cesari, G. Siri, G. Cenderello, V.M. Pinto, G.A. Rollandi; Genoa/IT (dott.luca.cevasco@gmail.com)

Purpose: Verify if TE, SWE and MRE obtain comparable results in the measurement of fibrosis in patients affected by chronic viral hepatitis.

Methods and Materials: We have evaluated 30 consecutive patients (of 100 expected) affected by HCV or co-infected by HCV+HIV. Acquisition of TE, SWE and MRE was performed the same day. Interdisciplinary consensus reference, performed by a panel of experts, determined the real fibrosis stage of each patient, taking into consideration clinical and laboratory features, serum biomarkers of fibrosis and a comprehensive assessment of all non-invasive stiffness imaging methods. Weighted kappa (with Landis & Koch categorization), Bland-Altman plot and Pearson correlation were adopted.

Results: All the techniques, compared independently with the interdisciplinary consensus reference, showed substantial agreement (at least 64%). In particular the agreement resulted almost perfect (93%) in case of MRE. Comparing the techniques with each other the agreement resulted at least moderate (46%) and, in the case of TE vs. MRE, substantial (66%). BMI (Pearson: 38.3%, $p=0.028$) and Dual-Dixon-Fat-Fraction (48.6%, 0.008) were positively correlated with a higher difference among values. Bland-Altman plot showed that the mean difference between obtained METAVIR scores ranged from a minimum of 0.0, 95%CI (-1.0; 1.0) MRE vs SWE, to a maximum of 0.1, 95%CI (-0.7; 0.8) fibroscan vs. MRE.

Conclusion: The preliminary data showed that TE, MRE and SWE obtain comparable results in the measurement of fibrosis in patients affected by chronic viral hepatitis. MRE showed the best agreement with our consensus reference. These data must be confirmed at completion of enrollment.

Author Disclosures:

L. Cevasco: Research/Grant Support; The study received a grant from General Electric.

14:00 - 15:30

Room X

Vascular

SS 315

Carotid and plaque imaging

Moderators:

D. Bos; Rotterdam/NL
N.N.

B-0212 14:00

Association of non-alcoholic fatty liver disease with increased carotid intima-media thickness considering other cardiovascular risk factors

A. Mohammadzadeh, M. Mohammadzadeh, V. Shahkarami, M. Shakiba, P. Sabetrasekh; Tehran/IR (psrpsr82@gmail.com)

Purpose: Non alcoholic fatty liver disease (NAFLD) is the most common liver disease (%6-35) while associated with cardiovascular risk factors and metabolic syndrome (age, diabetes, hyperlipidemia, hypertension and smoking). Here, we want to evaluate association of increased carotid intima-media thickness with NAFLD considering other cardiovascular risk factors to see if NAFLD is independently associated with increased carotid IMT.

Methods and Materials: Totally 300 patients [150 NAFLD - 150 normal] referred to 4 academic hospitals were enrolled. Patients with history of alcohol use, hepatitis, HIV, chemotherapy and other organ failures were excluded. A single radiologist performed abdominal sonographies[3-5MHz probe] and carotid sonography[7.5 MHz probe](measuring posterior wall of both common carotids and calculating mean value). NAFLD was diagnosed based on sonographic findings in absence of acute or chronic liver and kidney diseases and malignancies.

Results: Mean age was 51.2 ± 14.8 [20-97] and 184[%61.3] were male. Mean IMT was greater in patients with diabetes, hypertension, hyperlipidemia and NAFLD[all $P < 0.001$] and these variables with age were statistically significant in univariate models for estimating IMT. Among NAFLD patients, 38[%25.3] had increased IMT [unilateral or bilateral; considering 0.8 as cutoff point] while this frequency was 8 [%5.3] among normal subjects [$P < 0.001$, odds ratio=6, 95%CI=2.7-13.4]. In multivariate regression models[IMT as dependent variable], NAFLD, age and HLP were independent significant variables in linear model[$R^2=0.41$] and NAFLD showed highest odds ratio[16.4] among significant variables[age, BMI, NAFLD and HLP] in logistic model

Conclusion: Increase carotid IMT is highly associated with NAFLD independent of other cardiovascular risk factors and should be considered in these patients.

B-0213 14:08

Carotid intima-media thickness (CIMT) as a window to atherosclerosis

D.J. Petrovic; Belgrade/RS (dusanpetrovic736@gmail.com)

Purpose: The objective of the survey was to establish the relation between the carotid intima-media thickening (CIMT) and the coronary artery disease (CAD) among the patients tested by coronary angiography due to suspecting the coronary artery disease.

Methods and Materials: Eighty respondents with angiography-diagnosed coronary disease (40 men and 40 women varying between the age of 30 and 80) were tested by the ultra-sound Doppler angiography and compared to the identical number of healthy respondents of the same gender and age structure and without risk factors in terms of the coronary disease.

Results: Statistically, the thickness of CIMT is significantly higher for the respondents of both sexes with the presence of CAD ($p < 0.01$). The respondents with the multi-vessel coronary disease have significantly higher CIMT than the respondents with the one-vessel or two-vessel coronary disease ($p < 0.05$). Statistically, the cross-sectional surface area of the a. carotis communis (CSA) is significantly larger among the respondents with CAD in comparison with the control group.

Conclusion: The evaluation of CIMT is a reliable parameter for detecting the degree of vascular remodelling in the process of arteriosclerosis (pre-atherosclerosis or subclinical atherosclerosis) while changes on coronary and carotid arteries correlate to a high degree. Carotid duplex ultrasonography can be used as an important screening method owing to several advantages such as ease of use, reproducibility, no radiation exposure, and high correlation with atherosclerosis. Early diagnosis of carotid artery disease is of utmost importance, and ultrasound plays a pivotal role therein.

B-0214 14:16

Development and validation of a pathlength calculation for carotid-femoral pulse wave velocity

M. Bonnici-Mallia, J. Weir-McCall, L. Brown, J. Summersgill, P. Talarczyk, S. Chin, F. Khan, A.D. Struthers, G. Houston; *Dundee/UK* (mbonnicimallia@nhs.net)

Purpose: Carotid-femoral Pulse Wave Velocity (PWV) is the gold standard for measuring arterial stiffness and is predictive of future cardiovascular events. The purpose of this study was to generate a formula from easily obtainable clinical metrics in order to determine the carotid-femoral pathlength component of PWV calculation.

Methods and Materials: 1183 participants, free from cardiovascular disease, underwent whole-body MRI (WBMRI) as part of the TASCFORCE study. Distance between carotid and femoral vessels was obtained by tracing the arterial centreline from the bifurcation of the common carotid to that of the common femoral artery. A backward linear regression model was used to generate a formula for calculating pathlengths based on age, sex, heart rate, height and weight. This calculation was then validated in an external cohort of 128 participants from the SUMMIT study who had also undergone WBMRI.

Results: Applied within the TASCFORCE cohort, the formula provided moderate agreement with true distance ($r=0.59$, $p<0.001$), with a mean difference of 0.04mm (limits of agreement= -55.5 - 56.3 mm, $p=0.96$ for difference). Compared with the measured arterial pathlength on MRI in the SUMMIT cohort, there was a small underestimation of the pathlength distance by the formula with a mean difference of 10.1mm (limits of agreement= -39 - 59 mm), $p<0.001$, and a moderate correlation between the two measures ($r=0.61$, $p<0.001$).

Conclusion: Using simple allometric measures, arterial pathlength for PWV can be calculated with less variability and greater accuracy than current body surface techniques, holding promise for improving interstudy and intercentre reproducibility, thus expanding the utility of PWV calculation in clinical practice.

Author Disclosures:

J. Weir-McCall: Research/Grant Support; Guerbert Laboratories.

G. Houston: Research/Grant Support; Guerbert Laboratories, Cook Medical, Medtronic.

B-0215 14:24

Lumen dynamics of spontaneous arteries dissection

M. Dreval, L. Kalashnikova, M. Krotenkova, L. Dobrynina; *Moscow/RU* (dreval-marina83@yandex.ru)

Purpose: To estimate the possibility of recanalization of internal carotid (ICA) and vertebral arteries (VA) with spontaneous dissection treated with conservative management

Methods and Materials: The study included 46 patients (46% males, mean age 36.83 ± 7.61 years) with artery dissection manifested by ischaemic stroke or isolated head or neck pain. MRI was performed on 1.5 T scanner. Data of 3D-TOFMRA of the cervical arteries and T1fat-sat of the neck were obtained. The examinations were carried out twice: in the course of the first two weeks and after two months. The size of an internal lumen at the level of dissection and at the level of unchanged artery were measured, degree of the stenosis was evaluated

Results: At the 1st study lumen stenosis of ICA was revealed in 60% of cases, lumen stenosis of VA in 90% (35), occlusion in 40% (10) and 5% (2), respectively. The mean stenosis degree was 45% for ICAD and 50% for VA. MRI Follow-up study showed that in patients with initial stenosis lumen diameter of dissected arteries increased with the time in all cases. In patients with initial luminal occlusion due to dissection recanalization of VA occurred in

50%, spontaneous recanalization of ICA - in 40%. Residual stenosis in all cases was haemodynamically insignificant (20-25%).

Conclusion: Cervical arteries dissection is a dynamic process, stenosis is completely or partially resolved in all cases in two months. In contrast, occlusions are resolved in less than a half of cases and the residual stenosis is considered haemodynamically insignificant.

B-0216 14:32

Relationship between ICA geometry and plaque composition

G. Corrias¹, M. Porcu², M. Laino³, L. Saba¹, A. Mereu¹; ¹ *Monerrato/IT*, ² *Cagliari/IT*, ³ *Rome/IT* (ale.mereu7@studenti.unica.it)

Purpose: The aim of our study is to demonstrate whether there is a relationship between the geometry of the ICA and atherosclerotic plaque composition in terms of fat, mixed, calcific plaque and volume.

Methods and Materials: This is a prospective single institution pilot study enrolling 55 patients, for a total of 110 carotids, who were scheduled to perform a MDCTA of the supra-aortic vessels. The institutional review board approval for this study was obtained. Plaque composition was quantified either as absolute volume or as percentage of each different component to the total plaque. Associations between ICA curvature and plaque development were statistically investigated. The variables relationship was calculated using correlation coefficient r .

Results: There is a strong correlation between ICA curvature and the volume of each plaque component in absolute values. Fat plaque volume and curvature correlation coefficient r : 0.3390 (significance level p : 0.0006). Fibrous plaque volume and curvature correlation coefficient r : 0.2295 (significance level p : 0.0217). Calcium plaque volume and curvature correlation coefficient r : 0.2820 (significance level p : 0.0045).

Conclusion: We have found a strong correlation between the ICA curvature and the presence of a plaque in the proximal tract of ICA, of any composition. The bigger the curvature value, the highest is the probability to find a plaque, in terms of absolute volume representation. In particular, analysing the percentage of the plaque composition we have found that the higher the curvature value, the bigger the probability to find a plaque composed with mostly fat (with a significance level $p=0.0027$).

B-0217 14:40

Are there any differences in radiation-induced and non-radiation-induced carotid atherosclerosis?

T.-C.M. Ying¹, Y. Li¹, W.C.V. Wu¹, C. Yuan², L.W.D. Kwong¹, S.P. Yip¹, K.W.H. Law¹, W.Y.S. Lee¹; ¹ *Hong Kong/HK*, ² *Hunan/CN* (htmying@polyu.edu.hk)

Purpose: Carotid atherosclerosis is common in both post-radiotherapy (RT) nasopharyngeal carcinoma (NPC) patients and individuals with cardiovascular risk factors (CVRF). This study aimed to use ultrasound to investigate the differences in radiation-induced and non-radiation-induced carotid atherosclerosis with focus on the number of carotid plaque, carotid intima-media thickness (IMT) and plaque echogenicity.

Methods and Materials: Carotid ultrasound was performed on 20 post-RT NPC patients and 20 CVRF subjects. In each patient/subject, the IMT of common carotid arteries was measured. The common, internal and external carotid arteries were examined, and the number of carotid plaque detected was recorded. Ultrasound images of carotid plaques were analysed with a computer software to quantify the plaque echogenicity which was expressed as grey scale median (GSMedian) and mean (GSMean).

Results: Post-RT NPC patients (0.78 ± 0.24 mm) had significantly larger carotid IMT than CVRF subjects (0.69 ± 0.16 mm) ($p < 0.05$). Carotid plaques were more commonly found in post-RT NPC patients ($n=48$) than CVRF subjects ($n=36$). Carotid plaques in post-RT NPC patients (31.1 ± 11.8 and 35.3 ± 12.5 respectively) had significantly lower GSMedian and GSEMean than those in CVRF subjects (39.5 ± 16.2 and 43.6 ± 17.2 respectively) ($p < 0.05$).

Conclusion: Radiation-induced carotid atherosclerosis tended to be more severe than non-radiation-induced carotid atherosclerosis as evidenced by larger carotid IMT and higher incidence of plaque formation in post-RT NPC patients. When compared to CVRF subjects, carotid plaques in post-RT NPC patients were more hypoechoic as evidenced by the lower GSMedian and GSEMean, and thus were relatively more unstable leading to higher risk of cerebrovascular diseases.

B-0218 14:48

Carotid IMT and haemodynamic indices in evaluation of atherosclerosis in hypertensives

S.F. Kenis; *Zaria/NG* (shedrackkenis@yahoo.com)

Purpose: To evaluate carotid intima media thickness and haemodynamic indices as sonographic markers of atherosclerosis in a resource limited environment.

Methods and Materials: The study involved 130 hypertensive patients and 130 age-matched controls. All underwent carotid Doppler examination using

Mindray DC-8 ultrasound machine. Blood samples were taken after an overnight fast for lipid profile and blood sugar (FBS). The Framingham risk score (FRS) was calculated from patients' information. The data was analysed using SPSS version 20.0, and T-test was used to assess the difference between variables. Pearson correlation was used to determine correlation between duplex finding and FRS. $p < 0.05$ was considered statistically significant.

Results: The mean age of the hypertensive patients was 50.20 ± 10.30 years, and the mean age for control is 49.39 ± 9.89 years. The mean carotid intima-media thickness (CIMT) was significantly higher in hypertensives compared to control. Common carotid artery (CCA) pulsatility index (PI), CCA resistive index (RI), internal carotid (ICA) PI and ICARI were not significantly different between hypertensive patients and control. It was observed that the value of carotid haemodynamic indices increases with increasing age in the hypertensive, but the relationship of increasing age and haemodynamic indices was less clearly demonstrated in the control. There was a strong correlation between CIMT and FRS in the hypertensives and only in the ICA was there a moderate to weak correlation between haemodynamic parameters and FRS.

Conclusion: CIMT appears to be the best sonographic marker of atherosclerosis. Though carotid haemodynamic indices correlate less clearly than CIMT, there appears to be a gradual increase in the carotid haemodynamics with age, particularly in the hypertensives.

B-0219 14:56

Magnetic resonance imaging-based assessment of carotid atheroma: a comparative study of patients with and without coronary artery disease
A. Usman¹, U. Sadat, Z. Teng, M. Graves, J. Boyle, J. Gillard; *Cambridge/UK* (ammara.usman2013@gmail.com)

Purpose: Functional magnetic resonance (MR) imaging of atheroma using contrast media enables assessment of the systemic severity of atherosclerosis in different arterial beds. Whether black-blood imaging has similar ability remains widely unexplored. In this study, we evaluate whether black-blood imaging can differentiate carotid plaques of patients with and without coronary artery disease (CAD) in terms of morphological and biomechanical features of plaque vulnerability, thereby allowing assessment of the systemic severity nature of atherosclerosis in different arterial beds.

Methods and Materials: Forty-one patients with CAD and 59 patients without CAD underwent carotid black-blood MR imaging. Plaque components were segmented to identify large lipid core (LC), ruptured fibrous cap (FC), and plaque haemorrhage (PH). These segmented contours of plaque components were used to quantify maximum structural biomechanical stress.

Results: Patients with CAD and without CAD had comparable demographics and comorbidities. Both groups had comparable prevalence of morphological features of plaque vulnerability (FC rupture, 44% versus 41%, $P = .90$; PH, 58% versus 47%, $P = .78$; large LC, 32% versus 47%, $P = .17$), respectively. The maximum biomechanical stress was not significantly different for both groups (241 versus 278 kPa, $P = .14$) respectively.

Conclusion: Black-blood imaging does not appear to have the ability to differentiate between the morphological and biomechanical features of plaque vulnerability when comparing patients with and without symptomatic atherosclerotic disease in a distant arterial territory such as coronary artery.

B-0220 15:04

DCE-MRI demonstrates less microvasculature in symptomatic carotid atherosclerosis

G.A.J.C. Crombag¹, R. van Hoof¹, F.H. Schreuder², R.J. van der Geest³, W.H. Mess¹, R. van Oostenbrugge¹, P.A. Hofman¹, J.E. Wildberger¹, M. Kooi¹; ¹Maastricht/NL, ²Nijmegen/NL, ³Leiden/NL (g.crombag@maastrichtuniversity.nl)

Purpose: Rupture of a vulnerable carotid atherosclerotic plaque is an important underlying cause of stroke. Increased leaky plaque microvasculature may contribute to plaque vulnerability. These immature microvessels may facilitate the entrance of inflammatory cells into the plaque. As dynamic contrast-enhanced (DCE) magnetic resonance (MR) imaging is a non-invasive method to study leaky plaque microvasculature, we investigated the difference in plaque microvasculature between the symptomatic and contralateral asymptomatic carotid plaque.

Methods and Materials: 88 symptomatic patients with >2 mm carotid plaque underwent 3T MRI (including DCE-MRI) to identify the presence of a lipid-rich necrotic core (LRNC) and to assess plaque microvasculature. K^{trans} was calculated for the entire symptomatic and contralateral asymptomatic plaque, using a pharmacokinetic model (Patlak model). K^{trans} represents the contrast medium transfer rate from the microvasculature to the extracellular space. The presence of an LRNC was assessed on the post-contrast black-blood T1W MR images. Differences in K^{trans} between the symptomatic and asymptomatic side were assessed using a paired samples *T* test. Independent samples *T* test was used to compare the means between plaques with and without LRNC.

Results: A significantly lower K^{trans} was found in the symptomatic carotid plaque compared to the asymptomatic side ($0.062 \pm 0.0017 \text{ min}^{-1}$ versus

$0.057 \pm 0.0020 \text{ min}^{-1}$, $p = 0.033$). Furthermore, there was a significant lower K^{trans} in plaques with an LRNC ($0.061 \pm 0.017 \text{ min}^{-1}$ versus $0.054 \pm 0.014 \text{ min}^{-1}$, $p = 0.041$).

Conclusion: Unexpectedly, the symptomatic carotid plaques had a significantly lower K^{trans} , indicative of a decrease of leaky plaque microvasculature in symptomatic plaques. This may be related to a larger amount of necrotic tissue in symptomatic plaques.

B-0221 15:12

New 3D-arterial analysis software to evaluate carotid atherosclerotic plaque in comparison with CEUS, CTA and histological examination

V. De Soccio¹, V. Cantisani¹, M. Di Segni^{1,2}, N. Di Leo¹, A. Rubini¹, V. Forte¹, D. Fresilli¹, F. D'Ambrosio¹, C. Catalano¹; ¹Rome/IT, ²Civitavecchia/IT (valerio.forte@gmail.com)

Purpose: To assess the accuracy of ultrasonographic 3D-Arterial Analysis in characterizing stenosis percentage and vulnerability of carotid plaques.

Methods and Materials: Sixty seven patients were enrolled with the following criteria: (1) asymptomatic stenosis of carotid artery $\geq 70\%$ but $< 100\%$; or (2) recent transient ischemic attack or ischemic stroke, and ipsilateral carotid stenosis $\geq 50\%$. Eventually all patients underwent endarterectomy and samples were histologically assessed for instability features. 3D-Arterial Analysis provided a colour map to evaluate plaque vulnerability and a 3D volumetric stenosis evaluation. Its diagnostic performance has been compared to histological examination for plaque's vulnerability and to CEUS and CTA for stenosis' grading.

Results: Histological examination identified 47 vulnerable plaques with at least one of the following criteria: fibrous cap $\geq 200 \mu\text{m}$, presence of lipid core, intra-plaque haemorrhage, leukocyte recruitment or angiogenesis. 3D-Arterial Analysis software, CEUS and CTA were able to detect 42, 41 and 41 of these 47 vulnerable plaques respectively, with 89%, 87% and 87% sensitivity and 100% specificity. 3D-Arterial Analysis software and CEUS were able to evaluate stenosis percentage with 88% sensitivity and 100% specificity compared to CTA, identifying 59/60 severe stenosis.

Conclusion: 3D-Arterial Analysis software and CEUS seem effective tools to assess plaque's vulnerability and stenosis severity, providing useful information for surgery planning.

Author Disclosures:

V. Cantisani: Speaker; Bracco, Toshiba Medical Systems, Samsung Healthcare.

B-0222 15:20

MR imaging shows an inverse association between the microvasculature and intraplaque haemorrhage in atherosclerotic carotid lesions

G.A.J.C. Crombag¹, R. van Hoof¹, S. Heeneman¹, P. Nederkoorn², W.H. Mess¹, R. van Oostenbrugge¹, M.J. Daemen², J.E. Wildberger¹, M. Kooi¹; ¹Maastricht/NL, ²Amsterdam/NL (g.crombag@maastrichtuniversity.nl)

Purpose: Rupture of a vulnerable atherosclerotic plaque is an important cause of clinical ischaemic events. The presence of intraplaque haemorrhage (IPH) is associated with plaque rupture and plaque progression, and predicts cerebrovascular events. However, the underlying mechanisms contributing to IPH are not fully understood. The dominant view is that IPH is caused by leakage of erythrocytes from immature microvessels. Alternatively, it has been suggested that plaque rupture/fissures are important in the development of IPH. The goal of this study was to investigate the association between leaky atherosclerotic plaque microvasculature and the presence of IPH in a large prospective cohort study of patients with symptomatic carotid plaques.

Methods and Materials: 101 symptomatic patients underwent MRI of the symptomatic carotid plaque for detection of IPH and dynamic contrast-enhanced (DCE)-MRI for assessment of plaque microvasculature. K^{trans} , an indicator of microvascular flow, density and leakiness, was estimated using pharmacokinetic modeling. Statistical analysis was performed using an independent samples *T* test and logistic regression, correcting for clinical risk factors.

Results: A decreased vessel wall K^{trans} was found for IPH-positive patients ($0.033 \pm 0.001 \text{ min}^{-1}$ versus 0.040 ± 0.001 , $p = 0.001$), which remained significant after correction for confounding factors. No difference in adventitial K^{trans} was found in patients with and without IPH ($0.040 \pm 0.002 \text{ min}^{-1}$ versus 0.039 ± 0.001).

Conclusion: We identified an inverse association between IPH and the microvasculature in symptomatic carotid plaques. Alternative and additional factors, such as disrupted plaque surface and fissures, may contribute to the development of IPH.

14:00 - 15:30

Room Z

Interventional Radiology

SS 309

Aortic and arterial interventions

Moderators:

A. Massmann; Homburg a.d. Saar/DE
N.N.

K-05

Keynote lecture

N.N.

B-0223 14:09

Hybrid repair of aortic pathology involving aortic arch

Y. Xu, L. Huang; Beijing/CN (xueyuguo2006@163.com)

Purpose: To evaluate the safety and efficacy of hybrid repair for aortic lesions involving aortic arch.

Methods and Materials: From February 2009 to September 2016, 81 consecutive patients (70 men; mean age 63.4±7.9 years, range 32-79) underwent brachiocephalic bypass combined with stent-graft implantation ("hybrid") and were enrolled in the study. Aortic pathologies included Stanford type B aortic dissection (n=22), aortic arch aneurysm (n=26), aortic arch pseudoaneurysm (n=14), aortic arch penetrating ulcer (n=11) and proximal endoleak (n=5) or pseudoaneurysm formation (n=3) after TEVAR. Hybrid repair comprised 3 landing in zone 0, 44 landing in zone 1 and 34 landing in zone 2. Simultaneous procedures included left subclavian artery embolization (n=57), endovascular abdominal aortic repair (n=1), coronary artery bypass (n=1), left common carotid endarterectomy (n=1) and renal stenting (n=4). Follow-up was performed at 1 month, 3 months, 6 months, 1 year and annually thereafter to investigate endoleak, patency of vascular graft and exclusion of aortic pathology.

Results: Technical success was 100%. Instant endoleak was observed in 9 (11.1%), 7 type I, 2 type II cases on postoperative angiography. Early morbidity was 8.6% (7/81). Early death occurred in 5 cases (6.2%). Follow-up was complete in 100% for 39.4±14.5 months (range 1 -81 months). During follow-up, all the vascular grafts were patent. Late mortality was 6.2% (5/81) and morbidity was 14.5% (8/81).

Conclusion: Hybrid repair of aortic pathologies involving aortic arch is safe and effective with good short- and mid-term results, greatly expanding the indication of endovascular aortic repair.

B-0224 14:17

Overall survival and factors predicting long-term outcome after thoracic aortic endovascular repair

B. De Coster, S. Houthoofd, A. Laenen, I. Fourneau, G. Maleux; Leuven/BE (bruno.decooster@uzleuven.be)

Purpose: To assess overall survival and to determine factors predicting outcome after thoracic endovascular aortic repair.

Methods and Materials: This is a retrospective analysis including a cohort of 212 consecutive patients (165 males and 47 females; mean age 64 years) who underwent thoracic endovascular aortic repair (TEVAR) in a tertiary referral centre for aortic disease. Main indications were true thoracic aortic aneurysm (TTAA) (n=58; 27.6%), traumatic aortic rupture (n=33; 15.7%), anastomotic pseudoaneurysms (n=23; 10.9%), dissecting thoracoabdominal aneurysm (n=22; 10.5%) and symptomatic, acute type B dissection (n=21; 10.0%). In 79 patients (37.3%), a hybrid procedure, including supra-aortic rerouting, was performed. Kaplan-Meier estimates are used for overall survival and Cox regressions models are used for univariable analysis of the association between risk factors and survival.

Results: Proximal landing zone were predominantly zone 3 (n=66; 31.3%), zone 2 (n=63; 29.9%) and zone 1 (n=38; 18%). In-hospital mortality was n=18 (8.5%). Overall survival was 79.6%, 65.9% and 51.1% at 2, 5 and 10 years, respectively; better overall survival was revealed for traumatic aortic rupture, chronic posttraumatic pseudoaneurysms and anastomotic pseudoaneurysms (P<0.05). Clinical risk factors influencing overall survival include prior coronary bypass surgery, atrial flutter, arterial hypertension, renal failure, chronic obstructive pulmonary disease and associated abdominal aortic aneurysm (P<0.05).

Conclusion: TEVAR is an effective treatment option for various thoracic aortic diseases with highest survival rates for traumatic aortic rupture and anastomotic pseudoaneurysms. Several clinical parameters are identified as risk factors for overall survival.

B-0225 14:25

Analysis of remodeling in abdominal aortic branch perfusion patterns complicated by type B aortic dissection after thoracic endovascular aortic repair

T. Li, X. Han; Beijing/CN (litiezhengaz@163.com)

Purpose: To evaluate the efficiency of thoracic endovascular aortic repair in dealing with visceral malperfusion based on the image-analysis of type B aortic dissection.

Methods and Materials: Retrospective analysis to 32 patients from September 2015 to March 2016 in our department, who were diagnosed type B aortic dissection with visceral malperfusion, the information of clinic and image, as well as the following-up were collected. By observing the image of computed tomography angiography of aortic dissection in preoperative, we analyzed the type of branch perfusion patterns in four abdominal branches (celiac trunk, superior mesenteric artery, bilateral renal artery) in statistical.

Results: Four abdominal branches (total 128 branches), 78 branches (67%) expressed with Class I patterns, in which Class I-b presented with 1%, Class I-c presented with 5%; 14 branches (11%) expressed with Class II patterns, in which Class II-b-1 presented with 4%, Class II-b-2 presented with 3%; 16 branches (13%) expressed with Class III patterns, in which Class III-a presented with 13%, without Class III-b and III-c presentation; the remaining 12 branches with normal. Successful rate of TEVAR was 100%. The mean following-up was 4 months. Postoperative CTA showed that among 14 high-risk abdominal branches, 13 branches (92.9%) preserved improvement, the remaining one branch (7.1%) with I-b showed ischemic malperfusion in progress to I-c.

Conclusion: In comparison to the perfusion of ischemic branches complicated by aortic dissection in pre- and post-operative, there was profound benefit in the reconstruction of abdominal branches to extend the redefined branch type by Nagamine.

B-0226 14:33

Evaluating aortic endograft (EVAR) fate according to anatomical instruction (IFU) compliance: which anatomical feature has the most impact on graft fate?

N. Güner, A. Gulcu; Izmir/TR (baturalpguner@gmail.com)

Purpose: In today's practice, abdominal aortic aneurysms (AAA) are prevalently repaired endovascularly (EVAR). Because of its applicability on high-morbidity patients, a large group of EVAR patients have anatomic features that do not comply with endograft device specifications. Our research evaluates the follow-up complication rates of EVAR patients with device-compliant and device-non-compliant anatomical features.

Methods and Materials: Patients treated with EVAR between 2009 and 2015, and having follow-up studies in our institution are included in our study (50 patients). Patients were grouped according to their IFU (instructions for use) compliance, and later each of the seven IFU anatomic criteria individually. Treatment efficiency were observed by aortic/iliac enlargement, type 1 and 3 endoleaks and reintervention obligations during follow-up.

Results: Of patients, 48% had IFU compliant and 52% had non-compliant anatomy. Mean follow-up time was 23 months. There were not any differences between compliant and non-compliant groups in complication rates and treatment efficiency. When each of the IFU anatomic criterias was used for grouping, proximal properties and iliac diameter did not yield any statistical difference. In patients with inadequate iliac fixation (<15mm), endoleak and reintervention rates were statistically higher (P 0.002 and 0.008).

Conclusion: Proximal aneurysmal features were for long considered the most important factor in endograft fate. New design features in endografts may have changed this. Our study claims that distal fixation properties represent a very important and possibly strongest factor on the fate of an endograft. Small number of studies found on distal fixation properties had similar outcomes with our study.

B-0227 14:41

Role of intra-vascular ultrasound (IVUS) in EVAR planning

G. Falcone, C. Raspanti, G. Gabbani, E. Casamassima, F. Mondaini, M. Citone, F. Fanelli; Florence/IT (gianmarcofalcone@gmail.com)

Purpose: To evaluate accuracy and safety profile of Intravascular Ultrasound (IVUS - PhilipsVolcano) in pre-treatment EVAR planning for Aortic Abdominal Aneurysm(AAA)

Methods and Materials: In 36 consecutive patients(mean age 70.1 +/- 5.9; 15 male) with AAA pre-procedural EVAR evaluation was performed with CT angiography (CTA). IVUS intra-operative evaluation of proximal neck diameter, sac diameter , distal neck and iliac artery diameter was performed. Endoprosthesis sizing was grounded on CTA data in 18 pts and on IVUS data in 18. IVUS evaluation of endoprosthesis apposition was performed at the end of the procedure. A comparison between IVUS and CTA data was performed.

Results: IVUS was technically feasible in all cases. Mean proximal aortic neck diameter was 28mm (range 21-34mm) on CTA evaluation while on IVUS evaluation was 26mm (range 20-31); Mean iliac artery diameter on CTA was 12mm (range 11-15mm) and 12mm on IVUS (10-13mm). In 5 cases a mismatch >2.5mm between CT and IVUS measurement of the proximal neck was observed. Technical success was achieved in all EVAR cases. No type I endoleaks were observed in the IVUS group. In the CTA group one type I endoleak was observed due to infolding of the fabric. In this case proximal aortic neck diameter was 26 on CTA and 21mm on IVUS evaluation. No IVUS related complication were reported.

Conclusion: IVUS is a safe evaluation tool and allows a better measurement of aortic diameters in the EVAR planning, reducing the complication rate.

B-0228 14:49

Interventional treatment of visceral artery aneurysms: single centre experience over 16 years

P. Reidler, M. Lerchenberger, M. Rentsch, C.G. Trumm; *Munich/DE (Paul.Reidler@med.uni-muenchen.de)*

Purpose: To evaluate treatment efficacy, complications and short-term mortality after primary interventional treatment of visceral artery aneurysms (VAAs).

Methods and Materials: From 71 consecutive cases of treated VAAs during the years 1999-2015 we selected all patients who had undergone primary endovascular treatment in elective or emergency settings. Aneurysm location and size were assessed by CTA with multiplanar reconstructions. Complications were classified according to Clavien-Dindo (CD) from Grade 0 to V. Mortality was assessed at follow-up after 30 days.

Results: Thirty-two patients (mean age: 57.5 years, female/male: 12/20) who received primary emergency (12) or elective (19) endovascular treatment for single VAA were included. VAAs occurred at the coeliac trunk (1), splenic (8), gastroduodenal (8), hepatic (7), superior mesenteric (3), gastric (3), pancreatic (1) and pancreaticoduodenal artery (1). Aneurysm size varied between 7 and 116mm (Median: 23mm). Primary intervention was successful in 29 patients (91%). 25 patients (78%) did not show any or only insignificant postinterventional complications (CD 0 and I). Pharmacologically treatable complications (CD II) were found in 1 patient (3%). 6 patients (19%) needed further interventional (4) or surgical (2) treatment (CD III) due to residual aneurysm perfusion (1), re-bleeding (2), splenic infarction (2), hepatic abscess (1), stent dislocation (1) or complications due to severe pancreatitis (1). 30-day mortality was 0%.

Conclusion: Interventional therapy of VAA presented a high rate of primary therapeutic success and no to minor complications in a majority of cases. As more severe complications might require interventional or surgical approach, management should include both specialties.

B-0230 14:57

Endovascular repair of 40 Visceral Artery Aneurysms (VAAs) and Pseudoaneurysms (VAPAs) with the Viabahn Stent-Graft: technical aspects, clinical outcome and mid-term patency

P. Marra, M. Venturini, M. Colombo, G. Brembilla, M.M. Panzeri, M. Salvioni, S. Gusmini, F. De Cobelli, A. Del Maschio; *Milan/IT (marra.paolo@hsr.it)*

Purpose: Endovascular repair of VAAs and VAPAs with Stent-Grafting (SG) can simultaneously allow aneurysm exclusion and vessel preservation, minimizing the risk of ischemic complications. We report a single-center experience on SG of visceral aneurysms, focusing on technical aspects, clinical outcome and mid-term patency.

Methods and Materials: Patients affected by VAAs or VAPAs and treated between 2003 and 2017 with SG using a self-expandable peripheral Viabahn stent-graft were retrospectively reviewed. Aneurysm type, patient number, SG clinical setting, procedural data, peri-procedural complications, technical success, clinical success, 30-day mortality, and follow up (aneurysm exclusion, stent-graft patency, ischemic complications) were analysed.

Results: SG was performed in 40 patients (22 VAPAs/18 VAAs) with 44 procedures (25 in emergency, 19 in election), via transfemoral approach in 37 cases and transaxillary in 7. SG was associated with coil-embolization in 6 cases. One peri-procedural complication was recorded (a splenic artery dissection successfully converted to transcatheter embolization). The overall technical and clinical success rates were respectively 96% and 84%, with excellent trend in election procedures (both 100%). Overall 30-day mortality was 12.5% always due to septic shock after pancreatic surgery. Stent-graft thrombosis occurred in 2 patients within 3 months, with aneurysm exclusion and without ischemic complications. Stent-graft patency and aneurysm exclusion were confirmed at 6, 12 and 36 months in 18, 12 and 7 patients, respectively.

Conclusion: SG of VAAs and VAPAs was safe and effective, particularly in election setting. The Viabahn stent-graft, flexible and without shape memory, is suitable for endovascular repair of tortuous visceral arteries.

B-0231 15:05

Endovascular treatment of visceral artery aneurysms and pseudoaneurysms: extravascular stent graft migration as a possible long-term complication

L. Mascagni¹, M. Tiplaldi¹, M. Pignatelli¹, M. Cappucci¹, M. Krokidis², G. Orgera¹, M. Rossi¹; ¹Rome/IT, ²Cambridge/UK (luca.nero@hotmail.it)

Purpose: Immediate- and long-term result analysis of endovascular visceral aneurysm and pseudoaneurysm treatment with stent grafts.

Methods and Materials: From February 2006 to October 2011, we deployed 23 stent grafts in 21 patients (12 males and 9 females, mean age 58.2 years) affected by aneurysm or pseudoaneurysm of the splenic artery (n=13), hepatic artery (n=5), gastroduodenal artery (n=1) and renal artery (n=2). The aneurysmal sack dimensions ranged from 9 to 60 mm. We evaluated the technical success, stent patency, possible migration, breakage and aneurysmal reperfusion. The follow-up, performed with CECT, was repeated at 1, 6 and 12 months, then yearly (range 12-72 months).

Results: We achieved complete aneurysmal exclusion in 20/21 patients (95%). In one case, we had incomplete sealing and splenic artery's hilar branch fissuration during the procedure and thus treated with coils and ruled out of the follow-up. We reported complete aneurysmal exclusion in 20/20 patients in follow-up. In 4 cases, we observed stent occlusion, although without organ-related ischemia; in 3 of these 4 cases, stent occlusion was associated with stent graft migration: one inside the gastric antrum at the 36th month during follow-up (confirmed with endoscopy) and two in the lesser omentum at the 12th and 60th month follow-up.

Conclusion: Endovascular treatment of aneurysmal and pseudoaneurysmal pathology of visceral arteries with stent grafts is a safe and effective technique with good immediate- and long-term results. Extravascular migration of the stent graft after its occlusion is a rare, yet possible late complication. According to our evidence, we recommend follow-up even in case the stent is occluded.

B-0232 15:13

Multicentre experience in endovascular treatment of aorto-iliac-femoral anastomotic pseudoaneurysms: evaluation of long-term follow-up

G. Guzzardi¹, B. Del Sette¹, P. Cerini¹, G. Carrafiello², F. Fusaro¹, D. Laganà³, C. Stanca¹, A. Carriero¹; ¹Novara/IT, ²Milan/IT, ³Catanzaro/IT (guz@libero.it)

Purpose: The purpose of this study is to assess the effectiveness of anastomotic pseudoaneurysms (APAs) endovascular treatment following aorto-iliac-femoral surgical reconstruction confronting technical and clinical success in patients with aortic lesions versus iliac-femoral lesions.

Methods and Materials: Were retrospectively evaluated 54 patients that had undergone aorto-iliac-femoral by-pass (72APAs). All patients were evaluated before treatment with CTA to assess the characteristics of the lesions. Follow up was performed with Eco-color-Doppler and/or CTA at 1, 3, 6 months after the procedure and then yearly. Patients were divided in two groups if they presented pseudoaneurysms in aorta or only in iliac-femoral district.

Results: Immediate technical success was 100%. No periprocedural complications occurred. Six patients died during follow-up due to APA-non related causes and 5 for sepsis 3 months after the procedure. During a mean follow up of 25.5 months (range: 3-72), 3/47 occlusions of stent-graft leg occurred respectively 7 days, 3 days and 24 months after the procedure, 2 type I endoleak and 1 type III endoleak. Primary clinical success rate was 87.2% and secondary clinical success was 95.7%. We witnessed a higher mortality in patients with aortic pseudoaneurysms even though it did not reach statistical significance (P>0.05).

Conclusion: Endovascular treatment of APAs is a valid alternative to open surgery and could be proposed as treatment of choice especially in patients with high surgical risk.

14:00 - 15:30

Room O

Chest

SS 304

Quantitative CT: a new diagnostic and functional tool

Moderators:

M. Occhipinti; Florence/IT
M.-P. Revel; Paris/FR

B-0233 14:00

Correlation analysis of quantitative CT parameters and pulmonary function in COPD patients

Q. Yu¹, X. Quan¹, X. Lu²; ¹Guangzhou/CN, ²Shenyang/CN

Purpose: To explore the correlation between quantitative CT parameters and clinical pulmonary function in COPD patients using a new COPD automatic analysis software.

Methods and Materials: There were 60 patients with COPD (male 51, median age: 65.9y) who underwent thin-slice chest CT scans both at end-inspiratory and end-expiratory. Airway measurement was provided average values along center line between start and end in the bronchiole of right upper apica lobes by software. ① Indirect indicators of air trapping were measured (end-inspiratory/end-expiratory), which included relative volume change (RVC)_{-860 to -950}, the expiration to inspiration ratio of mean lung density (MLD_{E/I}); ② Direct indicators of airway were measured (end-inspiratory, filter D), which included the following parameters: wall thickness (WT), lumen diameter (LD), Pi10, wall area (WA), lumen area (LA), wall area ratio (WA%), lumen area ratio (Ai%), WA/LA. Spearman rank correlation test and multiple variable analysis were used to evaluate the relationship between the above quantitative CT parameters and pulmonary function (airflow limitation: FEV1%, FEV1/FVC; airway resistance: Z5, R5, R20, Fres; diffusion capacity: DLCOSB).

Results: ① The correlation between indirect index of air trapping (RVC_{-860 to -950}, MLD_{E/I}) and airflow limitation ($r=-0.898$ to -0.906 , $P<0.001$), diffusing capacity ($r=-0.830$, -0.802 , $P<0.001$), airway resistance ($r=0.725-0.815$, $P<0.001$) was statistically significant. ② The correlation between direct indicators and airflow limitation ($r=-0.305$ to -0.623 , <0.01), diffusing capacity ($r=-0.325$ to -0.482 , $P<0.01$), airway resistance ($r=0.280$ to 0.591 , $P<0.01$) also was significant. Obviously, the correlation between the indirect index and pulmonary function is good ($r^2>0.5$), which was better than the direct index ($r^2<0.5$), the best of those was -0.906 (between RVC_{-860 to -950} and FEV1/FVC).

Conclusion: COPD software provides accurate and reproducible measurement of quantitative CT parameters, in which the correlation between indirect indicators of air trapping (RVC_{-860 to -950}, MLD_{E/I}) and pulmonary function is good.

B-0234 14:08

Using a neuronal network-based software to predict lung function values from qCT parameters in patients with COPD

J.F.M. Gawlitza, T. Sturm, K. Spohrer, T. Henzler; Mannheim/DE
(joshua_gawlitza@yahoo.de)

Purpose: Quantitative computed tomography (qCT) is an emerging technique for diagnostics and research in patients with COPD. qCT parameters show strong correlation with lung function tests and symptoms. Nevertheless, it is often criticised that qCT only provides anatomical and not functional information. We evaluated a neuronal network-based tool to predict lung function parameters from qCT values against actual lung function tests.

Methods and Materials: 75 patients with diagnosed COPD underwent body plethysmography and a dose-optimised qCT examination on a third-generation dual-source CT (Somatom Force, Healthineers, Forchheim, Germany) in inspiration and expiration. Four qCT parameters were acquired and used within a neuronal-network based dashboard software (PrediCT, Mannheim, Germany) to predict FEV1, FEV1/VC and RV/TLC. The predicted lung function values were then evaluated against the actual tested lung function parameters from body plethysmography.

Results: The mean relative error of the predicted values compared to the lung function tests was 9% for FEV1/VC, 10% for RV/TLC and 17% for FEV1. The root mean squared error was 9.3 for FEV1/VC, 10.5 for RV/TLC and 16.9 for FEV1, respectively.

Conclusion: Novel neuronal-network based software allows the prediction of lung function values from static qCT parameters within a reasonable margin of error. Therefore, qCT parameters may contain more information than we currently utilise and can potentially augment standard functional lung testing.

B-0235 14:16

Quantitative assessment of lung volume and lung density distribution in lung transplant patients: progression pattern in chronic lung allograft dysfunction

S. Dettmer¹, H. Suhling¹, T. Kaireit¹, J.-M. Kuhnigk², J. Gottlieb¹, J. Vogel-Claussen¹, F. Wacker¹, H.-o. Shin¹; ¹Hannover/DE, ²Bremen/DE
(dettmer.sabine@mh-hannover.de)

Purpose: To evaluate lung volume and density distribution as quantitative CT parameters for progression of chronic lung allograft dysfunction (CLAD) following lung transplantation.

Methods and Materials: 120 lung transplant patients with 327 CT (baseline 6 months after transplantation and during follow up) were evaluated. Following calculation of lung volume and density histogram features (mean lung density, peak, full-width-at-half-maximum, percentiles) skewness and kurtosis were calculated. Longitudinal analysis was performed using the difference of measurements between baseline and follow-up examinations. Patients with and without CLAD (matched 1:3) were compared with independent t-test. Three different time points in regard to CLAD diagnosis were evaluated: the last examination (<1year) before CLAD onset, the first examination after CLAD onset (<1year), and the first examination with severe CLAD / BOS stage 3.

Results: Of these 120 lung transplant patients 16 patients developed CLAD during the follow-up period. Measurements were significantly different between patients with and without CLAD and increase with disease progression. Major differences are the expiratory and inspiratory lung volume ($p<0.001$ - $p=0.014$), the ratio of expiratory and inspiratory lung density ($p=0.001$ - $p=0.236$) and the percentiles on expiration ($p<0.001$ - $p0.36$). Measurements reveal a progressive hyperinflation of the lung and a reduced respiratory dynamic.

Conclusion: Longitudinal changes of lung volume and density distribution measured on CT were significantly different between patients with and without CLAD and reveal a progressive hyperinflation of the lung which begins in the lower lobes and expands to the whole lung with disease progression.

B-0236 14:24

Quantitative CT and machine learning methods can predict eventual development of bronchiolitis obliterans syndrome after lung transplantation

E.J.M. Barbosa Jr.¹, M. Lanclus², W. Vos², C. Van Holsbeke², W. De Backer³, J. De Backer³, J.C. Lee¹; ¹Philadelphia, PA/US, ²Kontich/BE, ³Antwerp/BE
(eduardo.mortani@gmail.com)

Purpose: Long term survival after lung transplantation (LTx) is limited by bronchiolitis obliterans syndrome (BOS), defined as sustained decline in FEV₁ not explained by other causes. Machine learning (Support Vector Machine - SVM) applied to baseline quantitative CT metrics (qCT) and pulmonary function testing (PFT) was used to predict eventual development of BOS.

Methods and Materials: Paired inspiratory-expiratory CT scans of 41 patients who underwent LTx were analysed retrospectively. All were disease free at initial CT; 15 patients developed BOS at follow up, whereas 26 patients remained BOS free (BOS was defined as sustained reduction in FEV₁>10% compared to baseline FEV₁ after LTx). SVM was applied to baseline qCT features and PFT, to predict LTx patients' probability of eventual development of BOS.

Results: A total of 23 baseline FRI parameters could significantly distinguish between non-BOS patients and eventual BOS developers ($p < 0.05$), whereas no PFT parameters could. Using machine learning methods (SVM), LTx patients with smaller lung volumes ($p<0.001$), smaller airway volumes ($p=0.01$) and surface ($p=0.04$) and higher airway resistance ($p=0.03$) had greater probability of developing BOS. A combination of lobar resistance, surface area of the central airways and regional lobar volumes could predict BOS development with an accuracy of 85%.

Conclusion: Baseline qCT biomarkers may allow, via machine learning methods, accurate prediction of eventual onset of BOS from baseline qCT features, whereas baseline PFT metrics cannot. This may optimise the management paradigm of LTx patients.

B-0237 14:32

Temporal subtraction of serial-computed tomography images for visualisation and quantification of disease progression in idiopathic pulmonary fibrosis

H.-O. Shin, M. Minkler, L. Jaeger, C. Caliskan, S. Dettmer, J. Vogel-Claussen, F. Wacker, A. Prasse; Hannover/DE (shin.hoen-oh@mh-hannover.de)

Purpose: To evaluate temporal subtraction (TS) as an imaging biomarker for monitoring disease in idiopathic pulmonary fibrosis (IPF).

Methods and Materials: In 54 paired volumetric computed tomography scans (CT) of 27 patients with IPF, a semi-automatic lobe-based segmentation and a non-linear registration were performed warping the follow-up CT scan to the baseline CT scan. A TS image was calculated by subtracting the baseline CT from the warped follow-up CT. A colour look-up table was used for visualisation

of the TS image showing areas of decreased/increased density in shades of blue and red, respectively. CT-quantification was performed calculating the percentage volume change (PVC) of areas with decreased/increased density using a threshold of ± 150 HU in the TS images together with density histogram measures (changes in skewness and kurtosis). CT measurements were correlated with changes in pulmonary function test (PFT): FVC%, FEV1%, and KCO.

Results: In TS images, even subtle changes in parenchymal patterns could be visualised. Considering the complementary nature of CT features and PFT, a good correlation was found between PVC (increased/decreased/ total density change) and KCO (-0.36/-0.56 /-0.5, $p < 0.1$). No significant correlation was found for FVC% and FEV1%. Density histogram features (skewness / kurtosis) showed no significant correlation with PFT for KCO, FEV1% and FVC%.

Conclusion: TS facilitates visual assessment of longitudinal CT scans displaying morphological changes in the colour-coded TS image. PVC may allow for objective quantification of regional morphological changes in IPF patients.

B-0238 14:40

Subtraction CT of the lungs: accuracy of motion correction software

D. Grob¹, L.J. Oostveen¹, J. R uhaak², S. Heldmann², B. Mohr³, M.M. Prokop¹, M. Brink¹, I. Sechopoulos¹; ¹Nijmegen/NL, ²L ubeck/DE, ³Edinburgh/UK (Dagmar.Grob@radboudumc.nl)

Purpose: To compare the performance in registration between pre- and post-contrast computed tomography (CT) chest images of two algorithms using an anthropomorphic digital phantom to evaluate the potential accuracy of temporal subtraction to generate pulmonary iodine maps.

Methods and Materials: We used a recent version of the XCAT phantom, with enhanced airway and pulmonary vessel structures, to simulate pre- and post-contrast CT images (voxel size: 0.6x0.6x1.0 mm³) at different inspiration levels with realistic system noise. We varied the difference in diaphragm position between the two scans from 0 to 20 mm because this value exceeded the 95th percentile found in 100 clinical subtraction CT datasets. Registration was performed using two different lung algorithms (SURE Subtraction Lung, Toshiba Medical Systems and NLR, Fraunhofer MEVIS). For each registration, we calculated the voxel-by-voxel difference between the true deformation and the algorithm-estimated deformation.

Results: Between respiratory phases, the median displacement in the phantom was 5.2mm (interquartile range: 2.3mm - 11.6mm). At 20 mm difference in diaphragm position, the median residual error in registration was 0.93mm (0.52mm - 1.58mm) with SURE Subtraction Lung, and 0.97mm (0.50 mm - 1.84 mm) with the NLR algorithm. The largest errors were seen in the paracardiac regions.

Conclusion: Both tested registration algorithms can compensate for respiratory motion with a median residual error below 1 mm. This level of accuracy opens up new applications such as direct detection of emboli in segmental arteries or evaluation of pulmonary nodule enhancement.

Author Disclosures:

D. Grob: Research/Grant Support; Toshiba medical systems. **L.J. Oostveen:** Research/Grant Support; Toshiba Medical Systems. **S. Heldmann:** Employee; Fraunhofer-Gesellschaft zur F orderung. **B. Mohr:** Employee; Toshiba Medical Visualization Systems. **M.M. Prokop:** Research/Grant Support; Toshiba Medical Systems. Speaker; Bracco, Bayer, Toshiba Medical Systems. Other; Thirona (Spinoff), Veolity. **M. Brink:** Research/Grant Support; Toshiba Medical Systems. **I. Sechopoulos:** Research/Grant Support; Toshiba Medical systems, Siemens. Speaker; Siemens.

B-0239 14:48

Quantitative CT assessment in patients with desquamative interstitial pneumonia: correlations with pulmonary function parameters

S. Hong, S. Lee, N. Kim, S. Lee, J. Seo; Seoul/KR (sanghyeop.hong@gmail.com)

Purpose: To evaluate the correlations between quantitative CT parameters and pulmonary function parameters in patients with desquamative interstitial pneumonia (DIP).

Methods and Materials: From April 2002 to April 2014, 40 patients with DIP were included in our study (39 men and 1 woman; mean age 58.5 years). For quantitative assessment on CT, a texture-based in-house software was used to quantify six regional CT patterns: normal, ground-glass opacity (GGO), reticular opacity (RO), honeycombing, emphysema, and consolidation. The total abnormal opacity was defined as the sum of extents of GGO, honeycombing, and emphysema. Correlations between the quantified CT parameters and the physiologic parameters were evaluated using the Pearson correlation coefficient.

Results: The mean values of FEV₁, FVC, FEV₁/FVC ratio, FEF_{25-75%}, and DLco were 85.0%, 86.7%, 74.9%, 79.2%, and 65.6%. The mean 6-minute walking distance and lowest SpO₂ during the 6-minute walking test were 514.2 m and 92.7%. The mean extents of GGO, consolidation, emphysema, RO, honeycombing, and total abnormal opacity were 14.3%, 3.0%, 3.6%, 8.9%,

2.6%, and 20.5%. The total abnormal opacity showed significant correlations with DLco ($r = -0.466$; $P = 0.002$) and SpO₂ ($r = -0.534$; $P = 0.001$), but no correlations with FEV₁, FVC, FEV₁/FVC ratio, and FEF_{25-75%} ($P = 0.391, 0.366, 0.281, \text{ and } 0.681$, respectively).

Conclusion: Quantitative assessment of regional disease patterns in DIP patients showed significant correlations with DLco and SpO₂.

B-0240 14:56

Use of quantitative computed tomography to assess post-interventional long-term changes after bronchial thermoplasty in patients with severe asthma

P. Konietzke, O. Weinheimer, M. Wielp utz, W. Wagner, P. Heussel, C. Heussel, H.-U. Kauczor, F.J. Herth, M. Schuhmann; Heidelberg/DE (p.konietzke@gmx.de)

Purpose: Bronchial thermoplasty (BT) can be considered in the treatment of severe asthma. By reducing smooth muscle mass, and thus reducing bronchial wall thickening and bronchoconstriction, asthmatic symptoms may be controlled. We hypothesized that quantitative computed tomography (QCT) is an appropriate tool to measure long-term effects of BT on airway dimensions and air-trapping.

Methods and Materials: 32 paired inspiratory and expiratory CT scans of 16 patients were acquired before and after BT. The fully automatic YACTA software calculated wall thickness (WT), wall percentage (WP), lumen area (LA) and total diameter (TD) in a generation-based as well as total lung volume (TLV) and air-trapping parameters (E/I, RVC₈₅₆₋₉₅₀, A1-A3) in a lobe-based approach, respectively.

Results: WT decreased after performing BT significantly by 3.75% ($p = 0.035$) with a subsequent significant increase in LA by 5.39% ($p = 0.046$) and a decrease of 3.67% in WP ($p < 0.001$) for the combined airways generations 2nd-7th. TD increased by 0.69% on average ($p = 0.706$). After BT media TLV decreased by 68 cm³ ($p = 0.459$), air-trapping had a significant reduction for the parameter IE ($p < 0.001$), RVC₈₅₆₋₉₅₀ ($p < 0.001$), and A1-A3 ($p < 0.003$, $p < 0.001$ and $p < 0.001$), respectively.

Conclusion: QCT was able to show long-term post-interventional changes in patients treated with BT. Significantly reduced WT and WP with an increase in the lumen can be interpreted as direct therapeutic effects caused by a reduction in airway-smooth muscle mass and changes in neuronal innervation. QCT also showed a significant reduction in air-trapping. QCT parameters may be used in therapy guidance and monitoring.

B-0241 15:04

Accuracy of emphysema volume and airway measurements according to FBP, HIR, MIR, and virtual monoenergetic reconstruction images at both low- and standard-dose settings

M. Ha¹, C. Kim¹, K.Y. Lee¹, C. Shin¹, E.-Y. Kang², Y.-W. Oh², C. Ko¹, J. Cha¹; ¹Ansan/KR, ²Seoul/KR (gkahdls89@gmail.com)

Purpose: To evaluate the accuracy of emphysema volume (EV) and airway measurements (AMs) produced by various iterative reconstruction (IR) and virtual monoenergetic images (VME) at both low- and standard-dose settings.

Methods and Materials: CT images were obtained on phantom at both low and standard doses (30mAs vs 100mAs at 120kVp). Each CT scan was reconstructed using filtered back-projection (FBP), hybrid IR (iDose⁴), model-based IR (IMR-R1, IMR-ST1, IMR-SP1), and VME at 70 keV (VME70). The EV of each air column and wall area percentage of each airway tube were measured in all algorithms. Absolute percentage measurement errors of EV (APE_{vol}) and AM (APE_{WA%}) were then calculated. Repeated measures analysis of variance (ANOVA) was performed on repeated measured data.

Results: EV was most accurately measured in IMR-R1, and AM was the most accurate in IMR-SP1 on both low- and standard-dose CT (all $P < 0.05$). There were no significant differences in the APE_{vol} of IMR-R1 between low and standard doses (all $P > 0.05$). VME70 showed a significantly higher APE_{vol} than iDose4, IMR-R1, and IMR-ST1 (all $P < 0.004$). VME70 also showed a significantly higher APE_{WA%} compared with the other algorithms (all $P < 0.001$).

Conclusion: The measurement of EV and AM via application of IMR on both low- and standard-dose CT showed reliable accuracy in a phantom study. However, VME did not result in any improvement of measurement accuracy. Among these algorithms, IMR was the most accurate modality for measurement of both emphysema volume and airway wall thickness.

B-0242 15:12

Qualitative and quantitative comparison of lung nodules in an ex-vivo system on a high-pitch dual source CT and a standard CT in free breathing

C.A. Burgard; Munich/DE (caroline.burgard@med.uni-muenchen.de)

Purpose: To analyse the image quality of lung nodules using two different CT protocols (high pitch dualsource or standard CT) in free breathing and in full inspiration and expiration stimulating a non-compliant patient.

Methods and Materials: Three porcine lungs were prepared with 28 artificial nodules (mean diameter 10.4 mm) and subsequently placed into a dedicated CT compatible chest phantom (PROdesign artiCHEST). Images were obtained in static full inspiration and expiration breath hold, and as well as in free breathing, with two different CT protocols. Quantitative analysis was carried out with a semiautomatic volumetric program (LungCARE, Syngo.via, Siemens, Erlangen, Germany). The reproducibility of nodule volumetry was calculated. Motion artifacts were semi quantitatively assessed by two readers (from 0 or absent to 3 or relevant and non-diagnostic).

Results: In the qualitative analysis, the artefacts in the examinations performed with standard CT intensified with increasing number of respiratory acts per minute, whereas they were negligible in the highpitch dualsource CT examinations. These differences were statistically significant ($P < 0.005$). In quantitative analysis, the relative differences (Δ between the value of the volume calculated with standard and high pitch minus the inspiration value divided by the inspiration value) in the volumetric volume measured in standard CT were statistically significant in the 9, 15 and 18 breaths per minute scans.

Conclusion: While a standard CT examination for nodule volumetry relies on a steady breath-hold of the subject, the presented study demonstrated the feasibility of a high-pitch, dualsource CT acquisition in free breathing i.e. in non-compliant patients.

B-0243 15:20

Quantitative CT as a one-stop shop to describe status and outcome of patients with acute respiratory distress syndrome (ARDS)

P. Leiser, J. Schoettler, F.S. Centner, T. Kirschning, J. Krebs, M. Hagmann, C. Weiß, S.O. Schönberg, H. Haubenreisser; Mannheim/DE
(p.leiser@stud.uni-heidelberg.de)

Purpose: The aim of this study was to establish quantitative CT (qCT) parameters for pathophysiological understanding and clinical use in patients with ARDS. The most promising parameter is introduced.

Methods and Materials: 28 intubated patients with ARDS obtained a conventional and dual-energy CT scan in end expiratory breathhold. Following manual segmentation, 138 volume-, perfusion- and lung weight-related qCT parameters were correlated with 71 anaesthesiological parameters such as applied ventilation pressures (PEEP, Pdrive) and established status and prognosis scores (SOFA, SAPS II). Multiple regression analysis was then performed to enable the prediction of these scores by a single CT scan.

Results: Of all examined qCT parameters, excess lung weight (ELW) displayed the most significant results. ELW correlates positively with the amount of extravascular lung water ($r=0.72$), atelectatic lung volume ($r=0.92$), applied PEEP ($r=0.37$) and negatively with the lung's mean CM enhancement ($r=-0.65$; all $p < 0.05$). More significantly than any other anaesthesiological parameter it correlates with the patient's SOFA- ($p < 0.0001$, $r=0.69$) and SAPS II-Score ($p=0.0005$, $r=0.62$). A combination of ELW, mean CM and Pdrive can predict SOFA up to $r^2=87.95\%$.

Conclusion: ELW constitutes the best parameter to assess pathophysiology, status and outcome of patients with ARDS and should be considered a first-range diagnostic tool during the first hours of ICU treatment, providing better correlation to relevant clinical parameters than the current standard Horowitz index ($\text{PaO}_2/\text{FiO}_2$).

14:00 - 15:30

Room N

Genitourinary

SS 307

Prostate cancer diagnosis

Moderators:

A. Guerra; Lisbon/PT
N.N.

B-0244 14:00

Analysis of clinical and economic management optimisation of multiparametric-MRI as the first line tool in men with high clinical suspicion of prostate cancer

M. Pecoraro¹, A. Padhani², R. Campa¹, M.C. Valerio¹, C. Catalano¹, V. Panebianco¹; ¹Rome/IT, ²Middlesex/UK (pecoraro.martina1@gmail.com)

Purpose: Determine diagnostic and treatment costs, and effectiveness of the pathways incorporating multiparametric MRI biopsy (mp-MRI/Bx), compared with transrectal ultrasound-guided biopsy (TRUS/Bx), in men at high risk of prostate cancer (PCa).

Methods and Materials: A cost and time analysis, based on data from a published randomized, single centre study. 1140 patients with total PSA > 4 ng/mL divided in 2 groups: 570 patients underwent a TRUS/Bx, while 570 patients underwent a mp-MRI/Bx.

Results: Mp-MRI/Bx diagnosis costs were 14.6% greater than TRUS strategy (228,946 € vs 199,750 €), and 5.2-6.0% higher for therapy (1,912,000 € vs 1,802,800 €). Mp-MRI/Bx strategy was highly effective for excluding clinically significant disease (Gleason ≥ 7); sensitivity and NPV both 100% (95% CI 98-100%). If verification of negative mp-MRI was not undertaken, differential cumulative therapy costs for mp-MRI/Bx strategy remained higher (8.4%), despite potential savings in active surveillance costs, because of increased radical therapies (mp-MRI/Bx = 409; TRUS/Bx = 373). Time-to-diagnosis was shorter for the mp-MRI/Bx strategy (median 4.0 months (IQR 3-6); TRUS/Bx (median 6 months (IQR 4-12); $p < 0.001$).

Conclusion: Our analyses suggest mp-MRI/Bx strategy is effective for diagnosing patients with suspected PCa, providing faster and more accurate diagnoses.

B-0245 14:08

Impact of upfront risk stratification on the negative predictive value of multiparametric MRI in patients with no history of prostate cancer

M. Abihanna¹, C. Melodelima², P.-C. Moldovan¹, R. Souchon¹, A. Ruffion³, M. Colombe¹, S. Crouzet¹, O. Rouviere¹; ¹Lyon/FR, ²Grenoble/FR, ³Pierre Benite/FR (m_abihanna@hotmail.fr)

Purpose: To assess the impact of upfront risk stratification on the negative predictive value (NVP) of multiparametric MRI (mpMRI) with patients without history of prostate cancer.

Methods and Materials: We retrospectively analysed a prospective database of 646 patients (456 biopsy naive, 189 referred for repeat biopsy) who underwent mpMRI before biopsy. The prediction of clinically significant prostate cancer (csPCa) at biopsy by clinical (age, digital rectal examination, PSA density [PSAd]), history of prior negative biopsy) and imaging (Likert score, extracapsular extension [ECE], magnetic field strength, experience of radiologist and presence of a concordant hypoechoic lesion [Concord-Echo]) variables was assessed by multivariate analysis. Significant clinical variables were included in a 'clinical model'. Three definitions for csPCa were used (csPCa1: USIP grade group ≥ 3 ; csPCa2: USIP grade group ≥ 2 ; csPCa3: csPCa2 and USIP grade group 1 with cancer invasion length ≥ 5 mm).

Results: Age, PSAd, history of prior negative biopsy, Likert score, ECE and Concord-Echo significantly predicted the presence of csPCa1-3. Adding the Likert score to the clinical models significantly increased the models' performance. Omitting biopsy in patients with negative mpMRI would have avoided 28.9% (Likert $\leq 3/5$) or 45.7% (Likert $\leq 4/5$) of biopsies while missing 9.2-11.5% of csPCa1, 11.9-18.5% of csPCa2 and 19.5-28% of csPCa3. mpMRI NPV decreased when the csPCa probability given by the clinical models increased. Therefore, considering clinical models' output allowed defining scenarios missing <5% of csPCa and omitting biopsies in 24.1-39.8% (csPCa1), 20.4-26.2% (csPCa2), and 10.2-12.8% (csPCa3) patients.

Conclusion: Upfront risk stratification of patients allows rational use of mpMRI NPV.

B-0246 14:16

Diagnostic performance of biparametric MR imaging for detection of prostate cancer: a systematic review and meta-analysis

X. Niu; Chengdu/CN (niu19850519@163.com)

Purpose: To perform a systematic review and meta-analysis to estimate the diagnostic performance of biparametric MR imaging (bp-MRI) for the detection of prostate cancer (PCa).

Methods and Materials: Two independent reviewers performed a systematic review of the literature published as of June 1, 2017, using predefined search terms. The standard of pathological reference was established at prostatectomy or prostate biopsy. The number of true- and false-positive, true- and false-negative results were extracted. The quality assessment of diagnostic accuracy studies tool was used to assess the quality of the selected studies. Statistical analysis included pooling of diagnostic accuracy, meta-regression, subgroup analysis, head-to-head comparison and identification of publication bias.

Results: Thirty-three studies were used for general data pooling. Overall sensitivity was 81% (95% confidence interval [CI]: 76%, 85%), and overall specificity was 77% (95% CI: 69%, 84%). As for clinically relevant prostate cancer (cr-PCa), multiparametric MRI (mp-MRI) maintained high diagnostic value [AUC=0.85 (95% CI: 0.82, 0.88)]. There was no evidence of publication bias ($P=0.673$). From head to head comparison, mp-MRI demonstrated significantly higher pooled sensitivity of 0.85 (95% CI: 0.78, 0.93) compared with 0.80 (95% CI: 0.71, 0.90) for bp-MRI ($P=0.01$). However, the pooled specificity was not significantly different [0.77 (95%CI: 0.58, 0.95) vs 0.80 (95%CI: 0.64, 0.96), respectively; $P = 0.82$].

Conclusion: Results of this meta-analysis suggest that bp-MRI has high diagnostic accuracy in detection of PCa, and maintained high detection rate for crPCa. However, owing to high heterogeneity among the included studies, caution is needed in applying our results.

B-0247 14:24

Diffusion-weighted MRI in prostatic lesions: diagnostic performance of normalised ADC using normal peripheral prostatic zone as a reference

T.F.T. Ali; Zagazig/EG (tamerfathi2008@yahoo.com)

Purpose: To evaluate the potential value of using the normal peripheral prostatic zone (PZ) as a reference site to improve the performance of DWI in the evaluation of prostatic lesions.

Methods and Materials: 38 patients with clinical suspicion of cancer prostate and who are scheduled to undergo a TRUS-guided biopsy were subjected to DW-MRI with ADC calculation. The normalised ADC (nADC) value was calculated by dividing the ADC of lesion by ADC of reference site (healthy peripheral zone). DWI-MRI results were compared to that of biopsy. Data were analysed and ROC was used to evaluate the performance of ADCs and nADCs.

Results: The patients were classified histopathologically into non-malignant group (16 patients) and malignant group (22 patients). Significant negative correlation between each of ADC and nADC and malignancy was detected. There was no significant difference between the mean ADC of peripheral healthy PZ in benign and malignant cases. There was significant difference between the mean ADC and mean nADC in benign and malignant lesions (1.049 ± 0.217 versus $0.659 \pm 0.221 \times 10^{-3} \text{mm}^2/\text{sec}$, $p < 0.001$) and (0.475 ± 0.055 versus 0.328 ± 0.044 , $p < 0.001$), respectively. There was a significant higher diagnostic performance of nADC than ADC with ADC cut-off value $0.75 \times 10^{-3} \text{mm}^2/\text{sec}$ and nADC cut-off value 0.39 could significantly differentiate between benign and malignant lesion with sensitivity, specificity, PPV, NPV of 86.36, 75, 82.61 and 80%, respectively, $p < 0.0001$ for ADC and 95.45, 93.75, 95.45 and 93.75%, $p < 0.0001$ for nADC.

Conclusion: The diagnostic performance of nADC using normal peripheral zone is higher than ADC in the discrimination between cancerous and non-cancerous lesions of the prostate.

B-0248 14:32

Dynamic contrast-enhanced MRI (DCE) for prostate cancer detection: are qualitative and quantitative analyses the key to success?

F. Ziayee, T. Ullrich, R. Rabenalt, P. Albers, G. Antoch, L. Schimmöller; Düsseldorf/DE (farid.ziayee@med.uni-duesseldorf.de)

Purpose: DCE remains an integral part of the multi-parametric MRI of the prostate. The aim of this study was to evaluate the importance of qualitative and quantitative analyses of dynamic contrast-enhanced MRI (DCE) with regard to prostate cancer (PCa) detection.

Methods and Materials: DCE data of 103 consecutive patients with multi-parametric MRI (T2WI, DWI, DCE) and subsequent MRI-(in-bore)-biopsy of the prostate were retrospectively analysed. Qualitative (curve type, PI-RADS v2) and quantitative (K_{trans} , K_{ep}) analyses of in total 206 lesions (87 cancer positive and 119 benign lesions) were performed. Cancer detection, discrimination of significant cancer, and localization was assessed and compared to histopathologic findings.

Results: Regarding discrimination between PCa and benign lesions, differences between K_{trans} , K_{ep} , and curve types were not statistically significant ($p = 0.2-0.9$). Subdivided in peripheral zone (PZ) and transition zone (TZ) K_{trans} ($p < 0.01$; $p = 0.04$) and K_{ep} ($p = 0.04$, $p < 0.01$) were significantly different between PCa and benign lesions. The PI-RADS v2 overall score could discriminate PCa and benign lesions in both, PZ and TZ ($p < 0.01$), whereas PI-RADS single scores of DCE could differentiate PCa better in PZ ($p < 0.01$) than in TZ ($p = 0.5$). All perfusion parameters could not differentiate between insignificant and significant ($\geq 4+3=7b$) prostate cancer ($p = 0.5-0.8$).

Conclusion: PI-RADS v2 criteria for DCE discriminate well between benign lesions and PCa in the peripheral zone. Qualitative (curve type) and quantitative parameters (K_{trans} , K_{ep}) provide no additional improvement in PCa detection compared to PI-RADS scoring alone. DCE-MRI alone did not allow differentiation between significant and insignificant PCa.

B-0249 14:40

Prostate tumour volume analysis on MRI as a predictor for aggressive disease

N.M. Hughes, C. O'Neill, F.M. O'Brein, N. Mayer, P. Kelly, J.G. Buckley, K. O'Regan; Cork/IE (nicolahughes@rcsi.ie)

Purpose: Patients with high Gleason grade (GG) prostate cancer have been shown to have radiological indicators of increased tumour aggressiveness on MRI. The aim of this study was to evaluate tumour volume on MRI as a potential predictor of aggressive disease by correlating with Gleason grade.

Methods and Materials: We performed a retrospective review of prostate MRI in patients with HG-PCa (GG8-10) over a three year period. An age-matched and PSA-matched number of patients with GG7 Pca (GG 3+4 and 4+3) was also reviewed. Volumetric tumour analysis was performed on T2-weighted (T2W) sequences and on diffusion-weighted MRI using Osirix® software.

Results: Seventy-five (n=38 GG7, n=17 GG8, n=17 GG9, n=3 GG10) MR studies were included in total. Average tumour volume for GG 7 disease was 1.96 cc on T2W sequences (range: 0.14-21.0159 cc) and 1.81 cc on ADC maps (range: 0.0763-17.1745 cc). HG-PCa (GG 8 and above) had an average tumour volume of 6.95 cc (3.29 cc GG8, 9.31 cc GG9, 14.39 cc GG10) on T2W sequences (range: 0.0891-54.3883) and 7.83 cc (3.27 cc GG8, 11.04 cc GG9, 15.47 cc GG10) on diffusion MRI (range: 0.0778-72.7619). There was a positive correlation between tumour volume and GG using both T2W sequences ($p < 0.001$) and ADC maps ($p < 0.001$).

Conclusion: This study has shown a positive correlation between tumour volume and Gleason grade. Volumetric analysis of prostate cancer on MRI may have a role in predicting more aggressive disease.

B-0250 14:48

Prostate volume estimation at MRI: reproducibility and limits

M. Bonatti¹, F. Lombardo¹, M. Simioni², G. Avesani¹, G. Bonatti¹; ¹Bolzano/IT, ²Verona/IT (matteobonatti@hotmail.com)

Purpose: To evaluate reproducibility of prostate volume estimated with the ellipsoid formula and to show its correlation with PSA density risk class.

Methods and Materials: We included in our IRB-approved retrospective study 60 consecutive patients who underwent prostate MRI for the detection of cancer at our Institution between July and September 2017. Two readers independently estimated prostate volume by means of the ellipsoid formula using axial and sagittal T2-weighted images. A third reader measured prostate volume by means of manual segmentation on axial T2-weighted images using commercially available software (iTK-SNAP). PSA density was calculated for each patient according both to the measured and estimated prostate volumes. Data were compared using paired t-test.

Results: Mean prostate volume calculated with manual segmentation was 54 ± 20 cc. Mean prostate volume estimated with ellipsoid formula was 50 ± 19 cc for reader 1 and 52 ± 20 cc for reader 2. Prostate volume estimated with the ellipsoid formula was significantly different between the two readers ($p = 0.015$). Prostate volume estimated with the ellipsoid formula was significantly different from prostate volume calculated with segmentation for reader 1 ($p = 0.0016$) and not significantly different for reader 2 ($p = \text{n.s.}$); the mean volume difference was 14% for reader 1 and 13% for reader 2. For both readers, 5/60 (8.3%) patients would have changed their PSA density risk class (< 0.15) when comparing data obtained from estimation with those obtained from measurement.

Conclusion: Prostate volume estimated with the ellipsoid formula shows poor reproducibility and might lead to errors in PSA density evaluation.

B-0251 14:56

Prevalence and significance of incidental extraprostatic findings in patients undergoing magnetic resonance imaging of the prostate for detection of prostate cancer

F.M. Schäfer, P. Asbach, M. Haas, B. Hamm, A. Baur; Berlin/DE (Frederik.Schaefer@charite.de)

Purpose: Multiparametric magnetic resonance imaging (mpMRI) of the prostate can detect prostate cancer with high accuracy. Imaging depicts a wide array of pelvic and abdominal tissues in addition to the prostate. In this study we evaluated the prevalence as well as the clinical significance of incidental extraprostatic findings that can be detected on mpMRI.

Methods and Materials: We retrospectively identified 300 patients (median age, 64 years; range, 46-76 years) who had undergone mpMRI of the prostate at 3 Tesla as a first-line test before prostate biopsy between October 2016 and August 2017 using a standardized examination protocol in accordance with the current Prostate Imaging - Reporting and Data System recommendations. One experienced reader blinded to clinical data analyzed imaging with a focus on incidental extraprostatic findings. Findings that necessitated further work-up were rated as clinically significant.

Results: Of all extraprostatic findings diverticulosis (n=103; 34.3%) and inguinal herniation of fat (n=85; 28.3%) were most common. In 13 patients (4.3%) extraprostatic findings were rated as clinically significant including suspicion for a neoplasm of the bladder (n=1), neoplasms of the sigmoid and rectum (n=3), femoral head necrosis (n=1), chronic diverticulitis of the sigmoid (n=5), and subacute inflammation of an aortic aneurysm (n=1).

Conclusion: Whilst incidental extraprostatic findings were commonly detected on mpMRI, findings rated as clinically significant were only found in a small number of patients. However, awareness of these findings as well as their correct description in imaging reports is important in order to initiate further work-up.

Author Disclosures:

B. Hamm: Research/Grant Support; Siemens AG, Bayer AG. Shareholder; Siemens AG. **A. Baur:** Speaker; Speaker for Bayer AG.

B-0252 15:04

Mp-MRI of the prostate: anti-peristaltic hyoscine butylbromide significantly decreases motion artefacts and allows better delineation of anatomic structures

T. Ullrich, L. Schimmöller, M. Quentin, K.A. Schmaltz, C. Rubbert, C. Arsov, R. Rabenalt, P. Albers, G. Antoch; *Düsseldorf/DE*
(Tim.Ullrich@med.uni-duesseldorf.de)

Purpose: To prospectively evaluate the effect of hyoscine butylbromide (HBB) on visualisation of anatomical details and motion-related artefacts in mp-MRI of the prostate at 3.0 Tesla.

Methods and Materials: One hundred and three consecutive patients (65±10years) received high-spatial resolution axial T2-weighted TSE sequences at 3.0T without a spasmolytic agent, repeated after application of 40mg HBB and followed by routine mp-MRI. Secondary endpoints were (1) susceptibility to side effects assessed on 5-point Likert scales by two blinded readers, (2) dependence of spasmolytic effect on patients' weight, and (3) prostate volume.

Results: In 68% of the patients, HBB significantly improved the anatomic score (mean 3.4±0.9 before and 4.4±0.7 after HBB for both readers, $p<0.001$). In 67% HBB significantly enhanced the artefact score (mean 3.2±1 before and 4.2±0.8 after HBB for reader 1, $p<0.001$; 3.2±1 and 4.1±0.8 for reader 2, $p<0.001$). Subgroup analyses revealed no statistically significant difference between patients with different bodyweight or prostate volume. Inter-reader agreement was excellent ($k=0.95-0.98$).

Conclusion: Administration of anti-peristaltic medication (hyoscine butylbromide) significantly improved image quality and relevantly reduced motion-related artefacts in mp-MRI of the prostate in over 2/3 of the patients. The anti-spasmolytic effect is independent of body weight and prostate volume. No side effects of HBB were reported.

B-0253 15:12

Texture analysis of prostate MRI: utility for differentiating patients combined intraductal carcinoma of the prostate from prostate adenocarcinoma

L. Chu, R. Liu; *Chengdu/CN* (710341139@qq.com)

Purpose: To investigate texture analysis of prostate MRI for cancer differentiation between patients combined intraductal carcinoma of the prostate (IDC-P) and prostate adenocarcinoma.

Methods and Materials: 3.0T multi-parametric MRI was performed on 41 significant prostate cancer patients prior to prostatectomy. Twenty-one patients had prostate adenocarcinoma and twenty patients combined intraductal carcinoma of the prostate. Histogram-based parameters and textural features were extracted from the region of interests delineated around tumor outline on T2 and the T1-TSE DCE sequence based on pathological information and diffusion weighted imaging (DWI). The resulting data were processed with Mann-Whitney U test and binary logistic regression models. Diagnostic accuracy was assessed by area under the receiver operating characteristic curves (ROC-AUC).

Results: Texture features have no significant difference on T2WI between two groups. IDC-P showed lower Skewness ($p=0.016$) with ROC-AUC 0.724, Cluster Shade ($p=0.013$) with ROC-AUC 0.732 and higher HaraEntropy ($p=0.015$) with ROC-AUC 0.726 compared to prostate adenocarcinoma. Combining Cluster Shade and HaraEntropy yielded ROC-AUC 0.803.

Conclusion: Several texture features on DCE series appear useful for differentiating intraductal carcinoma of the prostate from prostate carcinoma and GS assessment. The role of DCE in prostate MRI diagnosis may be underestimated for various DCE features in distinct pathology types of prostate cancer.

B-0254 15:20

Cell cycle progression genomics and MRI features of prostate cancer: radiogenomic correlation and prognostic synergism

A.G. Wibmer¹, N.L. Robertson¹, B. Ehdaie¹, S. Stone², M. Brawer³, H. Hricak¹, H. Vargas¹; ¹New York, NY/US, ²Salt Lake City, UT/US, ³Irvine, CA/US
(wibmera@mskcc.org)

Purpose: To explore correlations of the Prolaris® genetic test with magnetic resonance imaging (MRI) features of prostate cancer; and to assess both tests' capabilities to predict adverse features on prostatectomy histopathology.

Methods and Materials: 122 patients undergoing prostate biopsy, Prolaris® test, and MRI from 08/2013-11/2015 were included. The Prolaris® test encompasses 46 genes associated with cell cycle progression (CCP). MRI features included PI-RADSv2 scores, extracapsular extension (ECE), and quantitative metrics (i.e. tumour length, volume, apparent diffusion coefficient). In a sub-group analysis of 42 patients (34.4%) undergoing prostatectomy, results of both tests were correlated with adverse histopathologic features, i.e. Gleason Group ≥3, ECE, and lymph node metastases.

Results: According to the American Urologic Association guidelines, 54 (44.3%) were 'low risk', 64 (52.5%) 'intermediate risk', and 4 (3.3%) 'high risk' patients. Tumour volume ($p=0.032$) and ECE ($p=0.015$) on MRI were associated with higher CCP scores, while PI-RADSv2 scores were not. In the subgroup analysis, ECE on MRI ($p=0.009$) and Prolaris® CCP scores ($p=0.017$) were independently associated with Gleason group ≥3 on surgical specimen. ECE on MRI was the only independent predictor of histopathologic ECE ($p=0.003$) and nodal metastases ($p=0.025$).

Conclusion: We found a radiogenomic association of cell cycle progression genes with tumour volume and ECE on MRI. Gene expression levels and ECE on MRI were independent predictors of adverse histopathologic tumour features. Both tests may therefore provide synergistic prognostic information.

Author Disclosures:

S. Stone: Employee; Myriad Genetics, Inc. M. Brawer: Employee; MDxHealth.

14:00 - 15:30

Room L 8

Head and Neck

SS 308

Temporal bone, temporomandibular joint and maxillofacial imaging

Moderators:

U. Lamot; Ljubljana/SI
B. Ozgen Mocan; Ankara/TR

B-0255 14:00

The diagnostic value of ultrasonography in assessing temporomandibular joint disc position

D. Talmaceanu¹, L.M. Lenghel¹, G. Baciut¹, M. Baciut¹, H. Rotar¹, N. Bolog², S. Buduru¹, L. Daniel¹, S. Ducea¹; ¹Cluj-Napoca/RO, ²Munchenstein/CH
(manu_2416@yahoo.com)

Purpose: The purpose of this study was to assess the diagnostic value of high-resolution ultrasound (US) in temporomandibular joint (TMJ) disc displacements, compared to magnetic resonance imaging (MRI).

Methods and Materials: 74 patients (with 148 TMJs) with signs and symptoms of TMJ disorders were included in this study. All patients underwent US and MRI of both TMJs 1 to 5 days after the clinical exam. MRI examinations were performed using 1.5 T equipment. Ultrasonographic examination was performed using a high-resolution (13 MHz) linear transducer. The diagnostic characteristics of the tests (sensitivity, specificity, positive and negative predictive values, accuracy and Youden Index) were computed along with 95% confidence intervals.

Results: MRI depicted 68 (45.95%) normal joints, 47 (31.76%) with disc displacement with reduction, 33 (22.3%) with disc displacement without reduction and 34 (22.97%) with degenerative changes. US detected 78 (52.7%) normal joints, 37 (25%) with disc displacement with reduction, 33 (22.3%) with disc displacement without reduction and 21 (14.19%) with degenerative changes. Compared to MRI, US showed a sensitivity of 93.1%, specificity of 87.88%, accuracy of 90.32%, a positive predictive value of 87.1% and a negative predictive value of 93.55% for overall diagnosis of disc displacement. The Youden Index was 0.81.

Conclusion: Based on the results of the study, high-resolution ultrasonography showed high sensitivity, specificity and accuracy in the diagnosis of TMJ disc displacement, being a valuable imaging technique in assessing TMJ disc position.

B-0256 14:08

Is condyle morphology a factor for anterior temporomandibular disc displacement?

I. Camlidag, A.T. Sayit, M. Elmali; *Samsun/TR* (ilkayozaydin@hotmail.com)

Purpose: To investigate morphological features of the mandibular condyle and its association with anterior temporomandibular disk displacement.

Methods and Materials: 133 patients who underwent temporomandibular MRI examination with presumed diagnosis of temporomandibular dysfunction between January 2015 and December 2016 were retrospectively involved. Patients with marked osteoarthritis, posterior disk dislocation, tumour, abscess and motion artefacts that would hamper evaluation were excluded. Three radiologists evaluated all MR images in consensus. Temporomandibular disc locations were classified as normal, anteriorly displaced with reduction (ADr) and anteriorly displaced without reduction (ADwr). Condylar shapes were classified as flat, rounded and angled on sagittal oblique images. Condyle anteroposterior width (c-APW) was measured on sagittal oblique T1-weighted images in closed-mouth positions.

Results: 106 discs were in normal position, 80 discs were ADr, 80 discs were ADwr. 93 discs were flat, 109 were rounded and 64 were angled. Mean cAPW

was 6.9 mm in normal cases, 5.9 mm in ADr and 5.8 mm in ADwr patients. c-APW were significantly smaller than normal cases in patients with ADr and ADwr ($p=0.00$); however, no significant difference was found between ADr and ADwr patients. Flat and rounded type condylar shape was equally common among normal discs; however, rounded type was common among ADr and angled type was common among ADnr. ADr cases were significantly younger from normal cases; however, no age difference was found between normal and ADwr patients and ADr-ADwr patients. ADr and ADwr were more common among female gender.

Conclusion: Mandibular condyle shape and its anteroposterior width is associated with anterior disc displacement.

B-0257 14:16

Fast and accurate diagnosis of oval or round window perilymphatic fistula on CT and MRI without contrast injection on 101 patients with surgical confirmation

A. Venkatasamy, Z. Al Oghrani, A. Charriot, C. Debry, F. Veillon; *Strasbourg/FR (aina.vnkt@gmail.com)*

Purpose: We evaluated the usefulness of temporal bone CT and/or T2W steady-state free precession sequence (SSFP) MR images for the positive diagnosis of perilymphatic fistula (PFL) of the round (RW) and/or oval windows (OW), with surgery as gold standard.

Methods and Materials: We enrolled patients who presented for a suspicion of PLF after a barotrauma, imaged by either a temporal bone CT and/or a high-resolution T2W SSFP MR sequence. All patients underwent exploratory surgery and surgical findings served as gold standard. Two radiologists, analysed the RW and OW on the side of the clinical symptoms on CT and MR.

Results: A fluid filling of the RW and OW on non-contrast CT or T2W MR was a good sign of PFL with high sensitivity and specificity. For the OW, if a fluid filling was the best sign of PFL, indirect CT signs were also helpful. The combination of CT and MR had the best sensitivity (95.6%) and specificity (100%) for the diagnosis of PFL.

Conclusion: Non-injected CT or MRI is highly reliable for the fast and accurate diagnosis of PLF. Sensitivity and specificity increased when both techniques are combined, thus we recommend starting the explorations with CT, followed by a T2W sequence on MRI.

B-0258 14:24

Effect of varying tube potentials for the assessment of cochlear implants using advanced cone-beam CT

I. Burck, I. Yel, M.H. Albrecht, S.S. Martin, J.L. Wichmann, S. Balster, T. Stöver, B. Kaltenbach, T.J. Vogl; *Frankfurt a. Main/DE (iris.burck@gmx.de)*

Purpose: To evaluate the diagnostic value of 120 kilovolt (kV) compared to 96 kV acquired cone-beam CT images in patients after cochlear implantation (CI).

Methods and Materials: In this retrospective study, 75 postoperative cone-beam CT examinations obtained with 120 kV versus standard 96 kV were independently reviewed by four radiologists. Depiction of bone structures of the otocapsule were rated including the osseous spiral lamina, inner and outer wall of the cochlea, vestibule and semicircular canals. Furthermore, metal and motion artefacts, visualisation of single electrode contacts on the CI array, as well as overall image quality were assessed. Criteria were analysed using 5-point Likert-scales. Radiation dose was measured.

Results: Visualisation of bone structures of the otocapsule (mean score, 2.2 vs 3.1; $P<0.01$), and motion artefacts (mean score, 1.7 vs 2.4; $P<0.01$) were both rated higher using 120 vs 96 kV images. In addition, overall image quality showed higher scores for 120 kV settings (mean score, 2.1 vs 2.8; $P<0.01$). No significant differences were found for subjective evaluation of metal artefacts (mean score, 2.6 vs 2.7; $P=0.33$). Radiation dose of 96 kV images was significantly lower compared to 120 kV images (0.082 mSv vs 0.141 mSv, $P<0.01$).

Conclusion: Most recent cone-beam CT at 120 kV significantly improves the depiction of temporal bone structures and single electrode contacts compared to standard kV settings.

Author Disclosures:

J.L. Wichmann: Speaker; GE Healthcare; Siemens Healthcare.

B-0259 14:32

Radiation exposure imparted during multidetector and cone-beam CT scans for the perioperative cochlear implant evaluation

N. Guberina, U. Dietrich, D. Arweiler-Harbeck, M. Forsting, A. Ringelstein; *Essen/DE*

Purpose: To examine radiation doses imparted during 128-, 256-, 384-multislice CT-scanners (MSCT) and cone-beam computed tomography (CBCT) for the perioperative cochlear implant insertion.

Methods and Materials: Radiation doses were evaluated during standardized petrous bone CT protocols at different MSCTs ((I) single-source CT-scanner Somatom Definition AS+, (II) 2nd generation of dual-source CT-scanner Somatom Definition Flash, (III) 3rd generation of dual-source CT-scanner

Somatom Force (all Siemens Healthcare GmbH, Erlangen, Germany)) and at the CBCT Ziehm Vision RFD 3D (Ziehm Imaging GmbH, Nuremberg, Germany) ((IV) (a) RFD 3D (standard modifier) and (b) RFD 3D (low-dose modifier)). Image quality was independently examined by two experienced radiologists appraising various important parameters (electrode array placement, quality control of cochlear implant surgery and evaluation of the temporal bone in case of complications) based on real patients' examinations ($n=78$). Wilcoxon signed rank test was used to determine statistically significant differences ($p<0.05$). Interrater reliability was determined by calculating k values.

Results: In MSCT setting, the following radiation doses were assessed (CTDI_w, DLP_{mean} of different positions, top, center, bottom, right and left): (I) 21.5mGy; 216mGycm; (II) 19.7mGy; 195mGycm; (III) 12.7mGy; 127mGycm; in the CBCT setting, radiation doses were distributed as follows: (IV) (a) 1.9mGy; 19.4 mGycm; (b) 1.2mGy; 12.9mGycm. Overall, image quality was evaluated as good for both, MSCT- and CBCT-examinations, with a good interrater reliability ($r = 0.81$).

Conclusion: For the perioperative examination of cochlear implant insertion CBCT bears considerable dose-saving potential. Radiation doses are considerably lower during petrous bone CT protocols in the CBCT setting compared to MSCT setting while maintaining adequate image quality.

B-0260 14:40

Diagnostic performance of digital tomosynthesis as compared to conventional radiography in evaluation of craniovertebral junction

P. Kala, R. Avantsa, G. Gowda; *Bangalore/IN (prachi_kala@yahoo.com)*

Purpose: Overlying bony structures limit the assessment of CVJ anatomy. CT provides more precise information but with potential radiation hazards and high costs. Digital tomosynthesis (DTS) improves visualization by removing visual clutter of overlying anatomy. Purpose of the study is to assess the diagnostic performance of DTS in evaluation of CVJ.

Methods and Materials: In an approved prospective study, CT, conventional radiography and DTS were performed in 30 controls and 26 patients with CVJ pathology. Standard radiographs and DTS were performed on GE Discovery XR650 system with "VolumeRAD™". An automatic exposure control technique was used. Image quality was scored for conspicuity and pathology detection by two independent radiologists with experience of more than 3yrs in DT. Radiation dose of the all exams was compared.

Results: DTS was superior to radiography with sharper delineation of anatomy and detection of pathology of occipital condyles (89.6%), odontoid process (95%), C1 (86%) and C2 (100%) vertebrae in the coronal and atlanto-axial junction (92.4%) and dento-axial distance(92.4%) in sagittal slices. The results were found comparable to CT for the same. There was gross reduction in the radiation dose compared to CT (from 28 mGy to 3 mGy), and no significant rise compared to plain radiographs (from <2 mGy to 4 mGy).

Conclusion: DTS improved evaluation of CVJ anatomy. It has the potential to cut in number of views required, providing rapid diagnosis and savings on further imaging, radiation exposure, imaging costs that could mean reducing anxiety and discomfort for the patient.

Author Disclosures:

P. Kala: Research/Grant Support; GE Healthcare. G. Gowda: Research/Grant Support; GE Healthcare.

B-0261 14:48

Thesphenoid ostium and its relationship to other endoscopic landmarks in acromegaly: a CT-based morphological study

V. Hegde¹, N. Rajgopalan², S. Thakar²; ¹Chennai/IN, ²Bangalore/IN (verahegde@gmail.com)

Purpose: Acromegalic pituitary adenomas are known to cause disproportionate enlargement of the craniofacial and skull base structures (both soft tissue and bony) and thus complicate the trans-sphenoidal surgical approach. Morphological assessment of various landmarks, relevant to the endoscopic pituitary surgeon was done on thin section CT-PNS in operated cases of pituitary adenoma. The data was analysed with respect to growth hormone (GH) levels.

Methods and Materials: The medical records, thin section (1mm) CT-PNS images and their 2D reformations of 15 acromegalic patients (GH) were compared with 15 non-acromegalic patients (n-GH). Various morphological data (size of sphenoid ostium (SO), displacement of SO, depth of sphenoid and sella from piriform aperture, turbinates, sella and inter-carotid distance) and anatomical variations (middle turbinate, sphenoid sinus) were documented and compared between the two groups and in correlation with serum growth hormone levels. Image analysis was done using ImageJ software (ver 1.49).

Results: The ostium size in GH group was significantly larger than n-GH group ($p=0.005$). A moderate trend for an upward ($r=0.45$) and lateral ($r=0.34$) displacement of the SO in the sphenoid face was observed in patients with increasing GH values. The width of the sellar floor, sphenoid rostrum and inter-carotid distance positively correlated with GH levels ($r = 0.40, 0.43, 0.35$ respectively).

Conclusion: The anatomical distortion in acromegalic pituitary adenoma poses a challenge to endoscopic pituitary surgeon. Prior knowledge and anticipation may prevent failures and complications.

B-0262 14:56

Comparing subjective and objective image quality at two different radiation exposure ranges of the paranasal sinus CT examinations using a volumetric 320-row detector CT system

M. Kantarci, A. Levent, S. Eren, B. Pirimoglu; *Erzurum/TR (akkanrad@hotmail.com)*

Purpose: To evaluate image quality of protocol including 135 kVp, 5 mAs and 80 kVp, 5 mAs in the paranasal sinus CT examinations using single volumetric 320-row multidetector CT technique.

Methods and Materials: From September to December 2016, both of our control group including 135 kVp and 5 mAs and our study group including 80 kVp and 5 mAs paranasal CT protocols were simultaneously performed on 40 patients using single volumetric 320-row multidetector CT device. Image quality for bony structures, air-filled structures and soft tissues were independently assessed for each group by three blinded observers using a 3-point grading scale.

Results: The effective radiation dose calculated for the control group scans was 0.037 ± 0.003 mSv. But, it was 0.0099 ± 0.001 mSv for the study group scans. The effective radiation dose of study group was statistically significantly lower than control group ($p < 0.001$). Despite significant lowering of the radiation doses, image qualities were sufficient for evaluating all the bony structures, air-filled structures and soft tissues except for eye muscle, retrobulbar fat and eye bulb.

Conclusion: Our results present that our protocols for study and control group provide significant dose reduction without the loss of diagnostic image quality for paranasal sinus CT. Paranasal sinus CT imaging can be performed at very low radiation exposure maintaining high image quality using a single volume 320-row detector CT device using 135 kVp and 5 mAs.

B-0263 15:04

"How much radiation do my baby get sick?" Answering to worried moms about dental radiology in childhood

F. Testa, N. Angarano, M. Marchisio, R. Olivero, D. Fraire, V. Verna; *Bra/IT (frates@gmail.com)*

Purpose: To evaluate the impact on the pediatric population of radiological examinations such as OPT and cephalometry and to provide practical answers to parents often in trouble about radiation risk.

Methods and Materials: We considered a series of 345 OPTs and 165 cephalometries on children 4-12 yo, calculating the effective dose using an anthropomorphic phantom, according to MonteCarlo algorithms. We estimated the exposure rate of the pediatric population of our country. For each procedure, we optimized parameters in order to dose and image quality.

Results: OPTs not rightly optimized administered a cumulative effective dose of 34.368 mSv, that could be reduced of an amount of 4.096 mSv, (-11.9%); unoptimized cephalometries administered a cumulative dose of 14.15 mSv, that could be reduced of 0.49 mSv, (-3.46%). We calculated an Odds Ratio to undergo OPTs between children 0-12 and adults as 2.24 ($p < 0.0000$) ad to undergo to cephalometries as 15.08 ($p < 0.0000$). We estimated 31.5% of the children of our country undergo to an OPT during their childhood in public health service; nowadays it is impossible to estimate how many children are studied at private dental practice.

Conclusion: Empirically, considering an average annual Italian environmental dose of 3.3 mSv, an optimized cephalometry is estimated equal to about one week of environmental exposure, but it can reach the three months if not optimized; an OPT equals one month if optimized but until one year if unoptimized. Therefore, optimization is a must and, if implemented, the parents can be quietly relaxed.

B-0264 15:12

High-resolution dental MRI for planning palatal graft surgery: a clinical pilot study

T. Hilgenfeld, T. Kästel, A. Heil, P. Rammelsberg, S. Heiland, M. Bendszus, F.S. Schwinding; *Heidelberg/DE (tim.hilgenfeld@med.uni-heidelberg.de)*

Purpose: Because previous studies have revealed high variability of palatal masticatory mucosa thickness, preoperative evaluation before tissue graft harvesting is recommended e.g. by cone beam computed tomography. To evaluate whether high-resolution, non-contrast-enhanced dental MRI can be used for accurate determination of palatal masticatory mucosa thickness (PMMT) and to locate the greater palatal artery (GPA).

Methods and Materials: Two independent raters measured PMMT by use of dental MRI in 180 positions for five human volunteers. For comparison, clinical bone sounding was performed. To ensure identical measurement positions in MRI and bone sounding, tooth-supported resin splints were fabricated.

The GPA was identified in two MRI sequences. Intra- and inter-observer agreement for MRI measurements and agreement between MRI and bone sounding were calculated by using the intra-class correlation coefficient (ICC) and Cohen's kappa (κ).

Results: Reliability of dental MRI measurements was high (intra-observer ICC 0.962; inter-observer ICC 0.959). Agreement of MRI measurements with bone sounding was moderate (ICC 0.744) and the GPA could be identified in 85% of measurement points. Good intra-observer agreement was observed for GPA identification (κ 0.778).

Conclusion: PMMT thickness measured by high-resolution, non-contrast-enhanced dental MRI is comparable with that obtained by bone sounding. Dental MRI enables reliable, non-invasive, and radiation-free planning of palatal tissue harvesting and can also be used for precise location of the GPA, which might help reduce complications during surgery.

B-0265 15:20

MRI profile of sinonasal mucosal melanoma: analysis of 46 cases

E. Tononcelli, L. Calabretta, M. Ravanelli, D. Lombardi, D. Farina, R. Maroldi; *Brescia/IT (tononcelli.elena@gmail.com)*

Purpose: To assess the MR imaging profile of sinonasal mucosal melanoma (SMM) and to compare it with intestinal-type adenocarcinoma (ITAC) and squamous cell carcinoma (SCC).

Methods and Materials: Retrospective analysis of MRI signal pattern was performed in 46 patients affected by SMM, correlating with histology on surgical specimen in 41/46. In all lesions, quantitative assessment was performed on T1 sequences -normalising tumour signal to a pterygoid muscle- and on the ADC map, comparing findings with 28 ITAC and 9 SCC. Enhancement homogeneity and bone changes in SMM were qualitatively assessed. Statistical analysis was performed applying Student's T-test, exact-Fischer test and ANOVA-test.

Results: Statistically significant difference was seen between normalised T1 signal of amelanotic (avg.0.88) and melanotic (avg.1.23) SMM and between each subtype and SCC (avg.1.05) and ITAC (avg.1.06) ($p < 0.05$). No significant difference was seen between normalised T1-signal of ITAC and SCC. ANOVA with pairwise comparison showed significant difference between the ADC value of SMM (avg.0.875 mm²/s), ITAC (avg.1.125 mm²/s) and SCC (avg.0.941 mm²/s). Inhomogeneous enhancement was significantly more frequent in larger SMM ($p < 0.05$). Bone remodelling was significantly more frequent in primary than in recurrent SMM ($p < 0.05$), associated with focal erosion in primary and extensive erosion in recurrent SMM.

Conclusion: SMM is a rare and highly aggressive histotype displaying some specific MR signs that may differentiate it from the most common ITAC and SCC. MRI pattern is related to histology, particularly in the melanotic type.

14:00 - 15:30

Room E1

Breast

SS 302

Breast ultrasound

Moderators:

G. Esen; Istanbul/TR
M.A. Marino; Messina/IT

B-0266 14:00

Breast lesions characterisation: prospective comparison of strain and shear wave elastography as additional tool to BIRADS classification

V. De Soccio, V. Cantisani, G. Alagna, M. Di Segni, V. Forte, N. Di Leo, S. La Morte, F. D'Ambrosio; *Rome/IT*

Purpose: To evaluate the diagnostic performance of strain elastography (SE) and shear-wave elastography (SWE), in combination with US, to improve the differentiation of benign and malignant breast lesions

Methods and Materials: 130 histopathologically proven breast lesions were prospectively evaluated by using US, SE and SWE. Each lesion was classified according to the BIRADS lexicon and SE semi-quantitative dynamic features (strain ratio), and SWE through quantitative techniques (expressed in kPa). Histology was used as reference standard. 2x2 contingency tables and ROC curve analysis were used to assess the diagnostic performance and Pearson's χ^2 test was used to assess the significance of differences, with $p = 0.05$ significance threshold

Results: Histological examination revealed 83 benign and 47 malignant breast lesions. US showed 80% sensitivity and 70% specificity. SWE kPa yielded a sensitivity of 72%, a specificity of 66% and ROC area of 0.691. US plus SF showed a sensitivity of 88%, a specificity of 76.6% and ROC area of 0.823. US plus SWE m/s had a sensitivity of 74%, a specificity of 76% and ROC AUC of 0.750.

Conclusion: Our experience suggests that SE and SWE in combination with B-mode US, are valid tools to improve BIRADS category assessment and the differentiation of benign from malignant breast lesions. According to our results, SE was more accurate than SWE.

Author Disclosures:

V. Cantisani: Speaker; Toshiba, Samsung and Bracco.

B-0267 14:08

Meta-analysis of 3 methods to analyse breast strain elastography

R.G. Barr¹, A. DeSilvestri², V. Scotti², F. Manzoni², C. Tinelli²;

¹Rootstown, OH/US, ²Pavia/IT (rgbarr@zoominternet.net)

Purpose: There are 3 methods of interpreting strain breast elastography; E/B ratio, 5-point color scale and strain ratio. This meta-analysis was performed to determine if one methods was superior.

Methods and Materials: A systematic search of the medical literature was performed on July 2017. The following terms were used for the bibliographic strategy: Breast Neoplasm, Ultrasonography, mammary, elastic imaging techniques, strain elastography, real-time elastography, strain imaging, sensitivity, and specificity. Studies eligible for inclusion had biopsy proven results, utilised either E/B, 5-P, or SR and had at least 50 cases.

Results: 505 records were retrieved (220 after duplicates removal); of them 60 full-text were carefully examined and 46 papers were included in the metanalysis, publication year ranged from 2007 and 2017 (median year 2012). Quality of studies was generally high. Mean age of woman was 48 years; 12398 lesions (4242 malignant) were analysed. For the 5p methods the sens was 77%, spec 87%, LRP 5.3, LRN 0.24. For the strain ratio the sens was 87%, spec 81%, LRP 4.8, and LRN 0.16. For the E/B the sens was 96%, spec 87%, LRP 7.6 and LRN 0.03.

Conclusion: Of the three methods the E/B ratio has the highest sensitivity and E/B and 5P have the highest spec. With a LRN of 0.03 the E/B ratio can conclusively exclude a malignancy.

Author Disclosures:

R.G. Barr: Advisory Board; Bracco Diagnostic; Lantheus Medical. Equipment Support Recipient; Philips Ultrasound; Siemens Ultrasound; GE Ultrasound; SuperSonic Imagine. Speaker; Philips Ultrasound; Bracco Diagnostic.

B-0268 14:16

Anatomic factors affecting shear wave elastography of malignant and benign breast lesions

L. Plonski, E. Carmon, E. Chernovsky, G. Zeltzer, T. Sella; *Jerusalem/IL* (tamarse@hadassah.org.il)

Purpose: Shearwave elastography (SWE) characterizes breast lesion stiffness by measuring waves propagating through the surrounding tissue. The purpose of this study was to evaluate how anatomic factors of the breast affect the performance of SWE.

Methods and Materials: SWE was measured in 349 breast masses undergoing biopsy. Variables analyzed were density of the surrounding breast tissue (fatty n=130 or dense n=219) and depth of the lesion (superficial n=79, mid-breast n=137 or deep n=117). Data analysis evaluated the ability of SWE to differentiate benign from malignant as compared to histology. Statistical analysis included ROC curves, student's T test and the Kruskal-Wallis test.

Results: The optimal cutoff point to distinguish benign from malignant was 58.5kPa (AUC= 0.923) in dense tissue and 60.2kPa (AUC =0.932) in fatty tissue. Average Emax was higher for malignant masses: 144.4 kPa vs 34.8 kPa in dense tissue and 134.3 kPa vs 34.2 kPa in fatty tissue (p<0.001). There was no difference in PPV and NPV of SWE for dense vs fatty tissue (70.7% and 94.9% vs 87% and 90.2%). In all three depth groups ave Emax was higher for malignant compared to benign lesions (superficial 152.1 kPa vs 31.8 kPa, mid 129.1 kPa vs 30.6 kPa, deep 143.4 kPa vs 43kPa; p<0.001). PPV and NPV of SWE in superficial lesions were 72.4% and 93.9%, at mid-depth 81% and 92.4% and for deep lesions 78.1% and 94.3%.

Conclusion: SWE is not significantly affected by anatomic factors of the breast, differentiating malignant from benign lesions with high accuracy.

B-0269 14:24

Breast sonoelastography: comparison of the accuracy of the computer assisted diagnosis (CAD) classifier system using two values of different cut-off values with the visual classifier

E.F. Fleury¹, A.C. Gianini¹, V.J. Ayres², L. Ramalho¹, J. Sousa Neto¹, K.D. Marcomini³; ¹São Paulo/BR, ²Santo André/BR, ³São Carlos/BR (edulfleury@hotmail.com)

Purpose: To evaluate the diagnostic accuracy of a CAD system to classify breast masses by elastography, using cut-off values for 75% and 80% stiffness areas, comparing with the results of the visual analysis.

Methods and Materials: Prospective evaluations were performed in accordance to local ethical committee. It was included 85 consecutive breast masses evaluated by strain elastography, of which 33 were malignant and 52 were benign. The masses were classified according to stiffness: 1. Soft; 2.

Intermediate; 3. Rigid. The rigid lesions (3) were considered suspicious. First, the visual classification was performed. To evaluate the CAD system, the radiologist needs to delimit the edges of the lesion so that the computer automatically classifies the lesion. For classification with the CAD system the radiologist needs to delineate the mass margins so that the computer automatically classifies the lesion. For classification, the CAD system values the percentage of rigid area of the mass. Cutting values of 75% rigidity (CAD75) and 80% rigidity (CAD80) were compared. The ROC curves for the 3 classifiers were determined.

Results: The sensitivity and specificity obtained for each classifier were as follows: CAD75 90.9% and 67.3% respectively, CAD80 90.9% and 65.4%, and VISUAL 87.9% and 63.5%. The ROC curves were as follows: 0.837, 0.832, 0.817. There was no statistically significant difference for the ROC curves, however the CAD75 was the classifier that presented the best ROC curve.

Conclusion: Our results show that CAD using 75% cutoff for rigid area is the classifier with the best diagnostic accuracy.

B-0270 14:32

Role of elastography in the characterisation of subcentimeter breast lesions

S. Sampangi, S. Shivalingappa, M. Ashok Kumar, I. Desai, A. Kesari, D. Basavalingu, A. Verma, K. Kallur, P. Asokan; *Bangalore/IN* (dr_sudhakar79@yahoo.com)

Purpose: To characterize subcentimeter breast lesions on elastography and to determine its utility for differentiating benign from malignant lesions.

Methods and Materials: 60 patients aged between 25 to 60 years and a total of 65 subcentimeter isoechoic or hypoechoic breast lesions were evaluated with elastography (Siemens Acuson S2000) between 2014 to 2016. Elastography was performed using Virtual Touch imaging (VTI) and Virtual Touch quantification (VTQ) applications. E/B ratio (Elastography/B-mode size ratio) was recorded from the VTI image and an average VTQ value (average of 5 measurements in m/s) were obtained. All the lesions underwent percutaneous ultrasound guided core biopsy.

Results: Of the 65 lesions biopsied, 41 lesions were malignant and 24 lesions were benign. The mean E/B ratio of malignant masses (1.28± 0.21) was significantly higher than that of benign masses (1.07 ± 0.09), with p value less than 0.001. There was no statistically significant difference between the mean VTQ value of malignant masses (2.71 ± 0.75) and benign masses (2.79 ± 1.03), with p value more than 0.05. With the use of ROC curve, the cut off E/B ratio was estimated to be 1.2 with sensitivity of 73.2%, specificity of 82.7%, and accuracy of 79.2%.

Conclusion: Ultrasound elastography (VTI and VTQ) is a noninvasive technique to characterize tissue stiffness. E/B ratio of subcentimeter breast lesions can be used for differentiating between benign and malignant breast lesions and for potentially correlating with tumor desmoplastic reaction.

B-0271 14:40

Chemoresponse assessment in locally advanced breast cancer patients: comparison of grey scale ultrasound and ultrasound elastography

A. Katyan, M.K. Mittal, C. Mani, A.K. Mandal, S.B. Grover; *New Delhi/IN* (amitkatyan@icloud.com)

Purpose: The study was conducted to compare the role of grey scale ultrasound and strain wave elastography in evaluating the response to neo-adjuvant chemotherapy (NACT) in patients with locally advanced breast cancer (LABC).

Methods and Materials: In this IRB approved study, eighty three patients of LABC were investigated with greyscale ultrasound and strain wave elastography. Women receiving NACT had the affected breast scanned by greyscale ultrasound and elastography before each cycle of chemotherapy and immediately before surgery. Changes in ultrasound size and elastographic parameters (size ratio, strain ratio) were documented and then compared to clinical and pathologic tumour response as evaluated after mastectomy.

Results: Mean strain ratio and mean size ratio for responders was significantly lower in responders in comparison to non-responders. Elastographic strain ratio parameters demonstrated high sensitivity and specificity for determining response even after the first cycle of chemotherapy. Strain wave elastography was found to detect treatment response earlier as compared to greyscale ultrasound in patients of LABC receiving NACT.

Conclusion: Tumour strain ratio was found to be the best predictor of treatment response in patients of LABC. Elastographic parameters showed significant change in its parameters earlier as compared to change in greyscale ultrasound size measurements. Serial imaging with elastography has the potential to predict treatment response early during the course of NACT, which may prove vital in management of patients with breast cancer.

B-0272 14:48

Can a hyperechogenic breast lesion be malignant?

E. Horvath, E.H. [Castillo Balladarez](#), M.F. Pizzolon, C. Silva, M. Gallegos, M.A. Pinochet, M. Galleguillos, M. Uchida, P. Gonzalez; *Santiago/CL (eliette88@hotmail.com)*

Purpose: Hyperechogenic breast lesions have been described as generally benign and are rarely biopsied. The aim of this work was to evaluate the frequency of malignant hyperechogenic breast lesions, describe their imaging findings and histopathological characteristics.

Methods and Materials: IRB approved, retrospective, descriptive case series. Biopsied hyperechogenic lesions were selected from a database of 3,394 consecutive US-guided breast Core biopsies (1,020 malignant, 299 high-risk and 2,075 benign lesions) performed between 2006 and 2016. Any lesion that presented greater echogenicity than subcutaneous cellular tissue of more than 90% of its volume, was considered hyperechogenic. Demographical data, US and histopathological characteristics were recorded.

Results: In total 27 (1,08%) lesions biopsied were hyperechogenic: 21 (57%) of them had benign results. Sixteen patients (mean age: 52 years; range: 26-80) had hyperechogenic cancers, representing 1,5% (16/1,020) of all malignancies: 1 CDIS and 15 invasive carcinomas (81% ductal and 19% lobular histology). Mean size = 2 cm, range: 7-30 mm. All of them exhibited a small central hypoechoic foci and were partially or completely surrounded by fatty tissue. Shape, margins, orientation and vascular architecture were highly suggestive of malignancy on US, mammogram and MRI (features BI-RADS 4 and 5). In histopathological exam these cancers were surrounded by adipose tissue (not by fibroglandular tissue); also, they presented a hypocellular collagenous center and were hypercellular on its periphery, intermixing with fatty tissue, fibrous tracts and collagen.

Conclusion: Hyperechogenic cancers are very rare (less than 2% of breast cancers), but it is important to recognise them to avoid misdiagnosis.

B-0273 14:56

Texture feature analysis can support breast lesions identification and characterisation in images acquired by automated breast ultrasound systems

M. [Marcon](#), A. Becker, N. Berger, M. Wurnig, M. Wagner, T. Frauenfelder, A. Boss; *Zurich/CH (Magda.Marcon@usz.ch)*

Purpose: To demonstrate how texture feature analysis(TA) can support the management of breast imaging findings in automated breast ultrasound imaging.

Methods and Materials: In this prospective IRB-approved study 644 images acquired with an automated breast ultrasound system(ABUS) in 24 consecutive patients with biopsy-proven malignancy(230 images from cancer, 53 glandular tissue, 53 fat) and in 21 with fibroadenoma with follow-up longer than 18 months or biopsy(211 images from fibroadenoma, 49 glandular tissue, 48 fat) were evaluated. After ROI placement, TA was performed applying 19 features computed from histogram and higher-order features for differentiation of cancer, fibroadenoma, glandular tissue and fat.ANOVA was used for the evaluation of differences among the four categories. In case of significant differences, ROC curve calculation and logistic regression analysis were performed to determine sensitivity and specificity. Bonferroni correction was applied using a p-value<0.05.

Results: Entropy values were different among the four categories(mean+/-sd, cancer 5.27+/-0.40, fibroadenoma 5.67+/-0.15, glandular tissue 5.73+/-0.30, fat 5.56+/-0.23, p<0.00001) and the ROC curve obtained comparing malignant lesions versus other findings had AUC=0.84(C.I. 0.81-0.88); using a cut-off value of 5.48 a sensitivity of 86% and specificity of 70% was obtained. Using contrast and energy_mean to differentiate lesions (cancer and fibroadenoma) from normal tissue (fat and glandular tissue) AUC=0.86(C.I.0.83-0.89) and AUC=0.88(C.I.0.85-0.91) were obtained, respectively, and binary logistic regression of the two variables results in AUC=0.92(C.I.0.89-0.94).

Conclusion: Texture feature analysis has the potential to support the differentiation between breast lesions and normal tissue as well as to distinguish cancer from fibroadenoma in automated breast ultrasound imaging.

B-0274 15:04

Does breast cancer subtype affect the diagnostic performance of axillary ultrasound for nodal staging in breast cancer patients

M.L.G. Vane¹, T. [van Niinatten](#)¹, P.J. Nelemans¹, M.B. Lobbes¹, L. van Roozendaal², L. Kooreman¹, K. Keymeulen¹, M. Smidt¹, R. Schipper¹; *1Maastricht/NL, 2Heerlen/NL (thiemovnn@gmail.com)*

Purpose: Physical examination followed by axillary ultrasound is routinely performed to assess preoperative axillary lymph node status in breast cancer patients. However, the accuracy of axillary ultrasound to assess nodal status for different subtypes of breast cancer is unknown. The aim of this study was to determine whether the diagnostic performance of axillary ultrasound is affected by breast cancer subtype.

Methods and Materials: All newly diagnosed breast cancer patients between 2008 and 2016 in MUMC+ with axillary ultrasound prior to axillary surgery were retrospectively included. Diagnostic performance of the axillary ultrasound (sensitivity, specificity, positive predictive value (PPV), negative predictive value (NPV), false-negative rate (FNR) and accuracy) was determined for each of the following subtypes:ER+PR+HER2-, HER2+, and ER-PR-HER2-. Histopathology of axillary surgery specimens served as gold standard. Differences in diagnostic performance between breast cancer subtypes were calculated using Chi-squared test.

Results: A total of 1,129 breast cancer cases were included. Most common subtype was ER+PR+HER2- with 76.0% (858), followed by 13.3% in HER2+ (150) and 10.7% in ER-PR-HER2- tumors (121). The difference in NPV was significant between ER-PR-HER2- and HER2+ tumors (90.2% versus 80.6%, p=0.048) and HER2+ and ER+PR+HER2- tumors (90.2% versus 87.2%, p=0.04). Sensitivity, specificity, NPV, FNR and accuracy did not significantly differ per breast cancer subtype.

Conclusion: The NPV of axillary ultrasound differed per molecular subtype, and was highest in ER-PR-HER2- tumors. The clinical consequence of the difference in NPV between breast cancer subtypes is unknown. Other parameters of diagnostic performance did not significantly differ per breast cancer subtype.

B-0275 15:12

Can documenting the number of abnormal nodes at axillary ultrasound accurately predict axillary nodal burden

N. [Sharma](#)¹, M. Wallis², R.G. Newcombe³, S. Puri⁴, M. Al-Attar⁵, S. Pascaline⁶, M. Hajaj⁵, B. Elsberger⁷, A. Goyal⁴; ¹Leeds/UK, ²Cambridge/UK, ³Cardiff/UK, ⁴Derby/UK, ⁵Leicester/UK, ⁶Kettering/UK, ⁷Dundee/UK (Nisha.sharma2@nhs.net)

Purpose: The aim was to determine if for women with needle biopsy-proven positive node on preoperative axillary ultrasound (AUS), the number of abnormal nodes seen on AUS is a predictor of number of positive nodes at histology.

Methods and Materials: This prospective multicentre cohort study included consecutive patients with early breast cancer who had needle biopsy-proven positive node on AUS and underwent axillary lymph node clearance (ALND) between October2015 and July 2016. The number of abnormal nodes at preoperative AUS was recorded by the scanning radiologist/radiographer.

Results: 123 patients were included in the study. Median age of the women was 62 (range 30 to 93) years. 54/123 (44%) women had one abnormal node while 69 (56%) had multiple abnormal nodes on AUS. 40/123 (33%) women had two or less nodes with metastases at histology after ALND. Tumours 20 mm or less (P < 0.001) and one abnormal node on AUS (P < 0.001) were associated with two or less nodes with metastases at ALND. Both remained significant in logistic regression analysis. The likelihood of at least three metastases based on the combination of these two factors had 95% sensitivity (79 of 83), 35% specificity (14 of 40), negative predictive value of 78% (14 of 18) and positive predictive value of 75% (79 of 105).

Conclusion: Women with needle biopsy-proven positive nodes, around 3 in 4 women (78%) with invasive tumour size 2cm or less and one abnormal node on AUS have 2 or less positive nodes at ALND. These women are overtreated by upfront ALND and can be offered SNB.

B-0276 15:20

Specification of breast masses according to BI-RADS classification enforced with contrast-enhanced ultrasound

E. [Peniaeva](#)¹, A. Sencha², Y. Patrunov¹, E. Sencha²; ¹Yaroslavl/RU, ²Moscow/RU (Ellapenyeva@mail.ru)

Purpose: To define the diagnostic value of contrast-enhanced ultrasound (CEUS) in specification of BI-RADS category of breast lesions.

Methods and Materials: CEUS with intravenous bolus administration of 2.4ml of Sonovue® was performed in 67 patients of the age 28-67 years. Linear 7-15MHz probes with specialised "contrast" option were used for CEUS. Core needle biopsy after CEUS diagnosed 28 carcinomas and 39 benign lesions.

Results: The following patterns were registered. CEUS BI-RADS 1 - no change. CEUS BI-RADS 2 (conferred 30 benign lesions) - slow or synchronous isoenhancement without perfusion defects and feeding vessels, slow or synchronous hypoenhancement with distinct regular margins without feeding vessels, absence of contrast enhancement of the lesion with distinct regular margins. CEUS BI-RADS 3 (6 benign lesions and 2 carcinomas) - synchronous hyperenhancement without perfusion defects and feeding vessels that does not exceed the grayscale size of the lesion. CEUS BI-RADS 4 (3 benign lesions and 12 carcinomas) - fast hyperenhancement of irregular shape that exceeds the grayscale size. CEUS BI-RADS 5 (14 breast carcinomas) - fast hyperenhancement of regular/irregular shape with perfusion defects that does not exceed or exceeds the grayscale size, or hyper/isoenhancement with/without perfusion defects with feeding vessels. US BI-RADS scale had the sensitivity of 75%, specificity 82.4%, diagnostic accuracy 79.1% in diagnosis of

breast carcinoma. CEUS BI-RADS scale improved the sensitivity up to 92.8%, specificity - 92.3%, diagnostic accuracy - 92.5%.

Conclusion: CEUS improves the diagnostic value of ultrasound in differentiation of breast lesions.

14:00 - 15:30

Room E2

Neuro

SS 311

Neuroinflammation and neuroinfection

Moderators:

A. Rovira-Cañellas; Barcelona/ES

R. Woitek; Vienna/AT

B-0277 14:00

Histogram analysis of ADC maps and FLAIR MR imaging can predict active demyelination in multiple sclerosis

K.Y. Wang, J. Carlton, D. Guffey, F.E. [Moron](#); Houston, TX/US

(femoron@gmail.com)

Purpose: The aim is to evaluate the discriminatory power of apparent diffusion coefficient (ADC) values and FLAIR signal intensity histogram analysis in differentiating new acute demyelinating lesions (ADLs) and new non-acutely demyelinating lesions (N-ADLs) in multiple sclerosis (MS).

Methods and Materials: A total of 64 lesions from 32 MRIs of patients with clinically definite MS were analyzed. A new ADL was defined as an enhancing lesion. A new N-ADL was defined as a new non-enhancing lesion not present on a prior comparison MRI performed <1 year. Discrete lesions were selected for optimal region-of-interest (ROI) placement. Manual ROIs were drawn on FLAIR and ADC map by maximizing lesion coverage while avoiding volume averaging. Mean, max, min, 10th, 25th, 50th, 75th, and 90th percentile values were calculated. A second ROI was drawn in the contralateral normal-appearing white matter (WM). A ratio was obtained by dividing lesion value by contralateral WM value. Wilcoxon rank-sum test was used to compare ratios between ADL and N-ADL. Logistic regression was used to assess associations between FLAIR ratios and new ADLs. Receiver operating curve analysis evaluated discriminatory power of ADC map and FLAIR ratios. A $p < 0.05$ was considered statistically significant.

Results: The data skewness ranged from 1.11 (ratio of 10th percentile diffusivity) to -0.34 (ratio of min FLAIR value). The FLAIR ratios of all descriptive statistics (mean, max, min, and percentiles) were significantly higher for ADLs compared to N-ADLs ($p = 0.0002$ to < 0.0001). No significant associations between FLAIR ratios and ADLs were noted for all descriptive statistics with logistic regression. The diffusivity ratios of all descriptive statistics (mean, max, min, and percentiles) were also significantly higher for ADLs compared to N-ADLs ($p = 0.0309$ to 0.0117). ROC analysis of FLAIR demonstrated an area under the curve ranging from 0.792 (max ratio) to 0.833 (25th percentile ratio). A cutoff of 1.471 for the 25th percentile FLAIR ratio provides a 0.86 sensitivity, 0.70 specificity, and 0.81 accuracy. ROC analysis of ADC demonstrated an area under the curve ranging from 0.669 (min ratio) to 0.698 (90th percentile ratio). A cutoff of 1.543 for the 90th percentile ADC ratio provides a 0.75 sensitivity, 0.70 specificity, and 0.73 accuracy.

Conclusion: The signal intensity of FLAIR and diffusivity on ADC maps may have the potential to discriminate between new ADL and N-ADL in MS.

B-0278 14:08

Proton magnetic resonance spectroscopy (¹H-MRS) of the brain in patients with tick-borne encephalitis

R. [Zawadzki](#)¹, B. Kubas¹, M. Hladuński¹, J. Zajkowska¹, O. Zajkowska², D. Jurgilewicz¹, A. Garkowski¹, S. Pancewicz¹, U. Lebkowska¹; ¹Białystok/PL, ²Warsaw/PL (zaw.radoslaw@gmail.com)

Purpose: To study the metabolic changes of the brain by ¹H-magnetic resonance spectroscopy (¹H-MRS) in patients with tick-borne encephalitis (TBE).

Methods and Materials: 22 patients diagnosed with TBE and 24 healthy controls have been enrolled. All of them underwent routine magnetic resonance imaging (MRI) protocol using 3.0 T MRI scanner, which included T1-weighted images, T2-weighted images, fluid-attenuated inversion recovery (FLAIR), and diffusion weighted images (DWI). ¹H-MRS examinations were performed with the following acquisition parameters: repetition time (TR), 2000 ms; echo time (TE), 135 ms; number of excitations, 128. Single voxels were manually located bilaterally in the basal ganglia, thalami and in the hemispheres of cerebellum. Metabolites to creatine (Cr) ratios were analysed. The following peaks were assessed: N-acetylaspartate (NAA), choline-containing compounds (Cho), and glutamate/glutamine/γ-aminobutyric acid complex (Glx).

Results: Compared to controls we found statistically significant decrease of the NAA/Cr ratio bilaterally in the right and left thalamus ($p = 0.0002$ and $p = 0.0017$, respectively) and statistically significant increase of the Cho/Cr ratio in the right and left thalamus ($p = 0.03$ and $p = 0.0065$, respectively). We also observed statistically significant increase of the Cho/Cr ratio in the left hemisphere of cerebellum ($p = 0.04$). There were no statistically significant brain metabolite alterations within other evaluated areas.

Conclusion: A significant reduction in NAA/Cr ratio and statistically significant increase of the Cho/Cr ratio in comparison with the control group suggests the presence of neuronal damage in patients with TBE.

B-0279 14:16

Altered hippocampal GABA and glutamate levels and functional connectivity in multiple sclerosis

X. [Yin](#)¹, F. Gao², G. Wang²; ¹Chongqing/CN, ²Jinan/CN (xuntaoyin@gmail.com)

Purpose: There is growing evidence for dysfunctional glutamatergic excitation and/or gamma-aminobutyric acid (GABA)ergic inhibition in patients with multiple sclerosis (MS). Cognitive impairment may occur during the early stages of MS and hippocampal abnormalities have been suggested as biomarkers. However, researchers have not clearly determined whether changes in hippocampal GABA and glutamate (Glu) levels are associated with cognitive impairment and aberrant neural activity in patients with MS.

Methods and Materials: We used magnetic resonance spectroscopy to measure GABA and Glu levels in the left hippocampal region of 29 patients with relapsing-remitting MS and 29 healthy controls (HCs). Resting-state functional connectivity (FC) with the hippocampus was also examined. Partial correlation analyses of the cognitive performance, hippocampal GABA+ and Glu levels and FC strengths, were performed separately for patients with MS and HCs, while controlling for age and gender.

Results: Compared to HCs, patients exhibited significantly lower GABA+ and Glu levels, which were associated with verbal and visuospatial memory deficits, respectively. Patients also showed decreased FC strengths between the hippocampus and several cortical regions, which are located within the default mode network. Moreover, hippocampal GABA+ levels correlated with the FC strengths in HCs but not in patients with MS.

Conclusion: This study describes a novel method for investigating the complex relationships among excitatory/inhibitory neurotransmitters, brain connectivity and cognition in health and disease. Strategies that modulate Glu and GABA neurotransmission may represent new therapeutic treatments for patients with MS.

B-0281 14:24

Advanced MRI assessment during dendritic cell immunotherapy

A. [Gioppo](#), M. Eoli, D. Aquino, G. Finocchiaro, M.G. Bruzzzone, V. Cuccarini; Milan/IT (andrea.gioppo@istituto-besta.it)

Purpose: To examine advanced MRI findings encountered in first diagnosis glioblastoma patients treated with dendritic cell immunotherapy.

Methods and Materials: A retrospective analysis was performed on longitudinal MRIs obtained before the first vaccination and every two months, by 22 patients enrolled in the EUDRACT N°2008-005035-15 trial. Tumor volume, mean normalized tumoral CBV (rCBV), mean normalized tumoral ADC (rADCmean), ADC mode (ADCmode), ADC skewness (ADCskew) were collected.

Results: We identified 10 responders and 12 not-responders. In responders, basal rADCmean was significantly higher than in non-responder patients (1.34 ± 0.17 vs 1.14 ± 0.34 ; $p = 0.03$). After the first four vaccinations, responders showed a significant decrease in rADCmean (1.34 ± 0.17 vs 1.23 ± 0.23 ; $p = 0.028$) and not statistically differences in ADCskew, when compared to non-responders. A decrease in rADCmean value ≥ 0.13 and a change in ADCskew ≥ 0.14 were significant predictor of longer progression-free survival (PFS) (17.2 vs 10.2 ; $p = 0.04$ / 15.4 vs 9.3 ; $p = 0.02$) and overall survival (OS) (33 vs 19.9 ; $p = 0.003$ / 29 vs 12.4 ; $p = 0.002$). Regarding follow-up, MRI performed at progression demonstrated a significant increase of rCBV (4.25 vs 5.38 ; $p = 0.04$) and a significant decrease in rADCmean (1.17 vs 1.01 ; $p = 0.004$) when compared to basal MRI. MRI performed at pseudo-progression showed no modification of rCBV and rADCmean. A significant decrease in ADCmode was observed comparing value obtained at pseudo-progression time with those obtained at the following exams (0.0012 vs 0.0010 ; $p = 0.008$).

Conclusion: An early decrease in rADCmean and no significant changes in ADCskew are related to a better survival in GBM patients treated with DC immunotherapy. Modification of rCBV and rADCmean can be useful in distinguishing progression and pseudo-progression.

B-0282 14:32

Cortical vs juxtacortical lesions in multiple sclerosis: an analysis of PSIR performance in comparison to FLAIR

M.R. Lima¹, G. Furlin¹, A. Kupske¹, J.S. Muller¹, M.C.A. de Vecino¹, M.G. Longo², K.R.S.B. Nunes¹, B.B. Valentini¹, M.A.G. de Caneda¹;
¹Porto Alegre/BR, ²Boston, MA/US (Gabifurlin@gmail.com)

Purpose: Multiple sclerosis (MS) affects white and grey matter. Imaging differentiation between juxtacortical and cortical lesions can be challenging with the standard magnetic resonance (MRI) sequences. New sequences have demonstrated better performance, like phase-sensitive inversion recovery (PSIR). This study evaluates the performance of PSIR to detect and differentiate cortical plaques in patients with MS, in comparison to FLAIR.

Methods and Materials: Patients with MS confirmed by McDonald criteria (2010) who underwent MRI examination in our service between March 2016 and April 2017 were retrospectively evaluated by two radiologists that quantified the number of lesions detected first by FLAIR and then by PSIR. Later, they estimated how many lesions were reclassified using PSIR.

Results: 71 patients were included with an average of 12.7 years of disease. 52 patients (73.2%) presented juxtacortical lesions in FLAIR. Of these, 43 (82.7%) had lesions reclassified using PSIR, with a median number of 2.55 lesions per patient. 38 (54.3%) presented supratentorial lesions identified only in PSIR, with a median number of 1.44 lesions per patient. 23 (32.9%) presented infratentorial lesions identified only in PSIR, with a median number of 1.43 lesions per patient. PSIR showed better performance than FLAIR in identifying MS lesions in supratentorial and infratentorial compartments ($p < 0.001$ for both), detecting an average of 1.5 more lesions in supratentorial and 0.42 more in infratentorial compartment.

Conclusion: The evaluation of MS lesions with PSIR showed greater performance for diagnosis and classification in comparison to FLAIR and its use should be encouraged in the clinical practice.

B-0283 14:40

Neuroimaging manifestations of HIV-AIDS at a reference center in south of Brazil

G.F.D. Castanho, P. Yokoo, J. Geske, G. Michelis, A. Cremonese, B.C. Teixeira; Curitiba/BR (gabrielle.castanho@gmail.com)

Purpose: The nervous system is among the most frequent and serious targets of human immunodeficiency virus (HIV) infection, mainly in patients with profound immunosuppression. This group of patients presents particular aspects of neuroimaging that must be known and recognised by radiologists. We want to present illustrative magnetic resonance imaging (MRI) findings in HIV positive patients.

Methods and Materials: This was a retrospective observational study. We reviewed all orders of Brain MRI at our service, in a two year period (March 2015 to March 2017) with a total of 2089 exams. We included patients with a known HIV diagnosis described in the medical application or summary of hospital discharge. We identified 123 HIV patients (154 Brain MRI) and we studied and correlated with anatomopathological and clinical-laboratory findings.

Results: The majority of patients in our sample were hospitalised (61%). In this group 52% had CD4<200 and 14% was not available, also we observed some overlapping findings, infection was found in 56% (39% toxoplasmosis, 16% PML, 11% syphilis, 11% tuberculosis and 9% HIV encephalopathy), neoplasm in 10% (62% lymphoma and 25% metastasis), 26% had others lesions (45% microangiopathy, 20% infarcts and 5% IRIS) and 17% of patients evolved to death. In the outpatients only 8% had CD4<200 and 8% was not available, we found 6.3% with signs of active infections and 23% with chronic alterations (vascular and infectious), the remainder presented nonspecific or normal findings.

Conclusion: The hospitalised patients presented a more aggressive pattern than outpatients, as expected, because of the larger immunosuppression.

B-0284 14:48

Acute optic neuritis (ON): can magnetic resonance (MRI) in the acute setting help in determining the aetiology?

C. Rosti, M. Cellina, V. Fetoni, M. Pirovano, M. Ciocca, G. Oliva; Milan/IT (cristina.rosti@gmail.com)

Purpose: ON is an inflammatory disease of the optic nerve which can be idiopathic or associated with demyelinating or autoimmune diseases. Our aim was to investigate if MRI in the acute setting may help in establishing ON aetiology.

Methods and Materials: 60 previously healthy subjects presented to our emergency department with a first episode of ON, clinically diagnosed. Patients underwent ophthalmologic, neurologic examinations, blood tests and by brain and orbit basal CT. A 1.5T MRI of the orbit, brain and cervical spine was executed within 48 hours from the onset. The protocol included a 3D FLAIR, DWI, T1 and T2 weighted sequences, with fat saturation (FS) on the

orbit and, after contrast injection, a T1 3D MPRAGE on the brain, FS T1 SE on the orbit and cervical spine. Neuroradiologists, unaware of clinical data, made an ON aetiological diagnosis based on the MRI datasets. ON were classified as idiopathic or clinically isolated syndrome (CIS), multiple sclerosis (MS) or optic neuromyelitis (NMO) in case of T2 lesions, according to location, morphology, contrast enhancement (CE).

Results: All CT were negative. According to MRI, 22 ON were classified as idiopathic (19 negative MRI, 3 swelling of the optic nerve); 7 as MS (spatio-temporal disseminated T2 lesions); 29 as CIS (T2 lesions without CE with/without cervical and optic nerve involvement), 2 as NMO (brain and cervical lesions with typical characteristics). MRI results confirmed neuroradiologists' diagnosis. NMO was confirmed by the anti-aquaporin-4.

Conclusion: MRI findings perfectly matched neurologists' diagnosis confirming ON aetiological diagnosis.

B-0285 14:56

Evaluation of chronic MS lesions with T1 magnetic resonance fingerprinting

E. Springer¹, W. Bogner¹, P. Cardoso¹, M. Nittka², J. Pfeuffer², G. Koerzdoerfer^{2,2}, R. Kirsch², S. Trattnig¹; ¹Vienna/AT, ²Erlangen/DE (elizabeth.springer@meduniwien.ac.at)

Purpose: MR Fingerprinting (MRF) is a novel approach in data acquisition, post-processing and visualization[1]. Non-enhancing T1-hypointense lesions (black holes) in multiple sclerosis (MS) are chronic lesions characterized by severe axonal damage[2, 3], and with a persistent iron ring are considered slowly progressive lesions[4, 5]. Iron rings are in most cases only visible at 7T due to higher spatial resolution and stronger susceptibility effects[6, 7]. To investigate whether MRF T1 relaxation times may be used to differentiate chronic T1-hypointense lesions with iron ring-deposits from chronic T1-hypointense lesions without iron-deposits.

Methods and Materials: Ten relapsing remitting MS (RRMS) patients were measured on a 3T MAGNETOM-PRISMA MR-scanner with a 64-channel head/neck coil, and on a 7T-MAGNETOM MR-scanner (both Siemens Healthcare, Germany) with a 32-channel head coil (Nova Medical). The comprehensive routine MS protocol, including FLAIR, 3D-FLAIR, T2-TSE, MP2RAGE, diffusion-weighted imaging, post-contrast T1-weighted images, as well as a prototype MRF sequence[8] were performed at 3T, susceptibility-weighted imaging at 7T. MRF T1 relaxation times were measured in regions of interest in FLAIR-hyperintense, T1-hypointense lesions without contrast media uptake, containing iron ring-deposits on SWI, and non-containing iron-deposits, using Syngo Via. Multi-Level Analysis (MLA) was assessed to take clustered multiple measures per patient into account when comparing different regions.

Results: MRF T1 relaxation times were significantly higher in chronic T1-hypointense MS lesions containing iron ring-deposits than in non-iron-containing chronic T1-hypointense MS lesions ($p=0.002$).

Conclusion: MRF T1 relaxation times may be used to differentiate iron-containing from non-iron-containing chronic MS lesions, and thus may facilitate the depiction of a more progressive form of RRMS at 3T.

Author Disclosures:

M. Nittka: Employee; Siemens Healthcare GmbH. **J. Pfeuffer:** Employee; Siemens Healthcare GmbH. **G. Koerzdoerfer:** Grant Recipient; from Siemens Healthcare GmbH. **R. Kirsch:** Employee; Siemens Healthcare GmbH.

B-0286 15:04

Brain damage in early adult paediatric-onset MS with no or minimal disability

L. Nichelli¹, A. Giorgio², J. Zhang², M. Stromillo², F. Rossi², M. Battaglini², M. Mortilla³, M.P. Amato³, N. De Stefano²; ¹Modena/IT, ²Siena/IT, ³Florence/IT (lucianichelli@gmail.com)

Purpose: Paediatric-onset MS (POMS) patients seem to benefit from brain adaptive mechanisms in the short-medium term, although they reach clinical disability at a significantly younger age than adult-onset MS (AOMS) patients. To investigate such unfavourable long-term clinical outcome, we measured structural and functional brain damage in early adult POMS patients with no or minimal clinical disability.

Methods and Materials: 15 POMS patients (age=24.8±7 years; median EDSS=1), 14 age- and disability-matched AOMS patients and 20 normal controls (NC) underwent a 3T MRI examination. We obtained WM-lesion volume (LV) and probability maps (LPM), brain volumes (whole brain, WM, GM, neocortical, deep GM) with SIENAX and performed a voxelwise DTI and resting fMRI analyses with FSL tools, using the statistics of non-parametric permutation testing.

Results: No differences in LV and in brain volumes were found between POMS and AOMS. However, in comparison with AOMS patients, early adult POMS showed (i) at the level of posterior corona radiata (PCR), an eloquent area for motor disability, higher probability of lesion occurrence ($p=0.002$) and higher axial and radial diffusivity ($p<0.001$); and (ii) a reduced long-range functional connectivity between default mode network and secondary visual

network ($p=0.0016$), whose interaction supports important cognitive functions such as spatial attention and visual learning.

Conclusion: This pattern of structural damage and altered functional connectivity in early adulthood may give insight into long-term outcome of POMS.

B-0287 15:12

Comparison between grey matter-only and white matter-only imaging in the detection of brain multiple sclerosis lesions

Z. Abidi¹, F. Faeghi², Z. Mardanshahi³, J. Abdolmohammadi⁴, M. Haghighikaboudkola⁵, ¹Qaemshahr/IR, ²Tehran/IR, ³Sari/IR, ⁴Sanandaj/IR, ⁵Babolsar/IR (abidi4805@sbmu.ac.ir)

Purpose: We aimed to evaluate two different types of double inversion recovery sequence including grey matter-only (GM only) and white matter-only (WM only) imaging and routine brain MRI sequences in detection of multiple sclerosis (MS) lesions.

Methods and Materials: In this study, 30 patients including 19 patients with RRMS and 11 with SPMS were examined on a 1.5T Philips MRI scanner, using GM only, WM-only imaging and routine brain MRI sequences with same parameters, including field of view, matrix, slice thickness, voxel size and number of signal averaging (NSA). In GM-only imaging two inversion pulses with inversion delay times ($T_{I1}=3400$ and $T_{I2}=325$ ms) optimized to suppress signal of WM and cerebrospinal fluid (CSF) to image cortex alone and in WM-only imaging two different TI ($T_{I1}=3700$ and $T_{I2}=525$ ms) are used to suppress signal of GM and CSF to image the WM lonely.

Results: More total number of lesions were displayed on GM-only sequence compared with WM-only imaging ($p=0.0001$) and FLAIR ($p=0.014$) and T2W_TSE ($p=0.0001$). Higher contrast ratio has been observed between the white matter lesions and the normal-appearing white matter (NAWM) in most anatomical regions.

Conclusion: GM-only and WM-only imaging provide additional information compared to routine brain MRI sequences. Although GM-only imaging was superior to routine sequences, but WM-only imaging had a poor detection of MS lesions in brain. So, we highly recommend routine use of GM-only imaging for early detection of MS lesions.

14:00 - 15:30

Room F2

Emergency Imaging

SS 317

CT imaging in trauma

Moderators:

A. Agrawal; Delhi/IN
F.G. Mück; Munich/DE

B-0288 14:00

Improved image quality and reduced radiation dose in trauma CT using a custom arm rest pillow

V. Larsen, C.T. Traplay, B.R. Mussmann; Odense/DK (brz9ak@gmail.com)

Purpose: In multi-trauma CT, assessment of the liver is crucial for the diagnosis, but with current scan procedures the patients are often scanned with the arms down causing artifacts in the abdominal region. We developed a custom arm rest pillow allowing for scans with arms in overhead position. We hypothesized that the arms-over-head position would affect image quality in the parenchymal organs positively, while moderate image quality decrease in the cervical spine was expected. The purpose was to assess dose and image quality implications of the custom pillow in emergency CT.

Methods and Materials: We included 24 multi-trauma patients referred for chest-abdomen scans. Using the trauma pillow 12 patients were scanned feet first, arms over head and 12 were scanned head first, arms down (standard procedure). Subjective image quality was assessed in the parenchymal organs and cervical spine using a five-point scale. Image quality scores < 3 were considered unacceptable. Image scores and dose length products were compared using the two-sided unpaired t test.

Results: Mean DLP decreased from 2360 to 1800 mGy*cm ($p=0.06$) using the pillow. Mean image quality score in the parenchymal organs increased from 2.4 to 4.3 ($p<0.00001$). All patients with insufficient image quality were scanned with arms down. Cervical spine image quality decreased from 4.7 to 3.6 ($p<0.0001$) with no scores below cut-off.

Conclusion: Image quality can potentially be improved in the parenchymal organs and radiation dose can be reduced using the trauma pillow while image quality in the cervical spine is decreased, yet diagnostically acceptable.

B-0289 14:08

Evaluation of the diagnostic potential of the GCS for the indication of whole-body CT in paediatric polytrauma

C. Frellesen, J. Wichmann, P. Tischendorf, T.J. Vogl, K. Eichler; Frankfurt a. Main/DE (c.frellesen@gmail.com)

Purpose: To evaluate the diagnostic potential of the Glasgow Coma Scale (GCS) for the indication of whole-body CT (WBCT) in paediatric polytrauma.

Methods and Materials: 100 paediatric polytrauma patients with WBCT were compared according to age, gender, mechanism of injury (MOI), GCS, detected injury and injury severity score (ISS). Correlation between GCS and patient groups with (p+) and without (p-) injury was assessed using Mann-Whitney U Test and ROC analysis to evaluate its predictive potential.

Results: Average age was 9.13 years with predominance of male patients (72 vs 28%). Traffic accidents were the most frequent MOI (63%). Injury was detected in 71% of the patients, most commonly of the head (43%). There was no significant correlation between MOI and ISS. P+ and p- showed significant differences regarding GCS ($p<0.001$). ROC analysis revealed an optimum discrimination threshold of the GCS at 12.5 with an inaccuracy rate of 21% relating to craniocerebral injuries and 30% to whole-body injuries, respectively.

Conclusion: The indication of WBCT in paediatric polytrauma patients should not be based on the GCS alone. Focused CT of individual body regions is to be preferred. Cranial CT is recommended at a GCS less than or equal to 13.

Author Disclosures:

J. Wichmann: Speaker; Siemens Healthcare; GE Healthcare.

B-0290 14:16

Who needs a CT scan? Incorporating S100B into existing guidelines in the management of mild traumatic brain injury

L. van den Hauwe, M. Landen, F. Vandereyken, R. Vael, P. Bracke; Brasschaat/BE (lucvdhauwe@mac.com)

Purpose: To determine whether S100B, a protein biomarker of brain injury, can predict intracranial abnormalities CT in patients with mild traumatic brain injury (mTBI).

Methods and Materials: Consecutive adult patients with mTBI (GCS 14-15) were included in this study. Patients were managed according to existing guidelines for CT selection based on patient history and clinical examination. S100B was analysed within 4 hours after the traumatic event; results were available within 1 hour. Non-contrast CT was subsequently performed when elevated S100B levels were found.

Results: One hundred seven patients were included during a 12-month period (October 2016-September 2017). Thirteen patients (12%) showed traumatic abnormalities on CT, including skull/facial fractures ($n=9$), subarachnoid haemorrhage ($n=6$), cortical contusions ($n=4$), subdural haematoma ($n=3$), intracerebral haematoma ($n=2$), and epidural haematoma ($n=1$). No patients needed neurosurgical intervention; none died as a result of the TBI. Thirty-three patients (31%) had normal S100B levels and 74 patients (69%) showed elevated S100B levels ($\geq 0.105\mu\text{g/L}$). Compliance to the new guidelines was not always perfect. As a result over-triage occurred in 4 patients (4%) and under-triage occurred in 11 patients (10%). A false-negative test was observed in 1 demented patient who had a subarachnoid haemorrhage and a subdural haematoma on CT. A false-positive test was observed in a multitrauma patient (liver laceration and rib fractures) without head injury.

Conclusion: Used in combination with clinical decision rules, S100B may reduce the need for CT and as such reduce radiation exposure to the patient and save costs to the society.

B-0291 14:24

Can computed tomography (CT) help in predicting diplopia in orbital blowout fractures (BOFs)?

M. Cellina¹, M. Orsi¹, C. Floridi², G. Oliva¹; ¹Milan/IT, ²Perugia/IT (m.cellina@yahoo.it)

Purpose: The management of BOFs is controversial and the assessment of diplopia is the most important criterion for planning surgical repair. Our aim was to determine CT findings that can be used to predict diplopia in patients with BOFs.

Methods and Materials: We retrospectively evaluated orbital CT of all patients presented for blunt craniofacial trauma ($N=3500$) from January 2014 to June 2016, selecting patients with CT-proven BOFs. For each CT we assessed the following variables: fracture site, bone fragments displacement, extraocular muscle (EOM) swelling, EOM dislocation, EOM entrapment, EOM hooking, intraconal and extraconal emphysema, intraconal and extraconal hematoma, orbital fat herniation. All patients underwent Hess-Lancaster test to establish the presence of diplopia. After performing group comparison with Pearson χ^2 test, we derived our prediction model using logistic regression, with diplopia as the prediction and CT variables as predictors.

Results: We observed 299 patients with BOFs, 46 (15.4%) with diplopia. CT variables with statistically significant difference between the group with diplopia

and the group without diplopia were as follows: floor fracture ($p=.014$), bone fragments displacement ($p=.001$), EOM swelling ($p=.001$), EOM displacement ($p<.001$), EOM entrapment ($p<.001$), orbital fat herniation ($p=.003$). CT variables with significance as predictors of diplopia at multivariate analysis were only: floor location (odds ratio [OR], 2.87; 95% confidence interval [CI]: 1.22, 6.73; $p=.01$), muscle entrapment (OR, 10.69; 95% CI: 3.76, 30.4; $p<.001$) and muscle displacement (OR, 11.51; 95% CI: 3.05, 43.3; $p<.001$).

Conclusion: Diplopia can be predicted on CT findings after an orbital trauma.

B-0292 14:32

Multi-energy CT in patients with thoraco-abdominal bleeding: new techniques to facilitate image reading and to help save dose

J. Kahn¹, G. Böning¹, U. Fehrenbach¹, F. Feldhaus¹, D. Kaul¹, M.H. Maurer², D.M. Renz³, F. Streitparth¹; ¹Berlin/DE, ²Berne/CH, ³Jena/DE

Purpose: CT protocols for the detection of bleeding sources often include native CT series to distinguish between calcifications and contrast-agent extravasation. The study evaluates whether virtual native imaging (VNI) can replace real native imaging (RNI) in the reading of acute thoraco-abdominal bleeding and whether monoenergetic imaging can improve the detection of the bleeding's origin.

Methods and Materials: Out of a total of 107 data sets from patients with clinically suspected bleeding, 20 patients (14 men; age 65.4±14.1 years) showed active visceral or soft-tissue bleeding in multi-energy CT angiography. After acquisition of an RNI series, the multi-energy protocol included VNI, monoenergetic images at 40 and 140keV and iodine mapping. CT numbers of ROIs in liver, pancreas, aorta, kidney, muscle and the bleeding jet were measured for quantitative image analysis (contrast-to-noise ratios, CNR). Two radiologists rated detectability of the bleeding source in different series. Wilcoxon rank test was used to compare related samples.

Results: VNI series showed sufficient, but not complete suppression of iodine (CT number aorta RNI: 33.2±12.3, VNI: 44.8±9.5, $p<0.01$; bleeding jet RNI: 43.1±16.9, VNI: 56.2±16.7, $p<0.05$). VNI showed significantly higher CNR than RNI in all measured organ regions. 40keV images showed a CNR in bleeding jets 4 times higher than standard 140keV images and were the best series to detect bleeding sources in qualitative rating.

Conclusion: VNI can safely replace RNI in a CT protocol looking for bleeding sources with a potential dose reduction of 30%. Low keV series may improve detection of the bleeding's origin.

B-0293 14:40

Evaluation of CT and clinical features of bowel and/or mesenteric injury in blunt abdominal trauma: a case-control study

A. Lansier, C. Bourillon, R. Jantzen, E. Ragot, A. Follin, A. Berger, O. Clement, P. Halimi, C.A. Cuenod; Paris/FR (alexandre.lansier@gmail.com)

Purpose: To evaluate the multidetector CT and clinical features of bowel and/or mesenteric injuries in blunt abdominal trauma and evaluate the interobserver agreement according to the experience of the radiologist.

Methods and Materials: This retrospective case-control study included 30 cases with surgically confirmed bowel and/or mesentery requiring surgical repair and 52 consecutive controls with blunt abdominal or chest trauma and no surgically important bowel and/or mesenteric injury. CT findings were screened by two radiologists: an 8-year-experienced in abdominal imaging radiologist and a second-year resident blinded to the patients' outcome. Clinical outcomes were analysed by consulting the medical file. Sensitivity and specificity were calculated for each sign and a kappa coefficient were used to establish the interobserver variability.

Results: The CT signs with best positive likelihood ratio were extra luminal air (infinity), bowel wall defect (infinity) and thickening (38.13), decreased bowel wall enhancement (10.4) and mesenteric vessels abnormalities (9.01). The specificity of clinical seat belt sign associated with anterior abdominal wall injury on CT was 98%. The sensitivity of free intraperitoneal fluid was 100% and its density was higher in cases. More than 50% of patients with missed diagnosis on first CT had a visceral injury associated. Diagnosis of mesenteric and/or bowel injury depends on the experience of the radiologist (kappa = 0,6).

Conclusion: Multidetector CT is accurate for the diagnosis of bowel and/or mesenteric injuries in blunt abdominal trauma depending on the experience of the radiologist. The association of clinical seat belt sign and anterior abdominal wall injury on CT is highly specific.

B-0294 14:48

Prognostic and diagnostic value of hyperattenuating adrenal glands on contrast-enhanced computed tomography scans of polytraumatized patients

D. Kildal, T. Erben, M. Beer; Ulm/DE

Purpose: The adrenal gland with its endocrinal hormones relates to several reactions due to traumatic injury of the human body. Purpose of this study was to seek possible connections between hyperattenuating adrenal glands on

contrast-enhanced CT scans of polytraumatized patients and potentially lethal injuries.

Methods and Materials: This retrospective study includes 379 polytraumatized patients which had a biphasic contrast-enhanced CT. Two radiologists assessed the general pathologies, Hounsfield units (HU) measurements of the adrenal gland [AG], the V. cava inferior [VCI] and the erector spinae muscle [ESM] were registered. Patients were sorted into 2 groups [group 1: HU(AG) ≥ HU (VCI); group 2: HU (AG) ≤ HU (VCI)].

Results: 31 patients exhibited hyperattenuated AGs and were sorted into group 1. 348 patients were sorted into group 2 due to non-hyperattenuated AGs. Density in group 1 was 106.77 ± 29.29 HU, in group 2 density was 83.80 ± 26.50 HU. 11 patients of group 1 suffered from intracranial bleeding [ICB] (group 1: 11/31 ICB, 35.48%) whilst 54 patients of group 2 showed ICB (group 2: 54/348 ICB, 15.52%). Intracranial bleeding and hyperattenuating AGs were noticed in 11 out of 65 cases (11/65, 16.92%). A comparison between group 1 and 2 showed that it is significantly more likely to express/suffer from ICB while expressing hyperattenuated AGs (Fisher's exact test p value: 0.0104, Chi-square test p value: 0.0047).

Conclusion: Hyperattenuating AGs of polytraumatized patients are frequently linked to intracranial bleeding and, therefore, might function as a red flag in contrast-enhanced abdominal examinations of polytraumatized patients.

B-0295 14:56

Dual-phase CT protocol in the assessment of traumatic liver injuries

F. Iacobellis¹, I. Iadevito², A. Sorbo², M.G. Scuderi¹, S. Daniele¹, A. Sparano¹, G. Russo¹, L. Romano¹, M. Scaglione²; ¹Naples/IT, ²Castel Volturno/IT (iacobellis@gmail.com)

Purpose: To examine the role of dual-phase CT protocol in the assessment of traumatic injuries of liver, evaluating the prevalence of parenchymal contusion, active bleeding, and contained vascular injuries between arterial and portal venous phase.

Methods and Materials: Dual-phase CT examinations of 175 patients diagnosed with traumatic liver injury performed were retrospectively reviewed. For each examination, arterial and portal venous phase were compared in the identification of liver parenchymal injuries, active bleeding, and contained vascular injuries.

Results: Of 175 patient, 154 (88%) had parenchymal lesions and 21 (12%) showed associated vascular injuries. Out of these, 16/21 (76.2%) had active bleeding and 5/21 (23.8%) contained vascular injuries. Parenchymal lesions were evident in all the patients in the portal venous phase. In 5/16 patients with active bleeding (30%), the arterial phase was crucial to correctly identify the arterial origin of the bleeding. In 3/5 patients with contained vascular injuries (60%), the detection of vascular lesion was possible only in the arterial phase.

Conclusion: Dual-phase CT examinations increase the possibility, in the arterial phase, to detect contained arterial injuries and to identify the arterial origin of active bleeding, whereas the venous phase is essential to identify the parenchymal injuries, venous vascular injuries, to differentiate contained vascular injuries from active bleeding and to evaluate the bleeding entity.

B-0296 15:04

Correlation between CT-based liver injury scoring and subsequent management

M. Reim¹, A. Lomp¹, V. Mihnovits¹, P. Ilves¹, S. Saar², U. Lepner¹, P. Talving^{1,2}; ¹Tartu/EE, ²Tallinn/EE (Reimmartin@gmail.com)

Purpose: The liver is the second most commonly injured abdominal solid organ. The aim of the study was to determine correlation between CT scoring of liver injuries and subsequent operative management.

Methods and Materials: The data for consecutive trauma admissions to major trauma facilities with liver injuries between 1/2009 and 12/2013 were retrospectively included using ICD 10 codes (S36.10) and the images reviewed from the All-Estonian Picture Archive (PACS). CT scoring per American Association for the Surgery of Trauma organ injury scale stratified liver injuries into minor/moderate (grades I-III) vs. severe (grades IV-V) injuries. The primary outcomes were operative management and in-hospital mortality.

Results: Overall, 81 cases were included. The mean age of the cohort was 31.5 ± 12.2 years and 73.1% were male. Overall, grades I-III injuries 86.4% (n=70) and grades IV-V injuries 13.6% (n=11) were examined. The most common associated injuries involved chest wall (n=44; 54.4%), lung (n=42; 51.8%), lower ribs (n=32; 39.5%), and small bowel at (n=11; 13.6%), spleen (n=9; 11.1%), kidneys (n=7; 8.6 %). Nonoperative management was used in 82.7% (n=67), 84.3% (n=59) of the cases for grades I-III and in 72.7% (n=8) of the cases for grades IV-V. There was no correlation between CT scoring of liver injuries and surgical management ($p=0.196$). The mortality of the patients with CT scoring was 2.5% (n=2), including one grade V injury.

Conclusion: The majority of the liver injuries were minor or moderate and CT-scoring of liver injuries did not determine subsequent surgical management. Further prospective studies are warranted.

B-0297 15:12

Comparison of the inter-observer reliability of injury severity recording between unstructured and structured CT reports of blunt abdominal trauma

Y.-C. Wong, L.-J. Wang, C.-H. Wu; *Taoyuan/TW (ycwong@cgmh.org.tw)*

Purpose: To compare between unstructured and structured CT reports for the inter-observer reliability of injury severity recording in blunt abdominal trauma (BAT) among different readers.

Methods and Materials: In this IRB-approved study, we randomly selected 30 contrast-enhanced CT examinations of BAT from January 2013 to December 2013. All images were anonymised for viewing by six readers (two attending radiologists, two senior residents, two junior residents) who were blinded to clinical outcome. They recorded CT findings independently on unstructured and structured templates six months apart. We compared injury severity of each item on a 6-point Likert scale and intraclass correlation coefficient (ICC) of all readers between unstructured and structured reports.

Results: Active bleeders were recorded more critical on structured reports by 4 (4/6, 66.7%) readers. Solid organ injuries were recorded more critical on structured reports by 2 (2/6, 33.3%) junior residents. Pelvic and spine injuries were recorded more critical on structured reports by 1 (1/6, 16.7%) junior resident. In contrast, hollow organ injuries were recorded less critical on structured report by 1 (1/6, 16.7%) attending radiologist. The ICC values for hollow organ injuries on unstructured and structured reports were 0.837 and 0.821, respectively. The ICC values for active bleeders, solid organ injuries, pelvic and spine injuries on unstructured and structured reports were all > 0.900.

Conclusion: Structured reports could alter the injury severity recording of active bleeders and solid organ injuries from less to more critical especially among junior residents.

Author Disclosures:

Y. Wong: Grant Recipient; MOST104-2314-B-182A-090. L. Wang: Grant Recipient; MOST104-2314-B-182A-090. C. Wu: Grant Recipient; MOST104-2314-B-182A-090.

B-0298 15:20

Whole-body multidetector CT in polytrauma patients: incidence and clinical significance of missed diagnoses

F. Ruschi; *Bolzano/IT (francesco.ruschi@gmail.com)*

Purpose: To evaluate the incidence and significance of missed diagnoses at whole body MDCT in polytrauma patients.

Methods and Materials: Whole body (head to symphysis) MDCT reports of 169 polytrauma patients (study group) were retrospectively evaluated and compared with clinical/surgical management. The study group was divided into three subgroups: no missed injuries, missed injuries of no clinical significance, clinically significant missed injuries (requiring medical or surgical treatment). The MDCT exams of second and third subgroups were re-evaluated in order to determine whether the missed lesions were recognisable or truly non-detectable.

Results: The commonest types of injuries were intracranial bleeding (23%), rib fractures (32%), pneumothorax (17%), lung contusions (15%), spine fractures (23%) and midface-skull fractures (11%). In 94.1% of patients all injuries were diagnosed correctly. Eight patients (4.7%) had missed injuries that required no further treatment (non-displaced fractures, spleen/liver/cerebral contusions). Two patients (1.2%) had relevant missed injuries such as carotico-cavernous fistula and diaphragmatic rupture. With secondary interpretation the 80% of these lesions could be diagnosed. The carotico-cavernous fistula was missed probably because during the second survey (MDCT) there were concomitant life-threatening injuries (diffuse subarachnoid hemorrhage, internal carotid artery dissection) to focus on. On the other hand, as the diaphragmatic lesion was detected at laparotomy in a patient with CT diagnosis of complete spleen rupture, this had no additional therapeutic consequence (there was already an indication for an emergent laparotomy).

Conclusion: Missed injuries in CT reports of polytrauma patients have rarely clinical significance and they are often detected at follow up imaging.

14:00 - 15:30

Room D

Musculoskeletal

SS 310

Joint imaging

Moderators:

N.N.

M. Tzalonikou; Athens/GR

B-0299 14:00

Dose optimisation in digital radiography of the hands: evaluation of the GC85A low-dose technology

S. Siepmann, K. Ziegeler, A. Beck, T. Diekhoff, A. Bach, B. Hamm, K.-G. Hermann; *Berlin/DE (stefan.siepmann@charite.de)*

Purpose: Patients with rheumatic conditions are frequently required to undergo follow-up X-ray examinations to measure disease progression. Thus, reduced dose digital radiography may play a role to keep long-time exposure minimal. The aim of this study was to evaluate the GC85A low-dose technology in patients with suspected rheumatoid arthritis.

Methods and Materials: Fixed low-dose (LD) digital radiography protocols at 51.6 kVp were defined with 1.7 mAs and 1.2 mAs, that equal 80% and 64%, respectively, of the standard exposure (SE). LD images were processed further using the feature preserving noise reduction algorithm (S-Vue 3.02) implemented into the GC85A X-ray device (Samsung, Seoul, South Korea). Patients were consecutively enrolled. Randomly, one hand was X-rayed with one of the LD protocols while the opposite hand received the SE protocol. Images were scored independently by two readers blinded to X-ray protocol. Standardised scoring included evaluations of bony contours, spongy bone, joint spaces, soft tissues, image noise and contrast on 0-5 numeric weighting scales.

Results: X-ray images of both hands were acquired in 116 patients. Mean image quality scores were 29.1 ± 2.8 for SE and 28.9 ± 3.1 for LD (no significant difference) for the total population. This result remained when analysing only 80% and 64% LD images, respectively. No major artefacts occurred in any of the X-rays acquired.

Conclusion: Low-dose GC85A digital radiography down to 64% of the standard exposure is a suitable approach to reduce the lifetime X-ray radiation dose in patients with rheumatic conditions, that need to undergo follow-up X-ray examinations every other year.

B-0300 14:08

Heels: the higher, the better? Weight-bearing MRI evaluation of the forefoot in women during heeled-shoes wearing

C. Gianneramo, F. Bruno, S. Quarchioni, E. Cannizzaro, P. Palumbo, S. Mariani, F. Arrigoni, A. Barile, C. Masciocchi; *L'Aquila/IT (camillagianneramo@gmail.com)*

Purpose: To evaluate the possible physiological changes of the forefoot in women wearing heels using weight-bearing MRI.

Methods and Materials: We evaluated 22 healthy volunteers (mean age 32.3 years, range 28-36). All women were submitted to MRI examination of the foot in orthostatic weight-bearing position using a dedicated low-field scanner (0.3T). Each examination consisted of 3 acquisitions, respectively without heel (position1, P1), with a 2.3in (6cm)-heel (position2, P2) and with a 4.7in (12cm)-heel (position3, P3). We acquired a sagittal SSFP 3D sequences, with reconstructions on coronal and axial planes.

Results: For each position we measured, on the axial plane, the distance between the centre of the first and the centre of the fifth metatarsal heads (M1-M5D), the transverse arch height (TAL), the distance from the centre of the third metatarsal head to the plane passing from the base of the medial sesmoid to the base of the fifth metatarsal head, and the angle between the first and fifth metatarsal (M1-M5) measured on the coronal plane. Mean values of M1-M5D were 63.4mm (P1), 69.4mm (P2) and 74.8mm (P3) ($p < 0.005$). Mean values of TAL were 12.7mm (P1), 10.8mm (P2) and 8.1mm (P3) ($p < 0.005$). Mean values of M1-M5 were 21.68° (P1), 28° (P2) and 31° (P3) ($p < 0.005$). These alterations resulted into evident modifications of the anatomical relations of the forefoot structures.

Conclusion: Our MRI findings defined the physiological changes of the forefoot structures in women wearing heeled-shoes; these results could represent an important background to evaluate symptomatic subjects with foot pathology exacerbated by heeled-shoes wearing.

B-0301 14:16

MDCT arthrography assessment of the severity of cartilage damage and scapholunate dissociation in regard to specific component tears of the scapholunate ligament

J.-B. Quere, C. Phan, A. Miquel, L. Arrive, Y. Menu, M. Crema; *Paris/FR* (quere.jb@gmail.com)

Purpose: To evaluate the severity of cartilage damage assessed on MDCT arthrography in a sample of patients with scapholunate interosseous ligament (SLIL) tear, in regard to specific dorsal or volar component involvement. The relationships with assessment of scapholunate dissociation were also evaluated.

Methods and Materials: We retrospectively included 43 patients who underwent MDCT arthrography with SLIL tears. Dorsal and volar components of the SLIL were separately assessed for tears and graded as: normal, partial tear, or complete tear. Cartilage damage was assessed in 14 regions of the wrist using a modified WORMS system (grades 0-6). Cartilage damage score was obtained by summing WORMS grades from regions of the radial side. Staging of SLAC (0-3) was performed. Scapholunate dissociation was measured at the tenth of a millimeter. The Student's T and the Wilcoxon rank-sum tests were used to evaluate the differences in cartilage damage scores and scapholunate dissociation when assessing tears of dorsal and volar components of the SLIL.

Results: Cartilage damage scores were greater in patients with complete tears of the dorsal component (12.67; 95%CI 7.63, 17.72) than in patients with no or partial tears (2.83; 95%CI 1.25, 4.41); p values<0.001. Scapholunate dissociation values were also greater in these patients (p values<0.0001). Scapholunate dissociation was more severe in SLAC≥1 than in SLAC 0 (p values<0.0001), with a cut-off value of 3.9 mm for diagnosing SLAC≥1 (sensitivity 79.2%, specificity 94.7%).

Conclusion: The severity of cartilage damage and scapholunate dissociation is greater when the dorsal component of the SLIL is completely ruptured.

Author Disclosures:

M. Crema: Shareholder; Boston Imaging Core Lab, LLC.

B-0302 14:24

MRI patterns of locked metacarpophalangeal joints of the long fingers

L. Lassalle¹, F. Lapegue², H. Guerini¹, R. Campagna¹, V. Vuillemin¹, N.E. Regnard¹, A. Buisson¹, J.L. Drape¹; ¹Paris/FR, ²Narbonne/FR (louis.lassalle@gmail.com)

Purpose: Locked metacarpophalangeal (MCP) joints of long fingers may be clinically misdiagnosed with more common trigger fingers. The goal is to describe the MR patterns of locked fingers

Methods and Materials: MRI studies of 13 patients (12-65 yo) : 9 females (69%) and 4 males (31%), with clinical presentation of locked finger (loss of active and passive extension of the MCP joint with preserved interphalangeal joint mobility) were retrospectively reviewed by two MSK radiologists. MRI patterns were described according to the type of the lesion (dorsal or volar locking) and clinical presentation (further flexion possible: type 1 of impossible: type 2). Surgical correlation was available in 6 cases.

Results: In type 1 lesions MR demonstrated osseous prominences or osteophytes of the radial condyle of the MC head and entrapment of the accessory collateral ligament. In type 2 lesions MR depicted intra-articular entrapment of a torn volar plate following an acute trauma. In dorsal locking MRI highlighted an entrapment of either a dorsal interosseous tendon or a torn collateral ligament between the sagittal band and the dorsal interosseous expansion ("stener like" lesion).

Conclusion: MRI allows an accurate evaluation of the anatomical lesions in locked MCP joints. Several different lesions may have the same clinical presentation.

B-0303 14:32

Cartilage damage assessed with dGEMRIC occurs at the zone of 3D CT-based impingement simulation: a pilot study

F. Schmaranzer, T. Lerch, I. Todorski, P. Haefeli, M. Hanke, S. Werlen, K. Siebenrock, M. Tannast; *Bern/CH*

Purpose: For complex cases of femoroacetabular impingement (FAI), CT-based 3D impingement simulation is the current gold standard to determine the impingement location. Delayed gadolinium-enhanced MRI of cartilage (dGEMRIC) allows a noninvasive estimation of cartilage composition. (1) To compare T1 indices between clock-face positions with versus without simulated impingement; (2) to assess whether the clock-face position of lowest T1 index is located at the zone with highest prevalence of impingement.

Methods and Materials: This is a retrospective IRB-approved study. Twenty-one patients (mean age 30 years) with symptomatic FAI and preoperative indirect MR arthrography at 3.0 T (0.2 mmol/kg, Gd-DTPA²⁺) for dGEMRIC (3D T1 maps, dual-flip angle technique) and 3D CT scans of the pelvis with distal femoral condyles were included. Radial T1 images were reformatted. Regions

of interest were placed manually. CT-based 3D models of the bony hip were generated and impingement simulation was performed with in-house developed software. This served as the gold standard. (1) Mean T1 indices between clock-face positions with versus without impingement were compared. (2) Overlap between the clock-face position with lowest mean T1 indices with the zone of highest prevalence of impingement (% of hips) was assessed.

Results: (1) Mean T1 indices for clock-face positions with impingement (482±146 ms) were significantly (p<0.001) lower compared to those without impingement (594±180 ms). (2) Lowest mean T1 indices (472±140 ms) were at the zone of highest prevalence of impingement (2 o'clock position; 21/21 hips, 100%).

Conclusion: dGEMRIC may be used for impingement detection instead of CT scans in young patients with FAI.

B-0304 14:40

Diagnostic efficacy of a 3D sequence in the standard MR protocol among high risk patients for knee cartilage lesions

M. Vlychou¹, I. Kyriakis², K. Vassiou¹, I. Tsougos¹, S. Michalitsis¹, M. Hantes¹; ¹Larissa/GR, ²Milton Keynes/UK (mvlychou@med.uth.gr)

Purpose: Articular cartilage lesions is a common injury among patients between 20 and 40 years of age. 3T MR imaging is the method of choice for detecting traumatic knee lesions; however, its performance remains challenging especially for grade I and II cartilage defects. The purpose of the present study is to assess the diagnostic efficacy of a 3D sequence among high risk patients for knee cartilage lesions.

Methods and Materials: One hundred eleven patients (78 males, 33 females, mean age 34.8 years) were included in the study. All patients underwent the same MR protocol at a 3T MR scanner including T1-weighted and 2D proton density-weighted sequences in three planes and a 3D spoiled gradient-recalled echo (SPGR) sequence. Subsequently all patients underwent arthroscopy. Each articular surface was graded initially at the 2D sequences and subsequently at the 3D sequence and was graded accordingly by two independent radiologists blind to arthroscopic findings. Arthroscopic grading was used as the gold standard. The McNemar test was used to compare sensitivity, specificity, positive and negative predictive values.

Results: There was a statistically significant improvement in both specificity and sensitivity for detecting cartilage lesions by adding the 3D SPGR sequence and also a statistically significant (p < 0.05) improvement in the proportion of correctly graded cartilage lesions, especially in cartilage defects located in the femoral trochlea.

Conclusion: The routine protocol of knee may benefit from adding a 3D sequence since it may improve the diagnostic efficacy for detecting and grading cartilage lesions in high risk patients.

B-0305 14:48

Comparison of T2*-weighted gradient-echo sequence with magnetisation transfer contrast, to other MRI sequences in the diagnosis of gonarthrosis

U.Y. Ayaz¹, M.H. Ozturk², A. Dilli³, B. Hekimoglu³; ¹Mersin/TR, ²Trabzon/TR, ³Ankara/TR (umityasarayaz@yahoo.com)

Purpose: We compared the efficacy of T2*-weighted (W) gradient-echo (GE) sequence with magnetisation transfer contrast (MTC), to those of other MRI sequences in diagnosis of osteoarthritic chondral defects of the knee.

Methods and Materials: In this prospective study, 30 patients with gonarthrosis who would undergo total knee prosthesis operations were included. 1.5-T knee MRI was performed before surgery. T2*W GE with and without MTC, fat-saturated (FS) T1W GE and FS proton density (PD) sequences were obtained. Before surgery, images were evaluated by two radiologists together, in consensus. For verification of MRI, osteoarthritic chondral defects were evaluated and documented both intraoperatively (in vivo) and after their excision by two orthopedic surgeons, together in consensus. T2*W GE sequence with MTC was compared to other MRI sequences in distinguishing the lesioned cartilage. Statistical analysis was made.

Results: In distinguishing lesioned cartilage from the intact one, the sensitivities of FS PD FSE, T2*W GE with MTC, FS T1W GE and T2*W GE without MTC were 82%, 82%, 78% and 78%, respectively. There was no significant difference between FS PD FSE and T2*W GE with MTC (P> 0.05), while there were significant differences between these two sequences (FS PD FSE and T2*W GE with MTC) and the other two sequences (FS T1W GE and T2*W GE without MTC) (P <0.05).

Conclusion: The use of MTC with T2*W GE seems to increase the sensitivity of the sequence in diagnosis of osteoarthritic chondral defects. The contrast between cartilage and synovial fluid is more prominent with MTC.

B-0306 14:56

Knee derangement in the era of total knee replacement epidemic
M. Abd El Bagi, O. Alshehri, H. Alfaleh, S. Ahmed, F. Alorfi, N. Ashraf, A. Thomas, M. Reutener; *Riyadh/SA (othmanzayed@googlemail.com)*

Purpose: To determine the current causes of internal knee derangement that might lead to total knee replacement if not treated at an earlier stage.

Methods and Materials: A retrospective review of consecutive knee MRI scans performed at a tertiary care hospital. The reports and all images were reviewed. Indications were tabulated. Where plain films were performed, their results were registered.

Results: 404 consecutive knee MRI scans were reviewed. Age range was 41 to 81 with a mean age of 39.3 years. 247(61.1) were males. 157(38.8%) were females. Commonest age group was 21-40 (46.6%) of the 404 patients. The commonest abnormality was osteoarthritis in 182 (45%) of the 404 patients with equal number of affected males and females. Osteoarthritis was mild in 126(69.2%), moderate in 44(24.1%) and severe in 12 (6.5%) of the 182 cases. The second commonest abnormality was menisci derangement in 160(39.6%). 93(58.1%) of these 160 patients were males and 67(41.8%) were females. Anterior cruciate ligament abnormalities were detected in 146(36.1%), other ligaments injuries in only 34(8.4%). Joint effusion was seen in 110(27.2%). Cartilage lesions detected in 67(16.5%). Trochlear dysplasia was seen in 91 (22.5%) by groove depth. Lateral patellar tilt indicated a higher incidence of 114(28.2 %) possibly exaggerated by collateral ligaments degenerative laxity.

Conclusion: The common findings of current internal derangement are surgically or arthroscopically correctable by simpler and less expensive procedures than total knee replacement. MRI alone or in correlation with plain radiographs, can demonstrate these lesions at an earlier stage.

B-0307 15:04

Diagnostic imaging of haemophilic arthropathy in children: 3T MRI HAMRIS staging scale
K. Bokwa-Dabrowska, P. Łaguna, M. Brzewski; *Warsaw/PL (katarzyna.bokwa@gmail.com)*

Purpose: Haemophilia is a genetic bleeding disorder which leads to many complications including arthropathy. Precise MRI assessment provides valid clinical information and may lead to complementation of primary prophylaxis.

Methods and Materials: The study group included 16 boys (25 large joints) aged 5-19 years with haemophilia who were examined with 3T MRI within HAMRIS programme (haemophilic arthropathy in magnetic resonance imaging-staging programme). Each patient had had an episode of haemarthrosis affecting the examined joint and was supplemented with factor VIII or IX. Some examinations were performed in forced positions due to limited mobility. The HAMRIS protocol included basic sequences in three planes: T1 fse, T2-weighted fse, TIRM, PD, T2 mapping, T2 me2d and T2 fl2d gradient sequences were obtained in 3D. Each examination was complemented with DWI to reassess the osseous oedema.

Results: The HAMRIS scale includes 5 grades which gives a detailed classification of post-haemorrhagic complications. It classifies an injury according to the location and concerns the scope of endosteal oedema. The exacerbation of pathologies may be easily determined with the HAMRIS scale and make it possible to implement early orthopaedic prophylactic treatment.

Conclusion: The implementation of the HAMRIS programme may be a chance to avoid surgery and permanent disability. As MRI diagnostics is becoming more accessible, it is thought that it should be performed on a routine basis in patients with haemophilia.

B-0308 15:12

Fat saturated 3D-flash sequence improves erosion detection on the sacroiliac joints: results from the SIMACT study
T. Diekhoff, J. Greese, J. Sieper, D. Poddubnyy, B. Hamm, K.-G. Hermann; *Berlin/DE (kgghermann@gmail.com)*

Purpose: Detection of structural lesions of the sacroiliac joint improves the specificity of magnetic resonance imaging (MRI). Our study applies a three-dimensional 3D-flash sequence (volumetric interpolated breath hold examination; VIBE) for erosion detection to patients with suspicion of axial Spondyloarthritis (axSpA).

Methods and Materials: Low-dose computed tomography (IdCT) and MRI with T1 and VIBE of 110 prospectively included patients with low back pain were acquired and scored for erosions and joint space alterations by three readers. A contingency table analysis using IdCT as standard of reference, a comparison of sum scores using repeated measurements ANOVA with multiple comparisons and the calculation of interrater-reliability using Cohen's kappa was performed.

Results: The erosion sum score was higher for MR-VIBE (8.1 ± 9.3) as compared to MR-T1 (6.7 ± 8.4), $p = 0.003$, similarly, the total number of erosions (15.5 ± 21.8 vs 9.2 ± 12.1 , $p < 0.001$). The joint space sum score was 1.8 ± 2.2 for MR-VIBE and 0.8 ± 1.0 for MR-T1, $p < 0.001$. MR-VIBE showed a

higher sensitivity for erosions as compared to MT-T1 (95 % vs 79%, respectively) and joint space alterations (88 % vs 76%) without a decrease in the specificity for erosions (93 % each) and only a small decrease for joint space alterations (93% vs 99 %, respectively).

Conclusion: MR-VIBE detected erosions at the sacroiliac joints with higher sensitivity and similar specificity compared to a standard MR-T1 sequence. Therefore, MR-VIBE may be a valuable supplement to standard MR protocols.

B-0309 15:20

Prevalence of fat metaplasia and other structural changes of sacroiliac joints in patients without axial spondyloarthritis: a cross-sectional MRI study

K. Ziegeler, H. Eshkal, C. Schorr, J. Sieper, T. Diekhoff, M.R. Makowski, B. Hamm, K.-G. Hermann; *Berlin/DE (katharina.ziegeler@charite.de)*

Purpose: To determine the prevalence of fat metaplasia and other structural lesions of the sacroiliac joints associated with axial spondyloarthritis in a non-rheumatological patient population.

Methods and Materials: MRI examinations that included the pelvis of patients without known rheumatological disease were used for this retrospective cross-sectional study. These images were evaluated for sacroiliac fat deposition, sclerosis, osteophytes and joint space alterations such as erosions or ankylosis. Patients were divided into 7 age groups (from 15-24 to ≥ 75). Prevalence of lesions across age groups were calculated. Possible clinical confounders (e.g. status post-radiation, suspected inflammatory bowel disease) were investigated with regard to their impact on lesion prevalence and extent to exclude bias.

Results: A total of 485 patients were enrolled in this study. Fat deposition, was very common, showing a prevalence of 50.6% in the age group < 45 which increased with age to 94.4% in patients ≥ 75 years. Erosions were uncommon: 0.6% of patients < 45 and 2.6% of the entire study population exhibited this feature, with no detectable age-dependent increase. Sclerosis and osteophytes were detected in 13.7% and 37.0% of patients, respectively. None of the investigated clinical confounders showed a significant impact on lesion prevalence.

Conclusion: Our study shows a very high prevalence of periarticular fat deposition adjacent to the sacroiliac joint in asymptomatic patients, while erosions are extremely uncommon.

14:00 - 15:30

Room G

Physics in Medical Imaging

SS 313

Dose management and diagnostic reference levels

Moderators:

H. Bosmans; Leuven/BE
R. Villa; Monza/IT

K-06 14:00

Keynote lecture

V. Tsapaki; *Athens/GR*

B-0310 14:09

Online platform for fast and accurate calculation of fetus dose in CT
N. Saltybaeva, H. Alkadhi; *Zurich/CH (Natalia.Saltybaeva@usz.ch)*

Purpose: CT examination of pregnant patients is always a challenging task because of the concern about the radiation risk to the fetus (embryo). The methods estimating radiation dose to the fetus are either limited in their accuracy or require complicated measurements and calculations. The purpose of our study was to create online platform for fast and accurate fetal dose assessment.

Methods and Materials: The online tool for fetal dose assessment was based on precalculated data from Monte Carlo simulations (MSC). These simulations were performed on standard phantoms, representing 3-, 6- and 9-month of pregnancy, using generic x-ray spectrum, filtration and scanner geometry. To validate the tool we compared the dose values calculated by the algorithm on standard phantoms against those calculated for the real patients. For this purpose MCS were also performed on 11 pregnant patient (gestational ages 7-35 weeks) previously underwent clinically indicated abdominal CT, using individual kVp, mAs curves, collimation, and scanner geometry.

Results: The algorithm proposed in the study allows estimating dose to the fetus with an accuracy of 32 (STD~17%). The study has shown strong correlation ($p < 0.05$) between the accuracy of calculated dose and patients size. The algorithm tends to overestimate fetus dose by 41% in overweight

patients, however, this effect can be corrected (23±11% of accuracy) if patient effective diameter is used as an input parameter.

Conclusion: The proposed algorithm allows for fast and sufficiently accurate assessment of radiation dose to the fetus in CT. The prototype is available online.

B-0311 14:17

Radiation dose for digital breast tomosynthesis: influence of breast composition and breast thickness

N. van der Werf¹, E.-J. van Dijk², D. Dickenscheid¹, M.C. Kock¹; ¹Dordrecht/NL, ²The Hague/NL (n.r.vanderwerf@asz.nl)

Purpose: Compared to digital mammography (DM), average glandular dose (AGD) increases for digital breast tomosynthesis (DBT). However, the contribution of breast composition and compression thickness (CT) to the increase in AGD remains unknown. Therefore, the objective of this study was to evaluate the influence of breast composition and CT on differences in AGD between DM and DBT.

Methods and Materials: A total of 2,368 out-patients with low (n=479), medium (n=1689) and high (n=200) glandular fraction (GF) were scanned with the Selenia Dimensions as part of routine clinical practice. Each scan consisted of both DM and DBT acquisition within the same compression. ACR composition A and D correspond with the categories low GF and high GF, respectively. ACR composition B and C were combined and correspond with medium GF. Each GF was subdivided based on the CT into >40, 40-50, 50-60 or <60mm. Statistical significance was analysed using paired T tests between DM and DBT scans, where p<0.05 was deemed significant.

Results: For cranio-caudal (CC) views, overall AGD increased significantly (p<0.0005) by 0.99, 0.40 and 0.12 mGy for low, medium and high GF, respectively. Low and medium GF showed significant increased (p<0.0005) AGD for all CT. For high GF, AGD increased (p<0.0005) for 35 and 45 mm, whereas AGD decreased significantly (p<0.05) for 55 and 65mm.

Conclusion: Differences in AGD between DM and DBT depends on both GF and CT. AGD for high GF breast of 50-60 or >60mm CT was significantly lower for DBT than for DM.

B-0312 14:25

A national web-based tool for optimisation of radiological protocols

S.J. Thunberg, H. Båvenäs, T. Cederlund; Stockholm/SE (stefan.thunberg@ssm.se)

Purpose: All medical examinations using radiation for imaging must be optimized for both adult and paediatric patients. The purpose of this project was to develop a web-based national support for the optimization process for medical exposures.

Methods and Materials: Swedish Radiation Safety Authority has developed and launched DosReg, a web-based tool for registration of imaging protocols and local diagnostic reference levels (LDRL). The user receives a histogram in real-time illustrating other clinics' results as well as the national DRLs for each modality and procedure. DosReg has been developed for six different modalities: computed tomography, nuclear medicine, mammography, interventional procedures, conventional radiology, and dental CBCT.

Results: Five out of DosReg's six modalities were released in 2017. CT was released in September 2016. All the modalities contain registered LDRLs. CT has the most registrations, with 351 (as of October 2017), as this modality has been available for the longest period of time. Several clinics in Sweden have used DosReg in their optimization work in cases where their initially reported LDRLs were higher than those of other clinics. There have been several cases where DosReg's optimization tool has resulted in a dose reduction in the range of 50-80 per cent.

Conclusion: Immediate implementation of this tool by radiological departments needing to optimize some of their protocols will lead to substantially improved optimization of radiological protocols in Sweden, which in turn will result in less variation nationally in doses received by patients from the same kind of examination.

B-0313 14:33

Validation of the DACS-integrated radiation dose monitor skin dose mapping software using XR-RV3 Gafchromic films for fluoroscopically guided procedures

L. Hadid-Beurrier¹, B. Habib Geryes¹, M.-J. Waryn², A. Jean-Pierre¹, J. Farah³; ¹Paris/FR, ²Bondy/FR, ³Le Kremlin-Bicêtre/FR (bouchra.habib-geryes@aphp.fr)

Purpose: To determine the accuracy of a DACS-integrated patient skin dose mapping solution for fluoroscopically guided procedures using on-phantom and on-patient Gafchromic film measurements.

Methods and Materials: The DACS-integrated radiation dose monitor® (RDM, Medsquare) software uses radiation dose structured report (RDSR) to calculate cumulative patient skin dose distribution in 1 cm² area taking into account backscattered radiation, table and mattress attenuations. To determine their

accuracy, RDM skin dose maps were compared against measurements performed with XR-RV3 Gafchromic films on IGS530 and 540 (GEMS) and ArtisZee-VC21 (Siemens) systems. To validate RDM peak-skin-dose (PSD) calculations and 2D-skin-dose distributions, measurements were first performed considering a PMMA phantom and then in clinical settings for patients undergoing pulmonary angioplasties and AVM/aneurysm neuro-embolizations.

Results: Thanks to a careful calibration of XR-RV3 films using a clinical beam quality, a 11.4% overall measurement uncertainty was achieved. RDM PSD calculations and Gafchromic film measurements performed on the PMMA phantom agreed within 23% for all considered beam projections (PA, R/LAO20°-60°, RAO30°CAU20°, etc.), radiation qualities (60-85 kV), fields-of-view (16-30 cm), collimations and lateral/vertical table positions (-30 to +30 cm from isocenter). Skin dose distributions measured on patients show a 25% agreement with RDM mapping proving its accuracy in complex clinical settings.

Conclusion: This benchmarking study proves the accuracy of RDM skin dose mapping software as a key tool for interventional procedures with high risk of skin reactions. The software is being tested in clinical settings for cardiac and abdominal procedures extending the tests to Philips and Toshiba vascular equipment.

B-0314 14:41

Radiation dose impact of indication- and BMI-based CT protocols vs anatomy-based protocols: prospective multicentre study

H. Brat¹, F. Zanca², S. Imsand¹, B. Rizk³, S. Montandon⁴, H. Pasquier⁵, D. Fournier¹; ¹Sion/CH, ²Leuven/BE, ³Villars-sur-Glane/CH, ⁴Gland/CH, ⁵Creteil/FR (hugobene@gmail.com)

Purpose: To assess impact on dose metrics of indication- and BMI-based CT protocols vs anatomy-based protocols in a prospective multicentre dose optimisation study.

Methods and Materials: A protocol optimisation based on clinical indication and BMI with stepwise dose reduction was implemented on 5 CT scanners (Philips Healthcare, NL). 3215 abdomen CT examinations (mean BMI 26 (13-86)) were prospectively assessed for diagnostic image quality. All data were collected using a dose management software (DoseWatch, GE) after parameter uniformisation and protocol Radlex mapping. Anatomy- and indication-based institutional DRLs (median CTDIvol) were compared to each other as well as to national DRLs, according to BMI. Mann-Whitney tests were used to assess statistical significant differences (p<0.05).

Results: (1) All examinations were significantly lower than national P75 DRLs. (2) Per clinical indication, institutional DRLs were significantly lower than national abdomen P25 DRL (10 mGy) for BMI<25 patients. (3) BMI stratification enabled a significant dose impact (BMI<25/BMI>25): appendicitis 5.8/9mGy, colonography 4.1/9.5mGy, diverticulitis 5.9/9.5mGy, kidney stones 5.6/8.6mGy, liver 7.3/13mGy, pancreas 5.6/8.5mGy, renal infection 6.5/8.9mGy, renal tumour 5.8/9.4mGy. (4) Indication: compared to anatomy-based protocols were significantly lower for specific indications: CT colonography, kidney stones and pancreas for BMI<25 and pancreas, kidney stones, renal infection and renal tumour for BMI>25 patients.

Conclusion: This multicentre prospective study showed: (1) a statistically significant reduction in patient X-ray exposure when considering BMI and indication-based abdomen CT protocols compared to anatomical region protocols and national DRLs. (2) A p25 DRL target for BMI<25 abdomen CT achievable in all patients.

Author Disclosures:

F. Zanca: Employee; GE Healthcare. S. Montandon: Employee; Philips Healthcare.

B-0315 14:49

CT scan radiation dose evaluation by clinical indication: a multi-centric French study

A. Hornbeck¹, B. Habib Geryes², N. Pierrat², V. Jarrige³, S. Dreuil⁴, H. Ducou le Pointe²; ¹Strasbourg/FR, ²Paris/FR, ³Bourges/FR, ⁴Fontenay-aux-Roses/FR (amauryhornbeck@gmail.com)

Purpose: To propose dosimetric indicators representing French national practices for current adult CT-scan clinical indications.

Methods and Materials: 22 groups of clinical indications (GCI) for diagnostic CT-scan in adult patients were defined jointly by the French Society of Medical Physics (SFPMP) and the French Society of Radiology (SFR), based on their frequency and their requirements in terms of image quality. A national call for participation was sent to the medical physicists' community and a data sheet was emailed to the volunteers. Data collection took place from March to June 2017. For each scanner and each GCI, 15 to 30 consecutive exams performed between 2015 and 2017 were required. Collected data included scanner characteristics (model, year, maximum collimation), patient morphological data (age, gender, weight, height), technical settings (kV, scan length, contrast media, tube current modulation, reconstruction algorithm) and dosimetric data (CTDIvol, DLP) for each phase of the CT exam. A two-step validation was

performed: the global coherence of the collected data was checked and the pertinence of the selection method of the examinations was reviewed.

Results: 10753 CT-scan acquisitions, representing 7490 examinations, were collected from 53 public and private French radiology departments. Dosimetric indicators are proposed as examination DLP and acquisition CTDI and DLP for each GCI. Influence of patient morphology or examination technical settings is studied for selected GCIs.

Conclusion: CT-scan dosimetric indicators by clinical indication represent an attempt to provide a tool for CT dose optimization that is better adapted to the everyday clinical practices.

B-0316 14:57

Multicentre CT scanner dose excellence programme: strategies and results

H. Bra¹, C. Dias², S. Behzad Imsand³, C. Thouly¹, S. Montandon⁴, B. Rizk⁵, D. Fournier¹, F. Zanca⁶, ¹*Sion/CH*, ²*Buc/FR*, ³*Epalinges/CH*, ⁴*Gland/CH*, ⁵*Villars-sur-Glane/CH*, ⁶*Leuven/BE* (hugobene@gmail.com)

Purpose: To comply to the revised European Basic Safety Standards Directive to present a radiation dose optimisation and education programme through CT protocol harmonisation and optimisation in a multicentre setting.

Methods and Materials: A dose team was set up with one radiologist and one technologist in each center, a CT field engineer, a physicist and team leader. Data were collected in a dose management software (Dosewatch™, GE). Two-step strategy: 1. harmonisation by designing a clinical indication-based protocol map with 2 categories of patients according to body mass index (BMI < 25 and BMI > 25), after CT parameters uniformisation and protocol Radlex mapping. 2. Optimisation using a 12% step-wise mA reduction for all protocols. Low-contrast resolution was quantified by phantom analysis (QRM™ 401 abdomen phantom, Germany) to guarantee 5mm liver lesion detectability. Image quality was assessed using adapted European image quality guidelines and an electronic voting tool in the dose tracking software.

Results: Protocol harmonisation eliminated redundant protocols and reduced dose globally by 6% for chest and 7% for abdomen at institutional level. Protocol optimisation additionally reduced dose by 26% on average before hitting the low-contrast resolution limit (phantom measurements). Clinical indication- and BMI-based protocols allowed significantly lower dose levels than existing DRLs.

Conclusion: Homogenising CT protocols and optimising radiation doses without compromising image quality can be achieved with a clear road map, leadership, team work, education, regular communication, commitment, continuous dose monitoring and partnership with stakeholders. The use of automatic dose data collection and phantom tests during optimisation are key.

B-0317 15:05

Evaluation of diagnostic reference levels for conventional radiography in Austria

D. Wachbauer, F. Röthlin, P. Homolka, H.M. Moshammer, H. Ostermann; *Vienna/AT* (david.wachbauer@goeg.at)

Purpose: Evaluation of Austrian National Diagnostic Reference Levels (NDRLs).

Methods and Materials: A nationwide survey on common conventional radiography examinations was conducted. In line with Austrian radiation protection standards, all relevant Austrian hospitals and radiology practices were asked to report a minimum sample of 10 representative dose-area products (DAP) together with patient weight. Participants were invited via e-mail, followed up by reminders to increase participation rates. 59% of invited institutions (67% hospitals, 51% radiology practices) submitted DAP data (n=15305), 31% submitted additional data on patient weight. Case numbers presented varied from 1005 to 2121. Plausibility checks were performed to increase data quality. Third quartiles (Q75) of median DAP of participating institutions were calculated and compared to NDRLs.

Results: DAP values and interquartile ranges (IQR) are given in cGy*cm². Third quartiles (Q75) were considerably lower than existing NDRLs. Highest discrepancies (≥50%) were observed for skull AP/PA (Q75: 49, IQR:21, NDRL:100), skull LAT (Q75:49, IQR:21, NDRL:100), chest PA (Q75:13, IQR:6, NDRL:28) and LAT (Q75:42, IQR:21, NDRL:100). Discrepancies of ≥20% occurred for abdomen AP/PA (Q75:184, IQR:92, NDRL:300), pelvis AP (Q75:194, IQR:96, NDRL:300) and lumbar spine LAT (Q75:310, IQR:149, NDRL:400). For lumbar spine AP (Q75:176, IQR:90, NDRL:200) discrepancy was 12%. Q75 for bedside chest X-ray (Q75:20, IQR:10) was significantly (p<0.01) higher than thorax PA. Average patient weight was 74kg.

Conclusion: Q75 derived from the survey are on average 40% lower than Austrian NDRLs suggesting an update of NDRLs. Since Q75 correspond nicely to German and Swiss NDRLs, an update would be in accordance with European DRL harmonisation efforts.

B-0318 15:13

Diagnostic reference levels for interventional radiology: quantifying diagnostic cerebral angiography complexity

T. De Bondt¹, F. Zanca², X. Lopez Rendon², L. Brouhon¹, T. Van der Zijden¹, M. Voormolen¹, O. D'Archange¹, P.M. Parizel¹, ¹*Antwerp/BE*, ²*Buc/FR* (timo.debondt@gmail.com)

Purpose: To comply with the 2013/59/Euratom guidelines, diagnostic reference levels (DRL) for interventional radiology procedures need to be established. The complexity of procedures influences the delivered radiation dose; hence, a quantitative measure for complexity needs to be defined to stratify dose levels.

Methods and Materials: A complexity form was drafted through a collaboration of 3 interventionalists, a radiographer and a medical physicist. This form contains factors, with grading scale, that contribute to delivered radiation dose in diagnostic cerebral angiography. Complexity data from 27 interventions were acquired, along with automatically collected dosimetric data from a dose-tracking software system (DoseWatch, GE Healthcare). A multiple linear regression model was built to predict air kerma (Kair) and dose area product (DAP), which are the quantities in which DRLs are expressed.

Results: Statistically significant factors to predict Kair and DAP are fluoroscopy time (p=0.007; p<0.001) and presence of anatomical variant (p<0.001; p=0.002). Additional parameters are of significant value to predict DAP: weight (p=0.002), ease of catheterization (p<0.001) and peripheral vessel disease (p<0.001). A complexity index based on the regression coefficients was not able to categorize procedures as being easy, medium or difficult with a statistically significant difference.

Conclusion: Adding a complexity factor to define DRLs for interventional procedures poses a significant challenge. Our pilot study shows that relevant complexity factors differ between models for Kair and DAP, which is problematic. Larger datasets with standardized complexity forms need to be acquired to establish robust models to define DRLs for interventional radiology procedures.

Author Disclosures:

T. De Bondt: Consultant; GE Healthcare. **F. Zanca:** Employee; GE Healthcare. **X. Lopez Rendon:** Employee; GE Healthcare.

B-0319 15:21

Implementation of updated ACR size-specific CT diagnostic reference levels based on water-equivalent diameter and SSDE using automated dose monitoring software

P. Kröpil, C. Thomas, O.T. Bethge, Y. Klosterkemper, J. Aissa, E. Appel, C. Schleich, G. Antoch, J. Boos; *Düsseldorf/DE*

Purpose: To use automatic dose monitoring software to analyse institutional CT dose data regarding the updated American College of Radiology (ACR) diagnostic reference levels (DRLs) based on water-equivalent diameter (Dw) and size-specific dose estimates (SSDE) to detect patient-size subgroups in which dose can be optimised.

Methods and Materials: This retrospective study included all institutional chest CT, pulmonary CT-angiography and abdominopelvic CT from 06/2016 to 03/2017. Dw and SSDE were automatically calculated using in-house-developed Matlab software (The Mathworks, Natick) and stored into our dose monitoring system (DoseIntelligence®, Pulmocard). SSDE as CT dose parameter was analysed regarding updated ACR DRLs using Dw to group patients (size groups: 21-25cm, 25-29cm, 29-33cm, 33-37cm, 37-41cm).

Results: 30002 CTs were performed during the study period, n=4541 were included in the analysis (age 62.2±16.1 years, Dw 29.0±3.6cm). Mean SSDE relative to updated DRLs were 43.9±21.7% for non-contrast (n=655) and 51.2±24.5% for contrast-enhanced (n=719) chest CT, 66.9±30.6% for pulmonary CTA (n=371), 41.8±28.5% for non-contrast (n=635) and 55.1±21.7% for contrast-enhanced (n=2161) abdominopelvic CT. Lowest dose compared to ACR DRLs was found for Dw-group 21-25cm in non-contrast abdominopelvic CT (31.8±21.3%). The only transgression of ACR DRLs was found for Dw-group 37-41cm in non-contrast abdominopelvic CT (100.3±60.0%).

Conclusion: Mean SSDE of institutional CT protocols were lower than updated ACR DRLs. However, size-specific subgroup analysis revealed slight transgression of DRLs in non-contrast abdominopelvic CT of large patients. Updated ACR size-specific DRLs allow for a comprehensive analysis of CT dose data and help identifying patient subgroups in which dose can be optimised.

14:00 - 15:30

Room K

Radiographers

SS 314

Balancing dose and image quality in CT

Moderators:

S.D. Moerup; Odense/DK
N.N.

K-07 14:00

Keynote lecture

J. Santos; Coimbra/PT

B-0320 14:09

Image comparison of virtual non-contrast images and true non-contrast images obtained from dual-energy CT in latest generation dual-source and dual-layer CT for liver

B. Na, S.-J. Lee, H.-J. Jeong, D.-S. Kim; Seoul/KR (*passion3744@gmail.com*)

Purpose: To evaluate the reliability of virtual non-contrast (VNC) images obtained from two different dual-energy CT (DECT) which have different mechanism to produce VNC image.

Methods and Materials: Sixty patients underwent liver CT examination, using both dual-layer detector CT and third-generation dual source CT. Mean attenuation and contrast to noise ratio (CNR) for the relevant tissues were compared between true non-contrast (TNC) and VNC images. Paired student t tests were used for statistical analysis. Under same CT scan parameter, using the both DECT, performance phantom was scanned to evaluate background noise which could influence CNR.

Results: Mean attenuation difference between TNC and VNC image with dual-source CT and dual-layer CT were as follows, respectively: right liver lobe - 0.22 and -1.02, left liver lobe -0.99 and 2.12, psoas muscle -0.8 and 1.01, aorta 5.63 and 14.47, spleen 3.92 and 3.9, right kidney 5.17 and 6.59, left kidney 6.35 and 6.23. There was no significant difference in mean attenuation value of liver and psoas muscle from the both DECT scanner ($p > 0.05$). CNR on TNC image was higher than on VNC image because background noise of VNC was almost twice of higher than TNC. However, under same CT scan parameter, in the phantom experiment, same background noise values were shown between TNC and VNC from the both CT scanner.

Conclusion: VNC image obtained from both dual-source and dual-layer CT could potentially be an alternative to TNC image for liver examination.

B-0321 14:17

Acceptable noise levels in abdominal CT examinations of obese paediatric patients

M. O'Connor, J.G. Stowe, S.J. Foley; Dublin/IE (*michelle.oconnor@ucd.ie*)

Purpose: This research investigated acceptable noise levels in abdominal CT scans of obese paediatric patients

Methods and Materials: A MATLAB-based low dose simulation software was developed and validated in-house which enabled simulation of 50mAs stepwise increases in mAs. With ethical permission, a sample of 21 obese abdominal CT datasets, stratified by age (5-, 10- and 15-year olds) was retrospectively collected from Irish paediatric hospitals. Scans were performed on Philips 64 slice Brilliance scanners using weight-based protocols (80-120kVp, AEC, 64x0.625mm collimation, pitch0.891, iDose level 4). A single axial slice at the level of L1 from each scan was modified using the low dose simulation software to imitate scans obtained at lower mAs i.e. higher noise levels. This resulted in a total of 76 scans for review. Objective noise measurements were performed by the lead researcher using identical sized ROI's in three homogeneous locations; (1) liver, (2) subcutaneous adipose tissue, (3) air 2cm anterior to skin. Subjective image quality analysis was carried out by four experienced paediatric radiologists. Diagnostic acceptability, subjective image noise, contrast resolution, spatial resolution and visibility of anatomical structures were scored using a grading system devised from the European Guidelines on quality criteria for CT.

Results: The amount of noise considered acceptable in abdominal scans of obese paediatric patients by all four viewers was; 18.6HU in the 5-year-old group, 16.24HU in the 10-year-old group and 15.91HU in the 15-year-old group.

Conclusion: This research is the first to establish the maximum noise level (16HU) tolerated on abdominal CT scans of obese paediatric patients.

B-0322 14:25

Does body mass index affects radiation dose reduction in prospective electrocardiographic gating cardiac computed tomography?

B. Kara, M. Onur, A. Toker, S. Horoz, D. Akata; Ankara/TR (*tomografi@hotmail.com*)

Purpose: To evaluate the effect of body mass index (BMI) in radiation dose reduction in different cardiac computed tomography (CT) protocols.

Methods and Materials: We retrospectively evaluated cardiac CT examinations of 172 patients (79 female, 93 male; mean age: 64, ranging between 37-81) presented with cardiac symptoms. Patients were grouped according to BMI as group I (BMI < 30) and group II (BMI > 30). Cardiac CT examinations were performed with two different methods as conventional cardiac and prospective ECG gating (PECT) method. Radiation dose levels of patients were recorded as dose length product (DLP) values. We compared the DLP values of two cardiac CT protocols in group I and group II.

Results: PECT and conventional cardiac CT were performed in 32 and 56 patients, respectively in group I. Group II was consisted of 28 and 56 patients, respectively. There were statistically significant differences between mean DLP values of patients underwent PECT (DLP:111.88; DLP: 188.50) and conventional cardiac CT (DLP: 376.54; DLP: 858.54) in group I ($P < 0.0001$) and group II ($P < 0.0001$), respectively. Radiation dose reduction was more significant in group II.

Conclusion: Prospective ECG gated cardiac CT yields significant radiation dose reduction in patients with BMI < 30 and BMI > 30. Reduction of radiation dose is more prominent in patients with BMI > 30.

B-0323 14:33

Metal artefact reduction in the musculoskeletal system with dual-energy CT and spectral imaging

C. Fraga Piñeiro¹, M. González Vázquez¹, M. Monteiro²; ¹Vigo/ES, ²Coimbra/PT (*carlosfraga@gmail.com*)

Purpose: Metal artefacts have been an important limitation in musculoskeletal CT, but with the advent of dual-energy equipment new strategies to reduce metal artefact have been provided. We intended to compare metal artefact reduction and image quality in dual-energy computed tomography (DECT) using polychromatic and high-energy monochromatic images.

Methods and Materials: We collect data from 39 patients with metallic implants in extremities who underwent DECT polychromatic images with 80, 120 and 140kV and post-processing high-energy monochromatic images at 110, 130 and 150keV were used. Qualitative evaluation of the artefact and image quality was performed by two musculoskeletal radiologists using Likert scale. We use Spearman's Rho for inter-observer correlation. Artefact severity was assessed quantitatively.

Results: The best results were obtained at 140kV as well as in monochromatic series. The inter-observer agreement was (artefact $rs=0.73-0.95$ and quality image $rs=0.77-0.93$). Artefact severity (artefact index): 14.16 (80kV), 11.01 (120kV), 7.74 (140kV), 6.36 (110keV), 5.5 (130keV) and 4.94 (150keV). All results presented statistical significant differences ($p < 0.05$), except for 130 and 150keV which had comparable results.

Conclusion: Metal artefact reduction and image quality were rated superior in monochromatic high energies, compared with polychromatic images and, within these, those with 140kV were considered better than with energies of 80 and 120kV.

B-0324 14:41

Effective dose calculations of trunk CT scans in single-energy CT (SECT) and fast kVp switching dual-energy CT (FKS-CT)

K. Yagami¹, T. Miyoshi¹, S. Shigeyama¹, H. Okada¹, S. Suzuki², S.J. Foley³; ¹Gifu/JF, ²Toyooka/JF, ³Dublin/IE (*yagami@gifu-u.ac.jp*)

Purpose: To compare effective dose calculations based on dose-length product (DLP), size-specific dose estimate (SSDE) and measured organ doses in SECT and FKS-CT using an anthropomorphic phantom.

Methods and Materials: Two 64-detector row CT systems (Discovery CT750HD; GE and Brilliance 64; Philips) were used for dose measurement. An anthropomorphic phantom (Alderson Rando Phantom) with thermoluminescent dosimeters (BeO) was positioned inside (n=97) and on the surface (n=60) of various anatomical organs as per ICRP 103 for measuring the effective dose and calculating SSDE according to AAPM 204. The scanning conditions were the same as those used in clinical practice. The scanning range of FKS-CT was chest apices to symphysis pubis and SECT were three different examinations including chest apices to symphysis pubis (whole body), diaphragm to symphysis pubis (abdomen-pelvis) and chest apices to diaphragm (chest).

Results: Measured average effective dose between the two CT systems in whole-body CT was 13 mSv, in abdomen-pelvis CT was 9 mSv, chest CT was 5 mSv, and in FKS-CT was 13 mSv. For both CT systems, the difference between effective dose based on measured organ doses and calculations from

SSDE and k-factors was within 10% for all scan ranges and also FKS-CT. However, the use of DLP and k-factors resulted in 25% differences in effective dose compared to measured organ dose values.

Conclusion: For both SECT and FKS-CT, effective dose from measured organ doses closely approximated effective dose calculated from SSDE but DLP conversion to effective dose consistently underestimated both values.

B-0325 14:49

Impact of scanner type and acquisition parameters on the accuracy of displayed computed tomography dose index

C. Dionisi, B. Cannillo, R. Matheoud, L. Vigna, G. Fusco, M. Brambilla; Novara/IT (clizia.dionisi@gmail.com)

Purpose: According to the EU directive 2013/59, CT scanners shall be able to inform the practitioner of relevant parameters for assessing the patient dose. The aim of this study was to measure the accuracy of the displayed CTDI on ten different CT scanners of various vendors and to assess the impact of acquisition parameters on CTDI accuracy.

Methods and Materials: CT scanners from 4 vendors (16 slices n=6, 32 slices n=1, 64 slices n=3) were included in the study. The accuracy of the displayed CTDI was checked using a dosimeter. The impact of the independent variables, CT model (16, 32, 64 slices), phantom size (head/body), kVp (80, 100, 120, 140 kVp) and primary collimation (≤ 3 mm, 3-10mm, 10-20mm, >20 mm) on the dependent variable, accuracy of the displayed CTDI (derived from user manual), assessed by a four-way factorial ANOVA.

Results: All the factors had a statistically significant impact on CTDI accuracy ($p<0.01$). In a head to head comparison, the lower accuracies were found on average for 16 slices CT ($-10\pm 5\%$), for HeadPhantom ($-8\pm 8\%$), for 80kV ($-14\pm 11\%$) and for thick collimation ($-9\pm 12\%$), whereas maximum accuracies were found for 64 slices CT ($-5\pm 10\%$; $p<0.001$), BodyPhantom ($-5\pm 9\%$; $p=0.05$), 140 kV ($-5\pm 9\%$; $p<0.01$) and thin collimation ($-6\pm 7\%$; $p=NS$).

Conclusion: In the case of 16CTs and acquisition protocols involving the use of the HeadPhantom with low kV and a wide primary collimation, the displayed CTDI inaccuracies may be higher than 20% (suspension level in the EC RP N.162).

B-0326 14:57

Dose values in interventional computed tomography procedures: a multicentre study

A.R. Costa¹, I. Gomes¹, A.S. Pimenta², C. Oliveira¹, C.M. Almeida³, G.N. Paulo¹, J. Santos¹; ¹Coimbra/PT, ²Porto/PT, ³Lisbon/PT (araquel.costa@hotmail.com)

Purpose: The number of computed tomography (CT)-guided interventions had increased exponentially on the last decade. The aim of this study was to analyse the frequency of examinations, protocols and patient dose values.

Methods and Materials: The study was carried out in three Portuguese centres of reference of excellence. Retrospective analysis of the frequency of interventional CT procedures, patient data (age, gender and examination body region), exposure parameters and dose values, in terms of CT dose index (CTDIvol) and dose length product (DLP) were directly collected from picture archiving and communication system (PACS).

Results: Local DRLs were obtained for the most common interventional CT procedures per each centre (76% chest, 10% bone, 8% pelvic and 6% abdomen). Lung biopsy revealed to be the most frequent procedure. The exposure parameters and dose values vary across the centres. The found acquisition modes for intervention CT are 2D in (axial and helical mode) and CT fluoroscopy. The highest interventional acquisition dose values were found for CT fluoroscopy. The majority of the obtained dose values are similar to other studies.

Conclusion: The first national approach of interventional CT dose values was performed. Different approaches to these procedures were verified. A lack of standardisation of practice was identified justifying further research to protect the staff and decrease the risk of patient's over-exposure and procedure complications.

B-0327 15:05

One-stop imaging for triple-rule-out CT angiography using 16-cm wide-detector CT: a preliminary study

K. Liu, Z. Li; Chengdu, Sichuan/CN (634270986@qq.com)

Purpose: To investigate the feasibility of one-stop imaging for triple-rule-out (TRO) CT angiography (CTA) using 16-cm wide-detector CT in patients with acute chest pain.

Methods and Materials: Totally 23 patients with requests for examinations of thoracic vessels underwent TRO CTA on a 256-row, 16-cm wide-detector CT using a protocol consisting of an axial, ECG-gated cardiac acquisition followed by a spiral chest CT acquisition from the thoracic inlet to the diaphragm bottom in a free breathing condition. Heart rate was not controlled. The total volume of iodinated contrast medium (370mg/ml) for a biphasic injection protocol was 60-75ml (30-45ml based on the weight of patients; then another 30ml).

Attenuation values and standard deviations in pulmonary artery, thoracic aorta, coronary artery and muscle were measured to calculate contrast noise ratio (CNR) for vessels as objective indicators to evaluate the image quality. The subjective image quality was evaluated independently by two readers. Effective dose was recorded.

Results: All patients gained satisfactory image quality for diagnosis. There was no statistically significant difference between the scores of two readers ($P>0.05$). Mean attenuation values were adequate at 464.3 ± 146.1 HU in the pulmonary trunk, 313.1 ± 50.4 HU in the aortic arch, 378.5 ± 64.9 HU and 410.3 ± 58.3 HU in the right and left coronary artery, respectively. Noise was 16.6 ± 1.8 and CNR were 27.1 ± 8.6 in the pulmonary trunk, 18.0 ± 3.2 in the aortic arch, 22.1 ± 5.1 and 23.8 ± 3.7 in the right and left coronary artery, respectively. Effective radiation dose for the entire scan was 4.5 ± 0.9 mSv.

Conclusion: One-stop imaging for TRO CTA using 16-cm wide-detector CT can improve image quality, with low radiation dose and contrast medium volume.

B-0328 15:13

Optimisation of computed tomography practice: phantom and patient approach

F. Pires, T. Patrão, F. Alves, J. Santos; Coimbra/PT (fspires.11@gmail.com)

Purpose: Computed tomography examinations are responsible for a large proportion of effective collective dose across the countries, and concern about potential effects increased in the last years. The aim of this study was to analyse the exposure parameters and dose levels of the most common CT procedures to audit and implement optimisation measures.

Methods and Materials: This study was carried out in four phases: (1) establishment of local diagnostic reference levels (DRLs) base on the 75th percentile dose value of the most common CT examinations; (2) analyse of the practice and literature comparison; (3) anthropomorphic phantom experimental tests with PBU-60; (4) subjective and objective image quality analysis, based on visual grading characteristic (VGC) of the radiologist opinion of the guideline criteria and on the standard deviation value of the Hounsfield units in homogeneous regions of interest, respectively.

Results: Local DRLs were obtained for head, chest, abdomen and lumbar column. The majority of the values were higher than the recommendation. The optimisation experimental tests allowed the definition of new exposure parameters with radiologist approval. The optimised local DRLs are according to the recommend values in most of the body regions. Image quality analyses revealed an expected increase of noise; however, no significant differences were founded for the majority of criteria.

Conclusion: The most common CT procedures were optimised. Dose reductions were obtained with diagnostic imaging criteria fulfilment and radiologist approval.

B-0329 15:21

Assessment of image quality criteria from chest CT examinations

R. Carrasquinho¹, A.M. Ribeiro¹, L.P. Ribeiro¹, O. Lesyuk², R.P. Almeida¹, A.F. Abrantes¹; ¹Faro/PT, ²São Brás de Alportel/PT (oksanalesyuk@gmail.com)

Purpose: To assess the image quality criteria from chest CT examinations based in quality control charts and to demonstrate the importance of implementing an image quality control system.

Methods and Materials: A retrospective study was conducted in a public CT unit using a random sample of 750 chest CT examinations grouped into 30 smaller samples, each one with 25 exams. Using a checklist based on CT quality criteria, the conformities and non-conformities found were recorded and used to establish three types of quality control: (1) the proportion of conformities and non-conformities (p chart); (2) the total number of non-conformity exams (np chart) and (3) the total number of non-conformities in each sample (c chart), in order to suggest corrective actions for improvement.

Results: Considering all exams, 186 (24,80 %) are non-conformity exams. 265 non-conformities were identified and the "absence of data relating to examination" presented the highest number of non-conformities (55,09%), followed by the group "image quality criteria" (17,36 %), "artefacts" (13,96%) and the "incorrect positioning" (13,58 %).

Conclusion: This research allowed the identification of different types of non-conformities found in chest CT images, which have impact on image quality. Therefore, the existence of suitable quality control of the image is essential to achieve high quality standards in CT departments. It is recommendable to do training courses regularly improving radiographer's performance and strategies to improve image quality in CT must be implemented.

14:00 - 15:30

Room M 1

Cardiac

SS 303

Cardiac imaging in metabolic disease

Moderators:

A. de Roos; Leiden/NL
E. Pershina; Moscow/RU

B-0330 14:00

Obesity and type 2 diabetes: cardiovascular and cerebral aspects

R.L. Widya; Leiden/NL (R.L.Widya@lumc.nl)

Purpose: This thesis focuses on cardiovascular and cerebral dimensions and function in people with obesity and type 2 diabetes.

Methods and Materials: Extensive cardiovascular, abdominal and cerebral phenotyping by magnetic resonance imaging (MRI), magnetic resonance spectroscopy and functional MRI was performed in healthy, overweight and obese subjects, and type 2 diabetes patients. Statistical analysis included multivariate linear regression models to investigate the complex interrelationships between fatty liver, visceral and subcutaneous adiposity, metabolic syndrome, and several cardiovascular and cerebral outcome measures.

Results: In a large population-based cohort, hepatic triglyceride content was associated with left ventricular diastolic function and aortic pulse wave velocity after adjustments for several cardiometabolic risk factors. Studies with type 2 diabetes patients showed right ventricular remodeling and impaired systolic and diastolic function, in a similar manner as changes in left ventricular dimensions and function. A 6-month exercise intervention induced tissue-specific changes in ectopic fat compartments. Short-term caloric restriction normalized hypothalamic responsiveness to glucose ingestion in patients with type 2 diabetes. Obesity was associated with larger amygdalar and hippocampal volumes, and increased abdominal visceral adipose tissue rather than subcutaneous adipose tissue was associated with microstructural brain tissue damage.

Conclusion: Cardiovascular and cerebral impairments in obesity and type 2 diabetes are influenced by several metabolic abnormalities. Fatty liver itself could pose a risk of myocardial dysfunction and subclinical vascular impairment above and beyond known cardiovascular risk factors that are clustered within the metabolic syndrome. Exercise and caloric restriction show beneficial effects on ectopic fat deposition and hypothalamic glucose response.

B-0331 14:08

CT dose reduction for epicardial fat measurement in obese patients: effects of low-dose cardiac CT and adaptive statistical iterative reconstruction

S. Mirafzal, C. Lahaye, A. Mulliez, P. Morin, M.A. Vaz Touret, Y. Boirie, L. Boyer, L. Cassagnes; Clermont-Ferrand/FR (sonia_mirafzal@hotmail.fr)

Purpose: To evaluate the effects of radiation dose reduction—120 kV versus 100 kV—and the reconstruction algorithm used—adaptive statistical iterative reconstruction (ASIR)—on the variability and reproducibility of EFV (epicardial fat volume) in obese patients.

Methods and Materials: Standard dose CT (120 kV) and low-dose (100kV) calcium artery scoring CT (CAS-CT) examination were performed in 80 obese patients. The standard dose CT images were reconstructed using ASIR 30% (reference standard in our center); the low-dose CT images were reconstructed using ASIR 30%, 50% and 100%. In the 320 images series obtained, the EFV was measured using a semi-automatic software. Two observers independently quantified EFV and inter-observer agreement was evaluated.

Results: Radiation dose of the low-dose CAS-CT examinations was 67% (mean) lower than standard dose CT examinations. The mean noise on standard dose CT, ASIR 30 low-dose CT, ASIR 50 low-dose CT, ASIR 100 low-dose CT were 22.5, 35.5, 30.3, and 22.8, respectively. Excellent correlations were observed between the EFV measured on standard dose CT and EFV measured on low-dose CT ASIR 50/EFV measured on low-dose CT ASIR 100 ($r=0.96$, $p<0.01$ and $r=0.97$, $p<0.01$, respectively). Inter-observer agreement was excellent too: $r=0.97$, $p<0.01$.

Conclusion: A 67.0% reduction of the radiation dose would be possible in CT for the measurement of EFV in obese patients using low-dose CT and the reconstruction algorithm ASIR instead of 120 kV standard dose CT.

B-0332 14:16

Computer-aided semi-automatic quantification of epicardial fat volume on angio-CT images

M. Codari¹, C. De Angelis², M. Scarabello², F. Secchi¹, F. Sardaneli¹; ¹San Donato Milanese/IT, ²Milan/IT (marina.codari@grupposandonato.it)

Purpose: The quantification of epicardial adipose tissue (EAT) on angio-CT images is still limited in clinical routine due to the post-processing time. To this aim, we proposed a semi-automated method for EAT quantification and evaluated its reproducibility.

Methods and Materials: Twenty-one consecutive angio-CT, performed from February 2017 to May 2017, were retrospectively selected. Our local Ethics Committee approved this study. A semi-automatic approach was developed to detect the pericardial sac through the 3D interpolation of contours manually identified on different views and segment the EAT contained therein. Two operators segmented all images using a double-blinded approach. One operator performed it twice. The number of contours and EAT volume (cm^3) were recorded for all images. Data are presented as median and interquartile range. Wilcoxon signed rank test was used for comparisons while Bland-Altman analysis was used to assess operator reproducibility.

Results: Intra- and inter-operator analysis showed: a bias of 1.0 cm^3 , a coefficient of repeatability of 14.0 cm^3 , an average measurement of 90.2 cm^3 , and a reproducibility of 84%; 1.1 cm^3 , 21.0 cm^3 , 90.9 cm^3 , and 77% respectively. The median number of drawn contours was 12 (10-14), with statistically significant difference between the number of segmented contours by each operator ($p=0.018$), but not between the corresponding volume values ($p=0.875$).

Conclusion: The proposed method allows segmenting a whole angio-CT images, with submillimetric resolution, using few contours with an acceptable level of reproducibility. The significant difference in contours number seems to not affect volume segmentation accuracy, allowing to further reduce them.

B-0333 14:24

Epicardial fat volume as a potential imaging biomarker for coronary artery disease in symptomatic patients

G. Milanese¹, M. Silva¹, L. Bruno², M. Goldoni¹, E. Maffei³, F. Cademartiri⁴, N. Sverzellati¹; ¹Parma/IT, ²Palermo/IT, ³Urbino/IT, ⁴Rotterdam/NL (gianluca.milanese@studenti.unipr.it)

Purpose: Epicardial adipose tissue is a visceral fat depot with paracrine activity that may associate with increased coronary artery disease (CAD). We tested if individuals with increased epicardial fat volume (EFV) - as quantified by cardiac CT angiography (CCTA) - show a higher amount of coronary artery calcifications (CAC) and a higher prevalence of CAD.

Methods and Materials: Patients with clinical indication to CCTA were retrospectively selected. EFV was quantified as the sum of voxels with density between -190 and -30 HU, within the volume outlined by the epicardial sheet. CAC was quantified according to the Agatston score (AS) and patients were stratified in four groups: $AS=0$; $1 \leq AS < 100$; $100 \leq AS < 400$ and $AS \geq 400$. CAD was classified as absent, non-obstructive, and obstructive (lumen reduction $\geq 50\%$). Parameters were reported as median and interquartile range (IQR). Correlation was tested by Spearman test. Multivariable analysis tested association between CAD and morpho-clinical metrics.

Results: In 1,351 patients, median EFV was 90.92 ml (IQR=66,2); median CAC was 58 (IQR=452). CAD was absent in 848, non-obstructive in 325 and obstructive in 170 patients. EFV and CAC were moderately correlated ($r_s = 0.34$; $p < 0.001$). EFV was significantly higher in patients with higher CAC ($p < 0.001$) and in patients with obstructive CAD ($p < 0.001$). CAC ($p < 0.001$), but not EFV ($p > 0.05$), was a significant predictor of CAD category. When adjusting for traditional clinical cardiovascular risk factors, EFV was not a significant predictor of CAC.

Conclusion: EFV is higher in patients with obstructive CAD, its role in the development of CAD is probably due to shared risk factors.

B-0334 14:32

Intra- and interobserver variability of MR-based assessment of myosteatosis as a biomarker for metabolic diseases in subjects from the general population

L.S. Kiefer¹, J. Fabian¹, R. Lorbeer², J. Machann¹, C.L. Schlett³, S. Rosplecz⁴, A. Peters⁵, F. Bamberg¹; ¹Tübingen/DE, ²Munich/DE, ³Heidelberg/DE, ⁴Oberschleißheim/DE, ⁵Neuherberg/DE (lena.kiefer@med.uni-tuebingen.de)

Purpose: To determine the reproducibility of skeletal muscle adipose content quantification by magnetic resonance imaging (MRI) as a metabolic biomarker in subjects from the general population.

Methods and Materials: Subjects without cardiovascular disease from a population-based cohort study underwent a whole-body 3T MRI protocol, including a T2*-corrected, multi-echo 3D-gradient-echo Dixon (TR 8.90 ms, six echo times, flip angle 4°). Skeletal muscle adipose content was quantified as mean proton-density fat fraction in % in M. psoas major (MPM), M. quadratus

lumborum (MQL), autochthonous back muscles (ABM) and M. rectus abdominis (MRA) on the right (R) and left (L) side at level L3 by two independent readers. Variability was assessed using Bland-Altman plot analysis of absolute differences and intra-class-correlation coefficients (ICC) from two-way random-effects ANOVA.

Results: Among 40 subjects (mean age 54.8±8 years, 62.5% males, mean BMI 28.7±5.3) a total of 320 measurements were performed. Inter-reader agreement was excellent for all muscle compartments (MPMR: ICC 0.91, MPML: ICC 0.98, MQLR: ICC 0.98, MQLL: ICC 0.91, ABMR ICC 0.97, ABML: ICC 0.98, MRAR: ICC 1.00, MRAL: ICC 0.98) with only minor absolute differences (-0.3±1.0%, -0.1±0.5%, 0.2±0.7%, -0.2±0.8%, -0.9±1.5%, -0.4±1.3%, -0.3±1.5% and -0.3±1.5%; respectively). Similarly, intra-reader reproducibility was excellent for all included muscle compartments (ICC 0.95 to 1.00, absolute differences -0.2 to 0.3%). All agreement was independent of BMI and body height (ICC 0.90 to 0.99).

Conclusion: Skeletal muscle adipose content by MRI is highly reproducible and may therefore serve as a robust metabolic biomarker in larger cohort studies to determine its prognostic role.

B-0335 14:40

Cardiovascular function in relation to abdominal adipose tissue distribution

E.H.M. Paiman, R. de Mutsert, R.L. Widya, J.W. Jukema, F.R. Rosendaal, H.J. Lamb; *Leiden/NL (e.h.m.paiman@lumc.nl)*

Purpose: To assess the relation of abdominal subcutaneous (SAT) and visceral adipose tissue (VAT) with left ventricular (LV) remodeling, cardiac function and aorta stiffness.

Methods and Materials: This is a cross-sectional analysis of 1076 participants of the Netherlands Epidemiology of Obesity study, who underwent abdominal and cardiovascular MRI. We used linear regression to examine the associations of SAT and VAT area with LV ejection fraction (EF), LV mass/end-diastolic volume (concentricity), the ratio of mitral early and late filling rate (E/A) and aorta pulse wave velocity (PWV), adjusted for sex, age, ethnicity, education, smoking, menopausal status, use of hormone therapy and either VAT or SAT.

Results: Participants (47% men) had a mean (SD) age of 56 (6) years, SAT: 237 (97) cm², VAT: 91 (56) cm², LVEF: 64 (6)%, LV concentricity: 0.66 (0.13) g/ml, E/A ratio: 1.32 (0.50), PWV: 6.7 (1.4) m/s. Per SD of SAT, LV concentricity was 0.02 (95%CI: 0.01, 0.03) g/ml lower, and LVEF was 0.79 (0.30, 1.29)% lower. Per SD of VAT, LV concentricity was 0.02 (0.01, 0.03) g/ml higher, and E/A ratio was 0.07 (0.03, 0.11) lower. SAT and VAT were not associated with PWV (beta: 0.00 (-0.11, 0.11) m/s per SD SAT and 0.06 (-0.07, 0.19) m/s per SD VAT).

Conclusion: In this middle-aged population-based cohort, SAT was associated with LV eccentric remodeling and lower systolic function. In contrast, VAT was associated with LV concentric remodeling and lower diastolic function. For cardiovascular risk assessment, it is essential to differentiate between abdominal subcutaneous and visceral adiposity.

B-0336 14:48

MRI-based epi- and para-cardial fat depots in a cohort of prediabetics, diabetics and healthy controls from a general population without cardiovascular disease

S.D. Heber¹, R. Lorbeer², S. Gatidis¹, J. Machann¹, S. Auweter², S. Sellner², A. Peters³, F. Bamberg⁴, C.L. Schlett⁴, ¹Tübingen/DE, ²Munich/DE, ³Neuherberg/DE, ⁴Heidelberg/DE (*sophiaheber@web.de*)

Purpose: The quantification of the pericardial fat depots by MRI in a cohort of prediabetics, diabetics and healthy controls from a population without cardiovascular disease and relation to different fat depots and cardiovascular risk factors.

Methods and Materials: Assessment of the cardiac fat depots was conducted in the MR cine steady-state free precession (SSFP) sequence (TR 29.97 ms, TE 1.46 ms) in 400 subjects from the KORA FF4 cohort. Epi- and pericardial fat were segmented manually in a single slice at end-systole and end-diastole. Median regression was conducted to examine the relationship of epi- and paracardial fat to impaired glucose metabolism.

Results: Of 400 subjects, 372 (93%) were included in the analysis (median age 57 years; 59.4% male), including 220 healthy controls, 100 prediabetics, and 52 diabetics. Fat measurements correlated strongly between end-systolic and end-diastolic slices while measurements were on average slightly larger when derived from systolic (+11.3% for epicardial- and +10.8% for paracardial fat). Both, epi- and para-cardial fat increased stepwise from healthy controls to subjects with prediabetes and diabetes (7.7 vs. 9.2 vs. 10.3 cm² for epicardial- and 14.3 vs. 20.3 vs. 27.4 cm² for paracardial fat, retrospectively; both p<0.001). While paracardial fat is independent of BMI (p=0.03) or SAT (p=0.048) in diabetics, none of the cardiac fat depots are associated to the diabetic status independent of VAT.

Conclusion: There is an increase for epi- and paracardial fat from healthy controls to subjects with prediabetes and diabetes, which is only partially independent of other, abdominal MR-based fat depots.

B-0337 14:56

Coronary CT angiography-based fractional flow reserve in diabetic patients: results from the MACHINE consortium

F. Nous¹, A. Coenen¹, M. Kruk², J. De Geer³, U.J. Schoepf⁴, D. Yang⁵, A. Kurata⁶, R.P. Budde¹, K. Nieman¹; ¹Rotterdam/NL, ²Warsaw/PL, ³Linköping/SE, ⁴Charleston, SC/US, ⁵Seoul/KR, ⁶Ehime/JP (*f.nous@erasmusmc.nl*)

Purpose: Coronary CT angiography (CCTA)-derived fractional flow reserve (FFR) (CT-FFR) simulates the hyperaemic state to evaluate the haemodynamic impact of coronary artery disease (CAD), assuming a normal coronary microvascular response. Coronary microvascular dysfunction, however, is frequently present in diabetic patients. We assess the diagnostic performance of a machine learning (ML) application for on-site computation of CT-FFR in diabetic patients.

Methods and Materials: The diagnostic performance (sensitivity, specificity, negative predictive value, positive predictive value, accuracy) of ML-based CT-FFR was analysed per patient and per vessel in patients with and without diabetes, who were enrolled in the MACHINE consortium. Invasive FFR was used as a reference and FFR ≤0.8 was considered haemodynamically significant for CAD. Per-patient and per-vessel discrimination of lesion-specific ischaemia by CT-FFR were assessed by the area under receiver operating characteristic (ROC) curves.

Results: 75 out of 351 patients had diabetes (21%), involving 110 of the 525 vessels (21%). Per-vessel diagnostic accuracy of ML-based FFR in diabetic patients was 85% (95% CI: 72-91%) and 76% (72-80%) in non-diabetic patients (p=0.136). On a per-patient level, the accuracy of ML-based FFR in diabetic patients was 86% (77-94%) and in non-diabetic patients 85% (80-89%) (p=0.884). The area under curve of per-vessel and per-patient ROC curves of diabetic and non-diabetic patients was comparable (per-vessel: 0.88 (0.82-0.95) vs 0.82 (0.78-0.86); per-patient: 0.88 (0.80-0.96) vs 0.82 (0.77-0.87)).

Conclusion: The diagnostic performance and the discrimination of ischaemia by on-site ML-based CT-FFR analysis are similar in diabetic patients and non-diabetic patients.

Author Disclosures:

U.J. Schoepf: Consultant; Bayer Healthcare and Guerbet Inc..

Research/Grant Support: Astellas, Bayer Healthcare, GE Healthcare, Siemens Healthineers. **K. Nieman:** Research/Grant Support; Bayer Healthcare, GE Healthcare, Siemens Medical Solutions, HeartFlow.

B-0338 15:04

The right ventricular strain assessment in type 2 diabetes mellitus patients: insights from cardiac magnetic resonance feature tracking

B.-Y. Hu, Z.-G. Yang, X. Liu, K. Shi, H.-Y. Xu, Y.-K. Guo; *Chengdu/CN (237772342@qq.com)*

Purpose: To investigate the feasibility of cardiac magnetic resonance (CMR)-derived feature tracking for assessing right ventricle (RV) myocardial deformation in type 2 diabetes mellitus (T2DM), and to determine if these parameters are correlated to biochemical markers.

Methods and Materials: A total of 57 T2DM patients, including 14 with impaired right ventricle ejection fraction (RVEF), 43 with preserved RVEF and 22 healthy controls were studied. Cardiac volumes and function, right ventricular feature tracking parameters [the global longitudinal, circumferential, and radial peak strain (PS), peak diastolic strain rate (PDSR), and peak systolic strain rate (PSSR)] were determined by CMR. The intraclass correlation coefficient (ICC) was used to evaluate the inter- and intra-observer variabilities.

Results: Compared with controls, significantly lower values of longitudinal PS in the T2DM with impaired RVEF (-23.90±4.06% vs -27.22±2.37%, p=0.009) and preserved RVEF groups (-25.27±3.37% vs -27.22±2.37%, p=0.009) indicates impairment of RV function. Furthermore, the circumferential and radial PDSR in the impaired RVEF group decreased significantly compared with controls (both P<0.05). In the T2DM cohort, longitudinal PS correlated with HbA1c (r=0.470, P=0.001) and low-density lipoprotein (r=0.355, P=0.027), and had weak correlation with RV end-diastolic volume (r=0.279, P=0.013), RV end-systolic volume (r=0.262, P=0.020), and RV myocardial mass (r=0.226, P=0.045). The ICCs for intra- and inter-observer variabilities were 0.798-0.905 and 0.701-0.897.

Conclusion: In adults with T2DM, abnormal RV myocardial deformation can be monitored using CMR feature tracking, even in those with preserved RVEF; and the diastolic dysfunction was associated with HbA1c and low-density lipoprotein.

B-0339 15:12

Assessment of the left ventricular myocardial strain in type 2 diabetes mellitus patients with hypertension using MR tissue tracking
L. Xie, Y. Guo, Z. Yang; *Chengdu/CN (xielinjun2016@163.com)*

Purpose: To investigate the left ventricular myocardial strain in type 2 diabetes mellitus (T2DM) patients with hypertension using cardiac magnetic resonance tissue tracking.

Methods and Materials: Thirty-six T2DM patients with hypertension (Group 1), 39 cases of T2DM without hypertension (Group 2) and 26 normal control individuals were enrolled. All patients underwent cardiovascular magnetic resonance (CMR), including cardiac cine sequence (short-axis, long-axis two-chamber and four-chamber image). Cardiac function indexes and tissue tracking parameters were all measured by CVI42 and compared statistical. Pearson's correlation between the left ventricular ejection fraction (LVEF) and the left cardiac strain parameters were also investigated.

Results: All the patients recruited finished CMR and the baseline characteristics were recorded. The Group 1 presented lower LVEF than Group 2 and normal group (LVEF: Group 1: 57.17±9.30%, Group 2: 61.11±5.73%, normal group: 62.22±3.44%; $P=0.032$, 0.004). Compared with the normal group, the global radial, circumferential and longitudinal peak strain (PS) of the Group 1 were significantly reduced (all $P<0.05$). Group 2 presented with lower longitudinal PS value than control group (Group2: -16.50±2.27%; control group: -18.10±1.85%, $P=0.004$). Pearson correlation analysis indicated a significant and positive correlation between the LVEF and radial PS ($r = 0.746$, $P<0.001$) and circumferential PS ($r = 0.786$, $P<0.001$). A positive correlation existed between the longitudinal PS and LVEF ($r = 0.587$, $P<0.001$).

Conclusion: The myocardial strain decreased in T2DM patients with hypertension were more obvious than control group. The myocardial strain appears to be more sensitive than LVEF for assessing LV dysfunction in T2DM patients without hypertension.

B-0340 15:20

Phenotypic multi-component involvement of subclinical disease as quantified by MRI in subjects with prediabetes, diabetes and normal glucose tolerance

C. Storz¹, S. Rospolecz², R. Lorbeer³, W. Rathmann⁴, M.F. Reiser³, U. Hoffmann MD MPH⁵, A. Peters², C.L. Schlett⁶, F. Bamberg¹; ¹Tübingen/DE, ²Neuherberg/DE, ³Munich/DE, ⁴Düsseldorf/DE, ⁵Boston, MA/US, ⁶Heidelberg/DE (corinna.storz@med.uni-tuebingen.de)

Purpose: To compare whole-body subclinical disease phenotypes by magnetic resonance (MR) imaging to study differences between subjects with prediabetes, diabetes, and controls with normal glucose tolerance.

Methods and Materials: Overall, 400 subjects from a western general population without prior cardiovascular disease were enrolled in a prospective case-control study and underwent whole-body MR between June 2013 and September 2014. The MR protocol was tailored to the assessment of metabolic and arteriosclerotic alterations, including age-related white matter changes, hepatic proton-density-fat-fraction, visceral adipose tissue volume, left ventricular remodeling index, carotid plaque, and late-gadolinium enhancement. MR features were summarized in an ordinal phenotypic-based metric (score range: 0-6). Univariate, multivariate correlation, and unsupervised clustering were performed.

Results: 243 subjects with complete multi-component MR datasets were included in the analysis (55.6±8.9 years, 62% males), 48 were classified as subjects with prediabetes and 38 as subjects with diabetes. The MR phenotypic score was significantly higher in subjects with diabetes and prediabetes as compared to controls (mean score, 3.00±1.04 and 2.69±0.98 vs 1.22±0.98, $p<0.001$, respectively), also after adjustment for potential confounders. Clustering analysis identified two clusters of MR phenotype patterns associated with glycaemic status ($p<0.001$), independent of the MR phenotypic score (Cluster II: odds ratio: 2.49; 95%-CI: [1.00, 6.17], $p=0.049$).

Conclusion: Subjects with prediabetes and diabetes have significantly higher phenotypic-based metric as compared to subjects with normal glucose tolerance, and feature a diabetes-specific pattern of MR phenotypes.

14:00 - 15:30

Room M 2

Paediatric

SS 312

Muskuloskeletal and child abuse

Moderators:

A. Bartoloni; Rome/IT
R.R. Van Rijn; Amsterdam/NL

B-0341 14:00

Detection of bridging vein thrombosis at computed tomography: a specific sign of shaken baby syndrome?

S. Nahmani, D. Grevent, K. Beccaria, N. Boddart; Paris/FR
(sarah.nahmani@gmail.com)

Purpose: Shaken baby syndrome (SBS) also known as abusive head trauma (AHT) is a major cause of head trauma in infants. Bridging vein rupture caused by antero-posterior movements has proved to be responsible of subdural hematoma (SDH). The resulting thrombosis, following the rupture can be seen in CT and MRI. The objective is to evaluate the specificity of bridging vein thrombosis (BVT) seen in cranial CT (cCT) in SBS compared to a cohort of infants victims of accidental head trauma.

Methods and Materials: A total of 173 cCT of children under 36 months of age, performed between 2010 and 2016 in Necker hospital (92 who were diagnosed AHT and 81 with accidental head trauma) were analyzed retrospectively and independently by two radiologists who were blinded to the diagnosis.

Results: BVT were found in 69/92 AHT, sensitivity = 75%, (95% CI : 64.8-83.4%) and 6/81 accidental head trauma, specificity = 93% (95% CI : 84.6-97.2%) by the senior reader (and respectively 65, sensitivity = 71%, (95% CI : 60.2-79.6) and 11, specificity = 86% (95% CI : 76.9 - 93) by the junior reader), $p<0.05$. Further analysis showed that the 6 BVT in the accidental group were consecutive to 2 road traffic accidents, 1 defenestration, 1 polytraumatism, and 2 traumatism eventually reclassified as AHT.

Conclusion: BVT, seen in cCT, is a very sensitive and specific sign of AHT. This finding is not compatible with a minor alleged trauma and should suggest AHT in infants brought spontaneously to emergency room without polytrauma.

B-0342 14:08

The estimation of radiation dose in suspected child abuse imaging

H. Niiniviita, E. Saukko, J. Saunavaara; Turku/FI (hannele.niiniviita@tyks.fi)

Purpose: To assess the radiation doses related to imaging in suspected child abuse with patients under the age of 2 years and to estimate the additional radiation dose, if follow-up images are taken according to the new guidance of the Royal College of Radiologists.

Methods and Materials: There were 60 suspected child abuse patients, who were imaged between the years 2013 and 2016. The number of studies, radiation doses and image parameters for calculating effective dose (voltage, tube current-time product, image area, additional filtration) were collected from PACS. The radiation dose was recorded as DAP-value (dose area product, $mGycm^2$) and the effective dose of skeletal survey was estimated by PCXMC-software for nine patients. The effective dose of suggested follow-up images were estimated from these calculations.

Results: We reviewed 154 x-rays studies, where the main protocols used were skeletal survey (22%), femur (17%) and thorax (10%). In skeletal survey there were at mean 19 exposures and the mean DAP was 261 $mGycm^2$. The highest DAP-values were observed in skull (AP+LAT, 102.7 $mGycm^2$), spine (LAT, 34.8 $mGycm^2$), thorax (oblique, 17.1 $mGycm^2$) and pelvis (AP, 15.4 $mGycm^2$). The mean effective dose in skeletal survey was 61 μSv and the effective dose of follow-up images including extremities, thorax AP and two obliques was estimated to be approximately 25 μSv . The effective dose of extremities contribute 25% of total dose in control images.

Conclusion: The highest radiation doses related to suspected child abuse imaging are generated from skull and spine. The additional radiation dose of follow-up images is low.

B-0343 14:16

Optimising imaging in suspected child abuse: a five-year prospective study in a tertiary referral children's service

I. Moorthy, K. Iliadis, T. Diacon, L. Moon, L. Vitta; Brighton/UK
(kyriakos.ilias@bsuh.nhs.uk)

Purpose: Imaging teams are crucial in assisting paediatric and social service professionals when child abuse is suspected. This study aims to consolidate guidance on best practice in imaging these vulnerable children, while remaining sensitive to the rights of their carers.

Methods and Materials: Prospective data were collated for every skeletal survey performed over a five-year period (April 1, 2012 to March 31, 2017) as part of an ongoing audit, using a pre-designed data collection form. Accuracy of reporting of bony injury, and bony density and morphology were studied (audit standard: 100% compliance). As double reporting and timely follow-up imaging contribute to diagnostic accuracy, this was also studied (audit standard: 100% compliance). Our neuroimaging practice was also audited.

Results: Total number of children studied = 88 (100%); number of positive initial skeletal surveys = 48 (55%); number where bone morphology and density were commented on = 80 (91%); number of double reports of initial skeletal surveys = 80 (91%); number where second reporter disagreed with first reporter = 3 (3%); interval to follow-up imaging = 11 to 33 days (mode 14 days); number of follow-up surveys = 72 (82%); number of follow-up surveys with new findings = 4 (5%).

Conclusion: Multidisciplinary teamwork and clear imaging protocols (including double-reporting, follow-up imaging, and relevant neuroimaging) are crucial to making the correct diagnosis in suspected child abuse. Ongoing audit of imaging practice optimises diagnostic accuracy.

B-0345 14:24

Quantitative bone ultrasound: low sound wave propagation in cortical bone as a novel, non-invasive imaging biomarker in children and adolescents with hypophosphatemic rickets

J. Schneider¹, A. Raimann², A. Boni-Mikats², M. Krssak², R. Klepochová², G. Häusler², K. Raum¹, J.M. Patsch²; ¹Berlin/DE, ²Vienna/AT (janina.patsch@meduniwien.ac.at)

Purpose: The assessment of ultrasound wave propagation in cortical bone is a novel, non-invasive quantitative imaging tool in bone research. The purpose of this study was to determine sound wave propagation properties in the distal extremities of paediatric patients with hypophosphatemic rickets and healthy controls.

Methods and Materials: Following study approval by institutional review and written informed consent, we performed quantitative bone ultrasound in children, adolescents and young adults with xlh (n=8), and healthy controls (n=13). The majority of patients and controls also underwent high-resolution peripheral quantitative computed tomography (HR-pQCT) of the radius and tibia as a standard of reference. Bone ultrasound was performed at the distal radius and the distal tibia according to a structured examination protocol, using a dedicated 1MHz transducer with one receiver arrays and two transmitter array. Based on bidirectional axial transmission and propagation of ultrasound waves, the 'first arriving signal velocity' (vFAS) was measured and post-processed. HR-pQCT images were reviewed by a board-certified radiologist, data were evaluated by the manufacturer's quantification software.

Results: Quantitative bone ultrasound of wave propagation was feasible in all study participants. At the distal radius, we found vFAS to be significantly lower in XLH patients than in healthy controls (-6.8%; ANOVA: p = 0.0013). A similar reduction of vFAS was observed in the distal tibia (-6.5%; ANOVA: p = 0.0009). HR-pQCT scans revealed microstructural deficits in both cortical and trabecular bone.

Conclusion: Sound wave propagation in cortical bone is a promising imaging biomarker in children and adolescents with hypophosphatemic rickets.

B-0346 14:32

Evaluation of a new computer-aided diagnosis system for automated bone age assessment in comparison to the Greulich Pyle atlas method: advanced results of a multireader study

C. Booz, J.L. Wichmann, S. Böttger, A. Al Kamali, S.S. Martin, D. Leithner, L. Lenga, T.J. Vogl, B. Bodelle; Frankfurt a. Main/DE (boozchristian@gmail.com)

Purpose: To investigate a novel computer-aided diagnosis (CAD) software for bone age (BA) assessment in comparison to the Greulich Pyle (GP) method regarding its accuracy and precision. In addition, we evaluated the influence of carpals on bone age assessment.

Methods and Materials: Data from clinically indicated left hand and wrist radiographs of 305 children were included. Total BA, BA of the distal radius and BA of the carpals were determined by three radiologists using the GP method and additionally assessed by the CAD software (BoneXpert). Pearson product-moment correlation, Bland-Altman plot, root-mean-square (rms) deviation and further agreement analyses were calculated.

Results: Mean total BA was 9.76 years (CAD) and 9.81 years (GP) showing very high correlation between both approaches (r=0.985; rms deviation 0.49 years). Mean BA of the distal radius was 9.50 years (CAD) and 9.82 years (GP) (r=0.963). Mean BA of the carpals was 9.94 years (GP). Statistical analysis demonstrated a significantly higher correlation between total BA and BA of the distal radius (r=0.969) than between total BA and BA of the carpals (r=0.923). Assessment of the carpals showed only good inter-reader agreement (κ=0.79), while the agreement in analysing the distal radius was excellent (κ =0.98).

Conclusion: The evaluated CAD system allows for precise BA assessment compared with the GP method. Assessment of the carpals is challenging and leads to comparatively lower precision and inter-reader agreement. Methods assessing BA without analysing the carpals should be more accurate than methods including the carpals in analysis like the GP method.

Author Disclosures:

J.L. Wichmann: Speaker; GE Healthcare, Siemens Healthineers.

B-0347 14:40

Role of imaging in the diagnosis of glenohumeral deformity following obstetric brachial plexus injury

A.N. Parimalai¹, A. Chelladurai¹, K. Damodaran², P. Muthayan¹; ¹Chennai/IN, ²Coimbatore/IN (anand7687@gmail.com)

Purpose: To study the use of imaging in the assessment of glenohumeral deformity following obstetric brachial plexus injury. To study the usefulness of CT in the measurement of glenoid version angle and humeral head dislocation and to propose a grading for the severity of glenohumeral deformity.

Methods and Materials: This was a prospective study, conducted in the Department of Radiodiagnosis at Stanley Medical College between August 2015 and July 2016. The study group included 21 children below the age of 10 years presenting with posterior dislocation of the shoulder, with a past history of obstetric brachial plexus palsy. The children were examined with modified Mallet score and Naraka's neurological grading. CT of both shoulders using GE Optima 128 slice scanner and MRI using 1.5 Tesla Siemens unit were done. MR myelogram of the cervical spine was done.

Results: In our study, glenoscapular angle, percentage of humeral head anterior to the scapular line, scapular height and scapular width were analysed by paired Student's t test and were statistically significant [p<0.05]. We classified the children according to Waters and proposed radiological grading. We also classified according to the joint's stability. 3 affected joints were stable, 9 were subluxated and 9 dislocated. The higher the grade of deformity, the more difficult will be the shoulder movements and the scores worse in the Modified Mallet scale.

Conclusion: CT clearly identifies glenohumeral deformities such as increased glenoid retroversion, posterior subluxation or dislocation of the humeral head, smaller humeral head size and smaller size of the scapula as deviations from the normal status.

B-0348 14:48

Relationship between cranio-orbital volume changes and the severity of skull base dysmorphism in infants with anterior synostotic plagiocephaly: a quantitative analysis

M. Panfilii, R. Calandrelli, L. Massimi, S. Gaudino, C. Colosimo; Rome/IT (panfilimarco@gmail.com)

Purpose: The premature fusion of one coronal suture causes skull and orbital alterations in terms of side-to-side asymmetry. This study aimed to quantify the relationship between cranio-orbital complex changes and the severity of skull-base dysmorphism in patients with unicoronal synostosis.

Methods and Materials: We analysed CT images of 21 infants (mean age 156 days) with unicoronal synostosis, subdividing them into three subgroups according to severity of skull-base dysmorphism. Cranial fossae lengths, intracranial volume (ICV), each half-skull ICV (synostotic and non synostotic side), whole brain volume (WBV), orbital volumes (OV) were measured. ICV_{affected}/ICV_{unaffected side} and OV_{affected}/OV_{unaffected side} ratios were evaluated. Our results were compared with those of 21 age-matched healthy subjects.

Results: In all subgroups: reduced lengths and asymmetry of the anterior (CX) and the middle (XM) cranial fossae and asymmetry between ICV_{affected}/ICV_{unaffected} and between OV_{affected}/OV_{unaffected} were significant (p<0.05); ICV, WBV and ratio ICV/WBV were not significantly altered (p>0.05); OV on the affected side resulted significantly reduced only in group III (p<0.05). OV on the synostotic side were found to correlate with CX and XM lengths.

Conclusion: Skull and orbital changes revealed a side-to-side asymmetry but only the OV of the affected side, in group III, was found significantly reduced. It implies a relationship between the major severity of skull base dysmorphism and orbital alterations on affected side probably related to earlier timing of synostotic process; the lack of reduced ICV on synostotic side, in group III, suggests a different plasticity of skull cavity respect to orbital one.

B-0349 14:56

Detailed evaluation of a completely automatic, computer-assisted (CAD) analysis of hand X-ray examinations by including four different paediatric collectives

D.M. Renz¹, A. Schröder¹, J. Böttcher², A. Pfeil¹, F. Streitparth³, U.K. Teichgräber¹, H.-J. Mentzel¹; ¹Jena/DE, ²Gera/DE, ³Berlin/DE (diane.renz@med.uni-jena.de)

Purpose: The CAD system BoneXpert (Visiana) determines the bone age of children and adolescents on hand X-ray examinations. Furthermore, the CAD

method calculates bone parameters of the metacarpals, among others the „bone health index“ (BHI). The study purpose was a detailed evaluation of the CAD method, focusing on bone parameters, by including paediatric collectives with the following disorders: obesity, underweight, hypothyroidism, or chronic inflammatory bowel disease.

Methods and Materials: In the investigation, 325 children and adolescents (151 boys, 174 girls) between 3 and 18 years were included. All X-ray examinations were analysed visually and with the CAD system. The bone parameters of the CAD analysis were compared with age- and gender-matched normative values by using Z-scores; these Z-scores were calculated for the calendar as well as the skeletal age.

Results: High correlations were achieved between the visual determination of bone age and the CAD analysis, ranging between 0.848 and 0.956 ($p < 0.001$) for the different paediatric collectives. The Z-scores of the BHI were significantly reduced in all four cohorts (Student's t-tests, $p < 0.01$), if the bone age was the reference. In the case of using the calendar age, the BHI Z-scores were also significantly lower compared to the normative collective ($p < 0.01$), with one exception of female obese patients.

Conclusion: One major benefit of the CAD method is the calculation of parameters of bone health without using any additional radiation exposure. To early identify paediatric patients with osteopenia can induce prevention strategies to reduce the risk of developing osteoporosis, also in later life.

B-0350 15:04

Movie projection systems for paediatric CT examinations: effects on examination time, motion artefacts, and the need for restraints

N. Nagasawa, K. Kitagawa, K. Hashizume, A. Yamazaki, H. Maki, H. Sakuma; *Tsu/JP (nagasawa@clin.medic.mie-u.ac.jp)*

Purpose: It is important to reduce the anxiety of children for successful diagnostic and therapeutic procedures. The purpose of this study was to develop and assess the usefulness of a handy movie projection system for CT examinations.

Methods and Materials: We designed a handy movie projection system consisting of a mobile projector (MP-CL1; Sony, Tokyo, Japan) connected with a tablet device (iPad; Apple, Cupertino, USA) that was placed on the patient couch near the child's head. Movies were projected onto the upper wall of the CT gantry aperture with a projection size of 35 x 26 cm at 32 lumens. The system was implemented for head CTs in 54 paediatric patients aged 3-10 years (projection system group, 6.5 ± 2.6 y.o.) and animated movies were projected during the CT examination. Examination time, motion artefact, and the need for restraint were compared with 46 paediatric head CTs scanned without the system (conventional group, 6.6 ± 1.8 y.o., $p = ns$).

Results: Examination time (from topogram to end of scan) of the projection system group was significantly shorter compared to the conventional group (63.0 ± 37.1 sec vs 92.4 ± 42.4 sec, $p < 0.001$). The projection system group had no motion artefacts, while 15.2% (7/46 cases) of the conventional group had motion artefacts ($p < 0.001$). The projection system group less frequently required restraint to complete the examination, compared to the conventional group (3.8% (2/52) vs 15.2% (7/46), $p < 0.05$).

Conclusion: We developed a handy movie projection system that can shorten examination time, decrease motion artefacts, and reduce the need for restraint in paediatric CT.

B-0351 15:12

Parents wish more information on radiation exposure of their children

H. Oikarinen, H. Mahajan, A. Perttu, L. Ukkola, A.-L. Jussila, A. Henner; *Oulu/FI (helja.oikarinen@ppshp.fi)*

Purpose: To find out parents' experience and wishes for information in connection with their child's examination exposing to radiation.

Methods and Materials: A questionnaire was prepared and provided to parents of paediatric patients up to 12 years in a university hospital. Information received from the referring physician prior to their child's x-ray examination as well as wishes for future communication were enquired. Forty-one parents responded to the survey. Twenty-five children were referred for plain radiography of extremities, the others for dental, body or skull area examinations.

Results: Twenty-one patients had been referred from primary care and 17 from the hospital. Altogether 34/41 parents had received enough information on the purpose of the examination, 3/41 on the dose of radiation and 8/35 on other possible options. In all, 11/41 parents were aware of radiation use, and previous examinations were discussed in 7/41 of the cases. The parents scored the overall communication as 6.5 (mean) on a Likert scale from 4 (poor) to 10 (excellent). Altogether 38 out of 40 parents wish to receive information on the purpose, 35 on the dose and 31 on other possible options. Symbols of radiation and corresponding period of natural background radiation are preferred to reveal the dose. In all, 32 out of 38 parents would like to receive the information from the referring physician, 19 from a radiographer.

Conclusion: Parents wish to receive more information on radiation exposure prior to their child's radiography examination.

B-0344 15:20

Ultrasound of the limping child

D. Grant, E. Quinn, R. Gordon Boyd, C. Lee, K.A. Platt, K. Partington; *Oxford/UK (davidjamesgrant@live.co.uk)*

Purpose: Septic arthritis (SA) is an emergency with potential long-term sequelae if diagnosis/treatment is delayed. Kocher determined four predictors which help distinguish between SA and transient synovitis: nonweight-bearing (non-WB), fever, raised white cells (WC), and Erythrocyte Sedimentation Rate (ESR). Singhal showed that C-Reactive Protein (CRP) may also be predictive. Ultrasound with aspiration and microscopy remains the gold standard. Although not irradiating, ultrasound represents a time, resource and opportunity cost. Aspiration may prove upsetting for a child and poses its own risks. This study assesses whether clinical predictors may help determine the need for US.

Methods and Materials: Retrospective analysis of all paediatric lower limb ultrasound performed over 12 months at a Tertiary Hospital. Studies were manually filtered for clinical concern of SA. Data obtained from Electronic Patient Records and Radiology Information Systems.

Results: Of 142 cases, joint effusion was present in 46 (32.4%). 14 aspirations performed. There were 6 cases of SA. Pre-determined risk factors were as follows: 'non-WB' (6/6 in SA, 84/136 in non-SA); fever (SA 5/6, non-SA 54/136, $p = 0.035^*$); CRP > 20mg/L (SA 5/6, non-SA 35/128, $p = 0.004^*$); ESR > 40mm/hr (SA 3/5, non-SA 25/112); and WC > $12 \times 10^9/L$ (SA 4/6, non-SA 31/130, $p = 0.019^*$). All cases of septic arthritis demonstrated at least 2 risk factors. 68 (50%) of non-SA cases demonstrated fewer than 2 risk factors.

Conclusion: Requiring at least 2 SA clinical risk factors would have obviated the need for 68 ultrasounds, including 3 aspirations, whilst maintaining 100% sensitivity. We propose that this represents a resource-efficient addition to the diagnostic algorithm in a limping child.

14:00 - 15:30

Room M 3

Oncologic Imaging

SS 316

Cancer radiomics: adding value in cancer

Moderators:

A. Farchione; Rome/IT
S.M. Niehues; Berlin/DE

K-08 14:00

Keynote lecture

X. Montet; Geneva/CH

B-0352 14:09

Radiomics as a novel tool for primary nodal staging in rectal cancer

J.J.M. van Griethuysen^{1,2}, D.M. Lambregts¹, S. Trebeschi¹, M. Maas¹, M.J. Lahaye¹, G.L. Beets^{1,2}, F.C. Bakkers², R.G.H. Beets-Tan^{1,2}, H.J. Aerts³; ¹Amsterdam/NL, ²Maastricht/NL, ³Boston, MA/US (j.v.griethuysen@nki.nl)

Purpose: To assess the potential of quantitative MR-imaging analysis using radiomics for nodal characterization in primary rectal cancer staging.

Methods and Materials: 226 lymph nodes (from 34 rectal cancer patients who underwent MRI followed by surgical resection) were analyzed and matched node by node with histopathology. The short axis was measured for each node (on T2W-MRI) and nodes were manually segmented on T1W and T2W-MRI to extract 748 radiomic features (using PyRadiomics). Using principal feature selection, we selected the 25 features providing the best complementary information to routine nodal size measurements. Performance to distinguish between malignant and benign nodes was assessed with areas under the curve (AUC) per feature using a binomial mixed effects logistic regression model, correcting for patient number. False detection rate correction set at 10% was applied to correct for multiple testing.

Results: 17/226 nodes were malignant. The selected features were compared to (and combined with) nodal size measurements using a bootstrap method with 100 iterations; the model was trained on a random subset of patients and tested on the remaining patients (train:test ratio 80:20). The average performance for nodal size measurements was AUC 0.82. The best performing radiomic feature after FDR correction (GLCM-difference average; a measure of heterogeneity) resulted in an AUC of 0.83; the combination of this feature with nodal size resulted in an AUC of 0.85.

Conclusion: Radiomics may provide valuable quantitative information to characterize rectal cancer lymph nodes, particularly features reflecting nodal heterogeneity are promising. Although radiomics slightly improves staging performance, the added benefit compared to routine size-based staging appears to be limited.

B-0353 14:17

CT radiomics signature for preoperative esophageal cancer patients lymph node metastasis prediction

J. Qu¹, C. Shen²; ¹Zhengzhou/CN, ²Xi'an/CN (jqryq@126.com)

Purpose: To build and validate a radiomics signature for the prediction of pre-operation lymph node (LN) metastasis in esophageal cancer (EC).

Methods and Materials: A total of 189 EC patients were enrolled in this study, and their LN metastases have been pathologically confirmed. The data was collected from January 2016 to April 2016, patients in the first three months were set in the training cohort, and patients in April 2016 were set in the validation cohort. 789 radiomics features were extracted from CT images of patients. The lasso approach was exploited for dimension reduction and selection of the feature space. The multivariable logistic regression analysis was adopted to build the radiomics signature. The area under receiver operating characteristic curve (AUC) were adopted to estimate the signatures' discrimination power.

Results: Thirteen radiomics features were selected to build the radiomics signature. The radiomics signature was significantly associated with the LN metastasis ($P < 0.001$). The area under the curve (AUC) of radiomics signature performance in the training cohort is 0.763 (95% CI: 0.680-0.847), and in the validation cohort is 0.738 (95% CI: 0.677-0.793). The model showed good discrimination, with a C-index of 0.754 (95% CI: 0.686 to 0.822) in training cohort and 0.741 (95% CI: 0.663 to 0.819) in the validation cohort. Decision curve analysis showed the threshold probability is larger than 0.15, our model will receive benefit.

Conclusion: The present study proposed a radiomics signature, which can be potentially applied in the individual preoperative prediction of LN metastasis status in EC patients.

B-0354 14:25

CT texture features of adrenal tumours: the answer to indeterminate adrenal lesions?

J. Gariani, M.M. Siddique, G. Cook, V.J. Goh; London/UK (Joanna.Gariani@hcuge.ch)

Purpose: To identify the potential discriminating global and locoregional CT texture features of adrenal tumours.

Methods and Materials: Following an institutional review board waiver, portal-phase enhanced CT scans (120kV, variable mAs, soft tissue reconstruction, matrix 512, FOV 350mm, 2/5mm slice thickness) of 58 consecutive incidentally discovered adrenal lesions (>2.0cm, 21 benign adenomas and 37 malignant tumours) in 48 patients (28 male-20 female, mean age 66.35 years) were assessed with the final diagnosis based on imaging follow-up (>6months) or adrenal CT/MRI. Manual segmentation of each lesion was performed, using an in-house software, by a radiologist (>8 years experience) who was blinded to the final diagnosis, and 92 features encompassing histogram, fractal, second and high-order features were recorded.

Results: Significant differences were found for 46 features including histogram mean, median and skewness ($p=0.004$, $p=0.029$ and $p=0.013$); fractal dimension standard deviation and Hurst exponent ($p=0.014$, $p < 0.001$); GLCM (grey-level co-occurrence matrices) autocorrelation and cluster shade ($p=0.003$, $p=0.003$); and NGTDM (neighbourhood grey tone difference matrices) coarseness, contrast, busyness and complexity ($p < 0.001$, $p=0.001$, $p < 0.001$, $p=0.03$). There was a significant difference in volume between malignant and benign lesions (48.5cm^3 vs 13.3cm^3 , $p < 0.001$).

Conclusion: CT texture differs between benign and malignant adrenal lesions. Texture analysis may be a useful adjunct for the characterisation of indeterminate adrenal lesions.

B-0355 14:33

Machine learning and radiomics analysis of multi-parametric PET/MRI: characterisation of primary cervical cancers

J. Grueneisen, F. Nensa, A. Demircioglu, M. Forsting, K. Herrmann, L. Umultu; Essen/DE (johannes.grueneisen@uk-essen.de)

Purpose: To investigate the prediction potential of PET/MR-derived parameters of patients with cervical cancer assessed with radiomics and machine-learning algorithms.

Methods and Materials: A total of 30 patients with previously untreated cervical cancers underwent a simultaneous 18F-FDG PET/MR examination. The study protocol comprised the acquisition of morphological (T1w-, T2w-images), functional (DWI, DCE-MRI) and metabolic (18F-FDG PET) parameters. After tumour segmentation, quantitative imaging features (n=631) were extracted using the Radiomic Image Processing Toolbox. Statistical analysis and modeling were performed using Python 3.5 and the scikit-learn software machine learning library for the Python programming language.

Results: Correlation analysis of the full set of 631 image features revealed strong correlations between image features, representing redundant information. Therefore, feature selection methods were applied to identify the

20 highest ranking features, which were used for further analysis. For the determination of N-stage, receiver operating characteristic (ROC) analysis revealed an area under the curve (AUC) of 0.85 with a sensitivity and specificity of 79% and 75%. Furthermore, statistical analysis revealed a higher performance for the determination of the M-stage with a 94% sensitivity and 90% specificity and an AUC of 0.97.

Conclusion: The present data show strong correlations between certain PET and MRI-derived quantitative features and major prognostic factors of cervical cancers assessed with radiomics and machine learning algorithms. Therefore, radiomics analysis based on multiparametric PET/MR data offers a large number of non-invasive biomarkers, potentially facilitating a new platform for improved cancer detection, prediction of prognosis and determination of treatment response.

B-0356 14:41

Radiomics as a predictive biomarker of metastatic response to immunotherapy

S. Trebeschi¹, S.G. Drago^{2,1}, I. Kurilova¹, F. Lalezari¹, D.M. Lambregts¹, E. Smit¹, C.U. Blank¹, H.J. Aerts^{3,1}, R.G.H. Beets-Tan¹; ¹Amsterdam/NL, ²Monza/IT, ³Boston, MA/US (s.trebeschi@nki.nl)

Purpose: Immunotherapy represents a major breakthrough in cancer treatment. Various predictive biomarkers are currently under investigation, but none with conclusive results yet. With this study, we aim to evaluate the performance of radiomics imaging biomarkers to predict response to immunotherapy (PD-1 blockade) in specific to discriminate non-responders.

Methods and Materials: We retrospectively retrieved baseline and follow-up CE-CTs of 213 metastasized patients (131 NSCLC, 82 melanoma) undergoing immunotherapy at our institution. Patients were divided in a discovery (n=143) and independent validation set (n=70). Target lesions (1-43 lesions/patient, median 3, 1055 total) were delineated on baseline and first follow-up. Radiomics features were extracted from each lesion. Evolution in lesion diameter on FU-CT was the main response outcome (non-response > 20% increase). A random forest with wrapper feature selection was trained on the discovery set and optimized via sequential model-based optimization.

Results: The radiomic classifier revealed coarse texture features (GLCM), compactness, elongation and sphericity to be the best predictive features. When tested in the independent validation set, AUCs up to 0.83 were reached to predict non-response in the NSCLC group, with results better compared to predicting response based on routine pre-treatment lesion volume measurements (AUCs < 0.64). In the melanoma group, results were considerably poorer with similar results for radiomics features (AUCs < 0.65) and lesion volume (AUC < 0.65).

Conclusion: (1) Radiomics analysis of routine clinical CE-CT-imaging could provide viable biomarkers to predict non-response to immunotherapies in melanoma and NSCLC before treatment; (2) the differences in performance between melanoma and NSCLC suggest that both immune-generic and cancer-specific models are required.

B-0357 14:49

CT-derived texture analysis in predicting tumoral response to immunotherapy in patients with lung cancer and correlation with iRECIST

F. Rivosecchi, D. Caruso, D. De Santis, D.M. Bellini, N. Panvini, M. Rengo, A. Laghi; Latina/IT (flaminia.rivosecchi@gmail.com)

Purpose: To investigate whether CT-derived texture features (TFs) correlate with tumoral response in patients with lung cancer (LC) undergoing immunotherapy.

Methods and Materials: Twelve patients with lung adenocarcinoma who underwent contrast-enhanced CT before and after immunotherapy with Nivolumab were retrospectively analysed. Tumoral first-order TFs (mean, attenuation, standard deviation, mean value of positive pixels [MPP], entropy, skewness, and kurtosis) were assessed with TexRAD software using 5 scale filter (SF) as 0, 1, 1.5, 1.8, and 2. Response assessment was obtained by using Response Evaluation Criteria in Solid Tumours in Immunotherapeutic Trials (iRECIST) using appropriate software (mint lesionTM). Paired t-student test was performed to compare the texture results and Pearson correlation with iRecist was performed as well.

Results: Seven patients showed progressive disease (PD) and 5 patients showed stable disease (SD) with iRECIST. Kurtosis was significantly higher for all the SFs in patients with PD compared to SD ($P=0.007$). Mean attenuation at SF0 was higher in PD compared to SD (12.1 ± 12.2 and -67.7 ± 60.0 , $P < 0.001$). Standard deviation at SF1 and SF1.5 in PD (139.2 ± 1.9 and 192.8 ± 2.5) was lower than SD (387.8 ± 180.7 and 501.8 ± 214.1). MPP at SF1.5 in PD was lower than SD (121.5 ± 3.9 vs 457.1 ± 260.2) (all $P < 0.05$). No significant differences were found among the other TFs. A positive correlation was observed between kurtosis and PD using iRecist ($r=0.56$, $P < 0.05$).

Conclusion: CT-derived TFs could serve as imaging biomarkers of tumoral response to immunotherapy in patients with LC.

B-0358 14:57

Evaluating response to chemotherapy in colorectal liver metastases: correlation between CT texture analysis and RECIST criteria

N. Panvini, D. Caruso, D. De Santis, D.M. Bellini, F. Rivosecchi, M. Rengo, A. Laghi; *Latina/IT (npanvini88@gmail.com)*

Purpose: To evaluate potential role of CT texture analysis (TA) based quantitative imaging biomarkers in predicting response of colorectal liver metastases (CRLM) to chemotherapy in comparison to response evaluation criteria in solid tumours 1.1 (RECIST 1.1).

Methods and Materials: This preliminary study evaluated eleven patients who underwent MDCT before and after chemotherapy (FOLFIRI or FOLFOX). According to RECIST 1.1 criteria computer-aided response assessment of target lesions was performed as reference standard using appropriate software (mint lesion™). For each measured target lesion the software automatically derived statistical texture parameters (mean value of positive pixel (MPP), uniformity of distribution of positive pixel (UPP), skewness, kurtosis, uniformity and entropy). TA parameters were compared between patients with partial response (PR) and progressive disease (PD). Correlation analysis between % change in TA parameters and in sum of diameters (SOD) of target lesions was performed.

Results: Four patients were classified as PR based on RECIST 1.1 while seven patients showed PD at follow-up. Mean follow-up time was 63.4 ± 6.6 days. Kurtosis and skewness significantly increased in patients who showed PD and were reduced in those who responded to treatment (p<0.05). No correlation was observed between response to therapy and MPP, UPP, uniformity and entropy.

Conclusion: Kurtosis and skewness significantly correlated with variation of target lesions' largest diameters. These TA parameters may play a relevant role in predicting response to therapy of CRLM.

B-0359 15:05

Histogram analysis of T1-weighted, T2-weighted, and postcontrast T1-weighted images in primary CNS lymphoma: correlations with histopathological findings

H.-J. Meyer, S. Schob, B. Münch, C. Frydrychowicz, U. Quäsching, K.-T. Hoffmann, A. Surov; *Leipzig/DE (jonas90.meyer@web.de)*

Purpose: Previously, some reports mentioned that magnetic resonance imaging (MRI) can predict histopathological features in primary CNS lymphoma (PCNSL). The reported data analysed diffusion-weighted imaging findings. The aim of this study was to investigate possible associations between histopathological findings, such as tumour cellularity, nucleic areas and proliferation index Ki-67, and signal intensity on T1-weighted and T2-weighted images in PCNSL.

Methods and Materials: For this study, 18 patients with PCNSL were retrospectively investigated by histogram analysis on precontrast and postcontrast T1-weighted and fluid-attenuated inversion recovery (FLAIR) images. For every patient, histopathology parameters, nucleic count, total nucleic area, and average nucleic area, as well as Ki-67 index, were estimated.

Results: Correlation analysis identified several statistically significant associations. Skewness derived from precontrast T1-weighted images correlated with Ki-67 index (p=- 0.55, P=0.028). Furthermore, entropy derived from precontrast T1-weighted images correlated with average nucleic area (p=0.53, P=0.04). Several parameters from postcontrast T1-weighted images correlated with nucleic count: maximum signal intensity (p=0.59, P=0.017), P75 (p=0.56, P=0.02), and P90 (p=0.52, P=0.04) as well as SD (p=0.58, P=0.02). Maximum signal intensity derived from FLAIR sequence correlated with nucleic count (p=0.50, P=0.03).

Conclusion: Histogram-derived parameters of conventional MRI sequences can reflect different histopathological features in PCNSL.

B-0360 15:13

Added value of radiomics signature to predict pulmonary metastasis in colo-rectal cancer patients with lung nodules

T. Hu, T. Tong, S. Wang; *Shanghai/CN (h16211230001@163.com)*

Purpose: To evaluate the added value of radiomics signature in the development and validation of nomograms to predict pulmonary metastases in colorectal cancer (CRC) patients with lung nodules.

Methods and Materials: A total of 266 CRC patients with pulmonary nodules were identified between January 2010 and October 2016 to analyze the clinical characteristics and texture parameters from chest CT images. Clinical features identified by the logistic regression analysis were used to construct a clinical nomogram, radiomics signature built by a LASSO regression model were added to the selected clinical features to develop the clinical-radiomics nomogram. The nomograms performance was assessed through discrimination and calibration. Decision curve analyses were applied to compare the clinical usefulness.

Results: The logistic regression analysis identified the primary tumor site, chronicity, and carcinoembryonic antigen as independent predictors. The LASSO model built the radiomics signature with four predictive texture parameters. The clinical nomogram was developed with good discrimination (c-index of 0.808 in the primary set and 0.776 in the validation set) and poor calibration. The clinical-radiomics nomogram showed an incremental prognostic value with superior discrimination (c-index of 0.944 in the primary set and 0.922 in the validation set) and calibration. The decision curve analyses demonstrated that the clinical-radiomics nomogram showed clinical usefulness.

Conclusion: In CRC patients with pulmonary nodules, the clinical-radiomics nomogram which was created by the clinical features and radiomics signature had exhibited superior discriminatory ability and accuracy for a metastases prediction. The clinical-radiomics nomogram is a reliable clinical treatment tool to predict pulmonary metastases.

B-0361 15:21

Personalised radiogenomic medicine: prostate cancer gene 3 and PI-RADSv2 team up to predict clinically significant prostate cancer

M. Nguyentat¹, V. Bura², A. Ushinsky¹, S. Fardin¹, C. Green¹, E. Uchio¹, T.K. Lee¹, C. Lall¹, R. Houshyar¹; ¹Orange, CA/US, ²Cluj-Napoca/RO (vlad.t.bura@gmail.com)

Purpose: Multiparametric-MRI (mpMRI) utilizing PI-RADSv2 has been shown to detect prostate cancer (PCa) with high diagnostic accuracy. Genomic data, such as prostate cancer Gene 3 (PCA3) is known to be overexpressed in PCa. However, studies combining the two are lacking. We propose a radiogenomic model combining prostate imaging and PCA3 data for detecting clinically significant PCa (csPCa).

Methods and Materials: We retrospectively reviewed patient charts of those who underwent urinary PCA3 testing, mpMRI, and MRI/TRUS fusion-biopsy from 09/2014-12/2016. PI-RADSv2 was utilized for mpMRI. csPCa was defined as Gleason Score ≥ 7. PCA3 data were recorded as both qualitative (positive/negative) and quantitative (absolute number) results. Logistic regression and ROC analysis were performed to assess correlation and diagnostic accuracy of our radiogenomic model for detecting csPCa.

Results: A binomial logistic regression of 62 men with 96 prostate lesions was performed to ascertain the effects of PCA3 and PI-RADSv2 scores on the likelihood that subjects have csPCa. The logistic regression model was statistically significant, $\chi^2(3) = 33.029$, $p < .0005$. Sensitivity of our model was 53.3%, specificity was 95.1%, positive predictive value (PPV) was 66.7% and negative predictive value (NPV) was 91.7%. The AUC of quantitative-PCA3 was 0.720 (95% CI 0.585-0.855, $p = 0.009$), while for PI-RADSv2 was 0.818 (95% CI 0.705-0.931, $p < 0.001$). Combining the two into one multivariate model produced an AUC of 0.920 (95% CI 0.860-0.979, $p < 0.001$).

Conclusion: Combining PI-RADSv2 and quantitative-PCA3 into one radiogenomic model achieves an excellent specificity, NPV, and a larger AUC for detecting csPCa.

14:00 - 15:30

Sky High Stage

Oncologic Imaging

MY 3

Oncologic Imaging

Moderators:

G. Brancatelli; Palermo/IT
S. Gourtsyoyanni; Athens/GR

B-0362 14:00

Whole-body diffusion-weighted MRI in Hodgkin Lymphoma: 3D texture analysis for early treatment response assessment

K.N. De Paepe¹, I.F. Vieira², F. De Keyzer², P. Wolter³, O. Bechter², D. Dierickx², R. Oyen², G. Verhoef², V. Vandecaveye²; ¹London/UK, ²Leuven/BE, ³Verviers/BE (katjadepaepe@gmail.com)

Purpose: To evaluate feasibility and predictive utility of early treatment response assessment in Hodgkin lymphoma (HL) using 3D texture analysis of whole-body diffusion-weighted MRI (WB-DWI/MRI).

Methods and Materials: Twenty-six patients with HL underwent 3-T whole body (WB) DWI/MRI before and 4 weeks after start of chemotherapy (1 treatment cycle). Responses after 1 treatment cycle, were assessed by the apparent diffusion coefficient change relative to baseline (ΔADC_{avg}), change of first-order-statistics (FOS) ADC histogram features (ΔADC_{hist}) and change of second-order-statistics (SOS) textures (ΔADC_{text}), generated by grey-level co-occurrence matrices. The discriminative capability of ΔADC_{avg} , ΔADC_{hist} and ΔADC_{text} to identify refractory/recurrent lesions versus responding lesions was determined using Mann-Whitney U tests, supplemented by Monte Carlo (MC) permutation tests for statistical robustness. Correlation of the response

variables with progression-free survival (PFS) was assessed with Kaplan-Meier and log rank tests.

Results: At a median follow-up time of 43 months (range 3-79 m), 21/26 patients had complete remission and 5 patients persistent/ recurrent disease (8 non-responding and 47 responding lesions). The ΔADC_{avg} ($p=0.84$) and ΔADC_{hist} ($p>0.05$) didn't correlate significantly with lesion response. The ΔADC_{ext} showed significant differences for energy (ΔADC_E ; $p=0.001$), local homogeneity (ΔADC_{LH} ; $p=0.002$), and entropy (ΔADC_H ; $p=0.001$), which also correlated significantly with PFS (ΔADC_{LH} ; $p=0.031$; ΔADC_E ; $p=0.013$; ΔADC_H ; $p=0.002$).

Conclusion: Early response assessment after 1 cycle of chemotherapy by WB-DWI/MRI texture analysis (ΔADC_{ext}) correlates significantly with PFS, showing substantially stronger association with tumor response than ΔADC_{avg} or ΔADC_{hist} .

B-0363 14:04

Dynamic glucose-enhanced MRI: clinical perspectives and challenges

D. Paech¹, P. Schuenke¹, C. Köhler¹, P. Bachert¹, M. Ladd¹, M. Bendszus¹, H.-P. Schlemmer¹, M. Zaiss², A. Radbruch¹; ¹Heidelberg/DE, ²Tübingen/DE (d.paech@dkfz.de)

Purpose: To investigate dynamic glucose-enhanced (DGE) magnetic resonance imaging (MRI) at 7 Tesla (7T) in the healthy human brain and newly diagnosed untreated glioblastoma patients.

Methods and Materials: Eleven newly diagnosed glioblastoma patients and eight healthy volunteers were included in this prospective ethic approved study. DGE MRI was performed at a 7T whole-body scanner (Siemens, Healthcare, Erlangen, Germany) using an in-house developed adiabatically-prepared chemical exchange sensitive spin-lock (CESL) sequence (temporal resolution = 7 sec). 100ml of 20% D-glucose were injected intravenously during DGE MRI. Gadolinium contrast-enhanced T1-w images were obtained along the clinical standard MRI protocol at 3T. Mean signal intensities of (1)the tumor regions vs. normal appearing white matter, and (2)gray matter vs. white matter, were compared by using the *Student's t-test*.

Results: No adverse effects were observed in patients and volunteers related to glucose injections. The DGE contrast allowed for the identification of pathophysiologically increased glucose uptake in the tumor area in all patients. The mean signal intensity of the glucose enhancing tumor region over all patients ($DGE_p=3.57\pm 1.79\%$) was significantly higher than in contralateral normal appearing white matter ($DGE_p=0.22\pm 0.80\%$) ($p<0.01$). Further, DGE MRI revealed an increased glucose uptake in gray matter regions compared to white matter of the normal human brain ($p<0.001$).

Conclusion: DGE MRI may provide complementary information about the metabolic heterogeneity of tumors, with implications for biopsy targeting, patient therapy and response monitoring. Furthermore, glucose enhanced MRI could open up the field of metabolic imaging without the limitations set by ionizing radiation and high expenses associated with radioisotopes.

B-0364 14:08

Compressed sensing accelerated 3D magnetic resonance cholangiopancreatography: application in pancreatic diseases

L. Zhu, Z.-y. Sun, H.-d. Xue, T.-y. Qian, Z.-y. Jin; Beijing/CN (zhuliang_pumc@163.com)

Purpose: To prospectively evaluate image quality, duct visibility and diagnostic performance in duct-related pathologies of compressed-sensing (CS) accelerated 3D MRCP, and compare to conventional 3D MRCP in patients with suspected pancreatic diseases.

Methods and Materials: Eighty patients (47 men and 33 women, median age, 57 years, range, 24-87 years) underwent 3D MRCP at 3.0T. Three protocols were performed in each patient: CS breath-hold (BH) protocol, CS navigator-triggered (NT) protocol, and conventional NT protocol. Acquisition time of each protocol was recorded. Image quality and duct visibility were independently rated in random order on a 5-point scale by two radiologists, who were blinded to the protocols. Receiver operating characteristic curves were generated, and area under the curve (A_z value) was used to compare the diagnostic performance of each protocol in duct-related pathologies.

Results: Acquisition time was 17 seconds for CS-BH protocol and 134.1 ± 33.5 seconds for CS-NT protocol, both being significantly shorter than the conventional NT protocol (364.7 ± 78.4 seconds, both $p<0.01$). CS-BH protocol showed significantly less artefacts compared to both NT protocols (both $p<0.01$). Visualization of bile ducts was comparable with all three protocols, whereas CS-NT and conventional NT protocol depicted pancreatic duct better than CS-BH protocol (for proximal, middle and distal segment, all $p<0.05$). CS-NT MRCP had highest diagnostic performance for detecting ductal anomalies, long-segment duct stenosis, abnormal branch ducts, and communication between cystic lesion and pancreatic duct (mean A_z value 0.943 ± 0.983).

Conclusion: CS-MRCP is feasible in patients with suspected pancreatic diseases. CS-NT MRCP demonstrated superior diagnostic accuracy for duct-related pathologies.

B-0365 14:12

Multiparametric MRI to predict response to external beam radiotherapy in locally advanced cervical cancer: comparison of MRI volumetry, diffusion-weighted MRI and MR texture analysis

L.A. Min^{1,2}, L.L.G.C. Ackermans¹, M.E. Nowee¹, J.J. van Griethuysen^{1,2}, S. Trebeschi¹, W. Vogel^{1,1}, M. Maas¹, R.G.H. Beets-Tan^{1,2}, D.M. Lambregts¹; ¹Amsterdam/NL, ²Maastricht/NL (lisaannamin@gmail.com)

Purpose: Locally advanced cervical cancer (LACC) patients who respond very well to external beam radiotherapy (EBRT), i.e. with near-complete tumour regression, might be candidates for early start of subsequent brachytherapy and dose de-escalation in the future. Goal was to investigate if we can predict upfront which patients will achieve a near-complete response using multiparametric MRI.

Methods and Materials: N=41 LACC patients were retrospectively included. Two readers in consensus analysed the pre-treatment MRIs (3.0T) and delineated whole-tumour volumes on T2-weighted and high b-value diffusion-weighted imaging (DWI). The following parameters were calculated: T2W-volume, DWI-volume, apparent diffusion coefficient (ADC), and texture parameters mean, SD, entropy and uniformity (LoG-filter 1.5). Areas under the ROC curve (AUC) to predict a near-complete response (tumour volume reduction >90% on T2W-MRI after EBRT) were calculated.

Results: AUC to predict a near-complete response was 0.58 for T2W-volume and 0.54 for DWI-volume. ADC rendered an AUC of 0.66. Texture measurements resulted in AUCs of 0.53 (mean), 0.69 (SD), 0.65 (entropy) and 0.63 (uniformity). The improvement in AUCs for the ADC and texture measures compared to T2W-volumetry were not statistically significant. Combining volume with ADC and/or texture parameters did not improve performance.

Conclusion: Pre-treatment tumour volumetry (T2W- or DWI-based) is not useful to predict a near-complete response. Quantitative diffusion and texture parameters may help to improve predictive performance, although results were not statistically significant and remained suboptimal in this small cohort. For future research it would be worthwhile to see if combining quantitative MRI with FDG-PET/CT can further improve results.

B-0366 14:16

Is there rationale for the routine inclusion of chest CT in gastric cancer staging? Evidence from a single-institution cancer registry

A.-H. Chen¹, C.-M. Chen²; ¹Taoyuan/TW, ²Taipei/TW (angel08141@gmail.com)

Purpose: ESMO 2016 and AJCC 8th edition guidelines recommend routine inclusion of chest CT in gastric cancer staging. We assessed the necessity and clinical value for such routine inclusion.

Methods and Materials: This is a retrospective review of Chang Gung Memorial Hospital, Linkou, Taiwan gastric cancer registry (between 2008 and 2014). We evaluated the inclusion of chest CT at initial staging, patterns of metastases at initial presentation and at recurrence following surgery. Overall survival was calculated from Kaplan-Meier estimates.

Results: A total of 1675 cases were reviewed. Between the review period, there was a doubling trend in the inclusion of chest CT (18.0% - 32.0%); however, the incidence of pulmonary metastases (0.8% - 2.6%) is rare. 478 patients (28.5%) had metastatic disease at presentation. The most common metastases were intra-abdominal (90.0%). 27 (3.2%) and 20 (2.4%) patients had pulmonary and cytologic-proven pleural metastases, respectively. Of all pulmonary metastases, 11 patients (40.7%) had primary lesions located at cardia/fundus. There was no solitary metastasis to lung or pleura and all the lesions could be identified in lower lung fields. Of the 203 patients (16.2%) recurrence, 15 (4.4%) pulmonary and 7 (2.1%) pleural metastases were found. There was no isolated pulmonary metastasis. No demonstrated significant difference in the median overall survival with or without lung metastases at initial presentation ($p=0.78$) and at recurrence ($p=0.85$).

Conclusion: Our findings do not support routine inclusion of chest CT in gastric cancer staging because of the rarity of pulmonary metastasis, absence of solitary metastasis and lack of survival difference.

B-0367 14:20

MR texture analysis: potential imaging biomarker for prediction of chemotherapy response in patients with colorectal liver metastases

H. Zhang, T.T. Tong; Shanghai/CN (17081376182@163.com)

Purpose: The purpose of the study was to determine if pre-treated MR texture features of colorectal liver metastases (CRLMs) are predictive of chemotherapy response after the first-line chemotherapy.

Methods and Materials: The study included 26 consecutive patients (a total of 193 liver metastasis) with unresectable CRLMs at our institution from August 2014 to February 2016. All patients underwent baseline MRI within 3 weeks before chemotherapy. Lesions were classified as either responding group or non-responding group according to changes in size. Texture analysis was quantified on T2-weighted images by two radiologists with an agreement on

regions of interest which were manually drawn on the largest cross-sectional area of the lesions. Five histogram features (mean, variance, skewness, kurtosis, entropy1) and five grey level co-occurrence matrix features (GLCM; angular second moment (ASM), entropy2, contrast, correlation, inverse difference moment (IDM)) were extracted. The texture parameters were analysed statistically to find the differences between the two groups and receiver operating characteristic curves were depicted to characterize each parameter value for evaluating treatment outcome.

Results: 107 responding and 86 non-responding lesions were evaluated. Higher variance, entropy1, contrast, entropy2 and lower ASM, correlation and IDM were independently ($P < 0.05$) associated with good response to chemotherapy with area under the ROC curve (AUCs) of 0.602-0.784. However, mean ($P = 0.186$), skewness ($P = 0.311$) and kurtosis ($P = 0.763$) did not show a significant difference.

Conclusion: MR texture features on pre-treated T2 images seem to be a promising tool for predicting the chemotherapy response of patients with colorectal liver metastases.

B-0368 14:24

Patterns of responses in metastatic NSCLC during immunotherapy: comparison of RECIST 1.1, irRECIST and iRECIST criteria

M. [Tazdait](#), F. Bidault, S. Ammari, C.S. Baileysguier, D. Planchard, J.-C. Soria, A. Marabelle, B. Besse, C. Caramella; *Villejuif/FR (melodie.tazdait@orange.fr)*

Purpose: Immune checkpoint inhibitors are an important tool in the therapeutic strategy against metastatic non-small cell lung cancer (NSCLC), however radiological evaluation is challenging due to the emergence of atypical patterns of responses. Several evaluation criteria have been proposed, RECIST 1.1, irRECIST and iRECIST, but have not been systematically compared in a homogeneous population.

Methods and Materials: We conducted a monocentric retrospective analysis of consecutive advanced NSCLC patients treated with an anti-PD1 or anti-PD-L1. Response patterns and the discordance between RECIST 1.1, irRECIST and iRECIST guidelines were described, and associations of response patterns and clinical outcome were explored.

Results: Overall 160 patients treated between February 2013 and October 2016 were included. Atypical responses were observed in 20 patients (13%), including 8 pseudoprogressions (5%) and 12 dissociated responses (8%). Thirteen of the 20 patients demonstrated clinical benefit. Per RECIST 1.1, 37 patients (23%) showed an objective response or stable disease and 123 patients (77%) exhibited progression. Eighty progressive patients were assessable for irRECIST and iRECIST: 15 patients were assessed differently however only three (3.8%) mismatches with a theoretical impact on the therapeutic decision were identified. Patients with pseudoprogression or dissociated response had higher overall survival than patients with true progression.

Conclusion: Atypical responses (pseudoprogression/dissociated response) occurred in 13% of NSCLC patients under immune checkpoint inhibitors. Based on survival analyses, RECIST 1.1 evaluation underestimated the benefit of immune checkpoint inhibitors in 11% of progressive patients. irRECIST and iRECIST identified these unconventional responses, with a 3.8% discrepancy rate.

B-0369 14:28

Diagnostic value of automated breast volume sonography (ABVS) in breast cancer detection in women with different ACR types

M. [Efremova](#), V.E. Gazhonova; *Moscow/RU (frem13@mail.ru)*

Purpose: To evaluate ABVS diagnostic performance in comparison with hand-held ultrasound (HH-US) and X-ray mammography MMG for breast cancer detecting depending on ACR breast type.

Methods and Materials: 171 women with 251 morphologically verified lesions were examined. For each woman ABVS, HH-US, MMG were performed. Two independent examiners evaluated the ABVS data separately on different workstations without any prior knowledge of patients' history. Bi-RADS classification for ABVS examination was used.

Results: In patients with ACR III, ACR IV the sensitivity (SE) of ABVS was significantly higher among all the methods and amounted to 96.5%, specificity (SP) was 84.1%, the area under the curve (AUC) had the highest value of 0.9 which indicated an excellent quality of the method. For ACR III, ACR IV breast type patients MMG had significantly greater SE 92% and SP 84.6% versus ABVS diagnostic performance (SE-76%, SP-40%, AUC-0.58). Cohen's kappa for inter-rater agreement for BI-RADS evaluation for ABVS in total was $\kappa = 0.62 \pm 0.05$ - good. For malignant tumours $\kappa = 0.82 \pm 0.07$ - very good, for benign $\kappa = 0.39 \pm 0.05$ - satisfactory. Thus, the possibility of missing malignant tumour by ABVS is extremely low but the chance of getting false-positive result is high.

Conclusion: ABVS can be recommended as a reliable imaging method for breast cancer detecting in patients with dense breasts (ACR III, ACR IV). Second look follow-ups may be required in cases of benign findings.

B-0370 14:32

Prognostic significance of different MRI modalities for evaluation of neoadjuvant chemoradiation treatment of locally advanced rectal cancer

O. [Ganvch](#); *Kyiv/UA (ganich1@gmail.com)*

Purpose: In a current study we assess the prognostic significance of a widely used tumor regression grade (mrTRG) and the approach that uses grey-scale evaluation of T2 WI aided by the software developed by us (EmrTRG).

Methods and Materials: During the years 2016-2017, 74 patients with primary diagnosed locally advanced rectal cancer (LARC) (mrT3mr+4N1-2M0) had been enrolled. All patients completed a course of neoadjuvant chemoradiation therapy (NCRT) with a total dose of 50.4 Gy with capecitabine and underwent curative surgery. 8-10 weeks after completion of the NCRT course an MRI examination with mrTRG and EmrTRG for evaluation of NCRT response was performed. MRI data had been compared with pathological TRG (pTRG), calculated by Dworak grading system.

Results: We observed no cases of tumor progression. Pathologic complete response (pTRG-5) was observed in 6 (7%) of patients, pTRG-4 - 10 (13%), pTRG-3 - 20 (26%), pTRG-2 - 24 (37%), pTRG-1 - 10 (13%), pTRG0 - 4 (4%). There were 12 (16%) patients with complete radiologic response according to mrTRG and 8 (11%) according to EmrTRG, 20 (27%) and 12 (16%) ($p < 0.05$) with mrTRG and EmrTRG grade 4, 12 (15%) and 18 (24%) ($p < 0.05$) with grade 3, 10 (13%) and 22 (31%) ($p < 0.05$) - grade 2, 14 (22%) and 10 (14%) - grade 1, 6 (7%) and 4 (4%) - grade 0 respectively.

Conclusion: EmrTRG demonstrated superior accuracy in detecting pTRG-2-4 grade of response to NCRT comparing to mrTRG. Both mrTRG and EmrTRG showed insignificant accuracy level in detecting pathological complete response.

B-0371 14:36

Prediction of response to transarterial radioembolisation by means of MRI-based texture analysis as a potential radiomics tool

R. [Reimer](#)¹, P. Reimer², A. Mahnken¹; *Marburg/DE, ²Karlsruhe/DE (robertpeterreimer@gmail.com)*

Purpose: To evaluate whether assessment of tumor heterogeneity by means of MRI based texture analysis in patients with liver metastases may predict progress to transarterial radioembolization (TARE) earlier than by morphologic criteria.

Methods and Materials: 37 patients with liver metastases treated by TARE underwent dynamic contrast enhanced and hepatocellular phase MRI with gadoxetic acid after TARE (mean 2.2 days). Response was evaluated on follow-up imaging scheduled in intervals of 3 months (median follow-up, 221 days) based on Response Evaluation Criteria in Solid Tumors 1.1 (RECIST 1.1). Results of texture analysis (mean (m), standard deviation (sd), skewness (s), kurtosis (k), entropy (e), uniformity (u)) of the ROI were compared between patients with and without progressive disease. Receiver operating characteristics including the area under the curve (AUC) were calculated.

Results: According to RECIST 1.1, 24 patients (64.9%) had progressive disease and 13 (35.1%) stable disease or partial response. Median k (2.88vs.2.33) in arterial phase MRI and median s (0.48 vs.0.3) and median k (2.85vs.2.45) ($p < 0.05$) in venous phase MRI derived from texture analysis showed earlier significant differentiation ($p < 0.05$) than RECIST 1.1 between patients with and without progressive disease. The AUC for k in arterial phase was 0.77 ($p < 0.05$) and for s and k in venous phase 0.71 ($p > 0.05$) and 0.72 ($p < 0.05$).

Conclusion: Texture analysis indicating tumor heterogeneity of liver metastases after TARE has the potential to predict progressive disease earlier than by morphologic criteria. Earlier prediction of response to TARE may optimize individual therapy in clinical medical and interventional oncology.

B-0373 14:40

Comparison of whole-body MRI (wbMRI) and bone scintigraphy in oncologic follow-up

A. [Malich](#)¹, I. Papageorgiou¹, D. Kovacevic¹, A. Kott¹, D. Wiech¹, U.K. Teichgräber^{2,1}; *Nordhausen/DE, ²Jena/DE (ansgar.malich@shk-ndh.de)*

Purpose: Scintigraphy is still first line method in the detection of osseous metastases. Whole body MRI, however, is increasingly more available at various MR-scanners and thus could fill the gap of reduced availability of nuclear medicine departments. Only few data compare both technologies.

Methods and Materials: 1633 whole body MRI were retrospectively evaluated using a double blinded setting. An unsuspecting MRI was scored true in case of continued unsuspecting follow up, true positive results were accepted in case of histopathology, or initiation of treatment due to proven metastases with related clinical signs. All cases were evaluated regarding the existence and report of scintigraphic analyses within 1 year after MRI.

Results: 285/1633 wbMRI-cases had a bone scintigraphy; 264/285 had a verification of the imaging modalities. In 208/264 cases scintigraphy and wbMRI revealed same results (86tp, 122tn). In total WbMRI vs scintigraphy had

the following results: tp: n=102/n=88; tn: n=136/n=146; Fp: n=25/n=14; fn: n=1/n=16. Sensitivity, specificity, PPV, NPV, accuracy are (wbMRI/scinti): 99.0%/84.6%; 84.5%/91.3%; 80.3%/86.3%; 99.3%/ 90.1%; 91.8%/88.0%. Other than bone metastases were found in 18.3%, other incidentally detected tumor like structures were reported in 11.3%. Additional findings in scintigraphy were reported in 1.5%.

Conclusion: Whole body MRI is valuable in oncologic follow up and can replace bone scintigraphy in case of availability. Significant number of additional metastatic findings and incidental tumor like lesions could be found by wbMRI compared to scintigraphic analysis.

B-0374 14:44

Does second reader opinion affect pancreatic adenocarcinoma management?

G. Corrias¹, S. Huicochea Castellanos¹, V. Balachandran¹, L. Saba², L. Mannelli¹; ¹New York, NY/US, ²Monserato/IT (corriasgmd@gmail.com)

Purpose: Patients with pancreatic cancer frequently present to tertiary referral centers with imaging studies that have been performed and interpreted elsewhere. At our institution, these outside studies undergo formal second opinion reporting by a fellowship-trained oncologic radiologist with expertise in abdominal imaging. The purpose of this study was to determine the impact of this practice on cancer staging and patient management

Methods and Materials: Randomised original and second opinion reports for 65 consecutive cases of biopsy proven pancreatic adenocarcinomas in a 4 years period from 2009 to 2013 were considered. Discrepancy rates for recommended patient management, as recommended by two experienced abdominal surgeons, were calculated. For the 10,8% (7/65) of cases that subsequently went to surgery, the accuracies of the reports were determined relative to the pathologic staging gold standard. For all other patients, performed management, checked with clinical and imaging standard of reference at 6 months, was considered.

Results: Following oncologic radiologists second opinion review, the cancer stage changed in 13% (9/65) for surgeon 1 and in 18,4% (12/65) for surgeon 2. The recommended management changed in 38,4% (25/65) for surgeon 1 and in 20% (13/65) for surgeon 2. When compared to the pathologic staging gold standard, the second opinion was correct 85,7% (6/7) of the time for both surgeons' interpretation.

Conclusion: Specialist second opinion review of outside imaging studies resulted in an accurate change in cancer stage and this frequently led to a change in their management plan.

B-0375 14:48

Prognostic impact of body composition in patients with metastasised malignant melanoma with checkpoint-inhibitor therapy

J. Nattenmüller, L. Eller, S. Lücke, A. Lonsdorf, H.-P. Schlemmer, H.-U. Kauczor, O.L. Sedlaczek; Heidelberg/DE (johannawelzel@gmail.com)

Purpose: Checkpoint-inhibitors (CI) are a major breakthrough in the treatment of a variety of human malignancies and led to significant improvements in response and survival rates in metastatic melanoma patients. However, prognostic markers to select for patients that will respond to CI-therapy remain vastly elusive. As a close link between body composition (esp. fat distribution) and immune competence has been suggested, the aim of this study is to evaluate the prognostic impact of body composition on therapy response.

Methods and Materials: 82 stage IV malignant melanoma patients (41 female, mean age 66ys, mean BMI 26.2kg/m²) treated with CI (Ipilimumab, Nivolumab, Pembrolizumab) underwent staging-CT with densitometric quantification of total (TFA), visceral (VFA) and subcutaneous fat area (SFA) and skeletal muscle index (SMI) at the spinal level L3/4 to evaluate their impact on progression-free (PFS) and overall survival (OS).

Results: Median PFS and OS time were 293 and 913 days, respectively. On OS, a significant univariate negative impact of male gender (HR=2.88; p=0.018) and a beneficial multivariate impact of SFA (HR=0.64, p=0.044) was found. On PFS, a significant beneficial effect was found for SFA in univariate (HR=0.69, p=0.01) and multivariate (HR=0.49, p<0.001) analyses. These effects of SFA were independent of gender. No significant impact of BMI, VFA, TAT and SMI was detected.

Conclusion: SFA had a significant beneficial prognostic value on both PFS and OS in stage IV melanoma patients undergoing CI-therapy. Further studies are needed to validate body composition and SFA as candidate biomarkers of favorable efficacy in CI therapy.

B-0376 14:52

Influence of Trigger-PSA and molecular active tumour volume evaluated with 68Ga-PSMA PET/CT on detection rate and localisation of recurrence in patients with prostate cancer

S.S. Medina-Ornelas, F. Garcia-Perez; Mexico City/MX (dr.sevastian@outlook.com)

Purpose: Investigate the association between molecular active tumour volume (MATV) evaluate with ⁶⁸Ga-PSMA-PET/CT and levels of Trigger-PSA for patients with Prostate cancer (PC).

Methods and Materials: Eighty-four patients who underwent to evaluation of PSA levels on the same week of the ⁶⁸Ga-PSMA-PET/CT (Trigger-PSA) were studied. were included. Sixty patients had received ADT at last 6 months before the examination. The median of the Trigger-PSA was 8.9 ng/mL (range 0.2-127 ng/ml).

Results: The median MATV of bone metastatic disease was significantly higher than that in metastatic lymph nodes (LN) and prostate bed (139.5 versus 17.7; p<0.05). Respect to Trigger-PSA values, the median Trigger-PSA levels of patients with tumours that were limited to the prostate bed (median Trigger-PSA 2.8ng/ml); loco-regional and/or distant lymph node disease (median Trigger-PSA 6.8ng/ml) and metastatic bone disease (median 46.8ng/ml (p<0.05). Positive patients had a mean Trigger-PSA of 4.3ng/mL vs 1.5ng/mL in negative patients (p <0.05). We established several threshold points for Trigger-PSA level and studied the detection rate for each one: Trigger-PSA ≤1ng/mL, detection rate 47.3%; Trigger-PSA 1-4ng/mL, 68.4%; Trigger-PSA ≥4ng/mL, 96.7%. When analyzing the best association between Trigger-PSA and MATV, we found that when Trigger-PSA was >4ng/mL, was greater for patients with a higher MATV (p<0.001).

Conclusion: The correlation of a low MATV evaluate with ⁶⁸Ga-PSMA-PET/CT has greater influence than the level of Trigger-PSA, which may have an impact on the timely change of the therapeutics used. A detection of the site of metastatic disease could lead to an appropriate therapeutic strategy.

B-0377 14:56

Improved detection of skeletal muscle metastases in iodine-density overlay maps and virtual monoenergetic reconstructions provided by spectral detector CT

S. Lennartz¹, M. Le Blanc¹, N. Abdullayev¹, N. Grosse Hokamp^{1,2}, D. Maintz¹, J. Borggreffe¹, T. Persigehl¹; ¹Cologne/DE, ²Cleveland, OH/US (simon.lennartz@uk-koeln.de)

Purpose: To investigate if iodine density overlay maps (IDM) and/or virtual monoenergetic images at 40 keV (VM_{40keV}) acquired with dual layer spectral detector computed tomography (SDCT) can improve detection of skeletal muscle metastases (SMM) compared to conventional polyenergetic images (PI).

Methods and Materials: In total, 36 oncologic patients, 12 patients with confirmed SMM proven by prior or follow-up CT, FDG-PET or histopathology, and 24 patients without SMM who received SDCT staging examinations were included in this retrospective, IRB-approved study. Detection rate was determined in a blinded, randomised multi-reader analysis of PI, IDM and VM_{40keV}. Quantitatively, iodine density and contrast-to-noise-ratio (CNR) were determined using the following ROIs: metastasis, adjacent skeletal muscle, subcutaneous fat, and air. Size and localisation of ROIs were kept constant between IDM, VM_{40keV} and PI. Standard deviation within the fat was considered to be representative of image noise. Statistical analysis was performed using Wilcoxon test and ROC-analysis.

Results: Both, IDM (69.1%) and VM_{40keV} (49.2%) yielded a significantly increased sensitivity for SMM compared to PI (24.2%). Specificity slightly dropped by 3.1% in IDM (78.0%) compared to PI (81.4%), while in VM_{40keV}, it decreased to 68.4%. Quantitative image analysis revealed a significant higher CNR (14.3±8.0) of SMM in VM_{40keV} compared to PI (5.5±6.2, p<0.0001). Iodine density in SMM was significantly enhanced compared to adjacent muscle tissue (1.83±1.1 mg/ml vs. 0.28±0.22 mg/ml, p<0.0001).

Conclusion: Iodine density maps (IDM) provided by SDCT significantly improve detection rate of SMM in oncologic patients while maintaining an equivalent level of specificity.

B-0378 15:00

Comparison of biopsy and pathological Gleason score in patients with biopsy-proven prostate cancer

V. Romano¹, V. Doronzio¹, S. Pedalino¹, V. Giannini¹, S. Mazzetti¹, A. Giacobbe², G. Muto², F. Russo¹, D. Regge¹; ¹Candiolo/IT, ²Milan/IT (vittorio.romano@irc.it)

Purpose: To compare biopsy Gleason Score (bGS) with pathological Gleason score (pGS) after prostatectomy in patients with positive MRI finding and biopsy-proven PCa.

Methods and Materials: Men with biopsy-proven PCa from either MR-targeted biopsy or saturation TRUS-guided biopsy were included in this study and

underwent radical prostatectomy within 3 months from diagnosis. Overall, 24 men with positive MR-targeted biopsy, and 30 subjects with positive saturation biopsy were considered. Whole-mount histological sections resected from radical prostatectomy were used as the reference standard, and biopsy/pathological Gleason score (GS) were compared, assessing the proportion of correctly classified PCa, upgrading and downgrading rates.

Results: After surgery, biopsy GS was correctly identified in 67% and 43% of cases, in MR-targeted biopsy and saturation biopsy, respectively ($p=0.08$). Biopsy GS was upgraded in 29% of MR-targeted and 30% of saturation biopsy, respectively ($p=0.94$). Downgrading was registered in 4% and 27% of cases in MR-targeted biopsy and saturation biopsy, respectively ($p=0.03$). Stratifying patients according to bGS, a higher number of 4+4 PCa were detected in the saturation than in the MR-targeted biopsy (16% vs 2%, $p=0.13$), while considering the pGS, the two sampling techniques (MR-targeted or saturation) reported no statistical difference when men were stratified by pGS ($p>0.27$).

Conclusion: MR-targeted and saturation biopsy reported a similar rate of correctly classified bGS, while in-bore MR-targeted biopsy showed a significant lower rate of downgrading with respect to saturation biopsy.

B-0379 15:04

Efficacy of intravoxel incoherent motion MRI in discrimination of metastatic vs non-metastatic abdominal lymph nodes in hepatobiliary malignancies: a correlation study with PET-CT

S. Sabet, S. Server, I. Karalok, E.K. Namal, N. Inan, Y. Tokat; *Istanbul/TR (sohey_l_61@yahoo.com)*

Purpose: The aim of this study was to evaluate the diagnostic performance of IVIM MR parameters in differentiating metastatic from non-metastatic abdominal lymph nodes in hepatobiliary malignancies.

Methods and Materials: MR images of 34 consecutive patients harbouring 83 upper abdominal lymph nodes with diagnosis of hepatobiliary malignant tumor were evaluated retrospectively. IVIM parameters were calculated for each lymph node from MR images obtained with 16 different b factors (0, 50, 100, 150, 200, 300, 400, 500, 600, 700, 800, 900, 1000, 1100, 1200, 1300 s/mm²) by a 1.5 Tesla MR scanner (Siemens, Magnetom Symphony, Erlangen, Germany). These parameters were compared with SUV max. values of target lesions in FDG PET-CT studies.

Results: The mean value of D was lower, and mean value of f was higher significantly for metastatic group than those of non-metastatic group ($p<0.001$), while D* and ADC did not show significant difference. D and f had largest area under curve in the ROC analysis (0.649 and 0.984 respectively) compared to other individual IVIM parameters leading to sensitivity and specificity of %96 and %86 for f in identification of metastatic lymph nodes.

Conclusion: IVIM parameters, specially D and f, reflect the metabolic activity of lymph nodes, providing a reliable diagnostic tool in distinguishing metastatic from non-metastatic lymph nodes with a lower price, shorter scan time and radiation free modality instead of PET-CT and may be applicable not just in cervical and thoracic tumors but also in abdominal lymphadenopathies caused by hepatobiliary malignancies.

B-0380 15:08

T2 hyperintense myometrial tumours: can MRI features differentiate leiomyomas from leiomyosarcomas?

G. Rio¹, M. Lima², R. Gil², M. Horta², T.M. Cunha²; ¹Braga/PT, ²Lisbon/PT (giselario_123@hotmail.com)

Purpose: To establish MRI features that help differentiate atypical and degenerated leiomyomas that show hyperintensity on T2WI from leiomyosarcomas (LMS).

Methods and Materials: This retrospective study evaluated 51 women who performed MRI and had T2 hyperintense myometrial tumours, proved by histology as atypical or degenerated leiomyomas or leiomyosarcomas (21 leiomyomas; 20 leiomyosarcomas), before they underwent hysterectomy. The association between MRI features (contours; free pelvic fluid, intra-tumoural haemorrhagic areas, T2 heterogeneity; T2 dark areas; flow voids; signal intensity and heterogeneity after contrast administration; unenhanced areas, localization of unenhanced areas; necrosis; cystic areas) and the histology (leiomyoma vs leiomyosarcoma) were calculated using Fisher's exact test. For those features that showed a significant association, a multivariate linear regression was performed.

Results: Five MRI features demonstrated a significant correlation with malignant histology: lobulated borders ($p=0.002$); T2 dark areas ($p=0.02$); necrosis ($p=0.001$); hyperintensity relative to the myometrium after contrast administration ($p=0.007$) and central unenhanced areas ($p=0.016$). Three of these features demonstrated a significant result predicting a malignant histology: lobulated contours, central unenhanced areas and necrosis ($F(3;34)=8.95$; $p<0.001$; $R^2=0.506$).

Conclusion: The presence of lobulated borders, T2 dark areas, necrosis, hyperintensity relative to the myometrium after contrast administration and central unenhanced areas can help distinguish between leiomyoma and leiomyosarcoma. The association of lobulated borders, necrosis and central unenhanced areas can help predict a malignant histology.

B-0381 15:12

3D imaging biomarkers for the prediction of survival in patients with non-small cell lung cancer or melanoma brain metastases treated with stereotactic body radiation therapy

M. Della Seta, F. Colletini, D. Kaul; *Berlin/DE (marta.della-seta@charite.de)*

Purpose: To investigate the value of 3D-quantitative tissue enhancement as an early imaging biomarker for survival in patients with singular non-small cell lung cancer (NSCLC) and melanoma brain metastases (BM) treated with stereotactic body radiation therapy (SBRT).

Methods and Materials: 48 patients with a singular BM were treated with SBRT (27 NSCLC- and 21 melanoma patients). Baseline contrast-enhanced MRI (ceMRI) was used for image analysis using the qEASL tool (Philips Healthcare). A segmentation-based 3D-quantification was performed to measure the relative tumour enhancement. Survival was evaluated using univariable and multivariable cox regression models.

Results: Median overall survival (OS) of the cohort was 8.9 months. The stratification of the cohort according to a 65% cutoff for the relative enhancing tumour volume achieved statistical significance in univariable and multivariable analysis for OS (univariable regression: $p=0.005$, HR= 0.375 [95% CI, 0.168-0.744], multivariable regression: $p=0.006$, HR= 0.376 [95% CI, 0.186-0.757]). Patients with >65% enhancing lesion volume survived significantly longer than patients with less-enhancing tumour lesions (4.9 months vs 10.2 months). In subgroup analysis of NSCLC-patients adenocarcinoma showed significantly longer median OS than non-adenocarcinoma NSCLC patients in univariable and multivariable analysis (3.5 months vs 10.2 months).

Conclusion: Enhancement on baseline ceMRI in patients with singular NSCLC and melanoma BM is strongly associated with patient survival after SBRT. Specifically, patients with hyper-enhancing lesions demonstrated improved survival as compared to those with mainly hypo-enhancing lesions. Lesion enhancement may be a potential factor in future prognostic indices for the prediction of survival of patients with BM.

16:00 - 17:30

Sky High Stage

Genitourinary

MY 4

Genitourinary

Moderators:

A.K. Dixon; Cambridge/UK
S. Nougaret; Montpellier

B-0382 16:00

Radiomics of high-grade serous ovarian cancer: association between quantitative CT features and prognosis

F. De Piano, V. Buscarino, M. Femia, L. Tofaneli, S. Raimondi, D. Origgi, F. Botta, S. Rizzo; *Milan/IT (fran.depi@gmail.com)*

Purpose: To determine if radiomic features, alone or combined with clinical data, are associated with residual tumour (RT) at surgery, and predict the risk of disease progression within 12 months (PD12) in ovarian cancer (OC) patients.

Methods and Materials: This retrospective study enrolled 101 patients according to the following inclusion parameters: cytoreductive surgery performed at our Institution (05/09/2007-23/02/2016), assessment of BRCA mutational status, pre-operative CT available. Radiomic features of the ovarian masses were extracted from 3D structures drawn on CT images. A phantom experiment was performed to assess the reproducibility of radiomic features. The final radiomic features included in the analysis (516) were grouped into clusters using a hierarchical clustering procedure. The association of each radiomic feature with RT and PD12 was assessed by Chi-Square test. Multivariate analysis was performed using logistic regression models. P-values < 0.05 were considered significant.

Results: Patients with values of F2-Shape/Compactness1 below the median, values of F1- GrayLevelCooccurrenceMatrix25/0-1InformationMeasureCorr2 below the median, and values of F1-GrayLevelCooccurrenceMatrix25/-333-1InverseVariance above the median showed a higher risk of RT (36%, 36% and 35%, respectively, as opposed to 18%, 18% and 18%). Patients with values of F4-GrayLevelRunLengthMatrix25/-333RunPercentage above the median, values of F2 shape/Max3DDiameter below the median, and F1-GrayLevelCooccurrenceMatrix25/45-1InverseVariance above the median showed a higher risk of PD12 (22%, 24% and 23%, respectively, as opposed

to 6%, 5% and 6%). At multivariate analysis F2-Shape/Max3DDiameter remained significant (HR (95%CI)=11.86 (1.41-99.88)).

Conclusion: This study demonstrated significant associations between radiomic features and prognostic factors such as RT and PD12.

B-0383 16:04

Prostate cancer detection rate in patients with negative multi parametric (mp) MRI or negative biopsy after 2 years of follow up

E. Appendino¹, S. Pedalino¹, E. Tabone¹, V. Romano¹, S. Mazzetti¹, A. Giacobbe², G. Muto², F. Russo¹, D. Regge¹; ¹Candiolo-Turin/IT, ²Milan/IT (elena.appendino@gmail.com)

Purpose: To assess prostate cancer (PCa) detection rate among patients in follow-up after a negative mp-MRI or biopsy, and to assess the negative predictive value (NPV) of mpMRI in the detection of PCa.

Methods and Materials: 140 men with negative prostate mp-MRI (PI-RADS 1, 2 or 3 with lesion diameter <7 mm), and 10 men with positive mp-MRI (PI-RADS>3 or =3 with diameter >7 mm) but a negative biopsy (TRUS or RM-guided) were monitored periodically with PSA values and urological visit. In case of PSA doubling time < to 3 years or following urological indication, subjects underwent a second mpMRI (2nd MRI). After 2-year follow-up, we defined as negative patients with: a) no increase of PSA, or b) patients with negative 2nd-MRI, or c) patients with negative biopsy after a 2nd-MRI.

Results: During follow-up 44/150 patients underwent a 2nd-MRI. In 10/44 patients a prostate lesion was found, triggering a PCa. Presence of PCa was biopsy-confirmed in 8/10 patients (6 men with GS=3+4, 1 with GS=4+3 and 1 with GS=3+3). Among the 8 biopsy-proven PCa after the 2nd-MRI, 2 were already reported on the first MRI, although not confirmed by biopsy. No clinical or laboratory changes were observed in the remaining 106/150 patients (102 men with negative mpMRI and 4 men with negative biopsy) during the 2-year follow-up period (70,6%). Overall 142/150 patients were considered negative (NPV of 94,7%).

Conclusion: Biopsy can be safely avoided in subjects with a negative mp-MRI if follow-up is performed with clinical examination and PSA assessment.

B-0384 16:08

Which cancer-related factors are associated with prostate cancer missing when evaluating mpMRI with PI-RADS v2?

R. Girometti¹, F. Greco¹, L. Cereser¹, G. Como¹, V. Ficarra², G. Giannarini¹, A. Crestani¹, C. Zuiani¹; ¹Udine/IT, ²Messina/IT (rgirometti@sirm.org)

Purpose: To assess which prostate cancer (PCa)-related factors are associated with cancer missing (CM) on multiparametric magnetic resonance imaging when using prostate imaging reporting and data system version 2 (PI-RADS v2).

Methods and Materials: Between May 2016-February 2017 we prospectively enrolled patients with biopsy-proven prostate cancer who underwent staging 3.0T Multiparametric magnetic resonance imaging (mpMRI) before radical prostatectomy. Two readers with 6 and 8 years of experience, respectively, detected and scored mpMRI findings according to PI-RADS v2 criteria in a blinded fashion compared to final whole-mount pathology. Using PI-RADS ≥4 score as threshold, we calculated the per-lesion cancer detection rate (CDR) of each radiologist. We then performed multiple logistic regression to assess whether PCa-related factors (clinical significance according to Epstein criteria, Gleason score, prostate specific antigen (PSA) level, histological lesion size, extraprostatic extension and prostatic location) were predictors of CM.

Results: Included were forty-eight patients (median iPSA 7.2 ng/ml) with 71 cancers (median size 16 mm, median Gleason score 6, stage ≥T3 in 19/48 cases, 51/70 clinically significant cancers (csPCa)). CDR ranged 0.48-0.60 for all cancers and 0.61-0.72 for csPCa. On univariate analysis, the model of both readers showed significant association (p<0.01) between CM and non-csPCa, Gleason score <7, size <1.4-1.5 cm, and absence of extraprostatic extension. On multivariate analysis, lower lesion size was the only independent predictor of CM (p<0.01) for both radiologist 1 (OR 0.12) and 2 (OR 0.18).

Conclusion: Smaller cancer size is the most impacting factor in CM when assessing PCa with PI-RADS v2.

B-0385 16:12

Role of ureteric jet angle as measured by colour Doppler ultrasound in evaluating severity (grading) of VUR in patients presenting with urinary complaints

P. Maravi; Bhopal/IN (maravipoornima@gmail.com)

Purpose: To correlate ureteral jet angles (UJA), measured by colour Doppler USG with VUR grades on micturating cystourethrogram (MCU) and establish ureteral jet angle (UJA), as non-invasive screening tool for detecting high grade vesoureteral reflux (VUR).

Methods and Materials: Symptomatic children referred in Dept. of Imaging for MCU were examined by colour Doppler USG in order to get the bilateral ureteric jet angles (UJA). UJA was measured as angle between the direction of

the ureteral jet and inter-ureteral ridge. Patients, who showed VUR on MCU, UJA were then correlated to grades of VUR using excel data tool.

Results: In total 34 children (8 mon- 12 yrs) including 20 males (M) and 14 females (F) were examined. Mean age was 4.96 yrs {4.60 yrs (M) and 5.47 yrs in (F)}. 21 patients, (10 (F) and 11 (M) showed VUR on MCU. 8 patients showed higher grade (grade 4 -5) including 7 M, 1 F. Range of UJA in VUR negative patients was 27-59° on right side (R) and 23-60° on left side (L). VUR positive patients showed angle range 42-84°(R) and 40-84° (L). Mean ureteric jet angle was 62.61°(R) and 61.80° (L). Grade IV/V VUR seen above >70°. Positive correlation {r=0.88 on R and 0.73 on L} was noted between UJA and VUR grading.

Conclusion: Colour Doppler USG measurement of UJA can be used as simple and non-invasive screening tool to detect the grade of VUR in symptomatic children therefore minimising the need for MCU, which is invasive and imposes risks related to radiation/contrast media administration.

B-0386 16:16

Accuracy of multiparametric MRI of prostate cancer recurrence after high-intensity focused ultrasound (HIFU): is dynamic contrast enhancement still needed?

R. Lotte, A. Lafourcade, M. Ezziane, P.-H. Jouve de Guibert, S. Tavoraro, P. Mozer, F. Boudghene, O. Lucidarme, R. Renard Penna; Paris/FR (raissalotte@hotmail.com)

Purpose: To assess the added value of dynamic contrast-enhanced (DCE) imaging to the combination T2-weighted imaging (T2w) + diffusion-weighted imaging (Dw) in detecting recurrence of prostate cancer (PCa) after HIFU using multiparametric magnetic resonance imaging (mpMRI).

Methods and Materials: We retrospectively selected 45 patients with clinical and biological suspicion of recurrence of PCa after focal HIFU. All patients underwent mpMRI at 1.5 and 3 Tesla (T2w, Dw and DCE) before biopsies. Two readers independently assigned a Likert score (from 1 to 5) of cancer likelihood for each prostatic sector (divided on 6 sextants) on T2w + Dw + DCE and T2w + Dw images. Prostatic biopsies were taken as the gold standard.

Results: Recurrent PCa was identified at biopsy in 37 (82%) of 45 patients. Area under the receiver operating curve of T2w + Dw and T2w + Dw + DCE imaging were not significantly different for both readers, at patient level and at lobe level. Using a Likert score ≥3 for PCa diagnosis threshold, sensitivity at lobe level for (a) senior and (b) junior reader for T2w +Dw +DCE was (a) 0.97 (b) 0.94 vs (a) 0.94 (b) 0.97 for T2w + Dw, specificity was (a) 0.27 (b) 0.09 vs (a) 0.27 (b) 0.27, respectively.

Conclusion: Accuracy of mpMRI was not significantly improved with added DCE to T2w + Dw imaging. Sensitivity was high for T2w + Dw + DCE and T2w + Dw with no significant difference, either for the junior or the senior reader.

B-0387 16:20

Development of preoperative prediction of high Fuhrman grade in the patient with clear cell renal cell carcinoma

J. Ding, J. Chen, J. Sun, W. Xing; Changzhou/CN (dingjiule@163.com)

Purpose: To develop and validate a nomogram for the preoperative prediction of high Fuhrman grade ccRCC (III-IV).

Methods and Materials: The prediction model was developed in a training cohort that consisted of 114 patients with ccRCC. The pseudocapsule, intratumoural artery, morphological feature and tumour size were assessed by a radiologist. Radiomic features were extracted from the CT images of ccRCC at both arterial and portal venous phases. The least absolute shrinkage and selection operator was used for data dimension reduction and radiomics score calculation. A multivariate logistic regression model was used in training cohort to predict the high Fuhrman grade at nephrectomy. The predictors included pseudocapsule, intratumoural artery, morphological feature, tumour size and texture analysis of renal mass, and a nomogram was generated. The performance of the nomogram was assessed in an independent validation cohort contained 92 consecutive patients.

Results: The radiomics score, which consisted of 2 selected features, was significantly associated with Fuhrman grade (P < 0.05). Predictor contained in the individualized prediction nomogram included the features of radiomics score and morphological feature. The model showed the good discrimination with a concordance index of 0.859 (concordance index = 0.861 through the 80 samples in training cohort) and good calibration. Application of the nomogram in the validation cohort still gave good discrimination [concordance index = 0.782 (75%CI, 0.575 to 0.987)] and good calibration.

Conclusion: The nomogram that incorporated the radiomics and morphological features can be conveniently used to facilitate the preoperative individualized prediction of the high Fuhrman grade ccRCC.

B-0388 16:24

Prognostic value of diffusion-weighted imaging for clinical outcome prediction in uterine cervical cancer treated with radiotherapy
K. Gu, C.K. Kim, J. Lee; *Seoul/KR (kyowon.gu@gmail.com)*

Purpose: To investigate the prognostic value of diffusion-weighted imaging (DWI) in predicting clinical outcome in patients with cervical cancer after radiotherapy (RT).

Methods and Materials: Enrolled 124 patients with stage IB-IVB cervical cancer who received definitive RT with (n=117) or without (n=7) concurrent chemotherapy underwent MRI at 3T including DWI before and during (at 1 month) treatment. The mean apparent diffusion coefficient (ADC) value was measured on the tumour and the percentage change (ΔADC_{mean}) between 2 time points was calculated. Cox proportion hazard model was performed to evaluate the association of imaging and clinical variables with progression-free survival (PFS) and cancer-specific survival (CSS).

Results: During a median follow-up of 3.6 years, disease progression was found in 40 patients (32.2%) and 19 patients (15.3%) died of their disease. On multivariate analysis, ΔADC_{mean} (hazard ratio [HR]=0.98, P=0.015) and histologic type (HR= 2.66, P= 0.020) were significantly independent factors for PFS, and ΔADC_{mean} (HR=0.97, P=0.015) and parametrial invasion on MRI (HR=0.22, P=0.024) were significantly independent factors for CSS. Pretreatment ADC values were not associated with PFS and CSS (P>0.05). Using the optimal cutoff values of ΔADC_{mean} , the 3-year PFS was significantly lower for ΔADC_{mean} <38.7% than for ΔADC_{mean} \geq 38.7% (P<0.001). The 3-year CSS was significantly lower for ΔADC_{mean} <15.7% than for ΔADC_{mean} \geq 15.7% (P<0.001).

Conclusion: The percentage change of tumour ADC after RT may be a useful predictor of tumour progression and survival in patients with cervical cancer.

B-0389 16:28

Intravoxel incoherent motion and blood oxygen level-dependent of early iodinated contrast-induced acute kidney injury induced in a rabbit model
Y. Wang¹, K. Ren¹, L. Xie²; ¹Shenyang/CN, ²Beijing/CN
(wangyongfang1219@163.com)

Purpose: To assess if parameters in intravoxel incoherent motion (IVIM) and Blood oxygen level-dependent (BOLD) can be used to evaluate early Iodinated Contrast-Induced Acute Kidney Injury (CIAKI) in a Rabbit model.

Methods and Materials: 21 Zealand white rabbits weighing 2.5-3.0 kg were chosen and received iohexol at the dosage of 5.0g/kg. IVIM and BOLD were performed longitudinally at 24 h prior to and 1 h, 1 d, 2 d, 3 d and 4 d postinjection of iohexol. The parameters D, f, D* and ADC and R2* values were obtained. The expression of hypoxia inducible factor (HIF-1 α) in renal tissue was detected by immunohistochemistry. Repeated measure One-way analysis of variance was used for data analyses.

Results: BOLD and IVIM demonstrated distinct signals in all of the four renal regions, and inner stripes of the renal outer medulla showed the most pronounced modifications. For the measurements, an increased R2* value and strong attenuation of D and ADC were observed at 1-2 d after iohexol injection (p<0.05). As perfusion measurement, a significant decrease was shown for D* and f in 1 h-2 d (p<0.05) and an increase in 3-4 d. Compared with baseline levels, distinct elevation of R2* value were observed in all the anatomical compartments at 1 hour (p<0.05), to the maximum levels at 1 d (p<0.05), this observed trends were consistent with the expression of hypoxia inducible factor HIF-1 α .

Conclusion: The IVIM and BOLD techniques can be used as noninvasive tools to perform a time course study of the pathogenesis associated with CIAKI.

B-0390 16:32

Comparison of MRI and transvaginal ultrasonography in the diagnosis of retrocervical septum endometriosis
M. Wang, J. Lu, Y. Dai, Y. Xia; *Beijing/CN (wmd328@126.com)*

Purpose: To explore the clinical value of MRI and transvaginal ultrasonography (TVS) in the identification of retrocervical septum endometriosis.

Methods and Materials: Thirty-five patients with histologically confirmed endometriosis in retrocervical septum were retrospectively studied. All the patients underwent both MRI and TVS before laparoscopic surgery. Mapping of deep infiltrating endometriosis (DIE) in retrocervical septum was performed. MRI and TVS results were compared with surgical and pathological findings.

Results: The accuracy for MRI in the identification of endometriosis in retrocervical septum was 62.9% (22/35) and for TVS was 28.6% (10/35). Among 35 patients, the sensitivity, specificity and accuracy for MRI in the detection of posterior cul-de-sac obliteration and adhesion was 71.4% (10/14), 61.9% (13/21), 65.7% (23/35). The sensitivity, specificity and accuracy for MRI in the detection of DIE in uterosacral ligament was 47.6% (10/21), 87.8% (43/49), 75.7% (53/70).

Conclusion: MRI was superior to TVS for the diagnosis of DIE in retrocervical septum. MRI can demonstrate high sensitivity in the detection of cul-de-sac obliteration and adhesion, as well as evaluation the locations and extension of DIE. The information offered by MRI is helpful in determining surgical options and planning appropriate treatment.

B-0391 16:36

Clinical complications in percutaneous renal biopsy guided by ultrasound: 16 vs 18-gauge needles

P. Ramos Botelho Antunes¹, M.C. Barbosa Álvares¹, F. Franco Monteiro Prado¹, F. Tinôco Alvim de Souza¹, M. Álvares de Campos¹, E. Carvalho de Siqueira¹, R. Berindoague Neto¹, B. Carvalho Silva Rabelo²; ¹Belo Horizonte/BR, ²Itauna/BR
(brenorabelomed@gmail.com)

Purpose: Compare complications of percutaneous renal biopsy using two gauge(G) needles, 16G and 18G.

Methods and Materials: 238 individuals with renal biopsy(RB) indication were randomly separated into two groups according to the gauge of needle used. 134 patients(110 non-transplanted, and 24 renal transplanted) were biopsied with a 16G needle and 104(64 non-transplanted, and 40 renal transplanted) were biopsied with a 18G needle. Major and minor complications were analyzed immediately, and at 3 different times after procedure(4 hours, 12 hours and 7 days).

Results: The study presented a general index of 11.3% major complications. Patients who underwent RB with a 16G needle were more likely to complicate than 18G needle biopsies(17% vs. 3.8%; OR 5.1; 95% CI, 1.7-15.4; p=0.001). Although renal transplant patients submitted to 16G needle biopsies also presented higher complication rates when compared to patients submitted to 18G needle biopsies(OR 5.5; CI 95%, 0.5-56.9), there was no statistically significant association(p=0.14). On the other hand, non-transplanted renal patients had higher rates of complications in patients submitted to 16G needle biopsy in relation to patients submitted to 18G needle biopsy(OR 4.5; 95% CI, 1.3-15.8; p=0.01). The mean number of complete glomeruli harvested per biopsy for 16G and 18G needles was 22.1 and 17.5, respectively.

Conclusion: Our study findings suggest that there is a need to carefully weigh the potential risks for using a larger biopsy needle against the desire for more diagnostic tissue. Kidney biopsies taken by 18G needles resulted in lower frequency of complications compared to 16G.

B-0392 16:40

Developing a new PI-RADS v2-based nomogram for forecasting high-grade prostate cancer

X. Niu; *Chengdu/CN (niu19850519@163.com)*

Purpose: To establish a predictive nomogram for high-grade prostate cancer (HGPCa) in biopsy-naive patients based on the prostate imaging reporting and data system version 2, magnetic resonance imaging (MRI)-based prostate volume, MRI-based PV-adjusted prostate-specific antigen density, and other classical parameters.

Methods and Materials: Between August 2014 and August 2015, 158 men who were eligible for analysis were included as the training cohort. A prediction model for HGPCa was built using backward logistic regression and was presented on a nomogram. The prediction model was evaluated by a validation cohort between September 2015 and March 2016 (n=89). Histology of all lesions was obtained with MRI-directed transrectal ultrasound (TRUS)-guided targeted and sectoral biopsy.

Results: The multivariate analysis revealed that patient age, PI-RADS v2 score, and adjusted PSAD were independent predictors for HGPCa. The most discriminative cut-off value for the logistic regression model was 0.33; the sensitivity, specificity, positive predictive value, and negative predictive value were 83.3%, 87.4%, 88.4%, and 81.2%, respectively. The diagnostic performance measures retained similar values in the validation cohort (AUC=0.83).

Conclusion: The nomogram for forecasting HGPCa is effective and potentially reducing harm from unnecessary prostate biopsy and over-diagnosis.

B-0393 16:44

Diffusion-weighted MRI as a prognostic and response biomarker in patients with castration-resistant prostate cancer and bone metastases

R. Perez Lopez^{1,2}, N. Tunariu¹, D.-M. Koh¹, J.S. de Bono¹; ¹London/UK, ²Barcelona/ES (rperez@vhio.net)

Purpose: To correlate diffusion-weighted imaging (DWI) MRI features of bone metastases from castration-resistant prostate cancer (CRPC) with pathology (1), and evaluate whole-body DWI as prognostic (2) and response biomarker (3) in CRPC.

Methods and Materials: 1. 43 consecutive bone metastasis biopsies (33 patients) with DWI performed <12 weeks before bone biopsy and a reference cohort of 10 patients with no bone metastases were reviewed. DWI differences in bone biopsy positive/negative for tumour cells (Mann-Whitney) and DWI

cellularity correlations (Spearman's correlation "r") were assessed. 2. Prognostic value was evaluated in 43 consecutive patients. Total volume of bone metastases by DWI (tDV) was correlated with survival (Kaplan-Meier) and prognostic factors (r). 3. Utility as response biomarker was assessed in a clinical trial of olaparib in CRPC (n=21), comparing whole-body DWI at baseline and after 12 weeks of treatment. Regression analysis between tDV and median apparent diffusion coefficient (mADC) changes and treatment response were pursued.

Results: 1. mADC in bone metastases and non-metastatic bone was $993 \times 10^{-6} \text{mm}^2/\text{s}$ vs $601.8 \times 10^{-6} \text{mm}^2/\text{s}$, median normalized (n) nDWI signal was 4AU vs 1.6AU; $p < 0.001$. ADC and nDWI signal correlated with tumour cellularity; $p < 0.001$. 2. tDV correlated with all evaluated prognostic factors (haemoglobin; prostate-specific antigen; lactate dehydrogenase; alkaline phosphate; all $p < 0.001$) and CTC count ($p = 0.004$). tDV associated with overall survival (hazard ratio: 1.74; $p = 0.035$). 3. Change in tDV and mADC at 12 weeks associated with response to therapy ($p < 0.01$, $p = 0.04$, respectively).

Conclusion: DWI of bone metastases informs on prognosis and response to treatment in CRPC. DWI findings correlate with pathology. These data contribute towards DWI implementation in prostate cancer care.

B-0394 16:48

Tumour size at MRI association with lymph node metastasis and lymphovascular space invasion in resectable cervical cancer: a multicentre evaluation of surgical specimens

X.-I. Chen, P. Zhou, H. Li; *Chengdu/CN (penghyzhou@126.com)*

Purpose: To determine whether the gross tumour volume (GTV) and the maximum diameter of resectable cervical cancer at MRI could predict the presence of lymph node metastasis (LNM) and lymphovascular space invasion (LVSI).

Methods and Materials: 315 consecutive patients with cervical cancer who underwent surgery in 1 week after contrast-enhanced MRI were retrospectively identified from multiple hospitals. The tumour size including GTV and the maximum diameter of tumour were evaluated on MRI. Statistical analysis was performed to determine whether tumour size could predict LNM and LVSI. Cutoffs of GTV and the maximum diameter of tumour were first investigated in a cohort of 255 patients (group A) and then validated in an independent cohort of 60 patients (group B) using area under the receiver operating characteristic curve (AUC) analysis for predicting LNM and LVSI.

Results: Univariate analysis showed GTV and the maximum diameter of tumour could predict the presence of LNM and LVSI (all $P < 0.0001$). Multivariate analyses indicated GTV as an independent risk factor of LNM and LVSI (all $P < 0.0001$). In the group A, GTV and the maximum diameter of tumour could help identify the presence of LNM (AUC, 0.813 and 0.741, respectively) and LVSI (AUC, 0.806 and 0.751, respectively). In the group B, GTV and the maximum diameter of tumour could help identify the presence of LNM (AUC, 0.902 and 0.825, respectively) and LVSI (AUC, 0.771 and 0.748, respectively).

Conclusion: GTV and the maximum diameter of resectable cervical cancer at MRI demonstrated capability in predicting the presence of LNM and LVSI.

B-0395 16:52

NSsAfe: observational study on the incidence of nephrogenic systemic fibrosis in patients with renal impairment following gadoteric acid administration

A. Gottschalk, B. Kress; *Frankfurt a. Main/DE (andreas.gottschalk@gmx.net)*

Purpose: To prospectively determine the incidence of nephrogenic systemic fibrosis (NSF) in patients with renal impairment after administration of gadoteric acid (Dotarem, Guerbet, France).

Methods and Materials: Worldwide post-marketing study including 540 patients with moderate, severe or end-stage renal impairment, scheduled to undergo a routine contrast-enhanced MRI with gadoteric acid. Medical history, MRI indication(s) and adverse events (AEs) were recorded for each patient. Patients were followed up over 2 years after gadoteric acid administration with three visits to detect any signs/symptoms suggestive of NSF.

Results: Included patients had a mean age of 69.6 ± 12.7 years [range: 21-95], with a ratio male/female of 58.5%/41.5%. Renal impairment was graded as moderate for 69.3% of patients, severe for 16.1% and end-stage for 12.0%; 2.6% had undergone a kidney transplant. The mean (\pm SD) estimated glomerular filtration rate was $37.6 \pm 15.7 \text{ ml/min/1.73 m}^2$ [range: 4.0-74.2]. Central nervous system exploration was the main MRI indication (34.6%). The follow-up period was completed: 434 patients (80.4%) attended the first follow-up visit, 390 (72.2%) attended the second, and 354 (65.6%) attended the third. At the third follow-up visit, renal impairment was moderate for 40.1% of the patients, severe for 9.3% and end-stage for 14.4%. Overall, neither AEs related to the administration of gadoteric acid, nor signs of NSF were reported.

Conclusion: At the end of the 2-year follow-up period, the study shows no signs of NSF after gadoteric acid administration, confirming its good safety profile in this high-risk population.

B-0396 16:56

Staging of endometrial carcinoma with MRI: does the fusion T2-weighted and high b-value diffusion-weighted images improve diagnosis? An agreement study with histopathology

M. Correia¹, M.A. Serrado², M. Horta¹, T.M. Cunha¹, D. Virella¹; ¹Lisbon/PT, ²Funchal/PT (marianatomecorreia@gmail.com)

Purpose: To assess diagnostic accuracy of staging of endometrial carcinoma using MRI and evaluate the utility of fused T2-weighted (T2WI) and high b-value diffusion-weighted images (DWI).

Methods and Materials: This single-centre study includes 94 patients with endometrial carcinoma who underwent pretreatment MRI and subsequent surgery. One experienced radiologist assessed the grade of tumor invasion, according to FIGO system. The first evaluation was based on the T2WI, dynamic contrast enhance-MRI and DWI, afterwards the DWI and Fused T2-DWI images were considered for staging. These data were compared with the histopathologic findings as gold standard. The agreement was assessed by Cronbach Alpha test (kappa value) and interclass correlation coefficient (ICC).

Results: The diagnostic agreement of MRI without the fusion T2-DWI images was 85.7%, 50%, 22.2%, 30.8%, 50%, 40%, 28.6% and 25% for staging IA, IB, II, IIIA, IIIB, IIIC1, IIIC2 and IVB respectively (kappa=0.405 \pm 0.058; ICC=0.556, 95%CI 0.399-0.681). When fused T2-DWI images were considered, the agreement was instead 97.1%, 50%, 22.2%, 38.5%, 50%, 70%, 28.6% and 50% for IA, IB, II, IIIA, IIIB, IIIC1, IIIC2 and IVB respectively (kappa=0.537 \pm 0.057; ICC=0.695, 95%CI 0.574-0.786). The fused T2-DWI images improved the diagnostic agreement when evaluating tumor invasion of more than one-half of the myometrial thickness (kappa=0.787 \pm 0.063 vs. 0.617 \pm 0.063), the pelvic lymph node involvement (kappa=0.480 \pm 0.141 vs. 0.217 \pm 0.155) and the distant metastatic spread (kappa=0.569 \pm 0.166 vs. 0.378 \pm 0.192).

Conclusion: The use of fused T2-DWI images seems to improve the diagnostic performance for staging of endometrial carcinoma, particularly for assessing myometrial invasion, pelvic lymph node involvement and distant metastatic spread.

B-0397 17:00

Testicular microlithiasis: clinic-radiologic-pathologic correlation in 289 patients with germ cell tumour

M. De la Mora Malvez¹, A. Garza Gangemi¹, D.A. Sanchez Nava¹, M. Licano², O.C. Rico Rodriguez¹, C. Kauffman Ortega¹, R. Castillejos Molina¹; ¹Mexico City/MX, ²Tlalpan/MX (mariannedlm27@gmail.com)

Purpose: Testicular microlithiasis (TML) has been reported in 5.6% of asymptomatic patients in ultrasound examinations. Its association with primary testicular cancer (PTC) and extragonadal cell tumours (EGCT) is still controversial.

Methods and Materials: This is a retrospective observational study of prospectively collected data of 289 consecutive patients with germ cell tumours from a tertiary care centre between 2008 and 2017. Baseline characteristics (the presence of comorbidities, hypogonadism, primary tumour site, tumour histology, and clinical stage) and testicular ultrasonographic characteristics (testicular volume, tumour characteristics, and the presence of microlithiasis) were recorded for every patient. Imaging characteristics were analysed between groups according to primary tumour site and tumour histology.

Results: The median age at diagnosis was 27 ± 9 years and 12.7% of the patients had a history of cryptorchidia. Non-seminomatous tumours were more frequent (60.6%) than seminomas. Twenty two patients (7.6%) had EGCT and 267 had PTC. Unilateral TML was observed in 20.8% of the patients and bilateral microlithiasis was detected in 11.8% of the patients. Bilateral TML was more frequent in non-seminomatous tumours, 16.8% v.s. 6.5%, $p = 0.04$. Furthermore, the presence of bilateral TML was more common in patients with EGCT when compared with PCT patients 31.8% v.s. 10.1%, $p = 0.01$. Testicular atrophy (volume $< 12 \text{cc}$) was also associated with the presence of microlithiasis ($p < 0.01$).

Conclusion: TML is more common in non seminomatous histology and it is associated with testicular atrophy. Bilateral testicular microlithiasis is more common in EGCT.

B-0399 17:04

Differentiation and diagnosis of benign and malignant testicular lesions using ¹⁸F-FDG PET/CT

D. Shaq; *Guangzhou/CN (312368517@qq.com)*

Purpose: The purpose of this study was to evaluate the differential diagnostic value of ¹⁸F-fluorodeoxy glucose positron emission tomography/computed tomography (¹⁸F-FDG PET/CT) for benign and malignant testicular lesions.

Methods and Materials: The PET/CT scans of 53 patients with testicular lesions confirmed by biopsy or surgical pathology were retrospectively analysed. There were 32 cases of malignant tumours and 21 cases of benign lesions. Differences in the maximum standardised uptake value (SUVmax)

measurements and the SUVmax lesion/background ratios between benign and malignant lesions were analysed. The diagnostic value of this PET/CT modality for the differential diagnosis of benign versus malignant testicular lesions was calculated.

Results: The differences in the SUVmax measurements and the SUVmax lesion/background ratios between benign and malignant lesions were statistically significant (SUVmax: $Z=-4.295$, $p=0.000$; SUVmax lesion/background ratio: $Z=-5.219$, $p=0.000$); specifically, both of these indicators were higher in malignant lesions compared to benign lesions. An SUVmax of 3.75 was the optimal cutoff value to differentiate between benign and malignant testicular lesions. The diagnostic sensitivity, specificity, accuracy, positive predictive value, and negative predictive value of this PET/CT modality in the differential diagnosis of benign versus malignant testicular lesions were 90.6%, 80.9%, 86.8%, 87.9%, and 85.0%, respectively.

Conclusion: ^{18}F -FDG PET/CT can accurately identify benign and malignant testicular lesions.

B-0400 17:08

Ectopic pregnancies in caesarean section scars: five-years' experience

H.S. Darwish¹, Y. Habash¹, M. Habsah², ¹Ismailia/EG, ²Cairo/EG
(darwish.hoda@yahoo.com)

Purpose: To evaluate our 5 years experience in diagnosis and treatment of ectopic pregnancy developing in a caesarean section scar.

Methods and Materials: The study included twenty one women who were diagnosed with a caesarean scar ectopic pregnancy (CSEP) in the first trimester, which was confirmed by ultrasound and treated in our hospital during 5 years between 2012 and 2016. The clinical presentations, imaging findings, and treatment outcomes of all these pregnancies were recorded.

Results: All our 21 cases underwent successful early first trimester diagnosis with trans-vaginal colour Doppler ultrasonography and termination by a systemic methotrexate administration, or with aspiration of the gestational sac. Fourteen of them underwent systemic methotrexate treatment; and seven patients underwent trans-cervical aspiration of the gestational sac. Intraoperative bleeding occur in all 7 cases that treated with aspiration of the gestational sac, one of them end with hysterectomy. Uterine rupture occurs in one patient and treated conservatively. No complications occur in cases treated with systemic methotrexate injection. The cesarean scar mass followed with trans-vaginal ultrasound and regressed from 2 months to about 1 year after treatment.

Conclusion: Early imaging recognition, diagnosis of CSEP and effective treatment is critically important to improve outcome, minimise the need for emergency extended surgery, minimise maternal complications, maintain treatment options, and potentially preserve future fertility.

B-0401 17:12

Role of ultrasound and MR imaging in evaluation of patients at high risk of morbidly adherent placenta

G. Khatri, N. Antil, R. Misra, S.K. Bajaj; New Delhi/IN
(garvit_khatri@hotmail.com)

Purpose: To study the spectrum of ultrasound Doppler and MR Imaging findings in patients at high risk for adherent placenta; to compare the efficacy of ultrasound Doppler and MR Imaging in diagnosis of adherent placenta.

Methods and Materials: A total of 50 high risk pregnant patients (at least one caesarean section and low lying placenta) were included in the study. Ultrasound and MR imaging was performed. Specific Ultrasound and MR Imaging features were evaluated. All patients were followed up to delivery for confirmation of diagnosis. Categorical variables were presented in number and percentage (%) and continuous variables were presented as mean \pm SD and median. Normality of data was tested by Kolmogorov-Smirnov test. If the normality was rejected then non parametric test was used. A p value of <0.05 was considered statistically significant.

Results: Diagnostic accuracy of MR imaging was 94 % compared to 78 % for ultrasound Doppler. Both the modalities have similar high sensitivity (92.3 %). However MR imaging has better specificity (97%) compared to ultrasound Doppler (82 %). Most sensitive MR imaging feature is dark intraplacental band on T2 images. Most sensitive ultrasound Doppler imaging feature is intraplacental lacunae with turbulent flow.

Conclusion: All pregnant patients with previous caesarean section should be screened for low lying placenta in the first trimester. Ultrasound Doppler should be the initial modality for choice to diagnose adherent placenta. In equivocal cases MR imaging should be used as supplementary modality.

Thursday, March 1

08:30 - 10:00

Sky High Stage

Chest

MY 5

Chest

Moderators:

P. Franchi; Teramo/IT
J. Vilar; Valencia/ES

B-0402 08:30

Fully automated assessment of HRCT images for follow-up of IPF

R. Rubtsov, L. Kehler, A. Giannakis, M. Kreuter, M. Eichinger, O. Weinheimer, K. Maier-Hein, H.-U. Kauczor, C.P. Heussel; Heidelberg/DE
(roman.rubtsov.med@gmail.com)

Purpose: To quantify CT data using computer-aided diagnostic tool compared to pulmonary functional tests (PFT) longitudinally in patients with idiopathic pulmonary fibrosis (IPF).

Methods and Materials: 112 patients (M:F; 92:20) with IPF diagnosed through interdisciplinary approach, with either stable disease (n=73) or acute exacerbation (n=39) underwent 2 consecutive HRCT (6 months interval). "In-house" software, Lung Fibrosis Quantification Tool (LUFIT), based on a 3D-metamodel algorithm was used for fully automated lung segmentation and histograms analysis. Percentiles of lung histogram analysis, reflecting the amount of end-stage fibrosis (80th) and "ground-glass" (40th), derived from baseline HRCT and follow-up, were correlated to PFT and analysed according to Mann-Whitney.

Results: The strongest correlation was found between TLC measured by LUFIT and with body plethysmography (R2=0.95). Moderate negative correlations were observed between 80th and VCIN (-0.696) and DLCO SB (-0.649) in the "exacerbation-group" at baseline. In the stable group no relevant change of PFT or histogram parameters was found. In the "exacerbation" group 80th/40th percentile rise by 42/14 HU (p=0.0008/0.0047).

Conclusion: LUFIT proved to be accurate in quantifying the lung volume. In patients with exacerbation it detects the acute end-stage changes, developing in the course of the disease. Fully automated assessment of fibrosis extent and can be helpful as an additional tool in quantitative analysis of CT data in patients suffering from IPF.

B-0403 08:34

Quantitative prediction of malignancy on newly developed 3D computer-aided volumetry (CADv) with pulmonary nodule component evaluation on thin-section CT

Y. Ohno¹, A. Yaguchi², K. Aoyagi³, S. Kaminaga³, Y. Kishida¹, S. Seki¹, T. Yoshikawa¹; ¹Kobe/JP, ²Kawasaki/JP, ³Otawara/JP (yosirad@kobe-u.ac.jp)

Purpose: To evaluate the quantitative capability of newly developed 3D computer-aided volumetry (CADv) with pulmonary nodule component assessment for predicting malignancy and postoperative recurrence on thin-section CT.

Methods and Materials: 59 consecutive patients with 101 pulmonary nodules underwent repeated thin-section CT, pathological examination, surgical resection and/or follow-up examination. Then, all nodules were divided into malignant (n=64) and benign (n=37) nodule groups. In this study, CADv automatically assessed solid, ground-glass opacity, cavity and total nodule volumes from two serial CT data. Then, total volume change per day (TV/day), solid to total volume change ratio per day (S/T ratio/day) and doubling time (DT) were determined. Student's t test was performed to compare all indexes between malignant and benign groups. Then, ROC analyses were performed to compare differentiation capabilities of indexes as having significant differences between malignant and benign groups. Finally, each diagnostic performance was compared by McNemar's test.

Results: TV/day and DT had significant differences between malignant and benign nodule groups (p<0.05), although TV/day and S/T ratio/day had significant difference between recurrence and non-recurrence groups (p<0.05). On distinguishing malignant from benign groups, area under the curves (Azs) of TV/day (Az=0.94) was significantly larger than that of DT (Az=0.62, p<0.001). In addition, specificity (SP) and accuracy (AC) of TV/day were significantly higher than those of DT (p<0.001).

Conclusion: Newly developed 3D CADv system has quantitative capability for prediction of malignancy and postoperative recurrence on thin-section CT.

Author Disclosures:

Y. Ohno: Research/Grant Support; Toshiba Medical Systems Corporation. A. Yaguchi: Employee; Toshiba Corporation. K. Aoyagi: Employee; Toshiba Medical Systems Corporation. S. Kaminaga: Employee; Toshiba Medical Systems Corporation. S. Seki: Research/Grant Support; Toshiba Medical Systems Corporation. T. Yoshikawa: Research/Grant Support; Toshiba Medical Systems Corporation.

B-0404 08:38

Logistic regression analysis and a risk prediction model of tumour spread through air spaces (STAS) in patients with stage I lung adenocarcinoma

X. Wang; Beijing/CN (oliverwxy_zz@sina.com)

Purpose: Tumour spread through air spaces (STAS) is an important pattern of invasion and impacts the frequency and location of recurrence. The objective was to assess the correlation between STAS and metabolic tumour burden measured by PET/CT, and to establish a risk prediction model of STAS in patients with stage I lung adenocarcinoma.

Methods and Materials: We reviewed 121 consecutive patients. The standardised uptake value (SUV_{max}, SUV_{mean} and SUV_{peak}), metabolic tumour volume (MTV), total lesion glycolysis (TLG), diameter and computed tomography volume (CTV) were measured. All risk factors were analysed by multivariate logistic regression analysis; regression coefficients and odds ratios were calculated for independent risk factors. A STAS risk prediction model was created using the regression coefficients to determine the predictive probability (PP).

Results: There was significant difference of STAS distribution among different nodule types (P = 0.001). In the correlation analysis of STAS with the metabolic tumour burden parameters, SUV_{max} (P=0.020), SUV_{mean} (P=0.002), SUV_{peak} (P=0.002) and TLG (P=0.004) were significantly correlated with STAS. MTV (P=0.721), diameter (P=0.480) and CTV (P=0.651) showed no significant correlation with STAS. The predictive probability of STAS and the incidence of STAS were analysed using the ROC curve (AUC = 0.749, P = 0.000). The sensitivity, specificity, and accuracy of the predictive model for STAS were 67.3%, 70.8% and 69.4%, respectively.

Conclusion: The predictive model developed was accurate in predicting the incidence of STAS. SUV and TLG were valuable predictive indices in the prediction of STAS.

B-0405 08:42

Quantitative MRI assessment of interstitial lung disease

M.T.A. Buzan¹, A. Wetscherek², C. Heussel², M. Kreuter², J. Dinkel³, ¹Cambridge/UK, ²Heidelberg/DE, ³Munich/DE

Purpose: To evaluate the contribution of advanced quantitative magnetic resonance imaging (MRI) in the assessment of interstitial lung disease (ILD).

Methods and Materials: We prospectively included 34 patients (mean age: 68 years; M:F, 1:1) with pathologically proven usual interstitial pneumonia (UIP) and nonspecific interstitial pneumonia (NSIP). All patients underwent thin-section multislice computed tomography (CT) and MRI of the lung at 1.5T. The MRI protocol included entire lung T2 mapping based on ECG-gated multi-echo single shot turbo spin-echo sequence (TE: 20, 40, 79, 140, 179 ms), and a contrast-enhanced radial-VIBE sequence with golden-angle spacing acquired during 5 minutes of free-breathing, followed by 5D reconstructions of the data. For this study, we used the end-expiratory phase. The CT images were used to assess the patterns and severity of lung fibrosis.

Results: The T2 relaxation of normal lung showed significant difference to pathological areas (p<0.001). The T2 relaxation time increased with the increase in fibrotic tissue density. UIP and NSIP regional patterns could not be differentiated by T2 relaxation times. T2 relaxation showed a significant statistical difference between active-inflammatory and stable-fibrotic NSIP. Both in severe and non-severe disease, there is later peak enhancement in idiopathic pulmonary fibrosis (IPF) compared to non-IPF, p<0.01. In non-IPF, the more severe lesions had longer time to peak and slower washout rate as compared to non-severe lesions, p<0.05.

Conclusion: MRI is a non-invasive, non-irradiating method that allows advanced, quantitative tissue characterization in ILD both in chronic and active states.

B-0406 08:46

Primary and metastatic lung tumours treated with stereotactic body radiation therapy (SBRT): own experience

N. Martynova, N. Vorobyov, A. Mikhailov, J. Gutsalo, E. Smirnova, A. Kalesnik, G. Andreev, A. Kubasov, A. Lyubinskij; St. Petersburg/RU
(natlmartynova@gmail.com)

Purpose: Assessing SBRT efficiency and toxicity for primary lung cancer and lung metastases.

Methods and Materials: In a period from 12.2011 to 02.2017, 71 patients with primary and metastatic lung tumours were treated. SBRT was applied to 103 tumours: 33 primary tumours and 70 metastases of different tumour sites. Two linear accelerators with different respiratory motion tracking systems (RMTS) were used: CyberKnife (CK) with Synchrony RMTS and TrueBeam STx (TB) with gating.

Results: Clinical observation group includes 52 patients with 81 lung tumours. Average tumour volume was 44.7 cc (0.2-496.5 cc). Observation median was 7 months. Local control (LC) was achieved in all cases, median of LC was 6

months. For 19 (23.5%) tumours complete response was achieved, median was 5 months. There was a local relapse in 17 (21%) cases, 15 of which were squamous cell relapse. There was discovered a negative linear dependence of local relapse probability from BED₁₀ for squamous cell tumours. Disease progression was observed among 29 patients, 93% of them had a local control preserved during the whole observation period. TB demonstrated higher early toxicity rate than CK (19% vs 8%, p=0.01), grade 1-2 for most patients; 5 patients had grade 3 early toxicity. None of the patients had grade 4 early toxicity. Late toxicity did not exceed grade 2 for all the patients.

Conclusion: SBRT appears to be safe and effective treatment option for patients with lung lesions, including huge and central tumours. Potentially, higher radiation doses are needed to achieve better LC for squamous cell tumours.

B-0407 08:50

Diagnostic value of radiologic signs of pulmonary hypertension: pulmonary artery aortic ratio, pulmonary artery vertebral ratio and contrast regurgitation in hepatic veins

G. Zanirato Rambaldi, F. Niro, N. Galìè, M. Zompatori; *Bologna/IT*
(giuseppe.zanirato@gmail.com)

Purpose: To assess the diagnostic value of pulmonary artery (PA) aortic ratio (PAR), PA vertebral ratio (VR) and regurgitation of intravenous contrast medium (CM) into hepatic veins (HVR) as predictors of pulmonary hypertension (PH).

Methods and Materials: We retrospectively reviewed clinical characteristics, CT scans, echocardiograms, and right-sided heart catheterization of patients with suspected PH undergoing angio-CT scan of PA between 2005 and 2013. The PA, aortic and anteroposterior vertebral diameter from the same CT image were measured. HVR was evaluated based on reflux of CM into hepatic veins. Linear and logistic regression were used to examine the relationships between CT studied parameters and PA systolic (PASP), diastolic (PADP), mean pressure (mPAP) and PA resistances (PAR) by invasive haemodynamics.

Results: 359 patients (96 with primary PH, 77 and 98 with, respectively, connective tissue diseases and congenital heart diseases: Eisenmenger syndrome associated PH and 88 without PH) were enrolled. PAR and VR correlated linearly with PASP, PADP, mPAP and PAR (p<0.0001). PAR > 1 is 63.3% sensitive and 85.4% specific (area under the ROC curve (AUC)=0.83) for PH. VR > 1.33 is 71.53% sensitive and 80.9% specific (AUC=0.84) for PH. In younger subjects (<58 years), AUC for PAR and VR was 0.91 (respectively, p=0.0020 and p=0.0004). HVR was 89.6% specific for tricuspid regurgitation and correlated with increased PAP and PAR.

Conclusion: PAR, VR and HVR correlate with haemodynamic dysfunctions in PH, PAR > 1.07 and VR > 1.33 are valid predictors of possible PH, especially in subjects < 58 years old.

B-0408 08:54

Application of high-pitch scanning mode in low-dose lung-computed tomography screening for patients with chronic obstructive pulmonary disease: a pilot study

C. Li, M. Li, L. Jin; *Shanghai/CN* (licheng3456@sohu.com)

Purpose: This study was performed to evaluate the performance of high-pitch scanning mode in computed tomography (CT) examination of chronic obstructive pulmonary disease (COPD).

Methods and Materials: Chest CT scans were performed in 300 patients clinically diagnosed with COPD before which the subjects were divided into 3 experimental groups and 2 control groups; Siemens sensation 16 was employed to perform spiral CT scanning for experimental group 1, a GE lightspeed VCT was used for experimental group 2, a Siemens definition flash was used for experimental group 3, with the parameters of 100kV and automatic mAs and different pitch.

Results: The average of lung parenchyma CT in experimental group 3 was -918.18±6.57, which was significantly different from the other 4 groups (P<0.001). There was no significant difference between control groups 1, 2 and experimental groups 1, 2 (P>0.05), but the experimental group 3 was significantly different from those of the remaining groups (P<0.001).

Conclusion: The application of a high-pitch scanning mode for patients with COPD can effectively reduce their breath holding time, prevent complications, and reduce motion artefacts. As such, the approach has great scanning performance and is promising for clinical applications.

B-0409 08:58

Morphological study of blood vessels near lung tumour by the 3D quantitative CT technique

Y. Li, Y.-I. Dai, Y.-m. Guo; *Xi'an/CN* (yuyanyan_zi@126.com)

Purpose: The effect of non-enhanced CT on the changes of vascular morphology in lung cancer is investigated. A 3D quantitative CT measurement method based on differential geometry algorithm was found to be suitable for the morphological study of blood vessels adjacent to lung tumour.

Methods and Materials: Lung cancer ipsilateral and contralateral pulmonary vascular changes were assessed by the routine visual examination and FACT-digital lung TM quantitative CT measurement software. This study included 162 patients with lung cancer and 178 healthy subjects. All cases of lung cancer were confirmed by pathology. The number of blood vessels and area of blood vessels normal to cross sections of 5/6-generation bronchioles were selected as pulmonary vascular morphological parameters.

Results: The visual method has revealed the ratio of ipsilateral pulmonary vascular abnormalities in lung cancer (151/162) to be less than that of quantitative CT (162/162). The visualization time required to determine pulmonary vascular abnormalities (3.2 ± 1.5 min) exceeded that of quantitative CT measurements (2.5 ± 1.3 min) for P < 0.05. According to quantitative CT measurements, the number and area of pulmonary blood vessels in the ipsilateral lung cancer exceeded those in the contralateral side and in the control group (P = 0.00, 0.00).

Conclusion: A fully automated quantitative CT measurement method was successfully applied to the identification of pulmonary blood vessels and quantitative measurements of morphological changes of blood vessels near lung tumour.

B-0410 09:02

IPF: diagnosis and follow-up using CT fibrosis score, correlation with clinical and functional data in a cohort of patients in therapy with pirfenidone or nintedanib

S. Riva, G. Guzzardi, M. Barini, M. Valenti, A. Carriero, M. Pelle; *Novara/IT*
(silviariva.riva@gmail.com)

Purpose: The aim of this study was to evaluate the utility of a VISUAL CT-FIBROSIS SCORE in evaluation of extension of usual interstitial pneumonia (UIP) and in the 12-month follow-up after the start of antifibrotic therapy with pirfenidone or nintedanib.

Methods and Materials: Since 2015, in our institute 15 patients have received IPF diagnosis on the basis of clinical and radiological data. The inclusion criteria was only the radiological diagnosis of UIP DEFINITE. For each patient a CT-FIBROSIS SCORE (as suggested by previous experiences in the literature as those of Ichikado, Ley and Sverzellati) was calculated and the value of diffusing capacity of the lungs for carbon monoxide (DLCO) was collected, which correlates with the progression of the disease, at diagnosis and follow-up. We used McNemar's test for the correlation between CT-FIBROSIS SCORE and DLCO.

Results: The assigned FIBROSIS SCORE score was measured in absolute terms within the sample a minimum value of 123.3 and a maximum of 238.3. The mean DLCO value at diagnosis was 46.24 and at the follow-up of 40.75. McNemar's test showed a statistically significant difference between evolution over time of the FIBROSIS SCORE parameter and the clinical-instrumental parameter of the DLCO. The value of p, returned by the application of this test, was in fact above 0.05, resulting in 0.7.

Conclusion: The interpretation of the statistical result allows us to assert that there is a correlation between the score of fibrosis and the performance of the DLCO.

B-0411 09:06

Pulmonary embolism-induced perfusion defects on iodine maps: quantitative comparison of dual-energy CT and subtraction CT

D. Grob¹, L.J. Oostveen¹, M.M. Prokop¹, C. Schaefer-Prokop², I. Sechopoulos¹, M. Brink¹; ¹Nijmegen/NL, ²Amersfoort/NL (Dagmar.Grob@radboudumc.nl)

Purpose: To compare signal-to-noise ratios for pulmonary embolism-induced perfusion defects on iodine maps derived from dual-energy CT (DECT) and subtraction CT (SCT).

Methods and Materials: We recruited 27 consecutive patients diagnosed with acute PE from a prospective trial for comparison of DECT and SCT, in which 100 kV unenhanced scans and 140/100 kV DECT pulmonary angiography had been performed in patients with suspected PE. We included all perfusion defects seen on DECT in which there was an acute segmental PE with ≥75% vascular obstruction but no emphysema or consolidation present. Noise was measured on the iodine maps as the standard deviation in normal parenchyma. Signal was defined as the enhancement difference between the perfusion defect and the surrounding normal parenchyma in a triangular region of interest. Signal-to-noise ratios (SNRs) were compared for iodine maps derived from DECT and SCT using a Wilcoxon signed test.

Results: Median dose-length product was 154 mGy·cm for SCT and 162 mGy·cm for DECT. Noise was not significantly different between the two (p=0.86). Seventy perfusion defects in 45 lungs were included. The average SNR was 18.5 for SCT and 16.9 for DECT (p=0.09). Significant differences in SNR were only found in perfusion defects in the upper lobes, with an average SNR of 22.0 for SCT and 18.1 for DECT (p<0.05).

Conclusion: At similar radiation dose, perfusion defects on subtraction CT show similar or higher SNR than those on dual-energy CT. This implies that SCT is a viable alternative to DECT for depicting perfusion defects.

Author Disclosures:

D. Grob: Research/Grant Support; Toshiba Medical Systems. **L.J. Oostveen:** Research/Grant Support; Toshiba Medical Systems. **M.M. Prokop:** Research/Grant Support; Toshiba Medical Systems. **Speaker;** Bracco, Bayer, Toshiba Medical Systems. **Other;** Thirona, Veolity. **I. Sechopoulos:** Research/Grant Support; Toshiba Medical Systems, Siemens. **Speaker;** Siemens. **M. Brink:** Research/Grant Support; Toshiba Medical Systems.

B-0412 09:10

Advantages of spectral CT in staging of patients with non-small cell lung cancer (NSCLC)

U. Fehrenbach¹, K. Merz¹, G. Böning¹, J. Kahn¹, F. Feldhaus¹, M.H. Maurer², D. Renz³, B. Hamm¹, F. Streitparth¹; ¹Berlin/DE, ²Berne/CH, ³Jena/DE (uli.fehrenbach@charite.de)

Purpose: Imaging of NSCLC is based on morphological criteria in contrast-enhanced CT studies. Spectral CT(SCT) offers additional information by specific SCT values. We evaluated the SCT values' usefulness in staging of lung cancer patients.

Methods and Materials: 116 patients with confirmed NSCLC were included in a prospective cohort study. All patients received a single-phase contrast-enhanced SCT (80kV/140kV). SCT values (iodine content(IC), spectral slope pitch(k) and quantitative HU increase) of tumor tissue (primaries and metastases) and lymph nodes(LN) were acquired. Adrenal masses(AM) were evaluated in virtual native series(VNS). Additional lung structure changes were analyzed as secondary findings.

Results: 52 non-treated NSCLC primary tumors were sufficiently measurable. Adenocarcinoma showed significantly higher normalized IC than squamous cell carcinoma (18.8vs12.0;p=0,035). 126 LN were analyzed and metastases showed significantly lower IC and k than benign LN (20.8vs25.8;p=0,023;1.6vs2.5;p=0,000). Tumors in local control after radiochemotherapy showed significant lower IC in hot spot analysis than tumors in progressive disease (4.27vs2.06;p=0,000). In 34 AM, VNS identified adenomas with high sensitivity and specificity (96%,100%). Pulmonary metastases showed no significant differences to benign lung nodules (p=0,18-0,76). Secondary findings of atelectasis, pneumonia, scar tissue and pleural effusion showed heterogeneous IC. In 2 patients a perfusion defect through pulmonary embolism could be visualized.

Conclusion: SCT and its specific values may support the differentiation between histological NSCLC subtypes and may improve the identification of LN metastases. It can also improve evaluation of tumor response after radiochemotherapy. With VNS, adrenal adenomas can be differentiated to metastases. Pulmonary perfusion defects can be visualized in iodine maps.

B-0413 09:14

Longitudinal airway remodeling in active and past smokers in a lung cancer screening population

T.D. Buschulte, M.O. Wielpütz, B.J. Jobst, M. Trauth, J. Tremper, O. Weinheimer, S. Delorme, N. Becker, H.-U. Kauczor; *Heidelberg/DE (T.Buschulte@gmx.de)*

Purpose: Little is known on the longitudinal changes of airways on computed tomography (CT) depending on smoking status. Thus, we assessed CT-based airway metrics by quantitative post-processing repeatedly over a period of 4y in a group of heavy smokers.

Methods and Materials: CT scans in a lung cancer screening program were performed for 4y at 12mon intervals in 284 long-term ex-smokers (ES), 405 continuously active smokers (CS), and 31 subjects who quit smoking during 2y after baseline CT (recent quitters, RQ). CT were evaluated by airway analysis software, computing the total diameter (TD), luminal area (LA) and wall percentage (WP) from 5th-8th airway generation.

Results: At all time points, TD and LA were significantly higher in ES compared to CS, for example at baseline with 6.24mm vs. 5.93mm (p<0.001) and 15.23mm² vs. 13.51mm² (p<0.001), respectively. RQ also showed a tendency towards higher TD (6.15mm vs. 5.93mm, n.s.) and significantly higher LA (14.77mm² vs. 13.51mm², p<0.001) than CS after 3y, and also after 4y. Smoking status independently predicted TD, LA, and WP at baseline as well as at 3y and 4y follow-up (p<0.01-0.001) in a multivariate analyses, with a stronger impact than pack years.

Conclusion: Bronchial narrowing and wall thickening depend on the smoking status. Smoking-induced airway wall inflammation may partially be reversible after smoking cessation even in heavy smokers at risk of COPD. Therefore quantitative CT-based airway metrics within clinical trials should consider the current smoking status instead of pack years only.

B-0414 09:18

Bronchial wall changes after thermoplasty in the treatment of severe asthma: CT scan assessment at 3 months

Y.W. Kim¹, M.P. Debray², C. Fetita³, O. Fouque¹, M. Aubier², P.-Y. Brillet¹; ¹Bobigny/FR, ²Paris/FR, ³Evry/FR (wouk1805@gmail.com)

Purpose: Our goal is to assess by CT scan bronchial wall changes induced by thermoplasty, an endoscopic technique aiming at reducing airway smooth muscle mass.

Methods and Materials: This prospective study included 24 patients with severe asthma. For each bronchus, airway lumen area (LA), wall area (WA) and WA as a percentage of total bronchial area (WA%) were automatically generated from CT acquisitions by the software BronCare, before (M0) and after (M3) treatment. The measures were confronted to functional data and asthma control.

Results: After treatment, LA remained unchanged. By contrast, WA and WA% increased at M3 (M0/M3: 16.7/19.0 mm² for WA and 63.7/66.7% for WA%; p<0.0001). These variations were correlated to pre-thermoplasty values, with a negative linear correlation (r>-0.7, p<0.0001). The less thick bronchi tended to thicken more. The importance of this effect differed between patients (p=0.0004 for WA%). Thereby, the patients could be split into two clusters in relation to WA and WA% pre-thermoplasty values, their modifications after treatment and patient's height (p<0.0046). The clusters did not differ according to other initial clinical data or follow-up events.

Conclusion: Bronchial thermoplasty results in bronchial structural changes, reflecting a residual inflammation and might be adjusted to patient's morphotype.

B-0415 09:22

Optimisation of a chest CT protocol for the detection of ground glass opacity nodules: feasibility study with a computer-assisted detection system and a lung cancer screening phantom

S. Kang, T.H. Kim, I.K. Park, C.H. Park; *Seoul/KR (smkang13@gmail.com)*

Purpose: To optimise computed tomography (CT) parameters for the detection of ground glass opacity nodules (GGNs) using a computer-assisted detection (CAD) system and a lung cancer screening phantom.

Methods and Materials: A phantom containing GGNs (~600 HU) was examined with a 256-row multi-detector CT scanner. Three tube voltages (120, 100, 80kVp) were used in combination with five tube currents (400, 200, 100, 50, 25mA); three slice thickness (0.625, 1.25, 2.5mm); and four different reconstruction algorithms (ASIR-V) of 0, 30, 60, 90. For each protocol, the accuracy of the CAD system was evaluated for the 6 target GGNs that were 8, 10, or 12mm in size.

Results: Among the 180 combinations of CT parameters, 80kVp, 200mA, and 1.25mm had the best performance with 6 true positives (TP) and no false positives (FP). For 80kVp, 400mA, 1.25mm, there were 5TP, 1FP; and 100kVp, 100mA, 1.25mm had 4TP and 1FP; while 100kVp, 50mA, 1.25mm had 4TP and 1FP; and 120kVp, 25mA, 1.25mm had 4TP and 3FP. (All above combinations were with ASIR-V of 90.) Other combinations had fewer than 3TP and especially any combinations with a 0.625mm had 0TP and at least 1FP result.

Conclusion: Chest CT at low voltage with thin slice thickness and high iterative reconstruction algorithm might improve the detection rate of a CAD system for small GGNs in lung cancer screening.

B-0416 09:26

Diagnostic ability of the primary lung cancer by radiologists with chest x-ray

R. Nishino¹, H. Numasaki², N. Minamoto¹, S. Nakai¹, T. Uchigashima¹, A. Takahashi¹, S. Ehara¹, M. Sakai¹, S. Takashima¹; ¹Suita/JP, ²Osaka/JP (u686321c@ecs.osaka-u.ac.jp)

Purpose: The purpose of this study was to determine the factors that influence the diagnostic ability of pulmonary nodules with chest x-ray (CXR) and to assess the factors that influence the confidence on the diagnosis of the nodules that were correctly detected.

Methods and Materials: Five chest radiologists interpreted chest radiographs (non-nodule images: 200 and nodule images; 200 (subsolid nodule: 95 and solid nodule; 105)), and diagnostic ability was assessed using localized receiver operating characteristics (LROC) analysis. For nodule group, we studied statistical differences between the correctly diagnosed group and incorrectly diagnosed group in 9 factors, and assessed the factors that influence the diagnostic ability using logistic regression analysis. For the correctly diagnosed group, we performed statistical tests in 9 factors, and assessed the factors that influence the confidence on the diagnosis using multiple regression analysis.

Results: The mean area under the LROC curves was 0.73 ± 0.015 (accuracy: 70.3%, sensitivity: 48.7% and specificity: 91.9%). On logistic modelling, CT value of the nodule, diameter of the nodule and the overlap with other

structures were common significant factors for 5 radiologists. On multiple regression analysis, the overlap with other structures was common significant factor for 5 radiologists.

Conclusion: The significant factors that influence the diagnostic ability of CXR for primary lung cancer were CT value of the nodule, diameter of the nodule and the overlap with other structures. The significant factor that influences the confidence on the diagnosis of the nodules that were correctly detected was the overlap with other structures.

B-0417 09:30

Salivary gland tumours in the central airway: the comparison of CT features between adenoid cystic carcinoma and mucoepidermoid carcinoma

Y. Deng, Q. Zeng, X. Wu, X. Li, W. Luo; Guangzhou/CN
(hotden_1@hotmail.com)

Purpose: To compare the CT features between adenoid cystic carcinoma (ACC) and mucoepidermoid carcinoma (MEC) in the central airways.

Methods and Materials: This retrospectively study complying with HIPAA was approved by Institutional Review Board. A total of 10 patients with ACC (7 females, 3 males; median age, 33 years; age range, 21 to 59 years) and 9 patients with MEC (7 females, 2 males; median age, 21 years; age range, 15 to 37 years), who underwent contrast-enhanced CT before surgery or biopsy, were identified and included. The CT features of the tumour including location, maximum diameter, growth pattern, and enhancement were evaluated. The difference of tumour location and growth pattern between ACC and MEC was compared using Chi-squared test. The difference of maximum tumour diameter, enhancement between ACC and MEC were compared using Mann-Whitney U test.

Results: 8 of 10 ACC (80%) origin from trachea, while 2 of 9 MEC (22%) origin from trachea ($p=0.04$). 9 of 10 ACC (90%) and 3 of 9 MEC (33%) exhibited infiltrative growth pattern, while 1 of 10 ACC (10%) and 6 of MEC (67%) exhibited expansile growth pattern ($p=0.04$). There was no difference of maximum tumour diameter between two subtypes ($p=0.762$). The MEC showed significant greater enhancement than ACC (MEC: median, 62 HU; 25th-75th percentile, 55-67 HU; ACC: median, 30 HU; 25th-75th percentile, 26-37 HU; $p=0.002$).

Conclusion: ACC and MEC in the central airways has distinct CT features including the location, growth pattern and enhancement.

B-0418 09:34

Early residual tumour differentiation from benign periablation thermal injury after radiofrequency ablation by spectral analysis with dual-energy computed tomography

L. Yuekao; Shi Jiazhuang/CN (64502240@qq.com)

Purpose: To investigate the applicative value of dual-energy computed tomography (DECT) spectral analysis on the quantitative assessment of residual tumour after radiofrequency ablation.

Methods and Materials: With CT-guided percutaneous tumour tissue inoculation, we established rabbit VX2 tumour model and incomplete tumour ablation model. Triple-phase contrast-enhanced DECT data on 24 rabbits with VX2 carcinoma then were assessed at day 3 (n=6), 1 week (n=6), 2 weeks (n=6) and 3 weeks (n=6) after incomplete RFA independently by two readers. Under different KeV values, we determined the average CT value of the area of interest and the plot of spectra and compared the differences between the residual tumour and inflammation. The pathologic specimens were sectioned in the same plane as DECT imaging.

Results: With CT-guided percutaneous tumour tissue inoculation, we established a rabbit VX2 tumour model and an incomplete tumour ablation model. Triple-phase contrast-enhanced DECT data on 24 rabbits with VX2 carcinoma then were assessed at day 3 (n=6), 1 week (n=6), 2 weeks (n=6) and 3 weeks (n=6) after incomplete RFA independently by two readers. Under different KeV values, we determined the average CT value of the area of interest and the plot of spectra and compared the differences between the residual tumour and inflammation. The pathologic specimens were sectioned in the same plane as DECT imaging.

Conclusion: Spectral curve with DECT might help in differentiating benign periablation reactive tissue from residual tumour in VX2 carcinoma in rabbits after RF ablation.

B-0420 09:38

Assessment of survival in patients with idiopathic pulmonary fibrosis using Kurtosis and mean lung density HRCT indexes

A.G. Torcitto¹, D. Falsaperla¹, S.E. Torrisi¹, L.A. Mauro¹, M. Pavone¹, G. Russo², A. Stefano², C. Vancheri¹, S. Palmucci¹; ¹Catania/IT, ²Cefalù/IT (alfre.84@katamail.com)

Purpose: To investigate the diagnostic accuracy of Kurtosis and Mean Lung Density (MLD) in the assessment of survival in a cohort of patients with Idiopathic Pulmonary Fibrosis (IPF).

Methods and Materials: 42 patients with IPF diagnosis and a minimum follow-up time of 3 years were retrospectively collected; HRCT and pulmonary function tests (FVC and DLCO) performed at diagnosis time were analysed; the extent of fibrotic disease was quantified on HRCT using Kurtosis, MLD, percentage of HAA and Fibrotic areas. Patients were divided into 3 groups according to Kurtosis value (kurtosis index <3, 3-4 and >4) and according to MLD (MLD <-800, between -800 and -750, >-750). Survival analysis was performed according to these variables. Correlations between kurtosis and MLD indices and pulmonary function tests were also performed using Spearman's Rank correlation.

Results: Significant survival differences were found according to the kurtosis values ($p=0.002$) and MLD value ($p=0.003$) obtained from HRCT quantitative evaluation at the diagnosis time. Spearman's Rank correlation analysis showed also a positive correlation between kurtosis value and FVC ($r=0.57$, $p=0.0001$); a positive correlation between kurtosis value and DLCO ($r=0.52$, $p=0.0004$); a negative correlation between MLD value and FVC ($r=-0.53$, $p=0.0003$); a negative correlation between MLD value and DLCO ($r=-0.41$, $p=0.0069$).

Conclusion: Kurtosis index and MLD value may provide an accurate estimation of survival in a population of IPF patients from the time of diagnosis. These HRCT-derived indices demonstrate also a correlation with common pulmonary function values (FVC and DLCO) pointing out their possible use in clinical practice.

B-0421 09:42

Volumetric analysis of intravoxel incoherent motion diffusion-weighted MRI in predicting the invasiveness of non-small cell lung cancer

J. Jiang¹, L. Cui², Y. Fu¹, G. Xu¹; ¹Yancheng/CN, ²Nantong/CN (1021809719@qq.com)

Purpose: To investigate the value of intravoxel incoherent motion (IVIM) parameters D, D*, f and apparent diffusion coefficient (ADC) in preoperative prediction of tumour grade, lymph node metastasis and pleural invasion in non-small cell lung cancer (NSCLC) patients.

Methods and Materials: 39 surgically-diagnosed NSCLC patients (39 lesions) were enrolled in this study and underwent free-breathing DWI and IVIM (10 b-values, 0-1000 s/mm²) scans one week before the operation on a Siemens 3T MRI. ADC_{mean}, ADC_{min}, D, D* and f values were independently calculated by volumetric region of interest (ROI) by 2 observers. Inter-observer reproducibility was assessed. Differences of these parameters in tumors with different differentiation degree, with or without lymph node metastasis, and with or without pleural invasion were compared. Receiver operating characteristic (ROC) curves were generated to determine the diagnostic performance.

Results: Good inter-observer reproducibility was seen in all parameters except D*. D and ADC_{min} were significantly lower in poorly differentiated lung cancer ($P<0.001$ and 0.001, respectively) and so was D in patients with lymph node metastasis ($P=0.010$). While in patients with pleural invasion, D was significantly lower and f was significantly higher ($P=0.017$ and 0.005, respectively). According to ROC curve analysis, highest values of area under the curve (AUC) appeared when predicting tumor grade and lymph node metastasis with D (0.858, 0.761) and predicting pleural invasion with f (0.766).

Conclusion: IVIM diffusion parameter D can better predict tumor grade and lymph node metastasis whereas IVIM perfusion fraction f can better predict pleural invasion before operation in NSCLC patients.

10:30 - 12:00

Room B

Abdominal Viscera

SS 601a

Innovations in hepatobiliary imaging

Moderators:

B. Kaltenbach; Frankfurt a. Main/DE
J.M. Lee; Seoul/KR

B-0422 10:30

Potential ketamine-related cholangitis in severely ill burn patients: liver imaging features

M. Hajji, C. De Tymowski, P. Bourrier, V. Mallet, A.M. Zagdanski, M. Legrand, E. De Kerviller; Paris/FR (hajjimaha1989@gmail.com)

Purpose: The French national drug agency (ASM) has recently issued a warning regarding potential ketamine-related liver toxicity in burn patients, with cases of severe liver cholestasis. Our aim was to describe the radiological pattern of biliary tract abnormalities in this setting.

Methods and Materials: We included patients admitted in the St-Louis burn unit between 2012 and 2017 with liver cholestasis (Alkaline phosphatase and Gamma-glutamyltransferase more than 1.5N) and treated with intravenous ketamine. Liver imaging was analyzed for potential signs of bile duct abnormalities. Among 154 patients with liver imaging, 116 had scanner, 45 had US, and 10 had liver MRI.

Results: Liver imaging was most of times found normal except for hepatomegaly (n=15). Seven patients had cholangitis images with diffuse enlargement of intra and extra-hepatic bile ducts and abnormal heterogeneous intra-luminal material in bile ducts (fig). In 3 cases, small satellite abscesses were noticed. They received cumulative high doses of ketamine (mean 122 g [min 62-max 221g] during their hospitalization. They had a severe biological cholestasis = 5time N. Liver biopsies showed an aspect of cholangitis with overloaded bile without ischemic lesions in one patient and portal-lobular fibro-inflammatory lesions in another.

Conclusion: In severely ill burn patients receiving very high doses of ketamine, we observed bile duct images featuring cholangitis together with intra-luminal heterogeneous abnormal material. Imputability and mechanisms of liver toxicity of ketamine still requires further exploration. In the meantime, radiologist should specifically search for such features in patients exposed to high doses of ketamine.

B-0423 10:38

Gd-BOPTA excretion MRI analysis in patients with compromised and non-compromised bile ducts

M. Shorikov, M. Lapteva, P. Polyakov, D. Frantsev, O.N. Sergeeva, B. Dolgushin; Moscow/RU (mglapteva@inbox.ru)

Purpose: Magnetic resonance contrast agent (MRCA) Gd-BOPTA demonstrated dual excretion either by liver or kidneys. As it was previously shown in obstructive jaundice models, a bile duct ligation in the rodents significantly reduced the liver-to-kidneys excretion ratio compared to that in the animals after sham procedure. MRI assessment of the hepatic function based on Gd-BOPTA excretion shift is attempted in the study.

Methods and Materials: 25 patients that had MRI-examination with Gd-BOPTA in period 2015-2016 showing normal total serum bilirubin level were included in the study: 15 patients with cholestatic liver diseases (14-Klatskin tumour, 1-primary sclerosing cholangitis) after biliary decompression (group 1) and 10 patients without cholestasis (10-metastatic neuroendocrine tumours, group 2). They were studied on 1.5T MRI system. MRCP was also done in all the cases. T1VIBE-images were acquired before/after (arterial, portal, venous, delayed (1, 20, 40 minutes) phases) 10ml Gd-BOPTA i.v. injection. One patient from group 1 had an additional study with 7.5ml of Gd-DTPA a month later; T2WI, DWI+ADC-maps were also evaluated in this patient for liver fibrosis detection.

Results: Endobiliary Gd-BOPTA was registered in 3/10 patients in group 1 and in all group 2. Maximal diameter of bile duct correlated to SI (liver) at 20, 40min ($r^2=0.9$, $p<0.002$). SI(liver)/SI(kidney) was significantly lower in group 1 compared to group 2 ($p<0.02$) at 20, 40min phase. Additionally in patient who had two studies with different MRCA: 1)Gd-BOPTA: SI(liver)/SI(kidney) for segment with signs of liver fibrosis was lower than SI(liver)/SI(kidney) for segment without fibrosis ($p<0.05$); 2) Gd-DRPA: the ratio for segments was not significantly different ($p>0.05$) and higher than in case of the Gd-BOPTA injection ($p<0.05$).

Conclusion: Patients with cholestatic liver diseases demonstrated Gd-BOPTA excretion shift even after biliary decompression and serum bilirubin normalisation.

B-0424 10:46

Spectral CT and cholesterol content in gallbladder stone

E. Danse¹, N. Joudiou¹, G. Muccioli¹, N. Michoux¹, J. Collart¹, C. Hubert¹, A. Vlassenbroeck², B. Gallez¹, E. Coche¹; ¹Brussels/BE, ²Eindhoven/NL (etienne.danse@uclouvain.be)

Purpose: To assess whether dual energy CT measurements can predict the percentage of cholesterol in gallstones taking spectro-MR as reference.

Methods and Materials: In 18 patients operated for symptomatic gallbladder stone, the removed stones were evaluated in vitro using a spectral MDCT (IQon, Philips Healthcare, Cleveland, OH). These specimens were evaluated in the Biomedical MRI research lab with a Spectro-MR system, to assess the presence and the amount of cholesterol and Calcium respectively. Correlation between spectro-MR measurements and CT data was assessed using Spearman rank correlation coefficient. Relationship between CT attenuation (HU) and MR measurements was investigated for different voltages (40kVp, 70kVp, 80kVp and 200kVp) using linear regression. The correlation between effective atomic number (Zeff) and MR measurements was also investigated.

Results: The proportion of the variation in the dependent variable (%^{cholesterol}) explained by the regression model was found to be high at 40kVp (Equation: %^{cholesterol} = 56.4 - 0.15*HU, $p^{\text{intercept}} < 0.0001$, $p^{\text{slope}} = 0.0001$, coefficient of determination $R^2_{40kVp} = 0.76$). A linear model was found to describe well the relationship between Z_{eff} and the cholesterol content determined by RMN (Equation: %^{cholesterol} = 192 - 21.0*Z_{eff}, $p^{\text{intercept}} < 0.0001$, $p^{\text{slope}} < 0.0001$, coefficient of determination $R^2 = 0.73$).

Conclusion: At 40kVp, a linear model explains the relationship between the density of the stones measured in Hounsfield unit and the % of cholesterol in the stones measured in MR. Additionally, the Z number allows predicting the content in cholesterol within the stones.

Author Disclosures:

A. Vlassenbroeck: Employee; Philips HealthCare.

B-0425 10:54

Is cross-sectional imaging predictive of difficult hepatectomy in patients undergoing liver transplantation?

R. Girometti, D. Iorenzin, L. Montaldo, G. Como, A. Risaliti, C. Zuiani; Udine/IT (rgirometti@sirm.org)

Purpose: Dissecting the inferior vena cava (IVC) from the dorsal sector (DS) of the recipient's liver is a major cause of difficult hepatectomy (DH) in orthotopic liver transplantation (OLT). We investigated whether DS morphology is associated with DH (primary end point) or early postoperative complications (EPOC).

Methods and Materials: We retrospectively included 67 patients who underwent preoperative 64-row multidetector (CT) (n=57) or 1.5T magnetic resonance imaging (MRI) (n=10) before OLT. Two radiologists in consensus calculated the volume of the liver dorsal sector (V-LDS, including Couinaud segments I and IX), volume of caudate lobe (V-CL), degree of IVC encirclement (E-IVC), length of IVC-DS contact (L-IVC-DS), and caudate lobe-to-right lobe ratio (CL/RL). Imaging findings, clinical and operative features (including sex, age, aetiology of cirrhosis, model end-stage liver disease (MELD), IVC-related operative times, packed red blood cells and fresh frozen plasma) were entered into a logistic regression model to identify predictors of the study end points.

Results: DH and EPOC occurred in 19/67 (28.4%) and 15/67 patients (19.7%), respectively. On multivariate analysis, no imaging, clinical or operative features were predictors of DH ($p>0.05$), while a V-LDS $<33.6 \text{ cm}^3$, V-CL $<15.0 \text{ cm}^3$, and CL/RL <0.75 were found to be significant ($p<0.05$) protectors from EPOC (OR 0.08, 0.03 and 0.13, respectively). On receiving operating characteristic (ROC) analysis, the sensitivity/specificity for DH and POC of V-LDS, V-CL and CL/RL were 0.65/0.63, 0.70/0.51 and 0.70/0.4 for DH, and 0.46/0.71, 0.73/0.56 and 0.86/0.57 for EPOC.

Conclusion: While having no role in predicting DH, liver DS morphology can help in the preoperative stratification of the risk of EPOC.

B-0426 11:02

Improved visualisation of hepatic metastases in gadoxetate disodium-enhanced MRI: potential of contrast-optimised (phase-sensitive) inversion recovery imaging

U.L. Fahlenkamp, L.C. Adams, S.M. Böker, G. Engel, M. Huynh Anh, M. Wagner, B. Hamm, M.R. Makowski; Berlin/DE (ute.fahlenkamp@charite.de)

Purpose: To investigate the potential of a contrast-optimised (phase-sensitive) inversion recovery (IR) MR imaging technique in gadoxetate disodium-enhanced scans for detection of hepatic metastases.

Methods and Materials: The institutional review board approved this prospective study. After written informed consent, 31 patients (16 male, 15 female) with suspected or known hepatic metastases were examined on a 1.5 T MR system 20 minutes after administration of 10 ml gadoxetate disodium. A single-breath-hold T1-weighted gradient-echo volumetric-interpolated-breath-

hold (VIBE) sequence was acquired as part of the standard clinical imaging protocol. In addition, a contrast-optimised (phase-sensitive) IR sequence was acquired with an inversion time (TI) adjusted for optimal suppression of signal from metastases compared to surrounding liver parenchyma. In both sequences, number of metastases and lesion-to-liver contrast (LLC) was assessed.

Results: Overall, 302 liver metastases were identified in the investigated patient collective (n=31). A significantly ($p \leq 0.05$) higher LLC was measured on contrast-optimised (phase-sensitive) IR sequences (0.79 ± 0.13) compared to VIBE sequences (0.40 ± 0.17). Detection rate for metastases ≤ 0.5 cm was significantly higher ($p \leq 0.05$) based on (phase-sensitive) IR (n=106/117) compared to standard VIBE sequence (n=88/117). Detection rate for metastases > 0.5 cm was comparable ($p > 0.05$) between both sequences. Size measurement revealed a slightly larger lesion size (1.14 ± 0.80 , $p \leq 0.05$) of the metastases on (phase-sensitive) IR images compared to T1 VIBE.

Conclusion: Contrast-optimised (phase-sensitive) IR MR imaging improves the detection of small hepatic metastases in gadoxetate disodium-enhanced scans compared to a conventional T1 gradient-echo VIBE sequence.

B-0427 11:10

CT-based liver surface nodularity quantification for the detection of clinically significant portal hypertension in cirrhotic patients

R. Sartoris¹, V. Vilgrain², P.-E. Rautou², M. Ronot², ¹Genoa/IT, ²Clichy/FR (riccardo.sartoris@hotmail.it)

Purpose: To evaluate the diagnostic performance of non-invasive liver surface nodularity (LSN) quantification derived from CT images for the diagnosis of clinically significant portal hypertension (CSPH), with respect to hepatic venous pressure gradient (HVPG) and to compare it with other non-invasive measures and derived scores.

Methods and Materials: 203 cirrhotic patients [(mean 58 ± 10 years, women: 119); 102 of them with CSPH] with valid HVPG measurement and abdominal CT within 60 days were selected. Transient elastography (fibroscan) was performed in 91 patients. LSN was measured by drawing a ROI over the liver edge and the software calculated the margin irregularity. LSN and derived scores (LSN x spleen diameter and LSN/platelet count) were compared with other common non-invasive measures including liver-to-spleen volume, platelet count/spleen diameter, liver stiffness, PH-risk score and LSPS score.

Results: LSN valid measures were obtained in 189 patients (93.1%). LSN was significantly correlated with HVPG ($r=0.75$; $p < 0.001$). Patients with CSPH had a significantly higher LSN score (3.22 ± 0.59 vs 2.44 ± 0.34 ; $p < 0.001$), with AUROC of 0.884 ± 0.03 . Cut-off value of 2.76 allowed identifying CSPH with sensitivity, specificity, PPV and NPV of 80%, 87%, 88% and 79%. AUROC of LSN was significantly higher than that of all other non-invasive tests (all $p < 0.001$).

Conclusion: CT-based non-invasive LSN quantification is effective for the detection of patients with CSPH, with higher diagnostic performance than other non-invasive measurements and could improve the detection of CSPH.

B-0428 11:18

Improvement of diagnostic image quality of abdominal CT using a deep learning-based reconstruction: initial clinical trial targeting hepatic metastases

Y. Nakamura¹, T. Higaki¹, F. Tatsugami¹, J. Zhou², Z. Yu², N. Akino³, Y. Ito³, M. Iida¹, K. Awai¹; ¹Hiroshima/JP, ²Vernon Hills, IL/US, ³Otawara/JP

Purpose: We developed a new reconstruction method which could generate better image quality CT image using a deep learning-based reconstruction (DLR) trained by teaching dataset of higher dose CT image reconstructed with model-based iterative reconstruction. The purpose of this study was to confirm clinical feasibility of our method compared with conventional hepatic CT images targeting hepatic metastases.

Methods and Materials: We evaluated 51 hepatic metastases from colorectal cancer in 17 patients. A radiologist measured standard deviation of the attenuation measured in the paraspinous muscle as image noise, and calculated contrast-to-noise ratio (CNR) = $(ROI_L - ROI_T)/N$, where ROI_L is the mean attenuation of the liver parenchyma, ROI_T is the mean attenuation of the tumour, and N is noise. Each liver lesion was reviewed independently by other two radiologists and graded on a 5-point confidence scale ranging from 1 = cannot identify to 5 = can detect lesion without diagnostic compromise. The difference between conventional CT processed with hybrid iterative reconstruction (hybrid-IR) and CT processed with our new method using DLR was determined.

Results: Image noise was significantly lower on images with DLR compared to hybrid-IR ($p < 0.01$). In addition, CNR on images with DLR was significantly higher than those with hybrid-IR ($p < 0.01$). Confidence score for liver lesions was significantly higher with images with DLR compared to those with hybrid-IR ($p < 0.01$ for both radiologists).

Conclusion: DLR improved quantitatively and qualitatively image quality of abdominal CT for evaluation of hepatic metastases.

Author Disclosures:

J. Zhou: Employee; Toshiba Medical Research Institute USA, Inc. **Z. Yu:** Employee; Toshiba Medical Research Institute USA, Inc. **N. Akino:** Employee; Toshiba Medical Systems Corporation. **Y. Ito:** Employee; Toshiba Medical Systems Corporation. **K. Awai:** Advisory Board; GE Healthcare. Research/Grant Support; Toshiba Medical Systems Co., Ltd, Hitachi, Ltd, Bayer AG, Daiichi Sankyo, Ltd, Eisai, Ltd, Fujitsu, Ltd.

B-0429 11:26

Up to seven criteria for liver transplantation: a single-centre experience

K. Koryukova, M. Bezzi, M. Di Martino, S.G. Ginanni Corradini, M. Rossi, C. Catalano; Rome/IT (micdimartino@hotmail.it)

Purpose: To test "up to seven" criteria for HCC in liver transplant candidates, with emphasis on imaging role and patients outcome.

Methods and Materials: The study was approved by the Institutional Review Boards. In this prospective study were analysed patients who underwent liver transplantation (LT) between January 2012 and December 2015. Of 79 transplant procedures 31 patients reported HCC nodules (69 lesions of which 43 were treated before). Diagnosis of HCC was taken by two expert radiologists in liver imaging according to LI-RADS classification in MR or CT examinations. Radiological staging correlated with histological result (Pearson). One-year survival was also taken into account.

Results: Of 31 patients with HCC, 10 exceed Milan criteria for imaging analysis but were considered within "up-to-seven". On a patient-per-patient analysis, imaging reported a sensitivity of 60% (in explanted liver four patients were out of "up to seven" criteria). One-year after liver transplantation, four patients developed recurrence of HCC, of these 2 patients were out of Milan criteria.

Conclusion: "Up-to-seven" criteria for LT should replace Milan criteria and allow more patients with HCC to be candidates of this treatment.

B-0430 11:34

A deep-learning approach to the significant liver fibrosis binary classification problem using gender, morphologic and haemodynamic measurements derived from B-mode ultrasound images

A. Angelakis, I. Gatos, A. Soultatos, A. Kanavaki, E. Panteleakou, I. Theotokas, I. Vafiadis, E. Manesis, P. Zoumpoulis; Athens/GR (ath.angelakis@gmail.com)

Purpose: Traditional methods such as haematologic tests, e.g. FIBROMETER[®], strain, shear wave elastographic (SWE) stiffness cut-off values, e.g. FIBROSCAN[™], SuperSonic Imagine SWE, and parameters derived from image analysis, e.g. color clustering of SWE, are used for the significant liver fibrosis binary classification (SLFBC) problem. The AUC of the above methods is: 0.82, 0.82, 0.84 and 0.87 accordingly. The purpose of this study was to design and tune a deep neural network (DNN) to automate classification of a patient's liver fibrosis stage ($F \leq F1$, $F \geq F2$) with high accuracy, sensitivity, specificity and AUC.

Methods and Materials: Our data set consisted of 103 liver biopsy validated patients with chronic liver disease from which 62 were $F \leq F1$ and 41 were $F \geq F2$. Input parameters for our model were: {patient gender}, four B-mode morphologic longitudinal diameter (LD) measurements: {right lobe, caudate lobe, left lobe, spleen} and one haemodynamic parameter {portal vein LD}. We normalized the values of these features and designed a DNN with two hidden layers. A 10-fold cross validation (CV) technique was used to overcome underfitting, overfitting, bias and variance issues.

Results: 10-fold CV provided the following results: accuracy: 0.9364 +/- 0.0582, $F1$: 0.9136, sensitivity: 0.9024, specificity: 0.9365, AUC: 0.927 with 95% CI [0.817 - 1.000].

Conclusion: In this study, we proposed a different approach to solve SLFBC problem using deep learning. Our preliminary results demonstrate improved accuracy, sensitivity, specificity, and AUC (all > 0.90) compared to traditional diagnostic methods. Larger data sets are required to further validate our algorithm.

B-0431 11:42

Three-dimensional texture analysis technology in computed tomography: a new radiological marker in the pathology of liver cancer

H. Xu, Y. Gao; Chengdu/CN (xuhuisophia@163.com)

Purpose: Texture analysis is a new technology with many advantages such as non-invasive, quantized and economical. This research is performed to explore the relationship with the parameters of TA(texture analysis) and the pathological grade of liver cancer.

Methods and Materials: Patients were involved in the retrospective research from march of 2011 to November of 2014 who have primary liver cancer. According to the radiology and pathology, 47 patients who have contrast-enhanced CT imaging were involved in the study. Analysis software is CT Kinetics APP, in which includes GLH, grey-level histogram, GLCM, grey-level co-occurrence matrix and GLRLM, grey-level run-length matrix. CT imaging

(Siemens 128 multislice spiral CT, slice thickness=1mm; scan protocol: plain scan, arterial phase and venous phase). Region of interest (ROI) was drawn by 2 radiologists with at least 2 years of experience. ROI was drawn in three phases and merge to 3d imaging for texture analysis.

Results: All parameters were divided into 2 groups by high differentiation and poor differentiation in pathology, which calculated by Mann-Whitney U test from SPSS23.0. The area under curve (AUC) of inverse difference moment (arterial phase) in GLCM is 0.762 (cutoff=0.60097), which is tested by receiver operating characteristic. The AUC of correlation (arterial phase) in GLCM is 0.755 (cut off=0.3021). The AUC of energy and skewness in GLCM are 0.731 (cutoff=0.0679) and 0.672 (cutoff=-0.2186) respectively.

Conclusion: Texture analysis could predict the pathological grade of liver cancer from pre-treatment CT imaging. As a non-invasive and post-processing computer-aided diagnosis, TA could provide more information for clinic.

B-0432 11:50

Analysis of the relationship between imaging patterns of calcification and response to chemotherapy in patients with colorectal metastases

J. Zhang, B. Wu, Y. Zhou; Chengdu/CN (396297113@qq.com)

Purpose: The purpose of our study was to determine the relationship between the CT features (morphology, distribution and density) of colorectal cancer metastases calcification and response to chemotherapy (cetuximab combined).

Methods and Materials: A retrospective review of CT of 111 patients who were treated with cetuximab-combined chemotherapy between 2011 and 2016 revealed 27 cases of tumor calcifications. The Response evaluation was performed according to the standard of Response Evaluation Criteria in Solid Tumors 1.1 (RECIST 1.1). And the patients with metastases calcification was divided into two groups according to the response to the therapy. Analysis included the survival time between the two groups; the morphology and distribution of calcifications; and changes in number, density, morphology.

Results: The common site of metastatic calcification is the liver (70.4%), followed by lymph nodes (29.6%). The overall prognosis of patients with metastases calcification is better than those without calcification, 279 ± 37 VS 186 ± 18 days ($P=0.022$) respectively. In all patients with metastases calcification, the overall outcome of the effective group was better than that in the ineffective group, 385 ± 17 VS 244 ± 38 days ($P=0.042$) respectively. The density increases with time, the effective group compare to the ineffective group slope are 11.9 ± 4.0 VS 7.9 ± 1.6 , $P=0.025$. The calcification number changes between the two groups is significantly different. But the differences of morphology and distribution between the two groups are not significantly.

Conclusion: Metastasis of colorectal cancer with calcification predicts a favorable prognosis. Calcification density growth rate and increased calcification number, which correlated with the response to the chemotherapy.

LSTV numbers analysed the images. Interobserver agreement and accuracy of ICT sign were assessed.

Results: The interobserver agreement was good for determining ICT level (Cohen's kappa=0.78, $p<0.001$). The rate of correct numbering by ICT sign in LSTV group was significantly lesser than controls (43.1% vs 96.4%, respectively, $p<0.001$). Moreover, patients with sacralisation had significantly less rate of correct numbering than those with lumbarisation (33.3% vs 63.2%, respectively, $p=0.03$).

Conclusion: The ICT does not seem as a reliable landmark for correct numbering of LSTV in patients with no intervertebral disc degeneration.

B-0434 10:47

The termination level of dural sac relevant to caudal epidural block in lumbosacral transitional vertebrae: comparison between sacralisation and lumbarisation groups

J.Y. Jeon; Incheon/KR (mdjeonjy@gmail.com)

Purpose: Back and buttock pain can be associated with lumbosacral transitional vertebrae (LSTV). Appreciation of anatomical variations due to LSTV may impact safe performance of caudal epidural block (CEB). We investigated the termination level of the dural sac (DS) and anatomical features of lumbosacral region in patients with LSTV, and compared these findings between sacralisation and lumbarisation groups.

Methods and Materials: 494 LSTV were included and categorised into sacralisation ($n=201$) or lumbarisation groups ($n=293$). MRI of the all LSTV patients were reviewed to determine the termination level of DS, the presence and the caudal level of sacral perineural cyst. MRI findings in the both groups were compared and analysed.

Results: The distribution frequency of termination levels of DS demonstrated significant difference between the two groups. The mean caudal DS level in the lumbarisation group was significantly lower than the sacralisation group (lower third of S2 [131 {44.7%} of 293 patients] vs. lower third of S1 [78 {38.8%} of 201 patients]). The DS terminated at S3 in more than 19% of lumbarisation group, whereas in only one case of sacralisation group. The incidence of perineural cyst was not significantly different between two groups.

Conclusion: When planning CEB for patients with LSTV, especially in the lumbarisation cases, pre-procedural MR imaging to check the termination level of DS, presence of perineural cysts would be of great use for lowering the risk of unexpected dural puncture during the procedure.

B-0435 10:55

Modic changes: the association with low back pain and activity limitation - a systematic literature review and meta-analysis

C. Herlin¹, P. Kjaer¹, A. Espeland², J. Skouen², C. Leboeuf-Yde¹, J. Karppinen³, J. Niinimäki⁴, J.S. Sørensen⁴, T.S. Jensen⁵; ¹Odense/DK, ²Bergen/NO, ³Oulu/FI, ⁴Svendborg/DK, ⁵Silkeborg/DK (tuejen@rm.dk)

Purpose: To investigate if Modic Changes (MC) are associated with non-specific low back pain (LBP) and/or activity limitation and if such an association is modified by other factors.

Methods and Materials: The MEDLINE, CINAHL and EMBASE databases were searched for relevant cross-sectional and case-control studies including people of all ages from general, working or clinical study populations were eligible for inclusion. Data extraction for risk of bias assessment, associations and potential modifiers were completed independently by pairs of reviewers. Data were used to calculate odds ratio (OR) with for dichotomous outcomes or to perform t-tests for continuous outcomes. Meta-analysis was performed for homogeneous studies.

Results: In all, 5210 citations were identified and 31 studies were included. One study had low risk of bias. Fifteen studies (48%) reported statistically significant positive associations between MC and LBP. Meta-analysis resulted in an OR of 4.01 (1.52-10.61). Both pooled and individual study data showed no difference in the strength of association of MC1 and MC2 with LBP. One of seven studies reported a statistically significant positive association between activity limitation and MC. Lumbar disc level and disc degeneration were found to reduce the estimates of association between MC and LBP.

Conclusion: The results from this comprehensive systematic review indicate that the associations between MC and LBP related outcomes are inconsistent. This finding should call for caution when using "Modic changes" as a specific diagnosis, explanation for LBP, and indication for specific treatment in patients with non-specific LBP.

10:30 - 12:00

Room C

Musculoskeletal

SS 610a

Spine imaging

Moderators:

M. Epermane; Riga/LV
A. Loizides; Innsbruck/AT

K-09 10:30

Keynote lecture

I.-M. Noebauer-Huhmann; Vienna/AT

B-0433 10:39

Role of iliac crest tangent sign in correct numbering of lumbosacral transitional vertebrae

N. Gunduz, G. Durukan, M.B. Eser, A. Aslan, A. Kabaalioglu; Istanbul/TR (gulcin_dr_kan@hotmail.com)

Purpose: Iliac crest tangent (ICT) sign has recently emerged as a reliable landmark to correctly number the lumbosacral transitional vertebrae (LSTV) in patients with degenerated intervertebral disc disease. We retrospectively evaluated the usefulness of ICT in subjects without disc degeneration.

Methods and Materials: Fifty-eight patients with LSTV [19 (32.8%) female, 42±18 years] and 55 control subjects without LSTV [23 (41.8%) female, 42±19 years] who had undergone vertebral computed tomography in the emergency service for evaluation of suspected trauma were included. The ICT was drawn on the coronal images, with the cursor in the sagittal view set to the posterior one third of the vertebral body located one level above the LSTV. The last lumbar vertebra was used instead of LSTV in control group. When more than 1.25 vertebral body was counted below the ICT, the LSTV was considered as S1, otherwise as L5. The gold standard numbering was determined by counting the vertebrae craniocaudally. Two readers blinded to the correct

B-0436 11:03

Weight-bearing MRI evaluation of Modic changes: uncovering the "biomechanical stress" and "active discopathy" theories in low back pain

F. Bruno, C. Marsecano, M. Micelli, A. Splendiani, C. Masciocchi; *L'Aquila/IT* (federico.bruno.1988@gmail.com)

Purpose: To evaluate the MRI modifications of Modic 1 endplate changes under loading and the possible clinical correlation in patients with low back pain

Methods and Materials: We evaluated 38 patients (20 females, 16 males, mean age 48.3 years) with low back pain and MRI evidence of Modic 1 vertebral changes. Patients were examined on a low field MR scanner in standard supine and upright position. Patients with history of trauma, malformations, infectious-inflammatory diseases, spine tumours were excluded. For each patient, in each scan, two observers evaluated the endplate involvement by Modic changes (as percentage of vertebral body extension), the intervertebral disc height at the level of the endplate changes and the degree of intervertebral disc hydration (according to Pfirrmann). Pain evaluation in both supine and upright position was assessed by means of VAS score.

Results: In upright position Modic 1 changes increased in 24 patients (63.1%, $p < 0.001$). A reduction of disc height (89.5% of patients) and disc hydration (68.4%), respectively with negative ($r = -0.12$) and positive ($r = 0.46$, $p < 0.005$) correlation with Modic 1 changes was observed. 30 patients (78.9%) reported increase of pain in the upright position, and positive correlation with Modic 1 increase

Conclusion: Our imaging results suggest an instrumental evidence of the biomechanical stress theory for the development of Modic 1 changes. Moreover, upright scans under physiological loading represent an added value to standard sequences, being able to provide diagnostic information for answering clinical questions, such as pain due to "active discopathy" in patients with Modic 1 changes

B-0437 11:11

Oblique sagittal images prevent underestimation of neuroforaminal stenosis grade caused by disc herniation in cervical spine MRI

L. Kintzélé, C. Rehnitz, H.-U. Kauczor, M.-A. Weber^{2,1}; *Heidelberg/DE*, ²Rostock/DE (laurent.kintzele@med.uni-heidelberg.de)

Purpose: Identify whether sagittal MRI images (SMI) result in underestimation of neuroforaminal stenosis grade (NSG) compared to oblique sagittal MRI images (OSMI) in patients with cervical spine disc herniation.

Methods and Materials: 74 patients with 104 cervical disc herniations compromising the corresponding nerve root were evaluated. NSGs were evaluated in SMI and OSMI by one senior and one resident radiologist. OSMI were angled 30° towards the standard sagittal plane. NSGs were classified from 0 (no stenosis) to 3 (high-grade stenosis).

Results: Average NSG of both readers was significantly lower in SMI compared to OSMI (2.41 ± 0.65 and 2.92 ± 0.27). For 49 of 104 disc herniations (47.1%), one or both readers found a NSG which was at least 1 grade lower in SMI compared to OSMI. Significant difference maintained looking at patients who had neurological symptoms (2.50 ± 0.55 and 2.88 ± 0.32) or underwent cervical spine surgery subsequently (2.58 ± 0.49 and 2.90 ± 0.31). Based on location a significant difference between SMI and OSMI was found for foraminal herniations (2.36 ± 0.67 and 2.91 ± 0.27). In contrast, no significant difference was observed for recessal herniations (2.68 ± 0.46 and 2.91 ± 0.30) or herniations which caused myelopathy (2.74 ± 0.45 and 2.91 ± 0.29). Kappa values showed a very good interreader reliability for SMI (0.88) and OSMI (0.94).

Conclusion: SMI tends to underestimate NSG compared to OSMI for disc herniations in cervical spine MRI. OSMI should, therefore, be considered as a valuable option for selected patients.

B-0438 11:19

Disc and vertebral changes after spinal fusion at serial CT imaging: correlation with disc stability

N. Amini, E. Fomekong, C. Raftopoulos, B. Vande Berg; *Brussels/BE* (nadia.amini@uclouvain.be)

Purpose: To assess disc and vertebral changes after translaminar interbody fusion (TLIF) of lumbar discs by comparing MDCT examinations of the lumbar spine obtained immediately after surgery and 6 months later with comparison between stable and unstable discs.

Methods and Materials: Two radiologists independently analyzed 36 discs after TLIF (Peek cage and bone grafting) by comparing CT examinations obtained immediately after surgery and 6 months later. They assessed changes in disc height and they scored bone formation and graft resorption (0 : no bone formation/graft resorption, 1 : bone formation without bridging bone/partial graft resorption, 2 : bridging bone/complete graft resorption). Disc

stability was determined by consensus reading on follow-up CT (unstable disc: intradiscal vacuum or bone resorption around the pedicle screws).

Results: There were 19 stable and 17 unstable discs at 6 months follow-up. For both readers, the frequency of complete bony fusion was statistically significantly higher in stable than in unstable discs ($p = 0.003/0.02$ for reader 1/2). The frequency of trabecular bone thickening was statistically significantly higher in stable than in unstable discs ($p = 0.005$ for reader 1 only). For both readers, the frequency of bone graft resorption, of trabecular bone atrophy and of disc space narrowing was not statistically significantly different between stable and unstable discs.

Conclusion: Appearance of bridging bone and of trabecular bone thickening near the cages are associated with disc stability. Disc space narrowing, vertebral bone resorption and bone graft resorption are seen in similar frequency in stable and unstable disc.

B-0439 11:27

Evaluation of colour-coded virtual non-calcium images reconstructed from dual-energy CT for detection of lumbar disc herniation in comparison to MRI: initial results

C. Booz, J. Noeske, S.S. Martin, L. Lenga, D. Leithner, T. Gruber-Rouh, K. Eichler, T.J. Vogl, J.L. Wichmann; *Frankfurt a. Main/DE* (boozchristian@gmail.com)

Purpose: Detection of lumbar disc herniation in standard grey-scale computed tomography (CT) is challenging. The aim of this feasibility study was to evaluate the diagnostic accuracy of two dual-energy computed tomography (DECT)-based colour-coded virtual non-calcium (VNCA) image reconstruction algorithms for detection of lumbar disc herniation in comparison to magnetic resonance imaging (MRI) as standard of reference.

Methods and Materials: In this retrospective study, thirty-seven patients underwent clinically indicated third-generation dual-source DECT and MRI of the lumbar spine. Conventional linear-blended CT scans were obtained and two different corresponding colour-coded VNCA reconstructions were generated. First, three radiologists independently evaluated standard VNCA images for presence and degree of lumbar disc herniation and spinal nerve root affection. After 4 weeks, VNCA images optimized for analysis of intervertebral discs were examined by the same observers. Findings were compared with MRI evaluated by two separate observers serving as reference standard.

Results: A total of 222 intervertebral discs were analysed. VNCA images optimized for analysis of intervertebral discs showed a higher overall sensitivity (94.7% vs 78.0%), specificity (97.0% vs 92.3%), positive predictive value (96.3% vs 89.3%) and negative predictive value (95.7% vs 83.5%) for detection of lumbar disc herniation compared with standard VNCA images ($P < 0.001$). Receiver-operating characteristic analysis revealed areas under the curve of 0.958 (optimized VNCA) and 0.851 (standard VNCA).

Conclusion: Initial results showed that a novel DECT-based colour-coded VNCA image algorithm specifically optimized for analysis of intervertebral discs can substantially improve diagnostic accuracy for detection of lumbar disc herniation. Inexperienced observers showed the most benefit.

Author Disclosures:

J.L. Wichmann: Speaker; GE Healthcare, Siemens Healthineers.

B-0440 11:35

The effect of radiographically detected vertebral osteoarthritis (VO) on bone mineral density (BMD) and trabecular bone score (TBS)

A. Corazza¹, D. Albano², S. Rapisarda¹, V. Chianca², C. Messina¹, L.M. Sconfienza¹; ¹Milan/IT, ²Palermo/IT, ³Naples/IT (angelcoraz@libero.it)

Purpose: TBS is a recently developed textural score that provides an indirect index of vertebral trabecular microarchitecture from lumbar spine (LS) dual energy x-ray absorptiometry (DXA) scan. Our aim was to evaluate the effect of radiographically detected VO on BMD and TBS.

Methods and Materials: We retrospectively identified all patients who performed a LS DXA during the first six months of 2015, together with a LS x-ray (maximum interval between x-ray and DXA=4 months). Among them, we only included patients with VO visible on DXA and confirmed on LS x-ray (maximum two vertebrae involved). We calculate: 1. BMD/TBS difference between the vertebrae affected by VO and the adjacent vertebrae (AV) with the greater BMD/TBS value; 2. BMD/TBS difference between the vertebrae affected by VO and the average L1-L4 BMD/TBS (average value included the vertebrae with VO).

Results: Out of 542, we included 42 females (mean age=75±10y) with VO. Mean BMD (g/cm^2): vertebrae with VO= 1.120 ± 0.160 ; AV= 0.976 ± 0.152 ; L1-L4= 0.988 ± 0.127 . Mean TBS: vertebrae with VO/VF= 1.379 ± 0.138 ; AV= 1.298 ± 0.144 ; L1-L4= 1.310 ± 0.104 . BMD difference between VO and VA= $+14.8\%$; between VO and L1-L4= $+13.4\%$. TBS difference between VO and VA= $+6.2\%$; between VO and L1-L4= $+5.3\%$. All differences were significant ($p < 0.05$). We found a positive correlation between BMD and TBS for vertebrae with VO ($R = 0.6194$, $p < 0.05$).

Conclusion: Compared to adjacent-vertebrae and L1-L4, VO significantly impacts both on BMD and TBS, despite the variation in terms of TBS was lower was lower compared to BMD. BMD and TBS values are positively correlated.

B-0441 11:43

Vertebral bone marrow composition: assessment of age and gender dependency using chemical shift encoding-based water-fat MRI

A. Rohrmeier, J. Syväri, M. Diefenbach, D. Franz, S. Ruschke, M. Dieckmeyer, J.S. Kirschke, D. Karampinos, T. Baum; *Munich/DE*
(Alexander.Rohrmeier@t-online.de)

Purpose: Assessment of vertebral bone marrow composition has been recently proposed as an advanced imaging biomarker for osteoporosis-associated fracture risk prediction. We investigated the age and gender dependency of vertebral proton density fat fraction (PDFF) using chemical shift encoding-based water-fat MRI.

Methods and Materials: 156 subjects with no history of pathological bone changes were recruited (age range 20-29 years:12/30 males/females; 30-39:15/9; 40-49:4/14; 50-59:9/27; 60-69:5/19; 70-79:4/8). All subjects underwent 3T MRI with a sagittal spoiled gradient echo sequence for chemical shift encoding-based water-fat separation at the lumbar spine (pixel spacing: 0.98x0.98 mm²; slice thickness:4 mm). Vertebral bodies of L1-4 were manually segmented in the PDFF maps to extract PDFF values at each vertebral level.

Results: PDFF increased from L1 to L4 in all subjects (L1: 35.9±11.7%; L2: 36.2±10.9%; L3: 37.2±10.7%; L4: 39.5±11.2%; p<0.05). Mean PDFF was significantly (p<0.05) greater in males than females in their twenties (32.0±8.0% vs 27.2±6.0%) and thirties (35.3±6.7% vs 27.3±6.2%). With increasing age, females showed an accelerated fatty conversion of the bone marrow compared to men with no significant (p>0.05) PDFF differences in their forties (males: 32.4±8.4%; females: 34.5±6.8%) and fifties (males: 42.0±6.1%; women: 40.5±9.7%). The accelerated conversion process continued resulting in greater PDFF values in females than males in their sixties (males: 40.2±6.9%; females: 48.8±7.7%; p=0.033) and seventies (males: 43.9±7.6%; females: 50.5±8.2%; p=0.208).

Conclusion: Vertebral bone marrow composition is dependent on age and gender. An accelerated fatty conversion of the bone marrow was observed in females with increasing age. The results allow insights into physiological changes of the vertebral bone marrow and may serve as reference data.

B-0442 11:51

A preliminary study of dual-energy CT spectral curve equation for the diagnosis of osteoporosis

L. Wang, S. Gong; *Nantong/CN* (wanglin_nt@126.com)

Purpose: To investigate the diagnostic value of dual-energy CT (DECT) spectral curve equation for osteoporosis (OP).

Methods and Materials: The prospective study was approved by the institutional ethics committee. Informed consent was obtained from all patients. Sixty-seven patients with lumbago underwent both DECT and dual-energy x-ray absorptiometry (DXA) examinations. DECT images were reconstructed using iterative algorithm (ADMIRE) with strength level 3. Spectral curves were generated through measuring CT values from photon energy 40 keV to 190 keV with commercially available software (virtual monoenergetic plus, Syngo Via, version VB10A, Siemens Healthcare). Curve estimation was implemented for analysing correlations between photon energies and CT values under functions of linear, quadratic, cubic, inverse and power. In addition, degree of fittings was recorded to determine the optimal curve equation. Bone mineral density (BMD) and T-score of patient measured by DXA were set as the reference standard. Diagnostic value of curve equation was assessed by ROC analysis.

Results: 16 patients were diagnosed as OP and 51 patients were diagnosed as non-osteoporosis (NOP) under DXA. R² of cubic and inverse curve equation was significantly higher than linear, quadratic, and power (all P < 0.01). The average coefficients of inverse curve equation ($\bar{a}_{i-average}$) were correlated with BMD and T-score (r were 0.56 and 0.55, respectively). All P < 0.01). The sensitivity and specificity of $\bar{a}_{i-average}$ for diagnosing OP were 93.75% and 83.39% with a cut-off value of 10760.97.

Conclusion: The DECT spectral curve equation is clinically applicable for quantitative assessment of osteoporosis.

10:30 - 12:00

Room Z

Interventional Radiology

SS 609

Special image guidance in interventions

Moderators:

M. Tsitskari; Athens/GR
R. Uberoi; Oxford/UK

B-0443 10:30

CT-guided transluteal drainage of deep pelvic abscess

S.F. Murphy, C.J. Sullivan, P. McCormick, B.J. Mehigan, D. Kevans, I.M. Brennan, M.J. Guiney, N. Sheehy, J.F.M. Meaney; *Dublin/IE*
(stephenmurphy@rcsi.ie)

Purpose: Deep pelvic abscesses can be challenging to drain percutaneously. Transabdominal drainage, the simplest approach, may be precluded by overlying structures including bowel loops, bladder and iliac vessels. The greater sciatic foramen, an oval space in the posterolateral aspect of the pelvis lying inferior to the sacroiliac articulation, offers an effective alternative access route, but requires detailed anatomical knowledge of the region to avoid vessel and nerve injury. We describe a consecutive case series of CT-guided transluteal drainages from our institution.

Methods and Materials: We retrospectively reviewed all cases from January 2007 to August 2017 identified on our RISPACS database. Data collected included patient demographics, cause/size of abscess, catheter size, microbiology, inflammatory markers, follow-up scans and complications.

Results: 100 patients (65 female, 35 male) underwent CT-guided transluteal drainage. The mean age was 57.4 (range 20-89) years. Causes included post-operative anastomotic leak, perforated malignancy, inflammatory bowel disease, diverticulitis and appendicitis. The mean collection diameter was 7.6 cm (range 1.2-16). 78 patients had complete resolution following single (71) or 2 drainages (7), 9 failed to resolve and required surgical intervention and the remainder (13) had a partial resolution that was managed conservatively.

Conclusion: CT-guided transluteal drainage is a safe and effective technique and is the procedure of choice for deep pelvic abscesses when a transabdominal approach is not possible.

B-0444 10:38

Virtual guidance of percutaneous transthoracic needle biopsy with c-arm cone-beam CT: diagnostic accuracy, risk factors and effective radiation dose

D. Fior¹, D. Leni¹, F. Vacirca¹, D. Ippolito¹, S. Sironi², R. Corso¹; ¹Monza/IT, ²Bergamo/IT (davidefior85@gmail.com)

Purpose: C-arm cone-beam computed tomography (CT)-guided transthoracic lung core-needle biopsy (CNB) is a safe and accurate procedure for the evaluation of patients with pulmonary nodules. The purpose of our study was to retrospectively evaluate the diagnostic performance, complication rates and effective radiation dose of C-arm cone-beam CT-guided core-needle biopsy in a large monocentric XperCT-guided lung CNB series.

Methods and Materials: We retrospectively collected data regarding 514 C-arm cone-beam CT-guided CNBs from January 2010 to June 2017. Diagnostic performance, complication rate and effective radiation dose were investigated. Variables influencing diagnostic performance and complications were assessed using univariate logistic regression analyses.

Results: The sensitivity, specificity, positive and negative predictive value and accuracy for patients subjected to CNBs were, respectively, of 96.8%, 100%, 100%, 100% and 97.2%. Considering risk factors for pneumothorax, no significant differences were found regarding patient and lesion characteristics. Perilesional haemorrhage occurred more frequently in older patients (P=.046) and in smaller lesions (P=.001). Haemoptysis was more frequent in patients with perilesional haemorrhage, with a statistically significant P value (P=.01). Mean effective dose through CBCT-guided biopsies and CT-guided biopsies was 7.12 ± 8.78 mSv and 20.91 ± 8.12 mSv, respectively, with a statistically significant difference (p=0.024).

Conclusion: Our results demonstrate that C-arm cone beam CT biopsy combined with Xper-CT virtual guidance is a reliable and accurate technique that allows exact localisation of pulmonary lesions, effective preprocedural planning and real-time fluoroscopy altogether, potentially improving the accuracy of lung biopsies while reducing the effective radiation dose to the patient.

B-0446 10:46

Real-time 3D-guidance based on C-arm-acquired cone-beam CT (CBCT) in transjugular intrahepatic portosystemic stent shunt (TIPSS) placement

G. Böning¹, W. Lüdemann¹, J. Chapiro², M. Jonczyk¹, B. Gebauer¹, R.W. Günther¹, F. Streitparth¹; ¹Berlin/DE, ²New Haven, CT/US

Purpose: Placement of TIPSS is a technically challenging intervention. The aim of this study was to evaluate the feasibility of CBCT-based real-time 3-D guidance and its potential benefits compared to standard guiding methods.

Methods and Materials: 21 patients were prospectively included. We used real-time, 3-D guidance based on a C-arm-acquired CBCT. Feasibility, technical success, procedure/puncture time, applied dose of the intervention and the relative dose share of CBCT were determined. As control groups, we prospectively analyzed 15 TIPSS interventions with ultrasound (US) guidance, retrospectively 23 cases with US guidance and 23 cases with puncture utilizing anatomical landmarks.

Results: CBCT guidance was feasible in all patients. Additional US guidance was necessary in 7 cases, and in 2 of these cases TIPSS implantation was not successful (9.5%). TIPSS placement failure in the prospective US-guided group was 20% and 13% in both retrospective control groups. All failures were excluded from analysis. In the CBCT only group a median of 2 attempts and a mean of 11±14 minutes were needed for portal vein puncture. The mean procedure time in this group was 91±38 minutes with an applied dose of 426±208 Gy*cm and 4% mean dose share of CBCT in the intervention. Regarding to our results CBCT guidance is not significantly inferior to current standard guiding techniques.

Conclusion: CBCT-based guidance for TIPSS placement was feasible and comparable to standard guidance procedures regarding to puncture attempts, time and dose. The relative dose of CBCT is low compared to total dose of intervention.

B-0447 10:54

Impact of personality and experience of interventional radiologists in outcome of CT-guided percutaneous lung biopsies

M.-L. Kromrey¹, S. Schäfer¹, T. Iltermann¹, B. Mensel¹, J.-P. Kühn^{1,2}; ¹Greifswald/DE, ²Dresden/DE (marie-luise.kromrey@uni-greifswald.de)

Purpose: To investigate the influence of personality and experience of interventional radiologist itself on technical success and rate of complication in computer tomography-guided percutaneous transthoracic needle biopsies (PTNB) of suspicious pulmonary nodules.

Methods and Materials: Between 2006-2014, 38 interventional radiologists performed 1,056 PTNB. Technical success, rate of complications and interventional-related predictors of PTNB were determined. PTNB of radiologists with less than 20 interventions, lack of consent, and PTNB with missing variables were excluded, leaving 445 interventions performed by 14 radiologists. Interventionalists underwent a Big-Five personality trait and State-Trait Anxiety Inventory to quantitatively assess personality and psyche. Adjusted for predictors, factors to describe personality such as openness to experience, conscientiousness, extroversion, agreeableness, neuroticism (range 0-20), and anxiety (range 20-80) as well as experiences of interventional radiologists were compared to outcome of PTNB for each interventionalist.

Results: There was no significant difference in technical success of interventional radiologists, which ranged between 75.8-95.7%, P=0.428. Rate of complications ranged between 56.1-85.7%, P=0.12 (major complications: 15.0-24.1%, P=0.57; minor complications: 31.6-67.5%, P<0.05). Personality traits of interventionalists did not differ in technical success and rate of complications. Experience of interventional radiologists had no significant impact on technical success (P=0.132) or rate of complications (P=0.459).

Conclusion: Using a standard operation procedure for CT-guided lung biopsies, technical success and rate of complications are unaffected by the interventional radiologists itself, as well as their years of experience and personality traits such as openness to experience, conscientiousness, extroversion, agreeableness, neuroticism and anxiety.

B-0448 11:02

MR-guided transrectal prostate biopsy with robotic assistance: initial experience

F. Cornud¹, A. Lefevre¹, P. Camparo², P. Soyler¹; ¹Paris/FR, ²Amiens/FR (francois.cornud@imagerietourville.com)

Purpose: To show our preliminary results of MR-guided transrectal biopsies (MRGB) with a robotic assistance (Soteria, the Netherlands) for the diagnosis of prostate cancer.

Methods and Materials: 33 patients (67±33y/o, PSA level: 10±6ng/ml), with a single PI-RADS lesion score equal to or greater than 2, underwent MRGB. In 18 patients, MRGB was a repeat biopsy session following one to three series of systematic biopsies (15 patients) or three targeted biopsies (3 patients) with a software-based image fusion system, all showing no cancer or a microCa,

Gleason score 3+3. The remaining 15 patients had no prior biopsy. The success rate to sample the lesion, the cancer-detection-rate (CDR) and the occupation time of the MR-room were evaluated.

Results: The PI-RADS score was 2, 3, 4 and 5 in 3, 8, 13 and 9 cases, respectively. Sixteen lesions originated in the peripheral zone and 17 in the transition zone (one in the anterior stroma). Software-based adjustments of the robot allowed to align the needle guide with the target in all lesions. Two cores were obtained in 31 patients and 3 cores in 2 patients. The MR-room occupation time dropped from approximately 45-50mn to 20-30mn after 20 cases. The overall CDR was 64.7% and, according to the PI-RADS score, 0, 50, 64 and 100% for PI-RADS score 2, 3, 4 and 5 lesions, respectively. No complication was observed.

Conclusion: Robotic-assisted MRGB can be performed with a short MR-room occupation time. Sampling is possible whatever the lesion location, with two cores in the vast majority of cases.

B-0449 11:10

Volumetric magnetic resonance-guided high-intensity focused ultrasound ablation of adenomyosis: the influence of T1 perfusion in predicting treatment outcome

N.M. Duc¹, B. Keserci¹, H.Q. Huy¹, P.N. Hoa¹, P.M. Thong²; ¹Ho Chi Minh/VN, ²Ha Noi/VN (bsnguyenminhdud@pnt.edu.vn)

Purpose: We investigated the role of magnetic resonance (MR) T1 perfusion-based time-signal intensity (SI) curves of adenomyosis tissue compared to the myometrium in predicting the treatment outcome of MR-guided high-intensity focused ultrasound (HIFU) ablation of adenomyosis.

Methods and Materials: 30 adenomyosis patients (39.2 ± 5.1 years with a range of 30-56 years) who underwent MR-guided HIFU ablation were divided into 2 groups based on dynamic contrast-enhanced (DCE) MR images at screening: group A (n = 15) if the time-intensity curves of adenomyosis are lower than that of myometrium and group B (n = 15) if the time-intensity curves of adenomyosis are equal or higher than that of myometrium. The immediate post-HIFU non-perfused volume (NPV) ratio and adenomyosis volume reduction ratio at 6-month follow-up were assessed.

Results: The volume of adenomyosis was 101.2 ml ± 59.0 (32-189.0 ml) for group A and 98.3 ml ± 53.5 (27.0-186.0 ml) for group B. Immediate post-HIFU NPV ratio of adenomyosis was 84.5 ± 6.9 (80-100%) for group A and 42.7% ± 17.2 (11.3-59.6%) for group B (p<0.001). Adenomyosis volume reduction ratio at 6-month follow-up was 26.8% ± 15.2 (21.2-42.6%) for group A and 7.5% ± 8.2 (-8.9-21.6%) for group B (p<0.001).

Conclusion: Our findings suggest that T1 perfusion-based classification could be served as the MRI classification parameter before MR-guided HIFU ablation for predicting the treatment outcome of HIFU ablation.

B-0450 11:18

Transjugular renal biopsy in patients with impaired coagulation status

P. Heil, B. Tyczynski, M. Reinboldt, Y. Li, J. Theysohn, S. Suntharalingam, J. Grüneisen, A. Kribben, A. Wetter; Essen/DE (axel.wetter@uk-essen.de)

Purpose: To evaluate transjugular renal biopsy (TJRB) in patients with acute nephritic or nephrotic syndrome and impaired coagulation status.

Methods and Materials: 99 TJRB were performed in 42 patients (median age 58y, range 18-83y; 31 male/11 female) from August 2008 to September 2017. After ultrasound-guided puncture of the right jugular vein, a 9F-sheath was inserted in Seldinger technique and the lower branch of the right kidney vein was probed with a 5f multipurpose-catheter. Biopsies were performed under fluoroscopic control with a curved 9F-renal biopsy set and a 19G-Tru-Cut needle. The obtained samples were visually checked by an experienced nephrologist.

Results: Tissue of the renal cortex was extracted in 97 of 99 biopsies. The mean number of glomeruli obtained was eight per procedure. Two specimens contained renal medulla without glomeruli, however, one of those specimens was sufficient for histopathological diagnosis. Main diagnoses were IgA nephritis and glomerulosclerosis. We observed two complications: One patient developed haematuria and urinary bladder tamponade. Another patient suffered from a retroperitoneal haematoma.

Conclusion: In our large uncentered experience, TJRB enabled histopathological diagnosis in 41 of 42 Patients (98%). TJRB proves to be an effective procedure in patients at risk for bleeding complications.

B-0451 11:26

Development of a new image display system for angiography based on detection of electroencephalogram signals from operator's brain

M. Sato¹, T. OGURA¹, S. Yamanouchi¹, N. Hayashi¹, H. Watanabe¹, K. Doi²; ¹Maebashi/JP, ²Willowbrook, IL/US (mitubati.mitu.mitu@gmail.com)

Purpose: Various radiographic images obtained during interventional radiology are commonly used. Although radiographic images may be displayed by physicians, they could not use the console of the image display system to

Chest

SS 604

Optimisation of CT angiography: from single- to dual-energy CT

Moderators:

R.W. Bauer; St. Gallen/CH
T.R.C. Johnson; Munich/DE

B-0454 10:30

Oligaemia of tumour-involved lung displayed by Z-effect of dual-detector spectral CT

Y. Yue, X. Lu, Q. Guo; Shenyang/CN (*ghostaa2000@aliyun.com*)

Purpose: Tumour destruction of pulmonary vessels may result in reduced blood flow of distal or proximal lung tissue. Our purpose is to display blood flow change by Z-effect of dual-layer detector CT. Z-effect is an image in which the pixel values represent the effective atomic number of the displayed tissue.

Methods and Materials: We reviewed 29 cases with enhanced dual-detector spectral CT scan. In them, 23 were proved to have malignancy, with 5 cases of squamous cell carcinoma, 16 cases of adenocarcinoma and 2 cases of small cell carcinoma. Ten of these cases are central type tumour while other 19 cases are solid solitary nodules (SPN) or mass, including all 6 inflammatory cases. Conventional unenhanced lung window, virtual monoenergetic at 70keV and 40keV, Z-effect slices were saved for evaluation. Abnormal attenuation at distal or proximal part of the tumour in artery or delay phase were identified as positive for oligaemia.

Results: According to morphological type, all ten central type cases are positive for oligaemia in Z-effect images in both artery and delay phase. While 4 positive in monoenergetic slice. In the 13 malignant SPN or mass cases, 8 (72.7%) show oligaemia in artery phase and 4 in delay phase in Z-effect images. Two (33.3%) in the 6 inflammatory cases show oligaemia in Z-effect images in artery and delay phase.

Conclusion: Z-effect image is sensitive in detecting blood flow changes of lung caused by tumour invasion. These changes take places in most central type and peripheral type carcinomas but less likely to appear in inflammatory cases.

B-0455 10:38

Application value of dual-detector spectral CT in evaluation of metastatic lymph nodes in lung cancer

L. Gao, Y. Hou, Y. Ma, X. Lu, Z. Jia; Shenyang/CN

Purpose: To investigate the application value of dual-detector spectral CT in the evaluation of metastatic lymph nodes in lung cancer.

Methods and Materials: 24 patients with lung cancer undergoing dual-phase enhanced scan with dual-detector spectral CT were selected. Short diameter of lymph nodes, spectral curve, and iodine uptake were measured. According to pathological findings, lymph nodes were divided into metastatic group and non-metastatic group. The slope of the spectral Hounsfield unit curve (AHu), arterial enhancement fraction (AEF) and short diameter were calculated (AEF = iodine uptake in arterial phase/iodine uptake in venous phase × 100%) and compared. Additionally, receiver operating characteristic (ROC) curves were drawn to confirm the optimum threshold and diagnostic efficiency.

Results: A total of 50 lymph nodes were included, with 24 metastatic lymph nodes and 26 non-metastatic lymph nodes. Short diameter of lymph nodes, AHu and AEF in the 2 groups all showed significant differences (1.49 ± 0.69 vs 0.87 ± 0.22, 2.77 ± 0.24 vs 2.40 ± 0.17, 98.54 ± 15.83 vs 70.14 ± 16.38, respectively; *P* < 0.05). The optimum diagnostic efficiency of AEF was the largest (AUC_{AEF} = 0.928, AUC_{short diameter} = 0.809 and AUC_{AHu} = 0.889), and its threshold was 76.84%. The sensitivity, specificity, negative predictive value and positive predictive value were 88.00%, 76.00%, 90.48% and 75.00%, respectively.

Conclusion: Multiple quantitative parameters of dual-detector spectral CT provide an effective noninvasive method for accurate evaluation of metastatic lymph nodes in lung cancer, especially, AEF has the higher diagnostic efficacy in differentiating metastatic and non-metastatic lymph nodes.

B-0456 10:46

Evaluation of diagnostic value of iodine base material of dual-detector spectral CT for pulmonary aspergillosis invasion by ROC

B. Yuan, W. Zhang, X. Lu, Z. Jia; Shenyang/CN (*zhw65321@sina.com*)

Purpose: To explore the diagnostic value of iodine base material of dual-detector spectral CT for pulmonary aspergillosis invasion by receiver operating characteristic curve (ROC curve).

avoid their unsanitary hands. Therefore, we developed an image display system with use of an electroencephalogram (EEG) without use of hands.

Methods and Materials: We used Mindwave MOBILE (Neurosky Ltd., CA, US) as an EEG sensor. We programmed proper algorithms to provide suitable commands such as paging and zooming by use of EEG signal obtained. For observer study, we investigated the average response time required for paging due to observer's eye blink and the correct detection rate. We also investigated the average response time required for zooming due to the observer's concentration and the correct detection rate.

Results: The average response time required for paging which can be controlled by operator's eye blink was 0.43±0.02 s. The correct detection rate of 100% was achieved by 28 observers, whereas three observers provided 80%. The average response time required for zooming which can be controlled by operator's concentration on his/her mind was 5.85±0.56 s. The correct zooming rate of 100% was achieved by 27 observers, whereas three observers provided 90%, and one observer provided 80%. The correct detection rate of 100% was achieved by approximately 90% observers. The results seem to indicate that the image display system could be utilized for physicians properly.

Conclusion: Radiographic images can be displayed by use of EEG signals without use of physician's hands for angiography.

B-0452 11:34

Contrast enhancement improves PET-US fusion navigation for tumour ablation targeting

N. Gennaro¹, G. Mauri¹, S. de Beni², T. Ierace¹, D. Poretti¹, V. Pedicini¹, A. Chiati¹, L. Solbiati¹; ¹Milan/IT, ²Genoa/IT (*nicolo.gennaro@humanitas.it*)

Purpose: To assess if tumour targeting improves when US/¹⁸F-DG-PET/CT image fusion-guided percutaneous ablations of liver metastases inconspicuously seen or undetectable with US are performed using contrast enhanced PET-CT (PET-CECT) vs conventional unenhanced PET-CT.

Methods and Materials: Fifty-eight metastases mostly from colorectal cancer (38/58, 65.5%) in 23 patients (13 males/10 females, mean age 62.8±9 years) underwent percutaneous microwave ablation (MWA) guided by US/¹⁸F-DG-PET/CT image fusion, either with PET-CECT (28/58, 48.3%) (group 1) or with unenhanced PET-CT (30/58, 51.7%) (group 2). Lesion size (1.0-4.0 cm, mean 2.0 in group 1 and 0.6-4.5 cm, mean 1.9 in group 2) was comparable in the two groups. Time needed for co-registration and rates of technical success and complete ablation were evaluated in both groups.

Results: Time needed for co-registration was significantly shorter in group 1 (mean 4.5 vs 6.0-14.0 min, mean 10.9 in group 2). All lesions were targeted in group 1, while 5/30 were missed in group 2 (technical success 100% vs 83.3%)(*p* = 0.0237). Complete ablation was achieved in one session for 23/28 (82.1%) metastases of group 1 and for 17/30 (56.7%) of group 2 (*p* = 0.03).

Conclusion: Percutaneous ablation of liver metastases inconspicuously visible of totally undetectable with US, guided by US/¹⁸F-DG-PET/CT image fusion is feasible and effective. If PET-CECT is performed and used for co-registration with US, time needed for co-registration, technical success and completeness of ablation are significantly improved, since the visualisation of hepatic vascularity on CECT allows to achieve more accurate spatial registration and therefore more precise lesion targeting.

B-0453 11:42

Prospective comparison US vs. CEUS guided percutaneous biopsy in the diagnosis of large intra- and retroperitoneal tumors

Z. Spirchez, P. Radu, N. Al Hajjar, G. Kacso, T. Mocan; Cluj-Napoca/RO (*zspirchez@yahoo.co.uk*)

Purpose: Due to the presence of necrosis the accuracy of echoguided percutaneous biopsy (US-PB) in the diagnosis of large retro (RPT) and intra peritoneal tumors (IPT) is around 70-80%. CEUS is able to delineate necrotic from well perfused areas inside the tumors. The aim of this prospective study is to compare the sensitivity of US and CEUS guided PB in the diagnosis of these tumors.

Methods and Materials: 60 patients with 24 IPT and 36 RPT (mean diameter 7.5 cm, range 4-22 cm) were referred for PB. In 32 patients (11 IPT, 21 RPT) PB was performed using US guidance. 28 patients (13 IPT, RPT) were biopsied using real time CEUS guidance. The lesions in the CEUS -PB group were larger than those in US-PB group (mean diameter 8.1 cm vs. 6.8 cm) (*P* > 0.05). PB was performed with an 18G Bard needle coupled on Biopsy Gun.

Results: Real time CEUS-PB was technically successful in all procedures (100% technical success rate). The sensitivity of PB was significantly higher in CEUS -PB group than in conventional US -PB group for all lesions (96.4% vs. 78.1%, *p* < 0.05) and RPT (100% vs. 78.9%, *p* < 0.05). For IPT the sensitivity was also higher for CEUS-PB (90.9% vs. 76.9%) but without statistical significance (*p* = 0.36). No major complication occurred in both groups.

Conclusion: Percutaneous CEUS guided PB in intra and retroperitoneal tumors is a feasible and safe technique. It significantly improves the overall sensitivity of the procedure in patients with large lesions.

Methods and Materials: The patients who underwent chest contrast-enhanced scanning by dual-detector CT and confirmed with pathology results were enrolled (20 cases with pulmonary aspergillosis invasion and 30 cases with lung neoplasm). The normalised iodine concentrations (NIC-ROI iodine concentration/thoracic aorta iodine concentration) of all lesions on both arterial and venous phases were measured and calculated and the results were compared between the two groups. ROC curve was used to determine the best cut-off points of NIC on arterial and venous phases for pulmonary aspergillosis invasion group. Pathological diagnosis as gold standard, the diagnostic values of NIC on arterial and venous phases for pulmonary aspergillosis invasion were analysed.

Results: The differences of NICs on arterial and venous phases between the two groups were statistically significant (both $P < 0.01$). The areas under ROC of NICs on arterial and venous phases were 0.901 and 0.900, respectively, and the best cut-off points of NIC on arterial and venous phases obtained via analysis of the ROC were 0.90 and 0.85, respectively. Their sensitivities for the diagnosis of NPC were 88% and 86%, while the specificities were 85% and 83%, respectively.

Conclusion: With high values in the diagnosis of pulmonary aspergillosis invasion, the NICs on arterial and venous phases can be used as effective indicators for diagnosis of pulmonary aspergillosis invasion by dual-detector spectral CT.

B-0457 10:54

Are there suboptimal CTPE studies in the DECT era: low mono-energetic images for pulmonary artery assessment

N. Lev Cohain, I. Leichter, J. Sosna; *Jerusalem/IL*
(NAAMAL@HADASSAH.ORG.IL)

Purpose: Low mono-energetic images (MEI) of dual-energy CT (DECT) enable greater contrast density. We hypothesized that low-energy MEI could salvage suboptimal pulmonary emboli CT (CTPE) studies. Hence, the contrast enhancement of the pulmonary arteries (PA) on conventional CTPE and low MEI was compared.

Methods and Materials: 49 patients who underwent CTPE using DECT at 120kV and 90mAS (IQon, Philips Healthcare, Eindhoven, Netherlands) between 1 and 4/2017 were retrospectively reviewed. Early arterial enhanced series were evaluated using conventional images and MEI at 50-keV. Regions of interest (ROI) were marked in four locations: the main, left, right and right lower lobe PA. Any HU value below 220 was considered suboptimal. Paired t test determined the significance of difference in contrast density.

Results: Of the conventional images, 32.1% (63/196 ROIs) had HU values lower than 220, and considered limited for the evaluation of an emboli. 24.5% (12/49) were suboptimal in the main PA, 34.7% (17/49) in the left PA, 32.7% (16/49) in the right PA and 36.7% (18/49) in the right lower lobe PA. No low HU values were found on the MEI at 50-keV. The mean HU value on the 50-keV images was significantly higher ($p < 0.001$) compared to the conventional image (536.4 HU vs 257.5HU, respectively). The mean enhancement factor of the contrast density on the 50-keV images was 2.08.

Conclusion: Low mono-energetic DECT images significantly enhance the contrast density in the pulmonary vessels. The diagnostic yield of CTPE studies can be increased, by salvaging suboptimal studies and turning them into diagnostic studies.

B-0458 11:02

Transient interruption of contrast (TIC) in CT pulmonary angiography: frequency and impact on the diagnostic value of CT examinations using a dual-source CT system

J. Hennicaux, A. Hutt, M. Kyheng, J.-B. Faivre, J. Remy, M. Rémy-Jardin; *Lille/FR* (martine.remy@chru-lille.fr)

Purpose: To evaluate the incidence of transient interruption of contrast (TIC) during dual-source chest CT angiographic (CTA) examinations and its impact on the diagnostic value of examinations.

Methods and Materials: Retrospective review of 449 consecutive chest CTA examinations obtained on a 3rd generation DSCT system was undertaken to search for TIC on single- (SE) ($n=276$; 61.5%) and dual-energy (DE) ($n=173$; 38.5%) CT examinations. This physiological artifact was recognized on the basis of (a) decrease in opacification within pulmonary arteries (PAs); (b) concurrent depiction of unopacified blood from the inferior vena cava entering the right heart; and (c) adequate opacification of pulmonary veins and left cardiac cavities.

Results: TIC was identified on 19 examinations (19/449; 4%), more frequently seen on DE (14/19; 74%) than SE (5/19; 26%) examinations. Four types of TIC were depicted: (1) decreased opacification only within central PAs, observed in 4 patients (Group 1; 4/19; 21%); (2) decreased opacification within central and peripheral PAs in the remaining 15 patients (Group 2; 15/19; 79%) with TIC

depicted in the middle third of the chest (12/15), the initial (1/15) or late (1/15) part of the acquisition, or over the entire thorax (1/15). In both groups, the mean level of attenuation within PAs of the TIC zone was 228.7 ± 69.1 HU in central and 223.9 ± 54.8 HU in peripheral PAs, enabling confident analysis of PAs down to the segmental (2/19) or subsegmental (15/19) level.

Conclusion: TIC was identified in 4% of the study population, never responsible for indeterminate CTA examinations.

Author Disclosures:

J. Remy: Consultant; Research Consultant, Siemens Healthcare.

M. Rémy-Jardin: Research/Grant Support; Siemens Healthcare.

B-0459 11:10

Incidence of transient interruption of contrast (TIC): a retrospective single-centre analysis in 225 consecutive CT pulmonary angiography studies

S. Sudarski¹, T. Henzler¹, H. Haubenreisser¹, S.O. Schönberg¹, A. Gutzeit²; ¹Mannheim/DE, ²Zurich/CH (sonja.sudarski@medma.uni-heidelberg.de)

Purpose: To assess occurrence of transient interruption of contrast (TIC) phenomenon in pulmonary CT angiography (CTPA) studies performed to rule out pulmonary embolism.

Methods and Materials: In this retrospectively designed single-centre study, CTPA exams of 225 consecutive patients scanned between 9/1/2016 and 12/31/2016 on a 16-slice single-source CT scanner system were analysed. Exams were screened a priori to measurements and exams with non-adequate pulmonary artery contrast due to incorrect bolus tracking or failure of i.v. contrast administration were excluded from the analysis. HU values in the thoracic aorta and in the pulmonary trunk were assessed in duplicate measurements and the aorto-pulmonary ratio was calculated. An aorto-pulmonary ratio > 1 was defined as presence of TIC.

Results: 3 patients had to be excluded due to incorrect bolus tracking. Final analysis in 222 patients (mean age 65 ± 19 years, range 18 to 99 years) were analysed. Mean density in the pulmonary trunk was 275 ± 17 HU, in the aorta 208 ± 15 HU. Mean aorto-pulmonary ratio was 0.81 ± 0.29 . 48 patients (21.6%) had an aorto-pulmonary ratio > 1 .

Conclusion: TIC is a common phenomenon in CTPA studies with an incidence of 22% in our retrospective cohort.

B-0460 11:18

Assessment of optimal window settings for display of traditional and noise-optimised virtual monoenergetic imaging in dual-energy CTPA

J.L. Wichmann¹, A.M. Bucher¹, L. Lenga¹, C. Arendt¹, D. Caruso², T. D'Angelo³, A. Blandino³, G. Ascenzi³, T.J. Vogl¹; ¹Frankfurt a. Main/DE, ²Rome/IT, ³Messina/IT (docwichmann@gmail.com)

Purpose: To define optimal window settings for display of virtual monoenergetic images (VMI) of dual-energy CT pulmonary angiography (DE-CTPA) and assess impact on image quality in comparison to standard reconstruction and settings.

Methods and Materials: Data from 45 patients who underwent DE-CTPA were retrospectively evaluated. Three image dataset were assessed: standard linearly-blended (M 0.6), 70-keV traditional VMI (M70), and 40-keV noise-optimised VMI (M40+) reconstructions. For M70 and M40+, the subjectively best window setting (width and level, B-W/L) was initially assessed independently by two blinded observers and subsequently related with pulmonary artery attenuation to obtain calculated optimised values (O-W/L) using linear regression. Subjective evaluation of image quality between different W/L settings were assessed by two additional blinded readers.

Results: Best (B-W/L) settings for M70 and M40+ were 880/280HU and 1410/450HU, respectively. Regression analysis resulted in an O-W/L of 850/270HU for M70 and 1350/430HU for M40+. Significant differences for W/L were found between B-W/L and O-W/L for M40+, and between M70 and M40+ for both B-W/L and O-W/L (all $p < 0.001$). Subjective image quality was significantly increased for M70 and M40+ after application of O-W/L (all $p < 0.001$). Highest subjective scores were observed for M40+ regarding vascular contrast, embolism demarcation, and overall image quality (all $p < 0.001$).

Conclusion: Application of O-W/L settings is mandatory to optimise subjective image quality of VMI reconstructions of DE-CTPA. M40+ showed better subjective image quality than M70. A width slightly less than two times the pulmonary trunk attenuation and a level approximately of overall pulmonary vessel attenuation are recommended.

Author Disclosures:

J.L. Wichmann: Speaker; GE Healthcare, Siemens Healthcare.

B-0461 11:26

Optimal monochromatic energy levels in spectral CT pulmonary angiogram for the detection of pulmonary thromboembolism: using detector-based spectral CT

M. Ha, K.Y. Lee, C. Kim, S.-K. Kim, S.-J. Park, B.-K. Je, S.H. Lee, Y. Lee, J. Cha, A. Jeong-Cheon; *Ansan/KR (bearsksk@gmail.com)*

Purpose: The aim of this study was to investigate the optimal monochromatic level, in spectral CT pulmonary angiography, for the detection of pulmonary thromboembolism, using detector-based spectral CT.

Methods and Materials: 103 patients were referred to undergo pulmonary CTPA with spectral CT mode in the arterial phase. Images of both conventional (120 kVp) and multiple monochromatic energy level (VME) images from 40 keV to 100 keV at intervals of 10 keV were generated using Spectral CT viewer. Image noise, clot diameter and clot to artery contrast-to noise ratio (CNR), signal-to-noise ratio (SNR) at selected monochromatic levels were measured and compared. Subjective image quality was also assessed by two radiologists and compared. We analyzed data using Kruskal-Wallis test and correlation analyses.

Results: The lowest noise was obtained at VME level of 100 keV. There was no difference in the mean noise between the VME images of 50, 60, 70, 80, 90 and 100 keV. The CNR and SNR values were achieved at the 40 keV level and increased as energy decreased. The highest diagnostic confidence for the detection of pulmonary thromboembolism was at VME level of 70 keV, because two reader's agreement at this level had the highest kappa coefficient ($\kappa=0.68$). The clot diameter decreased with decreasing energy level.

Conclusion: Virtual monochromatic images at 100 keV yielded the lowest image noise. The highest CNR and SNR were obtained at 40 keV VME image. An optimal analysis of pulmonary thromboembolism can be achieved on virtual monochromatic spectral images at 70 keV.

B-0462 11:34

Right heart thrombi and acute pulmonary embolism: analysability of right cardiac cavities in the conditions of routine dual-source chest CT angiographic examinations

C. Fantini, J. Hennicaux, J.-B. Faivre, P. Felloni, J. Remy, M. Remy-Jardin; *Lille/FR (martine.remy@chru-lille.fr)*

Purpose: To evaluate the analysability of right cardiac cavities on dual-source chest CT angiographic (CTA) examinations positive for acute pulmonary embolism (PE) in the conditions of routine clinical practice.

Methods and Materials: Among 449 patients referred for suspicion of acute PE, chest CTA was found positive in 59 patients (13%). The analysability of the right atrium (RA) and right ventricle (RV) was based on the evaluation of (a) the homogeneity of contrast attenuation; (b) the presence & severity of beam-hardening artifacts. A second acquisition during the CT session was at the radiologist's discretion.

Results: The RA was deemed interpretable in 44 patients (44/59; 74.6%) (Group 1a: 31/39; 79%) (Group 2a: 13/20; 65%) with homogeneous or slightly heterogeneous opacification and no beam-hardening artifacts (mean attenuation: 340.5 ± 140.6 HU) while it was rated as not confidently interpretable in 15 patients (15/59; 25.4%) (Group 1b: 8/15; Group 2b: 7/15). The RV was always interpretable. In Group 1b, the RA became analysable on the delayed acquisition, obtained in all but one patient. In group 2b, the use of monochromatic images at 90 and 100 keV provided interpretable images (absence of beam-hardening artifacts; sufficient level of attenuation to depict intracardiac thrombi) in all but 2 patients, leading to a total of analysable cavities in 90% of Group 2 patients (18/20). Right intracardiac thrombi were depicted in two patients (2/59; 3%).

Conclusion: Right cardiac cavities were interpretable on a single acquisition in 79% and 90% of patients scanned with SE and DE, respectively.

Author Disclosures:

J. Remy: Consultant; Research Consultant, Siemens Healthcare.

M. Remy-Jardin: Research/Grant Support; Siemens Healthcare.

B-0463 11:42

Automatic spectral chest CT assist protocol: can the improvement of the noise index setting further decrease the radiation dose and optimise the image quality?

R. Wang, J. Gao, Y. Zhou; *Zhengzhou/CN (wr807115125@163.com)*

Purpose: To investigate the effect of automatic spectral imaging assist (ASIA) on radiation dose and image quality of enhanced chest CT examinations with low-dose contrast agent for patients with different body mass index (BMI).

Methods and Materials: 120 patients with dual-phase enhanced chest CT were randomly divided into experimental group (A) and control group (B). In each group, patients in three different BMI intervals were scanned at the noise index of 13, 18 and 22 respectively. By using 300 mgI/kg contrast agent, the group A used the ASIA combined with 50% adaptive statistical iterative reconstruction (ASIR) technique to obtain the spectral monochromatic images

(40-70 keV). The conventional 120 kVp CT with 450 mgI/kg contrast agent was adopted in the group B, and the filtered back-projection (FBP) algorithm was used to reconstruct images. Then, the index of radiation dose and image quality were calculated and evaluated.

Results: The images of the group A show better performance in reducing and maintaining image noise than that of group B ($p < 0.05$), especially for patients with BMI $< 18.5 \text{ kg/m}^2$ and BMI $> 24.9 \text{ kg/m}^2$. There are no statistical differences of CTDIvol, DLP and ED between two groups at all BMI levels with noise index of 13 ($p > 0.05$). However, the NI of 18 and 22 in group A were higher than that of group B.

Conclusion: The quality of images obtained by using ASIA combined with ASIR technique can meet the requirements of clinical diagnosis. However, its ability to reduce radiation doses is not satisfactory.

B-0464 11:50

Segmental and sub-segmental pulmonary embolism displayed by dual-detector spectral CT

Y. Yue, X. Lu, W. Zhang, Q. Guo; *Shenyang/CN (ghostaa2000@aliyun.com)*

Purpose: Pulmonary embolism involving segmental or sub-segmental artery is difficult to diagnosis in enhanced CT. Dual-detector spectral CT can promote detecting ability by display low perfusion area and small thrombi. We reviewed cases of segmental or sub-segmental embolism and correlate with their clinical background.

Methods and Materials: Enhanced dual-detector CT scans of lung were performed in 1200 cases. Lung and mediastinum slices along with iodine density and Z-effect map were reviewed (Z-effect is an image in which the pixel values represent the effective atomic number of the displayed tissue). Pulmonary embolism was described as artery thrombi with or without low perfusion in corresponding area in iodine density or Z-effect maps. Embolism involving pulmonary artery trunk or lobar branches is not included in this study. Clinical information including patient history, serum D-dimer level and revised Geneva score was recorded for analysis.

Results: Twenty-three cases were confirmed to have single or multiple segmental or sub-segmental embolisms. In them, 16 cases have a history of malignancy, including 5 cases of cervical cancer, 4 cases of esophageal cancer, 3 cases of lung cancer, 2 cases of liver cancer, 1 case of lymphoma and 1 case of pancreas cancer. In benign cases, 3 patients have brain stroke and 4 patients have no special history. Serum D-dimer level varied from 674 to 5440 (1520 ± 1313) mmol/l and revised Geneva score varied from 4-7 (5.28 ± 0.83).

Conclusion: Segmental or sub-segmental embolism is more likely to involve patients with malignancy and with mild symptoms or D-dimer levels.

10:30 - 12:00

Room N

Genitourinary

SS 607

Female pelvis

Moderators:

M. Basta Nikolic; Novi Sad/RS

N.N.

B-0465 10:30

Myometrial infiltration by deep pelvic endometriosis: MRI assessment

M. Francavilla¹, D. Resta¹, F. Lorusso², G. Angelelli¹, C. Tartaglia¹, P. Pignataro¹, M. Scioscia³, A.A. Stabile Ianora¹, A. Scardapane¹; ¹Bari/IT, ²Castellana Grotte/IT, ³Negrar, Verona/IT (mariano_fra@hotmail.it)

Purpose: Myometrial infiltration from peritoneal implants is often associated with endometriotic lesions in bowel, bladder, and with adenomyosis. Evaluation of the correlation between myometrial invasion and severity of deep pelvic endometriosis was made.

Methods and Materials: A retrospective survey of 198 women with previous laparoscopic surgery for pelvic endometriosis was carried out. A pelvic MRI was performed in all patients: it consisted in T2w-TSE sequences in axial, sagittal, and coronal planes and T1w and THRIVE sequences in the axial plane. The presence of endometriomas and endometriotic nodules in Douglas pouch, rectovaginal septum, torus uterinus and uterosacral ligaments was reported. Similarly, intestinal infiltrative nodules, vesical and ureteral implants and pelvic adhesions were recorded. Results were analysed with χ^2 test.

Results: Uterine infiltration was found in 26/198 (13%) patients, adenomyosis in 76/198 (38%) of cases, and their coexistence in 19/198 (9%) of women. Uterine invasion was detected in 19% of patients with Douglas pouch obliteration (vs 3% of women without Douglas involvement), in 24% of patients with rectovaginal septum lesions (vs 3% of women without RVS foci), in 28% and 38% of patients with bowel nodules and major intestinal resection

respectively (vs 2.5% of women that did not show these two findings). All the results demonstrated to be statistically significant, with $p < 0.05$.

Conclusion: Myometrial infiltration is associated with severe features of deep pelvic endometriosis, in particular with colorectal involvement and consequent bowel resection.

B-0466 10:38

Diffusion tensor imaging (DTI) for evaluation of sacral plexus abnormalities in patients with pelvic deep infiltrating pelvic endometriosis with pelvic pain: a pilot study

A.M. Kalovidouris, M.I. Vargas, B. Delattre, N. Pluchino, X. Montet, D. Botsikas; Geneva/CH (Anastasia-Marie.Kalovidouris@hcuge.ch)

Purpose: To prospectively investigate if fractional anisotropy (FA) or apparent diffusion coefficient (ADC) of the lumbosacral plexus roots, correlate with intensity of pelvic pain in patients with pelvic deep infiltrating endometriosis (DIE). A secondary aim was to compare FA and ADC values in patients with DPE documented on MRI with those with negative morphologic MRI.

Methods and Materials: A DTI sequence was performed in all patients (mean age 33.5 ± 8.9) referred for pelvic MRI with clinical suspicion or known DIE from June 2016 to July 2017. The patients filled in a questionnaire with self-evaluation of pelvic pain in a scale from 0-10. A radiologist tracked all roots of lumbosacral plexus, from L5 to S3. Mean FA and ADC for all roots were calculated. Correlation coefficient r between pain scale and FA and ADC was calculated. FA and ADC values between patients with MRI documented DIE and those without DIE lesions on MRI were compared.

Results: 149 patients (74 with endometriosis detected on MRI and 75 without) were included in the study. There was a statistically significant negative correlation between overall pain and ADC (mean $r = -0.1967$, $p = 0.0181$) and a weak positive correlation of FA mean and pain, with a statistical trend ($p = 0.0541$). There was no statistically significant difference between ADC and FA values for patients with and without DPE detected on morphological MRI ($p > 0.05$).

Conclusion: This study showed a negative correlation between ADC and positive correlation between FA of the lumbosacral plexus and pain. This could be explained by an intramyelinic oedema or microarchitectural abnormalities of the neural roots providing innervation to DIE lesions.

B-0467 10:46

Ovaries in patients with Mayer-Rokitansky-Küster-Hauser syndrome vs normal females: a retrospective cohort study with magnetic resonance imaging

Y. Wang, J. Lu, L. Zhu, R. Chen, B. Jiang, Z. Jin; Beijing/CN (wang_yue111@126.com)

Purpose: To explore the MRI appearances of ovaries in patients with Mayer-Rokitansky-Küster-Hauser (MRKH) syndrome as compared with a control group.

Methods and Materials: Pelvic MRI of 83 MRKH patients and 60 age-matched normal females were retrospectively reviewed by two experienced gynaecological radiologists in consensus. Characteristics including location of ovary, ovarian volume, and follicle counts were assessed. Ectopic ovary was established when it was located out of the pelvis, anterolaterally just behind the anterior pelvic wall, or far laterally in the paracolic gutter or near the lateral pelvic wall. Ovarian volume was calculated using the formula for the volume of an ellipsoid. Average numbers of follicle counts determined by two radiologists were recorded. The incidence of ectopic ovary was compared between MRKH patients and controls. The ovarian volume and follicle counts were compared among three groups: ectopic ovaries in MRKH patients, eutopic ovaries in MRKH patients, and normal controls.

Results: In total, 166 ovaries in 83 MRKH patients and 120 ovaries in 60 control females were evaluated. Thirty-seven ovaries in 23 MRKH patients (28%, 23/83) and 3 ovaries in three control females (5%, 3/60) were abnormally located ($P < 0.001$). The mean volume was 9.2 ± 6.3 ml of the ectopic ovaries in MRKH patients, 7.8 ± 4.0 ml of the eutopic ovaries in MRKH patients, and 8.9 ± 4.8 ml in control females ($P > 0.05$). No obvious difference was observed with regard to follicle counts.

Conclusion: MRKH patients associated with increased incidence of ectopic ovaries. Ovarian volumes and follicle counts were not differed statistically between MRKH patients and normal controls.

B-0468 10:54

Invasive placenta: MRI prognosticators for patients' clinical outcome

C. Bourgioti, K. Zafeiropoulou, E. Panourgias, K. Chatoupis, A. Antoniou, M. Nikolaidou, L.A. Mouloupoulos; Athens/GR (charisbourgioti@yahoo.com)

Purpose: To investigate any possible association between MRI features and maternal peripartum outcome in patients with abnormal placentation.

Methods and Materials: Between March 2016 and June 2017, 49 gravid patients (mean age: 35.7 years, mean gestational age: 32.5 weeks) with sonographically confirmed placenta previa were referred for dedicated prenatal MRI. All MRIs were reviewed prospectively by two radiologists experienced in genitourinary imaging. All patients underwent C-section within 6 weeks from MRI; perioperative or/and pathological findings were used as standard of reference. Logistic regression models were used to investigate which MRI features were predictive of adverse peripartum events including increased blood loss, prolonged duration of delivery or hysterectomy performance.

Results: Thirty-eight (77.6%) patients had invasive placenta (percreta, $n = 26$, accreta/increta, $n = 12$) on surgery; 22/38 patients had bladder involvement, while 11/38 patients had parametrial invasion. Stepwise linear regression analysis showed that evidence of bladder invasion on MRI and T2 dark intraplacental bands were independently associated with prolonged duration of delivery (> 60 min). Additionally, bladder invasion on MRI, serosal hypervascularity and T2 dark bands were independently associated with massive blood transfusion (> 10 units packed red blood cells) during surgery. Serosal hypervascularity (OR = 18.34, 95% CI: 1.53-219.0, $p = 0.021$) and T2 dark bands (OR = 11.32, 95% CI: 2.09-61.38, $p = 0.005$) were significantly associated with hysterectomy performance.

Conclusion: MRI evidence of bladder invasion, serosal hypervascularity or T2 dark intraplacental bands were independently associated with poor maternal outcome in patients with abnormal placentation.

B-0469 11:02

Colour Doppler unhappy surprise in transvaginal ultrasound evaluation of post-abortive vaginal bleeding: uterine arteriovenous malformations

S.A.H. Hassanein; Shebin el-kom/EG (shaimaahamid@hotmail.com)

Purpose: To assess the prevalence of uterine arteriovenous malformations and emphasize its presence as a cause of post-abortive bleeding.

Methods and Materials: A retrospective study was conducted reviewing the data acquired from transvaginal ultrasound combined with Doppler examination to patients presented by post-abortive bleeding at our institute during the last two years. The studied group included 548 patients presented clinically by post-abortive bleeding. All of them were examined by transvaginal ultrasound. Both grey-scale and Doppler examination were conducted in all cases.

Results: Reviewing the transvaginal ultrasound data revealed retained products of conception in 412 patients, normal scan in 118 patients and 18 cases of suspected uterine arteriovenous malformations which constitute the study population. Reviewing the patients' clinical data revealed post-abortive bleeding with duration ranging from 3 days to 3 weeks post-abortion. The mean age was 28.7 years. History of previous curettage was present in 16 cases. Doppler study showed the intense myometrial hypervascularisation with turbulent flow in 18/18 cases of AVM. The size of the intra-myometrial component exceeded 5 cm in 12/18 cases (66.7%). The largest vessel diameter ranged from 8 to 28 mm with a mean of 16.2 mm. The mean velocity detected was 22 cm/sec.

Conclusion: Uterine arteriovenous malformations are a serious cause for post-abortive bleeding and although their incidence is rare, it is very important to be identified using transvaginal ultrasound whether grey-scale or Doppler to avoid serious life-threatening bleeding.

B-0470 11:10

Ovarian ischaemia vs haemorrhagic infarction: differentiation by MRI in cases of adnexal torsion

Y. Ragab¹, H. Kheir¹, H. Hamza², S. Maher¹; ¹Cairo/EG, ²London/UK (yragab61@hotmail.com)

Purpose: To demonstrate the role of magnetic resonance (MR) imaging findings, in differentiating between ovarian infarction and ischaemia and consequently the rate of ovarian salvage in cases of adnexal torsion.

Methods and Materials: 25 patients with surgically proven ovarian torsion were evaluated by two radiologists regarding the following MR findings: pelvic fluid collection, uterine deviation, ovarian enlargement, ovarian parenchymal hypointensity on T2-weighted images (WI), hyperintensity on T1 (WI) with fat saturation, recognition of twisted pedicle, diffusion restriction and ovarian parenchymal enhancement. These MR findings were statistically correlated with the operative findings and histopathological results (for cases of ovarian infarction).

Results: Pathologically, ovarian haemorrhagic infarction was confirmed in 6 out of 25 cases. Ovarian hypointensity on T2 WI was seen in all cases with

infarction 6/6. Ovarian hyperintensity (compared to the contralateral sides) was observed in 4/6 and 5/6 cases with infarction on T1WI and DWI, respectively. Ovarian enlargement, fluid collections, uterine deviation and twisted pedicle were detected in most cases with or without haemorrhagic infarction. Poor parenchymal contrast enhancement was observed in all cases without or with necrosis.

Conclusion: Detection of ovarian infarction is of prognostic importance in cases of torsion to assess salvageability, and thus may affect the surgical decision. Swollen hypointense ovarian parenchyma on T2 WI with lack of contrast uptake are the most reliable MRI signs, followed by hypersignal on T1 WI fat sat and DWI.

B-0471 11:18

MRI predictive factors for vaginal stenosis in patients with cervical cancer after ChemoRadiation Therapy (CRT)

M. [Sbarra](#), M. Miccò, B. Gui, E. Rodolfo, A.L. Valentini, R. Manfredi; *Rome/IT* (sba.martina@gmail.com)

Purpose: Vaginal Stenosis (VS) is a toxicity after radiotherapy. Our purpose was to describe radiotherapy induced changes in the vagina after CRT for cervical cancer and to find any Magnetic Resonance Imaging (MRI) predictive factors for the development of stenosis.

Methods and Materials: This retrospective study included 43 patients (mean age 49,5 y) with FIGO IB2-IIIb cervical cancer treated with CRT administered with external beam radiation therapy. They underwent 1.5 T pelvic diffusion weighted DW-MRI before (baseline), at 2 weeks from the start (early) and at the end of the treatment (late). On all MRIs, tumor volume (TV), the length and the thickness of the vagina were measured. DWI were analysed qualitatively at each time point. VS was clinically graded at each follow-up using Common Terminology Criteria for Adverse Effect v.4.03. The statistical analysis were made with Mann-Whitney test. ROC curves were generated for statistically significant DW-MRI parameters.

Results: According to CTCAE: Grade1 had 15 pts and Grade≥2 had 28 pts. TV was higher in Grade1 (p= 0,013). The mean vaginal length and thickness decreased between baseline and final MRI from 82,0 to 71,6 mm and from 3,3 to 2,6 mm respectively. DWI had a lower signal intensity at the final MRI in Grade≥2 (p<0,0001). According to ROC analyses the AUC was 0,917 (p< 0,0001) for DWI and 0,731 (p= 0,013) for TV.

Conclusion: This is the first study that demonstrates the utility of DW-MRI to find predictive factors for VS in cervical cancer after CRT.

B-0472 11:26

Female Skene's gland diseases: CT and MR imaging evaluation

H. Wang, J. [Guan](#), Y. Guo; *Guangzhou/CN* (usefulkey0077@hotmail.com)

Purpose: To analyse the imaging characteristics of Skene's gland (periurethral gland) diseases on CT and MRI, further to improve the understanding and imaging diagnosis.

Methods and Materials: 15 female cases with Skene's gland disease confirmed by pathology were retrospectively analysed. Imaging features of Skene's gland disease were summarized.

Results: Skene's gland cysts (n=3) located in the distal and posterolateral urethra or close proximity to the urethra, presenting as cystic lesions with teardrop shape on sagittal images, appeared as hypo-attenuation on CT, and hypo-intensity on T1WI, hyper-intensity on T2WI, and without enhancement. One with infection presented as hyper-intensity on T1WI and gaseous intensity inside, and thickened cystic wall. Urethral diverticulum (n=10) located in the middle or distal and posterolateral urethra, and presented as a horseshoe-shaped cystic lesion partially surrounding the urethral (n=3) or spoke wheel-like cystic lesion with multiple septum completely surrounding the urethra (n=7). They appeared as fluid attenuation/intensity on CT and MRI without enhancement. Heterogenous signal or attenuation and enhanced septum or cystic wall were found in 6 cases with infection. Malignant tumour of Skene's gland (n=2, adenocarcinoma and neuroendocrine carcinoma) presented as cystic-solid mass surrounding the urethral, showing heterogeneous low attenuation on CT and iso- to hyper-intensity on T2WI and hypo- to iso-intensity on T1WI with enhancement. A "prostate" sign was specific for determining the lesion origin of the Skene's gland.

Conclusion: According to the lesion location and imaging features, we can make an accurate diagnosis and distinguish different types of female Skene's gland diseases.

B-0473 11:34

Diagnostic value of MR perfusion in characterisation of complex adnexal masses

H.A.S. [Sabet](#), R.M. El Kady, N.N. Omar, A.M. Abbas; *Assiut/EG* (bobaiez1989@gmail.com)

Purpose: To assess the role of MR perfusion weighted imaging (MR PWI) in characterisation of complex adnexal masses.

Methods and Materials: Twenty-seven patients underwent MR PWI using rapid dynamic contrast-enhanced T1-weighted gradient echo. Regions of interest (ROIs) were drawn in the solid part of the adnexal lesion and the outer myometrium. PWI was analysed using descriptive, time signal intensity curves and semiquantitative parameters (relative enhancement (RELENH), maximum enhancement (MAXENH), maximum relative enhancement (MAXRELENH), time to peak (TTP), and wash-in rate (WASHIN) and wash-out rate (WASHOUT). Time intensity curve and semiquantitative parameter results were correlated to the histopathological results.

Results: Curve type 1 was found to be 100% specific for benign ovarian tumours (p=0.017). Type III curve showed (76%) sensitivity and (60%) specificity for malignant tumours. MAXENH showed accuracy of 73.2%, sensitivity of 76.5% and specificity of 70% for malignant tumours. WIR showed the highest sensitivity (88.2%) while WOR with a cut-off value of 6.03 showed the highest specificity (90%).

Conclusion: PWI is useful in characterisation of adnexal masses. We can depend upon WIR in depicting malignant masses and applying the cut-off of WOR to exclude the false-positive cases and avoid radical surgery in unnecessary patients especially in women aiming at preserving fertility.

B-0474 11:42

MRI in endometriosis: a new platform

W.R.A. [Abdel Hamid](#); *Cairo/EG* (w.gforever@yahoo.com)

Purpose: The aim of this study is to validate the ability of MRI as an accurate tool in verifying the endometriotic load in patients with clinically suspected endometriosis. Our aim was also to verify the results of non-contrast MRI compared to contrast enhanced MRI through laparoscopic correlation.

Methods and Materials: 60 female patients within an age range of 27 and 44 years were included in the study. A thin slice high resolution MR study was performed for all patients with a protocol including Axial & sagittal T2W, T1W (with and without fat suppression), DWI images together with delayed post contrast T1W fat suppressed images in the three orthogonal planes. Findings were compared to results of laparoscopy.

Results: Based on our results, IV contrast didn't add much. The data acquired from T1W images with fat suppression and DWI's were sufficient and showed high sensitivity and specificity values when compared to laparoscopic findings. Each key finding was validated separately including endometriomas, adenomyosis, solid endometriotic implants, giving high sensitivity (94.59%, 100% & 95.35%), specificity (96.15%, 95.65% & 100%), PPV (97.22%, 88.89% & 100%) and NPV (92.59%, 100% & 90.48%) respectively.

Conclusion: Non-contrast MRI can be considered a highly accurate tool in screening for endometriotic load. It can be used as a roadmap prior to laparoscopic intervention to help guide gynecologists so as not to miss lesions.

B-0475 11:50

Utility of histogram analysis of apparent diffusion coefficient maps obtained using 3.0T MRI for distinguishing uterine endometrial carcinoma from endometrial polyps

W. [Wang](#), J. Cheng, Y. Zhang; *Zhengzhou/CN* (weijianwang520@163.com)

Purpose: We explored the role of histogram analysis of apparent diffusion coefficient (ADC) maps for discriminating uterine endometrial carcinoma and endometrial polyps.

Methods and Materials: We retrospectively evaluated findings in 40 patients with uterine endometrial polyps and 50 patients with endometrial carcinoma who underwent diffusion-weighted imaging (b = 0,800 s/mm²) at 3T with acquisition of corresponding ADC maps. We derived histogram data from regions of interest drawn on all slices of the ADC maps in which tumour was visualised, including areas of necrosis and haemorrhage in the tumour. We used the Mann-Whitney test to evaluate the capacity of histogram parameters (mean, skewness, kurtosis, 50th, 90th percentiles) to discriminate uterine endometrial carcinoma from endometrial polyps and analysed the receiver operating characteristic (ROC) curve to determine the optimum threshold value for each parameter and its corresponding sensitivity and specificity.

Results: Uterine endometrial carcinoma demonstrated significantly higher mean values of ADC, skewness, kurtosis, 50th, 90th percentiles than endometrial polyps (P < 0.05). ROC curve analysis of the 90th percentile yielded the best area under the ROC curve (AUC; 0.92), sensitivity of 90%, and specificity of 95%, with a cutoff value of 198.

Conclusion: Histogram analysis of ADC maps might be helpful for discriminating uterine endometrial carcinoma from endometrial polyps

10:30 - 12:00

Studio 2018

Imaging Informatics

SS 605

Radiomics and deep learning

Moderators:

A. Alberich-Bayarri; Valencia/ES
W.H. Sommer; Munich/DE

B-0476 10:30

Radiomics of metastatic clear-cell renal carcinoma: reproducibility and correlation for feature reduction

A. Bouchouicha, J. Deidier, K. Benac, D. Balvay, S. Oudard, R. Pirracchio, L.S. Fournier, B. Rance; Paris/FR (afef.bouchouicha@aphp.fr)

Purpose: To evaluate the robustness and redundancy of radiomics features extracted from CT images.

Methods and Materials: 28 metastatic clear-cell renal carcinoma patients were enrolled, before therapy initiation. Tumour was manually delineated by three expert physicians. Three categories of features were extracted: shape descriptors, intensity histogram statistics and textural features. Impact of filters and grey-level scales on features was studied. Concordance correlation coefficients (CCC) and inter-class correlation coefficients (ICC) were calculated to assess the reproducibility. Spearman correlations were performed to assess feature redundancy.

Results: 1564 radiomics features were extracted from each image. Different filters had little effect and grey levels no significant effect on extracted radiomics feature values. 231/1564 features showed high reproducibility for ICC (ICC \geq 0.8), and 198/1564 for CCC (CCC \geq 0.9). Features with an ICC \geq 0.8 and CCC \geq 0.9 were considered the most robust. This step reduced the number of relevant features to 158. Among these, highly correlated features with correlation \geq 0.9 were removed. This procedure yielded 23 features both robust and independent.

Conclusion: This study allows understanding feature stability and redundancy, and impact of pre-processing filters and grey-scales levels. These steps are mandatory to subsequently use radiomics features for prediction of therapy response and outcome in oncology.

B-0477 10:38

Application of radiomics and artificial intelligence in survival prediction of lung cancer patients

I. Shiri, P. Geramifard, H. Abdollahi, S. Shayesteh, G. Hajianfar, H. Pouraliakbar, A. Mohammadzadeh, A. Bitarafan-Rajabi; Tehran/IR (Isaac.sh92@gmail.com)

Purpose: Before initiation of therapy, accurate prediction of tumor's response to treatment enhance clinical care management. The aim of current study was to develop a predictive model based on lung cancer survival using artificial neural network (ANN) algorithm on image biomarkers.

Methods and Materials: Lung lesions from archived DICOM images (TCIA) of four hundred and sixty cancer patients were segmented using automatic region growing algorithm. Image preprocessing steps were performed by wavelet decompositions. Following image preprocessing and decompositions, eight images based on the wavelet, 632 quantitative 3D textures based on the GLRLM, GLCM and GLSZM, and 15 Shape features and 19 first order features were extracted from the 3D-tumor volumes segmentation. Supervised back-propagation ANN classifier was used to predict survival and dead status in lung cancer patients using radiomics features. Sixty-six percent of data was recruited as test and remained was used as training set.

Results: ANN was found as an effective method in prediction of survival in lung cancer patients. Our results showed this model with 73.4%, sensitivity, 79.1% specificity and 78.7% area under the curve (AUC) has a strong predictive power.

Conclusion: We discovered a novel prognostic model based on radiomics and artificial intelligent which can effectively predict survival in lung cancer patients. This study demonstrates that radiomics and artificial intelligent can provide valuable clinical information for advance personalized treatment in patients with lung cancer.

B-0478 10:46

Multimodality radiomics signature analysis improves prediction power against Stand-Alone analysis of PET, CT and MRI images

I. Shiri, P. Geramifard, H. Abdollahi, A. Bitarafan-Rajabi, A. Mohammadzadeh, H. Pouraliakbar; Tehran/IR (Isaac.sh92@gmail.com)

Purpose: Radiomics is a high-throughput computing process convert medical tomographic images to high dimensional data sets. These data is subsequently mined and can effectively contribute for improving decision support system.

Although radiomics signature was performed on different image modality systems, in this study, we assessed the possible improvement of prediction power of multi-modality analysis against stand-alone imaging systems.

Methods and Materials: Forty two soft tissue sarcoma (STS) patient from the Cancer imaging archive with MRI, CT, PET scans and information about lung metastases were subjected to current study. Image were preprocessed by different methods including image resampling, Laplacian of Gaussian (LOG) filtration with different sigma value, and wavelet. Following preprocessing and segmentation of GTV, 3D radiomics features based on shape, SUV (for PET) and intensity histogram, texture features including NGTDM, GLSZM, GLRLM, TFC were extracted. After feature selection and reduction, different supervised machine learning methods were used to predict lung metastases from stand alone and multimodality systems.

Results: Improvement in radiomics signature was observed in multimodality imaging system. The results of the prediction model using stand-alone analysis of CT, MRI and PET shows area under the curve (AUC) values of 0.731, 0.89, and 0.95 respectively. The corresponding value is 0.978 in multi-modality imaging systems analysis.

Conclusion: The results of this study indicate that multimodality radiomics signature analysis improves prediction power against stand-alone analysis of PET, CT and MRI images which lead to better predicting model of lung cancer in patients with STS.

B-0479 10:54

A new radiomics approach to predict the evolution of PI-RADS score 3/5 prostate areas in multiparametric MR

N.C. D'Amico, E. Grossi, G. Valbusa, A. Malasevski, G. Cardone, S. Papa; Milan/IT (damiconatascha@gmail.com)

Purpose: To characterize, through a radiomic approach, the nature of areas classified PI-RADS 3/5, recognized in multiparametric prostate magnetic resonance with T2-weighted (T2w), diffusion and perfusion sequences with paramagnetic contrast.

Methods and Materials: 24 cases undergoing multiparametric prostate MR and biopsy were admitted to this pilot study. The clinical outcome of the PI-RADS 3/5 was found through biopsy, which found eight malignant tumours. The analysed images were acquired with a Philips achieve 1.5T machine with a CE-T2-weighted sequence in the axial plane. Semi-automatic tumour segmentation was carried out on MR images using 3DSlicer image analysis software. 45 shape-based, intensity-based and texture-based features were extracted and represented the input for pre-processing. An evolutionary algorithm (a TWIST system based on KNN algorithm) was used to subdivide the dataset into training and testing set and select features yielding the maximal amount of information. After this pre-processing 20 input variables were selected and different machine learning systems were used to develop a predictive model based on a training testing crossover procedure.

Results: The best machine learning system (three-layer feed-forward neural network) obtained a global accuracy of 90% (80 % sensitivity and 100% specificity) with an ROC of 0.82.

Conclusion: Machine Learning systems coupled with radiomics show a promising potential in distinguishing benign from malignant tumours in PI-RADS 3/5 areas.

B-0480 11:02

Quantitative CT-based radiomics as predictor of local resectability of pancreatic ductal adenocarcinoma

J. Van der Putten¹, S. Zinger¹, P.H.N. De With¹, M.M. Prokop², J.J. Hermans²; ¹Eindhoven/NL, ²Nijmegen/NL (jjhermans@gmail.com)

Purpose: To compare the performance of an expert radiologist to that of quantitative radiomics for prediction of local resectability of pancreatic ductal adenocarcinoma on routine abdominal CT.

Methods and Materials: We included 66 patients (m:f=32:34; range 35-82 yrs) with histologically proven pancreatic ductal adenocarcinoma who were operated within 4 weeks of an initial routine portal-venous phase multidetector-row CT examination. An expert abdominal radiologists scored CT data for tumor resectability. Another expert abdominal radiologist drew tumor contours to obtain a volume of interest, from which we computed 90 intensity, shape and texture features. During training the feature vector was reduced with a feature selection algorithm and combined with several classifiers to predict local resectability using radiomics.

Results: There were 43 hypo- and 23 iso-attenuating tumors, of which 29 were resectable and 37 non-resectable. The best classification result was obtained with a logistic regression classifier with the feature vector reduced by regularized discriminative feature selection. Accuracy for predicting resectability was 67% for the radiologist, and 83% for radiomics. Sensitivity, specificity, positive and negative predictive value for resectability were 90%, 49%, 58% and 86%, respectively, for the radiologist and 79%, 86%, 84%, and 82%, respectively, for radiomics.

Conclusion: Quantitative CT-based radiomics for prediction of resectability of pancreatic adenocarcinoma on routine CT may outperform expert radiologists with respect to accuracy and positive predictive value but at a lower sensitivity.

B-0481 11:10

Radiomics: prediction of acoustic neuroma response to the CyberKnife treatment

N.C. D'Amico, I. Castiglioni, E. Grossi, G. Valbusa, G. D'Anna, F. Rigioli, I. Bossi Zanetti, G. Scotti, S. Papa; *Milan/IT (nataschaclaudia.d'Amico@cdi.it)*

Purpose: The objective of the study is to analyse MR images acquired before CyberKnife treatment, to predict the response and avoid unnecessary radiosurgery for patient.

Methods and Materials: T1-weighted MR images of 38 patients presenting an acoustic neuroma treated with CyberKnife® at the CDI (52.6% responders with volume reduction) were selected and analysed. Analysed images were acquired on 1.5T machines with contrast-enhanced T1-weighted sequences in the axial plane. Semi-automatic tumour segmentation was carried out on MR images using the 3DSlicer image analysis software. Shape-based, intensity-based and texture-based features were extracted. An evolutionary algorithm (a TWIST system based on KNN algorithm) was used to subdivide the dataset into training and test set and select features yielding the maximal amount of information. After this pre-processing, a predictive model based on a training-testing crossover procedure was developed. The best neural network obtained was a 3-layer feed forward back propagation algorithm with 8 input variables containing the maximal amount of information.

Results: The neural network was used twice inverting the training/testing set. In the first analysis, the sensitivity was 100%, while the specificity, was 77.78%. These two results gave a global accuracy of 88.89%. In the second analysis the sensitivity was 61.54% and the specificity 100%, with a global accuracy of 80.77%. The mean value of the global accuracy was 84.83%.

Conclusion: The obtained results show that machine learning coupled with radiomics has a great potential in distinguishing responders with volume reduction from responders without volume reduction to radiosurgery, before the treatment.

B-0482 11:18

Automated translation of radiologic reports with deep learning-powered translation engines: a feasibility study

T. Weikert¹, R. Wyttenbach², G. Nicolas¹, R. Hendel³, C. Glessgen¹, J. Bremerich¹, E.M. Merkle¹; ¹Basle/CH, ²Bellinzona/CH, ³Würzburg/DE (thomasjohannes.weikert@usb.ch)

Purpose: The quick, accurate and inexpensive translation of medical reports is a task of increasing importance in a globalised world with many patients crossing language borders during their treatment. Recently, deep learning-powered translation engines showed impressive results translating prose texts. The purpose of our study was to assess the utility of such engines in a radiological context.

Methods and Materials: 20 German radiology reports of oncologic follow-up examinations generated between March and September 2017 were randomly selected. The impression section was translated into English, French and Italian by two deep learning-powered translation engines (DeepL and Google Translate). The translations were then evaluated by three bilingual radiologists in the respective language (RH: English; NG: French; RW: Italian). Three error categories were labeled (stylistic error, content error without significance, potentially dangerous error).

Results: Overall, 79% of all words were translated correctly. However, only nine out of 120 translations were free of potentially dangerous errors and altogether 806 mistranslations were identified. Overall, the two translation engines showed a comparable performance. Of note, the quality of the translations into English was noticeably superior with 89% of all words correctly translated and 43% less potentially dangerous errors.

Conclusion: Deep learning-powered translation engines in their current version are not suitable for automated translation of complex oncologic radiology reports. However, considering the fact that the performance of neuronal networks depends heavily on the data they were trained on, training on medical texts holds an enormous potential for better results in the near future.

B-0483 11:26

Automated detection and localisation of skull fractures from CT scans using deep learning

R. Ghosh¹, S. Chilamkurthy¹, P. Rao¹, M. Biviji²; ¹Mumbai/IN, ²Nagpur/IN (rohit.ghosh@qure.ai)

Purpose: To develop and validate deep learning-based algorithm pipeline for fast detection and localisation of skull fractures from non-contrast CT scans. All kinds of skull fractures: undisplaced, depressed, comminuted, etc. were included as part of study.

Methods and Materials: Anonymized and annotated dataset of 350 scans (11750 slices) with skull fractures were used for generating candidate proposals for fractures. Stacked network pipeline was used for candidate generation - a fully convolutional network for ROI generation and another deep convolutional network for ROI classification. Final ROI classification model (ResNet18) yielded fracture probabilities for candidates generated through the fully convolutional (UNet) network. Separate deep learning model was trained to detect haemorrhages on scan level which was used as proxy for clinical information. Fracture candidate features like size, probabilities, depth for top 5 most probable fracture candidates along with haemorrhage model confidence (P_{haemorrhage}) were combined to train random forest classifier to detect fracture on scan level. In case of predicted fracture, most probable candidate(s) were used for localization.

Results: Separate set of 2971 scans, uniformly sampled from database with no exclusion criterion, was used for testing scan-level decisions with 108 scans reported as skull fracture cases. To evaluate scan-level decisions for fractures, area under receiver operating curve (AUC-ROC) was calculated as 0.83 with P_{haemorrhage} as feature and 0.72 without. Free receiver operating curve yielded 0.9 sensitivity at 2.85 false-positives-per-scan. Predictions on each patient takes <30s.

Conclusion: Deep learning-based pipeline can accurately detect and localize skull fractures. Pipeline can be used for triaging patients for presence of skull fractures.

Author Disclosures:

R. Ghosh: Employee; Qure.ai. S. Chilamkurthy: Employee; Qure.ai. P. Rao: Employee; Qure.ai.

B-0484 11:34

Fast estimation of kidney volumes and time courses in DCE-MRI using convolutional neural networks

A.S. Lundervold¹, K. Sprawka², A. Lundervold¹; ¹Bergen/NO, ²Łódź/PL (allu@hvl.no)

Purpose: We create a novel method for fast and accurate estimation of kidney volumes and signal intensity time courses in DCE-MRI, aiming at extracting both structural and functional quantitative information from the moving kidney.

Methods and Materials: Two repeated SPGR-DCE-MRI datasets were acquired from 20 healthy volunteers, resulting in 40 examinations, each consisting of 74 volumes recorded over ~6 min. We trained a 3D convolutional neural network (using a single standard NVIDIA GeForce 1080Ti GPU) for segmentation of left and right kidneys. The network has a dual-pathway architecture, incorporating both local and global information in the volumes. To create training data, we manually delineated 10 individual volumes from 10 different time-series, and extended the delineations to 740 volumes using image registration.

Results: Our implementation is able to segment all 74 volumes in a previously unseen, unregistered recording in less than 7 minutes. Mean segmentation accuracy (Dice) was 0.843 (SD=0.010). Mean (SD) left and right kidney volumes [ml] (incl. renal hilum) in one of the subjects (FF03) examined seven days apart (MR1 and MR2) was: MR1 L: 301.6 (15.9), R: 389.8 (16.9); MR2 L: 307.4 (17.8) R: 395.3 (23.6).

Conclusion: A CNN is able to quickly and accurately segment the moving kidneys in DCE-MRI, providing estimates of kidney volumes and mean signal intensity time courses. We are currently working to achieve sub-segmentation of the kidney (cortex, medulla, pelvis) and segmentation of the aorta (for AIF), enabling automated and fast estimation of GFR directly from the DCE-MRI.

B-0485 11:42

Automatic detection of intracranial calcifications in non-contrast CT

G. Bortsova, G. van Tulder, F. Dubost, A. van der Lugt, D. Bos, M. De Bruijn; *Rotterdam/NL (gerdabortsova@gmail.com)*

Purpose: Intracranial carotid artery calcification (ICAC) is a major risk factor for stroke, and might contribute to dementia and cognitive decline. Further research into the relationship between ICAC and neurological diseases is much demanded, but hampered by the time-consuming manual annotation of ICAC lesions. Therefore, we introduce the first fully automatic ICAC lesion detection method.

Methods and Materials: Non-contrast-enhanced CT scans were performed in 1882 participants of the Rotterdam Study, a population-based cohort study (mean age 69.6(6.8), 51.7% female). Two trained observers annotated the scans by indicating regions of interest on the intracranial carotid artery track (from the horizontal petrous segment to the circle of Willis) where calcifications were visible. ICAC lesion segmentations were obtained from these annotations by thresholding at 130 HU. We developed a deep learning based algorithm to automatically delineate ICAC lesions in CT scans. The algorithm was trained on scans of 882 subjects and validated on 1,000 scans of other subjects.

Results: The intraclass correlation between ICAC volumes computed from manual and automatic ICAC segmentations was 97.7%. This is close to the interrater agreement of 99%. The Bland-Altman bias (95% CI) was 197(-384, 778). (Mean ICAC volume is 1151±1624.)

Conclusion: Our algorithm can be used to automate the time-consuming manual annotation of ICAC in large epidemiological studies, whilst maintaining a comparable level of accuracy. This can facilitate research into causes and consequences of ICAC, which might result in development of new treatments and establishment of ICAC volume as a stroke risk estimator in clinical practice.

B-0486 11:50

Automated liver metastases detection on CT using multi-class patch based convolutional neural networks

E. Klang¹, M. Frid², I. Diamant², A. Ben Cohen², M. Di Segni³, E. Konen¹, H. Greenspan², M.M. Amitai¹; ¹Ramat Gan/IL, ²Tel Aviv/IL, ³Rome/IT

Purpose: To evaluate a patch based deep learning approach for liver metastases detection that models the variability between liver metastases, normal liver parenchyma and normal liver boundary.

Methods and Materials: This research was supported by the ISRAEL SCIENCE FOUNDATION (grant No. 1918/16). In this study we evaluate a patch based Convolutional Neural Networks (CNN) approach for liver metastases detection on portal phase CT studies. Patches (~32x32 pixels/patch) are extracted from each liver and then fed into a multi-class CNN, which classifies the patches into three categories: (1) liver metastases, (2) normal liver parenchyma, (3) normal liver boundaries. The networks decisions between the three categories are then fused to reach a binary lesion versus non-lesion decision. Data augmentation was applied to enrich the number of patches (flipping, rotation). A senior radiologist segmented all liver and metastases boundaries. True positive rate (TPR) and false positive per case (FPC) were compared to a binary patch based CNN classifier (metastases vs. liver).

Results: The entire dataset included CT images of 132 livers with 498 2D segmented liver metastases. The CNN was trained using ~140,000 patches for each class. Evaluation was performed on the 132 livers with 2-fold cross validation. TPR and FPC were 85.9% and 1.9 for the multi-class CNN and 80.0% and 2.8 for the binary CNN.

Conclusion: The multi-class deep learning algorithm shows promising results in liver metastases detection task. Using prior knowledge of medical data, such as differences between interior and boundaries, may enhance CNN results.

10:30 - 12:00

Room L 8

Head and Neck

SS 608

Head and neck ultrasonography

Moderators:

N. Chidambaranathan; Chennai/IN
K. Markiet; Gdansk/PL

K-10 10:30

Keynote lecture

G. Madani; London/UK

B-0487 10:39

In vivo evaluation of optic nerve and periorbital structures' biomechanical properties using shear-wave elastography in patients with glaucoma

M. Guazzaroni, S. Marsico, V. Girardi, T. Campagnuolo, S. Altobelli, R. Floris; Rome/IT (salvatore.marsico@hotmail.it)

Purpose: Glaucoma is an eye disease characterised by a slow and progressive damage of the optic nerve, retinal ganglion cell and visual field. The purpose of this study was to investigate shear-wave elastography use in the evaluation of the optic nerve and periorbital structures (orbital fat, lateral rectus and complex retinal-choroid).

Methods and Materials: An observational retrospective study, including 20 patients with glaucoma and 20 volunteers of the control group, was carried out. All of the participants had comprehensive ophthalmological exams (tonometry, OCT). In vivo evaluations of the biomechanical properties of the optic nerve and periorbital structures were performed with shear-wave elastography using a linear multifrequency probe (10-2 Mhz) in all participants. Differences of parameter stiffness of patients with and without glaucoma were evaluated using Student's t test.

Results: The mean stiffness of the optic nerve and periorbital structures (fat tissue, complex retinal-choroid) was significantly higher in glaucoma patients for each measured region (P<0.05). Statistical significance of these results increased by the evaluation of the "Strain Ratio", which is the relationship between the optic nerve and periorbital structure. Indeed, the "Strain Ratio", optic nerve/fat tissue, was significantly higher in patients with glaucoma.

Conclusion: Shear-wave elastography allows to identify stiffness variations of the optic nerve and periorbital structures in glaucomatous eyes.

B-0488 10:47

Ultrasound elastography of solid thyroid nodules: how far could we get?

N.F. El Ameen, M.F. Amin; El Minia/EG (nadia.elameen@yahoo.com)

Purpose: To evaluate the diagnostic accuracy of elastography in differentiation between benign and malignant solid thyroid nodules.

Methods and Materials: A prospective study, included 100 patients having 120 solid thyroid nodules. All patients were referred from surgery department between June 2016 and June 2017. All patient cohorts undergo routine ultrasonography and then elastography (USE). All radiological results were correlated with surgery and histopathology results.

Results: Using routine ultrasonography only showed sensitivity and specificity of 91% and 94%, respectively. Adding elastography to routine ultrasonography examination increases the sensitivity and specificity to 95% and 97.3%, respectively. Elastography confirmed that scores 4 and 5 were diagnostic for malignant nodules in examination of 40/48 nodules and scores 1 and 2 were diagnostic for benign nodules in the examination of 59/72 nodules.

Conclusion: Elastography is a promising technique if added to routine ultrasonography examination. It will improve the diagnostic accuracy of ultrasonography in differentiation between malignant and benign solid thyroid nodules. It will reduce the need for unnecessary biopsy and surgery.

B-0489 10:55

Complementary diagnostic role of shear wave elastography (SWE) in assessment of thyroid nodules during ultrasound examination

M. Schiavone; Monza/IT

Purpose: To evaluate the feasibility of the application of shear wave elastography (SWE) in the routine management of thyroid nodules, as a possible additional tool to the standard ultrasonography (US) triage.

Methods and Materials: A total of consecutive 214 patients, scheduled for US-guided thyroid fine-needle aspiration (FNA), were included in the study group. The presence of a pure colloid lesion was an exclusion criteria. The patients underwent conventional US examination and software 2D-SWE measurements. Absolute SWE stiffness measurements on color-coded elastograms, expressed in kPa and m/s, were correlated with radiological and pathological features and their discriminatory performances have been assessed and statistically analysed.

Results: The SWE values in thyroid nodules were significantly higher than normal thyroid tissue (p=0.0001), proving the different elastic properties of the pathological tissues. The SWE elasticity was not influenced by the characteristics of the bioptic smears, being unrelated to content and haematic composition of FNA. Regarding the radiological characteristics of the nodules, SWE highest values were associated with largest lesions (p=0.0105) but independent from ecographic and Doppler findings. The final correlation between the SWE results and the pathological diagnoses showed a trend in stiffness from tender tumours (follicular adenoma) to papillary thyroid carcinoma (p=0.0160).

Conclusion: SWE represents a quick, feasible, reproducible and helpful complementary diagnostic tool in routinely clinical practice in identifying the presence of thyroid nodules within normal parenchyma.

Author Disclosures:

M. Schiavone; Author; Davide Ippolito, Cammillo Tale-Franzese, Davide Leni, Fabio Pagni.

B-0490 11:03

Comparison of shear-wave elastography (SWE) and real-time elastography in the same thyroid nodules: which is more accurate?

Y. Fu; Beijing/CN (13699216067@163.com)

Purpose: Virtual touch tissue imaging (VTI), conventional US elasticity imaging (EI), virtual touch tissue imaging quantification (VTIQ), acoustic radiation force impulse (ARFI) are four elastographic forms available in one ultrasound machine. The purpose of this research is to establish the diagnostic accuracy of VTI, VTIQ, ARFI, EI in differentiating benign from malignant thyroid nodules.

Methods and Materials: All solid nodules identified on grey-scale imaging were subjected to elastography in 2016. Diagnostic performance was compared with histological findings as the gold standard. Receiver operating characteristics curves were applied to look for any significant differences. Univariate and multivariate analyses with potential variables were examined to identify independent variables for malignancy prediction.

Results: There were 85 patients (mean age, 42 years) with 90 pathologically proven thyroid nodules included in our research. There were 32 benign nodules and 58 malignant nodules. Forty nodules could not be assessed using ARFI for the lesion velocity was x.xx m/s. So, ARFI was not included for statistics. Four potential factors were found with significant effects on malignancy prediction and they were echogenicity, echogenic foci, VTI, VTIQ. After multivariate analysis, VTI was the only independent variable for

malignancy prediction ($P=0.001$). Area under the ROC curve for VTi was higher than that with other significant independent variables, and VTi of at least grade III was the best cutoff values for malignant thyroid nodules.

Conclusion: VTi is a useful tool for the differential diagnosis of thyroid nodules with higher diagnostic performance than shear-wave elastography and traditional EI.

Author Disclosures:

Y. Fu: Author; ligang cui.

B-0491 11:11

Comparison between the US vs MRI features of papillary thyroid carcinoma

S. Hu; *Zhenjiang/CN (hsd2001054@163.com)*

Purpose: This study aimed to evaluate the magnetic resonance imaging (MRI) and ultrasound (US) features of papillary thyroid carcinoma (PTC) and to compare the US and MRI features of PTCs.

Methods and Materials: Between January 2015 and April 2016, 86 consecutive patients underwent surgery for pathologically confirmed PTCs. All patients underwent neck US and MRI examination before thyroid surgery. For each case, the US and MRI features emphasized included the echogenicity/signal, margin, shape, anteroposterior to transverse diameter ratio (A/T), microcalcifications and lymph node metastasis. Statistical analysis was performed using the χ^2 test.

Results: In the comparison of US and MRI features, $A/T \geq 1$ (41.9% in US and 62.8% in MRI) and lymph node metastasis (88.0% in MRI; 56.0% in US) demonstrated a statistically significant difference ($P=0.009$, $P=0.025$) and there was no significant difference in the margin and shape ($P=0.724$, $P=0.316$).

Conclusion: The study results demonstrated that the MRI features of PTCs including A/T and lymph node metastasis were inferior to US.

B-0492 11:19

Role of ultrasound in management of indeterminate thyroid nodules (Bethesda III and IV)

E. Horvath, C. De la Barra, G. Aguilera, C. Silva, J. Slater, V. Skoknic, S. Majlis, M. Garcia, P. Gonzalez; *Santiago/CL (camidlb@gmail.com)*

Purpose: To evaluate the role of US in predicting benignity or malignancy of lesions Bethesda III and IV, to support medical decisions (follow-up, re-puncture or surgery).

Methods and Materials: IRB approved retrospective descriptive study. Thyroid fine needle aspirations (FNA) with clot technique, performed between 2010 and 2015 were reviewed. Nodules classified as Bethesda III (atypia of undetermined significance = AUS; follicular lesion of undetermined significance = FLUS) and IV (follicular neoplasm = FN and suspicion of follicular neoplasia = SFN) were selected. Only patients who underwent thyroidectomy were included for this analysis. Nodules were considered low risk on US when presenting as TIRADS score 2, 3, 4A and intermediate-high risk with TIRADS 4, 4B, 5. US risk was compared with the presence of malignancy in the surgical specimen.

Results: In total 3.738 FNAs were performed in the period studied; 269 (7.2%) were Bethesda III and 46 (1.2%) Bethesda IV. Ninety patients (65 FLUS, 11 AUS and 14 FN/SFN) underwent surgery. In TIRADS 4, 4B and 5 nodules malignancy was 12.2% (6/49) in FLUS, 100% (10/10) in AUS and 50% (6/12) in FN/SFN. Meanwhile, in TIRADS 2, 3 and 4A nodules, no malignancy was identified (0/19).

Conclusion: The high presence of AUS malignancy is highlighted. No malignancy was detected for Bethesda III-IV nodules presenting with low risk US TIRADS patterns. This information could assist the clinician in making therapeutic decisions.

B-0493 11:27

Prospective assessment of TIRADS US assessment and strain and Shear wave elastography to discriminate benign from malignant thyroid lesions

V. De Soccio, G. Alagna, V. Forte, M. Di Segni, V. Cantisani, E. Tassone, C. Catalano, F. D'Ambrosio; *Rome/IT*

Purpose: To determine the diagnostic performance of strain ratio elastography (SR) and shear wave elastography (SWE) associated with TIRADS based US classification, in order to differentiate benign from malignant thyroid nodules.

Methods and Materials: 210 consecutive, histopathologically proven nodules in 200 patients (55 males, 145 females; mean age: 42.2 years; range: 18-83 years) and were evaluated through B-mode US with Color-Doppler assessment, SR and SWE. Each lesion was classified according to the TIRADS lexicon - as proposed by Kwak et al. and evaluated for US features (size, B-mode and Color-Doppler features), SR semi-quantitative and SWE quantitative data. Imaging and histopathological findings were compared. Diagnostic performances of B-mode ultrasound, SR, SWE, and their combination were estimated using ROC analysis and 2x2 contingency tables.

Results: Histological examination identified 136 benign and 74 malignant thyroid lesions. US according to TIRADS, SR and SWE showed a sensitivity (Se) of 59.6%, 82.7% and 51.9% and a specificity (Spe) of 83.8%, 92.7%, 85.3%, respectively. SR with B-mode US increased the diagnostic performance (Se: 90.4%, Spe: 93%, AUC: 0.9 $p < 0.004$); SWE with B-mode US did not improve overall accuracy (Se: 58.3%, Spe: 84.2%), though representing a valid tool in selected cases

Conclusion: SWE and SR are useful additional US techniques. SE was, in general, more accurate than SWE - which proved useful only in selected cases. The combination of SR with B-mode US increased the diagnostic accuracy between benign and malignant nodules.

Author Disclosures:

V. Cantisani: Speaker; Toshiba, Samsung, Bracco.

B-0494 11:35

Ultrasonographic diagnosis of salivary gland atrophy after radio-iodine treatment for papillary thyroid cancer

E. Horvath, V.S. Skoknic, C. Silva, H. Tala, N. Sánchez, C. Whittle, J.P. Niedmann, S. Majlis, C. Schweinitz; *Santiago/CL (velimirskoknic@gmail.com)*

Purpose: To describe ultrasonographic (US) findings of mayor salivary glands (MSG) atrophy in patients who received radio-iodine (RAI) treatment for papillary thyroid cancer (PTC). Determine MSG damage prevalence and associated risk factors.

Methods and Materials: IRB approved, prospective non-concurrent cohort study. Patients that had CPT surgery with subsequent RAI between 2005-2015, were included. All had a preoperative US and at least one follow-up US 12months after RAI administration. Patients with prior MSG altered findings were excluded. Uni and multivariate analysis with logistic regression was performed using US gland damage as dependent variable and RAI dose, gender and age as independent variables. Statistical significance was defined as $p < 0.05$.

Results: In total 328 patients [average age: 42.47(IQR 34-53), female: 263 (80.2%)] met inclusion criteria, receiving a median dose of 105mCi (IQR 100-150). Follow-up period: 12-107months. In 103 patients (31.4%) US detected salivary gland atrophy (size reduction, wavy contours, hypoechogenicity and heterogeneous structure) in at least one MSG. Univariate analysis indicated that total RAI dose received was significantly associated with atrophy ($p < 0.01$). No actinic injury was present in patients treated with a total dose lower than 100mCi. Multivariate logistic regression revealed total radiation dose OR of 2.35 (IC95% 1.80 to 3.06) and women OR of 2.17 (IC 95% 1.07 to 4.42) for MSG atrophy.

Conclusion: Actinic sialoadenitis is common, affecting approximately one-third of patients. Cumulative dose is the main factor related to this damage. For the first time, US was used to prospectively and systematically evaluate the MSG of patients with RAI treatment.

B-0495 11:43

Sonographic evaluation of abdominal wall fat index, intima-media thickness and plaque score in obstructive sleep apnoea syndrome

N. Cetin, I. Gunes Tatar, O. Ergun, M. Yuceege; *Ankara/TR (mdnurcan@hotmail.com)*

Purpose: Visceral obesity is prevalent in obstructive sleep apnoea syndrome (OSAS) and it is an independent risk factor for cardiovascular diseases. The aim of this study was to investigate whether patients with OSAS have an increase in abdominal wall fat index (AFI), a new indicator of visceral fat deposition, intima-media thickness (IMT) and plaque score (PS), two indicators of cardiovascular risk.

Methods and Materials: 104 patients (73 females, 31 males) between ages 23-73 years without known atherosclerotic or metabolic disease were evaluated by ultrasonography to calculate AFWI, to measure IMTs and to determine plaque scores, who underwent polysomnography with suspect of OSAS. Maximum thickness of preperitoneal fat (P_{max}) and minimum thickness of subcutaneous fat (S_{min}) were measured to calculate AFI ($AFI = P_{max}/S_{min}$), IMTs were measured and carotid arteries were evaluated for the presence of atherosclerotic plaques to determine PS. Patients were grouped as no OSAS (< 5), mild OSAS (5-15), moderate OSAS (15-30) and severe OSAS (> 30) according to AHI.

Results: While AHI correlated with AFI ($p=0.019$), it was not with IMT_{mean} ($p=0.158$) and PS ($p=0.345$). There was no significant difference between four OSAS groups in terms of AFI ($P=0.179$).

Conclusion: This study suggests that AFI may reflect and be used in the follow-up of OSAS. AFI was correlated with AHI but not with OSAS groups. It was thought to be due to low numbers of patients in each group. AHI was also not correlated with IMT_{mean} and PS. This could be due to majority of newly diagnosed patients.

B-0496 11:51

Transverse and sigmoid sinus stenosis and pressure gradient in patients with pulsatile tinnitus

T. Su, L. Jin, Y. Han; *Beijing/CN*

Purpose: To investigate angiographic features in patients with pulsatile tinnitus (PT) and assess intravenous pressure gradient in venous sinus stenosis associated with PT.

Methods and Materials: This study retrospectively analyzed cerebral angiography in a group of patients with diagnosed PT. Besides conventional arterial images, all angiography included indirect 2D and 3D venography focusing on related venous sinus. A subgroup of venous stenosis in transverse and sigmoid sinus detected by venography was noted. Subsequent direct venography and intravenous pressure gradient in venous sinus stenosis was acquired.

Results: Our study included consecutive 37 PT patients with angiography. Except for four cases with dural arteriovenous fistula, all had normal arterial appearances. There were only two cases showing complete normal arterial and venous patterns. Among other 31 PT patients, there were nine with sigmoid sinus diverticulum (SSD) and ipsilateral upstream sinus stenosis (SS) and ipsilateral dominant venous sinus (DVS), nine with transverse and sigmoid SS and ipsilateral DVS, three with SSD and ipsilateral upstream SS, four with transverse and sigmoid SS, three with SSD, three with DVS, respectively. Besides 15 cases with SSD (48.4%) known as one of the causes for PT, 25 cases with transverse and sigmoid SS (80.6%) were found, and average intravenous pressure gradient in venous sinus stenosis was 906 Pa (130-2170 Pa). In addition, DVS in PT diseased side (67.7%) may have some relation with PT.

Conclusion: High rates of transverse and sigmoid Sinus abnormalities were observed in PT. Related sinus stenosis with pressure gradient may have connection with PT.

10:30 - 12:00

Room E1

Breast

SS 602

Breast MR/PET and PET/CT

Moderators:

I.-A. Gheonea; Craiova/RO
C.K. Kuhl; Aachen/DE

B-0497 10:30

Histogram analysis of apparent diffusion coefficients for monitoring early response in patients with breast cancer undergoing concurrent chemotherapy

W. Wang, J. Cheng, Y. Zhang; *Zhengzhou/CN (weijianwang520@163.com)*

Purpose: To explore the role of histogram analysis of apparent diffusion coefficient (ADC) related parameters in early assessment of treatment response during the concurrent chemotherapy(CCT) course of breast cancer.

Methods and Materials: We retrospectively evaluated findings in 42 patients with breast cancer who underwent diffusion-weighted imaging ($b = 0,800 \text{ s/mm}^2$) at 3T with acquisition of corresponding ADC maps before CCT, at the end of 2nd and 4th week during chemotherapy. Whole lesion ADC histogram analysis generated several histogram related parameters including skewness, kurtosis, mean, variance and percent. The ADC histograms of 42 patients were generated to visually observe dynamic changes of the histogram parameters following CCT.

Results: All parameters except mean and variance showed significant changes during CCT (all $P < 0.05$). Skewness and kurtosis both showed high early decline rate (25%, 32 %) at the end of 2nd week of CCT. The percent of ADC histogram also changed obviously following CCT.

Conclusion: ADC histogram analysis held the potential in monitoring early tumor response in patients with breast cancer undergoing CCT.

B-0498 10:38

Imaging of the hypoxic microenvironment in breast cancer using PET/MR

J.C. Carmona-Bozo, T. Torheim, R. Woitek, A.J. Patterson, O. Abeyakoon, C. Carraco, E. Provenzano, M.J. Graves, F.J. Gilbert; *Cambridge/UK (jcc83@cam.ac.uk)*

Purpose: To investigate relationships between hypoxia (^{18}F -FMISO-PET), tumour perfusion (DCE-MRI) and pathology in breast cancer.

Methods and Materials: Imaging was performed using a GE Signa PET/MR scanner on 13 patients with pathologically confirmed breast cancer. A 60-min simultaneous PET/MR scan was performed following injection of 300 MBq ^{18}F -FMISO and a 2-hour uptake period. Hypoxic status was assessed using the influx rate constant K_i determined through Patlak-plot analysis. Tumour hypoxic

fractions were estimated as the percentage of voxels with K_i values $>2\text{SD}$ of the mean in normoxic muscle. Perfusion was derived from DCE-MRI data using the extended Tofts model (K^{trans}). Pathological correlates included tumour type, grade, size, percentage of tumour-infiltrating lymphocytes, necrosis, nodal and receptor status.

Results: A total of 26 lesions were assessed (ER+: $n=25$; ER-: $n=1$). Linear mixed effects analysis indicated that tumour grade and necrosis were significant predictors of K_i ($p=0.014$ and 0.027 , respectively). Hypoxia was identified in 46% of the lesions, with hypoxic fractions ranging between 0-36%. Higher median hypoxic fractions were observed in lobular (6.7%) vs ductal (3.0%), HER2- (8.4%) vs HER2+ (3.6%), and positive (6.0%) vs negative (2.6%) nodal status, although these differences were not significant. A negative significant correlation was observed between tumour-infiltrating lymphocytes and hypoxic fraction ($\rho=-0.45$; $p=0.023$). An inverse, heterogeneous relationship was observed between K_i and K^{trans} ($\rho=-0.1$; $p>0.05$).

Conclusion: Necrosis, tumour grade and lymphocyte infiltration were strong predictors of hypoxic status. Hypoxia had a negative, heterogeneous relationship with perfusion and may also be influenced by tumour type, HER2 and nodal status.

B-0499 10:46

What is the diagnostic performance of 18-FDG-PET/MR and PET/CT in the initial staging of breast cancer?

D. Botsikas, I. Bagetakos, M. Picarra, S. Boudabbous, X. Montet, G.T. Lam, I. Mainta, A.M. Kalovidouri, M. Becker; *Geneva/CH (diomidis.botsikas@hcuge.ch)*

Purpose: To compare the diagnostic performance of 18-FDG-PET/MR and PET/CT for the initial staging of breast cancer.

Methods and Materials: Two independent readers blinded to clinical/follow-up data retrospectively reviewed PET/MR and PET/CT examinations performed for initial breast cancer staging in 80 consecutive patients (mean age $=55.3 \pm 7.7$ years). The diagnostic confidence for lesions in the contralateral breast, axillary and internal mammary regions, bones and other distant sites were recorded. Sensitivity, specificity, positive predictive (PPV) and negative predictive values (NPV) were calculated and results were compared with the gold standard (pathology and/or follow-up >24 months).

Results: 9/80 patients had bone metastases, 13/80 had other distant metastases, 46/80 had axillary, 9/80 had internal mammary metastases and 3/80 had contralateral breast tumours. Inter-reader agreement for lesions was excellent (weighted kappa=0.833 for PET/CT and 0.823 for PET/MR) with similar results regarding reader confidence between the two tests (ICC=0.875). In the patient-per-patient analysis, sensitivity and specificity of PET/MRI and PET/CT were similar ($p>0.05$). In the lesion-per-lesion analysis, the sensitivity of PET/MR and PET/CT for bone metastases, other metastases, axillary and internal mammary lymph nodes, and contralateral tumours was 0.924 and 0.6923 ($p=0.034$), 0.923 and 0.923 ($p=1$), 0.854 and 0.812 ($p=0.157$), 0.9 and 0.9 ($p=1$), 1 and 0.25 ($p=0.083$), respectively. The corresponding specificity was 0.953 and 1 ($p=0.081$), 1 and 1 ($p=1$), 0.893 and 0.92 ($p=0.257$), 1 and 1 ($p=1$) and 0.987 and 0.97 ($p=1$), respectively.

Conclusion: Diagnostic confidence with both examinations was similar. Although PET/MR had a superior sensitivity for bone metastases than PET/CT in the lesion-by-lesion assessment, the diagnostic performance in the patient-per-patient analysis was similar.

B-0500 10:54

A proposal diagnostic algorithm for F-18FDG PET/CT-detected breast incidental lesion based on BI-RADS and SUVmax criteria

M. Bakhshayeshkaram, S. Zahirifard, F. Aghahosseini, R. Hashemi Beni; *Tehran/IR (ktaghahosseini@gmail.com)*

Purpose: To propose a diagnostic algorithm for PET-detected breast incidental lesion by applying BI-RADS and SUVmax criteria.

Methods and Materials: A total of 58 breast incidental lesions from 51 patients contemporaneously investigated by BI-RADS within 1 month from PET study constituted the study cohort and verified by histopathologic results or a 2-year clinical follow up (malignant=10, benign=48). The performance characteristics were then calculated for $\text{SUVmax} \geq 2$, $\text{SUVmax} \geq 3.7$ and BI-RADS ≥ 4 , separately and conjunctively.

Results: Diagnostic performance of $\text{SUVmax} \geq 2$, $\text{SUVmax} \geq 3.7$ and BI-RADS ≥ 4 were calculated to be 70%, 60% and 80% for sensitivity, 73.2%, 82.9% and 92.7% for specificity and 72.54%, 88.23% and 90.19% for accuracy, respectively. Combined criteria using either $\text{SUVmax} \geq 2$ or $\text{SUVmax} \geq 3.7$ had 100% sensitivity, 73.2% and 87.8% specificity and 78.43% and 90.19% accuracy, respectively. The distribution of combined criteria in benign and malignant groups were found to be as the following: Benign group: double positive: 2 (4.87%), 1 (2.44%), PET-only positive: 9 (21.95%), 1 (2.44%), BI-RADS-only positive: 1 (2.44%), 2 (4.87%), double negative: 28 (68.29%), 37 (90.24%), respectively, Malignant group: double positive: 7 (70%), 4 (40%), PET-only positive: 2 (20%), 2 (20%), BI-RADS-only positive: 1 (10%), 4 (40%), double negative: 0, respectively.

Conclusion:

Malignancy can be confidently excluded in double negative lesions. Lesion with BI-RADS<4 and SUVmax≥3.7 and those with BI-RADS ≥4 and SUVmax <2 should prompt into histopathologic confirmation. BI-RADS negative lesions with 2<SUVmax<3.7 may benefit from a short term imaging follow up.

B-0501 11:02

Breast MRI and dedicated breast PET (dbPET): friends and foes

M. Herranz¹, S. Argibay-Vazquez¹, I. Dominguez-Prado¹, P. Ling Ling², L. Graña³, M. Vázquez Caruncho³, A. Ruibal¹; ¹Santiago de Compostela/ES, ²Shanghai/CN, ³Lugo/ES (michel.herranz.carnero@sergas.es)

Purpose: Breast MRI shows high sensitivity with non-ionizing radiation; however, significant disadvantages including its moderate specificity are also reported. Recently, dedicated breast PET (dbPET) system has emerged as an additional imaging tool for breast cancer diagnosis and follow-up. To compare FDG-dbPET with MRI on breast lesion characterization, we analysed sensitivity, specificity, positive predictive value (PPV) and negative predictive value (NPV).

Methods and Materials: Two hundred women with known or suspected breast carcinoma were enrolled in this study. Both a dbPET scan and breast MRI scans were performed. Sensitivity and specificity of MRI and dbPET scans were calculated on the basis of pathology reports.

Results: A total of 252 lesions were assessed. Lesion size range was 0.18 to 7.6 cm. In lesion-by-lesion analysis, specificity and sensitivity of MRI alone were 93% and 81%, respectively; meanwhile, the lesion-based sensitivity of dbPET was 96% and the breast-based specificity was 98%. The positive predictive value and the negative predictive value for MRI alone were 80% and 89%, respectively; however, for dbPET were 98% and 96%, respectively. In a significant number of cases, dbPET helped to disprove positive findings by resonance, and in 4% helped to define new positives that had gone unnoticed at resonance.

Conclusion: Dedicated breast PET scans increase the specificity of MRI. False positives are reduced. The results of the current study showed that FDG-dbPET is much more effective than MRI in detecting early breast cancer positives.

B-0502 11:10

Value of quantitative magnetic resonance imaging T1-relaxation time in predicting contrast-enhancement in breast cancer

X. Zhang, M. Li, L. Mao, C. Wang, S. He, M. Liu; Guangzhou/CN (764673239@qq.com)

Purpose: To evaluate the feasibility of T1 mapping in assessing the tissue properties equivalent to contrast-enhancement without the need for contrast agent.

Methods and Materials: Patients with newly-diagnosed breast cancer were selected for this study. The subtraction of T1 maps pre and post-contrast enhancement $\Delta T1$ maps: $\Delta T1$ maps: was used to determine areas of contrast-enhancement. With the contrast-enhancement on $\Delta T1$ maps as reference, ROC analysis served to detect an optimal T1 cut-off on T1 maps prior contrast agent injection to distinguish between contrast-enhancing tissue and its surroundings.

Results: 15 patients were included. A T1 value >2081ms predicted contrast-enhancing tumor tissue with a sensitivity of 83% and specificity of 71% $\Delta T1$: AUC, 0.89; $p < 0.0001$ gt: Interestingly, T1 prolongation >2081 ms that did not overlap with contrast-enhancing area transformed into contrast-enhancement later on.

Conclusion: T1- relaxation time may be a useful technique to assess tissue properties in breast disease equivalent to contrast-enhancement without the need for contrast agent. It may also provide information on sites with future tumour progression.

B-0503 11:18

MRI of invasive mass breast cancer: correlation of global vascularity and ADC with pathological features

A. Milani, R.M. Trimboli, L.A. Carbonaro, M. Codari, G. Di Leo, F. Sardaneli; Milan/IT (angelomilani9296@gmail.com)

Purpose: To investigate the association between breast global vascularity (GV), apparent diffusion coefficient (ADC) and pathological prognostic factors in invasive mass lesions.

Methods and Materials: Thirty invasive mass breast cancers were included: 27 (89%) ductal, 2 (8%) lobular and 1 (3%) mucinous. Vessels with ≥ 2 mm diameter and ≥ 30 mm length were identified on maximum intensity projections from contrast-enhanced subtracted MRI, then lengths of all selected vessels were summed and considered as GV, for each of the two breasts. ADC was obtained for each lesion placing a region of interest encompassing the mass. Grade, Ki67, human epidermal growth factor receptor 2 (HER2), estrogen and progesterone receptors, pT and pN were obtained from pathology reports. Spearman, Mann-Whitney U, Kruskal-Wallis and Jonckheere-Terpstra statistics were used.

Results: Women were aged 57.9 ± 10.6 (mean \pm standard deviation); median lesion size was 19.8 mm (interquartile range [IQR] 13-27 mm). A significant difference in GV was observed between cancerous and healthy breasts ($p < 0.001$). A trend for correlation of GV and ADC was observed ($r = 0.337$, $p = 0.08$). A higher GV was associated with HER2 positive tumors ($p = 0.027$) and lower ADC values were associated with a higher proliferation of Ki67 ($p = 0.017$).

Conclusion: In invasive mass breast cancers, GV is associated with HER2 overexpression, showing an interplay between receptor status and vascularization. The association of ADC with Ki67 proliferation subtends an increased cellularity of aggressive cancers. Multiparametric MRI, including GV, has a potential for defining the hallmarks of breast cancers.

B-0504 11:26

Utility of diffusion in evaluating chest wall invasion of breast tumours

N. Samreen, C. Lee, K. Adler, A. Bhatt, T. Hieken, S. Zingula, K.N. Glazebrook; Rochester, MN/US (samreen.naziya@mayo.edu)

Purpose: To investigate the sensitivity and specificity of diffusion-weighted imaging (DWI) in determining chest wall invasion of breast malignancies.

Methods and Materials: A retrospective search was performed on keywords including "chest wall invasion" in breast MRI reports at our institution over the last 12 years. The presence of chest wall invasion based on T2-weighted, DWI, and post-contrast acquisitions was evaluated through consensus readings by two board-certified breast imagers. Correlations with histopathology and neoadjuvant chemotherapy were made.

Results: Search results yielded 58 patients; 30 had no DWI and were excluded. The remaining 28 patients each showed loss of fat plane on T2-weighted and post-contrast acquisitions. 23/28 (82%) additionally showed enhancement within the chest wall, and 20/28 (71%) qualitatively showed restricted diffusion within the chest wall. The mean ADC values (automatically calculated by CAD software) in the chest wall (-0.4 ± 1.2 mm²/s, [-1.8, 1.5]) were similar to those in the breast tumour (-0.2 ± 1.3 mm²/s, [-1.5, 1.4]). Review of clinical notes showed 5/28 patients with unavailable follow-up, so 23 patients were used in subsequent data analysis. Sensitivity, specificity, and negative predictive value (NPV) were 100%, 33%, and 100% for DWI and 100%, 27%, and 100% for post-contrast MRI, respectively, in the assessment of chest wall invasion.

Conclusion: DWI when used in conjunction with post-contrast MRI suggests a high NPV for assessing chest wall invasion of breast cancers which can increase confidence for surgical planning.

B-0505 11:34

MR evaluation of fibroglandular tissue (FGT) and background parenchymal enhancement (BPE) in breast cancer and its association with receptor status

S.B. Grover¹, P. Jain¹, S.K. Jain¹, A.K. Mandal¹, H. Grover²; ¹New Delhi/IN, ²Bridgeport, CT/US (shabnamgrover@yahoo.com)

Purpose: Breast cancer encompasses a spectrum of several molecular subtypes with distinct epidemiological and pathophysiological profiles, leading to significant variations in treatment response. Fibroglandular tissue (FGT) proportion and background parenchymal enhancement (BPE) on breast MR have been proposed as predictors of tumour molecular subtypes, thereby affecting treatment protocol. The aim of our study was to evaluate the biomarker role of FGT and BPE in breast cancer, by correlating with oestrogen receptor (ER), progesterone receptor (PR) and HER2 receptor status.

Methods and Materials: 36 patients with newly diagnosed, biopsy-proven breast cancer underwent breast MR on 1.5T, in this IRB-approved study. FGT proportion and BPE were recorded and classified based on previously described criteria. Pathological analysis for receptor status was done. Association between the considered variables was evaluated using Pearson's chi-square, continuity correction chi-square, and Fisher's exact test. A $p < 0.05$ was considered statistically significant.

Results: Patients with increased FGT proportion were found to have ER- and PR-positive tumours ($p < 0.01$ for both). Higher extent of BPE was associated with ER positivity ($p = 0.002$); however, no significant association was found with PR status ($p = 0.310$). Both FGT and BPE showed no relation with HER2 status ($p = 0.536$ and $p = 0.226$, respectively).

Conclusion: Higher FGT proportions in breast cancer show association with both ER and PR positivity, whereas BPE showed association only with ER. Our work further substantiates research on the biomarker role of MR-assessed FGT and BPE in breast cancer, in predicting molecular subtypes and their individual treatment regimes.

B-0506 11:42

Implementation of imaging biomarkers of healthy breast tissue with multiparametric [18F]FDG-PET/MRI may aid breast cancer diagnosis

D. Leithner^{1,2}, G.J. Wengert², M. Weber², T.H. Helbich², P. Kapetas², P.A.T. Baltzer², E.A. Morris¹, G. Karanikas², K. Pinker^{1,2}; ¹New York, NY/US, ²Vienna/AT (doris.leithner@googlemail.com)

Purpose: To assess imaging biomarkers of breast tumors and contralateral healthy breast parenchyma with 3T multiparametric (mp) PET/MRI and to investigate which can be used for breast cancer diagnosis.

Methods and Materials: In this IRB-approved prospective study 125 women, who underwent fused 3T mpPET/MRI with dynamic contrast-enhanced MRI (DCE-MRI), diffusion-weighted imaging (DWI) and [18F]FDG-PET for a BI-RADS 0,4/5 lesion and histopathological verification were included. BI-RADS descriptors with DCE, ADC with DWI, and SUVmax with [18F]FDG-PET of the lesion were recorded. SUVmax, ADCmean, BPE (background parenchymal enhancement), and FGT (amount of fibroglandular tissue) for the contralateral healthy breast were noted. A stepwise logistic regression with forward selection to identify the combination of biomarkers for the differentiation of benign and malignant tumors and to assess diagnostic parameters was performed.

Results: There were 98 malignant lesions (81 IDC, 8 ILC, 5 DCIS, 4 other; 90 masses) and 27 benign lesions (16 masses). The biomarkers that were different between benign and malignant lesions and included in the equation were BI-RADS descriptor DCE margins ($P<0.001$), and tumor ADCmean ($P=0.008$). Other biomarkers of tumor and normal breast tissue did not reach significance. Based on the combination of these two imaging biomarkers, diagnostic accuracy was 96.2%, sensitivity was 98.9%, and specificity was 81.3% for separation of benign and malignant lesions.

Conclusion: The combination of qualitative and quantitative MRI imaging biomarkers (DCE margins, ADCmean tumor) show promise to improve differentiation of benign and malignant breast lesions. In this study, other mpPET/MRI imaging biomarkers did not add diagnostic accuracy.

B-0507 11:50

Are there differences in multiparametric breast [18F]FDG-PET/MR imaging biomarkers of contralateral healthy tissue in patients with and without breast cancer?

D. Leithner^{1,2}, T.H. Helbich², B. Bernard-Davila¹, G.J. Wengert², P. Kapetas², P.A.T. Baltzer², A. Haug², E.A. Morris¹, K. Pinker^{1,2}; ¹New York, NY/US, ²Vienna/AT (doris.leithner@googlemail.com)

Purpose: To evaluate whether there are differences in multiparametric (mp) [18F]FDG-PET/MR imaging biomarkers of contralateral healthy breast tissue in patients with benign and malignant breast tumors.

Methods and Materials: In this IRB-approved prospective study, 141 women underwent 3T mpPET/MRI with contrast-enhanced MRI, diffusion-weighted imaging (DWI), and [18F]FDG-PET for the assessment of abnormality (BI-RADS 0,4/5). The following imaging biomarkers were recorded for the contralateral tumour-free breast: background parenchymal uptake (BPU) with [18F]FDG-PET; apparent diffusion coefficients (ADCmean) with DWI; BPE (background parenchymal enhancement); and amount of fibroglandular tissue (FGT). Appropriate statistical tests were used to assess differences in imaging biomarkers between benign and malignant lesions.

Results: There were 100 malignant and 41 benign lesions. BPE was minimal in 61, mild in 56, moderate in 19, and marked in 5 patients. BPE differed significantly ($P<0.001$) between patients with benign and malignant lesions, with patients with cancer demonstrating decreased BPE in the contralateral breast. A borderline statistically significant difference was observed for FGT ($P=0.055$). BPU for patients with mild BPE was 1.5, for mild BPE 1.9, for moderate BPE 2.2, and for marked BPE 1.9. BPU differed significantly between patients with benign (mean, 1.9) and malignant lesions (mean, 1.8) ($P<0.001$), whereas ADCmean did not differ between groups ($P=0.19$).

Conclusion: Differences in mpPET/MR imaging biomarkers, obtained from contralateral healthy breast tissue, exist between patients with benign, and patients with malignant breast tumours. Contralateral BPE, BPU, and FGT are decreased in patients with cancer, and may potentially serve as imaging biomarkers for the presence of cancer.

10:30 - 12:00

Room E2

Neuro

SS 611

Stroke: diagnosis and intervention

Moderators:

P. Mordasini; Berne/CH
T. Struffert; Erlangen/DE

B-0508 10:30

Mechanical thrombectomy of M1 and M2 segment occlusions: a single-center experience with 546 patients

F. Seker, J. Pfaff, U. Neuberger, S. Nagel, P.A. Ringleb, M. Bendszus, M.A. Möhlenbruch; Heidelberg/DE

Purpose: Considering recent randomized controlled trials on mechanical thrombectomy (MT) in ischemic stroke, the American Heart Association guidelines state that MT in M2 occlusions may be reasonable, but with uncertain benefit. We, therefore, compared safety, angiographic and clinical results of M1 and M2 segment occlusions after MT in a retrospective study.

Methods and Materials: Between 2009 and 2016, patients with an acute occlusion of the M1 or M2 segment of the middle cerebral artery were retrospectively analyzed. Good outcome was defined as modified Rankin Scale score of 0-2 at 90 days. Successful recanalization was defined as a Thrombolysis in cerebral infarction score of 2b-3.

Results: In total, 546 consecutive patients with M1 (n=457) or M2 (n=89) occlusion were included. Compared to M1 occlusions, M2 occlusion presented with a significant lower baseline NIHSS score (15 vs. 17, $p=0.010$) and higher ASPECTS [9 (IQR 8-10) vs. 9 (IQR 7-9), $p=0.004$]. Endovascular treatment of M2 occlusions had a non-significant lower rate of symptomatic intracranial hemorrhages (2.2% vs. 8.1%, $p=0.068$). Furthermore, M2 occlusions showed a trend to higher recanalization rates (82.0% vs. 72.6%, $p=0.065$) and a significantly higher rate of good clinical outcome (49.4% vs. 34.8%, $p=0.026$).

Conclusion: This retrospective analysis adds evidence that MT in M2 occlusions is safe and achieves slightly better recanalization rates and significantly better clinical outcome compared to M1 occlusions with a lower rate of symptomatic intracranial hemorrhages after MT.

B-0509 10:38

Impaired cerebrovascular reactivity is at high risk of stroke in patients with intracranial stenosis

J. Papassin, A. Krainik, O. Heck, E. Condamine, J. Pietras, F. Tahon, O. Detante; Grenoble/FR (akrainik@chu-grenoble.fr)

Purpose: Impaired cerebrovascular reserve is suggested to explain haemodynamic stroke in symptomatic patients with intracranial atherosclerotic stenosis (IAS) in spite of intensive medical management. We studied relationships between baseline characteristics of patients with unilateral symptomatic IAS, recurrence of ischaemic events, basal perfusion, and cerebrovascular reactivity assessed by BOLD fMRI (CVR BOLD fMRI).

Methods and Materials: Twenty patients with symptomatic unilateral IAS of middle cerebral artery (MCA) or internal carotid artery were selected (61.0±11.5yo). We measured basal perfusion using DSC, and CVR elicited by hypercapnic challenge (8%CO₂) using BOLD contrast (3T AchievaTX, Philips, voxel=4x4x4mm, TR/TE/α=3000/35ms/90°, 240 dynamics in 12min during a block-design hypercapnia). Individual end-tidal CO₂ pressure was used as physiological regressor to conduct linear regression analysis. Post-processing was performed using AMIGOV0.9, an in-house software (Python3.6, Matlab8.6, SPM12), giving whole-brain and regional basal CBF, CBV, MTT and CVR. We calculated statistical relationships between individual clinical and biological baseline characteristics, recurrent ischaemic events, basal perfusion, and CVR BOLD fMRI in MCA territories (CVR_{MCA}) reported by laterality indices (LI).

Results: Nine patients (45%) had an abnormal LI CVR_{MCA} (|LI| CVR_{MCA}≥0.08). During follow-up (m=3.0years), recurrent ischaemic events occurred within the first year. They were more frequent in impaired CVR_{MCA} group (n=7/9) than in normal CVR_{MCA} group (n=1/11), with different survival curves (log rank, $p=0.001$). Baseline characteristics were similar in both groups.

Conclusion: Impaired CVR assessed by BOLD hypercapnic fMRI is associated with increased risk of stroke in patients with symptomatic IAS. CVR mapping should be proposed to select high-risk patients to discuss additional treatment.

B-0510 10:46

Dual-energy computed tomography for optimised visualisation of early cerebral infarctions after endovascular stroke therapy

A.E. Grams, T. Djurdjevic, T. Schiestl, M. Knoflach, F. Dazinger, E.R. Gizewski, B. Glodny; *Innsbruck/AT (astrid.grams@i-med.ac.at)*

Purpose: The aim of this study was to investigate if dual-energy computed tomography (DECT) series, optimised for edema visualisation, allows an advantageous identification of early infarctions after endovascular stroke therapy (EST). Therefore, a modified virtual non-contrast (VNC) series, named "edema map" (EM), was generated.

Methods and Materials: Forty-six patients (21 women and 25 men) with a mean age of 63 years (24-89 years) were included. Brain window (BW), VNC and EM series were evaluated. Density differences between infarctions and contralateral areas (CID), final infarct volume predictability, infarction identifiability and image noise were assessed with region of interest measurements. Follow-up imaging served as standard for comparison. For the statistical evaluation, Kruskal-Wallis, Dunn's multiple comparison tests and receiver operating curve analyses were performed.

Results: Highest CIDs were found in the EM (73.3±/49.3), compared to the BW (-1.72±/13.29) and the VNC (8.30±/4.74) series ($p < 0.0001$). The EM revealed highest infarction identification rates (area under the curve: 0.97, vs. 0.54 and 0.90, $p < 0.0001$) with a cut-off value of < 50.7 HU, despite slightly more pronounced image noise. A prediction of the future infarction size succeeded best with the EM series (area under the curve: 0.67, vs. 0.50 and 0.59, cut-off 16.74 HU).

Conclusion: With the EM series a higher contrast and better early infarct identifiability can be achieved than with VNC or BW series. This technique could feature the opportunity to modify early therapy decisions.

B-0511 10:54

Mechanical thrombectomy in basilar artery occlusion: the presence of bilateral posterior communicating arteries is a predictor of favorable clinical outcome.

V. Maus¹, A. Kalkan¹, C. Kabbasch¹, N. Abdullayev¹, U.B. Barnikol¹, T. Liebig², C. Dohmen¹, G.R. Fink¹, A. Mpotsaris³; ¹Cologne/DE, ²Berlin/DE, ³Aachen/DE (volker-maus@gmx.de)

Purpose: Mechanical thrombectomy (MT) in basilar artery occlusion (BAO) is a subject of debate. We investigated clinical outcome of MT in BAO and predictors of a favorable outcome.

Methods and Materials: 104 MTs in BAO (carried out between 2010 and 2016) were analyzed. Favorable outcome (modified Rankin Scale (mRS) ≤ 2) at 90 days was the primary endpoint; influence of following variables on outcome was investigated: number of detectable posterior communicating arteries (PcoAs), patency of basilar tip, completeness of BAO, and posterior circulation Alberta Stroke Program Early CT Score (PC-ASPECTS). Secondary endpoints were technical periprocedural parameters including symptomatic intracranial hemorrhage (sICH).

Results: Favorable clinical outcome at 90 days was 25% and mortality was 43%. Rate of successful reperfusion (modified Thrombolysis In Cerebral Infarction (mTICI) $\geq 2b$) was 82%. Presence of bilateral PcoAs (AUC: 0.81, $p < 0.0001$), low National Institute of Health Stroke Scale (NIHSS) on admission (AUC: 0.74, $p < 0.01$), PC-ASPECTS ≥ 9 (AUC: 0.72, $p < 0.01$), incomplete BAO (AUC: 0.66, $p < 0.001$), and basilar tip patency (AUC: 0.66, $p < 0.01$) were associated with favorable outcome. Stepwise logistic regression analysis revealed that the strongest predictors of favorable outcome at 90 days were bilateral PcoAs, low NIHSS on admission, and incomplete BAO (AUC: 0.923, $p < 0.0001$).

Conclusion: MT in BAO is safe with high rates of successful reperfusion. Aside from baseline NIHSS and incomplete vessel occlusion, both known predictors of favorable outcome in anterior circulation events, we found collateral flow based on the presence or absence of PcoAs had a decisive prognostic impact.

B-0512 11:02

Intracranial carotid artery calcification and endovascular treatment effect in acute stroke patients due to large vessel occlusion

K. Compagne¹, P. Clephas¹, C.B. Majoie², W. Van Zwam³, A. van Es¹, D.W. Dippel¹, A. Van der Lugt¹, D. Bos¹; ¹Rotterdam/NL, ²Amsterdam/NL, ³Maastricht/NL (c.compagne@erasmusmc.nl)

Purpose: Intracranial carotid artery calcification (ICAC) may interfere with the safety and efficacy of endovascular treatment (EVT). We assessed the influence of ICAC volume and pattern on the effect of EVT in patients with acute ischemic stroke.

Methods and Materials: All 500 patients included in the MRCLEAN trial on the effectiveness of EVT were analyzed. The volume (mm³) and pattern (located in tunica intima or tunica media) of ICAC were determined on baseline CT. Functional outcome at 90 days was assessed with the modified Ranking Scale.

Next, we investigated the association of ICAC volume and pattern with functional outcome using adjusted ordinal logistic regression models with an interaction term between treatment allocation and ICAC.

Results: We found no association of ICAC volume with functional outcome (acOR per unit increase ICAC volume 0.94 (95%CI 0.84-1.06). Moreover, we found no evidence for effect modification by ICAC volume ($p=0.56$). Predominantly medial ICAC pattern was nearly significant associated with poorer functional outcome (acOR 1.63; 95%CI 0.99-2.66). Yet, we found evidence for treatment effect modification by ICAC pattern ($p=0.02$): a better functional outcome after EVT in patients with predominantly medial calcification (acOR 2.55; 95%CI 1.38-4.72) and no effect of EVT in patients with predominantly intimal calcifications (acOR 0.76; 95%CI 0.39-1.50).

Conclusion: Predominantly medial calcification pattern of ICAC relates to poorer functional outcome in ischemic stroke patients, but the benefit of EVT in ischemic stroke patients with a medial calcification pattern is larger compared to the treatment effect in patients with a intimal calcification pattern.

Author Disclosures:

C.B. Majoie: Research/Grant Support; Stryker. **W. Van Zwam:** Research/Grant Support; Stryker, Codman. **D.W. Dippel:** Research/Grant Support; Stryker, Bracco Imaging. **A. Van der Lugt:** Research/Grant Support; Stryker.

B-0513 11:10

Ipsilateral thalamic diaschisis in acute ischaemic stroke: occurrence, perfusion characteristics, and association with morphologic and clinical outcome

P. Reidler, K. Thierfelder, M.P. Fabritius, F. Schuler, W.H. Sommer, W.G. Kunz; *Munich/DE (Paul.Reidler@med.uni-muenchen.de)*

Purpose: Ipsilateral thalamic diaschisis (ITD) describes the reduction of thalamic function, metabolism and perfusion resulting from a distant lesion to the ipsilateral hemisphere. Our aim was to evaluate its perfusion characteristics and clinical impact in acute ischemic stroke.

Methods and Materials: Subjects were selected from a cohort of 1,644 patients who underwent multiparametric CT including CT-perfusion (CTP) for suspected stroke. Inclusion criteria were: acute middle cerebral artery (MCA) territory ischemia, follow-up-confirmed infarction and absence of posterior circulation ischemia. Perfusion-deficit regions were delineated according to the Alberta Stroke Program Early CT Score (ASPECTS) regions. ITD was defined as reduced perfusion of the ipsilesional thalamus present on ≥ 2 CTP maps. Morphologic outcome and subacute complications were assessed on follow-up. Functional outcome was quantified using the modified Rankin Scale (mRS). Statistical analysis contained univariate linear and binary logistic regression.

Results: We included 154 patients. ITD was present in 32 subjects (20.8%, ITD+). Perfusion deficit regions in ITD+ subjects revealed a more frequent involvement of caudate, internal capsule and lentiform nucleus (each with $p < 0.001$). We observed larger perfusion-deficit volumes and smaller perfusion-mismatch ($p < 0.001$) in the ITD+ group. There was no significant independent association of ITD with final infarction volume ($\beta = -0.110$, $p = 0.135$) or functional outcome (mRS ≤ 2) after 90 days ($OR = 1.109$, $p = 0.987$). No differences in baseline characteristics or subacute complications were present ($p > 0.05$).

Conclusion: ITD is frequently observed in acute MCA stroke associated with a marked involvement of subcortical areas. This finding should neither be misdiagnosed as posterior circulation ischemia nor considered unfavorable in clinical management.

B-0514 11:18

Improved assessment and evaluation of arterial occlusion in acute ischaemic stroke with contrast-enhanced MR angiography

S. Dhundass, A. Collin, L. Duron, S. Escalard, M. Obadia, R. Blanc, J.-C. Sadik, J. Savatovsky, A. Lecler; *Paris/FR (sdhundass@gmail.com)*

Purpose: To compare in acute ischaemic stroke (AIS) patients, the accuracy of two techniques of MR angiography: contrast-enhanced magnetic resonance angiography (CEMRA) and Time Of Flight MRA (TOF MRA) for the detection of the clot and their value in predicting clot location and length.

Methods and Materials: 131 consecutive adult patients admitted to our center for confirmed acute ischaemic stroke from august 2014 to july 2016 were assessed. Clot visibility, location and length on CEMRA were compared to those on TOF MRA and SWI. It was compared to Digital subtraction angiography (DSA) for the subgroup that underwent thrombectomy. Clot burden score (CBS) was evaluated on TOF MRA and CEMRA in case of anterior arterial occlusion.

Results: 52 patients showed an occlusion on CEMRA and 63 on TOF MRA. CEMRA showed higher correlation to SWI regarding detection of the clot ($k = 0.68$ (0.55-0.81)) its length ($ICC = 0.72$ (0.61-0.79)) and location ($k = 0.69$ (0.57-0.79)), than TOF MRA ($k = 0.48$ (0.33-0.61); $ICC = 0.18$ (-0.03-0.38); $k = 0.5$ (0.36-0.62)). CBS was significantly higher on CEMRA ($p = 7e-06$). In the thrombectomy sub group (N=28), occlusion was detected on both

techniques for all patients, CEMRA had a higher correlation with DSA ($\kappa = 0.73$ (0.47-0.91) vs $\kappa = 0.62$ (0.35-0.85)) for determining clot's location.

Conclusion: Our results showed that CEMRA enabled a more accurate detection of arterial occlusion in patients with AIS in comparison with TOF MRA, as well as the evaluation of clot characteristics such as its length and location, adding valuable information to stratify patient's risk and management.

B-0515 11:26

Combined measurements of clot density in unenhanced and enhanced CT of acute ischaemic stroke in complete vessel occlusions of the medial cerebral artery predict 90 day patient outcome

J. Kottlors¹, C. Kabbasch¹, V. Maus¹, A. Mpotsaris², J. Borggrefe¹;
¹Cologne/DE, ²Aachen/DE (Jan.Borggrefe@uk-koeln.de)

Purpose: Ex-vivo CT-studies of blood thrombi (BT) showed, that contrast-enhancement (CE) is determined by fibrin-content while unenhanced density is associated with the fraction of red blood cells. This study investigates if CE BT measurements in CT of acute ischemic stroke (AIS) can enhance prediction of patient outcome.

Methods and Materials: This study includes 137 AIS patients treated with mechanical thrombectomy between 2010-2016, including M1 middle cerebral artery occlusions only. Outcome was determined with modified Rankin-Scale (mRS90). Differentiation of complete and incomplete large vessel occlusion (CLVO/ILVO) based on CT and angiography. Two blinded readers classified BT based on native CT (NECT); a) hypo-, b) iso-, and c) hyperdense as well as in CT angiography (CECT); d) not-enhancing, e) intermediate and f) enhancing.

Results: Twenty-three ILVO patients (16.8%) differed significantly from CLVO patients in mRS at admission (median: 4 vs. 5) and after 90 days (median: 1 vs. 4) ($p < .05$). Excluding ILVO, classification according NECT did not show statistical differences between hypo-, iso- and hyperdense CLVOs. Classification of CLVOs according CECT shows significant distinctions between the intermediate (median: 3) and enhancing BT-group (median: 4), also between the enhancing- and the not-enhancing BT-group (median: 3) (both $p < .05$). This is consistent with a correlation of .291 between CE and mRS after 90 days ($p < .001$).

Conclusion: As described in literature, NECT BT density is associated with good patient outcome. Increased contrast enhancement of the BT in CECT, shows a further significant association with unfavorable outcome. ILVO is a significant bias of thrombus characterization.

B-0516 11:34

The influence of CT perfusion on the selection of stroke patients for endovascular therapy

J.M. Ospel, G. Karwacki, K. Blackham; Basle/CH
(johannamaria.ospel@usb.ch)

Purpose: Determine whether CT perfusion changes patient selection for interventional therapy in acute stroke patients compared to combined native CT and CT angiography data.

Methods and Materials: 100 consecutive acute stroke CT examinations (non-contrast CT, CTA, CTP) from patients who received intravenous lysis at our hospital were retrospectively evaluated in a blinded fashion. An experienced neurointerventionalist reviewed the cases first without and, after a month delay, with the CTP data (Syngo.via, Siemens Healthineers). Clinical information such as NIHSS, age and side of neurologic deficit was provided to the reader. A questionnaire was used, including ASPECTS score, location of vessel occlusion and whether or not endovascular intervention was indicated. Differences in detection rate of vessel occlusion and interventional decision were compared. Criteria for intervention on CTP included <100 ml core infarct volume and > 1.2 mismatch ratio.

Results: ASPECTS score was ≥ 7 in all cases. Detection rates of proximal vessel occlusion ($n=33$) and the decision to intervene differed between the two interpretive sessions in only one case; in this group the average NIHSS was 16. Within the remaining group (distal or no vessel occlusion), there was discordance in 12 patients; average NIHSS was 8.

Conclusion: In selected acute stroke patients (NIHSS ≥ 10 and ASPECTS ≥ 7) presenting within the 4.5 hour intravenous lysis window, CTP is unnecessary for the detection rate of proximal vessel occlusion or the decision to proceed with endovascular intervention. CTP may be helpful in patients with NIHSS < 10 where distal occlusions are more common.

B-0517 11:42

Classification of CT perfusion infarct core in acute ischaemic stroke using automated measurements of tissue density on non-contrast CT

P. Reidler, K. Thierfelder, M.P. Fabritius, W.H. Sommer, W.G. Kunz;
Munich/DE (Paul.Reidler@med.uni-muenchen.de)

Purpose: To determine the diagnostic value of automated quantification of tissue density on non-contrast CT (NCCT) to classify CT perfusion (CTP) infarct core in acute ischaemic stroke.

Methods and Materials: Out of 1,644 consecutive cases of suspected ischaemic stroke, we selected patients with follow-up-confirmed middle cerebral artery infarction, admission NCCT and CTP, and absence of prior stroke. NCCT density in Alberta Stroke Program Early CT Score (ASPECTS) regions were quantified as average Hounsfield Unit (HU) values using automated segmentation and calculation of HU ratios (rHU) between ischaemic and non-ischaemic hemispheres (ASPECTS-Tool.v1.2, Siemens, Germany). CTP-deficit was rated separately on cerebral blood flow (CBF) and volume (CBV) maps per region. Infarct core was defined as coexisting CBF- and CBV-deficit. Receiver operating characteristic curves (ROC) with Youden's index and associated rHU cut-off values with highest discriminative power were calculated per region.

Results: A total of 129 patients were included. ROC analysis demonstrated that density measurements enabled a significant discrimination of infarct core in the regions Capsula interna (C) (AUC=0.797, $p < 0.001$), Insula (I) (AUC=0.663, $p = 0.002$), Lentiform nucleus (L) (AUC=0.726, $p < 0.001$), and M1 cortex (AUC=0.615, $p = 0.025$). Youden's Index calculations indicating the power to discriminate infarct core resulted in cut-off values of rHU=0.963 for C (sensitivity/specificity=0.767/0.727), rHU=0.960 for I (sensitivity/specificity=0.506/0.886), rHU=0.957 for L (sensitivity/specificity=0.706/0.674), and rHU=0.949 for M1 cortex (sensitivity/specificity=0.343/0.903).

Conclusion: Automated NCCT density measurements can identify ASPECTS regions with CTP infarct core in C, I, L and M1 cortex. This technique has the potential to improve decision support in case CTP is not available.

B-0518 11:50

Haemorrhagic transformation and aspirin therapy after thrombectomy: an inter- and intra-rater agreement study

A. Guenego^{1,2}, A. Leclerc¹, K. Premat¹, C. Ducroux¹, M. Roques², R. Blanc¹, M. Pottin¹, R. Fahed¹; ¹Paris/FR, ²Toulouse/FR (adrienguenego@gmail.com)

Purpose: We aimed to systematically review the literature and assess the reliability of haemorrhagic transformation (HT) diagnosis and classification on brain computed tomography performed 22-36 hours after mechanical thrombectomy in acute ischaemic stroke (AIS) patients with anterior circulation large vessel occlusion.

Methods and Materials: Studies assessing the reliability of HT diagnosis and/or ECASS classification were reviewed. Eighteen raters independently assessed twice 30 brain CT scans realized 22 to 36 hours after mechanical thrombectomy in patients included in a multicentric randomized trial. Agreement was measured with Fleiss' and Cohen's unweighted kappa statistics.

Results: The review yielded 4 studies reporting 19 measures of agreement. Populations, methods, analyses, and results were heterogeneous (moderate to excellent agreement), precluding a meta-analysis. In our study, interrater agreement for HT diagnosis was moderate for all raters ($\kappa = 0.55$, 95%CI [0.41-0.68]) and each subspecialty. The interrater agreement for ECASS classification was fair for all raters ($\kappa = 0.37$ [0.27-0.50]), but improved to a moderate level after dichotomization. Dichotomization of the ECASS classification also improved the number of raters to reach a substantial (or higher) intrarater agreement (from 7/18 [38.9%] to 14/18 [77.8%]). The interrater agreement for aspirin therapy decision was moderate for all raters ($\kappa = 0.52$ [0.40-0.66]), and substantial among the vascular neurologists ($\kappa = 0.70$ [0.57-0.84]).

Conclusion: The diagnosis and classification of HT according to ECASS criteria on brain CT scans performed 22 hours to 36 hours after thrombectomy might not be reliable among untrained physicians. Despite the lack of reliability, the interrater agreement for aspirin therapy decision among vascular neurologists was substantial.

10:30 - 12:00

Room F2

GI Tract

SS 601b

Colorectal imaging: CTC and beyond

Moderators:

V. Cappendijk; ^s Hertogenbosch/NL
D. Ramos-Andrade; Coimbra/PT

K-11 10:30

Keynote lecture

T. Mang; Vienna/AT

B-0519 10:39

Impact of radiologist experience on detection of colorectal neoplasms at CT colonography screening

L. Pusceddu¹, V. Vani¹, G. Giannetto¹, L. Morra², L. Correale², S. Delsanto², C. Senore², D. Regge²; ¹Candiolo/IT, ²Turin/IT (laura.pusceddu@gmail.com)

Purpose: To assess the relationship between radiologist experience and adenoma detection rate at CT colonography (CTC) screening.

Methods and Materials: Post-hoc analysis of a large RCT was performed, including 2593 CTCs read by 7 radiologists. Radiologist experience was classified according to the total number of CTC performed before the trial (i.e. <200, 200-1,000, >1,000). Multilevel logistic regression was used to model the influence of reading volumes on the probability to detect adenomas. Analyses were performed separately for each of the following lesions: all adenomas (ADR), distal adenomas (DADR), proximal adenomas (PADR), advanced histology (i.e. ≥10-mm, villous histology or high grade dysplasia). A 6-mm cut-off was used for post-CTC referral to colonoscopy.

Results: 1337 (51.5%), 584 (22.5%), and 672 (26.0%) CTCs were read by radiologists with reading volumes <200, 200-1000, and >1000, respectively. The average ADR, DADR and PADR were 8.0% (95% CI: 7.0-9.1%; range, 5.8-8.7%), 5.0% (95% CI: 4.3-5.9%; range, 2.1-8.4%), and 5.1% (95% CI: 4.2-6.3; range, 4.4-5.4%), respectively. Radiologist experience appeared to be related with DADR (OR, >1000 vs ≤1000: 1.49; 95% CI: 1.04-2.13), but not with PADR (OR, >1000 vs ≤1000: 0.91; 95% CI: 0.64-1.29). The association of radiologist experience with distal location appeared to be statistically significant also for advanced adenomas (OR, >1000 vs ≤1000: 1.73; 95% CI: 1.08-2.88).

Conclusion: High reading volumes, greater than 1000 CTCs, may be required to achieve high adenoma detection rates in the distal colon. Reading volume may be considered as a new quality indicator for CTC screening.

B-0520 10:47

Patients' experience with, and factors for participation in flexible sigmoidoscopy and CT colonography screening insight from the Proteus Colon Trial

V. Vani, G. Giannetto, L. Pusceddu, L. Morra, L. Correale, S. Del Santo, C. Senore, D. Regge; Turin/IT (vanina.vani87@gmail.com)

Purpose: To compare the acceptability of CTC and FS screening and the factors predicting CTC screening participation, targeting participants in the Proteus Trial.

Methods and Materials: 1984 eligible individuals, were randomly assigned to be invited to FS or CTC screening. All attendees and a 50% sample of CTC non-attendees were contacted 3-6 months after invitation for a phone interview, investigating screening experience and factors affecting participation. Odds ratios (OR) were computed by multivariable logistic regression.

Results: 239/264 (90.6%) FS attendees, 237/298 (79.5%) CTC attendees and 182/299 (60.9%) CTC non-attendees answered the interview. Attendees who would recommend the test to friends or relatives were 99.1% among FS and 93.3% among CTC attendees. Discomfort associated with bowel preparation was higher among CTC than FS attendees (OR: 2.77; 95% CI: 1.47-5.24). CTC non-attendees were less likely to be men (OR: 0.36; 95% CI: 0.18-0.71), retired (OR: 0.31; 95% CI: 0.13-0.75), to report regular physical activity (OR: 0.37; 95% CI: 0.20-0.70), or having read the information leaflet (OR: 0.18; 95% CI: 0.08-0.41); they were more likely to mention screening-related anxiety (mild - OR: 6.30; 95% CI: 2.48-15.97; moderate/ severe - OR: 3.63; 95% CI: 1.87-7.04), erroneous beliefs about screening (OR: 32.15; 95% CI: 6.26-165.19), or a recent FOBT (OR: 13.69; 95% CI: 3.66-51.29).

Conclusion: CTC and FS screening are well accepted. Further reducing the discomfort from bowel preparation may increase CTC screening acceptability. Negative attitudes, erroneous beliefs about screening and organizational barriers are limiting screening uptake. All these factors are modifiable and therefore potentially susceptible to interventions.

B-0521 10:55

Patient experience of screening CT colonography with reduced and full bowel preparation in a randomised trial

L. Sali¹, L. Ventura¹, A. Borgheresi¹, S. Delsanto², P. Mantellini¹, M. Mascalchi¹, M. Zappa¹, G. Grazzini¹; ¹Florence/IT, ²Turin/IT (lapo.sali@unifi.it)

Purpose: To assess patient experience of bowel preparation and procedure for screening CT colonography with reduced (r-CTC) and full preparation (f-CTC) in a randomised trial (SAVE study).

Methods and Materials: 4825 eligible subjects were randomly invited to screening r-CTC or f-CTC. Participants to r-CTC (n=674) and to f-CTC (n=612) were asked to complete a pre- and post-procedure questionnaire. Items were analysed separately and pooled with chi-square and t test.

Results: Pre-procedure questionnaire was returned by 531 (79%) subjects in the r-CTC group and by 465 (76%) in the f-CTC group, and post-procedure questionnaire by 525 (78%) in the r-CTC group and by 453 (74%) in the f-CTC group. In pre-procedure questionnaire 88% of subjects in the r-CTC group reported no preparation related disorders compared to 70% of those in the f-CTC group (p<0.001). In post-procedure questionnaire average scores for discomfort of the procedure were not significantly different between r-CTC (3.53±0.04) and f-CTC (3.59±0.04) groups (p=0.84).

Conclusion: Reduced bowel preparation is reported to be more tolerable than full preparation for screening CT colonography. Procedure related discomfort is not influenced by bowel preparation.

Author Disclosures:

S. Delsanto: Employee; im3D.

B-0522 11:03

Neoplasia yield with FIT two years after CTC screening

G. Giannetto¹, L. Pusceddu¹, V. Vani¹, L. Morra², L. Correale², C. Senore², S. Del Santo², D. Regge²; ¹Candiolo/IT, ²Turin/IT (ggiannetto27@gmail.com)

Purpose: We have conducted a trial (Proteus trial) comparing neoplasia yield of CTC and sigmoidoscopy in a population based screening setting among subjects aged 58-60. Screenees detected with polyps ≥ 6 mm at CTC were referred for colonoscopy (TC). We aim to assess the role of FIT screening among subject without polyps or with polyps < 6 mm at CTC screening.

Methods and Materials: According to the FIT screening protocol eligible screenees enrolled in the Proteus trial, were invited to undergo FIT screening (single sample, with a positivity cut-off at 20 µg/gr. faeces) two years after the screening CTC. The outcomes of interest were: participation rate (proportion of invitees examined), positivity rate (PR), positive predictive value of TC referral and detection rate (DR) of advanced adenomas or CRC (AN).

Results: Participation was 70.4% (1541/2331); the PR was 4.1% and 89.7% (57/64) of those referred for TC actually had the test. The PPV for AN was 17.5% (10/57, including 1 CRC) and the AN DR was 6.1%.

Conclusion: Participation in FIT screening among subjects having performed a CTC was lower than among subjects who had previous FIT tests. FIT is still detecting AN among subjects with diminutive polyps or negative CTC, although PR and PPV are lower as compared to subjects with previous negative FIT result.

B-0523 11:11

Focal colorectal uptake in ¹⁸F-DG-PET/CT: maximum standard uptake value as a trigger in a semi-automated screening setting

W. Luboldt; Munich/DE (luboldt@screening.org)

Purpose: Focal colorectal uptake in ¹⁸F-DG-PET/CT may be associated with a malignancy and can be quantified. This provides the basis for an automatic trigger threshold above which cases are flagged for colonoscopic evaluation and below which for individual assessment. The purpose is to determine the lowest maximum standard uptake (SUV_{max}) in colorectal cancer that could be used as a threshold to trigger endoscopic evaluation and to evaluate whether the SUV_{max} needs to be further normalised to a priori known extrinsic factors.

Methods and Materials: The SUV_{max} was measured in 54 colorectal carcinomas and correlated with gender, age, blood glucose level, injected activity, body mass index and time to scan using t test or correlation coefficients (Pearson and Spearman, according to distribution).

Results: There was no correlation between SUV_{max} and any of the extrinsic factors mentioned above. The lowest SUV_{max} value was 5 [mean ± SD (range): 11.1 ± 4.8 (5.0-24.6)].

Conclusion: In contrast to most other screening techniques, semi-automation in colorectal screening seems possible with PET/CT. This opens the door for further study into the feasibility of automated screening. Independent from extrinsic factors, an SUV_{max} ≥5.0 in a focal colorectal uptake in ¹⁸F-DG-PET/CT should automatically trigger for endoscopic evaluation, if not contraindicated. Cases with SUV_{max} <5 should be assessed individually before referral for endoscopy. Thus, more interpretation time could be spent on those cases with a lower uptake and more ambiguous diagnosis.

B-0524 11:19

MRI T2WI and fat-suppressed-T2WI image fusion technology in improving image quality for the evaluation of anal fistulas

Z. Dong, S.-T. Feng, M. Huang, Y. Jia, H. Cai, Z.-P. Li, B. Shen; Guangzhou/CN (asrachel@126.com)

Purpose: We aimed to develop a novel magnetic resonance (MR) image fusion technology (combined T2-weighted imaging [T2WI] and fat-suppressed T2WI [T2WI-FS]) to improve image quality for better display of both anal fistulas and the anatomical structure of the anus.

Methods and Materials: A total of 32 patients with proven anal fistula were retrospectively studied. All of the patients underwent anal MR imaging, including axial fast spin echo (FSE) T2WI and FSE T2WI-FS. T2WI and T2WI-FS were used to form the fusion image (T2WI-fusion) based on the addition of the gray values obtained from each pixel via a MR post-processing workstation. The signal intensities of the fistula, the peri-fistula sphincter and perianal fat in T2WI, T2WI-FS and T2WI-fusion were measured with the algorithm Fisher score= $(\mu-\mu_m)/\sqrt{(\sigma^2-\sigma_m^2)}$, where μ and σ are the mean and standard deviation (SD), respectively, of the tissue signal intensity. The difference in Fisher scores between T2WI, T2WI-FS and T2WI-fusion were compared.

Results: The mean Fisher scores of the fistula vs sphincters from T2WI-fusion (FS_{Fusion-fistula}=6.56) were significantly higher than those from T2WI (FS_{T2WI-fistula}=3.35) (P=0.001). The mean Fisher scores of sphincter vs fat from T2WI-fusion (FS_{Fusion-sphincter}=10.84) were also significantly higher than those from T2WI-FS (FS_{fat suppression-sphincter}=2.57) (P=0.001).

Conclusion: The T2WI and T2WI-FS fusion technology integrates the advantages of both T2WI and T2WI-FS. The combination has the ability to improve image quality and facilitate accurate evaluation of anal fistulas and sphincters.

B-0525 11:27

Preoperative assessment of simple and complex anorectal fistulas: tridimensional endoanal ultrasound? Magnetic resonance or both?

F. Iacobellis, L. Roberto, L. De Pascale, R. Rella, R. Natella, A. Reginelli, R. Grassi; Naples/IT (iacobellist@gmail.com)

Purpose: The purpose of this study was to evaluate the diagnostic value of 3D-EAUS and MR in the preoperative assessment of both simple and complex anorectal fistulas.

Methods and Materials: From Jan-2015 to Jan-2017, 124 patients with perianal fistulas underwent anamnestic evaluation, clinical examination, unenhanced and H2O2 enhanced 3D-EAUS and MRI. The results of imaging evaluation were compared with surgical findings, considered as reference standard.

Results: Perfect agreement between 3D-EAUS and surgery in the anal fistulas severity grading was found (K= 1). The fistulas were classified as simple in 68/126 (53.9%) and complex in 58/126 (46.03%) cases. In both simple and complex anal fistulas, 3D-EAUS showed a not significantly higher accuracy in the evaluation of internal openings, if compared with MRI (p= 0.47; McNemar Chi-Square Test). In the complex anal fistulas, MRI showed a significantly higher accuracy in the evaluation of secondary extensions if compared with 3D-EAUS (p= 0.041; McNemar Chi-Square Test) whereas, in the simple anal fistulas, not significantly difference was found.

Conclusion: In the preoperative work-up of patients with anorectal fistulas, 3D-EAUS may represent the first-line diagnostic tool. In the cases of fistulas classified as complex by 3D-EAUS, the MR may be indicated as adjunctive diagnostic imaging examination, to more carefully describe the fistulas complete anatomy.

B-0526 11:35

Identification of internal opening in perianal fistula: comparison of 3D cube vs 2D at 3.0 Tesla

V. Nyapathi; Rajahmundry/IN (drvainaynpathy@gmail.com)

Purpose: The hypothesis was that 3D T2FSE cube in comparison to 2D T2FSE sequence would be more accurate in detection of internal opening with perianal fistula.

Methods and Materials: A total of 100 (age 20-60yrs) patients with clinically suspected fistula-in-ano (72 men and 28 women) underwent pelvic MR examinations on a GE Signa HDxt 3.0 Tesla. All the patients had T2-weighted MR imaging at 3T with both 1-mm-thick 3D T2FSE cube and 5-mm-thick axial, coronal and sagittal 2D T2FSE sequences. The internal opening, side tracts and abscesses were evaluated on both sequences. Statistical analysis of detection rate was performed to compare 3D T2FSE with 2D T2FSE images using Fisher exact test and Chi-square test.

Results: Accuracy in detection of internal opening is higher on 3D cube than 2D images. A p value of 0.0004 in Fisher exact test and p value of 0.00023 in Chi-square test are considered to indicate a significant difference.

Conclusion: The advantage of 3D T2 FSE cube sequence is its accuracy in the identification of internal opening in a perianal fistula and secondary lesions with multiplane reconstruction in comparison with 2D T2 FSE sequence.

B-0527 11:43

Can we reliably identify the appendix on unenhanced ultra-low-dose CT in the era of iterative reconstruction?

D. Ordu, L.-P. Rollandi, K. Rippel, C. Scheurig-Muenkler, T. Kröncke, F. Schwarz; Augsburg/DE (deniz.ordu@klinikum-augsburg.de)

Purpose: To determine factors influencing the accuracy in the identification of the appendix on ultra-low-dose CT by residents with on-call experience.

Methods and Materials: We included 163 patients presenting to the ED over a 5-month period who were referred for an unenhanced ultra-low-dose CT of the abdomen for urolithiasis. A model-based iterative algorithm was used for image reconstruction. As reference standard, two faculty radiologists evaluated all datasets and information from the electronic health records. Two residents blinded towards this reference standard independently analysed all datasets for the presence of the appendix and digitally marked it if identified.

Results: 35 patients were excluded due to uncertain AE status. Of the remaining 128 patients (80 men, median age 47, median DLP 46mGy*cm), 56 had had prior appendectomy. Interobserver agreement was high (88%, $\kappa=0.75$). Readers had a sensitivity, specificity and accuracy of 91%, 88%, 90% and 92%, 91%, 91%, respectively. The subgroup of patients with incorrect identification of the appendix had lower BMI (23.5±4 vs 28±7kg/m², p=0.02) and tendencies towards lower CTDI (0.91±0.3 vs 1.21±0.6mGy, p=0.1) and lower DLP (43±13 vs 53±25mGy*cm, p=0.16) but there was no difference in image noise (15.9±3.8 vs 15.9±3.6HU, p=1.0). BMI had high predictive value for an incorrect identification of the appendix (AUC=0.73, p<0.01), while image noise lacked any measurable effect (AUC=0.52, p=0.84).

Conclusion: The normal appendix or its absence can be correctly identified on unenhanced ultra-low-dose CT scans in the vast majority of cases by residents with on-call experience. Low BMI is a strong predictor for misclassification, while image noise lacked any measurable effect.

B-0528 11:51

Use of conventional defecography or dynamic MRI defecography in patients with symptomatic pelvic floor dysfunction: a retrospective intraindividual trial

M.C. Langenbach, M. Kaup, M. Beeres, J.-E. Scholz, C. Park, C. Frellesen, T.J. Vogl, T. Gruber-Rouh; Frankfurt a. Main/DE (marcel.langenbach@me.com)

Purpose: Conventional defecography [CD] is a standard method in diagnostic of pelvic floor dysfunction. Since dynamic magnetic resonance imaging [MRI] has become more common, examinations are possible without X-ray and iodinated contrast media. Differences of both methods will be compared in this retrospective intraindividual trial.

Methods and Materials: 50 patients (44 females, 6 males; mean age: 57 years) were evaluated with CD and dynamic MRI defecography [MRD]. Iodinated contrast media was used for CD, ultrasound gel for MRD. Two radiologist with more than 5 years' experience evaluated the presence of rectal prolapse, rectocele, enterocele, sigma diverticula and Cul de sac [CdS] phenomenon/syndrome.

Results: In CD, rectal prolapse was observed in 45 patients, in MRD only in 8 patients (p<0.001). CD showed a rectocele in 37, MRD in 41 patients (p=0.337). No significant differences were documented for retention of rectoceles (p=0.188), but significant for the size (MRD: 2.40cm; CD: 1.91cm; p=0.016). For occurrence of enterocele and sigma diverticula (p=0.604; p=0.149), no significant differences were found. Identification of elongated sigma is more sensitive in CD than MRD (p=0.008). CdS phenomenon and syndrome were seen in CD in 8 and 9 cases, in MRD only in one patient, respectively (p=0.015; p=0.008).

Conclusion: MRD instead of CD is a strong alternative option for diagnosis of pelvic floor dysfunctions. Additionally, lack of radiation and possibility for direct evaluation of anterior and middle compartment puts MRI into a stronger role. Despite various advantages of MRD, the choice of the method is depending on the clinical question.

10:30 - 12:00

Room D

Musculoskeletal

SS 610b

Bone trauma

Moderators:

A. Barile; L'Aquila/IT

R. Mirón Mombiola; Valencia/ES

B-0529 10:30

Three-material decomposition with dual-layer spectral detector CT compared to MRI for the detection of bone marrow oedema in patients with acute vertebral fractures

B.J. *Schwaiger*, A. Gersing, J. Hammel, K. Mei, F.K. Kopp, E.J. Rummeny, K. Wörtler, T. Baum, P.B. Noel; *Munich/DE*

Purpose: To assess whether bone marrow oedema in patients with acute vertebral fractures can be accurately diagnosed based on three-material decomposition with dual-layer spectral detector CT (SDCT).

Methods and Materials: Acute (n=41) and chronic (n=19) osteoporotic thoracolumbar vertebral fractures in 28 subjects (70±14 years, 18 women) as diagnosed by MRI (hyperintense signal in STIR sequences) were assessed on a SDCT (Philips IQon). Data were processed using an in-house developed algorithm to decompose spectral data into calcium, oedema-equivalent and fat-equivalent density maps. Two radiologists, blinded to clinical and MR findings, assessed the images independently, using a Likert scale (1=no oedema; 2=likely no oedema; 3=likely oedema; 4=oedema). Accuracy, sensitivity and specificity for identifying acute fractures (Likert scale, 3 and 4) were analysed using MRI as standard of reference.

Results: For the identification of acute fractures, conventional CT images showed a sensitivity of 63% and specificity of 84%, whereas the sensitivity (95%) and specificity (90%) of decomposed SDCT images were substantially higher. Accuracy increased from 70% for conventional images to 93% using SDCT. Readers considered MRI necessary for fracture age determination in 60% (based on conventional images) and 28% (based on SDCT images), respectively. Interreader agreement was high for the classification of acute fractures in conventional (ICC, 0.79 [95% confidence interval, 0.68-0.87]) and SDCT images (ICC, 0.95 [0.92-0.97]).

Conclusion: Material decomposition of SDCT data substantially improved accuracy for the diagnosis of acute vertebral fractures, with a high interreader agreement. This may spare patients' additional examinations and facilitate the diagnosis of vertebral fractures.

B-0530 10:38

Single-source dual-energy computed tomography for the assessment of bone marrow oedema in vertebral compression fractures: a prospective diagnostic accuracy study

T. *Diekhoff*¹, N. Engelhard¹, M. Fuchs¹, M. Pumberger¹, M. Putzier¹, J. Mews², B. Hamm¹, K.-G. Hermann¹; ¹*Berlin/DE*, ²*Neuss/DE* (*torsten.diekhoff@charite.de*)

Purpose: The aim of this study was to evaluate the diagnostic accuracy of single-source dual-energy computed tomography (DECT) in patients with vertebral compression fractures.

Methods and Materials: Patients aged 50 or more years were prospectively included and underwent both DECT on a single-source machine (80/135 kVp sequential volume acquisition) and 1.5 Tesla MRI including T1 and STIR sequence that served as standard of reference. Virtual non-calcium images (VNCa) were reconstructed using a three-material decomposition algorithm. Only vertebrae with loss of height in CT were included in the analysis. Images were independently scored for bone marrow oedema by three blinded readers using a 0-3 rating scale. A contingency table analysis, test for inter-reader reliability using Cohen's kappa and measurements of signal-to-noise (SNR) and contrast-to-noise ratios (CNR) were performed.

Results: 70 patients and 192 vertebrae were included. DECT showed a reader-dependent sensitivity of 72% (62 to 80%) and a specificity of 70% (46 to 71%) for BME. Sensitivity increased with the oedema score in MRI (81% for grade 2 and 89% for grade 3). Cohen's kappa was inferior for DECT (0.32 to 0.48) compared to MRI (0.56 to 0.62). T1 provided a significantly better signal- and contrast-to-noise ratio compared to STIR, CT and VNCa (p < 0.0001); however, there were no differences between STIR and VNCa.

Conclusion: DECT is able to detect BME with substantial diagnostic accuracy and can be performed utilizing a single-source system. It provides sufficient image quality; however, trained readers are needed for image interpretation.

Author Disclosures:

J. Mews: Employee; Toshiba MS.

B-0531 10:46

Contribution of ultra-low dose CT in lumbar spine trauma

F. *Snene*, A. Hamard, J. Greffier, P. Viala, J. Beregi, A. Larbi; *Nîmes/FR* (*snenefehmi@gmail.com*)

Purpose: To evaluate the diagnostic power of ultra-low-dose CT (ULD-CT) of the lumbar spine compared to the X-ray in emergency room.

Methods and Materials: A preliminary study on anthropomorphic phantom made it possible to determine the level of reference dose and the iterative level for the ULD-CT. Then an ULD acquisition without contrast medium injection as well as an X-ray of the lumbar spine were performed in 28 patients consulting the emergency department of our institution from March to August 2017. Raw data were reconstructed with *Sinogram-Affirmed-Iterative-Reconstruction* (SAFIRE, Siemens) with bone (I70f) and soft tissue (I30f) reconstructions kernel.

The subjective analysis (image quality, diagnostic quality, characterization of the lesions with confidence level) was performed by double blind reading (1 senior and 1 junior radiologist). The diagnostic performance of the ULD-CT and X-ray were compared.

Results: Effective dose for ULD-CT were lower than the national X-ray Diagnostic Reference Level (DRL). Kappa Cohen test agreement among the two observers for the evaluation of traumatic lesions was substantial, ranging from 0.9 to 1. The analysis of data showed the absence of inferiority of the ULD-CT in the detection of traumatic lesions comparatively to the X-ray. The ULD-CT showed its superiority in the detection of disc disease (p<0.05). Readers recorded a significantly high score of diagnostic confidence level for ULD-CT compared to X-ray (p<0.05).

Conclusion: ULD-CT with iterative reconstructions allowed a reliable study of spine trauma patients with a lower irradiation dose than spine radiography. Reproducibility is independent of the level of experience of the readers.

B-0532 10:54

Evaluations of outcomes for drop in pain and analgesic use for kyphoplasty in the treatment of 249 patients with vertebral compression fractures: a single centre results

R. *Marcello*, G. Assegnati, A. Di Blasi, F. Cortese, S. Vitale; *Rome/IT* (*robermarcello@gmail.com*)

Purpose: Vertebral compression fractures (CF) resulting from osteoporosis, cancer and trauma are common and painful. QoL is at high risk and morbidity and mortality rates increase following a compression fracture (CF). Kyphoplasty is a minimally invasive procedure to stabilise a CF. The effectiveness and reliability to reduce pain and drop in pain killers use were considered.

Methods and Materials: 249 patients suffering from CF due to osteoporosis, trauma and malignancy receiving percutaneous trans-pedicle fluoro-guided balloon kyphoplasty were evaluated. The primary objective was to show significant improvement in two end points such as back pain relief (VAS score) and analgesic use at one week and three months after treatment. Pre-procedural workup was carried out on spinal unenhanced multiplanar MRI or CT.

Results: Back pain significantly decreased after treatment: the mean VAS pain score before treatment was 16.33 +/- 2.45 (range 13-20) versus 9.25 +/- 4.90 (range 2-18) one week after treatment and was 7.00 +/- 5.25 (range 1-14) three months after treatment. Analgesic use dropped after treatment. Device- and procedure-related complications were asymptomatic balloon rupture in three patients, asymptomatic to the skin cement leakage through monolateral pedicle access successfully removed with a clamp in one patient and possibly cement-related new CF within four weeks post-procedure in five patients.

Conclusion: Our large single centre evaluation shows that balloon kyphoplasty is a very effective and reliable procedure for the treatment of vertebral CF due to osteoporosis, trauma and malignancy.

B-0533 11:02

Vertebral body insufficiency fractures: detection of vertebrae at risk on clinical CT images using texture analysis and machine learning

U. *Mühlematter*, M. Mannil, T. Finkenstaedt, A.S. Becker, G. Osterhoff, R. Guggenberger, M. Fischer; *Zurich/CH* (*urs.muehlematter@gmail.com*)

Purpose: Osteoporotic insufficiency fractures of the spine are frequent complications in elderly patients. We introduce an alternative for bone quality measurements based on texture analysis (TA) with machine learning (ML) of CT scans of the trunk to identify vertebrae at risk for fracture.

Methods and Materials: Consecutive standard CT scans of 57 patients with insufficiency fractures of the spine were analyzed. Intact vertebrae in the first scan that either fractured ('instable') or remained intact ('reference') in the consecutive scan were manually segmented on mid-sagittal reconstructions. If available, a third scan was assessed to validate the reference vertebra over a longer period. Texture features for all vertebrae were extracted using open source software (MaZda). Multiple ML approaches, e.g. random forest and

support vector machines were used to classify instable and reference vertebrae as well as cases (instable and reference) and matched (gender, age and fracture level) controls from a prior study.

Results: 60 vertebrae were included. Mean time difference between the first and second scan was 237 days (SD \pm 117.5), between latter and third 548 days (SD \pm 386). ML based classification of cases vs. controls showed sensitivity, specificity and AUC of 0.91, 0.86 and 0.93 and of 0.63, 0.43 and 0.45 for instable vs. reference vertebrae, respectively.

Conclusion: TA combined with ML allows to distinguish healthy and diseased bone with a high accuracy. However, within the diseased spine the prediction of single vertebrae that will fracture at a future point in time remains challenging.

B-0534 11:10

Comparing trabecular bone score and serum bone biomarker in predicting vertebral fracture for diabetes

Y.-C. Lin¹, A.Y. Cheung², S.-F. Kuo¹, K.-H. Wu¹, C.-M. Sung¹, C.-M. Fan¹, F.-P. Chen¹; ¹Keelung/TW, ²Taoyuan/TW (yuching1221@gmail.com)

Purpose: Type 2 diabetes patients (T2D) have poor bone quality with increased vertebral fracture (VF) risk. There are two available methods for predicting fracture risk, trabecular bone score (TBS) and serum bone turnover biomarkers. This study compares the diagnostic performance and also studies the association between these two methods.

Methods and Materials: Postmenopausal T2D female patients were prospectively enrolled. All received image studies of bone densitometry for TBS calculation and lateral lumbar spine radiographs for VF assessment. Laboratory studies of vitamin D, intact parathyroid hormone (iPTH), bone-specific alkaline phosphatase (sBALP, bone resorption biomarker) and beta-C-terminal telopeptides (sCTX, bone formation biomarker) for bone turnover assessment. We compared the performance of each parameters with vertebral fracture using Student's *t* test, age-adjusted odds ratio (OR) and receiver operating characteristic (ROC) curve. Lastly, Pearson for correlation of different parameters was calculated.

Results: A total of 285 T2D patients were analysed with mean age of 61.1 years and total of 32 patients with VF (11.23%). Significantly lower TBS and higher sBALP ($p < 0.001$; $p = 0.030$) were shown in group with VF with OR of < 0.001 and 1.080 ($p < 0.001$; $p = 0.029$) and area under curve (0.820 and 0.746). Vitamin D, iPTH and CTx is not significantly associated with VF. TBS only significantly correlated to sBALP (-0.276, $p < 0.001$) but not to sCTX (-0.096, $p = 0.107$).

Conclusion: TBS has a better diagnostic performance than serum bone turnover biomarkers in predicting VF in T2D and lower the TBS are predisposed to unbalanced rate of bone turnover and resulted in bone fragility.

B-0535 11:18

Haemarthrosis of the knee and knee fracture: evaluation with high-resolution ultrasound

S.P. Ivanoski¹, V. Vasilevska Nikodinovska², ¹Ohrid/MK, ²Skopje/MK (slavcoivanoski@gmail.com)

Purpose: To evaluate the presence of knee fracture in patients with sonographic signs of knee haemarthrosis.

Methods and Materials: 31 patients with acute knee trauma and ultrasound signs of knee haemorrhagic effusion were evaluated for presence of bone fractures. High-resolution transducer was used for detecting haemorrhagic knee effusion within the suprapatellar and parapatellar knee recesses. Emergency radiography or CT was performed for establishing diagnosis of bone fracture. Control group consisted of 31 patients with acute knee trauma and anechoic, non-haemorrhagic knee effusion on ultrasound. Sensitivity, specificity, positive and negative predictive value of the method were evaluated.

Results: Radiography and CT findings were positive for bone fracture in 26 of 31 patients with knee haemarthrosis on ultrasound. In 12 cases patellar osteochondral fracture in acute dislocation were found, followed by fracture of femoral condyle (6 patients), platotibial fracture (5 cases), and tibial eminence fracture (2 patients). Avulsion fracture of the tibial tuberosity was present in 1 patient. In control group 4 avulsion fractures were detected (2 Pelegrini-Stieda, and 2 second fractures), without any intraarticular fracture. Sensitivity of the method for detection of intraarticular fractures was 83.9%. Specificity was 87.1%, positive and negative predictive value were 86.7% and 84.4%.

Conclusion: High resolution ultrasound is a good method for detecting even a small amounts of fluid within the knee recesses. Sonographic diagnosis of knee haemarthrosis can be a good predictor of intraarticular knee fracture. Further investigations should be performed for detecting small knee fracture in all cases of haemarthrosis detected by ultrasound.

B-0537 11:26

Anatomy-based MR classification of the iliopsoas muscle complex after petrochanteric femur fracture

M. Kaniewska¹, M. Schenkel¹, K. Eid¹, T. Bühler¹, R. Kubik-Huch¹, S. Anderson^{1,2}; ¹Baden/CH, ²Sydney/AU

Purpose: Petrochanteric femur fracture (PFF) with a dislocation of the lesser trochanter may lead to deterioration of quality of the iliopsoas muscle complex (IMC). In this prospective study, an anatomy-based evaluation of the IMC after PFF using MRI is proposed. Additionally, the inter-reader reliability of 2 classifications of fatty muscle degeneration (FMD) was determined.

Methods and Materials: Adult patients after surgery of PFF with a displaced lesser trochanter were included. Muscle quality was evaluated by means of MRI using Goutallier and Slabaugh classifications at 3 anatomic levels (L4/L5, L5/S1, spina iliaca anterior inferior). Two radiologists independently reviewed the images. Force measurement was performed on both hips. Linear mixed-effect models were used to determine the effect of fracture on muscle quality and strength. Cohen's kappa statistic was used to assess the inter-reader agreement.

Results: 18 patients were included. The IMC showed higher grades of FMD (grade 3 and 4 in Goutallier and grade 3 in the Slabaugh classification, respectively) on the fractured side (FS) than on the non-fractured side (NFS). The mean difference between muscle strength on FS and NFS was -12N (p value > 0.05). Inter-reader agreement for the Goutallier and Slabaugh classifications was good and very good, respectively (weighted K = 0.78 and 0.85).

Conclusion: Anatomy-based MR evaluation of the IMC provides a valuable tool for the assessment of muscle quality after PFF. FMD of the IMC is evident and results in a minimal reduction of muscle strength. In terms of inter-reader agreement, the Slabaugh classification is superior to the Goutallier classification.

Author Disclosures:

M. Kaniewska: Research/Grant Support; Young Researchers Grant European Society of Musculoskeletal Radiology (ESSR).

B-0538 11:34

Are fractures of the anterior calcaneal process indicative of a more advanced Chopart joint injury?

A. Hirschmann^{1,2}, W.R. Walter², E.F. Alaia², E. Garwood², Z.S. Rosenberg²; ¹Basle/CH, ²New York, NY/US (anna.hirschmann@usb.ch)

Purpose: To assess the co-existence of anterior calcaneal process (ACP) fractures with talonavicular joint injury, indicating advanced Chopart joint injury, and to correlate our findings with radiologic and clinicians' diagnosis.

Methods and Materials: Retrospective radiological data search ("avulsion fracture"; "anterior calcaneal process fracture") was performed. Inclusion criteria were imaging evidence of injury to ACP on radiographs and MRI within 8 weeks of ankle injury. Injuries at ACP and talonavicular component of Chopart joint, using radiographs and MRI, were assessed by three musculoskeletal radiologists. The prospective radiologic and clinical diagnosis were documented. McNemar and kappa statistics were used ($P < 0.005$).

Results: Final cohort had 21 patients. On radiographs, avulsion fractures of the ACP and at talonavicular joint were evident in 48% (10/21) and 38% (8/21), respectively. Concomitant fractures of both joints, indicating advanced Chopart joint injury, were evident in 14% (3/21). On MRI, avulsion fractures of the ACP and at the talonavicular joint were evident in 100% (21/21) and 76% (16/21), respectively. Thus, concomitant fractures at both joints were present in 76% of the cases. Differences between imaging modalities were significant ($p < 0.008$). Interrater agreement was 0.144-0.538 and 0.976-1 for ACP and 0.488-0.637 and 0.286-0.364 for talonavicular injuries on radiographs and MRI, respectively. 60% of ACP fractures were prospectively missed on radiographs (none on MRI), while 38% and 25% of talonavicular findings were prospectively missed on radiographs and MRI, respectively. 60% of Chopart joint injuries were clinically misdiagnosed as ankle sprains.

Conclusion: Radiological evidence of injury at either component of Chopart joint should draw attention to a more severe Chopart joint sprain.

Author Disclosures:

A. Hirschmann: Research/Grant Support; Stiftung Prof. Dr. Max Cloëtta and Uniscientia Foundation, Gottfried und Julia Bangerter-Rhyner-Stiftung, Helmut-Hartweg-Fonds of the Schweizerischen Akademie der Medizinischen Wissenschaften, Freie Akademie der Wissenschaften Basel.

B-0539 11:42

Comparing dGEMRIC and clinical outcome 6 years after FAI surgery with versus without microfracturing: a controlled pilot study

F. Schmaranzer¹, P. Haefeli¹, M. Hanke¹, T. Lerch¹, K. Siebenrock¹, S. Werlen¹, M. Tannast¹, L. Büchler², ¹Bern/CH, ²Biel/CH

Purpose: To compare (1) T1 indices and (2) clinical outcome in patients with a minimum 6-year follow-up who had undergone FAI surgery with versus without microfracturing.

Methods and Materials: After IRB approval patients with a minimum 6-year follow-up who had undergone surgical hip dislocation with or without microfracturing for treatment of FAI and of extensive chondral flaps and defects were searched. A total of 46 patients were identified, 17 in the 'Mfx group' and 29 in the 'no Mfx group'. All eligible patients underwent indirect MR arthrography (Gd-DTPA 2-0.2 mmol/kg) with a dual-flip angle GRE-technique for acquisition of 3D T1 maps at latest follow-up. (1) T1 indices of acetabular cartilage were assessed on radially reformatted images. Regions of interest were manually placed. (2) Patient-reported outcome was evaluated at latest follow-up using Western Ontario and McMaster Universities Osteoarthritis Index (WOMAC) and Harris Hip Score (HOOS). Unpaired Student's t tests and Mann-Whitney U tests were used ($p < 0.05$).

Results: There was no significant difference ($p > 0.05$) in the overall (438 ± 150 ms versus 434 ± 136 ms) and regional (superior [11-1 o'clock], anterior [2-4 o'clock], posterior [8-10 o'clock]) T1 indices between the two groups. WOMAC (52 ± 65 versus 39 ± 46) and HHS (71 ± 27 versus 87 ± 12) did not differ significantly ($p > 0.05$) between the two groups.

Conclusion: The results suggest that treatment of cartilage lesions with microfracturing during FAI surgery does not positively or negatively affect clinical or radiographic mid-term results compared to patients with no treatment of cartilage lesions.

10:30 - 12:00

Room G

Physics in Medical Imaging

SS 613

Innovations in medical imaging

Moderators:

M. Kortensniemi; Helsinki/FI
G. Sommer; Basle/CH

B-0540 10:30

Impact of software parameter settings on image quality of Virtual Grid processed radiography images: a contrast-detail study

T. Gossye, M. Peleman, P. Smeets, E. Achten, K. Bacher; Ghent/BE
(tim.gossye@ugent.be)

Purpose: The use of an anti-scatter grid is uncommon in bedside radiography. Dedicated software to compensate scatter in the images became recently available. The aim was to evaluate the influence of software parameter settings on the image quality using a contrast-detail study.

Methods and Materials: 2400 images of a CDRAD (Artinis) test object were acquired with a digital D-EVO II GOS detector accompanied with Virtual Grid (VG) post-processing software (Fujifilm Medical Systems). The test object was placed between PMMA to mimic patient scatter (total thickness range: 12-26 cm). For each phantom thickness images were acquired with a kVp range 81-125. 12 different VG software parameters combinations were investigated (2 grid ratios, 3 linepairs/cm, 2 types of interstitial material). The acquired images were analysed with the CDRAD Analyser software 2.1 and the relative Image Quality Figure inverse (IQFinv) was calculated. A linear mixed model statistical design was performed for data analysis (IBM SPSS 23).

Results: VG software significantly ($P < 0.001$) improved the digital images. Compared to non-VG images, mean relative IQFinv values significantly increased from 26% to 32% for grid ratio 6 and 10 respectively ($P < 0.001$). For the other two parameters no statistically significant differences are observed ($P > 0.05$). Small but significant interactions are noticed for: ratio*linepairs/cm and ratio*PMMA thickness*kV.

Conclusion: VG software is able to improve bedside radiography imaging significantly. The most important factor influencing the image quality improvement is the VG grid ratio setting. The other software parameter settings did not significantly affect the relative IQFinv.

B-0541 10:38

X-ray dark-field and phase-contrast images facilitate the detection of wooden and glass foreign bodies on radiographs

K. Hellbach¹, E. Beller¹, A. Schindler¹, F. Schoeppe¹, N. Hesse¹, A.B. Baumann¹, R. Schinner¹, C. Hauke², F. Meinel¹; ¹Munich/DE, ²Forchheim/DE

Purpose: The purpose of this study was to assess the value of dark-field and phase-contrast radiography for the detection of foreign bodies (FB) compared to transmission radiographs.

Methods and Materials: Ex vivo pig paws were prepared with metallic, wooden and glass FB (n=10 each). Paws without FB served as controls (n=30). Images were acquired with a prototype, preclinical grating-based large object radiography system (not commercially available). To investigate the diagnostic value of adding dark-field and/or phase-contrast images to transmission images a reader study was performed, asking five blinded readers to independently assess the images for the presence or absence of any FB.

Results: Sensitivity for the detection of metal FB was 100% for all readers. The sensitivity for the detection of wooden FB increased from 2% for transmission images to 78% for dark-field images ($p < 0.0001$), and to 16% when phase-contrast images were added ($p = 0.0264$). For the detection of glass FB, the sensitivity slightly increased from 84% for transmission images to 96% when adding phase-contrast images ($p = 0.041$). The sensitivity for the detection of any foreign bodies was highest when transmission, dark-field and phase-contrast images were assessed simultaneously: 91%, compared to 62% for the sole analysis of transmission images ($p < 0.0001$).

Conclusion: Detection of glass FB was significantly improved when phase-contrast images were analysed. Assessment of dark-field images resulted in a substantially improved detection of wooden FB compared to the sole analysis of transmission images.

Author Disclosures:

C. Hauke: Employee; Siemens Healthcare GmbH.

B-0542 10:46

High-fidelity vessel visualisation in diagnostic CT: low-dose dynamic CTA via singular value decomposition-guided filter (SVGF)

F. Pisana¹, T. Henzler², H. Haubenreisser², E. Klotz³, B. Schmidt³, M. Kachelrieß¹; ¹Heidelberg/DE, ²Mannheim/DE, ³Forchheim/DE

Purpose: To provide high-fidelity images of vessels in low-dose dynamic CT angiography (CTA).

Methods and Materials: Dynamic CTA provides additional unique information compared to conventional CTA. Low-dose acquisitions, however, typically result in noise and artefacts and small vessels may be hard to be visualised, particularly in the temporal MIP volume. We developed a non-linear filter to significantly improve image quality. After subtracting the baseline, the temporal redundancy of the dataset is enforced via singular value thresholding, which has the effect of reducing the temporal noise while preserving the temporal signal. The temporal MIP of the such-filtered volume is used to guide a spatial bilateral filter. Additionally, to preserve temporal coherence, we introduced a weight depending on the similarity of the smoothed temporal profiles. The SVGF was retrospectively tested on several low-dose dynamic CTA cases, acquired at 70 kV, with a Somatom Force CT scanner (Siemens, Forchheim, Germany).

Results: The CNR of small vessels was evaluated on the temporal MIP of both the unfiltered and filtered cases. The SVGF improved the CNR by 80% on average, resulting in a potential dose reduction of a factor of 3. Also, each temporal phase was significantly improved, allowing for higher details in the dynamic MPR, MIP and VRT visualisations.

Conclusion: Dynamic CTA could potentially replace conventional CTA given the significance of the additional information provided. Our new SVGF approach could allow for dynamic CTA at very low doses, roughly 1.5 mSv instead of 4.5 mSv, and restore detailed dynamic visualisation of the vessels.

Author Disclosures:

E. Klotz: Employee; Siemens Healthcare GmbH. B. Schmidt: Employee; Siemens Healthcare GmbH.

B-0543 10:54

Potential of spectral photon-counting CT for the differentiation between blood and iodine in a bovine brain

I. Riederer¹, D. Bar-Ness², F. Pfeiffer³, P. Douek², S.A. Si-mohamed², A.A. Fingerle^{1,3}, E.J. Rummeny¹, P.B. Noel^{1,3}, D. Muenzel^{1,3}; ¹Munich/DE, ²Bron/FR, ³Garching/DE (isabelle.riederer@tum.de)

Purpose: To evaluate the potential of Spectral Photon-Counting CT (SPCCT) for the differentiation between blood and iodine in a bovine brain.

Methods and Materials: Tubes with blood and a concentration series of iodine-based contrast agents were scanned with a preclinical SPCCT system (both in-vitro and in an ex-vivo bovine brain tissue sample) to obtain spectral

and conventional data. Iodine density maps and virtual non-contrast images were generated using the multibin spectral information to perform material decomposition. Region-of-interest (ROI) analyses were performed within the tubes to quantitatively determine the absolute content of iodine.

Results: In conventional CT images, ROI analysis showed similar HU density values for the tubes with blood and iodine (59.9 +/- 1.8 versus 59.2 +/- 1.5). Iodine density maps enabled clear differentiation between blood and iodine in-vitro, as well as in the bovine brain. Quantitative measurements of the different iodine concentrations matched well with those of actual prepared mixtures (measured: 0.57 +/- 0.09 mg/cm³, actual: 0.5 mg/cm³; measured: 0.77 +/- 0.16 mg/cm³, actual: 0.75 mg/cm³; measured: 0.93 +/- 0.15 mg/cm³, actual: 1 mg/cm³; measured: 2.11 +/- 0.21 mg/cm³, actual: 2mg/cm³; measured: 5.06 +/- 0.06 mg/cm³, actual: 5 gm/cm³; measured: 10.33 +/- 0.18 mg/cm³, actual: 10 mg/cm³; measured: 16.08 +/- 0.13 mg/cm³, actual: 15 mg/cm³).

Conclusion: Spectral Photon-Counting CT allows for multi-material decomposition and differentiation between blood and iodine in-vitro and within a bovine brain, providing reliable quantification of the iodine concentration.

B-0544 11:02

An automated alignment correction algorithm for CT imaging: evaluation based on a CT image quality phantom and application to sediment cores from cold-water coral mounds

S. Skornitzke¹, G. Pahn¹, A. Bahr¹, J. Raddatz², H.-U. Kauczor¹, W. Stiller¹;
¹Heidelberg/DE, ²Frankfurt a. Main/DE
(Stephan.Skornitzke@med.uni-heidelberg.de)

Purpose: Alignment of objects during computed tomography (CT) acquisition can be crucial for evaluation, e.g. for image quality assurance. An algorithm for automated alignment correction of scanned objects was developed, evaluated in a phantom, and applied to acquisitions of sediment cores, enabling extraction of geological samples.

Methods and Materials: A phantom (ConeBeam Phantom; QRM, Germany) was scanned at 120kVp/150mAs (SOMATOM Definition Flash; Siemens Healthineers, Germany). Image series were randomly rotated (up to ±2.86°) and translated (up to ±15mm) 1000 times and alignment was automatically corrected using the developed algorithm. Alignment parameters determined by the algorithm were compared to randomised parameters, and four regions of interest (ROIs) were placed in the low-contrast phantom segment, comparing mean values before and after correction. After validation, CT series of six sediment cores from cold-water coral mounds acquired at 140kVp/570mAs were corrected for alignment.

Results: Average absolute differences between detected and randomized parameters were 0.15±0.07° around x-axis, 0.02±0.02° around y-axis, 0.01±0.06mm in x, and 0.11±0.08mm in y. Mean values for ROI measurements averaged for corrected datasets were -148.54±1.40HU, -76.78±0.90HU, -48.16±0.86HU and -16.64±0.48HU, compared to original measurements of -149.76HU, -77.54HU, -48.61HU and -17.00HU. Alignment could be corrected for all six CT series of sediment cores. Average absolute rotation was 0.37±0.33° around x-axis, 0.21±0.22° around y-axis, and average absolute translation was 3.93±2.89mm in x and 7.21±2.37mm in y.

Conclusion: The algorithm allows to automatically correct alignment of imaged objects, e.g. in CT series of standard quality assurance phantoms as well as general cylindrical objects, enabling further evaluation.

Author Disclosures:

G. Pahn: Employee; Philips GmbH Market DACH.

B-0545 11:10

Correcting for acoustic and optical inaccuracies in photoacoustic imaging using multimodal priors

S. Mandal, D. Komljenovic; Heidelberg/DE (s.mandal@dkfz.de)

Purpose: Photoacoustic (PA) imaging depends on the principle of optical generation and acoustic detection of signals from tissue sample. However, biological tissue suffer from significant depth dependent optical fluence losses and acoustic attenuations. We aim to correct for these inaccuracies aided by extrinsic imaging priors obtained through concurrent high-frequency ultrasound (US) imaging of tissue samples.

Methods and Materials: A hybrid PA-US system (Vevo LAZR-X, VisualSonics) was employed for acquisition of fused multimodal data in real time. The temperature was monitored continuously using built-in temperature sensor, it was used as an initial estimate for speed-of-sound (SoS) calibration. We corrected for the small variations in SoS by incorporating multiple SoS in tissue and coupling medium, which was modelled using skin-line detection from the US image. The optical fluence correction was achieved through Monte Carlo modeling of light transport in multi-layered tissues (MCLM). The information regarding the different tissue layers were obtained through multi-label segmentation of US images. Finally, anisotropic diffusion was used for noise reduction in the images without loss of edge information.

Results: The corrected beamformed PA image showed an improvement of PSNR (43.289) and MSE (3.049). Further, fluence correction offers improved

resolution at greater depths in the PA images. Results were verified using phantom studies and *in vivo* kidney images of small animal (rat) models.

Conclusion: These experimental results demonstrate that mutual information from US and PA can significantly improve the imaging performance of the beamformed PA image, and reduce errors introduced by optical and acoustic attenuations.

B-0546 11:18

Improved contrast-enhanced time-resolved MR angiography on a small bore 3T MRI system

S. Riederer, E. Stinson, M. Bernstein, N. Campeau, J. Huston, J. Trzasko; Rochester, MN/US (riederer@mayo.edu)

Purpose: To describe the implementation of an improved time-resolved contrast-enhanced MR angiography sequence on a compact 3T MRI scanner.

Methods and Materials: Recently a 37-cm bore "compact" 3T MRI system has been developed, specifically targeted to imaging the head and extremities, with smaller bore size enabling improved-performance gradient hardware. Compared to typical gradient amplitude and slew rates (50 mT/m, 200 T/m/sec) of a 70 cm whole body MRI, the compact 3T system has specifications (80 mT/m, 700 T/m/sec). The smaller gradient diameter reduces peripheral nerve stimulation at higher switching limits than conventional diameter gradients. For this work, a reference time-resolved CE-MRA sequence was adapted to benefit from the compact 3T scanner's increased gradient performance. This enabled reduction of the TR/TE of the SPGR T1-weighted sequence from 4.2/1.9 msec to 2.9/1.3 msec. This technique was evaluated in five human volunteers under an IRB-approved protocol.

Results: Acceleration techniques enabled 1 mm isotropic resolution with 2.5 sec update time on the compact 3T. The improved CE-MRA technique was able to resolve multiple phases of the arterial-venous passage of blood through brain vasculature of the volunteers. Benefits of shorter TE imaging include increased SNR and fewer flow-related artefacts. None of the volunteers experienced peripheral nerve stimulation.

Conclusion: The enhanced gradient performance of the compact 3T MRI scanner permits 30% reduction in TR and TE parameters for contrast-enhanced MRA, affording increased SNR and improved spatial/temporal resolution compared to that achievable using a whole body MRI scanner.

B-0547 11:26

Fast field-cycling MRI for medical applications

L.M. Broche, J. Ross, G.R. Davies, D.J. Lurie; Aberdeen/UK
(l.broche@abdn.ac.uk)

Purpose: The relationship between T₁-relaxation time and field strength in MRI is known to be very informative on molecular dynamics but is not accessible by conventional MRI systems. Here we introduce a new technology that measures T₁ as a function of field strength, accessing that rich source of information to provide novel contrast.

Methods and Materials: Our prototype human-scale Fast Field-Cycling (FFC) measures T₁-dispersion by rapidly switching the main magnetic field (B₀) during the pulse sequence to reach any field strength between 25 uT and 0.2 T within 20 ms. Its resistive magnet is driven by power amplifiers giving full control of B₀ with a 15 ms stabilisation time. Additional coils outside the main magnet provide local cancellation of the Earth's field.

Results: The system has been fully commissioned and is capable of *in vivo* imaging using its full field range. Images of the head and knees were obtained from normal volunteers and patients within 40 minutes for a resolution of 4x4x8 mm over 250 mm field of view. T₁-dispersion images were obtained that agreed with measurements on excised tissues from a benchtop FFC instrument.

Conclusion: FFC-MRI allows us to explore and take advantage of the unique T₁-dispersion contrast. The use of a purely resistive magnet allows us to access ultra-low magnetic fields, providing information on slow molecular dynamics. Our work currently concentrates on demonstrating how this newly accessible region of the T₁ dispersion curve can be exploited for clinical diagnosis in stroke, osteoarthritis and Alzheimer's disease.

Author Disclosures:

D.J. Lurie: Grant Recipient; GE Healthcare.

B-0548 11:34

Radiopaque 3D printing of patient individual phantoms for computed tomography and radiation therapy

P. Jahnke, F.B. Schwarz, M. Ziegert, B. Hamm, M. Scheel; Berlin/DE
(paul.jahnke@charite.de)

Purpose: To develop a method for 3D printing realistic anthropomorphic phantoms of individual patients.

Methods and Materials: Conventional inkjet technology is used together with radiopaque ink to print CT images of individual patients on standard paper. Stacking of the printed sheets results in 3D objects that are examined in the CT scanner. Calibration of the printer and a gray scale correction procedure of

the CT images are necessary to achieve realistic Hounsfield units. Processing of the printed stack with a paper based 3D printer creates stable phantoms with the attenuation properties and the shape of the original patient.

Results: Radiopaque 3D printing allows transfer of patient anatomy and pathology into a detailed individual phantom. Gray scale analysis with ink containing potassium iodide solutions (0.6 g/mL) on a HP Deskjet 6940 inkjet printer (Hewlett Packard, Palo Alto, Calif) yields an exponential correlation between template gray scales and printer deposition. Correction of the print template allows to achieve a linear correlation ($r = 0.9946$; 95% CI: 0.9916, 0.9966). Application of the gray scale correction procedure to the CT image data set results in linear correlation of phantom and patient Hounsfield units ($r = 0.9925$; 95% CI: 0.9635, 0.9985).

Conclusion: Radiopaque 3D printing realizes detailed anthropomorphic phantoms of individual patients. Applications are in training, device and protocol optimization, quality assurance and dosimetric investigations.

Author Disclosures:

P. Jahnke: Patent Holder; DE202015104282U1, EP000003135199A1, US020170042501A1. Research/Grant Support; BIH TTF, BMWi EXIST.

F.B. Schwarz: Research/Grant Support; BMWi EXIST. **M. Ziegert:** Research/Grant Support; BMWi EXIST. **M. Scheel:** Patent Holder; DE202015104282U1, EP000003135199A1, US020170042501A1.

B-0549 11:42

Gallium Arsenide hybrid photon counting x-ray detectors: towards large area single-shot spectral mammography

S. Gkoumas, M. Habl, V. Radicci, M. Rissi, T. Thuering, S. Traut, P. Trueb, P. Zambon, C. Broennimann; *Baden-Daettwil/CH* (*spyridon.gkoumas@dectris.com*)

Purpose: This study presents the latest developments of two dimensional GaAs hybrid photon counting (HPC) detectors with respect to breast imaging applications. We discuss why direct conversion GaAs sensors combined with HPC technology is an optimum choice for fast exposure, single-shot and large area spectral mammography.

Methods and Materials: The two prototype HPC X-ray imaging detectors used for this study are based on the DECTRIS SANTIS 0804 HR design using IBEX technology. They employ GaAs and CdTe as direct conversion sensor materials. Each detector has an active area of $8 \times 4 \text{ cm}^2$, a pixel size of $75 \mu\text{m}^2$ and two fully calibrated and independently adjustable energy selective thresholds. The detectors' performance is assessed using mammography phantoms such as the ACR 156 and also imaging performance characteristics such as quantum efficiency (QE), modulation transfer function (MTF) and the newly introduced spectral efficiency (SE).

Results: Both GaAs and CdTe show an excellent 5/4/5 score when imaging the ACR 156 phantom. For the relevant energy range of screening and diagnostic mammography, or digital breast tomosynthesis, GaAs exhibits QE higher than 80%. Moreover, GaAs shows higher QE than CdTe for the 30-50 keV energy range which is significant in terms of dose efficiency for spectral mammography. Spectral efficiency in combination with preliminary material decomposition results are discussed.

Conclusion: GaAs HPC X-ray imaging detectors present very attractive characteristics optimally suited for large area, low dose single-shot spectral mammography. They exhibit excellent image quality and optimum QE for the energy range of breast imaging applications.

B-0550 11:50

Development of algorithms to degrade the image quality of mammograms for lesion detectability studies

J. Boita^{1,1}, A. Mackenzie², R. Van Engen¹, M.J. Broeders^{1,1}, I. Sechopoulos^{1,1}; ¹Nijmegen/NL, ²Guildford/UK (*joana.dossantosboita@radboudumc.nl*)

Purpose: To develop algorithms to degrade mammographic image quality for future studies of how varying image quality affects lesion detectability.

Methods and Materials: Algorithms were developed to reduce the contrast in specific image areas, decrease spatial resolution, and add correlated noise in digital mammograms: problems sometimes observed in processed images of several systems. First, an algorithm was developed to segment dark and bright areas on mammograms, reducing their contrast using a sigmoid function. To decrease resolution, images were multiplied by the difference between the standard and the desired, lower modulation transfer function (MTF). Correlated noise was created by enhancing the high spatial frequencies content in the image. The low contrast algorithm was tested by comparing mammograms to low-quality mammograms. Validation of resolution reduction was performed comparing the image of a 3D printed breast phantom placed on the support table corrupted by the MTF obtained 7 cm above the table, to an image of the phantom when placed there, using the Universal Quality Index (UQI). Addition of correlated noise was tested with breast phantom images using the Normalized Noise Power Spectrum (NNPS).

Results: Changes in contrast appeared realistic comparing to real low-quality mammograms. Comparison of phantom images and the simulated reduced

resolution images resulted, as expected, in a UQI of 1. Breast phantom images with added correlated noise showed, as expected, a higher NNPS.

Conclusion: The three algorithms appear to result in realistic images with degraded quality, allowing for flexible paired comparisons with high-quality mammograms when evaluating image quality and detectability.

10:30 - 12:00

Room K

Radiographers

SS 614

Fine tuning MRI practice

Moderators:

J. Castillo; Msida/MT
C. Catalano; Rome/IT

B-0551 10:30

MRI of children aged 4-9 without anaesthesia using communication at the children's cognitive level

S. Scheffmann Olloni, N. Villadsen; *Odense/DK* (*signe_scheffmann@hotmail.com*)

Purpose: The primary purpose was to assess if MRI can be performed without anaesthesia on children aged 4-9 using communication at their cognitive level. The secondary purpose was to evaluate the parents' perception of the children's confidence using an app to inform about the scan.

Methods and Materials: During a 3-month period, we asked 52 children aged 4-9 to show up 30 minutes before their MRI scan. 11 of the children were scheduled for MRI under general anaesthesia (GA). We welcomed each child in the waiting room and established a good relation with the child to provide the necessary information before the MRI scan. We used an app called 'HC And' with animated characters showing how MRI and other examinations are performed. Furthermore, we asked the parents to answer a questionnaire to assess if they thought their children were better informed and more confident after using the app.

Results: All children scheduled for GA completed the scan without GA. All parents rated the app either overall good or very good. All parents felt their child got more information about the scan using the app. All parents felt that their child was more confident before and during the scan using the app.

Conclusion: Using communication at the children's cognitive level, more children can complete MRI scan without GA. At the same time, the use of the app markedly improves the parents' perception of the children's confidence.

B-0552 10:38

Development of an fMRI linguistic paradigm to monitor PPA patients: a pilot study

C. Ferreira¹, I. Cadório², A. Barbosa², A. Freixo², B. Silva², D. Figueiredo², M. Lousada², M. Castelo-Branco¹, P.M. Martins²; ¹Coimbra/PT, ²Aveiro/PT (*pmartins@ua.pt*)

Purpose: Functional magnetic resonance Imaging (fMRI) is an emerging technique used to report therapy induced changes in primary progressive aphasia (PPA). However, there are no well-defined protocols and most studies only use picture naming tasks. This study aimed to develop and test an adequate fMRI paradigm for future use in PPA patients.

Methods and Materials: Five right-handed healthy volunteers were enrolled in this study. Three lists of stimuli were visually presented, one for each task. The naming task consisted of 40 black and white line drawings. Semantic task included 15 related word-pairs and 15 unrelated word-pairs. A total of 36 non-word pairs were specifically tailored to the phonological task, considering European-Portuguese syllabic structure. Image acquisition was carried out in a 3T scanner and general linear model analysis was performed using BrainVoyagerQx. Statistical findings were thresholded at the voxelwise level $p < .05$ and corrected for multiple comparisons.

Results: The naming task induced a left-sided activation of frontotemporal cortices accompanied by a bilateral activation of occipital regions. In the semantic task, participants recruited semantic processing areas located in the left frontotemporal and parietal lobes, as well as occipital lobe bilaterally. The phonological task revealed cortical activity in the left frontal lobe, right cerebellar areas, and bilateral occipital lobe. In general, cerebral activation patterns found in this study are supported by the literature.

Conclusion: This protocol can be used in future studies targeting PPA population. Diagnosis and treatment monitoring can be facilitated by comparing the activated areas of PPA individuals with a matched-control group.

B-0553 10:46

1.5T vs 7T in determining changes of white matter in multiple sclerosis: preliminary studies

A. Pankowska, K. Kochalska, K. Dyndor, A. Łazarczyk, R. Pietura; Lublin/PL (zubianna@gmail.com)

Purpose: Multiple sclerosis is a chronic, progressive neurological disease which causes disablement and cognitive impairment. The aim of this work is to reveal main advantages of examinations performed in the ultra-high magnetic field. More precise and detailed imaging may help in better understanding of mechanisms responsible for origination and progression of this disease.

Methods and Materials: MRI examinations were performed on 1.5 T Optima MR GE using 8-channel NV Head Array Coil and Discovery 950 GE 7T scanner with Nova Head 32-channel head coil. At 1.5 T we performed a 3D CUBE T2 FLAIR and 3D T1 SPGR sequence with inversion time of 1000ms. At 7 T we acquired 3D CUBE T2, 3D T1 BRAVO sequence with an inversion time of 1000ms and SWAN. All ten patients with a demyelinating disease with age in a range of 22 to 58 and EDSS scale in the range of 1 to 6 were imaged on the both MRI systems. Images of all patients group were analyzed by two radiologists working in consensus.

Results: Studies performed in 7T showed higher sensitivity and specificity in detecting the presence of demyelinating plaques in the subcortical white matter and changes in the cerebral cortex. SWAN sequence presented the characteristic course of the blood vessels through a demyelination plaque.

Conclusion: Ultra-high 7T field MR imaging contributes to the better detection and characterisation of MS lesions due to an increased signal to noise ratio (SNR) and improved contrast what allows clinician for better visualisation of white matter lesions.

B-0554 10:54

A multi-centre study: qualitative and quantitative comparison of liver MR image quality

S. Al Dahery, L.A. Rainford, A. McGee; Dublin/IE (shrooq_talal@hotmail.com)

Purpose: Quality evaluation of axial liver MR images acquired at 1.5T using two-dimensional (2D) breath-hold T2-weighted (T2W) fast spin-echo (FSE) and three-dimensional (3D) T1-weighted (T1W) gradient echo sequences, focusing on the clarity of visualisation of normal liver anatomy.

Methods and Materials: Axial 2D T2W FSE and T1W 3D GRE pre-contrast liver MR images from (n=96 cases) acquired at Irish (n=10) and Kingdom of Saudi Arabia (n=9) hospitals were analysed. SNR and CNR values were calculated for normal liver parenchyma, spleen and background noise. Images were evaluated qualitatively for the presence of motion artefacts, visualisation of liver parenchyma and vascular pattern and spleen parenchyma. Optimal sequence parameters were independently agreed by expert readers (n=8) and applied to 10 volunteers. Radiologists (n=3) and radiographers (n=2) qualitatively evaluated optimised liver MR images and indicated their preferred sequence (original/optimised).

Results: Differences in motion artefact within original T2W FSE images was noted between countries. Differences in 3D T1W GRE image quality criteria scores for spleen parenchyma visualisation, SNR and spatial resolution from protocol 1 using a slice thickness ≤ 3 mm compared to protocol 2 using slice thickness of ≥ 4 mm were noted ($p < 0.05$). SNR and CNR findings elicited significant differences following optimisation compared the original protocols ($p = 0.004$). Qualitative descriptive statistics were higher for the optimised protocols compared to the original protocols for all sequences.

Conclusion: Radiographers require appropriate knowledge of MR physics to fully optimise MR image quality. Quantitative and qualitative evaluation of MR images can usefully guide sequence parameter optimisation.

B-0555 11:02

Performance of single-use syringe versus multi-use MR contrast injectors: a prospective comparative study

F. Struik, J.J. Futterer, M. van der Graaf, M.M. Prokop; Nijmegen/NL (femkestruik@gmail.com)

Purpose: To compare performance parameters of a single-use syringe and a multi-use MR contrast injector.

Methods and Materials: We compared preparation time, cost for disposables and volumes of contrast material used for a single-use syringe (A; Mallinckrodt Optistar LE, Liebel-Flarsheim, USA) and a multi-use MR contrast injector (B; Max 3, Ulrich Medical, Germany) in a prospective cross-over trial. All consecutive patients eligible for dynamic MRI on two MR systems were included during a period of 20 working days. After 10 days, the injector was switched. Technician satisfaction was evaluated using a questionnaire.

Results: We could include 111 and 95 patients for systems A and B, respectively. Average preparation time was 4:55 min for A and 2:24 min for B ($p < 0.05$). Total injected volume was 752 ml for A and 695 ml for B (N.S.). Contrast waste for A was 10.7% using 7.5-ml syringes. Contrast waste for B was 4.5% for 7.5-ml containers. Costs for disposables were lower for B if more

than 5 patients per days were injected. Technicians satisfaction was higher for B (4.7 versus 2.8 on a 5-point scale; $p < 0.05$).

Conclusion: The multi-use MR contrast injector led to higher technician satisfaction, shorter preparation time, and lower cost if more than 5 patients were injected per day. In addition, cheaper contrast containers of 15 or 30 ml could be used for the first patients if more than 2 or more than 4 injections are performed per day.

Author Disclosures:

F. Struik: Research/Grant Support; Ulrich Medical. **J.J. Futterer:** Research/Grant Support; Ulrich Medical. **M. van der Graaf:** Research/Grant Support; Ulrich Medical. **M.M. Prokop:** Research/Grant Support; Ulrich Medical.

B-0556 11:10

Ambient experience in MRI

P. Pedersen¹, L. Fremmelevholm¹, S.H. Jørgensen², S. Moerup¹; ¹Odense/DK, ²Svendborg/DK (curly64@gmail.com)

Purpose: To investigate if radiographers can contribute to reduced anxiety during MRI scans for adults with the use of new developed Ambient Experience system.

Methods and Materials: In total, 102 patients were included in this study and randomized into two groups, 61 patients (61.8%) were scanned with the Ambient Experience system turned on and 41 (40.1%) were scanned with white light. Two validated questionnaires "The Magnetic Resonance Imaging-Anxiety Questionnaire" and "The Claustrophobia Questionnaire" were used to illustrate whether Ambient Experience (Philips Healthcare, Amsterdam) could reduce anxiety for adults during an MRI scan. Patients included in this study were all scanned with head first to get the perfect effect of the Ambient Experience system.

Results: Results showed that 83 of the 102 patients had a degree of claustrophobia. 29 patients had a mild degree, 33% of these patients scanned with Ambient Experience were more relaxed during the MRI scan, than patients scanned without the system (9%). Furthermore, six patients scanned with Ambient Experience described that previous scans were horrible or uncomfortable, but the use of Ambient Experience made it a better experience with reduced anxiety.

Conclusion: The questionnaire indicated that patients preferred to be scanned with Ambient Experience. It is difficult to conclude that Ambient Experience alone can reduce anxiety. Communication, time and previous experiences can also affect the patient; however, all 61 patients scanned with Ambient Experience had a better experience during the scan and felt less anxious than those who have been scanned with white light.

B-0557 11:18

Evaluation of occupational exposure from electromagnetic field radiation on mobile magnetic resonance imaging units

A.F.C. Sousa, J. Santos, A. Ferreira; Coimbra/PT (a.filipa.c.sousa@gmail.com)

Purpose: The health staff exposure to electromagnetic fields in Magnetic Resonance Imaging (MRI) has been increasing and no evidence is found regarding the mobile MRI units and their exposure measurement. This study intends to measure the staff exposure to static magnetic fields on these units to assess compliance with exposure limits.

Methods and Materials: This investigation was performed in the United Kingdom, in 5 mobile MRI units, Siemens Symphony 1.5T and was divided in three phases: analyses of the examinations frequency; Measurement of the first operator exposure using a TAOMA TS/001/UB combined with a TS/002/BLF probe during routine protocols (n=98); Quantification of the exposure variation in different locations using a homogenous phantom.

Results: The lumbar spine, knee and brain are the three most common anatomic regions examined. On the second phase, no significant differences were found between the anatomic region selected and the amplitude or frequency ($p > 0.05$). However, significant differences were found ($p = 0.001$) between the anatomic regions and the maximum value detected on the lumbar spine. On the third phase, the amplitude values shown significant differences between the amplitude value and the probe's position ($p = 0.015$).

Conclusion: The obtained results are in compliance with the Electromagnetic Field Directive. However, it would be interesting to promote training for MRI mobile workers, in order to present methods for their exposure reduction during patients attending. Further research on this subject would be helpful and interesting, not just on the mobile units but also at other facilities.

B-0558 11:26

Detection of colorectal cancer liver metastases with MRI: is diffusion-weighted imaging (DWI) solely as good as DWI + dynamic T1-weighted sequences after extracellular Gd?

M.N. Tettero; Alkmaar/NL (mereltettero@gmail.com)

Purpose: To compare the diagnostic performance of unenhanced liver magnetic resonance imaging (MRI) with diffusion-weighted MR (DWI) and Gd-

based enhanced liver MRI with DWI in patients with colorectal liver metastases (CRLM) on per-patient basis.

Methods and Materials: A query of our image database was performed between 2014 and 2016, identifying patients with histologically proven colorectal cancer, who were submitted to MRI for suspicion of CRLM. 24 patients were found with CRLM, and 24 patients without liver metastases were found to form the control group. All patients underwent dedicated liver MR protocol among others with DWI and T1-weighted GRE sequences after extracellular Gd. Comparison was performed between the entire dataset (extended protocol) and reduced dataset in which the post-contrast T1 GRE had been removed (reduced protocol). Three abdominal radiologists evaluated both datasets independently of each other, with a minimum time between the reading of 2 weeks. Images were correlated with the reference standard (consisting of histopathology/comparison imaging/follow-up).

Results: The diagnostic performance for the detection of CRLM, on per-patient basis is as follows. Reduced protocol: sensitivity 92% (CI 80.6-100), specificity 100%. Extended protocol: sensitivity 100%, specificity 100%.

Conclusion: DW-MRI is an excellent imaging tool for screening and surveillance of patients at risk of CRLM (sensitivity 92%, specificity 100%) with a short scan time of 10-15 minutes. The combination of DWI with enhanced T1-weighted MRI is the best screening modality for CRLM with 100% sensitivity and 100% specificity, however, with long scan times, 40-45 minutes and with the administration of intravenous contrast agent.

B-0559 11:34

A data mining approach to the SAR values over large MR image repositories

A.C.C. Murragas¹, P.M. Martins¹, C. Ferreira², T.M. Godinho¹, M. Castelo-Branco², A. Silva¹; ¹Aveiro/PT, ²Coimbra/PT (accm@ua.pt)

Purpose: In magnetic resonance imaging, the radiofrequency energy absorption arises as one of the main safety concerns, being mainly related with increased body temperature. Monitoring radiofrequency absorption is achieved by the estimation of specific absorption rate (SAR), whose implementation lies on equipment manufacturers, which in turn are not totally enlightening about its calculus. This work presents an exploratory approach of whole-body SAR values stored in DICOM metadata aiming to find correlation with body weight, body mass index (BMI), gender and pulse sequences for abdominal/pelvic (17.812 series) and head (29.907 series) studies.

Methods and Materials: All studies were acquired in a 3 Tesla scanner with high-performance gradients. Data were extracted using Dicoogle, a DICOM metadata mining tool. Several DICOM tags were analysed (e.g. patient weight, height, gender, sequence name). For each study type, specifically weighted pulse sequences were related with weight, BMI and gender through boxplot diagrams, statistical and effect size analysis.

Results: SAR limits were never exceeded. Generally, SAR values tended to decrease with increasing body weight and BMI values for abdominal/pelvic studies. On the other hand, head studies showed different trends regarding distinct pulse sequences. SAR values tend to be higher in male individuals (p<0.05). As expected, turbo spin echo sequences present the highest SAR values. The values found for echo gradient spoiled sequence (FLASH) were also high.

Conclusion: It is confirmed that SAR estimates are related with the analysed variables. An individual examination of pulse sequences is recommended to observe trends regarding weight, BMI or gender.

B-0560 11:42

Optimisation of the Blade technique in the cervical spine MRI

R.M. Lopes¹, D. Carvalho²; ¹Vila Nova de Gaia/PT, ²Coimbra/PT (rogeriolopes87@gmail.com)

Purpose: The Blade technique for MRI imaging of the cervical spine has proven to be a reliable tool for reducing artifacts typically for this anatomic region. The objective of the study is to evaluate the image quality, the contrast and diagnostic acuity between T2 TSE conventional and T2 Blade in the axial and sagittal planes.

Methods and Materials: The sample is composed of 14 patients in the sagittal plane and 12 patients in the axial, being acquired with similar acquisition parameters and evaluated by two neuroradiologist. Statistical evaluations were achieved using the X² test.

Results: The neuroradiologist A considered the images of the sagittal Blade excellent in 42.9% of the cases and only 14.3% in the TSE that relates the characterization of bone lesions. The neuroradiologist B considered the sagittal Blade technique excellent in 78.6% of the cases and only 35.7% in the TSE in the representation of herniated disc. In the axial plane, in the representation of bone lesions, the neuroradiologist A, considers the Blade technique excellent in 41.7% of the cases and only 25% in the TSE. The neuroradiologist A, select the Sagittal Blade technique in 42.86% and the TSE in 7.14% of the cases. The neuroradiologist B, in the axial plane prefers the Blade in 41.67% and only 8.33% in the TSE.

Conclusion: The quality of the images belonging to the T2 Blade sequences on the sagittal and axial plans were considered superior to the T2 TSE conventional.

B-0561 11:50

Comparing the detection rate of melanoma metastases on gadolinium-based contrast-enhanced MRI brain scan compared to a non-enhanced scan.

K. Thakor, V. Major, S. Patel, H.R. Bergman, W. McGuire, A. Lakhani; Northwood/UK (kirti_taylor@yahoo.co.uk)

Purpose: Malignant melanoma is the 3rd most common malignancy to metastasise to the brain. At our institution, patients with high-risk melanoma undergo surveillance with regular MRI brain scans with intravenous gadolinium-based contrast agents (GBCA). Research has recently shown that recurrent administration of GBCA can result in gadolinium deposition within the brain although the effects of this is yet unknown. The purpose of this study was to identify if intracranial metastatic melanoma deposits can be visualised on the pre-contrast scans to evaluate if these patients can undergo surveillance with unenhanced brain MRI scans.

Methods and Materials: A retrospective study was conducted. Consecutive patients attending for MRI brain scans with intravenous GBCA for metastatic melanoma were reviewed for the period of January 2016 to December 2016. The pre-contrast T1 coronal sequence was compared to the post-contrast 3D sequence.

Results: 195 patients were evaluated. An intracranial metastatic deposit was reported in 13.9% of the scans, out of which only 25.9% of the scans showed identifiable metastasis on the pre-contrast scan.

Conclusion: The results demonstrate that the use of GBCA is essential in brain scans for metastasis detection in patients with melanoma as the majority of lesions are not identifiable without contrast enhancement. However, at our institution the pre- and post-contrast sequences are not identical, this difference could account for some of the number of lesions detected. Using the same sequence for pre- and post-contrast scans for further investigation would help in a more accurate comparison.

10:30 - 12:00

Room M 1

Cardiac

SS 603

Update on large trials, registry and adverse event assessment

Moderators:

C.D. Claussen; Tübingen/DE
P. Toia; Palermo/IT

B-0562 10:30

Correlation of a new formula measuring carotid-femoral pulse wave velocity with cardiovascular risk factors, major adverse events and mortality

S. Chin, J. Weir-McCall, L. Brown, J. Summersgill, P. Talarczyk, M. Bonnici-Mallia, F. Khan, A.D. Struthers, G. Houston; Dundee/UK (sookcheng@doctors.org.uk)

Purpose: Carotid femoral pulse wave velocity (PWV) is a strong predictor of cardiovascular mortality and methods using external distance measurements are not reliable as they are prone to confounding factors. A new formula for PWV calculation was derived from whole-body magnetic resonance angiograms (WB-MRA) and we aim to examine if this formula correlates better with cardiovascular risk factors, major cardiovascular adverse event (MACE) and mortality.

Methods and Materials: Arterial pathlengths were measured from WB-MRA from the TASCFORCE study group and backwards linear regression was applied to derive the formula: carotid femoral pathlength=100.36+(0.70×age[years])+(137.81×height[m])+(0.51×weight[kg])-(0.18×pulse)+(46.25 [if female],53.89 [if male]). This was then applied to two population study groups. From this, correlation between the new PWV calculations (PWV_{NEW}) versus external measurements (PWV_{CAER} and PWV_{SUM}) and cardiovascular risk factors were calculated using Pearson and Spearman correlation co-efficients. Significant difference was assumed when p<0.05.

Results: There were 1242 SUMMIT study participants and 825 Caerphilly study participants. There were no loss of correlation between PWV_{NEW} with age, blood pressure or creatinine levels (p<0.01). In both the SUMMIT and Caerphilly cohort, the PWV_{NEW} showed a loss correlation with obesity and waist circumference. The hazard ratio was 1.11 and 1.17, respectively, for cardiovascular mortality and MACE and is unchanged for all PWV measurements.

Conclusion: The new formula based on the patient's height, weight, sex and pulse measurements demonstrates less variability and is more accurate compared to measurements using external distances without losing its association with cardiovascular risk factors, MACE and mortality.

Author Disclosures:

J. Weir-McCall: Grant Recipient; Guerbet Laboratories. **G. Houston:** Grant Recipient; Guerbet Laboratories, Cook Medical, Medtronic.

B-0563 10:38

Acute adverse events in cardiac MR imaging with gadolinium-based contrast agents: results from the European Society of Cardiovascular Radiology (ESCR) MRCT registry in 72,839 patients

J. Uhlig¹, C. Lücke², R. Vliegenthart³, C. Loewe⁴, M. Grothoff², A. Jacquier⁵, M. Francone⁶, J. Lotz¹, M. Gutberlet⁷; ¹Göttingen/DE, ²Leipzig/DE, ³Groningen/NL, ⁴Vienna/AT, ⁵Marseille/FR, ⁶Rome/IT (cluecke@gmx.de)

Purpose: To assess the incidence of acute adverse events (AAE) in gadolinium-enhanced cardiac magnetic resonance (CMR) imaging with statistical adjustment for potential confounders.

Methods and Materials: Gadolinium-based contrast agents (GBCA) enhanced CMR from the ESCR MR/CT registry were included. AAEs were classified according to the ACR manual on contrast media. Multivariable logistic regression was used to model the likelihood of AAEs in various GBCA, adjusting for pharmacological stressor, main indications, age and sex.

Results: In 72,839 CMR, 260 AAE occurred (0.36%), with a minority of severe adverse events (SAE) (n=24, 0.033%). Patients without pharmacological stress (PS) imaging had a lower AAE rate (n=120/54,285, 0.22%) than patients receiving PS (n=140/18,554, 0.75%). Highest AAE rates were reported for regadenoson (n=34/1,151, 2.95%), and dobutamine (n=7/482, 1.45%), mainly dyspnoea (n=24). Compared to the most frequently used gadobutrol [56%], AAE were more likely for gadoteridol [4%] (OR=3.16, 95% CI: 2.10-4.74, p<0.001), and less likely for gadoter acid [20%] (OR=0.64, 95% CI: 0.44-0.93, p=0.018). There was multiplicative interaction between GBCA and PS (p<0.01). Comparing adenosine to regadenoson, the AAE rate differed by the factor 9 for gadobutrol (0.52% vs 4.56%), while rates were comparable for gadoter acid (0.3% vs 0.47%), independent of PS. However, no significant difference in the frequency of AAEs depending on the molecular structure, ionicity or chelate stability of GBCAs was found.

Conclusion: GBCA-enhanced CMR is generally safe with event rates comparable to those of other body regions. The likelihood of AAE increases with stress imaging and depends on the pharmacological stressor and main indication.

B-0564 10:46

Prevalence and clinical relevance of extra-cardiac findings in CMR imaging

D. Mastrodicasa¹, C. Mantini², F. Bianco², F. Ricci², S. Gallina², G. Messalli³, F. Cademartini⁴, A.R. Cotroneo⁵; ¹Charleston, SC/US, ²Chieti/IT, ³Naples/IT, ⁴Rotterdam/NL (domenico.mastrodicasa@gmail.com)

Purpose: To estimate the prevalence of ECF detected from clinically indicated CMR scans, and to determine the associated downstream effect on clinical management and resource utilisation.

Methods and Materials: ECF were retrospectively evaluated in 500 consecutive patients undergoing CMR for different cardiovascular diseases. Two independent radiologists retrospectively reviewed transaxial bSSFP multi-slice images acquired with a field of view including thorax and upper abdomen. The ECF were classified as clinically non-significant (benign), clinically significant (potentially or absolutely considered to be of clinical significance, mandatory to be reported and monitored), and major (remarkable pathology, mandatory to be reported, further investigated and treated). A 15-month clinical follow-up was obtained from hospital records and referring physicians.

Results: Of 500 patients, 108 patients (21.6% of study population) had a total of 153 ECF, 59 (38.8%) non-significant, 76 (50%) significant and 18 (11.7%) major. Of 94 significant and major ECF, 46 (36 clinically significant and 10 major) were previously unknown and more common in older patients. The 10 newly diagnosed major ECF (2% of study population and 6.5% of all IEFs), including tumours in 5 patients (1% of study population), were confirmed by downstream evaluations and required specific treatment. Patients with major ECF were older than patients without. Significant and major newly diagnosed ECF both required additional diagnostic tests respectively in 44% and 100% of cases.

Conclusion: ECF are increasingly being spotted by radiologists and cardiologists on CMR scans. The detection of previously unknown major ECF has a strong impact on the course of patients' clinical history.

B-0565 10:54

Results from the Italian Registry of Contrast Material use in Cardiac Computed Tomography (IRCM-CCT)

L. La Grutta¹, A. Clemente², E. Maffei³, G. Privitera⁴, M. Rengo⁵, P. Toia¹, M. Francone⁶, M. Midiri¹, F. Cademartini^{7,8}, ¹Palermo/IT, ²Massa (MS)/IT, ³Urbino/IT, ⁴Catania (CT)/IT, ⁵Latina/IT, ⁶Rome/IT, ⁷Rotterdam/NL, ⁸Naples/IT (ludovicola.grutta@hotmail.it)

Purpose: The Italian Registry of Contrast Material use in Cardiac Computed Tomography (IRCM-CCT) is a retrospective, multicenter, multivendor, observational study on the use of contrast media (CM) in patients undergoing CCT. The aim of IRCM-CCT is to assess safety profile and influence on image quality of CM use.

Methods and Materials: IRCM-CCT enrolled 1894 consecutive patients (≥50 per site; CCT indicated for suspected coronary artery disease) at 20 cluster sites. Demographic characteristics, CT and CM protocols, clinical indications, safety markers, radiation dose reports, qualitative (i.e. poor vascular enhancement) and quantitative (i.e. HU attenuation values) image parameters were recorded. A core lab assessed all image parameters.

Results: The cohort includes 1117 men and 777 women (mean age 61±14 years, mean body mass index 26±4) studied with ≥64 detector rows CT scanners and several iodine contrast media protocols and molecules (iodixanol, iopamidol, iobitridol, iopromide, and iomeprol). The following adverse reactions to CM were recorded: 6 extravasations and 17 reactions (11 mild, 4 moderate, 2 severe). The core lab reading reported the following vascular attenuation: 537±160HU in the aorta, 472±160HU in the right coronary artery, 502±158HU in the left main, 475±156HU in the left anterior descending artery, and 458±158HU in the circumflex artery. In 4% of cases the image quality was not satisfactory due to poor enhancement.

Conclusion: In a multicenter registry on CM use during CCT the prevalence of CM-related adverse effects was very low. The appropriate use of CM is a major determinant of image quality.

B-0566 11:02

Frequency and spectrum of incidental findings in cardiovascular disease CT screening trial

M. Vonder¹, C.M. van der Aalst², R. Vliegenthart¹, M. Kaatee¹, J. Gratama³, D. Kuijpers⁴, H. de Koning², M. Oudkerk⁵; ¹Groningen/NL, ²Rotterdam/NL, ³Apeldoorn/NL, ⁴The Hague/NL (marleenvonder@gmail.com)

Purpose: To determine the frequency, spectrum, and potential clinical relevance of incidental findings found on computed tomography coronary artery calcium scans (CT-CAC) of screenees.

Methods and Materials: Incidental findings on CT-CAC scans of screenees from the ROBINSCT trial were recorded from January 2015 through September 2017. Informed consent for the ROBINSCT trial was obtained from all participants. Incidental findings were described individually and grouped based on potential clinical relevance and organ level. Incidental findings with a high potential of being clinically relevant were reported to the screenee's general practitioner.

Results: In total, 10,129 screenees underwent a CT-CAC scan, mean age was 61.6 (SD: 7.3) years and 52.1% were male. One or more incidental findings were recorded on 603 (6.0%) CT-CAC scans, the mean of age of screenees with an incidental finding was 64.1 (SD: 6.5) year and 40.7% were male. Of the incidental findings found, 46.1% was hepatic, 24.5% cardiovascular, 13.5% pulmonary, 12.0% gastrointestinal, 3.0% lymphatic and 0.7% splenic. Of all incidental findings, 9.0% were potentially clinically relevant and were reported to the general practitioner.

Conclusion: In 1:16 screenees one or more incidental findings are found on CT-CAC scans for cardiovascular screening, and 1:200 is potentially clinically relevant and reported to the general practitioner.

B-0567 11:10

Correlation between haptoglobin phenotypes and myocardial reperfusion injury in consecutive ST-elevation myocardial infarction as detected by cardiac magnetic resonance

M. Guglielmo¹, C. Banfi¹, E. Giannazza¹, A. Guaricci², A. Baggiano¹, D. Andreini¹, S. Mushtaq¹, M. Pepi¹, G. Pontone¹; ¹Milan/IT, ²Bari/IT (marco.guglielmo@cctm.it)

Purpose: Primary percutaneous coronary intervention (pPCI) has significantly reduced cardiovascular mortality of ST segment elevation myocardial infarction (STEMI) patients. Cardiac magnetic resonance (CMR) has emerged as the gold standard technique for the measurement of the myocardial salvage index (MSI) and microvascular obstruction (MVO). We sought to evaluate the correlation between variants of haptoglobin and myocardial reperfusion injury.

Methods and Materials: Consecutive STEMI patients reperfused by primary PCI were enrolled in this study with characterization of phenotypes of haptoglobin. A CMR was performed by 1 week after STEMI evaluating the following parameters: left ventricle ejection fraction (LVEF), MSI and

prevalence and amount of MVO. Primary endpoint of study was to evaluate the correlation between different phenotypes of haptoglobin and myocardial reperfusion injury as detected by CMR.

Results: 124 consecutive STEMI were enrolled. Three different phenotypes Hp 1-1, Hp 1-2, Hp 2-2 were observed in 10 (8%), 55(44%) and 59(48%) patients, respectively. CMR showed a LVEF and MSI of $49\pm 10\%$ and 0.38 ± 0.9 , respectively. The MVO was observed in 33 patients (27%) with a mean value of $2\pm 4\%$ of left ventricle myocardial mass. The patients with phenotype Hp 1-1 or Hp 1-2 showed no differences in terms of LVEF (p:0.18) and MSI (p:0.3) but higher prevalence (37% vs 17%, p<0.01) and amount ($2.7\pm 0.4\%$ vs $1.3\pm 0.4\%$ of left ventricle mass, p<0.05) of MVO as compared to phenotype Hp 2-2. Hp 2-2 was an independent predictor of MVO [HR:1.28 (1.08-2.4), p:0.20].

Conclusion: Different variants of haptoglobin may play a crucial role in cardiac repair responses. Further studies might evaluate if different therapeutic strategies should be developed based on phenotypes of haptoglobin of patients.

B-0568 11:18

Basic haematological biomarkers are associated with coronary calcification

A.M. den Harder¹, J.M. Wolterink¹, P.A. de Jong¹, M.C.H. de Groot¹, R.P. Budde², I. Isgum¹, S. Haitjema¹, I.E. Höfer¹, T. Leiner¹; ¹Utrecht/NL, ²Rotterdam/NL (t.leiner@umcutrecht.nl)

Purpose: Improved understanding of potential associations between basic haematological biomarkers and the coronary artery calcification (CAC) score may help unravel the pathophysiology of CAC and subclinical coronary artery disease. Therefore we investigated the association between basic haematological biomarkers and the CAC score.

Methods and Materials: A retrospective cross-sectional study was performed within the Utrecht Patient Oriented Database. Patients with suspected/known coronary artery disease who underwent CT CAC scoring and standard haematology analysis that was part of routine clinical care (within 3 months of CT acquisition) were included. Complete haematology datasets were extracted from haematology analyzers. Linear regression adjusted for clinical confounders was used to assess if haematological biomarkers were related to the CAC score.

Results: In total, 1,507 patients were included of which 43% (n=648) had a CAC score of 0. Mean age (\pm SD) was 53 ± 13 years, and 34% of patients were female. Red blood cell count ($\beta=-0.16$ [-0.25 - -0.04], p=0.011), red blood cell distribution width (RDW, $\beta=0.24$ [0.10 - 0.40], p=0.001), coefficient of variation of neutrophil lobularity ($\beta=0.13$ [0.01 - 0.26], p=0.028) and mean lymphocyte cell size ($\beta=0.24$ [0.11 - 0.38], p<0.001) were independently associated with the CAC score after adjustment.

Conclusion: RDW, coefficient of variation of neutrophil lobularity, and mean lymphocyte cell size are associated with a higher CAC score. While increased red blood cell count is associated with a lower CAC score. These biomarkers may further contribute to our understanding of the pathophysiology of CAC. Future studies should determine the pathophysiological significance of these associations.

Author Disclosures:

A.M. den Harder: Research/Grant Support; Abbott Diagnostics, BBMRI-NL.
J.M. Wolterink: Research/Grant Support; Abbott Diagnostics, BBMRI-NL.
P.A. de Jong: Research/Grant Support; Abbott Diagnostics, BBMRI-NL.
M.C.H. de Groot: Research/Grant Support; Abbott Diagnostics, BBMRI-NL.
R.P. Budde: Research/Grant Support; Abbott Diagnostics, BBMRI-NL.
I. Isgum: Research/Grant Support; Abbott Diagnostics, BBMRI-NL.
S. Haitjema: Research/Grant Support; Abbott Diagnostics, BBMRI-NL.
I.E. Höfer: Research/Grant Support; Abbott Diagnostics, BBMRI-NL.
T. Leiner: Research/Grant Support; Abbott Diagnostics, BBMRI-NL.

B-0569 11:26

Accuracy of an artificial intelligence deep learning algorithm for the detection of calcified plaques at coronary CT angiography

M. Eid¹, C.N. De Cecco¹, D. De Santis², A. Varga-Szemes¹, M.H. Albrecht³, D. Mastroiaca¹, P. von Knebel Doeberitz¹, P. Sahbee⁴, U.J. Schoepf¹; ¹Charleston, SC/US, ²Rome/IT, ³Frankfurt a. Main/DE, ⁴Malvern, PA/US (eidmarwen.md@gmail.com)

Purpose: Evaluate the accuracy of an artificial intelligence deep learning algorithm for the detection of coronary artery calcium in coronary CT angiography (CCTA) studies.

Methods and Materials: 194 patients who had undergone clinically indicated CCTA were retrospectively selected. Two readers independently evaluated the contrast-enhanced images noting the presence of calcified plaques in the right coronary artery (RCA), left anterior descending artery (LAD) and left circumflex coronary artery (LCx). In this analysis, the left main coronary artery (LM) was merged with the LAD. Evaluation discrepancies were solved by a third reader. For the automated analysis, the heart detection, coronary artery centreline detection, centreline labeling, and plaque detection was performed fully automatically. The presence of coronary calcified plaques was assessed by a

recurrent neural network with long short-term memory, previously trained for coronary artery calcium detection. Per-vessel and overall sensitivity, specificity and diagnostic accuracy of the algorithm were calculated.

Results: A total of 194 patients were analysed for a total of 565 vessels. No patient was excluded. On a per-vessel analysis, the algorithm achieved a sensitivity (Se), specificity (Sp), and diagnostic accuracy (DA) of 92.96% (CI 84.33%-96.67%), 82.76% (CI 74.64%-89.14%), and 86.63%, respectively, for the RCA, 93.07% (CI 86.24%-97.17%), 95.45% (CI 88.77%-98.75%), and 94.17%, respectively, for the LM/LAD, 89.86% (CI 80.21%-95.82%), 90.00% (CI 83.18%-94.73%), and 89.95%, respectively, for the LCx. The overall Se, Sp and DA were 92.12 (CI 92.12%-95.19%), 88.89% (CI 84.95%-92.10%), and 90.26%, respectively.

Conclusion: The proposed deep learning algorithm performs with high diagnostic accuracy for the automated detection of calcified plaques at CCTA.

Author Disclosures:

C.N. De Cecco: Research/Grant Support; Siemens Healthineers.
A. Varga-Szemes: Research/Grant Support; Siemens Healthineers.
U.J. Schoepf: Research/Grant Support; Astellas, Bayer, GE, Siemens Healthineers.

B-0570 11:34

Computer-aided detection of coronary plaques in cardiac CTA

L. Liu, J. Yang; Beijing/CN (tjdxxy@qq.com)

Purpose: Computed Tomography Angiography (CTA) is a widely used non-invasive imaging modality to diagnose and treat Cardiovascular diseases (CVD). Detection of coronary plaques (CP), especially non-calcified plaques with lower intensity values, from CTA data is a time-consuming and challenge task. In this work, we proposed and evaluated an automated segmentation system for plaques detection in CTA imagery.

Methods and Materials: We developed a machine-learning framework for plaque detection using 3D convolutional neural network (3D CNN). The system combined both a priori knowledge of CPs and data-driven learning method. CP candidates were generated using intensity, geometric features. The CP candidates in the form of 3D cubes are fed into a 3D CNN to classify plaque and non-plaque inputs. Due to the limited amount of CTA data, transfer learning was utilized to obtain highly discriminative features. The performance of the system on 52 CTA volumes with manually labeled plaques was investigated.

Results: The total detection accuracy was 90.4% with respect to the manual expert. Specifically, 86.3% of non-calcified and 92.4 of calcified plaques were achieved. The mean accuracy of plaque localization was 91.2% in term of the Dice similarity coefficient.

Conclusion: Using a priori knowledge in our computer-aided framework improved the accuracy of coronary detection. The overall performance of the proposed computer-aided frameworks demonstrates a good agreement with manual expert annotations.

Author Disclosures:

L. Liu: Employee; MedPai LLC. **J. Yang:** Employee; MedPai LLC.

B-0571 11:42

Comparison of coronary calcium distribution in large population-based screening trials: Dutch (ROBINSICA) vs multi-ethnic (MESA) population

M. Vonder¹, C.M. van der Aalst², R. Vliegenthart¹, M. Kaatee¹, J. Gratama³, D. Kuijpers⁴, H. de Koning², M. Oudkerk¹; ¹Groningen/NL, ²Rotterdam/NL, ³Apeldoorn/NL, ⁴The Hague/NL (marleenvonder@gmail.com)

Purpose: To compare coronary artery calcium (CAC) distribution of the Dutch ROBINSICA trial and with the multi-ethnic MESA trial.

Methods and Materials: ROBINSICA participants screened with CAC computed tomography (CT) were included in this study, and informed consent was obtained from all participants. The Agatston score was determined and CAC distribution based on the number of affected coronary arteries and diffusivity index was calculated. Diffusivity index (%) was defined as: $1 - \text{CAC in most affected vessel} / \text{total CAC}$. Agatston score-based risk categorization (1-100, 101-300, >300) was performed, and CAC distribution was analysed per risk category. The CAC score and distribution were compared for the Dutch ROBINSICA trial and multi-ethnic MESA trial as published by Blaha et al. (JACC Cardiovascular Imaging 2016).

Results: In total 59.8% of the 7,516 ROBINSICA participants (mean age 62.9 (SD 7.1)) had a positive Agatston score, being higher than in MESA (49.9%). The number of affected arteries increased for increasing age, calcium score and diffusivity index (p<0.001). The CAC distribution tended to be less diffuse for a similar number of affected arteries (2, 3, 4 arteries with CAC) in ROBINSICA (19.7%, 33.1%, 44.1%) compared to MESA (24.3%, 38.2%, 46.0%). On the contrary, a comparable distribution pattern for number of affected arteries over the risk groups was found for the two populations.

Conclusion: The amount of CAC tends to be less diffuse for similar number of affected arteries, while the distribution of the number of affected arteries over the risk categories is comparable for ROBINSICA compared to the multi-ethnic MESA population.

B-0572 11:50

Mitral annular plane systolic excursion assessed by cardiovascular magnetic resonance is an independent predictor of major adverse cardiac events after STEMI

M. Pamminer, T. Nalbach, M. Reindl, G. Klug, S.J. Reinstadler, W. Jaschke, B. Metzler, A. Mayr; Innsbruck/AT (Mathias.Pamminer@tirol-kliniken.at)

Purpose: We aimed to assess whether mitral annular plane systolic excursion (MAPSE) as assessed by cardiac magnetic resonance (CMR) imaging is a predictor of major adverse cardiac events (MACE) after ST-elevation myocardial infarction (STEMI).

Methods and Materials: CMR was performed in 322 consecutive patients within 3 days (IQR 2-4 days) after reperused first acute STEMI. MAPSE was determined in a 4-chamber CINE view by measuring the distance of mitral annulus position between the end diastole and the aortic valve closure. Patients were followed for major adverse cardiac events (MACE) - death, non-fatal myocardial re-infarction, stroke and congestive heart failure. Cox proportional hazards regression modelling was used to identify factors independently associated with MACE.

Results: Thirty-eight MACE (12%) occurred during a median follow-up of 18 months [IQR 12-19 months]. In ROC analysis, the AUC of MAPSE for the prediction of MACE was 0.72 (95%CI 0.64 - 0.80, $p < 0.0001$) with an optimal cut-off value of 8.6 mm. Univariate Cox regression analysis revealed a hazard ratio (HR) for reduced MAPSE of 4.45 (95%CI 2.21 - 9.15, $p < 0.0001$). After adjustment for age, left ventricular (LV) ejection fraction and infarct size the association between reduced MAPSE and MACE remained significant (HR: 3.74, 95%CI 1.51 - 9.22, $p = 0.004$). By Kaplan-Meier analysis, patients with MAPSE < 8.6 mm experienced significantly higher incidence of MACE than patients with a MAPSE ≥ 8.6 mm ($p < 0.0001$).

Conclusion: CMR assessed MAPSE represents an easily determinable parameter and is an independent predictor of MACE after acute STEMI.

B-0574 10:38

Fast acquisition abdominal MRI study for the investigation of suspected acute appendicitis in paediatric patients: prospective assessment of diagnostic accuracy and clinical efficacy

K. James, P. Duffy, R. Kavanagh, A. Feeley, D. Ryan, P. Murphy, C. Bogue, M. Maher, O.J. O'Connor; Cork/IE (richkavanagh@rcsi.ie)

Purpose: The purpose of this study was to investigate if a short duration, fast acquisition MRI scan of the lower abdomen is diagnostically superior and faster than ultrasound when investigating paediatric patients who present with suspected acute appendicitis.

Methods and Materials: After obtaining clinical research ethics committee approval, 17 patients aged between 7 and 16 were included in the study. All patients underwent US and MRI scanning. MRI protocol: Axial and coronal gradient echo T2 scans (SSFSE) from the renal hilum to the femoral heads followed by axial and coronal fat saturated SSFSE. Diffusion weighted imaging was also performed. Diagnostic accuracy, radiologist diagnostic confidence, and patient satisfaction were measured.

Results: Three males and fourteen females were included in the study. Mean age was 11.3 +/- 2.6 yrs. Mean BMI was 20.9 +/- 7 kg/m². The appendix was seen on only 12% of US scans but was seen on 88% of MRI scans ($p < 0.0005$). Appendicitis was diagnosed on 12% of US and on 41% of MRI ($p = 0.05$). Diagnosis remained uncertain after US in 88% of cases and after MRI in 12% ($p < 0.0005$). No difference was found between the mean time for US 16.8 +/- 10 mins [95% CI: 11.6-22] and MRI 18.2 +/- 4.1 mins [95% CI: 16.1-20] ($p = 0.6$). No significant difference was found in patient satisfaction between the modalities ($p = 0.87$).

Conclusion: This fast acquisition MRI abdomen protocol was superior to US in the investigation of paediatric patients with suspected appendicitis with superior diagnostic performance and diagnostic confidence and similar patient satisfaction.

10:30 - 12:00

Room M 2

Paediatric

SS 612

Paediatric abdominal imaging

Moderators:

K. Iliadis; Brighton/UK
D. Kljucsek; Ljubljana/SI

B-0573 10:30

Magnetic resonance enterography (MRE) surveillance of asymptomatic paediatric Crohn's disease patients

K. Wu, M. Gee, J. Kaplan; Boston, MA/US (kwu4@partners.org)

Purpose: Magnetic resonance enterography (MRE) has become the primary modality for the evaluation of symptomatic paediatric Crohn's disease (CD) patients. The role of MRE for surveillance in asymptomatic patients is not clear. We seek to analyse MRE studies performed on asymptomatic CD patients and to identify imaging features associated with clinical recurrence.

Methods and Materials: Retrospective search was performed to identify patients < 18 years of age with known CD and MRE performed while asymptomatic on therapy. Studies were reviewed by an experienced paediatric radiologist blinded to clinical data for the presence or absence of four imaging features: wall thickening, T2 hyperintensity, mural hyperenhancement, and vasa recta engorgement, as well as overall assessment of the presence or absence of active disease. Two paediatric gastroenterologists reviewed the electronic records to evaluate for clinical recurrence within six months of MRE.

Results: 37 MRE studies performed in 36 asymptomatic patients were identified. 10 patients demonstrated clinical recurrence within 6 months of MRE. Overall assessment of disease activity by MRE was observed in a higher proportion of patients with clinical recurrence (80%) compared to patients without recurrence (29.6%) ($p = 0.01$). Among individual imaging features, mural hyperenhancement demonstrated the highest accuracy (76%) and was observed in 80% of patients with 6-month clinical recurrence vs 26% without ($p < 0.01$).

Conclusion: MRE evidence of active inflammation in asymptomatic CD patients is associated with future clinical recurrence, with mural hyperenhancement having a statistically significant association with recurrence within 6 months. These suggest a role for imaging in surveillance of asymptomatic paediatric CD patients.

B-0575 10:46

Comparison of image quality of the abdominopelvic computed tomography in paediatric patients: low-osmolar contrast media vs less iodine-containing iso-osmolar contrast media

M. Kim¹, J.-Y. Hwang¹, K. Choo¹, H. Ryu², Y.-W. Kim¹; ¹Yangsan/KR, ²Seoul/KR (maeran.kim@gmail.com)

Purpose: The aim of this study was to evaluate the effect of iso-osmolar contrast media (CM) containing a low iodine dose on image quality for abdominal computed tomography in paediatrics.

Methods and Materials: The low-osmolar CM group and iso-osmolar CM group consisted of 101 and 102 CT scans, respectively, with patients less than 18 years old. Patient age, weight, radiation dose, peak tube voltage, and volume of CM were retrospectively reviewed. Objective measurement of the contrast enhancement and noise were analysed and contrast-to-noise ratios (CNRs) of the abdominal aorta, portal vein and liver were calculated. Four radiologists participated in subjective analysis. Regarding subjective measurement, a four-point scale system was devised to evaluate degrees of contrast enhancement, image noise, beam hardening artefact, and overall image quality. Reader performance for correctly differentiating the groups was evaluated.

Results: Regarding the objective measurement, contrast enhancement and noise were significantly higher in the low-osmolar CM group ($P < .02$). In subjective analysis, there was no significant difference in contrast enhancement, and overall image quality between groups. Image noise, however, was worse in the low-osmolar CM group ($P = .003$). Overall sensitivity and specificity for correctly differentiating iso-osmolar CM were 58.3% and 51.7%, respectively. Especially, among subjects that used 120kVp, contrast enhancement was significantly stronger in the low-osmolar CM group ($P = .008$), and sensitivity to differentiate the iso-osmolar CM was as high as 75%.

Conclusion: Application of iso-osmolar CM was found to be feasible for performing paediatric abdominopelvic CTs. Subjective contrast enhancement and image quality assessments were not statistically different between groups.

B-0576 10:54

CT colonography in the diagnostic algorithm of examination of children with defaecation dysfunction

V. Ermolaeva, N. Marochko, A. Pinigin; Khabarovsk/RU (ermolaeva.valent@gmail.com)

Purpose: The goal of the research was to analyse the anatomical features of the distal colon, pelvic muscle diaphragm by CT colonography in children with defaecation dysfunction.

Methods and Materials: We examined 121 patients, including 13 children after surgical correction of the anal atresia. CT colonography was performed using a CT Toshiba Aquilion64. Children were divided into three age groups: 0-4 years (young), 5-10 years (middle) and 11-17 years (older).

Results: The research showed a significant increase in anorectal angle in the group of children with encopresis: $115 \pm 8^\circ$ and in the group of operated children: $122 \pm 9^\circ$, as a sign of puborectalis muscle dysfunction. Anorectal angle was $94 \pm 2.5^\circ$ in the young and the middle-age groups and $86 \pm 5^\circ$ in the older group with constipation. External anal sphincter was considerably thicker in children with constipation, than in children with encopresis. The research revealed a significant shortening of the puborectalis muscle in patients with constipation and its lengthening in patients with encopresis. We offered to use the ratio of the length to width of the puborectalis muscle (PR coefficient) that was 10 ± 2 in the patients with encopresis and 19 ± 5.5 in operated patients, which was significantly different from the control group: 7.5 ± 0.6 .

Conclusion: CT colonography allows to determine the role of pelvic diaphragm and distal colon in the development of defecation disorders in children, including in patients after surgical correction of the anal atresia.

B-0577 11:02

Value of structured report form for appendix ultrasound in paediatric patients: can we reduce negative appendectomy and additional CT?

H. Kim, H. Kim, S. Jang; *Seongnam-si/KR (rabaftrap@naver.com)*

Purpose: To evaluate the rate of negative (unnecessary) appendectomy and additional CT exams after structured report (SR) versus free text report (FTR) for ultrasound (US) exams in paediatric patients with suspected appendicitis.

Methods and Materials: Between January 2009 and June 2016, 1150 paediatric patients with suspected appendicitis who underwent appendix US were included. On November 2012, we deployed a SR form delivering the likelihood of appendicitis in a 5-point Likert scale for appendix US. The patients were classified into two groups according to the US report form (SR and FTR). The patients of each group were categorised into three grades according to the likelihood of appendicitis (1=not appendicitis, 2=equivocal appendix, and 3= acute appendicitis) based on described US report. Primary outcome (percentage of appendectomy rate) and secondary outcome (percentage of additional CT exam following US to diagnose appendicitis) were compared between two groups.

Results: We identified 550 patients in the FTR group and 600 patients in the SR group. Negative appendectomy rates were decreased by 8.4% between two groups: 16.2% (19 of 117 patients) in FTR and 7.8% (8 of 102 patients) in SR ($p = 0.028$). And there was also decrease in the proportion of additional CT exam by 5.3% between two groups: 13.5% (74 of 550 patients) in FTR and 8.2% (49 of 600 patients) in SR ($p = 0.003$).

Conclusion: Using the SR based on the likelihood of appendicitis for paediatric appendix US can decrease the rate of negative appendectomy and additional CT exam.

B-0578 11:10

Liver regenerative nodules in paediatric patients: diagnostic value of Gd-EOB-DTPA

E. Petrush, E.V. Mikhaylova, D. Sevrjukov, A. Nikulina; *Moscow/RU (cherkun.ekaterina@gmail.com)*

Purpose: To describe radiological patterns of multiple liver lesions in hepatospecific phase in children after cytostatic and immunosuppressive therapy to analyse their nature.

Methods and Materials: Nine children aged 10 to 17 with multiple liver lesions were included in retrospective study with the following diagnoses: Ewing's sarcoma ($n=1$), vaginal rhabdomyosarcoma ($n=1$), neuroblastoma ($n=1$), nephroblastoma ($n=1$), dermatofibrosarcoma ($n=1$), Li-Fraumeni syndrome ($n=1$), glomerulonephritis ($n=2$), juvenile rheumatoid arthritis ($n=1$). 6 patients underwent chemotherapy, 2 high-dose chemotherapy, 1 radiation therapy on abdominal area, 3 immunosuppressive therapy. All children underwent MRI at 3T using body coil. Contrast agent Gd-EOB-DTPA was used at dose of 0.1ml/kg.

Results: Liver lesions appeared in the interval 2 to 14 years after special treatment for oncology patients, 2 to 9 years from the beginning of treatment for patients continuously receiving immunosuppressive therapy. Most of the nodules accumulated contrast agent in hepatospecific phase (i.e. have hepatocyte nature). Among multiple hepatocyte-nature lesions in patient with Li-Fraumeni syndrome the 3rd tumour (PEComa) has been revealed. It had different pattern of contrast enhancement compared to other lesions in hepatospecific phase. Diagnoses were confirmed histologically for non-hepatocyte lesions, by dynamic control for hepatocyte lesions.

Conclusion: Multiple liver hepatocyte nature lesions in children may be assigned to hepatotoxic therapy and were described as regenerative nodules. However, we should not forget about the possibility of appearance of new primary tumours in these patients. Hepatospecific contrast agent can explain nature of the liver lesions and provide the possibility to avoid biopsies in some cases.

B-0579 11:18

Simplified cystography protocol for dose exposure reduction in paediatric patients for the diagnosis of vesicoureteral reflux

G. Zanirato Rambaldi, M. Baldazzi, L. Pierotti, F. Carfagnini, M. Zompatori; *Bologna/IT (giuseppe.zanirato@gmail.com)*

Purpose: Vesicoureteral reflux (VUR) is the most common indication for voiding cystourethrography (VCUG) in paediatric patients. The aim of this study was to evaluate whether a simplified cystography (SC) protocol, consisting of only two images, can lead to the correct diagnosis of presence and degree of VUR, to save dose exposure.

Methods and Materials: We retrospectively reviewed VCUG from 243 patients (164 male, 79 female; aged between 2 days and 24 years, median 7 months) performed in our centre over a period of two years, from July 2015 to June 2017. The SC consisted of two images acquired at maximum filling and post-urination. The first image to reveal passive VUR and the second for active VUR. VUR was graded in the SC unaware of the result of the traditional VCUG. K Cohen and Chi-square tests were applied to analyse the agreement between the SC and traditional VCUG.

Results: The agreement between SC and VCUG was "very good" with k value of 0.952 (95%CI 0.91-0.99). SC, moreover, confirmed the exact degree of VUR in almost all cases ($p < 0.001$ at Chi-square test). Only 7 cases of grade 1 VUR were not diagnosed at SC. SC was 93.7% sensitive (95%CI 88.7-98.7) and 100% specific.

Conclusion: The SC protocol revealed to be accurate in the diagnosis of VUR in paediatric population. Acquiring only two images instead of a traditional VCUG can lead to a drastic reduction in dose exposure to paediatric patients, when the clinical indication is VUR.

B-0580 11:26

Non-contrast-enhanced MR angiography for detecting crossing renal vessels in infants and young children (< 6 years old): comparison with CE angiography and surgery

F. Sertorio¹, M. Damasio¹, V. Incarbono², M. Wong¹, A. Pistorio¹, G. Mattioli¹, G. Magnano¹; ¹Genova/IT, ²Varese/IT (fiammetta.sertorio@gmail.com)

Purpose: Evaluate a new non-contrast-enhanced MR sequence, the bTRANCE (balanced-SSFP-triggered angiography non-CE), for the identification of crossing renal vessels (CRVs) in children under 6 years of age, comparing with data obtained from contrast-enhanced MR angiography (CE-MRA) and surgery.

Methods and Materials: A retrospective review of pre-operative MR urography (MRU) of 29 children (1 month to 6 years old) with monolateral hydronephrosis was conducted by two independent readers. Presence or absence of CRVs at the ureteropelvic junction (UPJ) was identified with T2w, BTFE, bTRANCE sequences and 3D CE-MRA and compared with surgical findings. Intra- and inter-reader agreement was calculated using Cohen's kappa coefficient. Image quality, sensitivity, specificity, positive predictive value (PPV), negative predictive value (NPV), positive likelihood ratio (LR+) and negative likelihood ratio (LR-) were evaluated.

Results: Image quality was fair/good in more than 85% of cases for the bTRANCE, 95% for the CE-MRA. The agreement with surgical findings resulted 83% for the bTRANCE and 75% for the CE-MRA. The bTRANCE had a sensitivity, specificity, NPV, PPV, LR+, LR- of 70%, 92.9%, 81.3%, 87.5%, 9.8, 0.32, respectively, vs 55.6%, 90.9%, 71.4%, 88.3%, 6.11, 0.49 of the CE-MRA. Inter- and intra-reader agreements for the identification of CRVs were both 100% for the bTRANCE, and 88% and 90.9%, respectively, for CE-MRA.

Conclusion: The bTRANCE has proven to be superior to the contrast-enhanced sequences compared with the surgical gold standard in infants and young children under 6 years of age, with UPJ obstruction. Thus, it is a reliable, valid and safe alternative to CE-MRA for identifying CRVs.

B-0581 11:34

Coexistence and relation of congenital and acquired urinary tract pathologies in Jarcho Levin syndrome: comparison to spina bifida aperta

I. Karalok, I. Alatas, H. Canaz, S. Sabet, C. Sever, A. Gayef, N.I. Gurcan; *Istanbul/TR (dr.igulcan@hotmail.com)*

Purpose: Our aim was to evaluate the coexistence and relation of congenital and acquired urinary tract pathologies in Jarcho Levin Syndrome with comparison to spina bifida aperta.

Methods and Materials: 60 Jarcho Levin Syndrome and 55 spina bifida aperta patients, between 2013-2017, were evaluated and compared for congenital and acquired urinary tract pathologies by ultrasonography.

Results: There was a significant increased incidence of position anomaly secondary to rotocolysis ($p < 0.005$), horseshoe kidney ($p = 0.007$) and congenital anomaly ($p < 0.005$) in Jarcho Levin Syndrome compared to spina bifida aperta. We also depicted a significant correlation between renal scar and parenchymal thinning ($p = 0.001$), increased renal parenchymal echo ($p = 0.028$), atrophy ($p = 0.006$) and pelviectasis ($p = 0.049$). Increased echogenicity of renal

parenchyma was positively related with existence of parenchymal thinning ($p < 0.001$), scar ($p = 0.028$), atrophy ($p < 0.001$), hydronephrosis ($p < 0.001$) and bladder wall thickening ($p = 0.014$). Ectopic kidney anomaly was found to be related with renal hypogenesis ($p < 0.001$). Horseshoe kidney anomaly demonstrated a significant correlation with hydronephrosis ($p = 0.024$) and acquired renal pathologies ($p < 0.001$).

Conclusion: Position anomaly secondary to rotoscoliosis, horseshoe kidney and congenital anomaly are more frequent in Jarcho-Levin syndrome compared with spina bifida aperta. Renal scar and increased renal parenchymal echogenicity are the most important predictors of subsequent renal parenchymal disease. Horseshoe kidney is the only congenital anomaly which increases the risk of acquired renal pathologies. Congenital and acquired urinary tract pathologies are more frequent in Jarcho Levin Syndrome than normal population. Long term and careful follow-up is essential in order to reduce the risk of probable renal insufficiency in this group especially in cases with increased echogenicity of renal parenchyma and renal parenchymal scar.

B-0582 11:42

Quantitative evaluation of testicular stiffness with shear-wave elastography

Z. [Bavramoğlu](#), E. Çaliskan, R. Yılmaz, I. Adaletli; *Istanbul/TR*
(incezuhal@yahoo.com)

Purpose: We aimed to evaluate the testicular parenchyma in terms of stiffness in paediatric patients with testicular microlithiasis by shear-wave elastography and compare the values with normal control subjects.

Methods and Materials: Nineteen patients previously diagnosed with testicular microlithiasis under follow-up for 18±10 months were included in study group. In control group, 21 patients with no medical history that could affect testicular tissue were prospectively included. 38 testes in the study group and 42 testes in the control group were evaluated with grey-scale ultrasound and shear-wave ultrasonography.

Results: There were no differences in ages and testis volumes between the study and control groups. The mean SWE values of all testes based on elasticity and speed parameters in the study group were 8.24 ± 2.36 kPa and 1.56 ± 0.16 m/s, respectively; while in the control group mean SWE values were 4.66 ± 1.07 kPa and 1.21 ± 0.12 m/s, respectively. Elasticity values were significantly higher in testes with microlithiasis compared to the control group ($p < 0.001$).

Conclusion: Shear-wave elastography evaluation demonstrate effects of ultrastructural changes in elasticity that are not detected on grey-scale ultrasound. Shear-wave elastography is a further reliable method in follow-up examination of paediatric testicular microlithiasis.

B-0583 11:50

Application of ADC Value of MR DWI in the evaluation of children's renal function

W. [Bai](#), G. Ning, X. Li; *Chengdu/CN* ([huaxi_bwj@163.com](#))

Purpose: To discuss the application of ADC value of MR DWI in the evaluation of children's renal function.

Methods and Materials: 9 patients of 1 stage purpura nephritis (group A: 5 male and 4 female, 7~15 years old) and 6 healthy volunteers (group B: 3 male and 3 female, 6~11 years old) were underwent routine MRI and coronal DWI ($b = 600$ s/mm²). For every child, the ADC values of cortex and medulla in the two kidneys were measured in ADC images, with setting the region of interest (ROI) of about 20mm² to the upper, the middle, the lower regions and calculating the average values. Independent-samples t test was made in the ADC values of cortex and medulla from the two groups. And paired-samples t test was made in the ADC values of cortex and medulla from the same group.

Results: (1) the mean ADC value of cortex in group A (178.73×10^{-5} m²/s \pm 14.04) was lower than that in group B (202.78×10^{-5} m²/s \pm 11.11), with statistically significant differences ($P = 0.004$). (2) the mean ADC value of medulla in group A (161.48×10^{-5} m²/s \pm 20.33) was lower than that in group B (193.56×10^{-5} m²/s \pm 17.67), with statistically significant differences ($P = 0.008$). (3) In group A and B, the ADC value of cortex was higher than that of medulla, without statistically significant differences ($p = 0.114$ in group A and $p = 0.265$ in group B).

Conclusion: MR DWI is a noninvasive method to evaluate children's renal function. The ADC value can early detected the abnormality of renal function in the patient of 1 stage purpura nephritis, before the morphological change.

10:30 - 12:00

Room M 3

Oncologic Imaging

SS 616

Lung cancer: what's next?

Moderators:

M. Sánchez; Barcelona/ES
M. Simic; Zagreb/HR

B-0584 10:30

Comparison of ¹⁸F-FDG PET/CT and ¹⁸F-FDG PET/MRI for thoracic staging in lung cancer patients

J. [Kirchner](#)¹, L.M. Sawicki¹, A.F. Tschischka¹, L. Umutlu², K. Herrmann², B.M. Schaarschmidt¹, G. Antoch¹, P. Heusch¹; ¹Düsseldorf/DE, ²Essen/DE
([Julian.Kirchner@med.uni-duesseldorf.de](#))

Purpose: To compare the diagnostic potential of ¹⁸F-FDG PET/MRI and ¹⁸F-FDG PET/CT for primary and locoregional lymph node staging in lung cancer patients.

Methods and Materials: A total of 101 patients (64 men, 37 women, mean age 62.5±9 years) with histopathologically confirmed NSCLC were included. All patients underwent ¹⁸F-FDG PET/CT and subsequently ¹⁸F-FDG PET/MRI. Two readers performed T and N staging in separate sessions according to the eighth edition of the American Joint Committee on Cancer Staging manual for ¹⁸F-FDG PET/CT and PET/MRI, respectively. Histopathology served as the reference standard. The mean and maximum standardised uptake value (SUVmean and SUVmax) and the maximum diameter of the primary tumour were measured and compared in PET/CT and PET/MRI.

Results: PET/MRI and PET/CT agreed on T stages in 55 of 56 (98.2 %) patients. Compared with histopathology, PET/CT determined correct T-stage in 89.3% and PET/MRI in 87.5%, respectively. For definition of thoracic N stages, PET/MRI and PET/CT were concordant in 100 of 101 patients (99%). PET/CT determined the N stage correctly in 91 of 101 patients (90.1 %). PET/MRI determined the N stage correctly in 90 of 101 patients (89.1%). No statistically significant difference between PET/CT and PET/MRI for primary tumour or lymph node metastases detection was seen. The tumour size and SUVmax measurements derived from PET/CT and PET/MRI imaging exhibited an excellent correlation ($r = 0.968$ and $r = 0.817$, respectively; $p < 0.01$).

Conclusion: ¹⁸F-FDG PET/CT and ¹⁸F-FDG PET/MRI perform equally well for T and N staging in patients suffering from NSCLC.

B-0585 10:38

Impact of waiting times on tumour growth and pathological upstaging at surgery

I.H. [Bhat](#); *London/UK* ([insha.bhat24@gmail.com](#))

Purpose: There is no objective data on tumour growth or pathological upstaging in early lung cancers awaiting surgery. Our study aims to evaluate if the current waiting times under '62-day' lung cancer pathway are associated with tumour growth or pathological upstaging.

Methods and Materials: 121 consecutive patients with early stage NonSmall Cell lung cancer who underwent resection were analysed. The difference between maximum diameters at diagnostic & preoperative CTscans was calculated to obtain diameter change. Increase in size of ≥ 5 mm or $\geq 20\%$ was considered significant. Time interval between baseline & repeat CT (CT-int), & between baseline CT and surgery (Surg-int) were calculated. CT-int & Surg-int were compared between upstaged & non-upstaged patients. Other potential prognostic indices (SUVmax, smoking status etc.) were also evaluated as categorical variables, p value < 0.05 considered significant.

Results: Median CT-int and Surg-int were 2.6 and 2.4 months respectively. 44.6% patients had a tumour growth ≥ 5 mm, 22% had tumour growth $\geq 20\%$. 36% patients were upstaged at surgery due to nodal/pleural invasion, satellite nodules or increase in tumour diameter. There was no significant difference between median CT-intervals in patients who had a tumour growth $< 20\%$ or $\geq 20\%$: 2.4 months vs 2.6 ($p = 0.06$). Surg-int was not correlated with growth $\geq 20\%$ either ($p = 0.24$).

Conclusion: Current cancer pathway waiting time practices are not associated with significant tumour growth or pathological upstaging in this cohort. Adenocarcinomas have an increased risk of pathological upstaging, however when considering only tumour size, this risk was not significant.

B-0586 10:46

The 8th edition IASLC staging system for lung cancer, a step beyond current imaging accuracy?

M. Murphy, C. Barry, C. Cronin, D. Healy; *Dublin/IE*
(markmurphy1608@gmail.com)

Purpose: The International Association for the Study of Lung Cancer (IASLC) has recently developed an 8th edition of its lung cancer staging. This further sub divides the T-status component into ever smaller size ranges. This was developed on pathology specimen measurements from a large population database. Many clinical decisions are made in the pre-operative domain however, with the T status dependent on radiology measurement. We wanted to determine if contemporary clinical staging based on radiology would accurately predict the proposed T-status from post-operative specimens.

Methods and Materials: We performed a retrospective analysis of 150 primary lung cancer cases that proceeded to surgical resection. Determination of size on the diagnostic CT scan was compared with the post-operative pathological size. Factors such as interval between imaging and surgery were also assessed.

Results: There was a discrepancy between the pre-operative CT tumour size and the post-operative pathology. The average difference was 0.567cm. This had consequences on staging accuracy. Based on size alone, CT accurately assessed T status in 65.3% of patients using the 7th edition IASLC, whereas only 54% of patients were accurately staged with the 8th edition. There was no correlation between time to surgery and tumour size.

Conclusion: We conclude that although the 8th edition of the IASLC TNM lung cancer staging system is an evolution at a population level, in lung cancer management, implementing the 8th edition as proposed may reduce the staging accuracy to as low as 54%. This evolution may prove an obstacle to utilisation of neoadjuvant strategies

B-0587 10:54

Iodine density obtained with spectral detector CT is a predictor for lesion dignity of pleural thickening

S. Lennartz¹, M. Le Blanc¹, N. Grosse Hokamp^{1,2}, D. Maintz¹, T. Persigehl¹;
¹Cologne/DE, ²Cleveland, OH/US (simon.lennartz@uk-koeln.de)

Purpose: To examine whether iodine density (ID) provided by spectral detector computed tomography (SDCT) is a valid parameter for differentiation between benign pleural thickening (BPT) and pleural carcinomatosis (PC).

Methods and Materials: In total, 30 contrast-enhanced SDCT scans of the chest were included at this retrospective, IRB-approved study. In detail, 15 SDCT scans of oncologic patients with PC confirmed by histopathology, FDG-PET or change during treatment, as well as 15 SDCT scans of patients with BPT confirmed by prior or follow-up CT (≥6 months). ROI-based quantitative image analysis was performed by two radiologists that determined attenuation (HU) and standard deviation (SD) in conventional polyenergetic images (PI). ROIs were than copied to identical position in iodine density reconstructions to determine the iodine density (mg/ml). The following ROIs were used: pleural lesion, adjacent skeletal muscle (thoracic wall, diaphragm, myocardium), subcutaneous fat, air, aorta, lung, pleural effusion. Statistical analysis was performed using student's t-test and multivariate linear modelling.

Results: Iodine density was significantly higher in PC (2.26±0.83 mg/l) compared to BPT (0.58±0.49 mg/ml, p≤0.0001). Although attenuation in PI differed significantly between PC and BPT as well, multivariate linear modelling showed that ID was the more powerful predictor for lesion dignity (p≤0.05). Both contrast-to-noise ratio (CNR) and difference in ID of PC in relation to the adjacent skeletal muscle of the thoracic wall were significantly increased compared to BPT (p≤0.0001).

Conclusion: Iodine density reconstructions provided by SDCT are a powerful predictor for differentiation between benign pleural thickenings and pleural carcinomatosis in oncologic patients.

B-0588 11:02

Comparison of overall-survival in squamocellular-NSCLC patients treated with Nivolumab assessed with RECIST1.1 and iRECIST

E. Raimondi, L. Belluomini, A. Cartuan, M. Bassi, R. Rizzati, M. Tilli, A. Frassoldati, M. Giganti, G. Benea; *Ferrara/IT* (edoardo.raimondi@unife.it)

Purpose: To compare the survival data, consisting of overall-survival (OS), for squamocellular-NSCLC patients treated with Nivolumab with RECIST1.1 and iRECIST criteria response categorisation.

Methods and Materials: After IRB approval, the CT-images of 15 squamocellular-NSCLC patients treated with Nivolumab were retrospectively evaluated at baseline, 3-months and 6-months by RECIST1.1 and iRECIST criteria. Patients were categorised as responders and non-responders as per RECIST1.1. For iRECIST, patients showing complete-response, partial-response or 6-months ongoing stable-disease were considered responders, while those showing progressive-disease were considered non-responders. Unconfirmed progressive-disease by iRECIST was considered as stable-

disease for categorisation purposes. Kaplan-Meier analysis for these response categories was performed for OS.

Results: According to RECIST1.1, 5/15 (33.3%) patients were categorised as responders and 10/15 (66.6%) patients as non-responders. According to iRECIST, 11/15 (73.3%) patients were categorised as responders and 4/15 (26.6%) patients were categorised as non responders. Significant differences between responders and non-responders for OS were observed for both radiological response criteria (Log-rank test: p<0.05). Median OS following RECIST1.1 was 22 months for responders and 10 months for non-responders (HRs: 0.5796; 0.2101-1.5991). Median OS following iRECIST was 21 months for responders and 7 months for non-responders (HRs: 0.1774; 0.02127-1.4795).

Conclusion: The OS curves for RECIST1.1 were similar to the one observed in iRECIST. For non-responders, the OS observed in RECIST1.1 was longer than the one observed in iRECIST; this difference may suggest that iRECIST better identifies progression of disease.

B-0589 11:10

Can perfusion heterogeneity in CT perfusion maps of NSCLC flaw clinical considerations based on global mean blood flow values?

S. Malavasi¹, D. Barone², G. Gavelli¹, A. Bevilacqua¹; ¹Bologna/IT, ²Forli/IT
(s.malavasi@unibo.it)

Purpose: Tumour heterogeneity is one of the key features regarding progression disease, diagnosis, and therapeutic response. CT perfusion (CTp) studies are usually based on mean perfusion values, computed on a single slice or the whole tumour. The aim of this work is to determine to what extent the heterogeneity pouring out from single slices can flaw studies using global mean values only.

Methods and Materials: 10 patients with single NSCLC lesions (26 examinations) were enrolled and underwent CTp. ROIs were drawn on aorta and on five central slices of each lesion. Mean global BF values were calculated on each slice (mSBF) and for the whole tumour (mWBF). The entropy E (i.e., a direct measure of data information content) was computed on BF values to assess the hemodynamic heterogeneity. For each lesion, the equivalence between each mSBF and mWBF was checked to assess whether mWBF of a lesion could represent the perfusion characteristics of a slice.

Results: Five slices only, all pertaining to different lesions, were represented by the mWBF, none of them bringing the highest information content in its tumour (i.e., the maximum E). 11 couples of lesions having the same mWBF were found, but with slices with very different perfusion patterns, mSBF and E values.

Conclusion: While global perfusion values computed on whole tumours may improve reproducibility, they cannot allow for tumour haemodynamic heterogeneity. Tumours with same mWBF could have very different response to therapies. Accordingly, additional parameters like BF entropy are needed to support mWBF in clinical considerations.

B-0590 11:18

Single-source dual-energy CT as part of 18F-FDG PET/CT: direct comparison of iodine-related and metabolic parameters in lung cancer

J. Baxa¹, T. Matouskova¹, J. Ludvik¹, B. Schmidt², M. Sedlmair², J. Ferda¹;
¹Pizen/CZ, ²Forchheim/DE (baxaj@fnplzen.cz)

Purpose: To assess possible correlation of FDG uptake and iodine-related attenuation values derived from PET/CT using single-source dual-energy CT scan (DE-CT) in non-small cell lung cancer (NSCLC).

Methods and Materials: 48 patients with histologically proven NSCLC underwent 18F-FDG-PET/CT within the staging. PET/CT included single-source DE-CT in late post-contrast phase. Direct comparison of FDG uptake and DE-related values was performed. Sub-study regarding different histological types and various thresholds for volume metabolic values quantification was also performed.

Results: A strong correlation was found between volumetric FDG parameters (MTV - metabolic tumour volume and TLG - total lesion glycolysis) and total iodine content using Pearson correlation analysis with various thresholds for FDG lesion segmentation (r=0.965-0.983; p<0.0001). The strongest correlation of MTV and TLG with iodine content was reached using 10% threshold for segmentation. Only weak correlation was found between iodine content and SUVmax. Significant difference between adenocarcinomas and other histological subtypes was proved in selected parameters of metabolic and DE data.

Conclusion: Our study demonstrated the strong correlation of the iodine content calculated from single-source DE-CT with volumetric FDG parameters in NSCLC without a significant effect of the threshold value for FDG lesion segmentation. This fact indicates the possible prognostic value of iodine content that could be used as another parameter for therapy-response monitoring.

Author Disclosures:

B. Schmidt: Employee; Siemens Healthineers. **M. Sedlmair:** Employee; Siemens Healthineers.

B-0592 11:26

Value of the first day PET/CT in post thermal ablation of lung tumours

W. Tantawy, A. Zarea, A.S. Ibrahim, M. Abdel Kawi, Y. Hussein, M. Nasr, M. Barsoum; Cairo/EG (oyehiaomar@gmail.com)

Purpose: to evaluate the role of the first day PET/CT imaging done immediately post CT guided microwave thermal ablation (TA) of lung tumors.

Methods and Materials: Thermal Ablation of lung tumors by using microwave technique guided by CT was performed for all 26 patients followed by post ablation PET/CT that was done immediately within the first day. Twenty-six patients were included in the study (16 females, 10 males) including 32 lesions, two lesions were ablated in 6 cases and single lesion in 20 cases.

Results: PET/CT examination done within the first day post ablation for all cases following microwave ablation (MWA), showed complete loss of metabolic activity of whole ablated lesions (i.e. SUV= equal or lesser than the physiological background lung activity). Sensitivity and specificity of first day PET/CT following adequate ablation was 100%.

Conclusion: First day PET/CT examination is an excellent and accurate imaging modality for the evaluation of adequacy of microwave ablation of lung tumors and should be considered the modality of choice with a sensitivity and specificity of 100%.

B-0593 11:34

Predicting nodal activity and clinical outcome of non-small cell lung cancer using 18-FDG PET-CT in the age of EBUS-FNA: initial results

G. Chambers, S. Vaidyanathan, F.U. Chowdhury; Leeds/UK (g.chambers@nhs.net)

Purpose: 18F-FDG PET-CT has an established role in the staging of lung cancer and helps guide Endobronchial ultrasound-guided fine needle aspiration (EBUS-FNA), increasing the positive yield and informing management. This study aims to correlate FDG PET-CT with EBUS-FNA to assess patient outcomes in discordant cases.

Methods and Materials: Images of 177 patients who underwent both EBUS-FNA and 18-FDG PET-CT, between 2010 and 2012, were analysed for nodal disease status using maximum standardised uptake values (SUVmax) above mediastinal background as a marker for positivity. Assessors were blind to the EBUS-FNA outcomes during this analysis. 354 EBUS-FNA sampled nodes were then correlated with the PET-CT findings and categorised as concordant or discordant. Survival analysis was performed comparing the patients with concordant and discordant results to determine if discordant results (FDG PET-CT false positive) conferred a survival benefit over a 5 year follow-up period.

Results: FDG-positive nodal disease and EBUS-FNA were concordant in 91 patients (51%) and discordant in 86 (49%) patients (6 up-staged by EBUS, 80 down-staged by EBUS). Survival analysis showed that there was no significant survival benefit when EBUS-FNA down-staged nodal disease, compared to those with concordant findings (p=0.91). Overall sensitivity, specificity, positive predictive value and negative predictive value for PET-CT were 0.88, 0.60, 0.56 and 0.88 respectively, compared to EBUS-FNA.

Conclusion: Initial results suggest that even when EBUS-FNA downstages FDG PET avid disease, no statistically significant survival benefit is conferred over a 5 year follow up period. The reasons for this are likely to be multifactorial.

B-0594 11:42

DWI-based radiomics for prediction of chemotherapy outcomes in lung cancer: a pilot study

Z. Li; Kunming/CN (lizhenhui621@qq.com)

Purpose: To investigate the wealth of radiomics for pretreatment DWI in prediction of treatment response of lung cancer with chemotherapy.

Methods and Materials: Thirty patients with lung cancer confirmed by pathology were enrolled. According to the RECIST, all patients were divided into good response group (GR) and non-good response group (non-GR) after the second cycle of chemotherapy. ADC imaging (b=600, 800 and 1000 s/mm²) were collected. Totally, 19 985 radiomics features were extracted in the ADC imaging. The lasso was adopted in feature selection and used in classifier model. ROC was used to evaluate the capability of the three models to predict GR.

Results: 16 patients were divided into GR, while 14 patients were divided into non-GR. The AUC, sensitivity and specificity of the radiomics based on the ADC imaging (b=600, 800 and 1000 s/mm²) for GR prediction were 0.875, 0.895 and 0.750, 0.924, 0.947 and 0.938, 0.918, 0.895 and 0.875, respectively. The AUC among the three groups had no difference (P>0.05).

Conclusion: It is possible to predict GR after chemotherapy in lung cancers based on the radiomics of pretreatment DWI.

14:00 - 15:30

Room B

Abdominal Viscera

SS 701a

New developments in MRI of the liver

Moderators:

T. Bader; Vienna/AT
I.L. Gubskiy; Moscow/RU

B-0601 14:00

Added value of diffusion-weighted imaging in hepatic tumours and its impact on patient management

J. Taron, J. Johannink, M. Bitzer, K. Nikolaou, M. Notohamprojo, R. Hoffmann; Tübingen/DE (taronjana@yahoo.com)

Purpose: To investigate the diagnostic value of additional diffusion-weighted imaging (DWI) of the liver and its impact on therapy decisions in patients with hepatic malignancy.

Methods and Materials: Interdisciplinary gastrointestinal tumour board cases concerning patients with hepatic malignancies discussed between 11/2015 and 06/2016 were included in this retrospective, single-center study. Two radiologists independently reviewed the respective liver MR examination first without, then with DWI. The readers were blinded regarding number, position and size of hepatic malignancies. Cases in which DWI revealed further findings to conventional sequences on hepatic tumour status were presented to the members of the interdisciplinary tumour board. In this setting, the changes in treatment decisions based on these additional findings in the DWI sequences were recorded.

Results: A total of 87 patients were included. DWI revealed additional findings in 12 patients (13.8%) which had a direct effect on the therapy in 8 patients (9.2%): in 6 patients (6.9%) the surgical/interventional treatment was adapted (n=5: extended resection, n=1: with transarterial chemoembolization of a single hepatocellular carcinoma only detectable in DWI); 2 patients (2.3%) received systemic therapy (n=1: neo-adjuvant, n=1: palliative) based on the additional findings in DWI. In 4 patients (4.6%) additional findings did not affect the therapeutic decision. Definite confirmation of malignancy was not possible in two cases during follow-up.

Conclusion: DWI is a relevant diagnostic tool in oncologic imaging of the liver. By providing further information regarding tumour load in hepatic malignancies it can lead to a significant change in treatment.

B-0602 14:08

MRI liver surface nodularity score: optimising spline stiffness to non-invasively stage fibrosis

K. Cox¹, S. Nandwana¹, B. Olaiya², P. Mittal¹, O. Ibraheem¹, A. Smith³; ¹Atlanta, GA/US, ²Marshfield, WI/US, ³Birmingham, AL/US (klcox2@emory.edu)

Purpose: Determine ideal preprogrammed liver surface nodularity (LSN) spline stiffness (SS) for differentiating fibrosis stages in viral chronic liver disease (vCLD).

Methods and Materials: vCLD patients with 2009-2015 MRI were cross-referenced for liver biopsy within 6 months or prior to cirrhosis biopsy. LSN score was obtained on post-contrast MRI with increasing preprogrammed SS (S15, S18, S21, S24). Patients excluded for slice thickness >3mm, frequency matrix <256. Median LSN score calculated for fibrosis stages and splines. ANOVA and receiver operator characteristic curve (AUC) analysis for accuracy of LSN score per SS for differentiating fibrosis stages. Wilcoxon rank-sum test explored associations between LSN scores and Scheuer staging. Exploratory cutoff values were investigated.

Results: 244 patients (153 male); mean age 53.8 (range 24-79). Patients per fibrosis stage: F0=41, F1=16, F2=24, F3=29, F4=134. LSN scores increased with increasing SS (p<0.001). AUC increased with increasing fibrosis. S21 had the highest AUC for F0-1 versus F2-4 (AUC=0.794), F0-2 versus F3-4 (AUC=0.807), and F0-3 versus F4 (AUC = 0.855). Using S21, median LSN scores were higher in advanced versus early fibrosis (4.06 versus 3.54), and cirrhosis versus non-cirrhosis (4.26 versus 3.54), p <0.001. S21 advanced fibrosis cutoff LSN score 3.83 had 67% sensitivity and 88% specificity. Cirrhosis cutoff LSN score 3.99 had 66% sensitivity and 92% specificity.

Conclusion: LSN scores increase with increasing SS. S21 LSN score demonstrated highest AUC for most fibrosis stages and can differentiate early from advanced fibrosis; cirrhosis from non-cirrhosis. Optimizing SS may differentiate early stages of fibrosis with improved accuracy, potentially eliminating the need for liver biopsy.

Author Disclosures:

K. Cox: Grant Recipient; RSNA Seed Grant. A. Smith: Owner; Liver Nodularity LLC. Patent Holder; patent pending.

B-0603 14:16

Association between multi-phasic MRI radiomic features and treatment response after stereotactic body radiation therapy

R. Du, M.S. Alam, V.H. Lee, V. Vardhanabuthi; *Hong Kong/HK (du94@hku.hk)*

Purpose: In this study, we analyse the association of radiomic features extracted from multi-phasic MRI scans and treatment response of patients who underwent stereotactic body radiation therapy (SBRT) and overall survival (OS).

Methods and Materials: A prospective cohort of 24 patients diagnosed with hepatocellular carcinoma (HCC) who underwent SBRT was analysed. Each patient received multi-phasic MRI scans at pre-treatment and 3-months post-treatment using gadoteric acid (gadoterate) contrast agent. Several sequences were analysed including pre-contrast, dynamic phases, 10 minutes and 20 minutes post-contrast, and T2W for radiomic features (103 extracted features). Volumetric ADC values were also extracted for each lesion. Univariate logistic regression model was used to analyse the association between pre- and post-treatment radiomic features/ADC and treatment response (infield recurrence and overall survival). The performance of the features was assessed by ROC analysis using leave-one-out cross-validation.

Results: Radiomic features from GLCM texture features were found to be most associated with treatment response. Features extracted from 10-minute delayed phase scans were found to be highly associated with infield recurrence (AUC = 0.7-0.85). For OS, GLCM features extracted from arterial phase scans and portal venous phase scans were found to be the most associated (AUC = 0.65-0.76). No significant association was found with features extracted from pre-contrast, T2W and 20-minute delayed phases. No association was found between SBRT dose and changes in ADC values.

Conclusion: We have found a strong association in radiomic features extracted from different MRI phases and infield recurrence in HCC patients treated with SBRT and overall survival. No association was found between ADC values and treatment parameters.

B-0604 14:24

Liver fibrosis vs cholangiocarcinoma MRI appearance and distinguishing features based on the DWI and ADC map

A. Sciuk¹, R. Kidzinski², E. Frankowska²; ¹Houston, TX/US, ²Warsaw/PL (*adam.sciuk@bcm.edu*)

Purpose: Benign confluent hepatic fibrosis and cholangiocarcinoma can have a similar morphologic appearance at CT and MRI. DWI offers a new method for making this distinction more reliable.

Methods and Materials: We retrospectively reviewed 18 abdominal MRI done with conventional T2, T1-precontrast, and dynamic postcontrast as well as DWI performed using b values of 0 and 500 sec/mm². Diagnoses: 12 cholangiocarcinomas, 3 primary sclerosing cholangitis and 3 diffuse liver cirrhosis. Both quantitative (ADC values) and qualitative reviews of DWI data (comparing SI of lesion to liver and spleen) were performed.

Results: All 12 cases with cholangiocarcinoma demonstrated increased relative signal intensity (SI) of the lesion relative to liver on the b-500 DWI in comparison to the b-0; nine cases had SI equal or higher than the SI of the spleen. Three cholangiocarcinomas despite a relative increase in SI on the b-500 images were slightly darker than the spleen. All benign cases showed decrease in relative signal intensity on the b-500 images in relation to the b-0, and were similar to the spleen. Quantitative assessment demonstrated a significant overlap.

Conclusion: Preliminary work indicates that cholangiocarcinoma displays a "relative brightening" of SI on b-500 in relation to b-0, whereas the benign cases showed a "relative darkening". Furthermore, the SI of nine out of twelve malignant cases was equal or higher the SI of the spleen; three potential false positives can occur with PSC. A SI equal to liver on b-500 image has a high negative predictive value despite positive T2 and contrast-enhanced imaging results.

B-0605 14:32

Initial experience with magnetic resonance elastography of liver

I. Csemez, M. Ujlaki, M. Gödeny; *Budapest/HU (imcsemez@gmail.com)*

Purpose: Mechanical tissue properties of the liver can be quantitatively assessed using magnetic resonance elastography (MRE). These parameters change in pathological conditions of the liver. We aimed to investigate the potential benefits of MRE with focal liver lesions, post-treatment changes and cirrhosis in focus.

Methods and Materials: Scans were performed on a 3 Tesla GE Discovery MR750w MRI scanner using the MR Touch Standard sequence. The system produces elastograms, i.e. liver maps indicating tissue stiffness. MRE was performed on 43 patients: 20 patients with histologically confirmed malignant liver tumors, 7 patients undergoing intervention (5 metastasectomies and 2 radiofrequency ablations), 3 patients with hemangioma, 2 patients with cirrhosis, and 11 patients with chemotherapy followup.

Results: In 13 cases of malignant liver lesions, tissue stiffness was significantly higher compared to the surrounding liver parenchyma (> 4.5 kPa). No abnormal stiffness was measured in the case of benign lesions or post-treatment changes except one patient. In both cases of cirrhosis, significant increase in liver stiffness was observed. In 10 cases, the study was not interpretable, due to small lesion size (< 2 cm) or motion artifacts.

Conclusion: Areas of high tissue stiffness can be easily distinguished from soft tissue on elastograms. Unlike ultrasound-based elastography techniques, MRE provides quantitative information on tissue stiffness of nearly the whole liver. It may provide additional information to conventional MR sequences on focal liver lesions greater than 2 cm. By decreasing motion artifacts MRE may be used to estimate hepatic functional reserve in patients scheduled for major hepatectomy.

B-0606 14:40

Improved DWI of the liver at 3T using respiratory triggering with simultaneous multi-slice acceleration

A.A. Tavakoli, U. Attenberger, J. Budjan, S.O. Schönberg, P. Riffel; *Mannheim/DE (s.tavakoli@gmx.de)*

Purpose: To compare respiratory triggered diffusion weighted imaging with simultaneous multi-slice acceleration (SMS-RT-DWI) of the liver with a standard free-breathing echoplanar-DWI (s-DWI) protocol regarding a reduction of imaging artefacts associated with diffusion weighted imaging at 3T.

Methods and Materials: 23 patients who underwent an MRI study of the liver were included in this retrospective study. Examinations were performed on a 3T whole-body MR system (Magnetom Skyra, Siemens). In all patients both s-DWI and SMS-RT-DWI of the liver were obtained. Images were qualitatively evaluated by two independent radiologist with regard to overall image quality, liver edge sharpness, sequence related artefacts and overall scan preference. For quantitative evaluation signal-to-noise ratio (SNR) and apparent diffusion coefficient (ADC) values were measured in different areas of the liver. We performed the Chi²-test for statistical analysis of qualitative parameters and the paired students t-test for analysis of quantitative parameters.

Results: Overall image quality, liver edge sharpness and sequence related artefacts of SMS-RT-DWI were rated significantly better compared to s-DWI (for all p < 0.05). For 82.6% of the examinations (19/23), both readers preferred SMS-RT-DWI overall to s-DWI with excellent inter-reader agreement (kappa=0.83). SNR values were significantly higher for SMS-RT-DWI than for s-DWI (151±122 vs. 69±46, p=0.0006), while mean ADC values did not differ significantly between the two sequences (994±129x10⁶mm²/s vs. 1002±123 x10⁶mm²/s, p=0.75).

Conclusion: By exploiting a simultaneous multi-slice technique at 3T, respiratory triggered DWI of the liver could be acquired with substantial image quality improvements compared to s-DWI while maintaining acquisition time.

B-0607 14:48

How to avoid gadoteric acid-related artefacts? Prospective multi-institutional study in 1994 patients

U. Motosugi¹, M. Hori², S. Goshima³, K. Kozaka⁴, T. Hyodo⁵, Y. Nakamura⁶, A. Nishie⁷, T. Tamada⁸, A. Kanki⁹; ¹Yamanashi/JP, ²Suita/JP, ³Gifu/JP, ⁴Kanazawa/JP, ⁵Osakayama/JP, ⁶Hiroshima/JP, ⁷Fukuoka/JP, ⁸Kurashiki/JP (*umotosugi@nifty.com*)

Purpose: To prospectively investigate the potential solution of gadoteric disodium-induced imaging artefacts using the data from multi-institutional study in Japan.

Methods and Materials: This prospective observational study was performed in eight institutions in Japan. In total, 1,994 dynamic contrast-enhanced MR examinations of the abdomen were performed either with gadoteric disodium (gadoteric acid group, n = 1,647) or with other gadolinium-based contrast agents (other GBCA group, n = 347). MR technologists recorded breath-hold fidelity using a respiratory monitor on MR scanners. Breath-holding during the scan was classified as either a success or a failure based on the shape of the monitored respiratory motion. Any adverse effects (self-report) were also recorded. The severity of respiratory motion-related artefacts in the liver on the pre-contrast and arterial phase images were evaluated: substantial artefact or not. The risk of gadoteric acid-induced substantial artefacts was evaluated with multivariate logistic analysis.

Results: Substantial artefacts in the arterial phase were more frequently observed in the gadoteric acid group (8.3% [136/1647]) compared with the "other GBCA" group (3.2% [11/347], p=0.001). Gadoteric acid-induced substantial artefacts in patients who successfully held their breath in pre-contrast scans were independently related to older age (odds ratio [OR]=1.04, p<0.001), female (OR=0.57, p=0.032), longer acquisition time (OR=2, p=0.009), and multiple arterial phase acquisitions (OR=0.47, p=0.048).

Conclusion: Gadoteric acid induces breath-hold failure and substantial artefacts in arterial phase scans. Gadoteric acid-induced substantial artefacts can be avoided using a shorter acquisition time sequence and multiple arterial phase acquisitions.

B-0608 14:56

High-field-strength MR imaging of the liver at 3.0T: comparative study with 1.5 T in cirrhotic population

K. Koryukova¹, M. Rossi¹, M. Di Martino¹, L. Saba², S.G. Ginanni Corradini¹, C. Catalano¹, ¹Rome/IT, ²Cagliari/IT (micdimartino@hotmail.it)

Purpose: To prospectively evaluate whether magnetic resonance (MR) imaging of the liver at 3.0 T is comparable to that at 1.5 T in terms of detection and characterization of focal liver lesions in cirrhotic patients.

Methods and Materials: This prospective study was approved by the institutional review board. A comparative study between two groups of cirrhotic patients, composed, respectively, with 58 and 56 elements with 109 and 97 lesions, was conducted. Patients were examined at 1.5- and 3.0-T MR imaging. The imaging protocol consisted of T2-weighted turbo spin-echo (SE) sequences with or without fat suppression, as well as T1-weighted gradient-echo (GRE) sequences with or without gadoxetic acid contrast agent. All images were rated independently by two radiologists.

Results: Excellent interobserver agreement was found ($\kappa=0.86$ 1.5T and 0.81 3T). The mean sensitivity of MR was similar between 1.5T and 3T (85% vs 86.2%) as well as the mean positive predictive value (98% vs 97.8%). The diagnostic accuracy was significantly greater at 3T (0.88 vs 0.995).

Conclusion: MR imaging of the liver at 3.0 T, compared with that at 1.5 T, is feasible with equivalent diagnostic utility in terms of detection and characterization of focal liver lesions in cirrhotic patients.

B-0609 15:04

The influence of intravenous non-specific gadolinium-based contrast media application on image quality of T2-weighted MRC in preoperative evaluation of living liver donors

A. Jarczowski, I. Reimers, D. Geisel, T. Denecke; Berlin/DE (anne.frisch@charite.de)

Purpose: To investigate the influence of gadobutrol (Gd-DO3A-butrol, Gadovist®, Bayer-Schering Pharma AG, Germany), gadoterate dimeglumine (Gd-DOTA, Dotarem®, Guerbet GmbH, Germany) and gadofosveset trisodium (Vasovist®, Bayer-Schering Pharma AG) on image quality of heavily T2-weighted single-shot thick-slab and multisection-thin-slice MRC in preoperative evaluation of living liver donors.

Methods and Materials: In this retrospective study, 58 patients (30 female, 28 male, mean age 35 years) underwent MRC before and after intravenous injection of non-specific contrast agents at 1.5 and 3 Tesla (T). Assessment included the evaluation of signal to noise ratio (SNR) and contrast to noise ratio (CNR) performance of the left and right bile duct, hepatic hilum as well as common bile duct (CBD). The assessment of image quality and duct visualization (each 5-point Likert scale) was analysed independently by three blinded readers. Reasons for impairment of image quality (e.g. movement artefacts and superimposing signals) were noted, if applicable.

Results: SNR, CNR, image quality and degree of duct visualization do not differ significantly before and after intravenous injection of non-specific gadolinium-based contrast agents. Overlapping signals caused by intrahepatic vessels that diminish the image quality of MRC were reduced by 8% in single-shot thick-slab MRC and by 3% in multisection MRC, respectively.

Conclusion: T2-weighted MRC in preoperative evaluation of living liver donors should be acquired after an intravenous application of non-specific gadolinium-based agents since the pre-contrast MRC does not bring any benefit in image quality and the incidence of superimposing intrahepatic vessel signals are lower in post-contrast MRC.

B-0610 15:12

Transient arterial phase respiratory motion-related artefact in liver MR imaging gadoxetic acid vs extracellular gadolinium. A within-patient cohort comparative study

A. Darnell, J. Rimola, E. Belmonte, A. Forner, V. Sapena, C. Ayuso, J. Bruix; Barcelona/ES (ANDARNEL@clinic.cat)

Purpose: To compare the frequency and severity of transient arterial phase (TAP) respiratory motion-related artifact following gadoxetic acid (EOB) and extracellular gadolinium [(EC-Gd), Gadobutrol] in a cohort of cirrhotic patients.

Methods and Materials: Eighty-two cirrhotic patients from prospective series underwent liver MR with EC-Gd and EOB within 1 month. Two readers, blinded to all data assigned a respiratory motion-related artifact score (0 [none], 1 [mild, no impact on reader confidence interpretation], 2 [moderate, causing decrease in reader confidence interpretation], and 3 [severe, non-diagnostic]) for non-enhanced, arterial and portal-venous phase. Scores for each phase were averaged and definitions for TAP, severe TAP and post-contrast motion-related artifacts were established. The frequency of motion-related artifacts was compared for each pair of examinations.

Results: The mean motion scores for EC-Gd and EOB for non-enhanced phase were 0.68 vs. 0.73 ($p=0.3$), for arterial phase 0.91 vs. 1.26 ($p<0.0001$), and for portal-venous phase 0.73 vs. 0.87 ($p=0.04$). The frequency of TAP

observed on EOB was superior to EC-Gd (19.5% vs. 6%; $p=0.013$), but there were no differences in frequencies for severe TAP ($p>0.99$) between both contrast agents. EOB was associated to a higher frequency of post contrast motion-related artifacts (7.3% vs. 0%; $p=0.03$).

Conclusion: TAP respiratory motion-related artifact is more frequently observed on liver MRI with EOB than with EC-Gd and it may affect 19.5% of the patients. However, the rate of severe TAP was very low and similar for both contrast agents.

Author Disclosures:

J. Bruix: Consultant; Bayer HealthCare, BTG, Daichi, Bristol-Myers Squibb, Novartis, Gilead, AbbVie, Arquile, Sytex and Roche. Speaker; Bayer HealthCare, BTG.

B-0611 15:20

Respiratory motion artefact affecting hepatic arterial phase MR imaging: comparison between gadoxetate disodium and gadobenate dimeglumine

K. Koryukova¹, L. Saba², M. Di Martino¹, C. Catalano¹, ¹Rome/IT, ²Cagliari/IT (micdimartino@hotmail.it)

Purpose: To compare frequency and severity of arterial phase respiratory motion-related artefact following gadoxetate disodium and gadobenate dimeglumine in patients with cirrhosis.

Methods and Materials: This prospective study was approved by the institutional review board and was compliant with HIPAA. The requirement to obtain informed consent was waived. One-hundred and six consecutive MR examinations were evaluated, 48 performed with gadoxetate disodium and 58 performed with gadobenate dimeglumine. All examinations were performed with the same magnet (1.5 T) and acquisition protocol. Two radiologists blinded to the contrast material rated motion artefacts on a scale of 1 (no motion) to 5 (non-diagnostic images) for the pre-contrast, the arterial, the venous and the late dynamic phases. Mean motion scores were compared using the Wilcoxon signed rank test. The number of patients with TSM, as well as the number of those with "adequate" arterial phases, was compared with the χ^2 or Fisher's exact test, as appropriate.

Results: The arterial phase reported significantly more MTS compared to the other acquired sequences with both contrast agents. Mean motion scores in the arterial phases in the gadoxetate disodium cohort were significantly worse than those in the gadobenate dimeglumine cohort ($P=0.029$). TSM occurred at a higher rate with gadoxetate disodium than with gadobenate dimeglumine (20.8% [10 of 48 examinations] vs 3.4% [two of 58 examinations], $P<0.001$).

Conclusion: Motion-related artefact occurs significantly more often than after gadobenate dimeglumine in patients with cirrhosis.

14:00 - 15:30

Room C

Musculoskeletal

SS 710a

Muscle and nerve

Moderators:

H. Gruber; Innsbruck/AT
H. Platzgummer; Vienna/AT

K-12 14:00

Keynote lecture

M. Reijnen; Leiden/NL

B-0612 14:09

Diffusion tensor imaging (DTI) in the evaluation of peripheral nerve sheath tumours: is it valuable for surgeons?

I. Capretti¹, F. Bruno¹, S. Quarchioni², E. Cannizzaro¹, C. Gianneramo¹, S. Mariani¹, F. Arrigoni¹, A. Barile¹, C. Masciocchi¹; ¹L'Aquila/IT, ²Teramo/IT (ilaria_capretti@hotmail.it)

Purpose: To demonstrate the preoperative role of MR in the localization and characterization of tumoral peripheral nerve sheath lesions and the identification of nervous fibers and the relationship with adjacent structures.

Methods and Materials: Twenty-six patients, suspected of having tumoral lesions, underwent contrast enhanced MR (3Tesla). They were evaluated with morphological sequences such as PD, FSE T1, FSE T2, FSE T2-weighted fat-saturated and postcontrast T1-weighted fat-saturated, but also with Spin-echo-single-shot EPI sequences (b-value 1000 s/mm²; 25 diffusion gradient orientations). We used quantitative parameters derived from DTI: apparent diffusion coefficient (ADC) and fractional anisotropy (FA) and reconstructed the nervous fibers involved in the lesion. All patients were subjected to surgical treatment and we studied the correlation between MR imaging and surgical findings.

Results: In all the patients, morphological sequences showed that lesions involved peripheral nerves and they appeared hyperintense in T2-weighted

sequences with enhancement in postcontrast T1-weighted fat-saturated sequences. DTI techniques allowed the visualization and relationship between tumour and normal axons of peripheral nerves with high sensitivity (78.9%), specificity (71.4%) and positive predictive value (88.2%). During surgery, a good correlation between MR images and intraoperative aspects was observed with sensitivity of 90%, specificity of 83% and positive predictive value of 95%. **Conclusion:** According to our experience, preoperative DTI techniques are useful to plan the safest surgical resection in order to minimize post-operative neurological deficits.

B-0614 14:17

Feasibility of shear wave elastography (SWE) in diagnosing carpal tunnel syndrome (CTS)

S. Rauch; Innsbruck/AT (stefanrauch@gmx.at)

Purpose: To evaluate longitudinal and axial plane measurements of shear wave elastography (SWE) at a proximal and distal level in determining median nerve (MN) elasticity and diagnosing carpal tunnel syndrome (CTS).

Methods and Materials: 27 healthy volunteers (three male, mean 37 yrs., range 24-37; 24 female, mean 54 yrs., range 43-78) and one hand of 27 CTS patients (twelve male, mean 72.0 yrs., range 43-82; 15 female, mean 65 yrs., range 29-82) were examined by using a 18-5 MHz transducer. Cross sectional (CSA) area of MN was determined at the level of pronator quadratus muscle (CSAp) and at the level of the maximum CSA in the carpal tunnel (CSAd). Δ -CSA was determined as the difference between both measures. SWE measurements were performed for MN both at proximal and distal levels in axial and longitudinal orientations. Measures were compared between CTS patients and controls at both levels in both orientations (axial and longitudinal).

Results: Both the SWE values and CSA in CTS patients were significantly higher than that of healthy volunteers ($P < 0.001$). Longitudinal SWE was superior to axial SWE measurements ($P < 0.001$). The presence of CTS was predicted by a shear wave velocity of 10.41 cm/s (mean) ($P < 0.001$) with a cut-off value of 9.85 (sensitivity 0.93, specificity 0.63) and an area under the curve (ROC) of 0.85.

Conclusion: SWE proved to be sensitive in CTS patients and a single longitudinal SWE measurement at the carpal tunnel is sufficient for the diagnoses of CTS.

B-0615 14:25

Ultrasound of the Thenar Motor branch in Carpal Tunnel Syndrome

F. Zaottini, R. Picasso, S. Airdi; Genova/IT (federico.zaottini.fz@gmail.com)

Purpose: This study was aimed to investigate the ultrasound (US) appearance of the thenar motor branch (TMB) of the median nerve (MN) in patients with carpal tunnel syndrome (CTS) and thenar muscle weakness at physical examination and electrophysiology.

Methods and Materials: Twenty-two consecutive wrists from n=15 patients (mean age 61±5) who had clinical and electrophysiological diagnosis of CTS and signs of thenar muscle weakness were included. In each patient, the CSA of the MN and the caliber of the vertical segment of the TMB were measured with 17-5MHz US. In addition, the thenar muscles echotexture and the appearance of the intermuscular segment of the TMB were recorded. Electrophysiology included standard needle technique and sampling of motor and sensory conduction velocities of the MN. Correlation between US findings and electrophysiology was then obtained.

Results: US was able to identify the TMBs in all but one wrists. The mean TMB diameter was 0.9±0.28mm (95% CI). In 43% of cases, the vertical segment of the TMB resulted to be larger than normal, ranging between 0.7mm to 2mm. The intramuscular segment of the TMB appeared swollen in 9% of cases. Overall, the mean CSA of the MN at wrist was 16.1mm². No correlation was observed between TMB caliber and either CSA of the MN or electrophysiologic signs of denervation of thenar muscles.

Conclusion: The TMBs often appear swollen in patients with CTS and signs of thenar muscle weakness. There is no significant correlation, however, between thenar muscle weakness and abnormal appearance of the TMB.

B-0616 14:33

High resolution Ultrasound of the Motor Branch of the Ulnar Nerve beyond the Guyon tunnel

R. Picasso¹, F. Zaottini¹, S. Airdi²; ¹Genova/IT, ²Savona/IT (riccardo.picasso@gmail.com)

Purpose: To illustrate the ultrasound (US) findings of distal entrapment neuropathy of the motor branch of the ulnar nerve (UNMB) beyond the Guyon tunnel.

Methods and Materials: A dissection study was performed on n=3 cadaveric hands to assess the regional anatomy of the UNMB beyond the pisiform. US was performed in a group of n=10 healthy subjects to examine the nerve at the hamate hook, pisohamate ligament and within the palm. A series of n=10 consecutive patients with motor symptoms in the territory of innervation of the UNMB in the hand (zone 2) were examined with US using a linear 17-5MHz

transducer. These patients had neurophysiologic, 1.5T MR imaging and surgical correlations.

Results: US was reliable to depict the UNMB from its origin to the midpalm. Two levels of entrapment were identified. In five patients, the UNMB was compressed on the outside slope of the hamate hook by ganglion cysts. Four other patients had more distal compression in the palm by fibrous bands (n=1) and ganglion cysts (n=3). One had multiple neurofibromas affecting the nerve and its divisional branches. In midpalmar entrapments, there was selective denervation of the III/IV dorsal interosseous muscles. Overall, US gave useful preoperative information on the level of injury.

Conclusion: US may help the diagnostic work-up of distal ulnar neuropathies giving information on the level and nature of constricting findings. In patients with suspected zone II syndrome, US should include a thorough evaluation of the UNMB at the level of the hamate hook and the midpalm.

B-0617 14:41

MRI assessment of the microstructural integrity of the peripheral nerves in Charcot-Marie-Tooth disease

F.I. Rozalli, F. Fadzli, T. Krisnan, K. Rahmat, L.K. Tan, N. Shahrizaila, N. Ramli; Kuala Lumpur/MY (farhana.fadzli@yahoo.com)

Purpose: Charcot-Marie-Tooth (CMT) is one of the most common inherited causes of peripheral neuropathy. Our goal was to investigate the microstructural integrity of sciatic and peroneal nerves in CMT using diffusion tensor imaging (DTI), and evaluate muscle atrophy.

Methods and Materials: A total of 9 CMT patients and 9 age- and gender-matched healthy controls were recruited. DTI using 3-tesla MRI machine was performed to evaluate the sciatic and peroneal nerves. Post-processing produced DTI values for each nerve. Axial in-out phase of the calf was used to classify muscle atrophy (tibialis anterior) using Goutallier classification.

Results: The FA values were significantly reduced (0.330±0.036 vs 0.408±0.023, $p < 0.001$, for sciatic nerve; 0.3575±0.107 vs 0.5484±0.107, $p < 0.001$, for peroneal nerve) and RD values were significantly increased (1.149±0.102 vs 0.852±0.472, $p = 0.04$ for sciatic nerve; 2.291±0.6417 vs 1.103±0.329, $p < 0.001$ for peroneal nerve) in CMT patients. The mean muscle atrophy value was significantly increased in CMT patients (0.78±0.833 vs 3.33±0.707, $p < 0.001$). We also found correlation between DTI values (FA and RD) and muscle atrophy grading.

Conclusion: DTI was able to detect degenerative and demyelination changes in CMT, which corresponds to the nature of the disease. MRI also supports that there was significant muscle atrophy in CMT patients. MRI-DTI could emerge as a useful screening tool for asymptomatic high-risk patients with family history of CMT for early detection of neuropathy and as an adjunct to EMG in the prognostication of CMT.

B-0619 14:49

Core muscle composition and fat distribution in Parkinson's disease

C.-K. Wang, H.-L. Chen, W.-C. Lin; Kaohsiung/TW (moonrbi@gmail.com)

Purpose: Sarcopenia and alteration of fat distribution were known in PD patients, but the intramuscular fat distribution has not yet been well established. The aim of this study was to investigate fat distribution in core and extremity muscle and its relationship with clinical severity and frailty.

Methods and Materials: Twenty-five patients with PD and 20 age- and sex-matched healthy volunteers were recruited. All subjects underwent MRI study using IDEAL sequence to determine the fat distribution in core and extremity muscles (including psoas muscles and the thigh). PD patients received clinical survey to evaluate disease severity and frailty. The alteration in the fat content in core and extremity muscles, frailty and clinical severity were correlated.

Results: The fat content in measured muscles exhibited higher in PD patients (psoas muscles: $p = 0.014$, anterior compartment of thigh: $p = 0.006$, medial compartment of thigh: $p < 0.001$, posterior compartment of thigh: $p = 0.003$). The fat infiltration of measured muscle was significantly correlated with clinical severity and items of frailty. The average percentage of fat content of bilateral medial compartment of thigh showed correlation with UPDRS-1 ($r = 0.707$, $p < 0.001$) and average percentage of fat content of bilateral anterior compartment of thigh showed correlation with weakness and exhaustion ($r = 0.519$, $p = 0.019$).

Conclusion: Higher percentage of fat content in core and extremity muscles is a significant phenomenon in PD patients. The pathophysiology of sarcopenia and frailty in PD might be a consequent process of neuromuscular degenerative changes and, therefore, PD patients were limited their daily activity due to decreased muscle strength.

B-0620 14:57

Ultrahigh field (7T) diffusion tensor imaging of healthy skeletal muscles: a quantitative comparison with 3T

C. Giraud¹, S. Motyka¹, M. Weber¹, T. Feiweier², S. Trattning¹, W. Bogner¹;
¹Vienna/AT, ²Erlangen/DE (chiara_giraud@hotmail.it)

Purpose: To compare diffusion tensor imaging (DTI) with 7T and 3T of the human calf muscles.

Methods and Materials: Ten volunteers (5 males; mean age 29.1±4.7 years), without any history of muscle disease, were examined twice (i.e. during the same day, without repositioning) at 3T (MAGNETOM Prisma, Siemens Healthcare) and 7T (research scanner, Siemens Healthcare), using a STEAM-DTI sequence. SNR, DTI metrics (tracks' number (tracks_n), length (tracks_l), volume (tracks_v), fractional anisotropy (FA), and mean (MD), axial (AD) and radial diffusivity (RD)) of the entire datasets (*entire_calf*), of tibialis anterior (TA), gastrocnemius medialis (GM) and lateralis (GL) were collected. Student's T test was used to compare SNR and DTI metrics obtained at 3T and 7T. Intraclass-correlation coefficients (ICC) were derived to assess the reliability of DTI measurements at 3T and 7T.

Results: The SNR was higher at 7T (+105.11%; p<.001). At 7T, tracks_n, tracks_l, and tracks_v were higher for *entire_calf*, GM and GL (tracks_n: +5.5%, +3.1%, +8.5%; tracks_l: +12.1%, +12.2%, +14.7%; tracks_v: +13.3%, +16.4%, +19.2%; p<.05, each); TA showed only higher tracks_n and tracks_v (+6.3%, +16.4%; p<.05 each). MD and RD were higher at 7T for the *entire_calf* (+1.3%; +1.8%; p<.05, each) and for TA (+7.3%, 8.9%; p<.05, each). TA showed higher FA at 3T (+3.1%; p=.001) and higher AD at 7T (+5.6%; p<.001). GM demonstrated lower MD and RD at 7T (-2.8%; -3.4%; p<.05). ICC was excellent (>.750) for both 7T and 3T regarding GM's and GL's tracks_n, tracks_l, RD, *entire_calf*'s RD, TA's RD and FA. Excellent ICC values were obtained only at 3T for the *entire_calf*'s and GL's MD and AD, and GL's FA and GM's AD. GM's tracks_l and TA's tracks_l had excellent ICC only at 7T.

Conclusion: Ultrahigh field demonstrated higher SNR and an overall improvement in fibre tracking metrics. Further studies are necessary to better characterize the advantages and the challenges in specific muscles.

Author Disclosures:

T. Feiweier: Employee; Siemens Healthcare GmbH.

B-0621 15:05

Compression garments in delayed-onset muscle soreness (DOMS): randomised controlled trial with acoustic radiation force impulse (ARFI), contrast-enhanced ultrasound (CEUS) and MRI

R. Heiß¹, M. Kellermann¹, B. Swoboda¹, C. Grim², A.M. Nagel¹, M. Uder¹, T. Hottel¹;
¹Erlangen/DE, ²Osnabrück/DE (Rafael.Heiss@uk-erlangen.de)

Purpose: To investigate the influence of compression garments on changes in muscle perfusion, stiffness and oedema in DOMS.

Methods and Materials: DOMS was induced in fifteen healthy participants using an eccentric exercise protocol. After exercise, a conventional sports compression garment (class I) was worn on one randomized calf for 60h. ARFI (shear wave velocities (SWV)), CEUS (peak enhancement (PE) and wash-in area under the curve (WIAUC)) and MRI (normalized T2 signal intensity and T2 time) of the gastrocnemius muscle (GM) were assessed at baseline and 60 h after exercise at both calves.

Results: After exercise the normalized T2 signal intensity (1.0±0.30 vs 1.94±1.05, p=0.008) and the T2 time (37.52±9.67 vs 55.64±12.72 ms, p=0.015) were significantly higher in the GM in the compressed calf; but no change for WIAUC (p=0.88), PE (p=0.51) and ARFI SWV (p=0.60) were observed. For the non-compressed calf all assessed parameters changed significantly: T2: 1.0±0.16 vs 2.20±1.16, p=0.001; T2 time: 37.75±9.28 vs 55.67±14.78 ms, p=0.005, WIAUC: 2461±660 vs 5297±743, p=0.01, PE: 328±45 vs 753±31, p=0.005, ARFI SWV: 2.2±0.26 vs 1.78±0.24m/s, p=0.008. No significant difference was observed in normalized T2 signal intensity (p=0.397), T2 time value (p=0.953), WIAUC (p=0.93) and PE (p=0.730) in the GM comparing the compressed and non-compressed lower leg after exercise. Only ARFI SWV values in the same comparison revealed a statistically significant difference (p=0.001).

Conclusion: Wearing conventional compression garments after inducing DOMS may shorten the normalization of muscle stiffness, but have no significant effect on the degree of intramuscular oedema or perfusion of the gastrocnemius muscle.

Author Disclosures:

M. Uder: Speaker; Bracco Group, Siemens AG, Bayer AG.

14:00 - 15:30

Room Z

Interventional Radiology

SS 709

Non-liver ablation

Moderators:

D. Ilic; Novi Sad/RS
 N.N.

B-0622 14:00

Feasibility study of microwave ablation system: localisation and eradication of tumourous lesions

T.J. Vogl¹, C. Reimann², M. Puentes-Damm², F. Hübner¹, B. Bazrafshan¹;
¹Frankfurt a. Main/DE, ²Darmstadt/DE (t.vogl@em.uni-frankfurt.de)

Purpose: To investigate the difference between the dielectric properties of normal and malignant liver tissue by measuring the permittivity of freshly excised samples from liver resection.

Methods and Materials: A microwave ablation system is proposed with a microwave sensor at the tip of the applicator as an additional information source for accurate localization of the targeted tumour during the intervention. A measurement procedure was developed to evaluate the broadband dielectric properties of a liver sample containing healthy and tumour tissue. In total, 22 measurements were performed by touching the surface under test with a dielectric probe (2.1 mm in diameter) connected to a network analyser. Measurement points were recorded on normal (8), tumour (8), and tumour boundary (6) locations.

Results: At 12GHz, the permittivity mean value ± standard deviation of normal tissue was $\epsilon_r=33.8\pm0.86$ and of tumour tissue $\epsilon_r=44.33\pm5.49$, which results in a relative difference of =31.15%. The proposed applicator is able to distinguish between healthy and tumour tissue exhibiting a sensitivity of 10%. During thermal ablation measurements, a lesion zone of approximately 3 cm³ was obtained with an input power of 20W for 4 minutes when the functional model was inserted into the liver sample. By detecting tumour tissue, an additional source of information is provided for the interventional radiologist and could lead to a reduced number of insertions and readjustments. Moreover, the high operation frequency leads to an efficient heat generation for thermal ablation treatment.

Conclusion: The new microwave system possibly allows simultaneous diagnostic and therapeutic microwave application.

B-0623 14:08

Microwave ablation (MWA) of pulmonary neoplasms: clinical performance of MWA with spatial energy control vs conventional low-frequency MWA

T.J. Vogl¹, L. Basten, N.N.N. Naguib, N.-E.A. Nour-Eldin; Frankfurt a. Main/DE (t.vogl@em.uni-frankfurt.de)

Purpose: To evaluate the clinical performance of a new microwave ablation (MWA) technology with spatial energy control (SEC) for treatment of lung malignancies in comparison to a conventional low-frequency (LF) MWA technology.

Methods and Materials: In this retrospective study, 59 consecutive patients (mean: 58.9±12.7 years) were treated in 71 sessions using SEC-MWA. Parameters collected were technical success and efficacy, tumour diameter, tumour and ablation volume, time, energy, complication rate, 90-day mortality, local tumour progression (LTP) at 3-month follow-up, ablative margin size and ablation zone sphericity. Results were compared with the same parameters retrospectively collected from the last 71 conventional LF-MWA sessions (n=56 patients; mean 60.3±10.8 years). Statistical comparison was done using Wilcoxon-Mann-Whitney test.

Results: Technical success was 98.6% for both technologies; efficacy was 97.2% (SEC-MWA) and 95.8% (LF-MWA). The 90-day mortality rate was 4.2% (3/71) in both groups without any intraprocedural death. Complications were recorded in 21.1% (15/71) of SEC-MWA and in 31% (22/71) of LF-MWA, of which 4.2% (3/71) and 9.9% (7/71) were major (all p>0.182). The median deviation from ideal sphericity (1.0) was 0.195 (SEC-MWA) vs 0.376 (LF-MWA) (p<0.001). Absolute minimal ablative margins per ablation were on average 7.5±3.6 (SEC-MWA) vs 4.2±3.0 mm (LF-MWA) 8p<0.001. LTP until 3-month follow-up occurred in 5.6% (4/71) and 7.0% (5/71), respectively (p>0.7).

Conclusion: SEC-MWA of lung malignancies and conventional LF-MWA technology are safe and effective independent of the used system. However, SEC-MWA achieves more spherical ablation zones with larger ablative margins vs LF-MWA (p<0.001).

B-0624 14:16

Renal tumour cryoablation beyond T1a: outcomes for 56 T1b biopsy-proven RCC lesions

T.A. [Gibson](#), N. Patel, N. McGill, A. King, D. Breen; *Southampton/UK* (tagibson0@gmail.com)

Purpose: Percutaneous image-guided renal cryoablation (CRA) represents an alternative nephron-sparing technique for renal tumours. The majority of published data has focused on its application specifically to T1a disease. Hence, our purposes are to: a) provide results of a single-centre prospective study of the technical and oncological outcomes of CRA for T1b (<7cm) lesions and b) compare these results with our equivalent data for T1a (<= 4cm) renal masses.

Methods and Materials: 433 patients with 486 T1 renal lesions treated between 2008 and 2016 were identified from a prospectively maintained tumour registry. A subset of 56 patients with stage T1b (4-6.9cm) sporadic biopsy-proven RCC were selected for further analysis. Exclusion criteria: previous history of RCC or heritable disease; <3 months follow-up.

Results: a) Demographics: 39 male, 17 female; average age = 70yrs; average tumour size = 4.8cm. b) Technical outcomes: technical success i) primary ablation rate = 51/56 (91.1%), ii) secondary ablation rate (where performed) = 2/2 (100%); complications (Clavien-Dindo grade III+) = 3/56 (5.4%). c) Oncological outcomes: mean length of follow-up = 26 months. No significant difference between T1a and T1b cohorts in overall survival (p= 0.43), late local recurrence-free survival (p = 0.45), or metastasis-free survival (p = 0.50).

Conclusion: Our findings of no statistical difference for CRA in the treatment of T1a or T1b renal masses concur with those of other studies in the literature. CRA, therefore, seems a reasonable treatment option for sporadic RCC tumours of <7cm. Further (follow-up) data are needed for comparison with partial nephrectomy.

B-0625 14:24

CT-guided percutaneous cryoablation treatment of renal cancer: an outcome analysis from our experience

S. [Gitto](#), G. Calareso, T. Cascella, G. Greco, M. Vaiani, S. Stagni, R. Salvioni, C. Spreafico; *Milan/IT* (sal.gitto@gmail.com)

Purpose: To perform an outcome analysis from our experience in CT-guided percutaneous cryoablation (PCA) treatment of renal cancer (RC).

Methods and Materials: We evaluated patients with a minimum follow-up of one year after PCA of RC or extrarenal metastasis from RC performed between 10/2007 and 10/2016. All patients were inoperable or refused surgery and cases were discussed multidisciplinary. A biopsy was performed in patients without a previous diagnosis of RC. Post-operative monitoring included biochemistry 4, 8, 24 hours and a non-contrast CT scan 24 hours after PCA. Follow-up consisted of contrast CT scans 1, 3, 6, 9, 12 months after PCA and then every 6 months for 3 years. Absent/persistent mass contrast-enhancement indicated response/recurrence, respectively.

Results: Eighty-five patients were included (27F; mean age 68[35-86] years; 25 with a solitary kidney); 80 with RC and 5 with an extrarenal metastasis. Mean follow-up was 51(12-116) months. Mean mass diameter was 30(10-100) mm. Biochemical parameters were normal after PCA. Major early complications included: 1 sepsis, 1 ureteral fistula, 1 duodenal fistula, 1 arteriovenous fistula, 1 active arterial bleeding. No patients died for these complications. 93% of patients (79/85) showed complete response after PCA. Six patients had recurrent disease: 3 were successfully retreated with PCA, 1 underwent nephrectomy, 2 were not further treated and died for other causes. No significant difference in age (P=0.113;95%CI) and mass diameter (P=0.668;95%CI) was found between responsive and recurrent patients.

Conclusion: PCA is effective in the treatment of RC in patients ineligible for surgery and can be repeated in recurrent cases.

B-0626 14:32

Technical success and local control after image-guided microwave ablation (MWA) of T1a renal tumours with a new high-power generation system

M. [Colombo](#), M.M. Panzeri, P. Marra, G. Brembilla, M. Venturini, U. Capitanio, F. Montorsi, A. Del Maschio, F. De Cobelli; *Milan/IT* (colombo.michele@hsr.it)

Purpose: MWA is a novel thermal ablation technique which allows larger and more uniform ablation zones (AZ) with shorter procedure time compared to other ablative techniques. High-power MWA may present advantages in term of local renal tumor control. In the present study we evaluated safety, technical success, local control, and survival after MWA of RCC with a new high-power generation system.

Methods and Materials: From October 2014 to March 2017 twenty-three patients (mean age 65 y; range 45-86 y) with 26 renal cancers (clear cell RCC = 21; papillary RCC = 10; chromophobe RCC = 3, oncocytoma=1) not eligible for surgical treatment were treated with MWA procedures (US/CT guided percutaneous = 23 lesions; laparotomic = 1; laparoscopic = 2), with a 2450

MHz/100 W generator with Thermosphere™ Technology (Emprint™, Medtronic). At follow up (FU), contrast-enhanced CT or MR was performed after one, six and twelve months. Technical success, AZ, complete ablation (CA) and clinical success were assessed.

Results: Mean diameter of the lesions was 2.3 cm ± 1.1; (range, 0.9-4.2 cm). Technical success was achieved in 100% of cases and mean AZ was 28.7 mm at 1 month FU. CA at 1 year was 96%. No severe complications and 6 mild complications (19%, all perirenal haematoma) were observed. One year morbidity and mortality were both 0%.

Conclusion: In our experience, MWA with Thermosphere™ Technology is effective and safe to treat RCC.

B-0627 14:40

Our experience in percutaneous ablative treatment of renal T1a e T1b lesions: results from 90 patients treated with MWA, RFA and CRA

E. Faiella, D. Santucci, A. [Alfonsi](#), G. Pacella, C. Altomare, C. Bernetti, C. Rollo, R.F. Grasso, B. Beomonte Zobel; *Rome/IT* (a.alfonsi@unicampus.it)

Purpose: To evaluate efficacy and safety of ablation procedures for the treatment of kidney lesions <7cm.

Methods and Materials: 90 patients with single T1a and T1b lesions of the kidney, susceptible to ablative procedure, were retrospectively analyzed: 30 treated with Radiofrequency (RFA), 30 with Cryoablation (CA) and 30 with Microwave (MWA). Biopsy was performed for all the lesions. Complications rate, local control in terms of Disease Free Survival (DFS) and renal function, and survival in terms of Cancer Specific Survival (CSS) and Overall Survival (OS), were evaluated.

Results: Mean age of patients was 68.8 years (29-94 years); mean tumor size was 26.51mm (6-102mm). Eighty-two lesions (91%) were T1a and 8 (9%) T1b. In 19 cases artificial dissection was performed. The treatment was effective in 96% of cases, with peri-procedural complications in 6 patients (5 haemorrhages and 1 hydro-ureteronephrosis). Ten patients (11.1%) reported a recurrence of disease (9 T1a and 1 T1b) (p> 0.05) in a mean time of 3 months: 6 (20%) underwent MWA, 2 (6.7%) RFA and 2 (6.7%) CA (p <0.05). 1 case of renal failure in mono-kidney patient. The only significant predictor of DFS in the multivariate analysis, was the histotype, with a higher recurrence rate in RCC (p <0.05). Nine (10%) patients died for other causes.

Conclusion: Safety and efficacy in short and long-term control of the three procedures are comparable. However, long-term surveillance is required, especially after MWA. Patient selection, based on tumor characteristics (size and location), and patient comorbidities remain crucial.

B-0628 14:48

Percutaneous ablative treatment of pelvic rectal cancer recurrence

C. [Pusceddu](#); *Cagliari/IT* (clapusceddu@gmail.com)

Purpose: To retrospectively evaluate the technical feasibility, safety and efficacy of percutaneous ablative treatment of painful pelvic rectal cancer recurrent in patients unfit for surgery and no longer susceptible to radiotherapy or chemotherapy.

Methods and Materials: Fourteen patients, mean age 61 years, with pelvic recurrence of rectal carcinoma, mean size 4.7 (2.5-9cm) underwent RFA (11 cases) and cryoablation (2 cases) to reduce pain and to limit local progression of disease. All the procedures were performed under CT guidance using local anaesthesia and conscious sedation. The therapeutic outcomes were evaluated by CT or MRI at 1-, 3-, 6- and 12-month intervals. Complete lack of tumour enhancement images after injection of contrast media was considered an indication of complete tumour necrosis.

Results: Total necrosis of the tumour was observed in 7 patients, partial in the remaining 7. Complete pain relief was obtained in eight patients and a significant reduction of pain in the remaining patients (mean VAS score from 7.8 before treatment to 1.4 after treatment). In two patients an abscess in pre-sacral space and a bladder-rectal fistula after RFA was observed. During the mean follow-up of 40 months (7-55 months) 10 patients died due to local or distant tumour progression whereas four patients are still alive and 2 of them disease free.

Conclusion: In selected cases, percutaneous ablative treatment of pelvic rectal cancer recurrence can be considered a safe and effective treatment capable of obtaining satisfactory control of pain and stabilization of the relapse.

B-0629 14:56

Microwaveablation (MWA) of liver metastases from pancreatic neuroendocrine tumour (pNET): preliminary results with a new generation system

P. [Marra](#), P. Diana, F. Ratti, S. Partelli, M. Salvioni, S. Gusmini, M. Venturini, L. Aldrighetti, F. De Cobelli; *Milan/IT* (marra.paolo@hsr.it)

Purpose: MWA is in the panel of treatment for pNET liver metastases in symptomatic oligometastatic patients. Many case series in the literature, most based on radiofrequency ablation, report variable rates of efficacy with

relatively high rates of local tumor progression (LTP). We aimed to report our preliminary results, using a new generation high-power MWA system.

Methods and Materials: In the last two years, seven patients underwent liver MWA in our institution for the treatment of synchronous (n=4) or metachronous (n=11) pNET metastases (total nodules=15). MWA procedures were performed either percutaneously (n=5) or during surgery (n=10), using a 100W/2450MHz Microwave Generator (Emprint, Medtronic). Resection of the pancreatic neoplasm was performed synchronously to MWA treatment in 2 patients. DCE-CT or MRI were used to assess 1-month complete ablation (CA) and LTP at follow up.

Results: CA was achieved in 100% of cases. No complications occurred. Overall LTP was 0% at a mean observation time of 11.8 months (9-18). One patient developed liver disease progression after 15 months, however without recurrence at ablation site.

Conclusion: In our preliminary experience, MWA performed with a new generation system provided excellent results for the treatment of pNET liver metastases. During follow up, although limited, no LTP was observed. Even if the utility of loco-regional treatment of pNET liver metastases is still debated, we believe that MWA with a new generation system provide good cost-benefit ratio in oligo-metastatic patients.

B-0630 15:04

MR-guided focused ultrasound (MRgFUS) ablation of painful osteoid osteoma: perfusion imaging as predictors of clinical outcomes associated with complete bone integrity restoration

S. Bednarova, A. Napoli, R. Scipione, S. Dababou, C. Marrocchio, H.-P. Erasmus, C. Catalano; *Rome/IT (sandra.bednarova@gmail.com)*

Purpose: To correlate quantitative and semi-quantitative perfusion parameters of post-ablation osteoid osteoma (OO) nidus with treatment outcome and bone remodelling.

Methods and Materials: Thirty-nine subjects with radiologically confirmed symptomatic OO were treated with MRgFUS in an institutional review board-approved clinical trial, according to the intention-to-treat principle. Bone-forming changes were evaluated before and after MRgFUS procedure; annual CT and dynamic contrast-enhanced MRI (DCE-MRI) scans were performed over a period of 3 years. Quantitative and semi-quantitative parameters of OO nidus perfusion were analysed for significance with regard to post-procedural complete/partial bone restoration. Multivariate analysis was conducted to investigate imaging and demographic (age, sex, BMI) variables in relationship with clinical outcomes (VAS for pain).

Results: 31 of 36 patients underwent MRgFUS ablation of OO nidus; 29 encountered a complete clinical response (VAS score 0 during follow-up); 2 patients with residual pain at 1-month follow-up (VAS 1-3) required re-treatment using RFA. At 36-month follow-up, MRI showed no residual nidus perfusion in 76.7% of cases, with bone restitution-ad-integrum in 30% of cases. Multivariate statistical analyses demonstrate that both patients' age (<18 years) and no residual perfusion of nidus on post-procedural DCE-MRI are significant favorable prognostic factors in terms of clinical outcome and complete bone restoration. Variable relationship between clinical outcome and bone remodelling was found in older patients (>18 years).

Conclusion: MRgFUS is an effective and safe treatment for painful non-spinal osteoid osteoma; patients' age shows significant impact on clinical outcome as well as on bone integrity restoration when total nidus ablation is achieved.

B-0632 15:12

Percutaneous US- and CT-guided thermal ablation of 20 adrenal metastases: treatment effectiveness in short- and intermediate-term imaging follow-up with CT and MRI

G. Frauenfelder, E. Faiella, D. Santucci, B.B. Beomonte Zobel, R. Grasso; *Rome/IT (giulia.frauenfelder@gmail.com)*

Purpose: To retrospectively evaluate efficacy and safety of adrenal metastasis percutaneous ablation, in terms of clinical outcomes and imaging follow-up. To evaluate additional contribution of DWI and subtracted MR sequences during radiological follow-up.

Methods and Materials: A total of 20 adrenal metastases were treated through RTA, CA or MWA. Probes were inserted under US-CT-guidance. Type of ablation and treatments parameters were influenced by lesion size and location. Each patient was evaluated with a short-term (3 months) and intermediate-term (after 6 months) imaging follow-up through contrast-enhanced CT and/or MRI. Technical success, complications, local tumour progression and overall survival were analysed on a per-patient basis. Sensitivity, specificity, positive predictive value (PPV), negative predictive value (NPP) and accuracy of CT and MR enhancement, DWI and subtraction sequences were separately evaluated during short- and intermediate-term intervals.

Results: Technical success (within 24 hours) was obtained in 100% of cases. Complications were recorded in 20% of patients (15% hypertensive peak; 5% sub-glissonian haematoma). There were 15% cases of short-term progression (recidive): all these patients had undergone RTA (62.5% of efficacy). In short-

term follow-up, accuracy for CT enhancement, MR enhancement, DWI and subtraction was, respectively, 83.3%, 80%, 75% and 90% while in intermediate-term was 84.2%, 89.5%, 94.7% and 94.7%. Overall survival was 92% after 12 months.

Conclusion: Percutaneous US- and CT-guided thermal ablation may be a safe and effective procedure in metastatic adrenal lesion treatment. Short- and intermediate-term imaging follow-up could be performed with both CT and MR; DWI and subtracted sequences are essential to increase MR accuracy.

14:00 - 15:30

Room O

Chest

SS 704

CT dose reduction: technique and applications in chest

Moderators:

J. Biederer; Heidelberg/DE
A. Nair; London/UK

K-13 14:00

Keynote lecture

D. Tack; Baudour/BE

B-0633 14:09

Individual and specific dose-level selection using dual-source computed tomography of the chest and its impact on image quality and radiation dose

A. Wressnegger¹, C. Schestak¹, H. Prosch¹, G. Apfaltrer², H. Ringl¹, P. Apfaltrer¹; ¹Vienna/AT, ²Graz/AT
(alexander.wressnegger@meduniwien.ac.at)

Purpose: The purpose of this study was to evaluate the value of individual and specific dose-level selection in dual-source computed tomography (DSCT) of the chest and its impact on image quality and radiation dose.

Methods and Materials: This retrospective study included 105 patients (57.1% male, 52.5±13.3 years). All patients had received routine unenhanced chest CT for follow-up examination reasons on both, a 2nd-generation DSCT (2nd DSCT) (Somatom Definition Flash, Siemens Healthineers) and a latest generation DSCT (Somatom Drive, Siemens Healthineers). 2nd DSCT scans were performed with 120kV and 100-150ref mAs, Care dose enabled, and FBP. Latest generation DSCT were performed with variable kV (Care kV enabled) and 50-70ref mAs, Care dose enabled, and iterative reconstruction (Admire). Signal/noise (SNR) was assessed in 6 thoracic regions. Subjective image quality (IQ_{sub}) was graded on a 5-point Likert scale. Group comparisons were performed using t test or Wilcoxon-rank-sum-test as appropriate.

Results: Dose length product (DLP) and effective dose (ED) were 208.5±63.3mGy*cm and 3.8±1.1mSv versus 112.2±34.7mGy*cm and 2.0±0.6mSv for 2ndDSCT and latest generation DSCT, respectively (P<.001), corresponding to a radiation dose reduction of 54%. SNR was 5.4±3.5 versus 6.5±3.4 for 2nd DSCT and latest generation DSCT, respectively (P=0.01), indicating a superior IQ for the latest generation scanner despite significantly less dose. IQ_{sub} was excellent for both scanners with a median score of 1[1-1] [25th-75th percentile] (P=0.7).

Conclusion: Use of latest generation DSCT enables personalized and specific dose level selection with an overall consequent radiation dose reduction of 54% while maintaining or exceeding image quality of former CT hardware.

B-0634 14:17

Model-based iterative reconstruction algorithm in low-dose CT pulmonary angiography in emergency setting: dose reduction and diagnostic quality images

L. Riva¹, D. Ippolito¹, C. Talei Franzesi¹, A. de Vito¹, C. Cangiotti¹, C. Maino¹, S. Sironi²; ¹Monza/IT, ²Bergamo/IT (luca.riva89@gmail.com)

Purpose: To compare radiation dose and image quality of low-dose CT pulmonary angiography(CTPA) combined with Model-Based Iterative Reconstruction (IMR), with a standard dose CTPA-study, in patients with suspect of pulmonary embolism(PE).

Methods and Materials: Eighty-seven patients investigated for PE in emergency setting were enrolled. The study-group was evaluated using a 256-MDCT (iCT elite, Philips) with 80-kV, dose right index and automated tube-current modulation, low volume of CM (50mL;350mg/mL) and IMR algorithm to reconstruct raw data. Control-group underwent a standard CTPA-study on 16-MDCT scanner, with the same volume of CM(120kV;150-250mAs;FBP-reconstruction).Two radiologists performed quantitative evaluation measuring vessels contrast-enhancement and calculating SNR and CNR. A 4-point scale

was used to perform qualitative evaluation. Radiation dose exposure data was recorded as DLP and CTDIvol.

Results: The intra-vessel density, SNR and CNR were significantly higher in study-group than in control-group (i.e. CNR: IMR 43.56±21.81 vs FBP-CTPA 23.21±12.11; $p < 0.05$), while background noise was significantly lower ($p < 0.05$) in study-group in comparison with control-group. DLP and CTDIvol in IMR-CTPA were significantly lower than those in FBP-CTPA ($p < 0.05$), with a 56% reduction of CTDIvol (IMR-CTPA 6.41±1.41 mGy vs FBP-CTPA 14.68±3.42 mGy) for study-group. Raw data reconstruction time of the IMR was higher than FBP with a mean value of 2.08 minutes, otherwise acceptable for emergency setting. Moreover, the overall image quality rating score was higher for IMR-CTPA than FBP-CTPA both for the two readers ($p < 0.05$; $C_{\alpha} = 0.91$).

Conclusion: Low-kV setting combined with IMR can improve diagnostic image quality of CTPA in pulmonary embolism, compared to a standard CTPA reconstructed with FBP, allowing to reduce the radiation dose to patients.

B-0635 14:25

The impact of ASiR-V in different noise index in thorax CT imaging: comparison between normal dose and low dose

L. Jin, M. Li, Y. Sun; *Shanghai/CN (BrightDK@126.com)*

Purpose: To evaluate the impact of adaptive statistical iterative reconstruction-veo (ASiR-V) technique in thorax CT imaging between normal dose and low dose.

Methods and Materials: Randomly selected 42 patients sent to do thorax CT by clinical doctors from April-July 2017 were divided into three groups: (NI=14, 120KV) group A, (NI=28, 120KV) group B, (NI=28, 80KV) group C. All groups were reconstructed by ASiR-V technique: weight from 0%-100%, interval was 10%, image slice and reconstruction interval was 0.625mm. Signal intensity was measured by placing a region of interest in 3cm upon the corner of the sternum, noise was measured in the thoracic aorta. Image quality was visually assessed by two radiologists over 15 experience using a 5-point scale. The inter-observer differences were determined by kappa statistics.

Results: The image noise of each group decreases with the increase of ASiR-V weight, and the contrast noise increases with the increase of ASiR-V weight. The image quality of all sequences in image analysis was above 3 points and above which was satisfied with diagnosis, 40% weight ASiR-V got the highest image quality. The ED of each group was (3.03±1.63)mSv, (3.86±0.74)mSv, (3.62±0.63)mSv; the ED of low-dose group (B&C) was decreased by 75% compared with normal group (A). There was perfect inter-observer concordance in terms of image quality ($\kappa = 0.912$).

Conclusion: ASiR-V technique for image reconstruction was obviously better than FBP, 40% weight was the best choice, specially under low-dose scanning; the effect of noise on image quality could be well compensated, so images met the diagnosis in lower radiation dose.

B-0636 14:33

Study of image quality in chest CT using prospective ASiR-V

Q.Q. Yuan; *Zhengzhou/CN (yuanqian10@163.com)*

Purpose: To explore the optimal prospective ASiR-V percentage in chest CT with good image quality and low radiation dose.

Methods and Materials: A phantom containing solid pulmonary nodule examined on GE revolution CT was randomly divided into six groups using prospective ASiR-V technique (0%, 20%, 40%, 60%, 80%, 100%). The quantitative analyses included objective noise and CNR. The subjective image quality was graded on a scale from 1 (worst) to 5 (best). CTDIvol, CNR, noise and image score were compared with ANOVA.

Results: CTDIvol had statistically significant differences of all groups ($P < 0.05$). CNR, noise and image score of 40%, 60%, 80% and 100% ASiR-V were statistical difference between each group ($P < 0.05$). However, the image score of 60%, 80% and 100% ASiR-V could not meet the diagnostic requirement with 3.40±0.51 vs 2.40±0.51 vs 1.20±0.41. 40% ASiR-V image score basically met the diagnostic requirement with 4.40±0.51, meanwhile mean dose reduction relative to 0% ASiR-V was 44%. There was no significant difference in CNR and image score between 20% and 0% ASiR-V, CNR was 1.36±0.16 vs 1.22±0.22 ($P = 0.17$) and subjective image score was 4.80±0.41 vs 5.00±0.00 ($P = 0.21$), meanwhile mean dose reduction relative to 0% ASiR-V was 26%.

Conclusion: Images of prospective 60%, 80%, 100% ASiR-V provided the lower CTDIvol and noise, but the poor image quality could not meet the diagnostic requirement. Images obtained from 20% and 40% ASiR-V had the similar image quality with 0% ASiR-V producing lower radiation dose. 20% and 40% ASiR-V could be recommended for chest CT scan.

B-0637 14:41

Comparison of ultra-low-dose computed tomography (ULDCT) and standard-dose computed tomography (SDCT) for the detection of interstitial lung disease

S. Takehara¹, T. Iwasawa¹, T. Baba¹, T. Ogura¹, M.S. Oba²; ¹Yokohama/JP, ²Tokyo/JP (takehara198963@gmail.com)

Purpose: To compare the ability of ultra-low-dose computed tomography (ULDCT) and standard-dose computed tomography (SDCT) for detecting interstitial lung disease (ILD).

Methods and Materials: Fifty-one patients were recruited prospectively. Each patient underwent computed tomography (CT) examinations at standard dose (auto electric current; below 350 mA, 120 kV) and ultra-low-dose (20 mA, 120 kV). The average effective doses were 5.8 and 0.37 mSv, respectively. Three board-certified radiologists diagnosed ILD based on SDCT images. The volume of a normal lung (N-pattern) and fibrosis (F-pattern) were measured using a Gaussian histogram normalized correlation (GHNC) system; volume ratios to the whole lung volumes were calculated. Receiver operating characteristic (ROC) curve analysis of the F-pattern volume ratio was used to examine the ability of ULDCT and SDCT to detect ILD.

Results: Out of 51 patients, 30 were diagnosed with ILD. The GHNC was used to analyse the ULDCT results of all patients. In the GHNC analysis, the N-pattern volume ratio on ULDCT was significantly larger than that on SDCT [median, 86.19% in ULDCT and 83.58% in SDCT ($p < 0.001$)]. The F-pattern volume on ULDCT was significantly smaller than that on SDCT [median, 5.59% in ULDCT and 7.33% in SDCT ($p < 0.001$)]. The areas under the ROC curve for F-pattern were 0.946 (95% confidence interval, 0.89-1.0) in ULDCT and 0.927 (95% confidence interval, 0.87-1.0) in SDCT.

Conclusion: The area of fibrosis might be underestimated when ULDCT is used. However, the F-pattern volume ratio measured using ULDCT is similar to that by SDCT in its ability to detect ILD.

B-0638 14:49

Ultra-low-dose CT with tin filtration for lung densitometry and emphysema detection

Y. Gao, X. Zhai, L. Zhang, K. Huang; *Beijing/CN (gaoyanli1997@msn.com)*

Purpose: The purpose of this study was to determine whether ultralow-dose CT with tin filtration can be used for quantification of lung density and for emphysema detection.

Methods and Materials: Fifty-two patients were prospectively enrolled and underwent both low-dose CT (120 kV, 50 effective mAs) and ultralow-dose CT. Ultralow-dose CT was performed with single-energy at 100kV using tin filtration (Sn100 kV, 100 effective mAs). Images were reconstructed by filtered back projection (FBP) for low-dose CT and FBP and advanced modelled iterative reconstruction (ADMIRE, strength level 3 and 5) for ultralow-dose CT. Radiation dose was recorded. Emphysema index, 15th percentile of lung attenuation, mean lung attenuation, total lung volume and image noise were measured in each image series and compared.

Results: The effective dose of low-dose CT was 2.0 ± 0.6 mSv, and that of ultralow-dose CT was 0.2 ± 0.1 mSv. Compared with the findings for low-dose CT, emphysema index was significantly overestimated by 4% on ultralow-dose CT FBP images, 2% on ADMIRE step 3 images, but no significant difference was observed on ADMIRE step 5 images. The 15th percentile of lung attenuation was significantly underestimated by 6 HU on ultralow-dose FBP images, while no significant differences were exhibited on ADMIRE images compared with low-dose CT. No significant differences were observed in mean lung attenuation and total lung volume. Image noise was significantly reduced using ADMIRE compared to FBP.

Conclusion: Ultralow-dose CT with tin filtration is feasible for lung density quantification and emphysema detection. ADMIRE improves the accuracy of ultralow-dose CT.

B-0639 14:57

Impact of iterative model reconstruction on the correlation between CT quantification of emphysema and airway measurements and pulmonary function test in the normal study cohort

D. Kim¹, C. Kim², K. Lee¹, J.-Y. Choo², E.-Y. Kang², Y.-W. Oh²; ¹Ansan/KR, ²Seoul/KR (dj8827@naver.com)

Purpose: To compare the correlation between PFT and different reconstruction algorithms and to suggest useful guidance to optimize the reconstruction protocol in the CT quantification of the lung and airways in the normal study subjects.

Methods and Materials: Chest CT from 223 subjects were reconstructed using variable reconstruction algorithms including FBP, hybrid IR(HIR), and model-based IR(MIR) to determine the scan protocol best correlated with PFT. Measurements of each dataset were compared: emphysema index (EI) and wall area percentage (WA%). We compared the CT parameters between FBP, HIR and MIR with PFT parameters. Pearson correlation and linear regression

analysis were conducted to evaluate between different algorithms and PFT in the whole study subjects and subgroups according to smoking history.

Results: In the whole study subjects, EIs of all the reconstruction algorithms involving FBP, HIR, IMR-R1, and IMR-ST1 showed significant correlations with FEV1/FVC. Among these, EI of IMR-R1 showed the highest correlation with FEV1/FVC. WA% in IMR-SP1 showed significant correlation with both FEV1 and FEV1/FVC. In the subgroup analysis, EIs of all the reconstruction algorithms involving FBP, HIR, IMR-R1, and IMR-ST1 showed significant correlations with FEV1/FVC in both ever- and never-smokers. Among these, EI of IMR-R1 showed the highest correlation with FEV1/FVC in both ever- and never-smokers. WA% in IMR-SP1 showed also significant correlation with both FEV1 and FEV1/FVC in both ever- and never-smokers.

Conclusion: CT quantification of emphysema and airway using MIR showed best correlation with PFT compared to using HIR and FBP in the normal study cohort.

B-0640 15:05

Performance and radiation dose comparison of the recently introduced ultralow-dose chest computed tomography (CT), standard-dose CT and digital chest radiography

T. Svahn¹, T. Sjöberg², K. Shahgaldi¹, J. Nordström¹, ¹Gävle/SE, ²Hudiksvall/SE (tony.svahn@regiongavleborg.se)

Purpose: To evaluate diagnostic performance and absorbed radiation dose of ultra-low-dose CT (ULD-CT) in comparison to that of standard CT (SD-CT) and digital chest radiography (DR).

Methods and Materials: Pulmonary nodules were simulated in an anthropomorphic phantom (LungMan; Kyoto Kagaku). Thirty cases, 18 with lesions (45 lesions in total of 3-12 mm) and 12 without, were acquired at each imaging technique. Two radiologists interpreted the cases in a blinded detection study. Performance was assessed using the JAFROC figure-of-merit (FOM). Radiation absorbed dose to the lungs were measured using TLD-dosimeters. A systematic search was performed to identify patients examined by both ULD-CT and SD-CT for extraction and evaluation of radiation dose metrics.

Results: Performance was not significantly different between ULD-CT and SD-CT (FOMs: 0.824 vs 0.857; ΔFOM: 0.03). Significantly more lesions were detected with the two CT techniques in comparison to DR (FOM: 0.541; ΔFOM: 0.31 and 0.28). Depending on patient size, ULD-CT was found to yield two to twelve times higher dose to the lungs than DR (PA + lateral views), but only ~4-11% the dose from SD-CT. Paired radiation dose data was eligible for forty patients, which correlated with the measured dose differences, but with a wider dose range.

Conclusion: ULD-CT may serve as an alternative to both SD-CT and DR, considerably reducing dose in the first case and improving diagnostic accuracy in the second. Raised awareness of ULD-CT may lead to increased usage in the appropriate clinical setting at the local radiology department.

B-0641 15:13

Low-dose digital radiography in diagnosis of COPD's phenotypes

N. Gorbounov, A. Dergilev, V. Kochura, Y. Manakova, A. Sudarkina; Novosibirsk/RU (a.sudarkina@mail.ru)

Purpose: Determination of the features of low-dose digital radiography in the diagnosis of phenotypic variants of COPD.

Methods and Materials: 107 patients with COPD of varying severity were examined. The average age of the patients was 51.8 ± 1.5 years (46 - 59 years). All patients underwent low-dose digital radiography of the chest in the frontal projection in different phases of respiration. The electron optical density of the lungs was determined in the upper, middle and lower zones of both lungs.

Results: In patients with a predominance of emphysematous variant of COPD (n = 15) the most characteristic radiological symptom was lung emphysema (14% of 107 patients) and inspiratory electron optical density value was 748.18 ± 4.72 optical density units (ODU). In patients with a predominance of bronchitic variant of COPD (n = 43) the most common radiological symptom was the presence of amplification and deformation of lung pattern (40% of 107 patients) and inspiratory electron optical density value was 668.04 ± 12.26 ODU. For patients with mixed phenotypic variant of COPD (n = 49) it was characterized by a combination of X-ray symptom of amplification and deformation of lung pattern with lung emphysema (46% of 107 patients); the average value of inspiratory electron optical density value was 815.24 ± 17.25 ODU.

Conclusion: The technique of low-dose digital radiography can detect X-ray symptoms and determine electron optical density of the lungs in patients with COPD that allows optimizing the diagnosis of phenotypic variants of chronic obstructive pulmonary disease.

B-0642 15:21

Radiation protection: factors influencing compliance to referral guidelines in minor chest trauma

F. Louage¹, A. Van Muylem², N. Howarth³, P. Gevenois², D. Tack⁴; ¹Ath/BE, ²Brussels/BE, ³Chênes-Bougeries/CH, ⁴Braine-L'Alleud/BE (fabian.louage@ulb.ac.be)

Purpose: To test the hypothesis that referral guidelines are not sufficiently known by prescribers and that medico-legal concerns could influence the prescription of radiographs in minor chest trauma.

Methods and Materials: We submitted a questionnaire including a typical clinical history and questions on reasons for prescribing radiographs of the ribs in minor chest trauma to 112 prescribers (33 residents, 18 surgeons, 7 internists, 24 general practitioners and 30 ER physicians). All accepted to participate. Comparisons were performed by exact Fisher tests followed by a post hoc analysis and by a McNemar test.

Results: Fifty-eight percent of prescribers proposed rib radiographs, most (89%) being unaware of the guidelines. Only 11% of them changed their intention to order radiographs after information on referral guidelines and radiation dose (P=0.057). The mean dose delivered by rib radiographs was 38 times higher than that of a chest X-ray. Legal and medico-legal concerns (requirements from insurance policies and avoidance of lawsuits) were the main reasons for requesting radiographs.

Conclusion: Unsharpness of guidelines in addition to social and medico-legal issues, rather than medical reasons or the lack of knowledge of the guidelines, strongly influence the prescription of radiographs of the ribs in minor chest trauma. As stated by the 2013/59 Euratom Directive, legal issues should be addressed specifically in future versions of referral guidelines.

14:00 - 15:30

Room N

Genitourinary

SS 707

Gynaecologic cancers

Moderators:

S. Freeman; Cambridge/UK
N.N.

K-14 14:00

Keynote lecture

A.G. Rockall; London/UK

B-0643 14:09

Newly categorised seromucinous tumours of ovary: computed tomographic and magnetic resonance imaging features with pathological correlation

J. Han, K.A. Kim, C. Hyeyoon, J.W. Kim, Y. Park, J. Lee, J.W. Choi, C.H. Lee, C.M. Park; Seoul/KR (seryjooin@hanmail.net)

Purpose: To describe computed tomographic (CT) and magnetic resonance imaging (MRI) findings of newly established seromucinous ovarian tumors in the revised 2014 WHO classification, according to tumor type with pathological correlation.

Methods and Materials: We retrospectively reviewed the CT and MR images of 29 patients with seromucinous tumors of ovary for the following factors: size, configuration, signal intensity (SI), staging, and accompanying ovarian endometriosis.

Results: The mean age was 45.2 years (range, 20-84 years). 32 seromucinous tumors were found on CT or MRI (17 adenoma (A), 7 borderline (B), and 8 carcinoma (C)), and the mean size was 11.4 cm (A: 12.6 cm, B: 6.8 cm, C: 13.3 cm). Adenomas appeared as unilocular (n=10) or multilocular (n=7) cystic mass. Borderline tumors (n=6, 86%) and carcinomas (n=8, 100%) showed complex cystic and solid mass. The SI of solid portion on T2-weighted images (T2WI) was hyperintense in borderline and hypointense in carcinoma. The seromucinous carcinomas were FIGO stage IA (n=7, 88%) and stage IC (n=1). Endometriosis was accompanied with 18 tumors (A: 8; 46%, B: 5; 71%, C: 5; 63%).

Conclusion: The CT and MRI appearance of seromucinous tumors varied according to tumor type. T2WI high SI solid portion was useful for differentiating borderline tumor from carcinoma. Seromucinous tumors were frequently associated with endometriosis.

B-0645 14:17

Clinical value of low-kiloelectron volt monoenergetic images of dual energy computed tomography for evaluation of peritoneal seeding of ovarian cancer

T.M. Kim, S. Kim, J. Cho, S. Kim; Seoul/KR (kjambong@gmail.com)

Purpose: The purpose of this study was to compare the image quality of virtual low-kiloelectron volt (keV) monoenergetic (monoE) images with conventional images reconstructed from enhanced spectral computed tomography (CT) in detection of peritoneal implants.

Methods and Materials: Thirty patients who underwent serial pelvis CT scans due to ovarian cancer were included in this retrospective study. From spectral data, the two virtual low-keV monoE (40-keV and 50-keV) images were reconstructed. The conventional images using filtered back projection (FBP) and iterative reconstruction (IR) protocols were also evaluated. Two radiologists measured the attenuation and standard deviation of peritoneal implants, adjacent bowels and ascites. The mean attenuation, signal-to-noise ratio (SNR) and contrast-to-noise ratio (CNR) were calculated and compared using paired t-test.

Results: The 201 peritoneal implants were measured and evaluated. The virtual low-keV monoE (40-keV and 50-keV monoE) images showed significantly higher mean attenuation values of peritoneal implants than conventional images. The all SNR and CNR values showed significantly higher in the virtual 40-keV monoE images. The virtual 50-keV monoE images showed the similar SNR and CNR values to IR images. In terms of contrast between peritoneal implants and adjacent bowels, the virtual 40-keV monoE images showed significantly higher image quality than virtual 50-keV monoE images.

Conclusion: The virtual 40-keV monoE images significantly increase the contrast of peritoneal implants. The low-keV monoE reconstructions from spectral CT can demonstrate excellent clinical value for detection and management of peritoneal seeding in ovarian cancer patients.

B-0646 14:25

Prediction of histological grade of endometrial cancer by means of MRI

M. Bonatti, B. Pedrinolla, F. Lombardo, G. Avesani, G. Bonatti; Bolzano/IT (matteobonatti@hotmail.com)

Purpose: To evaluate the capability of MRI in predicting histological grade of endometrial cancer (EC).

Methods and Materials: IRB-approved retrospective study; requirement for informed consent was waived. 90 patients with histologically proven EC who underwent preoperative MRI and surgery at our Institution between Sept2011 and Nov2016 were included. Myometrial invasion (</>50%) was assessed on T2-weighted images in association with diffusion-weighted images. Neoplasm and uterus volumes were estimated according to the ellipsoid formula using sagittal and para-axial images. Neoplasm/uterus volume ratio (N/U) was calculated. ADC maps were generated and histogram analysis was performed using commercially available software. MRI parameters were compared with the definitive histological grade (G1=28 patients, G2=29, G3=33) using ANOVA and Tukey-Kramer tests.

Results: Deep myometrial invasion was significantly more frequent in G2-G3 lesions than in G1 ones (p<0,005). N/U ratio was significantly higher for high-grade neoplasms (mean 0,08 for G1, 0,16 for G2 and 0,21 for G3; P=0,002 for G1 vs. G2-G3); a cut off value of 0,13 enabled to distinguish G1 from G2-G3 lesions with 50% sensibility and 89% specificity. ADC values didn't show any statistically significant correlation with tumour grade.

Conclusion: N/U ratio >0.13 and deep myometrial invasion are significantly correlated with high grade EC, whereas ADC values are not useful for predicting EC grade.

B-0647 14:33

Prediction of pathologic upgrading in biopsy-proven low-grade endometrial cancer: utility of diffusion-weighted imaging

J. Park¹, C. Kim²; ¹Daejeon/KR, ²Seoul/KR (jjskku@naver.com)

Purpose: To investigate the utility of diffusion-weighted imaging (DWI) for predicting pathologic upgrading in endometrial cancer.

Methods and Materials: A total of 221 patients who underwent MRI before surgery for biopsy-proven grade I endometrial cancer were enrolled. The minimum apparent diffusion coefficient (ADC_{min}) was calculated using histogram analysis of the entire tumour. Clinical and imaging variables were compared between patients with and those without postoperative pathologic upgrading. The independent predictors of pathologic upgrading were determined using logistic regression analysis.

Results: Pathologic upgrading was identified in 42 patients (19.0%). Patients with pathologic upgrading had larger tumours, more frequently showed deep myometrial invasion on MRI, and had lower ADC_{min} values than those without pathologic upgrading (all P<0.001). The area under the receiver operating characteristic curve of ADC_{min} and tumour size was 0.812 (cut-off, 0.600×10³

mm²/s) and 0.758 (cut-off, 3cm), respectively. On multivariate analysis, tumour ADC_{min}≤0.600×10⁻³mm²/s (odds ratio [OR], 11.8; P<0.001) and tumour size on MRI>3 cm (OR, 3.24; P=0.009) were independently associated with pathologic upgrading. Upgrading occurred in 23 of 31 patients (74.2%) with ADC_{min}≤0.600×10⁻³mm²/s and tumour size>3cm, and in 7 of 114 patients (6.1%) with ADC_{min}>0.600×10⁻³mm²/s and tumour size ≤3cm.

Conclusion: Tumour ADC and tumour size on MRI may be useful parameters for predicting pathologic upgrading in biopsy-proven grade I endometrial cancer.

B-0648 14:41

Utility of histogram analysis of apparent diffusion coefficient maps in differential diagnosis of uterine sarcoma and degenerated uterine leiomyoma

M. Huang; Zhengzhou/CN (huangmengna1127@163.com)

Purpose: To investigate the value of histogram analysis of apparent diffusion coefficient (ADC) maps for discriminating uterine sarcoma and degenerated uterine leiomyoma.

Methods and Materials: 43 patients with uterine sarcoma and 46 patients with degenerated uterine leiomyoma who underwent MRI and DWI scanning were retrospectively evaluated. Histogram data from regions of interest drawn on all slices of the ADC maps of parenchyma of different tumours were derived and statistically analysed by independent samples t test. The receiver operating characteristic (ROC) curve was analysed to determine the optimum threshold value for each parameter and its corresponding sensitivity and specificity.

Results: Uterine sarcoma demonstrated significantly lower mean values of ADC: 5%, 10%, 25%, 50%, 75%, 90% and 95% than degenerated uterine leiomyoma (P < 0.05). ROC curve analysis of the 90% yielded the best area under the ROC curve (AUC; 0.941), sensitivity of 91.3%, and specificity of 90.2%, with a cutoff value of 1.155×10⁻³mm²/s.

Conclusion: Histogram analysis of apparent diffusion coefficient maps is beneficial in differential diagnosis of uterine sarcoma and degenerated uterine leiomyoma.

B-0649 14:49

Diagnostic performance of MRI for assessing parametrial invasion in cervical cancer: a head-to-head comparison between oblique and true axial T2-weighted images

S. Woo^{1,2}, S. Kim¹, J. Cho¹, S. Kim¹; ¹Seoul/KR, ²Daejeon/KR (j_crew7@hotmail.com)

Purpose: To investigate whether oblique axial T2-weighted images (T2WI) provide added value compared with true axial T2WI for assessing parametrial invasion (PMI) in cervical cancer.

Methods and Materials: This retrospective study included 71 women with treatment-naïve cervical cancer who underwent MRI (including oblique and true axial T2WIs) followed by radical hysterectomy. Two blinded radiologists (R1 and R2) independently assessed PMI on both sequences using a 5-point Likert scale. Receiver operative characteristic (ROC) curve analysis was performed. Subgroup analysis was done for tumours sized >2.5 and ≤2.5 cm. Inter-reader agreement was assessed with kappa (k) statistics.

Results: There were 15 patients (21.1%) with PMI at hysterectomy. Oblique axial T2WI showed significantly greater area under the curve (AUC) than true axial T2WI by R1 (0.941 [95%CI=0.858-0.983] vs 0.917 [95%CI=0.827-0.969], p=0.027) but not R2 (0.879 [95%CI=0.779-0.944] vs 0.827 [95%CI=0.719-0.906], p=0.153). In tumours >2.5 cm, AUC was greater using oblique than true axial T2WI (0.906 vs 0.860, p=0.046 and 0.839 vs 0.765, p=0.086). Agreement was almost perfect for oblique axial T2WI (k=0.810) and substantial for true axial T2WI (k=0.704).

Conclusion: Oblique axial T2WI may provide potentially greater diagnostic performance than true axial T2WI for determining PMI, especially in tumours >2.5 cm. The inter-reader agreement was greater when using oblique axial T2WI than when using true axial T2WI.

B-0650 14:57

Blood oxygenation level-dependent MRI for prediction of clinical outcome in uterine cervical cancer treated with radiotherapy

J. Lee, C. Kim, K. Gu; Seoul/KR (jiyeong25.lee@samsung.com)

Purpose: To investigate the value of blood oxygenation level-dependent (BOLD) magnetic resonance imaging (MRI) as a predictor of clinical outcome in cervical cancer patients treated with radiotherapy (RT).

Methods and Materials: Between October 2009 and August 2017, 98 patients with stage IB-IVB cervical cancer who received definitive RT with (n= 92) or without (n= 6) concurrent chemotherapy underwent BOLD MRI before treatment. BOLD MRI was obtained at 3T using a multiple fast field echo sequence to acquire 12 T2*-weighted images. The R2* value (rate of spin dephasing, sec⁻¹) was measured in the tumour. Cox proportion hazard model was used to evaluate the association of imaging and clinical variables with

Neuro

SS 711a Psychiatric disorders

Moderators:

E. Lotan; Tel-Aviv/IL
T.A. Yousry; London/UK

B-0653 14:00

Investigating direction of effective connectivity in obsessive compulsive disorder with resting state fMRI

H. Li, X. Hu, L. Zhang, L. Lu, X. Bu, S. Tang, X. Huang; Chengdu/CN
(979280614@qq.com)

Purpose: Obsessive-compulsive disorder(OCD) is a common psychiatric disorder characterized by disruption in functional connectivity of certain brain networks. This study aimed to investigate direction of effective connectivity(EC) in OCD by estimating anomalous cross-structure causal effects and to further investigate whether those connectivities would correlate with the severity of clinical symptoms.

Methods and Materials: A total of 88 OCD patients and 88 sex and age matched healthy control(HC) were recruited. We performed bivariate voxel-wise and multivariate ROI-wise Granger Causality(GC) Analysis using the REST-GCA in the REST toolbox. The multivariate GC analysis incorporating regions identified in the bivariate GC analysis. The comparison of group difference were performed using a linear mixed-effects model and the correlations between effective connectivity and clinical variables were performed by Pearson correlation analysis.

Results: Compared with HC, OCD patients showed excitatory EC from pallidum and cerebellum to dorsolateral prefrontal cortex(DLPFC), and from DLPFC to posterior cingulate cortex(PCC), from superior parietal lobule(SPL) to PCC. While inhibitory EC start from middle temporal gyrus(MTG) point to DLPFC. In addition, there is a positive correlation between inhibitory EC from MTG to DLPFC and Hamilton Score for Anxiety in OCD patients.

Conclusion: Our findings for the first time demonstrated the either excitatory or inhibitory effects among these structures implicated in OCD brain network alterations and its correlation with clinical symptom. These findings shed light on our understanding of the OCD pathology from a cerebral network point of view.

B-0654 14:08

Structural magnetic resonance imaging study on schizophrenic patients with violence risk

Y. Li, F. Fan, Z. Feng, W. Liang, S. Tan, F. Yang; Beijing/CN
(867840617@qq.com)

Purpose: This study utilized structural MRI with FreeSurfer to assess different brain cortical morphology changes (brain cortical thickness, surface area, volume and mean curvature) in schizophrenic patients with violence risk and to elucidate the correlation between the obtained brain characteristics and clinical parameters.

Methods and Materials: Sixty-six patients were classified into 2 groups (violence: nonviolence group =49:17) based on the MOAS to analyse the brain structure differences. Individuals in each group underwent structural MRI, then, FreeSurfer was used to carry out subsequent brain structure analysis. The statistical software used was SPSS22.0.

Results: There were no statistical differences in gender, age and other clinical information between two groups (P>0.05). Compared with nonviolence group, the violence group showed increased cortical mean curvature in left cingulate sulcus (0.0104±0.0132 vs 0.1131±0.0107, P=0.006), reduced cortical thickness in right postdorsal cingulate gyrus (3.2771±0.2993 vs 2.999±0.2637, P=0.001) and left occipital pole (2.2471±0.2237 vs 2.0971±0.1856, P=0.008). Brain volume showed reductions in left temporal middle gyrus (8734.12±1091.164 vs 7562.33±1195.055, P=0.001), left transverse temporal sulcus (567.71±143.795 vs 466.57±117.752, P=0.005) and right superior frontal sulcus (4503.53±737.935 vs 3856.24±799.814, P=0.005) in violence risk brains. The ROC demonstrated left cingulate and superior precentral sulcus mean curvature can diagnose the schizophrenic violence risk, the AUC is 0.715 (95%CI: 0.566-0.865, P=0.008) and 0.726 (95%CI: 0.578-0.875, P=0.006), respectively. The multinomial logistic regression model adjusting the general clinical information the right postdorsal cingulate gyrus cortical thickness is shown to be an independent factor predicting the violence risk of schizophrenia (OR: 0.003[0.000,0.174], P=0.005).

Conclusion: A reduction in the brain cortex thickness and volume and an increase in the cortical mean curvature may be associated with schizophrenia with violence risk. The right postdorsal cingulate gyrus cortex thickness could predict violence of schizophrenia as an independent factor.

progression-free survival (PFS), cancer-specific survival (CSS), and overall survival (OS).

Results: During a median follow-up of 3.8 years, disease progression was identified in 33 patients (33.7%) and 14 patients (14.3%) died of their disease. Tumour R2* value had a significant difference between with and without progression (P< 0.001). On multivariate analysis, tumour R2* value was significantly independent factor for PFS (hazard ratio [HR]= 1.18, P= 0.001), CSS (HR= 1.25, P= 0.003) and OS (HR= 1.22, P= 0.009), respectively. Of clinical variables, histologic type was significantly independent factor for PFS (HR= 1.02, P= 0.013). For predicting tumour progression, the area under receiver operating characteristic curve of R2* value was 0.724, which was significantly different with other variables (P< 0.001).

Conclusion: As an imaging marker, pretreatment BOLD MRI may be useful for predicting clinical outcome in patients with cervical cancer treated with RT.

B-0651 15:05

Primary vaginal malignancies: a single oncology centre experience

M. Lima¹, G. Rio², M. Horta¹, T.M. Cunha¹; ¹Lisbon/PT, ²Braga/PT
(mariana_talina@hotmail.com)

Purpose: Review the clinical and imaging features of primary vaginal neoplasms of a large oncologic referral centre.

Methods and Materials: Retrospective analysis of clinical and MR findings of primary vaginal cancers over a 11-year period (Feb/2006-Sep/2017).

Results: 35 cases were found. The most common histological type was squamous cell carcinoma (SCC) (77.1%), followed by adenocarcinoma (14.3%). Glassy cell carcinoma, melanoma and botryoid sarcoma occurred as single cases. There was no statistically significant difference (p=0,550) in the mean age at diagnosis between SCC (63y) and adenocarcinoma (58y), as well as in the mean size of the tumor (p=0,998; SCC:41.5mm; adenocarcinoma: 41.3mm). SCCs were homogeneous on T2-weighted images, while adenocarcinomas were heterogeneous (one also showed hyperintense areas on T1-weighted imaging). Regarding the location, both SCC(59%) and adenocarcinomas (80%) were predominantly confined to the upper third, while melanoma occurred in the lower third. All adenocarcinomas originated on the anterior vaginal wall, while the majority of SCC originated on the posterior wall (62.5%). The remaining SCCs preferentially involved the right (16.7%)/left vaginal wall (16.7%), however one case showed circumferential involvement. 54% of patients had previous hysterectomy. In the adenocarcinomas group, all were performed for benign pathology; in the SCCs group, 73% were associated with cervical dysplasia (83% CIN III).

Conclusion: The imaging distinction of histological subtypes of vaginal cancer is not possible, although their location and MR signal can provide some clues. Many patients with vaginal SCC had a previous hysterectomy with cervical dysplasia, probably because they may share HPV infection as a risk factor.

B-0652 15:13

Comparison of 18F-FDG PET/MRI and MRI alone for whole-body staging of 71 women with suspected recurrent pelvic cancer: a follow-up study

L.M. Sawicki¹, J. Kirchner¹, J. Gruenewald², V. Ruhlmann², B.M. Schaarschmidt¹, M. Forsting², K. Herrmann², G. Antoch², L. Umutlu²; ¹Düsseldorf/DE, ²Essen/DE (Linomorris.sawicki@med.uni-duesseldorf.de)

Purpose: To evaluate the diagnostic performance of 18F-FDG PET/MRI for whole-body staging of women with suspected recurrent pelvic cancers in comparison with MRI alone.

Methods and Materials: Seventy-one consecutive women (54±13 years) with suspected recurrence of cervical (32), ovarian (26), endometrial (7), vulvar (4), and vaginal (2) cancer underwent PET/MRI including a diagnostic contrast-enhanced MRI protocol. PET/MRI and MRI were separately evaluated regarding lesion count, localisation, categorisation (benign/malignant), and diagnostic confidence (3-point scale; 1-3) by two physicians. Reference standard was histopathology and follow-up imaging. Diagnostic accuracy and proportions of lesions rated correctly were retrospectively compared using McNemar's Chi² test. Differences in diagnostic confidence were assessed by Wilcoxon test.

Results: Fifty-five patients showed cancer recurrence. PET/MRI correctly identified more patients with cancer recurrence than MRI alone (100% vs 83.6%, p<0.01). Based on the reference standard, 241 lesions were detected in the study cohort (181 malignant, 60 benign). While PET/MRI provided correct identification of 181/181 (100%) malignant lesions, MRI alone correctly identified 135/181 (74.6%) malignant lesions, which was significantly less compared to PET/MRI (p<0.001). PET/MRI offered superior diagnostic accuracy (99.2% vs 79.3%, p<0.001) and diagnostic confidence in the categorisation of malignant lesions compared with MRI alone (2.7±0.5 vs 2.4±0.7, p<0.001).

Conclusion: PET/MRI demonstrates excellent diagnostic performance and outperforms MRI alone for whole-body staging of women with suspected recurrent pelvic cancer.

Author Disclosures:

L. Umutlu: Consultant; Bayer AG.

B-0655 14:16

Meta-analysis of resting-state functional connectivity of major depressive disorder in youth

S. Tang, X. Hu, Q. Gong, X. Huang; *Chengdu/CN (731781233@qq.com)*

Purpose: To investigate neural dysfunction in youth with major depressive disorder (MDD) reported in existing resting-state functional connectivity (rsFC) studies.

Methods and Materials: Seed-based rsFC studies comparing youth with MDD with healthy controls (HCs) (published before September 30, 2017) were retrieved from electronic databases (PubMed, Web of Science, and EMBASE). Articles that conducted a comparison of youth with MDD aged under 25 and HCs using seed-based rsFC were retained and coordinates of brain regions exhibiting different rsFC in youth with MDD compared with HCs were extracted. Anisotropic effect size-signed differential mapping (AES-SDM) meta-analysis was performed to assess rsFC alterations in 375 youth with MDD compared to 313 HCs.

Results: Compared with HCs, youth with MDD showed hyperconnectivity in the right postcentral gyrus (the main sensory receptive area), left superior frontal gyrus (in coordination with the action of the sensory system), and right heschl gyrus (processing incoming auditory information) and hypoconnectivity in the left middle orbital-frontal gyrus (referring to emotion and reward in decision making).

Conclusion: Increased connectivity in the right postcentral gyrus, left superior frontal gyrus and right heschl gyrus which all involve in sensory perception such as vision, hearing and touch may reflect the biased external to internal sense and cognition processing. Meanwhile, reduced connectivity in the left middle orbital-frontal gyrus implicated in emotion and reward in decision making may give an index to the deficits in internal to external emotion and salience executing. These findings paralleled to the core feature of MDD patients may underlie the cognitive and affective abnormalities in depressive disorder.

B-0656 14:24

Relationship between peripheral Interleukin 10 and white matter integrity in stable medicated schizophrenia

G. Fu¹, W. Zhang¹, J. Liu¹, Y. Xiao¹, L. Yao¹, J.A. Sweeney^{1,2}, S. Lui¹; ¹Chengdu/CN, ²Cincinnati, OH/US (*guiufu08011991@163.com*)

Purpose: Deficits of white matter integrity have been widely reported in patients with schizophrenia, while the cause of such changes remains unclear. Interleukin 10 (IL-10) was reported to be associated with white matter integrity in animal model. However, it is unknown whether there is any change of IL-10 and related white matter integrity in schizophrenia patients. We aimed to investigate the relationship between peripheral IL-10 level and fractional anisotropy (FA) in stable medicated schizophrenia patients.

Methods and Materials: Diffusion tensor data scanned with 3T SKYRA and IL-10 data tested via quantitative chemiluminescent assay were acquired from 47 stable medicated schizophrenia outpatients and 49 healthy subjects. FA map was processed using FSL 5.0.6 and Tract-Based Spatial Statistics. Correlation analyses controlling for age and gender were conducted to explore the relationships between FA values and IL-10 levels.

Results: There was no significant difference in age and sex between the two groups. Decreased FA was found diffusively distributed, mainly including corpus callosum, bilateral posterior thalamic radiation, right longitudinal fasciculus and left inferior fronto-occipital fasciculus in schizophrenia compared with healthy controls (TFCE $p < 0.05$). IL-10 level was higher in schizophrenia than healthy group ($p < 0.001$). Interestingly, IL-10 level was negatively correlated with FA among all subjects mainly involving corpus callosum, right posterior thalamic radiation, right superior longitudinal fasciculus, and left inferior fronto-occipital fasciculus ($p < 0.05$).

Conclusion: This study shows that dysregulation of IL-10 relates to the changes of white matter integrity in schizophrenia patients, which supports the role of the inflammatory processes in the pathogenesis of schizophrenia.

B-0657 14:32

Support vector machine-based classification of first-episode drug-naïve schizophrenia patients and healthy controls using structural MRI

Y. Xiao¹, Z. Yan², Y. Zhao³, B. Tao¹, Q. Gong¹, S. Lui¹; ¹Chengdu/CN, ²Wenzhou/CN, ³Cheng Du/CN (*xiaoyuancq@163.com*)

Purpose: Although regional brain deficits have been demonstrated in schizophrenia patients by structural MRI studies, one important question that remains largely unanswered is whether the complex and subtle deficits revealed by MRI could be used as objective biomarkers to discriminate patients from healthy controls individually.

Methods and Materials: To address this question, a total of 326 right-handed participants were recruited, including 163 drug-naïve first-episode schizophrenia (FES) patients and 163 demographically matched healthy controls. High-resolution anatomic data were acquired from all subjects and

processed via Freesurfer software to obtain cortical thickness and surface area measurements. Subsequently, the support vector machine (SVM) was used to explore the potential utility for cortical thickness and surface area measurements in the differentiation of individual patients and healthy controls.

Results: The accuracy of correct classification of patients and controls was 85.0% (specificity 87.0%, sensitivity 83.0%) for surface area and 81.8% (specificity 75.0%, sensitivity 88.2%) for cortical thickness ($p < 0.001$ after permutation testing). Regions contributing to classification accuracy mainly included the grey matter in default mode, central executive, salience, and visual networks.

Conclusion: Current findings, in a sample of never-treated FES patients, suggest that the patterns of ill-related grey matter changes has potential as a biomarker for identifying structural brain alterations in individuals with schizophrenia. Future prospective studies are needed to evaluate the utility of imaging biomarkers for research and potentially for clinical purpose.

B-0658 14:40

LHPP gene polymorphism affects spontaneous brain activity in major depressive disorder

L. Cui¹, F. Wang¹, X. Gong², M. Chang¹, Z. Yin¹, G. Fan¹, Y. Tang¹, K. Xu¹; ¹Shenyang/CN, ²Shanghai/CN (*cmu00ring@163.com*)

Purpose: A single-nucleotide polymorphism at the LHPP gene (rs35936514) has been reported in genome-wide association studies to be associated with major depressive disorder (MDD). However, the neural system effects of rs35936514 that mediate the association are unknown. The present work conducts a neuroimaging analysis to explore whether and which brain neural systems are affected by the LHPP rs35936514 polymorphism.

Methods and Materials: A total of 160 subjects were studied: a CC group homozygous for the C allele (23 individuals with MDD and 57 controls) and a T-carrier group carrying the high-risk T allele (CT/TT genotypes; 22 MDD and 58 controls). All participants underwent resting-state functional magnetic resonance imaging (rs-fMRI) scanning. Brain activity was assessed using the amplitudes of low-frequency fluctuations (ALFF).

Results: MDD patients showed a significant increased ALFF in the left middle temporal gyrus and occipital cortex. The T-carrier group showed increased ALFF in the left superior temporal gyrus. Significant diagnosis \times genotype interaction was noted in the bilateral lingual gyri, bilateral dorsal lateral prefrontal cortex (dlPFC) and left medial prefrontal cortex (mPFC) ($P < 0.05$, corrected).

Conclusion: MDD patients with LHPP rs35936514 CT/TT genotype may influence the regional brain activity. These findings implicate the effects of the rs35936514 variation on the neural system in MDD.

B-0659 14:48

Impaired mixed emotion processing in the right ventrolateral cortex in schizophrenia

A.G. Szabo, L.R. Kozák, K. Farkas, G. Rudas, G. Csukly; *Budapest/HU (szabadam@gmail.com)*

Purpose: My thesis is about the differences of brain activity between schizophrenic patients and healthy controls, when they are about to recognize mixed emotions. Schizophrenia has negative effect on the processing of emotional facial expressions, as proved by multiple previous studies. While most of these research used the standard Ekman dataset, we aimed to reflect on everyday life situations a more complex way than the limited set of facial expressions presented by Ekman's actors.

Methods and Materials: Age- and education-matched healthy controls (18) and patients with schizophrenia (19) were enrolled in an fMRI experiment, using a set of 10 fearful, 10 happy, 10 mixed fear (70% fear and 30% happy) and 10 mixed happy (70% happy and 30% fear) facial expressions, the mixed expressions created by the software Morph from Ekman images. The images were presented in a randomized order and subjects had to categorize expressions by button presses. Data analysis was performed in SPM, and resulting maps further analysed using *ICN Atlas*ing toolbox.

Results: The patient group showed decreased fMRI activation during fear, mixed fear and mixed happy conditions in the right ventrolateral prefrontal cortex (VLPFC) and the right anterior insula (RAI) at the voxel and cluster level after family-wise error correction. No difference was found between study groups in activations for happy faces.

Conclusion: Using mixed emotions opens a new avenue in schizophrenia research, pointing out the importance of VLPFC in emotion recognition and decision making, e.g. its decreased activation in schizophrenia affects fear recognition.

B-0661 14:56

A fMRI comparison of paediatric patients with obsessive-compulsive disorder and controls during a Stroop task

I. [Duman](#), G. Ekinici, A.R. Arman, H. Aslan, E.B. Usta, G.O. Bilim, M. Kavus; Istanbul/TR (edda_ikram@hotmail.com)

Purpose: It has been suggested that abnormal inhibitory networks may be implicated in the pathophysiology of obsessive-compulsive disorder (OCD) and could account for the disorder's core symptom. The study aimed to investigate abnormalities in brain regions mediating cognitive response inhibition and attention allocation (basic demanding task) during the performance of coloured-card Stroop task using functional magnetic resonance imaging (fMRI) in children and adolescent with OCD compared to healthy controls.

Methods and Materials: Block-design fMRI was used to compare brain activation in 7 children and adolescents with OCD with that of 8 matched controls during a Stroop task of response inhibition and basic demanding conditions.

Results: No patient had comorbidity besides OCD. During the basic demanding task, participants with OCD showed reduced activation in the bilateral frontal, insular, parietotemporal regions ($p < 0.05$, uncorrected). During response inhibition task, OCD group showed reduced activation in the left middle frontal gyrus (dlPFC), right frontal medial cortex (FMC), left anterior cingulate cortex (ACC), bilateral inferior frontal gyri, orbitofrontal cortices (OFC), insular, parietotemporal regions, basal ganglia, and thalamus ($p < 0.05$, uncorrected). When we compared the basic demanding status with the response inhibition condition, the OCD group showed decreased activation only during the response inhibition task in the right FMC, left ACC, bilateral OFC, basal ganglia and thalamus.

Conclusion: The results of the present study support the hypothesis that frontostriatohalamic regions and ACC play effective role in response inhibition in childhood OCD, and also demonstrate dysfunction of left dlPFC, temporoparietal regions, and insular cortices during attention allocation.

B-0662 15:04

Posttraumatic stress disorder-related alterations in modular characteristic and white matter connectivity of brain structural networks

X. [Suo](#)¹, D. [Lei](#)², Q. [Gong](#)¹; ¹Chengdu/CN, ²London/UK (1107229715@qq.com)

Purpose: Although previous studies reported altered topology of brain network in posttraumatic stress disorder (PTSD), the modular organization of brain network remains largely unknown. This study aims to examine the topologic alterations of brain white matter structural network in PTSD at global, modular and nodal levels.

Methods and Materials: Diffusion tensor imaging and graph theory approaches were used to investigate the topologic organization of the brain structural network in 76 PTSD patients and 76 age-, gender-, and years of education-matched trauma-exposed non-PTSD controls. Individual white matter networks were constructed for each participant, and the global, modular and nodal measurements of the networks between two groups were compared with nonparametric permutation tests.

Results: At global level, the PTSD showed lower clustering coefficient ($P = 0.0156$) and normalized characteristic path length ($P = 0.0348$) compared with non-PTSD controls. At modular level, the patients demonstrated significantly increased between-module connections between fronto-parietal module, fronto-striatal-temporal module and default mode network. At node level, increased nodal centralities in the common frontal, temporal and occipital regions were found ($P < 0.05$, FDR corrected). The clinician-administered PTSD scale score was positively correlated with the nodal efficiency of left inferior temporal gyrus ($r = 0.354$, $P = 0.002$).

Conclusion: The structural brain network showed a shift toward 'randomization' in the PTSD group, indicated by increased between-modular connections with increased nodal centralities involving frontal-temporal-occipital regions. The disassociation between the current structural and previous functional connectome studies suggests that the neural activity is shaped, but not limited by the underlying anatomy.

B-0663 15:12

Structural and functional brain abnormalities in schizophrenia: a cross-sectional study at different stages of the disease

C. [Zhao](#); Beijing/CN (zhaochaoy@163.com)

Purpose: To investigate the grey matter volume (GMV) and neural activity alterations in subjects at 4 different stages of schizophrenia.

Methods and Materials: The subjects comprised 53 genetic high-risk (HR) individuals, 26 ultrahigh-risk (UHR) individuals, 58 first-episode schizophrenia (FES) patients, 41 chronic schizophrenia (ChSz) patients and 39 healthy controls (HC). They underwent structural and resting-state functional MRI scanning. GMV, amplitude of low-frequency fluctuations (ALFF) and regional homogeneity (ReHo) values were compared among the 5 groups using voxel-based morphometry and the software REST. Relationships between these

alterations and symptoms in FES group were evaluated by partial correlation analysis.

Results: GMV decline was observed in the bilateral occipital lobe, left orbital frontal cortex, bilateral superior parietal lobule (SPL), right middle temporal gyrus (MTG), gyrus rectus and medial superior frontal gyrus (SFG) in FES group and in the bilateral occipital lobe in HR group. FES group showed increased ALFF in the caudate and decreased ReHo in the bilateral inferior parietal lobule (IPL) and precuneus. ChSz group showed increased ALFF in the right hippocampus. GMV of the right MTG and SPL and ReHo of the precuneus were negatively correlated with the general score, while GMV of the right MTG was negatively correlated with the total score on the positive and negative syndrome scale.

Conclusion: Structural and functional deficits are prior to symptoms and are more prominent at the onset of illness than other phases. The prefrontal cortex, right MTG, striatum and default mode network play important roles in the pathogenesis of schizophrenia.

14:00 - 15:30

Room L 8

Head and Neck

SS 708

Thyroid and parathyroid imaging

Moderators:

A. Borges; Lisbon/PT

E. Scapin; Monserrato/IT

B-0664 14:00

Sonographic features of medullary thyroid carcinoma: application of Thyroid Imaging Reporting and Data System (TIRADS) classification

G. [Yun](#), Y. Kim, S. Choi; Seongnam-Si/KR (gabinyun@gmail.com)

Purpose: To evaluate the performance of the Korean Thyroid Imaging Reporting and Data System (K-TIRADS) for medullary thyroid carcinoma (MTC) and to report the sonographic characteristics of MTC.

Methods and Materials: The ultrasound (US) images and medical records of MTC patients diagnosed on the basis of cytopathologic results from June 2003 to November 2016 were retrospectively reviewed. Four independent reviewers (two experienced radiologists and two 1st year residents) reviewed fifty-seven pre-operative US images of MTC patients for shape, composition, echogenicity, margin and calcification of the MTC nodules and categorized the nodules using K-TIRADS classification. The metastatic lymph nodes were assessed for cystic change, echogenicity, the presence of fatty hilum and microcalcification. Inter-observer agreement for K-TIRADS was assessed with weighted kappa statistics.

Results: Ninety-five percent of nodules were classified as having either high suspicion (68.4%) or intermediate suspicion (26.3%). K-TIRADS score was significantly higher in MTCs with lymph node metastasis ($p = .003$). The predominant sonographic findings of MTCs were solid content (87.7%) and hypoechoogenicity (99.5%). Suspicious lymph nodes were present in 28% of MTCs, which showed solid component (81.3%), heterogeneous echogenicity (50%), loss of fatty hilum (93.7%), microcalcification (68.8%) and hypervascularity (86%). MTCs showing irregular shape, microcalcification and presence of ETE were associated with lymph node metastases ($p = .008$, .001, .021, respectively). The inter-rater agreement was good (weighted kappa 0.82) between the two experienced reviewers, and the inexperienced reviewers also showed good agreement with the most experienced reviewer (weighted kappa 0.73 and 0.81).

Conclusion: The K-TIRADS classification performed well in MTC nodules with good inter-observer agreement.

B-0666 14:08

Can valuable information be derived from the exploitation of quality maps along elasticity maps in SWE of thyroid nodules?

L. [Chami](#)^{1,1}, G. Bera¹, M. Lefort¹, J. Griffon¹, O. Lucidarme^{1,1}, C. Pellot-Barakat²; ¹Paris/FR, ²Orsay/FR (linda.chami@yahoo.com)

Purpose: Quality maps are now provided together with elasticity maps on Shear wave elastography (SWE) Aixplorer systems (Supersonic Imagine, France). The purpose was to evaluate how to improve reliability and reproducibility of SWE measurements in thyroid nodules.

Methods and Materials: 50 thyroid nodules from 46 patients (33 w, 9 m, 56±15 yrs) scheduled for fine needle biopsy were prospectively included. 4 nodules with non-diagnostic cytology were excluded. 3 SWE measurements were obtained repetitively in longitudinal and transversal plane resulting in 300 measurements. Mean elasticity values (ME), mean quality coefficients (MQC), ratio ME nodule/thyroid and ME long/trans were computed. Coefficients of variation of elasticity values (CV_E) were computed for reproducibility study. Spearmans coefficients and Student T-tests were used for statistical analysis.

Results: Neither ME values nor the ratio ME nodule/thyroid were significantly different for benign (N= 34/50) and malignant (N=12/50) nodules (ME values: 18.4±9.7 kPa vs 21.1±8.6 kPa and 12.8±6.1 vs 8.5±3.5 kPa in the longitudinal and transversal plane respectively; ratio : 1.23±/-0.61 vs 1.25±/-0.72 (NS)). The ratio ME long/trans was significantly lower for benign nodules (1.55±0.91 vs 2.67±1.29 (p=0.05)). MQC values were significantly higher in the longitudinal plane than in the transversal one (0.73±0.11 vs 0.63±0.10, p < 0.001). A significant correlation was found between MQC and CV_E (r=0.46, p = 0.0015).

Conclusion: The ratio ME longitudinal/transversal was the only parameter that allowed to discriminate benign from malignant thyroid nodules. Quality maps were higher in longitudinal plane and SWE reproducibility was improved for the measurements with the highest quality.

B-0667 14:16

Atypical ultrasonographic patterns of papillary thyroid carcinoma: how to recognise them

E. Horvath, G. Aguilera, C. Silva, M. Droguett, V.S. Skoknic, H. Tala, S. Majlis, J. Slater, C. Whittle; *Santiago/CL (velimir.skoknic@gmail.com)*

Purpose: To analyse the atypical papillary thyroid carcinoma (PTC) US patterns, comparing them with typical cases, and to describe their main characteristics.

Methods and Materials: A retrospective review of thyroidectomies between 2013 and 2016 with PTC was conducted. Classical PTCs (Group A) were separated from those that showed atypical patterns (Group B). These were compared according to age, gender, size, histological subtype and association with Hashimoto's thyroiditis (HT). Shapiro-Wilk, chi-squared, Student's t tests or Mann-Whitney-Wilcoxon tests were used.

Results: A total of 453 PTC met inclusion criteria. In 51 cases (11.2%) [19 men (38%), median age 41 years (14-68)], an atypical pattern was observed. Median size: 14 mm (5-50 mm), 32 (63%) > 10 mm. 27% were associated with HT. A significant difference was found between Groups A and B in terms of gender (p < 0.025), size (p < 0.001) and histological subgroup (p < 0.01), with more men, larger lesions and more follicular variant of PTC with atypical pattern. The dominant characteristics observed in Group B were: solid-cystic mixed structure, similar to colloid nodule but without hyperechoic foci in 23 (45%), isoechoogenicity in 19 (37%) and presence of capsule in 20 (40%), findings that were shared in the majority of the cases, with or without association with calcifications. In addition, pooled microcalcifications without associated nodule were detected in 6 cases (12%).

Conclusion: One in every 10 PTCs has an atypical ultrasound appearance. It is important to recognise the characteristics described as concerning for malignancy to recommend FNAs in a timely manner, since 63% are macrocarcinomas.

B-0668 14:24

Can S-detect provide accurate differentiation of thyroid nodules? - assessing the impact on the assessment made by operators with different experience

G. Alagna, V. Cantisani, V. Forte, V. De Soccio, N. Di Leo, A. Rubini, M. Di Segni, F. D'Ambrosio, C. Catalano; *Rome/IT (gralagna@gmail.com)*

Purpose: To assess whether automatic TI-RADS assessment with S-Detect could be reliable in the differentiation of thyroid nodules.

Methods and Materials: One hundred seventy eight FNAB proven nodules in 106 patients (77 females, 29 males, aged 13-85 years, mean 55.3), were evaluated by a radiologist and a radiology resident. Operators assessed and categorized lesions without and with S-detect, using Kwak's TI-RADS. Sensitivity (SE), specificity (SPE), positive and negative predictive values (PPV, NPV), diagnostic accuracy through McNemar's test were calculated. Differences significance was assessed with Pearson's χ^2 test, with a p= 0.05 threshold.

Results: At FNAB, 13 nodules on 178 (7.3%) were malignant, 27 out of 178 (15.1%) at high risk, 110 on 178 (61.8%) probably benign and 28 out of 178 (15.7%) were certainly benign. Nodules categorization according to S-detect, radiologist and resident was as follows: TIRADS 2: 27, 26, 26; TIRADS 3: 112, 112, 105; TIRADS 4: 29, 30, 39; TIRADS 5: 10, 10, 8. When S-detect was not employed, SE, SPE, PPV and NPV were 83.5%, 93.5%, 85.2%, 89.6% for the experienced radiologist and 75.6%, 86.4%, 70.4% and 96.9% for the radiology resident, respectively. When S-detect was employed, SE, SPE, PPV and NPV 84.8%, 97.1%, 90.7%, 95.1%, for the experienced radiologist and 84.8%, 97.1%, 90.7%, 95.1% for the resident. No statistically significant difference in diagnostic performance was noted for the radiologist, whereas it resulted significant for the resident.

Conclusion: According to these results, S-Detect is a useful tool since it improves thyroid nodule differentiation accuracy of the non-experienced operator.

Author Disclosures:

V. Cantisani: Speaker; Bracco, Toshiba Medical Systems, Samsung Healthcare.

B-0669 14:32

Quantitative analysis of ADC values in differentiating papillary thyroid carcinoma and thyroid adenoma

S. Hu; *Zhenjiang/CN (hsd2001054@163.com)*

Purpose: To explore the differential diagnosis value of ADC value of PTC and thyroid adenoma (TA).

Methods and Materials: Routine MRI sequences and axial diffusion weighted sequences of neck with different b values (300,500,800 s/mm²) were performed in 34 patients with 43 nodules (including 37 PTCs and 6 TAs) confirmed by pathology. The ADC value of the solid component of each lesion was measured respectively. Independent samples t test was used to evaluate whether the ADC values had significant differences between the two lesions. Receiver operating characteristic (ROC) curves were drawn and used to evaluate the diagnosis value of ADC values in PTC and TA.

Results: The ADC value of PTC is lower than the one of TA with a significant difference statistically in all different b values. The average ADC values of PTC and TA were 1.791±0.544×10⁻³ mm²/s and 2.528±0.642×10⁻³ mm²/s (b-value 300 s/mm²), 1.510±0.453×10⁻³ mm²/s and 2.138±0.656×10⁻³ mm²/s (b-value 500 s/mm²), and 1.305±0.419×10⁻³ mm²/s and 1.906±0.643×10⁻³ mm²/s (b-value 800 s/mm²), respectively. The highest diagnostic accuracy can be obtained with a b-value of 300 s/mm² with the area under the curve of 0.815. When the b-value was selected as 300 s/mm² and the diagnostic threshold was 1.786×10⁻³ mm²/s according to the ROC curve, the sensitivity, specificity, positive predictive value, negative predictive value and Youden Index were 62.6%, 100%, 100%, 30.0% and 62.6, respectively.

Conclusion: The ADC value is helpful in the differentiation of PTC and TA, and a better result can be achieved by using a DWI with a b-value of 300 s/mm².

B-0670 14:40

A novel mobile phone app to minimise bias and aid the FNAC decision-making process

A. McDermott, P. Navin, T. Tarmey, A. Weir, D. Bergin, J.F. Bruzzi, B. Voisin, D. Sheppard; *Galway/IE (ailbhmcdermott@gmail.com)*

Purpose: Ultrasound is the modality of choice to help differentiate between benign and malignant thyroid nodules. The investigation algorithm on whether or not to perform FNAC takes into account several sonographic features of different weighting, and is not clear-cut. The decision is facilitated by a number of international guidelines. This study aims to address the sensitivity of the available guidelines in recommending FNAC. We then present and assess the clinical utility of a novel user-friendly mobile-phone 'app' to facilitate decision-making.

Methods and Materials: 200 consecutive thyroid FNAC cases between 2013 and 2014 were retrieved. Imaging was blindly reviewed by 4 subjects. The decision regarding FNAC was determined: 1. using guidelines (AAEC, ASRU, ATA, BTA, Korean) in read-only format; 2. using an interactive locally derived 'app' incorporating sonographic features and presenting various guideline recommendations, including TI-RADS. Statistical analysis was performed using 'R' and SPSS.

Results: In read-only format, the highest sensitivity was achieved with ATA (88.2%) and Korean (88.3%) guidelines. However, there was inter-user variability. The incorporation of specific sonographic features into an app (yes/no format) provides an overall sensitivity of 80% (new TI-RADS), 91% (AAEC) and 96% (Korean), thus increasing the appropriateness of FNAC. In addition, the app significantly reduced inter-user variability (p<0.001), thus minimising discrepancy.

Conclusion: Even when presented with international guidelines there are inconsistencies in the decision on when to perform FNAC. We describe the performance of widely-applied international guidelines in clinical practice, and present a novel 'app' to standardise the decision-making process and minimise the potential for human bias.

B-0671 14:48

Comparison of the clinical utility of international guidelines to aid the decision on when to perform FNAC for thyroid nodules

A. McDermott, P. Navin, A. Weir, T. Tarmey, J.F. Bruzzi, B. Voisin, D. Sheppard; *Galway/IE (ailbhmcdermott@gmail.com)*

Purpose: Thyroid nodules are a common finding. The decision on whether to perform fine-needle aspiration cytology to dissociate benign from malignant nodules is complex. A number of international guidelines, including the recent ACR TIRADS, incorporate sonographic features of different weighting to facilitate the decision-making process. This study compares commonly used international guidelines and their clinical utility for appropriate nodule FNAC.

Methods and Materials: Consecutive thyroid FNAC cases between 2013 and 2014 were retrieved. Sonographic features were reviewed and the recommendation on whether to perform FNAC or not based on international

guidelines (ACR TIRADS, AACE, ASRU, ATA, Kim and Korean) was analysed. Data were analysed using R statistical software package.

Results: 200 patients who underwent thyroid nodule FNAC during the study time period were included. The mean age was 55.1±15.6 years, with 83% women. The new ACR TIRADS guidelines provided a sensitivity of 81% and a specificity of 32%. The best sensitivity (appropriate sampling of cancer cases) was achieved from the application of the Korean guidelines (96%, specificity 0.075%). However, the best specificity (true-negative rate) was achieved from the ASRU guidelines (49%, sensitivity 64%).

Conclusion: Despite numerous internationally available guidelines, no guideline satisfactorily achieves a combination of high sensitivity and specificity. The new ACR TIRADS guidelines provide a sensitivity and specificity of 81 and 32%, respectively.

B-0672 14:56

Diagnostic performance of US-based fine-needle aspiration criteria for thyroid malignancy: comparison of three international society thyroid imaging reporting and data systems

S. Yoon, D. Na, H. Gwon; *Gangneung/KR (ysj-626@hanmail.net)*

Purpose: Thyroid imaging reporting and data system (TIRADS) is the quantitative scoring system for malignancy risk stratification of thyroid nodules. The aim was to compare the diagnostic performance of US-based FNA criteria for the detection of thyroid malignancy among recently proposed three international society TIRADS including Korean-TIRADS, ACR-TIRADS, and EU-TIRADS.

Methods and Materials: This study included a total of 1081 consecutive thyroid nodules (≥ 1 cm) in 898 patients with final diagnoses from January 2013 to December 2015. US features of thyroid nodules were retrospectively reviewed and classified according to the categories defined by the three international society TIRADS. The diagnostic performance of US-based FNA criteria for the detection of thyroid malignancy and unnecessary FNA rates were calculated and compared among the three TIRADS.

Results: Of the 1081 thyroid nodules, 940 (87%) were benign and 141 (13%) were malignant, with papillary carcinoma comprising 93.6% of all malignancies. The Korean-TIRADS (96.5%) and EU-TIRADS (92.9%) were more sensitive for the detection of malignancy than ACR-TIRADS (79.4%) ($p < 0.001$), while the ACR-TIRADS (67.4%) had a higher specificity than Korean-TIRADS (22.6%) or EU-TIRADS (23.2%) ($p < 0.001$). The unnecessary FNA rate was lower in the ACR-TIRADS (28.3%) than that in Korean-TIRADS (67.3%) or EU-TIRADS (66.8%). There was no significant difference in sensitivity, specificity, and the unnecessary FNA rate between Korean-TIRADS and EU-TIRADS ($p \geq 0.125$).

Conclusion: Korean-TIRADS and EU-TIRADS had a similarly higher sensitivity for malignancy than ACR-TIRADS; however, those had a lower specificity and higher unnecessary FNA rates than ACR-TIRADS.

B-0673 15:04

Ectopic parathyroids: incidence, localisation trends and diagnostic evaluation: retrospective study from a single tertiary institute

A.A. Singhal, S.S. Bajjal, D. Sarin, S.K. Arora, A. Mithal, S. Mishra; *Gurgaon/IN (DR.ALKAASINGHAL@GMAIL.COM)*

Purpose: Aim is to evaluate the incidence of ectopic parathyroids, their localisation, diagnostic evaluation and surgical confirmation.

Methods and Materials: Retrospective study conducted at a tertiary institution, where 400 patients operated for hyperparathyroidism from 2012 to 2017 was analysed. Diagnostic findings of Sestamibi and ultrasound were compared with surgical findings. SPECT CT was used in select cases.

Results: Of 400 patients single adenoma was seen in 350 patients (87.5%), two or more nodules in 41 patients (10.2%), and carcinoma in 3 cases. Of the 350 solitary adenomas, 291 were juxtaposed to thyroid (83.1%), and ectopic in 59 (16.8%) cases. Ectopic along the thymic tract in 38 cases (10.8%), upper mediastinum 8 cases (2.2%), angle of jaw in 2 cases (0.5%), carotid sheath 2 cases (0.5%), retroesophageal 2 cases (0.5%) and intrathyroidal in 7 cases (2%). Sestamibi was positive in localising parathyroid nodule in 297 (84.8%) cases, and ultrasound in 339 (96.8%) cases. Of the localised sestamibi nodules 82% were true and 3% were false localisation at surgery. Nodules localised by Ultrasound were true in 99% and false in 1% cases. Ultrasound localised the nodules in sestamibi negative cases in 12% patients.

Conclusion: Identification of ectopic parathyroids and differentiation from thyroid nodules and other neck lesions is the key role of imaging. Ultrasound is complimentary to MIBI and offers significant value addition by precision anatomical localisation, characterisation and finding additional nodules. Using two imaging modalities of MIBI and ultrasound, the diagnostic sensitivity is 99% and specificity is 98%.

B-0674 15:12

The diagnostic value of 4D MRI for the localisation of parathyroid adenomas

M. Ozturk, A.V. Polat, C. Celenk, M. Elmali, C. Polat; *Samsun/TR (dr.mesutozturk@gmail.com)*

Purpose: The aim of this study was to assess the feasibility of 4-dimensional magnetic resonance imaging (4D MRI) for the localisation of parathyroid adenomas in patients with primary hyperparathyroidism.

Methods and Materials: Preoperative 4D MRI including dynamic contrast-enhanced (DCE) sequence and T2-weighted multipoint Dixon (T2-mDixon) sequence with in-phase, out-phase and, fat-suppressed images in 31 patients with surgically proved parathyroid adenomas were evaluated retrospectively. Two readers blinded to surgical findings independently reviewed the images in two sessions (T2-mDixon sequence alone and T2-mDixon + DCE sequence). MRI localisation of the suspected adenoma in each session was compared with the surgical results and interobserver variability (weighted kappa [κ]) was assessed.

Results: By interpreting the T2-mDixon images alone, reader 1 correctly detected 26 parathyroid adenomas (sensitivity: 84%, positive predictive value: 90%) and reader 2 correctly detected 24 parathyroid adenomas (sensitivity: 77%, positive predictive value: 92%). With the addition of DCE sequence, reader 1 correctly identified 27 parathyroid adenomas (sensitivity: 87%, positive predictive value: 90%) while reader 2 correctly identified 26 parathyroid adenomas (sensitivity: 84%, positive predictive value: 93%). Interobserver agreement was also superior in T2-mDixon + DCE sequence compared to T2-mDixon sequence alone ($\kappa = 0.81$ and 0.74 , respectively).

Conclusion: 4D MRI with T2-mDixon and DCE sequence is a reliable method for identification of parathyroid adenomas.

14:00 - 15:30

Room E1

Breast

SS 702

Breast screening

Moderators:

C. Colin; Pierre-Bénite/FR
N.A. Healy; Cambridge/UK

B-0675 14:00

Incidence and tumour characteristics of bilateral and unilateral interval breast cancers at screening mammography

R.M.G. van Bommel; *Eindhoven/NL (rob_van_bommel@hotmail.com)*

Purpose: Detected by screening mammography, bilateral breast cancer has a different pathological profile compared to unilateral breast cancer. We investigated the incidence of bilateral interval breast cancers and compared their characteristics with those of unilateral interval breast cancers.

Methods and Materials: We included all screening mammograms of women who underwent biennial screening mammography in the South of the Netherlands between January 2005 and January 2015. We collected breast imaging reports, biopsy results and surgical reports of all referred women and of all women who presented with interval breast cancer. The tumour with the highest tumour stage (index cancer) was used for comparison with unilateral interval cancers.

Results: A total of 753 interval cancers were detected, of which 24 (3.2%) were bilateral. Among the invasive interval cancers, bilateral cancers more frequently showed a lobular histology than unilateral cancers (37.5% (9/24) vs. 16.1% (111/691), $P=0.01$). There is a trend towards a larger proportion of bilateral than unilateral interval cancers graded 1 (45.8% (11/24) vs. 27.8% (192/691), $P=0.08$). There were no other statistically significant differences in tumour characteristics. Also, the proportion of missed cancers on the latest screen was comparable for unilateral and bilateral interval cancers (23.0% vs. 25.0%, $P=0.9$).

Conclusion: Bilateral interval cancers comprise a small proportion of all interval cancers. Except of a higher proportion of invasive lobular cancers and a more favourable histological grade of invasive cancers, tumour characteristics are comparable for bilateral and unilateral interval breast cancers.

B-0676 14:08

Missed and true screen-detected and interval breast cancers in a population-based breast cancer screening programme

T. Hovda¹, A.S. Hølen², H. Bjørndal¹, S. Sebuødegård², S. Hofvind²;
¹Drammen/NO, ²Oslo/NO (tone.hovda@vestreviken.no)

Purpose: To describe the distribution of missed and true screen-detected (SDC) and interval (IC) breast cancer after a retrospective informed consensus review in a biennial population-based breast cancer screening programme.

Methods and Materials: We performed a consensus-based informed review of randomly selected cases of SDC and IC detected at eight breast centers in BreastScreen Norway. Prior screening and diagnostic digital mammograms were used. A panel of five breast radiologists (minimum 1 year experience with high volume screen-reading), reviewed and classified 648 SDC and 532 IC cases according to visibility of the breast tumor at prior screening mammograms (missed, minimal sign actionable, minimal sign non-actionable, true, and occult), and mammographic density (BI-RADS 5th edition, a-d). We used descriptive statistics to describe the distributions of classification, stratified by detection mode (SDC and IC).

Results: Among the SDC, 163 (25%) were classified as missed, 95 (15%) minimal sign actionable, 108 (17%) minimal sign non-actionable, 281 (43%) true, and one case as occult. For the IC: 133 (25%) were missed, 79 (15%) minimal sign actionable, 77 (15%) minimal sign non-actionable, 178 (34%) true, and 65 (12%) occult. 67% of the SDC were classified as BI-RADS a or b and 33% as c or d. For IC, 50% were BI-RADS a or b and 50% c or d.

Conclusion: In this retrospective informed review, 40% of cancers were visible at prior screening (missed or minimal sign actionable), regardless of detection mode. A higher mammographic density was observed among IC compared to SDC.

B-0677 14:16

Interval breast cancer rates and histopathologic tumour characteristics after false-positive screening result in a population-based screening programme

S. Sebuødegård, S. Hofvind; Oslo/NO (solveig.hofvind@krefregisteret.no)

Purpose: To compare rates and tumour characteristics of interval breast cancers (IBC) detected after a prior screening negative versus false-positive result among women who participated in BreastScreen Norway.

Methods and Materials: The study included 497,694 women aged 49-71 years who underwent 1,179,645 mammographic screening examinations during 2004-2014. Rates and odds ratio (OR) of IBC among women with a prior negative (reference group) versus false-positive result were estimated using logistic regression models, adjusting for age at diagnosis, year of screening and county of residence.

Results: Among 1,999 IBC, 32 (2%) and 86 (4%) were detected in women with a false-positive result with and without needle biopsy, respectively. The rate of IBC was 16.4 (95%CI: 15.7-17.2) for women with a prior negative result, and 45.6 (95%CI: 32.3-64.5) and 43.0 (95%CI: 34.8-53.0) for women with a prior false-positive result with and without needle biopsy, respectively. Adjusted ORs of IBC were 2.9 (95% CI: 2.1-4.2) and 2.8 (95% CI: 2.2-3.4) for women with a false-positive result with and without needle biopsy, respectively, relative to women with a negative result. Women with a prior negative result had a lower proportion of tumours ≤10 mm and Grade I tumours compared to women with a prior false-positive result with benign biopsy (15% [248/1,634] versus 40% [8/20], p<0.01, and 14% [243/1,725] versus 45% [9/20], p<0.01).

Conclusion: Women with a false-positive screening result had a higher odds of IBC, but more favorable tumour characteristics of IBC compared to women with a prior negative screening result.

B-0678 14:24

Comparison between interval breast cancer (IBC) and screen detected cancer (SDC) in a single centre

F. Curro¹, M. Tonutti, F. Giudici, F. Zanconati, M. Bortoli, M.A. Cova; Trieste/IT (francescacurro86@gmail.com)

Purpose: The introduction of the breast screening program (BSP) raised the problematic of interval breast cancer (IBC). The aim of this study was to evaluate the performance of BSP and the prognostic features of screen detected cancer (SDC) compared to IBC.

Methods and Materials: Women diagnosed with breast cancer (SDC and IBC) between January 2008 and December 2014 at a single unit of the BSP in Trieste (Italy) were included. We retrospectively collected data concerning patient's demographics, radiological patterns, tumour size, lymph node involvement, grading, and molecular biology. The proportional incidence of IBC was determined considering the incidence of expected breast cancers without BSP.

Results: There were 640 breast cancers included (626 women, 14 bilateral): 520 (81%) were SDC and 120 were IBC (19%). The proportional incidence of IBC was 15.3% and the sensitivity of the BSP was 83%. IBC presented more

aggressive features compared to SDC, such as tumor invasion (95% vs 85%; p=0.005), tumor size (≥T2 36% vs 20%; p=0.0003), grading (G3 38% vs 19%; p<0.001) and St.Gallen molecular subtype (triple negative 12% vs 6%; p<0.001). IBC were mostly diagnosed in women with dense breasts (density c and d: 45% vs. 24%; p<0.001) and were hardly detectable with mammography (R1 14% vs. 1%, p<0.001). There were no significant differences in lymph node involvement (p=0.4).

Conclusion: The proportional incidence of IBC and the sensitivity of the BSP, indicators of efficacy, were aligned to European standard. IBC had more adverse prognostic markers for overall survival when compared to SDC

B-0680 14:32

Detection of multiple cancers in a large UK screening population

S. Dumonteil, L.S. Wilkinson, S. Mohammadi, V. Scott; London/UK (scott.victoria@gmail.com)

Purpose: Imaging protocols at assessment of women recalled based on their screening mammograms are inconsistent across UK screening units. At our institution we carry out bilateral whole breast ultrasound on all women with a suspicious ultrasound lesion. The purpose of this study was to quantify the number of multiple cancers detected and how many of these were identified as a result of completion ultrasound imaging or further review of the screening mammogram.

Methods and Materials: The assessment results of 16,244 consecutive women assessed in screening clinic at the South West London Breast Screening Service between 2008 and 2016 were retrospectively analysed. Cancer detection rate and number of multiple cancers were calculated. Imaging from the multiple cancers was reviewed to assess how many extra cancers were detected due to local practice.

Results: From 2008 to 2016, 16,244 individual women were assessed in screening clinic and 8,136 (50%) women had at least 1 biopsy. 34% of assessment episodes (2,821 of 8,284) resulted in the detection of cancer. 351 (12%) were multiple cancers, 288 (10%) being ipsilateral and 63 (2%) being contralateral. A review of the imaging from the multiple cancers revealed that approximately one third of the extra cancers were identified as a result of our local protocols for women with a suspicious lesion on initial targeted ultrasound.

Conclusion: Bilateral whole-breast ultrasound and careful review of the screening mammograms in women with a suspicious lesion leads to significant increased detection rate of multiple breast cancers.

B-0681 14:40

Attendance in BreastScreen Norway by proportion of immigrants in a county

S. Bhargava, G. Mangerud, S. Hofvind; Oslo/NO (sameer.bhargava@krefregisteret.no)

Purpose: To examine whether the attendance rate among immigrants and non-immigrants in BreastScreen Norway was associated with the proportion of immigrants residing in the counties.

Methods and Materials: We selected invitations sent to women living in counties with a low (<5% of invitations sent to immigrants) or a high proportion of immigrants (>10% of invitations sent to immigrants), hereafter referred to as low- and high-density counties, respectively. We merged data about birth country and socio-demographic factors from Statistics Norway with screening data from the Cancer Registry of Norway. The study period was 2005-2015. For both immigrants and non-immigrants, unadjusted and adjusted rate ratios (RR) with 95% confidence intervals (95% CI) compared attendance rates in low- and high-density counties.

Results: Women in the six low-density counties received 852,193 invitations, and women in Oslo, the capital city and the only high-density county, received 277,229 invitations. Attendance rates were 76.9% in low-density counties and 63.1% in Oslo. Using Oslo as reference, RR of attendance was 1.26 (95% CI 1.24-1.28) for immigrants and 1.16 (95% CI 1.16-1.16) for non-immigrants in low-density counties. Adjusted RR was 1.16 (95% CI 1.14-1.17) for immigrants and 1.14 (95% CI 1.14-1.14) for non-immigrants.

Conclusion: Immigrants and non-immigrants in Oslo had lower attendance than the same groups of women living in low-density counties. Efforts to increase attendance in urban areas should target both immigrants and other low-attending groups.

B-0682 14:48

Comparison of phantom target detectability for digital mammograms, tomosynthesis and synthetic mammograms

L. Vancoillie, L. Cockmartin, N. Marshall, H. Bosmans; Leuven/BE (liesbeth.vancoillie@uzleuven.be)

Purpose: To compare target detectability in digital mammography (FFDM), digital breast tomosynthesis (DBT) and synthetic mammograms (SM) using two contrast detail phantoms: CDMAM (homogeneous background) and a 3D

phantom developed in-house with calcification and mass lesion-like inserts ('L1') in a structured background.

Methods and Materials: Detectability was measured for FFDM, DBT and SM acquisitions of the phantoms on a Siemens Inspiration Prime. Dose settings were derived from automatic exposure control (AEC), and then manually set at three levels: AEC/2, AEC and 2xAEC, with 10 acquisitions per dose level. Both phantoms were read manually using the 4 alternative forced choice (4-AFC) method. Threshold thickness (T_T) was established for CDMAM while threshold diameter (d_T) was found for L1, both calculated for a 62.5% correct score. Software (CDCOM-based) scoring of the CDMAM images was also performed. **Results:** CDCOM followed human reading and ranked threshold thickness as a function of dose the same way as did the human readers. Both the CDMAM T_T results for 0.1 mm diameter discs and the L1 d_T results showed small detail (~microcalcification) detectability was greatest for FFDM, followed by DBT and then SM ($p < 0.0001$). The L1 phantom (i.e. with structured background relevant to mass lesion detection) showed better mass-like lesion detection for DBT, followed by SM, with FFDM having the worst performance ($p < 0.0001$).

Conclusion: For detection of microcalcification-like details, both phantoms ranked imaging modality detectability as FFDM>DBT>SM. For detection of mass-like lesions in a structured background, the L1 phantom ranked detectability as DBT>SM>FFDM.

Author Disclosures:

H. Bosmans: Research/Grant Support; The medical physics team has a research agreement with Siemens-Healthineers.

B-0683 14:56

Screening mammography's pitfalls: a retrospective review of false positive recall

F. Leone, M. Orsi, A. Presazzi, D. Mariani, M. Cellina, G. Oliva; *Milan/IT (federica-leone@live.it)*

Purpose: To analyse the most common feature in false positive recall in order to suggest a strategy for assessment of challenging screening mammogram.

Methods and Materials: We reviewed a retrospective cohort of 6830 patients involved in screening program for breast cancer between November 2015 and September 2017. We included the false positive recall which at second level exam have been classified as BIRADS 1 or 2. We evaluated two different groups according to agreement recall(AR) or disagreement recall(DR). We compared the differences among tumoural imaging features between the two groups and considering also the overall findings prevalence in screening recall(SR).

Results: we obtained a final cohort of 1157 suspicious findings whose 416(35,9%) have been in AR group and 741(64,1%) in DR group. In the AR group we found, as single or one of multiple features in suspicious lesion, 287(69%) mass, 26(6,25%) calcifications, 78(18,75%) architectural distortion and 25(6%) asymmetric density; in the DR group we detected 578(78%) mass, 89(12%) architectural distortion, 43(6%) asymmetric density, 31(4%) calcifications. Differences in tumour imaging features between the two groups were statistically significant ($p < 0.05$).

Conclusion: Our results show how mass is the most common feature in false positive recall with no changes between one or two readers. Calcification, when classified as BIRADS 2, is a rare challenging feature, mostly due to the expertise of breast radiologist. Our study proves how screening program is a good tool to avoid false positive recall for architectural distortion and asymmetric density, considering the higher prevalence of these findings in recall group.

B-0684 15:04

The impact of image quality and mammographic breast density on missed cancers in organised screening

M. Abdollell, P. Brown, J. Caines, J.I. Payne, K. Tsuruda, P. Barnes, M. Rivers-Bowerman, S.E. Iles; *Halifax, NS/CA (Sian.Iles@nshhealth.ca)*

Purpose: The aim of this study was to explore the relationship between image quality and breast density with the risk of missing cancers in a breast screening practice.

Methods and Materials: The study sample included women diagnosed with missed interval cancers ($n=45$) and non-cancer controls ($n=2475$) identified from a 3:1 age- and screen-matched case-control study that included all breast cancer cases diagnosed between 2009-2015 in a provincial breast screening program offering digital mammography to women aged 40-75 ($n=9388$). Image quality and breast density were determined for each mammogram using fully automated algorithms (Densitas Inc.). Data were partitioned into training (two-thirds) and test (one-third) datasets. Women with inadequate (versus adequate) image quality were compared on their status of true missed cancers vs non-cancers, controlling for breast density. Logistic regression analysis was conducted, modeling cancer status as the dependent variable with image quality and percent mammographic density as independent variables. Odds ratios were estimated for risk of missed cancers using the test dataset.

Results: Women with mammograms of inadequate quality are 1.56 times more likely (OR=1.56, 95% CI(0.97,2.46), adjusted for breast density) to have a

missed cancer; including an interaction term of quality*density generates an OR=0.92, 95% CI(0.29,2.75).

Conclusion: Image quality affects risk of missing cancers in mammographic breast exams differentially by breast density. The results of this study indicate that it may be clinically important to evaluate both image quality and breast density routinely during mammographic screening.

Author Disclosures:

M. Abdollell: CEO; Densitas Inc. Founder; Densitas Inc. **K. Tsuruda:** Employee; Densitas Inc.

B-0685 15:12

Piloting an international self-test: assessment of international mammography screening skills (AIMSS)

M. Broeders¹, B. Yankaskas², J. Timmers¹, D.L. Miglioretti³, R.A. Smith⁴; ¹Nijmegen/NL, ²Chapel Hill, NC/US, ³Davis, CA/US, ⁴Atlanta, GA/US (m.broeders@lrbc.nl)

Purpose: To pilot a mammography self-test, developed to measure radiologists' screening performance and provide feedback, in different translations and international settings and evaluate the logistical challenges of implementing a self-test.

Methods and Materials: Nine countries varying in language and organisation, participated: USA, Canada, Norway, Italy, Spain, Mexico, Brazil, Taiwan and Japan. For each country, a local coordinator targeted recruiting 30 radiologists. A web-based system was developed to support the self-test and pre- and post-test questionnaires to gather information on radiologists, practice characteristics, feedback on experience and performance. Each site received IRB exemption or approval.

Results: To date, 133 radiologists have consented, 71 completed the self-test, 114 completed the pre-test questionnaire and 54 completed the post-test questionnaire. Early recruitment was good, however, currently, only 41 of 133 (31%) participants completed all pilot items, despite multiple reminders. The self-test, including teaching points, was well-received with 95% rating it a good tool for evaluating performance and 88% saying they would recommend it to others; 54% thought they performed better than the results indicated; 27% expected worse results. Main problems reported were downloading the images to the workstations, delays from IRBs, and in some countries, delay due to the technical testing and translation of the self-test. Performance was generally good with mean women-level sensitivity 85%, breast-level sensitivity 80% and specificity 82%.

Conclusion: The self-test was well-received, was considered a good teaching tool, and translations worked well. We experienced logistical and technical problems which resulted in inability for some radiologists to complete the self-test.

Author Disclosures:

M. Broeders: Research/Grant Support; American Cancer Society.

B. Yankaskas: Research/Grant Support; American Cancer Society.

J. Timmers: Research/Grant Support; American Cancer Society.

D.L. Miglioretti: Advisory Board; Hologic. Research/Grant Support; American Cancer Society. **R.A. Smith:** Research/Grant Support; American Cancer Society.

14:00 - 15:30

Room E2

Neuro

SS 711b

Vascular imaging

Moderators:

S.A.C. Squarza; Milan/IT

P. Vilela; Almada/PT

B-0686 14:00

Effect of carotid endarterectomy on the distribution and value of cerebral blood flow: evaluation by territorial arterial spin labelling

H. Xu, Y. Liu, H. Yuan; *Beijing/CN (84498843@qq.com)*

Purpose: To evaluate the cerebral blood flow(CBF) changes on distribution and value of brain feeding arteries after carotid endarterectomy(CEA) using territorial arterial spin labelling(t-ASL).

Methods and Materials: 1. Twelve patients diagnosed with carotid artery stenosis scheduled for CEA were recruited (mean age 60±7.8 males, 4 females). 2. MR imaging was performed with a 3.0T MR system 1 week before and after CEA. Cerebral perfusion territory maps were obtained by labelling bilateral internal carotid arteries and basilar artery using super-selective ASL. These images were then combined into a 3-colored territorial CBF maps. 3. The CBF values were obtained from the same size ROI (70mm²) respectively in the same position of different individual vascular perfusion images before

and after surgery. To assess the changes in CBF after CEA(Δ CBF), we calculated the following difference: Δ CBF=CBF_{postoperative}-CBF_{preoperative}.

Results: 1. The contribution to perfusion in the hemisphere via the collateral circulation is reduced after CEA. 2. The CBF values of both the lesion carotid artery perfusion sides and contralateral sides were increased after CEA($P<0.5$).

Conclusion: 1. CEA improves cerebral perfusion in patients with carotid artery stenosis, and patients with greater perfusion deficits prior to CAS have greater improvement in perfusion after CEA. 2. tASL has potential as a noninvasive imaging tool for the quantitative evaluation of hemodynamic changes after CEA, as well as demonstrate the relative role of collateral pathways before surgery and redistribution of blood flow after surgery.

B-0687 14:08

Added value of c-arm contrast-enhanced cone-beam CT to routine contrast-enhanced MRI in evaluation of sporadic intracranial cavernous malformations for detecting associated DVAs

B. Kocak, A. Zeynalova, O. Kizilkilic, N. Kocer, C. Islak; *Istanbul/TR* (*drburakkocak@gmail.com*)

Purpose: Association of intracranial cavernous malformations (CMs) and developmental venous anomalies (DVAs) has a significant impact on preoperative planning and postoperative prognosis. In routine clinical practice, T1-weighted contrast-enhanced MRI (CE-MRI) is generally considered the gold standard. C-arm contrast-enhanced cone-beam computed tomography (CE-CBCT) is a relatively new technique and increasingly used to investigate vascular pathologies. Our purpose was to explore the added value of CE-CBCT to CE-MRI in detecting associated DVAs.

Methods and Materials: Between July 2011 and September 2017, one hundred and fifty patients with intracranial CMs were evaluated with CE-CBCT in our department. Applying the inclusion and exclusion criteria, retrospective review revealed 56 patients with sporadic intracranial CMs (53 with single; 3 with double CMs) who had both CE-MRI and CE-CBCT studies. DVAs were evaluated first on CE-MRI, and then along with CE-CBCT. The diagnosis was made by consensus. McNemar's test was used in statistical analysis.

Results: Of 56 patients, 37 (66%) had associated DVAs on CE-MRI. On the other hand, 19 (33%) patients had no DVA. Of 19 patients with no DVA on CE-MRI, 10 (52.6%) had DVA on CE-CBCT as a new diagnosis. The remaining 9 patients had no DVA on CE-CBCT either. Differences in the proportions of associated DVAs on CE-MRI and CE-CBCT was statistically significant, $p<.05$.

Conclusion: C-arm CE-CBCT evaluation may be a useful imaging technique especially in patients with negative routine CE-MRI in terms of detecting associated DVA. Nearly in half of those particular patients, CE-CBCT can reveal an associated DVA as a new diagnosis.

B-0688 14:16

MRI agreement of SVS of thrombi

R. Bourcier¹, L. Détraz¹, J.-M. Serfaty¹, B. Guyomarç'h Delassale¹, M. Mirza², I. Derraz¹, F. Toulgoat¹, O. Naggara³, H. Desal¹; ¹Nantes/FR, ²Dublin/IE, ³Paris/FR (*lili.detrax@gmail.com*)

Purpose: The susceptibility vessel sign (SVS) on MRI is related to thrombus location, composition and size, in acute stroke. No study has questioned its inter-MRI agreement. We aimed to compare in vitro the diagnostic accuracy of 4 different MRI for thrombus histological characterisation.

Methods and Materials: 35 thrombi analogs of different composition that was histologically categorised as fibrin-dominant, mixed, or red blood cell (RBC)-dominant. We scanned these manufactured thrombi on four different MRI with T2* sequence constructor's parameters. Nine radiologists, blinded to thrombus composition and MRI scanner model, classified twice, in a two-week interval, the SVS of each thrombus as absent, questionable, or present. We calculated weighted kappa with 95% confident interval (CI), the sensitivity, specificity and accuracy of the SVS on each MRI scanner to detect RBC dominant thrombi and compared it between MRI scanners.

Results: The SVS was present in 42%, absent in 33%, and questionable in 25%. The inter-scanner agreements were moderate to good, ranging from 0.45 (CI : 0.37-0.52) to 0.67 (CI : 0.61 - 0.74). The correlation between the SVS and the thrombus composition was moderate κ : 0.50 (CI: 0.44 - 0.55) to good κ : 0.76 (CI: 0.72-0.80). Sensitivities, specificities and accuracy to identify RBC-dominant clots were significantly different between MRI ($p<0.001$).

Conclusion: The diagnostic accuracy of the SVS to determine thrombus composition varies significantly among MRI scanners. Normalization of T2* sequences between scanners may be needed to better predict thrombus composition in future multicenter studies.

B-0689 14:24

Dynamic evaluation of notch signaling-mediated angiogenesis in ischemic rat using magnetic resonance imaging

J. Tian, Y. Yang; *Shanghai/CN* (*tjqhehe@126.com*)

Purpose: Notch signaling pathway is involved in angiogenesis induced by brain ischemia and can be efficiently inhibited by the γ -secretase inhibitor DAPT. The aim of the present study was to non-invasively investigate the effect of DAPT treatment on angiogenesis in brain repair after stroke using MRI.

Methods and Materials: Sprague-Dawley rats were subjected to 90 minutes of transient middle cerebral artery (MCA) occlusion and treated with saline (n=20) or with DAPT (n=20) at 72 hours after onset of ischemia. MRI measurements including T2-weighted imaging (T2WI), susceptibility-weighted imaging (SWI) and cerebral blood flow (CBF) were performed at 24 hours after reperfusion and weekly up to 4 weeks using a 3-Tesla system. Histological measurements were obtained at each time point after MRI scans.

Results: Brain edema and ischemic lesions was significantly reduced in the DAPT-treated rats, as demonstrated by T2WI. SWI showed that DAPT treatment significantly enhanced angiogenesis in the ischemic boundary zone (IBZ) especially in the ipsilateral striatum compared to control group, with local cerebral blood flow in the angiogenic area elevated, along with increases in vascular density confirmed by histology.

Conclusion: Treatment of ischemic stroke with DAPT significantly augments angiogenesis, which promotes post-stroke brain remodeling by elevating CBF level, and these processes can be dynamically monitored and evaluated by MRI.

B-0690 14:32

Delayed postoperative changes after intracranial aneurysm surgery

E. Grigorieva, V. Krylov, V. Dashyan, V. Lukyanchikov; *Moscow/RU* (*iara333@yahoo.com*)

Purpose: Main strategies of intracranial aneurysms treatment are microsurgical clipping or coiling complicated by angiospasm and ischaemia and microcirculation deficits. Our purpose was to estimate the long-term changes after treatment both non-ruptured aneurysms and after angiospasm.

Methods and Materials: 69 patients (40 women, 29 men, 19-71y.o.) were examined more than 12 months after surgery with native brain CT, CT angiography and whole brain CT perfusion followed by estimating of cerebral blood flow, cerebral blood volume and mean transite time in similar areas of the cortex.

Results: 56 patients underwent surgical clipping, including 10 patients (14,5%) with ruptured aneurysms. In 13 cases (18,8%) aneurysms were coiled, in 1 patient with stent assisting. In 43 of 56 cases native CT revealed postoperative brain changes, in 90,7% at the access level with 36 cases (83,7%) of the perfusion deficits. The deformities of the parent artery was determined in 22 patients (31,9%) with hypoperfusion in 68,2% of cases. 11 patients demonstrated the residual aneurysm sac with hypoperfusion of temporal lobe in 54,5% ($p< 0,005$). 10 patients were treated after aneurysm rupture and angiospasm. In 50% of patients perfusion deficits were revealed with arteries deformity, independent of the aneurysm size, localization or treatment strategy. No residual sac was found.

Conclusion: The parent vessel postoperative deformity was more common after the ruptured aneurysm closure while the residual aneurysmal sac was revealed after non-ruptured aneurysms. Perfusion disturbances correlated with post-ischaemic changes and vessel deformity ($p<0,001$) but not with residual aneurysm or method of treatment.

B-0691 14:40

Epidemiology of intracranial vertebral artery calcification observed on computed tomography in a cohort of trauma patients

C. Lucci¹, R. Kockelkoren¹, D. Bos², A. Van der Lugt², M. Geerlings¹, J. Hendrikse¹, P.A. de Jong¹; ¹Utrecht/NL, ²Rotterdam/NL (*carlo.lucci@hotmail.com*)

Purpose: Intracranial vascular disease is the leading cause of ischemic stroke worldwide. In this light, substantial research has been performed on calcification in the carotid artery while data available on vertebral artery calcification (VAC) are limited. Considering its possible role in the development of symptomatic cerebrovascular disease, we examined VAC prevalence and distribution according to sex and age in a cohort of trauma patients.

Methods and Materials: Unenhanced head CT scans of patients admitted from July 2007 to August 2016 to the University Medical Center Utrecht for trauma were examined. We randomly selected 1016 patients (49.2% men) aged 0-99 years (mean \pm SD, 47.8 \pm 28.6; approximately 50 men/women per age decade). Calcifications were assessed visually (Modified Woodcock) and volumetrically (mm³) from the foramen magnum till the basilar artery bifurcation.

Results: The overall prevalence of VAC was 16% and the mean volume (\pm SD) was $11.27 \pm 57.06 \text{ mm}^3$. At logistic regression, increasing age was significantly associated with the presence of VAC ($p < 0.001$). Age was also related to VAC volume (Spearman's $\rho = 0.212$, $p = 0.007$). There was a statistically significant association between female sex and VAC prevalence (18.6% in women and 13.4% in men; Chi-Square = 5.107, $p = 0.024$).

Conclusion: Prevalence of VAC in our cohort is high and increments proportionally with ageing. It also seems to affect women more than men but further studies must investigate the aetiology behind this finding. VAC evaluation is easy on non-contrast head CT scans and could be implemented in clinical radiology in behalf of the creation of a stroke risk assessment scale.

B-0692 14:48

Standard diffusion-weighted imaging on the brain detects cervical internal carotid artery dissections

G.G.A. Adam, C. Cognard, F. Bonneville, *Toulouse/FR*
(gilles.adam31@gmail.com)

Purpose: To assess the capacity of a standard diffusion-weighted sequence performed on the brain and to detect dissecting haematoma related to cervical internal carotid artery (ICA) dissections.

Methods and Materials: Retrospective study of a cohort of 110 patients under 55 years of age (40 women, mean age: 46.79 years) admitted at the acute phase of a neurological deficit, headache or neck pain, and investigated by at least a standard 3 Tesla diffusion-weighted sequence on the brain. Among them were included 50 patients (14 women, mean age: 46.72) who subsequently had an internal carotid artery dissection, as confirmed by ultrasound, MRI or DSA. In the whole anonymized cohort, a senior and a junior radiologist separately assessed on the diffusion-weighted sequence only, the presence of a crescent-shaped or circular hypersignal projecting on the subpetrosal segments of the ICA arteries, assuming that it would correspond to a dissecting haematoma related to ICA dissection.

Results: The senior radiologist found 46 subpetrosal hyperintensities in 43/50 patients with ICA dissection, none in patients without dissection (sensitivity 86%, specificity 100%). The junior radiologist found 48 subpetrosal hyperintensities in 45/50 patients with dissection, none in patients without dissection (sensitivity 90%, specificity 100%). The interobserver kappa, calculated at 0.99, was excellent.

Conclusion: In our cohort, a standard diffusion-weighted sequence performed on the brain, at the acute phase of a stroke or a clinical suspicion of dissection detected nearly 90% of the ICA dissections.

B-0693 14:56

Diagnostic performance of three-dimensional high resolution magnetic resonance imaging for intracranial aneurysms: comparison with digital subtraction angiography

Y. Yim, J.Y. Kim, S.C. Jung, B.E. Lee, S.J. Kim, H.S. Kim, D.H. Lee, C.G. Choi, J.E. Park; *Seoul/KR* (youngheeyim@gmail.com)

Purpose: To evaluate diagnostic performance of three-dimensional high-resolution magnetic resonance imaging (3D HR-MRI) for intracranial aneurysms compared to digital subtraction angiography (DSA).

Methods and Materials: A total of 299 patients (M:F = 37:262; age range, 27-79) who underwent 3D HR-MRI, DSA, TOF-MRA from January 2012 to December 2016 were retrospectively enrolled. Two neuroradiologists independently evaluated TOF-MRA (3D MIP and axial source), CTA, 3D HR-MRI, and DSA for the determination of intracranial aneurysms or infundibula which were suspected of having on TOF-MRA within circle of Willis, bilateral ophthalmic arteries, bilateral posterior communicating arteries, bilateral anterior choroidal arteries, basilar artery and bilateral superior cerebellar arteries. Diagnostic performances for TOF-MRA, CTA, and 3D HR-MRI were assessed with DSA as the reference standard. Inter-observer agreements are calculated.

Results: Of 452 lesions on TOF MRA, aneurysms of 173 (38%) and infundibula of 276 (61%), and no aneurysm of 3 (1%) were diagnosed on DSA. Sensitivity, specificity, positive predictive value, and negative predictive value were 61%, 81.3%, 73.8%, 76% for TOF 3D MIP, 73.7%, 89.4%, 81.5%, 84.3% for TOF-MRA source, 65.9%, 99%, 97.7%, 82.7% for CTA, and 70.2%, 97.6%, 94.9%, 83.8% for 3D HR-MRI, and with the exception of ophthalmic arterial lesions, 53.7%, 87.3%, 60.9%, 83.6% for TOF 3D MIP, 65.1%, 92.5%, 76.2%, 87.7% for TOF-MRA source, 64.6%, 100%, 100%, 83.7% for CTA, and 90.6%, 98.5%, 95.6%, 96.6% for 3D HR-MIR. Readers showed good inter-observer agreement ($K = 0.637$).

Conclusion: 3D HR-MRI shows superior diagnostic performance for intracranial aneurysms except ophthalmic arterial lesions compared to TOF-MRA and CTA.

B-0694 15:04

Scannographic density of intracranial venous sinuses in healthy patients and diagnosed with venous thrombosis at 2600 meters above sea level from 2008 to 2016

S. Andrade, S. Velasco, S. Bermúdez, N. Useche, A.J. Morillo; *Bogota/CO*
(santiandrade_1985@hotmail.com)

Purpose: Intracranial venous sinus thrombosis is a rare pathology in which diagnostic imaging plays a crucial role. Simple brain scanning is the initial choice imaging study because it is a rapid method to evaluate the morphology and quantification of venous sinus density. Actually, only quantitative reference values of attenuation of sinus have been documented at geographic altitudes below 500 meters above sea level. According to the correlation between hematocrit and vascular density, the available values may be inaccurate for populations living at higher altitudes. The purpose of this research is to document the attenuation of venous sinuses in healthy patients and the intracranial venous thrombosis in Bogotá-Colombia (located at 2600 mts above sea level), to obtain quantitative information that allows an objective analysis in patients with suspicion of this pathology, values that could be used as reference in similar geographic altitude at world-wide level.

Methods and Materials: Cross-sectional, retrospective and analytical studies performed from January 2008 to June 2016. Accessible population were patients with a simple brain scannography with diagnosis of venous sinus thrombosis and healthy patients in Bogotá-Colombia.

Results: Hematocrit and intravascular scannographic attenuation has been demonstrated again. There were higher densities in healthy patients as previously reported in the literature (70 HU).

Conclusion: Reference values for patients living at higher altitudes than those already reported have a direct impact on diagnosis of intracranial venous thrombosis, decreasing neurological sequelae secondary to late diagnosis; these values also help to define which patients should be subjected to confirmatory studies.

B-0695 15:12

Virtual non-contrast CT derived from dynamic CTA in acute stroke

E.J. Smit, F.J.A. Meijer, M.M. Prokop; *Nijmegen/NL* (ewoudsmit@gmail.com)

Purpose: To assess if virtual non-contrast CT derived from dynamic CTA may obviate separately performed non-contrast CT images for acute stroke assessment.

Methods and Materials: In our hospital, all patients with suspected stroke undergo non-contrast CT and dynamic CTA/CT perfusion imaging if they 1) are eligible for i.v. thrombolysis or 2) have evidence of intracerebral hemorrhage on non-contrast CT (clinical trial). We selected 27 consecutive patients from this database. Virtual non-contrast images were reconstructed as the precontrast images of dynamic CTA after applying a 4D-similarity noise reduction filter. An experienced observer scored all images in a blinded manner for the presence and location of hemorrhage, midline shift, loss of gray white-matter differentiation, dens-vessel sign, old infarcts and hydrocephalus. Standard non-contrast images served as the reference standard.

Results: Virtual non-contrast images could not be derived in one case because of severe motion artefacts. Five patients had an intracranial hemorrhage which were all detected on virtual non-contrast CT. Also midline shift (four cases), loss of gray white-matter differentiation (one case), old infarcts (two cases) and hydrocephalus (none) were scored equal on both techniques. Dens vessel signs could not be reliably assessed on the virtual non-contrast images because of occasional artefacts or early contrast arrival.

Conclusion: It seems feasible to replace non-contrast CT by virtual non-contrast CT images for acute stroke assessment, allowing for a single-acquisition dynamic CTA stroke protocol from which haemorrhage, artery occlusion, and tissue perfusion can be evaluated.

Author Disclosures:

E.J. Smit: Research/Grant Support; Toshiba Medical Systems. Speaker; Toshiba Medical Systems. M.M. Prokop: Research/Grant Support; Toshiba Medical Systems. Speaker; Toshiba Medical Systems.

B-0696 15:20

Neuroimaging signs and features of brain lesions in patients with CADASIL

N. Kurochkina, A. Moroz, R. Kononov, M. Krotenkova, S. Illarionkin; *Moscow/RU* (nadia_sk@mail.ru)

Purpose: To evaluate specific changes in MRI of the human brain, associated with either cerebral autosomal dominant arteriopathy with subcortical infarcts and leukoencephalopathy (CADASIL) or hypertensive microangiopathy (HM).

Methods and Materials: We enrolled 24 patients with genetically confirmed CADASIL (19-81 y.o.) and 25 patients with HM (46-79 y.o.). The following MRI sequences were performed for every subject: T1 MPR, T2, FLAIR, DTI with calculation of fractional anisotropy (FA), mean, axial and radial diffusivity maps. Brain tissue lesions were assessed using Standards for Reporting Vascular

changes on nEuroimaging (STRIVE). Voxel-wise group analysis was carried out using SPM12 software to study the white matter microstructure.

Results: In the CADASIL group the following changes were observed (in % of patients): recent small subcortical infarcts - none; lacunes - 54%; white matter hyperintensities (WMH) by Fazekas 1 - 12%, Fazekas 2 - 17%, Fazekas 3 - 71% (sites of predilection: anterior temporal lobe and external capsule); cerebral microbleeds - 42%; enlarged perivascular spaces - 88%; brain atrophy - 27%. Morphometry analysis revealed differences in diffusivity maps and FA as well as volumes of brain structures in patients with moderate and severe WMH (Fazekas 2 and 3) between CADASIL and HM groups.

Conclusion: Neuroimaging signs of brain lesions are common for all types of cerebral small vessel disease, including CADASIL. However, the distribution of WMH and patterns of microstructural alterations specify the differences observed in CADASIL in comparison with HM, that reflects their various morphopathology.

14:00 - 15:30

Room F1

Oncologic Imaging

SS 716

Advances in oncologic imaging

Moderators:

E.G. Klompenhouwer; Eindhoven/NL
N.N.

B-0697 14:00

Can conventional MRI help to rectify grading of soft-tissue sarcomas (STS) on needle-core microbioscopy (NCB)?

A. Crombe¹, P.-J. Marcelin², F. Le Loarer¹, E. Stoeckle¹, A. Italiano¹, J.-M. Coindre¹, M. Kind¹; ¹Bordeaux/FR, ²Saint-Pierre/FR (amandine.crombe@ens-lyon.fr)

Purpose: Prognosis and management of STS strongly rely on histopathological grading. The European Society for Medical Oncology recommends NCB to assess grading, despite the risk of underestimation due to sampling. Our aim was to identify combination of MRI features associated with high-grade (III) and how it reclassified grade I-II STS on NCB into true high-grade STS on surgical specimen.

Methods and Materials: Of the 498 patients diagnosed with a STS in the ConNective Tissue in Cancer Network database) and followed-up in our sarcoma reference center between 2008 and 2015, we retrospectively included 130 patients with: available MRI with gadolinium-chelates injection, pathological grade on final surgical specimen, no neoadjuvant treatment. 66 had NCB. Visceral sarcomas, well-differentiated liposarcomas, angiosarcomas were excluded. Two radiologists evaluated: location, size, heterogeneity, margins, architecture, surrounding tissue and bone-vessel-nerve invasion.

Results: Final pathological grade was 69 grade III, 47 grade II, 14 grade I. On multivariate analysis, 3 criteria were associated with true grade III: ill-defined margins >10% of tumor surface on post-contrast T1-WI (p=0.026, OR=2.93, IC95%=(1.14-7.56)), necrotic signal (p=0.013, OR=2.28, IC95%=(1.24-6.43)), enhancement of surrounding oedema (p=0.004, OR=3.55, IC95%=(1.51-8.32)). Inter-observer agreements were 0.66(0.52-0.79), 0.78(0.65-0.90) and 1(1.00-1.00), respectively. Among the 43 patient with grade I-II on NCB, presence of at least 2 of these 3 criteria would correctly reclassify 12/14 (85.7%) true grade III but would ill-classify 15/29 (51.7%) true grade I-II (p=0.047).

Conclusion: Conventional MRI can help evaluate STS grading but additional features from other imaging modalities are required to improve reclassification after NCB.

B-0698 14:08

Machine learning approach on semantic and texture MRI features for early response evaluation in patients with high-grade soft-tissue sarcomas undergoing neoadjuvant chemotherapy

A. Crombe¹, C. Perier², O. Saut², B. Denis de Senneville¹, F. Le Loarer¹, E. Stoeckle¹, S. Cousin¹, A. Italiano¹, M. Kind¹; ¹Bordeaux/FR, ²Talence/FR (amandine.crombe@ens-lyon.fr)

Purpose: To evaluate the feasibility and added value of machine learning and radiomics approaches to early predict the response after 2 cycles of anthracycline-based neoadjuvant chemotherapy (NAC) in soft-tissue sarcomas (STS)

Methods and Materials: This retrospective single-center study included 52 uniformly patients (4-6 cycles NAC) with locally advanced high-grade STS, between 2008 and 2015. Good histological response (GHR) was defined as ≤10% stainable cells on final surgical specimen. All benefited from baseline (t0) and post-2 cycles 1.5T-MRI (t1) with gadolinium-chelates injection. MRI post-

processing consisted in histogram-based intensity normalisation and voxel standardisation. Random forest classifier was applied on: initial clinico-biological data, features from radiologist's visual assessment (semantic features: tumour architecture, margins, periphery), shape, histogram and textural features from T2-weighted-imaging at t1 and their changes (absolute or relative from t0 to t1). Areas under the receiver operating curve (AUC) and diagnostic performance of tested classifiers were compared.

Results: 17 GHR and 35 poor-responders (PHR) were analysed. According to RECIST1.1, 3/35 (8.6%) PHR showed progressive disease and 0/17 (0%) GHR showed partial or complete response at early evaluation. 77 features were assessed. The best classification performance was obtained using absolute changes of radiomics features giving: accuracy=75%, sensibility=91%, specificity=48%, positive predictive value=77%, negative predictive value=69%, AUC=0.67 (0.60-0.74).

Conclusion: Machine learning and radiomics approaches can substantially improve the NAC response prediction in high grade locally advanced STS and should be evaluated in prospective studies on additional imaging modalities.

B-0699 14:16

Calcium suppression in spectral detector computed tomography improves visualization of bone metastasis

N. Grosse Hokamp^{1,2}, N. Abdullayev¹, V. Neuhaus¹, J. Holz¹, D. Maintz¹, J. Borggreff¹; ¹Cologne/DE, ²Cleveland, OH/US (nils.grosse-hokamp@uk-koeln.de)

Purpose: To investigate a benefit from calcium suppression images (VNCa) in spectral detector computed tomography (SDCT) for assessment of bone metastases using MRI as a gold standard.

Methods and Materials: 24 patients with vertebral metastases that underwent SDCT for oncologic staging purpose and MRI examination of the spine were included in this retrospective, IRB-approved study. Images were reconstructed as conventional images (CI) and using a prototype algorithm for calcium suppression (Philips Healthcare) with 3 different presets (VNCa¹, VNCa² and VNCa³). In each patient, normal bone (as determined by MRI) served as intra-individual standard-of-reference. Circular regions of interest were drawn in metastatic bone, normal bone and subcutaneous fat in CI and copied to identical positions in VNCa¹⁻³, attenuation and standard deviation were recorded. Attenuation was compared using t test and receiver operator characteristics (ROC) were analysed to assess performance of the different VNCa algorithms.

Results: In conventional images attenuation in normal bone was higher than in metastatic bone (140.9±65.7 vs 86.1±33.6; p<0.05), after subtraction of calcium attenuation in metastatic bone was higher (e.g. VNCa¹: -240.0±60.6 vs -80.5±70.5, p<0.05); the absolute difference between normal and metastatic bone increased from 54.8 in CI to 159.5 (p<0.05), while noise remained constant (p≥0.05). This resulted in a significant increase of the area under the curves as depicted by ROC analysis in VNCa¹⁻² as compared to CI and VNCa³ (0.95/0.98 vs 0.74/0.73, respectively, p<0.05).

Conclusion: Virtual non-calcium images provided by SDCT can be helpful in differentiating bone metastasis and non-metastatic bone if calcium suppression is adjusted to an appropriate level.

B-0700 14:24

A deep learning-based radiomics model for classification of mammography mass lesions in breast cancer patient

I. Shiri, P. Geramifar, A. Bitarafan-Rajabi, A. Mohammadzadeh, H. Pouraliakbar, S.P. Shayesteh; Tehran/IR (Shayeste_sajad@yahoo.com)

Purpose: Breast cancer is the most commonly diagnosed cancer with high mortality and morbidity. There are different biomarkers which can be obtained from breast tissue to classify mass lesions. The main aim of this study was to classify malignant and benign breast cancer using convolutional neural network (CNN).

Methods and Materials: In this study, we used 315 mammography images of breast cases (148 benign and 167 malignant) from CBIS-DDSM database. Image patches are extracted around each lesion and used as train and test data set. The neural network consists of convolutional blocks composed of Convolutions, Batch Norm, ReLU, and Max Pooling Blocks followed by FC layers. The final layer is a soft-max layer for binary classification. We evaluate the CNN performance using free response receiver operating characteristic (FROC) analysis.

Results: CNN performance evaluation and accuracy of the model was performed using free response receiver operating characteristic (FROC) analysis. The analysis shows the deep learning approach achieves FROC value of 82.3% with accuracy of 85.3%.

Conclusion: CNN in hierarchically way uses a set of nonlinear transformations, to represent the visual content of an image automatically from scratch. Deep learning takes advantage of no need for segmentation, feature extraction, feature reduction and classification manually against conventional radiomics methods. Thus, deep learning-based radiomics model can be used instead of hand crafted texture feature analysis in radiomics processing.

B-0701 14:32

IVIM MRI of oestrogen-receptor-positive breast cancer: association with quantitative IVIM parameters and Ki-67 proliferation status

R. Balaji; Chennai/IN (ravikanthbalaji@gmail.com)

Purpose: Investigate association of IVIM MRI-derived quantitative parameters with Ki-67 proliferation index in patients with oestrogen receptor (ER)-positive breast cancers.

Methods and Materials: 67 patients with ER-positive breast cancer were included in the study. All patients underwent IVIM MR imaging along with regular diffusion and DCE MRI on 1.5 Tesla scanner. IVIM-derived parameters: f the perfusion fraction, D the pure diffusion coefficient, D^* perfusion-related pseudo-diffusion and IVIM-derived ADC were analysed and correlated with Ki-67 status. High (>14%) and low Ki-67 (<14%) proliferation indices were obtained.

Results: f values (perfusion fraction) were significantly elevated in high Ki-67 index group (P<0.001). D and ADC values were lower in high Ki-67 group (P <0.001). Low Ki-67 index tumours had lower f values but not statistically significant high D or ADC values. High f values (14%) were seen in grade 3 tumours which were larger (>2cm) and had greater propensity for axillary nodal metastases and were associated with high Ki-67 proliferation index. f fraction had greater confidence interval 1.756-42.24 for correlation with Ki-67 index.

Conclusion: f and true diffusion coefficient values can be used as independent biomarkers to correlate Ki-67 proliferation status in oestrogen receptor-positive breast cancers.

B-0702 14:40

Metastatic axillary lymph nodes in patients with breast cancer: value of quantitative shear wave elastography

Y. Kabin, O. Kostash, V. Kapustin, A. Gromov; Moscow/RU (www.kapustin@yandex.ru)

Purpose: To evaluate the usefulness of LN tissue elasticity quantitative assessment by shear wave elastography (SWE) for detection of axillary lymph node (LN) metastatic involvement in women with breast cancer (BC).

Methods and Materials: 172 women with verified BC were included in this study. In every case the most suspicious LN was chosen, using B-mode ultrasonography (BUS) for the further elasticity parameters assessment. Tissue elasticity (kPa) was measured at the most suspicious hypoechoic portion of LNs, detected by BUS. LN tissue changes type (benign or malignant) were subsequently proved by ultrasound-guided fine-needle aspiration biopsy or postoperative histological evaluation in all cases. These data were retrospectively compared for two groups of patients (with benign and metastatic LN) using Mann-Whitney test. Statistical measures of performances (Se, Sp) of SWE elasticity for LN metastases detection were calculated using receiver operating curve (ROC) analysis.

Results: "Tissue elasticity" value in metastatic LNs was significantly higher comparing to benign LN changes ($p=0.000$). This quantitative SWE parameter showed high diagnostic efficacy for axillary LN metastases detection [area under curve (AUC) - 0.924]. The best diagnostic performance (Se=0.87, Sp=0.81) was received at 31,5 kPa cut-off value.

Conclusion: Tissue elasticity parameter (kPa), assessed by SWE, gives valuable diagnostic information (adjunctive to the diagnostic performance of BUS) for the axillary LN metastasis detection in patients with BC.

B-0703 14:48

Quantitative PET parameters in predicting event free survival in patients with Hodgkin lymphoma

I. Kriachok¹, O. Novovsadi¹, T. Skrypets¹, A. Gorbach¹, Y. Kmetiyuk¹, O. Kozlova¹, M. Novikov¹, L. Mikhalska¹, V. Kozlov²; ¹Kiev/UA, ²Odessa/UA (nicknovi@gmail.com)

Purpose: To analyse whether quantitative metabolic PET parameters, their negative predictive value (negative PET scan and no treatment failure, NPV) and positive predictive value (positive PET scan and treatment failure, PPV) were associated with EFS.

Methods and Materials: SUVmean, MTV (computed with 41% threshold algorithm) and TLG were retrospectively calculated at baseline (PET-1), interim (PET-2) and end of treatment (PET-3) metabolic PET/CT studies of 45 patients with Hodgkin lymphoma. 53% of patients had stage I-II disease and 47% - stage III-IV disease. All patients were treated with ABVD or BEACOPP-14/esc chemotherapy regimens.

Results: The ORR in the group was 95.5%. There were 73% patients with negative and 27% with positive PET-2 studies, which yielded an NPV of 82% and PPV of 18%, $p < 0.05$. Multivariate analysis showed PPV to be the only variable significantly influencing EFS with HRs of 1.07 [95% confidence interval (CI) 1.0-1.15, $p = 0.00008$]. According to Cox regression, MTV and SUVmean at PET-3 were the variables significantly influencing EFS with HRs of 1.07 [95% confidence interval (CI) 1.0-1.13, $p = 0.005$] and 2.0 [95% (CI) 1.4-

2.82, $p = 0.0001$), respectively. Unfortunately, quantitative parameters at PET-1 and PET-2 were not statistically significant in predicting clinical outcome in this study.

Conclusion: Quantitative PET parameters may play a predictive role in identifying patients at high risk of treatment failure. Further studies will be conducted to investigate PET quantitative data predictive value.

B-0704 14:56

Diagnosis of diffuse spleen involvement in haematological malignancies using a spleen to liver attenuation ratio in CECT

C.P. Reinert, C. Hinterleitner, K. Nikolaou, M. Horger; Tübingen/DE (christian.reinert@med.uni-tuebingen.de)

Purpose: To assess the mean attenuation values of the normal spleens vs. involved spleens in haematological malignancies and to try to discriminate the two groups by using attenuation ratios to the normal liver parenchyma in the portal-venous enhancement phase on CECT.

Methods and Materials: Included were 60 (27 male; mean age 55.0y) consecutive patients with known malignant haematologic diseases who underwent CECTs for staging before and after chemotherapy and 60 controls (31 male; mean age 62.2y). We calculated in all patients the spleen index (Lx/BxDx0.5) and measured the attenuations of the spleen and liver in the portal-venous enhancement phase calculating the spleen-to-liver ratios. Standard-of-reference was the significant reduction (>20%) of the spleen index following successful chemotherapy or normalization of FDG-uptake in a subgroup undergoing 18F-FDG-PET/CT for staging.

Results: The spleen-to-liver attenuation ratios in involved spleens were significantly lower over the controls, respectively (0.94 vs. 0.98, $p < 0.0045$). The pre- to posttreatment attenuations in the spleen in the involved group were significantly lower (93.70 HU vs. 113.15 HU, $p < 0.0001$) as well as the pre- to posttreatment spleen to liver attenuation ratios (0.94 vs. 1.17, $p < 0.0001$). Using a cut-off-value of 100.9 HU the positive predictive value was 0.81 (95% confidence interval). The spleen index significantly dropped down after successful treatment (574.87 cm³ to 287.64 cm³, $p < 0.0001$).

Conclusion: Spleen-to-liver attenuation ratios in haematological malignancies with diffuse involvement of spleen are significantly lower as in controls and could therefore be used complementary to the spleen index as an indicator of spleen involvement at staging.

B-0705 15:04

Is whole body ¹⁸F-FDG-PET/CT including the extremities routinely warranted in melanoma patients?

C. Riedl¹, H. Schoder¹, G.A. Ulaner¹, T. Saidon¹, K. Juluru¹, W. Weber¹, K. Pinker²; ¹New York, NY/US, ²Vienna/AT (riedlc@mskcc.org)

Purpose: ¹⁸F-FDG-PET/CT of melanoma patients is often performed as a whole body (WB) study including the upper and lower extremities. This causes increased examination time and radiation dose and is of questionable clinical value. The aim of this study was to investigate the value of ¹⁸F-FDG-PET/CT imaging of the extremities in melanoma patients.

Methods and Materials: The hospital database was searched for melanoma patients who underwent WB ¹⁸F-FDG-PET/CT between 2012-2016. Imaging reports were searched for findings in the extremities that would not have been included in a scan ranging from the skull base to mid thighs, the range routinely used in most other malignancies. Findings in the extremities considered less likely to be malignant (<25%) were considered clinically irrelevant. Findings in an extremity related to the primary tumour were also considered clinically irrelevant.

Results: 1975 ¹⁸F-FDG-PET/CT scans in melanoma patients were identified. There were 276 (14%) findings in the extremities that were classified as a malignant (primary/recurrence, local or distant metastases). In 1.6% (32/1975) patients we identified metastases in an extremity that would not have been covered by an "eyes-to-thighs" scan or a scan of the extremity afflicted by the primary tumour. In 93.8% (30/32) of these patients there was disseminated disease. Thus WB ¹⁸F-FDG-PET/CT detected clinically relevant metastases in the extremities in only 0.1% (2/1975) of melanoma patients.

Conclusion: WB ¹⁸F-FDG-PET/CT almost exclusively detected metastases in the extremities in patients with disseminated disease or in the extremity afflicted by the primary tumour.

B-0706 15:12

Integrated ¹⁸F-FDG PET/MR for the initial detection of lymph node metastases in malignant melanoma: is sentinel lymph node biopsy still necessary?

B.M. Schaarschmidt¹, J. Grueneisen², V. Stebner², L.M. Sawicki¹, C. Buchbender¹, P. Heusch¹, L. Umutlu², G. Antoch¹, T. Poeppel²; ¹Düsseldorf/DE, ²Essen/DE

Purpose: To evaluate the performance of 18F-FDG PET/CT, 18F-FDG PET/MR and 18F-FDG PET/MR including diffusion-weighted imaging (DWI) in

sentinel lymph node metastasis detection after primary tumour resection in malignant melanoma patients.

Methods and Materials: In this retrospective analysis, 52 patients (female: n=30, male: n=22) that underwent 18F-FDG PET/CT and subsequent PET/MR including DWI 18F-FDG prior to radioguided SPECT/CT sentinel lymph node mapping and resection were included. In separate sessions, 87 sentinel lymph nodes were identified using SPECT/CT in PET/CT, PET/MR PET/MR+DWI datasets and their dignity (benign/malignant) was determined by increased tracer uptake (PET/CT), increased tracer uptake and suspicious morphological appearance (PET/MR) as well as reduced apparent diffusion coefficients in DWI (PET/MR+DWI). Histopathological results served as reference standard.

Results: Of 136 resected lymph nodes, 87 could be identified in SPECT/CT. Seventeen metastatic lymph nodes were detected by histopathology (size: <0.1mm: n=4, 0.1-1mm: n=7, >1mm: n=6). Sensitivity, specificity, positive predictive value and negative predictive value were 17.7%, 95.6%, 50.0% and 82.3% for PET/CT, 23.5%, 96.9%, 66.7% and 82.3% for PET/MR and 0%, 93.3%, 0%, 82.4% for PET/MR+DWI. PET/MR+DWI performed worse than the other methods as contradictory information between PET and DWI reduced the number of true-positive findings.

Conclusion: 18F-FDG PET/MR is unable to improve initial lymph node metastasis detection in malignant melanoma patients in comparison to PET/CT and will not be able to replace sentinel lymph node resection for diagnostic purposes in malignant melanoma patients. The additional analysis of DWI even worsened the performance of PET/MR due to contradictory information.

B-0707 15:20

Usefulness of spleen size and volume measured by computed tomography for predicting clinical outcome in chronic myeloid leukemia
M. Seo, S.-E. Lee, J.-I. Choi, D.-W. Kim; *Seoul/KR (minkook.seo@gmail.com)*

Purpose: Spleen size is one of well-known prognostic factors for chronic myeloid leukemia (CML) patients and many scoring systems include the spleen size as a parameter. The purpose of this study is to evaluate whether spleen diameter on axial (ASD) and coronal (CSD) CT imaging and spleen volume (SV) measured using CT images would accurately predict the prognosis of initially diagnosed CML patients.

Methods and Materials: A total of 89 CML patients who were initially diagnosed and treated by imatinib were enrolled. ASD and CSD were measured on axial and coronal CT imaging by measuring the longest diameter of spleen. SV was quantitated by the semi-automatic volume measurement software. Conventional measurement of spleen by palpation, ASD, CSD and SV were analyzed for cumulative incidence (CI) of complete cytogenetic response (CCyR), major molecular response (MMR), failure-free survival (FFS), progression-free survival (PFS) and overall survival (OS) using the Kaplan-Meier methods and the log rank test.

Results: Measurements by palpation and ASD were statistically significant for CI of CCyR and MMR ($p < 0.001$ for all parameters). However, they were not significant for FFS, PFS and OS. On the other hand, CSD was significant for CI of CCyR ($p = 0.003$), MMR ($p < 0.001$) and PFS ($p = 0.038$). SV was significant for CI of CCyR ($p < 0.001$), MMR ($p < 0.001$), FFS ($p = 0.040$) and PFS ($p = 0.033$). However, no measurement was significant for OS.

Conclusion: Spleen volume measurement using CT images is superior to conventional palpation or 2-dimensional measurement of spleen size for predicting the prognosis of CML patients treated by imatinib.

14:00 - 15:30

Room F2

GI Tract

SS 701b

Solving challenges in upper GI imaging

Moderators:

M. Radzina; Riga/LV

S. Schmidt Kobbe; Lausanne/CH

B-0708 14:00

Intravoxel incoherent motion diffusion-weighted MR imaging in gastro-esophageal cancer: correlation with ¹⁸F-FDG-PET and histopathology

K. Schawkat¹, B.-R. Sah^{1,2}, G. Delso³, E. Ter Voert¹, P. Schneider¹, C.S. Reiner¹, M. Huellner¹, P. Veit-Haibach⁴; ¹Zurich/CH, ²London/UK, ³Waukesha, WI/US, ⁴Toronto, ON/CA (khoschy.schawkat@usz.ch)

Purpose: To evaluate the relationship of multimodality parameters derived from intravoxel incoherent motion (IVIM) diffusion-weighted MR imaging and ¹⁸F-FDG-PET in patients with gastro-esophageal cancer and to investigate their histopathological correlation.

Methods and Materials: Twenty-two consecutive patients (19 male; mean age 64.9±11.7 years; range 37-84 years) with adenocarcinoma (n=15) and esophageal squamous cell carcinoma (n=7) were analyzed prospectively. PET-

parameters (SUVmax, mean tumor volume (MTV), total lesion glycolysis (TLG)) and IVIM parameters (pseudodiffusion (D*), perfusion fraction (fp), true diffusion (D), b-value (bval)) were determined, correlated to each other and to histopathology (staging, grading, regression). The relationship of these parameters was evaluated using Spearman's correlation with Bonferroni correction to exclude false positive results under multiple testing.

Results: IVIM and PET-parameters showed significant negative correlation for: MTV II bval ($r_s = -0.643$, $p = 0.002$), TLG II bval ($r_s = -0.699$, $p = 0.000$) and TLG II fp ($r_s = -0.577$, $p = 0.006$). Negative correlation was also found for bval II staging ($r_s = 0.590$, $p = 0.005$). TLG II Dt showed positive correlation ($r_s = 0.705$, $p = 0.000$). After Bonferroni correction no significant correlation was found for MTV II fp ($r_s = -0.527$, $p = 0.014$) and for MTV II Dt ($r_s = 0.487$, $p = 0.025$).

Conclusion: IVIM parameters (fp, Dt) provide useful quantitative information and correlate with the PET-parameter total lesion glycolysis (TLG). In addition, bval significantly correlates with staging. IVIM might be a valuable tool for non-invasive pre-therapeutic characterization of gastro-esophageal cancer.

B-0709 14:08

The concentration of iodine in perigastric adipose tissue: a novel index for assessment of serosal invasion in patients with gastric cancer after neoadjuvant chemotherapy

L. Yang; *Shijiazhuang/CN (64502240@qq.com)*

Purpose: This study aims to explore the association between iodine concentration (IC) in perigastric adipose tissue (PAT), quantified by dual-energy computed tomography (DECT), and serosal invasion (SI) in patients with gastric cancer after neoadjuvant chemotherapy (NAC)

Methods and Materials: 43 patients with T4-staged gastric cancer (with SI) were enrolled in the 4th Hospital of Hebei between January 2015 and December 2016. IC and standard IC in PAT (IC_{PAT} and SIC_{PAT}) were quantified by DECT pre- and post-NAC. Postoperative pathologic examination was performed to stage gastric cancer. IC_{PAT} and SIC_{PAT} between patients at T1-T3 stages (group A, without SI) and patients at T4 stage (group B, with SI) were compared subsequently, with receiver operating characteristic (ROC) curve applied for evaluating the accuracy of the ΔSIC_{PAT} in identifying post-NAC SI.

Results: The accuracy of conventional computed tomography (CT) in identifying SI was 72.09%. Differences of variations between pre- and post-NAC IC_{PAT}, SIC_{PAT}, ΔIC_{PAT} and ΔSIC_{PAT} were observed, respectively ($P < 0.05$). Intragroup IC_{PAT} and SIC_{PAT} also changed significantly after NAC ($P < 0.05$), except the SIC_{PAT} in group B ($P > 0.05$). The area under the ROC curve (AUC) was 0.929, with the threshold of ΔSIC_{PAT} reaching 0.095. The sensitivity, specificity and accuracy of SIC_{PAT} in identifying post-NAC SI were 92.30 %, 86.70 %, and 88.37%, respectively.

Conclusion: These results showed that SIC_{PAT} is an accuracy index for identifying post-NAC SI, by which it might be used to assess the effectiveness of neoadjuvant chemotherapy and the optimal timing for the operation.

B-0710 14:16

Use of CT perfusion parameters in assessment of early response of gastric cancer to neoadjuvant chemotherapy

P. Pilius, I. Shraimer, A. Klimentko, V.E. Sinityn; *Moscow/RU (polishka1903@gmail.com)*

Purpose: To assess whether the changes of CT Perfusion (CTP) parameters of gastric cancer could be used as biomarkers for evaluation of early response of gastric cancer to neoadjuvant chemotherapy.

Methods and Materials: 21 patients with local advanced adenocarcinoma of stomach were analyzed. The patients received 2-5 courses of neoadjuvant chemotherapy (EOX or XELOX schemes) before surgery. CTP scans were performed prior and after the first course of chemotherapy. CTP parameters (blood flow (BF), blood volume (BV) and permeability surface (PS)) of the tumor were computed on a dedicated workstation with a consensus between two radiologists.

Results: 7 patients (33.3%) with good pathological response to treatment (grade 1-2 accordingly to Mandar score) consisted the 1st group. Other 14 patients (66.6%) with poor response (grade 3-5) made the 2nd group. All studied CTP parameters decreased in the both groups after treatment, but all these changes were not significant. CTP values before and after chemotherapy in the 1st group: BV 5.5 and 5.2 ($p = 0.83$), BF 68.5 and 56.8 ($p = 0.21$), PS 39.5 and 31.3 ($p = 0.3$); in the 2nd group: BV - 7.3 and 5.9 ($p = 0.83$), BF - 73.2 and 68.6 ($p = 0.58$), PS - 35.0 and 30.7 ($p = 0.24$), corr.

Conclusion: CTP parameters of the gastric cancer decreased after the first course of chemotherapy both in patients with good and poor response. Further improvements in CTP protocols and analysis are needed in order to make it a valuable tool to assess results of chemotherapy in gastric cancer.

B-0712 14:24

The CTP for detection of primary oesophageal carcinoma

M. [Kantarci](#), A. Levent, R. Sade, S. Eren, H. Ogul, F. Guven, G. Bayraktutan; *Erzurum/TR (akkanrad@hotmail.com)*

Purpose: The purpose of this study was to investigate the efficiency of computed tomographic perfusion (CTP), contrast-enhanced computed tomography (CECT) and ^{18}F -fluorodeoxyglucose positron emission tomography (PET/CT) in the diagnosis of oesophageal cancer.

Methods and Materials: This prospective study consisted of 33 patients with pathologically confirmed oesophageal cancer of which 2 had oesophageal abscess. All the patients underwent CTP, CECT and PET/CT imaging and the imaging findings were evaluated. Sensitivity, specificity, positive predictive and negative predictive values were calculated for each of the three imaging modalities relative to the histological diagnosis.

Results: Thirty three tumours were visualized on CTP; on CECT:29, on PET/CT:27. Six tumours were stage 1 and the two and four tumours were missed by CECT and PET/CT, respectively. The significant differences were between the CTP and CECT ($p<0.02$), and CTP and PET/CT ($p<0.04$), for stage 1 tumours were found. Sensitivity, specificity, positive predictive. Corresponding values for and negative predictive value of CTP were 100%, 100%, 100% and 100%, respectively. Corresponding values for CECT were 93.94%, 0%, 93.94% and 0%, respectively, and those of PET/CT were 87.88%, 0%, 93.55% and 0%, respectively. Hence, the sensitivity, specificity, positive predictive and negative predictive values of CTP were better than those of CECT and PET/CT.

Conclusion: The CTP had an advantage over CECT and PET/CT in detecting small lesions. The CTP was valuable especially in stage 1 tumours.

B-0713 14:32

The value of dual-detector spectral CT imaging in the identification of gastric carcinoma and gastric lymphoma

S. [Jiang](#), Y. Ren, H. Yan, X. Lu; *Shenyang/CN (1904451977@qq.com)*

Purpose: To explore the value dual-detector spectral CT scan in the differential diagnosis of gastric cancer (GC) and gastric lymphoma (GL).

Methods and Materials: 32 patients with gastric cancer and 12 patients with gastric lymphoma were retrospectively analysed. All patients were performed enhanced abdominal CT scanning with spectral CT. The attenuation values of virtual monochromatic energy 40 ~ 140 keV, iodine concentration and effective atomic number (Z_{eff}) of the two groups were measured. The normalized iodine concentration (NIC, lesion iodine concentration / aorta abdominalis iodine concentration) and the slope of the spectral curve (λ_{HU}) were calculated in arterial phases and venous phases.

Results: In arterial phase, attenuation values of 40 ~ 70 keV of GL group were lower than that in GC group, the difference was significant at 40 keV, attenuation values of GC group was statistically higher than that in GL group (131.3 ± 67.6 HU vs 81.3 ± 40.4 HU; $t = 2.56$, $P < 0.05$). λ_{HU} on 40 ~ 100 keV monochromatic images was higher in GC group than that in GL group (1.37 ± 0.98 vs 0.65 ± 0.59 ; $t = 2.64$, $P < 0.05$). The NIC in GC group was higher than GL group (0.125 ± 0.1 vs 0.061 ± 0.06 ; $t = 2.34$, $P < 0.05$). The Z_{eff} in GC group was higher than GL group (8.1 ± 0.47 vs 7.6 ± 0.51 ; $t = 3.39$, $P < 0.05$).

Conclusion: Gastric cancer and gastric lymphoma have different energy spectrum CT characteristic parameters that can provide the reference value for clinical imaging to identify.

B-0714 14:40

Prognostic significance of systemic inflammation and FDG-PET bone marrow uptake in patients with oesophageal cancer

R.J. [Pallas](#), K.G. Foley, T. Crosby, P.A. Fielding; *Cardiff/UK (robbyfromtherock-2@yahoo.co.uk)*

Purpose: Systemic inflammation is regarded as a poor prognostic indicator in cancer patients. FDG uptake is increased in areas of inflammation. Early research suggests novel immunotherapy techniques may be beneficial in selected cancer patients and treatment decisions could be guided by PET/CT. The aim of the study is to investigate the prognostic significance of bone marrow (BM) uptake in patients with oesophageal cancer (EC) and correlate serum haematological results with recorded standardised uptake values (SUV).

Methods and Materials: Consecutive patients with biopsy-proven esophageal cancer staged with PET/CT between October 2010 and July 2015 were considered. All patients underwent definitive chemoradiotherapy. Patients with haematological disorders and BM metastases were excluded. Mean BM SUV was calculated from regions of interest placed in 5 adjacent vertebral bodies. Cox regression models assessed the prognostic significance of clinical, metabolic and haematological variables. P values < 0.05 were considered statistically significant. Primary outcome was overall survival (OS).

Results: Seventy-eight patients (median age 71 (range 35-81), 54 males, 38 adenocarcinomas, 35 squamous cell carcinomas) were included. Median OS was 25.0 months (95% confidence intervals 13.6-36.4). Radiological stage was

significantly associated with OS (X^2 14.735, df 6, $p=0.022$). Age, tumour location, SUVmax of primary tumour, mean SUV of vertebrae, Hb, WCC, neutrophils, lymphocytes, platelets and albumin were not associated with OS ($p=0.561$, 0.971 , 0.656 , 0.869 , 0.584 , 0.216 , 0.344 , 0.324 , 0.165 , 0.378 , respectively).

Conclusion: Radiological stage was significantly associated with OS. However, metabolic and haematological variables were not statistically significant. A larger cohort of EC patients is required to test this hypothesis.

B-0715 14:48

MRI of the gastric antrum for the quantification of gastric motility: comparison between obese and normal weight patients

S. [Picchia](#), M. Rengo, D. De Santis, D.M. Bellini, S. Badia, A. Laghi; *Latina/IT (simona.picchia87@gmail.com)*

Purpose: To compare gastric motility in obese and normal weight patients with magnetic resonance imaging (MRI).

Methods and Materials: This is a non-randomized single-centre study. CineMRI for motility analysis was obtained by 1.5T MRI using 2DtrueFISP (coronal and axial planes) after 650-ml liquid meal (Nutridrink) plus 2 yolks, 1 albumen and 150 ml of water over 10 minutes. This 525-kcal meal was composed of 25% fat, 25% protein, and 50% carbohydrate. Images were acquired before and immediately after the meal and every 20 minutes, for a total exam time of 100 minutes. Each gastric motility scan lasted 60 seconds, with 100 images acquired in free breathing. Antral length, maximal contraction amplitude and contraction frequency were evaluated on a dedicated software. Results obtained in obese and normal weight patients were compared.

Results: Twenty patients (10 obese and 10 normal weight) were included in the study. Motility antral scans showed that during fasting and postprandial period, in obese patients the three parameters evaluated were significantly lower (mean basal antral length in obese patients: 6.75 ± 0.8 cm/in normal weight patients: 8.12 ± 0.43 cm, p value < 0.05 ; mean postprandial antrum length in obese patients: 7.56 ± 1.03 cm/in normal weight patients: 9.4 ± 0.12 mm, p value < 0.05 ; mean basal maximal contraction amplitude in obese patients: 7.1 ± 0.72 mm/in normal weight patients: 8.97 ± 0.43 , p value < 0.05 ; mean postprandial maximal contraction amplitude in obese patients: 8.3 ± 1.5 mm/in normal weight patients: 9.76 ± 0.76 mm, p value < 0.05 ; mean basal contraction frequency in obese patients 8.7 ± 0.98 cpm/in normal weight patients: 10.3 ± 0.9 , p value < 0.05 ; mean postprandial contraction frequency in obese patients: 9.8 ± 1.4 cpm/in normal weight patients: 11.2 ± 1.2 cpm, p value < 0.05).

Conclusion: MRI is able to identify differences in antral motility between obese and normal weight patients.

B-0716 15:56

Prediction of gastric cancer with synchronous hepatic metastasis by enhancement pattern of primary lesion using multiphase contrast-enhanced computed tomography

D. [Tsurumaru](#), Y. Nishimuta, T. Muraki, Y. Asayama, H. Honda; *Fukuoka/JP (tsuru-d@radiol.med.kyushu-u.ac.jp)*

Purpose: To examine contrast-enhanced computed tomography (CECT) features of primary site of gastric cancers with synchronous hepatic metastasis.

Methods and Materials: One hundred and eleven consecutive patients with pathologically proven advanced gastric cancers who were evaluated with CECT were enrolled. CT images were obtained 40s (arterial phase), 70s (portal phase) and 240s (delayed phase) after injection of nonionic contrast material. Eleven patients were diagnosed having hepatic metastasis at the time of diagnosis. Two radiologists in consensus determined the "peak enhancement phase" in which the lesion showed the highest attenuation value among the three phases for each case. The readers traced the entire tumour as the region of interest (ROI) of the gastric lesion, and measured the CT attenuation value for each phase. We compared the peak enhancement phase of positive hepatic metastasis group ($n=11$) and negative hepatic metastasis group ($n=100$) using Chi-square tests, and compared the CT attenuation values of the two groups in each phase using analysis of variance (ANOVA).

Results: The peak enhancement was significantly different between the two groups ($p=0.0007$); most of the positive hepatic metastasis cases had peak enhancement in the arterial phase. The CT attenuation values of positive hepatic metastasis cases were significantly lower than those of negative hepatic metastasis cases in the delayed phase.

Conclusion: Hepatic metastasis of gastric cancer may be predictable according to enhancement pattern of primary lesion on multiphase CECT.

B-0717 15:04

MRI for response assessment after neoadjuvant chemoradiotherapy in oesophageal cancer: added value of diffusion-weighted imaging

S.E. Vollenbrock, F.E. Voncken, D.M. Lambregts, M. Maas, L.C. ter Beek, B.M. Aleman, R.G.H. Beets-Tan, A. Bartels-Rutten; *Amsterdam/NL* (s.vollenbrock@nki.nl)

Purpose: High accuracy is needed to select oesophageal cancer patients with a complete response (CR) after neoadjuvant chemoradiation (nCRT) for organ-preserving treatment instead of oesophagectomy. Performance of T2-weighted MRI (T2W-MRI) without and with diffusion-weighted MRI (DW-MRI) for response assessment after nCRT was determined.

Methods and Materials: Thirty-two patients with locally advanced oesophageal cancer underwent MRI (1.5T; T2W-MRI and DW-MRI (b-values=0,200,800 s/mm²)) before and after nCRT with a maximum of 21 days between MRI and surgery. Three radiologists first scored only T2W-MRI. Secondly they rescored with DW-MRI. A 5-point score was used (1=definite CR, 3=inconclusive, 5=definite residual tumour). Histopathology after oesophagectomy represented the reference standard (Mandard tumour regression grade 1=CR, 2-5=residual tumour). Area under the ROC (AUROC), sensitivity and specificity were calculated considering MRI scores 3-5 as tumour-positive.

Results: Two out of 32 patients were excluded due to poor image quality. Seven (23%) of 30 patients achieved a CR. AUROCs for the 3 radiologists individually were 0.57, 0.67, 0.64 for T2W-MRI only and 0.76, 0.69, 0.72 with DW-MRI (p=0.06, 0.57, 0.60). Sensitivity for detecting residual tumour was 100%, 91%, 87% on T2W-MRI and 96%, 96%, 87% with DW-MRI. Specificity was 14%, 43%, 43% on T2W-MRI and 57%, 43%, 57% with DW-MRI.

Conclusion: T2W-MRI with DW-MRI shows fair accuracy of response assessment after nCRT in oesophageal cancer patients while T2W-MRI only performs poorly. Sensitivity of the combination is high, indicating that the risk of missing residual tumour is minimal. However, specificity is lacking. Future studies investigate if addition of (echo-)endoscopy improves response assessment.

B-0718 15:12

Perivascular infiltration and histologic difference: is it helpful to determine T stage of advanced gastric cancer in CT?

J. Kim, W.S. Chung, H.Y. Jang, H.C. Kim, T.S. Kang, H.J. Lee, J.S. Sohn; *Daejeon/KR* (apple17171@naver.com)

Purpose: This study aims to determine whether morphologic and histologic features are useful for CT T stage of advanced gastric cancer.

Methods and Materials: A review of medical records yielded the 160 patients with advanced gastric cancer, who had available preoperative stomach CT scans for review and were pathologically confirmed. Individual review of stomach CT scans was subsequently performed by two radiologists, who were blinded to pathologic stage. Using CT, they were classified according to standard T stage, perivascular T stage, and histologic T stage. Diagnostic accuracy of each T stage and time to progression (TTP) between positive and negative perivascular infiltration group were analyzed.

Results: Diagnostic accuracy of standard T stage, perivascular T stage, and histologic T stage was respectively 65%, 68.75%, and 77.5%. There was significantly different between diagnostic accuracy of standard T stage and histologic T stage. There was no significantly different between standard T stage and perivascular T stage. However, in the subgroup analysis that was pathologically confirmed as T3 and T4a, there was significantly different between standard T stage and perivascular T stage. In pathologically confirmed T3 and T4a group, TTP of negative perivascular group was longer than positive perivascular group.

Conclusion: Considering histologic differentiation and perivascular infiltration could be useful option for pre-operative CT T staging of AGC. Especially, perivascular infiltration is more useful option for differentiation of T3 and T4a gastric cancer.

14:00 - 15:30

Room D

Musculoskeletal

SS 710b

Ankle and foot

Moderators:

M. Zanetti; Zurich/CH
N.N.

B-0719 14:00

Posterior tibial tendon dysfunction: clinical and magnetic resonance imaging findings having histology as reference standard

C. Messina¹, D. Albano², A. Corazza¹, S. Rapisarda¹, N. Martinelli¹, A. Bianchi¹, L.M. Scofnienza¹; ¹Milan/IT, ²Palermo/IT (carmelomessina.md@gmail.com)

Purpose: To investigate the correlation between MRI, clinical tests, histopathologic features of posterior tibial tendon (PTT) dysfunction in patients with acquired adult flatfoot deformity surgically treated with medializing calcaneal osteotomy and flexor digitorum longus tendon transposition.

Methods and Materials: Nineteen patients (11 females; age: 46years, range: 18-75) were pre-operatively evaluated using the single heel rise (HR) and the first metatarsal rise (FMR) sign tests. Two reviewers graded the PTT tears on a I-III scale and measured the hindfoot valgus angle on the pre-operative ankle MRI. The specimens of the removed portion of PTT were histologically analysed by two pathologists using the Bonar and Movin score. Linear regression, Spearman's rank order, and intraclass correlation coefficient (ICC) statistics were used.

Results: ICC for MRI was excellent (0.952). Correlation between FMR and HR tests was at limit of significance (r=0.454; P=0.051). HR and FMR significantly correlated to the Movin score (r=0.581; P=0.009 and r=0.538; P=0.018, respectively), not to the Bonar score (both with r=0.424; P=0.070). PTT tendinopathy grading at MRI significantly correlated to the FMR (p=0.041), but not to the hindfoot valgus angle (p=0.496), the HR (p=0.943), the Bonar (p=0.937) and Movin score (p=0.436). The hindfoot angle did not correlate to any of the other variables (p>0.264).

Conclusion: For PTT dysfunction, HR and FMR tests showed high correlation with histology evaluated using the Movin score, without correlation with the Bonar score. Semiquantitative grading of PTT dysfunction at MRI only correlates to the FMR and not to histology. The hindfoot valgus angle is not correlated to any of the considered variables.

B-0720 14:08

Factors related to bone marrow oedema of accessory navicular bone in the evaluation with MR imaging

M. Tsuchiya, T. Masui, M. Katayama, M. Sasaki, K. Kawamura, Y. Hayashi, T. Yamada, H. Sakahara; *Hamamatsu/JP* (D16018@hama-med.ac.jp)

Purpose: A symptomatic accessory navicular bone was reported to show bone marrow oedema pattern (BMEP) in magnetic resonance imaging (MRI), but the relationship between BMEP and the characteristics of the accessory navicular bone and feet might not be clear. This study examined the relationship between accessory navicular-related BMEP and MRI-based measurements.

Methods and Materials: Patients with accessory navicular bone were enrolled from January 2004 to September 2017, including 20 patients with BMEP (8 females; mean age ± SD, 22.2 ± 15.1 years) and 29 control subjects without BMEP (14 females; mean age ± SD, 32.9 ± 19.6 years). The maximum length of the accessory navicular bone, protrusion percent, and arch height index (AHI), an indicator of flat feet, were obtained from MRI. Two observers independently conducted these measurements. Uni-/multivariate analyses were performed.

Results: Univariate analysis revealed that patients with BMEP showed longer maximum length (p<0.001), higher protrusion percent (p<0.001), and lower AHI (p<0.001) than those without BMEP. Multivariate logistic regression analysis revealed that patients with BMEP were more likely to show larger accessory navicular bones (odds ratio, 1.695; 95% confidence interval [CI]: 1.130, 2.544; p=0.011) and lower AHI (odds ratio, 0.759; 95% CI: 0.619, 0.930; p=0.008) than those without BMEP. The area under the receiver operating characteristic curve was 0.922.

Conclusion: Patients with accessory navicular bone with BMEP have larger accessory navicular bones and are more likely to have flat feet than those without BMEP. This information can be an objective basis for therapeutic strategy.

Author Disclosures:

H. Sakahara: Grant Recipient; Bayer Yakuhin, Ltd, DAICHI SANKYO COMPANY, LIMITED, Eisai Co., Ltd, FUJIFILM RI Pharma Co., Ltd, Nihon Medi-Physics Co., Ltd, KONICA MINOLTA JAPAN. INC, Hamamatsu Photonics k.k..

B-0721 14:16

Detection of kinematic changes induced by sequential lateral ankle ligament section: a dynamic 4D-CT scan study

L. Buzzatti, B. Keelson, J. Apperloo, N. Buls, T. Scheerlinck, G. Van Gompel, J.P. Baeyens, J. De Mey, E. Cattrysse; *Brussels/BE*
(Luca.Buzzatti@vub.ac.be)

Purpose: To investigate the potential of 4D-CT to detect kinematic changes induced by sequential lateral ankle ligament section.

Methods and Materials: The tibia of two fresh frozen specimens were fixed on a custom-made device and the ankle joint was moved at a pace of 25 cycles/minute. The anterior talo-fibular ligament, the calcaneo-fibular ligament and the posterior talo-fibular ligament were cut sequentially. Dynamic-CT scan image datasets of the intact ankle and after each ligament cut were acquired with a 256-slice GE Revolution CT-Scanner (80kV, 25mA, tube rotation time 0.28s, z-axis coverage 120mm, scanning time 3.92s). Rigid registrations of single bones (tibia, talus and calcaneus) were performed and transformation matrixes were derived. Using the global reference frame of the CT (x, y, z), the talo-crural (motion of talus relative to the tibia) and sub-talar (motion of calcaneus relative to the talus) joint kinematics were described as displacement of the centroid of the talus and calcaneus, respectively. Radiation dose was also recorded.

Results: The difference between the displacement of the intact ankle and the cut scenarios was up to 2.90mm, 1.19mm, 1.37mm (sub-talar joint) and up to 2.63mm, 2.58mm, 5.46mm (talo-crural joint) for the x-, y-, z-axes, respectively. Comparing the intact and injured ankle, deflections in the centroid displacement curves occurred at different time points. Each acquisition required a radiation dose (CTDI_{vol}) of 1.9mGy.

Conclusion: The present study showed that low-dose 4D-CT may allow to detect motion changes of the talo-crural and sub-talar joint induced by lateral ankle ligament lesions. This highlights the potential of 4D-CT to investigate dynamic functional joint laxity.

B-0722 14:24

Value of b-mode ultrasonography and real time sonoelastography for detecting injury of the lateral ligaments of the ankle joints

A. Karadavi, T. Ozer, N. Voyvoda, B. Fariz; *Kocaeli/TR*
(aysegulkaradavi@hotmail.com)

Purpose: We aimed to demonstrate the effectiveness of Ultrasound Elastography(USE) in lateral collateral ligament (LCL) injury due to recurrent ankle sprain, to compare with LCL elastography findings of healthy individuals.

Methods and Materials: A total of 108 ankles in 54 patients with a clinical suspicion of ankle ligament injury and total of 60 ankles in 30 healthy volunteers were included. The LCL including ATFL, CFL, PTFL were divided into the following thirds for images evaluation: proximal, middle and distal. Longitudinal images of each tendon were obtained using ultrasonography (US) and USE. Each tendon were evaluated in four grades and measured for length and thickness in US images. USE images were evaluated in four grades for elasticity pattern, strain ratios(SR).

Results: The ATFL lengths were shorter in the patient group than the control group (p<0.05). The grades of ATFL, CFL, PTFL were found to increase in the patient group than the control group based on US findings (p<0.05). The elastogram types of ATFL and CFL were different from the control group (p<0.001). In the patient group, the values of SR and mean SR values for ATFL and CFL were found to be significantly lower than the control group (p<0.001)

Conclusion: US can be used as an effective non-invasive diagnostic method to demonstrate LCL injuries resulting from recurrent sprains of the ankle in active athletes. The USE examination is also a valuable US-based diagnostic method which can show alterations in the ligament structures during recurrent traumas of LCL in the asymptomatic period

B-0724 14:32

Subtalar instability and lateral ankle instability: the difference with emphasis on subtalar ligaments using 3-D isotropic MRI

D. Yoon, S. Moon; *Seoul/KR* (ydy0222@gmail.com)

Purpose: To investigate, using 3-D isotropic MRI, the difference between subtalar instability (STI) and lateral ankle instability (LAI) with emphasis on subtalar ligaments.

Methods and Materials: Preoperative MRIs of 10 patients with STI treated with arthroscopic subtalar reconstruction were compared with MRIs of 23 patients with LAI only. The thickness and width of the anterior capsular ligament (ACL), interosseous talocalcaneal ligament (ITCL), thickness of calcaneofibular ligament (CFL) and anterior talofibular ligament (ATFL) were measured (Mann-Whitney test). Abnormalities in the ACL, ITCL, CFL, ATFL, cervical ligament and inferior extensor retinaculum were analysed by two radiologists.

Results: Patients with STI had a significantly smaller ACL thickness (1.48mm vs 2.12mm in LAI; p=0.012) and smaller ACL width (7.30mm vs 8.64mm in LAI; p=0.007) compared with those with LAI. The ACL thickness of ≤1.8 mm had sensitivity of 80.0% and specificity of 75.0% and the ACL width of ≤8 mm had a sensitivity of 80.0% and a specificity of 85.0% for discriminating STI from LAI. The thickness of ATFL was significantly larger in patients with LAI (p=0.001). Absence or complete tear of ACL was more common in patients with STI (60.0% vs 13.0% in LAI; p=0.010). Complete tear of ATFL was more common in patients with LAI (60.9% vs 10.0% in STI; p=0.008).

Conclusion: Thin or narrow ACL in the tarsal sinus are suggestive of STI rather than LAI. Absence or complete tear of ACL was more common in patients with STI. Complete tear of ATFL is more common in patient with LAI.

B-0725 14:40

Usefulness of T2 mapping sequences for the evaluation of Achilles tendinopathy with 3T MRI

E. Cannizzaro, S. Quarchioni, F. Bruno, C. Gianneramo, S. Mariani, F. Arrigoni, L. Zugaro, A. Barile, C. Masciocchi; *L'Aquila/IT*
(estercannizzaro@hotmail.it)

Purpose: To investigate the capability of T2 mapping sequences on a 3T scanner in evaluating quantitatively Achilles tendon (AT) composition.

Methods and Materials: 13 patients (8 male, 5 female, mean age 34.7 years, range 24-61) with clinical and instrumental evidence of tendinopathy of the AT and 13 healthy volunteers (9 male, 4 female, mean age 36.4 years, range 26-59) were examined on a 3T MR scanner with standard morphological and T2 mapping sequences. The AT was divided into 3 clinically relevant subregions: insertion (INS), midportion (MID) and muscle-tendon junction (MTJ). Regions of interest (ROI) were used for quantitative assessment and mean values of T2 relaxation times were recorded.

Results: In asymptomatic volunteers, we obtained mean T2 values of 42.27ms at the insertional area, 36.24ms in the midportion and 45.91ms at the muscle-tendon junction. In patients with low-grade tendinopathy the mean T2 values were: 45.8 at the MTJ, 54.86 at the MID, 44.90 at the INS, with statistically significant higher values in the midportion compared to the matched healthy controls (p<0.05). In patients with high grade tendinopathy mean T2 values were significantly lower than the control group in all subregions: 25.90 at the MTJ, 16.56 at the MID, 23.85 at the INS (p<0.05).

Conclusion: Our study provides normal T2 values for asymptomatic AT and T2 values changes in degenerated tendons. These reference values can be used for comparison in order to diagnose subtle degeneration and can be a reliable tool to monitor treatment related tendon healing.

B-0726 14:48

Importance of sonoelastographic assessment of ruptured and contralateral achilles tendons - prevention of further injuries

I. Dumic Cule, G. Ivanac, D. Lemac, B. Brkljacic; *Zagreb/HR*
(ivodc1@gmail.com)

Purpose: The concept of assessing the mechanical properties of the Achilles tendon after reconstruction using ultrasound shear wave elastography (SWE) and its positive correlation with standardised questionnaires has been recently introduced in the clinical practice. Since it was demonstrated that about 6% of patients with ruptured Achilles tendon experience the rupture of contralateral tendon in the future, the aim of this study was to estimate the risk for rupture of contralateral tendon in patients who underwent surgical reconstruction of ruptured Achilles tendon by using subjective questionnaires and ultrasound SWE.

Methods and Materials: Twenty-four patients who underwent surgical repair of the ruptured achilles tendon and twelve aged matched healthy controls were examined with ultrasound SWE. Functional outcomes were assessed with American Orthopedic Foot and Ankle Society (AOFAS) scoring system and subjective rating system which we introduced and validated.

Results: The elasticity of injured tendon was markedly decreased (by 42%) compared to contralateral tendon of the patient, as expected. Both AOFAS score and our novel subjective assessment scale positively correlate with ultrasound SWE values in ruptured Achilles tendons. The elasticity of contralateral Achilles tendons in patients is 23% lower than among healthy individuals.

Conclusion: Irrespective of the lack of difference in the subjective feeling assessed by AOFAS, the contralateral tendon in the patients with reconstructed Achilles tendon has significantly lower elasticity than healthy individuals. Therefore, contralateral tendons in patients who suffered from rupture are more prone to future ruptures.

B-0727 14:56

MRI T2 mapping: a sensitive and reliable approach to examine changes in muscle metabolism of extrinsic foot muscles

G. Bratke, S. Willwacher, K. Weiss, D. Maintz, G.-P. Brüggemann; *Cologne/DE (grischa.bratke@uk-koeln.de)*

Purpose: The aim of the study was to examine the sensitivity and reliability of T2 mapping demonstrating changes in metabolism of the extrinsic foot muscles through experimentally varied foot and ankle biomechanics in running.

Methods and Materials: Twelve volunteers completed three 75-min treadmill running sessions at constant speed in a neutral shoe (NS) and two experimental shoes. Experimental shoe 1 (ESm) has posts on the medial aspect of the midsole increasing the stiffness to control the foot eversion and moves the point of ground reaction force application (PFA) medially. Shoe 2 has posts on the lateral border and shifts the PFA laterally. T2 mapping was taken with a Carr-Purcell-Meiboom-Gill-sequence on a 3T Philips Ingenia Scanner before the run, after 2.5, 45 and 75 minutes. ANOVA was applied to identify differences related to the biomechanical intervention and the duration of exercise.

Results: For all muscles, T2 mapping identified a significant increase in T2 times after 2.5 min ($p < 0.001$) and a decrease after 45 and 75 min ($p < 0.001$). ANOVA showed a significant smaller increase in T2 times for the NS compared to ESm in the lateral and medial (MG) head of the gastrocnemius muscle, soleus, extensor digitorum longus and peroneus (e.g. MG: NS +13.17%; ESm +15.27% ($P < 0.001$)).

Conclusion: T2 mapping documents sensitively experimentally induced changes in foot and ankle biomechanics during running and related muscle activation with higher spatial resolution than surface electromyography. The decrease of T2 times might be a correlate of an earlier described intramuscular lactate decrease during prolonged exercise.

Author Disclosures:

K. Weiss: Employee; Philips.

B-0728 15:04

Diabetic foot complicated by osteomyelitis: the role of multiparametric magnetic resonance tomography

M. Zamyshvskaya, V. Zavadovskaia, M. Zorkaltsev, V. Udodov, E. Grigoriev; *Tomsk/RU (Zamyshvskayamari@mail.ru)*

Purpose: To evaluate the possibilities of multiparametric magnetic resonance imaging for the identification of osteomyelitis (OM) in the diabetic foot (DF).

Methods and Materials: 90 patients (51 male (56.7%), 39 female (43.3%); mean age 56.43 ± 13.20) with suspected diabetic foot bone infections were studied. MRI was performed by using the Siemens MAGNETOM Essenza MRI-scanner (1.5T) in the T1, T2, FSat. After native images, MR angiography with contrast enhance was performed (Gadobutrol, 15ml). Delayed post-contrast MR study was performed in T1-SE.

Results: Pyoinflammatory processes in patients with diabetic foot syndrome according to CE MRA were associated not only with accelerated contrast travel time ($26.04 \pm 8.03s$), but in ischemic form of complicated DF - with delayed contrast travel time ($38.20 \pm 6.47s$), other features were early venous visualisation because of arteriovenous shunting, long-time local increase of the contrast accumulation in the area of interest. Osteomyelitis in patients with diabetic foot syndrome characterised by junction ulcer/fistula to the bone with increased marrow signal in T2 and FSat for native MRI followed by the appearance of constant local increased contrast accumulation in the soft tissue area of interest in conjunction with the long-term increase of bone marrow signal for postcontrast MRI.

Conclusion: Multiparametric MRI is informative diagnostic method in diagnostics of osteomyelitis in the diabetic foot, because complex morphofunctional vascular assessment in combination with bone inflammatory process detection should help to decrease amputations and volume of the resected fragment.

B-0729 15:12

T2 mapping of Achilles tendinopathy: our experience using T2 mapping sequences in the diagnosis and evaluation of treatment response after PRP therapy

I. Capretti¹, F. Bruno¹, S. Quarchioni², P. Palumbo¹, S. Mariani¹, F. Arrigoni¹, L. Zugaro¹, A. Barile¹, C. Masciocchi¹; ¹L'Aquila/IT, ²Teramo/IT (ilaria_capretti@hotmail.it)

Purpose: To evaluate the capability of T2 mapping in evaluating semiquantitatively changes in Achilles tendon after PRP treatment.

Methods and Materials: We evaluated 15 patients (10 males and 5 females with mean age of 35.2 years, range 26-51) with Achilles tendinopathy at different degrees (mild-intermediate, 7 patients, group A; moderate-severe 8 patients, group B). All patients were treated with US-guided intratendinous injection of Platelet-Rich Plasma (PRP). They were examined on a 3T MR

scanner with standard morphological and T2 mapping sequences before and after six months from treatment.

Results: In patients with mild-intermediate grade tendinopathy the mean T2 values before treatment were: 46.2 at the muscle-tendon junction(MTJ), 53.70 at the midportion(MID), 42.70 at the insertion(INS), with statistically significant higher values in the midportion compared to the matched healthy controls ($p < 0.05$). After six months to treatment with PRP they showed an improvement of T2 values in midportions similar to normal values (36,24 ms). In patients with moderate-severe grade tendinopathy mean T2 values were significantly lower than the control group in all subregions: 23.94 at the MTJ, 15.10 at the MID, 20.50 at the INS ($p < 0.05$) and after six months they didn't show significant variations of T2 values.

Conclusion: According to our preliminary results, T2 mapping shows an high capability to assess and follow-up Achilles tendon pathologies together with other standard morphologic sequences and is usefulness in predict Achilles tendon changes after PRP therapy.

14:00 - 15:30

Room G

Physics in Medical Imaging

SS 713

Quantitative imaging and neural networks

Moderators:

C. Cavedon; Verona/IT
M.J. Willeminck; Stanford, CA/US

B-0730 14:00

Automatic computation of liver and lung perfusion parameters through the analysis of CT image sequences

S. Malavasi¹, G. Gavelli², V. Vilgrain³, A. Bevilacqua¹; ¹Bologna/IT, ²Meldola/IT, ³Clichy/FR (s.malavasi@unibo.it)

Purpose: The goal of this PhD thesis work is contributing to advance Computed Tomography perfusion (CTp) towards standardization by improving the accuracy of perfusion results(1), the clinical relevance of studies where global perfusion parameters are commonly utilised(2) and the reproducibility of results in multicentre studies(3).

Methods and Materials: 315 liver CTp examinations from 14 Centres and 34 lung CTp studies were considered. First, through a voxel-based analysis of the time-concentration curves, an error index capable to *measure* the quality of perfusion results was set up and validated. Thereafter, an adaptive algorithm exploiting that error index was developed to automatically detect on CTp maps misleading perfusion values (1). Then, a measure of tumour functional heterogeneity was conceived(2). Finally, data pertaining to a large multicentre study on liver CTp (PIXEL) were analysed to also investigate the effects of the sources of protocol heterogeneity(3).

Results: The algorithm developed was correctly able to identify and exclude from the analysis vessels, bronchi, and artefacts, allowing to improve perfusion results reliability(1). Global values cannot take into account haemodynamic heterogeneity proving to even mislead clinical considerations(2). Tentative guidelines were provided to help planning protocols(3).

Conclusion: Reliability of results improved by detecting and removing unreliable CTp values. A measure of functional heterogeneity must be provided together with mean perfusion values to improve the clinical representativeness of the studies. In conclusion, the automatic methods implemented and the tentative guidelines for multicentre studies represent a clear step forwards to CTp translation in the standard clinic.

B-0731 14:08

Use of calcium chloride as a calibration phantom material to aid identification of clinically significant compounds with spectral CT

T.E. Kirkbride, N. Anderson, A.Y. Raja; *Christchurch/NZ (tracy.kirkbride@ara.ac.nz)*

Purpose: Material identification using spectral CT relies on scanning known concentrations of compounds of interest to enable calibration of the material decomposition software for spectral photon-counting CT (SPCCT). Clinically significant compounds, such as calcium hydroxyapatite (HAP), do not dissolve well and preparation requires creating a suspension, which may not be spatially stable. We show that calcium chloride can be used as a substitute for such compounds during this procedure, by comparing these solutions with commercial solid HAP rods, the advantage of the rods being the stable and uniform distribution of HAP.

Methods and Materials: A range of serially diluted concentrations of calcium chloride and commercially available solid inserts of HAP, with CT water as base material, were used. High-resolution images of the samples were generated using a preclinical MARS SPCCT scanner equipped with the Medipix3RX photon processing detector bonded to cadmium-zinc-telluride.

Images of the calibration phantom were obtained using energy thresholds 20, 30, 40 and 50 keV at 80 kVp. Theoretical attenuation coefficients of HAP and calcium chloride were used to determine the effective HAP concentration of the calcium chloride samples. This information, along with the MARS SPCCT signals from the calcium chloride, was used to calibrate the system.

Results: Concentrations of calcium chloride whose attenuation profile matches that of HAP have been determined. MARS SPCCT data from HAP rods shows calcium chloride can be used to substitute HAP.

Conclusion: Substitution of soluble compounds for insoluble compounds within a calibration phantom for spectral CT is possible, potentially improving material identification.

Author Disclosures:

N. Anderson: Research/Grant Support; Supported in part by project grant PROJ-13860-NMTS-UOC from the New Zealand Foundation for Research, Science, and Technology.. Shareholder; N. G. Anderson holds shares of MARS Bioimaging Ltd. **A.Y. Raja:** Research/Grant Support; Supported in part by project grant PROJ-13860-NMTS-UOC from the New Zealand Foundation for Research, Science, and Technology..

B-0732 14:16

The effect of motion blur and noise on the precision and accuracy of wrist joint kinematics detection from 4D-CT scans

G.J. [Streekstra](mailto:g.j.streekstra@amc.uva.nl), M. de Roo, S.D. Strackee, I. Dobbe; *Amsterdam/NL (g.j.streekstra@amc.uva.nl)*

Purpose: Recent developments in 4D CT acquisition techniques enable detection of kinematics of carpal bones in the wrist joint. Detection of carpal kinematics requires the patient to move the wrist, while multiple 3D CT scans are acquired. If the wrist motion is too fast, time frames in the 4D image sequence will become blurry and therefore, may become unusable for kinematics detection. We investigated the impact of motion blur and noise on kinematics estimates from 4D-CT images.

Methods and Materials: 4D CT images were acquired of a phantom representing a wrist joint, while moving with known rotational speed. For this purpose we used a dedicated 4D scan protocol on a regular Philips Brilliance 64 slice CT scanner. The wrist phantom was created by segmenting a wrists' anatomy from a CT-scan and subsequent 3D printing by additive manufacturing. Joint kinematics was estimated by 4D image analysis methods involving segmentation of wrist bones from a static CT scan and image registration of the segmented bones to the time frames in the 4D scan.

Results: The experiments reveal that, within a physiological range of carpal bone velocities, the accuracy of joint kinematics estimation are in the order of 1 degree for rotational and 0.2 mm for translational parameters. Systematic errors in kinematical parameters increase slightly with rotational speed.

Conclusion: The limited influence of wrist joint motion on kinematic parameters ensures sufficiently accurate estimation of carpal bone kinematics with regular 64 slice 4D CT scanners in patients.

B-0733 14:24

Context-sensitive organ-specific evaluation and analysis of dual-energy computed tomography (DECT)

S. Dorn¹, S. Chen², F. Pisana¹, M. Özdemir¹, J. Maier¹, S. Sawall¹, M. Knaup¹, A. Maier², M. Lell², M. [Kachelrieß](mailto:marc.kachelrieß@dkfz.de)¹; ¹Heidelberg/DE, ²Erlangen/DE, ³Nürnberg/DE (marc.kachelriess@dkfz.de)

Purpose: To combine various organ-dependent dual energy evaluation methods into an automatic and standardized analysis tool to facilitate radiologists' workflow.

Methods and Materials: There are many commercial DECT applications, which provide a multitude of information about the tissue type, material composition or function. However, all applications automatically process the entire dataset and the user needs to invoke each one separately. The proposed method automates and standardizes the DE applications using prior anatomical information. By means of a 3D convolutional neural network, the DECT data are classified into different organs. The ROIs that are required for patient-specific calibration of the algorithms can now be placed automatically into the corresponding anatomical structures and the applications are automatically selected and only applied to the specific organs. This context-sensitive analysis allows to simultaneously evaluate multiple organs and to show organ-specific dual energy overlays wherever appropriate.

Results: Ten contrast-enhanced DECT patient datasets are processed. The data are acquired with a dual source CT system. We are able to automate and standardize the spectral analysis of the DE data using prior anatomical information. Each tissue type is evaluated with its corresponding DE application simultaneously. The results are identical with those obtained by a user who manually calibrated, selected and applied the applications to various organs.

Conclusion: The proposed method is an important step towards the presentation of evermore increasingly complex information in spectral CT and

towards improving the radiologists' workflow significantly. The method can readily be generalized to the automatic evaluation of multi energy CT data.

B-0734 14:32

Deep convolutional neural network (D-CNN) for efficient and automatic lung cancer detection

I. Shiri, P. Geramifar, A. Bitarafan-Rajabi, A. Mohammadzadeh, H. Pouraliakbar; *Tehran/IR (Isaac.sh92@gmail.com)*

Purpose: Lung cancer is one of the most widely cause of cancer death in the world. One of the most challenging task is the early detection of lung cancer in full 3D CT-Scans. In this study we present a deep learning framework for efficient and fully automated lung cancer detection in 3D CT-Scan images.

Methods and Materials: 750 CT scan of patients (430 non-cancers and 320 cancerous) from KDSB17 were used in this study. Image preprocessing such as variance reduction image re-sampling to an isomorphic resolution, Lung segmentation, Normalization, and Zero centering in order to reduce the problem of space were performed. The 3D Convolution layers perform 3x3x3 convolutions with stride 1x1x1 and no padding, and of 3D Pool layers perform with 2x2x2 max pooling with stride 2x2x2 (and no padding). ReLU function was used as activation functions, and soft-max layer was applied for binary classification of cancerous and noncancerous patient.

Results: The 3D deep convolutional neural network were performed on different iterations and epochs and the best accuracy of D-CNN was reached to 69.7 percent.

Conclusion: Accuracy of model was acceptable at CAD study, however the radiologist needs more detailed information than just one single series of CT scan for diagnosis (e.g., time series of CT scan over a few month, biopsy information, and metabolic imaging). Deep learning model need to use more data-set and also more information than just one single series of CT scan to improve its performance and reaching human observer level.

B-0735 14:40

A noise-robust and accurate measurement method for the wall thickness of small airways in low-dose CT scans

Z. [Yang](mailto:yangzepa@snu.ac.kr)¹, H. Jin¹, J. Kim^{1,2}; ¹Suwon/KR, ²Seoul/KR (yangzepa@snu.ac.kr)

Purpose: Small airway dimensions are important biomarkers for evaluation of pulmonary diseases, such as asthma, COPD, etc. We present a novel method, attenuation profile matching (APM) technique, which provides accurate determination of small airway dimension as well as robustness to CT scan parameters.

Methods and Materials: The point spread functions of a CT were acquired and employed for generating synthetic attenuation profiles of an airway by taking convolution with the numerical airway models of varying wall thickness. Dimensions of a given airway were determined as those of the numerical model yielding minimum error between the measured and synthetic attenuation profiles across the airway.

Results: In a phantom study with airway tubes, proposed method was shown to be highly accurate in determining airway dimension. The measurement error for the 0.6 mm thick tube with 3 mm diameter was as small as 0.02 mm (3.3%) in wall thickness and 0.17 mm (5.6%) in lumen diameter. And for the wall thickness, error for the smallest (0.6 mm thick) tube was 0.02 mm (3.3%). In a pilot patient study, the proposed method could distinguish the airway thickness of COPD cases (1.16 ± 0.23 mm) from that of normal subjects (0.6 ± 0.18 mm) while the measurements with FWHM substantially overlapped (1.45 ± 0.32 mm vs. 1.28 ± 0.30 mm) and thus hardly be distinguished each other.

Conclusion: Our proposed APM technique has a potential to overcome the resolution limitations of current CT systems and determine the small airway dimensions of COPD patients accurately.

B-0736 14:48

Real-time x-ray scatter estimation for CT and CBCT using a deep convolutional neural network

J. Maier, S. Sawall, M. [Kachelrieß](mailto:marc.kachelrieß@dkfz.de); *Heidelberg/DE (marc.kachelriess@dkfz.de)*

Purpose: Scatter correction is crucial to maintain the diagnostic value and to obtain quantitative images in CT and CBCT. Current scatter correction approaches are either too inaccurate or too slow. Therefore, we developed the deep scatter estimation (DSE) algorithm: a deep convolutional neural network to derive accurate scatter estimates in real-time.

Methods and Materials: The gold standard of scatter correction is to subtract a scatter estimate derived by a Monte Carlo (MC) photon transport code. However, being computationally expensive, MC simulations cannot be used routinely. To combine high accuracy and real-time applicability, DSE uses a modified U-net that is trained to reproduce the outcome of MC simulations based on the acquired projection data. This study demonstrates the potential of DSE using simulations and measurements of an experimental CBCT system. Two conventional computationally efficient scatter estimation approaches were implemented as reference: A kernel based scatter estimation (KSE) and the hybrid scatter estimation (HSE).

Results: The mean absolute error (MAE) between MC and KSE, HSE and DSE was used as a performance measure. Considering the simulated data, we observe a MAE of 14.1 % (KSE), 7.2 % (HSE) and 1.1 % (DSE). Similar results are obtained for measured data with a MEA of 16.7 % (KSE), 7.8 % (HSE) and 2.8 % (DSE).

Conclusion: DSE clearly outperforms conventional scatter estimation approaches in terms of accuracy while requiring similar processing time. DSE performs nearly as accurate as Monte Carlo simulations but is superior in terms of speed by orders of magnitude.

B-0737 14:56

An innovative MRI harmonization method for multicentre radiomic analysis in glioblastoma

S. Reuzé¹, A.-S. Dirand¹, R. Sun¹, F. Orlhac², G. Louvel¹, S. Ammari¹, E. Deutsch¹, c. robert¹; ¹Villejuif/FR, ²Orsay/FR (sylvain.reuze@gustaveroussy.fr)

Purpose: MR-based radiomic features show a great correlation with tumour heterogeneity and treatment outcome, but also a strong dependence on acquisition parameters.

Methods and Materials: 190 glioblastoma patients with multicentre T1-Gd MRI were retrospectively included. Two spheres were delineated in the white matter (WM). Tumour (GTV) was manually segmented. Post-processing was performed as follows: an intensity rescaling to [0–32767] to erase inter-patient differences in intensity range, then a resampling on a 0.5x0.5x0.5mm³ grid. 39 radiomic features were extracted using LIFEx freeware. Wilcoxon analysis was performed between sets of feature values in WM to assess the robustness of features among different scanners. Different methods of discretization were investigated in GTV: relative (RD) or absolute (AD) with 32–256 levels. Spearman correlation coefficients ρ were computed in GTV between all features, and between each feature and tumour volume.

Results: Histogram characteristics extracted from WM highlighted a large scanner dependence ($p < 0.05$). RD (32 or 64 bins) limited this dependence for textural features. Only two histogram features were robust among all devices, whereas 7 histogram and 7 textural features were robust depending on magnetic field strength ($p > 0.05$). After postprocessing, RD highlighted correlations between features and tumour volume ($|\rho| > 0.5$, 8 features). AD decreased these correlations and reduced the dependence of features between devices. For 25 couples of devices, there were at least 25 robust features, and 11 textural features were robust among magnetic field strength ($p > 0.05$).

Conclusion: We proposed a simple and innovative MRI harmonization method which showed promising results on a large multicentre cohort.

B-0738 15:04

ROI-based phase analysis for neuronal current MRI

T. Yoneda, M. Iwata, H. Indo, N. Kurehana, S. Yoshinaga, M. Takeda, H. Terasawa; Kumamoto/JP (tyoneda@kumamoto-u.ac.jp)

Purpose: Functional MRI (fMRI) using BOLD effect is noninvasive tool for study of neuro activation in various areas. In this twenty years, alternative principle of BOLD was suggested so called Neuronal Current MRI (ncMRI). The ncMRI is designed so as to directly detect neuronal current on MRI. This study suggested an ROI-based analysis approach to sensitively detect neuronal current via MR-phase information.

Methods and Materials: We prepared axon imitated phantom in which cellophane tube with 1 mm diameter as axon was located. Potassium and Sodium were doped in the 20 %w gelatin and it was filled in the phantom to realise source of neuronal current. The neuronal current (5 uA) was induced by alternative voltage with 40 Hz. MRI scan were carried out on 7T-MRI (BioSpec 20/70 USR, Bruker BioSpin, Germany) with FLASH sequence with solenoid transmit-receiver coil. All MR-images were acquired a plane perpendicular to long axis of axon. Phase image was derived in DICOM format and unwrapped by high-pass filter to remove unwanted phase bias. Phase around the axon was measured by setting circular ring ROI and phase signal was statistically evaluated by student's-t test between current on and off.

Results: Statistics showed significant difference ($p < 0.05$) when the charge carried by current during scan was larger than 100 nC, but no significant difference less than 50 nC.

Conclusion: The ncMRI with phase information could detect very small but biologically reasonable current. Our study showed limit of sensitivity depended on total charge during scan.

B-0739 15:12

MRI delta-radiomics feature robustness and reproducibility: the impact of image registration and day-to-day repeat-ability in GBM cancer patient

I. Shiri, G. Hajianfar, H. Abdollahi, S. Shayesteh, h. pouraliakbar, A. Bitarafan-Rajabi, A. Mohammadzadeh, P. Geramifar; Tehran/IR (Isaac.sh92@gmail.com)

Purpose: Delta-radiomics features can be used as prognostic models during therapy courses and time series data analysis. As the image registration is one of the main process in time series and multi-modality image analysis, the purpose of this study is investigate the impact of image registration on delta radiomics features.

Methods and Materials: Ten patients' data with recurrent GBM who underwent brain MRI were used in this study. T2w, T1w Images were registered by different methods including, Full affine (12 DOF), Full scale (9 DOF), Global scale (7 DOF) and Rigid body (6 DOF). Following image registration, GBM lesions were segmented and delineated using semi-automatic 3D region growing algorithms. 94 quantitative 3D features were extracted from each lesion, corresponding to size, shape, Intensity histogram and textural feature. All radiomics features were categorised into 3 groups based on coefficient of variation (COV) including a small (COV $\leq 10\%$), intermediate (10 % < COV $\leq 25\%$) and large (COV $> 25\%$) range of variation with respect to the mean.

Results: All shape features such as compactness, elongation and spherical disproportion and 71 (73%) features have good reproducibility. Eleven intermediate reproducibility and 14 remain features including difference entropy, entropy, difference variance, cluster shade, cluster prominence, inverse variance from GLCM and GLV from GLRLM, and Entropy from intensity have low reproducibility.

Conclusion: Delta-radiomics feature robustness and reproducibility in brain MRI due to image registration is feature-dependent. Delta-radiomics features with low COV are better candidates for robust tumour quantification in time series data analysis and clinical practice.

B-0740 15:20

Wavelet-based radiomics texture features stability in MRI of GBM patients: a test-retest study

I. Shiri, G. Hajianfar, S. Shayesteh, H. Abdollahi, H.R. Pouraliakbar, A. Bitarafan-Rajabi, A. Mohammadzadeh, P. Geramifar, A. Sanaat; Tehran/IR (amir.sanaat@gmail.com)

Purpose: Radiomics texture features have been recently introduced as quantitative image bio-markers which can be used potentially for diagnosis, prognosis and prediction of response to therapy in cancer patient. One of major challenges in this era is validity of this quantitative parameters. The main aim of current study was to evaluate stability of radiomics features in test retest study.

Methods and Materials: Fifteen patients with recurrent GBM who underwent repeated MR imaging with approximately two day interval were included to current study. All lesions were segmented to whole tumor, necrosis area and active tumor area. Following wavelet decompositions of image, eight images were derived. Following segmentation and decompositions of images, 632 quantitative 3D textures based on GLRLM, GLCM and GLSZM, were extracted from the 3D-tumor volumes of each segmentation. For every radiomics feature, test-retest was assessed with the intra-class correlation coefficient (ICC) and the concordance correlation coefficient (CCC) and finally the most reproducible and robust radiomics features were selected.

Results: 455 texture feature (71%) such as GLNUN from HHH_glrml and Entropy from HHH_glcm had good reproducibility. 114 texture features (18%) had intermediate reproducibility and remain (11%) such as Autocorrelation from LLH_glcm, from LLH_glszm and Cluster Shade from LLL_glcm.

Conclusion: Test-retest and correlation analyses have identified redundant radiomics wavelet based textures which would be prone to errors if they employed as quantitative biomarker for GBM image analysis. Using reproducible texture warranted more advanced applications of this quantitative parameters as being used for treatment monitoring, outcome prediction or imaging biomarkers.

14:00 - 15:30

Room K

Radiographers

SS 714

Optimising radiographic practice

Moderators:

M. O'Connor; Dublin/IE
S. Savolainen; Helsinki/FI

B-0741 14:00

Relationships between image quality and radiation dose during paediatric pelvis radiography: a factorial phantom study

A.H. Mohammed Ali¹, P.H. Hogg¹, A. England², ¹Salford/UK, ²Manchester/UK
(p.hogg@salford.ac.uk)

Purpose: Paediatric pelvic radiography exposure factor selection is difficult due to age/size variations; this study evaluates image quality and dose for a range of acquisition parameters.

Methods and Materials: 2,016 DR images were acquired using a 5-year-old pelvis phantom. Acquisition parameters included: KVP (56-89, 3 kVp increments), mAs (1-16, 1 or 2 mAs increments), SID (100, 115, 130 and 145 cm) and filtration (0, 2 mm Al and 1mm Al + 0.1 mm Cu). Image quality (IQ) was assessed using physical and visual methods. Physical included SNR and CNR. Visual involved observers scoring sharpness and noise. Entrance surface dose was measured. Regression and main effect plots were conducted.

Results: Adjusted (R^2) was 0.76 for radiation dose; range = 0.31-0.78 for IQ. Increasing additional filtration had the greatest impact decreasing IQ (physical β =-6.72 and visual β =-1.13) and radiation dose (β =-50.0). mAs increased radiation dose (β =17.32) and IQ (physical β =0.63, visual β =17.32). Elevating KVP increases radiation dose (β =4.92); initially it increases IQ, then it reduces (physical β =-0.15, visual β =0.49). As SID increases dose reduces (β =-2.60) and IQ remained unchanged (physical β =-0.80, visual β =-0.09). Main effect plots for each exposure parameter showed different relationships when compared to others: either linear, or non-linear, with plateauing. SID=115cm produced the highest levels of image sharpness.

Conclusion: Paediatric optimisation studies should consider a full factorial design to identify the impact of all acquisition parameters. Increasing KVP whilst reducing mAs produces lower dose and maintains IQ, but only for specific levels of filtration and SID.

B-0742 14:08

PA vs AP positioning in digital radiography of lumbar spine: the impact of kVp in large-sized patient image quality

E.Y. Boateng^{1,2}, H.K. Shariati¹, R.K. Sharma², A. Sanderud², ¹Kongsvinger/NO, ²Oslo/NO (emmboa@ous-hf.no)

Purpose: Investigate differences in lumbar spine radiography when changing from AP to PA projection and impact of a large patient size and kVp.

Methods and Materials: The radiography was performed at a Canon Triathlon T3 with CXDI 401C detector using AEC with 100mAs cut-off, 50-100kVp to image a RS-113 pelvis phantom. Without modifications, the phantom had a 32-inch waistline. By adding 4 kg ox fat at the stomach region, and 1 kg on the back and buttock of the phantom, a large patient with a 44-inch waistline was simulated. With 10 observers, an absolute visual grading analysis (VGA) study using a 5-point Likert scale was performed to assess the images in sharpness, noise, and overall diagnostic quality. Effective dose was calculated using PCXMC.

Results: The VGA-study showed no significant difference between the image quality in AP and PA ($p = 0.084$). The best average VGA scores, AP=4.6 and PA=4.4, were at 70 kVp for the standard-sized images while effective dose was calculated to be reduced by 64% when changing from AP to PA projection. With the large-sized phantom the 80kVp had the best VGA scores, AP=3.8 and PA=3.7, and effective dose was reduced 44% in the PA projection. The PA projection magnification of the spine give a slight reduction in sharpness.

Conclusion: The result of the study shows that PA projection provides a lower effective dose to the patient compared with AP projection with no significant reduction in visible image quality. This is seen in both standard- and large-sized patient.

B-0743 14:16

Indexing DICOM metadata from medical imaging repositories: opportunities and challenges

M. Rodrigues dos Santos; Aveiro/PT (mrs@ua.pt)

Purpose: DICOM metadata, stored in medical image repositories, can be a very valuable source of information for the professional practice characterization. The enormous amount of data, as well as the diversity of

informational environments, can make very problematic the DICOM metadata access and usage. It is therefore very relevant to identify the potentialities associated with indexing DICOM metadata as well as the main challenges that arise from the acquisition and management of huge volumes of data.

Methods and Materials: A meta-analysis was performed on the results of works supported in the indexing of DICOM metadata from different hospitals PACS archives using the Dicoole application as a DICOM metadata indexing tool.

Results: Work supported by the indexation of metadata from several PACS of 7 health units was analyzed. The volume of data analyzed ranged from 85757 to 36562284 images, corresponding for the latter to more than 1324000 imaging studies performed on more than 438000 patients. The articles analyzed revealed the potential for the use of DICOM metadata, but also challenges associated with indexing and managing large volumes of metadata, namely the identification of medical imaging stakeholders, computational needs and information management, the quality of DICOM metadata, the analysis of individual and population exposure and the use of human and material resources.

Conclusion: It is possible to aggregate and consolidate huge amounts of DICOM metadata as a means to characterize professional practice. However, the success of its use depends on access and information management strategies as well as of the metadata quality.

B-0744 14:24

Patient radiation dose and fluoroscopy time during ERCP: a single-centre retrospective study of influencing factors

E. Saukko¹, J.M. Grönroos^{1,1}, P. Salminen^{1,1}, A. Henner², M.T. Nieminen^{2,2}, ¹Turku/FI, ²Oulu/FI (ekaterina.saukko@tyks.fi)

Purpose: The number and complexity with associated increased technical difficulty of therapeutic ERCP procedures have significantly increased resulting in longer procedural and fluoroscopy times. During ERCP, the patient is exposed to ionizing radiation and the consequent radiation dose depends on multiple factors. The aim of this study was to identify factors affecting fluoroscopy time and radiation dose in patients undergoing ERCP.

Methods and Materials: Data related to patient demographics, procedural characteristics and radiation exposure in ERCP procedures (n=638) performed between August 2013 and August 2015 were retrospectively reviewed and analysed. Statistically significant factors identified by univariate analyses were included in multivariate analysis with fluoroscopy time (FT) and dose area product (DAP) as dependent variables. Effective dose (ED) was estimated from DAP using conversion coefficient.

Results: The factors independently associated with increased DAP during ERCP were age, gender, radiographer, complexity level of ERCP, cannulation difficulty grade, bile duct injury and biliary stent placement. In multivariate analysis, the endoscopist, the complexity level of ERCP, cannulation difficulty grade, pancreatic duct leakage, bile duct dilatation and brushing were identified as predictors for a longer FT. The mean DAP, FT, number of acquired images and ED for all ERCP procedures were 2.33 Gy·cm², 1.84 min, 3 and 0.61 mSv, respectively.

Conclusion: Multiple factors had an effect on DAP and FT in ERCP. The awareness of these factors may help to predict possible prolonged procedures causing a higher radiation dose to the patient and thus facilitate the use of appropriate precautions.

Author Disclosures:

P. Salminen: Speaker; Lecture fees from Merck and Lilly.

B-0745 14:32

Dose reduction with PA projection in lumbar spine radiography

E. Alukic, D. Škrk, N. Mekis; Ljubljana/SI

Purpose: The aim of the research was to determine the effect on radiation dose to the patient in lumbar spine radiography when using the PA projection instead of the conventional AP projection and how does that effect the image quality.

Methods and Materials: The research was conducted both, on an anthropomorphic phantom and on 100 patients, randomly divided into two equal groups of 50. In the first group the lumbar spine imaging was conducted in the AP projection, whereas in the second group the imaging was conducted in the PA projection. The dose was measured with dose area product (DAP) meter. The level of tissue displacement and patient height and weight was measured and image size was obtained. The image quality assessment was performed by three experienced radiologists with the use of ViewDEX imaging software and the effective dose was calculated using PCXMC2.0. Prior to the study the National medical ethic committee approval was obtained.

Results: When using PA projection, the average thickness of abdomen was reduced by 2.4 cm ($p < 10^{-3}$) in the PA projection, as did DAP by 16.3 μ Gy m² ($p = 0.009$) and the effective dose by 0.09 mSv ($p < 10^{-3}$). We did not find any significant difference in image quality between AP and PA projection of lumbar spine radiography ($p = 0.690$).

Conclusion: The results showed that the use of PA projection of lumbar spine reduces DAP (26.7 %) and effective dose (53.3 %) while preserving the image quality.

B-0746 14:40

Construction of obese phantoms for dose optimisation and image quality purposes

S.J.M. [Alqahtani](#)^{1,2}, K. Knapp¹, R.M. Palfrey¹, J.R. Meakin¹; ¹Exeter/UK, ²Najran/SA (salbeshri@hotmail.com)

Purpose: To build obese phantoms that can be used in dose optimisation and image quality research.

Methods and Materials: Two sets of urethane based materials, along with other additives, priorly verified to be identical to fat and lean in terms of density, Hounsfield unit (HU) and linear attenuation coefficient, were used. Moulds were constructed using polystyrene design based on a 3D scan of a KYOTO phantom (PBU-50). The fat and lean mass in the abdominal region was calculated from DXA scans of 264 healthy female subjects. Two BMI groups, 38 and 46 kg/m², were constructed and tested for HU across different regions.

Results: The constructed phantom consisted of two layers of fat tissue-equivalent substitutes (FTES) which encircled the abdominal region of the KYOTO phantom anteriorly and posteriorly each weighed 9.3 kg. Additionally, two thin layers of lean tissue-equivalent substitutes (LTES), each 1.9 kg, were added anteriorly and posteriorly to the previous FTES layers. This represented a BMI group of 38 kg/cm². Another two layers of FTES, total weight of 7.5 kg, along with two LTES layers, total weight 3.9kg, represent a 46 kg/m² BMI group. Across 4 levels of kVp (70,80,100 and 120 kVp) the HU for FTES was -77.87 ± -16.7, in 9 different regions for each slab, while for the LTES, the HU was 23.25 ± 7.14, in 3 different regions for each slab.

Conclusion: Two obese phantoms were constructed. When used along with the KOYOTO phantom, dose optimisation work and image quality assessment can be conducted.

B-0747 14:48

Personalised patient protocol for radiostereometric analysis

O. [Muharemovic](#), A. Troelsen, M.G. Thomsen, T. Kallemsø, K.K. Gosvig; [Hvidovre/DK \(omarradiograf@hotmail.com\)](mailto:Hvidovre/DK (omarradiograf@hotmail.com))

Purpose: Increasing pressure in the clinic requires a more standardised approach to radiostereometric analysis (RSA) imaging. The aim of this study was to investigate whether implementation of personalised RSA patient protocols could increase image quality and decrease examination time and the number of exposure repetitions.

Methods and Materials: Forty patients undergoing primary total hip arthroplasty (THA) were equally randomised to either a case or a control group. Radiographers in the case group were assisted by personalised patient protocols containing information about each patient's post-operative RSA X-ray. Radiographers in the control group used a standard RSA protocol.

Results: At 3 months, radiographers in the case group significantly reduced (p<0.001) the number of exposures (NE) by 1.6, examination time (ET) with 19.2 minutes, and distance between centrum of prosthesis (CP) and centrum of calibration field (CCF) with 34.1 mm when compared to post-operative (baseline) results. At 12 months, the case group significantly reduced (p<0.001) NE by 2.0, ET with 22.5 minutes, and CP to CCF distance with 43.1 mm when compared to baseline results. No significant improvements were found in the control group at any time point.

Conclusion: There is strong evidence that personalised RSA patient protocols have a positive effect on image quality and radiation dose savings. Implementation of personal patient protocols as a RSA standard will contribute to the reduction of examination time, thus ensuring a cost-benefit for department and patient safety.

B-0748 14:56

Large-sized patient chest radiography: a relative visual grading analysis study

F.P. Soares¹, E. Aymon², A.M. Burke³, S. Dijkstra⁴, J. Fosshaug⁵, S.N. [Sanders](#)⁶, A.F.N. Silva⁶, A. Sanderud⁵; ¹Florianopolis/BR, ²Lausanne/CH, ³Dublin/IE, ⁴Groningen/NL, ⁵Oslo/NO, ⁶Lisbon/PT (s.n.sanders@st.hanze.nl)

Purpose: To investigate the impact of different kVp and mAs values on image quality and effective dose in large-sized patient chest radiography.

Methods and Materials: A chest phantom (Kyoto) with simulated lesions and additional 30mm plates to simulate a large-size patient was imaged at various kept and mass values using a Canon CXDI digital detector. With 20 observers, a relative visual grading analysis (VGA) study was performed to assess image quality and nodule visibility in five chest radiographs asking worse, equal or better on eight image criteria adapted from the EU guidelines. The VGA study reference image was of the phantom at standard size without the chest plates using 125kVp, 2.4mAs by AEC and 24µSv. Effective dose was calculated using PCXMC. VGA scores were compared against signal-to-noise ratio (SNR) and contrast-to-noise ratio (CNR).

Results: An image obtained with 125kVp/4.0mAs/43µSv had the highest SNR, and the 125kVp/2.0mAs/21µSv had the highest CNR. In the VGA study, the 125kVp/4.0mAs/43µSv was seen as the most optimal image with 51% of scores from the observers being equal or better than the reference image. The image using AEC 125kVp/6.88mAs/74µSv was given the lowest score in VGA study with 23% score of equal or better. The scores with different kVp, 117kVp/2.5mAs/22µSv and 133kVp/2.5mAs/31µSv were 41% and 34%.

Conclusion: It is possible to get higher SNR, CNR and VGA scores in large-sized patient chest radiography at lower mAs than that given using standard AEC, due to post-processing. Changing the kVp did not improve the image quality.

B-0749 15:04

Radiation dose reduction on thyroid in mammography

D.C. Entradas, S. Rodrigues, R.P.P. Almeida, L.P. Ribeiro, A.F. Abrantes, M.V.C. [Reis](#); [Faro/PT \(monica14@live.com.pt\)](mailto:Faro/PT (monica14@live.com.pt))

Purpose: To evaluate the entrance skin dose reduction in the thyroid using radiation protection in mammography exams.

Methods and Materials: In this experimental research, two anthropomorphic phantoms (full body and breast phantoms) were placed in the mammography equipment according with the standard positioning criteria. Optically stimulated luminescence (OSL) dosimeters were placed over the phantom thyroid region and a total of 40 radiation exposures were made for entrance skin dose measurements. The measurements were made on both standard projections for the breast study (cranio-caudal and medio-lateral oblique) with and without the use of the thyroid lead protection (0.5 mm).

Results: The entrance skin dose received by the thyroid was superior in medio-lateral oblique projection (44 µGy) compared to the cranio-caudal projection (36 µGy) without lead protection. With the lead protection there is a dose reduction of 83.3 % in the cranio-caudal projection (6 µGy) and 93.2% in the medio-lateral oblique projection (3 µGy). Therefore, in the mammography examination (total of four projections), the use of the lead protection reduces the entrance skin dose on thyroid by 89%.

Conclusion: The use of thyroid lead protection is highly recommended since it can reduce the radiation dose in this radiosensitive organ during mammography exams, attending the ALARA principle. However, we should also consider that the use of the shield might provide artefacts, making difficult the correct analysis of the breast tissue and leading to the examination repetition increasing the dose received in the mammary gland, as well as the other organs.

B-0750 15:12

Correlation measurements between positron emission tomography 18F-FDG dose and external exposure

Ž.R. [Janulcikas](#); Vilnius/LT

Purpose: To evaluate correlation between administered ¹⁸F - FDG dose and measured patient's emitted external exposure at different time.

Methods and Materials: In this study was analysed data of 101 adult patients: weight, administered ¹⁸F - FDG dose, external exposure. Patient's emitted external exposure was measured at distance of 0,3 m and 1 m, also at different time. Pearson correlation coefficient was used to determine correlation strength.

Results: 101 Patient's weight was from 42 kg to 109 kg and injected ¹⁸F - FDG was from 290 MBq to 438 MBq. Correlation between weight and dose was strong (r = 0,88) and statistically significant (p<0,00). Unfortunately, it is estimated that the correlation between the injected ¹⁸F - FDG dose and external exposure (immediately after the injection) is very weak (r = 0,17) and statistically insignificant (p = 0,07) Also, correlation between the administered dose and the emitted external exposure before patients being released to home is very weak (r = 0,03) and statistically insignificant (p=0,731), and more weaker than correlation immediately after injection.

Conclusion: Correlation between injected ¹⁸F - FDG dose and external exposure is estimated to be very weak and statistically insignificant. Radiation safety specialists and nuclear medicine radiographers should always gather external exposure data from patient at exactly same distance and body part. To testify this study results, there should be more further tests and data.

B-0751 15:20

Fabrication of fat tissue-equivalent substitutes (FTES) and lean tissue-equivalent substitute (LTES) to underpin obese phantom construction

S.J.M. [Alqahtani](#)^{1,2}, K. Knapp¹, R.M. Palfrey¹, J.R. Meakin¹; ¹Exeter/UK, ²Najran/SA (salbeshri@hotmail.com)

Purpose: The literature reports high doses delivered to obese patients in projection radiography. This suggests more dose optimisation work is required for this group of patients. However, to date, there is no commercially available phantom representing obese patients. Therefore, this study outlines a fabrication method to build an obese phantom.

Methods and Materials: A urethane-based material, PMC 121/30 dry, was used for fat and lean tissue-equivalent substitutes (FTES and LTES). For the LTES, a 2.8% by weight of calcium carbonate was added to the PMC and mixed by hand for 25 minutes, while 2% of phenolic microspheres by weight was used instead for the FTES. Both FTES and LTES were tested for density and Hounsfield unit and compared to the ICRU 44. For linear attenuation coefficient, they were compared to slabs of lard and Perspex with identical thickness across a wide range of kVp (40 to 120 kVp).

Results: The density was 1.04 and 0.90 g/cm³ for LTES and FTES, respectively. The Hounsfield unit for the FTES was -66.75 ± -4.26, and 30.08 ± 6.03 for LTES, both agreed with ICRU 44. The mass attenuation coefficient for the FTES against the lard and for the LTES against the Perspex was identical across the range of kVp.

Conclusion: The current study illustrates a method of constructing LTES and FTES that can be used in building different sizes of phantom for dose optimisation and image quality purposes.

14:00 - 15:30

Room M 1

Cardiac

SS 703

New CT protocols to assess coronary artery and myocardium

Moderators:

M. Francone; Rome/IT
C.L. Schlett; Heidelberg/DE

B-0752 14:00

Diagnostic accuracy between low and high tube voltage third-generation dual-source coronary CT angiography using tailored contrast medium injection protocols

M. Albrecht¹, C.N. De Cecco², K. Otani³, J.W. Nance², A. Varga-Szemes², D. De Santis⁴, P. von Knebel Doeberitz², T.J. Vogl¹, U.J. Schoepf²;
¹Frankfurt a. Main/DE, ²Charleston, SC/US, ³Tokyo/JP, ⁴Roma/IT (MoritzAlbrecht@gmx.net)

Purpose: To compare the diagnostic accuracy between coronary CT angiography (CCTA) using ≤100 vs >100 kV peak (kVp) settings and a kVp-tailored contrast medium injection protocol with catheter angiography as the reference standard.

Methods and Materials: One hundred-twenty patients were retrospectively enrolled in this study (mean age=62.6 years, mean BMI=29.0 kg/m²). Patients underwent CCTA and were separated into two cohorts (each n=60) based on the tube voltage (mean kVp=84.3 and 116.5, respectively). The contrast media was tailored to the kVp level: 70=40mL, 80=50mL, 90=60mL, 100=70mL, 110=80mL, and 120=90mL. Quantitative contrast-to-noise ratio (CNR) was measured. Two radiologists evaluated image quality and reported the presence of significant coronary stenosis (>50% luminal narrowing) in a segment-based fashion.

Results: Sensitivity/specificity for ≤100 vs >100 kVp CCTA were: per-patient=93.9/92.6% vs 90.9/92.6%, per-vessel=91.5/97.8% vs 94.0/96.8%, and per-segment=90.0/96.7% vs 90.7/95.2%, respectively, without significant differences (all P>0.64). Quantitative image quality was slightly higher (P>0.18) using lower kVp settings (mean CNR=12.0 and SNR=9.8) vs higher kVp CCTA (mean CNR=11.1 and SNR=8.9). No significant differences were found for subjective image quality among the cohorts (P=0.38). Contrast media requirements were reduced by 38.1% using low vs high kVp (53.6 vs 86.6mL, P<0.001). Radiation dose in ≤100 kVp was 59.6% less than >100 kVp examinations (4.3 vs 10.6 mSv, P<0.001).

Conclusion: Third-generation dual-source CCTA using a kVp-tailored contrast injection protocol can be robustly performed at ≤100 kVp in an overweight population while maintaining diagnostic accuracy for coronary stenosis detection compared to >100 kVp image acquisition, substantially reducing radiation and contrast dose.

Author Disclosures:

C.N. De Cecco: Consultant; Consultant for and/or receives research support from Guerbet and Siemens. **K. Otani:** Employee; Siemens.

A. Varga-Szemes: Consultant; Consultant for Guerbet. **U.J. Schoepf:** Consultant; Consultant for and/or receives research support from Astellas, Bayer, Bracco, GE, and Siemens.

B-0753 14:08

Dual-energy coronary CT angiography: improved vascular contrast using noise-optimised virtual monoenergetic imaging

C. Arendt, D. Leithner, L. Lenga, S.S. Martin, T.J. Vogl, J.L. Wichmann; Frankfurt a. Main/DE (crt.arendt@gmail.com)

Purpose: To evaluate the impact of different energy levels on image quality regarding visualization of coronary arteries and evaluation of coronary stenoses in traditional (VMI) and noise-optimized virtual monoenergetic imaging (VMI+).

Methods and Materials: Spectral DE-CCTA evaluation was performed in 50 cases by using standard linearly-blended (F_0.6), VMI and VMI+ algorithms at different energy levels (40-100 keV, 10 keV-increments). SNR and CNR of main coronary arteries were assessed for objective image quality analysis. Diagnostic confidence was determined by 4 observers using a 5-point Likert scale. Diagnostic accuracy for the detection of >50% stenoses was performed by the same observers, taking into consideration invasive coronary angiography.

Results: Objective image parameters peaked at 40-keV VMI+ reconstructions (SNR: 46.3 [29.6]; CNR: 36.2 [20.3]), significantly superior (all p<0.001) compared with highest results at 70-keV VMI series (29.0 [15.8]; 18.4 [14.8]) and with F_0.6 images (23.7 [14.0]; 15.7 [10.2]). Diagnostic confidence (all p-values < 0.05) was highest at 40-keV VMI+ series with good subjective image quality (median: 4; ICC: 0.81), low noise (4; 0.82) and optimal plaque delineation (5; 0.85). 16 patients (32%) underwent additional ICA. Sensitivity and specificity for the detection of >50% stenoses were highest in 40-keV VMI+ reconstructions (98% and 96%) compared with 70-keV VMI (95% and 94%) and standard F_0.6 (94% and 94%) image series.

Conclusion: DE-CCTA with VMI+ reconstructions at 40 keV significantly increases objective image quality of coronary arteries, leading to improvement of plaque delineation compared with VMI-technique and standard linearly-blended image series. Consequently, diagnostic accuracy and confidence were increased.

Author Disclosures:

J.L. Wichmann: Speaker; GE and Siemens.

B-0754 14:16

Napkin-ring plaques can be identified on coronary CT angiography images using radiomic analysis

M. Kolossvary¹, J. Karady¹, B. Szilveszter¹, P. Kitslaar², B. Merkely¹, P. Maurovich-Horvat¹; ¹Budapest/HU, ²Leiden/NL (marton.kolossvary@cirg.hu)

Purpose: Napkin-ring sign (NRS) is an independent prognostic imaging marker of major adverse cardiac events. However, identification of NRS is challenging due to its qualitative nature and, therefore, depends on reader experience. A more quantitative and reproducible approach is desirable. Therefore, our purpose was to assess whether radiomic parameters can differentiate between NRS and non-NRS plaques.

Methods and Materials: From symptomatic patients' coronary CT angiography images we identified 30 NRS plaques. We matched these with 30 non-NRS plaques with similar degree of calcification and stenosis, localization, tube voltage and image reconstruction settings. All plaques were segmented manually. 8 conventional (lesion length and volume, mean plaque burden, vessel wall remodeling index, lumen area stenosis, mean, minimum and maximum plaque attenuation) and 4440 radiomic parameters were calculated. We used permutation test of symmetry to assess differences between NRS and non-NRS plaques, while we calculated receiver operating characteristics' area under the curve (AUC) values to evaluate diagnostic accuracy. Bonferroni-corrected p<0.0012 was considered significant.

Results: None of the conventional quantitative parameters, while 20.6% (916/4440) of radiomic parameters showed a significant difference between NRS vs. non-NRS plaques. Almost half of these (418/916) reached an AUC value greater than 0.80. Short- and long-run low-grey-level emphasis and surface ratio of high-attenuation voxels to total surface had the highest AUC values (0.918, 0.894 and 0.890, respectively).

Conclusion: Radiomics can identify NRS plaques with excellent diagnostic accuracy. Radiomics could increase the reproducibility and accuracy of diagnostic image interpretation in the future.

Author Disclosures:

M. Kolossvary: Author; Márton Kolossvary is the software developer of Radiomics Image Analysis (RIA) program which was used for radiomic calculations. **P. Kitslaar:** Employee; Pieter Kitslaar is employed by Medis medical imaging systems bv. This software was utilized for the coronary segmentations and image export.

B-0755 14:24

Diagnostic accuracy of coronary CT angiography performed with a novel whole-heart coverage high-definition CT scanner in patients with coronary artery bypass graft

M. Andreini, S. Mushtaq, G. Pontone, A.D. Annoni, A. Formenti, M.E. Mancini, M. Guglielmo, A.L. Bartorelli, M. Pepi; Milan/IT (daniele.andreini@ccfm.it)

Purpose: To evaluate interpretability, radiation exposure and diagnostic accuracy of CCTA compared to invasive coronary angiography (ICA) in the assessment of grafts and non grafted or distal runoff coronary arteries performed with the latest generation of cardiac-CT scanner.

Methods and Materials: We enrolled 100 consecutive patients with CABG who underwent ICA and CCTA (16-cm z-axis coverage with 256 detector rows, 0.28 sec gantry rotation time). We assessed coronary segment interpretability, effective dose (ED) and diagnostic accuracy vs. ICA.

Results: Mean HR during the scan was 70±11 bpm. 26 patients were in atrial fibrillation and 74 in sinus rhythm. Among the latter, 27 patients had a HR>75bpm. CCTA CABG interpretability was 100%, independently from the type of graft (arterial or venous). After comparison with ICA, CCTA was able to correctly detect the occlusion or significant stenosis of all CABG. The overall interpretability of non-grafted and distal runoff coronary arteries was high (95.5%). Sensitivity, specificity, positive predictive value, negative predictive value and accuracy of native coronary arteries were 98.3%, 98.6%, 96.2%, 99.4%, and 98.5%, respectively. Mean effective dose was 2.5±0.8mSv.

Conclusion: The novel whole-heart coverage CT scanner allows to evaluate CABG and native coronary arteries with excellent diagnostic accuracy and low radiation exposure also in the presence of atrial fibrillation and high heart rate.

B-0756 14:32

Cardiac CT for demonstrating non-calcified coronary atherosclerotic plaque: effect of knowledge-based iterative model reconstruction on image quality

T. Li, L. Yang; Beijing/CN (litaofeivip@163.com)

Purpose: The purpose of this study was to assess image quality of demonstrating coronary plaques using iterative model reconstruction (IMR), a knowledge-based iterative reconstruction algorithm, the latest reconstruction technique.

Methods and Materials: Sixty-six patients (53 male and 13 female) with single-vessel disease with non-calcified plaques or non-calcified predominant plaques and significant coronary stenosis (≥50%) using prospective electrocardiogram-gated coronary 256-slice CT angiography were selected. Paired image sets were created using two types of reconstruction: hybrid iterative reconstruction (HIR) (iDose4; Philips Healthcare) and IMR. Signal-to-noise ratio (SNR) of image was calculated and contrast-to-noise ratio (CNR) between plaque and adjacent fat tissue was measured on a cross-sectional multi-planar reconstruction image of the plaque.

Results: Seventy-seven non-calcified plaques or non-calcified predominant plaques with significant coronary stenosis were detected. Two plaques were located on LM, 51 plaques on LAD, 23 on RCA and 1 on LCX. χ^2 test showed there was no significantly statistical difference to present positive remodeling, low density plaque and spotty calcification with HIR and IMR reconstructed method, still there was significantly statistical difference to discern napkin-ring sign between two algorithms (χ^2 12.12, $p < 0.001$). The image noise of IMR was lower than that of HIR (10±2 versus 13±2) ($p < 0.01$), and SNR of image and CNR between plaques and surrounding fat tissue on IMR were better than that on HIR (SNR: 46±15 versus 37±11) (CNR: 16.0±4.6 versus 12.0±3.6) ($p < 0.01$).

Conclusion: IMR can significantly decrease the image noise and improve image quality compared with HIR for the coronary atherosclerotic plaques demonstration on coronary 256-slice CT angiography.

B-0757 14:40

Iodine quantification at rest and stress to differentiate ischaemic, infarcted and normal myocardium using dual-energy CT

M. van Assen¹, C.N. De Cecco¹, R. Vliegenthart², M. Oudkerk², U.J. Schoepf¹; ¹Charleston, SC/US, ²Groningen/NL (m.van.assen@umcg.nl)

Purpose: The aim of this study was to evaluate the potential of rest-stress dual-energy CT (DECT) iodine quantification to discriminate between normal, ischemic, and infarcted myocardium.

Methods and Materials: Patients underwent rest-stress DECT on a second-generation dual-source scanner. Rest-stress perfusion single photon emission CT (SPECT) and rest-stress cardiac magnetic resonance (CMR) imaging with late gadolinium enhancement (LGE) were performed to identify ischemic and infarcted myocardium. Patients were categorized into an ischemic, infarcted, and control group based on SPECT and CMR results. Regions of interest (ROI) were placed in the septal area of the iodine maps to assess iodine concentrations in normal/remote myocardium. ROIs were sampled in ischemic and infarcted areas detected on perfusion and LGE-images. In addition,

variations in iodine concentration were analyzed on a per-segment basis according to the AHA-16-segment model in the control group.

Results: 42 patients were included: 10 ischemic, 17 infarcted, and 15 controls. There were no significant differences in iodine concentrations between segments. Iodine concentrations in both ischemic and infarcted myocardium were significantly lower than in normal myocardium (p value 0.005 and < 0.001), ranging from 1.3 mg/mL (0.9-1.8) and 0.6 mg/mL (0.4-0.8) at rest and stress in ischemic myocardium, and 0.3 mg/mL (0.3-0.5) and 0.5 mg/mL (0.5-0.7) at rest and stress in the infarcted myocardium, respectively. At rest, iodine concentration of ischemic myocardium was significantly higher compared to infarcted myocardium (p value < 0.001).

Conclusion: DECT quantification of iodine concentration from rest-stress imaging is able to distinguish between normal, ischemic, and infarcted myocardium and holds potential as an imaging biomarker for tissue characterization.

Author Disclosures:

C.N. De Cecco: Research/Grant Support; Siemens Healthineers.

U.J. Schoepf: Research/Grant Support; Siemens Healthineers, Bracco, GE, Bayer.

B-0758 14:48

The value of wide-detector helical CT combined with adaptive statistical iterative reconstruction-V in patients with high heart rate during coronary CT angiography

H. Zhao; Zhengzhou/CN (kindergirl@sina.cn)

Purpose: To compare the radiation dose and image quality of wide-detector helical CT combined with ASIR-V with stand-detector helical CT with ASIR in patients with high heart rate (HR) during coronary CT angiography (CCTA).

Methods and Materials: Eighty high heart rate patients (HR-during the CT scans ≥ 80 bpm) underwent CCTA were randomly divided into two scan groups (n=30 each): the study group: detector coverage of 160mm, 100 kVp, 50% pre-ASIR-V; the control group, detector coverage of 40mm, 120 kVp, 50% ASIR. Quantitative parameters [image noise (SD of AA), SNR, CNR, CT values of ascending aorta (AA), left main coronary artery (LM), proximal segment of left anterior descending (LAD-p), circumflex proximal segment (LCX-p), right coronary artery (RCA-p)] and effective dose (ED) were compared with two sample t tests. The image quality of coronary artery was evaluated using a four-point scale based on the 15-segment model after using SSF technique reconstructions when necessary and then compared with χ^2 test.

Results: The study group and control group showed no significant differences in image noise, SNR, CNR and CT values of AA, LM, LAD-p, LCX-p, RCA-p. No significant differences were found for the diagnostic image quality of coronary artery segments (546/551 VS 552/559) and the ratio of SSF technique reconstructions (27/40 VS 31/40) among the two groups. The ED for the study group and the control was (2.16±0.79)mSv and (9.74±3.89)mSv, respectively. There was significant difference in ED among this two groups.

Conclusion: Comparing with stand-detector helical CT in patients with high HR, the wide-detector helical CT combined with 50% pre-ASIR-V could reduce 78% radiation dose while maintain overall image quality.

B-0759 14:56

Study on the optimum keV and different contrast agent concentration in coronary stent imaging using spectral CT: in vitro study

L. Yang, Y. Hou, Y. Ma, Z. Jia, X. Lu; Shenyang/CN (8609469@qq.com)

Purpose: To investigate optimally visual combination of different keV and concentration of contrast agent (CT) in the coronary artery stent using spectral CT in vitro study.

Methods and Materials: Fifteen coronary artery stents (internal diameter of 2.5 - 4.0 mm) were randomly divided into artificial coronary artery, respectively filled six different concentrations of contrast agent (12.85, 6.59, 5.29, 4.43, 3.80 and 3.33 mg/ml). All artificial coronary artery scanned with dual-detector CT, obtain images from 40 to 200 keV (interval of 10 keV). Subjective image quality was evaluated by two doctors using Likert 5 method. Objective image quality assessment including artificial lumen narrowing (ALN), signal to noise ratio (SNR), contrast to noise ratio (CNR).

Results: The image quality of 6.59mg/ml+60 keV group was the highest total score ($P < 0.05$). The ALN value was (21.33 ± 12.48)% in 6.59mg/ml + 60 keV group, which was significantly lower than that in other groups ($P < 0.05$). In 6.59mg/ml + 60 keV group, the SNR of stent lumen was 26.08 ± 3.74, which was significantly higher than that of 3.93 ~ 12.85mg/ml + 70 ~ 200keV group ($P < 0.05$). The CNR of 6.59mg/ml + 60 keV group was significantly higher than that of 3.33 ~ 12.85mg/ml + 70 ~ 200keV group ($P < 0.05$).

Conclusion: In vitro scans, at concentration of 6.59 mg/ml + ml with 60 keV, image quality was better, stent diameter measurement results closer to real diameter, can be recommended for clinical diagnosis.

B-0760 15:04

Assessment of image quality of coronary artery and left ventricular function and volume using low kVp, mA modulation and advanced model based iterative reconstruction

K. Choo, Y.-J. Jeong, M. Kim; *Busan/KR (jyj107@hanmail.net)*

Purpose: To compare 3rd generation dual source CT (DSCT, Somatom force, Siemens Medical Solution, Forchheim, Germany) using 70 or 80 kVp and ECG-based maximum tube current modulation and advanced modeled iterative reconstruction with echocardiography (ECHO) for the determination of left ventricular ejection fraction (LVEF), end-diastolic volume (EDV), end-systolic volume (ESV) as well as assessing coronary artery image quality and patient radiation dose.

Methods and Materials: Forty consecutive patients (M:F = 32:8, mean age, 57.1 ± 6.4 years) with chest pain were enrolled in this study. EF, EDV and ESV were measured by both DSCT and ECHO, and the correlation coefficients were assessed. In addition, subjective image quality of coronary artery segment (1, excellent; 4, poor) and radiation dose were recorded.

Results: Comparison of LVEF, EDV, and ESV between DSCT and ECHO showed a significant correlation ($p < 0.01$) and the LVEFs measured by DSCT and ECHO were not statistically different. However, LV, EDV and ESV from DSCT were statistically higher than those from ECHO ($p < 0.05$). The average subjective image quality score of the coronary artery segment was 1.10 and the mean patient radiation dose was 2.07 ± 0.4 mSv.

Conclusion: DSCT with low kVp, mA modulation and advanced model based iterative reconstruction offers comparable results to ECHO for LVEF and LVV and good image quality of coronary artery with a low radiation dose.

B-0761 15:12

Effect of image reconstruction algorithms on cardiovascular radiomic features using coronary CT angiography

M. Kolossvary, B. Szilveszter, J. Karady, B. Merkely, P. Maurovich-Horvat; *Budapest/HU (martonandko@gmail.com)*

Purpose: Radiomic analysis is an emerging analytical approach to identify new imaging biomarkers of specific phenotypes and outcomes. Little is known how novel image reconstruction algorithms might affect radiomic characteristics. Therefore, our objective was to assess the effect of image reconstruction settings on radiomic features of coronary atherosclerotic lesions.

Methods and Materials: 60 coronary atherosclerotic lesions were reconstructed using filtered-back projection (FBP), hybrid iterative reconstruction (HIR) and model-based iterative reconstruction (MIR). Images were segmented using a semi-automated software. Segmentations were manually adjusted if needed. Voxels containing plaque tissue were exported as an original DICOM dataset. Overall, 114 grey level co-occurrence matrix (GLCM) and 11 grey level run length matrix (GLRLM) statistics were calculated using the Radiomics Image Analysis (RIA) software package. Using linear regression analysis, the effect of FBP and MIR as compared to the reference HIR technique corrected for additional imaging settings was investigated. A p value smaller than 0.05 was considered significant.

Results: Among GLCM statistics 14.0% (16/114) was differed between FBP-HIR, while 19.3% (22/114) showed a significant difference between HIR-MIR. However, among GLRLM statistics only short run emphasis, and run percentage was significantly different between HIR and MIR reconstructions.

Conclusion: Image reconstruction algorithms affect several radiomic statistics, therefore standardization of imaging protocols is needed to achieve robust and reproducible results.

Author Disclosures:

M. Kolossvary: Author; Márton Kolossvary is the software developer of Radiomics Image Analysis (RIA) program which was used for radiomic calculations.

B-0762 15:20

Motion elimination in low-dose 4D myocardial computed tomography perfusion (CTP) using the automated smooth temporal registration for analysis of 4D image data (ASTRA) algorithm

S. Lukas, S. Feger, M. Rief, E. Zimmermann, M. Dewey; *Berlin/DE*

Purpose: We propose a four-dimensional (4D) motion elimination algorithm for joint temporal alignment and denoising of a 4D CTP sequence to provide physiologically meaningful local time attenuation curves (TACs) for subsequent myocardial perfusion quantification.

Methods and Materials: Dynamic contrast-enhanced 320-row CTP was performed in 31 patients with suspected or confirmed coronary artery disease (CAD). In a unified approach we decouple cardiac deformation from temporal intensity changes due to contrast enhancement by iteratively performing a local polynomial kernel regression temporally and a 4D principal component analysis (PCA) spatially. A multi-resolution two-stage rigid and deformable B-spline registration model was applied by minimizing the temporal misalignment

measured by the weighted sum of the eigenvalues of the inter-volume correlation matrix. Registration performance was assessed by measuring temporal smoothness, spatial noise, and degree of local volumetric deformation (determinant of the spatial Jacobian) at four distinct regions at the left-ventricular wall for each patient. Solely PCA-based registration without temporal regression served as the reference standard.

Results: The proposed ASTRA registration algorithm provided superior registration performance when compared to the benchmark. The algorithm consistently improved temporal smoothness (32.5 ± 12.4 vs. 185.1 ± 103.8 , $p < 0.001$) and spatial noise (21.8 ± 13.2 vs. 27.6 ± 12.4 , $p < 0.001$) at the myocardial target regions at comparable local deformation behaviour ($0.997 \times / 1.073$ vs. $0.999 \times / 1.055$, $p = 0.169$, geometric average) and improved overall temporal alignment of the registered sequence (20.93 ± 2.60 vs. 21.86 ± 2.94 , $p < 0.001$).

Conclusion: The novel ASTRA registration algorithm for a 4D CTP sequence outperforms the benchmark with 80% temporal and 20% spatial noise reduction without introducing strong volumetric deformations.

Author Disclosures:

M. Dewey: Grant Recipient; Toshiba Medical Systems, Guerbet, Cardiac MR Academy Berlin, and Bayer (Schering-Berlex), Siemens Medical Solutions, Philips Medical Systems. Research/Grant Support; DE 1361/14-1, 603266-2, HEALTH-2012.2.4.-2, 20072013 2/05, 20072013 2/48, F/23/08, F/27/10, DFG, BMBF, 01KG1013, 01KG1110, 01KG1210. Speaker; Toshiba Medical Systems, Guerbet, Cardiac MR Academy Berlin, and Bayer (Schering-Berlex).

14:00 - 15:30

Room M 2

Paediatric

SS 712

Paediatric chest

Moderators:

T.R. Semple; London/UK
N.N.

B-0763 14:00

Fast magnetic resonance imaging (MRI) of invasive lung aspergillosis in immunocompromised children: comparison with HRCT

T. Akbas¹, S. Ulus², B.S. Karagun¹, T. Arpacı¹; ¹Adana/TR, ²Istanbul/TR (tugana.akbas@acibadem.edu.tr)

Purpose: To compare the diagnostic accuracy of fast lung MRI with high resolution computed tomography (HRCT) in immunocompromised children with invasive pulmonary aspergillosis.

Methods and Materials: Twenty seven children (14 boy, 13 girl, mean age = 12.8; range age 5-17 years) with suspected invasive pulmonary aspergillosis after chemotherapy and hematopoietic stem cell transplantation underwent 1.5 Tesla MRI and HRCT. Pulmonary MRI study protocol included T2 weighted half-Fourier single-shot turbo spin echo (HASTE) and T1 weighted volumetric interpolated breath hold examination (VIBE) sequences. The average MRI scanning time was three minutes. Both the location and the type of lesion (halo sign, air crescent sign, peribronchial consolidation, bronchopneumonia, centrilobular and tree in bud nodules) were assessed on MRI and HRCT blinded to patient's data by two radiologists. Kappa test, sensitivity, specificity, accuracy, positive and negative predictive values were used to determine the compliance.

Results: The location of the lesion in HRCT were concordant with T2 HASTE sequence ($\kappa_w: 0.550$ $p = 0.0001$) and T1 VIBE sequence ($\kappa_w: 0.550$ $p = 0.0001$) corresponding to a negative predictive value of 100%, positive predictive value of 95%, sensitivity of 100%, specificity of 40%, accuracy 95%. The type of lesion in HRCT were concordant with T2 HASTE sequence ($\kappa_w: 0.447$ $p = 0.0001$) and T1 VIBE sequence ($\kappa_w: 0.442$ $p = 0.0001$) corresponding to a negative predictive value of 33%, positive predictive value of 100%, specificity of 100% and accuracy 93%.

Conclusion: According to our study; MRI is a fast, radiation free examination for detecting of pulmonary invasive aspergillosis lesions with high accuracy rate in immunocompromised children.

B-0764 14:08

Pulmonary MRI: diagnostic performance and detection of structural abnormality using ultrashort echo time in cystic fibrosis patients

M.S. Kraus, M. Esser, M. Teufel, S. Fleischer, J. Riethmueller, C. Ruff, I. Tsiflikas, J.F. Schäfer; *Tübingen/DE (mareen.kraus@med.uni-tuebingen.de)*

Purpose: To evaluate the diagnostic performance of a coronal 3D Ultra Short Echo time sequence (UTE) in pulmonary magnetic resonance imaging in cystic fibrosis patients in comparison to the in-house standard; a morphological axial PDw Flash 3D in breath-hold, coronal T2w TSE with double triggering and functional sagittal PDw Flash 2D in submaximal in- and expiration.

Methods and Materials: Twenty five CF patients who underwent pulmonary MRI (1.5 Tesla scanner) were included. Coronal UTE sequences were acquired in submaximal in- and expiration as well as the standard pulmonary protocol. Two independent readers assessed overall image quality, cardiac respiratory motion artifacts (using a 3-point Likert scale), bronchiectasis abnormality and the degree to which airways and vessels were visible. For both MR protocols typical cystic fibrosis pathologies were semi-quantitatively assessed using the

"MRI-CF-Score" including bronchiectasis, mucus plugging, centrilobular opacity, consolidation, sacculcation and air trapping.

Results: Diagnostic performance based on overall image quality, motion artifacts and airway/vessel visibility was rated higher by the independent readers for the UTE sequence. There were no significant differences in total MR-CF-Scores considering the different protocols. Significant ($p < 0.001$) reduction of acquisition time was noted for the singular plane UTE in submaximal breathing conditions.

Conclusion: Pulmonary MRI with UTE offers increased depiction and delineation of peripheral pathologic lung manifestations in patients with cystic fibrosis with improved image quality compared to the conventional standard protocol, whilst significantly reducing the acquisition time, which is particularly relevant in the pediatric patient group.

B-0765 14:16

World Health Organization guidelines for achieving high-quality paediatric chest radiographs for use in epidemiological studies

S. Lacey^{1,2}, K. Mulholland¹, N. Fancourt¹, K. O'Brien², J. de Campo¹, M. de Campo¹; ¹Parkville/AU, ²Baltimore, MD/US (stephen.lacey@rch.org.au)

Purpose: Consistent high-quality chest radiographs are essential for reliable case definitions in epidemiological studies of childhood respiratory disease. However, there is no centralised resource on chest radiograph acquisition relevant to study investigators and site staff. Previous experience suggests that suboptimal quality radiographs can be minimised through early collaboration between radiology departments and research staff.

Methods and Materials: The World Health Organisation Chest Radiography in Epidemiological Studies or "WHO-CRES" project was formed in 2015. A major objective of the project was to develop appropriate resources for investigators and facility staff in remote and under-resourced regions to enable them to safely obtain high-quality paediatric chest radiographs. These resources were developed by the Quality and Safety co-investigator and finalised by a technical working group consisting of radiologists and investigators.

Results: The technical guidelines are divided into three sections: 1. The Pre-Study Survey evaluates the current technical parameters, capabilities and processes of individual radiology facilities and their suitability for participation in paediatric epidemiological studies. 2. The Study Guidelines review the major factors contributing to quality paediatric chest radiographs, identifying issues that are most important and/or require adjustment by a research team. Recommendations for achieving quality chest radiographs in studies involving children aged 0-59 months are provided. 3. The Quality Control Guidelines include the recommended performance and documentation of quality control measures for continual optimisation of equipment and facility processes.

Conclusion: These WHO-CRES guidelines provide an easily accessible and unique resource to better facilitate the acquisition of consistent, high-quality chest radiographs in epidemiological studies.

B-0766 14:24

Value of paediatric chest CT in a representative patient cohort of 2019 examinations

M. Esser, S. Hess, M. Teufel, S. Gatidis, I. Tsiflikas, J.F. Schäfer; Tübingen/DE

Purpose: To test if chest CT delivers useful results according to the clinical question and which examinations are possibly dispensable.

Methods and Materials: In this retrospective study at a clinic with maximum care facilities, 2019 chest CT examinations in 973 patients (median age, 10.5 years; range, 2 days to 17.9 years) were analysed over 7 years with regard to the application of contrast agents and information about the referring department including the clinical question and CT findings. For this purpose electronically stored documents were evaluated. For each examination it was identified if the clinical question was answered and if additional findings relevant for therapy were detected.

Results: Most CT scans were performed without contrast enhancement ($n=1251$; 62%). Most examinations ($n=987$) were requested from the Department of Haematology/Oncology. The most frequent indication was a suspected pneumonia ($n=380$; 19%). In 1411 CT scans (70%) anomalies according to the suspected diagnosis were found, 608 examinations (30%) gave a negative reply to the question. There were predominantly negative results (62%) when the question was for an infection process prior to bone marrow transplant. In 81 scans without relevant findings concerning the primary question, an additional finding relevant for therapy was detected (19% of all additional findings). Overall, CT provided findings with a conclusive result and clinical relevance in 97.6% of all scans.

Conclusion: Based on an appropriate clinical question, paediatric chest CT in specialised centres has a high informative clinical value. The strict indication and clinical evaluation appears crucial for the prevention of dispensable CT examinations.

B-0767 14:32

Influence of reconstruction algorithms to chest CT examination in children: comparison of image quality among standard-, reduced- and ultra-low-dose CTs in chest phantom study

E. Suehiro¹, T. Sekitani¹, W. Tani¹, N. Negi¹, K. Fujii², T. Yoshikawa¹, Y. Ohno¹; ¹Kobe/JP, ²Tokyo/JP

Purpose: To determine the influence of reconstruction algorithm to image quality and radiation dose reduction capability on chest CT in chest children phantom study.

Methods and Materials: A commercially available chest CT phantom was simulated as 5-year-old children were scanned with a 320-detector row CT with automatic exposure control (AEC). Performance of 3D AEC was performed by targeted SDs, which were tested from 10 (CTDIvol: 16.6mGy) to 110 (CTDIvol: 0.5mGy) at every 20 intervals, although other scan parameters were constant. Then, each SD data was reconstructed as 1mm and 5mm contiguous section thickness with filtered back projection (FBP), commercially available hybrid-type iterative reconstruction (IR) (i.e. AIDR 3D), and model-based IR (FIRST) methods. Then, actual image noise determined by ROI measurement was compared at each targeted SD data by Tukey's HSD test. Finally, mean visualization scores were compared between CT obtained at targeted SD as 10 and reconstructed by FBP (i.e. standard CT) and all other CT data by Wilcoxon signed-rank test.

Results: On both section thickness CT images at each targeted SD, image noise of FBP was significantly higher than that of AIDR 3D and FIRST ($p < 0.05$). When compared lung parenchyma visualization capability, both section thickness CT data obtained at targeted SD as 70, 90 and 110 and reconstructed by FBP had significant difference with standard CT ($p < 0.05$).

Conclusion: This phantom study shows reconstruction algorithm had significantly affected the radiation dose reduction at chest CT examination using 3D AEC in children.

B-0768 14:40

Technical challenges of quantitative chest MRI data analysis in a large cohort paediatric study

A. Nguyen¹, A. Perez-Rovira¹, L. Duijts¹, M. De Bruijne¹, A. Aliverti², F. Pennati³, T. Ivanovska³, H.A. Tiddens¹, P. Ciet¹; ¹Rotterdam/NL, ²Milan/IT, ³Göttingen/DE (354271an@student.eur.nl)

Purpose: To evaluate the effect of geometric distortion on MRI lung volume quantification and evaluate available manual, semi- and fully automated methods for lung segmentation.

Methods and Materials: A phantom was scanned with MRI and CT. GD was quantified as difference in phantom's volume between MRI and CT, with CT as gold standard. Dice scores were used to measure overlap in shapes. Furthermore, a subset of 11 subjects with MRI measurements from a large prospective population-based cohort study was used to test lung segmentation methods on 2D and 3D Gradwarp corrected scans. Intra-Class Correlation coefficient, Bland-Altman plots, Wilcoxon, Mann-Whitney U and paired t-tests were used for statistics.

Results: Using phantoms, volume differences between CT and MRI varied according to MRI positions and 2D and 3D Gradwarp correction. With the phantom located at isocenter, MRI overestimated the volume relative to CT by $5.56 \pm 1.16\%$ to $6.99 \pm 0.22\%$ with body and torso coils, respectively. Higher Dice scores and smaller intra-object volume differences were found for 3D Gradwarp corrected MR images. In subjects, semi- and fully automated segmentation tools had high agreement with manual segmentations (ICC=0.971-0.993 for end-inspiratory scans; ICC=0.992-0.995 for end-expiratory scans). Manual segmentation time per scan was approximately 4 hours and 2-3 minutes for automated methods.

Conclusion: Volume overestimation of MRI due to GD can be quantified. Existing semi- and fully automated segmentation methods allow accurate, reproducible and fast lung volume quantification. Chest-MRI can be a valid radiation-free imaging modality for lung segmentation and volume quantification in large cohort studies.

Author Disclosures:

L. Duijts: Research/Grant Support; ERA HDHL.

B-0769 14:48

Imaging findings of Loeyes-Dietz syndrome in paediatric population

H.O. [Özdemir](#), A. Sanchez-Montanez Garcia-Carpintero, A. Sabate Rotes, I. Delgado Alvarez, L. Riaza Martin, A. Coma, L. Riera Soler, A. Castellote, E. Vazquez Mendez; *Barcelona/ES (onurkont88@gmail.com)*

Purpose: Loeyes-Dietz syndrome is a rare autosomal-dominant connective tissue disorder with multisystemic radiological manifestations. The purpose of our study was to describe radiological findings of LDS in 3 groups; cardiovascular, neuroradiological and musculoskeletal findings which can help to correct diagnosis and follow-up.

Methods and Materials: Three paediatric radiologists retrospectively reviewed cardiovascular MRI, cranial MRI/MRA, cervical MRA/CTA and plain film studies of 12 patients all of whom had positive genetic testing and clinical characteristic of LDS. All patients were under 18 years old at diagnosis. All of them had cardiovascular MRI and nine had neurovascular imaging modalities.

Results: Eleven patients had aortic root dilatation which is the most common cardiovascular finding of the syndrome. 6 patients had also dilatation of the other parts of thoracic aorta, 2 had main pulmonary artery dilatation, 2 had coronary artery dilatation, 1 had abdominal aortic dilatation and 1 had bicuspid aortic valve. 2 patients had aortic dissection (cause of death). One patient had normal cardiovascular MRI. In between 9 patients who had cranial imaging, all patients had tortuosity of vertebral basillary and carotid arteries, hypertelorism and microretrognathia. Other neuroradiological findings: craniosynostosis (5 patients), upper cervical spine abnormalities (3), gliotic foci (2), ventriculomegaly (1), intracranial aneurysms and intracranial haemorrhage (1, cause of death). As musculoskeletal findings, 10 patients had scoliosis, 7 had pectus deformities and 1 had joint contractures.

Conclusion: Aortic root dilatation, neurovascular tortuosity, hypertelorism, microretrognathia are the most common imaging findings associated with LDS. Aortic dissection and intracranial haemorrhage are the most common causes of mortality.

B-0770 14:56

Aortic & carotid intima-media thickness in term small for gestational age newborns and term normal newborns

S.M.s.a. [Revanna](#), V. Kenchanahalli Rangaswamy, V. Devappa, V.K. Shamachar; *Bangalore/IN (sinumr25@gmail.com)*

Purpose: To compare the intima media thickness of abdominal aorta (aIMT) & carotid arteries (cIMT) in small for gestational age (SGA) term newborns with appropriate for gestation age term newborns

Methods and Materials: In our study the newborns are divided into 2 groups: Group I included 50 AGA normal term newborns with birth weight between 50-90th centile (control group) and group II included 50 SGA term newborns with birth weight less than 10th centile (patient group). All measurements are performed by a single observer by using high resolution ultrasonography.

Results: Mean abdominal aIMT and cIMT values of normal term newborns (AGA) were 0.40 ± 0.042 mm ($n = 50$) and 0.32 ± 0.031 mm ($n = 50$), respectively. Maximum and minimum aIMT and cIMT values of term newborns were 0.45 and 0.35 mm and 0.35 and 0.25 mm, respectively. The mean aIMT and cIMT were higher in SGA group (0.45 ± 0.058 mm) and 0.40 ± 0.047 compared with the control group.

Conclusion: Small for gestational age fetuses have a thicker aortic and carotid wall than AGA fetuses, which possibly represents preclinical atherosclerosis and a predisposition to later cardiovascular disease.

B-0771 15:04

What is the underestimation of radiation dose to the paediatric thyroid from contrast-enhanced CT, if contrast medium uptake is not taken into account?

K. Perisinakis, S. [Pouli](#), A. Tzedakis, K. Spanakis, A.A. Hatzidakis, M. Raissaki, J. Damilakis; *Iraklion/GR (stellapouli@gmail.com)*

Purpose: Administration of iodine-based contrast in CT has been shown to increase radiation dose in enhanced organs. The current dose calculation methods ignore contrast administration. The aim of our study was to assess the underestimation of radiation dose to the thyroid of children undergoing contrast-enhanced CT if contrast medium uptake is not taken into account.

Methods and Materials: Paediatric head/neck or chest CT examinations involving pre- and post-contrast imaging were retrospectively selected from our department database to identify those CT image series where the thyroid was visible. CT density of thyroid tissue in HU was measured in pre- and post-contrast images at the corresponding positions. The resulting Δ HU was recorded for each patient. Utilizing recently published data, Δ HU corresponded to % w/w iodine concentration and subsequently to % dose increase induced by contrast uptake.

Results: The thyroid gland was visible in 11 chest and 3 neck CT scans. The estimated increase in radiation dose absorbed by thyroid tissue due to contrast accumulation ranged from 12% to 46%, with a mean value of 23%.

Conclusion: The radiation dose to the paediatric thyroid gland due to contrast enhancement may be underestimated by up to 46% if contrast medium uptake is not taken into account. Scanning of the upper lung fields should be avoided during paediatric chest CT whenever possible to prevent thyroid exposure. Whenever this is unavoidable, estimation of radiation dose to the gland should take into consideration contrast medium uptake.

B-0772 15:12

Dose distribution to radiosensitive organs using advanced thoracic CT imaging techniques

A.F. [Halaweish](#)¹, M. Siegel², I. Duba¹, K. Grant¹, B. Schmidt³; ¹Malvern, PA/US, ²St. Louis, MO/US, ³Forchheim/DE

Purpose: To examine how various Thoracic CT techniques affect radiation dose distribution in pediatric-sized phantoms, with particular focus on especially radiosensitive organs like the lungs and breasts.

Methods and Materials: In two anthropomorphic phantoms (1- and 5-year-old equivalents), radiation doses in 38 sites (six organs) were measured using metal oxide semiconductor field effect transistors (MOSFETs) paired with a mobileMOSFET measurement system (model TN-RD-70-W, Best Medical Canada Ltd.). The phantoms were scanned using routine single-energy, dual-energy, ultra-fast pitch spiral and ultra-low dose tin-filtered CT imaging protocols. Organ dose distribution was calculated as a percentage of the dose length product, facilitating inter- and intra-protocol comparisons.

Results: Compared with single-energy scans, dual energy CT demonstrated lower relative organ doses for both phantoms. Dual-energy scanning reduced lung dose by 27.3% and 21.9% and breast dose by 37.8% and 31.3 % in the 1- and 5-year-old phantoms respectively. Ultra-low dose Sn100kV scans reduced lung dose by 31.63% (1-year-old phantom) and 14.74% (5-year-old phantom) when compared to 70kV scans, and 13.79% (1-year-old phantom) and 1.89% (5-year-old phantom) when compared to 80kV scans. Ultra-low dose Sn100kV imaging in combination with ultra-fast pitch spiral produced the largest dose reduction for lung and breast compared to single-energy CT at 70 kV in the 5-year-old phantom (25.66% and 48.44% for lung and breast respectively).

Conclusion: Dual-Energy CT, ultra-low dose tin-filtered and ultra-fast pitch spiral scanning demonstrated a decreased dose to the lungs and breasts of pediatric size phantoms when compared with routine single-energy scans, while providing clinically diagnostic image quality.

Author Disclosures:

A.F. Halaweish: Employee; Siemens Healthineers. **I. Duba:** Employee; Siemens Healthineers. **K. Grant:** Employee; Siemens Healthineers.

B. Schmidt: Employee; Siemens Healthineers.

B-0773 15:20

Study of the feasibility of DAP-to-body-weight ratio as diagnostic reference level in paediatric interventional cardiology

F. De Monte, L. [Riccardi](#), A. Boschini, B. Castaldi, L. Baffoni, O. Milanese, M. Paiusco; *Padova/IT*

Purpose: To investigate the feasibility of the dose-area product to body weight ratio (DAP/BW) as dose index for Diagnostic Reference Level (DRL) in paediatric Interventional Cardiology (IC) procedures.

Methods and Materials: IC procedures (91 diagnostic, 166 therapeutic) performed on patients <18 years old were stratified into BW classes every 10 kg. DAP values were extracted from the Structured Dose Report using a dose-tracking software. Mean, median, σ and 75th values of DAP and DAP/BW were calculated. ANOVA was used to determine whether there were any statistically significant differences between DAP corresponding to BW classes both for diagnostic and interventions. Correlations DAP vs. BW were investigated for diagnostic and therapeutic procedures and also for homogeneous subgroups of interventions. DAP/BW ratios were compared between procedure groups (Mann-Whitney test).

Results: When diagnostic and therapeutic procedures are considered as a whole, DAP differences among BW classes were not statistically significant and, in addition, a low correlation DAP vs. BW was found ($R=0.533$ and $R=0.265$, respectively). Strong correlations did appear when procedures were stratified by type: R coefficient varied from 0.730 (angioplasty) to 0.859 (PDA closures). Highest DAP values resulted for highly complex interventions (angioplasty) performed on <10 kg babies. DAP/BW values derived from ASD closures were statistically different from all the other investigated interventions.

Conclusion: When a robust correlation between DAP and BW exists, the DAP/BW ratio is a reliable DRL in IC procedures overcoming BW stratification method. An effort is necessary in order to define appropriate criteria of procedures stratification, considering different implanted devices.

14:00 - 15:30

Sky High Stage

Cardiac

MY 7

Cardiovascular

Moderators:

A. Tóth; Budapest/HU

M. Zins; Paris/FR

B-0774 14:00

The image quality of turbo high-pitch dual-source CT coronary angiography in patients with free-breathing, free heart rate and any BMI
K. Sun, B. Lu; Beijing/CN (Henryska@163.com)

Purpose: To evaluate the image quality and effective radiation dose of turbo high-pitch dual-source CCTA in patients with free-breathing, free heart rate and any body mass index.

Methods and Materials: Between July 2015 and December 2015, 1179 consecutive patients (body mass index (BMI) range: 14.53-37.65 kg/m²) (597 female, mean age: 58±10 years) undergoing clinically indicated CCTA were included. No β-blockers were administered for all patients before the examinations. CCTA was performed with a 3rd-generation dual-source CT system. The image acquisition phase was manually set at 60% of the RR interval for patients with HR≤70 beats per minute (bpm) and at 30% of the RR interval for the patients with HR>70bpm. The image noise, contrast-to-noise ratio (CNR), image quality scores and effective radiation dose were assessed.

Results: The average heart rate was 76±12 bpm (range: 40-133 bpm). A total of 3537 coronary arteries were evaluated in 1179 patients. The mean image quality scores was 1.21±0.72 for all coronary arteries. Based on patient analysis, the proportion of non-diagnostic coronary artery segments was 8.54%. The average image noise and CNR of aortic root were 24.6±6.7 HU (range:7-52 HU) and 30.8±9.8 (range 8.3-110.8), respectively. The effective radiation dose was 0.61±0.16 mSv (range: 0.14-1.41 mSv).

Conclusion: In conclusion, in patients with free-breathing, free heart rate and any body mass index, the turbo high-pitch dual-source CT coronary angiography provides a good image quality and low rate of non-diagnostic coronary segments, while being associated with significant reduction of radiation exposure.

Author Disclosures:

K. Sun: Author; Bin lu.

B-0776 14:04

Machine-learning on-site CT-derived fractional flow reserve (FFR) compared to invasive FFR: influence of myocardial mass on accuracy
M. Albrecht¹, S. Baumann², J.W. Nance³, C.N. De Cecco³, A. Varga-Szemes³, R. Vliegenthart⁴, C. Schwemmer⁵, T.J. Vogl¹, U.J. Schoepf³, S.S. Martin¹;
¹Frankfurt a. Main/DE, ²Mannheim/DE, ³Charleston, SC/US, ⁴Groningen/NL, ⁵Erlangen/DE (simartin@outlook.com)

Purpose: To investigate the impact of myocardial mass on accuracy of on-site machine-learning CT-derived fractional flow reserve (CT-FFRml) for the determination of lesion-specific ischaemia using invasive FFR as the reference standard.

Methods and Materials: In total, 458 vessels from 301 patients were evaluated. The correlation of myocardial mass was correlated to the discrepancy of CT-FFRml and FFR. Diagnostic accuracy of CT-FFRml for the detection of lesion-specific ischaemia (FFR < 0.8) was analysed according to the amount of myocardial mass.

Results: Greater myocardial mass was associated with an underestimation of CT-FFRml values ($r = 0.307$, $P < 0.001$). The incremental value of CT-FFRml in diagnostic accuracy compared to visual CCTA assessment was greater ($P = 0.04$) in the cohort with higher myocardial mass (increase in accuracy, 18.0 %) in comparison with lower myocardial mass values (increase in accuracy, 16.8 %).

Conclusion: Machine-learning on-site CT-FFRml has greater incremental value for the detection of lesion-specific ischaemia compared to CCTA evaluation in patients with higher myocardial mass. Simultaneously, higher myocardial mass is correlated to a slight underestimation of CT-FFRml values.

Author Disclosures:

C.N. De Cecco: Consultant; Guerbet and Siemens. **A. Varga-Szemes:** Consultant; Guerbet. **C. Schwemmer:** Employee; Siemens. **U.J. Schoepf:** Consultant; Astellas, Bayer, Bracco, GE, and Siemens.

B-0777 14:08

Extra-cardiac findings at cardiac MR imaging: a single-center retrospective study over 14 years

F.C. Sokolowski, P. Karius, A. Lembcke, P.M. Wagner, A. Rodríguez Sánchez, M. Dewey; Berlin/DE (felix.sokolowski@gmail.com)

Purpose: To determine the prevalence and significance of extra-cardiac findings (ECF) in a large set of cardiac magnetic resonance (MR) imaging-examinations.

Methods and Materials: The institutional review board approved this retrospective, single-center study. A total of 4376 cardiac MR imaging reports of 3553 patients (age 37.4 ± 20 years, 60.8 % male) from 2000 to 2014 were included. Findings with a recommendation for follow-up were considered "major ECF". To analyze the association of indication, age and gender of patients with ECF, Poisson regression and computed incidence rates ratios (IRR) were evaluated.

Results: The overall prevalence of ECF was 34% (95% confidence interval (CI) 32.5-35.6). Major ECF were present in 3.4% (95% CI 2.9-4.1) while findings that changed patient management were found in 0.9% (95% CI 0.7-1.3). In the cases of congenital heart disease (CHD), the prevalence of ECF was higher as compared to myocarditis (IRR 6.0, $p < 0.001$) while the prevalence for major ECF was lower (IRR 0.2, $p < 0.05$). Increased patients' age was associated with more non-vascular ECF ($p < 0.001$). Female patients had the same probability of having an ECF as male patients (IRR 1.04 (95% CI 0.95 - 1.14)).

Conclusion: ECF in cardiac MR are present in about every third examination while relevant ECF that change patients' management can be found in about one in hundred patients. Our data suggest that it is important to involve well-trained radiologists in reading cardiac MR images, which often contain ECF if congenital heart disease is the clinical indication.

Author Disclosures:

M. Dewey: Author; Dewey is the editor of Coronary CT Angiography and Cardiac CT, both published by Springer, and offers hands-on workshops on cardiovascular imaging (www.ct-kurs.de), Associate editor of Radiology and European Radiology. Consultant; He is a consultant to Guerbet and one of the principal investigators of multi-center studies (CORE-64 and 320) on coronary CT angiography sponsored by Toshiba Medical Systems.. Patent Holder; PCT/EP2016/071551. Research/Grant Support; Heisenberg Program of the DFG for a professorship (DE 1361/14-1), the FP7 Programme of the European Commission for the randomized multicenter DISCHARGE trial (603266, HEALTH-2012.2.4.-2), The European Regional Development Fund (20072013 2/05, 20072013 2/48), the German Heart Foundation/German Foundation of Heart Research (F/23/08, F/27/10), The Joint Program from the German Research Foundation (DFG) and the German Federal Ministry of Education and Research (BMBF) for meta-analyses (01KG1013, 01KG1110, 01KG1110), GE Healthcare, Bracco, Guerbet, and Toshiba Medical Systems. Speaker; Lecture fees from Toshiba Medical Systems, Guerbet, Cardiac MR Academy Berlin, and Bayer (Schering-Berlex). Other; Institutional master research agreements exist with Siemens Medical Solutions, Philips Medical Systems, and Toshiba Medical Systems..

B-0778 14:12

Incremental diagnostic value of myocardial perfusion stress testing for intermediate obstructive lesions on coronary CT angiography in acute chest pain

E. Feldman, J. Bai, E. van Staaldin; Stony Brook, NY/US (eric.feldmann@stonybrookmedicine.edu)

Purpose: The purpose of our study is to evaluate the diagnostic yield of nuclear medicine stress testing in acute chest pain patients deemed to have borderline obstructive (50-69%) stenosis by coronary CT angiography (CCTA).

Methods and Materials: We retrospectively reviewed 4769 patients who presented to our emergency department (ED) with acute chest pain and had a CCTA. All patients had normal initial troponin levels, EKG and no prior history of obstructive coronary artery disease. The interpreting physicians' recommendations and any subsequent testing such as myocardial stress/rest perfusion imaging and coronary artery catheterization were recorded.

Results: Patient demographics included a mean age of 53.3 years and 53.3% (N= 2544) were female. The interpreting CCTA physicians recommended stress testing 8% (385/4769) of the time with 54% (209/385) of these patients receiving nuclear medicine myocardial perfusion imaging (MPI) within 30 days of the coronary CT. Of the patients receiving MPI, 93.8% (N=196) were interpreted as normal and 6.2% (N=13) abnormal. Of the patients with an abnormal MPI 62% (N=8) had a coronary catheterization with 37.5% (N=3) of these requiring percutaneous coronary intervention (PCI).

Conclusion: The vast majority of acute chest pain patients (93.8%) with intermediate (50-69%) obstructive lesions on CCTA will have normal findings on contemporaneous MPI.

Thursday

B-0779 14:16

Subclinical coronary and carotid atherosclerosis in asymptomatic high-risk patients

M. Guglielmo¹, A. Guaricci², V. Lorenzoni¹, S. Mushtaq¹, G. Muscogiuri¹, E. Maffei³, F. Cademartini⁴, R. Mark⁵, G. Pontone¹, ¹Milan/IT, ²Bari/IT, ³Monastier di Treviso/IT, ⁴Montreal, ON/CA, ⁵Maywood, IL/US (marco.guglielmo@ccfm.it)

Purpose: The aim of the study was to evaluate the incremental prognostic benefit of carotid artery disease and subclinical coronary artery disease (CAD) features in addition to conventional clinical evaluation in asymptomatic population.

Methods and Materials: Over a six-year period, 10-year-Framingham risk score (FRS) together with carotid ultrasound (CUS) and coronary computed tomography angiography (CCTA) were evaluated for the prediction of coronary heart disease (CHD) events.

Results: We enrolled 517 consecutive asymptomatic patients (63% male, 64±10 years of age). Median CACS was 34 [0-100]. Over a median follow-up of 4.4 [3.4-5.1] years there were a total of 53 CHD events (10%). Patients experiencing CHD had higher CACS, higher incidence of carotid disease, presence of CAD≥50%, and remodeled plaque as compared to patients without CHD events. At multivariable analyses, presence of CAD≥50% (HR=5.14, 95%CI: 2.1-12.4) and percentage of segment with remodeled plaque (HR=1.04, 95%CI: 1.03-1.06) independently predict CHD risk (P<0.001). The models adding CAD≥50% or percentage of segments with remodeled plaque resulted in higher discrimination and reclassification ability compared to a model based on 10-year FRS, carotid disease and CACS. Specifically, the C-statistic improved up to 0.75 with the addition of CAD and 0.84 when adding percentage of segments with remodeled plaque, while net reclassification improvement index was 0.86 and 0.92, respectively.

Conclusion: In an asymptomatic population, carotid disease assessment and CACS provide incremental prognostic value as compared to FRS. CAD- and plaque-positive remodeling further increase the CHD events prediction as compared to a model based on 10-year-FRS, carotid disease, and CACS estimation.

B-0780 14:20

Comparison of sports activity between ambitious triathletes with and without myocardial late gadolinium enhancement

J. Stáreková¹, B. Scherz, E. Tahir, M. Avanesov, M. Patten, J.M. Weinrich, K. Müllerleile, G. Adam, G.K. Lund; *Hamburg/DE (j.starekova@uke.de)*

Purpose: Long-term intensive training leads to functional and morphological adaptation of the heart. Incidence of myocardial fibrosis detected by cardiac MRI (CMR) is variable in competitive athletes. The purpose of this study was to analyse the differences in sports activity between triathletes with and without LGE.

Methods and Materials: 54 competitive healthy male triathletes (44±10 years) underwent a CMR performed on 1.5T Achieva (Philips), including LGE imaging. Image analysis was performed on cvi42 (Circle). CMR parameters are given as the mean of two independent observers. Physical fitness was determined by an exercise test. Competition history was reported using a standardised questionnaire with information about the number, distance and duration of completed events.

Results: In 9 out of 54 triathletes (17%) a non-ischaemic focal myocardial fibrosis of the left ventricle (LGE+) was detected. LGE+ triathletes had higher peak exercise systolic blood pressure (213±24 vs 194±26mmHg, p<0.05) and higher LV mass index (93±7 vs 84±11g/m², p<0.05) compared to LGE-triathletes. They participated more often in middle- and long-distance competitions and completed longer cumulative race distances at cycling (4418±3094 vs 1490±1114km, p<0.0001) and swimming (64±32 vs 31±25km, p<0.01).

Conclusion: There is high prevalence (17%) of focal non-ischaemic myocardial fibrosis among male triathletes. An increased systolic blood pressure during exercise, the amount and extent of race distances as well as unapparent myocarditis might be cofactors in the genesis of myocardial fibrosis. The clinical relevance of myocardial fibrosis in triathletes is currently unclear; however, it might be a foundation for future heart failure and arrhythmia leading to sudden cardiac death.

B-0781 14:24

Evaluation of dark blood LGE in assessing sub-endocardial MI and papillary muscle scar

L. Song¹, X. Ma¹, X. Zhao², L. Zhao¹, Y. Fan¹, B. Wu¹, Z. Wang¹, H. Chen¹; ¹Beijing/CN, ²Kunming/CN (linsheng.s1992@yahoo.com)

Purpose: To investigate whether modified dark blood late gadolinium enhancement (DB-LGE) technique can provide complementary diagnostic information in patients with subendocardial myocardial infarction (MI) and papillary muscle scars.

Methods and Materials: 37 patients (52±10 years, 34 male) with definitely diagnosed MI, were prospectively included. All patients underwent 3.0 T-cardiac-MR (Discovery MR 750W, GE, WI) with conventional LGE and DB-LGE acquisition. The image quality and infarcted size quantitative measurement were compared using paired T test and Bland-Altman analysis. The level of agreement between reviewers was assessed using intraclass correlation coefficients.

Results: Modified DB-LGE performed better on a visual assessment of the ability to differentiate MI from the blood pool. The images provided significantly higher contrast to noise ratio (6.3±2.3 vs 2.1±1.4, P<0.001) and a 4-fold higher signal intensity ratio (4.9±1.8 vs 1.3±0.3, P<0.001) between MI and blood pool signals. DB-LGE detected more subendocardial MI (26 segments, 263 vs 237) and papillary muscle with scars (21 vs 7). Combined with echocardiography, papillary muscle with scars was associated with potential mitral valve insufficiency. Infarcted size compared between conventional LGE and DB-LGE showed no statistically significant difference (18.7±10.1 vs 19.4±10.5, P=0.096). The interobserver agreement was good to excellent for MI detection.

Conclusion: DB-LGE improves the contrast between the MI and blood pool and helps in the identification of subendocardial MI and papillary muscle scars. The quantitative and qualitative comparison in this study revealed that DB-LGE may be an alternative method to LGE in clinical use.

Author Disclosures:

L. Song: Author; First author. **X. Ma:** Author; Corresponding Author. **X. Zhao:** Author; First author.

B-0782 14:28

Stress-rest CMR for the assessment of myocardial perfusion reserve index modification after coronary sinus stent implantation

A. Palmisano, G. Benedetti, F. Giannini, L. Baldetti, A. Del Maschio, F. De Cobelli, A. Esposito; *Milan/IT (palmisano.anna@hsr.it)*

Purpose: The management of patients with angina refractory to revascularisation procedures and medical therapy is a challenge. The implantation of a hourglass-shaped coronary sinus stent named "Reducer" seems to improve patients' symptoms. However, the physiopathological mechanism underlying clinical benefit is not clear. Aim of the study was to evaluate the modification in myocardial perfusion reserve occurring after "Reducer" implantation using a stress-rest CMR study.

Methods and Materials: 11 patients eligible for implantation of the "Reducer" underwent clinical evaluation (CCS Angina Class and 6minutesWT) and a stress-rest CMR study with dipyridamole before the implantation and after 3 months. Segmental and transmural distribution of inducible hypoperfusion and LGE was visually assessed. Myocardial perfusion reserve index (MPRI) of each segment and each myocardial layer (endocardium, midwall and epicardium) was measured using stress-rest CMR.

Results: All patients reported an improvement of ≥2CCS (p <0.0001) and a 60% increase in the average distance during the 6 minutes WT (p=0.004). MPRI significantly increased after "Reducer" implantation (1.29 vs 1.48; p<0.05). The analysis per cardiac segments showed an increase of MPRI in the ischemic territories (p=0.02334 for subendocardial ischaemia, and p=0.0001 for transmural ischaemia) while post-infarction necrotic area and healthy myocardial did not show significant changes (p=0.14 and p=0.12, respectively).

Conclusion: These preliminary data provide a new insight about the physiopathological mechanism of action of coronary sinus stent, suggesting its ability to determine a reduction of the inducible ischaemia of viable myocardial segments, associated to an improvement of angina symptoms and exercise tolerance.

B-0783 14:32

Myocardial fibrosis imaging based on T1-mapping and ECV measurement in diabetics: diagnostic value compared with LGE imaging

Y. Gao, Z. Yang, X. Liu; *Chengdu/CN (304789161@qq.com)*

Purpose: The objects of this study were: (i) evaluate the sensitivity and extent of myocardial fibrosis by extracellular volume fraction (ECV) and late gadolinium enhancement (LGE) in diabetes mellitus (DM) patients; (ii) ECV in diabetic individuals would be associated with the level of glycosylated hemoglobin (HbA1c) and duration of diabetes.

Methods and Materials: Thirty-six DM patients and 15 health controls who underwent cardiovascular magnetic resonance (CMR) including ECV measurement and LGE imaging were included. The 36 DM patients were classified in two group: a higher HbA1c group (HbA1c (%) ≥7.0; n=15) and a lower HbA1c group (HbA1c (%) <7.0; n=21). The independent-samples T test and Spearman rank correlation test were used for comparison and evaluated the relation.

Results: CMR measured ECV value was significantly higher in DM group compared with control group (36.1±3.8% vs. 31.1±1.7%, p<0.05), while the LGE percent was no difference in the two group (p=0.234). Between the higher HbA1c group and lower HbA1c group, the value of ECV was higher in the higher group (36.2±4.72 vs. 32.67±2.61, p<0.05). The spearman test showed a

moderate relationship between ECV and high HbA1c ($r=0.331$, $p<0.05$) and the same between ECV and duration of diabetes ($r=0.348$, $p<0.05$).

Conclusion: For DM patients, ECV might be more sensitive to early detect myocardial fibrosis than LGE. In addition, ECV was associated with HBALC and duration disease time, which could help to early heart condition monitoring.

B-0785 14:36

Prevalence of subclinical coronary artery disease by coronary computed tomography among low risk women after preeclampsia

G.A. Zoet¹, L. Benschop², R.P. Budde², C.J.M. de Groot³, A.H.E.M. Maas⁴, J.E. Roeters van Lennep², B.B. van Rijn¹, B.K. Velthuis¹, A. Franx¹; ¹Utrecht/NL, ²Rotterdam/NL, ³Amsterdam/NL, ⁴Nijmegen/NL (gzoet@umcutrecht.nl)

Purpose: The risk of coronary artery disease (CAD) is increased after preeclampsia, although traditional cardiovascular risk models often classify these women as low risk. This study compared prevalence of coronary artery atherosclerosis in low risk women with a history of preeclampsia to a population-based reference cohort.

Methods and Materials: Formerly preeclamptic women aged 45-55 years and low risk according to National Cholesterol Education Program (NCEP) were included in this analysis of a multicenter, prospective cohort study. Data were compared with women of similar age and ethnicity in the Multi-Ethnic Study of Atherosclerosis (MESA). Coronary artery calcium score (CACS) was calculated and contrast-enhanced coronary computed tomography angiography (CCTA) was performed in addition to routine cardiovascular risk assessment. Primary outcome was prevalence of CACS ≥ 0 Agatston Units (AU) and/or any coronary atherosclerotic plaques on CCTA. CACS were converted to adjusted MESA percentiles. Increased cardiovascular risk was defined according to the 2016 European guideline definition as CACS ≥ 300 AU or ≥ 75 th MESA percentile.

Results: Of 131 asymptomatic low risk women (mean age 48.3 \pm 2.8 years) with prior preeclampsia; 28% had CACS ≥ 0 , 46% had coronary atherosclerotic plaques on CCTA, and 3.9% showed $\geq 50\%$ luminal stenosis. Compared with the reference group, women after preeclampsia showed increased prevalence of CACS ≥ 0 AU (OR 2.3; 95% CI 1.4-3.8), any plaque on CCTA and increased cardiovascular risk (28% versus 15%; OR 2.2, 95% CI 1.4-3.7).

Conclusion: Asymptomatic women after preeclampsia aged 45-55 years commonly show subclinical CAD with increased cardiovascular risk compared with women from a population-based reference cohort.

B-0786 14:40

Quantitative oedema and late gadolinium enhancement thresholds for the diagnosis of myocarditis in suspect cases

M. Ali, C.B. Monti, F.S. Carbone, F. Secchi, P.M. Cannao', F. Sardaneli; Milan/IT (marco.ali90@gmail.com)

Purpose: To quantify and evaluate left ventricle oedema and late gadolinium enhancement (LGE) percentages in patients with acute myocarditis in order to establish thresholds for Lake Louise Criteria in cardiac magnetic resonance (CMR).

Methods and Materials: A total of 96 patients, 48 of which having a diagnosis of myocarditis and two CMR examinations from acute phase and follow-up (at least 3 months apart), and 48 age- and sex- matched healthy subject as control group with one CMR examination, were retrospectively analyzed. For both groups left ventricle oedema and LGE percentages were quantified after manual contouring using the semi-automated Medis Suite MR Software. After the assessment of data distributions' normality, parametric and non-parametric tests were used for comparison among groups. Thresholds were established using ROC curves formed comparing data from acute phase and controls.

Results: Comparison between oedema in acute phase (12.76%, IQR 8.73%-19.10%) and follow-up (6.69%, IQR 5.41%-9.00%), or with controls (6.41%, IQR 5.27%-7.67%), showing significant differences with both $p<0.001$. The comparison between LGE in acute phase (6.30%, IQR 4.51%-9.08%) and follow-up (4.29%, IQR 3.22%-7.19%), or with controls (4.27%, IQR 3.00%-5.09%), showed significant differences with a p-value of 0.001 and <0.001 , respectively. Thresholds were established for oedema at 7.9% with 93% sensitivity and 73% specificity, and for LGE at 4.30% with a sensitivity of 80% and specificity of 55%.

Conclusion: Quantitative thresholds of oedema and LEG may be used as clinical information useful in case of suspected myocarditis.

B-0787 14:44

Correlation between liver density and epicardial fat volume: biomarkers of coronary artery disease

C. Ferrari¹, G. Milanese¹, M. Silva¹, N. Giovanardi¹, M. Goldoni¹, E. Maffei², F. Cademartiri³, N. Sverzellati¹; ¹Parma/IT, ²Urbino/IT, ³Rotterdam/NL (cate.ferr@gmail.com)

Purpose: To test correlation between liver density and metabolic visceral adipose depot of epicardial fat, and whether it can act as biomarker of coronary artery disease (CAD) in patients undergoing cardiac computed tomographic angiography (CCTA).

Methods and Materials: The mean liver density (MLD) was quantified averaging density of three manual regions of interest (ROI); one in the left and two in the right lobe of the non-contrast computed tomography (CT) scans. Patients were stratified in steatotic (MLD ≤ 40 HU) and non-steatotic (MLD >40 HU). Epicardial fat volume (EFV) was quantified as the sum of voxels with density between -190 and -30 HU, within the volume outlined by the epicardial sheet. CAD was qualitatively evaluated and stratified in three groups: no CAD, non-obstructive CAD, and obstructive CAD. Continuous variables were reported as median and its interquartile range (IQR).

Results: In 1,181 patients, median MLD was 51.71 HU (IQR=13); median EFV was 87.19 ml (IQR=63.36). No CAD, non-obstructive CAD, and obstructive CAD were defined in 721 (61%), 296 (25.1%) and 164 (13.9%) patients, respectively. MLD and EFV were negatively correlated ($r_s=-0.364$; $p<0.001$); EFV was significantly higher in steatotic (114.21, IQR=84.02) compared with non-steatotic patients (82.03, IQR=58.23) ($p<0.001$). MLD was lowest in patients with obstructive CAD ($p<0.001$). In multivariate analysis, after adjustment for traditional clinical cardiovascular risk factors, MLD was associated with EFV ($p<0.001$) and with the presence of CAD ($p<0.001$).

Conclusion: MLD correlates with EFV and it can act as a potential biomarker for the stratification of CAD risk.

B-0788 14:48

Semi-quantitative evaluation of coronary microvascular dysfunction in paediatric patients with leukaemia using magnetic resonance first-pass perfusion imaging

Q. Zhao, X. Rong, Z. Yang, K. Diao, Y. Gao, Y. Guo; Chengdu/CN (zhaoqin626@foxmail.com)

Purpose: To evaluate the regional coronary microvascular dysfunction discrepancies in paediatric leukaemia patients with or without daunorubicin therapy by cardiac magnetic resonance (CMR) first-pass perfusion imaging.

Methods and Materials: Twenty-six paediatric patients with leukaemia, including 13 with daunorubicin therapy (treatment group) and 13 without daunorubicin therapy (non-treatment group) underwent CMR at rest. Imaging protocols included short axis cine, first-pass myocardial perfusion and late gadolinium enhancement (LGE). Left ventricular ejection fraction (LVEF), degree of LGE, perfusion parameters including maximal slope (Slopemax), time to peak (Tpeak) and peak signal intensity were all measured and compared by independent-sample t-test. The Spearman correlation test was used to calculate the relationships between LVEF, LGE, cumulative dose of daunorubicin and perfusion parameters.

Results: A total of 416 myocardial segments were analysed. Compared with non-treatment group, Slopemax decreased in treatment group (12.62 \pm 4.80 vs. 8.53 \pm 2.64, $p < 0.05$), while Tpeak increased (30.85 \pm 12.89 vs. 116.78 \pm 38.95, $p < 0.001$) in apical segments alone. LVEF and peak signal intensity were not shown significant difference in two groups. LGE was identified in 6 patients with daunorubicin therapy. In mid-ventricular segments, the cumulative dose of daunorubicin (mean 165.13 \pm 54.43 mg) was moderately associated with the degree of LGE ($r = 0.682$, $p < 0.05$).

Conclusion: Combined with LGE, CMR resting first-pass myocardial perfusion may help to achieve early diagnosis and clinical intervention of coronary microvascular dysfunction in paediatric patients with leukaemia, especially after the daunorubicin therapy.

B-0789 14:52

Cardiac magnetic resonance in prognostic stratification of patients with acute myocardial infarction and preserved ejection fraction

G. Daquino, I. Carbone, N. Galea, L. Agati, G. De Rubeis, C. Catalano, M. Francone; Rome/IT (gianmarcodacquino@gmail.com)

Purpose: This study was designed to investigate the prognostic role of early post-infarction CMR on long-term risk stratification of STEMI patients with preserved ejection fraction (LVEF $> 50\%$).

Methods and Materials: 55 PCI-reperfused STEMI patients were included. The median time between STEMI and CMR was 5 days (IQR 3 - 7). LV volumes and function, infarct size, early and late microvascular obstruction (MVO), and haemorrhage were measured. The primary endpoints were the incidence and CMR determinants of MACE at 5-year follow-up.

Results: During median follow-up of 2.5 years (range 1 to 5 years), 7 patients experienced MACE, yielding an annualized event rate of 2.71%. All CMR-based prognostic markers were no significantly different between MACE and no MACE patients, except for late MVO extent (0.9 ± 1.0 g vs. 0.07 ± 0.10 g; $p = 0.003$). Late MVO extent and the incidence of MACE at 5 years correlated moderately ($r = 0.411$; $p = 0.003$). ROC analysis identified late MVO extent > 1.4 g (AUC 0.647; 95% CI, 0.374 - 0.920; $p = 0.036$) as the best cut-off value for predicting the primary endpoint. Late MVO cut-off value > 1.4 g was a strong independent predictor of MACE at long-term follow-up (HR = 8.31; 95% CI, 1.52 - 45.65; $p = 0.015$).

Conclusion: CMR-based late MVO extent after primary PCI is a strong predictor of MACE at 5-year follow-up in patients with LVEF $> 50\%$. Remarkably, late MVO extent > 1.4 g provided prognostic insights leading to improved long-term risk stratification.

B-0790 14:56

4D flow MRI for the analysis of celiac trunk and mesenteric artery stenoses

F. Siedek, D. Giese, K. Weiss, S. Ekdawi, S. Brinkmann, W. Schröder, C. Bruns, D. Maintz, S. Haneder; *Cologne/DE (f.siedek@gmail.com)*

Purpose: This study aims to assess the feasibility of 4D-flow-MRI measurements in complex vascular territories; namely, the celiac artery(CA) and superior mesenteric artery(SMA).

Methods and Materials: In this prospective study, 22 healthy volunteers(HV) and 10 patients(PAT) were scanned at 3T. Blood flow parameters were compared between HV and PAT with stenosis of the CA and/or SMA as a function of stenosis grade characterised by prior contrast-enhanced computed tomography(CE-CT). 4D-flow-MRI acquisition covered the CA, SMA and adjusting parts of the aorta(AO). Measurements of velocity- (peak velocity[PV], average velocity[AV]) and volume-related parameters (peak flow[PF], stroke volume[SV]) were conducted. Further, stenosis grade and wall shear stress(WSS) in the CA, SMA and AO were evaluated.

Results: In PAT, prior evaluation by CE-CT revealed 11 low- and 5 mid-grade stenoses of the CA and/or SMA. PV and AV were significantly higher in PAT than in HV [PV: $p < 0.0001$; AV: $p = 0.03$, $p < 0.001$]. PF and SV did not differ significantly between HV and PAT; however, a trend towards lower PF and SV could be detected in PAT with mid-grade stenoses. Comparison of 4D-flow-MRI with CE-CT revealed a strong positive correlation in estimated degree of stenosis (CA: $r = 0.86$; SMA: $r = 0.98$). PAT with mid-grade stenoses had a significantly higher average WSS magnitude than HV ($p = 0.02$).

Conclusion: This study suggests that 4D-flow-MRI is a robust technique for the evaluation of complex flow characteristics in small vessels such as the CA/SMA. It approves comparable to the morphologic assessment of complex vascular territories using CE-CT but in addition offers the functional evaluation of flow parameters that goes beyond the morphology.

Author Disclosures:

K. Weiss: Employee; Philips Healthcare, Germany.

B-0791 15:00

Comparison of biphasic DE-CT with virtual unenhanced dual energy reconstruction and triphasic CT with true unenhanced images in patients with suspected acute bleeding

S. Walter, S. Schneeweiß, M. Maurer, M. Lescan, F. Bamberg, K. Nikolaou, A.E. Othman; *Tübingen/DE (sven.walter@uni-tuebingen.de)*

Purpose: The comparison of biphasic DE-CT with arterial and venous phase and conventional triphasic CT in patients with suspected active hemorrhaging.

Methods and Materials: With suspected active bleeding, ninety-seven consecutive patients underwent routine triphasic CT with true unenhanced (TNE), arterial and venous dual-energy phase. For simulation of virtual unenhanced images (VNE), which were generated using dual-energy venous phase, we used commercially available software. Both noncontrast datasets were assessed on image quality, noise, artifacts, sharpness and diagnostic confidence on a 5-point-scale (5 = best possible outcome) by two blinded readers, individually. Furthermore, datasets with conventional triphasic CT and biphasic DE-CT with VNE were compared in respect to presence/absence of active bleeding and type of bleeding.

Results: Acute hemorrhage was diagnosed in 37.1% (75% arterial) of the included subjects (mean age: 66.3 ± 14.5 years, 62% male). VNE images showed significantly lower overall image quality ($p < .001$) while compensation for artifacts was superior ($p < .001$) compared to TNE. No significant difference was seen in diagnostic confidence, both rated highly ($p \leq .012$). Hematoma was found in 48.6% in virtual and true unenhanced scans with no discordant findings by the radiologists (Kappa=1.0). Regarding presence and type of hemorrhage, triphasic and biphasic CT datasets showed almost perfect agreement with concordant findings in almost all cases (Kappa > 0.96).

Conclusion: VNE images showed comparable diagnostic confidence and an almost perfect agreement regarding presence and type of acute hemorrhage as TNE images. This indicates that biphasic DE-CT with VNE could replace triphasic CT for suspected acute bleeding, thus reducing scan time and radiation dose.

B-0792 15:04

Virtual monochromatic imaging improves the stent visualisation in lower extremity run-off CT angiography by dual-layer spectral detector CT

D. Zhang, Z. Jin, H. Xue, S. Yu, R. Wu; *Beijing/CN (cadina1984@163.com)*

Purpose: To evaluate the image quality and optimise keV level of VMI on stent visualisation in lower extremity CT angiography (CTA) compared with conventional 120 kVp image.

Methods and Materials: 24 patients undergoing run-off CTA on a dual-layer spectral detector CT were enrolled. All images were acquired at 120-kVp and monochromatic images from 40 to 150 keV with 10 keV increment and conventional 120 kVp images were reconstructed from the same scan due to the nature of spectral detector CT. The image quality was analysed on 12 monochromatic and conventional image sets. In-stent luminal diameter was measured twice using a calibre by 2 radiologists. The attenuation, noise, SNRs and CNRs were measured. Image quality was determined using a five-point scale.

Results: 30 stents were present. CNR and SNR were significantly higher with ≤ 70 keV-VMI (CNR: 16.0 ± 5.9 - 61.1 ± 27.5 ; SNR: 23.2 ± 11.7 - 48.6 ± 29.6) compared to conventional CT (CNR: 21.0 ± 8.6 ; all $p = 0.000$; SNR: 8.9 ± 10.4 ; all $p < 0.003$); there was no significant difference between 80keV-VMI (CNR: 16.0 ± 6.4 , $p = 0.197$; SNR: 17.4 ± 6.0 , $p = 0.417$) and conventional CT on CNR and SNR. Luminal stent diameters were increased at ≥ 70 keV (5.26 ± 1.27 - 5.43 ± 1.32 vs. 5.09 ± 1.34 , all $p < 0.001$). The score of image quality was highest at 80-90 keV-VMI (3.94 ± 0.25 - 4.00 ± 0.03 vs. 3.31 ± 0.48 , both $p = 0.000$).

Conclusion: 80 keV-VMI improves image quality and accuracy for stent evaluation at run-off CT angiography by dual-layer spectral detector CT.

B-0793 15:08

Magnetic particle imaging: safe use of endovascular stents

F. Wegner, T. Friedrich, N. Panagiotopoulos, J.P. Goltz, F.M. Vogt, M.A. Koch, T.M. Buzug, J. Barkhausen, J. Haegerle; *Lübeck/DE (franz.wegner@uksh.de)*

Purpose: Magnetic particle imaging (MPI) is a new three-dimensional imaging method. Cardiovascular imaging is seen as a promising future application of MPI. The purpose of this study was to evaluate the heating behaviour of endovascular stents as a safety aspect of cardiovascular MPI.

Methods and Materials: 21 commercially available endovascular stents of different sizes (diameter: 3-10mm, length: 11-99mm) and materials (stainless steel, nitinol, platinum-chromium, cobalt-chromium) were evaluated. They were implanted in silicone tubes matching the stent diameter and placed into a preclinical MPI scanner. The temperature change was measured with fiber optic thermometers over a period of 431 seconds of a standard imaging protocol.

Results: An increase of temperature of 0.1K (absolute accuracy of the temperature measurement) or more in relation to the reference temperature was defined as heating of the material. 12 stents showed heating of at least 0.1K or more. Four stents showed heating of more than 3.0K. The biggest temperature difference was 12.4K. The only significant predictor for the heating behaviour of the stents was their diameter. Pearson's correlation coefficient between the stent diameter and the square root of the temperature difference was $r = 0.96$.

Conclusion: In principle, MPI in the presence of endovascular stents is safely possible as most of the stents showed no or mild increase in temperature. If the increase of temperature of stents with a larger diameter is still measurable under (blood) flow conditions and thus relevant in vivo has to be further evaluated.

16:00 - 17:30

Sky High Stage

Neuro

MY 8

Neuro

Moderators:

Z. Merhemic; Sarajevo/BA
M. Vernooij; Rotterdam/NL

B-0794 16:00

Trajectories of imaging markers of the ageing brain: the Rotterdam study

E.J. Vinke, M. de Groot, V. Venkatraghavan, S. Klein, W.J. Niessen, M.A. Ikram, M.W. Vernooij; Rotterdam/NL (e.vinke@erasmusmc.nl)

Purpose: Brain changes in ageing may aid in better understanding of the ageing process and to distinguish normal ageing from age-related pathology. Longitudinal data in a broad age range are scarce, whereas these can provide important information on the rate of change. We estimated trajectories of several MRI markers based on longitudinal data and determined the sequence of these changing markers in ageing.

Methods and Materials: On 11,020 MRI scans (1.5T) from 5,428 persons aged 45 years and older from the population-based Rotterdam study, the following imaging markers were assessed: volumetric measures (total brain volume (TBV), grey matter (GM), white matter (WM), normal appearing white matter (NAWM), white matter lesion (WML), hippocampus), diffusion measures (fractional anisotropy (FA), mean diffusivity (MD)) and focal vascular lesions. Linear mixed models were used to estimate trajectories of change, for males and females separately. The sequence of changing MRI markers in ageing was determined by comparing these trajectories.

Results: Most markers show an exponential change with advancing age in the whole brain and per lobe, except for GM, which showed a more linear decrease with age. In general, females showed lower rates of change compared to males. The sequence in ageing markers was: TBV-MD-NAWM-WML-WM-hippocampus-GM-FA. The presence of vascular lesions shows an exponential increase with age, where males have a higher probability of having cortical and lacunar infarcts.

Conclusion: These data provide insight into the normal ageing process in the brain and its variability. Future studies can use this as a background to study pathology.

B-0795 16:04

The neural substrate of retinal neurodegeneration: the Rotterdam study

U. Mutlu, M. Ikram, G.V. Roshchupkin, P.W.M. Bonnemaier, J.M. Colijn, W.J. Niessen, M. Ikram, C.C.W. Klaver, M.W. Vernooij; Rotterdam/NL (u.mutlu@erasmusmc.nl)

Purpose: There is a growing evidence that markers of retinal neurodegeneration such as thinner retinal nerve fiber layer (RNFL) and ganglion cell layer (GCL), assessed on optical coherence tomography (OCT), are reflective of global brain atrophy. Yet, little is known on the relation of these layers with specific brain regions. Using voxel-based analyses (VBA) of both grey matter density and white matter microstructure, we aimed to unravel which specific brain regions are associated with these retinal layers.

Methods and Materials: We included 2235 persons (mean age: 67.3 years, 55% women) from the Rotterdam Study (2007-2012), who had gradable retinal OCT images and brain magnetic resonance (MRI) scans. Thickness of RNFL and GCL were measured on OCT images. Voxel-based morphometry protocols were applied to process MRI data. We investigated the association of retinal sublayers with voxels in brain MRI by performing linear regression models adjusted for age, sex, subcohort, education, axial length of the eye, intracranial volume, and cardiovascular risk factors.

Results: We found that thinner RNFL and GCL were associated with lower grey matter density of the visual cortex, and with lower fractional anisotropy and higher mean diffusivity in white matter tracts that are part of the optic radiation. Furthermore, thinner GCL was associated with lower grey matter density of the thalamus.

Conclusion: Thinner RNFL and GCL are associated with grey and white matter changes in the visual pathway suggesting that retinal degeneration on OCT may be specific for atrophy in the visual pathway rather than global brain atrophy.

B-0796 16:08

Multi-parametric 11C-methionine-MR/PET for brain tumour imaging utilising MR fingerprinting

L. Umutlu¹, M. Nittka², R. Kirsch², H. Quick¹, K. Herrmann¹, M. Gratz¹, M. Forsting¹, M. Forsting¹, ¹Essen/DE, ²Erlangen/DE (Lale.Umutlu@uk-essen.de)

Purpose: To investigate a novel approach of multiparametric tissue characterization of brain tumours based on morphologic, functional, metabolic and relaxometric properties utilizing integrated MR/PET and MR fingerprinting.

Methods and Materials: 25 patients with suspected brain tumours were enrolled in this trial. Examinations were performed on an integrated 3-tesla PET/MR system (Biograph mMR). PET and MR imaging was obtained simultaneously in one bed position after injection of 18F-FET. The (PET)MRI protocol included the following sequences: (1) TIRM, (2) FLAIR, (3) DWI, (4) SWI, (5) post-contrast MPRAGE imaging, (6) single-voxel spectroscopy and (7) MR fingerprinting. Histopathology served as the reference standard.

Results: An increase in malignancy from low-grade (grade 1-2) to high-grade glioma (grades 3, 4) was associated with increasing/positive PET uptake, contrast enhancement, increasing values in choline and choline/creatine as well as increasing T1 and T2 values. While low-grade astrocytoma did not show any pathologic tracer uptake or contrast enhancement, grade 3 gliomas showed increasing tracer uptake and increasing T1 and T2 values in MRF, respectively (mean values, grade 3 tumours: SUV_{max}:1.8 T/N: 1.3; T1: 1442/ T2: 122.9; mean values, grade 4 tumours: SUV_{max}: 3.4 T/N: 2.1; T1: 1752/ T2: 93.8).

Conclusion: The results of this novel approach of multi-parametric PET/MR imaging of brain tumours including MR fingerprinting demonstrate corresponding changes in tissue property based on the combined assessment of morphologic, functional, metabolic and relaxometric properties, indicating a correlation to the grading of brain tumours and leveraging tissue characterization to a unique level of multi-parametric assessment.

Author Disclosures:

M. Nittka: Employee; Siemens Healthineers. **R. Kirsch:** Employee; Siemens Healthineers.

B-0797 16:12

Sum score of cerebral small vessel disease relates to risk of stroke, dementia and mortality in the Rotterdam study

P. Yilmaz, M. Ikram, W.J. Niessen, M. Ikram, M.W. Vernooij; Rotterdam/NL (p.yilmaz@erasmusmc.nl)

Purpose: Cerebral small vessel disease (CSVD) is a major cause for brain damage leading to disability, morbidity and mortality. Markers of CSVD on magnetic resonance imaging (MRI) include white matter hyperintensities, lacunes, cerebral microbleeds and perivascular spaces. These have been separately associated with stroke, cognitive decline and dementia. However, combining the individual CSVD markers into a sum score might better capture the global CSVD burden. We investigated the association of CSVD sum scores with stroke, dementia and mortality.

Methods and Materials: 1655 stroke-free and non-demented participants (mean age 73.3 years, 54.4% women) of the prospective population-based Rotterdam Study underwent brain MRI (1.5 T) in 2005-2011 and were followed for major outcomes until 2015-2017. The CSVD sum score was composed by counting presence of each CSVD MRI marker (range 0-4). We determined the association of CSVD sum scores with risk of stroke, dementia and mortality using Cox models, adjusting for age, sex and also the Framingham Stroke Risk Profile (FSRP).

Results: During mean follow-up of 7.0 years, 66 participants developed stroke, 67 dementia and 308 died. CSVD sum scores ≥ 2 were associated with a higher risk of stroke and mortality (FSRP-adjusted hazard ratios (HR) 3.3, 95% CI 1.5-7.2; HR 1.5, 95% CI 1.0-2.0, respectively). A CSVD sum score of 3 showed an increased risk of dementia (FSRP-adjusted HR 2.8, 95% CI 1.1-7.3).

Conclusion: Higher CSVD sum scores on MRI are associated with a higher risk of stroke, dementia and mortality. Future steps are optimising the CSVD score including advanced imaging biomarkers.

B-0798 16:16

MRI brain atrophy can predict dementia in cognitively normal Parkinson's patients: a 7 year follow-up study

V. Pozdnyakova¹, R. Zivadinov², T.O. Dalaker¹, I. Dalen¹, N. Bergsland², K. Oppedal¹, K. Pedersen¹, O. Tysnes³, G. Alves¹; ¹Stavanger/NO, ²Buffalo, NY/US, ³Bergeb/NO

Purpose: Dementia has a significant impact on mortality and prognosis in patients with Parkinson's disease (PD). Previous magnetic resonance imaging (MRI) studies have demonstrated cross-sectional associations of hippocampal atrophy and lateral ventricle enlargement with cognitive impairment in PD. In

this 7-year population-based prospective longitudinal study of an incident PD cohort, we explored whether early volume loss in these anatomic areas can predict future dementia development in cognitively normal Parkinson's patients.

Methods and Materials: This MRI study enrolled 123 newly-diagnosed and drug-naïve PD patients without mild cognitive impairment according to Movement Disorder Society (MDS) level 1 criteria. All underwent standardised 3D-T1 weighted brain MRI on a 1.5T or 1.0T scanners at baseline. MRI images were segmented using SIENAX and FIRST software. Patients were followed prospectively over a 7-year period. Dementia was diagnosed according to MDS criteria. Multiple logistic regression analysis with adjustment for age, sex and education was performed to calculate odds ratios (ORs) with 95% confidence intervals (CIs) for incident dementia during follow-up.

Results: We found that total hippocampal volume (OR 0.54 [CI 0.32-0.91], $p=0.02$), right hippocampal volume (OR 0.29 [CI 0.11-0.78], $p=0.01$) and lateral ventricle volume (OR 1.03 [CI 1.00-1.05], $p=0.04$) at time of diagnosis were significant predictors of dementia development during follow-up, independently of age, sex and education.

Conclusion: Hippocampal atrophy and lateral ventricular enlargement in patients with PD are early signs of evolving cognitive decline. Volumetric MRI may be helpful in the prediction of dementia associated with PD.

B-0799 16:20

Quantitative study of noninvasive prediction of glioma IDH1 gene status by APT combined with ASL imaging

J. Wen; Shanghai/CN (wen123jianbo@163.com)

Purpose: The purpose of the study was to explore whether amide proton transfer (APT) and arterial spin labeling imaging (ASL) helped to noninvasively predict isocitrate dehydrogenase 1 (IDH1) gene status of glioma.

Methods and Materials: MTRasym (3.5 ppm) values (APT values) and CBF values were measured in the tumour parenchyma region. Normalised CBF was calculated according to the formula $nCBF = CBF_{tumour}/CBF_{cerebellum}$. Independent samples t-test and ROC analysis were used in this study. Logistic regression analysis was combined with the effective parameters of APT and ASL to calculate the overall correct prediction rate.

Results: 90 patients with both APT and ASL data. In LGG, the APT and nCBF values of wild-type IDH1 gene were higher than those of IDH1 mutant group ($p = 0.027$, $p < 0.001$). AUC = 0.802, 0.844, APT cutoff = 1.35 (%) and nCBF cutoff = 1.74, the sensitivity was 97% and 81.80%, the specificity was 60.2% and 62.2%. In HGG, the APT and CBF have statistical significance ($p = 0.004$, $p = 0.005$); AUC = 0.695, 0.712, respectively. APT cutoff = 3.24 (%), the sensitivity and specificity were 67.4% and 72.2%, respectively. When $CBF = 76.83 \times ml/100 \text{ g/min}$, sensitivity and specificity were 64.2% and 69.4%, respectively. Logistic regression combined with APT values and nCBF values to obtain the overall correct prediction rate is 78.7% and 86.8%, respectively.

Conclusion: APT and ASL provide a valuable new method for the noninvasive diagnosis of the IDH1 gene state of brain glioma. Combination of APT and ASL can improve the overall IDH1 gene prediction rate of glioma.

B-0800 16:24

Sex differences in resting-state cerebral activity alterations in internet gaming disorder

Y. Sun, Y. Zhou, Y. Wang, X. Han, W. Ding, J. Xu; Shanghai/CN (cjs1119@hotmail.com)

Purpose: Although there is evidence that the prevalence rates of internet gaming disorder (IGD) differs between males and females, no studies have examined whether such sex differences extend to brain function. This study was to explore the sex differences in resting-state cerebral activity alterations in IGD.

Methods and Materials: Thirty male participants with IGD (IGDm), 23 female participants with IGD (IGDf), and 30 male and 22 female age-matched healthy controls (HC) were recruited and underwent resting-state functional MR imaging. Maps of amplitude of low-frequency fluctuation (ALFF) and seed-based functional connectivity (FC) were constructed. A two-factor ANCOVA model was specified using SPM8, with sex (male, female) and diagnosis (IGD, HC) as the between-subject factors. When interaction effects occurred, post hoc pair-wise comparisons were performed using two-sample t tests within the interaction masks. We used Barratt impulsiveness scale-11 (BIS-11) to assess the behavioral inhibition function and Chen internet addiction scale (CIAS) to evaluate the severity of IGD. The correlations between the values of ALFF/FC and clinical scores were assessed using partial correlation analysis, respectively.

Results: The amount of ALFF in the orbit part of left superior frontal gyrus (SFG) significantly decreased selectively in IGDm, which was negatively correlated with BIS-11 score. Furthermore, orbit part of left SFG also showed decreased connectivity with posterior cingulate cortex, right angular gyrus, and right dorsolateral prefrontal cortex in IGDm.

Conclusion: Our findings suggest that sex-specific cerebral activity alterations existed in IGD, and these alterations have clinical relevance as a biomarker for the behavioral inhibition function of IGD.

B-0801 16:28

3D neuromelanin imaging for differential diagnosis between Parkinson disease and essential tremor: a multicenter retrospective study

Y. Kwon¹, W.-J. Moon¹, M. Park¹, H. Kim¹, J. Choi²; ¹Seoul/KR, ²Suwon/KR (quan01@gmail.com)

Purpose: Differentiation between Parkinson disease (PD) and essential tremor (ET) can be difficult. As neuromelanin-containing SN can be visualised on 3D-neuromelanin-sensitive imaging, we aimed to evaluate SN T1 hyperintensity and its diagnostic accuracy in patients with PD and ET.

Methods and Materials: This retrospective study enrolled 36 patients with PD and 22 patients with ET from two hospitals, between August 2016 and February 2017. 3D neuromelanin-sensitive T1-weighted sequence was obtained using two 3-T scanners. Two observers evaluated the SN T1 hyperintensity of each side of SN using a seven-point scale (with 0.5 increments from 0 to 3) according to the extent and degree of signal reduction of neuromelanin. Diagnostic performance of visual assessment was investigated using receiver operating characteristic analyses. Intra-rater and inter-rater agreement were calculated by weighted kappa.

Results: Reduction of SN T1 hyperintensity was significantly more prominent in PD than in ET ($p < 0.001$). The sum of neuromelanin scale from both sides provided AUC of 0.924 (95% CI, 0.823-0.977; sensitivity of 80.6% and specificity of 90.9%) with a threshold of at least 1.0. Inter-rater and intra-rater agreement was 0.902 and 0.900, respectively.

Conclusion: Visual assessment of SN T1 hyperintensity by expert reviewers provides high diagnostic accuracy in differential diagnosis between PD and ETs. We suggest that 3D neuromelanin imaging with a simple visual grading system can be helpful in clinically challenging cases.

B-0802 16:32

Ischaemic optic neuropathy: using track-weighted imaging to detect changes in the neuroretina

A. Attye¹, C. Jean¹, P. Remond¹, A. Lecler², F. Aptel¹, C. Chiquet¹, L. Lamalle¹, A. Krainik¹; ¹Grenoble/FR, ²Paris/FR (aattye@chu-grenoble.fr)

Purpose: Track-Weighted Imaging (TWI) was recently introduced as a tractography-based method with high anatomical contrast. We report the use of this method to explore the human retina in healthy volunteers and patients with anterior ischemic optic neuropathy (AION).

Methods and Materials: Twenty patients who had undergone MRI were included, and compared with 20 healthy volunteers. For the diffusion-weighted acquisition, we used a b-value of 1000 s/mm^2 and 60 directions distributed over four scans. We performed a constrained spherical deconvolution-based volumetric tractography method, whereby 10 million streamlines are initiated from seed points randomly distributed throughout the orbital area. We then reconstructed TWI maps with isotropic voxel size of 300 μm . We tested the effect of number of diffusion-weighted directions, ocular laterality, ocular dominance on healthy retinal fascicles distribution and the effect of the presence/absence of the fascicles on the visual field defect in patients with factorial analysis of variance.

Results: We found influence of ocular laterality, ocular dominance and number of diffusion-weighted directions on the neuroretinal healthy fascicle distribution. 8 out of 20 AION patients presented with complete absence of neuroretinal fascicle, side of the disease, which was correlated with visual field mean deviation at the 6 month-visit [$F_{(1, 17)} = 6.97$, $p = 0.016$]. 7 patients presented with a temporal fascicle in the injured eye, this fascicle presence was linked to visual field mean deviation at the 6 month-visit [$F_{(1, 17)} = 8.43$, $p = 0.009$].

Conclusion: The initial distribution of neuroretinal fascicle correlated with AION patients' visual outcome.

B-0804 16:36

Intracranial atherosclerotic plaque enhancement associated with ischaemic stroke: a study with three-dimensional high-resolution magnetic resonance vessel wall imaging

X. Bai, J. Lin; Shanghai/CN (baixueqin1@126.com)

Purpose: To evaluate the reproducibility of three-dimensional high-resolution magnetic resonance vessel wall imaging (HR-MRI) for demonstration of intracranial atherosclerotic plaque enhancement and to explore the relationship between plaque enhancement and ischemic stroke.

Methods and Materials: 52 patients with ischemic stroke underwent traditional head MRI, 3 dimensional-time of flight magnetic resonance angiography and HR-MRI on a 3.0T MRI scanner. Each identified intracranial plaque was classified as either culprit or non-culprit. The degree of plaque enhancement was graded by two independent radiologists, the degree of plaque enhancement and luminal stenosis were compared between culprit and non-culprit groups by using Mann-Whitney U test. Binary logistic regression

analysis was performed to assess the relation between the degree of plaque enhancement and culprit plaques.

Results: 118 plaques were identified in 52 patients with ischemic stroke (52 culprit and 66 non-culprit plaques). The degree of enhancement was rated as strong, moderate and none in 40, 9 and 3 culprit plaques, and in 4, 24 and 38 non-culprit plaques. Both intra-observer and inter-observer agreement were high for identification of plaque enhancement ($\kappa > 0.75$). For the group of culprit plaques, the degree of plaque enhancement ($Z = -7.787, P < 0.01$) and luminal stenosis ($Z = -5.327, P < 0.01$) were significantly higher than those in non-culprit group. Binary logistic regression analysis revealed that strong enhancement of plaques was independently associated with culprit plaques (OR: 74.3, 95%CI: 15.0-367.1, $P < 0.01$).

Conclusion: Three-dimensional HR-MRI detects enhancement of intracranial plaques with high reproducibility. Enhancement is more common in culprit plaques and is associated with the likelihood of ischemic stroke.

B-0805 16:40

Quantitative measurement of brain iron deposition in patients with peritoneal dialysis using susceptibility mapping

A.-N. Lin; *Kaohsiung/TW (miracoli1126.ai@gmail.com)*

Purpose: To evaluate different susceptibility of brain structures between patients with chronic kidney disease who underwent peritoneal dialysis & healthy controls using quantitative susceptibility mapping (QSM) & their correlations with clinical data.

Methods and Materials: For twenty-six patients (13 men & 13 women, mean age 54.46 year old) with peritoneal dialysis and twenty-six age & sex matched controls (12 men & 14 women, mean age 55.65 year old) were included in this prospective study. Magnitude image & phase image were reconstructed for susceptibility mapping to quantitate difference of iron deposition between patients & healthy controls. Partial correlation & stepwise multiple regression analysis between susceptibility & clinical parameters were calculated.

Results: The result confirmed that increased brain iron deposition in bilateral caudate nucleus, putamen, substantia nigra, red nucleus & right dentate nucleus in the patient group. There is no significant correlation between brain susceptibility & serum iron profile or dialysis efficiency. Also, negative correlation were found between susceptibility of basal ganglia and executive function, speech and language function and visuospatial function but positive correlation with Beck depression inventory which indicates increased iron deposition leads to cognitive impairment.

Conclusion: It is concluded that increased brain iron deposition in peritoneal dialysis patient was associated with cognitive dysfunction.

B-0806 16:44

Increased cerebral GABA concentration measured using ¹H MRS in the acute paediatric mTBI

P.E. Menshchikov, N. Semenova, I. Melnikov, M. Ublinskiy, T. Akhadov; *Moscow/RU (peeterem@gmail.com)*

Purpose: The vast majority of mild traumatic brain injury (mTBI) cases do not lead to abnormalities of brain structures. The correlation between early structural neuroimaging findings and long-term clinical outcomes is weak. The main aim of this work was to estimate changes in *in vivo* cerebral GABA and glutamate concentrations after acute mTBI using ¹H MRS.

Methods and Materials: Two groups of participants were included in the study: patients (n=11, mean age - 16±2 years, Glasgow Coma Score (GCS) - 15) with acute mTBI (mean time between trauma and MRI examination 40±20 hours); 8 healthy children (mean age - 16±1 years) without history of any TBIs. ¹H MR spectra were acquired on scanner Philips 3.0T Achieva TX using PRESS (NAA, creatine, choline signals) and MEGA PRESS (GABA and glutamate signals) pulse sequences. All voxels in size of 25x25x30 mm were located in the frontal lobe.

Results: The main effect on the [GABA] was found ($Z = 2.03, p < 0.05$), with the patients having higher [GABA] as compared to the control group (36%) (Fig. 2). Absolute concentrations of NAA, tCho, tCr and glutamate were unchanged.

Conclusion: This study for the first time revealed increased cerebral [GABA] as well as disorders in the [GABA]/[GLX] balance in the paediatric acute mTBI. The most likely cause of [GABA] increase is growth of free pool of GABA (non-related to GABA receptors). Postconcussion changes of neurotransmitter revealed in the present study could be promising for understanding of functional consequences of MRI-negative TBI.

B-0807 16:48

A preliminary study on non-invasive prediction of IDH1 gene status in glioblastoma by intravoxel incoherent motion MR imaging

J. Wen; *Shanghai/CN (wen123jianbo@163.com)*

Purpose: To investigate the value of intravoxel incoherent motion MR imaging (IVIM) in non-invasive judgment of IDH1 gene status of diffuse glioblastoma.

Methods and Materials: Prospective collection of diffuse glioma patients in 95 cases, the tumour real area of the IVIM imaging parameters: (F), average

apparent diffusion coefficient (ADCmean), fast apparent diffusion coefficient (fastADC), diffusion coefficient (DDC), and pseudo-diffusion coefficient (D*). Calculate the parameters of the contralateral white matter area after the parameters: (NrF, nrD, nrD*nrADC). The effective parameters were used to plot the ROC curve. The correct predictive rate of IDH1 gene was calculated by logistic regression analysis.

Results: The values of F, ADCmean, nrADCmean and DDC were significantly higher in the low-level group than in the wild-type low-grade group ($P < 0.05$). The F value and fastADC values of the mutant high-level group were significantly lower than those of the wild-type high-level group ($P < 0.05$). The sensitivity and specificity of ROC AUC were 0.125, 0.67, 0.65 and 0.780; ADCmean were 1.182, 0.750, 0.875 and 0.842, respectively, and nrADCmean were 1.481, 0.762, 0.875 and 0.899, respectively, DDC were 1.193, 0.792, 0.750, 0.774, respectively. High-grade glioma combined with F and fastADC concluded that the correct predictive rate of IDH1 gene was 82.5% and the likelihood ratio was 46.07.

Conclusion: IVIM examination provides a new method for non-invasive diagnosis of diffuse glioblastoma IDH1 gene status before surgery.

B-0808 16:52

In vivo molecular profiling of human glioma using dynamic susceptibility contrast magnetic resonance perfusion imaging

J.-M. Hempel, J. Schittenhelm, B. Bender, M. Skardelly, G. Tabatabai, S. Castaneda Vega, U. Ernemann, U. Kloese, C. Brendle; *Tübingen/DE (johann-martin.hempel@uni-tuebingen.de)*

Purpose: To assess the diagnostic performance of dynamic susceptibility contrast perfusion magnetic resonance perfusion imaging (DSC-MRI) for in vivo human glioma molecular profiling.

Methods and Materials: One hundred patients with histopathologically confirmed glioma who provided written informed consent were retrospectively assessed between 01/2016 and 02/2017 in two prospective trials that were approved by the local institutional review board. Cerebral blood volume (CBV) metrics from DSC-MRI were assessed, and histogram parameters of rCBV results were compared among WHO 2016-based histological findings and molecular characteristics. A classification and regression tree (CART) algorithm with 10-fold cross-validation was used to calculate the diagnostic accuracy.

Results: The 90th percentile (C90) of rCBV was significantly lower in patients with the isocitrate-dehydrogenase 1/2 (IDH1/2) mutation (2.86 ± 1.21 ; $p < 0.001$) and loss of alpha-thalassaemia/mental retardation syndrome X-linked (ATRX) expression (2.23 ± 0.91 ; $p < 0.001$) than in those with the IDH1/2 wild type (4.78 ± 2.34) and who maintained ATRX expression (4.30 ± 2.02), respectively. The C90 of rCBV correctly predicted ATRX expression in 86.4% and the IDH1/2 mutation in 70.4% of patients. The standard deviation (SD) of rCBV was significantly higher in glioblastoma with methylated O6-methylguanine DNA methyltransferase (MGMT; 1.99 ± 0.73 ; $p = 0.001$) than in those with unmethylated MGMT (1.20 ± 0.45). The SD of rCBV correctly predicted MGMT methylation status in 81.8% of all primary glioblastomas.

Conclusion: DSC-MRI may provide insight into the human glioma molecular profile regarding IDH1/2 mutation status, ATRX expression, and the MGMT methylation profile. Thus, rCBV is a promising potential biomarker for glioma.

Author Disclosures:

J. Schittenhelm: Grant Recipient; Else Übelmesser Foundation (30.19845).

B-0810 16:56

Prediction of postoperative cerebral hyperperfusion: a study using territory arterial spin labelling (tASL)

T. Lin, Y. Lyu, Z. Zuo, H. You, J. Qu, B. Hou, F. Feng; *Beijing/CN (jasminelly@163.com)*

Purpose: Cerebral hyperperfusion (CH) or hyperperfusion syndrome (CHS) is a rare complication after revascularisation, but may lead to intracranial haemorrhage. The objective of this study was to investigate the relationship between postoperative hyperperfusion and perfusion territories change.

Methods and Materials: We retrospectively reviewed 22 patients with severe unilateral or bilateral carotid stenosis. The perfusion volume and cerebral blood flow of each brain feeding vascular (left/right internal carotid artery and vertebralbasilar artery) before and within 3 days after carotid endarterectomy (CEA) were measured using tASL and ASL, respectively. Volume fraction (perfusion volume/brain volume) of each territory was calculated. Patients were classified into three groups: only with postoperative CBF increase $\geq 100\%$ (CH group, n=7), CBF increase with headache right after surgery on the ipsilateral side and/or with deteriorated consciousness, focal neurological deficits or seizure (CHS group, n=2) and normal perfusion group (n=13), both CH and CHS group were considered as hyperperfusion group (n=9).

Results: Perfusion volume fraction before CEA was significantly smaller in the hyperperfusion group compared to normal perfusion group ($14.05\% \pm 11.51\%$ vs $31.55\% \pm 11.45\%$, $P = 0.02$). And perfusion fraction significantly increased after surgery in the hyperperfusion group compared to normal perfusion group ($19.53\% \pm 9.76\%$ vs $4.75\% \pm 7.65\%$, $P = 0.001$).

Conclusion: Postoperative markedly increased CBF is associated with smaller perfusion volume before surgery and large perfusion volume increase after surgery in the stenosis side, which may be predictors for postoperative hyperperfusion.

B-0811 17:00

Characteristics of plaques and lenticulostriate arteries in stroke patients by whole-brain vessel wall

F. Wu, Q. Yang, C. Zhang; Beijing/CN (chaozhang0328@hotmail.com)

Purpose: The aim of the present study was to evaluate atherosclerotic plaque characteristics and lenticulostriate arteries (LSA) together by novel whole-brain high-resolution magnetic resonance imaging (WB-HRMRI) and to establish their relationship with different infarction patterns.

Methods and Materials: Stroke patients with artery-to-artery (A-to-A) embolism or branch atheromatous disease (BAD) were prospectively enrolled and WB-HRMRI was performed. The characteristics of the intracranial atherosclerotic plaques and distribution of LSA branches were compared between the two groups.

Results: Fifty-eight first-time stroke patients were finally enrolled including 32 A-to-A embolism and 26 BAD. Hyperintensity plaques (HIP) and plaque surface irregularity were more frequently observed in A-to-A embolism group than in the BAD group ($P < 0.001$ and $P = 0.028$, respectively). Patients with A-to-A embolism infarction had severer stenosis degree than patients with BAD infarction ($P = 0.001$). The average number and length of visualized LSA branches significantly reduced in patients with BAD compared with A-to-A embolism ($P = 0.025$ and $P = 0.029$). Logistic regression analysis showed that HIP was independently associated with A-to-A embolism infarction, while reduction in the numbers of LSA branches was independently associated with BAD infarction. Odds ratios for HIP and the numbers of LSA branches were 12.21 and 2.07 (95% confidence interval 2.41 - 61.83 and 1.06 - 4.07; $P = 0.002$ and 0.034) respectively.

Conclusion: A-to-A embolism infarction has distinct vascular pathophysiologies in terms of plaque and LSA characteristics compared with BAD. WB-HRMRI enables the combination of vessel wall and LSA imaging which can predict future stroke.

B-0813 17:04

MRI assessment of brain grey matter structural changes in severe nicotine dependency

A. Dong; Zhengzhou/CN (845516273@qq.com)

Purpose: To evaluate brain structure changes in mild nicotine dependency by voxel-based morphological method.

Methods and Materials: In this study, 77 severe nicotine-dependent (FTND < 6 score) and 37 non-smoking healthy volunteers were scanned with Siemens Skyro 3.0T magnetic resonance scanner. Subjects were routinely MRI (to exclude intracranial lesions) sequence and 3D-MPRAGE sequence. SPM8 pretreatment based on Matlab was used to analyse the data. The SPM8 software was used to analyse the independent sample t test (FWE correction, $P < 0.001$) with the smoking group and the control group. The spearman correlation analysis was used to analyse the difference between severe nicotine-dependent group and smoking data with SPSS 17.0.

Results: Compared with the control group, the mild nicotine-dependent group exhibited decreased GMV in bilateral thalamus, bilateral supramarginal gyrus (right supramarginal gyrus, left supramarginal gyrus), and the area with elevated GMV was not found (FWE corrected, $P < 0.05$, cluster size > 318 voxels). Bilateral thalamus, right supramarginal gyrus GMV were significant negatively correlated with smoking index and tobacco years, and right thalamus was negatively correlated with daily smoking ($\alpha = 0.05$, $P < 0.05$).

Conclusion: The changes of brain structure among smokers mainly focused on reward-related pathways and marginal systems, and part of the grey matter volume of brain regions is related to smoking behaviour data. The results would help for further study into the mechanism of brain function in chronic smokers.

Scientific Sessions

Friday, March 2

08:30 - 10:00

Sky High Stage

Interventional Radiology

MY 9

Interventional Radiology

Moderators:

R.F. Dondelinger; Liège/BE
P.M. Kitrou; Patras/GR

B-0814 08:30

Two year follow-up: results after acute stroke endovascular thrombectomy

A. Balodis, M. Radzina, K. Kupcis, E. Milglane, J. Savlovskis, H. Kidikas, A. Veiss; *Riga/LV (arturs.balodis@gmail.com)*

Purpose: Endovascular thrombectomy (ET) in acute ischemic stroke treatment with large artery occlusion after 3 months has shown a good neurological result, however there are only few long term results available. The aim of our study was to analyze ET functional outcome after 2-years from initial treatment, in patients with acute ischemic stroke due to large artery occlusion.

Methods and Materials: The prospective study included 91 patients hospitalized within time window of 8 hours with middle cerebral artery M1 or internal carotid artery occlusion. Sixty-one (67%) of them received thrombolysis followed by ET, 30(33%) - thrombectomy solely. Modified Rankin scale (mRS) was used to evaluate early therapy results and late results at 3 months and 2 years.

Results: There were 44(48%) women and 47(52%) men analyzed with mean age 67.66±11.9(SD) years. Successful recanalization rate after ET was 90% (TICI-2b,3). Median mRS (0-2): after discharge was 29(32%), 3 months mRS was 36(40%), p=0.01 and 2 years mRS (0-2) was 34(37%), respectively. No statistical difference between 3mo and 2y, p=0.32. Two years follow up mortality was 32(35%) compared to 13(15%) in 3 months, difference was statistically significant. 44% of patients with severe disability mRS 4-5 at 3 months were with the same status after 2 years (3mo vs 2y: 23(25%) and 10(11%), respectively).

Conclusion: Our results show that after 2 years ET can show high number of good long term functional outcome. The majority of high mortality rates after 2 years resulted from patient group with severe neurological deficit mRS(4-5) at 3 months.

B-0815 08:34

Comparison between not-stent retriever and stent retriever mechanical thrombectomy for the intra-arterial acute ischemic stroke treatment

E. Puoglielli, R. Lattanzi, V. Di Mizio, S. Roiati, F. Navarra, V. Di Egidio; *Teramo/IT (edopug@hotmail.com)*

Purpose: The objective of this work is to compare the ability to remove of the thrombus, the final TICI and outcomes for non-stent retriever nST and stent retriever ST thrombectomy for the AIS treatment.

Methods and Materials: between April 2009 and September 2017, 220 patients (mean age 62,7y) were treated for AIS with mechanical thrombectomy, fulfilled the classic inclusion criteria of EST, using retrievable stents or aspiration. NCCT, CTP-CTA and DSA were used for imaging. Primary outcomes were: the 90 days ≤ 2 mRS, the TICI recanalization rate, the incidence of symptomatic intracranial hemorrhages (ICHs). Patient's age, sex, etiology of occlusion, time of treatment, median NIHSS at presentation, mRS at discharge were correlated using univariate analysis and multivariate regression.

Results: mNIHSS at presentation was 24 (ranged 9-33). Sites of arterial occlusion before treatment were: M1-M2 156/220 (70.90%), intracranial carotid 8/220 (0.03%), M2-M3 14/220 (6.36%), tandem occlusion 6/220 (2.72%), extracranial internal carotid isolated occlusion 5/220 (2.27%), P1 7/220 (3.18%), basilar trunk 24/220 (10.90%). Statistical significant differences were observed between ST group 123/220 patients (55.90%) and nST 97/220 (44.09%) one in terms of ≤ 2 mRS at discharge [21.24% [nST] vs 64.73% [ST]; p<0.005] and high TICI Score 2b-3 recanalization rates (77.32% [NSR] vs 98.51% [SR]; p < 0.005).

Conclusion: clot composition and anatomic factors could explain the difference on nST vs ST outcomes. A combined multimodal approach for AIS treatment using the two different methods could lead to very high recanalization rates with low complications.

B-0816 08:38

Endoscopic ultrasound-guided hybrid therm ablation in patients with stage III pancreatic adenocarcinoma: a clinical study with radiological perspectives

M. Barbera, S. Testoni, E. Dabizzi, S. Gusmini, M. Petrone, A. Esposito, A. Del Maschio, P. Arcidiacono, F. De Cobelli; *Milan/IT (barbera.maurizio@hsr.it)*

Purpose: A third of cases of pancreatic cancer is locally advanced and unresectable (LAPC) at diagnosis. Endoscopic ultrasound-guided hybrid cryotherm ablation (EUS-HTP) combines radiofrequency with cryogenic cooling, reaching the pancreas also when inaccessible through percutaneous approaches. Aim of this ongoing study was to evaluate the feasibility, safety and post-procedural imaging findings of this novel therapy.

Methods and Materials: 35 consecutive patients with LAPC were prospectively enrolled at the Gastrointestinal Endoscopy Unit of our tertiary referral Center for a singular or repeated EUS-HTP session. The absolute tumor volume (ATV) and ablation necrotic volume (ANV) were measured in timely close follow-up CECT scans and, if suitable, MR images by an advanced visualisation tool. Data were analysed by descriptive and non-parametric statistics.

Results: EUS-HTP resulted feasible in 26 patients (74.3%), except in 9 cases due to tumor stiffness or vessel interposition. CT identified the ANV in 25 patients (96%), whereas MR in all cases when performed; no statistical difference was found in the ANV measure between CT and MRI (P = 0.664). The mean ANV was 12.44 mm³ (range 1.3-56) with an average ablation percentage of 34.9% (range 3-65). The median post-HTP overall survival (OS) time was 6 months (range 1-22), increasing from 5 to 9 months with more than one session (P = 0.066). Early complications occurred in 11 patients (37%), all mild except one moderate, conservatively treated.

Conclusion: EUS-HTP is a safe and feasible therapy for patients with LAPC; both CT and MRI result useful for follow-up after treatment.

B-0817 08:42

Impacts of related risk factors on the efficacy of interventional treatment towards intractable postpartum haemorrhage

C. Zhao; *Beijing/CN (zhaochaoxy@163.com)*

Purpose: To investigate the risk factors that impact the efficacy of interventional treatment of intractable postpartum haemorrhage (IPH).

Methods and Materials: A total of 64 IPH patients were admitted and received interventional treatment, among whom 57 cases were successfully treated (bleeding stopped), while 7 cases failed. The clinical data of the success group and the failure group were observed for the multivariate analysis of the possible reasons that might cause haemostatic failure.

Results: The univariate analysis of each suspected factor of haemostatic failure showed that history of uterine scar, combined use of uterotonics, uterine inertia, and placenta exhibited statistically significant differences between the 2 groups (p<0.05); the multivariate logistic regression analysis showed that history of uterine scar and combined use of uterotonics were the risk factors for the interventional treatment failure of IPH, with OR values of 11.23 (95% CI 1.26~100.22) and 12.83 (95% CI 1.05-156.34), respectively.

Conclusion: History of uterine scar and combined use of uterotonics were the risk factors for interventional treatment failure of IPH.

B-0818 08:46

Is portal vein embolisation of liver segment IV mandatory before extended right hemihepatectomy?

C. Loberg, S. Keil, F. Goerg, C.K. Kuhl, P.L. Bruners; *Aachen/DE (cloberg@ukaachen.de)*

Purpose: Portal vein embolisation (PVE) is an established procedure to introduce hypertrophy of the future liver remnant (FLR) in patients scheduled for extended right hemihepatectomy (ERH). There is uncertainty as to whether PVE needs to include the branches to the left medial segment (S4), or whether induction of hypertrophy is sufficiently achieved if right PV branches (S5-8) are occluded. We analysed hypertrophy rates of patients undergoing PVE of S5-8 branches only.

Methods and Materials: PVE was done prior to ERH when the anticipated volume of FLR was < 30% of the total liver volume in patients with compromised, or < 25% of the total liver volume in patients with normal liver function. PVE of the right portal venous system (S5-8) was performed. Liver volumetry was done on contrast-enhanced CT acquired within 1 week before and 3-4 weeks after PVE.

Results: 140 patients were included. Technical success was achieved in (99%) of patients. At follow-up CT volumetry showed sufficient hypertrophy by an average of 36% (range, 25-39%) in (97%) . A total 98 of the 135 patients with sufficient hypertrophy (73%) went on to ERH. In 37/135 patients (27%), hepatectomy was ultimately not performed because of extrahepatic tumour spread. A total 8/135 patients (6%) had new lesions in the left liver (FLR) at

post-PVE-CT; these patients underwent ERH with additional percutaneous local ablation.

Conclusion: PVE of portal vein branches to segments 5-8 is sufficient to induce satisfactory hypertrophy of the FLR to allow extended right hepatectomy.

B-0820 08:50

Combined antegrade and retrograde approach in iatrogenic ureteral injuries: the rendez-vous technique

G. Pacella, E. Faiella, D. Santucci, A. Alfonsi, C. Altomare, B. Beomonte Zobel, R.F. Grasso; *Rome/IT (giuseppina.pacella23@gmail.com)*

Purpose: Ureteral injuries are the most common urologic complications occurring during abdominal and pelvic surgery, with an incidence ranging from 1% to 10%. The choice treatment is generally open surgery, but the rendez-vous technique represents an alternative strategy. Our study evaluates the feasibility and effectiveness of the rendez-vous technique in case of complete iatrogenic ureteral injuries.

Methods and Materials: From 2012 to 2017 we treated 20 patients with the rendez-vous technique for complete iatrogenic ureteral injuries: 12 patients underwent to radical hysterectomy, 3 to radical cystectomy, 5 to rectal anterior resection. The diagnosis was supported by CT-urography and antegrade pielography. The rendez-vous technique was performed by the introduction of a gooseneck snare through the nephrostomic access to capture the end of the retrograde ureteral wire, which was retrieved from the percutaneous sheath to gain a through-and-through access. A double J stent was antegradely inserted and a nephrostomy tube was kept in place.

Results: The rendez-vous technique was successful in all cases with resolution of the ureteral leak. In all patients the nephrostomy tube was removed after 30 days. After performing CT-urography the stent was removed permanently in 16 patients after 6 months and in 4 after 9 months. Only three cases showed a locale post-treatment stenosis treated with surgical ureteral reimplantation. In the other cases there was no ureteric stricture at the site of the previous injury.

Conclusion: The rendez-vous technique is an effective minimally invasive procedure that can be used to restore the continuity of the ureter avoiding open surgical.

B-0821 08:54

MR-guided focused ultrasound (MRgFUS) thalamotomy for the treatment of medically refractory essential tremor

S. Dababou¹, C. Marrocchio¹, C. Halpern², J. Henderson², A. Napoli¹, C. Catalano¹, K. Butts Pauly², V. Santini², P. Ghanouni²; ¹Rome/IT, ²Stanford, CA/US (susy150791@gmail.com)

Purpose: Clinical outcome assessment of MRgFUS thalamotomy for the treatment of medically-refractory essential tremor.

Methods and Materials: 8 patients underwent unilateral transcranial MRgFUS(ExAblate-InSightec)ablation within the ventral intermediate nucleus of the thalamus for the treatment of medically refractory essential tremor. The primary endpoint was the reduction in the dominant hand tremor score, evaluated by Part A and Part B of the Clinical Rating Scale for Tremor(CRST) at 3 months. The secondary endpoints were the changes at 3 months in the quality of life(Questionnaire for Essential Tremor(QUEST)), and in the subject daily functionalities(Part C of the CRST); and in the durability of these changes at 6 and 12-month follow-up visits.

Results: At 3-month follow-up 8 patients were assessable. The dominant hand tremor decreased by 57% from a mean baseline score of 20.5+/-3.4 to 8.8+/-4.6(P=0.01). Quality of life scores improved by 25% from a pre-treatment value of 57.1+/-17.7 to 42.9+/-14.1(P=0.01), and disability scores also reduced by 65% from a baseline value of 18.9+/-4.4 to 6.6+/-4.0(P=0.01). Symptom improvement was durable with 9.0+/-3.6(P=0.01) and 9.3+/-5.0(P=0.01) dominant hand tremor score at 6 and 12 months respectively. The most common immediate adverse events were related to frame placement. At 12 months, 2 patients reported a mild sense of imbalance.

Conclusion: MRgFUS thalamotomy has shown positive and promising results in reducing dominant hand tremor in medication-refractory essential tremor.

B-0822 08:58

CT-guided percutaneous synovial cyst rupture using a 11G Jamshidi needle: early experience and results of a novel technique

S. Islam, D. Johnson; *London/UK (s.islam@imperial.ac.uk)*

Purpose: Lumbar synovial cysts are an increasingly reported cause of radiculopathy and back pain. Percutaneous treatment offers a minimally invasive alternative to high-risk surgery. Percutaneous techniques involve imaging to guide a small calibre needle into the facet joint. In our experience this leads to a high rate of recurrence requiring future surgery. We trialled a novel approach using a large bore needle under CT guidance in the hope of achieving increased disruption of the fibrocartilaginous wall and reducing

recurrence. The purpose of the study was to review the early results of percutaneous synovial cyst treatment using a 11G Jamshidi needle.

Methods and Materials: 9 sedated patients underwent percutaneous synovial cyst rupture through a translaminar approach, using a 11G Jamshidi needle under CT guidance. Following rupture as demonstrated by contrast injection, 80mg depomedrone + 1ml bupivacaine was injected into the rupture bed. Patients were followed up from 6 weeks to 4.5 years post-procedure.

Results: At 6-week follow-up there were no significant complications and only 1 patient had required surgery for persistent symptoms. At long-term follow-up, 5 patients remained asymptomatic, with 3 patients requiring a repeat intervention.

Conclusion: There is currently no standardised technique for percutaneous synovial cyst treatment and the previously published outcome data are based on using small 20/22G needles. The number of patients requiring future surgery in these studies varies from 10 to 55%. This is the first time a large bore needle has been used to achieve cyst rupture, demonstrating its safety and efficacy.

B-0823 09:02

Performance and safety of pancreas biopsy: are there more complications made by routes of risk?

J.M. Sastoque G, S. Lombardo, J.J. Espejo Herrero, I. Domínguez Paillacho, M. Perez Montilla, L.J. Zurera Tendero; *Cordoba/ES (jorgem4402@hotmail.com)*

Purpose: Retrospective analysis of pancreas CNB performance and overall safety assessment comparing biopsies performed through risk routes (liver, gastrointestinal tract) in relation to a direct route (peritoneal or retroperitoneal).

Methods and Materials: Biopsies of pancreatic lesions performed between April 2010 and September 2017 were retrospectively analysed. Biopsies were performed with 16 and 18G needles. The CT images, histopathological results and details of the procedure as route of approach and the associated complications were evaluated. If the biopsy was negative for malignancy, the clinical history was reviewed to evaluate the final etiology of the pancreatic lesion.

Results: CNB was performed on 83 patients (50 men, 33 women) with mean age of 62.65 years through different routes with 16G (n = 35) and 18G (n = 48) needles. The sensitivity, specificity, positive and negative predictive value of the total study were 82.53%, 100%, 100% and 64.51%, respectively. A total of 24 biopsies were performed with transperitoneal approach, 1 retroperitoneal and 58 with risk routes (colon (n = 3), stomach (n = 34), duodenum (n = 1), jejunum = 8), pleura (n = 1) and the remainder combining these routes (n = 10). The rate of major complications was 4.81% (n = 4) and minor 3.61% (n = 3); without finding a significant difference between the direct peritoneal approach (n = 3) and through risk routes (n = 4), neither with the needle size.

Conclusion: Pancreatic percutaneous CNB using the trans-organ approach is a safe and effective technique to diagnose malignant pancreatic lesions.

B-0824 09:06

TACE using mitomycin with or without irinotecan for HCC in European patients

T. Gruber-Rouh, K. Eichler, N.-E. Nour Eldin, N.N.N. Naguib, M.C. Langenbach, T.J. Vogl; *Frankfurt a. Main/DE*

Purpose: To evaluate survival data and local tumour control in two groups with different chemotherapeutic agents in TACE treatment of HCC patients.

Methods and Materials: A total of 28 patients (mean age: 67.3 years) with HCC were repeatedly treated with chemoembolisation in four-week intervals. Twenty patients suffered of BCLC-stage-B, while eight patients obtained chemoembolisation for bridging purpose (BCLC-Stage-A). In total, 98 chemoembolisations were performed (mean 3.4 treatments/patient). The administered chemotherapeutic agent included either mitomycin only (n=14; 50%) or mitomycin in combination with irinotecan (n=14; 50%). Lipiodol plus DSM was used for all embolisations. Local tumour response was assessed by MRI using mRECIST criteria. Progression-free survival (PFS) was evaluated.

Results: In the mitomycin-irinotecan group, the CR was encountered in 21.4%, PR in 42.9% and SD in 28.6%, and PD in 7.1%. The local tumour control in the mitomycin group was: PR in 57.2%, SD in 21.4%, and PD in 21.4% (p=0.043). The PFS of patients after chemoembolisation with mitomycin was four months compared to the significantly higher PFS of twelve months in the mitomycin-irinotecan group (p=0.003).

Conclusion: Chemoembolisation of HCC with mitomycin and irinotecan is the preferred treatment option for achieving local control and PFS.

B-0825 09:10

Randomised controlled trial of free-hand vs robotic-guided needle positioning in CT-guided thermoablation of liver tumours

W.J. Heerink¹, S.J.S. Ruiter¹, M. Arnolli², J. Pennings¹, B. Lansdorp², R. Vliegenthart¹, M. Oudkerk¹, K.P. de Jong¹; ¹Groningen/NL, ²Enschede/NL (w.j.heerink@umcg.nl)

Purpose: Accurate needle placement and minimal needle manipulation is critical in microwave ablation (MWA) of liver tumours. In this randomized controlled trial, a novel robotic-guided needle positioning system (NPS) is compared to free-hand positioning.

Methods and Materials: 42 liver tumours were randomized in a free-hand group and a robotic-guided NPS (DEMCON Advanced Mechatronics, Enschede, the Netherlands) group. Primary endpoint was the number of needle repositionings before start of ablation. Secondary endpoints included Euclidian and lateral positioning error. Stratification between in-plane and out-of-plane (needle angle from axial plane ≥ 10 degrees) procedures was performed.

Results: For in-plane procedures, the median number of needle repositionings in the free-hand (n=13) and NPS group (n=10) was 1 (0-5) and 0 (0-0, p=0.012), the mean Euclidian error was 12.7 \pm 6.8mm and 11.0 \pm 4.7mm (p=0.514), and the mean lateral error was 6.1 \pm 2.9mm and 7.2 \pm 5.3mm (p=0.518), respectively. For out-of-plane procedures, the median number of needle repositionings in the free-hand (n=8) and NPS (n=11) group was 1 (0-7) and 0 (0-1, p=0.011), the mean Euclidian error was 15.7 \pm 5.7mm and 8.4 \pm 3.3 (p=0.003), and mean lateral error was 11.6 \pm 2.8mm and 6.0 \pm 3.2mm (p=0.001), respectively. Tumour size and depth were comparable in all groups.

Conclusion: For all procedures, robotic-guided needle positioning required no needle repositioning before start of ablation. It is associated with a higher positioning accuracy, though only in out-of-plane approaches. Especially in these cases, the use of the novel robotic-guided NPS is advantageous.

Author Disclosures:

M. Arnolli: Employee; DEMCON Advanced Mechatronics. **B. Lansdorp:** Employee; DEMCON Advanced Mechatronics.

B-0826 09:14

Vertebroplasty with trajectory planning and 3D road map applications: first experiences

M. Inecikli; *Rize/TR (drinecikli@yahoo.com)*

Purpose: Trajectory planning and 3-dimensional road map (TP&3D-RM) advanced applications are two important software programmes installed in new-generation angio devices. The purpose of this study is to show that the x-ray exposure in vertebroplasty (VP) cases is reduced by the TP&3D-RM technique.

Methods and Materials: All VP operations were performed using a biplane angiography device. 52 patients were included in the study and divided into two groups. The TP&3D-RM technique of the angio device was used at 26 VP. In 26 VP cases, conventional VP operation was performed. The amount of dose used during the procedure was recorded. Complications during the procedure were noted. The data were analysed statistically. $P < 0.05$ was determined to be statistically significant.

Results: The age of 22 female and 30 male patients was on average 67.5 years. In 39 cases left transpedicular, in 4 cases right transpedicular and in 9 cases bipedicular approach was used. VP treatment was performed between thoracic 5 and lumbar 5 vertebrae. VP operation was performed mostly in the L3 vertebra (%17.3). The decrease in x-ray exposure in VP cases made with TP&3D-RM technique was statistically determined ($p < 0.001$). There was no statistically significant difference in complication rates during the procedure ($p > 0.05$).

Conclusion: VP processing with TP&3D-RM technique increases the reliability of the process, reduces radiation exposure, and provides profit in terms of time and cost. Especially in cases with rotoscoliosis, for L5 vertebra and thoracic vertebrae on T8 and above, and traumatic vertebral fractures, this technique can contribute to a more controlled treatment.

B-0827 09:18

Stent retriever single shot study (4S): multivariable analysis for first-pass recanalization in acute stroke

F.J. Melendez^{1,1}, S. Rosati^{2,2}, S. Aixut Lorenzo^{1,1}, S. Remollo Friedemann^{3,1}, M.F. Werner Reyes^{1,1}, M. Ribó Jacobi^{1,1}, D. Hernández Morales^{1,1}, M. Martínez^{1,1}, A. Tomasello Weitz^{1,1}; ¹Barcelona/ES, ²Madrid/ES, ³Riells I Viabrea/ES (fermandomelendezun@gmail.com)

Purpose: First-pass recanalization have been described as a predictor factor for the clinical outcome and mortality in acute stroke. It is necessary to identify optimal techniques that maximise recanalization in the first-pass. A multivariable analysis of technical aspects in thrombectomy is introduced.

Methods and Materials: 228 patients were treated by thrombectomy. A multivariable analysis was carried out in order to achieve recanalization in the

first-pass. Stent-retriever, aspiration catheter, balloon catheter, adapt technique, combined techniques, diameter and length of devices were considered. TIC1 2B-3 was the aim. A statistical analysis was done to find the best possible combination to get first-pass recanalization.

Results: We found statistically significant difference in the diameter of the stent but not the length, diameter less than 4 mm (.772 U.Mann-Whitney) when compared to more than 4 mm (.49 U.Mann-Whitney). Distal aspiration catheter (48.6%) vs without distal aspiration catheter (62.2%) ($X^2 = 3.884$ p=.049). Bypass effect (61.1%) vs without bypass effect (52.4%) ($X^2 = 7.057$ p=.029) and thrombus protrusion into cell stent (65.3%) vs without protrusion (34.8%) ($X^2 = 10.477$ p=.005) also showed difference statistically significant.

Conclusion: In our study, we found that smaller diameters of stent, protrusion of thrombus into the cell stent with bypass effect and without aspiration catheter have better first-pass effect. Further manoeuvres may be helpful as the balloon catheter. This combination should increase the accuracy and successful recanalization after the first-pass.

B-0828 09:22

US-guided percutaneous renal biopsy: a 10 year retrospective analysis

J.A. Sheehan, R. Durganau, T. Tarmey, G.J. O'Sullivan, D. Sheppard; *Galway/IE (sheehan24@gmail.com)*

Purpose: To evaluate the indication and safety of US-guided percutaneous renal biopsy at our institution over a 10 year period.

Methods and Materials: A retrospective analysis was performed of 749 patients whom underwent renal biopsy between March 2006 and September 2016. All US-guided biopsies were performed with free hand technique, using a 5mhz curvilinear probe, and an 18-gauge core biopsy needle. Patient's vital signs were monitored during the procedure and 6 hours post biopsy to evaluate for signs of haemodynamic instability. All patients underwent a post procedure full blood count to ensure stable haemoglobin levels. In the case of ongoing pain or a drop in haemoglobin levels, further investigation with Ultrasound or Computed Tomography(CT) was performed to evaluate for the presence of acute haemorrhage.

Results: 749 patients underwent biopsy with a mean age of 53 and a range of 15 to 90. 443(59%) were male. 785 total biopsies were performed on both native(n=737) and allograft(n=48) kidneys. The majority (54.4%) of biopsies were indicated for renal impairment(n=408) followed by proteinuria(n=204), Haematuria(n=74), and renal mass (n=64). 11(1.4%) patients had a major complication requiring blood transfusion. 53(7%) patients had minor complications requiring subsequent imaging, but were managed conservatively without further intervention.

Conclusion: US guided renal biopsy is indicated for multiple reasons the majority of which are renal impairment. The procedure is safe with an acceptable low risk of both major and minor complications.

B-0829 09:26

Treatment of intramural and submucosal uterine fibroids (UFs) using MRgFUS (magnetic resonance-guided focused ultrasound surgery)

S. Iafrate, I. Capretti, E. Cannizzaro, F. Arrigoni, M. Di Luzio, A.V. Giordano, S. Mascaretti, G. Mascaretti, C. Masciocchi; *L'Aquila/IT (sonia.iafrate87@gmail.com)*

Purpose: To evaluate the reduction of volume of submucosal and intramural uterine fibroids (UFs) by MRgFUS treatment and subsequent possible reduction of symptoms, during 1 years of follow-up.

Methods and Materials: Twenty-six women, (mean age 42), affected by symptomatic UF underwent MRgFUS between July 2015 and July 2016. All the patients were assessed by MRI and UFs were classified according to FIGO staging system. Twelve/26 patients showed submucosal UFs (GROUP 1, 5 of type 0, 4 of type 1 and 3 of type 2) experiencing reproductive problems, dysmenorrhea. Fourteen/26 patients showed intramural fibroid (GROUP 2, 5 of type 3, 3 of type 4 and 6 of type 5) experiencing "bulk symptoms". We analysed non-perfused volume (NPV) that represent the treated area after treatment; reduction of UFs volume, Symptoms severity score questionnaire (UFS-QOL), clinical symptomatology improvement.

Results: A good outcome was observed in all patients underwent MRgFUS, the mean initial value of the NPV was about 80-90 %. At the end of follow-up (1 year), in the GROUP 1, 7/12 displayed a decrease of the UFs volume associated with a recovery of uterine wall morphology. A disappearance of the UF was observed in 5/12. In the GROUP 2 we observed a decreased in UFs volume, (5/14 about 70%, and 9/14 about 50%). All the patients showed a reduction of UFS-QOL with an improvement around 90%. No severe adverse events were recorded during the follow-up.

Conclusion: Patients affected by both submucosal and intramural UFs may benefit from MRgFUS, during follow-up of 1 year. A progressive reduction of UFs volume and a symptomatic improvement may be observed.

B-0830 09:30

Evaluation of a 3D printed anthropomorphic phantom for simulation of CT-guided procedures

P. Jahnke, F.B. Schwarz, M. Ziegert, O. Abdelhadi, T. Almasi, M. Nunninger, B. Hamm, M. Scheel; Berlin/DE (paul.jahnke@charite.de)

Purpose: Radiopaque 3D printing realizes detailed anthropomorphic phantoms of individual patients. We further developed this method to allow CT-guided needle placement. The aim was to evaluate such a phantom for realistic simulation of CT-guided procedures.

Methods and Materials: Experienced interventional radiologists (n = 10) performed periradicular infiltration on a radiopaque 3D printed phantom and rated different aspects regarding suitability of the phantom to simulate CT-guided procedures in a questionnaire. Additionally, quantitative parameters of their simulation procedures (number of images acquired, procedure time, needle tip visibility, and needle corrections) were compared with a retrospective cohort of 50 clinical cases performed by the same interventionalists. Descriptive statistics and Mann-Whitney U test were used for data analysis.

Results: Simulation procedures on the phantom were rated highly realistic for anatomic detail, needle navigation, and overall course of the procedure. Phantom haptics were characterized as most comparable to tight muscle tissue. All participants found the phantom suitable for training and learning purposes. Strong similarity of the simulation procedures to clinical procedures was supported by the comparative analysis of quantitative procedure parameters, with no significant differences in overall number of images acquired (p > 0.5), procedure time (p > 0.5) and needle corrections (p > 0.05) between procedures on the phantom and on patients.

Conclusion: A radiopaque 3D printed anthropomorphic phantom allows highly realistic simulation of CT-guided procedures and can be used for training, procedure optimization, and development of interventional techniques.

Author Disclosures:

P. Jahnke: Patent Holder; DE202015104282U1, EP000003135199A1, US020170042501A1. Research/Grant Support; BIH TTF, BMWi EXIST.

F.B. Schwarz: Research/Grant Support; BMWi EXIST. **M. Ziegert:** Research/Grant Support; BMWi EXIST. **M. Scheel:** Patent Holder; DE202015104282U1, EP000003135199A1, US020170042501A1.

B-0831 09:34

Recurrence and survival following image-guided percutaneous microwave ablation in primary lung malignancy

M. Tsakok, M. Little, R. Millington, G. Hynes, F. Gleeson, M. Anderson; Oxford/UK (mariatsakok1@gmail.com)

Purpose: Microwave ablation (MWA) is a relatively new alternative to radiofrequency ablation (RFA), that has been shown to produce larger ablation zones within a shorter time compared to RFA. There is a paucity of literature regarding recurrence and survival for this technique in primary lung cancer (LC).

Methods and Materials: Retrospective review yielded 53 patients with LC treated with MWA over a 6-year period at our tertiary referral centre. We defined LC on the basis of biopsy sample (45%) or imaging features (PET avidity/size increase, 55%). Patients were unsuitable for surgical resection or stereotactic body radiation therapy (SBRT) due to medical co-morbidities or tumour characteristics, and MWA was recommended by the MDT. The median age of patients was 76.3 (55-91), mean size of ablated lesion 25mm (12-50mm) and mean follow-up was 14 months (1-33 months).

Results: Local recurrence was identified in 11% (6/53), however in three patients, local control was subsequently achieved by re-ablation. Local recurrence was significantly more likely for larger tumour size >25mm (p=0.002). 78% patients demonstrated no evidence of recurrence at follow-up imaging (mean 14 months; 1-33). There were six cases of distant recurrences: three occurring to liver, one intrapulmonary recurrence, one nodal recurrence and two mixed recurrence (lung+liver, lung+peritoneum). 32/53 patients have deceased, median survival was 13 months (1-32) - cause of death was not cancer in 60% of cases.

Conclusion: MWA of primary LC is able to achieve local control rates that are equivalent to SBRT and superior to the literature using RFA.

B-0832 09:38

Sampling errors in image-guided liver biopsies: depiction of the biopsy site on immediate post-interventional CE MRI

G. Schneider, A. Bucker, L. Fenzl; Homburg/DE (Lisa.Fenzl@uniklinikum-saarland.de)

Purpose: Sampling errors in image-guided biopsies of focal liver lesions are a common problem in clinical routine. The purpose of our study was to evaluate if MRI may detect the exact location where a liver biopsy was taken and confirm sampling of representative tissue.

Methods and Materials: MRI-guided liver biopsy was performed in a total of 35 patients. Immediately post-biopsy unenhanced and CE-MRI (0.05 mmol/kg MultiHance) was performed in order to depict the exact biopsy site. Imaging included T1- and T2-weighted unenhanced sequences (T2-TSE, HASTE, T1w-flash-2D and 3D-VIBE-DIXON Sequences) as well as dynamic 3D-VIBE-DIXON imaging post-bolus CM injection. Furthermore a T1w-flash-2D sequence and a 3D-VIBE-DIXON sequence in the equilibrium phase and in the hepatobiliary phase (hb-phase) were acquired.

Results: In all patients the biopsy tract could be detected on post-biopsy imaging. On unenhanced imaging the biopsy tract was best detected on the T1w flash-2D sequences (30/35) followed by the 3D-VIBE-DIXON sequence (27/35). T2w-TSE and HASTE images could not delineate the biopsy tract sufficiently. On CE images the biopsy tract was depicted best in the equilibrium phase both on the T1w flash 2D and 3D-VIBE-DIXON sequence (34/35). In the biliary phase depiction of the sampling area (33/35) together with a more adequate depiction of the lesion that underwent biopsy was noted.

Conclusion: Immediate post-liver biopsy MRI allows for depiction of the biopsy tract both on unenhanced and CE MRI with advantages seen for CE images. T2w imaging does not reliably depict the biopsy tract.

Author Disclosures:

G. Schneider: Advisory Board; Bracco. Research/Grant Support; Bracco, Siemens, Guerbet. Speaker; Bracco, Siemens, Guerbet. **A. Bucker:** Research/Grant Support; Bracco, Siemens.

B-0833 09:42

Contrast-enhanced ultrasound (CEUS) as guidance system for ablative treatments of primary and secondary liver tumours: a multicenter study

G. Francica¹, F. Meloni², M. Pompili³, F. Terracciano⁴, E. Caturelli⁵, I. de Sio⁶; ¹Castel Volturno/IT, ²Milan/IT, ³Rome/IT, ⁴San Giovanni Rotondo/IT, ⁵Viterbo/IT, ⁶Naples/IT (giampierofrancica@gmail.com)

Purpose: To retrospectively characterise the prevalence of CEUS-guided ablation (CEUS-ABL) of liver tumours at six interventional ultrasound centres.

Methods and Materials: The six participating centres retrospectively selected all patients in whom therapeutic needles for percutaneous ethanol injection (PEI), radiofrequency (RF), microwave (MW) have been positioned into target lesions during CEUS. The prevalence of CEUS-ABL of each centre between 2008 and 2016, contrast agent consumption and safety, procedure indications, ablation effectiveness and complication rate were assessed.

Results: CEUS-ABL was carried out in 148 patients (103 M/45 F, median age 74 yrs.) with 151 liver targets (median size 15 mm) of which 86.7% were HCC tumours. PEI, RF and MW were performed in 35.2%, 46.3% and 18.5% of cases, respectively. CEUS-ABL represented 7.4% (range 2.5%-13.8%) of 2015 ablative sessions performed at the participating centres. Indications to the procedure were: improvement of conspicuity of the target (28.5%), target undetectable on non-enhanced ultrasound (29.8%), detection of vital area/s in nodules with either incomplete ablation or recurrent tumour (41.7%). A single dose (2.4 ml) of contrast agent was used in 72.2% of cases. No major complications or death occurred after CEUS-ABL. Complete ablation was obtained in 113 nodules (74.8%). Altogether hyperthermic techniques (RF and MW) performed better than PEI (86.7% vs. 51% of complete ablation).

Conclusion: The indications for CEUS-ABL for liver tumours are limited, but this procedure can be useful in challenging clinical scenarios, e.g. poorly visualised or invisible lesions, choice of vital area/s in nodules with previous incomplete ablation or local tumour progression.

10:30 - 12:00

Room A

Abdominal Viscera

SS 1001a

Advances in hepatobiliary CT and MRI

Moderators:

F. Agnello; Palermo/IT
B.I. Choi; Seoul/KR

B-0834 10:30

MRI imaging of branch-duct IPMN: evaluation of agreement between observers with different degrees of experience

L. Bertuzzo, G. Zamboni, R. Negrelli, R. Pozzi Mucelli; Verona/IT

Purpose: The Sendai and Fukuoka consensus guidelines have defined the characteristics of high-risk mucinous lesions. Purpose of our study was to assess the agreement between an experienced and a non-experienced reader in recognising the main features defined by the guidelines in a series of IPMN.

Methods and Materials: IRB approval was waived for this retrospective study. We included 118 patients (45 M, 73 F, average age 68 years) affected by IPMN who underwent MRI and MRCP in our institution. Two readers, respectively with 10 and 4 years of experience in abdominal imaging, reviewed independently the scans assessing all cysts >5 mm for wall/internal septa thickening, solid mural nodules, dilation of the main pancreatic duct (MPD) and contrast enhancement. The readers were blinded to clinical and laboratory information. Kappa statistics was calculated.

Results: 10 patients had mixed-type IPMN and 108 branch-duct IPMN. Patients had a median of 2 cysts >5 mm each (range 1-20; mean 2.6). A total of 307 cystic lesions were reviewed, with a mean size of 11.8 mm (5-50 mm). The two readers showed very good agreement regarding MPD dilation ($k=0.908$), wall thickening ($k=0.893$), and presence of mural nodules ($k=0.856$). The agreement was good for presence of filling defects ($k=0.721$), wall enhancement ($k=0.725$) and presence of mural nodules ($k=0.663$).

Conclusion: Readers with different experience in abdominal imaging, when assessing IPMN at MRI-MRCP, show an interobserver agreement ranging between good (0.663) and very good (0.908) when applying the Fukuoka criteria, confirming their usefulness for lesion evaluation standardisation.

B-0835 10:38

Intra-individual interscanner variation of virtual unenhanced attenuation values derived from twin-beam dual-energy CT in comparison to dual-source dual-energy CT in 126 patients

A. Cosentino¹, M. Obmann², J. Gehweiler², V. Kelsch², V. Hofmann², T.J. Re², D. Boll², M. Benz²; ¹Turin/IT, ²Basle/CH (aurelio.cosentino@gmail.com)

Purpose: The purpose of this study was to evaluate the comparability of virtual unenhanced (VUE) attenuation values derived from a novel technique for single-source twin-beam dual-energy CT using a split-filter (tbDECT; two equal parts of gold and tin) and a dual-source dual-energy CT (dsDECT).

Methods and Materials: A total of 126 patients were retrospectively analysed. Each patient underwent an abdomino-pelvic CT on a tbDECT and a second-generation dsDECT scanner (SOMATOM Definition Edge and Flash, Siemens, Germany). Virtual unenhanced images were reconstructed off of venous phase series using commercially available software (Syngo.via, Siemens, Germany). Attenuation values of the liver, spleen, kidneys, blood, fat and muscle were recorded. Disagreement of VUE attenuation values >10HU between the two scans was defined as inadequate.

Results: The intrapatient interscanner analysis showed significant differences between VUE attenuation values derived from tbDECT and dsDECT ($p<0.01$) in 6 of 7 organs. The percentage of patients with differences in VUE attenuation values >10HU between tbDECT and dsDECT ranged between 15% (left kidney) and 62% (spleen).

Conclusion: This study showed significant differences in VUE attenuation values derived from different dual-energy techniques (tbDECT vs dsDECT) in the same patient. Thus, to ensure reliable VUE attenuation measurements, it is advisable to perform patient follow-up studies using the same dual-energy technology.

B-0836 10:46

Diffusion-weighted magnetic resonance imaging in uveal melanomas: validation of early chemotherapeutic monitoring of targeted therapy

N. Guberina, S. Bauer, H. Richtig, M. Scheulen, A. Wetter; Essen/DE (nika.guberina@uk-essen.de)

Purpose: The aim of this study was to explore the feasibility of diffusion-weighted magnetic resonance imaging (MRI) sequences (DW-MRI) as a non-invasive technique for monitoring of therapeutic response to targeted therapy in patients with metastatic uveal melanoma.

Methods and Materials: In retrospective analysis the chemotherapeutic response to targeted therapy was evaluated in 47 patients with metastatic uveal melanoma using diffusion-weighted MRI (DW-MRI) and ADC maps at 1.5T MRI [$b=100,500,1000s/mm^2$]. The apparent diffusion coefficient (ADC) was assessed in metastatic liver lesions prior to therapy [w0] as well as two [w2] and eight weeks [w8] after therapy initiation. The examination protocol included fat-saturated, dynamic T1- and T2-weighted sequences. Correlation with clinical response was performed. Responders were defined as stable-disease. The results were analysed using the analysis of variance (ANOVA) and the paired-sample t-test.

Results: The apparent diffusion coefficient measured by DW-MRI increased in hepatic lesions which showed no tumour progress under targeted therapy (w8 $p8<0.05$). Lesions with no therapeutic response revealed a decrease of ADC within w8 (w8 $p8<0.02$). Furthermore, ratio of ADC0/ADC2 and ADC0/ADC8 between patients with stable-disease and non-responders proved to be significant (w2 $p2<0.05$; w8 $p8=0.006$). Baseline ADC values showed no significant relationship to therapeutic response.

Conclusion: Notably, the results illustrate that DW-MRI allows a non-invasive monitoring of therapeutic response to targeted therapy in patients with metastatic uveal melanoma at an early stage of therapy. An early monitoring of therapeutic response is crucial to determine whether the therapy benefits outweigh the risks associated to treatment toxicity of targeted therapy.

B-0837 10:54

MRI liver adenoma subtyping in animal models of glycogenesis type Ia

F. Rosa, L. Basso, R. Resaz, L. Secondini, I. Verardo, F. Grillo, V. Prono, A. Eva, C. Neumaier; Genoa/IT (francescarosa892@gmail.com)

Purpose: Hepatocellular adenomas (HCA) are benign tumours and their major complication is malignant transformation to hepatocellular carcinoma (HCC). Among various subtypes of HCA, β -catenin-activated (β HCA) have a greater risk of malignant transformation. In preclinical studies dedicated MRI protocols suitable to characterize and monitor liver lesions are requested to allow research on their oncogenesis and progression. The aim of this study is to validate a new MRI protocol for HCA subtyping to distinguish low-risk from high-risk tumours.

Methods and Materials: An experimental animal model of glycogen storage disease 1a in which HCC and different types of HCA represent late and severe complications has been previously designed. The experiments were carried out on a 3T scanner performing T2-weighted imaging and T1 spoiled gradient echo-weighted imaging before and after administration of gadobenate dimeglumine. A total of 40 mice were studied for focal lesions detection and a group of 15 was monitored every 4 weeks for 3 months to evaluate lesion growth. Mice were sacrificed after last MRI and lesions were classified using immunohistochemistry.

Results: Our protocol was able to detect liver lesions with a minimum diameter of 1 mm. MRI identified 4 different patterns after contrast administration (isointense, hyperintense, hypointense lesions and lesions with a peripheral contrast enhancement) which corresponded to different HCA subtypes.

Conclusion: β HCA displayed MRI features (hyperintensity on T2WI and hypointensity after contrast administration) clearly distinguishable from those exhibited by other subtypes, indicating that MRI is a reliable method to identify high-risk HCA.

B-0838 11:02

The role of visceral and subcutaneous adipose tissue measurements and their ratio by MRI in subjects with prediabetes, diabetes and healthy controls from a general population

C. Storz¹, S.D. Heber¹, S. Rosplecz², J. Machann¹, K. Nikolaou¹, R. Lorbeer³, A. Peters², C.L. Schlett⁴, F. Bamberg¹; ¹Tübingen/DE, ²Neuherberg/DE, ³Munich/DE, ⁴Heidelberg/DE (corinna.storz@med.uni-tuebingen.de)

Purpose: Different adipose tissue compartments are associated with metabolic risk. The aim of this study was to study the relationship of visceral and subcutaneous adipose tissue (VAT and SAT, respectively) by magnetic resonance imaging (MRI) and their ratio in subjects with impaired glucose metabolism from the general population.

Methods and Materials: Subjects from a population-based cohort with established prediabetes, diabetes and healthy controls without prior cardiovascular diseases underwent 3 Tesla MRI. VAT and SAT were quantified from isotropic VIBE-Dixon as total volume and area on a single slice, and their ratio was calculated. Clinical covariates and cardiovascular risk factors were assessed in a standardized fashion. Univariate and adjusted analyses were carried out to determine group differences.

Results: Among 384 subjects (age: 56.2 ± 9.2 years, 58.1% male), volumetric and single-slice VAT, SAT and VAT/SAT ratio measurements were strongly correlated (all $>r=0.89$). Similarly, VAT/SAT_{volume} ratio was strongly correlated with VAT_{volume} but not with SAT_{volume} ($r=0.72$ and $r=-0.21$, respectively). Significant higher levels of VAT_{volume}, SAT_{volume} and VAT/SAT_{volume} ratio were found in subjects with impaired glucose metabolism (all $p \leq 0.01$). After adjustment for potential cardiovascular confounders, VAT_{volume} and

VAT/SAT_{volume} ratio remained significantly higher in subjects with impaired glucose metabolism (all <0.02), whereas the association for SAT_{volume} attenuated. In addition, there was a decreasing effect of glycemic status on VAT/SAT_{volume} ratio with increasing body mass index and waist circumference.

Conclusion: VAT_{volume} and VAT/SAT_{volume} ratio are associated with impaired glucose metabolism, independent of cardiovascular risk factors, with a decreasing effect of VAT/SAT_{volume} ratio in obese subjects.

B-0839 11:10

Non-invasive preoperative quantification of pancreatic fibrosis and lipomatosis: correlation of magnetisation transfer imaging and multi-gradient echo MRI with histopathology

K. Schawkat, D. Eshmunin, D. Lenggenhager, K. Endhardt, B. Vrugt, A. Boss, H. Petrowsky, P.-A. Clavien, C.S. Reiner; Zurich/CH (khoschy.schawkat@usz.ch)

Purpose: To investigate the correlation of magnetization transfer (MT) imaging and multi-gradient-echo magnetic resonance imaging (MRI) with histopathology to quantify pancreatic fibrosis and lipomatosis in patients prior to pancreatoduodenectomy.

Methods and Materials: 24 patients (age, 68±8ys, 16 males) prospectively underwent quantitative MT imaging with a 2D gradient-echo sequence and multi-gradient-echo imaging on a 3T MRI one day prior to pancreatoduodenectomy due to pancreatic adenocarcinoma (n=14), duodenal adenocarcinoma (n=6), neuroendocrine tumor (n=3) or IPMN (n=1). MT-ratio (MTR) and proton density fat fraction (PDFF) were measured in pancreatic tail (PT) and at the resection margin (RM). Pancreatic fibrosis was graded as mild, moderate or severe (F1-3), lipomatosis was graded as 0-10%, 11-30%, and >30% fat deposition (L1-3) on histopathology. Mann-Whitney-U-test and Spearman's correlation was used.

Results: Patients with advanced pancreatic fibrosis (F3) showed a significant higher MTR compared to the F1-group at the RM and PT (38±4 vs. 32.3±1.6, p=.018 and 39.7±5.5 vs.31.2±1.7, p=.001). Spearman's correlation coefficient of MTR and fibrosis grade was r=.532 for RM (p=.011) and r=.554 for PT (p=.008). Pancreatic parenchyma with advanced fat deposition (L2-3) showed significantly higher PDFF compared to lipomatosis grade L1 (RM: p=.002 and PT: p=.001). PDFF of pancreatic parenchyma showed a moderate and significant correlation with histopathological lipomatosis grade (RM: r=.668 and PT: r=.707, p=.000). MTR was significantly higher in pancreatic tumor compared to pancreatic parenchyma (44±5.5 vs. 37.4±5.4, p=.000).

Conclusion: Multiparametric MRI of the pancreas including MTR and PDFF maps may yield quantitative information to preoperatively quantify pancreatic fibrosis and lipomatosis noninvasively.

B-0840 11:18

Conventional liver fat quantification MRI vs complex chemical shift-encoded MRI in an oncologic population

G. Corrias¹, S. Eskreis-Winkler², S. Krebs¹, J. Zheng¹, L. Saba², L. Mannelli¹; ¹New York, NY/US, ²Monserrato/IT (corriasgmd@gmail.com)

Purpose: MRI is the most accurate imaging technique in diagnosing steatosis. It can also be used to quantify hepatic fat content. There are two main ways in which steatosis can be quantified with MRI: conventional IOP and proton density fat fraction (PDFF). The aim of this study is to compare IOP with an innovative type of PDFF, called IDEAL-IQ, in quantifying fat fraction in an oncological population.

Methods and Materials: A total of 50 consecutive patients were included in the study. Two radiologists reviewed the images and placed 3 elliptical ROIs of 10 mm of diameter in the liver. Intra-class correlation coefficient (ICC) was estimated to evaluate agreement on fat fraction between conventional MRI and IDEAL, as well as between 2 readers. Exact Wilcoxon signed rank test was used to compare iron level and fat fraction between conventional MRI and IDEAL, in all patients, patients with normal iron level, and patients with above normal iron level.

Results: The agreement on fat fraction using conventional MRI was poor (ICC=0.372). The agreement on iron level and IDEAL IQ fat fraction was excellent (ICC=0.935). A statistical difference was demonstrated in fat fraction estimation in low iron group between the fat fractions calculated by IDEAL-IQ and IOP (p<0.001 for reader 1 and 2).

Conclusion: Our results show that fat fraction calculated from IDEAL-IQ maps and from T1-weighted-in-and-out-of-phase (IOP) imaging are significantly different in a population without pathologic liver iron levels. IDEAL IQ had an excellent inter-reader agreement.

B-0841 11:26

Ability to diagnose disorders of liver haemodynamics in conditions of biliary hypertension with perfusion computed tomography

V. Malakhanov, P.V. Seliverstov; Irkutsk/RU (malakhanow@mail.ru)

Purpose: The possibility of detection of haemodynamic disorders of the liver in patients with obstructive jaundice syndrome.

Methods and Materials: The study included 37 patients (median 59 years). Duration of jaundice from 3 days to 1 month from the onset of the disease. Patients according to the classification by V. D. Fedorov (2000) were divided into three groups: mild (n = 14), moderate (n = 12) and severe (n = 11). Used Ultravist-370 (50 ml), the infusion rate 5.5 ml/s. Evaluated: arterial liver perfusion (ALP), portal liver perfusion (PLP). The total liver perfusion (TLP) were calculated by summing up blood (ALP) and portal perfusion (PLP).

Results: In patients with mild, decrease PLP to 15.0%, increase ALP up to 10.0%, TLP is not reduced. In patients with a medium degree of reduced PLP to 40.0%. ALP is increased to 80.0% of TLP is reduced from 15 to 30.0%. In patients with a severe degree there is a decrease in PLP to of 73.0%, with an increase in ALP to 26.0%, TLP was reduced by more than 50.0%.

Conclusion: CT perfusion can be used as a method of assessing haemodynamic instability in the liver in patients with biliary hypertension to assess the severity of liver failure. The obtained information will allow you to properly optimise the treatment of patients.

B-0842 11:34

Comparison of stiffness values of peripheral and central liver tissues with MR elastography in patients with primary sclerosing cholangitis

D. Kuru Öz, E. Peker, M. Kul, A. Erden; Ankara/TR (digdem_k@hotmail.com)

Purpose: In primary sclerosing cholangitis (PSC), peripheral vascular and / or lymphatic drainage disturbances resulting from periductal inflammation of peripheral bile ducts are seen as peripheral subcapsular triangular hyperintense areas in T2-weighted images. In the progressive phase, fibrosis may develop in this tissue of impaired perfusion. This study aims to compare the tissue stiffness values of liver peripheral and central segments with MR elastography based on T2 signal differences in liver parenchyma in patients with PSC.

Methods and Materials: A total of 10 patients with PSC were included in this study (5 males, 5 females, mean age 50.6 years, median age 49 years (range 38-59)). The stiffness values of the 1/3 peripheral section and the remaining central section of the liver were measured on confidence map of MR elastography (1.5 Tesla MR system). The 'Wilcoxon signed rank test' was used to compare the peripheral and central measurements determined as mean kPa.

Results: The median stiffness values were 4.3 kPa and 3.35 kPa in peripheral and central sections, respectively. Significant difference between the peripheral and central tissue stiffness values was detected (p=0.008).

Conclusion: In PSC, tissue stiffness in the periphery of the liver is greater than in the central. This finding is consistent with the observation that ductal dilatation, periductal inflammation and fibrosis are predominantly seen at the periphery.

B-0843 11:42

Portal hypertension associated with oxaliplatin administration: incidence and natural history

M. Di Martino, K. Koryukova, C. Catalano; Rome/IT (micdimartino@hotmail.it)

Purpose: To establish incidence and clinical manifestations of non-cirrhotic portal hypertension in patients affected by gastrointestinal neoplasm treated with oxaliplatin.

Methods and Materials: This is a retrospective single-center study. From a database of 570 patients we considered eligible for the study 94 patients with GI tract neoplasm (57 colon, 28 rectum, 5 stomach, 4 other) who underwent chemotherapy (mean duration therapy 5.7 months) according to specific selective criteria. Two expert radiologists in liver imaging reviewed in consensus three computed tomography examinations (baseline, at the end of therapy and 6 months after the end of therapy) looking for features of portal hypertension (ascites and varices) and measuring portal vein and spleen parameters (long axis, area and volume). T Student's test and χ^2 Person were used for statistical analysis.

Results: Mean long-axis diameter of portal vein and spleen and spleen volume were significantly higher at the end of therapy (p=.0009; p < .0001; p < .0001, respectively). At the end of therapy, two patients developed varices (2.1%), ten cases of portal vein increase in size (10.6%) and 26 cases of splenomegaly (28%) were reported. Seven patients reported both splenomegaly and portal vein enlargement. After six months the end of therapy, in 4 patients signs of portal hypertension disappeared.

Conclusion: Patients who undergo chemotherapy with oxaliplatin should be also observed for portal hypertension and its evolution.

B-0844 11:50

Learning from our errors: what are the common clinically important errors that radiologists repeatedly make in the UK's largest teaching hospital and how can we best address them?

A. Koo, J.T. Smith; Leeds/UK (andrew.koo@doctors.org.uk)

Purpose: To review the attendance, activity and outcomes of 5 years of Radiology departmental educational/discrepancy meetings in our hospital. This is a meeting attended by sub-speciality radiologists, radiographers, nurses, support staff and managers.

To review the clinically important cases and categorise them in an attempt to identify recurring patterns of errors (or educational themes). To identify how many of these themes could be addressed by a more positive and less pejorative method of presenting cases rather than simply reviewing people's "errors".

Methods and Materials: All the attendance records and cases discussed in the 30 consecutive meetings from November 2011 under a single chairman were reviewed retrospectively. Cases had been selected by team members who had noticed a discrepancy / educational case and were presented anonymously.

Results: Mean consultant attendance per meeting was 29 and 69% attended at least 3 meetings per year (Royal College of Radiology recommendation). 628 cases were reviewed. 98% consultants in the department had contributed at least one case over 5 years. 7 common themes were identified; missed lung cancers, missed fractures and their mimics, missed incidental cancers, incorrect cancer staging, incorrect characterisation of disease, missed clinically significant non-cancer diagnoses and uncommon but clinically important disease processes with image-specific signs. Good spots could be identified to illustrate each of these seven common themes.

Conclusion: The fact that many errors in our department fell into several common themes could facilitate rolling audits and targeted teaching. "Good spots" address these themes in a more positive way than "errors".

Author Disclosures:

J.T. Smith: Author; The authors would like to acknowledge Catherine Parchment Smith in helping write and edit our abstract.

10:30 - 12:00

Room C

GI Tract

SS 1001b

Rectal cancer: old problems, new tools

Moderators:

L. Curvo-Semedo; Coimbra/PT
A. Plumb; London/UK

B-0846 10:30

Diffusion-weighted MR-volumetry and high-resolution MR-volumetry association with lymphovascular invasion and N-stages in resectable rectal cancer

H. Li, G.W. Chen, X.-L. Chen; Chengdu/CN (522696619@qq.com)

Purpose: To determine whether diffusion-weighted imaging (DWI)-volumetry and high-resolution T2-weighted imaging (T2WI) MR-volumetry could predict lymphovascular invasion (LVI) and N-stages in resectable rectal cancer.

Methods and Materials: 50 consecutive patients with rectal cancer who underwent radical surgery in 1 week after DWI and high-resolution T2WI were retrospectively identified. Gross tumour volume (GTV) was evaluated on DWI and high-resolution T2WI. Univariate and multivariate analyses were performed to determine whether GTV could predict LVI and lymph node metastasis (LNM). Mann-Whitney U test was performed to compare GTV among N-stages. Cut-offs of GTV were investigated using area under the receiver operating characteristic curve (AUC) analysis for predicting LVI and N-stages.

Results: DWI-GTV and T2WI-GTV increased with LVI ($r=0.750$ and 0.710 , $P<0.0001$, respectively) and increasing of N stage ($r=0.780$ and 0.755 , $P<0.0001$, respectively). Univariate analysis showed DWI-GTV and T2WI-GTV could predict LVI ($P<0.0001$). Multivariate analyses indicated only DWI-GTV as an independent risk factor of LVI ($P=0.005$, odds ratio=1.207) and LNM ($P=0.005$, odds ratio=1.420). The Mann-Whitney U test showed DWI-GTV and T2WI-GTV could distinguish N0 from N1, N0 from N1-2, N0-1 from N2 ($P<0.0001$). DWI-GTV could predict LVI (cut-off 11.05cm^3 ; AUC 0.899), and distinguish N0 from N1 (cut-off 10.86cm^3 ; AUC 0.865), N0 from N1-2 (cut-off 10.46cm^3 ; AUC 0.934), N0-1 from N2 (cut-off 17.7cm^3 ; AUC 0.932). T2WI-GTV could predict LVI (cut-off 13.74cm^3 ; AUC 0.877), and distinguish N0 from N1 (cut-off 12.25cm^3 ; AUC 0.827), N0 from N1-2 (cut-off 13.36cm^3 ; AUC 0.911), N0-1 from N2 (cut-off 20.43cm^3 ; AUC 0.927).

Conclusion: High-resolution T2WI-GTV and DWI-GTV of resectable rectal cancer were correlated well with the LVI and LNM, but the latter is a potentially more promising non-invasive technique that can help predict the preoperative LVI and distinguishing N-stages.

B-0847 10:38

Could perfusion heterogeneity assessed at DCE-MRI predict rectal cancer sensitivity to chemoradiotherapy?

A. Di Chiara, A. Palmisano, A. Esposito, P. Rancoita, P. Passoni, A. Del Maschio, F. De Cobelli; Milan/IT

Purpose: To evaluate whether the rectal cancer's perfusion heterogeneity prior to chemoradiotherapy (CRT) evaluated using histogram analysis of DCE-MRI quantitative parameters can predict response to treatment.

Methods and Materials: Twenty-one patients with histologically proven rectal adenocarcinoma underwent DCE-MRI before CRT. Tumour volumes were drawn on Ktrans and Ve maps using T2W-images as reference and 25th, 50th, 75th percentile, mean, standard deviation, skewness and kurtosis calculated. After CRT, all patients underwent surgery and, according with histopathological Rödel's tumour regression grade (TRG), patients were classified in poor responder "non-GR" (TRG 0,1,2) and good responders "GR" (TRG3-4). Mann-Whitney's test was used to compare measurement between GR and non-GR and ROC curves to identify parameters predictive of response. All p-values were adjusted for multiple comparisons using the Bonferroni's correction.

Results: 16 (76%) patients resulted GR and 5 (24%) non-GR. Skewness and kurtosis of Ve resulted significantly higher in non-GR (4.886 ± 1.320 and 36.402 ± 24.486 , respectively) than in GR (1.809 ± 1.280 , $p=0.003$ and 6.268 ± 8.130 , $p=0.011$). Ve skewness < 3.635 was able to predict GR with an AUC of 0.988, sensitivity 93.8%, specificity 80% and accuracy 90.5%. Ve kurtosis < 21.095 was able to predict response with an AUC of 0.963, sensitivity 93.8%, specificity 80% and accuracy 90.5%. Other parameters showed no significant differences, and were not predictive of response.

Conclusion: Ve skewness and kurtosis seem promising in the prediction of rectal cancer's response to CRT.

B-0848 10:46

Radiomics analysis for preoperative prediction of lymph node metastasis in patients with rectal cancer

H. Liu, C. Zhang, J. Li, D. Wang; Shanghai/CN (liuhuanhuan0117@163.com)

Purpose: To investigate the value of radiomics analysis for preoperative prediction of lymph node metastasis in patients with rectal cancer.

Methods and Materials: A total of 183 patients with histopathologically confirmed rectal cancer who underwent high-resolution MR imaging without chemoradiotherapy were divided into the primary cohort ($n=128$) and the validation cohort ($n=55$). Radiomics features were extracted from oblique axial T2-weighted images of each patient. The independent two-sample t test, Kruskal-Wallis test, and Pearson correlation analysis were used for feature selection. A radiomics signature was built and multivariable logistic regression analysis was used to develop the radiomics model including radiomics features and independent clinico-radiologic risk factors. The performance of the radiomics model was assessed by its calibration, discrimination, and clinical usefulness.

Results: A total of 385 radiomic features were extracted from each patient, and 6 radiomics features were selected for the radiomics signature. The radiomics model included radiomics signature, MR-reported lymph node status, and carcinoembryonic antigen (CEA) level. The model showed good discrimination and moderate calibration in the primary cohort and validation cohort, with a C-index of 0.842 (95% confidence interval (CI), 0.770-0.914) and 0.722 (95% CI, 0.643-0.884), respectively. Decision curve analysis confirmed the clinical utility of the radiomics model.

Conclusion: We developed a radiomics model based on the MR radiomics features in combination with independent clinico-radiologic risk factors. The model could be helpful for predicting the lymph node metastasis in patients with rectal cancer.

B-0849 10:54

Locally advanced rectal cancer: the value of whole-tumour histogram-based texture analysis of baseline ADC map in predicting tumour response to neoadjuvant chemoradiotherapy

I. Yang, B. Wu; Chengdu/CN (lqyang95@163.com)

Purpose: To determine the diagnostic performance of ADC map before treatment in predicting pathological complete response (pCR) after neoadjuvant chemoradiotherapy (nCRT) in patients with locally advanced rectal cancer (LARC) using whole-tumour histogram-based texture analysis.

Methods and Materials: 26 patients with LARC who completed nCRT and surgery were enrolled retrospectively. Histopathologic tumour regression grade was the reference standard. Whole-tumour ROIs were manually drawn twice (two weeks interval) on pre-CRT ADC maps performed with the same imaging unit ($b=0, 600, 1000 \text{ s/mm}^2$) by one radiologist. Intraclass correlation coefficient

(ICC) was calculated to evaluate intraobserver variability. Independent t test was used to compare histogram-based texture parameters between two groups. Receiver operating characteristic (ROC) analysis was performed to evaluate their diagnostic performance.

Results: For both measurements the standard deviation, variance, entropy, quantile 75%, 90% and 95% of whole-tumour pre-CRT ADC values were significantly lower in pCR group ($P=0.001-0.046$). And the uniformity and energy were higher ($P=0.007-0.027$). Since the intraobserver agreement was good between two measurements (ICC, 0.850-0.957), the first-time data were used to following analyses. Respective AUCs of quantile 75%, 90% and 95% values when determining pCR were 0.739, 0.770, and 0.806, with the optimal cut-off point of 1.04×10^{-3} (sensitivity=86.7%, specificity=63.6%), 1.204×10^{-3} (sensitivity=86.7%, specificity=63.6%), and 1.339×10^{-3} mm²/s (sensitivity=86.7%, specificity=72.7%), respectively.

Conclusion: The pCR group appeared less heterogeneous on pre-CRT ADC map and had lower high percentile ADC values than non-pCR group. Whole-tumour histogram-based texture analysis of pre-CRT ADC map could effectively predict pCR after neoadjuvant CRT in LARC patients.

B-0850 11:02

T2-weighted signal intensity to predict complete and good response after neoadjuvant chemoradiation therapy in patients with rectal cancer

R.A.P. [Dijkhoff](mailto:rebeccadjkhoff@hotmail.com); Maastricht/NL (rebeccadjkhoff@hotmail.com)

Purpose: To determine whether T2-weighted signal intensity (T2W-SI) can predict complete and good response after neoadjuvant chemoradiation (CRT) in patients with rectal cancer.

Methods and Materials: 171 consecutive patients with rectal cancer treated with neoadjuvant CRT underwent MRI before and 8-10 weeks post-CRT. The primary tumour and remnant after CRT were manually delineated on T2W-MRI. Histogram analyses were performed on these volumes of interest with pyramids. Extracted parameters were mean, median, SD, range, minimum, maximum T2W-SI before and after CRT. Change between pre- and post-CRT T2W-SI parameters was calculated. Heterogeneity of T2W-SI was assessed by the coefficient of variance (CoV=SD/mean). T2W-SI parameters were compared between complete (CR; ypT0), good responders (GR; ypT0-1) and non-responders (NR; ypT2-4). Reference standard was either surgery or a wait-and-see programme with at least 2 years of recurrence-free follow-up.

Results: 36/135 patients had a CR and 49/171 a GR. Maximum SI (941.62 vs 1149.63, $p=0.028$), heterogeneity of the SI (0.265 vs 0.291, $p=0.017$) and SI range (828.56 vs 1074.52, $p=0.009$) at primary staging were significantly lower in CR than in NR. Minimum SI at primary staging was significantly higher in both CR (113.06 vs 75.10, $p=0.017$) and GR (117.02 vs 69.46, $p=0.001$) compared to NR. The mean difference in SI between primary and restaging was larger in both CR and GR compared to NR, although not statistically significant in the CR patients (CR: -14257 vs NR: -105.44, $p=0.114$ and GR: 176.83 vs NR: -87.72, $p=0.001$).

Conclusion: The pre-CRT T2W-SI is significantly higher in CR and GR with a larger decrease in mean SI after CRT. These parameters could be a potential non-invasive marker for predicting complete/good response in patients with rectal cancer before and after CRT.

B-0851 11:10

Predictive value of functional imaging markers derived from PET/CT and diffusion-weighted MRI in response assessment of rectal cancer treatment

S. [Drago](mailto:silvia.drago@hotmail.it), C. Talei Franzesi, S. Lombardi, A. Casiraghi, L. Guerra, S. Sironi, D. Ippolito; Monza/IT (silvia.drago@hotmail.it)

Purpose: To assess the clinical diagnostic value of functional imaging for tumor response prediction in rectal cancer, combining quantitative parameters of ADC and SUV max before and after chemo-radiation therapy, with tumor regression grade at histology

Methods and Materials: Forty-five patients with biopsy rectal adenocarcinoma were enrolled in this study. All patients underwent whole body 18-FDG-PET/CT scan and pelvic MRI examination before (PET1, MR1) and after neoadjuvant chemo-radiation therapy (PET2, MR2). MRI was performed on 1.5T magnet (Philips, Achieva), adding DWI sequences (b-value 0 and 1000 mm²/sec) to the standard protocol. On PET/CT the SUVmax of rectal lesions was calculated in PET1 and PET2. The different SUVmax (Δ SUV) and ADC (Δ ADC) values, between baseline and pre-surgical scan, were assessed and correlated with pathologic tumor regression grade (Mandard's criteria; TRG 1=complete regression, TRG5=no regression)

Results: Twenty-nine tumors (68%) showed complete or subtotal regression (TRG1-2) at histology and classified as responders; 16 tumors (32%) were classified as non-responders (TRG3-5). The mean values of SUV max in PET1 were higher than in PET2 ($p<0.001$), whereas mean ADC values were lower in MR1 than MR2 ($p<0.001$). The best predictors for TRG response were SUV2 (threshold 4.4) and ADC2 (1.28×10^{-3} mm²/s). Moreover, combining the median quantitative values in a single analysis, the PPV for different response groups

related to TRG system, showed an overall AUC of 96%, higher than DWI (88.2%) or SUVmax (93.3%)

Conclusion: In era of PET/MRI scanner, combining DWI value and PET/CT could be the most feasible method to evaluate tumor response in rectal cancer, with accuracy values higher than other imaging techniques

B-0852 11:18

Texture analysis of magnetic resonance imaging in differential diagnosis of rectal tumours

M. [Huang](mailto:huangmengna1127@163.com); Zhengzhou/CN (huangmengna1127@163.com)

Purpose: To analyse magnetic resonance images of rectal villous tubular adenoma and T1-T2 rectal adenocarcinoma, and evaluate the texture characteristics of two kinds of rectal tumours by "nearest neighbour algorithm".

Methods and Materials: From March 2014 to January 2017, 30 patients with rectal villous tubular adenoma and 43 patients with T1-T2 rectal adenocarcinoma in our hospital were retrospectively analysed; texture analysis was performed on the ROIs of two types of tumours.

Results: Totally 24 texture parameters were extracted based on statistical methods, of which 14 parameters had statistically significant difference between the two kinds of data sets ($P<0.05$). The sensitivity, specificity and accuracy of "nearest neighbour algorithm" of texture parameters of rectal villous tubular adenoma and T1-T2 rectal adenocarcinoma were $79.87 \pm 7.55\%$, $53.89 \pm 10.16\%$ and $69.24 \pm 5.52\%$, respectively.

Conclusion: Texture analysis can extract more features for the differential diagnosis of rectal villous tubular adenoma and T1-T2 rectal adenocarcinoma, which would be conducive to the development of clinical treatment and provide a new method for the differential diagnosis of rectal tumours.

B-0853 11:26

Whole tumour texture analysis based on ADC maps as quantitative imaging biomarker in patients with locally advanced rectal cancer "responders" to neoadjuvant chemoradiotherapy

A. [Grassi](mailto:andrea.grassi14@alice.it), A. Cirigliano, S. Carbone, M. Biondi, V. Nardone, L. Pirtoli, L. Volterrani; Siena/IT (andrea.grassi14@alice.it)

Purpose: To evaluate the predictivity of Texture Analysis (TA) parameters extrapolated by the whole tumour analysis on ADC maps in tumoural response and recurrence in patients with locally advanced rectal cancer (LARC) treated with neoadjuvant chemoradiotherapy (CRT).

Methods and Materials: We retrospectively analysed 35 pre-CRT MR imaging examinations. After complete surgical resection, only 23 patients with tumour regression grade (TRG) 1-2, considered "responders" according to Mandard TRG, were finally enrolled. Texture features (mean, standard deviation, skewness, kurtosis, entropy and uniformity) were assessed using a filtration-histogram technique and were independently correlated, by univariate and multivariate analysis, with TRG and the onset of metastasis. ROC curve analysis was performed and DFS was assessed with Kaplan-Meier method.

Results: Nine patients showed TRG1 (pathological complete response: pCR) and fourteen TRG2 whereas six patients (one TRG1, five TRG2) developed metastatic disease. Kurtosis was significantly lower in TRG1 in comparison with TRG2 ($p=0.016$) and significantly higher in patient who had recurrence from those who did not have metastasis ($p=0.013$). The optimal cut off values were ≤ 3.5 (78% sensitivity, 86% specificity in predicting pCR) and ≥ 4.6 (67% sensitivity, 100% specificity in predicting metastatic disease) respectively.

Conclusion: Texture ADC Kurtosis seems to be a promising parameter in discriminating both rectal cancer responsiveness to CRT and tumoural aggressiveness (metastatic risk). Further investigations are needed to confirm usefulness TA kurtosis in customised management of patients with LARC.

B-0854 11:34

Accurate localization of rectal cancer on preoperative magnetic resonance imaging: a prospective study using an anal verge marker

Y. [Han](mailto:yeonny0714@naver.com), B. Park, M. Kim, D. Sung, N. Han, K. Sim, S. Cho; Seoul/KR (yeonny0714@naver.com)

Purpose: To determine an approach for rectal cancer localization using MRI, with the anal verge as a landmark.

Methods and Materials: Fifty patients scheduled for MRI evaluation of rectal cancer were evaluated. Two markers were attached to the anal verge at 6 and 12 o'clock positions. On sagittal T2WI, the distance between the lowest margin of cancer and upper tangent of the two markers was measured by two radiologists in 6 different ways, and compared with that obtained using rigid sigmoidoscopy. The intraclass correlation coefficient (ICC) was used for the correlation verification. Precise localization of the anal verge was evaluated based on the anal verge markers.

Results: Among 6 different measurement methods, the "direct centre" method showed the highest correlation with rigid sigmoidoscopy (ICC = 0.81) and good interobserver correlation (ICC = 0.98). This method measures the linear distance between the centre of the line segment abutting the lowest margin of the tumour and perpendicular to the longitudinal axis of the rectum, and the

upper tangent of the anal verge markers, on mid-sagittal T2WI. The anal verge identified by the marker was located within a range of -1.4 ~1.5 cm (mean -0.24 cm) from the lowest margin of the external sphincter.

Conclusion: The "direct centre" method is an accurate and relatively easy way for tumour localization using preoperative rectal MRI. The anal verge is located between 1.4 cm above and 1.5 cm below the lowest margin of the external sphincter and is usually in the upper portion of the lowest margin of the external sphincter.

B-0855 11:42

Predictive factors of recurrence at MR examination performed before and after preoperative chemoradiotherapy in patients with rectal cancer: a retrospective study

F. Prampolini, S. Taschini, A. Pecchi, F. Sani, F. Gelsomino, A. Spallanzani, S. Kaleci, P. Torricelli; *Modena/IT (prampolini.francesco@tiscali.it)*

Purpose: To evaluate whether MRI performed before and after neoadjuvant chemoradiotherapy (NACRT) could predict the risk of recurrence in patients with rectal cancer.

Methods and Materials: This study included 87 patients with rectal cancer who had undergone pre- and post-NACRT local staging MRI, with dedicated protocol, between 2005 and 2016. Two radiologists independently reviewed all MR examinations retrospectively and assessed the T-stage, nodal involvement (>5 mm), distance from mesorectal fascia and extramural venous invasion (EMVI scoring system 0-4). Correlation between these parameters and patients' risk of recurrence was evaluated with statistical analysis.

Results: In our analysis all four assessed parameters correlated significantly with the risk of recurrence (*P* value range 0.002-0.026) when evaluated in MRI performed after NACRT, but not in MRI performed before NACRT. The specific analysis of EMVI score (0-4) showed a statistically significant correlation with recurrence only when evaluated at MRI post-NACRT, while extramural venous invasion, if considered as present or absent, regardless of its score, correlated significantly with the risk of recurrence also in pre-NACRT MR examination (*P*=0.011).

Conclusion: MRI performed after NACRT has a significant value in predicting the risk of recurrence in patients with rectal cancer. EMVI strongly correlated with the risk of recurrence and its presence in pre-NACRT MRI should be considered as an early predictive factor of disease relapse.

10:30 - 12:00

Room Z

Interventional Radiology

SS 1009

Vascular interventions: intra- and extracranial

Moderators:

C. Binkert; Winterthur/CH
N.N.

B-0856 10:30

Outcomes of endovascular treatment for acute large vessel ischaemic stroke more than 6 hours after symptom onset

R. Motyer¹, H. Kok², H. Asadi³, A. O'Hare¹, P. Brennan¹, P. Sarah¹, S. Looby¹, P. Nicholson¹, J. Thornton¹; ¹Dublin/IE, ²London/UK, ³Melbourne, Victoria/AU (ronanmotyer@gmail.com)

Purpose: Benefit from endovascular thrombectomy (EVT) for large vessel occlusion (LVO) acute ischaemic stroke (AIS) is well demonstrated. Furthermore, emerging evidence supports efficacy in appropriately selected patients treated beyond current recommendations of 6 hours. We evaluated clinical outcomes in patients undergoing late EVT at our institution.

Methods and Materials: Retrospective review of prospectively collected clinical database on 355 patients who underwent EVT for LVO AIS. Data collected consisted of patient demographics, radiological findings and outcome details. Outcomes, including 90-day functional status, recanalisation, symptomatic intracranial haemorrhage (sICH) and 90-day mortality, for patients undergoing EVT <6 hours, >6 hours and >7.3 hours were compared.

Results: 355 patients underwent EVT for LVO AIS at our institution during the review period, with 74 (21%) patients treated >6 hours from symptom onset. Successful recanalisation was achieved in 285 (80%) patients, with 228 (81%) achieving a mTICI ≥2b in <6 hour group, and 57 (77%) in >6 hour group (*p*=0.429). 90-day functional independence (mRS 0-2) was achieved in 162 (46%) patients, with 130 (46%) achieving a mRS of 0-2 in <6 hour group, and 32 (43%) in >6 hour group (*p*=0.643). No significant differences were found in rates of sICH or 90-day mortality. No significant differences in functional independence, recanalisation rates, sICH, or mortality were identified in patients treated with EVT >7.3 hours compared to <7.3 hours.

Conclusion: In appropriately selected patients, EVT >6 hours was associated with comparable outcomes to those treated <6 hours. These data support a physiological approach to patient selection.

B-0857 10:38

Endovascular thrombectomy beyond 12 hours of stroke onset: a stroke network's experience of late intervention

R. Motyer, J. Thornton, S. Power, P. Brennan, A. O'Hare, S. Looby, D. Williams, B. Moynihan, S. Murphy; *Dublin/IE (ronanmotyer@gmail.com)*

Purpose: The benefit of late endovascular thrombectomy (EVT) in correctly selected patients presenting with large vessel occlusion acute ischaemic stroke has been demonstrated, with positive outcomes achieved up to 24 hours from symptom onset. As a tertiary stroke service, we reviewed our outcomes in cases of EVT performed >12 hours from symptom onset.

Methods and Materials: Retrospective review of prospectively maintained database of all EVT cases performed for management of AIS with LVO of the anterior circulation at our institution. Patients were evaluated using ASPECTS on non-contrast CT brain and collateral grade on multiphase CT angiogram (mCTA) to aid selection for intervention. Data, including patient demographics, neuroimaging findings, procedural details, recanalization rates and 90-day functional outcomes, from all EVT cases performed >12 hours was collected.

Results: Of the 542 consecutive EVT cases reviewed, 25 (4.6%) were performed >12 hours from symptom onset. Median age was 69 (IQR, 55-80), median NIHSS on presentation 14 (IQR, 11-18.5), median ASPECTS was 8 (IQR, 8-9) and moderate-good cerebral collateral status in 96% of patients (*n*=24). Median time to groin puncture was 880 minutes (IQR, 753.5-977.5), with a rate of successful recanalization (mTICI 2b-3) of 88% (*n*=22). The rate of 90-day functional independence (mRS 0-2) was 52% (*n*=13). There were no cases of symptomatic intracranial haemorrhage and 90-day mortality rate was 12% (*n*=3).

Conclusion: With careful patient selection, guided by ASPECTS and collateral status, EVT may be performed safely and effectively, with good functional outcomes achieved in patients with delayed presentation acute ischaemic stroke.

B-0858 10:46

Acute ischaemic stroke due to tandem occlusions of the internal carotid artery: results of endovascular recanalisation and clinical outcome

M. Voormolen, T. Van der Zijden, O. D'Archangeau, L. Yperzeele, P. Vanacker, I. Baar, M. Muto, T. Menovsky, P.M. Parizel; *Antwerp/BE (maurits.voormolen@uza.be)*

Purpose: Tandem occlusion of internal carotid artery (ICA) is defined as proximal ICA (near) occlusion combined with distal (embolic) occlusion of ICA and/or middle cerebral artery (MCA). We assessed endovascular recanalisations and clinical outcome in acute ischaemic stroke (AIS) patients due to ICA tandem occlusions.

Methods and Materials: We evaluated immediate angiographic results and prospective clinical outcomes of 19 consecutive patients with tandem ICA occlusions, treated with mechanical thrombectomy (MT) between January 2014 and July 2017, involving 15 men and 4 women, with a median age of 69 years (range 52-87). They comprised 15% of total anterior circulation stroke recanalisations in this period. Thirteen patients had left ICA occlusion (68%). Fifteen patients (79%) received intravenous thrombolysis before endovascular recanalisation.

Results: Successful recanalisation (TICI 2b/3) was seen in 14 patients (74%) and no recanalisation (TICI 0) in three patients (16%). Median procedure time was 65 minutes (range 20-120). Median number of passages was one (range 0-5). In 7 patients (37%) balloon angioplasty of ICA was performed; 1 carotid stent was placed (5%). Median NIHSS was 19 (range 9-29) at admission and 13 (range 2-30) at discharge. Only six patients (32%) had favorable clinical outcome at 3 months (mRS≤2); 9 patients (47%) had major cerebral infarcts, 6 patients died (32%).

Conclusion: In our series, endovascular recanalisation of tandem ICA occlusions in patients with acute ischaemic stroke showed high rates of successful recanalisation, but unfavorable clinical outcomes. Further studies are needed to determine which patients might benefit from endovascular recanalisation.

B-0859 10:54

Bronchial artery embolisation: tuberculosis patients with haemoptysis

K. Muhammad, I.A. Lutfi; *Karachi/PK (dr.khairmuhammad@gmail.com)*

Purpose: The goal of this study is to present our experience of bronchial artery embolization for the treatment of life threatening haemoptysis in patients with pulmonary tuberculosis. This study focuses on overall clinical success rate of this procedure and its cost effectiveness.

Methods and Materials: Our study is based on four year retrospective cross-sectional data from March 2013 to Feb 2017. In our study, fifty patients underwent bronchial artery embolization for the treatment of life threatening

haemoptysis secondary to pulmonary tuberculosis. These patients were referred to radiology department from pulmonary clinics/ emergency. As a part of our departmental protocol, CT aortogram/pulmonary angiogram was performed on almost every patient to evaluate the bleeding bronchial artery for embolization.

Results: We found out in our study bronchial artery embolization was successful in forty eight patients (96 %) and followed up till six months. Recurrence occurred in four (8%) patients after six months in whom there developed new lung cavity or recanalization of artery in previous lesion. In two patients (4%) embolization procedure was abandoned due to tortuous course of bronchial artery. Out of total fifty patients, some of our patient developed complications such as chest pain in fifteen patients (30%) and one patient (2%) developed lower limb weakness (spinal cord related complication). However, there was no mortality due to this procedure in our study.

Conclusion: Bronchial artery embolization is life saving procedure for patient with haemoptysis with no procedure related mortality in our study and cost effective compared to surgery.

B-0860 11:02

Pulmonary arterial occlusion treatment in patients with haemoptysis: a 32-case single-centre study

Z.C. [Charline](mailto:charline.zadro@gmail.com), M. Jaffro; *Toulouse/FR (charline.zadro@gmail.com)*

Purpose: Pulmonary arterial bleeding is a rare cause of haemoptysis, which requires a specific endovascular treatment. Herein, we report the feasibility and effectiveness of pulmonary artery occlusion treatment (PAOT) in our centre.

Methods and Materials: Thirty-two patients treated by PAOT between January 2010 and May 2017 in Toulouse Rangueil University Hospital were retrospectively included. We performed a thoracic angio scan for each patient looking for an argument pointing to a pulmonary arterial origin (PAO) of the bleeding.

Results: Nineteen patients (59 %) had a neoplasia and seven (22%) an active infectious disease. Signs contradicting to a PAO were irregularities (88%) and occlusion (31%) of the pulmonary artery, a lung parenchyma necrosis (59%) and pseudoaneurysms (44%). We used steel coils in 23 cases (72%) and plugs in 12 (38%). The feasibility of PAOT was 100% and the clinical efficacy, defined by early and sustained interruption of bleeding for 1 month, was 78% with a recurrence rate at the last follow-up of 31%. Seven patients had recurrence in the first month, and three later with additional embolisations (5) or surgeries (2). Only one patient with active infection experienced recurrence. Twenty-five patients (78%) had received an exclusive PAOT and 7 (22%) a combined occlusion of pulmonary and bronchial or systemic non-bronchial arteries. There was no significant difference between the two interventions concerning recurrence or survival.

Conclusion: PAOT by steel coils or/and plug is feasible and efficacious with little recurrence in the long term.

B-0861 11:10

Renal artery embolisation for vascular lesions following Nephron-sparing surgery: a five-year experience

E. [Amodeo](mailto:enriamo@gmail.com), A. Contegiacomo, N. Attempati, A. Paladini, C. Di Stasi, R. Manfredi; *Rome/IT (enriamo@gmail.com)*

Purpose: Indications to Nephron-Sparing Surgery (NSS) are extending overtime, resulting in improved renal function and parenchymal preservation. On the other hand, NSS is burdened by potentially life-threatening vascular lesions (NSS-VL). Renal Artery Embolization (RAE) is emerging as a mini-invasive alternative to surgery for NSS-VL management. This observational retrospective study describes our experience in the treatment of NSS-VL.

Methods and Materials: Thirty-six patients, from January 2012 to December 2016, with a NSS-VL diagnosed on Computed Tomography Angiography (CTA) before RAE were retrospectively enrolled. Type (pseudo-aneurysm; arteriovenous fistulas; active bleeding) and site (proximal; segmental; distal) of NSS-VL were assessed on CTA images and confirmed during RAE procedure. Technical (intra-procedural VL exclusion) and clinical (patient clinical stability >5 days) success, type of embolic agents (Coils; Glue; Polyvinyl-alcohol particles, PVA; Absorbable Gelatine Sponge, AGS) and intra/ peri-procedural complications were assessed by clinical charts and radiological reports analysis.

Results: Patients had 24/36 (66,6%) pseudo-aneurysms, 6/36 (16,7%) arteriovenous fistulas and 6/36 (16,7%) active bleeding. RAE was performed with Glue (25/3; 69,4%), PVA (6/36; 16,7%), Coils (5/36; 13,9%), AGS (3/36; 8,3%) or a combination of materials (7/36; 19,4%). Technical and clinical success was achieved in 36/36 (100%) and 33/36 (91,7%) patients, respectively. Glue migration occurred in 1/36 (2,8%) patient and was managed by intra-procedural fragmentation with angioplasty balloon. 3/36 (8,3%) patients encountered post-procedural bleeding successfully re-treated with RAE.

Conclusion: RAE is a feasible, effective and safe, mini-invasive alternative to surgery in NSS-VL management.

B-0862 11:18

Alternative techniques in splenic artery embolisation in blunt splenic trauma

M. [Citone](mailto:michele.citone@gmail.com), F. Mondaini, C. Raspanti, G. Gabbani, E. Casamassima, G. Falcone, F. Fanelli; *Florence/IT (michele.citone@gmail.com)*

Purpose: Splenic artery embolisation (SAE) has been increasingly employed as adjunctive tool in non operative management (NOM) in blunt splenic trauma (BST). Despite high technical success, controversies still exist on technique and materials employed, being coils the most utilised tool. We report our experience with Amplatzer Vascular Plug (AVP) and Onyx in splenic artery embolisation for trauma.

Methods and Materials: Between 2015 and 2017, 11 patients, 7 male, (mean age 47yo range 16-67) received SAE treatment as part of NOM for isolated BST with embolic agent different from coils. Indication to treatment was grounded on contrast blush or active bleeding (AB) or AAST injury score >3 on CECT. In 6 patient proximal embolisation with AVP (20-30% oversized) for injury grade >III without active bleeding (AB) was performed while in 5 patients distal SAE with Onyx 34 was performed for AB and (4pts) or extensive laceration (1pt). All procedures were performed under local anesthesia while deep sedation was required for the onyx group.

Results: Technical success (intended as bleeding cessation or splenic artery occlusion) was achieved in 100%. Embolisation was achieved in less than 1min. No migration of embolic agent was observed. None of the patients required splenectomy. No major complication or re-bleeding were reported. No evidence of abscess or major infarction was observed at CT scan performed within 48h.

Conclusion: SAE with AVP or Onyx is a safe and effective procedure in splenic artery embolisation for blunt splenic trauma alternative to traditional coils.

B-0863 11:26

Management of acute occlusion of the superior mesenteric artery by local thrombolysis (multidisciplinary approach)

M.M.A.H. [ElShafei](mailto:mohamedshafei@yahoo.com), A. Elgendi; *Alexandria/EG (mohamedshafei@yahoo.com)*

Purpose: To evaluate the effectiveness of endovascular local thrombolysis management in acute superior mesenteric artery (SMA) occlusion as alternative or neo-adjunctive treatment modality to surgery in a multidisciplinary approach strategy.

Methods and Materials: The study was conducted on 12 patients presented by acute abdomen in the emergency department and diagnosed by CT as acute superior mesenteric artery occlusion. In all cases the main stem of the SMA was involved. The median time from admission to attempted endovascular revascularisation was 6-12 hours except for one case (36h). Superselective catheterisation of the SMA was done using Cobra 5fr catheter for control angiogram and a hydrophilic guidewire was introduced passing the occlusive thrombus or embolus and an initial bolus dose of rt-PA or streptokinase was injected, after that exchanged the Cobra catheter by Simmond' catheter for infusion over 12-24 hours. Re-checking the flow after the infusion period was done before removal of the catheter. Close monitoring of the patient was done by multidisciplinary team.

Results: Successful revascularisation of the SMA was achieved in all patients. Only one patient needed further open laparotomy and bowel resection. No significant post-procedure bleeding was reported in any of the cases. One month follow up was done.

Conclusion: Local thrombolysis for acute SMA occlusion is a minimally invasive procedure that can be effective as alternative treatment in selected group of patients without peritonitis. Early intervention (golden time) is the key for better results.

B-0864 11:34

Endovascular treatment of haemodialysis arteriovenous fistula with vessel preparation and drug-coated balloon angioplasty: a single-centre study

J. [Lucev](mailto:jernej.lucev@gmail.com), S. Breznik, D. Dinevski, R. Ekart, M. Ruprecht; *Maribor/SI (jernej.lucev@gmail.com)*

Purpose: To evaluate the effect of PTA of haemodialysis fistulas utilizing drug-coated balloons with plain balloon vessel preparation (VP DCB).

Methods and Materials: From 2012 to 2015, 31 patients (16 men; mean age 62.81+/-17.2 years) with failing arteriovenous fistula were treated. All stenoses were dilated with regular high-pressure PTA balloons. After achieving angiographic success (<10% residual stenosis), drug-coated balloons were used for drug administration. Observation period was 6, 12 and 24 months. Results were compared with plain balloon PTA performed from 2006 to 2011 (31 patients; 15 men; mean age 67.03+/-8.44 years). Target lesion primary patency, primary-assisted patency and secondary patency were compared. T test, Mann-Whitney U test, Fisher's exact test, Kaplan-Meier survival curve and

log-rank test were used for statistical analysis. The significance was set at 0.05.

Results: Target lesion primary patency for VP DCB and plain balloon group was significantly different at 6 months (90.3% vs 61.3%; $p=0.016$), 12 (77.4% vs 29%; $p=0.000$) as well as 24 months (45.2% vs 16.1%; $p=0.026$). Kaplan-Meier survival curve also showed significant difference for target lesion primary patency (534.2 vs 315.7 days; $p=0.000$). Target lesion primary assisted patency could not be compared because both groups were too different. However, only 38.7% of patients in VP DCB group were treated twice or more vs 80.6% in plain balloon group ($p=0.002$). There were no significant differences in target lesion secondary patency.

Conclusion: VP DCB PTA decreases the rate of reinterventions and increases target lesion primary patency during the first 24 months.

B-0865 11:42

Lysis-assisted balloon (LAB) thrombectomy - a method for declotting thrombosed arteriovenous dialysis grafts: results from a retrospective analysis of 241 endovascular procedures

P. Kitrou¹, P. Papadimitos¹, K. Katsanos¹, S.C. Spiliopoulos², N. Christeas¹, D. Karnabatidis¹; ¹Patras/GR, ²Athens/GR (panoskitrou@gmail.com)

Purpose: To retrospectively investigate the results of a percutaneous lysis-assisted balloon (LAB) thrombectomy procedure for the treatment of thrombosed arteriovenous dialysis grafts (AVGs).

Methods and Materials: Within 5 years (January 2012 to December 2016), 291 declotting procedures were performed for the treatment of thrombosed dialysis arteriovenous fistulas and grafts. Data were available for 129 patients (75 men, 58.1%) with an AVG, undergoing 241 procedures [1.87procedures/patient (1-10)]. Procedure includes initial lysis with 5mg recombinant tissue plasminogen activator followed by thrombectomy with a high pressure balloon for thrombus maceration using "facing sheaths" technique. 61 patients had ≥ 2 declotting procedures. In 80 cases (80/241; 33.2%) a stent graft (SG) was used for treatment of persistent stenosis. Main primary outcome measures were clinical success and postintervention assisted primary patency (PAPP). Secondary outcome measures included procedural complications and investigation of independent factors that could influence circuit survival.

Results: Median PAPP was 434 days according to Kaplan Meier survival analysis. Clinical success was 96.26%. In 6 cases (6/241, 2.49%) declotting failed and a catheter was placed. There were 16 minor (16/241, 6.64%) and no major complications. There was no significant difference in circuit survival regardless of SG use (No SG 406 days vs. SG 349 days; $p=0.24$). There was a significant difference in favor of the 2nd declotting compared to the 1st in 61 patients (1st: 162 days vs. 2nd: 447 days; $p<0.0001$).

Conclusion: LAB thrombectomy resulted in higher circuit survival rates with increased technical success and minimum complications without the use of thrombectomy devices.

B-0866 11:50

Cumulative patency rate of forearm vs upper arm arteriovenous dialysis fistulae

A. Almehmi, V. Narasimha Krishna, A.M. Abdel Aal; Birmingham, AL/US (aalmehmi@uabmc.edu)

Purpose: Both upper arm (UA) and forearm (FA) arteriovenous fistulas (AVF) are utilised as a permanent hemodialysis access. The aim of this study was to compare the cumulative patency rate of FA-AVFs and UA-AVFs and to explore the predictors of access survival.

Methods and Materials: We retrospectively analysed 286 hemodialysis patients who underwent AVF creation at our institution between January 2005 and December 2015. Cumulative access patency was defined as the time from access creation to permanent failure, regardless of the number of interventions required to maintain long-term patency for dialysis. The cumulative patency rate was calculated in UA-AVF and FA-AVF groups using Kaplan-Meier survival methods and log-rank tests. Backward stepwise Cox regression model was utilised to determine predictors of hemodialysis access survival.

Results: The total number of patients included in the UA-AVF and FA-AVF groups were 121 and 165 cases, respectively. Baseline characteristics included: 39% were females; 88% were blacks; 50% were diabetics; 96% and 28% of patients had hypertension and congestive heart failure, respectively. Cumulative patency rate of UA-AVF and FA-AVF during the follow up time was 74% and 59%, respectively ($p=0.008$). In multivariate analysis of AVF survival, we found that hemodialysis access failure was higher in FA-AVF than UA-AVF (HR: 1.97 [1.28-3.06]; $p=0.002$). Further, female gender was associated with increased AVF failure (HR: 1.58 [1.05-2.37]; $p=0.03$).

Conclusion: FA-AVFs have a lower cumulative patency rate as compared to UA-AVFs. Further, UA-AVFs and male gender are associated with a better hemodialysis access survival.

10:30 - 12:00

Room O

Chest

SS 1004

Artificial intelligence in chest imaging

Moderators:

J. Jacob; London/UK
N.N.

K-15 10:30

Keynote lecture

J. Jacob; London/UK

B-0867 10:39

Artificial intelligence applied on the national lung screening trial dataset: a radiomics study

S. Martin, J. Hofmeister, S. Burgermeister, C.D. Becker, X. Montet; Geneva/CH (steve.martin@hcuge.ch)

Purpose: To investigate the added value of radiomics applied on the National Lung Screening Trial (NLST) dataset in estimating solitary pulmonary nodule malignancy risk compared to the PanCan model.

Methods and Materials: Lung adenocarcinoma ($n=227$) and squamous cell carcinoma ($n=94$) with a long axis greater than 8 mm obtained from the NLST dataset were included and matched with benign lung nodules ($n=299$). Features extraction ($n=124671$) was performed using an open-source python package after automatic segmentation of the 620 lung nodules from low-dose unenhanced computer tomography (CT). Benign versus malignant classification based on radiomics and clinical data was achieved via features selection, dimension reduction (using principal component analysis), and classification (using a support vector machine classifier). The demographic data, part of the NLST dataset and combined to the extracted features from the CT images for the radiomics analysis, were also evaluated solely according to the PanCan model. Sensitivity, specificity, positive predictive value (PPV) and negative predictive value (NPV) of the radiomics were calculated based on the histological diagnostic given in the NLST dataset. The diagnostic performances of the two models were compared on their area under the receiver operating characteristic curve (AUC) analysis.

Results: Radiomics model: sensitivity 96.9%, specificity 93.3%, PPV 93.9%, NPV 96.6%, AUC: 0.983. PanCan model: AUC: 0.797.

Conclusion: Artificial intelligence and data mining in chest CT raise the diagnostic confidence higher than any other models in the field of non-invasive characterisation of lung nodules.

B-0868 10:47

Lung nodule risk stratification using Deep Learning on the complete US National Lung Screening Trial dataset

C. Arteta, L. Pickup, P. Novotny, Z. Sandford, J. Brabec, D. Dufek, J. Kunst, J. Declerck, T. Kadir; Oxford/UK

Purpose: Correct classification of screen or incidentally detected indeterminate pulmonary nodules is essential to avoid excessive follow-up. Prior work on limited datasets has shown the potential of computer aided risk stratification but validation on large datasets is required prior to use as a rule-out test. For the first time, we demonstrate validation of a Deep Learning risk stratification system on the complete US National Lung Screening Trial (NLST) dataset.

Methods and Materials: The NLST dataset was manually curated such that each reported nodule and cancer was located and diagnostically characterised. Training and testing sets were built from the full set of patients with solid/mixed nodules of 6mm and above (6132). A Convolutional Neural Network (CNN) was trained with four-fold cross-validation, withholding approximately 370 nodules (class-balanced) in each test set. Performance was evaluated using Area-Under-the-ROC analysis and also the fraction of benign nodules correctly rejected at 0%, 1% and 2% of misclassified malignant nodules (FNR). Similar analysis was performed using nodule size as a classifier.

Results: Using the CNN, Benign Rejection Fraction (min, variance) at 0%, 1%, 2% FNR was 19% (14%, 8%), 32% (16%, 12%), 37% (18%, 13%) respectively. Using size, benign rejection fraction values were 0% at all threshold. AUC for the CNN and size was 0.87 and 0.82 respectively.

Conclusion: Using the CNN, a significant proportion of patients with benign nodules can be correctly identified while keeping the rate of missed cancers at extremely low, thereby avoiding unnecessary follow-up.

Author Disclosures:

C. Arteta: Employee; Optellum Ltd. **L. Pickup:** Employee; Optellum Ltd. Founder; Optellum Ltd. Shareholder; Optellum Ltd. **P. Novotny:** Employee; Optellum Ltd. **Z. Sandford:** Employee; Optellum Ltd. **J. Brabec:** Employee; Optellum Ltd. **D. Dufek:** Employee; Optellum Ltd. **J. Kunst:** Employee; Optellum Ltd. **J. Declerck:** Board Member; Optellum Ltd. Employee; Optellum Ltd. Founder; Optellum Ltd. Shareholder; Optellum Ltd. **T. Kadir:** Employee; Optellum Ltd. Founder; Optellum Ltd. Shareholder; Optellum Ltd.

B-0870 11:55

Automatic prediction of emphysema extent in low-dose CT by deep learning

G. **Bortsova**¹, S.N. Ørting², F. Dubost¹, I. Katramados³, L. Hogeweg³, M.M. Wille⁴, L.H. Thomsen⁴, M. De Bruijne¹; ¹Rotterdam/NL, ²Copenhagen/DK, ³Groningen/NL, ⁴Hellerup/DK (gerdabortsova@gmail.com)

Purpose: Emphysema is commonly quantified using CT densitometry measures, which however correlate only moderately with visual assessment of emphysema extent according to trained observers. We propose a deep learning approach to automatically quantify emphysema extent based on its CT patterns rather than on density alone, mimicking visual assessment.

Methods and Materials: Two low-dose CT scans (baseline and 5th annual follow-up) were acquired at full inspiration from 1934 participants of the Danish Lung Cancer Screening Trial (inclusion criteria: age 50-70, at least 20 pack-years of smoking and FEV₁ of at least 30% of predicted). Two observers independently scored emphysema extent from 0 (no emphysema) to 5 (75-100% of lung affected) in the upper, middle and lower lung regions. We trained our algorithm on scans of 993 subjects and evaluated it on 941 subjects.

Results: Agreement between automated and expert's assessment of emphysema presence was good (area under the ROC curve 0.89, accuracy 90.4% - similar to interobserver agreement of 91%). The intraclass correlation coefficient was 0.757 (Pearson: 0.823) for emphysema extent scoring and 0.835 (Pearson: 0.852) between the observers. The Pearson correlation of the expert's scores and densitometry based on -950HU threshold was 0.436. Only in 1.5% of the scans the predicted score was more than one category off.

Conclusion: Our emphysema quantification method's performance is promising. This method may replace time-consuming visual assessment in large-scale studies and, eventually, in clinical practice.

Author Disclosures:

I. Katramados: Founder; COSMONIO. **L. Hogeweg:** Employee; COSMONIO.

B-0871 11:03

Fully automated segmentation of pulmonary fibrosis using different software tools

A. **Giannakis**¹, T. Norajitra¹, L. Kehler¹, J. Dinkel², O. Weinheimer¹, C. van Lunteren¹, M. Kreuter¹, K. Maier-Hein¹, C. Heussel¹; ¹Heidelberg/DE, ²Munich/DE (a-giannakis@hotmail.com)

Purpose: Evaluation of software tools for segmentation of fibrotic pulmonary parenchyma will strengthen the role of multidetector CT as biomarker of disease extent, evolution, and response to therapy in patients with pulmonary fibrosis.

Methods and Materials: 418 non-enhanced thin section MDCT of 127 patients with idiopathic pulmonary fibrosis and 78 MDCT of 78 healthy individuals were analysed through three fully automated, completely different software tools: YACTA, LUFIT, and IMBIO. The agreement between YACTA and LUFIT on segmented lung volume, 80th (reflecting fibrosis) and 40th (reflecting ground glass opacity) percentile of lung density histogram was analysed using Bland-Altman plots. The fibrosis and ground glass opacity segmented by IMBIO (lung texture analysis software tool) were included in specific regression analyses.

Results: In the IPF-group, LUFIT performed better than YACTA by segmenting more lung volume (mean difference 242 ml, 95% limits of agreement -54 to 539 ml), as well as quantifying higher 80th (76 HU, -6 to 158 HU) and 40th percentile (9 HU, -73 to 90 HU). No relevant differences were revealed in the control group. The 80th/40th percentile as quantified by LUFIT showed positive correlation with the percentage of fibrosis/ground glass opacity calculated by IMBIO ($r = 0.784/r = 0.918$).

Conclusion: In terms of segmentation of pulmonary fibrosis, LUFIT as shape model-based segmentation software tool is superior to YACTA, which works based on threshold, because the density of severe fibrosis is similar to that of the surrounding soft tissues. Therefore, LUFIT may serve as a valid tool in the quantification of pulmonary fibrosis, since this disease mainly affects the subpleural space.

Author Disclosures:

L. Kehler: Advisory Board; LK received compensation for advisory boards from Roche. **C. Heussel:** Consultant; Consultation or other fees Schering-Plough 2009, 2010 Pfizer 2008-2014 Basilea 2008, 2009, 2010 Boehringer Ingelheim 2010-2014 Novartis 2010, 2012, 2014 Roche 2010 Astellas 2011, 2012 Gilead 2011-2015. Employee; •Head of Diagnostic and Interv Radiology with Nuclear Medicine, Thoraxklinik Heidelberg •Member of the German Center

for Lung Research. Owner; Stock ownership in medical industry: GSK. Patent Holder; Method and Device For Representing the Microstructure of the Lungs. IPC8 Class: AA61B5055FI, PAN: 20080208038, Inventors: W Schreiber, U Wolf, AW Scholz, CP Heussel. Research/Grant Support; Research funding: Siemens 2012-2014 Pfizer 2012-2014 MeVis 2012, 2013 Boehringer Ingelheim 2014 German Center for Lung Research. Speaker; Lecture Fees: Gilead 2008-2014 Essex 2008, 2009, 2010 Schering-Plough 2008, 2009, 2010 AstraZeneca 2008-2012 Lilly 2008, 2009, 2012 Roche 2008, 2009 MSD 2009-2014 Pfizer 2010-2014 Bracco 2010, 2011 ME. Other; Comitee membership, Chest working group of the German Roentgen society, National guidelines: bronchial carcinoma, mesothelioma, COPD, screening for bronchial carcinoma, CT and MR imaging of the chest.

B-0872 11:11

Clinical validation of a deep learning algorithm for quantification of the idiopathic pulmonary fibrosis pattern

T.R. Nimmada¹, P. Rao¹, P.S. Sanghavi¹, V. Venugopal², P. Warier¹, Z. Udawadia¹, B. Jankharia¹; ¹Mumbai/IN, ²New Delhi/IN (pooja.rao@qure.ai)

Purpose: Radiologists are currently ill equipped to precisely estimate disease burden and track the progression of idiopathic pulmonary fibrosis (IPF). Development of an automated method for IPF segmentation is challenging, due to the complexity of the fibrosis pattern and degree of variation between patients. Deep neural networks are machine learning algorithms that overcome these challenges. We describe the development and validation of a novel deep learning method to quantify the IPF pattern.

Methods and Materials: We used high-resolution chest CT scans from 23 patients with IPF as training data. The fibrosis pattern was marked out on 60 slices per scan. Annotated scans, with 6 additional normal scans were used to train a convolutional neural network to outline the IPF disease pattern. Segmentation accuracy was measured using Dice score. For each patient, percentage of lungs affected by IPF was calculated. An independent set of 50 scans was used for clinical validation. Disease volume was independently estimated by 2 thoracic radiologists blinded to the algorithm estimate. Algorithm-derived estimates were correlated with radiologist estimates of disease volume.

Results: A 3-dimensional neural network architecture coupled with 2-dimensional post-processing of each slice produced the most accurate segmentation, with a Dice score of 0.77. The correlation between algorithm-derived disease volume estimate and average radiologist estimates was 0.92. Inter-radiologist correlation was 0.89. Radiologist estimates of disease volume varied by 5.5% (range 0-15%).

Conclusion: We demonstrate that a deep neural network, trained using expert-annotated images, can accurately quantify the percentage of lung volume affected by IPF.

Author Disclosures:

T.R. Nimmada: Employee; Qure.ai. **P. Rao:** Employee; Qure.ai. **P. Warier:** Employee; Qure.ai.

B-0873 11:19

Risk assessment of lung cancer development in Idiopathic Pulmonary Fibrosis (IPF) patients using quantitative HRCT analysis

D. **Falsaperla**¹, S.E. Torrisi¹, A. Torcitto¹, G. Russo², A. Stefano², A. Vancheri¹, A. Basile¹, C. Vancheri¹, S. Palmucci¹; ¹Catania/IT, ²Cefalù/IT (danielefalsaperla@gmail.com)

Purpose: To investigate the diagnostic accuracy of Kurtosis, High Attenuation Area (HAA) and Fibrotic Area (FA) HRCT indexes in risk assessment of lung cancer development in patients with Idiopathic Pulmonary Fibrosis (IPF).

Methods and Materials: 42 IPF patients were retrospectively analysed; patients were divided into subjects that developed lung cancer (Group A n=9) and patients without lung cancer development (Group B n=33). HRCT and pulmonary function tests were reviewed; the extent of fibrotic disease was quantified on HRCT using Kurtosis, HAA and FA. For group A, measurements were obtained from HRCT acquired before cancer development - medially performed 26 months after IPF diagnosis; for group B, we analysed HRCT acquired medially 18 months from IPF diagnosis. HRCT indexes, FVC and DLCO values were compared between groups using Mann-Whitney U-test.

Results: No difference was recorded for FVC and DLCO values. No statistical difference was found among groups for median values of Kurtosis (3.76 versus 4.26), HAA (27.85 versus 23.16) and FA (15.77 versus 13.89). ROC analysis for prediction of lung cancer development using a threshold value of Kurtosis index ≤ 5.31 showed sensibility of 100% and specificity of 24.2%; for FA index, using a threshold value >26.375 , ROC analysis obtained sensibility of 66.7% and specificity of 69.7%. For HAA index, a threshold value >14.59 reported sensibility and specificity of 77.8% and 60.6%.

Conclusion: Kurtosis, FA and HAA provide limited diagnostic accuracy in risk assessment of cancer development in IPF patients; FA and HAA showed the best sensitivity/specificity ratio in predicting lung cancer.

Friday

B-0874 11:27

Radiomics signature for non-small cell lung cancer recurrence risk prediction after surgery: quantitative analysis of the tumour and peritumoural lung parenchyma on presurgical MDCT

T. Akinci D'Antonoli, A. Farchione, J. Lenkiewicz, M. Chiappetta, G. Cicchetti, A.R. Larici, V. Valentini, L. Bonomo, R. Manfredi; *Rome/IT (drtugba@hotmail.com)*

Purpose: To estimate recurrence risk after surgery in non-small cell lung cancer (NSCLC) patients by employing a prediction model with radiomics signature (RS) and clinical parameters.

Methods and Materials: 124 NSCLC patients (stages I to IIIA) who received surgery (2008-2013) at our hospital were retrospectively enrolled. Tumour recurrence (TR), local recurrence (LR) and distant metastasis (DM) was diagnosed on follow-up imaging (3-5 years). The region of interests (ROI) for the tumour (GTV), the peritumoural lung parenchyma 2 cm around the tumour (PTV) and the involved lobe (LB) were semiautomatically contoured. 90 features (statistical, morphological, textural) were extracted from each ROI with an in-house developed software (Moddicom). RS was computed with the best-performed radiomics model's coefficients for each outcome (features selection: "fscaret" and step-wise selection on the top 10 features; model selection: highest AUC in 10-fold cross-validation), then significant clinical features (Cox regression analysis: tumour-node-metastasis stage [TNMS], histology, age, smoking status and gender) were added. Predictive nomograms were created at 1-, 2-, 3-year survival.

Results: Median time-to-recurrence was 44 months; 25 patients developed LR, 31 patients developed DM. For TR and DM outcomes GTV+PTV (AUC 0.750 for both), for LR outcome GTV (AUC 0.731) were found to be the best performed models; adding TNMS improved all models' performance (TR, DM, LR: AUC 0.760, 0.759, 0.750, respectively). The nomogram with RS and TNMS discriminated high-risk better than TNMS alone.

Conclusion: Utilizing radiomics on pre-treatment MDCT images, extracting peritumoural and intratumoural radiomics features could be a useful tool to stratify NSCLC patients at different recurrence risk and to define a personalised treatment.

Author Disclosures:

T. Akinci D'Antonoli: Grant Recipient; ESOR.

B-0875 11:35

Lung adenocarcinoma radiogenomics predicts clinical outcome

A. Leonardi, A. Napoli, R. Scipione, M. Anzidei, S. Dababou, C. Catalano; *Rome/IT (andrea.leonardi1988@gmail.com)*

Purpose: To statistically correlate CT features, quantitative texture analysis (QTA), epidermal growth factor receptor (EGFR) mutations and clinical outcome in patients with lung adenocarcinoma.

Methods and Materials: We retrospectively enrolled eighty-one patients affected by lung adenocarcinoma to evaluate conventional CT features and assess QTA analysis. Correlations between CT features, QTA, EGFR mutations and clinical outcome were determined through univariate analysis, unpaired Student t test, chi-square and Mann-Whitney tests. A multiple logistic regression analysis and Receiver Operating Characteristics (ROC) curve analysis versus death and EGFR status was performed for CT features and QTA.

Results: EGFR mutation was detected in 31/81 tumors (38.3%). EGFR mutation demonstrated a correlation with emphysema ($p < 0.0001$) and a positive association with necrosis ($p = 0.017$). At multivariate analysis air-bronchogram and locoregional infiltration were proved to be positively and negatively associated with EGFR-mutated status ($p = 0.0304$ and $p = 0.0018$ respectively). No significant correlation was observed between the conventional CT features and overall survival. Mean, SD and skewness were found to have a significant correlation with EGFR mutation ($p = 0.0001$; $p = 0.0001$; $p = 0.0459$). The only parameter correlated with the event of death was entropy ($r = 0.2708$; $p = 0.0329$).

Conclusion: CT and QTA features of lung adenocarcinoma demonstrated a significant relationship with EGFR mutations and clinical outcome.

B-0876 11:43

Can texture analysis predict non small cell lung cancer recurrence after surgery ?

R.S.R. Lopes do Rosario, N. Michoux, V. Lacroix, B. Ghaye; *Brussels/BE (ritar1@hotmail.com)*

Purpose: To predict the aggressiveness of NSCLC (in terms of recurrence) using morphology and texture analysis on a pre-surgical CT.

Methods and Materials: This retrospective study included 46 consecutive patients with NSCLC (T1 or T2N0M0) treated by surgery. A preoperative acquisition obtained using the same reconstruction parameters on the same CT scanner was used to extract tumor morphological properties, to assess intra-tumoral texture parameters from the *Grey Level Co-occurrence and Run-*

Length matrices. Eight patients presented with tumor recurrence during a mean follow-up of 4.5 years after surgery. Different predictive models either based on individual parameters or on a small set of parameters embedded in a logistic regression were reconstructed. Receiver operating characteristic analysis was performed to assess the predictive performance of these models. Then, the best multiparametric models were submitted to a *leave-one-patient-out-cross-validation (LOOCV)*.

Results: Individual morphological parameters Surface Area and Aspect Ratio displayed a good performance in identifying patients with tumor recurrence (Area: Se=88%, Sp=88%, AUC=0.86, Aspect Ratio: Se=88%, Sp=60%, AUC=0.73). After LOOCV, models based on 4 texture parameters (Homogeneity, Sum Variance, Grey-Level Nonuniformity, Run Percentage) or on (Sum Average, Grey-Level Nonuniformity, Run Percentage, Short Run Low Grey-Level Emphasis) displayed a very good performance in identifying patients with tumor recurrence (Se=100%, Sp=91%, Acc=91% for both models).

Conclusion: These preliminary results confirm the growing evidence that lung cancers have texture features related to their tumoral aggressiveness. Combining morphological and texture parameters may allow improved tumor recurrence prediction. Further work is required to understand how to optimally implement texture analysis of these CT images.

10:30 - 12:00

Room N

Genitourinary

SS 1007

Renal and adrenal imaging

Moderators:

G. Aringhieri; *Pisa/IT*

J. Belfield; *Liverpool/UK*

B-0877 10:30

Diagnostic accuracy of primary macronodular adrenal hyperplasia on CT: a quantitative and qualitative study

S.M. Ando, F.M. Coelho, P.C. Viana, L.G. Gomes, M.B.V. Fragoso, F.I. Yamauchi; *São Paulo/BR (sabrina.ando78@gmail.com)*

Purpose: To determine the accuracy of computed tomography (CT) in diagnosis of primary macronodular adrenal hyperplasia (PMAH).

Methods and Materials: This retrospective IRB approved study included 122 patients divided into 4 groups: PMAH (n=9), congenital adrenal hyperplasia (CAH) (n=21), primary hyperaldosteronism (PH) (n=52) and control group (CG) (n=40). CT images were evaluated by two blinded observers, who subjectively classified adrenals as definitive or not for PMAH, based on bilateral adrenal enlargement with nodules. Measurements of adrenal body and limbs width and length in axial plane were also recorded.

Results: Sensitivity, specificity, positive and negative predictive values for subjective analysis were 89%, 95%, 57% and 99% for observer 1 and 89%, 91%, 44% and 99% for observer 2. The interobserver agreement was 0.99 by kappa statistics. All measurements demonstrated significant difference between PMAH and others groups ($p < 0.05$ ANOVA). Mean body, medial and lateral limbs width and adrenal length measurements in right and left adrenals were respectively on PMAH 1.5, 0.9, 0.8 and 4.9 cm and 1.7, 1.0, 1.3 and 4.9 cm. On CG, 0.6, 0.3, 0.3 and 3.5 cm and 0.7, 0.5, 0.4 and 3.6 cm. On CAH and PH, 0.8, 0.5, 0.5 and 4.0 cm and 0.9, 0.6, 0.5 and 4.1 cm. The cut off ≥ 1.5 cm of right body width had 100% of specificity and 55.5% of sensitivity for the diagnosis of PMAH.

Conclusion: Qualitative CT features have high accuracy for diagnosis of PMAH. Quantitative analysis may also be useful in indeterminate cases with high specificity.

B-0878 10:38

Hollowed adrenal gland sign in patients of septic shock: prevalence, CT appearance and consequence

Q. Xie, H. Wang, J. Guan; *Guangzhou/CN (usefulkey0077@hotmail.com)*

Purpose: To investigate the prevalence, CT appearance and consequences of hollowed adrenal gland sign in septic shock patients.

Methods and Materials: From September 2014 to May 2017, there were 152 consecutive patients with septic shock in ICU (mean 60.6 years; range 19-89 years; 95 males, 57 females). All the patients received dual-phase contrast-enhanced CT scan in one week after diagnosis. CT findings and clinical records were reviewed retrospectively. Single factor analysis was performed. The hollowed adrenal gland sign was defined as: (1) diffuse enlargement of bilateral adrenal gland; (2) in arterial phase, the central area of adrenal gland shows much lower attenuation; (3) in venous phase, the central "hollowed" area shows further enhancement and is similar to the peripheral area.

Results: All the patients showed various degrees of and diffuse enlargement in bilateral adrenal gland. 52 patients (52/152) showed hollowed adrenal gland sign (positive group) while the remaining 100 patients were negative. The prevalence of hollowed adrenal gland sign in septic shock patients was 34.2% and finally 43 patients died from MODS (82.7%, 43/52). In negative group, 50 patients finally died from MODS (50.0%, 50/102). There was significant difference between two groups ($P < 0.01$). The result of single factor analysis showed that the hollowed adrenal gland sign was an independent factor to predict prognosis (death) for septic shock patients.

Conclusion: Hollowed adrenal gland sign is common on CT in septic shock patients and predicts a dim prognosis.

B-0879 10:46

Histogram analysis of adrenal lesions with a single measurement: feasibility and incremental value for diagnosing adenomas

T.O. Rocha¹, T.C.V. Albuquerque¹, J.C. Nather¹, C.S. Garrido¹, J. Elias Jr¹, S. Tucci Jr¹, Z. Wang², A.C. Westphalen², V.F. Muglia¹; ¹Ribeirao Preto/BR, ²San Francisco, CA/US (talescva@gmail.com)

Purpose: Our purpose was to assess if histogram analysis of adrenal lesions, from a single measurement of mean and standard deviation (SD), using threshold of 10% of negative voxels can replace voxel counting while keeping diagnostic accuracy.

Methods and Materials: In a four-year period, 308 consecutive patients had 325 adrenal lesions diagnosed on CT exams. After exclusions, 91 patients (108 lesions), 20 malignant and 88 adenomas (confirmed by histology or follow-up) were enrolled. Two observers retrospectively measured size, mean attenuation, SD and generate histogram. The voxel distribution was assessed for normality. The 10th percentile was calculated from voxel counting (P10obs) and estimated from the formula: $P10est = mean - (1.282 \times SD)$. Diagnostic accuracy of mean attenuation and histogram analysis using P10obs and P10est were compared.

Results: 74 patients had 88 adenomas and 17 patients had 20 malignant lesions, 7 adrenocortical carcinomas, 13 metastasis. 93.1% of histograms had a normal distribution. The correlation among P10obs and P10est was perfect, $r = 0.9827$ (reader 1) and 0.9843 (reader 2) ($p < 0.00001$ for both). For both readers, sensitivity, specificity of the mean attenuation analysis was 65.9% (55.0-75.7%) and 100.0% (83.2-100%), and for P10obs and P10est was the same, for both observers, 87.5% (78.7-93.6%) and 95% (75.1-99.8%), respectively. The increment in sensitivity was significant ($p < 0.0001$), while the drop of specificity was not ($p = 0.15$).

Conclusion: The majority of voxels histograms from adrenal lesions follows normal distribution allowing an estimation using mean and SD. The accuracy of histogram was superior to mean attenuation analysis, either using P10est or P10obs.

B-0880 10:54

CT numbers of kidneys in virtual noncontrast images acquired from dual-source dual-energy dynamic CT of kidney: comparison with standard noncontrast CT

Y.-M. Lin; Taipei/TW (garbato@gmail.com)

Purpose: To compare virtual noncontrast (VNC) images derived from dynamic dual-source, dual-energy CT (dsDECT) of kidney with standard noncontrast (SNC) images, and determine the optimal phase for generating virtual noncontrast images.

Methods and Materials: Twenty-nine men and sixteen women underwent dynamic dsDECT (100/Sn140kVp) of kidney that included noncontrast, corticomedullary (CMP), nephrographic (NP), and excretory phases (EP). CT numbers were measured in the cortex and medulla. Image noise was measured on SNC and VNC images. Expected dose saving by removing the SNC phase was calculated.

Results: The difference in mean attenuation between SNC and VNC images was ≤ 4 HU. VNC attenuation values of the cortex in the CMP and medulla in the NP did not significantly differ from SNC values. VNC attenuation of the cortex was higher than that of the medulla in the CMP ($p < 0.05$), while there was no significant difference in NP. In the EP, inadequate iodine subtraction was obvious in the urinary collecting system. Image noise was significantly greater in SNC images ($p < 0.001$). Mean radiation dose reduction achievable by removing the SNC phase was $12.3\% \pm 0.9\%$.

Conclusion: VNC images from dynamic dsDECT of kidney were similar to SNC images, with greater attenuation variability. We recommend the NP as the optimal phase for creating VNC images in dynamic dsDECT of kidney.

B-0881 11:02

Optimal energy level for renal lesion detection and characterisation on virtual monoenergetic images

C. Schabel^{1,2}, F. Vernuccio³, J. Ramirez Girlando⁴, K. Nikolaou¹, D. Marin²; ¹Tübingen/DE, ²Durham, NC/US, ³Palermo/IT, ⁴Malvern, PA/US (christoph.schabel@med.uni-tuebingen.de)

Purpose: Dual energy-reconstructed virtual monoenergetic images (VMIs) can yield more stable CT numbers and improved image quality compared to conventional single energy CT imaging. The aim of our study was to investigate the best VMI energy for the detection and characterization of renal lesions.

Methods and Materials: This retrospective, HIPAA-compliant study was IRB approved, with a waiver of informed consent. Between June 2012 and July 2016, a total of 194 renal lesions (62 solid, 132 cystic) underwent unenhanced single-energy and enhanced dual-energy CT during the nephrographic phase. VMI datasets were created from 70 to 100 keV. Lesion enhancement was measured by calculating the difference in attenuation (ΔHU) between the contrast-enhanced VMI and unenhanced single-energy images. Receiver-operating-characteristics were determined.

Results: The area-under-the-curve (AUC) was highest at 70keV (0.96) and decreased significantly with higher energies (0.94 at 80keV [$P = 0.004$]; 0.86 at 90 keV [$P < 0.0001$], and 0.79 at 100keV [$P < 0.0001$]). Number of missed minimally-enhancing solid renal lesion was lowest at 70keV(13/62) and increased with higher energies (19/62 at 80keV, 25/62 at 90keV, and 29/62 at 100keV) using a threshold of 15HU lesion enhancement. However, 12 of the 132 confirmed renal cysts were incorrectly classified at 70 keV VMI due to spurious levels of enhancement, compared to 5, 3, and 7 false positive cases at 80, 90, and 100keV, respectively.

Conclusion: Our study demonstrated that VMI at 70 keV may represent the optimal energy level for renal lesion detection and characterization.

Author Disclosures:

C. Schabel: Speaker; Siemens Healthcare. **J. Ramirez Girlando:** Employee; Siemens Medical Solutions USA. **D. Marin:** Speaker; Siemens Healthcare.

B-0882 11:10

Diffusion weighted magnetic resonance imaging in assessment of parenchymal damage in chronic kidney disease

K. Sulkowska, P. Palczewski, A. Furmanczyk-Zawiska, A. Perkowska-Ptasinska, W. Szeszkowski, M. Durlik, M. Golebiowski; Warsaw/PL (k.sulkowska@outlook.com)

Purpose: The aim of our study was to evaluate the feasibility of using diffusion weighted magnetic resonance imaging (DW-MRI) for noninvasive assessment of pathologic changes in CKD.

Methods and Materials: Thirty-four patients in different stages of CKD were examined on a 1.5 T MR unit. The examination consisted of morphologic sequences and respiratory triggered multislice diffusion-weighted echo-planar sequence with 10 b values. Diffusion parameters were calculated with the use of mono- (total apparent diffusion coefficient, ADC_T) and biexponential model (pure diffusion coefficient-D and perfusion fraction-Fp). In 31 patients, ultrasound guided biopsy was performed in less than 30 days from MRI (18 ± 4 days). Histopathological assessment was performed by an experienced nephropathologist who separately scored changes in glomeruli and tubulointerstitium. Pearson's correlation coefficients (PCCs) were calculated by bivariate correlation to investigate relationship between diffusion parameters and histopathological assessment of renal damage. P -value < 0.05 indicated statistical significance.

Results: We observed a moderate negative correlation between D and the percentage of glomeruli with focal global sclerosis (PCC -0.52, $p = 0.003$). D also reversely correlated with combined parameters reflecting chronic changes in glomeruli (PCC -0.48, $p = 0.006$) and tubulo-interstitium (PCC -0.47, $p = 0.007$). ADC_T showed significant negative correlation only with interstitial infiltrations (PCC -0.44, $p = 0.013$). Fp showed very high standard variation and no significant correlation with histopathological assessment.

Conclusion: DWI-MR allows for a noninvasive assessment of parenchymal damage and glomerular loss in CKD. Using biexponential fitting of DW-signal is advantageous over monoexponential fitting owing to the elimination of negative influence of Fp on obtained results.

B-0883 11:18

Towards renal metabolic imaging of fatty kidney

I. Dekkers¹, P. de Heer², A.P.J. de Vries¹, H.J. Lamb¹; ¹Leiden/NL, ²Amsterdam/NL (I.A.Dekkers@lumc.nl)

Purpose: Elevated renal triglyceride content (fatty kidney) is a potential biomarker for obesity-related renal disease. However, non-invasive measurement techniques for the assessment of renal triglyceride content (TG) are currently limited. Here we report the results of the technical development of

renal metabolic imaging for the quantification of renal TG using proton-magnetic resonance spectroscopy (1H-MRS).

Methods and Materials: Renal metabolic imaging was performed in healthy human volunteers using a 3T MRI. Quantitative intra- and inter-examination single-voxel point resolved spectroscopy (PRESS) spectra were obtained in healthy human renal parenchyma using 1H-MRS with respiratory motion triggering. In total, 23 healthy participants (mean age 30.1±13.4 years, mean BMI 22.8±5.2 kg/m²) underwent 1H-MR spectroscopy, of which 19 participants underwent intra-examination reproducibility and 9 participants underwent inter-examination reproducibility. Renal TG content was calculated via in-house-developed post-processing script and corresponding reproducibility was determined using Pearson's correlation and Bland-Altman analysis.

Results: Overall mean renal TG content was 0.19±0.12% (range 0.07 to 1.02%). There were no significant differences between first TG% and repeated measurements (p=0.96 for intra-examination; p=0.75 for inter-examination). Both intra-examination (r=0.91) and inter-examination (r=0.73) measurements were highly correlated with first TG measurements. Intra-examination and inter-examination limits of agreement of renal log TG% were, respectively [-1.36%, +0.34%] and [-0.77%, +0.62%].

Conclusion: Renal proton MR spectroscopy is a reproducible technique for measuring renal triglyceride content non-invasively. This technique can be applied in future studies to further investigate the development of obesity-related renal disease.

B-0884 11:26

DKI of microstructural alterations in the kidneys of patients with hyperuricemia

X. Cai, Z. Chen; Guangzhou/CN (caixran@jnu.edu.cn)

Purpose: To evaluate the feasibility of diffusion kurtosis imaging (DKI) for early detection of renal microstructural alterations in patients with hyperuricemia.

Methods and Materials: A total of 75 subjects including 25 asymptomatic hyperuricemia (AH) patients, 25 gouty arthritis (GA) patients and 25 age- and sex-matched healthy volunteers were enrolled in this study. MR examinations were performed on a 3T MR scanner. DKI data were acquired to derive axial, radial, and mean kurtosis, as well as fractional anisotropy (FA), axial, radial, and mean diffusivity for comparisons among the 3 groups. Also, they were correlated with estimated glomerular filtration rate (eGFR).

Results: Mean MK and Kr values in the renal cortex and medulla significantly increased from control subjects to the AH and GA patients (p < 0.05). GA patients showed statistically greater cortical and medullary Ka values as compared with the other two groups (p < 0.05). Mean medullary FA value significantly decreased across the three groups (p < 0.05). The mean MD and Da values in the cortex and medulla and Dr value in the medulla were found to be significantly different between GA patients and control subjects (p < 0.05). No correlation was found between any DKI parameters with eGFR.

Conclusion: DKI demonstrates comparably stronger potential than diffusion tensor imaging in terms of early detection of renal cortex and medulla changes in patients with hyperuricemia. MK and Kr may be more sensitive to detect early-stage injury.

B-0885 11:34

Can renal artery resistive index predict disease activity in lupus nephritis?

S.M. Mehana; Alexandria/EG (sayedmehana9@gmail.com)

Purpose: To evaluate the predictive value of Doppler renal resistance index (RRI) in comparison with disease activity score, serologic and biology parameters in lupus nephritis.

Methods and Materials: The study included 43 patients with SLE fulfilling the Systematic Lupus International Collaborating Clinics Classification 2012 Criteria; group I included 33 patients with lupus nephritis, group II included 10 SLE patients without lupus nephritis and group III included 10 healthy subjects as control group. Determination of the activity and chronicity indices performed according to the scheme of the International Society of Nephrology/Renal Pathology Society (ISN/RPS) 2003 classification of lupus nephritis.

Results: • The mean value of Doppler-Based RRI in the healthy group is significantly lower than the lupus nephritis and SLE patients who showed also a significant difference. • The mean age of those who had resistive index of 0.7 and above was significantly higher than those below 0.7. The same pattern was observed for blood urea, creatinine and renal biopsy chronicity index. • The Area under the ROC curve (AUC) of Doppler-Based Renal Resistive index as a marker of renal biopsy chronicity index was 0.769 (95% confidence interval). • A renal resistive index of 0.70 threshold is better than 0.65 cut-off to predict renal biopsy chronicity index • No significant correlation was found between renal resistive index and activity index in renal biopsy.

Conclusion: Renal resistive index can be used as a non invasive reliable marker of chronicity in cases of lupus nephritis.

B-0886 11:42

Deep learning for automated MRI-based cyst load determination in PKD patients

M. Gattoni, A. Hartenstein, E. Siewert, T. Denecke, B. Hamm, D. Geisel, T. Penzkofer; Berlin/DE

Purpose: Quantification and follow-up of cyst load in polycystic kidney disease (PKD) patients through radiological imaging can be arduous to perform, especially in MRI. We applied deep learning to facilitate this task.

Methods and Materials: We collected 51 datasets of patients with polycystic kidney disease, standardized imaging and good image quality. Manual segmentation of the liver and liver cysts was performed on T2 Imaging. The data were divided into cases for training, for validation and for independent testing. A deep learning network was trained using the DeepMedic 3D-CNN platform. The results were compared to manual threshold segmentation of the same dataset using the DICE coefficient for segmentation similarity.

Results: Average cyst load in the datasets was 42.4 ± 21.7 percent in livers with a volume of 3404 ± 1705ml. DICE similarity coefficients were 0.84 ± 0.07 between manual and deep learning segmentations and 0.80 ± 0.10 between thresholding and manual segmentation (p=0.038). Typical segmentation times in PKD patients are 30+ min for manual segmentation, compared to ~5min for threshold segmentation and less than a minute (24.9 ± 14.6s) for the deep learning segmentation.

Conclusion: Automated liver cyst load measurement using a deep learning approach can be performed using a 3D-CNN approach on a single MRI sequence. Application of this method could lead to markedly reduced assessment time enabling consistent follow-up and potentially abbreviated MRI protocols for PKD patients.

Author Disclosures:

B. Hamm: Consultant; Toshiba Medical Services Corporation. Equipment Support Recipient; Elbit Imaging Ltd. Grant Recipient; Toshiba Medical Services, Koninklijke Philips NV, Siemens AG, General Electric Company, Elbit Imaging Ltd, Bayer AG, Guerbet SA, Bracco Group, B. Braun Melsungen AG, KRAUTH medical KG, Boston Scientific Corporation. Investigator; CMC Contrast AB. Shareholder; Siemens AG, General Electric.

B-0887 11:50

An integrated CAD system of DWI MRI and laboratory biomarkers in the diagnosis of kidney transplant dysfunction

M. Shehata¹, M.E. Abou El-Ghar², T. El-Diasty², A. EL-Baz³,
¹Louisville, KY/US, ²Mansoura/EG, ³Louisville, KY/US
(maboelghar@yahoo.com)

Purpose: Accurate non-invasive assessment of kidney transplant dysfunction (KTDF) is crucial for the identification of proper treatment. Therefore, we introduce a novel fully automated computer-aided diagnostic (CAD) system for KTDF assessment using 4D (3D + b-value) DW-MRI data integrated with laboratory-based biomarkers.

Methods and Materials: The proposed CAD system integrates both clinical (e.g. SPCr and CrCl) and image-based biomarkers. To extract the latter, our CAD system aligns the DW-MRI data to handle motion effects and then segments kidney from surrounding tissues, after that, estimates ADCs to construct the discriminatory features for transplant status classification, finally, image and clinical biomarkers are fused together to assess transplant status by cascading two stages of deep learning-based classifiers. The first stage distinguishes non-rejection (NR) from rejection and its mimics; the second stage classifies this rejection and its mimics as early rejection (ER) or other kidney diseases (OD) (e.g. acute tubular injury, etc.).

Results: DW-MRI datasets have been collected from 58 biopsy-proven cohort. All subjects, NR (16), ER (37), and OD (5), were assessed with SPCr laboratory values. Approximately, 50 coronal DW-MR images were acquired to cover the whole kidney before any biopsy procedure using a GE 1.5T scanner at different b values. Using leave-one-subject-out experiments, our CAD system achieved a 95% accuracy (sensitivity = 95% and specificity = 94%) between NR and rejection and its mimics, and a 95% accuracy between ER and OD transplants.

Conclusion: Our initial diagnostic results hold promise of the proposed CAD system as a reliable, inexpensive, and noninvasive diagnostic tool.

10:30 - 12:00

Studio 2018

Oncologic Imaging

SS 1016a

Improving practice in oncologic imaging

Moderators:

T. Pfammatter; Zurich/CH

M. Seidensticker; Munich/DE

B-0888 10:30

A 2 minute, ultra-fast wholebody PET/CT enabled by digital photon counting PET detector technology

M.I. Knopp¹, C.L. Wright¹, K. Binzel¹, F.L. Giesel², J. Zhang¹, P. Maniawski³, M.V. Knopp¹; ¹Columbus, OH/US, ²Heidelberg/DE, ³Cleveland, OH/US (knopp.29@osu.edu)

Purpose: To assess the clinical feasibility of a 10x reduction in whole body PET acquisition time with comparable diagnostic and quantitative characteristics to current clinical PET acquisition enabled by digital photon counting PET (dPET).

Methods and Materials: Thirty-eight patients scheduled for FDG whole body PET/CT were imaged using three separate acquisitions as part of intra-individual comparison study with a pre-commercial release dPET/CT (Vereos) and cPET/CT (Gemini). Standard cPET imaging was performed at ~75 min p.i. of ~450 MBq FDG with investigational dPET imaged at ~55 min p.i. The first dPET acquisition was performed using 90s/bed position, immediately followed by a 9s/bed position acquisition lead to average table times of ~15 and ~2 min and compared with 90s/bed position cPET. The 9s/bed dPET were reconstructed using a previously optimised methodology. All other aspects of image acquisition were kept identical. Three blinded reviewers evaluated the data sets regarding visual characteristics, diagnostic confidence and semi-quantitative readouts.

Results: Visual assessment scores were significant higher for 90s/bed dPET whole body (p<.01) with no significant difference between 9s/bed dPET and 90s/bed cPET. Quantitatively, the 9s/bed dPET presented slightly increased background noise, however there was no impact on diagnostic confidence or SUV measures.

Conclusion: Next generation digital photon counting detector technology enabled a radical reduction in wholebody acquisition time with comparable diagnostic confidence and quantitative precision to current generation cPET acquisitions taking 10 times longer. This allows for new PET workflow concepts, improved patient comfort, minimised patient motion and whole-body pseudo dynamic imaging of tracer uptake.

Author Disclosures:

P. Maniawski: Employee; Philips.

B-0889 10:38

Practice-based evidence for clinical benefit of PET/CT - results of the first oncologic PET/CT registry in Germany

C. Pfannenberg, L. Wang, B. Gückel, S. Gatidis, S.-C. Olthof, M. Reimold, C. La Fougère, K. Nikolaou, P. Martus; Tuebingen/DE (christina.pfannenberg@med.uni-tuebingen.de)

Purpose: To evaluate the impact of PET/CT on clinical management based on a prospective data registry. The registry was developed to meet the requirements for PET/CT coverage by health insurance.

Methods and Materials: We evaluated a prospective patient cohort having a non-investigational PET/CT at one university center from 4/2013 till 08/2016. The registry collected questionnaire data from requesting physicians on intended patient management before and after PET/CT. 4504 patients with 5939 PET/CT examinations were enrolled in the registry, including evaluable data from 3724 patients with 4754 studies. The impact of PET/CT was assessed across various cancers for different indications and categories of non-treatment (watching, additional imaging, biopsy) and treatment.

Results: The most frequent PET/CT indication was cancer staging (60.5%). Melanoma, lung, lymphoma, NET and prostate cancers accounted for 70% of cases. Overall, PET/CT was associated with a 36.9% change (OR 4.4; 95% CI, 3.8-5.0) in decision to treat or not to treat, including 30.4% change to treatment from non-treatment. The frequencies of changes ranged from 46.0% for melanomas to 28.3% for head and neck cancers. The impact of PET/CT was highest in reducing demands for additional imaging which decreased from 50.9% to 5.8%. Pre-PET/CT planned invasive biopsy could be avoided in 73.3% of cases. When the intended management was treatment, the therapeutic goal (curative vs.palliative) changed after PET/CT in 21.6% of cases.

Conclusion: The data of this large representative registry confirmed that physicians often change their intended management on the basis of PET/CT consistent across different cancer types.

B-0890 10:46

Patients' perception of radiologists in an oncologic imaging department

C. Giaconi, F. Cerimele, A. Bulleri, C. Basile Fasolo, E. Neri; Pisa/IT (radiodiagnostica3.aoup@gmail.com)

Purpose: To analyse the patients' perception of the radiologist role in an oncologic imaging Department.

Methods and Materials: Between June and July 2017, two surveys have been addressed to 400 patients admitted to an Oncologic Imaging Department. The "Entry" survey was handed out to patients waiting for their turn in the radiology unit and included questions related to the environment and reception workflow. The "Exit" survey, instead, was given at the end of the examination to patients waiting for their report or that were just about to leave the department. It included questions related to the visibility of radiologist, to the clarity of medical consultation, the perception of the different professional roles (radiologist and radiographer).

Results: Ninety percent (369/400) of patients declared that the Radiologist did not clearly introduced himself to the patient, but were satisfied by the quality of consultation in the entry and exit phases. Eighty-four patients who had ultrasound, that were asked to rate the helpfulness and kindness of the radiologist, responded very satisfied in 68 cases (80.25%) satisfied in 10 (11.9%), somewhat satisfied in 6. Most patients (294/400; 93.04%) recognized that the diagnosis was carried out by the radiologist, but 13 patients (4.11%) answered "the technician" and 9 (2.85%) "the machine".

Conclusion: The survey demonstrate that the vast majority of patients have a correct perception of the radiologists' roles in the imaging department. However such well recognized value of the radiologist seems to be less balanced by an appropriate doctor to patient communication.

B-0891 10:54

How to structure the attendance of radiologists to oncologic multidisciplinary team meetings

C. Giaconi, F. Cerri, C. Arena, A. Bulleri, E. Neri; Pisa/IT (claudiagiaconi@tiscali.it)

Purpose: In XX University Hospital there is a strong demand of attendance of radiologists to oncologic multidisciplinary teams (MDTs). The aim of the study is to analyse the additional workload of radiologists attending MDTs.

Methods and Materials: The oncologic imaging Unit of the xx University Hospital fulfill the imaging requests of the Oncologic Unit with 8 board certified radiologists. Each staff member is committed to perform US, CT and MRI on a 38 hours x week working time. However, in the last 3 years a strong demand of attendance of radiologists to MDTs has been raised by the Oncology Department, on a weekly basis, for the following cancer types (GI tract, head and neck, melanoma, pediatric, lymphoma, prostate, gynecology). Radiology staff commitments and workload has been re-scheduled accordingly.

Results: The mean weekly workload increase by each radiology staff was 7 hours (+20%). The time allocated by each radiologist to participate MDTs included 3 hours for MDTs preparation (prior review of patient's images, and clinical information) and 4 hours mean attendance. The workload increase was not compensated by a reduction in imaging acquisition and reporting time.

Conclusion: Attendance of radiologists to MDTs is mandatory for the management of oncologic patients, and represents a value-based professional role. However, the time allocated to prepare and attend MDTs is not accounted as indicator of radiologists workload and performance.

B-0892 11:02

Open access prescription in oncologic imaging: one-year trial

F. Cerri, C. Giaconi, C. Arena, A. Bulleri, E. Neri; Pisa/IT (claudiagiaconi@tiscali.it)

Purpose: To implement an open access prescription system (Pleiade) to allow order entries from the Oncologic to the Imaging Unit in an Academic Hospital.

Methods and Materials: In the last 3-years the oncologic imaging demand in XX University Hospital raised rapidly, with specific request of Total Body CT for primary staging and follow-up in various cancer groups; the Oncologic Imaging Unit could not itself fulfill the entire CT request. Therefore since January 2017 a so called "open access" hospital information system, called "Pleiade", was implemented, allowing the electronic prescription of CT exams from the Oncologic to the Imaging Department on a 365 day scheduled agenda, that included 54 patients slots per week. A clinical decision support system is not yet implemented.

Results: To date the agenda is fully booked since December 2017, with 218 patients scheduled per month. A retrospective analysis of a 6 months activity that included 1308 patients, showed that the vast majority of CT (1110/1308 patients; 84%) was performed with the clinical indication of oncologic follow-up. Therefore the strong demand of CT exams for the follow-up impacted on the availability of primary staging slots.

Conclusion: The Pleiade system unburdened the administrative workload of the oncologic imaging Department. However the open access to the imaging schedule, and the absence of appropriateness criteria, generated a significant prescription of follow-up CT, that impacted on the availability of primary staging CT.

B-0893 11:10

Integrated versus separate reporting of FDG-PET/CT and MRI for abdominal malignancies: effect on diagnostic confidence and staging outcomes

L.A. Min^{1,2}, W. Vogel¹, M.J. Lahaye¹, M. Maas¹, M. Donswijk¹, E. Vegt¹, R.G.H. Beets-Tan^{1,2}, D.M. Lambregts¹; ¹Amsterdam/NL, ²Maastricht/NL (*l.min@nki.nl*)

Purpose: Increasing numbers of patients receive multimodality imaging (FDG-PET/CT and MRI) to stage abdominal malignancies, with potential implications for optimal image interpretation. This study evaluates effects of integrated reporting of FDG-PET/CT and abdominal MRI on diagnostic confidence and staging outcomes.

Methods and Materials: 149 cases where abdominal MRI and FDG-PET/CT were performed within a 14-day interval were retrospectively included. Original MRI and PET reports were retrieved from the hospital database and reported findings (per lesion; total 1228) translated into a 5-point confidence score (1=definitely benign to 5=definitely malignant). Teams of 2 readers (radiologist + nuclear physician) together performed integrated re-assessment of the images, blinded for the initial reports.

Results: Integrated re-assessment led to discrepant findings in ≥ 1 lesions compared with either the original FDG-PET/CT or MRI reports in 62/149 cases, which would have had no clinical impact in 26 (17.4%), minor impact in 17 (11.4%) and potential major impact in 19 (12.8%). On a per lesion basis, the integrated approach resulted in increased/decreased diagnostic confidence in 8.7%/6.2% compared to the initial FDG-PET/CT and 11.5%/11.0% compared to the initial MRI reports. Inconclusive (confidence 3) scores were comparable: 8.3% (FDG-PET/CT) and 8.1% (MRI) for the initial reports vs 6.9% for the integrated approach.

Conclusion: Integrated assessment of FDG-PET/CT and MRI by a nuclear physician and radiologist together leads to discrepant findings compared to separate imaging assessment in a substantial number of cases, which could have potential major clinical impact in 12.8%. Impact on overall diagnostic confidence and number of inconclusive outcomes appears to be limited.

B-0894 11:18

New insights for spectral CT imaging in staging of patients with hypervascularised abdominal tumours

G. Böning¹, S. Adelt¹, U. Fehrenbach¹, J. Kahn¹, F. Feldhaus¹, M.H. Maurer², D.M. Renz³, B. Hamm¹, F. Streitparth¹; ¹Berlin/DE, ²Berne/CH, ³Jena/DE

Purpose: In oncologic imaging, spectral CT based parameters of iodine concentration and spectral slope over virtual mono-energetic levels may deliver information superior to standard CT. Aim of this study was to analyse potential differences of spectral CT parameters in hypervascularised abdominal tumours to improve lesion characterisation.

Methods and Materials: 111 patients with hypervascularised abdominal tumours were included. We analysed 77 cases with neuroendocrine tumours/carcinomas (NET/NEC), 18 cases with hepatocellular carcinoma (HCC) and 16 cases with renal cell carcinoma (RCC). Patients underwent a standardised multiphase abdominal CT with spectral mode arterial phase. We analysed iodine concentrations of the tumours, the increase slope of mean HU in tumors between 40keV and 140keV as well as the applied dose.

Results: The iodine concentrations of the tumours were $2.5 \pm 1.5 \text{ mg/cm}^3$ (NET/NEC), $2.2 \pm 0.7 \text{ mg/cm}^3$ (HCC) and $3.8 \pm 1.8 \text{ mg/cm}^3$ (RCC). The increases slope of mean HU in tumours between 40keV and 140keV were 2 (NET/NEC), 1.8 (HCC) and 3 (RCC). In a subgroup of 41 patients (26 NET/NEC, 9 HCC, 6 RCC) with strong tumour hypervascularisation the mean HU values at 40 keV were significantly ($p < 0.001$) different between RCC (421 ± 167 HU) and HCC/NET (245 ± 70 HU/ 266 ± 140 HU). The mean CTDI_{vol} of the spectral mode arterial phase was $9.6 \pm 4 \text{ mGy}$ and $9.9 \pm 4.3 \text{ mGy}$ / $9.9 \pm 4.6 \text{ mGy}$ for portal venous and hepatic venous phases.

Conclusion: Spectral CT based parameters are promising to deliver additional information for characterisation of hypervascularised abdominal tumours at dose levels comparable to standard CT. To determine whether they can be used in clinical routine potential confounding factors should be analysed.

B-0896 11:26

Application of 80-kVp scan and raw data-based iterative reconstruction for reduced iodine load PET/CT in an oncological setting: a win-win technique

R. Balaji; Chennai/IN (*ravikanthbalaji@gmail.com*)

Purpose: To evaluate the image quality, radiation dose, and renal safety of contrast medium (CM)-reduced abdominal-pelvic CT combining 80 kVp and advanced Iterative Reconstruction (IR) in patients with renal dysfunction being worked up or followed up in an oncological setting.

Methods and Materials: The study included 30 patients with renal dysfunction (estimated glomerular filtration rate [eGFR] $\leq 45 \text{ mL/min/1.73 m}^2$) who underwent PET/CT with low dose of contrast medium (Iodixanol 320, 360 mg/kg, 80 kVp, IR). 30 other patients without renal dysfunction (eGFR $\geq 60 \text{ mL/min/1.73 m}^2$) who underwent standard PET/CT (120 kVp, filtered-back projection) with normal contrast dose (Iodixanol 320, 600 mg/kg) were included as controls. The following image criteria were compared - CT attenuation, image noise, and contrast-to-noise ratio (CNR). Size-specific dose estimate (SSDE) and renal function 1-3 months after CT were measured.

Results: The SSDE and iodine load of the 80-kVp protocol were 30% and 45%, respectively, lower than of the 120-kVp protocol ($p < 0.01$). CT attenuation and CNR of solid viscera and vessels in 80-kVp images were better than those of 120-kVp images ($p < 0.05$). There were no significant differences in quantitative or qualitative image noise or subjective overall quality ($p > 0.05$). No significant contrast induced renal parenchymal injury was observed.

Conclusion: 80-kVp scans combined with advanced Iterative Reconstruction result in 40-50% reduction in radiation dose and 40% iodine load with no compromise on diagnostic image quality. At the same time risk of contrast induced renal damage was also reduced.

B-0897 11:34

Improved image quality of whole body low-dose CT study combined with iterative model reconstruction algorithms for follow-up of oncologic patients

I. Salemi¹, D. Ippolito¹, C.R. Talei Franzesi¹, C. Maino¹, C. Cangini¹, S. Sironi²; ¹Monza/IT, ²Bergamo/IT (*i.salemi@campus.unimib.it*)

Purpose: To compare radiation dose and image quality of low-dose CT protocol combined with iterative model reconstruction algorithm (IMR) with standard-dose approach combined with hybrid-iterative reconstruction algorithm (iDose) for follow-up of oncologic patients.

Methods and Materials: Seventy-three patients with known oncological diseases who underwent, during their clinical follow-up, both low-dose CT, performed on 256-row scanner (iCT Elite, Philips) with 100 kV and automated mAs modulation (depending on patient weight), and standard-dose CT, performed on 256-row scanner with 120 kV and automated mAs modulation, were enrolled. Images were reconstructed with IMR algorithm for low-dose CT examination and iDose algorithm for standard-dose CT examination. We evaluated density values and signal-to-noise ratio (SNR), along with image noise, dose parameters and diagnostic quality with 5-point scale.

Results: Noise of images expressed as SD values, measured in liver and spleen, was significantly lower in IMR images (liver 10.98 vs 14.05, $p < 0.001$) whereas SNR was statistically higher (9.03 vs 8.47) compared to iDose reconstructions. Volumetric-Computed-Tomographic-Dose-Index (CTDIvol) and Dose-Length-Product (DLP) were significantly lower in IMR compared to iDose reconstructions (DLP 491.48 vs 856.92 $\text{mGy} \cdot \text{cm}$, $p < 0.001$), with overall dose reduction of 42.6%. Qualitative analysis did not reveal significant differences in diagnostic quality ($p = 0.04$).

Conclusion: Automatic tube-current modulation combined with IMR algorithm and low kV setting allows dose reduction (42.6%) in whole body CT imaging without loss of diagnostic quality, thus representing a useful diagnostic approach in reducing dose exposure in oncologic patients who underwent several follow-up studies.

B-0898 11:42

Slowly injected unsplit bolus protocol for the reduction of contrast medium (CM) and mean radiation dose exposure (SUPREME Protocol)

A. Contegiacomo, N. Attepatil, E. Amodeo, D. Coppolino, A. Cina, R. Manfredi; Rome/IT (*andrea.contegiacomo@policlinicogemelli.it*)

Purpose: To validate SUPREME protocol in terms of vascular/parenchymal enhancement, image quality, contrast medium (CM) administration and radiation exposure (RE), in oncological patients.

Methods and Materials: SUPREME Protocol was adopted for prospective examination of 40 consecutive patients with a previous standard protocol CT examination, performed in our institution. SUPREME protocol: patient weight: $>70 / <70$ kg; CM volume: 130/120; CM injection-rate: 2/1.8 mL/s; Saline solution volume: 60/50 mL; Saline solution injection-rate: 3 mL/s; Acquisition delay: 80s; body surface: thorax-abdomen. Two radiologists in consensus compared SUPREME Protocol examinations with both immediately previous

and next follow-up CT examinations of the same patient performing: images qualitative (0/3=poor/excellent) and quantitative (Hounsfield Units sampling at aorta, great vessels and liver/spleen parenchyma) assessment; CM administration and RE comparison between the two protocols. Statistical analysis was performed with T-student test and Cohen's k coefficient.

Results: The agreement between the two protocols for the images qualitative assessment was good (k-Cohen>0.6) for the two radiologists in consensus. No quantitative differences were observed between the two protocols with only a better enhancement of the inferior mesenteric artery in the standard protocol (p<.05). A global 15% of CM volume and 37.8% of dose exposition reduction was observed in the SUPREME protocol with respect to standard protocol (p<.05).

Conclusion: SUPREME Protocol is a valid tool in oncological patients, for CM administration and RE reduction, providing the same image quality of standard protocol.

10:30 - 12:00

Room L 8

Head and Neck

SS 1008

Tackling challenges in head and neck cancer imaging

Moderators:

M. Lell; Nürnberg/DE
E. Vassallo; Msida/MT

B-0899 10:30

Metal artefact reduction in computed tomography (Smart MAR): improvement of image quality and diagnostic confidence in patients with metallic dental implants

F. Feldhaus¹, G. Böning¹, U. Fehrenbach¹, J. Kahn¹, M.H. Maurer², D.M. Renz³, B. Hamm¹, F. Streitparth¹; ¹Berlin/DE, ²Berne/CH, ³Jena/DE (felix.feldhaus@charite.de)

Purpose: To determine whether the metal artefact reduction tool - a three-stage, projection-based, postprocessing algorithm - improves subjective and objective image quality and diagnostic confidence in patients with dental artefacts.

Methods and Materials: 100 consecutive patients with nonremovable oral implants or dental fillings were included. Indications were oropharyngeal tumours. CT scans were performed on a single-source, 64-row multislice CT scanner (MS-CT, Evolution, GE Healthcare). CT raw data were postprocessed using Smart MAR. Image quality of Smart MAR-based reconstruction series was evaluated both quantitatively (5 ROIs) and qualitatively (two independent raters) and compared to standard reconstructions. Dose was analysed in terms of dose-length-products (DLP) and computed tomography dose indices (CTDIvol).

Results: In Smart MAR reconstructions, both attenuation and noise were significantly reduced in areas adjacent to implants and in more distant areas (all p<0.001) compared to standard reconstructions. There was statistically significant improvement in signal-to-noise ratio (SNR; p=0.001) and contrast-to-noise ratio (CNR; p=0.001). Smart MAR significantly improved visualization of tumour (detected in 36 of 100 patients, 36%) and representative oropharyngeal tissue (p<0.001). In 8 of 36 patients (22%), tumour was only detected in reconstructed series using Smart MAR. The mean DLP of the entire scan was 506.8mGy*cm; average CTDIvol was 5.5mGy for oropharyngeal region.

Conclusion: Smart MAR significantly improved both objective and subjective image quality of oropharyngeal CT scans even in the presence of severe artefacts, resulting in higher diagnostic confidence. Allowing automated imaging postprocessing without increasing radiation exposure compared to standard CT scans, Smart MAR appears to be well suitable for clinical routine.

B-0900 10:38

Next generation imaging of head and neck cancer using dual-layer spectral CT

F. Lohöfer, G. Kaissis, F. Köster, M. Rasper, I. Einspieler, C. Gerngross, A. Fichter, E.J. Rummeny, R. Braren; Munich/DE

Purpose: The aim of this study was to evaluate the performance of dual-layer spectral CT (DLSCCT) in the detection and staging of head and neck cancer (HNC) compared to conventional contrast enhanced CT (CECT).

Methods and Materials: 39 patients with histopathologically proven diagnosis of HNC were examined with a DLSCCT scanner and retrospectively analyzed. A 50-patient healthy control group was used. Images were acquired in the portal venous phase. Monoenergetic 40kV-equivalent (*MonoE40*) images and iodine maps were compared to CECT images. Diagnostic confidence for tumor identification and margin detection was rated independently by 4 experienced

observers. The steepness of the Hounsfield Unit (HU)-increase at the tumor margin was analyzed. External carotid artery branch image reconstructions were performed and their contrast compared to conventional arterial phase imaging.

Results: *MonoE40* images were superior to CECT images in tumor detection and margin delineation. *MonoE40* showed significantly higher attenuation differences between tumor and healthy tissue compared to conventional CT images (p<0.0001) The HU-increase at the boundary of the tumor was significantly steeper in *MonoE40* images compared to conventional CT images (p<0.0001). Iodine uptake in the tumor was significantly higher compared to healthy tissue (p<0.0001). *MonoE40* images allowed depiction of the external carotid artery and its branches in the portal venous phase.

Conclusion: DLSCCT enables improved detection of primary and recurrent HNC as well as quantification of tumor iodine uptake. Improved contrast between tumor and background compared to CECT provides diagnostic confidence concerning tumor margin detection and vessel identification, which can facilitate surgical planning.

B-0901 10:46

Staging of head and neck cancer by dual energy CT: comparison of dual and single source dual energy

M. Wiesmüller, W. Wüst, M.S. May, M. Uder; Erlangen/DE (marco.wiesmueller@uk-erlangen.de)

Purpose: Aim of this study was to compare image quality of third-generation Single-Source Dual-Energy CT (SS-DECT) with third-generation Dual-Source dual energy CT (DS-DECT) in staging examinations of head and neck cancer.

Methods and Materials: 102 patients with histologically proven head and neck cancer were prospectively randomized to undergo radiation dose matched SS-DECT (n=51, 120 kV, split filter technique, 384 ref. mAs) or DS-DECT (n=51, 80/Sn150 kV, tube A 100/ tube B 67 ref. mAs) for tumor staging. Inline weighted average images (WAI) and virtual monoenergetic images (VMI) for two different low energies (40 and 60 keV) were reconstructed. Objective image quality was evaluated as dose normalized contrast to noise ratio (CNRD) and subjective image quality was rated on a 5-point Likert-scale.

Results: In both groups highest CNRD for vessel and tumor attenuation was obtained on 40 keV VMI. CNRD for tumor attenuation was comparable between SS-DECT and DS-DECT while CNRD for vessel attenuation was on average 1.4 times higher with DS-DECT for low energies (40 and 60 keV). Overall subjective image quality in the SS-DECT group was highest on the WAI followed by 40 keV and 60 keV. Subjective image quality was significantly better with DS-DECT.

Conclusion: In SS-DECT as well as DS-DECT highest overall image quality in head and neck imaging can be obtained with a combination of WAI and low keV reconstructions. DS-DECT is superior to SS-DECT in terms of subjective image quality and vessel attenuation, but comparable for tumor attenuation.

B-0902 10:54

Oral cavity cancer staging by CT for the new TNM-8: using an extrapolated measurement to evaluate the depth of invasion

J.M.M.M. Santos, A. Mourão de Abreu, M.R.T. Garcia, L. Franceschi, L.L. Matos, C.J. Silva, E.M.M. Gebrim, R.L.E. Gomes; São Paulo/BR (joao_ssa@hotmail.com)

Purpose: To retrospectively compare computed tomography oral cavity primary cancer staging, comparing the 7th and 8th edition of TNM, based on an imaging extrapolated measurement of the new pathological depth of invasion criteria.

Methods and Materials: The records of 100 patients with oral cavity primary cancer operated in our institution from 2009 to 2015 were reviewed retrospectively. Pathological and imaging tumor and nodal staging were reclassified according to 8th edition of TNM (TNM-8), and correlated to the previous TNM-7. TNM-8 changes implemented extranodal extension and depth of invasion (DOI), which was based on the pathological specimen measure from the level of outer line of the closest adjacent normal mucosa to the deepest point of the tumor. Here, we proposed a post-contrast CT extrapolation of the pathological DOI criteria using the measure from the transition line between lesion and adjacent normal mucosa to the deepest point of the tumor (extrapolated depth).

Results: Among T1 or T2 patients, there was a discrepancy between 7th and 8th TNM staging in 70%. Of these, 67 (95.8%) were up-staged (p < 0.0001). The nodal factor was up-staged in 10% of the patients. Locoregional recurrence-free survival and oral cavity cancer-specific survival prediction of TNM-8 was significantly more accurate (p < 0.0001).

Conclusion: Compared with the 7th edition, TNM-8 provides valuable results regarding tumor and nodal staging. Post-contrast CT is a great tool to analyze the depth of the lesion and perform the correct staging, provided that the measurements are made in the right way.

B-0903 11:02

Does performing staging MRI for lateral tongue tumours after biopsy of the primary tumour overestimate tumour dimensions and staging?

B. [Dhillon](#), D. Pawaroo; *Norwich/UK* (baljeet.dhillon@doctors.org.uk)

Purpose: Tumour (T) staging of oral cavity carcinoma is dependent upon the maximal dimension of the tumour. The majority of the staging MRIs for lateral tongue tumours in our institution are performed after the biopsy of the primary tumour. It can be difficult to discern whether the abnormal T2 high signal and contrast enhancement at the primary tumour site is due to malignancy or whether part of it may be due to the biopsy. This makes T staging of the tumour difficult. It is important for the surgeons to have accurate T staging particularly the thickness of the tumour to ensure the correct operation is carried out for complete excision.

Methods and Materials: 35 patient who underwent hemiglossectomy for lateral tongue carcinoma were identified. Tumour dimensions on T2-weighted MRI and contrast-enhanced MRI were measured in AP and lateral planes. Corresponding tumour measurements from histology reports of the surgical specimen were compiled. Paired t test was used to compare the MRI and histological measurements.

Results: All patients had biopsy before staging MRI. Paired t test showed no significant difference between the MRI and histologic measurements ($p=0.3978$ for AP dimension, $p=0.4364$ for lateral dimension). Only 3 cases (of 35) had their T-staging downstaged based on histology post-operatively. 6 cases actually had their T-staging upstaged based on histology post-operatively.

Conclusion: Performing MRI post-biopsy does not significantly increase the tumour measurements and hence does not affect the tumour staging preoperatively.

B-0904 11:10

Assessment of mandibular involvement by oral cavity and oropharyngeal squamous cell carcinoma: CT scan and MRI evaluation

R.K.N. [Solanki](#), I.N. Patel; *Ahmedabad/IN* (solankim@yahoo.co.in)

Purpose: To identify CT and MRI findings to predict mandibular involvement by oral cavity and oropharyngeal squamous cell carcinoma. To establish MRI as a superior modality to CT scan for mandibular involvement.

Methods and Materials: MR and CT images in 36 patients with SCC of the oral cavity (Ca buccal mucosa, retromolar trigone, gingivobuccal sulcus, floor of mouth) were evaluated for the presence and extent of mandibular cortex, bone marrow invasion and inferior alveolar canal involvement. The results were correlated with histopathologic findings. Using a multidetector spiral CT scanner & 1.5 T MRI in all patients with T1 W1, T2W1 and fat suppressed images were obtained

Results: We analyzed location of tumor on lower alveolus, tumor within 1 cm of mandible, sensory distribution of inferior alveolar nerve and identified periosteal stripping like subperiosteal reaction, cortical expansion and pathologic fracture as predictor of bone invasion. CT scan detects mandibular invasion grossly, missing it in 27% cases and is also associated with pitfalls of dental amalgam artifact. T1 W1, T2 W1 and contrast-enhanced T1-weighted images are of highest value detection of involvement of bone marrow, inferior alveolar canal and soft tissue extent. Detection of tumour signal replacing the hypointense cortical rim was considered the main MRI finding

Conclusion: MRI is now commonly considered the modality of choice for bony involvement, extension to retromolar trigone, alveolar ridge and inferior alveolar canal invasion with additional information about recurrent or residual disease in oral cavity and oropharyngeal squamous cell carcinoma, even more sensitive than CT scan.

B-0905 11:18

Automatic adaptive iterative metal artifact reduction

A.F. [Halaweish](#)¹, B. Schmidt², K. Grant¹, T. Flohr², C. Hofmann²; ¹*Malvern, PA/US*, ²*Forchheim/DE*

Purpose: Current metal artifact reduction (MAR) algorithms either present the user with a list of application specific presets, resulting in varying image impressions based on usage, or forgo the flexibility for simplicity and provide one processing option regardless of scenario. The objective of this work is to evaluate the performance of an automatic-adaptive MAR algorithm, aimed at automating the metal detection and artifact reduction processing and eliminating end result variability.

Methods and Materials: Building upon the currently implemented iterative MAR (IMAR) algorithm, automatic IMAR incorporates an automated online adaption of MAR parameters into the post-processing pipeline. This is accomplished through slice-by-slice adaption of the parameters based on image and sinogram metrics. In addition to the adaptive parameterisation, dedicated z-filtering and sinogram mixing improvements facilitate the incorporation of a more accurate sinogram restoration, by preserving as much of the original information as possible. Finally, an adaptive high-frequency streak reduction solution is incorporated into the workflow. To give the user

additional flexibility, rather than relying on predetermined application specific presets, strength of artifact reduction was incorporated as an option for processing.

Results: Automatic IMAR processed images from Head and Neck, Thoracic, Abdominal and MSK specific scans demonstrated excellent image quality and significantly reduced streak artifacts through the imaged region of interest, when compared to their WFBP and traditional IMAR processed equivalents.

Conclusion: The automation of the metal artifact reduction process, through adaptive parameter selection and improved metal artifact reduction efforts, facilitates an application which specifically tailors image quality with minimal user interaction.

B-0906 11:26

Virtual monoenergetic images can reduce metal artefacts caused by dental implants in computed tomography

N. [Grosse Hokamp](#)^{1,2}, K.R. Laukamp¹, S. Lennartz¹, D. Zopfs¹, D. Maintz¹, J. Borggreffe¹; ¹*Cologne/DE*, ²*Cleveland, OH/US* (nils.grosse-hokamp@uk-koeln.de)

Purpose: To compare the extent of metal artefact reduction by use of high-keV virtual monoenergetic images (VMI) from spectral detector computed tomography (SDCT).

Methods and Materials: 40 consecutive patients with dental implants were included in this retrospective, IRB-approved study. All examinations were performed using a SDCT (IQon, Philips Healthcare). Images were reconstructed as conventional images (CI) and as VMI in a range of 40-200 keV (10 keV increment). Quantitative image analysis was performed ROI-based by measurement of attenuation (HU) and standard deviation (SD) in most pronounced hypo- and hyperdense artefact, fat and soft tissue with presence of artefacts. Qualitatively, extent of artefact reduction, assessment of soft palate and cheeks were rated on 5-point Likert scales by 2 radiologists. Statistically data were assessed using ANOVA and Wilcoxon test with correction for multiple comparisons; interrater agreement was determined by intraclass correlation coefficient (ICC).

Results: The hypo- and hyperattenuating artefacts showed an increase and decrease of HU values in high-keV VMI (CI/ VMI_{200keV}: -218.7/-174.4 HU, $p=0.1$; and 309.8/119.2, $p<0.05$, respectively). Artefacts in the fat, as depicted by image noise did also decrease in high-keV VMI (CI/VMI_{200keV}: 23.9/16.4, $p<0.05$). Qualitatively, hyperdense artefacts were decreased significantly in VMI \geq 100keV (e.g. VMI_{200keV}/CI: 3(1-5)/2(1-3), $p<0.05$). Artefact reduction resulted in improved assessment of the soft palate and cheeks (e.g. VMI_{200keV}/CI: 3(1-5)/2(1-4) and 3(1-5)/2(1-5), $p<0.05$). Overall interrater agreement was good (ICC=0.78).

Conclusion: VMI as provided by SDCT allow for reduction of artefacts caused by dental implants and improves diagnostic assessment of soft tissue.

B-0907 11:34

Diagnostic accuracy of FDG-PET and contrast-enhanced CT in patients with head and neck cancer of unknown primary origin

D. [de Haan](#)^{1,2}, A. van der Hoorn², H.E. Westerlaan²; ¹*Almelo/NL*, ²*Groningen/NL* (ddhaan@gmail.com)

Purpose: To assess the diagnostic accuracy of FDG-PET and contrast-enhanced CT in patients with a malignant cervical lymph node of unknown primary origin. We propose that additional imaging techniques could improve the diagnostic accuracy in these patients.

Methods and Materials: We retrospectively analysed 48 patients who presented with a malignant cervical lymph node, without presence of a clinically apparent primary tumour. Patients underwent an total body FDG-PET scan or total body FDG-PET combined with a contrast-enhanced CT-scan of the head and neck. The imaging studies were correlated with biopsy or surgical pathology results of the suspected primary tumour if detected in clinical follow-up.

Results: FDG-PET detected a primary tumour in 21 out of 48 patients (44%), while contrast-enhanced CT detected a primary tumour in 13 patients (29%). 3 patients had a negative FDG-PET and a positive CT, and 9 patients had a positive FDG-PET and a negative CT. The combined sensitivity of FDG-PET and CT was 50%. Out of 23 patients with negative imaging (50%), 13 had a confirmed site of primary tumour during treatment and follow-up (27%), confirming malignancy in 34 patients (71%). In 14 patients, no primary site was confirmed (29%).

Conclusion: Patients with cancer of unknown primary often have negative findings on oncologic imaging workup. A primary site may be detected during follow-up. We demonstrate the diagnostic accuracy of FDG-PET and contrast-enhanced CT-scan. Adding other imaging modalities might also improve the sensitivity of initial imaging.

B-0908 11:42

Can MR textural analysis improve detection of extracapsular nodal spread in patients with oral cavity cancer?

R. Frood, E.Y.A. Palkhi, M. Barnfield, R. Prestwich, S. Vaidyanathan, A. Scarsbrook; Leeds/UK (russell.frood@doctors.org.uk)

Purpose: To explore the utility of MR texture analysis (MRTA) for detection of extracapsular nodal spread (ECS) in oral cavity squamous cell carcinoma (SCC).

Methods and Materials: 115 patients with node-positive oral cavity SCC treated surgically between 2008 and 2016 who received radiotherapy in a single centre were evaluated; 45 patients (39%) had pathological evidence of ECS. Two experienced radiologists independently reviewed baseline MRI blinded to histology. Presence/absence of MR features associated with ECS were agreed in consensus. Region of interests (ROI) encompassing the largest node on T2 and post-contrast T1-weighted images were defined. First-order texture parameters (entropy, skewness and kurtosis) were extracted using proprietary software (TexRAD) with fine, medium and coarse filters. Sensitivity, specificity and positive and negative predictive values (PPV and NPV) of MR predictors of ECS were compared with histology as the gold standard. Areas under the curve (AUC) calculated by receiver operating characteristics (ROC) analysis and optimal threshold was calculated for texture parameters.

Results: Sensitivity, specificity, PPV and NPV (%) for MR predictors were: flare sign (38%, 95%, 86%, 66%); irregular capsular contour (69%, 45%, 42%, 63%); local infiltration (31%, 92%, 77%, 63%); nodal necrosis (72%, 41%, 49%, 65%). Nodal entropy had a statistically significant correlation with ECS on both MR sequences independent of filtration level; the most significant being medium filtration T1 nodal entropy ($p=0.001$), AUC = 0.70, with a threshold > 5.26.

Conclusion: First-order MRTA may improve ECS prediction in oral cavity SCC.

B-0909 11:50

Comparison of local shim coils and slice-specific integrated shimming in EPI-based DWI of the head and neck region

S. Walter¹, M. Notohamiprodjo¹, M. Keil², K. Nikolau¹, P. Martirosian¹, S. Gatidis¹; ¹Tübingen/DE, ²Erlangen/DE (sven.walter@uni-tuebingen.de)

Purpose: Echo-planar (EPI) diffusion weighted imaging is a widely used MR method for (non-)oncological diseases because of its short acquisition-time and defiance against motion induced phase errors. Nevertheless, static field inhomogeneities cause artefacts at higher field strengths in the head/neck region. The purpose was to assess the implementation of additional shim coils into the head/neck surface coil to homogenize the magnetic field, thus improving image quality, compared to single-shot and slice-specific integrated dynamic shimming EPI.

Methods and Materials: sEPI, iEPI and cEPI with additional shim coils (cEPI) of the head/neck region was performed in 10 healthy volunteers (6 male, mean age: 29±4 years) on a clinical 3 Tesla MR-scanner (MAGNETOM Vida, Siemens). Additionally, B0 field maps were acquired using T1w GRE sequence. Assessment of image quality, geometric distortions, ghosting artefacts and signal loss was performed visually by two radiologists in consensus on a 4-point-scale (1 = best possible outcome). Apparent diffusion coefficients (ADC) were compared using ROIs in the spinal fluid, spinal cord and the trapezius muscle.

Results: Additional shim coils showed improved homogenization of the static field, foremost of the lower, posterior neck. Image quality, geometric distortions, signal loss and fat saturation were reduced in iEPI and cEPI. Mean ADC values showed no significant differences in all three compartments; sEPI: 3507, 793 and 1663, iEPI: 3722, 797 and 1765, cEPI: 3597, 839 and 1690.

Conclusion: Additional shim coils in the surface coils of the head/neck showed improved overall image quality compared to sEPI and comparable results to iEPI.

Author Disclosures:

M. Keil: Employee; Employee of Siemens Healthineers.

10:30 - 12:00

Room E1

Breast

SS 1002

Breast MRI

Moderators:

G. Forrai; Budapest/HU

F. Kilburn-Toppin; Cambridge/UK

K-16 10:30

Keynote lecture

C.K. Kuhl; Aachen/DE

B-0910 10:39

Malignant breast lesions typing with diffusion tensor imaging: could fractional anisotropy considered a preoperative 'imaging biomarker'?

F. Pipan¹, P. Clauser², C. Zuiani¹, T.H. Helbich², P.A.T. Baltzer²; ¹Udine/IT, ²Vienna/AT (francesca.pipan@gmail.com)

Purpose: To assess the relationship between apparent diffusion coefficient (ADC) and fractional anisotropy (FA) derived from diffusion tensor imaging (DTI) and breast cancer biomarkers Estrogen Receptor (ER), proliferation index Ki67 and human epidermal growth factor receptor2 (HER-2).

Methods and Materials: The Ethics Committee approved this retrospective study. 359 consecutive patients performed 3T MRI with an additional DTI sequence. Included in our analysis were 154 patients (mean age 54 years, range 26-87) with 159 new diagnosed histologically verified malignant lesions. The ADC and FA values were retrospectively measured using a region of interest positioned in the suspicious lesion. Immunohistochemical analysis with evaluation of ER (>11% ER+, ≤11% ER-), Ki67 (>14% Ki67+, ≤14% Ki67-) and HER-2 was performed on the biopsy specimens according to current standards. Mann-Whitney U-test and receiver operating characteristics (ROC) analysis were applied.

Results: FA values were higher in ER+ (0.152±0.004; ER- 0.117±0.006 $p<0.05$) and lower in Ki67+ (0.138±0.004; Ki67- 0.164±0.009, $p<0.05$). There were no significant differences in ADC in ER+/ER- ($p=0.22$) and Ki67+/Ki67- ($p=0.47$) or ADC and FA values in HER2+/HER2- ($p=0.88$ and $p=0.36$, respectively). The area under the ROC curve showed two cut off values: FA>0.17 (identification of 34.7% of ER+, specificity 90.9%) and FA<0.10 (identification of 23.3% of Ki67+, specificity 94.19%).

Conclusion: FA were significantly higher in ER+ and lower in Ki67+ tumours. FA seems to be more reliable than ADC in characterizing malignant breast lesions. FA could be used as a preoperative "imaging biomarker" and considered an additional tool for therapeutic planning.

B-0911 10:47

Breast lesion detection and characterisation with MRI: intra-individual comparison of gadoterate meglumine and gadobenate dimeglumine at 3 Tesla

P. Clauser¹, T.H. Helbich¹, P. Kapetas¹, K. Pinker², M. Bernathova¹, P.A.T. Baltzer¹; ¹Vienna/AT, ²New York, NY/US (paola.clauser@meduniwien.ac.at)

Purpose: To compare a halved dose of the high-relaxivity contrast agent gadobenate dimeglumine, 0.075 mmol/kg, with a two-fold higher dose of gadoterate meglumine, 0.15 mmol/kg, for breast lesion detection and characterization on contrast-enhanced MRI at 3 Tesla.

Methods and Materials: Eligible for this IRB-approved prospective, randomized, intra-individual comparative study were patients with imaging abnormalities (BI-RADS 0, 4 or 5) on conventional imaging. Each patient underwent two examinations, 24-72h apart, one with gadobenate and the other with gadoterate administered in randomized order. Examinations were performed at 3T using identical sequence and timing parameters including high spatiotemporal resolution dynamic-CE, T2w-TSE, STIR-T2w and DWI. Histopathology was the standard of reference. Three blinded, off-site readers evaluated the examinations using BI-RADS. Detection, sensitivity, specificity, and accuracy were calculated per-lesion and per-region and compared by univariate and multivariate analysis.

Results: 109 patients were recruited. Five were excluded due to technical problems or lack of reference standard leaving 104 women with 142 histologically verified lesions (109 malignant, 33 benign) for evaluation. The detection with gadobenate (84.5-88.7%) was not inferior to gadoterate (84.5%-90.8%), $P>0.165$. At per-region analysis, gadobenate demonstrated higher specificity (96.4%-98.7% vs. 92.6-97.3%, $P<0.007$) and accuracy (96.3-97.8% vs. 93.6-96.1%, $P<0.001$), for all three readers. Gadobenate allowed a reduction in false positives of up to 58%. Multivariate analysis demonstrated a reader-independent superior accuracy with gadobenate.

Conclusion: Halved dose of gadobenate (0.075, mmol/kg) is not inferior to a two-fold higher dose of gadoterate (0.15 mmol/kg) for lesion detection. Gadobenate allows improved lesion characterization with an increased specificity and accuracy.

Author Disclosures:

T.H. Helbich: Grant Recipient; The current study (PI T.H.H.) was supported by Bracco Imaging, Milan, Italy.

B-0912 10:55

A formalised clinical decision rule applied to breast MRI: can we rule-out malignancy in lesions presenting as suspicious mammographic microcalcifications?

J. Al Mohanna¹, F. Pipan², P. Clauser³, A. Bumberger³, A. Stöttinger³, P. Kapetas³, C. Zuiani², T.H. Helbich³, P.A.T. Baltzer³,¹Riyadh/SA, ²Udine/IT, ³Vienna/AT (dr.jalilah@hotmail.com)

Purpose: To investigate whether a clinical decision rule (the Kaiser score, formerly *Tree* flowchart) applied to breast MRI in patients with lesions presenting as suspicious mammographic microcalcifications can rule-out malignancy.

Methods and Materials: IRB-approved retrospective single-center study. 150 consecutive patients (mean age 52 years, range 24-85) undergoing breast MRI (protocol in accordance with EUSOBI/EUSOMA recommendations) for lesions presenting as suspicious mammographic microcalcifications (BI-RADS 4) were investigated. Breast MRI were interpreted by two independent readers that localized the area of microcalcifications in the MRI images and applied the Kaiser score. In short, this rule consists of a formalized flow chart that guides the reader through a 3-step diagnostic process. A resulting score indicates the probability of malignancy ranging from 1 (minimal) to 11 (maximal). A cut-off of ≤ 4 was suggested to avoid unnecessary biopsies. Each reader's results were tested against the reference standard (vacuum-assisted breast biopsy) using Receiver Operating Characteristics (ROC) analysis.

Results: Histopathology revealed 96 malignant and 54 benign lesions (malignancy rate 64%). Areas under the ROC curves (AUC) were measured: 0.810 (95%-CI: 0.738-0.869), R1 and 0.779 (95%-CI: 0.704-0.842), R2. Both readers AUC's did not differ ($P=0.479$). At a cut-off of >4 , sensitivity was 97.9% (R1) and 100% (R2). Applying this cut-off could have reduced unnecessary biopsies by 50% (95%-CI: 36.1-63.9%) for R1 and 22.2% (95%-CI: 12.0-35.6%).

Conclusion: The formalized Kaiser score applied to breast MRI in patients with lesions presenting as suspicious mammographic microcalcifications can rule-out malignancy, allowing a potential reduction of unnecessary biopsies by 22.2-50%.

B-0913 11:03

Selecting treatment options in patients with ductal carcinoma in situ (DCIS) using MRI

A. ter Braak, P.W. Plaisier, M. Menke-Pluijmers, P.J. Westenend; *Dordrecht/NL* (bpmterbraak@yahoo.com)

Purpose: Ductal carcinoma in situ (DCIS) is diagnosed in a needle biopsy. In 20-25% of the patients underestimation occurs, i.e. invasive breast cancer is detected in the surgical specimen. In patients with invasive cancer, nodal staging is performed by sentinel node biopsy. Patients without invasive cancer could be candidates for active surveillance. MRI is sensitive in detecting invasive cancer and thus could be helpful in selecting patients with a biopsy diagnosis DCIS for one of these options.

Methods and Materials: Prospective observational study in which MRI was offered to all subsequent patients with a biopsy DCIS diagnosis in addition to standard diagnosis and treatment between april 2012 and march 2017.

Results: 157 of 228 (69%) subsequent patients with DCIS were included. Biopsies were performed using a 9G needle. 71 patients were not included, mainly because patients declined participation. Five patients, two of which were included, were not operated. The underestimate rate both in included and not included patients was 25%, thus excluding selection bias. The positive predictive value of MRI for detecting invasion was 0.57 (26 of 46 patients). The negative predictive value of MRI was 0.90 (98 of 109 patients). Sensitivity and specificity for detecting invasive cancer on MRI were 0.70 and 0.83.

Conclusion: In patients with DCIS diagnosed by needle biopsy, negative MRI could reliably identify patients without invasive cancer. MRI could be used to select patients with DCIS for active surveillance. However, MRI can not reliably predict the presence of invasive cancer in patients with DCIS.

Author Disclosures:

A. ter Braak: Research/Grant Support; Supported by a grant from Pink Ribbon. **P.J. Westenend:** Research/Grant Support; Supported by a grant from Pink Ribbon.

B-0914 11:11

Contribution of preoperative breast MRI study to pure DCIS

E. Horvath, C. Darrás Ismael, C. Silva, E. Castillo, M.A. Pinochet, C. Galleguillos, E. Droguett, M. Villalon, F. Pizzolon; *Santiago/CL* (darrascarla@gmail.com)

Purpose: To evaluate the usefulness of preoperative MRI study in patients with pure ductal carcinoma in situ (DCIS).

Methods and Materials: IRB approved a retrospective, descriptive observational study of a series of cases. Patients with breast cancer operated between January 2015 and March 2017 were reviewed and pure DCISs with mammography (Mx), ultrasound (US) and preoperative MRI available in PACS were selected. Bland-Altman test was used to describe the size concordance considering the histopathology of the surgical specimen as the reference standard. The MRI contribution was classified into 4 groups. Group 1: MRI provided the same information as conventional studies. Group 2: improved the description of tumour size without changing the surgical approach. Group 3: generated unnecessary procedures. Group 4: correctly changed the surgical management.

Results: Of 467 cancers operated, 77 (16.5%) were DCIS, 41 (53.2%) pure and 36 with microinvasion (46.8%). Thirty-three patients met inclusion criteria. The average age was 52.78 ± 12.55 years. The detectability of the lesions was 90.9%, 30.3% and 74.2% for the Mx, US and MRI, respectively. Concordance index of tumour size: MRI=73.3%, US=70% and Mx=58.1%. MRI contribution in preoperative staging: Group 1=18 cases (58%), Group 2= 3 cases (9.7%), Group 3=0 and Group 4=2 cases (6.5%).

Conclusion: Undoubtedly, Mx is the main method of detection of pure DCIS. However, MRI proved to be the best technique to evaluate tumour size, allowing better preoperative staging than conventional studies in 15% of the cases, and even to correctly change surgical management in 6%.

B-0915 11:19

Is it worth to perform preoperative MRI after the combination of digital mammography, digital breast tomosynthesis and US?

I. González de la Huebra Rodríguez, A. García Baizán, M. Calvo Imirizaldu, A. Ezponda Casajús, P. Bartolomé, A. Quilez, A.M. Elizalde Pérez, L.J. Pina Insausti; *Pamplona/ES* (igonzalez.6@unav.es)

Purpose: To compare the sensitivity (ST) of preoperative breast MRI and the combination digital mammography (DM) + tomosynthesis (DBT) + US in all cancers and in specific subtypes.

Methods and Materials: We reviewed the records of 280 breast cancers in 192 women, diagnosed between October 2011 and September 2016. All of the patients underwent DM, DBT, US and MRI. This was designed as a lesion-by-lesion study. The lesions were classified according to the BI-RADS categories (1-3 were considered negative, while 4-5 positive). The gold standard was the surgical specimen. We compared the sensitivities of the different combinations DM+DBT+US vs DM+DBT+US+MRI using a McNemar test (SPSS 20.0).

Results: 280 breast cancers (32 ductal carcinomas in situ, 210 invasive ductal carcinomas, 38 invasive lobular carcinomas) were reviewed in 192 patients. Among the 248 invasive cancers, 207 were luminal (129 luminal A, 78 luminal B) and 41 were non-luminal (32 triple negative and 9 pure Her2). The ST for the combination DM+DBT+US was 86.4% while the ST for MRI was 94.3% ($p<0.001$). For DCIS the ST were, respectively, 82.3% vs 85.3% ($p=1$), for IDC the ST were 87.9% vs 96.2% ($p<0.001$), for ILC the ST were 81.6% vs 92.1% ($p=0.219$). Regarding the immunohistochemical patterns, for luminal cancers the ST was 85.8% vs 94.6% ($p<0.001$) and for non-luminal cancers 92.7% vs 97.6% ($p=0.5$).

Conclusion: According to our data, the addition of breast MRI significantly increased the sensitivity of the combination DM+DBT+US for all cancers, except for DCIS, invasive lobular cancers and non-luminal cancers.

B-0916 11:27

The incremental value of preoperative MRI for evaluation of extent of disease in IDC vs ILC

T. Alster, E. Carmon, B. Maly, T. Sella; *Jerusalem/IL* (tamarse@hadassah.org.il)

Purpose: ILC is more commonly multifocal/multicentric compared to IDC, with a high discordance rate between imaging and pathology. However, most studies were conducted before the era of breast MRI. The purpose of this study was to assess the incremental value of pre-operative breast MRI over mammography (MG) and US in depicting the accurate extent of disease in IDC compared to ILC.

Methods and Materials: Retrospective analysis of pre-operative MG, US and MRI was performed in 239 patients with either IDC (n=193) or ILC (n=46). Images were evaluated for solitary, multifocal or multicentric disease and compared for concordance with post-surgical pathology. Discordance was documented as either overestimation or underestimation. Two tailed paired T and Fischer's exact tests were used for analysis.

Results: Multifocality was present on pathology in 35% and 61% of patients with IDC and ILC ($p < 0.05$) and multicentricity in 23% and 42% respectively ($p = 0.84$). For IDC, concordance with pathology for all modalities was similar (65-76%). In ILC, MRI was more commonly concordant than MG and US (89%, 44%, 49% for multifocality ($p < 0.05$) and 80%, 63%, 71% for multicentricity ($p = 0.3$)). Among discordant cases, underestimation was significantly more common for MG and US. MRI equally overestimated multifocal and multicentric disease in IDC (21 and 22%), but very rarely overestimated multifocal disease in ILC (2%).

Conclusion: The added benefit of MRI for evaluation of extent of disease is greater in ILC than IDC. Demonstrating an 80-90% concordance rate with pathology, ILC should be regarded as a relative indication for pre-operative MRI.

B-0917 11:35

The role of MRI in predicting irradical surgery and local recurrence after breast conserving surgery in T3 breast cancer patients after neoadjuvant chemotherapy

I. Ioan^{1,2}, J. van Urk², D.K. Schouten², M.E. van der Noordaa², M. Vrancken Peeters², R.G.H. Beets-Tan², G. Winter-Warnars², C. Loo²; ¹San Donato Milanese/IT, ²Amsterdam/NL (ileana.ioan@libero.it)

Purpose: To investigate the role of MRI in predicting irradical surgery and local recurrence (LRR) after breast conserving surgery (BCS) in patients with extensive breast cancer (>5 cm) treated with neoadjuvant chemotherapy (NAC).

Methods and Materials: Dynamic Contrast Enhanced MR images of 45 patients with T3 breast cancer, treated with NAC and BCS were retrospectively reviewed. Morphology, size, enhancement kinetics were assessed before and after NAC and the accuracy of MRI to predict pathological CR (pCR). Clinical, surgical and histological information after NAC and during long term follow up was obtained.

Results: Median follow up was 4.6 years (min 0.8y - max10.2y). Seventeen (38%) patients had positive margins after BCS. Of these, only seven (15%) had mastectomy, two (4%) had re-excision and eight (18%) had more extensive radiotherapy. There were no local recurrences. Two patients died of distant metastasis. Clinical Complete Response (cCR) on MRI was achieved in 24 (53%) patients and pCR in only 14 (31%). Sensitivity, specificity, NPV and PPV of MRI to predict pCR was: 55%, 71%, 42% and 81%. The risk of irradical surgery was equal for patients with 37% (9/24) and without 38% (8/21) cCR on MRI after NAC. The risk of irradical BCS was higher in patients with non mass enhancement on MRI before NAC 45% (11/24) or ILC 60% (6/10) than in mass enhancement 28% (6/21) or IDC 34% (12/35).

Conclusion: Non mass enhancement on MRI before neoadjuvant chemotherapy is associated with higher risk of irradical breast conserving surgery in T3 breast cancer.

B-0918 11:43

Accuracy of breast magnetic resonance imaging compared to mammography in the preoperative detection and measurement of pure ductal carcinoma in situ

H. Preibsch, J. Beckmann, G. Blumenstock, A. Staebler, B. Wietek, K. Nikolaou, B. Wiesinger; *Tübingen/DE* (Heike.Preibsch@med.uni-tuebingen.de)

Purpose: Ductal carcinoma in situ (DCIS) hinders detection by imaging methods due to multifocal appearance and discontinuous growth. Preoperative determination of its extent is therefore challenging. Aim of this study was to investigate the additional benefit of breast magnetic resonance imaging (MRI) to mammography (MG) in the diagnosis of DCIS according to size and grading.

Methods and Materials: Retrospective analysis of 295 patients with biopsy-proven, pure DCIS. Mean patient age was 57.0 years (27-87 years). In 41.7% (123/295) MRI was performed additional to MG. Mammographic breast density, benign breast parenchymal enhancement (BPE), tumour size and grading were analyzed.

Results: Mean tumour size of DCIS was 35.3mm. DCIS was occult on MG in 14.6% (43/295) and on MRI in 1.6% (2/123). Size was underestimated by 4.6mm (mean) mammographically. Regarding breast density MG overestimated tumour size by 16mm (median) in density a, was exact in density b and underestimated by 5.5 and 8mm in density c and d, respectively. DCIS was high grade in 46.8% (138/295), intermediate grade in 41.1% (123/295) and low grade in 11.9% (35/295). MG was exact regarding tumour size in low grade DCIS, underestimated intermediate grade by 1mm (median) and high grade by 10.5mm (median). MRI overestimated low grade DCIS by 1mm (median), was exact regarding intermediate grade and underestimated low grade by 1mm (median). BPE did not significantly influence tumour detection and measurement.

Conclusion: MRI outperforms MG in the detection and size estimation of DCIS with a benefit for surgical planning and reduction of positive margin rates.

B-0919 11:51

Non-mass enhancement in breast-MRI: which BI-RADS descriptors for distribution and internal enhancement patterns have the highest likelihood of malignancy?

M. Lunkiewicz¹, S. Forte², B.K. Freiwald¹, G. Singer¹, R.A. Kubik-Huch¹; ¹Baden/CH, ²Basle/CH (magdalena.lunkiewicz@ksb.ch)

Purpose: The purpose of this study was to evaluate the positive predictive values for malignancy of non mass enhancement (NME) descriptors, using the revised BI-RADS Atlas (5th Edition), with focus on clustered ring internal enhancement pattern.

Methods and Materials: We reviewed Breast MRIs of patients on which an MRI-guided VAB-Biopsy had been performed between 2012 and 2016. All studies were independently reevaluated by two experienced radiologists, blinded to the histopathological results. Distribution modifiers and pattern of internal enhancement was recorded. Consensus was reached by involving a third radiologist. The findings were correlated with the histopathological results.

Results: 142 women were included. 72 biopsied lesions were assessed as NME. Pathology results for NME included 53 (73.6%) benign lesions and 19 (26.4%) malignant lesions. Among all internal enhancement patterns, clustered ring enhancement (7/14, PPV 50%) and clumped enhancement (7/30, PPV 23.3%) had the highest malignancy rate. Among all distribution patterns, segmental distribution (5/9, PPV 55.6%) and linear distribution (5/20, PPV 25%) had the highest malignancy rate. The combination of segmental distribution and clustered ring internal enhancement pattern had the highest malignancy rate (4/6, PPV 66.7%). The overall interobserver agreement rate for distribution modifiers was 0.67 and 0.69 (CI 95%) for internal enhancement pattern. The biggest discrepancy occurred between focal distribution of non mass enhancement vs mass lesions. Interreader agreement was lowest for the segmental distribution and clumped internal enhancement pattern.

Conclusion: Using the revised 5th edition of BI-RADS Atlas, clustered ring internal enhancement pattern and segmental distribution had the highest PPV for malignancy.

10:30 - 12:00

Room E2

Neuro

SS 1011a

Stroke: prediction of outcome

Moderators:

F. Bozzetti; Parma/IT
K.D. Kurz; Stavanger/NO

K-17 10:30

Keynote lecture

B.K. Velthuis; Utrecht/NL

B-0920 10:39

Covert brain ischaemia and its impact on cognition in the Polish population: preliminary results of the PURE - mind (Prospective Urban and Rural Epidemiological) cohort study

J. Jacków, A. Zimny, P. Podgórski, M. Siasidek, D. Szczesniak, J. Rymaszewska, K. Poltyn-Zaradna, K. Zatońska, A. Szuba; *Wrocław/PL* (jagodajackow@yahoo.pl)

Purpose: Assessment of incidence of covert brain ischaemia and its impact on cognition in the Polish population as a part of Polish and international PURE-mind (Prospective Urban and Rural Epidemiological) cohort study after one year of the project.

Methods and Materials: The study group consisted of 249 subjects (mean age: 56.1 yrs range: 42-66 yrs, F/M: 155/94, urban/rural: 197/52). All participants were examined using international PURE-mind protocols including questionnaires about their life-style, laboratory blood tests and psychological assessment measured with Montreal Cognitive Assessment (MOCA) followed by structural brain MRI. Axial T2-, PD-weighted, FLAIR and DWI images were used to assess the number of white matter hyperintensities (WMHs) and SWI for microbleeds. Imaging findings were correlated with cardiovascular risk factors and cognitive state.

Results: WMHs were found in 97/249 (38.9%) subjects (mean number: 16.1, range: 1-89). No large territorial infarcts and microbleeds were found. 176/249 (70.6%) participants showed normal cognitive state while 73/249 (29.4%) revealed mild cognitive impairment (MCI). There was a significant positive correlation between WMHs and age ($p < 0.05$). There were no correlations among WMHs and gender, weight, urban/rural living environment, contact with heavy metals, smoking, alcohol consumption, hypertension, diabetes, myocardial ischaemia and cognitive impairment ($p > 0.05$). 61/176 (34.6%) normal and 36/73 (49.3%) MCI subjects showed similar amount of WMHs (mean number: 15.0, range: 1-73; mean number: 14.0, range: 1-89, respectively).

Conclusion: Incidence of WMHs is strongly related to age, less dependent on their life-style or accompanying diseases. WMHs have no important impact on cognitive state in the relatively young screened population.

B-0921 10:47

Clinical and MRI characteristics of patients with pontine hyperintense lesions in a series of ischaemic strokes

M. Maier, S. Colombani, M. Mejdoubi; *Fort De France/FR*

Purpose: Pontine hyperintense lesions (PHL) are sometimes detected on brain Magnetic Resonance Imaging (MRI) in asymptomatic patients. They are therefore considered a form of small vessel disease (SVD) with possibly the same pathophysiology as white matter hyperintensities (WMH). Because this imaging sign is rarely seen in the general population, the aim of our study was to investigate the relationship between PHL and clinical/MRI data in a series of stroke patients.

Methods and Materials: Patients' medical history was obtained regarding age, gender, the presence of arterial hypertension, diabetes mellitus, hypercholesterolemia, coronary heart disease, atrial fibrillation, peripheral arterial obstructive disease, current smoking and alcohol consumption. WMH grade, presence of microbleeds, infarcts type and PHL presence were reported after MRI analysis. Potential predictors of PHL presence were investigated using logistic regression modelling.

Results: PHL were found in 110 (20.6%) of the 534 prospectively included stroke patients. In univariate analysis, a significant association was demonstrated between PHL and age ($p < 0.0001$), female gender ($p = 0.04$), microbleeds ($p < 0.0001$), high WMH grade (Fazekas classification 2-3; $p = 0.0001$), hypertension ($p = 0.02$) and diabetes ($p = 0.03$). In multivariate analysis, only age ≥ 60 years (OR [95% CI]: 3.44 [1.17-10.15], $p < 0.025$), female gender (OR [95% CI]: 1.78 [1.11-2.87], $p = 0.0175$), microbleeds (OR [95% CI]: 1.97 [1.18-3.30], $p = 0.0098$) and high WMH grade (OR [95% CI]: 7.54 [4.17-13.62], $p < 0.0001$) remained independently associated with PHL.

Conclusion: Several clinical and imaging factors are independent predictors of PHL presence in stroke patients. To our knowledge, significant association between PHL occurrence and microbleeds has never been reported before. This might suggest that SVD is the principle pathophysiologic process in PHL. We suggest that PHL be considered as a subgrade in the Fazekas classification.

B-0922 10:55

Collateral filling velocity predicts malignant oedema development in acute ischaemic stroke

M.F. Froelich, P. Reidler, M.P. Fabritius, L. Rotkopf, F. Schuler, W.H. Sommer, K.M. Thierfelder, W.G. Kunz; *Munich/DE*

Purpose: To assess the predictive value of collateral filling velocity on malignant edema development (MED) in acute ischemic stroke.

Methods and Materials: Subjects were selected from a cohort of 1,845 consecutive patients with suspected ischemic stroke who underwent CT including whole-brain CT perfusion. Inclusion criteria were: (1) isolated pre-bifurcation M1 segment occlusion, and (2) available follow-up imaging within 72 hours. Time to peak (TTP) enhancement was measured distal to the occlusion in the M2 segment branches in the Sylvian fissure. Collateral filling velocity was defined as the difference in TTP enhancement between the ischemic and non-ischemic hemisphere. MED was defined as development of midline shift of ≥ 5 mm in follow-up imaging. Multivariable binary logistic regression analysis was performed to adjust for clinical and imaging parameters.

Results: Ninety-nine patients (56.6% female, mean age 73 years) were included. 18 patients (18.2%) suffered from MED. Longer TTP enhancement was significantly associated with MED (odds ratio [OR]=1.627; 95% confidence interval [CI], 1.044-2.536; $p=0.032$). Lower values of the Alberta Stroke Program Early CT Score (OR=0.370; 95% CI, 0.152-0.898; $p=0.028$) were also associated with MED. The analysis was further adjusted for intravenous thrombolysis treatment, neurological deficit on admission based on the National Institutes of Health Stroke Scale, and the volume of cerebral blood flow-cerebral blood volume mismatch, which were not associated with MED (all $p > 0.05$).

Conclusion: Slower collateral filling velocity independently predicts malignant edema development in acute large-vessel occlusion stroke. As an objective, threshold-independent quantitative parameter, it may allow standardized risk prediction in acute stroke imaging.

B-0923 11:03

Collateral scores and perfusion parameters for outcome prediction in acute ischaemic stroke: how many scans are needed?

K. Schregel, I. Tsogkas, D. Behme, C. Peter, I. Maier, J. Liman, M. Knauth, M.-N. Psychogios; *Göttingen/DE (katharina.schregel@med.uni-goettingen.de)*

Purpose: Collateral circulation is an important determinant for outcome in endovascularly treated patients with acute ischaemic stroke (AIS). Several

collateral scores to support triage and outcome prediction exist. We applied different scoring systems on single- and multi-phase CTA (sp-/mpCTA) and compared them to CT perfusion (CTP) to identify the best method for collateral evaluation in AIS.

Methods and Materials: A total of 102 patients with AIS due to large vessel occlusion (LVO) in the anterior circulation who underwent multimodal CT imaging and who were treated endovascularly were included. Collateral status was assessed on spCTA and on mpCTA derived from CTP using four different scoring systems and compared to CTP parameters.

Results: Collateral scores correlated well with each other and with CTP ($p < 0.01$ for each). Collateral scores stratified by extent of perfusion deficit were significantly different between groups ($p < 0.01$ for each). Stepwise logistic regression showed that probability of a favorable outcome was highest, when patients were not hypertensive, had high baseline ASPECTS and good collaterals on spCTA (OR 5.82, 1.53 and 1.47, respectively; 95% CI 1.83-18.51, 1.03-2.27 and 1.11-1.94, respectively). In ROC analysis, a spCTA collateral score discriminated best between favorable and unfavorable outcome and was equal to CTP parameters.

Conclusion: Collateral status evaluated on spCTA may suffice for outcome prediction and decision making in AIS patients, potentially obviating further imaging modalities like mpCTA or CTP.

Author Disclosures:

M. Psychogios: Speaker; Speakers' honoraria from Siemens Healthineers.

B-0924 11:11

The utility of CAD software in acute stroke protocol workflow for automatic evaluation of infarct core size

D. Juskanic, A. Petrovicova, S. Holly; *Nitra/SK (juskanic@gmail.com)*

Purpose: Triage acute stroke patients for appropriate treatment is often carried out in a high-pressure setting, which is a potential source of interpretative variability. Use of decision supportive tools appears to be promising in reducing interpretation and management errors. Without prior systematic use of ASPECTS, we describe the single centre experience while implementing the CAD software during night shifts.

Methods and Materials: During two months study period, all 95 patients with suspected stroke referred during night shifts were examined under standard CT stroke protocol with subsequent automatic post-processing using the CAD tool e-ASPECTS (Brainomix, Oxford, UK). In patients with ICA or MCA strokes, logistic regression was used to evaluate the relationship between entry variables and treatment decisions. The correlation between ASPECTS with mRS on discharge was performed.

Results: The greatest influence on treatment decision had entry NIHSS ($p = 0.01$), ASPECTS was not significant ($p = 0.294$). In the treatment group, none of the patients had ASPECTS lower than 7, median ASPECTS was 9 (interquartile range [IQR] 8-9). In patients with no specific treatment, median ASPECTS was 10 (interquartile range [IQR] 9-10). Moderate correlation between ASPECTS and mRS on discharge was found ($r = 0.518$).

Conclusion: In the treatment group, where no other contraindications were present, ASPECTS played more of an external role in validating decisions made during standard routine protocol. Conversely, in the subset of patients outside the 4.5-hour window or patients with wake-up stroke, ASPECTS could potentially serve as a factor favoring revascularization, or as a quantitative alternative for CT perfusion.

B-0925 11:19

Voxel-based lesion symptom mapping of NIHSS scores in patients with acute media infarction

J. Jesser¹, B. Dinse¹, J. Baldo², A. Arévalo³, M. Bendszus¹, K. Schlamp¹; ¹Heidelberg/DE, ²Martinez, CA/US, ³São Paulo/BR (Jesser.Jessica@gmail.com)

Purpose: The aim of this study was to find key areas in the brain that cause a severe clinical situation when damaged in patients with an acute infarction of the middle cerebral artery.

Methods and Materials: In retrospect we identified 126 patients with acute media infarction. Inclusion criteria: symptom onset < 24 h before MRI, no mismatch between stroke lesion in diffusion- and perfusion-weighted imaging (DWI vs. PWI) in the MRI session, accessible NIHSS records ("National Institute of Health Stroke Scale"). The NIHSS is used for quantification of stroke severity. The stroke lesion was manually traced in the DWI-sequence and normalized to standard space. VLSM-analysis ("voxel-based lesion symptom mapping"): In the process a t-test is conducted in every voxel using the lesioned versus non-lesioned voxel as independent variable and the total NIHSS score (at the time of the MRI) as dependent variable.

Results: We found three highly significant clusters ($p < 0.001$) associated with high NIHSS scores in acute media infarction. These clusters are localised in the left brain hemisphere: subcortical in the supramarginal gyrus, in the corona radiata where the corticospinal tract and the arcuate fascicle cross and below the basal ganglia in the inferior frontooccipital fascicle.

Conclusion: The areas associated with high NIHSS scores in acute media infarction are involved in functions like language, visual attention and movement. We think that these areas are important for integrating several functions and therefore cause a dramatic clinical situation even when only a small volume of brain tissue is damaged.

B-0927 11:27

Clinical outcome after mechanical thrombectomy in diabetic patients with major ischaemic stroke of the anterior cerebral circulation

J. Borggrefe¹, B.K. Glück¹, C. Kabbasch¹, O. Onur¹, N. Abdullayev¹, V. Maus¹, G.R. Fink¹, A. Mpotsaris²; ¹Cologne/DE, ²Aachen/DE
(Jan.Borggrefe@uk-koeln.de)

Purpose: Diabetic patients (DP) with acute ischaemic stroke (AIS) show a poorer outcome than non-diabetic patients (NDP). This study provides a comprehensive analysis of factors associated with unfavourable outcome in DP receiving MT for AIS of the anterior circulation.

Methods and Materials: This monocentric study includes 317 consecutive patients receiving MT for AIS in the terminal internal carotid artery and/or middle cerebral artery, including 46 DP. The study included pretreatment stroke CT with perfusion and collateral status, comprehensive treatment data, pre-existing comorbidities, laboratory parameters, and medication. Neurological status was assessed at baseline (NIHSS/mRS) and after 90 days (mRS 90).

Results: Compared to NDP, DP showed a significantly poorer outcome (mRS90 >2) (p<0.05). Collateralization and infarct core size did not differ between groups while the penumbra was significantly smaller in DP than in NDP (p<0.05). The poorer mRS 90 outcome (mRS90 > 2) in DP was associated with poor collaterals (p=0.01) and hyperglycemia on admission (aHG) (p<0.05). Shorter time to recanalization (TTR) was associated with favourable mRS 90 in the NDP group (p<0.001) but not in DP (p=0.49). In univariate logistic regression, following parameters were significantly associated with mRS 90: diabetes, aHG, TTR, and the NIHSS (p<0.05 each). In multivariate analyses and partition regression models DP with admission hyperglycemia (≥ 132 mg/dl) and older age (≥ 66 years) showed a particularly poor outcome.

Conclusion: The main factors for a less favourable outcome of DP after MT are admission hyperglycemia, age, NIHSS, and prolonged times to recanalization.

B-0928 11:35

MRI morphometry of the corpus callosum in patients with small vessel diseases of the brain

D. Bazhenova, V.E. Sinitsyn, R.N. Kononov; Moscow/RU
(bazhenova.darya@gmail.com)

Purpose: The purpose of this study was to compare the area of corpus callosum (CC) segments in healthy subjects and patients with small vessel disease of the brain (SVDB) using MRI morphometry.

Methods and Materials: Three groups of subjects (N = 109, 29-83 years, 42 male) took part in the study: 1st group - hypertensive microangiopathy (n=73), 2nd - cerebral autosomal dominant arteriopathy with subcortical infarcts and leukoencephalopathy (CADASIL) (n=9), 3rd - healthy volunteers (n=27). Subjects underwent MRI of the brain and neuropsychological assessment. The areas of CC and each of 7 segments were calculated using the MultiVox software (Fig.1).

Results: The areas of the 1st, the 6th, the 7th segments, and the total area of CC in patients with hypertensive microangiopathy were significantly less than in the control group and CADASIL (p<0.005). The severity of cognitive impairment of the examined individuals positively correlated with the area of the 1st, the 2nd segments and the total area of CC (p<0.05). The grade of the cerebrospinal space expansion correlated inversely with the areas of the 1st, the 2nd, and the 6th CC segments (p<0.05).

Conclusion: The study discovered differences in the area of the CC and some of its segments between studied groups. The severity of cognitive impairment correlated with a volume decrease in the anterior part of CC. The expansion of cerebrospinal space volume in patients with SVDB was associated with decrease of the grey and white matter volume, including CC. Morphometry of CC can be used as a biomarker of SVDB.

B-0929 11:43

The aspect of intracranial haemorrhage of cranial CT at the moment of admission is useful to predict the clinical and radiological evolution

S. Bonilla, E. Pascual Goni; Barcelona/ES (santibonilla22@gmail.com)

Purpose: To determine which neuroradiology signs were able to predict the growth (HG), the early neurological impairment and the functional prediction.

Methods and Materials: Retrospective study of consecutive patients diagnosed with spontaneous intracranial hemorrhage [IHC] (2013-2016). The study includes the patients with cranean CT < 6 hours and exclusion criteria. Two blind assessors analyzed the form, density, presence of intraliesional

hypodensities, swirl-sign, blend-sign & black hole in basal CT. Interobserver variability for each sign (Cohen's kappa) was analyzed. Clinical and radiological variables associated to growth, DNP (decrease of the scale of Glasgow (GCS) of >1p and/or NIHSS ≥4p increase) and functional prediction at 3 months were evaluated through univariate and multivariate analysis.

Results: 98 out of 313 patients fulfilled criteria. The irregular form frequency, heterogeneous density, presence of hypodensities, "swirl-sign", "blend-sign" and "black hole" were 57%, 32%, 51%, 36%, 9% and 34% respectively. Interobserver concordancy was good for all of them (K>6). The growth was observed in 42% of cases. The growth was associated regardless the form and the presence of hypodensities. The DNP was associated regardless the GCS at the admission, the form and the swirl-sign. The functional prediction was associated regardless the form.

Conclusion: The morphological characteristics of intracranial haemorrhage (IHC) in the cranean CT at the admission predict the risk of growth, the early neurological impairment and the functional prediction. The analysis of the form of the haemorrhage in our patients was the sign of the best predictive power of the clinical & radiological evolution.

10:30 - 12:00

Room F1

Oncologic Imaging

SS 1016b

Improvements in neuro-oncology imaging

Moderators:

L. Hermoye; Brussels/BE

L. Jacobi-Postma; Maastricht/NL

B-0930 10:30

Whole tumour histogram analysis of T2-weighted, diffusion-weighted, and postcontrast T1-weighted images in medulloblastoma: assessment risk of recurrence

Q. Lv; Zhengzhou/CN (478071645@qq.com)

Purpose: To explore the value of MRI whole-tumour histogram in the risk assessment of medulloblastoma recurrence.

Methods and Materials: Retrospective analysis of 32 patients which were pathologically confirmed medulloblastoma. These patients were divided into two groups, which were defined as the recurrent group and the non-recurrent group. Using the software Mazda, whole-tumour regions of interest were drawn on all slices of diffusion-weighted, T2-weighted, and postcontrast T1-weighted images to obtain histogram parameters, including the average value, variance, skewness, kurtosis, perc.01%, perc.10%, perc.50%, perc.90% and perc.99%. The histogram parameters were analysed statistically to find out the characteristics of the significant differences between the two groups. Next, we drew the ROC curve to assess diagnostic efficiency in medulloblastoma recurrence.

Results: The variance, the kurtosis derived from precontrast T1-weighted images have the statistical significance (P<0.05). The variance showed the sensitivity and the specificity of the risk of medulloblastoma recurrence were 81.36% and 60.0%, respectively; the kurtosis were 86.7% and 62.5%. The variance and the 99th percentiles derived from T2-weighted images have the statistical significance (P<0.05). The sensitivity and the specificity were 66.7%, 87.2% and 66.7%, 76.5%, respectively. However, there is no difference of parameters between two groups in the ADC (P>0.5).

Conclusion: MRI whole-tumour histogram analysis can be used as an important supplementary method to assess the risk of medulloblastoma recurrence. The variance derived from T2-weighted images has the potential to be the most significant parameter for assessing the risk of medulloblastoma recurrence.

B-0932 10:38

The role of diffusion weighted imaging for the differentiation of malignant and benign peripheral nerve sheath tumours

L. Well¹, K.I. Geier¹, M. Kaul¹, L. Späth¹, T. Derlin², J. Herrmann¹, G. Adam¹, J. Salamon¹; ¹Hamburg/DE, ²Hannover/DE (l.well@uke.de)

Purpose: To evaluate the role of diffusion-weighted-imaging (DWI) for the differentiation of malignant and benign peripheral nerve sheath tumours (MPNST/BPNST) in patients with Neurofibromatosis 1 using intravoxel incoherent motion (IVIM) and standard apparent diffusion coefficient (ADC) models.

Methods and Materials: Prospectively, n=26 patients with neurofibromatosis 1 were subjected to magnetic resonance imaging; n=67 tumours (n=12 MPNST / n=55 BPNST). Imaging was performed at 3T, acquired sequences were T2w with and without fat-saturation, 3D-T1w and DWI. Eleven b-values (0-800 s/mm²) were fitted with a biexponential model to extract perfusion fraction f, diffusion coefficient D and pseudo-diffusion coefficient D*. Additionally, the

apparent diffusion coefficient (ADC) was calculated. ROIs were manually drawn in the center and periphery of tumours to determine signal intensities. Seven morphological features were selected for visual differentiation. Mann-Whitney-U, Fisher's exact test and receiver operating characteristic (ROC) analyses were performed.

Results: Signal intensities of MPNST were significantly different from BPNST in IVIM (mean f: 21022 vs 13608 $p=0.0028$; mean D*: 971613 vs 1756326 $p<0.0001$) and ADC (mean 1232182 vs 2108616; $p<0.0001$). Signal intensities between center and periphery of tumours were significantly different for the perfusion fraction in BPNST but not in MPNST ($p=0.0171$; all other $p>0.05$). ROC showed good levels of sensitivity and specificity for ADC and D* (Sensitivity vs specificity: ADC 91.67%vs98.18%, AUC 0.9833; D* 91.67%vs90.91%, AUC 0.9318). Morphological features were applicable for identification of MPNST (all $p<0.05$).

Conclusion: Diffusion weighted imaging allows identification of MPNST in patients with Neurofibromatosis 1 with high levels of sensitivity and specificity.

B-0933 10:46

Relaxation-compensated multi-pool CEST signal at 7T MRI of glioblastomas is dependent on the anatomic localisation

C. Dreher¹, J. Windschuh¹, F. Sahn¹, P. Bachert¹, M. Ladd¹, M. Zaiss², H.-P. Schlemmer¹, A. Radbruch¹, D. Paech¹; ¹Heidelberg/DE, ²Tübingen/DE (c.dreher@dkfz-heidelberg.de)

Purpose: To investigate the localization dependence of relaxation-compensated multi-pool Chemical-Exchange-Saturation-Transfer (CEST) MRI at 7T and histopathological parameters in newly diagnosed untreated WHO IV^o glioma patients.

Methods and Materials: Twenty patients with newly diagnosed WHO IV^o gliomas were prospectively included in this study and investigated at a 7T whole-body scanner (Siemens Healthcare, Erlangen, Germany). Mean CEST signal intensities (Nuclear-Overhauser-Effect(NOE), Amide-Proton-Transfer(APT), Downfield_NOE-suppressed APT(DNS_APT)), ADC parameters and histopathological parameters of the tumor volumes were evaluated with regard to extension, localization (brain hemisphere and lobe) and contact to the subventricular zone using non-parametric Mann-Whitney tests, ANOVA on ranks test and Spearman correlation.

Results: Mean CEST APT&DNS_APT signal intensities (0,156±0,118 & 0,137±0,116) were significantly increased in right vs. left hemisphere glioblastomas (0,072±0,014 & 0,048±0,014), ($p=0,044$ and 0,010). Mean ADC parameter were significantly decreased in right vs. left hemisphere glioblastomas ($1,04*10^7\pm0,08*10^7$ vs. $1,18*10^7\pm0,12*10^7$) ($p=0,046$). Mean CEST NOE signal intensity didn't differ significantly between both hemispheres, but was significantly increased in case of subventricular zone contact (0,101±0,015 vs. 0,118±0,015) ($p=0,037$). The lobe localization and extension of the tumor had no significant effect on CEST and ADC signals. CEST APT&DNS_APT and ADC signal intensities did significantly correlate (-0,67 and -0,56) ($p<0,01$), but not CEST NOE and ADC parameters. Histopathological parameters were not significantly different with regard to different localizations.

Conclusion: Relaxation-compensated multi-pool CEST MRI signal depends on the anatomic localization. Amide CEST and ADC are positively correlating - NOE parameters are solely different with regard to subventricular zone contact, possibly showing complementary information to Amide CEST and ADC.

B-0934 10:54

Metabolic imaging of tumours employing dynamic ¹⁷O MRI: initial results in glioma patients

D. Paech, N. Behl, R. Umatham, M. Ladd, H.-P. Schlemmer, A. Nagel, S. Niesporek; Heidelberg/DE (d.paech@dkfz.de)

Purpose: To investigate cerebral metabolic rate of oxygen consumption (CMRO₂) in brain tumours employing dynamic ¹⁷O magnetic resonance imaging (¹⁷O-MRI).

Methods and Materials: In this ongoing IRB approved study one untreated glioma patient (male, 26 y.-o. astrocytoma WHO grade II) was included. ¹⁷O MRI was conducted at a 7 Tesla whole-body scanner (Siemens Healthcare, Erlangen, Germany) with a nominal spatial resolution of (7.5mm)³ employing a density-adapted radial sequence with Golden Angle acquisition scheme. 3.8±0.1L of 70%-enriched ¹⁷O gas were administered using a remotely controllable closed circuit breathing system. High-resolution T1 MPRAGE (0.6mm)³ and T2 TSE (0.4x0.4x0.5mm)³ sequences were additionally acquired and used for tumour and normal brain segmentation. Post-processing of ¹⁷O-MRI data was conducted with a partial volume correction algorithm to account for spilling-effects at low resolution. Signal intensities in the investigated volumes were compared using the Wilcoxon rank-sum tests.

Results: ¹⁷O-MRI MRI revealed significantly decreased CMRO₂ in tumour tissue (0.59-0.66±0.16 μmol/g/min) compared to contralateral normal appearing brain tissue (1.10-1.22±0.08 μmol/g/min) ($p<0.01$). Further, CMRO₂

was significantly increased in gray matter (2.34-2.58±0.20 μmol/g/min) compared to white matter tissue (0.56-0.62±0.06 μmol/g/min) ($p<0.01$).

Conclusion: ¹⁷O-MRI may provide new insights into tumour metabolism through the localised quantification of the cerebral metabolic rate of oxygen consumption. Our results agree with the Warburg-effect describing decreased CMRO₂ of tumours due to the shift in glucose metabolism from oxidative phosphorylation to lactate production for energy generation.

B-0935 11:02

Histogram analysis of apparent diffusion coefficient maps for distinguishing lateral ventricle central neurocytoma from ependymoma

W. Wang, J. Cheng, Y. Zhang; Zhengzhou/CN (weijianwang520@163.com)

Purpose: We explored the role of histogram analysis of apparent diffusion coefficient (ADC) maps for discriminating lateral ventricle central neurocytoma from ependymoma.

Methods and Materials: We retrospectively evaluated findings in 35 patients with lateral ventricle central neurocytoma and 20 patients with ependymoma who underwent diffusion-weighted imaging (b = 0,800 s/mm²) at 3T with acquisition of corresponding ADC maps. We derived histogram data from regions of interest drawn on all slices of the ADC maps in which tumor was visualized, including areas of necrosis and hemorrhage in the tumor. We used the t test to evaluate the capacity of histogram parameters (variance, kurtosis, 1th, 10th percentiles) to discriminate central neurocytoma from ependymoma and analyzed the receiver operating characteristic (ROC) curve to determine the optimum threshold value for each parameter and its corresponding sensitivity and specificity.

Results: Lateral ventricle central neurocytoma demonstrated significantly lower variance, kurtosis, 1th, 10th percentiles than ependymoma ($P < 0.05$). ROC curve analysis of the variance yielded the best area under the ROC curve (AUC; 0.83), sensitivity of 80%, and specificity of 82%, with a cutoff value of 2012.

Conclusion: Histogram analysis of ADC maps might be helpful for discriminating lateral ventricle central neurocytoma from ependymoma.

B-0936 11:10

Nedd4-1 expression promotes tumour progression in gliomas and relationship between nedd4-1 expressions and DKI features in gliomas

X. Cheng, J. Cheng; Zhengzhou/CN (chengxiaoyaz@163.com)

Purpose: The aim of this study was to investigate whether Nedd4-1 is present in glioma and to evaluate the correlation of Nedd4-1 expression with the progression, prognosis and DKI manifestation of the disease.

Methods and Materials: 60 patients with gliomas, who underwent preoperative DKI at 3 T after written informed consent. Normalized mean kurtosis (MKn) and mean diffusivity (MDn) metrics from DKI were assessed in these patients. Immunohistochemistry and western blot were used to investigate the expression of Nedd4-1 protein in these patients.

Results: Immunohistochemistry levels and western blotting analysis discovered that the expression of Nedd4-1 was increased with WHO grade ($P<0.05$). In addition, a non-parametric analysis revealed that the attenuated Nedd4-1 expression was significantly correlated with a large tumour diameter ($P<0.05$), frequent intra-tumour necrosis ($P<0.05$), and that high expression of Nedd4-1 is closely consistent with poor prognosis of glioma. MKn was significantly higher (but MDn decreased) in higher glioblastoma (0.56 ± 0.11) than in primary glioblastoma (0.38 ± 0.10 , $p < 0.05$). Significant correlations were found between nedd4-1 and MKn ($r = 0.623$, $P < 0.001$); as well as for MDn ($r = -0.418$, $P < 0.05$). In contrast, FA had no obvious correlation with nedd4-1 ($r = 0.065$, $P = 0.603$).

Conclusion: Our results provide convincing evidence that the expression of Nedd4-1 is up-regulated in human gliomas. The glioma patients with higher Nedd4-1 expression have a worse prognosis. Considering the diagnostic and prognostic significance of these molecular markers, MK appears to be a promising in vivo biomarker for glioma.

B-0937 11:18

Visually AcceSable Rembrandt Image (VASARI) assessment features predict GBM recurrence patterns

D. Xuesong, W. Zhang; Chongqing/CN (duxs1966@126.com)

Purpose: To estimate Visually AcceSable Rembrandt Image (VASARI) assessment features in predicting GBM recurrence patterns.

Methods and Materials: Sixty-five patients who suffered from GBM recurrence were included. Pre-surgery MRI and survival data were collected retrospectively. Semantic features were extracted using the VASARI feature-set criteria by three experienced neuro-radiologists independently. Recurrence patterns defined as "local" and "distant" with enhanced T₁WI at the time recurrence was proven. Survival analysis was done using the Kaplan-Meier analysis.

Results: Patients' recurrence was proven either by pathology or by the RANO criteria. Patient number of "local" was 49 (71.1%), while "distant" was 16

(28.9%). Clinical data such as age, Ki-67 and KPS showed no significant differences in the two groups. Semantic feature based on VASARI set indicated that tumour necrosis (F7), definition of the non-enhancing (F13), cortical involvement (F20), extent of resection of enhancing tumour (F26) and extent resection of nCET (F27) showed significant difference in unique recurrence patterns. Results revealed PFS was much longer when tumour necrosis ratio was low and patients suffered cortical involvement survived a shorter PFS and so it did in F26 and F27 subgroups.

Conclusion: VASARI features could predict GBM recurrence patterns and these features were associated with patients' PFS.

B-0938 11:26

Using multiple linear regression to investigate IDH1 gene mutation in glioma by joint application of DCE-MRI and DSC-MRI

W. Xu¹, J. Wen², Y. Li², ¹Shanghai, SH/CN, ²Shanghai/CN (xuweixingzi@163.com)

Purpose: To explore whether quantitative analysis of DCE-MRI and DSC-MRI could detect IDH1 gene status in glioma.

Methods and Materials: Patients (Dec. 2014-Oct. 2016) underwent DCE-MRI and DSC-MRI. The associations between each parameters and IDH1 gene status were analyzed by independent sample t test. The effective parameters were analyzed by multiple linear regression to calculate the prediction accuracy (PA).

Results: 57 LGG (43 IDH1 mutation type vs 14 IDH1 wild type) and 71 HGG cases (12 IDH1 mutation type vs 43 IDH1 wild type) underwent DCE-MRI. 56 LGG (45 IDH1 mutant type vs 11 IDH1 wild type) and 74 HGG cases (14 IDH1 mutant type vs 60 IDH1 wild type) had DSC-MRI. 120 patients took both scanning. All cases were pathologically confirmed. In LGG group, the K_{ep} , K^{trans} , TTP, Ve, rCBV, rCBF had statistical difference between IDH1 mutant and wild type ($P < 0.05$). AUC was 0.945, 0.904, 0.934, 0.827, 0.818 and 0.79, respectively. Combined rCBV, K_{ep} and K^{trans} obtained PA as high as 96.4%, OR= 9.22. Model: $y = 19.11 - 0.89 rCBV - 60.6 K_{ep} + 11.22 K^{trans}$. The K_{ep} , K^{trans} , Ve, MAXSlope, AUC, rCBV and rCBF had significant associations with IDH1 status in HGG ($P < 0.05$). AUC was 0.838, 0.816, 0.827, 0.832, 0.862, 0.826 and 0.774, respectively. Combined rCBV, K_{ep} and K^{trans} obtained 90.5% IDH1 PA, OR=42.34. Model: $y = 2.44 - 0.43 rCBV - 5.05 K_{ep} - 4.93 K^{trans}$.

Conclusion: Combined use of DCE-MRI and DSC-MRI could benefit the judgement of IDH1 gene mutation in glioma.

B-0939 11:34

Evaluation of the apparent diffusion coefficient in patients with recurrent glioblastoma under treatment with bevacizumab with radiographic pseudoresponse

T.A. Auer, F. Marini, M. Renovanz, M.A. Brockmann, Y. Tanyildizi; Mainz/DE

Purpose: Response assessment in neuro-oncology criteria (RANO) are used to assess response to first-line treatment of glioblastoma (GBM). Differentiation between response and pseudoresponse under treatment with bevacizumab (BVZ) remains challenging. This study evaluates ADC changes in patients with radiographic pseudoresponse under treatment with (BVZ).

Methods and Materials: Patients (n=40) with recurrent GBM under treatment with BVZ underwent MRI before, two and four months after treatment with BVZ. In patients with radiological pseudoresponse (n=11), ADC analyses were performed. Areas with T1 contrast enhancement (CE) decrease and FLAIR signal decrease were manually selected and compared with size and position-matched healthy contralateral brain parenchyma.

Results: Histogram-based ADC ($10^{-6} \times \text{mm}^2/\text{s}$) of these patients decreased significantly ($p < 0.005$) from baseline MRI (T1-CE, FLAIR: 1124.9±160.3, 1098.4±226.2, respectively) to 2 months (781.3±110.7, 783.3±103.3) and remained stable during 4 months (777.0±138.5, 784.4±155.4, all mean±SD), despite progressive disease. Mean ADC values of the healthy contralateral brain tissue remained stable ($p > 0.05$) (ADC values: baseline: 786.2±110.7, 2 months: 781.1±76.2, 4 months: 804.1±86.2).

Conclusion: Treatment of GBM with BVZ leads to a decrease of ADC values in areas of pre-treatment T1-CE/FLAIR signal hyperintensity to levels of comparable with normal brain tissue. ADC values remained normal, even when progressive tumour growth was reported.

B-0940 11:42

The predictive capacity of DWI vs perfusion imaging in response assessment of brain metastases following stereotactic radiosurgery

P. Arcuri¹, S. Rocca¹, G. Fodero¹, R. Mole¹, A. Destito¹, C. Bertucci², D. Lagana³; ¹Catanzaro/IT, ²London/UK (arpa@alice.it)

Purpose: The purpose of this study was to compare the predictive capacity of the apparent diffusion coefficient (ADC) with perfusion imaging distinguishing tumour recurrence or progression from treatment effects in brain metastasis, following stereotactic radiosurgery (SRS).

Methods and Materials: We retrospectively reviewed 32 brain metastases from 24 patients treated with SRS (3x10 Gy), imaged at baseline, one month

and three months post-treatment using DWI and perfusion imaging. At one year post-treatment or last available follow-up MRI, volume criteria determined final tumour response status. Gd-DTPA was injected intravenously at a rate of 4 mL/s. To assess differences in tumour blood volume during radiotherapy and among patients, all CBV maps were normalized to CBV values in the contralateral NAWM (rCBV). Youden's index test was used for statistical analysis to define optimal thresholds that distinguished responders from non-responders as well as sensitivity and specificity.

Results: Sensitivity of an increase in the ADC ratio to make an early (1 month) prediction of tumour control was 81.7% and specificity was 86.5%. When using rADC values of metastases measured in the follow-up of 3 months, sensitivity and specificity were 83.5 and 70.7%, respectively. Progressive lesions showed a significant reduction in rCBV values at the 1-month follow-up with a sensitivity and specificity of 85.3% and 80.0%. At the 3-month follow-up, sensitivity and specificity were 83.5 and 70.7%, respectively.

Conclusion: An increased rADC values and a significant reduction in rCBV values at the 1-month follow-up are indicators of good tumour control, and reflect the beneficial effect of SRS.

10:30 - 12:00

Room F2

Emergency Imaging

SS 1017

Non-traumatic emergencies

Moderators:

R.M.M. Hinzpeter; Zurich/CH

D.J.M. Tolan; Leeds/UK

K-18 10:30

Keynote lecture

D.R. Kool; Amsterdam/NL

B-0941 10:39

Simulation-based training for radiology professionals in the management of acute emergencies following contrast media reactions

R. Taoussi, Z. Qechchar, M. Fehdi, M. Mouhaoui, N. Touil, O. Kacimi, N. Chikhaoui, G. Lembarki; Casablanca/MA

Purpose: The purpose of our study was to assess the effectiveness of simulation-based medical education in the management of radiological emergencies among Radiologists and technicians and to compare this teaching method to the traditional theoretical clinical education.

Methods and Materials: Our study was a prospective, observational, single-centered study including the radiologist and technicians of Casablanca Ibn Rochd University Hospital including Professors in Radiology. The study undertaken in five phases: First a pre-test followed by a theoretical and practical training on emergencies following the administration of iodinating contrast medias, then the students were separated in two groups, one undergoing the medical simulation training and one that doesn't, and then a post-test concerning the two groups.

Results: 40 professionals were enrolled in the study: 20 (Group 1) benefited from the medical simulation and 20 (Group 2) who didn't. The pre-test results were comparable between the two groups (6,05/20 ± 2,68 for groupe 1 versus 5,88/20 ± 2,52 for groupe 2). The post test results were better for group 1 (18,83/20 ± 1,27 versus 17,13/20 ± 2,01 for group 2, $p < 0,0001$). The average satisfaction rate was 8,79/10 ± 2,17. The results of the satisfaction survey were in favor of the effectiveness of simulation-base medical teaching in the improvement of the theoretical knowledge (100%) as well as the medical reasoning when faced with a Radiological emergency (100%).

Conclusion: This study emphasis the benefit of simulation-based medical teaching and learning as an innovating teaching tool in front of Radiology emergencies.

B-0942 10:47

Clinical impact of iterative model reconstruction algorithm in a department of emergency radiology in a large series of patients

A. Pecorelli¹, D. Ippolito¹, A. de Vito¹, S. Lombardi¹, L. Riva², C. Talei Franzesi³, S. Sironi³; ¹Monza/IT, ²Missaglia/IT, ³Bergamo/IT (pecorelli.anna@gmail.com)

Purpose: To compare the radiation dose exposure of low dose Computed Tomography (CT) examinations using iterative model reconstruction (IMR) algorithm with standard CT equipment in an Emergency Radiology Department (ERD), with trauma center.

Methods and Materials: We reviewed more than 7000 CT scan examinations performed with new 256row CT scan (iCT Elite, Philips) combined with new IMR algorithm, in several anatomical district (i.e.: brain, thorax, abdomen and whole body) in patients referred to our ERD with different clinical emergency settings

(trauma, embolism, vascular disease). For each exam we analyzed the CT dose index (CTDI, expressed in mGray) and the dose length product (DLP, expressed in mGray.cm) and compared with dose of our previously CT scan equipment.

Results: The means values of CTDI were lower with IMR compared with our previous CT equipment: brain 59.3 vs 42.4 (-29%), thorax 8.8 vs 5.6 (-36%), abdomen 17.7 vs 6.3 (-64%) and whole body 16.8 vs 12.4 (-26%). In the same way the totals DLP were lower with IMR compared with standard CT: brain 949.2 vs 794.7 (-17%), thorax 324.3 vs 242.5 (-25%), abdomen 911.0 vs 361.5 (-60%) and whole body 1118.0 vs 893.0 (-20%).

Conclusion: The radiation dose can be significantly reduced using LDCT with IMR algorithm instead standard CECT for the diagnostic evaluation of patients admitted in an ERD.

B-0943 10:55

Age dependency of the Wells Score for pulmonary embolism

S. Nagel, I. Steffen, T. Elgeti; Berlin/DE (sebastian.nagel@charite.de)

Purpose: To evaluate a possible age dependency of the classic Wells Score (WS) in patients with suspected pulmonary embolism (PE).

Methods and Materials: 1000 consecutive patients from our emergency department were included into this IRB approved retrospective study. WS were re-calculated from electronic patient records. CT-pulmonary angiography (CTPA) served as standard of reference for the diagnosis of PE. Logistic regression models and receiver operating characteristic (ROC) curves were used to analyze the effect of patient age, D-Dimer, WS and INR on PE. Best cut-off values in ROC analyses were determined using Youden-Index.

Results: Pulmonary embolism was present in 25.6% of cases. Univariate ROC analysis showed a significant effect of D-Dimer (AUC=0.8; $p<0.001$) and WS (AUC=0.78, $p<0.001$). The multivariate logistic regression model showed a significant association of PE with D-Dimer ($p<0.001$), WS ($p<0.001$) and INR ($p<0.05$) whereas patient age showed a tendency to significance ($p=0.070$). A significant interaction was observed for WS and patient age ($p=0.006$). ROC analysis of the multivariate logistic regression model predictor revealed an AUC of 0.84 ($p<0.001$) with a sensitivity of 79.4% and a specificity of 73.5% for the best cut-off value.

Conclusion: The results of this exploratory study show a significant interaction of the patients' age and the Wells Score for the diagnosis of PE. This may indicate the use of age dependent cut-off values for WS to undertake CTPA.

B-0944 11:03

Ruling out acute kidney injury (AKI) with "admission" reno-caval ultrasound (ARCUS) examination

N. Attempati, A. Contegiacomo, E. Amodeo, M. Barone, A. Cina, R. Manfredi; Rome/IT (nicoatt89@gmail.com)

Purpose: Acute Kidney Injury (AKI) requires fast and effective diagnostic workup, but no tools are available for ruling out all possible aetiologies (pre-renal/renal/post-renal) at one time. This study aims to evaluate whether examination of Inferior Cava Vein (IVC) collapsibility (hydration index) and hydronephrosis (obstruction index), with the integration of doppler Resistivity Index (RI), as first diagnostic tool (ARCUS), allows AKI aetiology identification.

Methods and Materials: from January 2016 to July 2017, ARCUS examination was prospectively performed on 30 patients with sudden oligo-anuria or estimated Glomerular Filtration Rate (eGFR) reduction. Maximal inspiration IVC collapse $>50\%$ was considered suggestive of pre-renal AKI and presence of hydronephrosis suggestive of post-renal AKI; in all the other cases RI >0.70 was considered diagnostic for renal AKI. ARCUS examination outcome was compared with final medical diagnosis to assess tool specificity and sensitivity.

Results: 17/30 patients had IVC collapse $>50\%$, with 85.7% specificity and 93.7% sensitivity for pre-renal AKI; hydronephrosis was observed in 10/30 patients, with a 100% specificity and sensitivity for post-renal AKI. In 3/30 patients RI evaluation was performed: 2 patients had RI >0.70 and 1 <0.70 (pre-renal AKI), with a sensitivity and specificity of 50% and 100% respectively for Renal AKI.

Conclusion: our pilot study suggests that ARCUS examination is a very good tool for AKI initial and rapid evaluation, with excellent specificity and good sensitivity.

B-0945 11:11

When ultrasound is not enough: predicting downstream utilisation of CT after ultrasound in patients with acute abdomen

K. Rippel, D. Ordu, L.-P. Rollandi, T. Kleffel, C. Scheurig-Muenkler, T. Kröncke, F. Schwarz; Augsburg/DE (Katharina.Rippel@klinikum-augsburg.de)

Purpose: To analyse whether markers of systemic inflammation predict the utilisation of additional CT after ultrasound in ED patients presenting with acute abdominal pain.

Methods and Materials: We analyzed 506 patients who presented to the ED over a three-month period with acute abdominal pain and were referred for an

ultrasound examination of the abdomen. We analysed electronic health records for prior medical history and laboratory tests of systemic inflammation (WBCC and CRP) at the time of presentation. Furthermore, all abdominal CT scans performed within a 36-hour window following the ultrasound exam were registered. Receiver-Operating-Characteristic (ROC) statistics were used to analyse the predictive value of CRP and WBCC for additional utilisation of CT. We performed subgroup analyses for patients without recent hospital admission and with known malignancy.

Results: 71 patients were excluded due to various reasons. Of the remaining 435 patients, 65 (15%) underwent additional abdominal CT. Differences in WBCC and CRP between patients who underwent CT vs. those who did not were highly significant (WBCC: 12.4 [9.2;17.6] vs. 9.6 [7.5;12.9]; CRP: 8.2 [0.93;20.4] vs. 1.1 [0.28;6.0], both $p<0.01$). On ROC analysis, WBCC and CRP had similar moderate predictive values for subsequent utilisation of additional CT (AUC: 0.69±0.04 vs. 0.66±0.04, $p=0.66$). Predictive values were highest in the subgroup of patients without hospital admission in the preceding 12 months (AUC: 0.89±0.06 vs. 0.75±0.05, $p=0.06$).

Conclusion: Across all patients presenting with acute abdomen, CRP and WBCC has moderate predictive value for subsequent CT utilisation after ultrasound. However, in patients without recent hospital admission, predictive value is excellent.

B-0946 11:19

How accurate are we and how can we get better in diagnosing acute appendicitis by unenhanced multidetector computed tomography: a large meta-analysis and literature review

A. Mishra, R. AlSaady, S. Patel, S.A. Mahemood, T.S. Abdulla, A.A.W. Hussain; Doha/QA (dranjumish@yahoo.com)

Purpose: To analyse CT criteria and determine best CT parameter(s) for diagnosing acute appendicitis.

Methods and Materials: Retrospective analysis of patients diagnosed with acute appendicitis was done. 800 patients underwent unenhanced abdominal CT (UACT) within 24-48 hours of onset of acute pain, were analysed (male 563 (70.4%); female 237 (29.6%); mean age 36 years; range 5-86 years). UACT assessment of appendix was based on: appendix diameter, periappendiceal inflammatory fat-stranding (PIFS), fluid collection, free air and appendicolith.

Results: Appendiceal diameter correlated to the inflammation of the appendix ($p=0.001$) with sensitivity (Sn)=94.4%, specificity (Sp)=90.3%, negative predictive value (NPV)=93.2% and positive predictive value (PPV)=91.6%. 767 (95.9%) patients had appendiceal diameter ≥ 7 mm, of which 43 (5.6%) did not have histopathological diagnosis of acute appendicitis. The patients with acute appendicitis had a mean appendiceal diameter of 8.5 mm (range 6-16; SD 2.7) whereas patients with normal appendix had mean appendix diameter of 4.1 mm (range 2-6; SD 0.8). There was correlation between CT criteria for presence of PIFS, fluid, appendicolith and inflammation of the appendix ($p=0.01$). In patients with normal appendix, mild-to-moderate PIFS was noted in 16 (48.5%) and severe PIFS in 10 (30.3%) patients. In patients with acute appendicitis, PIFS was observed in 682 (85.3%) patients with Sn=96.2%, Sp=87.4%, NPV=92.8% and PPV=89.6%. None of the patients with normal appendix had appendicolith whereas 309 (38.6%) with acute appendicitis demonstrated appendicolith with Sn=96.1%, Sp=78.2%, NPV=76.7%, PPV=74.3%. 17 (2.1%) had periappendiceal fluid. 6 (0.8%) had extraluminal air around the appendix out of which 1 (5.9%) did not have histopathological perforation. Combining appendiceal diameter and PIFS yielded Sn=98.4%, Sp=99.8%, NPV=94.5% and PPV=99.2%.

Conclusion: Appendiceal diameter ≥ 7 mm and PIFS have high sensitivity but relatively lower specificity individually, but when combined together has almost 100% specificity with 99.2% positive predictive value.

B-0947 11:27

Comparing diagnostic performance of ultra-low-dose CT compared to abdominal plain films

J. Lee¹, S. Bruni¹, S. Kennedy¹, V. Swami¹, E. Chen¹, R. Menezes¹, D. Borrego², C. Lee², P. Rogalla¹; ¹Toronto, ON/CA, ²Rockville, MD/US (ljjohn.lee@mail.utoronto.ca)

Purpose: To determine relative diagnostic performance of ultra-low-dose CT (ULD-CT) and abdominal plain films (APF) with regard to sensitivity, specificity, positive predictive value (PPV) and negative predictive value (NPV) in the emergency setting.

Methods and Materials: As per new institutional protocol, all patients with acute abdominal pain who would be referred to APF were automatically converted to ULD-CT. Target exposure values were set to achieve 1 mSv equivalent exposure to a standard 75 kg individual. Our study examined 196 consecutive ULD-CT ordered since initiation of the new protocol and 196 consecutive APF from the emergency department prior to inception of new protocol over a period of 9 weeks. Final diagnosis was compared to the gold standard diagnosis comprising of lab values, clinical notes, additional imaging tests, endoscopy, and surgery. Each patient was followed up for a minimum of one month.

Results: There were no statistical difference between age (63.3 vs 60.8, $p=0.5$) and gender (49% vs 51% male, $p=0.7$) between ULD-CT and APF groups. When comparing ULD-CT to APF, sensitivity (0.86 vs 0.40, $p<0.01$), specificity (0.98 vs 0.81, $p=0.02$), PPV (0.94 vs 0.50, $p<0.01$) and NPV (0.92 vs 0.74, $p=0.02$) were higher for ULD-CT.

Conclusion: ULD-CT has statistically higher sensitivity, specificity, PPV and NPV compared to APF. ULD-CT has the potential to replace APF by delivering significantly better diagnostic information despite a radiation dose profile comparable with conventional APF. This is the largest study to date comparing the diagnostic performance of ULD-CT compared to APF.

B-0948 11:35

CT signs of bowel necrosis in CL-SBO

C. Rondenet¹, I. Millet², L. Corno¹, I. Boulay Coletta¹, P. Taourel², M. Zins¹; ¹Paris/FR, ²Montpellier/FR

Purpose: To identify computed tomography (CT) findings associated with bowel necrosis in patients with surgically confirmed strangulating closed-loop small-bowel obstruction (CL-SBO) due to adhesions or internal hernia.

Methods and Materials: This retrospective study was approved by our institutional review board and informed consent was waived. To identify specific signs of bowel necrosis, two gastrointestinal radiologists performed blinded, independent, retrospective reviews of 41 CT studies from consecutive patients who had CL-SBO due to adhesions or internal hernias and who underwent surgery within 48 h. Based on surgical and pathological findings, patients were classified as having reversible ischaemia or histologically documented necrosis. Univariate statistical analyses were performed to assess associations between CT signs and bowel necrosis. K statistics were computed to assess interobserver agreement.

Results: We included 25 (61%) women and 16 (39%) men with a median age of 79 years. Bowel necrosis was found in 25/41 (61%) patients and ischaemic but viable bowel in 16/41 (39%) patients. Increased unenhanced bowel-wall attenuation was the only CT finding significantly associated with bowel necrosis ($P=0.0002$). This sign had 58% (95%CI, 37-78) sensitivity and 100% (95% CI, 79-100) specificity for necrosis. Interobserver agreement was fair (0.59; 95%CI, 0.37-0.82).

Conclusion: Increased unenhanced bowel-wall attenuation is specific of bowel necrosis and should lead to prompt laparotomy for bowel resection.

B-0949 11:43

Contribution of ultra low-dose CT in extremities trauma

F. Snene, T. Addala, J. Greffier, P. Viala, J.P. Beregi, A. Larbi; Nimes/FR (snefefhmi@gmail.com)

Purpose: To evaluate the diagnostic power of ultra-low-dose CT (ULD-CT) of the extremities (wrist/hand or ankle/foot) compared to the X-ray in emergency room.

Methods and Materials: An ULD acquisition without contrast medium injection as well as an X-ray of the injured extremities were performed in 76 patients consulting the emergency department of our institution from March to August 2017. Raw data were reconstructed with Sinogram-Affirmed-Iterative-Reconstruction (SAFIRE, Siemens) with soft tissue (I30f) and bone (I70f) reconstructions kernel. The subjective analysis (image quality, diagnostic quality, characterization of the lesions with confidence level) was performed by double blind reading (1 senior and 1 junior radiologist). The diagnostic performance of the ULD-CT and X-ray were compared.

Results: Effective dose for ULD-CT were lower than the recommendations of the IRSN 2012(National Institute for Radiation Protection and Nuclear Safety). Kappa Cohen test agreement among the two observers for the evaluation of traumatic lesions was substantial, ranging from 0.8 to 0.95. The analysis of data showed the absence of inferiority of the ULD-CT in the detection of traumatic lesions comparatively to the X-ray. The ULD-CT showed its superiority in the characterization of associated anomalies ($p<0.05$). Readers recorded a significantly high score of diagnostic confidence level for ULD-CT compared to X-ray ($p<0.05$).

Conclusion: ULD-CT with iterative reconstructions allowed a reliable study of extremities trauma patients with an equivalent or lower irradiation dose than plain X-ray. Reproducibility is independent of the level of experience of the readers.

B-0950 11:51

Diagnostic performance of quiescent interval single-shot (QISS) non-contrast MRA at 3 Tesla for the diagnosis of acute lower limb ischaemia

Y. Raqab¹, A. Al Marakby¹, H.M. Hamza², A. Hasani¹; ¹Cairo/EG, ²London/UK (yragab61@hotmail.com)

Purpose: To assess the diagnostic performance and limitations of ECG-gated non-contrast-enhanced quiescent interval single-shot (QISS) magnetic resonance angiography at a magnetic field strength of 3 Tesla in patients with acute peripheral arterial occlusive disease (PAOD).

Methods and Materials: 29 patients with manifestations of acute lower limb ischaemia, referred for lower limb gadolinium-based contrast enhanced magnetic resonance angiography (MRA) were included. Imaging was performed on a 3T whole-body MR. Non-contrast MRA series using QISS technique were initially performed. Image quality and stenoses diameters were compared to contrast-enhanced MRA (CE-MRA) as standard of reference. Two blinded readers rated the image quality and the degree of stenosis for both ECG-gated QISS and CE-MRA in 26 predefined arterial vessel segments on 5-point Likert scales.

Results: Compared with CE-MRA, QISS MRA technique showed high sensitivity (93%), specificity (95%), positive (95.1%), and negative predictive value (96%) for the detection of significant ($\geq 50\%$) stenosis or occlusion. Interreader agreement for stenosis and occlusion assessment of both QISS and CE-MRA was excellent (κ -values of 0.94 and 0.95, respectively). As compared to CR-MRA, image quality of QISS was significantly lower for the distal aorta, the femoral and iliac arteries (each with $p<0.01$), while no significant difference was found in the popliteal ($p=0.07$) and lower leg arteries ($p=0.9$).

Conclusion: Non-contrast QISS MRA has been shown to be technically comparable to CE-MRA in the assessment of femoropopliteal and leg arteries; however, it has limitations during evaluation of the lower aorta and iliac arteries.

10:30 - 12:00

Room D

Musculoskeletal

SS 1010

Shoulder imaging and intervention

Moderators:

J.-L. Drapé; Paris/FR
N.N.

B-0951 10:30

Inferior glenohumeral vertical distance: a novel radiographic marker better suited for detection of rotator cuff tears involving the infraspinatus tendon

M. Alfaqih, S. Soni, S. Flacke, Y. Andrabi, D. Elentuck, R. French; Burlington, MA/US (mohammad.alfaqih@lahey.org)

Purpose: Evaluate the association between the radiographically determined inferior glenohumeral vertical distance (IGHVD) and rotator cuff tears (RCT) involving infraspinatus (IS) tendon and compare the sensitivity and specificity of acromiohumeral distance (AHD) and IGHVD for RCT involving IS tendon.

Methods and Materials: 140 patients with MRI proven full thickness rotator cuff tear were included after they met the inclusion and exclusion criteria. Patients were divided into two groups, group A: RCT involving full or partial IS tears, and group B: RCT not involving IS. Radiographs were analysed blinded to MRI findings. IGHVD determined by measuring vertical distance from anatomical neck to inferior glenoid level in anteroposterior (AP) view; distance of more than 2mm was considered positive. AHD was assessed by measuring vertical interval between inferior border of acromion process and humeral head in (AP) view; distance less than 7 mm was considered positive.

Results: Group A included 89 patients and Group B involved 51 patients. A strong association was found between IGHVD and rotator cuff tears involving infraspinatus tendon ($p < 0.001$). IGHVD was found to have increased sensitivity, PPV and NPV (66%, 92%, 60%, respectively) compared to AHD (20%, 85%, 40%, respectively). The specificity of both was comparable (90% for IGHVD and 94% for AHD).

Conclusion: There is a strong association between radiographically determined IGHVD and infraspinatus tear and is more sensitive than AHD.

Author Disclosures:

S. Flacke: Consultant; BTG International Ltd, Surefire Medical, Inc, Koninklijke Philips BV, XACT Robotics.

B-0952 10:38

Imaging of aponeurotic expansion of supraspinatus tendon by 3.0 T MRI and its association with biceps brachii long head, supraspinatus and subscapularis tendon pathologies

Z. Akkaya, H. Bas, D. Oztuna, G. Sahin; Ankara/TR (zehraakkaya@gmail.com)

Purpose: The purpose of this study was to identify the prevalence of the aponeurotic expansion of the supraspinatus tendon (SSa) by 3.0 T MRI and to search for possible associations with the pathologies of the supraspinatus (SS), biceps brachii long head (BB) and subscapularis (Sub) tendons.

Methods and Materials: A total of 154 patients and 157 shoulders (3 cases with bilateral examinations) between the ages of 18 and 45 years, examined by 3.0 T scanner between July 2011 and March 2017, were re-examined for the presence of SSa. When present, it was further categorised according to its

size. The exclusion criteria were history of shoulder trauma, surgery, deformity, inflammatory arthropathy, end-stage rotator cuff disease, major systemic illness, and technically inadequate imaging. The pathologies of BB, SS and Sub tendons were evaluated separately and using Mann-Whitney U and Kruskal-Wallis tests tendon pathologies were compared to SSa types

Results: A total of 82 male and 72 female cases with a mean age of 34 (± 8.2) were included. There were 126 cases (80.3%) without a visible SSa and the incidence of BB pathologies in this group was significantly lower than the other types where a visible SSa was noted ($p < 0.05$). No significant correlations were found between pathologies of SS and Sub and SSa types. For pathologies of all three tendons, age was found to be a significant variable ($p < 0.01$).

Conclusion: BB tendon pathologies were significantly more common in cases with SSa which might indicate a risk factor on its own.

B-0953 10:46

Reliability of strain elastography in the supraspinatus tendon

K. [Bragø](#); [Odense M/DK](#) (kabr2@ucl.dk)

Purpose: Sonoelastography (SEL) is used to measure tissue elasticity, and individual studies show good reliability; however, this study investigates the reliability of SEL, when used in the supraspinatus tendon. The aim of this study was to test the intra-examiner reliability of a novel SEL protocol for supraspinatus tendon elasticity in participants with supraspinatus tendinosis diagnosed with MRI and in asymptomatic participants.

Methods and Materials: Ten participants with no shoulder complaints and 10 participants with supraspinatus tendinosis were examined independently by the project leader (KB). GE LOGIQ S7 fitted with a quasi-static strain imaging software was used to create elastograms as ratios between the supraspinatus tendon and reference regions of muscle (deltoid), and a gel pad, respectively. Elastograms were also evaluated qualitatively according to the structure (homogeneous, relatively homogenous, and heterogeneous), the colour (blue, blue with 1-25% green, blue with 26-50% green, green with 1-25% blue, and green), and the number of lesions was counted.

Results: The intra-class correlation (ICC 2.3) of measurements with the reference of muscle was excellent 0.92 (95%CI: 0.80-0.97), as well as for the gel pad 0.87 (95%CI: 0.67-0.95) and number of lesions 0.98 (95%CI: 0.96-0.99). Moderate kappa (k) was found for estimation of colour ($k = 0.58$) and structure ($k = 0.60$).

Conclusion: Intra-rater reliability was moderate to excellent when a standardized procedure was applied for measuring tissue stiffness in the supraspinatus tendon. Future studies should test inter-rater reliability in addition to validation against conventional ultrasound and MRI.

B-0954 10:54

Evaluation of tendinopathy of the long head of the biceps tendon by strain and shear wave elastography

M.H. Sahan, M. Inal, V. [Buruldav](#), T. Kultur; [Kirikkale/TR](#) (vedoctor@hotmail.com)

Purpose: The purpose of this study was to investigate strain (SE) and shear wave elastography (SWE) characteristics of the long head of the biceps tendon (LHBT) tendinopathies in comparison with magnetic resonance imaging (MRI).

Methods and Materials: Twenty patients with a diagnosis of tendinopathy and twenty healthy subjects with a normal LHBT in MRI were enrolled. A total of 40 shoulders were examined prospectively by SE and SWE. LHBT SE color mapping was divided into four types in accordance with elasticity designs: type I predominantly blue (hardest tissue), type II predominantly blue-green (hard tissue), type III predominantly green (intermediate tissue), type IV predominantly green-yellow-red (soft tissue). Quantitative measurements of LHBT hardness with SWE were analyzed in kilopascals (kPa).

Results: SE images from the tendinopathy group: transverse: type I (24%), type II (50%), type III (25%); longitudinal: type I (15%), type II (75%), type III (10%); control group images: transverse: type II (10%), type III (55%), type IV (35%); longitudinal: type II (10%), type III (55%), type IV (35%). SWE values: transverse: 38.32 ± 7.2 kPa, 18.6 ± 3.1 kPa and longitudinal: 39.42 ± 7.4 kPa, 20.62 ± 4.6 . There was a statistically significant difference in terms of elasticity patterns between the tendinopathy and control groups ($p < 0.001$). The receiver operating characteristic curve analysis was perfect and a cut-off value of transverse, 25.8 kPa, longitudinal, 24.6 kPa shear had very high sensitivity and specificity for tendinopathy.

Conclusion: SE and SWE may be useful diagnostic tools for LHBT tendinopathy when considering usability, cost effectiveness and patient preference compared to MRI.

B-0955 11:02

How, when, why in magnetic resonance arthrography: an international survey by the European Society of Musculoskeletal Radiology

D. [Albano](#)¹, C. Messina², A. Tagliafico³, L.M. Sconfienza²; ¹Palermo/IT, ²Milan/IT, ³Genoa/IT (albanodomenico@me.com)

Purpose: To perform an online survey among all members of the European Society of Musculoskeletal Radiology (ESSR) to understand how, when, and why magnetic resonance arthrography (MRA) is used in clinical practice.

Methods and Materials: We administered an online survey to all 1,550 members of the ESSR about the use of MRA in clinical practice asking ten different questions. Subgroup analysis was performed between general and orthopaedic hospitals. Mann-Whitney U and χ^2 statistics were used.

Results: A total of 148 answers were included in our analysis, representing 9.5% (148/1,550) of ESSR members. A median of 3,000 (25th-75th percentiles: 1,567.5 - 5,324.5) musculoskeletal MR examinations per single institution were performed in 2016 and a mean of 125.5 MRAs (50.75 - 249). Ratio between MRA and musculoskeletal MR was 4.7% (1.6%-9.0%). Using MRA, the most investigated joint was the shoulder followed by the hip. The most common indications were the evaluation of instability, labrum, and rotator cuff. Fluoroscopy represented the preferred guidance to inject joints in 61.0% of cases. A self-prepared mixture of gadolinium and saline solution is preferred in general hospitals, while pre-diluted gadolinium-based syringes are mainly used in orthopaedic hospitals ($P = .010$). The number of MRA performed at orthopaedic hospitals (284; 83.75-449.50) was significantly higher ($P = .006$) than that performed at general hospitals (115.50; 44.75-234.25).

Conclusion: One out of twenty MR examinations is a MRA, with higher prevalence in orthopaedic hospitals. The shoulder and the hip are the most investigated joints. Instability and labrum are the most common reasons to perform MRA.

B-0956 11:10

The diagnostic accuracy of diffusion-weighted imaging for the detection of partial-thickness rotator cuff tears

O. [Mansour](#); G. Jafarinosar; [Tehran/IR](#) (mansour.omid@yahoo.com)

Purpose: The aim of our study was to investigate the accuracy of DWI sequence in diagnosis of partial thickness tears of rotator cuff tendon in compare with routine sequences.

Methods and Materials: We collected the data of 60 patients who referred to our imaging centre for shoulder MRI. Imaging was performed with a 1.5 Tesla MRI unit (Ingenia CX, Philips medical systems). The following imaging protocol was used: coronal oblique T2W TSE (TR/TE 3200/90ms), thickness 3.5mm, coronal oblique T1W TSE (TR/TE 460/16ms), thickness 3.5mm, coronal, sagittal and axial PD fat suppressed (TR/TE 1800/24ms), thickness 3.5mm. All sequences were acquired with a fov 16cm and matrix size 256x228. DWI sequence (b factors 0 and 600s/mm²) was performed in coronal oblique plane (TR/TE 3200/60ms), thickness 3.5mm, fov 20cm, matrix size 128x128. Of 60 patients, 32 patients underwent shoulder arthroscopy within 3 months after MR examination. Two radiologists reviewed MRI studies.

Results: Imaging findings at MRI studies and arthroscopic results were compared in 22 of 32 patients were diagnosed with partial thickness tears in arthroscopy. The results showed DWI sequence was superior to routine sequences in diagnosing partial thickness tears of rotator cuff.

Conclusion: According to the results of our study, DWI sequence plays a effective role to diagnose the partial thickness tears of rotator cuff than routine sequences (DWI accuracy 88%, routine sequences accuracy 76%).

B-0957 11:18

Ultrasound imaging of muscle contraction of the tibialis anterior in patients with facioscapulohumeral dystrophy

K. [Gijbertse](#)¹, R. Goselink¹, S. Lassche¹, M. Nillesen¹, A. Sprengers¹, N. Verdonschot^{1,2}, N. van Alfen¹, C.L. de Korte¹; ¹Nijmegen/NL, ²Enschede/NL (kaj.gijbertse@radboudumc.nl)

Purpose: The pathophysiological mechanisms leading to muscle weakness in most neuromuscular disorders are not completely understood. Dynamic ultrasound imaging in combination with a speckle tracking method is introduced to visualize and quantify muscle deformation.

Methods and Materials: Ultrasound image sequences were acquired from 16 legs (4 patients with facioscapulohumeral dystrophy (FSHD) and 4 healthy controls) during voluntary contractions of the tibialis anterior muscle. A cross correlation method was applied to estimate muscle tissue deformation from the ultrasound images. The resulting deformation patterns were compared with muscle ultrasound echo intensity analysis (a measure of fat infiltration and dystrophy) and clinical outcome measures.

Results: Ultrasound speckle tracking revealed a distinctively different tissue motion patterns between patients with peroneal weakness and healthy controls. Patients with severe peroneal weakness showed a homogeneous displacement pattern of the tibialis anterior with small motion of the central

aponeurosis (2.1 ± 1.0 mm), contrary to healthy subjects that showed a large non-uniform displacement (9.7 ± 1.8 mm), increasing from the periphery of the muscle to the central aponeurosis. Furthermore, the difference in muscle deformation patterns of patients shows good agreement with clinical measures (e.g. decrease in force generation) and ultrasound echo intensity analysis.

Conclusion: This work provides a tool to quantify muscle motion and evidence of changing functional behaviour of the affected muscles in FSHD patients. The quantitative characterization of muscle contraction provides new insights into the way pathologic muscle tissue deforms, leading to a better understanding of the underlying mechanisms related to weakness in muscle disease.

B-0958 11:26

Adhesive capsulitis of the shoulder: a new ultrasound-guided and rehabilitation multidisciplinary treatment protocol to restore shoulder girdle kinesis

G. Ferrero, V. Amico, F. Lacelli, E. Fabbro, N. Perrone, G. Serafini; *Pietra Ligure/IT (giulio.ferrero@gmail.com)*

Purpose: To examine the effectiveness in short and medium terms of a new multidisciplinary treatment protocol (ultrasound guided and rehabilitative) of adhesive capsulitis of the shoulder (AC).

Methods and Materials: 12 patients with clinical diagnosis of AC were treated with a protocol including ultrasound-guided capsular hydrodistension, intra-articular steroid and hyaluronic acid (HA) injection, suprascapular and axillary nerves US-guided block and physiotherapy (PKT) within two hours. Intensive PKT was then administered for 20 sessions. Evaluation was made before and after the first treatment, at the fifth, tenth and twentieth session using Constant-Murley scale and measuring ROM. The results were compared with a control group of 15 patients treated without nerve block. T test was used to evaluate differences in Constant-Murley scale and ROM before and after treatment.

Results: Prompt ROM improvement ($P < 0.001$) was observed after the first treatment session in both groups, with better C-M score and ROM values in patients who underwent nerve block. In both groups, a gradual and constant ROM recovery was observed.

Conclusion: The study demonstrates that the proposed treatment can be effective, with better results compared to conventional treatment both in terms of ROM recovery and pain. AC can be treated with a multidisciplinary approach to obtain a shorter recovery time and better clinical results.

B-0959 11:34

US-guided percutaneous double needle lavage in the treatment calcific tendinopathy of the rotator cuff performed with or without US-guided block of the suprascapular nerve

D. Maietini, R. Torre, S. Mosca, A. Rebonato; *Perugia/IT (danielemaietini@gmail.com)*

Purpose: To compare the outcome of ultrasound-guided percutaneous double needle irrigation (US-PICT) in the treatment of calcific tendinopathy of the rotator cuff performed with or without ultrasound-guided block of the suprascapular nerve in terms of pain control and shoulder mobility.

Methods and Materials: We retrospectively enrolled 47 patients treated with US-PICT during 2015 and 2016 diagnosed with calcific tendinitis of the rotator cuff. Twenty-seven patients were treated with US-PICT alone while the remaining 20 were treated after the ultrasound-guided block of the suprascapular nerve of the same shoulder, using Lidocaine. The Visual Analogy Scale (VAS) and the Constant score were assessed before and immediately after the procedure and at 7 days, one and three months.

Results: Overall patients the VAS and Constant scores showed a significant improvement after the procedure, during the follow-up ($p < 0.0001$). The block group showed a significant reduction of the VAS immediately after the procedure with respect to the non-block group (mean values 4,4 vs 5,6) ($p = 0.01$). At one week, one and three month follow-up there was no significant difference between groups considering VAS score ($p > 0.05$). Constant score values didn't show any statistical difference during follow up between the block and non-block group. No major or minor complication were encountered.

Conclusion: Ultrasound-guided percutaneous double needle irrigation in the treatment calcific tendinopathy confirmed to be effective both considering pain control and shoulder recovery. Ultrasound-guided block of the suprascapular nerve is effective in peri-procedure pain control while doesn't improve shoulder mobility recovery.

B-0960 11:42

Another breach in the wall: efficacy of sodium hexametaphosphate (SHMP) solution vs simple saline in percutaneous treatment of calcific tendinitis of the shoulder: 6-months follow-up

S. Mariani¹, F. Bruno¹, S. Quarchioni², E. Cannizzaro¹, C. Gianneramo¹, F. Arrigoni¹, L. Zugaro¹, A. Barile¹, C. Masciocchi¹; ¹L'Aquila/IT, ²Teramo/IT (*mari.silvia@hotmail.it*)

Purpose: Calcific tendinitis of the shoulder is a common cause of pain and articular disability. The aim of our study was to evaluate the efficacy of percutaneous US-guided lavage in treatment of calcific tendinitis using a sodium hexametaphosphate (SHMP) solution (0.5%), in comparison with the same technique using simple saline.

Methods and Materials: We evaluated 32 symptomatic patients with calcific tendinitis of the rotator cuff. Patients were randomly divided into 2 groups and treated by percutaneous fragmentation and lavage using SHMP (Group 1, 16 patients) or simple saline (Group 2, 16 patients). In all patients, clinical and instrumental evaluation morphologic changes were assessed before and 2 weeks, 1 month and 6 months after treatment. Imaging evaluation included conventional radiography and ultrasound, while clinical follow-up was performed using Constant Shoulder Score for functional improvement and VAS Score for pain.

Results: In Group 1, 11 patients showed almost complete dissolution of calcifications (68,75%), while the remaining 5 just partial dissolution (31,25%); of these, 3 (60%) showed subtotal dissolution after 1 month. In Group 2, 9 patients (56,25%) showed almost complete dissolution and partial in the remaining 7 (43,75%) ($p \leq 0.05$), of these 1 patient (14,29%) showed subtotal dissolution after 1 month. VAS and Constant Score showed a significant improvement in 100% of patients in both groups ($p \leq 0.05$) after 4 weeks and 6 months.

Conclusion: The use of SHMP showed superior results compared to the treatment with simple saline solution especially in single session treatment and short-term follow-up. After 6 months in fact, both groups showed matched results.

B-0961 11:50

Improvement of image quality and diagnostic confidence using Smart MAR - a projection-based CT protocol in patients with orthopaedic metallic implants in hip and shoulder

F. Feldhaus, G. Böning, U. Fehrenbach, J. Kahn, B. Hamm, F. Streitparth; *Berlin/DE (felix.feldhaus@charite.de)*

Purpose: To determine whether the metal artifact reduction tool - a three-stage, projection-based, postprocessing algorithm - improves subjective and objective image quality and diagnostic confidence in patients with orthopaedic implants.

Methods and Materials: 20 patients with orthopaedic screws/replacement of hip or shoulder were included. CT scans were performed on a single-source, 64-row multislice CT scanner (MSCT, Evolution, GE Healthcare). CT raw data were postprocessed using Smart MAR. Image quality of standard and Smart-MAR-based reconstruction series was evaluated both quantitatively (in ROIs) and qualitatively (two independent raters) and compared to standard reconstructions. Dose was analyzed in dose-length products (DLP) and computed tomography dose indices (CTDIvol).

Results: Smart MAR reconstructions of shoulder and hip (each $n = 10$) showed significantly reduced attenuation and noise of regions adjacent to metallic implants (all $p < 0.005$). Smart MAR improved subjective visualization of adjacent trabecular and cortical bone and adjacent soft tissue (all $p < 0.02$). Subjective diagnostic confidence was also improved in hip ($p = 0.01$) and shoulder region ($p = 0.02$). There was no significant improvement in signal-to-noise ratio (SNR; $p < 0.72$). Mean DLP of hip region was 515,7 SD 192,2 HU (shoulder: 295,6 SD 144,0), mean CTDIvol 13,5 SD 4,6 (shoulder 13,7 SD 6,4).

Conclusion: Smart MAR significantly improved image quality of hip and shoulder CT scans even in the presence of severe artifacts, resulting in higher diagnostic confidence. Especially for the evaluation of periprosthetic tissues of the hip and shoulder, this automated postprocessing technique appears to be well suitable for clinical routine without increasing radiation exposure compared to standard CT scans.

10:30 - 12:00

Room K

Radiographers

SS 1014

Quality issues in ultrasound and CT

Moderators:

O.P. Bansal; New Delhi/IN
A. England; Salford/UK

B-0962 11:18

Reduction of contrast agent using virtual monochrome image in haemodynamics aortic phantom

F. Washizuka, T. Kitamura, T. Hatakeyama, H. Nakano; Tokyo/JP
(fuyuki.washizuka@med.toho-u.ac.jp)

Purpose: It is possible to reduce the contrast agent in the fixed type phantom using virtual monochrome images (VMI). Consider whether reduction of the amount of contrast agent is possible even using haemodynamic aortic phantom.

Methods and Materials: Using the CT scanner (Somatom Definition Flash; Siemens Healthcare), haemodynamic phantom was scanned in the dual energy scan (80-Sn140kV). The kernel used for image reconstruction is "B30". Injection condition was 24mg/ml/kg/s (assuming a weight of 60 kg, 370mg/ml syringe, and 10-second injection). After that the contrast agent was reduced by 10% and scanned. The reconstructed images are 54 keV, 57 keV, 60 keV, 63 keV, 66 keV, 69 keV, and 72 keV and MIX images. Contrast to noise ratio (CNR) and shape reproducibility was calculated, and visual evaluation was performed.

Results: The CNR was highest at around 66 keV, and CT value was increased at lower keV. Using VMI (66keV), if the CNR is made equivalent, the contrast agent can be reduced by 20% and equivalent images can be obtained. Considering the noise of the background and using further low keV, the CT value increases, it is possible to reduce 40% of the contrast agent.

Conclusion: Using VMI in not only fixed phantom but also haemodynamic phantom, we could reduce contrast agent by up to 40%.

B-0963 10:30

Development and reliability of an ultrasound protocol to evaluate quadriceps muscle mass and diaphragm structure: a pilot study

A. André¹, J. Pinto², D. Oliveira², C. Aguiar², S. De Francescos², A. Oliveira², A. Marques², P. Martins²; ¹Coimbra/PT, ²Aveiro/PT
(alexandra.andre@estescoimbra.pt)

Purpose: This study aimed to evaluate the intra and inter-operator reliability of an ultrasound (US) protocol, to assess quadriceps muscle mass and diaphragm structure in healthy people, for future monitoring of patients with respiratory disease.

Methods and Materials: Twelve volunteers (6♀, 31.8±10.6 years; BMI=23.4±3.7 kg/m²) participated. An US equipment (Logiq P6 PRO, GE) with a multifrequency linear probe (11L) was used. Three measures of Quadriceps (Q_{TK}) and Rectus Femoris thickness (RF_{TK}), RF cross sectional area (RF_{Area}), bilateral diaphragmatic thickness at maximal inspiration (D_{TKI}) and at end expiration (D_{TKE}) were obtained by one operator. Six volunteers were randomly evaluated by two operators. Mann Whitney test was used to assess differences between inspiration and expiration and the right and left hemi-diaphragm. The Intraclass Correlation Coefficient ($ICC_{2,1}$) was used to explore reliability.

Results: Mean RF_{TK} were 1.72cm, 8.19cm² for RF_{Area} and 3.23cm for Q_{TK} . Significant differences were found between D_{TKI} and D_{TKE} both at right (0.31±0.17cm vs 0.23±0.19cm, p=0.01) and left hemi-diaphragm (0.37±0.18cm vs 0.24±0.14cm, p=0.01). No significant differences between the right and left hemi-diaphragms were observed during inspiration or expiration. Intra and inter-operator reliability were all Excellent: D_{TKE} (intra: $ICC_{2,1}$ =0.977; inter: $ICC_{2,1}$ =0.822), D_{TKI} (intra: $ICC_{2,1}$ =0.903; inter: $ICC_{2,1}$ =0.805), Q_{TK} (intra: $ICC_{2,1}$ =0.976; inter: $ICC_{2,1}$ =0.940), RF_{Area} (intra: $ICC_{2,1}$ =0.973; inter: $ICC_{2,1}$ =0.981) and RF_{TK} (intra: $ICC_{2,1}$ =0.998; inter: $ICC_{2,1}$ =0.762).

Conclusion: Results showed the feasibility and reliability of this US protocol in healthy people. One single measurement by one operator seems to be adequate. Bilateral diaphragmatic measurements might not be necessary in respiratory patient's evaluation

B-0964 10:38

Orbital ultrasound evaluation of the optic nerve sheath diameter

H.I.M.G. Ferraz¹, R.A. Santos²; ¹Peso da Régua/PT, ²Coimbra/PT
(helenaimgferraz@gmail.com)

Purpose: The human eye is one of the most complex organs in our body. The fact that the eye is a liquid-filled superficial structure allows an optimal appreciation of the ocular structures on ultrasound. There has been an

increase in the use of this modality in the evaluation of the diameter of the optic nerve sheath (ONSD). To purpose of the study is to analyse the reproducibility of the ONSD diameter measures, to characterise the ONSD by ultrasound, to verify the existence of correlation with body mass index (BMI), blood pressure (BP) and glucose values.

Methods and Materials: 370 ultrasound images of ONSD were collected from 84 individuals, divided into 2 groups. The ICC was obtained to evaluate the reproducibility of the ultrasound measurements. The BMI, BP and glucose values were also collected from all subjects. The correlation of data was also evaluated with the Pearson test and the Student's T test for independent samples.

Results: The ONSD ICC values showed satisfactory reproducibility (0.73). BMI and age showed a positive correlation with BP (p<0.05). No significant differences were found between the group with pathology (myopia, astigmatism or hypermetropia) and without.

Conclusion: Ultrasonography showed a satisfactory reproducibility to assess the ONSD and could help with new ocular disease evaluation.

B-0965 10:46

Effects of smoking on carotid artery structures and haemodynamics: role of the radiographer in ultrasound assessment

D.M.B. Simão, L.P. Ribeiro, A.F. Abrantes, J.P. Pinheiro, R.P. Almeida, A.Q. Brito, S. Rodrigues; Faro/PT (diogo_simao93@hotmail.com)

Purpose: Currently, tobacco is a behaviour associated with the appearance of several pathologies, such as atherosclerosis or stroke and qualified radiographers in sonography field should be able to detect premature vascular changes due to smoking. The goal of this study was to assess and compare structural and haemodynamic parameters on carotid arteries in smokers and non-smokers by ultrasound.

Methods and Materials: Several parameters on the carotid artery were evaluated by a trained radiographer: intima-media thickness (IMT), peak systolic velocity (PSV) and end-diastolic velocity (EDV). Measurements were performed using a sample of 103 volunteer participants (52 non-smokers and 51 smokers) aged between 20 and 40 years. B-mode images were acquired in longitudinal and transverse sections of the common carotid arteries. Inclusion criteria contains healthy participants with unknown diseases. The smokers group was divided into four different categories depending on the number of cigarettes smoked by day.

Results: It were observed higher mean values for all of the structural and haemodynamic parameters in the smokers group (IMT=0,706mm; PSV=104,94cm/s and DV=30,20cm/s) comparing with non-smokers (IMT=0,512mm; PSV=72,47cm/s and DV=19,29cm/s). Also, the female smokers group presents higher values when compared with the male smokers group (x=0,758 vs x=0,652, respectively).

Conclusion: The data from this study suggest that smoking has negative effects on carotid artery structure and haemodynamics. Therefore, smoking is a risk factor for alterations in carotid artery haemodynamics and female smokers are more likely to develop vasculares changes. Radiographers can play a key role in the detection of pathophysiological changes in a preventive perspective.

B-0966 10:54

Abdominal and lumbar muscle evaluation by ultrasound

R.A.M. Santos, R. Barreiro; Coimbra/PT (rutemartinssantos@gmail.com)

Purpose: The aim of this study is to characterize the muscular ultrasound of two postural muscles (rectus abdominis and lumbar multifidus) in healthy individuals and in individuals with postural alterations (namely hyperlordosis).

Methods and Materials: 30 young adults were submitted to an ultrasound evaluation of the rectus abdominis and multifidus lumbar muscles in rest and contraction and an angle measurement of the lumbar spine through a photometry equipment. They were divided into groups: one of control and other with non-congenital posture. The sample was composed of 11 participants with postural deviations and 19 without. 360 images were analysed with Image J software to obtain muscle thickness and echo-intensity values from the two muscles in two conditions and the angle of the lumbar spine was calculated also for all participants.

Results: There were significant differences between rest and contraction on muscle thickness and echo intensity of both muscles. There were no significant differences between the two groups of participants and there was no correlation between the angle and the ultrasound measurements.

Conclusion: The postural deviations do not influence the ultrasound characteristics of the studied muscles. However, more studies must be performed to analyse the relation between the lumbar and abdominal muscles and the postural changes.

B-0967 11:02

Vastus lateralis stiffness assessed by SSI elastography
R.A. Santos¹, P. Armada-da-Silva²; ¹Coimbra/PT, ²Lisbon/PT
(rutemartinsantos@gmail.com)

Purpose: To assess changes in VL's shear modulus with knee position and after a session of maximal isometric and isokinetic Conc and Ecc contraction and to analyse the relationship between VL's shear elasticity and submaximal knee extension torque with supersonic shear wave imaging (SSI).

Methods and Materials: Sixteen subjects were submitted to acute changes in VL's stiffness associated with passive stretching, performance of short but intense contractile activity, and muscle isometric contractions that were investigated by means of SSI.

Results: The results demonstrated an acute increase of around 10% in VL's shear modulus as a result of performing maximal isometric, concentric, and eccentric contractions. The shear modulus of the VL also increased when the knee moved from 10° to 50° and then to 90° flexion. Finally, a linear relationship between the shear modulus and the level of isometric muscle contraction was observed.

Conclusion: SSI proved to be a good method to investigate muscle mechanical property changes associated with muscle function. These results emphasise the value of an objective and quantifiable muscle US evaluation for studying muscle adaptation to exercise training and muscle function, in general.

B-0968 11:10

Use of ultrasound for diagnosis of schistosomiasis mansoni
H.M.K. Masha; Nairobi/KE (hildakadzo@yahoo.com)

Purpose: To establish the role of ultrasound in the diagnosis of Schistosoma mansoni.

Methods and Materials: Ultrasound was used to scan a group of 400 individuals in obtaining sonographic grading. The study was done in an area called Nzoia in Kenya and included adults and children both males and females. The age range considered for the study was 8-45 years. Characteristic sonographic features of schistosoma to be observed were periportal fibrosis noted along the long axis of the intrahepatic portal veins. Scanning along central and peripheral bifurcation points of the portal veins produced branching pattern of high echogenicity. From this sonographic pattern, grading was done as follows: A- Normal, B-Early peripheral fibrosis, C-Clear cut pipestems and rounded density bands, D-Central fibrosis of main portal vein and gallbladder wall thickening, E-Advanced stages of fibrosis forming patches on the liver parenchyma, F-extreme advanced fibrosis extending to the liver surface, distorting its shape, XYZ other pathology not schisto related. Wall thickness of the portal veins was measured. Other sonographic abnormalities were noted (splenomegaly, oesophageal and splenic varices and ascites). A portable ultrasound machine with curvey linear probe was used. Portable generator, warm gel, Pinter with glossy printing paper and recording material.

Results: The grading observed were as follows; pattern B-65%, C-5.4%, E-1.5%, F-4.6%, X Y Z- 0.7%. It was also noted that advanced sonographic abnormalities seen in children differed significantly from those of adults.

Conclusion: Ultrasound is an ideal tool for classification of liver fibrosis in schistosomiasis and can also be used in a country control programme.

B-0969 11:26

Point of care creatinine testing: a feasibility study in an outpatient CT setting
B. Snaith^{1,2}, M.A. Harris¹, B. Shinkins³, M. Jordaan¹, A. Lewington³, M. Messenger³, N. Spencer¹; ¹Wakefield/UK, ²Bradford/UK, ³Leeds/UK
(bev.snaith@midyorks.nhs.uk)

Purpose: There remains controversy around the relationship between iodinated contrast media and contrast-induced acute kidney injury (CI-AKI), but international guidance endorses renal function screening. Point of care (PoC) testing may reduce inefficiencies, improve patient safety and optimise capacity, but evaluation of their implementation within this context is limited.

Methods and Materials: Following ethical approval, this feasibility study was performed across two UK hospital sites. A PoC creatinine analyser was added as an adjunct to the standard laboratory blood test. Patients having contrast-enhanced CT consented to a risk screening questionnaire and two samples of blood for PoC and laboratory analysis for evaluation of serum creatinine (SCr) and estimated glomerular filtration rate (eGFR). Follow-up testing 48-72 hours post-contrast was also offered. The analytical performance and clinical concordance of PoC was assessed.

Results: 300 patients were recruited with a mean age of 65 years (range 23-91). Pre-scan blood test timing varied (mean 3.7 weeks; range 0- 59.6); however, four patients had bloods available despite fail-safe procedures. Three patients had an unexpected drop in eGFR; all indicated acute illness. Screening questionnaire responses showed a statistically significant relationship between reduced eGFR and renal (p=0.010) or cardiac (p=0.032)

problems. At follow-up, five patients (5/102; 4.9%) registered CI-AKI (≥25% increase in SCr). Positive and negative bias was seen with the PoC device, with mean bias close to zero.

Conclusion: PoC technology exhibits acceptable clinical performance. The implementation of a risk screening questionnaire partnered with PoC technology may streamline services and enable direct access to imaging; however, multi-centre evaluation is required.

Author Disclosures:

B. Snaith: Grant Recipient; NHS England Cancer Diagnostic Capacity Fund.

B-0970 11:34

Implementation of a multi-phase contrast injection: single-pass acquisition trauma CT protocol

D.J. Biddle, S. Freeman, A. Barker, C. Walker, R. Higgins, S. Upponi; Cambridge/UK (david.biddle@nhs.net)

Purpose: Can the radiation dose for trauma CT be reduced utilising a multiphase contrast injection, single-pass acquisition, whilst maintaining the overall image quality?

Methods and Materials: 50 consecutive trauma CTs using the established two-pass protocol were retrospectively analysed (arterial thoracoabdominal imaging and portal venous abdominopelvic imaging). Retrospective analysis was also made of 50 consecutive trauma CTs utilising the new single-pass, multiphase injection protocol (mixed arterial and venous phase of chest, abdomen and pelvis). Patients were imaged on a Siemens Definition AS+ 128 slice scanner. Both trauma protocols were triggered using a region-of-interest (ROI) placed over the descending thoracic aorta. Hounsfield unit measurements were obtained with a ROI drawn over the main pulmonary artery, descending thoracic aorta and portal vein. Two consultant radiologists assessed the overall quality of the studies, rating the studies as diagnostic or non-diagnostic, and evaluating contrast density. Splenic enhancement was specifically assessed as a marker of solid organ enhancement. Radiation dose was compared.

Results: The single-pass cohort had significant dose reduction compared with the two-pass method (DLP 935.60 vs 1849.58 mGycm; p=0.000000005506), and a lower kV (p = 0.0029). Pulmonary artery enhancement was comparable (p = 0.401), whilst the aortic and portal vein attenuation was significantly higher in the single-pass cohort. Both cohorts had excellent diagnostic quality: 100% in two-pass method and 98% in single-pass method. Both cohorts maintained diagnostic splenic attenuation (100%).

Conclusion: The single-pass, multiphase technique significantly reduces the radiation dose in trauma patients, compared with the established technique, whilst maintaining diagnostic accuracy.

B-0971 11:42

CT hepatic contrast enhancement adjusted for body type versus lean body weight

T. von der Fehr, V. Hjelle, J.M. Erdal, T. Helle, A.P. Parkar; Bergen/NO (janne.erdal@gmail.com)

Purpose: The optimal contrast enhancement for detection of liver lesions on CT is 50 HU. We aimed to study if switching from administered contrast amount based on body type to a lean body weight (LBW) calculator (according to Hume) could improve the quality of hepatic contrast enhancement (HCE).

Methods and Materials: The age, gender, height and weight, contrast amount, flow rate and tube voltage (kV) of 200 consecutive patients who underwent the same CT protocol were recorded. The first 100 patients (group A) were administered contrast amount (80-100-120 ml) according to their body type (normal-overweight-muscular). The next 100 patients (group B) were administered contrast according to their LBW (0.75 g iodine/kgLBW). As delay was fixed at 70s and all other parameters remained constant, flow rate varied in group B. CT density (HU) on the first smart-prep image and post-contrast were measured on the same slice and anatomic area. Density increase ≤49 HU was considered "inadequate".

Results: After image review, 183 patients were included (group A= 95, group B=88). Inadequate HCE scans fell between group A (29.31%) and group B (16.18%), but not significantly (X₂, p=0.053). Age, gender, body weight and flow rate did not significantly affect HCE. kV significantly affected HCE, with 91% adequate scans with 100 kV and 61% with 120 kV (X₂, p<0.001). LBW >60 kg significantly affected kV (p=0.006) and HCE (p=0.004).

Conclusion: The LBW calculator only slightly, but not significantly, improved HCE. Increasing LBW warrants imaging at 120 kV to achieve acceptable image quality, but also reduces the iodine attenuation. Future optimisation process must address improving HCE in patients with LBW>60 kg.

B-0972 11:50

Optimisation of contrast delivery using quantitative and qualitative analysis in a clinical based CTPA setting

C. McKay, S. Maguire, P. Gilligan, C. Walsh, J. Matthews, S.J. Eustace; Dublin/IE (ce.mckay5@gmail.com)

Purpose: Current practice in our hospital involves bolus tracking with subjective manual cessation of contrast administration for CT Pulmonary Angiography. This has implications for contrast usage in certain vulnerable patient cohorts. The purpose of the study was to assess the effect of varying the volume of contrast administered on the enhancement of the pulmonary arteries.

Methods and Materials: CTPA (n=100) images from a dual tube definition scanner (Siemens, Erlangen) were evaluated using objective and subjective parameters. The average Hounsfield units were assessed in the pulmonary artery at central, segmental and subsegmental levels. The clinical analysis was based on the experienced radiologists' reports which include a commentary on image quality including the level of contrast opacification of the pulmonary arteries.

Results: There was a significant variation in the volumes of contrast administered for CTPA exams (Range 35-90 ml of Optiray 350 (Guerbet, France), Median: 66 ml, Mode :90 ml). Contrast enhancement of the pulmonary arteries were maintained above the set threshold of 210 Hounsfield units even at low contrast volumes. All exams in the cohort were considered sufficient for diagnosis, however 7% were noted as suboptimal in the clinical reports. A lower kVp setting was found to improve vascular enhancement.

Conclusion: It is possible to deliver adequate CTPA images with lower contrast volumes in a clinical setting and a protocol of a maximum volume of 70 ml is proposed.

heterogeneity. Our aim is to perform analyses of influencing factors on established and novel parameters of myocardial tissue characterization.

Methods and Materials: 55 cardiovascular magnetic resonance examinations were performed at 3T (Magnetom Skyra®, Siemens Healthineers) in carefully chosen healthy volunteers. A dedicated software (CVI42, Circle®) analysed the produced T1 Maps. Tissue heterogeneity parameters were calculated and included analysis of dispersion like mean and standard deviation (SD), dynamic range and mean absolute deviation (MAD) of mean T1-values and their SD. These values were subsequently tested for influencing factors like age, sex and their combination using an analysis of variance (ANOVA). Post-hoc testing using the Bonferroni correction was performed for subgroup analyses.

Results: Established parameters like median T1 were influenced by gender (p=.001), but not by age (p=.777). Myocardial dispersion parameters, e.g. MAD or dynamic range showed no statistically significant differences with regard to age and gender (p=.559 and .665 respectively p=.416 and .105). The combination of both factors did not reveal a significant influence.

Conclusion: Published data on the influence of age and gender on established T1-Map parameters in healthy volunteers is controversial. These controversies could be caused by selection bias, differences in sequence types or post-processing software. Sophisticated post-processing analysis of myocardial tissue heterogeneity are not influenced by age and gender and could be beneficial to establish myocardial tissue characterization as a method for clinical use.

B-0975 10:46

Artefacts in myocardial mapping

C. Eilers, J. Eichstädt, K.-H. Schmidt, C. Düber, T. Emrich, K.-F. Kreitner; Mainz/DE (tilman.emrich@gmail.com)

Purpose: Cardiac magnetic resonance (CMR) imaging in general and myocardial mapping in particular provide valuable insights into the structure of myocardial tissue and help in discriminating healthy from diseased myocardium. However, artefacts and insufficient motion correction remain an existing but rarely addressed problem in CMR mapping imaging.

Methods and Materials: In this study, 66 patients with miscellaneous heart diseases and 80 healthy volunteers underwent T1 and T2 myocardial mapping at 3T. All maps were evaluated with regard to frequency of artefacts. The type of artefacts and the involved myocardial segments according to American Heart Association (AHA) classification were recorded. Furthermore, we evaluated in how far the artefact prevented clinical evaluation of the involved segment. The artefacts were classified as: chemical shift artefacts, off-resonance artefacts, susceptibility artefacts, partial volume artefacts and artefacts due to insufficient motion correction.

Results: In native T1- and T2-mapping, artefacts occurred in 7% of the myocardial segments, 6% had to be excluded from further analysis. Most common artefacts were off-resonance and susceptibility artefacts. Myocardial segments most often affected by artefacts were located inferolateral, anteroseptal and apical. There was no statistical significant difference in the amount, type and distribution of artefacts between T1 and T2 mapping and between the mapping of healthy volunteers and patients.

Conclusion: The frequency of artefacts in T1 and T2 mapping prevented further analysis in 6% of segments. The distribution of artefacts among segments is not random. Instead, it follows the same recurring pattern in patients and healthy volunteers and in both T1 and T2 mapping.

B-0976 10:54

Myocardial T1 and T2 mapping in severe aortic stenosis: novel insights into the pathophysiology of myocardial remodelling

A. Fehrmann Efferoth, M. Treutlein, T. Rudolph, V. Rudolph, K. Weiss, D. Giese, A. Bunck, D. Maintz, B. Baessler; Cologne/DE (anafehrmann@googlemail.com)

Purpose: Severe aortic stenosis (AS) is known to be associated with substantial myocardial remodelling, leading to diffuse myocardial fibrosis (DMF). The purpose of the present study was to combine native T1 and T2 mapping in a comprehensive cardiac magnetic resonance (CMR) examination to characterize myocardial tissue changes in the setting of severe AS.

Methods and Materials: 26 prospectively selected patients with severe AS and 17 healthy controls underwent CMR imaging on a clinical 3T scanner. The CMR protocol included a native modified Look-Locker T1-mapping and a gradient-spin-echo T2-mapping sequence in three short-axis slices and one long-axis view. After segmentation, myocardial T1 and T2 values were averaged over the entire myocardium.

Results: Global native myocardial T1 was significantly increased in AS patients when compared with controls (1305±39 vs 1272±21 ms, p=.005). Similarly, mean myocardial T2 was significantly elevated in AS patients (51±4 vs 46±2 ms, p<.001) and showed a strong correlation with native T1 (r=.60, p<.001). An overlap was observed between T1 values of both groups, whereas T2 times discriminated nearly perfectly between the two groups (area under the curve: 0.76 for T1, 0.87 for T2).

10:30 - 12:00

Room M 1

Cardiac

SS 1003

Myocardial tissue characterisation: mapping, texture analysis and spectral CT

Moderators:

O. Stukalova; Moscow/RU
N.N.

B-0973 10:30

T1 based myocardial tissue characterisation in healthy volunteers: reference values for novel parameters of tissue dispersion

S. Rueppel, S. Lyschik, M.C. Halfmann, S. Benz, J. Eichstädt, C. Düber, K.-F. Kreitner, T. Emrich, F. Hahn; Mainz/DE

Purpose: Data on reference values of healthy adults concerning novel markers of myocardial tissue heterogeneity based on T1 Maps does actually not exist. We aim to provide these reference values for analysis of myocardial tissue heterogeneity to strengthen this approach for clinical use.

Methods and Materials: In this study, 55 carefully chosen healthy volunteers, matched in age and sex, underwent CMR imaging at 3 Tesla (Magnetom Skyra®, Siemens Healthineers). We evaluated Modified Look-Locker inversion recovery (MOLLI) based T1 Maps by using a dedicated software (CVI42, Circle®) after accurate elimination of artifacts. Beside established parameters like mean segmental and global T1 values, parameters of myocardial tissue dispersion as maximum and minimum T1 (max and minT1), dynamic range (dyn), standard deviation (SD) and mean absolute deviation (MAD) of mean T1 and SD were calculated.

Results: The measurements lead to the following values (median and interquartile range): Global T1 1190 ms (1148 ms/ 1217 ms), SD 85,2 ms (70.9 ms/ 98,7 ms), MADT1 25,3 ms (16,7 ms/ 35,5 ms), MADSD 12,8 ms (9,6 ms/ 21,0 ms), minT1 931 ms (864 ms/ 1013 ms), maxT1 1710 ms (1595 ms/ 1810 ms) and Dyn 777 ms (696 ms / 928 ms).

Conclusion: To our knowledge, our study provides first reference values for novel markers of myocardial tissue heterogeneity in healthy adults. Further studies are needed to establish this approach for clinical use.

B-0974 10:38

Novel T1 map parameters of tissue heterogeneity are not influenced by age and gender in healthy volunteers

S. Lyschik, S. Rueppel, S. Benz, M.C. Halfmann, J. Eichstädt, C. Düber, K.-F. Kreitner, T. Emrich, F. Hahn; Mainz/DE

Purpose: Data concerning the influence of gender and age on myocardial T1-values is controversial or not existing, especially for novel parameters of tissue

Conclusion: Patients with severe AS exhibit significantly elevated native myocardial T1 times, which has previously been shown to correlate with the amount of myocardial collagen. The present study is the first to show that native T1 and T2 values are both significantly elevated and correlated in AS patients, pointing towards a potential role of oedematous/inflammatory processes in the pathophysiology of myocardial remodelling associated with AS.

Author Disclosures:

K. Weiss: Employee; Philips Healthcare. **B. Baessler:** Research/Grant Support; Wilhelm Vaillant-Stiftung.

B-0977 11:02

Myocardial tissue characterisation by cardiac magnetic resonance imaging in left ventricular non-compaction: new insights with T1 mapping and extracellular volume quantification

J.A.B. Araújo-Filho, A.N. Assuncao-Jr, M.D. Tavares de Melo, R.N. Dantas Jr, C.H. Nomura, J.R. Parga Filho; São Paulo/BR (ariaraujocg@hotmail.com)

Purpose: This study aimed to characterize myocardial T1 mapping and extracellular volume (ECV) fraction by cardiovascular magnetic resonance (CMR), and investigate how these biomarkers relate to left ventricular ejection fraction (LVEF) and ventricular arrhythmias (VA) in patients with left ventricular non-compaction (LVNC).

Methods and Materials: We prospectively recruited 36 patients with LVNC and 18 controls to perform a cardiovascular magnetic resonance (CMR) with T1 mapping from July 2013 to September 2016. ECV was quantified in LV segments without late gadolinium enhancement (LGE) areas to investigate diffuse myocardial fibrosis. Differences in CMR parameters between patients and controls were assessed using t test or Wilcoxon rank-sum test, and a linear regression model was built for LVEF to test the association with ECV and clinical characteristics.

Results: Patients with LVNC had higher native T1 (1024±43ms vs. 995±22ms, p=0.01) and expanded ECV (28.0±4.5% vs. 23.5±2.2%, p<0.001) compared to controls. ECV was independently associated with LVEF (β =-1.3, p=0.003). Moreover, among patients without LGE, VA were associated with higher ECV (27.7% with VA vs 25.8% without VA, p=0.002).

Conclusion: In LVNC patients, tissue characterization by T1 mapping suggests an extracellular expansion in myocardium without LGE, which was associated with myocardial dysfunction and VA, possibly related to diffuse myocardial fibrosis. These findings lend support to the potential role of T1 mapping in refining LVNC risk stratification.

B-0978 11:10

ECV mapping without HCT: comparison between two different synthetic ECV-calculation methods and clinical applicability

L. Bottoni¹, E. Gavazzi¹, M. Ravanelli¹, M. Zanirato², A. Greiser², D. Farina¹, R. Maroldi¹; ¹Brescia/IT, ²Erlangen/DE (luca.bottoni87@hotmail.com)

Purpose: To assess the accuracy and clinical applicability of two different synthetic-ECV mapping methods.

Methods and Materials: 47 consecutive cardiac MRI scans were performed applying three different ECV mapping techniques: 8/47 patients were discarded for poor image quality. In 15/39 automated ECV mapping (Siemens, Germany), incorporating the Hct measured in lab. This method was set as the reference standard. In 24/39 cases was applied automated synthetic ECV mapping (with software-calculated Hct) (Siemens, Germany). In all patients in-house calculated ECV was performed applying the formula $[(1-Hct)/(1/\square\text{myocardium}-1/\square\text{blood})]$ with $Hct=[0,88-(T1\text{blood}/3240)]$. Image were analysed placing ROIs on blood pool and myocardium, rigidly in the same position in all cases.

Results: The software-calculated Hct was compared with the lab-measured Hct in 17 cases: software-calculated Hct was significantly higher (p=.0089). The in-house calculated Hct was compared with the lab-measured Hct in 29 cases: no significant difference was seen. However, no statistically relevant difference between the ECV measured with automated-ECV, synthetic-ECV and in-house calculated ECV was found.

Conclusion: Synthetic-ECV mapping bases its measurement on a software-calculated Hct which is significantly different from real, whereas in-house calculation offers a more reliable estimate. However, the ECV values measured with three techniques show no statistical difference. Synthetic-ECV mapping is a clinically applicable alternative in cases when lab-measured Hct is unavailable.

B-0979 11:18

Diagnostic potential of texture analysis applied on cardiac magnetic resonance T1 and T2 mapping in patients with biopsy-proven chronic myocarditis

B. Baessler¹, C. Lücke², K. Klingel³, R. Kandolf³, G. Schuler², D. Maintz¹, M. Gutberlet², H. Thiele², P. Lurz²; ¹Cologne/DE, ²Leipzig/DE, ³Tubingen/DE (bettina.baessler@uk-koeln.de)

Purpose: To apply texture analysis (TA) for the first time on T1 and T2-maps derived from cardiac magnetic resonance (CMR) T1 and T2 mapping and to test its diagnostic performance in patients with "DCM-like" chronic myocarditis.

Methods and Materials: Forty patients with clinical chronic heart failure (EF<50%, symptom duration >14 days) and suspicion for underlying chronic myocarditis were prospectively included. Patients underwent biventricular endomyocardial biopsy (EMB), cardiac catheterization and CMR imaging at 1.5T including native T1 and T2-mapping as well as standard Lake Louise criteria (LLC). TA was applied on T1 and T2-maps using a freely available software package by drawing a region of interest encompassing the entire myocardium. Step-wise dimension reduction and texture feature selection was performed for selecting texture features enabling the diagnosis of DCM-like chronic myocarditis, using EMB as the reference standard.

Results: Mean symptom duration was 121±164 days and mean EF was 26±11%. EMB confirmed the presence of myocarditis in 26 patients (EMB+), whereas 14 patients had no signs of inflammation (EMB-). Similar to standard LLC, mean myocardial T1 and T2 demonstrated poor diagnostic performance in receiver operating curve (ROC) analyses (area under the curve [AUC]: 0.52 for LLC, 0.54 for T1 and T2, respectively). The combination of two texture features derived from T2 maps, T2_Kurtosis and T2_SumEntrp, yielded a superior diagnostic performance with an AUC of 0.75 and a sensitivity/specificity of 77/71%.

Conclusion: TA is feasible when being applied on myocardial T1 and T2-maps and delivers interesting novel parameters for the diagnosis of chronic myocarditis.

B-0980 11:26

Texture analysis of myocardial infarction of CT: impact of iterative reconstruction

M. Mannil, J. von Spiczak, U. Mühlematter, A. Thanabalasingam, R. Manka, H. Alkadhi; Zurich/CH (Manoj.Mannil@usz.ch)

Purpose: To compare machine learning-based texture analysis (TA) with subjective visual diagnosis of myocardial infarction (MI) in CT of the heart, and to evaluate the impact of iterative reconstruction (IR) on the results.

Methods and Materials: Ten patients with confirmed chronic MI and twenty controls with no cardiac abnormality underwent the same contrast-enhanced ECG-gated cardiac CT protocol. Images were reconstructed with filtered back projection (FBP) and advanced modelled IR at strength levels 3-5. Subjective diagnosis of MI was made by two independent, blinded readers. Classification of MI was performed using machine-learning based decision tree models for the entire dataset and after splitting into training and test data to avoid overfitting.

Results: Subjective visual analysis for diagnosis of MI showed excellent intrareader (kappa:0.93) and poor interreader agreement (kappa:0.3), with variable performance at different reconstruction types. TA showed similarly high performances for all image reconstructions (correct classifications 94-97%, areas-under-the-curve 0.94-0.99). After splitting into training and test data, overall lower performances were observed with best results for IR level 5 (correct classifications 73%, area-under-the-curve 0.65).

Conclusion: As compared to subjective visual image analysis, machine learning-based TA enables objective and reproducible diagnosis of MI in CT with high accuracy, showing best results at highest IR levels.

B-0981 11:34

Texture analysis and machine learning for detecting myocardial infarction in non-contrast low-dose CT

M. Mannil, J. von Spiczak, R. Manka, H. Alkadhi; Zurich/CH (Manoj.Mannil@usz.ch)

Purpose: To test whether texture analysis (TA) and machine learning enable the detection of myocardial infarction (MI) on non-contrast enhanced low radiation dose cardiac computed tomography (CCT) images.

Methods and Materials: In this IRB-approved retrospective study, we included non-contrast enhanced electrocardiography-gated low radiation dose CCT image data (effective dose 0.5mSv) acquired for the purpose of calcium scoring of 27 patients with acute MI, 30 patients with chronic MI, and in 30 subjects without cardiac abnormality (hereafter termed *controls*). TA of the left ventricle was performed using free-hand regions-of-interest and texture features were classified twice. Model I: controls vs. acute MI vs. chronic MI; Model II: controls vs. acute and chronic MI. For both classifications, five commonly used machine learning classifiers were used: decision tree C4.5

(J48), k-nearest neighbors (k-NN), locally weighted learning (LWL), sequential minimal optimization (SMO), and an artificial neural network. Additionally, two blinded, independent readers visually assessed non-contrast CCT images for the presence or absence of MI.

Results: In model I, best classification results were obtained using the k-NN classifier (sensitivity 69%, specificity 85%). In model II, best classification results were found with the LWL classification (sensitivity 86%, specificity 81%) with an area-under-the-curve from receiver operating characteristics analysis of 0.78. In comparison, both readers were not able to identify MI in any of the non-contrast, low radiation dose CCT images.

Conclusion: This study indicates the ability of TA and machine learning for detecting MI on non-contrast low radiation dose CCT images, being not visible for the radiologists' eye.

B-0982 11:42

Myocardial textural analysis and machine learning for differentiating normal myocardium vs chronic infarct on non-contrast CT scan

A.A. Albweady¹, S. Raja², S. George³, M. Alharbi², K. Aldossari², ¹Qassim/SA, ²Riyadh/SA, ³Houston, TX/US (ALBWEADY88@GMAIL.COM)

Purpose: Prior sparse literature suggests that a couple of soft findings on plain CT such as hypodensity, calcium deposits etc can favor chronic infarction. Recent developments in Radiomics- texture analysis (TA) and machine learning (ML) can tease out such occult features on medical imaging including CT. We explored if TA and ML can differentiate normal myocardium from prior infarcts.

Methods and Materials: We retrospectively analysed 24 patients (M=18, F=6), having both FDG PET-CT and MPI (cardiac perfusion SPECT) for myocardial viability from 2015 to 2017. Utilising the ground truth (scar Vs. normal myocardium) on the co-registered PET and SPECT transverse slices (matched defect-infarct, mismatch-viable myocardium), we flagged 3 to 4 representative 3D VOI (volume of interest) on each pt. on a dedicated workstation. The voxel level data from the flagged VOI were exported to EXCEL and MATLAB for TA computation.

Results: Utilising a Training subset 50% (no=18), Testing subset 50% (no=18), for developing the predictive model and testing respectively. A prediction classification accuracy of 82%, AUC 0.875 in the training set was achieved with C5.1 decision tree algorithm to classify scar vs. normal myocardium. Using one way ANOVA the single most important feature had a statistically significant p-value of 0.009 in the differentiation of scar Vs normal myocardium.

Conclusion: Texture analysis and machine learning can dissect normal myocardium from chronic infarcts, on non-contrast CT. The novel technique could potentially be used as a screening tool in patients at high risk for unrecognised chronic infarcts.

B-0983 11:50

Initial in vitro comparison of a spectral photon counting CT and a spectral dual-layer CT system for non-invasive evaluation of soft-plaque-restenosis in coronary artery stents

T. Hickethier¹, D. Bar-Ness², A. Bunck¹, D. Maintz¹, G. Pahn³, P. Coulon⁴, S.A. Si-mohamed², P. Douek², M. Sigovan²; ¹Cologne/DE, ²Lyon/FR, ³Hamburg/DE, ⁴Suresne/FR (tilman.hickethier@uk-koeln.de)

Purpose: Even when compared to latest spectral-dual-layer-CT-systems (SDLCT) future spectral-photon-counting-detector-CT-systems (SPCCT) promise improved spatial resolution and decreased (stent related) blooming artifacts. We investigated the influence of conventional (Conv) and monoenergetic (MonoE) reconstructions from SDLCT and SPCCT on delineation of soft-plaque-restenosis in coronary stents.

Methods and Materials: Artificial stenosis (~30HU) were implanted into 10 different coronary stents (~3mm) embedded in plastic tubes filled with contrast agent (~400HU). CT data was acquired with a SDLCT (IQon, Philips) and a SPCCT (Prototype, Philips). Sharp kernels were used for reconstructions with Conv and MonoE at 50, 70, 100 and 140keV. Visibility of the stenosis and the remaining lumen was evaluated by 2 readers for each stent and reconstruction using a Likert scale reaching from 1 (image quality impedes lumen assessment) to 5 (stenosis and remaining lumen are clearly visible).

Results: Interrater agreement was very good (kappa=0.9). Stenosis delineation was best in Conv, 50 and 70keV MonoE SPCCT images (median score=5). Differentiation was significantly more difficult in corresponding SDLCT images (median score=3;p<0.01). Despite visibly lower blooming artifacts, 100 and 140keV MonoE images showed significantly poorer results than the corresponding 50keV MonoE images due to reduced contrast enhancement resulting in impaired visualisation of the unaltered lumen (median score=2 for 100keV and 1 for 140keV on both scanners;p<0.01).

Conclusion: Evaluation of soft-plaque-restenosis can be significantly improved by using conventional and low keV MonoE reconstructions of future SPCCT. High keV MonoE reconstructions are not recommended for coronary stent assessment with SPCCT or SDLCT due to impeded stenosis delineation.

Author Disclosures:

G. Pahn: Employee; Philips. P. Coulon: Employee; Philips.

10:30 - 12:00

Room M 3

Molecular Imaging

SS 1006

Molecular imaging of biology and pathology

Moderators:

A. Esposito; Milan/IT
N.N.

B-0984 10:30

To evaluate the role of 68Ga DOTA NOC receptor PET CT in detection of unknown primary neuroendocrine tumours

S.M. Shaikh; Hyderabad/IN (drsikandar_s@yahoo.co.in)

Purpose: The aim of our study was to evaluate the role of receptor PET/CT using 68Ga-DOTA-NOC in the detection of undiagnosed primary sites of neuroendocrine tumours (NETs).

Methods and Materials: Overall 29 patients (M:F 15:14, age 55±9 yr) with histopathologically proven NET and unknown primary were included. PET/CT was performed after injection of 100 MBq (46-260 MBq) of 68Ga-DOTA-NOC. The (SUVmax) was calculated and compared with SUVmax in known pancreatic NET (pNET) and ileum/jejunum/duodenum (SI-NET). The results of PET/CT were also correlated with CT alone.

Results: In 17/29 (59%) of patients, 68Ga-DOTA-NOC PET/CT localised the site of the primary: ileum/jejunum (7), pancreas (6), rectum (1), lungs (1) and paraganglioma (2). CT alone (on retrospective analyses) confirmed the findings in 6/29 (20%) patients. The mean SUVmax of identified previously unknown pNET and SI-Net were 15.6 ± 9.8 (range 7.8-34.8) and 8.1 ± 6.0 (range 4.2-27.8), respectively. SUVmax in patients with previously known pNET and SI-NET were 26.1±14.5 (range 8.7-42.4) and 11.3±3.7 (range 5.6-17.9). The SUVmax of the unknown pNET and SI-NET was significantly lower (p< 0.05) as compared with known primary tumour sites. 19% of the patients had high-grade and 81% low-grade NET. In 3/29 patients the primary tumour was subsequently resected (1 pancreatic, one ileal and one rectal tumour).

Conclusion: 68Ga- DOTA-NOC PET/CT is highly superior to 111In Octreoscan (17% detection rate for CUP according to the literature) and plays a major role in the management of patients with CUP-NET.

B-0985 10:38

PET/MR of biliary tract malignancies: impact on treatment planning

O.A. Catalano¹, U. Mahmood¹, C. Ferrone¹, L. Blaszkowsky², L. Goyal¹, T. Hong¹, C. Catana³, D. Gervais¹, B.R. Rosen³; ¹Boston, MA/US, ²Newton, MA/US, ³Charlestown, MA/US (onofriocatalano@yahoo.it)

Purpose: To compare the impact of PET/MR versus PET/CT on treatment planning in biliary malignancies.

Methods and Materials: 18 consecutive patients with biliary malignancies underwent whole-body contrast-enhanced (CE)-FDG-PET/CT, 13 of them underwent CE-FDG-PET/MR and 5 non-CE-FDG-PET/MR. Two readers evaluated PET/CT and PET/MR for local extension, resectability and metastases. Impact of findings on treatment planning was discussed with the referring clinicians.

Results: PET/MR and PET/CT were concordant and correct in 8/18 patients: disclosing metastases in 4 and ruling out metastases and confirming resectability in 4. However, in 1/4 of resectable cases PET/MR demonstrated additional regional lymphadenopathy mandating changes in surgical technique. PET/MR and PET/CT were concordant and incorrect in 1/18 patient, missing peritoneal disease. PET/MR and PET/CT were discordant in 9/18, with PET/MR being correct: PET/MR disclosed metastases missed at PET/CT in 4, diaphragmatic infiltration missed on PET/CT in 1, and interpreted benign findings, confused with metastases on PET/CT, in 4 (inflammatory enlarged non-regional lymph nodes in 1, focal cholangitis in 2, perfusion abnormalities in 1) making them resectable.

Conclusion: PET/MR imaging of biliary malignancies is useful in staging and assessment for resectability. PET/MR did not mis-stage any patient when compared to PET/CT, correctly diagnosed all 9 discordant cases, and mandated changes in treatment plan in 10 cases (p<0.05). PET/MR might represent a valid tool for treatment planning of biliary malignancies.

B-0986 10:46

Implications of 2-hydroxyglutarate in gliomas with IDH1/2 mutations

L. Wang^{1,2}, Y. Zhang¹, Z. Liu^{3,1}, H. Mao²; ¹Shenzhen/CN, ²Atlanta, GA/US, ³Nanchang/CN (2718377613@qq.com)

Purpose: Mutated isocitrate dehydrogenase 1 or 2 (mIDH1/2) occur in 80% of low grade gliomas. Onco-metabolite, R(-)-2-hydroxyglutarate (2HG) is a biomarker for mIDH on molecular classification of tumors and can be detected with magnetic resonance spectroscopy (MRS) for predicting prognosis. To determine whether MRS measurement of 2HG can provide more prognostic and therapeutic information, we investigated the correlations of 2HG level with tumour progressions and other metabolites.

Methods and Materials: 2HG concentrations were measured from tissue specimens of 47 gliomas with mIDH by 2D Correlation Spectroscopy using solid state NMR. All tumours were categorised into three WHO grades. Progression free survival (PFS) of patients with mIDH/wild type (WT) IDH was determined. 2HG levels were compared with WHO grades, PFS, and selected metabolites, such as lactate (Lac), glutamate (Glu) and glutamine (Gln). Non-parametric Mann-Whitney correlation for comparison/Spearman was used for statistical analysis.

Results: 2HG level is elevated in tumours of higher grades. mIDH gliomas has increased PFS compared to those with WT IDH. However, PFS is negatively correlated with 2HG concentration. Metabolite measurements showed that increased 2HG level is related to increases of Glu and Gln, indicating that 2HG may trigger a metabolic shift since Glu/Gln can be converted to α -ketoglutarate, the substrate of mIDH. Furthermore, the levels of Lac and 2HG are found to be positively correlated, possibly due to increase of glucose consumption related to high mutant enzyme activity.

Conclusion: Imaging methods capable of monitoring 2HG level may enable non-invasive and longitudinal assessment of prognosis and treatment responses.

B-0987 10:54

Magnetic resonance spectroscopy of the placenta: a feasibility study

C.M.J. Beaumont, E.H. Whitby; Sheffield/UK (charlottebeaumont@gmail.com)

Purpose: Placental proton magnetic resonance spectroscopy (¹H MRS) is a newly emerging technique with the potential to non-invasively assess the function of the placenta in vivo. Previous studies utilising this technique have been limited. This study aimed to investigate whether this tool could be feasible for routine clinical use.

Methods and Materials: In utero-placental MR spectra were obtained from women (n=43) referred for foetal MRI following abnormal ultrasound scans. Participants were of varying gestational age (GA) and exhibited a wide range of foetal pathologies unrelated to placental function. Spectra quality was assessed both qualitatively and quantitatively, with the potential influence of GA and placental Grannum grade (GG) also considered.

Results: Almost 75% of spectra obtained were considered good quality, with substantial agreement between assessors (Fleiss Kappa: K=0.646) and were, therefore, considered suitable for diagnostic interpretation. Neither GA (Anova: P>0.05) nor GG significantly influenced visual spectra quality. Signal-to-noise ratio also appeared unaffected by the GA (regression: P>0.05) and GG (Anova: P>0.05) of participants. Lipid contamination due to foetal movement negatively affected spectra obtained from participants of low GA. No visible trend was observed between GA or GG and spectral metabolites.

Conclusion: In vivo placental ¹H MRS is feasible in routine clinical practice and warrants further investigation. The spectra obtained do not appear to be influenced by either the GA or GG in terms of quality or spectral metabolites. Future studies establishing metabolite threshold profiles for conditions, and confirming our conclusions regarding the influence of potential confounding variables would be beneficial.

B-0988 11:02

Imaging glycolytic heterogeneity of HCC in real time using dynamic hyperpolarised magnetic resonance spectroscopy: a personalised medicine approach

G. Kaissis, F. Lohöfer, E. Bliemsrieder, G. Topping, F. Schilling, E.J. Rummeny, M. Schwaiger, R. Braren; Munich/DE

Purpose: To demonstrate glycolytic heterogeneity of hepatocellular carcinoma in a homograft model using hyperpolarised ¹³C-Pyruvate dynamic magnetic resonance spectroscopy (MRS) and response to PARP14 inhibition therapy as in vitro validation.

Methods and Materials: Cell clones were derived from diethyl nitrosamine (DEN)-induced tumors and implanted into the hindquarters of Wistar rats. Dynamic hyperpolarised ¹³C-Pyruvate-MRS was performed. Real-time conversion of pyruvate to lactate was measured and modelled using a two-compartment model. Results were correlated with IC₅₀ values of the corresponding cell lines for PARP14 inhibition in vitro.

Results: Cell clone isolation and reimplantation from DEN-induced HCC was successful. Dynamic MRS provided excellent SNR and showed linear kinetic characteristics for pyruvate to lactate conversion (R²= 0.98, p<0.001, n=6). Kinetic constants correlated inversely with IC₅₀ values of the same cell lines for in vitro PARP14 inhibition (R²= -0.9384, p=0.0015, n=6).

Conclusion: This is the first study to demonstrate successful cell isolation and reimplantation in the DEN/Wistar model and the first to demonstrate feasibility of dynamic hyperpolarised ¹³C-Pyruvate-MRS for kinetic modelling of pyruvate-to-lactate conversion for identification of metabolic subgroups. In vitro results correlate with MRS measurements demonstrating higher sensitivity to antiglycolytic therapy in tumors with high lactate production from pyruvate (i.e. higher glycolytic activity). Our approach can be utilised for imaging metabolic heterogeneity of HCC (e.g. differentiating glycolytic vs. nonglycolytic tumors) in the setting of personalised medicine applications as well as pharmacodynamic studies and novel inhibitor development.

B-0989 11:10

The early study of DWI and 1H-MRS in rabbit VX2 transplanted tumours after radiation comparison with pathology changes

Y.-M. Li, D.-D. Lin, Z. Xing, Y. Chuan, X. Xu; Fuzhou/CN (fjmulym@163.com)

Purpose: To analyse the role of DWI and 1H-MRS in evaluating the sensitivity of early radiotherapeutic effects by comparing the features of DWI and 1H-MRS with pathology changes in VX2 transplanted tumour.

Methods and Materials: Sixty rabbits were implanted VX2 tumour in unilateral thigh muscle to establish the experimental models. 2 weeks later, the rabbits were randomly divided into 10 groups according to whether accepting the radiation therapy and the different observation time. The groups were performed MR scans include T1WI, T2WI, DWI, and ¹H-MRS on 3.0T before radiotherapy and 1,3,5,7days after radiotherapy, respectively. Tumour volume, ADC values, Cho/Cr ratios and Lip/Cr ratios of rabbit VX2 transplanted tumour in radiation group and control group at different observed day were analysed using a factorial design statistical method.

Results: 1. After radiation, ADC values in radiation group increased gradually (P<0.05). 2. Cho peak tended to descend and the Lip peak tended to climb in radiation group. There were statistically changes of Cho/Cr, Lip/Cr ratios in different group and times. 3. The expression of the bax gene in radiation group tended to increase gradually.

Conclusion: DWI and 1H-MRS could detect the internal structure changes of tumour early after radiation in the level of molecule and biochemistry. There were some correlations between the tumour volume, the ADC values, Cho/Cr ratios and Lip/Cr ratios and the expression of bax gene after early radiotherapy, DWI and 1H-MRS may be valuable means in predicting early radiotherapeutic effect.

B-0990 11:18

BAT activity in Type I and Type II diabetes mouse models: multimodal imaging study using 7T MRI and intravital microscopy

C.S.L. Jung, M. Heine, N. Mangels, M. Kaul, G. Adam, H. Itrich, J. Heeren; Hamburg/DE

Purpose: Purpose was to determine metabolic activity of brown adipose tissue (BAT) in type I and type II diabetes mouse models using superparamagnetic iron oxide nanoparticles (SPIO) or quantum dots (QD - for intravital microscopy (IVM)) embedded into triglyceride-rich lipoproteins (TRL).

Methods and Materials: C57BL/6J wild-type mice were either treated iv with Alloxan (Abcam) which is toxic to pancreatic beta cells or received a high fat diet to induce diabetes (type I and II). BAT activity was stimulated using CL316,243, a β_3 receptor agonist. MRI at 7T ClinScan (Bruker) was performed before and 20min after iv injection of TRL-SPIOs using a T2*w Multiecho-GRE sequence. IVM analysis was performed for real time imaging of TRL-QD uptake into BAT. To quantify TRL clearance, the fate of radioactively labelled TRLs were analysed under same experimental conditions.

Results: While control mice show a significant signal drop after CL treatment, no signal difference in BAT before and after TRL-SPIO injection was detectable neither for type I nor for type II diabetes mouse model. Real time IVM analyses showed a reduction of TRL-QD uptake in case of diabetes. MRI and IVM results were confirmed quantitative by metabolic studies using radioactive TRL. In both setups diabetes disease leads to a reduction of TRL uptake into BAT.

Conclusion: β_3 -receptor activation via CL with following acute insulin release lead to BAT activation, which can be visualised *in vivo* by MRI. In case of diabetic disease, the uptake of TRL into BAT is diminished, indicating a loss of BAT activity.

B-0991 11:26

In vivo tracing of superparamagnetic iron oxide-labelled bone marrow mesenchymal stem cells transplanted for traumatic brain injury by susceptibility weighted imaging in a rat model

Y. Zhang; Zhengzhou/CN (109496417@qq.com)

Purpose: To label rat bone marrow mesenchymal stem cells (BMSCs) with superparamagnetic iron oxide (SPIO) in vitro, and to monitor the survivorship and location of these labelled BMSCs in a rat model of traumatic brain injury (TBI) by susceptibility weighted imaging (SWI) sequence.

Methods and Materials: BMSCs were cultured in vivo and then labeled with SPIO. The rat TBI model was developed in the left hemisphere following Feeney's method. Twenty-four hours after TBI, we stereotactically transplanted the BMSCs into the region nearby the contusion site. Monitoring of these SPIO-marked BMSCs by SWI was performed at one day, one week and three weeks after implantation.

Results: Numerous BMSCs were successfully labeled with SPIO and positive for Prussian blue staining. Scattered iron particles were observed in the cytoplasm by electron microscopy. MRI of the transplanted sites demonstrated a low signal intensity on every image of SWI sequence.

Conclusion: SWI sequence in vivo can consecutively and noninvasively trace and demonstrate the status and distribution of BMSCs labelled with SPIO in the brain of TBI model rats.

B-0992 11:34

Molecular imaging heterogeneity study of breast tumours as a new diagnosis parameter

M. Herranz¹, P. Ling Ling², P. Aguiar¹, W. Liang², L. Albaina Latorre³, M. Juaneda⁴, A. Ruibal⁵; ¹Santiago de Compostela/ES, ²Shanghai/CN, ³A Coruña/ES (michel.herranz.camero@sergas.es)

Purpose: The concept of tumour heterogeneity corresponds to different levels of expression, cellularity, hypoxia or other parameters interested in being measured into a single tumour. We describe relationship between tumour heterogeneity concept uses in radiology with PET parameters and if any biological characteristics of the breast tumours have a structure-function correlation.

Methods and Materials: 500 consecutive patients with breast cancer were analysed in a dedicated breast PET. Different parameters have been defined to find a pattern of texture and heterogeneity (TeHe), for this, and following the rules of the radiological descriptions we have described a series of structural templates. A mathematical pattern has been defined for their correlation. Patterns of heterogeneity have been correlated with clinical values of the tumours, such as molecular classification, size, type, histology, progression, relapses, etc.

Results: 7 different patterns divided into 5 large groups of values for TeHe are described, and classified as: 1: homogeneous diffuse, 2: lobular, 3: annular and spindle, 4: eccentric and focused; and 5: speckled. A numerical value has been assigned between 1 and 5 for this classification with 1 being the most homogeneous and 5 being the most heterogeneous. This value is achieved through a mathematical relationship: $\text{medSUV}/\text{maxSUV} / [(\text{MedSUV}/\text{maxSUV})\text{Qmax}/(\text{medSUV}/\text{maxSUV})\text{Qmin}]$.

Conclusion: Studies of tumour heterogeneity based on metabolism show us different patterns that correlate with molecular subtypes and predict response to treatments.

B-0993 11:42

Small animal imaging using a clinical PET/CT system: high throughput imaging enabled by next-generation digital PET

M.V. Knopp, K. Briley-Saebo, M.I. Menendez, A. Siva, K. Binzel, J. Zhang; Columbus, OH/US

Purpose: Preclinical imaging, particularly of rodents, is a key aspect of development of new molecular imaging approaches. We sought to develop the capability of multi-subject, simultaneous whole-body PET/CT imaging using a next generation, digital PET detector based, clinical PET system.

Methods and Materials: A pre-commercial release, next-generation, digital photon counting clinical PET/CT system (Philips Vereos, dPET) was used. Enabled by the excellent count sensitivity and time of flight timing resolution (325 ps) of the dPET system, we have previously optimized an ultra-high definition reconstruction utilizing a 1 mm³ voxel size. CT imaging was reconstructed with a 1024x1024 matrix, 0.5 mm voxel length. A mouse hotel that can be variably configured to accommodate up to 6 animals at once was constructed.

Results: Both CT and PET imaging was achievable within a single acquisition volume achieving excellent image quality with an initial acquisition time of 10 minutes. We additionally found that imaging for 3 minutes produced adequate image quality as well. No cross-interference from the multiple beds was observed. While the 6 bed layout appears practical, a higher number of beds is feasible without loss of spatial or quantitative quality from the PET perspective.

The CT field of view is limited to about 6 mice if high resolution imaging is required.

Conclusion: Next-generation clinical PET/CT systems can feasibly be used for high throughput, whole-body imaging of rodents, here with 6 animals simultaneously. This approach could benefit large rodent population imaging with efficient radiotracer management, particularly for short lived isotopes.

B-0994 11:50

Preliminary analysis of ultrasound imaging-based thermometry in ex vivo biological tissues

F. Giurazza, G. Frauenfelder, C. Massaroni, G. Galati, A. Picardi, E. Schena, B.B. Beomonte Zobel, S. Silvestri; Rome/IT (francescogiurazza@hotmail.it)

Purpose: Real-time monitoring of tissue temperature during percutaneous tumour ablation improves treatment efficacy, leading clinicians to adjustment of treatment settings. This study aims at assessing the feasibility of ultrasound-thermometry during laser ablation of biological tissue using a specific ultrasound imaging techniques based on elastography (ARFI).

Methods and Materials: ARFI uses high-intensity focused ultrasound pulses to generate 'radiation force' in tissue; this causes tissue displacements trackable using correlation-based ultrasound methods: the sensitivity of shear waves velocity is able to detect temperature changes. Experiments were carried out using a Nd:YAG laser (power: 5W) in three ex vivo pig livers. In each organ was placed a thermocouple close to the applicator tip (distance range: 1.5-2.5cm) used to record a reference temperature. Positioning of laser applicator and thermocouple was eco-guided. The organ was scanned by an echography system (Siemens ACUSON-S3000); propagation velocity was measured in a region of interest (ROI) of 1x0.5cm located close to the thermocouple, to investigate the influence of tissue temperature on shear wave velocity.

Results: Shear wave velocity has a very low sensitivity to temperature up to 55-60°C, and in all cases velocity is <5m·s⁻¹; for temperature >55-60°C velocity shows a steep increment. The system measures a value "over limit", meaning a velocity >10 m·s⁻¹.

Conclusion: Ultrasound thermometry during laser-ablation of biological tissue based on elastography shows an abrupt output change at temperatures >55-60°C. This issue can have a significant clinical impact, considering tumour necrosis when temperature crosses 55°C to define the boundary of the damaged volume.

10:30 - 12:00

Room M 5

Neuro

SS 1011b

Contrast media and perfusion imaging

Moderators:

H.R. Jäger; London/UK
A. Radbruch; Heidelberg/DE

B-0995 10:30

Gd presence in the brain: impact of daytime and anaesthesia

T. Taoka¹, G. Jost², S. Naganawa¹, H. Pietsch²; ¹Nagoya/JP, ²Berlin/DE (ttaoka@med.nagoya-u.ac.jp)

Purpose: The purpose of the current study is to investigate the influence of the circadian rhythm associated with the glymphatic activity on the presence of gadolinium the rat brain after repeated administration of gadolinium-based contrast agents (GBCA).

Methods and Materials: Twenty-four Han-Wistar rats were divided into four groups: Group 1; morning injection, Group 2; evening injection, Group 3; morning injection under short-duration anaesthesia and Group 4; morning injection under long-duration anaesthesia. Every subject received gadodiamide (1.8mmol/kg x 8 times over 2 weeks). 5 weeks after the last injection the brains were dissected and the Gd concentration in the cerebellum, pons and cerebrum was quantified by inductively coupled plasma mass spectrometry.

Results: In cerebellum, mean Gd concentrations were 3.58, 5.77, 2.95 and 2.51 (nmol/g tissue) in Groups 1, 2, 3 and 4, respectively. Likewise, mean Gd concentrations were 2.86, 5.04, 2.37 and 1.92 (nmol/g) in cerebrum, and 1.63, 1.76, 1.61 and 1.22 (nmol/g) in pons.

Conclusion: In the cerebellum and cerebrum, Gd concentration was highest in the group with evening injection, followed by morning injection, morning injection with short anaesthesia and morning injection with long anaesthesia GBCA administration. As rats are nocturnal animals, glymphatic system is expected to be more active during daytime. The results of this study might be explained by the higher glymphatic clearance following the morning injection, while a reduced glymphatic activity is present after the injection in the evening. Anaesthesia seemed to facilitate the glymphatic clearance of GBCA especially for longer durations.

Author Disclosures:

G. Jost: Employee; Bayer AG. **H. Pietsch:** Employee; Bayer AG.

B-0996 10:38

Quantitative assessment of spatial and temporal gadolinium deposition within the deep brain nuclei

G. Marie, P. Pożeg, J. Son Forget, J.P. Maeder, R. Meuli; *Lausanne/CH* (guillaume.marie@chuv.ch)

Purpose: Gadolinium is known to deposit in the deep brain nuclei, but no quantitative study has been done yet. This study aims to quantify the spatial and temporal dissemination of gadolinium in deep brain nuclei after repeated injections of linear GBCA.

Methods and Materials: We analysed retrospectively MRIs from a cohort of 30 patients at CHUV, who received at least 10 injections of non-ionic linear gadodiamide (Omniscan, GE healthcare, Piscataway, New Jersey). We calculated the difference of native T1 mean SI ratios of DN, GP, posterior thalamus, SN, superior colliculus and anterior putamen, to pons, not known to accumulate significantly gadolinium. We analysed the change rates in the SI ratios over the successive GBCA's administrations, using linear mixed effects modelling (Bernal-Rusiel et al., *NeuroImage*, 2013).

Results: We observed a significant, gradual and differential increase of SI ratios in ROIs after successive injections ($P < 0.001$), suggesting a gradual deposition in space and time where faster profiles of deposition in GP, DN and SN are demonstrated in comparison to superior colliculus, posterior thalamus and anterior putamen.

Conclusion: The deposit may occur gradually in space and time following the first injection of linear GBCAs, as quantitative measures show differential profiles of T1 hypersignals in basal ganglia structures. The different slopes observed in SI ratios may correlate with respective inner iron content of different nuclei and subsequent increased probability of transmetallation reactions with the GBCA ligand and of gadolinium unchelation.

B-0997 10:46

Gadolinium retention in the brain: an MRI relaxometry study comparing linear and macrocyclic types of gadolinium-based agents

Y. Forslin, J. Martola, S. Shams, S. Fredrikson, M. Kristoffersen Wiberg, T. Granberg; *Stockholm/SE* (yngve.forslin@ki.se)

Purpose: Gadolinium retention in the brain after administrations of gadolinium-based contrast agents (GBCA) has recently been demonstrated, predominantly in the dentate nucleus (DN) and globus pallidus (GP). This retention is associated with lasting high T₁-weighted signal and has been consistently shown for linear GBCAs. It is debated if the more stable macrocyclic GBCAs lead to in vivo-detectable alterations of the T₁. We aimed to quantitatively investigate T₁ in relation to linear and macrocyclic GBCA administrations in DN and GP by relaxometry in MS patients.

Methods and Materials: A multi-parametric MRI sequence was used to obtain longitudinal relaxation rates on a 3 T Siemens Magnetom Trio MRI scanner. In 89 consecutively recruited patients with multiple sclerosis (MS), regions of interest were drawn in the DN and GP by a resident in radiology blinded to the clinical information.

Results: Patients without previous exposure to GBCAs and those who had only received macrocyclic GBCA had longer T₁ relaxation, in DN and GP, in comparison with those patients who had received >1 linear GBCA (unpaired t test: $P = 0.036$ and $P = 0.021$, respectively). Higher number of administered linear (but not macrocyclic) GBCA was associated with faster T₁ relaxation in DN and GP (multiple regression analysis: $\beta = 0.32$, $P = 0.006$ and $\beta = 0.24$, $P = 0.046$). These results remained significant after correction for the MS disease duration.

Conclusion: Multiple GBCA administrations lead to shorter relaxation rates in GP and DN. Patients only receiving the macrocyclic type gadoterate meglumine have a longer relaxation rates in comparison with patients who received linear types of GBCA.

Author Disclosures:

S. Fredrikson: Other; has received honoraria for lectures, educational activities or consultancy from Allergan, Bayer, Biogen Idec, Genzyme, Merck Serono, Novartis, Sanofi and Teva.

B-0998 10:54

Increased signal intensity of dentate nucleus in multiple sclerosis patients with history of higher gadolinium-enhanced MRI scans

H. Naghibi, M. Mohammadzadeh, A. Fallahian, M. Shakiba, P. Sabatrasekh, H. Soroush; *Tehran/IR* (mm1361@yahoo.com)

Purpose: It has been mentioned that there is an increased probability of hyperintensity of dentate nucleus [DN] with more gadolinium [GAD]-enhanced MRI exams. Here, we have assessed this event in a group of multiple sclerosis [MS] patients with history of multiple GAD-enhanced MRI exams.

Methods and Materials: Totally 140 MS patients [mean age: 36.1±9.3 years (19-64); 86% female] with history of multiple GAD-enhanced MRI scans and 21 healthy controls were enrolled. DN hyperintensity was assessed visually in unenhanced T1-weighted MRI; signal intensity ratio [SIR] was calculated by setting region of interests [ROIs] on DN and pons and dividing DN SI into pons SI. Two groups of patients and controls and different patient subgroups [classified based on total number of MRI scans (more than 4 times versus others)] were compared regarding mean SIR and visual hyperintensity.

Results: Totally, 83 patients received contrast more than 4 times [68%]; among them, 26 showed DN hyperintensity [31.3%] while there was not hyperintensity in other patients and controls [both $P < 0.02$]. Mean SIR in patients and controls was 1.10±0.07 and 1.04±0.02, respectively [$P < 0.001$]. Mean SIR was 1.14±0.04 in DN hyperintense patients and 1.09±0.07 in other patients [$P < 0.001$]. Mean SIR in patients with higher contrast injection (>4) was 1.12±0.7 while it was 1.06±0.04 in other patients [$P < 0.001$]; after deleting patients with DN hyperintensity, these figures were 1.11±0.08 and 1.06±0.04, respectively [$P < 0.001$]. Correlation coefficient of SIR with contrast injection time was 0.66 [$P < 0.001$].

Conclusion: SI and visual DN hyperintensity are increased in more contrast injections. This could be due to tissue deposition of GAD. The clinical importance of this phenomenon should be assessed in future studies.

B-0999 11:02

USPIO-enhanced MRI study on electroacupuncture alleviating inflammatory response of permanent focal subacute-stage cerebral ischaemia in rats

S. Yang, F. Lu, S. Zhan; *Shanghai/CN*

Purpose: To evaluate the effectiveness of acupuncture on alleviating inflammatory response derived by macrophages recruitment during subacute period after permanent middle cerebral artery occlusion (pMCAO) in rats on enhanced MRI with ultrasmall superparamagnetic particles of iron oxides (USPIO).

Methods and Materials: Thirty-nine SD ischaemia rats with USPIO injection were established including sham-operation group (group A), pMCAO group without acupuncture (group B) and electroacupuncture pMCAO group (group C). Each group was further divided into 3 subgroups on 72h, 5d and 7d after ischaemia modeling. The signal intensity of the darkest area of infarction with corresponding mirror area was measured on T2W images after MR scanning. Then the darkest area of infarction and mirror area on SWI of groups B and C were measured and the ratios were calculated. Correlations between signal intensity ratios of the darkest area on T2W images and proportion of positive iron particles in anti-CD68 macrophages were analysed.

Results: The ratios of darkest area with 7d on T2W images were significantly higher in group C than in group B ($P < 0.05$). The ratios of darkest area with 5d and 7d subgroups were significantly higher in group C than that in group B on SWI ($P < 0.05$). The signal intensity ratios of the darkest area on T2WI were positively correlated with proportion of positive iron particles in anti-CD68 macrophages of 5d ($r = 0.483$, $P = 0.047$) and 7d ($r = 0.525$, $P = 0.033$).

Conclusion: With USPIO-enhanced MRI, we found electroacupuncture could alleviate inflammatory response derived by macrophages recruitment at the subacute stage in pMCAO rats.

B-1000 11:10

MRI perfusion weighted imaging and von Willebrand factor antigen (VWF:Ag) as predictors of prognosis in grade IV gliomas (GBM)

F.M. Doniselli, G. Marfia, S.E. Navone, L. Guarnaccia, R. Campanella, P. Summers, A. Costa; *Milan/IT* (fabio.doniselli@gmail.com)

Purpose: The prognostic significance of VWF:Ag and dynamic contrast-enhanced (DCE) and dynamic susceptibility contrast (DSC) MRI parameters in brain tumours is unknown. The aim of the study is to investigate the correlation of MRI-perfusion parameters and VWF:Ag with patient prognosis in GBM.

Methods and Materials: We reviewed a series of twenty-six patients with biopsy-proven GBM (males/females 18/8; median age 63 years) who underwent pre-operative DCE-MRI and DSC-MRI. VWF:Ag was analysed from pre-operative collected plasma sample (expressed as IU/dL). We measured the mean and maximum values of DSC-derived relative cerebral blood flow (rCBF) and volume (rCBV), DCE-derived volume transfer constant (K^{trans}), plasma volume (V_p) and reflux rate constant between the fractional volume of the extravascular space and blood plasma (K_{ep}). Non-parametric Mann-Whitney test was used.

Results: The median overall survival was 7 months (interquartile range=5-12). The distribution of vWF:Ag was bimodal, for which the median value (247 IU/dl) was used to separate the patients into two equally sized groups: a low vWF:Ag group (vWF:Ag<248; median=165, IQR=137-201) and a high vWF:Ag group (vWF:Ag>=248; median=410, IQR=329-528). When we compared the two groups, the median follow-up duration was 10 (IR=7-15) and 6 months (IR=3-7.5), respectively ($p = 0.02$). The median K^{trans} values were 0.31 (IR=0.16-0.50) and 0.53 min⁻¹ (IR=0.34-1.19), respectively ($p = 0.02$). The median K_{ep}

values were 1.79 (IR=1.23-2.70) and 3.89 min⁻¹ (IR=2.42-7.15), respectively (p=0.005). No significant differences in overall survival or correlation with VWF:Ag were found for other parameters.

Conclusion: These findings in a small group of patients suggest a role for VWF:Ag, K^{trans}, and K_{ep} as a prognostic indicator of post-operative survival of patients with GBM.

B-1001 11:18

3D high-resolution post-contrast imaging at 3T for the delineation of enhancing brain tumours: a comparison of three different techniques

L. Danielli¹, D. Distefano¹, E. Prodi¹, E. Ventura¹, G.C. Riccitelli¹, M. Reinert¹, A. Kaelin¹, A. Cianfoni^{1,2}, E. Pravata¹; ¹Lugano/CH, ²Bern/CH (lucia.danielli@eoc.ch)

Purpose: To prospectively investigate three different post-contrast 3D-T1-MRI techniques [Magnetization-Prepared-Rapid-Gradient-Echo (MPRAGE), Volumetric-Interpolated-Brain-Examination (VIBE), Sampling-Perfection-with-Application-optimised-Contrasts-using-different-flip-angle-Evolutions (SPACE)] in the assessment of contrast-to-noise-ratio (CNR), total volume (TV) and margins extent delineation (MED) of brain primitive tumours (pT) and metastases potentially amenable to surgical and/or conformal radiotherapy treatment.

Methods and Materials: Fifty contrast-enhancing lesions (38 pT and 12 metastases) were detected in 36 patients using 3T MRI with 1-mm MPRAGE, VIBE and SPACE sequences randomly acquired 5 minutes after 0.1ml/kg administration of gadobutrol. Lesions CNR and TV segmentation were performed by an experienced neuroradiologist using a validated semi-automated tool (SmartBrush, Brainlab) followed by manual refinement. For each combination of sequence pairs, MED mismatch was quantified using subtraction volumetric maps of the segmented lesions. Mann-Whitney and paired-samples Wilcoxon non-parametric tests were used to investigate between-sequences discrepancies in CNR, TV and MED subtraction volumes.

Results: In both pT and metastases, CNR was higher for SPACE compared to VIBE and MPRAGE (p-range<0.001-0.045) and for VIBE compared to MPRAGE (p-range<0.001-0.004). Larger TVs for pT were obtained with SPACE compared to VIBE (p=0.006), and for metastases with SPACE compared to MPRAGE (p=0.012). Discrepancy in MED was also found, with SPACE exceeding both VIBE (p=0.004) and MPRAGE (p=0.01) in pT, and MPRAGE only (p=0.005) in metastases.

Conclusion: We found technique-related differences in the CNR, TV and MED estimates of both brain pT and metastases. The relatively higher CNR seen with SPACE may account for the larger TV and MED. These findings may be relevant for treatment planning and response assessment.

Author Disclosures:

L. Danielli: Research/Grant Support; Scientific Research Advisory Board of the EOC (ABREOC).

B-1002 11:26

Comparison of arterial spin-labeling and dynamic susceptibility contrast MRI in detecting crossed cerebellar diaschisis in patients after glioma resection

T. Lin, F. Feng, Y. Lv, H. You; Beijing/CN (jasminelly@163.com)

Purpose: To compare two clinical most common used methods: arterial spin-labeling (ASL) and dynamic susceptibility contrast (DSC) MRI in detecting CCD in patients after glioma resection.

Methods and Materials: 145 patients with perfusion deficit in one hemisphere after glioma resection and radiotherapy were reviewed. Lesion locations were recorded. Visual qualitative analysis was performed by two neuroradiologists on ASL CBF map. Signal intensity asymmetry of bilateral cerebellar hemisphere was classified into three grades: grade I, isointense; grade II, slightly hypointense; grade III, markedly hypointense. Quantitative analysis by calculating asymmetry index (AI) of bilateral cerebellar hemispheres was performed on all 145 patients on ASL CBF, DSC rCBF and rCBV maps. One-way ANOVA was used to compare differences between the AIs in each method. Chi-squared or Fisher exact test was used for finding correlations between CCD and the locations of supratentorial lesions.

Results: The interrater agreement was excellent (kappa value = 0.852) in qualitative analysis. Thirty-nine (26.9%) patients were CCD positive (27 in grade II and 12 in grade III). Lesions affecting corona radiata (P<0.001), basal ganglia (P<0.001), temporal lobe (P=0.038) and insular lobe (P=0.031) were significantly associated with CCD. The mean AI of ASL CBF (27.59%±8.60%) was significantly larger than that of DSC rCBV (15.27%±12.66%) (P<0.001) and DSC rCBF (10.84%±8.56%) (P<0.001).

Conclusion: ASL is more sensitive than DSC rCBV and rCBF map in detecting CCD among patients after glioma resection. CCD is more likely to be associated with supratentorial lesion involved with corona radiata, basal ganglia, temporal lobe and insular lobe.

B-1003 11:34

MR-perfusion characteristics and PET/CT comparison in patients with gliomas after radiotherapy

A.V. Smirnova¹, O.V. Lukina², M. Cherkashin², N. Plakhotina², A. Tkachev³, M. Anishkin¹, M. Rukhlenko¹; ¹St. Petersburg/RU, ²Saint-Petersburg/RU, ³Volgograd/RU (smirnova_alina@bk.ru)

Purpose: To evaluate gliomas perfusion changes after radiotherapy in comparison with PET/CT data.

Methods and Materials: In our study 125 gliomas patients treated by different radiation modalities were initially included. 51 were excluded on different stages because they did not survive at month 24. All patients were divided into two groups: group A - gliomas I-II (n=21), group B - gliomas III-IVG (n=53). MR-perfusion and PET/CT (methionine) were performed before radiotherapy, and after 6, 12, 18 and 24 months.

Results: In group A initially increase CBV, methionine UI≥2.0; in follow-up 1 high CBV in 93%, UI≤2.2; decrease CBV in 7%, UI≤1.8; in follow-up 2 high CBV in 74%, UI≤2.7; reduction CBV in 26%, UI≤1.8; in follow-up 3 high CBV in 57%, UI≤3.2; in follow-up 4 reduction CBV in 43%, UI≤1.8; in follow-up 5 high CBV in 31%, UI≤4.1; reduction CBV in 69%, UI≤1.6 were detected. In group B initially not increased CBV, methionine UI≤1.5; in follow-up 1 low CBV in 83%, UI≤1.5; in follow-up 2 increase CBV in 17%, UI≤1.7; in follow-up 3 low CBV in 91%, UI≤1.5; increase CBV in 8%, UI≤1.7; in follow-up low CBV in 98%, UI≤1.5; increase CBV in 2%, UI≤1.5; in follow-up 5 low CBV in 100%, UI≤1.5.

Conclusion: Gliomas metabolism and perfusion in first year after radiotherapy characterised by multidirectional changes. Just after 2 years of surveillance we have detected strong CBV and UI reduction. We suggest that future investigations with strong study power will generate evidence for clear differentiation the gliomas relapse and postradiation brain damage.

B-1004 11:42

Can unenhanced brain magnetic resonance imaging be used in routine follow-up of meningiomas to avoid gadolinium deposition in the brain?

F. Kural Rahatli, F. Yildirim Donmez, Ç. Kesim, k. Haberal, H. Turnaoglu, A. Agildere; Ankara/TR (drkural@hotmail.com)

Purpose: We speculated that unenhanced brain MRI can be used in routine follow-up of patients with intracranial meningioma to avoid gadolinium deposition in the brain and allow measurement of meningioma dimensions from precontrast T2-weighted images. We investigated whether measurements on pre-contrast T2-weighted images and post-contrast T1-weighted images are correlated.

Methods and Materials: Thirty meningiomas with multiple enhanced brain MRI using linear non-ionic GDBCA (gadoversetamide) were analysed. The dimensions of meningiomas were measured on both axial precontrast T2-weighted images and axial postcontrast T1-weighted images. Signal intensity ratios were calculated for dentate nucleus-to-pons (DN/pons), dentate nucleus-to-cerebellar white matter (DN/cerebellum) and globus pallidus-to-thalamus (GP/thalamus).

Results: Size of six meningiomas increased, as determined from measurements on both axial precontrast T2-weighted images and axial postcontrast T1-weighted images. The signal intensity ratios showed a significant increase (p<0.005) from the first to last brain MRI. The mean DN/pons ratio at first MRI was 1.055±0.38 and 1.149±0.86 at the last MRI. The mean DN/cerebellum ratio at first MRI was 1.068±0.42 and 1.156±0.78 at the last MRI. The mean GP/thalamus ratio at first MRI was 1.077±0.24 and 1.136±0.58 at the last MRI.

Conclusion: Size of meningiomas in post-contrast axial T1-weighted images was correlation with that in pre-contrast axial T2-weighted images, that is, both showed tumour growth. DN/pons, DN/cerebellum, and GP/thalamus signal intensity ratios increased with multiple administrations of linear non-ionic GBAs in patients with normal renal function. Gadolinium deposition could be avoided in patients with meningioma using unenhanced brain MRI for follow-up scans.

B-1005 11:50

Perfusion abnormality in posterior inferior cerebellar artery termination of vertebral artery on arterial spin labelling and dynamic susceptibility contrast perfusion MRI

D. Park, T. Kim; Guri/KR (dwpark@hanyang.ac.kr)

Purpose: A posterior inferior cerebellar artery (PICA) termination of vertebral artery has been regarded as a normal variation of vertebrobasilar circulation. However, the perfusion condition of PICA territory in the cerebellum has not been evaluated. This study aims to present the perfusion abnormality in PICA termination of vertebral artery (PICA-VA) on arterial spin labelling (ASL) and dynamic susceptibility contrast (DSC) perfusion MRI.

Methods and Materials: Sixteen patients (M:F=8:8, 49-90 years old) who conducted brain MRI including MR angiography, and ASL and DSC perfusion MR studies and are found to have PICA-VA, are evaluated in this study. PICA-

Scientific Sessions

VA are associated with ipsilateral hypoplastic vertebral artery in 14 patients, and bilateral foetal type posterior cerebral artery in 2 patients.

Results: Hypoperfusion in PICA territory is detected on both ASL and time to peak (TTP) map of DSC perfusion MRI in 11 patients (68.7%), on only TTP perfusion MRI in 2 patients (12.5%), on only ASL perfusion MRI in 1 patient (6.3%) and not on both perfusion MRI in 2 patients (12.5%). Any clinical manifestations of vertebrobasilar insufficiency are not accompanied in 2 patients (12.5%).

Conclusion: PICA-VA that is regarded as normal variation, considerably have hypoperfusion in PICA territory of cerebellum. PICA-VA could have the clinical significance, especially in vertebrobasilar insufficiency, so perfusion study such as ASL or DSC perfusion MRI may help to evaluate the clinical status of vertebrobasilar insufficiency.

Scientific Sessions

Saturday, March 4

08:30 - 10:00

Sky High Stage

Musculoskeletal

MY 13

Musculoskeletal

Moderators:

M.S. Posadzky; Poznan/PL
M.F. Reiser; Munich/DE

B-1012 08:30

Spectral detector-computed tomography iodine density thresholds for the detection of vertebral metastases

N. Abdullayev, V. Neuhaus, M. Le Blanc, N. Grosse Hokamp, V. Maus, S. Lennartz, D. Maintz, J. Borggrefe; *Cologne/DE (Jan.Borggrefe@uk-koeln.de)*

Purpose: To evaluate quantitative iodine density mapping (IDM) from spectral detector computed tomography (SDCT) as a quantitative parameter for the separation of vertebral trabecular bone metastases (BM) and healthy trabecular bone (HTB).

Methods and Materials: This retrospective study includes portal venous SDCT datasets of cancer patients with and without known bone metastasis (n=43 and n=40, respectively). Target lesions as well as non-affected control vertebrae were defined by two radiologists in consensus using follow-up CT imaging, MRI and/or bone scintigraphy. IDM and its standard deviation (SD) were determined based on ROI measurements in BM and HTB of patients with and in HTB of patients without bone metastasis, and various reference tissues/vessels in both. Phantomless bone mineral density (vBMD) measurements of the lumbar spine were conducted.

Results: We found a significant difference between IDM of BM and HTB (mean 5.55 ± 0.98 vs. 3.57 ± 0.96) ($p < 0.0001$); however, there was a considerable overlap and a vBMD bias. A trivariate analysis including IDM, the inhomogeneity of the IDM as determined by the SD, and the normalization to the vertebral venous sinus improved the statistical separation of metastasis to a specificity of 100.0% and a sensitivity of 95.4% (AUC 0.98, $p < 0.05$ compared to univariate models).

Conclusion: SDCT allows for quantification of iodine in bone lesions which appears promising to serve as a parameter for the detection of bone metastases.

B-1013 08:34

Combining fractal- and entropy-based bone texture analysis for the prediction of osteoarthritis: data from the multicentre osteoarthritis study (MOST)

Z. Bertalan¹, S. Nehrer², R. Ljuhar¹, A. Fahrleitner-Pammer³, D. Ljuhar¹, H.-P. Dimai²; *Vienna/AT, ²Krems/AT, ³Graz/AT (rljuhar@gmail.com)*

Purpose: Osteoarthritis (OA) is the leading cause of long-term pain and disabilities associated with musculoskeletal disorders. Effective treatment depends on early detection and quantification of risk. Current disease parameters, like joint space width (JSW), have proven to be insufficient for the prediction of OA. The purpose of the present study was to investigate if combining bone texture analyses with JSW and joint space area (JSA) may improve prediction of OA.

Methods and Materials: Conventional posterior-anterior (PA) knee radiographs were obtained from the multicentre osteoarthritis study (MOST) database. Oriented texture algorithms were developed, using specific machine-learning algorithms. Selected areas used for textural analyses included 4 regions of interest (ROI) in the proximal tibia and one on each condyle of the distal femur. Furthermore, JSW/JSA were assessed using newly developed and fully automated software.

Results: 1092 radiographs obtained from one study centre were screened. 230 women, 344 men met the inclusion criteria, i.e. a Kellgren & Lawrence (KL) score of 0 at baseline. At month 84, 41 female, 79 male patients had developed $KL \geq 1$, and 189 female, 265 male patients remained at $KL = 0$. Area under the curve (AUC) for incident OA using JSW/JSA/clinical features was 0.67 ± 0.08 for women, 0.61 ± 0.1 for men. In contrast, combining texture, JSW/A and clinical features resulted in significantly improved AUC (0.80 ± 0.07 for women and 0.69 ± 0.1 for men, respectively).

Conclusion: This study provides strong evidence that a combination of textural analyses of plain radiographs together with JSW/A and clinical features is superior to JSW/A and clinical features alone in predicting incident OA.

B-1014 08:38

Delayed gadolinium-enhanced MRI of menisci and cartilage (dGEMRIM/dGEMRIC) in overweight patients with knee osteoarthritis

S. Hangaard¹, H. Gudbergson¹, C.L. Daugaard¹, H. Bliddal², J.D. Nybing¹, V. Casula³, M.T. Nieminen³, C.J. Tiderius⁴, M. Boesen²; *¹Frederiksberg/DK, ²Copenhagen/DK, ³Oulu/FI, ⁴Lund/SE (stine.hangaard.01@regionh.dk)*

Purpose: Changes in the menisci are associated with development of knee osteoarthritis (KOA). The aim of this study was to examine the delayed-gadolinium-enhanced-MRI-of-menisci (dGEMRIM) and its relationship with Kellgren-Lawrence grade (KLG) and with articular cartilage dGEMRIC.

Methods and Materials: 86 overweight patients with KOA (mean KLG 3) from the CAROT study had an intra-articular injection of Gd contrast. Four invasion times (50, 350, 650, 1410 ms) dGEMRIC and dGEMRIM were performed in 1.5 T. T1 relaxation time values were calculated for posterior weight-bearing femoral cartilage in the lateral knee compartment, and for the posterior horn of the lateral and medial menisci.

Results: For femoral cartilage (N=86) the mean T1 value was 441ms. The mean T1 value in the lateral menisci (N=85) was 498ms and for the medial menisci (N=62) mean T1 value was 484ms. A positive correlation was found between posterior medial and lateral menisci $R=0.62$ ($p < 0.0001$) and a similar trend was seen between lateral femoral cartilage and lateral menisci with $R=0.26$ ($p=0.02$). Comparing the meniscus from the most affected knee compartment to KLG showed trends toward increasing T1 values for KLG 1-3 and a decreasing T1 value for KLG 4.

Conclusion: The positive correlation between lateral and medial menisci indicates parallel degeneration processes in both knee compartments. The correlation between menisci and cartilage suggests concomitant, but different, degeneration in the two tissues in OA. The interpretation of inverse U-shaped relation between meniscal T1 values and KLG is in accordance with findings comparing various degrees of meniscal degeneration with dGEMRIM and proteoglycan content.

B-1015 08:42

Ultrasound of the posterior interosseous nerve in the arcade of Frohse

C. Tulay, S. Aubry, A. Podda, J. Behr; *Besancon/FR (wonder_angel15@hotmail.com)*

Purpose: To accurately assess the diameter of the posterior interosseous nerve (PIN) as it passes through the arcade of Frohse and to demonstrate that exist a physiological difference in anteroposterior diameter between the upstream, the entry point and downstream of the arcade.

Methods and Materials: Prospective monocentric study of the PIN in 30 healthy volunteers (sex ratio = 1) which have been examined bilaterally by ultrasound with a high frequency probe (18 MHz) in longitudinal section. The anteroposterior diameter of the PIN was measured at the entry point in the arcade of Frohse, 5mm upstream and 5mm downstream.

Results: The anteroposterior diameter of the PIN was $0.833 \text{ mm} \pm 0.208$, $0.6 \text{ mm} \pm 0.173$ and $0.486 \text{ mm} \pm 0.131$ respectively upstream, at the entry and downstream of the Arcade of Frohse. It significantly decreases by 27.2% between the upstream and entry point (-0.233 mm ; $p < 0.001$), by 16.6% between the entry point and downstream (-0.114 mm ; $p < 0.001$), and by 39% between the upstream and downstream (0.357 mm ; $p < 0.001$).

Conclusion: There is a physiological decrease in the anteroposterior diameter of the PIN as it passes through the arcade of Frohse, not to be wrongly considered as a compression of the nerve in the arcade.

B-1016 08:46

Safety and efficiency of treatment of partial supraspinatus tendon tear with injection of PRP and HA

C. Lupo¹, A. Meli², V. Incarboni², N. Casamassima², L. Callegari²; *¹Palermo/IT, ²Varese/IT (claudialu@live.it)*

Purpose: Evaluate safety and efficiency of treatment of partial supraspinatus tendon tears with intralesional injection of autologous platelet-rich plasma (PRP) associated with low molecular weight hyaluronic acid (HA 0.8%) under ultrasound guidance.

Methods and Materials: Between January and September 2016, we selected 84 patients, mean age 57, with an ultrasound diagnosis of partial tear of supraspinatus tendon; 48/84 confirmed with MRI. Before the treatment (T0), all patients were evaluated the pain with the visual analogue scale (VAS). After local ultrasound guided anaesthesia with lidocaine, an injection of glenohumeral joint with a 22G needle with lateral access was given, followed by needling of supraspinatus tendon and subsequent intratendineous injection with 2.5cc of (PRP) and 2cc of (HA0.8%), 3 injections, one every three weeks. The safety of the procedure was considered by the analysis of complications; efficacy was considered by clinical follow-up at six weeks after the procedure and imaging follow-up at six months in 84/84 patients with US and in 35/84 with MRI.

Results: 84/84 patients improved pain with a statistically significant difference ($p < 0.001$) of VAS scale before and after treatment without major complications. 55/84 patients showed some modification of the ultrasound and RM patterns.

Conclusion: Injection of (PRP) with (HA0.8%) is a well-tolerated procedure in treatment of partial the supraspinatus tendon tear with a marked improvement on pain.

B-1017 08:50

Improving the sensitivity of bone mineral density assessment using spectral detector CT

S. van Heden¹, K.-H. Su, F. Liang, J.-W. Kuo, D.W. Jordan, B. Eck, P.R. Ros, R. Muzic; *Cleveland, OH/US (svheden@vub.ac.be)*

Purpose: Bone mineral density (BMD) analysis by Dual-Energy x-ray Absorptiometry (DEXA) is complicated by false negatives due to overlapping densities in the projection area. Spectral Detector CT (SDCT) can overcome these limitations, while providing volumetric information. We investigated its performance for BMD assessment and compared it to DEXA and phantom-less Quantitative CT (QCT).

Methods and Materials: Ten uniform solutions of bone-like material, K_2HPO_4 ranging 0-600 mg/ml, were scanned in an acrylic phantom using the SDCT in four varying clinically relevant scan conditions. Images were processed to estimate the K_2HPO_4 concentrations. A model representing a human lumbar spine (European spine phantom) was scanned and used as calibration for linear regression analysis, so that our method could be retrospectively applied to abdominal SDCT scans of 20 patients who also had a QCT and DEXA. Performance of QCT, DEXA and our SDCT method were compared.

Results: There was excellent correlation ($R^2 > 0.99$, $p = 0.00$) between true and measured K_2HPO_4 concentrations for all scan conditions. Overall mean measurement error ranged from -11.49 ± 4.70 mg/ml ($-2.78 \pm 6.01\%$) to -12.34 ± 6.26 mg/ml ($-4.77 \pm 3.00\%$) depending on scan conditions. Using DEXA as gold standard, sensitivity and specificity for detecting decreased BMD in the scanned patients was 100 and 73.3%, and 100 and 40% for SDCT and QCT respectively.

Conclusion: SCDT has excellent sensitivity and high specificity for detecting decreased BMD, allowing its use for opportunistic screening or pre-operative planning.

B-1018 08:54

Virtual bone mineral density imaging with third-generation dual-energy CT for diagnosis of osteoporosis: a preliminary study

L. Wang, G. Shenchu, B. He, J. Chen; *Nantong/CN (wanglin_nt@126.com)*

Purpose: To quantitatively assess the diagnostic value of virtual bone mineral density (VBD) imaging at DECT for osteoporosis (OP).

Methods and Materials: Forty-five patients with vertebral trauma underwent DECT and DXA examinations of the lumbar 1-4. VBD images were derived from three-material decomposition algorithm using post-processing software ('Liver VNC', Syngo Via Dual Energy, Siemens), while the default CT values of fat, soft tissues, iodine and iodine slope were corrected to the yellow marrow, red marrow, calcium and calcium slope which were recommended in another software ('Bone Marrow', Syngo Via Dual Energy). CT attenuation values (VBD_Att), calcium density (VBD_CaD) and fat fraction (VBD_Fat) were measured for quantitative analyses. CT numbers on mixed images (LB_0.5) reconstructed with a merging coefficient 0.5 at DECT were recorded. Bone mineral density and T scores of lumbar measured with DXA served as the gold standard. Pearson correlation analysis was performed to compare DECT and DXA results. Diagnostic performance of VBD imaging was assessed by ROC analysis.

Results: A total of 166 lumbar were evaluated. LB_0.5 and VBD_Att were significantly different between OP and non-OP vertebral bodies (all $P < 0.01$). VBD_Att and VBD_CaD both had significant correlations with T scores (all $P < 0.01$). However, no significant correlation existed between VBD_Fat and T scores ($P = 0.08$). Furthermore, sensitivity and specificity for assessment of OP were 86.00%, 80.17% for VBD_Att and 84.00%, 81.03% for VBD_CaD. Diagnostic performance was significantly higher in VBD_Att and VBD_CaD compared to LB_0.5 (all $P < 0.01$).

Conclusion: Dual-energy VBD imaging shows acceptable diagnostic performance for OP in patients with vertebral trauma.

B-1019 08:58

Quantitative MRI of knee articular cartilage in hyperuricemia

X. Cai, X. Liu; *Guangzhou/CN (caixran@jnu.edu.cn)*

Purpose: To identify the changes of knee articular cartilage in patients with gout and with asymptomatic hyperuricemia.

Methods and Materials: Forty-three patients with gouty arthritis, 30 with asymptomatic hyperuricemia and 30 age- and sex-matched controls were included in this study. Multiple-TE FSE sagittal images of the knee were acquired using a 3T MRI scanner. T2 values of the superficial and deep zones

of the tibiofemoral and patellofemoral cartilages were analysed in sub-compartmental areas and compared among the three groups. Also, they were correlated with the serum uric acid level in those gout patients without taking any uric-acid-lowering drug.

Results: Cartilage thinning was observed in 13 out of 57 (22.81%) involved knees in patients with the symptomatic gout and 3 out of 36 (8.33%) examined knees with asymptomatic hyperuricemia. Significantly higher T2 values were observed at the superficial and deep zones of the cartilage in the gout patients compared to the normouricemic controls. However, no significant difference was found in T2 values of superficial and deep zones of the cartilage between the asymptomatic hyperuricemia patients and normouricemic controls. Moderate positive correlation was found between the T2 value of superficial zone of the cartilage with serum uric acid level.

Conclusion: Patients with gout demonstrate increased T2 value at the superficial and deep zones of the knee cartilage indicative of early change in cartilage matrix composition. Cartilage thinning also occurs more frequently in those patients. The high serum uric acid level could accelerate the cartilage injuries in gouty patients.

B-1020 09:02

In vivo quantitative 4D-CT analysis of carpal kinematics with radioscapoid and luno-capitate angles during radio-ular deviation: feasibility and clinical interest

A. Rauch; *Nancy/FR (aym.rauch@gmail.com)*

Purpose: To study the variation of radioscapoid (RSA) and lunocapitate (LCA) angles during wrist radio-ular deviation (RUD) using semi-automatic quantitative 4D-CT in patients with and without scapholunate-ligament tears (SLT).

Methods and Materials: 37 patients with suspected scapholunate instability were prospectively evaluated with 4D-CT and CT-artrography of the wrist. The study was approved by the local ethics committee and all patients signed an informed consent. Various dynamic parameters (mean, amplitude, maximal angle, standard deviation (SD), angular coefficient of variation (ACV)) describing RSA and LCA variation during wrist RUD were calculated and compared in patients with and without SLT by two readers.

Results: The mean values for RSA and LCA in the control group varied, respectively, from $102.98^\circ \pm 7.6^\circ$ to $104.47^\circ \pm 8.89^\circ$ and $85.92^\circ \pm 9.37^\circ$ to $90.09^\circ \pm 10.56^\circ$ with ACV from 10.78% to 11.03% and 13.49% to 13.52% for readers one and two, respectively. The inter-observer variability was excellent for RSA (ICC = 0.82) and substantial for LCA (ICC = 0.79). LCA amplitude, SD and maximal angle were significantly smaller in SLT group (p varied from 0.0001 to 0.0026), respectively, from 36% to 44%, 37% to 44% and 13% to 19%. RSA amplitude tended to be smaller in SLT group (18% to 27%, p varied from 0.0295 to 0.1328). LCA yielded the best sensitivity for SLT (71-91%) while RSA yielded the best specificity (87-100%).

Conclusion: 4D-CT can quantitatively assess carpal kinematics during RUD which could improve the diagnosis and prognostic evaluation of patients with SLT.

B-1021 09:06

Detection of osseous metastases using dual-energy CT with material decomposition algorithms: phantom development and preliminary clinical validation

H.-C. Huang¹, B.M. Yeh², R. Srinivasan², Y. Sun²; ¹Taipei City/TW, ²San Francisco, CA/US (hjround@gmail.com)

Purpose: Meta-analysis studies have shown that the conventional single-energy computed tomography (SECT) has limited ability in detecting subtle bone metastases. The purpose of this study was to use dual-energy CT (DECT) with bone-water material decomposition algorithms to detect nearly isodense bone metastases in phantoms, and to validate its use with retrospective patient DECT scans which were initially read as negative for bone metastases, but later detected by other imaging modalities or at follow-up CT.

Methods and Materials: We constructed 51 semi-anthropomorphic lumbar spine phantoms randomly embedded with 75 simulated tumours (25 mild lytic, 25 isodense, and 25 mild sclerotic). These phantoms were scanned in a rapid-kilovoltage-switching DECT scanner. Two radiologists independently reviewed images from 70 keV virtual monochromatic reconstruction and 4 material decomposition algorithms (hydroxyapatite-water, water-hydroxyapatite, cortical bone-water, water-cortical bone). We recorded reviewer's response regarding the presence of tumours. The sensitivity and specificity of different reconstruction algorithms were evaluated with McNemar test. The tumour conspicuity scores were recorded in 3-point Likert scales and then evaluated by Wilcoxon signed rank test. Finally, we validated our testing algorithms by retrospectively reviewing patients' images in our institution.

Results: Hydroxyapatite-water material decomposition algorithm achieved higher sensitivity in detecting isodense lesions (38% vs 18%, $p = 0.013$) and possessed higher tumour conspicuity score ($p < 0.0001$) as compared to the 70

keV reconstruction in the phantom study. Hydroxyapatite-water algorithm also detected more tumours in the retrospective patients' studies.

Conclusion: DECT with hydroxyapatite-water material decomposition may help detect subtle spine metastases. Further study in prospective clinical scans is warranted.

Author Disclosures:

B.M. Yeh: Author; Author with Royalties, Oxford University Press. Shareholder; Nextrast, Inc. **R. Srinivasan:** Grant Recipient; Seed Grant, Department of Radiology and Biomedical Imaging, UCSF.

B-1022 09:10

High diagnostic accuracy of k_{ep} on dynamic contrast-enhanced MRI perfusion in identifying vertebral malignancy

M. Verma, S. Sood, B. Singh, M. Thakur, S. Sharma, S. Sharma; *Shimla/IN (mansiverma1608@gmail.com)*

Purpose: Vertebral lesions are not easily amenable to biopsy due to inherent risks associated with this invasive procedure. There is considerable overlapping of radiologic features of benign and malignant lesions on conventional MRI. We performed this study to evaluate the role of dynamic contrast-enhanced (DCE) MRI perfusion parameters in differentiating malignant from benign lesions.

Methods and Materials: We studied all patients presenting to our hospital with a radiologic evidence of vertebral lesions from July 2016 through June 2017. We performed DCE-MRI of spine on 1.5 T scanner using 3D VIBE sequence after intravenously injecting 0.1mmol/kg body weight of gadopentetate dimeglumine. We used Tofts model to calculate DCE parameters that included K^{trans} , k_{ep} , V_e and $iAUC$. We compared the means of each perfusion parameters by type of lesion (benign/malignant) at 0.05 significance level and performed ROC curve analysis.

Results: We could confirm histologic/cytologic diagnosis in 35 of the 45 patients recruited. Of these 19 were tubercular and 16 malignant lesions. The mean (\pm sd) of k_{ep} (min^{-1}) was significantly higher (2.89 ± 3.3) in malignant compared to benign lesions (0.81 ± 0.19), whereas V_e (ml/g) was significantly lower in malignant (0.27 ± 0.13) compared to benign lesions (0.47 ± 0.12) at 0.05 significance level. k_{ep} cut-off of $\geq 1.17 min^{-1}$ had a sensitivity of 93.8% and specificity of 100% with a diagnostic accuracy of 94.4% in detecting malignant disease.

Conclusion: High k_{ep} is highly suggestive of malignant lesions. We recommend k_{ep} cut-off of $\geq 1.17 min^{-1}$ that was found to have high diagnostic accuracy in identifying malignant lesions.

B-1023 09:14

Complementary metal artefact reduction of total hip replacements by monoenergetic and O-MAR reconstructions in spectral-detector computed tomography

K.R. Laukamp, S. Lennartz, V. Neuhaus, N. Grosse Hokamp, R. Rau, M. Le Blanc, N. Abdullayev, D. Maintz, J. Borggreffe; *Cologne/DE (kai.laukamp@uk-koeln.de)*

Purpose: This study compares metal artefact (MA) reduction in imaging of total hip replacements (THR) using virtual monoenergetic images (VMI), for MA reduction specialised iterative reconstructions (O-MAR) and conventional images (CI) from spectral-detector computed tomography (SDCT).

Methods and Materials: 27 SDCT datasets of patients carrying THR were included. CI, O-MAR and VMI with different energy levels (60-200keV) were reconstructed from the same scans. MA width was measured. Attenuation (HU), noise (SD) and contrast-to-noise ratio (CNR) were determined in: extinction artefact, adjacent bone, muscle and bladder. Two radiologists assessed artefact reduction and image quality subjectively.

Results: In comparison to CI, VMI (200keV) and O-MAR showed a strong artefact reduction (MA width: CI 29.9 ± 6.8 mm, VMI 17.6 ± 13.6 mm, $p<0.01$; O-MAR 16.5 ± 14.9 mm, $p<0.001$; MA density: CI -412.1 ± 204.5 HU, VMI -279.7 ± 283.7 HU; $p<0.01$; O-MAR -116.74 ± 105.6 HU, $p<0.001$). In strong artefacts reduction was superior by O-MAR. In moderate artefacts VMI was more effective. O-MAR showed best noise reduction and CNR in bladder and muscle ($p<0.05$), whereas VMI were superior for depiction of bone ($p<0.001$). Subjective assessment confirmed that VMI and O-MAR improve artefact reduction and image quality ($p<0.001$).

Conclusion: O-MAR and VMI (200keV) yielded significant MA reduction. Each showed distinct advantages regarding effectiveness of artefact reduction and assessment of adjacent bone, muscle and pelvic organs.

B-1024 09:18

Ultra-high field 7 Tesla MRI and biomechanical investigation of vertebral bone microarchitecture

D. Guenoun, A. Foure, M. Pithioux, S. Guis, T. Le Corroller, V. Pauly, P. Chabrand, P. Champsaur, D. Bendahan; *Marseille/FR (daphne.guenoun@ap-hm.fr)*

Purpose: to investigate bone microarchitecture parameters of human ex-vivo vertebrae using ultra-high field 7Tesla MRI (7T MRI).

Methods and Materials: Twenty four vertebrae (L2, L3, and L4) from eight cadavers were studied using 7T MRI. Their Bone mineral densities (BMD) were investigated using dual energy x-ray absorptiometry. Then, all specimens underwent mechanical compression tests to failure. The failure load (in Newton) and constraint (in megapascal) were measured. Bone volume fraction (BV/TV), trabecular thickness (Tb.Th), and trabecular spacing (Tb.Sp) were measured in MRI using a digital topological analysis (Bone J). Measurements were recorded by two observers to characterize the interrater reliability. Statistical analyses were performed using SPSS. Correlations between variables were analyzed using Spearman correlations and stepwise regression. A p value of 0.05 was considered as significant.

Results: the inter-rater reliability for bone microarchitecture parameters quantification was very good. The failure load and constraint measured during the compression tests were significantly correlated with BV/TV, Tb.Sp and BMD while Tb.Th was correlated with constraint only ($p<0.05$). Stepwise regression with backward elimination demonstrated that combining BV/TV and BMD improved the relationship with the constraints from an adjusted $r^2=0.384$ for BMD alone to an adjusted $r^2=0.414$ for BMD+BV/TV.

Conclusion: we demonstrated for the first time that the variables characterizing the vertebral bone microarchitecture in 7T MRI were significantly correlated with biomechanical parameters. In addition, we illustrated that combining BMD and 7T MR, trabecular bone analysis provided additional information regarding vertebral bone strength in comparison with DXA alone.

B-1025 09:22

Postoperative evaluation of a arthroscopic coracoid bone block surgery with CT-Scan.

O. Andreani¹, P. Gendre², C. Dekimpe¹, A. Rudel¹, N. Amoretti¹, P. Boileau¹; ¹Nice/FR, ²Cagnes sur Mer/FR (andreani.olivier@gmail.com)

Purpose: To know and use the criteria of good positioning and bone consolidation of a coracoid bone block. To evaluate the results in terms of positioning and bone consolidation of an arthroscopic technique of Latarjet coracoid bone block.

Methods and Materials: A retrospective monocentric study of 161 patients who underwent a Latarjet coracoid bone block surgery under arthroscopy by a senior operator for management of anterior chronic shoulder instability. All patients were monitored at 15 days and 6 months by CT-scan. The positioning of the stop was evaluated in the horizontal and vertical plane. Bone consolidation was evaluated at 6 months.

Results: The bone block was sub-equatorial in 151 (93%) patients, equatorial in 9 (5%) and supra-equatorial in 2 (1%). The bone block was flush in 153 patients (94%), overflowing in 8 (4.5%) and medial in 1 patient (0.5%). At 6 months postoperative, complete bone consolidation was obtained in 147 patients (90.5%). 14 (9%) had a bone block pseudarthrosis, one a fractured of the bone block, one a complete lysis and one a bone block migration. The clinical prognostic factor of lack of consolidation was smoking. Five patients had recurrent instability.

Conclusion: CT-scan is an easy and reproducible tool for postoperative osseous evaluation of Latarjet arthroscopic surgery. This technique gives good results in terms of positioning and consolidation of the coracoid bone block.

B-1026 09:26

Volumetric bone mineral density assessment of the lumbar spine using a novel phantomless dual-energy CT postprocessing algorithm in comparison to dual x-ray absorptiometry

C. Booz¹, P.C. Hofmann², M. Sedlmair¹, T. Flohr², B. Schmidt², S.S. Martin¹, D. Leithner¹, T.J. Vogl¹, J.L. Wichmann¹; ¹Frankfurt a. Main/DE, ²Forchheim/DE (boozchristian@gmail.com)

Purpose: Current techniques for the evaluation of bone mineral density (BMD) commonly require phantom calibration. The purpose of this study was to evaluate a novel algorithm for phantomless in vivo dual-energy computed tomography (DECT)-based volumetric assessment of BMD of the lumbar spine in comparison to dual x-ray absorptiometry (DXA).

Methods and Materials: This retrospective study was approved by the institutional review board. The requirement to obtain informed consent was waived. Data from clinically indicated DECT and DXA examinations within 2 months of 47 patients were evaluated. Using a novel automated dedicated postprocessing algorithm for DECT, the trabecular bone of lumbar vertebrae L1-L4 was analysed after five volumes of interest on different slices had been

manually defined for each vertebral body. Pearson product-moment correlation, Bland-Altman plot and further regression analyses were calculated for statistical analysis.

Results: A total of 186 lumbar vertebrae in 47 patients (24 male, 23 female) were analysed. Mean BMD of L1-L4 determined by DXA was 0.986 g/cm², and 20 patients (42.6%) showed an osteoporotic BMD according to guidelines of the World Health Organisation. Average DECT-based BMD of L1-L4 was 88.68 mg/cm³. According to CT guidelines of the American College of Radiology DECT measurements identified seventeen patients (36%) with an osteoporotic BMD. Statistical analysis showed a moderate correlation between volumetric and areal BMD values based on DECT and DXA with a Pearson's product-moment correlation coefficient of $r=0.421$.

Conclusion: A novel DECT-based postprocessing algorithm allows for phantomless volumetric BMD assessment of the trabecular bone of lumbar vertebrae.

Author Disclosures:

P.C. Hofmann: Employee; Siemens Healthineers. **M. Sedlmair:** Employee; Siemens Healthineers. **T. Flohr:** Employee; Siemens Healthineers.

B. Schmidt: Employee; Siemens Healthineers. **J.L. Wichmann:** Speaker; GE Healthcare, Siemens Healthineers.

B-1027 09:30

Learning curve of an ultrasound-guided percutaneous release of carpal tunnel: a cadaveric study

O. Andreani, C. Dekimpe, C.-P. Raffaelli, N. Amoretti; *Nice/FR*
(andreani.olivier@gmail.com)

Purpose: The aim of our study was to evaluate the feasibility and the learning curve of an ultrasound-guided percutaneous carpal tunnel release.

Methods and Materials: 14 carpal tunnel releases were carried out, on unembalmed cadavers, 7 by a senior and 7 by a junior radiologist. Sonographic evaluation, with 18 MHz probe, was first performed to detect the anatomical variant and length of the retinaculum. After hydrodissection by Xylocaine of the carpal tunnel, we used an Acufex knife (2,5 mm; Smith and Nephew®) to cut the retinaculum, under ultrasonographic guidance. We evaluated the time (from the first injection of Xylocaine until the knife was taken off); success of the procedure: complete release of retinaculum and absence of complication (lesion of the median nerve and its branch, especially the thenar motor branch, or vascular structure, especially the arterial palmar arch), checked by dissection after procedure; and size of cutaneous incision.

Results: The mean time of the procedure was 14 minutes. (11 min senior versus 17 min junior). The section was complete at the 4th procedure for the senior and at the 5th procedure for the junior radiologist. No lesion of the median nerve or vascular structure was observed. The release was incomplete in 7 firsts' wrists, due to an incomplete section of the distal retinaculum (lack of 10 mm on average). Several passages were associated with more frequent complete section. The mean size of the incision was 3 mm.

Conclusion: We observed a rapid learning curve of carpal tunnel release with ultrasound guidance, for a senior or junior radiologist, without difference in the term of success. This procedure seems to be safe, reproducible and minimally invasive.

B-1028 09:34

The accuracy of ultrasound with and without sonoelastography in the diagnosis of partial-thickness rotator cuff tears with MDCT arthrography and arthroscopic verification

V.E. Gazhonova, M. Emelianenko, M. Onishchenko; *Moscow/RU*
(vx969@yandex.ru)

Purpose: To compare the diagnostic accuracy of conventional US and sonoelastography (SE) for the diagnosis of partial-thickness rotator cuff tears (RCTs) with MDCT-arthrography and arthroscopic correlation.

Methods and Materials: 50 shoulders with suspected partial RCT based on MRI or US findings were assessed with conventional US and SE. SE images were evaluated by reviewers using experimentally proven colour grading system (grade 2, red colour - RCT, grade 1, green - tendonitis, grade 0, blue - normal). Strain ratios (SR) in the affected region of the tendon were calculated in comparison to the deltoid muscle. MDCT arthrography and arthroscopy were used as reference methods for verification.

Results: Using conventional US, 75% (24 of 32) of the partial RCTs were found correctly. Using SE, 28 RC tendons were categorised as grade 2, 15 as grade 1, and 7 as grade 0. SR in RCT regions <1.2 was in 30 shoulders, and SR >1.2 in 20 patients. Evaluation of interobserver reliability of the SE findings showed "almost perfect agreement" with a weighted kappa coefficient of 0.83 for colour SE grades. By comparing SE with the reference methods, colour grading system had a positive correlation ($r=0.84$, $p<0.001$), and SR values <1.2 were characteristic for RCT with positive correlation ($r=0.93$, $p<0.001$). In diagnosing a partial RCT, SE was more sensitive than conventional US ($p<0.05$).

Conclusion: SE using colour grading scale and quantification of SR values in the affected tendon's regions is a more sensitive and specific technique for diagnosing partial-thickness RCT than conventional US.

B-1029 09:38

Iterative reconstruction improves image quality in virtual non-calcium images of the spine for the detection of bone marrow edema in patients with vertebral compression fractures

N. Engelhard¹, K.-G. Hermann¹, M. Fuchs¹, M. Pumberger¹, M. Putzier¹, J. Mews², B. Hamm¹, T. Diekhoff¹; ¹Berlin/DE, ²Neuss/DE
(nils.engelhard@charite.de)

Purpose: Dual-energy computed tomography (DECT) allows detection of bone marrow edema (BME) after vertebral compression fractures using virtual non-calcium imaging (VNCa). The aim of this study was to evaluate, which reconstruction offers the best image quality.

Methods and Materials: 18 patients over 50 years of age with available CT raw-data were retrospectively included. DECT was performed on a single-source machine (80/135 kVp sequential volume acquisition) and reconstructed using filtered back projection (FBP) and iterative reconstructions (IR) with three different iteration levels (IR1-IR3). VNCa images were generated using a raw-data (RD) and an image-data (ID) based software. Target vertebrae (TV) with fracture and BME in STIR sequence and normal appearing reference vertebrae (RV) were defined. Signal-to-noise ratio (SNR) and contrast-to-noise ratio (CNR) were calculated. Intervertebral ratio (IVR) served as measurement for the detectability of BME. Friedman-Test with multiple comparisons was applied.

Results: 39 TV and 18 RV were included. RD showed significantly inferior SNR ($p = 0.0001-0.0003$) compared to ID. CNR differences were only significant for FBP vs IR3 ($p = 0.002$). In ID, IR gradually improved SNR values, however, differences were only significant for FBP vs IR3 ($p = 0.005$). For CNR there was no significant difference. IVR improved with increasing iteration levels, however, differences were only significant for the comparison to FBP ($p = 0.03-0.0008$). We found no differences of IVR comparing RD and ID.

Conclusion: IR improved the image quality and detectability of BME in DECT. The ID was superior to the RD based approach.

Author Disclosures:

J. Mews: Employee; Toshiba MS.

B-1030 09:42

T2 relaxometry of cartilage and meniscus and semi-quantitative assessment of the knee using DESS: a 5-minute MRI scan

S. Eijgenraam¹, A. Chaudhari², G. Gold², M. Reijman¹, E. Oei¹, B. Hargreaves²; ¹Rotterdam/NL, ²Stanford, CA/US (s.eijgenraam@erasmusmc.nl)

Purpose: Quantitative MRI measures such as T2 relaxation times of cartilage and meniscus, and semi-quantitative assessments such as MRI Osteoarthritis (OA) Knee Score (MOAKS), are commonly used to track spatial and temporal changes of knee-OA. Acquiring these biomarkers currently requires multiple MR sequences, resulting in long acquisition-times. We evaluated the double-echo steady-state (DESS) sequence with an acquisition-time of only five minutes for simultaneous T2 relaxometry of cartilage and meniscus, and MOAKS scoring, in patients with no, mild and moderate knee-OA.

Methods and Materials: 54 patients (20, 18 and 16 with Kellgren-Lawrence (KL) grades 0, 2, and 3 resp.) were scanned using DESS and a clinical multisequence knee-protocol. MOAKS was performed with only DESS (with multiplanar reformatting). Mean T2-values of cartilage and meniscus were calculated on single slices. Statistical testing between KL-groups was performed using Students T-Tests. Correlation between T2-values and MOAKS was assessed using linear regression analysis.

Results: Mean T2-values in cartilage, obtained with DESS, were 37.7 ± 4.1 , 44 ± 8 and 50.8 ± 8.4 ms for KL0, KL2 and KL3 resp. ($p < 0.001$). In menisci, mean T2-values of 15.4 ± 3.3 , 18 ± 3.3 and 21 ± 6.4 ms were found for KL0, KL2 and KL3 resp. ($p < 0.001$). T2-values showed a good correlation with corresponding MOAKS-cartilage findings ($r = 0.61$, $p = 0.002$).

Conclusion: Simultaneous quantitative T2 and morphological assessment of cartilage and meniscus with a 5-minute DESS-sequence show consistent outcomes with increasing stages of degeneration, making this sequence a promising tool for OA research.

B-1031 09:46

Correlation of body mass index with paraspinal muscle fatty degeneration in non-diabetic patients with lumbar spinal canal stenosis: results from 685 patients

S. Winkhofer¹, J. Burgstaller¹, U. Held¹, T. Finkenstaedt¹, F. Del Grande², G. Andreisek³, J. Steurer¹, N. Bolog⁴; ¹Zurich/CH, ²Lugano/CH, ³Münsterlingen/CH, ⁴Münchenstein/CH (Sebastian.Winkhofer@usz.ch)

Purpose: Purpose of this study was to investigate the correlation between lumbar muscle fatty degeneration assessed by magnetic resonance imaging (MRI) and body mass index (BMI) in a large non-diabetic patient group with lumbar spinal stenosis (LSS).

Methods and Materials: MRI images of 685 patients (52% female, mean age 74 years, interquartile range 67 - 80 years) with LSS were analysed in this institutional review board-approved study. Muscle degeneration was assessed by two independent readers on axial T2 weighted images using a modified 5-grades Goutallier classification. The correlation between muscle degeneration and BMI was calculated using the non-parametric Spearman coefficient test.

Results: The following distribution of muscle degeneration was found in the 685 patients: grade 0: 136 (20%), grade 1: 265 (39%), grade 2: 220 (32%), grade 3: 41 (6%), grade 4: 23 (3%). The mean BMI was 26.6 kg/m², interquartile range 23.8 to 29.7. Correlation analysis between BMI and the muscle stage degeneration in 5 ordinal categories was 0.060 for female patients (p = 0.26), 0.148 for male patients (p = 0.007), and 0.067 for all patients (p = 0.08).

Conclusion: The weak correlation between BMI and the degree of muscle degeneration indicates that overweight might not be an important potential source of paraspinal muscle degeneration in non-diabetic patients with LSS.

10:30 - 12:00

Room C

Neuro

SS 1411a

Neurodegeneration/dementia

Moderators:

E. Gangemi; Rome/IT
M. Vasco Araújo; Recife, PE/BR

K-19 10:30

Keynote lecture

M. Vasco Araújo; Recife, PE/BR

B-1032 10:39

Diffusion tensor imaging in idiopathic normal-pressure hydrocephalus: clinical and CSF flowmetry correlations

I. Grazzini, G. Cuneo, F. Redi, C. Caccialupi, K. Sammartano, C. Ciccostoto; Arezzo/IT (irene.grazzini@gmail.com)

Purpose: Diffusion tensor imaging (DTI) is a non-invasive magnetic resonance (MR) technique that provides information about the orientation and the anisotropy of the white matter tracts, and may delineate microstructural changes in cerebral white matter. We analysed DTI quantitative parameters in idiopathic normal-pressure hydrocephalus (INPH) patients and investigated the relationship between DTI findings and clinical scores and CSF flow velocity.

Methods and Materials: 15 consecutive patients with INPH and Evans Index >0.3 and 15 age-matched controls underwent MR CSF flowmetry and DTI using a 1.5T system. Fractional anisotropy (FA), mean diffusivity (MD), axial diffusivity (AD) and radial diffusivity (RD) values were calculated using a region-of-interest (ROI) atlas-based tract mapping in 9 cerebral areas and compared among the two groups. In addition, for INPH patients, DTI parameters were correlated to clinical scores (Mini-Mental State Examination (MMSE) and Frontal Assessment Battery (FAB)) and CSF flow velocity.

Results: Mean FA was significantly lower in the INPH group than in the control group for the forceps minor; the INPH group had significantly higher mean AD for the genu of the corpus callosum (p<0.05). We did not find significant correlation between the DTI parameters and CSF flow velocity and MMSE, whilst we observed a negative correlation between forceps minor FA and FAB.

Conclusion: Our findings suggest that DTI will provide a non-invasive biomarker of white matter changes in patients with INPH. Moreover, DTI may offer a prognostic tool, over CSF flow velocity, to help identify INPH patients who may benefit from surgical intervention.

B-1033 10:47

A survey for neuroimaging harmonization needs for large-scale neurodegenerative biomarker studies

J. Jovicich¹, F. Barkhof^{2,3}, C. Babiloni⁴, K. Herholz⁵, B.N. van Berckel², C. Mulert⁶, G. Frisoni^{7,8}, SRA-NED JPNP Working Group¹; ¹Mattarello/IT, ²Amsterdam/NL, ³London/UK, ⁴Rome/IT, ⁵Manchester/UK, ⁶Hamburg/DE, ⁷Brescia/IT, ⁸Geneva/CH (jorge.jovicich@unitn.it)

Purpose: The European Joint Programme on Neurodegenerative Disease Research committed to our working group SRA-NED (<http://www.sraned.org/>) the survey of the international community for identifying (1) current barriers for a harmonized use of MRI/PET/EEG biomarkers of neurodegenerative diseases and (2) community-driven solutions to overcome them.

Methods and Materials: A 10-minute survey was developed to gather information from relevant communities (neuroimaging consortia, industry, and more than 30 international researcher and medical associations). The survey evaluated high-level barriers to participate in multicentric studies, biomarkers to be prioritized and current challenges for modality-specific harmonization issues.

Results: 459 participants completed the survey (MRI 53.6%, EEG 30.3%, and PETSPECT 16.1%). Participants represented a strong multidisciplinary community, dominated by research and academia including industry and clinical settings (Europe 75%, North and South America 20%, and Asia, Oceania and Africa 5%). In all modalities (MRI/PET/EEG), more than 60% of the participants reported significant difficulties for including neuroimaging markers in multicentric clinical studies, indicating barriers for each neuroimaging modality. Survey participants converged to specific requests about support needs for a more productive use of MRI/PET/EEG biomarkers. Results allowed making concrete suggestions for potential solutions, inspiring a roadmap for the future investments of international sponsors for clinical trials in the neurodegenerative diseases.

Conclusion: To our knowledge, this survey represents the largest in the clinical neuroimaging community in the field of neurodegenerative diseases. The results support a strategic research agenda of future investments to exploit the potential of the MRI/PET/EEG biomarkers in large multicentric studies in neurodegenerative diseases.

B-1034 10:55

Subcortical nuclei in Alzheimer's disease: a volumetric and diffusion kurtosis imaging study

M.-L. Wang, W. Li; Shanghai/CN (doctor-mingliang@sjtu.edu.cn)

Purpose: To investigate the volumetric and DKI parameter changes of subcortical nuclei in AD, and their relationship with cognitive function.

Methods and Materials: A total of 17 mild AD patients, 15 moderate to severe AD patients, and 16 controls underwent examinations of neuropsychological tests, MRI scans. Volume, mean kurtosis (MK), mean diffusivity (MD), and fractional anisotropy (FA) were measured in subcortical nuclei including the hippocampus, thalamus, caudate, putamen, pallidum, and amygdala. MRI parameters were compared among groups. Correlation analysis was performed between subcortical nuclei volume, DKI parameters, and MMSE score.

Results: Significant volume reduction was seen in left hippocampus in mild AD, and bilateral hippocampus, thalamus, putamen, left caudate and right amygdala in moderate to severe AD (P<0.05). Increased MD values were observed in left hippocampus, left amygdala and right caudate in mild AD, and bilateral hippocampus and right amygdala in moderate to severe AD (P<0.05). Decreased MK values were observed only in bilateral hippocampus in moderate to severe AD (P<0.05). No group significances were found in FA value. MMSE score was positively correlated with volume of bilateral hippocampus, thalamus, and putamen, and MK value of left hippocampus (P<0.05). A negative correlation was found between MMSE score and MD value of bilateral hippocampus and left amygdala (P<0.05).

Conclusion: Mild AD mainly has microscopic subcortical changes revealed by increased MD value, and moderate to severe AD mainly has macroscopic subcortical changes revealed by volume reduction. MK is more sensitive in the late AD than mild AD.

B-1035 11:03

Structural and functional changes in resting brain activity in neurodegeneration according to VBM and rsfMRI comparison

E. Seliverstova, Y. Seliverstov, M. Krotenkova, R. Kononov, A.N. Sergeeva, S. Illarionshkin, S. Morozova; Moscow/RU

Purpose: To study structural and functional pattern in resting brain network (default mode network) in early stages Parkinson's disease (PD) comparing to healthy controls by voxel-based MRI (VBM) and resting-state fMRI (rsfMRI) data analysis.

Methods and Materials: We have examined and compared 3 independent groups. Forty patients with PD in early steps in pharmacological treatment and

newly diagnosed and 22 healthy volunteers were investigated and underwent 1.5 T T1-MPR, rsfMRI scanning for VBM and rsfMRI data acquisition. All participants were right-handed.

Results: In group of newly diagnosed PD patients we observed significant ($p < 0.005$) greater volume of right precuneus (part of DMN) comparing to patients in pharmacological treatment and healthy volunteers. We perform the ROC-test with estimation of sensitivity and specificity of right precuneus changes with receipt of threshold values of this index. Comparing rsfMRI data and volume changes in precuneus in group of newly diagnosed PD patients we observed direct correlation: than higher volume of precuneus that greater area of spontaneous neuronal activity in left anterior prefrontal cortex.

Conclusion: Our findings may be part of functional cortical reorganization with functional connectivity changes between brain regions and indicate about compensatory hypertrophy of precuneus as compensatory mechanisms of neuroplasticity phenomena in early stages of PD with sensitivity (77.8 %) and specificity (76.5%) probably achieve to beginning PD and be an additional early marker of neurodegeneration.

B-1036 11:11

Determining leader nodes in dementia networks

Y. Yazicioglu¹, K. Pinker², A. Tahmassebi³, A. Meyer-Baese^{3,4},
¹Boston, MA/US, ²Vienna/AT, ³Tallahassee, FL/US, ⁴Maastricht/NL
 (ameyerbaese@fsu.edu)

Purpose: Fusing modern network theory and control strategies yields a novel transformational paradigm in dementia research. One research direction is determining the leader nodes in disease networks that can be directly manipulated via external inputs to influence the overall network trajectory and simulate the disease progression.

Methods and Materials: We examine 249 subjects with FDG-PET and T1-weighted MRI images consisting of 68 control, 111 mild cognitive impairment (MCI) and 70 Alzheimer's disease (AD). We consider only 42 out of the 116 from the AAL in the frontal, parietal, occipital and temporal lobes. Different from previous work on controllability of disease networks, we determine the disease leader nodes by relying only on the network's structure, particularly the graph distances between the nodes, and not on the existing connection weights.

Results: We show that there is a common leader node in structural and functional brain networks reflecting the changes from controls over MCI to AD. For functional data, we see one leader node in the frontal lobe present in all three networks and a decreasing number of leader nodes from controls to AD. The same situation is observed for structural data with one node in the temporal lobe, however there are more nodes in common between controls/MCI and MCI/AD.

Conclusion: We have established a new method to determine the leader nodes that can be directly manipulated to change the trajectory of the dementia networks. Implicitly, we can gain an understanding of dementia evolution and the subsequent development of therapeutic solutions.

B-1037 11:19

Differential functional connectivity changes of subregions of the dorsal premotor cortex in healthy ageing

B. Sigl¹, C. Jockwitz², S. Eickhoff², F. Hofstaedter², C. Rubbert¹, K. Amunts², S. Caspers², B. Turovski¹, J. Caspers¹, ¹Düsseldorf/DE, ²Jülich/DE
 (benjamin.sigl@med.uni-duesseldorf.de)

Purpose: The dorsal premotor cortex (PMd) is the interface between the motor and higher cognitive networks and shows several structural and functional changes in healthy ageing as well as in various neurodegenerative diseases such as Parkinson's disease. Here, we investigate the resting-state functional connectivity (RSFC) and age effects of the PMd with respect to three recently identified cytoarchitectonic subregions (6d1-3).

Methods and Materials: Resting-state fMRI of 848 healthy adults from the population-based cohort study 1000BRAINS was analysed (age=55-88 years, mean-age=67.22 years; 459 males; 3T-MRI). Cytoarchitectonic maximum probability maps of PMd areas served as seed regions for RSFC analyses. After preprocessing of fMRI data using SPM, voxel-wise whole-brain RSFC was assessed for each seed and correlated with age ($p < 0.05$, cluster-level FWE corrected).

Results: All PMd areas of both sides showed connectivity decline with left anterior insula (AI) with increasing age. Area-specific connectivity loss was found for the right area 6d1 in the bilateral primary motor cortex, for the left area 6d2 in the inferior parietal lobule, for the right area 6d2 in the right dorsolateral prefrontal cortex (dlPFC), and for the left area 6d3 in the left ventral premotor cortex. An age-dependent increased connectivity was found for bilateral area 6d3 in the sensorimotor areas on both sides.

Conclusion: PMd subregions show divergent RSFC changes during ageing, which support their functional diversity. Connectivity loss with the motor cortex, dlPFC and AI could explain the decline in sensorimotor and cognitive abilities in older age. Increase of area 6d3's RSFC with sensorimotor areas might hint at compensatory mechanisms regarding its interface function within the motor system.

B-1038 11:27

Automatic quantification of enlarged perivascular spaces on brain MRI

F. Dubost¹, H.H. Adams¹, G. Bortsova¹, M. Ikram¹, W.J. Niessen^{1,2}, M.W. Vernooij¹, M. De Bruijne^{1,3}, ¹Rotterdam/NL, ²Delft/NL, ³Copenhagen/DK
 (floriandubost1@gmail.com)

Purpose: Enlarged perivascular spaces (EPVS) are an emerging biomarker for cerebral small vessel disease. An automatic quantification of EPVS is introduced, as manual scoring of EPVS is a tedious and error-prone task.

Methods and Materials: T2-weighted MR images (voxel size 0.49 x 0.49 x 0.8mm³) were acquired from 2000 subjects (mean age 74 years, range 60-90) from a population-based study. An experienced rater (2 years experience) counted the number of EPVS on a single slice in the centrum semiovale and basal ganglia and on the whole volume in hippocampi and midbrain. A deep learning algorithm, based on convolutional network regression, was developed to reproduce the visual scoring. The algorithm was trained on 1600 and evaluated on 400 MRI scans. Intraclass correlation coefficients (ICCs) were computed to assess agreement between automatic and visual scores and we compared to inter-rater (105 scans) and intra-rater (85 scans) reliabilities.

Results: The ICC between visual and automatic scores was 0.87 (+/- 0.02) for centrum semiovale, 0.80 (+/- 0.02) for basal ganglia, 0.81 (+/- 0.03) for hippocampi and 0.62 for midbrain (+/- 0.04). Except for the midbrain, these values were equal to or higher than inter-rater reliability (ICCs 0.80, 0.62, 0.82 and 0.75, respectively), and intra-rater reliability (0.88, 0.80, 0.85 and 0.82, respectively).

Conclusion: The automatic scoring of EPVS shows good agreement with visual scoring, at the level of intrarater agreement for the centrum semiovale, basal ganglia and hippocampi. This method can facilitate quantitative EPVS analysis in large clinical studies.

B-1039 11:35

Dementia imaging in Europe: results from the European Society for

Neuroradiology (ESNR) Diagnostic Subcommittee Survey

M.W. Vernooij¹, S. Haller², G. Frisoni³, F. Pizzini⁴, T.A. Youssry⁵, N. Bargallo Alabart⁶, M. Smits¹, R. Schmidt⁷, F. Barkhof⁸, ¹Rotterdam/NL, ²Geneva/CH, ³Brescia/IT, ⁴Verona/IT, ⁵London/UK, ⁶Barcelona/ES, ⁷Graz/AT, ⁸Amsterdam/NL (m.vernooij@erasmusmc.nl)

Purpose: The purpose of this survey was to assess current practices throughout Europe, with respect to standardised imaging, evaluation and reporting of brain imaging in clinical practice of patients suspected of dementia.

Methods and Materials: Survey invitations were emailed to ESNR members (n=1662) and known associates (n=6400). The questionnaire featured 45 individual items, divided into multiple choice, single best choice and free text answers. Information was gathered on personal practice, imaging technique and protocol, scan rating and reporting and communication with clinicians.

Results: 193 individuals from unique institutes (28 European countries) had responded by 1 July 2017. Of these, 75% were neuroradiologists, 12% general radiologists, 11% (neuro)radiologists in training, 38% of responding centres perform > 5 scans/week for suspected dementia (48% 1-5 scans). MRI is primarily used in 72% of centres, 25% use primarily CT. >90% of centres acquire a combination of T2w, FLAIR, non-contrast T1w, DWI and T2*w sequences. 75% of centres use visual rating scales in reporting, primarily Fazekas and medial temporal atrophy scale. 32% of respondents note they are not fully confident in using rating scales. Only 23% of centres extract volumetric information from dementia scans. A minority of centres (28%) uses structured reports.

Conclusion: Results show homogeneity in imaging modality and protocol, but more heterogeneity in application of volumetric processing and structured reporting and communication. Though likely subject to selection bias, this survey yields valuable information on current practices in dementia imaging, and forms the basis for future recommendations.

B-1040 11:43

Sulcal-based morphometry for the diagnosis of normal-pressure hydrocephalus in patients with ventriculomegaly

G. Kuchcinski, C. Jacquiez, M. Baroncini, J. Dumont, C. Delmaire, L. Defebvre, J.-P. Pruvo, X. Leclerc; Lille/FR (gregkuch@msn.com)

Purpose: To determine the diagnostic accuracy of automated sulcal morphometry to differentiate patients with idiopathic normal-pressure hydrocephalus (iNPH) from patients with ventriculomegaly secondary to other conditions in comparison to standard visual rating scales.

Methods and Materials: The local institutional ethics review board approved the study. Written informed consent was obtained from all patients. Thirty-one consecutive patients with iNPH, 35 with vascular dementia, 23 with chronic noncommunicating hydrocephalus and 24 healthy controls prospectively underwent a 3T MR examination. Sulcal opening of ten sulci of interest throughout the brain convexity was measured using an automated surface-based approach from the 3D T1-weighted images. High-convexity tightness

and lateral sulcus dilatation were independently evaluated by 2 observers using visual rating scales. The interobserver reliability was calculated with linear weighted kappa and intraclass correlation coefficient for visual rating scales and sulcal opening, respectively. ROC curve analysis determined the best parameter to identify iNPH patients.

Results: Automated sulcal morphometry achieved a higher reproducibility and diagnostic accuracy than visual rating scales ($P < 0.05$). The best parameter to discriminate iNPH from other conditions was the ratio between opening lateral sulcus opening and intraparietal sulcus opening (AUC=0.85 [95%CI=0.74-0.95] and 0.87 [95%CI=0.74-0.96] for the left and right hemisphere, respectively). A cut-off value $> 1.25/1.20$ in the left/right hemisphere provided a sensitivity of 81%/84% and a specificity of 89%/84%.

Conclusion: Automated sulcal morphometry is a suitable method to analyse the modifications of the subarachnoid spaces of iNPH patients and may help the radiologist to discriminate iNPH from ventriculomegaly secondary to brain atrophy or noncommunicating hydrocephalus.

B-1041 11:51

3D detection of cellular neurodegeneration in Alzheimer's disease via multi-scale x-ray phase-contrast micro- and nano-CT

G.E. Barbone¹, P. Di Pietro², M. Eckermann¹, A. Mittone³, A. Bravin³, P. Romanelli⁴, G. Battaglia², P. Coan⁵; ¹Garching/DE, ²Pozzilli/IT, ³Grenoble/FR, ⁴Milan/IT, ⁵Großhadern/DE
(Giacomo.Barbone@physik.uni-muenchen.de)

Purpose: Experimental x-ray phase-contrast CT (PCI-CT) provides soft-tissue sensitivity without application of stains or contrast agents. Most interestingly, this technique can visualize nervous tissue structure at multiple scales, from full-organ anatomy to single cells without the need for sample dissection. We thus choose PCI-CT for the analysis of AD pathology in the brain of 3xTgAD mice, an experimental model of AD expressing three mutant alleles, *Psen1*, *APP* and *tau*, and displaying both amyloid- β plaque and tangle pathologies.

Methods and Materials: Multi-scale 3D images of brain samples extracted from wild-type mice (n=6) and 3xTgAD mice (n=6, all at 13 months of age) were obtained by synchrotron PCI-CT. We used 17-30 keV x-rays and sCMOS-sensor PCO camera, and switched between optics systems with voxel sizes from $3^3 \mu\text{m}^3$ to $0.1^3 \mu\text{m}^3$.

Results: Full-organ 3-micron brain CTs showed the PCI's sensitivity to microscopic amyloid deposits within both hippocampal and cortical cell layers. Moreover, localized $0.3 \mu\text{m}$ CTs detect single neuronal cells, intra-neuronal aggregates, and extracellular deposits. We observed both healthy and altered pyramidal neurons and recognized them alongside agglomerates. Image contrast allows quantification of aggregate load and of cell layers-specific plaque size 3D distributions. Last, sub-cellular structures (cone-shaped soma, circular high-density nuclei) are visible at $0.1^3 \mu\text{m}^3$.

Conclusion: PCI-CT detects amyloid plaques in aged healthy and diseased 3xTgAD mice, and provides unique 3D mappings of neuronal tissues, their surrounding angio-structures, and of single neurons down to the nanometer scale. PCI-CT thus provides a novel high-resolution 3D virtual histology technique for *postmortem* neuroimaging of neurodegenerative diseases.

10:30 - 12:00

Room X

Vascular

SS 1415

Peripheral arteries/arteritis

Moderators:

E. Dosa; Budapest/HU
C. Herzog; Munich/DE

B-1042 10:30

Preliminary results of DWI sequences in detecting arterial wall inflammation in patients with giant cell arteritis

A. Napolitano, G. Ironi, E. Tombetti, E. Incerti, S. Leoni, M. Picchio, L. Gianolli, L. Dagna, F. De Cobelli; Milan/IT (napolitano.angela@hsr.it)

Purpose: The usefulness of techniques of vessel wall imaging is still debated and novel tools are required. We aimed to verify if MRI diffusion-weighted imaging can provide a novel characterisation of vasculitic lesions.

Methods and Materials: T1 weighted, T2-weighted STIR and DWI (b0 -b600) MRI sequences were performed to evaluate the aorta and its primary branches in 5 GCA patients with a recent positive FDG-PET examination. From a clinical point of view, two patients were classified as "active", while three as "grumbling". The same sequences were performed in 5 healthy subjects, as controls.

Results: All five patients showed arterial wall hyperintensity in STIR (median arterial-to-muscle ratio 4.1, range 3.6-5.1) and DWI b-600 images, with restricted arterial wall diffusivity in the ADC maps (median ADC 2.3, range 1.6 - 3.3). Conversely, in the healthy control group no abnormalities in the aortic wall were found with STIR sequences (median T2 ratio 1.8, range 1.1-2.2, $p=0.016$), as well as no high signal was detectable in DWI. Considering individual arteries of the GCA patients, the ADC values correlated both with wall thickness (r 0.607, $p=0.016$) and the arterial-to-muscle ratio at the STIR sequences (r 0.709, $p=0.015$), while did not correlate with SUV (r 0.065, $p=0.819$).

Conclusion: Vessel wall characterisation by DWI is feasible in GCA and can reveal ongoing wall oedema in patients with grumbling disease. DWI might thus help define the activity status of patients. Further studies are warranted to better define the role of DWI imaging in GCA.

B-1043 10:38

Ultrasound biomicroscopy in the diagnosis of giant cell arteritis

C.-P. Raffaelli, A. Hombieux, N. Tieulie, S. Lassalle, N. Azulay, P. Giordana; Nice/FR (raffaelli.c@chu-nice.fr)

Purpose: The purpose of this study was to evaluate the value of ultrasound biomicroscopy (UBM) in the diagnosis of giant cell arteritis (GCA).

Methods and Materials: 19 patients with classical clinical criterias of GCA were included. Both temporal arteries were explored using an ultra-high frequency transducer (Vevo MD, Visualsonics, 70 MHz) providing an axial resolution of $20 \mu\text{m}$. Wall artery analysis relayed on : (i) Wall thickness and ratio wall thickness/artery diameter. (ii) Characteristic GCA features as intima hyperplasia. All the patients underwent a temporal artery biopsy (TAB) as a gold standard with histologic and biomicroscopic correlations.

Results: The feasibility of UBM was complete in all the patients. 11 patients were diagnosed with GCA by TAB. The UBM wall thickness ratio ($p = 0.001$) and intimal hyperplasia ($p = 0.001$) were highly correlated with GCA. A wall thickness cut-off ($210 \mu\text{m}$) had an accuracy of 100%.

Conclusion: The UBM seems a new and promising device for early diagnosis and monitoring of GCA, requiring further studies.

B-1044 10:46

Dynamic 4D CT angiography (DCTA) of the lower extremities with a 256-slice CT

N. Buls¹, Y. De Brucker¹, H. Devos², D. Aerden³, G. Van Gompel¹, P.T. Boonen³, K. Nieboer¹, J. de Mey³; ¹Brussels/BE, ²Wemmel/BE, ³Jette/BE (nico.buls@uzbrussel.be)

Purpose: To investigate the benefit of additional dynamic 4D CT series (DCTA) on the lower extremities in the evaluation of patients suspected with periphery arterial disease (PAD).

Methods and Materials: Seventeen patients received a dynamic sequence next to their runoff CTA. Acquisition was performed on a 256-slice CT (GE Healthcare) with following scan protocol: 18x repeated series at the level of the calves at 2s interphase delay and 160mm collimation. The CTA injection protocol was: 90mL contrast and 40mL saline, the dynamic sequence used 50mL contrast and 40mL saline. Two readers rated following items on a four point Likert scale: arterial enhancement; stenosis assessment; diagnostic confidence; vessel calcification; venous overlay. Enhancement (HU) was

measured in major vessels from time enhancement curves. Effective radiation dose was also estimated.

Results: A total of 102 vessels were analyzed. Enhancement was considered better with DCTA (66% of vessels) than CTA (44%) and vessels with insufficient enhancement dropped from 24% to 8%. Optimal diagnostic confidence increased from 31% to 58% with DCTA. The DCTA information changed stenosis assessment in 25% of the cases. Venous overlay was higher with DCTA (15%) than CTA (6%). Interreader variability was moderate (κ 0.42). Compared to runoff CTA, mean HU values were higher ($p < 0.001$) with DCTA in all arteries: ATA (+48%), APer (+53%), ATP (+42%). The additional dose of the DCTA (0.2mSv) was 3.9% of the CTA (5.1mSv).

Conclusion: The addition of dynamic CT angiography could improve diagnostic confidence in the evaluation of patients with PAD.

B-1045 10:54

Establishing a new protocol for aortofemoral CT angiography using the lowest possible contrast media with the advent of faster scanners

A. Hatem¹, B.K. Hazaimah¹, I. Alhyari¹, A. Jalaleh¹, S. Salman², A. Al-Omari¹; ¹Amman/JO, ²Beirut/LB (bhazaimah@gmail.com)

Purpose: To establish low-contrast-dose protocol for imaging of lower extremity arteries adjusting scan parameters without affecting image quality. This is particularly important in diabetics, elderly and patients with renal impairment.

Methods and Materials: 81 patients have been examined in this study on 64 slice CT scanners or higher from different vendors. Double test bolus technique was used to calculate time to peak (TTP) in descending aorta and in popliteal artery using 5 and 8mL of contrast for each patient consequently. Scan time was calculated subtracting TTP1 from TTP2. Total scan time and delay values were adjusted according to a formula related to scan length and TTP-interval. Machine parameters were adjusted to fit with the scan length and time needed. CT density was measured in 4 consecutive levels to ensure satisfactory enhancement within the aorta, iliac, popliteal and distal posterior tibial (PTA) arteries.

Results: Contrast volume used was 40ml for 72% of case and 50ml for 24% of the cases. In two cases, 60mL of contrast was used due to prolonged TTP2/TTP1 interval. Average CT densities were 529, 430, 379 and 224HU at aorta, iliac, popliteal and PTA levels respectively. 92.5% of cases had density values more than 200HU at popliteal level and 97.5% were more than 115HU at level of PTA. All studies revealed satisfactory enhancement at all scan levels.

Conclusion: Volume of contrast media needed to do angiography studies can be lowered with the advent of faster CT machines.

B-1046 11:02

Combined assessment of peripheral artery disease by MRI-based vascular calcification visualisation and quiescent interval single-shot (QISS) MRA

A. Varga-Szemes¹, T. Duguay¹, T. Todoran¹, S. Fuller¹, C.N. De Cecco¹, P. Suranyi¹, R.R. Edelman², I. Koktuzoglu², U.J. Schoepf¹; ¹Charleston, SC/US, ²Evanston, IL/US (vargaasz@musc.edu)

Purpose: To investigate the added value of calcification visualisation on the diagnostic confidence and accuracy of detecting peripheral artery disease (PAD) and to compare the accuracy of calcium quantification between prototype proton density weighted, in-phase 3D stack-of-stars gradient-echo (PDIP-GRE) MRI in patients undergoing quiescent interval single shot (QISS)-MRA and CTA.

Methods and Materials: Fourteen patients (68±9 years) referred for lower extremity CTA prior to digital subtraction angiography (DSA) were prospectively enrolled for a same-day 1.5T MRI. PDIP-GRE MRI and QISS-MRA were acquired covering the iliofemoral region. Two readers rated diagnostic confidence (3-point scale) and graded stenosis (< or >50%) on QISS-MRA without and with the visualisation of calcification. Sensitivity and specificity were calculated using DSA as reference. Intra-arterial calcium was quantified using ImageJ (NIH) and compared between MRA and CTA using paired t test and Bland-Altman analysis.

Results: Of the 84 segments available for calcification assessment, >50% stenosis was detected in 37 (44%), while calcium was present in 58 (69%). The diagnostic confidence (2.1 [1.9-2.3] vs 2.3 [2.1-2.5]; $P < 0.0001$) and the sensitivity and specificity of QISS-MRA in the detection of >50% stenosis (83.2% and 97.6% vs 86.4% and 98.0%, respectively) were improved when calcification data were available. Calcium quantification showed no statistical difference between MRI and CTA ($121 \pm 77 \text{mm}^3$ vs $127 \pm 84 \text{mm}^3$; $P = 0.0249$). Bland-Altman analysis revealed excellent agreement with a mean of difference at -5.8mm^3 .

Conclusion: Based on our initial results, QISS-MRA combined with PDIP-GRE MRI seems to be promising for the complex assessment of vascular anatomy in PAD, which could be beneficial in interventional procedure planning.

Author Disclosures:

A. Varga-Szemes: Research/Grant Support; Siemens Healthcare.

C.N. De Cecco: Research/Grant Support; Siemens. **U.J. Schoepf:** Consultant; Bayer, General Electric, Guerbet, Siemens. Research/Grant Support; Astellas, Bayer, General Electric, Siemens. Speaker; Bayer, General Electric, Guerbet, Siemens.

B-1047 11:10

Quiescent-interval single-shot (QISS) MRA for interventional procedure planning: a feasibility study in patients with peripheral artery disease

A. Varga-Szemes¹, T. Duguay¹, T. Todoran¹, M. Penmetsa¹, S. Fuller¹, P. Suranyi¹, C.N. De Cecco¹, D. Mastrodicasa², U.J. Schoepf¹; ¹Charleston, SC/US, ²Chieti/IT (vargaasz@musc.edu)

Purpose: To investigate the feasibility of interventional procedure planning using quiescent-interval single-shot (QISS) MRA in patients with peripheral artery disease (PAD).

Methods and Materials: Twenty-one PAD patients (67±8 years) underwent lower extremity CTA and QISS-MRA at 1.5T (prototype QISS sequence) prior to digital subtraction angiography (DSA). Segmental vascular diameter was compared among QISS-MRA, CTA, and DSA using the Friedman test. For each significant stenosis observed on QISS-MRA, intravascular stent length and diameter needed to reinstate flow in the vessel was estimated. The estimated stent size was compared to the stent implanted using the Wilcoxon test and Bland-Altman analysis.

Results: Of the 346 segments analysed with QISS-MRA, significant stenosis was detected in 82 (23.6%). Vascular diameters showed good agreement among QISS-MRA, CTA, and DSA (overall $P > 0.05$). Based on DSA evaluation, 25 stents were implanted involving 31 segments. Average estimated stent diameter was in good agreement with the average actual diameter ($8.4 \pm 2.8 \text{mm}$ vs $8.1 \pm 3.7 \text{mm}$, respectively; $P = 0.0934$; Bland-Altman mean of differences 0.3mm). However, QISS-MRA-based stenosis length measurement underestimated the length of the stent necessary to bridge the stenosis ($35.5 \pm 11.9 \text{mm}$ vs $40.1 \pm 13.9 \text{mm}$, $P = 0.0215$, respectively; Bland-Altman mean of differences -4.6mm).

Conclusion: The prediction of stent diameter required to treat stenosis in patients with PAD was feasible using QISS-MRA. QISS-MRA slightly underestimated the actual stent length, which is most likely attributed to the fact that implanted stents usually extend beyond the proximal and distal ends of a stenosis. Based on these preliminary results, QISS-MRA seems promising for the non-contrast evaluation of vascular anatomy in PAD patients prior to intervention.

Author Disclosures:

A. Varga-Szemes: Research/Grant Support; Siemens. **C.N. De Cecco:** Research/Grant Support; Siemens. **U.J. Schoepf:** Consultant; Bayer, General Electric, Guerbet, Siemens. Research/Grant Support; Astellas, Bayer, General Electric, Siemens. Speaker; Bayer, General Electric, Guerbet, Siemens.

B-1048 11:18

Accuracy of diameter measurement of vascular model: comparison of virtual monochromatic imaging in dual-energy CT with conventional 120-kVp scan

H. Sugawara, S. Suzuki, Y. Katada, T. Ishikawa, R. Fukui, Y. Yamamoto; Tokyo/JP (capy.sugawara@gmail.com)

Purpose: To compare the performance of virtual monochromatic imaging (VMI) in dual-energy CT and conventional 120-kVp scan in measurement of the inner diameter of vascular models.

Methods and Materials: We compared 50-keV VMI, 70-keV VMI, and conventional 120-kVp scan using images of an acrylic phantom for MTF calculation and another vascular phantom. The vascular phantom contains 12 vascular models with 4 diameter (1.5, 2.0, 2.5, 3.0 mm) and filled with 3 densities of contrast material (high, 20-fold dilution; middle, 40-fold dilution; low, 60-fold dilution). We evaluated intraluminal peak CT value and full width at half maximum (FWHM) for each 3.0-mm vascular model on CT attenuation profile. The diameters of all 12 vascular models were measured by software automation. Analysis of variance with repeated measures was used for statistics.

Results: Calculated MTF indicated 120-kVp scan has better spatial resolution than VMI. Intraluminal peak CT value and FWHM were 50-keV VMI > 120-kVp scan > 70-keV VMI. Measurement errors of 70-keV VMI were significantly larger or comparable than that of 120-kVp scan in all 12 vascular models. Measurement errors of 50-keV VMI were significantly smaller than that of 120-kVp scan in low-density vascular models, but larger in most of high/middle density vascular models.

Conclusion: In comparison with conventional 120-kVp scan, VMI at low keV can improve the accuracy of diameter measurement of poorly enhanced vessels. However, in other conditions, VMI can increase the measurement errors with decreased spatial resolution, and should be applied carefully in evaluating vessel diameter.

B-1049 11:26

Modified calcium subtraction in dual-energy CT angiography of the lower extremity runoff: impact on diagnostic accuracy for stenosis detection

D. De Santis¹, C.N. De Cecco¹, M.H. Albrecht², B.A. Thomas¹, B.E. Jacobs¹, U.J. Schoepf¹, K. Otani³, K. Grant⁴, A. Laghi⁵; ¹Charleston, SC/US, ²Frankfurt a. Main/DE, ³Tokyo/JP, ⁴Rochester, MN/US, ⁵Latina/IT (domenico.desantis@hotmail.it)

Purpose: To investigate the diagnostic accuracy of a modified three-material decomposition calcium subtraction (CS) algorithm for arterial stenosis detection in dual-energy (DE) computed tomography angiography (CTA) of the lower extremity runoff compared to standard images using digital subtraction angiography (DSA) as the reference standard.

Methods and Materials: Eighty-eight patients (53 males; mean age, 65.9±11 years) with peripheral artery disease (PAD) who had undergone DE-CTA of the lower extremity runoff were included in this IRB-approved, HIPAA-compliant retrospective study. Linearly blended (M_0.5) and CS datasets were reconstructed. Contrast-to-noise ratios (CNR) for both datasets were quantified. Two independent readers assessed subjective image quality using 5-point Likert scales. A subgroup of 45 patients with DSA was used to assess the diagnostic accuracy of the two datasets for ≥50% stenosis detection. Diagnostic performance parameters were estimated using random-effects logistic regression analysis and compared using generalized estimating equations.

Results: The overall diagnostic accuracy (sensitivity, specificity, positive and negative predictive values) for CS reconstructions was 96.5% (97.5%, 95.6%, 90.9%, and 98.1%) and for M_0.5 images 93.1% (98.8% 90.4%, 82.3%, and 99.1%). CS datasets showed higher CNR (15.3±7.3) compared to M_0.5 images (13.5±6.5, $P<0.001$). Both reconstruction series showed comparable subjective image quality scores (CS, 4.64; M_0.5, 4.57; $P=0.220$).

Conclusion: The modified three-material decomposition CS algorithm provides greater diagnostic accuracy for stenosis detection of the lower extremity runoff compared with standard linearly-blended images.

Author Disclosures:

C.N. De Cecco: Research/Grant Support; Siemens. **U.J. Schoepf:** Consultant; Bayer, Guerbet. Research/Grant Support; Astellas, Bayer, GE, Siemens. **K. Otani:** Employee; Siemens. **K. Grant:** Employee; Siemens.

B-1050 11:34

Quantification of blood velocity from time-resolved CT angiography on a 256-slice CT

P.T. Boonen¹, N. Buls¹, J. Vandemeulebroucke², G. Van Gompel¹, Y. De Brucker¹, D. Aerden¹, J. De Mey¹; ¹Jette/BE, ²Etterbeek/BE (pieter.thomas.boonen@vub.be)

Purpose: To quantify the blood velocity in the arteries of the lower extremities and to investigate the correlation with peripheral arterial disease (PAD).

Methods and Materials: 7 Patients with suspicion of PAD underwent time-resolved Computed Tomography Angiography (CTA) in addition to their standard run-off CTA, consisting of 18 repeated axial acquisitions at 2s interphase delay at the level of the calves with 16cm collimation (Revolution CT, GE Healthcare). Image data was processed using in-house developed processing tools. Motion during the acquisitions was compensated by applying registration, after which the anterior tibial artery, posterior tibial artery and peroneal artery were automatically segmented by identifying large intensity changes over time. Subsequently, blood velocity was quantified in the arteries by creating time attenuation curves (TAC) of the arterial cross-sections in every slice and determining the time to peak (TTP).

Results: The described method led to plausible velocity estimations in all arteries (n=18) for patients that were considered healthy (n=3). For pathological patients (n=4), only 12 out of 22 arteries could be quantified due to suboptimal bolus arrival, severe calcification or occlusions. For arteries of healthy patients, blood velocity was normally distributed ($p=0.282$) with a median value of 82.3 mm/s (95% CI= 55.5- 89.9 mm/s). Blood velocity in arteries of pathological patients was observed to be significantly lower, 30.7 mm/s (95% CI= 27.4-45.7 mm/s), $p<0.01$.

Conclusion: Time-resolved CT data allows to quantify blood velocity in the arteries of the lower extremities. In heavily occluded arteries, the contrast was insufficient in order to quantify velocity.

B-1051 11:42

Resveratrol treatment does not reduce vascular inflammation in male subjects at risk of developing type 2 diabetes: an ¹⁸F-FDG PET/CT study

E. Boswijk¹, M. de Ligt, M.-F. Habets, W. van Marken Lichtenbelt, J.E. Wildberger, F. Mottaghy, P. Schrauwen, J. Bucerius; *Maastricht/NL* (eboswijk@gmail.com)

Purpose: Resveratrol has shown anti-inflammatory effects in in vitro and animal studies. We investigated the effect of resveratrol on vascular

inflammation and systemic inflammatory activation in the spleen and bone marrow in humans.

Methods and Materials: This was a sub-study of a double-blind randomized crossover trial and included eight men with decreased insulin sensitivity undergoing an ¹⁸F-FDG PET/CT after, respectively, 34 days of placebo and resveratrol treatment (150 mg/day) to evaluate its effect on brown adipose tissue activity. ¹⁸F-FDG uptake was analysed in the carotids, ascending aorta, aortic arch, descending and abdominal aorta, as well as in adipose tissue regions, spleen and bone marrow to investigate resveratrol's effect on these structures. Mean and maximum target-to-background ratios (TBRs; TBR_{mean} and TBR_{max}) were compared between periods (paired T test or Wilcoxon signed-rank test).

Results: In all arterial territories, TBR_{mean} and TBR_{max} were slightly higher after resveratrol treatment compared to placebo treatment (n.s.). The TBR_{max} of the most diseased segment and the percentage of active segments ($TBR_{max} \geq 1.6$) were also higher after resveratrol treatment (n.s.). A similar trend was seen for the spleen (n.s.), bone marrow (n.s.) and visceral adipose tissue (TBR_{max} 0.3 ± 0.1 vs. 0.5 ± 0.2 , $p=0.011$), but not for subcutaneous adipose tissue (n.s.).

Conclusion: Arterial inflammation was not reduced by resveratrol in subjects at risk of developing type 2 diabetes as assessed with ¹⁸F-FDG PET/CT. In addition, systemic inflammatory activation in the spleen, bone marrow and adipose tissue was not attenuated by resveratrol. Our results could underline findings of recent studies questioning the effects of resveratrol in humans.

B-1052 11:50

Automated tube potential selection of the lower extremity runoff: comparison to fixed kV with mAs modulation

M. Beeres¹, K. Juhee, A.M. Bucher, C. Frellesen, M.H. Albrecht, J.L. Wichmann, J.-E. Scholtz, T.J. Vogl, T. Gruber-Rouh; *Frankfurt a. Main/DE* (beeres@gmx.net)

Purpose: To evaluate the impact of automated attenuation-based tube potential selection (ATPS) on image quality and radiation dose exposure parameters by a computed tomography angiography (CTA) lower extremity runoff.

Methods and Materials: Two hundred and forty patients (156 men, 84 women) underwent CTA examinations of the lower extremity runoff on a second-generation dual-source CT system: 120 patients at a fixed tube potential of 120 kV and a tube current of 180 reference mAs, another 120 patients using automated attenuation-based tube potential selection (ATPS). Volume CT dose index (CTDIvol), dose-length-product (DLP), body diameters, noise, signal-to-noise ratio (SNR) and subjective image quality were compared.

Results: In the ATPS group, 80 kV was automatically selected in 102 patients, 100 kV in 15 patients and 120 kV in 3 patients. 140 kV was not chosen in any of the cases. The median CTDIvol 4.81 (2.2-10.6) mGy and DLP 568 (203 - 1324) mGy·cm in the ATPS group were significantly lower compared to the fixed 120 kV group with CTDIvol 8.1 (4.4-14.4) mGy and DLP 1027.5 (509 - 1806) mGy·cm; $p < 0.01$. Image quality was comparable ($p>0.05$).

Conclusion: Automated attenuation-based tube potential selection allows for significant dose savings in lower extremity runoff CTA while image quality remains constant at a high level.

10:30 - 12:00

Room Z

Interventional Radiology

SS 1409

Embolisation techniques for liver tumours

Moderators:

J.I. Bilbao; Pamplona/ES
M. Dioguardi Burgio; Clichy/FR

B-1053 10:30

Treatment of non resectable HCC: SIRT vs TACE liver toxicity comparison with MELD score

J. Delicque¹, C. Allimant, C. Cassinotto, L. Piron, L. Escal, A.-D. Ilonca, E. Assenat, B. Guiu; *Montpellier/FR* (j-delicque@chu-montpellier.fr)

Purpose: To evaluate and compare liver toxicity of trans-arterial chemoembolization (TACE) and selective internal radiation therapy (SIRT) in non resectable hepatocellular carcinoma (HCC).

Methods and Materials: 158 TACE treatments (80 patients) and 37 SIRT treatments (31 patients) performed from August 2012 to July 2015 were included and analysed. Pre and post treatment (1month) MELD score were calculated and compared. Datas about technical points of TACE and SIRT, liver disease and HCC were noted. Post treatment evaluation was about MELD score variation (Delta MELD) and post treatment score >15, with calculation models that integrated possibility of multiple treatments (Generalized Estimating Equations).

Results: SIRT patients had higher tumor burden (AFP score > 2) and portal vein thrombosis (PVT) rate than TACE patients ($p < 0.005$). In univariate analysis, there were a trend ($p=0.11$) to a higher MELD variation with TACE than with SIRT and a statistical association with a post treatment MELD >15 with TACE than with SIRT. In multivariate analysis, factors associated with Delta MELD and MELD > 15 were all related to liver disease.

Conclusion: There is a trend to a lower degradation in liver function with SIRT compared with TACE in the treatment of non-resectable HCC, taking into account the possibility of multiple treatments. Further investigations should be performed due to a higher tumor burden and PVT in our SIRT population.

B-1054 10:38

TACE of HCC using mitomycin and lipiodol with or without DSM for HCC: comparative study

T. Gruber-Rouh, K. Eichler, N.N.N. Naguib, M.C. Langenbach, B. Kaltenbach, T.J. Vogl; *Frankfurt a. Main/DE*

Purpose: Evaluation of survival data and local tumour control after TACE in two groups with different embolisation protocols in the treatment of HCC patients.

Methods and Materials: 99 patients (mean age: 63.6 years), 78 male (78.8%) and 21 female (21.2%) with HCC were repeatedly treated with chemoembolisation in 4-week intervals. Eighty-eight patients had BCLC-stage-B, in 11 patients chemoembolisation was performed for bridging (BCLC-Stage-A). In total, 667 chemoembolisation treatments were performed (mean 6.7 treatments/patient). The administered chemotherapeutic agent included mitomycin. For embolisation, lipiodol only ($n=51$; 51.5%) or lipiodol plus degradable starch microspheres (DSM) ($n=48$; 48.5%) was used. The local response of the tumours was assessed by MRI using response evaluation criteria in solid tumours 1.1 (RECIST 1.1) Patient survival times were evaluated using Kaplan-Meier curves and log-rank tests.

Results: The local tumour control in the lipiodol group was: PR (partial response) in 11 (21.6%), SD (stable disease) in 32 (62.7%) and PD (progressive disease) in 8 cases (15.7%). In the lipiodol DSM group, the PR was encountered in 14 cases (29.2%), SD in 22 (45.8%) and PD in 12 (25.0%) ($p=0.211$). The median survival of patients after chemoembolisation with lipiodol was 25 months and in the lipiodol DSM group 28 months ($p=0.845$).

Conclusion: There was no statistical significant benefit reported of using lipiodol and DSM in comparison of using lipiodol-only for chemoembolisation of HCC in achieving local control and survival data. Only a slight trend for benefit of using lipiodol and DSM was shown.

B-1055 10:46

Safety and efficacy of transarterial chemoembolization using very small drug-eluting beads for advanced stage hepatocellular carcinoma

A.M.K. Abdel Aal^{1,2}, S. Tatum¹, K. Mahmoud¹, S. Moawad¹, N. Ertel¹, R. Oser¹, S. Saddekni¹, N. A. Aboueldahab¹, A. Gunn¹; ¹Birmingham, AL/US, ²Cairo/EG (akamel@uabmc.edu)

Purpose: To evaluate the safety and efficacy of transarterial chemoembolization (TACE) in the treatment of advanced stage hepatocellular carcinoma (HCC) using very small drug-eluting beads (DEB).

Methods and Materials: We retrospectively reviewed the medical records of 47 patients with advanced-stage HCC (BCLC-C) who underwent TACE using 75um DEB as their first therapy for HCC between November 2013 and March 2016. Patients were evaluated for median hospital stay, 30-day adverse events, 30-day mortality, toxicity profile, radiologic response, progression-free survival (PFS) and overall survival (OS).

Results: The study included 36 (78.2%) males with a mean age of 65.5 (SD=9.4) years. HCV and alcoholic cirrhosis were present in 56.5% and 30.4% of the patients, respectively. Child-Pugh A, ECOG 1 and portal vein invasion were seen in 71.7%, 69.7% and 19.6% of the patients, respectively. Segmental TACE was performed in 91.3% of the patients. The median hospital stay was 1 day (range: 1-4). There were no 30-day mortality. There was a single occurrence of hepatic abscess. Grades 1 and 2 toxicities were seen in 21.7% of the patients. There was no grade 3, 4 or 5 toxicity recorded. Complete response, objective response and disease control were 21%, 61% and 79%, respectively. The PFS and OS were 7.2 and 14.3 months, respectively. The 6, 12 and 24 months survival were 93%, 89% and 71%, respectively.

Conclusion: TACE using very small (75um) DEB is safe and effective in the treatment of patients with advanced stage HCC, with OS of 14.3 months and very low toxicity.

B-1056 10:54

Comparing HCC tumour vascularisation on baseline imaging and after Lipiodol cTACE: how do estimations of enhancing tumour volumes differ on contrast-enhanced MR and CT?

W. Lüdemann¹, F. Colletini¹, D. Geisel¹, D. Schnapauff¹, G. Wieners¹, B. Gebauer¹, J. Chapiro², J. Kahn¹; ¹Berlin/DE, ²New Haven, CT/US (willie-magnus.luedemann@charite.de)

Purpose: Arterial tumour vascularisation and Lipiodol deposition after cTACE of HCC are known to be associated. Nature and strength of the correlation between enhancing tumour volume on baseline imaging and Lipiodol deposition after cTACE were analyzed. Estimations of enhancing tumour volumes on contrast enhanced (CE)-CT or MRI were compared using Lipiodol deposition as a benchmark for arterial tumour vascularisation.

Methods and Materials: 78 HCC patients who underwent their first cTACE procedure were retrospectively enrolled. A segmentation-based quantification of overall and enhancing target lesion volumes (qEASL) was performed on baseline arterial phase CE-CT (55 patients) or MR (23 patients), post treatment Lipiodol deposition was quantified on native CT imaging. Correlations were analyzed using scatter plots, the Pearson correlation coefficient (PCC) and linear regression analysis. Subgroup analysis was performed according to lobar, segmental and subsegmental execution of cTACE.

Results: The PCC for each of the baseline imaging modalities and Lipiodol deposition as dependent variable was 0.91, after stratification according to selectivity of cTACE the PCCs ranged between 0.91 and 0.98. The linear regression equations for the non-stratified data sets were $y=1.39x+15.44$, $R^2=0.83$ for CT and $y=0.33x+12.58$, $R^2=0.82$ for MR imaging, hence, the regression coefficient for CT as baseline modality was 4.21 times greater.

Conclusion: There is a highly linear correlation for both MR and CT baseline enhancing tumour volume and Lipiodol deposition after TACE. Using Lipiodol deposition as a benchmark, it could be objectified that MR imaging is more sensitive for the detection and estimation of arterial tumour vascularisation than CT imaging.

B-1057 11:02

Tumour targeting and 3D voxel-based dosimetry to predict tumour response, toxicity and survival after Y-90 resin microsphere radioembolisation in HCC

C. Allimant, M. Kafrouni, J. Delicque, A.-D. Ilonca, M. Fourcade, D. Mariano-Goulard, C. Cassinotto, L. Piron, B. Guiu; *Montpellier/FR* (carole.allimant@gmail.com)

Purpose: To evaluate the impact of complete targeting and 3D-voxel-based dosimetry on post-treatment Y90-PET/CT to predict tumour response, survival and toxicity in patients with advanced HCC treated with Y90-resin microspheres.

Methods and Materials: 42 Sir-sphere® treatments administered in our centre from February 2012 to December 2015 were retrospectively analysed. 3D-dosimetry was calculated using a treatment planning system to obtain dose-volume histogram and the area under the DVH (AUDVH, in Gy) to measure Y90 dose deposition in different liver volume (tumour, non-tumoural). Tumour control was defined upon mRECIST criteria at 6 months. We documented toxicity by radioembolization-induced liver disease (REILD) occurrences. Uni- and multivariate logistic regressions were used to compute corresponding odds ratios [95%CI] according to tumour complete targeting and $AUDVH_{Tumour}$. Second endpoints were survival analysis using the Kaplan-Meier method and compared using log-rank tests and toxicity analysis comparing mean dose deposition in non-tumoural irradiated liver in REILD versus non-REILD patients using Mann-Whitney test.

Results: The 6-month tumour control rate was 40.5%. Complete targeting was observed in 60% of cases. By univariate logistic regression, tumour targeting and $AUDVH_{Tumour}$ were significantly associated with tumour control ($p < 0.001$ and $p = 0.008$ resp.). By multivariate analysis, both factors independently predicted tumour control (OR=36.97 [1.83-747] $p < 0.001$ and OR=1.027 [1.002-1.071], $p = 0.0325$ resp.). Overall survival was significantly higher for both factors ($p < 0.002$). We observed 4 REILD (9.5%) with significantly higher dose to the normal irradiated liver ($p = 0.004$).

Conclusion: Complete targeting and Y90-dose to the tumour, for the first time represented by $AUDVH_{Tumour}$ are independent factors associated with tumour control.

B-1058 11:10

Transarterial Radio-embolisation with 131I-Lipiodol for Hepatic metastases: experience in tertiary care oncology centre in India

V. Bhargavi, I. Subbanna, S.S. Swamy; Bangalore/IN
(bhargavi_vidya@yahoo.in)

Purpose: Surgical resection is often not feasible in metastatic hepatic disease. To analyse the response and survival benefits of Transarterial Radioembolization (TARE) with Iodine-131(I131) Lipiodol for hepatic metastases.

Methods and Materials: Prospective study of 65 patients (between May 2011 to December 2016) with pathologically proven hepatic metastases from varying groups of primary carcinomas having poor response to other treatments. All patients fulfilling the inclusion/exclusion criteria underwent transarterial radioembolization (TARE) with I131 Lipiodol. All patients were isolated for at least 5 days for radiation safety purpose. Post procedure the patients were reviewed after one month with a follow up PET CT and tumour marker levels to evaluate response of treatment. Overall survival for each patient was calculated.

Results: At the end of follow up period, 17 of 65 patients died with 48 alive. Mean overall survival was 34.415 ± 3.0 months. Mean survival duration was 38.88 ± 5 months in NET, 35.118 ± 3.95 in GI, 27.21 ± 8.3 with pancreatico-biliary and 20.685 ± 5.2 with other malignancies ($p=0.17$). Overall survival after 45 months was 70%. 45 months survival in NET was 76%, 75% in GI, 57% in pancreatico-biliary and 50% in other malignancies. Response evaluation in 22 patients, 7 (32%) showed partial response, 3 (14%) showed stable disease and 12 (54%) showed progressive diseases. All patients showed reduction in serum tumour marker levels.

Conclusion: TARE with 131I-Lipiodol is highly effective with significant survival benefit in patients with hepatic metastases, refractory to other treatments.

B-1059 11:18

Prospective randomised trial: tumour response of colorectal liver metastasis after transarterial chemoembolisation with two different protocols using MRI

T.J. Vogl, M.C. Langenbach, R. Hammerstingl, J. Scholz, T. Gruber-Rouh; Frankfurt a. Main/DE (t.vogl@em.uni-frankfurt.de)

Purpose: To prospectively evaluate therapy response of third-line transarterial chemoembolisation (TACE) for colorectal liver metastases with either degradable starch microspheres (DSM) or lipiodol using regular and diffusion MRI.

Methods and Materials: In total, 50 patients (35 males, 15 females, mean 62 years, range 40-79) underwent TACE. They were randomly assigned into two groups: group A receiving DSM and group B receiving lipiodol as embolisation agents. Chemotherapy consisted of a combination of cisplatin, irinotecan and mitomycin. Therapy response was evaluated using MRI with diffusion imaging and unenhanced MRI sequences, which were performed before each of the three TACE cycles to obtain tumour volume and apparent diffusion coefficient (ADC). Moreover, contrast-enhanced MRI sequences were performed before the first and after the last TACE cycle. Tumour response was evaluated using the RECIST criteria. Differences in tumour volume response between the lipiodol and DSM group were calculated with BIAS using the Friedman test and the Mann-Whitney U test.

Results: The DSM group showed statistically significant reduction in the average tumour volume compared with lipiodol during the course of the therapy (mean -59%, $p=0.006$). Additionally the dynamics of ADC values during the therapy correlated significantly with therapy response, stating partial response as responders and stable disease with progressive disease as nonresponders ($p=0.046$). No statistically significant difference in tumour response was found comparing the lipiodol and DSM group.

Conclusion: A statistically significant reduction in tumour volume was found in the DSM group. No significant difference in tumour response was found comparing the Lipiodol and DSM group.

B-1060 11:26

Idarubicin-loaded beads for chemoembolisation of HCC: interim analysis of IDASPHERE II (FFCD 1307) multicentre single-arm phase II trial

B. Guiu¹, P. Chevallerier², A. Rode³, A. Bouvier⁴, P.-J. Valette⁵, C. Cassinotto¹, L. Piron¹, M. Boulain⁵; ¹Montpellier/FR, ²Nice/FR, ³Lyon/FR, ⁴Angers/FR, ⁵Dijon/FR (b-guiu@chu-montpellier.fr)

Purpose: The primary end point was to assess the objective response (OR) rate at six months after trans-arterial chemoembolisation (TACE) for HCC using idarubicin-loaded beads.

Methods and Materials: TACE sessions (1-4) were performed using 10 mg of idarubicin loaded in 100-300 micron DC Bead. Toxicity was assessed according to NCI-CTCAE v4.0. The objective response (primary end point) was evaluated (mRECIST) using MRI (centralized review). The study was a 2-

step Fleming design (H0: 25% of OR at 6 months vs H1: 40%, power=90%, one sided; $\alpha=5\%$). 46 patients were included for the interim analysis.

Results: 46 patients (median age: 71y; range: 44-89y) were enrolled in seven centres at interim analysis. Performance status was 0 in 83%, 1 in 15% and 3 in 2%. BCLC status was A in 10.9%, B in 76.1% and C in 13%. Bilobar disease was reported in 51% with >3 HCC nodules in 53.5% patients. Complete response, partial response and stable disease were observed in 6 (13.6%), 16 (36.4%) and 4 (9.1%) patients, respectively. OR rate at 6 months was 50% (90%CI: 36.8-63.2%). The trial was stopped at interim analysis because of its efficacy.

Conclusion: TACE of HCC using idarubicin-loaded beads is well tolerated and provides a 50% objective response rate at 6 months. A randomised phase 3 trial is warranted.

B-1061 11:34

Transradial versus transfemoral access for hepatic chemo-embolisation: intrapatient prospective single-center study

A. Posa, R. Iezzi, F. Carchesio, C.A. Barone, A. Gasbarrini, R. Manfredi; Rome/IT (alessandro.posa@gmail.com)

Purpose: To compare transfemoral approach (TFA) and transradial approach (TRA) in patients undergoing hepatic chemoembolization in terms of safety, feasibility, and procedural variables, including fluoroscopy time, radiation dose (reference air kerma [RAK]), and patient preference.

Methods and Materials: A single-center prospective intrapatient comparative study was conducted with 42 consecutive patients with hepatic malignancies who received 2 consecutive treatment sessions of unilobar hepatic chemoembolization within a 4-week interval over a 6-month period with both TRA and TFA. All procedures were performed by 1 interventional radiologist who assessed the eligibility of patients for inclusion in the study. The primary endpoint was intraprocedural conversion rate. Secondary endpoints were access site complications, angiographic and procedural variables, and evaluation of patient discomfort and preferences.

Results: A 100% technical success rate and a crossover rate of 0% were recorded. There were no major vascular complications and similar rates of minor complications (4.8% for TRA, 7.1% for TFA; $P=.095$), which were self-limited and without any clinical sequelae. TRA treatments required a significantly longer preparation time for the procedure ($P=.008$) with no significant differences for other procedural variables. Greater discomfort at the access route and patient inability to perform basic activities after the procedure were recorded for TFA ($P<.001$). TRA was preferred by 35 patients (35/42) for potential future transarterial procedures.

Conclusion: TRA is safe and feasible for transarterial hepatic chemoembolization, with high technical success, low overall complications, and improved patient comfort.

B-1062 11:42

A comparative study of a new generation robotic angiography system based on patient dose and image quality during transarterial chemoembolisation

T.J. Vogl, L. Alizadeh, M.H. Albrecht, P. Tischendorf; Frankfurt a. Main/DE (t.vogl@em.uni-frankfurt.de)

Purpose: Comparison of patient dose and diagnostic image quality between two generations of robotic angiographic systems for transarterial chemoembolization (TACE) therapy of malignant liver tumours.

Methods and Materials: 159 patients undergoing TACE treatment were divided randomly into three groups: generation one, generation two before and generation two after the protocol update. Patient imaging was performed with fluoroscopy and digital subtraction angiography (DSA) acquisition protocols. Radiation dose was measured using an ionization chamber, measuring dose-area-product (DAP) in Gy·cm² and reference-point-air-kerma (RP) in mGy. Image quality was analysed by three radiologists through a blinded evaluation, considering clinically relevant image parameters.

Results: The second-generation system provided significantly ($p < 0.05$) better clinical image quality (IQ) of 30% in DSA and 81% before and 76% after digital fluoroscopy protocols vs the older generation system. The new generation system also showed a lower radiation exposure, by RP -48% and -40% DAP in DSA acquisition. In fluoroscopy protocols a decrease of RP -3% and -5% DAP before, and RP -50% and -49% DAP after update was found for second-generation systems, compared to first-generation systems.

Conclusion: Recent generation angiography systems allow significant dose reductions, while improving image quality in fluoroscopy and DSA during TACE treatment.

B-1063 11:50

Generation I vs new-generation cone-beam CT, digital subtraction angiography and digital fluoroscopy in patients undergoing TACE: comparison of radiation dose and image quality

T.J. Vogl, L. Alizadeh, K. Graef, N.-E.A. Nour-Eldin; Frankfurt a. Main/DE (t.vogl@em.uni-frankfurt.de)

Purpose: To compare radiation dose, clinical image quality (IQ) and aspects of workflow and usability in a clinical environment for patients and radiologists during transarterial chemoembolization (TACE) of hepatic malignancies using generation I (A.Zeego) C-arm cone-beam CT (CBCT) or the new generation II (A.Pheno) CBCT.

Methods and Materials: 153 patients with liver malignancies underwent preprocedural MRI and TACE in a 4- to 6-week interval. During TACE generation I and generation II CBCT were both operated by the same experienced radiologists and patients were randomized. From 02/17 onwards a software patch was applied on the generation II system for reducing the radiation dose in fluoroscopy. Radiation dose and image data were collected as DICOM (SR, XA) system data from each CBCT. Radiation doses were measured with the built-in standardized measuring units of the CBCTs (Siemens-Healthineers/Forchheim) measuring DAP and SED. Afterwards qualitative image quality was compared in a blinded trial of three individual experienced readers through a scale-based evaluation.

Results: Generation II system provided a significantly better IQ of $\bar{x}=30\%$ before and $\bar{x}=25\%$ after patch in digital subtraction angiography (DSA) and of $\bar{x}=81\%$ before and $\bar{x}=76\%$ after patch in digital fluoroscopy protocols vs the older generation. Moreover, detectability of guidewire and microcatheters in fluoroscopy protocols was improved. It also showed a lower radiation exposure after patch fluoroscopy and in DSA acquisitions vs generation I system.

Conclusion: Generation II vs generation I system provides better IQ and workflow with lower radiation dose. Further, it facilitates very low-dose radiation spectrum for clinical use.

10:30 - 12:00

Room N

Genitourinary

SS 1407

Prostate cancer staging and active surveillance

Moderators:

F. Cornud; Paris/FR.

M. de Rooij; Nijmegen/NL

B-1070 10:30

To evaluate the role of 68Ga-PSMA PET-CT in patients with newly diagnosed high-risk prostate cancer

S.M. Shaikh; Hyderabad/IN (drsikandar_s@yahoo.co.in)

Purpose: The aim of the current study was to assess the use of 68Ga-PSMA (prostate-specific membrane antigen) in patients with prostatic cancer.

Methods and Materials: 68Ga-PSMA PET-CT was performed after injection of radiotracer and scan done after one hour. 27 patients with diagnosed prostate cancer, Gleason score of 7 or higher were included in inclusion criteria. The study is retrospective.

Results: All 27 patients had increased 68Ga-PSMA uptake in the prostate. In 8 patients (32%) uptake was localized. In 6 patients PET-CT findings suggested capsular involvement, in 3, seminal vesicles involvement and in 2, uptake was not separated from the rectum or urinary bladder wall which was suggestive of infiltration. Nineteen patients (72%) had increased lymph node uptake. In 14 patients nodal uptake was detected only in the pelvis (3 perirectal, 10 iliac, 1 superior rectal), in 3 also in retroperitoneal nodes and in 2 in mesenteric nodes. In 6 patients (23%) skeletal increased uptake intramedullary=1, cortical and intramedullary=2, and cortical =9. In 2 of the 6 patients the bone was the only site of uptake other than the primary tumour site. There was a single patient with lung nodules suggestive of metastasis. Of the 23, 6 had surgery (26%); 5 patients (in 2 with combination of radiation (R) and hormonal therapy (H)) and 1 with uptake also in pelvic lymph node dissected at surgery. 12 patients (54%) received hormonal therapy and one patient received chemotherapy.

Conclusion: 68Ga-PSMA PET-CT has a potential impact on treatment approach.

B-1064 10:38

Prediction of minimal extraprostatic extension with MRI: correlation with whole-mount histological sections

S. Pedalino, E. Appendino, E. Tabone, S. Mazzetti, D. Regge, F. Russo; Candiolo/IT (salvatore.pedalino@ircr.it)

Purpose: To differentiate with MRI organ-confined prostate cancers (PCas) that infiltrate the fibrous capsule from PCAs with minimal extracapsular extension (mECE).

Methods and Materials: 70 prostatectomized patients with a total of 73 lesions were enrolled in this study. Of the 73 lesions, 57 were organ confined but with infiltration of the fibrous capsule (T2f); 16 had mECE (i.e. ≤ 0.7 mm in radial extension; T3m). An experienced urologist retrospectively reviewed T2w images (axial, coronal, sagittal) of all 73 lesions to assess the presence/absence of mECE. For each tumour the contact length with the fibrous capsule in mm, the presence/absence of bulging, the presence/absence of plaque-like morphology without bulging were recorded. Receiver operating characteristic (ROC) curves were used to determine the contact length cut-off to differentiate T2f from T3m.

Results: Presence of bulging was found in 12% (7/57) and 44% (7/16) of T2f and T3m, respectively ($p < 0.01$). Plaque-like morphology was present in 14% (8/57) T2f and in 19% (3/16) T3m tumours ($p = 0.70$). Both plaque-like morphology and bulging were absent in 74% (42/57) of T2f and 37% (6/17) of T3m tumours ($p = 0.02$). The median contact between lesion and prostatic capsule was 11mm (IQR 7-15) and 14mm (IQR 13-16) for T2f and T3m tumours, respectively ($p = 0.02$). With ROC analysis a sensitivity of 75% and a specificity of 65% were obtained in the prediction of the T3f at the best cut-off value (12mm).

Conclusion: Presence of bulging and a of broad contact (> 12 mm) of the tumour with the fibrous capsule are predictive of mECE.

B-1065 10:46

Added value of MRI tractography of periprostatic nerve plexus to conventional T2-WI in detection of extra-capsular extension of prostatic cancer

A. Cybulski, M. Catania, R. Negrelli, E. Boninsegna, S. Brancato, A. Tafuri, G. Zamboni, S. Siracusano, R. Pozzi Mucelli; Verona/IT (matteocatania89@gmail.com)

Purpose: To evaluate the role of MRI in detection the extra-capsular extension (ECE) of prostatic tumor through T2-WI, tractography of periprostatic nerve plexus and a combination of both.

Methods and Materials: 36 patients with diagnosis of prostatic neoplasia performed MRI and underwent radical prostatectomy. Histopathological analysis showed ECE in 15/36 and capsule sparing in 21/36. By means of T2-WI, ECE was evaluated in a qualitative manner: a score (1 to 4) was assigned to each lesion; sensitivity and specificity were calculated for each score group. We performed a quantitative analysis on 2 tractographic parameters, fractional anisotropy (FA) and apparent diffusion coefficient (ADC), and computed the ratio between the lesion quadrant and its contralateral (L/H ratio). We compared L/H ratios of patients with and without ECE; ROC analyses were performed to determinate ECE cut-off values of tractographic parameters. These cut-off values were used in association with T2-WI to reassess patients and to evaluate if specificity and sensitivity of ECE detection change.

Results: T2-WI showed a sensitivity of 80% and a specificity of 71% in detection of ECE. Tractography displayed a significant difference in L/H ratio for FA and ADC between patients with and without ECE. The simultaneous use of T2-WI and tractography revealed high sensitivity (100%) on patients with low suspect of ECE (score:1-2) and high specificity (80-100%) on patients with medium-high suspect of ECE (score:3-4).

Conclusion: MRI tractography combined with T2-WI is able to identify tumor ECE with higher sensitivity and specificity than conventional T2-WI alone.

B-1066 10:54

How to predict anterolateral extracapsular tumour extension in patients with prostate cancer

H. Ahn, S.I. Hwang, H.J. Lee; Seongnam/KR (ahnhyungwoo@naver.com)

Purpose: To investigate imaging markers indicating anterolateral extracapsular extension (ECE) of anteriorly located prostate cancer.

Methods and Materials: Among 505 anteriorly located prostate cancers on histopathological mapping between 2011 and 2016, 221 lesions of category 4 and 5 in prostate imaging reporting and data system on multiparametric MRI were enrolled. Two radiologists independently measured the largest tumour dimension, the length of the border where the tumour contacts the anterolateral prostate capsule if present and apparent diffusion coefficient value, and assessed the capsular morphology in five categories (intact, focal thinning, bulging, disrupted, or measurable extracapsular disease). Intraclass correlation coefficient (ICC) and Cohen's κ statistics were used to assess inter-reader agreement. Logistic regression analysis was done to assess the meaningful

indicator of ECE, along with Gleason score and prostate-specific antigen level with each measurement. The cutoff value of measurement in the prediction of ECE was obtained using Youden Index.

Results: Inter-reader agreement was excellent for the largest tumour dimension (ICC 0.81, 95% CI 0.76-0.85) and capsulotumoural border length (ICC 0.80, 95% CI 0.75-0.85), and was good in the categorisation of capsular morphology (κ 0.64, 95% CI 0.55-0.74). The capsulotumoural border length (odds ratio [OR], 1.1) and the preservation of capsular contour (OR 0.3) were found to be statistically significant in the prediction of ECE. A capsulotumoural border of 1.0 cm demonstrated a sensitivity and specificity of 82.6% (57/69) and 71.1% (108/152), respectively.

Conclusion: Anterolateral ECE should be suspected when the tumour is in contact with the anterolateral capsule with its border measuring 1.0 cm or longer, or when the capsular contour is disrupted.

B-1067 11:02

T-staging of prostate cancer: prevalence and predictive value of frequently used signs of extracapsular extension on prostate MRI

F. [Pesapane](mailto:filippopesapane@gmail.com), C. Standaert, P. De Visschere, G. Villeirs; *Ghent/BE*

Purpose: To evaluate the staging performance of frequently used signs of extracapsular extension (ECE) on prostate magnetic resonance imaging.

Methods and Materials: The presence of ECE in index lesions visible on prebiopsy mpMRI (consisting of T2w images, DWI and DCE on a 3 Tesla system) of 46 patients (mean age 63 years, mean PSA 17.2 ng/mL) with biopsy-proven prostate cancer, who underwent subsequent radical prostatectomy between 11/2011 and 12/2014, was retrospectively assessed by two radiologists (15 and 8 years of experience) on the basis of 8 criteria selected from literature. For each sign, the prevalence and positive predictive value (PPV) for histopathologically proven ECE was calculated as the average of both readers.

Results: Tumour-capsule contact was the most prevalent sign (56.9%), but with the lowest PPV (51.9%), although increasing with broader capsular contact (57.9% if ≥ 10 mm and 81.3% if ≥ 20 mm). Prevalence and PPV were 18.6% and 69.0% for capsular signal-intensity disruption, 14.7% and 75% for contour bulging, 11.8% and 75.0% for unsharp margin, 8.8% and 85.7% for irregular contour, 6.9% and 87.5% for periprostatic fat infiltration, and 2.9% and 100% for both rectoprostatic angle obliteration and periprostatic mass, respectively.

Conclusion: Broad tumor-capsular contact length, irregular contour, periprostatic fat infiltration, rectoprostatic angle obliteration and periprostatic mass are associated with the highest chance of ECE of the index lesion. All other signs are more prevalent, but less predictive of ECE. Reporting the chance of ECE can add important information to the treatment decision-making.

B-1068 11:10

Development of an extraprostatic extension imaging score based on multiparametric MRI and histopathology correlations

R. [Campa](mailto:riccardocampa23@gmail.com), V. Salvo, M. Pecoraro, M. Del Monte, V. Panebianco, C. Catalano;

Purpose: To develop an extraprostatic extension imaging score (EPEIS) based on multiparametric magnetic resonance (mpMRI) of prostate cancer (PCa). It may give the urologist an easily comprehensible information, either alone or embedded into a nomogram, that can be helpful for local staging and proper therapeutic planning.

Methods and Materials: A cohort of 32 consecutive patients with clinically localised PCa who underwent preoperative mpMRI and then radical prostatectomy (RP) were enrolled in the study from January 2015 to August 2017. Patients underwent staging 3T MpMRI (T2WI on axial and coronal planes, DWI with b values up to 2000 s/mm², DCE images). Two expert radiologists retrospectively evaluated the exams assigning a T-stage, according to ESUR MR prostate guidelines, and the EPEIS, ranging from 0 to 5, based on PIRADSV2 staging criteria. Histopathological prostatectomy data were used as standard reference.

Results: Extraprostatic extension (EPE) was present in 13/32 (41%) patients. ROC curves analysis shows How EPEIS proved to be a good indicator in the staging (AUC=0.76 [0.65-0.85]); better than the assignment of a T-stage (AUC=0.71 [0.60-0.82]). Youden's J statistic was made to select the best EPEIS cut-off. EPEIS proved good sensitivity (0.65-0.87) and specificity (0.73-0.95), especially if compared to the T-stage assignment sensitivity (0.58-0.80) and specificity (0.67-0.89).

Conclusion: EPEIS proved to be a promising mpMRI indicator of PCa micro- and macroscopic extracapsular extension. Its usefulness could be increased if included within appropriate nomograms.

B-1069 11:18

Whole-body MRI for bone metastasis detection in prostate cancer: the roles of static field intensity and contrast media in focus

D. Kovacevic, I. [Papageorgiou](mailto:papageorgiou@gmail.com), R.L. Chelaru, S. Winzler, A. Malich; *Nordhausen/DE*

Purpose: The purpose of this study is to define whether the static field intensity (1.5T vs 3T) and the use of gadolinium enhancer influence the diagnostic accuracy of whole-body magnetic resonance imaging (WB-MRI) for osseous metastasis in prostate cancer.

Methods and Materials: The study was retrospective for 96 patients scanned between 05/2007 and 08/2017. 49 patients were imaged at 1.5T and 47 at 3T with a T1-w FFE and a STIR or a Dixon at the coronal level. The slice thickness was 6 mm at 1.5T and 3 mm at 3T. In 24 (25%) patients, the scan was enhanced with gadoteridol (ProHance) 0.2 mmol/kg. Clinical or bioptic confirmation served as the gold standard.

Results: The sensitivity (Se) and specificity (Spe) for 1.5T was 88%/100%, and the positive predictive value (PPV)/negative predictive value (NPV) was 100%/88%. The static field strength of 3T showed Se/Spe 96.15%/90.48% and a PPV/NPV of 92.59%/95%. Binary logistic regression with Fisher's exact test revealed no significant difference between 1.5T and 3T WB-MRI (P 1.0). The Se/Spe of WM-MRI (merged 1.5T and 3T) without enhancement was 92.5%/96.87%, with PPV/NPV 97.37%/91.18%. With administration of gadoteridol, the Se/Spe was 92.31%/90.91% and the PPV/NPV was 92.31%/90.91%. Binary logistic regression with Fisher's exact test returned no significant effect for gadoteridol (P 1.0, odds ratio 1.545).

Conclusion: The diagnostic accuracy of WB-MRI for osseous metastatic disease in prostate cancer is equal for the most commonly used static field strengths, 1.5T and 3T, and independent of gadolinium enhancer administration.

B-1071 11:26

Multiparametric magnetic-resonance to confirm eligibility to an active surveillance programme for low-risk prostate cancer: intermediate time results of a high-volume centre protocol

S. [Luzzago](mailto:stefanoluzzago@gmail.com), M. Catellani, A. Russo, E. Di Trapani, F. Mistretta, G. Musi, P. Pricolo, G. Petralia, O. De Cobelli; *Milan/IT*

Purpose: To evaluate confirmatory multiparametric magnetic resonance imaging (mpMRI) of the prostate at the time of active surveillance (AS) enrollment to reduce disease misclassification.

Methods and Materials: From 2012 to 2016, 383 patients with low-risk disease respecting PRIAS criteria underwent confirmatory 1.5-T mpMRI. AS was proposed to patients with PI-RADS scores ≤ 3 and no extraprostatic extension (EPE) at mpMRI, whereas patients with PI-RADS score ≥ 4 and/or EPE were treated actively. Kaplan-Meier analyses quantified progression-free survival (PFS) in patients enrolled in AS program. Logistic regression analyses tested the association between confirmatory mpMRI and clinically-significant-prostate-cancer (csPCa) at radical prostatectomy (RP). Diagnostic performance of mpMRI was calculated in patients submitted to immediate RP.

Results: Median time of persistence in AS protocol was 24 months (IQR 13-38). Progression-free-survival rate was 99%, 90%, and 86% at 1, 2 and 3 years, respectively. At multivariable analysis, PI-RADS 3, PI-RADS 4, PI-RADS 5 and EPE increased the probability of having csPCa at immediate RP (PI-RADS 3 [OR]: 1.2, $p=0.26$; PI-RADS 4 [OR]: 5.1, $p=0.02$; PI-RADS 5 [OR]: 6.7; $p=0.009$; EPE [OR]: 11.8, $p<0.001$). Confirmatory positive mpMRI showed sensibility, specificity, PPV and NPV of 85%, 55%, 68% and 76%, respectively.

Conclusion: Confirmatory mpMRI at the time of AS enrollment reduces misclassification rate of csPCa. We suggest to perform target biopsies in patients with PI-RADS score 3 and 4 lesions.

B-1072 11:34

Evaluation of MRI parameters for prediction of prostate cancer upgrading in active surveillance

D. Portalez, M. [Jaffro](mailto:jaffro.m@chu-toulouse.fr); *Toulouse/FR*

Purpose: To evaluate MRI parameters for Gleason score progression in patients with low-risk prostate cancer managed with active surveillance.

Methods and Materials: 125 patients enrolled in AS for prostate cancer with a PI-RADSV2 score 3 or higher underwent systematic biopsies (SB) and MRI-TRUS targeted-fusion biopsies (TB). MRI findings (PI-RADS v2 scoring, ADC value measurements, quantitative DCE parameters, tumour's volume, tumour's visibility on the high b value images) were correlated to pathological results for each lesion. The final study population included 111 patients with Gleason 3+3 on initial biopsies and MRI's target in the peripheral zone (PZ). Statistics consisted in Chi-squared or Fisher's exact test for categorical variables and Mann-Whitney test for continuous variables with a multivariate logistic regression between Gleason 7 and MRI parameters.

Results: Overall upgrade concerned 50/125 patients with 45/111 in the PZ and 1/14 in the transitional zone. Disease was upgraded in 23/125 patients on SB

and in 50/125 patients on TB. Sensitivity, specificity, positive and negative predictive values of ADC value for confirmatory biopsy upgrade in the PZ of 111 patients were 82.2%, 81.8%, 75.5% and 87.1% respectively. A higher performance of ADC value in the prediction of Gleason score upgrading was found compared to other MRI parameters. This upgrading was clearly associated with a lower tumour's ADC value and tumour visibility on the high b value Images.

Conclusion: ADC value tumour's measurement and tumour visibility on the high b value images provided greater accuracy in predicting upgrading on confirmatory biopsies than other MRI parameters.

B-1073 11:42

Added value of multiparametric magnetic resonance (mpMR) and transrectal ultrasound-MR fusion biopsy in active surveillance for prostate cancer

F. Ciccicarese, B. Corcioni, C. Gaudiano, M. Garattoni, F. Busato, R. Golfieri; Bologna/IT (ciccicarese.f@gmail.com)

Purpose: Active surveillance is currently reserved for selected low-risk patients affected by prostate cancer with a Gleason Score =6; at initial diagnosis, mpMR is considered for the high negative predictive value and to reduce misclassification. The aim of this study was to evaluate mpMR findings in patients in active surveillance, with focus on suspected lesions submitted to transrectal ultrasound-MR fusion biopsy.

Methods and Materials: We retrospectively reviewed mpMR scans performed from January 2016-June 2017; on a total of 744 exams, we selected 88 patients submitted to MR for a previous diagnosis of prostate cancer Gleason Score 3+3 suitable for active surveillance. MR data were expressed by using PIRADS classification. In case of PIRADS ≥ 3 , we considered patients that underwent adjunctive transrectal ultrasound-MR fusion biopsy and we analyzed histological results.

Results: mpMR documented benign findings (i.e. PIRADS 1-2) in 39/88 patients (44.3%), while in the others 49/88 (55.7%) the presence of a clinically significant cancer was considered to be equivocal (PIRADS 3 in 35/88-39.8%) or probable (PIRADS 4-5 in 14/88-15.9%). 20/49 patients were submitted to fusion biopsy in our Institute; in 12/20-60.0% a higher Gleason score was detected (7-9)

Conclusion: Almost 50% of patients in active surveillance shows MR abnormalities. Prostate mpMR combined with target fusion biopsies reduce downstaging and help in correct management.

B-1074 11:50

Impact of upfront risk stratification on the negative predictive value of multiparametric MRI in patients under active surveillance

M. Abihanna¹, C. Melodelima², P.-C. Moldovan¹, R. Souchon¹, A. Ruffion¹, M. Colombel¹, S. Crouzet¹, O. Rouviere¹; ¹Lyon/FR, ²Grenoble/FR (m_abihanna@hotmail.fr)

Purpose: To assess the impact of upfront risk stratification on the negative predictive value (NPV) of multiparametric MRI in patients under active surveillance (AS).

Methods and Materials: We retrospectively analysed a prospective database of 326 patients under AS who underwent multiparametric MRI before biopsy. The prediction of clinically significant prostate cancer (csPCa) at biopsy by clinical (age, digital rectal examination, PSA density [PSAd], history of prior negative biopsy) and imaging (Likert score, extracapsular extension [ECE], magnetic field strength, experience of radiologist and presence of a concordant hypochoic lesion [Concord-Echo]) variables was assessed by multivariate analysis. Significant clinical variables were included in a 'clinical model'. Three definitions for csPCa were used (csPCa1: grade group ≥ 3 ; csPCa2: grade group ≥ 2 ; csPCa3: csPCa2 and grade group 1 with cancer invasion length ≥ 5 mm).

Results: Age, PSAd and Likert score significantly predicted the presence of csPCa1-3. In addition, ECE significantly predicted the presence of csPCa1-2. Adding the Likert score to the clinical models significantly increased the model's performance for csPCa1-3. Omitting biopsy in patients with negative mpMRI would have avoided 37.4% (Likert $\leq 3/5$) or 53.1% (Likert $\leq 4/5$) of biopsies while missing csPCa in 7.1% (csPCa1), 20.2-33.7% (csPCa2) and 35.8-48.9% (csPCa3) patients. mpMRI NPV decreased when the probability of csPCa given by the clinical models increased. Therefore, considering clinical models' output allowed defining scenarios missing <5% of csPCa and omitting biopsies in 33.4-45.4% (csPCa1), 13.5-16.6% (csPCa2), and 7.1-8.9% (csPCa3) patients.

Conclusion: Upfront risk stratification of patients can allow rational use of mpMRI NPV.

10:30 - 12:00

Studio 2018

Oncologic Imaging

SS 1416

Advances in oncologic imaging of the abdomen

Moderators:

T.K. Helmberger; Munich/DE
S. Jovanovic; Belgrade/RS

B-1075 10:30

Combined diffusion-weighted MRI with conventional T2 and T1 in-phase/out-of-phase sequences: a short screening protocol for liver metastases

S. De Vuysere^{1,2}, V. Vandecaveye¹, R. Dresen¹; ¹Leuven/BE, ²Bonheiden/BE (sofie.devuysere@gmail.com)

Purpose: To evaluate whether a short magnetic resonance imaging (MRI) protocol consisting of diffusion-weighted imaging (DWI), T1 in-phase/out-of-phase and T2-weighted sequences can accurately detect liver metastases without the need of post-contrast imaging.

Methods and Materials: Liver MRI was performed in 124 consecutive patients with various primary cancers. Three independent readers with different experience level (1 year, 10 years and 15 years respectively) retrospectively reviewed the DWI, T2 and T1 in-phase/out-of-phase sequences. All observers used confidence levels for the prediction of metastases (1 = definitely no metastases, 2 = probably no metastases, 3 = inconclusive, 4 = probably metastases, and 5 = definitely metastases). Sensitivity, specificity, positive predictive value, and negative predictive value were calculated with the cut-off level between 2 and 3 (rating 1) and 3 and 4 (rating 2). Histopathology or 2-years imaging follow-up were the reference standard.

Results: Reader 1 had a sensitivity and NPV of 100% in both ratings. Specificity was respectively 72% versus 96%, PPV of 61% versus 92%. Reader 2 had a sensitivity of 100%, specificity 98%, PPV 97%; NPV 100% in rating 1; sensitivity 94%, specificity 100%, PPV 100%, NPV 97% in rating 2. Reader 3 had no inconclusive results. In both ratings sensitivity was 100%, specificity 97%, PPV 97%, NPV 100%.

Conclusion: DWI, T2 and T1 in-phase/out-of-phase sequences allowed accurate detection of liver metastases in an experienced reader. In future, this time-efficient protocol could be used for screening of liver metastases, without the need for post-contrast imaging.

B-1076 10:38

CT attenuation of liver metastases of colorectal cancer is a prognostic factor of overall survival

M.F. Froelich, V. Heinemann, W.H. Sommer, J. Holch, J. Ricke, D. Modest, F.O. Hofmann; Munich/DE

Purpose: To investigate the prognostic value of mean CT-attenuation of liver metastases for overall survival (OS) in metastatic colorectal cancer (mCRC).

Methods and Materials: Patients with histologically confirmed mCRC from a clinical phase III trial who received 5-FU, leucovorin and irinotecan with cetuximab or bevacizumab were included into the analysis. In a baseline CT in portal venous phase the mean attenuation of liver metastases was assessed using semi-automated volumetry. ROC analysis was used to determine an optimal threshold identifying long-term survivors. Its influence on OS was investigated in Kaplan-Meier and Cox proportional hazard regression.

Results: Of a total of 592 patients, 347 were eligible for volumetric segmentation of liver metastases. Mean attenuation was 60.09HU. A higher attenuation was associated with longer OS (per 10HU: HR 0.85 (0.75; 0.93), $p < 0.001$). 61.62HU was found as optimal threshold to predict longer OS (median 21.3 vs 30.6 month; HR 0.61 (0.47; 0.80), $p < 0.001$) and was confirmed in multivariate regression (HR 0.61 (0.46; 0.82), $p < 0.001$).

Conclusion: Increased mean baseline CT attenuation of liver metastases may be utilised to identify mCRC patients with longer OS.

Author Disclosures:

V. Heinemann: Advisory Board; Merck KGaA, Roche AG, Amgen, Sanofi, Lilly, SIRTEX, Boehringer Ingelheim, Baxalta, Taiho, Merrimack. Consultant; Merck KGaA, Roche AG, Amgen, Sanofi, SIRTEX, Baxalta. Other; Merck KGaA, Roche AG, Amgen, SIRTEX, Baxalta. **J. Holch:** Consultant; Roche. Other; Novartis. **D. Modest:** Consultant; Merck KGaA, Amgen, Bayer, Servier, Roche. Other; Merck KGaA, Roche AG, Amgen, Bayer, Sanofi, Servier.

B-1077 10:46

Predicting the response of colorectal cancer liver metastases (CRCLM) to preoperative chemotherapy using gadoteric acid-enhanced MRI

N.V.V.P. Costa¹, N. Bastati², S. Pötter-Lang², Z. Guengoern², Y. Bican², A. Ba-Ssalamah², ¹Lisbon/PT, ²Vienna/AT (nunovpc@gmail.com)

Purpose: The aim of the study was to create a scoring system based upon gadoteric acid-enhanced magnetic resonance imaging (⁹⁸MRI) features to predict the treatment response (TR) to chemotherapy.

Methods and Materials: This was a retrospective study of 30 consecutive patients (65.2±11.2years) with CRCLM, who underwent ⁹⁸MRI after chemotherapy and before hepatic resection. Metastases were classified according to a suggested scoring system (0-6 points) in three groups of response: optimal (≤2 points); partial (2-4 points); and no-response (≥4 points). The scoring system comprised three features: overall homogeneity (homogeneous=0, mixed=1, heterogeneous=2); tumour-liver interface (sharp=0, mixed=1, ill defined=2); and peripheral rim enhancement (≤2 mm=0, 2-4 mm=1, ≥4 mm=2). Apparent diffusion coefficient (ADC) values were measured. The primary outcome was residual vital tumour (RVT). The scoring system, response groups, and ADC values were calculated and compared with the RVT percentage. Demographic, laboratory, and imaging findings were included in a multivariate statistical analysis. The three groups of response were correlated with patient survival and the log-rank test was used to compare two survival distributions (optimal/partial response vs no-response groups).

Results: Forty-one CRCLM showed good inter-observer agreement (κ=0.86). Multiple regression demonstrated an association between RVT (32.9±11.2) and the scoring system (p<0.001), the response group (p<0.001), and the ADC values (p<0.021). The survival distributions between optimal/partial response and no-response showed a trend to be different (p=0.066).

Conclusion: ⁹⁸MRI correlated well with our scoring system, different response groups, and ADC values in patients with CRCLM treated with chemotherapy, and may be used to assess the RVT percentage.

B-1078 10:54

MRI-based treatment response assessment for liver metastasis stereotactic radiotherapy

D.I. Kuplevatskaya, A. Babiy, N. Vorobyov, V.I. Kuplevatsky, N. Berezina, M. Cherkashin; St. Petersburg/RU (dkup@ldc.ru)

Purpose: To develop MRI criteria for stereotactic body radiation therapy (SBRT) treatment response assessment in patients with liver metastases.

Methods and Materials: In our study 39 patients with liver metastasis, treated by SBRT were included. Abdominal MRI (1.5T scanner) was performed before radiation and after 1, 4, 6, 12 months. The protocols include: T2 Cor, T2 CorFS, T2 Sag, T2 tra, T1 tra in a phase-antiphase, DWI (b 50, 400, 1000), T2 Ax TSE BLADE FS 3 mm on the liver area, dynamic contrast T1tra VIBE FS 1.5 mm. Analysis included target measurement by RECIST 1.1 criteria, necrotic area volume measurement by "Segmentation volume" (OleaSphere V2.3 SP1), DWI, dynamic contrast enhancement and parenchymal postradiation change assessment.

Results: Tumour response after SBRT was revealed in 62% in month 1 and in 49% in month 4. Size decreasing by 30% or more was maximal in 76.9% patients (month 1) and maximal tumour necrosis (25 to 50% lesions) was detected in month 4. In 6 and 12 months after radiation, stabilization was observed in 64% and 71% of cases. Necrotic changes (more than 50% of target volume) were revealed in 61.2% of patients. Complete tumour response after 12 months of SBRT was detected in 13% of patients.

Conclusion: Multiparametric MRI allows to assess morphological characteristics and functional status of radiated metastases and liver parenchyma after SBRT. Complex imaging support radiation oncologist with clear treatment response assessment and is a helpful tool for timely treatment strategy changing.

Author Disclosures:

D.I. Kuplevatskaya: Speaker; Siemens. M. Cherkashin: Speaker; Siemens.

B-1079 11:02

Multi-parametric MRI assessment of acute response to stereotactic body radiation therapy in patients with hepatocellular carcinoma or non-small cell lung cancer

X. Yang, E. Miller, P. Subramanian, T.M. Williams, M.V. Knopp; Columbus, OH/US

Purpose: To study tumour's acute response to stereotactic body radiation therapy (SBRT) with multi-parametric functional MRI.

Methods and Materials: Patients with unresectable hepatocellular carcinoma (HCC) or non-small cell lung cancer (NSCLC) received multi-parametric MRI prior to and within 24 hours after a single fraction of SBRT. BOLD, DWI (NSCLC: b=0/600; HCC: b=0/50/600), and DCE-MRI (Gadobenate, 0.5mL/s infusion) sequences were acquired on a 3T scanner. BOLD response to an

oxygen challenge (15L/min) was measured with the R2* difference between air-breathing and oxygen-breathing cycles. Apparent Diffusion Coefficient (ADC) was calculated from the DWI data. DCE-MRI was analyzed with the modified Brix's pharmacokinetic model. Linear mixed effects model was used for statistical analysis.

Results: Sixteen lesions (9 HCC/7 NSCLC) were identified for analysis. BOLD/DWI/DCE data were available for 16/15/11 lesions. Statistically significant BOLD response to the oxygen challenge was observed in 5 HCCs but in only 1 NSCLC. SBRT induced significant decreases in air-breathing R2* in both HCC (2.1 s⁻¹, P<0.001) and NSCLC (3.4 s⁻¹, P=0.006). This decrease in R2* was positively correlated with an increase in DCE parameter k_{ep} (r=0.74/0.70 for HCC/NSCLC). The correlation between R2* decrease and ADC increase was negative for NSCLC (r=-0.68), and close to zero for HCC (r=0.1).

Conclusion: SBRT induces an acute decrease in R2* within 24 hours post-treatment in different types of lesions regardless of their BOLD responses. This change cannot be explained by radiation-induced vasogenic edema. It is more likely to be an indicator of improved tumour oxygenation due to a temporary increase in perfusion.

B-1080 11:10

Impact of the MRI sequence and observer on the gross tumour volume (GTV) in patients with oesophageal and gastro-oesophageal junction (GOJ) cancer

K. Owczarczyk, C. Kelly-Morland, S. Mcelroy, J. Winfield, M.M. Siddique, A. Qureshi, G. Cook, V.J. Goh; London/UK (christian.kelly-morland@kcl.ac.uk)

Purpose: Target volume definition for oesophageal/GOJ cancer is challenging and guided by a combination of diagnostic modalities. The high contrast-to-noise of MRI may be of value for radiotherapy treatment planning (RTP). Our aim was to compare the gross tumour volume (GTV) using T2-weighted (T2w) and diffusion weighted (DWI) MRI and to evaluate the agreement between a radiation oncologist and radiologist.

Methods and Materials: Following ethics approval and consent, 26 oesophageal/GOJ cancer patients underwent prospective 1.5T MRI. The GTV was delineated on both T2-w and high b-value (b-900s/mm²) DWI images by a radiation oncologist and subspecialty radiologist independently. GTV was compared for each reader and sequence using the paired t-test (comparing means); and Dice Coefficient (DC), and Jaccard Similarity Index (JSI; assessing volume congruity). Inter-observer agreement was assessed using Bland-Altman statistics.

Results: DWI GTV was larger by a mean of 14.8% (95% CI -6.7%-36.6%) when delineated by the radiation oncologist while T2w GTV was larger by 18.2% (95%CI -48.2%-4.8%) when delineated by the radiologist, p>0.05. DC and JSI were higher for the T2w than DWI GTV (DC: 0.46±0.19 vs 0.56±0.16; JSI: 0.41±0.15 vs 0.31±0.16). Bland-Altman limits of agreement were similar (DWI: -137.7 to -130.5%; T2-w: -146 to -149.5% respectively).

Conclusion: Sequence selection and reader affects GTV measurements. These results emphasize the importance of sub-specialty radiologist input in RTP of oesophageal cancer as well as combining the information from multiple sequences at the time of target volume delineation.

B-1081 11:18

Comparison of 4'-[methyl-¹¹C] thiothymidine (4DST) PET/CT and FDG PET/CT for predicting response to neoadjuvant therapy in patients with oesophageal cancer

M. Hotta¹, R. Minamimoto¹, K. Yamada¹, K. Yokoyama¹, J. Toyohara²; ¹Shinjyuku-ku, Tokyo/JP, ²Itabashi-ku, Tokyo/JP (masatoshihotta@yahoo.co.jp)

Purpose: Imaging of DNA synthesis can be achieved using 4'-[methyl-¹¹C] thiothymidine (4DST) PET/CT, which shows a high correlation with cell proliferation. The aim of this study was to evaluate the diagnostic value of 4DST PET/CT for predicting response to neoadjuvant therapy in patients with oesophageal cancer, compared with FDG PET/CT.

Methods and Materials: Twenty-five patients (23 males, 2 females; mean age, 64.8±9.2 years) with histologically diagnosed oesophageal cancer underwent 4DST and FDG PET/CT after completion of neoadjuvant chemotherapy or chemoradiation therapy. All patients subsequently underwent oesophagogastrectomy after neoadjuvant therapy. Based on pathological findings, patients were divided into responder and non-responder groups. The maximum standardized uptake value (SUVmax) of the primary lesion was measured for 4DST and FDG, and compared between responder and non-responder groups. Receiver operating characteristics (ROC) analysis was used to evaluate the diagnostic performance of 4DST and FDG SUVmax for predicting response.

Results: The pathological diagnosis revealed 13 responders and 12 non-responders. The responder group showed lower 4DST and FDG SUVmax than the non-responder group, which was statistically significant for 4DST (4.0±1.6 vs 6.8±3.1 for 4DST, p=0.01; 4.3±1.2 vs 7.3±4.3 for FDG, p=0.07). Area under

the curve (AUC) was higher for 4DST SUVmax (0.82; CI, 0.66-0.98) than for FDG SUVmax (0.72; CI, 0.50-0.93).

Conclusion: 4DST PET/CT has a potential for predicting response to neoadjuvant therapy in patients with oesophageal cancer compared with FDG PET/CT. Higher uptake of 4DST after neoadjuvant therapy may indicate inadequate response to neoadjuvant therapy.

Author Disclosures:

M. Hotta: Research/Grant Support; Grant-in-Aid for Young Scientists (B) No. 17K18396 from the Japan Society for the Promotion of Science, Grant of the Japan Radiological Society from Bayer.

B-1082 11:26

Efficiency of perfusion CT in pancreatic mass characterisation

S. Aslan, M. Nural, I. Camlidag, M. Danaci; *Samsun/TR (serdaraslan28@hotmail.com)*

Purpose: To evaluate the efficacy of perfusion CT (PCT) in pancreatic lesion detection and characterisation.

Methods and Materials: 56 patients with tumour or tumour suspicion on dynamic MDCT underwent PCT. Perfusion parameters (BV, BF, MTT, PS) of the tumour and normal parenchyma was calculated separately by two different readers. Lesions were grouped as adenocarcinoma, neuroendocrine tumour (NET) and mass-forming chronic pancreatitis (MFCP) according to histopathological diagnoses. Isoattenuating lesions were evaluated as a subgroup.

Results: All perfusion parameters in 42 adenocarcinoma cases were significantly different from normal pancreatic parenchyma and MFCP cases ($p < 0.001$ and $p < 0.001$, respectively). 5 MFCP cases had significantly prolonged MTT and lower BV, BF, and PS ($p < 0.05$) whereas 5 NET cases had higher BV, BF, and PS compared with normal parenchyma ($p < 0.05$). When BV, BF, PS, and MTT were chosen as 6.84 ml, 64.43 ml, 28.08 ml/100 ml/min and 7.47 sec, respectively, differentiation between adenocarcinoma and MFCP were made with high sensitivity (%100, %100, %97.8 and %100, respectively) and specificity (%92.3, %100, %80 and %100, respectively). 11 isoattenuating lesions also had prolonged MTT and lower BV, BF, and PS compared with normal parenchyma ($p < 0.05$). Of isoattenuating lesions, 6 adenocarcinomas had significantly lower BV, BF, PS and prolonged MTT compared with 5 MFCP cases ($p < 0.001$). Interreader agreement was high-very high (ICC = 0.76 - 0.99).

Conclusion: PCT is a reliable method for diagnosis and characterisation of pancreatic masses and in cases of the diagnostic dilemma.

B-1083 11:34

Pancreatic ductal adenocarcinoma: association of RECIST1.1 and Choi criteria with survival data and clinical outcome

E. Raimondi^{1,2}, K. Young², K. Kouvelakis², D.-M. Koh², V. Calamai², N. Starling², M.A. Bali²; ¹Ferrara/IT, ²London/UK (edoardo.raimondi@unife.it)

Purpose: To compare overall survival (OS) and progression-free survival (PFS) of pancreatic ductal adenocarcinoma (PDA) patients treated with FOLFIRINOX chemotherapy with RECIST1.1 and Choi criteria response categorisation.

Methods and Materials: After IRB approval, 32 patients with locally advanced (LAPDA) and 35 patients with metastatic (MPDA) PDA treated with FOLFIRINOX were retrospectively included. Pre and post-treatment CT studies were analysed using Mint Lesion™. Within each group, patients were categorised as responder (R) and non-responder (NR) according to RECIST1.1 and Choi criteria. Kaplan-Meier analysis was performed for R and NR categories for each radiological criteria for OS and PFS.

Results: Significant differences between R and NR for OS and PFS were observed in both groups for both radiological response criteria (Log-rank test: $p < 0.05$). For LAPDA median OS was 34.57 vs 13.82 months by RECIST1.1 (HRs: 2.62-32.59) and 21.12 vs 12.34 months by Choi (HRs: 1.44-12.12). Median PFS was 27.07 vs 11.74 months for RECIST1.1 (HRs: 1.89-13.79) and 15.10 vs 10.59 by Choi (HRs: 1.16-8.98). For MPDA, median OS was 20.89 vs 8.88 months by RECIST1.1 (HRs: 1.34-6.66) and 18.49 vs 8.22 months by Choi (HRs: 2.47-15.26). Median PFS was 13.82 vs 5.56 months by RECIST1.1 (HRs: 1.59-7.95) and 13.39 vs 2.76 months by Choi (HRs: 4.95-55.56).

Conclusion: Response categorisation by RECIST1.1 was superior to Choi criteria in LAPDA in stratifying patient outcomes, but Choi criteria better associated with OS and PFS in MPDA. These observations may suggest differences in the disease imaging phenotypes.

B-1084 11:42

Virtual touch quantification technology in differentiation between benign and malignant solid small pancreatic tumors: initial results

Y. Dong, F. Mao, J. Cao, P. Fan, W. Wang; *Shanghai/CN (dr_mimi@163.com)*

Purpose: To evaluate the feasibility of differentiating between pancreatic ductal adenocarcinomas (PDA) and other solid benign pancreatic tumors with virtual touch quantification (VTQ) shear wave technology.

Methods and Materials: Over the periods of January 2016 to October 2017, a total of 78 patients with unclassified solid small pancreatic lesion ≤ 20 mm were prospectively evaluated. ACUSON AXONA US system (Siemens Medical Solutions, Mountain View, CA, USA), equipped with a C6-1 transducer was used. VTQ were performed, shear wave velocity (SWV) and the differences in SWV ratio of solid pancreatic lesion to surrounding parenchyma were evaluated. In all patients VTQ elastography results were compared with cytology or histology findings as the gold standard.

Results: A total of 78 pancreatic lesions including 58 (74.3 %) PDA, 13 (16.7 %) solid pseudopapillary tumors (SPT) and 7 (8.9 %) pancreatic neuroendocrine tumors (NET) were analysed. The mean SWV values obtained were (3.59 ± 0.32) m/s for PDA, (2.61 ± 0.11) m/s for SPT and (2.47 ± 0.54) m/s for NET ($P < 0.05$). The SWV ratios were 2.43 ± 0.22 for PDA and 1.19 ± 0.21 for benign lesions ($P < 0.05$). For the diagnosis of PDA, while using the cut off value 3.67 m/s for SWV and 2.51 for SWV ratio, good sensitivity (81.3%) and specificity (77.5%) were obtained for the characterization of PDA.

Conclusion: VTQ is a new elastography method that shows promising clinical application for the quantification of PDA elasticity. Increasing tissue stiffness of PDA is represented by greater SWV values.

B-1085 11:50

Dedicated DW-MR imaging as an accurate selection tool for hyperthermic intraperitoneal chemotherapy (HIPEC) in patients with peritoneal carcinomatosis (PC) from colorectal origin

I. van't Sant-Jansen, M. Engbersen, S. Chandrasegaram-Shanmuganathan, D.M. Lambregts, N.F. Kok, G.L. Beets, R.G.H. Beets-Tan, A.G. Aalbers, M.J. Lahaye; *Amsterdam/NL (M.Lahaye@nki.nl)*

Purpose: The peritoneal cancer index (PCI) is a surgical scoring system to quantify the extent of PC. It is used to select patients who might benefit from cytoreductive surgery (CRS)/HIPEC. To prevent unnecessary surgery in patients whose peritoneal tumour burden is too extensive, patient selection based on preoperative imaging is highly desirable. Computed tomography is inaccurate in predicting PCI. In order to assess whether DW-MRI can select potentially operable patients we compared PCI estimated preoperatively by DW-MRI with PCI found at surgery.

Methods and Materials: Forty-seven consecutive patients (M/F=21/26) with histologically proven colorectal cancer and suspected or confirmed PC were included. All patients underwent preoperative dedicated whole-body DW-MRI (scantime=35min) before exploratory laparoscopy or CRS/HIPEC. PCI was prospectively assessed by two independent radiologists on MR-imaging and was compared to PCI at surgery (=reference standard). Based on PCI patients were categorised as operable (PCI 0-20) or inoperable (PCI 21-39).

Results: Mean PCI at surgery was 11.6(range 0-31). Mean radiological PCI for reader 1 was 10.8 (range 2-33) and 9.2(range 0-31) for reader 2. Radiologist 1 and 2 staged respectively 44/47 and 41/47 patients correctly (accuracy 94%/87%). Both radiologists detected all operable patients with a PCI<21 at surgery (sens=100%). Respectively, 3 and 6 patients were understaged by DW-MRI. There were no false negatives results. The intraclass correlation between the two radiologists was excellent (ICC=0.91, 95%CI:0.765-0.956).

Conclusion: DW-MRI is an accurate and reproducible selection tool to non-invasively select patients who could potentially benefit from CRS/HIPEC. DW-MRI may replace surgical PCI staging in selected patients.

10:30 - 12:00

Room E1

Breast

SS 1402a

B3 lesions

Moderators:

P. Clauser; Vienna/AT

V. Lehotska; Bratislava/SK

B-1086 10:30

Role of one-pass breast lesion excision system in complete excision of high-risk breast lesions expressed as clusters of microcalcifications

A. Christou¹, V. Koutoulidis², D. Koulocheri², K. Zografos², G. Zografos²;
¹Doncaster/UK, ²Athens/GR (alexandrachristou@gmail.com)

Purpose: To assess the role of the breast lesion excision system (BLES) in complete removal of clusters of microcalcifications found on mammogram proved histologically to be high-risk lesions.

Methods and Materials: 394 consecutive women with 400 cases of suspicious clusters of microcalcifications underwent stereotactic biopsy using the intact BLES device between January 2014 and January 2016. 38/400(9.5%) cases proved histologically to be high-risk lesions and were subsequently assessed for underestimation and complete removal.

Results: Mean size was 9.75mm (1.5mm-18mm) which was within the size that BLES needle can excise (20 mm). 4 papillomas with atypia (10.5%), 14 cases with flat epithelial atypia (FEA) (36.8%), 10 cases with lobular neoplasia (LN-atypical lobular neoplasia [ALN], lobular carcinoma in situ [LCIS]) (26.3%), 8 with atypical ductal hyperplasia (ADH) (21.2 %) and 2 cases with mucocoele-like lesions (MLL) with atypia (5.3%) were found. 29/ 38 lesions had subsequent surgery and all 38 had a 2-year follow up. Complete excision was achieved in 23/29 lesions (79.3%). No underestimation was found. 2-years mammographic stability was found in all lesions. Mann Whitney test showed that clear BLES specimen margins over 1mm was statistically significant predictive factor for complete removal (p=0,041).

Conclusion: One-pass BLES intact stereotactic technique is a safe and accurate biopsy method with high rates of complete removal of small high-risk lesions which could be potentially used as an alternative excision method to diagnostic surgery and avoid subsequent surgical excision.

B-1087 10:38

Prognostic characteristics of B3 lesions detected by mammographic screening programmes in the Veneto region

I. Brilli¹, E. Tosi¹, M. Zorzi¹, A. Rizzo², C. Fedato³, E. Orvieto¹, M. Lo Mele¹, M. Baracco¹, A. Fiore¹; ¹Padua/IT, ²Treviso/IT, ³Dorsoduro/IT (isa.brilli@libero.it)

Purpose: Breast lesions with uncertain malignant potential (B3) are extremely heterogeneous and have a mean predictive value (PPV) for cancer of 31.7%. We retrospectively analysed a case series of B3 detected by screening programmes of Veneto region to identify selection criteria for surgery.

Methods and Materials: Among the 2.239.137 women screened from 2003 to 2015, 7.179 performed a biopsy (VAB or CNB) and 757 had a B3 outcome, 542 of which confirmed at histological revision. We evaluated the PPV for cancer of age, mammographic and/or ultrasound findings, radiological suspicion (R), biopsy diagnosis, presence of atypia.

Results: B3 cases referred to surgery were 447/542 (82%). Out of the 419 with available outcome, 133 (31.7%) were positive for carcinoma (43 invasive - PPV 10.3%, and 90 in situ - PPV 21.5%). At preoperative mammography, 57% of B3 lesions showed cluster of microcalcifications, 30% opacity and 13% distortions. PPV for invasive lesions was higher for distortions (RR 3.63; 95% CI 1.39-9.14) and for R4 radiological classification (RR 2.15; 95% CI 1.06-4.43). PPV was reduced in the absence of atypia (RR 0.49; 95% CI 0.23-0.99) and for the B3 class of papillary lesion (RR 0.12; 95% CI 0.003-0.81). Age was not significantly associated with PPV.

Conclusion: Radiological distortion, R4 classification and the presence of epithelial atypia could be considered as valid selection criteria for surgical excision. The low risk for malignant neoplasm suggests to select the B3 cases to refer for surgery through discussion in multidisciplinary team to limit overtreatment.

B-1088 10:46

A prospective study on uncertain biological potential lesion (B3) overtreatment in tomosynthesis breast screening: role of tomosynthesis-guided biopsy (DBT-VAB)

G. Romanucci¹, S. Brunelli¹, A. Caneva², S.A. Montemezzi¹, F. Caumo³;
¹Verona/IT, ²San Bonifacio/IT, ³Padua/IT (giovi.romanucci@libero.it)

Purpose: DBT in screening practice improves the detection of architectural distortions, often associated with B3 lesions. B3 category represents a clinical dilemma due to the significant risk of associated malignancy with often subsequent surgical excision to histologically examine the entire lesion. Aim of this study is to assess the accuracy of DBT-VAB in reducing overtreatment of B3 lesions, detected with tomosynthesis as architectural distortions.

Methods and Materials: 265 DBT-VAB were performed from 1st April 2015 to 31st March 2017, 97 of them on architectural distortions. At least 24 biopsy specimens were obtained in each procedure. Radial scars and papillary lesions, usually considered B3 lesions, if <20 mm and completely removed after DBT-VAB, were downgraded to B2 and sent to yearly follow-up.

Results: Microhistological result of architectural distortions was malignant in 22/98 cases (22.4%). According to the new proposed categorization, B3 lesions lowered from 61/98 (62.2%) to 21/98 (21.4%) with the subsequent management: 9 were sent to yearly follow up; the remaining 12 lesions underwent surgical excision which revealed 3 malignancies, both seen only on DBT. Similarly, B2 lesions raised from 15.3% (15/98) to 56.1% (55/98), all sent to yearly follow-up.

Conclusion: DBT-VAB ensures the patient the most precise diagnostic and therapeutic workup for architectural distortion. It accurately characterizes architectural distortions and allows a B3 risk stratification to reduce overtreatment.

B-1089 10:54

Radial scars detected at screening mammography: is surgical excision always indicated?

T. Tarmey, P. McGreal, A. McDermott, M. Sheehan, A. O'Connell; Galway/IE (tarattarmey@gmail.com)

Purpose: Radial scars (RS) diagnosed at percutaneous biopsy can be associated with ductal carcinoma in situ (DCIS) and invasive carcinoma and current management involves surgical excision. The occurrence of DCIS and invasion is increased when there is associated atypia at biopsy. We assessed any histological features at biopsy that may warrant more conservative management.

Methods and Materials: We retrospectively reviewed all cases from a National Breast Cancer Screening Program centre over a ten-year period (2007-2016) to identify all patients with a histological diagnosis of a RS made by percutaneous biopsy. All women underwent excision. For all cases, the core biopsy reports were analysed for the presence of atypia, carcinoma in situ or invasive carcinoma. Any progression in histological grade from a lesion on initial biopsy to the surgically excised specimen was considered an upgrade. Data were statistically analysed with SPSS V.23.

Results: 185,766 women were screened and 91 pure RS were identified at percutaneous biopsy giving an incidence of 0.05%. 9 (10%) cases were upgraded to atypia, 8 (9%) cases were upgraded to DCIS and 7 (8%) cases were upgraded to invasive carcinoma giving an overall upgrade rate of 26%. Therefore, initial core biopsy has a sensitivity of 37% and specificity of 92%.

Conclusion: In patients with RS, the overall histological upgrade rate of 26% from percutaneous biopsy to surgical excision suggests that lack of invasion, DCIS or even atypia at biopsy does not help differentiate between RS that warrant excision versus those that may be managed more conservatively.

B-1090 11:02

Atypical ductal hyperplasia: our experience in the management and long-term clinical follow-up in 71 patients

L. Nicosia¹, A. Latronico¹, A. Faggiani², C. Cannataci³, S. Penco¹, E. Cassano¹;
¹Milan/IT, ²Acerra/IT, ³Msida/MT (lucanicosia88@gmail.com)

Purpose: Atypical ductal hyperplasia (ADH) is a high-risk benign lesion found in approximately 1-10% of breast biopsies and associated with a variable incidence of carcinoma after surgical excision. The main goal of our study is to present our experience in the management and long-term follow-up of 71 patients with ADH diagnosed on breast biopsy.

Methods and Materials: Results of 3808 breast biopsy specimens from 1 January 2000 to 31 December 2005 were analysed to identify all biopsies which resulted in a diagnosis of ADH. The histopathological results of the 45 patients who underwent surgery were analysed. Long-term follow-up for the remaining patients was carried out.

Results: 45 of 71 (63.4%) patients with histological diagnosis of ADH on breast biopsy underwent surgery. Definitive histological results revealed invasive carcinoma in 7 (15.6%), high-grade ductal carcinoma in situ (DCIS) in 10 (22.2%) patients, lobular carcinoma in situ (LCIS) in 4 cases

(8.9%) and benign findings in 24 cases (53.3%). 12 of 71 (16.9%) patients underwent only long-term follow-up; one (8.3%) of these developed invasive breast carcinoma after 6 years.

Conclusion: Atypical ductal hyperplasia diagnosed on breast biopsy is associated with a relatively high incidence of invasive carcinoma and high-grade ductal carcinoma in situ at the time of surgical excision. Certain radiological and cytological criteria can be used to help determine which patients should forgo surgery and be followed up with good results. Long-term follow-up is always crucial for patients who have not undergone surgery.

B-1091 11:10

Intraductal papilloma without atypia in breast biopsies: rate of upgrades to carcinoma at excision and radiological features predictive of an upgrade

D. Leithner^{1,2}, B. Kaltenbach¹, C. Park¹, K. Pinke^{2,3}, P. Hoedl¹, F. Stephan¹, V. Moebus¹, T.J. Vogl¹, M.P. Müller-Schimpfle¹; ¹Frankfurt a. Main/DE, ²New York, NY/US, ³Vienna/AT (doris.leithner@googlemail.com)

Purpose: While excision of atypical papilloma of the breast is mandatory, the management of intraductal papilloma without atypia (IDP) diagnosed with biopsy remains controversial. This study sought to investigate the rate of upgrade to carcinoma at surgical excision of IDPs, and identify clinical and radiological features predictive of an upgrade.

Methods and Materials: Patients with a core-needle or vacuum-assisted biopsy diagnosis of papilloma without atypia and surgical excision of this lesion at a breast centre between 2007 and 2017 were enrolled in the study. Cases with radiologic-pathologic discordance and history of breast carcinoma were excluded. Appropriate statistical tests were performed to correlate clinical characteristics and radiologic features with an upgrade to malignancy at excision.

Results: For 60 women with 62 surgically removed IDPs, the upgrade rate to malignancy was 16.1% (10 upgrades; 4 IDC, 6 DCIS). Vacuum-assisted biopsy was used for 14 IDPs, while 46 were sampled by core-needle biopsy. IDP with upgrade to carcinoma showed a significantly greater distance to the nipple than benign papilloma after excision (63.5 vs. 36.8, P=0.013). No significant associations were found between upgrade to carcinoma and age, menopausal status, lesion size, presence of microcalcifications, BI-RADS descriptors, initial BI-RADS category, and biopsy modality.

Conclusion: The upgrade rate at surgical excision for IDPs diagnosed with biopsy was 16.1%, suggesting that observation only might not be appropriate for all patients with a biopsy diagnosis of IDP. For patients with peripheral IDP, excision of the lesion should be considered.

B-1092 11:18

Imaging findings of papillary lesions of the breast with histopathologic correlation: a five-year study from Instituto Nacional de Ciencias Médicas y Nutrición "Salvador Zubirán"

D. Lara Nuñez, P. Gonzalez Balboa, M. Chapa Ibarquengoitia, R.E. Fuentes Corona, F. Candanedo González, M. Licano Zubiate, K.P. Castro German; *Mexico/MX* (dennylaran5@gmail.com)

Purpose: To establish the radiologic characteristics of benign and malignant papillary lesions of the breast.

Methods and Materials: A descriptive, cross-sectional study was used to examine all patients who underwent percutaneous or excisional breast biopsy between July 2012 and July 2017 at Instituto Nacional de Ciencias Médicas y Nutrición "Salvador Zubirán". All radiologic and histopathological images were rechecked for the study.

Results: Of the 94 papillary lesions, 47.3% were intraductal papilloma, 33.3% intraductal papillomatosis, 11.8% micropapillary ductal carcinoma in situ and 7.5% papillary carcinoma. 24.7% corresponded to BIRADS 4A, 41.5% to BIRADS 4B, 16.8% to BIRADS 4C, 9% to BIRADS 5, and 7.8% to BIRADS 6. Of these lesions, only 17% were located in a retroareolar region. 66% of the lesions corresponded to nodules with an average size of 13 mm(± 7.8 SD) and 24.5% contained calcifications.

Conclusion: It is difficult to differentiate between benign and malignant papillary lesions by their appearance, this is why the final diagnosis is done with radiologic-pathologic correlation.

B-1093 11:26

Probably benign findings (BI-RADS 3) at breast MRI: frequency and malignancy rate

M. Iodice¹, V. Pittari¹, R.M. Trimboli², N. Berger³, L.A. Carbonaro², F. Sardaneli¹; ¹Milan/IT, ²San Donato Milanese/IT, ³Zurich/CH (maidice@gmail.com)

Purpose: Retrospectively evaluate the frequency of BI-RADS3 lesions on breast MRI and determine the rate of malignancy in women at average, intermediate and high risk of breast cancer.

Methods and Materials: Consecutive breast MRI examinations performed from July 2010 to February 2017 were retrospectively reviewed to identify

lesions prospectively assigned with BI-RADS3 category. Women with histopathology or a minimum 2-year imaging follow-up entered the analysis. Findings reported as BI-RADS3 were reviewed. The frequency of BI-RADS3 assessment, the rate of cancer and negative predictive value (NPV) were calculated. 95% confidence interval (CI) were calculated using the binomial distribution.

Results: A total of 682 women underwent breast MRI in the study period. 444 women who underwent MRI before March 2015 were considered for this study. 47 lesions in 38 women were assigned with BI-RADS3 category (38/444, 8.5%, 95% CI 0.1%-2.0%). Outcomes were available for 44 lesions in 36 women: 19/44 (43%, 95% CI 28.3%-59.0%) were biopsied, 8/44 (18%, 95% CI 8.2%-32.7%) were operated, 17/44 (38.6%, 95% CI 24.4%-54.5%) did not have evidence of malignancy at 22-81 months. Malignancy was found in 3/44 lesions (6.8%, 95% CI 1.4%-18.7%), in 2/36 women (5.5%, 95% CI 0.7%-18.7%). NPV was 93.2% (41/44 lesions%, 95% CI 81.3%-98.6%) and 94.4% (34/36 women, 95%, CI 81.3%-99.3%). There were one invasive ductal carcinoma (IDC) and 2 IDC with in situ component; they appeared on MRI as masses (n=2) and focus (n=1).

Conclusion: The rate of women who received a BI-RADS3 assessment at breast MRI was 8.5% with a cancer rate higher of 5.5%. Careful adherence to lesion criteria is necessary to maintain a low malignancy rate for BI-RADS category 3 lesions. The presence of a unique suspicious feature deserves an up-graded rating.

B-1094 11:34

Optoacoustic imaging increases the sensitivity of mammography and specificity of US: implications for practice

O. Abevako¹, R.A. Woitek², M. Wallis¹, P.L. Moyle¹, S. Morscher³, N. Malchus³, R. Manavaki¹, I.A. Mendichovszky¹, J. Joseph¹, J. Quiros-Gonzales¹, S. Bohndiek¹, F.J. Gilbert¹; ¹Cambridge/UK, ²Vienna/AT, ³Munich/DE (oshi.creativity@googlemail.com)

Purpose: Optoacoustic (OA) imaging fused with ultrasound (OPUS) can provide novel functional and anatomical information on breast tissue microenvironment. The aim of our study was to develop a clinically useful OA feature set to differentiate benign and malignant breast lesions and investigate its usefulness in image interpretation.

Methods and Materials: Female patients with benign, indeterminate or suspicious lesions were recruited from our institution's symptomatic and breast screening clinics and imaged at 800nm (total haemoglobin wavelength) mapping vascularity. An OA imaging feature set was developed using the first 38 lesions. Features for malignancy were (1) irregular high signal lesion cap, (2) feeding vessel, (3) high signal rim and (4) claw sign; for benignity (1) splayed/displaced vessels sign and (2) absence of OA signal were used, in combination with the ultrasound BIRADS lexicon. Two radiologists (5 and 25 years breast-imaging experience) trained initially on feature set examples. They then independently, blindly and randomly scored the mammography, ultrasound and OA images of the remaining 44 lesions.

Results: Of 92 lesions, 10 were excluded due to technical errors. The feature set had 12 malignant and 26 benign lesions; the test set included 31 malignant and 13 benign lesions. Sensitivity pairs for readers 1 and 2 for mammography, US and OPUS were (90.3%, 90.3%), (96.5%, 96.5%) and (96.5%, 96.5%), respectively, with specificities of (71.4%, 71.4%), (53.8%, 46.1%) and (84.6%, 84.6%). The weighted Kappa inter-reader agreement was 0.91, 0.79 and 0.997 for mammography, US and OPUS.

Conclusion: Combining OA with US information has the potential to improve reader specificity and decrease biopsy rates.

B-1095 11:42

Phyllodes tumours of breast: histogram analysis of the apparent diffusion coefficient for assessment of tumour grade

W. Tang, Y. Zhang, J. Cheng; *Zhengzhou/CN* (597744255@qq.com)

Purpose: Investigating the value of histogram analyses of apparent diffusion coefficient (ADC) values for determining phyllodes tumour grades.

Methods and Materials: In all, 48 patients with phyllodes tumours (PTs) of breast included low-grade (Group 1; n = 30), intermediate-grade (Group 2; n = 12), and high-grade (Group 3; n = 6) tumours. Diffusion-weighted imaging (DWI) was performed in the axial plane. The ADC maps were generated, regions of interest were drawn on the middle section of lesion. Calculated histogram parameters included mean, 0.1th, 10th, 50th, 90th, and 99th percentiles of ADC, skewness, and kurtosis. Histogram parameters were correlated with tumour grade. We divided intermediate-grade and high-grade tumours into Group 2, low-grade tumours into Group 1. The parameters of two groups were calculated and the diagnostic performance for distinguishing different pathologic features was assessed.

Results: The ADC mean, 50th, 90th, and 99th percentiles of ADC, skewness showed significant differences among the two groups. The ROC analysis between low-grade, intermediate-grade and high-grade tumours showed that the 90th percentile ADC achieved the highest area under curve (AUC) at 0.806.

Conclusion: ADC histogram analyses are able to differentiate histologic grades of PTs.

B-1096 11:50

Variations in BI-RADS mammographic density classification between radiologists at three breast centres

T. Hovda¹, Å.S. Hølen², H. Bjørndal¹, S. Sebuødegård², S. Hofvind²;
¹Drammen/NO, ²Oslo/NO (tone.hovda@vestreviken.no)

Purpose: Mammographic density is a risk factor for breast cancer and may serve as a basis for implementation of stratified screening. We explored variations in mammographic density classification performed by radiologists at three breast centres in BreastScreen Norway.

Methods and Materials: The initial classification of mammographic density according to BI-RADS 5th edition (a-d) for a total of 1617 screening examinations was performed in consensus at three different breast centres by local radiologists. Subsequently, the same examinations were re-viewed and re-classified by a consensus panel of two radiologists from each centre. We used descriptive statistics to compare the initial and subsequent classifications of mammographic density.

Results: The initial density classification yielded the following distribution: a: 13%; b: 43%; c: 35%; and d: 9%, while subsequent classification resulted in the distribution a:12%; b: 45%; c: 32%; and d:12%. For classification a), the percentage of examinations classified in the same density category initially and subsequently was 64% (n=132), ranging from 39 to 92% among the three centres; for b): 76% (n=523, range 58-82%); for c) 52% (n=359, range 55-64%); and for d): 67% (n=98, range 59-89%). When grouping the density categories a+b and c+d, 88% (range 74-96%) initially classified as category a or b remained in category a or b, while 82% (range 80-92%) initially classified as c or d remained in category c or d.

Conclusion: Mammographic density classification is subject to great variability among radiologists. This makes comparisons demanding and may complicate the use of density as a factor for stratification of mammographic screening.

10:30 - 12:00

Room E2

Neuro

SS 1411b

Peripheral nerve and spine

Moderators:

C. Lukas; Bochum/DE
 M.I. Vargas; Geneva/CH

B-1097 10:30

Preliminary clinical application of high-resolution MRI of the optic nerve using a small loop coil combined with head coil

Q. Dai^{1,2}, Z. Yang², G. Hong², L. Rao², M. He², P. Geng²; ¹Shenzhen/CN, ²Guangzhou/CN (dqunyaod@163.com)

Purpose: To preliminary explore the clinical application of high resolution MRI of the optic nerve using a small loop coil combined with head coil.

Methods and Materials: 102 optic nerves from optic neuritis and optic nerve radiation injury patients from October 2015 to February 2017 were prospectively collected. Transverse, coronal and sagittal images of optic nerves were obtained using a loop coil combined with head coil (group A) and single head coil (Group B), respectively. Whole brain 3D enhanced scan and optic nerve reconstruction were also performed. Image quality was scored and images were analysed by two neuroradiologists. The non-parametric Wilcoxon signed rank test was used to compare the difference of quality scores between group A and B, and $P < 0.05$ was statistically significant. Compared with the gold standard, sensitivity and specificity of displaying optic nerve lesions using different coils were calculated.

Results: The difference of FS-T2W image quality scores between two groups was statistically significant ($P < 0.05$) in three planes, and group A was better than group B. Sensitivity of displaying optic nerve lesions of group A was 86%, and specificity was 100%; while sensitivity of group B was 38.7%, and specificity was 88.9%.

Conclusion: High resolution MRI of the optic nerve using a small loop coil combined with head coil is suitable for clinical application and has certain clinical application value, with better image quality and higher sensitivity and specificity in displaying optic neuritis and optic nerve radiation injury, compared with conventional MRI using single head coil.

B-1098 10:38

Selection of coil for high-resolution MRI of the optic nerve

Q. Dai^{1,2}, Z. Yang², G. Hong², L. Rao², P. Geng²; ¹Shenzhen/CN, ²Guangzhou/CN (dqunyaod@163.com)

Purpose: To compare MR image quality of the optic nerve using a small loop coil combined with head coil, single head coil, and single small loop coil to choose the best coil for high-resolution MRI of the optic nerve.

Methods and Materials: Imaging was performed on 12 healthy volunteers with a 3.0T MR scanner using single 7-cm-diameter loop coil (group A), single head coil (group B) and a combination of these 2 coils (group C). Transverse, coronal and sagittal images of optic nerves were obtained. 3 groups of images were independently reviewed and scored according to an image quality scoring criterion by 2 neuroradiologists. The Kappa test, paired χ^2 test and nonparametric Wilcoxon signed rank test were used. $P < 0.05$ was statistically significant.

Results: 24 optic nerves were included. Group A can only display part of the intraorbital optic nerve and no quality scoring was performed. The Kappa values of scores of group B and C between the 2 radiologists were 0.880, 0.778, 0.600; 1.000, 0.882, 0.619, respectively. There was no significant difference between the scores by the 2 radiologists ($P > 0.05$). Scores of transverse, coronal and sagittal FS-T2WI of group B and C were 2.250±0.909, 1.250±0.417, 2.521±0.499; 3.750±0.442, 3.771±0.417, 3.875±0.304. The difference between the two groups was statistically significant ($P < 0.05$), with group C better than B.

Conclusion: Optic nerve MRI using a small loop coil combined with head coil is better than using single head coil or single small loop coil and can display the whole optic nerve with high resolution.

B-1099 10:46

The impact of trigeminal nerve atrophy and vascular compression on outcomes of trigeminal neuralgia after stereotactic radiosurgery

Y.-S. Hu, C.-C. Lee, W.-Y. Guo, C.-J. Lin, H.-C. Yang, H.-M. Wu, K.-D. Liu, W.-Y. Chung; Taipei/TW (sam6526@hotmail.com)

Purpose: Trigeminal nerve atrophy and neurovascular compression (NVC) are frequently observed in symptomatic nerves of classical trigeminal neuralgia (TN). The purpose of this study was to determine whether these nerve characteristics on MRI contribute to gamma knife surgery (GKS) outcomes in classical TN.

Methods and Materials: From 2006 to 2012, 67 patients of unilateral classical TN without previous surgery received GKS with a maximal dose of 90 Gy delivering to the trigeminal nerve proximal to the brainstem. Two evaluators, blinded to the side of pain, analysed the MRI before GKS to obtain the parameters, including proximal nerve cross-sectional area (CSA), vessel type of NVC, and site of NVC along the nerve. Correlations of the parameters with pain relief (Barrow Neurologic Institute [BNI] Grades I-IIIb) and pain recurrence (BNI Grades VI-V) after GKS were made using Cox regression and Kaplan-Meier analyses.

Results: The median CSA of the symptomatic nerves was significantly smaller than that of asymptomatic nerves (4.95 mm² vs 5.9 mm², $p < 0.001$). After adjustment for age and sex, only the nerve CSA was predictive of initial pain relief (hazard ratio 0.81, $p = 0.032$) and pain recurrence (hazard ratio 0.58, $p = 0.028$) after GKS. Patients with nerve atrophy (defined as CSA ≤ 4.4 mm²) had a lower 5-year probability of maintaining pain relief than those without nerve atrophy (65% vs 86%, $p = 0.044$).

Conclusion: Trigeminal nerve atrophy may predict pain recurrence in classical TN after GKS. Future studies are required to determine optimal treatment for long-term pain relief in classical TN with nerve atrophy.

B-1100 10:54

Measurement of normal optic nerve sheath diameter and nerve diameter on high resolution MRI

Q. Dai^{1,2}, Z. Yang²; ¹Shenzhen/CN, ²Guangzhou/CN (dqunyaod@163.com)

Purpose: To measure normal optic nerve sheath diameter (ONSD) and nerve diameter (OND) on high resolution MR images using a small loop coil combined with head coil.

Methods and Materials: 33 normal optic nerves underwent MR scanning using a small loop coil combined with head coil. ONSD and OND (transverse and superior inferior) at levels 3, 6, 9, 12, 15, 18, 21mm after the eyeball were measured on coronal FS-T2W images. Nonparametric Wilcoxon signed rank test was used to compare transverse and superior inferior diameters on the same level, and Friedman test was used to compare diameters among different levels.

Results: (1) Transverse and superior inferior ONSD and OND on coronal images was statistically different ($P < 0.05$) on levels 3, 6, 9mm after the eyeball. There was no statistical significance in difference between transverse and superior inferior ONSD and OND on levels 12, 15, 18, 21mm ($P > 0.05$). (2) Difference of ONSD among levels 3, 6, 9mm was statistically significant

($P < 0.001$, both transverse and superior inferior). There was no statistical significance in difference of OND among levels 3, 6, 9mm ($P > 0.05$), while OND among levels 3, 6, 9, 12mm was statistically different ($P < 0.05$). No significant difference was in ONSD among levels 12, 15, 18, 21mm ($P > 0.05$), similarly in OND ($P > 0.05$).

Conclusion: Normal optic nerve shows oval on levels 3-9mm after the eyeball and nearly circular on levels 12-21mm on coronal plane. Subarachnoid space on levels 3-9mm decreases gradually. Consistent results of ONSD and OND among different levels can be obtained on levels 12-21mm.

B-1101 11:02

Diagnostic efficiency of ultrasonography in case of peripheral nerve traumatic injuries

E. Zhurbin, A. Gayvoronskiy, I. Zheleznyak, V. Dekan; *St. Petersburg/RU* (Zhurbin-90@mail.ru)

Purpose: To estimate the use and diagnostic efficiency of ultrasonography in case of peripheral nerve traumatic injuries.

Methods and Materials: The research includes 154 patients with post-traumatic peripheral nerve neuropathy. All patients underwent ultrasonography on the expert class machine with the linear transducer with frequency range of 5 to 15 MHz. For ultrasonography efficiency evaluation, a statistical analysis of sensibility, specificity and accuracy was used, by the procedure of a referential (surgical interference or positive conservative treatment) and studied method (ultrasonography) qualified assessment.

Results: It was discovered that ultrasonography is an efficient diagnostic method for peripheral nerve traumatic injuries. It allows assessing injury localisation and the type to the full extent and to decide on further treatment tactics. According to ultrasonography results, 122 patients were operated and 32 patients treated conservatively. After comparative analysis of pre-operative ultrasonography data with the changes detected during the surgical interference and the results of conservative treatment, the diagnostic efficiency of ultrasonography in case of limb peripheral nerve traumatic injuries was estimated.

Conclusion: Ultrasonography is an efficient diagnostic method for limb peripheral nerve traumatic injuries. Ultrasonography with a sensitivity of 93.6% and specificity of 68.2% allows to detect injuries which always demand surgical interference, or prove the nerve trunk anatomical integrity, which does not demand a surgery as the injury appears to be reversible. The accuracy of ultrasonography is 86.4%, which makes it one of the leading methods of the given pathology diagnostics.

B-1102 11:10

Opportunities for the combined use of ultrasonography and neuromonitoring during the intra-operative phase of ultrasound guidance for the surgical treatment of radial nerve injury

V. Dekan, E. Zhurbin, A. Grishchenkov; *St. Petersburg/RU* (dekanvs@mail.ru)

Purpose: To assess the opportunities for the use of ultrasonography and neuromonitoring for ultrasound guidance during radial nerve surgical treatment.

Methods and Materials: A combination of ultrasound and neuromonitoring was applied to 37 patients during surgical treatment of radial nerve injuries. The research included patients with post-traumatic neuropathy of varying severity levels and duration.

Results: Intra-operative ultrasonography reduces operational trauma by 25% on average in each case, due to application of neurolysis from the nerve trunk injury in the direction of native anatomical structures and ending within the cicatricial adhesion. In five cases of radial nerve neurotmesis, proved visually afterwards, applying neuromonitoring in the nerve proximity test mode led to exposure of the safe muscular branches of the brachioradialis muscle, which were situated in the cicatricial conglomerate of the modified tissue and did not come in sight of the ultrasound detector. In the closing stage of neurolysis, due to the use of ultrasonography combined with neuromonitoring, in four cases an intrastem neuroma, undiscovered during the pre-operative percutaneous diagnostics, was detected.

Conclusion: The use of ultrasonography and neuromonitoring represents the opportunity of nerve trunk direct visualization and simultaneous nerve conduction assessment, which leads to a reduction in operational trauma and the number of early post-operative complications. It helps to increase the patient rehabilitation tempo. Intra-operative ultrasonography and neuromonitoring measurements are able to give a qualified failure mode assessment of all the nerve trunk structures and allows choosing more efficient and less traumatic surgical treatment tactics.

B-1103 11:18

Preliminary application study of optic nerve DTI in non-neoplastic lesions

Q. Dai^{1,2}, Z. Yang², G. Hong², L. Rao²; ¹Shenzhen/CN, ²Guangzhou/CN (dqunyao@163.com)

Purpose: To analyze DTI findings of normal optic nerve and measure normal ADC and FA values to offer reference for clinical application, and to explore clinical application value of DTI in non-neoplastic lesions of the optic nerve.

Methods and Materials: DTI was prospectively performed on 24 normal optic nerves and 73 optic nerves with non-neoplastic lesions from October 2015 to February 2017 using 3.0T MR scanner. Signal characteristics were observed and ADC, FA values were measured respectively. The difference of values between normal and lesion group was compared using independent sample t test. Ability of ADC and FA value in displaying non-neoplastic lesions was analyzed with ROC curve.

Results: Normal optic nerves showed slightly low signal on ADC maps and high signal on FA maps. Normal ADC value ($\times 10^{-3} \text{mm}^2/\text{s}$) was 1.102 ± 0.202 , and FA value was 0.540 ± 0.073 . Signal of lesions slightly increased on ADC maps and decreased on FA maps. ADC value of lesion group significantly increased ($P = 0.03$), and FA value significantly decreased ($P < 0.001$). Area under the ROC curve of ADC was 0.642, and that of FA was 0.768. When the cut-off point of FA value was ≤ 0.4827 , Youden index being the biggest, sensitivity was 64.4% and specificity was 87.5%.

Conclusion: Normal optic nerve shows slightly low signal on ADC maps and high signal on FA maps. Signal of non-neoplastic lesions slightly increases on ADC maps and decreases on FA maps, with ADC value increasing and FA value decreasing. In displaying non-neoplastic lesions of the optic nerve, FA value is better.

B-1104 11:26

High-resolution MRI findings of the normal optic nerve using a small loop coil combined with head coil

Q. Dai^{1,2}, Z. Yang², L. Rao², G. Hong², P. Geng²; ¹Shenzhen/CN, ²Guangzhou/CN (dqunyao@163.com)

Purpose: To observe the morphology and signal characteristics of normal optic nerve on high-resolution MR images and analyse the anatomical and histological basis.

Methods and Materials: 33 normal and 2 cadaveric optic nerves underwent MR scanning using a small loop coil combined with head coil. The cadaveric optic nerves were separated and pathologically examined. The morphology and signal characteristics of the optic nerves were analysed by two neuroradiologists, and those of the cadaveric optic nerves were observed and compared with the histological findings.

Results: 31 normal optic nerves (2 were abandoned because of obvious artefact) and 2 cadaveric optic nerves were included. The normal optic nerve was round and showed mixed isointensity and hypointensity surrounded by hyperintense subarachnoid space on coronal FS-T2WI and elongated isointensity on transverse and sagittal FS-T2WI, and the optic nerve sheath showed hypointensity. MRI findings of the cadaveric optic nerves were similar, and histology showed that the optic nerve fibers were separated into bundles by connective tissue including vessels. Compared with MRI, the optic nerve fibers showed isointensity and septae showed hypointensity.

Conclusion: High-resolution MRI of the optic nerve using a small loop coil combined with head coil can show the anatomical details and signal characteristics on coronal images. The normal optic nerve is round and shows mixed isointensity and hypointensity similar to a chessboard on high-resolution coronal T2WI, which is consistent with cadaveric optic nerve MR findings and relative to nerve bundles and connective tissue septae in histology.

B-1105 11:34

Automated three-dimensional detection of dural ectasia in Marfan syndrome by means of isotropic MRI and shape-based machine learning

F. Rengier¹, O. Naas¹, T. Norajitra¹, M. Messerli², K. Kallenbach¹, M. Karck¹, K. Maier-Hein¹, H.-U. Kauczor¹; ¹Heidelberg/DE, ²Zurich/CH (fabian.rengier@web.de)

Purpose: To investigate automated three-dimensional detection of dural ectasia in Marfan syndrome using isotropic MRI and shape-based machine learning.

Methods and Materials: 211 patients being evaluated for Marfan syndrome during 2012-2016 underwent MRI including single slab 3D T2-weighted TSE sequence of the lumbosacral spine with a spatial resolution of $1 \times 1 \times 1 \text{mm}$ in 5:06 min. A random sample of 40 patients (32.5 ± 11.2 years, 22 female) was included, thereof 21 patients diagnosed with Marfan syndrome according to the 2010 Revised Ghent Nosology. A shape-based machine learning algorithm was developed for 3D segmentation of dural sac and vertebral bodies L4, L5 and S1. For comparison with current clinical standard, anteroposterior diameters of vertebral bodies and dural sac were assessed at mid-level

Breast

SS 1402b DWI of the breast

Moderators:

P.A.T. Baltzer; Vienna/AT
I. Thomassin-Naggara; Paris/FR

B-1108 10:30

Apparent diffusion coefficient at 3T MRI in differentiating benign and malignant breast lesions: a quantitative analysis

P. Gupta, M. Popli, K. Diwan; *New Delhi/IN (dr.pranavg@gmail.com)*

Purpose: The purpose of this research work was to establish role of quantitative assessment of apparent diffusion coefficient (ADC) in distinguishing benign breast lesions (BBL) from malignant breast lesions (MBL).

Methods and Materials: In a cross sectional study from September 2013 to August 2016, 200 patients with palpable or mammographically detected breast lesions underwent 3T MRI. Of these, 120 patients with 126 lesions underwent specimen histologic examination and were included in the study for retrospective analysis. ADC values were calculated at b values of 0, 400 and 800 s/mm² after identification of maximally enhancing component on dynamic contrast enhanced images. ADC value and histopathology correlation was then done using appropriate statistical tools.

Results: Of the 126 lesions, 84 lesions were malignant and 42 were benign on histopathology. The mean ADC value varied significantly (*p* value < 0.01) between BBL ($1.52 \pm 0.45 \times 10^{-3}$ mm²/s) and MBL ($0.98 \pm 0.21 \times 10^{-3}$ mm²/s). An ADC cut-off value of 1.2×10^{-3} mm²/s for MBL was calculated by drawing ROC curve and it achieved a sensitivity of 92.9% and specificity of 81%. The study showed a sensitivity of 94%, specificity of 83.3%, positive predictive value (PPV) of 91.8% and negative predictive value (NPV) of 87.5% upon using ADC cut off value 1.2×10^{-3} mm²/s.

Conclusion: Diffusion weighted imaging (DWI) along with quantitative ADC value proves to be an effective complimentary parameter in differentiating MBL from BBL and needs to be integrated into the diagnostic algorithm of breast lesions.

B-1109 10:38

High reproducibility of breast lesion ADC values based on fixed size and shape region of interest in diffusion-weighted imaging

M. Wielema, M. Dorrius, H. Dijkstra, E. Langius, G. De Bock, M. Oudkerk, P. Sijens; *Groningen/NL (m.wielema@umcg.nl)*

Purpose: To evaluate three fixed-size region of interest (ROI) methods and the largest oval ROI positioned within breast lesions, in apparent diffusion coefficient (ADC) analysis of diffusion-weighted imaging (DWI) data.

Methods and Materials: Included were 98 consecutive women with 110 lesions (95 malignant) undergoing breast DWI between 11/2008 and 06/2014. Reproducibility of three smaller fixed-size circular ROIs in the middle of each lesion (ROI₂, 0.3 cm²) and at lowest ADC (ROI₃, 0.3 cm²; ROI₄, 0.6 cm²) was compared with maximum oval ROI positioned within the lesion contours (ROI₁). ROIs were positioned by three independent observers at the largest cross section on the T1-weighted image and copied to the DW images, using b values 0 and 1000 s/mm² to obtain ADC maps. Intraclass-correlation coefficients (ICCs) were calculated to evaluate intra- and inter-observer agreement for each ROI method. ROC analysis was performed.

Results: Inter- and intra-observer ICCs were strong (0.80-0.94) in ROI₂-4, and similar to ROI₁ (0.82-0.90). Highest agreement between observers (0.84-0.94) and highest accuracy (0.80) was reported for ROI₄.

Conclusion: Breast lesion ADCs derived from fixed-size subregion ROIs are highly reproducible. The proposed user-friendly methodology is equal or better in clinical performance as compared with whole lesion assessment, as assessed by ROC analysis and false-positive outcomes.

B-1110 10:46

A comparative study of the DKI model and the traditional DWI model in the diagnosis of breast cancer

T. Li, K. Li, Y. Xiong; *Shanghai/CN (kanganli@sina.com)*

Purpose: To compare the value of the diffusion kurtosis imaging model with the traditional single-index diffusion-weighted imaging model parameters in the differential diagnosis of breast lesions.

Methods and Materials: 64 cases of breast lesions were examined by DKI (b = 0, 500, 1000, 1500, 2000, 2500, 3000 s/mm²) and traditional DWI (b = 0, 1000 s/mm²). The diagnostic efficacy of the DKI parameters (MK and MD) and the traditional DWI parameters (ADC) in benign and malignant breast lesions

between the superior and inferior endplates and dural sac diameter ratios were calculated.

Results: Dural sac volumes for Marfan patients/controls were in ml: at L4 $10.8 \pm 2.9/7.5 \pm 1.1$ (*p*=0.013), L5 $9.2 \pm 3.5/5.7 \pm 1.2$ (*p*<0.001), and S1 $10.2 \pm 8.4/3.3 \pm 1.3$ (*p*<0.001). Sensitivity, specificity, positive predictive value and negative predictive value for diagnosis of Marfan syndrome were: for 3D segmentation using L4 >9.1ml or S1 >5.6ml as cut-off 81%/94%/94%/80%, for criteria of Habermann et al. 71%/65%/71%/65%, for criteria of Oosterhof et al. 57%/88%/86%/63%, and for dural sac diameter ratios with highest AUC 67%/94%/93%/70%. The false-positive rate was reduced to 6% using 3D segmentation compared to 35%/12% using criteria of Habermann/Oosterhof et al., respectively.

Conclusion: Automated three-dimensional detection of dural ectasia using isotropic MRI and shape-based machine learning is feasible and potentially superior to the current clinical standard of dural sac diameter ratios.

B-1106 11:42

The role of diffusion tensor imaging parameters in characterisation and differentiation of the spinal cord tumours

B. Szemplinska¹, E. Maj², W. Szeszkowski², M. Prokopienko¹, A. Cieszanowski², A. Marchel², O. Rowinski²; ¹Warszawa/PL, ²Warsaw/PL (bszemplinska@yahoo.com)

Purpose: The aim of this study was to differentiate between infiltrating and non-infiltrating nature of the intramedullary spinal tumours using diffusion tensor imaging (DTI) derived metrics from the enhancing parts of tumour and peri-tumoural regions.

Methods and Materials: 18 patients were included in the study: 6 with infiltrating (3 Astrocytomas, 2 Glioblastomas, 1 PNET) and 12 with non-infiltrating (Ependymomas) spinal cord tumours. Conventional MRI before and after IV Gadolinium administration was done followed by DTI. Fractional anisotropy (FA), diffusivity (TRACE) and apparent diffusion coefficient (ADC) were measured in the enhancing tumour parts, peritumoural margin (oedema most adjacent to the tumour), peritumoural oedema and normal-appearing spinal cord (24 DTI values per patient). ROI of a fixed size of 0.15 cm² was used in all measurements. The results were compared between the two groups of tumours.

Results: FA values measured in the peritumoural margin were significantly higher in the non-infiltrating compared to the infiltrating tumours (*p*<0.007), whereas TRACE values were significantly lower (*p*<0.009). The differences were smaller in peritumoural oedema (*p*<0.03 and *p*<0.04 respectively). FA values measured in the enhancing tumour parts and in normal-appearing spinal cord showed no significant differences between the two groups of tumours.

Conclusion: The information provided by DTI may be used to help differentiate between infiltrating and non-infiltrating intramedullary spinal tumours by characterisation of surrounding spinal cord tissue. Our preliminary results showed that this technique, applied previously for the imaging of brain tumours, could also improve the preoperative assessment of spinal cord lesions.

B-1107 11:50

Three years of experience with magnetic resonance spectroscopy in spinal cord

P. Wawrzyniak, A. Hebda, B. Bobek-Billewicz; *Gliwice/PL (pawel.wawrzyniak@io.gliwice.pl)*

Purpose: Usefulness of MRS of spinal cord-own experience.

Methods and Materials: 1H MRS of spinal cord was performed in 44 patients with spinal cord lesion between 09.2014 and 09.2017 (total of 55 studies). Spinal cord lesions were localized: 42/55 in C spine, 3/55 in C-Th, 10/55 in Th. Mean lesion volume was 1.75 cm³. 8 patients had resection done with 5 cases of ependymoma 2 cases of pilocytic astrocytoma and one case of hemangioblastoma. Patients were divided into groups: presumed neoplastic lesion (n=28, 36 studies), proven tumours (n=8, 11 studies) and presumed non-neoplastic lesion (n=8, 8 studies). All spectra were analyzed in LCModel (version 6.1-4F) software. Spectra was deemed good quality when LCModel calculated SNR was above 1. Metabolite ratios were calculated as follows: Cho/Cr, NAA/Cr, Cho/NAA for long echo time and ml/Cr for short echo. 1H MRS study of spinal cord was performed on Siemens 3T MAGNETOM Prisma as a part of standard spinal cord imaging protocol. Sequence parameters: SVS PRESS; TE 30 and 135 ms; NEX, respectively, 256 and 320, FA 90°; water signal saturation; TR 1700 ms; total acquisition window: 2000 ms.

Results: There was no statistically significant difference between these groups. From total of 110 spectra 57 were of good quality.

Conclusion: Spinal cord spectroscopy is very demanding technique for both patient and operator. No reference spectra was taken into account in this study which might help with proper evaluation, however, it is too time consuming for standard protocol

was compared, and the correlation between MK, MD and ADC values and the prognostic factors of breast cancer was analysed.

Results: The difference of MK, MD and ADC between the benign and malignant groups was statistically significant ($P < 0.05$). The area under the ROC curve of MK, MD and ADC was 0.897, 0.827 and 0.776, respectively. According to the Youden index, the sensitivity, specificity and accuracy of the MK were 83.3%, 85.3% and 84.4%, respectively. The combination of the three parameters could increase the AUC to 0.935. The MK of ER-positive lesions was higher than negative ($P = 0.024$). The correlation analysis showed that ER was low positively correlated with MK ($r = 0.417$, $P = 0.022$), and there was no significant correlation between the other prognostic factors and the parameters ($P > 0.05$).

Conclusion: The parameters of the DKI model and the traditional DWI model can be used to differentiate benign from malignant breast lesions. The diagnostic value of MK in the DKI model is the largest. There is a certain correlation between the DKI model parameters and the prognostic factors.

B-1111 10:54

Preoperative diagnostic value of DKI combined with quantitative dynamic contrast-enhanced MRI in breast lesions

T. Li, Y. Xiong, K. Li; *Shanghai/CN (kanganli@sina.com)*

Purpose: To evaluate the diagnostic efficacy of MRI diffusion kurtosis imaging and quantitative dynamic contrast enhancement in benign and malignant breast lesions.

Methods and Materials: Sixty-four females were enrolled in the study of MRI diffusion kurtosis imaging and quantitative dynamic contrast enhancement between November 20 and 2017 in May, respectively. All of them were confirmed benign and malignant after surgical resection or puncture. The MK and MD values were calculated by the DKI model, and the hemodynamic parameters were obtained by quantitative dynamic contrast enhancement, including Ktrans, Kep, Ve and Vp.

Results: The MK and MD values of breast cancer were 0.879 ± 0.176 and $1.248 \pm 0.380 \times 10^{-3} \text{mm}^2/\text{s}$ respectively in the DKI model. The MK and MD values of benign lesions were 0.577 ± 0.142 and $1.792 \pm 0.505 \times 10^{-3} \text{mm}^2/\text{s}$, the difference was statistically significant ($P < 0.05$). In the DCE model, the Ktrans and Kep mean values of breast cancer were $0.101 \pm 0.039 \text{min}^{-1}$ and $0.398 \pm 0.194 \text{min}^{-1}$, respectively. The mean values of Ktrans and Kep of benign lesions were $0.062 \pm 0.067 \text{min}^{-1}$ and $0.210 \pm 0.121 \text{min}^{-1}$, respectively. The difference was statistically significant ($p < 0.05$), and the other DCE parameters were not statistically significant. The highest sensitivity, specificity and accuracy of MK in all parameters were 91.3%, 80.5% and 84.4% respectively.

Conclusion: MRI diffusion kurtosis imaging and dynamic contrast-enhanced quantitative hemodynamic parameters are of great value in the differential diagnosis of benign and malignant breast lesions. The combination of both can significantly improve the diagnostic efficiency.

B-1112 11:02

Non-mass-like enhancement in MR imaging of the breast: lesion characterisation with morphologic criteria and diffusion-weighted imaging

W. Buchberger, K. Gautsch, W. Oberaigner; *Innsbruck/AT (wolfgang.buchberger@tirol-kliniken.at)*

Purpose: The purpose of this study was to assess the accuracy of contrast-enhanced magnetic resonance imaging and diffusion weighted imaging in distinguishing benign from malignant non-mass-like breast lesions.

Methods and Materials: 76 lesions showing non-mass-like enhancement in 74 consecutive patients were analyzed. Distribution, internal enhancement patterns, and contrast kinetic curve patterns were classified according to the BI-RADS lexicon. Apparent diffusion coefficient (ADC) values were obtained from manually placed ROIs on diffusion weighted images. Univariate and multivariate analysis was performed to find indicators for malignancy. The probability of malignancy was calculated for various combinations of findings. Histological diagnosis obtained by means of vacuum-assisted core biopsy was used as gold standard.

Results: Clumped enhancement ($p < 0.001$), heterogeneous or clustered ring enhancement ($p = 0.031$), and ADC less than $1.3 \times 10^{-3} \text{mm}^2/\text{s}$ ($p = 0.028$) were the strongest indicators of malignancy. Non-mass lesions with homogeneous internal enhancement and ADC values more than $1.3 \times 10^{-3} \text{mm}^2/\text{s}$ had a probability of malignancy of 5%, while all other combinations of findings had a probability of malignancy of 31- 85%.

Conclusion: The combination of internal enhancement characteristics and ADC showed a high accuracy in the characterization of non-mass-like lesions in contrast-enhanced breast MR imaging.

B-1113 11:10

DTI of the breast: is it worth the hassle?

W.R.A. AbdelHamid; *Cairo/EG (w.gforever@yahoo.com)*

Purpose: The aim of this study is to assess the role of diffusion tensor imaging in characterization of equivocal breast lesions.

Methods and Materials: 30 female patients with 36 equivocal breast lesions were subjected to an MR study including T2W, STIR, DTI and dynamic post contrast study. DTI maps including direction, ADC and FA maps were assessed both qualitatively and quantitatively. All lesions were biopsied and verified histopathologically.

Results: The mean acquisition time of DTI was 14 min and its mean post processing time was 22 minutes. Based on histopathology the 36 lesions were 21 benign and 15 malignant. Based on time/intensity curves, 20 were considered suspicious with types IIb and III curves, while 16 were considered benign with types I and IIa curves with 7 false positive lesions and 2 false negative. Addition of DTI significantly improved the accuracy of characterization with only 2 false positive lesions and only 1 false negative with a sensitivity of 94.12% and specificity of 89.47%. Direction map proved beneficial in overcoming the pitfalls of ADC and FA value overlaps between benign and malignant entities.

Conclusion: Although DTI requires long acquisition and post processing times, yet our initial results are promising warranting further research over a larger scale of patients to confidently establish it as a diagnostic tool that can replace contrast and reduce the need for unwanted biopsies.

B-1114 11:18

Comparison of FOCUS (field-of-view optimised and constrained undistorted single-shot)-DWI with standard DWI-MRI and DCE-MRI in the qualitative assessment of breast lesions

L. Vassallo, V. Doronzio, G. Cappello, E. Tabone, D. Regge, L. Martincich; *Candiolo/IT (lorenzo.vassallo1987@libero.it)*

Purpose: To compare the performance of FOCUS-DWI with standard DWI-MRI and DCE-MRI in detecting breast lesions.

Methods and Materials: 50 consecutive women undergoing pre-surgical breast MRI from January to December 2016 were enrolled in the study. Exams were carried out with 1.5T magnet and dedicated 8-channel coil following the recommended technical requirements. FOCUS-DWI was performed on the axial plane with limited shimming to the rectangular area target. DCE-MRI was considered as the standard reference. The type (mass and non-mass) of each suspicious lesion detected at DCE-MRI was evaluated and then compared to similar findings identified at both standard DWI-MRI and FOCUS-DWI. The diagnostic confidence of FOCUS-DWI and DCE-MRI was compared by the following point scale: +1 (FOCUS-DWI > DCE-MRI), 0 (equal) and -1 (FOCUS-DWI < DCE-MRI). The same evaluation was performed between FOCUS DWI and standard DWI.

Results: DCE-MRI identified 59 malignant pathologically proven lesions, 48 mass and 11 non-mass (size range 6-90mm). All the lesions were correctly detected at standard DWI. 5 lesions (all mass; size range 7-15 mm) were not identified at FOCUS-DWI. In no case, diagnostic confidence with FOCUS-DWI was higher than that with DCE-MRI, while it was comparable in only 10/54 cases (18%). The diagnostic confidence between FOCUS-DWI and standard DWI was higher in 37% of cases (20/54), similar in 28% (15/54) and worse in 35% (19/54).

Conclusion: Our series shows that FOCUS-DWI has potential clinical utility since it can identify 85% of suspicious breast lesions. Because of better spatial resolution, FOCUS-DWI reached higher diagnostic confidence when compared with standard DWI-MRI.

B-1115 11:26

Breast MRI: circularity metrics in mass shape assessment of benign and malignant breast tumours

M. Nadrljanski, Z. Milosevic; *Belgrade/RS (dr.m.nadrljanski@gmail.com)*

Purpose: Mass shape metrics on breast MRI include parameters of tumour geometry reflecting the lesion growth pattern. Differences between benign and malignant breast masses in terms of circularity metrics (tumour ellipticity, linear eccentricity, tumour area surface, tumour volume, circulatory ratio, compactness, circularity, Cmax value) were tested in order to define the significance and potential use for better mass shape characterisation and differentiation between benign and malignant lesions.

Methods and Materials: Thirty histologically confirmed mass lesions were evaluated with MRI (1.5T) - benign tumours (n1=15) and carcinoma (n2=15) based on the mathematical expressions (volume, ellipticity, linear eccentricity, circulatory ratio, compactness, Cmax value) and (in)complete elliptic integrals (circumference assessment, surface area definition).

Results: Difference in linear eccentricity proved to be highly statistically significant between benign and malignant lesions ($6.91+/-1.81$ vs. $12.39+/-$

3.75, $p=0.0001$). The same applied to tumour compactness (0.42 ± 0.08 vs. 0.27 ± 0.07 , $p=0.001$) and C_{max} value (0.96 ± 0.02 vs. 0.82 ± 0.12 , $p=0.001$). Ellipticity was not considered highly significant in differentiation between benign and malignant mass lesions (0.65 ± 0.09 vs. 0.56 ± 0.18 , $p=0.04$). Expectedly, linear eccentricity and compactness were considered correlated only in benign lesions ($r=0.79$, $p=0.0004$) and ellipticity and compactness only in malignant lesions ($r=0.54$, $p=0.038$).

Conclusion: Computed parameters of circularity metrics in mass shape assessment on breast MRI (tumour compactness, C_{max} value and linear eccentricity), enabled binary classification: benign vs. malignant mass lesion. Possible compound mass-shape-score may be of help in better mass shape assessment, should the results of larger trials support these preliminary data.

B-1116 11:34

Background parenchymal enhancement at breast magnetic resonance imaging: association with tumour response to neoadjuvant chemotherapy

E. Horvath, E.H. Castillo Balladarez, C. Silva, C. Darrás, M. Uchida, M.A. Pinochet, A. Altamirano, E. Droguett, C. Galleguillos; *Santiago/CL (eliette88@hotmail.com)*

Purpose: Analyse neoadjuvant chemotherapy (NAC) effect on breast MRI background parenchymal enhancement (BPE). Determine association between BPE changes and tumour response.

Methods and Materials: IRB-approved, analytic retrospective study. All breast cancer patients who underwent NAC and had pre-treatment and follow-up 3T MRI studies between December 2013 and September 2017 were included. BPE was analysed on subtraction images and axial and sagittal MIP images, and categorised with BI-RADS lexicon. Tumours were classified according to histology as invasive ductal carcinoma (IDC) or invasive lobular carcinoma (ILC) and grouped by immunohistochemical (IHC) subtype: Luminal A, Luminal B, HER-Luminal (HL), HER2-enriched and Triple negative (TN). Imaging response was evaluated using *RECIST* 1.1 criteria.

Results: 40 patients were included, mean age of 47 ± 9.9 years, 67,5 % were premenopausal. Histopathological analysis revealed 37 cases of IDC, two ILC and one IDC+ILC. IHC assessment showed 12 TN, 10 Luminal A, 10 Luminal B and 8 (HL). There was a global reduction of BPE after NAC in all subgroups, larger in premenopausal women ($P_v=0.01$). TN and HL had higher initial BPE, and postmenopausal patients had an OR of 6.4 for having a mild BPE prior to NAC. 32,5% of patients had complete imaging response. A prior absent-mild BPE, IDC tumour or Luminal A/B IHC subtype were associated with higher OR for partial tumour response (OR 1.8, 2 y 5.7, respectively), although only IHC subtype reached statistical significance.

Conclusion: Decrease in BPE signal after NAC may be used as a predictive factor of tumour response.

B-1117 11:42

Ultra-high field dynamic contrast-enhanced MRI (DCE-MRI) of the breast at 7T with pharmacokinetic (PK) modeling accurately differentiates between benign and malignant breast tumours

R.E. Ochoa Albiztegui¹, J.V. Horvat¹, S. Thakur¹, B. Bernard-Davila¹, S. Trattnig², T.H. Helbich², E.A. Morris¹, K. Pinker¹; ¹New York, NY/US, ²Vienna/AT (eochoa.albiztegui@gmail.com)

Purpose: To investigate whether ultra-high field dynamic contrast-enhanced magnetic resonance imaging (DCE-MRI) of the breast at 7T with pharmacokinetic (PK) modeling using the quantitative biomarkers can be used for differentiation of benign and malignant tumors.

Methods and Materials: Thirty-seven patients with 43 lesions with a suspicious imaging finding on mammography or sonography were included in this IRB-approved study and underwent DCE-MRI of the breast at 7T using a high spatial and temporal resolution sequence (spatial resolution of 0.7 mm³ voxel size, temporal resolution of 14 s). Quantitative PK imaging biomarkers (K_{Trans} & k_{ep}) were assessed using the DCE-Tool OsiriX plugin (http://kyungs.bol.ucla.edu/software/DCE_tool/DCE_tool.html). A whole tumor 2D-ROI (wtROI) and a 10mm standardized 2D-ROI (sROI) were manually drawn by two readers independently in the slice with the maximum lesion diameter and the most enhancing part of the lesion. Appropriate statistics were used to assess inter-rater agreement.

Results: Mean (μ) and standard deviation (σ_x) for K_{Trans} of malignant lesions for wtROI and sROI were $\mu=0.322$ ($\sigma_x=0.14$), $\mu=0.379$ ($\sigma_x=0.126$) respectively. K_{ep} of malignant wtROI and sROI was $\mu=0.553$ ($\sigma_x=0.508$), $\mu=0.613$ ($\sigma_x=0.50$) respectively. K_{Trans} for malignant and benign lesions were significantly different in the wtROI ($p=0.0070$) and sROI ($p=0.0023$). K_{ep} for malignant and benign lesions were also significantly different in the wtROI ($p=0.0050$) and sROI ($p=0.0149$). There was excellent inter-reader correlation between the 2 readers, with a (91%, 88%, 84%, 76%) $p<0.01$.

Conclusion: DCE-MRI at 7T using PK modeling can differentiate between benign and malignant breast tumors using both wtROI or sROI.

B-1118 11:50

Characterisation of breast lesions by whole lesion texture analysis of high b value diffusion-weighted imaging (DWI)

A. Christou¹, A. Ghiatas², K. Veliou³, D. Priovolos², H. Bougias³; ¹Doncaster/UK, ²Athens/GR, ³Ioannina/GR (alexandrachristou@gmail.com)

Purpose: To retrospectively investigate texture parameters in distinguishing breast lesions using high b-value DWI.

Methods and Materials: 30 women with 34 breast lesions underwent breast MRI in 1.5T MRI unit. DWI was applied as part of the standard protocol. The b-value 800 images were analysed and classified by whole lesion texture analysis (TA). 21 features derived from the histogram, grey-level-co-occurrence matrix (GLCM) and grey-level-run-length-matrix (GLRLM) were analysed and compared between benign and malignant lesions with Mann-Whitney U test ($p=0.05$). ROC analysis was used to evaluate the most effective cut-off values.

Results: 19 cases were malignant and 15 benign. Statistically significant difference between malignant and benign lesions was found in contrast, correlation, dissimilarity and homogeneity regarding GLCM texture metrics. No significant difference found in entropy and energy metrics. Short-run low grey-level emphasis (SRLGE) regarding the GLRLM metrics showed significant difference. No statistical difference found in any feature from histogram metrics. Univariate logistic regression showed that contrast and dissimilarity yielded the highest area under curve (AUC) 0.836 and 0.845, respectively, whereas energy and entropy yielded the lowest AUC 0.576 and 0.561, respectively.

Conclusion: High b-value DWI whole lesion texture analysis is able to differentiate breast pathologies with contrast and dissimilarity from GLCM texture metrics being the most effective discriminators.

10:30 - 12:00

Room D

Musculoskeletal

SS 1410

Advanced imaging techniques, algorithms and measurements

Moderators:

M. Froeling; Utrecht/NL

J. Hodler; Zurich/CH

K-20 10:30

Keynote lecture

C. Weidekamm; Vienna/AT

B-1119 10:39

Reduction of metal artefacts in patients with spinal fusions: metal artefact reduction algorithms and virtual monoenergetic images from spectral detector computed tomography

N. Grosse Hokamp^{1,2}, N. Abdullayev¹, V. Neuhaus¹, A. Mpotsaris¹, D. Maintz¹, J. Borggrefe¹; ¹Cologne/DE, ²Cleveland, OH/US (nils.grosse-hokamp@uk-koeln.de)

Purpose: To compare the extent of metal artefact reduction by use of dedicated metal artefact reduction algorithms (MAR) and high keV virtual monoenergetic images (VMI) from spectral detector computed tomography (SDCT).

Methods and Materials: 25 patients with spinal fusion were included in this IRB-approved study. All examinations were performed using a SDCT (IQon, Philips Healthcare). Images were reconstructed as conventional images (CI), with a MAR algorithm and as VMI in range of 40-200keV (10keV increment). Quantitative image analysis was performed ROI-based by measurements of attenuation (HU) and standard deviation in most pronounced hypo- and hyperdense artefacts and posterior subcutaneous fat. Qualitatively, assessment of metal-bone interface, spinal canal and soft tissue were rated on 5-point Likert scales. Further, extent of artefact reduction was evaluated by two radiologists. Statistical analysis was performed using ANOVA and Wilcoxon test with correction for multiple comparisons.

Results: The hypo- and hyperattenuating artefacts showed a significant increase and decrease of HU values in both high keV VMI and MAR reconstructions (CI/MAR/VMI_{200 keV}: -397/-115/-48 HU and 470/211/74 HU, respectively; $p\leq 0.05$). Artefacts in the subcutaneous fat, as depicted by image noise, did decrease in high keV VMI ($p=0.09$) and MAR ($p\leq 0.05$; CI/MAR/VMI_{200keV}: 27.0/20.2/17.6). Qualitatively, metal-bone interface was better assessable in high keV VMI ($p\leq 0.05$), while soft tissue was better assessable in MAR ($p\leq 0.05$). Artefacts were reduced in 24/28 examinations.

Conclusion: SDCT allows for metal artefact reduction through MAR algorithms and computation of virtual monoenergetic images in patients with spinal fusion. Thus, the combination of both techniques is promising to yield further artefact reduction.

B-1120 10:47

MR imaging with metal artefact reduction for the differentiation between patients with and without infected total hip arthroplasty

B.J. [Schwaiger](#), A. Gersing, D. Münzel, J. Dangelmaier, P.M. Prodingler, C. Suren, E.J. Rummeny, K. Wörtler; *Munich/DE*

Purpose: To evaluate imaging parameters obtained from MRI with metal artefact reduction to differentiate between patients with and without infected total hip arthroplasty (THA).

Methods and Materials: In 46 patients (65±11 years; 25 women) with THA, 1.5T MRI was acquired with view angle tilting (VAT) and slice-encoding metal artefact correction (SEMAC). Parameters describing changes of metal/bone interface, surrounding bone and soft tissue including synovial response patterns were assessed independently by three radiologists. All patients underwent revision surgery, and signs of infection and loosening were assessed according to AAOS criteria. Chi-squared tests and sensitivity/specificity analyses were performed with intraoperative findings as standard of reference.

Results: At surgery, an infection was confirmed in 12 patients, 21 patients showed an implant loosening and 13 showed conditions not related to infection/loosening. Presence of the following findings was significantly more common in patients with infection compared to those without: T2-hyperintense lining at the metal/bone interface (p=0.037; sensitivity, 92%; specificity, 41%), periostitis (p=0.027; 58%; 77%), an oedema (p=0.001; 75%; 77%), contrast enhancement (p=0.030; 75%; 70%) or an abscess (p=0.026; 38%; 95%) in the surrounding soft tissue, enlarged lymph nodes (p=0.020; 25%; 97%) and lamellated synovial response (p=0.020; 25%; 97%).

Conclusion: The differentiation between patients with and without infected total hip arthroplasty may be possible using a set of parameters derived from MR with metal artefact reduction. The most sensitive parameter was a T2-hyperintense lining at the metal/bone interface, while the most specific findings were presence of an abscess, enlarged lymph nodes and lamellated synovial response.

B-1121 10:55

Comparison of metal artifact reduction by OMAR, MonoE or combined techniques derived from dual-layer spectral CT

J. [Dangelmaier](#), B.J. [Schwaiger](#), A.S. Gersing, A. Sauter, I. Riederer, D. Muenzel, A.A. Fingerle, E.J. Rummeny, P.B. Noel; *Munich/DE*

Purpose: To compare image quality using virtual monoenergetic images (MonoE), the orthopedic metal artifact reduction (OMAR) algorithm and a combination of both techniques in patients with arthroplasty or spondylodosis.

Methods and Materials: 30 patients (70±12 years; 19 women) with total hip/shoulder arthroplasty (n=20) or spondylodosis (n=10) were examined on a dual-layer spectral CT. Axial reconstructions (0.9 mm) of standard CT images, MonoE (160keV and 200keV), OMAR and combined techniques (MonoE+OMAR) were calculated in soft and hard convolution kernels. Image quality in all reconstructions was rated by four radiologists, blinded for the type of artifact reduction technique, using a 5-point Likert scale. Hounsfield units (HU) were measured within the most pronounced hypodense streak artifact as well as in the reference tissue. Friedman's analyses and Wilcoxon-signed rank test were performed for each observer separately and the mean of all observers for each reconstruction. Inter-reader agreement was calculated with ICCs.

Results: Image quality was rated significantly higher in all artifact-reduced images, compared to standard CT (p<0.001; MonoE160 soft tissue kernel p=0.001). Images reconstructed with MonoE+OMAR were rated significantly better than MonoE or OMAR alone (p<0.001). HU measurements within artifacts were significantly closer to reference values in all artifact-reduced images, with a superior artifact reduction obtained with MonoE+OMAR (88 % vs. 80% for OMAR or 45% for MonoE). Inter-reader agreement was good to excellent (ICCs).

Conclusion: Both, the qualitative assessment and quantitative measurements, demonstrated superior artifact reduction using virtual monoenergetic images in combination with OMAR, suggesting a clinical advantage in patients with arthroplasty or spondylodosis.

B-1122 11:03

Bone marrow adiposity assessed by 3T MR-spectroscopy in the hip of women with anorexia nervosa

S. [Badr](#)¹, V.M. Pansini¹, I. Legroux-Gérot¹, J. Vignau¹, R. Stefan², D.C. Karampinos², C. Chauveau³, B. Cortet¹, A. Cotten¹; ¹Lille/FR, ²Munich/DE, ³Boulogne-sur-Mer/FR (sammy@badr.fr)

Purpose: Bone marrow adiposity (BMA) in women with anorexia nervosa is paradoxically increased, contrasting with a reduction of the subcutaneous and visceral fat compartment volumes. As BMA may contribute to bone fragility in anorexic patients, we studied its relationship with bone mineral density and body composition.

Methods and Materials: 82 anorexic patients were included between January 2014 and June 2017. BMA of the hip was quantified using 3 tesla MR spectroscopy, by calculating signal-weighted bone marrow fat fraction (BMFF) in 4 different locations: the acetabulum, greater trochanter, femoral neck and proximal femoral diaphysis. Bone mineral density of the hip and body composition (body mass index, percentage of lean body mass and body fat percentage) were determined using dual-energy x-ray absorptiometry.

Results: With the exception of the greater trochanter, correlations were significant between BMFF and bone mineral density in the different locations of the hip (Spearman's rank correlation coefficients: pfemoral neck=-0.24, pacetabulum=-0.28, pdiaphysis=-0.28; p<0.05). Regarding body composition, BMFF was significantly correlated with the percentage of lean body mass and the body fat percentage only in the femoral neck (pfat=0.29 and plean=-0.27; p<0.05). No significant correlation was found between body mass index and BMFF in the hip.

Conclusion: BMFF is negatively correlated with bone mineral density in the acetabulum, femoral neck and proximal femoral diaphysis of the hip of women with anorexia nervosa. However, correlations between BMFF and body composition were only found in the femoral neck, suggesting location-dependent relationships with the other fat compartments.

Author Disclosures:

D.C. Karampinos: Research/Grant Support; Philips Healthcare.

B-1123 11:11

Augmented reality-guided lumbar facet joint injections

C.A. [Agten](#), C. Dennler, A.B. Roskopf, L. Jaberg, C.W. Pfirrmann, M. Farshad; *Zurich/CH* (christoph.agten@balgrist.ch)

Purpose: To assess accuracy of augmented reality-guided lumbar facet joint injections.

Methods and Materials: A spine phantom completely embedded in hardened opaque agar with three ring markers was built. A 3-D model of the phantom was uploaded to an augmented reality headset (Microsoft HoloLens). Two radiologists, independently performed twenty augmented reality-guided and 20 CT-guided facet joint injections each: for each augmented reality-guided injection, the hologram was manually aligned with the phantom container using the ring markers. The radiologists targeted the virtual facet joint and tried to place the needle tip in the holographic joint space. CT was performed after each needle placement to document final needle tip position. Time needed from grabbing the needle to final needle placement was measured for each simulated injection. An independent radiologist rated images of all needle placements in a randomized order blinded to modality (augmented reality vs CT) and performer as: perfect, acceptable, incorrect, unsafe. Accuracy and time to place needles were compared between augmented reality-guided and CT-guided facet joint injections.

Results: In total, 39/40 (97.5%) of augmented reality-guided needle placements were either perfect or acceptable compared to 40/40 (100%) CT-guided needle placements (P=.5). One augmented reality-guided injection missed the facet joint space by 2 mm. No unsafe needle placements occurred. Time to final needle placement was substantially faster with augmented reality guidance (mean 14 ± 6 s vs 39 ± 15 s, P<.001 for both readers).

Conclusion: Augmented reality-guided facet joint injections are safe and accurate in an experimental setting.

B-1124 11:19

3D MR-based simulation of hip impingement is as accurate as 3D CT-based impingement simulation

F. [Schmaranzer](#), C. Degonda, T. Lerch, I. Todorski, K. Siebenrock, J.L. Cullmann, M. Tannast, G. Zheng; *Bern/CH*

Purpose: For complex cases of femoroacetabular impingement (FAI), CT-based 3D impingement simulation is the current gold standard for impingement detection. 3D MRI-based impingement simulation would offer a radiation-free alternative. We asked: (1) How many surface points of 3D models derived from 3D CT versus 3D MRI differ by <1mm? (2) Do impingement-free range of motion values correlate between 3D models derived from CT/MRI?

Methods and Materials: IRB-approved comparative, retrospective study of 20 symptomatic hips with FAI. 3D CT scans (isovoxel: 1mm³) of the entire pelvis

and the distal femoral condyles were obtained. Preoperative MR arthrograms of the hip were obtained including 0.8mm³ isovoxel T1 3D VIBE- and 1mm³ isovoxel 3D T1 VIBE DIXON sequences of the entire pelvis and the distal femoral condyles. Threshold-based manual segmentation was performed using commercial software (AMIRA). Both 3D models were compared with in-house developed software to calculate (1) percentage of the surface points with < 1mm difference between the CT-/MR-based 3D models and to assess (2) the correlation in impingement-free range of motion (in: flexion; extension; internal rotation 90° of flexion; external rotation in 90° of flexion; abduction; adduction) and location of impingement on CT/MRI.

Results: (1) 83%/79% of the surface points of the proximal femur, respectively, of the acetabulum differed by <1mm between the CT-based and MRI-based 3D models. (2) Correlation for the range of motion values was excellent (Spearman rho=0.993, p<0.05) between CT/MRI.

Conclusion: MR-based 3D models of the hip joint can replace CT-based 3D models for impingement simulation in young FAI patients.

B-1125 11:27

Performance of an automated vs manual MR scanner workflow of whole-body MRI

D. Stocker¹, T. Finkenstaed¹, B. Kuehn², D. Nanz¹, M. Klarhöfer¹, B. Kiefer², C.S. Reiner¹; ¹Zurich/CH, ²Erlangen/DE (daniel.stocker@usz.ch)

Purpose: To evaluate the performance of an automated magnetic resonance imaging (MRI) scanner workflow reducing user interactions compared to the manual MRI workflow for whole-body (WB) MRI.

Methods and Materials: This prospective study was approved by the local ethics committee. 20 patients underwent WB-MRI for myopathy evaluation on a 3T MRI-scanner. 10 patients (7 females; age, 52±13ys; body mass index [BMI], 23.2±3.0) were examined with a prototypical automated scanner workflow (automated whole-body segmentation) and 10 patients (6 females; age, 35.9±12.4ys; BMI, 24.9±5.6) with a manual scan. For each sequence (coronal T2-weighted turbo inversion recovery magnitude [TIRM] and axial T1-weighted contrast-enhanced sequence with volume interpolated breath-hold examination [VIBE]) overall image quality (IQ; 5, excellent; 1, poor) and completeness of examination volume were assessed by two readers. Examination time, number of user interactions and the MR-technicians' planning effort (1, highest; 10, lowest) were compared.

Results: Overall IQ was similar between automated and manual MRI (TIRM: 4.00±.94 vs 3.45±1.19, p=.264; VIBE: 4.20±.88 vs 4.55±.55, p=.423). Total examination time was significantly shorter for automated MRI (30.0±4.2min vs 41.5±3.4min, p<.0001) with significantly shorter planning time (2.5±.79min vs 14.0±7.0min, p<.0001). Planning time was 8% vs 34% of total examination time for automated vs manual workflow (p<.0001). The number of user interactions and rated planning efforts with automated MRI were significantly lower compared to manual MRI (10.2±4.4 vs 48.2±17.2, p<.0001 and 2.20±.92 vs 4.80±2.39; p=.005, respectively).

Conclusion: The automated MRI workflow significantly reduced examination time and user interactions while producing comparable IQ in WB-MRI for evaluation of myopathies.

Author Disclosures:

B. Kuehn: Employee; Siemens Healthcare. **M. Klarhöfer:** Employee; Siemens Healthcare. **B. Kiefer:** Employee; Siemens Healthcare.

B-1126 11:35

CAM type femoroacetabular impingement: correlations between alpha angle vs volumetric measurements and surgical findings

R.A.K. Dessouky^{1,2}, J. Wells², L. Zhang³, A. Gleason², R. Chopra², Y. Chatzinoff², N.P. Fey², Y. Xi², A. Chhabra²; ¹Zagazig/EG, ²Dallas, TX/US, ³Beijing/CN (rihamedessouky@gmail.com)

Purpose: To determine the correlation of 3DCT measurements of CAM type femoro-acetabular impingement [FAI] with surgical findings of labral tear and cartilage loss.

Methods and Materials: Digital search of symptomatic FAI patients who underwent hip surgery for a CAM-type FAI from July 2013 to August 2016 yielded 43 patients. Demographic data, clinical and surgical findings were recorded. Two readers evaluated 3DCT images to calculate volumes of the femoral head and bump as well as alpha angles. Correlations between CT and surgical findings were obtained. Inter-reader reliability was determined using intraclass correlation [ICC].

Results: Thirteen men and fourteen women were included with a mean age of 37.3 ± 10.4 years. The most common clinical finding was positive FADIR [19/27, 70.4%]. Twenty-seven labral tears and twenty cartilage defects were found on surgery. Significant correlations between the femoral bump and head volumes with the extent of the labral tear [p values = 0.008 and 0.003, respectively] existed. No significant correlations were found between alpha angles at 1 and 2 O'clock and extent of the labral tear [p values >0.05] or any measurement with cartilage loss [p>0.05]. Inter-reader reliability was excellent to moderate [ICC= 0.85 and 0.52] for femoral head and bump volumes, and fair to poor [ICC = 0.40 and 0.05] for alpha angles at 1 and 2 o'clock, respectively.

Conclusion: Volumetric measurements of CAM type FAI significantly correlate with the extent of the labral tear with superior inter-reader reliability than alpha angle, rendering it a more clinically relevant method to quantify CAM morphology.

Author Disclosures:

A. Chhabra: Consultant; ICON Medical, unrelated to this presentation. Other; Book Royalities; Jaypee, Wolters, unrelated to presentation.

B-1128 11:43

FDG-PET/CT for diagnosis of infection in post-traumatic non-unions

L. Antunovic, M. Catalano, L. Di Mento, E. Malagoli, L. Balzarini, A. Chiti, A. Kirienco, M. Berlusconi, N. Trenti; *Rozzano/IT (lidija.antunovic@humanitas.it)*

Purpose: To assess the diagnostic performance of FDG-PET/CT in the evaluation of infection causing post-traumatic bone non-unions.

Methods and Materials: 47 patients treated in our trauma center, who underwent pre-operative FDG-PET/CT for suspected infection, were retrospectively reviewed. Clinical history, diagnostic examinations, laboratory and microbiology results, patient outcome, were collected and analyzed. FDG PET/CT images were evaluated with the addition of semi-quantitative analysis using SUVmax. Imaging findings, as assessed by an experienced nuclear medicine physician and a musculoskeletal radiologist, were correlated with microbiological examination of the intraoperative specimens. Finally, diagnostic performance of FDG-PET/CT was assessed.

Results: 22 patients were not infected, while remaining 25 had positive intraoperative microbiological results. Infection was correctly detected on FDG-PET/CT images in 23 cases, while 2/25 infected patients had no significant FDG uptake and were considered as false negatives. In 6 cases FDG-PET/CT showed false positive results; 16/22 disease-free patients were correctly diagnosed. The diagnostic accuracy of FDG-PET/CT in the final diagnose of infection was 83% (39/47). Sensitivity, specificity, positive predictive value and negative predictive value of FDG-PET/CT were 92%, 73%, 79% and 88% respectively. Likelihood ratio for a positive test(LR+) 3.41. Likelihood ratio for a negative test resulted 0.11. Pre-test probability of disease was 53%. Post-test probability based on LR+ resulted 79%, while post-test probability based on LR- was 11%.

Conclusion: Our data indicate FDG-PET/CT is a valuable diagnostic tool in the evaluation of post-traumatic infection.

10:30 - 12:00

Room G

Physics in Medical Imaging

SS 1413

Image quality evaluation and optimisation in CT

Moderators:

I. Hernandez-Giron; Leiden/NL
O. Rampado; Turin/IT

B-1129 10:30

Iterative reconstruction algorithms in computed tomography: is it possible to go beyond Fourier metrics for image quality assessment?

N. Paruccini, R. Villa, S. Morzenti, C. Spadavecchia, M. Signoriello, D. Ippolito, A. Crespi; *Monza/IT (n.paruccini@asst-monza.it)*

Purpose: Iterative reconstruction algorithms (IR) have been introduced in clinical practice. In this condition, the Fourier analysis requirements are not completely satisfied because of the effects of non-linearity and non-stationarity produced by the iterative reconstruction process. Alternative metrics, not based on Fourier transform, have been used to evaluate image quality.

Methods and Materials: A cylindrical water filled phantom was equipped with central cylindrical inserts of various densities and then scanned changing CTDIvol, reconstruction algorithm, filter and slice thickness. Blur was investigated with a simple metric based on the comparison of the original images with the same images after a low pass filter application. A statistical method was employed to evaluate low contrast detectability (LCD) in a homogeneous region. Results were then used to characterise noise amount and texture. Furthermore, the relationship between Noise Power Spectrum (NPS) and LCD was investigated.

Results: The image quality improvement obtained with IR is underline with both metrics. Blur metric is able to detect the different sharpness degree. The relationship between noise and Blur underlines a different behaviour for IR; Blur increases with lower dose levels or with higher reconstruction thickness. LCD curves underline an averaged improvement of 35-45%. Through evaluation of the LCD curves, information regarding colour and texture of noise are obtained. Furthermore, the shapes of LCD and NPS curves are in accordance.

Conclusion: The metrics proposed can be applied to any kind of reconstruction algorithms and with few requirements. Results are in accordance with metrics based on Fourier analysis.

B-1130 10:38

Image quality of conventional images of dual-layer spectral CT: a phantom study

F. van Ommen¹, E. Bennink¹, A. Vlassenbroek², J.W. Dankbaar¹, A. Schilham¹, M.A. Viergever¹, H.W. De Jong¹; ¹Utrecht/NL, ²Brussels/BE (f.vanommen@umcutrecht.nl)

Purpose: As dual-layer spectral CT scanners are mainly used for routine non-spectral imaging, these images should not come with a dose or image quality penalty as compared to a conventional CT scanner. The influence of a dual-layer detector on the image quality of conventional CT images is evaluated by comparison with a conventional CT scanner.

Methods and Materials: A CATPHAN600 phantom was scanned on an IQon Spectral CT and a Brilliance iCT scanner (Philips Healthcare, Best, The Netherlands). Four protocols, and three tube voltages were used to assess image quality at equalized dose levels. Noise and spatial resolution were characterized. Furthermore, contrast-to-noise-ratio, image uniformity, CT number linearity, slice thickness, slice spacing, and spatial linearity were evaluated.

Results: Noise levels were equivalent for both scanners. Resolution levels showed small but significant differences up to 0.3 lp/cm in favour of the dual layer. Contrast-to-noise ratio was equivalent at 80 and 120 kVp, but at 140 kVp significant differences up to 0.4 in favour of the dual-layer detector were found. Both scanners showed perfect CT linearity for body scans, but both showed an underestimation of the CT numbers for high-opacity materials for head scans. Slice thickness was slightly overestimated, but slice spacing was reconstructed correctly. In addition, spatial linearity was excellent with a maximum error of 0.1 mm.

Conclusion: The performance of the IQon in routine non-spectral imaging is comparable to the performance of the iCT. The similar performance suggests that the introduction of a dual-layer detector does not compromise image quality of conventional CT images.

Author Disclosures:

F. van Ommen: Research/Grant Support; Dutch heart foundation, Netherlands Organization for Scientific Research (NWO), Philips Healthcare. A. Vlassenbroek: Employee; Philips Healthcare. J.W. Dankbaar: Grant Recipient; TTW grant: 14732. M.A. Viergever: Grant Recipient; TTW grant: 14732. H.W. De Jong: Grant Recipient; TTW grant: 14732.

B-1131 10:46

Evaluation of the effect of image noise on CT perfusion measurements using digital perfusion phantoms

S. Skornitzke, H.-U. Kauczor, W. Stiller; Heidelberg/DE (Stephan.Skornitzke@med.uni-heidelberg.de)

Purpose: Models used for computed tomography (CT) perfusion studies might react differently to image noise present in CT acquisitions. Different algorithms from one commercially available CT perfusion software were evaluated for susceptibility to image noise.

Methods and Materials: Digital perfusion phantoms were generated using a deconvolution model for simulating time-attenuation curves (TACs) for 16 different combinations of the perfusion parameter blood flow (BF: 30/60/90/120 ml/100 ml/min) and flow extraction product (FEP: 10/20/30/40 ml/100 ml/min) corresponding to values encountered in clinical studies. TACs were distorted with additive Gaussian noise at 50 different strengths to approximate various levels of image noise, performing 200 repetitions for each noise level. 160000 TACs were evaluated in total by measuring BF and FEP, and comparing results for the maximum-slope and Patlak model to those obtained with a deconvolution model (syngo.via Body Perfusion; Siemens Healthineers, Germany).

Results: All evaluated perfusion models show a dependence on image noise: means and standard deviations of BF and FEP over repetitions increase with increasing image noise. The increase in means is larger for low values of BF and FEP and nearly vanishes for high values. Deviations are below 50% under all conditions only for noise levels below 20 HU (BF) or 10 HU (FEP). BF measurements performed with the deconvolution model show a larger standard deviation than those performed with the maximum-slope model.

Conclusion: Measurements of perfusion parameters depend heavily on the magnitude of image noise, which has to be taken into account during the interpretation of results, e.g. as a quantitative imaging biomarker.

Author Disclosures:

H.-U. Kauczor: Grant Recipient; Siemens Healthineers.

B-1132 10:54

The optimal energy level of virtual monochromatic images from spectral CT for reducing beam-hardening artefacts due to contrast media in the thorax

D. Kim¹, C. Kim², K. Lee¹, E.-Y. Kang³, Y.-W. Oh³, H. Kim¹, J. Cha¹; ¹Ansan/KR, ²Ulsan/KR, ³Seoul/KR (dj8827@naver.com)

Purpose: To determine the optimal energy level of virtual monoenergetic images (VME) from spectral CT compared to that of conventional polychromatic images (COV) for reducing beam-hardening artefacts caused by contrast media in the thorax.

Methods and Materials: A total of 101 consecutive patients who underwent chest CT were retrospectively included in this study. The same contrast media and injection protocols were applied to the whole study population. VME image data sets ranging from 70 to 200 keV and COV were obtained. Readers' subjective image quality scores were recorded in COV and VME at 70 keV (VME70), 100 keV (VME100), 130 keV (VME130), and 200 keV (VME200). Image noise, CT number difference, contrast-to-noise ratio (CNR), and signal-to-noise ratio (SNR) were also obtained in each algorithm. The Kruskal-Wallis test with Bonferroni correction was used compared to the differences in subjective image scores, CT numbers, image noise, SNR values, and CNR values between the reconstruction techniques.

Results: The best subjective image quality score and the lowest image noise were observed in VME130 compared to COV (all P<0.001). CT number differences were significantly lower in both VME100 and VME130 than in COV (all P<0.001). SNR was similar between VME130 and COV, although both SNR and CNR decreased as the energy level increased.

Conclusion: Optimal evaluation of chest CT was best achieved at 100-130 keV. VME130 offered the best image quality score and image noise. VME100 and VME130 showed significantly lower CT number differences than in COV.

B-1133 11:02

Sub-millisievert multiphase acquisitions for coronary CT angiography of congenital coronary anomalies in paediatric patients

J. Le Roy, H. Vernhet Kovacsik, H. Zargane, M. Vincenti, A. Lacampagne, P. Amedro; Montpellier/FR (le.roy-julien@hotmail.com)

Purpose: To assess feasibility and performance of selective multiphase coronary CT angiography (CCTA) at very low dose for paediatric patients with coronary artery anomaly

Methods and Materials: 50 paediatric patients with coronary artery anomalies underwent a cardiac CT between December 2015 and October 2017. Several parameters were recorded, including age (6.1y± 4.9), BMI (15.8kg.m-2±2.5), heart rate (89bpm±26) and heart rate variability (14bpm±11). Depending on these parameter combinations, specific protocols were designed to target the best theoretical cardiac phase in every situation; giving best compromise between image quality and reduced radiation dose. Acquisitions were realized on last generation single-source CT (Revolution CT, GEHC). Image quality was assessed qualitatively on a four point scale by two radiologists.

Results: All acquisitions fully answered the diagnostic question (100% - 50/50). Image quality was considered as "good" or "excellent" in ninety percent of cases (90%-45/50). Ten percent (10%-5/50) were scored as "adequate" while no exam were "not assessable". Looking at these five patients, movement artefacts were principal causes of average -but still diagnostic-image quality. No significant visualisation differences were reported between the different coronary segments with a global score of 3.5±0.6 on a 4 point scale (200 segments analysed in total). No correlation between image quality and cardiac parameters were reported (r=-0.17 and r=-0.10 respectively for Heart rate and HR variability). Mean effective dose was 0.98 mSv.

Conclusion: Infra-millisievert multiphase CCTA acquisitions could be performed with diagnostic quality for a dose equivalent to only 20% of a paediatric chest CT dose.

B-1134 11:10

A preliminary study about the robustness of quantitative CT features of pancreatic NEN: inter-observer variability assessment in delineation of lesions contours on CT images

G. Benedetti¹, M. Panzeri¹, M. Mori¹, C. Sini², M. Barbera¹, S. Partelli¹, M. Falconi¹, C. Fiorino¹, F. De Cobelli¹; ¹Milan/IT, ²Potenza/IT (benedetti.giulia@hsr.it)

Purpose: Radiomic is a promising field to build predictive models relating imaging features to clinical outcomes, especially for neoplasms. Nevertheless, its robustness is still under investigation. Especially, a reliable delineation of the lesions is of fundamental importance for Radiomic Features (RF) extraction. Our aim was to assess interobserver variability in delineating pancreatic neuroendocrine neoplasms (NEN) on CT images, and its impact on RF.

Methods and Materials: 10 histologically confirmed pancreatic NEN were contoured on CT images by 3 blinded observers. Contours were delineated on arterial or venous phase, depending on where the tumour was best seen, and

then projected onto the pre-contrast acquisition and adjusted to correct small anatomical discrepancies. Interobserver contouring variability was assessed by DICE-index and volume distribution among contours; significance of differences between observers was tested with Wilcoxon. Paired analysis between observers was performed. 72 RF were extracted from each observer's contours; their robustness was investigated against contour variability with Spearman-R and Intra-Class Correlation (ICC).

Results: Volume mean and median were 7.6cc and 1.5cc. A satisfactory agreement was found, with mean DICE=0.77±0.075 and no significant differences between observers. 50/72 RF were very robust (ICC>0.9); 10/72 showed an ICC<0.8, mostly in the 'Neighbourhood intensity-difference' RF family. Average R-values were 0.89 for RF with ICC>0.9 and 0.84 for the others RF. Only 'sphericity' (i.e. external shape of the lesion) R-value was<0.6. **Conclusion:** Results show a relatively small inter-observer variability in delineating pancreatic NEN with little impact on RF, suggesting the possibility of a robust CT-based RF extraction on larger population.

B-1135 11:18

Comparison of clinical and phantom image quality for low-contrast liver lesions in a prospective multicentre dose optimisation protocol

H. Brat¹, D. Racine², S. Montandon³, S. Behzad Imsand⁴, B. Rizk⁵, D. Fournier¹, ¹Sion/CH, ²Lausanne/CH, ³Gland/CH, ⁴Epalinges/CH, ⁵Villars-sur-Glane/CH (hugobene@gmail.com)

Purpose: To compare diagnostic performance for low-contrast liver lesions on patient and phantom images in a prospective multicentre CT scanner dose optimisation protocol.

Methods and Materials: A protocol optimisation based on clinical indication and BMI with stepwise dose reduction was implemented on 5 CT scanners (PhilipsTM). 3035 abdomen CT examinations were prospectively assessed for diagnostic image quality (radiologist vote). 33 patients who underwent a CT examination for liver tumour or cancer staging before and after optimization were evaluated for image quality (European guidelines). In parallel, phantom (QRMTM 401 abdomen) acquisition with 2.5 (size M) and 5cm (size L) soft-tissue ring was performed before and after dose reduction using the liver tumour follow-up protocol. A channelized Hotelling (CHO) model observer was used to assess lesion detectability using the ROC paradigm with the area under the ROC curve (AUC) as figure of merit.

Results: Median patient CTDI_{vol} value decreased from 6.8 to 5.2mGy (-24%) and from 10.8 to 8.5mGy (-22%), respectively, for BMI<25 and >25. For phantom images, mean CTDI_{vol} value decreased from 8.8 to 6.3mGy (-28%) for M-sized and from 15.9 to 11.8mGy (-26%) for L-sized phantom. No negative vote was registered and no loss of image quality was observed in the 33 paired patients' subgroup. Phantom analysis showed constant low-contrast lesion detectability until 26% dose reduction. However, additional dose reduction impaired detectability of 5mm lesions.

Conclusion: Combining clinical and phantom diagnostic image quality enabled dose reduction according to the ALARA principle without impairing low-contrast liver lesion detectability.

B-1136 11:26

Endoleak detection with ultra-low radiation exposure CT based on sparse sampling and reduced tube current

F.K. Kopp¹, R.-D. Bippus², K. Mei¹, A. Sauter¹, B.J. Schwaiger¹, A. Gersing¹, J. Dangelmaier¹, E.J. Rummeny¹, P.B. Noel¹; ¹Munich/DE, ²Hamburg/DE (felix.kopp@tum.de)

Purpose: To assess the diagnostic performance of sparse sampling computed tomography with significantly reduced radiation dose regarding the detection of endoleaks after endovascular aortic repair (EVAR).

Methods and Materials: 11 patients (seven positive and four negative for the diagnosis of an endoleak after EVAR) were examined using a 256-slice CT scanner and were retrospectively included in this study. A reduced radiation exposure was simulated by combining tube current reduction and sparse sampling. Three datasets were calculated, hereby each dataset showed the same radiation dose (20% of clinical radiation dose): dataset A with continuous sampling, dataset B with 2-times sparse sampling (keeping every 2nd view) and dataset C with 4-times sparse sampling. Four blinded radiologists, evaluated each dataset for the presence of an endoleak, with at least seven days between the consecutive readings. Sensitivity, specificity, negative predictive value (NPV), positive predictive value (PPV) and the area under the ROC curve (AUC) were calculated with the clinical diagnosis as standard of reference.

Results: Sensitivity, specificity, NPV and PPV were 71%, 69%, 81% and 58% for dataset A; 75%, 81%, 88% and 65% for dataset B; and 82%, 75%, 87% and 75% for dataset C. AUC values, averaged over the four readers, were 0.80, 0.82 and 0.86 for dataset A, B and C, respectively.

Conclusion: Using sparse sampling, sensitivity, specificity, NPV, PPV and AUC is increased compared to continuous sampling at the investigated dose level (dose reduction of 80%), suggesting that sparse sampling may allow significant radiation dose reduction for follow-up examinations.

Author Disclosures:

R. Bippus: Employee; Philips Research.

B-1137 11:34

Optimisation of abdominal CT examinations across different scanners in one hospital using a new liver phantom

S.F. Svensson¹, H. Heier-Baardson², B.E. Nielsen², E.B. Herud², L.O. Holmen², H.K. Andersen¹, A.C.T. Martinsen¹; ¹Oslo/NO, ²Grålum/NO (siriff@ous-hf.no)

Purpose: To optimize a CT abdomen protocol using a newly developed liver phantom.

Methods and Materials: An anthropomorphic liver phantom with hyperdense lesions, designed for receiver operating characteristic (ROC) analysis, was scanned using three CT scanners, each with its own iterative reconstruction method: a Philips Ingenuity Elite with IMR, a Philips Brilliance with iDose⁴ and a GE Revolution Evo with ASiR-V. The phantom was scanned at CTDI_w 5, 10, 15 and 20 mGy, and the images were reconstructed using levels 3 and 5 of iDose⁴, IMR 1 routine, IMR 2 routine and IMR 1 soft tissue, and ASiR-V 20%, 40%, 60% and 80%. Three radiologists interpreted the images independently, and a ROC analysis was performed.

Results: Generally, the area under curve (AUC) increased and the confidence interval (CI) narrowed with higher dose levels for all scanners. All reconstructions at 15 and 20 mGy had AUC values > 0.8. IMR scans at 10 mGy or higher had AUC > 0.9. At 10 mGy, IMR 2 routine had the highest score, 0.96 (CI 95%: 0.91-1.0). At 5 mGy, only IMR scored better than AUC 0.5. The interpreters are most familiar with Philips CT images, and preferences may have influenced image quality scoring.

Conclusion: In general, IMR had higher score than iDose⁴ and ASiR-V for all dose levels. This was a phantom study, so a future clinical validation of the results is necessary.

B-1138 11:42

Feasibility of whole-body low-dose CT using spectral shaping for detection of osteolytic lesion in patients with multiple myeloma

S. Suntharalingam¹, C. Mikat, A. Wetter, N. Guberina, A. Salem, P. Heil, M. Forsting, K. Nassenstein; Essen/DE (Saravanabavaan.Suntharalingam@uk-essen.de)

Purpose: The aim of this study was to investigate radiation dose and image quality of a whole-body low-dose CT (WBLDCT) with tin filtration at 100 kV (Sn100 kV) for the assessment of osteolytic lesions in patients with multiple myeloma.

Methods and Materials: Thirty consecutive patients were retrospectively selected, who underwent a WBLDCT on a third generation DSCT (Sn100 kV, ref. mAs: 130). They were matched with patients, who were examined on a second generation DSCT with a standard low-dose protocol (100 kV, ref. mAs: 111). Objective and subjective image quality, radiation exposure as well as the frequency of osteolytic lesions were evaluated.

Results: All scans were of diagnostic image quality. Subjective overall image quality was significantly higher in the study group (p=0.0003). Objective image analysis revealed that signal intensities, signal-to-noise and contrast-to-noise of the bony structures were equal or significantly higher in the control group. There was no significant difference in the frequency of osteolytic lesions (p=0.259). The median effective dose of the study protocol was significantly lower (1.45 mSv vs. 5.65 mSv; p < 0.0001).

Conclusion: WBLDCT with Sn100 kV can obtain sufficient image quality for the depiction of osteolytic lesions while reducing radiation dose by approximately 74%.

B-1139 11:50

A procedure towards optimised prenatal CT scan protocols for low dose imaging of suspected skeletal dysplasia

I. Indestege¹, L. Cockmartin, J. Binst, W. Coudyzer, H. Bosmans, M. Aertsen; Leuven/BE (ingeindesteeg@gmail.com)

Purpose: To work out a procedure for low dose computed tomography (CT) protocols allowing diagnosis and evaluation of prenatal skeletal dysplasia.

Methods and Materials: Three anthropomorphic phantoms were constructed with a fresh-frozen female lumbar spine and pelvis, in combination with the (Leeds Test Objects) sedentexCT phantom at the theoretical position of the fetus, and water and fat slabs to simulate different sizes of mother and fetus. Scans were performed on a Somatom Force CT (Siemens) under tube current and kV modulation to verify with which patients the 3 phantoms would match (dose data collection with DOSE by Qaelum). The phantoms were also compared to patients in perimeter and size-specific dose estimate (SSDE). Scans were acquired for 5 kV settings at 5 dose levels each to find threshold detectability of hydroxyl-apatite inserts in the phantom and subsequently graded for several criteria by 2 readers.

Results: Perimeters, kV, CT Dose Index (CTDI) and SSDE confirmed that the phantoms covered the complete range of patients, with the perimeter being a

practical criterium for future patient categorisation. The following dose settings guaranteed proper quality (visual grading minimally 4 on a scale of 5) and lowest CTDI: perimeter 100.4 cm: 80 kVp, 18 mAs, CTDI 0.34mGy; perimeter 119.7 cm: 110kV, 34 mAs, CTDI 1.76 mGy, and perimeter 126.6 cm: 140 kVp, 18 mAs, CTDI 1.75mGy. The procedure worked out well in a first patient case.

Conclusion: A procedure for low dose prenatal CT scans with satisfactory image quality for skeletal evaluation was successfully established.

Author Disclosures:

H. Bosmans: Other; co-founder of Qaelum.

10:30 - 12:00

Room K

Radiographers

SS 1414

Radiography education

Moderators:

K. Knapp; Exeter/UK

D. Miletić; Rijeka/HR

B-1140 10:30

Development of a radiological anatomy free software as a teaching tool

M.V.L. Oliveira, P. Geambastiani, G.A. Lopez, M. Cambuí; *Salvador/BR*
(marcusradiology@gmail.com)

Purpose: To develop a learning environment for radiologic anatomy education to assist radiographers/radiologic technologists students and professionals.

Methods and Materials: This study was divided into two phases: 1) image acquisition and 2) software development. The first step was to perform a tomographic scan and radiographic images from a tissue-equivalent phantom of the head and neck, containing the same density and atomic number as bone tissue. In addition, an anthropomorphic phantom of the chest was used for radiographic imaging. The radiographs were held using a computed radiography (CR) digitizer system. The second step consisted in the development of a macro using the ImageJ free software. In this digital environment, radiologic anatomy reference points were inserted and multiple questions were applied.

Results: The software presented radiologic anatomy from 1) skull projections: Waters view, Caldwell view, Towne view, lateral, submentovertex, PA view, 2) thoracic spine projections: AP view and lateral view, and 3) chest (PA view, lateral and oblique). Tomographic imaging presented hundred anatomic points of the skull. Multiple choice questions and a report containing the number of correct answers, as well as the user ID and date of the test were presented. The tests were applied in three languages (Portuguese, Spanish, and English).

Conclusion: An user-friendly and inexpensive software was presented. Radiographers/radiologic technologists, students and professionals from several countries are able to practice, repeatedly, the identification of radiologic anatomic points. This method can be applied as a feasible technological tool for enhancing learning by interactive learning environment.

B-1141 10:38

Pregnancy and radiation: video as a tool for health professionals communicating knowledge and risks

A.F. Reitan¹, H.M. Olerud², A. Borthne³; ¹*Oslo/NO*, ²*Kongsberg/NO*, ³*Lorenskog/NO* (anita.reitan@hioa.no)

Purpose: To ensure that health care professional have the necessary basic knowledge of radiation protection recommendations by producing the information film "Pregnancy and radiation". Pregnancy and radiation is a subject that can cause concern to both healthcare professionals and pregnant women. There is a lot of uncertainty about how much radiation a foetus is capable of taking and the risk of foetal damage after an x-ray examination.

Methods and Materials: Qualitative survey: semi-structured interviews of two general practitioners (GPs) to map which topics were relevant in an information film and how these should be conveyed in film. Video production: produce a short, research-based film with the aim of making existing knowledge more accessible and easier to understand.

Results: The information video is based on recommendations and available knowledge. The take-home message is delivered through dialogue, narration and text. The film consists of five cases that show examples of how x-ray examinations of pregnant women can be justified. Using focused, research-based knowledge, in a video as a tool, we can raise the knowledge of GPs on the subject of pregnancy and radiation.

Conclusion: Using focused, research-based knowledge, in a film as a tool, we are most likely to raise the knowledge of GPs on the subject of pregnancy and radiation. A quantitative survey showed that knowledge among GPs increased after them seeing the video.

B-1142 10:46

Application of the cognitive load theory in simulation experiences to stimulate critical thinking in 2nd year radiography students

A. Louw; *University of Johannesburg/ZA* (amandai@uj.ac.za)

Purpose: To explore the significance of the cognitive load theory as pedagogical strategy to enhance critical thinking in radiography students who participate in a high-fidelity simulation experience.

Methods and Materials: An inter-professional, high-fidelity simulation scenario was specifically designed to stimulate students' higher cognitive skills such as critical thinking, multi-level communication, teamwork and prioritisation in a stress loaded scenario involving chest and elbow imaging. An authentic scenario setting, various role players, life-like sound effects and the demand of multiple cases realistically increased the cognitive load of students and exposed them to the pressures often encountered in casualty settings in South African hospitals. In line with the cognitive load theory, essential basic knowledge and skills were revised and layered well in advance of the simulation experience to be stored in students' long-term memory for easy retrieval when immersed in a non-routine scenario.

Results: Students managed the demands of the scenario fairly well, performed up to the standard expected at their level of training and came to new insights not previously addressed in a classroom context. During the reflective debriefing session steered by student observers, four themes, namely prioritisation, communication, team roles and situational and mental preparedness emerged.

Conclusion: Students who were given explicit guidance regarding supportive knowledge and skills prior to being involved in a multi-case stress-loaded simulation experience achieved the targeted learning outcomes when allowed to reflect on their actions and decisions immediately after the simulation experience.

B-1143 10:54

Enhancing radiographer threshold CT competencies through simulation

M. Hardy¹, M.A. Harris²; ¹*Bradford/UK*, ²*Wakefield/UK*
(M.L.Hardy1@bradford.ac.uk)

Purpose: The last decade has seen extensive growth of computed tomography (CT) placing greater expectations on radiographers to participate in CT image acquisition early in their careers. Pre-qualification technical skills development is achieved through the integration of academic and clinical learning but pressures on service capacity limit opportunities for students to obtain practical experience. Practice simulation has been shown to be beneficial to learning but limited opportunities exist in relation to CT skills development. This proof of concept study explored whether a bespoke CT simulation web platform could increase student confidence and competence in non-contrast head acquisition.

Methods and Materials: Supported by funding from Health Education England, an integrated CT simulation programme distributed through the internet was developed. This programme reflected current clinical CT practice taking student from patient registration through to discharge and requiring decision-making on image acquisition and reconstruction processes. Both practice and assessment modes were incorporated for monitoring student CT skills development and errors in decision-making.

Results: The CT simulation programme enabled students to practice their clinical skills and see the consequence of errors in parameter choice on image quality. Students reported greater confidence in CT processes prior to clinical placement and ability to question clinical radiographers from a wider knowledge base.

Conclusion: CT simulation technologies that enable errors in judgement to be made, and consequences appreciated, increase fundamental knowledge and understanding of the technology. Expansion of the CT simulation programme to include chest imaging is being explored.

B-1144 11:02

A systematic methodology for the development and validation of inventories of biomedical imaging physics learning outcomes for radiography and radiology specialities

J. Castillo¹, C. Caruana², A. Mizzi³, P.S. Morgan⁴, C. Westbrook⁵;
¹*San Gwann/MT*, ²*Mside/MT*, ³*Attard/MT*, ⁴*Nottingham/UK*, ⁵*Cambridge/UK*
(josecast@melita.com)

Purpose: To develop a research methodology for developing local CPD outcomes in imaging physics for radiographers and radiologists.

Methods and Materials: An extensive literature review on learning outcomes development and multi-stakeholder consensus validation approaches was carried out and best practices were identified. A methodology was developed and tested by application to the development of a physics learning outcomes (LO) for local MRI radiographers.

Results: The method follows: (a) a multi-stakeholder Delphi process was used to forecast the MRI service portfolio for the year 2020; (b) a multi-stakeholder

nominal group technique was used to optimise the MRI care pathway/service quality criteria; (c) a survey of MRI competence profiles (CP) from the major English-speaking countries was used to identify good practices in CP design; (d) an MRI CP was set up based on the results of steps (a)-(c) and validated with a multi-stakeholder group; (e) an inventory of biomedical imaging physics LO required to deliver the CP was developed via an analysis of textbooks and research literature and validated by a multi-stakeholder expert group. The multi-stakeholder group agreed that the current MRI service catalogue should be maintained, whilst proposing new specific services. The care pathway/associated quality criteria were optimised. CP from 6 countries were studied. A CP consisting of 43 competence statements was developed and validated. An inventory of physics LO closely integrated with the CP was developed and validated.

Conclusion: The process is sufficiently generic to be applicable to the development of physics learning outcomes for all radiography and radiology specialities.

B-1145 11:10

Periodic refresher course for the radiographers of multimodal radiology department: the role of IT technologies

A. Fedorov, M. Cherkashin; St. Petersburg/RU (fedorov@ldc.ru)

Purpose: To assess electronic-based educational programs' effectiveness in radiographers' professional development plan.

Methods and Materials: 18 MRI radiographers were included in study. We have used electronic testing system with ID binding, MR examination simulator. Electronic platform was created by IT specialist under MR technologist overview. On the first step, initial experience was evaluated by testing and interview and staff was divided in 3 groups (by knowledge level). Educational course was 2 days (12 hours in total) and includes lectures, MR simulator practice with case studies and final examination. After 6 months we have performed interim review (interview) and after 12 months final review with electronic testing and interview with feedback form.

Results: Based on 3 groups' scoring, radiographers were divided into qualification classes. 2 technicians were assigned to the highest qualification group. Moderate group was assigned to 11 employees. 5 radiographers were assigned to the lowest group of qualifications. All employees have passed re-certification in months 12 and the strong positive dynamic was revealed. 5 technicians from the lowest group increased their knowledge level and upgraded into group 2. 2 employees, received the highest qualification, were transferred to an expert multimodal centre for working with advanced technologies and to act as coaches. Personal satisfaction rate was revealed in 89%.

Conclusion: Electronic platform with face-to-face interviews, regular follow-ups and employees' motivation is the effective tool for staff development. For high-quality and full-fledged training of healthcare personnel it is obvious to use educational and development plans based on electronic technologies.

B-1146 11:18

Eyes on the future of mammography education and training: what needs to be focused to match the demands of the clinical practice?

A. Henner¹, E. Metsälä², N. Richli Meystre³, C. Sá dos Reis¹, B. Strøm⁴, J. Pires Jorge³, T. Kukkes⁵, ¹Oulu/FI, ²Helsinki/FI, ³Lausanne/CH, ⁴Bergen/NO, ⁵Tartu/EE (eija.metsala@metropolia.fi)

Purpose: The purpose of this study was to identify areas that require update on specific knowledge to allow the progression of radiographers' practice in mammography.

Methods and Materials: This study was a cross sectional online survey based on online questionnaire addressed to clinical radiographers in five European countries about training including perceived challenges and continuous professional development (CPD). The questions were closed-ended with possibility to add comments. Answers were dichotomous, multiple choice or with a five point Likert Scale. The data collected (N= 140) was analysed and redundant data was disregarded. Statistical data analysis was performed using the software packages SPSS (version 21, IBM) by using descriptive methods, Chi square and independent samples t-test.

Results: Regardless of country, radiographers considered positioning (86%) and coping with pain (88%), anxiety (83%) and imaging breast implants (71%) as the most challenging tasks. Respondents participated on CPD training about mammography (88%). However, 62% had less than 10 hours CPD per year. Congresses (70%) and conferences (41%) were the most common sources to update knowledge.

Conclusion: The majority of the radiographers reported the need of more training in mammography. The lack of evidence-based knowledge especially related to clinical image quality appropriateness criteria and related to optimal breast compression suggest the importance of well-designed studies on these topics. Variability found could encourage radiographers and teachers to question their own practice and to revise the training programs.

B-1147 11:26

Comparison of curricula, clinical experiences and attributes of radiography programmes delivered by four European educational institutions

C.S. Reis¹, S. Mæhle², J.A. Pires Jorge³, H. York⁴, L. Flaction³, S. Johansen²; ¹Perth/AU, ²Oslo/NO, ³Lausanne/CH, ⁴Herts/UK (Jose.JORGE@hesav.ch)

Purpose: To compare the curricula, teaching/learning strategies, skills, clinical practice outcomes and research of radiography programmes delivered by four different European educational institutions.

Methods and Materials: This study was developed in two phases: one focused on curricula analysis using an observation grid and another involving a survey performed on students and teaching staff. Questionnaires were design to explore teaching and learning strategies, skills and outcomes of clinical practice.

Results: ECTS dedicated per core area (natural sciences, clinical practice, research, imaging technology, humanities) differed between institutions. Research practice was similar for three institutions out of four. Students classified technical, practical and communication skills as the most important, while teaching staff highlighted critical thinking. The majority of students defined as "very good" their experience in radiography (58.5%) and computed tomography (45%). Magnetic resonance imaging training was considered "average" by 53% of the UK students and "good" by the others (40%). Mammography, nuclear medicine and radiotherapy were not always available for some students. For 71% (55/78) of the students, the research work contributed to the development of critical/reflective thinking.

Conclusion: The four radiography programmes analysed in this study presented variations on curricula, contact hours and clinical experiences with impact on the outcomes. The critical thinking was emphasised as one of the most important skills that a radiographer should develop and, for that reason, research should be considered as a core unit in radiography/medical imaging education. Further work is needed to assess the real impact of different programmes on professional and academic mobility across Europe.

B-1148 11:34

The development of a CAD tool employing TELTA, designed to support the training of radiographers in chest pattern recognition

S. Mdeletshe¹, A. Nel¹, L. Rainford², H.A. Lawrence¹; ¹Johannesburg/ZA, ²Dublin/IE (sibusisom@uj.ac.za)

Purpose: Radiography is a dynamic profession that has undergone rapid technological advancements in recent years. The use of technology-enhanced learning, teaching and assessment (TELTA) to support innovative training options for radiographers to enhance their radiographic image evaluation and pattern recognition skills is warranted. However, a gap in current practice exists in the availability of custom designed computer-aided detection (CAD) tools to augment TELTA use in radiography.

Methods and Materials: A CAD tool for teaching pattern recognition in chest imaging was designed as a collaborative project between the Mechanical Engineering Science and Medical Imaging and Radiation Sciences Departments, the University of Johannesburg. A Design Science Research (DSR) paradigm was used. An initial needs analysis was performed involving a focus group interview of eight practising radiography educators. The findings of a systematic literature review coupled with the needs analysis outcomes were used to compile a software requirements specification document to guide the CAD tool development process.

Results: A CAD prototype was designed to function as a live tool for LTA purposes. The CAD tool design facilitates the collection of data on student tool usage, performance in automated assessments and managed progress based on user-tracked data. Important to the tool was that the students should be able to apply standard pattern recognition tools to manipulate the image without altering the original.

Conclusion: Details of how the prototype was developed will be given; the development base provides an evidence based mechanism for further prototype innovations. Initial data from prototype testing will be provided.

B-1149 11:42

Internship supervisors' perception of the radiography students in clinical environment

A.F. Abrantes¹, V.L. Gaspar¹, L.P. Ribeiro¹, O. Lesyuk², A.M. Ribeiro¹, R.P. Almeida¹, C.A. da Silva³; ¹Faro/PT, ²São Brás de Alportel/PT, ³Evora/PT (oksanalesyuk@gmail.com)

Purpose: To identify and describe the perception of internship supervisors of the radiography students in clinical environment about their competencies, skills and characteristics.

Methods and Materials: A quantitative descriptive, correlational design was used. Data were collected through an adapted version of the Clinical Learning Assessment Inventory-Mentor (CLASI-M) questionnaire with a final sample of

34 radiographer supervisors of the last year undergraduated radiography students from a public university.

Results: The training and education provided to the undergraduated radiography students prior to their internship is sufficient to assure the gradual development of the competencies and characteristics of the future radiographers. Additionally, the effective integration into the multidisciplinary team and a relationship of trust with the supervisor are also fundamental for the student's development. The majority of the supervisors are very satisfied with the students' availability (93,6%) and the levels of supervision (96,7%) throughout the radiography clinical internship.

Conclusion: The pedagogical atmosphere is considered pivotal, with reference to students' learning activities and competent development within the clinical setting. The most desired competencies in a student by supervisors are communication skills with both patients and other team members, a high level of theoretical knowledge and performance in practice, fast learning and the overall motivation exhibited throughout the internship. Furthermore, supervisors are satisfied with both their own and students' availability, showing great expectations for the future radiographers.

B-1150 11:50

The use of moulage to prepare first year diagnostic radiography students for the sight of open wounds: initial findings of a doctoral pilot study
N. Shiner; Derby/UK (N.shiner@derby.ac.uk)

Purpose: Transitioning to clinical placement is challenging for first year diagnostic radiography students; specifically working with ill patients. Focus groups held with students following their first clinical placements indicated issues comprehending the sight of open wounds. Witnessing the result of trauma is linked with anxiety and psychological trauma. Simulated practice offers experiential learning to students in a safe environment. Active participation and the debrief stage offers opportunity for analysis, problem solving and reflection. The use of moulage (make-up) increases fidelity and immersion of participants in simulated practice. A gap in the literature was identified and led to this pilot study for a doctoral thesis; preparing students for open wounds prior to clinical placement.

Methods and Materials: Ethical approval was gained. A mixed method quasi-experimental study was designed. Twelve first year radiography students were randomly assigned to control and experimental groups. The experimental group attended a simulation of a patient suffering open wounds (moulage). Quantitative data was gathered from both groups at the same time points using visual analogue scales. Focus groups will be held post clinical placement to gather qualitative data.

Results: It is hypothesised that the experimental group will value the opportunity to explore and discuss experiencing patients with open wounds. The control group will have similar experiences to previous cohorts indicating difficulties in this area.

Conclusion: As work is in progress the findings of this study will be reported. This is an innovative use of moulage in this context, contributing to the evidence base supporting transitioning students.

10:30 - 12:00

Room M 1

Cardiac

SS 1403

Myocardial MRI: perfusion, tissue tracking and fibrosis

Moderators:

F. Secchi; Milan/IT
E.J.R. van Beek; Edinburgh/UK

K-21 10:30

Keynote lecture

R. Vliegenthart; Groningen/NL

B-1151 10:39

Impact of local native T1 times on pixel-wise quantification of myocardial blood flow

C. Kräuter, U. Reiter, C. Reiter, A. Schmidt, M.H. Fuchsjäger, R. Stollberger, G. Reiter; Graz/AT (corina.kraeuter@medunigraz.at)

Purpose: To investigate the impact of local native T1 time variations on pixel-wise quantification of myocardial blood flow (MBF) from dynamic contrast-enhanced magnetic resonance imaging (DCE-MRI).

Methods and Materials: 15 patients with coronary heart disease underwent 3T pre-contrast T1 mapping and cardiac DCE-MRI at rest using a saturation recovery fast low angle shot sequence. Gadolinium-based contrast agent was administered as bolus at a dose of 0.05 mmol/kg. After coil sensitivity and motion correction of DCE series, signal intensity was converted to contrast agent concentration employing a signal intensity model and incorporating measured native T1 times. MBF was calculated pixel-wise using Fermi modelling. Segmental mean MBF values calculated with global and local native myocardial T1 times, respectively, were compared using paired t-test. Myocardial segments exhibiting perfusion deficits were identified by visual analysis of DCE series.

Results: Segmental mean MBF values calculated with global and local native T1 times, respectively, did not yield a significant difference (MBF global T1, 0.61 ± 0.16 ml/min/g; MBF local T1, 0.62 ± 0.16 ml/min/g; $p=0.4354$). However, considering segments with and without perfusion deficits individually revealed a decrease in MBF for segments with perfusion deficits if local instead of global native T1 times were employed (MBF global T1, 0.47 ± 0.17 ml/min/g; MBF local T1, 0.43 ± 0.16 ml/min/g; $p=0.0016$); segments without perfusion deficits showed the opposite behavior (MBF global T1, 0.64 ± 0.14 ml/min/g; MBF local T1, 0.65 ± 0.14 ml/min/g; $p=0.0083$).

Conclusion: Local instead of global native T1 times should be used in pixel-wise MBF quantification to avoid overestimation of MBF in myocardial regions with perfusion deficits.

Author Disclosures:

G. Reiter: Employee; Siemens Healthineers.

B-1152 10:47

Cardiac magnetic resonance T1 reactivity in coronary artery disease

M. van Assen, R. van Dijk, D. Kuijpers, R. Vliegenthart, M. Oudkerk; Groningen/NL (m.van.assen@umcg.nl)

Purpose: To assess the potential of rest and stress T1-mapping for differentiating normal and diseased myocardium without Gadolinium in patients with suspected coronary artery disease (CAD).

Methods and Materials: Patients underwent 1.5T magnetic resonance imaging (MRI) as part of clinical work-up due to suspicion of CAD. To identify ischemic and infarcted myocardium adenosine stress perfusion and late gadolinium enhancement (LGE) MRI were performed. Patients were categorized into an ischemic, infarct, and control group based on perfusion and LGE images. Patients were excluded if they had both ischemic and infarcted myocardium. At rest and stress, a native Modified Look-Locker Inversion Recovery (MOLLI) T1-mapping acquisition was performed. Short-axis pixel-wise myocardial T1-maps were acquired with inline motion-correction. Regions of interest (ROI) were placed in the septal (normal myocardium), ischemic and infarcted areas.

Results: 64 patients were included: 10 with myocardial ischemia, 15 with myocardial infarction, and 39 controls. Rest and stress native T1-values were significantly higher in infarcted myocardium (median 1044ms [interquartile range (IQR) 985-1076] and 1053ms [IQR 989-1088]) compared to ischemic myocardium (median 961ms [IQR, 939-988] and 958ms [IQR, 945-988]). T1-reactivity was significantly lower in ischemic and infarcted myocardium (median 0.00% [IQR,-0.18-0.16] and 0.41% [IQR, 0.09-0.86]) compared to remote myocardium (median 3.54% [IQR, 1.48-5.78] and 3.21% [IQR, 1.95-4.79]).

Conclusion: T1-mapping in rest and stress is able to distinguish between normal, ischemic, infarcted and remote myocardium using native T1-values and T1-reactivity, and holds potential as an imaging biomarker for tissue characterization using MRI.

B-1153 10:55

Myocardial microvascular dysfunction in patients with end-stage renal disease: assessment with 3.0T cardiac magnetic resonance

R. Xu, H. Xu, Z. Yang, Y. Guo; *Chengdu/CN (Xrongdoctor@163.com)*

Purpose: To quantitatively evaluate the left ventricular regional myocardial microvascular function in patients with end-stage renal disease (ESRD), and to clarify the feasibility of first-pass perfusion imaging for detection myocardial microvascular dysfunction in patients with ESRD.

Methods and Materials: In total, 67 patients with ESRD and 19 healthy subjects were enrolled and the first-pass perfusion was analysed. The ESRD patients were divided into two groups including 16 patients with systolic dysfunction (EF<50%) and 51 patients with preserved systolic function (EF≥50%). The LV myocardial perfusion parameters included Upslope, time to maximum signal intensity (TTM) and max signal intensity (MaxSI) which were compared among the patient groups and controls. Continuous variables were compared using independent one-way analysis of variance (ANOVA).

Results: The ESRD patients with impaired LVEF had significantly lower SV than that of the normal subjects, and the LV mass was markedly increased (all P < 0.001). The patients with ESRD had significantly reduced first-pass perfusion MaxSI in the all segment compared with the normal subjects (all P < 0.001). For the Upslope and TTM, the patients with ESRD (impaired EF) had lower Upslope in the basal segment (2.53±1.21 vs 2.04±0.81, P < 0.05) than the patients with ESRD (preserved EF); all patients had lower Upslope in the mid-segment and shorter TTM in the apical segment than the controls P < 0.05).

Conclusion: The first-pass perfusion CMR can discover and monitor the myocardial microvascular dysfunction in ESRD patients.

B-1154 11:03

Impaired segmental myocardial microvascular dysfunction in chronic kidney diseases patients: assessed by cardiac magnetic resonance first-pass perfusion imaging

H. Xu, Z. Yang, Y. Guo, W. Peng, W. Peng; *Chengdu/CN (xuhuayan89@sina.com)*

Purpose: This research is aimed to access the myocardial microvascular dysfunction in chronic kidney disease (CKD) patients by using cardiac magnetic resonance (CMR) first-pass perfusion imaging, and investigate its association with left ventricular (LV) dysfunction.

Methods and Materials: Seventy-five CKD patients and 29 normal controls were enrolled. All subjects were underwent 3.0T CMR examination. First-pass perfusion imaging in three standard short-axis slices (apical, middle, and basal) and one the 4-chamber view were obtained immediately after intravenous injecting gadobenate dimeglumine. All imaging were calculated on the offline dedicated software (cvi42). Perfusion slope, time to peak (TTP) and max signal intensity (mSI) were obtained. LV dysfunction were defined as LV ejection fraction (EF) <50%.

Results: The slope and mSI of basal, middle and apical segment in CKD patients with LV dysfunction was lower than those without LV dysfunction and normal controls; and those preceding slope of CKD patients without LV dysfunction were also reduced comparing with normal controls (all P≤0.05). For the TTP, only basal segment of patients with LV dysfunction were elongated comparing with those without LV dysfunction and normal controls (37.52±16.10s vs. 26.92±14.02s and 28.30±8.29s). LVEF were positively correlated with basal and middle slope (r=0.293 and 0.129, P≤0.05). In addition, LVEF is significantly related to basal mSI (r=0.301, P≤0.05). Logistic regression analysis demonstrated that myocardial perfusion slope is the independent risk factor of LV dysfunction.

Conclusion: Segmental myocardial microvascular dysfunction was found in CKD patients without LV dysfunction. Segmental slope and basal mSI were significantly associated with LVEF. Perfusion slope was demonstrated the independent risk factor of LV dysfunction.

B-1155 11:11

Semi-quantitative and quantitative magnetic resonance perfusion analysis: a meta-analysis

R. van Dijk¹, M. van Assen², R. Vliegenthart¹, G. de Bock¹, P. van der Harst¹, M. Oudkerk¹; ¹Groningen/NL, ²Charleston, SC/US (r.van.dijk02@umcg.nl)

Purpose: To assess the diagnostic accuracy of semi-quantitative and quantitative magnetic resonance perfusion (MR) analysis.

Methods and Materials: Pubmed, WebOfScience, and Embase were systematically searched using the following eligibility criteria: study domain - patients with known or suspected CAD. Index test - quantitative or semi-quantitative MR perfusion. Reference standard - ICA+/-FFR or QCA. Outcome

- diagnostic accuracy of index test compared to reference standard. Study design - observational. The summary measures used to assess diagnostic accuracy were sensitivity, specificity, and area under the receiver operating curve (AUC). Data were pooled according to analysis territory, reference standard and perfusion parameter. Significant heterogeneity was defined as Q-statistic <0.10 and/or I² of >50%.

Results: After removal of duplicates 1967 articles were screened based on title and abstract. 137 articles were selected for full text assessment and 22 studies were included in the final analysis. Pooled diagnostic accuracy for segment-, territory- and patient-based analyses showed good diagnostic performance with sensitivity of 0.88, 0.82, and 0.83, specificity of 0.72, 0.83, and 0.76 and AUC of 0.90, 0.84, and 0.87, respectively. Only per territory analysis pooled sensitivity, per territory anatomical reference standard sensitivity and per territory semi-quantitative specificity did not show significant heterogeneity.

Conclusion: Overall, the diagnostic performance of both semi-quantitative and quantitative MR perfusion analysis is quite good. However, the real clinical value of semi-quantitative and quantitative MR perfusion analysis remains uncertain due to extensive inter-study heterogeneity and large differences in MR perfusion acquisition protocols, reference standards, and methods of assessment of myocardial perfusion parameters.

B-1156 11:19

Compressed sensing real-time cine imaging in patients with cardiac arrhythmia: does it help to reduce mistriggering artefacts?

P.-E. Allard¹, A. Bridoux¹, B. Longere¹, V. Silvestri¹, M. Schmidt², C. Forman², F. Pontana¹; ¹Lille/FR, ²Erlangen/DE (pauledouardallard@hotmail.fr)

Purpose: To evaluate the impact of a compressed sensing (CS) real-time prototype cine sequence (sparse 2D cine, Siemens Healthineers) on mistriggering artefacts in patients with arrhythmia, in comparison with the reference cine-imaging technique.

Methods and Materials: 71 consecutive patients (41 males; mean age=59±20.6 years), referred for cardiac magnetic resonance (CMR) examination with concomitant irregular heart rate (defined by R-R interval variation >10%), were prospectively enrolled. For each patient, a standard segmented multi-breath-hold steady-state free precession (bSSFP) sequence (Group 1) and a real-time CS single-breath-hold prototype sequence (Group 2) were systematically acquired. Two radiologists independently assessed mistriggering artefacts, objective and subjective image quality for both acquisition techniques.

Results: The mean heart rate variation was 38% ±22.6 (range: 12-122). A total of 599 cine slices were evaluated in each Group (mean number of slices per patient=8.4 ±1.9). The number of slices with mistriggering artefacts per patient was higher in Group 1 than in Group 2 (7.2 ±2.4 vs 0.03 ±0.08, p<0.0001). The European CMR registry standardised artefact score was lower in Group 2 than in Group 1 (1.6 ±1.5 vs 2.9 ±0.5, respectively, p<0.0001). Subjective image quality score was improved in Group 2 compared to Group 1 (2.6 ±0.7 vs 1.9 ±0.8, respectively, p<0.0001).

Conclusion: Compressed sensing real-time cine imaging drastically reduces mistriggering artefacts and improves image quality of CMR cine acquisition in patients with arrhythmia.

Author Disclosures:

M. Schmidt: Employee; Siemens Healthcare. **C. Forman:** Employee; Siemens Healthcare.

B-1157 11:27

Strain parameters for the right ventricle in cardiac MRI: the forgotten child?

S. Benz, M.C. Halfmann, J. Eichstädt, A. Lollert, C. Düber, K.-F. Kreitner, T. Emrich; *Mainz/DE (sbenz@students.uni-mainz.de)*

Purpose: Since the original work from Zerhouni et al. in 1988, strain analysis in cardiac magnetic resonance (CMR) imaging has been dwelling under the surface of clinical routine. Recently, through the development of post-processing approaches such as feature tracking, strain analysis is in the focus of interest. In a meta-analysis by Vo et al., only 9 out of the 17 publications included the right ventricle by just measuring global longitudinal strain (GLS_{RV}). The purpose of our study was to establish the reference values of the RV in healthy volunteers.

Methods and Materials: In this study, 62 healthy volunteers underwent CMR imaging at 3T (Magnetom Skyra®, Siemens Healthineers). We manually traced the endocardial and epicardial contours for both late systolic and diastolic phases in both ventricles on the short- and long-axis cine images. The software (Cvi42 Circle®) then subsequently tracked the movement of these contours.

Results: We measured all three strains for both ventricles, leading to the following values for right ventricle: global radial strain (GRS_{RV}) 13.47% (± 6.46), global circumferential strain (GCS_{RV}) -7.61% (± 3.92) and median global longitudinal strain (GLS_{RV}) -24.35% (± 5.22). There was a significant difference

between GLS_{RV} in the present study from the pooled mean value of meta-analysis.

Conclusion: The amount of variance between our and the published data might be explained by the use of different tracking softwares and the absence of standardized protocols. However, there is a need for establishment of those as a basis for assessment of RV strains in cardiac diseases in future studies.

B-1158 11:35

Global and segmental cardiac magnetic resonance tissue tracking of hypertrophic cardiomyopathy: how do hypertrophy and fibrosis contribute to myocardial deformation?

R.-Y. Shi, R. Wu, D. An, B. Chen, L. WU, J.-R. Xu; *Shanghai/CN* (ryshicn@hotmail.com)

Purpose: In hypertrophic cardiomyopathy (HCM), both heterogeneous left ventricular hypertrophy and focal fibrosis influence regional deformation. The goal of this study was to assess global strain, native T1 and extracellular volume (ECV) changes to differentiate the extent of hypertrophy, and to measure the contribution of hypertrophy and fibrosis in segmental strain deformation.

Methods and Materials: Forty early-stage HCM patients were examined by a 3.0 Tesla magnetic resonance scanner. We analysed circumferential, longitudinal and radial strain, systolic and diastolic strain rates using 2D and 3D modes. Native T1, ECV values and focal fibrosis were assessed. The generalised equation estimating (GEE) module was applied to evaluate in segmental levels.

Results: At the global level, ECV significantly correlated with conventional LV function and strain parameters, but not native T1 values. Global strain parameters in 3 directions were found to correlate best with the extent of hypertrophy (LV mass/BSA). At the segmental level, LGE presence significantly correlated with segmental hypertrophy ($P < 0.0001$). The GEE module suggested that LGE presence and segmental hypertrophy (thickness ≥ 15 mm) were observed antagonistic in 2D radial strain ($\beta = 12.756$, $P = 0.006$) and diastolic radial strain rate ($\beta = 1.314$, $P = 0.005$).

Conclusion: Subtle LV deformations can be observed and measured by strain before the manifestation of LV functional changes. Our study demonstrated 2D CS is a stable global parameter correlated with LV functional and ECV changes. At the segmental level, hypertrophy and LGE presence are antagonistic in 2D RS and diastolic RSR.

B-1159 11:43

Taking CMR strain into the next dimension

S. Benz, M.C. Halfmann, J. Eichstädt, A. Lollert, C. Düber, K.-F. Kreitner, T. Emrich; *Mainz/DE* (sbenz@students.uni-mainz.de)

Purpose: Cardiac magnetic resonance (CMR) imaging and post-processed tissue tracking are evolving for characterisation of a wide variety of pathologies. Though the images are captured two-dimensionally, tissue tracking algorithms allow for accurately visualised and measured 3D movements. We therefore analysed similarities and differences between 2D and 3D strain analysis.

Methods and Materials: CMR was performed on 62 healthy volunteers at 3T (Magnetom Skyra®, Siemens Healthineers). Based on cine images, endocardial and epicardial contours were manually traced on late systolic and diastolic images in both ventricles. This comprised multiple slices in the short axis and four chamber views for both ventricles, respectively two chamber view for the left ventricle. The tissue tracking software (CVI42 Circle®) then subsequently tracked the movement of the drawn contours and calculated 2D and 3D strain parameters.

Results: We found significant differences between 2D and 3D in global values concerning radial and longitudinal strains ($p < .0001$, respectively), while the circumferential strain was not significantly different. After adjusting for gender and age we were not able to explain the differences.

Conclusion: Due to the complex myocardial architecture and the three-dimensional movements of the heart, it appears plausible that the 3D strain comes closer to measuring the physiological motion. Therefore we suggest adding it to standard protocol, especially as long as superiority of either 2D or 3D strains has not been proven. Furthermore, there is a need for general standardisation in CMR tissue tracking.

B-1160 11:51

Age and sex dependency of myocardial strain in CMR: an urgent need to standardise

M.C. Halfmann, S. Benz, J. Eichstädt, A. Lollert, C. Düber, K.-F. Kreitner, T. Emrich; *Mainz/DE* (Moritz.Halfmann@gmx.de)

Purpose: Data concerning feature tracking strain analyses are still rare. Therefore, it is difficult to perform reliable analyses of influencing factors. We aim at providing additional data to consolidate feature tracking cardiac magnetic resonance imaging (FT-CMR) as a method eligible for clinical use.

Methods and Materials: We performed 62 FT-CMR examinations for the left and right ventricles in healthy volunteers using semi-automatic tracking software (CVI42 Circle®). The calculated global strain values were subsequently tested for influencing factors like age, sex and their combination using an analysis of variance (ANOVA). Post-hoc testing using the Bonferroni correction was performed for the various subgroup analyses.

Results: The left ventricular global strains (radial, circumferential and longitudinal) both in 2D and 3D showed statistically significant differences with regard to sex but not with regard to age. The combination of both factors did not reveal a significant influence. Interestingly, in the right ventricle we found statistically significant differences of strain values between old and young individuals, while sex had a smaller impact. Again, the combination of the subgroups did not yield any significant results.

Conclusion: Our results contrast those of a recently published meta-analysis of Vo *et al.*, where sex or age did not have a significant influence. These differences might be explained by use of different software, number of slices used for tracking and measured strain parameters. This shows the urgent need of standardisation for feature tracking algorithms before we can effectively employ FT-CMR in clinical routine.

10:30 - 12:00

Room M 2

Paediatric

SS 1412

Foetal and neonatal imaging

Moderators:

F.E. Avni; Lille/FR

D. Piotrowska-Kownacka; Warsaw/PL

K-22 10:30

Keynote lecture

D. Prayer; Vienna/AT

B-1161 10:39

Establishing age-specific reference values of lung volume in preterm born infants using MR-based volumetry

G. Negrao de Figueiredo, F. Schöppe, A. Pomschar, K. Förster, A. Hilgendorff, S. Stöcklein, B. Ertl-Wagner; *Munich/DE* (gofigueiredo@yahoo.de)

Purpose: Although reference values of total lung volume (TLV) exist for foetal MRI, age-specific normal values of TLV in preterm infants based on MRI are not yet available. We aimed to evaluate the influence of gestational age (GA) at birth, and severity of bronchopulmonary (BPD) on TLV in preterm infants establishing age-specific values of TLV.

Methods and Materials: 38 preterm neonates with no (n=20) and mild (n=18) BPD (grades 0 and 1, respectively) were evaluated. GA at scan ranged between 34 and 38 gestational weeks (GW) and GA at birth from 24 to 31 weeks. The whole lung was segmented manually on axial T2w images. TLV across BPD grades was compared using the t-test. Multivariate linear regression was used to evaluate the influence of GW at birth, at scan and BPD grade on TLV.

Results: The median (IQR) TLV was 56.76cm³ (47.07-68.12). There was no significant difference in TLV between BPD 0 vs. 1 ($P=0.987$). Neither GW at birth, nor BPD grade had a significant influence on TLV ($P=0.637$ and $P=0.958$). Only GW at scan was significantly associated with TLV ($P=0.015$). Therefore, reference values for GA at scan around term (36±2 weeks) were established. The TLV increased with GW at scan, with the median TLV ranging from 48.71cm³ at 34 GW to 78.11cm³ at 38 GW.

Conclusion: We demonstrated that manual MR-based volumetry of TLV in preterm neonates is a feasible approach. The established age-specific reference values of TLV may provide an important basis to detect alterations of TLV.

B-1162 10:47

Towards an elastographic atlas of the neonatal brain

E.F. Garcés Iñigo, L. Marti-Bonmati, R. Llorens, M. Vento Torres; *Valencia/ES* (engari@alumni.uv.es)

Purpose: To define the normal elasticity values of the grey and white matter in the neonate.

Methods and Materials: Randomised healthy term born neonates were recruited from our maternity ward between their 2nd and 3rd day of live. A total of 57 cerebral ultrasound elastography were archived. All examinations were performed using a Siemens Acuson S2000 ultrasound system with a multifrequency 4-9 MHz probe. In all cases, a quantitative shear wave imaging method (Virtual Touch™ Imaging Quantification) was applied. Protocol included bilateral sagittal planes of the thalamus and of the corona radiata.

Elastograms with at least 5 non-overlapping quantitative measurements were obtained from each anatomic location.

Results: Statistical analysis was made from a total of 1.885 quantitative measurements of the shear wave velocity (493 from right thalamus, 513 from left thalamus, 434 from right corona radiata and 445 from left corona radiata). The estimated mean value of the velocity in the thalamus is 1,184 m/s with a IC95% [1,147 - 1,221] and that of the corona radiata is 1,608 m/s with a IC95% [1,573 - 1,642]. No significant association was found with laterality, gestational age, cephalic perimeter, sex, height, or type of delivery.

Conclusion: There is a clear difference in the elasticity of the grey and white matter in healthy term neonates. Knowledge of the normal values is essential since changes from normal elasticity are expected in pathological tissues.

B-1163 10:55

Respiratory distress syndrome in neonates-comparison between lung ultrasound and chest x-ray

I. Sefic-Pasic, A. Džananovic, M. Bukvic, S. Terzic, M. Agovic, S. Vegar-Zubovic; Sarajevo/BA (irmina.sefic@gmail.com)

Purpose: The aim of this paper is to introduce basic principles of lung ultrasound, technique and ultrasound findings in neonatal respiratory distress syndrome and to compare it with chest X-ray.

Methods and Materials: Lung ultrasound examinations were performed prospectively in 49 neonates (25 boys, 24 girls) with positive clinical and laboratory signs of respiratory distress syndrome and ultrasound findings were compared with chest X-ray. All ultrasound examinations were performed with a high frequency linear-array probes of 7,5 and 10 MHz. Interpretation of findings have been done by two radiologists. Interpretation of chest x-ray was based on 4-grade scale and ultrasound findings were classified into 3-stage profiles. Results were compared with statistical analysis.

Results: In the cohort of 49 patients we calculated Pearson Correlation Coefficient and the value of R was -0.5161. This is a moderate negative correlation, but these results correlate with grading system of RDS (respiratory distress syndrome) - high x-ray score and low ultrasound score refers to most severe grade of RDS and vice versa. Sensitivity of ultrasound was 98,4% and PPV 93%. We have found pathological findings on ultrasound presented with confluent B-lines-white lungs, subpleural consolidation of lung parenchyma, pneumothorax, abnormalities of pleural line and A lines in resolution of disease.

Conclusion: Lung ultrasound is a reliable tool for diagnosing and follow up of respiratory distress syndrome in neonates. Introducing lung ultrasound in diagnostic algorithm, number of x-ray examinations can be decreased and exposure of neonates to ionizing radiation.

B-1164 11:03

The role of lung ultrasound in the differential diagnosis of respiratory distress syndrome and transient tachypnoea in preterm and newborn infants

M. Mughetti¹, G. Gardelli¹, E. Giampalma¹, M. Zompatori²; ¹Cesena/IT, ²Bologna/IT (martinamughetti@gmail.com)

Purpose: Respiratory distress syndrome (RDS) and transient tachypnoea (TTN) are the most common causes of respiratory distress in premature and newborn infants. The diagnosis of RDS and TTN is based on clinical diagnosis and chest x-ray, but sometimes these entities show overlapping radiographic patterns. For this reason, pulmonary ultrasound is emerging as a reliable diagnostic tool to integrate radiography. The aim of our study was to evaluate the role of pulmonary ultrasonography in the differential diagnosis of RDS and TTN in the newborn.

Methods and Materials: From September 2016 to June 2017, 62 preterm or newborn infants with respiratory distress admitted to the Neonatal Intensive Care Unit were studied with chest x-ray and lung ultrasound.

Results: The white lung was demonstrated exclusively in patients with RDS ($p = 0,000$) and the simultaneous presence of a white lung and pleural irregularities and absence of spared areas showed high specificity (100%) and discrete sensitivity (76%) in identifying RDS. The double lung point was detected in both lung fields in 16 out of 21 TTN patients and in no patients with RDS ($p = 0,000$), exhibiting 100% sensitivity, 76% sensitivity, 100% positive predictive value and 88% negative predictive value.

Conclusion: The results of this study show that pulmonary ultrasound is a reliable and accurate tool for the differential diagnosis of RDS and TTN. However, chest RX remains the first-level diagnostic tool and can be integrated by ultrasound examination, which also allows a radiation-free follow-up.

B-1165 11:11

Italian guidelines for diagnostic exposure in neonatal intensive care units

A. del Vecchio^{1,1}, S. Salerno^{1,2}, M. Barbagallo^{3,1}, M. Campoleoni^{1,1}, V. Cannata^{4,1}, G. Chirico^{1,5}, C. Granata^{1,6}, A. Loria^{1,1}, A. Magistrelli^{1,4}; ¹Milan/IT, ²Palermo/IT, ³Catania/IT, ⁴Rome/IT, ⁵Brescia/IT, ⁶Genoa/IT (loria.alessandro@hsr.it)

Purpose: In the recent years, clinical progress and better medical assistance for pregnant women, together with the introduction of sophisticated technologies, have improved the survival of preterm infants. However, this result requires frequent radiological investigations mostly represented by thoracic and abdominal radiographs in incubators. The aim of this document is to help public and private health-care operators in taking choices involving radiation exposures of newborns.

Methods and Materials: The guideline has been written and shared by four scientific societies: AIFM (Italian Association of Physics in Medicine), SIN (Italian Neonatology Society), SIP (Italian Paediatric Society), and SIRM (Italian Medical Radiology Society) to guarantee good standard practices for every professional involved in neonatal intensive care units (NICUs). The report is divided into clinical and physical dosimetric sections as follows: clinical indications (thorax x-ray indications; abdominal x-ray indications); good practice in radiological exposures (devices; exposure parameters and modalities; x-ray field collimation; patient positioning and immobilisation; diagnostic reference levels); radiation protection (patient, operators and environmental protection; shieldings); incubators (commercial incubators and their characteristics; the results of attenuation measurements).

Results: Taking into account the experience and expertise of 10 Italian centres, the guideline set out the criteria to ensure a high standard of neonatal care in NICU about procedures, facilities, recommended equipment, quality assurance, radiation protection measures for children and staff members and communication on radiation risk.

Conclusion: This document will allow a standardisation of the approach to the exposures in NICU.

B-1166 11:19

Magnetic resonance imaging of congenital lung lesions

C. Amaxopoulou¹, J. Geiger¹, P. Grethen¹, R. Gnannt², P. Bode¹, U. Moehrlen¹; ¹Zurich/CH, ²Zollikoberg/CH (camaxopulu@hotmail.com)

Purpose: To evaluate the performance of magnetic resonance imaging (MRI) for assessment of congenital pulmonary malformations.

Methods and Materials: Retrospective review of consecutive lung MRI performed (2013-2017) in 29 children (median age 0.4y, range 2d-15y) for suspected congenital lung anomalies with detection of 31 lesions: congenital pulmonary airway malformation (n=15), sequestration (n=3), hybrid lesion (n=3), hypogenetic lung syndrome (n=3), congenital lobar hyperinflation (n=3), bronchogenic cyst (n=1), and bronchial atresia (n=3). Respiratory-gated fast-spin-echo and dynamic contrast-enhanced images obtained at 1.5 T (free-breathing) were assessed for parenchymal, vascular and perfusion abnormalities. MRI findings were compared to results obtained from computed tomography (CT) and pathology following surgery.

Results: Lung parenchyma was delineated as normal (n=5; 16%), solid (n=8; 26%), cystic (n=13; 42%), hyperinflated (n=6; 19%), or mixed (n=7; 23%). Mucus plugs were seen in 5 cases. Systemic arterial supply was evident in 10 cases, systemic or anomalous venous drainage in 7 cases. All parenchymal lesions showed altered perfusion, either defects (n=22;71%), delayed systemic perfusion (n=8;26%) or both (n=2;7%). Perfusion was helpful for lesion characterization in 18 cases (58%). Parenchymal findings were confirmed by CT in 11/11 cases. The type of congenital lesion was verified by pathological findings in 17/17 cases. No correlation is available in 13 patients managed conservatively and in 2 patients awaiting surgery.

Conclusion: A dedicated MRI lung protocol is able to reliably delineate not only vascular but also parenchymal abnormalities. As characterization of congenital lung lesions has become feasible, lung MRI should be considered as radiation-free alternative to CT for evaluation of these lesions.

B-1167 11:27

The meconium sign in foetal MRI performed for the diagnosis of diaphragmatic hernia

C. Sofia¹, M. Tropea¹, L. Di Grazia¹, P. Spillare¹, N. Boscolo Bariga¹, M. Marino², A. Tregnaghi¹; ¹Venice/IT, ²Messina/IT (car.m.sofia@tiscali.it)

Purpose: To assess the presence of T1 hyperintensity due to meconium in the herniated bowel of fetuses with diaphragmatic hernia. **Background:** Meconium is the material retained in the intestine of foetus from the 13 weeks gestation. It is composed of paramagnetic substances as minerals (Fe, Mn and Mg) and of free fatty acids, carbohydrates and minerals that explain its hyperintense signal on T1 sequences. Meconium slowly migrates from the small bowel to the colon and rectum, increasing in T1 brightness and amount throughout the gestation.

Methods and Materials: 56 foetal MRI examinations were reviewed by two different readers, with different expertise in foetal MRI, in consensus. All the examinations were performed using both T1 and T2 weighted acquisitions. Among the studies 9 diaphragmatic hernias were found. Intestine filled with meconium was considered present in the thorax when a bowel-shaped T1 hyperintensity was seen. The final diagnosis was made by surgical or pathological follow-up. Sensitivity and specificity of the "meconium" sign as diagnostic feature for diaphragmatic hernia were calculated.

Results: 8 fetuses showed the meconium sign. In one case of diaphragmatic hernia no bowel-shaped T1 hyperintensity was seen in the thorax. The sensitivity and specificity of meconium sign alone in the diagnosis of diaphragmatic hernia were 88.89 and 100 %.

Conclusion: Meconium sign can reliably detect diaphragmatic hernia in foetal MRI examinations. However, the evaluation of all the other MRI diagnostic criteria and features is mandatory.

B-1168 11:35

Fetal-MRI based segmentation of the diaphragm in fetuses with congenital diaphragmatic hernia: a retrospective pilot study

F. Prayer, W. Krois, M. Metzelder, G. Kasprian, P. Brugger, G.M. Gruber, M. Weber, D. Prayer, J.M. Patsch; Vienna/AT (florian.prayer@gmail.com)

Purpose: Characterization of congenital diaphragmatic hernia (CDH) type and extent during fetal development may provide an opportunity for personalised therapy planning. This pilot study investigates the feasibility of fetal MRI-based manual diaphragmatic segmentation in fetuses with CDH.

Methods and Materials: Routine fetal MRI data of 22 fetuses with CDH (GW 22-36), who later underwent diaphragmatic repair surgery, were utilised to perform manual segmentation of the diaphragm and diaphragmatic defect using ITK-SNAP. Three-dimensional visualisation and surface area measurements of the normal diaphragm and diaphragmatic defect were obtained. Ratios of diaphragmatic and diaphragmatic defect surface areas, as well as diaphragmatic defect surface area and lung volume were calculated. Three-dimensional visualisations and surface area measurements were used to determine type and size of the diaphragmatic defect, and findings were compared with information extracted from diaphragmatic repair surgery reports regarding diaphragmatic defect location, size, and possible use of a patch.

Results: Diaphragmatic segmentation, subsequent three-dimensional visualisation and diaphragmatic (defect) surface area measurements were feasible in 20 of 22 (90.91%) fetuses with CDH. In two cases diaphragmatic segmentation was not possible due to excessive fetal movement. Findings regarding diaphragmatic defect type and size showed good accordance with information extracted from diaphragmatic repair surgery reports.

Conclusion: Fetal MRI-based diaphragmatic segmentation is feasible in a majority of CDH cases. Three-dimensional visualisation and surface area measurements of the diaphragm and diaphragmatic defect may support therapeutic decision-making and promote a personalised approach in CDH.

B-1169 11:43

Post-mortem magnetic resonance imaging appearances of foeticide in perinatal deaths

S.C. Shelmerdine, M. Hickson, N.J. Sebire, O.J. Arthurs; London/UK (susie_c_s@yahoo.co.uk)

Purpose: Determine the imaging features of foeticide at post-mortem MRI findings to eliminate confusion at post-mortem where mode of death is unknown.

Methods and Materials: A retrospective review over a 5.5-year period was performed comparing two groups of post-mortem foetal cases, cases which underwent termination of pregnancy matched to a group of controls which had undergone spontaneous miscarriage or stillbirth. The groups were matched according to gestational ages, weight and time since death. Two readers blinded to the patient's antenatal history recorded the presence of gas, blood and fluid in different body compartments. Statistical analysis was conducted using a Fisher's exact test.

Results: 26 cases of foeticide (mean age 25wks (range: 20 - 36)) and 75 non-terminated fetuses (mean GA 26.7wks (19 - 36)) were compared. A higher proportion of foeticide cases had pneumothoraces (23.1% vs 1.3%, p = 0.001), haemothoraces (42.3% vs 4%, p = 0.001), pneumopericardium (30.8% vs 5.3%, p = 0.002) and haemopericardium (34.6% vs 0%, p = 0.0001) compared to controls. The presence of intracardiac gas and abdominal findings (ascites, haemoperitoneum and free gas) were higher in the foeticide group but did not reach statistical significance. Pericardial and pleural effusions and soft tissue oedematous changes were not statistically different and are likely to represent post-mortem change.

Conclusion: Characteristic imaging features of foeticide can help the reporting radiologist differentiate iatrogenic from physiological and pathological causes of body fluid and gas disturbance on post-mortem perinatal MRI.

B-1170 11:51

High-resolution isotropic diffusion-weighted imaging in neonatal death investigation

S.C. Shelmerdine, A. McDowell, D. Carmichael, O.J. Arthurs; London/UK (susie_c_s@yahoo.co.uk)

Purpose: To develop/assess a new multi-band diffusion imaging at 3T for perinatal post-mortem MRI (PMMR).

Methods and Materials: We acquired PMMR brain and body imaging in 7 neonates, mean gestational age 33 weeks (range 30-37 weeks) at 3T. Whole-body 3T quantitative DWI imaging scan parameters were TE 53.4ms; TR 5600ms; voxel size 1.8mm isotropic; multi-band factor 2. One unweighted image and four diffusion-weighted images at b=250, 750, 1250 and 1750mm² with gradients applied in 12 uniformly distributed directions, and a reversed phase encoding scan were acquired and corrected for distortion. Image quality was scored by one radiologist blinded to acquisition technique on a visual analogue scale (1 to 5, unacceptable to excellent, respectively) at individual b values and on combined b-score mean diffusivity (MD) map.

Results: There was good image quality for the multiband, multislice DWI PMMR, attributable to increased resolution and signal-to-noise ratio. The average mean quality score increased with increasing b values with score of 2.7 for b=250, 3.6 for b=750, 4.1 for b=1250, 4.7 for b=1750 and 4.9 for combined b-value map. This improved quality allowed separation between average MD and fractional anisotropy signal values in all major body organs at 3T.

Conclusion: Multi-slice multi-band quantitative DWI is feasible for whole-body perinatal post-mortem imaging. Our optimised sequence utilising higher field strength and gradient performance gave improved whole-body isotropic high-resolution imaging compared to the current clinical approach, reducing partial volume effects and allowing detailed future PMMR investigation.

10:30 - 12:00

Room M 3

Molecular Imaging

SS 1406

Contrast agents and molecular imaging

Moderators:

F.A. Gallagher; Cambridge/UK
N.N.

K-23 10:30

Keynote lecture

F.A. Gallagher; Cambridge/UK

B-1171 10:39

Orthotopic lung cancer: molecular imaging-monitored intratumoural radiofrequency heat-enhanced HSV-TK gene therapy

Q. Weng^{1,2}, F. Zhang¹, F. Xiong¹, Y. Jin¹, J. Song², M. Chen², J. Hui², J. Ji², X. Yang¹; ¹Seattle, WA/US, ²Lishui/CN (wengqy99@gmail.com)

Purpose: To validate the feasibility and efficacy of intratumoural radiofrequency hyperthermia (RFH)-enhanced herpes simplex virus thymidine kinase (HSV-TK)/ganciclovir (GCV) gene therapy for non-small cell lung cancer (NSCLC).

Methods and Materials: Animal protocols were approved by the Institutional Animal Care and Use Committee. The study included: (1) in vitro experiments using human NSCLC cells to establish the "proof of principle" of the new RFH-enhanced HSV-TK/GCV gene therapy; (2) in vivo experiments using mouse models with NSCLC to further demonstrate the principle; and (3) in vivo experiments using rat models with orthotopic NSCLC to validate feasibility of the new technique. Cells and animals were divided into four groups (n=6/group): (i) combination therapy (HSV-TK/GCV gene therapy plus RFH); (ii) RFH alone; (iii) HSV-TK/GCV gene therapy; and (iv) PBS. Molecular imaging findings were confirmed by subsequent pathology.

Results: For the in vitro experiments, the confocal microscopy, MTS assay, and bioluminescent imaging demonstrated significantly diminished viable cells and cell proliferation with the combination therapy, compared to the other three treatments (P<0.05). For the in vivo experiments, the optical and/or ultrasound imaging demonstrated significantly decreased relative bioluminescence signals and sizes of tumours, respectively, with the combination therapy, compared to other treatments (P<0.05). These results were confirmed with pathology.

Conclusion: This study demonstrates the feasibility and efficacy of intratumoural RFH-enhanced HSV-TK/GCV gene therapy for NSCLC, as guided and monitored by molecular imaging. This technical development may introduce a new paradigm for effective management of unresectable lung cancer by integrating the advantages of interventional molecular imaging, RF technology, and direct intratumoural gene therapy.

B-1172 10:47

Radiofrequency hyperthermia-enhanced intratumoral herpes simplex virus-thymidine kinase (HSV-TK) gene therapy of ovarian cancer: monitored by ultrasound and optical imaging

Y. Li¹, F. Zhang², S. Zhao², G. Jin³, L. Zhao⁴, Y. Zhou², P. Li², X. Yang²;
¹Guiyang/CN, ²Seattle, WA/US, ³Shanghai/CN, ⁴Wenzhou/CN
 (Liyang1120@163.com)

Purpose: To investigate the feasibility of using imaging-guided RF hyperthermia (RFH) to enhance intratumoural HSV-TK/ganciclovir (GCV) suicide gene therapy of ovarian cancers, monitored by optical and ultrasound imaging.

Methods and Materials: Human ovarian cancer cells (SK-OV-3) labelled with luciferase/lentivirus and rats with luciferase-positive orthotopic ovarian cancers in four groups received different treatments: (i) combination treatment with HSV-TK/GCV-mediated gene therapy plus RFH; (ii) gene therapy; (iii) RFH and (iv) control. MTS assay and confocal microscopy were used to evaluate the cell viability. Bioluminescence optical and ultrasound imaging were used to monitor the changes of tumour size and bioluminescence signal intensities at different time points. The imaging findings were correlated with subsequent pathology confirmation.

Results: MTS assay demonstrated the lowest cell proliferation in the group with combination therapy, compared with three control treatments (41.0% vs 47.8% vs 97.3% vs 100%), as corresponded to the smallest number of survived cells by confocal microscopy and the lowest bioluminescence signal by optical imaging. Ultrasound imaging showed the smallest relative tumour volume with combination therapy, compared with the other three groups (0.23 vs 1.26 vs 5.43 vs 6.74). Bioluminescent optical imaging demonstrated a significantly decreased relative bioluminescence signal in combination therapy, compared with the other three treatments (0.35 vs 1.26 vs 3.43 vs 3.90). Both imaging findings were confirmed by pathology, demonstrated as the significantly increased apoptotic cells in the combination therapy group.

Conclusion: Image-guided intratumoural RFH could enhance HSV-TK/GCV gene therapy of rat ovarian cancers, which provides a new opportunity for effectively managing ovarian cancers.

B-1173 10:55

In vivo tracking of the tropism of mesenchymal stem cells to malignant gliomas using reporter gene-based MR imaging

M. Cao; Guangzhou/CN (caominghui1019@163.com)

Purpose: Mesenchymal stem cells (MSCs) have emerged as a promising cellular vehicle for gene therapy of malignant gliomas due to their property of tumour tropism. However, MSCs may show bidirectional and divergent effects on tumour growth. Therefore, a robust surveillance system with a capacity for noninvasive monitoring of the homing, distribution and fate of stem cells in vivo is highly desired for developing stem cell-based gene therapies for tumours.

Methods and Materials: In this study, we used ferritin gene-based magnetic resonance imaging (MRI) to track the tumour tropism of MSCs in a rat orthotopic xenograft model of glioma. MSCs were transduced with lentiviral vectors expressing ferritin heavy chain (FTH) and enhanced green fluorescent protein (eGFP). Intra-arterial, intravenous and intertumoural injections of these FTH transgenic MSCs (FTH-MSCs) were performed in rats bearing intracranial C6 gliomas.

Results: The FTH-MSCs were detected as hypointense signals on T2- and T2*-weighted images on a 3.0 T clinical MRI. After intra-arterial injection, 17% of FTH-MSCs migrated toward the tumour and gradually diffused throughout the orthotopic glioma. This dynamic process could be tracked in vivo by MRI up to 10 days of follow-up, as confirmed by histology. Moreover, the tumour tropism of MSCs showed no appreciable impact on the progression of the tumour.

Conclusion: These results suggest that FTH gene-based MRI can be used to reliably track the tropism and fate of MSCs after their systemic transplantation in orthotopic gliomas. This in vivo tracking system will facilitate the development of stem cell-based therapies for malignant gliomas.

B-1174 11:03

Tumour microenvironment-responsive intelligent nanocomposites for efficient theranostics of glioma

H. Liu, W. Zhang; Chongqing/CN (303609940@qq.com)

Purpose: To evaluate the applicability of an intelligent nanocomposite for tumour microenvironment (TME)-responsive multi-modality imaging and enhanced photodynamic therapy of glioma in vivo.

Methods and Materials: Bovine serum albumin (BSA)-stabilized manganese dioxide (MnO₂) and gold nanoclusters (AuNCs) hybrid nanocomposites (BSA-MnO₂-AuNCs, BMANCs) were synthesized via a facile and environmentally friendly one-pot biomimetalization approach. The response of BMANCs to acidic hydrogen peroxide (H₂O₂) was evaluated in vitro. The applicability of BMANCs for MRI/NIRF/CT multi-modality imaging was performed in glioma-

bearing nude mice. The efficacy of BMANCs on TME regulation tumour and photodynamic therapy were also investigated.

Results: BMANCs with suitable size, desirable water dispersibility and excellent biocompatibility were prepared. The AuNCs exhibited an intense red fluorescence (Ex/Em=520/720 nm) and a satisfactory CT contrast ability. The high reactivity of MnO₂ towards endogenous H₂O₂ within the acidic TME could release Mn²⁺ ions and realize TME-responsive MR imaging. Owing to the efficient tumour accumulation of BMANCs and generated O₂ in situ resulting from the reaction between MnO₂ and H₂O₂, tumour hypoxia, acidification and tumour angiogenesis were effectively alleviated. Furthermore, the BMANCs exhibited remarkably enhanced photodynamic therapy than that of BSA-AuNCs, due to the improved oxygenation at the tumour site.

Conclusion: The as-prepared BMANCs hold great potential for comprehensive TME regulation and enhanced theranostics against hypoxic solid tumours.

B-1175 11:11

Fluorescence molecular imaging of infection and inflammation utilizing a novel probe specific for myeloperoxidase

B. Pulli, C. Wang, G.R. Wojtkiewicz, J. Chen; Boston, MA/US
 (pulli.benjamin@mgh.harvard.edu)

Purpose: Myeloperoxidase (MPO) is an important oxidative enzyme that is crucial for defence against pathogens, but also contributes to tissue damage in inflammation. We sought to develop a molecular imaging probe sensitive and specific to MPO that is suitable for fluorescence imaging applications.

Methods and Materials: Sixteen female C57BL/6J (wild-type) mice and 6 MPO-knockout mice were either injected subcutaneously with purified MPO, treated topically with PMA to induce irritant contact dermatitis, injected intracerebrally with *Salmonella* to induce brain abscess, or injected subcutaneously with *Streptococcus pneumoniae* to induce bacterial cellulitis. 6 hours after induction, mice were injected with the MPO sensor or a non-specific control analogue. Mice underwent fluorescence reflectance imaging. Brains were cut into sections on a cryotome, and immunohistochemistry for MPO was performed.

Results: A linear increase in signal is observed with increasing concentrations of purified MPO (R²=0.991). In irritant contact dermatitis and bacterial cellulitis, increased fluorescence signal was detected in wild-type mice injected with MPO sensor (P<0.01). In MPO-knockout mice injected with MPO sensor and in wild-type mice injected with control analogue, no signal increase was detectable (P>0.05). In cerebral abscess, MPO activity (MPO sensor) was only observed within the abscess, whereas MPO protein (immunohistochemistry) was detected in adjacent brain areas as well.

Conclusion: The fluorescent MPO sensor can specifically detect MPO activity in vivo at relevant biological concentrations. This was validated in mouse models of infection and inflammation. Importantly, we found that MPO activity does not always colocalize with MPO protein, differentiating between active and latent inflammation.

B-1176 11:19

Integrin-targeted multispectral optoacoustic tomography with MRI correlation for monitoring a BRAF/MEK inhibitor combination therapy in a murine model of human melanoma

P.M. Kazmierczak, N.C. Burton, G. Keinrath, H. Hirner-Eppeneder, M. Schneider, R.S. Eschbach, M.F. Reiser, J. Ricke, C.C. Cyran; Munich/DE
 (Philipp.Kazmierczak@med.uni-muenchen.de)

Purpose: To investigate $\alpha_v\beta_3$ -integrin-targeted multispectral optoacoustic tomography (MSOT) and MRI for monitoring a BRAF/MEK inhibitor combination therapy in a murine model of human melanoma.

Methods and Materials: Human BRAF V600E-positive melanoma xenograft (A375)-bearing Balb/c nude mice (n=10) were imaged before (day 0) and after (day 7) a BRAF/MEK inhibitor combination therapy (encorafenib, 1.3 mg/kg/d; binimetinib, 0.6 mg/kg/d, Array BioPharma Inc.; n=5) or placebo (n=5), respectively. MSOT was performed on a preclinical system (inVision 256-TF, iThera Medical GmbH) unenhanced and 5 h after i. v. injection of an $\alpha_v\beta_3$ -integrin-targeted fluorescent probe (IntegriSense 750, Perkin Elmer; 4 nmol). The $\alpha_v\beta_3$ -integrin-specific tumor signal was derived by spectral unmixing. T2w MRI data sets were acquired on a clinical 3 Tesla scanner (MAGNETOM Skyra, Siemens Healthineers). The imaging results were validated by multiparametric immunohistochemistry (β_3 -integrin expression, CD31-microvascular density, Ki-67-proliferation).

Results: The $\alpha_v\beta_3$ -integrin-specific tumour signal was significantly reduced under therapy showing a unidirectional decline in all animals (from 7.98±2.22 to 1.67±1.30; p=0.043). No significant signal change was observed in the control group (from 6.60±6.51 to 3.69±1.93; p=0.155). Immunohistochemistry revealed a significantly lower integrin expression (β_3 : 0.20±0.02 vs. 0.39±0.05; p=0.008) and microvascular density (CD31; 119±15 vs. 292±49; p=0.008) in the therapy group. Tumour volumes increased with no significant intergroup difference (therapy: +107±42 mm³; control +112±44mm³, p=0.841). In vivo blocking

studies using the $\alpha_v\beta_3$ -integrin antagonist cilengitide (Selleck Chemicals) confirmed the target specificity of the fluorescent probe.

Conclusion: $\alpha_v\beta_3$ -integrin-targeted MSOT allowed for the early non-invasive monitoring of a BRAF/MEK inhibitor combination therapy in a murine model of human melanoma.

Author Disclosures:

P.M. Kazmierczak: Grant Recipient; Förderprogramm für Forschung und Lehre, LMU. **N.C. Burton:** Employee; iThera Medical GmbH. **C.C. Cyran:** Speaker; Speakers bureau Siemens Healthineers.

B-1178 11:27

Molecular MR imaging of myeloperoxidase reveals a new myeloid cell treatment effect of interferon-beta in experimental multiple sclerosis

B. Pulli¹, R. Forghani², C. Wang¹, G.R. Wojtkiewicz¹, J. Chen¹;
¹Boston, MA/US, ²Montreal, QC/CA (pulli.benjamin@mgh.harvard.edu)

Purpose: Treatment effects of interferon-beta (IFN) and glatiramer acetate (GA), two first-line agents used in multiple sclerosis (MS), are similar as evaluated by conventional MRI. We investigated the effects of these two drugs on myeloid cells with MPO-Gd, an activable molecular MR probe specific to the pro-inflammatory enzyme myeloperoxidase (MPO).

Methods and Materials: Fifty female wild-type or MPO knockout mice were induced with EAE, a mouse model of MS, and treated with IFN (1 µg/day), GA (150 µg/day), MPO inhibitor ABAH (0.8 mg/day), or saline. The mice underwent MRI at 4.7T with MPO-Gd at disease peak (day 12). Lesion volume, number, contrast-to-noise ratio (CNR), and total MPO-Gd enhancement were quantified, and mechanistic in vitro experiments were performed.

Results: MPO-Gd CNR (representing MPO activity in vivo) decreased after ABAH and IFN administration, but not with GA. Lesion volume, lesion number, and total MPO-Gd enhancement decreased with all three agents. These findings suggest that IFN may have the imaging signature of a MPO inhibitor. However, direct enzymatic inhibition was only found with ABAH. When isolated myeloid cells were stimulated to secrete MPO, IFN decreased MPO activity, similar to ABAH. Inhibition of superoxide anion production resulted in the restoration of MPO activity from stimulated cells. Spectrophotometry revealed that IFN destroys the iron-containing prosthetic group of MPO and thus inactivates the enzyme.

Conclusion: Molecular imaging profiling revealed a novel myeloid cell-specific treatment effect of IFN, a first-line treatment of MS. IFN irreversibly inactivates MPO via a superoxide-dependent pathway, which improves clinical disease.

B-1179 11:35

Naluf, for spectral CT in the diagnosis of osteosarcoma

Y. Jin, L. Gao, F. Han, Y. Lv, J. Zhang; Shanghai/CN (yingyingjin@yahoo.com)

Purpose: To investigate the potential of spectral computed tomography (CT), used in combination with a Lutecium-based upconversion nanoparticles (UCNPs), for characterization of osteosarcoma and bone.

Methods and Materials: Spectral CT which can enrich conventional CT images with the capability to image and quantify certain elements based on their distinctive K-edge energies was chosen as a powerful tool. Lutecium-based upconversion nanoparticle (UCNPs) had higher spectral CT performance compared with clinically used iohexol. Spectral CT performance was investigated by testing gradient concentration of these contrast agents (CAs) in vitro. Balb/c nude mice were used as model for imaging osteosarcoma in vivo. Cellular uptake of Lutecium-based UCNPs was further evaluated by using confocal microscopy. Toxicity tests were also carried out including cellular toxicity tests, blood routine examinations, hepatorenal function, body weight and some other indexes.

Results: Spectral CT enabled differentiation of Lutecium-based UCNPs, iohexol and bone. Different materials were presented as colorized voxels against the normal grayscale X-ray background, distinguishing the high attenuation of calcium from the osteosarcoma tumor tissues that contained the Lutecium-based CAs. The results of in vivo and in vitro experiments demonstrated that Lutecium-based CAs had higher spectral CT performance and could still be obviously observed at higher KeV (120-140 KeV) images while the signals of iohexol and bone were relatively weak. The toxicity was proven to be low which made it potential for clinical application in the future.

Conclusion: Spectral CT imaging, combined with Lutecium-based CAs, provided a promising opportunity for effectively distinguishing bone and osteosarcoma in vivo.

B-1180 11:43

Ultrasound molecular imaging of breast cancer in mcf-7 orthotopic mice model using a novel dual-targeted ultrasound contrast agent

L. Xu, F. Li, J. Du; Shanghai/CN (ly230502@163.com)

Purpose: To prospectively evaluate ultrasound molecular imaging with dual-targeted gold nanoshelled poly(lactide-co-glycolic acid) nanocapsules carrying p53 and vascular endothelial growth factor receptor type 2 (VEGFR2) antibodies (V&p53-PLGA@Au NCs) in MCF-7 orthotopic mice model.

Methods and Materials: V&p53-PLGA@Au NCs were fabricated with an inner PLGA and outer gold nanoshell spherical structure. Its targeting capabilities were evaluated in targeted cells (HUVEC, MCF-7 cells) and control cells (4T1, MDA-MB-231 cells). Contrast-enhanced ultrasound imaging with V&p53-PLGA@Au NCs was evaluated qualitatively and quantitatively in vitro and in MCF-7 orthotopic mice model by two different systems. The biodistribution of NCs in mouse was preliminarily investigated. Differences were calculated using analysis of variance. Expression of p53 and VEGFR2 in mice tumour tissues were tested with immunofluorescence.

Results: The V&p53-PLGA@Au NCs showed well-defined spherical shape with the average diameter of 276.90±110.50 nm. In cell culture, targeted cells showed higher fluorescence signals and targeting rate than control cells (79.01±5.63% vs 2.11±1.07%, P<0.01; 75.54±6.58% vs 5.21±3.12%, P<0.01). In vivo, contrast-enhanced ultrasound imaging showed significantly higher video intensity when using V&p53-PLGA@Au NCs compared with non-targeted NCs. There were more V&p53-PLGA@Au NCs in tumours in mice than non-targeted NCs (P<0.05).

Conclusion: V&p53-PLGA@Au NCs are demonstrated to be novel dual-targeted ultrasound molecular contrast agents and may have potential applications in early noninvasive visualization of breast cancer.

10:30 - 12:00

Sky High Stage

Head and Neck

MY 14

Head and Neck

Moderators:

S.J. Golding; Oxford/UK
B. Verbist; Leiden/NL

B-1181 10:30

Evaluation of the differentiation in head and neck squamous cell carcinoma with PET/MR

H. Dang, Y. Chen, Z. Jin, H. Xue, B. Hou, F. Li; Beijing/CN (shengdai23@126.com)

Purpose: To preoperatively evaluate the performance of discrimination with integrated positron emission tomography/magnetic resonance imaging (PET/MR) in the tumour differentiation of head and neck squamous cell carcinoma(HNSCC).

Methods and Materials: 18F-FDG PET imaging was performed with ToF method. MR imaging included the anatomic and functional sequences of T1-weighted and T2-weighted imaging, diffusion-weighted imaging and dynamic contrast enhanced imaging. The values of standardise uptake value(SUV_{mean}) which was measured based on 42% contour lines, apparent diffusion coefficients(ADC_{mean}), and the volume transfer coefficient (K^{trans}) were used as the qualitative analysis measurements. Pearson correlation coefficients were calculated between each pair of the three parameters. One-way ANOVA was used to evaluate the discrimination of each parameter among different differentiation groups. The PET/MR multi parameters were combined with Logistic Regression. ROC was used to evaluate the diagnostic efficiency of tumour differentiation with individual parameters and the combination of PET/MR.

Results: Finally, a total of 23 subjects included in this study. The correlations between each of the three individual parameters are weak. The statistic differences are significant in different degrees of tumour differentiation for all three individual parameters, and the value of ADC_{mean} is the best one. The accuracy of SUV_{mean}, ADC_{mean} and K^{trans} are 74.3%, 77.1%, 57.1%. The combination of PET/MR demonstrated an improved diagnostic efficiency with an accuracy of 85.7%.

Conclusion: This preliminary integrated PET/MR study demonstrated that compared with the individual parameters of PET/MR, the combination of PET/MR can improve the diagnostic efficiency of tumour differentiation in HNSCC.

B-1182 10:34

Is it benign or malignant? Assessing isolated lymphadenopathy of the head and neck using textural analysis

S. Chin, A. Kamalasanan, S. Henderson, T.A. Sudarshan; Dundee/UK (sookcheng@doctors.org.uk)

Purpose: Isolated lymphadenopathy can be the only initial presentation of squamous cell cancer (SCC) of the head and neck. Accurate identification of benign lymphadenopathy from malignant nodal disease and lymphoma is difficult. Due to this, patients are subjected to invasive nodal biopsies, majority of which will be benign disease and a small proportion will be non-diagnostic. We aim to analyse if the use of textural analysis can help identify malignant disease and aid differentiation between lymphoma and metastatic disease.

Methods and Materials: Twenty patients each with normal lymph nodes, histology-proven lymphoma and SCC with nodal involvement were retrospectively selected. Lymph node textural analysis on computed tomography (CT) images was analysed using MaZda software (Technical University of Lodz, Poland). Statistical differences were assessed using the Mann-Whitney U test.

Results: From the eleven textural features analysed, there were significant differences in entropy, contrast, correlation, difference entropy and inverse difference moment between metastatic nodes, lymphoma nodes and normal nodes (all $p < 0.001$). Entropy has been shown to be a good differentiator between pathology; entropy of normal nodes was 1.448, metastatic nodes 2.163 and lymphoma nodes 0.143.

Conclusion: Significant differences in the various textural features between lymphoma, metastatic and normal lymph nodes exist. This suggests an avenue for the use of lymph node textural analysis to aid diagnosis and reduce the number of benign nodal biopsies.

B-1183 10:38

Head and neck cancer heterogeneity assessed by CT texture analysis: can it predict the human papilloma virus status?

F. Mungai, M. Pietragalla, L. Bonasera, M. Bartolucci, V. Berti, V. Miele; Florence/IT (f.mungai@gmail.com)

Purpose: Human papillomavirus-positive (HPV+) head and neck (HN) squamous cell carcinoma represents a different molecular, clinical and prognostic entity from HPV-negative (HPV-) disease. The purpose of this study was to determine if analysis of texture features of primary lesion on contrast-enhanced CT (CECT) images can be useful in predicting the HPV status.

Methods and Materials: Pre-treatment CECT images of 50 patients with primary HN carcinoma and known HPV status were retrospectively reviewed. The primary tumour was delineated within a manually drawn volume of interest (VOI). Six first-order and 34 higher order textural features were extracted from each VOI; the latter parameters were derived from analysis of: grey-level co-occurrence matrix (GLCM), neighbourhood grey-level different matrix (NGLDM), grey-level run length matrix (GLRLM) and grey-level zone length matrix (GLZLM). T test was used to evaluate differences in textural features between HPV+ and HPV- lesions. Logistic regression was performed to ascertain the effects of different textural features on the likelihood that a lesion is related or not to HPV.

Results: Of the 50 examined lesions, there were 30 HPV+ and 20 HPV-. Statistically significant ($p < 0.05$) differences were seen in, respectively, 5 GLRLM, 2 NGLDM and 4 GLZLM extracted parameters. The logistic regression model was statistically significant for these parameters and correctly classified lesions with accuracies of 77-95%.

Conclusion: HPV+ HN cancers have different textural characteristics than HPV- lesions and are correlated with higher textural coarseness. CT texture analysis of the primary HN carcinoma may be used as a tool for predicting the HPV status.

B-1184 10:42

Estimation of the irradiation dose of children exposed to CBCT for various dental pathologies

M. Marcu, M. Hedesiu; Cluj-Napoca/RO (marcumaria88@gmail.com)

Purpose: The aim was to estimate the effective, cumulative and organ doses in children exposed to CBCT.

Methods and Materials: A prospective study was conducted in 561 children aged between 0 and 18 years exposed to CBCT in two European centres, over two years. The radiation doses were estimated for the following dental pathologies: orofacial cleft, impacted teeth, bone pathology, dental anomalies, dentoalveolar trauma, orthognathic surgery, and endodontics. The effective and organ doses were calculated by Monte Carlo simulation in paediatric voxel phantoms. The doses obtained were extrapolated and normalized to age and for the CBCT exposure protocol.

Results: The median of the effective dose was 137.9 μ Sv and median of cumulative dose was 231.4 μ Sv. Children with dental anomalies had statistically significant higher radiation doses compared to other pathologies ($p < 0.05$). The effective dose was influenced by the field of view (FOV) and age at exposure. The highest doses were found for salivary glands (Q3 was 4.5 mGy) followed by brain (2.4 mGy), thyroid (1.0 mGy) and bone marrow (0.2 mGy). Organ doses were significantly influenced by dental pathology with a lower exposure for brain, thyroid and bone marrow (RBM) in clinical cases that used a small FOV (impacted teeth, endodontic evaluation) compared to cases that required a large FOV (dental anomalies, orofacial cleft and orthognathic surgery). The radiation exposure of salivary glands does not vary with dental pathology.

Conclusion: The results revealed the influence of dental pathology, FOV dimension and age on CBCT doses of children.

B-1185 10:46

Disrupted brain functional network architecture in long-term sensorineural hearing loss patients

X.-M. Xu, G. Teng; Nanjing/CN (xmxu15@163.com)

Purpose: Resting-state functional magnetic resonance imaging (fMRI) studies have demonstrated the disruptions of multiple brain networks in sensorineural hearing loss (SHL) patients. Nonetheless, several studies found no differences in network processing between HL patients and healthy controls (HCs). Its neural bases are poorly understood. To identify aberrant brain network architecture involved in long-term hearing loss, we compared the resting-state fMRI (rs-fMRI) patterns of SHL patients and HCs.

Methods and Materials: Long-term SHL patients ($n = 22$) with abnormal hearing abilities and age-, sex-, education-matched HCs ($n = 21$) participated in the current study and underwent the rs-fMRI scanning. We used degree centrality (DC) to investigate functional connectivity (FC) strength of the whole-brain network and functional connectivity analysis to explore aspects involved in sensorineural HL.

Results: Compared to HCs, we found significantly increased network centrality in left angular gyrus and left precuneus (GFR corrected, $P < 0.025$ for voxel level; $P < 0.05$ for cluster level). What's more, the left angular gyrus revealed increased connectivity to the right parietal lobe while the precuneus exhibited enhanced connectivity to the right angular gyrus (GFR corrected, $P < 0.025/2$).

Conclusion: Rs-fMRI provides a new and novel method for identifying aberrant brain network architecture. Long-term HL patients have disrupted FC in visual and non-auditory areas. The current findings will provide a new perspective for understanding the neuropathophysiological mechanisms and neural plasticity in long-term SHL.

B-1186 10:50

Elastography shear wave contribution when evaluating thyroid follicular nodules comparing to histological findings

P.H.D. Moraes, M. Chammas, M. Schelini; São Paulo/BR (pedrohenrique.mmoraes@gmail.com)

Purpose: Follicular lesion is found in about 10-30% of all FNAB of thyroid nodules. 20% have a diagnosis of follicular carcinoma in the final histological analysis, although 80% of them are benign. Motivated by unnecessary surgeries performed, we studied with shear-wave elastography (SWE) to distinguish benign from malignant nodules (BETHESDA III and IV) before the histological analysis.

Methods and Materials: We included nodules with Bethesda III or IV on cytological analysis. The equipment used was Logic E9, GE, with SWE elastography. We classified follicular nodules according to strain pattern (1-5) - 1: high deformity, lower risk for malignancy and 5: low strain, high risk for malignancy. SWE deformation indexes (SWE index) were defined by two ROIs: one including most of the nodule and the other at pre-thyroid muscles. The arithmetic average of three different SWE indexes of each nodule was calculated. A deformation ratio (RDM) was calculated by dividing the SWE index of the pre-thyroid musculature (sternocleidomastoid) by the SWE index of the nodule, both using Kpa. All patients were submitted to surgical removal, with histological analysis.

Results: 16 patients were studied. 11/16 had histological diagnosis of carcinoma. 7/11 had an elastogram pattern > 2 . Statistical analysis, however, failed to show a significant association between carcinoma diagnosis and the elastogram pattern ($p = 0.611$). $RDM > 1.32$ suggest an increased risk for the diagnosis of carcinoma (sensitivity 81.8% and specificity 80%) ($p = 0.015$).

Conclusion: $RDM > 1.32$ is related to increased risk for the histological diagnosis of carcinoma in nodules with follicular pattern at cytology (BETHESDA III and IV).

B-1187 10:54

Metrics and textural features of MRI diffusion to improve classification of common parotid gland tumours

Z. Zhang, J. Cheng; Zhengzhou/CN (yinierzhang@sina.com)

Purpose: This study aimed to improve the identification ability of benign and malignant parotid gland tumours using support vector machine classifiers on quantitative MR imaging features.

Methods and Materials: 52 patients with parotid gland tumours (28 pleomorphic adenoma, 16 mucoepidermoid carcinoma, and 8 Warthin tumour) were included in this retrospective study without previous biopsy or surgery. Shape, histogram, and textural features were computed from T2WI and contrast-enhanced T1WI and the apparent diffusion coefficient (ADC) map. Combinations of features were used to train tumour-type-specific classifiers for pleomorphic adenoma, Warthin tumour, and mucoepidermoid carcinoma types in separation and as a joint classifier. The performance of different classifiers was assessed and compared using randomly selected subsets of training and test data.

Results: ADC histogram features (50th and 90th percentiles and skewness) yielded the best classification of tumour type (on average >92.3% of pleomorphic adenoma, >96.1% of Warthin tumour, and >84.7% of mucoepidermoid carcinoma). The resulting joint classifier correctly assigned >90.3% of the parotid gland tumours.

Conclusion: Support vector machine-based classifiers using ADC histogram features yielded very good discrimination among common parotid gland tumour types, and ADC textural features show promise for further subtype discrimination.

B-1188 10:58

The diagnostic value of combination of US < MRI preoperative prediction for the extrathyroidal extension of papillary thyroid carcinoma
S. Hu, Zhenjiang/CN (hsd2001054@163.com)

Purpose: The purpose of the present study was to evaluate the diagnostic performance of preoperative ultrasonography (US), magnetic resonance imaging (MRI) and US combined with MRI for the prediction of extrathyroidal extension (ETE) in patients with papillary thyroid carcinoma (PTC).

Methods and Materials: Between January 2013 and December 2016, 83 consecutive patients underwent surgery for pathologically confirmed PTCs with ETE. We analysed all patients with PTC with ETE preoperative combination of US and MRI scan to evaluate ETE.

Results: For T3 (minimal ETE), the accuracy was 92.2% (47/51) for US, 74.5% (38/51) for MRI, and their combination was 98.0% (50/51). The difference in the three methods for T3 was statistically significant (P=0.000). For T4 (extensive ETE), the accuracy was 62.5% (20/32) for US, 87.5% (28/32) for MRI, and their combination was 93.8% (30/32). The difference in the three methods for T4 was statistically significant (P=0.000). For the total accuracy of ETE, US was 80.7% (67/83), MRI was 79.5% (66/83), and their combination was 96.4% (80/83). The difference of the three methods for ETE was statistically significant (P=0.001).

Conclusion: The combination of US and MRI can improve the accuracy of ETE for PTC.

B-1189 11:02

Use of the previously proposed (2013) ultrasound total malignancy score (TMS) in the management of thyroid nodules
S. Zannoni¹, G. Pompili¹, S. Tresoldi¹, G. Di Leo¹, A. Ravelli¹, A. Primolevo², G. Spadarella¹, G. Carrafiello¹, ¹Milan/IT, ²Altamura/IT (stefaniazannoni@hotmail.com)

Purpose: To validate the role of the Total Malignancy Score (TMS) previously proposed (Pompili et al.2013) in identifying thyroid nodules suspicious for malignancy by means of the sum of their ultrasound features.

Methods and Materials: The local ethical committee approved this prospective observational study. We examined 231 nodules in 231 consecutive patients (164 females; age range 20-87 years; median age 59 years; IQR 48-70 years) who underwent ultrasound followed by fine needle aspiration cytology (FNAC). Nodules had been further classified using the TMS considering ultrasound features (number, echogenicity, structure, halo, margins, Doppler-signal, calcifications, growth) and the Bethesda System for Reporting Thyroid Cytopathology (TBSRTC) considering cytological features. Patients with nodules considered non-negative (categories III-VI TBSRTC) underwent histological analysis, repeated FNAC or 2 years strict ultrasound follow-up. Association between final diagnosis, each of the ultrasound features and TMS was estimated using the Chi-square test, the Mann Whitney U test and a multivariate logistic regression. A ROC curve was obtained for TMS diagnostic accuracy.

Results: At ultrasound 47%(108/231) of the nodules had TMS<3, 18%(42/231) TMS=3 and 35%(81/231) TMS>3. At FNAC 85%(196/231) of the nodules resulted benign and 15%(35/231) non-negative. Hypoechoogenicity, solid structure, presence of microcalcifications and nodule's number resulted independent predictors of the final diagnosis and TMS diagnostic accuracy was good (area under the ROC curve: 0.82).

Conclusion: The TMS system is simple to use, reliable, easy reproducible and strongly relates to malignancy risk. According to our results, FNAC could be limited to nodules with TMS >=3, without missing any carcinoma.

B-1190 11:06

A multivariate analysis combining DCE and IVIM derived parameters to improve parotid tumours differential diagnosis
F. Patella¹, G. Franceschelli¹, M. Petrillo², M. Sansone², R. Fusco², G. Carrafiello¹, ¹Milan/IT, ²Naples/IT (battellina@gmail.com)

Purpose: To evaluate the diagnostic value of a MRI protocol combining dynamic contrast-enhanced(DCE-MRI) and diffusion-weighted imaging (DW-MRI) in patients with parotid tumours.

Methods and Materials: 14 histopathological proven parotid tumours(7 Warthin tumours,WT, and 7 Pleomorphic Adenomas, PA) in 11 patients were included. For both DCE-MRI and DW-MRI model free and model based

parameters were computed pixel by pixel on manually segmented regions of interest(ROIs) drawn on entire lesion's volume. Extracted parameters were: Ktrans, kep, vp, MRE, TTP, WIS, WOS, f, D, D*. For each parameter median and standard deviation values on segmented ROIs were calculated for each lesion with a Matlab environment. Statistical evaluations included univariate and multivariate analysis using conventional linear analysis and advanced techniques to separate PA by WT. Furthermore, for the 153 possible couples of parameters specificity, sensibility, PPV and NPV were computed.

Results: No single variable could differentiate WT by PA. Only 4 couples presented AUC = 1: 1) Ktrans(std) and f(std); 2) Ktrans(std) and D(std); 3) Kep(std) and D(std); 4) MRE(av) and TTP(av). The linear combination of these coupled variables provided 4 new parameters: $Y1 = 46.0 * Ktrans(std) + 34.7 * f(std)$; $Y2 = 34.8 * Ktrans(std) + 8368 * D(std)$; $Y3 = 0.525 * kep(std) + 7223 * D(std)$; $Y4 = 0.0361 * MRE(av) + 1.5 * TTP(av)$ -Optimal cut-off resulted 7.2973; 6.8202; 1.0210; 6.0205 respectively. In all cases sensitivity, specificity, PPV e NPV were 100% (misclassification error rate = 0%).

Conclusion: New coupled variables provided by a linear combination of DCE-MRI and IVIM derived parameters potentially could help in differential diagnosis between WT and PA.

B-1191 11:10

Does RFA induce neoplastic change of benign thyroid nodules
S. Ha, J. Shin, J. Baek, D. Song, S. Chung, Y. Choi, J. Lee; Seoul/KR (su3ha5@hanmail.net)

Purpose: With increase in detection of thyroid nodules, radiofrequency ablation (RFA) has been investigated for the treatment of symptomatic thyroid nodules, and has been shown to represent acceptable alternative to surgery. Currently, there has been no data whether RFA promote neoplastic transformation of undertreated peripheral portion of the benign nodules through biopsy. The aim of our study was to evaluate during 5-year follow-up, whether RFA treated benign thyroid nodules is associated with malignancy through biopsy, along with clinical efficacy and cytomorphological alteration after treatment.

Methods and Materials: The data were retrospectively collected between April 2008 and June 2013 and core needle biopsy (CNB) was performed on 16 benign thyroid nodules who were treated using RFA. Parameters were compared between the time of each patient's enrollment and the last follow-up examination using a linear mixed model statistical analysis. The slides were reviewed again by two pathologists.

Results: No atypical cells or neoplastic transformation were detected in undertreated peripheral portion of treated benign nodules on CNB specimen. RFA neither altered thyroid capsule nor changed the thyroid tissue adjacent to the treated area. In the histopathological examinations, we observed 82.3% acellular hyalinization, which was the most common finding. After mean follow-up period of more than 5 years, mean volume had decreased to 6.4±4.2 ml, with volume reduction rate of 81.3%±5.8% (p<0.0001).

Conclusion: RFA is effective for treatment of benign nodules without carcinogenic effect or tissue damage in the normal thyroid tissue adjacent to the RFA treated zone.

B-1192 11:14

Prognostic significance of PET-based radiomic image features in locally advanced laryngeal and hypo-pharyngeal squamous cell carcinoma
H.L. Nelstrop, R. Prestwich, M. Barnfield, G.M. McDermott, A. Scarsbrook; Leeds/UK (hannah.nelstrop@nhs.net)

Purpose: To determine whether radiomic features derived from 18F-FDG positron emission tomography (PET) are prognostic predictors in patients with locally advanced laryngeal and hypo-pharyngeal squamous cell carcinoma (SCC) and explore the relationship between radiomic features and tumour volume.

Methods and Materials: Retrospective analysis of 43 consecutive patients with laryngeal and hypo-pharyngeal squamous cell carcinoma (SCC) treated at a single institution was performed. Tumours were segmented using specialised software: RTx Advanced (Mirada Medical) and Advantage workstation (GE Healthcare). Radiomic analysis was performed on tumour and background volumes using Chang-Gung Image Texture Analysis toolbox (CGITA). Entropy derived from the grey-level histogram (Entropy_{hist}), entropy and dissimilarity derived from the grey-level co-occurrence matrix and zone percentage derived from the grey-level size zone matrix were assessed. Univariate Cox regression was performed on the results with respect to disease-specific survival (DSS) and progression-free survival (PFS) with significance taken as P<0.05. Spearman's rank correlation was used to assess the correlation between parameters.

Results: None of the radiomic features were prognostic predictors of DSS or PFS following correction for multi-hypothesis testing; however, all texture features were significantly correlated with tumour volume (p<0.002). This correlation reduced for Entropy_{hist} and zone percentage when only the larger tumours (10-15cm³) were included in the analysis.

Conclusion: Patients with laryngeal/hypopharyngeal tumour sizes greater than 10-15cm³ are more suited for radiomic analysis due to the reduced correlation between texture features and tumour size.

B-1193 11:18

Lateralisation effects on functional connectivity of the auditory network in patients with unilateral pulsatile tinnitus as detected by functional MRI
H. Ly, P. Zhao, Z. Liu, X. Liu, H. Ding, S. Gong, Z. Wang; *Beijing/CN*
(chrishvan@126.com)

Purpose: Unilateral pulsatile tinnitus (PT) was proved to be a kind of disease with brain functional abnormalities within and beyond the auditory network (AN). However, changes in patterns of the lateralisation effects of PT are yet to be established.

Methods and Materials: We recruited 23 left-sided, 23 right-sided PT (LSPT, RSPT) patients and 23 normal controls (NC). We combined applied independent component analysis and seed-based functional connectivity (FC) analysis to investigate alteration feature of the FC of the AN using resting-state functional magnetic resonance imaging (rs-fMRI).

Results: Compared with NC, LSPT patients demonstrated disconnected FC within the AN in both sides. Disrupted network integrity between AN and executive control network, self-perceptual network and limbic network was also demonstrated bilaterally. In contrast, RSPT demonstrated decreased FC within the AN on the left side, but significant increased FC within the AN in the right side (symptomatic side). Enhanced FC between AN and executive control network, self-perceptual network and limbic network was also found mainly on the right side. Positive FC between the auditory network and the limbic network may be a reason to explain why RSPT patients are willing to be in clinic.

Conclusion: LSPT exhibits disrupted network integrity in brain functional networks. But RSPT are featured by enhanced FC within AN and between networks, especially on the right (symptomatic) side. Corroboration of featured FC helps to reveal the pathophysiological changing process of the brain in patients with PT, providing imaging-based biomarker to distinguish PT from other kind of tinnitus.

B-1194 11:22

Shear wave elastography in the evaluation of level VI lymph nodes in papillary thyroid carcinoma
W. Chang, M. Chen; *Shanghai/CN* (cwy_jiayou@126.com)

Purpose: This study aimed at exploring the value of shear wave elastography (SWE) in ultrasound evaluation for level VI lymph nodes in papillary thyroid carcinoma (PTC).

Methods and Materials: 87 level VI lymph nodes from 22 consecutive patients with PTC were evaluated by grey-scale ultrasound and SWE in condition of ex vivo before rapid frozen section. Grey-scale ultrasound and SWE indexes of metastatic and non-metastatic lymph nodes were evaluated by statistical analysis separately in all patients and in patients without Hashimoto's thyroiditis (HT). Indexes included transverse diameter, longitudinal diameter, longitudinal-to-transverse diameter ratio (L/T ratio), E_{mean} , E_{min} , E_{max} and E_{SD} . The rapid frozen section result of each lymph node was used as gold standard to evaluate the diagnostic performance of grey-scale ultrasound and combination method which combined grey-scale ultrasound and SWE.

Results: In all patients, significant indexes included longitudinal diameter ($p=0.009$), L/T ratio ($p=0.003$), E_{max} ($p=0.016$) and E_{SD} ($p=0.006$). In patients without HT, significant indexes included longitudinal diameter ($p=0.002$), L/T ratio ($p=0.003$), E_{mean} ($p=0.030$), E_{max} ($p<0.001$) and E_{SD} ($p=0.001$). Combining grey-scale ultrasound with SWE, combination method had higher AUC than grey-scale ultrasound both in all patients (0.887 vs 0.841) and patients without HT (0.925 vs 0.866). Grey-scale ultrasound had higher AUC in patients without HT than in all patients (0.866 vs 0.841), which was the same with combination method (0.925 vs 0.887).

Conclusion: Shear wave elastography can provide additional information for ultrasound evaluation of level VI lymph nodes in papillary thyroid carcinoma, especially in papillary thyroid carcinoma without Hashimoto's thyroiditis.

B-1195 11:26

Diagnostic value of dual-energy CT imaging for cervical lymph node metastasis in patients with papillary thyroid cancer
M. He; *Fuzhou/CN* ([hemuzhen@sina.com](mailto:hemizhen@sina.com))

Purpose: To quantitatively assess the diagnostic value of dual-energy computed tomography(CT) imaging for cervical lymph nodes metastasis in patients with papillary thyroid cancer.

Methods and Materials: Fifty-five consecutive patients with suspected of thyroid cancer were prospectively enrolled and underwent enhanced dual-energy spectral CT scan. The normalised iodine concentration (NIC) and the slope of the spectral Hounsfield unit curve (λ_{HU}) during both arterial and venous phases were measured, respectively, from iodine overlay images and spectral curves. Two-sample t test was performed to compare quantitative parameters at dual-energy CT between the histopathologically proven benign and

metastatic lymph nodes. Receiver operating characteristic curves were generated for sensitivity and specificity analyses as well as evaluating the diagnostic value of dual-energy CT imaging and conventional CT features.

Results: Using the conventional CT features for detection of metastatic lymph nodes, sensitivity, specificity and accuracy were 4%-79.0%, 63.6%-100% and 43.9%-72.6%, respectively. Both arterial and venous phase NIC and λ_{HU} were significantly higher in metastatic than in benign lymph nodes (all $p<0.001$). The best quantitative parameter for detection of lymph nodes metastasis was arterial phase NIC with optimal threshold value of 25.8%, sensitivity, specificity were 90.3% and 96.6%. The area under curve (AUC) of arterial phase NIC and λ_{HU} was significantly higher than those of venous phases (all $P<0.001$).

Conclusion: Compared with qualitative conventional CT features, quantitative parameters associated with NIC and λ_{HU} at dual-energy CT showed higher accuracy and better diagnostic performance for cervical lymph node metastasis in patients with papillary thyroid cancer.

B-1196 11:30

Multiphasic CT vs dynamic contrast-enhanced MRI in the characterisation of parotid gland tumours

N. Charwat Mohammed El-Sayed; *Mansoura/EG* (nehaltharwat83@gmail.com)

Purpose: Salivary gland tumours are challenging with regard to preoperative diagnosis. The aim of our study was to highlight the value of multiphasic CT and contrast-enhanced dynamic MRI in characterisation of benign and malignant parotid tumours as well as to compare the diagnostic accuracy of both modalities.

Methods and Materials: The study group included 45 patients (54 lesions), 26 males and 19 females, and their age ranged from 24 to 78 years. All patients underwent both CT and MRI examinations. The time intensity (or attenuation) curve for each lesion was analysed and compared with the final post-operative pathology.

Results: The type of the curve on dynamic contrast-enhanced MRI had high sensitivity, specificity, positive predictive and negative predictive values, and accuracy in characterisation of benign and malignant parotid tumours (94.4%, 97.2%, 94.4%, 97.2%, and 96.3%, respectively). Also, curve analysis on multiphasic CT revealed similar high sensitivity, specificity, positive predictive and negative predictive values, and accuracy as compared to DCE-MRI (92.6%, 96.3%, 92.6%, 96.3%, and 95.1%, respectively).

Conclusion: Both dynamic contrast-enhanced MRI and multiphasic CT have comparable high accuracy in characterising the different histological types of parotid gland tumours.

B-1197 11:34

An innovative 3D-3D superimposition for assessing anatomical uniqueness of frontal sinuses (FS) through segmentation on CT scans

M. Cellina, D. Gibelli, C. Sforza, G. Oliva; *Milan/IT* (m.cellina@yahoo.it)

Purpose: Uniqueness in shape and size is the most relevant anatomical characteristic of FS and finds a prominent application in personal identification of skeletons and human remains. This study aims at assessing anatomical uniqueness of FS through 3D registration and automatic calculation of point-to-point distances between 2 models.

Methods and Materials: We selected 30 subjects who underwent 2 maxilla CT scans (interval time: 1-5 months; acquisition parameters: kV: 120, mAs: 320, collimation: 40 × 0.6 mm, tube rotation: 1 s; reconstruction thickness: 3 mm; reconstruction filter: H60 sharp). FS were automatically segmented through ITK-SNAP software; the 3D models belonging to the same patient were automatically superimposed according to the least point-to-point difference between the 2 surfaces. Then, we executed the same procedure on 200 randomly selected maxilla CT of other patients to perform 100 superimpositions of FS belonging to different individuals (mismatches). Average root mean square (RMS) point-to-point distances observed in the group of matches and mismatches were assessed through Student's t test. Logistic regression was calculated to provide a diagnostic tool for the recognition of FS.

Results: In the group of matches, RMS value was on average 0.35 mm (SD: 0.25), and 2.90 mm (SD: 1.63) in the group of mismatches, with a statistically significant difference ($p<0.0001$). A logistic formula was developed according to the RMS values from matches and mismatches and was applied to a novel set of 100 superimpositions, with an accuracy of 100%.

Conclusion: This approach to the assessment of anatomical uniqueness provides reliable morphological and quantitative evaluation.

B-1198 11:38

Diagnostic efficacy of dynamic manoeuvres in computed tomographic evaluation of oral cavity lesions

R.V. Mathilakath; *Davangere Karnataka/IN* (rajesh.venunath@gmail.com)

Purpose: To evaluate the diagnostic efficacy of dynamic manoeuvres in CT for better delineation of oral cavity lesions as compared to conventional scans to assess the origin and extent of oral cavity lesions.

Interventional Radiology

SS 1509

Liver, lung and thyroid ablation

Moderators:

F. Colletini; Berlin/DE

K.A. Hausegger; Klagenfurt/AT

B-1201 14:00

Microwave ablation (MWA) in the treatment of colorectal liver metastases (CRLM): an eight-year follow-up study

T.J. Vogl, M. Zitsch, W. Bechstein, J. Trojan; Frankfurt a. Main/DE
(t.vogl@em.uni-frankfurt.de)

Purpose: To evaluate survival time and the progression-free survival of patients with colorectal liver metastases (CRLM) in curative and palliative intention depending on different parameters.

Methods and Materials: In this retrospective study, 132 patients (59 women, 73 men; mean 61.86; range 35-88) were treated with microwave ablation (MWA) for CRLM between 2010 and 2017. A total of 257 lesions were investigated regarding location of the metastases, technical success, used power, diameter, volume and ablation zone volume. Pre-treatment and follow-up were also documented. Moreover, patients were divided into two different groups based on the indication of the treatment (palliative or curative).

Results: The mean diameter and volume of the intrahepatic metastases were 18.6 mm±10.1 mm and 4.54 cm³±3.4 cm³. MWA was performed with an average power of 45 kJ. The follow-up MR images showed a mean post-ablation volume of 38.0 cm³. Three patients had a local recurrence (3/132; 2.2%) and 13 patients had new intrahepatic metastases (13/132; 9.8%). The average survival was 520 days (1.42 years). In the curative group, mean survival was 637 days (1.74 years) and in the palliative group 250 days (0.68 years), respectively. All MWAs were without any serious complications. Mild side effects were local haematoma and pain symptoms.

Conclusion: MWA for treatment of CRLM is an effective therapeutic treatment procedure with excellent local control rates and improved survival in the curative group.

B-1202 14:00

Comparison between microwave and radiofrequency ablation in local control of colorectal liver metastases

E. Raimondi^{1,2}, K.N. De Paepe², D.-M. Koh², J. McCall², N. Fotiadis²;
¹Ferrara/IT, ²London/UK (edoardo.raimondi@unife.it)

Purpose: To retrospectively analyse the safety and efficacy of radiofrequency ablation (RFA) and microwave ablations (MWA) in the treatment of colorectal cancer liver metastases (CRC-LM).

Methods and Materials: 193 patients with unresectable CRC-LM treated with RFA or MWA in a single centre between March 2006 and December 2016 were retrospectively evaluated. Medical records and imaging studies were reviewed for demographic data, technical deployment, associated complications, tumour recurrence and overall survival. Rate of tumour recurrence, complication rates and patient survival were compared between RFA and MWA treatments.

Results: 456 procedures were performed in 193 patients (123 male, 70 female) with a median age of 66 years (range 32-91 years). Of these, 343/456 (75.2%) were RFA and 113/456 (24.8%) were MWA. The median number of procedures per patient was 2 (range 1-10). Median lesion size was 17mm (range 3-80mm). The local tumour recurrence rate was 45% for RFA and 28% for MWA, with a hazard ratio of 0.6 in favour of MWA (95%CI 0.4-0.9). Two and five year overall survival for RFA vs MWA were 88% vs 89% (p>0.05) and 35% vs 66% (p<0.05) respectively. Complications were reported in 43/456 procedures (9.4%); in 28/343 (8.1%) of RFA and 15/113 (13.3%) of MWA. One patient died due to multi-organ failure post RFA.

Conclusion: MWA achieved better local tumour control compared with RFA in the treatment of CRC-LM, with a slightly higher complication rate.

B-1203 14:16

Risk factor-based prediction algorithm for liver function damage in patients with hepatocellular carcinoma after microwave ablation

Y. Zhou, X. Jing, J. Ding; Tianjin/CN (dr.jingxiang@aliyun.com)

Purpose: To investigate the influence of liver function damage in patients with hepatocellular carcinoma (HCC) after microwave ablation (MWA) on prognosis and establish a risk factor-based algorithm to predict liver function damage.

Methods and Materials: A total of 745 patients with HCC undergoing MWA were enrolled in this study and were classified into modelling and validation group. The progression-free survival (PFS) and overall survival (OS) were

Methods and Materials: 52 patients with histologically proven diagnosis of various oral cavity lesions referred for CT evaluation were included in this hospital-based prospective cross-sectional study conducted over a period of two years from December 2013 to November 2015. The consented subjects were subjected to a preliminary conventional plain and contrast study followed by puffed cheek CT scans as described by Weissman and Carrau. The images were compared simultaneously by an experienced radiologist for evaluation of origin and extent of the lesion.

Results: Puffed cheek manoeuvre was highly useful in 71.2% of cases and was not much helpful in 28.8% in evaluation of oral lesions. Puffed cheek CT has a sensitivity of 69% and a specificity of 43% in accurately staging oral malignancies. Puffed cheek CT had a positive predictive value of 36% and a negative predictive value of 81% and an accuracy rate of 51% compared to conventional CT in staging oral malignancies.

Conclusion: Puffed cheek CT scans provide a clearer and more detailed evaluation of mucosal surfaces of the oral cavity than do conventional (non-puffed) images. In selected patients, like those with lesions of retromolar trigone, the puffed cheek technique may serve as a worthy supplement to conventional CT in the evaluation of bony invasion and proper delineation of tumour extent.

B-1199 11:42

Diagnostic value of contrast-enhanced 3D FLAIR sequence in acute optic neuritis

P. Tunlayadechanont, T. Panyaping, P. Cheecharoen, P. Jindahra; Bangkok/TH (fangpt123@gmail.com)

Purpose: Contrast enhancement and hypersignal T2W of the optic nerve are abnormal findings in acute optic neuritis. Contrast-enhanced FLAIR sequence has both T2W and T1W effects. We aimed to study the diagnostic accuracy of whole-brain CE 3D FLAIR sequence in our routine brain protocol in detecting acute optic neuritis compared with clinical diagnosis.

Methods and Materials: This was retrospective cross-sectional study including optic nerves from twenty-two patients who first-time diagnosis of acute optic neuritis from clinical data and neuro-ophthalmological examination. All patients underwent brain MRI imaging with CE 3D FLAIR imaging at 3T. The hypersignal CE-FLAIR of optic nerve was assessed independently by 2 neuroradiologists. The optic nerve to white matter of the frontal lobe signal intensity ratio was also calculated as maximum SIR and mean SIR.

Results: 30 pathologic nerves of acute optic neuritis from twenty-two patients were diagnosed by neuroophthalmologist. 23 hypersignal of optic nerves were found on CE-FLAIR. Interrater agreement was substantial (K=0.73). The consensus optic nerve signal abnormality on CE-FLAIR has 82% accuracy, 77% sensitivity, 93% specificity, 96% positive predictive value and 65% negative predictive value. Optic nerve to frontal white matter SIR of the affected optic nerves showed statistically significant higher than those normal optic nerves. Using a cut-off maximum SIR of 1.24 and cut-off mean SIR of 1.16 with 93% sensitivity and 86% specificity have 89% and 91% accuracy, respectively.

Conclusion: Hypersignal of optic nerve on whole-brain CE 3D FLAIR sequence has diagnostic potential in acute optic neuritis.

B-1200 11:46

Radiological diagnosis of desomorphine-associated osteonecrosis

A. Babkova, N.S. Serova, S.P. Pasha, M. Shariya; Moscow/RU (an4i1@ya.ru)

Purpose: Atypical osteonecrosis cases have been noted from 2003 in Russia due to abuse of synthetic drugs, such as desomorphine, which is one of the most widespread drug because of its low cost, quick production process from codeine pills with red phosphorus and other toxic substances.

Methods and Materials: From 2010 to 2017, 165 desomorphine addicts were evaluated at the Sechenov University. Patients underwent skull X-ray, panoramic radiography, multispiral computed (MSCT) and cone-beam computed tomographies (CBCT), radionuclide diagnostics. As a result of this evaluation, 165 patients were diagnosed with "Toxic phosphorus necrosis" of skull bones. Patients underwent different surgical interventions.

Results: Conventional radiography, MSCT, CBCT revealed empty tooth sockets in 165 patients, sclerotic end plates in 76 patients (46%). Massive diffuse periosteal deposits in the lower jaw region were in 97 patients (59%). Alterations in the upper jaw were in 39 subjects (24%). A pathological mandible fracture was observed in 38 cases (23%). Bone scintigraphy and SPECT showed excessive accumulation of the 99mTc-Pyrophosphate in the skull bones in 30 cases (100%): in the maxilla, mandible, in the eye-pits (n=11;31%), in the cheekbones (n=8;26%), in the sternum (n=11;31%), in the clavicles and humeral heads (n=7;23%), in the crests of the ilium (n=6;20%), in the knee areas (n=5;17%).

Conclusion: Complex radiological diagnostic technologies used to evaluate the skeletal system in patients taking desomorphine allow full identification of the nature of this disorder, presence of concomitant complications, help in the determination of the surgical strategy and planning of further reconstructive treatments.

analysed using Kaplan-Meier and log-rank tests. The β -coefficients derived from a logistic regression model were used to calculate the risk score.

Results: 69 of 498 patients in modelling group suffered from liver function damage. The 1-, 2- and 3-year OS were 93.7%, 88.0%, 79.8% and 89.2%, 79.6%, 57.8% for patients without and with liver function damage ($p=0.043$), respectively. A total of five risk factors were filtrated by logistic regression model, namely Child-Pugh classification before treatment, tumour numbers, ablation volumes, relative position between the tumour and portal vein (PV) and APRI. These factors were used to calculate the risk score to predict liver function damage. The AUC of the risk score for predicting liver function damage was 0.798 in modelling group and 0.832 for validation group. The sensitivity and specificity to identify liver function damage were 65.22%, 84.38% in modelling group and 60.61%, 88.32% in validation group, respectively.

Conclusion: Liver function damage after MWA is an unfavourable factor for prognosis. The algorithm based on risk factors is a stabilized assessment model to predict liver function damage in patients with HCC after MWA.

B-1204 14:24

CT texture parameters to evaluate outcome after thermal ablation for colorectal liver metastases

E. Klompenhouwer, R.G.H. Beets-Tan, M. De Boer, S. Trebeschi, W. Prevoo, D.M. Lambregts, G.L. Beets, M. Maas; *Amsterdam/NL* (*l.klompenhouwer@nki.nl*)

Purpose: Early detection of incomplete ablation or local tumour progression (LTP) after thermal ablation is challenging. Aim of this retrospective pilot study is to determine whether liver CT texture is valuable to evaluate the completeness of ablation and to early detect LTP after thermal ablation in patients with colorectal liver metastases.

Methods and Materials: Texture parameters were extracted from CT scans of 27 patients (38 lesions; 23 RFA and 15 MWA) 1 month post-ablation. Ablation zones were delineated in 3D-slicer and texture parameters were calculated with an internal tool programmed in Python for the total lesion and for the ablation margin. This ablation margin of 3 mm inwards and outwards was added by the Python tool after delineating the total lesion. Evaluated texture parameters were mean, median, entropy, skewness and kurtosis, which were compared with outcome post-ablation: no LTP, LTP during follow-up or incomplete ablation. Median follow-up was 12 (5-48) months.

Results: 25 lesions were completely ablated, 4 were incompletely ablated and 9 showed LTP during follow-up. In lesions that were incompletely ablated or showed LTP ($N=13$), the median and mean texture density were significantly higher than in patients without LTP, both for the total lesion texture ($p=0.032$ and $p=0.036$, respectively) and the texture of the ablation margin ($p=0.026$ and $p=0.034$, respectively).

Conclusion: The mean and median texture density of the total lesion and ablation margin 1 month post-ablation might be valuable non-invasive markers to evaluate incomplete ablation and detect early LTP after thermal ablation for colorectal liver metastasis before they are visible on CT during follow-up.

B-1205 14:32

Microwave ablation (MWA) of liver malignancies: outcomes and prognostic factors of local tumour progression (LTP) with a new generation system

P. Marra, P. Diana, F. Ratti, F. Cipriani, M. Salvioni, S. Gusmini, M. Venturini, L. Aldrighetti, F. De Cobelli; *Milan/IT* (*marra.paolo@hsr.it*)

Purpose: High-power MWA may present advantages in term of local tumor control, compared with other ablative techniques, but data in the literature are conflictual. We analyzed the outcomes and investigated potential prognostic factors of LTP in the treatment of hepatocellular carcinoma (HCC) and colorectal cancer liver metastases (CRLM), using a new generation MWA system.

Methods and Materials: From November 2014 to June 2017, 50 patients (HCC=30; CRLM=20) underwent percutaneous, laparoscopic or open surgical MWA of 61 liver nodules with a 100W/2450MHz Microwave Generator (Emprint, Medtronic). DCE-CT or MRI were used to assess 1-month complete ablation (CA) and LTP at follow up.

Results: Overall CA rate was 97.3%. Overall LTP in HCC and CRLM metastases was respectively 18% (mean observation time, 15.3 months, interval 6-31 months) and 10% (mean observation time 10.8 months, interval 6-21). For HCC, BCLC-stage >0, multiple nodules, viral etiology and relapsing disease were associated to LTP without statistical significance; LTP was not influenced by age, nodule size and vessels/capsule proximity. For CRLM, a lesion size >20mm was associated to higher LTP ($p=0.027$). Nodule number >5 showed increased LTP without statistical significance. LTP was not influenced by age, KRAS mutation, synchronous/metachronous metastases and vessels/capsule proximity. LTP did not differ among percutaneous and surgical approaches.

Conclusion: LTP rates after liver MWA for HCC and CRLM are comparable with the literature. CRC mets >20mm are associated with higher LTP. Our initial experience with high-power MWA is promising and further development of this technique will probably provide even better results.

B-1206 14:40

Microwave ablation therapy of giant hepatic cavernous haemangiomas

S. Cakir, M. Baykara Ulsan, I.N. Mutlu, N. Kiliçkesmez, C. Turan Bektas, A. Yardimci; *Istanbul/TR* (*mehmetsemihcakir@gmail.com*)

Purpose: Endovascular embolisation therapy used as a classical method in the treatment of hepatic giant cavernous haemangiomas does not yield the desired results like dimensional diminution and a decrease in symptoms. It is aimed to demonstrate the effectiveness of treatment with microwave ablation (MWA) therapy.

Methods and Materials: Between October 2016 and April 2017, patients ($n=10$; 5 female, 5 male) with liver giant cavernous haemangioma underwent MWA therapy and followed for a mean of 6 months. 3 patients presented with gastric complaints, 5 patients had abdominal pain and 2 patients had thrombocytopenia. Patient pain scoring was noted according to the 10-point visual analog scale. MWA therapies were performed by using an 18-gauge electrode (Accu2i pMTA Applicator, AngioDynamics, Inc. Hampshire, UK) under ultrasound guidance in the presence of analgesia and sedation. Mean ablation time was 8.5 minutes.

Results: All ablations were terminated with technical success and there were no major complication. Abdominal pain, especially localised at right upper quadrant, developed after procedure due to ablation therapy and additional analgesia support was given. Average pain score decreased from 5.1 to 1.3 after the first month. Mean tumour volume decreased 66.1% after sixth months.

Conclusion: Therapy of microwave ablation for hepatic haemangiomas with a high-powered microwave device appears to be safe and effective in providing tumour shrinkage, devascularisation and pain relief. While transarterial chemoembolisation alone cannot cause significant tumour shrinkage, the effect of MWA is excellent for haemangioma destruction. Therefore MWA can be used for the treatment of large hepatic haemangiomas.

B-1207 14:48

The effect of oesophageal varices on the outcome of RF ablation in patients with HCC

M. Ahmad; *Sohag/EG* (*mandw20022002@hotmail.com*)

Purpose: To determine the therapeutic efficacy of radiofrequency ablation and the impact of oesophageal varices on the survival final results.

Methods and Materials: 121 of 168 patients with portal hypertension had oesophageal varices, underwent RF ablation as a treatment for a single HCC (≤ 5 cm). Therapeutic efficacy was evaluated. Logistic regression analyses of risk factors for occurrence of complication and multivariate cox-regression analyses for overall survival were detected.

Results: Patients with HCC and oesophageal varices had a complete ablation rate of 88.4%. Portal vein thrombosis was the most type of complication. By univariate analysis, thrombocytopenia ($P=0.032$) was an independent risk factor of complications. By multivariate analysis, left lobe location of HCC ($P=0.015$) was an independent risk factor of complications and subcapsular location of HCC ($P=0.019$) was an independent prognostic factor for survival.

Conclusion: This current study has proven that patients with portal hypertension and oesophageal varices can tolerate RF ablation of HCC. Dealing caution as regards correction of thrombocytopenia and professionally as regards location of HCC, we can improve the outcome of RF ablation.

B-1208 14:56

Feasibility, effectiveness and safety of percutaneous MR-guided ablation of small hepatic malignancies

J. Weiß, R. Hoffmann, E. Kessler, H. Rempp, K. Nikolaou, S. Clasen; *Tübingen/DE* (*jakob.weiss@med.uni-tuebingen.de*)

Purpose: To investigate the feasibility, effectiveness and safety of percutaneous MR-guided ablation of small hepatic malignancies.

Methods and Materials: Between January 2012 and December 2016, 45 patients were included in this IRB-approved retrospective study. All patients were scheduled for percutaneous MR-guided tumour ablation (radiofrequency $n=27$; microwave $n=16$) due to primary (HCC $n=11$; CCC $n=2$) or secondary hepatic malignancies with a lesion diameter of ≤ 12 mm. A 1.5T MR system was used for planning, targeting and therapy monitoring. Technical success and long-term effectiveness were assessed by dynamic contrast-enhanced MR imaging. Mean follow-up was 17.1 ± 11.6 months (range: 4-42 months).

Results: Tumour ablation was successfully completed in 43 patients. In six patients (13%), planning imaging revealed new, unexpected lesions, which were either treated in the same session ($n=4$) or changed therapy management ($n=2$) due to diffuse tumour progress. Thus, incomplete treatment or non-indicated local ablation could be avoided. Planning imaging was

conducted without contrast agent administration in 82% (n=37) of the ablation procedures. In 66% (n=30), target tumours were visible in real-time MR-fluoroscopy during the intervention. Post-procedural imaging revealed a technical success of 100% with no major complications. During follow-up, no local tumour recurrence was observed although twelve patients presented with new tumours distant to the ablation zone.

Conclusion: MR-guided ablation is a feasible approach for effective and safe treatment of small hepatic malignancies. In addition, MR planning imaging is helpful to account for unexpected changes of the oncological situation to avoid inappropriate treatment in favor of patient safety.

B-1209 15:04

A new software for immediate volumetric assessment of tumour ablation completeness: could it allow to spare local retreatments?

R. Muglia¹, M. Solbiati², L. Solbiati³; ¹Pieve Emanuele/IT, ²Milano/IT, ³Rozzano (Milano)/IT

Purpose: To retrospectively evaluate accuracy of a software (AblationFit®), R.A.W. Endosight, Milan, Italy) in assessing complete ablation of tumours with percutaneous thermal ablation.

Methods and Materials: Out of 320 HCCs treated with microwave ablation (AMICA, HS, Aprilia, Italy) from 2010 to 2016, 90 patients in which ablations were technically successful were selected. Imaging follow-up of at least one year was performed. With AblationFit® the ceCT volumes of the 90 HCCs before ablation and the corresponding achieved volumes of necrosis were segmented, co-registered and superimposed, to estimate complete target inclusion into the necrosis volume. Predictions of complete vs partial ablation provided by the software were verified analysing presence or absence of local tumour progression (LTP) on 1-yr follow-up ceCT.

Results: Two experienced radiologists confirmed the ablation in 90/90 cases. With AblationFit® reconstructions, only 73/90 HCCs were entirely included into the volumes of necrosis, while 17/90 were partially included. At 1-yr follow-up, ceCT showed no-LTP in 69/90 and LTP in 21/90. With AblationFit® no-LTP and LTP were correctly predicted, respectively, in 65/73 and 13/17. 8/73 cases of complete ablation according to AblationFit® developed LTP and in 4/17 of partial ablation according to AblationFit® LTP did not develop. Sensitivity of AblationFit® was 62% and specificity 94%. In 13/13 cases of correct prediction of LTP, tumour regrowth in the location where AblationFit® showed residual tumour.

Conclusion: AblationFit® used at the time of ablations, in 13/90 HCCs local re-treatment could have been spared thanks to the immediate detection of non-ablated tumour.

Author Disclosures:

M. Solbiati: Founder; R.A.W., Endosight, Milan, Italy. Shareholder; R.A.W., Endosight, Milan, Italy.

B-1210 15:12

Ablation therapy of non-colorectal cancer lung metastases: retrospective analysis of tumour response post LITT, RFA and MWA

N.-E.A.N. Mohammed, N.N.N. Naguib, T. Gruber-Rouh, I. Burck, T.J. Vogl; Frankfurt a. Main/DE (nour410@hotmail.com)

Purpose: To retrospectively compare the local tumour response and survival rates in patients with non-colorectal-cancer-lung-metastases post-ablation-therapy using laser-induced thermo-therapy-(LITT), radiofrequency ablation-(RFA) and microwave ablation-(MWA).

Methods and Materials: Retrospective analysis of 175 CT-guided ablation sessions performed on 109 patients (43 males and 66 females, mean age: 56.6 years). 17 patients with 22 lesions underwent LITT treatment (tumour size: 1.2-4.8 cm), 29 patients with 49 lesions underwent RFA (tumour size: 0.8-4.5 cm) and 63 patients with 104 lesions underwent MWA treatment (tumour size: 0.6-5 cm). CT-scans were performed 24-hours post-therapy and on follow-up at 3, 6, 12, 18 and 24 months.

Results: The overall-survival rates at 1-, 2-, 3- and 4-year were 93.8%, 56.3%, 50.0% and 31.3% for patients treated with LITT, 81.5%, 50.0%, 45.5% and 24.2% for patients treated with RFA and 97.6%, 79.9%, 62.3% and 45.4% for patients treated with MWA respectively. The mean survival-time was 34.14 months for MWA, 34.79 months for RFA and 35.32 months for LITT. In paired comparison a significant difference could be detected between MWA versus RFA (p=0.032). The progression-free survival showed a median of 23.49 ± 0.62 months for MWA, 19.88 months ± 2.17 months for LITT and 16.66 ± 0.66 months for RFA (p=0.048). The lowest recurrence rate was detected in lesions ablated with MWA (7.7%; 8 of 104 lesions) followed by RFA (20.4%; 10 of 49 lesions) and LITT (27.3%; 6 of 22 lesions) p-value of 0.012. Pneumothorax was detected in 22.16% of MWA ablations, 22.73% of LITT ablations and 14.23% of RFA ablations.

Conclusion: LITT, RFA and MWA may provide an effective therapeutic option for non-colorectal cancer lung metastases with an advantage for MWA regarding local tumour control and progression-free survival rate.

B-1211 15:20

Application of contrast-enhanced ultrasound during microwave ablation for large benign thyroid nodules

W. Wang, F. Mao, J.Y. Cao, P. Fan, Y. Dong; Shanghai/CN (puguang61@126.com)

Purpose: We aimed to evaluate the value of contrast-enhanced ultrasound (CEUS) during both pre- and post-treatment evaluation of microwave ablation (MWA) for large benign thyroid nodules.

Methods and Materials: Between Jan 2017 and Oct 2017, 65 patients with a total of 65 large benign thyroid nodules admitted to our hospital for MWA treatment were included. Mean diameter of nodules is 54 ± 14 (mm). The generator of microwave system is designed with a frequency of 2450 MHz and a maximum output power of 100W. The ablation procedures were monitored by real-time ultrasound. Before MWA, dynamic CEUS examinations were performed to make pre-treatment assessment, including blood perfusion of nodules and their relationship with surrounding large vessels. One day and six month after ablation, the post-treatment CEUS were conducted to evaluate whether the original nodules were completely ablated.

Results: During pre-ablation CEUS evaluation, peripheral hyperenhanced rings were detected during arterial phase of all nodules, with mean thickness 1.3 ± 0.5 mm. MWA were conducted successfully in all 65 thyroid nodules. Post-ablation CEUS showed that 62 (95.4%) nodules with complete ablation had no enhancement. The peripheral hyperenhanced ring disappeared in all nodules. The volume reduction of 63 ± 3.1 % was achieved with benign thyroid nodules after six months follow-up. No major complications occurred.

Conclusion: Microwave ablation with real time ultrasound guidance is an effective and safe method in treatment of large benign thyroid nodules. CEUS is a sensitive and effective method to make both pre-treatment evaluation and post-treatment efficacy of MWA.

14:00 - 15:30

Room L 8

Head and Neck

SS 1508

Cancer and lymph node imaging

Moderators:

N.I. Traykova; Plovdiv/BG
N.N.

K-24 14:00

Keynote lecture

S. Connor; London/UK

B-1212 14:09

Proposal of imaging reporting and data system for cervical lymph node based on computed tomography

K. Lee¹, J. Baik²; ¹Ras Al Khaima/AE, ²Busan/KR (lkh770429@naver.com)

Purpose: To compare computed tomography (CT) features of benign and malignant cervical lymphadenopathy and to propose a CT-based, structural reporting system for cervical lymph node: lymph node reporting and data system on CT (LNRADS-CT).

Methods and Materials: The Institutional Review Board approved and informed patient consent was waived. Between January 2014 and August 2016, a total of 1337 subjects underwent neck CT examination at a single institution. The study included consecutive 407 (malignant lymphadenopathy: 170, benign lymphadenopathy: 237) cases with pathologic diagnosis or sufficient follow-up. CT features of cervical lymph nodes were retrospectively analysed: longest diameter, shortest diameter, shape, necrosis, perinodal fat infiltration, conglomeration, invasion of adjacent structures and enhancement pattern. Regression equation was utilized, and a score was assigned for each significant factor. Risk of malignancy was determined according to the number of suspicious CT features.

Results: Malignant lymphadenopathy revealed larger shortest diameter, round shape, necrosis, conglomeration and well enhancement more frequently (P < .05). As the number of suspicious features increased, fitted probability of malignancy increased. Risk stratification of LNRADS-CT was 12.2% in category I (no suspicious features), 38.2% in category II (one suspicious feature), 80.6% in category III (two suspicious features), and 92.4-99.3% in category IV (more than three suspicious features).

Conclusion: LNRADS-CT was proposed based on a 4-point category and can be used to assess the risk of malignancy in cervical lymph nodes.

B-1213 14:17

Diagnostic value of real-time ultrasound image fusion compared to ultrasound-only-guided lymph node fine-needle aspiration in head and neck cancer patients

P. De Koekkoek-Doll, M. van den Brekel, W. Vogel, L. Smit, J.J. van Griethuysen, M. Maas; *Amsterdam/NL (p.doll@nki.nl)*

Purpose: Aim was to evaluate the feasibility of real-time fusion of ultrasound (US) with available tomographic image data for the assessment and guidance of fine-needle aspiration (fused-FNA) for nodal staging in head and neck cancer.

Methods and Materials: 55 patients were prospectively included. Fused-FNA was performed after routine US-FNA, using the electromagnetic navigation system Percunav on a Philips EPIQ-US machine. Live US was fused with PET/CT, MRI, or CT-data. FNA was performed on additional suspicious nodes identified by image fusion. Reference standard consisted of cytological evaluation of the FNAs and histology from node dissection if performed.

Results: Fusion was performed with PET/CT (n=53, 96%), MRI (n=1, 2%) and CT (n=1, 2%). In 6 patients (11%) without suspicious lymph nodes fused-FNA was not performed. On the remaining 49 patients (89%), FNA was performed in 120 nodes. For 97 nodes, FNA was performed based on routine US. Their location was confirmed with accurate image fusion in 88 cases, for the remaining 9 nodes adequate image fusion was not achieved. After US-FNA, 23 additional nodes were identified based on image fusion and fused-FNA was performed. Of all nodes undergoing FNA 46/111 (41%) had malignant cytology, and of the 23 additional fused-FNA nodes 7 were proven malignant (30%). In total, 42% of all PET-positive nodes were malignant.

Conclusion: Real-time US image fusion with FNA is feasible in head and neck cancer, leads to an increased detection of malignant nodes, and allows for more accurate identification of the location of PET-positive nodes.

Author Disclosures:

P. De Koekkoek-Doll: Author; M. van den Brekel, MD PhD, W. Vogel, MD PhD, L. Smit, MD PhD, J. van Griethuysen, MD, M. Maas, MD PhD.

B-1214 14:25

Computer-aided quantification of intranodal vascularity enhanced the accuracy of ultrasound in distinguishing metastatic and tuberculous cervical lymph nodes

T.-C.M. Ying, S. Cheng, A. Ahuja; *Hong Kong/HK (htmying@polyu.edu.hk)*

Purpose: Ultrasound features of tuberculous nodes are varied and simulated metastatic nodes. This study presents a novel computer-aided method that can quantify intranodal vascularity and enhance the accuracy of ultrasound in distinguishing metastatic and tuberculous cervical lymph nodes.

Methods and Materials: Grey scale and power Doppler sonograms of 100 patients with palpable cervical nodes were reviewed (60 metastases, 40 tuberculous lymphadenitis). Ultrasound images of cervical nodes were evaluated for the shape, echogenic hilus, necrosis and vascular distribution of lymph nodes (conventional assessment). Intranodal vascularity index (VI) was quantified using a customised computer program. The diagnostic accuracy of using conventional assessment and its combination with intranodal VI was evaluated.

Results: Metastatic and tuberculous nodes tended to be round (75% vs 50%), without echogenic hilus (90% vs 72.5%) and have peripheral vascularity (73.3% vs 85%). Intranodal necrosis is more common in tuberculous nodes (27.5%) than metastatic nodes (8.3%). The diagnostic accuracy of conventional assessment in distinguishing metastatic and tuberculous nodes was 59% with sensitivity, specificity, positive predictive value (PPV) and negative predictive value (NPV) of 87%, 18%, 61% and 47% respectively. Results showed that metastatic nodes (23.4±2.1%) tended to have higher VI than tuberculous nodes (12±1.6%) (p<0.05). The optimal cut-off of VI was 20%. By combining conventional assessment and intranodal VI quantification, the diagnostic accuracy was 69% with sensitivity, specificity, PPV and NPV of 72%, 65%, 75% and 60% respectively.

Conclusion: Combining intranodal VI quantification and conventional assessment enhances the diagnostic accuracy of ultrasound in distinguishing metastatic and tuberculous cervical lymph nodes.

B-1215 14:33

Cervical adenopathies: diagnostic efficacy of DCEMR

L. Aghaghazvini, F. Hashemi, H. Sharifian, B. Rasuli, N. Yazdani; *Tehran/IR (aghaghazvini.leila@gmail.com)*

Purpose: Pre-operative differentiation of benign from malignant cervical adenopathies (CN) remains a challenge. We assessed the efficacy of dynamic contrast MRI (DCEMR) for differentiation between benign and malignant CN.

Methods and Materials: DCEMR were performed in patients with CN who were candidates for surgical resection, before radiotherapy or chemotherapy. In all patients we used 3 Tesla MRI with fast spin echo T2- and T1-weighted images in axial and coronal planes and T1 weighted after contrast medium

administration. We recorded dynamic curves and values every 30 seconds up to 10-15 minutes after contrast injection. Data were evaluated in a mixed model analysis and findings were compared with postoperative histopathologic results.

Results: 49 cervical lymph nodes (17 benign and 32 malignant) were included in this study. In time-intensity curves there were significant differences between benign and malignant groups in two parameters: 5-minute washout slope (p value: 0.008) and 5-minute washout ratio (p value: 0.013). For 5-minute washout slope there were 96% sensitivity and 27% specificity at cut-off point: 1.7, 100% specificity and 40% sensitivity at cut-off point: 7.4, 70% sensitivity and 70% specificity at cut-off point: 3. Other DCEMR parameters, lymph nodes sizes and T2w heterogeneity were different but not significant statistically. Also necrosis only was present in malignant lymph nodes.

Conclusion: DCEMR only for washout ratio and slope at 5 minutes after contrast injection could be helpful in differentiation between benign and malignant CN in this study but larger studies are necessary.

B-1216 14:41

Role of RI (resistive index) value as imaging bio marker in differentiating benign and malignant cervical lymphnodes

K.A. Bhagwat; *Davangere/IN (bhagwatkishan@gmail.com)*

Purpose: To assess the role of resistive index , RI value as imaging bio marker in differentiating benign and malignant cervical lymph nodes. To correlate routine ultrasonography features of enlarged nodes with resistive index on Doppler and cytological correlation.

Methods and Materials: Type of study: prospective study. Sample size: 50; Inclusion criteria: patients presenting with clinically palpable cervical lymphadenopathy referred for Ultrasonography. Exclusion criteria: patients who have been treated earlier for cervical lymphadenopathy. Method: all patients underwent high resolution sonography of neck with Colour Doppler and following results were recorded. Only the largest node in each patient was included for study. Morphology: 1. shape of node; 2. size; 3. echotexture; 4. roundness index; 5. necrosis; 6. loss of hilar architecture. Doppler: Hilar flow pattern. Resistivity index of vascularity. The above findings were recorded. Morphologically the nodes were classified as benign and malignant and their RI values were studied. FNAC results were correlated wherever possible.

Results: Out of 50 patients , about 30 patients had benign lymph nodes and 20 patients had malignant secondary nodes. Most of the lymph nodes which were benign on morphological criteria had RI value less than 0.7. All malignant nodes had RI value of 0.8 and above. The unequivocal cases had RI value between 0.7 and 0.8. In these cases FNAC finally concluded that nodes with RI value of 0.75 are malignant.

Conclusion: Thus resistivity index of vascularity of lymph nodes is a reliable cost effective imaging bio marker in differentiating benign and malignant cervical lymphadenopathy.

B-1217 14:49

The use of micro-flow imaging (MFI, Philips Medical Systems) in ultrasound guided tissue sampling of head and neck masses

H. Toghyan, A. Al-Khatib, B. Stenberg, A. McQueen; *Newcastle upon Tyne/UK (hamid.toghyan101@gmail.com)*

Purpose: Ultrasound (US) guided tissue sampling of neck masses is an essential component of a head & neck imaging service. One reason for non-diagnostic US guided lymph node sampling is necrosis of the target lesion (particularly in head & neck squamous cell carcinoma and lymphoma) and this can lead to additional samples being required via repeat percutaneous procedures or surgical excision. Standard Doppler flow is primarily used for diagnostic assessment of vascular architecture within neck masses, but a more detailed perfusion map could enable the ultrasound practitioner to identify and target viable, non-necrotic tissue and reduce the number of samples required to achieve diagnostic sample quality for pathological interpretation.

Methods and Materials: Patients presenting with a neck mass requiring tissue sampling were assessed with MFI, a new technology designed to detect small vessel blood flow with high resolution and minimal artifact, facilitating assessment of lesion perfusion. Samples were obtained from each target lesion, under direct ultrasound guidance using an e18-4 linear US probe and Epiq 7 US machine (Philips Medical Systems). Pathology results, including the pathologist's comments about the adequacy and quality of the samples were obtained from our hospital's intranet.

Results: In this case series/technical evaluation, we present our early experience in utilising MFI and its superiority to standard Doppler flow imaging in depicting vascularity in head and neck masses.

Conclusion: We propose that increased diagnostic confidence in detecting viable regions within abnormal cervical nodes guides tissue sampling, with the potential for fewer procedures and greater adequacy rates.

B-1218 14:57

Higher definition head and neck imaging enabled with digital photon counting PET/CT: an intra-individual comparison with conventional photomultiplier PET/CT

C.L. Wright¹, K. Binzel¹, J. Zhang¹, P. Maniawski², M.V. Knopp¹;
¹Columbus, OH/US, ²Cleveland, OH/US

Purpose: To assess the clinical impact and potential clinical benefit of digital photon counting PET (dPET) for higher definition PET/CT imaging in head/neck by intra-individual comparison to conventional photomultiplier tube detector (cPET) PET.

Methods and Materials: Thirty oncology patients participated in an intra-individual comparison of FDG PET using pre-commercial release dPET/CT (Vereos) and cPET/CT (Gemini). Standard cPET imaging was performed at ~75 min p.i. of 481 MBq FDG, investigational dPET imaging either at ~55 min or ~95 min p.i. All other aspects of image acquisition were kept identical. Digital PET images were reconstructed using Time-of-Flight with 4mm3 (standard definition/SD), 2mm3 (high definition/HD), and 1mm3 (ultra-high definition/UHD) voxel volumes and compared with SD cPET images. Blinded readers evaluated image sets in regard to overall quality, lesion/tissue characterization, and quality of background in head/neck region.

Results: All cPET/dPET data sets were evaluable. When compared with cPET, higher definition dPET demonstrated improved image quality for qualitative assessment and detection of small FDG-avid head/neck lesions. There was also improved image quality for normal structures/tissues without an appreciable effect on the background FDG activity. FDG activity in lesions and normal tissues/structures were better characterized with HD/UHD dPET. Kappa scores were consistently higher.

Conclusion: Higher definition dPET improved visualization and characterization of FDG-avid lesions and normal tissues/structures in the head/neck including higher kappa scores for agreement. The improved image quality and lesion/tissue characterization appears to be enabled by the faster timing resolution of dPET (~325ps) compared with cPET (~550ps) and higher definition reconstruction reducing partial volume.

Author Disclosures:

P. Maniawski: Employee; Philips Healthcare.

B-1219 15:05

Correlation between apparent diffusion coefficient and standardised uptake values in head and neck carcinomas

S. Türk, S. Bayraktaroglu, E. Ramo, Ö. Akagündüz, R. Savaş; Izmir/TR
 (sevcanturk.ege@hotmail.com)

Purpose: Head and neck carcinoma may cause a decreased apparent diffusion coefficient (ADC) on diffusion-weighted magnetic resonance imaging (DW MRI) and an increased standardised uptake value (SUV) on fluorodeoxyglucose (FDG) positron emission tomography (PET/CT). We analysed the reproducibility and treatment-related changes of ADC and SUV measurements in head and neck carcinoma and evaluated whether these biomarkers are correlated or independent.

Methods and Materials: This retrospective analysis of DW MRI and FDG PET/CT data series included 36 head and neck carcinoma. Kruskal-Wallis, one-way ANOVA and Mann-Whitney U methods were used to detect any statistical correlation and prognostic significance of ADC and SUV values in responders and non-responders to radiotherapy.

Results: Mean ADC_{min}, ADC_{mean} and ADC_{max}/mean in head and neck carcinoma were 0.68±0.17×10⁻³mm²/s, 0.82±0.17×10⁻³ mm²/s and 0.83 ± 0.10 mm²/s, respectively. Mean SUV_{mean} and SUV_{lbm} were 14.65±5.5 and 10.96±5.1, respectively. Spearman's correlation analysis showed no significant correlation between ADC and SUV measurements. Although statistically not significant, a trend towards higher SUV and lower ADC was observed in head and neck tumours. Statistically, not significant, a trend towards higher SUV and higher ADC was observed in non-responders to radiotherapy.

Conclusion: Our data suggest that ADC and SUV values are reproducible and independent biomarkers in head and neck carcinomas.

B-1220 15:13

MRI-based surveillance for patients with recurrent head and neck cancer after hypofractionated stereotactic (SBRT) re-irradiation

N. Plakhotina, A. Mikhailov, A.V. Smirnova, D.I. Kuplevatskaya, N. Vorobyov; St. Petersburg/RU (plakhotinadezhda@gmail.com)

Purpose: To assess MRI value for SBRT treatment response evaluation in patients with recurrent head and neck cancer.

Methods and Materials: 23 patients with head and neck cancer relapse primarily treated by SBRT were enrolled (age range: 33-79 years). Patients were re-irradiated with SBRT (35 Gy in 5 fractions). MRI protocol included T2 and T1 WI, with/without FS, axial DWI, T1FS after gadolinium enhancement, with slice thickness 1-3 mm. MRI were performed before initiating SBRT and then each 3 months.

Results: In 86.9% (20 patients) we have found disease stabilization (by RECIST criteria) and the absence of progression during the 24 months. After 3-9 months tumour contours became more uneven, structure became heterogeneous, signs of the necrosis appeared, which were replaced by fibrous tissue after 9-12 months. In all patients in months 3-9 significant oedema at 1 cm margin around tumour focus was revealed. However, after 6 months, the distant oedema signs (mucositis, muscles and fat swelling) were decreasing. In 3 patients (13.1%) we could not assess the long-term results due to death from disease progression.

Conclusion: MRI-based treatment response assessment in head and neck cancer relapse provides adequate information for clinical decision but characterized by some features, demanding multidisciplinary evaluation. Local tissues swelling after SBRT in first months do not allow accurate tumour evaluation and simulate disease increase. To exclude false errors radiologist needs to know RT method, compare MR results with treatment plans and review images in close collaboration with radiation oncologist.

B-1221 15:21

Perineural spread of fungal sinonasal infections: CT scan and MRI findings

M. Mohammadzadeh¹, A. Mohammadzadeh¹, Z. Haghghi¹, H. Sharifian¹, V. Mohammadzadeh², S. Kadivar²; ¹Tehran/IR, ²Rasht/IR
 (mralimohammadzadeh@yahoo.com)

Purpose: To study imaging features and anatomic pathways of perineural spread (PNS) in head and neck fungal infections.

Methods and Materials: Imaging findings of 25 patients diagnosed with sinonasal fungal infection evaluated. Perineural tumour spread was defined as foraminal enlargement, foraminal destruction, nerve enlargement, abnormal enhancement of the evaluated nerves and obliteration of the perineural fat pad.

Results: 52% of patients revealed definitive signs of perineural spread. All of patients with PNS had Infra Orbital Fissure and pterygopalathine obliteration. Maxillary branch of trigeminal nerve was involved in 100% of PNS cases. Sinus cavernous involvement in 69% and Meckels cave in 30% of these cases were identified.

Conclusion: Perineural spread is a common mechanism of extension in sinonasal fungal infections and the most common pathway is spread along mandibular division of trigeminal nerve.

14:00 - 15:30

Room M 1

Cardiac

SS 1503

Children and 3D printing

Moderators:

G. Bastarrika; Pamplona/ES
 T. Yalynska; Kyiv/UA

B-1222 14:00

3D-assessment of RVOT dimensions prior to percutaneous pulmonary valve implantation

S. Ebel¹, S. Gottschling², M.T.A. Buzan³, M. Grothoff¹, I. Dähnert¹, R. Wagner¹, D. Gräfe¹, M. Gutberlet¹, C. Lücke¹; ¹Leipzig/DE, ²Halle/DE, ³Cluj-Napoca/RO
 (sebastian.ebel@icloud.com)

Purpose: To evaluate which cardiac MRI technique allows for better assessment of the RVOT in patients with pulmonary valve disease after tetralogy of Fallot (TOF) repair: contrast-enhanced MR-angiography (ceMRA) or 3D steady-state free precession (SSFP) during systole and/or diastole.

Methods and Materials: We retrospectively evaluated 89 patients (male:female:45:44 mean age 19 ± 8 years), who underwent cardiac-MRI (1.5 T) after surgical TOF repair. Data sets covering the whole heart in systole and diastole were obtained using a ECG-gated 3D SSFP and a non-gated ceMRA. Measurements were performed in the narrowest diameter of the RVOT and MPA to obtain the mean minimal, maximal and effective diameter.

Results: The mean minimal diameters in diastolic SSFP, systolic SSFP and ceMRA were 21.4 mm (± 6.1 mm), 22.6 mm (± 6.2 mm) and 22.6 mm (± 5.96 mm), respectively. The mean maximal diameters were 29.9 mm (± 9.5 mm), 29.98 mm (± 6.98 mm) and 28. mm (± 8.1 mm) respectively. The mean effective diameter was 23.2 mm (± 5.7 mm), 27.4 mm (± 6.7 mm) and 24.4 mm (± 6.2 mm), with a significant difference between diastole and systole (p<0.0001). Measurements in ECG-gated SSFP showed a better inter- and intraobserver variability compared to measurements in ungated ceMRA sequences.

Conclusion: Patients with TOF repair who could benefit from PPVI should undergo non-invasive CMR for preprocedural assessment. There are significant differences regarding the size of the RVOT and pulmonary trunk between systole and diastole; therefore, it is essential to obtain ECG-gated

sequences for precise measurements. We show that 3D SSFP sequences acquired during systole are best to identify a potential landing zone for PPVI.

Author Disclosures:

S. Ebel: Author; Sebastian Gottschling, Maria TA Buzan, Matthias Grothoff, Ingo Dähnert, Robert Wagner, Daniel Gräfe, Matthias Gutberlet, Christian Lücke.

B-1223 14:08

3D-printed heart model to guide LAA closure: preliminary results

A.-L. [Hachulla](#), S. Noble, G. Guglielmi, D. Agulleiro, H. Muller, J.-P. Vallee; *Geneva/CH (anne-lise.hachullalemaire@hcuge.ch)*

Purpose: Percutaneous left atrial appendage (LAA) occlusion is as an alternative therapeutic approach to medical therapy for stroke prevention in patients with atrial fibrillation. The correct sizing of the occluding device remains challenging due to the variable LAA shape. We investigated the use of personalised 3D-printed model to guide the selection of the device size.

Methods and Materials: Fifteen patients scheduled for an occlusion of the LAA underwent a cardiac CT. The left atrium was segmented by semiautomatic algorithms and a 1.5 mm thick shell of the left atrium was exported in STL format and printed using a flexible material. A new CT scan of the 3D-printed model with and without inserted Amplazer® Amulet cardiac plugs was acquired. The size of the Amulet predicted with CT, transechocardiography (TEE) and 3D-printed model was compared to the size of the device implanted in the patient.

Results: The segmentation process was fast (less than 15 min). The device size was correctly predicted in 8/15 cases with TEE, in 10/15 cases with Cardiac CT, in all of the 15 cases with 3D-model. On the 3D-printed model CT, the proximal disc sealing the ostium of the LAA and the close contact of the distal lobe with the LAA wall could be seen very well. In case of incorrect sizing, absence of contact with the LAA wall or device deformation was easily identified.

Conclusion: We introduced a fast and robust protocol using personalized 3D-printed LAA model to select the correct size of the occluding device.

B-1224 14:16

Left atrial appendage closure guided by 3D-printed patient-specific models

M. [Guglielmo](#)¹, A. Guaricci², D. Andreini¹, M. Conti¹, S. Marconi¹, F. Auricchio³, M. Pepi¹, C. Tondo¹, G. Pontone¹; ¹Milan/IT, ²Bari/IT, ³Pavia/IT (marco.guglielmo@cchm.it)

Purpose: Percutaneous left atrial appendage (LAA) occlusion has been proposed as an alternative therapeutic approach for stroke prevention in patients affected by atrial fibrillation. 3D printing allows reconstruction of patient-specific models of the heart using computed tomography angiography (CTA). We sought to assess whether the sizing of the implanted occluder device is in accordance with the sizing obtained using the 3D printing models.

Methods and Materials: We used 3D printing to create patient-specific LAA models, reconstructed by CTA, as supporting tool of the pre-operative stage of the LAA occlusion procedure with endovascular devices, such as the Wave Crest device (Coherex Medical, Inc, USA) and the Amplatzer Amulet device (St Jude Medical, St Paul, MN).

Results: 13 patients, undergoing percutaneous LAA occlusion, were retrospectively analysed; for each of them a patient-specific 3D LAA-printed model was manufactured using pre-operative CTA images. We observed that: i) in 54% of the cases (n=7) the actual sizing was underestimated when compared to the 3D-printed model; ii) in 38% of the cases (n=5) the two sizing approaches matched; iii) only in 1 case (8%) an overestimation of the actual size compared to the 3D-printed model was detected. In all underestimated cases a drawback, such as leakage or device migration was observed.

Conclusion: This report demonstrates that 3D printing LAA model may contribute in sizing the device, finding its correct position and guiding the choice of the device, providing additional data to angiography and TEE.

B-1225 14:24

3D printing of the aortic root based on cardiac computed tomography and cardiac magnetic resonance imaging: preliminary experience on pre-procedural planning for aortic valve stenting

M. [Gatti](#), R. Faletti, A. Cosentino, G. Pennisi, A. De Paoli, A. Di Chio, S. Fiore, L. Pavan, P. Fonio; *Turin/IT (marcogatti17@hotmail.it)*

Purpose: To determine the feasibility of using CCT and CMRI to print individual models of the aortic root complex for aortic annulus measurement.

Methods and Materials: Retrospective study on 20 patients who underwent aortic valve replacement with available records of pre-surgery annulus assessment by CCT and CMRI and of intra-operative assessment by Hegar dilators. The imaging DICOM data were loaded into an imaging processing software (OsirixMD) to obtain Standard Tessellation Language (STL) files that were exported to a model-editing software (Meshmixer®) and edited to retain only the aortic root from the left ventricular outflow tract to the sinotubular

junction. 40 aortic annuli were printed using a fusion deposition modelling printer (Ultimaker 2 Extended+®) with flexible polylactic acid filaments. The same cardiac surgeon performed both the intra-operative and the 3D model measurements. A time-cost analysis was performed. Data were analysed using Wilcoxon signed-rank test.

Results: There were no significant differences when compared the annulus dimensions measured by 3D models derived from CCT (p=0.33) and CMRI (p=0.44) to the surgical reference of intra-operative sizing. Valve sizing for CoreValve® by intra-operative measurement had the same good agreement with 3D model-based measurement, with a 95% match rate; for SAPIEN XT® the agreement was slightly better (95%) for CMR-derived model than for CCT (90%). Time and cost per model were: STL creation ~30min; printing time ~30min; post-processing ~5min; material cost <1€.

Conclusion: The 3D models performed well when compared to the surgical reference of intraoperative sizing. This approach may be a reliable, not expensive, patient-specific pre-operative planning opportunity.

B-1226 14:32

Fusion of coronary CT angiography and whole-heart 3D CMR myocardial perfusion: building a framework for comprehensive 3D cardiac imaging

J. [von Spiczak](#), R. Manka, A. Gotschy, S. Oebel, S. Hamada, H. Alkadhi; *Zurich/CH*

Purpose: To develop a high-quality framework for hybrid three-dimensional imaging of coronary CT angiography (CCTA) and dynamic whole-heart 3D cardiovascular magnetic resonance stress perfusion (CMR-Perf) image data to correlate coronary artery stenoses to stress-induced myocardial perfusion deficits.

Methods and Materials: 23 patients underwent CCTA and CMR-Perf. For CCTA, image quality and stenoses >50% were documented. For CMR-Perf, image quality and stress-induced perfusion deficits were noted. A new software framework was developed to allow for three-dimensional image fusion of patient data revealing relevant stenoses and corresponding perfusion deficits. Computation steps included: 1) automated segmentation of CT coronary arteries and heart contours; 2) manual segmentation of the left ventricle in CMR-Perf images; 3) automatic co-registration of CT and CMR datasets; 4) projection of the CMR-Perf values on the CT left ventricle. A dedicated algorithm for high-quality interpolation and co-registration was developed to avoid frequently occurring image artefacts. Results of the hybrid 3D analysis were compared to separate readouts from CCTA and CMR-Perf data.

Results: CT and CMR image quality was rated as good to excellent (scores 3.5±0.5 and 3.7±0.4, respectively, scale 1-4, 1=poor, 4=excellent). Multimodal three-dimensional image fusion was feasible in all patients. Perfusion deficits could be correlated to culprit coronary lesions in all cases.

Conclusion: Three-dimensional fusion of morphological high-resolution CCTA and functional CMR-Perf image data is feasible using the imaging framework presented in this work. Hybrid imaging can ease the anatomic correlation of stress induced myocardial perfusion deficits and their culprit lesions.

B-1227 14:40

3D image fusion of whole-heart dynamic cardiac MR perfusion and late gadolinium enhancement: identifying areas for revascularisation

J. [von Spiczak](#), M. Mannil, H. Alkadhi, R. Manka; *Zurich/CH*

Purpose: To develop a framework for three-dimensional image fusion of whole-heart dynamic 3D cardiac MR perfusion (3D-PERF) and 3D late gadolinium enhancement (3D-SCAR) to delineate stress-induced myocardial perfusion deficits and areas of scar.

Methods and Materials: Five patients with coronary artery disease (54±20 years) undergoing cardiac MR were included. A software framework was developed for 3D fusion of 3D-PERF and 3D-SCAR data revealing perfusion deficits along with myocardial scar. Computation steps included: 1) manual segmentation of the left ventricle in 3D-PERF and 3D-SCAR images; 2) semi-automatic thresholding of perfusion and scar data; 3) automatic calculation of ischaemic and scar burden; 4) projection of perfusion and scar values on an artificial template of the left ventricle; 5) semi-automatic co-registration to an exemplary heart contour easing 3D orientation; 6) 3D rendering of the combined datasets using automatically defined color tables. All tasks were performed by two independent, blinded readers. Interreader agreement was determined by calculating intraclass correlation coefficients.

Results: Image acquisition, post-processing, and 3D fusion was feasible in all cases. All patients showed stress-induced perfusion deficits in 3D-PERF; three patients showed late gadolinium enhancement in 3D-SCAR. Average ischaemic burden was 16% and average scar burden was 8%. Interreader agreement was excellent for both 3D-PERF (ICC=0.95) and 3D-SCAR (ICC=0.99). 3D fusion allowed intuitive visual assessment of perfusion deficits, scar, their overlap, and areas possibly accessible to revascularisation.

Conclusion: 3D fusion of 3D-PERF and 3D-SCAR facilitates anatomic correlation of stress-induced myocardial perfusion deficits and scar tissue for identifying areas for potential revascularisation.

B-1228 14:48

Prognostic impact of myocardial perfusion single-photon-emission computed tomography in patients with major extracardiac findings by computed tomography for attenuation correction

Z.C. Charline; Toulouse/FR (charline.zadro@gmail.com)

Purpose: Attenuation correction computed tomography (CT) contributes to an improvement in the diagnostic accuracy of myocardial perfusion imaging (MPI) by single-photon-emission tomography (SPECT). The aim of this study was to explore the prognosis of patients with major findings by CT according to the results of MPI.

Methods and Materials: 1506 patients who underwent MPI by SPECT between January 2010 and June 2011 in the CHU of Toulouse Rangueil were retrospectively included. Attenuation correction CT images were systematically analysed for major and minor abnormalities.

Results: 830 (55.1%) and 212 (14.1%) patients had minor and major extracardiac findings, respectively. Among patients with major extracardiac findings, the abnormality was previously unknown in 113 (53.3%) patients. 90 (41.9%) had abnormal MPI, 73 (34.4%) had a myocardial infarction scar, 55 (25.9%) had myocardial ischaemia, and 38 (17.7%) patients had both myocardial infarction scar and myocardial ischaemia. Among the 201 patients available for survival analysis, there were 67 (31.2%) deaths over a follow-up period of 3.2 ± 1.3 years. There was no significant impact on survival arising from MPI, whatever the result. The results were the same among the 103 patients with previously unknown major extracardiac findings.

Conclusion: Extracardiac findings by CT during MPI are frequent. Patients with major extracardiac findings have a poor mid-term outcome, whatever the results of the myocardial perfusion imaging. Extracardiac findings should be systematically checked when attenuation correction CT is performed.

B-1229 14:56

3D analysis and planning of septal reduction therapy based on CT coronary angiography in patient with hypertrophic cardiomyopathy

B. Batsak; Kiev/UA (dr.batsak@gmail.com)

Purpose: The aim of our study was to develop non-invasive method for preoperative 3D analysis and planning of septal reduction therapy.

Methods and Materials: Were performed CT coronary angiography with 320-MDCT (Aquilion ONE) in 45 patients with obstructive form of hypertrophic cardiomyopathy (mean age- 41 ± 7.3 , mean weight- 70 ± 13.2). We performed reconstruction of the 3D anatomy of coronary artery and myocardium of interventricular septum with the help of a post processing software package. For alcohol septal ablation we define the area of blood supply by septal branch of LCA. For planning surgical myectomy we perform 3d anatomical reconstruction of LV myocardium and zone of obstruction for determine level and amount of myocardium resection. Obtained data was analyzed.

Results: We found that septal branch supply the hypertrophic region of interventricular septum which caused obstruction in 21 patients. In 15 patient, no septal branches larger than 1 mm. In 9 patient, the 1st septal branch supplies area below site of obstruction. In patients with an appropriate anatomy of septal branches we performed alcohol ablation. During procedure we confirm area of blood supply by contrast echocardiography with perfloran. In patients with a non-appropriate anatomy of septal branches we performed myectomy after preoperative 3D planning

Conclusion: 3D analysis and planning of septal reduction therapy based on CT coronary angiography helps in choosing optimal methods of treatment in patient with obstructive form of hypertrophic cardiomyopathy.

B-1230 15:04

Assessment of post-operative pulmonary regurgitation by pre-operative RV and pulmonart artery imaging characteristics in pediatric TOF repaired with trans-valve surgert

Y. Gao, Z. Yang, K. Shi, K. Diao; Chengdu/CN (304789161@qq.com)

Purpose: Pulmonary regurgitation (PR) is most common complications after tetralogy of Fallot (TOF) surgical repair, the long-term PR might result in cardiovascular events. The aim of this study was to assess the influence of post-operative right ventricle(RV) and pulmonary artery(PA) parameters on post-operative PR by dual-source computed tomography(DSCT).

Methods and Materials: A total of 41 patients had TOF repaired with trans-valve surgery were retrospectively recruited. All diameters were measured using the computer caliper during systole. The RV and PA parameters evaluated by pre-operative DSCT were compared between the PR and non-PR groups used non-parametric test and Spearman test.

Results: The result showed that the PA parameters (McGoan ratio, Nakata index and LPA diameter) and RV parameters (RV length diameter and RV short diameter) all had significant differences between the two groups (all $p < 0.05$). There was a significant correlation between PR and LPA diameter ($r = 0.35$), McGoan ratio ($r = 0.32$), and Nakata index ($r = 0.43$), and the same as PR between RV length diameter ($r = -0.46$) and RV short diameter ($r = -0.34$).

ROC analysis also revealed that moderate sensitivity and specificity were obtained for predicting the occurrence of PR with LPA (66.33%; 82.60%), McGoan ratio (83.33%,56.52%), Nakata index (83.33%; 60.87%), RV length diameter 66.67%; 82.61%) and RV short diameter (77.78%; 60.87%).

Conclusion: This study indicated that these pre-operative indexes by DSCT are associated with post-operative PR, and these pre-operative PA and RV parameters could be new predictive factors for the occurrence of PR.

B-1231 15:12

Modified myocardial performance index for evaluation of foetal cardiac function in small for gestational age fetuses

A. Taori; Indore/IN (abhijitaaori@gmail.com)

Purpose: To test the validity of modified myocardial performance index for foetal cardiac function assessment and explore the sequence of changes in modified MPI, umbilical artery and ductus venosus flow in SGA fetuses.

Methods and Materials: Singleton pregnancies between 24 and 36 weeks gestation with 'small for gestational age fetuses' as assessed by foetal biometry were included. Umbilical artery and ductus venosus waveforms were obtained. Myocardial performance index was calculated as $MPI = (ICT+IRT)/ET$ with appropriate placement of Doppler gate to include both the lateral wall of the ascending aorta and the mitral valve, where the clicks corresponding to the opening and closing of the two valves could be clearly visualised.

Results: All fetuses with early-onset IUGR and abnormal umbilical artery indices had abnormal MPI values. Significant percentage of fetuses with late-onset IUGR and normal umbilical artery PI also had an elevated MPI. In IUGR fetuses, MPI is one of the earliest parameters affected and remains elevated throughout the different stages of IUGR. MPI is a direct measurement of myocardial performance while DV flow patterns are an indirect reflection, thus abnormal myocardial function becomes evident in DV only in advanced stage of deterioration.

Conclusion: Modified MPI is the earliest and reliable marker for global cardiac dysfunction in response to hypoxia. It can detect true growth-restricted fetuses amongst SGA fetuses with normal UA flow velocities. It has immense potential in late-onset IUGR fetuses where even a short period of hypoxia can cause severe morbidity.

B-1232 15:20

Diagnostic accuracy of non-contrast self-navigated free-breathing MRA in paediatric patients with coronary anomalies using CTA as reference standard

M. Albrecht¹, A. Varga-Szemes², C.N. De Cecco², T.J. Vogl¹, J.W. Nance², D. De Santis³, M. Eid², D. Piccini⁴, U.J. Schoepf²; ¹Frankfurt a. Main/DE, ²Charleston, SC/US, ³Rome/IT, ⁴Lausanne/CH (MoritzAlbrecht@gmx.net)

Purpose: To evaluate the diagnostic accuracy of a non-contrast, free-breathing, self-navigated 3D (SN3D) coronary MR angiography (cMRA) technique for coronary artery (CA) anatomy assessment in children with coronary abnormalities, using coronary CT angiography (cCTA) as the reference standard.

Methods and Materials: We prospectively enrolled 21 pediatric patients (15 male, 12.3 ± 2.6 years) undergoing same-day unenhanced SN3D cMRA and contrast-enhanced cCTA. Two radiologists scored the depiction of CA segments and reader confidence using a 3-point scale: 1=insufficient, 2=moderate, and 3=excellent. Readers assessed CAs for anomalies, high CA origin, and both inter-arterial and intra-mural CA course. Sensitivity, specificity, positive and negative predictive values (PPV, NPV) were calculated to evaluate diagnostic accuracy. Inter-observer agreement was assessed using Intra-class Correlation Coefficients (ICC).

Results: Fourteen children showed CA anomalies or pathologies on cCTA images. Depiction of CA segments was scored higher for cCTA compared to cMRA ($P < 0.015$), except regarding the left main CA ($P = 0.301$), with good ($ICC = 0.62$) to excellent ($ICC = 0.94$) inter-observer agreement. Diagnostic confidence was higher for cCTA evaluation ($P = 0.046$). Sensitivity, specificity, PPV and NPV of cMRA were 92%, 92%, 96% and 87% for the detection of CA anomalies, 85%, 85%, 74% and 92% for high CA origin, 71%, 92%, 82% and 87% for inter-arterial course, and 41%, 96%, 87% and 80% for intra-mural course.

Conclusion: SN3D cMRA is highly accurate for the detection of CA anomalies and inter-arterial course in children without radiation exposure, contrast administration, or need for breathing commands. Diagnostic confidence and CA visualisation, however, are still inferior in comparison with cCTA.

Author Disclosures:

A. Varga-Szemes: Consultant; Akos Varga-Szemes is a consultant for Guerbet. **C.N. De Cecco:** Consultant; Carlo N. De Cecco is a consultant for and/or receives research support from Guerbet and Siemens. **D. Piccini:** Employee; Siemens. **U.J. Schoepf:** Consultant; U. Joseph Schoepf is a consultant for and/or receives research support from Astellas, Bayer, Bracco, GE, and Siemens.

14:00 - 15:30

Room M 2

Neuro

SS 1511

Movement disorders and neurodegeneration

Moderators:

P. Demaerel; Leuven/BE
M. Vernooij; Rotterdam/NL

B-1233 14:00

MR imaging of the Parkinson's syndrome: a pictorial essay

E.D. Alves, C.d.F. Zorzenon, G.H.A.A. Bienes, H.B. Ferraz, H. Carrete Jr;
Sao Paulo/BR (ealves23@hotmail.com)

Purpose: The Parkinson syndrome is a worldwide condition that affects millions of people. This syndrome has a broad aetiology, but mostly are caused by unknown neurodegenerative process. Some of these diseases, including the most common one, the Parkinson disease, have been a usual challenge diagnosis to radiologist around the world. We intend to show that this situation can change under the new MRI sequences that have been developed and applied to the diagnosis of these conditions.

Methods and Materials: 40 patients suffering from Parkinson's syndromes underwent brain MRI non-contrast studies in a 3 Tesla system. We have applied the usual T1 and T2 images associated with a T1-weighted neuromelanin-sensitive image and to a multiecho susceptibility image to evaluate the substantia nigra and nigrosome-1. These patients all have already a clinical diagnosis, with a diverse aetiology. Among these group of aetiologies are Parkinson disease, Parkinson plus syndromes, vascular diseases, medication-related conditions and Parkinson-like processes (essential tremor). It was also done studies of 15 voluntary healthy control patients.

Results: Some of the diseases that cause Parkinson syndrome have presented typical findings in regular MRI studies. Others, like Parkinson disease, that a few years ago would have presented no conclusive MRI signs, have showed reliable findings in the T1 neuromelanin-sensitive images and in multiecho susceptibility images.

Conclusion: The use of the new developed sequences to evaluate the morphology and signal of the *substantia nigra* can provide reliable information for the differential diagnosis of the conditions that causes the Parkinson syndromes.

B-1234 14:08

Phase value assessment reveals iron accumulat in Parkinson disease

A.N. Sirin Özcan, E.B. Dirik; Ankara/TR (aysenursirinozcan@gmail.com)

Purpose: As a progressive neurodegenerative disorder Parkinson disease demonstrated iron accumulation in substantia nigra. In daily neuroradiology practice neuroimaging still have supplied limited information and used particularly only to exclude parkinson plus syndromes. Iron accumulation prediction was made with different methods and phase value assessment from susceptibility weighted imaging phase data is one of them.

Methods and Materials: 20 parkinson and 21 healthy control group patient included in the prospective study. MRI examination consisted Susceptibility weighted imaging with phase and magnitude imaging. Phase value quantified via SPIN software. Phase value evaluated from substantia nigra from three level at axial section for each side as right and left. Parkinson disease clinically effected and non effected side analyzed individually. Both side of Parkinson group compared with control group and also with each other. Statistical analysis was performed on SPSS with ANOVA test.

Results: Phase values were statically different in Parkinson and control group. But inside the Parkinson group although clinically effected side demonstrated higher phase values than non effected side it didn't showed statically significant difference.

Conclusion: Phase value assessment is useful to demonstrate iron accumulation effect at substantia nigra in Parkinson disease.

B-1235 14:16

Within- and across-network alterations of the sensorimotor network in Parkinson's disease

J. Caspers¹, S.B. Eickhoff², F. Hoffstaedter², C. Rubbert¹, J. Aissa¹, M. Südmeyer³, B. Turowski¹, A. Schnitzler¹, C. Mathys⁴; ¹Düsseldorf/DE, ²Jülich/DE, ³Potsdam/DE, ⁴Oldenburg/DE (Julian.Caspers@med.uni-duesseldorf.de)

Purpose: Neuroimaging studies repeatedly demonstrated alterations in sensorimotor areas related to Parkinson's disease (PD). As a systematic evaluation of the sensorimotor network (SMN) in PD is yet missing, we

investigate the within- and across-network functional connectivity (FC) of the SMN in PD based on independent component analysis (ICA) of resting-state fMRI.

Methods and Materials: Resting-state fMRI (3T, EPI, TR=2.2s, TE=30ms, flip-angle=90°, resolution=3.1x3.1x3.1mm, acquisition time=11min) was evaluated in 38 PD patients, acquired under regular medication (ON) and after withdrawal of dopaminergic drugs (OFF), and 43 age-, gender-, and movement-matched healthy controls. Preprocessed fMRI time series were decomposed into 20 intrinsic connectivity networks using ICA in FSL. We tested for group differences in FC between patients and controls within the SMN using dual regression (p<0.05, FWE corrected), and between SMN and the remaining 19 networks using FSLNets (p<0.05, FDR corrected).

Results: Within the SMN, PD patients (OFF) showed decreased connectivity in left inferior parietal lobule compared to controls and, additionally, in left postcentral gyrus compared to their ON scan. There were no group differences between patients (ON) and controls. Across networks, SMN was decoupled from (primary) motor and visual networks in PD OFF, which partially normalized in medical ON.

Conclusion: PD is associated with SMN connectivity impairments, both, within and across networks. These dysfunctions in short- and long-range sensorimotor connections are at least partially alleviated by dopaminergic treatment. Connectivity decrease within the network and to primary motor networks is directly linked to PD-related motor symptoms. Decoupling from visual networks hints to deficits in visuospatial integration for motor planning.

B-1236 14:24

Peculiarities of brain activation during dominant-hand tactile perception in lateralised Parkinson's disease

O. Omelchenko, Z. Rozhkova, M. Makarchuk, I. Karaban; Kiev/UA (Ol.Omelchenko@gmail.com)

Purpose: We propose brain activation and connectivity analysis during the unilateral tactile stimulation in primary and non-primary hand motor symptom lateralised Parkinson's disease (PD) patients for the motor PD symptom asymmetry impact study on the somatosensory processing in PD.

Methods and Materials: Three groups of right-handed subjects (G1/G2/G3) were studied with 1.5T Signa MR scanner (GE, USA). G1 consisted of 7 healthy subjects (4F, 51-83y.o.). G2 consisted of 6 PD patients with left-side (non-primary hand) motor symptoms (2F, 53-74y.o.). G3 consisted of 6 PD patients with right-side (primary hand) motor symptoms (2F, 56-74y.o.). Index finger tactile stimulation successively alternating for right and left hand was used for somatosensory fMRI activation. Data processing was made by FSL.

Results: For G1/G2/G3 activation of contralateral postcentral gyrus was shown. In G2/G3 primary (right) hand stimulation evoked more activation in bilateral postcentral gyri, contralateral superior parietal lobule, supramarginal gyrus, inferior part of pre/postcentral gyri. In G3 activation of contralateral ventral premotor area was found. Increased functional connectivity was shown for left globus pallidus, right dorsal premotor cortex, right dorsolateral prefrontal cortex in G2 and bilateral premotor, right prefrontal, bilateral superior parietal lobule in G3.

Conclusion: Primary somatosensory cortex remains steadily active during tactile stimulation in PD, while primary hand tactile stimulation in primary hand lateralised PD patients also evoke activation of primary and associative sensory, motor and executive nodes of the cortex. Tactile stimuli processing evokes increased connectivity of globus pallidus, premotor, prefrontal and parietal cortex, which might reveal tactile-evoked motion suppression in PD.

B-1237 14:32

Detection of Parkinson's disease based on resting-state inter-network functional connectivity using machine learning

C. Rubbert¹, C. Mathys^{1,2}, S.B. Eickhoff^{3,1}, F. Hoffstaedter^{3,1}, M. Südmeyer⁴, C.J. Hartmann^{1,1}, B. Turowski¹, A. Schnitzler^{1,1}, J. Caspers^{1,3,1}; ¹Düsseldorf/DE, ²Oldenburg/DE, ³Jülich/DE, ⁴Potsdam/DE (christian.rubbert@med.uni-duesseldorf.de)

Purpose: Parkinson's disease (PD) is a clinical diagnosis, which may be challenging in certain cases. Resting-state functional connectivity has been reported to show alterations in PD and may prove to be a valuable biomarker in those cases. We evaluated an unsupervised, data-driven classification approach to identify PD patients based on between-network connectivity in whole-brain resting-state fMRI (rs-fMRI).

Methods and Materials: Whole-brain rs-fMRI (Siemens Trio 3T, EPI/TR=2.2s/TE=30ms/flip angle=90°/resolution=3.1x3.1x3.1mm/acquisition time=11min) was assessed in 42 PD patients (medical OFF) and 47 healthy controls (HC) matched for age and gender. Between-network connectivity based on full and partial correlation measures were computed for each subject based on a canonical functional network architecture at different levels of granularity (Human Connectome Project, "recon2" subjects, 03/2017 dataset). A boosted logistic regression model was trained on the correlation matrices using 20 repeats of 10-fold cross-validation. The number of iterations was fixed

at 100, then optimized for the best set of components. Accuracy was averaged over the validation folds to evaluate model performance.

Results: The median accuracy over the different granularities was as following: 15 components = 61.9% (full correlations)/66.4% (partial correlations), 25=75.8%/73.1%, 50=71.4%/65.6%, 100=66.0%/62.5%, and 200=67.0%/52.5%. 160 iterations were found to be optimal for the best model (25 components), yielding a median accuracy of 75.9% (SD=3.5) for full correlations and 74.5% (SD=3.9) for partial correlations.

Conclusion: The accuracy for predicting PD in rs-fMRI is overall acceptable. It is varying with the number of components and better at a lower number of components, which should be explored in more detail.

B-1238 14:40

Volumetric analysis of the pattern of brain atrophy in Wilson's disease
J.P. Chu, Y. Song, X. Tang, L. Zou; *Guangzhou/CN (15692009037@163.com)*

Purpose: To quantitatively evaluate brain atrophy pattern in Wilson's disease (WD) using a novel and validated fully automated whole brain segmentation method.

Methods and Materials: 3D-T1-weighted MRI scans were obtained from 27 WD patients (M: 17, F: 10, median: 31.3y) with neurological manifestations and 25 health controls (M: 8, F: 17, median: 25.1y). The volumetric segmentations of each structure were obtained automatically by using a multi-atlas processing pipeline to segment T1-weighted images into 289 anatomical regions of interest (ROI). In the volumetric group difference analyses, multiple comparison correction was carried out by controlling the family-wise error rate (FWER) at 0.05.

Results: In WD patients, significant volumetric decrease was found in 59 ROIs. Deep nuclei including bilateral putamen, substantia nigra, red nucleus, globus pallidus, caudate nucleus and thalamus showed obvious atrophy. For neuroanatomically defined white matter, we found significant atrophy of bilateral superior fronto-occipital fasciculus, external capsule in the claustrum, subcortical white matter of the subgenual anterior cingulate cortex, corticospinal tract, then followed by anterior corona radiata and cerebral peduncle ($P < 0.001$). More notably, volumetric reduction detected in deep nuclei was more severe than white matter. Among basal ganglia, the putamen showed the most obvious atrophy. Moreover, eight ROIs including lateral and third ventricles had volumetric increase, which indicated a larger ventricular system secondary to brain atrophy.

Conclusion: Volumetric data obtained with automated segmentation of cerebral regions showed a significant atrophy of different brain structures in WD. Our study demonstrated that the atrophy of deep nuclei was more obvious than whiter matter.

B-1239 14:48

A 3 Tesla MRI brain atlas for Parkinson's disease as diagnostic and interventional tool

I. Papageorgiou^{1,2}, L. Angelidakis³, C. Damianou³, M.-N. Psychogios², P. Lingor², K. von Eckardstein², A. Malich¹, S. Hadjidemetriou³,
¹Nordhausen/DE, ²Goettingen/DE, ³Limassol/CY
(ismini.e.papageorgiou@gmail.com)

Purpose: Parkinson's disease (PD) is a chronic degenerative disorder of the central nervous system. The aim of this work is to develop an MRI-based brain atlas representative of the PD-brain alterations for diagnostic and interventional medical applications.

Methods and Materials: The data were 3.0 T MRI brain images from 16 PD patients and 10 matched controls. The brain atlases with multiple contrasts have been computed with the open platform 3D Slicer® using T1-weighted (T1w), T2-weighted (T2w) images, as well as susceptibility weighted images (SWI). Anatomic co-registration with a labeled atlas in BrainSuite® was done, refined with the level-set segmentation method by ITK-Snap®. Target structures were analysed for their volume and signal intensity.

Results: Comparison with the control group unravels a significant PD-related T1w signal loss in the caudate nucleus (CN) and putamen (Put) compared to age-matched controls (CTL). The T1w signal intensity is significantly reduced in PD patients in the CN/Put by approximately 8%/4% on the average CTL value ($p < 0.001$, rank-sum test), albeit without associated volume loss. The diagnostic efficacy of the T1w signal intensity is high according to the ROC analysis with an AUC 0.93/0.88. T1w, T2w and SWI atlas data, as well as average 3D volume rendering reconstructions for the substantia nigra, red nucleus, subthalamic nucleus and thalamus, are provided in detail.

Conclusion: We establish a disease-specific, PD MRI brain atlas for the midbrain structures and the striatum using the 3D Slicer®. T1w signal loss in the striatum may be a promising PD imaging biomarker.

B-1240 14:56

Asymptomatic T1 pallidal hyper intensity in patients with chronic liver disease

F. Costa, J.P. Filipe, C. Reis; *Porto/PT*

Purpose: T1 pallidal hyperintensity is believed to be caused by the deposits of neuroactive substances in the brain, particularly manganese. These changes may precipitate Acquired Hepatocerebral Degeneration (AHD), a rare chronic encephalopathy that may follow any form of chronic liver disease (CLD). Its clinical spectrum comprises motor signs, cognitive impairment, short term memory loss and in some cases mielopathy. It is believed that its prevalence is approximately from 1 to 2% in patients with CLD. Little is known about the prevalence of T1 pallidal hyperintensity in chronic liver patients population that bare no symptoms and may therefore be wrongfully labeled as AHD.

Methods and Materials: We retrospectively analyzed the medical records and imaging studies of CLD patients, for whom brain MRI data was available. The presence of T1 hyperintensity, its location and signal intensity was registered. We used non-parametric tests and Fisher's exact test to evaluate the association between symptomatic and asymptomatic patient and T1 signal intensity, hyperintensity location and Child-Pugh scores.

Results: We identified 250 patients, of which 16 (6.4%) had T1 pallidal hyperintensity, and among them only 7 (2.8%) presented with AHD clinical spectrum symptoms, meaning that 56% of patients with T1 pallidal hyperintensity showed no symptomatology whatsoever. Comparing symptomatic and asymptomatic patients, we observed no significant univariate association between the two groups and Child-Pugh score, signal intensity or location.

Conclusion: The T1 hyperintense pallidal signal is not predictive of AHD in this exploratory study, raising the question of its exact role in the clinical diagnosis of AHD.

B-1242 15:04

T2* hypointensity of the bulbar segment of the primary motor cortex in ALS patients with bulbar impairment

G. Donatelli, E. Caldarazzo Ienco, G. Migaletto, P. Cecchi, G. Aringhieri, G. Siciliano, M. Cosottini; *Pisa/IT*

Purpose: In amyotrophic lateral sclerosis (ALS) the disruption of bulbar function as speech and swallowing is a possible clinical manifestation and to distinguish between the contribution of UMN and LMN degeneration to bulbar impairment is difficult. Recent 7T-MR studies suggested T2*-hypointensity as a possible marker of UMN impairment in ALS patients. We assessed the cortical T2* signal intensity of the bulbar segment of the primary motor cortex (fM1) in ALS patients, and its relationship with bulbar impairment.

Methods and Materials: Forty-seven ALS patients underwent 3D multi-echo T2*-weighted sequence at 3T-MR. Two neuro-radiologists visually assessed fM1 signal intensity using a score system (0=signal intensity similar to that of the postcentral gyrus; 1=mild hypointensity; 2=marked hypointensity). The bulbar impairment was evaluated using the items I-III of ALSFRS-R.

Results: Thirteen patients had bulbar impairment. In 15 patients fM1 was rated bilaterally hypointense: 10 patients received score=2 and had bulbar impairment; 5 patients received score=1 and have not bulbar impairment. fM1 of two patients without bulbar symptoms had score=1 only in one side. Thirty patients received score=0; three of them had bulbar impairment. Considering score=2 as pathological, sensitivity, specificity, PPV, NPV and accuracy of fM1 hypointensity were 0.77, 1, 1, 0.92 and 0.94. Considering bilateral score>0 as pathological, they were 0.77, 0.85, 0.67, 0.90 and 0.83. The interobserver agreement was 0.78.

Conclusion: The marked bilateral fM1 hypointensity seems the typical finding in ALS patients with bulbar impairment. The follow-up of patients without bulbar symptoms could provide information about the prognostic role of fM1 hypointensity.

B-1243 15:12

Role of qualitative and quantitative parameters in differentiation of PSA from other atypical parkinsonian syndromes in MRI

P. Hota¹, T. Dhibar², A. Biswas²; ¹Bangalore/IN, ²Kolkata/IN
(meparamitahota@gmail.com)

Purpose: Overlapping atrophic features without specific radiological signs complicate the diagnosis of various atypical parkinsonian syndromes. A method of differentiating progressive supranuclear palsy from other atypical Parkinsonian syndromes with qualitative and quantitative measurement of midbrain volume loss is introduced.

Methods and Materials: T1 mid-sagittal MRI image of 35 patients with clinically diagnosed PSP (n=6), MSA (n=4), DLB (n=2), CBD (n=3) and IPD (n=20) were acquired and measurements were taken as depicted below. Elliptical region of interest was placed over the pons and the midbrain in mid-sagittal slice. Two lines were drawn to define the major axes of the ellipses, corresponding to superior - inferior axis. The maximum measurement

perpendicular to the major axis was taken as the absolute pons and midbrain diameter for calculation.

Results: The absolute midbrain diameter and the midbrain to pons ratio were measured. Statistical significance of midbrain measurement $< 9.35\text{mm}$ calculated from two columns and rows contingency table by Fisher's exact probability test gives the P value that is < 0.001 . 100% of clinically diagnosed MSA and PSP cases had a midbrain diameter measured as previously shown $< 9.35\text{mm}$. 100% of clinically diagnosed PSP cases showed midbrain to pons ratio as described before < 0.52 .

Conclusion: Midbrain to pons ratio < 0.52 is 100% specific for detection and differentiation of PSP from other atypical parkinsonian syndromes. This sign is reproducible, simple and correlates with other previously published results.

14:00 - 15:30

Room M 3

Oncologic Imaging

SS 1516

Prostate cancer: what's next?

Moderators:

I. Blazic; Belgrade/RS
U.G. Mueller-Lisse; Munich/DE

B-1244 14:00

Radiological Wheeler staging system: a valid tool to improve the local staging of organ-confined prostate cancer with mp-MRI

E. Tabone¹, V.M. Doronzio¹, E. Appendino¹, V. Romano¹, S. Pedalino¹, M. Manfredi², S. Mazzetti¹, D. Regge¹, F. Russo¹; ¹Candiolo/IT, ²Orbassano/IT (emanuele.tabone@gmail.com)

Purpose: To determine a new multiparametric-MRI staging system based on pathology for the assessment of capsular invasion in PCa.

Methods and Materials: This retrospective single center multi-reader study included consecutive patients with preoperative mp-MRI who underwent non nerve-sparing radical prostatectomy. Three radiologists with different experience and blinded to pathology, reported all examinations, classifying lesions according to a 5-point score based on radiological Wheeler (rW), derived from the pathological Wheeler (pW). Whole-mount histological sections were used as the reference standard and the pathologist defined the extent of capsular invasion using pW. PCa classified as L0,L1,L2 (respectively without contact, with contact or with infiltration of fibrous capsule) were grouped in the T2 stage class, while L3F and L3E (respectively with radial extracapsular infiltration $\leq 0.7\text{mm}$ and $> 0.7\text{mm}$) in the T3 stage class. The accuracy of mp-MRI in predicting the pathological group T2 or T3 was assessed and AUC analysis was performed for each and overall readers.

Results: 105 patients were included for a total of 130 PCas. Sensitivity of the most experienced reader was 49% (17/35 T3 PCas), specificity 95.8% (91/95 T2 PCas), PPV 81% (17/21), and NPV 83% (91/109). Overall sensitivity was 60%, specificity 77%, PPV 50%, and NPV 84%. The AUC of the two most experienced readers in the detection of capsular invasion was 0.72-0.74.

Conclusion: In experienced hands organ-confined PCa is well recognized by mp-MRI and allows pre-treatment decision to tailor surgical approach (i.e., nerve-sparing radical prostatectomy). The understaging of T3 tumours remains a limitation, independently of radiologist expertise.

B-1246 14:08

Comparison of prostate cancer detection rates between MR-targeted and saturation TRUS-guided biopsy

V. Romano¹, E. Tabone¹, E. Appendino¹, S. Mazzetti¹, V. Giannini¹, A. Giacobbe², G. Muto², F. Russo¹, D. Regge¹; ¹Candiolo/IT, ²Milan/IT (vittorio.romano@ircc.it)

Purpose: To compare PCa detection rate of in-bore MR-targeted biopsy and of saturation TRUS-guided biopsy in men with clinical suspicion of PCa and a positive MRI finding.

Methods and Materials: Diagnostic mp-MRI was performed using a 1.5T magnet and a phased-array coil combined with an endorectal coil. Acquisition protocol included T1- and T2-weighted, diffusion-weighted, and dynamic contrast-enhanced imaging. Subjects with at least one region with suspicion of PCa were considered positive at MRI, and randomly allocated (ratio 1:1) to MR-targeted biopsy (arm A) or saturation TRUS-guided biopsy (arm B). In MR-targeted biopsy only index lesions were sampled, using at least 2 cores, while in saturation TRUS-guided biopsy at least 28 cores were retrieved. Biopsy Gleason score (bGS) was used as the reference standard.

Results: PCa detection rate was 71% and 76% in arm A and arm B, respectively. No statistical significant difference was observed between the detection rates of the two study arms ($p=0.58$). In arm B, we observed higher overall PCa detection rate in the biopsy-naïve group than in patients with at

least one previous negative biopsy (88% vs 62%, $p=0.03$). Sampling efficiency was in favour of arm A with 59.7% of core detecting PCa versus 22.3% of the arm B ($p < 0.0001$).

Conclusion: In-bore MR-targeted biopsy has a comparable PCa detection rate to TRUS-guided saturation biopsy, but reached a significant higher positivity rate of biopsy cores. Using a lower number of sampling cores could reduce pain perceived by patients, increasing acceptance and tolerability of the targeted procedure.

B-1247 14:16

Targeted MRI/TRUS fusion-guided biopsy in patients with suspicious pararectal lymph nodes after radical prostatectomy

V. Kapustin, A. Gromov, V. Shirokorad, Y. Subbotin; Moscow/RU (www.kapustin@yandex.ru)

Purpose: To determine a possibility of simultaneous transrectal ultrasound and MR imaging technique (sensor-based MR-TRUS Fusion) for biopsy guidance in patients with biochemical recurrence (BR) after radical prostatectomy when metastatic involvement of pararectal LN is suspected.

Methods and Materials: 18 patients with BR after radical prostatectomy (RP) and suspicious pararectal LN were included in this study. Multiparametric 1.5T MRI with a surface coil were performed. Initial MR examinations showed suspicious pararectal LN in 16 cases. In 2 cases pararectal LN-mts were primarily suspected by PET-CT findings and subsequent retrospective MRI data review. Simultaneous MR and TRUS image formations were performed. High accuracy level (0.3-0.4 cm) of "Fusion" images superposition was achieved in 11 cases. In these cases core-needle targeted biopsies (TB) of suspicious LN were performed. In 3 cases achieved accuracy level was too low, however areas of suspicious LN localization for further TRUS-guided TB were detected. Eventually, in 2 cases LN-mts were localized at the level of rectosigmoid junction, thus they were unachievable for TRUS approach. In these cases fine-needle aspiration biopsies (FNAB) were performed with cognitive Fusion navigation under endosonoscopic control.

Results: Use of MRI/TRUS-Fusion technique allowed us to verify metastatic involvement of pararectal LN in 13 out of 18 cases. In the remaining 5 cases fragments of pelvic fat with no evidence of tumor growth or LN tissue were histologically revealed.

Conclusion: MRI/TRUS-Fusion proves to be a promising technique for targeted core-needle biopsies in patients after RP when a pararectal lymph nodes mts-involvement is suspected.

B-1248 14:24

Could mpMRI really improve the detection of clinical recurrence of prostate cancer with low PSA value and efficacy of radiation treatment?

F. Kosssov, P. Bulychkin, D. Romanov, M.A. Shorikov, E. Tarachkova, V. Panov, S. Tkachev, B. Dolgushin, G. Hagverdiyeva; Moscow/RU (fil-doc@yandex.ru)

Purpose: Salvage radiation therapy (SRT) is the main treatment modality for patients with prostate cancer recurrence (PCaR) after radical prostatectomy (RP). Clinical PCaR (tumour substrate appearance at area of prostate bed or regional lymph nodes metastasis) early detection improves SRT efficiency. Medical imaging plays minor role in clinical PCaR diagnostic due to low accuracy of routine radiological approaches (TRUS-CT-MRI). Multiparametric MRI (mpMRI) would significantly improve clinical PCaR detection even in patients with low PSA values and small sizes of tumour substrate.

Methods and Materials: 142 men (54-71 years, median - 62) with biochemical recurrence (PSA $> 0.2\text{ ng/ml}$) after RP were examined by mpMRI before and 6 months after SRT with every 3 months PSA control. There were 2 groups of patients with clinical PCaR: 1) PCaR size $> 5\text{ mm}$ (PSA 0.9 ng/ml); 2) PCaR size $< 5\text{ mm}$ (PSA 0.5 ng/ml). Prescribed dose of SRT to regional lymphatic nodes was 44 Gy, to prostate bed - 66 Gy (72 Gy - if region of clinical PCaR was identified).

Results: Clinical PCaR was found in 121 cases. 8 patients had distant metastasis. 13 patients had no significant mpMRI data of clinical PCaR. mpMRI sensitivity/specificity for clinical PCaR at I group were 89%/96%; at II group - 78%/87%, respectively. In all cases, PSA progression decreases after SRT was evaluated. Size of clinical PCaR significantly correlated with PSA level ($p < 0.001$). Higher SRT doses to PCaR areas associated with fast PSA level decrease ($p < 0.004$).

Conclusion: mpMRI showed high sensitivity and specificity in clinical PCaR detection. SRT escalation dose to area of clinical PCaR effected to more progressive PSA reduction.

B-1249 14:32

11C-Choline PET/CT in the detection of oligometastatic prostate cancer recurrence

D. Poursanova, I. Aslanidis, O. Mukhortova, I. Ekaeva, T.A. Trifonova, V.I. Shirokorad, D.A. Roshchin; *Moscow/RU (dipoursanidou@gmail.com)*

Purpose: To investigate the diagnostic value of 11C-Choline PET/CT in the detection of oligometastatic prostate cancer (PCa) recurrence, which is essential in determining the personalized therapeutic approach.

Methods and Materials: This retrospective analysis included results of 11C-Choline PET/CT examinations performed in 217 PCa patients with rising PSA after radical treatment. The mean PSA value in the group was 2.1 ± 2.5 (0.2-9.7) ng/ml. Examinations were done on PET/CT scanner (Biograph-64, Siemens) 10 min after 11C-Choline injection (400-550Mbcq).

Results: Overall, PET/CT detected PCa relapse in 56% (121/217) patients, of which 68% (82/121) had oligometastatic process (1-3 lesions). Local relapse was revealed in 62% (51/82) patients, distant oligometastatic lesions were identified in 33% (27/82), both local and distant metastases in 5% (4/82) cases. Oligometastases to lymph nodes were diagnosed in 35 patients, of which 71% (25/35) had single foci, and of these 57% (20/35) were presented by normal-size lymph nodes (median 6 mm). Oligometastases to skeleton were revealed in 23 patients, of which 78% (18/23) had single foci, and the rest had several - two (n=4) and three (n=1) foci. Importantly, that 5 of 23 PET-positive patients with bone metastases had no structural abnormalities on CT images, corresponding to isolated involvement of bone marrow.

Conclusion: 11C-Choline PET/CT has been shown to be a noninvasive accurate technique for detection of recurrent PCa in patients with rising PSA after radical treatment, which allows to differentiate patients with local and distant metastases in one study, as well as identify oligometastatic process and, therefore, is useful in determining the further personalized therapeutic approach.

B-1250 14:40

Comparisons of imaging biomarkers on simultaneous choline PET and multiparametric MRI between TNM staging in high-risk prostate cancer patients

L.-J. Wang, J.-R. Tseng, Y.-C. Lin; *Taoyuan/TW (lijenwang0918@gmail.com)*

Purpose: To compare imaging biomarkers between TNM staging on simultaneous C11 choline PET (chPET) and multiparametric prostate MRI (mpMRI) in high-risk prostate cancer (PCA) patients.

Methods and Materials: From January 2015 to December 2016, we prospectively enrolled 31 PCA patients undergoing simultaneous chPET and mpMRI. Of each patient, total lesion glycolysis and metabolic tumour volume of standardized uptake values (SUV_{TLG} and SUV_{MTV}), maximum values of perfusion parameters ($k_{trans,max}$ and kep_{max}), and minimum value of apparent diffusion coefficient (ADC_{min}) of PCA were recorded. The presence or absence of extra-prostate or adjacent organ extension (T3-4), regional lymph node metastasis (N1) and distant metastasis (M1) of each patient was determined by histological results, imaging findings, clinical examinations and follow-up. Imaging biomarkers between patients with and without T3-4, N1 and M1 were compared using Mann-Whitney U test.

Results: Of the 31 patients, there were 27 patients (87.1%) with T3-4, 13 patients (41.9%) with N1, and 17 patients (54.8%) with M1 diseases. Significant differences of SUV_{TLG} , SUV_{MTV} , $k_{trans,max}$, kep_{max} and ADC_{min} between patients without and with T3-4 as well as of SUV_{TLG} and SUV_{MTV} between patients without and with M1 were shown (all $p < 0.05$). Nonetheless, there were no significant differences of all 5 imaging biomarkers between patients without and with N1 as well as of $k_{trans,max}$, kep_{max} and ADC_{min} between patients without and with M1 diseases.

Conclusion: Imaging biomarkers on chPET and mpMRI are good indicators of primary tumour status of PCA.

B-1251 14:48

Prospective evaluation of extent of disease in prostate cancer biochemical relapse by ^{68}Ga PSMA-HBED-CC PET/CT

G. Chong, D. Barahona Z., A. Balcells, D. Hasson, G. Schiappacasse, A. Labra Weitzler; *Santiago de Chile/CL (danibarahona@gmail.com)*

Purpose: Accurately determining the extent of disease on biochemical relapse of prostate cancer (PCa) can have important therapeutic implications. The lesion detection rate of ^{68}Ga PSMA-HBED-CC-PET/CT and its relation to prostate-specific antigen (PSA) level and Gleason score is evaluated.

Methods and Materials: All patients subjected to ^{68}Ga PSMA-HBED-CC-PET/CT with PCa biochemical relapse, from November 2014 to December 2016 were included. Laboratory exams performed prior to PSMA-PET-CT were retrieved from electronic medical records, and histopathology results were extracted from surgical specimens. All high-uptake regions were identified by two experienced readers. Regional involvement was defined as urethrovesical anastomosis lesions or pelvic lymphadenopathies.

Results: 102 patients were recruited. Mean age was 70.3 years (SD: 9.2), and median PSA Score was 2.52 ng/ml (IQR: 7.1), with a minimum value of 0.04 ng/ml, and 35% of PSA values under 1 ng/ml. PSMA-PET/CT was positive for 70% of patients. Among PSMA-PET/CT positive cases, 55% had regional involvement and 2.5% had suprapelvic lymphadenopathies without regional involvement. PSMA-PET/CT was positive in 43% of studies with PSA levels of < 1 ng/ml. The lowest PSA level related to a positive finding was 0.11 ng/ml. 16% of lymphadenopathies detected were under 0.5 cm, and 69% were under 1 cm. 28% of studies showed bone metastases. A high Gleason score (9-10) was non-significantly associated with a higher number of pelvic metastases.

Conclusion: ^{68}Ga PSMA-HBED-CC-PET/CT can identify secondary lesions in PCa biochemical relapse even in patients with very low PSA levels and can accurately identify small intra- and extra-pelvic lymphadenopathies, which can substantially influence treatment planning.

B-1252 14:56

The impact of ^{68}Ga PSMA I&T PET/CT on radiotherapy planning in patients with biochemical cancer relapse after radical prostatectomy in prostate cancer.

C. Berliner, T. Frenzel, M. Tienken, M. Abdel, S. Klutmann, D. Beyersdorff, G. Adam, A. Krüll, P. Bannas; *Hamburg/DE (caberberliner@gmail.com)*

Purpose: To determine the impact of ^{68}Ga PSMA I&T PET/CT on radiotherapy planning of biochemical cancer relapse of prostate cancer.

Methods and Materials: We performed a retrospective analysis of 75 patients who underwent ^{68}Ga PSMA I&T PET/CT scans prior to scheduled radiotherapy treatment. All patients had a documented biochemical relapse after radical prostatectomy. The age distribution was median 69 (range 52-86) years. The PSA level was median 0.2 (range 0.02-653.2) ng/ml. We compared the impact of ^{68}Ga PSMA I&T PET/CT on lesion detection and treatment decision.

Results: ^{68}Ga PSMA I&T PET/CT revealed a total of 47 positive lesions, whereas CT detected 18 lesions. The therapeutic regimen was changed in 32 of 75 cases (43%) based on the ^{68}Ga PSMA I&T PET/CT. In 31 cases (41%) it upstaged to an enhanced tumour extension. Twenty-five cases (33%) received an additional boost to the ^{68}Ga PSMA I&T PET/CT-positive findings.

Conclusion: ^{68}Ga PSMA I&T PET/CT is an advanced hybrid imaging technique prior radiotherapy treatment for prostate cancer patients with proven biochemical relapse. It is significantly impacting the radiotherapy planning and enables individualized therapy for prostate cancer patients.

B-1253 15:04

Clinical utility of ^{18}F -NaF and ^{68}Ga -PSMA PET-CT as prognostic marker in patients with metastatic prostate cancer treated with Radium-223

S.S. Medina-Ornelas, F. Garcia-Perez; *Mexico City/MX (dr.sebastian@outlook.com)*

Purpose: Determine if ^{18}F -NaF and ^{68}Ga -PSMA PET/CT can predict response to ^{223}Ra treatment in patients with metastatic prostate cancer (mPC).

Methods and Materials: Twenty patients with metastatic castration-resistant PC (mCRPC), and seven patients with high-grade PC (hgPC), were evaluated with ^{18}F -NaF and ^{68}Ga -PSMA PET-CT prior to receipt ^{223}Ra therapy a standard dose (55kBq/kg), and 4-6 weeks after the last dose, with simultaneous measurements of PSA and alkaline phosphatase (AP). A semiquantitative bayesian analysis of each patient allowed to establish 3 study groups based on the molecularly active volume: low-burden (< 1000 cm³), medium-burden (1001-3000 cm³); and high burden (> 3001 cm³). Ten patients were classified as high-burden, 7 patients as medium-burden and 10 patients as low-burden.

Results: Fifteen patients completed 6 cycles (7-hgPC, 8-mCRPC). Nine were of low burden and six of medium-burden, which showed a decrease in PSA and AP levels ($p < 0.05$); the rest of patients according to the number of doses variable results was obtained; the value of ^{18}F -NaF and ^{68}Ga -PSMA as a predictive tool in response therapy according to the degree of tumour burden. Patients with low-burden treated with ^{223}Ra showed to be a predictor of good prognosis in response to treatment ($p < 0.05$); while patients with high-burden have a high probability of do not complete 6 cycles.

Conclusion: The PET-CT in the evaluation of response to ^{223}Ra is useful tool in the selection of those patients who are likely to improve according to their degree of overall tumour burden, in addition to timely evaluation of therapeutic efficacy.

B-1254 15:12

Assessment of response to therapy in bone metastases from prostatic malignancy beyond mono-exponential diffusion imaging

R. Balaji; *Chennai/IN (ravikanthbalaji@gmail.com)*

Purpose: To evaluate performance of intra-voxel incoherent motion model of diffusion imaging in monitoring treatment response in bone metastases from prostatic malignancy and possible identification of early androgen resistance.

Methods and Materials: 36 patients with histologically proven prostatic malignancy with bone metastases on whole body diffusion imaging (using

DWIBS sequence) with no prior treatment with anti-androgens were included in the study. Imaging was performed on Achieva 1.5 Tesla scanner (Philips Healthcare, Best, The Netherlands) the day after commencement of antiandrogen therapy and thereafter at 3 time points: 2 weeks, 3 months and 6 months. Lesions in iliac bones or sacrum were analysed. Images were acquired in an axial plane with 11 b values. IVIM parameters (perfusion fraction [f], molecular diffusion coefficient [D], and perfusion-related D [D^*]) and apparent diffusion coefficient (ADC) were obtained.

Results: D values (P 0.001) were the most sensitive, robust and reproducible indicator for response. D values increased in the first 2 weeks of therapy and continued to rise and plateaued off after 3 months. f values increased after one month and remained stable till 3 months but showed further increase at 6 months. ADC values derived from mono-exponential equation also showed elevation after therapy.

Conclusion: D values derived from IVIM model demonstrated very good measurement repeatability and sensitive to treatment response. f values provide complimentary data to identify tumour response. Thus, a combination of ADC, D and f values would provide non-invasive monitoring of therapy and possibly predict early resistance to treatment.

14:00 - 15:30

Sky High Stage

Abdominal Viscera

MY 15

Abdominal and Gastrointestinal

Moderators:

M. Dewey; Berlin/DE
M. Zins; Paris/FR

B-1255 14:00

The efficacy of MRI in the diagnostic work-up of cystic fibrosis-associated liver disease

S. Pötter-Lang, K. Stauer, P.A.T. Baltzer, D. Tamandl, D. Muin, N. Bastati-Huber, E. Halilbasic, L. Kazemi-Shirazi, A. Ba-Ssalamah; Vienna/AT (sarah.potter-lang@meduniwien.ac.at)

Purpose: To identify independent imaging features and establish a diagnostic algorithm for early diagnosis of cystic fibrosis-associated liver disease (CFLD) in CF patients as compared with a control group (CG) on gadoxetic acid-enhanced MRI.

Methods and Materials: 90 adult patients were enrolled, 50 with CF and 40 of the CG. The CF group was divided in two subgroups, the retrospective or test subgroup ($n = 33$) and the prospective or validation subgroup ($n = 17$). The CG (patients with normal liver enzymes, but no more than benign focal liver lesions) was divided also accordingly (27:13). MRI variables including quantitative and qualitative parameters were used to distinguish those with CFLD from the CG using the clinical criteria by Debray. Fifteen qualitative single-lesion CF descriptors were defined. Two readers independently evaluated the images. Univariate statistical analysis was performed to obtain the significant imaging features that differentiate CF patients from the CG. Subsequently, a multivariate classification analysis using the chi-squared automatic interaction detector (CHAID) methodology was performed to identify the most important descriptors. Diagnostic performance was assessed by receiver-operating characteristic (ROC) analysis.

Results: Three independent imaging descriptors distinguished CFLD from CG: a) the presence of altered gallbladder morphology (GBAM); b) periportal tracking (PPT) and c) periportal fat deposition (PPFD). Prospective validation of the classification algorithm demonstrated a sensitivity of 94.1 % and specificity of 84.6 % for discriminating CFLD from the control cohort.

Conclusion: We identified 3 independent imaging features that could potentially diagnose early-stage CFLD on unenhanced MRI.

B-1256 14:04

T₁ mapping on gadoxetic acid-enhanced MR imaging potentially predicts recurrence of HCC after hepatectomy

W.T. Wang, S. Zhu, Y. Ding, L. Yang, C.-Z. Chen, Q.-H. Ye, M.-S. Zeng, S.-X. Rao; Shanghai/CN (787356268@qq.com)

Purpose: The enhancement on hepatobiliary phase on gadoxetic acid-enhanced magnetic resonance imaging (MRI) could reflect biological properties of hepatocellular carcinoma (HCC). The retrospective study aimed to evaluate the prognostic significance of T₁ mapping on gadoxetic acid-enhanced MRI in prediction of recurrence of single nodular HCC (≤ 3 cm) after hepatectomy.

Methods and Materials: A total of 107 patients with single nodular HCC (≤ 3 cm) who underwent preoperative gadoxetic acid-enhanced MRI followed by hepatectomy was included retrospectively. Independent prognostic MR imaging findings were identified on multivariate analysis. Based on the optimal

cut-off value of the receiver operating characteristic (ROC) curve analysis, cumulative recurrence rates were compared between groups of low and high reduction rate of T₁ relaxation time.

Results: Reduction rate of T₁ relaxation time ($P = 0.001$; hazard ratio = 0.08; 95% confidence interval [CI]: 0.02-0.38) and non-hypervascular hypointense nodules ($P = 0.042$; hazard ratio = 2.21; 95% CI: 1.03-4.77) in preoperative gadoxetic acid-enhanced MRI were independently related to recurrence of HCC after hepatectomy. The area under ROC curve analysis of reduction rate of T₁ relaxation time was 0.802. Patients with lower reduction rates ($\leq 44.8\%$) group had higher cumulative recurrence rates. A combination of these two risk factors in patients with single HCC had significantly higher recurrence rates compared to those with either or none of the two risk factors during the years of follow-up.

Conclusion: Reduction rate of T₁ relaxation time in combination with the presence of non-hypervascular hypointense nodules can potentially predict recurrence of HCC after hepatectomy.

B-1257 14:08

Magnetic resonance imaging of hepatitis B virus-related hepatocellular carcinoma: correlations with imaging features and molecular marker glypican-3

S. Wang, J.H. Li; Beijing/CN (wangsudn815@163.com)

Purpose: To investigate whether imaging features from dynamic contrast-enhanced magnetic resonance imaging (DCE-MRI) could aid in the prediction of pathological grading of hepatocellular carcinoma (HCC) related to hepatitis B virus (HBV) cirrhosis, by correlation analysis between lesion signal intensity variation in MRI and glypican (GPC)-3 immunohistochemistry.

Methods and Materials: Seventy-four patients with HBV-related HCC (22 cases well-differentiated HCC, 33 cases moderately differentiated, and 19 poorly differentiated) underwent DCE-MRI and biopsy before any targeted therapy. Signal intensity variance ratio was used to assess the image contrast between the region of interest (ROI) of tumours and liver parenchyma, by two radiologists who independently drew the ROI and calculated signal variance ratio on MRI images. GPC-3 expression grading was evaluated with immunohistochemistry.

Results: Low GPC-3 expression level was observed predominantly in well-differentiated HCC, whereas high GPC-3 expression level was observed predominantly in poorly and moderately differentiated HCC ($p < 0.05$). We observed a significant correlation between GPC-3 expression and lesion signal intensity variance ratio in the arterial enhancement phase ($r = 0.323$, $p = 0.005$), as well as between GPC-3 expression and lesion signal intensity variance ratio from T2-weighted images ($r = 0.276$, $p = 0.017$). However, no correlation was found between GPC-3 grade and signal variance ratio in hepatic portal venous and late phases.

Conclusion: GPC-3 expression level of HCC showed a favorable diagnostic performance in differentiating well-differentiated from poorly differentiated HCC. Signal intensities in arterial phase and T2WI were well correlated with the degree of GPC-3 expression in HBV-cirrhosis-related HCC. Consequently, some MRI parameters are expected to non-invasively predict differentiation stages of HCC before biopsy or surgery.

B-1258 14:12

Differentiation of inflammatory pseudo-tumour from colorectal liver metastases on gadoxetic acid-enhanced magnetic resonance imaging

S. Ichikawa, U. Motosugi, T. Suzuki, T. Shimizu, H. Onishi; Chuo-shi/JP

Purpose: To determine the differential features of inflammatory pseudo-tumour (IPT) from colorectal liver metastases (CLM) on gadoxetic acid-enhanced magnetic resonance imaging (MRI).

Methods and Materials: This retrospective study was approved by the institutional review board, and waived informed patient consent. One hundred and thirty-four patients with pathologically proven or clinically diagnosed IPT ($n = 25$) and CLM ($n = 109$) who had undergone gadoxetic acid-enhanced MRI were enrolled. Images were analysed for the shape, enhancement pattern on hepatic arterial phase (HAP), persistent rim-enhancement during HAP to late phase, blood vessel penetration, peri-tumoural enhancement on HAP, peri-tumoural hypointensity on hepatobiliary phase (HBP), peri-tumoural hyperintensity on T2-weighted imaging (T2WI), biliary dilatation, target appearance (central hypointense area with peripheral hyperintense rim) on HBP, signal pattern of diffusion-weighted imaging (DWI) and T2WI, and lesion-to-liver signal intensity ratio (LLR) on HBP and DWI. Univariate and multivariate analyses were performed to identify relevant differentiating features between IPT and CLM.

Results: Univariate analysis revealed that the following significant parameters favour IPT over CLM: irregular shape, hyperenhancement on HAP, blood vessel penetration, target appearance on HBP, peri-tumoural hyperintensity on T2WI, absence of persistent rim-enhancement, high LLR on HBP, and low LLR on DWI ($P < 0.0001$ - 0.0361). Multivariate analysis revealed that target appearance on HBP, high LLR on HBP, and low LLR on DWI were predictive of IPT ($P = 0.0220$ - 0.0330).

Conclusion: Target appearance on HBP and LLR on HBP and DWI were the reliable imaging features for distinguishing IPT from CLM on gadoteric acid-enhanced MRI.

B-1259 14:16

Dynamic-enhanced CT of multiple solid pancreatic lesions: prevalence and features of non-malignancies

L. Zhu, J. Li, Z.-y. Sun, H.-d. Xue, Z.-y. Jin; *Beijing/CN*
(zhuliang_pumc@163.com)

Purpose: To determine the prevalence of multiple solid pancreatic lesions on dynamic enhanced CT in a large cohort of patients with suspected pancreatic diseases, and to describe CT features of non-malignant disease entities.

Methods and Materials: We investigated 8096 consecutive patients who underwent dynamic enhanced CT pancreas protocol at a tertiary pancreatic disease center (June 2014 to August 2017). The final clinical diagnosis was used to determine the prevalence of malignant and non-malignant courses. The diagnostic accuracy of dynamic enhanced CT for non-malignancies was calculated. Univariate and multivariate analyses were conducted to identify clinical and CT findings (age, gender, symptoms, serum biomarkers and CT morphological and enhancement features) that predict non-malignancy.

Results: Multiple solid pancreatic lesions were seen in 1.5% of patients with suspected pancreatic diseases (121/8096). The prevalence of non-malignancies was 19.8%(24/121). The most common non-malignancy was autoimmune pancreatitis (17.4%, 21/121). The most common malignancies were neuroendocrine tumours (51.2%, 62/121), pancreatic adenocarcinoma (as the dominant lesion, 12.4%, 15/121), metastases (7.4%, 9/121) and lymphoma (5.8%, 7/121). In patients with multiple solid pancreatic lesions, dynamic enhanced CT had a sensitivity of 79.2% and a specificity of 92.8% for diagnosing non-malignancies. Elevated serum IgG4 level ($p<0.001$), hypoenhancement in arterial phase ($p=0.001$), non-hypoenhancement in later phases ($p=0.009$) and location in both proximal and distal pancreas ($p=0.036$) were found to be predictors of non-malignancies.

Conclusion: Multiple solid pancreatic lesions were rare, with a wide disease spectrum. Dynamic enhanced CT provides clues for determining disease nature.

B-1260 14:20

Diagnostic accuracy and interobserver agreement: CEUS-LI-RADS vs MRI-LI-RADS

B. Schellhaas, M. Hammon, D. Strobel, R. Görtz, A. Cavallaro, R. Janka, M.F. Neurath, M. Uder, H. Seuss; *Erlangen/DE*
(hannes.seuss@uk-erlangen.de)

Purpose: We compared diagnostic accuracy and interobserver-agreement for the recently introduced contrast-enhanced ultrasound (CEUS)-based algorithm CEUS-LI-RADS (liver imaging reporting and data system) versus the well-established magnetic resonance imaging (MRI)-LI-RADS for non-invasive diagnosis of hepatocellular carcinoma (HCC) in high-risk patients.

Methods and Materials: Focal liver lesions in 50 high-risk patients (mean age 66.2 ± 11.8 years; 39 male) were assessed retrospectively with CEUS and MRI. Two independent observers reviewed CEUS and MRI examinations, respectively, classifying observations according to CEUS-LI-RADsv.2016 and MRI-LI-RADsv.2014. Interobserver agreement was assessed with Cohen's Kappa. Diagnostic accuracy for histologically proven lesions ($n=36$) was compared between CEUS-LI-RADS and MRI-LI-RADS.

Results: 43 lesions were HCCs; two were ICCs; five were benign lesions. Diagnostic accuracy was 64%/50% (observer 1/2) for CEUS-LI-RADS and 81%/75% (observer 1/2) for MRI-LI-RADS. Washout was observed more frequently with MRI. Interobserver-agreement for arterial hyperenhancement was $\kappa=0.511/0.565$ (CEUS/MRI), for washout it was $\kappa=0.490/0.582$ (CEUS/MRI), and for CEUS-LI-RADS category it was $0.309/0.609$ (CEUS/MRI).

Conclusion: CEUS-LI-RADS in its current form is inferior to MRI-LI-RADS for definite diagnosis of HCC (LR-5). Arterial hyperenhancement is the key feature for diagnosis of HCC with CEUS. Combining the LR-4 and LR-5 categories in CEUS-LI-RADS would improve diagnostic accuracy, sensitivity and interreader agreement.

B-1261 14:24

Evaluating autoimmune pancreatitis under corticosteroid treatment with T1 mapping

L. Zhu, H.-D. Xue¹, Z.-Y. Sun¹, D. Nickel², T.-Y. Qian¹, Z.-Y. Jin¹; ¹*Beijing/CN*, ²*Erlangen/DE* (zhuliang_pumc@163.com)

Purpose: To evaluate the T1 relaxation time of autoimmune pancreatitis (AIP) in the native state and its change after corticosteroid treatment (CST).

Methods and Materials: The institutional review board approved this prospective study and all patients provided written informed consent. Twelve patients with focal AIP and 22 patients with diffuse AIP received pancreatic MR including T1 mapping on a 3T scanner, both before and after steroid treatment.

Twenty patients without pancreatic diseases who received T1 mapping of the pancreas served as control. In each patient, T1 relaxation time of pancreatic parenchyma in the head, body and tail was measured.

Results: The T1 relaxation time of normal pancreatic parenchyma was 785.4 ± 49.5 msec. For both focal and diffuse AIP, the T1 relaxation time was significantly elongated compared to the control (both $p<0.001$). After 4-12 weeks of CST, the T1 relaxation time of the pancreas shortened significantly towards normalization, compared to the baseline value (for focal AIP: from 1220.7 ± 139.3 msec to 931.7 ± 86.4 msec; and for diffuse AIP: from 1104.5 ± 121.8 msec to 893.8 ± 108.4 msec, both $p<0.01$). The visually uninvolved parenchyma in focal AIP had longer T1 relaxation time compared to normal pancreas ($p<0.01$), which also shortened significantly after steroid treatment (from 918.7 ± 128.9 msec to 831.1 ± 94.3 msec, $p<0.01$).

Conclusion: T1 mapping could accurately depict the inflammatory state and extent in patients with AIP, and monitor parenchyma change with treatment. T1 mapping detects more extensive parenchyma involvement in focal AIP, compared to visual inspection.

B-1262 14:28

Non-hypervascular pancreatic neuroendocrine tumours: spectrum of MDCT imaging findings and differentiation from pancreatic ductal adenocarcinoma

E. Belousova, G. Karmazanovsky; *Moscow/RU* (mestre@inbox.ru)

Purpose: To determine contrast-enhanced MDCT features to differentiate nonhypervascular pancreatic neuroendocrine tumors (PNETs) from pancreatic ductal adenocarcinomas (PDACs).

Methods and Materials: We included 74 patients with PNETs and 80 patients with PDACs who underwent preoperative MDCT. Two radiologists evaluated the morphologic characteristic and enhancement patterns of the tumors. Tumor-to-pancreas enhancement ratio was defined as the HU value of the tumor divided by the HU value of the pancreas. The possibilities of PNET or PDAC were estimated for nonhypervascular PNETs.

Results: On the basis of arterial enhancement, 43 PNETs were hypervascular and 31 were nonhypervascular. When compared to PDAC, nonhypervascular PNETs more frequently had well-defined tumor margins, intratumoral cystic components, calcifications and blood vessels and less frequently had main pancreatic duct dilatation, peripancreatic infiltration and vascular invasion ($p<0.01$ for all). Nonhypervascular PNETs had higher tumor-to-pancreas enhancement ratio in venous phase (1.02 vs 0.78 , $p<0.05$). Nonhypervascular PNETs more often had portal-venous hyperenhancement or persistent iso-enhancement, while PDAC more often had persistent hypo-enhancement or gradual delayed enhancement ($p<0.001$). The most accurate MDCT-findings to predict nonhypervascular PNET were the absence of MPD dilatation and peripancreatic infiltration (79% and 92% accuracy), portal-venous phase hyperenhancement or persistent iso-enhancement (77%), the presence of intratumoral blood vessels (77%) and relative enhancement intensity in venous phase >0.9 (76%). Using these criteria, the area under curve for differentiation of PNET from PDAC was $0.906-0.846$.

Conclusion: Combined assessment of the enhancement and morphologic characteristics can improve the diagnosing of nonhypervascular PNETs at contrast-enhanced MDCT, reducing the rate of false diagnoses of nonhypervascular PNETs as PDAC.

B-1264 14:32

Application of CT texture analysis in evaluating histologic grade of pancreatic neuroendocrine tumours

S.-h. Cheng^{1,2}, L. Zhu¹, H. Xue¹, Z. Jin¹; ¹*Beijing/CN*, ²*Chengdu/CN*
(1025518057@qq.com)

Purpose: To explore the application of CT texture analysis (CTTA) to differentiate between G1 versus G2 and G3 pancreatic neuroendocrine tumours (PanNETs).

Methods and Materials: A total of 36 patients with G1 PanNETs ($n = 18$) and G2+G3 PanNETs ($n = 18$) were included in this retrospective study. Both unenhanced and enhanced CT images were chosen for CTTA. Texture parameters including mean grey-level intensity (mean), standard deviation (SD), entropy, mean of positive pixels (MPP), skewness, and kurtosis were compared between G1 and G2+3 PanNETs. Receiver operating characteristic (ROC) analysis was performed and the area under the ROC curve (AUC) was calculated. Sensitivity (Se), specificity (Sp), positive predictive value (PPV), negative predictive value (NPV), and accuracy were calculated using the cut-off value of texture parameter with the highest AUC.

Results: Compared to G2+G3 PanNETs, G1 PanNETs had significantly lower skewness ($P = 0.031$) on unenhanced images and lower skewness ($P < 0.05$), higher mean ($P = 0.047$) and MPP ($P < 0.05$) on enhanced images. A skewness <0.23 at medium texture scale on enhanced images identified G1 PanNETs from G2+G3 PanNETs with the highest AUC of 0.724 ± 0.091 (Se = 61.1%, Sp = 94.4%, PPV = 91.6%, NPV = 70.8%, and accuracy = 77.8%).

Conclusion: CTTA proved to be a feasible tool for differentiating G1 PanNETs from G2+G3 PanNETs. Skewness quantified from medium texture scale on enhanced images was the optimal diagnostic parameter for estimating histologic grade of PanNETs.

B-1265 14:36

The efficacy of superb microvascular imaging for diagnosing acute cholecystitis: comparison with conventional ultrasonography

J. Ra, E. Lee, H. Park, J. Lee, S. Park, B. Choi; *Seoul/KR*
(joonbi89@naver.com)

Purpose: To evaluate the diagnostic performance of ultrasonography (US) plus superb microvascular imaging (SMI) compared to conventional US alone for diagnosing acute cholecystitis.

Methods and Materials: We retrospectively investigated 54 patients with right upper quadrant abdominal pain who underwent US with SMI. The pixel count of SMI showing flow signal was measured in the region of interest of the gallbladder bed of the liver. Two radiologists independently evaluated the imaging features and rated the five-point diagnostic likelihood level before versus after the addition of SMI using the optimal cut-off SMI pixel count obtained by the receiver operating characteristic (ROC) curve. Multivariate logistic regression analysis identified predictive factors for acute cholecystitis. Pairwise comparison of ROC was performed to compare the diagnostic performance of US before versus after the addition of SMI.

Results: Of the 54 patients, 29 had acute cholecystitis confirmed by cholecystectomy or percutaneous cholecystostomy. The SMI pixel count was significantly higher in acute than in non-acute cholecystitis (169.84 versus 27.48, $p < 0.001$). The optimal SMI cut-off pixel count for predicting acute cholecystitis was 56.67 with 82.8% sensitivity and 92.0% specificity. In multivariate analysis, SMI pixel count and gallbladder wall thickening were significant predictive factors ($p < 0.05$). Area under the curve values were significantly higher after the addition of SMI than before (0.850 versus 0.729, $p = 0.022$).

Conclusion: Quantitative SMI values were significantly higher in acute than in non-acute cholecystitis. US plus SMI could objectively improve diagnostic performance compared with conventional US alone for acute cholecystitis.

B-1266 14:40

MR T2 mapping of hepatocellular carcinoma: sequence parameters optimisation and its correlation with Ki-67 proliferation status, histological grades and microvascular density

L. Cao, B. Song; *Chengdu/CN* (clk2089@icloud.com)

Purpose: To optimise T2 mapping imaging parameters in liver and explore the relationship between T2 relaxation time of HCC and histological results.

Methods and Materials: (I) Ten healthy volunteers were examined to optimise T2-prepared TrueFISP parameters to acquire the best quality of T2 map. (II) Thirty-five HCC patients were included. T2 map was acquired through T2-prepared TrueFISP on a 3T scanner. Freehand ROI was placed in HCC solid regions to measure T2 value. The relationship between Ki67 indices, microvascular density (MVD) and T2 was determined by correlation analysis. ANOVA was used to evaluate the statistical differences of T2 among histopathological groups. ROC analysis of discriminating well-differentiated (grade I) from moderately-(grade II) and poorly-differentiated (grade III and IV) HCC was performed for T2.

Results: (I) Three T2-prepared images with length of 0, 25 ms, 55 ms could provide the best quality of T2 map and meanwhile the shortest breath-holding time. (II) T2 value of poorly-, moderately- and well-differentiated HCC were (40.6±3.2) ms, (42.9±2.8) ms and (49.6±3.9) ms, respectively, and there were significant differences among them ($p < 0.001$). T2 value demonstrated good diagnostic performance (AUC = 0.94) for discriminating well-differentiated HCC from the others, with sensitivity of 83.3% and specificity of 72.4% respectively. T2 value were significant negatively correlated with Ki67 indices ($\rho = -0.546$, $p = 0.037$) and MVD ($\rho = -0.679$, $p = 0.009$).

Conclusion: T2 value demonstrated moderate correlations with tumour proliferation status and neovascularisation. Quantitative measurement of T2 value offers a potential way for non-invasive evaluation of HCC malignancy.

B-1267 14:44

Readout-segmented echo-planar diffusion-weighted MR for the evaluation of aggressive characteristics of rectal cancer

X. Chunchao, Z.-L. Li; *Chengdu/CN* (xiachunchao@126.com)

Purpose: To evaluate whether aggressive characteristics of rectal cancer can be predicted by the apparent diffusion coefficient (ADC) obtained using readout-segmented echo-planar imaging (rs-EPI) diffusion-weighted magnetic resonance.

Methods and Materials: One hundred and fifteen patients were enrolled. The image quality of ADC maps obtained using rs-EPI was compared with that using traditional single-shot echo-planar imaging (ss-EPI), and ADC measurement was performed on the rs-EPI based ADC maps. Differences in

ADC values of tumors grouped according to differentiation grade, clinical T stage and plasmatic carcinoembryonic antigen (CEA) level were tested. The correlation between each aggressive characteristic and the corresponding ADC values was evaluated.

Results: The image quality of ADC maps obtained by rs-EPI was superior to that of ss-EPI ($P < 0.05$). The ADC values of tumor were categorized based on the following differentiation grades: poor ($0.89 \pm 0.12 \times 10^{-3} \text{ mm}^2/\text{s}$), moderate ($1.13 \pm 0.25 \times 10^{-3} \text{ mm}^2/\text{s}$), and good ($1.31 \pm 0.19 \times 10^{-3} \text{ mm}^2/\text{s}$); $P < 0.001$. Tumors with lower differentiation grades corresponded to lower ADC values ($r = 0.59$, $P < 0.001$). However, significant differences were not observed in different clinical T stage ($1.16 \pm 0.19 \times 10^{-3} \text{ mm}^2/\text{s}$ vs. $1.15 \pm 0.28 \times 10^{-3} \text{ mm}^2/\text{s}$ vs. $1.08 \pm 0.21 \times 10^{-3} \text{ mm}^2/\text{s}$ vs. 1.15 ± 0.20 ; $P = 0.47$) and plasmatic CEA level ($1.14 \pm 0.26 \times 10^{-3} \text{ mm}^2/\text{s}$, vs. $1.03 \pm 0.35 \times 10^{-3} \text{ mm}^2/\text{s}$, $P = 0.06$).

Conclusion: rs-EPI sequence-based ADC values represent a potential imaging marker for the assessment of aggressive rectal cancer characteristics.

B-1269 14:48

Comparison of liver stiffness measurements between point shear wave elastography (ElastQ) and two-dimensional shear wave elastography (ElastQ Imaging) equipped on a same machine

W. Hong¹, S.M. Lee¹, M.J. Kim¹, H. Ha¹, K. Lee¹, D. Lee², S. Lee¹;
¹Anyang/KR, ²Seoul/KR (wj.jenny29@gmail.com)

Purpose: To prospectively compare applicability rate between point shear wave elastography (pSWE, ElastPQ) and a new two-dimensional shear wave imaging (2D-SWE, ElastQ Imaging) and to correlate liver stiffness (LS) values measured by the two elastographic techniques equipped on a same machine in the same population.

Methods and Materials: We prospectively enrolled 152 patients (82 men, 70 women; age 20-83 years), 62 of whom were previously diagnosed with chronic liver disease. LS values were measured in the same session using two techniques equipped on a same ultrasound machine (EPIQ7G). The applicability rates of the two techniques were compared by Chi square test. LS values obtained by the two techniques were correlated and compared using Spearman correlation coefficient and Wilcoxon signed-rank test. For the assessment of agreement of LS value measurement, we used 95% Bland-Altman limit of agreement.

Results: The applicability rate of ElastQ Imaging (139/152, 91.4%) was significantly higher than that of ElastPQ (115/152, 75.7%) ($P = 0.001$). The LS values obtained by the two techniques showed strong correlation ($r = 0.866$, $P < 0.001$). The 95% limit of agreement of the two techniques was ranged from -53.7% to 36.2%. The mean LS value of ElastQ Imaging ($6.49 \pm 3.95 \text{ kPa}$) was significantly higher than that of ElastPQ ($5.88 \pm 3.29 \text{ kPa}$) ($P < 0.001$).

Conclusion: ElastQ Imaging showed better applicability rate than ElastPQ. However, LS values obtained by ElastQ Imaging was significantly higher than those obtained by ElastPQ. In addition, the two techniques are not interchangeable due to the large limit of agreement.

B-1270 14:52

MRI-detected extramural vascular invasion is one of the strongest risk factors in predicting distant metastasis in rectal cancer

P. Tripathi¹, S. Rao¹, W. Guo¹, B. Rai², M.-S. Zeng¹;
¹Shanghai/CN, ²Wuhan/CN (pratik9_band@hotmail.com)

Purpose: Extramural vascular invasion (EMVI) has been recommended as an independent prognostic factor for poor overall survival rate in rectal cancer. We aimed to evaluate the MRI-detected extramural vascular invasion (mrEMVI) in predicting distant metastasis in T3 rectal cancer.

Methods and Materials: Post-operative histopathologically confirmed T3 rectal cancer patients without previous treatment from July 2014 to December 2016 were enrolled for this study. Two blinded radiologists evaluated location of the tumour, the degree of mesorectal extension and MRI detected extramural vascular invasion (mrEMVI). mrEMVI was further categorized into EMVI positive and EMVI negative in T2-weighted image using mrEMVI scoring system. The results along with other clinical characteristics (age, sex, tumour location, MRI detected distance of mesorectal extension, lymphatic invasion, perineural invasion, mrEMVI score and CEA) were then correlated with synchronous metastases to determine the risk factors using univariate and multivariate analyses.

Results: In 180 patients, 38 patients were confirmed to be mrEMVI positive, 142 patients mrEMVI negative. There were totally 34 patients with synchronous metastasis in which 25 were mrEMVI positive and 9 were mrEMVI negative. Three factors were significantly associated with synchronous metastasis: mrEMVI ($p = 0.001$; odds ratio=8.665), histopathological lymphatic invasion ($p = 0.001$; odds ratio=12.940) and preoperative CEA ($p = 0.026$; odds ratio=4.124). mrEMVI score 4 was more liable for synchronous metastasis ($p = 0.044$; odds ratio=9.429) than mrEMVI score 3 in rectal cancer.

Conclusion: mrEMVI positive is an independent risk factor for synchronous distant metastasis in rectal cancer. mrEMVI score 4 is a strong risk factor for synchronous metastasis than mrEMVI score 3 in rectal cancer.

B-1271 14:56

Radiomics analysis for preoperative prediction of synchronous distant metastasis in patients with rectal cancer

H. Liu, C. Zhang, J. Li, D. Wang; *Shanghai/CN (liuhuanhuan0117@163.com)*

Purpose: To investigate the value of radiomics analysis for preoperative prediction of synchronous distant metastasis in patients with rectal cancer.

Methods and Materials: A total of 177 patients with histopathologically confirmed rectal cancer who underwent high-resolution MR imaging before any treatment were divided into the primary cohort (n=123) and the validation cohort (n=54). Radiomics features were extracted from oblique axial T2-weighted images of each patient. The independent two-sample t test, Kruskal-Wallis test, and Pearson correlation analysis were used for feature selection. A radiomics signature was built and multivariable logistic regression analysis was used to develop the radiomics model including radiomics features and independent clinico-radiologic risk factors. The performance of the radiomics model was assessed by its calibration, discrimination, and clinical usefulness.

Results: A total of 385 radiomic features were extracted from each patient, and 9 radiomics features were selected for the radiomics signature. The radiomics model included radiomics signature, MR-reported lymph node status, and CA199. The model showed good discrimination and moderate calibration in the primary cohort and validation cohort, with a C-index of 0.840 (95% confidence interval (CI), 0.768-0.912) and 0.782 (95% CI, 0.648-0.916), respectively. Decision curve analysis confirmed the clinical utility of the radiomics model.

Conclusion: We developed a radiomics model based on the MR radiomics features in combination with independent clinico-radiologic risk factors. The model could be used to predict synchronous distant metastasis in patients with rectal cancer, which could be helpful for individual treatment strategy.

B-1272 15:00

CT-based radiomics for prediction of neoadjuvant chemotherapy outcomes in locally advanced gastric cancer: a pilot study

Z. Li; *Kunming/CN (lizhenhui621@qq.com)*

Purpose: To investigate the wealth of radiomics for pretreatment CT in prediction of pathological response of locally advanced gastric cancer with preoperative chemotherapy.

Methods and Materials: Thirty consecutive patients with CT-staged II/III gastric cancer receiving neoadjuvant chemotherapy were enrolled. All patients underwent unenhanced, late arterial phase (AP) and portal venous phase (PP) of the abdomen CT scans. In total, 19,985 radiomic features were extracted in AP and PP for each patient, respectively. Four methods were adopted in feature selection and 6 methods were used in the process of building the classifier model. Twenty-four combinations of feature selection and classification methods were examined. ROC curves were used to evaluate the capability of each combination of feature selection and classification method to predict non-good response evaluated with tumour regression grade.

Results: The mean AUC ranged from 0.760 to 0.954 in AP and from 0.671 to 0.925 in PP according to different combinations of feature selection and the classification method. For both AP and PP, the feature selection method of lasso + classifier of lasso achieved the highest prognostic performance (AUC, 0.954 ± 0.064 and 0.925 ± 0.073 , respectively). For the combination of AP and PP (AP+PP), the AUC was 0.965. There was no statistical difference between AP and PP, AP and AP+PP, PP and AP+PP in the highest prognostic performance (all $P > 0.05$).

Conclusion: It is possible to predict non-GR after neoadjuvant chemotherapy in locally advanced gastric cancers based on the radiomics of CT.

B-1273 15:04

Can emergency CT reliably detect significant blunt bowel and mesenteric injury?

N. Keller, T. Zingg, F. Agri, J.-F. Knebel, S. Schmidt Kobbe; *Lausanne/CH (keller.nathalie@chuv.ch)*

Purpose: To evaluate and compare two previously validated imaging-based scoring systems for the detection of significant blunt bowel and mesenteric injury (sBBMI) by emergency computed tomography (CT).

Methods and Materials: We consecutively included all our polytrauma patients addressed from 2008 to 2015 to our emergency department (trauma registry cohort) following a road traffic accident provided that they had undergone abdominal CT before surgery. In consensus, two radiologists, blinded to patients' outcome, reviewed all the CT examinations in view of 6 mesenteric, 4 intestinal and 9 other abdominal trauma CT findings. The latter were then correlated with patients' surgical outcome or clinical follow-up (>24h). Furthermore, two previously validated imaging-based bowel-injury scoring systems were compared with each other by applying them on our cohort (t test, Chi-square test).

Results: Among 681 analysed patients 21 (3.1%) had sBBMI, confirmed by emergency laparotomy. Pneumoperitoneum, small hemoperitoneum, diffuse

bowel wall thickening, mesenteric or pericolic stranding, vascular extravasation, and anterior abdominal wall injury were significantly correlated with sBBMI, as were each of the two scoring systems, the Faget and Mc Nutt score ($p < 0.001$).

Conclusion: The prevalence of sBBMI among polytrauma patients is low; however, early diagnosis is necessary. Certain CT-features are pathognomic; thus, they must not be overlooked. Scoring systems may be helpful, but do not seem mandatory for the detection of significant blunt bowel and mesenteric injury.

B-1274 15:08

MRI vs FDG PET-CT for response assessment after neoadjuvant chemoradiotherapy in oesophageal cancer

S.E. Vollenbrock, F.E.M. Voncken, D.M. Lambregts, M. Maas, E. Vegt, L.C. ter Beek, B.M.P. Aleman, R.G.H. Beets-Tan, A. Bartels-Rutten; *Amsterdam/NL (s.vollenbrock@nki.nl)*

Purpose: The debate nowadays is whether patients with oesophageal cancer who show clinical complete response (cCR) after neoadjuvant chemoradiotherapy (nCRT) could be deferred from resection. Critical is an accurate response assessment tool. FDG-PET-CT is current clinical routine to rule out distant metastases, but is suboptimal for local tumour restaging. We determined the performance of MRI compared with FDG-PET-CT for response assessment after nCRT.

Methods and Materials: Twenty-three patients with locally advanced oesophageal cancer underwent FDG-PET-CT and MRI (1.5T; T2W&DWI; b-values=0,200,800s/mm²) before and after nCRT with a maximum of 21 days between imaging and surgery. One radiologist scored MRIs and one nuclear medicine physician scored FDG-PET-CTs, both using a 5-point score (1=definite cCR, 3=inconclusive/equivocal, 5=definite residual tumour). Histopathology of the resection specimen was the reference standard (Mandard tumour regression grade 1=pCR, 2-5=residual tumour). Areas under the ROC (AUROC), sensitivity and specificity were calculated considering imaging scores 3-5 tumour-positive.

Results: Two patients were excluded due to poor image quality. Six (29%) of 21 patients achieved a pCR. AUROC was 0.58 on PET-CT versus 0.80 on MRI ($p = 0.056$). Sensitivity for residual tumour was 67% on FDG-PET-CT and 93% on MRI, whereas specificity was 50% on FDG-PET-CT versus 57% on MRI. The number of equivocal scores was 6 on FDG-PET-CT and 3 on MRI.

Conclusion: MRI shows a tendency towards higher accuracy than FDG-PET-CT for the local assessment of tumour response. MRI shows a lower number of equivocal scores than FDG-PET-CT which may be because of better discrimination between treatment-related effects and residual tumour.

16:00 - 17:30

Sky High Stage

Breast

MY 16

Breast

Moderators:

P. Clauser; Vienna/AT
A. Oktay; Izmir/TR

B-1275 16:00

Comparison of double-reading of mammography-2D with single-reading of tomosynthesis plus synthesised mammography: is it time to change the way we work in breast-screening programme?

S. Romero, J.L. Raya Povedano, M. Cara Garcia, A.L. Santos, M. Pedrosa Garriguet; *Cordoba/ES*

Purpose: To evaluate single reading of tomosynthesis plus synthesised mammography compared with double-reading of mammography-2D as new screening strategy.

Methods and Materials: Women (50-69) were invited to participate in this prospective study between January 2015 and December 2016, written informed consent was provided. Those who agreed underwent combined mammography plus tomosynthesis at the same time. The reading models were: 1) double-reading of mammography-2D (double-2D); 2) single-reading of tomosynthesis + synthesised mammography (single-3D). Each participant had three blind and independent readings. Five radiologists with exclusive dedication to breast imaging participated.

Results: 16067 women participated. 98 cancers were detected in 97 participants (one bilateral cancer), because we present data for 16068 screens. 69 cancers were detected with both techniques (double-2D and single-3D), 7 cancers detected only at double-2D (4.7/1000) and 18 cancers only at single-3D (5.4/1000), showing a significant increase of 12.6% (95%CI: 7.2%-21.2%, $p=0.043$). 1196 women were recalled, 250 recalls occurred with both techniques, 560 only at double-2D (5.0%) and 232 only at single-3D

(2.9%), significant decrease of 40.5% (95%CI: 37.2-43.9%, $p < .001$). Both techniques detected similar cancer number in 3341 women baseline screened (23 double-2D and 22 single-3D). In 12727 women previously screened, 53 cancers were detected at double-2D (4.2/1000) and 65 cancers at single-3D (5.1/1000), a significant increase in 18.5% (95%CI: 10.9-29.5%, $p = .004$).

Conclusion: Single reading of tomosynthesis plus synthesised mammography allows a significant increase in cancer detection and decrease in recalls compared to double reading of mammography-2D, so it could be considered as new screening strategy.

B-1276 16:04

Radiomics signature from enhanced T1-weighted MR image helps to improve the differential diagnosis performance of sub-1cm breast mass

L. Wang¹, D. Wang¹, X. Li²; ¹Shanghai/CN, ²Guangzhou/CN (wanglijun@xinhua.com.cn)

Purpose: To investigate the value of magnetic resonance imaging (MRI)-based radiomics signature for differentiation of malignant from benign masses that manifest as sub-1cm breast masses.

Methods and Materials: We enrolled 130 patients with 130 pathologically confirmed solitary and solid sub-1cm breast masses (training cohort: $n=90$; validation cohort: $n=40$) on MRI. The 130 masses included 94 benignities and 36 malignancies. A total of 388 radiomic features were extracted from the second post-contrast enhanced T1-weighted MR image. A model 1 including the clinical and conventional MRI features was established. A model 2, which incorporated model 1 with radiomic features was constructed. Feature selection and model building were performed by logistic regression.

Results: The radiomics signature, which consisted of seven selected features, was a significant diagnostic indicator in the differential diagnosis of the sub-1cm breast mass in the training cohort ($p=0.016$). The model 2 yielded a C-index of 0.885 in the training cohort and 0.862 in the validation cohort. The model 2 had a higher accuracy in differential diagnosis of sub-1cm masses than the model 1 both in the training cohort (80% vs. 75.6%) and the validation cohort (85% vs. 70%). Decision curve analysis demonstrated that the model 2 had a higher overall net benefit than the model 1 with a significant difference ($p=0.001$).

Conclusion: The radiomics signature is an independent diagnostic factor for the differential diagnosis of sub-1cm breast masses. Incorporating radiomics signature into clinical and conventional MRI features performed better in the differential diagnosis of sub-1cm breast masses.

B-1277 16:08

Correlation between optoacoustic imaging and molecular subtypes of malignant breast masses

G. Menezes¹, R.M. Pijnappel¹, C. Meeuwis², B. Bisschops³, J. Veltman⁴, P. Lavin⁵, M. van de Vijver⁶, R.M. Mann⁷; ¹Utrecht/NL, ²Arnhem/NL, ³Dordrecht/NL, ⁴Almelo/NL, ⁵Framingham, MA/US, ⁶Amsterdam/NL, ⁷Nijmegen/NL (giselalgm@gmail.com)

Purpose: OA/US fuses real time gray-scale ultrasound imaging with optoacoustic imaging using laser light. This enables simultaneous functional (relative de-oxygenation of hemoglobin) and morphologic imaging of breast masses using a hand-held duplex OA/US probe. In this study we assessed the correlation between OA/US features and histopathological findings of malignant breast lesions.

Methods and Materials: For OA/US 3 internal and 2 external features were scored per lesion. Spearman correlation was used to analyze the relationship between these OA/US features and mitotic index. Pearson correlation coefficient was used to evaluate the correlation with percentages of ER, PR and Ki-67. One-way ANOVA was used to evaluate the correlation between the OA/US features and molecular subtypes.

Results: Of 215 breast masses included in this prospective multicenter study, 67 were malignant. A significant correlation was observed between the sum of 3 OA/US internal feature scores and the mitotic index ($p = 0.0352$). There was a significant correlation between summed OA/US internal feature scores and Ki-67 percentages ($p = 0.0250$), and between summed OA/US internal feature scores and ER percentages ($p = 0.0307$). OA/US Internal Vessel Scores significantly distinguished Luminal A from Luminal B masses ($p = 0.0221$) and triple negative from HER-2 positive masses ($p = 0.0440$). Both summed internal and external OA/US Features helped to differentiate between Luminal A and triple negative masses ($p = 0.0134$).

Conclusion: OA/US features may be used to differentiate among breast cancer molecular subtypes. They may also help to identify triple negative breast cancers.

Author Disclosures:

P. Lavin: Consultant; Provided study design and analysis services to Seno Medical Instruments, Inc. (sponsor of the research project).

B-1278 16:12

Diagnostic values of magnetic resonance imaging in mammography detected BI-RADS 4 category calcifications

Y. Jiang, H.-U. Kauczor; Heidelberg/DE (peggy_jiang@hotmail.com)

Purpose: To assess the diagnostic value of magnetic resonance imaging (MRI) in suspicious calcification which were negative on ultrasound.

Methods and Materials: A total of 338 suspicious calcification lesions were included in the study. Those calcifications were classified above BI-RADS 4 category and negative on ultrasound between January 2013 and June 2016. 277 lesions were sent to breast magnetic resonance imaging (MRI). Then evaluate mammography (MG) and MRI features of suspicious calcification lesions and correlate with pathologic results.

Results: A total of 338 lesions, benign lesions 284 (84.0%), malignant lesions 54 (16.0%). Benign calcifications were most presented as amorphous calcifications 74.3% (211/284), while malignant calcifications were most presented as fine pleomorphic calcifications 40.7% (22/54). In malignant calcifications 67.4% lesions were presented as non-mass enhancement, and mass enhancement were more common in malignant lesions than in benign lesions, (20.9% VS 3.4%, $P < 0.001$). 11.6% lesions were presented as non enhancement while 75.2% benign calcifications were presented as non enhancement, ($P < 0.001$). Persistent time-signal intensity curve (TIC) suggest benign lesions (82.8% VS 34.2%, $P < 0.001$) while wash-out curve suggest malignant lesions (57.9% VS 13.8%, $P < 0.001$). The detect sensitivity for ultrasound negative calcifications were 60.5% for MG and 88.4% for MRI, ($P = 0.003$). The negative predictive value were 92.3% for MG and 97.5% for MRI, ($P = 0.015$).

Conclusion: MRI has higher sensitivity and negative predictive value (NPV) than MG. For ultrasound negative suspicious calcifications, the combination of MRI could improve the diagnostic efficiency.

B-1279 16:16

Characterising mammographic calcification as a prognostic biomarker for breast tumour phenotypes

J. Li, Y. Song, Y. Wu, H. Cai, L. Li; Guangzhou/CN (lijiao@sysucc.org.cn)

Purpose: To identify the relationship between histological types and calcification characteristics on mammography in breast carcinomas.

Methods and Materials: Between January 2012 and January 2016, 755 consecutive patients with calcified lesions on mammography were recruited, including 160 (21.2%) with ductal carcinoma in situ (DCIS), 272 (36.0%) with DCIS with invasion component (DCIS-I), and 323 (42.8%) with pure invasive ductal carcinoma (IDC). 568 features were extracted from microcalcification clusters. We applied the 10-fold cross-validation as the criterion for feature selection and classification. We compared the performance of seven classification methods based on clinical features alone. For radiomics alone or combined clinical features and radiomics signatures, five feature selection methods and the same seven classification methods were evaluated in terms of their performance. Probability estimates for the three prediction models in test cohort were compared by multivariate analysis of variance (MANOVA).

Results: The mean age of pure-IDC patients was statistically older than DCIS-I and pure-IDC ($P < .001$); the proportion of dense breast in DCIS-I was higher than for other histological types ($P < .001$); mass prevalence was most frequent in pure IDC ($P < .001$). ROC curve analysis showed that clinical variables combined with radiomics signatures (AUC, 0.8463) was superior to clinical variables alone (AUC, 0.8161) and to radiomics signatures (AUC, 0.7060) ($P < .001$) in discrimination pure-DCIS from pure-IDC. The combination methods XGBoost + logistic regression gave the highest prognostic performance.

Conclusion: Microcalcifications on mammograms can help predict histopathological phenotypes.

B-1280 16:20

Intravoxel incoherent motion diffusion-weighted magnetic resonance imaging in characterisation of axillary lymph nodes: preliminary animal experience

Y. Zhu, X. Li, F. Wang, Z. Ye; Tianjin/CN (zhuyueqiang1985@126.com)

Purpose: To investigate the diagnostic value of intravoxel incoherent motion (IVIM) diffusion-weighted imaging (DWI) for discriminating axillary metastatic from non-metastatic lymph nodes (LNs) in rabbit models.

Methods and Materials: The institutional animal care and use committee approved this study. Forty New Zealand white rabbits were randomly divided into two groups. The axillary LN models were created by inoculating VX2 cell suspension and complete Freund's adjuvant in the mammary glands of 20 female rabbits of each group, respectively. Conventional MRI and IVIM DWI were performed after animal models were successfully established. Images of axillary LNs were analysed with regard to long-axis diameter (L), short-axis diameter (S), apparent diffusion coefficient (ADC) and IVIM parameters (D, D*,

f). Receiver operating characteristic analyses were conducted to determine the diagnostic performance of aforementioned criteria.

Results: A total of 42 metastatic and 30 non-metastatic LNs were successfully isolated. ADC and D of metastatic LNs were significantly lower than those of non-metastatic ones (all $P < 0.001$), whereas D^* was statistically higher ($P = 0.033$). L, S, and f showed no significant difference between the two groups ($P = 0.089, 0.058, 0.054$, respectively). Optimal cutoff values, area under the curve, sensitivity, and specificity for differentiation were as follows: ADC= $1.101 \times 10^{-3} \text{ mm}^2/\text{s}$, 0.886, 78.6%, 90.0%; D = $0.938 \times 10^{-3} \text{ mm}^2/\text{s}$, 0.927, 83.3%, 93.3%; and $D^* = 12.635 \times 10^{-3} \text{ mm}^2/\text{s}$, 0.657, 52.4%, 80.0%.

Conclusion: IVIM DWI is useful to distinguish metastatic from non-metastatic LNs in axilla. D was the most discriminative variable for predicting metastatic LNs.

B-1281 16:24

Radiomics with MRI for early prediction of the response to neo-adjuvant chemotherapy in breast cancer patients

A. Tahmassebi¹, A. Meyer-Baese¹, G.J. Wengert², T.H. Helbich², K. Pinker-Domenig², ¹Tallahassee, FL/US, ²Vienna/AT
(katja.pinker-domenig@meduniwien.ac.at)

Purpose: In patients undergoing neoadjuvant chemotherapy for breast cancer, the achievement of a pathological complete response (pCR) is associated with a significantly improved disease-free and overall survival. The aim of this study was to assess radiomics with dynamic contrast-enhanced (DCE) MRI for the early prediction of pathological complete response (pCR) in breast cancer patients undergoing neoadjuvant chemotherapy.

Methods and Materials: In this IRB-approved prospective study, 41 women (median age 50 years; range 25-80 years) with breast cancer scheduled for NAC were included and underwent mpMRI using DCE MRI prior to and after two cycles of NAC. For each lesion a total of 14 features were extracted ranging from morphological, enhancement and ADC parameters. Recursive feature elimination method along with five different classifiers including linear support vector machine (SVM), linear discriminant analysis (LDA), logistic regression (LR), random forest (RF), and stochastic gradient descent (SGD) was employed to rank the features.

Results: Radiomics analysis and classification accuracy of mpMRI achieved AUCs for residual cancer burden (RCB) score (AUC 0.85), metastases (AUC 0.89) based on RF and death (AUC 0.95) based on SVM. The most relevant parameters for prediction of RCB score were mass internal enhancement, shape and margins with DCE, for metastasis peritumoural oedema, mass margins and internal enhancement, and for death high signal intensity on T2-weighted imaging, mass margins, and internal enhancement.

Conclusion: Radiomics with DCE-MRI enables prediction of response to NAC with high accuracy and thus can provide predictive information and guide treatment decisions.

B-1282 16:28

The role of arterial spin labelling (ASL) and diffusion tensor imaging (DTI) and to differentiate between malignant and benign breast lesions

A.N. Kamble¹, A. Kamble², M. Popli¹, ¹New Delhi/IN, ²Mumbai/IN
(akshaykumar.kamble92@gmail.com)

Purpose: Diffusion tensor imaging picks up the architectural distortions. Arterial spin labelling give perfusion maps by utilising the water as a contrast medium itself. Both of these techniques do not require contrast, therefore, clinically significant where contrast is contraindicated. We applied these techniques to differentiate between malignant and benign breast lesions.

Methods and Materials: 44 women with breast lesion detected on mammography, USG or MR underwent advanced MR imaging. DTI was performed at 3Telsa (Skyra Siemens) in 12 directions using a diffusion-weighted echo planar sequence. 2D ASL (Arterial Spin Labelling) protocol was modified with T1 of 1800ms and TR of 4000. Analysis of DTI and ASL data was done by dedicated post processing team using MATLAB-2017a, FSL and ASL 2.0 toolbox. Taking histopathology as Gold Standard, ROC curves were plotted.

Results: Total of 44 lesions were detected on MRI. ROC curve showed ASL has 72% sensitivity, 89.5% specificity, 79.5% accuracy, 10% FPR. The blood flow to the malignant lesions was significantly higher (350 ml/100gm tissue/sec, SD: 100ml) compared to benign lesions (150ml/100gm tissue/sec, SD: 90ml) ($p \text{ value} < 0.05$). ROC curve for DTI showed 80% sensitivity, 78% specificity, 79% accuracy, 21 % FPR. Combined DTI and ASL had increased sensitivity of 84%.

Conclusion: This study demonstrates advanced MR imaging using ASL and DTI has good specificity for differentiating breast cancer from benign lesions. With ASL quantification of blood flow to malignant and benign lesion is possible. The sensitivity of combined ASL and DTI method is better than the sensitivity of both independently.

B-1283 16:32

Earlier detection of breast cancer using artificial intelligence

A. Watanabe¹, W. Bradley², V.D. Lim², C.Y.R. Chim²,
¹Manhattan Beach, CA/US, ²San Diego, CA/US (alyssa90266@gmail.com)

Purpose: It is known that up to 50% of breast cancers may be seen on previous mammograms. The purpose of this study was to evaluate the potential benefit of using a deep learning based breast CAD in earlier detection of breast cancer.

Methods and Materials: A 3 year retrospective audit was performed of an archive of mammograms obtained from a community based practice. 125 cases of confirmed breast cancers with prior studies were identified. All of the mammograms were processed using a deep learning based CAD (cmAssist, CureMetrix, La Jolla, CA). The cancer cases were evaluated by 2 radiologists who identified retrospective findings and then classified them as actionable vs nonactionable. The type of lesion (calcification, density, or mass) was also tabulated. The ROC and AUC of the entire data base was calculated as well as the false positive per image rate to demonstrate overall accuracy of the CAD.

Results: The artificial intelligence trained CAD flagged 100% of the breast cancers that were detected by the original interpreting radiologists. In addition, the CAD flagged actionable findings on prior mammograms in 76% of the cases. The true negative rate for the CAD also showed high accuracy. There were few false flags.

Conclusion: This deep learning based CAD flagged a majority (76%) of breast cancers on prior studies that showed retrospective findings. This CAD could be a powerful tool in enhancing earlier detection of cancer on mammography and reducing false negative mammography.

Author Disclosures:

A. Watanabe: Consultant; Curemetrix. W. Bradley: Advisory Board; Curemetrix. V.D. Lim: Consultant; Curemetrix. C.Y.R. Chim: Employee; Curemetrix.

B-1284 16:36

Sensitivity of contrast-enhanced spectral mammography (CESM) versus digital mammography (DM) for detecting breast cancer in dense or extremely dense breasts

E. Gioutlaki, C. Tzimas, E. Feida, A.N. Chalazonitis; Athens/GR
(egiou@hotmail.gr)

Purpose: Contrast-enhanced spectral mammography (CESM) is a quite new imaging method for neo-angiogenesis detection by tracking iodinated contrast agent uptake and washout in suspicious breast lesions. Our aim was to compare mammography findings of CESM and DM, in dense or extremely dense breasts.

Methods and Materials: From October 2012 to May 2017, 283 women, aged from 24 to 88 years, (mean age 54.6 years) with dense or extremely dense breasts, underwent CESM examination. Evaluation of CESM examination was based on enhancement intensity of the lesion according to a qualitative scale categorized into 4 steps as follows: type -1 (negative enhancement), type 0 (no enhancement), type 1 (moderate enhancement), type 2 (intense enhancement). Histopathology reports were compared with imaging assessment.

Results: Out of 283 women, 20 of them had bilateral lesions. From a total sample of 189 breasts positive in CESM, 164 were diagnosed with breast cancer at histopathology. According to our study, the sensitivity of this method was 91%, specificity 71.4%, and accuracy 82%. On the contrary, conventional MMG had a sensitivity of 73%, a specificity of 62%, and diagnostic accuracy 67%. As a result, sensitivity, specificity and accuracy were significantly higher on CESM compared to MMG.

Conclusion: Many factors may affect the diagnostic accuracy of DM. One of them is breast density. Cancer may be occult in dense breast. It seems that CESM is superior to DM in detecting breast cancer with high accuracy, especially in dense breasts.

Author Disclosures:

E. Gioutlaki: Speaker; E.Gioutlaki.

B-1285 16:40

MRI analysis after neoadjuvant chemotherapy on breast cancer: correlation between radiological and pathological response

E.M.S. Negrao, A. Bitencourt, J.A. Souza, E. Ferreira Marques, C. Souza Guatelli, L. Graziano, M.L.L. Albuquerque; São Paulo/BR
(brenda_kika@yahoo.com.br)

Purpose: Breast cancer is classified into molecular subtypes (MS), which differ in clinical presentation, response to treatment and survival. Triple-negative (TN) and HER2 expression (HER2+) are known to be more aggressive and potentially metastatic. Complete pathological response (pCR) after neoadjuvant systemic treatment (NST) is considered predictor of clinical benefit. The aim of this study was to compare radiological response at magnetic resonance imaging (MRI) and pathological response after NST.

Methods and Materials: 310 breast tumours were analysed retrospectively in a cancer centre between October 2014 and July 2017. Radiological response (MRI after NST) was compared to the pathological response (surgical specimen) and stratified the different MS to define the ability of MRI to predict the pCR.

Results: Patients' age ranged between 27 and 85 years (mean age 47 years). The predominant Luminal B in 189 cases (of these, 55 cases hybrid Luminal B: HER2+). TN in 90 cases and HER2+ (hormone negative) in 31 cases. There were 126 cases (41%) of pCR (10 cases had only residual CDIS). The sensitivity, specificity and accuracy of the MRI was 82%, 74% and 79%, respectively. Stratifying by MS, the highest indexes were HER2+ (89%, 82% and 83%) and the TN subtype (78%, 78% and 70%). The Luminal B subtype presented specificity of 56% (Luminal B hybrid obtained 78%).

Conclusion: MRI has remained a good method to investigate the pCR, especially in the HER2+, TN and Luminal B hybrid subtypes, demonstrating greater accuracy in the pCR in the more aggressive subtypes.

B-1286 16:44

Screen-detected breast cancer: differences in mammographic tumour features between agreement and disagreement recall

M. Orsi, M. Cellina, F. Leone, D. Mariani, A. Presazzi, C. Floridi, G. Oliva; Milan/IT (marcello.orsi@asst-fbf-sacco.it)

Purpose: To analyse how radiological features of breast cancer are correlated with agreement and disagreement recall, in a single-centre independent double reading population-based screening program.

Methods and Materials: Between November 2014 and February 2017, screening mammograms positive for breast cancer were retrospectively evaluated by two radiologists, in consensus, to assess the tumoural imaging features (mass, calcifications, asymmetric density or architectural distortion). We evaluated two different groups according to agreement recall (AR) or disagreement recall (DR). We compared the differences among tumoural imaging features between the two groups.

Results: 113 consecutive screen-detected histologically proved breast cancer mammograms were reviewed, there were 76 AR and 37 DR. In the AR group, we found, as single or part of multiple features in a suspicious lesion, 51 (67%) mass, 24 (32%) calcifications, 24 (32%) architectural distortion and 18 (23%) asymmetric density; in the DR group, we depicted 20 (54%) architectural distortion, 11 (30%) mass, 9 (24%) calcifications, 7 (19%) asymmetric density. Differences in tumour imaging features between the two groups were statistically significant ($p < 0.05$).

Conclusion: Our results show that architectural distortion is the most frequent tumour imaging feature in the DR group, which includes a false-negative result; the detection of architectural distortion requires a good practice of mammography and any technical improvements focused on depicting architectural distortion could increase the overall sensitivity of mammographic screening.

B-1287 16:48

Interpretation of patterns of enhancement on contrast-enhanced digital mammography: an approach to a standardised scheme

S. Gareer, Y. Mounir, M.H. Helal, O. Mokhtar, A. Abdel Aziz, H. Kassas, L. Bassam; Cairo/EG (sherhangareer@gmail.com)

Purpose: Applying the morphological descriptors described in the MRI breast imaging and reporting data system (BIRADS) in characterising enhancing breast lesions seen on CESM.

Methods and Materials: Methods: 178 breast lesions in patients with mean age 46 years in a prospective study were included. Morphological categorisation of the included lesions was presented into focus, mass and non-mass forms. Furthermore classifications included the margin, enhancement intensity for "focus", the shape, margin and internal enhancement for "mass" and the distribution and internal enhancement for "non-mass". Each morphology descriptor was evaluated separately (irrespective of the other descriptors) by calculating its sensitivity, specificity, (PPV) and (NPV)

Results: This study included 104 malignant lesions versus 74 benign. Diagnostic accuracy parameters for CEDM were sensitivity 98 % (102/104) and specificity 76% (56/74). Irregular margin intense enhancement focus (1/8) was diagnosed malignant, (7/8) while regular margin faint enhancing foci were benign. Irregular shape, spiculated margin and heterogeneous internal enhancement descriptors of mass lesion descriptors conformed to malignancy (PPV 92.5% of the former and 88.7% of the latter, p value ≤ 0.001). Asymmetry with segmental distribution, (17/27) (70.8%) heterogeneous and clumped internal enhancement patterns were indicative for malignancy in non mass enhancement (PPV < 0.001)

Conclusion: MRI lexicon morphology descriptors can be applied (yet with few exceptions) in the characterization of enhancing breast lesions on CESM. The most sensitive descriptors for malignant lesions regarding masses are irregular, margins yet for NME the focal, ductal and segmental distribution with heterogeneous or clumped enhancing patterns. Foci are still controversial.

B-1288 16:52

Screen-detected breast cancer: an argument for starting screening mammography at age 40 in the community-based setting

R. Benjamin¹, M. Aujero¹, K.S. Traylor¹, M. Gerges², J. Holt¹; ¹Newark, DE/US, ²Philadelphia, PA/US (Rbenjamin@christianacare.org)

Purpose: Current screening guidelines are contradicting. An argument for starting screening mammography at age 40 is introduced.

Methods and Materials: A total of 38,393 screening mammograms, additional imaging studies, and relevant biopsy results were compiled and analysed at our institution from August 2015 to December 2016. 72.5% of the studies were performed with tomosynthesis. No stratification was based on imaging modality, race, breast density, or risk assessment.

Results: 38,393 patients were stratified into different age ranges including 40-49, 50-64, and over 65. 10,267 patients were within the 40-49 age range and 31 cancers were detected, 20 invasive. 16,735 patients were within the 50-64 age range and 97 cancers were detected, 64 invasive. 10,680 patients were within the greater than 65 age range and 93 cancers were detected, 75 invasive.

Conclusion: In our screening populations, 14% of all screen-detected cancers were found in women aged 40-49 and 65% of these (21/30) were invasive. Although, the USPSTF agrees that there is a "net benefit" to screening women age 40-49, it gives a "C" recommendation for screening in this age group. Data obtained by the task force come predominantly from randomised and observational studies and trials which date as far back as 1963. Furthermore, film mammography, not digital mammography or tomosynthesis (DBT), was the basis for their recommendations. With growing research on the benefits of DBT, the USPSTF recommendations should be updated according to current data. This study supports the ACR and ACOG recommendation that annual screening mammography begin at age 40.

B-1289 16:56

Abbreviated breast MRI: do we still need contrast media?

A. D'Angelo¹, J. Al Mohanna², P. Clauser³, P. Kapetas³, P. Rinaldi¹, C. Zuiani⁴, T.H. Helbich³, K. Preidler³, P.A.T. Baltzer²; ¹Rome/IT, ²Riyadh/SA, ³Vienna/AT, ⁴Udine/IT (anna.dangelo05@gmail.com)

Purpose: To compare the diagnostic performance of two abbreviated breast MRI protocols for the characterisation of breast lesions: Diffusion Weighted Imaging (Non-contrast MRI, NC-MRI) and early enhanced T1w (first contrast enhanced measurement, CE-MRI).

Methods and Materials: IRB-approved retrospective single-center study. 57 consecutive patients (median age 55, range 29-84 years) were eligible, who underwent biopsy of BI-RADS 4/5 findings after full diagnostic workup including mammography, ultrasound and MRI. The MRI protocol (3T Siemens Magnetom Skyra; 16-channel coil) included a readout-segmented DWI (b 0, 800 and calculated b1400 s/mm²) and Dynamic-Contrast-Enhanced (DCE) images (T1w VIBE with fatsat; single-dose Gadoteridol (ProHance), temporal resolution 72 seconds). Two fellowship-trained breast radiologists (R1, R2) independently assigned a BI-RADS and visibility score (ordinal 5-point scale) to NC-MRI and CE-MRI using MIP reconstructions and original acquisitions. Receiver Operating Characteristics (ROC) and Visual Grading Characteristics (VGC) analysis were applied.

Results: Histopathology revealed 36 malignant and 21 benign lesions. Areas under the ROC curves were similar: CE-MRI: 0.825 (95%-CI: 0.702-0.913), R1 and 0.810 (95%-CI: 0.684-0.901), R2; NC-MRI: 0.721 (95%-CI: 0.573-0.841), R1 and 0.730 (95%-CI: 0.582-0.847), R2. The lower AUC in NC-MRI was mainly due to a lower sensitivity. In both readers, NC-MRI could not rule-out malignancy while CE-MRI could. VGC analysis revealed a superior lesion conspicuity by CE-MRI ($P < 0.001$, R1, R2).

Conclusion: The comparison of abbreviated NC-MRI and CE-MRI revealed a superiority of CE-MRI for characterisation of breast lesions. NC-MRI readings could not rule-out malignancy, stressing the necessity of contrast media in breast MRI for breast cancer diagnosis.

B-1290 17:00

Mammography, breast MRI and histopathological features of pure ductal carcinoma in situ

Y. Jiang, H.-U. Kauczor; Heidelberg/DE (peggy_jiang@hotmail.com)

Purpose: To analyze the imaging and histopathological features of pure ductal carcinoma in situ (DCIS). To evaluate the sensitivity of breast MRI and mammography (MG) in the detection of pure DCIS.

Methods and Materials: A total of 131 pure DCIS lesions between January 2013 and June 2016 were included. According to 2013 BI-RADS to evaluate MG and MRI features of calcified and non-calcified DCIS. All lesions were divided into different cancer subtypes determined by immunohistochemistry (IHC) and fluorescence in situ hybridization (FISH). Correlate molecular subtypes and nuclear grade of pure DCIS with MG and MRI features.

Results: Most pure DCIS (68.0%) presented with suspicious calcifications (including other abnormal expression: mass, FAD and architectural distortion). 32.0% presented without suspicious calcifications. For DCIS presented with suspicious calcifications on MG, diagnostic accuracy for MRI was 95.1% (P=0.001). Diagnostic accuracy of MG and MRI for DCIS without suspicious calcifications on MG were 62.2% and 91.9% (P=0.002). On MRI, 69.7% pure DCIS presented as non-mass enhancement. HER2 positive DCIS were more commonly associated with calcifications than ER positive and triple negative DCIS (54.0%, 45.5% VS 81.4%, P=0.002). High nuclear grade DCIS more presented with calcification compared to middle and low grade DCIS (42.1%, 67.2% VS 77.8%, P=0.015). The diagnostic accuracy for MG and MRI were 80.6% and 94.1% (P=0.002).

Conclusion: The most typical MG and MRI features of pure DCIS were suspicious calcification and non mass-like enhancement. MG was better than MRI in diagnosing calcified DCIS, while MRI was better in diagnosing non-calcified DCIS

B-1291 17:04

Molecular subtypes of invasive breast cancer: correlation between PET/CT and MRI findings

M. Akin, I.S. Örgüç, F. Aras, A. Kandiloglu; *Manisa/TR (meloakin@gmail.com)*

Purpose: In our study, we investigated the diagnostic value of F18-FDG PET/CT and MRI findings in determining molecular subtypes of invasive breast cancer. In addition, the relationships between the volume measurements in PET/CT and MRI and the pathological volume of the mass were evaluated.

Methods and Materials: A total of 55 primary invasive breast cancer masses in 51 female patients who had histopathological diagnosis and underwent FDG PET/CT and MRI before therapy were retrospectively analysed. The correlations between molecular subtypes and SUVmax, SUVmean, Mlmean, MTV and HU values from FDG PET/CT findings; shape, margin, intratumoral enhancement, kinetic curve type and ADC values (based on 2013 BI-RADS MRI classification) from MRI findings were evaluated. In addition, the relationships between the pathologic tumor volume and the tumor volume measured by MRI and PET/CT were evaluated.

Results: The SUVmax and SUVmean values of the luminal B subtype of invasive breast cancer were higher than the luminal subtype A (p = 0.002, p = 0.017, respectively); the triple negative subtype had a higher SUVmax value than the luminal subtype A (p = 0.028). There were statistically significant strong positive correlations between MTV and FTV (p= 0.000; r= 0.857); MTV and the pathologic tumor volume (p= 0.006, r= 0.796); FTV and the pathologic tumor volume (p= 0.006, r= 0.921).

Conclusion: Our findings suggested that SUVmax value was superior to MRI findings in predicting molecular subtypes. In addition, we determined that MRI was superior to PET/CT in predicting the pathologic tumor volume.

B-1292 17:08

Focal breast categorisation according to the BI-RADS-US lexicon: role of a computer-aided decision-making support

A. Orlando, F. Amato, M. Di Vittorio, C. Lupo, L. Spatafora, M. Safina, F. Ienzi, R. Ienzi, T.V. Bartolotta; *Palermo/IT (orlandoalexiamed@hotmail.it)*

Purpose: To assess a computer-guided decision-making software (S-Detect) in the sonographic characterisation of focal breast lesions (FBLs).

Methods and Materials: According to BI-RADS-US lexicon, 300 FBLs (size: 2.6-47.2mm) in 255 patients were prospectively assessed in consensus by two experienced radiologists without and with S-Detect. To evaluate intra and inter-observer agreement, two residents assessed independently the same 300 FBLs at baseline and after 3 months. All the FBLs classified as BI-RADS-4 or 5 underwent core-biopsy, all the lesions classified as BI-RADS-3 were followed-up.

Results: 120/300 FBLs were malignant, 2/300 high-risk and 178/300 benign. Experts reviewers showed higher Sensitivity, Specificity, PPV and NPV with S-Detect (97.5%, 86.5%, 83.2%, 98.1%) than without (91.8%, 81.5%, 77.2%, 93.6%) (p>0.05), as confirmed by ROC curve analysis (0.95 with and 0.92 without [p=0.0735]). A significant higher area under the ROC curve was found for Resident#1 (0.85 without and 0.88 with S-Detect [p=0.0067]) and Resident#2 (0.83 without and 0.87 with S-Detect [0.0302]). Intra-observer agreement (k score) improved with S-Detect from 0.69 to 0.78 for Resident#1 (p>0.05) and from 0.69 to 0.81 for Resident#2 (p>0.05). Inter-observer agreement improved with S-Detect from 0.67 to 0.7 (baseline; p>0.05) and from 0.63 to 0.77 (after 3 months; p>0.05). According to S-Detect-guided reclassification, 25/64 (39.1%; 95%CI=[25.1;51.0]) FBLs underwent no change in clinical management (CM), 27/64(42.2%; 95%CI=[30.0;52.3]) and 12/68(18.7%; 95%CI=[27.1; 51.1]) underwent respectively a positive and a negative change in CM.

Conclusion: S-Detect is an effective tool for the classification of FBLs according to BI-RADS-US lexicon, improving cancer detection rate, especially for less experienced physicians.

B-1293 17:12

Comparison of automated vs bilateral handheld whole-breast US in screening patients regarding efficacy and patient preference

B. Tutar, G. Esen, H. Kara, N. Guldogan, C. Uras; *Istanbul/TR (gulesenicten@gmail.com)*

Purpose: To evaluate the efficacy and patient satisfaction for automated breast volumetric scanning (ABVS) compared to handheld breast US (HHUS).

Methods and Materials: From May 2014 to July 2015, 338 screening patients underwent bilateral technician performed ABVS followed by physician performed HHUS (ACUSON S2000™; Siemens, Germany). Acquisition and evaluation time, patient satisfaction, image interpretability, lesion number and BIRADS scores were recorded. Chi square test was used for statistical analysis.

Results: Mean examination time was 20 minutes for ABVS and 10 minutes for HHUS. Mean interpretation time for ABVS was 8 minutes. The ratio of patients who experienced severe pain during the procedure was 8% for ABVS and 3% for HHUS. With ABVS, 19 patients (5.6%) were recalled because of areas of shadowing (BIRADS 0) but were normal on second look US. ABVS detected more solid lesions in 10 patients, while HHUS detected more in 4. The difference was statistically significant. The final category for ABVS was BIRADS 4 in 11 and BIRADS 5 in 1 patient. With HHUS, there were 2 BIRADS 4 and 2 BIRADS 5 results. US guided biopsy was performed in 4 patients and cancer was diagnosed in 2.

Conclusion: ABVS is superior to HHUS in lesion detection with no false negative results. Patient satisfaction is good and physician time is shorter. It can be an alternative to HHUS in breast clinics. It should be kept in mind that the recall rate is higher and positive predictive value is lower with ABVS as stated in previous reports.

B-1294 17:16

Breast cancer staging with automated breast volume scanner (ABVS) and digital breast tomosynthesis (DBT): a comparison with magnetic resonance imaging (MRI)

R. Girometti, L. Tomkova, M. Zanoteli, M. Lorenzon, A. Linda, V. Londero, C. Zuiani; *Udine/IT (rgirometti@sirm.org)*

Purpose: To investigate whether the combination of ABVS and DBT (ABVS+DBT) is comparable to MRI in staging breast cancer.

Methods and Materials: We retrospectively included seventy-three patients with histologically proven breast cancer who underwent preoperative ABVS, DBT and 1.5T MRI in the period July 2015-January 2017. Two radiologists in consensus recorded the number, site and BI-RADS category of breast findings during two independent reading strategies, namely using DBT+ABVS or MRI (complemented with hand held ultrasound second look images, if indicated). Using histology or 1-year follow up as the standard of reference, we calculated sensitivity and specificity for breast cancer of both imaging strategies.

Results: Patients showed a total of 160 lesions (109 malignant and 51 benign). Malignant lesions were multifocal, multicentric and bilateral in 53, 16, 3 and 1 cases, respectively. Sensitivity and specificity of ABVS+DBT versus MRI were 88.1% and 86.2% vs. 94.5% and 88.2%, respectively, with no significant differences in cancer detection (p>0.05; McNemar's test). Compared to MRI, ABVS+DBT missed 9 lesions, including 5/9 DCIS or DCI with DCIS, 3 DCI and 1 Paget disease. Compared to ABVS+DBT, MRI missed 2 lesions (DCIS).

Conclusion: ABVS+DBT approaches MRI in staging breast cancer, and might represent a diagnostic alternative in selected cases.

Scientific Sessions

Sunday, March 4

08:30 - 10:00

Sky High Stage

Radiographers

MY 17

Radiographers

Moderators:

C. Beardmore; London/UK
D. Katsifarakis; Athens/GR

B-1295 08:30

Clinical value of dynamic contrast-enhanced MRI and diffusion-weighted imaging on diagnosis of central gland prostate carcinoma

W. Jing, X. Zhang; *Shenyang/CN*

Purpose: To study the clinical value of dynamic contrast-enhanced MRI (DCE-MRI) and diffusion-weighted imaging (DWI) on diagnosis of central gland prostate cancer (CG-PCa).

Methods and Materials: A retrospective analysis was performed based on the clinical data of 63 patients who were admitted in the Hospital and confirmed to have central gland disease through pathological diagnosis. There were 34 cases of CG-PCa and 29 of CG-BPH. According to the pathological Gleason scores, the 34 patients with PCa were divided into three groups: the low (GS 3+3), moderate (GS 3+4) and high (GS 4+3, 4+4, 4+5, 5+4, 5+5) malignancy groups. The DCE-MRI semi-quantitative parameters (TTP, MSI), quantitative parameters (K_{trans}, K_{ep} and V_e) and ADC of the PCa and the BPH were measured and compared. These parameters were used for ROC curve analysis to calculate the PCa diagnosis susceptibility and specificity. The correlations between the ADC value and Gleason score grouping were assessed.

Results: The TTP and MSI values of the BPH patients were both higher than those of the PCa ones (P<0.05). Meanwhile, statistically significant differences were found in the K_{trans}, K_{ep} and ADC values between the PCa and the BPH whereas the differences in the V_e values showed no statistical significance. The largest area of K_{trans} under the ROC curve reached 0.82 with the susceptibility and specificity of 82.4% and 67.6%. There were significant differences in the ADC values among the three groupings (F=14.04, P>0.05). The ADC values of the low and the moderate malignancy groups showed no significant differences (P>0.05). The results suggested negative correlations between the ADC value and the Gleason score grouping.

Conclusion: Hence, DCE-MRI and DWI have important clinical value on CG-PCa identification.

B-1296 08:34

Development and validation of a low-cost paediatric pelvic phantom for digital radiography dose optimisation

A.H. Mohammed Ali¹, P.H. Hogg¹, A. England²; ¹Salford/UK, ²Manchester/UK (*p.hogg@salford.ac.uk*)

Purpose: Imaging phantoms can be cost prohibitive and a need, therefore, exists to produce low-cost alternatives which are fit for purpose. Consequently, this paper outlines the development and validation of a low-cost dose/image-quality pelvic phantom for a 5-year-old child.

Methods and Materials: Tissue equivalent materials representing paediatric bone (plaster) and soft tissue (PMMA) were used. PMMA was machined to match the bony anatomy identified from a CT scan of a 5-year-old child and cavities were created for plaster infusion. Phantom validation comprised physical and visual measures. Physical included CT density (HU) comparison between a CT scan of a 5-year-old male one of the phantom, a signal to noise ratio (SNR) comparative analysis of AP DR phantom X-ray images against a commercially anthropomorphic phantom. Visual analysis used a psychometric image quality scale.

Results: For HUs, the percentage difference between cortical bone and soft tissue and the equivalent tissue phantom substitutes were 88.4% and 86.1%, respectively. For SNR (mAs response) there was a strong positive correlation between the two phantoms (r>0.95 for all kVps). For kVp response, there was a strong positive correlation (1-8mAs (r>0.85)), this decreased as mAs increased (r=-0.21 at 20 mAs). Psychometric scale results produced a Cronbach's alpha of almost 0.8.

Conclusion: Physical and visual measures suggest the low-cost phantom has suitable anatomical characteristics for X-ray imaging. Our method produces a low-cost phantom which could have utility in dose and image quality optimisation studies.

B-1297 08:38

80kV vs 100kV in the CT pulmonary angiography protocol: an evaluation of the impact on patient dose and image quality on two CT machines

A. Rusandu^{1,2}, A. Ødegård¹, G.C. Engh¹, H.M. Olerud²; ¹Trondheim/NO, ²Kongsberg/NO (*albertina.rusandu@ntnu.no*)

Purpose: The aim of this study was to analyse the dose reduction and image quality achieved using 80kV instead of 100kV in CT protocols for pulmonary arteries.

Methods and Materials: 80 examinations of non-obese patients were analysed (40 consecutive patients for each protocol, equally distributed on two CT scanners). Objective image quality was assessed by measurements of HU values (average and standard deviation) in five ROIs in pulmonary arteries and calculations of signal-to-noise (SNR) and contrast-to-noise ratio (CNR). Subjective image quality was independently evaluated by two radiologists in terms of perceived noise, sharp reproduction of pulmonary arteries and overall diagnostic quality. Radiation dose parameters (CTDI_{vol}, DLP, SSDE and effective dose) were compared. Differences in dose and objective image quality for the two protocols were assessed using the independent t test; comparison of subjective grading of image quality was performed with Mann-Whitney U test.

Results: Use of 80kV significantly increased arterial contrast enhancement. Both measured and subjectively rated image noise was higher at 80 kV. Differences in SNR, CNR and subjective diagnostic image quality between protocols were not statistically significant (p = 0.177, p=0.88, p=0.703). The dose reduction achieved by using 80kV was significant on both scanners (SSDE reduction 33% and 45%, p<0.001; effective dose reduction 40% and 52%, p<0.001).

Conclusion: Use of 80kV protocols for CT examinations of pulmonary arteries in non-obese patients with body weight below 80 kg results in significant reduction of patient doses without compromising diagnostic image quality.

B-1298 08:42

Atypical functional connectivity between cerebral and cerebellar resting state networks in autism spectrum disorder

Y. Wang, W. Zhang, S. Lui; *Chengdu/CN (970805975@qq.com)*

Purpose: Motor impairment has been repeatedly documented in autism spectrum disorder (ASD). However, it is unclear what brain mechanisms contribute to this impairment. Our purpose is to examine the correlation between motor data and brain resting-state functional imaging and identify the functional connectivity (FC) alteration in ASD individuals using seed-driven approach.

Methods and Materials: We acquired resting-state functional magnetic resonance imaging scans from 43 subjects (24 ASD) 10-33 years old. ROIs were identified by examining the correlations between motor data and whole brain ALFF in control and ASD separately. Whatever correlation of motor data with brain ALFF showed statistical significance, its specific brain region was selected as one of the ROIs and further used for FC analysis. Brain-behaviour relationships were assessed by regressing FC measures with social deficit severity and repetitive behaviours.

Results: Relative to typically developing control participants, individuals with ASD showed a mixed pattern of both over- and under-connectivity in the cerebral-cerebellar network, including increased connectivity of posterior cerebellum with left superior parietal, bilateral superior occipital and left middle occipital gyrus but decreased connectivity with prefrontal cortex and superior temporal gyrus. Decreased connectivity was also identified within cerebellar network, and was negatively correlated with repetitive behaviour score (P<0.05, uncorrected).

Conclusion: Individuals with ASD showed a mixed pattern of over- and under-connectivity with cerebral-cerebellar network and decreased connectivity within cerebellar network, these findings are consistent with emerging evidence of disrupted network segregation and integration in ASD. Further, abnormal decreased connectivity within cerebellar network implicates relation with restricted and repetitive behaviours in ASD.

B-1299 08:46

Morphological characteristics of carotid atherosclerotic plaques: comparison based on CTA and MRI

N. Giannotti, J. McNulty, S.J. Foley, P. Kelly; *Dublin/IE (nicola.giannotti@ucd.ie)*

Purpose: Risk stratification of atherosclerotic plaque is based on the degree of stenosis. However, classification of plaque components (fibrous tissue, lipid, and calcium) can be associated with plaque vulnerability and may be used as a predictor of cerebrovascular events.

Methods and Materials: CT Angiography (CTA) and High-resolution MRI (HRMRI) datasets of 30 patients with confirmed internal carotid artery stenosis were analysed by a single observer using two software tools (TeraRecon iNtuition™ and MRI-Plaque View2.1) to measure the volume of plaque components. Plaque volume was assessed through semi-automatic

segmentation of the vessel wall from the lumen. Three Hounsfield unit ranges were defined in the CTA analysis, while an algorithm based on morphology enhanced probabilistic plaque segmentation was used for the HRMRI analysis. The Wilcoxon signed-ranked test assessed whether statistical differences exist between CTA and HRMRI plaque components measurements and Spearman's correlation test investigated their level of agreement. Bland-Altman plots assessed proportional bias.

Results: Although a significant difference was found between fibrous tissue measurements; measurements of lipid and calcium did not statistically change ($Z=-2.026$, $p=0.43$) ($Z=-2.448$, $p=0.14$) and Spearman's tests showed moderate agreement $rs=0.446$ ($p=0.013$), 0.444 ($p=0.014$). Bland-Altman plot confirmed no proportional bias between lipid and calcium measurements ($t=0.359$, $p=0.722$) ($t=1.354$, $p=0.187$).

Conclusion: Lipid and calcium measurements did not statistically differ between CTA and HRMRI. Although limitations affect these analyses, further investigations are necessary in order to validate these approaches since the presence of certain components within atherosclerotic lesions can lead to plaque vulnerability and cerebrovascular events.

B-1300 08:50

The impact of the smartphone application (app) on MR radiographers' knowledge and confidence in relation to MR image-quality-related errors

W. Alsharif, M. Davis, L.A. Rainford, A. McGee; *Dublin/IE* (walaa.alsharif@ucdconnect.ie)

Purpose: This study aimed to evaluate the impact of a smartphone app prototype on the level of MR radiographers' knowledge and confidence in recognising and rectifying MR image-quality-related errors.

Methods and Materials: The study used the comparison-experimental approach (pre- and post-test). Thirty-five MR radiographers independently reviewed a prepared series of MR images ($n=25$). The participants were requested to identify image-quality-related errors, to specify error-correction strategies and score how confident they were in relation to their responses. Participants were then divided into experimental ($n=19$) and control cohorts ($n=16$). The app was provided to the experimental cohort for three months, after this period both cohorts re-reviewed the MR images and retested.

Results: During pre-test, a low level of MR radiographer knowledge was noted in terms of correct identification of the type of image quality error and specification of an appropriate error-correction strategy ($p<0.05$). The confidence level of radiographers in their ability to name the types of error varied significantly ($p<0.05$). During post-test, the results showed a statistically significant difference between control and experimental cohorts relative to participants' pre- to post-test knowledge level. For the experimental cohort, years of experience, qualification and type of hospital were not associated with radiographer knowledge level and confidence in recognising the presence of an image quality error, naming the error and specifying appropriate correction strategies ($p>0.05$).

Conclusion: The study identified the potential of the smartphone app as an effective educational tool to support MR radiographers' knowledge in recognising and characterising MR image quality errors.

B-1301 08:54

Role of renal ultrasound in pelvic imaging: to scan or not to scan?

K. Cronin, S.J. Foley, S. Simpson, A. Kelly; *Dublin/IE* (kevin.cronin@ucd.ie)

Purpose: Ultrasound is a highly sought after imaging tool with consequent resource pressures. Kidneys are often routinely scanned when female patients present for pelvic imaging. The objective of this audit was to identify the frequency of abnormal renal findings when imaged following pelvic examinations and determine the clinical significance of the patient. The results would be used to inform the local imaging protocol.

Methods and Materials: A retrospective study was carried out over a four-month period in a single university teaching hospital. Radiology reports were reviewed from the hospital radiology information system. Renal findings were recorded as normal/abnormal based on local double reporting system and clinical significance recorded according to pre-agreed criteria reached via consensus between two sonographers. The average kidney scan time was estimated based on all departmental sonographers' input ($n=10$).

Results: The results for 286 scans were analysed, and 31 (11%) abnormal scans were identified, most of which were benign cysts ($n=15$). Just 16 (6%) were deemed clinically significant (13 complicated cysts, 1 carcinoma, 1 calculus, 1 mild hydronephrosis). The estimated mean time to scan the kidneys was 20 min, which equates to 98 hours and 40 min of scanning kidneys where findings were normal during this period.

Conclusion: Routine scanning of the kidneys with pelvic examinations is not recommended and significant time/resources can be saved from an evidence-based scanning protocol.

B-1302 08:58

Implementing mobile radiography services: a qualitative study of managers' experiences of success criteria and barriers to overcome

E. Kjelle, K.B. Lysdahl, H.M. Olerud, A. Myklebust; *Kongsberg/NO* (elin.kjelle@usn.no)

Purpose: The objective of this qualitative study was to evaluate success criteria and barriers in the process of implementing mobile radiography services, from managers' point of view.

Methods and Materials: 11 semi-structured interviews were conducted with managers from five hospitals and six municipalities in Norway with mobile radiography services. Core issues in the interview guide were barriers and facilitators in the different implementation phases. The framework method of thematic analysis was used for inductive data analysis.

Results: Five main categories were developed: national health policy, regional and municipal policy and conditions, inter-organizational implementation projects, experienced outcome, and professional skills and personal characteristics. These categories were allocated into three higher order classifications macro-, meso- and micro-level. The main barriers experienced by the managers were financial, structural and procedural. In particular, the reimbursement system, crossing of healthcare levels and incompatible information systems. The main facilitators were external funding, collaboration and enthusiastic individuals.

Conclusion: The main success criteria were external funding and the support and engagement from individuals in the collaborating organizations. To facilitate mobile services and services across healthcare levels, changes in management and the financial system are needed. In addition, there is a need for compatible information systems across healthcare levels. This study have been submitted to BMC health services research.

B-1303 09:02

Paediatric lifetime cancer risk for head CT protocols of a 1-year-old child

M.R. Benhalim, P.H. Hogg, A. England, L.A. Walton, K. Szczepura; *Salford/UK* (P.Hogg@salford.ac.uk)

Purpose: To compare effective risk (ER) for a range of paediatric CT brain scanning protocols.

Methods and Materials: An ATOM phantom representing a one-year-old child was implanted with MOSFET radiation detectors. Helical CT scans were undertaken using 162 protocols. Protocols included changes in rotation times, gantry angulation, pitch, mA and detector configuration. Absorbed tissue doses were read from MOSFET and used to estimate ER, using BEIR VII report, for males and females aged 0-5 years.

Results: ER ranged from 20-102 and 8-46 for females and males, respectively. ER increased consistently by approximately 38% for females and 17% for males when the pitch factor changed from fast to detail (mean ER 102 versus 64 and 46 versus 29, respectively). Changing mA modulation from high to low dose resulted in a 48% risk reduction for both female and male (mean ER 102 versus 36 and 46 versus 16, respectively). Changing detector configuration from 0.5x16 to 1.0x16 resulted in approximately 33% reduction for both female and male, respectively. The gantry angulation and rotation time had no effect on ER. When CT gantry angle changed from 0° to 27° and the rotation time from 0.5 to 0.75 (S), the percentage change in effective risk was 0.03% and 0.0% for female and male, respectively.

Conclusion: CT protocol selection has a significant effect on ER and it is important to consider this when implementing protocols. Risks are lower for older children and males.

B-1304 09:06

How can we improve the patient experience of nuclear medicine hybrid imaging procedures? A systematic review of the evidence

S. King; *Bristol/UK* (simon5.king@uwe.ac.uk)

Purpose: Patients attending complex imaging examinations may suffer from anxiety and discomfort resulting in reduced satisfaction and perceptions of a suboptimal experience. A systematic literature review was performed on the patient experience of nuclear medicine hybrid imaging procedures.

Methods and Materials: A systematic search of relevant databases including MEDLINE, EMBASE, AMED and CINAHL was conducted. Articles identified during the search process as meeting pre-determined inclusion criteria were then subjected to quality appraisal. A process of narrative synthesis followed in which key themes were identified and could be used to inform any recommendations for practice.

Results: Five studies were identified that met the predetermined inclusion criteria. The studies were evaluated within two separate strands: the quantifiable evidence relating to the effectiveness of an intervention in improving patient experience, and a thematic analysis of the qualitative evidence. Four key themes were identified relating to: prior knowledge of the procedure, anxiety levels, standards of care and physical comfort levels. The review demonstrates some promising areas for further investigation and early

evidence to show which interventions may have a positive impact on patient experience.

Conclusion: The findings of the review highlight the diverse and challenging ways that patients experience nuclear medicine hybrid imaging. All health professionals involved in this type of imaging need to be aware of the experiences of their patients and provide them with ongoing support. This could be through the use of accurate patient information resources and/or ensuring that staff-patient communication is able to reduce feelings of isolation and anxiety.

B-1306 09:10

Air embolism on coronary computed tomography angiography: its incidence associated with the preparation of intravenous infusion

S. Kavano¹, K. Ono¹, T. Yamaguchi², H. Ota¹; ¹Sendai/JP, ²Sapporo/JP (skavano.ism@gmail.com)

Purpose: Air embolism can be observed in the right heart system following injection of contrast media with power injector system on coronary CT angiography. Although almost all air embolism is asymptomatic, it has potential risks of paradoxical embolism. The study aimed to evaluate whether its incidence on coronary CT angiography was associated with the process of preparation for intravenous infusion.

Methods and Materials: We retrospectively evaluated a total of 693 coronary CT examinations in three institutions. Trained CT nurses placed an intravenous cannula in the forearm. Tubes connected to the cannula were prepared in the following ways: A, an interposed three-way cock and 20-ml syringe filled with normal saline to collect air contamination in the tube; B, direct connection to the power injector system without interposed three-way cock; C, an interposed three-way cock and 50-ml normal saline drip infusion bottle system to keep the tube patency. The incidence and location of air emboli and preparation of intravenous injection were assessed.

Results: The overall incidence of air embolism was 54.9% (381/693), most frequently observed in the right atrium (81.9%, 312/381). Its incidence was significantly different among the three methods of preparation (A, 21% (34/162), B: 62.9% (237/376) and C, 71% (110/155), respectively, $p < 0.05$). No patient demonstrated any symptom associated with air embolism.

Conclusion: Using a three-way cock with syringe demonstrated the lowest incidence of air embolism on coronary CT angiography. It is recommended to reduce the potential risks of complications related to intravenous contrast medium injection.

B-1308 09:14

Evaluating the roles of CT radiographers in the UK

M.A. Harris¹, M. Hardy²; ¹Wakefield/UK, ²Bradford/UK (martine.harris@midyorks.nhs.uk)

Purpose: Computed tomography (CT) technologies have advanced significantly over the last decade resulting in faster patient throughput and greater utility. However, threshold radiographer competencies, as defined by the UK Health and Care Professions Council (HCPC), are limited and no certification and registration requirements for operating CT exist. Instead, generic person and professional skills and knowledge frameworks have been published but these are inconsistent in their role expectations. As a result, a unified knowledge and skills analysis tool has been developed. This study reports the application of this tool to UK CT radiographer role descriptors to compare current clinical roles with theoretical framework standards.

Methods and Materials: A convenience sample of UK advertised radiographer role descriptors requiring participation in CT were surveyed and analysed using systematic structured content analysis to determine correlation with themes within the unified framework tool.

Results: A total of 114 radiographer role descriptors were analysed. Role grades and experience required, as well as type of recruiting organization, were varied. While key knowledge, skills and behaviors were evident across all roles, we noted discrepancies in role expectations. Further, the language used to describe role characteristics was inconsistent and open to interpretation.

Conclusion: Small changes in language were identified between recognized levels of radiography practice and these have a significant impact on expected radiographer decision-making, responsibility and autonomy of clinical practice. However, the majority of these competencies reflect generic professional standards and CT clinical task competencies remain largely undefined potentially placing patients at risk of inconsistent CT imaging practice.

B-1309 09:18

Digital radiography: impact of a lower tube voltages on image quality and radiation dose in chest phantom radiography

I. Hauge¹, I.-J. Aandahl¹, J.-P. Baranzelli², P.M. Coelho³, L. Eriksen¹, N. Hadebe⁴, G. Kahl⁵, S. van Schagen⁶, M. O'Connor⁷; ¹Oslo/NO, ²Lausanne/CH, ³Lisbon/PT, ⁴Bloemfontein, Free State/ZA, ⁵Santa Catarina/BR, ⁶Groningen/NL, ⁷Dublin/IE (vs_steven@hotmail.com)

Purpose: A tube voltage of 120 kVp is the standard in chest radiography. However, three studies have found that a lower kVp (e.g. 80 kVp) may provide better image quality for visualizing lung tissue and the cardiac silhouette. The aim of this study is to investigate the impact of tube voltage reduction on dose and image quality of DR chest phantom radiographs.

Methods and Materials: An anthropomorphic chest phantom, without and with additional plates, to simulate a normal and large person, was imaged in PA and lateral projections using stepwise increases of 10 kVp, from 60 to 130 kVp. Subjective image analysis was conducted by doing visual grading analysis (VGA). Six observers rated the image quality score (IQS). In addition, objective image analysis was performed by using ImageJ analysis software by finding the contrast-to-noise ratio for six and 3 regions of interest (ROI) in the image, for the PA and lateral view, respectively. To optimize with regard to both image quality and dose, the figure of merit (FOM) = (contrast-to-noise-ratio squared/DAP) was estimated at each selected kVp.

Results: 91 kVp had highest IQS for PA without plates and 110 kVp for the PA with plates, lateral without plates and lateral with plates. However, 130 kVp had the best FOM.

Conclusion: The VGA analysis showed that it is possible to reduce the kVp and still get good image quality. However, more extensive VGA is needed to come to a definite conclusion.

B-1310 09:22

Patient doses in plain chest x-ray compared to national DRLs

A. Henner, K. Paalimäki-Paakki; Oulu/FI (anja.henner@oamk.fi)

Purpose: Finnish Radiation and Nuclear Safety Authority set updated diagnostic reference levels (DRLs) in 2017 (both ESD and DAP) for adult's plain chest x-ray. These DRLs are: pa projection 0.12mGy (0.1Gy*cm²) and lateral projection 0.5mGy (0.2Gy*cm²). There is also achievable level for DR: pa 0.05mGy (0.07Gy*cm²) and lateral 0.14Gy*cm². Purpose of this study was to find out doses of chest examination and compare them to updated national DRLs.

Methods and Materials: The data (526 patients) was collected by student radiographers during their clinical practice in spring 2016 and 2017 all over Finland. Imaging protocols, equipment and doses/parameters were documented. Entrance surface doses were calculated with formula $ESD=Y(U,F) \cdot (FDD/FSD)^2 \cdot Q \cdot BSF$. Measurements of radiation output were done by vendors or hospital engineers. DAP meter was available only in few places and, therefore, is not included in data.

Results: Source to image distance 200cm, focal spot size 1mm or 1.2mm, grid 10:1 ; 12:1, 17:1, kV 125 and AEC were used. Added filtration varied according to the manufacturer. Mean ESD was 0.08mGy in pa and 0.31mGy in lateral projection.

Conclusion: The mean ESD 0.08mGy in pa projection compared to DRL 0.12mGy and in lateral ESD 0.31mGy compared to 0.5mGy are below DRLs. Both CR and DR detectors are included in the mean. With DR the mean ESD in pa was 0.05mGy which is same as the achievable level.

B-1311 09:26

Radiography on wheels for nursing home residents may reduce healthcare costs

E. Kjelle¹, L. Kleven², H. Olerud¹, H. Melberg^{2,2}; ¹Kongsberg/NO, ²Oslo/NO (elin.kjelle@usn.no)

Purpose: To determine whether mobile radiography service for nursing home residents reduce cost from a societal perspective.

Methods and Materials: To do the cost analyses a model was constructed based on current knowledge of organization of radiology services for nursing home residents. The model included two different organizational alternatives, hospital-based services alone and hospital-based services combined with a mobile radiography service. In addition to the x-ray examination, the model included the immediate treatment given based on the results of the examination. The treatment could be given either in the hospital (in or outpatient) or at the nursing home. Transition probabilities in the model are based on data collected from hospitals in southeast Norway and earlier research. Cost data have been collected in reports, Norwegian regulations and Statistics Norway. Costs are presented in Euro (annual average of daily rates in 2016).

Results: The preliminary analysis indicates that the mean cost of examining and treating one resident in the case of hospital-based services would be approximately € 2 116 (95% CI: 1 908 - 2 313). In the case of combination of

hospital-based and mobile services the mean cost would be € 1 378 (95% CI: 1 342-1 410).

Conclusion: Mobile radiography services reduce costs by approximately 35% when x-ray examining and treating nursing home residents in southeast Norway.

B-1312 09:30

Evidence-based practice in diagnostic imaging departments - involving the patients in procedure-development

L. Hammerström; Sarpsborg/NO (linda.hammerstrom@hioa.no)

Purpose: In an effort to increase patient safety and reduce adverse events in health care, there is a strong focus on developing and utilising evidence-based clinical guidelines or protocols. The purpose of this study has been to investigate radiographers' views on involving the patients in developing procedures in imaging departments.

Methods and Materials: The study has a qualitative inductive design with phenomenological approach. Data collection took place in individual, semi-structured interviews. Inclusion criteria: Radiographers with experience in developing guidelines or protocols in imaging departments. Managers in eight imaging departments received information about the study and inclusion criteria by email, to help in recruitment by suggesting participants. Fourteen suggested participants received information about the study by email. Seven radiographers in five different imaging departments who met the inclusion criteria choose to participate in the study. The author transcribed and analysed all interviews.

Results: The study suggests that brief encounters with patients and complex high-tech equipment are factors that can complicate patient involvement in procedure development in imaging diagnostics. The study shows that radiographers perceive patient involvement in developing procedures difficult and confusing, due to few guidelines on how to involve the patients.

Conclusion: The findings suggests that further training and research on EBP must be a focus in future procedure development. New ways of thinking is in order to involve the patients according to the governments' intentions

B-1313 09:34

Relationship between body fat by DEXA and cardiovascular risk factors

R.A.M. Santos, A.C. Girão, J.P. Figueiredo; Coimbra/PT (rutemartinsantos@gmail.com)

Purpose: To evaluate the relationship between % body fat (%BF) and % abdominal fat (%ABDF) evaluated by bone densitometry (DEXA) and risk factors for cardiovascular diseases in young adult's students.

Methods and Materials: 214 individuals (aged between 18-25 years), were submitted to a DEXA for the determination of %BF and android fat (AF) classified in four groups using the Bray criteria (1998); and submitted to blood sampling for biochemical analyses: glycemia, triglycerides, total cholesterol and HDL, and insulin resistance. Correlation was assessed by the Pearson coefficient. Fat parameters and biochemical analysis were compared by Student's t-test. The association between anthropometric variables and cardiovascular risk factors was analysed by gender using the χ^2 test. The multivariate linear regression allowed to identify the predictors of %BF and AF.

Results: The prevalence of obesity was 9.09% in boys and 16.6% in girls, with the average of the ABDF (AF) respectively of 17.49% and 29.27% ($p=0.000$). There was a positive correlation of insulin resistance with BF ($p=0.023$), with total cholesterol ($p=0.001$) and triglycerides ($p=0.019$) only in girls. Also in girls, a positive correlation was observed between TF and triglycerides ($p=0.030$). With the multivariate linear regression, we verified that both predictive models of BF and AF expressed a modest explanatory model ($R^2=0.4$) associated to predictors gender and BF ($p<0.05$).

Conclusion: This study shows that gender and triglycerides are one of the predictors for BF and AF, in girls.

B-1314 09:38

Exposure to electromagnetic fields during a gradient echo sequence in a 3T MRI scanner along z-axis

V.M.F. Silva, I. Ramos, M. Marques, J. Moreira; Porto/PT (vitorsoft@gmail.com)

Purpose: Occupational staff, volunteers and patients' accompanying sometimes are exposed to electromagnetic fields (EMF) during magnetic resonance imaging (MRI) procedures, inside MRI room. This study aims at evaluating the propagation of the electromagnetic field associated with a T2 gradient echo brain sequence along the z-axis from the magnet entrance up to the room limits in a 3T scanner.

Methods and Materials: A well 200 MHz oscilloscope (Agilent DS01024A), that was positioned outside the MRI room, was used with a receiving rectangular loop connected through a double-shielded coaxial cable, allowing measurements of the induced voltage due to RF-magnetic field. Six independent measurements of induced voltage were taken at different fixed

points in the MRI room along the z-axis from the bore, using a T2 gradient echo brain sequence.

Results: Values obtained ranged from 55 mV to 382 mV and a sinusoidal z-dependence of the induced voltage was ascertained, due to interference of the income and wall reflected RF-wave. Lowest values were reached at the bore entrance (0 cm) and at 150 cm from the entrance. Highest values were reached at 105, 210, 225, 240 and 255 cm from the bore entrance. Values measured on the back of the equipment were at 380 mV range at different points.

Conclusion: Values measured from all six measurements showed a "sinusoidal" waveform shape, demonstrating that highest values are not located in points closer to the magnet isocenter. Professionals must be aware to that for better practices in terms of exposure to EMF in MRI.

10:30 - 12:00

Room C

Abdominal Viscera

SS 1801

Liver: beyond morphology

Moderators:

P. Bonaffini; Monza/IT
N. Elmas; Izmir/TR

B-1323 10:30

Diagnostic performance in the stage of liver fibrosis: comparison of magnetic resonance T1 rho and acoustic radiation force impulse

J. Li, C. Zhang, H. Liu, S. Yang, Y. Wang, W. Chen, D. Wang; Shanghai/CN (lijinning117@163.com)

Purpose: To compare the diagnostic performance of magnetic resonance (MR) T1 relaxation time in rotating frame (T1 rho) and ultrasound-based elastography (acoustic radiation force impulse imaging, ARFI) for staging liver fibrosis in rat models.

Methods and Materials: Thirty-two rats were injected with carbon tetrachloride (CCl₄) to induce liver fibrosis and fifteen rats were injected without CCl₄ as control. Both T1 rho and ARFI imaging were performed for all rats, and T1 rho values and ARFI velocities were measured. The stage of liver fibrosis was identified based on METAVIR scoring system (F0-4). The Pearson correlation coefficient was obtained between the two imaging techniques and pathological staging. Diagnostic performance was determined by calculating areas under receiver operating characteristic curves (AUCs).

Results: There is moderate correlation between T1 rho values and ARFI velocities ($r = 0.624$, $P < 0.001$). T1 rho values showed stronger correlation with the stage of liver fibrosis ($r = 0.82$, $P < 0.001$) than that of ARFI velocities ($r = 0.618$, $P < 0.001$). AUCs of diagnosing fibrosis of $\geq F1$, $\geq F2$, $\geq F3$, $\geq F4$ for T1 rho imaging was 0.923, 0.901, 0.898, 0.961, respectively, which was higher than 0.862, 0.825, 0.815, 0.860 of ARFI imaging, and there is significant difference of AUCs between two imaging techniques for detecting fibrosis of $\geq F3$ ($P = 0.046$) and $\geq F4$ ($P = 0.019$).

Conclusion: MR T1 rho value is a better biomarker than ultrasound ARFI velocity for staging liver fibrosis, especially for diagnosing obvious fibrosis ($\geq F3$).

B-1315 10:38

Evaluation of T1 measurement methods of the liver in chronic liver disease

A. Yamada, T. Nonaka, M. Nakamura, T. Suzuki, D. Komatsu, S. Fujita, Y. Fujinaga, M. Kadoya; Matsumoto/JP (a_yamada@shinshu-u.ac.jp)

Purpose: The purpose of study is to validate reproducibility and clinical usefulness of T1 measurement by variable flip angle method (VFA) and saturation recovery method (SR) in chronic liver disease.

Methods and Materials: Consecutive sixty-four patients with chronic liver diseases who underwent MR elastography (MRE) and T1 measurement of the liver from April 2015 to April 2016 in our institution were included in this IRB approved prospective study. Plastic bottle phantoms filled with various concentration of Gd-EOB-DTPA (0, 0.1, 0.2 mmol/mL) were scanned together with patients. T1 of the liver and phantoms were measured by VFA in 43 patients, by SR in 21 patients, before and 20 minutes after contrast media administration. Correlation coefficient between Gd-EOB-DTPA concentration and measured 1/T1 in phantoms (rC), normalized absolute difference in repeated measurement of T1 in phantoms (dT1), correlation coefficient between liver stiffness obtained by MRE and native T1 of the liver (rLS) were statistically analyzed between VFA and SR.

Results: Mean and standard deviation (SD) of rC and dT1 were 0.9084 ± 0.3103 and 0.3058 ± 1.0881 for VFA, 0.9997 ± 0.0006 and 0.0379 ± 0.0201 for SR, respectively ($P = 0.0105$ and 0.0262). Mean and 95%

confidence intervals of rLS were 0.0658 (-0.3531, 0.4848) for VFA, -0.7779 (-0.9461, -0.6098) for SR, respectively.

Conclusion: T1 measurement by SR is more reproducible and well correlated to Gd-EOB-DTPA concentration and liver stiffness than that by VFA.

B-1317 10:46

Assessment of histological stage of fibrosis using relative liver enhancement in patients with primary sclerosing cholangitis

J. Yamamura, A. Aigner, C. Schramm, R. Zenouzi, G. Adam, S. Keller; Hamburg/DE (j.yamamura@uke.de)

Purpose: To assess if relative liver enhancement (RLE) of extracellular gadolinium-based contrast agent (GBCA) enhanced magnetic resonance imaging (MRI) could be used as a marker of hepatic fibrosis and inflammation in patients with PSC.

Methods and Materials: 40 patients (41.2±7.1 years) underwent 3-tesla (T) MRI examination of the liver as well as liver biopsies in a mean time of 54±55 days between liver biopsy and MRI. Ishak modified hepatic activity index (mHAI) and Scheuer grading/staging of inflammation/fibrosis were used to categorize the specimen. T2w1 and multiphase T1w1 were performed, where T2 signal intensities, contrast enhancement and RLE were assessed. Interobserver agreement tests, and mixed effects regression models were applied to derive effect estimates for the association between histopathology and MRI parameters.

Results: A fibrosis stage >2/4 was found in n=26/66 of liver histologies. Regression models revealed a significant positive correlation of delayed-phase RLE and fibrosis staging (e.g. 69.2 times (95%-CI: 45.8-92.8) higher RLE for fibrosis 3 or 4 compared to 0. Interobserver agreement for quantification of RLE was excellent (portalvenous RLE R=0.93; delayed RLE R=0.97). Interobserver agreement was good both for detection of T2 signal alterations and contrast enhancement (Cohen's Kappa T2 >0.77; contrast enhancement >0.92). No significant association between portalvenous/delayed RLE and mHAI was observed.

Conclusion: Delayed RLE of multiphase MRI may provide a reproducible and accessible evaluation of hepatic fibrosis in patients with PSC.

B-1318 10:54

Assessing liver fibrosis with diffusion-weighted MRI: comparison between conventional and kurtosis models

L. Yang, M. Zeng, S. Rao; Shanghai/CN

Purpose: To assess liver fibrosis in patients with chronic liver disease using diffusion kurtosis imaging (DKI), in comparison with conventional diffusion-weighted imaging.

Methods and Materials: This prospective study was conducted with a 1.5T MR scanner. DKI with b-values of 0, 200, 500, 1000, 1500 and 2000 sec/mm² was performed in 81 patients with chronic liver disease. Mean diffusivity (MD), mean kurtosis (MK) and apparent diffusion coefficient (ADC) maps were calculated. Correlations of MK and MD with fibrosis stages and ADC were computed. The diagnostic efficacy of MD, MK and ADC for predicting stage 2 fibrosis or greater, and stage 3 fibrosis or greater was compared.

Results: The MD (rho=-0.475, P<0.001), MK (rho=0.526, P<0.001) and ADC (rho=-0.480, P<0.001) correlated significantly with fibrosis stages, and ADC exhibited a strong negative correlation with MK (rho=-0.967; P<0.001) and a moderate association with MD (rho=0.601, P<0.001). Areas under the curves (AUCs) for predicting stage 2 fibrosis or greater were not significantly different (P>0.05) between MK (0.809,95%CI: 0.709-0.909) and ADC (0.797,95%CI: 0.695-0.899) as well as between MD (0.715,95%CI: 0.598-0.832) and ADC. AUCs were also similar for MD (0.710,95%CI: 0.599-0.822), MK (0.768,95%CI: 0.665-0.870) and ADC (0.747,95%CI: 0.641-0.853) for predicting stage 3 fibrosis or greater.

Conclusion: DKI is feasible for predicting liver fibrosis in patients with chronic liver disease, but MD and MK offer similar diagnostic performance to ADC values.

B-1319 11:02

The potential role of Gadoxetate disodium (Gd-EOB-DTPA) and diffusion-weighted magnetic resonance imaging in primary sclerosing cholangitis

J. Yamamura¹, J. Sedlacik¹, T. Schuler¹, R. Buchert², H. Kooijman-Kurfuerst¹, C. Schramm¹, J. Fiehler¹, G. Adam¹, S. Keller¹; ¹Hamburg/DE, ²Berlin/DE (s.keller@uke.de)

Purpose: To assess the diagnostic effectiveness of both dynamic contrast-enhanced (DCE) and diffusion-weighted (DWI) magnetic resonance imaging (MRI) in patients with primary sclerosing cholangitis (PSC).

Methods and Materials: After measuring the hepatic fibrosis classified according to METAVIR fibrosis score with ultrasound-elastography within an interval of 0±6 months, 47 patients (43.4 ± 14.5 years) with known PSC were examined by DCE-MRI using Gd-EOB-DTPA and by DWI on a 3.0-tesla scanner. DCE-parameters were calculated using a dual-inlet two-compartment uptake model. ROI covering the right liver lobe were drawn by two observers

independently. Pearson correlation and univariate analysis of variance was used to test quantitative ADC and DCE-parameters for differences between the fibrosis stages.

Results: Both ADC and hepatocellular uptake rate (Ki) correlated significantly to hepatic fibrosis (r=-0.610; P<0.001 and r=-0.368; P=0.01). Multiple comparison testing of ADC confirmed significant difference in discrimination of F0/1 from F2 (p=0.02), F3 (p=0.008), and F4 (p=0.001). The optimal cut-off value of ADC=1.17 mm²/sx10⁻³ for discrimination of F0/1 from F3 showed a sensitivity 0.1 and specificity of 0.826. The cut-off value ADC=1.13 mm²/sx10⁻³ discriminated F0/1 from F4 with a sensitivity of 0.875 and specificity of 0.87. Ki only discriminates F0/1 from F4 (p=0.034), but not F2 or F3. The cut-off value Ki=0.353/100/min and Ki=0.355/100/min showed a sensitivity of 0.857 and specificity of 0.5 to discriminate F0/1 from F3 and F4, respectively.

Conclusion: DWI showed a higher sensitivity to differentiate several stages of fibrosis and might be more preferable than DCE-MRI for diagnosis and staging of fibrosis in PSC.

B-1320 11:10

Tumour response to preoperative chemotherapy in patients with colorectal liver metastases: can ADC values evaluated at 3T MRI replace RECIST criteria?

F. Donati, P. Boraschi, R. Cervelli, F. Pacciardi, G. Tarantini, M. Castagna, L. Urbani, D. Caramella, F. Falaschi; Pisa/IT (francescamaria69@gmail.com)

Purpose: To evaluate tumour treatment response in colorectal liver metastases (CRLM) after preoperative chemotherapy (pCT) at 3T MRI, focusing on the role of ADC values.

Methods and Materials: Twenty-five patients with CRLM, who underwent 3T MRI before and after fluorouracil-based pCT and subsequently treated by parenchymal-sparing liver surgery, were retrospectively included in our study. Diffusion weighted-MRI (DW-MRI) was performed using a spin-echo echo-planar sequence with multiple b-values, obtaining an ADC map. Fitted ADC values were calculated by two radiologists in conference for each lesion before and after pCT, by drawing on the ADC map a ROI around the tumour burden of the lesion. Maximum diameter of each lesion in both examinations was recorded. Diameter variations and RECIST 1.1 criteria were assessed. All MRI findings were histopathologically related to Tumour Regression Grading (TRG) of resected liver metastases. Statistical analysis was performed on a per-lesion basis.

Results: A total of 58 CRLM were analyzed. According to RECIST 1.1, 8 lesions were classified as CR, 24 as PR and 25 as SD. In only one lesion PD was found. In 8 lesions both ADC and TRG was not evaluated due to the lesion disappearance. TRG 1, TRG 2, TRG 3, TRG 4 and TRG 5 were observed in 6, 12, 12, 13 and 7 lesions, respectively. ADC_{post}, Δ ADC values (both p<0.0001), RECIST 1.1 criteria (p=0.0009) were significantly different based on TRG classes.

Conclusion: 3T DW-MRI, using ADC values, can be a reliable tool to assess tumour treatment response after pCT in CRLM.

B-1321 11:18

Liver function estimation using gadoxetic acid-enhanced liver MRI

J.-H. Yoon¹, E. Kim¹, T. Okuaki², J. Lee¹; ¹Seoul/KR, ²Tokyo/JP

Purpose: To determine whether hepatocyte fraction derived from gadoxetic acid-enhanced liver MRI can estimate liver function.

Methods and Materials: In this IRB approved prospective study analysed 50 patients who underwent gadoxetic acid MRI at 3T and ICG R₁₅. T1 maps of the liver using Look-Locker sequence were obtained before contrast (preT1 map) media injection and 10 minutes (post T1 map) after a standard dose of gadoxetic acid (0.025mmol/kg). Hepatocyte fraction and liver volume were calculated. The relationships were evaluated between MR parameters and ICG R₁₅. The parameters were also compared between patients with different Child-Pugh class, and with different ICG R₁₅ results (≥15% or <15%).

Results: Hepatocyte fraction (r=-0.78) and liver volume (r=-0.42) showed a negative correlation with ICG R₁₅. Compared with patients with chronic liver disease (CLD) or Child A (88%, 44/50), hepatocyte fraction (238.6±106.3%, 77.0±34.6%, P<0.0001) was significantly lower in Child B patients (12%, 6/50). In 44 patients with CLD or Child A, hepatocyte fraction (298.17±69.81% vs. 160.12±95.28%, P<0.0001) was significantly higher in patients with ICG R₁₅<15% (n=25), compared with patients with ICG R₁₅≥15% (n=19), whereas liver volume did not (1059.7±129.8mL vs. 991.7±207.0mL, P=0.19). Compared with liver volume, hepatocyte fraction showed a better performance to detect patients with ICG R₁₅> 20%, which is a contraindication of major hepatectomy (area under the curves were 0.70, and 0.98).

Conclusion: Hepatocyte fraction derived from gadoxetic acid-enhanced liver MRI showed a significantly negative correlation with ICG R₁₅, and showed a better performance to identify contraindicative patients of major hepatectomy than liver volumetry.

Author Disclosures:

J. Yoon: Research/Grant Support; Bayer Healthcare. E. Kim: Employee; Philips Healthcare Korea. T. Okuaki: Employee; Philips Healthcare Japan.

J. Lee: Advisory Board; Bayer Schering Pharma.. Research/Grant Support; Acuzen, Guerbet.

B-1322 11:26

Pathologic alterations in hepatic vasculature in primary sclerosing cholangitis: correlation with morphologic spectrum and abnormal hyperintensity in T2-weighted MR images

M. Kul, D. Kuru Öz, A. Erden; *Ankara/TR (melahatkul@yahoo.com)*

Purpose: To correlate both the spectrum of hepatic morphology and abnormally high signal intensity in T2-weighted (T2w) MR images in primary sclerosing cholangitis (PSC) with pathologic alterations in major hepatic vessels.

Methods and Materials: A total of 34 patients with PSC were included in this study. Two radiologists retrospectively analyzed the image sets in consensus regarding the presence of any pathologic finding in portal and hepatic veins, abnormally T2-hyperintense areas, and spectrum of hepatic morphologic changes. Patients were divided into hepatic vascular pathology group (HPG) and control group (CG). Hepatic morphology and T2-hyperintensity were correlated between both groups. In HPG, correlation was also made in terms of location between affected vessel and both morphologic changes and T2-hyperintensity. Additionally, time since diagnosis and total bilirubin levels were compared between both groups.

Results: In 12 out of 34 patients (35%) at least in one of the hepatic vessels pathologic alteration was present (HPG). No significant difference was detected between HPG and CG in terms of abnormal morphologic spectrum and T2-hyperintensity ($p > 0.05$). Total bilirubin levels, time since diagnosis did not differ between HPG and CG ($p > 0.05$). No significant correlation was found between hepatic vascular pathology and both hepatic morphologic changes and T2-hyperintensity in terms of location ($p > 0.05$).

Conclusion: Abnormal hepatic morphology and T2-hyperintensity do not appear to be primarily affected by pathologic alterations of hepatic and portal veins in PSC. Thus, the heterogenous spectrum of hepatic morphology/T2-hyperintensity in PSC seems rather to derive from heterogeneity in microperfusional alterations due to periductal inflammatory and fibrotic changes.

B-1324 11:34

The positive effects of bariatric surgery on NAFLD at early postoperative period: proof with ideal IQ sequences obtained by 3.0 Tesla MRI

Y. Metin¹, N. Orhan Metin¹, S. Kalcan¹, O. Ozdemir¹, M. Çolakoğlu¹, A. Küpelî², ¹Rize/TR, ²Mus/TR (ymetin53@gmail.com)

Purpose: To investigate the early effects of bariatric surgery on liver fat fraction (LFF), pancreas fat fraction (PFF) and liver length at 3T MRI using ideal IQ sequences.

Methods and Materials: Body mass index (BMI), body weight, liver fat fraction, pancreas fat fraction and craniocaudal length of liver were measured preoperatively (one week before surgery) and postoperatively (one month after surgery) in 39 consecutive patients (25 female, 14 male; age range, 25-60 years; mean age, 41 years) who underwent bariatric surgery [laparoscopic Roux-Y-gastric-bypass (4) or laparoscopic sleeve gastrectomy (35)] between May 2016 and April 2017.

Results: At the end of first month of bariatric surgery a significant decrease in mean values of pancreas and liver fat fraction has been observed along with a decrease of body weight and BMI. A moderate positive linear correlation was observed between LFF and PFF, liver length while a weak positive linear correlation was noticed between LFF, BMI and body weight.

Conclusion: Ideal IQ MRI sequences enables quantitative analysis of fatty infiltration within the liver and pancreas, and thus may be use as a non-invasive tool to monitor the positive effects of the surgery on fatty infiltration of these organs.

B-1325 11:42

Contrast-enhanced MR imaging 3D texture analysis as a potential tool for preoperative prediction of microvascular invasion in hepatocellular carcinoma

Y. Zhu, X. Ma, X. Zhao; *Beijing/CN (zhuyj04@126.com)*

Purpose: To explore the value of contrast-enhanced MR imaging (MRI) texture analysis in predicting the microvascular invasion (MVI) status of hepatocellular carcinoma (HCC) preoperatively.

Methods and Materials: A retrospective study of 90 pathologically confirmed cases was conducted. Studies were divided into two groups: the MVI-positive group (n=45) and MVI-negative group (n=45) based on pathology. 58 texture parameters of HCC were extracted using baseline MRI on both arterial phase (AP) and portal phase (PP) by a 3D method. The clinical radiological features were also included. Univariable logistic regression identified potentially predictive parameters, which were tested in multivariable logistic regression together with clinical features to predict development of MVI.

Results: In the clinical features, only max tumour diameter (MTD) showed significant difference between the two groups ($P=0.001$). Multivariable logistic regression revealed that MTD, 3 MR texture features in AP model and 3 in PP model might be predictors to MVI. AP model showed a better diagnostic performance than PP model using ROC analysis, with area under the curve (AUC) 0.921 (0.864-0.977) vs 0.815 (0.727-0.904), sensitivity 88.9% vs 80.0%, specificity 84.4% vs 71.1%.

Conclusion: The contrast-enhanced MRI 3D texture analysis can predict MVI of HCC preoperatively and noninvasively; the arterial phase showed better performance.

10:30 - 12:00

Room X

Vascular

SS 1815

Pulmonary circulation and venous imaging

Moderators:

N.J. Screation; Cambridge/UK

W.H. Sommer; Munich/DE

K-25 10:30

Keynote lecture

N.J. Screation; Cambridge/UK

B-1326 10:39

Virtual monoenergetic image reconstruction from spectral detector CT improves objective image quality and subjective assessment of pulmonary emboli

N. Grosse Hokamp^{1,2}, R. Kessner², R. Gilkeson², A. Gupta²; ¹Cologne/DE, ²Cleveland, OH/US (niels.grosse-hokamp@uk-koeln.de)

Purpose: To investigate objective and subjective image quality of virtual monoenergetic images (VMI) provided by spectral detector computed tomography (SDCT) for assessment of pulmonary vessels regarding emboli (PE).

Methods and Materials: 40 consecutive patients that underwent contrast-enhanced SDCT (IQon, Philips Healthcare) with PE-protocol were included in this IRB-approved study. Two regions of interest were placed in each of the following regions in conventional images (CI) and copied to VMI (40-200keV; 10keV increment): pulmonary trunk and arteries, lobar arteries, and segmental arteries. Attenuation (HU) and standard deviation (SD) were recorded, SDMuscle was considered representative of image noise. Signal- [SNR = HU(x) / SD(x)] was calculated. Subjectively, 40keV, 70keV, 110keV and CI images were assessed using 5-point Likert scale regarding large/intermediate/small vessel assessment and diagnostic confidence. ANOVA and Wilcoxon test were used for statistical assessment.

Results: Attenuation in vessels was higher in low-keV images ($p \leq 0.05$) while image noise remained constant throughout all reconstructions ($p \leq 0.05$); this resulted in a significant increase of SNR in VMI40-70keV compared to CI (e.g. lobar arteries, 40keV/CI: 40.7±14.6/13.9±4.8; $p \leq 0.05$). Segmental arteries' SNR in VMI40keV was equivalent to the SNR of the pulmonary arteries in CI (15.1±9.8 and 15.3±5.2, respectively). Subjectively, 40keV images significantly improved the assessment of vessels (e.g. intermediate, 4(4-5) vs 4(2-5), $p \leq 0.05$) resulting in a higher diagnostic confidence regarding PE (4.5(3-5) vs 4(2-4), $p \leq 0.05$).

Conclusion: Low-keV VMI from SDCT yields a significant increase in SNR of pulmonary vessels while maintaining low image noise. Accordingly, subjective vessel assessment and diagnostic confidence is improved in these reconstructions.

B-1327 10:47

CT pulmonary angiography at reduced radiation exposure and contrast material volume in obese patients using IMR and iDose⁴ in comparison to FBP

A. Quitzke, J. Schmidt-Holtz, C. Behzadi, G. Adam, M. Regier; *Hamburg/DE (a.laqmani@uke.de)*

Purpose: To intrindividually assess the image quality of CT pulmonary angiography (CTPA) in obese patients at reduced radiation exposure (RD-CTPA) and contrast medium (CM) volume using two different iterative reconstruction (IR) algorithms (iDose⁴ and iterative model image reconstruction (IMR)) in comparison to filtered back projection (FBP).

Methods and Materials: 17 obese patients (mean BMI: 37.6) with suspected pulmonary embolism (PE) underwent RD-CTPA (tube voltage: 100 kV; mean CTDIvol: 6.15 mGy; mean effective dose: 2.94 mSv) using 60 ml CM. The raw data were reconstructed using FBP and two different IR algorithms, iDose4 (levels 4 and 6) and IMR (levels 1-3) (Philips Healthcare). Subjective and objective image quality, image appearance and conspicuity of PE were

assessed in central, segmental, and subsegmental arteries. The objective image noise (OIN) was measured; contrast-to-noise ratio (CNR) was calculated.

Results: Noise reduction of up to 65% was achieved with iDose⁴ level 3 and of 85% with IMR level 3. CNR significantly increased with iDose⁴ and IMR compared to FBP ($p < 0.05$). Subjective image quality was rated significantly higher at IMR reconstructions in comparison with iDose⁴ and FBP. Moderate blotchy image appearance was observed when the highest strength of IMR was obtained, mildly limiting the diagnostic confidence. The conspicuity of central and segmental PE improved with the use of IMR. In subsegmental arteries, IMR was inferior to iDose⁴.

Conclusion: IMR enables CTPA at reduced radiation exposure and contrast medium volume in obese patients by the superior reduction of image noise and improvement of conspicuity of pulmonary embolism compared to FBP and iDose⁴.

B-1328 10:55

Model-based iterative reconstruction on low-dose CT pulmonary angiography: image quality and radiation dose saving compared with hybrid iterative reconstruction CTPA

A. de Vito¹, D. Ippolito¹, C.R. Talei Franzesi², L. Riva², S. Drago¹, S. Sironi¹; ¹Monza/IT, ²Milan/IT (a.devito@campus.unimib.it)

Purpose: To evaluate the dose reduction and image quality of low-dose pulmonary angiography (CTPA) reconstructed with model-based iterative reconstruction (IMR), and compared with standard CTPA with hybrid iterative reconstruction (iDose⁴).

Methods and Materials: 139 patients were prospectively enrolled and investigated for pulmonary embolism; a study group of 75 patients underwent low kV setting (80 kV, automated mAs) CTPA study, while a control group of 64 patients underwent standard CTPA protocol (100 kV; automated mAs); all patients were examined on 256 MDCT scanner (Philips iCT elite). In the study group, images were reconstructed using IMR technique, while in the control group we used iDose⁴ technique. CTDIvol, DLP and ED were evaluated in both groups. Region of interests were drawn in the three main pulmonary vessels to evaluate vascular enhancement (HU); signal-to-noise ratio (SNR) and contrast-to-noise ratio (CNR) were also calculated.

Results: Compared to iDose⁴-CTPA, low kV IMR-CTPA presented lower CTDIvol (6.41±0.84 vs 9.68±3.5 mGy) and DLP (248.24±3.2 vs 352.4±3.59 mGy*cm), with ED of 3.48±1.2 vs 4.93±1.8 mSv. Moreover, IMR-CTPA showed higher attenuation values (670.91±9.09HU vs 292.61±15.5HU) and a significantly higher SNR and CNR. The subjective image quality of low kV IMR-CTPA was also higher compared with iDose⁴-CTPA.

Conclusion: Low-dose CTPA (80 kV and automated mAs modulation) reconstructed with model-based algorithm represents a feasible protocol for the diagnosis of pulmonary embolism in the emergency setting, achieving high image quality with extremely low noise and a significant dose reduction within adequate reconstruction times (less than 120 seconds).

B-1329 11:03

High temporal resolution dynamic CE MRA in detection of reperfused pulmonary arteriovenous malformations (PAVMs) in HHT-patients

G. Schneider, A. Bucker, A. Massmann; Homburg/DE (dr.guenther.schneider@uks.eu)

Purpose: The recommended treatment of PAVMs in HHT patients (Hereditary Hemorrhagic Telangiectasia / Osler disease) is catheter embolization. Although immediate postinterventional imaging may show complete success of therapy, reperfusion may occur. We evaluated time-resolved contrast-enhanced MR-Angiography for detection of reperfused PAVMs.

Methods and Materials: 65 patients post embolization of PAVMs with platinum-coils or Amplatzer-vascular-plugs underwent follow-up studies for detection of reperfused PAVM. First, a time-resolved MRA-study was performed with injection of a small contrast medium bolus (0.025 mmol/kg BW (Gd-BOPTA) MultiHance, Bracco). The temporal resolution of the sequence was 3 sec/dataset with a total number of 72 slices. Thereafter a high resolution CE-MRA (0.075 mmol/kg BW MultiHance) with a timing based on the findings from the time-resolved study was performed. Images were evaluated regarding simultaneous enhancement of feeding artery and draining vein on dynamic CE-MRA.

Results: Time-resolved MR-Angiography was technically adequate in 61/65 cases. In 26/61 patients 32 reperfused PAVMs were detected. In those cases in which diagnosis of reperfused PAVM was unclear on high resolution images, evaluation of the enhancement kinetics of the draining vein on dynamic CE-MRA was used for diagnosis and could confirm 14 reperfused PAVM. All reperfused PAVM diagnosed on CE-MRA were confirmed by DSA and underwent reembolization.

Conclusion: Time resolved CE-MRA is a helpful adjunct to standard high resolution anatomic imaging, allowing for the evaluation of the enhancement kinetics of the draining vein as an indicator of recanalization of PAVM.

Compared with CT imaging of embolized PAVM, this is an important advantage of CE-MRA.

Author Disclosures:

G. Schneider: Advisory Board; Bracco. Research/Grant Support; Bracco, Siemens, Guerbet, Bracco, Siemens, Guerbet. Speaker; Bracco, Siemens, Guerbet. A. Bucker: Research/Grant Support; Bracco, Siemens, Guerbet. A. Massmann: Research/Grant Support; Bracco, Siemens, Guerbet.

B-1330 11:11

The frequency of coexistence of renal artery and vein variations on abdominal CT

S. Gurel, Ö. Yılmaz, A. Kiyani; Bolu/TR (safiyegurel@gmail.com)

Purpose: Our aim is to determine the frequency of coexistence of renal artery and vein variations.

Methods and Materials: Abdominal CT examinations of 505 patients (217 female and 288 male) were evaluated for the presence of renal artery variations [early branching, multiple renal arteries (hilar-polar-supplementary artery)], right renal vein variations (multiple right renal vein, split of right renal vein, gonadal vein connected to right renal vein) and left renal vein variations (circumaortic left renal vein, retroaortic left renal vein, multiple left renal vein). Presence of accompanying IVC anomaly (duplication and transposition) was evaluated as well. The frequency of renal artery and vein variations were calculated in percentages.

Results: The frequency of uni- or bilateral early branching of main renal artery were found to be 0.6% and 2.97% whereas uni- or bilateral multiple renal arteries were found to be 12.3% and 2.97% respectively. On the right side, the frequency of multiple renal veins, split renal vein and gonadal vein draining to renal vein were found to be 20.4%, 0.2%, 8.9% respectively. On the left side, the frequency of circumaortic renal vein and retroaortic renal vein were 6% and 3.96% respectively. No left-sided multiple renal veins and accompanying IVC anomaly were detected.

Conclusion: The frequency of coexistence of renal artery and vein variations were found to be 7.5%. Within this group, presence of left hilar artery and double renal vein on the right side in nine (1.78%) of 38 patients were found to be the most frequent coexistent variations.

B-1331 11:19

Evaluation of pelvic congestion syndrome with time-resolved MR angiography

S. Wassef, A. Stolpen; Iowa City, IA/US (shafik.wassef@gmail.com)

Purpose: The purpose of this educational exhibit is to review the role of time-resolved MR angiography (TR-MRA) in evaluation of pelvic venous congestion.

Methods and Materials: Although non-invasive imaging techniques, such as ultrasound and static CT and MRI, can be helpful, they cannot accurately determine the timing and direction of venous blood flow, which is essential for accurate diagnosis and treatment planning. Conventional angiography has been considered the gold standard for diagnosis and potential embolisation therapy. Recently, TR-MRA has proved to be a useful tool for the assessment of ovarian vein reflux eliminating the invasiveness and ionising radiation of conventional angiography.

Results: TR-MRA is a useful sequence for the assessment of ovarian vein reflux, which may aid the evaluation of pelvic congestion syndrome. Pelvic congestion syndrome (PCS), the female counterpart of male varicocele, is caused by incompetence of the left ovarian vein, often in combination with left renal vein compression. This results in venous reflux, pelvic venous engorgement, and chronic pelvic pain.

Conclusion: TR-MRA has been proven to be a quick and non-invasive technique that allows evaluation of the physiological blood flow. It can be useful in detecting ovarian vein reflux which help evaluating PCS. MRI also provides details of the anatomy and can evaluate for other possible causes of pelvic pain in addition to providing dynamic imaging of the pelvic vasculature.

B-1332 11:27

Determination of inferior vena caval diameter: is it true on cavography?

C. Ma; Changsha/CN (mcismc@126.com)

Purpose: The geometries and the orientations of IVC are various and variable, which may lead to an inaccurate diameter measurement. The purpose of this study was to (a) type the geometries and the orientations of IVC on cross-sectional CT imaging; (b) compare the discrepancy between anteroposterior projection diameter (PD) on cross-sectional CT imaging and hypothetical diameter based on caval circumferences calculation (CD); (c) if difference between PD and CD exists, how often it can affect IVC filter selection.

Methods and Materials: 1619 patients who underwent abdominal contrast-enhanced CT were included. The following parameters were measured on cross-sectional CT: (a) the anteroposterior PD and (b) the caval circumference. PD and CD were compared using Mann-Whitney U test. Cohen's kappa test was used to evaluate the agreement of measurement consistency between PD

and CD, where one yielded a diameter of >28mm and the other yielded a diameter of <28mm.

Results: PD was significantly larger than CD (22.3±3.5 vs 20.4±2.8, P<0.05) in the entire study population. With the PD rule, the prevalence of megacava was 5.5% in our study, but only 0.67% patients in our series had an IVC diameter greater than 28 mm according to the CD rule. When performing a Cohen's kappa test, an agreement of consistency for the diameter of 28 mm was poor with a kappa coefficient of 0.186.

Conclusion: As the geometry of IVC may not be circular, HD calculation based on circumference may be a more appropriate approach for IVC diameter determination.

B-1333 11:35

Evaluation of radiation dose and image quality of dual-detector spectral CT portal venography of swine using a low-concentration iodinated contrast agent and low tube current

C. Chen, X. Lu, H. Liu, Z. Lu; *Shenyang/CN (475395751@qq.com)*

Purpose: To investigate image quality and radiation dose of the low-iodine-load contrast agents for portal venography by dual-detector spectral CT.

Methods and Materials: Five swines (weighing 42.5±3.1 kg) underwent portal venography by dual-detector spectral CT (120 kVp; current: dose right index 22) with the following four different contrast media injection protocols: total iodine dose 40ml, 50ml, 60ml for 270 mg I/ml and 80ml for 350 mg I/ml (control group). The data were reconstructed in monochromatic images at 40, 50, 60, 70 keV (spectral iterative reconstruction level 3). The image noise (IN) (standard deviation, SD) of portal vein (PV) and the contrast-to-noise-ratio (CNR) of PV-to-liver parenchyma were measured. Subjective score of the sharpness of PV boundaries and the diagnostic acceptability (DA) were performed by two radiologists independently using a 5-point scale (1 very poor to 5 excellent).

Results: The radiation dose (CTDIvol) for low-iodine-load contrast groups was 60% lower than for control group (7.4mGy vs 18.4mGy, P < 0.05). The IN, CNR, DA and sharpness of PV of all groups were statistically different (P < 0.05). For each low-iodine-load contrast group, the IN decreased and CNR increased from 40 keV to 70 keV, respectively. Compared with control group, monochromatic images 50 keV + 50 ml contrast dose combination demonstrated the acceptance image quality.

Conclusion: At less than 40% of the conventional radiation dose, by the dual-layer detector spectral CT, 50ml isotonic iodine contrast agents still clearly show the portal vein, at the same time, to meet the diagnostic needs.

B-1334 11:43

Treatment of varicose veins with endovenous laser ablation using low linear endogenous density

S. Sangma¹, U. Gorski¹, M. Yadav², T. Yadav¹, N. Khandelwal¹; ¹Chandigarh/IN, ²New Delhi/IN (ujjwalgorski@gmail.com)

Purpose: To assess the efficacy of EVLA with 1470 nm laser using low linear energy density (LEED) less than 80 J/cm

Methods and Materials: A prospective study was conducted in a total of 58 limbs with GSV incompetence using low LEED below 80 J/cm. The occlusion rate, improvement in CEAP and VCSS, ulcer healing rate, improvement in symptoms were assessed. The complication rate and recurrence of disease were also assessed.

Results: The occlusion rate was 96.1%; there was up gradation of CEAP score by one or two grades by a period of one month in 75 % cases and rest by a maximum period of 3 months. Ulcer healing rate was seen in more than 91 % patients. Over 95 % confirmed improvement of symptoms. The post procedure pain was minimal and less than 50 % requiring NSAIDs immediately post procedure. DVT was encountered in 2% of patients. No major complications like pulmonary embolism and arterio-venous fistula were encountered. Two patients had segmental recanalisation of GSV after a period of 18 months. One patient had recurrence of symptoms and down gradation of CEAP score.

Conclusion: EVLA with 1470 nm using low LEED is an effective mode of treatment for varicose veins with lesser complications and similar venous occlusion rate with higher LEED>90 J/cm. No significant recanalisation of GSV was encountered; however a longer period of follow up will be required to determine incidence of recanalisation and recurrence of disease.

B-1335 11:51

Multiparameter ultrasound in the diagnosis of deep vein thrombosis of the lower extremities

A. Demidova, I. Rychkova, N. Krivosheeva, E.A. Zubareva, A. Kuznecova; *Moscow/RU*

Purpose: With the advent of the latest visualisation technologies such as acoustic structure quantification (ASQ), ultrasound elastography (USEG) and superb microvascular imaging (SMI), we get an opportunity to detect hypoechoic thrombotic masses in the deep veins of the lower extremities, hardly visualised in B-mode and colour duplex or power Doppler imaging modes. The combined use of new technologies, based on different variants of echo signal processing, allowed us to qualitatively assess the ageing of deep vein thrombosis (DVT).

Methods and Materials: 32 patients aged 43 to 85 years with DVT underwent ultrasound examination (B-mode, CD, PD) and additional examination using ASQ, USEG and SMI. All examinations were provided with Toshiba Aplio 500 ultrasound systems with high-frequency linear transducers.

Results: Visualisation of thrombi with USEG had advantages over B-mode in the acute phase of thrombus formation. Thrombi were coded as homogeneous hard elastic structure in the vein lumen. Thrombi after the retraction phase were coded as soft elastic structure; later, the stiffness of the structure increased and the signs of elastic inhomogeneity appeared. Within the zone of recanalisation, we detected soft elastic parts. Using SMI allowed us to detect early signs of the recanalisation process (before appearance of classic color Doppler signs). ASQ technology determines inhomogeneity of thrombi which were homogeny hypoechoic structures in the B-mode.

Conclusion: New ultrasound technologies allow us to reliably assess the echo structure of thrombi within different DVT stages and determine early signs of the recanalisation processes. Moreover, these technologies are simple to use and can be provided within a short time.

10:30 - 12:00

Room Z

Interventional Radiology

SS 1809

Bone and spine interventions

Moderators:

V. Chianca; Naples/IT

B.A. Radeleff; Hof/DE

K-26 10:30

Keynote lecture

A.D. Kelekis; Athens/GR

B-1336 10:39

Percutaneous combined treatment for lumbar disc herniation: how we do it

G. Galvano¹, M. Raciti², G. Scavone¹, S. De Luca¹, A. Cannella¹, C. Di Lorenzo¹, G. Tigano¹, A. Scavone¹; ¹Catania/IT, ²Pavia/IT (mariavittoria.raciti@libero.it)

Purpose: To show percutaneous combined treatment, coblation and oxygen-ozone nucleus pulposus ablation, for lumbar disc decompression under fluoroscopic guidance and local anaesthesia.

Methods and Materials: Retrospective single-centre study has been performed. Inclusion criteria included patients with back pain (visual analogue scales VAS > 6), unsuccessful conservative treatments at least six weeks and protruded disc without calcifications. Main exclusion criteria were extruded disc herniation, black disc, spinal stenosis, spondylolisthesis, instability, neoplastic disease, metabolic bone disease, infection and haemorrhagic diathesis. Since July 2015, 150 patients (82 male, 68 female, from 26 to 69 years) were enrolled. Disc disease was studied with MR or TC and electromyography in doubt cases. Interventions have been performed with postero-lateral access under fluoroscopic guidance in local anaesthesia. All patients were treated with coblation and oxygen-ozone nucleus pulposus ablation, and simultaneously with transforaminal periganglionic steroid injection. The clinical outcomes were evaluated using VAS score at 1, 6 and 12 months of follow-up.

Results: There was a significant reduction of back pain in 80% of patients. The average preoperative VAS score was 7.1±0.3; VAS score was decreased down to 2.1±0.3 1 months after the procedure; the final follow-up VAS score was 2.6±0.1. The treatment showed a complication rate <1%. Only 1 patient showed an early complication, extruded disc herniation.

Conclusion: The advantage of percutaneous combined treatment, coblation and oxygen-ozone nucleus pulposus ablation, is that it is a single minimally invasive procedure which allows for a double treatment with a synergistic effect. Combination treatment is more effective than single procedures without increasing complications.

B-1337 10:47

CT-guided pulsed radiofrequency treatment of the lumbar dorsal root ganglion in patients with acute radicular low back pain

A. Napoli, S. Dababou, H.-P. Erasmus, C. Marrochio, R. Scipione, C. Catalano; *Rome/IT (alessandro.napoli@uniroma1.it)*

Purpose: To determine the clinical impact of CT-guided Pulsed Radiofrequency (PR) in the management of patients with acute or sub-acute neuro-radicular pain from lumbar disc herniation, refractory to usual therapeutic strategies.

Methods and Materials: Patients were eligible for this single-center prospective study if they presented acute or sub-acute neuro-radicular low back pain (EMG confirmed), refractory to usual treatments (drugs and injections), and if they could safely undergo PR-procedures. Treatment was performed using a 22-20G needle-electrode with probe tip directed to the symptomatic DRG under CT-guidance; E-pulsed radiofrequency (Cosman G4) was administered for 10min at 45V with constant local temperature of 42°C. Clinical evaluation was conducted with Visual Analogue Scale (VAS), Oswestry Disability Index (ODI) and Roland-Morris score (RM) for quality of life assessment; all questionnaires were obtained at baseline and at 1-week, 1-month and 3-month follow-up. Analyses were performed on a per-protocol basis.

Results: Over a 3-year period, 80 patients were treated with PR. Median VAS decreased from 7.8 to 3.5 to 2.6 to 1.3, median ODI from 78.0 to 12.5 to 6.0 to 5.5 at baseline, 1 week, 1 month and 3 months, respectively; RM decreased from 16 to 3 to 1.5 at baseline, 1 month and 3 months, respectively ($p < 0.001$). Overall, 90.0% of patients reached a 0 VAS score within the first month after treatment; 97.5% had a decrease of ≥ 20 points in ODI score in the same interval. 6 patients were considered partial responders requiring a second PR session.

Conclusion: CT-guided PR has shown to be a minimally invasive, effective and repeatable percutaneous treatment option for patients with acute or sub-acute neuro-radicular low back pain.

B-1338 10:55

Clinical outcome of rotational angiography in percutaneous laser disc decompression

D.N. Srivastava, V. Ha, A. Monga, R. Malhotra; *Ansari Nagar/IN (drdeepsrivastava@gmail.com)*

Purpose: 1. To evaluate the use of 3D rotational angiography technique in the percutaneous laser disc decompression (PLDD) treatment. 2. To evaluate the role of PLDD in patients with low back pain due to disc herniation.

Methods and Materials: We performed a prospective study of 46 patients who underwent PLDD for chronic discogenic low back pain. The PLDD procedure was performed under fluoroscopic guidance using flat panel DSA unit with 3D rotational x-ray imaging facility. For PLDD 980-nm diode laser was used. Follow-up clinical outcomes were assessed by the modified MacNab criteria.

Results: Excellent to fair response was seen in 30 out of 46 patients with overall success rate of 65%. In a group of patients with disc herniation smaller than 1/3 of the spinal canal diameter (34/46), success rate was 73.9% and in patients with disc herniation more than 1/3 of the spinal canal diameter (12/46), success rate was 26%.

Conclusion: Preoperative imaging studies and selection of patients with disc herniation smaller than 1/3 of the spinal canal diameter predict the clinical outcome of PLDD. 3D rotational angiography technique with Dyna CT is useful in target selection to maximise the efficacy of the technique. PLDD is a valid alternative for those selected patients with contained lumbar disc herniation, who do not respond to conservative treatment.

B-1339 11:03

Evaluation of magnetic resonance guided focused ultrasound (MRgFUS) as a first-line treatment of bone metastases with the intention of local treatment and pain palliation

H.-P. Erasmus, A. Napoli, S. Dababou, C. Marrochio, R. Scipione, C. Catalano; *Rome/IT (hansperasmus@gmail.com)*

Purpose: To evaluate MRgFUS as a first-line treatment of metastatic bone disease for the purpose of tumor control and pain palliation.

Methods and Materials: 40 patients with naïve (no previous treatment) symptomatic skeletal metastases, suitable for MRgFUS, were enrolled. Imaging (CT/MRI) was performed before and 3, 6 and 12 months after treatment. The primary endpoint was the number of lesions with partial or complete response at 3 months according to MD Anderson criteria. Clinical outcomes were evaluated over the same time period using a VAS score.

Results: Out of 40 patients, 7 were lost and missed the 3-month imaging check. 33 patients with 41 lesions were evaluated. The procedure was successful in terms of local control at 3 months in 20 lesions (49%) - complete in 12, partial in 8. Stable disease was observed in 5 lesions and a progression in 2. VAS score dropped from an average of 9 to 6 to 3 to 1.5 to 1 before, immediately after and 3, 6 and 12 months after treatment. Results were

statistically independent of histology (primary cancer). The only element influencing the outcome was the size of the lesion (up to 16 cm), with 7 cm as a reasonable cutoff for successful ablation - $p < 0.01$. BMI, age and sex did not play a role in the final outcome. No major adverse events occurred.

Conclusion: MRgFUS for painful bone metastases appears to achieve a local control of the lesion and satisfactory pain control.

B-1340 11:11

Drill-assisted bone tissue sampling: do we need to care about heat?

S. Niehues, J.L. Vahldiek, B. Geyer, B. Hamm, F. Poch, K.S. Lehmann; *Berlin/DE*

Purpose: Battery-powered drill-assisted bone tissue sampling has become a value alternative to manual drilling. Due to enhanced rotation speed and improved material, sampling of bone lesions has become more comfortable in lesser time. The question if enhanced drilling results in an increased heating of the system and the bone sample, leading to temperature-related sample affection, remains unclear.

Methods and Materials: Eight experimental drillings using a battery-powered drilling system (Arrow OnControl, Teleflex, Shavano Park, TX, USA) were carried out in an in vivo model using large pigs (15 sec. drilling time) with a temperature probe placed adjacent to the drilling canal. Continuous temperature measurements during the drilling was recorded to identify possible heating of the tissue.

Results: During the drilling process, we encountered a slight heating effect of median 0.65 degrees Celsius (SD 0.33, min. 0.1, max. 1.4 degrees Celsius). Initial heating reached a plateau phase during the drilling process.

Conclusion: Battery-powered drilling causes a slight heating of the tissue not exceeding 1.4 degrees Celsius. Initial heating is limited mainly due to the heat-sink effect preventing from thermal damage of the bone probe.

B-1341 11:19

The clinical impact of a novel low-dose protocol for minimal-invasive CT-guided musculoskeletal interventions

Z. Alagic, H. Alagic, R. Bujila, M.C. Wick; *Stockholm/SE (zlatan.alagic@sll.se)*

Purpose: CT-guided biopsies are important to establish the diagnoses of musculoskeletal lesions. They have a low morbidity and high cost-effectiveness but high levels of radiation. This prospective study compares our low-dose protocol for CT-guided musculoskeletal biopsies on a latest generation 16-cm detector 258-slice multi-detector CT (MDCT) scanner with advanced dose-reduction techniques to a protocol on a 64-slice MDCT scanner.

Methods and Materials: Between October 2016 and April 2017, 115 patients met the inclusion criteria and 58 of these underwent a CT-guided intervention utilising our novel low-dose protocol on a 258-slice MDCT (group A). The remainders underwent CT-guided intervention on a 64-slice MDCT without modern radiation-dose reduction (group B). Between-group comparisons comprised radiation dose, success rate, image quality parameters and workflow.

Results: In group A, the mean total DLP was 41.2 ± 2.9 mGy*cm and statistically significantly lower than of group B (257.4 ± 22.0 mGy*cm), corresponding to a mean dose reduction of 84% ($p < 0.001$). For group A, the mean CTDI_{vol} for the localizer scan was 1.34 ± 0.08 mGy and for the puncture scan 1.88 ± 0.09 mGy. Corresponding values for group B were 5.88 ± 0.14 mGy and 13.16 ± 0.40 mGy and statistically significantly higher than for group A ($p < 0.001$, respectively). The success rate in group A was 91.2% and in group B 87.9% ($p = N.S.$). No negative effect on quantitative- and qualitative image-quality parameters, time of intervention and number of biopsy scans was found.

Conclusion: We developed and successfully utilised a low-dose protocol for CT-guided musculoskeletal biopsies on a 258-slice MDCT that markedly reduces the radiation dose without affecting success rate, image quality and workflow.

B-1342 11:27

MR-guided high-intensity focused ultrasound (MRgFUS) for the treatment of oligometastatic prostate cancer bone metastases: can sound waves downstage cancer spread?

C. Marrochio, A. Napoli, R. Scipione, S. Dababou, H.-P. Erasmus, C. Catalano; *Rome/IT (cristinamarrochio@gmail.com)*

Purpose: With improvements in diagnostic modalities such as functional imaging, oligometastatic prostate cancer is being diagnosed with greater frequency than ever before. Our aim was to determine MRgFUS ability to downstage patients with oligometastatic bone disease with a single session of non-invasive metastasis-directed therapy.

Methods and Materials: The study was designed with intention-to-treat metastatic bone lesions. Patients were enrolled if they had accessible bone metastasis and could safely undergo MRgFUS (InSightec, Israel). Baseline measurable characteristics included dynamic contrast-enhanced MRI study

(Gd-BOPTA, Bracco; GE 750 3T magnet) with semiquantitative perfusion analysis, PSA level (ng/ml) and choline PET (SUV). Measurable variables were obtained at treatment time, and 3 months, 12 months and 24 months follow-up. **Results:** 18 patients fulfilled the inclusion criteria and safely underwent MRgFUS procedure of metastatic bone ablations. Lesions were located in the pelvis (11), scapula (3) and long bones (4). At baseline, all lesions showed a significant DCE perfusion (highly vascular) with a mean perfusion reduction of 88% at the 3 months follow-up (CI:100-50; $p < 0.001$) and stable at subsequent follow-up scans. Similarly, PSA levels decreased from a mean baseline of 19 (ng/ml) to 7.1, 2.9 and 2.1, at 3-12 and 24 months, respectively. SUV values showed a similar trend with reduction from baseline (mean 8.9 to 3.0, 2.3 and 1.7; $p < 0.001$). In all patients, a single MRgFUS session was appropriate without any major or minor adverse events reported. **Conclusion:** MRgFUS is a totally non-invasive procedure that can obtain nearly complete bone ablation in patients with oligometastatic prostate disease. The technique features a radiation-free approach that can be of incremental value in the long-survivor subset of oncological patients, significantly reducing the risk of toxic effects.

B-1343 11:35

Focused ultrasounds for the treatment of bone metastases: efficacy and feasibility

A. Iannessi, A.-S. Bertrand, H. Beaumont, R. Natale, G. Baudin, A. Thyss; Nice/FR (asbertrand3@hotmail.com)

Purpose: To evaluate the efficacy and feasibility of high intensity focused ultrasounds (HIFU) for the treatment of bone metastases.

Methods and Materials: A single-centre prospective study involving 11 consecutive patients with symptomatic bone metastases were done (8 women, 3 men). Patients were treated by Focused Ultrasounds performed with MR-guidance applied to bone metastases. Surgical treatment or radiotherapy treatment were not indicated for the patients who underwent FUs. The lesions were located in the appendicular and axial skeleton, consisting of secondary symptomatic lesions resulting from metastatic disease. The clinical course of pain was evaluated using the Visual Analog Scale (VAS) before treatment, at one week, and one month after treatment. We used Wilcoxon signed rank test to assess change in patient's pain (R CRAN software V 3.1.1).

Results: Patient follow-ups in our series show supportive results: within 11 patients, 10 patients were satisfied with a long-lasting result after the procedure had been performed, and would recommend the intervention to relatives. The average evaluation of pain was 7.9/10 (SD: 1.3) before treatment, 2.8/10 (SD: 1.7) one week after treatment, and 2.3/10 (SD: 2.1) one month after treatment. Our results show a significant decrease of the pain felt by patients between -before procedure and one week after the procedure- ($p = 0.003$), -before procedure and one month after the procedure- ($p = 0.004$).

Conclusion: HIFU under MR-guidance seems to be an effective and safe procedure in the treatment of symptomatic bone lesions for patients suffering from metastatic disease with a significant decrease of patient's pain.

B-1344 11:43

How to carry out follow-up studies in patients with osteoid osteoma treated with minimally invasive procedures (MRgFUS and RFA).

Evaluation of imaging findings and clinical outcome

C. Gianneramo¹, S. Quarchioni², P. Palumbo¹, F. Arrigoni¹, S. Mariani¹, L. Zugaro¹, A. Barile¹, C. Masciocchi¹; ¹L'Aquila/IT, ²Teramo/IT (camillagianneramo@gmail.com)

Purpose: To evaluate the main diagnostic CT and MRI findings after treatment of osteoid osteoma (OO) with radiofrequency ablation (RFA) or MRgFUS, and their relationship with clinical outcome with a follow-up period that lasted up to 24 months

Methods and Materials: We retrospectively evaluated follow-up CT and MRI examinations of 35 patients treated with minimally invasive procedures (MRgFUS and RFA) (23 and 12 patients respectively). We analysed imaging findings that proved the good clinical outcome, in particular bone marrow oedema, perilesional flogistic reaction, disappearance of the nidus, "needle signs", periosteal reaction and "ring signs". We identified the follow-up period when this imaging signs disappeared, according to clinical improvement (evaluated by VAS score).

Results: Clinical improvement was exhibited by VAS reduction (from 8 to 1) after 6 months from treatment. Imaging analysis showed decrease of bone marrow oedema in 65% of patients and decrease of perilesional flogistic reaction in 50% of cases in the 6 months follow-up. After one year from treatment, resolution of bone marrow oedema and perilesional flogistic reaction, was observed in 86% and 70% of cases respectively. We also noted significant decrease of periosteal reaction in 60% of patients. Two-years control was important to evaluate the disappearance of the nidus (80% of cases).

Conclusion: According to our results, follow-up CT and MRI examinations after treatment of OO should be performed at 6, 12 and 24 months, since in this time we have statistically significant correlations between clinical outcome and variations in imaging findings.

B-1345 11:51

Ablation zones after radiofrequency ablation in 16 patients with atypical cartilaginous tumours

R. Rivas Loya, J. Overbosch, J. Kraeima, R.A.J.O. Dierckx, P.C. Jutte, P.M. Van Ooijen; Groningen/NL (r.rivas.loya@umcg.nl)

Purpose: Local bone tumour treatment using Radiofrequency Ablation (RFA) is increasing, but mostly clinical outcomes are reported. There is a lack of radiology data regarding ablation zones in bone, needed for reliable planning and predictability. The purpose is to report ablation zones in 16 RFA procedures in Atypical Cartilaginous Tumours (ACT).

Methods and Materials: A retrospective study of 16 patients with ACT in long bones underwent a single placement CT-guided temperature controlled RFA. Tumours <10 mm (n=1) were treated with 10 mm needles; tumours 10-20 mm (n=9) with 20 mm needles, and tumours 20-30 mm (n=6) with 30 mm needles. The ablation zone was measured three months later in a follow-up MRI scan.

Results: All ablations were successful and without complications. Mean total ablation time was 9.25 minutes (range 8-12 minutes), in which the tip of the needle was at 90°C for a mean time of 7.62 minutes (range 6-10 minutes). Mean ablation zone diameters and standard deviations (SD) were: 24 mm for 10 mm needles, 41.37 mm (range 35-48 mm and SD 3.9 mm) for 20 mm needles, and 46.66 (range 42-64 mm and SD 7.88 mm) for 30 mm needles.

Conclusion: Clinical success obtained reaffirm that RFA can be effectively performed in the treatment of ACT. Ablation zones are ellipsoids 10-20 mm larger than the tip of the needle, with a SD <10 mm. However, there were outliers. Thus, stressing the need for better real-time monitoring techniques and better planning to develop safe and effective bone tumour ablations.

10:30 - 12:00

Room O

Chest

SS 1804

Bronchopulmonary diseases: new trends in CT and MR

Moderators:

J. Ley-Zaporožhan; Munich/DE
N.N.

B-1346 10:30

High-resolution lung MRI: 1.5 or 3 Tesla?

G. Chassagnon¹, C. Martin¹, W. Ben Hassen², A. Stemmer³, S. Bennani¹, M.-P. Revel-Dubois¹; ¹Paris/FR, ²Saint-Denis/FR, ³Erlangen/DE (gchassagnon@gmail.com)

Purpose: To compare high-resolution lung MR images acquired at 1.5 and 3 Tesla.

Methods and Materials: 3D spiral VIBE sequences were performed in 10 healthy volunteers on a 1.5 Tesla unit with an isotropic resolution of 1.2 mm³ and then at 3 Tesla with isotropic resolutions of 1.0 and 1.2 mm³. Assessment of bronchi up to the subsegmental level and signal measurements were performed. Signal and contrast-to-noise ratios (SNR, CNR) were calculated. Images acquired with the 1.2 mm³ resolution at 1.5 and 3 Tesla were compared to assess the effect of the magnetic field strength on image quality. Images with 1mm³ and 1.2mm³ resolution acquired at 3 Tesla were also compared to assess the effect of image resolution. Comparisons were performed using paired t-tests.

Results: Mean acquisition and reconstruction times respectively ranged from 4.9 ± 0.4 to 6.1 ± 3.1 minutes and from 9.1 ± 2.1 to 14.3 ± 7.5 minutes. They were significantly longer for the 1mm³ resolution. Ninety-five to 99% and 33 to 45% of the segmental and subsegmental bronchi were detected, respectively. The number of visible subsegmental bronchi was significantly higher with the 1mm³ resolution ($p = 0.04$) and significantly lower at 3 Tesla ($p = 0.04$). Mean SNR and CNR ranged from 133 to 165% and from 5.7 to 9.6%, respectively. Both were significantly lower at 3 Tesla ($p = 0.016$ and 0.003, respectively).

Conclusion: High-resolution lung MRI is feasible at 1.5 and 3 Tesla. However, bronchial visibility as well as SNR and CNR are significantly better at 1.5 Tesla.

Author Disclosures:

W. Ben Hassen: Employee; Siemens Healthineers. A. Stemmer: Employee; Siemens Healthineers.

B-1347 10:38

Preliminary application of PETRA sequence in lung nodule screening

H. Feng; Shijiazhuang/CN (hellofh1984@163.com)

Purpose: To assess lung MRI with a respiratory-gated pointwise encoding time reduction with radial acquisition (PETRA) sequence at 3T and compare it with computed tomography (CT) on the visibility of lung nodules.

Methods and Materials: Patients were imaged with PETRA sequence, T2-haste sequence, T2-blade sequence, T1-vibe and CT. Taking the image of CT as the gold standard, the total detectable rate of nodules, the detection rate of solid nodules, the detection rate of glass nodule and the difference of CNR and maximum diameter were compared. SPSS21.0 software was used for statistical analysis. Comparisons were made using the Wilcoxon-signed rank test for means and the McNemar test for ratios. Agreement between CT and MR imaging was assessed using the kappa test.

Results: Good agreement was found between CT and PETRA image ($k = 1.0$). Compared with other sequences, Petra sequence has a higher detection rate, the total detection rate is 85%, the detection rate of solid nodules, glass nodules and some solid nodules are 80%, 74% and 100%, respectively. For nodules with diameter greater than 5mm, the detection rate was 85%, and the CT value was higher than that of 600HU. The detection rate was 83%, and the nodules located in the middle and upper lung fields were better than those in the lower lung fields.

Conclusion: PETRA enables free-breathing and submillimeter imaging of lung nodules with high CNR and may be an alternative to CT for patients with lung nodules.

B-1348 10:46

Chemical exchange saturation transfer (CEST) imaging vs diffusion-weighted imaging vs FDG-PET/CT: single- and multiparametric approach for diagnosis of pulmonary nodules

Y. Ohno¹, M. Yui², Y. Kishida³, S. Seki¹, T. Yoshikawa¹; ¹Kobe/JP, ²Otawara/JP (yosirad@kobe-u.ac.jp)

Purpose: To directly and prospectively compare the capability for diagnosis of pulmonary nodules between single- and multi-parametric approaches by chemical exchange saturation transfer (CEST) imaging, diffusion-weighted imaging (DWI), and FDG-PET/CT.

Methods and Materials: Fifty-six consecutive patients with 65 pulmonary nodules underwent CEST imaging and DWI at a 3T MR system, FDG-PET/CT, and pathological and/or follow-up examinations. According to final diagnoses, all lesions were divided into lung cancer (n=44) and benign nodule (n=21) groups. Then, magnetization transfer ratio asymmetry (MTR_{asym}) was calculated from z-spectra at 3.5ppm, ADC and SUV_{max} were assessed by ROI measurements. To compare each index between two groups, Student's t test was performed. Multivariate logistic regression analysis was performed to investigate the discriminating factors of malignant lesions from benign lesions. ROC analysis was performed to compare diagnostic performance among all methods. Finally, sensitivity, specificity and accuracy were compared among all methods by McNemar's test.

Results: Mean MTR_{asym} , ADC and SUV_{max} of malignant group had significant difference with those of benign group ($p < 0.05$). Multivariate regression analysis identified MTR_{asym} (odds ratio [OR]: 0.62), ADC (OR: 1.01) and SUV_{max} (OR: 0.15) as a significant differentiator of malignancy. ROC analysis showed area under the curve (Az) of multiparametric method (Az=0.96) was significantly larger than that of SUV_{max} (Az=0.84, $p < 0.05$). Sensitivity and accuracy of multiparametric method were significantly higher than those of SUV_{max} ($p < 0.05$).

Conclusion: Multiparametric approach by CEST imaging, DWI and PET/CT has a potential to improve diagnosis performance of PET/CT for diagnosis of pulmonary nodules.

Author Disclosures:

Y. Ohno: Research/Grant Support; Toshiba Medical Systems Corporation.

M. Yui: Employee; Toshiba Medical Systems Corporation. S. Seki: Research/Grant Support; Toshiba Medical Systems Corporation.

T. Yoshikawa: Research/Grant Support; Toshiba Medical Systems Corporation.

B-1349 10:54

Active surveillance of subsolid nodules detected by screening: safe strategy to reduce overtreatment

M. Silva¹, C. Jacobs², G. Capretti², F. Ciompi², B. Van Ginneken², C.M. Schaefer-Prokop^{3,2}, A. Marchionò⁴, U. Pastorino⁴, N. Sverzelati¹; ¹Parma/IT, ²Nijmegen/NL, ³Amersfoort/NL, ⁴Milan/IT (mariosilvamed@gmail.com)

Purpose: Lung cancer derived from subsolid nodule (SSN) can show extremely slow growth rate having no impact on patient outcome. Active surveillance might reduce the rate of overtreatment. The aim of this study was to determine long-term evolution of SSN, survival and cause of death of screenees with SSN, in a large lung cancer screening trial.

Methods and Materials: SSNs underwent active surveillance by low-dose computed tomography. Risk of developing lung cancer, overall mortality, and mortality from lung cancer were calculated by Cox proportional hazards model. Rates of potential overdiagnosis and potential overtreatment were calculated according to the National Comprehensive Cancer network guidelines for lung cancer screening.

Results: SSNs were found in 16.9% (389/2,303) of screenees. During 9.3 ± 1.2 years, the hazard ratio (HR) of developing any lung cancer in subjects with SSN was 6.77, with more cancers not derived from SSN. HR of overall mortality in screenees with SSN was 1.34 and HR of lung cancer mortality was 3.80; no death was associated with lung cancer derived from SSN. Potential overdiagnosis was seen in 28.5% (81/284) and potential overtreatment in 3.5% (10/284). Screenees with a high-risk SSN had an increased risk of lethal lung cancer not derived from SSN compared with screenees with low-intermediate risk ($p = 0.023$).

Conclusion: Active surveillance of SSN does not increase risk of lung cancer mortality due to local progression of the lesion. Active surveillance by long-term annual low-dose computed tomography is a safe strategy to reduce overdiagnosis and overtreatment in lung cancer screening.

Author Disclosures:

C. Jacobs: Research/Grant Support; MeVis Medical Solutions AG.

B. Van Ginneken: Grant Recipient; Mevis Medical Solutions. Shareholder; Thirona BV. U. Pastorino: Research/Grant Support; Italian Ministry of Health RF 2004, Italian Association for Cancer Research AIRC 2004 IG 1227, Italian Association for Cancer Research AIRC 5xmille IG 12162, Fondazione Cariplo 2004-1560.

B-1350 11:02

Lung cancer screening with MRI: characterisation of nodules with different non-enhanced MRI sequences

M. Meier-Schroers, R. Homsj, H. Schild, D. Thomas; Bonn/DE (michael.meier@ukbonn.de)

Purpose: To analyse MRI characteristics of pulmonary nodules in lung cancer screening.

Methods and Materials: 82 participants of a lung cancer screening were included for this prospective study. MRI datasets of 32 subjects with 46 nodules ≥ 6 mm were prospectively evaluated together with 50 controls. Acquired MRI sequences were T2-STIR, T2, bSSFP, 3D-T1, and DWI. Each sequence was randomly and separately viewed blinded to low-dose CT (LDCT). Size, shape and contrast of nodules were evaluated on each sequence. Findings were correlated with LDCT and with histopathology if available.

Results: There were eight carcinomas with a size of 7-35 mm. Detection rates for malignant nodules were 100% for T2-STIR, T2 and bSSFP, and 87.5% for 3D-T1. Contrast was significantly higher for malignant nodules on all sequences. Seven of eight carcinomas showed restricted diffusion, positive predictive value of diffusion restriction as an indication of malignancy was 41.2%. Size measurement by MRI significantly correlated with LDCT. Sensitivity/specificity for nodules ≥ 6 mm was 89.1%/94.2% for T2-STIR, 87.0%/94.2% for T2, 69.9%/98.0% for bSSFP, and 67.4%/96.0% for 3D-T1. Seven of eight subsolid nodules were visible on T2-sequences with lesion contrast being significantly lower compared to solid nodules. Two of eight subsolid nodules were detected by bSSFP and none by 3D-T1. All three calcified nodules were detected by 3D-T1, one by bSSFP, and none by T2-sequences.

Conclusion: Malignant nodules, as well as calcified and subsolid nodules seem to have distinctive characteristics on different MRI sequences. T2-imaging was most suitable for the detection of pulmonary nodules ≥ 6 mm.

B-1351 11:10

Variation of tube electric current (mA) in lung CT screening for glass ground nodules (GGNs) bigger than 3 mm: phantom study

L. Jin; Shanghai/CN (BrightDK@126.com)

Purpose: To explore and assess the feasibility analysis and evaluation for lung mini-nodule thorax CT screening.

Methods and Materials: Two kinds of lung nodules with different distance (3mm, 5mm) and density (-630HU, -800HU), totally four nodules, were randomly placed in phantom. The phantom was scanned under different mA and KV setting by both Lightspeed VCT and Discovery HD750. All the images were scored by 2 experienced radiologists including detection and diagnosis of the lung nodules and image quality. The differences of the inter-observer were determined by kappa statistics.

Results: There was perfect concordance of inter-observers in image quality and diagnostic acceptability ($\kappa = 0.819$, $\kappa = 0.847$). There was no statistical difference in CT value of the air ($P = 0.056 > 0.05$). For (3mm, -630HU), under HDCT (120KV, 20mA) for detection, the lowest ED was 0.6mSv; for (120 KV, 40mA) the lowest ED was 1.21mSv; under VCT (120KV, 80mA), the lowest ED was 1.19mSv; for (120 KV, 160 mA), the lowest ED was 3.57mSv. For (3mm, -800HU), under HDCT (80KV, 120mA), the lowest ED was 1.22mSv; for (80 KV, 280mA), the lowest ED was 2.84mSv; under VCT (120KV, 120mA), the lowest ED was 2.37mSv; for (120 KV, 240mA), the lowest ED was 5.95mSv.

Conclusion: In this phantom study, using (120KV, 20mA, HDCT) scanning parameters could be satisfied with the detection for (3mm, -630HU) or over (5mm) lung mini-nodule, but if involving differential diagnosis, the lowest

scanning parameters could be (120KV, 40mA, HDCT). For (3mm, -800HU), detection scanning parameters could be (80KV, 120mA, HDCT), diagnosis scanning parameters could be (80 KV, 280 mA, HDCT).

B-1352 11:18

Semiquantitative visual assessment of sub-solid pulmonary nodules ≤ 3 cm in differentiation of lung adenocarcinoma spectrum

F.-Z. Wu; *Kaohsiung/TW (cmvuu1029@gmail.com)*

Purpose: We aimed to analyze the CT features of persistent subsolid nodules (SSN) ≤ 3 cm diagnosed pathologically as adenocarcinoma spectrum to investigate whether parameters enable distinction between invasive and preinvasive lesions.

Methods and Materials: A total of 129 patients with 141 SSNs confirmed with surgically pathologic proof were retrospectively reviewed. SSNs were classified into three categories: pure ground-glass nodules (pure GGNs), heterogeneous GGNs, and part-solid nodules. Of 141 SSNs, there were 57 pure GGNs, 22 heterogeneous GGNs, and 62 part-solid nodules.

Results: SSN subclassification showed a significant linear trend with the invasive degree of the adenocarcinoma spectrum (pure GGNs 7%; heterogeneous GGNs 36.4%; part-solid nodules 85.5%, P for trend <0.0001). For invasive lesions detection in 141 SSNs, a solid part of ≥ 3 mm was the most specificity (sensitivity, 76.9%; specificity, 94.7%), followed by air-bronchogram sign (sensitivity, 53.8%; specificity, 89.5%), SSN subclassification (sensitivity, 81.5%; specificity, 88.2%), and a lesion size ≥ 12 mm (sensitivity, 84.6%; specificity, 76.3%). For invasive lesion detection in 79 pure or heterogeneous GGNs, the heterogeneous GGN sign was the most useful finding, with most specificity (sensitivity, 66.7%; specificity, 79.1%), followed by CT attenuation (HU) of ≥ -493 (sensitivity, 75%; specificity, 74.6%) and a lesion size ≥ 10 mm (sensitivity, 83.3%; specificity, 70.1%).

Conclusion: In conclusion, this simple combined visual and semiquantitative analysis of CT features helps distinguish invasive from preinvasive lesions.

B-1353 11:26

Analysis of pulmonary fibrosis, using an elastic registration technique in a model of fibrosis: systemic sclerosis

C. Martin¹, G. Chassagnon¹, R. Marini², A. Regent¹, L. Mouthon¹, N. Paragios², M.-P. Revel¹; ¹Paris/FR, ²Gif-sur-Yvette/FR (*chachmartin@hotmail.com*)

Purpose: To evaluate the feasibility of pulmonary fibrosis detection in scleroderma patients by using magnetic resonance imaging (MRI) and an elastic registration algorithm.

Methods and Materials: Full inspiratory and expiratory spiral VIBE (Volume Interpolated Breath-hold Examination) sequences were performed on a 3T-MRI unit. Depending on High Resolution Computed Tomography results, 3 patient groups were considered: no infiltrative lung disease (ILD), ILD without fibrosis and ILD with fibrosis. A control group of healthy volunteers was also evaluated. An elastic registration algorithm was applied to all examinations in order to get Jacobian maps for each subject. Regions with the most important volume changes between inspiration and expiration were compared in the 3 patient groups and healthy volunteers, using Dice coefficients. Pearson correlation coefficient was calculated between Dice coefficient and Forced Vital Capacity (FVC).

Results: 33 subjects were prospectively evaluated. Jacobian distributions were visually different between subjects with and without ILD. ROC curves analysis was performed for the whole cohort and for a subgroup composed by healthy volunteers and fibrotic patients. The best Dice coefficient cut-off value was 0.44 for both analysis, with sensitivities of 92% and 86% and specificities of 75% and 100% for the presence of fibrosis, respectively. No significant correlation was found between Dice coefficient and FVC ($R=0.12$, $p=0.6$).

Conclusion: Elastic registration of inspiratory and expiratory MR images shows significant differences between subjects with and without ILD. High specificity for the presence of fibrotic changes is reported even though no correlation was found with FVC, in this preliminary study.

Author Disclosures:

C. Martin: Research/Grant Support; Société Française de Radiologie, Bourse CARDIF - L'assistance respiratoire.

B-1354 11:34

Finding the right spot: where to measure airway parameters in patients with COPD?

J.F.M. Gawlitza, A.M. Fischer, I. Akin, M. Borggreffe, S.O. Schönberg, H. Haubenreisser, T. Henzler, F. Trinkmann; *Mannheim/DE (joshua_gawlitza@yahoo.de)*

Purpose: The importance of spirometry for diagnosing and treating COPD was reduced in the 2017 revision of the GOLD report. While spirometry does not reflect the complexity of the disease, quantified computed tomography (qCT) may gain further relevance. Airway measurements show strong correlations with lung function tests and symptoms. However, these correlations are specific to the airway localization, and currently there is no evidence for the

ideal spot. Therefore, the aim of this prospective study was to systematically correlate airway measurements with extensive lung function testing.

Methods and Materials: 65 patients with diagnosed COPD underwent body plethysmography, impulse oscillometry and dose-optimized qCT examination (Somatom Force, Healthineers, Germany) in inspiration and expiration. Eight airway parameters were acquired for both scans in every lobe for the third- to fifth-generation bronchus and correlated with the lung function tests.

Results: The most significant correlations between airway parameters were found for the third-generation bronchus of the upper left lobe during expiration (25 out of 48 correlation pairs, mean $r = -0.39$) and for the third-generation bronchus of the upper right lobe during inspiration (9 out of 48 correlation pairs, mean $r = -0.25$). No significant correlations were for example found for the upper right lobe in expiration.

Conclusion: Correlations between airway parameters and lung function tests vary widely between lobes, bronchus generations and breathing states. Our work suggests that the third-generation bronchus of the upper left lobe in expiration could be the preferred localization for airway quantification in future studies.

B-1355 11:42

Prospective quantification of respiratory mechanics in COPD patients before and after lung volume reduction surgery on dynamic MRI

K. Martini, C. Caviezel, G. Milanese, W. Weder, T. Frauenfelder; *Zurich/CH*

Purpose: To prospectively evaluate respiratory mechanics in chronic obstructive pulmonary disease (COPD) patients pre- and post-lung volume reduction surgery (LVRS) on dynamic magnetic resonance imaging (MRI).

Methods and Materials: 24 patients (11 female, median age 63y) suffering from COPD and scheduled for LVRS were included. MRI was performed on a 3T MR-scanner and dynamic sequences of the lung were acquired in a sagittal plane during two breath-cycles for both lungs the day before and 3 months after LVRS, herein termed as pre- and post-LVRS-MRI. Quantitative measurements were performed on sagittal planes for left and right lung in pre- and post-LVRS-MRI: lung height, anteroposterior (AP) diameter, hemidiaphragm height and lung area as well as hemidiaphragm area were measured. Additionally, lung areas during one breath cycle were measured. Student's t test was used to test for statistically significant differences between pre- and post-LVRS-MRIs. A p value <0.05 was considered as statistically significant.

Results: In expiration, mean lung and hemidiaphragmatic area on both sides ($p_{\text{right}}=0.002$ and $p_{\text{left}}=0.043$) as well AP diameter of both lungs ($p_{\text{right}}=0.003$ and $p_{\text{left}}<0.001$) improved significantly in patients undergoing LVRS. Dynamic measurements showed significant differences pre- and post-LVRS on the right lung, but not on the left ($p_{\text{right}}=0.032$ and $p_{\text{left}}=0.606$). There were no significant changes in lung and hemidiaphragmatic high pre- and post-LVRS. Additionally, there was no difference of the measured variables in inspiration.

Conclusion: By increasing the elastic recoil of the lung LVRS improves significantly impaired respiratory mechanics caused by increased airflow resistance and reduces pulmonary compliance in patients with COPD.

B-1356 11:50

MR-based lung volume segmentation in population-based whole-body MR imaging: correlation with clinical characteristics, pulmonary function testing and obstructive lung disease

J. Mueller¹, R. Lorbeer², R. von Krüchten¹, A. Pomschar³, H.-U. Kauczor¹, F. Bamberg⁴, H. Schulz⁵, S. Karrasch⁵, C.L. Schlett¹; ¹Heidelberg/DE, ²Munich/DE, ³München/DE, ⁴Tuebingen/DE, ⁵Neuherberg/DE (*Ricarda.vonKruechten@med.uni-heidelberg.de*)

Purpose: Whole-body magnetic resonance imaging (MRI) is increasingly performed as part of clinical service and research. The value of lung volume derived from non-dedicated MRI sequences is unknown.

Methods and Materials: As part of a population-based KORA FF4 study, 400 subjects aged 56.4 (± 9.2) years underwent whole-body MRI. Lung volumes were derived semi-automated and related to common predictors, pulmonary function tests (PFT, available in $n=214$) and obstructive lung disease (FEV1/FVC $<70\%$ or self-reported physician diagnosis of COPD/emphysema).

Results: The average MRI-based lung volume (MRLV) was 4.0 ± 1.1 L, which was $64.8 \pm 14.9\%$ of the predicted total lung capacity (TLC) and $124.4 \pm 27.9\%$ of the predicted functional residual capacity. In multivariate analysis, MRLV was positively associated with age, male gender, current smoking, and height. Among PFT indices, MRLV correlated best with TLC, alveolar volume (VA), and residual volume (RV; $r=0.57$ each), while it was negatively correlated to FEV1/FVC ($r=-0.36$) and lung diffusing capacity (TLCO/VA; $r=-0.16$). Combining the most strongly associated PFT parameters in a multivariate model, RV and FEV1/FVC remained independently associated with MRLV ($\beta=0.50$, $p=0.04$, and $\beta=-0.02$, $p=0.02$, respectively) explaining up to 45% of the variability of the MRI data. In subjects with obstructive lung disease, higher MRLVs were observed yielding an AUC of 0.673 for a FEV1/FVC below 0.7 and of 0.654 for a diagnosis of COPD/emphysema.

Conclusion: Lung volumes derived from non-dedicated whole-body MRI were independently associated with RV and FEV1/FVC after accounting for well-known predictors and typical risk factors of respiratory function and show moderate accuracy for detection of obstructive lung disease.

10:30 - 12:00

Room N

Genitourinary

SS 1807a

Prostate imaging reporting and data system (PI-RADS)

Moderators:

B.K. Barth; Zurich/CH
J.C. Vilanova; Girona/ES

K-27 10:30

Keynote lecture

J. Venancio; Lisbon/PT

B-1357 10:39

Learning the language of PI-RADS version 2: correlation between prostate MRI lexicon terms and malignancy

M. Rudolph, A. Baur, M. Haas, S. Mahjoub, H. Cash, P. Asbach, B. Hamm, T. Penzkofer; Berlin/DE

Purpose: To assess the value of PI-RADS 2 lexicon terms for predicting prostate cancer using lesion shape, border and diffusion characteristics.

Methods and Materials: Prostate lesions of 160 patients that received multiparametric prostate MRI and subsequent MRI/TRUS-biopsy including systematic biopsy were examined in a blinded and randomized setting by two experienced radiologists. Every lesion was examined with regard to imaging characteristics as defined by PI-RADS v2 lexicon terms. The histopathological result of the respective lesion was correlated to the assigned morphological features and positive and negative predictive values (PPV and NPV) were calculated.

Results: 174 lesions were identified of which 102 (58.6%) were histopathologically confirmed malignant. Predictive values of lexicon terms describing lesion characteristics were reported as follows (PPV/NPV): "restricted diffusion" (76%/74%), "DWI hyperintensity" (80%/86%), "ADC hypointense" (74%/90%), "round" (53%/40%), "oval" (66%/43%), "lenticular" (83%/43%), "lobulated" (71%/43%), "water drop shaped" (91%/44%), "wedge shaped" (29%/37%), "linear" (7%/37%), "irregular shape" (63%/43%), "circumscribed" (57%/40%), "non-circumscribed" (83%/43%), "indistinct" (63%/42%), "obscured" (85%/49%), "irregular border" (71%/43%), "spiculated" (100%/42%), "encapsulated" (12%/36%), "organized chaos" (31%/30%), "erased charcoal sign" (86%/45%).

Conclusion: Out of 20 examined PI-RADS lexicon items, the terms associated with restricted diffusion had a favorable combination of both high PPV and NPV to correctly predict and exclude malignant lesions. The shape and border terms associated with inflammation or BPH "wedge shaped", "linear", "encapsulated" and "organized chaos" showed a potential to predict benign lesions with low PPV/NPV. The remaining lexicon terms had mediocre predictive values indicating potential for refinement in further iterations of the PI-RADS lexicon.

Author Disclosures:

A. Baur; Speaker; Bayer. B. Hamm; Consultant; Toshiba Medical Services Corporation. Equipment Support Recipient; Elbit Imaging Ltd. Grant Recipient; Toshiba Medical Services Corporation, Koninklijke Philips NV, Siemens AG, General Electric Company, Elbit Imaging Ltd, Bayer AG, Guerbet SA, Bracco Group, B. Braun Melsungen AG, KRAUTH medical KG, Boston Scientific Corporation. Investigator; CMC Contrast AB. Shareholder; Siemens AG, General Electric Company.

B-1358 10:47

Diagnostic performance of PI-RADS version 2 in detecting prostate cancer using whole-mount histology after radical prostatectomy as the standard of reference

R. Girometti¹, S. Bednarova¹, S. Sioletic¹, V. Ficarra², F. Greco¹, A. Crestani¹, C. Zuiani¹; ¹Udine/IT, ²Messina/IT (rgirometti@sirm.org)

Purpose: To assess the accuracy of prostate imaging reporting and data system version 2 (PI-RADS v2) in detecting prostate cancer (PCa) on multiparametric magnetic resonance imaging (mpMRI).

Methods and Materials: During May 2016-February 2017 we prospectively included patients with PCa undergoing staging 3.0T mpMRI before radical prostatectomy. One experienced pathologist performed whole-mount histology on prostate specimens. mpMRI images were analysed independently by three

radiologists (2-8 years of experience) who detected, mapped and scored imaging findings following PI-RADS v2. After an mpMRI-to-whole-mount histology matching, we calculated sensitivity and specificity in detecting PCa and clinical significant PCa (csPCa) using PI-RADS ≥ 3 and ≥ 4 thresholds. Inter-reader agreement in attributing the PI-RADS score was calculated with Cohen's weighted-kappa statistic.

Results: Included were forty-eight patients (median iPSA 7.2 ng/ml) with 71 cancers on final histology (median size 16 mm, median Gleason score 6, stage $\geq T3$ in 19/48 cases). On a per-lesion basis, sensitivity was slightly higher with PI-RADS ≥ 3 vs. ≥ 4 threshold (range 0.55-0.62 vs. 0.48-0.60 for all PCAs, and 0.67-0.74 vs. 0.61-0.72 for csPCAs, respectively), at expenses of lower specificity (range 0.11-0.30 vs. 0.56-0.71 for all PCAs, and 0.28-0.30 vs. 0.55-0.71 for csPCAs, respectively). Accuracy improved on a per-patient basis, with 0.64-0.77 sensitivity and 0.73-0.83 specificity for csPCa with a PI-RADS ≥ 4 threshold. Inter-reader agreement was moderate to substantial ($\kappa=0.47-0.72$ vs. 0.51-0.71 for PI-RADS thresholds ≥ 3 and ≥ 4 , respectively).

Conclusion: PI-RADS v2 showed good diagnostic performance in detecting PCa, with acceptable inter-reader agreement. PI-RADS ≥ 4 threshold offered a better balance between sensitivity and specificity.

B-1359 10:55

Diagnostic yield of prostate biopsies and PI RADS version 2 scoring of MRI prostates

G. Chilvers, U. Udeshi; Worcester/UK (geoffreyschilvers@gmail.com)

Purpose: Current literature assessing the accuracy of PI-RADS v2 scoring of MRI prostates demonstrates variable outcomes. This study investigates this further with the largest reported population to date. We also determine if the addition of cognitive targeted biopsies to systematic biopsies of the prostate improves diagnostic yield for prostate cancer.

Methods and Materials: A retrospective study was performed comparing all prostate biopsy results in 2016 with PI-RADS v2 score on the pre-biopsy MRI. Two populations were identified: those with PI-RADS v2 score of 4 or 5 (significant cancer identified) and those with PI-RADS v2 score of 1, 2 or 3. A significant cancer was defined histologically as a Gleason score ≥ 7 . The histology results were analysed to determine whether the diagnosis of prostate cancer was made via systematic biopsies or cognitively targeted biopsies.

Results: 464 patients were included. 166 scored PI-RADS 4 or 5. 63% of these had histologically proven significant cancer, whilst 90% of 298 patients scored 1, 2 or 3 had no histologically proven significant cancer. Overall, sensitivity 77%, specificity 81%, positive predictive value 63% and negative predictive value 90%. 49.4% of systematic prostate biopsies demonstrated prostate cancer, whilst 51.1% of systematic plus cognitively targeted prostate biopsies demonstrated prostate cancer.

Conclusion: This study demonstrates that PI-RADS v2 scoring can help identify which patients require further investigation with prostate biopsy. PI-RADS v2 scores of 1, 2 or 3 correlate well with histologically non-significant biopsy results. Cognitively targeted biopsies in addition to systematic prostate biopsies slightly improve the diagnostic yield for prostate cancer.

B-1360 11:03

Clinical value of the PIRADS score in predicting benign and malignant conditions at MRI-guided prostate biopsy: a correlation of 54 patients with suspicion of prostate cancer

K. Engelhard, K. Bogner, F. Schneider; Nürnberg/DE (karl.engelhard@martha-maria.de)

Purpose: To evaluate the sensitivity and positive predictive value of the PIRADS score 4 and 5 (version 2) in determining positive histological tumour results and the impact of PIRADS score 3 score in differentiating these nondistinctive lesions as benign or malignant at MRI-guided prostate biopsy in patients with the suspicion of prostate cancer.

Methods and Materials: 54 patients with an elevated PSA value >4 ng/ml and a cancer suspicious region in multiparametric MRI underwent MRI-guided biopsy in a standard 1.5T magnet. 34 men were biopsy naïve, 20 patients had prior tumour-negative biopsies. A mean of 2.2 cores were taken from each tumour-suspected lesion. The PIRADS scores of the tumour-suspected lesions were compared with the histological results of the biopsy.

Results: Applying the PIRADS system 54% of cancers were detected by MRI-guided biopsy with a rate of 90% significant tumours. The sensitivity of PIRADS score 4, 5 was 90%, by a positive predictive value of 70%. In 25 men with PIRADS score 3 no cancerous tissue was found at histology. In one of these lesions a high-grade PIN was detected.

Conclusion: In this study the PIRADS score system was highly sensitive and shows a fair positive predictive value in detecting significant prostate cancers at MRI-guided biopsy. Including PIRADS 3 lesions into the biopsy procedure in our population the score can be helpful as a predictive tool in the estimating whether a PIRADS 3 lesion should undergo a targeted biopsy.

B-1361 11:11

Audit of diagnostic yields of prostate cancer in biopsy naive patients at high risk of cancer on the London Cancer Alliance Best Practice Prostate Pathway (LCABPPP)

H.K. Sokhi¹, S. Patel¹, A. Padhani², A. Pope¹; ¹London/UK, ²Northwood/UK

Purpose: To document multiparametric MRI (mpMRI) diagnostic yields of the 2013 LCABPPP involving pre-biopsy mpMRI followed by TRUS biopsies in patients at high risk of prostate cancer (PCa).

Methods and Materials: 214 pre-biopsy PI-RADS compliant mpMRI studies performed between April 2014 & April 2017. 195 (91%) patients had PSA >10ng/mL and/or abnormal digital rectal examination. 180 scans evaluated with the PI-RADS scoring systems. mpMRI findings were correlated with TRUS +/- targeted biopsy histology.

Results: Prevalence of all PCa and clinically significant cancer (csPCa: Gleason>3+3) was 72% and 58% respectively in 199 of 214 patients. Of 180 PI-RADS assessed mpMRIs, 121 contained focal index lesions (PI-RADS 3-5); 33 demonstrated non-measurable extensive/diffuse changes (PI-RADS 3-5); 26 were negative (PI-RADS 1-2). Overall diagnostic yield of all PCa and csPCa was 4/26 (15%) & 1/26 (4%) for PI-RADS 1/2; 6/19 (32%) & 3/19 (16%) for PI-RADS 3; 20/27 (74%) & 14/27 (52%) for PI-RADS 4 and 102/108 (94%) & 87/108 (81%) for PI-RADS 5 categories respectively. Rule out ability (Sen 99%, NPV 96%, LR-ve 0.03) was better than rule in performance (Spec 33%, PPV 68%, LR+ve 1.49) for csPCa.

Conclusion: There is a high prevalence of positive mpMRI (PI-RADS 3-5) in higher risk biopsy naive patients. Positive mpMRI (PI-RADS 3-5) is associated with all PCa and csPCa detection rate of 83% & 68% respectively using TRUS +/- targeted biopsy. Systematic TRUS biopsy has negligible yields in mpMRI negative patients.

B-1362 11:19

PI-RADS version 2-based assessment of prostate in patients with borderline-elevated prostate-specific antigen levels: a prospective study

A. Yadav, M. Bagarhatta, U. Jaipal; Jaipur/IN (arushiy403@gmail.com)

Purpose: To predict clinically significant prostate cancer (CSPca) in patients with borderline-elevated prostate-specific antigen (PSA) levels.

Methods and Materials: Fifty patients with PSA levels of 4-10 ng/ml were prospectively evaluated by 3.0 T multiparametric MRI (mpMRI). Evaluation was done by 2 independent radiologists using PI-RADS v2 scoring system. Region-based analysis with sectoral mapping followed by 12 core systematic biopsy was done. CSPca was defined as Gleason score \geq 3+4 or tumour volume \geq 0.5 ml. Histopathology by expert uropathologist was considered gold standard. Statistical analysis was done with SPSS 20 and diagnostic accuracy was calculated separately for PI-RADS score 3 and 4 as cutoff. Youden index was used for best diagnostic cutoff. Kappa test was used for diagnostic concordance among radiologists.

Results: 95% cores of biopsy specimen were reported satisfactory. Mean age was 62 \pm 1 years, with mean PSA of 7.86 \pm 2.79 ng/ml. The diagnostic accuracy (95% CI) of PI-RADS v2 with score of 3 as cutoff in diagnosing CSPca was: sensitivity, 0.93 (0.77-0.99); specificity, 0.94 (0.92-0.96); LR+, 17.40 (12.05-25.13); LR-, 0.07 (0.02-0.28), respectively. The PPV were from 0.39 to 0.57 and NPV from 0.98 to 0.99. ROC curve showed a score of 3 as the best diagnostic cutoff (AUC - 0.949). The diagnostic concordance among two radiologists was good (kappa=0.719).

Conclusion: PI-RADS v2 has very high NPV in predicting CSPca in patients with borderline PSA, reducing the number of useless biopsy and morbidity. A score of 3 seems to be the best cutoff to diagnose CSPca.

B-1363 11:27

When does biopsy make sense in patients with an overall PI-RADS score of 3?

T. Ullrich, L. Schimmöller, M. Quentin, N. Laqua, D. Blondin, C. Arsov, R. Rabenalt, P. Albers, G. Antoch; Düsseldorf/DE (Tim.Ullrich@med.uni-duesseldorf.de)

Purpose: To systematically analyse patients with 'equivocal' (PI-RADS-3) lesions in multiparametric prostate MRI (mp-MRI) and MR-targeted plus systematic transrectal ultrasound-guided (TRUS-GB) biopsies as reference standard and define conditions under which biopsy is recommended.

Methods and Materials: One hundred and twenty consecutive patients with a PI-RADS overall score of 3 after mp-MRI (T2WI, DWI, DCE-MRI) at 3T and subsequent targeted MRI/US fusion-guided (FUS-GB) plus systematic 12-core TRUS-GB were retrospectively included in this study. Endpoints were prostate cancer (PCa) detection rates, distribution of Gleason scores and location of PCa.

Results: PCa was detected in 13 of 118 patients (detection rate 11%) including five patients with a Gleason score (GS) of \geq 3+4=7 (4.2%). 1.4% (3/212) of the transitional lesions and 9.4% (6/64) of the peripheral zone lesions were positive for PCa. 54% of the PCa patients showed MRI patterns of peripheral prostatitis combined with diffuse stromal hyperplasia. Prostate

volume was significantly lower in PCa patients ($p=0.015$), whereas differences in PSA levels were not statistically significant ($p=0.87$). PSA density (PSAD) was higher in patients with PCa (0.19 vs 0.12ng/ml/ml).

Conclusion: In patients with PI-RADS overall score of 3 low-grade PCa (GS 3+3=6) can occur. PCa with a GS \geq 3+4=7 can reliably be detected in mp-MRI. GS \geq 4+3=7 PCa is very unlikely in PI-RADS-3-lesions. Therefore, these patients primarily should receive follow-up MRI. In patients with a combination of MRI aspects of extensive prostatitis and diffuse stromal hyperplasia, low prostate volume, and high PSA density a combination of targeted and systematic biopsy might be considered.

B-1364 11:35

How to prevent patients with a false-positive overall score of PI-RADS 4

T. Ullrich, L. Schimmöller, M. Quentin, N. Laqua, F. Dietzel, C. Arsov, R. Rabenalt, P. Albers, G. Antoch; Düsseldorf/DE (Tim.Ullrich@med.uni-duesseldorf.de)

Purpose: To characterize patients with an overall PI-RADS score of 4 in mp-MRI of the prostate and negative histology after combined targeted and systematic biopsy in a large cohort based on clinical conditions and PI-RADS decision rules.

Methods and Materials: 170 consecutive patients with a PI-RADS v2 overall score of 4 after multi-parametric MRI (T2WI, DWI, DCE) at 3T and subsequent targeted MR/US fusion-guided plus systematic transrectal ultrasound-guided biopsy were retrospectively included in this study. Endpoints were detection rates and subgroup analyses.

Results: PCa detection rate was 62% (106/170) including 87 patients (51%) with a Gleason score (GS) of \geq 3+4=7 (csPCA). PSA density (PSAD) was significantly higher in PCa patients (0.22 \pm 0.12ng/ml/ml; $p<0.01$). 135/287 (47%) index lesions in the peripheral zone (PZ) were positive for PCa whereas 28/143 (20%) transitional lesions revealed PCa. 58/107 (54%) PZ lesions with PI-RADS single score of 3 in DWI and upgrade to overall PI-RADS 4 due to positive DCE contained PCa. 4/10 (40%) transitional lesions with upgrade to overall PI-RADS 4 due to positive DWI (score 4 or 5) contained PCa.

Conclusion: Patients with an overall PI-RADS score of 4 possess a high likelihood of PCa/csPCA and index lesions need (additional) targeted biopsy. In case of negative histology results, targeted re-biopsy should be considered in patients with high PSAD and index lesion located in the PZ. Existing PI-RADS decision rules for upgrading lesions from 3 to 4 reveal PCa in many cases. DCE is essential not to miss significant PCa, especially in the peripheral zone.

B-1365 11:43

Is it possible to reduce the number of false positive cases of PI-RADS v.2 classification? Role of quantitative analysis of DCE-MRI in prostate lesions' characterisation

G. Cristel, A. Esposito, A. Damascelli, S. Antunes, G. Brembilla, A. Briganti, A. Del Maschio, F. De Cobelli; Milan/IT (cristel.giulia@hsr.it)

Purpose: To test the potential impact of pharmacokinetic dynamic contrast-enhanced MRI parameters on the multiparametric MRI (mpMRI) diagnostic performance, using PI-RADSv.2 as standard of reference.

Methods and Materials: From our Data-Base of 666 prostate mpMRI (1.5T) acquired between January 2016 and July 2017, we retrospectively evaluated a group of 103 patients, with available corresponding histological specimen obtained through target biopsies. Perfusion study included multiple flip-angle T1W-images (5°, 8°, 12°, 15°) for T1-mapping and contrast enhanced 3D-FFE-T1W sequence. Images were evaluated using PI-RADS score v.2 and pharmacokinetic parameters (Ktrans, Kep, Ve, Vp) were calculated with commercially available permeability software (population-based AIF). We evaluated the diagnostic performance of MRI for Gleason Score (GS) \geq 7 tumours, considering PI-RADS \geq 3 as pathological.

Results: The 103 lesions were classified as follows: 8 PI-RADS2, 23 PI-RADS3, 57 PI-RADS4 and 15 PI-RADS5. 59 lesions presented GS \geq 7 at histological evaluation. Sensitivity and PPV of mpMRI using PI-RADSv.2, were 98% and 61%, respectively. GS \geq 7 lesions showed higher Ktrans ($p<0.01$) and Kep ($p=0.01$) compared to GS<7. ROC curve analysis was used to identify a Ktrans cut-off value of 191x10⁻³/min (AUC 0.75) that predicted the presence of GS \geq 7 with sensitivity of 95% and specificity of 61%. Considering only PI-RADS \geq 3 lesions, the application of Ktrans cut-off shifted 22 false positives to true negatives with 3 false negative findings, resulting in an increase of PPV (79%) without a significant drop of sensitivity (93%, $p=0.25$).

Conclusion: DCE-MRI pharmacokinetic parameters, especially Ktrans, may improve PI-RADSv.2 diagnostic performance and its capability in prostate lesions' characterisation, decreasing the number of false positive results.

B-1366 11:51

Chronic prostatitis: distinction from prostate cancer and benign prostatic hyperplasia by means of PIRADS version-2 descriptors

U.G. Mueller-Lisse¹, M. Kuhn¹, M. Scherr², U.L. Mueller-Lisse¹, S. Murer¹, M.F. Reiser¹, J. Scheidler¹; ¹Munich/DE, ²Murnau a. Staffelsee/DE (ullrich.mueller-lisse@med.uni-muenchen.de)

Purpose: Chronic prostatitis (CP) is common and potentially difficult to distinguish from both benign prostatic hyperplasia (BPH) and prostate cancer (PCA) in mpMRI of the prostate. We hypothesized that prostate imaging reporting and data system-version-2 (PIRADSv2) descriptors for T2-weighted magnetic resonance imaging (T2WI) and diffusion-weighted magnetic resonance imaging (DWI) would not distinguish CP from BPH or PCA.

Methods and Materials: With ethics committee approval, consecutive 3.0T-multi-channel surface coil mpMRIs of 19 CP patients (previous clinical and MRI diagnosis, negative prostate biopsy, NBX), 17 BPH patients (NBX), and 16 patients with high-grade PCA (biopsy Gleason scores 4+3 to 4+5, n=7) or low-grade PCA (biopsy Gleason scores 3+3 and 3+4, n=9) were independently scored by two blinded observers (O1, O2) applying respective PIRADSv2 descriptors for T2WI and DWI. Two-tailed Fisher's exact tests assessed scoring contingency tables and two-tailed Student's T tests potential confounders (significance, p<0.05).

Results: Both observers distinguished BPH and high-grade-PCA. Despite significant statistical differences, PIRADSv2 scores implying malignancy overlapped between CP patients versus low-grade PCA patients in T2WI (O1: 1/19 versus 5/9; O2: 4/19 versus 6/9), standard pelvic DWI (O1: 0/19 versus 3/9; O2: 3/19 versus 5/9), and optimized DWI zoomed to the prostate (O1: 0/19 versus 4/9; O2: 4/19 versus 6/9), respectively. Between CP and low-grade PCA, prostate-specific antigen levels (PSA, 9.4±2.6 versus 8.4±5.2 ng/ml), PSA density (0.13±0.06 versus 0.17±0.10 ng/ml/ccm), and age (64±7 versus 65±9 years) did not differ significantly, while prostate volume differed (88.9±60.2 versus 48.4±10.0 ccm, p=0.01).

Conclusion: PIRADSv2 descriptors for T2WI and DWI of PIRADSv2 peripheral or central zone regions appear to overlap between CP and low-grade PCA.

10:30 - 12:00

Studio 2018

Oncologic Imaging

SS 1816

Latest imaging of gynaecological cancers

Moderators:

M.-L. Riibak; Tallinn/EE
A.G. Rockall; London/UK

B-1367 10:30

Whole-body tumour staging of cervical cancer patients using 18F-FDG PET/MRI: does it change therapeutic decisions when compared to MRI alone?

J. Gruenisen¹, T. Sarabhai¹, B.M. Schaarschmidt², A. Wetter¹, M. Forsting¹, K. Herrmann¹, L. Umutlu¹; ¹Essen/DE, ²Dusseldorf/DE (johannes.gruenisen@uk-essen.de)

Purpose: To investigate whether differences in local and whole-body tumour staging between integrated PET/MRI and MRI alone lead to different therapeutic decisions in patients with primary cervical cancer.

Methods and Materials: 53 consecutive patients with a primary cervical cancer were prospectively enrolled for a whole-body 18F-FDG PET/MRI examination. A radiologist and nuclear medicine physician analysed the MRI data, in consensus, followed by a second reading session of the PET/MR datasets. The readers were asked to perform a dedicated TNM staging (7th edition of the AJCC staging manual). Subsequently, the results of MRI and PET/MRI were discussed in a simulated interdisciplinary tumour board and therapeutic decisions based on both imaging modalities were recorded.

Results: Staging results of MRI and PET/MRI revealed discrepant findings in 17/53 (32%) cases, which led to differences in treatment recommendations for 11 patients (21%). PET/MRI over- (n=1) and underestimated (n=1) the actual tumour stage in two patients, which affected therapy decisions. Conversely, MR readings led to incorrect staging results in 9 patients (n=3, upstaging; n=6 downstaging). PET/MRI enabled determination of the correct tumour stage in 7 of those 9 patients. In the two other cases, false ratings in PET/MRI did not result in changes in therapy management. In the remaining 6 patients (11%), different imaging findings in MRI and PET/MRI did not lead to changes in therapeutic decisions.

Conclusion: Our results demonstrate the successful application and diagnostic advantage of integrated PET/MRI imaging over MRI alone for whole-body tumour staging of cervical cancer patients, enabling more accurate treatment planning.

B-1368 10:38

The prognostic value of pre-treatment FDG-PET/CT metabolic parameters in cervical cancer patients

V. Bollineni^{1,2}, S. Ytre-Hauge², A. Gulati², M. Halle², K. Woie², Ø. Salvesen³, C. Krakstad², J. Trovik², I. Haldorsen², ¹Brussels/BE, ²Bergen/NO, ³Trondheim/NO (bollineniv@yahoo.com)

Purpose: To explore quantitative metabolic and microstructural primary tumour parameters at pre-treatment FDG-PET/CT and diffusion-weighted MRI (DW-MRI) in relation to clinical FIGO stage and outcome in cervical cancer patients.

Methods and Materials: Fifty-three patients with histopathologically verified cervical carcinoma with clinical FIGO stage IB1-IV were subjected to FDG-PET/CT and for a subgroup also DW-MRI (n=30) prior-to-treatment. Maximum standardized uptake value (SUV_{max}), total lesion glycolysis (TLG) and metabolic tumour volume (MTV) were estimated from the entire primary tumour at FDG-PET/CT. On MRI, longest tumour diameter (MRI-LD), tumour volume (MRI-TV) and mean tumour apparent diffusion coefficient (ADC_{mean}) values were measured. FDG-PET/CT-parameters were explored in relation to clinical prognostic factors at diagnosis and progression/recurrence-free survival and compared to MRI parameters.

Results: The metabolic tumour parameters TLG and MTV were highly positively correlated to MRI-LD and MRI-TV (r=0.72-0.82; p<0.001 for all), whereas tumour SUV_{max} was only moderately correlated (r=0.29-0.36; p<0.04). High tumour TLG, MTV, MRI-LD and MRI-TV predict advanced-FIGO-stage, whereas high tumour-SUV_{max} does not. No significant correlations were observed between tumour-ADC_{mean} and the other imaging parameters or FIGO-stage. High primary tumour-MTV (> 56.7 cm³), high-TLG (> 412) and large MRI-TV (>36 cm³) as well as advanced FIGO-stage (> IIIA) predicted reduced progression/recurrence-free survival yielding corresponding hazard ratios [HR] of 7.8 (P=0.002), 6.9 (P=0.004), 4.6 (P=0.022) and 6.9 (P=0.004), respectively. In multivariate analysis, advanced FIGO-stage (> IIIA) and high-MTV (> 56.7 cm³) both had an independent unfavourable impact on progression/recurrence-free survival with adjusted HRs of 5.5 (P=0.02) and 7.8 (P=0.025), respectively.

Conclusion: High MTV at pre-treatment FDG-PET/CT and high clinical FIGO stage independently predict reduced progression/recurrence-free survival in cervical cancer patients.

B-1369 10:46

Quantitative MRI analysis of cervical cancer parametrium invasion

M. Shorikov, E. Tarachkova, V. Panov, I. Tyurin; Moscow/RU (vopanov@gmail.com)

Purpose: It is well known that MRI is a good method for evaluation of cervical cancer (CC) extent to parametrium. However, in the literature mostly the evaluation was qualitative and it was pointed out that MRI tends to overestimate the extent due to peritumoural inflammation. The purpose of the study is to correlate quantitatively measured on different MR-images the extent of the CC to parametrium to the results of the histological analysis performed after surgery.

Methods and Materials: 40 patients with histologically verified CC were enrolled in the study. The parametrium invasion maximal distance was measured in mm by two radiologists on different MR images (axial images, thickness=3mm): T2w/T2wfs, DWI+ADC-maps, contrast-enhanced T1TWISTfs at 90-120sec after i.v. injection of the MRCA (1.0mmol/ml solution of Gd-DO3A-butrol in standard dose). All the patients underwent surgery and the parametrium invasion of the tumour was measured in mm by a histologist.

Results: The MR measurements were significantly different to the histological findings (p<0.05) and tended to overestimate the invasion. The sen/sp for actual presence of the invasion and not peritumoural inflammation was estimated, the best results were on: T1WI+CE with sen/sp=0.96/0.92 for a 3mm distance on MRI and DWI sen/sp=0.91/0.92 for 4mm. MR results showed high correlation to histological measurements for all images (r²=0.79-0.93, p<0.05) with the best results for T1WI+CE and DWI. The actual distance can be calculated as: invasion (histology) = 0.8*invasion (T1WI+CE) - 0.8 or invasion (histology) = 0.7*invasion (DWI) - 1.0.

Conclusion: The critical distances to detect the presence of invasion with high sen/sp are determined in this study (best results for T1WI+CE and DWI). The actual distance can be calculated using our results.

B-1370 10:54

MRI findings of post-IGBT-treated cervical tumour

E. Wong¹, T. Chang², F. Cho¹, M. Lai¹, S. Soong¹, L. Law¹, M. Yeung¹, K. Tang¹; ¹Chai Wan/HK, ²Pok Fu Lam/HK (esthermfong@gmail.com)

Purpose: To study the accuracy of MRI as surveillance tool in locally advanced cervical cancer who has received MRI-image-guided brachytherapy (IGBT).

Methods and Materials: Consecutive cases of locally advanced cervical tumour receiving concurrent chemoradiation with whole pelvic radiotherapy were included. Pelvic MRI was performed 3-6 months post-radiotherapy.

Cervical biopsies were performed near the time of MRI. Images on post-radiotherapy MRI were retrospectively reviewed by 2 radiologists and scored as 1 = frank residual tumour signal, 2 = equivocal residual tumour signal, 3 = mainly fibrotic signal, no residual disease. The resulting scores were compared with the biopsy findings.

Results: 29 patients were retrospectively reviewed. The mean time interval between the last fraction of brachytherapy and post-treatment MRI was 20 weeks. Three cases were subsequently proven to have residual/recurrent disease at cervix or upper vagina. Out of the 15 cases rated as MRI negative (score 1) by both reviewers, none of their respective biopsies were positive. The other 14 cases were rated as either indeterminate (score 2) or frank residual disease (score 3) by either or both of the two reviewers. Three out of these are subsequently proven positive recurrent disease. Overall good interobserver agreement was found ($k=0.75$). Using residual disease detection as endpoint, MRI reached 100% for sensitivity and negative predictive value. Specificity was 73%.

Conclusion: MRI is highly sensitive in detection and ruling out of residual disease. It guides biopsy in dubious case.

B-1371 11:02

Simultaneous multiparametric PET/MRI for the assessment of therapeutic response to chemotherapy or concurrent radiochemotherapy of cervical cancer patients: preliminary results

T. Sarabhai, V. Stebner, A. Wetter, R. Kimmig, M. Forsting, L. Umutlu, J. Gruenewald; Essen/DE (theresia-catharina.sarabhai@uk-essen.de)

Purpose: To assess the response to chemotherapy or chemoradiotherapy in patients with primary cervical cancer, using simultaneous multiparametric PET/MR analysis.

Methods and Materials: 8 patients with a histopathologically confirmed primary cervical cancer were prospectively enrolled for a simultaneous 18F-FDG PET/MRI examination prior and after initial treatment strategy (chemotherapy, n=6; chemoradiotherapy, n=2). For the assessment of therapeutic response several morphological, functional and metabolic parameters of the primary tumors were determined in pre- and post-treatment PET/MR examinations. Histopathological correlation after subsequent tumor resection (n=7) or biopsy (n=1) served as the reference standard for the determination of therapeutic response.

Results: In accordance with the RECIST- and PERCIST-criteria, 7 of the 8 patients were classified as therapy responders (RECIST: CR=1, PR=6; PERCIST: CR=2; PR=5), while one patient showed stable disease. The responder group showed a significant reduction in tumor size (60%) and metabolic activity (SUVmax: 64%; SUVmean: 62%). Furthermore, a valuable increase of ADC values (ADCmin: 38%; ADCmean: 39%) and a significant decrease of certain perfusion parameters (Ktrans: 39%, Kep: 47%, iAUC: 57%) was found. Conversely, the non-responder revealed a slight decrease in tumor size (9%) and metabolic activity (SUVmax: 6%; SUVmean: 15%), accompanied with an increase of post-treatment perfusion parameters (Ktrans: 15%, Kep: 22%, iAUC: 22%). In addition, ADC values showed a slight (ADCmean: 24%) to moderate (ADCmin: 35%) increase during treatment.

Conclusion: These preliminary results demonstrate the feasibility of simultaneous multiparametric PET/MR analysis, which may function as a useful diagnostic tool for response assessment of initial treatment strategies in cervical cancer patients.

B-1372 11:10

Predicting early response in cervical malignancies to concurrent chemoradiation using intravoxel incoherent motion (IVIM) MRI

R. Balaji; Chennai/IN (ravikanthbalaji@gmail.com)

Purpose: To evaluate the use of intravoxel incoherent imaging diffusion MRI in assessing early response of cervical malignancies treated with concurrent chemoradiation.

Methods and Materials: 36 patients with cervical malignancies decided by the tumour board for concurrent chemoradiation were included in the study. Patients underwent routine diagnostic pelvic MRI for staging purpose in a 1.5T scanner. IVIM imaging was also performed with 11 b values 0 to 1000 s/mm^2 . Follow-up imaging was then performed a week after start of treatment, 3 weeks later and within 3 days of completing therapy. The apparent diffusion coefficient (ADC) maps were derived from the mono-exponential model, while the diffusion coefficient (D), perfusion fraction (f) and pseudo-diffusion coefficient (D*) maps were calculated from the bi-exponential model. Changes in ADC, D, f and D* in cervical cancers were investigated as bio-imaging markers for treatment response.

Results: ADC and D values showed progressive elevation after commencing treatment which persisted after completion. Mean D values after completion of therapy were $1.4 \pm 0.16 \times 10^{-3} mm^2/s$. f values, however, increased in the first week of treatment, started to decline by third week with significant fall in post-treatment scans ($0.14\% \pm 0.67$).

Conclusion: IVIM-derived D and f parameter values have significant potential in assessing treatment response non-invasively without use of contrast and without use of radionuclides.

B-1373 11:18

Evaluating the MR scoring system ("ADNEX MR score") for characterisation of sonographically indeterminate adnexal masses

H. Rajani, S.B. Grover, P. Mittal, G. Khanna; New Delhi/IN (heena.rajani@gmail.com)

Purpose: The critical role of imaging in adnexal masses is to differentiate between benign and malignant pathologies, as it has a crucial role in deciding the management: radical surgery versus fertility preserving laparoscopic surgery. Although ultrasound is the primary modality for evaluation of adnexal masses, the results are often inconclusive. The present study aimed to evaluate the "ADNEX MR score" for classification of sonographically indeterminate adnexal masses as benign or malignant.

Methods and Materials: MR imaging (1.5 T) was performed in 34 adnexal masses in 30 patients, presenting with sonographically indeterminate adnexal masses. Routine sequences were followed by Dynamic contrast enhanced study. The adnexal masses were assigned an "ADNEX MR score" between 1 to 5, as devised by Thomassin-Naggara et al. ROC curve analysis was done to determine the cut-off ADNEX MR Score for prediction of malignancy. All patients underwent laparoscopic or surgical excision. Statistical analysis was done using histopathology as gold standard.

Results: Using ROC analysis, we obtained the optimal "ADNEX MR score" cut-off value of 4. The sensitivity, specificity, NPV, PPV and accuracy of "ADNEX MR score", using cut off score ≥ 4 for prediction of malignancy was 100%, 90%, 100%, 87.5% and 94.% respectively with area under curve being 0.96.

Conclusion: In the present study, the "ADNEX MR score" value of 4 was found to have good sensitivity and specificity for malignancy prediction in sonographically indeterminate adnexal masses. Hence, "ADNEX MR score" should be included in the standardised MRI reporting format for adnexal masses.

B-1374 11:26

Adnexal masses: diagnostic value of DCE-MRI

S. Parviz; Tehran/IR (srparviz@gmail.com)

Purpose: To evaluate the utility of the dynamic contrast-enhanced magnetic resonance imaging (DCE-MRI) parameters in differentiating the malignant adnexal masses from the benign ones.

Methods and Materials: 43 patients with 49 complex adnexal masses (27 benign, 3 borderline, and 19 malignant) underwent preoperative DCE-MRI examinations, on a 3 Tesla MRI. Using extended Tofts' model, quantitative analysis was done in the solid parts of all tumours. Three PK parameters were defined as volume transfer coefficient (Ktrans), the rate constant (Kep), and the plasma volume (Vp). Semi-quantitative analysis was also performed and the values of relative signal intensity (SI_{rel}), wash-in-rate (WIR), the initial area under the curve (iAUC₆₀), time-to-peak (TTP) and wash-out-rate (WOR) were calculated. Using logistic regression and receiver operating characteristic (ROC) curve, we compared the mean values of individual parameters between the two groups.

Results: The mean value of Ktrans and the plasma volume (Vp) were significantly higher in malignant adnexal masses (P value < 0.0001 and P value = 0.001, respectively). Semi-quantitative analysis showed that SI_{rel} (P value < 0.0001), WIR (P value < 0.0001) and iAUC₆₀ (P value = 0.001) had higher values in malignant adnexal tumours compared to the benign ones. The pairwise comparison among the receiver operating characteristic (ROC) curves showed that the area under the curve (AUC) of Ktrans was significantly larger than the AUCs of all the other DCE-MRI parameters.

Conclusion: DCE-MRI is a relevant tool for differentiating benign from malignant adnexal masses. Among all pharmacokinetic and semi-quantitative parameters, Ktrans is the most accurate discriminator.

Author Disclosures:

S. Parviz; Author; Masoumeh Gity, Hamidreza Saligheh Rad, Anahita FathiKazerooni, Madjid Shakiba, Maryam Shirali.

B-1375 11:34

MR-imaging of neoplastic and non-neoplastic lesions of the vagina

S. Aksenova, N. Nudnov, J. Kreynina; Moscow/RU (fabella@mail.ru)

Purpose: Capabilities of MRI in detecting tumour lesions of the vagina using of the whole panel of modern features of MRI: DWI, DCE. Identify difficult moments in the diagnostic assessment of the vagina in operated patients with gynaecologic cancer.

Methods and Materials: 196 MRI examinations of pelvic with contrast enhancement were done in 137 patients. Complex MRI pelvic examinations with contrast enhancement were evaluated in 83 (60.6%) patients aged 34–82 (mean age 58 ± 4.7) with vagina neoplastic lesion suspicion, consisted of native

scanning, diffusion-weighted imaging, dynamic contrast enhanced examination with additional endovaginal MR suitable applicator introduction.

Results: Neoplastic lesions in vagina were found during MRI in 83 (60.6%) patients, at lower third – in 8 (9.7%), as endometrial and vulvar cancer progression, at middle third – in 20 (24.1%) patients, at upper third – in 55 (66.2%), included 30 (36.1%) patients with vaginal cuff relapse. It was revealed as a zone with increasing signal in T2WI and contrast accumulation in the arterial and venous phases. Non-tumour changes were observed in 54 patients. The greatest difficulty was to make the differentiation of early manifestations vaginal cuff relapse with residual fibrotic changes after radiation therapy. Differential diagnosis with post-radiation fibrosis demanded image fusion of T2WI fat sat, DWI and DCE with endovaginal MR-suitable applicator, which created conditions for better visualisation of vaginal wall structure and tumour localisation because of fold smoothing.

Conclusion: MRI allows a good visualisation of the tumour, as well as the differential diagnosis of neoplastic and non-neoplastic lesion.

B-1376 11:42

Diagnostic value of imaging for the detection of peritoneal metastases: a meta-analysis

I. van't Sant-Jansen, M. Engbersen, D.M. Lambregts, A.G. Aalbers, W. van Driel, R.G.H. Beets-Tan, M.J. Lahaye; *Amsterdam/NL (M.Lahaye@nki.nl)*

Purpose: To determine the diagnostic value of imaging in detecting peritoneal carcinomatosis (PC) in staging cancer patients.

Methods and Materials: A literature search in Pubmed, Embase (Ovid) and Scopus was performed (January 1997- July 2017) to identify studies reporting on the accuracy of imaging of PC in newly diagnosed primary gastrointestinal or ovarian cancers. Data extraction was performed by two observers in consensus. The sensitivity, specificity, and diagnostic odds ratio (DOR) were calculated using a bivariate random effects model and hierarchical summary operating curves (HSROC) were generated.

Results: The original search resulted in 4177 articles. Twenty relevant studies fulfilled all the required inclusion criteria of > 15 patients and surgery/histology/radiological follow-up as reference standard. From these articles 30 datasets could be extracted for analysis; 18 for CT, 8 for PET(CT) and 4 for MRI. The pooled sensitivity, specificity, DOR for detection of PC were 71% (CI:58-81%); 94% (CI:88-97%); 35.1 (CI:15.7-78.5) for CT. For PET(CT): 80% (CI:56-93%); 89% (CI:79-94%); 31.7(CI: 16.2-130.4). Due to the limited amount of MRI studies these datasets could not be analysed.

Conclusion: This meta-analysis shows that CT and PET(CT) demonstrate almost similar results in detecting peritoneal metastasis. More research is needed to investigate the diagnostic performance of MRI for peritoneal metastasis.

B-1377 11:50

Ovarian cancer staging: prospective comparison among ultrasound, CT and whole-body-MRI

V. Buscarino¹, S. Rizzo¹, A. Colarieti², M. Femia¹, E. Pagan¹, V. Bagnardi¹, M. Bellomi¹; ¹Milan/IT, ²Rome/IT (*valentinabuscarino@gmail.com*)

Purpose: The standard treatment of OC is primary cytoreductive surgery with resection of macroscopic disease; although, according to recent studies, interval debulking surgery after neoadjuvant chemotherapy allows comparable outcomes in advanced OC. The role of pre-operative staging is to select patients who may undergo up-front cytoreduction or may benefit from a neoadjuvant treatment. The objective of this study is a prospective comparison of diagnostic performance among WB-DW-MRI, US and CT.

Methods and Materials: All patients included underwent to US, CT and WB-DW-MRI as pre-surgical imaging evaluation before diagnostic or therapeutic surgery. Every imaging reader and the surgeon, reported on a specific report site of disease. Diagnostic performance of WB-DW-MRI, TC and US was calculated for each site, using the surgical evaluation as gold standard. The accuracy of WB-DWI-MR and CT were compared using the McNemar's test.

Results: Thirty-eight patients met the inclusion criteria. Imaging studies included for evaluation were: 31 CT, 36 US, 38 MRI examinations. WB-DWI-MR showed higher values of sensitivity, specificity and accuracy for crucial sites such as peritoneal carcinosis, mesenteric involvement and retraction, lombo-aortic and celiac nodes, although there was no significant statistical difference among WB-DWI-MRI and CT.

Conclusion: WB-DW-MRI is able to assess OC staging in satisfactory concordance with surgical findings, especially for sites considered crucial to indicate optimal resectability.

10:30 - 12:00

Room L 8

Imaging Informatics

SS 1805

Deep learning

Moderators:

S. Bisdas; London/UK

J. Fernandez-Bayó; Sabadell/ES

K-28 10:30

Keynote lecture

W. Kim; Los Angeles, CA/US

B-1378 10:39

Identifying pulmonary consolidation in chest x rays using deep learning

T.R. Nimmada, P. Putha, M. Tadepalli, S. Jain, P. Rao, P. Warier; *Mumbai/IN (tarun.raj@qure.ai)*

Purpose: Chest x-rays are widely used to identify pulmonary consolidation because they are highly accessible, cheap and sensitive. Automating the diagnosis in chest x-rays can reduce diagnostic delay, especially in resource limited settings.

Methods and Materials: Anonymised dataset of 423,218 chest x-rays with corresponding reports (collected from 166 centres across India spanning 22 x-ray machine variants from 9 manufacturers) is used for training and validation. x-rays with consolidation are identified from their reports using natural language processing techniques. Images are preprocessed to a standard size and normalised to remove source dependency. These images are trained using deep residual neural networks. Multiple models are trained on various selective subsets of the dataset along with one model trained on entire data set. Scores yielded by each of these models is passed through a 2-layer neural network to generate final probabilities for presence of consolidation in an x-ray.

Results: The model is validated and tested on a test dataset that is uniformly sampled from the parent dataset without any exclusion criteria. Sensitivity and specificity for the tag has been observed as 0.81 and 0.80, respectively. Area under the Receiver Operating Curve (AUC-ROC) was observed as 0.88.

Conclusion: Deep learning can be used to diagnose pulmonary consolidation in chest x-rays with models trained on a generalised dataset with samples from multiple demographics. This model performs better than a model trained on controlled dataset and is suited for a real world setting where x-ray quality may not be consistent.

B-1379 10:47

Efficacy of deep learning for screening pulmonary tuberculosis

P. Putha, M. Tadepalli, S. Jain, J. Chiramal, T.R. Nimmada, P. Warier; *Mumbai/IN (preetham.putha@qure.ai)*

Purpose: Chest X-rays(CXR), being highly sensitive, serve as a Screening tool in TB diagnosis. Though there are no classical features diagnostic of TB on CXR, there are a few patterns that can be used as supportive evidence. In Resource limited settings, developing Deep Learning algorithms for CXR based TB screening, could reduce diagnostic delay. Our algorithm screens for 8 abnormal patterns(TB tags)- Pleural effusion, blunted CP, Atelectasis, Fibrosis, Opacity, Nodules, Calcification and Cavity. It reports 'No Abnormality Detected' if none of these patterns are present on CXR.

Methods and Materials: An anonymized dataset of 423,218 CXRs with matched radiologist reports across (22 models, 9 manufacturers, 166 centres in India) was used to generate training data for the deep learning models. Natural Language Processing techniques were used to extract TB tags from these reports. Deep learning systems were trained to predict the probability of the presence/absence of each TB tag along with heat-maps that highlight abnormal regions in the CXR for each positive result.

Results: We validated the screening algorithm on 3 datasets external to our training set- two public datasets maintained by NIH(from Montgomery and Shenzhen) and a third from NIRT, India. The Area under the Receiver Operating Curve (AUC-ROC) for TB prediction was 0.91, 0.87 and 0.83 respectively.

Conclusion: Training on a diversified dataset enabled good performance on samples from completely different demographics. After further validation of its robustness against variation, the system can be deployed at scale to improve the current systems for TB screening significantly

Author Disclosures:

P. Putha: Employee; qure.ai. **M. Tadepalli:** Employee; qure.ai.

S. Jain: Employee; qure.ai. **J. Chiramal:** Employee; qure.ai. **T.R. Nimmada:** Employee; qure.ai. **P. Warier:** CEO; qure.ai.

B-1380 10:55

Automatic localisation and identification of vertebrae in spine CT scans by combining Deep Learning with morphological image processing techniques

A. Jiménez-Pastor, A. Alberich-Bayarri, B. Fos Guarinos, F. Garcia-Castro, L. Marti-Bonmati; Valencia/ES (anajimenez@quibim.com)

Purpose: In spine pathologies, the proper detection and identification of vertebrae is a need to perform diagnosis. This is a manual task that delays radiologists' workflow. The main goal of this work is to assist radiologists by detecting and identifying automatically vertebrae in spine CT scans.

Methods and Materials: To locate the spine centerline, a detection of the spinal canal was done by using a thresholding and a dilation using a cylindrical structuring element. Once the spine was located, the position of each vertebral body was detected and identified. This procedure was divided into 4 steps. First each axial 2D image was classified into 4 different regions: upper-thoracic, lower-thoracic, lumbar or sacrum. Thereafter, for each region, axial 2D images were classified into vertebra or non-vertebra. All these classifiers were designed using a pre-trained Convolutional Neural Network (CNN) to extract characteristics of each image followed by a Support-Vector-Machine (SVM) classifier and distribute them into the different groups. Finally, the centroid of each vertebra was calculated and identified.

Results: The mean localization error (distance between the estimated and real vertebra position) obtained was 7,37±8,69mm on the thoracic region and 9,21±8,70mm in the lumbar region; and the identification rate obtained was 89,20% in the thoracic region and 92,90% in the lumbar zone.

Conclusion: By combining deep learning with image processing techniques it is possible to automatically locate and identify vertebrae in spine CT scans. CNN are a good candidate to extract complex characteristics from the images in order to classify radiological images.

B-1381 11:03

Fully automatically staging of lung cancer using deep neural networks

K.S. Mader¹, A.W. Sauter², G. Sommer², T. Weikert², F. Trolese¹, J. Hagger¹, B. Stieltjes²; ¹Zurich/CH, ²Basel/CH (kevinmader@4quant.com)

Purpose: The standard diagnostic protocol for Lung Cancer involves an FDG-PET/CT to stage the patient. Both over- and undertreating the stage lead to drastic consequences for the patient's health and comfort. The full examination of these images takes up to 90 minutes per patient and requires the expertise of both a radiologist and a nuclear medicine physician. We aim to support physicians by automatically and quantitatively evaluating this reading and interpretation process.

Methods and Materials: Using a retrospective study with 179 patients, we collect the first PET-CT scan, manually annotate the suspicious lesions, and record the radiological TNM stage. We train a deep neural network using augmentation including transformed versions of the original images to avoid overfitting.

Results: The accuracy of the network was evaluated by using a validation group. The accuracy of the network was for very high: over 90% of lesions area was overlapping and a misclassification rate of 20%. Once the network was trained, detecting the suspicious lesions and computation of stage for a new patient can be done in a few seconds.

Conclusion: Staging and reading PET-CT images is a challenging task with large degrees of heterogeneity in both the patients and images. Given this heterogeneity, this initial study shows great promise in terms of speed and accuracy of the proposed set-up and could make this a valuable asset in the clinical environment and clinical trials.

Author Disclosures:

K.S. Mader: Founder; 4Quant AG. F. Trolese: Founder; 4Quant AG. J. Hagger: Founder; 4Quant AG. B. Stieltjes: Founder; HQImaging.

B-1382 11:11

Discrimination between distal ureteral stones and pelvic phleboliths in CT using a deep neural network: more than local features needed

M. Lidén, J.K. Jendeborg, M. Långkvist, A. Loutfi, P. Thunberg; Örebro/SE (matsliden@yahoo.com)

Purpose: To develop a deep learning method for assisting radiologists in the discrimination between distal ureteral stones and pelvic phleboliths in thin slice CT images, and to evaluate whether this differentiation is possible using only local features.

Methods and Materials: A limited field-of-view image data bank was retrospectively created, consisting of 5x5x5cm selections from 1-mm-thick unenhanced CT images centred around 218 pelvis phleboliths and 267 distal ureteral stones in 336 patients. 50 stones and 50 phleboliths formed a validation cohort and the remainder a training cohort. Ground truth was established by a radiologist using the complete CT examination during inclusion. The limited field-of-view CT stacks were independently reviewed and classified as containing a distal ureteral stone or a phlebolith by seven radiologists. Each cropped stack consisted of 50 slices (5x5cm field-of-view

and was displayed in a standard PACS reading environment. A convolutional neural network using three perpendicular images (2.5D-CNN) from the limited field-of-view CT stacks was trained for classification.

Results: The 2.5D-CNN obtained 89% accuracy (95% confidence interval 81%-94%) for the classification in the unseen validation cohort while the accuracy of radiologists reviewing the same cohort was 86% (range 76%-91%). There was no statistically significant difference between 2.5D-CNN and radiologists.

Conclusion: The 2.5D-CNN achieved radiologist level classification accuracy between distal ureteral stones and pelvic phleboliths when only using the local features. The mean accuracy of 86% for radiologists using limited field-of-view indicates that distant anatomical information that helps identifying the ureter's course is needed.

B-1383 11:19

Deep learning for liver segmentation and volumetry in late phase MRI

A. Schenk¹, G. Chlebus¹, H. Meine¹, S. Thoduka², N. Abolmaali²; ¹Bremen/DE, ²Dresden/DE (andrea.schenk@mevis.fraunhofer.de)

Purpose: Radioembolisation in the liver requires the computation of organ and tumor volumes for dosimetry planning. The purpose of this study was to investigate the accuracy of a new, fully-automated deep learning approach for liver segmentation in MRI data.

Methods and Materials: Images of 70 patients who underwent MRI to evaluate liver tumors were retrospectively analyzed. Data was acquired on two different scanners (Signa HDxt or Discovery 750, GE) applying a volume sequence and Gd-EOB-DTPA as contrast agent. Segmentation was performed on late phase images with a slice thickness of 2-3 mm.

Ground truth liver contours were accurately defined by experienced technicians using contouring and interpolation software and checked by a radiologist. Additionally, one radiologist and two residents defined routine segmentations for 28 patients scheduled for radioembolisation. A deep learning network was trained on the remaining 42 data sets and automatic organ boundaries were computed for the radioembolisation cases.

Results: Compared to the ground truth, relative volume error was 5.37%±4.38%, 3.63%±4.57% and 4.33%±4.62% for the three clinical users, and 6.95%±5.73% for the deep learning approach. DICE coefficient was 0.94±0.02, 0.95±0.02, 0.95±0.02, and 0.92±0.04 for the automatic method. Interactive ground truth segmentation took 24±8 minutes compared to approximately 10±4 minutes by the clinicians, and 20±7 seconds for the deep learning method.

Conclusion: Automated deep learning based liver segmentation in MRI data of radioembolisation patients was much faster with sufficient accuracy compared to interactive contouring and interpolation. The new method will support automated tumor load computation based on MRI in the future.

B-1384 11:27

Evaluation of a multiparametric deep learning model for glioblastoma segmentation

M. Perkuhn^{1,2}, F. Thiele^{1,2}, G. Shakinir^{1,2}, D. Gampis¹, P. Stavrinou¹, J. Borggreffe¹; ¹Cologne/DE, ²Aachen/DE (michael.perkuhn@uk-koeln.de)

Purpose: MRI is commonly used to non-invasively evaluate location, size, spread, oedema and the biological status of glioblastoma (GBM). Automatic, reliable and reproducible tumour segmentation can enable volumetric response assessment and effective integration of volumetric multimodal tumour characterization. The objective of this study was to apply a state-of-the-art deep learning algorithm for fully automatic GBM-compartment segmentation on clinical routine data from multiple centres, and to compare the results to ground truth manual expert segmentation.

Methods and Materials: 64 patients from 15 institutions with newly diagnosed, primary GBM were included. T1, T2, FLAIR and contrast-enhanced (CE) T1 sequences (Philips and Siemens scanners) underwent preprocessing and were fed to a deep-learning model based on DeepMedic. This model was trained on 220 cases of the BRATS database. Acquired segmentations were compared to manual segmentations of whole tumour (WT), necrosis (NC), and contrast-enhanced tumour (CET) performed by experienced radiologists as part of this study.

Results: The CET and WT were automatically detected in all patients. The automatic/manual segmentation dice similarity coefficients (DSC) were 0.86±0.09 (WT), 0.78±0.15 (CET), 0.62±0.30 (NC). For NC we found a correlation (R=-0.622, p<0.01) between surface-to-volume ratio and DSC. No correlation was found between resolution and DSC.

Conclusion: The proposed approach is robust on routine clinical data and has high accuracy comparable to interrater variability. This makes it a suitable building block for automatic tumour segmentation reviewed by the radiologist in pre-operative characterisation of GBM. Training the network on data with small/complex shape tumours might further increase the NC segmentation accuracy.

Author Disclosures:

M. Perkuhn: Employee; Philips Healthcare. **F. Thiele:** Employee; Philips Healthcare. **G. Shakirin:** Employee; Philips Healthcare.

B-1385 11:35

Peering into the darkness: visualising what neural networks learn through generative deep learning

J.C.Y. Seah, J.S.N. Tang, F. Gaillard; Melbourne/AU (J.Seah@alfred.org.au)

Purpose: To demonstrate the application of generative deep learning in visually representing what neural networks learn. The specific example explored is the prediction of B-type natriuretic peptide (BNP) levels as a marker of heart failure from chest radiographs.

Methods and Materials: 106,290 chest radiographs from 48,532 unique patients were extracted from a PACS database for this ethics approved study. 7,390 radiographs had a corresponding BNP result within 36 hours. The remainder 98,900 did not have a corresponding BNP result and formed the unlabelled dataset. The unlabelled dataset was used to create a generative model to convert radiographs to and from a low dimensional latent space. Simulated reconstructions for chest radiographs with high BNPs were then performed to visualise the same radiograph if it had a normal BNP. These were used to obtain a visual rationale which represent features the model has identified as important in this specific predictive task.

Results: A linear regression shows that the latent representations are logarithmically correlated with the accompanying BNP result. At a cut-off BNP value of 100 ng/L, the linear classifier obtained an AUC of 0.82. Qualitative assessment of the generated visual rationales confirms that the algorithm learns radiographic findings compatible with traditional human teaching. It also allows identification of unexpected features.

Conclusion: Generative learning can be applied to create visual representations of features learned by an algorithm. These visual representations could improve radiologists' understanding of deep learning algorithms and help enable the safe and appropriate application of deep learning in medicine.

B-1386 11:43

Automated detection of intra- and extra-axial haemorrhages on CT brain images using deep neural networks

S. Chilamkurthy¹, R. Ghosh¹, P. Rao¹, M. Biviji²; ¹Mumbai/IN, ²Nagpur/IN (rohit.ghosh@qure.ai)

Purpose: To develop and validate a deep neural network-based algorithm for automated, rapid and accurate detection from head CT for the following haemorrhages: intracerebral (ICH), subdural (SDH), extradural (EDH) and subarachnoid (SAH).

Methods and Materials: An anonymised database of head CTs was searched for non-contrast scans which were reported with any of ICH, SDH, EDH, SAH and those which were reported with neither of these. Each slice of these scans is manually tagged with the haemorrhages that are visible in that slice. In all, 3040 scans (116227 slices) were annotated, of which number of scans(slices) with ICH, SDH, EDH, SAH and neither of these are 781(6957), 493(6593), 742(6880), 561(5609) and 944(92999), respectively. Our deep learning model is a modified ResNet18 with 4 parallel final fully connected layers for each of the haemorrhages. This model is trained on the slices from the annotated dataset to make slice-level decisions. Random forests are trained with ResNet's softmax outputs for all the slices in a scan as features to make scan-level decisions.

Results: A different set of 2993 scans, uniformly sampled from the database without any exclusion criterion, is used for testing the scan-level decisions. Number of scans with ICH, SDH, EDH and SAH in this set are 123, 58, 41 and 62, respectively. Area under the receiver operating curve (AUC) for scan-level decisions for ICH, SDH, EDH and SAH are 0.91, 0.90, 0.90 and 0.90, respectively. Algorithm takes <1s to produce the decision for a scan.

Conclusion: Deep learning can accurately detect intra- and extra-axial haemorrhages from head CTs.

Author Disclosures:

S. Chilamkurthy: Employee; Qure.ai. **R. Ghosh:** Employee; Qure.ai. **P. Rao:** Employee; Qure.ai.

B-1387 11:51

Automatic detection of generalised cerebral atrophy using deep neural networks from head CT scans

S. Tanamala¹, R. Ghosh¹, S. Chilamkurthy¹, P. Rao¹, M. Biviji²; ¹Mumbai/IN, ²Nagpur/IN (rohit.ghosh@qure.ai)

Purpose: Features of generalised cerebral atrophy on brain CT images are the marker of neurodegenerative diseases of the brain. Our study aims at automated diagnosis of generalised cerebral atrophy on brain CT images using deep neural networks thereby offering an objective early diagnosis.

Methods and Materials: An anonymised dataset containing 78 head CT scans (1608 slices) was used to train and validate a skull-stripping algorithm.

The intracranial region was marked out slice by slice in each scan. Then a U-Net-based deep neural network was trained on these annotations to strip the skull from each slice. A second anonymised dataset containing 2189 CT scans (231 scans with atrophy) was used to train and validate an atrophy detection algorithm. First, an image registration technique was applied on the predicted intracranial region to align all scans to a standard head CT scan. The parenchymal and CSF volume was calculated by thresholding Hounsfield units from the intracranial region. The ratio of CSF volume to parenchymal volume from each slice of the aligned CT scan and the age of the patient were used as features to train a random forest algorithm that decides if the scan shows generalised cerebral atrophy.

Results: An independent set of 3000 head CT scans (347 scans with atrophy) was used to test the algorithm. Area under the receiver operating curve (AUC) for scan-level decisions is 0.86. Predictions on each patient takes time < 45s.

Conclusion: Deep convolutional networks can accurately detect generalised cerebral atrophy given a CT scan.

Author Disclosures:

S. Tanamala: Employee; Qure.ai. **R. Ghosh:** Employee; Qure.ai.

S. Chilamkurthy: Employee; Qure.ai. **P. Rao:** Employee; Qure.ai.

10:30 - 12:00

Room E1

Breast

SS 1802a

Image-guided biopsy/treatment

Moderators:

G. Ivanac; Zagreb/HR

S. Perez Rodrigo; Madrid/ES

B-1388 10:30

Features of MRI after cryoablation of primary breast cancer without surgical resection

Y. Machida¹, A. Shimauchi¹, T. Igarashi², H. Okuma², E. Fukuma³; ¹Chuo/JP, ²Tokyo/JP, ³Kamogawa/JP (machida.yoichi@kameda.jp)

Purpose: To retrospectively evaluate the features of serial magnetic resonance imaging (MRI) after cryoablation for breast cancer lesions without subsequent surgical resection.

Methods and Materials: This study was approved by the institutional review board. Requirement to obtain informed consent was waived. Ductal carcinoma in situ or invasive carcinoma \leq 15mm, nuclear grade 1 or 2, estrogen receptor positive/human epidermal growth factor 2 negative without lymph node metastasis were treated with cryoablation without subsequent excision. Two observers independently reviewed the first and second post-cryoablation MRI for shape (none, linear, or nodular) and suspicion for residual disease (positive or negative). Fisher's exact test or the Mann-Whitney U test was performed for variables. Interobserver agreement of findings was evaluated by calculating kappa values.

Results: Fifty-four cases were enrolled. The first and second post-cryoablation MRIs were performed 22-171 days and 82-487 days after cryoablation, respectively. The interobserver agreement for descriptor ranged fair to moderate ($\kappa = 0.331 - 0.434$). There were 7 cases (13.0%) for which either observer 1 or 2 evaluated positive suspicion on the first post-cryoablation MRI. There was a significant association between nodular shape compared to non-nodular (linear or none) and positive suspicion for residual disease or recurrence in both two observers' results ($p < 0.001$). On the second post-cryoablation, there were no cases with suspicious findings based on both of the two observers.

Conclusion: There were some cases with suspicious findings within treated area at the first post-cryoablation MRI, which can resolve during subsequent adjuvant therapies and follow-up management.

B-1389 10:38

Combined ultrasound-guided high-intensity focused ultrasound and vacuum assisted biopsy for treatment of large sized breast fibroadenoma

N.M. Abdel Razek, M. Hamed; Cairo/EG (naglaabdelrazek@yahoo.com)

Purpose: To assess the efficiency of ultrasound guided HIFU & VAB as non surgical technique for complete excision of large sized breast fibroadenoma

Methods and Materials: The study is a prospective one conducted in a single center during the period from February 2017 to September 2017. The ethical committee approval and patients written consents were obtained. The study included 20 patients with large sized breast fibroadenomas in one or both breasts were selected for treatment with US guided HIFU followed by VAB excision after 2 months. Patients' age ranged from 16 to 52 years ;mean 32 years. All patients with FA underwent core needle biopsy with histological confirmation. HIFU treatment was performed as an outpatient procedure under conscious sedation. After the treatment, follow up US with volume evaluation

was performed at 1 & 2 months and then percutaneous ultrasound guided VAB was performed to the residual lesion after HIFU

Results: The FA mean baseline size ranged between 3.5-6 cm diameter. At 1 month follow up, the mean volume reduction was $33.2\% \pm 19.1\%$ and achieved significance at 2 month $49.2\% \pm 16.2\%$, $p < 0.001$. After 2 months, the residual part was then excised using ultrasound guided VAB thus achieving complete excision.

Conclusion: Combined Ultrasound guided HIFU followed by VAB is an efficient well tolerated non invasive two step procedure for non-surgical complete excision of large fibroadenoma. Preliminary results are encouraging and show that the combined HIFU & VAB could be an alternative to surgery for large breast fibroadenoma. further work is still on progress.

B-1390 10:46

Digital breast tomosynthesis-guided vacuum-assisted biopsy (DBT-guided VAB): initial experience with patients positioned on a dedicated armchair

E. Venturini, M. Panzeri, C. Losio, M. Rodighiero, S. Tacchini, E. Schiani, P. Panizza; Milan/IT (venturini.elena@hsr.it)

Purpose: To evaluate the success rate and the tolerability of DBT-guided VAB with patients positioned on a dedicated armchair.

Methods and Materials: Sixty-four women with a suspicious breast finding (BIRADS 4) detectable only by mammography or DBT underwent DBT-guided VAB (Selenia Dimensions, Hologic). Patients were positioned in lateral decubitus or in sitting position on a dedicated armchair. DBT was acquired to determine lesion coordinates. Pre and post fire images were acquired with 2D-full field digital mammography to limit artifacts related to the needle (9G vacuum device). At least 12 biopsy specimens were obtained. Mammography of biopsy specimens was performed to verify the presence of microcalcifications.

Results: From 10/2016 and 09/2017 64 women (mean age 52 years; 39-81 years) with 66 suspicious (BI-RADS 4) mammographic findings underwent DBT-VAB. Overall, 66 DBT-guided biopsies were performed: 37 procedures with patient in sitting position, 29 in lateral decubitus. The technical success rate was 98.5% (65/66). Twenty-five breast carcinomas were diagnosed (4 invasive, 21 in situ) and 2 high-risk lesions were found at histological examination on biopsy specimens. Fifteen women underwent surgery at our Institution. One case of upgrade at final pathology was registered (from DCIS to 5 mm CDI with extensive in situ component). No serious complications were observed; 4 patients developed a small hematoma and 5 women a slight vasovagal reaction, which resolved spontaneously.

Conclusion: DBT-VAB with patients positioned on a dedicated armchair are a procedure with high success rate and well-tolerated.

Author Disclosures:

E. Venturini: Investigator; Philips, Novaura. Research/Grant Support; Philips, Novaura. P. Panizza: Investigator; Philips, Novaura. Research/Grant Support; Philips, Novaura. Speaker; Philips, Bayer, Hologic.

B-1391 10:54

Impact of MRI/ultrasound fusion-guided biopsy for breast lesions detected on MRI alone

S. Nakano¹, K. Fujii², J. Kousaka², Y. Mouri², T. Ando¹, M. Ido¹, M. Goto¹, Y. Ito¹, T. Ishiguchi¹; ¹Aichi/JP, ²Nagakute/JP (snakano1@aichi-med-u.ac.jp)

Purpose: When MRI-detected breast lesion can be identified by second-look US, US-guided biopsy is recommended. However, the detection rate of second-US is very heterogeneous because of the lack of reproducibility. The aim of this study was to examine the safety and outcomes of MRI/ultrasound fusion-guided biopsy using real-time virtual sonography (RVS) for breast lesions detected on MRI alone.

Methods and Materials: 39 lesions in 39 consecutive patients who underwent second-look US to identify MRI-detected lesions on prone MRI were enrolled in this retrospective study. For MRI-detected lesions that were not identified using conventional B-mode, second-look US using RVS and RVS-guided biopsy were performed after an additional supine MRI. The detection rate, lesion characteristics, and complication were assessed.

Results: The mean lesion size on MRI was 8.0 mm (3-46mm). Of the 39 lesions, 33 (85%) were detected and subjected to biopsy with second-look US using RVS. The MRI morphology types of these lesions were as follows: mass, 16; non-mass, 5; and focus, 12. 25 (76%) were benign and 8 (24%) were malignant. Of the 33 lesions, those with non-circumscribed margins and hypoechoogenicity were significantly more likely to be malignant ($p < 0.05$). The remaining 6 (15%) US-occult lesions could be judged to be benign after 24 months follow-up under RVS. There were no procedure-related complications.

Conclusion: Our results suggest that RVS-guided biopsy is a useful modality for the tissue sampling of breast lesions detected on MRI alone and may contribute to identifying cases in which MRI-guided biopsy is absolutely necessary.

B-1392 11:02

What can affect tomosynthesis-guided vacuum-assisted breast biopsy (TVAB) procedures? Clinical and technical challenges

G. Negro, M. Durando, G. Mariscotti, B. Desana, E. Regini, P. Isoardi, M. Garolla, P. Fonio, G. Gandini; Turin/IT (giulietta.negro@gmail.com)

Purpose: To evaluate clinical and technical performances of tomosynthesis-guided vacuum-assisted breast biopsy (TVAB), considering different breast compositions and mammographic lesion features.

Methods and Materials: All TVABs performed at our Breast Service between June 2016-July 2017 with an upright system and using VAB 9G-needles were retrospectively reviewed. We recorded all data about patient age, breast density, lesion type, dimension and localization, histology, breast thickness, breast positioning, number of projections, procedure time, average glandular dose (AGD), entrance surface dose (ESD). TVAB procedures were classified according to the number of performed projections (≤ 8 or ≥ 9), as less or more difficult proceedings. Uni- and multi-varied analyses of data were performed (significant p values < 0.05).

Results: 145 TVABs were included. Mammographic findings were: microcalcifications (115;79%), architectural distortions (14;10%), focal asymmetries (6;4%) and masses (11;7%). At microhistological examination, lesions were classified as B1 (1;1%), B2 (74;51%), B3 (38;26%), B4 (3;2%), B5 (29;20%). Average procedure time was 17 ± 4 minutes. Average number of projections per procedure was 8 ± 2 . TVAB with ≤ 8 projections were 95 (66%) and 50 (34%) with ≥ 9 . No associations were observed ($p > 0.05$) between easier technical feasibility (procedures ≤ 8 projections) and breast density or thickness, lesion dimension or localisation. Considering lesion type, microcalcifications correlated with a higher number of projections ($p = 0.01$). Median total AGD for TVAB with ≤ 8 projections was 10.8 mGy and 14.3 mGy with ≥ 9 ($p < 0.0001$) and correlated with median total ESD (35.6 mGy and 45.2 mGy respectively; $p < 0.0001$).

Conclusion: TVAB, in our experience, is a rapid, safe and accurate technique. The evaluation of microcalcifications correlated with a greater number of projections, as they can represent a more difficult target in tomosynthesis-images.

B-1393 11:10

Digital breast tomosynthesis (DBT) guided biopsy of thin breast patients: how tomosynthesis and special maneuvers contribute to the technical success

L.H.Y. Sinn, J.C.M. Sitt, C.Y. Fong, C.Y. Lui; Central/HK (lorriesinn@gmail.com)

Purpose: To evaluate how rapid target depths identification by DBT contribute to the improvement in workflow and successful rate in performing biopsies in thin breast patients, which minimize the need for open surgical biopsy.

Methods and Materials: Patients referred to our centre for tomosynthesis guided biopsies (core biopsy with 14G needle or vacuum assisted biopsy (VAB) with 9G/10G needle) from January 2016 to July 2017 with compressed thickness ≤ 30 mm were included. All biopsies were carried out under DBT guidance in upright position or with prone table system by dedicated radiologists. The compressed breast thicknesses, z value of the target coordinates, microcalcifications retrieval, histological diagnosis, and special maneuvers during the procedure were recorded.

Results: 33 patients (6 VAB, 27 core biopsies) were included, compressed breast thickness ranged 17-30mm. All (100%) biopsies were technically successful with target lesions (31 microcalcifications group: confirmed by specimen radiographs, 2 architectural distortions) removed. Different maneuvers including air-gap technique (n=4), lateral approach with lateral arm (n=1, VAB), petite needle (n=1, VAB) and application with peripheral pressure to increase breast thickness (ring technique, n=1, VAB) were used. No significant complications developed. 6 DCIS and 1 invasive ductal carcinoma were identified. No pathological discordance with final pathology identified in operated cases. Mean time of procedure was 22 (range 8-42) minutes.

Conclusion: DBT guided biopsies in thin breast patients provided better planning of approach before and during the procedures, with known anticipated target depths which allowed optimal positioning and special manipulations for successful lesion retrieval in short time.

B-1394 11:18

Diagnosis and treatment of suspected high-grade lesions using ultrasound-guided vacuum-assisted breast biopsy

J. Vucetic, J. Palao Errando, C. Barber Hueso, J.S. Cárdenas Herrán, M. Ortega Millán, R. Garcia Garcia; Valencia/ES (vucetic_jelena@yahoo.com)

Purpose: The purpose is to share our two-year experience in performing vacuum-assisted breast biopsy (VABB) for diagnosis and treatment of benign and potentially malignant breast lesions.

Methods and Materials: We received patients from outpatient clinics (68%), primary care (17%) and screening centers (15%). Eligible for VABB are considered lesions BI-RADS 4A and higher, high risk histology (B3 and

higher), radio-pathologic discordance (benign histology but suspicious lesion on image), and special cases such as patients with confirmed cancer and high anesthetic risk or BI-RADS 3 lesions at patient's request. We use Bard Encord vacuum system with 7G and 10 G needles. Biopsies are performed in supine position. We do follow up ultrasound and mammogram the next day for possible complications.

Results: A total of 76 lesions were biopsied from March 2015 to September 2017. The most of the lesions were BI-RADS 4A (63 lesions, 83%). Regarding histological classification, there were 35 (46%) of B3 lesions (papillary and/or atypical lesions on core needle biopsy). Five cancers were diagnosed (6.6%), three of them corresponding to BI-RADS 4A lesions, one 4B lesion and one BI-RADS 3 lesion BRCA+ patient.

Conclusion: Although longitudinal studies are still needed, the excision of high-risk lesions and lesions with radio-pathologic discordance is possible with VABB system. There is generally a very good tolerance among patients with a low complication rate. The surgical intervention is avoided in 95% of the cases in our series. It is essential to have multidisciplinary collaboration for the selection of cases.

B-1395 11:26

Design, development and validation of the first 3D PET manual breast-guided biopsy system

M. Herranz¹, G. Abou-Jaoude², W. Liang³, P. Aguiar¹, A. Ruibal¹;
¹Santiago de Compostela/ES, ²Lausanne/CH, ³Shanghai/CN
 (michel.herranz.carnero@sergas.es)

Purpose: Some of the problems reported with breast-specific PET imaging technology lies in those lesions able to detect but invisible to other techniques, or those that, because of their heterogeneity, are difficult to characterize, or tumours with functional resistance to chemotherapy. How we can be able to validate or demonstrate the correct diagnosis of these lesions?

Methods and Materials: The PROne BiOpsy System: ProBioS™ consists 1. a resistive resin adapter with fixed or mobile grids of 1, 3 or 6 racks. 2. A disposable holding system with receptacle for blood and other fluids, sterile and detachable. 3. A specific software. The system is adapted to be able to be used with any type of manual biopsy system.

Results: Test with PROBioS: 1. calibration of the 3D positioning. 2. Checking the theoretical calibration values. 3. Verification of empirical calibration values using point sources. Accuracy definition. 4. Verification of empirical calibration values using sources mimicking tumours. 5. Verification of empirical calibration values using breast phantoms. 6. Comparison with stereotaxic biopsy. 7.- Mathematical study of correlation between the values of biopsy in stereotaxic and MAMMI corrections. 8. Compression software studies. 9. Compression hardware studies. 10. Viability and sterilization studies. 11. Biopsies on patients.

Conclusion: We present the first 3D manual biopsy system guided by dedicated breast PET, its design, and its clinical utility. The development of this technique will allow the diagnosis of breast pathology to be much more precise and provide image services with an additional tool.

B-1397 11:34

Does breast MRI have a high negative predictive value for identifying residual axillary metastases in patients treated with neoadjuvant chemotherapy

N. Sharma, S. Rajan, B. Dall; Leeds/UK (Nisha.sharma2@nhs.net)

Purpose: It has been well documented that Breast MRI has a high negative predictive value (95%) for axillary metastases in women being staged for breast cancer. The question being asked is how good is breast MRI in determining complete pathological response in the malignant axilla in those women treated with neoadjuvant chemotherapy (NACT) and monitored with breast MRI. The end of treatment MRI T1 and T2 weighted sequences were reviewed to assess the axilla.

Methods and Materials: From October 2013-July 2015 49 patients who had breast cancer and biopsy proven malignant axillary lymph nodes treated with NACT were identified. All patients had an end of treatment MRI scan prior to axillary surgery. The lymph nodes were classified as normal or abnormal based on the T1 and T2 W sequences.

Results: 49 patients had axillary surgery. 57%(28/49) had malignant nodes at axillary clearance and 86% were correctly identified by MRI. 43%(21/49) had pathological complete response in the axilla and MRI correctly identified 71% of the cases. MRI overcalled 6 cases as being positive that were negative at surgery - all these lymph nodes showed evidence of tumour regression at histology.

Conclusion: MRI has a lower negative predictive value in assessing the axilla in women treated with NACT. This maybe related to the fact that these lymph nodes show evidence of tumour regression in the nodes which would account for signal and morphological changes seen on MRI which categorises the lymph nodes as being equivocal rather than normal.

B-1398 11:42

Comparison between standard specimen mammography and intraoperative specimen mammography (Faxitron®) located in the surgical block: has anything changed?

L.J. Pavan, M. Durando, G. Mariscotti, S. Martinello, G. Cappello, A. Ala, I. Castellano, P. Fonio, G. Gandini; Turin/IT

Purpose: To compare standard specimen mammography (SSM) with remote intraoperative specimen mammography (ISM)(Faxitron®), carried out by surgeons and remotely interpreted by radiologists, assessing operative times, intraoperative additional excision (IAE) and re-intervention rates for breast conserving surgery (BCS).

Methods and Materials: We retrospectively collected 129 consecutive patients (mean age 62±11 years, 136 lesions) who had BCS with SSM at our centre between 11/2011 and 02/2013 and 138 consecutive patients (mean age 60±11 years, 144 lesions) who underwent BCS with ISM between 08/2014 and 02/2015. We excluded patients treated in the first 6 months since ISM introduction, to avoid low-experience bias. Mammographic lesions were: 88 masses, 26 microcalcifications and 22 architectural distortions in SSM group, and 95, 23 and 26 in ISM group, respectively. Diagnostic reliability of SSM and ISM was evaluated considering pathology as gold standard, using Chi-square or Fisher's tests for categorical variables, and Mann-Whitney test for continuous variables.

Results: The two groups did not statistically differ for age (p=0.2), lesion sizes (p=0.29) and tumour histotypes (p=0.75). Intraoperative time was significantly (p<0.00001) higher for SSM (132±43min) than for ISM (90±42min). In SSM group, 39/136 (29%) lesions required IAE and 53/144 (37%) in ISM group, with no significant differences (p=0.16), even at a stratified analysis by each mammographic sign. Re-intervention rates were not statistically different between the two groups [SSM: 19/136 (14%), ISM: 11/144 (8%); p=0.08]. At pathology, 9/39 (23%) IAE specimens were positive for cancer in SSM group and 18/53 (34%) in ISM group, not statistically different (p=0.25).

Conclusion: The introduction of ISM significantly reduced surgical time without significant changes in IAE rates and surgical accuracy, corroborating the comprehension between surgeons and radiologists.

10:30 - 12:00

Room E2

Neuro

SS 1811a

Epilepsy

Moderators:

E. Achten; Gent/BE

A.M. Casado Lopez; Edinburgh/UK

K-29 10:30

Keynote lecture

L. Stenberg; Lund/SE

B-1399 10:39

Volumetric interpolated breath-hold MRI sequence: value and reliability in diagnosis of mesial temporal sclerosis

N.F. El Ameen, M.F. Amin; El Minia/EG (nadia.elameen@yahoo.com)

Purpose: To evaluate the role of 3D volumetric interpolated breath-hold sequence (VIBE) MRI of the brain in diagnosis of mesial temporal lobe sclerosis (MTS).

Methods and Materials: A prospective study included 45 patients with intractable epilepsy and suspected to have MTS. The patients were recruited between June 2015 and April 2016. All patients were referred from neurology department to radiology department in our institution. They underwent VIBE MRI in addition to the routine MRI protocol of the brain. Inter-observer reliability was done to the results to evaluate the reliability of VIBE sequence in diagnosis of MTS.

Results: Conventional T2WI was positive and diagnosed MTS in 34/45 (75.6%) and negative in 11/45 (24.4%) with sensitivity 90%, specificity 70% and accuracy 78%, while VIBE sequence was positive and diagnosed MTS in 39/45 (86.7%) and negative in 6/45 (13.3%) patients with sensitivity 92%, specificity 77% and accuracy 82%.

Conclusion: VIBE is a novel 3D gradient-echo sequence that offers several promising advantages if the object moves during the scan. Patients with intractable epilepsy could get much benefit from application of this sequence in routine imaging practice. It gives more clear images than T2WI and reduces the need for anaesthesia especially in children population.

B-1400 10:47

Description of white matter damage in patients with mesial temporal sclerosis evaluated by diffusion tensor imaging (DTI)

L.L. Resende, K. Lyra, C. Lôbo, L. Castro, V. Passarelli, R. Valerio, C. Jorge, C.D. Leite, M. Otaduy; São Paulo/BR (carlosfelipett2@gmail.com)

Purpose: Mesial temporal sclerosis (MTS) is a common cause of focal epilepsy. Although epilepsy is considered a grey-matter disease, white matter abnormalities have also been described. Describing white matter abnormality extension might help to understand different surgical outcomes. Our purpose is to describe the tracts affected and to evaluate differences in patients with right or left MTS.

Methods and Materials: 51 patients and 30 healthy controls were submitted to brain MRI and Diffusion tensor imaging (DTI) sequences with 32 gradient encoding direction. DTI images were post-processed with the FSL software and mean and median values of fractional anisotropy (FA) were obtained from 20 tracts. We grouped patients in left and right-sided MTS and compared FA between patients and controls for commissural, association and projection tracts, grouping tracts in ipsilateral and contralateral, regarding the laterality of MTS. We considered a p value <0.05 as statistically significant.

Results: In the comparison of commissural tracts, MTS patients showed a significant lower FA for forceps minor tract. In the comparison of association and projection tracts, we observed that right-sided MTS patients had a significantly lower FA in 7 of 9 right tracts (ipsilateral) and a lower FA in 6 of 9 left tracts (contralateral). Left-sided MTS patients had a significant lower FA in 3 of 9 left tracts (ipsilateral) and 6 of 9 right tracts (contralateral).

Conclusion: This study revealed diffusional abnormalities in 14 of the 20 tracts analysed. Curiously, MTS patients presented more damage on right-sided tracts, regardless the laterality of the hippocampal sclerosis.

B-1401 10:55

Incomplete hippocampal inversion does not affect the hippocampal volume in neurologically healthy subjects

D. Bajic¹, E. Kumlien¹, M. Milivojevic², R. Raininko¹; ¹Uppsala/SE, ²Uzice/RS (drabaj02@yahoo.se)

Purpose: In cases with incomplete hippocampal inversion (IHI), also called hippocampal malrotation, the hippocampus always looks narrow in axial images. In coronal images, it is difficult to compare the volumes of the hippocampi, which can be important in epilepsy, if there is IHI in one side. The aim of the study was to evaluate if IHI affects the hippocampal volume.

Methods and Materials: Hippocampal volumes were measured semiautomatically on MRIs of 99 neurologically healthy subjects aged 1-67 years. Asymmetry indices (AI) were calculated. AI was considered positive if the right hippocampus was larger and negative if the left was larger.

Results: 25/99 (25%) of the neurologically healthy subjects had IHI: 19 left-sided, 6 bilateral. The right hippocampus was larger in 63/74 (85%) subjects without IHI and in 86 (86%) of all subjects. The volumes of the left hippocampus in subjects without and with IHI did not differ statistically significantly. AI was 0.042±0.049 (mean±SD) in the 74 subjects without IHI and it was not age-dependent. AI was 0.029±0.036 in the 19 subjects with left-sided IHI, and 0.061±0.048 in the six subjects with bilateral IHI. Differences were not statistically significant. The ±2SD limits for AI were 0.14 and -0.05 in all subjects.

Conclusion: IHI does not seem to affect the hippocampal volume in neurologically healthy subjects. Consequently, AI is not affected by IHI. AI is not age-dependent and the same criteria for normal asymmetry can be used in the evaluation of the patients at all ages.

B-1402 11:03

Utility of volumetric assessment of the hippocampal substructures in hippocampal sclerosis

A.M. Granados, J.F. Orejuela; Cali/CO (anamaria.granados@gmail.com)

Purpose: Pathological classification of hippocampal sclerosis (HS) is based on neuronal loss of hippocampal substructures, which has been correlated with disease duration, memory function performance, and postoperative prognosis. The purpose of this work is to evaluate the usefulness of an automated method for the assessment of hippocampal substructures on MRI studies.

Methods and Materials: Twenty-five patients with unilateral-HS and twenty-five healthy subjects were included. Volumes of the whole hippocampus and hippocampal subfields were obtained using FreeSurfer. A p value less than 0.05 was considered statistically significant.

Results: A statistically significant decrease in the ipsilateral hippocampus was found in 22 cases (88.0%). With the exception of the fissure, there was a decrease in all ipsilateral hippocampal substructures in right-HS (CA1, p=0.0223; CA2-CA3, p=0.0066; CA4-DG, p=0.0066; fimbria, p=0.0046; presubiculum, p=0.0087; subiculum, p=0.0017), and left-HS (CA1, p<0.0001; CA2-CA3, p<0.0001; CA4-DG, p<0.0001; fimbria, p=0.0183; presubiculum, p<0.0001; subiculum, p<0.0001). No decrease in overall volume was observed in three patients; however, one case showed a decrease in the

volume of CA1, CA2-CA3, and CA4-DG, the second case of CA1, CA2-CA3, and subiculum; and in the other case, CA4-DG, fimbria, and presubiculum volumes were decreased.

Conclusion: The automated method used in this work could improve the predictive values of quantitative MRI analysis in the diagnosis of HS as it allows to identify focal alterations before global structural changes occur. Moreover, the good correlation found with the last ILAE classification suggests that this method could also play an important role as a prognosis tool.

B-1403 11:11

Prefrontal lobe cortex-thalamus pathway impairment in intractable temporal lobe epilepsy with executive control function abnormal: evidence from structural and functional MRI study

C. Zhang, N. Chen, K. Li, H. Yang; Beijing/CN (chaozhang0328@hotmail.com)

Purpose: The aim of this study was to investigate structure and functional connectivity of prefrontal lobe cortex (PFC)-thalamus pathway in unilateral intractable temporal lobe epilepsy (TLE) patients with impaired executive control function (ECF).

Methods and Materials: Thirty-seven intractable left TLE patients and twenty-three volunteers were recruited for diffusion tensor imaging and resting-state fMRI scanning. The patients were divided into two subgroups according to ECF performance which judged by Wisconsin card sorting test (WCST): ECF decreased group (18 subjects) as G1 and ECF normal group (21 subjects) as G2. The healthy control group (HC) included all 23 volunteers. The region of interest (ROI) was set in bilateral prefrontal cortex and bilateral thalamus. A general linear model (GLM) was employed to analyse fibres and functional connectivity (FC) between each pair of ROI among G1, G2 and HC (p<0.05). Pearson correlation between FC, fibre number and WCST score was also observed through partial correlation analysis (p<0.05).

Results: Fibre number and FC between left dorsolateral frontal gyrus and left thalamus of G1 were increased significantly when compared with G2 and HC (p=0.017). Both fibre number and FC had significantly negative correlation with WCST score (p<0.05).

Conclusion: This study demonstrated that decreased ECF was related to PFC-thalamus pathway. Furthermore, such alternation may potentially act as an important imaging feature for differentiating TLE patients with ECF impairment.

B-1404 11:19

Comparison between different post-processing techniques in the identification of focal cortical dysplasias in children with pharmacoresistant epilepsy

M. Rossi Espagnet, E. Bassanelli, A. Napolitano, N. Pietrafusa, L. De Palma, N. Specchio, D. Longo; Rome/IT (camilla.rossiespagnet@gmail.com)

Purpose: Different techniques have been developed to improve identification of malformations of cortical development such as focal cortical dysplasias (FCD) in MRI-negative patients affected by pharmacoresistant epilepsy (PRE). However, no studies investigated the reliability of these methods for the paediatric population so far. The purpose of this prospective on-going study is to compare the MAP and the SUPR-FLAIR techniques for the pre-surgical evaluation of the paediatric brain in children with PRE.

Methods and Materials: A group of 90 healthy subjects (age range 8-16 years) was used as a control group, while 10 patients (4 RMN positive and 6 RMN negative) with drug-resistant epilepsy, and histological proof of FCD, were analysed to compare the two methods. All subjects were scanned with a 3T Siemens Skyra (Erlangen, Germany). The original Map method has been optimised (Opti-MAP) by creating a specific template for paediatric subjects (90 healthy subjects), and inserting two tools into the algorithm: BET and N4ITK. For the SUPR-FLAIR Analysis the original algorithm was followed.

Results: The Opti-Map approach was successful in the 90% of cases despite the fact that most of the FCDs were type I. Conversely, the SUPR-FLAIR approach succeeded only in 20% of cases. In no cases, there was any overlap between the 2 methods.

Conclusion: From these preliminary results optimised MAP post-processing seems to be a more reliable tool compared to the SUPR-FLAIR technique in the pre-surgical evaluation of pharmacoresistant epilepsy in children. Further data are necessary to further optimise the template and validate these results.

B-1405 11:27

Mesial temporal sclerosis: is standard MRI protocol enough?

J. Ponnatapura Satyanarayana; Bangalore/IN (psjanardhan@yahoo.com)

Purpose: Evaluation of the different protocols of MR imaging in MTS and correlation with EEG findings. Pearls and pitfalls of MRI.

Methods and Materials: A prospective study was conducted of 52 mesial temporal sclerosis patients who underwent dedicated epilepsy protocol MRI and volumetric MRI on 1.5T within 7 days from the onset of seizures. A routine EEG from the scalp electrodes was obtained 3 days before or after the MRI.

Results: Thirty-six patients (69%) presented with partial seizure, and 31% presented with generalized clonic tonic seizure. 26% had childhood history of febrile illness. 62% diagnosed with MTS on MRI showed abnormal EEG findings and 10 showed normal EEG findings. The lateralisation of EEG in MTS patients was 70-76% ($p>0.5$). 98% of patients with MTS showed positive MR volumetric study ($p<0.5$), of which 36% showed normal EEG study ($p<0.5$). 100% of patients with hippocampal sclerosis were detected using "epilepsy protocol" MRI, which would have been missed if only "standard protocol" MRI was done.

Conclusion: Mesial temporal findings on MRI did not always result in abnormal EEG findings and hence newer imaging modalities like MR volumetric study, functional MRI, MR spectroscopy, SPECT and PET should be done in medically refractory seizures, especially before planning surgery.

B-1406 11:35

Comparison between BOLD-fMRI and Stereo-EEG in the pre-surgical evaluation of language dominance in children affected by pharmaco-resistant epilepsy

M. Rossi Espagnet, E. Bassanelli, N. Pietrafusa, L. Figà-Talamanca, L. De Palma, D. Longo, A. Napolitano; Rome/IT
(camilla.rossiespagnet@gmail.com)

Purpose: The optimal pre-surgical management of patients with pharmaco-resistant epilepsy (PRE) has the aim to correctly identify the seizure onset zone and to verify the localisation of "critical" regions to avoid post-surgery deficits. Both task-based fMRI and Stereo-EEG demonstrated good correlation in the identification of language dominance compared to WADA test. The purpose of this preliminary study is to verify the correlation between Stereo-EEG and fMRI results in the identification of language dominance in children with PRE.

Methods and Materials: Language Task-based fMRI obtained from a 3T scanner (Siemens Skyra, Erlangen, Germany) in 5 patients with PRE were retrospectively analysed to calculate lateralisation index (LI) for all the tasks applied (semantic task, verb generation and story listening). Stereo-EEG data obtained from all patients after electrode stimulation during language-related tasks were also reviewed to verify language dominance.

Results: Language dominance obtained from SEEG and fMRI was concordant in all patients. 4/5 patients demonstrated a left language lateralisation whilst 1/5 patient with a left fronto-temporo-parietal perinatal stroke demonstrated right language lateralisation. The location of language-related areas obtained from fMRI tasks demonstrated a good correlation with those that determined a block in language tests during electrode stimulation.

Conclusion: task-based fMRI and stereo-EEG provided good correlation in the evaluation of language dominance and can be considered reliable tools in the pre-surgical evaluation of children affected by PRE.

B-1407 11:43

The role of conventional MRI-based scale in distinguishing chronic disorders of consciousness

S. Morozova, E.I. Kremneva, L. Legostaeva, E. Mochalova, D. Sinitsyn, D. Sergeev, M. Krotenkova, N. Suponeva, M. Piradov; Moscow/RU
(kulikovasn@gmail.com)

Purpose: To evaluate predictive role of new suggested conventional MRI-based scale in distinguishing chronic disorders of consciousness (DOCDS-disorders of consciousness distinguishing scale).

Methods and Materials: Data were acquired from 24 patients with clinically assessed chronic disorders of consciousness (12 with minimal consciousness state (MCS) and 12 with unresponsive wakefulness syndrome (UWS)) due to anoxia or trauma age ranged 21-56. All patients underwent conventional MRI on Siemens Verio 3.0 T scanner, scanning protocol included conventional T2 sequence, T1 multiplanar sequence, which were used for scaling. The following parameters were suggested for DOCDS: general cortical atrophy, inner and external hydrocephalus, leukoencephalopathy, brainstem degeneration, corpus callosum degeneration and lesions. T2WI and T1WI of all patients were assessed according to the scale resulting in a total score. Images were analysed by two experts blinded to diagnosis and its cause. Statistical analysis was performed using SPSS 20.0.0.

Results: Total DOCDS score ranged 2-9. ROC-analysis showed threshold score 5.5, which means that patients with total DOCDS score 6 and more refer to UWS, 5 and less refer to MCS with sensitivity 76.9%, specificity 90.9% (area under the curve (AUC) = 82.9%, $p=0.006$).

Conclusion: Taking into consideration relatively high sensitivity and specificity, DOCDS could be used as an additional instrument in distinguishing chronic disorders of consciousness. The study was supported by Russian Science Foundation under grant 16-15-00274.

B-1408 11:51

Utility of MRI brain epilepsy protocol in new onset seizures: how is it different in developing countries?

J. Ponnatapura Satyanarayana; Bangalore/IN (psjanardhan@yahoo.com)

Purpose: To evaluate the diagnostic efficacy of standard MRI brain in patients with first-onset seizures and to identify whether there is an increase in the diagnostic yield with addition of a dedicated seizure protocol.

Methods and Materials: 129 cases were studied for a period of 18 months. Chi-square test was used to test for the difference in proportion. The correlation between MRI brain and EEG was studied using McNemar test. Patients underwent both standard protocol and dedicated epilepsy protocol MRI brain scanning on 1.5T within 7 days from the onset of seizures. A routine EEG from the scalp electrodes obtained 3 days before or after the MRI and after presentation with the index seizure, preferably within 48 hours.

Results: The diagnostic yield of MRI was 47%. Infection and inflammation was most common (28%). Of the 59 patients with potential epileptogenic lesions, 63% were detected using "standard protocol" MRI and remaining 37% lesions were detected using "dedicated epilepsy protocol" MRI. Of the epileptogenic lesions, all 11 patients (100%) with hippocampal sclerosis were detected using "epilepsy protocol" MRI which would have been missed if only "standard protocol" MRI was done. Patients with focal-onset seizures had a higher proportion of potentially epileptogenic lesions (81%) compared with the patients with generalized clonic tonic seizures.

Conclusion: A dedicated epilepsy protocol MRI should be done in all patients who present with first-onset seizures, which allows identification of a lesion and earlier consideration of epilepsy surgery especially in patients with focal-onset seizures.

10:30 - 12:00

Room F2

Breast

SS 1802b

Contrast-enhanced mammography and phase-contrast CT

Moderators:

O. Abeyakoon; Cambridge/UK
A. Vourtsis; Athens/GR

B-1409 10:30

Is there a difference in the degree of enhancement in contrast-enhanced spectral mammography between invasive lobular carcinomas and invasive ductal carcinomas?

T. van Nijnatten¹, M.B. Lobbes¹, K. Pinker², D.M. Keating², J.S. Sung², M. Morrow², J.E. Wildberger¹, M. Smid¹, M.S. Jochelson²; ¹Maastricht/NL, ²New York, NY/US (t.vannijnatten@maastrichtuniversity.nl)

Purpose: To investigate the differences in the degree of lesion enhancement of invasive lobular carcinomas (ILC) and invasive ductal carcinomas in contrast-enhanced spectral mammography (CESM).

Methods and Materials: This two-centre HPAA-compliant retrospective study included consecutive patients with ILC or IDC who underwent preoperative CESM between 2010 and 2017. Three independent readers (one expert CESM reader, one reader with greater than 4 years of experience in CESM and one inexperienced reader) assessed the degree of lesion enhancement of the cancers, blinded to histology. Enhancement was scored as: possible, weak, moderate or strong. Interobserver agreement was calculated by using quadratic-weighted kappa (including 95% confidence intervals) to compare the results of the expert CESM reader with the other readers.

Results: A total of 44 patients were included: 22 patients with ILC and 22 patients with IDC. The degree of lesion enhancement was classified significantly more often as possible or weak in patients with ILC compared to IDC (reader 1: 31.8% versus 4.5%, $p=0.045$; reader 2: 36.4% versus 18.2%, $p=0.310$; reader 3: 22.7% versus 4.5%, $p=0.185$). All other lesions were considered moderate or strong enhancement. Inter-observer agreement was good for the two experienced CESM readers ($\kappa=0.723$ (0.584 - 0.862) as well as for the expert CESM reader compared to the non-experienced CESM reader ($\kappa=0.728$ (0.598 - 0.858)).

Conclusion: There is a difference in the degree of enhancement between ILC and IDC, with ILC significantly more often presenting with weak enhancement. In case of weak lesion enhancement, radiologists should consider ILC for the final diagnosis.

Author Disclosures:

M.B. Lobbes: Research/Grant Support; GE. J.E. Wildberger: Research/Grant Support; Bayer, Agfa, BRACCO, GE, Philips, Siemens. Speaker; Bayer, Siemens.

B-1410 10:38

Quantification of enhancement in contrast-enhanced spectral mammography using a custom-made quantifier tool: a proof-of-concept study

H.K.P. Mulder, C.R. Jeukens, M. Rousch, J.E. Wildberger, M.B. Lobbes; Maastricht/NL (harmen.mulder@mumc.nl)

Purpose: Contrast-enhanced spectral mammography (CESM) is superior to conventional mammography and is able to show contrast agent uptake (enhancement) in breast lesions, increasing its diagnostic accuracy. A major step forward would be the ability to quantify enhancement, perhaps allowing discrimination between malign and benign tumours. In this proof-of-concept study, we present a novel quantification method for rating CESM enhancement.

Methods and Materials: We developed a novel, custom-made quantifier tool (*I*-STRIP) filled with different concentrations of contrast agent, which is positioned near the breast during acquisition. The measured CESM signal in the *I*-STRIP is used to quantify iodine mass thickness (IMT) in the breast. We evaluated the accuracy and precision using a dedicated phantom containing lesions with known IMT. Furthermore, we tested its effect on image quality and clinical use in five breast cancer patients.

Results: Phantom experiments showed that measured enhancement scales linearly with IMT. Furthermore, enhancement in a medium-thick (4.6 cm) breast phantom corresponded within 11.8%, 9.0% and 13.2% to enhancement in the *I*-STRIP for IMT's of 1.5, 3.0 and 7.5 mg/cm², respectively. Only for lesions near the periphery of the phantom the so-called breast-within-breast artefact resulted in overestimation of enhancement. In five clinical experiments, the workflow and the image quality were not influenced by the *I*-STRIP. The mean IMT of five invasive breast cancers was 2.1 mg/cm² (range 1.3-3.4 mg/cm²).

Conclusion: We showed in both phantom and clinical experiments that we could accurately quantify the CESM enhancement on recombined CESM images without affecting image quality.

Author Disclosures:

J.E. Wildberger: Research/Grant Support; Siemens, Philips, GE, BRACCO, Bayer, Agfa. Speaker; Siemens, Bayer.

B-1411 10:46

Contrast-enhanced spectral mammography and diffusion-weighted image with backward signal suppression: which is more effective in breast cancer detection?

N.A.E. ElDeib, F.M.E.S. Singer, S.M.M.T. Talaat, M. Anas, M. Rezk; Cairo/EG (nohasaid.rad@hotmail.com)

Purpose: The purpose of this study is to assess diagnostic accuracy of diffusion weighted imaging with background signal suppression (DWIBS) compared with contrast-enhanced mammography in the diagnosis of breast lesions and correlate the findings with the histopathological results.

Methods and Materials: 52 female patients have enrolled in this prospective study their age ranged between 23-77 years old, mean age is about (47.83,+/-SD=11.55)years. The patients presented with breast lesions by mammography were assessed by both contrast-enhanced mammography and DWIBS MR. Written consent was taken from the patients. The maximum dimension of the lesion or lesions was measured in both studies. Findings assessed by two radiologists, one for each modality without knowing pathologic results.

Results: The primary unit of analysis was the lesion, 54 lesions were detected in 52 cases. 39/54 of the lesions were histopathologically proven as malignant and 15/54 were benign. The calculated sensitivity, specificity, total accuracy, PPV and NPV for CEDM were (100.00%, 73.30%, 92.60%, 90.70% and 100.00%) respectively. The calculated sensitivity, specificity, total accuracy, PPV and NPV for DWIBS MRI were (94.90%, 93.30%, 94.40%, 97.40% and 87.50%) respectively. DWIBS MRI showed the highest diagnostic performance and accuracy due to improved specificity by reducing number of false positive results, compared to CEDM.

Conclusion: The DWIBS is a new non-contrast imaging technique with an improved specificity when compared to CEDM. DWIBS is superior to CEDM in the detection of both malignant and benign lesions. CEDM is less expensive, easier and quicker examination compared to MRI.

B-1412 10:54

Feasibility of contrast-enhanced spectrum mammography in breast cancer diagnosis

L. Zheng, C. Zhang, K. Li; Shanghai/CN (zhenglinfeng04@aliyun.com)

Purpose: To study feasibility of contrast-enhanced spectral mammography (CESM) in the diagnosis of breast cancer.

Methods and Materials: Institutional review board approved this study. Ninety-one cases clinically diagnosed with breast cancer were underwent CESM, mammography (MG) and contrast-enhanced magnetic resonance imaging (CE-MRI). Detectable rate of CESM, MG and CE-MRI were compared, respectively. Then average maximum dimension of suspicious lesions on CESM image was measured and compared with pathological specimen.

Finally, morphologic features of CESM images were analysed for four different molecular subtypes of breast cancer cases.

Results: CESM has high detectable rate than MG and CE-MRI for breast cancer (97.0% vs 83.3% vs 91.0%; P<0.05). For the measurement of mass average maximum dimension, no difference was found between CESM and pathology (P>0.05). However, CESM image features of the four different molecular subtype cases, including average maximum dimension of mass, shape, margin, enhancement and enlargement of lymph node, were of statistical difference (P<0.05).

Conclusion: CESM may play an important role in the breast cancer clinical practice.

B-1413 11:02

Features from computerised texture analysis of breast cancer on contrast-enhanced spectral mammography to predict tumour aggressiveness

C. Bassi, L.S. Fournier, M. Bouaboula, C. Rousseau, A.-S. Jannot, C. Ngo, H. Roussel, F. Chamming's; Paris/FR (clotilde.bassi@gmail.com)

Purpose: To evaluate whether heterogeneity as evaluated by texture analysis on contrast enhanced spectral mammography (CESM) was associated with breast cancer features on pathology.

Methods and Materials: Institutional review board was obtained. 79 patients with 79 breast cancers who underwent CESM between January 2015 and May 2017 were included in this retrospective monocentric study. 2D texture analysis was performed using TexRAD software. Quantitative texture parameters were compared with pathological features. Eigen value analysis was used to determine the number of independent parameters. Univariate analysis was performed to determine texture parameters significantly associated with tumour pathology. After Bonferroni correction, P less than 0,0014 was considered statistically significant.

Results: On univariate analysis, Kurtosis for Spatial scale filter (SSF) 0,5 (P = 0,0015) and 4 (P = 0,0006), skewness for SSF2 (P = 0,003) and mean proportion of positive pixels (MPP) for SSF2 (P = 0,004) showed significant association with mitotic index. There was also a trend for association between MPP SSF2 (P = 0,003) and SSF4 (P = 0,004) and tumour grade.

Conclusion: On CESM, heterogeneity of breast cancers as measured by texture analysis is associated with mitotic index and could be a promising biomarker of tumour aggressiveness.

B-1414 11:10

Impact of mammographic features and level of tumour-infiltrating lymphocytes on prognosis of triple-negative breast cancer

S. Casella, G. Mariscotti, M. Durando, I. Castellano, E. Vissio, F. Esposito, S. Osella Abate, P. Fonio, G. Gandini; Turin/IT (loricri@inwind.it)

Purpose: Triple-negative breast cancer (TNBC) is known to be associated with aggressive clinical behaviour and poor clinical outcomes. Elevated levels of tumor-infiltrating lymphocytes (TILs) positively correlate with the pathologic complete response and increased survival in patients with TNBC. The purpose of this study was to investigate associations between mammographic features, TIL levels and prognosis in patients with TNBC.

Methods and Materials: We conducted a retrospective observer study that includes 81 patients (mean age 56,6 years; range:36,6-88,1) with pathologically confirmed TNBC, who consecutively underwent preoperative digital mammography between January 2010 and March 2017. All mammographic lesions were evaluated by radiologists and classified in accordance with the BI-RADS lexicon. Tumors were divided into two groups: those with a TIL level of less than 10% and those ≥10%. Univariate and multivariate analysis were performed on the data.

Results: TNBCs were predominantly mass lesions (73/81, 90,1%), subgrouped in 16(21,9%) masses associated with microcalcifications, 3(4,1%) with architectural distortions and 1 with microcalcifications and architectural distortion. Out of 73 masses, 22(30%) had circumscribed margins, statistically associated with favourable clinical behaviour (IC 0.02-1.00, p=0.05); considering the 20/81(24.7%) cases with recurrence, only in 1 case the TNBC was a mass with circumscribed margins. In 36/81(44.5%) TNBC TILs level was ≥10% and in 45(55.5%) <10%. TILs ≥ 10% proved to be a positive prognostic biomarker for disease free-survival (HR 0.30; p=0.05).

Conclusion: In the TNBCs, circumscribed margins at mammography, as well TILs≥10% could provide added diagnostic benefit for the identification and treatment planning of TNBC with a good prognosis.

B-1415 11:18

Low-dose perfusion CT for quantification of tumour vascularity in breast cancer: correlation with prognostic biomarkers

B.K. Seo¹, E.K. Park¹, M. Kwon¹, C.S. Ko¹, J. Cha¹, K.R. Cho², O.H. Woo²;
¹Ansan/KR, ²Seoul/KR (seoboky@korea.ac.kr)

Purpose: To investigate the feasibility of low-dose perfusion computed tomography (CT) in breast cancers for quantification of tumor vascularity and to correlate perfusion indexes with prognostic biomarkers.

Methods and Materials: Low-dose perfusion CT was performed in 70 patients with invasive breast cancers. CT was performed in the prone position with a spectral CT (iQon, Philips Healthcare) after contrast media (Xenetix350, Guerbet) injection. On CT perfusion maps, perfusion (mL/100g/min), blood volume (mL/100g), time to peak (sec) and peak enhancement (HU) were measured in the tumor, normal breast glandular tissues and fat. Pathologically, tumor grade, estrogen receptor (ER), progesterone receptor (PR), human epidermal growth factor receptor 2 (HER2), and Ki67 level were evaluated. Statistically, CT perfusion indexes of the tumor and normal glandular tissues or fat was compared using the Wilcoxon signed rank test and CT indexes were correlated with histological characteristics with the Mann-Whitney or Kruskal-Wallis test.

Results: In breast cancers, perfusion, blood volume and peak enhancement values were significantly higher and time to peak was shorter than these values in normal glandular tissues and fat ($P < .05$). Perfusion significantly increased in breast cancers with high grade, ER- or HER2+ ($P < .05$). Time to peak decreased in cancers with high grade, ER-, HER2+ or high Ki67 level ($P < .05$). Peak enhancement significantly increased in high grade cancers ($P < .05$).

Conclusion: Low-dose perfusion CT in the prone position is feasible to quantify tumor vascularity in breast cancers and CT perfusion indexes may predict prognostic biomarkers.

B-1416 11:26

A visual grading analysis of propagation-based phase-contrast CT mammography

S. Tavakoli Taba¹, P. Baran², S. Lewis¹, R. Heard¹, S. Pacile³, Y.I. Nesterets², S.C. Mayo², C. Dullin⁴, D. Dreossi³, F. Arfelli³, D. Thompson², M. McCormack², M. Alakhra¹, F. Brun³, M. Pinamonti³, C. Nickson², C. Hall², F. Zanconati³, D.J. Lockie², H. Quiney², G. Tromba³, T.E. Gureyev², P.C. Brennan¹;
¹Sydney/AU, ²Melbourne/AU, ³Trieste/IT, ⁴Göttingen/DE

Purpose: While all current X-ray based breast imaging modalities rely on differences in soft tissue X-ray attenuation (absorption contrast), phase-contrast imaging (PCI) has capacity to also visualise variations in X-ray refraction (phase contrast). To successfully translate the preclinical results of PCI technology into clinical implementation, the imaging variables of the technology must first be optimised through radiological assessments by breast radiologists and medical imaging experts. We conducted a series of assessments to establish the optimum imaging conditions of X-ray propagation-based imaging (PBI), which is experimentally the simplest PCI technique for clinical purposes.

Methods and Materials: We investigated 161 synchrotron-based CT reconstructions of one full-size section of a breast specimen produced by adjusting the following five imaging parameters: sample-to-detector distance, X-ray energy, CT reconstruction method, phase retrieval algorithm applied to the CT projection images and maximum intensity projection in image reconstruction. A visual grading analysis was conducted in two stages (13 assessors in stage I and 15 assessors in stage II) by comparing various radiological image quality attributes of PBI CT scans with reference images approximating conventional CT images.

Results: The results showed that the application of the longest sample-to-detector distance (9.31 m in our experiments), the lowest employed X-ray energy (32 keV), full application of the phase retrieval algorithm and the use of maximum intensity projection could substantially improve the image quality compared with conventional imaging.

Conclusion: The results from this study should provide a strong basis for future radiological assessments and clinical testing of this advanced X-ray imaging technology.

Author Disclosures:

S. Tavakoli Taba: Research/Grant Support; This research was supported by a grant from the National Breast Cancer Foundation (Australia), We acknowledge travel funding provided by the International Synchrotron Access Program (ISAP) managed by the Australian Synchrotron and funded by the Australian Government, This research was undertaken on the SYNchrotron Radiation for MEDical Physics (SYRMEP) beamline of Elettra Synchrotron.

B-1417 11:34

Exploring contrast agents in phase-contrast x-ray mammography: an ex vivo pilot study

K. Lang¹, C. Arboleda², S. Forte³, Z. Wang², R. Kubik-Huch³, M. Stampanoni⁴;
¹Zurich/CH, ²Villigen/CH, ³Baden/CH, ⁴Zürich/CH (kristina.lang@med.lu.se)

Purpose: Phase contrast x-ray mammography (PCM) is an experimental breast imaging method, at the edge of clinical implementation, that besides absorption can measure the refraction and scattering of x-rays resulting in differential-phase-contrast (DPC) and dark-field (DF) images. We assessed the feasibility of using microbubbles and iodine contrast agents in PCM.

Methods and Materials: An ex vivo phantom of a fresh chicken breast (5x5x3cm) with fragments of eggshells simulating calcification clusters was used. Native and post-contrast images were acquired with a clinically compatible grating-interferometry-based mammography setup, based on a modified Philips MicroDose mammography system, operated at 38 kVp, 14 sec acquisition time, with an estimated dose of 1.3 mGy. 2 mL of sulphur hexafluoride microbubbles (SonoVue 8 µL/mL, Bracco) used for contrast-enhanced ultrasound, and iodine (Iopamiro 370 mg/mL, Bayer) were, respectively, injected into the phantom. The visibility of the contrast agents in the absorption, DPC and DF images were analysed in a side-by-side comparison and the contrast-to-noise-ratio (CNR) between the contrast agent and surrounding tissue was calculated.

Results: The microbubbles were clearly visible in the DF image (CNR=2.5), but not in the absorption or DPC images. The iodine was visible in the absorption image (CNR=15.8) and as noise in both the DF and DPC images.

Conclusion: This is a first proof-of-principle that microbubbles can be used as a contrast agent in clinically compatible PCM, due to their scattering properties, which implies a potential use of a contrast agent with a high safety profile in x-ray-based breast imaging.

Author Disclosures:

K. Lang: Other; Research collaboration with Philips. **C. Arboleda:** Other; Research collaboration with Philips. **Z. Wang:** Board Member; GratXray. **M. Stampanoni:** Board Member; GratXray.

B-1418 11:42

Effectiveness of superb microvascular imaging (SMI) in differentiating intraductal breast lesions

S. Bakdik, S. Arslan, F. Öncü, M.S. Durmaz, A. Altunkeser, M.A. Eryilmaz, Y. Unlu; Konya/TR (oncufatih@gmail.com)

Purpose: The aim of this study is to compare the diagnostic performance of Superb Microvascular Imaging (SMI) and power Doppler imaging (PDI) for differentiation of intraductal breast lesions.

Methods and Materials: A total of 54 intraductal breast lesions (13 solidified debris, 26 benign, 10 atypical and 5 malignant) in 53 patients were examined with B-mode ultrasonography, PDI and SMI. Vascularity grading, distribution of microvessels and penetrating vessels were evaluated with each doppler technique. Diagnostic performances of both methods were compared.

Results: SMI is more efficient in detecting flow signals than PDI. The highest diagnostic accuracy rates were achieved with SMI by using vascular grading. When hypervascularity was used as a cut-off value to differentiate malign and atypical lesions from benign lesions, sensitivity, specificity, positive predictive value, negative predictive value, and accuracy were 66.6%, 80.7%, 66.6%, 80.7%, and 75.6% for PDI, 86.6%, 76.9%, 68.4%, 90.9% and 80.4% for SMI respectively.

Conclusion: SMI is more sensitive than PDI in detecting subtle blood flow of intraductal breast lesions. The novel and promising vascular imaging technique can be helpful to B-mode ultrasonography to distinguish intraductal breast lesions.

B-1419 11:50

Usefulness of automated breast volume scanner to evaluate the early response to neoadjuvant therapy in breast cancer patients: a prospective study

A. D'angelo¹, P. Rinaldi¹, R. Rella¹, M. Giuliani¹, P. Belli¹, G. Carlino¹, C. Grippo¹, M. Romani¹, R. Manfredi²; ¹Rome/IT, ²Verona/IT (anna.dangelo05@gmail.com)

Purpose: To investigate the accuracy of ABVS compared with conventional ultrasound (US) to evaluate the early assessment of response to neoadjuvant therapy (NADT, chemotherapy/hormone therapy).

Methods and Materials: IRB-approved prospective single-center study. 35 consecutive patients (range 25-65 years), eligible for NADT, were enrolled. They underwent ABVS, US, MRI and mammography at the beginning of NADT, at the mid-therapy and before the surgery. MRI has been considered the gold standard. Two breast radiologists independently assigned a BI-RADS score to ABVS, MRI, US and MG, and they evaluated tumour response using RECIST criteria. Cohen's kappa coefficient was used to assess the agreement between ABVS and US.

Results: The comparison of ABVS and US showed that ABVS had a sensitivity of 86.7% [26 positive cases at ABVS/30 positive cases at US; 95% confidence interval (CI) 70.3%-94.7%], and a specificity of 80.0% (4 negative cases at ABVS/5 negative cases at US; 95% CI 37.6%-96.4%). Positive and negative predictive values (PPV and NPV) were, respectively, 96.3% (26 positive cases at ABVS and US/27 total positive cases at ABVS; 95% CI 81.7%-99.3%) and 50% (4 negative cases at ABVS and US/8 total negative cases at ABVS; 95% CI 21.5%-78.5%). The agreement between ABVS and US was 53.3% (Cohen's kappa p value=0.001).

Conclusion: Diagnostic performance of ABVS is high, indicating a potential use of it, in addition to MRI, as a useful tool for early prediction of response to NADT.

10:30 - 12:00

Room D

Musculoskeletal

SS 1810

Hip and knee

Moderators:

M. Fernandez Hernando; Santander/ES
M. Shahabpour; Brussels/BE

B-1420 10:30

3D printed model based on knee MRI as a new tool in surgical planning of anterior cruciate ligament reconstruction

L.J. Pavan, R. Faletti, L. Nicolet, A. Cosentino, A. Di Chio, M. Gatti, S. Fiore, F. Bonino, P. Fonio; Turin/IT (lucajpavan@gmail.com)

Purpose: The aim of the study was to compare measurement of transepicondylar femoral axis (TFA) and planned length of the surgical graft, both calculated on 3D printing models and on multiplanar reconstruction (MPR) of knee MRI, in view of anterior cruciate ligament (ACL) surgical reconstruction.

Methods and Materials: Sixteen healthy volunteers with no ACL lesions (6 females, 10 males, mean age 27 years, range 22-34y) underwent standard knee MRI examination on a 1.5T scanner (Philips Achieva 2.6T) with a complimentary T1-weighted volumetric gradient echo sequence. Knee bones were isolated and elaborated with open source softwares (Osirix®, Meshmixer®, Cura®, Slic3r®) to obtain a STL file for a Ultimaker2+® 3D extrusion printer. TFA measurement and ACL graft length were blindly calculated by an orthopaedic on 3D-printed models and by a radiologist on MPR images and compared using Wilcoxon signed-rank test.

Results: Mean values of TFA were 82,2±7 mm on 3D model and 83,1±7 mm on MPR images, with no significant difference ($p=0.056$). Mean values of graft lengths were significantly lower ($p<0.001$) on 3D printed models (136.6±13 mm) than on MPR images (146.1±13 mm), with a mean difference of 9.5±4 mm. Mean printing time was 11±1.8 hours and mean material cost 4.33±0.5 €.

Conclusion: 3D printing is a reliable, non-expensive technique with good anatomical correlation that needs further studies for a better assessment. A 9.5 mm difference in the planned length of ACL graft may still be acceptable from an orthopaedic point of view, on an average 140-160-mm graft.

B-1421 10:38

Anterior inferior iliac spine morphology: quantitative and qualitative assessment in an asymptomatic population

F.F. Ergen¹, O. Topcuoglu^{1,2}, S. Ardalı¹, T. Cankurtaran¹, A. Dolgun Barak¹, U. Aydingoz¹; ¹Ankara/TR, ²Istanbul/TR (omtopcuoglu@gmail.com)

Purpose: To assess the prevalence of anterior inferior iliac spine (AIIS) types, and to investigate the quantitative measurements that characterise AIIS morphology in an asymptomatic adult population.

Methods and Materials: In this prospective study, 358 hips from 179 consecutive subjects (age range, 19-82 years; 91 males, 88 females), who underwent CT examination for reasons other than hip problems and were negative for hip impingement test, were analysed. AIIS types were determined (1, flat wall of the ilium between distal end of AIIS and acetabular rim; 2, bony eminence between distal end of AIIS and acetabular rim; and 3, extension of AIIS to the anterior superior acetabular rim) and AIIS tip angle (TA), direct distance (DD) of the anterior acetabular rim to AIIS as well as projectional distances in vertical (VD) and horizontal (HD) planes were measured. Age- and gender-related factors were searched using two-way ANOVA test under three age groups (18-39, 40-59, and ≥60 years).

Results: There were 238 (66.5%) type 1, 118 (33.0%) type 2, and 2 (0.5%) type 3 AIISs, with significant difference between AIIS types among age groups and genders ($P<0.001$). VD and DD showed age- and gender-related ($P<0.001$, $P=0.001$), and TA demonstrated gender-related differences ($P=0.001$). Inter-observer variability was good for TA and moderate to poor for other measurements.

Conclusion: Type 1 AIIS is the most common shape across all age groups in adult females and in young and middle-aged adult males. TA, DD, and VD might be reliably used for the evaluation of AIIS morphology.

B-1422 10:46

Association between cam type femoroacetabular impingement and osteitis pubis on MR images

A.S. Akgun, M. Agirman; Istanbul/TR (drayserap80@gmail.com)

Purpose: Retrospectively to search whether there is an increase prevalence of osteitis pubis by MR imaging in patients with cam femoroacetabular impingement (FAI).

Methods and Materials: The study included 178 subjects; 90 patients with cam-type FAI diagnosed by magnetic resonance imaging and 88 subjects used as a control group. Additionally their MR data were analyzed for the characteristics of osteitis pubis, with severity graded from minimal to severe (4-point scale).

Results: A statistically significant increase in the prevalence of osteitis pubis was found in patients with femoroacetabular impingement compared with age-matched control subjects, with a prevalence of 45.6 % in the femoroacetabular impingement group compared with 5.7 % in the control group ($p=0.000$).

Conclusion: Femoroacetabular impingement results in restriction of internal rotation of the hip joint. This abnormal biomechanical stress lead to increased stresses at the pubis symphysis.

Keywords: Femoroacetabular impingement, Alpha angle, Osteitis pubis.

B-1423 10:54

Gouty knee arthritis: ultrasound findings compared to dual-energy CT

M.M.H. Abd Allah^{1,2}, S. Strobl¹, S. Rauch¹, E.J. Halpern³, C. Kremser¹, W. Jaschke¹, A. Klausner¹, ¹Innsbruck/AT, ²Assiut/EG, ³Philadelphia, PA/US (dr_m_hamdy2006@hotmail.com)

Purpose: To describe and compare findings of ultrasound (US) and dual-energy computed tomography (DECT) in patients with gouty knee arthritis.

Methods and Materials: Sixty-five patients (52 males and 13 females, mean age 61.7 years) with gouty knee arthritis underwent DECT examination using 128-multidetector CT scanner (Somatom Definition Flash, Siemens Healthcare, Forchheim, Germany) followed by US examination using a 5-18 MHz linear array transducer (Hitachi Aloka Medical, HI Vision Preirus, LTD, Tokyo). Both intra- and extra-articular findings of each modality were tabulated and the accuracy of imaging was compared to clinical diagnosis.

Results: The overall diagnosis of gout was positive in 52/65 patients (80%) by DECT versus 33/65 patients (50.8%) by US ($P=0.0016$). Among positive exams, DECT demonstrated intra-articular gouty deposits in 43/52 patients (cartilage 51.9%, lateral meniscus 65.4% and medial meniscus 42.3%), while US demonstrated intra-articular deposits in 31/33 patients (double contour 69.7%, tophi 51.5%, aggregates 27.3%), $P=0.059$. DECT demonstrated extra-articular deposits in 44/52 patients (quadriceps tendon 48.1%, patellar tendon 42.3%, lateral collateral ligament 15.4% and medial collateral ligament 23.1%), while US demonstrated extra-articular deposits in 11/33 patients ($P<0.0001$).

Conclusion: Although DECT and US both can detect gouty deposits in the knee, DECT is more sensitive than US for detection of gouty deposits. However, US still has a role as a cost-effective and widely available imaging modality in gout diagnosis especially upon detection of certain findings as double contour.

B-1424 11:02

Influence of meniscus tears on cartilage T2 relaxation time in subjects with and without knee osteoarthritis

R. Kijowski, K. Woo, F. Liu; Madison, WI/US (rkijowski@uwhealth.org)

Purpose: To investigate the influence of meniscus tears on cartilage T2 relaxation time in subjects with and without knee osteoarthritis.

Methods and Materials: Cartilage T2 was measured in the medial and lateral compartments of the knee in 93 subjects with 87 medial and 27 lateral meniscus tears and in a control group of 30 subjects without meniscus tears. Radiographs were reviewed to determine the Kellgren-Lawrence (KL) grade of knee osteoarthritis. Linear regression models adjusted for age and gender were used to compare cartilage T2 between groups of subjects and between meniscus tear types (vertical, horizontal, complex, and root).

Results: KL-0 (n=46), KL-1 (n=27), and KL-2 (n=20) subjects with meniscus tears had significantly higher ($p<0.001$) cartilage T2 within the medial compartment than KL-0 control subjects without meniscus tears (n=30). KL-1 and KL-2 subjects with meniscus tears had significantly higher ($p<0.01$) cartilage T2 within the lateral compartment than KL-0 control subjects. KL-0 subjects with medial meniscus tears (n=44) had significantly higher ($p<0.001$) cartilage T2 in the medial compartment than KL-0 control subjects. There was no significant difference ($p=0.09-0.84$) in cartilage T2 within the medial and lateral compartments between KL-0, KL-1, and KL-2 subjects with meniscus tears. Cartilage T2 in the same compartment as the meniscus tear was not significantly different ($p=0.06-0.81$) between tear types.

Conclusion: Subjects with meniscus tears had significantly higher cartilage T2 within the knee than subjects without meniscus tears controlling for age, gender, and KL grade which indicates that meniscus tears are an independent risk factor for cartilage degeneration.

B-1425 11:10

Subchondral bone/cartilage: a functional unit? Bone density and cartilage thickness are correlated

P. Omoumi, H. Babel, B. Jolles, J. Favre; *Lausanne/CH*
(patrick.omoumi@chuv.ch)

Purpose: To test whether subchondral bone mineral density (sBMD) and cartilage thickness (CTh) of femoral condyles are correlated in knees without and with severe medial femorotibial osteoarthritis (OA), using a subregional analysis with CT arthrography.

Methods and Materials: Knee CT arthrograms of 80 patients, divided into groups of non-OA (n=40, 13 males, 61.4±6.2 years) and severe medial OA (n=40, 19 males, 64.2±10.8 years) knees, were retrospectively analyzed. Cartilage and subchondral bone contours were segmented on a custom-designed software, leading to 3D models on which each point of the articular surface is given a CTh and sBMD (average signal intensity over the most superficial 3mm of subchondral bone) value. 3D property maps were produced by calculating average values for the entire weight-bearing regions as well as standard subregions of interest. Multiple regression analyses were performed to test for relationships between sBMD and CTh (regional and subregional values, as well as medial-to-lateral ratios), with covariates of age, gender and femoral bone size in any of the groups and regions/subregions (alpha<5%).

Results: For non-OA knees, sBMD medial-to-lateral ratios were significantly positively correlated with CTh medial-to-lateral ratios for the total regions ($R^2=0.23, p<0.01$), the external ($R^2=0.35, p<0.01$), and internal ($R^2=0.12, p<0.03$) subregions. For OA knees, sBMD medial-to-lateral ratios were significantly negatively correlated with CTh ratios for all regions/subregions (all $R^2 \geq 0.33, p<0.01$), except for the internal subregion ($R^2=0.08, p=0.08$).

Conclusion: The positive correlation between sBMD and CTh in non-OA knees, and the negative one in OA knees brings support to the theory of a subchondral bone/cartilage functional unit, which could help to better understand the pathophysiology of OA.

B-1426 11:18

Increased perfusion in subchondral bone marrow lesions in knee osteoarthritis measured with quantitative DCE-MRI

B. De Vries, J. Verschuere, D. Poot, E. Oei, G.P. Krestin; *Rotterdam/NL*
(b.devries@erasmusmc.nl)

Purpose: Knee osteoarthritis (OA) on MRI is characterized by articular cartilage degeneration, synovial inflammation, and subchondral bone marrow lesions (BMLs). Altered blood perfusion in subchondral bone is also considered an important OA process which may be associated with altered fluid dynamics, inflammation, bone remodeling, and cartilage degeneration. Since it is unknown whether BMLs directly represent altered blood perfusion, our aim was to quantitatively analyze perfusion in subchondral BMLs with dynamic contrast-enhanced MRI (DCE-MRI).

Methods and Materials: 16 patients with unicompartmental knee OA were prospectively included. Multisequence MRI including DCE-MRI was performed at 3T (GE Discovery MR750) using an 8-channel knee coil. DCE-MRI was acquired using a sagittal fat-suppressed 3D SPGR sequence (35 phases of 10 seconds) after intravenous contrast administration (0.2 mmol/kg gadopentetate dimeglumine, 2 ml/s). On fat-saturated T2-weighted images, regions-of-interest (ROIs) were defined in tibial or femoral subchondral bone containing BMLs and in surrounding subchondral bone without BMLs. Ktrans, a measure of capillary permeability, was calculated in each ROI. Mean Ktrans was mapped and compared between subchondral bone with and without BMLs using the Wilcoxon signed rank test.

Results: Subchondral BMLs were present in all patients. Perfusion maps and analysis of Ktrans consistently showed significantly ($p<0.001$) higher Ktrans values within subchondral BML ROIs compared to surrounding subchondral bone without BMLs.

Conclusion: Subchondral BMLs are associated with increased blood perfusion compared to subchondral bone regions without BMLs. This finding may aid in the understanding of OA pathogenesis and further research is needed to elucidate temporal relationships and correlation with symptoms.

B-1427 11:26

Who runs further? Intra-articular Platelet Rich Plasma (PRP) vs Viscosupplementation (HA) and PRP in the treatment of knee osteoarthritis: six-months follow-up study using T2 mapping

E. Cannizzaro, F. Bruno, S. Quarchioni, I. Capretti, S. Mariani, F. Arrigoni, L. Zugaro, A. Barile, C. Masciocchi; *L'Aquila/IT* (estercannizzaro@hotmail.it)

Purpose: To evaluate clinical outcomes and the degree of knee cartilage repair using T2 mapping sequences in patients with knee condropathy treated with intrarticular injection of Platelet Rich Plasma (PRP) or combined Viscosupplementation (HA) and PRP.

Methods and Materials: We analyzed 58 patients (33 males and 25 females; mean age 32,6±11,5 years) who underwent to intrarticular injection procedures in our center, with diagnosis of knee condropathy. All patients underwent to MRI (3T) and were evaluated before and after treatment (6 months) using images findings (WORMS score and T2 mapping values) and clinical outcomes (WOMAC index). All patients were randomly divided into two groups: Group A (29 patients) treated with PRP and Group B (29 patients) treated with PRP and HA.

Results: Group A showed an improvement of WOMAC index of 40%; the WORMS score showed improvement with decrease of the mean values (from 8,6 pre-treatment to 6,9 post-treatment). T2 mapping evaluation showed mean values of 46,7ms post-treatment (51,86 ms pre-treatment). Group B showed a clinical improvement of WOMAC index of 65%, with a decrease of WORMS score from 8,4 to 6,7. Mean T2 mapping values were 51,39 pre-treatment vs 45,19 post-treatment. All results showed statistical significance ($p<0.005$).

Conclusion: Both treatments showed similar results in terms of morphological improvement as showed by T2 mapping evaluation. Combined therapy PRP and HA showed higher efficacy in terms of clinical improvement compared to PRP therapy.

B-1428 11:34

The patella-shape: is it relevant to the analysis of patella malalignment?

A. Kolb, C. Chiari, R. Windhager; *Vienna/AT*
(alexander.kolb@meduniwien.ac.at)

Purpose: The tibial-tubercle-trochlear-groove-distance (TT-TG) is an established risk factor for patellar instability. However, it was criticised that TT-TG-measurements might be increased due to trochlear dysplasia despite a normal tibial tubercle position. To avoid this problem, the tibial-tubercle-posterior-cruciate-ligament-distance (TT-PCL) was suggested. Our study aimed to analyse, whether the patella shape represented as patellar-ridge-offset (PRO), is suitable to correct the TT-TG-distance in cases of trochlear dysplasia.

Methods and Materials: A retrospective analysis of 20 routine MRIs of patients with mixed patellar shapes and history of patellar instability was performed (mean age 24yrs). The PRO was defined as distance between the patellar-ridge and the patella-midpoint parallel to the inclined patella, measured on axial MRI slices. In contrast to the TT-TG-distance the combined PRO-TT-TG-distance gives information on the position of the knee extensor complex relative to the tibial tubercle.

Results: Mean RPO was 4.0mm (STD=2.00; range -1.5 to 7.6mm). TT-TG showed a very strong correlation to TT-PCL and PRO-TT-TG ($p<0.001$; $r=0.847$ and $r=0.915$); TT-PCL and PRO-TT-TG showed a strong correlation ($p<0.001$; $r=0.777$). PRO showed no significant correlation to the difference between TT-TG and TT-PCL ($p=0.801$; $r=-0.062$). In cases with PRO above 6mm, trochlear angle tends to be decreased (not significant, $p=0.174$).

Conclusion: The PRO is a promising parameter to adjust the TT-TG-distance to different trochlear and patellar shapes. Interestingly the effect of PRO is not correlated to the difference between TT-TG and TT-PCL, suggesting that TT-PCL is not only independent from trochlear dysplasia, but moreover influenced by other factors.

B-1429 11:42

The association of patellar maltracking with infrapatellar fat pad oedema and chondromalacia patella: a quantitative morphologic MRI analysis

M. Gursoy¹, B. Dirim Mete¹, Y.K. Cetinoglu¹, O. Oyar¹, N. Erdogan¹, M. Uluc¹, T. Bulut¹, G. Safa²; ¹Izmir/TR, ²Ankara/TR (kenancetinoglu@hotmail.com)

Purpose: Oedema in the superolateral portion of infrapatellar fat pad and chondromalacia patella (CP) could be related to impingement of fat between the patellar tendon or lateral patellar facet and the lateral femoral condyle. Due to the lack of extensive literature on the association of patellar maltracking with infrapatellar fat pad oedema, the evidence supporting this view remains suspicious. The aim of this study is to investigate the relationship of patellofemoral joint morphology with infrapatellar fat pad oedema and CP using patellar maltracking parameters on MRI.

Methods and Materials: Fifty patients with oedema in the superolateral portion of the infrapatellar fat pad (the study group) and control group (50 patients) with a normal infrapatellar fat pad were identified on MRI to compare with regard to five patellar maltracking parameters retrospectively. These

parameters were trochlear depth, the trochlear sulcus angle (TSA), patellar translation, the lateral patellofemoral angle (PFA) and the Insall-Salvati ratio. The relationship between patellar maltracking and the CP was also evaluated using the same parameters.

Results: In the study group the Insall-Salvati index and TSA were significantly high ($p=0.001$), the trochlear depth and PFA were low ($p=0.001$, $p=0.01$), while patellar translation showed no difference ($p=0.957$). In the CP group the Insall-Salvati index and TSA were significantly high ($p=0.001$), the trochlear depth was low ($p=0.001$). No statistically significant difference was found in PFA and patellar translation ($p=0.292$, $p=0.446$).

Conclusion: Oedema in the superolateral portion of infrapatellar fat pad and CP are associated with patellar maltracking.

B-1430 11:50

3D-printed models of the knee for evaluation of trochlear dysplasia in comparison to standard radiographs and computed tomography

B. Fritz¹, S. Fucntese¹, S. Zimmermann¹, P.M. Tscholl², R. Sutter¹, C.W. Pfirrmann¹; ¹Zurich/CH, ²Geneva/CH (benjamin.fritz@gmx.net)

Purpose: To test the hypothesis that 3D-printed specimens improve diagnosis of trochlear dysplasia and Dejour's classification in comparison to radiographs and computed tomography (Rx/CT).

Methods and Materials: This retrospective study was approved by the local ethics committee. 50 patients were included. 3D-models of the distal femur were printed after segmentation of CT-datasets. An expert panel consisting of a senior musculoskeletal radiologist and a senior knee surgeon classified the knees into normal or Dejour grade A-D, which served as the standard of reference. Therefore, the experts reviewed radiographs, CT, the 3D-specimens and patients' clinical history. The 3D-specimens and Rx/CT were evaluated by two readers independently and separately at the interval of 3 weeks for trochlear dysplasia and Dejour A-D. Statistics included general descriptive statistics, ROC-analysis and inter-reader reliability.

Results: The expert panel diagnosed a trochlear dysplasia in 28/50 patients. In comparison to the panel's diagnoses, the diagnostic accuracy for the presence/absence of trochlear dysplasia after evaluation of 3D-specimens and Rx/CT was for reader1 0.937 and 0.823 ($p=0.029$) and for reader2 0.982 and 0.946 ($p=0.147$). Inter-reader reliability was excellent for 3D-specimens and substantial for Rx/CT (Kappa: 0.920 and 0.788). For Dejour-classification, the proportion of exact matches for 3D- and Rx/CT-analysis were for reader1 36% and 59% and for reader2 48% and 52%. Inter-reader reliability was poor for 3D-specimens and fair for Rx/CT (Kappa: 0.148 and 0.368).

Conclusion: 3D-models can improve detection of trochlear dysplasia in comparison to radiographs and CT, whereas no additional value for grading into Dejour A-D could be demonstrated.

10:30 - 12:00

Room G

Physics in Medical Imaging

SS 1813

Developments in volumetric imaging

Moderators:

K.N. Bolstad; Bergen/NO
N.N.

B-1431 10:30

Task-based radiation dose assessment for paediatric dental CBCT imaging

A. Stratis, G. Zhang, R. Jacobs, R. Bogaerts, H. Bosmans; Leuven/BE (andreas.stratis@uzleuven.be)

Purpose: to calculate organ doses, effective dose-ED and LAR-incidence (cases/100,000 persons) for paediatric patients undergoing the most frequently applied dental-cone-beam-CT (CBCT) protocols in 5 scanners via Monte Carlo (MC) simulations.

Methods and Materials: An EGSnrc-MC framework and an in-house-built voxel-model-database (8 male and 10 female paediatric heads, 3 to 14 y.o) were employed. The MC-framework was customized and validated for Promax-3D-Max (Planmeca, FI), NewTom VGi-evo and NewTom 5G (QR srl, IT), CS9300 (Carestream, USA) and Accutomo 170 (Morita, JP) scanners. Organ doses were assessed for single-tooth, upper/lower-jaw, cleft, maxillofacial complex, sinus, face and skull imaging by simulating the respective scanner-specific and age-dependent FOVs-protocols.

Results: Females were slightly more radiosensitive in all cases (3% to 5% depending on the protocol), with organ-dose and radiation-risk increasing with decreasing age-at-exposure. The lowest risk protocol was for central-incisor-tooth imaging (14 y.o male, ED=13µSv, LAR=0.29) whereas the highest one was for skull imaging (5 y.o female, ED=323µSv, LAR=13.8). Salivary glands and oral mucosa were the highest irradiated organs in all cases, followed by

the Extra-thoracic-tissue (ET) in protocols where the entire nasal cavity was inside the primary field. The dose to thyroid was considerably high for young patients (max=1.1 mGy-5y.o-female-skull-protocol). The lowest doses were observed in scanners with tube-current-modulation and added-Cu-filtration.

Conclusion: Thyroid-lead-aprons are recommended for young patients. Small FOV-scans reach the dose levels of conventional panoramic acquisitions. The unavailability of manual collimation results in dose increase, especially for young patients, as the preset FOVs can extend the radiation field beyond the clinical volume of interest.

B-1432 10:38

Sliding organ motion regularisation for motion-compensated cone-beam CT (CBCT) in image-guided radiation therapy (IGRT)

S. Sauppe¹, J. Kuhm¹, M. Brehm², P. Paysan², D. Seghers², M. Kachelrieß¹; ¹Heidelberg/DE, ²Baden-Dättwil/CH (marc.kachelriess@dkfz.de)

Purpose: To improve the accuracy of motion estimation and motion compensation in CBCT of the thorax.

Methods and Materials: Respiratory-gated images minimize the motion artefacts, but yield severe sparseness artefacts. We propose a 4D motion-compensation (MoCo) algorithm with an enhanced underlying motion model that handles sliding organ motion. Our MoCo removes both motion artefacts and sparse view artefacts and ensures 100% data usage [MedPhys 40(10):101913,2013]. Image quality depends on the underlying motion model. Due to strong streak artefacts, regularization of the motion vector fields (MVFs) during motion estimation for continuity is necessary. Our guided regularization filter inputs a bone and lung segmentation. The algorithm handles sliding organ motion such as it occurs between the diaphragm and the lung wall. The filter passes motion perpendicular to the sliding organ boundary. We thus prevent non-physiological motion of the rib cage. For validation, we use an artificially deformed clinical CT scan and patient data acquired with a TrueBeam™ 4D CBCT system (Varian Medical Systems).

Results: Our guided regularization filter yields realistic high-fidelity thorax MVFs. Hereby, we can reconstruct 4D respiratory motion-compensated images, almost free of motion artefacts. Moreover, our proposed sliding organ motion model prevents unphysiological bone motion in motion-compensated images. We significantly improve spatial resolution and noise level by our 4D MoCo approach, preserving high temporal resolution for respiratory motion.

Conclusion: Our patient data demonstrate that good image quality is achievable at identical x-ray dose levels and at acquisition times as for today's 3D CBCT. Lung tumour treatments may benefit from our motion-compensated images.

B-1433 10:46

Material-guided scatter correction in cone-beam-computed tomography using spectroscopic information

C. Egan, P. Scott, N. Loxley; Sedgfield/UK (c.egan@ibexinnovations.co.uk)

Purpose: Scatter is a major problem in cone-beam-computed tomography (CBCT), causing reconstruction artefacts and reduced contrast. A material-guided scatter correction algorithm is introduced using spectral information generated from pixel-wise attenuation modulation of the x-ray beam.

Methods and Materials: A metal plate which is designed to cause a pixel-wise attenuation modulation of the x-ray beam is placed directly in front of a flat panel detector in a CBCT system. This modulation yields spectroscopic information, which is decomposed to give thickness and composition information about the sample. These data used to predict scatter using a Monte Carlo model, which is subtracted from the x-ray image. The material information is updated based upon this new scatter-corrected image. An iterative procedure then operates to converge to a solution where the scatter estimate and materials estimate no longer changes, leaving the final scatter-corrected image. This procedure is applied to every projection in a CBCT dataset which can be reconstructed using conventional algorithms.

Results: Applying the material-guided scatter correction algorithm to a water phantom removes the cupping artefact leaving a flat cross-sectional profile and at the same time improves mean contrast by 18%. Other phantom and cadaver samples have been processed, again showing reduced artefacts and enhanced contrast.

Conclusion: The material-guided scatter correction algorithm can accurately predict and correct scatter yielding superior quality images without the use of anti-scatter grids and no impact on dose.

Author Disclosures:

C. Egan: Employee; IBEX Innovations Ltd. P. Scott: Employee; IBEX Innovations Ltd. N. Loxley: CEO; IBEX Innovations Ltd.

B-1434 10:54

Moving metal artifact reduction (MMAR) for cone-beam CT (CBCT) scans of the thorax region

A. Hahn, S. Sauppe, M. Knaup, M. Kachelrieß; Heidelberg/DE
(andreas.hahn@dkfz.de)

Purpose: Established metal artifact reduction (MAR) methods are insufficient in cone-beam CT (CBCT) scans with moving metal implants such as fiducial gold markers. A method for moving metal artifact reduction (MMAR) is introduced.

Methods and Materials: Standard inpainting-based MAR methods do not account for respiratory patient motion and fail in cases with strong metal motion. MMAR resolves this issue by applying a motion compensation (MoCo) algorithm [MedPhys 40(10):101913, 2013]. This results in a 4D volume without motion blurring but with metal artifacts. They are corrected using a normalized MAR (NMAR) [Med Phys. 2010 Oct;37(10):5482-93]. A simulation was created by adding 5 analytical cylindrical gold markers of different sizes to a thorax scan that was acquired using a TrueBeam™ 4D CBCT system (Varian Medical Systems). Realistic deformation vector fields of different magnitudes were applied to simulate cases of different motion. The proposed algorithm was compared to standard linear interpolation MAR and was applied to CBCT data of a patient with metal markers.

Results: Using the MMAR algorithm, a 4D volume with a high temporal resolution is reconstructed. Remaining metal artifacts are almost completely removed in the 4D volume for all motion magnitudes. Simple MAR was able to reduce artifacts in cases of small motion but failed for large motion.

Conclusion: MMAR is able to properly account for motion of moving metal markers and is able to remove metal artifacts where classical linear interpolation MAR fails. The advantage of MMAR compared to MAR increases for larger motion.

B-1435 11:02

Focal spot blur correction for cone-beam CT (CBCT)

N.K. Waltrich, S. Sawall, M. Kachelrieß; Heidelberg/DE
(nadine.waltrich@dkfz.de)

Purpose: To correct for the spatial resolution mismatch caused by anode angulation in CBCT.

Methods and Materials: The combination of anode angulation and large fan and cone angles causes a position-dependent focal spot blur in CBCT data. This results in a variation of spatial resolution along the u- and v-direction of the flat detector and a resolution mismatch within the reconstructed volume. To assess the spatial resolution, a metal edge was measured at different u-v-positions close to the focal spot. The full width at half maximum of the line spread function is measured for each u-v-position and inter- and extrapolated to be available for each detector position. A projection-domain deconvolution iteratively achieves a user-prescribed (e.g. uniform) spatial resolution across the whole detector. Noise is reduced using a bilateral filter in the image domain with a position-dependent domain filter shape. The proposed method is validated using data from a line pattern phantom, an anthropomorphic head phantom, and patient measurements acquired with a CBCT system in short scan mode. This scan mode results in images with higher spatial resolution on the right side compared to the left side.

Results: On the right side, five iterations of the deconvolution algorithm increase the line pattern contrast from 198 HU to 442 HU. On the left side, 460 HU is measured before and after blur correction. This indicates a nearly complete spatial resolution restoration. The findings were confirmed in patient measurements.

Conclusion: The proposed method results in a homogeneous resolution throughout the complete volume.

B-1436 11:10

Spectroscopic cone-beam-computed tomography using pixel-wise attenuation modulation

C. Egan, P. Scott, N. Loxley; Sedgfield/UK (c.egan@ibexinnovations.co.uk)

Purpose: Quantitative information can be extracted from dual-energy-computed tomography (DECT) such as precise electron densities and effective atomic numbers, which can be used for accurate dose planning in radiotherapy, for example. DECT is normally implemented either using dual-source scanners or via rapid kV switching. Here we introduce a technique for obtaining spectroscopic information from a CBCT system using pixel-wise attenuation modulation of the x-ray beam, without the need for kV switching or dual sources.

Methods and Materials: A metal plate which is designed to cause a pixel-wise attenuation modulation of the x-ray beam is placed directly in front of a flat panel detector in a CBCT system. The differential attenuation of the x-ray beam over a group of pixels yields spectroscopic information, which can be decomposed to give quantitative composition information about the sample. This data is then run through a standard iterative reconstruction algorithm. The

reconstructed materials information is examined in 2D scatter plots, similar to standard DECT systems.

Results: A quantitative phantom containing tissue equivalent material inserts was scanned to yield 2D scatter plots in a materials space. Data in this space are classified using a Mahalanobis distance measure. The accuracy of this approach is quantified, and, compared to the literature values from standard DECT systems, yields analogous results.

Conclusion: Spectroscopic information can be extracted from a CBCT system without the need for kV switching or multiple sources, yielding comparable results to standard DECT systems.

Author Disclosures:

C. Egan: Employee; IBEX Innovations Ltd. P. Scott: Employee; IBEX Innovations Ltd. N. Loxley: CEO; IBEX Innovations Ltd.

B-1437 11:18

Stack transition motion compensation in sequential and in cardiac CT

S. Lebedev^{1,2}, K. Stierstorfer², M. Kachelrieß¹; Heidelberg/DE, ²Forchheim/DE (marc.kachelriess@dkfz.de)

Purpose: Sequential CT scans and cardiac CT scans result in image stacks whose overlapping regions may be inconsistent due to patient motion. We thus propose a motion compensation method for stack transition artefact removal (STAR).

Methods and Materials: To estimate stack-to-stack patient motion, STAR uses a novel symmetric deformable image registration algorithm to register stack overlap regions of adjacent stacks. The registration algorithm scans the surroundings of control points situated within stack overlaps for matching sub-volume pairs and finds the pair that maximizes a similarity metric. The optimal displacement for a control point yields the deformation vector at the respective position. To get a densely sampled motion vector field (MVF), a trilinear interpolation between the control points is performed within the transition areas. The MVFs are then extrapolated across the whole stack to minimise distortions. Cardiac CT patient data from a Somatom Definition Flash and a Somatom Definition Edge CT system (Siemens Healthineers, Forchheim, Germany) were used to validate the STAR algorithm.

Results: STAR is able to reduce the stacks transition artefacts and displace/deform structures in a size range of multiple millimetres and make small adjustments in the millimetre range. In all cases, the images become sharper and the information in the stack transition regions becomes consistent between adjacent stacks. The coronary arteries are much better defined even in cases with strong stack-to-stack patient motion.

Conclusion: Artefacts at stack transitions due to irregular motion can be addressed using symmetric registration. STAR was able to considerably improve image quality.

Author Disclosures:

S. Lebedev: Employee; Siemens Healthcare GmbH. K. Stierstorfer: Employee; Siemens Healthcare GmbH.

B-1438 11:26

First evaluation of new photon counting CT technology

J. Da Silva, M. Yveborg, F. Grönberg, M. Sjölin, S. Holmin, J. Lundberg, M. Danielsson; Stockholm/SE (jds@kth.se)

Purpose: We are developing a new photon-counting edge-on silicon detector with 0.2x0.3 mm² detector elements at the isocenter and 8 energy bins for clinical CT applications. The purpose of this work is to present the first images using our detector technology, and show significantly improved spectral and spatial resolution compared to current state-of-the-art. In addition, we demonstrate the feasibility of projection based three-material basis decomposition based on the novel technology.

Methods and Materials: For this work, several objects were imaged using a spectrally resolved silicon detector. The reconstructed CT images were compared to images using current state-of-the-art CT scanners at the Karolinska University hospital. Specifically, we compared spatial resolution, artefact visibility and identification of iodine. In addition, we performed projection based three-material basis decomposition using recent developments in forward model calibration.

Results: The results demonstrate improved spatial and spectral resolution, compared to current state-of-the-art. Specifically, we demonstrate improved visibility of small details, decreased visibility of artefacts and improved identification of iodine. In addition, reconstructed un-biased iodine basis images are presented.

Conclusion: Several objects have successfully been imaged using a novel spectrally resolved photon counting silicon detector with sub-millimetre resolution. Compared to current state-of-the-art, reconstructed CT images demonstrate a potential improvement for clinical CT applications by improved spectral and spatial resolution.

Author Disclosures:

J. Da Silva: Other; Financial interests Prismatic Sensors AB. M. Yveborg: Shareholder; Prismatic Sensors AB. F. Grönberg: Shareholder; Prismatic Sensors AB. M. Sjölin: Shareholder; Prismatic Sensors AB. S. Holmin: Other;

Medical advisor for Prismatic Sensors AB. **J. Lundberg**: Other; Financial Interest, Smartwise AB. **M. Danielsson**: Other; Stockholder, Prismatic Sensors AB President, Prismatic Sensors AB Stockholder, Innovicum AB President, Innovicum AB Stockholder, Biovica International AB Board Member, Biovica International AB Research.

B-1439 11:34

Phase-contrast monochromatic breast-CT: a feasibility study

R. Longo¹, M.A. Cova¹, P. Delogu², B. Golosio³, G. Mettievier⁴, A. Taibi⁵, M. Tonutti¹, G. Tromba¹, F. Zanconati¹; ¹Trieste/IT, ²Siena/IT, ³Cagliari/IT, ⁴Naples/IT, ⁵Ferrara/IT (renata.longo@ts.infn.it)

Purpose: To develop methods and the facility to perform the first study in phase-contrast (PhC) breast computed tomography (breast-CT) exploiting the monochromatic beam available at the Elettra synchrotron radiation (SR) laboratory.

Methods and Materials: Images of test objects and large breast specimens were acquired at the SR facility used for the first clinical study of PhC mammography and up-dated for breast-CT. The CdTe detector was a state-of-the-art dead-time-free single-photon-counting with a 60 µm pixel size. The monochromatic x-ray beam was set in the energy range 32-38 keV and the delivered mean glandular dose (MGD) was in the range 5-20 mGy. Since the SR provides high energy resolution and spatial coherence, the free-propagation PhC imaging technique was used and the phase-retrieval algorithm was applied on the projections before the image reconstruction. Contrast-to-noise ratio (CNR) and resolution performances were evaluated for both absorption and phase-retrieved images by considering fat and glandular tissue.

Results: The phase-retrieval approach resulted in a remarkable CNR increase with respect to the absorption image (from 0.5 to 3.5), while the resolution loss is significantly lower than the one obtained by applying common de-noising filters. Furthermore, the full volume reconstructions of a breast lumpectomy (about 9 cm diameter and 3 cm thickness) are presented (MGD about 5 mGy).

Conclusion: This investigation indicates that PhC monochromatic breast-CT, evaluated so far in terms of CNR, spatial resolution and scan volume, is feasible.

B-1440 11:42

Digital breast tomosynthesis: flat panel and photon counting detectors comparison

A. Loria¹, P. Signorotto¹, M. Campoleoni¹, N. Paruccini², R. Villa², E. Venturini¹, P. Panizza¹, A. del Vecchio¹; ¹Milan/IT, ²Monza/IT (loria.alessandro@hsr.it)

Purpose: In this study three digital breast tomosynthesis (DBT) devices equipped with different flat panel detectors (FPD) and a prototype equipped with a scan-spectral photon counting detector (PCD) are compared. The aim is to evaluate if a PCD device can guarantee comparable or even better image quality (IQ) delivering lower radiation doses than FPD devices.

Methods and Materials: Image quality performances were evaluated exposing two IQ DBT phantoms, Tomophan and Agatha, the CDMAM phantom and a homemade phantom for low-contrast detectability (LCD). Exposures were performed in automatic exposure control mode. Images with the lowest achievable post-processing were analysed. Geometric distortion, signal-difference-to-noise ratio (SDNR), LCD, in-plane resolution as modulation transfer function (MTF) in scan and sub-scan directions, slice-sensitivity profile (SSP), noise power spectrum (NPS) and artefact spread function (ASF) were evaluated.

Results: Geometric distortion, SDNR and NPS resulted comparable. PCD device showed the best LCD. In-plane resolution was higher for PCD device: FPD devices exhibit a reduction in MTF_{0.1} between 38% and 62%, both in scan and sub-scan direction. SSP showed comparable results for PCD and one of the FPD devices, while it was up to 60% worse for the others. PCD device had the worst ASF. Delivered dose with PCD device was 50% lower than doses delivered with FPD devices.

Conclusion: PCD device ensures a comparable or even better IQ than FPD devices, especially for spatial resolution and detectability of low-contrast objects, delivering much lower radiation dose. Photon counting seems to be really an impressive approach to DBT.

B-1441 11:50

Digital breast tomosynthesis index (DBTI): a score to evaluate digital breast tomosynthesis (DBT) device performance

A. Loria¹, P. Signorotto¹, E. Venturini¹, P. Panizza¹, A. del Vecchio¹; Milan/IT (loria.alessandro@hsr.it)

Purpose: The aim of this study is to combine image quality (IQ) and dosimetric parameters into a score to evaluate the goodness of a digital breast tomosynthesis (DBT) device.

Methods and Materials: Digital Breast Tomosynthesis Index (DBTI) is derived from two figure of merit (FoM) introduced to evaluate CT devices (Rose and ImPACT). These FoMs include parameters as contrast-to-noise ratio (CNR),

spatial resolution in terms of modulation transfer function (MTF), slice thickness and a dosimetric quantity (CTDI). In the same way, DBTI is designed to be dependent on signal-difference-to-noise ratio (SDNR), MTF, slice-sensitivity profile (SSP) and average glandular dose (AGD). IQ parameters were measured using the Tomophan phantom. SDNR was evaluated with the 0.2-mm-thick aluminum insert. MTF was calculated for scan and sub-scan directions from the point spread function of the 0.18mm tungsten bead. SSP evaluation was performed with the two reversing angled bead ramps method. These parameters were evaluated for two different DBT devices at seven different values of AGD, obtained manually setting the tube current time product.

Results: Each DBT device showed a characteristic value of DBTI. These values were constant as the tube current time product changes, with a standard deviation of 2% and 6% for the two devices.

Conclusion: Independence of DBTI from exposure parameters could make it a good FoM to benchmark DBT devices. Compared to CT, DBT have less clinical questions, so a single score could provide a reliable estimation of the goodness of the DBT device.

10:30 - 12:00

Room K

Radiographers

SS 1814

Quality improvement in radiography

Moderators:

J. Grehan; Dublin/IE
N.N.

B-1442 10:30

Does the post-processing annotation of images become a standard practice in digital radiography today?

E. Saukko¹, M. Wirtanen², K. Kortelainen²; ¹Turku/FI, ²Helsinki/FI (ekaterina.saukko@tyks.fi)

Purpose: Digital radiography allows post-processing annotation of images, which enables radiographers to apply markers electronically onto images post-exposure. This advancement has led to a decrease in use of lead anatomical side markers (ASMs), although the best practice has always been to place markers within primary beam. The aim of this study was to assess the radiographers' perception on the use of lead ASMs in Finland.

Methods and Materials: A self-designed questionnaire was sent in April 2017 to all members of the Society of Radiographers in Finland using the society's e-mail list (n=1696). In total, 278 responses were received.

Results: Among all respondents, only 32% reports that there were guidelines for lead ASMs use in their radiological department. About 88% of radiographers stated that lead ASMs were sufficiently available in the x-ray rooms and 18% had personal markers. The preference of ASMs use within primary beam over the post-processing annotation varied depending on the type of anatomy examined. Radiographers prefer using ASMs pre-exposure in radiographs demonstrating both sides of unilateral anatomy (72%, n=199), while in examinations performed outside the imaging departments the lead ASMs use was very scarce (21%, n=57). Longer work experience was associated with increased lead ASMs use in radiography of the skull and face (p=0.004), chest (p=0.006), bones and joints (p=0.021), spine (p=0.002) and in radiographs showing both sides of unilateral anatomy (p=0.019).

Conclusion: Overall, the use of ASMs post-exposure is predominated among radiographers. Written protocols, regular audits of practice and continuous staff education are recommended.

B-1443 10:38

Implementation of DR detectors for paediatric chest x-ray in NICU

D. Pekarovic¹, U. Zdesar, P.A. Jesih, M. Pungrcar; Ljubljana/SI (dean.pekarovic@kclj.si)

Purpose: Development of exposure charts when changing image detectors from imaging plates (CR) to digital detectors (DR).

Methods and Materials: After commissioning of a new mobile DR system in NICU, a group of radiographers, radiologist and medical physicist were established to optimise exposure technique. Patients were divided into seven age groups from neonates to the age of 18. Anode voltage (kV) and exposure (mAs) were changed in small steps from the factory settings and radiologist was consulted about image quality. Exposure index (EI) was used as a measure of detector exposure and dose area product (DAP) as a measure of patient exposure. As the last step, the DAP values for each group was compared to proposed EU diagnostic reference levels (PiDRL-paediatric dose reference levels). During the process, the gaps in knowledge regarding DR systems were identified and training curriculum for radiographers was prepared.

Results: A target exposure index (TEI) of 300 was set and radiographers were instructed to follow deviation index (DI). Data from 1816 patients were analysed in the period of 11 months. Average DI was 0.35 being largest (0.8) at the youngest age group (0-7 days). 5.8% of patients had DI larger than ± 3 (1.6% underexposed and 4.2% overexposed). Measured DAP were compared to diagnostic reference levels PiDRL. Third quartile DAP values for all groups were far below PiDRLs.

Conclusion: Introduction of new imaging equipment in radiology department often requires adoption of new exposure techniques required for optimised imaging. Technique changes should be followed by additional training of radiographers operating the equipment.

B-1444 10:46

Practitioner variability in collimation and centring for AP shoulder projections

D. Browne¹, K. Szczepura², A. England¹; ¹Manchester/UK, ²M6 6PU/UK (A.England@salford.ac.uk)

Purpose: Radiographic positioning textbooks recommend AP shoulder projections using either a square- or diamond-shaped radiation field. Recommendations reflect the likely differences in radiation dose to breast tissue but this is unproven. Within these texts there are also variations in the centring points proposed. The aim of this study was to assess differences in collimation field and centring point, and their effect on breast dose and image quality (IQ).

Methods and Materials: Six volunteers were invited to position and expose a PIXY phantom for an AP shoulder projection using both square- and diamond-shaped field. Entrance surface doses (ESD) were measured at four locations around a simulated breast to determine which scenario delivered the lowest overall ESD.

Results: Study findings demonstrated that switching from a square to a diamond X-ray field shape increased (24.5%) the total ESD to the breast (55.1 mGy vs 72.9 mGy; $P < 0.0001$). Positional accuracy results (IQ) indicated that practitioners can use either field shape accurately ($P > 0.05$). Evaluation of centring points suggests that practitioners showed a tendency to centre more medially and inferiorly when compared to textbooks.

Conclusion: Evidence from this study suggests that the absorbed dose to the breast could increase by moving from a square field to a diamond shape. Both techniques can be performed with similar accuracy and centring points used by participants did differ slightly from positioning texts. Findings from this pilot study warrant further investigation.

B-1445 10:54

Study of scattered radiation during fluoroscopy in hip surgery

O. Lesyuk¹, L.P. Ribeiro², A.F. Abrantes², P. Sousa², S. Rodrigues², R.P. Almeida², K.B. Azevedo², J.P. Pinheiro²; ¹São Brás de Alportel/PT, ²Faro/PT (oksanalesyuk@gmail.com)

Purpose: To measure the scattered radiation dose at different positions simulating hip surgery.

Methods and Materials: We simulated fluoroscopy-assisted hip surgery in order to study the distribution of scattered radiation in the operating room. To simulate the patient, we used an anthropomorphic whole-body phantom and a X-ray-specific detector to quantify the scattered radiation. Radiographs were obtained with a mobile C-arm X-ray system in continuous scan mode, with the tube at 0° (configuration 1) or 90° (configuration 2). The operating parameters employed (voltage, current, and exposure time) were determined by a statistical analysis based on the observation of orthopedic surgical procedures involving the hip.

Results: For all measurements, higher exposures were observed in configuration 2. In the measurements obtained as a function of height, the maximum dose rates observed were 1.167 (± 0.023) μ Sv/s and 2.278 (± 0.023) μ Sv/s in configurations 1 and 2, respectively, corresponding to the chest level of health care professionals within the operating room. Near to the patient, the maximum values were recorded in the position occupied by the surgeon.

Conclusion: We can conclude that, in the scenario under study, health care professionals workers are exposed to low levels of radiation, and that those levels can be reduced through the use of personal protective equipment.

B-1446 11:02

An investigation of the impact of image viewing parameter settings on the performance of 2.4 MP colour monitor in visualising low contrast detail using the CDRAD phantom

S.H. Al-Murshedi, P.H. Hogg, M.M. Benhalim, M. Alrowily, A. England; Manchester/UK (p.hogg@salford.ac.uk)

Purpose: To investigate the relation between the observer performance for low contrast details detection and the image viewing settings (magnification, window setting) for a wide range of image quality on 2.4 MP colour monitor

Methods and Materials: Six images of CDRAD phantom were generated, using adults chest radiography protocols with different image quality. Five observers evaluated the images on 2.4 MP colour monitor. The images were assessed in four different ways: firstly, the observers were not free in adjusting the contrast, intensity, and magnification of the image; secondly, only the magnification was allowed to be adjusted; thirdly, only the contrast and intensity were allowed to be adjusted; finally, the observers were free to adjust the contrast, intensity and magnification of the image

Results: Data analysis was conducted via repeated measures of variance (ANOVA). For the images with high quality, using magnification only has no significant difference on improvement of image scoring $p=0.10$, whereas significant difference was noted between employing windowing solely and using both windowing and magnification with $p=0.03$ and $p=0.00$ respectively. Furthermore, it was found image viewing manipulation has negative influence on image scoring for the ones characterised by low quality

Conclusion: The study demonstrates that adopting both magnification and windowing is of a significant impact on improving image scoring; employing windowing solely has the second highest impact. Hence, this study recommends the utilisation of image viewing manipulation only with the images that are of high image quality, while it should be avoided with the images that are of low quality

B-1447 11:10

The optimised location to assist patient during imaging of scoliosis with EOS system device

H.M.S. Laitinen, H. Niiniviita, E. Saukko, E. Svedström; Turku/Finland (helen.laitinen@edu.turkuamk.fi)

Purpose: With challenging scoliosis patients, it is occasionally necessary to assist patient in the examination room during exposure for patient safety and preventing movement. EOS system is a slot-scanning technique specialised to orthopaedic imaging, especially scoliosis. Finland's first EOS system installation was made at Turku University Hospital in 2017. The aim of this study was to measure scattered radiation during imaging of scoliosis with this new technique and thereby find the optimized place for the assistance.

Methods and Materials: An anthropomorphic phantom was set at the isocenter and scanned using standard scoliosis protocol, with both AP and LAT views. The scattered dose rates were measured at seven points from one meter above the floor level with ion chamber survey meter. At three points measurements were made also with lead shields. For reliability and repeatability measurements were repeated three times and average dose rates were calculated.

Results: The dose rate at the closest point (45 cm from isocentre) was 10.5 mSv/h, but lead apron reduced the dose significantly to 263 μ Sv/h. At the most distant point (175 cm from isocentre) the dose was 0.73 mSv/h and with lead shield 8.0 μ Sv/h. There was more scattered radiation on the lateral side than the AP/PA side.

Conclusion: Assistant should wear lead apron if holding the patient is necessary. If only presence in the same room is sufficient, assistant should be on the AP/PA side, behind lead shield, wear lead apron, and take distance, but keep the eye-contact to patient.

B-1448 11:18

A tool for automated assessment of imaging system resolution

R. Us, A. Matjažič, R. Bizjak, T. Hribar, Z. Malinova, N. Mekis; Ljubljana/Slovenia

Purpose: To develop and deploy a software solution for automatic, consistent and quantitative characterisation of an imaging system's spatial resolution.

Methods and Materials: We used an ETR-1 test plate, a Siemens Multix/Vertix system, AGFA CR MD 4.0 general cassettes and an AGFA 25.0 scanner. The study was conducted in two parts. The first series of exposures was done using the small focal spot while the second series utilised the large focal spot. All exposures were conducted in line with QC guidelines. Parameters including SID, tube voltage as well as the product of exposure time and tube current were held constant throughout. 20 exposures were done at different z axis positions to record system performance under each set of conditions, for a total of 40 images. We moved the test plate by 20 mm toward the cathode end of the FOV between successive exposures. An ImageJ macro was developed to carry out consistent characterisation of ETR-1's line pair segments. This data was used to chart an approximate MTF curve for each position along the z axis.

Results: Our results take the form of 2 spreadsheets containing MTF values for 20 different frequencies in the vertical direction and 19 different z axis positions in the horizontal direction. The sampling resolution limit was clearly visible in the first series at between 3,1 and 3,4 lp/mm which is consistent with our scanner specifications.

Conclusion: Our macro consistently produced a comprehensive quantitative characterisation of system performance using images from test plate exposures.

B-1449 11:26

Scattering in dental cone-beam computed tomography

J. Heikkinen, P. Sepponen, A. **Henner**; *Oulu/FI (anja.henner@oamk.fi)*

Purpose: The aim of this study was to produce information of scattered radiation that can be utilized in aforesaid situations and possibly in future CBCT applications and radiation protection. The measurement system and the presentation of the results can also be commonly utilized for scattering measurements. Therefore it's important to figure out doses, dose rates and directions of scattered radiation around the CBCT machine during the examination.

Methods and Materials: The scattering was measured using a RaySafe X2 X-ray measurement system and its survey-sensor. The studied CBCT machine was Scanora 3D (Soredex). CIRS ATOM 711-HN was used as an anthropomorphic patient-phantom. Measurements were performed on three different heights with normal dental imaging parameters (dental infection) and on one height with the largest FOV and highest resolution.

Results: Four scattering maps that represent the X-ray scattering in the X-ray simulation room were obtained. The highest doses were naturally measured in the vicinity of the CBCT machine on the height of the isocenter of the x-ray beam. Increasing the FOV and resolution led to increased scattered radiation. In addition to dose and dose rate measurements the dose rate as a function of time during the rotation of the gantry was examined.

Conclusion: The dose rates in the examination room were significant and regarding radiation protection. The scattering maps show the safest areas in the examination room

B-1450 11:34

Overview of CT throughput in a radiology department: drawbacks and solutions

B. **Kara**¹, A. Toker¹, S. Horoz¹, M. Onur¹, S. Sanje², D. Akata¹; ¹Ankara/TR, ²Istanbul/TR (tomografi@hotmail.com)

Purpose: The aim of this study to investigate the productivity of computed tomography (CT) units in a radiology department and to draw conclusions on how to achieve efficient outcomes.

Methods and Materials: A total number of 69.865 CT scans performed in four different multislice CT scanners (Scanner A, B,C,D) between May 2016 and April 2017 were analysed in terms of equipment utilization rate against institutional entitlement and industry benchmarks, staff utilization, adoption to protocol standardization, patient flow and end to end radiology value stream leveraging Lean Six Sigma methodology.

Results: Utilization rate of overall CT units was found as 61% against industry benchmarks (85%, 80%, 120%, 35% for scanners A, B, C and D, respectively). Based on data; 57% of CT requests were scanned at the same day whereas for 25% of patients it takes more than 5 days. Although CT examinations are mostly scheduled in office hours (between 8 am to 6 pm), utilization rates decreased significantly during lunch and staff shift change times. Patient preparation time was increased when there is single radiographer per scanner. Unnecessary activities in scanner room including manual entrance of patient information, patient questions, and opening route for intravenous contrast agent administration constituted 13% of total observed time in CT rooms.

Conclusion: Overview of radiology departments in guidance with professional partners using bench-markings is helpful for management and improvement of CT throughput. Changed behaviours of staff in accordance with innovative perspective of radiology departments will be helpful for overcoming drawbacks in CT throughput.

Author Disclosures:

S. Sanje: Employee; General Electric.

B-1451 11:42

Eye-lens dose in head CT examinations: evaluation of different methods through the use of gantry angulation and barium shields

M.V.C. **Reis**, S. Rodrigues, A.F. Abrantes, L.P. Ribeiro, R.P.P. Almeida, O. Lesyuk; *Faro/PT (monica14@live.com.pt)*

Purpose: To evaluate the effect of gantry angulation, scanning techniques (spiral vs sequential) and barium eye shielding on radiation dose to the eye lens during head CT examinations.

Methods and Materials: An anthropomorphic phantom was scanned with a routine head CT protocol using a 16-slices CT equipment. Three exposures were performed for each of the following settings with different combinations: (1) spiral and sequential scanning techniques, (2) with and without barium shields and (3) gantry angulation at 12°, 0°, -12° and -22° using the orbitomeatal line as reference. Thermoluminescent dosimeters (TLD) were used to measure the entrance skin dose (ESD) in eye lens.

Results: An ESD reduction range from 15% to 21% was verified in all configurations with barium shields. The lower ESD value was observed in configuration with barium shields and gantry angulation at -12° (28,86mGy). In terms of effective dose, it was found that the sequential scanning technique at 0° with no barium shield presents the higher value (0.43mSv), although below

the dose threshold. The lower effective dose (0.29mSv) was verified with the use of barium shield in combination with -12° of gantry angulation.

Conclusion: These results may be used to provide more adequate procedures and to ensure that protocols are operated safely below thresholds. Tilting the gantry to avoid the orbits and using the barium eye shielding are effective measures for reducing radiation dose to the eye lens in clinical practice. These actions should be considered when they are consistent with the clinical task and patient anatomy.

B-1452 11:50

Patients' experiences in coronary angiography

A. **Henner**, A. Lahdenperä, H. Suutari, K. Koivunen, K. Paalimäki-Paakki; *Oulu/FI (anja.henner@oamk.fi)*

Purpose: The purpose of this study was to find out patient's experiences after coronary angiography.

Methods and Materials: Patients' experiences were studied with group and individual theme interviews. 12 persons (aged 59-84 years) were interviewed in Autumn 2016. The data were analysed with inductive content analysis. Purpose of this study was to describe the patients' experiences in coronary angiography.

Results: According to the data, the patients felt that they are not encountered as individuals, but they still trust on the professionalism of the care team. Invasive nature of the coronary angiography affects strongly to the experience. Patients felt they have got very good care. On the other hand, the patients felt they are on conveyor belt and they are medicated too heavily. The invasive examination rises anxiety and fear. Patient's background and personality affects to what kind of and how much counselling they require before, during and after examination. According to patients, nobody told them about the use of radiation. The possibility to discuss and share the experiences with other patients is highly valued.

Conclusion: This study gives additional information about the patient's experience in coronary angiography. This study gave to interviewees a possibility to participate in the development of the future care pathway and also gives them a possibility to share their experiences. Results of our study can be used in the development of the coronary angiography procedure, more personalized patient counseling and patient profiles.

10:30 - 12:00

Room M 1

Cardiac

SS 1803

Deep learning in coronary and myocardium CT

Moderators:

V.E. Sinitsyn; Moscow/RU
N.N.

B-1453 10:30

Computed tomography CT: derived fractional flow reserve improves reader confidence for coronary CT angiography

C. **Schabel**¹, K. Nikolaou¹, L. Hurwitz²; ¹Tübingen/DE, ²Durham, NC/US (christoph.schabel@med.uni-tuebingen.de)

Purpose: To assess the impact of fractional flow reserve computed tomography (FFR_{CT}) on reader confidence and time efficiency for interpretation of coronary computed tomography angiography (CCTA).

Methods and Materials: This IRB-approved, HIPAA-compliant, consent waived, retrospective quality-assessment study included 50 patients (23 women, age 67±12years, body mass index 28.7±5.3kg/m²). CCTA was acquired on 2nd & 3rd generation dual-source MDCT with use of beta-blockers and nitroglycerin, and FFR_{CT} was calculated (HeartFlow, Redwood City, CA). Two readers with experience level COCATS2 (Core-Cardiology-Training-Symposium) and two with COCATS3 assessed CCTA alone and CCTA plus FFR_{CT}. Readers' confidence to diagnose or exclude coronary artery disease (CAD) and hemodynamically significant stenosis (HS) was rated on a 4-point Likert-scale (1=high, 2=good, 3=limited, 4=none) for the four major epicardial coronary artery vessels (CAV). Time to interpret was recorded.

Results: The severity of CAD in the cohort population was CAD-RADS1 (Coronary-Artery-Disease Reporting-and-Data-System) n=15, CAD-RADS2 n=8, CAD-RADS3 n=11, and CAD-RADS4 n=16. Sixty-four CAV in 33 patients had FFR_{CT} values <0.8. Readers' confidence when FFR_{CT} was available increased for CAD and HS (p=0.0001) with a reduction of "non-confident" patient reads (rank 3&4) by 27% and 75%, respectively. The change in confidence was not associated with CAD-RADS (p>0.1) but correlated with readers' experience (p=0.0001). The median time-to-read a CCTA study decreased by 5 minutes when FFR_{CT} was available (p<0.0001).

Conclusion: Interpretation of CCTA in conjunction with FFR_{CT} improved readers' confidence to identify or exclude CAD and HS with reduction of "non-confident" reads by 27% and 75%, respectively, and decreased the median time-to-interpret a CCTA by 5 minutes.

Author Disclosures:

C. Schabel: Speaker; Siemens Healthcare.

B-1454 10:38

Effect of coronary calcium on the diagnostic performance of machine learning-based coronary CT angiography-derived fractional flow reserve: results from the machine registry

C. Tesche¹, K. Otani², M. Albrecht³, C.N. De Cecco³, T. Duguay³, S. Baumann⁴, M. Renker⁵, A. Varga-Szemes³, U.J. Schoepf^{3,1}, ¹Munich/DE, ²Tokyo/JP, ³Charleston, SC/US, ⁴Mannheim/DE, ⁵Bad Nauheim/DE (tesche.christian@googlemail.com)

Purpose: To investigate the effect of coronary artery calcium (CAC) on the diagnostic performance of machine learning-based coronary CT angiography (cCTA)-derived fractional flow reserve (CT-FFR).

Methods and Materials: 481 vessels from 314 patients (62.3±9.3 years, 77% male) who had undergone cCTA followed by invasive fractional flow reserve (FFR) were investigated in this retrospective analysis of the MACHINE registry (Machine leArning-based CT angiograpHy-derived FFR: a Multi-ceNtEr Registry) data. CAC was quantified using the Agatston convention. The diagnostic performance of CT-FFR to detect lesion-specific ischaemia was assessed across all Agatston score quartiles with invasive FFR as the reference standard.

Results: The diagnostic accuracy of CT-FFR vs invasive FFR was superior to that of cCTA alone on a per-vessel (78% vs 58%) and per-patient (83% vs 73%) basis across all Agatston score quartiles. CT-FFR demonstrated high discriminatory power in vessels with high Agatston scores (250-2066) and a low to intermediate Agatston scores (0-249) without a statistically significant difference in the area under the receiver-operating characteristic curve (AUC) (AUC: 0.77 [95%CI 0.68-0.86] vs 0.86 [95%CI 0.82-0.90], *p*=0.76). CT-FFR showed incremental diagnostic value over cCTA in vessels with high Agatston scores (AUC 0.77 vs 0.55, *p*<0.001) and low to intermediate Agatston scores (AUC 0.86 vs 0.66, *p*<0.001).

Conclusion: Machine learning-based CT-FFR demonstrated superior diagnostic performance over cCTA alone in calcified coronary arteries on a per-lesion and per-patient level with no difference in the performance of CT-FFR between patients with low to intermediate and patients with high Agatston scores.

Author Disclosures:

K. Otani: Employee; Siemens Healthineers. **C.N. De Cecco:** Consultant; Guerbet. **A. Varga-Szemes:** Consultant; Guerbet. **U.J. Schoepf:** Consultant; Guerbet. Research/Grant Support; Astellas, Bayer, GE, Bracco, Medrad, Siemens.

B-1455 10:46

Artificial intelligence deep-learning-based coronary CT fractional flow reserve: the impact of iterative and filtered back projection reconstruction techniques

D. Mastrodicasa¹, C.N. De Cecco¹, A. Moritz², A. Varga-Szemes¹, G. Muscogiuri³, M. van Assen⁴, M. Eid¹, F. Lavra⁵, U.J. Schoepf¹; ¹Charleston, SC/US, ²Horb/DE, ³Milan/IT, ⁴Groningen/NL, ⁵Cagliari/IT (domenico.mastrodicasa@gmail.com)

Purpose: To evaluate the influence of CT reconstruction algorithms on machine-learning-based computed tomography-derived fractional flow reserve (CT-FFR_{ML}) results and processing time.

Methods and Materials: Iterative reconstruction in image space (IRIS) and filtered back-projection (FBP) datasets were retrospectively included from 40 patients who underwent coronary CT angiography (CCTA) on a 3rd generation dual-source scanner. Using a machine-learning software prototype, CT-FFR was computed on a per-vessel and per-segment basis, as well as proximal and distal to lesions with ≥50% luminal stenosis according to CCTA. Invasive FFR comparison was performed when available. Significant ischaemia was defined as invasive FFR and CT-FFR values ≤0.80. Computational times were recorded. Pearson correlation, Wilcoxon, and McNemar testing were used for data analysis.

Results: A total of 320 vessels were analysed to calculate CT-FFR. Per-vessel analysis of IRIS and FBP reconstructions showed significantly different CT-FFR values (*p*≤0.05). Correlations between the two algorithms for the left main (*r*=0.74), left anterior descending (*r*=0.76) and right coronary artery (*r*=0.70) were high. A per-segment analysis revealed significantly different CT-FFR values (*p*≤0.05) and high correlation for all proximal and middle segments (*r*=0.73 and *r*=0.70, *p*≤0.001, respectively). No difference in diagnostic accuracy was observed between algorithms (81.8%, *p*=1.000). Per-lesion correlation with invasive FFR values was moderate for both IRIS (*r*=0.53, *p*=0.117) and FBP (*r*=0.49, *p*=0.142). CT-FFR computational time was significantly shorter using IRIS reconstruction (15.9 vs 19.8 minutes, *p*≤0.05).

Conclusion: IRIS improves CT-FFR_{ML} post-processing speed, likely owing to reduced image noise. However, the reconstruction algorithm influences CT-FFR results with potential implications on patient management.

Author Disclosures:

C.N. De Cecco: Research/Grant Support; Siemens. **A. Varga-Szemes:** Research/Grant Support; Siemens. **U.J. Schoepf:** Consultant; Bayer, Guerbet. Research/Grant Support; Astellas, Bayer, GE, Siemens.

B-1456 10:54

Gender differences in machine learning-based coronary CT angiography-derived fractional flow reserve: results from the machine registry

B.E. Jacobs¹, S. Baumann^{1,2}, M. Renker^{1,3}, C. Tesche^{1,4}, T. Duguay¹, M.H. Albrecht^{1,5}, A. Coenen⁶, K. Nieman⁶, U.J. Schoepf¹; ¹Charleston, SC/US, ²Mannheim/DE, ³Bad Nauheim/DE, ⁴München/DE, ⁵Frankfurt/DE, ⁶Rotterdam/NL (jacobsbr@muscedu)

Purpose: Coronary computed tomography angiography (cCTA)-derived fractional flow reserve (cFFR) is a non-invasive FFR approach that improves diagnostic accuracy in detecting haemodynamically relevant lesions over cCTA alone. An artificial intelligence deep machine-learning method of calculating cFFR (ML-cFFR) has recently been introduced. Currently, no data exist regarding the influence of patient sex on the accuracy of artificial intelligence ML-cFFR.

Methods and Materials: Five centres enrolled 351 patients (73.5% male) with 525 vessels in the retrospective MACHINE (Machine leArning Based CT angiograpHy derived FFR: a Multi-ceNtEr) registry (NCT02805621). ML-cFFR and invasive FFR ≤0.80 were considered haemodynamically significant, whereas cCTA luminal stenosis ≥50% was considered obstructive.

Results: Compared with invasive FFR on a per-lesion basis, ML-cFFR reached a pooled sensitivity, specificity, positive predictive value, and negative predictive value of 83.0% (95%CI: 76.6-88.2), 73.4% (95%CI: 67.1-79.1), 71.2% (95%CI: 66.3-75.7), and 84.5% (95%CI: 79.5-88.4) in men vs 69.4% (95%CI: 51.9-83.7, *p*=0.0009), 83.5% (95%CI: 74.3-90.5, *p*=0.0207), 62.5% (95%CI: 50.0-73.5, *p*=0.0650) and 87.4% (95%CI: 80.7-91.9, *p*=0.4234) in women, respectively. The AUC of ML-cFFR was not significantly superior to cCTA alone on a per-vessel basis [0.83 (95%CI: 0.75-0.90) vs 0.79 (95%CI: 0.70-0.87), *p*=0.4752] in women, but showed a statistically significant improvement in men [0.83 (95%CI: 0.79-0.87) vs 0.74 (95%CI: 0.69-0.79), *p*<0.0001].

Conclusion: ML-cFFR significantly improves the diagnostic performance over cCTA alone for the detection of haemodynamically relevant lesions, using invasive FFR values as the reference standard. The incremental value is greater in men than in women.

Author Disclosures:

M. Renker: Author; Receives consulting fees/honoraria from Symetis. **A. Coenen:** Research/Grant Support; Receives financial research support from Siemens Healthcare. **K. Nieman:** Research/Grant Support; Receives institutional research support from Bayer Healthcare, GE Healthcare, Siemens Medical Solutions, and Heartflow. **U.J. Schoepf:** Author; Receives research support from Astellas, Bayer, Bracco, GE, and Siemens and is a consultant for Bayer, Guerbet, and Siemens.

B-1457 11:02

Noninvasive CT-derived FFR based on structural and fluid analysis with low radiation dose using a full iterative reconstruction

H. Takagi, K. Kikuchi, R. Tanaka, K. Yoshioka, Morioka/JP (hdnb69tkg@gmail.com)

Purpose: The purpose of this study was to evaluate the diagnostic performance for functional significance of coronary artery stenosis (i.e. ischaemia) of CT-derived fractional flow reserve (CT-FFR) at low radiation dose using a full iterative reconstruction (IR) technique.

Methods and Materials: This retrospective study included 19 vessels in 16 patients with suspected coronary artery disease (CAD) who underwent coronary CT angiography (CCTA), followed by invasive fractional flow reserve (FFR). All CCTA examinations were performed with a 320-row MDCT scanner, and all CT data were reconstructed with a full IR technique. CT-FFR was derived using a reduced order model performed with dedicated software on a standard desktop computer. Ischaemia was defined as a CT-FFR and FFR ≤0.80. The diagnostic performance with 95% confidence interval (95%CI) of CT-FFR was assessed with invasive FFR as the reference standard. The effective radiation dose of CCTA was calculated by a dose-length product (mGy·cm) and a standard conversion factor of 0.014 (mSv/mGy·cm).

Results: Ischaemia was observed in 58% (11/19) vessels during invasive FFR. On a per-vessel basis, sensitivity, specificity, accuracy, and area under the curve were 82% (95%CI, 63-89), 88% (95%CI, 62-98), 84% (95%CI, 63-93) and 0.85 (95%CI, 0.60-0.95) for CT-FFR. The CT-FFR and FFR were well correlated (*r*=0.79, *p*<0.01), and there was no significant difference between CT-FFR and FFR (-0.01±0.07, *p*=0.68). The mean effective radiation dose for CCTA was 1.9±1.0 mSv.

Conclusion: Noninvasive CT-FFR with low radiation dose using a full IR demonstrated a high diagnostic performance for the detection of ischaemia.

Author Disclosures:

K. Yoshioka: Research/Grant Support; Toshiba Medical Systems.

B-1458 11:10

Intermodel agreement of myocardial blood flow quantification in dynamic myocardial perfusion CT

M. van Assen¹, G. Pelgrim², M. Stijnen³, S. Van Tuijl³, U.J. Schoepf¹, R. Vliegenthart², M. Oudkerk²; ¹Charleston, SC/US, ²Groningen/NL, ³Eindhoven/NL (m.van.assen@umcg.nl)

Purpose: To assess intermodel agreement of tracer kinetic models to determine myocardial blood flow (MBF) and ischemia in dynamic CT myocardial perfusion imaging (CTMPI).

Methods and Materials: Three porcine hearts perfused in Langendorff mode (Physioheart®, LifeTec Group, Eindhoven, The Netherlands) and 8 patients with suspected CAD and rest-stress perfusion single photon emission CT (SPECT) were included. Dynamic CTMPI was performed in shuttle-mode (70kVp, 350mAs/rot, z-range 10.2cm) on 3rd-generation dual-source CT. In porcine hearts and patients, myocardial segments were drawn according to the AHA-16-segment model. Tissue attenuation curves were calculated per segment. The arterial input function was derived from the aorta. True MBF was calculated in the porcine model based on input flow and weight of the heart. In patients, ischemic segments were defined based on previous SPECT results. MBF (ml/g/min) quantification was performed using the upslope, Extended Toft (ET), Two-compartment (TC) and Fermi models.

Results: For the non-ischemic segments in the porcine hearts, the upslope method resulted in lower MBF (median 1.23, interquartile range[IQR]:1.07-1.46) compared to the Fermi, ET and TC model, which had median values of 1.93 (1.37-2.63), 2.78 (1.56-3.81) and 2.26 (1.64-3.29). True global MBF was calculated at median 1.88 (IQR:1.80-2.80). In patients all models showed a significant difference between ischemic and non-ischemic segments (p-value<0.001). Again the upslope model showed the lowest MBF values.

Conclusion: The most commonly used upslope method yielded lower absolute MBF values compared to other models and true MBF in porcine hearts. In patients all models were able to discriminate between ischemic and non-ischemic segments.

Author Disclosures:

M. Stijnen: Employee; LifeTec. **S. Van Tuijl:** Employee; LifeTec.

U.J. Schoepf: Research/Grant Support; Siemens Healthineers, GE, Bracco, Bayer

B-1459 11:18

Additional diagnostic value of CT perfusion over coronary CT angiography in stented patients with suspected in stent restenosis or coronary artery disease progression: Advantage study

D. Andreini¹, S. Mushtaq¹, J. Sonck², G. Pontone¹, E. Conte¹, M. Mancini¹, A. Baggiano¹, A.L. Bartorelli¹, M. Pepi¹; ¹Milan/IT, ²Brussels/BE (daniele.andreini@cctm.it)

Purpose: Aim of the study is to assess the diagnostic performance of CCTA alone, CTP alone and CCTA plus CTP when compared to invasive coronary angiography (ICA) in patients with coronary stents.

Methods and Materials: A cohort of consecutive patients referred to ICA were enrolled. The feasibility of CCTA, CTP and the combined evaluation CCTA plus CTP were calculated. Sensitivity, specificity, positive predictive value, negative predictive value and diagnostic accuracy of CCTA, CTP, combined evaluation CCTA-CTP (considered as positive when CCTA indicated a >50% stenosis or ISR and/or CTP indicated a perfusion defect) and concordant evaluation CCTA-CTP vs. ICA were calculated. Radiation exposure was recorded.

Results: Sixty nine patients were enrolled. CTP feasibility was significantly higher than CCTA feasibility in a stent-, territory- and patient-based analysis. The feasibility of the combined evaluation CCTA-CTP was significantly higher than CCTA feasibility. The diagnostic accuracy of CCTA was 78%, 81%, and 78%, respectively; the diagnostic accuracy of CTP was 90%, 92% and 84%, respectively; the diagnostic accuracy of combined CCTA-CTP was 84%, 88%, and 83%, respectively; the diagnostic accuracy of concordant CCTA-CTP was 95%, 97% and 96%, respectively. The diagnostic accuracy of concordant CCTA-CTP was higher than that of CCTA and CTP in a patient-based analysis. The mean effective dose of CCTA-CTP was 3.89±1.35 mSv.

Conclusion: The CTP assessment appears more feasible accurate than the anatomical evaluation alone by CCTA in patients with coronary stents. When results of CCTA and CTP are concordant the diagnostic accuracy of the combined evaluation is very high.

B-1460 11:26

Accuracy of CCTA to detect obstructive CAD using stress vs rest dataset in patients referred to stress CTP

M. Guglielmo¹, A. Guaricci², A. Baggiano¹, F. Fazzari³, D. Andreini¹, F. Fabiocchi¹, A. Lualdi¹, A. Bartorelli¹, G. Pontone¹; ¹Milan/IT, ²Bari/IT, ³Palermo/IT (marco.guglielmo@cctm.it)

Purpose: We sought to compare diagnostic accuracy of CCTA (coronary computed tomographic angiography) to detect obstructive CAD (coronary artery disease) between stress versus rest dataset as compared to invasive coronary angiography (ICA).

Methods and Materials: 66 symptomatic patients with intermediate to high pre-test probability of CAD and scheduled for clinically indicated ICA were prospectively enrolled. All patients underwent rest-CCTA followed by stress-CTP protocol with adenosine (revolution CT scanner, GE Healthcare, Milwaukee, WI) with injection of 70 ml of iodixanol 320 (Visipaque 320 mg/ml, GE Healthcare, Oslo, Norway). For both datasets, the image quality was evaluated with Likert score. The severity of coronary lesions was quantified by identifying the minimum diameter and reference diameter for all stenoses, and the percentage of stenosis will be derived according to the following formula: (Dref-Dmin)/Dref*100, where Dref is the reference diameter and Dmin is the minimum diameter. For CCTA and ICA, the obstructive CAD was defined as the presence of coronary artery stenosis ≥50%.

Results: Obstructive CAD was found in 61% of patients at ICA. In vessel-based model, the stress dataset showed a higher heart rate as compared to the rest dataset (p<0.001) with similar image quality. Stress dataset showed similar sensitivity (95% [CI95%: 89-100]) vs 93% [CI95%: 89-100]) but slightly lower specificity (75% [CI95%: 69-82]) vs 80% [CI95%: 74-86], p: 0.05] as compared to rest dataset. In both vessel and patient-based model, stress and rest dataset showed similar area under the curve (AUC) (0.84 vs 0.82 and 0.84 vs 0.84).

Conclusion: In static stress CTP, the new-generation scanner allows to perform the coronary artery imaging in the stress dataset with the same accuracy of rest dataset.

B-1461 11:34

The impact of a tiered cardiac CT protocol compared to functional testing on cardiovascular risk management in patients with suspected coronary artery disease

F. Noug¹, M.M. Lubbers¹, J. Akkerhuis¹, T. Bruning¹, B. Krenning¹, M. Kofflard², B.L. Kietselaer³, R.P. Budde¹, K. Nieman¹; ¹Rotterdam/NL, ²Dordrecht/NL, ³Maastricht/NL (f.noug@erasmusmc.nl)

Purpose: To assess the impact of a tiered cardiac CT protocol, compared to functional testing, on cardiovascular risk factors and life style changes in patients evaluated for coronary artery disease (CAD).

Methods and Materials: Patients with suspected CAD, who participated in the CRESENT I or CRESENT II trials, who were randomly assigned to cardiac CT or functional testing, were assessed. The protocol included a calcium scan and when indicated a coronary CT angiography (CCTA) (calcium score >0/high pre-test probability) and a CT myocardial perfusion (CRESENT II, CCTA: stenosis >50%), or functional-testing according to European guidelines. The use of preventive medication was registered at baseline and at 6 months (CRESENT I) or 1 year (CRESENT II) and patients were asked to fill out a questionnaire about their health status (smoking, diet, exercise, weight change, blood pressure and cholesterol level) at follow-up.

Results: Patients who underwent a cardiac CT (n=372) were more likely to improve at least one of the risk factors or life style changes compared to patients who underwent functional-testing (n=246) (78% vs. 67%, p<0.01). They were more likely to increase their exercise (p<0.05), to gain less weight (p<0.001) and to normalise their cholesterol levels (p<0.01). Fewer patients used antiplatelet agents and/or statins after diagnostic testing, from 31% to 24% (p<0.01) after CT, and from 45% to 39% (p<0.05). No differences were found between both groups.

Conclusion: A tiered cardiac CT protocol is associated with more change in life style in patients evaluated for CAD compare to functional testing.

Author Disclosures:

B.L. Kietselaer: Research/Grant Support; Astra Zeneca and Bayer. Speaker; Astellas and AMGEN. **K. Nieman:** Research/Grant Support; Siemens, General Electric, Bayer, Heartflow. Speaker; Siemens.

B-1462 11:42

Deep learning-based analysis of the left ventricular myocardium in coronary CTA images improves specificity for detection of functionally significant coronary artery stenosis

R.W. van Hamersvelt¹, M. Zreik¹, M. Voskuil¹, I. Isgum¹, T. Leiner¹; ¹Utrecht/NL (R.w.vanhamersvelt-3@umcutrecht.nl)

Purpose: To evaluate the added value of fully automatic deep learning-based analysis of left ventricular myocardium (LVM) in addition to routine stenosis

10:30 - 12:00

Room M 4

Genitourinary

SS 1807b

Contrast media, urography and stone disease

Moderators:

C. Roy; Strasbourg/FR
A.J. van der Molen; Leiden/NL

B-1464 10:30

Updated evidence-based European Society of Urogenital Radiology (ESUR) Contrast Media Safety Committee (CMSC) Guidelines for prevention of post-contrast acute kidney injury (PC-AKI)

A.J. Van Der Molen¹, P. Reimer², I. Dekkers¹, G. Bongartz³, H.S. Thomsen⁴;
¹Leiden/NL, ²Karlsruhe/DE, ³Basle/CH, ⁴Herlev/DK
(A.J.van_der_Molen@lumc.nl)

Purpose: To update current ESUR CMSC guidelines for prevention of PC-AKI after administration of iodine-based contrast media (CM).

Methods and Materials: Ten answerable clinical questions were phrased by the writing group. A systematic literature search was performed for each of the questions using PubMed, Medline, Embase and Web of Science databases. Literature was selected with help of published quality metrics (PRISMA, CONSORT, STROBE), and scientific evidence was graded using Oxford CEBM levels of evidence. Scientific evidence was combined with logistic and economic aspects into practical clinical recommendations.

Results: CM are much less nephrotoxic than previously defined. PC-AKI is the preferred terminology as in most instances the causative relation with CM can't be established. The CKD-EPI and updated Schwarz equations are recommended for estimation of glomerular filtration rate (eGFR). Patients are at increased risk for PC-AKI if eGFR <30ml/min/1.73m² if CM is administered intravenously or intra-arterially with second pass renal exposure. For maximum safety, eGFR <45ml/min/1.73m² is employed if CM is administered intra-arterially with first pass renal exposure and in ICU patients. Hydration with normal saline or bicarbonate remains the primary preventive measure, using shortened protocols. Other measures in addition to hydration have not been found sufficiently effective. Metformin should be stopped temporarily if eGFR <30ml/min/1.73m² and prescribing physician should be informed. It is not needed to align contrast-enhanced procedures with schedules of chronic renal dialysis.

Conclusion: Updated CMSC guidelines for prevention of PC-AKI lowered the cut-off for preventive measures to eGFR <30ml/min/1.73m² and shortened hydration protocols, resulting in reduced costs.

Author Disclosures:

A.J. Van Der Molen: Speaker; Guerbet, Bayer, Bracco.

B-1465 10:38

Intravenous contrast media administration: is there a risk of acute kidney injury?

M.D. Ferrer Puchol, E. Sanz-Rodrigo, P. Montesinos Garcia, E. Taberner Lopez, E. Blanco Pérez, M. Forment Navarro; Alzira/ES
(lolesferrer@ono.com)

Purpose: To assess whether intravenous contrast media administration (IVCMA) is associated with an increase in creatinine levels and risk for acute kidney injury.

Methods and Materials: This is a retrospective cohort analysis that included all patients who attended the Emergency Department (ED) during 6-year period (2010-2015) with a baseline creatinine (C1) and other creatinine (C2) 24-72 hours later. The Ethics Committee approved this study. An experienced systems analyst extracted all clinical information from the available data-base stored in the institution. Exclusion criteria: patients less 18 years, serum creatinine less 0.04 mg/dL or more 4.0 mg/dL and IVCMA in the 6 months before the study. Our mean annual census in ED was 105,435 visits. There were 3 groups: 1. Patients undergoing contrast-enhanced CT (n=6,662), 2. Patients undergoing non-contrast-enhanced CT (n=6,193), 3. Not CT received patients (n=33,802). We used both criteria for "Contrast-induced Nephropathy" (CIN) and for "Acute Kidney Injury Network/Kidney Disease" (AKI). Results were presented as odds ratios using Stata 15.

Results: We analysed 52,411 patients and, after applying exclusion criteria 46,637. Mean-age 67.95 years. C1 values: 1.16 mg/dL (SD:0.61), C2 values: 1.14 mg/dL (SD:0.66). Multivariable logistic regression revealed: Using AKI and CNI criteria: CT with IVCMA was not associated with increased incidence of acute injury (OR:0.9, 95% CI 0.83-0.99 and OR:0.89, 95% CI 0.81-0.98, respectively). The value of baseline creatinine conditioned nephropathy (OR:1.41) independently of CT being performed or not.

degree assessment for the detection of functionally significant coronary artery stenosis in resting coronary computed tomography angiography (CCTA).

Methods and Materials: We retrospectively studied 126 consecutive patients (76.9% male) who received a CCTA within one year prior to an invasive fractional flow reserve (FFR) measurement. An FFR \leq 0.80 and/or PCI performed was used as a reference to indicate a functionally significant stenosis. Resting CCTA scans were performed on a 256-slice CT. Stenosis degree was categorised as 0%, 1-30%, 31-49%, 50-69% and \geq 70% by visual assessment. Patients with stenosis \geq 70% were considered significant and \leq 30% non-significant. Patients with intermediate stenosis (31-69%) were referred for deep learning analysis of the LVM evaluating presence of functionally significant stenosis. LVM was automatically segmented using a multiscale convolutional neural network and subsequently characterised using a convolutional auto-encoder. Using these encodings, patients with functionally significant stenosis were identified using a support vector machine classifier. Diagnostic performance of the combined method was compared with stenosis degree evaluation on CCTA alone (\geq 50% stenosis indicating functional significance).

Results: In 84 patients (66.7%) a functionally significant stenosis was present. Sensitivity and specificity of stenosis degree evaluation alone (cut-off \geq 50%) were 91.7% and 31.0%. The combined method resulted in an increase in specificity to 50% with only minor decrease in sensitivity (82.1%).

Conclusion: Adding deep learning-based analysis of the LVM to stenosis grading improves specificity with only minor decrease in sensitivity.

Author Disclosures:

R.W. van Hamersvelt: Research/Grant Support; This study was financially supported by the project FSCAD (104003009), funded by the Netherlands Organization for Health Research and Development (ZonMw) with participation of Pie Medical imaging BV. M. Zreik: Research/Grant Support; This study was financially supported by the project FSCAD (104003009), funded by the Netherlands Organization for Health Research and Development (ZonMw) with participation of Pie Medical imaging BV. I. Isgum: Research/Grant Support; This study was financially supported by the project FSCAD (104003009), funded by the Netherlands Organization for Health Research and Development (ZonMw) with participation of Pie Medical imaging BV. T. Leiner: Research/Grant Support; This study was financially supported by the project FSCAD (104003009), funded by the Netherlands Organization for Health Research and Development (ZonMw) with participation of Pie Medical imaging BV.. Speaker; Speakers Bureau, Koninklijke Philips NV.

B-1463 11:50

A meta-analysis on functional CT for diagnosing haemodynamically significant coronary artery disease: ready for prime time?

C. Celeng¹, T. Leiner¹, P. Maurovich-Horvat², B. Merkely², P. de Jong¹, J.W. Dankbaar¹, B. Ghoshhajra³, U. Hoffmann³, R.A. Takx¹; ¹Utrecht/NL, ²Budapest/HU, ³Boston, MA/US

Purpose: Coronary CT angiography (CCTA) provides excellent anatomical albeit limited functional information about coronary artery disease (CAD). Various CT techniques have emerged for the assessment of myocardial ischemia. We performed a meta-analysis to determine the diagnostic accuracy of myocardial perfusion (CTP), CT derived fractional flow reserve (FFR_{CT}) and coronary transmural attenuation gradient (TAG) for the detection of hemodynamically significant CAD.

Methods and Materials: This meta-analysis was performed according to the PRISMA guidelines. We systematically searched PubMed, EMBASE and Web of Science for studies using invasive FFR as a reference standard for the assessment of CAD. Results were pooled to compute summary sensitivity, specificity and the diagnostic odds ratio on vessel level. Since stenosis degree on CCTA as a standalone technique has an excellent sensitivity, specificity was considered most relevant.

Results: Thirty-four studies reported on CCTA, 12 on CTP, 17 on FFR_{CT} and 6 on TAG. With CCTA 6225, with CTP 2170, with FFR_{CT} 2372 and with TAG 726 vessels were analyzed. For the assessment of hemodynamically significant stenosis at vessel level the specificity of CCTA was 65% [95% CI: 63-66%], of CTP was 79% [95% CI: 77-81%], of FFR_{CT} was 76% [95% CI: 74-79%] and of TAG was 64% [95% CI: 60-69%]. Combining CTP with CTA resulted in a slight improvement in specificity of 84% [95% CI: 81-86%] compared to CTP alone.

Conclusion: Functional CT (CTP and FFR_{CT}) yielded a substantial improvement in the identification of hemodynamically significant CAD, therefore it is ready to be integrated into the clinical routine.

Author Disclosures:

C. Celeng: Research/Grant Support; EACVI research grant.

Conclusion: These findings demonstrate that in our context, contrast media administration is not associated with an increase in incidence of acute kidney injury.

B-1466 10:46

Survey of contrast-induced nephropathy after CT scan in patients who stayed in Sari Imam Khomeini Hospital from 2016 to 2017

H. Majidi, F. Godazandeh, R. Abdi, F. Espahbodi, R. Alimohammadpur, M. Tayebi; *Sari/IR (farnaz_godazandeh@yahoo.com)*

Purpose: With the growing use of contrast agents in diagnostic imaging techniques, the contrast-induced nephropathy (CIN) has become a major source of hospital morbidity. The aim of this study was to determine the incidence of CIN after a CT scan with contrast and identifying its risk factors.

Methods and Materials: This cross-sectional study was induced on 100 patients who had CT scan with contrast. Predictors of CIN were evaluated in four general categories: demographic variables, underlying disease, concomitant medications, and laboratory findings (level of Cr, BUN and eGFR). Cr measurement was performed 24 and 48 hours after receiving contrast agent and increment of its baseline level to more than 25% or 0.5mg/dl after 48 hours was considered as an indicator of the CIN.

Results: The incidence of CIN was 7% and it was significantly associated with hypertension ($P=0.028$) and use of ARBs ($P=0.019$). BUN and eGFR parallel to each other were observed as more accurate markers than Cr in prediction of CIN incidence. However, BUN showed higher sensitivity (71.4% vs 57.1%), eGFR indicated higher specificity (75.3% vs 65.6%).

Conclusion: Hypertension and use of ARBs are the most important risk factors for CIN. BUN has been found to be a better marker compared to eGFR and Cr in CIN prediction. Thus, attention to marker BUN in initial assessments of the CIN incidence in patients undergoing CT with contrast is highly recommended.

B-1467 10:54

Multiphase urinary tract imaging with dual contrast using spectral photon-counting CT

S.A. Si-Mohamed¹, M. Sigovan², G. Normand², P. Coulon³, D. Bar-Ness², L. Bussel¹, P. Douek¹; ¹Bron/FR, ²Lyon/FR, ³Suresne/FR (*salimaymeric@gmail.com*)

Purpose: To demonstrate the feasibility of dual contrast multiphase imaging of urinary tract using a spectral photon-counting computed tomography (SPCCT).

Methods and Materials: SPCCT with 5 energy bins (Philips Healthcare, Haifa, Israel) was used at 120 kVp, 100 mA to acquire the urinary tract in 3 rabbits, following approval by an ethics committee. The protocol was to inject at 6 minutes apart first an iodine contrast agent (Xenetix, 350 mg/ml, 1 mg/kg, Guerbet) followed by a macrocyclic gadolinium contrast agent (Dotarem, 0.5 M, 3 ml/kg, Guerbet) in order to benefit from two different phases imaging, i.e. urinary for iodine and renal for gadolinium. Acquisitions were made at 10 and 30 seconds after second injection. SPCCT provided conventional HU and quantitative material decomposition iodine and specific K-edge gadolinium maps.

Results: The conventional CT images could not allow to discriminate the specific contrast agent pharmacokinetics opposite to the gadolinium and iodine maps. We observed a dual-phase imaging with urinary cavity enhancement by the first contrast media injected and a cortical and medullar enhancement resulting from the second contrast media injected, matching the expected pharmacokinetics of the contrast media. Moreover, the water images allowed visualisation of a non-enhanced-like image.

Conclusion: SPCCT allows in vivo dual contrast quantitative multi-phase imaging in a single acquisition. This finding pinpoints major clinical applications in multiphase imaging with no registration issues and with the additional value of reducing radiation dose to patients by reducing the number of acquisitions.

Author Disclosures:

P. Coulon: Employee; Philips employee.

B-1468 11:02

Split-bolus vs single-bolus MDCT urography: comparison of urinary tract opacification, radiation dose exposure and diagnostic capability

C. Valle¹, P. Bonaffini², F. Invernizzi³, A. Barletta¹, A. Casiraghi², A. Pappini³, S. Sironi¹; ¹Bergamo/IT, ²Monza/IT, ³Desio/IT (*clarissa.valle1987@icloud.com*)

Purpose: To compare urinary tract opacification, radiation dose exposure and diagnostic capability of split-bolus MDCT urography (CTU) as compared to single-bolus protocol.

Methods and Materials: Forty-eight patients (18-83 years), undergone CTU on a 64-row scanner (Aquilion, Toshiba) after IV administration of 90-110 mL of iodinated CM (350 mg/mL), were retrospectively analyzed: 24 (study group) performed a split-bolus CTU (combined nephrographic-excretory phase) and 24 (control group) a single-bolus protocol. Quantitative analysis of intraluminal opacification (HU) was achieved by placing ROIs in renal pelvis, ureters and bladder. Qualitative analysis was performed by two radiologists (1-

consultant;2-resident) using a 4-point scale (0:none;3:excellent); inter-observer agreement was calculated. The radiation dose exposure was calculated as DLP (mGy*cm) and CTDIvol (mGy). The diagnostic capability was evaluated using a 2-point scale (0:no answer;1: question satisfied) and considering histology, further imaging and endoscopy.

Results: The split-bolus protocol demonstrated significantly lower mean urinary attenuation (HU) as compared to the control group (L pelvis 909 vs 1326, R pelvis 877 vs 1253, L ureter 810 vs 1114, R ureter 655 vs 1127, bladder 605 vs 939); no differences were observed in quality of intraluminal opacification. The mean DLP was significantly lower (1869 vs 3002 mGy*cm; $p=0.045$) in the study group (dose exposure reduction of 37%). Split-bolus protocol answered to the clinical question in almost all the cases (2 diagnoses missed).

Conclusion: With a qualitatively comparable urinary tract opacification as compared to single-bolus protocols, split-bolus CTU results in a proper ability to answer the clinical question with a significant dose reduction of 37%.

B-1469 11:10

Evaluation of parenchymal and vascular enhancement in split-bolus MDCT urography compared to standard single-bolus protocol: a feasibility study

M. Balbi¹, F. Invernizzi², P.A. Bonaffini³, G.C. Preziosa¹, D. Nicoletta², C. Valle¹, A. Pappini², S. Sironi¹; ¹Bergamo/IT, ²Desio/IT, ³Monza/IT (*balbi.m@libero.it*)

Purpose: To evaluate parenchymal and vascular enhancement in split-bolus MDCT urography (CTU) studies compared to standard single-bolus protocol.

Methods and Materials: A total of 20 split-bolus (study group, a) and 20 single-bolus (control group, b) CTU studies were retrospectively reviewed. All examinations were performed in adult patients (19-84 years) following i.v. injection of 90-110 mL of iodinated contrast medium (CM; 350 mg/mL), on a 64-row scanner (Aquilion, Toshiba). Two radiologists (1-consultant, 2-resident) independently analyzed parenchymal and vascular enhancement in both groups on combined nephro-urographic (a) and portal venous phase (b) respectively. ROIs (regions of interest) were placed on: kidneys, liver, spleen, abdominal aorta and inferior vena cava (IVC). The corresponding mean HU and radiation dose exposure values (CTDIvol and DLP) were compared between the groups and statistically analyzed.

Results: In terms of HU values there were no statistically significant differences ($p > 0.05$) between the study and the control group. The mean attenuation values for split-bolus and single-bolus CTU were respectively: 187 vs 176 HU (R kidney), 188 vs 180 HU (L kidney), 109 vs 105 HU (liver), 114 vs 106 HU (spleen), 162 vs 152 HU (aorta) and 132 vs 121 HU (IVC). CTDIvol and DLP values in the study group were significantly lower ($p < 0.05$; mean values, 54 vs 104 mGy and 1663 vs 3065 mGy*cm, respectively).

Conclusion: Split-bolus CTU may provide studies potentially useful for the evaluation of extra-renal findings due to proper vascular and parenchymal enhancement, coupled to an overall dose reduction of about 47%.

B-1470 11:18

Diagnostic value of virtual monoenergetic urographic phase images in the assessment of urothelial carcinoma

D. Zopfs, S. Lennartz, D. Maintz, T. Persigehl; *Cologne/DE (david.zopfs@uk-koeln.de)*

Purpose: To compare virtual monoenergetic images of the urographic phase (U-VMI) with polyenergetic images of the venous (V-PI) and the urographic phase (U-PI) regarding image quality, organ and vessel contrast as well as diagnostic assessment of urothelial carcinoma using a spectral-detector CT (SDCT).

Methods and Materials: Contrast-enhanced SDCT of 13 patients with histologically confirmed urothelial carcinoma were included at this retrospective study. Attenuation (HU), image noise (SD) as well as signal- and contrast-to-noise-ratio (SNR, CNR) in V-PI, U-PI and U-VMI (40-200keV) were obtained from ROI-based measurements in following regions: liver, pancreas, renal cortex and medulla, psoas muscle, subcutaneous fat, renal vein and artery, portal vein, wall of urinary bladder, lymph node, prostate and uterus. Moreover, subjective assessment of vessel contrast, parenchymal organs, urothelial carcinoma and corticomedullar differentiation of the kidneys was rated using a 5-point Likert scale.

Results: Attenuation and SNR in U-VMI at 40keV were equivalent or higher compared to V-PI (p-range: 0.69 - 0.01). Regarding image noise, no significant difference was found between V-PI and U-VMI at 40keV ($p \geq 0.05$ each). CNR of urothelial carcinoma was significantly higher in U-VMI at 40keV than in V-PI (8.24 vs. 3.80, $p \leq 0.01$). Subjective vessel contrast, assessment of parenchymal organs, carcinoma and corticomedullar differentiation received equivalent or higher Likert scores in U-VMI at 40keV compared to V-PI (p-range: 0.06 - 0.6).

Conclusion: U-VMI at 40keV yield equivalent SNR of parenchymal organs and an even increased CNR of malignant lesions in comparison to V-PI, allowing for a better delineation of urothelial carcinoma.

B-1471 11:26

CT urography: dependence of distal ureter opacification on excretory-phase timing and urinary-bladder volume

U.L. Mueller-Lisse, R. Ebner, S. Seifert, C. Stief, J. Ricke, M.F. Reiser, U.G. Mueller-Lisse; *Munich/DE*

Purpose: CT urography (CTU) is challenged by distal ureter opacification in the excretory phase (DUO). Potential dependence of DUO on excretory-phase timing after venous-phase scanning (EPT) and urinary-bladder volume (UBV) were retrospectively analysed.

Methods and Materials: Ethics committee approval was obtained for an institutional picture-archiving-and-communication-system (PACS) search of CTU-examinations from 2007 to 2016 (three sites, nine different CT-scanners) in patients with extra-urinary abdominal or pelvic tumour or trauma or suspicion of tumour and reports of unremarkable native urinary tracts bilaterally. A random sample of 147 adult patients (age \pm -standard-deviation, 63 \pm -14 years, 66 females) was reviewed by two researchers who consented on DUO of each pelvic ureter (>80% opacified). EPT-intervals (3-34 minutes) were retrieved from PACS. Venous-phase and excretory-phase UBV were estimated in multi-planar image-reconstructions (ellipsoid formula). Two-tailed statistical tests were significant for $p < 0.05$.

Results: DUO was positive bilaterally in more than 75% and failed bilaterally in less than 10% of patients for EPT 8-11 minutes (1/50 failed, versus 19/59 <8 minutes, and 12/28 12-18 minutes, 3x2-chi-square, 9.51, 0.005 $p < 0.010$). DUO frequently failed (5/7) in venous-phase UBV <120 ml and associated excretory-phase UBV increase <50 ml after 12-18 minutes (versus 9/32, Fisher's exact test, $p = 0.0442$). Technical parameters (tube-charge, CTDI, DLP, slice thickness) did not differ significantly (all T tests, $p > 0.05$).

Conclusion: DUO appears to be most successful for EPT 8-11 minutes. EPT 12-18 minutes is likely to fail DUO when venous-phase UBV is <120 ml and excretory-phase UBV-increase <50 ml.

B-1472 11:34

Kinking of the upper ureter in CT urography: anatomic and clinical significance

M. Kamio, T. Nozaki, K. Yoshida, U. Tateishi, K. Akita; *Tokyo/JP*
(kamomino@luke.ac.jp)

Purpose: Although the course of the ureter is described as a straight descent in the retroperitoneum, kinking of the upper ureter is often seen at imaging. The aim of this study was to investigate kinking of the ureter and its underlying anatomic-clinical significance.

Methods and Materials: We evaluated 176 computed tomography (CT) images and classified kinking into three grades: no/mild kinking as Grade 1, moderate as Grade 2, and severe as Grade 3. We defined the "crossing point" (CP) as where the ureter crosses over the gonadal vein and assessed its relation to the kinking. Fourteen halves from seven cadavers were used for examination. Approaching anteriorly, we macroscopically observed the ureter and surrounding structures.

Results: On CT, the rate of the radiologically "significant" kinking classified into either Grade 2 or 3 was 18.4% on the right and 21.8% on the left. All kinking was either at or above the level of the CP. In cadavers, the ureter was relatively mobile in the perirenal fat and then beginning at approximately the level of the CP became firmly fixed to the anteromedial aspect of the psoas major muscle.

Conclusion: Kinking of the upper ureter is not a clinically significant finding and arises from the ureter having a relatively mobile portion in the perirenal space compared to its caudal portion. The fixation boundary can be identified by observing the CP.

B-1473 11:42

Characterisation of renal stones using spectral detector computed tomography using normal and low-dose protocols

N. Grosse Hokamp^{1,2}, J. Salem¹, J. Holz¹, G. Dervishi¹, M. Ritter³, A. Heidenreich¹, D. Maintz¹, S. Haneder¹; ¹Cologne/DE, ²Cleveland, OH/US, ³Mannheim/DE (nils.grosse-hokamp@uk-koeln.de)

Purpose: To investigate the feasibility of renal stone composition analysis using a spectral detector computed tomography scanner with normal and low-dose imaging protocols (SDCT).

Methods and Materials: 180 stones harvested from nephrolithotripsy or nephrolithotomy with a known composition as determined by infrared spectroscopy were examined in a non-anthropomorphic phantom on a SDCT (IQon, Philips Healthcare, The Netherlands), imaging was performed with 120kVp and a) 40mAs and b) 200mAs, resulting in an CTDIvol of 2mGy and 10mGy, respectively. Besides conventional CT images (CI), SDCT enables reconstruction virtual monoenergetic images (40-200keV). Spectral coefficient images (SC) were calculated performing a voxel-by-voxel subtraction of 40keV and 200keV images (Matlab R2017b, Mathworks Inc, USA). All stones were semi-automatically 3D-segmented on CI using a threshold-based algorithm

implemented in an offline Dicom-viewer. Statistic assessment was performed applying ANOVA with Tukey-HSD post hoc for multiple comparisons.

Results: Whewellite (n=73), weddellite (n=13), brushite (n=32), cysteine (n=19) struvite (n=15) and uric acid stones (n=28) were included in the analysis. Stone volume ranged from 10.0 to 599.2mm³. While on CI attenuation differed significantly between calcified and non-calcified stones only (whewellit/weddellit/brushite vs others: 393HU vs 173HU, $p \leq 0.05$), the spectral coefficient differed significantly between (//): whewellite, weddellite/brushite/struvite, cysteine/uric acid in 10mGy protocol (all $p \leq 0.05$; 95% confidence intervals 3.4-4.3/2.6-3.6/1.4-2.2//0.5-0.9). The same results were found for the 2mGy protocol, except differentiation of brushite from whewellite and weddellite concretions was not possible ($p = 0.6$).

Conclusion: SDCT allows for differentiation of renal stones using semi-automatic segmentation and spectral coefficient images, even in low-dose imaging protocols.

B-1474 11:50

Diagnostic performance of advanced modelled iterative reconstruction-applied images for detecting urinary stones on submillisievert low-dose computed tomography

J. Ahn, S. Kim, S. Kim, I. Nam, S.-J. Lee; *Busan/KR* (radiresi@gmail.com)

Purpose: To compare the sensitivities among the variable advanced modelled iterative reconstruction (ADMIRE) strengths applied to submillisievert (sub-mSv) low-dose CT (LDCT) and standard-dose CT (SDCT) for the detection of urinary stones.

Methods and Materials: A total of 92 consecutive patients (62 men and 30 women, mean age 50.8 years, range 17-79 years) with urinary stones underwent non-enhanced abdomino-pelvic CT that consisted of SDCT (120 kVp, 200 mAs) and LDCT (80 kVp, 60 mAs). The LDCT images were reconstructed separately with 5 different strengths of ADMIRE (hereafter, S1-S5) and filtered back projection (FBP). Two blinded radiologists independently recorded a number of urinary stones in the 6 LDCT data sets and SDCT. The sensitivity of each set for detecting urinary stones was compared using the McNemar test.

Results: A total of 309 urinary stones were analysed. The sensitivities of the 6 LDCT data sets showed no significant difference (FBP, S1-S5, for reader 1: 61%, 61%, 61%, 62%, 63%, and 62%; for reader 2: 47%, 49%, 50%, 50%, 51%, and 51%, $P > 0.05$, respectively), which were lower than those of SDCT for both readers (reader 1: 88%; reader 2: 81%, $P < 0.05$, respectively).

Conclusion: The sensitivities for detecting urinary stones showed no significant differences among sub-mSv LDCT with variable ADMIRE strengths and were lower than those of SDCT.

10:30 - 12:00

Room M 5

Neuro

SS 1811b

Paediatric and adult brain tumours

Moderators:

K. Dolic; Split/HR
M. Smits; Rotterdam/NL

B-1475 10:30

The value of whole tumour volume-based T2 histogram analysis of differential diagnosis in paediatric posterior fossa tumours

K. Xu, Y. Zhang; *Zhengzhou/CN* (15188367223@163.com)

Purpose: To study the value of whole tumour T2 histogram analysis of differential diagnosis in three common paediatric posterior fossa tumours (ependymoma, astrocytoma, medulloblastoma).

Methods and Materials: A retrospective analysis was conducted by brain MRI examination and pathology diagnosis of 133 cases of posterior fossa tumours in children patients in our hospital. Among them, there are 49 cases of ependymoma (there are 25 males and 24 females), 36 cases of astrocytoma (there were 19 males and 17 females), 48 cases of medulloblastoma (there were 36 males and 12 females), respectively, to draw the region of interest (ROI) in the T₂ MR transaxial images of three groups on each layer of tumour level using Mazda software and analyse the whole tumour gray histogram, performing a statistical analysis on the three sets of parameters obtained from histograms to find out statistical significance of each parameter.

Results: Through histogram analysis of 9 parameters, these 9 parameters were statistically significant (all $P < 0.05$), including mean, variance, kurtosis, skewness, Perc.01%, Perc.10%, Perc.50%, Perc.90% and Perc.99%.

Conclusion: The whole tumours T2 grey histogram analysis of three kinds of paediatric posterior fossa tumours in the differential diagnosis has certain value. It can be used as a new auxiliary method of diagnosis in three paediatric posterior fossa tumours.

B-1476 10:38

Predicting medulloblastoma genomic subtypes by exploiting MRI morphologic phenotypes

M.S. [Alahmadi](#), M. Alharbi, N. Mobark, A.N. Alsaad, A. Daghriri, A.B. Anver, M.S.J. Althagafi, S. Raja; *Riyadh/SA (mo.alahmadi@gmail.com)*

Purpose: Standard of care mandates classification of medulloblastomas into 4 genomic subtypes (SHH, WNT, grade III and grade IV) at presentation. However, the subtyping is done invasively. Recent work suggests that MRI features may classify the subtypes non-invasively. We postulate that a combination of morphologic MRI features may be more accurate, for subtype prediction.

Methods and Materials: A retrospective review of baseline MRI of all patients already having Medullaobastoma genomic subtyping (no=22) were reviewed blindly and the MRI features were categorized by 3 radiologists (expert, intermediate, novice), based on modified Vasari criteria for example contrast enhancement, morphologic features such as location, hemorrhage, cystic component etc. using Access data-sheet, and subsequently exported to SPSS modeler for subsequent analysis.

Results: Out of 22 cases with genomic subtypes of SHH, WNT, Group III and Group IV (6,3,3 and 10). We performed a binary classification by combining into two separate groups, more aggressive Group III+IV (morAg), and less aggressive SHH+WNT (lesAg). The best discriminator was peritumoral oedema, and the 2nd best was length of lesion. The classification accuracy of the model was 90%, the model classified all lesAg correctly.

Conclusion: Our results strongly suggest that peritumoral oedema and length of lesion on MRI can accurately discriminate medulloblastoma genomic subtypes non-invasively. The unique ability of peritumoral oedema to separate between the two groups, has not yet been described in the literature. Our results show significant peritumoral oedema around lesAg lesions contrary to what is expected, we observed that the aggressive medulloblastomas show minimal peritumoral oedema.

B-1477 10:46

Application of MRI whole-tumour histogram analysis in assessment risk of medulloblastoma recurrence

Q. [Lv](#); *Zhengzhou/CN (478071645@qq.com)*

Purpose: To explore the value of MRI whole-tumour histogram in the risk assessment of medulloblastoma recurrence.

Methods and Materials: Retrospective analysis of 26 patients which were pathologically confirmed medulloblastoma. These patients were divided into two groups, which were defined as the recurrent group and the non-recurrent group, each of the groups has 13 cases. Drawing the region of interest (ROI) on each slice of enhanced MR sagittal image including and doing the histogram analysis, the two steps were both conducted by the software Mazda. The histogram parameters were analysed statistically to find out the characteristics of the significant differences between the two groups. Next, we drew the ROC curve to assess diagnostic efficiency in medulloblastoma recurrence.

Results: As for the 9 parameters extracted from histogram, the differences of the variance, the 90th and 99th percentiles between the two groups have statistical significance ($P<0.05$). Areas under the ROC curve were 0.799, 0.728 and 0.746, respectively. The variance showed the sensitivity and the specificity of the risk of medulloblastoma recurrence which were 84.6% and 61.5%, respectively; the 90th percentile suggested both the sensitivity and the specificity were 69.2%, and by the 99th percentile, they were 69.2% and 61.5%, respectively. The cutoff of variance, the 90th percentile and 99th percentile were 414.66, 128.4, 159.235, respectively.

Conclusion: MRI whole-tumour histogram analysis can be used as an important supplementary method to assess the risk of medulloblastoma recurrence.

B-1478 10:54

Paediatric astrocytic tumour grading: comparison between ASL and DSC MRI perfusion

S. [Stagliano](#)¹, D. Tortora², M. Severino², C. Martinetti², M. Garrè², A. Rossi², G. Morana²; ¹Rome/IT, ²Genova/IT (*sere.stagliano@gmail.com*)

Purpose: The aim of this study was to compare arterial spin labelling (ASL) and dynamic susceptibility contrast (DSC) MRI perfusion with respect to diagnostic performance in tumour grading in paediatric patients with low- and high-grade astrocytic tumours (AT).

Methods and Materials: We retrospectively analysed 37 children with histologically proven treatment-naïve low- and high-grade AT who underwent pre-operative ASL and DSC MRI perfusion. Studies were performed on a 1.5 T scanner and a pulsed technique was used for ASL. DSC data were post-processed with a leakage correction software. Normalisation of tumour perfusion parameters was performed with contralateral normal-appearing gray matter. Normalised ASL-derived cerebral blood flow (nASL-CBF) values in the most perfused area of each neoplasm were compared with normalised DSC-

derived cerebral blood flow (nDSC-CBF) and cerebral blood volume (nCBV) data and correlated with WHO tumour grade. Statistics included Pearson's chi-square and Mann-Whitney U tests, Spearman's rank correlation and receiver operating characteristic (ROC) analysis.

Results: A significant correlation was demonstrated between ASL and DSC data ($p<0.001$). Significant differences in terms of ASL and DSC data were found between low- and high-grade AT ($p<0.001$). ROC analysis demonstrated similar performances between all parameters in predicting tumour grade (nASL-CBF: AUC 0.98, $p<0.001$; nDSC-CBF: AUC 0.97, $p<0.001$; nCBV: AUC 0.97, $p<0.001$).

Conclusion: Normalised pulsed ASL performed with a 1.5 T scanner provides comparable results to DSC MRI perfusion in paediatric AT and allows distinction between high- and low-grade AT.

B-1479 11:02

Differentiation of medulloblastoma and astrocytoma in children using histogram analysis of enhancement MRI

W. Wang¹, Y. Zhang¹, J. Cheng¹, Z. Zhang²; ¹Zhengzhou/CN, ²Henan/CN (*252936888@qq.com*)

Purpose: To investigate the diagnostic value of the histogram analysis derived from enhancement MR imaging in differentiating medulloblastomas from astrocytomas.

Methods and Materials: Retrospective analysis of 47 patients which were pathologically confirmed posterior fossa tumours, including 29 cases of medulloblastoma and 18 cases of astrocytoma. Drawing the region of interest (ROI) on the maximum level of enhanced MR sagittal image and going on histogram analysis, these two steps are all performed on the software named Mazda. A statistical analysis was performed on the histogram parameters to find out the characteristics of the significant differences between the two groups.

Results: In the 9 parameters which are extracted from histogram, C99 has the statistical significance. The maximum area under the ROC curve was 0.85. The optimum C99 to distinguish medulloblastomas from astrocytomas was 176.5 (76% specificity and 61% sensitivity).

Conclusion: Histogram analysis of enhancement MR imaging can provide reliably objective basis for differentiating medulloblastomas from astrocytomas.

B-1480 11:10

3D fast spin-echo T1 black-blood imaging for the preoperative detection of venous sinus invasion of meningioma: comparison with contrast-enhanced MRV

D. Wang; *Shanghai/CN (wangddfsk@126.com)*

Purpose: A comprehensive understanding of venous situation is helpful for optimised treatment decisions and for managing the severe complications of meningiomas adjacent to venous sinuses. To prospectively evaluate the diagnostic value of 3D FSE T1 CUBE MR imaging in comparison with contrast-enhanced MRV in the detection of sinus invasion by meningiomas.

Methods and Materials: Forty consecutive patients with suspected meningiomas adjacent to venous sinus underwent conventional MR imaging, CE-MRV and 3D CUBE T1WI scanning. Two neuroradiologists independently assessed images for (1) wall invasion and (2) lumen invasion of target venous sinus.

Results: 3D CUBE T1WI imaging was found to afford an easy way to detect the venous wall invasion by para-venous lesions. The inter-observer agreement was excellent ($\kappa=0.851$; 95% CI, 0.769-0.933) and the result was basically aligned with the surgical findings (sensitivity of 90.91%, specificity of 94.44%, PPV of 95.23%, NPV of 89.47% and Youden Index of 0.85). In the analysis of the lumen invasion, the inter-observer agreement obtained by 3D CUBE T1WI sequence was excellent ($\kappa=0.958$; 95% CI, 0.917-0.999) with a diagnostic accuracy of 92.5% based on surgical findings, which surpassed CE-MRV not only in inter-observer agreement ($\kappa=0.717$; 95% CI, 0.622-0.812) but also in diagnostic value (accuracy=65%). Among all 40 patients, no correlation was found between the extent of peritumoural oedema and venous invasion.

Conclusion: 3D CUBE T1WI sequence is a reliable technique to provide accurate assessment about the venous sinus invasion by meningioma. Meanwhile, CE-MRV is more suitable in the evaluation of the bypass draining veins around the tumour.

B-1482 11:18

Quantitative T1rho-weighted magnetic resonance imaging in gliomas: a preliminary study of its biochemical mechanism

Y. Yu, Y. Ren, H. Pang, Z. Yao; *Shanghai/CN (yy_0324@126.com)*

Purpose: To evaluate the utility of quantitative T1rho value for differentiating between low-grade and high-grade gliomas, and make a preliminary exploration of its possible molecular basis.

Methods and Materials: Thirty-six patients (28 males and 8 females; 43.9 ± 13.7 years) with pathologically verified gliomas were included in this study. MRI was performed for each patient on a 3.0T MRI system. An echo-planar

imaging-based T1rho-weighted MR pulse sequence (spin-lock times 20, 40, 60, and 80 ms) was employed to obtain single-slice images of maximum lesion. T1rho value maps were created using MATLAB software. The T1rho value of glioma parenchyma was measured on a manually drawn region of interest and correlated with the pathological grade of the gliomas. Furthermore, we calculated the hyaluronan intensity of each pathologic sections and analysed the correlation between intensity of hyaluronan and T1rho value.

Results: There were a total of 37 lesions (0, 22, 3 and 12 tumours of grades I, II, III, and IV, respectively) in the study. Low-grade (grades I and II) gliomas had significantly higher T1rho value than high-grade (grades III and IV) gliomas (179.22 ± 44.93 ms vs. 126.24 ± 22.91 ms; $P < 0.001$). With a cutoff T1rho value of 147.68 ms, the sensitivity for glioma grading was 81.8% and the specificity was 93.3%. Pathologically, T1rho value has a poor correlation with hyaluronan intensity in glioma.

Conclusion: Quantitative T1rho value can be a reliable imaging biomarker of the malignancy of brain gliomas. The cellular and molecular basis of T1rho is still unknown.

B-1483 11:26

DCE-MRI in human gliomas: a surrogate for assessment of invasive hypoxia marker HIF-1 α based on MRI-neuronavigation stereotactic biopsies

Q. Xie¹, J. Wu², Y. Ren¹, H. Pang¹, H. Zhang¹, T. Jin¹, Y. Wu¹, Z. Yao¹, X. Feng¹; ¹Shanghai/CN, ²Nantong/CN (xieqianjames@foxmail.com)

Purpose: The purpose of this study was to correlate dynamic contrast-enhanced magnetic resonance imaging (DCE-MRI) parameters with data from a specific marker of hypoxia, hypoxia-inducible factor 1 α (HIF-1 α), in human gliomas on a point-to-point basis using coregistered MRI and frameless stereotactic biopsies.

Methods and Materials: Thirty-four patients with treatment-naive gliomas underwent DCE, axial T1-weighted (T1W), T2-weighted (T2W), T2-weighted fluid acquisition of inversion recovery (T2FLAIR), and three-dimensional T1-weighted brain volume with gadolinium contrast enhancement (3D T1BRAVO+C) sequences on a 3.0-T MR scanner before stereotactic surgery. Quantitative perfusion indices such as endothelial transfer constant (K^{trans}), fractional extravascular extracellular space volume (V_e), fractional plasma volume (fpV), and reflux rate (k_{ep}) were measured at corresponding stereotactic biopsy sites. Each sample was considered an independent measurement, and its histology grade was diagnosed. HIF-1 α expression was quantified from the point-to-point biopsy tissues. Analyses of receiver operating characteristic (ROC) curves were done for HIF-1 α to discriminate different grades of glioma. To look for correlations between immunohistochemical (IHC) parameters and DCE indices, Spearman's correlation coefficient was used.

Results: Seventy biopsy samples from 34 subjects were included in the analysis. Mean immunoreactivity scores of HIF-1 α were 2.75 ± 1.11 for grade II ($n=24$), 6.20 ± 2.33 for grade III ($n=20$) and 10.46 ± 2.42 for grade IV ($n=26$). HIF-1 α showed very good-to-excellent accuracy in discriminating grade II from III, III from IV, and II from IV (area under the curve = 0.838, 0.862 and 0.994, respectively). K^{trans} and V_e showed a significantly positive correlation with HIF-1 α expression ($r = 0.686$, $P < 0.001$; $r = 0.549$, $P < 0.001$, respectively).

Conclusion: Our study demonstrated HIF-1 α to be a significant predictor of different grades of gliomas with high sensitivity and specificity. DCE-MRI is a useful, non-invasive imaging tool for quantitative evaluation of HIF-1 α , and its parameters may be used as a surrogate for HIF-1 α expression.

B-1484 11:34

3D MRSI biomarkers of glial tumour

T. Anastasia, I. Pronin, L. Fadeeva, V. Kornienko; Moscow/RU (alfa.net@list.ru)

Purpose: To evaluate metabolite ratio in the whole tumour volume on the base of 3D 1H-MP spectroscopy in patients with glial brain tumours.

Methods and Materials: 20 healthy volunteers (age 26-65 years), 20 patients (age 28-65 years) with low-grade gliomas and 20 patients (age 25-60 years) with high-grade gliomas were examined in our study. We assessed the following metabolites: choline, creatine and N-acetylaspartate.

Results: In control group of healthy volunteers, we measured the metabolite ratio in white and grey brain matter. There were following ratios in white matter: Cho/NAA - 1.45 ± 0.30 , Cho/Cr - 1.15 ± 0.11 , NAA/Cr - 2.70 ± 0.20 and grey matter: Cho/NAA - 0.52 ± 0.09 , Cho/Cr - 1.14 ± 0.11 , NAA/Cr - 2.53 ± 0.19 . In glial brain tumours the good correlation between an elevation of Cho/Cr ratio, decreases of NAA/Cr ratio and degree of malignancy were found. High-grade gliomas demonstrated an elevation of Cho/Cr (3.41 ± 0.79) and Cho/NAA (2.27 ± 1.3), compared with low-grade tumours Cho/Cr (2.54 ± 1.44) and Cho/NAA (2.76 ± 1.2). NAA/Cr ratio was higher in low-grade gliomas (1.44 ± 0.57) in comparison with grade III-IV lesions (0.95 ± 0.41).

Conclusion: 3D MRSI provides the clinicians qualitative and quantitative markers of brain biochemistry in normal brain and in gliomas. Precisely to evaluate the tumour malignancy.

B-1485 11:42

Brain tumour-induced alterations in haemodynamic responses of BOLD fMRI

L. Wang^{1,2}, Y. Zhang³, Z. Liu⁴, D. Chen⁵, L. Liu¹, H. Mao²; ¹Shenzhen/CN, ²Atlanta, GA/US, ³ShenZhen/CN, ⁴Nanchang/CN, ⁵Suzhou/CN (2718377613@qq.com)

Purpose: To investigate the effect of brain tumours on the haemodynamic responses and its impact on BOLD MRI signal time course to better understand tumour-induced alterations in haemodynamic responses and for accurate mapping in brain tumour patients.

Methods and Materials: fMRI data from 42 glioma patients who underwent presurgical mapping of primary motor cortex (PMC) with a block-designed fingertapping paradigm were analysed, retrospectively. Cases were divided into high- ($n=24$) and low- ($n=18$) grade groups based on pathology. Tumour volume and distance to the activated PMCs were measured. BOLD signal time courses from selected regions of interest (ROIs) in the PMCs of tumouraffected and contralateral unaffected hemispheres were obtained from each patient. Tumour-induced changes of BOLD signal intensity and time to peak (TTP) were analysed statistically.

Results: BOLD signal intensity and TTP in the tumour-affected PMCs are altered when compared with that in the unaffected hemisphere. The average BOLD signal level is statistically significantly lower in the affected PMCs. The average TTP in the affected PMCs is shorter in the high-grade group, but longer in the low-grade group compared to the contralateral unaffected hemisphere. The degrees of alterations in BOLD signal time courses are related to both the distance to activated foci and tumour volume, with a stronger effect in tumour distance to activated PMC.

Conclusion: Alterations in BOLD signal time courses are strongly related to tumour grade, tumour volume, and distance to the activated foci. Such alterations may impair accurate mapping of tumour-affected functional areas when using conventional fixed models.

10:30 - 12:00

Sky High Stage

Paediatric

MY 18

Paediatric

Moderators:

M. Haliloglu; Ankara/TR
P. Tomà; Rome/IT

B-1486 10:30

Volumetric histogram-based analysis of SUV and ADC values for the assessment of paediatric sarcomas at staging: preliminary results of a PET/MR study

A. Varotto¹, G. Orsatti¹, F. Crimi¹, D. Cecchin¹, P. Zucchetta¹, M. Weber², R. Stramare¹, C. Giraud¹; ¹Padua/IT, ²Vienna/AT (ale.varotto86@gmail.com)

Purpose: Previous studies showed heterogeneous results about the correlation between metabolic activity and cell density in sarcomas. Thus, our aim was to assess the relationship between ADCs and SUVs in paediatric sarcomas at staging, using histograms obtained by volumetric analyses.

Methods and Materials: Paediatric patients with histologically proven sarcoma, referring to our tertiary centre for a whole-body [18F]-FDG-PET/MR for staging and including DWI in the MR protocol were investigated. First, TIRM and PET images were re-sliced and resampled according to the ADC maps (i.e. Osiris Software). Regions of interest were drawn along tumour margins on TIRM images and then copied on PET and ADC datasets. Pixel-based SUVs and ADCs were collected from the entire volume of each lesion. Mean, median, skewness, kurtosis of SUVs and ADCs values were computed and Pearson correlation coefficient was applied (i.e. for the entire population and separately, for histological subgroups including more than five patients).

Results: Ten patients met the inclusion criteria (five males; mean age 8.9 ± 5.7 years). Histology revealed six rhabdomyosarcoma (i.e. three alveolar and three embryonal), two Ewing-sarcoma, one diffuse myofibromatosis and one chondroblastic osteosarcoma. The mean volume of the lesions was 135.46 ± 172.16 cm³. A significant negative correlation between ADCs' and SUVs' mean ($r_{\text{mean}} = -0.326$, $p < 0.001$), median ($r_{\text{median}} = -0.393$, $p < 0.001$) and skewness ($r_{\text{skewness}} = -0.623$, $p < 0.001$) emerged for the entire population and for rhabdomyosarcomas ($r_{\text{mean}} = -0.365$, $p = 0.002$, $r_{\text{median}} = -0.467$, $p < 0.001$, $r_{\text{skewness}} = -0.691$, $p < 0.001$) whereas a significant positive correlation was found for kurtosis ($r_{\text{kurtosis}} = 0.412$, $p < 0.001$ and $r_{\text{kurtosis}} = 0.395$, $p < 0.001$, respectively, for the entire population and for rhabdomyosarcomas).

Conclusion: Our preliminary results demonstrate that, using volumetric histograms, SUVs and ADCs are dependent biomarkers in paediatric sarcomas. Further studies, on a larger population, are necessary to confirm this evidence and assess its clinical implications after therapeutic treatment.

B-1487 10:34

Computer-assisted detection of acute pulmonary embolism in children and young adults: inter-observer effect

C. Tang¹, C. Zhou¹, U.J. Schoepf², D. Mastrodicasa³, Y. Zhao¹, L. Lu¹, X. Li¹, M. Lu¹, L. Zhang¹; ¹Nanjing/CN, ²Charleston, SC/US, ³Chieti/IT (522956587@qq.com)

Purpose: To evaluate the effect of a CAD algorithm on the identification of acute PE on CTPA studies in children and young adults by readers with varying experience levels.

Methods and Materials: In this retrospective study, six readers with differing levels of experience evaluated 303 patients' CTPA studies (range, 6-25 years) on per-emboli basis. Observers were asked to independently determine the presence of PE and rank their diagnostic confidence on a five-point scale with and without CAD. Reading time was recorded and sensitivities, specificities, accuracies, PPVs and NPVs were calculated.

Results: For all readers, there was no diagnostic performance difference in detecting central PE in the first to the third levels of the pulmonary arteries with or without the CAD (all P values >0.05). However, significant differences were found in the detection of peripheral PE with CAD versus without CAD. Except the most experienced reader, the sensitivities and NPVs differed significantly between with CAD and non-CAD readings. Additionally, the accuracies of all readers differed significantly between readings done with or without CAD. For each reader, the time with CAD was longer than those without CAD. Significant differences were found for confidence scores in inter-group measurements with CAD ($P=0.045$) and without CAD ($P<0.001$), but no difference in the confidence scores of any individual readers between CAD and non-CAD readings ($P>0.05$).

Conclusion: At the expense of longer reading time, the use of CAD improves sensitivities and NPVs for most readers and the accuracies of all readers in peripheral PE detection.

Author Disclosures:

U.J. Schoepf: Consultant; Bayer, Bracco, GE Healthcare, Medrad, and Sieme. Research/Grant Support; Bayer, Bracco, GE Healthcare, Medrad, and Sieme.

B-1488 10:38

Clinical equivalence assessment of T2 synthetic paediatric brain MRI

B. Kerleroux¹, T. Kober², T. Hilbert³, D. Sirinelli¹, B. Morel¹; ¹Tours/FR, ²Zurich/CH, ³Lausanne/CH (basile.kerleroux@gmail.com)

Purpose: Automated synthetic MR imaging (SyntMRI) provides different image contrasts as well as quantitative information from one scan. It would well suit paediatric neuroradiology for various applications such as analysis of white matter disorders. However, SyntMRI has been poorly evaluated in this population. The purpose of this study was to compare the image quality of synthetic T2 with conventional TSE T2 in paediatric brain MRI.

Methods and Materials: This was a mono-centre prospective study. Synthetic and conventional MRI acquisitions at 1.5 Tesla were performed for each patient during the same session using a prototype accelerated T2 mapping sequence package ($TA_{\text{synthetic}}=3:07$ min, $TA_{\text{conventional}}=2:33$ min). Image sets were blindly and randomly analysed by senior and fellow paediatric neuroradiologists. Global image quality, morphologic legibility of standard structures and artefacts were assessed using a 4-point Likert scale. Inter-observer kappa agreements were calculated. The capability of SyntMRI and conventional T2 to discern normal and pathological cases was evaluated.

Results: Sixty patients were enrolled. The diagnostic quality of SyntMRI was non-inferior to conventional imaging scale ($p=0.06$). There was no significant difference in the legibility of normal and pathological anatomic structures of synthetic and conventional T2 (all $p > 0.05$) as well as for artefacts except for phase encoding ($p=0.008$). Interobserver agreement was good to almost perfect (kappa between 0.66 and 1).

Conclusion: T2 SyntMRI, which provides quantitative T2 information that could be used to build normative databases of healthy subjects, could be suggested as an equivalent technique in paediatric neuro-imaging, compared to conventional TSE T2.

Author Disclosures:

T. Kober: Employee; Siemens.

B-1489 10:42

Effect of a child-adjusted method for brain volume quantification on group comparisons in dyslexia

T. Phan, D. Smeets, M. Vandermosten; Leuven/BE (van.phan@icometrix.com)

Purpose: A child-adjusted method for the quantification of grey matter (GM) and white matter (WM) volumes in young children is introduced, and its impact on group comparisons between healthy controls and dyslexia is assessed.

Methods and Materials: T1-weighted images were acquired from children of 5-6 years old (21 controls, 15 children with dyslexia) and checked for motion artefacts. For brain volume quantification, the brain segmentation was adjusted to children by the use of an age-specific atlas and probabilistic model-based

algorithm (referred to as childmetrix). Group comparisons based on GM and WM volumes estimated by this method are compared to results obtained with a method using the same segmentation algorithm, but based on an adult atlas (icobrain) and a method using a surface model-based segmentation based on an adult atlas (Freesurfer).

Results: Subtle differences between healthy controls and children with dyslexia were better captured by childmetrix that showed a higher effect size (Cohen's d of 0.40 for GM and 0.45 for WM) compared with icobrain (GM: 0.27, WM: 0.40) and Freesurfer (GM: 0.31, WM: 0.38). Compared to the literature, the results obtained with childmetrix on children of 5-6 years old were similar to differences measured in older populations (GM: 0.40, WM: 0.40).

Conclusion: The choice of segmentation method has an impact on group comparisons. Brain segmentation is adapted to young children (under 6 years old) by the use of an age-specific atlas, which enables measuring the subtle differences that might not be observed using standard methods based on adult atlas.

Author Disclosures:

T. Phan: Employee; employee at icometrix. Research/Grant Support; European Union H2020 MSCA-ITN-2014-ETN Programme, ChildBrain, #641652. **D. Smeets:** Employee; employee at icometrix.

B-1490 10:46

Enhancement of MRI histogram in the identification of children with medulloblastoma and ependymoma

W. Wang, J. Cheng, Y. Zhang; Zhengzhou/CN (weijianwang520@163.com)

Purpose: To investigate the diagnostic value of the histogram analysis derived from enhancement MR imaging in differentiating medulloblastomas from ependymoma.

Methods and Materials: Retrospective analysis of pathologically confirmed 36 cases of posterior fossa tumors, including 20 cases of medulloblastoma, 16 cases of ependymoma. The collection of the two kinds of tumor T1, T2 and enhanced T1 weighted magnetic resonance images, extraction of tumor region of interest using the software of MaZda (region of interest, ROI), histogram analysis for the maximum level of tumor region of interest, using the average value, variance, skewness, kurtosis, the 1,10,50,90,99 percentile characteristics, find out the significant differences between the two kinds of tumors.

Results: Histogram analysis of ADC including the mean, variance, skewness, kurtosis, the 1,10,50,90,99 percentile characteristics. The mean, variance, skewness, 90th and 99th percentile were detected statistical significance. ROC curve analysis of the variance yielded the best area under the ROC curve (AUC: 0.90), sensitivity of 92%, and specificity of 90%, with a cutoff value of 820.

Conclusion: Histogram analysis can provide more quantitative information characteristics, which provides a new method for the differential diagnosis of children with medulloblastoma and ependymoma.

B-1491 10:50

Prenatal imaging of anorectal malformations

L. Rohrer, Y. Vial, R. Meuli, L. Alamo-Maestre; Lausanne/CH (lysiane.rohrer@gmail.com)

Purpose: Anorectal malformations (ARM) are usually classified as low, intermediate and high type. Most of them are first discovered after birth. The purpose of this study is to describe the imaging signs suggesting ARMs at prenatal US and MRI exams in order to improve early diagnosis and optimize perinatal care.

Methods and Materials: All available prenatal imaging studies performed on children treated for ARM at the University Hospital of Lausanne between 2001-2016 were retrospectively reviewed and compared with the final diagnosis (low or intermediate-high ARM), obtained from postnatal imaging studies, surgery and/or autopsy records.

Results: We identified 54 children treated for ARM. Only 5 cases (9.2%) were diagnosed *in utero*. Prenatal exams were available in 17 cases (15 US, 7 MRI) corresponding to 5 low- and 12 intermediate-high type ARM, including 5 cloaca. Diagnosis was prenatally suspected in 5/17 (29.4%) and associated anomalies, mainly vertebral and renal, present in 15/17 cases (88%). Retrospectively evaluation identified imaging findings suggesting ARMs in 11/17 cases (64.7%, 1/5 low and 10/12 intermediate-high type ARMs). Findings include small or no anus identification and distal digestive dilatation in ARMs without fistula; rectal echogenic fluid and rectal hyperintense signal in T2-WI MRI images in ARMs with fistula and genital duplication and pelvic cystic masses in cloaca.

Conclusion: Prenatal diagnosis of ARMs requires a routine and systematic examination of the fetal pelvis and perineal area, especially in presence of vertebral, renal or genital anomalies. However, low type malformations remain extremely difficult to recognize.

B-1492 10:54

Prognostic value of radiological response assessment after induction therapy in paediatric soft tissue sarcomas

G. Orsatti¹, A. Varotto¹, F. Crimi², G. Bisogno¹, I. Zanetti¹, C. Giraudo¹, R. Stramare¹; ¹Padua/IT, ²Vicenza/IT (*giovanna_orsatti@hotmail.it*)

Purpose: Previous studies showed controversial results about the correlation between the dimensional modification, due to induction therapy, of paediatric soft tissue sarcomas (pSTS) and patients' outcome. Thus, our aims were to compare three methods of pSTSs dimensional assessment and evaluate their prognostic value.

Methods and Materials: Forty-five paediatric patients with non-metastatic STS (26 rhabdomyosarcomas and 19 non-rhabdomyosarcomas) who underwent MR or CT imaging at staging and after three cycles of chemotherapy were included. Three observers measured the tumour size using three different methods: maximal diameter, estimated volumetric assessment (the product of the three-maximal diameters and $\pi/6$) and software-assisted volumetric assessment. To investigate the interobserver agreement, the Overall Concordance Correlation Coefficient (OCCC) was calculated. Regarding tumour response, each patient was classified as "Good responder" (i.e., including Very good and Partial Response) or "Poor responder" (i.e., including Stable and Progressive Disease) according to each radiological method. To assess the inter-method agreement, Cohen's kappa coefficient was calculated. The Kaplan-Meier method was used to estimate the event-free survival (EFS) distribution. Differences between survival curves were analysed by the log-rank test.

Results: Interobserver agreement was very high for each method (OCCC > 0.9). The three methods showed a poor agreement regarding the classification of tumour response (i.e., highest value, $k=0.56$ between the two volumetric techniques). In rhabdomyosarcomas, the three-years EFS resulted to be significantly higher in "Good Responders" than in "Poor responders" using the estimated (76.2% vs 40%, $p=0.02$) and the software-assisted volumetric assessment (80% vs 33.3%, $p=0.002$) whereas no significant differences emerged for the "non-rhabdomyosarcomas" ($p>0.05$, for each method).

Conclusion: The volumetric assessment, especially when software-assisted, demonstrated to be a significant prognostic factor for paediatric STSs. Larger future studies are necessary to confirm these preliminary results.

B-1493 10:58

Central nervous system (CNS) involvement in congenital heart diseases (CHD): value of foetal MRI

R. Petrillo, A. Antonelli, S. Bernardo, S. Satta, V. Vinci, L. Manganaro, C. Catalano; *Rome/IT (roberta.petrillo@hotmail.it)*

Purpose: To demonstrate the diagnostic value of foetal MRI in the detection of CNS impairment in prenatally echocardiographic diagnosed CHD.

Methods and Materials: We retrospectively examined 24 fetuses (mean gestational age: 19-33), between February 2012 and April 2017, who underwent MRI in our institution at 1.5 T (Siemens Magnetom Avanto), without maternal sedation, after a foetal echocardiography. Prenatal findings were compared to fetopsy results, foetal MRI after 30 GW or postnatal MRI.

Results: On 24 cases, 7/24 had interatrial septal defect (IASD), interventricular septal defect (IVSD), and atrioventricular canal defect (CAVC), 6/24 had cardiac rhabdomyomas, 3/24 had hypoplastic left heart syndrome and hypoplastic aorta, 2/24 had transposition of the great vessels, 2/24 had Fallot tetralogy, 2/24 had aorta coarctation and 2/24 had intracardiac masses of uncertain significance. Magnetic resonance imaging was able to detect CNS impairment: we recognise 11/24 corpus callosum (CC) dysgenesis (4/13 CC hypoplasia, 4/13 complete CC agenesis, 3/13 partial CC agenesis), 7/24 ventriculomegalies or hydrocephalus, 3/24 subtentorial anomalies (Dandy-Walker, vermian hypoplasia and vermian malrotation), and 3/24 gyration anomalies.

Conclusion: Due to the high risk of CNS involvement in prenatal congenital heart diseases, it is essential to suggest an MRI study of the evolving foetal brain, especially in complex forms that suggest a syndromic background. Foetal MRI of the CNS is mandatory in the study of congenital heart disease due to the high rate of encephalic anomalies associated, particularly in IASD, IVSD and CAVC.

B-1494 11:02

Vermis-to-Pons ratio in the differential diagnosis of Vermian malformations: a foetal MRI study

A. Antonelli, S. Bernardo, R. Petrillo, S. Satta, S. Ciulla, V. Vinci, L. Manganaro, C. Catalano; *Rome/IT (amanda.antonelli@hotmail.it)*

Purpose: To assess the feasibility of Vermis-to-Pons Ratio in helping the prenatal MR diagnosis of isolated Dandy-Walker Malformation (DWM), in fetuses with a Ultrasonographic (US) suspicion of Posterior Cranial Fossa (PCF) abnormalities.

Methods and Materials: A total of 38 fetal MRI, performed in our department between April 2013 and June 2017 after a US examination, were retrospectively reviewed. All MRI examinations were performed using a 1.5 Tesla Magnetom Avanto (Siemens, Erlangen, Germany) without maternal sedation. Gestational Age (GA) range was 20-31 weeks. The study sample included fetuses with a US suspicion of PCF malformations such as DWM, vermian hypoplasia/agenesis, vermian malrotation and Walker Warbourg Syndrome (WWS); fetuses with Chiari Malformation type II, cerebellar hemorrhage and rhombencephalosynapsis were excluded. Vermis-to-Pons Ratio was manually measured in all cases.

Results: Fetal Magnetic Resonance Imaging found 16/38 cases of DWM, 6/38 of vermian malrotation, 2/38 of WWS and 4/38 isolated vermian hypoplasia; 10/38 fetuses had normal PCF anatomy and sub-tentorial morphology. In DWM the Vermis-to-Pons ratio was <1, while in normal fetuses was ≥ 1 . Depending on the maternal decision to continue the pregnancy, prenatal MRI findings matched with both fetopsy results and postnatal MRI.

Conclusion: The Vermis-to-Pons Ratio could be an additional parameter and a helpful tool in the assessment of PCF malformations, with a special focus on the differential diagnosis between DWM and vermian malrotation.

B-1495 11:06

Radiation use in paediatric age: are paediatricians updates of the state of the art legislation?

S. Salerno¹, C. Tudisca¹, C. Granata², D. Origgi³, L. Moro⁴, M. Barbagallo⁵, G. Corsello¹, A. Villani²; ¹Palermo/IT, ²Genoa/IT, ³Milan/IT, ⁴Pavia/IT, ⁵Catania/IT, ⁶Rome/IT (*ssalerno@sirm.org*)

Purpose: To assess the opinion on use of radiation in paediatric age and radiation protection knowledge by paediatricians members of the Italian Paediatric Society (SIP) via an online survey.

Methods and Materials: All members received an email invitation to join the survey as an initiative by the "Radiation in Paediatrics" project involving SIP, Italian Society of Medical Radiology (SIRM) and Italian Association of Medical Physics (AIFM) Scientific Societies. The survey included 11 questions about general knowledge on radiation protection and new legislation on the theme/issue of the respondents and eventual criticisms found in radiation protection field in the everyday practice.

Results: 877 SIP members participated in the survey and have entirely fulfilled the questionnaire. The most significant results of the survey were: 57.6% of the participants ignore the existence of guidelines that can help them in choosing the most appropriate diagnostic examination according to patient's symptoms, and the 47.1% has difficulties to evaluate the risk related to the use of examination using ionizing radiation. 43% do not know the European Directive 2013/59 Euratom. 98% of the participants believe it is necessary to grow their knowledge on the topic of radiation protection, considering useful a specific training on practical issues.

Conclusion: Most paediatricians were interested in radiation protection theme and considered their knowledge inadequate for their daily practice. Aim of the radiological society should be to organize a large-scale information campaign to spread the theme of radiation protection in a paediatric environment.

B-1496 11:10

Histogram analysis of apparent diffusion coefficients may predict molecular subgroups of medulloblastoma in children

W. Wang, J. Cheng, Y. Zhang; *Zhengzhou/CN (weijianwang520@163.com)*

Purpose: The aim is to verify if ADC histogram is able to predict new subgroups of MB.

Methods and Materials: sixty-five patients with diagnosis of MB (30 classic, 8 desmoplastic/nodular, 7 extensive nodularity, 20 large cell/anaplastic), with pretreatment MR imaging, histologic, genomic characterisation after surgery, were retrospectively selected. ADC maps were coregistered with T1w post-contrast and T2 images. Drawing the region of interest (ROI) on the maximum level of ADC maps and going on histogram analysis, these two steps are all performed on the software named Mazda. We used the Mann-Whitney test to evaluate the capacity of histogram parameters to discriminate among paired MB subgroups.

Results: Desmoplastic/nodular and extensive nodularity were detected no statistical significance. A trend in differences was found between classic and large cell/anaplastic. 9 texture parameters using histogram extracted, with statistical significance (mean, variance, 1 percent, 10 percent). ROC curve analysis of the 10th percentile yielded the best area under the ROC curve (AUC: 0.96), sensitivity of 98%, and specificity of 96%, with a cutoff value of 90.

Conclusion: The study shows histograms analysis of apparent diffusion coefficient can provide reliably objective basis for molecular subgroups of medulloblastoma in children.

B-1497 11:14

The role of prenatal diffusion weighted MRI in the evaluation of the fetal CNS condition in patients who received intrauterine blood transfusion as the hemolytic disease treatment

A.A. Berman¹, A. Ageev¹, O. Chernova², A. Vazhenin², ¹Ekaterinburg/RU, ²Chelyabinsk/RU (ageev.artem@gmail.com)

Purpose: The purpose of the study is to evaluate the appropriateness of prenatal MRI using diffusion weighted sequences in the evaluation of fetal brain focal lesions in cases of mother's hemolytic anemia before and after treatment of fetuses by intrauterine blood transfusion.

Methods and Materials: The focus group included 30 pregnant women with presence of haemolytic fetal disease by Rh- factor, which required treatment who underwent intrauterine blood transfusion, and further their 30 newborns with hemolytic disease and perinatal hypoxic-ischemic brain injury. The control group included 15 pregnant women without hemolytic disease with concomitant pathology of pregnancy comparable in gestational age, and further their 15 newborns. Prenatal MRI were performed at 1,5 T scanner. MRI protocol included DWI sequences with b0 and b700 s/mm². The local lesions in the fetal brain detected on MRI were defined as focal zones of hyperintensive signal at the T2 and DWI sequences accompanied by the signal restriction on the ADC maps.

Results: 45 focal lesions in 30 patients in focus group were revealed before therapy and only 12 focal lesions were revealed after therapy before birth. Average size of lesions was 1,8x1,9x2,1 mm and 0,4x0,4x0,5 mm respectively. No lesions were revealed in control group.

Conclusion: A statistically significant difference in the MRI data in focus and control group and before and after intrauterine blood transfusion was obtained thus prenatal MRI with DWI sequences was considered to be appropriate for pathomorphological evaluation of fetal focal brain lesions and evaluation of effectiveness of intrauterine hemotransfusion.

B-1498 11:18

Hepatobiliary ultrasonographic abnormalities and clinical severity score of paediatric sickle cell anaemia patients in a resource-poor setting

D. Ibe; Kaduna/NG (church.donaldo@yahoo.com)

Purpose: To determine the relationship between hepatobiliary ultrasonographic abnormalities and clinical severity score of paediatric sickle cell anaemia patients.

Methods and Materials: A cross-sectional descriptive study of hepatobiliary ultrasonographic findings of 420 steady-state paediatric sickle cell anaemia patients aged 1-18 years was conducted using Mindray (DC8) ultrasound machine. Clinical severity score was assessed based on 3 parameters: (a) the present state of the child: splenic (0-2) and hepatic (0-2) enlargement, current haematocrit (0-2) and total white blood count (0-2); (b) frequency of significant painful episodes (0-3), blood transfusion (0-3), and hospitalization (0-3) in the previous 12 months and (c) lifetime cumulative incidence of complications for each patient: cerebrovascular accident (5), acute chest syndrome (3), pneumococcal meningitis (3), avascular necrosis (2), gallstone (1), chronic leg ulcer (1), osteomyelitis (1), or priapism (1). A total score calculated ranged from 0 to 34 and the disease categorized as: mild (<8), moderate (8-17) and severe (>17). Chi-square test and Fisher's exact test were used to test for statistical relationship between variables.

Results: One hundred and forty-seven (35%) patients had hepatobiliary abnormalities with hepatomegaly (66.7%), biliary sludge (28.6%) and gallstones (17%) as the common findings. Mild and moderate forms of clinical severity of sickle cell anaemia were seen in 45.6% and 54.5%, respectively. None of the patients had a severe form of clinical severity. There was a statistically significant association between hepatobiliary abnormalities and the clinical severity of steady-state paediatric sickle cell anaemia patients (p value <0.001).

Conclusion: Hepatobiliary abnormalities have a statistically significant association with clinical severity score of paediatric sickle cell anaemia patients.

B-1499 11:22

Ultrasound diagnostics of the respiratory distress syndrome in premature infants

O. Sorochan; Kharkiv/UA (Sorochanop@gmail.com)

Purpose: To identify capabilities of lung ultrasound (LUS) in the diagnostics of respiratory distress syndrome (RDS) in premature infants.

Methods and Materials: We studied 54 preterm infants (32 boys, 22 girls) gestation age 25-34 weeks with diagnosis of RDS with varying severity grades. Ultrasound was performed at the bedside of a patient using the device Logiq E, GE Medical Systems, linear transducer with a frequency of 5-12 MHz. Chest x-ray (CXR) was performed for all patients the same day.

Results: The basic patterns of the lung tissue changes we found was B-line and consolidation ("white lung"). Evaluation was carried out according to the number of B-lines in the intercostal spaces. The most serious degree

manifested pattern of "white lung". On the base of this pattern premature infants with RDS were divided into four groups by degree of severity: 1st - 20.0%, 2nd - 40%, 3rd - 36.1%, and 4th - 13.9%. There was high correlation in CXR and LUS severity data that indicates possibility of its using in medical practice.

Conclusion: Ultrasound could not replace CXR to estimate all changes of the lungs, but can complement it. Also it can be useful for monitoring already established RDS to reduce radiation exposure.

B-1500 11:26

Role of MR enterography in evaluation of disease activity and treatment response in paediatric Crohn's disease correlation between MRE and PCDAI scores

A. Chellathurai, A. Narasingam, S. Radhakrishnan, S. Sankaranarayanan, D. Arun; Chennai/IN (amar02@yahoo.co.in)

Purpose: The aim of the study was to assess the role of MR enterography in the diagnosis and follow-up of children with Crohn's disease and to correlate disease activity indices with known MR enterography features of active disease.

Methods and Materials: This was a retrospective study including 24 patients (median age 11yrs, male 17) with clinically and histologically proven CD who underwent MRE. Two previously validated MRE scores - MR enterography global score (MEGS) and CD MRI index (CDMI) were calculated. A correlative analysis was made between the PCDAI score and MRE scores as well as individually with each MR variable. Comparison of both the MR scores was made between patients with different disease activity.

Results: MEGS and PCDAI scores showed strong positive correlation (r equals 0.724, p equal to or less than 0.001) CDMI and PCDAI scores showed moderate positive correlation (r equal to 0.661, p equal to 0.0004). There was a statistically significant difference in the MR scores between patients grouped by clinical activity. Among individual MR variables, mural thickness and enhancement best predicted the disease activity.

Conclusion: MR enterography-based scores and findings correlate with clinical activity in paediatric Crohn's. Thereby, MRE can be considered a valuable tool in the management of CD, predicting disease activity and offering a potential alternative to endoscopy in monitoring patients during follow-up.

B-1501 11:30

Transverse comparisons between ultrasound and radionuclide parameters in children with pelviureteric junction obstruction

N.O. Shwaky; Cairo/EG (norhanmedecine@yahoo.com)

Purpose: Correlation between ultrasound parameters and dynamic scintigraphic parameters in pelviureteric junction obstruction, the importance of each factor, and which of the ultrasound parameters most reflect the renal function, and if we can predict, on the basis of ultrasound parameters, the patient in whom radionuclide renography can be avoided. The role of ultrasound and radionuclide parameters in deciding on surgery was studied.

Methods and Materials: Ultrasound and renographic studies were compared. Anteroposterior pelvic diameter (APD) and calyceal size were divided into three levels of dilatation. Parenchymal thickness was considered either normal or significantly decreased. Acquisition of renograms with quantification of DRF, quality of renal drainage and cortical transit was carried out.

Results: The low DRF and poor drainage were higher among those with major hydronephrosis, severe calyceal dilatation or parenchymal thinning. Impaired cortical transit, which is a major risk factor for functional decline, was seen more frequently among those with very severe calyceal dilatation. However, none of the structural ultrasound parameters was able to predict whether the level of renal function or the quality of drainage was normal or abnormal. Alternatively, an APD <30 mm, a calyceal dilatation of <10 mm and a normal parenchymal thickness were associated with a low probability of decreased renal function.

Conclusion: Nuclear medicine examinations may be postponed in those with an APD <30 mm, a calyceal dilatation of <10 mm and a normal parenchymal thickness. On the contrary, precise estimation of DRF and renal cortical transit should be performed in APD >30 mm, major calyceal dilatation and/or parenchymal thinning.

B-1502 11:34

Spectrum of malformations of cortical development with clinicoradiological correlation and analysis of associated abnormalities: experience from a tertiary care centre in Egypt

D.M. El-Mossly, S.A. Mohammad, E.M. Abelhafez, N. Osman, K.A. Ahmad; Cairo/EG (dollyelmossly@yahoo.com)

Purpose: Malformations of cortical development (MCD) usually cause developmental disability, focal neurological deficits and seizures in children which are frequently resistant to anticonvulsant treatment. The structural neuroimaging technique especially MRI is the most important non-invasive method in their diagnosis and other associated brain abnormalities, thus

smaller lesions can be identified. So, it is important to exclude MCD in every case of developmental delay, congenital neurological signs and intractable epilepsy.

Methods and Materials: All paediatric cases with MCD diagnosed on MRI at Ain Shams University Hospital during the period from January 2015 till January 2017 were retrospectively reviewed with correlation to their presenting symptoms.

Results: Among 4300 paediatric patients referred for MRI brain, 72 cases with MCD were identified with prevalence of 1.67%. Epilepsy was the main presenting symptom (72%) and focal epilepsy was seen in 19.5% of the cases. There was an association between focal cortical dysplasia and focal epilepsy ($P=0.005$), polymicrogyria and global developmental delay ($P=0.008$) and also between tuberous sclerosis and epilepsy ($P=0.007$). The most common type of MCD was polymicrogyria (25%), followed by tuberous sclerosis (21%). MCD was seen in association with other neuroimaging findings, or as a part of syndromes as congenital muscular dystrophy spectrum especially Walker-Warburg syndrome and also it was seen in Sturge Weber and chronic infantile neurological cutaneous articular (CINCA) syndromes.

Conclusion: MCD showed relatively high prevalence among Egyptian children being associated with epilepsy and developmental delay. MCD was infrequently isolated, also occurred in association, or as a part of syndromes.

B-1503 11:38

Role of MRI vs CT in staging and decision making in paediatric renal masses

E. Nasr, A. Youssef, W. Zekry, T. Raafat, A. Younis, H.A. Elkiki; *Cairo/EG (emannasr84@yahoo.com)*

Purpose: To determine whether MRI can replace CT in local staging of newly diagnosed renal tumours in paediatric age group renal masses to avoid radiation exposure and contrast material administration.

Methods and Materials: 50 children with newly diagnosed renal masses were included. Contrast-enhanced CT and non-contrast MRI were done in all patients. Local staging was done in both studies separately. The surgical and pathological findings were the reference standard.

Results: The sensitivity of CT and MRI for detecting capsular penetration was 68.6% and 62.9%, respectively, while specificity was 86.5% and 83.8%. The sensitivity of CT and MRI for detecting lymph node metastasis was 76.5% and 52.9%, and specificity was 90.4% and 92.3%. Synchronous contra-lateral lesions were identified by CT in 4/9 cases and by MRI in 7/9 cases.

Conclusion: CT and MRI have similar diagnostic performance for detection of lymph node metastasis and capsular penetration. MR detected more contra-lateral synchronous lesions; however, these were present in a very small number of cases. Either modality can be used for initial loco-regional staging of paediatric renal tumours.

B-1504 11:42

Closed spinal dysraphisms: how to improve prenatal diagnosis

T. Nguyen, V. Houfflin-Debarge, M. Vinchon, N. Boutry, F.E. Avni; *Lille/FR (nguyentoan5989@gmail.com)*

Purpose: Prenatal diagnosis of closed spinal dysraphisms (CSDs) is difficult and not well studied. The purpose was to study the contribution of prenatal imaging in the diagnosis of CSD to improve their screening.

Methods and Materials: Patients with postnatally diagnosed CSD by spinal MRI or surgery in Lille University Hospital were included. Ultrasound signs, proportion of positive and negative prenatal diagnosis and the contribution of prenatal imaging techniques were analysed.

Results: 38 patients with CSD were included, 17 of whom were diagnosed prenatally. Ultrasound signs were a posterior soft tissue mass in 9 cases, low position of the conus medullaris in 8 cases, vertebral anomalies in 7 cases and spinal cord anomalies in 4 cases. Ultrasound was excellent in screening and characterizing cystic masses (8 diagnosed on 8 included), unlike fatty masses (1 only on 11). It was less successful in screening (7 on 14) and characterizing vertebral anomalies. In these cases, foetal CT scan permitted a full diagnosis. Foetal MRI was performed in 12 cases, allowing to characterize posterior soft tissues mass (100% of concordance between ultrasound and MRI). It was less accurate than ultrasound in studying the wall of the mass, the conus medullaris level and the spinal cord morphology.

Conclusion: Ultrasound must remain the first-line imaging technique and its study has to contain three parts: vertebral, spinal cord and posterior soft tissue study. Foetal MRI seems to be useful in characterizing a posterior soft tissue mass when ultrasound is difficult. Foetal CT scan is useful to characterize vertebral anomalies.

B-1505 11:46

Radiological appearance and follow up results of diaphragmatic mesothelial cysts during childhood

I. Akdulum¹, M. Öztürk², S. Karatoprak³, A. Sığırcı³; ¹Ankara/TR, ²Konya/TR, ³Malatya/TR (iakdulum@yahoo.com)

Purpose: Diaphragmatic mesothelial cysts (DMC) are rare congenital benign lesions. DMC often cannot be distinguished from liver cystic lesions and cause management failure. The aim of this study is to describe radiologic findings of DMC and to evaluate our follow-up results.

Methods and Materials: Ultrasound (US), computed tomography (CT) or magnetic resonance imaging (MRI) of DMCs were acquired from 20 children. Patients' age, gender, indication for imaging, size of cyst and follow-up times were evaluated prospectively.

Results: The patients were aged between 4 months to 13 years. Eight of 20 patients were female and 12 were male. The most common indication for imaging was abdominal pain. All patients had US exam. The long diameter of the DMC was between 14 and 39 mm. All DMC were located near to liver segment 6-7, extraparenchymal and bilobular. In addition, a triangular echogenic area of fatty tissue extending between the supra-lateral segment of the DMC and the liver parenchyma, which we have described as the "lateral fat sign", was detected. We confirmed the lateral fat sign in 6 patients with CT and in 2 patients with MRI. Patients were monitored for 12-36 months and the size of the lesions was stable in 13 patients. The lesion dimensions in 7 patients were reduced, but this was not statistically significant.

Conclusion: Cysts were treated with ablation techniques in the literature. We followed asymptomatic patients. With typical localization, bilobular form and lateral fat sign, diagnosis is clear. US is useful for diagnosis and follow-up of DMC.

14:00 - 15:30

Room B

Abdominal Viscera

SS 1901a

New development in CT of the liver

Moderators:

H. Ringl; Vienna/AT

G. Tardaguila de la Fuente; Vigo/ES

B-1506 14:00

Meta-analysis of spectral CT image analysis tools and multi-phase CT enhancement in diagnostic accuracy of hepatic cell carcinoma

Y. Zhou; Zhengzhou/CN

Purpose: To assess and compare the overall diagnostic value of spectral CT image analysis tools and multi-phase CT enhancement with hepatic cell carcinoma using meta-analysis.

Methods and Materials: Relevant English articles published on PubMed, EMBASE, Cochrane library database and Chinese articles published on CNKI and Wanfang database were searched. Characteristics of included articles were summarised and extracted. Statistical analyses were performed using Meta Disc version 1.4 and Review Manager 5.3. Heterogeneities of included articles were tested and selected using proper effect model. Pooled sensitivity, specificity, 95% CI, summary receiver operating characteristics (SROC) curve and area under curve (AUC) were calculated. The heterogeneity and sub-group analyses were explored.

Results: 12 of 101 retrieved articles were included, in which 3 articles used two methods of imaging modalities at the same time. Spectral CT image analysis tools consist of four articles of monochromatic image, three articles of spectral curve and four of spectral quantitative parameters, respectively. The pooled sensitivity, specificity (95% CI) and AUC of SROC for spectral CT image analysis tools and DECT were 0.91 (0.88-0.94), 0.78 (0.73-0.83), 0.9022 and 0.85 (0.78-0.90), 0.71 (0.60-0.80), 0.874. Sub-group analysis showed that category of spectral CT image analysis tools was the essential factor for diagnosis of HCC. The pooled sensitivity, specificity (95% CI) and AUC of SROC for monochromatic image, spectral curve and spectral quantitative parameters were 0.83 (0.74-0.91), 0.75(0.65-0.84), 0.8935; 0.87 (0.81-0.92), 0.73 (0.65-0.80), 0.9412 and 0.99 (0.96-1.00), 0.94 (0.85-0.98), 0.9877.

Conclusion: Spectral CT image analysis tools showed higher sensitivity, specificity and better diagnostic performance compared to conventional DECT, especially for spectral quantitative parameters.

B-1507 14:08

Perfusion CT vs triphasic CT in evaluation of hepatic masses

V. Laxmi, V. Chowdhury, R. Dixit, A. Agarwal; *New Delhi/IN*
(drvijaylaxmi25@gmail.com)

Purpose: Compare the diagnostic accuracy of triphasic and perfusion CT in characterisation of focal liver lesions as benign and malignant lesions. Correlation of radiological findings with histopathology.

Methods and Materials: Total of 50 patients with a clinical suspicion of focal liver lesions were included. Clinical and lab findings were recorded followed by CT examination on 128 slice scanner. Hepatic perfusion CT of entire liver volume was performed followed by routine scan of whole abdomen. Perfusion maps of the liver were generated using dedicated hepatic CT perfusion software. Various perfusion parameters like blood flow, blood volume, time to peak, permeability, arterial liver perfusion, portal venous perfusion and hepatic perfusion index were evaluated. The data set of perfusion CT was used to generate arterial phase images. The whole abdomen scan was taken as portal venous phase. Delayed phase scans were obtained wherever indicated. These images were analysed for presence of focal lesions and their enhancement pattern/perfusion parameters to characterise them. Findings were compared with histopathological/operative diagnosis/clinical follow up.

Results: Sensitivity of both Triple phase CT and perfusion CT for characterisation of lesion as malignant was equal at 97%. Specificity and positive predictive value of triple phase was 88.89% and 97% respectively. Both specificity and positive predictive value of perfusion CT was 100%.

Conclusion: Perfusion CT with a high sensitivity, specificity and positive predictive value is a useful tool for characterisation of liver lesions

B-1508 14:16

Iterative reconstruction in "virtual non-contrast" with dual-energy CT: is it an alternative to conventional unenhanced phase?

S. Jamali, C. Dragean, N. Michoux; *Brussels/BE* (sanaa.jamali@uclouvain.be)

Purpose: To compare attenuation values and image quality of virtual non-contrast (VNC) with conventional true non-enhanced phase (TNC), on dual-energy double-detector computed tomography (CT) and to assess potential radiation dose reduction.

Methods and Materials: 286 patients with the pre- and post-contrast imaging in dual-layer spectral detector CT were retrospectively analysed. Quantitative analysis was performed for 247 patients by the measurements of the mean attenuation value in different regions of the abdomen for VNC and TNC. Qualitative analysis was performed for 48 patients using a graded scale for image quality. The radiation dose delivered to patients was compared with dose of protocols without TNC.

Results: Difference of mean attenuation values between TNC and VNC is less than 15 UH in 98.3% and less than 10 UH in 92.3%. The higher difference was found for perineal fat. VNC overestimated attenuation in fat and underestimated it in aorta comparatively to TNC. Image quality was evaluated as good or excellent in 77% of TNC and 54% of VNC. VNC was in most cases an alternative acceptable for the replacement of TNC. Using VNC, the radiation dose can be diminished by 32%.

Conclusion: VNC reconstructions demonstrate good correlation with TNC images in different abdominals tissues. VNC image quality is satisfying and acceptable in most cases; technical improvement is needed to correct imperfect iodine removal. VNC seems one interesting alternative to TNC with reduction in irradiation dose. However, further studies are needed to evaluate VNC in the pathological cases.

B-1509 14:24

Segmental variation of CT liver attenuation index in living-related liver donors: correlation with histopathological findings

A. Rana¹, A. Jang¹, M. Jehangir¹, M. Asghar¹, R. Nazir¹, S. Burki², K. Shakeel¹;
¹Islamabad/PK, ²Rawalpindi/PK (aisha_jang@yahoo.com)

Purpose: To find out the variation in CT liver attenuation index between anterior and posterior liver segments on non-enhanced CT scan and correlate it with histological degree of steatosis.

Methods and Materials: A radiologist blinded to histological grading calculated mean anterior and posterior segments CT hepatic attenuation in 74 potential living-related liver donors.

Results: Significant association (with p value of 0.00) is found between anterior segment liver attenuation index and histopathological findings, whereas no significant association is seen between posterior and combined CT liver attenuation index with histopathological findings.

Conclusion: The results of our study suggest that mean liver attenuation index of posterior liver segments does not correctly predict the degree of steatosis and rather results in significant over estimation of steatosis due to beam hardening. Hence, while calculating CT liver attenuation index, only the anterior segments of liver should be sampled to quantify steatosis.

B-1512 14:32

Evaluation of tumour response in patients with neuroendocrine hepatic metastasis treated using transarterial chemoembolisation (TACE) on MRI

M. Lapteva, M. Shorikov, D. Frantsev, O.N. Sergeeva, E. Virshke, B. Dolgushin; *Moscow/RU* (mglapteva@inbox.ru)

Purpose: The purpose of the paper is to develop suitable TACE evaluation criteria in liver metastatic neuroendocrine tumour (mNET) patients on MRI.

Methods and Materials: 23 liver mNET patients (G1-9, G2-10, G3-2, unknown grade-2) who underwent 36 TACE procedures were enrolled in the study. 68 MRI studies performed 3-86 days before (median 28 days) and 23-147 days (median 61 days) after TACE were analysed retrospectively. Using 1.5T MRI scanner, we acquired: 1) 3DT1WIFS in the axial plane before i.v. contrast injection and after in the portal and delayed phases; 2) diffusion weighted images with ADC maps. We measured before/after TACE: (1) maximum necrotic/fibrotic zone diameter and solid component thickness on its periphery in the largest targeted lesion; (2) ADC and MR contrast agent accumulation dynamics (dSI) in regions of interest in tumour solid component.

Results: TACE effect according to RECIST (1.1) was evaluated as progressive disease in 8.3% cases, stabilised in 83.3% cases and partial response in 8.3% cases. The diameter of the fibrosis/necrosis areas before/after TACE demonstrated no changes (p=0.614), but solid component thickness on its periphery decreased significantly (p=0.003, median 16%). ADC values increased significantly in solid portions of mNETs after TACE (p=0.003). MR contrast agent accumulation of the lesions in portal phase decreased significantly after TACE (p=0.003, median 8.5%). Decrease of MR contrast agent accumulation in the solid part of the target lesions by more than 10% after TACE is associated with a longer time to progression of the disease (p=0.025). There is an increase in MR contrast agent washout time in the solid part of the target lesions after TACE (p=0.032).

Conclusion: Parameters changed in liver mNET after TACE: (1) solid component thickness in cases of central necrosis/fibrosis (decrease); (2) ADC (increase); (3) SI T1WI in portal phase (decrease) and this is the positive prognostic factor; 4) MR contrast agent washout time (increase).

B-1513 14:40

Perfusion CT imaging: diagnostic biomarker tool for survival predictor of tumour in response to antiangiogenic treatment in patients with advanced HCC lesions

D. Ippolito¹, G. Querques¹, C.R. Talei Franzesi², S. Lombardi¹, A. Pecorelli³, S. Sironi¹; ¹Monza/IT, ²Milan/IT, ³Bergamo/IT (davide.atena@tiscalinet.it)

Purpose: To investigate whether perfusion-CT (p-CT) imaging could depict the inhibition of tumour neoangiogenesis induced by sorafenib in advanced hepatocellular carcinoma (HCC), and whether it could be useful in determining the efficacy of anti-angiogenic therapy and predicting survival during treatment.

Methods and Materials: Ninety-eight p-CT examinations were performed among 29 cirrhotic patients, with advanced HCC, before and every 2 months after Sorafenib administration. Perfusion-CT protocol was performed on a 256-slice MDCT scanner, during injection of 50 ml of contrast medium. Perfusion parameters were considered (hepatic perfusion; arterial perfusion; hepatic perfusion index and time to peak) and statistically compared, at baseline and follow-up, between responders (complete response, stable disease or partial response) and non-responders (progressive disease). Kaplan-Meier analyses estimated the time to survival in overall population, after stratifying patients according to mRECIST.

Results: Percentage variation of perfusion parameters (Δ HP and Δ AP), from baseline to follow-up study was assessed and correlated with response classified according to mRECIST criteria. The group that responded to sorafenib showed a significant reduction of values in HCC target lesions after anti-angiogenic therapy (HP 29.4 \pm 23.7 vs 51.9 \pm 16.8; AP 29.8 \pm 25.5 vs 52.2 \pm 17.9; p<0.01), in comparison with progressor group that demonstrated an increase or no significant variation after treatment. When patients were stratified into mRECIST, higher survival rate was observed in the non-progressor group compared to the progressor (48.6% vs 28.6%), and statistically significant correlation was found between mRECIST- Δ HP (p=0.04) and mRECIST- Δ AP (p=0.01) and overall survival rate.

Conclusion: Quantitative analysis of perfusion parameters represents prognostic indicators useful in assessment of response to anti-angiogenic therapy, allowing for optimization of individualized treatment.

B-1514 14:48

Diagnostic value and radiation dose reduction of model-based iterative reconstruction compared with hybrid iterative reconstruction in abdominal CT study

A. de Vito¹, D. Ippolito¹, C.R. Talei Franzesi², L. Riva², S. Drago¹, S. Sironi¹;
¹Monza/IT, ²Milan/IT (a.devito@campus.unimib.it)

Purpose: To evaluate dose reduction and image quality of routinely abdominal CT images reconstructed with model-based iterative reconstruction (IMR) and low-kV setting compared with hybrid iterative reconstruction (iDose4) and standard kV protocol.

Methods and Materials: We prospectively enrolled 72 patients who underwent entire abdominal CT scan; 36 patients were examined using a low-kV setting (100kV) while the other 36 patients were investigated using standard kV setting (120 kV), on the same 256-row CT scanner (iCT Elite). In the study group images were reconstructed using IMR algorithm while in the control group we used iDose4 technique. CTDIvol and DLP were evaluated. Region of interests were drawn in three different levels in the liver and in spleen to evaluate absolute enhancement values (HU), SNR and CNR.

Results: Compared to standard dose iDose4-CT study the low kV IMR-CT presented lower CTDIvol (9.2 ± 1.2 vs 17.7 ± 2.5 mGy) and DLP (570.5 ± 8.3 vs 911 ± 10.2 mGy x cm) with ED of 6.3 ± 1.8 vs 9.44 ± 1.8 mSv. Low kV IMR images yielded higher attenuation values (HU) and higher SNR and CNR in liver and spleen, compared with standard dose iDose4 images. The subjective image quality of low-kV IMR CT was also higher compared with iDose4-CT.

Conclusion: Low dose CT scan (100kV and automated mAs modulation) reconstructed with IMR algorithm represents a feasible protocol for routinely daily examination of the abdomen, achieving excellent image quality with extremely low noise, and a significant dose reduction within acceptable reconstruction times (mean time of 3 minutes).

B-1515 14:56

Dual-energy CT in patients with abdominal malignant lymphoma: impact of noise-optimised virtual monoenergetic imaging on objective and subjective image quality

L. Lengua, D. Leithner, M.H. Albrecht, C. Booz, J.L. Wichmann, T.J. Vogl, S.S. Martin; Frankfurt a. Main/DE (lukas.lengua@gmail.com)

Purpose: To evaluate the impact of the noise-optimised virtual monoenergetic imaging (VMI+) technique on objective and subjective image quality in patients with malignant lymphoma undergoing abdominal dual-energy computed tomography (DECT).

Methods and Materials: 35 consecutive patients (mean age, 53.8 ± 18.6 years; range, 21-82 years) with histologically proven malignant lymphoma of the abdomen were enrolled in this IRB-approved retrospective study. DECT image series were reconstructed using standard linearly blended (M_0.6), as well as traditional VMI, and VMI+ reconstructions at 40 to 100 keV in 10-keV intervals. Attenuation measurements were performed in lymphoma lesions to calculate signal-to-noise (SNR) and contrast-to-noise ratios (CNR). Three independent radiologists assessed the overall image quality, lesion delineation, and image noise using five-point Likert scales.

Results: Assessment of objective image parameters showed the highest SNR and CNR values for 40-keV VMI+ (SNR, 15.77 ± 7.74 ; CNR, 18.27 ± 8.04) compared to standard linearly blended (SNR, 7.96 ± 3.26 ; CNR, 13.55 ± 3.47) and all traditional VMI series ($P < 0.001$). Regarding the subjective image evaluation, overall image quality peaked in the 60-keV VMI+ series (median, 5) with significant differences to all other series ($P < 0.001$). Evaluation of lesion delineation was superior in 40-keV VMI+ series (median, 5), whereas image noise showed best rating scores for 100-keV VMI+ (median, 5).

Conclusion: Low-keV VMI+ series significantly increase objective image quality of malignant lymphoma lesions in abdominal DECT examinations compared to standard DECT and VMI series. In addition, the highest lesion delineation can be achieved using 40-keV VMI+ reconstructions.

B-1516 15:04

Sarcopenia index as a predictor of post-transplant morbidity and mortality

S. Singhal¹, B.K. Saranga², D. Balakrishnan²; ¹Bangalore/IN, ²Kochi/IN (drsoumilsinghal75@gmail.com)

Purpose: Nutrition assessment in chronic liver disease is a challenge as the common indices such as anthropometric measurements and body mass index are inaccurate and overexpressed; hence, the use of sarcopenia index has shown to solve this problem. The primary aim of my study is to assess morbidity and mortality in post-transplant patient using sarcopenia index.

Methods and Materials: A cross-sectional prospective study was performed between October 2014 and November 2016, at Amrita Institute of Medical Sciences. The study was approved by the ethical committee. 60 patients (59 male, 1 female) were included in the study. Sarcopenia was assessed by calculating psoas volume and psoas index using volumetric software Aquarius

Intuition Terrarecon version 4.4.11. All statistical analyses were done using IBM SPSS version 20.0.

Results: Among the 60 patients included in the study 6 belonged to class 0, 16 to class 1 and 38 to class 2, patients who had normal psoas index (class 0 - as per European working group on sarcopenia in older people guideline of 2010) had nil mortality. Mean comparison analysis showed high risk of ICU stay in patients with sarcopenia. Correlation analysis of psoas index with ICU stay showed a negative correlation which was statistically significant. On associational analysis, the reintubation was found to have a significant correlation with mortality 72% (p value < 0.001).

Conclusion: Sarcopenia index acts as an important prognostic tool in post-transplant patients.

14:00 - 15:30

Room C

Abdominal Viscera

SS 1901b

Imaging of cystic and solid pancreatic lesions

Moderators:
N.N.

B-1517 14:00

Carcinoma pancreas: how good is multi-detector-computed tomography: a single-center experience

S. Singhal¹, N.K. Prabhu²; ¹Karnataka/IN, ²Kochi/IN (drsoumilsinghal75@gmail.com)

Purpose: To compare the staging of pancreatic carcinoma assessed by MDCT with surgery in a tertiary referral centre in Kerala.

Methods and Materials: A cross-sectional observational study was performed between November 2014 and October 2016, 25 patients (12 male and 13 female patients) were evaluated with a mean age of 54.2 years. CT was performed on all patients. The gold standard for diagnosis was operative and histopathology data. All statistical analyses were done using IBM SPSS version 20.0. Validity parameters like sensitivity, specificity, accuracy, positive and negative predictive value were computed for CT with respect to surgery.

Results: Of the 25 patients who were evaluated for surgery, 15 cases (60%) were classified as resectable tumours, 3 (12%) as borderline resectable and 7 (28%) as unresectable tumours. CT showed a sensitivity of 82.3% with a specificity of 87.5%. On assessing vascular invasion CT showed a sensitivity and specificity of 100% and 93.3%, respectively. Three patients who were classified as having borderline resectable tumour underwent vascular reconstruction during the surgery.

Conclusion: Contrast-enhanced multiphase pancreatic imaging using CT plays a pivotal role in diagnosing and assessing the resectability and vascular invasion of pancreatic tumours. It is very useful for determining borderline resectable tumours pre-operatively, which aids for better treatment planning.

B-1518 14:08

The diagnostic role of 256 multidetector-row CT in the detection and characterisation of incidental pancreatic cystic lesions: comparison with MR colangiopancreatography

S. Drago, D. Ippolito, C. Talei Franzesi, A. Nasatti, A. Parlati, A. Casiraghi, S. Sironi; Monza/IT (silvia.drago@hotmail.it)

Purpose: To compare the diagnostic accuracy of contrast-enhanced MDCT scan with MRI with MRCP sequences, in the detection of pancreatic cystic lesions and those features useful for their characterisation.

Methods and Materials: Fifty patients with no history of pancreatitis, neoplasm and prior surgical procedures in pancreas, who underwent both MDCT and MRI with MRCP (time interval lower than 90 days) for pancreatic cysts characterisation, were evaluated. All CT and MRI examinations were performed, respectively, on a 256 slice CT (Brilliance iCT; Philips) and on a 1.5 T magnet (Achieva, Philips). The reviewer recorded the number of lesions in each patient and the main morphologic features of the defined target lesions: location (head, uncinat process, neck, body, tail), number, size, communication with main pancreatic duct (MPD), maximum MPD diameter, presence of septa, mural enhancing nodules and calcifications. Data were analysed to compare the diagnostic performance of MDCT and MRI.

Results: A greater number of pancreatic cysts were identified on MRI than CT examinations (227 vs 128); however, the ICC value was 0.76, suggesting a good agreement. Very good agreement (ICC 0.98) was found regarding the diameter of target lesions (21.4mm on CT vs 21.8mm on MRI), location of target lesion ($\kappa=0.90$), detection of MPD dilatation ($\kappa=1.00$) and septa ($\kappa=0.86$). Fair agreement on the evaluation of MPD communication ($\kappa=0.33$) and calcifications ($\kappa=0.22$) was found.

Conclusion: MDCT can be considered almost equivalent to MRI with MRCP in the evaluation of pancreatic cystic lesion, offering detailed morphologic features helpful for their characterisation and correlation with a high risk of malignancy.

B-1519 14:16

CT features of primary pancreatic lymphoma: experience from three referral centres for pancreatic diseases

E. Boninsegna¹, G. Zamboni¹, D. Facchinelli¹, C. Triantopoulou², S. Gourtsoyianni³, M.C. Ambrosetti¹, R. Pozzi Mucelli¹; ¹Verona/IT, ²Athens/GR, ³London/UK (boninsegnae@gmail.com)

Purpose: To describe CT characteristics of primary pancreatic lymphoma (PPL), a rare disease with features in common with adenocarcinoma.

Methods and Materials: Fourteen patients were enrolled. CT: unenhanced scan, contrast-enhanced pancreatic and venous phases. Image analysis: tumour location; peri-pancreatic vessels encasement; necrosis; enlarged lymph nodes; fat stranding; enlarged bile duct and pancreatic duct; neoplasm longest dimension, volume and density.

Results: Histopathological diagnoses: follicular non-Hodgkin lymphoma (5/14), diffuse large B-cell lymphoma (6/14), high-grade B-cell lymphoma not otherwise specified (3/14). 6/14 PPLs were located in the pancreatic head, 7/14 in the body-tail and 1/14 involved the whole gland. In 5/14 cases superior mesenteric artery and vein were encased; splenic vein and artery encasement was depicted in 2 PPLs. Necrosis was present in 2/14. Enlarged retroperitoneal lymph nodes were found in 11 cases; fat stranding in all patients. Bile duct was dilated in 6 cases, pancreatic duct in 5. Mean neoplasm longest diameter and volume were 8.05 cm and 210.8 cm³. Mean tumour attenuation values were 39.1 HU at baseline, 60.6 HU in the pancreatic phase and 71.4 HU in the venous phase.

Conclusion: PPL presents as a large lesion with delayed homogeneous enhancement; peri-pancreatic fat stranding and vessel encasement are present, without vascular infiltration; pancreatic duct dilatation is rare.

B-1520 14:24

CT and pathologic correlation in pancreatic cancer after neoadjuvant chemoradiotherapy

J.R. Ayuso, M. Cuatrecasas, J. Maurel, O. Reig, C. Conill, A. Darnell, M. Pages, S. Rodríguez, S. Sanchez; Barcelona/ES (JRAYUSO@clinic.cat)

Purpose: To correlate morphologic changes observed in CT after neoadjuvant chemoradiotherapy (CRT) with the pathologic piece in patients with pancreatic cancer (PC).

Methods and Materials: Eleven patients with resectable pancreatic cancer (RPC) (Group1) who underwent surgery after CRT and nine with borderline pancreatic cancer (BPC) (Group2), selected from those included in the GEMCAD1003 trial, who completed the CRT treatment and underwent tumour resection were evaluated by CT before and after treatment. CT changes in tumour volume were determined by three orthogonal measurements and a semiautomatic tool. Tumour density measured in the portal venous phase and changes in vascular infiltration (only in group 2) were compared to pathologic tumour volume and tumour regression grade (TRG). Spearman coefficient and Wilcoxon test were used to compare results.

Results: The Spearman's correlation coefficients were 0.92 and 0.95, respectively, for manual and semiautomatic tumour volumes measured before and after CRT, but only 0.231 for post-CRT CT and pathologic tumour volume measurements. It was 0.39 for the correlation between CT volume reduction and tumour/fibrosis ratio. No correlation was observed between the CT volume reduction and pathologic TRG (p=0.96), or between variations in tumour density in the portal venous phase and the percentage of tumoural fibrosis (p=0.15). In group 2 patients, the percentage of radial and longitudinal tumour/vessel contact remained unchanged in 10/11 patients.

Conclusion: CT changes in size, density and extension in vascular infiltration in PC after CRT do not correlate with pathological tumour response.

B-1521 14:32

Lobar distribution of liver metastases based on the site of pancreatic neuroendocrine tumours

C. Fabris, G. Zamboni, M.C. Ambrosetti, R. Negrelli, R. Pozzi Mucelli; Verona/IT (cristina.fabris@yahoo.it)

Purpose: The presence of liver metastases from neuroendocrine tumours does not preclude surgery; the distribution of the metastases is important for treatment planning. Our purpose was to assess whether the location of the primary neuroendocrine tumour (pNET) in the pancreas influences the lobar distribution of metastases within the liver.

Methods and Materials: This is a retrospective review of the CTs performed on 49 patients with pNETs (27 males, 22 females) and liver metastases. Of these patients, 11 had a primary tumour in the head (group A: mean age 50,3 years) and 38 in the body-tail (group B: mean age 59,3 years). We evaluated tumour site, diameter, vascular invasion and number of metastases within each

lobe. We used an unpaired t-test to compare the total number of metastases between the two groups and Fisher's test to evaluate the number of metastases in the two lobes.

Results: Group B primary tumours were larger than group A (59,55 vs 39,82 mm; p 0.043). The number of liver metastases was higher in the right lobe in both groups (p=ns). The ratio of metastases in the right-to-left hemi-liver was 2,5:1 for group A compared with 1,79:1 for group B (p=0,0423). The splenic vein was more commonly involved in patients in group B.

Conclusion: Tumours from all locations in the pancreas will give a higher number of metastases in the right lobe. The right-to-left ratio is however significantly different based on the site of the primary tumour.

B-1522 14:40

MRI and MRCP features of chronic pancreatitis in patients with or without pancreas divisum abnormality and their relationship to patients age

M. Monti, G. Zamboni, L. Bertuzzo, R. Pozzi Mucelli; Verona/IT (marialaura.monti@hotmail.it)

Purpose: To compare the MRI and MRCP features of chronic pancreatitis (CP) in patients with or without pancreas divisum (PD) and to determine their relationship to patient age.

Methods and Materials: We retrospectively reviewed the MRI/MRCPs of 175 patients (mean age 53years) with symptomatic CP. 86 had CP associated with PD, and 89 had CP without PD. Both patients with PD and without PD were stratified by age: <40 years (26 PD; 33 non-PD), 41-60 years (27 PD; 28 non-PD), >60 years (33 PD; 32 non-PD). Two readers reviewed the scans for: morphological changes, signal intensity abnormalities, pancreatic ducts changes, filling defects. All MRI features were compared between age groups by using Chi-square test.

Results: No difference was observed in mean patient age between PD and non-PD patients (p=ns). Parenchymal intensity was significantly more often reduced in non-PD than in PD patients (p<0,001). The degree of parenchymal thinning, and irregularity of margins were significantly higher in non-PD patients in the groups aged <40 and 41-60 (p<0,001). No difference was observed between PD and non-PD patients aged >60 for irregularity of parenchymal margins (p=0,3). In non-PD patients, main pancreatic duct (MPD) and branch-ducts were significantly more often dilated (p=0,0031), and filling defects were more common (p<0,0007). A significant association was found between parenchymal T1-hypointensity, MPD dilation and filling defects and increasing age in non-PD patients compared to PD patients in all the age groups (p<0,001).

Conclusion: Patients with PD show less severe morphological alterations as compared with patients affected by other forms of CP.

B-1523 14:48

MRI evaluation of pathologically confirmed IPMNs of the pancreas using Fukuoka Guidelines: can we differentiate between invasive/high-grade IPMNs and low/moderate-grade IPMNs?

C. Fabris, G. Zamboni, R. Negrelli, E. Boninsegna, R. Pozzi Mucelli; Verona/IT (cristina.fabris@yahoo.it)

Purpose: IPMNs of the pancreas are intraductal mucin-producing cystic neoplasms with malignant potential. The Fukuoka criteria are commonly used to assess the risk of malignancy. Our purpose was to assess if these criteria can differentiate between invasive/high grade IPMNs and low/moderate grade IPMNs.

Methods and Materials: We reviewed the preoperative MRIs from 42 patients (25 males, 17 females; mean age 63,62 years) with a confirmed pathologic diagnosis of IPMN (invasive= 7; non invasive= 35). Two readers analyzed in consensus the MRIs for tumor size (>/< 3 cm), diameter of the main pancreatic duct (MPD) (>10 mm, <10 mm), presence of enhancing solid components, radiologic signs of pancreatitis, enhancing or nonenhancing nodules, thickened/enhancing walls, abrupt change in MPD caliber with distal atrophy, lymphadenopathy. MRI and pathology findings were compared using Fisher's test dividing the patients in two groups: invasive/high grade IPMNs vs low/moderate dysplasia IPMNs.

Results: A MPD >10 mm was significantly more common in patients with invasive/ high grade dysplasia IPMN than in patients with low/moderate dysplasia (p=0,0026). No significant difference was observed between the two groups for the tumor diameter, presence of solid nonenhancing or enhancing nodules, thickened enhancing walls, pancreatitis, abrupt change in MPD and presence of lymphadenopathy.

Conclusion: Fukuoka criteria are being commonly used to assess the risk of malignancy in patients with IPMN. The only criterion that appears to be helpful in differentiating between invasive/high grade IPMNs and low/moderate grade IPMNs is a MPD >10 mm.

B-1524 14:56

Preoperative classification of resectability of pancreatic cancer using multi-detector row CT: a study of interobserver reliability

I. Joo¹, J. Lee¹, E. Lee¹, D. Lee¹, J.-Y. Son¹, W. Chang², S. Lee³, H. Yang¹;
¹Seoul/KR, ²Seongnam/KR, ³Anyang/KR (hijijin@gmail.com)

Purpose: To investigate the interobserver reliability in the preoperative classification of resectability of pancreatic cancer using multi-detector row CT (MDCT).

Methods and Materials: In this retrospective study, we included 110 patients with pathologically confirmed pancreatic cancer who underwent baseline multiphase contrast-enhanced MDCT. Eight board-certified radiologists with different levels of experience (more experienced, n=4; less experienced, n=4) reviewed MDCT images to score the likelihood of local resectability using a 5-point Likert scale based on each reviewer's impression and to determine categories of resectable, borderline resectable, or unresectable based on given MDCT criteria. Diagnostic performance and interobserver agreement were determined by receiver operating characteristic (ROC) curve analysis and Fleiss kappa statistics, respectively.

Results: Overall interobserver agreements were fair in Likert scale (kappa = 0.360 [95% confidence interval (CI): 0.344-0.375]) and moderate in categories (kappa = 0.477 [95% CI: 0.452-0.502]). More experienced reviewers showed higher agreement in the determination of categories than those with less experience (kappa = 0.548 [95% CI: 0.495-0.600] vs 0.432 [95% CI: 0.377-0.487]) while there was no significant difference in Likert scale according to experience level (kappa = 0.395 [95% CI: 0.361-0.428] vs 0.347 [95% CI: 0.312-0.382]). In patients with reference standard for local resectability (n=82), area under the ROC curves were 0.845-0.978 on 5-point Likert scale and 0.833-0.960 on 3 categories.

Conclusion: In the resectability assessment of pancreatic cancer, MDCT shows only fair to moderate interobserver agreement. Radiologists with higher experience level would be more likely to make consistent classifications of resectability.

B-1525 15:04

Application of CT texture analysis in quantification of pancreatic cystadenoma phenotype images

Z. Feng, Z. Hu; Hangzhou/CN (gerxyuan@126.com)

Purpose: Pancreatic serous cystadenoma and pancreatic mucinous cystadenoma differ greatly in biological characteristics, as well as their treatment and prognosis. We quantified the special imaging features of pancreatic cystadenomas and to provide new parameters for identifying of pancreatic cystic tumours using computed tomography texture analysis (CTTA).

Methods and Materials: We retrospectively analysed contrast-enhanced CT data from patients who were admitted and had pathologically confirmed pancreatic serous cystadenomas (N = 48) and mucinous cystadenomas (n = 34) in our hospital from January 2009 to December 2016. Regions of interest were drawn manually on the parenchymal phase CT images according to the border of the tumours. A Laplacian of Gaussian band-pass filter was chosen to highlight the characteristics of the image. Mean grey-level intensity (M), variance (V), entropy (E), skewness (Ske) and kurtosis (Kur) were derived with different spatial scales from fine texture ($\sigma = 1.0$) to coarse texture ($\sigma = 2.5$).

Results: There were no statistically significant differences ($p > 0.05$) in value M, but statistically significant difference ($p < 0.05$) in value $V_{2.5}$, $E_{2.5}$, $Kur_{2.5}$ and $Ske_{0.25}$ between the two sets of serous cystadenomas and mucinous cystic tumours. Areas under the ROC curve for the two sets based on the texture parameters above ranged between 0.56 and 0.84.

Conclusion: CTTA can quantify and extract the specific and abstract texture features of medical images, and reveal the inherent heterogeneity between tumours, which facilitates objective evaluation of pancreatic cystadenoma image, and greatly improve clinical diagnosis and prognostic analysis.

B-1526 15:12

Microcystic serous pancreatic cystic neoplasms: the added diagnostic value of contrast-enhanced ultrasound

Y. Dong, F. Mao, J. Cao, P. Fan, W. Wang; Shanghai/CN (drdaisydong@hotmail.com)

Purpose: Preoperative diagnosis of microcystic serous pancreatic cystic neoplasms (MPN) is clinical challenges. The purpose of current study is to analyse contrast-enhanced ultrasound (CEUS) features of histologically proven MPN, in comparison to pancreatic ductal adenocarcinomas (PDA).

Methods and Materials: The present study was approved by the institutional ethics committee and informed consent was waived. Twenty-five patients with histologically proven MPN lesions and 30 patients with histologically proven PDA lesions were retrospectively analyzed. The CEUS features of pancreatic lesions were compared to the surrounding normal pancreatic parenchyma. Two radiologists assessed the CEUS enhancement pattern in consensus.

Results: All MPN and PDA lesions were hypoechoic on B-mode ultrasound. Twenty (80 %) MPN present as solitary multilocular microcystic lesion. With colour Doppler imaging (CDI), typical 'spoke wheel' macrovessels were identified in 64 % of lesions. On CEUS, most MPN lesions displayed hyper- (96 %) or isoenhancement (4 %) in the arterial phase with 'honeycomb' architectures. In contrast, all PDA lesions showed hypoenhancement in the arterial phase ($P < 0.01$).

Conclusion: CEUS of the pancreas has the potential to aid differentiation of MPN from other neoplastic lesions. The differential diagnosis to the typically hypovascularised pancreatic adenocarcinoma was always possible.

B-1527 15:20

Assessment of local vascular invasion in pancreatic carcinoma by MDCT using the angle measuring tool

D. Šaponjski, A. Djuric Stefanovic; Belgrade/RS (saponjski.d@gmail.com)

Purpose: According to the NCCN criteria, resectability of pancreatic carcinoma (PC) is commonly assessed by MDCT and depends on tumour's relation to neighbouring blood vessels, such as celiac trunk (CT), hepatic artery (HA), superior mesenteric artery (SMA), portal vein (PV) and superior mesenteric vein (SMV). The aim of study was to investigate methodology of the assessment of local vascular invasion of pancreatic carcinoma by MDCT using the angle measuring tool.

Methods and Materials: Fifty consecutive 64-MDCT scans of patients with the PC were retrospectively analysed. Maximal angle of blood vessel's circumference that was in direct contact with the tumour was measured using the angle measuring tool on axial section, and length of direct contact on MPR-reconstructed section. Accordingly, resectability was estimated using the NCCN criteria. Frequencies and correlations were statistically analysed using Spearman's (r_s) and Pearson's correlation coefficient (r).

Results: Average size of tumour was 36 ± 13 mm (10-68 mm). Majority of PCs were in advanced stage (60% T3 and 36% T4), located in the head of the pancreas (62%). 22% tumours were estimated as resectable, 48% borderline resectable, and 30% unresectable. SMV and PV were invaded most frequently (50% and 46%), and surrounding arteries in lower percent (SMA in 26%, HA in 22% and CT in 16%). Location, size and T-stage correlated with the frequency of local vascular invasion ($r_s > 0.450$). Maximal angle correlated with the length of the vascular infiltration ($r > 0.450$).

Conclusion: Precise estimation of vascular invasion in PC by MDCT is possible using the angle measuring tool.

14:00 - 15:30

Room X

GI Tract

SS 1901c

Inflammatory bowel disease: what next?

Moderators:

S. Kinner; Essen/DE
 N.N.

B-1528 14:00

7 T MR imaging for fibrosis evaluation in a radiation-induced murine model of colitis

M. Zappa¹, S. Dolas², D. Cazals-Hatem¹, F. Milliat³, P. Garteiser², M. David¹, V. Vilgrain¹, B. Van Beers¹, E. Ogier-Denis²; ¹Clichy/FR, ²Paris/FR, ³Fontenay-aux-Roses/FR (magaly.zappa@netc.fr)

Purpose: Crohn's disease transmural bowel wall inflammation can lead to fibrosis causing luminal narrowing and fistula which are the main indications to surgery. The aim of our study was to evaluate MR imaging to distinguish submucosal from transmural fibrosis using an original murine model of radiation-induced colitis.

Methods and Materials: Colitis was induced with localised single-dose radiation (27 Gy). We included an inflammation group of 24 rats with pathological features of severe acute inflammation associated with minimal submucosal fibrosis and a mixed group of 39 rats with pathological features of severe inflammation associated with transmural fibrosis, obtained two and twelve weeks after irradiation, respectively. Fat suppressed T2- and T1-weighted, diffusion-weighted, magnetisation transfer and perfusion using ASL technique 7 T MR imaging was performed.

Results: MR imaging showed significant differences between inflammation and mixed groups in normalised to muscle signal intensity on T2-weighted images (4.2 vs 3.1, $P < 0.0001$) and T1-weighted images (1.4 vs 1.3, $P = 0.0003$), ADC (2.17×10^{-3} vs 1.69×10^{-3} mm²/s, $P < 0.0001$), magnetisation transfer ratio (35 vs 42%, $P < 0.0001$) and perfusion (60 vs 38 mL/min/100g, $P = 0.0009$). Monoparametric analysis with the best AUC to differentiate the two groups included T2-weighted signal intensity, ADC and magnetisation transfer

ratio. The combination with the best global predictive value (94%) included all parameters but T1-weighted parameter (AUC 0.94).

Conclusion: MR multiparametric analysis was able to distinguish transmural from submucosal fibrosis in our radiation-induced model. This model could be used to evaluate antifibrotic treatments currently under development.

B-1529 14:08

Accuracy of multi-parametric magnetic resonance imaging in the diagnosis and grading of intestinal acute Graft-versus-Host disease after allogeneic bone marrow transplantation

D. Vitale, F. Maccioni, V. Buonocore, D. Bencardino, M. Lopez, A. Iori, C. Catalano; *Rome/IT (davide.vitale@uniroma1.it)*

Purpose: The diagnosis of the intestinal acute Graft-versus-Host disease (a-GvHD) after allogeneic bone marrow transplantation is based on clinical symptoms, CT findings and biopsies. We assessed Magnetic Resonance Imaging (MRI) diagnostic accuracy.

Methods and Materials: We performed a prospective study on 35 patients (range 9-69 years) with clinical suspicion of intestinal a-GvHD, who underwent clinical-endoscopic, histological and multi-parametric MRI evaluation. Inclusion criteria: intestinal symptoms within 100 days from transplantation, <2 weeks between MRI and clinical-endoscopic evaluation. The following MRI features were evaluated: small and large bowel wall thickening, T2 signal and Gadolinium-enhancement of the intestinal wall, mesenteric lymph nodes, peritoneal effusion, comb-sign and restricted diffusion. Histology, clinical-endoscopic data and follow-up were considered as gold standard for diagnosis and staging. Sensibility, specificity, accuracy and Cohen's kappa were calculated.

Results: In 21/35 (60%) a-GvHD was confirmed at histology and follow-up. In true positive patients, MRI showed significant continuous wall thickening in 76.2%, stratified wall contrast-enhancement in 90%, comb-sign in 76%, increased number of mesenteric lymph nodes in 19%, and free intra-peritoneal fluid in 57.2%. A significant correlation was found between number of pathological intestinal segments and clinical grade of a-GvHD ($r=0.54$, $p=0.009$). The distal ileum was the segment most frequently involved (85.7%). MRI sensitivity was 90.5%, specificity 78%, the PPV 86%, NPV 84%, accuracy 85%. Furthermore, MRI detected early disease in 82% of patients without intestinal symptoms.

Conclusion: In patients with intestinal a-GvHD, MRI can diagnose and grade the disease with high accuracy, in both early and more advanced or severe stages.

B-1530 14:16

DWI ADC values are influenced not only by bowel distention degree but also the presence of osmotically active agent: results from research in healthy subjects

I. Apine, M.P.M. Angerer, M. Baduna, G. Kruminia; *Riga/LV (dr.ilze.apine@gmail.com)*

Purpose: To assess dependence of bowel distention and presence of mannitol in MRE examinations on ADC values.

Methods and Materials: ADC values of small and large bowel walls with high SI in DWI images at b=600 and b=800 grading bowel filling as "distended" and "collapsed" were measured before and after oral ingestion of 2.5% mannitol (1-1.5 l) in 54 patients with no evidence of IBD. ADC differences between bowel filling grades and presence of mannitol were assessed with t-test and Wilcoxon signed-rank test.

Results: Statistically significant differences ($p<0.05$) were gained in jejunum after preparation where ADC values were lower in wall of collapsed bowel than of distended one (the mean ADC in collapsed bowel at b=600 and b=800 was 1.76×10^{-3} mm²/s (SD=0.48) and 1.10 (SD 0.32), respectively, whereas in distended bowel at b=600 and b=800 being 2.56×10^{-3} mm²/s (SD=0.63) and 1.95 (SD 0.41), respectively). Regarding presence of mannitol, higher ADC was achieved in collapsed jejunum for b 600 and 800, respectively, being 1.35 (SD 0.51) and 1.10 (SD 0.32) before preparation, 1.76 (SD 0.51) and 1.47 (SD 0.36) after preparation as well as in distended colon ascendens for ADC 600 and 800, being 1.56 (SD 0.26) and 1.36 (SD 0.27) before preparation and 2.48 (SD 0.59) and 2.10 (SD 0.44) after preparation.

Conclusion: ADC is influenced by both bowel distention degree and presence of mannitol which has to be considered in diagnosis of IBD.

B-1531 14:24

Magnetisation transfer MRI can characterise the degree of intestinal fibrosis in patients with Crohn's disease: comparing with contrast-enhanced and diffusion-weighted MRI

X. Li, S. Huang, Z. Fang, Z. Li; *Guangzhou/CN (lixuehua803@163.com)*

Purpose: To evaluate the role of magnetisation transfer imaging (MTI) for characterisation of intestinal fibrosis compared with contrast-enhanced (CE) imaging and DWI and its capability for differentiating fibrotic from inflammatory strictures in humans with Crohn's disease (CD).

Methods and Materials: Abdominal MTI, CE and DWI of 31 consecutive CD patients were analysed before elective surgery. Bowel wall MT ratio (MTR) normalised to skeletal muscle, ADC and the percentage of enhancement gain were calculated and region-by-region correlation with surgical specimen was performed for histologic degree of fibrosis and inflammation. The performance of MTI was validated on 5 new patients.

Results: Normalised MTRs correlated with fibrosis scores ($r=0.769$, $P<0.001$) but did not correlate with inflammation scores ($r=0.034$, $P=0.740$). Significant differences in normalised MTRs were found among non-fibrotic, mildly, moderately and severely fibrotic walls (all $P<0.05$). Normalised MTRs of mixed fibrotic and inflammatory bowel walls were significantly higher than that of purely inflammatory bowel walls ($P<0.001$). High accuracy of normalised MTRs was shown with an AUC of 0.919 ($P<0.001$) for differentiating moderately-severely fibrotic from non-fibrotic and mildly fibrotic bowel walls, followed by ADC (AUC=0.747, $P=0.001$) and the percentage of enhancement gain (AUC=0.592, $P<0.001$). Sensitivity, specificity and AUC of MTI for diagnosing moderate-severe fibrosis in the validation dataset were 80%, 100% and 0.9 ($P=0.033$), respectively.

Conclusion: MTI outperforms ADC and CE imaging in detecting and distinguishing varying degrees of bowel fibrosis with or without coexisting inflammation. It could potentially be used as a method to differentiate fibrotic from inflammatory intestinal strictures in CD.

B-1532 14:32

Biomarkers derived from time-intensity curves in patients with Crohn's disease

E. Quai¹, A. Gennari², M.A. Cova², E.J. Van Beek¹; ¹Edinburgh/UK, ²Trieste/IT (equaia@exseed.ed.ac.uk)

Purpose: To assess the best predictors of response to therapy in patients with Crohn's disease calculated from time - intensity curves after microbubble injection.

Methods and Materials: One-hundred-and-fifteen consecutive patients (66 male and 49 female; 45.76 years \pm 11) with a proven diagnosis of Crohn's disease involving the terminal ileal loop and scheduled to begin or under therapy with corticosteroids or biologics (infliximab or adalimumab) and with stricture of the terminal ileal loop were scanned after sulphur hexafluoride-filled microbubble injection. In each patient the terminal ileal loop was scanned with CEUS before the beginning and at the end of week 6 of pharmacologic treatment. In each patient the percent change (Post - Pre x 100/Pre) of each kinetic parameter - peak enhancement, wash-in and washout rate, mean transit time, area under the whole time-intensity curve (AUC), AUC during wash-in (AUCWI), and AUC during wash-out (AUCWO) were automatically calculated from time intensity curves. Percent changes of responders and non-responders were compared by Mann Whitney test. Separate univariate logistic regressions were conducted to determine the relationship between the percent change of each kinetic parameter (independent variables), and the therapeutic outcome as responder (dependent outcome variable).

Results: Responders (n=72 patients) and non-responders (n=43) differed ($P<0.05$) in the percent change of peak enhancement, and area under the curve. Percent change of AUC, AUCWI, AUCWO were found predictors of therapeutic outcome.

Conclusion: Area under time-intensity curve obtained after microbubble contrast agent injection is predictor of response to therapy in patients with Crohn's disease.

Author Disclosures:

E. Quai: Advisory Board; Bracco Imaging. Speaker; Bracco imaging.

B-1533 14:40

Performance of PET/MR enterography vs MR enterography alone vs PET alone in evaluating active inflammation in Crohn's disease

O.A. Catalano^{1,1}, V. Wu¹, U. Mahmood¹, A. Soricelli², A. Signore³, M. Salvatore², D. Gervais¹, B.R. Rosen⁴; ¹Boston, MA/US, ²Naples/IT, ³Rome/IT, ⁴Charlestown, MA/US (alberto.signore@uniroma1.it)

Purpose: To explore the performance of PET/MR enterography (PET-MR-E) versus MR enterography (MR-E) alone and PET alone in evaluating active inflammation in Crohn's disease patients.

Methods and Materials: 21 Crohn's disease patients underwent PET/MR-E followed by surgery within 8 weeks, and constitute our study population. The gastrointestinal tract was divided into 5 segments in each patient. Two readers evaluated MR-E alone, PET alone, and PET/MR-E for active inflammation in each segment.

Results: 59/105 bowel segments were positive for active inflammation at surgery. Sensitivity of PET (91.5%) and of PET/MR-E (88%) were statistically significantly higher than MR-E alone (80%) ($p=0.02$ and $p=0.08$, respectively). No statistically significant differences were found between sensitivity of PET and PET/MR-E ($p=0.48$). Specificity of MR-E (87%) and PET/MR-E (93%) were statistically significantly higher than PET (74%) ($p=0.01$ and 0.04, respectively) but no statistically significant difference was found between MR-E and PET/MR-E ($p=0.37$). Accuracy of PET/MR-E (91%) was statistically

significantly higher than PET (84%) and MR-E (83%) ($p=0.02$ and 0.01 , respectively). No statistically significant difference was found between PET and MR-E ($p=1.00$).

Conclusion: PET/MR-E is significantly more accurate than sub-modality alone and more specific than PET alone in the detection of active inflammation in patients with Crohn's disease.

B-1534 14:48

Detection of inflammatory bowel segments with [18F]-FDG PET/MR enterography by Crohn's disease: which surrogate marker is better? MaRIA, Clermont score or PET?

Y. Li, K.J. Beiderwellen, F. Nensa, K. Herrmann, L. Jost, L. Umutlu; *Essen/DE (yan.li@uk-essen.de)*

Purpose: To compare the diagnostic accuracy of magnetic resonance index of activity (MaRIA), Clermont score and PET parameter in detecting ileocolonic inflammation in Crohn's disease (CD) with an integrated whole-body PET/MR scanner.

Methods and Materials: 50 patients with known CD and recurrent symptoms underwent ileocolonoscopy with biopsy (reference standard) as well as PET/MR enterography. The average time interval between endoscopy and PET/MR scan was 3 days. The endoscopic activity of inflammation was determined by simplified endoscopic activity score for Crohn's disease (SES-CD) and categorized in absent, mild to moderate and severe (ulcerative inflammation).

Results: A total of 309 ileocolonic segments could be analysed. To detect active inflammatory segments, area under the curve (AUC) of receiver operating characteristic (ROC) for MaRIA was 0.93, sensitivity 0.86 and specificity 0.92 (cutoff ≥ 11.5); for Clermont score 0.89, 0.82 and 0.91 (cutoff ≥ 13); for SUVmax_ratio (SUVmax of the segment divided by SUVmax of liver) 0.87, 0.77 and 0.89 (cutoff ≥ 1.2), respectively. In detecting severe ulcerative inflammatory segments, AUC of ROC for MaRIA was 0.97, sensitivity 1.0 and specificity 0.89 (cutoff ≥ 14); for Clermont score 0.98, 1.0 and 0.93 (cutoff ≥ 17); for SUVmax_ratio 0.95, 0.86 and 0.91 (cutoff ≥ 1.5). MaRIA, Clermont score and SUVmax_ratio all correlated significantly with global SES-CD ($\rho = 0.76, 0.56$ and $0.52, p < 0.001$).

Conclusion: Both MR parameters were superior to PET in detecting active inflammatory segments. All of the three surrogate markers facilitate high diagnostic accuracy in detecting severe ulcerative inflammation.

B-1535 14:56

Magnetisation transfer and conventional MRI for characterisation of intestinal fibrosis and inflammation in patients with Crohn's disease

Z. Fang¹, X. Li¹, S. Huang¹, Z. Zhang², C.C. Sun¹, S.-T. Feng¹, Z. Li¹; ¹Guangzhou/CN, ²Winston-Salam, NC/US (fangzn05@126.com)

Purpose: An accurate and non-invasive technique to identify inflammation or fibrosis predominant strictures in Crohn's disease (CD) patients is crucial for treatment strategy. The aim of this study is to evaluate the value of magnetic transfer imaging as well as conventional MRI in characterizing types of CD strictures, using surgical histopathology as a reference standard.

Methods and Materials: Seventeen CD patients with 56 specimens who had MRI studies within 15 days before surgery were enrolled in this study. MRI findings and variables included MTR, normalized MTR, T2WI high signal intensity, wall thickness, changes of enhancement pattern over time, enhancement pattern and enhancement gain ratio in each phase of the dynamic contrast-enhanced study. Correlation analysis, group difference analysis and logistic regression analysis were performed to find specific MRI variables as predictors for moderate-severe inflammation and fibrosis.

Results: The severity of inflammation was significantly associated with the following MRI variables: T2WI high signal intensity and wall thickness (both $P < 0.05$). The degree of fibrosis was significantly associated with the following MRI variables: MTR, normalized MTR and wall thickness (all $P < 0.05$). Using T2WI high signal intensity as a predictor, MRI is able to differentiate mild and moderate-severe inflammation with a sensitivity of 0.913 and a specificity of 0.800. Using normalized MTR to discriminate mild and moderate-severe fibrosis, the sensitivity and specificity were 0.875 and 0.875, respectively.

Conclusion: T2WI high signal intensity and normalized MTR may serve as MRI markers for predicting moderate-severe inflammation and fibrosis, respectively, which can provide information for clinical treatment options.

B-1536 15:04

A simulated fast magnetic resonance enterography protocol in patients with Crohn's disease: a retrospective, randomised, double-blind study

G. Cicero, S. Mondello, A. Blandino, G. Ascenti, T. D'Angelo, S. Mazzotti; *Messina/IT (gcicero87@gmail.com)*

Purpose: Magnetic resonance enterography (MRE) is a radiation-free and accurate technique in the assessment of Crohn's disease, mainly impaired by high costs and prolonged scanning times. Our purpose is to compare the

diagnostic performance of standard MRE vs a "fast" protocol consisting of only three sequences.

Methods and Materials: 73 standard MRE examinations of patients with Crohn's disease performed over a 7-month period were retrospectively evaluated. The images of the two protocols were separated and evaluated by two radiologists with 12 and 2 years of experience in MRE. Statistical analysis was performed using the Cohen kappa value, the Lin's concordance correlation, Bland-Altman plot, and the nonparametric Mann-Whitney U test.

Results: Inter-protocol agreement was excellent for the presence and number of lesions, assessment of intestinal complications, and excellent in recognising inflammation pattern and extra-intestinal complications (kappa value 0.94-0.096). The assessment of fibrosis had lower agreement with a kappa value of 0.84, while an almost perfect concordance ($p < 0.999$) was found in the assessment of lesion extension. Inter-observer agreement was excellent for the presence and number of lesions, inflammation and intestinal and extra-intestinal complications; the assessment of fibrosis showed a lower agreement (93%; $\kappa = 0.84$; 95% CI, 0.69 to 0.96). A concordance coefficient of 0.997 (95% CI 0.995-0.999) between the readers was obtained for the lesion extensions. Moreover, time spent in the evaluation of the fast protocol was significantly lower.

Conclusion: The fast protocol achieves comparable performance with standard MRE. Furthermore, it has potentially enormous benefits in terms of patient's comfort, time and health-care cost savings.

B-1537 15:12

Established bowel damage detected on MR enterography in patients with Crohn's disease in complete endoscopic remission

J. Rimola, I. Alfaro, D. Vas, I. Ordás, E. Ricart, J. Panes; *Barcelona/ES (jrimola@clinic.cat)*

Purpose: To identify the MRE lesions that persist in patients with Crohn's disease (CD) in endoscopic remission as indicators of established damage and to determine its relationship with pre-treatment MRE lesions.

Methods and Materials: Patients with CD who had been included in prospective studies on autologous haematopoietic stem cell transplant and/or anti-TNF drugs were evaluated for this study. Inclusion criteria were: presence of at least one segment with severe inflammatory lesions on endoscopy (CDEIS >8.5) or MRE (MaRIA >11) before treatment and achievement of endoscopic remission after 1 year of treatment. Baseline and 1-year MRE were reviewed.

Results: 73 intestinal segments with severe inflammatory lesions from 28 patients achieved endoscopic remission. The prevalence of creeping fat and bowel mural fat did not change in association with achievement of endoscopic remission ($p=0.34$ and $p=0.35$, respectively). Furthermore, luminal stenosis persisted in 50% of initial stenosis and mural thickness >3 mm remained in 29% of segments. At least one of the aforementioned residual lesions was present in 30/73 segments with endoscopic remission. Regression analysis showed that the predictive factors on MRE for established residual mural lesions after achieving endoscopic remission were the presence of bowel fat deposition (OR=48.3, $p=0.001$) and stenosis (OR=15.96, $p=0.004$), whereas creeping fat was the predictive factor for persistent extramural lesions (OR=35.8, $p < 0.001$) and for either mural or extramural lesions (OR=16.25, $p < 0.001$).

Conclusion: Up to 41% of bowel segments in endoscopic long-standing remission after treatment had residual lesions at MRE. The presence of bowel fat deposition, stenosis and creeping fat may predict the development of established damage.

B-1538 15:20

Dual-energy CT enterography in evaluation of Crohn's disease: the role of virtual monochromatic images

E. Güler, N.G. Ünal, I. Hekimsoy, T. Köse, M. Harman, Z.N. Elmas; *Izmir/TR (gulerezgi@yahoo.com)*

Purpose: The purpose of this study is to evaluate the performance of virtual monochromatic images (VMI) in differentiating diseased and non-diseased bowel segments in Crohn's disease (CD). The second aim is to compare mural enhancement between patients with and without CD by using VMI.

Methods and Materials: Dual-energy CT enterography (CTE) of 61 patients (47 with CD and 14 without CD) were retrospectively reviewed. Images were reconstructed at VMI energy levels from 40 to 110keV in 10 keV increments. Attenuation, signal-to-noise ratio(SNR), and contrast-to-noise ratio(CNR) were obtained from diseased and non-diseased bowel segments. Subjective analysis of image quality of VMI and polychromatic images(PCI) was performed by two radiologists in consensus. Repeated measures ANOVA and Wilcoxon tests were used in the assessment of quantitative and subjective analyses, respectively.

Results: Attenuation, SNR, and CNR were found to be higher with a statistical significant difference in diseased segments than non-diseased segments in patients with CD at each energy level of VMI. In the evaluation of patients with and without CD, optimal attenuation, SNR, and CNR values were observed at 40keV (area under ROC curve (AUC):0.913;95% confidence interval(CI):0.843-

0.984), 40keV (AUC:0.807;95%CI:0.679-0.935), and 70keV (AUC:0.906;95%CI:0.82-0.987), respectively. For subjective analysis, there was a statistically significant difference between the comparison of VMI and PCI ($p < 0.05$).

Conclusion: VMI of dual-energy CTE provide information in differentiating diseased bowel segments in CD by assessing mural enhancement quantitatively. In the evaluation of CD and controls, VMI at 40keV and 70keV allow for the optimal attenuation and CNR of bowel segments, respectively.

14:00 - 15:30

Room Z

Interventional Radiology

SS 1909

Urogenital interventions

Moderators:

S. Bongiovanni; Cuneo/IT
J. Kettenbach; St. Pölten/AT

K-30 14:00

Keynote lecture

T.J. Kroencke; Augsburg/DE

B-1539 14:09

Interventional radiology approach in the treatment of symptomatic uterine fibroids: from diagnosis to treatment: our experience

P. Palumbo, S. Quarchioni, F. Bruno, M.V. Micelli, A. Giordano, M. Varrassi, S. Carducci, M. Di Luzio, C. Masciocchi; L'Aquila/IT
(palumbopierpaolo89@gmail.com)

Purpose: Uterine fibroids (UF) are the most common benign uterine neoplasm. Uterine artery embolization (UAE) and Magnetic Resonance guided Focused Ultrasound (MRgFUS) have been demonstrated to be safe and effective as uterus-sparing therapeutic option. Our purpose is to demonstrate the efficacy of both procedures in the treatment of symptomatic UF.

Methods and Materials: We retrospectively analysed 105 women. 58/105 were treated with MRgFUS and 47/105 were treated with UAE. They were screened by magnetic resonance imaging (MRI) to evaluate Non-Perfused-Volume (NPV) and Perfused Volume (PV) of remains fibroids. The UFs questionnaire (UFS-QOL) is used in order to assesses clinical symptoms severity before and after one year post procedure.

Results: After one year, the NPV mean value was of 95% using UAE and of 91% using MRgFUS. The post-treatment UFS-QOL has shown a significant reduction of score when compared to pre-treatment score. High efficacy of MRgFUS depends on the correct selection criteria (better efficacy for type 0 and 1 UFs when compared to other). The UFS-QOL too, show high value in case of inappropriate MRgFUS treatment (post-treatment score near to pre-treatment values, with mean value between 40 to 60), with necessity of retreatment or other treatment as UAE or myomectomy.

Conclusion: UAE is more radical compared to MRgFUS, but it is necessary to consider the age of patients and their wishing to conceive; considering controversial aspect about pregnancy after UAE, we consider always MRgFUS as first treatment option especially in young patients.

B-1540 14:17

A comparative study of quantitative T1 perfusion parameters in magnetic resonance-guided high-intensity focused ultrasound ablation of uterine fibroids

N.M. Duc¹, B. Keserci¹, H.Q. Huy¹, P.N. Hoa¹, P.M. Thong²; ¹Ho Chi Minh/VN, ²Ha Noi/VN (bsnguyenminhduc@pnt.edu.vn)

Purpose: To investigate the predictive role of quantitative perfusion parameters in magnetic resonance-guided high-intensity focused ultrasound (MR-HIFU) ablation of uterine fibroids.

Methods and Materials: 100 uterine fibroid patients (39.4 ± 5.9 years with a range of 22-52 years) underwent MR-HIFU were accessed in this study. The population was divided into 2 groups based on dynamic contrast-enhanced MR images at screening: group A (n = 75) if the time-intensity curves of uterine fibroids is lower than that of myometrium and group B (n = 25) if the time-intensity curves of uterine fibroids is equal or higher than that of myometrium. K_{trans} , area under the curve (AUC) of both fibroids and myometrium and the ratio K_{trans} and AUC of uterine fibroids relative to myometrium were investigated.

Results: K_{trans} , AUC, K_{trans} ratio and AUC ratio were 83.1 ± 59.0 (30.1-315.2); 20.7 ± 16.1 (3.2-69.8); 0.56 ± 0.18 (0.2-1.0); 0.6 ± 0.2 (0.3-1.0); for group A and 189.1 ± 87.9 (55.2-372.4); 38.4 ± 27.1 (9.2-99.1); 1.8 ± 0.7 (0.7-3.8); 1.8 ± 0.5 (1.3-2.9) for group B ($p < 0.05$), respectively. Immediate post-treatment non-perfused volume (NPV) ratio of uterine fibroids was 95.71% ± 5.9 (80-100%) for group A and 54.26% ± 25.77 (4.26-80.17%) for group B ($p < 0.05$).

Multiple linear regression manifested that there were K_{trans} ratio and AUC ratio parameters had significant effect on NPV ratio ($p < 0.05$).

Conclusion: The K_{trans} ratio and AUC ratio parameters could be served as a potential criteria in patient selection for an improved NPV ratio.

B-1541 14:25

MR-guided focused ultrasound (MRgFUS) compared to the main current therapeutic approaches for the treatment of uterine fibroids

S. Dababou, F. Andrani, A. Napoli, R. Scipione, C. Marroccchio, H.-P. Erasmus, C. Catalano; Rome/IT (susy150791@gmail.com)

Purpose: To prospectively evaluate the clinical outcome of magnetic resonance focused ultrasound (MRgFUS), uterine artery embolization (UAE) and surgery for symptomatic uterine fibroids.

Methods and Materials: 585 symptomatic uterine fibroids underwent pre-treatment MR evaluation to assess myoma characteristics and MRgFUS eligibility. 187(32%) were considered eligible for MRgFUS and treated with ExAblate-InSightec 2100 system, while 398 were ineligible and directed toward other therapeutic strategies. Of these, 137 patients underwent UAE, 143 myomectomy and 61 hysterectomy. The clinical outcome was evaluated by comparing the pre-treatment Symptoms Severity Score (SSS) with post-treatment SSS at the 3-month and 12-month follow-up. Data concerning the number and type of complications, days of hospitalization and days of convalescence were also collected and compared.

Results: The mean SSS reduction at 3 and 12 months was respectively 27,4% and 56,3% for the MRgFUS group; 48,7% and 56,9% for the UAE group; 69,8% and 67,1% for the myomectomy group; 96,6% and 94,5% for the hysterectomy group. The MRgFUS group demonstrated fewer complications (4 patients, 2,3%), while the major adverse events rate was reported in the UAE group (33 patients, 25,4%). All MRgFUS patients were treated in an outpatient setting, while the mean days for hospitalization and convalescence were, respectively, 3,4+/-2 and 11,7+/-9 days for the UAE group; 4,1+/-2 and 16,9+/-12 days for the myomectomy group; 4,5+/-1 and 24,6+/-14 days for the hysterectomy group.

Conclusion: The clinical efficacy of MRgFUS for uterine fibroids treatment is comparable to UAE, but slightly lower than that for myomectomy. However, MRgFUS is feasible in an outpatient setting and adverse events rate is significantly lower than that of other therapeutic strategies.

B-1542 14:33

Follow-up studies of uterine fibroids (UFs) treated with MRgFUS: who are the best candidates for treatment?

I. Capretti, S. Iafrate, E. Cannizzaro, F. Arrigoni, M. Di Luzio, A. Giordano, S. Mascaretti, G. Mascaretti, C. Masciocchi; L'Aquila/IT
(ilaria_capretti@hotmail.it)

Purpose: To investigate the individual variables that can influence a good clinical result in patients affected by symptomatic UFs and treated with MRgFUS.

Methods and Materials: A population of 110 women with symptomatic UFs (aged between 27 and 49) and treated with MRgFUS was retrospectively analyzed. These women were submitted to c.e.MRI immediately after treatment and after twelve months in order to evaluate the Non-Perfused Volume (NPV). Clinical outcome was investigated by means of a questionnaire about symptoms and health-related quality of life (UFS-QOL). Acoustic window, patients' BMI and distance from skin tissue to fibroid in the anterior or posterior uterine wall were considered as individual characteristics.

Results: All patients presented a mean value of NPV extension ranging between 68% and 81% after treatment and a reduction of 50% at twelve months. In 94 patients an improvement of symptomatology was observed: mean UFS-QOL value of 51.6 before treatment and 16.7 at the follow-up. Some women (70) became asymptomatic during the follow-up. Women with higher NPV ratio, appropriate and wide acoustic window, lower BMI and less distance between skin tissue and fibroid, in particular UFs of anterior uterine wall, achieved good clinical success.

Conclusion: MRgFUS may be considered a valid alternative therapy in patients affected by UFs. Some favorable conditions such as appropriate acoustic window and lower BMI and distance from the skin may be related to a better clinical success.

B-1543 14:41

Tips and tricks to treat difficult cases of uterine fibroids (UFs): how to increase eligibility in MRgFUS (magnetic resonance-guided focused ultrasound surgery)

S. Iafrate, I. Capretti, E. Cannizzaro, F. Arrigoni, M. Di Luzio, A. Giordano, S. Mascaretti, G. Mascaretti, C. Masciocchi; L'Aquila/IT
(sonia.iafrate87@gmail.com)

Purpose: To increase eligibility of uterine fibroids(UFs) treatment by MRgFUS, via some practical strategies, in order to obtain an adequate acoustic window for the ultrasound beam in difficult cases.

Methods and Materials: Fourteen patients affected by UFs, displaying an inadequate acoustic window to MRgFUS, were assessed from May 2014 to September 2016. Additionally to the common techniques used to obtain an adequate acoustic window, we tried to evaluate some strategies to increase the eligibility to the procedure. Inversion table together with abdominal massages were used to move up the bowel loops with the patients in antigravity position. To minimise intestinal bloating and peristalsis a low-fibre diet for a week before the MRgFUS was advised. Filling bladder to move-up bowel loops and filling rectum to outdistance the UFs from the sacrum were also used. The volume of treated UFs and Non perfuse volume (NPV) were calculated, while symptom outcome was assessed with a symptom severity score questionnaire (UFS-QOL).

Results: Fourteen patients, affected by UFS and with inadequate acoustic window, were evaluated. After using inversion table (20%), filling bladder and rectum (50%), low-fibre diet (30%) inadequate acoustic window was obtained and 10 patients underwent MRgFUS. A mean extension of NPV of 50-65% with a good effectiveness of the treatment was observed in all treated UFs. Furthermore, patients experienced a reduction of UFS-QOL around 70%, when compared with the pre-treatment score. No severe side effects were observed. Despite these practical strategies, 4 patients were not treated due to inadequate acoustic window.

Conclusion: Some practical strategies may increase eligibility to MRgFUS obtaining an adequate acoustic window for the ultrasound beam; in these patients, MRgFUS may improve clinical outcome.

B-1544 14:49

Combined uterine artery embolisation with intra-arterial chemoinfusion as a sole management for scar and cervical ectopic pregnancy

A. Elmokadem, R. Abdel-Wahab, A.A. El-Zayadi, M. ElRakhawy; *Mansoura/EG (mokadem83@yahoo.com)*

Purpose: To evaluate the technical and clinical outcomes of uterine artery embolization (UAE) along with the chemoinfusion of methotrexate (MTX) for cesarean scar (CSP) and cervical pregnancy (CP) as an alternative nonsurgical treatment to control bleeding and uterine preservation.

Methods and Materials: This study included eleven patients (age range between 25-40 year, mean; 31.8) with 7 CSP & 4 CP. They presented with vaginal bleeding and elevated β -HCG levels (mean 31.245 mIU/mL). The diagnosis of ectopic pregnancy was confirmed by sonography and magnetic resonance imaging. They were treated with UAE using embolic particles (500-700 microns) and gelatin sponge particles. In all patients, the infusion of MTX (50mg/m²) was performed before UAE. Angiographic features as contrast extravasation and utero-ovarian anastomosis were reported. Follow-up periods after UAE ranged between 6 to 24 months included weekly sonography and β -HCG level assessment with MRI scan after 2 months.

Results: All patients had prior history of cesarean section. The gestational sac age range between 6-11 week. In ten patients, UAE controlled active vaginal bleeding and postprocedural HCG levels were reduced significantly by the second week. One patient presented with persistent elevated HCG level and vaginal rebleeding was encountered. The rebleeding was successfully controlled by second UAE procedure. The ectopic pregnancies were dramatically resolved & uterus was preserved in all patients. No major complications were detected. Normal menses resumed within 2 months after UAE.

Conclusion: UAE along with chemoinfusion of MTX is effective non surgical alternative for treating SCP and CP with uterine preservation.

B-1545 14:57

Transperineal ultrasound-guided laser ablation for the treatment of benign prostatic hyperplasia in interventional radiology: preliminary results

G. Patelli¹, A. Ranieri¹, G.A. Paganelli¹, A. D'Alessio², F. Besana¹, G. Mauri³, C.M. Pacella⁴; ¹Seriante/IT, ²Osio Sotto-Zingonia/IT, ³Milan/IT, ⁴Albano Laziale/IT (gianluigi.patelli@asst-bergamoest.it)

Purpose: To assess the safety and efficacy of ultrasound-guided (US-g) transperineal laser ablation (TPLA) in treating benign prostatic hyperplasia (BPH).

Methods and Materials: fifty-five patients (age 72.6±10.4 years, range 58-93) suffering from obstructive syndrome secondary to BPH underwent TPLA using continuous wave (CW) diode laser source operating at 1064 nm (Echolaser Soractel Lite, Elesta s.r.l., Calenzano (FI), Italy). Under US-g, depending on basal volume, up to two 21 G introducer needles for each lobe were inserted via transperineal approach. Each treatment was performed with a fixed power protocol (3W) changing the illumination time case by case according to the prostate volume. The efficacy of the treatment was evaluated considering the changes of International Prostate Symptoms Score (IPSS), Quality of Life (QoL), post-void residual (PVR), peak urinary flow rate (Qmax) and prostate volume. The mean hospital stay and mean catheterization time were measured.

Results: In all patients, the treatment was successful without intraoperative and perioperative complications. The mean operation time was 43.3±8.7 min, mean ablation time 15.9±3.9 min, mean energy deployed 11,470.0±3,570.6J, mean hospital stay 1.5±0.4 days and mean catheterization time after the procedure 14.4±7.7 days. The mean follow-up was 11.5 months (range 4-36). IPSS improved from 22.2 to 7.7 (P<0.001), QoL from 4.5 to 1 (P<0.001), Qmax from 7.6 to 13.3 ml/s (P=0.001), PVR from 148.0 to 58.2 ml (P<0.001) and mean prostate volume from 80.6 to 52.6 ml (P<0.001). No major complications occurred.

Conclusion: TPLA is a novel option to treat patients affected by BPH. The study demonstrated that this approach was efficacious and safe with significant and durable results.

B-1546 15:05

MRI-guided percutaneous transgluteal ablation of unilateral prostate carcinoma: initial experiences and results

J. Figiel, A. Koenig, A. Hegele, A. Mahnken; *Marburg/DE (figiel@med.uni-marburg.de)*

Purpose: To evaluate safety, periprocedural imaging features and short-term outcome of MRI-guided percutaneous transgluteal cryo-ablation of focal prostate carcinoma in a 1.5T MR-scanner.

Methods and Materials: The analysis includes 10 consecutive Patients (age 46-75, average 60) with 11 interventions performed between 06/2016 and 07/2017. All patients had histologically proven unilateral prostate carcinoma (5 low risk, 6 intermediate risk). Pre- and postinterventional PSA-levels were measured. MRI-guided semigland-ablation was performed under general anesthesia via a transgluteal access. Realtime-imaging was used for positioning of the cryo-needle. Periprocedural imaging was used to monitor ice-ball formation. Rectum, urethral sphincter and bladder-tissue were spared. Postprocedural multiparametric MRI was performed to assess results after 1 day, 6 months and 12 months.

Results: Average procedure time was 2:41 h (2:07 h - 3:49 h). There were no major complications. One patient suffered hematuria for 4 weeks requiring no further treatment, one patient had a clinically irrelevant mucosal defect in the rectum and one patient had postinterventional urinary retention requiring prolonged transurethral catheterization. Peri- and postinterventional MRI showed full coverage of 9 lesions. In 1 lesions postinterventional biopsy revealed residual tumor and the intervention was repeated 10 months after initial procedure. PSA-levels declined by an average of 71.5% (18.2-99.5%). During follow-up no death or distant metastasis occurred.

Conclusion: Initial results show, that percutaneous MRI-guided cryoablation of focal prostate carcinoma is a safe and effective minimal-invasive therapy for a selected group of patients with prostate carcinoma. It may provide a viable alternative in patients under active surveillance.

B-1547 15:13

MR-guided focused ultrasound treatment for management of organ-confined intermediate-risk prostate cancer: evaluation of safety and effectiveness

S. Bednarova, A. Napoli, R. Scipione, S. Dababou, C. Marroccchio, H.-P. Erasmus, V. Panebianco, C. Catalano; *Rome/IT (sandra.bednarova@gmail.com)*

Purpose: To evaluate the safety and effectiveness of MR-guided focused ultrasound (MRgFUS) ablation of organ-confined intermediate-risk prostate cancer (PCa) in patients seeking urogenital functional preservation while controlling tumour growth, postponing or avoiding the need of definitive treatment.

Methods and Materials: This prospective single-arm study was approved by the institutional review board, and informed consent was obtained from all subjects. Sixteen treatment-naïve patients (age range 50-74 years) with histologically proven organ-confined intermediate-risk PCa (Gleason score $\leq 7=3+4/4+3$, T1-T2b, NO, M0 stage, PSA ≤ 20 ng/ml) underwent pre-treatment 3T multiparametric MR imaging (mpMRI) and for MR visible lesions MRgFUS treatment with ExAblate (InSightec) was performed. Safety of treatment was determined by evaluation of the incidence and severity of device-related complications while clinical efficacy was evaluated in terms of prostate MRI changes and serum PSA (sPSa) levels at 3, 6 and 12 months follow-up.

Results: MRgFUS shows low operative morbidity and no systemic side effects: one patient reported urinary incontinence and two patients referred erectile dysfunction after treatment. Contrast-enhanced MRI (DCE-MRI) at 3, 6 and 12 months follow-up showed no recurrence/residual disease in treated patients. Progressive decrease of sPSA levels was encountered; an average value of 17.1 ng/ml before treatment dropped to 2.2 ng/ml at 12 months follow-up. Yet all patients included in this study are considered free of clinically significant PCa with no present need of definitive treatment.

Conclusion: MRgFUS can reduce the need of surgery or radiation therapy in patients with intermediate-risk prostate cancer representing a safe and effective treatment.

B-1548 15:21

MR-guided in-bore prostate biopsy for clinically significant cancer detection in patients with negative TRUS biopsies and rising PSA level

N. Matinyan¹, V. Kuplevatsky², I. Minasyan¹, M. Cherkashin², N. Berezina², D. Sahakyan¹; ¹Yerevan/AM, ²St. Petersburg/RU (matinyan@doctor.com)

Purpose: To evaluate the potential of MRI-guided prostate biopsy in individuals with negative TRUS biopsy and rising PSA level.

Methods and Materials: This study covered 91 patients (aged 40-70), with negative TRUS biopsy and rising PSA level, who underwent multiparametric MRI, with high-field 3T scanner (MAGNETOM Verio) or 1.5T scanners (MAGNETOM Aera and Symphony). Quantitative and qualitative assessment of changes were carried out in accordance with the recommendations of PI-RADSv2. MRI-guided in-bore biopsy was performed using a MRI-compatible "In vivo" biopsy set, with a 150mm/16g needle gun. To navigate and control the location of the needle, T2 WI was used in the sagittal and coronal projection.

Results: Based on the results of multiparametric MRI, 40 patients were graded as PI-RADS 3, 32 patients as PI-RADS 4 and 19 patients as PI-RADS 5. Based on the histological data after the MRI-guided biopsy, in the group of patients with PI-RADS 3 score, 32 were diagnosed with adenocarcinoma (in one case clinically insignificant cancer was diagnosed, in the rest Gleason score did not exceed 3+4=7). In the group of patients with PI-RADS 4 score, 28 were diagnosed with adenocarcinoma (with average Gleason score 4+3=7). In the group of patients with PI-RADS 5 score, 19 were diagnosed with adenocarcinoma (with average Gleason score 4+3=7).

Conclusion: The MRI-guided biopsy is an efficient procedure for detecting clinically significant prostate cancer in patients with previous negative TRUS biopsies results and rising PSA level.

14:00 - 15:30

Room O

Chest

SS 1904a

Pulmonary vessels

Moderators:

F. Pontana; Lille/FR
J. Vlahos; London/UK

B-1549 14:00

Automated volumetry of peripheral pulmonary vessels based on CT angiography in suspected pulmonary hypertension

C. Melzig¹, O. Weinheimer¹, B. Egenlauf¹, M. Messerli², E. Grünig¹, H.-U. Kauczor¹, C. Heussel¹, F. Rengier¹; ¹Heidelberg/DE, ²Zurich/CH (claudius1.melzig@med.uni-heidelberg.de)

Purpose: To assess automated volumetry of the peripheral lung vasculature based on pulmonary CT angiography (CTPA) for the detection of pulmonary hypertension (PH).

Methods and Materials: 74 consecutive patients (mean 66.2 years, 50 female) who underwent right heart catheterization (RHC) and CTPA for suspected PH at our institution were included. Patients with chronic thromboembolic PH were excluded. In-house developed software was used for automated vessel segmentation. Vascular volumes within 10 mm, 15 mm and 20 mm of the lung borders were calculated.

Results: 42 out of 74 patients had PH (mean pulmonary arterial pressure (mPAP) 37±11 mmHg, 57%), while 32 had normal mPAP (17±4 mmHg). Peripheral vessel volumes were significantly enlarged in patients with PH compared to patients without PH: 86±29 vs. 66±23 cm³ within 20 mm, 59±24 vs. 42±19 cm³ within 15 mm and 31±17 vs. 19±14 cm³ within 10 mm of the lung borders (all p < 0.003). ROC analysis showed AUC for the detection of PH of 0.73 for 20 mm, 0.74 for 15 mm and 0.75 for 10 mm of the peripheral vascular volume. A cutoff value of 19.4 cm³ for the 10 mm peripheral vascular volume identified PH with 74% sensitivity, 72% specificity, 78% positive and 67% negative predictive value.

Conclusion: Automated volumetry of peripheral pulmonary vasculature is feasible and demonstrated significantly enlarged vessel volumes in patients with confirmed PH with the highest diagnostic accuracy within 10 mm of the lung periphery. The technique may facilitate non-invasive detection of PH.

B-1550 14:08

CT evaluation of small pulmonary vessel area in patients with bronchiolitis obliterans syndrome after lung transplantation

Y. Sato, J. Tominaga, N. Mori, Y. Matsuda, Y. Okada, K. Takase; Sendai/JP (maroty0507@gmail.com)

Purpose: To evaluate the cross-sectional area (CSA) of small pulmonary vessels measured on CT for detection of bronchiolitis obliterans syndrome (BOS) in patients who have undergone bilateral lung transplantation.

Methods and Materials: The institutional review board approved this study and waived informed consent. The study comprised consecutive 26 patients who underwent bilateral lung transplantation. The patients were divided into two groups: non-BOS and BOS on the basis of spirometry test. We measured CSA less than 5 mm² and calculated the percentage of total CSA for the lung area (%CSA<5) using plain chest CT. Three CT slices were selected for the measurement of CSA. The upper slice was taken 1 cm above the upper margin of the aortic arch, the middle slice was taken 1 cm below the carina, and the lower slice was taken 1 cm below the right inferior pulmonary vein. These three CT slices were analysed using ImageJ. The values of %CSA<5 were compared between the non-BOS and the BOS groups using the Mann-Whitney U test. P<0.05 indicated statistical significance.

Results: Six patients had BOS grade 0-p, two patients had BOS grade 2, and two patient had BOS grade 3. The remaining 16 patients had no BOS. Median %CSA<5 of the BOS group was significantly lower than that of the non-BOS group (0.49 versus 0.66, P=0.047). The ROC curve revealed that the area under the curve was 0.74.

Conclusion: CSA of small pulmonary vessels measured by CT may be useful for diagnosis of BOS after lung transplantation.

B-1551 14:16

High-resolution computerised tomography (HRCT) features of Group 1 pulmonary arterial hypertension (PAH): a case series of 21 lung transplant patients

M.S. Juárez-García, E. Pallisa, M. López-Meseguer, D. Varona Porres, A.L. Sanchez Martinez, E. Maciag, L. Cabanzo Campos, J. Andreu, O. Persiva Morenza; Barcelona/ES (anchante.juarez@gmail.com)

Purpose: Characterise HRCT features of PAH in a case series of patients who posteriorly received a uni-bilung graft between the years 2010 and 2017.

Methods and Materials: We retrospectively evaluated a case series of 21 PAH patients and described the last pre-transplant thoracic/HRCT features. These features were analysed by two independent thoracic-radiologists at five levels: origin of great vessels; main carina; pulmonary venous confluence; halfway between the third and fifth section; above the right hemidiaphragm. We defined the disease extension and the extent of the primary and secondary radiological features at each level. Primary features were centrilobular nodules, ground-glass opacities, and interlobular septal smooth thickening. Secondary features were enlargement of mediastinal lymph nodes, pleural/pericardial effusion, and egg-banana sign.

Results: Eight patients had idiopathic/heritable PAH, five had scleroderma, four had pulmonary veno-occlusive disease/Group 1 (PVOD), and four had left heart disease. Almost all idiopathic/heritable PAH patients had all the primary and secondary HRCT features, except interlobular septal thickening, which was only described in one patient (12.5%). All scleroderma patients had more than 50% of disease extension and positive egg-banana sign; however, no patient had interlobular septal thickening. All PVOD patients had centrilobular nodules, interlobular septal thickening and mediastinal lymph node enlargement, but none had positive egg-banana sign. All left heart disease patients had centrilobular nodules and interlobular septal thickening, but none had lymph node enlargement or pleural/pericardial effusion.

Conclusion: In our case series, the scleroderma patients had the greatest lung disease extension and the highest positivity of egg-banana sign. All PVOD patients showed the classical radiological features as described in the literature.

B-1552 14:24

Dual-energy CT (DECT) lung perfusion in chronic thromboembolic pulmonary hypertension (CTEPH): diagnostic accuracy and concordance with radionuclide scintigraphy

M. Masy, J. Giordano, C. Hossein-Foucher, G. Petyt, J. Remy, M. Remy-Jardin; Lille/FR (martine.remy@chru-lille.fr)

Purpose: To evaluate the concordance rate of DECT lung perfusion and ventilation/perfusion (V/Q) scintigraphy in diagnosing chronic thromboembolic pulmonary hypertension (CTEPH) amongst patients with proven pulmonary hypertension (PH).

Methods and Materials: 80 patients with proven PH underwent V/Q scintigraphy and DECT lung perfusion. Diagnosis of CTEPH was established by the presence of at least one segmental triangular perfusion defect on DECT perfusion images and by characteristic V/Q mismatch on scintigraphic examinations.

Results: The study population comprised 36 patients with CTEPH ("CTEPH group") and 44 patients with other aetiologies of PH (i.e. "non CTEPH group"). On DECT perfusion images alone, 35 were true positive, 6 false positive and 1 false negative (sensitivity: 0.97; specificity: 0.86; positive predictive value: 0.85; negative predictive value: 0.97). On V/Q scans, there were 36 true positives and 1 false positive (sensitivity: 1; specificity: 0.97; positive predictive value: 0.97; negative predictive value: 1). There was excellent agreement between DECT perfusion and scintigraphy in diagnosing CTEPH (kappa: 0.80). Combined information from DECT lung perfusion and CT angiographic images

enabled reclassification of (a) the 6 false-positive cases into the "non CTEPH group", triangular defects being related to small airway disease; (b) the false-negative case into the "CTEPH group", based on the finding of mild central and extensive peripheral chronic PE.

Conclusion: There is excellent agreement between DECT perfusion and V/Q scintigraphy. The diagnostic accuracy of DECT is reinforced by the morpho-functional analysis of datasets.

Author Disclosures:

J. Remy: Consultant; Research Consultant, Siemens Healthcare.

M. Remy-Jardin: Research/Grant Support; Siemens Healthcare.

B-1554 14:32

Overdiagnosis of PE in pregnancy? Interpretative discrepancy in the diagnosis of pulmonary embolism in pregnant patients undergoing CTPA
D.P. Mitchell, C.D. Gillespie, H. Moriarty, C.A. Ridge, P.J. MacMahon;
Dublin/IE (dpmitchell@gmail.com)

Purpose: To evaluate the rate of discrepancy in the diagnosis of PE in pregnant patients undergoing CTPA.

Methods and Materials: Retrospective review of all CTPA studies performed on pregnant patients referred to a tertiary referral centre over a two-year period. CTPA studies reported as positive for PE were matched with negative CTPA studies. This mixed subset was blindly reviewed by two subspecialist radiologists. CTPA study quality and thrombus volume was recorded.

Results: 98 CTPA studies were performed on pregnant patients over the two-year period. 14% (14/98) of studies were initially read as positive for PE. A subset of 30 studies (14 PE-positive and 16 PE-negative studies) were blindly assessed by two sub-specialist reviewers. There was 97% agreement between reviewers (29/30 studies). 1 study was considered nondiagnostic and 3 studies were determined to be suboptimal but sufficient for the diagnosis of a large- or medium-sized PE. The diagnostic agreement between the reviewers and the initial reporting radiologist in 83% (25/30). 36% (5/14) of "PE positive" studies were reclassified as false positives.

Conclusion: There was a higher than expected rate of discrepancy in the interpretation of positive CTPA studies. By raising awareness of this issue of PE over-diagnosis, the percentage of CTPAs reported as positive for PE dropped from 14% to 2% in our institution. We strongly recommend the addition of "MDT review" to the diagnostic treatment algorithm for all positive PE cases in pregnancy to ensure a subspecialty double read of all positive CTPA studies.

B-1555 14:40

Indeterminate CT pulmonary angiograms (CTPA) with dual-source CT (DSCT): prospective evaluation in 449 patients suspected of acute pulmonary embolism (PE)

J. Hennicau, A. Hutt, J.-B. Faivre, S. Khung, J. Remy, M. Remy-Jardin;
Lille/FR (martine.remy@chru-lille.fr)

Purpose: To evaluate (a) the rate of indeterminate CTPA acquired with a 3rd-generation DSCT system; and (b) the impact of correcting factors immediately applicable.

Methods and Materials: 449 patients underwent a DSCT angiogram with single- (SE) (n=276; 61.5%) or dual-energy (DE) CT (n=173; 38.5%). An indeterminate study was defined by (a) a totally nondiagnostic examination; or (b) an examination limiting the level of analyzability of pulmonary arteries to central vessels.

Results: Twelve CTPAs (12/449; 2.7%) were deemed indeterminate with a proportion that did not differ between examinations acquired with SE (9/276; 3.2%) and DE (3/173; 1.73%) (p=0.38). The contributing factors comprised (a) motion artifacts due to the lack of patient cooperation (1/12); (b) a poor level of enhancement (6/12); or (c) patient-related limitations (5/12). In the case of indeterminate SE examination (n=9): (a) a second acquisition was immediately obtained after correction of the presumed contributing factor: (i) repeated instructions to maintain apnea (1/9); (ii) selection of a lower kVp, higher iodine concentration or both (7/9); (iii) no change in the repeat CTPA (1/9); (b) the second acquisition was subsequently diagnostic in all but one patient. In the case of DE indeterminate acquisitions (n=3), the reading of low-kVp images restored a diagnostic image quality. After correction, the final rate of indeterminate CTPA was 0.2% (1/449).

Conclusion: The rate of indeterminate CTPA decreased from 2.7% to 0.2% after a second acquisition (SE) or the reading of low-kVp images of the initial acquisition (DE).

Author Disclosures:

J. Remy: Consultant; Research Consultant, Siemens Healthcare.

M. Remy-Jardin: Research/Grant Support; Siemens Healthcare.

B-1556 14:48

Significant reduction of contrast agent dose for venous phase chest CT scans: first experiences using monoenergetic reconstructions from a novel spectral detector scanner

T. Hickethier, J. Kröger, B. Baessler, D. Maintz, D.-H. Chang; Cologne/DE (tilman.hickethier@uk-koeln.de)

Purpose: Monoenergetic reconstructions (MonoE) from Dual-Energy-CT systems can elevate iodine attenuation and therefore might permit a significant reduction of contrast agent dose. In this study, we investigated the influence of MonoE from a novel Spectral-Detector-CT (SDCT) on delineation of mediastinal structures and overall image quality in chest CT examinations with significantly reduced contrast agent dose (>50%).

Methods and Materials: 41 patients underwent venous phase CT scans of the chest on a SDCT (IQon, Philips) and 35 instead of 75ml contrast agent followed by a NaCl flush of 60 ml. Images were calculated conventionally (Conv) and with MonoE at 40 keV. Contrast-to-noise-ratio (CNR) was measured for a hilar lymph-node (LN) as well as its attenuation difference to the adjacent pulmonary artery (LNPA). Image quality (IQ) was evaluated by 2 readers with respect to overall diagnostic certainty (ODC) and LN delineation (LND) using a 5-point-Likert-scale: 1=non-diagnostic; 2=barely diagnostic; 3=fair; 4=adequate; 5=excellent.

Results: Both subjective IQ parameters were significantly improved using MonoE compared to Conv (ODC 4.2 vs. 2.7; p<.01 / LND: 3.8 vs. 2.3; p<.01). The IQ of all MonoE reconstructions was rated at least as adequate without any non-diagnostic results. Objectively measured CNR and LNPA were superior using MonoE compared to Conv (CNR 14.18 vs. 5.96; p<.01 / LNPA 111.99 vs. 38.02 HU; p<.01).

Conclusion: In venous phase chest CT scans with markedly reduced contrast agent dose subjective image impression and objective IQ parameters can be significantly improved by using monoenergetic reconstructions from a novel SDCT.

B-1557 14:56

Investigation of a roll pump contrast media injector for individually adapted iodine concentrations

I. Rychina¹, T. Riemüller², V. Makarenko¹, V. Berezniyskiy¹, A. Tikhonov¹, J.A. Oreshkova¹, P. Frank³, L. Bockeria¹, R. Riemüller²; ¹Moscow/RU, ²Graz/AT, ³Ulm/DE (rainer@riemueller.net)

Purpose: To investigate the precision of different iodine concentrations obtained using an automatic contrast media (CM) injector and commercially available CM with higher iodine concentration.

Methods and Materials: Starting from an initial concentration of 320 (Iodixanol, blood iso-osmolality) and 350 mgI/ml (Iohexol, low osmolality) the CM were sequentially mixed with physiological NaCl-solution using the CT motion XD 8000 ulrich medical automatic CM injector with an injection speed of 2, 5, and 8 ml/s. The iodine concentration was reduced in steps of 10% down to 50% of the starting concentrations. Calibration standards were prepared diluting the initial solutions with distilled water. High-performance liquid chromatography (HPLC) measurements of the probes were performed on Agilent 1290 Infinity instrument equipped with ZORBAX Eclipse Plus C18 column maintained at 30°C and UV/Vis detector. The relative deviation of probes from the desired concentration was computed.

Results: For Iodixanol 320 an average relative deviation of 6.91% (min 1.5, max 12.63%) at an injection speed of 2 ml/s, 6.03% (min: 0.88, max: 16.89%) at 5 ml/s and 3.38% (min: 0.07, max: 9.37%) at 8 ml/s was obtained. Iohexol 350 showed an average relative error of 4.26% (min 0.3, max 7.8%) at 2 ml/s, 5.13% (min 1.2, max 9.6%) at 5 ml/s and 2.9% (min 1.1, max 5.1%) at 8 ml/s.

Conclusion: Our data confirm the feasibility of obtaining the desired iodine concentration using the automatic roll pump CM injector under investigation.

Author Disclosures:

P. Frank: Employee; Ulrich Medical. **R. Riemüller:** Consultant; Ulrich Medical.

B-1558 15:04

Lesion detection on the "all-in-one" window: is it as good as on conventional window settings? A feasibility study

A. Snoeckx¹, B. Broeckx², K. Carpentier¹, R. Corthouts¹, E. Luyckx¹, S. Nicolay¹, M.J. Spinhoven¹, A. Van Hoyweghen¹, J. Cant²; ¹Edegem/BE, ²Merelbeke/BE, ³Mortsel/BE (annemie.snoeckx@uza.be)

Purpose: Historically, CT studies are always viewed in several window settings, optimized to evaluate specific anatomic structures and regions (mediastinal, lung, bone and vascular window). A newly developed image processing technique fuses these conventional windows into a single "all-in-one" window. Our purpose was to compare lesion detection on this "all-in-one" window versus conventional window settings.

Methods and Materials: In this study, 50 consecutive thoracic oncology chest CT examinations, containing 417 documented lesions and features, were reviewed by 6 radiologists, subdivided into 2 groups of 3 radiologists each, with

similar levels of expertise in each group (experienced, junior and radiology resident). All scans were reviewed in conventional window settings (as in routine daily practice), by one group, and in the "all-in-one" window by the other group. Lesions were listed as 'missed' when they were not seen by at least two out of three observers and as 'well diagnosed' when seen by at least two out of three observers.

Results: Out of the 417 lesions, 68 lesions were missed: 21 on the "all-in-one" window, 30 on conventional views and 17 on both views. Statistical analysis with linear mixed model showed that use of the "all-in-one" window did not result in an increase of missed lesions ($p=1$). Conversely, we found a tendency towards better lesion detection on the "all-in-one" window, though not strongly significant ($p=0.07$). Inter-observer agreement in both groups was similar ($p=0.462$).

Conclusion: In chest CT examinations, lesion detection on the "all-in-one" window is at least as good as on conventional window settings.

Author Disclosures:

J. Cant: Employee; Agfa Healthcare.

B-1559 15:12

The influence of intelligent optimum tube voltage-combined low dose of contrast medium injection based on BMI on radiation dose and image quality of chest CT enhancement

Y. Zhou; *Zhengzhou/CN (zhouyue779@163.com)*

Purpose: To investigate influence of intelligent optimum tube voltage-combined low dose of contrast medium based on BMI on radiation dose and image quality of chest CT enhancement.

Methods and Materials: 104 patients who received spectral chest CT enhancement were randomly divided into groups A and B: group A with conventional 120 kVp, 450mgI/Kg contrast medium injection; group B with intelligent optimum tube voltage, 300mgI/Kg contrast medium injection. Patients were divided into three sub-groups based on BMI. Subjective image quality score, SNR, CNR of descending aorta at different layers and radiation dose were compared.

Results: Image quality scores of A1, A2 were higher than that of B1, B2 during arterial phase, while no significant difference during venous phase. A3 and B3 showed no statistical difference during arterial and venous phase. CNR of descending aorta at tracheal bifurcation, right pulmonary artery layer in A1 and B1, left/right atrium layer in A2 and B2, left/right atrium layer in A3 and B3 during venous phase have no statistical difference, other layers in group B were higher than that of group A. SNR in group B was superior to that of group A. Radiation dose in A1, A2 were lower vs B1, B2, dropped by 16.39% and 14.50%, respectively; however, there was no significant difference between A3 and B3.

Conclusion: Optimal tube voltage can be selected according to BMI using intelligent optimum tube voltage technique, which can reduce radiation dose and improve CNR. Combined low-contrast medium injection can reduce contrast agent injection and maintain image quality.

14:00 - 15:30

Room N

Genitourinary

SS 1907a

Prostate biopsy and (post-)intervention

Moderators:

A. Baur; Berlin/DE

V. Panebianco; Rome/IT

B-1560 14:00

A prospective study to compare the outcomes of MRF-TB and 12-core SB in different PSA groups

J.-M. Xu, Y.Q. Chen; *Shanghai/CN (junmei_510@126.com)*

Purpose: To assess and compare the rate of detection of clinically significant prostate cancer (csPCa) between magnetic resonance imaging (MRI)-ultrasound fusion-targeted prostate biopsy (MRF-TB) and 12-core systematic biopsy (SB) in the different prostate-specific antigen (PSA) groups.

Methods and Materials: This prospective study included 156 patients who underwent pre-biopsy MRI and 12-core SB between September 2014 and August 2016. In the patients with MRI-suspicious lesions ($n=123$), MRF-TB was performed before SB. In the clinically suspicious patients with normal MRI ($n=33$), SB was performed without MRF-TB. The detection rates for any cancer and csPCa were compared between MRF-TB and SB.

Results: Detection rate for any cancer was not significantly different between MRF-TB (64/123, 52.0%) and SB (66/156, 42.3%; $p=0.106$). For csPCa, the detection rate of MRF-TB (61/123, 49.6%) was significantly higher than that of SB (46/156, 29.5%; $p=0.001$). In a subset analysis of patients with PSA<10ng/ml, csPCa detection rate of MRF-TB (26/67, 38.8%) was

significantly higher than that of SB (16/83, 19.3%; $p=0.008$). In 10≤PSA<20ng/ml group, csPCa detection rate of MRF-TB (20/38, 52.6%) was also significantly higher than that of SB (15/52, 28.8%; $p=0.022$). In PSA≥20ng/ml group, csPCa detection rate of MRF-TB (15/18, 83.3%) was higher than that of SB (15/21, 71.4%), but no significant difference was found ($p=0.379$).

Conclusion: Our prospective study revealed a similar rate of prostate cancer detection between MRF-TB and SB, and MRF-TB could improve the overall detection of csPCa compared to SB. We also found that MRF-TB was superior to SB for csPCa detection in subset patients with PSA<10ng/ml and 10≤PSA<20ng/ml, but was similar in patients with PSA≥20ng/ml. Therefore, the traditional SB may be replaced by MRF-TB for detection of csPCa.

B-1561 14:08

The accuracy of MRI/TRUS fusion biopsy in detection of high-risk prostate cancer vs random biopsies: advertisement or necessary innovation?

F. Kossov¹, I.I. Abdullin¹, B. Kamolov¹, B. Olimov¹, O. Orlov¹, V. Panov¹, I. Tyurin¹, E. Fedorenko¹, V. Kapustin²; ¹Moscow/RU, ²Moscow Oblast/RU (*fil-doc@yandex.ru*)

Purpose: Systematic biopsies (SB) are an integral part of prostate cancer (PCa) diagnostics. SB PCa detection rate varies from 31% to 42%; however, the number of false-negative results is high. MRI/TRUS fusion target biopsy (MRI/TRUS FTB) probably would improve the detection of high-risk cancer (HRC) both in initial biopsy and in patients with preliminary negative SB results.

Methods and Materials: 82 patients with suspected PCa were examined. The criteria of patients inclusion was the presence of: 1) PSA>4 ng/ml and positive results of the digital rectal examination; 2) mpMRI data. The examination includes: 1) prostate mpMRI; 2) MRI/TRUS FTB; 3) SB.

Results: PCa was detected in 66 cases (including 12 cases with previously negative SB). MRI/TRUS FTB PCa detection rate includes: 1) 13.3% cases with Gleason=6; 2) 33.5% with Gleason=7; 3) 53.2% with Gleason=8-10. SB evaluates PCa in: 1) 27.8% patients with Gleason=6; 2) 38.9% with Gleason=7; 3) 27.8% with Gleason=8-10. MRI/TRUS FTB data is significantly highly competitive in high malignancy potential nodes detection with SB ($p<0.0001$). The HRC detection accuracy using MRI/TRUS FTB appears higher in comparison with SB data ($p<0.0001$). MRI data (estimated by PI-RADS v.2) showed significant correlation with the MRI/TRUS FTB results ($p<0.02$, correlation coefficient 0.7).

Conclusion: The MRI/TRUS FTB provides an opportunity to decrease the necessary number of punctures in PCa patients for detection of the histological material with the highest malignancy rate. MRI/TRUS FTB exposes low sensibility to insignificant PCa. It increases the detection of clinically relevant forms of PCa.

B-1562 14:16

MRI/US fusion prostate biopsy a single-centre experience

C. Cicero, E. Lievore, A. Casarin, B. De concilio, A. Celia, L. Genesio, A. Guarise; *Bassano del Grappa/IT (aircalo@yahoo.it)*

Purpose: MRI-US fusion biopsy system is a diagnostic procedure which permits the withdrawal of prostate specimens directly from a suspected lesion seen at MRI, bypassing random prostate biopsies. We studied the efficacy of the method among the patients evaluated in our facility.

Methods and Materials: 150 patients with findings suspicious for PCa (mean age 65.5 years, median PSA 5,533ng/mL and median prostate volume 59cc) underwent mpMRI. All the mpMRI were evaluated by a specialised urologist. The suspected lesions were classified according to the PI-RADS and marked. Data were transferred in the Biopsee® system and, with superimposition of MRI on real-time transrectal US, three-dimensional biopsy planning was conducted and transperineal biopsies were performed according to the planning. We conducted statistical evaluation of cancer detection in these patients.

Results: 58 out of 150 patients (39%) were found positive for PCa. The correlation between mpMRI findings and histologic evaluation was satisfactory for lesion marked as PI-RADS 5 or highly suspicious for PCa (34 over 52 or 65%) but mild for lesions classified as PI-RADS 4 or moderately suspicious for PCa (28 over 106 or 26,5%). Regarding complications, three patients were affected by acute urinary retention and one experienced haematuria.

Conclusion: Transperineal stereotactic prostate biopsy combining US/MR enables targeted evaluation of suspected lesions. The method is safe with few complications. The correlation between PI-RADS and histologic lesion approximates the results of similarly-conducted studies. The procedure is overall promising, and opens to other utilisations beyond the detection of PCa, such as focal therapy and active surveillance.

B-1563 14:24

Transrectal ultrasound-guided targeted biopsy of transition zone prostate cancer: usefulness of across midline sign

S. Park, S. Won; Seoul/KR (WSY0622@yuhs.ac)

Purpose: To retrospectively evaluate diagnostic performance of transrectal ultrasound (TRUS)-guided targeted biopsy (TB) of transition zone (TZ) prostate cancer (PCa) in patients with prebiopsy magnetic resonance imaging (MRI).

Methods and Materials: Consecutive series of 38 patients who underwent TRUS-guided TB of TZ lesions were evaluated. TB (mean core number, 2.4±0.6; range, 2-4) was performed by a single experienced radiologist under cognitive registration between prebiopsy MRI and TRUS. Across midline sign was defined by a focal lesion traversing the midline of prostatic TZ on MRI and TRUS, leading to discontinuity of the midline. Prostate Imaging-Reporting and Data System version 2 (PI-RADSv2) scoring for targeted TZ lesions was also conducted with T2-weighted and diffusion-weighted MRI by the same radiologist.

Results: PI-RADSv2 categories from 2 to 5 for TZ lesions consisted of 4, 14, 7, and 13. Cancer detection rate of TRUS-guided TB for TZ lesions was 78.9% (30/38). Across midline sign was identified in 50.0% (19/38). Cancer detection rate of TRUS-guided TB for TZ lesions showing across midline sign on both MRI and TRUS was 94.7% (18/19).

Conclusion: Under cognitive registration, TRUS-guided TB for TZ lesions showing across midline sign on both MRI and TRUS may be highly predictive of TZ PCa.

B-1564 14:32

In-bore biopsies of the prostate assisted by a remote-controlled manipulator at 1.5 T

N.P. Linder, A. Schaudinn, T.-O. Petersen, R. Stange, M. Moche, P. Stumpp, T. Kahn, H. Busse; Leipzig/DE (linder@uniklinik-leipzig.de)

Purpose: To evaluate technical and clinical performance of a fully MRI-compatible, pneumatically driven remote-controlled manipulator (RCM, "robot") for 1.5-T in-bore biopsies of the prostate.

Methods and Materials: This preliminary prospective study included the first 15 patients that underwent robotic (Sotera Medical, Arnhem, Netherlands), in-bore biopsies of the prostate in a wide-bore 1.5 T MRI (Magnetom Aera, Siemens Healthcare, Erlangen, Germany). Targeting and control of the transrectal needle guide were realized by rapid MR imaging (balanced SSFP sequence with acquisition times around 10 s). Biopsies were performed by two radiologists, each with 4 years of experience with prostate interventions. Analysis involved pre-biopsy MRI reports (PIRADS version 2), procedure times (between planning and final control MRI), periprocedural complications and histopathologic results of the samples.

Results: Mean age (range) was 67 (54 - 80) years and mean PSA level was 11.1 (0.7 - 21.5) ng/dl. Twelve patients (80%) had received prior biopsies under transrectal ultrasound guidance. Prebiopsy MRI reports involved 12 cases with a single suspicious finding (2x PIRADS 3, 5x "P4" and 5x "P5") and 3 cases with two ones (2x "P3" and 1x "P5"). Histopathologic examination revealed prostate cancer in 7 of 15 cases. One patient developed urosepsis which was successfully treated with antibiotics. Procedure times ranged between 26 and 85 min.

Conclusion: In-bore, transrectal prostate biopsies could be successfully performed with a robotic manipulator at a field strength of 1.5 T. Unlike with passive interventional devices, the patient may remain inside the bore for needle-guide adjustments.

B-1565 14:40

Experience with MRI guided prostate biopsies using the 3D Navigo system in an oncologic referral centre

S. Heijmink, R. van den Bergh, E. Wit, H. van der Poel; Amsterdam/NL (swheijmink@live.com)

Purpose: Multiparametric (mp) MRI has the potential to increase biopsy yield of prostate cancer detection. This study presents experiences with the Navigo system for MRI-TRUS fusion.

Methods and Materials: Navigo MRI-TRUS fusion biopsies was performed from 2015-2017. All patients received prebiopsy 3TmpMRI. Dependent on biopsy indication, random non-guided biopsies were taken in the same session. We recorded any encountered problems, compared Navigo and NG biopsy cancer detection rates, and explored predictors for positive biopsy outcome.

Results: Navigo biopsies were planned in 228 patients for diverse indications, of whom 26 (11%) could not be performed. In 18 (9%) of the remaining patients a problem was reported during the procedure. Any of the guided biopsies was positive in 24-85%, dependent on indication. Of the 202 Navigo procedures, additional non-guided cores were taken in 99 patients. Similar results between Navigo and non-guided biopsies were found for any positive biopsy rate, %positive cores, and mean Gleason score (all p>0.05), but the absolute number of cores taken was almost half for the Navigo biopsies.

Lowest lesion mean ADC was a persistent predictor in multivariable analysis for positive biopsy outcomes.

Conclusion: The benefit of 3TmpMRI targeted Navigo fusion biopsies was seen in the lower number of biopsy cores needed, but not in cancer detection rate or mean Gleason score. In patients without primary diagnosis, guided biopsies did not obviate the need for additional random biopsies. ADC was the main biopsy outcome predictor for guided and non-guided biopsies.

B-1566 14:48

Typical MR imaging findings after HIFU-hemiblation of the prostate

N.P. Linder¹, J. Michaelis¹, J. Gawlitza¹, H. Busse¹, P. Ho-Thi¹, T. Kahn¹, P. Stumpp¹, R. Ganzer², A. Schaudinn¹; ¹Leipzig/DE; ²Bad Tölz/DE (linder@uniklinik-leipzig.de)

Purpose: To evaluate MR imaging features of the prostate after high-intensity focused ultrasound (HIFU) treatment of the hemigland.

Methods and Materials: Eighteen patients with a mean age of 67.1 (48.9-78.5) years, mean Prostate-specific-Antigen level of 6.35 (4.0-9.8) ng/dl and biopsy-proven unilateral Prostate Cancer (PCa) received MRI before and 12 months after HIFU (Hemiblation, Focal One). MR/ultrasound fusion-guided Biopsy was performed after 12 months to exclude recurrent/contralateral cancer. MRI (3T) followed PIRADS version 2 guidelines with T2 TSE, diffusion-weighted imaging (DWI) and dynamic-contrast enhanced-T1 imaging (DCE). MR-analysis included quantitative and qualitative imaging characteristics, such as T2-volumetry, DCE and DWI signal-intensity measurements.

Results: Treatment resulted in a mean volume reduction of the target lobe by 49.1% (27.9-69.5%) and of the whole gland by 28.1% (1.0-45.6%), respectively. The typical image patterns of the ablated lobe consisted of a centrally positioned, T2-hyperintense, well circumscribed area, defined as seroma and/or a T2-hypointense area with heterogeneous DWI signal intensity, interpreted as scar, mainly adjacent laterally to the seroma. The combination seroma/scar was observed in 16 of 18 patients, whereas only scar was observed in 2 cases. In 50% of the cases a rim-like contrast media uptake around the ablation area was observed. MRI detected one of four cases of biopsy-proven low grade contralateral PCa and none of two cases of ipsilateral recurrent PCa (Ø Gleason: 6.5).

Conclusion: MRI analysis revealed distinct image patterns at 12 months after hemiblation, such as seroma, scar and volume reduction. However detection rate of recurrent or contralateral prostate cancer was low.

B-1567 14:56

Six months follow-up of periprostatic nerve plexus changes after robot-assisted radical prostatectomy using MRI tractography.

A. Cybulski, S. Brancato, V. Di Paola, R. Negrelli, E. Boninsegna, M. Catania, A. Tafuri, S. Siracusano, R. Pozzi Mucelli; Verona/IT (sarix_89@hotmail.it)

Purpose: To evaluate early and late modifications of periprostatic nerve plexus (PNP) after robot-assisted radical prostatectomy (RARP) with MRI tractography and their clinical correlations.

Methods and Materials: 34 patients (mean age:64,8) candidate to RARP performed 3 MRI examinations completed with 32-directions DTI sequences respectively before, 1 (mean:39,4 days) and 6 months (mean:201,7 days) after RARP. Tractography reconstructions were performed by positioning 6 ROIs of PNP, evaluating the following parameters: number of fibers(N), number of voxels(V), fractional anisotropy(FA), apparent diffusion coefficient(ADC), fiber length(L). Before each MRI, 2 questionnaires were administered to investigate urinary continence(ICIQ-SF) and erectile function(IEEF-5). Each tractography parameter of the 3 examinations was compared using Student's T-test and was correlated with urinary incontinence and erectile dysfunction using Kendall's-tau test.

Results: Reduction of N and V was observed 1 month after RARP, without any increment at 6 months. 1 month-MRI demonstrates reduction of FA, which returns to pre-surgery values at 6 months-control. Reduction of ADC was observed at 6 months-MRI compared with the previous examinations (p<0,001). No modification of L emerged. Positive correlation has been established between N(τ=0,297), V(τ=0,282), FA(τ=-0,249) and potency and between N(τ=-0,257), V(τ=-0,231) and urinary continence(p<0,001).

Conclusion: MRI tractography is able to identify complex changes regarding the number of fibers(N and V reduction post-RARP) and fiber patterns of PNP(FA reduction at 1 month, growing up back to pre-surgery values at 6 months). These changes correlate both with potency and urinary continence.

B-1568 15:04

Predicting and improving postprostatectomy urinary continence by pelvic floor measures on MR

S. Heijmink, N. Grivas, C. Tillier, R. van der Roest, E. van Mullekom, H. van der Poel; Amsterdam/NL (swheijmink@live.com)

Purpose: Urinary incontinence is a frequent complication of prostatectomy. MRI imaging of pelvic floor musculature has learned that several anatomical characteristics predict postprostatectomy continence function. We used this

information to attempt reconstruction of the pelvic floor after prostatectomy to improve continence outcome.

Methods and Materials: In 439 patients preprostatectomy MRI images were correlated to functional outcome continence scores (ICIQ-SF) for 10 pelvic measurements. Based on the obtained measures we changed the pelvic floor reconstruction from median fibrous raphe reconstruction only and added medialisation of the anterior muscle fibers of the levator ani muscle behind the urethra. In a prospective comparative analysis we studied the 6 months postoperative ICIQ-SF score in men with median fibrous raphe reconstruction with or without levator suspension and standard urethral-bladder anastomosis.

Results: A longer membranous urethral length (MUL), smaller interlevator distance (ILD) and more extensive fascia preservation score were predictive of earlier continence recovery. We developed an algorithm to predict continence outcome after prostatectomy based on these predictors. Since we hypothesized that narrowing of the pelvic floor exit by medializing anterior fibers of the levator ani muscle would artificially decrease ILD and elongate MUL and therefore improve postprostatectomy continence we performed this procedure in 211 men undergoing RARP. In comparison to standard (n=1375) or median fibrous raphe reconstruction (n=271) bladder-urethral anastomosis, MALF addition improved early (3w) (p=0.01) but not late (6m) continence recovery.

Conclusion: MRI-based pelvic floor prostaticometry individualizes prediction of postprostatectomy continence. Increasing pelvic floor support of the urethra improves early, but not overall continence.

B-1569 15:12

Correlation of short- and long-term urinary continence after radical prostatectomy with findings of preoperative multiparametric prostate MRI
M. Sauer, R. Pompe, P. Tennstedt, L. Budaeus, G. Salomon, G. Adam, D. Beyersdorff; *Hamburg/DE (m.sauer@uke.de)*

Purpose: To evaluate whether preoperative multiparametric prostate MRI (mpMRI) can help to stratify the risk of urinary continence (UC) after radical prostatectomy (RP) based on specified image findings.

Methods and Materials: Our institutional review board approved this retrospective study. 233 patients (median age 66.1 years) underwent standardized mpMRI at 3T prior to prostatectomy, including high-resolution T2w-TSE-imaging in 3 planes, T1w-TSE, DWI with ADC map, PD-TSE and Gd-DCE. Membranous urethra length, urethra angle and apex shape were measured systematically in T2w sequences in the sagittal plane. Prostate volume was determined during transrectal sonography. Image findings and clinical data (age, type of surgery) were correlated to UC as evaluated by a standardized questionnaire determining the amount of necessary hygiene pads one week (response rate 100%) and one year after surgery (response rate 61.4%; n=143 patients).

Results: Of all clinical parameters, there was a small yet significant positive correlation of age with UC one week (Spearman $r=0.27$, $p=0.0001$) and one year after surgery ($r=0.20$, $p=0.02$). Urethra angle and apex shape as measured in mpMRI did not correlate significantly with UC at neither time point. Correlation of the membranous urethra length with UC was small negative after one week ($r=-0.22$, $p=0.001$) and close to medium negative after one year ($r=-0.29$, $p=0.001$). Sonographic prostate volume did not correlate with UC and will be complemented by outstanding MRI volumetries.

Conclusion: Measurements of the membranous urethra length in mpMRI correlate with short- and long-term UC after radical prostatectomy and should be acknowledged during preoperative risk stratification.

B-1570 15:20

Additional value of early imaging of ⁶⁸Ga-PSMA-11 PET/CT in the assessment of local recurrence in prostate cancer patients with biochemical relapse

C. Uprimny, A. Kroiss, C. Decristoforo, J. Fritz, B. Nilica, W. Horninger, I. Virgolini; *Innsbruck/AT (Christian.UPRIMNY@tirol-kliniken.at)*

Purpose: Evaluation of local recurrence (LR) in prostate cancer patients with biochemical recurrence is hampered by high physiologic urinary bladder activity present on ⁶⁸Ga-PSMA-11 PET/CT exams, usually conducted 60 min after tracer injection (p.i.). This study aims to investigate whether additional early static PET scans could enhance diagnostic performance of ⁶⁸Ga-PSMA-11 PET/CT in the evaluation of LR.

Methods and Materials: 213 prostate cancer patients with biochemical recurrence referred to ⁶⁸Ga-PSMA-11 PET/CT were analysed retrospectively (median PSA: 1.47 ng/ml). In all patients an early static scan of the pelvis was performed with a median starting time of 281 sec p.i., followed by a whole-body PET/CT 60 min p.i. Image interpretation was based on visual analysis. Furthermore, calculation of maximum standardized uptake value (SUV_{max}) of pathologic lesions was performed.

Results: On standard PET images 60 min p.i. a LR-suggestive lesion (median SUV_{max}: 11.0) could be detected in 28 patients (13.1%), whereas an equivocal finding was present in 36 patients (16.9%). In contrast, on early PET scans a pathologic lesion compatible with LR was revealed in 52 patients (median

SUV_{max}: 5.9) and an unclear finding in only nine patients (4.2%). Early PET images led to a significant rise in the detection rate ($p<0.001$) as well as a significant reduction of equivocal findings ($p<0.001$) compared to PET-imaging 60 min p.i.

Conclusion: Assessment of local recurrence in prostate cancer patients with biochemical relapse referred to ⁶⁸Ga-PSMA-11 PET/CT is improved by additional early PET imaging.

14:00 - 15:30

Studio 2018

Chest

SS 1904b

MRI in chest oncology

Moderators:

J. Broncano; Córdoba/ES

J. Ley-Zaporozhan; Munich/DE

B-1571 14:00

Lung cancer screening with MRI: application of Lung-RADS in the first two screening rounds

M. Meier-Schroers, R. Homs, H. Schild, D. Thomas; *Bonn/DE (michael.meier@ukbonn.de)*

Purpose: To evaluate if Lung-RADS can be applied for MRI based on the results of the first two rounds of a lung cancer screening.

Methods and Materials: 224 participants of a lung cancer screening were examined with MRI and low-dose CT (LDCT). Acquired sequences were T2-MVXD, balanced-FFE, 3D-T1, and DWI. MRI was prospectively analysed regarding nodules blinded to LDCT (minimum nodule size 4mm). Nodules were assigned a Lung-RADS score based on their appearance and size at baseline and in follow-up examinations after 3, 6, and 12 months. MRI findings were correlated with LDCT.

Results: The early recall rate dropped from 13.8% at baseline to 1.9% in the second round with biopsy rates of 3.6% in the first round and 0.5% in the second round. All eight lung cancers were accurately depicted by MRI. The following categories were assigned on MRI with results of LDCT in parentheses: 4B/4X in 10 (10) cases, 4A in 16 (15) cases, 3 in 13 (12) cases, 2 in 77 (92) cases, 1 in 140 (126) cases. Lung-RADS scoring significantly correlated between MRI and CT ($p<0.001$). The score was overestimated by MRI in one case for category 4A, in two cases for category 3, and in five cases for category 2. The MRI-based Lung-RADS score was only underestimated for category 1 in 20 cases.

Conclusion: Lung-RADS might be applied for lung cancer screening with MRI, since findings significantly correlated with LDCT. Relevant findings with a Lung-RADS score of ≥ 3 were never missed or underestimated by MRI.

B-1572 14:08

The value of diffusion-weighted imaging based on monoexponential and biexponential model in the diagnosis of benign and malignant lung nodules and masses

J. Jiang¹, L. Cui², X. Gu³, Q. Hong¹, Y. Fu¹, G. Xu¹; ¹Yancheng/CN, ²Nantong/CN, ³Suzhou/CN (1021809719@qq.com)

Purpose: To compare the value of lesion-to-spinal cord signal-intensity ratio (LSR), apparent diffusion coefficient (ADC) and intravoxel incoherent motion (IVIM) parameters in the differentiation of pulmonary nodules and masses, and to explore the preferred region-of-interest (ROI) method.

Methods and Materials: 63 lesions (18 benign cases and 45 malignant cases) in forms of pulmonary nodules (n=26) or masses (n=37) were enrolled. DWI and IVIM scans were performed on a 3T MRI machine. LSR₉₀₀ was drawn and ADC_{mean}, ADC_{min}, D, D*, f were measured using single-slice ROI_s and volumetric ROI_v. ICCs were assessed. Parameters obtained by these two ROIs were compared using paired t-test and independent t-test was adopted to compare parameters between benign and malignant lesions. ROC curves were generated to identify the best parameters and thresholds to distinguish the benign and malignant lung nodules and masses.

Results: The inter-observer reproducibility of D* was relatively poor. There were no significant differences in ADC_{mean}, ADC_{min}, D and f values obtained by different ROI methods (P=0.029). Between benign and malignant lung nodules, only ADC_{mean}(ROI_s) showed difference while for lung masses, ADC_{mean}, ADC_{min}(ROI_v), D and f(ROI_s) all had diagnostic value, the highest belonging to D(ROI_v).

Conclusion: DWI can better diagnose pulmonary masses than pulmonary nodules. For the latter only ADC_{mean} obtained by single-slice ROI has the diagnostic value. For the former, ADC_{mean}, ADC_{min}, D and f all could do, but D obtained by volumetric analysis was preferred.

B-1573 14:16

Computed diffusion-weighted image: utility for differentiation of malignant from benign pulmonary nodules as compared with actually obtained diffusion-weighted image

Y. Kishida¹, S. Shinichiro¹, T. Yoshikawa¹, M. Yui², Y. Kassai², K. Kyotani¹, Y. Ohno¹; ¹Kobe/JP, ²Ōtawara/JP (yjk121@med.kobe-u.ac.jp)

Purpose: To determine the utility of computed diffusion-weighted image (DWI) for differentiation of malignant from benign pulmonary nodules as compared with actually obtained DWI (aDWI).

Methods and Materials: 61 consecutive patients with 82 pulmonary nodules (41 malignant and 41 benign nodules) underwent 3T MRI. All DWI were obtained using fast advanced spin-echo (FASE) sequence with b-values at 0 and 1000s/mm² (aDWI_{0, 1000}). Computed DWIs (cDWIs) were generated as 400, 600, 800, 1000, 1500 and 2000 (cDWI₄₀₀₋₂₀₀₀) s/mm² by commercially available software. Then, signal-to-noise ratio (SNR) and contrast ratio (CR) between nodule and thoracic muscles were determined by ROI measurement at each nodule. To compare image quality between aDWI₁₀₀₀ and each cDWI, SNR and CR were compared among all DWIs by Dunnett multiple comparison test. To compare diagnostic performance of pulmonary nodule and determine the threshold values of each DWIs, receiver operating characteristic (ROC) analyses were performed. Sensitivity, specificity and accuracy were compared among all DWIs and aDWI₁₀₀₀ combined with each cDWI by McNemar's test.

Results: SNRs of cDWI₄₀₀ and cDWI₆₀₀ were significantly higher than that of aDWI₁₀₀₀ (p<0.05). AUCs of cDWI₆₀₀ and cDWI₁₀₀₀ were significantly larger than that of cDWI₂₀₀₀ (p<0.05). There were no significant differences of diagnostic performance among all DWIs and aDWI₁₀₀₀ with each cDWI (p>0.05). However, specificity and accuracy of aDWI₁₀₀₀ were improved, when combined with cDWI₆₀₀.

Conclusion: Computed DWI is suggested as useful for differentiating malignant from benign pulmonary nodules, when added with actual DWI in routine clinical practice.

Author Disclosures:

S. Shinichiro: Research/Grant Support; Toshiba Medical Systems Co.
T. Yoshikawa: Research/Grant Support; Toshiba Medical Systems Co.
M. Yui: Employee; Toshiba Medical systems Co. **Y. Kassai:** Employee; Toshiba Medical Systems Co. **Y. Ohno:** Research/Grant Support; Toshiba Medical Systems Co., Bayer Pharma, Guerbet, Daiichi-Sankyo Co., Ltd., Eisai Co., Ltd., Fuji Pharma, Philips Electronics Japan.

B-1574 14:24

Functional MRI evaluation of b-2000 images improve mediastinal lesion characterisation

J. Coolen, F. De Keyzer, E. Verbeke, A. Dubbeldam, C. Dooms, P. De Leyn, W. De Wever, D. Van Raemdonck, J.A. Verschakelen; *Leuven/BE* (johan.coolen@uzleuven.be)

Purpose: Invasive surgical procedures are at the moment the cornerstone of mediastinal staging. We attempted to use a noninvasive MRI approach to differentiate benign from malignant mediastinal lesions and at the same time attempt to provide an imaging-based preoperative evaluation of lesion resectability.

Methods and Materials: 100 consecutive patients (58 male, 42 female), with a suspicious mediastinal lesion on clinical or on imaging-based (CT, PET or EBUS) examinations, were included. Additional to the anatomical MRI sequences on a 3 Tesla scanner DWI-acquisition was performed. All MR images were evaluated by visual inspection and by calculating the ADC values (mean) of the whole lesion (WL) (based on b-1000) and of the hyperintens b-1000 zones (based on b-2000). Histological examinations of operative specimens served as reference.

Results: A total of 43 benign and 57 malignant lesions were included. Diagnosis based on the mean ADC calculated from the WL (b-1000) was rather disappointing (sens.75.4%, spec.60.5% and acc.69.0%) and showed an optimal threshold of $1.97 \times 10^{-3} \text{ mm}^2/\text{s}$ between benign and malignant lesions. The ADC calculation on b-1000 images (b-2000) was much better (sens.94.7%, spec.88.4% and acc.92.0%) with an optimal cut-off value of $1.79 \times 10^{-3} \text{ mm}^2/\text{s}$. Over all patients, a very good correlation was found between MR-signs of local invasion and surgical resectability ($\kappa = 0.87$, p<0.0001).

Conclusion: This MR imaging technique with DWI might provide additional information for preoperative lesion characterization and assessment of lesion resectability. Volume and especially heterogeneity of the WL seem to preclude a b-1000 evaluation for diagnosis, but b-2000 rating allow better accuracies.

B-1575 14:32

Characterisation of mediastinal anterior masses with magnetic resonance imaging (MRI) using diffusion-weighted imaging

M. Gavrel, E. Auclin, C.S. Balleyguier, C. Caramella; *Villejuif/FR* (gavrelmarie@gmail.com)

Purpose: To characterise mediastinal anterior masses (MAM) in a qualitative and quantitative MRI evaluation using diffusion-weighted imaging (DWI). To

correlate imaging features of epithelial thymic malignancies with the World Health Organization (WHO) and Masaoka-Koga classifications.

Methods and Materials: A retrospective analysis of patients referred for an MAM between 2000 and 2017 was made. Correlation with histopathological examinations was performed except for patients with typical thymic hyperplasia or rebound. Chi-square, Fisher and Student's tests were used for data description. Logistic regression models and areas under the ROC curves were estimated.

Results: Out of 94 patients, 66 were included. 21 patients had a benign MAM and 45 had a malignant MAM including 25 thymomas and 10 thymic carcinomas. Qualitative assessment demonstrated significant differences for contours, shape, septas, capsule, calcifications, cystic or necrotic areas, invasiveness, homogeneity and pattern of enhancement (p<0,05). Mean chemical shift ratio (CSR) differed significantly between benign and malignant MAM ($0,66 \pm 0,26$ and $1,45 \pm 1,36$, respectively, p=0,003). Cutoff point for CSR was 0,880 (sensitivity 94%, specificity 84%). Mean apparent diffusion coefficient (ADC) differed significantly between benign and malignant MAM ($2,31 \times 10^{-3} \text{ sec}/\text{mm}^2 \pm 1,1$ and $1,17 \times 10^{-3} \text{ sec}/\text{mm}^2 \pm 0,64$, respectively, p=0,001). Cutoff point for ADC was $1,39 \times 10^{-3} \text{ sec}/\text{mm}^2$ (sensitivity 87%, specificity 68%). High-risk thymomas showed stronger enhancement than low-risk thymomas (p=0,04). Qualitative assessment demonstrated significant differences between thymomas according to the Masaoka-Koga classification for shape, contours, capsule, septas, invasiveness, homogeneity and pattern of enhancement (p<0,05).

Conclusion: DWI-MRI is a useful non-invasive technique for the characterisation of MAM.

B-1576 14:40

Quantitative analysis of diffusion weighted magnetic resonance imaging for characterization of mediastinal lymphadenopathy

A. Sudarkina, A. Dergilev, N. Gorbunov; *Novosibirsk/RU* (a.sudarkina@mail.ru)

Purpose: To evaluate the possibilities of diffusion-weighted imaging (DWI) with different scan parameters for the characterisation of mediastinal lymphadenopathy.

Methods and Materials: 30 patients with metastases (n=12), lymphoma (n=3), sarcoidosis (n=8) and reactive hyperplasia (n=7) of mediastinal lymph nodes were underwent DWI of the chest on 1.5T machine. Two series of DWI with different types of data acquisition (during free breathing and synchronised with breathing) and scan parameters (repetition time, slice thickness, values of acquired b-factors et al.) were obtained for all patients. The apparent diffusion coefficient (ADC) maps were calculated automatically. Altogether, 371 measurements of ADC were performed in the solid area of the lymph nodes in consecutive slices.

Results: The mean ADC values in metastases, lymphoma, sarcoidosis and reactive hyperplasia of mediastinal lymph nodes were $0.97 \pm 0.31 \times 10^{-3} \text{ mm}^2/\text{s}$, $0.89 \pm 0.07 \times 10^{-3} \text{ mm}^2/\text{s}$, $1.54 \pm 0.24 \times 10^{-3} \text{ mm}^2/\text{s}$, $1.66 \pm 0.32 \times 10^{-3} \text{ mm}^2/\text{s}$, respectively. The mean ADC value in benign lymphadenopathy ($1.62 \pm 0.28 \times 10^{-3} \text{ mm}^2/\text{s}$) was significantly higher (p<0.001) when compared to malignant lymphadenopathy ($0.95 \pm 0.29 \times 10^{-3} \text{ mm}^2/\text{s}$). The differences between the mean ADC values obtained with different scan parameters were insignificant (p>0.05) within all types of the lesions. According to the ROC-analysis the cut-off value of $1.36 \times 10^{-3} \text{ mm}^2/\text{s}$ can be used for differentiation of benign from malignant lymphadenopathy with a sensitivity of 80% and a specificity of 92%. The area under the curve was 0.947.

Conclusion: Quantitative analysis of ADC maps is a promising tool which can be used for noninvasive differentiation of malignant from benign mediastinal lymphadenopathy regardless of scan parameters and type of data acquisition of DWI.

B-1577 14:48

Value of computed tomography perfusion and diffusion-weighted imaging in predicting the efficacy of non-small cell lung cancer chemoradiotherapy

L. Cui; *Nantong/CN* (cuigeleili@126.com)

Purpose: To evaluate computed tomography perfusion (CTP) and diffusion-weighted imaging (DWI) parameters in estimating the efficacy of non-small cell lung cancer (NSCLC) chemoradiotherapy in terms of two-year progression-free survival (PFS) and overall survival (OS).

Methods and Materials: This prospective study was approved by our institutional review board. All 23 pathologically-confirmed NSCLC patients underwent CTP and DWI scans before the standard concurrent chemoradiotherapy. A series of pseudo-color perfusion images were produced, such as BF (blood flow), BV (blood volume) and PMB (permeability). DWI scan used three b values and generated three ADC images, i.e., ADC₁ (b=0, 300s/mm²), ADC₂ (b=0, 800s/mm²), and ADC₃ (b=300, 800s/mm²). Fixed area of ROI_l and maximum area of ROI_m were drawn. Kaplan-Meier survival curves were used to estimate PFS and OS while Cox regression with multiple variables was applied to identify independent predictors, significant level being 0.05.

Results: No significant correlation was found between clinical stages and two-year PFS and OS ($P=0.223$ and 0.112). The regression analysis showed that parameters with independent predictive value for PFS and OS were BF(ROI_m), PMB(ROI_m), and $ADC_2(ROI_m)$. A prediction scoring model was established accordingly: 0 for $BF(ROI_m) \geq 46.10 \text{ ml}/100 \text{ ml}/\text{min}$, $PMB(ROI_m) \geq 30.95 \text{ ml}/100 \text{ ml}/\text{min}$ or $ADC_2(ROI_m) \leq 1.52 \times 10^{-3} \text{ mm}^2/\text{s}$ whereas 1 for the otherwise. Three groups were yielded and the differences in two-year PFS and OS between them had statistical significance (Hazard Ratio=6.712 to 19.921, $P < 0.001$).

Conclusion: CTP parameters BF(ROI_m), PMB(ROI_m) and $ADC(b=0, 800 \text{ s}/\text{mm}^2, ROI_m)$ had independent predictive value for PFS and OS, and the prediction scoring model based on which had higher value in estimating treatment efficacy.

B-1578 14:56

Multiparametric approach by dynamic contrast-enhanced perfusion MRI with FDG-PET/CT: capability for conservative therapeutic response prediction in NSCLC patients

Y. Ohno¹, Y. Kishida¹, S. Seki¹, M. Yui², S. Ohyu², T. Yoshikawa¹; ¹Kobe/JP, ²Otawara/JP (yosirad@kobe-u.ac.jp)

Purpose: To directly compare the capability for quantitative therapeutic response prediction among dynamic CE-perfusion MRI, FDG-PET/CT and multiparametric approach by both modalities in non-small cell lung cancer (NSCLC) patients treated with chemoradiotherapy.

Methods and Materials: 43 consecutive Stage IIIB NSCLC patients (25 men, 18 women; mean age 67 years) underwent PET/CT, dynamic CE-perfusion MRI, chemoradiotherapy, and follow-up examination. Then, all patients were divided into two groups by RECIST guideline as follows: 1) responders (CR+PR cases: n=23) and 2) non-responders (SD+PD cases: n=20). In each patient, total perfusion (TP) and tumour perfusions from pulmonary (TPP) and systemic (TPS) circulations calculated from dynamic CE-perfusion MR data and SUV_{max} on PET/CT were assessed at each targeted lesion, and averaged to determine final values. Multivariate logistic regression analysis was performed to investigate the discriminating factors of responders. In addition, ROC analysis was performed to compare diagnostic performance among all methods. Finally, sensitivity, specificity and accuracy were compared among all methods by McNemar's test.

Results: Multivariate regression analysis identified SUV_{max} (odds ratio [OR]: 2.56) and TP (OR: 0.68) as significant differentiator of responder. ROC analysis showed area under the curve (Az) of multiparametric approach (Az=0.95) was significantly larger than that of TPP (Az=0.72, $p=0.001$). Sensitivity (95.7%) of multiparametric approach was significantly higher than that of TP (69.6%, $p=0.03$) and TPP (65.2%, $p=0.02$).

Conclusion: Multiparametric approach by dynamic CE-perfusion MRI and PET/CT can improve the capability for therapeutic response prediction as compared with each modality alone in NSCLC patients after conservative therapy.

Author Disclosures:

Y. Ohno: Research/Grant Support; Toshiba Medical Systems Corporation, Guerbet. S. Seki: Research/Grant Support; Toshiba Medical Systems Corporation. M. Yui: Employee; Toshiba Medical Systems Corporation. S. Ohyu: Employee; Toshiba Medical Systems Corporation. T. Yoshikawa: Research/Grant Support; Toshiba Medical Systems Corporation.

B-1579 15:04

Blood volume-based MR imaging with ultra-short TE: capability for prediction of postoperative lung function in NSCLC patients as compared with CT and perfusion SPECT

Y. Ohno¹, M. Yui², Y. Chen³, S. Ohyu², Y. Kishida¹, S. Seki¹, T. Yoshikawa¹; ¹Kobe/JP, ²Otawara/JP, ³Beijing/CN (yosirad@kobe-u.ac.jp)

Purpose: To directly compare the capability of semi-quantitatively assessed blood volume-based pulmonary MR imaging with ultra-short TE (BV-MRI with UTE) for prediction of postoperative lung function in non-small cell lung cancer (NSCLC) patients as compared with CT and perfusion SPECT.

Methods and Materials: 29 NSCLC patients underwent unenhanced and contrast-enhanced pulmonary MR imaging with UTE at a 3T system, CT, perfusion SPECT, and measurements of FEV₁% before and after lung resection. In each patient, BV MRI was generated as percent signal change between unenhanced and CE-MR imaging. On BV-MRI with UTE and perfusion SPECT, postoperative FEV₁% (poFEV₁%) was predicted from semi-quantitatively assessed blood volumes within total and resected lungs. Quantitatively predicted poFEV₁% using CT was determined from the functional lung volumes within total and resected lungs. Qualitatively predicted poFEV₁% using CT was determined from the number of segments of total and resected lungs. On each method, correlation with actual poFEV₁% and the limits of agreement between actual and each predicted poFEV₁% were statistically evaluated.

Results: BV-MRI with UTE ($r=0.82$, $p < 0.0001$) and quantitative CT ($r=0.86$, $p < 0.0001$) showed better correlation than qualitatively assessed CT ($r=0.79$,

$p < 0.0001$) and SPECT ($r=0.78$, $p < 0.0001$). The limits of agreement by BV-MRI with UTE (4.3±12.7%) and quantitatively assessed CT (3.5±10.8%) were smaller than those by qualitatively assessed CT (5.1±13.9%) and SPECT (4.2±14.5%).

Conclusion: BV-MRI with UTE can more accurately predict postoperative lung function than qualitatively assessed CT and perfusion SPECT, and is at least as valuable as quantitatively assessed CT in NSCLC patients.

Author Disclosures:

Y. Ohno: Research/Grant Support; Toshiba Medical Systems Corporation, Guerbet Japan. M. Yui: Employee; Toshiba Medical Systems Corporation. Y. Chen: Employee; Toshiba Medical Systems (China) Co., Ltd. S. Ohyu: Employee; Toshiba Medical Systems Corporation. S. Seki: Research/Grant Support; Toshiba Medical Systems Corporation. T. Yoshikawa: Research/Grant Support; Toshiba Medical Systems Corporation.

B-1580 15:12

A 3T MRI with radial T1-weighted 3D spoiled gradient echo sequence can clarify pleural invasion classification of primary lung cancer

H. Lee, W. Kwon, Y. Zhang; *Worju/KR (jeenylee@yonsei.ac.kr)*

Purpose: To clarify the pleural invasion of primary lung cancer by a 3T MRI with free-breathing radial T1-weighted 3D spoiled gradient echo sequence.

Methods and Materials: The study was approved by the institutional review board and the local ethics committee. All subjects provided written informed consent. Twelve patients (7 men and 5 women, average 73.0 years old) with primary non-small cell lung cancer had suspicion for pleural invasion on CT. Cases were reviewed by retrospective interpretation of prospectively acquired data from January 2016 to August 2017 and confirmed by pathology. A 3T MRI was performed with fat suppression and contrast enhancement with 0.9 mm slice thickness, TR=3.36 msec, and TE=1.66 msec. It was compared with 64 MDCT and conventional MRI sequence. Pleural invasion (PL) was graded as smooth and irregular margin of pleural enhancement.

Results: Six adenocarcinoma and six squamous cell carcinoma cases were enrolled. Five T3 stage (5 PL0) and six T4 stage (5 PL1 and 1 PL2) were involved. All cases with proven PL0 and PL1 had smooth and curvilinear high signal intensity of pleura. One case with PL2 had irregular signal intensity of tumour interface of pleura against the chest wall suggesting tumour invasion beyond the visceral pleural surface. Well-enhancing high signal intensity of pleural adhesion is well visible on enhanced radial T1-weighted spoiled gradient echo sequence by MRI and can estimate resectable visceral pleural invasion of primary lung cancer.

Conclusion: MRI with radial T1-weighted 3D spoiled gradient echo sequence can assess pleural invasion for T classification of lung cancer in routine clinical practice.

B-1581 15:20

MRI with DWI vs FDG-PET/MRI vs FDG-PET/CT vs conventional radiological examination: capability for TNM staging in patients with malignant pleural mesothelioma

Y. Ohno¹, Y. Kishida¹, S. Seki¹, M. Yui², K. Aoyagi², S. Kaminaga², T. Yoshikawa¹; ¹Kobe/JP, ²Otawara/JP (yosirad@kobe-u.ac.jp)

Purpose: To compare the TNM staging capability among MRI with diffusion-weighted imaging (DWI), FDG-PET/MRI, FDG-PET/CT and conventional radiological examination in patients with malignant pleural mesothelioma (MPM).

Methods and Materials: 23 consecutive and pathologically diagnosed MPM patients underwent whole-body MRI including DWI, PET/CT, conventional radiological and pathological examinations and surgical reports as well as follow-up examinations. TNM staging was evaluated by three different reader groups. Kappa statistics were determined for evaluations of agreements of each factor and the clinical stage between each method and final diagnosis. Finally, the diagnostic accuracy of each factor and of determination of the clinical stage was statistically compared with each other using McNemar's test.

Results: T factor agreements were determined as substantial (PET/CT and conventional examination: kappa value=0.61) or almost perfect (PET/MRI and MRI: kappa value=0.86). N factor agreements were also determined as substantial (PET/CT: kappa value=0.73, conventional examination: kappa value=0.61) or almost perfect (PET/MRI and MRI: kappa value=1.00). M factor assessment, agreements were also determined as moderate (conventional examination: kappa value=0.47), substantial (MRI: kappa value=0.78) or almost perfect (PET/MRI and PET/CT: kappa value=1.00). In addition, clinical stage agreements were determined as substantial (PET/CT and conventional examination: kappa value=0.70) or almost perfect (PET/MRI and MRI: kappa value=0.87). Finally, accuracies of N factor evaluation on PET/MRI and MRI were significantly higher than that of conventional examination ($p=0.03$).

Conclusion: Whole-body MRI with DWI and PET/MRI are potentially more useful than conventional radiological examination, and can be considered at least as effective as PET/CT in this setting.

Author Disclosures:

Y. Ohno: Research/Grant Support; Toshiba Medical Systems Corporation,

Bayer Pharma. **S. Seki**: Research/Grant Support; Toshiba Medical Systems Corporation. **M. Yui**: Employee; Toshiba Medical Systems Corporation. **K. Aoyagi**: Employee; Toshiba Medical Systems Corporation. **S. Kaminaga**: Employee; Toshiba Medical Systems Corporation. **T. Yoshikawa**: Research/Grant Support; Toshiba Medical Systems Corporation.

14:00 - 15:30

Room L 8

Imaging Informatics

SS 1905

Structured reporting and CAD

Moderators:

E. Neri, Pisa/IT

N. Pyatigorskaya, Paris/FR

B-1582 14:00

Structured reporting supports junior readers and improves PI-RADS conformity of multi-parametric MRI reports of the prostate-based on cross-lingual RADLEX annotations

M.E. Maros¹, B. Kämpgen², A. Förster¹, C. Groden¹, W.H. Sommer³, S.O. Schönberg¹, T. Henzler³, H. Wenz^{1,4}, ¹Mannheim/DE, ²Rimpar/DE, ³Munich/DE (matt.maros@gmail.com)

Purpose: Prostate cancer (PC) represents an enormous burden as the second most common cancer in men. Therefore, the Prostate Imaging Reporting and Data System (PI-RADS v2) was developed to provide imaging and reporting standards of multi-parametric prostate MRI (mpMRI) in accordance with terminologies of RSNA's Radiologic Lexicon (RADLEX). We present a proof of concept study to assess the effect of (1) structured reporting (SR) and (2) to use automatic RADLEX content annotation as a quality measure for prostate MRI-reports.

Methods and Materials: A cohort of 294 consecutive patients (02/2017-08/2017; mean age 66.6, range 34-89yrs) with suspected PC and mpMRI were retrieved from local RIS archives and reassessed by two independent blinded readers. All reports were generated using an online SR tool (www.smart-radiology.com). An automatic, cross-lingual annotation of German reports and English PI-RADS guideline with RADLEX terms was performed using a proprietary information extraction software (www.empolis.com). Structured reports of junior (n=110;37.4%) and senior (n=184;62.6%) radiologists were compared with the extracted PI-RADS RADLEX terms as a query using a free web-tool (radreport-query.com) and Wilcoxon rank-sum test.

Results: Annotation of PI-RADS guideline identified 394 RADLEX terms. Reports of junior and senior radiologists had similar number of key terms (W=10700, p=0.416). Comparing PI-RADS guideline confirm RADLEX content of both findings (W=10266, p=0.837) and impressions (W=11103, p=0.164) sections showed that junior readers achieved comparable scores as senior ones.

Conclusion: Automatic guideline-based RADLEX content extraction could serve as an important quality measure of reports of PC MRIs. SR templates support junior readers to produce high-quality PI-RADS conform mpMRI reports.

Author Disclosures:

B. Kämpgen: Employee; Empolis Information Management GmbH, Kaiserslautern, Germany. **W.H. Sommer**: Founder; co-founder of Smart Reporting GmbH. **T. Henzler**: CEO; managing director of Diagnostik München.

B-1583 14:08

Opportunities in automatically annotating radiology reports with RadLex terms

B. Kämpgen¹, M.E. Maros², T. Stening¹, W.H. Sommer³, A. Klüter⁴, ¹Rimpar/DE, ²Mannheim/DE, ³Munich/DE, ⁴Kaiserslautern/DE (benedikt.kaempgen@empolis.com)

Purpose: With the development, subsequent refinement and translation of RadLex, there is a trend in radiology towards the use of standardised terms for all information resources. As a result, there will be greater opportunities for Natural Language Processing (NLP) to automatically collect data with a high degree of accuracy. This work investigates the gap in coverage between the vocabulary used in non-English radiology reports and the controlled vocabulary of RadLex.

Methods and Materials: 300 MR prostate cancer, 280 CT haemorrhage, and 75 MR stroke suspected cases were randomly selected from two radiological institutions. Findings sections of anonymised German reports were annotated with RadLex terms using a proprietary web service that includes stemming, compounds, abbreviations and automatic inference of more general terms (average no of annotations=71). An ID3 decision tree with (pre-)pruning (criterion=gain ratio; maximal depth=20; minimal leaf size=2) was trained, 10-

fold cross-validated, and tested on subsets of the data to automatically classify case type (300/280/75) and level of reader experience (unexperienced: yrs>2, no=149; experienced: yrs>6, no=225).

Results: For case type, there is a macro-averaged f-score of 98% (precision: 97%, recall: 98%). For experience level, there is an f-score of 75% (precision: 65%, recall: 96%). Each test shows a 95% binomial confidence Wilson score interval no wider than 5%.

Conclusion: Radlex annotations of reports are sufficiently specific for basic data analysis and decision support. The more complex the information extraction task, the more additional information (e.g., beyond localised synonyms) need to be considered, e.g., negation detection, disambiguation and relation extraction.

Author Disclosures:

B. Kämpgen: Employee; Empolis Information Management GmbH.

T. Stening: Employee; Empolis Information Management GmbH.

W.H. Sommer: Founder; Smart Radiology GmbH. **A. Klüter**: Employee; Empolis Information Management GmbH.

B-1584 14:16

Quality assurance in CT: using automated CT dose monitoring software to implement updated national diagnostic reference levels

E. Appel, P. Kröpil, C. Thomas, J. Aissa, Y. Klosterkemper, N. Heinzler, J. Boos; ¹Düsseldorf/DE (elisabeth.appel@med.uni-duesseldorf.de)

Purpose: To evaluate the implementation of the updated computed tomography (CT) diagnostic reference levels (DRLs) from the German Federal Office for Radiation Protection into clinical routine using an automatic CT dose monitoring system.

Methods and Materials: CT radiation exposure was analysed before and after implementing the updated national DRLs into clinical routine in 2016. After the implementation process, institutional CT protocols were mapped to the anatomic regions for which DRLs were provided. Systematically exceeded protocols were optimised and analysed in detail. Analysed CT radiation output parameters were volumetric computed tomography dose index (CTDIvol) and dose length product (DLP). Three radiologists evaluated subjective image quality using a 3-Point-Likert-Scale.

Results: 94258 CT series (from 27103 CT examinations) in adult patients performed in 2016 were included. Averaged over all body regions with available DRL, institutional CTDIvol/DLP were always below the DRLs (65.2 ± 32.9 %/67.3 ± 41.5 % initially; 59.4 ± 32.0 %/60.5 ± 39.9 % after optimisation). Thus, incipiently exceeding protocols were seen for pelvis (CTDIvol 107.7 ± 65.7 %/DLP 106.3 ± 79.3 %), lumbar spine (160.8 ± 74.7 %/175.2 ± 104.1 %) and viscerocranium (108.0 ± 39.0%/152.7 ± 75.7%). After optimisation, radiation dose was 87.9 ± 73.0 %/87.8 ± 80.8 % for the pelvis, 67.8 ± 33.2 %/74.5 ± 50.6 % for the lumbar spine and 95.1 ± 45.8 %/133.3 ± 74.6 % for the viscerocranium.

Conclusion: An automatic CT dose monitoring system enabled not only comprehensive monitoring of a DRL implementation process but can also help optimising radiation exposure.

B-1585 14:24

Investigating potential gadolinium toxicity to gadoterate meglumine (Dotarem) in local renally insufficient adult and paediatric populations using bioinformatics data linkage

L.K. Young, S. Matthew, G. Houston; ¹Dundee/UK (lkyoung@dundee.ac.uk)

Purpose: Although current guidelines restrict the use of some gadolinium-based contrast agents in patients with renal insufficiency (RI) (eGFR<60ml/min/1.73m²), they may be administered when the clinical benefit-risk ratio is favourable. This study uses routine electronic health records to investigate the incidence of potential gadolinium toxicity to the agent gadoterate meglumine within a local RI population.

Methods and Materials: Adult and paediatric patients who underwent contrast-enhanced MRI were identified, stratified by renal function and followed using health data. The following were identified: confirmed cases of NSF; onset of chronic pain, a symptom of NSF and potentially gadolinium deposition disease (GDD) (identified by new, regular pain medication prescriptions within 7 days post-MRI) and contrast-induced nephropathy (CIN) (>25% increase in creatinine within 3 days post-MRI). Comparisons were made via chi-square tests to non-RI and non-contrast MRI populations.

Results: From 2004 to 2016, 22,325 and 572 contrast-enhanced scans were performed on adult and paediatric patients, respectively. 14% of scans were undertaken while the patient had RI (30≤eGFR<60, n=2,622; 15≤eGFR<30, n=464; eGFR<15, n=123). Zero resulted in NSF diagnosis with an average follow-up time of 6.0 ± 2.5years (range, 8months - 15years). For all scans, there was no statistically higher rate of chronic pain onset post-MRI (adults: p=0.777, paediatrics: p=0.578), nor rate of CIN (adults: p=0.566, paediatrics: p=0.841), regardless of renal function or whether contrast was administered.

Conclusion: These data indicate that gadoterate meglumine administered to adult and paediatric RI patients does not result in a higher rate of potential gadolinium toxicity symptoms.

Author Disclosures:

L.K. Young: Research/Grant Support; **Guerbet. S. Matthew:** Research/Grant Support; **Guerbet. G. Houston:** Research/Grant Support; **Guerbet.**

B-1586 14:32

Machine learning in radiology operations management

O. [Pianykh](mailto:Pianykh@gmail.com); *Newton Highlands, MA/US* (opiany@gmail.com)

Purpose: Radiology workflow presents a complex mixture of planned events and random deviations. The old management approach was to set certain expectations and hope that they would be met. Instead, we propose to employ machine learning algorithms for predicting and managing Radiology workflow.

Methods and Materials: To optimize radiology workflow at Massachusetts General Hospital, we developed an event-tracking system ("Tempus Fugit", or TF for short), entirely based on RIS, PACS, and reporting data. The system was implemented as a real-time process (3-minute updates), querying radiology databases for the most recent year of data (nearly 1,000,000 records per query), to identify each study status in the current processing chain. Capturing this complex data enabled us to build machine-learning models for predicting and analyzing radiology operations.

Results: We applied machine learning algorithms to several major operational problems such as predicting patient wait times, predicting facility delays, and identifying operational bottlenecks. Decision-based models such as regression trees proved efficient for identifying bottlenecking logic - Predictive models such as elastic nets achieved high accuracy in forecasting wait/delay times. As a result, we achieved: - Accurate prediction of wait/delay times: 80% within a 5-min error. Ability to objectively identify the real sources of our operational bottlenecks.

Conclusion: Machine learning is only a tool, but it can help when applied to a right problem. Large, noisy radiology workflow data, too complex to be analyzed manually, presents a perfect target for such applications, and can lead to visible improvements in operations management.

B-1587 14:40

Automated assessment of Sarcopenia on CT studies

J.E. [Burns](mailto:jburns@uci.edu)¹, J. Yao², J. Chen¹, R.M. Summers²; ¹*Orange, CA/US*, ²*Bethesda, MD/US* (jburns@uci.edu)

Purpose: Central sarcopenia is an adverse risk factor for mortality in cancer, liver transplantation, cirrhosis, and older trauma patients. The purpose is to validate a fully-automated system to opportunistically analyze lumbar paraspinal muscles for sarcopenia on CT.

Methods and Materials: Watershed, graph cut, and level set algorithms obtain initial segmentation of lumbar vertebrae. Paraspinal muscles are localized and segmented by holistically nested neural networks through image-to-image training and classification. The system is tested on two data sets, CTs from PET/CT examinations of 40 patients with metastatic cancer and abdominal CTs from an elder cohort of 25 patients, to assess performance variation and generalizability of results. Manually segmented paraspinal muscles served as reference standard. Sarcopenia is defined through meta-analysis of publications as normalized L3 total psoas muscle index (L3TPI) of < 3.62 cm²/m² for women and <4.92 cm²/m² for men. Segmentation accuracy is assessed via Dice Similarity Coefficient.

Results: Dice coefficients for detecting psoas and posterior paraspinal muscle groups were 0.877±0.073 and 0.919±0.031 for PET/CT, and 0.886±0.089 and 0.948±0.018 for abdominal CT, respectively. L3TPI was 5.6 ±/ 2.5 and 4.9 ±/ 2.1 cm²/m² (women) and 8.6 ±/ 3.2 and 7.9 ±/ 3.6 cm²/m² (men) for automatic and manual measurement respectively. Sarcopenia was present in 21.2% (7/33) and 24.2% (8/33) of women, and 9.3% (3/32) and 15.6% (5/32) of men from automatic and manual measurement respectively.

Conclusion: This fully-automated system accurately determines paraspinal muscle volume on CT for sarcopenia detection and monitoring, with potential to predict prognosis and guide patient management.

B-1588 14:48

COPD phenotyping with parameter response maps based on paired inspiratory/expiratory low-dose computed tomography

O. [Weinheimer](mailto:weinheimer@uni-heidelberg.de)¹, C.J. Galban², T.E. Robinson³, M. Wjelpütz¹, C. Heussel¹, H.-U. Kauczor¹, B.J. Jobst¹; ¹*Heidelberg/DE*, ²*Ann Arbor, MI/US*, ³*Palo Alto, CA/US* (weinheimer@uni-heidelberg.de)

Purpose: Patients suffering from chronic obstructive pulmonary disease (COPD) can be subdivided using computed tomography (CT) into an airway-dominant or emphysema-dominant phenotype. The parametric response map (PRM) method, a voxel-wise image analysis technique may detect distinct functional differences between these phenotypes.

Methods and Materials: 169 paired inspiratory/expiratory low-dose CT scans (120 kV, 30-35 mAs, ~3.5 mSv) from the multicentre COSYCONET study were visually classified as airway-dominant (67%) and emphysema-dominant (33%). PRM was computed fully automatically employing a deformable volumetric

registration and lung segmentation, classifying lung voxels as normal parenchyma (PRM^{Normal}), functional small-airway disease (PRM^{fSAD}) and emphysema (PRM^{Emph}). For comparison the emphysema index (EI) was calculated on the inspiratory scans.

Results: Average PRM^{Normal}, PRM^{fSAD}, PRM^{Emph} and EI were 66.9%, 26.4%, 6.9% and 9.2% in the airway-dominant group and 46.9%, 32.3%, 19.8% and 23.1% in the emphysema-dominant group, respectively. The differences were significant between the groups with p=1.8e-07, p=0.006, p=3.6e-08 and p=2.8e-08. The Pearson correlation coefficient r between PRM^{Normal} and forced expiratory volume in 1s (FEV₁) was 0.63 (p<2.2e-16), for PRM^{fSAD} -0.54 (p=3.1e-14), for PRM^{Emph} -0.55 (p=5.1e-15) and for EI -0.55 (p<2.2e-16) across all patients, which was similar for airway-dominant and emphysema-dominant phenotypes.

Conclusion: PRM identified fSAD regions, which would have been missed by emphysema quantification just on inspiratory CT scans. The results show that in emphysema-dominant COPD there is a large fraction of fSAD besides irreversible emphysema, which may be addressed by therapy. Additionally, the combination of PRM^{fSAD} and PRM^{Emph} leads to a higher correlation with FEV₁.

B-1589 14:56

Model for improved correlation of BMD values between abdominal routine dual-energy CT data and DXA scans

M. [Woisetschlaeger](mailto:woisetschlaeger@spangeus.com), A. Spängeus; *Linköping/SE*

Purpose: In this study, we evaluated a new software solution to calculate volume bone mass densities (vBMD) from dual-energy CT studies (DECT) and correlated them to DXA. We constructed a model where influencing factors for differences between vBMD and aBMD were taken into account.

Methods and Materials: A total of 20 patients, i.e. 80 vertebrae, were examined with abdominal DECT (in three contrast phases) where the L1-L4 were analysed with a software delivering vBMD. Within 1 month after the DECT, a DXA scan was performed. The amount of calcifications in the abdominal aorta (ACS) and of spondylarthritis (SAS) was evaluated.

Results: The median age was 70.5 years (43 - 85) where 60% were women and 40% men. A significant correlation was found between DXA BMD and vBMD from DECT without contrast (WNC), and with venous contrast (WVC), but no significant correlation was found with arterial contrast. After combining DECT WNC, ACS and SAS in Model 1, a correlation is achieved with an R² = 0.616. The Pearson correlation between Model 1 predictive value and DXA is 0.785 (p=0.001). The respective values in Model 2 for the DECT WVC are R² = 0.612 and predictive value of 0.782 (p=0.001).

Conclusion: The shortcomings of DXA in predicting true BMD values compared to DECT, as being susceptible for confounding factors like calcifications in the abdominal aorta and osteoarthritis changes can be overcome by quantifying the amount of confounding factors and taking these into account in an explanatory model.

B-1590 15:04

Computer-aided detection of sonographic features for thyroid nodules and its effects on readers' performance

A. [Chen](mailto:achen@ntu.edu.tw), C.-N. Chen, H.-C. Tai, M.-H. Wu, K.-Y. Chen, M.-C. Ho, K.-J. Chang; *Taipei/TW* (achen@ntu.edu.tw)

Purpose: This study is to evaluate the performance of an FDA-cleared computer-aided detection (CADE) device for thyroid nodules and its effects on readers' performance.

Methods and Materials: A total of 130 images of thyroid nodules were randomly selected from a case pool of 372 patients with 472 thyroid nodules. The ground truth for the presence of each sonographic feature was determined by a panel of three specialists. Detection of feature presence was evaluated by AUROC's and t-test p-values. For assessment of the effects on readers' performance, diagnostic decisions were compared to the pathology results (74 benign and 56 malignant). Seven physicians were recruited to read the 130 ultrasound images. The reader performance was then evaluated by the multiple reader multiple case (MRMC) study design and Dorfman-Berbaum-Metz method.

Results: The study first showed that the computed values of the anechoic area, echogenic foci, hypoechogenicity, heterogeneity, and ill-defined margin were all tested significant in detecting their presence with p-values <0.0001 for the first three features, 0.033 and 0.0014 for the last two and the AUC=0.882, 0.788, 0.817, 0.71 and 0.686, respectively. The MRMC study showed that the average AUC (=0.796) with CAde was significantly larger (p-value=0.0077) than the average AUC (=0.724) without CAde.

Conclusion: The tested CAde device was shown significant in detecting presence of the five sonographic characteristics. The diagnostic interpretations by physicians reading the ultrasound images with the CAde device were also shown significantly improved when compared to interpretations without the device.

Author Disclosures:

A. Chen: Author; receive research grant from AmCad BioMed. **C. Chen:** Author; receive research grant from AmCad BioMed. **H. Tai:** Author; receive

research grant from AmCad BioMed. **M. Wu:** Author; receive research grant from AmCad BioMed. **K. Chen:** Author; receive research grant from AmCad BioMed. **M. Ho:** Author; receive research grant from AmCad BioMed. **K. Chang:** Author; receive research grant from AmCad BioMed.

B-1591 15:12

Newly developed curvelet-based noise reduction algorithm for volume CT data

M.S. Usanov, N.S. Kulberg, A.V. Petraikin, S.P. Morozov; *Moscow/RU (m.usanov@npcmr.ru)*

Purpose: Estimate the effectiveness of newly developed noise reduction algorithm by means of analysis of acquired volume CT data, obtained from phantoms and patient studies of various anatomical areas.

Methods and Materials: A new 3D noise reduction algorithm was developed based on wavelet curvlet transformation and bilateral filter. Estimation of noise reduction quality was made based on volume CT data, obtained from various CT scanners and study objects, including phantoms, brain, chest, abdominal area. 30 % of analysed studies are low dose CT. Overall, 113 studies were analysed. After data processing the results were assessed by radiologists, who made valuable notices in the algorithm presets. The following parameters were taken into consideration: standard deviation (SD), determination coefficient. Special attention was paid to speed of data processing.

Results: SD is improved in phantom study by 58.08%, and in patient study by 76.89%. Confidence interval for SD value difference = 0.0003. Determination coefficient between mean native and processed values = 0.99 for phantom study and = 0.97-0.99 for patient study, which means the data remains unspoiled, without any value loss or border deformation. Estimated processing time of 500 slices is around 20 seconds.

Conclusion: Proposed algorithm has shown its effectiveness in the field of various CT data processing without data spoilage, comparing to standard methods. This method requires only DICOM files, without manipulating raw data. High speed processing allows the algorithm to be used both on workstations and PC. This new technology will enhance quality of CT diagnostic, as well as lowering x ray dose for patients during the study. The work is supported by RFBR, project 17-01-00601.

B-1592 15:20

Multiparametric magnetic resonance imaging of the prostate with computer-aided detection: non-experienced observer performance study

G. Cappello, V. Giannini, S. Mazzetti, F. Russo, L. Vassallo, V. Doronzio, D. Regge; *Turin/IT (giovanni.cappello@ircc.it)*

Purpose: To understand how non-experienced readers interacts with likelihood map generated by a computer-aided detection (CAD) for prostate cancer (PCa) detection and to compare their sensitivity, specificity and reading time obtained with and without the color-coded map.

Methods and Materials: 90 multiparametric magnetic resonance imaging (mp-MRI) prostate cases (45 negatives and 45 with at least one significant PCa) were reviewed twice by three radiology residents. First, suspected PCa were detected on the basis of CAD marks observed on a likelihood map superimposed to the T2w image, as anatomical reference. After 6 weeks, readers reviewed the same cases analyzing mp-MRI unassisted. Sensitivity, specificity, and reading time were compared for the two reading paradigms.

Results: The stand-alone CAD sensitivity was equal to 94.3%. Considering all readers, sensitivity was 66.7% (95% CI 58.0-74.5%) and 70.4% (95% CI 61.9-77.9; p=0.236) for unassisted and CAD paradigm, respectively. Sensitivity was higher with CAD for lesions with GS>6 (79.6% vs 71.0%; p=0.0287), but not for lesion with diameter ≥10 mm (76.5% vs 79.0%; p=0.395). Specificity was not affected by CAD (94.8% for CAD vs 89.6%; p=0.071). The average reading time was significantly lower (170s vs 66s; p<0.001) when using the CAD system.

Conclusion: Using the CAD system, non-experienced readers can detect more patients with GS>6 PCa than unassisted MRI interpretation; overall reporting time is shorter. However, CAD stand-alone sensitivity was significantly higher, demonstrating that operators were somewhat uncomfortable when using CAD systems. However, other reading paradigms should be tested to evaluate the clinical usability of CAD systems.

14:00 - 15:30

Room E2

Neuro

SS 1911a

Trauma and encephalopathies

Moderators:

A.S. Gersing; Munich/DE
D. Goldsher; Haifa/IL

B-1593 14:00

Saliently alteration of hub profiles following acute mTBI

X. Wang¹, C. Sun¹, S. Wang¹, J. Cao¹, H. Xu¹, S. Gan¹, B. Yin², G. Bai², L. Bai¹; ¹*Xi'an/CN*, ²*Wenzhou/CN (lemon124w@outlook.com)*

Purpose: To investigate altered network hubs following acute mild traumatic brain injury (mTBI) in a large homogenous sample compared with healthy controls.

Methods and Materials: 74 mTBI patients (46 males, ages of 36.3 ± 12.7 years) within 7 days post-injury and 51 matched healthy controls (26 males, ages of 36.7 ± 12.2 years) were enrolled in this study. Functional brain networks were constructed using resting state fMRI. Hub disruption index κ was also calculated across the whole network and for each functional network. SVM was applied to test whether participation coefficient can be used as a neurobiomarker to identify mTBI patients from controls.

Results: Our results indicated evidence for a radical reorganization of highly efficient hub nodes following mTBI. Specially, hubs for mTBI patients distributed in more extensive networks such as the default mode network (DMN), ventral attention network (VAN) and frontoparietal network (FPN), somatomotor network (SMN) and the visual network (VN), compared with healthy controls limited to the first three. Hubs in healthy controls typically became non-hubs in patients and vice versa defined by a novel hub disruption index. Participation coefficients for mTBI presented significantly decreased in the DMN (P=0.015) and FPN (P=0.02), while increased in the VN (P=0.035). Additionally, SVM trained with participation coefficient metrics identified mTBI patients from controls with 78% accuracy, providing for its diagnostic potential in clinical settings.

Conclusion: These evidence suggested a saliently spatial transition of hub profiles even in the very early stage of mTBI, associated with functional network reorganization in these patients.

B-1594 14:08

Automatic vs human detection of traumatic cerebral microbleeds on susceptibility-weighted imaging

A.W. van der Eerden^{1,2}, T.L.A. van den Heuvel¹, B.H. Geurts¹, B. Platel¹, T. Vande Vyvere^{3,4}, L. van den Hauwe^{3,4}, T.M.J.C. Andriessen⁵, B.M. Góraj^{1,6}, R. Manniesing¹; ¹*Nijmegen/NL*, ²*Venlo/NL*, ³*Edegem/BE*, ⁴*Leuven/BE*, ⁵*Gorinchem/NL*, ⁶*Warsaw/PL (ankevandereerden@gmail.com)*

Purpose: To evaluate the performance of computer-aided traumatic cerebral microbleed detection (CAD) with and without human interference.

Methods and Materials: 33 adult patients admitted to our emergency department with moderate or severe TBI (mean age 33 years, 21 males) underwent a standardised trauma 3T MRI-protocol at 28 weeks. The microbleeds in their SWI-scans were annotated by an expert. A CAD system was developed, based on this training set. Six experts, blind to the CAD-results, annotated a subset of ten patients. In two experiments, we compared the performance of the CAD system to each of these six experts, using the majority voting results of the other five experts as the reference standard for the calculation of performance characteristics (paired t-test). In the first experiment, the performance of fully automatic microbleed detection was assessed. In the second experiment, one expert removed CAD-annotations she considered false positives from the automatically detected microbleeds, and briefly screened the CAD-annotated SWI-scans to complete the dataset with missed definite microbleeds.

Results: Fully manual evaluation took one hour per patient with an average sensitivity of 77% (SD 12.4%). The sensitivity of fully automatic detection of candidate microbleeds was 89% (SD 0.8%). Evaluation of the CAD results by an expert took 13 minutes per patient with a sensitivity of 93% (SD 1.0%) (p < 0.05 versus fully manual evaluation).

Conclusion: This CAD system allows detecting more microbleeds in a reduced reading time. This may facilitate the execution of otherwise too time-consuming large studies on the clinical relevance of microbleeds.

Author Disclosures:

T. Vande Vyvere: Employee; Icometrix. **L. van den Hauwe:** Consultant; Icometrix.

B-1595 14:16

Looking for association between blood pressure, imaging severity and complications - MR imaging study in posterior reversible encephalopathy syndrome

S.B. Hiremath, A.A. Gautam, G. Benjamin; *Thiruvalla/IN*
(shivaprakashbh@gmail.com)

Purpose: To evaluate for significance of association between blood pressure and imaging severity with hemorrhage and cytotoxic edema in PRES.

Methods and Materials: This retro - prospective study included the medical records and imaging involving 35 consecutive patients with PRES from 2010 - 2016. The clinical data was analyzed for blood pressure recorded at the ictus with MR imaging including a spin-echo echo planar diffusion weighted imaging (DWI) and susceptibility weighted angiography (SWAN) with conventional sequences. The presence of haemorrhage and cytotoxic edema was assessed for significance of correlation and association with each other and with BP and imaging severity (IS).

Results: Hemorrhage was found in 25.7 % of patients and cytotoxic edema was in 20 % of patients. There was no statistically significant association of hemorrhage ($p = 0.403$) and cytotoxic edema ($p = 0.162$) with BP. There was statistically significant association of hemorrhage ($p < 0.001$) and cytotoxic edema ($p = 0.011$) with IS and with each other ($p = 0.002$). There was significant correlation of hemorrhage (Cramer's V - 0.672) and cytotoxic edema (Cramer's V - 0.506) with IS and with each other (Cramer's V - 0.523).

Conclusion: There is significant association of hemorrhage and cytotoxic edema with imaging severity and among each other. The endothelial injury secondary to hyperperfusion or hypoperfusion is the basic mechanism of changes in PRES. Vasculopathy and decreased perfusion results in ischemia and restricted diffusion; rupture of pial vessels due to impaired autoregulation causes subarachnoid hemorrhage and post-ischemic reperfusion leads to microhemorrhages.

B-1596 14:24

Atypical inter-hemispheric communication following subacute mild traumatic brain injury

Z. Wang¹, S. Wang¹, C. Sun¹, B. Yin², G. Bai², X. Niu¹, Y. Sun¹, M. Zhang¹, L. Bai¹; *Xi'an/CN, Wenzhou/CN* (wangzhuonan424@stu.xjtu.edu.cn)

Purpose: To examine the structural integrity of the corpus callosum (CC) in subacute phase of mild traumatic brain injury (mTBI) patients and its related inter-hemispheric functional connectivity changes.

Methods and Materials: Forty two patients with mTBI (29 male, ages of 37.8 ± 11.9 years) and 42 matched healthy controls (male 22, 36.2 ± 9.9 years) underwent comprehensive neuropsychological evaluations as well as both diffusion tensor imaging (DTI) and resting state scanning. The specific division of the CC was conducted by using DTI in combination with a tract-tracing algorithm. Fractional anisotropy (FA) for each subsection of the CC was generated by the Tract-Based Spatial Statistics (TBSS) and inter-hemispheric functional connectivity (FC) was analyzed by using voxel-mirrored homotopic connectivity (VMHC) approach. These analysis were also compared between patients with mTBI and controls, covarying for age, sex, and education with multiple comparison corrections.

Results: MTBI patients showed significantly decreased FA in the splenium and marginally reductions in the mid anterior body part of CC compared with controls ($P < 0.01$, corrected for multiple comparisons). The increased FC were shown in the pre-supplementary motor area and supplementary motor area, while decreased in the default-mode network (DMN) (precuneus/ posterior cingulate and inferior parietal lobule), salience network (SN) (fronto-insular cortex) and orbitofrontal cortex (OFC) ($P < 0.05$, FDR corrected).

Conclusion: As a conduit in mediating inter-hemispheric communications, the structural loss in the specific section of the CC may, therefore, influence the corresponding projection fibers and its related inter-hemispheric functional connectivity following mTBI.

B-1599 14:32

Subcortical nuclei and cognitive impairment in sub-acute mild traumatic brain injury: a diffusion kurtosis imaging and volumetric study

M.-L. Wang, W. Li; *Shanghai/CN* (doctor-mingliang@sjtu.edu.cn)

Purpose: To investigate the volumetric and diffusional kurtosis imaging (DKI) changes of subcortical nuclei in sub-acute mTBI, and to assess the relationship between subcortical nuclei volume, DKI parameters and cognitive function.

Methods and Materials: A total of 23 mTBI patients and 24 control participants underwent examinations of neuropsychological tests, MRI-based morphological and DKI scans. Volume, mean kurtosis (MK), mean diffusivity (MD), and fractional anisotropy (FA) were measured in bilateral hippocampus, thalamus, caudate, putamen, pallidum, and amygdala. Neuropsychological tests and MRI parameters were compared between mTBI and control group. Correlation analysis was performed to examine the relationship between subcortical nuclei volume, DKI parameters and cognitive function.

Results: There were no significant differences in the volume of any subcortical nuclei between mTBI and control group. The mTBI group had higher MK value in right hippocampus, left thalamus, left caudate, right putamen, and right pallidum ($P < 0.05$), and lower MD value in right pallidum ($P < 0.05$). mTBI participants had worse performance in the domains of verbal memory, attention and executive function. In the mTBI group, the declined verbal memory function was correlated with higher MD value in left thalamus ($r = -0.678$, $P = 0.022$) and lower FA value in left amygdala ($r = 0.611$, $P = 0.016$). The attention deficit was correlated with lower MK value in left amygdala ($r = 0.625$, $P = 0.010$), right thalamus ($r = 0.634$, $P = 0.008$), right putamen ($r = 0.582$, $P = 0.018$), right hippocampus ($r = 0.576$, $P = 0.020$) and right amygdala ($r = 0.503$, $P = 0.047$).

Conclusion: DKI is more sensitive than conventional DTI for detecting subcortical nuclei microstructural changes that might underlie the pathology of cognitive impairment in sub-acute mTBI.

B-1600 14:40

Resting-state functional connectivity in the visual network: a possible predictor of treatment response in chronic migraine

D. Kies, J.A. Pijpers, M.D. Ferrari, M.C. Kruij, G.M. Terwindt; *Leiden/NL*
(d.a.kies@lumc.nl)

Purpose: Up to 25% of episodic migraine patients progress to chronic migraine (headache on more than 15 days per month). The mechanisms behind chronicification and reversion are still uncertain, although overuse of acute headache medication plays an important role. We investigated whether resting-state functional connectivity (RS-fc) can predict favourable outcome of treatment.

Methods and Materials: RS-fMRI was conducted in 112 participants with chronic migraine and medication overuse before and 3 months after treatment. Responders to treatment (greater than 50% reduction in headache days) were compared with non-responders, using RS-fc within ten functional networks. Data were preprocessed using a standard FSL pipeline with addition of the AROMA motion correction tool. Results were corrected for multiple comparisons.

Results: Data of 99 participants was complete and useable for analysis. The mean number of headache days at baseline was 21.2 per month. At baseline, the lateral visual network showed a higher connectivity in areas in the bilateral occipital cortex in responders vs non-responders ($p = .015$). Only in responders this higher functional connectivity decreased after treatment ($p = .001$). No differences in connectivity were detected at baseline or during follow-up in any of the other 9 evaluated networks.

Conclusion: Chronic migraineurs who responded to treatment showed a significantly higher RS-fc within the lateral visual network as compared to non-responders at baseline, as well as a significant decrease of RS-fc in this area after treatment. RS-fc might serve as a prognostic tool in selecting responsive patients for treatment.

B-1601 14:48

Prognostic role of CT imaging in coup and contrecoup injuries of brain

M. Jayakumar, A. Rangari, M.J. Rodriguez; *Vaniamkulam/IN*
(meghpsbb@gmail.com)

Purpose: Coup and contrecoup contusions are a set of focal brain injuries. Since the pathogenesis of the two are different, the outcome in the two also would be expected to be different. Present study aims to evaluate role of CT in predicting prognosis in coup-contrecoup injuries.

Methods and Materials: 103 consecutive cases presenting with coup and contrecoup injuries over a 1-year period were retrospectively analyzed. They were divided into three groups: Coup injuries with intraparenchymal injury ($n = 53$), contrecoup injuries ($n = 25$) and coup-contrecoup injuries ($n = 25$). The groups were comparable with respect to age and GCS. Site of primary impact was determined clinically. All patients underwent CT scan of brain. The mortality rates in each group were compared with respect to age, GCS and CT pattern. Significance was calculated using the chi-square test.

Results: Fractures, extraxial hemorrhage and intraparenchymal hemorrhage were the common findings identified on CT brain scan. There was a statistically significant difference in mortality between patients with coup injuries and patients with contrecoup ($p < 0.005$) and coup-contrecoup injuries ($p < 0.001$). There was no significant difference in mortality between contrecoup and coup-contrecoup injuries.

Conclusion: CT is able to identify coup and contrecoup injuries effectively. Presence of a contrecoup component on CT scan predicts a worse outcome in head injuries and warrants aggressive management and thus can help in deciding course of management.

B-1603 14:56

Vision-related structural and functional reorganisation after incomplete acute cervical cord injury

Q. Chen, N. Chen, W. Zheng, X. Chen, X. Li, K. Li, C. Zhang; Beijing/CN
(chaozhang0328@hotmail.com)

Purpose: The aim of this study was to explore possible vision-related structural and functional reorganisation of the brain after acute incomplete cervical cord injury (ICCI), which often leads to motor dysfunction, using multi-modal MR imaging study, and to further study their associations with motor and other clinical variables.

Methods and Materials: Eleven patients with ICCI and eleven matched healthy controls (HCs) were recruited. All participants underwent structural and functional MRI scans. Voxel-based morphometry analysis was carried out to investigate the differences in brain structure between ICCI and HCs, the fractional amplitude of low-frequency fluctuations (fALFF) was used to characterise changes in regional neural activities, and the independent component analyses (ICA) were used to explore alterations in resting-state network after spinal cord injury (SCI). Finally, we also investigate the correlations between brain imaging metrics and clinical variables.

Results: Compared with HCs, patients with ICCI showed significant grey matter (GM) atrophy in the left hippocampus and parahippocampal gyrus, and right superior frontal gyrus (SFG) and right middle frontal gyrus (MFG), and decreased fALFF in the left OFC. Moreover, ICCI patients exhibited decreased intra-network functional connectivity (FC) in the medial vision network (mVN). Finally, the mean fALFF value was correlated with the clinic motor scores.

Conclusion: Our findings provide evidence that acute ICCI can induce significant structural and functional alterations in vision-related regions of the brain. These reorganisations may suggest a potentially vital role for vision-related rehabilitation training in SCI patients with sensorimotor dysfunction, such as virtual reality (VR)-augmented training, brain-computer interfaces (BCI).

14:00 - 15:30

Room F2

Breast

SS 1902a

Risk-based screening

Moderators:

L.A. Carbonaro; San Donato Milanese/IT
D. Dijlas-Ivanovic; Sremska Kamenica/RS

B-1604 14:00

Risk-based strategies for supplemental breast cancer screening

D.L. Miglioretti¹, B. Sprague², C. Gard³, G. Rauscher⁴, J. Tice⁵, K. Kerlikowske³; ¹Davis, CA/US, ²Burlington, VT/US, ³Las Cruces, NM/US, ⁴Chicago, IL/US, ⁵San Francisco, CA/US (dmiglioretti@ucdavis.edu)

Purpose: Supplemental screening of women with dense breasts has been promoted given the low sensitivity of mammography in these women; however, screening ultrasound and MRI are limited by high false-positive rates. We evaluated the efficiency of basing supplemental screening decisions on a risk model for screening failures versus breast density.

Methods and Materials: We included 1,808,514 million screening mammograms on women 40-74 years in the U.S. Breast Cancer Surveillance Consortium. Risk factors were collected at the screen. Screening failures were defined as interval invasive cancers (<12 months after a normal mammogram) and screen-detected cancers AJCC stage IIb or higher. We used logistic regression to develop a risk model to predict the probability of a screening failure given a woman's age, BI-RADS breast density, family history, race/ethnicity, and history of benign breast disease.

Results: Screening failures occurred in 1.36/1000 and 1.71/1,000 screens performed on women with heterogeneously and extremely dense breasts, respectively. Supplemental screening of women with dense breasts (46% of population) would potentially avert 64% of screening failures. To potentially avert 64% of failures based on our risk model, only the 41% of women with failure risk >1.05/1000 would receive supplemental screening, resulting in fewer supplemental screens per failure (601 vs. 705). Supplemental screening of the 23% of women with failure risk >1.36/1000 would to potentially avert 46% of failures, further lowering the supplemental screens per failure to 476.

Conclusion: A risk model for screening failures more efficiently identifies women who might benefit from supplemental imaging than breast density.

Author Disclosures:

D.L. Miglioretti: Advisory Board; Hologic. K. Kerlikowske: Investigator; Grail, Google.

B-1605 14:08

Feasibility of risk assessment and personalised breast screening recommendations delivery in community radiology practice: a national prospective study (NCT02997384)

C.S. Balleyguier¹, E. Bayou¹, B. Boyer², S. Canale¹, I. Ewencyk-Biton², R. Gilles³, L. Rotenberg⁴, J. Viala⁵, S. Delalogue¹; ¹Villejuif/FR, ²Paris/FR, ³Bordeaux/FR, ⁴Neuilly-Sur-Seine/FR, ⁵Antony/FR

Purpose: Stratified breast cancer (BC) prevention is a major option for the future but requires adapted and relevant tools to assess BC risk and communicate with the women. The prospective "Riviera" trial (NCT02997384) aimed to evaluate the feasibility of a BC prevention consultation using a dedicated software, in private community practices in France. We report results obtained among participating radiologists.

Methods and Materials: Riviera was conducted from December 2016 to July 2017 and involved 8 community radiologists. Women aged 40-74 were proposed to have their BC risk assessed and a personalized screening program (PSP) provided using the Mammorisk™ software. Primary end point was the % of women accepting to participate. Secondary objectives were women's awareness, anxiety and satisfaction, and physicians' satisfaction. The participants filled questionnaires at accrual and 48h later. The radiologists' point of view was evaluated with a standardized questionnaire.

Results: 189 women were included. Median age was 51 (41% between 40 and 49). The BC risk assessment acceptance rate was 100%. 31 % of women were reclassified at high risk. 70% of women returned the H48 questionnaires. 93% found that the information and the PSP were clear or very clear. Anxiety levels after the consultation were low. The mean score for radiologists' satisfaction was good.

Conclusion: A BC prevention consultation with risk assessment and delivery of a PSP is feasible in community radiology practices. The next step is to evaluate the feasibility at a European level taking into consideration the different BC screening organizations.

B-1606 14:16

Mammographic density, age and family history: a minimally sufficient set of parameters to risk stratify average-risk women for follow-up screening

M. Abdolell, K. Tsuruda, J.I. Payne, P. Brown, J. Caines, P. Barnes, M. Rivers-Bowerman, S.E. Iles; Halifax, NS/CA (Sian.Iles@nshealth.ca)

Purpose: This study evaluated the consistency and discriminatory power of several short-term breast cancer risk models within a general screening population.

Methods and Materials: This 3:1 age- and screen-matched case-control study sampled all breast cancer cases diagnosed among digitally screened women aged 40-75 years (2009-2015) within a provincial breast screening programme. Clinical risk factor data and fully automated percent mammographic density assessments were obtained for 2,347 cases and 7,041 controls. The data were partitioned such that risk models were developed using a training dataset and validated using a test dataset. Patient-specific risk estimates were derived from models that included density and clinical risk factors alone and in combination. Agreement between models was assessed using intraclass correlation coefficient (ICC) and kappa; the predictive performance was assessed using the area under the receiver operating curve (AUROC).

Results: The agreement between risk estimates was highly variable (ICC=0.016-0.962, kappa=0.025-0.823). The risk model performance varied highly (AUROC=0.485-0.602). Agreement was almost perfect between a model including density, family history and age versus a model that additionally included menopausal status, HRT use and parity (ICC=0.962, kappa=0.823); the predictive performance was similar (AUROC =0.594,0.598).

Conclusion: Risk models can generate significantly different risk estimates for the same woman depending on the risk factors included, thus altering follow-up recommendations, especially for higher-risk women. A short-term risk model incorporating mammographic density, family history and age provides a practical solution for risk stratification of the average-risk population.

Author Disclosures:

M. Abdolell: CEO; Densitas Inc. Founder; Densitas Inc. K. Tsuruda: Employee; Densitas Inc.

B-1607 14:24

Mammographic breast density analysis with automated volumetric breast density in a single centre of Taiwan women

H.-K. Wu, W.-P. Wu; Changhua/TW (139496@cch.org.tw)

Purpose: Women with increased mammographic breast density are known to be at higher risk of developing breast cancer. The changes of breast density among diverse age groups in Asian women is still elusive. We aimed to investigate the distribution of breast density in Taiwanese women.

Methods and Materials: A retrospective review of data collected from 130,237 women who underwent digital mammography from 2011 to 2016 was conducted. On the basis of ACR BI-RADS 5th edition breast composition, breast density analysis based on fully-automated volumetric breast density

estimates (Volpara) were determined on four density grades (a, b, c, d) and a binary classification of fatty (a-b) vs. dense (c-d) breast.

Results: In Taiwan women, the frequency of dense breast was 94.0% (30-39 years old), 93.4% (40-49), 82.8% (50-59), 67.5% (60-69), 63.1% (70-79), and 63.5% (80-89), *p*-trend <0.001. Taiwanese women has a higher frequency of dense breast, but this frequency decreased abruptly between the ages of 50 and 69. Even in 70-89-year-old women, dense breasts are majority.

Conclusion: Our results indicate the higher frequency of dense breast among Taiwanese women.

B-1608 14:32

Assessing the diagnostic accuracy of a 3D functional infrared imaging as adjunct screening for women at high risk for breast cancer

M. Sklair-Levy¹, E. Friedman¹, O. Halshtok Neiman¹, A. Shalmon¹, M. Gotlieb¹, R. Faermann¹, J. Oaknin², D. Izhaky²; ¹Ramat Gan/IL, ²Airport City/IL (david@realimaging.com)

Purpose: Three-dimensional functional infrared imaging (3DIRI) has been shown before to provide high-accuracy risk assessment for the likelihood of breast cancer based on multiparametric evaluation of metabolic imaging biomarkers. In this prospective one-arm clinical study, 3DIRI is added twice yearly to a screening program which includes annual breast MRI and breast ultrasound or mammography surveillance. The aim of this study was to determine diagnostic accuracy of 3DIRI.

Methods and Materials: Following Ethics Approval, 230 females at high risk for breast cancer due to genetic predisposition, mainly known carriers of BRCA 1/2 mutation, signed informed consent for this study. They underwent 465 screening rounds between January 2015 and June 2016. Screening included 3DIRI scan (prototype Real Imager 8) and MRI or breast ultrasound or mammography. Accuracy of 3DIRI was determined by ROC curve using histopathological confirmation for cancer cases and one-year follow-up for non-cancer.

Results: Of 230 women who underwent 465 standard care screening procedures, 63 women underwent biopsy of which, 55 proved to be benign while 8 were malignant on histopathology. In addition, one interval cancer was observed during the follow-up. AUC of 3DIRI was 82.32%.

Conclusion: Three-dimensional functional infrared imaging can provide risk assessment for the likelihood of breast cancer with high accuracy in a population of women that are at high risk for breast cancer. Additional studies are necessary to evaluate its clinical utilisation as adjunct to mammography in screening population.

Author Disclosures:

J. Oaknin: Employee; Real Imaging Ltd. **D. Izhaky:** Employee; Real Imaging Ltd..

B-1609 14:40

Correlation of breast MRI screening with 3D functional infrared imaging

U. Fischer¹, F. Baum¹, J. Oaknin², D. Izhaky²; ¹Göttingen/DE, ²Air Port City/IL (david@realimaging.com)

Purpose: Three-dimensional functional infrared imaging (3DIRI) has been shown before to provide high-accuracy risk assessment for the likelihood of breast cancer in women based on multiparametric evaluation of metabolic imaging biomarkers. The aim of this study was to investigate the relationship between risk assessment score derived from 3DIRI and BI-RADS classification result derived from breast MRI.

Methods and Materials: In this prospective, ethically approved study, written informed consent was obtained from 120 women who underwent 3DIRI exam and breast MRI between September 2016 and September 2017. 3DIRI risk assessment score (on a scale of -100 to 100, with positive score indicating likelihood for malignancy) was used to determine area under the receiving operating characteristics in which MRI assessment (BI-RADS lexicon classification) was used as the gold standard. We used a Fisher's exact test to further compare association of MRI BI-RADS classification with 3DIRI scores.

Results: Seventy-three women (mean age, 58) were enrolled, recruited and had bilateral contrast-enhanced MRI screening and valid 3DIRI (Real Imager 8) imaging scan at day of analysis. Of 73 women, 32 women (44%) had positive MRI (BI-RADS≥3). AUC for 3DIRI was 0.70 (U test *p*<0.005). A Fisher's exact test of association between positive/negative MRI and positive/negative 3DIRI risk assessment score further corroborated this association (*p*<0.01).

Conclusion: Three-dimensional functional infrared imaging risk assessment score may serve as a predictor of positive breast screening MRI and may be utilized for selection of women for breast MRI screening.

Author Disclosures:

J. Oaknin: Employee; Real Imaging Ltd. **D. Izhaky:** Employee; Real Imaging Ltd.

B-1610 14:48

Interest of breast MRI surveillance in women with a personal history of breast invasive lobular carcinoma

J. Sanchez, C. de Bazelaire; Paris/FR

Purpose: Our purpose was to evaluate if breast MRI (BMRI) had an interest in the follow-up of patients after pure invasive lobular carcinoma (ILC).

Methods and Materials: From a retrospective review from January 2006 to February 2016, we recorded patients' and tumours' characteristics at the initial and second breast cancer (BC): systemic recurrence, disease-free survival (DFS) and overall survival (OS).

Results: 308 of 727 patients were included with a mean follow-up of 75.5 months: 217 with a conventional follow-up (mammography and ultrasound) and 91 with additional BMRI. There was no difference between the groups in locoregional recurrence (LR) (13 vs 22, *p* = 0.561). 306 BMRI were performed to detect 12 LR with 4 occult BC. BMRI had 4.2% cancer detection rate, 100% sensitivity, 88.7% specificity and 11.8% false positives. The DFS after exclusion of patients with distant recurrence was not significantly different: 184.7 months (IC 95% : 145.6-223.8) without MRI and 156.3 months (125.5-187.2) with MRI (*p* = 0.132). The mean OS did not differ significantly between the groups, being 318 months with MRI and 301.8 months without MRI (IC 95% = 275.5 - 328; log rank = 0.087).

Conclusion: BMRI surveillance did not increase the detection of LR and appeared not to be associated with an improvement in OS.

B-1611 14:56

How early can MRI diagnosis of breast cancer be in BRCA mutated women?

A. Pecchi, G. Musacchia, M. Verrusio, R. Battista, B. Canossi, L. Cortesi, P. Torricelli; Modena/IT (pecchi.annarita@policlinico.mo.it)

Purpose: Genes mutations increase the risk of developing breast cancer in women by approx. 50%. In the literature, evidence has consistently reported the importance of MRI screening for early diagnosis of breast cancer in these patients. Primary endpoint was to describe morphological and dynamic patterns of breast cancer diagnosed by MRI during an intensive surveillance multi-imaging protocol. Secondary endpoint was to retrospectively analyse the MRI examination obtained during the round prior to diagnosis to identify the early signs of cancer.

Methods and Materials: Our study involves 224 high-risk women studied with a multi-imaging screening protocol that includes mammography, ultrasound and MRI, differently matched according to woman's age.

Results: 25/224 women developed breast cancer: 4/25 diagnosed in the interval between a round and the next; 21/25 during multi-imaging follow-up. Among these, MRI enhancement pattern was non mass-like in 4 cases, mass-like in 17 cases, 4 of which showed a typical ring enhancement. In 9/21 of tumours detected during MRI screening, at the MRI performed one year before the diagnosis can be detected 3-6 millimetre neoangiogenic foci, early sign of cancer not visible with the other imaging modality.

Conclusion: In high-risk women, MRI showed a higher sensibility than mammography and ultrasound, confirming as the more efficient screening method. Repeated annually, MRI offers the advantage of comparing with previous exams from which you can detect the appearance of small enhancement foci that may be an early sign of tumour and, therefore, must be considered suspicious.

B-1612 15:04

Single-centre experience with breast MRI maximum intensity projection (MIP) views: sensitivity, specificity and accuracy of the stand-alone evaluation

M. Orsi, M. Cellina, C. Floridi, F. Leone, E. Battaglia, F. Barmettler, G. Oliva; Milan/IT (marcello.orsi@asst-fbf-sacco.it)

Purpose: Breast MRI has been proposed as a reliable screening tool for young high-risk patients for breast cancer. MIP reconstruction is a simple, reproducible and comparable view. The aim of our study was to test MIP views as a stand-alone tool for the detection of suspicious findings.

Methods and Materials: From September 2013 to February 2017, 159 consecutive breast MRI scans, performed in a single centre with a 1.5 Tesla scanner, were retrospectively evaluated by an expert radiologist that analysed the MIP coronal and axial views to assess the presence of suspicious findings (SF+ or SF-). The diagnostic accuracy of the MIP views was tested taking as gold standard of the complete radiologic evaluation (breast MRI, US and mammography), considering BI-RADS 1-2 as true negative and BI-RADS 3-5 as true positive.

Results: We analysed 159 breast MRI scans performed in women of a median age of 51(+/-24) years. 11 exams were excluded from the study for motion artefacts. In 89/148 MIP evaluation result was SF+; in 59/148 SF-. MIP evaluation showed sensitivity and specificity of 90.5% and 94.3%, respectively, and accuracy of 0.92. False-negative results were 9: 4 BI-RADS3, 2 BI-RADS4 and 3 BI-RADS5; mean diameter of non-depicted lesions was 8mm (+/-4mm).

Conclusion: MIP reconstruction view showed high sensitivity and specificity in assessing the presence of suspicious findings. Single image comparison with previous analogues helps the readers to notice the appearance or growing of the suspicious findings in the screening setting.

B-1613 15:12

Assessment of background parenchymal enhancement on breast MRI: which sequence shows the best agreement?

B. Bignotti¹, M. Calabrese¹, S. Tosto¹, F. Valdora¹, M. Durando², A. Tagliafico^{1,1}, G. Mariscotti²; ¹Genoa/IT, ²Turin/IT (bignottibianca@gmail.com)

Purpose: To evaluate inter- and intrareader agreement among different sequences for assessment of background parenchymal enhancement (BPE) on breast MRI.

Methods and Materials: Two independent readers qualitatively categorized BPE on ninety-eight breast MRI using a four-point scale (minimal, mild, moderate or marked) in accordance with the BI-RADS category system. According to MR sequence used for the assessment of BPE categorization, interreader and intrareader agreement across four reading strategies were performed: (1) initial contrast-enhanced fat-suppressed T1-weighted; (2) initial contrast-enhanced subtracted images; (3) MIP images; (4) combination of the initial contrast-enhanced fat-suppressed T1-weighted, initial contrast-enhanced subtracted and MIP images. Readers repeated BPE assessment of twenty-eight breast MRI four weeks after the initial assessment. K statistics was used to calculate the agreement.

Results: Interreader agreement was moderate (k=0.44) using initial contrast-enhanced fat-suppressed T1-weighted, substantial (k=0.69) using initial contrast-enhanced subtracted images, substantial (k=0.67) using MIP images, substantial (k=0.71) using a combination of the initial contrast-enhanced fat-suppressed T1-weighted, initial contrast-enhanced subtracted and MIP images. Mean intra-reader agreement among the two readers was moderate (k=0.55) using a combination of contrast-enhanced fat-suppressed T1-weighted, initial contrast-enhanced subtracted and MIP images.

Conclusion: Overall, the combination of the initial contrast-enhanced fat-suppressed T1-weighted, initial contrast-enhanced subtracted and MIP images showed the highest inter- and intrareader agreement.

B-1614 15:20

Background parenchymal enhancement in MRI, mammographic density and risk of breast cancer

F. Amato¹, A. Orlando¹, M. Di Vittorio¹, M. Safina², T.V. Bartolotta¹, R. Ienzi¹; ¹Palermo/IT, ²Castellammare del Golfo/IT (amaciccio89@gmail.com)

Purpose: Evaluate the relationship between "background parenchymal enhancement" (BPE) on magnetic resonance imaging (MRI), mammographic density (MD) and breast cancer (BC).

Methods and Materials: According to BIRADS, two radiologists have classified BPE on MRI (minimal/mild/moderate/marked) and mammographic density (A/B/C/D) of 231 patients (age: 29-91 aa) underwent MR and Mammography examination. Patients with (111/231; 48 %) and without (120/231 ; 52 %) family history of BC were included, and patients with BRCA positivity were excluded. Patients were divided into four groups: Group I: BPE minimal/mild and DM A-B; Group II: BPE minimal/mild and DM C-D; Group III: BPE moderate/marked and DM A-B; Group IV: BPE moderate/marked DM and C-D. Using the chi-square test was calculated the Relative Risk (RR) of BC in the various groups.

Results: 75/231 (32,5%) patients were in Group I, 131/231 (56,7%) in the second, 11/231 (4,8%) in the third and 14/231 (6,1%) in the fourth. Diagnosis of BC was made in 35/75 (46,7% %) of cases in group I, in 60/131 (45,8%) in Group II, in 8/11 (72,7%) in Group III and in 5/14 (35,7%) in group IV. Prevalence of BC was significantly greater among the patients of group III, who had a moderate/marked BPE and DM Grade A-B (p = 0.0181; RR = 1.60; 95% CI: 1.08-2.36), regardless of familiarity and age.

Conclusion: The degree of BPE isn't directly related to the degree of mammographic density or to the relative risk of BC. The association between high BPE and low DM was significantly correlated with a higher prevalence of BC.

14:00 - 15:30

Room D

Musculoskeletal

SS 1910

Chronic inflammatory diseases

Moderators:

E. Inarejos; Esplugues de Llobregat/ES
I. Sudol-Szopińska; Warsaw/PL

B-1615 14:00

Detection of osteitis at the sacroiliac joint in patients with chronic low back pain by STIR and T2-weighted fat-suppressed turbo spin echo sequences: results from the SIMACT study

J. Greese, T. Diekhoff, J. Sieper, C. Schwenke, M.R. Makowski, D. Poddubnyy, B. Hamm, K.-G. Hermann; Berlin/DE (juliane.greese@charite.de)

Purpose: To compare short tau inversion recovery (STIR) and T2-weighted fat-suppressed turbo spin echo (T2-FS) sequences to detect osteitis lesions at sacroiliac joints (SIJ) in patients with chronic low back pain (CLBP).

Methods and Materials: This prospective study included 110 patients with CLBP and suspicion of spondyloarthritis and 18 healthy volunteers. All 128 participants (age range 19 to 57 years) underwent 3.0 Tesla MRI of the SIJ including STIR and T2-FS. Two readers independently evaluated osteitis in STIR and T2-FS in separate scoring sessions. Sum score values, signal-to-noise (SNR) and contrast-to-noise (CNR) ratios were calculated. Images were further analysed whether they fulfilled the Assessment of SpondyloArthritis international Society (ASAS) criterion of a "positive MRI" (MRI+). Inter-reader agreement was calculated by intra-class correlation coefficients (ICC).

Results: Overall, sum score values for osteitis lesions were significantly higher (p=0.02) for T2-FS (reader 1: 3.90±5.67; reader 2: 7.10±8.69) compared to STIR (reader 1: 2.55±4.41; reader 2: 3.95±5.79). Mean SNR was measured 16.54 for STIR and 37.30 for T2-FS (p=0.03). Likewise, mean CNR was 4.14 for STIR and 20.20 for T2-FS (p=0.02). ASAS MRI+ definition was significantly more often fulfilled for T2-FS compared to STIR (p=0.0003) by both readers. Inter-reader ICC values were very good both for STIR (0.91) and T2-FS (0.86).

Conclusion: T2-FS sequences detect more MRI+ patients with superior image quality in cohorts with CLBP compared to STIR. Therefore, we recommend T2-FS as addition to STIR for MRI protocols of the SIJ.

B-1616 14:08

T2-mapping of the sacroiliac joints at 1.5T: a reproducibility study

D. Albano¹, V. Chianca², M. Galia¹, R. Cuocolo², R. Bignone¹, C. Messina³, L.M. Sconfienza³, A. Brunetti², R. Lagalla¹; ¹Palermo/IT, ²Naples/IT, ³Milan/IT (vitochianca@gmail.com)

Purpose: T2-mapping of the sacroiliac joints has shown to be feasible at 3T, but feasibility at 1.5T has never been tested. We evaluated the reproducibility of T2 relaxation time measurements of the sacroiliac joints at 1.5T.

Methods and Materials: Healthy volunteers underwent an oblique axial multislice multiecho spin-echo T2-weighted sequence of the sacroiliac joints at 1.5 T. The regions of interest were manually drawn with Olea Sphere[®] 3.0 software (Olea Medical[®], La Ciotat, France) by two musculoskeletal radiologists to include the cartilaginous part of the sacroiliac joints. Intra- and inter-observer reproducibility was tested using the Bland-Altman method. Association between sex and T2 relaxation times was tested using the Mann-Whitney U test. Correlation between T2 relaxation times and body mass index (BMI) was tested using the Spearman's rho.

Results: Eighty sacroiliac joints of 40 subjects (mean age: 28±4.8 years, range: 20-43; mean BMI: 23.3±3.1, range: 18.9-30) were imaged. The mean T2 value calculated by the senior radiologist in the first series of measurements was 42±4.4ms, whereas in the second series was 40.7±4.5ms. The mean T2 value obtained by the radiology resident was 41.1±4.2ms. Intra-observer reproducibility was 88% (coefficient of repeatability=3.8; bias=1.28; p<0.001), while inter-observer reproducibility was 86% (4.7; -0.88; p<0.001). There was significant association between sex and T2 relaxation times (p=0.024) and significant inverse correlation between T2 relaxation times and BMI (r=-.340, p=0.002).

Conclusion: The assessment of T2 relaxation time measurements of sacroiliac joints seems reproducible to be performed at 1.5T. Further studies could investigate the potential clinical application of this tool.

B-1617 14:16

MRI findings of sacroiliac joint disorders in SAPHO syndrome

X. Shao, W. Xu, C. Li, X. Zhao, W. Zhang; Beijing/CN (sxl669594@sina.com)

Purpose: To retrospectively evaluate the MRI features of sacroiliac joint disorders in 38 SAPHO patients, thus increasing the awareness of SAPHO syndrome among clinicians.

Methods and Materials: 38 SAPHO patients (female: male, 26:12; mean±SD age, 46.3±10.1 years) were enrolled. The frequency of sacroiliac joint disorders was calculated and MRI features were evaluated.

Results: 23 patients (41 joints) were involved, with a frequency of 60.5%(23/38). 52.2% (12/23) of these patients were bilaterally involved. Among the involved 41 joints, lesions distributed with a predilection on the sacrum in 58.5% (24/41). 87.8% (36/41) of the involved sacroiliac joints were affected by the cartilaginous portion, and 90.2%(37/41) by the ligamentous portion. Inflammatory changes including bone marrow oedema, capsulitis, effusion and enthesitis were observed in 80.5% (33/41), 29.3%(12/41), 24.4%(10/41) and 80.5%(33/41) of the involved sacroiliac joints, respectively. While chronic changes including post-inflammatory fatty deposition, erosion and sclerosis were observed in 92.7% (38/41), 70.7% (29/41) and 70.7% (29/41) of the involved sacroiliac joints, respectively. Joint space was widened in 19.5% (8/41) joints, narrowed in 17.1% (7/41) and ankylosis in 14.6% (6/41). Soft tissue involvement was observed in 14.6% (6/41) of the involved sacroiliac joints.

Conclusion: Sacroiliac joints were more bilaterally involved in SAPHO patients, with predilection on the sacrum. Active lesions and chronic lesions usually coexist, with a lower prevalence of ankylosing and soft tissue involvement. These MRI features could provide certain information of SAPHO syndrome. Consultation of skin lesions should be taken into consideration for a comprehensive evaluation and definite diagnosis.

B-1618 14:24

Sacroiliitis due to early ankylosing spondylitis, inflammatory bowel disease and Behçet's disease: could sacroiliac MRI play a role in differentiation?

Z. Akkaya, E. Peker, F.S. Ozalp Ates, G. Sahin; Ankara/TR (zehraakkaya@gmail.com)

Purpose: The purpose of this study was to investigate whether sacroiliitis due to early ankylosing spondylitis (AS), inflammatory bowel disease (IBD)-related spondyloarthropathy and Behçet's disease (BD) were distinguishable by MRI.

Methods and Materials: Sacroiliac MR images of 88 patients (52 with AS, 17 with BD, 12 with Crohn's disease (CD) and 7 with ulcerative colitis (UC) including 65 females and 23 males (mean age: 41.8 ±11.3) were retrospectively evaluated by two radiologists who were blind to the diagnoses. The evaluation parameters consisted of soft tissue-related changes (thickness of perirectal fat, presence of perirectal lymph node or submucosal fatty infiltration) and sacroiliac joint changes (joint surface irregularities-erosions, bone marrow edema, subchondral sclerosis-fatty change and laterality of involvement). Statistical analyses were performed to search for distinguishing parameters between the AS and IBD-Behçet's disease combined group. Additionally, the findings for the Behçet's disease group were compared to those of the IBD group.

Results: Marrow edema, chronic subchondral marrow changes, surface irregularities-erosions and bilateral involvement of the sacroiliac joints were significantly more common in the AS group ($p < 0.05$). No statistically significant results were found for either parameter between the IBD and Behçet's disease groups.

Conclusion: Both active and chronic joint changes were more pronounced in the AS group. Behçet's disease is a multisystem disorder but not an IBD-associated spondyloarthropathy. However, the analyzed Behçet's disease group displayed bowel and joint changes similar to those of the IBD group.

B-1619 14:32

Osteitis distribution on MRI of the sacroiliac joints in patients with osteitis condensans compared to axial spondyloarthritis

K.-G. Hermann¹, S. Mercan¹, K. Ziegeler¹, T. Diekhoff¹, J. Greese¹, B. Hamm¹, M. Bollow²; ¹Berlin/DE, ²Bochum/DE (kgghermann@gmail.com)

Purpose: Osteitis condensans (OC) is a non-inflammatory disorder affecting the sacroiliac joints (SIJ) and is attributed mainly to mechanical stress, such as pregnancy and delivery or frequent sports activities. In later stages, it can be readily diagnosed on conventional X-rays. However, frequently MRI is the sole imaging modality and confusion exists whether the distribution and frequency of MRI findings.

Methods and Materials: 119 MRI examinations of the SIJ from a single center specialized in MSK imaging were retrospectively analyzed independently by two experienced readers. Clinical data was collected prior to MRI acquisition via standardized patient questionnaires. A third reader (senior MSK expert) made a decision between either OC or SpA as the leading diagnosis, taking all available imaging data and clinical data into account. Scoring of osteitis was

done in a quadrantic scheme and in addition, the predominant site of findings in the anterior-posterior orientation was recorded (anterior, middle, and posterior positions).

Results: 71 patients with OC and 48 with SpA were identified. Osteitis was evident in 73% and 79% of patients, respectively, with mean osteitis sum scores of 1.75±2.55 and 4.13±4.62 ($p < 0.001$). While the distribution of osteitis was in the anterior position in 94% of OC patients only 38% of SpA patients demonstrated osteitis in the anterior position and 52% in the middle position.

Conclusion: Different osteitis distribution patterns can be identified to distinguish OC and SpA at SIJ, with OC demonstrating the lesser amount of osteitis compared to SpA, but most frequently located in the anterior inferior position.

B-1620 14:40

Relative maximum apparent diffusion coefficient: a potential biomarker of disease activity in axial spondyloarthritis

K. Lee, W. Lau, H. Tsang, C. Lau, H. Chung; Hong Kong/HK (viclkh88@gmail.com)

Purpose: To evaluate the correlation between diffusion-weighted imaging (DWI)-derived parameters of disco-vertebral lesions and clinical parameters in axial spondyloarthritis (SpA).

Methods and Materials: Two hundred and seventy-five patients with expert diagnosed axial SpA were recruited from 3 rheumatology centres. Clinical, biochemical and radiological parameters were collected. All patients underwent whole spine and sacroiliac (SI) joints MRI using short tau inversion recovery (STIR) sequence and diffusion weighted imaging (DWI). The presence of disco-vertebral lesions was defined by positive identification by two independent readers. Apparent diffusion coefficients (ADC) of disco-vertebral lesions and normal marrow were measured for determination of relative mean ADC (rADC_{mean}) and relative maximum ADC (rADC_{max}) of the disco-vertebral lesions. These were then compared with clinical parameters using Spearman and Pearson correlation coefficients.

Results: Twenty-six (9.5%) patients had disco-vertebral lesions. Forty-two (23 thoracic, 17 lumbar) lesions were identified. Inter-observer agreement was excellent ($\kappa = 0.895$). rADC_{max} correlated positively with intensity of back pain (CC=0.46; $p=0.02$), morning stiffness (CC=0.47; $p=0.02$), duration of stiffness (CC=0.44; $p=0.03$), and stiffness score (CC=0.49; $p=0.01$). No significant correlations were found between the number of lesions, ADC_{mean}, rADC_{mean}, CRP, ESR, and BASDAI score. There were no significant differences in the BASDAI score, CRP, and ESR in patients with or without disco-vertebral lesions.

Conclusion: In axial SpA, rADC_{max} of disco-vertebral lesions correlates significantly with degree of back pain and intensity of morning stiffness. This parameter could be a potential imaging biomarker.

B-1621 14:48

Examination of association of inflammatory activity in psoriatic arthritis and vascular calcification metabolism based on integrated ¹⁸F PET/MRI

N. Guberina, A. Körber, M. Forsting, L. Umutlu, A. Bockisch, K. Herrmann, T.D. Poeppel; Essen/DE

Purpose: To examine the association between vascular calcification metabolism and musculoskeletal manifestations in patients with active psoriatic arthritis.

Methods and Materials: In a prospective clinical trial 21 patients with psoriatic arthritis were included in the study. Participants were examined according to a standardized whole-body protocol on the PET/MRI-scanner MagnetomBiograph_mMR (Siemens Healthcare, Germany) within a single session. Joint inflammation based on ¹⁸F-NaF PET/MRI images was assessed according to 8 different variables (SUV_{max}, tenosynovitis, bone and soft tissue oedema, bone erosions, joint-space narrowing, joint-subluxation, and interphalangeal ankylosis). Vascular calcification metabolism was evaluated based on ¹⁸F-NaF-PET/MRI images in terms of ¹⁸F-NaF-uptake in large (aorta ascendens, aortic arch, thoracic and abdominal aorta descendens) and medium vessels (supraaortic arteries, a. mesenterica superior, iliac arteries, a. femoralis superficialis). SUV_{max} was normalized for the mediastinal blood pool. Furthermore, association with laboratory parameters (CRP, CCP, leukocytes, rheuma factor, triglycerides and cholesterol) was examined.

Results: A total of 21 subjects (71.4% men, 28.6% women, age range 23 - 77 years) were evaluated. Vascular calcification metabolism of large and medium vessels showed a significant positive correlation with changes observed in advanced stage of psoriatic joint manifestation ($p < 0.05$). Moreover, arthritic changes were not associated and showed no correlation with laboratory markers of inflammation ($p > 0.05$).

Conclusion: The severity of psoriatic joint manifestations in advanced stage of psoriatic arthritis does significantly correlate with vascular calcification metabolism. Patients with psoriatic arthritis with clinical mild arthritic changes may present severe atherosclerotic changes. Both psoriatic changes and vascular inflammation may precede the actual onset of clinical symptoms.

B-1622 14:56

Subclinical psoriatic arthritis detection in patients with psoriatic onychopathy

V. Linovs, M. Radzina, T. Linova, A. Rubins, S. Rubins; *Riga/LV (dr.viktors.linovs@gmail.com)*

Purpose: Find correlation between psoriatic onychopathy and subclinical enthesitis.

Methods and Materials: The prospective study included 97 patients: 25 patients with nail psoriasis (clinically confirmed) with no history of previous rheumatological disease, 47 patients with psoriasis without onychopathy with no history of previous rheumatological disease and 25 control cases (healthy individuals). Clinical evaluation and ultrasonographic assessment was performed in 12 entheses and 8 nails in each patient by a dermatologist and a radiologist (ultrasonographic assessment using modified Madrid Sonographic Enthesis Index (MASEI) protocol). Inflammatory activity in enthesitis (active enthesitis) was defined as the presence of power Doppler signal, tendon thickening and/or hypoechogenicity.

Results: There was correlation between enthesitis and psoriatic nail involvement ($p < 0.05$), as well as correlation between psoriasis and enthesitis ($p < 0.05$). No correlation between clinical evaluation of the enthesitis and enthesitis was observed ($p > 0.05$). Nail matrix thickness was significantly increased in patients with nail disease (1.89 mm vs. 1.75 mm; $p < 0.05$). The loss of the trilaminar nail plate appearance and increased Power Doppler signal in the matrix were also significantly associated with nail psoriasis ($p < 0.05$). There is correlation between clinical evaluation of the nail and ultrasound findings in the nail organ ($p < 0.05$). No pathological findings were seen in control group.

Conclusion: Ultrasound could be a valuable diagnostic tool for detection of subclinical enthesitis in patients with psoriatic onychopathy, which is proved to be predisposing factor of psoriatic arthritis. Ultrasound screening in psoriatic onychopathy patients may be considered as early stratification method for early treatment initiation.

B-1623 15:04

Hypodermal adipose tissue sonoelastography for monitoring different treatment responses in patients with plaque psoriasis

M. Guazzaroni, S. Altobelli, S. Marsico, A.U. Cavallo, A. Bozzi, R. Floris; *Rome/IT (salvatore.marsico@hotmail.it)*

Purpose: To evaluate hypodermal adipose tissue inflammation underneath psoriasis plaques quantifying tissue elasticity with sonoelastography before and after treatment with topic therapy, systemic therapy or with biologic drugs.

Methods and Materials: From September 2015 to September 2017, we enrolled 120 patients with plaque psoriasis with a mean age of 51 years (range 18-80) (38F, 22M) with plaque psoriasis and a PASI score of > 5 . They were divided into 3 groups of treatment depending on the prescribed drug: topic therapy (Group A), systemic therapy with DMARDs (Group B) and biologic drugs therapy (Group C). A baseline (T0) ultrasound examination with sonoelastography was performed before the beginning of drugs assumption. At this time the mean strain ratio was recorded on normal and pathologic skin. A follow-up clinical and ultrasonographic examination (T1) was performed after one month of treatment to evaluate therapy response.

Results: At T0 lesional mean strain ratio was significantly higher than non-lesional one, thus documenting an high grade of stiffness of the hypodermal fat underneath psoriasis evaluated plaques. T1 examination data obtained from the 3 selected groups of patients documented a significant decrease in stiffness when comparing groups B and C together with groups A and group C with both groups A and B. Mean strain ratio decrease correlated with clinical PASI improvement in all the responder patients in the considered groups.

Conclusion: Sonoelastography is able to identify hypodermal adipose tissue involvement in plaque psoriasis and it represents a valid method to assess early therapy response.

B-1625 15:12

Correlation between central adiposity distribution measured by DXA and inflammatory markers in the Italian cohort of the NU-AGE project

D. Mercatelli¹, A. Santoro¹, G. Guidarelli¹, M. Aparisi Gomez², G. Guglielmi³, C. Franceschi¹, G. Battista¹, A. Bazzocchi¹; ¹Bologna/IT, ²Valencia/ES, ³Andria/IT (abazzo@inwind.it)

Purpose: Adipose tissue is a source of hormones and cytokines, in particular visceral adipose tissue (VAT) and subcutaneous adipose tissue (SAT) have been linked to systemic inflammation. Both modifications in body composition (BC) and a low-grade chronic inflammation characterise human ageing. This study evaluates the changes of fat distribution, measured by dual-energy X-ray absorptiometry (DXA), and the correlation with some inflammatory markers in a group of Italian elderly people that increased BMI but reduced fat and vice-versa after one-year.

Methods and Materials: 271 sex-balanced volunteers free of major overt diseases, aged 65-79 years, were enrolled in the Italian cohort of the NU-AGE

study, a one year randomised, single-blind, controlled trial with two parallel groups (control vs. diet). Whole-body DXA scans to assess BC, and blood samples were taken at T0 and T1. Comparison of variables was performed using Wilcoxon rank-sum test.

Results: In 42 patients showing reduction of SAT but increase or no change in BMI, significantly lower levels of pro-inflammatory cytokines leptin ($p = 0.02801$) and TGF- β ($p = 0.04676$) were found, compared to 28 patients who gained SAT with no changes or reduced BMI. In 47 patients showing a reduction of VAT but an increase or no changes in BMI, significantly lower levels of leptin ($p = 0.02736$) were found compared to 23 patients who gained VAT but reduced their BMI.

Conclusion: DXA scans are useful to monitor BC changes over time, especially in patients where changes in BMI do not reflect changes in central adiposity distribution. Both VAT and SAT reduction were positively correlated with a decreased inflammatory status, despite an increase or no change in BMI.

14:00 - 15:30

Room G

Breast

SS 1902b

AI and CAD in breast imaging

Moderators:

J. van Zelst; Nijmegen/NL
S.J. Vinnicombe; Dundee/UK

B-1627 14:00

Determination of breast parenchymal enhancement (BPE) in breast MRI using a deep convolutional neural network

N. Berger, C. Rossi, A. Ciritis, M. Marcon, A.S. Becker, A. Boss; *Zurich/CH (Nicole.Berger@usz.ch)*

Purpose: Breast parenchymal enhancement (BPE) is rated in each breast MRI in the categories minimal, mild, moderate and marked. If elevated, BPE may hamper the evaluation of the acquired images. The aim of this study was to train a deep convolutional neural network (dCNN) for automatic classification of BPE according to the American College of Radiology Breast Imaging Reporting and Data System (ACR BI-RADS) Atlas.

Methods and Materials: In this IRB-approved retrospective study, breast-MRI data (1200 images) from 106 different patients were downloaded from the picture archiving and communications system (PACS) and labelled by a board certified radiologist according to the enhancement category. A dCNN with 13 convolutional layers followed by 4 dense layers and one fully connected layer implemented in Keras 2.0.8 was trained with 70% of the data, whereas 30% were used for validation. Minimal, mild and moderate BPE were compared in a one-vs-one fashion computing the probability for the suitability of each category. The classification was determined from the highest probability.

Results: Validation accuracy for BPE category minimal vs. mild was 0.63 and minimal vs. moderate was 0.69.

Conclusion: Even with limited training data, dCNN shows promising results for distinguishing the first three categories of the BPE in breast-MRI based on the ACR BI-RADS system. The proposed technique may in future be useful for accurate, standardized, and observer-independent BPE rating.

B-1628 14:08

Can the breast cancer screening case-load be reduced by deep-learning based identification of normal cases? An international multi-centre retrospective analysis

A. Rodriguez Ruiz¹, A. Gubern-Mérida¹, G. Gennaro², M. Chevalier³, S. Zackrisson⁴, I. Andersson⁴, I. Sechopoulos¹, R.M. Mann¹; ¹Nijmegen/NL, ²Padua/IT, ³Madrid/ES, ⁴Malmö/SE (alejandrorz@gmail.com)

Purpose: To study the feasibility of reducing the screening case load by automatically identifying digital mammography (DM) exams without abnormalities.

Methods and Materials: Three datasets used in previously published multi-reader studies, performed across four countries and using systems from three vendors, were collected. Each dataset consisted of DM exams, radiologists' BI-RADS[®] scores and ground truth, yielding 1122 exams (257 malignant) interpreted by 15 readers. A deep learning based computer system (Transpara 1.3.0, ScreenPoint Medical) automatically analyzed each exam, providing a cancer suspiciousness score (1-10). For each dataset, a modified set was created in which pre-selection was simulated by setting the radiologists' scores to BI-RADS 1 for all cases with cancer suspiciousness score ≤ 5 . The area under the reader-averaged receiver operating characteristic curve (AUC) was calculated for the original and modified sets, and compared using bootstrapping.

Results: After pre-selection, we observed only non-significant AUC changes; a slight increase in two sets: 0.785 (95% CI: 0.671-0.865) to 0.807 (0.696-0.887) [$P=0.095$], and 0.870 (0.819-0.912) to 0.883 (0.836-0.921) [$P=0.197$]; and a slight decrease in one: 0.821 (0.752-0.877) to 0.804 (0.723-0.871) [$P=0.473$]. Averaging among readers on each dataset, 27%, 20%, 8% of false positives were excluded; and 1%, 1%, 5% of true positives. Across datasets, pre-selection discarded 44%, 40%, 51% of non-malignant cases and 8%, 6%, 17% of malignant cases.

Conclusion: Automated identification of mammograms that are most likely normal, and therefore might not need to be read, is feasible without significantly affecting the reading performance. This may nearly halve the workload for screening radiologists.

Author Disclosures:

A. Gubern-Mérida: Employee; Screenpoint Medical BV. **R.M. Mann:** Consultant; Screenpoint Medical.

B-1629 14:16

A novel open-access neural network to evaluate suspicious mass lesions detected in breast MRI for direct integration into clinical workflows

S. Ellmann, E. Wenkel, M. Hammon, R. Janka, P.A. Fasching, R. Schulz-Wendtland, A. Maier, M. Uder, T. Bäuerle; Erlangen/DE (stephan.ellmann@uk-erlangen.de)

Purpose: To develop a novel machine learning algorithm for classification of suspicious mass lesions detected in breast MRI that can be readily integrated into clinical workflows and is based on objective image features only.

Methods and Materials: This retrospective study included 176 BIRADS 4 and 5 mass lesions in breast MRI with available histopathology as gold standard. 138 lesions were used to train a neural network for classification (benign vs malignant) using different objective parameters (lesion diameter, diffusion restriction, T2w-fs signal intensity, patient age, dynamic contrast enhancement curve type and washout ratio and number of lesions in the affected breast). 38 lesions were randomly selected and retained as a test set. Receiver operating characteristic analyses were used to determine the predictive abilities of the single predictors, and compared to the diagnostic accuracy of the neural network with McNemar tests. The neural network was made available as an open-access internet application using Shiny for R.

Results: The neural network achieved a sensitivity of 90.1% (95% CI 87.8-92.4) and a specificity of 82.6% (78.8-86.4) during training and validation, featuring significantly higher diagnostic accuracy compared to all single parameters alone ($p < .0001$). Regarding the test set lesions, sensitivity and specificity of the neural network were within the 95% confidence intervals (92.0% and 84.6%, respectively).

Conclusion: Here we present a machine learning algorithm for evaluation of suspicious mass lesions in breast MRI based on objective parameters that can only be directly applied in clinical workflows using an open-access online form.

B-1630 14:24

Advancements in computer-aided BI-RADS US characterisation of focal breast lesions: clinical assessment of a new software release of S-Detect

M.L. Di Vittorio, A. Orlando, F. Amato, L. Spatafora, M. Safina, A. Taibbi, F. Ienzi, R. Ienzi, T.V. Bartolotta; Palermo/IT (marialaura.divittorio@gmail.com)

Purpose: To compare version 2.0 (V2) to 1.0 (V1) of a computer-guided decision-making software (S-Detect) in the sonographic characterisation of focal breast lesions (FBLs).

Methods and Materials: 73 FBLs (mean size 15.9 mm) in 73 women detected by high frequency US (RS80A with Prestige, Samsung, Seoul) were retrospectively assessed by five independent reviewers with different years of experience (YOE) in breast sonography: one experienced radiologist (ER, >20 YOE), two general radiologists (GR#1 and GR#2, 5-10 YOE) and two radiology residents (RR#1 and RR#2). FBLs were randomly evaluated twice according to BI-RADS US lexicon with V1 and V2. US-guided core-biopsy was the standard of reference for BI-RADS category 4 or 5 FBLs. US follow-up at 6 and 12 months has been available for BI-RADS 3 category lesions both before and after S-detect assessment.

Results: 33/73 were malignant and 40/73 were benignant. Diagnostic accuracy, sensitivity, specificity values for the ER were 0.90, 1.00, 0.83 with V1 and 0.89, 1.00, 0.80 with V2 ($p>0.05$). Corresponding values were: 0.71, 0.83, 0.64 with V1 and 0.71, 0.79, 0.65 with V2 ($p>0.05$) for GR#1; 0.74, 0.76, 0.72 with V1 and 0.74, 0.76, 0.72 with V2 ($p>0.05$) for GR#2; 0.70, 0.95, 0.60 with V1 and 0.75, 0.87, 0.67 with V2 ($p>0.05$) for RR#1; 0.67, 0.77, 0.60 with V1 and 0.73, 0.76, 0.69 with V2 ($p=0.009$) for RR#2.

Conclusion: S-Detect V2 showed a better performance than V1 in lesion boundary segmentation, offering a more accurate tool for decision-making in the characterisation of FBLs, especially for less experienced physicians.

B-1632 14:34

Selection of parameters for computer model of breast anatomy through human observer experiments

D. Pokrajac¹, Z. Radovanovic^{2,2}, T. Milosavljevic², V. Stokanovic², S. Weinstein³, A. Imran Al-Zubaer¹, A.D.A. Maidment³, P.R. Bakic³; ¹Dover, DE/US, ²NiS/RS, ³Philadelphia, PA/US (dpokrajac@desu.edu)

Purpose: Human observers have evaluated the influence of software breast phantom parameters on the realism of synthetic mammography and tomosynthesis images.

Methods and Materials: Previously, we developed a recursive partitioning algorithm to simulate breast anatomy. The simulation parameters were selected using a volumetric analysis of reconstructed CT images of a mastectomy specimen. To validate selected parameters, we performed an observer study with clinical radiologists. Mammography and reconstructed tomosynthesis images of phantoms with various simulation parameters were synthesised, and used in 2-alternative forced choice experiments. The varied parameters included the number of simulated tissue compartments and the relative size and shape of compartments. In a preliminary study, we presented 16 synthetic image pairs (8 mammographic and 8 tomosynthesis) to a clinical radiologist. The observer was asked to indicate a more realistic image in each pair. We compared the observers' preference with parameters selected from the mastectomy specimen images.

Results: In the preliminary study, consistently for both mammography and tomosynthesis images, the observer preferred images of phantoms with the larger number of compartments, and with a wider variation in the compartment shape and size. While the number of compartments may be relatively easy to notice, the visual difference in parenchymal pattern due to the range of speed parameters is more subtle.

Conclusion: Our preliminary study supported the anatomy simulation parameters selected from the analysis of mastectomy specimen CT images. A full observer study with two additional radiologists and a larger image set is ongoing.

B-1633 14:40

S-detect as a teaching tool in the characterisation of breast lesions: a preliminary study

M. Di Segni, V. De Soccio, G. Bonito, A. Rubini, V. Magri, V. Cantisani, C. De Felice, F. D'Ambrosio, C. Catalano, G. Alagna; Rome/IT (gralagna@gmail.com)

Purpose: To assess the value of S-detect as a teaching tool in the characterisation of breast lesions.

Methods and Materials: One hundred twenty two female patients, aged 21 to 84 years, with 135 breast lesions were prospectively imaged with baseline US by a 32 years experienced radiologist and analysed with S-detect; 4 residents with different experience in breast imaging, blinded to clinical and pathological results, completed the exam with elastography. Then, the residents retrospectively described and categorised lesions according to BIRADS 2013 lexicon and to the scheme proposed by Jales et al. When lesions were categorised as BIRADS 4a by the residents, their readings were compared to the readings of S-detect and in case of disagreement, priority was given to S-detect (Samsung Healthcare, Seoul, South Korea). Diagnostic performance was analysed with 2x2 contingency tables and differences were assessed with Pearson's χ^2 test.

Results: Residents' sensitivity values varied from 95.5% to 100%, whereas specificity values varied from 54.2% to 70.8%; S-detect showed 91.1% sensitivity and 70.8% specificity. In case of BIRADS 4a lesions, using S-detect for 2 of the residents significantly increased from 54 to 75% and from 50% to 75%, whereas it was not significant for the most experienced one (from 70.8% to 75%, $p<0.005$) and for the remaining resident with weak performance ($p>0.05$).

Conclusion: S-detect has a potential as a teaching tool for the less experienced operators.

Author Disclosures:

V. Cantisani: Speaker; Bracco, Toshiba Medical Systems, Samsung Healthcare.

B-1636 14:48

Evaluation of a CAD (computer-aided detection)-enhanced 2D synthetic mammogram: comparison with a standard synthetic 2D mammogram and conventional 2D digital mammography

J. James¹, E. Giannotti¹, Y. Chen²; ¹Nottingham/UK, ²Loughborough/UK (jonathan.james@nuh.nhs.uk)

Purpose: CAD-enhanced mammograms utilise an algorithm identifying potential abnormalities on tomosynthesis slices blending them onto a synthetic image. The aim was to evaluate the diagnostic performance of CAD enhanced 2D synthetic mammograms in comparison with standard 2D synthetic mammograms generated from a tomosynthesis data set and conventional 2D digital mammography.

Methods and Materials: A CAD-enhanced synthetic 2D mammogram, a standard synthetic 2D mammogram and 2D digital mammogram were available in 68 breast screening recall cases. Two radiologists, blinded to image type and final assessment outcome, retrospectively read a single-side oblique and cranio-caudal projection for each of the three conditions. The resulting 204 pairs of 2D images were presented in random order and scored on a 1-5 scale (1: normal to 5: malignant) without access to the DBT slices. ROC analysis was performed with area under the curve (AUC) compared using Hanley's two-tailed test.

Results: There were 34 biopsy-proven malignancies and 34 normal/benign cases. Diagnostic accuracy was significantly improved for the CAD enhanced synthetic mammogram compared to the standard synthetic mammogram (AUC=0.846 and AUC=0.683, respectively, $p=0.004$) and compared to the conventional 2D digital mammogram (AUC=0.724, $p=0.027$). For all 68 cases, there was an average of 3.2 areas enhanced per image. For the 34 cancer cases, 97.4% of lesions were correctly enhanced, with 2.1 false areas enhanced per image.

Conclusion: CAD enhancement significantly improves performance of synthetic 2D mammograms and also exhibits improved diagnostic accuracy compared to conventional 2D digital mammography.

14:00 - 15:30

Room K

Radiographers

SS 1914

Professional issues in radiography

Moderators:

S.O. Schönberg; Mannheim/DE
N.H. Woznitza; London/UK

B-1637 14:00

The impact of shift work on life, psychological and physical health of radiographers: a comparison between fixed and rotating shifts

A.F.V. Cardoso¹, A.F. Abrantes¹, L.P. Ribeiro¹, S. Rodrigues¹, R.P. Almeida^{1,1}, C.A. da Silva²; ¹Faro/PT, ²Evora/PT (ana.fv.cardoso@hotmail.com)

Purpose: Shift work is necessary to ensure continuity of care in healthcare facilities where radiographers play an increasingly key role in patient care and patient safety. The aim of this study was to analyse the influence of rotating shift work on social and domestic life and on the health of radiographers as compared to the fixed shift.

Methods and Materials: This cross-sectional and correlational study was conducted in several public and private imaging departments using a combination of four instruments (Sleep Questionnaire, General Health Questionnaire, Physical Health Questionnaire and Scale of Social and Domestic life) consisting of 183 questions. A total sample of 102 radiographers was included and the questionnaires were interpreted and statistically analysed through descriptive statistics and correlation tests.

Results: Using *Mann-Whitney* test it was observed statistically significant differences between fixed and rotating shifts regarding the psychological disorders, social and domestic life ($p<0.05$). The rotating shifts have a moderate influence on psychological disturbances ($X=26.6$; $p=0.016$) as well on the social and domestic life ($X=9.5$; $p=0.005$). Moderate sleep disturbances were found for both groups and no statistically significant differences were found regarding the sleep disturbances, gastrointestinal and cardiovascular disorders.

Conclusion: Rotating shifts have consequences on the psychological health and social and domestic life of the radiographer. It is important to regulate and implement strategies to minimise biological, physical and social impact in the radiographer life to allow that these professionals keep working without significant health impairment.

B-1638 14:08

Patient perceptions of radiographer communication skills in general radiology

L. Soares¹, L.P. Ribeiro¹, A.F. Abrantes¹, A.M. Ribeiro¹, K.B. Azevedo¹, R.P. Almeida¹, O. Lesyuk², C.A. da Silva^{3,1}; ¹Faro/PT, ²São Brás de Alportel/PT, ³Evora/PT (oksanalesyuk@gmail.com)

Purpose: The improvement of results in healthcare through the transmission of information to the patient within a relation of empathy and trust is already a verified hypothesis. Healthcare professionals should base themselves on interpersonal competences throughout their daily work routine, to promote quality in medical imaging, patient safety and technical excellence. The aim of this study was the exploration of patient's perceptions regarding the performance of radiographer in terms of interpersonal communication skills during general radiology procedures.

Methods and Materials: The instrument used was the questionnaire "communication Assessment Tool" (Makoul et al. 2007) adapted to the professional reality of the radiographers. A total of 225 valid questionnaires (including 14 questions with a five-point Likert scale) from patients aged between 24 to 85 years old. The paper-based instrument was delivered and filled by the patients after the performance of general radiology procedures in two public hospitals

Results: The internal consistency of the questionnaire was excellent (Cronbach's alpha = 0.98). Highest ratings were for radiographer behaviour items, such as "greet the patients" (3.88), "respect for the patients" (4.04) and "time available to patient-centred care" (3.80). Lowest ratings were "encouraged to make questions," (3.65), "involved patients in decision-making process" (3.34) and "talk with patients about the next following steps" (3.49).

Conclusion: Radiographers communication skills were evaluated with good levels of patient confidence with the radiological examinations. Despite the overall positive results, this area of health service delivery must be accorded the attention it deserves to continually improve on patient satisfaction through improved communication.

B-1639 14:16

An account of silences in diagnostic radiography: a cultural quilt stitched together with the threads of social defences

T.J. O'Regan^{1,2}, L. Robinsion², A. Newton-Hughes², R. Strudwick³; ¹London/UK, ²Salford/UK, ³Ipswich/UK (Tracyo@sor.org)

Purpose: Multi-professional disciplines contribute typologies of silence that theorize approximately 50-70 different forms, functions and motives for silence. This study provides an account of cultures of silence that present at three UK clinical imaging departments.

Methods and Materials: A qualitative methodology of visual ethnography produced an account of silence in radiography practice. Main methods of creative collage workshops and twelve interviews were supplemented with observations of twenty five staff working in accident and emergency and general practice radiography.

Results: Thematic analysis demonstrates five overarching themes grounded in the data. Silence in radiography clinical practice is related to 1) Emotional labour and social defences; 2) Workload; 3) Avoidance of conflict; 4) Legal and ethical dilemma and dichotomy; 5) Hierarchy. Silence strategies were used to facilitate the smooth every day running of the imaging departments. Silence functioned to reflect and enact empathy towards patients and colleagues, it facilitated staff and patient well being and was also a strategy used to keep waiting times to the minimum. Silence reduced threats of litigation, promoted harmonious teamwork, decreased emotional anxiety and diminished the demands of emotional labour.

Conclusion: The study results in knowledge of silence and silencing strategies used in radiography. In particular data in the form of images and words raise awareness of the emotional labour and social defences employed within radiography. The conclusion is that silence is both help and hindrance to services in a clinical setting. The results should be used to inform health service development and change in cultures of practice.

B-1640 14:24

Job satisfaction of radiographers

S. Souto¹, A.F. Abrantes¹, C.A. da Silva², L.P.V. Ribeiro¹, R.P. Almeida¹, K.B. Azevedo¹; ¹Faro/PT, ²Evora/PT (lpribeiro@ualg.pt)

Purpose: The main objective of this study was to determine the relationship between job characteristics and job satisfaction among radiographers to determine which of the dimensions of the job characteristics model contribute most to job satisfaction among radiographers.

Methods and Materials: A self-applied questionnaire was used based in the basic task dimensions tool developed primarily by Hackman e Oldham. This paper-based survey was made available to the radiographers (n=63) working in two local public hospitals to assess the work content (variety of skills (VS), identity (I), Task Meaning (TM), Autonomy (A), Intrinsic feedback (IF), extrinsic feedback (EF), interrelationship (IR)) and the work context (satisfaction with the social environment (SE), satisfaction with supervision (SS), satisfaction with the possibilities of growth (SPG), satisfaction with the physical environment (SPE), satisfaction with payment and compensation (SPC), Satisfaction with Work Organization (SWO) and Satisfaction with Safety at Work (SSW)).

Results: The internal consistency of the questionnaire was good (Cronbach's alpha = 0.88). The lowest satisfaction scores were identified in IR (61.9%), EF (59%), SSW (71%), SPC (31.7%), SS (74.6%) and (77.8%). All the other dimensions scored higher than 80%.

Conclusion: In general, it is possible to say that radiographers are professionally satisfied. However, it is of major importance to show to the managers that human resources policies and management related problems still need major attention and improvement. In order to further strengthen and validate the findings of the study, interviews can be carried out in addition to the distribution of questionnaires.

B-1641 14:32

Evaluation of burnout syndrome in radiographers

V.R. Luiz, L.P.V. Ribeiro, A.F. Abrantes, K.B. Azevedo, R.P. Almeida, S. Rodrigues, N.F. Pinto; *Faro/PT (lpribeiro@ualg.pt)*

Purpose: Evidence demonstrates that health care professionals are more prone to burnout than other professionals due to the emotionally taxing interactions they have with their patients on a daily basis. The aim of this study was to measure occupational burnout levels among radiographers.

Methods and Materials: This research used a sample characterisation survey in addition to the *Maslach Burnout Inventory* (MBI), translated and validated to the professional's native language. The evaluated dimensions were emotional exhaustion (EE), depersonalisation (D) and reduced personal accomplishment (RPA). The MBI survey is composed by 22 questions where the professional should mark the answer in a 0 (never) to 6 (daily) Likert scale. A total of 119 radiographers from 9 different healthcare facilities agreed to participate.

Results: In this study, 99.2% of radiographers worked in a facility with emergency department. The EE, D and RPA dimensions revealed moderate levels of burnout. Statistically significant differences were found between dimension D and the hospital and between dimension RPA and the work in rotational shifts ($p < 0.05$). The variable job satisfaction interferes significantly with the three dimensions of the MBI.

Conclusion: This research allow us to conclude that the burnout may reach disturbing levels, since professionals often do not recognise this phenomenon and do not seek for help, thus becoming a chronic problem. Therefore, it is vital to develop further research in this area to strengthen the demonstration that healthcare may be endangered by health professionals in burnout.

B-1642 14:40

A survey on the attitude towards research among radiographers

I. Conceição, A.F. Abrantes, L.P. Ribeiro, S.I. Rodrigues, R.P. Almeida; *Faro/PT (inesconceicao.ic@gmail.com)*

Purpose: Research is a key component of evidence-based medical imaging and good knowledge and attitude towards research is important in implementing the paradigm shift from traditional model of practice to evidence-based practice. Therefore, the aim of this study was to assess the radiographers attitudes towards scientific research.

Methods and Materials: A cross-sectional, non-experimental research design was adopted, using a self-applied questionnaire and assigned to 115 radiographers from public and private imaging departments in order to verify important barriers and attitudes regarding research in clinical practice. The questionnaire includes 5 main sections with a total of 43 items. Data were interpreted and statistically analysed through descriptive statistics. Chi-square, Spearman and Mann-Whitney tests were also performed.

Results: Currently, most radiographers (78.3%) are not involved in research activities, but 80% presented interest in this field. It were observed statistically significant correlations between the radiographer involvement in research activities and the academic degree ($p = 0.027$) as well with the participation in research training programs ($p = 0.046$). Also, it were observed statistically significant differences between the radiographers involved and not involved in research activities, namely in the items: "Radiographer role includes the promotion of research activities" ($p = 0.019$), "Radiographer uses the research findings in clinical practice" ($p = 0.016$), "The need for research training programs" ($p = 0.001$) and all the items related to research competences ($p < 0.05$).

Conclusion: The data suggest positive attitudes among radiographers. However, some barriers to participation were identified and institutional support and provision of research related courses are needed to increase radiographers involvement in research activities.

B-1643 14:48

A comparative study about motivations, expectations and professional development in four European radiography programmes

C.S. Reis¹, J. Pires Jorge², S. Mæhle³, H. York⁴, L. Flaction², S. Johansen³; ¹*Perth/AU*, ²*Lausanne/CH*, ³*Oslo/NO*, ⁴*Herts/UK (Jose.JORGE@hesav.ch)*

Purpose: To compare motivations, expectations and work plans of recent graduated students and teaching-staff from different European radiography programmes.

Methods and Materials: A survey was performed to collect data about motivations, expectations, challenges, potentials of radiography education and plans for further professional development addressing students and teaching-staff. The questions were closed ended and answers were dichotomous, multiple choice, five- or nine-point Likert Scale. To explore further perspectives, open questions were introduced into the questionnaires. Content analysis was performed to analyse the data.

Results: Response rate varied between 16% to 93%. The motivations referred by students to pursue radiography education were the opportunity to work in a health-care organisation helping those that need help, performing different tasks and combining different areas of knowledge such as physics, patient

care, physiology and anatomy. 75% of students did not reach all of their own expectations for radiography, mainly due to the content and poor specialisation. An enlargement of radiographers' role was expected for the future by the teaching-staff. As further professional developments, the participants identified also the extension of studies (postgraduations, masters), more research and international collaborations.

Conclusion: In general, the participants have similar motivations, expectations and plans for the future even having different curricula. There is a need for improvements in education due to the permanent technological developments, changes and demands observed in the workplace/job markets. Further studies need to be performed to identify an approach that considers, at the same time, the specificities of each country and proving strategies to harmonise radiography in Europe.

B-1644 14:56

Where is the radiography profession heading? Plausible scenarios for the profession in Sweden in 2025

B. Bjorkman¹, K. Fridell², P. Tavakol Olofsson³; ¹*Jönköping/SE*, ²*Huddinge/SE*, ³*Stockholm/SE (berit.bjorkman@ju.se)*

Purpose: The aim of the study was to analyse and describe plausible scenarios for the radiography profession in 2025.

Methods and Materials: The study has a qualitative design with an inductive approach. Data collection is based on eleven focus group interviews, with 48 registered radiographers, working in eleven different diagnostic radiology departments throughout Sweden. The study builds on the scenario-planning method, which has the potential to predict four plausible scenarios for the radiography profession in the future.

Results: Two trends were considered as the most uncertain scenarios for the future, hence having the greatest impact on the radiography profession if they should occur. These trends were labelled: "Access to career advancement" and "A sufficient number of radiographers". Following four plausible scenarios unfolded: "The happy radiographer", "The specialist radiographer", "The dying profession" and "The assembly line".

Conclusion: The direction of the radiography profession within the Swedish context can probably be changed in a positive way. Hence, future opportunities and threats should be identified and incorporated into the strategic planning. Following, appropriate actions should be taken. It is suggested, that "The dying profession" scenario could be turned in the opposite direction by facilitating career development opportunities for radiographers. This direction would probably lead to a profession composed of "happy radiographers", who are specialists and competent to carry out advanced tasks. Heading towards this scenario, may as well lead to a more visible profession and consequently, radiographers being proud of their profession.

B-1645 15:04

Radiographers and non-accidental injury in children

A.F. Abrantes¹, D.M. Sobral², L.P.V. Ribeiro¹, K.B. Azevedo¹, R.P. Almeida¹, O. Lesyuk¹; ¹*Faro/PT*, ²*Cercal do Alentejo/PT (lpribeiro@ualg.pt)*

Purpose: The purpose of this research was to evaluate the capabilities and competences of radiographers with regard to situations of non-accidental injury in children.

Methods and Materials: On the medical environment, particularly in two public radiology departments from two hospitals, a self-applied questionnaire was applied to a total of 42 radiographers in order to study their capabilities and competences within the non-accidental injury in children.

Results: The internal reliability of the questionnaire was good (Cronbach's alpha = 0.84). Most of the radiographers (78.6%) referred to have had formal formation in paediatrics, during the academic training. The remaining have had post-graduated formation. Despite this fact, there was no statistical significance correlation ($p > 0.05$). 42.5% of the radiographers declared to have an acceptable level of competence to recognise the radiological signs of non-accidental trauma in children, although 47.6% referred to not know exactly the national guidelines on this matter. Most of the radiographers said to have excellent capacity to do these examinations, but most of them do not feel comfortable to give testimony in the court.

Conclusion: This research allowed to conclude that during the procedure of imaging examinations in cases of non-accidental injury in children, radiographers attribute a more significant valuation to clinical practice and direct contact with this type of situation, compared to specific training, as a means of attain the skills to engage in this area. Further education and training for radiographers dealing with children and non-accidental trauma is recommended.

B-1646 15:12

Evaluating the use of detector dose indicators in digital x-ray imaging systems

S. Lewis¹, T. Pieterse², L.A. Rainford³, H. Lawrence¹; ¹Johannesburg/ZA, ²Doornfontein, Johannesburg/ZA, ³Dublin/IE (shantell@uj.ac.za)

Purpose: Detector dose indicators (DDI) are the only indicator of correct exposure technique in digital x-ray imaging systems but the use of such indicators remains largely unexplored in a South African setting. The study investigated radiographers' familiarity and use of DDI and compared the actual DDI obtained in practice to the manufacturer's recommended standards which provided insight into current exposure technique practices in this setting.

Methods and Materials: An explorative and descriptive quantitative study was conducted in two phases at randomly selected radiography clinical training facilities (n=10). Phase one of the study investigated the radiographers' familiarity with and use of DDI (n=105) at selected sites by means of a questionnaire. In phase two of the study, actual DDI values were collected retrospectively from the same sites and compared to the manufacturer's recommended standards (n= 1422).

Results: 54.3% of respondents had a correct understanding of DDI and 55.7% of respondents used the DDI correctly. Of the 1422 retrospectively collected actual DDI values only 50% of DDI evaluated were within the manufacturer's recommended range and 27% of DDI evaluated indicated overexposure.

Conclusion: An observable lack of familiarity and the questionable use of DDI by radiographers coupled with some evidence of overexposure in the clinical setting suggest that improvements could be made to the training radiographers' receive on digital imaging systems. Moreover, retrospective auditing of DDI is advocated as a dose optimisation, radiation protection and quality improvement strategy in clinical departments in a South African setting.

B-1647 15:20

Evaluation of radiation protection knowledge among hospital employees

T.Ø. Holter¹, S. Torp², A. Martinsen¹; ¹Oslo/NO, ²Kongsberg/NO (uxtaho@ous-hf.no)

Purpose: Radiation protection regulations emphasize the importance of knowledge as a preventive factor in radiation safety. Employees occupationally exposed to ionizing radiation in hospitals are required to possess adequate competence regarding radiation protection and possible health hazards from radiation exposure. Besides, knowledge may prevent unnecessary concern. In this study, the reliability of self-assessment was compared to quantitative tests to evaluate the different methods for measuring the level of employees' knowledge on radiation protection.

Methods and Materials: A quantitative cross-sectional survey was performed to evaluate self-reported competence compared to quantitative test results. The results from the survey were tested for correlations using Cohen's Kappa. All staff members in the hospital carrying dosimeters were invited to participate. 528 respondents (52% of the invited respondents) answered the electronic questionnaire.

Results: Findings from this study demonstrate that there were discrepancies between the respondents tested and self-reported radiation protection knowledge (kappa = 0.27). Personnel with a high tested score tended to underestimate their knowledge, while personnel with a lower level of tested knowledge, tended to overrate themselves.

Conclusion: To evaluate the level of radiation protection knowledge among hospital workers, it is not sufficient to map their personal perception, as a large proportion of the informants either overrate or underestimate their level of knowledge. Supplementary analyses are needed to give an accurate impression of the level of competence, and should be implemented in further competence-raising efforts.

14:00 - 15:30

Room M 1

Cardiac

SS 1903

Cardiac imaging: from diagnosis to prognosis

Moderators:

F. Cademartiri; Rotterdam/NL

B. Dubourg; Rouen/FR

B-1648 14:00

Performance of native T1 and T2 mapping cardiovascular magnetic resonance to detect myocardial oedema in patients with dilated cardiomyopathy

W. Peng, Z.-L. Li, C. Xia; Chengdu/CN (yimaerlin@163.com)

Purpose: To evaluate the performance of native T1 and T2 mapping techniques to identify myocardial oedema in patients with dilated cardiomyopathy (DCM).

Methods and Materials: Twenty DCM patients and 10 healthy volunteers were enrolled in and underwent CMR examination. Modified Look-Locker Inversion recovery T1 maps and Balanced Steady-State Free Precession (bSSFP) T2 maps were acquired on matching short axis of basal, middle and apex segments. The native T1 values of T1 maps and T2 values of T2maps were measured and compared. Receiver operating characteristic analysis was performed to determine whether T2 values could be used in discriminating myocardial oedema between DCM patients and normal subjects.

Results: In DCM patients, T2 values were significantly increased in comparison with normal controls (45.61 ± 4.30 vs. 39.57 ± 5.01, p < 0.05). T1 values of DCM subjects were increased (1095.21 ± 266.73 vs. 991.99 ± 229.90), but no statistical significance (P=0.458). For the segmental heterogeneity, T2 values of basal, middle and apical segments in DCM patients were higher comparing with normal ones (all P<0.05). A cutoff value for global myocardial T2 of ≥ 42.91 ms provided a sensitivity, specificity, accuracy, negative and positive predictive value of 71% (42%-92%), 80% (30%-95%), 81.4% (57%-95%), 91% (59%-100%), and 50% (16%-84%) for DCM, respectively.

Conclusion: T2 mapping seems to be superior when compared with native myocardial T1 values for assessing myocardial oedema in patients with DCM. The threshold values of global T2 values may be used as indicators for differentiating myocardial oedema between DCM patients and normal subjects.

B-1649 14:08

The multidisciplinary "endocarditis team": results on imaging utilisation and diagnostic and therapeutic changes in the first 100 patients

L.E. Swart, M.M. Henneman, T.W. Galema, J.A. Bekkers, R. Valkema,

C.A.M. Schurink, N.J. Verkaik, J.W. Roos-Hesselink, R.P.J. Budde;

Rotterdam/NL (r.budde@erasmusmc.nl)

Purpose: The most recent European Society of Cardiology guidelines on endocarditis strongly advise to set-up a multidisciplinary "endocarditis team" including imaging specialists to guide diagnostic and therapeutic decisions. These guidelines now also include Cardiac CTA and PET-CT as major diagnostic criteria next to blood cultures and echocardiography. We present the first 100 patients discussed in our "endocarditis team".

Methods and Materials: Starting January 1st 2016, patients with suspected endocarditis were discussed in our "endocarditis team". At least one radiologist, nuclear medicine physician, cardiologist, cardiac surgeon and infectious diseases specialist/medical microbiologist were present every meeting. Data of patients were retrieved from the structured reports of these meetings and electronic patient files, including imaging technique utilization as well as diagnostic and therapeutic changes.

Results: One hundred patients (66 males; age 64±19y) with (suspicion of) native (n=43) or prosthetic (n=48) heart valve endocarditis or cardiac implantable device infection (n=9) were discussed (total amount of discussions: 143). At the time of initial discussion, the following diagnostics had been performed: TTE (n=82), TEE (n=76), cardiac CT (n=22), PET-CT (n=35) and MRI (n=10). Additional imaging was advised in 19 patients (19%) (16 cardiac CT, 7 PET-CT). During the "endocarditis-team" meetings, diagnosis changed in 13 patients (13%), and therapy in 53 (53%); surgical intervention recommended in 34, change in antimicrobial therapy recommended in 42).

Conclusion: A multidisciplinary "endocarditis team"-approach to patients with (suspected) endocarditis results in increased utilization of additional imaging techniques and a change in both diagnosis and treatment in a substantial numbers of patients.

B-1650 14:16

Six months follow-up after triple rule-out using second-generation dual-source CT in patients with acute chest pain

M. Fusaro¹, G. Balestrieri¹, A. Dorigo², G. Battistella¹, C. Bortolanza¹, G. Tessarin¹, L. Doni¹, A. De Leo¹, G. Morana¹; ¹Treviso/IT, ²Santa Maria di Sala/IT (fusaro341@gmail.com)

Purpose: To determine the prognostic value at six months of a low-dose protocol triple-rule-out CT using second-generation dual-source CT vs standard evaluation in acute chest pain.

Methods and Materials: A blinded prospective observational cohort study was conducted. We enrolled patients with acute chest pain, negative ECG, negative troponin test and low-intermediate cardiovascular risk, arriving at ED from March 7, 2016 to December 31, 2016. CT was performed in all patients with a standardized low-dose prospective ECG-trigger triple rule-out. Patients were classified with CAD >50%, <50% or without: all patients were treated by a standard protocol of our hospital without knowledge of the CT results. A follow-up phone call was conducted after 6 months to determine the occurrence of MACE (death, ACS, and coronary revascularization). Total DLP and contrast-enhanced phase DLP were assessed. The analysis of the data was performed with SPSSv13 and WinPEPI v11.5.

Results: 125 consecutive patients (53.2 yo ± 9.7), 83 (66.4%) males, were enrolled: 76 (60.8%) were free of CAD, 40 (32%) had <50% CAD and 9 (7.2%) had a >50% CAD. No pulmonary embolism or aortic dissection was observed. At 6 months, no MACE was observed. 4 patients were not traceable during follow-up. The total and the single contrast-enhanced phase DLP were, respectively, 250.7±90.8 and 195.2 ±82.5.

Conclusion: The triple-rule-out protocol with second-generation dual-source CT in properly stratified acute chest pain patients allows safe discharge and may be an ideal diagnostic tool in all hospitals with the necessary technology and experience.

B-1651 14:24

The prognostic value of late gadolinium enhancement in non-ischaeamic dilated cardiomyopathy

P.M. Cannao¹, F. Secchi, M. Scarabello, M. Ali, F. Sardaneli; Milan/IT (paola.m.cannao@gmail.com)

Purpose: To evaluate the prognostic value of late gadolinium enhancement (LGE) amount for the stratification risk in patients with non-ischaeamic dilated cardiomyopathy (DCM).

Methods and Materials: We retrospectively evaluated 58 DCM patients who underwent 1.5-T CMR at our Institution from July 2008 to April 2016. Of these, only 30 patients followed up for at least 10 months (median follow-up was 46 months). For each patient, segmentation and volume analysis were performed. LGE images were processed, after a semi-automated endocardial and epicardial segmentation of the slices, choosing 6 standard deviation threshold. Spearman's correlation was used to correlate the EDVi, ESVi, EF and SV of both ventricles with the amount of LGE. The ROC analysis was performed between the amount of LGE and the ICD implantation.

Results: There was a positively significant correlation between LV EDVi and LGE (r=0.550, P<.001), LV ESVi and LGE (r =0.590, P<.001) and LGE and LV SV (r=0.379, P=.004), while there was a negatively significant correlation between LVEF and LGE (r =-0.479, P=.002). In 10 patients implanted ICD or PM, a receiver-operator characteristic (ROC) curve analysis revealed a cutoff value of 20.4 g for the LGE amount and this cutoff was determined to have 80% sensitivity and 100% specificity.

Conclusion: An association between myocardial LGE and ICD implantation may be possible to identify high-risk patients. The cutoff found of 20.4 g could be an innovative method to guide the selection of patients eligible for device therapy with a sensitivity 80% and specificity 100%.

B-1652 14:32

The feasibility of dual-energy-computed tomography in cardiac contusion imaging for mildest blunt cardiac injury

M. Kantarci, A. Levent, S. Eren; Erzurum/TR (akkanrad@hotmail.com)

Purpose: The purpose of this study was to evaluate the efficiency and feasibility of DECT used in the diagnosis of cardiac contusion with the mildest blunt cardiac injury (BCI).

Methods and Materials: This study was performed between February 2014 and September 2015, a total of 17 consecutive patients (10 men and 7 women; median age 51 years [range: 20-78]) were enrolled in the study. DECT was performed within 48 hours of the trauma and a subsequent follow-up DECT was performed a little less than one year after the first examination. All examinations were analysed on iodine map images by two experienced radiologists. Interobserver and intraobserver agreement was calculated. The correlation of initial troponin level, age and gender with number of contusion areas in the left ventricle and complete recovery of contusion were measured.

Results: The contusion areas were amorphous, with considerable variation in their size, shape, and density. Contusions were primarily located in the left free

wall of ventricle, the ventricular septum, and the apex, respectively. In 10 patients, contusion areas disappeared upon follow-up examination. In four patients, the contusion areas decreased but were still present in the follow-up examination. The interobserver agreements were almost perfect with respect to the presence of cardiac contusion, the anatomic location of contusions, and the contusion areas.

Conclusion: DECT can show cardiac contusion and could be useful and feasible for the diagnosis and follow-up of BCIs. DECT is a new, user-independent and valuable imaging technique.

B-1653 14:40

Morbus Fabry: new insights from CMR strain imaging

M.C. Halfmann, S. Benz, J. Eichstädt, A. Lollert, C. Düber, K.-F. Kreitner, T. Emrich; Mainz/DE (Moritz.Halfmann@gmx.de)

Purpose: Although Morbus Fabry is widely acknowledged as a systemic disease, the focus of research concerning myocardial involvement has been focused on the left ventricle. Through the measurement of strains, we want to encourage the close examination of right ventricle (RV) as well.

Methods and Materials: In our study, 62 healthy volunteers and 10 patients with a diagnosis of Morbus Fabry and proven cardiac involvement underwent cardiac magnetic resonance (CMR) imaging at 3T. Using a semi-automatic tissue tracking software (CVI Circle®), we measured global strains for both ventricles from multiple axes.

Results: The left ventricular strain parameters (radial, circumferential and longitudinal strains) showed statistically significant differences between Morbus Fabry patients and healthy volunteers (p = .027 and .003). There were also significant differences concerning right ventricular strains (p = .012) with mean of RV global radial strains for Fabry patients of 19.13% (±6.35) and healthy volunteers of 13.47% (±6.46).

Conclusion: Despite the still limited patient number, we found significant evidence for right ventricular involvement of Fabry's disease. This should be the motivation to take a closer look and expand research also on the right ventricle in Fabry patients.

B-1654 14:48

Late gadolinium enhancement patterns in patients with hypereosinophilia: can CMR help identifying the aetiology?

D. Morgan¹, J. Pagniez¹, G. Lefevre¹, L. Averlant¹, J.-E. Kahn², B. Longere¹, V. Silvestri¹, F. Pontana¹; ¹Lille/FR, ²Suresnes/FR (dubois.morgan.59@gmail.com)

Purpose: The aim of this study was to assess the prevalence and patterns of cardiac abnormalities detected by cardiac magnetic resonance (CMR) in patients with hypereosinophilia according to the underlying disease.

Methods and Materials: Thirty consecutive patients without history of coronary artery disease (15 males; mean age = 47.7 ± 21) referred for hypereosinophilia were prospectively included. Hypereosinophilia was related to: idiopathic hypereosinophilic syndrome (HES) n=13; eosinophilic granulomatosis with polyangiitis (EGPA) n=6; parasitic infection n=3; hemopathy n=4; and allergy n=4. Cine functional parameters, T1 and T2 values on parametric mapping and late gadolinium enhancement (LGE) were independently assessed by two readers.

Results: Left ventricle (LV) and right ventricle (RV) ejection fractions were impaired in 19 patients (63%) and 7 patients (23%) respectively. LV and RV dilatation was observed in 7 patients (23%) and 2 patients (7%) respectively. Increased myocardial T1 and T2 values were found respectively in 10/21 patients (48%) and 4/21 patients (19%). LGE was detected in 13 patients (43%). Among them, 5 patients presented a myocarditis enhancement pattern (HES n=2, EGPA n=2, parasitic infection n=1), 5 patients presented a vasculitis enhancement pattern (EGPA n=3, parasitic infection n=1, hemopathy n=1) and 3 patients presented an endomyocardial fibrosis pattern (HES n=2, EGPA n=1); p = 0.59.

Conclusion: LGE was observed in almost half of the patients with hypereosinophilia with three different patterns (myocarditis, vasculitis and endomyocardial fibrosis) independently of the etiological diagnosis, suggesting a non-specific myocardial toxicity of the eosinophils.

B-1655 14:56

The effect of myocardial bridge on the presence and extent of coronary artery disease: case-control study

S. Papp, J. Karady, M. Kolossvary, Z. Drobni, B. Szilveszter, G. Barczy, B. Merkely, P. Maurovich-Horvat; Budapest/HU (papp.sara94@gmail.com)

Purpose: Previous studies have suggested that the presence of myocardial bridge (MB) increases the risk of atherosclerosis proximal to the MB. Our aim was to assess the effect of MB on the quantity and composition of plaques proximal to MBs.

Methods and Materials: Patients who underwent coronary CT-angiography due to suspected coronary artery disease were enrolled into this retrospective case-control study. We selected patients with MB on their left anterior

descending (LAD) coronary artery and a control group matched to age, sex, BMI and cardiovascular risk factors such as smoking, hypertension, diabetes mellitus and dyslipidaemia. Using semiautomated plaque quantification software we segmented the LAD segment proximal to the bridge in the cases and an identical length segment of the LAD in each control patient. We compared the plaque volume and plaque composition between the case and control groups (Wilcoxon signed-rank test).

Results: In total, we assessed 25 case-control pairs (mean age: 59.0±10.9 versus 59.0±10.9 years, p=0.946; males: 88%). The average length of the analysed segments proximal to MBs were 43.5±9.3mm in the case and 43.3±9.3mm in the control group (p=0.412). The total plaque volume did not differ between the groups (178mm² [IQR:146.9-198.9] versus 154mm² [IQR:124.4-204.9], p=0.638). We found no significant difference in the calcified plaque volume (19mm² [IQR:7.3-37.4] versus 12mm² [IQR:5.1-24.8], p=0.861), and in the non-calcified plaque volume (109mm² [IQR:66.3-131.7] versus 107mm² [IQR:79.0-139.1], p=0.527) between the groups.

Conclusion: Our results suggest that the MB has no effect on plaque volume and composition in coronary segment proximal to the MB.

B-1656 15:04

Atrial dysfunction in arrhythmogenic right ventricular cardiomyopathy: value of quantitative MR analysis in predicting atrial arrhythmias

M. Bourfiss¹, T. Zghaib², R.N.W. Hauer¹, H. Tandri², H. Calkins², S. Nazarian³, A.S.J.M. te Riele¹, B.K. Velthuis¹, S.L. Zimmerman², ¹Utrecht/NL, ²Baltimore, MD/US, ³Philadelphia, PA/US (m.bourfiss-2@umcutrecht.nl)

Purpose: Arrhythmogenic Right Ventricular Cardiomyopathy (ARVC) is an inherited cardiomyopathy that predominantly affects the ventricles. Evidence for direct atrial involvement remains limited and few studies have characterized atrial arrhythmias (AA) in ARVC. We aimed to characterize atrial involvement in ARVC using Cardiac Magnetic Resonance (CMR) and to identify CMR-based predictors of AA in ARVC.

Methods and Materials: We analyzed cine-CMR images of 66 definite ARVC patients without a history of AA or severe heart failure (NYHA≥3) and 24 healthy controls. Using tissue-tracking, we evaluated phasic bi-atrial volumes, ejection fractions (EF), peak longitudinal-strain (PLAS) and strain rates (SR). The primary outcome was the occurrence of AA during 6.8 [3.0-10.8] years of follow-up.

Results: Compared to controls, ARVC patients had higher bi-atrial volumes and lower right atrial (RA) passive-EF, RA-PLAS, systolic and early RA-diastolic SR and systolic left atrial (LA)-SR (p<0.05). Although worsening in ventricular size and function was associated with increased bi-atrial volumes and decreased function, variation in atrial parameters was only partially explained by ventricular changes (r² 5-29%). Using multivariable analysis, predictors of increased risk of AA during follow-up were higher atrial volumes (10% increased risk of AA per mL, p<0.05), decreased LA reservoir function (total LA-EF and LA-PLAS) and decreased RA conduit function (passive RA-EF and RA early diastolic SR).

Conclusion: ARVC is characterized by enlarged atria with decreased function, which is only partially explained by ventricular changes. Bi-atrial parameters predict incident AA after adjusting for clinical and ventricular characteristics, which suggests primary atrial involvement in ARVC.

B-1657 15:12

The role of cardiac magnetic resonance imaging (MRI) in the diagnostic work-up after aborted sudden cardiac death

L. Szabó, C.L. Czibalmos, I. Csécs, A. Tóth, F.I. Suhai, K. Heltai, E. Zima, L. Gellér, D. Becker, B. Merkely, H. Vágó; Budapest/HU (sz.liliana.e@gmail.com)

Purpose: The aim of our study was to assess the added value of cardiac magnetic resonance (CMR) imaging in the diagnostic work-up of aborted SCD in absence of coronary artery disease and to determine commonness to the myocardial abnormalities in this patient population.

Methods and Materials: During a 7.5-year period (between 2010 and 2017) at the Heart and Vascular Center of the Semmelweis University we performed CMR examinations in 78 patients (37.9±13.8 y, 37 male) after aborted SCD with normal coronary angiography. Among them, 10 were athletes (28.4±10.3 y, 8 male). We measured the left and right ventricular parameters and the presence of myocardial scar/necrosis. We assessed whether CMR changed the provisional diagnosis.

Results: In 65% of the cases (n=51) the CMR proved structural myocardial abnormality as follows: dilated (DCM n=12), arrhythmogenic right ventricular (ARVC n=4), hypertrophic (HCM n=4), Tako-tsubo (n=1) and noncompaction cardiomyopathy (n=1); myocarditis (n=4), acute myocardial infarction (n=3), mitral valve prolapse (n=4), endomyocardial fibrosis (n=1) and aspecific structural alterations (n=16). In the last group, myocardial fibrosis with nonischemic pattern could be identified in 7 patients. Age group specific incidence rates show that the most common structural heart disease over 35 years was DCM (n=9), while ARVC occurred more frequently under 35 years in our patient population, and was the most common structural disorder in

athletes (n=3). CMR examination changed the provisional diagnosis in 50% of the patients.

Conclusion: CMR provides an advanced diagnostic yield in the diagnostic work-up of the excessively variable aetiology of SCD.

B-1658 15:20

Cardiac MRI for a better identification of structural heart disease in patients with ventricular arrhythmia

D. Andreini, S. Mushtaq, G. Pontone, A.D. Annoni, A. Formenti, M.E. Mancini, E. Conte, M. Guglielmo, M. Pepi; Milan/IT (daniele.andreini@cclm.it)

Purpose: Aim of this study is to evaluate whether in patients with ventricular arrhythmia and normal echocardiography, cardiac MRI may identify patients with structural heart disease whose risk has been underestimated by transthoracic echocardiography

Methods and Materials: We enrolled a cohort of consecutive patients with VA who underwent to cardiac MRI after a negative echocardiography. For every patient the presence of cardiovascular symptoms were evaluated. Ventricular ectopic beats (VEBs) was graded as follow: >1000 VEBs/24h; >10000 VEBs/24h; non-sustained ventricular tachycardia (NSVT); sustained ventricular tachycardia (SVT) and history of resuscitated cardiac arrest. End-point of the study was the presence of structural heart disease at MRI.

Results: We enrolled 946 patients (age 41±16 years; 609 male 64.4%). Among them, 241 patients (25.5%) were found to have structural heart disease at cardiac MRI. More specifically, 91 (37.7%) patients had a diagnosis of previous myocarditis, 50 (20.7%) of arrhythmogenic right ventricular cardiomyopathy, 39 (16.2%) of dilated cardiomyopathy, 22 (9.1%) of previous myocardial infarction, 11 (4.6 %) of congenital heart disease, 13 (5.4%) of hypertrophic cardiomyopathy, 5 (2.1%) of left-dominant arrhythmogenic cardiomyopathy, 5 (2.1%) pericarditis and 5 (2.1%) of left ventricular non-compaction cardiomyopathy. Among clinical variable at multivariate analysis only previous SVT (OR 2.23 95%CI 1.26-3.9) and reported chest pain (OR 2.38 95%CI 1.55-3.64) are associated with MRI positive for structural heart disease.

Conclusion: Among patient with ventricular arrhythmia and normal transthoracic echocardiogram almost 25% had cardiac MRI positive for structural heart disease. Among clinical variable previous chest pain and SVT were associated to positive cardiac MRI.

14:00 - 15:30

Room M 4

Genitourinary

SS 1907b

Genital and obstetric imaging

Moderators:

B. Ahuja; Agra/IN
F. Giganti; London/UK

B-1659 14:00

"Avascular" hypoechoic testicular lesions on colour Doppler ultrasound: can they be considered benign? what is the added value of contrast-enhanced ultrasound?

D. Huang, M.R. Alsadiq, M. Sellars, R. Eckersley, P. Sidhu; London/UK (m.alsadiq@nhs.net)

Purpose: Although most avascular hypoechoic testicular lesions on colour Doppler US (CDUS) are often considered benign, the diagnosis may be unreliable due to inherent limitation of CDUS. The purpose of this study is to determine the added value of contrast-enhanced US (CEUS) to conventional CDUS in assessing hypoechoic testicular pathology in differentiating benign from malignant aetiology detected at scrotal US.

Methods and Materials: This retrospective study included 102 avascular hypoechoic testicular lesions detected at colour Doppler testicular ultrasound. The sonographic features recorded include lesion size and presence of vascularity on CEUS and CDUS. The reference standard was pathologic results or at least 6 months stability documented with serial follow-up ultrasound studies.

Results: 102 lesions with no vascular signal on CDUS were identified. 18 of these lesions (17.6%) showed enhancement on CEUS despite lack of signal on CDUS. 6 of lesions with CEUS enhancement were malignant (6/18, 33.3%). The remaining lesions (12) include pathology such as sarcoidosis, post biopsy change, intra-testicular adenomatoid tumour, focal scarring with history of previous orchiopexy, and focal atrophy in patient with Klinefelter syndrome. All lesions with no enhancement on CEUS (84) were of benign nature.

Conclusion: Although most avascular hypoechoic testicular lesions on CDUS are benign, a proportion of these lesions are malignant and demonstrate CEUS enhancement. CEUS provides a more definitive characterisation of vascularity

of a focal testicular lesion and would therefore add value to conventional CDUS in differentiating malignant from benign lesions.

Author Disclosures:

D. Huang: Speaker; Bracco. **M. Sellars:** Speaker; Bracco. **P. Sidhu:** Speaker; Bracco.

B-1660 14:08

A comparison of testicular tissue stiffness using shear wave elastography

M.R.V. Pedersen¹, H. Møller², P. Osther¹, P. Vedsted³, R. Holst⁴, S.R. Rafaelsen¹; ¹Vejle/DK, ²London/UK, ³Aarhus/DK, ⁴Oslo/NO (Malene.Foland.Vils.Pedersen@rsyd.dk)

Purpose: To compare elastography measurements in different testis tissues.

Methods and Materials: A total of 248 consecutive patients were included during the period between 2013 and 2016 from our department of radiology. All patients were outpatients referred by their general practitioner to a clinical US scrotal examination due to symptoms such as pain, discomfort, lump or testicular mass. Exclusion criteria were patients with torsion, inflammation, previously diagnosed with testicular cancer or any linguistic difficulties to understand the informed consent. All men provided written informed consent. Testicular stiffness was assessed using shear wave elastography (SWE). Three SWE velocity measurements were assessed in each testicle. All patients underwent B-mode US investigation followed by SWE. The patients were divided into three groups: men with normal testicular tissue, men with testicular microlithiasis and men with testicular cancer.

Results: We found a higher mean velocity in the group of patients with testicular cancer (1.92 m/s (95% CI 1.82-2.03)) compared to both the group with normal tissue (0.76 m/s (95% CI: 0.75-0.78)) (p<0.001) and the group with testicular microlithiasis 0.79 m/s (95% CI: 0.77-0.81) (p<0.001).

Conclusion: The presence of testicular microlithiasis increased stiffness slightly, but within the range of variation in normal testicles. Increased stiffness may indicate testicular malignancy in testicular lesions. Ultrasound elastography may be a very useful tool when investigating scrotum.

B-1661 14:16

Diffusion-weighted imaging combined with ADC in the diagnosis of testicular lesions

M. Huang; Zhengzhou/CN (huangmengna1127@163.com)

Purpose: The purpose of this study is to identify the diagnostic value of ADC combined with DWI in benign lesions and malignant lesions of testis.

Methods and Materials: 35 patients with testicular lesions confirmed by operation and pathological examination in our hospital were retrospectively analysed, including 18 benign lesions and 17 malignant lesions. The mean ADC values of normal tissue and parenchyma of testicular lesions were measured and statistically analysed by Kruskal-Wallis test and receiver operating characteristic (ROC) curve was delineated. The optimum ADC value for differential diagnosis of malignant testicular lesions was analysed and determined.

Results: In 33 cases of normal testicular tissue, DWI showed homogeneous high signal, mean ADC was $(1.137 \pm 0.119) \times 10^{-3} \text{ mm}^2/\text{s}$. 18 cases of benign lesions mostly showed unrestricted diffusion, mean ADC was $(1.104 \pm 0.463) \times 10^{-3} \text{ mm}^2/\text{s}$. In 17 cases of malignant lesions, DWI showed high signal, mean ADC was $(0.778 \pm 0.198) \times 10^{-3} \text{ mm}^2/\text{s}$. The comparison of ADC mean values between malignant testicular lesions and normal tissue as well as benign lesions of testis showed significant difference (P<0.05). The optimum ADC to distinguish malignant testicular lesions from benign testicular lesions was $0.911 \times 10^{-3} \text{ mm}^2/\text{s}$ (82.4% sensitivity and 82.4% specificity).

Conclusion: DWI combined with ADC value is beneficial to the preoperative diagnosis and differential diagnosis between malignant testicular lesions and benign lesions of testis.

B-1662 14:24

Diffusion tensor imaging parameters in the identification of spermatogenesis in men with non-obstructive azoospermia

A. Tsili¹, A. Ntorkou^{1,2}, L.G. Astrakas¹, A. Goussia¹, E. Panopoulou¹, N. Sofikitis¹, M. Argyropoulou¹; ¹Ioannina/GR, ²Paris/FR (atsili@cc.uoi.gr)

Purpose: To assess possible differences of testicular apparent diffusion coefficient (ADC) and fractional anisotropy (FA) values in different histological states of spermatogenesis in men with non-obstructive azoospermia (NOA).

Methods and Materials: Twenty infertile men with NOA and 21 age-matched controls were retrospectively evaluated. All subjects underwent 1.5 T MRI of the scrotum, including diffusion tensor imaging (DTI). ADC and FA in NOA and normal testes were measured. NOA testes were classified as NOA with highest Johnsen score (JS) ≥ 8 (group 1) and JS <8 (group 2), based on the presence of tubules with spermatozoa at histologic analysis. The same classification was used for mean JS (mJS). Parametric and non-parametric statistical tests were used to compare ADC and FA between NOA groups and normal testes (group 3).

Results: Statistical analysis showed differences in ADC and FA between groups 1 and 3 (P=0.047 and P<0.001, respectively) and between groups 2 and 3 (P=0.003 and P<0.001), but not between groups 1 and 2 (P=0.241 and P=0.976), when using the highest JS. When classification was based on mJS, ADC (P=0.014) and not FA (P=0.849) enabled the discrimination between groups 1 and 2.

Conclusion: Our preliminary data show promising results in the identification of spermatogenesis in NOA testes using DTI parameters. Both ADC and FA are increased in NOA testes compared to controls. However, ADC and not FA proved useful in differentiating NOA testes, based on histology.

B-1663 14:32

High-resolution MR imaging with small surface coil in diagnosis of slight penile lesions after penile injury

J. Guan, Y. Peng, H. Wang, Y. Guo; Guangzhou/CN (py9165@163.com)

Purpose: To investigate the diagnostic value for micro-penile lesions after penile injury using high-resolution MR imaging with small surface coil.

Methods and Materials: There were 13 patients with history of penile injury including intense intercourse or masturbation recently without clinical manifestations of penile fracture. In all patients, the complaints were mild and the sonographic results were negative. MR scan with both small surface coil (loop coil, diameter 11 cm) and body coil was performed in all 13 cases, respectively. MR findings were analysed by two experienced radiologists.

Results: Only 2 cases with suspected lesions were found by MR scan with body coil. 10 cases with slight lesions of penis were detected by MR scan with small surface coil. 8 out of 10 cases with slight albuginea tear presented as focal interruption (about 1-2mm) of the hypointensity tunica albuginea and a small amount overlying effusion. Tiny haematomas with diameter 2-3mm between tunica albuginea and the buck fascia were seen in the remaining 2 cases, presenting as a small nodule with hyperintensity on T2WI, hypo- or iso-intensity on T1WI without enhancement. MR scan with small surface coil detected more tiny lesions of penis than routine scan with body coil (P<0.05), and showed the MR imaging features for diagnosis.

Conclusion: MR scan with small surface coil can provide higher diagnostic sensitivity for slight penile lesions after penile injury, and avoid misdiagnosis.

B-1664 14:40

Neoclititoris size and location: a preliminary pelvic MRI study

E. Serena, F. Vedovo, S. Bucci, C. Trombetta, M. Bertolotto, M.A. Cova; Trieste/IT (elena.serena1986@libero.it)

Purpose: To evaluate whether MR investigation of neoclititoris size and location can help predict sexual function after male-to-female sex reassignment surgery (MtF-SRS).

Methods and Materials: The Female Sexual Function Index (FSFI) was calculated in 40 consecutive transsexual women who had postoperative MRI after MtF-SRS. An investigator blinded to sexual function data measured the distance between the neoclititoris and the neovagina and calculated the coronal and sagittal area of the neoclititoris and the volume from the three axes using the ellipsoid formula.

Results: 22 patients completed the study. The mean age was 34 ± 7.44 years. The majority were Caucasians (n=20, 91%) and in a relationship (n=13, 51%). The volume of the neoclititoris was $1.18 \pm 0.43 \text{ cm}^3$. Coronal and sagittal areas were $6.80 \pm 2.4 \text{ cm}^2$ and $5.33 \pm 1.34 \text{ cm}^2$, respectively. There was an inverse relationship between the distance of the neoclititoris from the neovagina and the FSFI total score (p < 0.0001). Neoclititoris size did not significantly correlate with FSFI total score (p=0.76).

Conclusion: In patients with MtF-SRS MRI allows evaluation of the neoclititoris. Our data suggest that neoclititoris localisation affects sexual function, with reduction of the distance between the neovagina and the neoclititoris associated with greater sexual satisfaction. Conversely, neoclititoris size does not to affect sexual function.

B-1665 14:48

US-guided sclerotisation of the cavernosal stumps following male-to-female sex reassignment surgery

M. Muca, M. Bertolotto, I. Zorzenon, M. Iannelli, C. Sachs, M.A. Cova; Trieste/IT (bertolot@units.it)

Purpose: In early male-to-female sex reassignment surgery (MtF-SRS) operations a variable portion of the cavernosal crura was preserved. This residual erectile tissue undergoes engorgement during sexual arousal, causing dyspareunia and limiting patient's life. Surgical removal is the most commonly used treatment. It consists in a wide dissection of the perineum with significant morbidity and a high risk of complications. Development of mini-invasive techniques is therefore necessary. The aim of this study is to describe US-guided sclerotherapy of the cavernosal stumps as an alternative to surgery, and to illustrate the results obtained in a series of 3 consecutive patients treated with this technique.

Methods and Materials: US-guided sclerotherapy was performed in 3 patients (mean age 29-38 years) with severe dyspareunia after MtF-SRS caused by residual cavernosal stumps. 2.5 micrograms of PGE1 were injected in each stump under US guidance to achieve erection. A 3% sodium tetradecyl sulphate (Fibrovein®) solution diluted 1/5 with saline was injected bilaterally. A variable amount (max.3.5 cc) was injected depending on the volume of the erectile tissue. In 2 patients, the treatment was repeated monthly for 7 and 8 sessions, respectively. The 3rd patient developed an abscess after the 5th session with prompt resolution of clinical symptoms after drainage.

Results: A good aesthetic and functional result was achieved in all patients with disappearance of the erections during sexual arousal and improvement of the sexual quality of life.

Conclusion: In patients with MtF-SRS US guided sclerotisation is a suitable mini-invasive alternative to surgical excision of the cavernosal stumps.

B-1666 14:56

Role of diffusion MR imaging and 3D/4D ultrasound in the assessment of placental insufficiency in gestational hypertension

S.A. Mansour, S.T. Hamed, S. Hosny, S.B. Elsayed; *Cairo/EG (sohathamed@yahoo.com)*

Purpose: To assess the role of diffusion-weighted MRI and 3D/4D ultrasound and power Doppler scanning in the detection of placental insufficiency in high-risk pregnancies with hypertension.

Methods and Materials: This prospective analysis included 50 pregnant females; 40 hypertensive and 10 control with the gestational age range from 20 to 34 weeks. All cases had undergone 3D/4D transabdominal ultrasound aided by power Doppler scanning and diffusion-weighted MR imaging. No contrast administration was used.

Results: There was a significant relation between right uterine artery RI (mean) of both cases and control groups when measured by power Doppler ultrasound ($P=0.014$). There was also a positive correlation between the presence of diastolic notch and RI value (P value= 0.012). There was also a significant difference between patients with normal and those with the abnormal placental signal in diffusion images as P value is significant (0.047). The mean of placental volume by MRI was 500.5 ± 223.12 with median (IQR) 507.08 (311.22-721.85) and by 3D ultrasound was 374.11 ± 251.52 with median (IQR) 329.02 (162.66-596.75). There was a significant difference between the measurement of placental volume by MRI and US among both cases and control groups where P value < 0.001 and 0.017, respectively. There was significant relation between results of both US and diffusion imaging in cases group (P value=0.006 and kappa value=0.318).

Conclusion: Diffusion-weighted imaging can detect early subtle findings of placental dysfunction more than detected with 3D/4D ultrasound, so it can add to the diagnostic accuracy of imaging in pregnancies at high risk of placental insufficiency.

B-1667 15:04

Placenta accreta index: what a radiologist should know about an imaging update in detection of morbidly adherent placenta

A. Agarwal, S. Agarwal, S. Sharma, S. Chandak; *Moradabad/IN (drarjit26@gmail.com)*

Purpose: To study the role of placenta accreta index (PAI) in detection of morbidly adherent placenta and to analyse the inter-observer reliability in its calculation.

Methods and Materials: 42 pregnant females with sonographically confirmed placenta previa in their third trimester and history of ≥ 1 caesarean section were subjected to ultrasonography for calculation of placenta accreta index (PAI). The index was calculated on the basis of placental morphology, retro-placental zone, uterine-bladder interface, myometrial thickness, bridging vessels and previous history of caesarean sections. Each parameter was weighted to produce a 9-point score (PAI) which predicted the probability of adherent placenta. PAI score of <5 was considered unfavourable and ≥ 5 as favourable for accreta. Statistical analysis was done to find the sensitivity, specificity and predictive values of PAI. The PAI was calculated by two radiologists separately, to determine the reproducibility of the technique. Cohen's Kappa and intra-class correlation co-efficient (ICC) were calculated for categorical and scale variables, respectively, to determine the inter-rater agreement in calculation of scores.

Results: Among 42 patients, 15 were placenta accreta on caesarean section. PAI ≥ 5 (favourable for accreta) was found in 17 and 14 patients by the two radiologists, respectively. The index showed highest sensitivity of 93.3% and specificity of 92.6% with negative predictive value of 96%. A perfect agreement was also found in calculation of PAI by the two radiologists with ICC of 0.959; p value < 0.001.

Conclusion: PAI can be utilised as a standard criterion for prediction of adherent placenta and thus decreasing maternal and foetal morbidity.

B-1668 15:12

Implementing strategies for a better quality fetal MRI by technologist training and the effect on radiologist satisfaction

S. Sefidbakht, L. Mina, R. Ravanfar Haghighi, B. Zeinali, M. Saeedi-Moghadam, F. Zarei, S. Haseli; *Shiraz/IR (sarahaseli@gmail.com)*

Purpose: To simplify and implement limited strategies for a improving quality of performing fetal MRI and to evaluate the effect on exam time and radiologist satisfaction

Methods and Materials: We designed a limited extra education strategy for MRI technicians which included a limited fetal brain MRI anatomy, practical solutions for obtaining perfect orthogonal images using a knowledge of the anatomy of the corpus callosum and vermis as key sagittal landmarks. We also included an extra orientation to motion insensitive MRI protocols tailored to our 1.5 Seimens Avanto and 8channel body coil. We measured the duration of the study with retrospective evaluation of the metadata on our PACS database. In addition we measured radiologist satisfaction of the quality of the images on a scale of 1 to 10 and recorded the time spent by the radiologist at the scanner before and after implementing the strategies. Independent samples T test was used to compare results.

Results: Last 100 patients before implementing the quality measures and first 100 patients with fetal MRI's performed immediately after implementing the qualities entered the study. Mean exam duration time changed from 36.57 ± 9.69 minutes to 24.86 ± 5.39 minutes ($p=0.002$). Mean radiologist supervision time was reduced from 9.58 ± 5.76 minutes to 5.43 ± 2.74 minutes ($p=0.020$). Radiologist satisfaction score with the quality of the images increased significantly from 7.35 ± 2.65 to 8.98 ± 2.31 .

Conclusion: Implementing a limited extra education strategy for technologists involved in fetal MRI can significantly improve the quality of the images and in the meantime reduce the exam time.

B-1669 15:20

Added value of foetal MRI in evaluation of lung anomalies

S. Sefidbakht, S. Bagheri, Z. Etemadi, B. Zeinali, M. Saeedi-Moghadam, N. Asadi, H. Vafaee; *Shiraz/IR (SepidehSefidbakhti@yahoo.com)*

Purpose: To retrospectively correlate all foetal MRI's performed over the last 5 years in our center with lung anomalies detected either primarily in ultrasound or unexpectedly in MRI with post-delivery results.

Methods and Materials: From a total of 456 foetal MRI's performed 53 studies (GA=30+/-8 wks) were performed either for evaluation of a lung finding detected in ultrasound or had an incidental lung finding detected in MRI. In 36 patients post delivery confirmation in form of phone calls, national registry search results or post-delivery CT scans, operation notes or pathology results was available.

Results: Patients included 11 cases of pure CPAM, 3 patients with hybrid lesions (two of which were correctly identified by MRI as such), 3 cases of bronchopulmonary sequestration (correctly diagnosed both by ultrasound and MRI, one fetus with pulmonary blastoma, one case of CHAOS, one case of LAM, 3 cases of pleural effusion, including one proven chylothorax. MRI ruled out focal lung abnormality suspected in ultrasound in 3 suspected cases, all asymptomatic after birth, showed two unsuspected cases of possible CO, both of which subsequently resolved spontaneously. Other patients had some form of uni or bilateral pulmonary hypoplasia.

Conclusion: Foetal MRI detected unsuspected non-significant foetal lung pathology in a small number of cases and also more accurately characterized two lesions. This detailed characterization however did not alter patient management or course.

14:00 - 15:30

Room M 5

Neuro

SS 1911b

Quantitative imaging techniques

Moderators:

O. Föslleitner; Vienna/AT
I. Tsougos; Larissa/GR

B-1670 14:00

Evaluation of pituitary micro-lesions using 3D space: the large sample analysis

H. Zhang, Y. Tang; Shanghai/CN (wozhanghua@126.com)

Purpose: To evaluate the diagnostic yield of the 3D-T2 SPACE sequences compared to a standard MR protocol concerning the pituitary micro-lesions at 3.0T with large sample analysis.

Methods and Materials: Magnetic resonance imaging (MRI) findings of 664 patients with clinically suspected pituitary lesions were retrospectively analysed in this study, some of them confirmed by pathology. Of all patients, post-contrast coronal 3D-SPACE sequence was performed, besides conventional scanning sequences (coronal T1 weighted image (T₁WI) and post-contrast enhanced T₁WI). The images were evaluated by two-experienced neuroradiologists independently in a retrospective fashion. The inter-observer agreement was analysed with kappa statistics.

Results: Compared to conventional sequences, there was an increase of 60.3% in confidence level on diagnosing pituitary micro-lesions with addition of 3D-SPACE sequence. The scores of combined conventional and 3D-SPACE sequences were significantly higher than that of conventional ($z=-6.403$, $P<0.01$) and 3D-SPACE ($z=-4.243$, $P<0.01$) alone. In addition, there was good inter-observer agreement for 3D-SPACE sequence ($k=0.826$).

Conclusion: Combined with routine sequence, 3D-SPACE sequence is reliable in improving the diagnostic confidence for evaluation of pituitary micro-lesions.

B-1671 14:08

Fully automated meningioma detection and segmentation using deep learning on routine multiparametric MRI

K.R. Laukamp, F. Thiele, G. Shakirin, M. Perkuhn, D. Zops, A. Faymonville, M. Timmer, J. Borggrete; Cologne/DE (kai.laukamp@uk-koeln.de)

Purpose: MRI is a key method for meningioma imaging. Clear indications regarding detection and tumour volume are needed for primary assessment, resection planning and monitoring along therapy. Monitoring meningioma volumetrically is superior to conventional diameter methods. We used a multiparametric deep learning model (DLM) on routine MR data including images from referring institutions to investigate performance in automated detection and segmentation.

Methods and Materials: MRI data (T₁-T₂-weighted, T₁-weighted contrast-enhanced [T₁CE], FLAIR) of n=38 grade I and n=18 grade II non-treated meningioma were available. Nine patients had been excluded earlier due to leucoencephalopathy, prevalent secondary tumours or strong artefacts. Tumour grade was determined by histopathology. The DLM was trained on an independent dataset of 249 cases of glioma and segments different tumour classes as defined in the BRATS-benchmark. Preprocessing included registration, skull stripping, resampling to isotropic resolution, and normalisation. The DLM was based on the DeepMedic-architecture (Kamnitsas2016) using a 3D-convolutional neural network for segmentation and a 3D-post-processing step to remove false positives. Results were compared to manual segmentation by an experienced radiologist in FLAIR and T₁CE tumour.

Results: The DLM detected meningioma in 55 of 56 cases. Further, automated segmentation correlated strongly with manual segmentation: average dice coefficients were 0.81±0.10 (range, 0.46-0.93) for the total tumour volume (union of tumour volume in FLAIR and T₁CE) and 0.78±0.19 (range, 0.27-0.95) for contrast-enhancing tumour volume in T₁CE.

Conclusion: The DLM yielded accurate automated detection and segmentation of meningioma tissue despite diverse scanner data and thereby may improve and facilitate future clinical management of this highly frequent tumour entity.

Author Disclosures:

F. Thiele: Employee; Philips employee. G. Shakirin: Employee; Philips employee. M. Perkuhn: Employee; Philips employee.

B-1672 14:16

²³Na-MRI demonstrates a sodium gradient within gliomas as a biomarker of tumour heterogeneity

F. Zaccagna¹, F. Riemer¹, M.A. McLean¹, J.T. Grist¹, R. Schulte², C. Watts¹, S.J. Price¹, M.J. Graves¹, F.A. Gallagher¹; ¹Cambridge/UK, ²Munich/DE (f.zaccagna@gmail.com)

Purpose: The increase in mitotic activity within gliomas is associated with a decrease in Na⁺/K⁺-ATPase activity and gain in concentration of these ions. ²³Na-MRI quantifies sodium concentration and can probe cell morphology and membrane function within the tumour microenvironment, as well as heterogeneity. The purpose of this study was to evaluate sodium distribution within glioma and in the surrounding tissue.

Methods and Materials: 33 patients were imaged on a 3T clinical scanner (GE Discovery MR750) using a Rapid Biomedical (Rimpar) dual-tuned ²³Na/¹H birdcage head coil. Sodium imaging was performed using an UTE sequence with 3D-cones readout (nominal isotropic resolution = 3mm). Intracellular-weighted sodium imaging was obtained using fluid suppression by inversion recovery (adiabatic inversion, T₁ = 30ms). Differences between tumour, grey matter (NAGM) and white matter (NAWM) in total sodium concentration (TSC) and intracellular sodium concentration (IW-SC) were tested using the paired samples t-test ($p<0.05$).

Results: All the patients completed the examination (age 57.8±17.5 yrs). TSC in the lesion was 50.2±16.9mM in the high grade gliomas (HGG), 43.1±28.6mM in the low grade gliomas (LGG) and 52.3±0.5mM in the metastases. The IW-SC was 22.4±17.4mM in the HGGs; 12.9±8.8mM in the LGGs and 7.5±2.3mM in the metastases. TSC was significantly higher in tumours when compared to NAGM ($p=0.0001$) and NAWM ($p=0.0001$).

Conclusion: In all cases, TSC was higher in the entire lesion and in the enhancing tumour compared to the NAGM and NAWM. In conclusion, we demonstrated a sodium concentration gradient across gliomas that is consistent with the expected underlying histopathology.

Author Disclosures:

R. Schulte: Employee; GE Healthcare.

B-1673 14:24

Brain aging in chronic HIV infection: a comparative multivoxel MR spectroscopy study

J. Boban^{1,2}, S. Brkic^{1,1}, D. Lendak^{1,1}, J. Ostojic¹, M. Bjelan², D. Kozic²; ¹Novi Sad/RS, ²Sremska Kamenica/RS (jasmina.konstantinovic@gmail.com)

Purpose: Studies of cognitive changes during the course of HIV infection resulted in hypothesis of accelerated brain aging. The aim of this study was to compare age-related changes in chronic neuroasymptomatic HIV+ patients, with age-related changes in age, gender and education-level-matched healthy subjects using magnetic-resonance spectroscopy (MRS).

Methods and Materials: Study included 60 chronically-infected HIV+ patients on combination antiretroviral therapy and 60 age- and education-matched healthy male subjects, who underwent standard magnetic resonance imaging and long-echo time multivoxel MRS protocol on 3T unit (Trio Tim, Siemens, Germany). Voxels were placed in grey matter of frontal and parietal cortices, and in posterior cingulate gyrus. We analyzed N-acetyl aspartate and creatine (Cr) peaks, expressed as NAA/Cr ratios. Statistical analysis included stratification of the sample according to age (in decades) and comparison of correspondent groups of HIV+ and healthy subjects using ANOVA. Significance was set at value $p<0.05$.

Results: ANOVA with stratified sample revealed significant differences in all locations when youngest groups were compared (20-29 years), while there were no significant differences between the youngest HIV+ subjects (20-29) and the oldest controls (50-59).

Conclusion: Our results imply an initial rapid decrease in NAA/Cr level early in the course of HIV infection, followed by relatively stable level of NAA/Cr over time. However, levels of NAA/Cr in healthy subjects were stable at younger age, with progressive decrease in the oldest group. Brain aging process in chronic, stable HIV infection shows signs of accentuation compared to healthy, with early and rapid decrease in neuron marker.

B-1674 14:32

Empty sella and inferior sella impression are frequently associated and characteristic in patients with growth hormone-secreting pituitary adenomas

G. Bier, J.-M. Hempel, U. Ernemann, B. Bender, J. Honegger; Tübingen/DE (georg.bier@med.uni-tuebingen.de)

Purpose: To assess the prevalence of a sellar floor lowering and empty sella phenomenon in patients with GH (growth hormone)-secreting pituitary adenoma in comparison to an age-matched control cohort.

Methods and Materials: 159 acromegalic patients were included in this study and compared to a control group (150 patients with non-GH-secreting adenomas and 50 patients without pituitary pathology). Magnetic resonance images of all patients were evaluated for the presence of an empty sella,

downward tumour extension and maximum superoinferior diameter of the mass.

Results: The empty sella phenomenon was detected significantly more often in patients with a GH-secreting adenoma (22% vs 7%; $p=0.003$). Moreover, GH-secreting adenomas presented with a significant rate of downward tumour extension (74.8% vs 35.5%; $p<0.0001$). A comparably decreased superoinferior diameter and higher ratio of intrasellar to suprasellar extension are predictive for the presence of a GH-secreting adenoma (AUC, 0.712).

Conclusion: The association of GH-secreting pituitary adenomas and an empty sella phenomenon is frequent. Moreover, GH-secreting adenomas are frequently accompanied by an enhanced impression of the sellar floor. Hypothetically, this is caused by tumour-induced bone remodelling processes.

B-1675 14:40

Role of phase contrast MR CSF flowmetry study in the evaluation of normal pressure hydrocephalus

S. Kumari¹, M. Mohammad Zakir², Y. Kirubha¹, K. Sudhakar¹, P. Chatterjee¹, R. Ranjan³, J. Kumari⁴, S. Kumar⁵, S. Khan²; ¹Chennai/IN, ²Nagpur/IN, ³Rohatak/IN, ⁴New Delhi/IN, ⁵Patna/IN (surbhinmch@gmail.com)

Purpose: To study role of cerebrospinal fluid (CSF) flowmetry indices in patients with symptoms of normal pressure hydrocephalus (NPH) and to establish its diagnostic value.

Methods and Materials: In this prospective case-control study, 44 patients (age range = 45-83 years) were evaluated by phase contrast (PC) MR CSF flowmetry in a 3T MRI equipment. 22 patients of NPH (with clinical and MRI diagnosis) and 22 age-matched control were evaluated. The CSF flow parameters studied include aqueductal stroke volume (ASV), peak systolic velocity (PSV), mean systolic velocity (MSV), forward flow (FF) and backward flow (BF). Statistical significance of these parameters was studied and comparisons were made between the parameters.

Results: CSF flow parameters reliably differentiated NPH patients from controls in this study. Cerebral aqueduct in patients with NPH showed increased ASV. ASV parameters also showed marked difference in the values between NPH and controls. In patients with NPH above 45 years of age, mean values of ASV, PSV, MSV, FF and BF flow were 0.190(ml), 9.0(cm/s), 4.8cm/s, 0.098(ml) and 0.091(ml), respectively. In the control group above 45 years of age, mean values of ASV, PSV, MSV, FF and BF were 0.032(ml), 5.0(cm/s), 3.3 cm/s, 0.022(ml) and 0.020 (ml). CSF flow parameters including ASV, PSV, MSV, FF and BF reliably differentiated NPH patients from controls in the above 45 years age group (p values were 0.0001, 0.0001, 0.003, 0.0001 and 0.0001 ml, respectively).

Conclusion: Phase-contrast MR CSF flowmetry is a non-invasive means of calculating CSF flow in patients with NPH. In patients with clinical and MRI evidence of NPH, CSF flow parameters including ASV, PSV, MSV, FF and BF can be reliably used as an additional diagnostic tool.

B-1676 14:48

Cognitive decline in ageing and cerebrovascular reactivity assessed by ASL fMRI of perfusion

N. Boudiaf, A. Krainik, J. Warnking, J. Pietras, O. Moreaud, M. Baciu; Grenoble/FR (akrainik@chu-grenoble.fr)

Purpose: Cerebral blood flow (CBF) and cerebral vascular reactivity (CVR) decrease with age and might affect cognitive functions. This study aimed at investigating their correlations with cognitive abilities during normal and pathological ageing.

Methods and Materials: We performed neuropsychological assessments on 13 healthy younger subjects (44.1±9.5yo), 10 older subjects without cognitive complaint (72.1±5.7yo), 11 older subjects with cognitive complaint (73.4±7.9yo). We tested cognitive functions (attention, short-term and working memories, executive functions, language). We measured basal CBF and CVR elicited by hypercapnic challenge (7%CO₂) using pCASL (3T Achieva TX, Philip, post-label delay=1525ms; voxel=3x3x6mm³; 20 slices; TE 12 ms; TR=4s for a total of 180 control and tag volumes acquired in 12 min during block-designed hypercapnia; s). Individual end-tidal CO₂ pressure was used as physiological regressor to conduct linear regression analysis. Post-processing was performed using AMIGOV0.9, an in-house software (Python3.6, Matlab8.6, SPM12), giving whole-brain and regional basal CBF, CBV, MTT, CVR. We tested correlations between global and regional CBF and CVR with cognitive scores.

Results: We found a decrease in attention and inhibition in older participants. Impaired-older subjects showed specific decreases in global cognitive functioning, executive functions, short-term and working memory. Global CBF decreased with age, only. Regional CBF decreased with attention and inhibition processes in anterior regions. Global CVR decreased with age and executive functions. Regional CVR decreased with lower performances in all cognitive tests, especially in posterior regions.

Conclusion: CBF and CVR decrease with ageing. Unlike CBF, regional CVR decrease is specifically associated with cognitive impairment during ageing.

B-1677 14:56

Comparative study of activation during color-word Stroop test and new suggested counting test performance

S. Morozova, E.I. Kremneva, Z. Gadzhieva, A.N. Sergeeva, B. Akhmetzianov, M. Zabitova, E. Kashina, M. Krotenkova, L. Dobrylina; Moscow/RU (kulikovasn@gmail.com)

Purpose: To explore fMRI-based activation in healthy subjects performing the Stroop color-word test, widely used for executive functions mapping, and new suggested counting test, which is simpler to explain and perform.

Methods and Materials: Data were acquired from 12 healthy subjects age ranged 45-63. MRI was performed on Siemens Verio 3.0 T scanner, scanning protocol included conventional T2-weighted sequence, T1 multiplanar sequence and simple block task-fMRI sequences using the Stroop color-word test and new suggested counting test as paradigms. Statistical analysis was performed using SPM8.

Results: FMRI-based analysis using modified Stroop test paradigm showed activation of constituent regions of executive network (anterior insular and anterior cingulate cortex, dorsolateral prefrontal cortex, premotor cortex, supplementary motor area and inferior parietal lobules) and also of medial parts of lenticular nuclei, of regions in occipital cortex and cerebellar hemispheres. FMRI analysis using new suggested counting test paradigm also showed activation of constituent regions of executive network, including angular gyri, and also activation of cerebellar hemispheres but without activation of occipital cortex. Significant differences between the series were found in occipital cortex.

Conclusion: Similar areas of activation during examination with Stroop test and counting test allow using new suggested counting test as an alternative paradigm for executive functions mapping, especially in patients with vision problems.

B-1678 15:04

Comparing normative subcortical volume distributions across cohorts

E.J. Vinke¹, W. Huizinga¹, M. Bergtholdt², M.A. Ikram¹, W.J. Niessen¹, F. Wenzel², M.W. Vernooij¹; ¹Rotterdam/NL, ²Hamburg/DE (e.vinke@erasmusmc.nl)

Purpose: More and more brain imaging data are publicly accessible and may serve as normative data for individual patient comparison. However, different normative cohorts differ in field strength, sequence parameters, and population. We assessed the differences in subcortical structure volumes between population and case-control studies, and the effects of using different cohorts for individual patient assessment.

Methods and Materials: Segmentation of subcortical structures was performed using a shape-constrained deformable surface model. Then, percentile curves were fitted on the volume distributions using the LMS method on healthy subjects from three different studies: (1.) the population-based Rotterdam Study (n=1000), (2.) the case-control study, Alzheimer's Disease Neuroimaging Initiative (ADNI) (n=430), and (3.) the United Kingdom Biobank population study (UKBB) (n=904), with an overall age range of 40 to 95 years. The percentiles for 50 AD and 50 MCI patients (from ADNI) based on the distributions of the three datasets served for assessing the impact on individual patient classification. Here, differences between these percentiles were tested using a Welch's two-sample T test.

Results: Overall, LMS percentile curves were highly overlapping between the three different datasets: for AD and MCI patients, there were no significant differences between percentiles for the putamen, thalamus, hippocampus and the nucleus caudate. Globus pallidus and amygdala revealed small differences, with mainly the Rotterdam Study data showing slightly lower normative values.

Conclusion: Overall, we found that the subcortical volume normative data from these three cohorts is interchangeable, suggesting more flexibility in clinical implementation.

B-1679 15:12

Are cerebral DTI changes correlated with degree of disability and cognitive dysfunction in patients with multiple sclerosis?

J. Bladowska, A. Pokryszko-Dragan, A. Banaszek, A. Zacharzewska-Gondek, M. Nowakowska-Kotas, E. Gruszka, M. Sasiadek; Wroclaw/PL (asia.bladowska@gmail.com)

Purpose: The aim of the study was to evaluate the microstructural changes within normal-appearing brain regions in multiple sclerosis (MS) patients using diffusion tensor imaging (DTI) as well as their association with disability and cognitive dysfunction.

Methods and Materials: Fifty patients with clinically definite, relapsing-remitting MS, according to McDonald's criteria (mean age 36.4 yrs) and 40 age- and sex-matched control subjects were enrolled in the study. DTI examinations were performed on a 1.5T MR scanner. Fractional anisotropy (FA) and apparent diffusion coefficient (ADC) values were obtained with a small ROI method within: genu (GCC) and splenium of the corpus callosum

(SCC) as well as within right and left thalami. There were no demyelinating lesions within the ROIs in any of the patients included in the study. Degree of disability was assessed using Expanded Disability Status Scale (EDSS) and cognitive function using Paced Auditory Serial Addition Test (PASAT) and Symbol Digit Modalities Test (SDMT).

Results: Significant decrease of FA ($p < 0.05$) and significant increase of ADC ($p < 0.05$) values were found in MS patients in GCC, SCC and both thalami compared to the normal subjects. There were significant correlations between FA values in GCC, SCC and SDMT results in MS subjects. ADC values in SCC and right thalamus were also significantly correlated with SDMT score. No correlations were found between FA or ADC values and EDSS.

Conclusion: Microstructural tissue damage assessed with DTI measurements within normal-appearing corpus callosum and thalamus shows significant relationship with cognitive dysfunction in MS patients.

B-1680 15:20

Optimising pre-surgical fMRI language mapping using knowledge derived from intrinsic connectivity brain networks for personalised therapy planning

L.R. Kozák¹, G. Gyebnár¹, A.G. Szabo¹, A.L. van Graan^{2,3}, P. Barsi¹, L. Lemieux^{2,3}, G. Rudas¹; ¹Budapest/HU, ²London/UK, ³Chalfont St. Peter/UK (lrkozak@gmail.com)

Purpose: Blood-oxygenation level dependent functional MRI (fMRI) became an important tool of pre-surgical workup of tumors and/or other epileptogenic lesions within or near eloquent brain areas. Still, there are almost as many paradigms in use as MRI centers using them. We aimed to investigate whether language mapping paradigms can be fine-tuned in a neuropsychologically meaningful way using inference based on intrinsic connectivity (also referred as resting-state) brain networks (ICNs).

Methods and Materials: fMRI language mapping results of 40 consecutive patients scanned using picture naming, synonym matching, speech comprehension, and word/non-word decision tasks in 2016-2017 on a Philips Ingenia 3T scanner were re-evaluated using our recently published ICN Atlas framework[1]. Correspondence information between ICNs and pertinent cognitive/behavioral domains derived from BrainMap[2,3] were used to infer the specific cognitive processes involved by the different paradigms based on the fMRI activation maps.

Results: There were paradigm-dependent differences both in the categorical label output of ICN_atlas toolbox (e.g. 'Perception.Vision.Shape' and 'Naming (Overt)' for picture naming; 'Perception.Audition', 'Passive Listening' and 'Pitch Monitor/Discrimination' for word/non-word decision), and in the weights associated with labels; within-task effects being smaller than between-tasks effects (Friedman's test, $p < 0.05$). These labeling differences reflected those expected for paradigms and patients based on prior neuropsychology.

Conclusion: fMRI-based inference may be used to fine-tune mapping paradigms for specific symptoms, lesion loci and/or specific sub-functions deemed necessary by neuropsychological evaluation, thus opening personalized ways for paradigm optimization and therapy planning.

[1]Kozák et al., NeuroImage (2017) 163C:319-341, [2]Laird, J Cogn Neurosci (2011) 23(12):4022-37. [3]Ray, Front Neurosci (2013) 7:237.

Wednesday, February 28

11:55
Discussant
H.A. [Deutschmann](#); Graz/AT

10:30 - 12:00

Sky High Stage

Interventional Radiology

CT 2

Clinical Trials in Radiology 1

Moderators:

M. Dewey; Berlin/DE
R.L. Ehman; Rochester, MN/US

B-0184 10:30

A two-center phase III, randomised, controlled study of MRgFUS vs EBRT in patients with metastatic non-spinal bone disease: palliative strategy for cancer-induced bone pain

A. [Napoli](#), R. Scipione, A. Leonardi, H.-P. Erasmus, S. Dababou, C. Marrocchio, C. Catalano; Rome/IT (alessandro.napoli@uniroma1.it)

10:40

Discussant

M. [Szczerbo-Trojanowska](#); Lublin/PL

B-0185 10:45

Percutaneous microwave thermal ablation (MWA) for patients with malignant lung tumors: mid-term results of a prospective multicenter study (MALT study)

A. [Posa](#)¹, R. Iezzi¹, F. Carchesio¹, A. Veltri², R. Cioni³, R. Manfredi¹, L. Bonomo¹; ¹Rome/IT, ²Orbassano/IT, ³Pisa/IT (alessandro.posa@gmail.com)

10:55

Discussant

F. [Gleeson](#); Oxford/UK

B-0186 11:00

Use of electromagnetic navigation improves performances in CT-guided interventions: a multicentric, prospective and randomised clinical trial

A. [Mounier](#), R.-C. Rouchy, M. Medici, E. Chipon, A. Moreau-Gaudry, I. Bricault; Grenoble/FR (amounier1@chu-grenoble.fr)

11:10

Discussant

T. [Penzkofer](#); Berlin/DE

B-0187 11:15

Randomised clinical trial of portal vein embolisation using n-butyl-cyanoacrylate vs polyvinyl alcohol particles plus coils for liver hypertrophy before major hepatectomies

J.H.M. [Luz](#)¹, E. Coimbra¹, T. Bilhim¹, F.V. Gomes¹, N.V. Costa¹, M.T. Correia¹, P. Luz², E. Barroso²; ¹Lisbon/PT, ²Rio de Janeiro/BR (jhugoluz@gmail.com)

11:25

Discussant

K.A. [Hausegger](#); Klagenfurt/AT

B-0188 11:30

Paclitaxel-coated balloon angioplasty for the treatment of symptomatic central venous stenosis in dialysis access: results from a prospective randomised control trial

P. [Papadimatos](#), P. Kitrou, K. Katsanos, N. Christeas, D. Karnabatidis; Patras/GR (pnpapadimatos@yahoo.gr)

11:40

Discussant

H. [Portugaller](#); Graz/AT

B-0189 11:45

Comparing different thrombectomy techniques in five large-volume centres: a 'real world' observational study

A.C. [Hesse](#)¹, A. Zapf¹, J. Liman¹, J. Fiehler², A. Mpotsaris³, P. Schramm⁴, A. Berlis⁵, M. Knauth¹, M.-N. Psychogios¹; ¹Göttingen/DE, ²Hamburg/DE, ³Aachen/DE, ⁴Lübeck/DE, ⁵Augsburg/DE (amelie.hesse@med.uni-goettingen.de)

Clinical Trials will be presented at ECR 2018; the abstracts will be published afterwards

Thursday, March 1

B-0600 11:45

The accurate non-invasive staging of liver fibrosis using deep learning radiomics of shear wave elastography for a multicenter study
H. [Zhou](#), K. Wang, J. Tian; *Beijing/CN* (zhouhui2015@ia.ac.cn)

11:55

Discussant

D. [Regge](#); *Turin/IT*

10:30 - 12:00

Sky High Stage

Cardiac

CT 6

Clinical Trials in Radiology 2

Moderators:

M. Dewey; *Berlin/DE*

R.L. Ehman; *Rochester, MN/US*

B-0595 10:30

MEDIRAD EARLY-HEART study: early clinical and biological predictors of radiotherapy-induced cardiac toxicity in breast cancer

M.-O. [Bernier](#)¹, S. Jacob¹, A.P.G. Crijns², J.A. Langendijk², R. Vliegenhart², S.E. Combs³, M. Mayinger³, A. Eraso⁴, F. Guedea⁵, M. Fiuza⁶, S. Constantino Rosa Santos⁶, E. Mousseaux⁷, E. Cardis⁸, G. Frija⁷; ¹Fontenay-aux-Roses/FR, ²Groningen/NL, ³Munich/DE, ⁴Girona/ES, ⁵L'Hospitalet del Llobregat/ES, ⁶Lisbon/PT, ⁷Paris/FR, ⁸Barcelona/ES (marie-odile.bernier@irsn.fr)

10:40

Discussant

V.E. [Sinitzyn](#); *Moscow/RU*

B-0596 10:45

Low-dose chest CT vs conventional chest x-ray prior to cardiac surgery: the CRICKET study

R.P.J. [Budde](#)¹, A.M. den Harder², T. Leiner², P.A. de Jong², J. Karady³, C. Chun³, A. Bogers¹, P. Horvat-Maurovich³, L. de Heer²; ¹Rotterdam/NL, ²Utrecht/NL, ³Budapest/HU (r.budde@erasmusmc.nl)

10:55

Discussant

J. [Bremerich](#); *Basle/CH*

B-0597 11:00

Computed tomography (CTA) vs invasive coronary angiography (ICA) in patients with atypical chest pain and suspected coronary artery disease (CAD): gender analysis of a randomised study

M. [Bossert](#)¹, S. Feger¹, M. Rief¹, D. Preuß¹, P. Ibes¹, P. Martus², K. Kofoed³, M. Laule¹, M. Dewey¹; ¹Berlin/DE, ²Tübingen/DE, ³Copenhagen/DK

11:10

Discussant

R. [Marano](#); *Rome/IT*

B-0598 11:15

Effect of coronary computed tomography vs invasive coronary angiography on statin adherence and serum lipid levels in patients with atypical chest pain: a randomised controlled trial

L. [Elzenbeck](#)¹, S. Feger¹, P. Martus², N. Rieckmann¹, K. Stangl¹, A. Marek¹, H. Dreger¹, M. Beling¹, E. Zimmermann¹, M. Rief¹, B. Chow³, P. Maurovich-Horvat⁴, M. Laule¹, M. Dewey¹; ¹Berlin/DE, ²Tübingen/DE, ³Ottawa, BC/CA, ⁴Budapest/HU (laura.elzenbeck@charite.de)

11:25

Discussant

R. [Vliegenthart](#); *Groningen/NL*

B-0599 11:30

The role of intraprostatic antibiotic injection for reducing infectious complications of transrectal ultrasound-guided biopsy

F. [Shobeirian](#), M. Darabi, S.M. Bagheri, M. Zare Mehrjardi, A. Rezayi; *Tehran/IR* (farzaneh.shobeirian@gmail.com)

11:39

Discussant

R.H. [Oyen](#); *Leuven/BE*

Friday, March 1

11:55

Discussant

P. [Aspelin](#); Stockholm/SE

10:30 - 12:00

Sky High Stage

Breast

CT 10

Clinical Trials in Radiology 3

Moderators:

M. Dewey; Berlin/DE

R.L. Ehman; Rochester, MN/US

B-1006 10:30

Breast cancer screening with tomosynthesis: distribution of cancer subtypes in the Malmö Breast Tomosynthesis Screening Trial

K.S. [Johnson](#)¹, S. Zackrisson¹, A. Rosso¹, H. Sartor¹, I. Andersson¹, L.H. Saal², K. Lang³; ¹Malmö/SE, ²Lund/SE (kristin.johnson@med.lu.se)

10:40

Discussant

F.J. [Gilbert](#); Cambridge/UK

B-1007 10:45

Digital breast tomosynthesis vs digital mammography: recall rate by mammographic density, interim analyses

H. [Aase](#)¹, Å.S. Holen², B. Hanestad¹, S. Hofvind²; ¹Bergen/NO, ²Oslo/NO (hildegunn.aase@helse-bergen.no)

10:55

Discussant

E.M. [Fallenberg](#); Berlin/DE

B-1008 11:00

Reduction in infarct volume on CT and functional outcome after endovascular treatment for acute ischaemic stroke: a causal mediation analysis

K. [Compagne](#)¹, M. Boers², H. Marquering², C.B. Majoie², W. Van Zwam³, D.W. Dippel¹, A. van Es¹, A. Van der Lugt¹, H. Lingsma¹; ¹Rotterdam/NL, ²Amsterdam/NL, ³Maastricht/NL (c.compagne@erasmusmc.nl)

Discussant

I. [Szikora](#); Budapest/HU

B-1009 11:15

Radiologic follow-up of the NU-AGE trial: body composition changes detected by dual-energy x-ray absorptiometry show a correlation with laboratory markers of inflammation

D. Mercatelli¹, A. Santoro¹, G. Guidarelli¹, C. Fabbri¹, R. Ostan¹, A. Berendsen², B. Pietruszka³, A. Jennings⁴, N. Meunier⁵, M. Aparisi Gomez⁶, E. Caumon¹, S. Fairweather-Tait⁴, A. Bialecka³, C. de Groot¹, G. Guglielmi⁸, G. Battista¹, C. Franceschi¹, A. [Bazzocchi](#)¹; ¹Bologna/IT, ²Wageningen/NL, ³Warsaw/PL, ⁴Norwich/UK, ⁵Clermont-Ferrand/FR, ⁶Auckland/NZ, ⁷Wageningen/IT, ⁸Andria/IT (abazzo@inwind.it)

Discussant

F. [Bamberg](#); Tübingen/DE

B-1010 11:30

An international randomised controlled trial of two interventions for reducing doses for computed tomography through audit feedback and sharing best practices

R. [Smith-Bindman](#)¹, P. Chu¹, Y. Wang¹, R. Chung¹, A. Einstein², D. Miglioretti³; ¹San Francisco, CA/US, ²New York, NY/US, ³Davis, CA/US (rebecca.smith-bindman@ucsf.edu)

11:40

Discussant

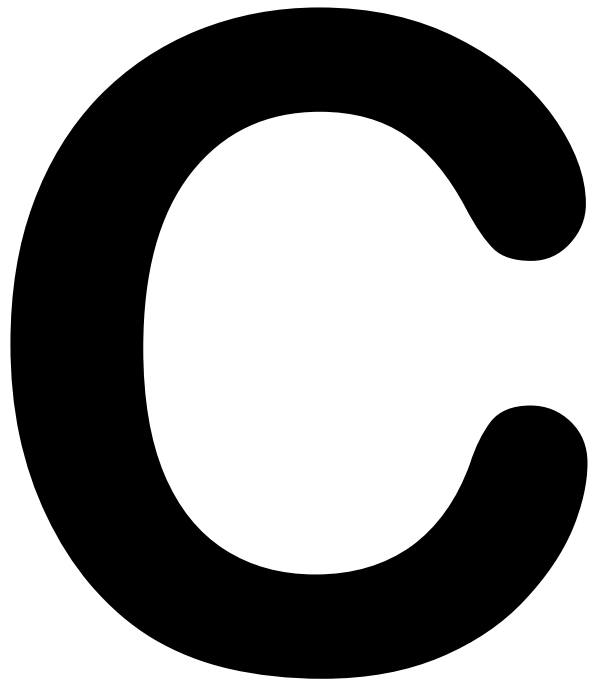
A. [Trianni](#); Udine/IT

B-1011 11:45

Prophylactic hydration to prevent contrast-induced nephropathy (AMACING): long-term results of a prospective, randomised, controlled, non-inferiority trial

E.C. [Niessen](#); Maastricht/NL (estelle.nijssen@mumc.nl)

Clinical Trials will be presented at ECR 2018; the abstracts will be published afterwards



**Scientific and
Educational
Exhibits
(C)**

Full EPOS™ presentations are published at epos.myESR.org and can be cited by a Digital Object Identifier (DOI), if selected so during poster submission.

D

Satellite Symposia (D)

Wednesday, February 28....	540
Thursday, March 1	544
Friday, March 2.....	546
Saturday, March 3.....	548

ECR/ESR takes no responsibility for the content of the Satellite Symposia, and the opinions expressed therein do not necessarily reflect those of the ECR/ESR

Wednesday, February 28

10:30 - 12:00

Studio 2018

jointly organised by Siemens Healthineers and Bayer HealthCare

SY 1a

High-risk screening with breast MRI: today and in the future

Moderator:

C. Van Ongeval; Leuven/BE

Phenotype-genotype correlation and radiological screening for breast cancer in gene mutation carriers

C. Van Ongeval; Leuven/BE

Approximately 5%-10% of breast cancers (BC) are hereditary; the most common mutation is BRCA 1, BRCA 2 and CHEK2. It has been shown that breast cancer gene mutation carriers (BCGM) have different clinical, histological and immune-phenotypic features. In BRCA1 BC presents at younger age (<40y) compared to BRCA2 and CHEK2 and is often more aggressive, presenting as medullary-like, triple negative breast cancers. Notwithstanding some studies reporting different mammographical characteristics of BC in BCGM, a study on imaging characteristics of BC in BRCA 1/ 2 and CHEK2 performed in University Hospitals Leuven (poster EUSOBI 2016) did not prove any difference compared to BC in non-mutation carriers. Breast tumour recurrence (first, second and contralateral) risk is significantly higher in BCGM carriers compared to non-mutation carriers, with CHEK2 most frequently showing an early and contralateral recurrence. Age at first breast cancer is also a strong risk factor for cumulative contralateral BC in BRCA1/2 carriers. Annual MRI alternating mammography and/or ultrasound is probably the most effective screening strategy in BCGM. Screening benefits, associated risks, and acceptance of false-positive results should be discussed.

Learning Objectives:

1. To learn about the immunohistochemical and radiological characteristics of breast cancer in BRCA 1, BRCA 2 and CHEK2 gene mutation carriers.
2. To understand the radiological follow-up program for breast cancer detection in gene mutation carriers.

Ten-year experience of population-based dynamic breast MR Imaging: the Study of Health in Pomerania (SHIP)

R. Bülow; Greifswald/DE

Purpose: To present 10-year results of dynamic breast MRI in the population-based Study of Health in Pomerania (SHIP).

Methods and Materials: Between 2008 and 2012, 774 women (51±12.9 years (range 20 to 83 years) participated in dynamic breast MRI with T1-weighted three-dimensional MR images (repetition time msec/echo time msec, 8.86/4.51; flip angle, 25°) acquired with a 1.5-T MR unit before and 1 to 5 minutes after a gadobutrol bolus injection of 0.1 mmol per kilogram of body weight. Images were analysed by two radiologists independently using the American College of Radiology BI-RADS-MRI Classification Form. In case of disagreement a consensus reading was performed. BI-RADS IV and V breast lesions were disclosed to the women with individual recommendations for follow-up. Between 2013 and 2017, MRI follow-up was realised in 275 (35.5%) women and 228 women participated additionally.

Results: At baseline 113/774 women (recall rate 14.6%) had breast lesions of category BI-RADS IV (n=106) or BI-RADS V (n=7): 84 mass lesions, 15 foci and 29 non-mass lesions. Diagnostic follow-up was completed in 111/113 (97.3%) women. In 21/113 (18.6%) women breast biopsy was performed confirming malignancy in 7/774 (0.9%) women. In the 5-year-follow-up group 3/275 women with new mass lesions (BI-RADS IV) have been detected (recall rate 1.1%) and malignancy was confirmed in 2/275 (0.73%).

Conclusion: Population-based dynamic breast MRI is feasible and has a recall rate of 14.6% at baseline and 1.1% during 5-year-follow-up. Mass lesion was the most detected lesion type. Malignancy was confirmed in 0.9% women at baseline.

Gadolinium retention: impact on breast MRI?

J. Barkhausen; Lübeck/DE

More than 30 years ago, contrast-enhanced MRI emerged as a new technique in clinical breast imaging and over the last three decades numerous clinical studies have shown excellent results for the detection and characterisation of breast lesions. Despite the most recent improvement of high-resolution and

diffusion-weighted MRI, dynamic contrast-enhanced sequences are still considered as the key component of any breast MRI examination. The applied gadolinium-based contrast agents (GBCAs) were considered as very safe compounds until the association between nephrogenic systemic fibrosis and GBCAs was suspected in 2006. Additionally, in late 2013 Kanda and colleagues described increased signal intensity in the dentate nucleus on unenhanced T1-weighted MR images as a consequence of repetitive previous GBCA administrations. Although no clinically relevant adverse events have yet been associated with the detection of gadolinium in the brain, the results of these studies must be taken seriously. With respect to breast MRI, these issues are especially important for repetitive breast cancer screening in high-risk patients for example with BRCA mutations. In this lecture the results of the most recent clinical trials addressing this topic and the regulatory recommendations will be presented and discussed in a comprehensive manner.

Learning Objectives:

1. To gain knowledge of the pharmacokinetics of different MR contrast agents.
2. To discuss the potential risks of gadolinium based contrast agents.
3. To learn about the most recent recommendations and guidelines.

Radiomics in breast imaging

L. Umutlu; Essen/DE

12:15 - 13:45

Studio 2018

jointly organised by Siemens Healthineers and Bayer HealthCare

SY 1b

Multimodality Lunch Symposium: Reading approaches and protocols

Moderator:

R.M. Mann; Nijmegen/NL

ABVS and personalised breast cancer screening

A.-R. Grivegnée; Brussels/BE

Dense fibroglandular tissue has an important impact on breast cancer screening. While mammography remains the gold standard in breast cancer screening (BCS), the approach has evolved and more personalised programs are now emerging. We will present our experience in BCS including ultrasound (Hand Held (HH) and/or Automated 3D) for patients having heterogeneously and extremely dense breasts. The conclusions of this study conducted in the ASSURE PROJECT (EU funded) show a higher cancer detection with an acceptable recall rate. The personalised workflow for BCS in our clinic has been defined as: Mammography (including DBT) followed by ABVS decided on the basis of volumetric density evaluation; then rapid overview by the radiologist of the examinations. If any positive or doubtful finding is seen, HHUS or dedicated mammogram is immediately performed. In addition, the use of CAD for mammography and ABVS is programmed as an evaluation process in our clinic.

Learning Objectives:

1. Ultrasound examination increases breast cancer detection rate with an acceptable recall rate.
2. ABVS is at least equivalent to HHUS in this application; furthermore it allows a quality assurance which is mandatory in BCS.
3. ABVS can be utilised in personalised breast cancer screening workflow in a reasonable cost-effective approach.

Approaches to accelerating and standardising DBT reading in screening: what's new? Final results of the Malmö Breast Tomosynthesis Screening Trial

S. Zackrisson; Malmö/SE

The superiority of digital breast tomosynthesis (DBT) compared to digital mammography (DM) for cancer detection in screening is undoubted, as indicated by the results from several large, prospective screening trials. One of the challenges for implementation of DBT in screening is that longer reading times are reported for DBT, up to twice as long as for DM. In high-volume screen reading, ways to improve reading times with sustained sensitivity and specificity are warranted. The image protocols vary between trials, from two-view DM+DBT, two-view synthetic DM+DBT and one-view DBT, although with quite similar results on detection and somewhat mixed effects on recalls. This presentation will include a discussion on what is the optimal image protocol. Further, does the use of narrow- versus wide-angle DBT make a difference? Do we need double reading with DBT? Will artificial intelligence systems replace one reader? Are thicker slices, slabbing, a way forward? How much

does experience add? Finally, some of the final results from the Malmö Breast Tomosynthesis Screening Trial will be presented.

Learning Objectives:

1. To be familiar with the different image protocols used in prospective trials.
2. To acknowledge ways to accelerate and standardise DBT screen-reading.

Breast elastography: examination protocol and imaging interpretation

C. Gkali; Athens/GR

In recent years the use of elastography in addition to sonography has become a routine clinical tool for the characterisation of breast masses. Studies have investigated the improvement of specificity in differentiating benign from malignant breast masses. Therefore, additional use of elastography could help to reduce the number of unnecessary biopsies in benign breast lesions especially in category IV lesions of the ultrasound breast imaging reporting data system (US-BI-RADS). Ultrasound elastography is a cheap, readily available, useful, quick, non-invasive method in the diagnosis of breast lesions but it needs specific training as well as acknowledging the technical and pathological factors which may influence it. Both Strain and ARFI (Shear Wave Elastography) methods have been evaluated. Whereas Strain elastography results in qualitative imaging of tissue stiffness due to induced compression, ARFI (SWE) elastography displays quantitative and qualitative information of tissue displacement. A standardised protocol is essential for an adequate and effective examination, also helping reducing the dependence from operators. Furthermore, knowledge of pitfalls that can be encountered when ultrasound elastography is performed may help to avoid erroneous images interpretation. Interesting and rare cases will be presented and interpreted.

Progress on whole-body MRI use for advanced breast cancer

A.R. Padhani; London/UK

Learning Objectives:

1. To learn how WB-MRI addresses limitations of current imaging for bone metastatic detection and response.
2. To understand how the biology of metastatic bone disease affects imaging findings.
3. To enumerate patient care.

12:30 - 13:30

Room F2

organised by GE Healthcare

SY 2

Clinical impact of GE Healthcare's latest innovations

Moderator:

O. Adda; Buc/FR

AIR Coil Technology: the next breakthrough in MRI

F.J. Robb; Cleveland, OH/US

Spectral imaging: the future of CT?

M. Zins; Paris/FR

Contrast-media considerations during complex MRI examinations

N.N.

12:30 - 13:30

Room K

organised by Canon

SY 3

The role of cross-modality imaging in oncology diagnostics and treatment

Moderator:

A. Denys; Lausanne/CH

MRI-US fusion for diagnostic assessment of the prostate and treatment guidance

T. Fischer; Berlin/DE

Published data on TRUS-guided repeat biopsy reveal markedly declining detection rates. The combination of high-resolution 3T magnetic resonance

imaging (MRI) with multi-parametric ultrasound (B-mode, elastography, Doppler, CEUS) can be implemented in the form of MRI/US fusion biopsy of the prostate. Our studies show this approach to be able to increase the detection rate of PCa in general and also of significant PCa (\geq cT2b and/or \geq Gleason score of 7). Since mainly patients with clinically significant PCa benefit from prostatectomy, the foremost diagnostic aim should be to identify these patients and separate them from patients with non-significant PCa. Our working group focuses on prostate cancer treatment by irreversible electroporation (IRE) which spares not only the nerves but also the large blood vessels and the urethra.

Learning Objectives:

1. Understand the basic technique of TRUS-guided prostate biopsy.
2. Understand the basics of MRI/US image fusion using clinical examples.
3. Understand the advantages of multi-parametric ultrasound compared with MRI.
4. Understand the benefits of focal treatment of prostate cancer using IRE.

Improving clinical pathways with angio CT in abdominal IR

B. Guu; Daix/FR

Minimally invasive techniques, such as liver ablation, are recommended for almost 50% of primary liver cancer cases. Thermoablation of tumours of the liver using multi-modality imaging, combining CT, ultrasound and angiography is a promising technique being developed. Almost 40% of liver tumours are not detectable with ultrasound and 20% are not identified in CT scanning. The combination of these imaging modalities, however, as well as the ability to mark the tumours endovascularly, has enabled us to perform three times more thermoablation treatments over the last three years with interventional follow-up.

Learning Objectives:

1. Understand the components of a modern Angio CT system.
2. Learn how Angio CT can change practice in abdominal IR.
3. Appreciate the benefit of Angio CT in terms of radiation exposure.
4. Learn about 4D imaging.

Interventional oncology in a state-of-the-art angio CT environment

A. Gangi; Strasbourg/FR

The combination of CT scan and C-arm fluoroscopy has been used since the 1990s. Expanding this set-up with high-end CT and angiography, a milestone in interventional radiology (IR) and oncology, has been shown to provide the most precise imaging in liver tumour management. In this presentation we will explore further applications in oncology and IR that might benefit from the combination of the high-end imaging modalities. We will furthermore discuss the minimal requirements for the installation of such a system, including technical and financial challenges.

Learning Objectives:

1. Identify the best indications for an Angio CT set-up.
2. Recognise the advantages of Angio CT.
3. Plan the installation of such a combination, transparency and accuracy in treatment decisions.

12:30 - 13:30

Room M 3

organised by SuperSonic Imagine

SY 4

Programme not available by date of publication

14:00 - 15:30

Studio 2018

organised by Siemens Healthineers

SY 1c

Digital mammography: from improving morphological assessment to functional imaging

Moderator:

L.J. Pina Insausti; Pamplona/ES

Impact of tomosynthesis angular range on mass conspicuity in patients with dense breasts: experiences from a radiologist's view

P.R. Fisher; Stony Brook, NY/US

Purpose: Recent studies have suggested that cancer detection rates for digital breast tomosynthesis (DBT) are poor for patients with heterogeneously to extremely dense breasts. These studies have been predominantly conducted on narrow-angle DBT. Increasing angular range (AR) reduces breast structural noise and increases image contrast for masses, potentially improving mass detection in dense breasts. We investigate the effect of AR on mass detectability using a previously validated cascaded linear system model (CLSM) for DBT, and compare theoretical results with clinical findings in an IRB-approved study.

Materials and Methods: Mass conspicuity in DBT was modelled as a function of AR using a normalised detectability index d' , incorporating breast structural noise and image contrast. DBT images were acquired for 6 patients with heterogeneously or extremely dense breasts on both the Hologic Selenia Dimensions (AR = 15°) and the Siemens MAMMOMAT Inspiration (AR = 50°). Two breast radiologists were presented with both sets of images for each patient and compared lesion conspicuity on a five-point scale (-2: lesion much more conspicuous on narrow-angle DBT, to +2: lesion much more conspicuous on wide-angle DBT).

Results: Mass detectability was predicted to increase with increasing AR due to reduced structural noise and increased contrast in the reconstructed image slices. Increasing AR from 15° to 50° would increase detectability of 2, 5 and 10 mm masses by 85.3%, 87.5% and 87.9%, respectively. Clinical findings corroborated simulation results, with mass conspicuity shown to be superior for wider-angle DBT, with a mean score of 0.89 (95% CI: 0.44, 1.44). Importantly, masses found in areas with high masking risk (defined as high local density as characterised by the radiologist) were more conspicuous on wider-angle DBT. **Conclusion:** Using a normalised detectability index d' , mass conspicuity was shown to increase with increasing AR. These results were corroborated by a pilot clinical study, and motivate an ongoing larger scale study to demonstrate whether DBT with wider AR provides superior mass conspicuity for patients with heterogeneously to extremely dense breasts.

Learning Objectives:

1. To understand the imaging science of the impact of AR in DBT image quality.
2. To compare the mass conspicuity in DBT with wide and narrow AR for patients with dense breast.

Impact of tomosynthesis angular range on mass conspicuity in patients with dense breasts: experiences from a physicist's view

W. Zhao; Stony Brook, NY/US

Purpose: Recent studies have suggested that cancer detection rates for digital breast tomosynthesis (DBT) are poor for patients with heterogeneously to extremely dense breasts. These studies have been predominantly conducted on narrow-angle DBT. Increasing angular range (AR) reduces breast structural noise and increases image contrast for masses, potentially improving mass detection in dense breasts. We investigate the effect of AR on mass detectability using a previously validated cascaded linear system model (CLSM) for DBT, and compare theoretical results with clinical findings in an IRB-approved study.

Materials and Methods: Mass conspicuity in DBT was modelled as a function of AR using a normalised detectability index d' , incorporating breast structural noise and image contrast. DBT images were acquired for 6 patients with heterogeneously or extremely dense breasts on both the Hologic Selenia Dimensions (AR = 15°) and the Siemens MAMMOMAT Inspiration (AR = 50°). Two breast radiologists were presented with both sets of images for each patient and compared lesion conspicuity on a five-point scale (-2: lesion much more conspicuous on narrow-angle DBT, to +2: lesion much more conspicuous on wide-angle DBT).

Results: Mass detectability was predicted to increase with increasing AR due to reduced structural noise and increased contrast in the reconstructed image slices. Increasing AR from 15° to 50° would increase detectability of 2, 5 and 10 mm masses by 85.3%, 87.5% and 87.9%, respectively. Clinical findings

corroborated simulation results, with mass conspicuity shown to be superior for wider-angle DBT, with a mean score of 0.89 (95% CI: 0.44, 1.44). Importantly, masses found in areas with high masking risk (defined as high local density as characterised by the radiologist) were more conspicuous on wider-angle DBT. **Conclusion:** Using a normalised detectability index d' , mass conspicuity was shown to increase with increasing AR. These results were corroborated by a pilot clinical study, and motivate an ongoing larger scale study to demonstrate whether DBT with wider AR provides superior mass conspicuity for patients with heterogeneously to extremely dense breasts.

Learning Objectives:

1. To understand the imaging science of the impact of AR in DBT image quality.
2. To compare the mass conspicuity in DBT with wide and narrow AR for patients with dense breast.

Synthetic 2D mammography with digital breast tomosynthesis: the new mammography

P. Clauser; Vienna/AT

The introduction of digital breast tomosynthesis (DBT) in conjunction with digital mammography (DM) is rapidly changing clinical practice. DBT is becoming the new mammography, and therefore the new first-line examination - in conjunction with DM - for women in the screening and assessment setting. The need to perform two examinations (DM and DBT) has raised concerns regarding the increased radiation exposure. Synthetic 2D mammography (SM) is a 2D image reconstructed from the DBT projections. SM is similar to DM and it could be used instead of DM to avoid the need for two examinations.

Learning Objectives:

1. Radiation dose of DM and DBT.
2. What is synthetic 2D mammography?
3. Current evidence in favor of the introduction of SM mammography to replace DM as an adjunct to DBT in clinical practice.

Clinical utility of contrast-enhanced dual energy mammography (CEDEM)

L.J. Pina-Insausti; Pamplona/ES

Contrast-enhanced dual energy mammography (CEDEM) is a development of digital mammography. By using dual energy (conventional low energy mammography plus high energy mammography) after the administration of a bolus of intravenous iodinated contrast medium, a morpho-functional image of the breast is acquired. This technique joins the high spatial resolution of conventional digital mammography with functional information based on neoangiogenesis. The indications of this technique for clinical use include: Problem-solving technique after inconclusive mammography, preoperative assessment of breast cancer, follow-up of scars after conservative treatment, follow-up of intermediate risk patients (borderline histological lesions, such as lobular carcinoma in situ, atypical ductal or lobular hyperplasia, as well as positive family history of breast cancer). In fact, the majority of indications are those of MRI, including the contraindications for MRI (pacemakers, claustrophobic patients, etc.). Furthermore, CEDEM has fewer false negative results than MRI. Nevertheless CEDEM has some limitations: The sensitivity is lower for ductal carcinomas in situ, lesions out of the field of view of the detector are missed and some benign lesions can enhance after contrast administration. CEDEM is contraindicated for patients allergic to iodine as well as for patients with renal insufficiency.

Learning Objectives:

1. To become familiar with contrast-enhanced dual energy mammography (CEDEM).
2. To learn the main indications for this technique.
3. To learn the main limitations of CEDEM.

Comparison of contrast-enhanced dual energy mammography and contrast-enhanced digital breast tomosynthesis for lesion assessment and radiation dose

P.R. Fisher; Stony Brook, NY/US

Purpose: Digital breast tomosynthesis combined with contrast-enhanced dual energy mammography (DBT+CEDEM) is being investigated for diagnostic accuracy. Contrast-enhanced digital breast tomosynthesis (CEDBT) provides coregistered low energy DBT and 3D contrast enhancement map. Synthetic CEDEM may also be generated and paired with synthetic mammogram. This study compares CEDBT with CEDEM for lesion assessment and dose efficiency.

Method and materials: A Siemens MAMMOMAT Inspiration DBT system modified for dual energy contrast-enhanced imaging is used. Patients with BIRAD 4 and 5 lesions and scheduled for biopsy were recruited for an IRB-approved CE imaging study. CEDEM images were acquired 120 seconds after injection of iodine contrast agent, followed by CEDBT acquisition under the same breast compression. Eleven malignant lesions from 12 patients were confirmed by pathology result. A reader study of side-by-side comparison between CEDEM and CEDBT is performed to assess lesions on 1) Contrast

enhancement level and 2) Margin identification, using a 5-point scale from -2 (CEDEM much better) to 2 (CEDBT much better). The radiation dose recorded by the DBT system is reviewed for DBT+CEDEM and CEDBT.

Synthetic CEDEM is created with dual-energy subtracted projections from CEDBT using software developed by Siemens Healthineers.

Results: For malignant lesions, CEDEM shows higher enhancement level than CEDBT slices (mean score=-0.64; 95% CI: -1.09, -0.18). CEDBT shows lesion margin better than CEDEM (mean score=0.78; 95% CI: 0.11, 1.44). In CEDBT slices, background parenchymal enhancement is less intense, and motion artifact is less severe than that in CEDEM. On average, CEDBT reduces dose by 32.8% ± 9.9% compared to DBT+CEDEM (average dose 1.91 ± 0.74 mGy vs. 2.86 ± 1.04 mGy). Synthetic CEDEM has similar mammographic appearance to CEDEM, and shows the same enhanced lesions.

Conclusion: CEDBT provides better lesion margin identification and reduces structural noise due to background parenchymal enhancement and motion compared to CEDEM, while the intensity of lesion enhancement is lower. CEDBT uses lower dose than DBT+CEDEM. Synthetic CEDEM can be created from CEDBT to quickly identify lesion enhancement. Clinical relevance/application: With the advent of DBT replacing FFDM, contrast imaging can potentially be done in full 3D setting (CEDBT) facilitated by synthetic 2D images (synthetic mammogram and synthetic CEDEM).

Personalised therapy through optimisation of diagnostic data in multi-disciplinary team decisions

R.M. [Mann](#); *Nijmegen/NL*

How can the use of diagnostic data in multi-disciplinary team decisions be optimised to enable more personalised therapy? Dr. Mann will walk us through this, using a specific breast cancer case as an example, covering everything from the complexity of preparation and patient empowerment to data Thursday, March 1

16:00 - 17:00

Studio 2018

organised by Siemens Healthineers

SY 1d

Big data and precision medicine in breast care

Moderator:

T. Manoharan; *Forchheim/DE*

Integrated decision support for improved patient outcome

T. [Manoharan](#); *Forchheim/DE*

In this segment we'll focus on value-based healthcare, exploring how Integrated Decision Support (IDS) can help make more precise diagnosis and therapy decisions in multi-disciplinary teams, improving patient health outcome, while keeping the clinical pathway cost-efficient. Emphasis will be placed on multi-modal data integration, including imaging, pathology, lab, genomics and other relevant clinical information.

Improving the clinical utility of digital breast tomosynthesis using novel software applications

R.M. [Mann](#); *Nijmegen/NL*

Digital breast tomosynthesis (DBT) is rapidly replacing mammography as standard of care due to its higher sensitivity and specificity. In clinical practice, in contrast to the screening situation, images are scrutinised in depth. Furthermore, the availability of ultrasound and MRI, if needed, require the DBT findings to be appreciated in a multimodality context. To deal with the large amount of data and the demanding requirements, software applications are indispensable to aid reading. To ensure detection of all lesions within the DBT dataset, novel CAD applications may help, not only localising abnormalities on synthetic 2D slices, but also navigating directly to the most relevant slice in the tomosynthesis volume. For the rapid evaluation of findings within the tomo dataset, synthetic 3D images offer unique possibilities; showing tissue composition of possibly abnormal areas and clearly locating suspicious lesions in the breast. Novel tools that automatically segment and measure relevant findings further aid in reporting and in addition may reduce inter-reader variability. Finally, coupling studies from one modality to the next integrates the findings and allows for multimodal assessment of lesions. Consequently, current software developments have a powerful impact on the usefulness of DBT and multimodality imaging.

The future of MR mammography: radiomics?

C.G.N. [Kaiser](#); *Mannheim/DE*

Recently, terms like big data, radiogenomics and radiomics as a basis for precision-based medicine are an increasingly common topic for discussion. In MR mammography there is also more information to be retrieved from the images than the sole question of whether invasive carcinoma is present. However, MR mammography presents more challenges than the "optimisation of the diagnostic return on investment" as the indications for MR mammography are still limited.

Thursday, March 3

12:30 - 13:30

Room O

organised by Philips

SY 5

The next MR wave

Welcome to MR with a new point of view: new perspective, bigger impact

A. [Radder](#); *Best/NL*

Philips next generation wide-bore 3.0T: body oncology imaging

R. [Braren](#); *Munich/DE*

Advanced and accelerated neuro imaging on a next generation wide-bore 3.0T MRI to simultaneously address clinical and research needs

J.S. [Kirschke](#); *Munich/DE*

Philips Prodiva 1.5T: bringing performance and productivity together

H. [Mahajan](#); *New Delhi/IN*

12:30 - 13:30

Room N

organised by Samsung

SY 6

Multiparametric ultrasound imaging

Moderator:

P.S. [Sidhu](#); *London/UK*

CEUS and 3D US for assessment of carotid plaque morphology

V. [Cantisani](#); *Rome/IT*

Diagnosis and treatment of hepatocellular carcinoma by CEUS

D.A. [Clevvert](#); *Munich/DE*

Comparison of US strain elastography and entero-MRI to typify the mesenteric and bowel wall changes during Crohn's disease

T.V. [Bartolotta](#); *Palermo/IT*

12:30 - 13:30

Studio 2018

organised by Siemens Healthineers

SY 7

Paving the way for MRI in precision medicine

Programme not available by date of publication

12:30 - 13:30

Room E 1

organised by Bracco

SY 8

Programme not available by date of publication

12:30 - 13:30

Room G

organised by Bayer HealthCare

SY 9

Time to look at the bigger picture ...

Presence of gadolinium in the brain and body being put into context, including NSF

Moderator:

V. [Runge](#); *Berne/CH*

Clinical perspective: what to consider and to know when interpreting the clinical literature on Gd presence in the brain and body

A. [Radbruch](#); *Heidelberg/DE*

Latest pre-clinical findings and potential consequences of gadolinium presence in brain

H. [Pietsch](#); *Berlin/DE*

10 years of NSF: a critical review in the context of gadolinium in brain and body

T. [Balzer](#); *Whippany, NJ/US*

Clinical recommendations in context to current health authority regulations

V. [Runge](#); *Berne/CH*

12:30 - 13:30

Room K

organised by Hologic

SY 10

Transforming breast biopsy with real time imaging: impact on clinical practice

Moderator:

L. [Fontaine](#); *Marlborough, MA/US*

Changing the breast biopsy approach in a national cancer institute: impact on clinical routine

G. [Scapperotta](#); *Milan/IT*

How much is enough? Quantity vs quality: our initial experience with a new vacuum assisted breast biopsy device in the UK

W. [Teh](#); *London/UK*

A new biopsy technology combined with tomosynthesis guidance: our experience and initial results

A. [Tejerina](#); *Madrid/ES*

12:30 - 13:30

Room M 3

organised by Siemens Healthineers

SY 11

Personalised ultrasound: advanced applications for customised patient care

Moderator:

G.T. Yusuf; London/UK

A paediatric cost and safety analysis of contrast-enhanced ultrasound

G.T. Yusuf; London/UK

Because of concern over medical ionising radiation exposure of children, contrast-enhanced ultrasound (CEUS) has generated interest as an inexpensive, ionising radiation-free alternative to CT and MRI. CEUS has received approval for paediatric hepatic use but remains off-label for a range of other applications. A retrospective study was performed to analyse adverse incidents encountered in paediatric CEUS and to assess the financial benefits of reducing the number of CT and MRI examinations performed. The records of 305 paediatric patients (187 boys, 118 girls; age range, 1 month-18 years) undergoing CEUS were reviewed. Most of the studies were for characterising liver lesions (147/305 [48.2%]) and trauma (113/305 [37.1%]); the others were for renal, vascular, and intracavitary assessment (45/305 [14.8%]). No immediate adverse reactions occurred. Delayed adverse reactions occurred in two patients (2/305 [0.7%]). These reactions were transient hypertension and transient tachycardia. Neither was symptomatic, and both were deemed not due to the underlying disorder. The potential cost savings of CEUS were \$74 per examination over CT and \$180 over MRI. Paediatric CEUS is a safe and potentially cost-effective imaging modality. Using it allows reduction in the ionising radiation associated with CT and in the gadolinium contrast administration, sedation, and anesthesia sometimes required for MRI.

Learning Objectives:

1. To acknowledge that paediatric CEUS is off label, but safe and useful in a wide variety of scenarios without exposure to radiation, iodinated contrast or the need for anaesthetic drugs.
2. To understand that the use of paediatric CEUS over conventional imaging pathways can result in significant cost reduction.
3. To learn about the characterisation of focal liver lesions and follow up post trauma represent two of the commonest reasons for paediatric CEUS usage.

The benefits of Shear Wave elastography in the liver

N.N.

The clinical advantages of advanced applications in the abdomen

M. D'Onofrio; Verona/IT

Shear Wave Elastography (SWE/ARFI) allows the assessment of the tissue stiffness. It is very important to consider that ARFI is implemented in the ultrasound scanner. Strength of the ARFI Virtual Touch Quantification technique relies in obtaining a number (meter/second or kilopascals) for the shear wave velocity generated in the explored tissue: the stiffer a tissue, the greater the numeric value. Several non-invasive methods are used for assessing liver fibrosis in order to avoid biopsy. Liver function tests and transient elastography are other non-invasive, sensitive and accurate tools. Many published studies analyse ARFI performance and feasibility in studying diffuse liver diseases and compare them to other diagnostic imaging modalities such as conventional US and transient elastography. Fewer papers describe the application of ARFI technology in the study of solid focal liver or pancreatic lesions, with different results. Contrast enhanced ultrasound can enhance the diagnosis of lesions and the use of SWE/ARFI can then improve the characterisation of these ultrasound detected pancreatic masses. Image fusion (CT/MRI & US) using eSieFusion can then be used in follow up and treatment to aid in more successful interventional exams, such as ablation procedures and response to therapies.

Learning Objectives:

1. To understand where using SWE can help in assessing tissue stiffness.
2. To understand the benefits of contrast enhanced ultrasound imaging and where it is useful in clinical practice.
3. To understand how the combination of SWE, CEUS and CT/MRI image fusion can be used to improve both detection and ablation of abdominal malignancies.

Friday, March 2

12:30 - 13:30

Room O

organised by Philips

SY 12

Advances in iterative reconstruction and spectral CT: transforming the use of CT in routine practice

Moderator:

A. Vlassenbroek; Anderlecht/BE

Iterative model-based reconstruction: basis of new imaging era

D. Ippolito; Monza/IT

Model-based iterative reconstruction is a new image reconstruction method which models the acquisition process, leading to image optimisation acting not only in the image domain but also in the projection domain (i.e. during the acquisition process). As a result, this algorithm can better deal with low signal levels in the setting of modern low dose acquisitions; in fact IMR can provide a significant reduction in image noise and streak artifacts, an increment of contrast-to-noise ratio and a significant improvement in spatial resolution, creating virtual "noise free" diagnostic images. Therefore the use of IMR may further improve the sensitivity and specificity of lesion's detection also in follow-up CT studies in different clinical setting (i.e. angiographic study, oncologic fields, emergency examinations), due to the increase of small details evidence. In summary, the main advantages of IMR in clinical practice are represented by high contrast resolution, subtle attenuation differences, applications in no compliant patients or patients with limited IV access or suboptimal acquisition timing, use of reduced radiation and contrast dose.

Spectral CT for emergency imaging: luxury or necessity

E. Danse; Brussels/BE

This lecture is focused on the interest of dual layer spectral scanner detectors for its routine use in the visceral emergency spectrum, including severe traumatised patient, bowel obstruction and ischemic disorders, genitourinary, pancreatic and hepatobiliary situations. Spectral CT for acute aortic and peripheral arteries disorders will be also presented. Additionally, we propose to share our way of process for the analysis and the report of CT examinations done with the spectral system, compared to the conventional CT.

The clinical validation of spectral benefits

D. Maintz; Cologne/DE

Spectral Detector CT offers new possibilities regarding image quality, dose reduction and diagnostic performance in clinical computed tomography. Using virtual monoenergetic images the contrast-to-noise ratio can be significantly increased and using material decomposition maps, such as e.g. iodine-maps, quantitative measurements of tissue components can be obtained. Over the last years systematic studies have been performed to evaluate the benefits in image quality, lesion detection and lesion characterisation. This lecture presents the scientific state-of-the-art and also gives an outlook on future spectral benefits.

12:30 - 13:30

Room N

organised by Hitachi

SY 13

Diverse and innovative imaging solutions, creating new value through innovation and digital technologies

Moderator:

P.S. Sidhu; London/UK

Clinical usefulness of new fusion imaging for interventional kidney/liver procedures

J.-M. Correas; Paris/FR

The role of combi-elasto and attenuation measurement in the assessment of diffuse liver disease

G. Ferraioli; Pavia/IT

Value of high-field open MRI and ultrasound image fusion for the detection of prostate cancer

C. Figge; Paderborn/DE

12:30 - 13:30

Studio 2018

organised by Samsung

SY 14

Innovations in Samsung's Digital Radiography Technologies

Experiences with Samsung's Digital Radiography at Freiburg University Hospital

E. Kotter; Freiburg/DE

Initial experiences with Samsung's Digital Radiography (DR) technology at Freiburg University Hospital will be presented. Two specific DR technology utilising the deep-learning (DL) algorithms and their preliminary results will be introduced - bone suppression imaging (BS) and computer-aided detection (CAD) for lung cancer nodules. First, application of bone suppression imaging (BS) for various subtle lung lesions will be shown. Second, computer-aided detection (CAD) technology for lung cancer nodule detection will be introduced. The detection accuracies of CAD system, radiologists, and radiologists with CAD assistance in reading chest PA digital radiography images will be compared.

Value of x-ray in the diagnosis and follow-up of rheumatic diseases

K.-G.A. Hermann; Berlin/DE

Initial experiences with Samsung's low-dose Digital Radiography technology will be presented. The speaker will share preliminary impressions from applying S-vue (TM) technology to diagnosis and follow-up of patients with rheumatic diseases of hands and feet.

Innovations in digital radiography dose reduction by Samsung

N.N.

12:30 - 13:30

Room E1

jointly organised by Bayer HealthCare and Siemens Healthineers

SY 15

Clear direction in CT: new standards for better patient care

Moderator:

J.E. Wildberger; Maastricht/NL

The China CT standardisation initiative

Z.Y. Jin; Beijing/CN

CT imaging on the edge: kV adapted contrast administration

U.J. Schoepf; Charleston, SC/US

12:30 - 13:30

Room G

organised by Bracco

SY 16

Programme not available by date of publication

Satellite Symposia

12:30 - 13:30

Room K

organised by Guerbet

SY 17

From Gd contrast-media stability to recommendations of the European Medicines Agency

Moderator:

O. Clément; Paris/FR

Gd retention: back to basics

R.E. [Lenkinski](#); Dallas, TX/US

Methodological approach for a correct interpretation of the gadolinium retention studies

J.-S. [Raynaud](#); Roissy/FR

From evidence to the new recommendations of the European Medicines Agency

O. Clément; Paris/FR

12:30 - 13:30

Room M 1

organised by Bayer Russia

SY 18

MR-perfusion in neuro-oncology: survival guide for daily practice

Moderators:

I.E. Tyurin; Moscow/RU

S. Morozov; Moscow/RU

I.N. Pronin; Moscow/RU

DSC and DCE: what does it mean and how to cook it?

H.R. [Jäger](#); London/UK

Primary diagnosis: when and why to use perfusion?

E.I. [Shults](#); Moscow/RU

Evaluation after treatment: Q&A

I. [Trofimenko](#); St. Petersburg/RU

12:30 - 13:30

Room M 2

organised by Philips

SY 19

First impressions of new ultrasound developments

Moderators:

M. Claudon; Vandoeuvre-les-Nancy/FR

R.G. Barr; Campbell, OH/US

New eL18-4 PureWave transducer with shear wave elastography for breast exams

R.G. [Barr](#); Campbell, OH/US

New Philips anatomical intelligent breast ultrasound solution

K. [Kinke](#); Chêne-Bougeries/CH

Potential of micro-flow imaging in bowel application

P.-J. [Valette](#); Pierre-Bénite/FR

eL18-4 in small parts, musculoskeletal and abdominal exams

A. [McNeill](#); Newcastle Upon Tyne/UK

12:30 - 13:30

Room M 3

organised by Siemens Healthineers

SY 20

Medical image interpretation in the age of artificial intelligence

Programme not available by date of publication

14:00 - 15:30

Room X

organised by GE Healthcare Russia

SY 21

Programme not available by date of publication

14:00 - 15:30

Room Z

organised by Carestream

SY 25

Carestream OnSight 3D Extremity System - Point Of Care CBCT

Moderator:

J.A. Carrino; Baltimore, MD/US

Evolution of CBCT

J.A. [Carrino](#); Baltimore, MD/US

The use of CBCT in clinical settings: the experience of Geneva University Hospital

X. [Montet](#); Geneva/CH

Use of OnSight 3D in emergency settings

T. [Jacques](#); Lille/FR

Clinical indications for weight-bearing CBCT

M. [Boesen](#); Copenhagen/DK

Different generations of metal artefact reduction algorithms

M. [Kortesniemi](#); Helsinki/FI

OnSight 3D workflow and usability

R. [Dobbin-Stacey](#); Cheltenham/UK

Saturday, March 3

12:30 - 13:30

Room X

organised by Nocimed, Inc.

SY 27

The future is now: advancing lumbar spine diagnostics for better outcomes

Advanced MR in the spine: a radiologist's view of the advanced techniques you need to know

L. [Tanenbaum](#); *New York, NY/US*

Lumbar Disc MRS: can it help my daily practice? An integrated spine surgeon's perspective and experience with NOCISCAN-LS exams using a Siemens 1.5T scanner

S. [Becker](#); *Vienna/AT*

12:30 - 13:30

Room Z

organised by Kheiron Medical Technologies

SY 26

How new technology can support radiologists: the benefits and challenges of advanced machine learning in mammography

Moderator:

S. [Tan](#); *London/UK*

How learnings and best practices from digital health can help radiology

V. [Gulati](#); *London/UK*

Perspectives on the challenges in developing ML for radiology: how ML can save breast screening

H. [Harvey](#); *London/UK*

Deep learning in mammography

P. [Kecskemethy](#); *London/UK*

12:30 - 13:30

Room L 8

organised by Philips

SY 22

Enhanced diagnostic confidence with digital fluoroscopy

Moderator:

S. [Mintert](#); *Hamburg/DE*

Together with clinical experts we will outline, how a fully digital workflow and our innovations in image quality contribute to meet the day-to-day challenges in your radiology department.

Real-time dose control, real-time image processing

A. [Gooßen](#); *Hamburg/DE*

12:30 - 13:30

Room G

organised by Bracco

SY 23

CEUS: evolving roles and uses

Moderator:

V. [Cantisani](#); *Rome/IT*

Vesicouretral reflux: the role of contrast ultrasound

F. [Papadopoulou](#); *Ioannina/GR*

Update on the EFSUMB guidelines for the use of CEUS

P.S. [Sidhu](#); *London/UK*

CEUS, a powerful diagnostic tool in daily practice: clinical case presentation

D.A. [Clevvert](#); *Munich/DE*

12:30 - 13:30

Room O

organised by Siemens Healthineers

SY 24

Programme not available by date of publication

E

Authors' Index (E)

Authors' Index

A

Aadnevik D.

Dose reduction: tips and tricks: A. Dose reduction in paediatric CT (RC 912), A-389

Abd El Bagi M., Alshehre O., Alfaleh H., Ahmed S., Alorfi F., Ashraf N., Thomas A., Reutener M.

Knee derangement in the era of total knee replacement epidemic (SS 310), B-0306

Abd Ellah M.M.H., Strobl S., Rauch S., Halpern E.J., Kremser C., Jaschke W., Klauser A.

Gouty knee arthritis: ultrasound findings compared to dual-energy CT (SS 1810), B-1423

Abdel Aal A.M.K., Mahmoud K., Kim S., Heeke B., Moawad S., Massoud M., Saddekni S., A. Aboueldahab N., Gunn A.
Outcomes of transjugular intrahepatic portosystemic shunt using 12-mm-diameter stent for portal hypertension with refractory ascites (SS 209), B-0034

Abdel Aal A.M.K., Tatum S., Mahmoud K., Moawad S., Ertel N., Oser R., Saddekni S., A. Aboueldahab N., Gunn A.

Safety and efficacy of transarterial chemoembolization using very small drug-eluting beads for advanced stage hepatocellular carcinoma (SS 1409), B-1055

Abdel Hamid W.R.A.

MRI in endometriosis: a new platform (SS 607), B-0474

Abdel Hamid W.R.A.

DTI of the breast: is it worth the hassle? (SS 1402b), B-1113

Abdel Razek N.M., Hamed M.

Combined ultrasound-guided high-intensity focused ultrasound and vacuum assisted biopsy for treatment of large sized breast fibroadenoma (SS 1802a), B-1389

Abdolell M., Brown P., Caines J., Payne J.I., Tsuruda K., Barnes P., Rivers-Bowerman M., Iles S.E.

The impact of image quality and mammographic breast density on missed cancers in organised screening (SS 702), B-0684

Abdolell M., Tsuruda K., Payne J.I., Brown P., Caines J., Barnes P., Rivers-Bowerman M., Iles S.E.

Mammographic density, age and family history: a minimally sufficient set of parameters to risk stratify average-risk women for follow-up screening (SS 1902a), B-1606

Abdullayev N., Neuhaus V., Le Blanc M., Grosse Hokamp N., Maus V., Lennartz S., Maintz D., Borggreffe J.

Spectral detector-computed tomography iodine density thresholds for the detection of vertebral metastases (MY 13), B-1012

Abeyakoon O., Woitek R.A., Wallis M., Moyle P.L., Morscher S., Malchus N., Manavaki R., Mendichovszky I.A., Joseph J., Quiros-Gonzales I., Bohndiek S., Gilbert F.J.
Optoacoustic imaging increases the sensitivity of mammography and specificity of US: implications for practice (SS 1402a), B-1094

Abidi Z., Faeghi F., Mardanshahi Z., Abdolmohammadi J., Haghghikaboudkola M.
Comparison between grey matter-only and white matter-only imaging in the detection of brain multiple sclerosis lesions (SS 311), B-0287

Abihanna M., Melodelima C., Moldovan P., Souchon R., Ruffion A., Colombel M., Crouzet S., Rouviere O.

Impact of upfront risk stratification on the negative predictive value of multiparametric MRI in patients with no history of prostate cancer (SS 307), B-0245

Abihanna M., Melodelima C., Moldovan P., Souchon R., Ruffion A., Colombel M., Crouzet S., Rouviere O.

Impact of upfront risk stratification on the negative predictive value of multiparametric MRI in patients under active surveillance (SS 1407), B-1074

Abrantes A.F., Gaspar V.L., Ribeiro L.P., Lesyuk O., Ribeiro A.M., Almeida R.P., da Silva C.A.

Internship supervisors' perception of the radiography students in clinical environment (SS 1414), B-1149

Abrantes A.F., Sobral D.M., Ribeiro L.P.V., Azevedo K.B., Almeida R.P., Lesyuk O.

Radiographers and non-accidental injury in children (SS 1914), B-1645

Adam E.J.

Euratom Basic Safety Standards Directive: a comprehensive approach for radiation protection: Panel discussion: Is the Basic Safety Standards Directive a step forward for patients, clinical professionals and regulators? (part 4) (EU 1)

Adam E.J.

Value-based radiology: Panel discussion: A European - US debate on the value of "value-based radiology" (part 5) (PI 3)

Adam E.J.

Euratom Basic Safety Standards Directive: a comprehensive approach for radiation protection: The clinical audit: the missing link (EU 1), A-148

Adam G.G.A., Cognard C., Bonneville F.

Standard diffusion-weighted imaging on the brain detects cervical internal carotid artery dissections (SS 711b), B-0692

Adams L., Ralla B., Engel G., Diederichs G., Busch J., Fuller F., Hamm B., Makowski M.R.

Assessing venous thrombus in renal cell carcinoma: preliminary results for non-contrast enhanced magnetic-resonance 3D-SSFP (SS 207), B-0061

Adriaensen M.

ESR and UEMS: a united European voice: Chairpersons' introduction (part 2) (ESR/UEMS 1), A-179

Agarwal A., Agarwal S., Sharma S., Chandak S.

Placenta accreta index: what a radiologist should know about an imaging update in detection of morbidly adherent placenta (SS 1907b), B-1667

Aghaghazvini L., Hashemi F., Sharifian H., Rasuli B., Yazdani N.

Cervical adenopathies: diagnostic efficacy of DCMR (SS 1508), B-1215

Agten C.A., Dennler C., Roskopf A.B., Jaberg L., Pfirrmann C.W., Farshad M.

Augmented reality-guided lumbar facet joint injections (SS 1410), B-1123

Ahmad M.

The effect of oesophageal varices on the outcome of RF ablation in patients with HCC (SS 1509), B-1207

Ahn H., Hwang S.I., Lee H.J.

How to predict anterolateral extracapsular tumour extension in patients with prostate cancer (SS 1407), B-1066

Ahn J., Kim S., Kim S., Nam I., Lee S.

Diagnostic performance of advanced modelled iterative reconstruction-applied images for detecting urinary stones on submillisievert low-dose computed tomography (SS 1807b), B-1474

Ahuja B.

MRI for gynaecologic imaging: how I do it: Chairperson's introduction (RC 1207), A-544

Akata D.

Imaging of HCC: C. Mimickers and pitfalls (E³ 520), A-244

Akbas T., Ulus S., Karagan B.S., Arpacı T.

Fast magnetic resonance imaging (MRI) of invasive lung aspergillosis in immunocompromised children: comparison with HRCT (SS 712), B-0763

Akdulum I., Öztürk M., Karatoprak S., Sığircı A.

Radiological appearance and follow up results of diaphragmatic mesothelial cysts during childhood (MY 18), B-1505

Akgun A.S., Agirman M.

Association between cam type femoroacetabular impingement and osteitis pubis on MR images (SS 1810), B-1422

Akhan O.

Image-guided therapies in oncology: Kidney (BS 6), A-411

Akin M., Örgüc I.S., Aras F., Kandiloglu A.

Molecular subtypes of invasive breast cancer: correlation between PET/CT and MRI findings (MY 16), B-1291

Akinci D.

Percutaneous interventional procedures: a practical guide: A. How to safely perform US-guided procedures (RC 809), A-365

Akinci D'Antonoli T., Farchione A., Lenkowicz J., Chiappetta M., Cicchetti G., Larici A.R., Valentini V., Bonomo L., Manfredi R.

Radiomics signature for non-small cell lung cancer recurrence risk prediction after surgery: quantitative analysis of the tumour and peritumoural lung parenchyma on presurgical MDCT (SS 1004), B-0874

Akkaya Z., Bas H., Oztuna D., Sahin G.

Imaging of aponeurotic expansion of supraspinatus tendon by 3.0 T MRI and its association with biceps brachii long head, supraspinatus and subscapularis tendon pathologies (SS 1010), B-0952

Akkaya Z., Peker E., Ozalp Ates F.S., Sahin G.

Sacroiliitis due to early ankylosing spondylitis, inflammatory bowel disease and Behçet's disease: could sacroiliac MRI play a role in differentiation? (SS 1910), B-1618

Aksakal M., Ozhan Oktar S., Esendagli Yılmaz G., Özenirler S., Cindoruk M., Hızal K., Baran Aksakal F.N., Yuçel C.

Use of 2D shear-wave elastography in predicting different stages of liver fibrosis according to METAVIR scoring system: a histopathological correlation study (SS 301b), B-0205

Aksenova S., Nudnov N., Kreynina J.

MR-imaging of neoplastic and non-neoplastic lesions of the vagina (SS 1816), B-1375

Al Dahery S., Rainford L.A., McGee A.

A multi-centre study: qualitative and quantitative comparison of liver MR image quality (SS 614), B-0554

Authors' Index

- Al Mohanna J., Pipan F., Clauser P., Bumberger A., Stöttinger A., Kapetas P., Zuiani C., Helbich T.H., Baltzer P.A.T.**
A formalised clinical decision rule applied to breast MRI: can we rule-out malignancy in lesions presenting as suspicious mammographic microcalcifications? (SS 1002), B-0912
- Al-Murshedi S.H., Hogg P.H., Benhalim M.M., Alrowily M., England A.**
An investigation of the impact of image viewing parameter settings on the performance of 2.4 MP colour monitor in visualising low contrast detail using the CDRAD phantom (SS 1814), B-1446
- Alagic Z., Alagic H., Bujila R., Wick M.C.**
The clinical impact of a novel low-dose protocol for minimal-invasive CT-guided musculoskeletal interventions (SS 1809), B-1341
- Alagna G., Cantisani V., Forte V., De Soccio V., Di Leo N., Rubini A., Di Segni M., D'Ambrosio F., Catalano C.**
Can S-detect provide accurate differentiation of thyroid nodules? - assessing the impact on the assessment made by operators with different experience (SS 708), B-0668
- Alahmadi M.S., Alharbi M., Mobark N., Alsaad A.N., Dagherri A., Anver A.B., Althagafi M.S.J., Raja S.**
Predicting medulloblastoma genomic subtypes by exploiting MRI morphologic phenotypes (SS 1811b), B-1476
- Albano D., Messina C., Tagliafico A., Sconfienza L.M.**
How, when, why in magnetic resonance arthrography: an international survey by the European Society of Musculoskeletal Radiology (SS 1010), B-0955
- Albano D., Chianca V., Galia M., Cuocolo R., Bignone R., Messina C., Sconfienza L.M., Brunetti A., Lagalla R.**
T2-mapping of the sacroiliac joints at 1.5T: a reproducibility study (SS 1910), B-1616
- Alberich-Bayarri A.**
Everything you need to know about 3D post-processing: A. 3D post-processing in 2018 (RC 105), A-047
- Alberich-Bayarri A.**
Artificial intelligence and big data in medical imaging: IT infrastructure, data sharing methods and data analysis aspects (PC 15), A-734
- Albrecht M., De Cecco C.N., Otani K., Nance J.W., Varga-Szemes A., De Santis D., von Knebel Doeberitz P., Vogl T.J., Schoepf U.J.**
Diagnostic accuracy between low and high tube voltage third-generation dual-source coronary CT angiography using tailored contrast medium injection protocols (SS 703), B-0752
- Albrecht M., Baumann S., Nance J.W., De Cecco C.N., Varga-Szemes A., Vliegenthart R., Schwemmer C., Vogl T.J., Schoepf U.J., Martin S.S.**
Machine-learning on-site CT-derived fractional flow reserve (FFR) compared to invasive FFR: influence of myocardial mass on accuracy (MY 7), B-0776
- Albrecht M., Varga-Szemes A., De Cecco C.N., Vogl T.J., Nance J.W., De Santis D., Eid M., Piccini D., Schoepf U.J.**
Diagnostic accuracy of non-contrast self-navigated free-breathing MRA in paediatric patients with coronary anomalies using CTA as reference standard (SS 1503), B-1232
- Albweady A.A., Raja S., George S., Alharbi M., Aldossari K.**
Myocardial textural analysis and machine learning for differentiating normal myocardium vs chronic infarct on non-contrast CT scan (SS 1003), B-0982
- Alcalá-Galiano A.**
MR imaging of the knee: A. Cruciate ligaments: what to know and do (RC 1710), A-920
- Alfaqih M., Soni S., Flacke S., Andrabi Y., Elentuck D., French R.**
Inferior glenohumeral vertical distance: a novel radiographic marker better suited for detection of rotator cuff tears involving the infraspinatus tendon (SS 1010), B-0951
- Alfayate Sáez E., de la Cámara Egea M.A., Vega de Andrea N.I.**
Making the most of social media: The value of social media to professional societies (EFRS WS), A-789
- Ali M., Monti C.B., Carbone F.S., Secchi F., Cannao' P.M., Sardaneli F.**
Quantitative oedema and late gadolinium enhancement thresholds for the diagnosis of myocarditis in suspect cases (MY 7), B-0786
- Ali R.M.K.M., England A., Mercer C.E., Tootell A.K., Hogg P.H.**
Impact of contralateral breast shielding on the risk of developing radiation-induced cancer from full field digital mammography (FFDM) screening (SS 214), B-0135
- Ali T.F.T.**
Diffusion-weighted MRI in prostatic lesions: diagnostic performance of normalised ADC using normal peripheral prostatic zone as a reference (SS 307), B-0247
- Alison M.**
Paediatric MRI: can we make gadolinium superfluous?: Chairperson's introduction (SF 13b), A-648
- Alkadhi H.**
Emergency radiology I: A. Acute aortic syndrome (E³ 121), A-001
- Alkadhi H.**
Dose reduction and image quality implications of iterative image reconstruction in CT: B. Iterative image reconstruction in clinical practice (dos and don'ts) (RC 1513), A-784
- Allard P., Bridoux A., Longere B., Silvestri V., Schmidt M., Forman C., Pontana F.**
Compressed sensing real-time cine imaging in patients with cardiac arrhythmia: does it help to reduce mistriggering artefacts? (SS 1403), B-1156
- Allen C.**
Focal treatment of prostate cancer: Imaging of prostate cancer: how accurately can prostate cancer be localised? (SF 9a), A-397
- Allimant C., Kafrouni M., Delicque J., Ilonca A., Fourcade M., Mariano-Goulard D., Cassinotto C., Piron L., Guiu B.**
Tumour targeting and 3D voxel-based dosimetry to predict tumour response, toxicity and survival after Y-90 resin microsphere radioembolisation in HCC (SS 1409), B-1057
- Almehmi A., Narasimha Krishna V., Abdel Aal A.M.**
Cumulative patency rate of forearm vs upper arm arteriovenous dialysis fistulae (SS 1009), B-0866
- Alqahtani F., Messina F., Offiah A.C.**
Assessment of a 33-point software programme for the identification of vertebral fractures in children (SS 212), B-0158
- Alqahtani S.J.M., Knapp K., Palfrey R.M., Meakin J.R.**
Construction of obese phantoms for dose optimisation and image quality purposes (SS 714), B-0746
- Alqahtani S.J.M., Knapp K., Palfrey R.M., Meakin J.R.**
Fabrication of fat tissue-equivalent substitutes (FTES) and lean tissue-equivalent substitute (LTES) to underpin obese phantom construction (SS 714), B-0751
- Alsharif W., Davis M., Rainford L.A., McGee A.**
The impact of the smartphone application (app) on MR radiographers' knowledge and confidence in relation to MR image-quality-related errors (MY 17), B-1300
- Alster T., Carmon E., Maly B., Sella T.**
The incremental value of preoperative MRI for evaluation of extent of disease in IDC vs ILC (SS 1002), B-0916
- Altamash M., Grover S.B., Suman S., Katyan A., Kumar A., Mandal A.K.**
Contrast-enhanced ultrasound in evaluation of renal masses: a preliminary experience (SS 207), B-0054
- Altay Ç.M., Düsünceli Atman E., Uzun C., Arslan M.F.**
Should breast artery calcifications be graded? (SS 202b), B-0098
- Altman A.**
Single-dual-multi-energy CT: B. Photon counting detectors in diagnostic CT (RC 113), A-035
- Alukic E., Škrk D., Mekis N.**
Dose reduction with PA projection in lumbar spine radiography (SS 714), B-0745
- Alves E.D., Zorzenon C.d.F., Bienes G.H.A.A., Ferraz H.B., Carrete Jr H.**
MR imaging of the Parkinson's syndrome: a pictorial essay (SS 1511), B-1233
- Amarnath C.**
State-of-the-art paediatric neuroradiology: Chairperson's introduction (RC 811), A-335
- Amato F., Orlando A., Di Vittorio M., Safina M., Bartolotta T.V., Ienzi R.**
Background parenchymal enhancement in MRI, mammographic density and risk of breast cancer (SS 1902a), B-1614
- Amaxopoulou C., Geiger J., Grehten P., Gnannt R., Bode P., Moehrlen U.**
Magnetic resonance imaging of congenital lung lesions (SS 1412), B-1166
- Amini N., Fomekong E., Raftopoulos C., Vande Berg B.**
Disc and vertebral changes after spinal fusion at serial CT imaging: correlation with disc stability (SS 610a), B-0438
- Amodeo E., Contegiaco A., Attempati N., Paladini A., Di Stasi C., Manfredi R.**
Renal artery embolisation for vascular lesions following Nephron-sparing surgery: a five-year experience (SS 1009), B-0861
- Anastasia T., Pronin I., Fadeeva L., Kornienko V.**
3D MRSI biomarkers of glial tumour (SS 1811b), B-1484
- Andersson B.**
Radiography research: a how to guide: How to avoid ethical issues (BR 1), A-549

Authors' Index

Andersson B.T.

Patient-doctor relationship and interdisciplinary communication in the radiology department: A radiographer's point of view (PA 1), A-695

Ando S.M., Coelho F.M., Viana P.C.,

Gomes L.G., Fragoso M.B.V., Yamauchi F.I. Diagnostic accuracy of primary macronodular adrenal hyperplasia on CT: a quantitative and qualitative study (SS 1007), B-0877

Andrade S., Velasco S., Bermúdez S., Useche N., Morillo A.J.

Scannographic density of intracranial venous sinuses in healthy patients and diagnosed with venous thrombosis at 2600 meters above sea level from 2008 to 2016 (SS 711b), B-0694

André A., Pinto J., Oliveira D., Aguiar C., De Francesco S., Oliveira A., Marques A., Martins P.

Development and reliability of an ultrasound protocol to evaluate quadriceps muscle mass and diaphragm structure: a pilot study (SS 1014), B-0963

Andreani O., Gendre P., Dekimpe C., Rudel A., Amoretti N., Boileau P.

Postoperative evaluation of an arthroscopic coracoid bone block surgery with CT-Scan. (MY 13), B-1025

Andreani O., Dekimpe C., Raffaelli C., Amoretti N.

Learning curve of an ultrasound-guided percutaneous release of carpal tunnel: a cadaveric study (MY 13), B-1027

Andreini D., Mushtaq S., Pontone G., Annoni A.D., Formenti A., Mancini M.E., Guglielmo M., Bartorelli A.L., Pepi M.

Diagnostic accuracy of coronary CT angiography performed with a novel whole-heart coverage high-definition CT scanner in patients with coronary artery bypass graft (SS 703), B-0755

Andreini D., Mushtaq S., Sonck J., Pontone G., Conte E., Mancini M., Baggiano A., Bartorelli A.L., Pepi M.

Additional diagnostic value of CT perfusion over coronary CT angiography in stented patients with suspected in stent restenosis or coronary artery disease progression: Advantage study (SS 1803), B-1459

Andreini D., Mushtaq S., Pontone G., Annoni A.D., Formenti A., Mancini M.E., Conte E., Guglielmo M., Pepi M.

Cardiac MRI for a better identification of structural heart disease in patients with ventricular arrhythmia (SS 1903), B-1658

Andreisek G.

Small joints: C. Temporomandibular joint (E³ 1119), A-514

Angelakis A., Gatos I., Soultatos A., Kanavaki A., Panteleakou E., Theotokas I., Vafiadis I., Manesis E., Zoumpoulis P.

A deep-learning approach to the significant liver fibrosis binary classification problem using gender, morphologic and haemodynamic measurements derived from B-mode ultrasound images (SS 601a), B-0430

Annoni A.D., Formenti A., Andreini D., Guglielmo M., Muscogiuri G., Pontone G., Consiglio E., Conte E., Pepi M.

Low-dose CT angiography for thoracaorta: optimal combination between 80kV and last generation iterative reconstruction algorithm levels (SS 215), B-0031

Antonelli A., Capuani S., Guerreri M., Bernardo S., Petrillo R., Vinci V., Manganaro L., Catalano C.

Apparent diffusion coefficient (ADC) and its correlation with gestational age (GA) in normal developing foetal brain: preliminary results of a prenatal MRI study (SS 212), B-0151

Antonelli A., Bernardo S., Petrillo R., Satta S., Ciulla S., Vinci V., Manganaro L., Catalano C. Vermis-to-Pons ratio in the differential diagnosis of Vermian malformations: a foetal MRI study (MY 18), B-1494

Antunovic L., Catalano M., Di Mento L., Malagoli E., Balzarini L., Chiti A., Kirienko A., Berlusconi M., Trenti N.

FDG-PET/CT for diagnosis of infection in post-traumatic non-unions (SS 1410), B-1128

Anzidei M.

Post-treatment evaluation: what every radiologist should know: C. Peripheral arterial disease (RC 815), A-359

Apine I., Angerer M.P.M., Baduna M., Krumina G.

DWI ADC values are influenced not only by bowel distention degree but also the presence of osmotically active agent: results from research in healthy subjects (SS 1901c), B-1530

Appel E., Kröpil P., Thomas C., Aissa J., Klosterkemper Y., Heinzler N., Boos J.

Quality assurance in CT: using automated CT dose monitoring software to implement updated national diagnostic reference levels (SS 1905), B-1584

Appendino E., Pedalino S., Tabone E., Romano V., Mazzetti S., Giacobbe A., Muto G., Russo F., Regge D.

Prostate cancer detection rate in patients with negative multi parametric (mp) MRI or negative biopsy after 2 years of follow up (MY 4), B-0383

Araujo Martins D., Ruiz Salmeron R., Rivera A., Caparros Escudero C., Cueto Álvarez L., Mateo Carballo F.

Angio-CT: key for landing zone reconstruction in TAVI (SS 203), B-0145

Araújo-Filho J.A.B., de Santis A., Nomura C.H., Tarasoutchi, F., Vieira M.C., Katz M., Brown J., Edelman E.R., Lemos P.A.

The role of topography of valve calcification in degenerative aortic stenosis: a new marker in CT evaluation (SS 203), B-0142

Araújo-Filho J.A.B., Assuncao-Jr A.N., Tavares de Melo M.D., Dantas Jr R.N., Nomura C.H., Parga Filho J.R.

Myocardial tissue characterisation by cardiac magnetic resonance imaging in left ventricular non-compaction: new insights with T1 mapping and extracellular volume quantification (SS 1003), B-0977

Arcuri P., Roccia S., Fodero G., Mole' R., Destito A., Bertucci C., Lagana' D.

The predictive capacity of DWI vs perfusion imaging in response assessment of brain metastases following stereotactic radiosurgery (SS 1016b), B-0940

Arendt C., Leithner D., Lenga L., Martin S.S., Vogl T.J., Wichmann J.L.

Dual-energy coronary CT angiography: improved vascular contrast using noise-optimised virtual monoenergetic imaging (SS 703), B-0753

Argyropoulou M.I.

Paediatric: A. Paediatric neuro imaging (E³ 1823), A-953

Argyropoulou M.I.

Imaging of the brain in preterm infants: The role of cerebral ultrasound (SF 12b), A-537

Argyropoulou M.I.

Brain tumours: A. Paediatric brain tumours (E³ 1421), A-682

Arkipova I.

Abdominal emergencies: friends and enemies: Chairperson's introduction (SF 17b), A-900

Aronen H.

ESR and UEMS: a united European voice: ETAP 2.0 (part 1): history of ETAP (ESR/UEMS 1), A-185

Arora A.

Liver and bile duct pathologies: A. Inflammatory and infectious disease (E³ 820), A-373

Arteta C., Pickup L., Novotny P., Sandford Z., Brabec J., Dufek D., Kunst J., Declerck J., Kadir T.

Lung nodule risk stratification using Deep Learning on the complete US National Lung Screening Trial dataset (SS 1004), B-0868

Asbach P.

Imaging strategies in renal tumours: C. Staging and organ-preserving strategies (RC 1707), A-899

Ashikhmin Y.

The heart team: coronary imaging and treatment: Multidisciplinary case presentation and discussion (MS 4), A-132

Aslan S., Nural M., Camlidag I., Danaci M. Efficiency of perfusion CT in pancreatic mass characterisation (SS 1416), B-1082

Athanasidou A.

My three top tips for breast imaging: US-guided biopsy (SF 8b), A-331

Athanasidou A.

Minimally-invasive local treatment of breast cancer: the time is now: Chairperson's introduction (RC 902), A-404

Athanasidou A.

Contrast-enhanced spectral mammography: Chairperson's introduction (SF 15b), A-752

Attempati N., Contegiacomo A., Amodeo E., Barone M., Cina A., Manfredi R.

Ruling out acute kidney injury (AKI) with "admission" reno-caval ultrasound (ARCUS) examination (SS 1017), B-0944

Attye A., Jean C., Remond P., Lecler A., Aptel F., Chiquet C., Lamalle L., Krainik A.

Ischaemic optic neuropathy: using track-weighted imaging to detect changes in the neuroretina (MY 8), B-0802

Auer C.M.

eHealth in radiology: policies, practices, pitfalls, potential: Member States Joint Action on eHealth (ESR/EU), A-774

Auer T.A., Marini F., Renovanz M., Brockmann M.A., Tanyildizi Y.

Evaluation of the apparent diffusion coefficient in patients with recurrent glioblastoma under treatment with bevacizumab with radiographic pseudoresponse (SS 1016b), B-0939

Aukland S.M.

Understanding paediatric neuroradiology: A. Imaging of the premature brain (RC 1712), A-889

Avenarius D.

Paediatric musculoskeletal imaging: A. How to distinguish normal variants from pathology on musculoskeletal MRI in children (RC 112), A-010

Authors' Index

Aviram G.

Updates on lung cancer management:
C. Lung cancer staging (E³ 918), A-449

Avni F.E.

Paediatric MRI: can we make gadolinium superfluous?: Safety issues of intravenous gadolinium in children (SF 13b), A-649

Ayaz Ü.Y., Ozturk M.H., Dilli A., Hekimoglu B.

Comparison of T2*-weighted gradient-echo sequence with magnetisation transfer contrast, to other MRI sequences in the diagnosis of gonarthrosis (SS 310), B-0305

Aydingoz U.

Musculoskeletal radiology: inflammation:
B. Arthropathies (E³ 221), A-062

Aydingoz U.

MR imaging of the knee: C. Looking around the corners: posteromedial and posterolateral (RC 1710), A-922

Ayuso C.

Imaging of the complicated postoperative abdomen: A. Liver (RC 401), A-096

Ayuso C., Darnell A., Rimola J., Garcia-Criado A., Vilana Puig R., Forner A., Bruix J.

Prospective evaluation of dynamic MR with gadoxetic acid for the non-invasive diagnosis of HCC in newly detected nodules smaller than two centimetres on US in cirrhotic patients (SS 301a), B-0191

Ayuso C.

Imaging of HCC: B. Early HCC and well-differentiated HCC (E³ 520), A-243

Ayuso J.R., Cuatrecasas M., Maurel J., Reig O., Conill C., Darnell A., Pages M., Rodríguez S., Sanchez S.

CT and pathologic correlation in pancreatic cancer after neoadjuvant chemoradiotherapy (SS 1901b), B-1520

Azarine A.A.

Cardiac MRI: from sequence to bedside:
A. 4D flow imaging: how and when can it help? (E³ 1326a), A-618

B

Ba-Ssalamah A.

Imaging of benign liver lesions: still difficult?:
C. FNH or adenoma? (RC 901), A-384

Ba-Ssalamah A.

Peritoneum and mesentery:
Chairperson's introduction (E³ 1622), A-866

Babkova A., Serova N.S., Pasha S.P., Shariya M.

Radiological diagnosis of desomorphine-associated osteonecrosis (MY 14), B-1200

Badia S., Bellini D., Marigliano C., Rengo M., Osimani M., Picchia S., Petrozza V., Laghi A.

CT texture analysis in clear cell renal cell carcinoma: a radiogenomics prospective (SS 207), B-0060

Badr S., Pansini V.M., Legroux-Gérot I., Vignau J., Stefan R., Karampinos D.C., Chauveau C., Cortet B., Cotten A.

Bone marrow adiposity assessed by 3T MR-spectroscopy in the hip of women with anorexia nervosa (SS 1410), B-1122

Baessler B., Lücke C., Klingel K., Kandolf R., Schuler G., Maintz D., Gutberlet M., Thiele H., Lurz P.

Diagnostic potential of texture analysis applied on cardiac magnetic resonance T1 and T2 mapping in patients with biopsy-proven chronic myocarditis (SS 1003), B-0979

Bai W., Ning G., Li X.

Application of ADC Value of MR DWI in the evaluation of children's renal function (SS 612), B-0583

Bai X., Lin J.

Intracranial atherosclerotic plaque enhancement associated with ischaemic stroke: a study with three-dimensional high-resolution magnetic resonance vessel wall imaging (MY 8), B-0804

Bajic D., Kumlien E., Milivojevic M., Raininko R.

Incomplete hippocampal inversion does not affect the hippocampal volume in neurologically healthy subjects (SS 1811a), B-1401

Bakdik S., Arslan S., Öncü F., Durmaz M.S., Altunkeser A., Eryilmaz M.A., Unlu Y.

Effectiveness of superb microvascular imaging (SMI) in differentiating intraductal breast lesions (SS 1802b), B-1418

Bakhshayeshkaram M., Zahirifard S., Aghahosseini F., Hashemi Beni R.

A proposal diagnostic algorithm for F-18FDG PET/CT-detected breast incidental lesion based on BI-RADS and SUVmax criteria (SS 602), B-0500

Balaji R.

IVIM MRI of oestrogen-receptor-positive breast cancer: association with quantitative IVIM parameters and Ki-67 proliferation status (SS 716), B-0701

Balaji R.

Application of 80-kVp scan and raw data-based iterative reconstruction for reduced iodine load PET/CT in an oncological setting: a win-win technique (SS 1016a), B-0896

Balaji R.

Assessment of response to therapy in bone metastases from prostatic malignancy beyond mono-exponential diffusion imaging (SS 1516), B-1254

Balaji R.

Predicting early response in cervical malignancies to concurrent chemoradiation using intravoxel incoherent motion (IVIM) MRI (SS 1816), B-1372

Balbi M., Invernizzi F., Bonaffini P.A., Preziosa G.C., Nicoletta D., Valle C., Pappini A., Sironi S.

Evaluation of parenchymal and vascular enhancement in split-bolus MDCT urography compared to standard single-bolus protocol: a feasibility study (SS 1807b), B-1469

Baleva D.

Highlighted Lectures: Imaging of paediatric gastrointestinal emergencies (TF 1), A-691

Bali M.A.

New challenges of pancreatitis: C. Tough clinical cases of cystic pancreatic lesions (E³ 1322), A-677

Balleyguier C.S.

Basic breast imaging: A. Calcifications in mammography (E³ 621), A-245

Balleyguier C.S.

Management of incidental findings in the genitourinary tract: C. Adnexa (RC 1307), A-627

Balleyguier C.S., Bayou E., Boyer B., Canale S., Eweczyk-Bitton I., Gilles R., Rotenberg L., Viala J., Delaloue S.

Feasibility of risk assessment and personalised breast screening recommendations delivery in community radiology practice: a national prospective study (NCT02997384) (SS 1902a), B-1605

Balzer T.

10 years of NSF: a critical review in the context of gadolinium in brain and body (SY 9)

Balodis A., Radzina M., Kupcs K., Milglane E., Savlovskis J., Kidikas H., Veiss A.

Two year follow-up: results after acute stroke endovascular thrombectomy (MY 9), B-0814

Bamberg F.

CT of the heart made easy: Non-invasive coronary (CT) angiography made easy (E³ 24D), A-719

Bamberg F.

What a radiologist needs to know about imaging of myocardial viability: C. CT (RC 1503), A-748

Bancroft L.W.

Postoperative imaging of sports injuries: A. Postoperative shoulder MRI after instability surgery (TC 1628), A-870

Bancroft L.W.

Postoperative imaging of sports injuries: C. Interactive case discussion (part 1) (TC 1628), A-872

Bankier A.A.

Updates on lung cancer management:
B. Lung nodule management (E³ 918), A-448

Barber I.

Paediatric musculoskeletal imaging:
C. Skeletal trauma in children (RC 112), A-012

Barbera M., Testoni S., Dabizzi E., Gusmini S., Petrone M., Esposito A., Del Maschio A., Arcidiacono P., De Cobelli F.

Endoscopic ultrasound-guided hybrid therm ablation in patients with stage III pancreatic adenocarcinoma: a clinical study with radiological perspectives (MY 9), B-0816

Barbone G.E., Di Pietro P., Eckermann M., Mittone A., Bravin A., Romanelli P., Battaglia G., Coan P.

3D detection of cellular neurodegeneration in Alzheimer's disease via multi-scale x-ray phase-contrast micro- and nano-CT (SS 1411a), B-1041

Barbosa Jr. E.J.M., Lanclus M., Vos W., Van Holsbeke C., De Backer W., De Backer J., Lee J.C.

Quantitative CT and machine learning methods can predict eventual development of bronchiolitis obliterans syndrome after lung transplantation (SS 304), B-0236

Bargellini I.

Portal hypertension and interventional radiology (IR): A. Imaging of portal hypertension (RC 109), A-051

Barkhausen J.

Gadolinium retention: impact on breast MRI? (SY 1a)

Barnacle A.

Peripheral vascular malformations: what every radiologist should know: C. Paediatric vascular malformations: diagnosis and treatment (RC 115), A-045

Barnacle A.

Vascular and interventional radiology in children: A. Common IR procedures in children: state-of-the-art (RC 412), A-107

Barr R.G.

New eL18-4 PureWave transducer with shear wave elastography for breast exams (SY 19)

Barr R.G., DeSilvestri A., Scotti V., Manzoni F., Tinelli C.

Meta-analysis of 3 methods to analyse breast strain elastography (SS 302), B-0267

Authors' Index

Bartolotta T.

Comparison of US strain elastography and entero-MRI to typify the mesenteric and bowel wall changes during Crohn's disease (SY 6)

Basile A.

Musculoskeletal interventions: what every radiologist should know: A. Musculoskeletal ablation and embolisation (RC 509), A-235

Basilico R.

Emergency radiology I: B. Abdominal trauma (E³ 121), A-002

Basilico R.

Emergencies following tumour therapy: C. Abdomen (E³ 1726b), A-943

Bassi C., Fournier L.S., Bouaboula M., Rousseau C., Jannot A., Ngo C., Rousset H., Chamming's F.

Features from computerised texture analysis of breast cancer on contrast-enhanced spectral mammography to predict tumour aggressiveness (SS 1802b), B-1413

Bastarrika G.

Coronary CT angiography: how to start practice, perform and evaluate the exam?: C. Beautiful cases from clinical practice: stents and bypasses (RC 1603), A-812

Bastos-Leite A.J.

Altered mental state: B. Imaging in altered mental state (RC 1311), A-638

Batalov A., Zakharova N., Pronin I., Pogosbekyan E.

Noncontrast ASL-perfusion in pre-surgical glioma diagnostics (SS 211), B-0086

Batsak B.

3D analysis and planning of septal reduction therapy based on CT coronary angiography in patient with hypertrophic cardiomyopathy (SS 1503), B-1229

Bäuerle T.

The radiological investigation of musculoskeletal tumours: C. CT and hybrid imaging (RC 1610), A-843

Baur A.

A multidisciplinary approach to prostate cancer: can we make a difference?: Chairperson's introduction (RC 1716), A-916

Baxa J., Matouskova T., Ludvík J., Schmidt B., Sedlmair M., Ferda J.

Single-source dual-energy CT as part of 18F-FDG PET/CT: direct comparison of iodine-related and metabolic parameters in lung cancer (SS 616), B-0590

Bayraktaroglu S.

Thoracic manifestations of systemic disease: B. Granulomatosis and polyangiitis (RC 1704), A-881

Bayramoglu Z., Çaliskan E., Yilmaz R., Adaletli I.

Quantitative evaluation of testicular stiffness with shear-wave elastography (SS 612), B-0582

Bazhenova D., Sinitsyn V.E., Kononov R.N.

MRI morphometry of the corpus callosum in patients with small vessel diseases of the brain (SS 1011a), B-0928

Beale T.

Imaging of the skull base: B. Tumours of the skull base (E³ 521), A-169

Beaumont C.M.J., Whitby E.H.

Magnetic resonance spectroscopy of the placenta: a feasibility study (SS 1006), B-0987

Becker C.D.

Functional imaging in oncology beyond morphology: where are we now?: Chairperson's introduction: What are the problems of morphologic evaluation (RC 516), A-215

Becker C.D.

Radiology will survive, but will the radiologist still be there?: The value of the radiologist in the evolving digital environment: challenges for leadership (PI 2), A-510

Becker C.D.

Difficult challenges in imaging the acute abdomen: C. Acute biliary conditions (RC 1301), A-607

Becker C.D.

Big data: implications for medical imaging and the need for data protection and cyber security: Implications of protection of medical imaging data: a European perspective (PA 2), A-819

Becker M.

New imaging approaches for radiotherapy: Multiparametric MR-PET for differentiation of residual disease vs treatment-induced inflammatory changes (ESR/ESTRO), A-888

Becker M.

Radiology and Swiss chocolate: a sweet combination: Truffle No. 3: multiparametric imaging in head and neck oncology (EM 1), A-455

Becker M.

Head and neck emergencies: It is red and swollen . . . (SF 12c), A-542

Becker M.

Head and neck: C. Oral cavity, oro- and hypopharynx and larynx (E³ 1423), A-702

Becker S.

Lumbar Disc MRS: can it help my daily practice? An integrated spine surgeon's perspective and experience with NOCISCAN-LS exams using a Siemens 1.5T scanner (SY 27)

Bedlington N.

Patient-doctor relationship and interdisciplinary communication in the radiology department: Chairpersons' introduction (part 1) (PA 1), A-692

Bedlington N.

eHealth in radiology: policies, practices, pitfalls, potential: Patient perspective on EU eHealth policies (ESR/EU), A-777

Bedlington N.

Big data: implications for medical imaging and the need for data protection and cyber security: Chairpersons' introduction (part 1) (PA 2), A-817

Bednarova S., Napoli A., Scipione R., Dababou S., Marrocchio C., Erasmus H., Catalano C.

MR-guided focused ultrasound (MRgFUS) ablation of painful osteoid osteoma: perfusion imaging as predictors of clinical outcomes associated with complete bone integrity restoration (SS 709), B-0630

Bednarova S., Napoli A., Scipione R., Dababou S., Marrocchio C., Erasmus H., Panebianco V., Catalano C.

MR-guided focused ultrasound treatment for management of organ-confined intermediate-risk prostate cancer: evaluation of safety and effectiveness (SS 1909), B-1547

Beeres M., Juhee K., Bucher A.M., Frellesen C., Albrecht M.H., Wichmann J.L., Scholtz J., Vogl T.J., Gruber-Rouh T.

Automated tube potential selection of the lower extremity runoff: comparison to fixed kV with mA modulation (SS 1415), B-1052

Beets-Tan R.G.H.

Gastrointestinal: 'the gut': Colon (BS 2), A-066

Beigelman C.

Imaging of the chest: B. Pleural disease (E³ 1221), A-517

Bell J.K.

Establishing competence in radiology: How to manage the incompetent professional? (PI 1), A-465

Belousova E., Karmazanovsky G.

Non-hypervascular pancreatic neuroendocrine tumours: spectrum of MDCT imaging findings and differentiation from pancreatic ductal adenocarcinoma (MY 15), B-1262

Benedetti G., Panzeri M., Mori M., Sini C., Barbera M., Partelli S., Falconi M., Fiorino C., De Cobelli F.

A preliminary study about the robustness of quantitative CT features of pancreatic NEN: inter-observer variability assessment in delineation of lesions contours on CT images (SS 1413), B-1134

Benhalim M.R., Hogg P.H., England A., Walton L.A., Szczepura K.

Paediatric lifetime cancer risk for head CT protocols of a 1-year-old child (MY 17), B-1303

Benjamin R., Aujero M., Traylor K.S., Gerges M., Holt J.

Screen-detected breast cancer: an argument for starting screening mammography at age 40 in the community-based setting (MY 16), B-1288

Benjaminov O.

Characterisation of focal liver lesions: B. Fat-containing lesions (E³ 620), A-262

Benjaminov O.

Radiologic anatomy: abdomen: Biliary tree (ESR/ESOR 2), A-340

Benz S., Halfmann M.C., Eichstädt J., Lollert A., Düber C., Kreitner K.-F., Emrich T.

Strain parameters for the right ventricle in cardiac MRI: the forgotten child? (SS 1403), B-1157

Benz S., Halfmann M.C., Eichstädt J., Lollert A., Düber C., Kreitner K.-F., Emrich T.

Taking CMR strain into the next dimension (SS 1403), B-1159

Berger F.H.

The latest update in imaging of polytrauma patients: B. CT: is it always whole body? (RC 1517), A-780

Berger N., Rossi C., Ciritsis A., Marcon M., Becker A.S., Boss A.

Determination of breast parenchymal enhancement (BPE) in breast MRI using a deep convolutional neural network (SS 1902b), B-1627

Berliner C., Frenzel T., Tienken M., Abdel M., Klutmann S., Beyersdorff D., Adam G., Krüll A., Bannas P.

The impact of [⁶⁸Ga]PSMA I&T PET/CT on radiotherapy planning in patients with biochemical cancer relapse after radical prostatectomy in prostate cancer. (SS 1516), B-1252

Berman A.A., Ageev A., Chernova O., Vazhenin A.

The role of prenatal diffusion weighted MRI in the evaluation of the fetal CNS condition in patients who received intrauterine blood hemotransfusion as the hemolytic disease treatment (MY 18), B-1497

Authors' Index

- Bernardi D., Gentilini M., De Nlsi M., Pellegrini M., Fantò C., Valentini M., Sabatino V., Houssami N.**
Digital breast tomosynthesis (DBT) as a primary screening test in a population-based screening programme: interim results of the Trento DBT pilot study (SS 202a), B-0077
- Bertalan Z., Nehrer S., Ljuhar R., Fahrleitner-Pammer A., Ljuhar D., Dimai H.**
Combining fractal- and entropy-based bone texture analysis for the prediction of osteoarthritis: data from the multicentre osteoarthritis study (MOST) (MY 13), B-1013
- Bertelli E., Agostini S., Addeo G., Verna S., Parretti F., Raspanti C., Minervini A., Mari A., Miele V.**
Contrast-enhanced ultrasonography (CEUS) and time/intensity curves for the active surveillance of small renal masses (SS 207), B-0056
- Bertolotto M.**
Elastography of superficial structures: where are we now?: Scrotal elastography: hype or real? (WG/EFSUMB 1), A-106
- Bertuzzo L., Zamboni G., Pozzi Mucelli R.**
MRI follow-up of IPMN: can we limit the use of gadolinium administration? (SS 201b), B-0018
- Bertuzzo L., Zamboni G., Negrelli R., Pozzi Mucelli R.**
MRI imaging of branch-duct IPMN: evaluation of agreement between observers with different degrees of experience (SS 1001a), B-0834
- Beyer T.**
Motion artefacts and their management in medical imaging: Chairperson's introduction (RC 1313), A-653
- Bezzi M.**
Image-guided therapies in oncology: Lungs (BS 6), A-412
- Bhagwat K.A.**
Role of RI (resistive index) value as imaging bio marker in differentiating benign and malignant cervical lymphnodes (SS 1508), B-1216
- Bhargava S., Mangerud G., Hofvind S.**
Attendance in BreastScreen Norway by proportion of immigrants in a county (SS 702), B-0681
- Bhargavi V., Subbanna I., Swamy S.S.**
Transarterial Radio-embolisation with 131I-Lipiodol for Hepatic metastases: experience in tertiary care oncology centre in India (SS 1409), B-1058
- Bhat I.H.**
Impact of waiting times on tumour growth and pathological upstaging at surgery (SS 616), B-0585
- Bick U.**
Screening for breast cancer: C. Screening with tomosynthesis (RC 402), A-119
- Biddle D.J., Freeman S., Barker A., Walker C., Higgins R., Upponi S.**
Implementation of a multi-phase contrast injection: single-pass acquisition trauma CT protocol (SS 1014), B-0970
- Bier G., Hempel J., Ernemann U., Bender B., Honegger J.**
Empty sella and inferior sella impression are frequently associated and characteristic in patients with growth hormone-secreting pituitary adenomas (SS 1911b), B-1674
- Bignotti B., Calabrese M., Tosto S., Valdora F., Durando M., Tagliafico A., Mariscotti G.**
Assessment of background parenchymal enhancement on breast MRI: which sequence shows the best agreement? (SS 1902a), B-1613
- Bilbao J.I.**
Image-guided therapies in oncology: Liver (BS 6), A-414
- Bilbao J.I.**
Interventional: B. Image-guided interventions in oncology (E³ 1923), A-972
- Bilhim T.**
Discovering Portuguese radiology: past, present, future: Prostate artery embolisation (PAE) for benign prostate obstruction (BPO): the paradigm shift (EM 2), A-686
- Birch J.**
Patient-doctor relationship and interdisciplinary communication in the radiology department: Patients' point of view (part 1) (PA 1), A-696
- Bisdas S.**
Stroke: emergent large vessel occlusion (ELVO): C. Is endovascular thrombectomy and medical therapy better than medical therapy alone? (E³ 1326b), A-668
- Bjorkman B., Fridell K., Tavakol Olofsson P.**
Where is the radiography profession heading? Plausible scenarios for the profession in Sweden in 2025 (SS 1914), B-1644
- Bjørnstad A.**
Closing the gap between education and clinical practice for radiographers: Education vs clinical practice (PC 13), A-659
- Bladowska J., Pokryszko-Dragan A., Banaszek A., Zacharzewska-Gondek A., Nowakowska-Kotas M., Gruszka E., Sasiadek M.**
Are cerebral DTI changes correlated with degree of disability and cognitive dysfunction in patients with multiple sclerosis? (SS 1911b), B-1679
- Blazic I., Campbell N.M., Knezevic A., Gonen M., Lynn P., Weiser M., Garcia-Aguilar J., Saltz L., Gollub M.J.**
Pelvic MRI after induction chemotherapy and before long-course chemoradiation therapy: what are the imaging findings? (SS 216), B-0167
- Bloem J.L.**
Musculoskeletal: bones and soft tissues: Bone tumours (BS 5), A-214
- Bloem J.L.**
New treatments for musculoskeletal tumours: Chairperson's introduction: What is changing? (SF 17a), A-892
- Blystad I., Warntjes J.B., Smedby Ö., Lundberg P., Larsson E.-M.B., Tisell A.**
qMRI using relaxometry detects non-visible peritumoural contrast enhancement in malignant gliomas (SS 211), B-0096
- Boateng E.Y., Shariati H.K., Sharma R.K., Sanderud A.**
PA vs AP positioning in digital radiography of lumbar spine: the impact of kVp in large-sized patient image quality (SS 714), B-0742
- Boban J., Brkic S., Lendak D., Ostojic J., Bjelan M., Kozic D.**
Brain aging in chronic HIV infection: a comparative multivoxel MR spectroscopy study (SS 1911b), B-1673
- Boccalini S., Bons L.R., van den Hoven A.T., Krestin G.P., van den Bosch A.E., Roos-Hesselink J., Budde R.P.**
Dynamic morphological changes of the aortic annulus in patients with bicuspid aortic valves (SS 203), B-0143
- Boekestijn B., Wasser M.**
Optimisation of MRI screening in hereditary pancreatic adenocarcinoma (SS 201b), B-0011
- Boer D.d., Dam-Vervloet L.A., Boomsma M.F., van Dalen J., Poot L.**
Validation of applied pressures after clinical introduction of pressure-standardised compression mammography (SS 214), B-0131
- Boesen M.**
Clinical indications for weight-bearing CBCT (SY 25)
- Bogaert J.**
Cardiac and vascular: C. Cardiovascular imaging: myocardium and pericardium (E³ 1323), A-643
- Bogaert J.**
What a radiologist needs to know about imaging of myocardial viability: A. MRI (RC 1503), A-746
- Bogveradze N., Mayer P., Klauss M., Lashkhi K., Kauczor H.-U., Weber T.F.**
Is MRCP necessary to diagnose pancreas divisum? (SS 201b), B-0014
- Boita J., Mackenzie A., Van Engen R., Broeders M.J., Sechopoulos I.**
Development of algorithms to degrade the image quality of mammograms for lesion detectability studies (SS 613), B-0550
- Bokwa-Dabrowska K., Łaguna P., Brzewski M.**
Diagnostic imaging of haemophilic arthropathy in children: 3T MRI HAMRIS staging scale (SS 310), B-0307
- Bollineni V., Ytre-Hauge S., Gulati A., Halle M., Woie K., Salvesen Ø., Krakstad C., Trovik J., Haldorsen I.**
The prognostic value of pre-treatment FDG-PET/CT metabolic parameters in cervical cancer patients (SS 1816), B-1368
- Bolstad K.N.**
Dose reduction and image quality implications of iterative image reconstruction in CT: Chairperson's introduction (RC 1513), A-782
- Bonatti M., Lombardo F., Simioni M., Avesani G., Bonatti G.**
Prostate volume estimation at MRI: reproducibility and limits (SS 307), B-0250
- Bonatti M., Pedrinolla B., Lombardo F., Avesani G., Bonatti G.**
Prediction of histological grade of endometrial cancer by means of MRI (SS 707), B-0646
- Bonilla S., Llauger Rossello J., Nuñez Peralta C., Valverde Lavirgen S., Palmer Sancho J.**
Radiological changes of giant cell tumour of bone in treatment with Denosumab (SS 210), B-0116
- Bonilla S., Pascual Goni E.**
The aspect of intracranial haemorrhage of cranial CT at the moment of admission is useful to predict the clinical and radiological evolution (SS 1011a), B-0929
- Böning G., Lüdemann W., Chapiro J., Jonczyk M., Gebauer B., Günther R.W., Streitparth F.**
Real-time 3D-guidance based on C-arm-acquired cone-beam CT (CBCT) in transjugular intrahepatic portosystemic stent shunt (TIPSS) placement (SS 609), B-0446
- Böning G., Adelt S., Fehrensbach U., Kahn J., Feldhaus F., Maurer M.H., Renz D.M., Hamm B., Streitparth F.**
New insights for spectral CT imaging in staging of patients with hypervascularised abdominal tumours (SS 1016a), B-0894

Authors' Index

- Boninsegna E., Zamboni G., Facchinelli D., Triantopoulou C., Gourtsoyianni S., Ambrosetti M.C., Pozzi Mucelli R.**
CT features of primary pancreatic lymphoma: experience from three referral centres for pancreatic diseases (SS 1901b), B-1519
- Bonnici-Mallia M., Weir-McCall J., Brown L., Summersgill J., Talarczyk P., Chin S., Khan F., Struthers A.D., Houston G.**
Development and validation of a pathlength calculation for carotid-femoral pulse wave velocity (SS 315), B-0214
- Bonomo L.**
ESR and UEMS: a united European voice: Chairpersons' introduction (part 1) (ESR/UEMS 1), A-178
- Booij R.**
Optimising computed tomography: B. Optimising radiation dose and image quality (RC 1614), A-850
- Boonen P.T., Buls N., Vandemeulebroucke J., Van Gompel G., De Brucker Y., Aerden D., De Mey J.**
Quantification of blood velocity from time-resolved CT angiography on a 256-slice CT (SS 1415), B-1050
- Booz C., Wichmann J.L., Böttger S., Al Kamali A., Martin S.S., Leithner D., Lenga L., Vogl T.J., Bodelle B.**
Evaluation of a new computer-aided diagnosis system for automated bone age assessment in comparison to the Greulich Pyle atlas method: advanced results of a multireader study (SS 312), B-0346
- Booz C., Noeske J., Martin S.S., Lenga L., Leithner D., Gruber-Rouh T., Eichler K., Vogl T.J., Wichmann J.L.**
Evaluation of colour-coded virtual non-calcium images reconstructed from dual-energy CT for detection of lumbar disc herniation in comparison to MRI: initial results (SS 610a), B-0439
- Booz C., Hofmann P.C., Sedlmair M., Flohr T., Schmidt B., Martin S.S., Leithner D., Vogl T.J., Wichmann J.L.**
Volumetric bone mineral density assessment of the lumbar spine using a novel phantomless dual-energy CT postprocessing algorithm in comparison to dual x-ray absorptiometry (MY 13), B-1026
- Borges A.**
Pathways for tumour spread: A. Pathways for oral cavity and oropharynx tumour spread (RC 408), A-110
- Borggrefe J., Glück B.K., Kabbasch C., Onur O., Abdullayev N., Maus V., Fink G.R., Mpotsaris A.**
Clinical outcome after mechanical thrombectomy in diabetic patients with major ischaemic stroke of the anterior cerebral circulation (SS 1011a), B-0927
- Boric I.**
Shoulder MRI: mastering technique and making my report relevant: Chairperson's introduction (RC 1210), A-568
- Bortsova G., van Tulder G., Dubost F., van der Lugt A., Bos D., De Bruijne M.**
Automatic detection of intracranial calcifications in non-contrast CT (SS 605), B-0485
- Bortsova G., Ørting S.N., Dubost F., Katramados I., Hogeweg L., Wille M.M., Thomsen L.H., De Bruijne M.**
Automatic prediction of emphysema extent in low-dose CT by deep learning (SS 1004), B-0870
- Bos P., Jasperse B., Balm A.J.M., ter Beek L.C., van Leeuwen F.W., van den Brekel M.W.M., Beets-Tan R.G.H., Buckle T.**
D-prep magnetic resonance imaging for the visualisation of the facial nerve (SS 208), B-0068
- Boswijk E., de Ligt M., Habets M., van Marken Lichtenbelt W., Wildberger J.E., Mottaghy F., Schrauwen P., Bucerius J.**
Resveratrol treatment does not reduce vascular inflammation in male subjects at risk of developing type 2 diabetes: an ¹⁸F-FDG PET/CT study (SS 1415), B-1051
- Botelho N.**
Discovering Portuguese radiology: past, present, future: The soul of Portugal: Facts and sounds of the Portuguese guitar (part 4) (EM 2)
- Botsikas D., Bagetakos I., Picarra M., Boudabbous S., Montet X., Lam G.T., Maita I., Kalovidouri A.M., Becker M.**
What is the diagnostic performance of 18-FDG-PET/MR and PET/CT in the initial staging of breast cancer? (SS 602), B-0499
- Bottoni L., Gavazzi E., Ravanelli M., Zanirato M., Greiser A., Farina D., Maroldi R.**
ECV mapping without HCT: comparison between two different synthetic ECV-calculation methods and clinical applicability (SS 1003), B-0978
- Bouchouicha A., Deidier J., Benac K., Balvay D., Oudard S., Pirracchio R., Fournier L.S., Rance B.**
Radiomics of metastatic clear-cell renal carcinoma: reproducibility and correlation for feature reduction (SS 605), B-0476
- Boudiaf N., Krainik A., Warnking J., Pietras J., Moreaud O., Baciu M.**
Cognitive decline in ageing and cerebrovascular reactivity assessed by ASL fMRI of perfusion (SS 1911b), B-1676
- Bouëtté A., Karoussou-Schreiner A., Ducou Le Pointe H., Grieten M., de Kerviler E., Rausin L., Bouëtté J., Majerus P.**
National audit on the appropriateness of CT and MRI examinations in Luxembourg (SS 213), B-0120
- Bourcier R., Détraz L., Serfaty J.M., Guymarc'h Delassalle B., Mirza M., Derraz I., Toulgoat F., Naggara O., Desal H.**
MRI agreement of SVS of thrombi (SS 711b), B-0688
- Bourfiss M., Zghaib T., Hauer R.N.W., Tandri H., Calkins H., Nazarian S., te Riele A.S.J.M., Velthuis B.K., Zimmerman S.L.**
Atrial dysfunction in arrhythmogenic right ventricular cardiomyopathy: value of quantitative MR analysis in predicting atrial arrhythmias (SS 1903), B-1656
- Bourgoti C., Zafeiropoulou K., Panourgias E., Chatoupis K., Antoniou A., Nikolaïdou M., Mouloupoulos L.A.**
Invasive placenta: MRI prognosticators for patients' clinical outcome (SS 607), B-0468
- Brader P.**
Novelties in oncologic imaging: A. Imaging and response assessment of immune-related therapies (E³ 126), A-027
- Brader P.**
Monitoring response: the essential guide for all radiologists: Chairperson's introduction (RC 816), A-342
- Brady A.**
Audit across Europe: directive and perspective: Chairpersons' introduction (part 1) (ESR Audit), A-82
- Brady A.**
Artificial intelligence (AI) applications: Chairperson's introduction (SF 10), A-990
- Brage K.**
Reliability of strain elastography in the supraspinatus tendon (SS 1010), B-0953
- Brambilla M.**
CT screening: benefits, doses and associated risks: Dose and risk assessment (ESR/EFOMP), A-228
- Brambilla M.**
Dose management systems and repositories: part B: Chairperson's introduction (EF 2), A-456
- Brancatelli G.**
Hepatocellular carcinoma: diagnosis, staging and current guidelines: Chairperson's introduction (SF 1), A-016
- Brancatelli G.**
Imaging of HCC: A. CT or MRI for diagnosis and follow-up? (E³ 520), A-242
- Brancatelli G.**
Radiologic anatomy: abdomen: Liver (ESR/ESOR 2), A-339
- Braren R.**
Philips next generation wide-bore 3.0T: body oncology imaging (SY 5)
- Brat H., Zanca F., Imsand S., Rizk B., Montandon S., Pasquier H., Fournier D.**
Radiation dose impact of indication- and BMI-based CT protocols vs anatomy-based protocols: prospective multicentre study (SS 313), B-0314
- Brat H., Dias C., Behzad Imsand S., Thouly C., Montandon S., Rizk B., Fournier D., Zanca F.**
Multicentre CT scanner dose excellence programme: strategies and results (SS 313), B-0316
- Brat H., Racine D., Montandon S., Behzad Imsand S., Rizk B., Fournier D.**
Comparison of clinical and phantom image quality for low-contrast liver lesions in a prospective multicentre dose optimisation protocol (SS 1413), B-1135
- Bratke G., Willwacher S., Weiss K., Maintz D., Brüggemann G.**
MRI T2 mapping: a sensitive and reliable approach to examine changes in muscle metabolism of extrinsic foot muscles (SS 710b), B-0727
- Braun F., Hadlich T., Ruhnke H., Jehs B., Thilo C., Scheurig-Muenkler C., Kroencke T.J., Schwarz F.**
Two novel methods for an objective quantification of iliac artery tortuosity derived from CT-angiography datasets in patients prior to transcatheter aortic valve implantation (TAVI) (SS 215), B-0023
- Breda S., De Vries B.A., Bessems G., Schiphof D., Heeringa J., Krestin G.P., Vernooij M.W., Bierma-Zeinstra S.M., Oei E.**
Follow-up of incidental cartilaginous tumours in the knee of middle-aged women (SS 210), B-0118
- Bremerich J.**
Novel ways to characterise myocardial tissue: T1 and T2 mapping: C. Clinical use of T1 and T2 mapping (RC 903), A-394
- Briers E.**
Big data: implications for medical imaging and the need for data protection and cyber security: Importance of data protection from a patient's view (PA 2), A-821

Authors' Index

Brilli I., Tosi E., Zorzi M., Rizzo A., Fedato C., Orvieto E., Lo Mele M., Baracco M., Fiore A.
Prognostic characteristics of B3 lesions detected by mammographic screening programmes in the Veneto region (SS 1402a), B-1087

Brink J.A.
Value-based radiology: Panel discussion: A European - US debate on the value of "value-based radiology" (part 1) (PI 3)

Brink J.A.
Value-based radiology: Basic concepts of value-based radiology: US perspective (PI 3), A-584

Brink J.A.
Big data: implications for medical imaging and the need for data protection and cyber security: Experiences from the US (PA 2), A-822

Brink M.
The polytrauma patient: Chairperson's introduction (MS 17), A-935

Brink M.
The polytrauma patient: Guidelines and game changers: the radiologist's perspective (MS 17), A-936

Brito J.
GI bleeding: how to solve the problem?: B. Occult and overt GI bleeding: the role of radiology (RC 101), A-005

Brkljačić B.
Minimally-invasive local treatment of breast cancer: the time is now: B. Radiofrequency ablation therapy (RC 902), A-406

Brkljačić B.
eHealth in radiology: policies, practices, pitfalls, potential: ESR eHealth tools (ESR/EU), A-775

Brkljačić B.
Trends in quality education in radiology: Introduction (ESOR), A-283

Brkljačić B.
US and vascular disease: a perfect match: B. Upper and lower limb: arterial district (RC 1315), A-664

Broche L.M., Ross J., Davies G.R., Lurie D.J.
Fast field-cycling MRI for medical applications (SS 613), B-0547

Broeders M., Yankaskas B., Timmers J., Miglioretti D.L., Smith R.A.
Piloting an international self-test: assessment of international mammography screening skills (AIMSS) (SS 702), B-0685

Brookes A.L.
Forensic imaging: C. The importance of the radiographer's role in forensic imaging (RC 114), A-041

Brountzos E.
TEVAR/EVAR: where we are and where we are going: B. EVAR (E³ 526b), A-239

Brown G.
Gastrointestinal radiology: B. Rectal cancer staging: key findings (E³ 721), A-282

Browne D., Szczepura K., England A.
Practitioner variability in collimation and centring for AP shoulder projections (SS 1814), B-1444

Bruno F., Marsecano C., Micelli M., Splendiani A., Masciocchi C.
Weight-bearing MRI evaluation of Modic changes: uncovering the "biomechanical stress" and "active discopathy" theories in low back pain (SS 610a), B-0436

Buchberger W., Gautsch K., Oberaigner W.
Non-mass-like enhancement in MR imaging of the breast: lesion characterisation with morphologic criteria and diffusion-weighted imaging (SS 1402b), B-1112

Buissink C.
Radiographers in preclinical imaging research: Chairpersons' introduction (part 1) (SF 9b), A-422

Bulakbasi N.
Diffuse low-grade gliomas: new things you should know: C. Advanced imaging in low-grade gliomas (RC 1711), A-911

Bülő R.
Ten-year experience of population-based dynamic breast MR Imaging: the Study of Health in Pomerania (SHIP) (SY 1a)

Buls N., De Brucker Y., Devos H., Aerden D., Van Gompel G., Boonen P.T., Nieboer K., de Mey J.
Dynamic 4D CT angiography (DCTA) of the lower extremities with a 256-slice CT (SS 1415), B-1044

Bura V., Nguyen H., Lee S., Tirkes T., Lall C.
Differences in liver imaging reporting and data system categorisation between MRI with hepatobiliary-specific vs primary-extracellular agents (SS 301a), B-0190

Burck I., Yel I., Albrecht M.H., Martin S.S., Wichmann J.L., Balster S., Stöver T., Kaltenbach B., Vogl T.J.
Effect of varying tube potentials for the assessment of cochlear implants using advanced cone-beam CT (SS 308), B-0258

Burgard C.A.
Qualitative and quantitative comparison of lung nodules in an ex-vivo system on a high-pitch dual source CT and a standard CT in free breathing (SS 304), B-0242

Burk K.S., Patino M., Canellas R., Patel M.J., Sahani D.V.
Use of CT texture analysis as a predictive biomarker of response to neoadjuvant FOLFIRINOX chemotherapy and chemoRT in pancreatic ductal adenocarcinoma (SS 201b), B-0016

Burns J.E., Yao J., Chen J., Summers R.M.
Automated assessment of Sarcopenia on CT studies (SS 1905), B-1587

Buscarino V., Rizzo S., Colarieti A., Femia M., Pagan E., Bagnardi V., Bellomi M.
Ovarian cancer staging: prospective comparison among ultrasound, CT and whole-body-MRI (SS 1816), B-1377

Buschulte T.D., Wielpütz M.O., Jobst B., Trauth M., Tremper J., Weinheimer O., Delorme S., Becker N., Kauczor H.-U.
Longitudinal airway remodeling in active and past smokers in a lung cancer screening population (MY 5), B-0413

Buzan M.T.A., Wetscherek A., Heussel C., Kreuter M., Dinkel J.
Quantitative MRI assessment of interstitial lung disease (MY 5), B-0405

Buzzatti L., Keelson B., Apperloo J., Buls N., Scheerlinck T., Van Gompel G., Baeyens J.P., De Mey J., Catrysse E.
Detection of kinematic changes induced by sequential lateral ankle ligament section: a dynamic 4D-CT scan study (SS 710b), B-0721

C

Cáceres J.
Errare humanum est: A. Errors in chest radiograph (E³ 1621), A-805

Cademartiri F.
The heart of the matter: imaging the myocardium: MR in ischaemic cardiomyopathies (E³ 24E), A-959

Cai X., Chen Z.
DKI of microstructural alterations in the kidneys of patients with hyperuricemia (SS 1007), B-0884

Cai X., Liu X.
Quantitative MRI of knee articular cartilage in hyperuricemia (MY 13), B-1019

Çakir S., Baykara Ulusan M., Mutlu I.N., Kiliçkesmez N., Turan Bektas C., Yardimci A.
Microwave ablation therapy of giant hepatic cavernous haemangiomas (SS 1509), B-1206

Caldar A.D.
Imaging in abdominal emergencies: an (evidence-based) update: B. The acute abdomen in young children (RC 512), A-191

Calli C.
Neurologic emergencies: Subarachnoid haemorrhage (BS 3), A-081

Calli C.
Emergencies following tumour therapy: A. Neuro (E³ 1726b), A-941

Calliada F.
Tips and tricks for abdominal ultrasound: Doppler imaging (WG 2), A-439

Camlidag I., Sayit A.T., Elmali M.
Is condyle morphology a factor for anterior temporomandibular disc displacement? (SS 308), B-0256

Campa R., Salvo V., Pecoraro M., Del Monte M., Panebianco V., Catalano C.
Development of an extraprostatic extension imaging score based on multiparametric MRI and histopathology correlations (SS 1407), B-1068

Camps Herrero J.
My three top tips for breast imaging: Post-therapy evaluation (SF 8b), A-334

Camps Herrero J.
MRI for early detection, staging and management of breast cancer: Chairperson's introduction (RC 1202), A-553

Cannao' P.M., Secchi F., Scarabello M., Ali M., Sardanelli F.
The prognostic value of late gadolinium enhancement in non-ischaemic dilated cardiomyopathy (SS 1903), B-1651

Cannizzaro E., Quarchioni S., Bruno F., Gianneramo C., Mariani S., Arrigoni F., Zugaro L., Barile A., Masciocchi C.
Usefulness of T2 mapping sequences for the evaluation of Achilles tendinopathy with 3T MRI (SS 710b), B-0725

Cannizzaro E., Bruno F., Quarchioni S., Capretti I., Mariani S., Arrigoni F., Zugaro L., Barile A., Masciocchi C.
Who runs further? Intra-articular Platelet Rich Plasma (PRP) vs Viscosupplementation (HA) and PRP in the treatment of knee osteoarthritis: six-months follow-up study using T2 mapping (SS 1810), B-1427

Cantisani V.
CEUS and 3D US for assessment of carotid plaque morphology (SY 6)

Authors' Index

Cantisani V.

Elastography of superficial structures: where are we now?: Thyroid US elastography: indications and limitations (WG/EFSUMB 1), A-103

Cao L., Song B.

T2 mapping and diffusion-weighted imaging of hepatocellular carcinoma: prediction of tumour histological grades (SS 301a), B-0199

Cao L., Song B.

MR T2 mapping of hepatocellular carcinoma: sequence parameters optimisation and its correlation with Ki-67 proliferation status, histological grades and microvascular density (MY 15), B-1266

Cao M.

In vivo tracking of the tropism of mesenchymal stem cells to malignant gliomas using reporter gene-based MR imaging (SS 1406), B-1173

Cappello G., Giannini V., Mazzetti S., Russo F., Vassallo L., Doronzio V., Regge D.

Multiparametric magnetic resonance imaging of the prostate with computer-aided detection: non-experienced observer performance study (SS 1905), B-1592

Capretti I., Bruno F., Quarchioni S., Cannizzaro E., Gianneramo C., Mariani S., Arrigoni F., Barile A., Masciocchi C.

Diffusion tensor imaging (DTI) in the evaluation of peripheral nerve sheath tumours: is it valuable for surgeons? (SS 710a), B-0612

Capretti I., Bruno F., Quarchioni S., Palumbo P., Mariani S., Arrigoni F., Zugaro L., Barile A., Masciocchi C.

T2 mapping of Achilles tendinopathy: our experience using T2 mapping sequences in the diagnosis and evaluation of treatment response after PRP therapy (SS 710b), B-0729

Capretti I., Iafrate S., Cannizzaro E., Arrigoni F., Di Luzio M., Giordano A., Mascaretti S., Mascaretti G., Masciocchi C.

Follow-up studies of uterine fibroids (UFs) treated with MRgFUS: who are the best candidates for treatment? (SS 1909), B-1542

Cardoso A.F.V., Abrantes A.F., Ribeiro L.P., Rodrigues S., Almeida R.P., da Silva C.A.

The impact of shift work on life, psychological and physical health of radiographers: a comparison between fixed and rotating shifts (SS 1914), B-1637

Carlsen J.

Elastography of superficial structures: where are we now?: Elastography of the breast: when should we assess tumour stiffness? (WG/EFSUMB 1), A-104

Carmona-Bozo J.C., Torheim T., Woitek R., Patterson A.J., Abeyakoon O., Carraco C., Provenzano E., Graves M.J., Gilbert F.J.

Imaging of the hypoxic microenvironment in breast cancer using PET/MR (SS 602), B-0498

Caroço R.

Planning your career: Radiography: your passport to travel (BR 3), A-929

Carrasquinho R., Ribeiro A.M., Ribeiro L.P., Lesyuk O., Almeida R.P., Abrantes A.F.

Assessment of image quality criteria from chest CT examinations (SS 314), B-0329

Carrié D.

Patient-doctor relationship and interdisciplinary communication in the radiology department: A radiologist's point of view (PA 1), A-694

Carrino J.

Evolution of CBCT (SY 25)

Caseiro Alves F.

Personalised medicine in liver tumours: A. Focal liver lesions in oncology patient (E³ 720), A-293

Caseiro Alves F.

Discovering Portuguese radiology: past, present, future: Introduction: SPRMN President address (EM 2), A-684

Caseiro Alves F.

Abdicating Portuguese radiology: past, present, future: The soul of Portugal: Facts and sounds of the Portuguese guitar (part 1) (EM 2), A-688

Caseiro Alves F.

Abdominal MRI: from standard to advanced protocols: Chairperson's introduction (RC 1701), A-876

Casella C., Mariscotti G., Durando M., Castellano I., Vissio E., Esposito F., Osella Abate S., Fonio P., Gandini G.

Impact of mammographic features and level of tumour-infiltrating lymphocytes on prognosis of triple-negative breast cancer (SS 1802b), B-1414

Caspers J., Eickhoff S.B., Hoffstaedter F., Rubbert C., Aissa J., Südmeyer M., Turowski B., Schnitzler A., Mathys C.

Within- and across-network alterations of the sensorimotor network in Parkinson's disease (SS 1511), B-1235

Cassar-Pullicino V.N.

Musculoskeletal: bones and soft tissues: Soft tissue tumours (BS 5), A-213

Castañer E.

CT of vascular pulmonary diseases: B. Evaluating the pulmonary vasculitis (E³ 218), A-069

Castañer E.

Pneumonia: B. Tuberculosis (RC 1204), A-531

Castanho G.F.D., Yokoo P., Geske J., Michellis G., Cremoneze A., Teixeira B.C.

Neuroimaging manifestations of HIV-AIDS at a reference center in south of Brazil (SS 311), B-0283

Castellano E.

Strategies for dose reduction in computed tomography: from technical concepts to clinical practice: Dose reduction strategies in paediatric CT (EU 2), A-250

Castillo J., Caruana C., Mizzi A., Morgan P.S., Westbrook C.

A systematic methodology for the development and validation of inventories of biomedical imaging physics learning outcomes for radiography and radiology specialities (SS 1414), B-1144

Catalano O.A., Mahmood U., Ferrone C., Blaszkowsky L., Goyal L., Hong T., Catana C., Gervais D., Rosen B.R.

PET/MR of biliary tract malignancies: impact on treatment planning (SS 1006), B-0985

Catalano O.A., Wu V., Mahmood U., Soricelli A., Signore A., Salvatore M., Gervais D., Rosen B.R.

Performance of PET/MR enterography vs MR enterography alone vs PET alone in evaluating active inflammation in Crohn's disease (SS 1901c), B-1533

Catania D.

Radiation protection from A to Z: Chairperson's introduction: The radiographers' role in radiation protection (BR 2), A-628

Caumo F., Romanucci G., Zorzi M., Brunelli S.

A prospective study on sensitivity and reading time of different reading strategies with DBT + synthetic 2D in breast cancer screening (SS 202a), B-0078

Caumo F., Romanucci G., Zorzi M., Brunelli S.

Breast screening with synthetic 2D and digital breast tomosynthesis (DBT): is it really more expensive? (SS 202a), B-0082

Celeng C., Leiner T., Maurovich-Horvat P., Merkely B., de Jong P., Dankbaar J.W., Ghoshhajra B., Hoffmann U., Takx R.A.

A meta-analysis on functional CT for diagnosing haemodynamically significant coronary artery disease: ready for prime time? (SS 1803), B-1463

Cellini M., Orsi M., Floridi C., Oliva G.

Can computed tomography (CT) help in predicting diplopia in orbital blowout fractures (BOFs)? (SS 317), B-0291

Cellini M., Gibelli D., Sforza C., Oliva G.

An innovative 3D-3D superimposition for assessing anatomical uniqueness of frontal sinuses (FS) through segmentation on CT scans (MY 14), B-1197

Cereser L., Greco F., Zanelli E., D'Angelo P., De Carli M., Zuiani C., Girometti R.

Chest HRCT findings in adult patients with different subtypes of humoral primary immunodeficiencies and correlation with lung function test results (SS 204), B-0046

Cerri F., Giaconi C., Arena C., Bulleri A., Neri E.

Open access prescription in oncologic imaging: one-year trial (SS 1016a), B-0892

Çetin N., Gunes Tatar I., Ergun O., Yücege M.

Sonographic evaluation of abdominal wall fat index, intima-media thickness and plaque score in obstructive sleep apnoea syndrome (SS 608), B-0495

Cevasco L., Perugin Bernardi S., Bacigalupo L., Paparo F., De Cesari M., Siri G., Cenderello G., Pinto V.M., Rollandi G.A.

Transient elastography (TE), shear wave elastography (SWE) and magnetic resonance elastography (MRE) for fibrosis assessment in chronic viral hepatitis: preliminary data (SS 301b), B-0211

Chambers G., Vaidyanathan S., Chowdhury F.U.

Predicting nodal activity and clinical outcome of non-small cell lung cancer using 18-FDG PET-CT in the age of EBUS-FNA: initial results (SS 616), B-0593

Chami L., Bera G., Lefort M., Griffon J., Lucidarme O., Pellot-Barakat C.

Can valuable information be derived from the exploitation of quality maps along elasticity maps in SWE of thyroid nodules? (SS 708), B-0666

Chang H., Park H., Kim Y., Yu M., Jung S., Jeon H.

Liver imaging reporting and data system (LI-RADS) version 2017 with gadoteric acid-enhanced MRI: utility of ancillary features in diagnosis of hepatocellular carcinoma (SS 301a), B-0195

Chang W., Chen M.

Shear wave elastography in the evaluation of level VI lymph nodes in papillary thyroid carcinoma (MY 14), B-1194

Authors' Index

Charline Z.C., Jaffro M.

Pulmonary arterial occlusion treatment in patients with haemoptysis: a 32-case single-centre study (SS 1009), B-0860

Charline Z.C.

Prognostic impact of myocardial perfusion single-photon-emission computed tomography in patients with major extracardiac findings by computed tomography for attenuation correction (SS 1503), B-1228

Chassagnon G., Martin C., Ben Hassen W., Stemmer A., Bennani S., Revel-Dubois M.-P.

High-resolution lung MRI: 1.5 or 3 Tesla? (SS 1804), B-1346

Chellathurai A., Narasingam A., Radhakrishnan S., Sankaranarayanan S., Arun D.

Role of MR enterography in evaluation of disease activity and treatment response in paediatric Crohn's disease correlation between MRE and PCDAI scores (MY 18), B-1500

Chen A., Chen C.

Is there rationale for the routine inclusion of chest CT in gastric cancer staging? Evidence from a single-institution cancer registry (MY 3), B-0366

Chen A., Chen C., Tai H., Wu M., Chen K., Ho M., Chang K.

Computer-aided detection of sonographic features for thyroid nodules and its effects on readers' performance (SS 1905), B-1590

Chen B., Shih T.T., Tien Y., Chang M., Cheng M.

Multiparametric PET/MR imaging biomarkers are associated with overall survival in patients with pancreatic cancer (SS 201b), B-0019

Chen C., Lu X., Liu H., Lu Z.

Evaluation of radiation dose and image quality of dual-detector spectral CT portal venography of swine using a low-concentration iodinated contrast agent and low tube current (SS 1815), B-1333

Chen Q., Chen N., Zheng W., Chen X., Li X., Li K., Zhang C.

Vision-related structural and functional reorganisation after incomplete acute cervical cord injury (SS 1911a), B-1603

Chen X., Zhou P., Li H.

Tumour size at MRI association with lymph node metastasis and lymphovascular space invasion in resectable cervical cancer: a multicentre evaluation of surgical specimens (MY 4), B-0394

Chen Y., Zhang X.

Predicting the relapse of acute pancreatitis based on radiomics signature of contrast-enhanced computed tomography (SS 201b), B-0015

Cheng S., Zhu L., Xue H., Jin Z.

Application of CT texture analysis in evaluating histologic grade of pancreatic neuroendocrine tumours (MY 15), B-1264

Cheng X., Cheng J.

Nedd4-1 expression promotes tumour progression in gliomas and relationship between nedd4-1 expressions and DKI features in gliomas (SS 1016b), B-0936

Chilamkurthy S., Ghosh R., Rao P., Biviji M.

Automated detection of intra- and extra-axial haemorrhages on CT brain images using deep neural networks (SS 1805), B-1386

Chilvers G., Udeshi U.

Diagnostic yield of prostate biopsies and PI RADS version 2 scoring of MRI prostates (SS 1807a), B-1359

Chin S., Weir-McCall J., Brown L., Summersgill J., Talarczyk P., Bonnici-Mallia M., Khan F., Struthers A.D., Houston G.

Correlation of a new formula measuring carotid-femoral pulse wave velocity with cardiovascular risk factors, major adverse events and mortality (SS 603), B-0562

Chin S., Kamalasanan A., Henderson S., Sudarshan T.A.

Is it benign or malignant? Assessing isolated lymphadenopathy of the head and neck using textural analysis (MY 14), B-1182

Choi Y., Park C.H., Hye Mi G., Kim T.H., Son E.

Incidental breast lesions on chest computed tomography: prevalence, clinical significance, and differential features for referral (SS 202b), B-0102

Chong G., Barahona Z. D., Balcells A., Hasson D., Schiappacasse G., Labra Weitzler A.

Prospective evaluation of extent of disease in prostate cancer biochemical relapse by [⁶⁸Ga]PSMA-HBED-CC PET/CT (SS 1516), B-1251

Chong V.

Differential diagnoses you don't want to miss: A. Differential diagnoses of orbital masses (RC 108), A-013

Choo K., Jeong Y., Kim M.

Assessment of image quality of coronary artery and left ventricular function and volume using low kVp, mA modulation and advanced model based iterative reconstruction (SS 703), B-0760

Chou I.C., Kuo Y., Lao I.H.W., Hsieh P., Su Y., Mak C., Sun D., Sheu M., Kuo H.

Can gadoteric acid-enhanced MRI predict that a solitary HCC (cT1) is pT1 or pT2? (SS 301a), B-0194

Christou A., Koutoulidis V., Koulocheri D., Zografos K., Zografos G.

Role of one-pass breast lesion excision system in complete excision of high-risk breast lesions expressed as clusters of microcalcifications (SS 1402a), B-1086

Christou A., Ghiatas A., Veliou K., Priovolos D., Bougias H.

Characterisation of breast lesions by whole lesion texture analysis of high b value diffusion-weighted imaging (DWI) (SS 1402b), B-1118

Chu J.P., Song Y., Tang X., Zou L.

Volumetric analysis of the pattern of brain atrophy in Wilson's disease (SS 1511), B-1238

Chu L., Liu R.

Texture analysis of prostate MRI: utility for differentiating patients combined intraductal carcinoma of the prostate from prostate adenocarcinoma (SS 307), B-0253

Chunchao X., Li Z.

Readout-segmented echo-planar diffusion-weighted MR for the evaluation of aggressive characteristics of rectal cancer (MY 15), B-1267

Ciccarese F., Corcioni B., Gaudio G., Garattini M., Busato F., Golfieri R.

Added value of multiparametric magnetic resonance (mpMR) and transrectal ultrasound-MR fusion biopsy in active surveillance for prostate cancer (SS 1407), B-1073

Cicero C., Lievore E., Casarin A., De concilio B., Celia A., Genesio L., Guarise A.

MRI/US fusion prostate biopsy a single-centre experience (SS 1907a), B-1562

Cicero G., Mondello S., Blandino A., Ascenti G., D'Angelo T., Mazzotti S.

A simulated fast magnetic resonance enterography protocol in patients with Crohn's disease: a retrospective, randomised, double-blind study (SS 1901c), B-1536

Ciet P.

Chest imaging of cystic fibrosis: from infants to adults: CT: information content vs dose? (SF 13a), A-610

Citone M., Mondaini F., Raspanti C., Gabbani G., Casamassima E., Falcone G., Fanelli F.

Alternative techniques in splenic artery embolisation in blunt splenic trauma (SS 1009), B-0862

Claudon M.

Tips and tricks for abdominal ultrasound: Chairpersons' introduction (part 1) (WG 2), A-437

Clauser P., Baltzer P.A.T., Kapetas P., Woitek R.A., Weber M., Leone F., Bernathova M., Helbich T.H.

Synthetic 2D mammography can replace digital mammography as an adjunct to digital breast tomosynthesis: experience with a wide angle DBT system (SS 202a), B-0079

Clauser P., Helbich T.H., Kapetas P., Pinker K., Bernathova M., Baltzer P.A.T.

Breast lesion detection and characterisation with MRI: intra-individual comparison of gadoterate meglumine and gadobenate dimeglumine at 3 Tesla (SS 1002), B-0911

Clauser P.

Synthetic 2D mammography with digital breast tomosynthesis: the new mammography (SY 1c)

Clément O.

How to foster clinical research in imaging departments: Results of the ESR Survey on European Research (ESR Research), A-400

Clément O.

Radiomics: what is it and how can we use it?: Chairperson's introduction (NH 12), A-572

Clément O.

From evidence to the new recommendations of the European Medicines Agency (SY 17)

Clevert D.A.

US and vascular disease: a perfect match: A. Abdominal aorta (RC 1315), A-663

Clevert D.A.

Diagnosis and treatment of hepatocellular carcinoma by CEUS (SY 6)

Clevert D.A.

CEUS, a powerful diagnostic tool in daily practice: clinical case presentation (SY 23)

Clevert D.A.

Tips and tricks for abdominal ultrasound: Elastography (WG 2), A-441

Codari M., Scarabello M., Secchi F., Sforza C., Baselli G., Sardanelli F.

Fully automated segmentation of ascending aorta on phase-contrast cardiac MR images: application in healthy and aneurysmatic patients (SS 215), B-0029

Codari M., De Angelis C., Scarabello M., Secchi F., Sardanelli F.

Computer-aided semi-automatic quantification of epicardial fat volume on angio-CT images (SS 303), B-0332

Authors' Index

- Cohen J., Kritter S., Hirt P., Ghelfi J., Reymond E., Ferretti G.R.**
Performance of a software prototype for ILD patterns recognition: how does it compare to chest radiologists? (SS 204), B-0050
- Cohen J., Ferretti G., Benmerad M., Bailly S., Ozcelik C., Reymond E., Jankowski A., Bayat S., Pepin J.**
CT quantitative and semi-quantitative thoracic and extra-thoracic biomarkers in COPD patients: how reliably can they predict patients' outcomes? (SS 204), B-0052
- Collettini F.**
Focal treatment of prostate cancer: Image-guided focal treatment using irreversible electroporation (IRE) (SF 9a), A-399
- Colombo M., Panzeri M.M., Marra P., Brembilla G., Venturini M., Capitanio U., Montorsi F., Del Maschio A., De Cobelli F.**
Technical success and local control after image-guided microwave ablation (MWA) of T1a renal tumours with a new high-power generation system (SS 709), B-0626
- Compagne K., Clephas P., Majoie C.B., Van Zwam W., van Es A., Dippel D.W., Van der Lugt A., Bos D.**
Intracranial carotid artery calcification and endovascular treatment effect in acute stroke patients due to large vessel occlusion (SS 611), B-0512
- Conceição I., Abrantes A.F., Ribeiro L.P., Rodrigues S.I., Almeida R.P.**
A survey on the attitude towards research among radiographers (SS 1914), B-1642
- Connor S.**
Cancer and lymph node imaging: Keynote lecture (SS 1508), K-24
- Contegiacomo A., Attempati N., Amodeo E., Coppolino D., Cina A., Manfredi R.**
Slowly injected unsplit bolus protocol for the reduction of contrast medium (CM) and mean radiation dose exposure (SUPREME Protocol) (SS 1016a), B-0898
- Cook G.**
Hybrid imaging in oncology: Role of hybrid imaging in thoracic malignancies (SF 15a), A-741
- Cook G.**
When to use hybrid imaging: What can we expect as future targets for new radiopharmaceuticals? (ESR/ESH), A-203
- Coolen J., De Keyzer F., Verbeke E., Dubbeldam A., Dooms C., De Leyn P., De Wever W., Van Raemdonck D., Verschakelen J.A.**
Functional MRI evaluation of b-2000 images improve mediastinal lesion characterisation (SS 1904b), B-1574
- Corazza A., Albano D., Rapisarda S., Chianca V., Messina C., Sconfienza L.M.**
The effect of radiographically detected vertebral osteoarthritis (VO) on bone mineral density (BMD) and trabecular bone score (TBS) (SS 610a), B-0440
- Corbi Bellot A., Albiol F., Albiol A.**
Combination of environment recognition sensors and conventional x-ray settings (SS 213), B-0121
- Cornford E.J.**
My three top tips for breast imaging: Stereotactic-guided biopsy (SF 8b), A-330
- Cornud F., Lefevre A., Camparo P., Soyer P.**
MR-guided transrectal prostate biopsy with robotic assistance: initial experience (SS 609), B-0448
- Correas J.-M.**
Ultrasound-guided interventional procedures: new techniques and applications: Kidney (WG 1), A-825
- Correas J.-M.**
Clinical usefulness of new fusion imaging for interventional kidney/liver procedures (SY 13)
- Correia M., Serrado M.A., Horta M., Cunha T.M., Virella D.**
Staging of endometrial carcinoma with MRI: does the fusion T2-weighted and high b-value diffusion-weighted images improve diagnosis? An agreement study with histopathology (MY 4), B-0396
- Corrias G., Porcu M., Laino M., Saba L., Mereu A.**
Relationship between ICA geometry and plaque composition (SS 315), B-0216
- Corrias G., Huicochea Castellanos S., Balachandran V., Saba L., Mannelli L.**
Does second reader opinion affect pancreatic adenocarcinoma management? (MY 3), B-0374
- Corrias G., Eskreis-Winkler S., Krebs S., Zheng J., Saba L., Mannelli L.**
Conventional liver fat quantification MRI vs complex chemical shift-encoded MRI in an oncologic population (SS 1001a), B-0840
- Cosentino A., Obmann M., Gehweiler J., Kelsch V., Hofmann V., Re T.J., Boll D., Benz M.**
Intraindividual interscanner variation of virtual unenhanced attenuation values derived from twin-beam dual-energy CT in comparison to dual-source dual-energy CT in 126 patients (SS 1001a), B-0835
- Costa A.R., Gomes I., Pimenta A.S., Oliveira C., Almeida C.M., Paulo G.N., Santos J.**
Dose values in interventional computed tomography procedures: a multicentre study (SS 314), B-0326
- Costa B.**
Discovering Portuguese radiology: past, present, future: The soul of Portugal: Facts and sounds of the Portuguese guitar (part 2) (EM 2)
- Costa F., Filipe J.P., Reis C.**
Asymptomatic T1 pallidal hyper intensity in patients with chronic liver disease (SS 1511), B-1240
- Costa N.V.V.P., Bastati N., Pötter-Lang S., Guengoern Z., Bican Y., Ba-Ssalamah A.**
Predicting the response of colorectal cancer liver metastases (CRCLM) to preoperative chemotherapy using gadoxetic acid-enhanced MRI (SS 1416), B-1077
- Cotten A.**
Degenerative disorders: Degenerative disorders (E³ 25A), A-079
- Cova M.A.**
Imaging strategies in renal tumours: A. Imaging methods, CT and MRI: the best out of two (RC 1707), A-897
- Cox K., Nandwana S., Olaiya B., Mittal P., Ibraheem O., Smith A.**
MRI liver surface nodularity score: optimising spline stiffness to non-invasively stage fibrosis (SS 701a), B-0602
- Cradock A.**
Contrast media in imaging: C. How safe really are gadolinium agents? (RC 814), A-355
- Cristel G., Esposito A., Damascelli A., Antunes S., Brembilla G., Briganti A., Del Maschio A., De Cobelli F.**
Is it possible to reduce the number of false positive cases of PI-RADS v.2 classification? Role of quantitative analysis of DCE-MRI in prostate lesions' characterisation (SS 1807a), B-1365
- Crombag G.A.J.C., van Hoof R., Schreuder F.H., van der Geest R.J., Mess W.H., van Oostenbrugge R., Hofman P.A., Wildberger J.E., Kooi M.**
DCE-MRI demonstrates less microvasculature in symptomatic carotid atherosclerosis (SS 315), B-0220
- Crombag G.A.J.C., van Hoof R., Heeneman S., Nederkoorn P., Mess W.H., van Oostenbrugge R., Daemen M.J., Wildberger J.E., Kooi M.**
MR imaging shows an inverse association between the microvasculature and intraplaque haemorrhage in atherosclerotic carotid lesions (SS 315), B-0222
- Crombe A., Marcelin P., Le Loarer F., Stoeckle E., Italiano A., Coindre J., Kind M.**
Can conventional MRI help to rectify grading of soft-tissue sarcomas (STS) on needle-core microbioscopy (NCB)? (SS 716), B-0697
- Crombe A., Perier C., Saut O., Denis de Senneville B., Le Loarer F., Stoeckle E., Cousin S., Italiano A., Kind M.**
Machine learning approach on semantic and texture MRI features for early response evaluation in patients with high-grade soft-tissue sarcomas undergoing neoadjuvant chemotherapy (SS 716), B-0698
- Cronin K., Foley S.J., Simpson S., Kelly A.**
Role of renal ultrasound in pelvic imaging: to scan or not to scan? (MY 17), B-1301
- Crouzet S.**
Focal treatment of prostate cancer: Image-guided focal treatment using high-intensity ultrasound (HIFU) (SF 9a), A-398
- Csemez I., Ujlaki M., Gödeny M.**
Initial experience with magnetic resonance elastography of liver (SS 701a), B-0605
- Cui L.**
Value of computed tomography perfusion and diffusion-weighted imaging in predicting the efficacy of non-small cell lung cancer chemoradiotherapy (SS 1904b), B-1577
- Cui L., Wang F., Gong X., Chang M., Yin Z., Fan G., Tang Y., Xu K.**
LHPP gene polymorphism affects spontaneous brain activity in major depressive disorder (SS 711a), B-0658
- Cunha T.M., Horta M.**
Gynaecological and obstetrics: B. Disorders of the adnexa (E³ 1523), A-769
- Currò F., Tonutti M., Giudici F., Zanconati F., Bortol M., Cova M.A.**
Comparison between interval breast cancer (IBC) and screen detected cancer (SDC) in a single centre (SS 702), B-0678
- Cybulski A., Catania M., Negrelli R., Boninsegna E., Brancato S., Tafuri A., Zamboni G., Siracusano S., Pozzi Mucelli R.**
Added value of MRI tractography of periprostatic nerve plexus to conventional T2-WI in detection of extra-capsular extension of prostatic cancer (SS 1407), B-1065

Authors' Index

Cybulski A., Brancato S., Di Paola V., Negrelli R., Boninsegna E., Catania M., Tafuri A., Siracusano S., Pozzi Mucelli R.
Six months follow-up of periprostatic nerve plexus changes after robot-assisted radical prostatectomy using MRI tractography (SS 1907a), B-1567

Cyran C.C.

Monitoring response: the essential guide for all radiologists: B. PERCIST: PET response criteria (RC 816), A-344

Czerny C.

Head and neck: B. Nose, paranasal sinuses and nasopharynx (E³ 1423), A-701

Czerny C.

Differential diagnoses you don't want to miss: B. Differential diagnoses of the jaw masses (RC 108), A-014

Czerny C.

Case-Based Diagnosis Training - Part 2: Head and neck (CB 2), A-974

D

D'Amico N.C., Grossi E., Valbusa G., Malasevski A., Cardone G., Papa S.
A new radiomics approach to predict the evolution of PI-RADS score 3/5 prostate areas in multiparametric MR (SS 605), B-0479

D'Amico N.C., Castiglioni I., Grossi E., Valbusa G., D'Anna G., Rigioli F., Bossi Zanetti I., Scotti G., Papa S.
Radiomics: prediction of acoustic neuroma response to the CyberKnife treatment (SS 605), B-0481

D'Angelo A., Al Mohanna J., Clauser P., Kapetas P., Rinaldi P., Zuiani C., Helbich T.H., Preidler K., Baltzer P.A.T.
Abbreviated breast MRI: do we still need contrast media? (MY 16), B-1289

D'angelo A., Rinaldi P., Rella R., Giuliani M., Belli P., Carlino G., Grippo C., Romani M., Manfredi R.
Usefulness of automated breast volume scanner to evaluate the early response to neoadjuvant therapy in breast cancer patients: a prospective study (SS 1802b), B-1419

D'Onofrio M.

Innovations in pancreatic imaging: Keynote lecture (SS 201b), K-02

D'Onofrio M.

The clinical advantages of advanced applications in the abdomen (SY 11)

D'Onofrio M.

Tips and tricks for abdominal ultrasound: CEUS (WG 2), A-440

D'Onofrio M.

Ultrasound-guided interventional procedures: new techniques and applications: Pancreas (WG 1), A-824

Da Silva J., Yveborg M., Grönberg F., Sjölin M., Holmin S., Lundberg J., Danielsson M.

First evaluation of new photon counting CT technology (SS 1813), B-1438

Dababou S., Marrocchio C., Halpern C., Henderson J., Napoli A., Catalano C., Butts Pauly K., Santini V., Ghanouni P.
MR-guided focused ultrasound (MRgFUS) thalamotomy for the treatment of medically refractory essential tremor (MY 9), B-0821

Dababou S., Andrani F., Napoli A., Scipione R., Marrocchio C., Erasmus H., Catalano C.

MR-guided focused ultrasound (MRgFUS) compared to the main current therapeutic approaches for the treatment of uterine fibroids (SS 1909), B-1541

Dacquino G., Carbone I., Galea N., Agati L., De Rubeis G., Catalano C., Francone M.

Cardiac magnetic resonance in prognostic stratification of patients with acute myocardial infarction and preserved ejection fraction (MY 7), B-0789

Dai Q., Yang Z., Hong G., Rao L., He M., Geng P.

Preliminary clinical application of high-resolution MRI of the optic nerve using a small loop coil combined with head coil (SS 1411b), B-1097

Dai Q., Yang Z., Hong G., Rao L., Geng P.

Selection of coil for high-resolution MRI of the optic nerve (SS 1411b), B-1098

Dai Q., Yang Z.

Measurement of normal optic nerve sheath diameter and nerve diameter on high resolution MRI (SS 1411b), B-1100

Dai Q., Yang Z., Hong G., Rao L.

Preliminary application study of optic nerve DTI in non-neoplastic lesions (SS 1411b), B-1103

Dai Q., Yang Z., Rao L., Hong G., Geng P.

High-resolution MRI findings of the normal optic nerve using a small loop coil combined with head coil (SS 1411b), B-1104

Damilakis J.

Clinical diagnostic reference levels for x-ray medical imaging: Panel discussion (part 1) (EU 3)

Damilakis J.

CT screening: benefits, doses and associated risks: Quantitative benefit-risk analysis (ESR/EFOMP), A-229

Damilakis J.

CT examination of pregnant patients: a dilemma for the radiologist and the mother: Dosimetry methods available (SF 8a), A-311

Damilakis J.

Dose management systems and repositories: part A: Chairperson's introduction (EF 1), A-418

Damilakis J.

Clinical diagnostic reference levels for x-ray medical imaging: Chairpersons' introduction and update on the project on clinical DRLs for x-ray medical imaging (part 1) (EU 3), A-500

Damilakis J.

Clinical diagnostic reference levels for x-ray medical imaging: An update on current European diagnostic reference levels (DRLs) in adult imaging (EU 3), A-504

Dang H., Chen Y., Jin Z., Xue H., Hou B., Li F.

Evaluation of the differentiation in head and neck squamous cell carcinoma with PET/MR (MY 14), B-1181

Dangelmaier J., Schwaiger B.J., Gersing A.S., Sauter A., Riederer I., Muenzel D., Fingerle A.A., Rummeny E.J., Noel P.B.

Comparison of metal artifact reduction by OMAR, MonoE or combined techniques derived from dual-layer spectral CT (SS 1410), B-1121

Danieli L., Distefano D., Prodi E., Ventura E., Riccitelli G.C., Reinert M., Kaelin A., Cianfoni A., Pravatà E.

3D high-resolution post-contrast imaging at 3T for the delineation of enhancing brain tumours: a comparison of three different techniques (SS 1011b), B-1001

Danse E., Joudiou N., Muccioli G., Michoux N., Collart J., Hubert C., Vlassenbroeck A., Gallez B., Coche E.
Spectral CT and cholesterol content in gallbladder stone (SS 601a), B-0424

Danse E.

Spectral CT for emergency imaging: luxury or necessity (SY 12)

Darnell A., Rimola J., Belmonte E., Forner A., Sapena V., Ayuso C., Bruix J.

Transient arterial phase respiratory motion-related artefact in liver MR imaging gadoxetic acid vs extracellular gadolinium. A within-patient cohort comparative study (SS 701a), B-0610

Darwish H.S., Habash Y., Habsah M.

Ectopic pregnancies in caesarean section scars: five-years' experience (MY 4), B-0400

Das M.

Every step counts: imaging and treatment of peripheral arterial disease: Endovascular treatment in peripheral arterial disease (E³ 24B), A-279

De Beaurepaire I., Grevent D., Levy R., Dangoulouff-Ros V., Munnich A., Rötig A., Boddart N.

High predictive value of MRI imaging in mitochondrial disease (SS 212), B-0154

De Bondt T., Zanca F., Lopez Rendon X., Brouhon L., Van der Zijden T., Voormolen M., D'Archembeau O., Parizel P.M.

Diagnostic reference levels for interventional radiology: quantifying diagnostic cerebral angiography complexity (SS 313), B-0318

de Bruijne M.

Artificial intelligence: a strategic view: Deep learning: basic principles (SF 6), A-982

de Bruijne M.

Artificial intelligence and big data in medical imaging: Machine learning in the biomedical domain: challenges and opportunities (PC 15), A-735

De Coster B., Houthoofd S., Laenen A., Fournéau I., Maleux G.

Overall survival and factors predicting long-term outcome after thoracic aortic endovascular repair (SS 309), B-0224

de Graaf R.

Interventional radiology in the venous system: vessel and eye opening: C. Lower limb chronic deep vein occlusion (E³ 1626a), A-860

de Haan D., van der Hoorn A., Westerlaan H.E.

Diagnostic accuracy of FDG-PET and contrast-enhanced CT in patients with head and neck cancer of unknown primary origin (SS 1008), B-0907

De Jonge M.C.

Upper extremity: Chairperson's introduction (E³ 919), A-443

De Koekoek-Doll P., van den Brekel M., Vogel W., Smit L., van Griethuysen J.J., Maas M.

Diagnostic value of real-time ultrasound image fusion compared to ultrasound-only-guided lymph node fine-needle aspiration in head and neck cancer patients (SS 1508), B-1213

De la Mora Malvárez M., Garza Gangemi A., Sánchez Nava D.A., Licano M., Rico Rodríguez O.C., Kauffman Ortega C., Castillejos Molina R.

Testicular microlithiasis: clinic-radiologic-pathologic correlation in 289 patients with germ cell tumour (MY 4), B-0397

Authors' Index

- De Monte F., Riccardi L., Boschini A., Castaldi B., Baffoni L., Milanese O., Paiusco M.**
Study of the feasibility of DAP-to-body-weight ratio as diagnostic reference level in paediatric interventional cardiology (SS 712), B-0773
- De Paepe K.N., Bonne L., Raimondi E., Fotiadis N., Koh D.-M., Starling N., Chau I., Brown G., Cunningham D.**
How safe are percutaneous liver biopsy procedures? Complication rate and seeding risk in an oncological setting (SS 301b), B-0209
- De Paepe K.N., Vieira I.F., De Keyzer F., Wolter P., Bechter O., Dierckx D., Oyen R., Verhoef G., Vandecaveye V.**
Whole-body diffusion-weighted MRI in Hodgkin Lymphoma: 3D texture analysis for early treatment response assessment (MY 3), B-0362
- De Piano F., Buscarino V., Femia M., Tofanelli L., Raimondi S., Origgi D., Botta F., Rizzo S.**
Radiomics of high-grade serous ovarian cancer: association between quantitative CT features and prognosis (MY 4), B-0382
- De Robertis R., Cardobi N., Martini Tinazzi P., Grimm R., Stemmer A., Zanirato M., Tortora G., D'Onofrio M.**
Intravoxel incoherent motion diffusion-weighted MR imaging of solid pancreatic masses: reproducibility and usefulness for characterisation (SS 201b), B-0017
- De Santis D., De Cecco C.N., Albrecht M.H., Thomas B.A., Jacobs B.E., Schoepf U.J., Otani K., Grant K., Laghi A.**
Modified calcium subtraction in dual-energy CT angiography of the lower extremity runoff: impact on diagnostic accuracy for stenosis detection (SS 1415), B-1049
- De Soccio V., Cantisani V., Di Segni M., Di Leo N., Rubini A., Forte V., Fresilli D., D'Ambrosio F., Catalano C.**
New 3D-arterial analysis software to evaluate carotid atherosclerotic plaque in comparison with CEUS, CTA and histological examination (SS 315), B-0221
- De Soccio V., Cantisani V., Alagna G., Di Segni M., Forte V., Di Leo N., La Morte S., D'Ambrosio F.**
Breast lesions characterisation: prospective comparison of strain and shear wave elastography as additional tool to BIRADS classification (SS 302), B-0266
- De Soccio V., Alagna G., Forte V., Di Segni M., Cantisani V., Tassone E., Catalano C., D'Ambrosio F.**
Prospective assessment of TIRADS US assessment and strain and Shear wave elastography to discriminate benign from malignant thyroid lesions (SS 608), B-0493
- de Vito A., Ippolito D., Talei Franzesi C.R., Riva L., Drago S., Sironi S.**
Model-based iterative reconstruction on low-dose CT pulmonary angiography: image quality and radiation dose saving compared with hybrid iterative reconstruction CTPA (SS 1815), B-1328
- de Vito A., Ippolito D., Talei Franzesi C.R., Riva L., Drago S., Sironi S.**
Diagnostic value and radiation dose reduction of model-based iterative reconstruction compared with hybrid iterative reconstruction in abdominal CT study (SS 1901a), B-1514
- De Vries B., Verschueren J., Poot D., Oei E., Krestin G.P.**
Increased perfusion in subchondral bone marrow lesions in knee osteoarthritis measured with quantitative DCE-MRI (SS 1810), B-1426
- De Vuysere S., Vandecaveye V., Dresen R.**
Combined diffusion-weighted MRI with conventional T2 and T1 in-phase/out-of-phase sequences: a short screening protocol for liver metastases (SS 1416), B-1075
- Decoster R.**
Radiography research: a how to guide: How to write a good scientific abstract (BR 1), A-551
- Dedulle A., Moussalli P., Jacobs J., Fytousi N.**
Evaluating the effect of image truncation in the calculation of water equivalent diameter (SS 213), B-0124
- Dehairs M., Marshall N.**
Validation of a task based automatic dose rate control (ADRC) method for interventional cardiology and radiology x-ray systems (SS 213), B-0126
- Dekan V., Zhurbin E., Grishchenkov A.**
Opportunities for the combined use of ultrasonography and neuromonitoring during the intra-operative phase of ultrasound guidance for the surgical treatment of radial nerve injury (SS 1411b), B-1102
- Dekkers I., de Vries A., de Roos A., Rabelink T., Rosendaal F.D., Lamb H.J., de Mutser R.**
Associations between liver fat, visceral fat and microalbuminuria in the general population (SS 301b), B-0204
- Dekkers I., de Heer P., de Vries A.P.J., Lamb H.J.**
Towards renal metabolic imaging of fatty kidney (SS 1007), B-0883
- Del Chiaro M.**
Cystic pancreatic lesions: how to differentiate, how to manage?: When not to operate and when to operate an incidental cystic pancreatic lesion (SF 5), A-222
- del Rosario Perez M.**
Clinical diagnostic reference levels for x-ray medical imaging: Panel discussion (part 5) (EU 3)
- del Vecchio A., Salerno S., Barbagallo M., Campoleoni M., Cannata V., Chirico G., Granata C., Loria A., Magistrelli A.**
Italian guidelines for diagnostic exposure in neonatal intensive care units (SS 1412), B-1165
- Delicque J., Allimant C., Cassinotto C., Piron L., Escal R., Ilonca A., Assenat E., Guiu B.**
Treatment of non resectable HCC: SIRT vs TACE liver toxicity comparison with MELD score (SS 1409), B-1053
- Della Seta M., Colletini F., Kaul D.**
3D imaging biomarkers for the prediction of survival in patients with non-small cell lung cancer or melanoma brain metastases treated with stereotactic body radiation therapy (MY 3), B-0381
- Demaerel P.**
Inflammatory and infectious CNS pathology: A. Autoimmune encephalitis (RC 1211), A-558
- Demetter P.**
Cystic pancreatic lesions: how to differentiate, how to manage?: The evolving role of pathology: can we improve patient stratification? (SF 5), A-221
- Demidova A., Rychkova I., Krivosheeva N., Zubareva E.A., Kuznecova A.**
Multiparameter ultrasound in the diagnosis of deep vein thrombosis of the lower extremities (SS 1815), B-1335
- den Harder A.M., Wolterink J.M., de Jong P.A., de Groot M.C.H., Budde R.P., Isgum I., Haitjema S., Höfer I.E., Leiner T.**
Basic haematological biomarkers are associated with coronary calcification (SS 603), B-0568
- Denecke T.**
Imaging of abdominal tumours: A. Liver tumours (E³ 1921), A-967
- Deng Y., Zeng Q., Wu X., Li X., Luo W.**
Salivary gland tumours in the central airway: the comparison of CT features between adenoid cystic carcinoma and mucoepidermoid carcinoma (MY 5), B-0417
- Denjoy N.**
Euratom Basic Safety Standards Directive: a comprehensive approach for radiation protection: The industry's perspective and work needed to comply with the Basic Safety Standards (EU 1), A-151
- Denjoy N.**
Euratom Basic Safety Standards Directive: a comprehensive approach for radiation protection: Panel discussion: Is the Basic Safety Standards Directive a step forward for patients, clinical professionals and regulators? (part 5) (EU 1)
- Derchi L.E.**
Value-based radiology: Panel discussion: A European - US debate on the value of "value-based radiology" (part 4) (PI 3)
- Derchi L.E.**
Management of incidental findings in the genitourinary tract: A. Adrenals (RC 1073), B-0255
- Derchi L.E.**
Big data: implications for medical imaging and the need for data protection and cyber security: Chairpersons' introduction (part 2) (PA 2), A-818
- Desai S.R.**
Patterns of pulmonary toxicity: B. Smoking-related lung disease (E³ 1526a), A-738
- deSouza N.M.**
MRI for gynaecologic imaging: how I do it: A. Basics of patient preparation and T2W-imaging (RC 1207), A-545
- Dessouky R.A.K., Xi Y., Zuniga J.R., Chhabra A.**
Role of magnetic resonance neurography [MRN] for the diagnosis of peripheral trigeminal nerve injuries in patients with prior molar tooth extraction (SS 208), B-0071
- Dessouky R.A.K., Wells J., Zhang L., Gleason A., Chopra R., Chatzinoff Y., Fey N.P., Xi Y., Chhabra A.**
CAM type femoroacetabular impingement: correlations between alpha angle vs volumetric measurements and surgical findings (SS 1410), B-1126
- Detmer S., Ringshausen F., Vogel-Claussen J., Fuge J., Faschkami A., Shin H.O., Welte T., Wacker F., Rademacher J.**
Computed tomography in primary ciliary dyskinesia: typical imaging findings in the cohort of adult patients with bronchiectasis (SS 204), B-0051
- Detmer S., Suhling H., Kaireit T., Kuhnigk J., Gottlieb J., Vogel-Claussen J., Wacker F., Shin H.**
Quantitative assessment of lung volume and lung density distribution in lung transplant patients: progression pattern in chronic lung allograft dysfunction (SS 304), B-0235

Authors' Index

Devaraj A.

Cavitary and cystic diseases of the lung:
B. Langerhans cell histiocytosis (LCH)
(E³ 418), A-162

Develter W.

Mass casualties: High-end CT imaging in
forensic medicine: experience after recent
Brussels terror attacks (PC 4), A-124

Dewey M.

Wilhelm Conrad Röntgen Honorary Lecture:
Value-based radiology: the future is now!
(HL 1), A-273

Dhillon B., Pawaroo D.

Does performing staging MRI for lateral tongue
tumours after biopsy of the primary tumour
overestimate tumour dimensions and staging?
(SS 1008), B-0903

Dhundass S., Collin A., Duron L., Escalard S., Obadia M., Blanc R., Sadik J., Savatovsky J., Lecler A.

Improved assessment and evaluation of arterial
occlusion in acute ischaemic stroke with
contrast-enhanced MR angiography
(SS 611), B-0514

Di Chiara A., Palmisano A., Esposito A., Rancoita P., Passoni P., Del Maschio A., De Cobelli F.

Could perfusion heterogeneity assessed at
DCE-MRI predict rectal cancer sensitivity to
chemoradiotherapy? (SS 1001b), B-0847

Di Maira T., Torregrosa Andres A., Navarro Aguilar V., Sánchez Mateos D., Fornes V., Berenguer Haym M.

Liver volumetry: a useful tool to predict
functional improvement after antiviral treatment
in cirrhotic chronic hepatitis C patients
(SS 201a), B-0006

Di Martino M., Koryukova K., Catalano C.

Portal hypertension associated with oxaliplatin
administration: incidence and natural history
(SS 1001a), B-0843

Di Segni M., De Soccio V., Bonito G., Rubini A., Magri V., Cantisani V., De Felice C., D'Ambrosio F., Catalano C., Alagna G.

S-detect as a teaching tool in the
characterisation of breast lesions: a preliminary
study (SS 1902b), B-1633

Di Vittorio M.L., Orlando A., Amato F., Spatafora L., Safina M., Taibbi A., Ienzi F., Ienzi R., Bartolotta T.V.

Advancements in computer-aided BI-RADS US
characterisation of focal breast lesions: clinical
assessment of a new software release of
S-Detect (SS 1902b), B-1630

Diaz Candamio M.J.

Making the most of social media: Enhancing
communication and collaboration through social
media (EFRS WS), A-787

Dick E.

Imaging of 'foreign bodies': A. Surgical and
orthopaedic devices: are they really properly
positioned? (RC 1317), A-645

Diekhoff T., Greese J., Sieper J., Poddubnyy D., Hamm B., Hermann K.

Fat saturated 3D-flash sequence improves
erosion detection on the sacroiliac joints: results
from the SIMACT study (SS 310), B-0308

Diekhoff T., Engelhard N., Fuchs M., Pumberger M., Putzier M., Mews J., Hamm B., Hermann K.

Single-source dual-energy computed
tomography for the assessment of bone marrow
oedema in vertebral compression fractures: a
prospective diagnostic accuracy study
(SS 610b), B-0530

Dijkhoff R.A.P.

T2-weighted signal intensity to predict complete
and good response after neoadjuvant
chemoradiation therapy in patients with rectal
cancer (SS 1001b), B-0850

Dillenseger J.

Radiographers in preclinical imaging research:
Radiographers in preclinical research:
challenges and chances (SF 9b), A-424

Ding J., Chen J., Sun J., Xing W.

Development of preoperative prediction of high
Fuhrman grade in the patient with clear cell renal
cell carcinoma (MY 4), B-0387

Dinkel J.

MR imaging of the lungs: B. Evaluating lung
neoplasms (E³ 318), A-085

Dioguardi Burgio M., Imbault M., Ronot M., Faccineto A., Van Beers B., Rautou P.E., Castera L., Tanter M., Vilgrain V.

Ultrasonic adaptive sound speed estimation for
the diagnosis and quantification of hepatic
steatosis (SS 301b), B-0202

Dioguardi Burgio M.

Radiologic anatomy: abdomen:
Pancreas (ESR/ESOR 2), A-341

Dionisi C., Cannillo B., Matheoud R., Vigna L., Fusco G., Brambilla M.

Impact of scanner type and acquisition
parameters on the accuracy of displayed
computed tomography dose index
(SS 314), B-0325

Bluzewski S.L., Patel N., Tincey S.R., Hare S.

Early treatment for PE diagnosed on CTPA:
does electronic critical report labelling make a
difference? (SS 205), B-0173

Dobbin-Stacey R.

OnSight 3D workflow and usability (SY 25)

Dodd J.D.

CT of vascular pulmonary diseases:
Chairperson's introduction (E³ 218), A-067

Doellinger F.

Chest imaging of cystic fibrosis: from infants to
adults: MRI: value of routine MRI?
(SF 13a), A-611

Dominguez A.

Forensic imaging: B. The role of CT angiography
in forensic imaging (RC 114), A-040

Donatelli G., Caldarazzo Ienco E., Migaleddu G., Cecchi P., Aringhieri G., Siciliano G., Cosottini M.

T2* hypointensity of the bulbar segment of the
primary motor cortex in ALS patients with bulbar
impairment (SS 1511), B-1242

Donati F., Boraschi P., Cervelli R., Pacciardi F., Tarantini G., Castagna M., Urbani L., Caramella D., Falaschi F.

Tumour response to preoperative chemotherapy
in patients with colorectal liver metastases: can
ADC values evaluated at 3T MRI replace
RECIST criteria? (SS 1801), B-1320

Dong A.

MRI assessment of brain grey matter structural
changes in severe nicotine dependency
(MY 8), B-0813

Dong Y., Mao F., Cao J., Fan P., Wang W.

Virtual touch quantification technology in
differentiation between benign and malignant
solid small pancreatic tumors: initial results
(SS 1416), B-1084

Dong Y., Mao F., Cao J., Fan P., Wang W.

Microcystic serous pancreatic cystic neoplasms:
the added diagnostic value of contrast-enhanced
ultrasound (SS 1901b), B-1526

Dong Z., Feng S., Huang M., Jia Y., Cai H., Li Z., Shen B.

MRI T2WI and fat-suppressed-T2WI image
fusion technology in improving image quality for
the evaluation of anal fistulas (SS 601b), B-0524

Doniselli F.M., Marfia G., Navone S.E., Guarnaccia L., Campanella R., Summers P., Costa A.

MRI perfusion weighted imaging and von
Willebrand factor antigen plasmatic levels
(VWF:Ag) as predictors of prognosis in grade IV
gliomas (GBM) (SS 1011b), B-1000

Donoghue V.

Paediatric: Chairperson's introduction
(E³ 1823), A-952

Donoso L.

Value-based radiology: Panel discussion:
A European - US debate on the value of "value-
based radiology" (part 2) (PI 3)

Donoso L.

Value-based radiology: Basic concepts of value-
based radiology: European perspective
(PI 3), A-585

Donoso L.

The new horizon for radiology: Chairpersons'
introduction (part 1) (NH 14), A-721

Dorn S., Chen S., Pisana F., Özdemir M., Maier J., Sawall S., Knaup M., Maier A., Lell M., Kachelrieß M.

Context-sensitive organ-specific evaluation and
analysis of dual-energy computed tomography
(DECT) (SS 713), B-0733

Dournes G.

MR imaging of the lungs: C. Evaluating the
airways (E³ 318), A-086

Doweidar A.A.A., Nouh M.R., Khalil A.M., Dashti K.

Can quantitative diffusion weighted imaging
segregate malignant from benign bone lesions?
A 3-T MRI feasibility study (SS 210), B-0109

Drago A., Alberotanza V., Massarelli C., Mappa L., Carbone M., de Ceglie M., Ventrella E., Stabile Ianora A.A., Scardapane A.

Does the heart cycle phase of cardiac-MSCT
influence the measurement of the aortic root in
patients undergoing TAVI placement?
(SS 203), B-0144

Drago S., Talei Franzesi C., Lombardi S., Casiraghi A., Guerra L., Sironi S., Ippolito D.

Predictive value of functional imaging markers
derived from PET/CT and diffusion-weighted
MRI in response assessment of rectal cancer
treatment (SS 1001b), B-0851

Drago S., Ippolito D., Talei Franzesi C., Nasatti A., Parlati A., Casiraghi A., Sironi S.

The diagnostic role of 256 multidetector-row CT
in the detection and characterisation of
incidental pancreatic cystic lesions: comparison
with MR colangiopancreatography
(SS 1901b), B-1518

Drahanowsky W.

Case-Based Diagnosis Training - Interlude:
Normal variant or disease? (CB), A-969

Dreher C., Windschuh J., Sahn F., Bachert P., Ladd M., Zaiss M., Schlemmer H.-P., Radbruch A., Paech D.

Relaxation-compensated multi-pool CEST signal at
7T MRI of glioblastomas is dependent on the
anatomic localisation (SS 1016b), B-0933

Dreval M., Kalashnikova L., Krotenkova M., Dobrynina L.

Lumen dynamics of spontaneous arteries
dissection (SS 315), B-0215

Authors' Index

Dreyer K.J.

Radiology will survive, but will the radiologist still be there?: Big-data, artificial intelligence, machine learning, deep learning etc.: what radiologists should know (PI 2), A-508

Dreyer K.J.

Artificial intelligence and big data in medical imaging: How will AI change radiology (PC 15), A-736

Dromain C.

Immunotherapy: a revolution in cancer care?: CT: looks bigger, but it's better (NH 9), A-386

Dromain C.

Contrast-enhanced spectral mammography: Finding the killer cancers? Can it replace MRI? (SF 15b), A-755

Dromain C.

Peritoneum and mesentery: A. Understanding primary tumours (E³ 1622), A-867

Drzegza A.

Non-oncological hybrid imaging: case-based: Non-oncological intracranial indications for hybrid imaging: case-based (ESH1), A-582

Du R., Khong P., Yuan H., Kwong D.L., Lee V.H., Vardhanabhuti V.

Shape-based and quantitative MRI radiomic features in the assessment of non-metastatic nasopharyngeal carcinoma (SS 208), B-0075

Du R., Alam M.S., Lee V.H., Vardhanabhuti V.

Association between multi-phasic MRI radiomic features and treatment response after stereotactic body radiation therapy (SS 701a), B-0603

Dubost F., Adams H.H., Bortsova G., Ikram M., Niessen W.J., Vernooij M.W., De Bruijne M.

Automatic quantification of enlarged perivascular spaces on brain MRI (SS 1411a), B-1038

Duc N.M., Keserci B., Huy H.Q., Hoa P.N., Thong P.M.

Volumetric magnetic resonance-guided high-intensity focused ultrasound ablation of adenomyosis: the influence of T1 perfusion in predicting treatment outcome (SS 609), B-0449

Duc N.M., Keserci B., Huy H.Q., Hoa P.N., Thong P.M.

A comparative study of quantitative T1 perfusion parameters in magnetic resonance-guided high-intensity focused ultrasound ablation of uterine fibroids (SS 1909), B-1540

Duman I., Ekinci G., Arman A.R., Aslan H., Usta E.B., Bilim G.O., Kavus M.

A fMRI comparison of paediatric patients with obsessive-compulsive disorder and controls during a Stroop task (SS 711a), B-0661

Dumic Cule I., Ivanac G., Lemac D., Brkljacic B.

Importance of sonoelastographic assessment of ruptured and contralateral achilles tendons - prevention of further injuries (SS 710b), B-0726

Dumonteil S., Wilkinson L.S., Mohammadi S., Scott V.

Detection of multiple cancers in a large UK screening population (SS 702), B-0680

E

Ebdon-Jackson S.

Euratom Basic Safety Standards Directive: a comprehensive approach for radiation protection: Chairperson's introduction (EU 1), A-145

Ebdon-Jackson S.

Euratom Basic Safety Standards Directive: a comprehensive approach for radiation protection: Panel discussion: Is the Basic Safety Standards Directive a step forward for patients, clinical professionals and regulators? (part 2) (EU 1)

Ebdon-Jackson S.

Euratom Basic Safety Standards Directive: a comprehensive approach for radiation protection: The regulatory approach (EU 1), A-149

Ebdon-Jackson S.

Audit across Europe: directive and perspective: HERCA and Audit: Inspection vs Clinical Audit. What's the difference? (ESR Audit), A-857

Ebel S., Gottschling S., Buzan M.T.A., Grothoff M., Dähnert I., Wagner R., Gräfe D., Gutberlet M., Lücke C.

3D-assessment of RVOT dimensions prior to percutaneous pulmonary valve implantation (SS 1503), B-1222

Edyvean S.

Patient-specific dosimetry: B. Patient dosimetry in CT and CBCT (RC 1713), A-925

Efremova M., Gazhonova V.E.

Diagnostic value of automated breast volume sonography (ABVS) in breast cancer detection in women with different ACR types (MY 3), B-0369

Egan C., Scott P., Loxley N.

Material-guided scatter correction in cone-beam-computed tomography using spectroscopic information (SS 1813), B-1433

Egan C., Scott P., Loxley N.

Spectroscopic cone-beam-computed tomography using pixel-wise attenuation modulation (SS 1813), B-1436

Eggesbø H.B.

Post-treatment imaging of the head and neck: Chairperson's introduction (RC 1308), A-621

Eid M., De Cecco C.N., De Santis D., Varga-Szemes A., Albrecht M.H., Mastrodicca D., von Knebel Doeberitz P., Sahbee P., Schoepf U.J.

Accuracy of an artificial intelligence deep learning algorithm for the detection of calcified plaques at coronary CT angiography (SS 603), B-0569

Eijkenraam S., Chaudhari A., Gold G., Reijman M., Oei E., Hargreaves B.

T2 relaxometry of cartilage and meniscus and semi-quantitative assessment of the knee using DESS: a 5-minute MRI scan (MY 13), B-1030

Eilers C., Eichstädt J., Schmidt K., Düber C., Emrich T., Kreitner K.-F.

Artefacts in myocardial mapping (SS 1003), B-0975

Eisenblätter M.

Quantitative imaging in oncology: A. Intra- and interindividual tumour heterogeneity and the impact for cancer diagnostics (E³ 1626b), A-862

El Ameen N.F., Amin M.F.

Ultrasound elastography of solid thyroid nodules: how far could we get? (SS 608), B-0488

El Ameen N.F., Amin M.F.

Volumetric interpolated breath-hold MRI sequence: value and reliability in diagnosis of mesial temporal sclerosis (SS 1811a), B-1399

El-Mossly D.M., Mohammad S.A., Abdelhafez E.M., Osman N., Ahmad K.A.

Spectrum of malformations of cortical development with clinicoradiological correlation and analysis of associated abnormalities: experience from a tertiary care centre in Egypt (MY 18), B-1502

ElDeib N.A.E., Singer F.M.E.S., Talaat S.M.M.T., Anas M.

Contrast-enhanced spectral mammography and diffusion-weighted image with backward signal suppression: which is more effective in breast cancer detection? (SS 1802b), B-1411

Eliezer M., Poillon G., Gillibert A., Maquet C., Horion J., Gerardin E., Trintignac A., Magne N., Attye A.

Sensorineural hearing loss in vestibular schwannoma relies on the presence of utricular hydrops, as diagnosed with heavily weighted T2 sequences (SS 208), B-0066

Ellmann S., Wenkel E., Hammon M., Janka R., Fasching P.A., Schulz-Wendtland R., Maier A., Uder M., Bäuerle T.

A novel open-access neural network to evaluate suspicious mass lesions detected in breast MRI for direct integration into clinical workflows (SS 1902b), B-1629

Elmokadem A., Abdel-Wahab R., El-Zayadi A.A., ElRakhawy M.

Combined uterine artery embolisation with intra-arterial chemoinfusion as a sole management for scar and cervical ectopic pregnancy (SS 1909), B-1544

EIShafey M.M.A.H., Elgendi A.

Management of acute occlusion of the superior mesenteric artery by local thrombolysis (multidisciplinary approach) (SS 1009), B-0863

Engelhard K., Bogner K., Schneider F.

Clinical value of the PIRADS score in predicting benign and malignant conditions at MRI-guided prostate biopsy: a correlation of 54 patients with suspicion of prostate cancer (SS 1807a), B-1360

Engelhard N., Hermann K., Fuchs M., Pumberger M., Putzier M., Mews J., Hamm B., Diekhoff T.

Iterative reconstruction improves image quality in virtual non-calcium images of the spine for the detection of bone marrow edema in patients with vertebral compression fractures (MY 13), B-1029

Engelhorn T.

Cerebrovascular disease: A. Vascular distribution territories: arterial and venous (RC 911), A-408

Engelhorn T.

Radiologic anatomy: neuro: Vascular distribution territories: arterial and venous (ESR/ESOR 3), A-562

Entradas D.C., Rodrigues S., Almeida R.P.P., Ribeiro L.P., Abrantes A.F., Reis M.V.C.

Radiation dose reduction on thyroid in mammography (SS 714), B-0749

Enzinger C.

Current guidelines and diagnostic criteria in multiple sclerosis (MS): Update on new clinical diagnostic criteria (SA 5b), A-209

Erasmus H., Napoli A., Dababou S., Marrocchio C., Scipione R., Catalano C.

Evaluation of magnetic resonance guided focused ultrasound (MRgFUS) as a first-line treatment of bone metastases with the intention of local treatment and pain palliation (SS 1809), B-1339

Ereno Ealo M.J.

State-of-the-art imaging of postoperative joints: C. Postoperative ankle and foot (E³ 526a), A-234

Authors' Index

Ergen F.F., Topcuoglu O., Ardali S., Cankurtaran T., Dolgun Barak A., Aydingoz U.

Anterior inferior iliac spine morphology: quantitative and qualitative assessment in an asymptomatic population (SS 1810), B-1421

Ermolaeva V., Marochko N., Pinigin A.

CT colonography in the diagnostic algorithm of examination of children with defaecation dysfunction (SS 612), B-0576

Ertl-Wagner B.

State-of-the-art paediatric neuroradiology: B. Imaging of developmental disorders (RC 811), A-337

Ertl-Wagner B.

My three top tips for neuroimaging: Leukodystrophies (SF 15c), A-757

Ertl-Wagner B.

Psychoradiology: a blend of molecular, functional and structural imaging with a taste of psychology: Chairperson's introduction (MS 16), A-827

Esen G.

My three top tips for breast imaging: MRI-guided biopsy (SF 8b), A-332

Esser M., Hess S., Teufel M., Gatidis S., Tsiflikas I., Schäfer J.F.

Value of paediatric chest CT in a representative patient cohort of 2019 examinations (SS 712), B-0766

Eustace S.J.

Lower extremity: A. Hip and pubic symphysis (E³ 819), A-369

Ewertsen C.

Tips and tricks for abdominal ultrasound: Fusion imaging (WG 2), A-442

F

Fabris C., Zamboni G., Ambrosetti M.C., Negrelli R., Pozzi Mucelli R.

Lobar distribution of liver metastases based on the site of pancreatic neuroendocrine tumours (SS 1901b), B-1521

Fabris C., Zamboni G., Negrelli R., Boninsegna E., Pozzi Mucelli R.

MRI evaluation of pathologically confirmed IPMNs of the pancreas using Fukuoka Guidelines: can we differentiate between invasive/high-grade IPMNs and low/moderate-grade IPMNs? (SS 1901b), B-1523

Faggioni L., Gabelloni M., Bianchi M., Costa G., De Carlo M., Petronio A.S., Caramella D.

One-stop high definition 64-row CT coronary angiography in patients with severe aortic stenosis candidate to transcatheter aortic valve implantation (TAVI): a pilot feasibility study (SS 203), B-0146

Fahlenkamp U.L., Adams L.C., Böker S.M., Engel G., Huynh Anh M., Wagner M., Hamm B., Makowski M.R.

Improved visualisation of hepatic metastases in gadoxetate disodium-enhanced MRI: potential of contrast-optimised (phase-sensitive) inversion recovery imaging (SS 601a), B-0426

Faiella E., Santucci D., Alfonsi A., Pacella G., Altomare C., Bernetti C., Rollo C., Grasso R.F., Beomonte Zobel B.

Our experience in percutaneous ablative treatment of renal T1a e T1b lesions: results from 90 patients treated with MWA, RFA and CRA (SS 709), B-0627

Falcone G., Raspanti C., Gabbani G., Casamassima E., Mondaini F., Citone M., Fanelli F.

Role of intra-vascular ultrasound (IVUS) in EVAR planning (SS 309), B-0227

Fallenberg E.M.

New mammography: tomosynthesis and future techniques: Chairperson's introduction (RC 502), A-174

Fallenberg E.M.

My three top tips for breast imaging: Contrast-enhanced spectral mammography (SF 8b), A-329

Fallenberg E.M.

Contrast-enhanced spectral mammography: Evidence for efficacy and implementation (SF 15b), A-754

Falsaperla D., Torrisi S.E., Torcitto A., Russo G., Stefano A., Vancheri A., Basile A., Vancheri C., Palmucci S.

Risk assessment of lung cancer development in Idiopathic Pulmonary Fibrosis (IPF) patients using quantitative HRCT analysis (SS 1004), B-0873

Fan S., Li X., Ye Z.

Correlations between the iodine concentrations from dual-energy computed tomography and molecular markers Ki-67 and HIF-1 α in rectal cancer: a preliminary study (SS 216), B-0170

Fanelli F.

Drug elution or drug illusion in vascular disease: Drug-eluting balloons and stents in femoropopliteal and crural lesions: pro (SF 13c), A-671

Fang Z., Li X., Huang S., Zhang Z., Sun C.C., Feng S., Li Z.

Magnetisation transfer and conventional MRI for characterisation of intestinal fibrosis and inflammation in patients with Crohn's disease (SS 1901c), B-1535

Fantini C., Hennicaux J., Faivre J., Felloni P., Remy J., Remy-Jardin M.

Right heart thrombi and acute pulmonary embolism: analysability of right cardiac cavities in the conditions of routine dual-source chest CT angiographic examinations (SS 604), B-0462

Farina D.

Differential diagnoses you don't want to miss: C. Differential diagnoses of soft tissue masses (RC 108), A-015

Farina D.

Pitfalls in interpretation of head and neck disease: B. Anatomical variants posing surgical risks (RC 808), A-314

Faruch M.

Advances in musculoskeletal techniques: whole-body MR: B. Non-oncologic applications (E³ 1821), A-945

Fedorov A., Cherkashin M.

Periodic refresher course for the radiographers of multimodal radiology department: the role of IT technologies (SS 1414), B-1145

Feger S.

Coronary CT angiography: how to start practice, perform and evaluate the exam?: A. Beautiful cases from clinical practice: coronary arteries (RC 1603), A-810

Fehrenbach U., Merz K., Böning G., Kahn J., Feldhaus F., Maurer M.H., Renz D., Hamm B., Streitparth F.

Advantages of spectral CT in staging of patients with non-small cell lung cancer (NSCLC) (MY 5), B-0412

Fehrmann Efferoth A., Treutlein M., Rudolph T., Rudolph V., Weiss K., Giese D., Bunck A., Maintz D., Baessler B.

Myocardial T1 and T2 mapping in severe aortic stenosis: novel insights into the pathophysiology of myocardial remodelling (SS 1003), B-0976

Feier D.S., Bastati-Huber N., Beer A.,

Fragner R.M., Einspieler H., Ba-Ssalamah A. Molecular features, histological parameters and enhancement measurements in NASH patients using gadoxetic acid-enhanced MR imaging (SS 201a), B-0003

Feldhaus F., Böning G., Fehrenbach U., Kahn J., Maurer M.H., Renz D.M., Hamm B., Streitparth F.

Metal artefact reduction in computed tomography (Smart MAR): improvement of image quality and diagnostic confidence in patients with metallic dental implants (SS 1008), B-0899

Feldhaus F., Böning G., Fehrenbach U., Kahn J., Hamm B., Streitparth F.

Improvement of image quality and diagnostic confidence using Smart MAR - a projection-based CT protocol in patients with orthopaedic metallic implants in hip and shoulder (SS 1010), B-0961

Feldman E., Bai J., van Staaldouin E.

Incremental diagnostic value of myocardial perfusion stress testing for intermediate obstructive lesions on coronary CT angiography in acute chest pain (MY 7), B-0778

Feng H.

Preliminary application of PETRA sequence in lung nodule screening (SS 1804), B-1347

Feng Z., Hu Z.

Application of CT texture analysis in quantification of pancreatic cystadenoma phenotype images (SS 1901b), B-1525

Fernandez Valverde F., Romero Martin S.,

Raya Povedano J.L., Gordillo Arnaud J.E. Breast screening 2D-mammography or breast tomosynthesis: comparison in terms of cancer detection and recalls (SS 202a), B-0085

Ferraoli G.

The role of combi-elasto and attenuation measurement in the assessment of diffuse liver disease (SY 13)

Ferrari C., Milanese G., Silva M.,

Giovanardi N., Goldoni M., Maffei E.,

Cademartiri F., Sverzellati N.

Correlation between liver density and epicardial fat volume: biomarkers of coronary artery disease (MY 7), B-0787

Ferrari R., Voena C., Mancini C., Zerunian M.,

Rivosecchi F., Marè V., Paramatti R.,

Faccini R., Laghi A.

MRI texture analysis of rectal cancer with mono- and multivariate analysis using machine learning artificial intelligence (SS 216), B-0162

Ferraz H.I.M.G., Santos R.A.

Orbital ultrasound evaluation of the optic nerve sheath diameter (SS 1014), B-0964

Ferreira C., Cadório I., Barbosa A., Freixo A.,

Silva B., Figueiredo D., Lousada M.,

Castelo-Branco M., Martins P.M.

Development of an fMRI linguistic paradigm to monitor PPA patients: a pilot study (SS 614), B-0552

Ferrer C.

How can radiologists expand their role in peripheral vascular intervention?: How to improve your relationship with the vascular surgeon (PC 9), A-431

Authors' Index

- Ferrer Puchol M.D., Sanz-Rodrigo E., Montesinos García P., Taberner Lopez E., Blanco Pérez E., Forment Navarro M.**
Intravenous contrast media administration: is there a risk of acute kidney injury? (SS 1807b), B-1465
- Ferrero G., Amico V., Lacelli F., Fabbro E., Perrone N., Serafini G.**
Adhesive capsulitis of the shoulder: a new ultrasound-guided and rehabilitation multidisciplinary treatment protocol to restore shoulder girdle kinesis (SS 1010), B-0958
- Figge C.**
Value of high-field open MRI and ultrasound image fusion for the detection of prostate cancer (SY 13)
- Figiel J., Koenig A., Hegele A., Mahnken A.**
MRI-guided percutaneous transluteal ablation of unilateral prostate carcinoma: initial experiences and results (SS 1909), B-1546
- Filippiadis D.**
Vascular and interventional radiology in children: C. Percutaneous treatment of osteoid osteoma (RC 412), A-109
- Filippiadis D.**
Musculoskeletal interventions: what every radiologist should know: B. Vertebral augmentation and discectomy techniques: can we challenge surgery? (RC 509), A-236
- Fior D., Leni D., Vacirca F., Ippolito D., Sironi S., Corso R.**
Virtual guidance of percutaneous transthoracic needle biopsy with c-arm cone-beam CT: diagnostic accuracy, risk factors and effective radiation dose (SS 609), B-0444
- Fischer S., Maeder R., Denysenkov V., Terekhov M., Zangos S., Prisner T., Vogl T.J.**
MR angiography in small animals using hyperpolarised water (SS 215), B-0030
- Fischer T.**
MRI-US fusion for diagnostic assessment of the prostate and treatment guidance (SY 3)
- Fischer U., Baum F., Oaknin J., Izhaky D.**
Correlation of breast MRI screening with 3D functional infrared imaging (SS 1902a), B-1609
- Fisher P.R.**
Impact of tomosynthesis angular range on mass conspicuity in patients with dense breasts: experiences from a radiologist's view (SY 1c)
- Fisher P.R.**
Comparison of contrast-enhanced dual energy mammography and contrast-enhanced digital breast tomosynthesis for lesion assessment and radiation dose (SY 1c)
- Fleury E.F., Gianini A.C., Ayres V.J., Ramalho L., Sousa Neto J., Marcomini K.D.**
Breast sonoelastography: comparison of the accuracy of the computer assisted diagnosis (CAD) classifier system using two values of different cut-off values with the visual classifier (SS 302), B-0269
- Foley S.J.**
Radiation protection from A to Z: The Basic Safety Standards Directive: all you need to know (BR 2), A-629
- Forbrig R., Patzig M., Trumm C.G., Stahl R., Dorn F.**
Radiation dose optimisation in intraoperative computed tomography of the brain (SS 213), B-0122
- Forrai G.**
Digital breast tomosynthesis (DBT): Keynote lecture (SS 202a), K-03
- Forrai G.**
The high-risk patient enigma: A. Lesions with an elevated risk for breast cancer (E³ 1726a), A-906
- Forslin Y., Martola J., Shams S., Fredrikson S., Kristoffersen Wiberg M., Granberg T.**
Gadolinium retention in the brain: an MRI relaxometry study comparing linear and macrocyclic types of gadolinium-based agents (SS 1011b), B-0997
- Forstner R.**
MRI for gynaecologic imaging: how I do it: C. Diffusion and ADC (RC 1207), A-547
- Fournier L.S.**
Monitoring response: the essential guide for all radiologists: C. Assessment of response using functional MR and CT imaging: the essentials (RC 816), A-345
- Fournier L.S.**
Radiomics: what is it and how can we use it?: Radiomics: what is it and how does it work? (NH 12), A-573
- Fraga Piñero C., González Vázquez M., Monteiro M.**
Metal artefact reduction in the musculoskeletal system with dual-energy CT and spectral imaging (SS 314), B-0323
- Fraga Rivas P., García del Salto L., de Miguel Criado J., Aguilera del Hoyo F., Benito Vicente C., Marco Sanz A.**
Preliminary analysis of a computer tool to avoid repetition of radiological tests (SS 205), B-0175
- França M.M.**
Diffuse liver disease: B. Congenital diffuse liver diseases and iron overload (E³ 320), A-089
- França M.M.**
Discovering Portuguese radiology: past, present, future: Imaging biomarkers for diffuse liver disease (EM 2), A-685
- Francavilla M., Resta D., Lorusso F., Angelelli G., Tartaglia C., Pignataro P., Scioscia M., Stabile Ianora A.A., Scardapane A.**
Myometrial infiltration by deep pelvic endometriosis: MRI assessment (SS 607), B-0465
- Francica G., Meloni F., Pompili M., Terracciano F., Caturelli E., de Sio I.**
Contrast-enhanced ultrasound (CEUS) as guidance system for ablative treatments of primary and secondary liver tumours: a multicenter study (MY 9), B-0833
- Francone M.**
From diagnosis to prognosis: how does cardiac imaging affect patient outcome?: A. In myocarditis (RC 503), A-193
- Francone M.**
Memorable cases in cardiovascular imaging: how to avoid common mistakes: Right ventricular myocarditis diagnosed with CMR: the great imitator (SF 12e), A-598
- Frauenfelder G., Faiella E., Santucci D., Beomonte Zobel B.B., Grasso R.**
Percutaneous US- and CT-guided thermal ablation of 20 adrenal metastases: treatment effectiveness in short- and intermediate-term imaging follow-up with CT and MRI (SS 709), B-0632
- Frauenfelder T.**
Everything you need to know about 3D post-processing: C. Interpretation of 3D processing results: from image to volume reading (RC 105), A-049
- Frauenfelder T.**
CT - patterns in chest radiology: back to basics and beyond: A. Secondary pulmonary lobule anatomy: essential to tackle with the nodular pattern (RC 404), A-100
- Frellesen C., Wichmann J., Tischendorf P., Vogl T.J., Eichler K.**
Evaluation of the diagnostic potential of the GCS for the indication of whole-body CT in paediatric polytrauma (SS 317), B-0289
- Friedrich K.M.**
Case-Based Diagnosis Training - Part 2: Spine (CB 2), A-976
- Friedrich K.**
Making the most of social media: Social media at ECR (part 2) (EFRS WS), A-791
- Frigerio A.**
Rethinking ductal carcinoma in situ (DCIS): A. New radiologic-pathologic knowledge on DCIS (RC 1302), A-633
- Frija G.**
Euratom Basic Safety Standards Directive: a comprehensive approach for radiation protection: Panel discussion: Is the Basic Safety Standards Directive a step forward for patients, clinical professionals and regulators? (part 1) (EU 1)
- Frija G.**
Clinical diagnostic reference levels for x-ray medical imaging: Panel discussion (part 2) (EU 3)
- Frija G.**
Euratom Basic Safety Standards Directive: a comprehensive approach for radiation protection: The clinical approach: the gap to be closed (EU 1), A-147
- Frija G.**
Dose management systems and repositories: part A: The 'EuroSafe Imaging' campaign's point of view (EF 1), A-419
- Frija G.**
Clinical diagnostic reference levels for x-ray medical imaging: Chairpersons' introduction and update on the project on clinical DRLs for x-ray medical imaging (part 2) (EU 3), A-501
- Frija G.**
Clinical diagnostic reference levels for x-ray medical imaging: The concept of clinical diagnostic reference levels (DRLs) (EU 3), A-503
- Fritz B., Fucentese S., Zimmermann S., Tscholl P.M., Sutter R., Pfirrmann C.W.**
3D-printed models of the knee for evaluation of trochlear dysplasia in comparison to standard radiographs and computed tomography (SS 1810), B-1430
- Froelich M.F., Reidler P., Fabritius M.P., Rotkopf L., Schuler F., Sommer W.H., Thierfelder K.M., Kunz W.G.**
Collateral filling velocity predicts malignant oedema development in acute ischaemic stroke (SS 1011a), B-0922
- Froelich M.F., Heinemann V., Sommer W.H., Holch J., Rieke J., Modest D., Hofmann F.O.**
CT attenuation of liver metastases of colorectal cancer is a prognostic factor of overall survival (SS 1416), B-1076
- Froeling M.**
Exploring the microscopic from macroscopic: the strengths of multiparametric MRI: MRI of cardiac muscle microstructure (ESR/ESMRMB 1), A-115

Authors' Index

Frøkjær J., Kipp J., Mark E., Drewes A., Olesen S.

CT volumetry of the pancreas: gland size in a normal population and its relation to age, gender and body composition (SS 201b), B-0012

Frood R., Palkhi E.Y.A., Barnfield M., Prestwich R., Vaidyanathan S., Scarsbrook A.

Can MR textural analysis improve detection of extracapsular nodal spread in patients with oral cavity cancer? (SS 1008), B-0908

Fu G., Zhang W., Liu J., Xiao Y., Yao L., Sweeney J.A., Lui S.

Relationship between peripheral Interleukin 10 and white matter integrity in stable medicated schizophrenia (SS 711a), B-0656

Fu Y.

Comparison of shear-wave elastography (SWE) and real-time elastography in the same thyroid nodules: which is more accurate? (SS 608), B-0490

Fuchsjaeger M.H.

New imaging approaches for radiotherapy: Chairpersons' introduction (part 2) (ESR/ESTRO), A-884

Fuchsjaeger M.H.

My three top tips for breast imaging: Chairpersons' introduction (SF 8b), A-324

Fuchsjaeger M.H.

Minimally-invasive local treatment of breast cancer: the time is now: C. Cryotherapy (RC 902), A-407

Fuchsjaeger M.H.

Patient-doctor relationship and interdisciplinary communication in the radiology department: Chairpersons' introduction (part 2) (PA 1), A-693

Fuchsjaeger M.H.

Case-Based Diagnosis Training - Part 2: Breast (CB 2), A-978

Fusaro M., Balestriero G., Dorigo A., Battistella G., Bortolanza C., Tessarin G., Doni L., De Leo A., Morana G.

Six months follow-up after triple rule-out using second-generation dual-source CT in patients with acute chest pain (SS 1903), B-1650

Fütterer J.J.

Do we need dynamic contrast enhancement (DCE) in prostate mpMRI?: Chairpersons' introduction (part 2) (PS 527), A-205

G

Galea N., Francone M., Coco S., Mancuso G., Martinelli O., Belli C., Carbone I., Gossetti B., Catalano C.

Magnetic resonance assessment of thrombus remodeling after endovascular aortic sealing of abdominal aortic aneurysms using the Nellix endosystem (SS 215), B-0027

Gallagher F.A.

Merging the best: hybrid imaging: C. Hyperpolarised MRI (RC 106), A-060

Gallagher F.A.

Contrast agents and molecular imaging: Keynote lecture (SS 1406), K-23

Galmiche C.

Is multiparametric MRI useful for differentiating oncocytomas from chromophobe renal cell carcinomas (SS 207), B-0059

Galvano G., Raciti M., Scavone G., De Luca S., Cannella A., Di Lorenzo C., Tigano G., Scavone A.

Percutaneous combined treatment for lumbar disc herniation: how we do it (SS 1809), B-1336

Gangi A.

Interventional oncology in a state-of-the-art angio CT environment (SY 3)

Gangi A.

Image-guided therapies in oncology: Bones (BS 6), A-413

Ganych O.

Prognostic significance of different MRI modalities for evaluation of neoadjuvant chemoradiation treatment of locally advanced rectal cancer (MY 3), B-0370

Gao L., Hou Y., Ma Y., Lu X., Jia Z.

Application value of dual-detector spectral CT in evaluation of metastatic lymph nodes in lung cancer (SS 604), B-0455

Gao Y., Zhai X., Zhang L., Huang K.

Ultra-low-dose CT with tin filtration for lung densitometry and emphysema detection (SS 704), B-0638

Gao Y., Yang Z., Liu X.

Myocardial fibrosis imaging based on T1-mapping and ECV measurement in diabetes: diagnostic value compared with LGE imaging (MY 7), B-0783

Gao Y., Yang Z., Shi K., Diao K.

Assessment of post-operative pulmonary regurgitation by pre-operative RV and pulmonart artery imaging characteristics in pediatric TOF repaired with trans-valve surgert (SS 1503), B-1230

Garces Iñigo E.F., Marti-Bonmati L., Llorens R., Vento Torres M.

Towards an elastographic atlas of the neonatal brain (SS 1412), B-1162

García Figueiras R.

Quantitative imaging in oncology: B. Quantitative image biomarkers for targeted tumour therapies (E³ 1626b), A-863

García Marcos R.

Percutaneous interventional procedures: a practical guide: B. How to safely perform CT-guided procedures (RC 809), A-366

García-Peña M.P.

Thoracic manifestations of systemic disease: C. Early manifestations in children and young adults (RC 1704), A-882

Gardarsdottir M.

All about TAVI: pre- and post-procedural assessment: Keynote lecture (SS 203), K-04

Gårdling J.

Successful paediatric imaging: C. Reducing the need for sedation and anaesthesia in MRI: the role of play therapy and other techniques (RC 514), A-227

Gareer S., Mounir Y., Helal M.H., Mokhtar O., Abdel Aziz A., Kassas H., Bassam L.

Interpretation of patterns of enhancement on contrast-enhanced digital mammography: an approach to a standardised scheme (MY 16), B-1287

Gariani J., Siddique M.M., Cook G., Goh V.J.

CT texture features of adrenal tumours: the answer to indeterminate adrenal lesions? (SS 316), B-0354

Gatti M., Faletti R., Cosentino A., Pennisi G., De Paoli A., Di Chio A., Fiore S., Pavan L., Fonio P.

3D printing of the aortic root based on cardiac computed tomography and cardiac magnetic resonance imaging: preliminary experience on pre-procedural planning for aortic valve sizing (SS 1503), B-1225

Gattoni M., Hartenstein A., Siewert E., Denecke T., Hamm B., Geisel D., Penzkofer T.

Deep learning for automated MRI-based cyst load determination in PKD patients (SS 1007), B-0886

Gavrel M., Auclin E., Balleyguier C.S., Caramella C.

Characterisation of mediastinal anterior masses with magnetic resonance imaging (MRI) using diffusion-weighted imaging (SS 1904b), B-1575

Gawlitz J.F.M., Sturm T., Spohrer K., Henzler T.

Using a neuronal network-based software to predict lung function values from qCT parameters in patients with COPD (SS 304), B-0234

Gawlitz J.F.M., Fischer A.M., Akin I., Borggreffe M., Schönberg S.O., Haubenreisser H., Henzler T., Trinkmann F.

Finding the right spot: where to measure airway parameters in patients with COPD? (SS 1804), B-1354

Gazhonova V.E., Emelianenko M., Onishchenko M.

The accuracy of ultrasound with and without sonoelastography in the diagnosis of partial-thickness rotator cuff tears with MDCT arthrography and arthroscopic verification (MY 13), B-1028

Gebauer B.

Novelties in oncologic imaging: C. Imaging-guided liver interventions in oncology (E³ 126), A-029

Geers-van Gemenen S.

Radiographers' challenge: informing patients about radiation risk: Chairperson's introduction: The European BSS (Basic Safety Standards) Directive and current legal requirements (SF 12d), A-577

Gennaro N., Mauri G., de Beni S., Ierace T., Poretti D., Pedicini V., Chiti A., Solbiati L.

Contrast enhancement improves PET-US fusion navigation for tumour ablation targeting (SS 609), B-0452

Georg D.

A multidisciplinary approach to prostate cancer: can we make a difference?: C. The radiation oncologist (RC 1716), A-919

Gershan V.

CT examination of pregnant patients: a dilemma for the radiologist and the mother: Chairperson's introduction (SF 8a), A-308

Gersing A.S.

The degenerative cervical spine: B. Cervical spinal stenosis and cervical spondylotic myelopathy (RC 111), A-021

Ghaye B.

MR imaging of the lungs: A. Diagnosing pulmonary embolism (E³ 318), A-084

Ghaye B.

Pulmonary embolism: a joint challenge for diagnostic and interventional radiology!: A. Imaging algorithm for pulmonary embolism (RC 1209), A-588

Ghosh R., Chilamkurthy S., Rao P., Biviji M.

Automated detection and localisation of skull fractures from CT scans using deep learning (SS 605), B-0483

Giaconi C., Cerimele F., Bulleri A., Basile Fasolo C., Neri E.

Patients' perception of radiologists in an oncologic imaging department (SS 1016a), B-0890

Authors' Index

- Giaconi C., Cerri F., Arena C., Bulleri A., Neri E.**
How to structure the attendance of radiologists to oncologic multidisciplinary team meetings (SS 1016a), B-0891
- Giannakis A., Norajitra T., Kehler L., Dinkel J., Weinheimer O., van Lunteren C., Kreuter M., Maier-Hein K., Heussel C.**
Fully automated segmentation of pulmonary fibrosis using different software tools (SS 1004), B-0871
- Gianneramo C., Bruno F., Quarchioni S., Cannizzaro E., Palumbo P., Mariani S., Arrigoni F., Barile A., Masciocchi C.**
Heels: the higher, the better? Weight-bearing MRI evaluation of the forefoot in women during heeled-shoes wearing (SS 310), B-0300
- Gianneramo C., Quarchioni S., Palumbo P., Arrigoni F., Mariani S., Zugaro L., Barile A., Masciocchi C.**
How to carry out follow-up studies in patients with osteoid osteoma treated with minimally invasive procedures (MRgFUS and RFA). Evaluation of imaging findings and clinical outcome (SS 1809), B-1344
- Giannetto G., Pusceddu L., Vani V., Morra L., Correale L., Senore C., Del Santo S., Regge D.**
Neoplasia yield with FIT two years after CTC screening (SS 601b), B-0522
- Giannotti E.**
New mammography: tomosynthesis and future techniques: C. The future of mammography: my predictions (RC 502), A-177
- Giannotti N., McNulty J., Foley S.J., Kelly P.**
Morphological characteristics of carotid atherosclerotic plaques: comparison based on CTA and MRI (MY 17), B-1299
- Gibaud B.**
Dose management systems and repositories: part B: Organisation of dose management systems and repositories for radiation protection and biomedical research: possibilities and limitations of current implementations and standards (EF 2), A-457
- Gibaud B.**
Linking imaging biobanks to -omics: the role of BBMRI and ESR: Integrating an imaging biobank in a BBMRI biobank (ESR/BBMRI-ERIC), A-616
- Gibaud B.**
Artificial intelligence (AI) applications: Imaging biobanks (SF 10), A-991
- Gibson T.A., Patel N., McGill N., King A., Breen D.**
Renal tumour cryoablation beyond T1a: outcomes for 56 T1b biopsy-proven RCC lesions (SS 709), B-0624
- Gijsbertse K., Goselink R., Lassche S., Nillesen M., Sprengers A., Verdonshot N., van Alfen N., de Korte C.L.**
Ultrasound imaging of muscle contraction of the tibialis anterior in patients with facioscapulohumeral dystrophy (SS 1010), B-0957
- Gilbert F.J.**
Screening for breast cancer: Chairperson's introduction (RC 402), A-116
- Gilligan P.**
CT examination of pregnant patients: a dilemma for the radiologist and the mother: Dose and risk communication to doctors and patients (SF 8a), A-312
- Gioppo A., Eoli M., Aquino D., Finocchiaro G., Bruzzone M.G., Cuccarini V.**
Advanced MRI assessment during dendritic cell immunotherapy (SS 311), B-0281
- Gioutlaki E., Tzimas C., Feida E., Chalazonitis A.N.**
Sensitivity of contrast-enhanced spectral mammography (CESM) versus digital mammography (DM) for detecting breast cancer in dense or extremely dense breasts (MY 16), B-1284
- Girardo C., Motyka S., Weber M., Feiweier T., Trattng S., Bogner W.**
Ultrahigh field (7T) diffusion tensor imaging of healthy skeletal muscles: a quantitative comparison with 3T (SS 710a), B-0620
- Girometti R., Greco F., Cereser L., Como G., Ficarra V., Giannarini G., Crestani A., Zuiani C.**
Which cancer-related factors are associated with prostate cancer missing when evaluating mpMRI with PI-RADS v2? (MY 4), B-0384
- Girometti R., Iorenzin D., Montaldo L., Como G., Risaliti A., Zuiani C.**
Is cross-sectional imaging predictive of difficult hepatectomy in patients undergoing liver transplantation? (SS 601a), B-0425
- Girometti R., Tomkova L., Zanotel M., Lorenzon M., Linda A., Londero V., Zuiani C.**
Breast cancer staging with automated breast volume scanner (ABVS) and digital breast tomosynthesis (DBT): a comparison with magnetic resonance imaging (MRI) (MY 16), B-1294
- Girometti R., Bednarova S., Sioletic S., Ficarra V., Greco F., Crestani A., Zuiani C.**
Diagnostic performance of PI-RADS version 2 in detecting prostate cancer using whole-mount histology after radical prostatectomy as the standard of reference (SS 1807a), B-1358
- Gitto S., Calareso G., Cascella T., Greco G., Greco G., Vaiani M., Stagni S., Salvioni R., Spreafico C.**
CT-guided percutaneous cryoablation treatment of renal cancer: an outcome analysis from our experience (SS 709), B-0625
- Giurazza F., Frauenfelder G., Massaroni C., Galati G., Picardi A., Schena E., Beomonte Zobel B.B., Silvestri S.**
Preliminary analysis of ultrasound imaging-based thermometry in ex vivo biological tissues (SS 1006), B-0994
- Gkali C.**
Breast elastography: examination protocol and imaging interpretation (SY 1b)
- Gkoumas S., Habi M., Radicci V., Rissi M., Thuering T., Traut S., Trueb P., Zambon P., Broennimann C.**
Gallium Arsenide hybrid photon counting x-ray detectors: towards large area single-shot spectral mammography (SS 613), B-0549
- Glocker B.**
Artificial intelligence: a strategic view: Machine learning for analysing medical images (SF 6), A-983
- Goh V.J.**
Molecular imaging in oncology: A. Imaging of hypoxia (RC 406), A-156
- Goh V.J.**
Functional imaging in oncology beyond morphology: where are we now?: A. Functional MRI techniques (RC 516), A-216
- Goh V.J.**
Personalised medicine in liver tumours: C. Assessment of response to treatment (E³ 720), A-295
- Goh V.J.**
Immunotherapy: a revolution in cancer care?: Chairperson's introduction: What the radiologist needs to know (NH 9), A-385
- Goldberg S.N.**
Immunotherapy: a revolution in cancer care?: Systemic and immunologic effects of image-guided interventions in oncology (NH 9), A-388
- Golding S.J.**
Head and neck: inflammation, tumour or something else?: Salivary glands (BS 1), A-025
- González de la Huebra Rodríguez I., García Baizán A., Calvo Imirizaldu M., Ezponda Casajús A., Bartolomé P., Quilez A., Elizalde Pérez A.M., Pina Insausti L.J.**
Is it worth to perform preoperative MRI after the combination of digital mammography, digital breast tomosynthesis and US? (SS 1002), B-0915
- Goßen A.**
Real-time dose control, real-time image processing (SY 22)
- Gorbounov N., Dergilev A., Kochura V., Manakova Y., Sudarkina A.**
Low-dose digital radiography in diagnosis of COPD's phenotypes (SS 704), B-0641
- Gore R.M.**
Imaging of the complicated postoperative abdomen: B. Pancreas (RC 401), A-097
- Gossye T., Peleman M., Smeets P., Achten E., Bacher K.**
Impact of software parameter settings on image quality of Virtual Grid processed radiography images: a contrast-detail study (SS 613), B-0540
- Gottschalk A., Kress B.**
NSsFaE: observational study on the incidence of nephrogenic systemic fibrosis in patients with renal impairment following gadoteric acid administration (MY 4), B-0395
- Gourtsoyannis N.**
Trends in quality education in radiology: ESOR in action 2018 (ESOR), A-284
- Grainger A.J.**
Upper extremity: A. Elbow (E³ 919), A-444
- Grainger A.J.**
Shoulder MRI: mastering technique and making my report relevant: C. Patterns of instability: what does the MRI show? (RC 1210), A-571
- Grainger A.J.**
Lower extremity sports injuries: B. Multimodality imaging of foot and ankle injuries in the athlete (TC 1428), A-708
- Grainger A.J.**
Lower extremity sports injuries: C. Interactive case discussion (part 2) (TC 1428), A-710
- Grams A.E., Djurdjevic T., Schiestl T., Knoflach M., Dazinger F., Gizewski E.R., Glodny B.**
Dual-energy computed tomography for optimised visualisation of early cerebral infarctions after endovascular stroke therapy (SS 611), B-0510
- Granados A.M., Orejuela J.F.**
Utility of volumetric assessment of the hippocampal substructures in hippocampal sclerosis (SS 1811a), B-1402

Authors' Index

- Granata C.**
Clinical diagnostic reference levels for x-ray medical imaging: An update on current paediatric diagnostic reference levels (DRLs) (EU 3), A-505
- Grant D., Quinn E., Gordon Boyd R., Lee C., Platt K.A., Partington K.**
Ultrasound of the limping child (SS 312), B-0344
- Granziera C.**
Exploring the microscopic from macroscopic: the strengths of multiparametric MRI: How quantitative MRI reveals brain microstructure (ESR/ESMRMB 1), A-114
- Grassi A., Cirigliano A., Carbone S., Biondi M., Nardone V., Pirtoli L., Volterrani L.**
Whole tumour texture analysis based on ADC maps as quantitative imaging biomarker in patients with locally advanced rectal cancer "responders" to neoadjuvant chemoradiotherapy (SS 1001b), B-0853
- Grazzini I., Cuneo G., Redi F., Caccialupi C., Sammartano K., Ciccotosto C.**
Diffusion tensor imaging in idiopathic normal-pressure hydrocephalus: clinical and CSF flowmetry correlations (SS 1411a), B-1032
- Greese J., Diekhoff T., Sieper J., Schwenke C., Makowski M., Poddubnyy D., Hamm B., Hermann K.**
Detection of osteitis at the sacroiliac joint in patients with chronic low back pain by STIR and T2-weighted fat-suppressed turbo spin echo sequences: results from the SIMACT study (SS 1910), B-1615
- Grenier N.**
Radiographers in preclinical imaging research: Chairpersons' introduction (part 2) (SF 9b), A-423
- Grenier N.**
Update on functional genitourinary MRI: A. Kidney (E³ 1526b), A-749
- Grenier N.**
Urogenital: A. Renal and adrenal imaging (E³ 1623), A-833
- Grenier N.**
Imaging strategies in renal tumours: B. Differential diagnosis of renal masses (RC 1707), A-898
- Grenier P.A.**
Mass casualties: Lesson learned from the Paris attacks (PC 4), A-122
- Grenier P.A.**
Chronic obstructive pulmonary disease (COPD): A. CT phenotyping and visual assessment (RC 804), A-305
- Grigorieva E., Krylov V., Dashyan V., Lukyanchikov V.**
Delayed postoperative changes after intracranial aneurysm surgery (SS 711b), B-0690
- Grimm J.**
Functional imaging in oncology beyond morphology: where are we now?: C. Assessment by molecular imaging (RC 516), A-218
- Grivegnée A.**
ABVS and personalised breast cancer screening (SY 1b)
- Grob D., Oostveen L.J., Rühak J., Heldmann S., Mohr B., Prokop M.M., Brink M., Sechopoulos I.**
Subtraction CT of the lungs: accuracy of motion correction software (SS 304), B-0238
- Grob D., Oostveen L.J., Prokop M.M., Schaefer-Prokop C., Sechopoulos I., Brink M.**
Pulmonary embolism-induced perfusion defects on iodine maps: quantitative comparison of dual-energy CT and subtraction CT (MY 5), B-0411
- Grosse Hokamp N., Abdullayev N., Neuhaus V., Holz J., Maintz D., Borggreffe J.**
Calcium suppression in spectral detector computed tomography improves visualization of bone metastasis (SS 716), B-0699
- Grosse Hokamp N., Laukamp K.R., Lennartz S., Zopfs D., Maintz D., Borggreffe J.**
Virtual monoenergetic images can reduce metal artefacts caused by dental implants in computed tomography (SS 1008), B-0906
- Grosse Hokamp N., Abdullayev N., Neuhaus V., Mpotsaris A., Maintz D., Borggreffe J.**
Reduction of metal artefacts in patients with spinal fusions: metal artefact reduction algorithms and virtual monoenergetic images from spectral detector computed tomography (SS 1410), B-1119
- Grosse Hokamp N., Kessner R., Gilkeson R., Gupta A.**
Virtual monoenergetic image reconstruction from spectral detector CT improves objective image quality and subjective assessment of pulmonary emboli (SS 1815), B-1326
- Grosse Hokamp N., Salem J., Holz J., Dervishi G., Ritter M., Heidenreich A., Maintz D., Haneder S.**
Characterisation of renal stones using spectral detector computed tomography using normal and low-dose protocols (SS 1807b), B-1473
- Grover S.B., Jain P., Jain S.K., Mandal A.K., Grover H.**
MR evaluation of fibroglandular tissue (FGT) and background parenchymal enhancement (BPE) in breast cancer and its association with receptor status (SS 602), B-0505
- Gruber-Rouh T., Eichler K., Nour Eldin N., Naguib N.N.N., Langenbach M.C., Vogl T.J.**
TACE using mitomycin with or without irinotecan for HCC in European patients (MY 9), B-0824
- Gruber-Rouh T., Eichler K., Naguib N.N.N., Langenbach M.C., Kaltenbach B., Vogl T.J.**
TACE of HCC using mitomycin and lipiodol with or without DSM for HCC: comparative study (SS 1409), B-1054
- Grueneisen J., Nensa F., Demircioglu A., Forsting M., Herrmann K., Umutlu L.**
Machine learning and radiomics analysis of multi-parametric PET/MRI: characterisation of primary cervical cancers (SS 316), B-0355
- Grueneisen J., Sarabhai T., Schaarschmidt B.M., Wetter A., Forsting M., Herrmann K., Umutlu L.**
Whole-body tumour staging of cervical cancer patients using 18F-FDG PET/MRI: does it change therapeutic decisions when compared to MRI alone? (SS 1816), B-1367
- Gruszczynska K.**
Memorable cases in cardiovascular imaging: how to avoid common mistakes: Hypertrabeculation vs non-compaction of the left ventricle: treat or don't touch? (SF 12e), A-602
- Gu K., Kim C.K., Lee J.**
Prognostic value of diffusion-weighted imaging for clinical outcome prediction in uterine cervical cancer treated with radiotherapy (MY 4), B-0388
- Guan J., Peng Y., Wang H., Guo Y.**
High-resolution MR imaging with small surface coil in diagnosis of slight penile lesions after penile injury (SS 1907b), B-1663
- Guazzaroni M., Altobelli S., Marsico S., Cavallo A.U., Bozzi A., Floris R.**
Hypodermal adipose tissue sonoelastography for monitoring different treatment responses in patients with plaque psoriasis (SS 1910), B-1623
- Guazzaroni M., Marsico S., Girardi V., Campagnuolo T., Altobelli S., Floris R.**
In vivo evaluation of optic nerve and periorbital structures' biomechanical properties using shear-wave elastography in patients with glaucoma (SS 608), B-0487
- Guberina N., Dietrich U., Arweiler-Harbeck D., Forsting M., Ringelstein A.**
Radiation exposure imparted during multidetector and cone-beam CT scans for the perioperative cochlear implant evaluation (SS 308), B-0259
- Guberina N., Bauer S., Richly H., Scheulen M., Wetter A.**
Diffusion-weighted magnetic resonance imaging in uveal melanomas: validation of early chemotherapeutic monitoring of targeted therapy (SS 1001a), B-0836
- Guberina N., Körber A., Forsting M., Umutlu L., Bockisch A., Herrmann K., Poeppel T.D.**
Examination of association of inflammatory activity in psoriatic arthritis and vascular calcification metabolism based on integrated ¹⁸F PET/MRI (SS 1910), B-1621
- Guenego A., Leclerc A., Premat K., Ducroux C., Roques M., Blanc R., Piotin M., Fahed R.**
Haemorrhagic transformation and aspirin therapy after thrombectomy: an inter- and intrarater agreement study (SS 611), B-0518
- Guenoun D., Foure A., Pithioux M., Guis S., Le Corroller T., Pauly V., Chabrand P., Champsaur P., Bendahan D.**
Ultra-high field 7 Tesla MRI and biomechanical investigation of vertebral bone microarchitecture (MY 13), B-1024
- Guerini H.**
Musculoskeletal ultrasound in the management of sports injuries: C. Ultrasound-guided intervention in the athlete: indications and techniques (RC 810), A-348
- Guerri S., Mercatelli D., Gasperini C., Aparisi Gomez M., Rimondi E., Albinetti U., Napoli A., Battista G., Bazzocchi A.**
MRgFUS treatment for painful bone metastases, analysis of non-responders: are there imaging features associated with poor clinical response? (SS 210), B-0114
- Guglielmo M., Banfi C., Giannazza E., Guaricci A., Baggiano A., Andreini D., Mushtaq S., Pepi M., Pontone G.**
Correlation between haptoglobin phenotypes and myocardial reperfusion injury in consecutive ST-elevation myocardial infarction as detected by cardiac magnetic resonance (SS 603), B-0567
- Guglielmo M., Guaricci A., Lorenzoni V., Mushtaq S., Muscogiuri G., Maffei E., Cademartiri F., Mark R., Pontone G.**
Subclinical coronary and carotid atherosclerosis in asymptomatic high-risk patients (MY 7), B-0779
- Guglielmo M., Guaricci A., Andreini D., Conti M., Marconi S., Auricchio F., Pepi M., Tondo C., Pontone G.**
Left atrial appendage closure guided by 3D-printed patient-specific models (SS 1503), B-1224

Authors' Index

Guglielmo M., Guaricci A., Baggiano A., Fazzari F., Andreini D., Fabiocchi F., Lualdi A., Bartorelli A., Pontone G.
Accuracy of CCTA to detect obstructive CAD using stress vs rest dataset in patients referred to stress CTP (SS 1803), B-1460

Guidi E., Giaconi C., Arena C., Neri E.
Tumour volume vs RECIST criteria in re-staging rectal cancer (SS 216), B-0168

Guimaraes L.S.
Dual-energy CT of the abdomen: the time is now: A. Basic principles and different approaches (E³ 1226), A-533

Guiu B., Chevallier P., Rode A., Bouvier A., Valette P., Cassinotto C., Piron L., Boulin M.
Idarubicin-loaded beads for chemoembolisation of HCC: interim analysis of IDASPHERE II (FFCD 1307) multicentre single-arm phase II trial (SS 1409), B-1060

Guiu B.
Improving clinical pathways with angio CT in abdominal IR (SY 3)

Gulati V.
How learnings and best practices from digital health can help radiology (SY 26)

Güler E., Ünal N.G., Hekimsoy I., Köse T., Harman M., Elmas Z.N.
Dual-energy CT enterography in evaluation of Crohn's disease: the role of virtual monochromatic images (SS 1901c), B-1538

Gulino P., Bianchi A., Scionti A., Diciotti S., Bartolini E., Papadopulos P., Defilippi C., Mascacchi M.
Dentate and basal ganglia T1-hyperintensity in pediatric patients who had received both linear and macrocyclic Gadolinium-based MRI contrast agents; evidence of a "carry-over" effect (SS 212), B-0161

Gullien R., Haakull A., Nyborg T., Sollid B., Stensvoll M., Ali S.M., Andersen J.
Tomosynthesis-guided vacuum-assisted breast biopsy: a survey of the patient's experience (SS 214), B-0140

Gunduz N., Durukan G., Eser M.B., Aslan A., Kabaalioglu A.
Role of iliac crest tangent sign in correct numbering of lumbosacral transitional vertebrae (SS 610a), B-0433

Güner N., Gulcu A.
Evaluating aortic endograft (EVAR) fate according to anatomical instruction (IFU) compliance: which anatomical feature has the most impact on graft fate? (SS 309), B-0226

Günther R.W.
Drug elution or drug illusion in vascular disease: Chairperson's introduction (SF 13c), A-669

Gupta P., Popli M., Diwan K.
Apparent diffusion coefficient at 3T MRI in differentiating benign and malignant breast lesions: a quantitative analysis (SS 1402b), B-1108

Gurel S., Yılmaz Ö., Kiyan A.
The frequency of coexistence of renal artery and vein variations on abdominal CT (SS 1815), B-1330

Gursoy M., Dirim Mete B., Cetinoglu Y.K., Oyar C., Erdogan N., Uluc M., Bulut T., Safa G.
The association of patellar maltracking with infrapatellar fat pad oedema and chondromalacia patella: a quantitative morphologic MRI analysis (SS 1810), B-1429

Guseva E., Morozov S., Burenchev D.V., Trofimenko I., Ledikhova N., Rostovtseva T.
Remote radiological audit: a regional quality assurance system (SS 205), B-0182

Gutberlet M.
Memorable cases in cardiovascular imaging: how to avoid common mistakes: Misleading CMR LGE artefact in cardiomyopathies (SF 12e), A-601

Gutberlet M.
Cardiac and vascular: A. Cardiovascular imaging: the basics (E³ 1323), A-641

Guthrie J.A.
My three top tips for abdominal imaging: Bile duct stones (SF 12a), A-521

Gutzeit A.
Patient-adapted communication between radiologist and patient: should radiologists rethink their patient care? (SS 205), B-0179

Guzzardi G., Del Sette B., Cerini P., Carrafello G., Fusaro F., Laganà D., Stanca C., Carriero A.
Multicentre experience in endovascular treatment of aorto-iliac-femoral anastomotic pseudoaneurysms: evaluation of long-term follow-up (SS 309), B-0232

H

Ha M., Kim C., Lee K.Y., Shin C., Kang E., Oh Y., Ko C., Cha J.
Accuracy of emphysema volume and airway measurements according to FBP, HIR, MIR, and virtual monoenergetic reconstruction images at both low- and standard-dose settings (SS 304), B-0241

Ha M., Lee K.Y., Kim C., Kim S., Park S., Je B., Lee S.H., Lee Y., Cha J., Jeong-Cheon A.
Optimal monochromatic energy levels in spectral CT pulmonary angiogram for the detection of pulmonary thromboembolism: using detector-based spectral CT (SS 604), B-0461

Ha S., Shin J., Baek J., Song D., Chung S., Choi Y., Lee J.
Does RFA induce neoplastic change of benign thyroid nodules (MY 14), B-1191

Haage P.
Post-treatment evaluation: what every radiologist should know: Chairperson's introduction (RC 815), A-356

Hachulla A., Noble S., Guglielmi G., Agulleiro D., Muller H., Vallee J.
3D-printed heart model to guide LAA closure: preliminary results (SS 1503), B-1223

Hadid-Beurrier L., Habib Geryes B., Waryn M., Jean-Pierre A., Farah J.
Validation of the DACS-integrated radiation dose monitor skin dose mapping software using XR-RV3 Gafchromic films for fluoroscopically guided procedures (SS 313), B-0313

Hagberg G.
Demystifying MRI: things you always wanted to know: C. Practical MRI: a toolkit of standard MR pulse sequences (RC 1613), A-846

Hahn A., Sauppe S., Knaup M., Kachelrieß M.
Moving metal artifact reduction (MMAR) for cone-beam CT (CBCT) scans of the thorax region (SS 1813), B-1434

Hahn H.K.
Quantitative imaging in oncology: C. Requirements for quantitative data extraction and analysis (E³ 1626b), A-864

Hajji M., De Tymowski C., Bourrier P., Mallet V., Zagdanski A.M., Legrand M., De Kerviller E.
Potential ketamine-related cholangitis in severely ill burn patients: liver imaging features (SS 601a), B-0422

Halaweish A.F., Siegel M., Duba I., Grant K., Schmidt B.
Dose distribution to radiosensitive organs using advanced thoracic CT imaging techniques (SS 712), B-0772

Halaweish A.F., Schmidt B., Grant K., Flohr T., Hofmann C.
Automatic adaptive iterative metal artifact reduction (SS 1008), B-0905

Halfmann M.C., Benz S., Eichstädt J., Lollert A., Düber C., Kreitner K.-F., Emrich T.
Age and sex dependency of myocardial strain in CMR: an urgent need to standardise (SS 1403), B-1160

Halfmann M.C., Benz S., Eichstädt J., Lollert A., Düber C., Kreitner K.-F., Emrich T.
Morbus Fabry: new insights from CMR strain imaging (SS 1903), B-1653

Haller S.
My three top tips for neuroimaging: Dementia (SF 15c), A-762

Halligan S.
Cancer screening: B. Colorectal cancer screening: what is the radiologist's role? (RC 1216), A-566

Halligan S.
The anal canal: does MRI make it easy?: Chairperson's introduction (E³ 1522), A-793

Hamm B.
The new horizon for radiology: Chairpersons' introduction (part 2) (NH 14), A-722

Hammerstrøm L.
Evidence-based practice in diagnostic imaging departments - involving the patients in procedure-development (MY 17), B-1312

Hammond C.
Placental imaging: how, when and why?: Abnormally invasive placenta: vascular anatomy and interventional radiology approaches to management (SF 16), A-816

Han J., Kim K.A., Hyeyoon C., Kim J.W., Park Y., Lee J., Choi J.W., Lee C.H., Park C.M.
Newly categorised seromucinous tumours of ovary: computed tomographic and magnetic resonance imaging features with pathological correlation (SS 707), B-0643

Han Y., Park B., Kim M., Sung D., Han N., Sim K., Cho S.
Accurate localization of rectal cancer on preoperative magnetic resonance imaging: a prospective study using an anal verge marker (SS 1001b), B-0854

Hangaard S., Gudbergensen H., Daugaard C.L., Bliddal H., Nybing J.D., Casula V., Nieminen M.T., Tiderius C.J., Boesen M.
Delayed gadolinium-enhanced MRI of meniscus and cartilage (dGEMRIM/dGEMRIC) in overweight patients with knee osteoarthritis (MY 13), B-1014

Harden S.
Coronary CT angiography: how to start practice, perform and evaluate the exam?: B. Staff training and technical requirements (RC 1603), A-811

Hardy M.
Radiography research: a how to guide: Chairperson's introduction: Why is radiography research important (BR 1), A-548

Authors' Index

Hardy M., Harris M.A.

Enhancing radiographer threshold CT competencies through simulation (SS 1414), B-1143

Harris E.

New imaging approaches for radiotherapy: Ultrasound imaging in radiotherapy: "old" technology with new applications in RT? (ESR/ESTRO), A-886

Harris M.A., Hardy M.

Evaluating the roles of CT radiographers in the UK (MY 17), B-1308

Hartmann I.

Pneumonia: A. Community-acquired pneumonia (RC 1204), A-530

Harvey H.

Perspectives on the challenges in developing ML for radiology: how ML can save breast screening (SY 26)

Hassanein S.A.H.

Colour Doppler unhappy surprise in transvaginal ultrasound evaluation of post-abortive vaginal bleeding: uterine arteriovenous malformations (SS 607), B-0469

Hatem A., Hazaimh B.K., Alhyari I., Jalaileh A., Salman S., Al-Omari A.

Establishing a new protocol for aortofemoral CT angiography using the lowest possible contrast media with the advent of faster scanners (SS 1415), B-1045

Hauge I., Aandahl I., Baranzelli J., Coelho P.M., Eriksen L., Hadebe N., Kahl G., van Schagen S., O'Connor M.

Digital radiography: impact of a lower tube voltages on image quality and radiation dose in chest phantom radiography (MY 17), B-1309

He M.

Diagnostic value of dual-energy CT imaging for cervical lymph node metastasis in patients with papillary thyroid cancer (MY 14), B-1195

Heber S.D., Lorbeer R., Gatidis S., Machann J., Auweter S., Sellner S., Peters A., Bamberg F., Schlett C.L.

MRI-based epi- and para-cardial fat depots in a cohort of prediabetics, diabetics and healthy controls from a general population without cardiovascular disease (SS 303), B-0336

Heerink W.J., Ruiters S.J.S., Arnolli M., Pennings J., Lansdorp B., Vliegthart R., Oudkerk M., de Jong K.P.

Randomised controlled trial of free-hand vs robotic-guided needle positioning in CT-guided thermoablation of liver tumours (MY 9), B-0825

Hegde V., Rajgopalan N., Thakar S.

Thesphenoid ostium and its relationship to other endoscopic landmarks in acromegaly: a CT-based morphological study (SS 308), B-0261

Heijmink S., van den Bergh R., Wit E., van der Poel H.

Experience with MRI guided prostate biopsies using the 3D Navigo system in an oncologic referral centre (SS 1907a), B-1565

Heijmink S., Grivas N., Tillier C., van der Roest R., van Mullekom E., van der Poel H.

Predicting and improving postprostatectomy urinary continence by pelvic floor measures on MR (SS 1907a), B-1568

Heikkinen J., Sepponen P., Henner A.

Scattering in dental cone-beam computed tomography (SS 1814), B-1449

Heil P., Tyczynski B., Reinboldt M., Li Y., Theysohn J., Suntharalingam S., Grüneisen J., Kribben A., Wetter A.

Transjugularrenal biopsy in patients with impaired coagulation status (SS 609), B-0450

Heiß R., Kellermann M., Swoboda B., Grim C., Nagel A.M., Uder M., Hotfiel T.

Compression garments in delayed-onset muscle soreness (DOMS): randomised controlled trial with acoustic radiation force impulse (ARFI), contrast-enhanced ultrasound (CEUS) and MRI (SS 710a), B-0621

Helbich T.H.

Screening for breast cancer: B. Screening with mammography and ultrasound (RC 402), A-118

Helbich T.H.

EIBIR Research Session: European imaging researchers united in diversity: Testing hybrid MR/PET (HYPMED) device for enhanced breast diagnosis in a multicentre clinical trial (EIBIR 1), A-321

Hellbach K., Beller E., Schindler A., Schoeppe F., Hesse N., Baumann A.B., Schinner R., Hauke C., Meinel F.

X-ray dark-field and phase-contrast images facilitate the detection of wooden and glass foreign bodies on radiographs (SS 613), B-0541

Helmberger T.K.

Personalised medicine in liver tumours: B. Treatment options and strategies for liver tumours (E³ 720), A-294

Helmberger T.K.

Interventional: A. Basic principles of angiography and image-guided interventions (E³ 1923), A-971

Hempel J., Schittenhelm J., Brendle C., Skardelly M., Bender B., Tabatabai G., Castaneda Vega S., Ernemann U., Klose U.

In vivo assessment of tumour heterogeneity in WHO 2016 glioma grades using diffusion kurtosis imaging (SS 211), B-0090

Hempel J., Schittenhelm J., Brendle C., Bender B., Skardelly M., Tabatabai G., Castaneda Vega S., Ernemann U., Klose U.

Histogram analysis of diffusion kurtosis imaging estimates for in vivo assessment of 2016 WHO glioma grades (SS 211), B-0093

Hempel J., Schittenhelm J., Bender B., Skardelly M., Tabatabai G., Castaneda Vega S., Ernemann U., Klose U., Brendle C.

In vivo molecular profiling of human glioma using dynamic susceptibility contrast magnetic resonance perfusion imaging (MY 8), B-0808

Henner A., Richli Meystre N., Sá dos Reis C., Strøm B., Pires Jorge J., Kukkes T., Metsälä E.

Mammography performance and quality assurance practice among five European countries (SS 214), B-0130

Henner A., Metsälä E., Richli Meystre N., Sá dos Reis C., Strøm B., Pires Jorge J., Kukkes T.

Eyes on the future of mammography education and training: what needs to be focused to match the demands of the clinical practice? (SS 1414), B-1146

Henner A., Paalimäki-Paakki K.

Patient doses in plain chest x-ray compared to national DRLs (MY 17), B-1310

Henner A., Lahdenperä A., Suutari H., Koivunen K., Paalimäki-Paakki K.

Patients' experiences in coronary angiography (SS 1814), B-1452

Hennicaux J., Hutt A., Kyheng M., Favier J., Remy J., Rémy-Jardin M.

Transient interruption of contrast (TIC) in CT pulmonary angiography: frequency and impact on the diagnostic value of CT examinations using a dual-source CT system (SS 604), B-0458

Hennicaux J., Hutt A., Favier J., Khung S., Remy J., Remy-Jardin M.

Indeterminate CT pulmonary angiograms (CTPA) with dual-source CT (DSCT): prospective evaluation in 449 patients suspected of acute pulmonary embolism (PE) (SS 1904a), B-1555

Herlin C., Kjaer P., Espeland A., Skouen J., Leboeuf-Yde C., Karppinen J., Niinimäki J., Sørensen J.S., Jensen T.S.

Modic changes: the association with low back pain and activity limitation - a systematic literature review and meta-analysis (SS 610a), B-0435

Hermann K.-G.

Value of x-ray in the diagnosis and follow-up of rheumatic diseases (SY 14)

Hermann K., Mercan S., Ziegeler K., Diekhoff T., Greese J., Hamm B., Bollow M.

Osteitis distribution on MRI of the sacroiliac joints in patients with osteitis condensans compared to axial spondyloarthritis (SS 1910), B-1619

Hermans R.

Post-treatment imaging of the head and neck: A. Normal findings after radiotherapy (RC 1308), A-622

Herranz M., Argibay-Vazquez S., Dominguez-Prado I., Ling Ling P., Graña L., Vázquez Caruncho M., Ruibal A.

Breast MRI and dedicated breast PET (dbPET): friends and foes (SS 602), B-0501

Herranz M., Ling Ling P., Aguiar P., Liang W., Albaina Latorre L., Juaneda M., Ruibal A.

Molecular imaging heterogeneity study of breast tumours as a new diagnosis parameter (SS 1006), B-0992

Herranz M., Abou-Jaoude G., Liang W., Aguiar P., Ruibal A.

Design, development and validation of the first 3D PET manual breast-guided biopsy system (SS 1802a), B-1395

Herrera I.

The degenerative cervical spine: C. The postoperative cervical spine (RC 111), A-022

Heskamp S.

Radiographers in preclinical imaging research: SPECT/CT (SF 9b), A-426

Heussel C.P.

Pneumonia: C. Fungal pneumonia in immunocompromised hosts (RC 1204), A-532

Heuvelmans M.A.

Updates on lung cancer management: A. Lung cancer screening (E³ 918), A-447

Hickethier T., Bar-Ness D., Bunck A., Maintz D., Pahn G., Coulon P., Si-mohamed S.A., Douek P., Sigovan M.

Initial in vitro comparison of a spectral photon counting CT and a spectral dual-layer CT system for non-invasive evaluation of soft-plaque-restenosis in coronary artery tortuosity (SS 1003), B-0983

Authors' Index

- Hickethier T., Kröger J., Baessler B., Maintz D., Chang D.**
Significant reduction of contrast agent dose for venous phase chest CT scans: first experiences using monoenergetic reconstructions from a novel spectral detector scanner (SS 1904a), B-1556
- Hilgenfeld T., Kästel T., Heil A., Rammelsberg P., Heiland S., Bendszus M., Schwindling F.S.**
High-resolution dental MRI for planning palatal graft surgery: a clinical pilot study (SS 308), B-0264
- Hinzpeter R.M.M.**
Thoracic emergencies: Acute coronary syndrome (BS 4), A-127
- Hiremath S.B., Gautam A.A., Benjamin G.**
Looking for association between blood pressure, imaging severity and complications - MR imaging study in posterior reversible encephalopathy syndrome (SS 1911a), B-1595
- Hirschmann A., Walter W.R., Alaia E.F., Garwood E., Rosenberg Z.S.**
Are fractures of the anterior calcaneal process indicative of a more advanced Chopart joint injury? (SS 610b), B-0538
- Hodel J.**
Current guidelines and diagnostic criteria in multiple sclerosis (MS): MRI in monitoring treatment complications (SA 5b), A-211
- Hoefel C.**
The anal canal: does MRI make it easy?: A. MRI of the anal canal: from normal anatomy to local tumour staging (E³ 1522), A-794
- Hofvind S., Moshina N., Waade G.G., Sebuødegård S.**
Breast compression and experience of pain: comparing two compression paddles (SS 214), B-0133
- Hogg P.H.**
Radiation protection from A to Z: The latest optimisation techniques in conventional radiography (BR 2), A-631
- Hojreh A., Kasprian G., Göral K.A., Klebermass-Schrehof K., Vergesslich Rothschild K., Weber M., Patsch J.M.**
SML ultrasound of the neonatal brain: comparison with MRI (1.5 T) in a clinical case series (SS 212), B-0155
- Holla M.**
The polytrauma patient: The secondary survey: from head to toe (MS 17), A-938
- Holter T.Ø., Torp S., Martinsen A.**
Evaluation of radiation protection knowledge among hospital employees (SS 1914), B-1647
- Holub P.**
Linking imaging biobanks to -omics: the role of BBMRI and ESR: Types of biobanks in the BBMRI network (ESR/BBMRI-ERIC), A-614
- Hong S., Lee S., Kim N., Lee S., Seo J.**
Quantitative CT assessment in patients with desquamative interstitial pneumonia: correlations with pulmonary function parameters (SS 304), B-0239
- Hong W., Lee S.M., Kim M.J., Ha H., Lee K., Lee D., Lee S.**
Comparison of liver stiffness measurements between point shear wave elastography (ElastPQ) and two-dimensional shear wave elastography (ElastQ Imaging) equipped on a same machine (MY 15), B-1269
- Hoppe H.**
US and vascular disease: a perfect match: C. Upper and lower limb: venous district (RC 1315), A-665
- Hornbeck A., Habib Geryes B., Pierrat N., Jarrige V., Dreuil S., Ducou le Pointe H.**
CT scan radiation dose evaluation by clinical indication: a multi-centric French study (SS 313), B-0315
- Horvath E., Castillo Balladarez E.H., Pizzolon M.F., Silva C., Gallegos M., Pinochet M.A., Galleguillos M., Uchida M., Gonzalez P.**
Can a hyperechogenic breast lesion be malignant? (SS 302), B-0272
- Horvath E., De la Barra C., Aguilera G., Silva C., Slater J., Skoknic V., Majlis S., Garcia M., Gonzalez P.**
Role of ultrasound in management of indeterminate thyroid nodules (Bethesda III and IV) (SS 608), B-0492
- Horvath E., Skoknic V.S., Silva C., Tala H., Sánchez N., Whittle C., Niedmann J.P., Majlis S., Schweinitz C.**
Ultrasonographic diagnosis of salivary gland atrophy after radio-iodine treatment for papillary thyroid cancer (SS 608), B-0494
- Horvath E., Aguilera G., Silva C., Droguett M., Skoknic V.S., Tala H., Majlis S., Slater J., Whittle C.**
Atypical ultrasonographic patterns of papillary thyroid carcinoma: how to recognise them (SS 708), B-0667
- Horvath E., Darrás Ismael C., Silva C., Castillo E., Pinochet M.A., Galleguillos C., Droguett E., Villalon M., Pizzolon F.**
Contribution of preoperative breast MRI study to pure DCIS (SS 1002), B-0914
- Horvath E., Castillo Balladarez E.H., Silva C., Darrás C., Uchida M., Pinochet M.A., Altamirano A., Droguett E., Galleguillos C.**
Background parenchymal enhancement at breast magnetic resonance imaging: association with tumour response to neoadjuvant chemotherapy (SS 1402b), B-1116
- Hota P., Dhibar T., Biswas A.**
Role of qualitative and quantitative parameters in differentiation of PSA from other atypical parkinsonian syndromes in MRI (SS 1511), B-1243
- Hotta M., Minamimoto R., Yamada K., Yokoyama K., Toyohara J.**
Comparison of 4'-[methyl-¹¹C] thiothymidine (4DST) PET/CT and FDG PET/CT for predicting response to neoadjuvant therapy in patients with oesophageal cancer (SS 1416), B-1081
- Hovda T., Holen Å.S., Bjørndal H., Sebuødegård S., Hofvind S.**
Digital breast tomosynthesis vs digital mammography: early performance measures in a population-based screening programme (SS 202a), B-0076
- Hovda T., Holen Å.S., Bjørndal H., Sebuødegård S., Hofvind S.**
Missed and true screen-detected and interval breast cancers in a population-based breast cancer screening programme (SS 702), B-0676
- Hovda T., Holen Å.S., Bjørndal H., Sebuødegård S., Hofvind S.**
Variations in BI-RADS mammographic density classification between radiologists at three breast centres (SS 1402a), B-1096
- Howarth N.**
Cavitary and cystic diseases of the lung: Chairperson's introduction (E³ 418), A-160
- Howlett D.C.**
Audit across Europe: directive and perspective: Chairpersons' introduction (part 2) (ESR Audit), A-853
- Hricak H.**
Do we need dynamic contrast enhancement (DCE) in prostate mpMRI?: B. No we don't! (PS 527), A-207
- Hu B., Yang Z., Liu X., Shi K., Xu H., Guo Y.**
The right ventricular strain assessment in type 2 diabetes mellitus patients: insights from cardiac magnetic resonance feature tracking (SS 303), B-0338
- Hu S.**
Comparison between the US vs MRI features of papillary thyroid carcinoma (SS 608), B-0491
- Hu S.**
Quantitative analysis of ADC values in differentiating papillary thyroid carcinoma and thyroid adenoma (SS 708), B-0669
- Hu S.**
The diagnostic value of combination of US < MRI preoperative prediction for the extrathyroidal extension of papillary thyroid carcinoma (MY 14), B-1188
- Hu T., Tong T., Wang S.**
Added value of radiomics signature to predict pulmonary metastasis in colo-rectal cancer patients with lung nodules (SS 316), B-0360
- Hu Y., Lee C., Guo W., Lin C., Yang H., Wu H., Liu K., Chung W.**
The impact of trigeminal nerve atrophy and vascular compression on outcomes of trigeminal neuralgia after stereotactic radiosurgery (SS 1411b), B-1099
- Huang D., Alsadiq M.R., Sellars M., Eckersley R., Sidhu P.**
"Avascular" hypoechoic testicular lesions on colour Doppler ultrasound: can they be considered benign? what is the added value of contrast-enhanced ultrasound? (SS 1907b), B-1659
- Huang H., Yeh B.M., Srinivasan R., Sun Y.**
Detection of osseous metastases using dual-energy CT with material decomposition algorithms: phantom development and preliminary clinical validation (MY 13), B-1021
- Huang K.**
Prediction of pathological differentiation for hepatocellular carcinoma: preoperative Gd-EOB-DTPA-enhanced MRI and histopathological correlation (SS 301a), B-0200
- Huang M.**
Utility of histogram analysis of apparent diffusion coefficient maps in differential diagnosis of uterine sarcoma and degenerated uterine leiomyoma (SS 707), B-0648
- Huang M.**
Texture analysis of magnetic resonance imaging in differential diagnosis of rectal tumours (SS 1001b), B-0852
- Huang M.**
Diffusion-weighted imaging combined with ADC in the diagnosis of testicular lesions (SS 1907b), B-1661
- Huber S.**
Planning your career: Chairperson's introduction: What employers are looking for from new graduates (BR 3), A-927

Authors' Index

Huber T., Rotkopf L., Kunz W.G., Bette S., Wiestler B., Gempt J., Zimmer C., Sommer W.H., Thierfelder K.

Wavelet-based reconstructions of dynamic susceptibility MR perfusion: a new method to visualize hypervascular brain tumours (SS 211), B-0088

Hughes N.M., O'Neill C., O'Brein F.M., Mayer N., Kelly P., Buckley J.G., O'Regan K.
Prostate tumour volume analysis on MRI as a predictor for aggressive disease (SS 307), B-0249

Huijgen W., van Rijswijk C.S., Bloem J.L.
mDixon is superior to frequency-selective fat suppression in musculoskeletal tumour imaging (SS 210), B-0110

Humphries P.D.
Paediatric MRI: can we make gadolinium superfluous?: The role of intravenous gadolinium in paediatric oncology (SF 13b), A-650

I

Iacobellis F., Iadevito I., Sorbo A., Scuderi M.G., Daniele S., Sparano A., Russo G., Romano L., Scaglione M.
Dual-phase CT protocol in the assessment of traumatic liver injuries (SS 317), B-0295

Iacobellis F., Roberto L., De Pascale L., Rella R., Natella R., Reginelli A., Grassi R.
Preoperative assessment of simple and complex anorectal fistulas: tridimensional endoanal ultrasound? Magnetic resonance or both? (SS 601b), B-0525

Iafrate F.
My three top tips for abdominal imaging: Colon polyp (SF 12a), A-525

Iafrate S., Capretti I., Cannizzaro E., Arrigoni F., Di Luzio M., Giordano A.V., Mascaretti S., Mascaretti G., Masciocchi C.
Treatment of intramural and submucosal uterine fibroids (UFs) using MRgFUS (magnetic resonance-guided focused ultrasound surgery) (MY 9), B-0829

Iafrate S., Capretti I., Cannizzaro E., Arrigoni F., Di Luzio M., Giordano A., Mascaretti S., Mascaretti G., Masciocchi C.
Tips and tricks to treat difficult cases of uterine fibroids (UFs): how to increase eligibility in MRgFUS (magnetic resonance-guided focused ultrasound surgery) (SS 1909), B-1543

Iannessi A., Bertrand A., Beaumont H., Natale R., Baudin G., Thyss A.
Focused ultrasounds for the treatment of bone metastases: efficacy and feasibility (SS 1809), B-1343

Ibe D.
Hepatobiliary ultrasonographic abnormalities and clinical severity score of paediatric sickle cell anaemia patients in a resource-poor setting (MY 18), B-1498

Ichikawa S., Motosugi U., Suzuki T., Shimizu T., Onishi H.
Differentiation of inflammatory pseudo-tumour from colorectal liver metastases on gadoteric acid-enhanced magnetic resonance imaging (MY 15), B-1258

Iezzi R.
No time to lose: aortic dissection - revisited: Acute diagnosis and imaging in aortic dissection (E³ 24A), A-077

Iezzi R.
Percutaneous interventional procedures: a practical guide: Chairperson's introduction (RC 809), A-364

Iezzi R.
How can radiologists expand their role in peripheral vascular intervention?: Chairperson's introduction (PC 9), A-428

Imhof H.
Head and neck: inflammation, tumour or something else?: Thyroid and parathyroid (BS 1), A-024

Indestege I., Cockmartin L., Binst J., Coudyzer W., Bosmans H., Aertsen M.
A procedure towards optimised prenatal CT scan protocols for low dose imaging of suspected skeletal dysplasia (SS 1413), B-1139

Inecikli M.
Vertebroplasty with trajectory planning and 3D road map applications: first experiences (MY 9), B-0826

Ioan I., van Urk J., Schouten D.K., van der Noordaa M.E., Vrancken Peeters M., Beets-Tan R.G.H., Winter-Warnars G., Loo C.
The role of MRI in predicting irradical surgery and local recurrence after breast conserving surgery in T3 breast cancer patients after neoadjuvant chemotherapy (SS 1002), B-0917

Ioannidis G.
Optimising computed tomography: A. Optimising access to CT in stroke (RC 1614), A-849

Iodice M., Pittari V., Trimboli R.M., Berger N., Carbonaro L.A., Sardaneli F.
Probably benign findings (BI-RADS 3) at breast MRI: frequency and malignancy rate (SS 1402a), B-1093

Iotti V., Giorgi Rossi P., Ravaioli S., Nitrosi A., Bertolini M., Bacchini E., Vacondio R., Pescarolo M., Pattacini P.
Comparing two visualisation protocols for tomosynthesis in screening: specificity and sensitivity of slabs vs planes plus slabs (SS 202a), B-0083

Ippolito D.
Iterative model-based reconstruction: basis of new imaging era (SY 12)

Ippolito D., Querques G., Talei Franzesi C.R., Lombardi S., Pecorelli A., Sironi S.
Perfusion CT imaging: diagnostic biomarker tool for survival predictor of tumour in response to antiangiogenic treatment in patients with advanced HCC lesions (SS 1901a), B-1513

Irion K.
Chronic obstructive pulmonary disease (COPD): Chairperson's introduction (RC 804), A-304

Islam S., Johnson D.
CT-guided percutaneous synovial cyst rupture using a 11G Jamshidi needle: early experience and results of a novel technique (MY 9), B-0822

Ivanoski S.P., Vasilevska Nikodinovska V.
Haemarthrosis of the knee and knee fracture: evaluation with high-resolution ultrasound (SS 610b), B-0535

J

Jacków J., Zimny A., Podgórski P., Sasiadek M., Szczesniak D., Rymaszewska J., Poltyn-Zaradna K., Zatońska K., Szuba A.

Covert brain ischaemia and its impact on cognition in the Polish population: preliminary results of the PURE - mind (Prospective Urban and Rural Epidemiological) cohort study (SS 1011a), B-0920

Jacob J.
Artificial intelligence in chest imaging: Keynote lecture (SS 1004), K-15

Jacobs B.E., Baumann S., Renker M., Tesche C., Duguay T., Albrecht M.H., Coenen A., Nieman K., Schoepf U.J.
Gender differences in machine learning-based coronary CT angiography-derived fractional flow reserve: results from the machine registry (SS 1803), B-1456

Jacobson J.
Musculoskeletal interventional procedures: B. Injectables, percutaneous tendon fenestration and tenotomy: clinical outcomes and current evidence (TC 1528), A-798

Jacobson J.
Musculoskeletal interventional procedures: C. Interactive case discussion (part 2) (TC 1528), A-800

Jacques T.
Use of OnSight 3D in emergency settings (SY 25)

Jacquier A.
From diagnosis to prognosis: how does cardiac imaging affect patient outcome?: B. In non-ischaemic cardiomyopathy (RC 503), A-194

Jacquier A.
Memorable cases in cardiovascular imaging: how to avoid common mistakes: Dyspnea with an abnormal right ventricle: role of MR imaging (SF 12e), A-600

Jaermann Y.
EFRS meets Switzerland and Portugal: Radiographers in Switzerland: challenges and chances (EM 4), A-496

Jäger H.R.
Cerebrovascular disease: C. Cerebral perfusion studies in cerebrovascular disease: techniques, indications and applications (RC 911), A-410

Jäger H.R.
DSC and DCE: what does it mean and how to cook it? (SY 18)

Jahnke P., Schwarz F.B., Ziegert M., Hamm B., Scheel M.
Radiopaque 3D printing of patient individual phantoms for computed tomography and radiation therapy (SS 613), B-0548

Jahnke P., Schwarz F.B., Ziegert M., Abdelhadi O., Almási T., Nunninger M., Hamm B., Scheel M.
Evaluation of a 3D printed anthropomorphic phantom for simulation of CT-guided procedures (MY 9), B-0830

Jäkel O.
New imaging approaches for radiotherapy: MR-LINAC technological advances and potential usability in clinical setting (ESR/ESTRO), A-887

Jamali S., Dragean C., Michoux N.
Iterative reconstruction in "virtual non-contrast" with dual-energy CT: is it an alternative to conventional unenhanced phase? (SS 1901a), B-1508

James J., Giannotti E., Chen Y.
Evaluation of a CAD (computer-aided detection)-enhanced 2D synthetic mammogram: comparison with a standard synthetic 2D mammogram and conventional 2D digital mammography (SS 1902b), B-1636

James K., Duffy P., Kavanagh R., Feeley A., Ryan D., Murphy P., Bogue C., Maher M., O'Connor O.J.
Fast acquisition abdominal MRI study for the investigation of suspected acute appendicitis in paediatric patients: prospective assessment of diagnostic accuracy and clinical efficacy (SS 612), B-0574

Authors' Index

James S.L.J.

The radiological investigation of musculoskeletal tumours: B. MRI and whole-body MRI (RC 1610), A-842

Jansen O.

Stroke: emergent large vessel occlusion (ELVO): B. Advanced thrombectomy techniques (E³ 1326b), A-667

Janulcikas R.

Correlation measurements between positron emission tomography 18F-FDG dose and external exposure (SS 714), B-0750

Jarczewski A., Reimers I., Geisel D., Denecke T.

The influence of intravenous non-specific gadolinium-based contrast media application on image quality of T2-weighted MRC in preoperative evaluation of living liver donors (SS 701a), B-0609

Jargiello T.

Thoracic emergencies: Acute aortic syndrome (BS 4), A-125

Jargiello T.

US and vascular disease: a perfect match: Chairperson's introduction (RC 1315), A-662

Jayakumar M., Rangari A., Rodriguez M.J.

Prognostic role of CT imaging in coup and contre coup injuries of brain (SS 1911a), B-1601

Jeon J.Y.

The termination level of dural sac relevant to caudal epidural block in lumbosacral transitional vertebrae: comparison between sacralisation and lumbarisation groups (SS 610a), B-0434

Jesser J., Dinse B., Baldo J., Arévalo A., Bendszus M., Schlamp K.

Voxel-based lesion symptom mapping of NIHSS scores in patients with acute media infarction (SS 1011a), B-0925

Ji Q., Chu Z., Li J.Y.

Evaluation of hepatic warm ischaemia-reperfusion injury and intervention effect of Lipo-PGE1 in rabbit models: 3.0T BOLD MRI study (SS 301b), B-0201

Jiang J., Cui L., Fu Y., Xu G.

Volumetric analysis of intravoxel incoherent motion diffusion-weighted MRI in predicting the invasiveness of non-small cell lung cancer (MY 5), B-0421

Jiang J., Cui L., Gu X., Hong Q., Fu Y., Xu G.

The value of diffusion-weighted imaging based on monoexponential and biexponential model in the diagnosis of benign and malignant lung nodules and masses (SS 1904b), B-1572

Jiang S., Ren Y., Yan H., Lu X.

The value of dual-detector spectral CT imaging in the identification of gastric carcinoma and gastric lymphoma (SS 701b), B-0713

Jiang Y., Kauczor H.-U.

Diagnostic values of magnetic resonance imaging in mammography detected BI-RADS 4 category calcifications (MY 16), B-1278

Jiang Y., Kauczor H.-U.

Mammography, breast MRI and histopathological features of pure ductal carcinoma in situ (MY 16), B-1290

Jiménez-Pastor A., Alberich-Bayarri A., Fos Guarinos B., Garcia-Castro F., Marti-Bonmati L.

Automatic localisation and identification of vertebrae in spine CT scans by combining Deep Learning with morphological image processing techniques (SS 1805), B-1380

Jin L., Li M., Sun Y.

The impact of ASiR-V in different noise index in thorax CT imaging: comparison between normal dose and low dose (SS 704), B-0635

Jin L.

Variation of tube electric current (mA) in lung CT screening for glass ground nodules (GGNs) bigger than 3 mm: phantom study (SS 1804), B-1351

Jin Y., Gao L., Han F., Lv Y., Zhang J.

Naluf₄ for spectral CT in the diagnosis of osteosarcoma (SS 1406), B-1179

Jin Z.

The China CT standardisation initiative (SY 15)

Jin Z.Y.

A glance of China through images: Introduction (EM 3), A-946

Jing W.

Clinical value of dynamic contrast-enhanced MRI and diffusion-weighted imaging on diagnosis of central gland prostate carcinoma (MY 17), B-1295

Jobst B.J.

Chronic obstructive pulmonary disease (COPD): C. Is there a role for MRI? (RC 804), A-307

Jofré H., Planas L., Luburich P., Conejero A., Molina M.

Description of interstitial findings in patients with diverse severity of telomere shortening (SS 204), B-0048

Johnson G.

Contrast media in imaging: A. Contrast-enhanced ultrasound: principles and applications (RC 814), A-353

Johnson K.J.

Paediatric radiology for the general radiologist: A. Fractures in children (E³ 1521), A-731

Joo I., Lee J., Lee E., Lee D., Son J., Chang W., Lee S., Yang H.

Preoperative classification of resectability of pancreatic cancer using multi-detector row CT: a study of interobserver reliability (SS 1901b), B-1524

Jovicich J., Barkhof F., Babiloni C., Herholz K., van Berckel B.N., Mulert C., Frisoni G., JPND Working Group S.J.

A survey for neuroimaging harmonization needs for large-scale neurodegenerative biomarker studies (SS 1411a), B-1033

Juárez-García M.S., Pallisa E., López-Meseguer M., Varona Porres D., Sanchez Martinez A.L., Maciag E., Cabanzo Campos L., Andreu J., Persiva Morenza O.

High-resolution computerised tomography (HRCT) features of Group 1 pulmonary arterial hypertension (PAH): a case series of 21 lung transplant patients (SS 1904a), B-1551

Jung C.S.L., Heine M., Mangels N., Kaul M., Adam G., Ittrich H., Heeren J.

BAT activity in Type I and Type II diabetes mouse models: multimodal imaging study using 7T MRI and intravital microscopy (SS 1006), B-0990

Jungmann P.M.

Knee: C. Postoperative (E³ 1019), A-469

Juskanic D., Petrovicova A., Holly S.

The utility of CAD software in acute stroke protocol workflow for automatic evaluation of infarct core size (SS 1011a), B-0924

K

Kabin Y., Kostash O., Kapustin V., Gromov A. Metastatic axillary lymph nodes in patients with breast cancer: value of quantitative shear wave elastography (SS 716), B-0702

Kachelrieß M.

Motion artefacts and their management in medical imaging: A. Managing motion in CT: conventional approaches and motion compensating techniques (RC 1313), A-654

Kahn J., Böning G., Fehrenbach U., Feldhaus F., Kaul D., Maurer M.H., Renz D.M., Streitparth F.

Multi-energy CT in patients with thoraco-abdominal bleeding: new techniques to facilitate image reading and to help save dose (SS 317), B-0292

Kainberger F.

Case-Based Diagnosis Training - Part 1: Musculoskeletal (CB 1), A-965

Kaiser C.G.N.

The future of MR mammography: radiomics? (SY 1d)

Kaissis G., Lohöfer F., Bliemsrieder E., Topping G., Schilling F., Rummeny E.J., Schwaiger M., Braren R.

Imaging glycolytic heterogeneity of HCC in real time using dynamic hyperpolarised magnetic resonance spectroscopy: a personalised medicine approach (SS 1006), B-0988

Kala P., Avantsa R., Gowda, G.

Diagnostic performance of digital tomosynthesis as compared to conventional radiography in evaluation of craniovertebral junction (SS 308), B-0260

Kalender W.A.

Euratom Basic Safety Standards Directive: a comprehensive approach for radiation protection: The technical approach: achievements and future of dose reduction (EU 1), A-146

Kalender W.A.

CT screening: benefits, doses and associated risks: Breast CT (ESR/EFOMP), A-230

Kalender W.A.

Euratom Basic Safety Standards Directive: a comprehensive approach for radiation protection: Panel discussion: Is the Basic Safety Standards Directive a step forward for patients, clinical professionals and regulators? (part 3) (EU 1)

Kalovidouri A.M., Vargas M.I., Delattre B., Pluchino N., Montet X., Botsikas D.

Diffusion tensor imaging (DTI) for evaluation of sacral plexus abnormalities in patients with pelvic deep infiltrating pelvic endometriosis with pelvic pain: a pilot study (SS 607), B-0466

Kamble A.N., Popli M.

Comparing computer-aided diagnosis (CAD) system with manual method for detecting breast arterial calcification (BAC) (SS 202b), B-0100

Kamble A.N., Kamble A., Popli M.

The role of arterial spin labelling (ASL) and diffusion tensor imaging (DTI) and to differentiate between malignant and benign breast lesions (MY 16), B-1282

Kamis M.F.A., Rahmat K., Ramli Hamid M.T.

Role of diffusion-weighted MRI (DWI) and intravoxel incoherent motion (IVIM) in monitoring treatment response to neoadjuvant chemotherapy in locally advanced breast cancer (SS 202b), B-0105

Authors' Index

Kamo M., Nozaki T., Yoshida K., Tateishi U., Akita K.

Kinking of the upper ureter in CT urography: anatomic and clinical significance (SS 1807b), B-1472

Kämpgen B., Maros M.E., Stening T., Sommer W.H., Klüter A.

Opportunities in automatically annotating radiology reports with RadLex terms (SS 1905), B-1583

Kang H., Jang S.

Differentiation of glioblastoma multiforme and single brain metastasis by the distribution pattern of intratumoral susceptibility sign derived from susceptibility-weighted imaging (SS 211), B-0089

Kang S., Kim T.H., Park I.K., Park C.H.

Optimisation of a chest CT protocol for the detection of ground glass opacity nodules: feasibility study with a computer-assisted detection system and a lung cancer screening phantom (MY 5), B-0415

Kaniewska M., Schenkel M., Eid K., Bühler T., Kubik-Huch R., Anderson S.

Anatomy-based MR classification of the iliopsoas muscle complex after petrochanteric femur fracture (SS 610b), B-0537

Kantarci M., Levent A., Eren S., Pirimoglu B.

Comparing subjective and objective image quality at two different radiation exposure ranges of the paranasal sinus CT examinations using a volumetric 320-row detector CT system (SS 308), B-0262

Kantarci M., Levent A., Sade R., Eren S., Ogul H., Guven F., Bayraktutan G.

The CTP for detection of primary oesophageal carcinoma (SS 701b), B-0712

Kantarci M., Levent A., Eren S.

The feasibility of dual-energy-computed tomography in cardiac contusion imaging for mildest blunt cardiac injury (SS 1903), B-1652

Kapetas P.

My three top tips for breast imaging: Complex cystic and solid lesions (SF 8b), A-327

Kapustin V., Gromov A., Shirokorad V., Subbotin Y.

Targeted MRI/TRUS fusion-guided biopsy in patients with suspicious pararectal lymph nodes after radical prostatectomy (SS 1516), B-1247

Kara B., Onur M., Tokar A., Horoz S., Akata D.

Does body mass index affects radiation dose reduction in prospective electrocardiographic gating cardiac computed tomography? (SS 314), B-0322

Kara B., Tokar A., Horoz S., Onur M., Sanje S., Akata D.

Overview of CT throughput in a radiology department: drawbacks and solutions (SS 1814), B-1450

Karadayi A., Ozer T., Voyvoda N., Fariz B.

Value of b-mode ultrasonography and real time sonoelastography for detecting injury of the lateral ligaments of the ankle joints (SS 710b), B-0722

Karalok I., Alatas I., Canaz H., Sabet S., Sever C., Gayef A., Gurcan N.I.

Coexistence and relation of congenital and acquired urinary tract pathologies in Jarcho Levin syndrome: comparison to spina bifida aperta (SS 612), B-0581

Karantanas A.H.

Radiologic anatomy: lower extremities: Hip (ESR/ESOR 1), A-253

Karantanas A.H.

Chronic trauma: spectrum of bone response (E³ 25B), A-280

Karantanas A.H.

Advanced MR techniques and imaging biomarkers: Chairperson's introduction (E³ 719), A-288

Karavasilis E., Karatopis A., Szatmari P., Illing R., Papanikolaou N.

Standardisation and optimisation of MRI examination protocols (SS 213), B-0129

Karcaaltincaba M.

Advanced MR techniques and imaging biomarkers: C. MR contrast agents in liver imaging (E³ 420), A-167

Karcaaltincaba M.

Dual-energy CT of the abdomen: the time is now: C. Applications for abdominal organs (E³ 1226), A-535

Karli Oguz K.

Paediatric MRI: can we make gadolinium superfluous?: Brain imaging: when is intravenous gadolinium necessary? (SF 13b), A-652

Kartalis N.

Cystic pancreatic lesions: how to differentiate, how to manage?: Diagnostic accuracy of non-invasive imaging modalities for characterising cystic pancreatic lesions (SF 5), A-220

Kartalis N.

The ten-minute abdominal MRI: make the dream come true!: Pancreas (SF 8c), A-351

Kartalis N.

Pancreatic tumours: A. Staging adenocarcinoma (E³ 1422), A-704

Katsanos K.

How can radiologists expand their role in peripheral vascular intervention?: How to improve your technical/procedural skills (PC 9), A-432

Katsanos K.

Drug elution or drug illusion in vascular disease: Effect of drug-eluting balloons and stents in haemodialysis access lesions: where is the evidence? (SF 13c), A-673

Katsifarakis D.

Radiation protection from A to Z: The importance of justification (BR 2), A-630

Katuliska K.

The latest update in imaging of polytrauma patients: C. Where is the proper place for MRI? (RC 1517), A-781

Katyan A., Mittal M.K., Mani C., Mandal A.K., Grover S.B.

Chemoresponse assessment in locally advanced breast cancer patients: comparison of grey scale ultrasound and ultrasound elastography (SS 302), B-0271

Kauczor H.-U.

The machines are coming: how will they change our future?: Chairperson's introduction (NH 5), A-170

Kauczor H.-U.

Cancer screening: A. Lung cancer screening: the evidence (RC 1216), A-565

Kavanagh R., Carroll A., Purcell Y.M., Smyth A.E., Khoo S.G., McNeill G., Malone D.E., Killeen R.P.

Is post-contrast MRI imaging necessary in the investigation of cholesteatoma recurrence when non-echo planar diffusion-weighted imaging is available? A diagnostic accuracy study (SS 208), B-0070

Kayano S., Ono K., Yamaguchi T., Ota H.

Air embolism on coronary computed tomography angiography: its incidence associated with the preparation of intravenous infusion (MY 17), B-1306

Kazmierczak P.M., Burton N.C., Keinrath G., Hirner-Eppeneder H., Schneider M., Eschbach R.S., Reiser M.F., Ricke J., Cyran C.C.

Integrin-targeted multispectral optoacoustic tomography with MRI correlation for monitoring a BRAF/MEK inhibitor combination therapy in a murine model of human melanoma (SS 1406), B-1176

Kecksemethy P.

Deep learning in mammography (SY 26)

Keeser D.

Psychoradiology: a blend of molecular, functional and structural imaging with a taste of psychology: Neuroimaging and neuromodulation: where are we heading (MS 16), A-831

Keil V.C.

Diffuse low-grade gliomas: new things you should know: A. Molecular basis for classification, treatment and predicting outcome in low-grade gliomas (RC 1711), A-909

Kelekis A.D.

Bone and spine interventions: Keynote lecture (SS 1809), K-26

Keller N., Zingg T., Agri F., Knebel J., Schmidt Kobbe S.

Can emergency CT reliably detect significant blunt bowel and mesenteric injury? (MY 15), B-1273

Kelly B.E.

ESR and UEMS: a united European voice: The European Perspective (part 2): clinical audit and its implementation in view of the European BSS Directive (ESR/UEMS 1), A-184

Kelly B.E.

Audit across Europe: directive and perspective: The Esperanto Audit Project: results from the pilot project and roll out (ESR Audit), A-854

Kelly B.S., Heffernan E., McNally S.

Breast arterial calcification on screening mammography can predict significant coronary artery disease in women (SS 202b), B-0099

Kelly E.

Planning your career: The dos and don'ts of preparing your curriculum vitae (BR 3), A-928

Kenis S.F.

Carotid IMT and haemodynamic indices in evaluation of atherosclerosis in hypertensives (SS 315), B-0218

Kerleroux B., Kober T., Hilbert T., Sirinelli D., Morel B.

Clinical equivalence assessment of T2 synthetic paediatric brain MRI (MY 18), B-1488

Kettenbach J.

Interventional radiology in the venous system: vessel and eye opening: B. Lower limb acute deep vein thrombosis (E³ 1626a), A-859

Keussen I.E.

Portal hypertension and interventional radiology (IR): B. Embolisation of varices and splenic artery in portal hypertension (RC 109), A-052

Khatri G., Antil N., Misra R., Bajaj S.K.

Role of ultrasound and MR imaging in evaluation of patients at high risk of morbidly adherent placenta (MY 4), B-0401

Authors' Index

Khouri Chalouhi C., Vernuccio F., Tuscano B., Duca P., Brancatelli G., Vanzulli A.

Comparison of two liver specific contrast agents in patients with different degrees of liver cirrhosis (SS 201a), B-0008

Kiefer L.S., Fabian J., Lorbeer R., Machann J., Schlett C.L., Rosplecz S., Peters A., Bamberg F.

Intra- and interobserver variability of MR-based assessment of myosteatosis as a biomarker for metabolic diseases in subjects from the general population (SS 303), B-0334

Kies D., Pijpers J.A., Ferrari M.D., Kruit M.C., Terwindt G.M.

Resting-state functional connectivity in the visual network: a possible predictor of treatment response in chronic migraine (SS 1911a), B-1600

Kiessling F.M.A.

Merging the best: hybrid imaging: B. Hybrid imaging with MR/PET (RC 106), A-059

Kijowski R., Woo K., Liu F.

Influence of meniscus tears on cartilage T2 relaxation time in subjects with and without knee osteoarthritis (SS 1810), B-1424

Kilburn-Toppin F.

My three top tips for breast imaging: Imaging the axilla (SF 8b), A-328

Kildal D., Schmidt S., Beer M., Schöffski O., Blasenbrey T.

Study of the current situation of patient information in the example of a CT scan: what are improvement options? (SS 205), B-0178

Kildal D., Schmidt S., Beer M., Schöffski O., Blasenbrey T.

Significant quality improvement of results and patient satisfaction in medical information for radiological examinations applying video information techniques (SS 205), B-0180

Kildal D., Erben T., Beer M.

Prognostic and diagnostic value of hyperattenuating adrenal glands on contrast-enhanced computed tomography scans of polytraumatised patients (SS 317), B-0294

Kim D., Kang B., Ko Y.

Can we diagnose T1 stage UB (urinary bladder) cancer from T2 stage with an inchworm/stalk sign on 3T-MRI? (SS 207), B-0062

Kim D., Kim C., Lee K., Choo J., Kang E., Oh Y.

Impact of iterative model reconstruction on the correlation between CT quantification of emphysema and airway measurements and pulmonary function test in the normal study cohort (SS 704), B-0639

Kim D., Kim C., Lee K., Kang E., Oh Y., Kim H., Cha J.

The optimal energy level of virtual monochromatic images from spectral CT for reducing beam-hardening artefacts due to contrast media in the thorax (SS 1413), B-1132

Kim D., Park S.

Percutaneous cryoablation for renal cell carcinoma using US-guided targeting and CT-guided ice-ball monitoring: procedure time, radiation dose and mid-term outcomes (SS 207), B-0058

Kim H., Yoon S.H., Hong H., Hahn S., Goo J.M.

A meta-analysis of a UIP pattern on CT: is surgical lung biopsy necessary in patients with a possible UIP pattern? (SS 204), B-0044

Kim H., Kim H., Jang S.

Value of structured report form for appendix ultrasound in paediatric patients: can we reduce negative appendectomy and additional CT? (SS 612), B-0577

Kim J., Chung W.S., Jang H.Y., Kim H.C., Kang T.S., Lee H.J., Sohn J.S.

Perivascular infiltration and histologic difference: is it helpful to determine T stage of advanced gastric cancer in CT? (SS 701b), B-0718

Kim M., Hwang J., Choo K., Ryu H., Kim Y.

Comparison of image quality of the abdominopelvic computed tomography in paediatric patients: low-osmolar contrast media vs less iodine-containing iso-osmolar contrast media (SS 612), B-0575

Kim M., Park J., Kim H.

Building an apparent diffusion coefficient radiomics to yield high diagnostic performance in identifying atypical primary CNS lymphoma mimicking glioblastoma (SS 211), B-0087

Kim S.W., Ryu H., Kim Y.R., Lee Y.H., Yoon K.

Quantitative evaluation of liver function using coefficient of variation value and contrast enhancement index (CEI) on gadoxetic acid-enhanced MR imaging in preoperative evaluation (SS 201a), B-0005

Kim T.M., Kim S., Cho J., Kim S.

Clinical value of low-kiloelectron volt monoenergetic images of dual energy computed tomography for evaluation of peritoneal seeding of ovarian cancer (SS 707), B-0645

Kim W.

The new horizon for radiology: What will the radiologist's job look like in 2025? (NH 14), A-723

Kim W.

Deep learning: Keynote lecture (SS 1805), K-28

Kim Y.W., Debray M.P., Fetita C., Fouque O., Aubier M., Brillet P.-Y.

Bronchial wall changes after thermoplasty in the treatment of severe asthma: CT scan assessment at 3 months (MY 5), B-0414

King A.D.

Post-treatment imaging of the head and neck: C. Treatment monitoring for early detection of recurrence (RC 1308), A-624

King A.D.

Distant metastases of head and neck cancer: A. Incidence and prognosis of synchronous cancer or distant metastases from head and neck tumours (E³ 926), A-434

King S.

How can we improve the patient experience of nuclear medicine hybrid imaging procedures? A systematic review of the evidence (MY 17), B-1304

Kinkel K.

New Philips anatomical intelligent breast ultrasound solution (SY 19)

Kinkel K.

Gynaecological and obstetrics: Chairperson's introduction (E³ 1523), A-767

Kintzelé L., Rehnitz C., Kauczor H.-U., Weber M.-A.

Oblique sagittal images prevent underestimation of neuroforaminal stenosis grade caused by disc herniation in cervical spine MRI (SS 610a), B-0437

Kirchner J., Sawicki L.M., Tschischka A.F., Umutlu L., Herrmann K., Schaarschmidt B.M., Antoch G., Heusch P.

Comparison of ¹⁸F-FDG PET/CT and ¹⁸F-FDG PET/MRI for thoracic staging in lung cancer patients (SS 616), B-0584

Kirkbride T.E., Anderson N., Raja A.Y.

Use of calcium chloride as a calibration phantom material to aid identification of clinically significant compounds with spectral CT (SS 713), B-0731

Kirschke J.

Advanced and accelerated neuro imaging on a next generation wide-bore 3.0T MRI to simultaneously address clinical and research needs (SY 5)

Kishida Y., Shinichiro S., Yoshikawa T., Yui M., Kassai Y., Kyotani K., Ohno Y.

Computed diffusion-weighted image: utility for differentiation of malignant from benign pulmonary nodules as compared with actually obtained diffusion-weighted image (SS 1904b), B-1573

Kitao A., Matsui O., Yoneda N., Kita R., Kozaka K., Kobayashi S., Minami T., Koda W., Gabata T.

Differentiation between hepatocellular carcinoma showing uptake of gadoxetic acid and focal nodular hyperplasia (SS 301a), B-0198

Kitrou P., Papadimitos P., Katsanos K., Spiliopoulos S.C., Christeas N., Karnabatidis D.

Lysis-assisted balloon (LAB) thrombectomy - a method for declotting thrombosed arteriovenous dialysis grafts: results from a retrospective analysis of 241 endovascular procedures (SS 1009), B-0865

Kjaer A.

Molecular imaging in oncology: B. Imaging of proliferation (RC 406), A-157

Kjelle E., Lysdahl K.B., Olerud H.M., Myklebust A.

Implementing mobile radiography services: a qualitative study of managers' experiences of success criteria and barriers to overcome (MY 17), B-1302

Kjelle E., Kleven L., Olerud H., Melberg H.

Radiography on wheels for nursing home residents may reduce healthcare costs (MY 17), B-1311

Klang E., Frid M., Diamant I., Ben Cohen A., Di Segni M., Konen E., Greenspan H., Amitai M.M.

Automatic liver metastases detection on CT using multi-class patch based convolutional neural networks (SS 605), B-0486

Klauser A.

Elastography of superficial structures: where are we now?: Is there any value in tendon and nerve assessment? (WG/EFSUMB 1), A-105

Klauser A.

Musculoskeletal ultrasound in the management of sports injuries: B. Ultrasound of the hip and knee: what is it good for and what are its limitations? (RC 810), A-347

Kleber F.

Drug elution or drug illusion in vascular disease: Drug-eluting balloons and stents, technology and biological interaction: lessons learned from the coronaries (SF 13c), A-670

Authors' Index

Klompshouwer E., Beets-Tan R.G.H.,

De Boer M., Trebeschi S., Prevoo W., Lambregts D.M., Beets G.L., Maas M.

CT texture parameters to evaluate outcome after thermal ablation for colorectal liver metastases (SS 1509), B-1204

Klontzas M.

Radiologic anatomy: lower extremities: Knee (ESR/ESOR 1), A-254

Knopp M.V., Briley-Saebo K., Menendez M.I., Siva A., Binzel K., Zhang J.

Small animal imaging using a clinical PET/CT system: high throughput imaging enabled by next-generation digital PET (SS 1006), B-0993

Knopp M.I., Wright C.L., Binzel K., Giesel F.L., Zhang J., Maniowski P., Knopp M.V.

A 2 minute, ultra-fast wholebody PET/CT enabled by digital photon counting PET detector technology (SS 1016a), B-0888

Kocak B., Zeynalova A., Kizilkilic O., Kocer N., Islak C.

Added value of c-arm contrast-enhanced cone-beam CT to routine contrast-enhanced MRI in evaluation of sporadic intracranial cavernous malformations for detecting associated DVAs (SS 711b), B-0687

Köcher M.

Peripheral vascular malformations: what every radiologist should know: A. The diagnostic assessment (RC 115), A-043

Koh D.-M.

Advanced MR techniques and imaging biomarkers: Chairperson's introduction (E³ 420), A-164

Koh D.-M.

Immunotherapy: a revolution in cancer care?: The MR armory in follow-up (NH 9), A-387

Kohler R.

Head and neck emergencies: Chairperson's introduction (SF 12c), A-540

Kohler R.

Pathways for tumour spread: C. Pathway for laryngeal and hypopharyngeal tumour spread (RC 408), A-112

Kolb A., Chiari C., Windhager R.

The patella-shape: is it relevant to the analysis of patella malalignment? (SS 1810), B-1428

Kolbitsch C.

Motion artefacts and their management in medical imaging: C. Motion compensation in MR and PET imaging (RC 1313), A-656

Kolossvary M., Karady J., Szilveszter B., Kitslaar P., Merkely B., Maurovich-Horvat P.

Napkin-ring plaques can be identified on coronary CT angiography images using radiomic analysis (SS 703), B-0754

Kolossvary M., Szilveszter B., Karady J., Merkely B., Maurovich-Horvat P.

Effect of image reconstruction algorithms on cardiovascular radiomic features using coronary CT angiography (SS 703), B-0761

Konietzke P., Weinheimer O., Wielpütz M., Wagner W., Heussel P., Heussel C., Kauczor H.-U., Herth F.J., Schuhmann M.

Use of quantitative computed tomography to assess post-interventional long-term changes after bronchial thermoplasty in patients with severe asthma (SS 304), B-0240

Koo A., Smith J.T.

Learning from our errors: what are the common clinically important errors that radiologists repeatedly make in the UK's largest teaching hospital and how can we best address them? (SS 1001a), B-0844

Kool D.R.

Emergencies following tumour therapy: Chairperson's introduction: The role of imaging in the early detection of complications in oncologic treated patients (E³ 1726b), A-940

Kool D.R.

Non-traumatic emergencies: Keynote lecture (SS 1017), K-18

Kopp C.W.

How can radiologists expand their role in peripheral vascular intervention?: How to improve your clinical knowledge (PC 9), A-429

Kopp F.K., Bippus R., Mei K., Sauter A., Schwaiger B.J., Gersing A., Dangelmaier J., Rummeny E.J., Noel P.B.

Endoleak detection with ultra-low radiation exposure CT based on sparse sampling and reduced tube current (SS 1413), B-1136

Kortesniemi M.

CT examination of pregnant patients: a dilemma for the radiologist and the mother: How to reduce radiation dose and keep CT diagnostics (SF 8a), A-310

Kortesniemi M.

Different generations of metal artefact reduction algorithms (SY 25)

Kortesniemi M.

Dose reduction and image quality implications of iterative image reconstruction in CT: A. Basics of iterative image reconstruction in CT (RC 1513), A-783

Koryukova K., Bezzi M., Di Martino M., Ginanni Corradini S.G., Rossi M., Catalano C.

Up to seven criteria for liver transplantation: a single-centre experience (SS 601a), B-0429

Koryukova K., Rossi M., Di Martino M., Saba L., Ginanni Corradini S.G., Catalano C.

High-field-strength MR imaging of the liver at 3.0T: comparative study with 1.5 T in cirrhotic population (SS 701a), B-0608

Koryukova K., Saba L., Di Martino M., Catalano C.

Respiratory motion artefact affecting hepatic arterial phase MR imaging: comparison between gadoxetate disodium and gadobenate dimeglumine (SS 701a), B-0611

Kossov F., Bulychkin P., Romanov D., Shorikov M.A., Tarachkova E., Panov V., Tkachev S., Dolgushin B., Hagverdyyeva G.

Could mpMRI really improve the detection of clinical recurrence of prostate cancer with low PSA value and efficacy of radiation treatment? (SS 1516), B-1248

Kossov F., Abdullin I.I., Kamolov B., Olimov B., Orlov O., Panov V., Tyurin I., Fedorenko E., Kapustin V.

The accuracy of MRI/TRUS fusion biopsy in detection of high-risk prostate cancer vs random biopsies: advertisement or necessary innovation? (SS 1907a), B-1561

Kotter E.

Daily use of mobile devices in radiology: A. What did mobile devices change in radiology education? (RC 805), A-361

Kotter E.

Experiences with Samsung's Digital Radiography at Freiburg University Hospital (SY 14)

Kottlors J., Kabbasch C., Maus V., Mpotsaris A., Borggrefe J.

Combined measurements of clot density in unenhanced and enhanced CT of acute ischaemic stroke in complete vessel occlusions of the medial cerebral artery predict 90 day patient outcome (SS 611), B-0515

Koutsouleris N.

Psychoradiology: a blend of molecular, functional and structural imaging with a taste of psychology: Can images predict psychiatric diagnosis and treatment response? (MS 16), A-830

Kovacevic D., Papageorgiou I., Chelaru R.L., Winzler S., Malich A.

Whole-body MRI for bone metastasis detection in prostate cancer: the roles of static field intensity and contrast media in focus (SS 1407), B-1069

Kozák L.R., Gyebnár G., Szabo A.G., van Graan A.L., Barsi P., Lemieux L., Rudas G.

Optimising pre-surgical fMRI language mapping using knowledge derived from intrinsic connectivity brain networks for personalised therapy planning (SS 1911b), B-1680

Krainik A.

Altered mental state: C. MRI in the diagnosis of Alzheimer's disease (RC 1311), A-639

Krajina A.

Portal hypertension and interventional radiology (IR): C. Transjugular intrahepatic portosystemic shunt (TIPS): critical appraisal of techniques and guidelines for treatment (RC 109), A-053

Kramer J.

Knee: Chairperson's introduction (E³ 1019), A-466

Kraus B.

Radiography research: a how to guide: How to critically appraise a research article (BR 1), A-550

Kraus M.S., Esser M., Teufel M., Fleischer S., Riethmueller J., Ruff C., Tsiflikas I., Schäfer J.F.

Pulmonary MRI: diagnostic performance and detection of structural abnormality using ultrashort echo time in cystic fibrosis patients (SS 712), B-0764

Kräuter C., Reiter U., Reiter C., Schmidt A., Fuchsjäger M.H., Stollberger R., Reiter G.

Impact of local native T1 times on pixel-wise quantification of myocardial blood flow (SS 1403), B-1151

Kreitner K.-F.

Shoulder: A. Post-traumatic (E³ 719), A-289

Kreitner K.-F.

Shoulder MRI: mastering technique and making my report relevant: B. Rotator cuff tears: what are they and what do they look like? (RC 1210), A-570

Krestin G.P.

EIBIR Research Session: European imaging researchers united in diversity: Chairperson's introduction (EIBIR 1), A-319

Kriachok I., Novovsod O., Skrypets T., Gorbach A., Kmetyuk Y., Kozlova O., Novikov M., Mikhalska L., Kozlov V.

Quantitative PET parameters in predicting event free survival in patients with hodgkin lymphoma (SS 716), B-0703

Authors' Index

Kroencke T.J.

Urogenital interventions: Keynote lecture (SS 1909), K-30

Kroll J.

Forensic imaging: A. Disaster victim identification (RC 114), A-039

Krombach G.A.

Peritoneum and mesentery: C. From misty mesentery to mesenteritis (E³ 1622), A-869

Kromrey M., Schäfer S., Ittermann T., Mensel B., Kühn J.

Impact of personality and experience of interventional radiologists in outcome of CT-guided percutaneous lung biopsies (SS 609), B-0447

Kröpil P., Thomas C., Bethge O.T., Klosterkemper Y., Aissa J., Appel E., Schleich C., Antoch G., Boos J.

Implementation of updated ACR size-specific CT diagnostic reference levels based on water-equivalent diameter and SSDE using automated dose monitoring software (SS 313), B-0319

Kubik-Huch R.A.

MRI for gynaecologic imaging: how I do it: B. Contrast agents (RC 1207), A-546

Kubik-Huch R.A.

Gynaecological and obstetrics: A. Imaging of the uterus (E³ 1523), A-768

Kuchcinski G., Jacquiez C., Baroncini M., Dumont J., Delmaire C., Defebvre L., Pruvo J.-P., Leclerc X.

Sulcal-based morphometry for the diagnosis of normal-pressure hydrocephalus in patients with ventriculomegaly (SS 1411a), B-1040

Kuhl C.K.

MRI for early detection, staging and management of breast cancer: C. Screening with abbreviated protocols (RC 1202), A-556

Kuhl C.K.

Breast MRI: Keynote lecture (SS 1002), K-16

Kul M., Kuru Öz D., Erden A.

Pathologic alterations in hepatic vasculature in primary sclerosing cholangitis: correlation with morphologic spectrum and abnormal hyperintensity in T2-weighted MR images (SS 1801), B-1322

Kumar S.

My three top tips for neuroimaging: Hydrocephalus (SF 15c), A-758

Kumari S., Mohammad Zakir M., Kirubha Y., Sudhakar K., Chatterjee P., Ranjan R., Kumari J., Kumari S., Khan S.

Role of phase contrast MR CSF flowmetry study in the evaluation of normal pressure hydrocephalus (SS 1911b), B-1675

Kuplevatskaya D.I., Babiy A., Vorobyov N., Kuplevatsky V.I., Berezina N., Cherkashin M.

MRI-based treatment response assessment for liver metastasis stereotactic radiotherapy (SS 1416), B-1078

Kural Rahatli F., Yildirim Donmez F., Kesim Ç., Haberal K., Turnaoglu H., Agildere A.

Can unenhanced brain magnetic resonance imaging be used in routine follow-up of meningiomas to avoid gadolinium deposition in the brain? (SS 1011b), B-1004

Kurochkina N., Moroz A., Konovalov R., Krotenkova M., Ilarionov S.

Neuroimaging signs and features of brain lesions in patients with CADASIL (SS 711b), B-0696

Kuru Öz D., Peker E., Kul M., Erden A.

Comparison of stiffness values of peripheral and central liver tissues with MR elastography in patients with primary sclerosing cholangitis (SS 1001a), B-0842

Kurz K.D.

Inflammatory and infectious CNS pathology: B. Infectious encephalitis (RC 1211), A-559

Kwon Y., Moon W., Park M., Kim H., Choi J.

3D neuromelanin imaging for differential diagnosis between Parkinson disease and essential tremor: a multicenter retrospective study (MY 8), B-0801

L

La Grutta L., Clemente A., Maffei E., Privitera G., Rengo M., Toia P., Francone M., Midiri M., Cademartiri F.

Results from the Italian Registry of Contrast Material use in Cardiac Computed Tomography (IRCM-CCT) (SS 603), B-0565

Lacey S., Mulholland K., Fancourt N., O'Brien K., de Campo J., de Campo M.

World Health Organization guidelines for achieving high-quality paediatric chest radiographs for use in epidemiological studies (SS 712), B-0765

Lahaye M.J.

Tumour response assessment in abdominal imaging: B. Rectal carcinoma (RC 1601), A-808

Laitinen H.M.S., Niiniviita H., Saukko E., Svedström E.

The optimised location to assist patient during imaging of scoliosis with EOS system device (SS 1814), B-1447

Lamb H.J.

Cardiac MRI: from sequence to bedside: B. Spectroscopy: implications of myocardial metabolism? (E³ 1326a), A-619

Lang K., Arboleda C., Forte S., Wang Z., Kubik-Huch R., Stampanoni M.

Exploring contrast agents in phase-contrast x-ray mammography: an ex vivo pilot study (SS 1802b), B-1417

Langenbach M.C., Kaup M., Beerers M., Scholz J., Park C., Frellesen C., Vogl T.J., Gruber-Rouh T.

Use of conventional defecography or dynamic MRI defecography in patients with symptomatic pelvic floor dysfunction: a retrospective intraindividual trial (SS 601b), B-0528

Laniado M.

Gastrointestinal: 'the gut': Stomach (BS 2), A-064

Lansier A., Bourillon C., Jantzen R., Ragot E., Follin A., Berger A., Clement O., Halimi P., Cuenod C.A.

Evaluation of CT and clinical features of bowel and/or mesenteric injury in blunt abdominal trauma: a case-control study (SS 317), B-0293

Lapteva M., Shorikov M., Frantsev D., Sergeeva O.N., Virshke E., Dolgushin B.

Evaluation of tumour response in patients with neuroendocrine hepatic metastasis treated using transarterial chemoembolisation (TACE) on MRI (SS 1901a), B-1512

Lara Nuñez D., Gonzalez Balboa P., Chapa Ibarquengoitia M., Fuentes Corona R.E., Candanedo González F., Licano Zubiate M., Castro German K.P.

Imaging findings of papillary lesions of the breast with histopathologic correlation: a five-year study from Instituto Nacional de Ciencias Médicas y Nutrición "Salvador Zubirán" (SS 1402a), B-1092

Larici A.R.

Updates on lung cancer management: Chairperson's introduction (E³ 918), A-446

Larici A.R.

Oncologic imaging: A. Lung cancer: key signs in the new TNM (E³ 1321), A-603

Larsen V., Traply C.T., Musmann B.R.

Improved image quality and reduced radiation dose in trauma CT using a custom arm rest pillow (SS 317), B-0288

Larsson E.-M.B.

When to use hybrid imaging: Differentiating radiation necrosis from tumour recurrence: do we need hybrid imaging? (ESR/ESHI), A-202

Lassalle L., Eminian S., Buisson A., Pessis E., Campagna R., Regnard N.E., Khaled W., Moya L., Drape J.L.

MRI characteristics of 26 onychomatricomas (SS 210), B-0117

Lassalle L., Lapegue F., Guerini H., Campagna R., Vuillemin V., Regnard N.E., Buisson A., Drape J.L.

MRI patterns of locked metacarpophalangeal joints of the long fingers (SS 310), B-0302

Lauenstein T.C.

The ten-minute abdominal MRI: make the dream come true! Liver (SF 8c), A-350

Lauenstein T.C.

Pancreatic tumours: C. Tough clinical cases (E³ 1422), A-706

Laukamp K.R., Lennartz S., Neuhaus V., Grosse Hokamp N., Rau R., Le Blanc M., Abdullayev N., Maintz D., Borggreffe J.

Complementary metal artefact reduction of total hip replacements by monoenergetic and O-MAR reconstructions in spectral-detector computed tomography (MY 13), B-1023

Laukamp K.R., Thiele F., Shakirin G., Perkuhn M., Zopfs D., Faymonville A., Timmer M., Borggreffe J.

Fully automated meningioma detection and segmentation using deep learning on routine multiparametric MRI (SS 1911b), B-1671

Laverman P.

Contrast media in imaging: B. Radiotracers in PET/RNI (RC 814), A-354

Laxmi V., Chowdhury V., Dixit R., Agarwal A.

Perfusion CT vs triphasic CT in evaluation of hepatic masses (SS 1901a), B-1507

Le Roy J., Vernhet Kovacsik H., Zargane H., Vincenti M., Lacampagne A., Amedro P.

Sub-millisievert multiphase acquisitions for coronary CT angiography of congenital coronary anomalies in paediatric patients (SS 1413), B-1133

Leander P.

Radiology will survive, but will the radiologist still be there?: The landscape in radiology is changing: the radiologists need to adapt (PI 2), A-507

Lebedev S., Stierstorfer K., Kachelrieß M.

Stack transition motion compensation in sequential and in cardiac CT (SS 1813), B-1437

Authors' Index

Lecouvet F.E.

Whole-body MRI: ready for prime time?: Chairperson's introduction (SA 5a), A-196

Lecouvet F.E.

Advances in musculoskeletal techniques: whole-body MR: A. Oncologic application (E³ 1821), A-944

Lederlin M.

Lung cancer in the era of molecular oncology and immune therapy: A. Lung adenocarcinomas with EGFR mutations (E³ 118), A-055

Lee H., An C., Kim M.

Diagnostic accuracy of LR-M criteria for differentiating combined hepatocellular cholangiocarcinoma on gadoxetate-enhanced MRI (SS 301a), B-0192

Lee H., Kwon W., Zhang Y.

A 3T MRI with radial T1-weighted 3D spoiled gradient echo sequence can clarify pleural invasion classification of primary lung cancer (SS 1904b), B-1580

Lee J.M.

Hepatocellular carcinoma: diagnosis, staging and current guidelines: Atypical appearance of HCC and mimics: how to solve the challenging cases (SF 1), A-019

Lee J., Kim C., Gu K.

Blood oxygenation level-dependent MRI for prediction of clinical outcome in uterine cervical cancer treated with radiotherapy (SS 707), B-0650

Lee J., Bruni S., Kennedy S., Swami V., Chen E., Menezes R., Borrego D., Lee C., Rogalla P.

Comparing diagnostic performance of ultra-low-dose CT compared to abdominal plain films (SS 1017), B-0947

Lee K.H., Tse M.L.D., Cheng A.K.C., Wong H.Y.F., Yu M.L., Li Y.L., Chien P.Y.C., Ho Y.C., Chu F.

An imaging and clinical scoring system to predict early mortality in spontaneous ruptured hepatocellular carcinoma treated with transarterial embolisation (SS 301a), B-0193

Lee K., Lau W., Tsang H., Lau C., Chung H.

Relative maximum apparent diffusion coefficient: a potential biomarker of disease activity in axial spondyloarthritis (SS 1910), B-1620

Lee K., Baik J.

Proposal of imaging reporting and data system for cervical lymph node based on computed tomography (SS 1508), B-1212

Lee S.

Making the most of social media: Social media at ECR (part 1) (EFRS WS), A-790

Lee S.

Audit across Europe: directive and perspective: Quality improvement and change management: Audit in industry (ESR Audit), A-856

Leen E.

Ultrasound-guided interventional procedures: new techniques and applications: Liver (WG 1), A-823

Leijenaar R.

Radiomics: what is it and how can we use it?: Radiomics: technical validation (NH 12), A-574

Leiner T.

Every step counts: imaging and treatment of peripheral arterial disease: State-of-the-art: non-invasive imaging of peripheral arteries (E³ 24B), A-278

Leiner T.

Post-treatment evaluation: what every radiologist should know: A. Thoracic aorta (RC 815), A-357

Leiner T.

How can radiologists expand their role in peripheral vascular intervention?: How to improve your diagnostic skills (PC 9), A-430

Leiser P., Schoettler J., Centner F.S., Kirschning T., Krebs J., Hagmann M., Weiß C., Schönberg S.O., Haubenreisser H.

Quantitative CT as a one-stop shop to describe status and outcome of patients with acute respiratory distress syndrome (ARDS) (SS 304), B-0243

Leithner D., Wengert G.J., Weber M., Helbich T.H., Kapetas P., Baltzer P.A.T., Morris E.A., Karanikas G., Pinker K.

Implementation of imaging biomarkers of healthy breast tissue with multiparametric [18F]FDG-PET/MRI may aid breast cancer diagnosis (SS 602), B-0506

Leithner D., Helbich T.H., Bernard-Davila B., Wengert G.J., Kapetas P., Baltzer P.A.T., Haug A., Morris E.A., Pinker K.

Are there differences in multiparametric breast [18F]FDG-PET/MR imaging biomarkers of contralateral healthy tissue in patients with and without breast cancer? (SS 602), B-0507

Leithner D., Kaltenbach B., Park C., Pinker K., Hoedl P., Stephan F., Moebus V., Vogl T.J., Müller-Schimpfle M.P.

Intraductal papilloma without atypia in breast biopsies: rate of upgrades to carcinoma at excision and radiological features predictive of an upgrade (SS 1402a), B-1091

Lell M.

Pathways for tumour spread: B. Pathways for nasopharyngeal tumour spread including perineural spread (RC 408), A-111

Lenga L., Leithner D., Albrecht M.H., Booz C., Wichtmann J.L., Vogl T.J., Martin S.S.

Dual-energy CT in patients with abdominal malignant lymphoma: impact of noise-optimised virtual monoenergetic imaging on objective and subjective image quality (SS 1901a), B-1515

Lenkinski R.

Gd retention: back to basics (SY 17)

Lennartz S., Le Blanc M., Abdullayev N., Grosse Hokamp N., Maintz D., Borggrefe J., Persigehl T.

Improved detection of skeletal muscle metastases in iodine-density overlay maps and virtual monoenergetic reconstructions provided by spectral detector CT (MY 3), B-0377

Lennartz S., Le Blanc M., Grosse Hokamp N., Maintz D., Persigehl T.

Iodine density obtained with spectral detector CT is a predictor for lesion dignity of pleural thickening (SS 616), B-0587

Leonardi A., Napoli A., Scipione R., Anzidei M., Dababou S., Catalano C.

Lung adenocarcinoma radiogenomics predicts clinical outcome (SS 1004), B-0875

Leone F., Orsi M., Presazzi A., Mariani D., Cellina M., Oliva G.

Screening mammography's pitfalls: a retrospective review of false positive recall (SS 702), B-0683

Leuchbaumer M.H., Rübenthaler J., Putz F.J., Slowinski T., Clevert D.A., Jung E., Fischer T.

Value of contrast enhanced ultrasound in evaluation of cystic renal lesions compared to computed tomography and magnetic resonance imaging (SS 207), B-0055

Lesyuk O., Ribeiro L.P., Abrantes A.F., Sousa P., Rodrigues S., Almeida R.P., Azevedo K.B., Pinheiro J.P.

Study of scattered radiation during fluoroscopy in hip surgery (SS 1814), B-1445

Lev Cohain N., Leichter I., Sosna J.

Are there suboptimal CTPE studies in the DECT era: low mono-energetic images for pulmonary artery assessment (SS 604), B-0457

Lewis S., Pieterse T., Rainford L.A., Lawrence H.

Evaluating the use of detector dose indicators in digital x-ray imaging systems (SS 1914), B-1646

Li C., Li M., Jin L.

Application of high-pitch scanning mode in low-dose lung-computed tomography screening for patients with chronic obstructive pulmonary disease: a pilot study (MY 5), B-0408

Li H., Hu X., Zhang L., Lu L., Bu X., Tang S., Huang X.

Investigating direction of effective connectivity in obsessive compulsive disorder with resting state fMRI (SS 711a), B-0653

Li H., Chen G.W., Chen X.L.

Diffusion-weighted MR-volumetry and high-resolution MR-volumetry association with lymphovascular invasion and N-stages in resectable rectal cancer (SS 1001b), B-0846

Li J., Song Y., Wu Y., Cai H., Li L.

Characterising mammographic calcification as a prognostic biomarker for breast tumour phenotypes (MY 16), B-1279

Li J., Zhang C., Liu H., Yang S., Wang Y., Chen W., Wang D.

Diagnostic performance in the stage of liver fibrosis: comparison of magnetic resonance T1 rho and acoustic radiation force impulse (SS 1801), B-1323

Li T., Yang L.

Cardiac CT for demonstrating non-calcified coronary atherosclerotic plaque: effect of knowledge-based iterative model reconstruction on image quality (SS 703), B-0756

Li T., Han X.

Analysis of remodeling in abdominal aortic branch perfusion patterns complicated by type B aortic dissection after thoracic endovascular aortic repair (SS 309), B-0225

Li T., Li K., Xiong Y.

A comparative study of the DKI model and the traditional DWI model in the diagnosis of breast cancer (SS 1402b), B-1110

Li T., Xiong Y., Li K.

Preoperative diagnostic value of DKI combined with quantitative dynamic contrast-enhanced MRI in breast lesions (SS 1402b), B-1111

Li X.

A glance of China through images: Interventional therapy for hepatocellular carcinoma: Chinese experiences (EM 3), A-949

Li X., Huang S., Fang Z., Li Z.

Magnetisation transfer MRI can characterise the degree of intestinal fibrosis in patients with Crohn's disease: comparing with contrast-enhanced and diffusion-weighted MRI (SS 1901c), B-1531

Li Y., Dai Y., Guo Y.

Morphological study of blood vessels near lung tumour by the 3D quantitative CT technique (MY 5), B-0409

Authors' Index

- Li Y., Beiderwellen K.J., Nensa F., Herrmann K., Jost L., Umutlu L.**
Detection of inflammatory bowel segments with [18F]-FDG PET/MR enterography by Crohn's disease: which surrogate marker is better? MaRIA, Clermont score or PET? (SS 1901c), B-1534
- Li Y., Zhang F., Zhao S., Jin G., Zhao L., Zhou Y., Li P., Yang X.**
Radiofrequency hyperthermia-enhanced intratumoral herpes simplex virus-thymidine kinase (HSV-TK) gene therapy of ovarian cancer: monitored by ultrasound and optical imaging (SS 1406), B-1172
- Li Y., Ren C., Cheng J.**
Feasibility study of intra-voxel incoherent motion MR imaging for the differentiation of benign and malignant soft tissue tumours (SS 210), B-0111
- Li Y., Fan F., Feng Z., Liang W., Tan S., Yang F.**
Structural magnetic resonance imaging study on schizophrenic patients with violence risk (SS 711a), B-0654
- Li Y., Lin D., Xing Z., Chuan Y., Xu X.**
The early study of DWI and 1H-MRS in rabbit VX2 transplanted tumours after radiation comparison with pathology changes (SS 1006), B-0989
- Li Z.**
DWI-based radiomics for prediction of chemotherapy outcomes in lung cancer: a pilot study (SS 616), B-0594
- Li Z.**
CT-based radiomics for prediction of neoadjuvant chemotherapy outcomes in locally advanced gastric cancer: a pilot study (MY 15), B-1272
- Lidén M., Jendeborg J.K., Långkvist M., Loutfi A., Thunberg P.**
Discrimination between distal ureteral stones and pelvic phleboliths in CT using a deep neural network: more than local features needed (SS 1805), B-1382
- Lima M., Rio G., Horta M., Cunha T.M.**
Primary vaginal malignancies: a single oncology centre experience (SS 707), B-0651
- Lima M.R., Furlin G., Kupske A., Muller J.S., de Vecino M.C.A., Longo M.G., Nunes K.R.S.B., Valentini B.B., de Caneda M.A.G.**
Cortical vs juxtacortical lesions in multiple sclerosis: an analysis of PSIR performance in comparison to FLAIR (SS 311), B-0282
- Lin A.**
Quantitative measurement of brain iron deposition in patients with peritoneal dialysis using susceptibility mapping (MY 8), B-0805
- Lin T., Lyu Y., Zuo Z., You H., Qu J., Hou B., Feng F.**
Prediction of postoperative cerebral hyperperfusion: a study using territory arterial spin labelling (tASL) (MY 8), B-0810
- Lin T., Feng F., Lv Y., You H.**
Comparison of arterial spin-labeling and dynamic susceptibility contrast MRI in detecting crossed cerebellar diaschisis in patients after glioma resection (SS 1011b), B-1002
- Lin Y., Cheung A.Y., Kuo S., Wu K., Sung C., Fan C., Chen F.**
Comparing trabecular bone score and serum bone biomarker in predicting vertebral fracture for diabetes (SS 610b), B-0534
- Lin Y.**
CT numbers of kidneys in virtual noncontrast images acquired from dual-source dual-energy dynamic CT of kidney: comparison with standard noncontrast CT (SS 1007), B-0880
- Linder N.P., Schaudinn A., Petersen T., Stange R., Moche M., Stumpp P., Kahn T., Busse H.**
In-bore biopsies of the prostate assisted by a remote-controlled manipulator at 1.5 T (SS 1907a), B-1564
- Linder N.P., Michaelis J., Gawlitza J., Busse H., Ho-Thi P., Kahn T., Stumpp P., Ganzer R., Schaudinn A.**
Typical MR imaging findings after HIFU-hemablation of the prostate (SS 1907a), B-1566
- Linovs V., Radzina M., Linova T., Rubins A., Rubins S.**
Subclinical psoriatic arthritis detection in patients with psoriatic onychopathy (SS 1910), B-1622
- Liu H., Zhang W.**
Tumour microenvironment-responsive intelligent nanocomposites for efficient theranostics of glioma (SS 1406), B-1174
- Liu H., Zhang C., Li J., Wang D.**
Radiomics analysis for preoperative prediction of lymph node metastasis in patients with rectal cancer (SS 1001b), B-0848
- Liu H., Zhang C., Li J., Wang D.**
Radiomics analysis for preoperative prediction of synchronous distant metastasis in patients with rectal cancer (MY 15), B-1271
- Liu K., Li Z.**
One-stop imaging for triple-rule-out CT angiography using 16-cm wide-detector CT: a preliminary study (SS 314), B-0327
- Liu L., Yang J.**
Computer-aided detection of coronary plaques in cardiac CTA (SS 603), B-0570
- Liu Y.**
How to foster clinical research in imaging departments: Implementing quality imaging in multicentre trials (ESR Research), A-403
- Liu Z.**
A glance of China through images: Radiomics nomogram to predict lymph node metastasis in colorectal cancer (EM 3), A-951
- Llopis E.**
Small joints: A. Fingers (E³ 1119), A-512
- Llopis E.**
Shoulder MRI: mastering technique and making my report relevant: A. The normal MRI: techniques and anatomy (RC 1210), A-569
- Lo Re G.**
Mass casualties: Postmortem imaging of migrant victims drowned in the Mediterranean Sea (PC 4), A-123
- Llobes M.B.I.**
Contrast-enhanced spectral mammography: Technique and comparative approaches (SF 15b), A-753
- Loberg C., Keil S., Goerg F., Kuhl C.K., Bruners P.L.**
Is portal vein embolisation of liver segment IV mandatory before extended right hemihepatectomy? (MY 9), B-0818
- Loewe C.**
Thoracic emergencies: Pulmonary embolism (BS 4), A-126
- Loewe C.**
Post-treatment evaluation: what every radiologist should know: B. Abdominal aorta (RC 815), A-358
- Loewe C.**
Memorable cases in cardiovascular imaging: how to avoid common mistakes: Coronary fistula mimicking a cystic paracardiac tumour (SF 12e), A-597
- Loewe C.**
Cardiac and vascular: B. Cardiovascular imaging: valves, endocardium and aorta (E³ 1323), A-642
- Logager V.**
Emergency radiology II: A. Urinary system trauma (E³ 921), A-379
- Lohöfer F., Kaissis G., Köster F., Rasper M., Einspieler I., Gerngross C., Fichter A., Rummeny E.J., Braren R.**
Next generation imaging of head and neck cancer using dual-layer spectral CT (SS 1008), B-0900
- Lomas D.J.**
Advanced MR techniques and imaging biomarkers: B. MR and US elastography (E³ 420), A-166
- Loney E.**
Head and neck emergencies: What is broken? (SF 12c), A-541
- Longo R., Cova M.A., Delogu P., Golosio B., Mettivier G., Taibi A., Tonutti M., Tromba G., Zanconati F.**
Phase-contrast monochromatic breast-CT: a feasibility study (SS 1813), B-1439
- Lopes R.M., Carvalho D.**
Optimisation of the Blade technique in the cervical spine MRI (SS 614), B-0560
- Lopes do Rosario R.S.R., Michoux N., Lacroix V., Ghayé B.**
Can texture analysis predict non small cell lung cancer recurrence after surgery? (SS 1004), B-0876
- Lord C., King L.**
Percutaneous image-guided cryoablation of musculoskeletal metastases to the chest wall: a single-centre experience (SS 210), B-0115
- Loria A., Signorotto P., Campoleoni M., Paruccini N., Villa R., Venturini E., Panizza P., del Vecchio A.**
Digital breast tomosynthesis: flat panel and photon counting detectors comparison (SS 1813), B-1440
- Loria A., Signorotto P., Venturini E., Panizza P., del Vecchio A.**
Digital breast tomosynthesis index (DBTI): a score to evaluate digital breast tomosynthesis (DBT) device performance (SS 1813), B-1441
- Lotte R., Lafourcade A., Ezziane M., Jouve de Guibert P., Tavoro S., Mozer P., Boudghene F., Lucidarme O., Renard Penna R.**
Accuracy of multiparametric MRI of prostate cancer recurrence after high-intensity focused ultrasound (HIFU): is dynamic contrast enhancement still needed? (MY 4), B-0386
- Lotz J.**
Cardiac MRI: from sequence to bedside: C. Feature tracking: what to conclude from strain and torsion? (E³ 1326a), A-620
- Louagé F., Van Muylem A., Howarth N., Geveno P., Tack D.**
Radiation protection: factors influencing compliance to referral guidelines in minor chest trauma (SS 704), B-0642

Authors' Index

Louw A.

Application of the cognitive load theory in simulation experiences to stimulate critical thinking in 2nd year radiography students (SS 1414), B-1142

Loy Rodas N., Ghimire P., de Mathelin M., Gangi A., Padoy N.

Teaching radiation safety intuitively with a head-mounted display (SS 213), B-0119

Luboldt W.

Focal colorectal uptake in ¹⁸FDG-PET/CT: maximum standard uptake value as a trigger in a semi-automated screening setting (SS 601b), B-0523

Lucci C., Kockelkoren R., Bos D., Van der Lugt A., Geerlings M., Hendrikse J., de Jong P.A.

Epidemiology of intracranial vertebral artery calcification observed on computed tomography in a cohort of trauma patients (SS 711b), B-0691

Lucev J., Breznik S., Dinevski D., Ekart R., Ruprecht M.

Endovascular treatment of haemodialysis arteriovenous fistula with vessel preparation and drug-coated balloon angioplasty: a single-centre study (SS 1009), B-0864

Lucic M.A.

ESR and UEMS: a united European voice: CME/CPD in Europe (part 3): the many ways to gain European CME/CPD credits (ESR/UEMS 1), A-189

Lüdemann W., Collettini F., Geisel D., Schnapauff D., Wieners G., Gebauer B., Chapiro J., Kahn J.

Comparing HCC tumour vascularisation on baseline imaging and after Lipiodol cTACE: how do estimations of enhancing tumour volumes differ on contrast-enhanced MR and CT? (SS 1409), B-1056

Luiz V.R., Ribeiro L.P.V., Abrantes A.F., Azevedo K.B., Almeida R.P., Rodrigues S., Pinto N.F.

Evaluation of burnout syndrome in radiographers (SS 1914), B-1641

Lukas C.

Gadolinium: image wisely: B. Do we need gadolinium in imaging MS? Pros and cons (part 1) (PS 1227), A-592

Lukas S., Feger S., Rief M., Zimmermann E., Dewey M.

Motion elimination in low-dose 4D myocardial computed tomography perfusion (CTP) using the automated smooth temporal registration for analysis of 4D image data (ASTRA) algorithm (SS 703), B-0762

Lundervold A.S., Sprawka K., Lundervold A.

Fast estimation of kidney volumes and time courses in DCE-MRI using convolutional neural networks (SS 605), B-0484

Lunkiewicz M., Forte S., Freiwald B.K., Singer G., Kubik-Huch R.A.

Non-mass enhancement in breast-MRI: which BI-RADS descriptors for distribution and internal enhancement patterns have the highest likelihood of malignancy? (SS 1002), B-0919

Lupescu I.

Optimising computed tomography: Chairpersons' introduction (part 2) (RC 1614), A-848

Lupo C., Meli A., Incarbone V., Casamassima N., Callegari L.

Safety and efficiency of treatment of partial supraspinatus tendon tear with injection of PRP and HA (MY 13), B-1016

Lurie D.J.

Demystifying MRI: things you always wanted to know: B. MR imaging basic concepts: how to turn signals into images (RC 1613), A-845

Luyckx E., Bosmans J.M.L., Broeckx B., Ceysens S., Parizel P.M., Snoeckx A.

Radiologists as co-author in case reports containing radiological images: does their presence influence quality? (SS 205), B-0181

Luzzago S., Catellani M., Russo A., Di Trapani E., Mistretta F., Musi G., Pricolo P., Petralia G., De Cobelli O.

Multiparametric magnetic-resonance to confirm eligibility to an active surveillance programme for low-risk prostate cancer: intermediate time results of a high-volume centre protocol (SS 1407), B-1071

Lv H., Zhao P., Liu Z., Liu X., Ding H., Gong S., Wang Z.

Lateralisation effects on functional connectivity of the auditory network in patients with unilateral pulsatile tinnitus as detected by functional MRI (MY 14), B-1193

Lv Q.

Whole tumour histogram analysis of T2-weighted, diffusion-weighted, and postcontrast T1-weighted images in medulloblastoma: assessment risk of recurrence (SS 1016b), B-0930

Lv Q.

Application of MRI whole-tumour histogram analysis in assessment risk of medulloblastoma recurrence (SS 1811b), B-1477

Lyschik S., Rueppel S., Benz S., Halfmann M.C., Eichstädt J., Düber C., Kreitner K.-F., Emrich T., Hahn F.

Novel T1 map parameters of tissue heterogeneity are not influenced by age and gender in healthy volunteers (SS 1003), B-0974

M

Ma C.

Determination of inferior vena caval diameter: is it true on cavography? (SS 1815), B-1332

Maas M.

Paediatric MRI: can we make gadolinium superfluous?: Assessment of musculoskeletal disorders: when is intravenous gadolinium necessary? (SF 13b), A-651

Maccioni F.

The anal canal: does MRI make it easy?: C. My tough cases (E³ 1522), A-796

Machida Y., Shimauchi A., Igarashi T., Okuma H., Fukuma E.

Features of MRI after cryoablation of primary breast cancer without surgical resection (SS 1802a), B-1388

Macho J.

Interventional treatment of stroke: a game changer: Stroke, endovascular treatment: beyond proximal occlusion and six-hour time window (SA 17), A-915

Mack M.G.

Pitfalls in interpretation of head and neck disease: C. Distinct head and neck disease or systemic disease? (RC 808), A-315

Mack M.G.

Head and neck: Chairperson's introduction (E³ 1423), A-699

Madani G.

Head and neck ultrasonography: Keynote lecture (SS 608), K-10

Mader K.S., Sauter A.W., Sommer G., Weikert T., Trolese F., Hagger J., Stieltjes B.
Fully automatically staging of lung cancer using deep neural networks (SS 1805), B-1381

Madoff R.

How to write a scientific paper and how to get it published: The review process in other clinical journals (ESR Publication), A-933

Madureira A.J.B.S.

Difficult challenges in imaging the acute abdomen: B. Bowel obstruction (RC 1301), A-606

Mahajan H.

Philips Prodiva 1.5T: bringing performance and productivity together (SY 5)

Mahesh M.

Dose management systems and repositories: part B: The ACR dose index registry: setting a benchmark (EF 2), A-459

Maier J., Sawall S., Kachelrieß B.

Real-time x-ray scatter estimation for CT and CBCT using a deep convolutional neural network (SS 713), B-0736

Maietini D., Torre R., Mosca S., Rebonato A.

US-guided percutaneous double needle lavage in the treatment calcific tendinopathy of the rotator cuff performed with or without US-guided block of the suprascapular nerve (SS 1010), B-0959

Maillet B.

ESR and UEMS: a united European voice: Differences and similarities between ESR and UEMS (part 2) (ESR/UEMS 1), A-181

Maillet B.

ESR and UEMS: a united European voice: The European Perspective (part 1): advocacy at the EU Level (part 2) (ESR/UEMS 1), A-183

Maintz D.

The clinical validation of spectral benefits (SY 12)

Majer M., Colombani S., Mejdoubi M.

Clinical and MRI characteristics of patients with pontine hyperintense lesions in a series of ischaemic strokes (SS 1011a), B-0921

Majidi H., Godazandeh F., Abdi R., Espahbodi F., Alimohammadpur R., Tayebi M.

Survey of contrast-induced nephropathy after CT scan in patients who stayed in Sari Imam Khomeini Hospital from 2016 to 2017 (SS 1807b), B-1466

Makowski M.R.

Novel ways to characterise myocardial tissue: T1 and T2 mapping: A. T1 mapping: technical considerations (RC 903), A-392

Makowski M.R.

Hybrid imaging in oncology: Prostate cancer: the "killer application" for MR/PET? (SF 15a), A-742

Maksimović R.

Liver and bile duct pathologies: C. Gallbladder pathologies (E³ 820), A-375

Malakhanov V., Seliverstov P.V.

Ability to diagnose disorders of liver haemodynamics in conditions of biliary hypertension with perfusion computed tomography (SS 1001a), B-0841

Malamateniou C.

Maximising outputs from research: C. Winning research grants (RC 414), A-144

Authors' Index

Malavasi S., Barone D., Gavelli G., Bevilacqua A.

Can perfusion heterogeneity in CT perfusion maps of NSCLC flow clinical considerations based on global mean blood flow values? (SS 616), B-0589

Malavasi S., Gavelli G., Vilgrain V., Bevilacqua A.

Automatic computation of liver and lung perfusion parameters through the analysis of CT image sequences (SS 713), B-0730

Malich A., Papageorgiou I., Kovacevic D., Kott A., Wiech D., Teichgräber U.K.

Comparison of whole-body MRI (wbMRI) and bone scintigraphy in oncologic follow-up (MY 3), B-0373

Malinauskaite L., Hofmeister J., Burgermeister S., Martin S., Montet X., Boudabbous S.

An artificial intelligence approach for the automatic diagnosis of lipoma and liposarcoma: a pilot radiomics study (SS 210), B-0112

Mallard S.

How to foster clinical research in imaging departments: How to structure a research management unit in an imaging department (ESR Research), A-402

Maly Sundgren P.C.

Establishing competence in radiology: The value of the European Diploma (PI 1), A-463

Maly Sundgren P.C.

Imaging of the brain in preterm infants: Chairperson's introduction (SF 12b), A-536

Maly Sundgren P.C.

Brain tumours: B. Adult brain tumours (E³ 1421), A-683

Maly Sundgren P.C.

My three top tips for neuroimaging: Assessment of tumour response/progression (SF 15c), A-766

Mamisch-Saupe N.

Small joints: B. Forefoot and midfoot (E³ 1119), A-513

Mandal S., Komljenovic D.

Correcting for acoustic and optical inaccuracies in photoacoustic imaging using multimodal priors (SS 613), B-0545

Manfredi R.

Characterisation of focal liver lesions: A. Hypervascular lesions (E³ 620), A-261

Manfredi R.

My three top tips for abdominal imaging: Dilated pancreatic duct (SF 12a), A-522

Manfredi R.

Pancreatic tumours: B. Neuroendocrine tumours (E³ 1422), A-705

Manfredi R.

Abdominal MRI: from standard to advanced protocols: A. Suspected pancreatic tumour (RC 1701), A-877

Mang T.

Colorectal imaging: CTC and beyond: Keynote lecture (SS 601b), K-11

Maniatis V.

Difficult challenges in imaging the acute abdomen: A. Perforation of the GI tract (RC 1301), A-605

Mann R.M.

My three top tips for breast imaging: Automated breast ultrasound (SF 8b), A-326

Mann R.M.

The high-risk patient enigma: B. Value of breast MRI. Rate of underestimation and impact on treatment decision: is breast MRI increasing the number of high-risk lesions? (E³ 1726a), A-907

Mann R.M.

Personalised therapy through optimisation of diagnostic data in multi-disciplinary team decisions (SY 1d)

Mann R.M.

Improving the clinical utility of digital breast tomosynthesis using novel software applications (SY 1d)

Mannil M., von Spiczak J., Mühlematter U., Thanabalasingam A., Manka R., Alkadhi H.

Texture analysis of myocardial infarction of CT: impact of iterative reconstruction (SS 1003), B-0980

Mannil M., von Spiczak J., Manka R., Alkadhi H.

Texture analysis and machine learning for detecting myocardial infarction in non-contrast low-dose CT (SS 1003), B-0981

Manoharan T.

Integrated decision support for improved patient outcome (SY 1d)

Mansour O., Jafarinosar G.

The diagnostic accuracy of diffusion-weighted imaging for the detection of partial-thickness rotator cuff tears (SS 1010), B-0956

Mansour S.A., Hamed S.T., Hosny S., Elsayed S.B.

Role of diffusion MR imaging and 3D/4D ultrasound in the assessment of placental insufficiency in gestational hypertension (SS 1907b), B-1666

Maravi P.

Role of ureteric jet angle as measured by colour Doppler ultrasound in evaluating severity (grading) of VUR in patients presenting with urinary complaints (MY 4), B-0385

Marcello R., Assegnati G., Di Blasi A., Cortese F., Vitale S.

Evaluations of outcomes for drop in pain and analgesic use for kyphoplasty in the treatment of 249 patients with vertebral compression fractures: a single centre results (SS 610b), B-0532

Marcon M., Becker A., Berger N., Wurnig M., Wagner M., Frauenfelder T., Boss A.

Texture feature analysis can support breast lesions identification and characterisation in images acquired by automated breast ultrasound systems (SS 302), B-0273

Marcu M., Hedesiu M.

Estimation of the irradiation dose of children exposed to CBCT for various dental pathologies (MY 14), B-1184

Marcy P.-Y.

Distant metastases of head and neck cancer: Chairperson's introduction (E³ 926), A-433

Mariani S., Bruno F., Quarchioni S., Cannizzaro E., Gianneramo C., Arrigoni F., Zugaro L., Barile A., Masciocchi C.

Another breach in the wall: efficacy of sodium hexametaphosphate (SHMP) solution vs simple saline in percutaneous treatment of calcific tendonitis of the shoulder: 6-months follow-up (SS 1010), B-0960

Marie G., Poeg P., Son Forget J., Maeder J.P., Meuli R.

Quantitative assessment of spatial and temporal gadolinium deposition within the deep brain nuclei (SS 1011b), B-0996

Maroldi R.

Head and neck: inflammation, tumour or something else?: Sinuses (BS 1), A-023

Maroldi R.

Distant metastases of head and neck cancer: C. Is functional imaging necessary to detect distant metastases in head and neck cancers? (E³ 926), A-436

Maros M.E., Kämpgen B., Förster A., Groden C., Sommer W.H., Schönberg S.O., Henzler T., Wenz H.

Structured reporting supports junior readers and improves PI-RADS conformity of multi-parametric MRI reports of the prostate-based on cross-lingual RADLEX annotations (SS 1905), B-1582

Marques H.

Discovering Portuguese radiology: past, present, future: Cardiac CT from anatomy to functional information: comprehensive CAD evaluation (EM 2), A-687

Marra P., Venturini M., Colombo M., Brembilla G., Panzeri M.M., Salvioni M., Gusmini S., De Cobelli F., Del Maschio A.

Endovascular repair of 40 Visceral Artery Aneurysms (VAAs) and Pseudoaneurysms (VAPAs) with the Viabahn Stent-Graft: technical aspects, clinical outcome and mid-term patency (SS 309), B-0230

Marra P., Diana P., Ratti F., Partelli S., Salvioni M., Gusmini S., Venturini M., Aldrighetti L., De Cobelli F.

Microwave ablation (MWA) of liver metastases from pancreatic neuroendocrine tumour (pNET): preliminary results with a new generation system (SS 709), B-0629

Marra P., Diana P., Ratti F., Cipriani F., Salvioni M., Gusmini S., Venturini M., Aldrighetti L., De Cobelli F.

Microwave ablation (MWA) of liver malignancies: outcomes and prognostic factors of local tumour progression (LTP) with a new generation system (SS 1509), B-1205

Marrocchio C., Napoli A., Scipione R., Dababou S., Erasmus H., Catalano C.

MR-guided high-intensity focused ultrasound (MRgFUS) for the treatment of oligometastatic prostate cancer bone metastases: can sound waves downstage cancer spread? (SS 1809), B-1342

Martí-Bonmatí L.

Imaging of benign liver lesions: still difficult?: Chairperson's introduction (RC 901), A-381

Martí-Bonmatí L.

Diffuse liver disease: C. Diagnosis and staging of liver fibrosis (E³ 320), A-090

Martí-Bonmatí L.

Trends in quality education in radiology: Integration of big data in radiological education (ESOR), A-287

Martí-Bonmatí L.

How to write a scientific paper and how to get it published: Important papers other than original articles (ESR Publication), A-934

Martí-Bonmatí L.

Case-Based Diagnosis Training - Part 1: Liver (CB 1), A-962

Marticorena Garcia S.R., Guo J., Tzschätzsch H., Althoff C.E., Dürr M., Halleck F., Hamm B., Fischer T., Sack I.

Long-term follow-up magnetic resonance elastography after novel direct antiviral therapy in chronic hepatitis C virus induced liver fibrosis (SS 201a), B-0001

Authors' Index

Martin C., Chassagnon G., Marini R., Regent A., Mouthon L., Paragios N., Revel M.-P.

Analysis of pulmonary fibrosis, using an elastic registration technique in a model of fibrosis: systemic sclerosis (SS 1804), B-1353

Martin S.

Musculoskeletal radiology: inflammation: A. Inflammatory and infections in the soft tissues (E³ 221), A-061

Martin S., Hofmeister J., Burgermeister S., Becker C.D., Montet X.

Artificial intelligence applied on the national lung screening trial dataset: a radiomics study (SS 1004), B-0867

Martinelli M., Chincarini M., Zamboni G., Fabris C., Conti C., Pedrazzani C., Pozzi Mucelli R.

Prognostic value of bodycomposition parameters assessed at the preoperative CT in patients with colorectal carcinoma (SS 216), B-0166

Martini K., Caviezel C., Milanese G., Weder W., Frauenfelder T.

Prospective quantification of respiratory mechanics in COPD patients before and after lung volume reduction surgery on dynamic MRI (SS 1804), B-1355

Martinoli C.

Musculoskeletal ultrasound in the management of sports injuries: A. Ultrasound of ankle injuries: technique and diagnosis (RC 810), A-346

Martynova N., Vorobyov N., Mikhailov A., Gutsalo J., Smirnova E., Kalesnik A., Andreev G., Kubasov A., Lyubinskij A.

Primary and metastatic lung tumours treated with stereotactic body radiation therapy (SBRT): own experience (MY 5), B-0406

Mascagni L., Tiplaldi M., Pignatelli M., Cappucci M., Krokidis M., Orgera G., Rossi M.

Endovascular treatment of visceral artery aneurysms and pseudoaneurysms: extravascular stent graft migration as a possible long-term complication (SS 309), B-0231

Masha H.M.K.

Use of ultrasound for diagnosis of schistosomiasis mansoni (SS 1014), B-0968

Masselli G.

Emergency radiology II: B. Non-traumatic urinary tract emergencies (E³ 921), A-380

Masselli G.

Placental imaging: how, when and why?: Placental abnormalities, timing of imaging, methods and diagnosis (SF 16), A-815

Mastrodicasa D., Mantini C., Bianco F., Ricci F., Gallina S., Messalli G., Cademartiri F., Cotroneo A.R.

Prevalence and clinical relevance of extra-cardiac findings in CMR imaging (SS 603), B-0564

Mastrodicasa D., De Cecco C.N., Moritz A., Varga-Szemes A., Muscogiuri G., van Assen M., Eid M., Lavra F., Schoepf U.J.

Artificial intelligence deep-learning-based coronary CT fractional flow reserve: the impact of iterative and filtered back projection reconstruction techniques (SS 1803), B-1455

Masy M., Giordano J., Hossein-Foucher C., Petyt G., Remy J., Remy-Jardin M.

Dual-energy CT (DECT) lung perfusion in chronic thromboembolic pulmonary hypertension (CTEPH): diagnostic accuracy and concordance with radionuclide scintigraphy (SS 1904a), B-1552

Mathilakath R.V.

Diagnostic efficacy of dynamic manoeuvres in computed tomographic evaluation of oral cavity lesions (MY 14), B-1198

Matinyan N., Kuplevatsky V., Minasyan I., Cherkashin M., Berezina N., Sahakyan D.

MR-guided in-bore prostate biopsy for clinically significant cancer detection in patients with negative TRUS biopsies and rising PSA level (SS 1909), B-1548

Matos C.

Cystic pancreatic lesions: how to differentiate, how to manage?: Chairperson's introduction (SF 5), A-219

Matos C.

Liver and bile duct pathologies: B. Cholangiocarcinoma: diagnosing and staging (E³ 820), A-374

Matos C.

Imaging of abdominal tumours: B. Pancreatic tumours (E³ 1921), A-968

Mauri G.

Ultrasound-guided interventional procedures: new techniques and applications: Thyroid (WG 1), A-826

Maus V., Kalkan A., Kabbasch C., Abdullayev N., Barnikol U.B., Liebig T., Dohmen C., Fink G.R., Mpotaris A.

Mechanical thrombectomy in basilar artery occlusion: the presence of bilateral posterior communicating arteries is a predictor of favorable clinical outcome. (SS 611), B-0511

Mayerhöfer M.E.

Molecular imaging in oncology: D. Biomarker imaging with MR (RC 406), A-159

Mayerhöfer M.E.

Whole-body MRI: ready for prime time?: The case of lymphoma (SA 5a), A-199

Mayerhöfer M.E.

Hybrid imaging in oncology: Chairperson's introduction (SF 15a), A-740

Mayr A., Kranewitter C., Klug G., Kremser C., Feuchtnr G., Jaschke W., Metzler B.

Comparison of cardiovascular magnetic resonance imaging and computed tomography to guide transcatheter aortic valve replacement: a pilot study (SS 203), B-0148

Mayrhofer M.T.

Linking imaging biobanks to -omics: the role of BBMRI and ESR: Secondary use of existing data: ethical issues, sharing and data protection (ESR/BBMRI-ERIC), A-613

Mazzei M.A.

CT - patterns in chest radiology: back to basics and beyond: Chairperson's introduction (RC 404), A-099

Mazzei M.

Highlighted Lectures: Non-occlusive mesenteric ischaemia: CT diagnosis and signs of reperfusion (TF 1), A-690

McDermott A., Navin P., Tarmey T., Weir A., Bergin D., Bruzzi J.F., Voisin B., Sheppard D.

A novel mobile phone app to minimise bias and aid the FNAC decision-making process (SS 708), B-0670

McDermott A., Navin P., Weir A., Tarmey T., Bruzzi J.F., Voisin B., Sheppard D.

Comparison of the clinical utility of international guidelines to aid the decision on when to perform FNAC for thyroid nodules (SS 708), B-0671

McDonald R.J.

Gadolinium deposition: is it harmful?: Gadolinium deposition in the brain: from preclinical studies to clinical implications (SF 4), A-137

McGill M., Paterson A.

A pain in the neck: imaging of the paediatric cervical spine (c-spine) in isolated neck trauma (SS 212), B-0152

McGinty G.

Value-based radiology: Panel discussion: A European - US debate on the value of "value-based radiology" (part 3) (PI 3)

McGinty G.

Value-based radiology: New metrics are required for value-based radiology (PI 3), A-586

McKay C., Maguire S., Gilligan P., Walsh C., Matthews J., Eustace S.J.

Optimisation of contrast delivery using quantitative and qualitative analysis in a clinical based CTPA setting (SS 1014), B-0972

McLenachan S.L., Williams M., Camilleri F., Newby D.E.

Vascular calcification on mammography and coronary artery disease identified by computed tomography (SS 202b), B-0097

McNeill A.

eL18-4 in small parts, musculoskeletal and abdominal exams (SY 19)

McNulty J.

Forensic imaging: Chairpersons' introduction (part 1) (RC 114), A-037

McNulty J.

How to foster clinical research in imaging departments: An overview of the roles of radiographers in research (ESR Research), A-401

McNulty J.

EFRS meets Switzerland and Portugal: Introduction (EM 4), A-493

McNulty J.

Making the most of social media: Chairperson's introduction: Social media in healthcare (EFRS WS), A-786

Mdletshe S., Nel A., Rainford L., Lawrence H.A.

The development of a CAD tool employing TELTA, designed to support the training of radiographers in chest pattern recognition (SS 1414), B-1148

Medina-Ornelas S.S., Garcia-Perez F.

Influence of Trigger-PSA and molecularactive tumour volume evaluated with 68Ga-PSMA PET/CT on detection rate and localisation of recurrence in patients with prostate cancer (MY 3), B-0376

Medina-Ornelas S.S., Garcia-Perez F.

Clinical utility of ¹⁸F-NaFand ⁶⁸Ga-PSMA PET-CT as prognostic marker in patients with metastatic prostate cancer treated with Radium-223 (SS 1516), B-1253

Mehana S.M.

Can renal artery resistive index predict disease activity in lupus nephritis? (SS 1007), B-0885

Meier-Schroers M., Homsy R., Schild H., Thomas D.

Lung cancer screening with MRI: characterisation of nodules with different non-enhanced MRI sequences (SS 1804), B-1350

Authors' Index

- Meier-Schroers M., Homsí R., Schild H., Thomas D.**
Lung cancer screening with MRI: application of Lung-RADS in the first two screening rounds (SS 1904b), B-1571
- Meijer F.J.A.**
The polytrauma patient: The neuroradiologist's perspective (MS 17), A-939
- Melendez F.J., Rosati S., Aixut Lorenzo S., Remollo Friedemann S., Werner Reyes M.F., Ribó Jacobí M., Hernández Morales D., Martínez M., Tomasello Weitz A.**
Stent retriever single shot study (4S): multivariable analysis for first-pass recanalization in acute stroke (MY 9), B-0827
- Melzig C., Weinheimer O., Egenlauf B., Messerli M., Grünig E., Kauczor H.-U., Heussel C., Rengier F.**
Automated volumetry of peripheral pulmonary vessels based on CT angiography in suspected pulmonary hypertension (SS 1904a), B-1549
- Menezes G., Pijnappel R.M., Meeuwis C., Bisschops B., Veltman J., Lavin P., van de Vijver M., Mann R.M.**
Correlation between optoacoustic imaging and molecular subtypes of malignant breast masses (MY 16), B-1277
- Meng-Na H., Jiang T.**
Preliminary exploration of the application of super microvascular imaging in focal liver lesions (SS 301b), B-0206
- Menshchikov P.E., Ublinskiy M., Manzhurtsev A., Akhadov T., Semenova N.**
Simultaneous decrease of aspartate and NAA levels in the brain after severe TBI: ¹H MRS study (SS 212), B-0156
- Menshchikov P.E., Semenova N., Melnikov I., Ublinskiy M., Akhadov T.**
Increased cerebral GABA concentration measured using ¹H MRS in the acute paediatric mTBI (MY 8), B-0806
- Menu Y.**
Trends in quality education in radiology: The beauty of face-to-face teaching (ESOR), A-285
- Menu Y.**
My three top tips for abdominal imaging: Liver metastases follow-up (SF 12a), A-528
- Menu Y.**
How to write a scientific paper and how to get it published: The review process in radiology (ESR Publication), A-932
- Mercatelli D., Santoro A., Guidarelli G., Aparisi Gomez M., Guglielmi G., Franceschi C., Battista G., Bazzocchi A.**
Correlation between central adiposity distribution measured by DXA and inflammatory markers in the Italian cohort of the NU-AGE project (SS 1910), B-1625
- Merhemic Z.**
Neurologic emergencies: Ischaemic stroke (BS 3), A-082
- Mershin K.**
The heart team: coronary imaging and treatment: The role of coronary imaging in the coronary artery bypass and valve surgery (MS 4), A-131
- Mershina E.**
The heart team: coronary imaging and treatment: Chairperson's introduction (MS 4), A-128
- Messina C., Albano D., Corazza A., Rapisarda S., Martinelli N., Bianchi A., Sconfienza L.M.**
Posterior tibial tendon dysfunction: clinical and magnetic resonance imaging findings having histology as reference standard (SS 710b), B-0719
- Messiou C.**
New treatments for musculoskeletal tumours: Multimodality imaging in treatment and surveillance of soft tissue sarcoma (SF 17a), A-895
- Metin Y., Orhan Metin N., Kalcan S., Ozdemir O., Çolakoglu M., Küpeli A.**
The positive effects of bariatric surgery on NAFLD at early postoperative period: proof with ideal IQ sequences obtained by 3.0 Tesla MRI (SS 1801), B-1324
- Meyer H., Schob S., Münch B., Frydrychowicz C., Quäschling U., Hoffmann K., Surov A.**
Histogram analysis of T1-weighted, T2-weighted, and postcontrast T1-weighted images in primary CNS lymphoma: correlations with histopathological findings (SS 316), B-0359
- Miglioretti D.L., Sprague B., Gard C., Rauscher G., Tice J., Kerlikowske K.**
Risk-based strategies for supplemental breast cancer screening (SS 1902a), B-1604
- Milanese G., Silva M., Seletti V., Galeone C., Bartholmai B., Palmucci S., Piciucchi S., Karwoski R., Sverzellati N.**
Follow-up of idiopathic pulmonary fibrosis: computed tomography vs functional metrics (SS 204), B-0045
- Milanese G., Mannil M., Martini K., Maurer B., Alkadhi H., Frauenfelder T.**
Effect of different radiation doses and reconstruction kernels of HRCT on texture analysis-based artificial neural network classification of patients with systemic sclerosis (SS 204), B-0047
- Milanese G., Silva M., Bruno L., Goldoni M., Maffei E., Cademartiri F., Sverzellati N.**
Epicardial fat volume as a potential imaging biomarker for coronary artery disease in symptomatic patients (SS 303), B-0333
- Milani A., Trimboli R.M., Carbonaro L.A., Codari M., Di Leo G., Sardaneli F.**
MRI of invasive mass breast cancer: correlation of global vascularity and ADC with pathological features (SS 602), B-0503
- Miller T.T.**
Lower extremity sports injuries: A. Sports-related injuries of the knee: what does the orthopaedic surgeon need to know? (TC 1428), A-707
- Miller T.T.**
Lower extremity sports injuries: C. Interactive case discussion (part 1) (TC 1428), A-709
- Min L.A., Ackermans L.L.G.C., Nowee M.E., van Griethuysen J.J., Trebesch S., Vogel W., Maas M., Beets-Tan R.G.H., Lambregts D.M.**
Multiparametric MRI to predict response to external beam radiotherapy in locally advanced cervical cancer: comparison of MRI volumetry, diffusion-weighted MRI and MR texture analysis (MY 3), B-0365
- Min L.A., Vogel W., Lahaye M.J., Maas M., Donswijk M., Vegt E., Beets-Tan R.G.H., Lambregts D.M.**
Integrated versus separate reporting of FDG-PET/CT and MRI for abdominal malignancies: effect on diagnostic confidence and staging outcomes (SS 1016a), B-0893
- Mirafzal S., Lahaye C., Mulliez A., Morin P., Vaz Touret M.A., Boirie Y., Boyer L., Cassagnes L.**
CT dose reduction for epicardial fat measurement in obese patients: effects of low-dose cardiac CT and adaptive statistical iterative reconstruction (SS 303), B-0331
- Miraglia R., Maruzzelli L., Petridis I., Marrone G., Luca A.**
Preliminary experience of TIPS creation using the new controlled expansion e-PTFE covered stent (SS 209), B-0033
- Mishra A., AlSaady R., Patel S., Mahemood S.A., Abdulla T.S., Hussain A.A.W.**
How accurate are we and how can we get better in diagnosing acute appendicitis by unenhanced multidetector computed tomography: a large meta-analysis and literature review (SS 1017), B-0946
- Mitchell D.P., Gillespie C.D., Moriarty H., Ridge C.A., MacMahon P.J.**
Overdiagnosis of PE in pregnancy? Interpretative discrepancy in the diagnosis of pulmonary embolism in pregnant patients undergoing CTPA (SS 1904a), B-1554
- Mitreska N.**
Successful paediatric imaging: Chairpersons' introduction: Paediatrics: more than just 'small adults' (part 2) (RC 514), A-224
- Mizandari M., Azrumelashvili T., Habib N.**
VesOpen procedure: the new percutaneous image-guided treatment option of HCC-induced portal vein thrombosis (SS 209), B-0037
- Mizandari M., Azrumelashvili T., Habib N.**
Image-guided percutaneous drainage of pancreatic duct: what for and how (SS 209), B-0040
- Mizandari M., Azrumelashvili T., Habib N.**
Fluoroscopy-guided percutaneous interventions via pancreatic duct percutaneous drainage track for diagnosis and treatment: feasibility and technique (SS 209), B-0041
- Mizzi A.**
Portal hypertension and interventional radiology (IR): Chairperson's introduction (RC 109), A-050
- Mohammadzadeh A., Mohammadzadeh M., Shahkarami V., Shakiba M., Sabetrasekh P.**
Association of non-alcoholic fatty liver disease with increased carotid intima-media thickness considering other cardiovascular risk factors (SS 315), B-0212
- Mohammadzadeh M., Mohammadzadeh A., Haghghi Z., Sharifian H., Mohammadzadeh V., Kadivar S.**
Perineural spread of fungal sinonasal infections: CT scan and MRI findings (SS 1508), B-1221
- Mohammed N.-E.A.N., Naguib N.N.N., Gruber-Rouh T., Burck I., Vogl T.J.**
Ablation therapy of non-colorectal cancer lung metastases: retrospective analysis of tumour response post LITT, RFA and MWA (SS 1509), B-1210
- Mohammed Ali A.H., Hogg P.H., England A.**
Relationships between image quality and radiation dose during paediatric pelvic radiography: a factorial phantom study (SS 714), B-0741
- Mohammed Ali A.H., Hogg P.H., England A.**
Development and validation of a low-cost paediatric pelvic phantom for digital radiography dose optimisation (MY 17), B-1296

Authors' Index

Molinari F.

CT - patterns in chest radiology: back to basics and beyond: B. Linear and reticular pattern (RC 404), A-101

Molinari F.

Imaging of the chest: A. Fibrosing lung diseases (E³ 1221), A-516

Monaco C.G., Parker G., Little R., Watson Y., Cheung S., O'Connor J., Marchianò A.V., Scaramuzza D.

Evaluation of diagnostic accuracy of diffusion weighted (DW) MRI in mesorectal lymph node staging of rectal carcinoma (ReNoRis) (SS 216), B-0165

Montet X.

The use of CBCT in clinical settings: the experience of Geneva University Hospital (SY 25)

Monti M., Zamboni G., Bertuzzo L.,**Pozzi Mucelli R.**

MRI and MRCP features of chronic pancreatitis in patients with or without pancreas divisum abnormality and their relationship to patients age (SS 1901b), B-1522

Moorthy I., Iliadis K., Diacon T., Moon L.,**Vitta L.**

Optimising imaging in suspected child abuse: a five-year prospective study in a tertiary referral children's service (SS 312), B-0343

Moraes P.H.D., Chammas M., Schelini M.

Elastography shear wave contribution when evaluating thyroid follicular nodules comparing to histological findings (MY 14), B-1186

Morana G.

New challenges of pancreatitis: B. Autoimmune pancreatitis and its relatives (E³ 1322), A-676

Mordasini M.

EFRS meets Switzerland and Portugal: Introduction: Across Switzerland (EM 4), A-494

Moreira I.C., Ventura S.R., Ramos I., Rodrigues P.P.

Learner's perception, knowledge and behavior assessment within a breast imaging eLearning course for radiographers (SS 214), B-0137

Morgan D., Pagniez J., Lefevre G.,**Averlant L., Kahn J., Longere B., Silvestri V., Pontana F.**

Late gadolinium enhancement patterns in patients with hypereosinophilia: can CMR help identifying the aetiology? (SS 1903), B-1654

Morozova S., Kremneva E.I., Legostaeva L.,**Mochalova E., Sinitsyn D., Sergeev D.,****Krotenkova M., Suponeva N., Piradov M.**

The role of conventional MRI-based scale in distinguishing chronic disorders of consciousness (SS 1811a), B-1407

Morozova S., Kremneva E.I., Gadzhieva Z.,**Sergeeva A.N., Akhmetzianov B.,****Zabitova M., Kashina E., Krotenkova M.,****Dobrynina L.**

Comparative study of activation during color-word Stroop test and new suggested counting test performance (SS 1911b), B-1677

Morris E.A.

MRI for early detection, staging and management of breast cancer: B. MR imaging biomarkers for the clinical setting (RC 1202), A-555

Mostbeck G.H.

GI bleeding: how to solve the problem?: A. Acute GI bleeding (RC 101), A-004

Motosugi U., Hori M., Goshima S., Kozaka K., Hyodo T., Nakamura Y., Nishie A., Tamada T., Kanki A.

How to avoid gadoteric acid-related artefacts? Prospective multi-institutional study in 1994 patients (SS 701a), B-0607

Mottet N.

A multidisciplinary approach to prostate cancer: can we make a difference?: A. The urologist: evidence-based clinical decision making (RC 1716), A-917

Motyer R., Kok H., Asadi H., O'Hare A.,**Brennan P., Sarah P., Looby S., Nicholson P., Thornton J.**

Outcomes of endovascular treatment for acute large vessel ischaemic stroke more than 6 hours after symptom onset (SS 1009), B-0856

Motyer R., Thornton J., Power S., Brennan P.,**O'Hare A., Looby S., Williams D.,****Moynihan B., Murphy S.**

Endovascular thrombectomy beyond 12 hours of stroke onset: a stroke network's experience of late intervention (SS 1009), B-0857

Moulopoulos L.

Whole-body MRI: ready for prime time?: The case of multiple myeloma (SA 5a), A-198

Muca M., Bertolotto M., Zorzenon I.,**Iannelli M., Sachs C., Cova M.A.**

US-guided sclerotherapy of the cavernosal stumps following male-to-female sex reassignment surgery (SS 1907b), B-1665

Mueller J., Lorbeer R., von Krüchten R.,**Pomschar A., Kauczor H.-U., Bamberg F.,****Schulz H., Karrasch S., Schlett C.L.**

MR-based lung volume segmentation in population-based whole-body MR imaging: correlation with clinical characteristics, pulmonary function testing and obstructive lung disease (SS 1804), B-1356

Mueller-Lisse U.G., Kuhn M., Scherr M.,**Mueller-Lisse U.L., Murer S., Reiser M.F.,****Scheidler J.**

Chronic prostatitis: distinction from prostate cancer and benign prostatic hyperplasia by means of PIRADS version-2 descriptors (SS 1807a), B-1366

Mueller-Lisse U.L., Ebner R., Seifert S.,**Stief C., Ricke J., Reiser M.F.,****Mueller-Lisse U.G.**

CT urography: dependence of distal ureter opacification on excretory-phase timing and urinary-bladder volume (SS 1807b), B-1471

Mueller-Peltzer K., Rübenthaler J.,**Clevert D.A.**

Contrast-enhanced ultrasound (CEUS) as a new technique to characterise suspected malignancies in renal transplants in comparison to standard imaging modalities (SS 207), B-0057

Mughetti M., Gardelli G., Giampalma E.,**Zompatori M.**

The role of lung ultrasound in the differential diagnosis of respiratory distress syndrome and transient tachypnoea in preterm and newborn infants (SS 1412), B-1164

Muglia R., Solbiati M., Solbiati L.

A new software for immediate volumetric assessment of tumour ablation completeness: could it allow to spare local retreatments? (SS 1509), B-1209

Muhammad K., Lutfi I.A.

Bronchial artery embolisation: tuberculosis patients with haemoptysis (SS 1009), B-0859

Muharemovic O., Troelsen A., Thomsen M.G., Kallemose T., Gosvig K.K.

Personalised patient protocol for radiostereometric analysis (SS 714), B-0747

Mühlematter U., Mannil M., Finkenstaedt T.,**Becker A.S., Osterhoff G., Guggenberger R., Fischer M.**

Vertebral body insufficiency fractures: detection of vertebrae at risk on clinical CT images using texture analysis and machine learning (SS 610b), B-0533

Mulder H.K.P., Jeukens C.R., Rousch M.,**Wildberger J.E., Lobbes M.B.**

Quantification of enhancement in contrast-enhanced spectral mammography using a custom-made quantifier tool: a proof-of-concept study (SS 1802b), B-1410

Mungai F., Pietragalla M., Bonasera L.,**Bartolucci M., Berti V., Miele V.**

Head and neck cancer heterogeneity assessed by CT texture analysis: can it predict the human papilloma virus status? (MY 14), B-1183

Murphy D.J.

The heart between the lungs: A. Cardiomyopathies (E³ 618), A-257

Murphy M., Barry C., Cronin C., Healy D.

The 8th edition IASLC staging system for lung cancer, a step beyond current imaging accuracy? (SS 616), B-0586

Murphy S.F., Sullivan C.J., McCormick P.,**Mehigan B.J., Kevans D., Brennan I.M.,****Guiney M.J., Sheehy N., Meaney J.F.M.**

CT-guided transgluteal drainage of deep pelvic abscess (SS 609), B-0443

Murraças A.C.C., Martins P.M., Ferreira C.,**Godinho T.M., Castelo-Branco M., Silva A.**

A data mining approach to the SAR values over large MR image repositories (SS 614), B-0559

Musmann B.R.

Successful paediatric imaging: B. Suspected non-accidental injury: best practice and advice (RC 514), A-226

Mutlu U., Ikram M., Roshchupkin G.V.,**Bonnemaijer P.W.M., Colijn J.M.,****Niessen W.J., Ikram M., Klaver C.C.W.,****Vernooij M.W.**

The neural substrate of retinal neurodegeneration: the Rotterdam study (MY 8), B-0795

Muto M.

My three top tips for neuroimaging: Low back pain (SF 15c), A-760

N

Na B., Lee S., Jeong H., Kim D.

Image comparison of virtual non-contrast images and true non-contrast images obtained from dual-energy CT in latest generation dual-source and dual-layer CT for liver (SS 314), B-0320

Nadrjlanski M., Milosevic Z.

Breast MRI: internal thoracic artery lymph node assessment in patients with invasive breast carcinoma (SS 202b), B-0103

Nadrjlanski M., Milosevic Z.

Breast MRI: circularity metrics in mass shape assessment of benign and malignant breast tumours (SS 1402b), B-1115

Nagasawa N., Kitagawa K., Hashizume K.,**Yamazaki A., Maki H., Sakuma H.**

Movie projection systems for paediatric CT examinations: effects on examination time, motion artefacts, and the need for restraints (SS 312), B-0350

Authors' Index

Nagel S., Steffen I., Elgeti T.

Age dependency of the Wells Score for pulmonary embolism (SS 1017), B-0943

Naghibi H., Mohammadzadeh M., Fallahian A., Shakiba M., Sabetrashk P., Soroush H.

Increased signal intensity of dentate nucleus in multiple sclerosis patients with history of higher gadolinium-enhanced MRI scans (SS 1011b), B-0998

Nahmani S., Grevent D., Beccaria K., Boddaert N.

Detection of bridging vein thrombosis at computed tomography: a specific sign of shaken baby syndrome? (SS 312), B-0341

Nakamura Y., Higaki T., Tatsugami F., Zhou J., Yu Z., Akino N., Ito Y., Iida M., Awai K.

Improvement of diagnostic image quality of abdominal CT using a deep learning-based reconstruction: initial clinical trial targeting hepatic metastases (SS 601a), B-0428

Nakano S., Fujii K., Kousaka J., Mouri Y., Ando T., Ido M., Goto M., Ito Y., Ishiguchi T.

Impact of MRI/ultrasound fusion-guided biopsy for breast lesions detected on MRI alone (SS 1802a), B-1391

Nanni C.

Molecular imaging in oncology: C. Imaging of metabolism (RC 406), A-158

Napoli A., Dababou S., Erasmus H., Marrocchio C., Scipione R., Catalano C.

CT-guided pulsed radiofrequency treatment of the lumbar dorsal root ganglion in patients with acute radicular low back pain (SS 1809), B-1337

Napolitano A., Ironi G., Tombetti E., Incerti E., Leoni S., Picchio M., Gianolli L., Dagna L., De Cobelli F.

Preliminary results of DWI sequences in detecting arterial wall inflammation in patients with giant cell arteritis (SS 1415), B-1042

Nasr E., Youssef A., Zekry W., Raafat T., Younis A., Elkiki H.A.

Role of MRI vs CT in staging and decision making in paediatric renal masses (MY 18), B-1503

Natale L.

Cardiac MRI: from sequence to bedside: Chairperson's introduction (E³ 1326a), A-617

Nattenmüller J., Eller L., Lücke S., Lonsdorf A., Schlemmer H.-P., Kauczor H.-U., Sedlaczek O.L.

Prognostic impact of body composition in patients with metastasised malignant melanoma with checkpoint-inhibitor therapy (MY 3), B-0375

Negrao E.M.S., Bitencourt A., Souza J.A., Ferreira Marques E., Souza Guatelli C., Graziano L., Albuquerque M.L.L.

MRI analysis after neoadjuvant chemotherapy on breast cancer: correlation between radiological and pathological response (MY 16), B-1285

Negrao de Figueiredo G., Schöppe F., Pomschar A., Förster K., Hilgendorff A., Stöcklein S., Ertl-Wagner B.

Establishing age-specific reference values of lung volume in preterm born infants using MR-based volumetry (SS 1412), B-1161

Negro G., Durando M., Mariscotti G., Desana B., Regini E., Isoardi P., Garolla M., Fonio P., Gandini G.

What can affect tomosynthesis-guided vacuum-assisted breast biopsy (TVAB) procedures? Clinical and technical challenges (SS 1802a), B-1392

Nelstrop H.L., Prestwich R., Barnfield M., McDermott G.M., Scarsbrook A.

Prognostic significance of PET-based radiomic image features in locally advanced laryngeal and hypo-pharyngeal squamous cell carcinoma (MY 14), B-1192

Nerad E., Lahaye M.J., Beets-Tan R.G.H.

Staging of colon cancer, best technique/modality, a PhD thesis (SS 216), B-0172

Neri E.

Dose management systems and repositories: part B: Imaging and dose repositories: tools to boost radiation protection and research? (EF 2), A-458

Neri E.

eHealth in radiology: policies, practices, pitfalls, potential: ESR eHealth SC and eHealth policy positions (ESR/EU), A-772

Neri E.

Artificial intelligence: a strategic view: Chairperson's introduction (SF 6), A-979

Neubauer C., Neubauer J., Windfuhr-Blum M., Langer M.

Microcalcifications in breast tomosynthesis including synthesised mammography, multiple angulated reconstructions and standard stack reconstructions (SS 202a), B-0081

Nguyen A., Perez-Rovira A., Duijts L., De Bruijne M., Aliverti A., Pennati F., Ivanovska T., Tiddens H.A., Ciet P.

Technical challenges of quantitative chest MRI data analysis in a large cohort paediatric study (SS 712), B-0768

Nguyen T., Houfflin-Debarge V., Vinchon M., Boutry N., Avni F.E.

Closed spinal dysraphisms: how to improve prenatal diagnosis (MY 18), B-1504

Nguyentat M., Bura V., Ushinsky A., Fardin S., Green C., Uchio E., Lee T.K., Lall C., Houshyar R.

Personalised radigenomic medicine: prostate cancer gene 3 and PI-RADSv2 team up to predict clinically significant prostate cancer (SS 316), B-0361

Nichelli L., Giorgio A., Zhang J., Stromillo M., Rossi F., Battaglini M., Mortilla M., Amato M.P., De Stefano N.

Brain damage in early adult paediatric-onset MS with no or minimal disability (SS 311), B-0286

Nicolau C.

Imaging strategies in renal tumours: Chairperson's introduction (RC 1707), A-896

Nicosia L., Latronico A., Faggian A., Cannataci C., Penco S., Cassano E.

Atypical ductal hyperplasia: our experience in the management and long-term clinical follow-up in 71 patients (SS 1402a), B-1090

Niehues S., Vahldiek J.L., Geyer B., Hamm B., Poch F., Lehmann K.S.

Drill-assisted bone tissue sampling: do we need to care about heat? (SS 1809), B-1340

Niessen W.J.

Artificial intelligence and big data in medical imaging: Chairperson's introduction (PC 15), A-733

Niiniviita H., Saukko E., Saunavaara J.

The estimation of radiation dose in suspected child abuse imaging (SS 312), B-0342

Nikolaou K.

Molecular imaging in oncology: Chairperson's introduction (RC 406), A-155

Nikolaou K.

Memorable cases in cardiovascular imaging: how to avoid common mistakes: Chairperson's introduction (SF 12e), A-596

Nikupaavo U.

Optimising computed tomography: Chairpersons' introduction (part 1) (RC 1614), A-847

Nimmada T.R., Rao P., Sanghavi P.S., Venugopal V., Warier P., Udwadia Z., Jankharia B.

Clinical validation of a deep learning algorithm for quantification of the idiopathic pulmonary fibrosis pattern (SS 1004), B-0872

Nimmada T.R., Putha P., Tadepalli M., Jain S., Rao P., Warier P.

Identifying pulmonary consolidation in chest x rays using deep learning (SS 1805), B-1378

Nishino R., Numasaki H., Minamoto N., Nakai S., Uchigashima T., Takahashi A., Ehara S., Sakai M., Takashima S.

Diagnostic ability of the primary lung cancer by radiologists with chest x-ray (MY 5), B-0416

Niu X.

Diagnostic performance of biparametric MR imaging for detection of prostate cancer: a systematic review and meta-analysis (SS 307), B-0246

Niu X.

Developing a new PI-RADS v2-based nomogram for forecasting high-grade prostate cancer (MY 4), B-0392

Noebauer-Huhmann I.

Spine imaging: Keynote lecture (SS 610a), K-09

Noël P.B.

Strategies for dose reduction in computed tomography: from technical concepts to clinical practice: Iterative image reconstruction for dose reduction in CT: technical background and concepts for clinical practice (EU 2), A-249

Norris D.G.

Demystifying MRI: things you always wanted to know: A. Basic MR: the building blocks of pulse sequences (RC 1613), A-844

Nous F., Coenen A., Kruk M., De Geer J., Schoepf U.J., Yang D., Kurata A., Budde R.P., Nieman K.

Coronary CT angiography-based fractional flow reserve in diabetic patients: results from the MACHINE consortium (SS 303), B-0337

Nous F., Lubbers M.M., Akkerhuis J., Bruning T., Krenning B., Kofflard M., Kietselaer B.L., Budde R.P., Nieman K.

The impact of a tiered cardiac CT protocol compared to functional testing on cardiovascular risk management in patients with suspected coronary artery disease (SS 1803), B-1461

Nyapathi V.

Identification of internal opening in perianal fistula: comparison of 3D cube vs 2D at 3.0 Tesla (SS 601b), B-0526

O

O'Connor J.

Quantitative imaging in oncology: Chairperson's introduction (E³ 1626b), A-861

O'Connor M., Stowe J.G., Foley S.J.

Acceptable noise levels in abdominal CT examinations of obese paediatric patients (SS 314), B-0321

O'Hara L.R.

Radiographers' challenge: informing patients about radiation risk: How to effectively communicate radiation risks (SF 12d), A-580

Authors' Index

O'Regan T.J., Robinsion L.,**Newton-Hughes A., Strudwick R.**

An account of silences in diagnostic radiography: a cultural quilt stitched together with the threads of social defences (SS 1914), B-1639

Ochoa Albiztegui R.E., Horvat J.V., Thakur S., Bernard-Davila B., Trattig S., Helbich T.H., Morris E.A., Pinker K.

Ultra-high field dynamic contrast-enhanced MRI (DCE-MRI) of the breast at 7T with pharmacokinetic (PK) modeling accurately differentiates between benign and malignant breast tumours (SS 1402b), B-1117

Oei E.H.G.

State-of-the-art imaging of postoperative joints: B. Postoperative knee (E³ 526a), A-233

Offiah A.C.

Why do I miss fractures in emergency?: A. Missed fractures in children (RC 1617), A-837

Oguzkurt L.

Interventional radiology in the venous system: vessel and eye opening: A. Varicose vein (E³ 1626a), A-858

Ohno Y., Fujisawa Y., Kishida Y., Seki S., Sugihara N., Yoshikawa T.

Inspiratory/expiratory xenon-enhanced area-detector CT (ADCT): capability for pulmonary functional loss and clinical stage evaluations in smokers (SS 204), B-0043

Ohno Y., Yaguchi A., Aoyagi K., Kaminaga S., Kishida Y., Seki S., Yoshikawa T.

Quantitative prediction of malignancy on newly developed 3D computer-aided volumetry (CADv) with pulmonary nodule component evaluation on thin-section CT (MY 5), B-0403

Ohno Y., Yui M., Kishida Y., Seki S., Yoshikawa T.

Chemical exchange saturation transfer (CEST) imaging vs diffusion-weighted imaging vs FDG-PET/CT: single- and multiparametric approach for diagnosis of pulmonary nodules (SS 1804), B-1348

Ohno Y., Kishida Y., Seki S., Yui M., Ohyu S., Yoshikawa T.

Multiparametric approach by dynamic contrast-enhanced perfusion MRI with FDG-PET/CT: capability for conservative therapeutic response prediction in NSCLC patients (SS 1904b), B-1578

Ohno Y., Yui M., Chen Y., Ohyu S., Kishida Y., Seki S., Yoshikawa T.

Blood volume-based MR imaging with ultra-short TE: capability for prediction of postoperative lung function in NSCLC patients as compared with CT and perfusion SPECT (SS 1904b), B-1579

Ohno Y., Kishida Y., Seki S., Yui M., Aoyagi K., Kaminaga S., Yoshikawa T.

MRI with DWI vs FDG-PET/MRI vs FDG-PET/CT vs conventional radiological examination: capability for TNM staging in patients with malignant pleural mesothelioma (SS 1904b), B-1581

Oikarinen H., Mahajan H., Perttu A., Ukkola L., Jussila A.L., Henner A.

Parents wish more information on radiation exposure of their children (SS 312), B-0351

Oikonomou A.

Cavitary and cystic diseases of the lung: C. Lymphangioliomyomatosis (E³ 418), A-163

Olchoway C.

Gadolinium deposition: is it harmful?: Assessing tissue integrity in the presence of gadolinium deposition in the brain (SF 4), A-138

Oleaga Zufiria L.

Establishing competence in radiology: Achieving homogeneity in radiology education: linking content to competence through the European training curriculum (PI 1), A-460

Oleaga Zufiria L.

ESR and UEMS: a united European voice: ETAP 2.0 (part 2): modernisation of ETAP (ESR/UEMS 1), A-186

Oliveira M.V.L., Geambastiani P., Lopez G.A., Cambui M.

Development of a radiological anatomy free software as a teaching tool (SS 1414), B-1140

Omelchenko O., Rozhkova Z., Makarchuk M., Karaban I.

Peculiarities of brain activation during dominant-hand tactile perception in lateralised Parkinson's disease (SS 1511), B-1236

Omoumi P.

Shoulder: B. Chronic pain (E³ 719), A-290

Omoumi P., Babel H., Jolles B., Favre J.

Subchondral bone/cartilage: a functional unit? Bone density and cartilage thickness are correlated (SS 1810), B-1425

Omoumi P.

MR imaging of the knee: B. Meniscal tears: obvious and subtle (RC 1710), A-921

Onal T., Afacan G.O., Akansel G., Arslan A.S., Anik Y., Inan N., Muezzinoglu B., Corapcioglu F.

The performances of radiographic criteria for bone malignancy when applied to computed tomography and magnetic resonance imaging (SS 210), B-0108

Op De Beeck B.J.

Personalised medicine in liver tumours: Chairperson's introduction (E³ 720), A-292

Ording Müller L.-S.

Juvenile idiopathic arthritis (JIA): C. MRI and role of contrast in the assessment of synovitis (E³ 426), A-154

Ordu D., Rollandi L., Rippel K., Scheurig-Muenkler C., Kröncke T., Schwarz F.

Can we reliably identify the appendix on unenhanced ultra-low-dose CT in the era of iterative reconstruction? (SS 601b), B-0527

Orlando A., Amato F., Di Vittorio M., Lupo C., Spatafora L., Safina M., Ienzi F., Ienzi R., Bartolotta T.V.

Focal breast categorisation according to the BI-RADS-US lexicon: role of a computer-aided decision-making support (MY 16), B-1292

Orsatti G., Varotto A., Crimi F., Bisogno G., Zanetti I., Giraud C., Stramare R.

Prognostic value of radiological response assessment after induction therapy in paediatric soft tissue sarcomas (MY 18), B-1492

Orsi M., Cellina M., Leone F., Mariani D., Presazzi A., Floridi C., Oliva G.

Screen-detected breast cancer: differences in mammographic tumour features between agreement and disagreement recall (MY 16), B-1286

Orsi M., Cellina M., Floridi C., Leone F., Battaglia E., Barmettler F., Oliva G.

Single-centre experience with breast MRI maximum intensity projection (MIP) views: sensitivity, specificity and accuracy of the stand-alone evaluation (SS 1902a), B-1612

Osiev A.

The heart team: coronary imaging and treatment: Interventional treatment/percutaneous (MS 4), A-130

Ospe J.M., Karwacki G., Blackham K.

The influence of CT perfusion on the selection of stroke patients for endovascular therapy (SS 611), B-0516

Owczarczyk K., Kelly-Morland C., Mcelroy S., Winfield J., Siddique M.M., Qureshi A., Cook G., Goh V.J.

Impact of the MRI sequence and observer on the gross tumour volume (GTV) in patients with oesophageal and gastro-oesophageal junction (GOJ) cancer (SS 1416), B-1080

Owens C.

Chest imaging of cystic fibrosis: from infants to adults: X-ray: is there still a value in CF? (SF 13a), A-609

Owens C.

Paediatric: B. Paediatric chest imaging (E³ 1823), A-954

Oyen R.H.

Urogenital: Chairperson's introduction (E³ 1623), A-832

Özbek S.S.

Head and neck: inflammation, tumour or something else?: Lymph nodes (BS 1), A-026

Özdemir H.O., Sanchez-Montanez Garcia-Carpintero A., Sabate Rotes A., Delgado Alvarez I., Riaza Martin L., Coma A., Riera Soler L., Castellote A., Vazquez Mendez E.

Imaging findings of Loeys-Dietz syndrome in paediatric population (SS 712), B-0769

Ozgen Mocan B.

Imaging of the skull base: A. Non-tumoural pathology of the temporal bone (E³ 521), A-168

Özmen M.N.

Urogenital: B. Imaging of the ureter and bladder (E³ 1623), A-834

Ozturk M., Polat A.V., Celenk C., Elmali M., Polat C.

The diagnostic value of 4D MRI for the localisation of parathyroid adenomas (SS 708), B-0674

P

Pacella G., Faiella E., Santucci D., Alfonsi A., Altomare C., Beomonte Zobel B., Grasso R.F.

Combined antegrade and retrograde approach in iatrogenic ureteral injuries: the rendez-vous technique (MY 9), B-0820

Pacifici S., Giudice D.

Outpointing breasts and hallux valgus: correlation and implications in mammography quality (SS 214), B-0136

Padberg F.

Psychoradiology: a blend of molecular, functional and structural imaging with a taste of psychology: A psychiatrist's view on neuroimaging (MS 16), A-828

Padhani A.R.

Progress on whole-body MRI use for advanced breast cancer (SY 1b)

Padhani A.R.

Whole-body MRI: ready for prime time?: The case of metastatic bone disease (SA 5a), A-197

Padhani A.R.

Imaging of the prostate: A. MRI diagnosis of prostate cancer (RC 807), A-316

Paech D., Schuenke P., Köhler C., Bachert P., Ladd M., Bendszus M., Schlemmer H.-P., Zaiss M., Radbruch A.

Dynamic glucose-enhanced MRI: clinical perspectives and challenges (MY 3), B-0363

Authors' Index

- Paech D., Behl N., Umatham R., Ladd M., Schlemmer H.-P., Nagel A., Niesporek S.** Metabolic imaging of tumours employing dynamic ¹⁷O MRI: initial results in glioma patients (SS 1016b), B-0934
- Pagonidis K.** Memorable cases in cardiovascular imaging: how to avoid common mistakes: Congenital elastic band of the aortic valve: a "multimodality" diagnosis (SF 12e), A-599
- Paiman E.H.M., de Mutsert R., Widya R.L., Jukema J.W., Rosendaal F.R., Lamb H.J.** Cardiovascular function in relation to abdominal adipose tissue distribution (SS 303), B-0335
- Palkó A.** Imaging of HCC: Chairperson's introduction (E³ 520), A-241
- Pallas R.J., Foley K.G., Crosby T., Fielding P.A.** Prognostic significance of systemic inflammation and FDG-PET bone marrow uptake in patients with oesophageal cancer (SS 701b), B-0714
- Palmisano A., Benedetti G., Giannini F., Baldetti L., Del Maschio A., De Cobelli F., Esposito A.** Stress-rest CMR for the assessment of myocardial perfusion reserve index modification after coronary sinus stent implantation (MY 7), B-0782
- Palmucci S., Torrisi S.E., Falsaperla D., Torcitto A., Basile A., Rosso R., Stefano A., Russo G., Vancheri C.** Correlation between pulmonary function tests and HRCCT indexes in idiopathic pulmonary fibrosis (IPF) patients (SS 204), B-0049
- Palumbo P., Quarchioni S., Bruno F., Micelli M.V., Giordano A., Varrassi M., Carducci S., Di Luzio M., Masciocchi C.** Interventional radiology approach in the treatment of symptomatic uterine fibroids: from diagnosis to treatment: our experience (SS 1909), B-1539
- Pameijer F.A.** Pitfalls in interpretation of head and neck disease: A. Anatomical variants without clinical consequence (RC 808), A-313
- Pamminger M., Nalbach T., Reindl M., Klug G., Reinstadler S.J., Jaschke W., Metzler B., Mayr A.** Mitral annular plane systolic excursion assessed by cardiovascular magnetic resonance is an independent predictor of major adverse cardiac events after STEMI (SS 603), B-0572
- Panfili M., Calandrelli R., Massimi L., Gaudino S., Colosimo C.** Relationship between cranio-orbital volume changes and the severity of skull base dysmorphology in infants with anterior synostotic plagiocephaly: a quantitative analysis (SS 312), B-0348
- Pankowska A., Kochalska K., Dyndor K., Łazorzyc A., Pietura R.** 1.5T vs 7T in determining changes of white matter in multiple sclerosis: preliminary studies (SS 614), B-0553
- Panvini N., Caruso D., De Santis D., Bellini D.M., Rivosecchi F., Rengo M., Laghi A.** Evaluating response to chemotherapy in colorectal liver metastases: correlation between CT texture analysis and RECIST criteria (SS 316), B-0358
- Papadopoulou F.** Vesicouretral reflux: the role of contrast ultrasound (SY 23)
- Papageorgiou I., Angelidakis L., Damianou C., Psychogios M., Lingor P., von Eckardstein K., Malich A., Hadjidemetriou S.** A 3 Tesla MRI brain atlas for Parkinson's disease as diagnostic and interventional tool (SS 1511), B-1239
- Papanikolaou N., Papaioannou G., Iliopoulos A., Szatmari P., Illing R.** Affidea imaging metrics platform: a comprehensive dashboard providing key performance indicators for optimisation of image quality and throughput (SS 205), B-0183
- Papanikolaou N.** Gastrointestinal: 'the gut': Small bowel (BS 2), A-065
- Papanikolaou N.** Advanced MR techniques and imaging biomarkers: A. Diffusion-weighted imaging (E³ 420), A-165
- Papanikolaou N.** The ten-minute abdominal MRI: make the dream come true!: Chairperson's introduction (SF 8c), A-349
- Papassin J., Krainik A., Heck O., Condamine E., Pietras J., Tahon F., Detante O.** Impaired cerebrovascular reactivity is at high risk of stroke in patients with intracranial stenosis (SS 611), B-0509
- Papp S., Karady J., Kolossvary M., Drobní Z., Szilveszter B., Barczy G., Merkely B., Maurovich-Horvat P.** The effect of myocardial bridge on the presence and extent of coronary artery disease: case-control study (SS 1903), B-1655
- Parimalai A.N., Chelladurai A., Damodaran K., Muthayan P.** Role of imaging in the diagnosis of glenohumeral deformity following obstetric brachial plexus injury (SS 312), B-0347
- Parizel P.M.** Gadolinium deposition: is it harmful?: Chairperson's introduction (SF 4), A-136
- Parizel P.M.** ESR and UEMS: a united European voice: Differences and similarities between ESR and UEMS (part 1) (ESR/UEMS 1), A-180
- Parizel P.M.** My three top tips for neuroimaging: Acute ischaemic stroke (SF 15c), A-759
- Park D., Kim T.** Perfusion abnormality in posterior inferior cerebellar artery termination of vertebral artery on arterial spin labelling and dynamic susceptibility contrast perfusion MRI (SS 1011b), B-1005
- Park J., Kim C.** Prediction of pathologic upgrading in biopsy-proven low-grade endometrial cancer: utility of diffusion-weighted imaging (SS 707), B-0647
- Park K.** Prediction of treatment response after immunotherapy in metastatic or recurrent urothelial carcinoma: potential imaging biomarker using CT texture analysis-a preliminary study (SS 207), B-0064
- Park S., Won S.** Transrectal ultrasound-guided targeted biopsy of transition zone prostate cancer: usefulness of across midline sign (SS 1907a), B-1563
- Parker A.P.** Cavitory and cystic diseases of the lung: A. Cavitory lung lesions (E³ 418), A-161
- Parker A.P.** Knee: A. Post-traumatic (E³ 1019), A-467
- Paruccini N., Villa R., Morzenti S., Spadavecchia C., Signoriello M., Ippolito D., Crespi A.** Iterative reconstruction algorithms in computed tomography: is it possible to go beyond Fourier metrics for image quality assessment? (SS 1413), B-1129
- Parviz S.** Adnexal masses: diagnostic value of DCE-MRI (SS 1816), B-1374
- Patella F., Franceschelli G., Petrillo M., Sansone M., Fusco R., Carrafiello G.** A multivariate analysis combining DCE and IVIM derived parameters to improve parotid tumours differential diagnosis (MY 14), B-1190
- Patelli G., Ranieri A., Paganelli G.A., D'Alessio A., Besana F., Mauri G., Pacella C.M.** Transperineal ultrasound-guided laser ablation for the treatment of benign prostatic hyperplasia in interventional radiology: preliminary results (SS 1909), B-1545
- Paulo G.** Maximising outputs from research: B. Collaborating across Europe (RC 414), A-143
- Paulo G.** CT screening: benefits, doses and associated risks: How to communicate (ESR/EFOMP), A-231
- Paulo G.** EFRS meets Switzerland and Portugal: The Portuguese NHS: the structural pillar that strengthens Portuguese democracy (EM 4), A-497
- Paulo G.** Radiographers' challenge: informing patients about radiation risk: So whose role is it? What different professionals can and should do (SF 12d), A-578
- Paulo G.** Audit across Europe: directive and perspective: Engaging in the Pilot: The Eurosafe Imaging Star Perspective (ESR Audit), A-855
- Pavan L.J., Durando M., Mariscotti G., Martinello S., Cappello G., Ala A., Castellano I., Fonio P., Gandini G.** Comparison between standard specimen mammography and intraoperative specimen mammography (Faxitron[®]) located in the surgical block: has anything changed? (SS 1802a), B-1398
- Pavan L.J., Faletti R., Nicolet L., Cosentino A., Di Chio A., Gatti M., Fiore S., Bonino F., Fonio P.** 3D printed model based on knee MRI as a new tool in surgical planning of anterior cruciate ligament reconstruction (SS 1810), B-1420
- Paysan P.** Motion artefacts and their management in medical imaging: B. Managing motion in cone-beam CT (CBCT): conventional approaches and motion compensating techniques (RC 1313), A-655
- Pecchi A., Musacchia G., Verrusio M., Battista R., Canossi B., Cortesi L., Torricelli P.** How early can MRI diagnosis of breast cancer be in BRCA mutated women? (SS 1902a), B-1611

Authors' Index

- Pecoraro M., Padhani A., Campa R., Valerio M.C., Catalano C., Panebianco V.**
Analysis of clinical and economic management optimisation of multiparametric-MRI as the first line tool in men with high clinical suspicion of prostate cancer (SS 307), B-0244
- Pecorelli A., Ippolito D., de Vito A., Lombardi S., Riva L., Talei Franzesi C., Sironi S.**
Clinical impact of iterative model reconstruction algorithm in a department of emergency radiology in a large series of patients (SS 1017), B-0942
- Pedalino S., Appendino E., Tabone E., Mazzetti S., Regge D., Russo F.**
Prediction of minimal extraprostatic extension with MRI: correlation with whole-mount histological sections (SS 1407), B-1064
- Pedersen M.R.V., Møller H., Osther P., Vedsted P., Holst R., Rafaelsen S.R.**
A comparison of testicular tissue stiffness using shear wave elastography (SS 1907b), B-1660
- Pedersen P., Fremmelevholm L., Jørgensen S.H., Moerup S.**
Ambient experience in MRI (SS 614), B-0556
- Pediconi F.**
Minimally-invasive local treatment of breast cancer: the time is now: A. High-intensity focused ultrasound (HIFU) therapy (RC 902), A-405
- Peebles C.**
What a radiologist needs to know about imaging of myocardial viability: Chairperson's introduction (RC 1503), A-745
- Peebles C.**
The heart of the matter: imaging the myocardium: MR in non-ischaemic cardiomyopathies (E³ 24E), A-960
- Peetrons P.**
Musculoskeletal interventional procedures: A. Diagnostic and therapeutic injections in the athlete: pearls and pitfalls (TC 1528), A-797
- Peetrons P.**
Musculoskeletal interventional procedures: C. Interactive case discussion (part 1) (TC 1528), A-799
- Pekarovíc D., Zdesar U., Jesih P.A., Pungřar M.**
Implementation of DR detectors for paediatric chest x-ray in NICU (SS 1814), B-1443
- Peng W., Li Z., Xia C.**
Performance of native T1 and T2 mapping cardiovascular magnetic resonance to detect myocardial oedema in patients with dilated cardiomyopathy (SS 1903), B-1648
- Peniaeva E., Sencha A., Patrunov Y., Sencha E.**
Specification of breast masses according to BI-RADS classification enforced with contrast-enhanced ultrasound (SS 302), B-0276
- Penzkofer T.**
Radiomics: what is it and how can we use it?: Radiomics: clinical challenges (NH 12), A-576
- Perez Lopez R., Tunariu N., Koh D.-M., de Bono J.S.**
Diffusion-weighted MRI as a prognostic and response biomarker in patients with castration-resistant prostate cancer and bone metastases (MY 4), B-0393
- Perisinakis K., Pouli S., Tzedakis A., Spanakis K., Hatzidakis A.A., Raissaki M., Damilakis J.**
What is the underestimation of radiation dose to the paediatric thyroid from contrast-enhanced CT, if contrast medium uptake is not taken into account? (SS 712), B-0771
- Perisinakis K.**
Single-dual-multi-energy CT: A. Basics of dual- and multi-energy CT (RC 113), A-034
- Perkuhn M., Thiele F., Shakirin G., Garmis D., Stavrinou P., Borggreffe J.**
Evaluation of a multiparametric deep learning model for glioblastoma segmentation (SS 1805), B-1384
- Pesapane F., Standaert C., De Visschere P., Villeirs G.**
T-staging of prostate cancer: prevalence and predictive value of frequently used signs of extracapsular extension on prostate MRI (SS 1407), B-1067
- Peters J.**
The polytrauma patient: The primary survey: talking ABC (MS 17), A-937
- Petrash E., Mikhaylova E.V., Sevriukov D., Nikulina A.**
Liver regenerative nodules in paediatric patients: diagnostic value of Gd-EOB-DTPA (SS 612), B-0578
- Petrillo R., Antonelli A., Bernardo S., Satta S., Vinci V., Manganaro L., Catalano C.**
Central nervous system (CNS) involvement in congenital heart diseases (CHD): value of foetal MRI (MY 18), B-1493
- Petrovic D.J.**
Carotid intima-media thickness (CIMT) as a window to atherosclerosis (SS 315), B-0213
- Peynircioglu B.**
Peripheral vascular malformations: what every radiologist should know: B. Percutaneous or endovascular treatment: when and how? (RC 115), A-044
- Pezzotti S., Borghesi A., Nocivelli G., Scrimieri A., Maroldi R.**
Solid indeterminate pulmonary nodules less than 300 mm³: application of the British Thoracic Society guidelines in clinical practice (SS 204), B-0053
- Pezzullo M.**
Imaging of 'foreign bodies': Chairperson's introduction (RC 1317), A-644
- Pfahler V., D'Anastasi M., Duerr H., Ricke J., Baur-Melnyk A.**
Tumour load in patients with multiple myeloma: β_2 -microglobulin levels vs low-dose whole-body CT (SS 210), B-0113
- PfannenberG C., Wang L., Gückel B., Gatidis S., Olthof S.C., Reimold M., La Fougère C., Nikolaou K., Martus P.**
Practice-based evidence for clinical benefit of PET/CT - results of the first oncologic PET/CT registry in Germany (SS 1016a), B-0889
- Pfirrmann C.W.A.**
State-of-the-art imaging of postoperative joints: A. Postoperative shoulder (E³ 526a), A-232
- Pfirrmann C.W.A.**
Lower extremity: Chairperson's introduction (E³ 819), A-368
- Pfirrmann C.W.A.**
Radiology and Swiss chocolate: a sweet combination: Truffle No. 2: hip preservation surgery: a fast evolving field also for imaging (EM 1), A-453
- Pfirrmann C.W.A.**
Upper extremity sports injuries: B. Soft tissue wrist injury in the athlete (TC 1328), A-679
- Pfirrmann C.W.A.**
Upper extremity sports injuries: C. Interactive case discussion (part 2) (TC 1328), A-681
- Phan T., Smeets D., Vandermosten M.**
Effect of a child-adjusted method for brain volume quantification on group comparisons in dyslexia (MY 18), B-1489
- Piankyh O.**
Machine learning in radiology operations management (SS 1905), B-1586
- Picasso R., Zaottini F., Airdali S.**
High resolution Ultrasound of the Motor Branch of the Ulnar Nerve beyond the Guyon tunnel (SS 710a), B-0616
- Picchia S., Rengo M., De Santis D., Bellini D.M., Badia S., Laghi A.**
MRI of the gastric antrum for the quantification of gastric motility: comparison between obese and normal weight patients (SS 701b), B-0715
- Pichler F., Zeilinger M.**
Radiographers in preclinical imaging research: Small animal imaging studies (SF 9b), A-427
- Pieper C.C., Schild H.**
Interstitial transpedal MR lymphangiography in pre-interventional work-up for lymphatic interventions in patients with chylous effusions (SS 209), B-0042
- Pietsch H.**
Latest pre-clinical findings and potential consequences of gadolinium presence in brain (SY 9)
- Piha T.**
eHealth in radiology: policies, practices, pitfalls, potential: EU Strategy for Digital Transformation of Health and Care (ESR/EU), A-773
- Pijnappel R.M.**
Screening for breast cancer: A. Screening with mammography only (RC 402), A-117
- Pilius P., Shrainer I., Klimenko A., Sinitsyn V.E.**
Use of CT perfusion parameters in assessment of early response of gastric cancer to neoadjuvant chemotherapy (SS 701b), B-0710
- Pina Insausti L.J.**
Basic breast imaging: B. Asymmetry and architectural distortion (E³ 621), A-246
- Pina-Insausti L.J.**
Clinical utility of contrast-enhanced dual energy mammography (CEDEM) (SY 1c)
- Pinker-Domenig K.**
Hybrid imaging in oncology: MR/PET of breast tumours (SF 15a), A-743
- Pinto A.**
Why do I miss fractures in emergency?: B. Missed fractures in adults (RC 1617), A-838
- Pinto dos Santos D.**
Artificial intelligence (AI) applications: Big data and structured reporting (SF 10), A-992
- Pipan F., Clauser P., Zuiani C., Helbich T.H., Baltzer P.A.T.**
Malignant breast lesions typing with diffusion tensor imaging: could fractional anisotropy considered a preoperative 'imaging biomarker'? (SS 1002), B-0910
- Pires F., Patrão T., Alves F., Santos J.**
Optimisation of computed tomography practice: phantom and patient approach (SS 314), B-0328

Authors' Index

- Pisana F., Henzler T., Haubenreisser H., Klotz E., Schmidt B., Kachelrieß M.**
High-fidelity vessel visualisation in diagnostic CT: low-dose dynamic CTA via singular value decomposition-guided filter (SVGF) (SS 613), B-0542
- Pitton M., Moddemann M., Zimmermann T., Schotten S., Galle P., Düber C.**
Risk factors of survival after TIPS using ePTFE covered stentgrafts in refractory ascites (SS 209), B-0036
- Pitton M., Becker F., Schotten S., Kloeckner R., Zimmermann T., Mittler J., Galle P.R., Otto G., Düber C.**
Role of interventional radiology in the scope of liver transplantation (SS 301b), B-0210
- Pizzini F.B.**
Gadolinium: image wisely: C. Do we need gadolinium in imaging vestibular schwannomas? Pros and cons (part 2) (PS 1227), A-595
- Plakhotina N., Mikhailov A., Smirnova A.V., Kuplevatskaya D.I., Vorobyov N.**
MRI-based surveillance for patients with recurrent head and neck cancer after hypofractionated stereotactic (SBRT) re-irradiation (SS 1508), B-1220
- Platz Batista da Silva N., Beyer L.P., Hornung M., Brunner S., Schliitt H.J., Wiggemann P., Jung E.**
Intraoperative shear wave elastography for assessment and staging of liver fibrosis and cirrhosis during open liver tumour surgery in correlation with histopathology: first results (SS 301b), B-0207
- Platz Batista da Silva N., Hornung M., Brunner S., Hackl C., Schliitt H.J., Stroszczyński C., Jung E.**
Intraoperative CEUS for localisation and characterisation of liver lesions during open liver tumour surgery: a single centre's 7 years experience (SS 301b), B-0208
- Plonski L., Carmon E., Chernovsky E., Zeltzer G., Sella T.**
Anatomic factors affecting shear wave elastography of malignant and benign breast lesions (SS 302), B-0268
- Pokrajac D., Radovanovic Z., Milosavljevic T., Stokanovic V., Weinstein S., Imran Al-Zubaer A., Maidment A.D.A., Bakic P.R.**
Selection of parameters for computer model of breast anatomy through human observer experiments (SS 1902b), B-1632
- Poletti P.-A.**
The latest update in imaging of polytrauma patients: A. Ultrasound: when, why and by whom? (RC 1517), A-779
- Ponnapatpura Satyanarayana J.**
Mesial temporal sclerosis: is standard MRI protocol enough? (SS 1811a), B-1405
- Ponnapatpura Satyanarayana J.**
Utility of MRI brain epilepsy protocol in new onset seizures: how is it different in developing countries? (SS 1811a), B-1408
- Pontana F.**
The heart between the lungs: C. Fat and calcium in the heart (E³ 618), A-259
- Portalez D., Jaffro M.**
Evaluation of MRI parameters for prediction of prostate cancer upgrading in active surveillance (SS 1407), B-1072
- Portelli J.**
Radiographers' challenge: informing patients about radiation risk: What do patients want to hear and need to be told? (SF 12d), A-579
- Portelli J.**
Radiation protection from A to Z: The radiographers' role in benefit-risk communication (BR 2), A-632
- Posa A., Iezzi R., Carchesio F., Barone C.A., Gasbarrini A., Manfredi R.**
Transradial versus transfemoral access for hepatic chemo-embolisation: inpatient prospective single-center study (SS 1409), B-1061
- Pötter-Lang S., Staufer K., Baltzer P.A.T., Tamandl D., Muin D., Bastati-Huber N., Halilbasic E., Kazemi-Shirazi L., Ba-Ssalamah A.**
The efficacy of MRI in the diagnostic work-up of cystic fibrosis-associated liver disease (MY 15), B-1255
- Poupon C.**
Exploring the microscopic from macroscopic: the strengths of multiparametric MRI: Modelling brain multicompartiment microscopic diffusion (ESR/ESMRMB 1), A-113
- Pozdniakova V., Froehlich J., Gutzeit A.**
Appropriateness and pattern of imaging modality choice amongst radiologists from different countries (SS 205), B-0174
- Pozdniakova V., Zivadinov R., Dalaker T.O., Dalen I., Bergsland N., Oppedal K., Pedersen K., Tysnes O., Alves G.**
MRI brain atrophy can predict dementia in cognitively normal Parkinson's patients: a 7 year follow-up study (MY 8), B-0798
- Pozzi Mucelli R.**
Pancreatic tumours: Chairperson's introduction (E³ 1422), A-703
- Pradella S., Vignoli C., Acquafresca M., Grossi F., Fusi I., Miele V.**
Paradoxical low-flow, low-gradient severe aortic stenosis: cardiac magnetic resonance (CMR) evaluation (SS 203), B-0141
- Prampolini F., Taschini S., Pecchi A., Sani F., Gelsomino F., Spallanzani A., Kaleci S., Torricelli P.**
Predictive factors of recurrence at MR examination performed before and after preoperative chemoradiotherapy in patients with rectal cancer: a retrospective study (SS 1001b), B-0855
- Prassopoulos P.K.**
Peritoneum and mesentery: B. Peritoneal carcinomatosis (E³ 1622), A-868
- Prayer D.**
Foetal and neonatal imaging: Keynote lecture (SS 1412), K-22
- Prayer D.**
Gynaecological and obstetrics: C. Fundamentals of foetal imaging (E³ 1523), A-770
- Prayer D.**
Case-Based Diagnosis Training - Part 1: Neuro (CB 1), A-963
- Prayer F., Krois W., Metzelder M., Kasprian G., Brugger P., Gruber G.M., Weber M., Prayer D., Patsch J.M.**
Fetal-MRI based segmentation of the diaphragm in fetuses with congenital diaphragmatic hernia: a retrospective pilot study (SS 1412), B-1168
- Preibsch H., Beckmann J., Blumenstock G., Staebler A., Wietek B., Nikolaou K., Wiesinger B.**
Accuracy of breast magnetic resonance imaging compared to mammography in the preoperative detection and measurement of pure ductal carcinoma in situ (SS 1002), B-0918
- Prokop M.**
Strategies for dose reduction in computed tomography: from technical concepts to clinical practice: Systems for dose reduction in CT: more than automated exposure control (EU 2), A-248
- Prokop M.**
CT examination of pregnant patients: a dilemma for the radiologist and the mother: Radiation risks vs clinical benefits (SF 8a), A-309
- Prosch H.**
Lung cancer in the era of molecular oncology and immune therapy: Chairperson's introduction (E³ 118), A-054
- Prosch H.**
Emergencies following tumour therapy: B. Chest (E³ 1726b), A-942
- Prosch H.**
Case-Based Diagnosis Training - Part 2: Chest (CB 2), A-975
- Puglielli E., Lattanzi R., Di Mizio V., Roiati S., Navarra F., Di Egidio V.**
Comparison between not-stent retriever and stent retriever mechanical thrombectomy for the intra-arterial acute ischemic stroke treatment (MY 9), B-0815
- Pulli B., Wang C., Wojtkiewicz G.R., Chen J.**
Fluorescence molecular imaging of infection and inflammation utilizing a novel probe specific for myeloperoxidase (SS 1406), B-1175
- Pulli B., Forghani R., Wang C., Wojtkiewicz G.R., Chen J.**
Molecular MR imaging of myeloperoxidase reveals a new myeloid cell treatment effect of interferon-beta in experimental multiple sclerosis (SS 1406), B-1178
- Pursanova D., Aslanidis I., Mukhortova O., Ekaeva I., Trifonova T.A., Shirokorad V.I., Roshchin D.A.**
11C-Choline PET/CT in the detection of oligometastatic prostate cancer recurrence (SS 1516), B-1249
- Pusceddu C.**
Percutaneous ablative treatment of pelvic rectal cancer recurrence (SS 709), B-0628
- Pusceddu L., Vani V., Giannetto G., Morra L., Correale L., Delsanto S., Senore C., Regge D.**
Impact of radiologist experience on detection of colorectal neoplasms at CT colonography screening (SS 601b), B-0519
- Putha P., Tadepalli M., Jain S., Chiramal J., Nimmada T.R., Warier P.**
Efficacy of deep learning for screening pulmonary tuberculosis (SS 1805), B-1379
- Puylaert J.B.C.M.**
My three top tips for abdominal imaging: Appendicitis (SF 12a), A-520
- Puylaert J.B.C.M.**
Imaging of 'foreign bodies': B. Foreign bodies in the gastrointestinal tract: the role of radiographs, US and CT (RC 1317), A-646
- Pyra K.K.**
Abdominal emergencies: friends and enemies: When to call the interventional radiologist and when to call the surgeon? (SF 17b), A-902

Authors' Index

Q

Qanadli S.D.

CT of vascular pulmonary diseases: C. Rendu-Osler disease (E³ 218), A-070

Qi R.

Comparison of aortic annulus dimensions by multimodal measurement before transcatheter aortic valve replacement (SS 203), B-0147

Qu J., Shen C.

CT radiomics signature for preoperative esophageal cancer patients lymph node metastasis prediction (SS 316), B-0353

Quaia E., Gennari A., Cova M.A., Van Beek E.J.

Biomarkers derived from time-intensity curves in patients with Crohn's disease (SS 1901c), B-1532

Quere J., Phan C., Miquel A., Arrive L., Menu Y., Crema M.

MDCT arthrography assessment of the severity of cartilage damage and scapholunate dissociation in regard to specific component tears of the scapholunate ligament (SS 310), B-0301

Quitze A., Schmidt-Holtz J., Behzadi C., Adam G., Regier M.

CT pulmonary angiography at reduced radiation exposure and contrast material volume in obese patients using IMR and iDose⁴ in comparison to FBP (SS 1815), B-1327

R

Ra J., Lee E., Park H., Lee J., Park S., Choi B.

The efficacy of superb microvascular imaging for diagnosing acute cholecystitis: comparison with conventional ultrasonography (MY 15), B-1265

Radbruch A.

Clinical perspective: what to consider and to know when interpreting the clinical literature on Gd presence in the brain and body (SY 9)

Radder A.

Welcome to MR with a new point of view: new perspective, bigger impact (SY 5)

Raffaelli C., Hombreux A., Tieulie N., Lassalle S., Azulay N., Giordana P.

Ultrasound biomicroscopy in the diagnosis of giant cell arteritis (SS 1415), B-1043

Ragab Y., Kheir H., Hamza H., Maher S.

Ovarian ischaemia vs haemorrhagic infarction: differentiation by MRI in cases of adnexal torsion (SS 607), B-0470

Ragab Y., Al Marakby A., Hamza H.M., Hasanin A.

Diagnostic performance of quiescent interval single-shot (QISS) non-contrast MRA at 3 Tesla for the diagnosis of acute lower limb ischaemia (SS 1017), B-0950

Raimondi E., Belluomini L., Cartuan A., Bassi M., Rizzati R., Tilli M., Frassoldati A., Giganti M., Benea G.

Comparison of overall-survival in squamocellular-NSCLC patients treated with Nivolumab assessed with RECIST1.1 and iRECIST (SS 616), B-0588

Raimondi E., Young K., Kouvelakis K., Koh D.-M., Calamai V., Starling N., Bali M.A. Pancreatic ductal adenocarcinoma: association of RECIST1.1 and Choi criteria with survival data and clinical outcome (SS 1416), B-1083

Raimondi E., De Paepe K.N., Koh D.-M., McCall J., Fotiadis N.

Comparison between microwave and radiofrequency ablation in local control of colorectal liver metastases (SS 1509), B-1202

Rainford L.A.

Maximising outputs from research: A. Designing robust research projects (RC 414), A-142

Rainford L.A.

Dose reduction: tips and tricks: C. The impact of dose management systems (RC 912), A-391

Rainford L.A.

Closing the gap between education and clinical practice for radiographers: Tools for success: academic and clinical practice working together (PC 13), A-661

Rainford L.A.

Radiography research: a how to guide: How to produce a high-quality scientific or educational poster (BR 1), A-552

Raissaki M.

Maximising outputs from research: Chairpersons' introduction (part 2) (RC 414), A-141

Raissaki M.

Imaging in abdominal emergencies: an (evidence-based) update: C. Polytrauma: differences between adult and paediatric protocols (RC 512), A-192

Raissaki M.

Closing the gap between education and clinical practice for radiographers: Chairpersons' introduction (part 2) (PC 13), A-658

Rajani H., Grover S.B., Mittal P., Khanna G.

Evaluating the MR scoring system ("ADNEX MR score") for characterisation of sonographically indeterminate adnexal masses (SS 1816), B-1373

Ramos Botelho Antunes P., Barbosa Álvares M.C., Franco Monteiro Prado F., Tinôco Alvim de Souza F., Álvares de Campos M., Carvalho de Siqueira E., Berindoague Neto R., Carvalho Silva Rabelo B.

Clinical complications in percutaneous renal biopsy guided by ultrasound: 16 vs 18-gauge needles (MY 4), B-0391

Ramsden W.

Establishing competence in radiology: Establishing competence in radiology: a UK perspective (part 2) (PI 1), A-462

Rana A., Jang A., Jehangir M., Asghar M., Nazir R., Burki S., Shakeel K.

Segmental variation of CT liver attenuation index in living-related liver donors: correlation with histopathological findings (SS 1901a), B-1509

Ranschaert E.R.

Daily use of mobile devices in radiology: C. Security and ethical issues of mobile device technology (RC 805), A-363

Ratib O.

Daily use of mobile devices in radiology: Chairperson's introduction (RC 805), A-360

Ratib O.

What a radiologist needs to know about imaging of myocardial viability: B. Hybrid imaging (RC 1503), A-747

Rauch A.

In vivo quantitative 4D-CT analysis of carpal kinematics with radio-scaphoid and luno-capitate angles during radio-ulnar deviation: feasibility and clinical interest (MY 13), B-1020

Rauch S.

Feasibility of shear wave elastography (SWE) in diagnosing carpal tunnel syndrome (CTS) (SS 710a), B-0614

Raymakers D., Coudyzer W., Cornelissen S.A., Maleux G.

Contrast volume reduction for aortic CT angiography using a volume calculator and a spiral flow device: a prospective randomised study (SS 215), B-0021

Raynaud J.-S.

Methodological approach for a correct interpretation of the gadolinium retention studies (SY 17)

Redheuil A.

Open and closed: the role of radiology in treatment of valvular heart disease: How to approach valvular heart disease using MRI (E³ 24C), A-483

Reekers J.A.

Peripheral vascular malformations: what every radiologist should know: Chairperson's introduction (RC 115), A-042

Reekers J.A.

Drug elution or drug illusion in vascular disease: Drug-eluting balloons and stents in femoropopliteal and crural lesions: contra (SF 13c), A-672

Reekers J.A.

Interventional: C. Vascular interventions (E³ 1923), A-973

Regge D.

Multiparametric liver imaging: Keynote lecture (SS 201a), K-01

Reidler P., Lerchenberger M., Rentsch M., Trumm C.G.

Interventional treatment of visceral artery aneurysms: single centre experience over 16 years (SS 309), B-0228

Reidler P., Thierfelder K., Fabritius M.P., Schuler F., Sommer W.H., Kunz W.G.

Ipsilateral thalamic diaschisis in acute ischaemic stroke: occurrence, perfusion characteristics, and association with morphologic and clinical outcome (SS 611), B-0513

Reidler P., Thierfelder K., Fabritius M.P., Sommer W.H., Kunz W.G.

Classification of CT perfusion infarct core in acute ischaemic stroke using automated measurements of tissue density on non-contrast CT (SS 611), B-0517

Reijnierse M.

Muscle and nerve: Keynote lecture (SS 710a), K-12

Reim M., Lomp A., Mihnovits V., Ilves P., Saar S., Lepner U., Talving P.

Correlation between CT-based liver injury scoring and subsequent management (SS 317), B-0296

Reimer R., Reimer P., Mahnken A.

Prediction of response to transarterial radioembolisation by means of MRI-based texture analysis as a potential radiomics tool (MY 3), B-0371

Reinert C.P., Hinterleitner C., Nikolaou K., Horgner M.

Diagnosis of diffuse spleen involvement in haematological malignancies using a spleen to liver attenuation ratio in CECT (SS 716), B-0704

Authors' Index

- Reis C.S., Mæhle S., Pires Jorge J.A., York H., Flaction L., Johansen S.**
Comparison of curricula, clinical experiences and attributes of radiography programmes delivered by four European educational institutions (SS 1414), B-1147
- Reis C.S., Pires Jorge J., Mæhle S., York H., Flaction L., Johansen S.**
A comparative study about motivations, expectations and professional development in four European radiography programmes (SS 1914), B-1643
- Reis M.V.C., Rodrigues S., Abrantes A.F., Ribeiro L.P., Almeida R.P.P., Lesyuk O.**
Eye-lens dose in head CT examinations: evaluation of different methods through the use of gantry angulation and barium shields (SS 1814), B-1451
- Reitan A.F., Olerud H.M., Borthne A.**
Pregnancy and radiation: video as a tool for health professionals communicating knowledge and risks (SS 1414), B-1141
- Rémy-Jardin M.**
When and how to use perfusion imaging in pulmonary vascular and airway disease?: A. CT (RC 104), A-007
- Rengier F., Naas O., Norajitra T., Messerli M., Kallenbach K., Karck M., Maier-Hein K., Kauczor H.-U.**
Automated three-dimensional detection of dural ectasia in Marfan syndrome by means of isotropic MRI and shape-based machine learning (SS 1411b), B-1105
- Renz D.M., Schröder A., Böttcher J., Pfeil A., Streiptarth F., Teichgräber U.K., Mentzel H.-J.**
Detailed evaluation of a completely automatic, computer-assisted (CAD) analysis of hand X-ray examinations by including four different paediatric collectives (SS 312), B-0349
- Resende L.L., Lyra K., Lôbo C., Castro L., Passarelli V., Valerio R., Jorge C., Leite C.D., Otaduy M.**
Description of white matter damage in patients with mesial temporal sclerosis evaluated by diffusion tensor imaging (DTI) (SS 1811a), B-1400
- Reuzé S., Dirand A., Sun R., Orhac F., Louvel G., Ammari S., Deutsch E., Robert C.**
An innovative MRI harmonization method for multicentre radiomic analysis in glioblastoma (SS 713), B-0737
- Revanna S.M.s.a., Kenchanahalli Rangaswamy V., Devappa V., Shamachar V.K.**
Aortic & carotid intima-media thickness in term small for gestational age newborns and term normal newborns (SS 712), B-0770
- Revel M.-P.**
Oncologic imaging: B. Incidental findings in oncologic patients (E³ 1321), A-604
- Ricci P.**
ESR and UEMS: a united European voice: CME/CPD in Europe (part 1): EACCME 2.0 (ESR/UEMS 1), A-187
- Ricci P.**
ESR and UEMS: a united European voice: CME/CPD in Europe (part 2): the Accreditation Council in Imaging (ESR/UEMS 1), A-188
- Riederer I., Bar-Ness D., Pfeiffer F., Douek P., Si-mohamed S.A., Fingerle A.A., Rummeny E.J., Noel P.B., Muenzel D.**
Potential of spectral photon-counting CT for the differentiation between blood and iodine in a bovine brain (SS 613), B-0543
- Riederer S., Stinson E., Bernstein M., Campeau N., Huston J., Trzasko J.**
Improved contrast-enhanced time-resolved MR angiography on a small bore 3T MRI system (SS 613), B-0546
- Riedl C., Schoder H., Ulaner G.A., Saidon T., Juluru K., Weber W., Pinker K.**
Is whole body ¹⁸FDG-PET/CT including the extremities routinely warranted in melanoma patients? (SS 716), B-0705
- Riibak M.**
Abdominal emergencies: friends and enemies: Life teaches us case by case (SF 17b), A-905
- Riklund K.**
Marie Curie Honorary Lecture: Hybrid imaging: the story so far and what to expect next (HL 2), A-486
- Riklund K.**
eHealth in radiology: policies, practices, pitfalls, potential: Chairperson's introduction (ESR/EU), A-771
- Rimola J., Alfaro I., Vas D., Ordás I., Ricart E., Panes J.**
Established bowel damage detected on MR enterography in patients with Crohn's disease in complete endoscopic remission (SS 1901c), B-1537
- Rimola J.**
Gastrointestinal radiology: A. Inflammatory bowel disease (E³ 721), A-281
- Rimola J.**
My three top tips for abdominal imaging: Crohn's disease (SF 12a), A-527
- Ringl H.**
Dual-energy CT of the abdomen: the time is now: B. Applications for genitourinary system (E³ 1226), A-534
- Rio G., Lima M., Gil R., Horta M., Cunha T.M.**
T2 hyperintense myometrial tumours: can MRI features differentiate leiomyomas from leiomyosarcomas? (MY 3), B-0380
- Riondel F.**
EFRS meets Switzerland and Portugal: (Helv)ethic: from a project to a new culture (EM 4), A-498
- Rippel K., Ordu D., Rollandi L., Kleffel T., Scheurig-Muenkler C., Kröncke T., Schwarz F.**
When ultrasound is not enough: predicting downstream utilisation of CT after ultrasound in patients with acute abdomen (SS 1017), B-0945
- Rischpler C.**
Non-oncological hybrid imaging: case-based: Cardiac hybrid imaging indications: case-based (ESHI), A-581
- Riva L., Ippolito D., Talei Franzesi C., de Vito A., Maino C., Cangiotti C., Santalco A., Sironi S.**
Image quality and radiation dose sparing of CT angiography for TAVI planning with low-kV, low contrast medium volume and model-based iterative reconstruction compared to standard CTA (SS 215), B-0024
- Riva L., Ippolito D., Talei Franzesi C., de Vito A., Cangiotti C., Maino C., Sironi S.**
Model-based iterative reconstruction algorithm in low-dose CT pulmonary angiography in emergency setting: dose reduction and diagnostic quality images (SS 704), B-0634
- Riva S., Guzzardi G., Barini M., Valenti M., Carriero A., Pelle M.**
IPF: diagnosis and follow-up using CT fibrosis score, correlation with clinical and functional data in a cohort of patients in therapy with pirfenidone or nintedanib (MY 5), B-0410
- Rivas Loya R., Overbosch J., Kraeima J., Dierckx R.A.J.O., Jutte P.C., Van Ooijen P.M.**
Ablation zones after radiofrequency ablation in 16 patients with atypical cartilaginous tumours (SS 1809), B-1345
- Rivosecchi F., Caruso D., De Santis D., Bellini D.M., Panvini N., Rengo M., Laghi A.**
CT-derived texture analysis in predicting tumoral response to immunotherapy in patients with lung cancer and correlation with iRECIST (SS 316), B-0357
- Rizzo S.**
Novelties in oncologic imaging: B. Radiomics: the role of imaging (E³ 126), A-028
- Robb F.J.**
AIR Coil Technology: the next breakthrough in MRI (SY 2)
- Robben S.G.F.**
Paediatric: C. Paediatric abdominal imaging (E³ 1823), A-955
- Robinson L.**
Making the most of social media: Improving patient engagement through social media (EFRS WS), A-792
- Robinson P.**
Imaging the hip and thigh: B. Groin pain in the athlete: what causes it and what does imaging contribute? (RC 910), A-416
- Robinson P.**
Small joints: D. Pubic symphysis (E³ 1119), A-515
- Robinson S.**
Case-Based Diagnosis Training - Part 1: Maxillofacial (CB 1), A-964
- Rocha T.O., Albuquerque T.C.V., Nather J.C., Garrido C.S., Elias Jr J., Tucci Jr S., Wang Z., Westphalen A.C., Muglia V.F.**
Histogram analysis of adrenal lesions with a single measurement: feasibility and incremental value for diagnosing adenomas (SS 1007), B-0879
- Rockall A.G.**
Monitoring response: the essential guide for all radiologists: A. RECIST made easy (RC 816), A-343
- Rockall A.G.**
Gynaecological cancers: Keynote lecture (SS 707), K-14
- Rodrigues dos Santos M., Rocha N., Silva A.**
Dose analytics over large DICOM datasets: a case study in mammography and a quest for meta data quality (SS 214), B-0139
- Rodrigues dos Santos M.**
Indexing DICOM metadata from medical imaging repositories: opportunities and challenges (SS 714), B-0743
- Rodriguez Ruiz A., Gubern-Mérida A., Gennaro G., Chevalier M., Zackrisson S., Andersson I., Sechopoulos I., Mann R.M.**
Can the breast cancer screening case-load be reduced by deep-learning based identification of normal cases? An international multi-centre retrospective analysis (SS 1902b), B-1628

Authors' Index

Roemer F.W.

MRI of articular cartilage and bone: areas of imaging confusion and practical solutions: B. Osteochondral injury, subchondral fractures and traumatic bone oedema: what is important and how do I describe it (RC 110), A-031

Rohde S.

Distant metastases of head and neck cancer: B. Is morphologic imaging enough to stage patients with head and neck tumours before therapy? (E³ 926), A-435

Rohrer L., Vial Y., Meuli R., Alamo-Maestre L.

Prenatal imaging of anorectal malformations (MY 18), B-1491

Rohrmeier A., Syväri J., Diefenbach M., Franz D., Ruschke S., Dieckmeyer M., Kirschke J.S., Karampinos D., Baum T.

Vertebral bone marrow composition: assessment of age and gender dependency using chemical shift encoding-based water-fat MRI (SS 610a), B-0441

Romano S.

Gastrointestinal: 'the gut': Oesophagus (BS 2), A-063

Romano V., Doronzio V., Pedalino S., Giannini V., Mazzetti S., Giacobbe A., Muto G., Russo F., Regge D.

Comparison of biopsy and pathological Gleason score in patients with biopsy-proven prostate cancer (MY 3), B-0378

Romano V., Tabone E., Appendino E., Mazzetti S., Giannini V., Giacobbe A., Muto G., Russo F., Regge D.

Comparison of prostate cancer detection rates between MR-targeted and saturation TRUS-guided biopsy (SS 1516), B-1246

Romanucci G., Brunelli S., Caneva A., Montemezzi S.A., Caumo F.

A prospective study on uncertain biological potential lesion (B3) overtreatment in tomosynthesis breast screening: role of tomosynthesis-guided biopsy (DBT-VAB) (SS 1402a), B-1088

Romero S., Raya Povedano J.L., Cara Garcia M., Santos A.L., Pedrosa Garriguet M.

Comparison of double-reading of mammography-2D with single-reading of tomosynthesis plus synthesised mammography: is it time to change the way we work in breast-screening programme? (MY 16), B-1275

Rondenet C., Millet I., Corno L., Boulay Coletta I., Taourel P., Zins M.

CT signs of bowel necrosis in CL-SBO (SS 1017), B-0948

Ronot M.

Diffuse liver disease: A. Assessment and quantification of fat in NAFLD (E³ 320), A-088

Ros P.R.

Imaging of benign liver lesions: still difficult?: B. Liver haemangiomas and mimickers (RC 901), A-383

Ros P.R.

Hybrid imaging in oncology: MR/PET of pelvic cancers (SF 15a), A-744

Ros P.

The new horizon for radiology: Transforming the integrated diagnosis (ID) opportunity into the Diagnostic Institute (DI) innovative change management (NH 14), A-724

Rosa F., Basso L., Resaz R., Secondini L., Verardo I., Grillo F., Prono V., Eva A., Neumaier C.

MRI liver adenoma subtyping in animal models of glycogenosis type Ia (SS 1001a), B-0837

Rosendahl K.

Paediatric radiology for the general radiologist: B. Typical MRI applications in paediatric musculoskeletal imaging (E³ 1521), A-732

Rossi Espagnet M., Bassanelli E., Napolitano A., Pietrafusa N., De Palma L., Specchio N., Longo D.

Comparison between different post-processing techniques in the identification of focal cortical dysplasias in children with pharmacoresistant epilepsy (SS 1811a), B-1404

Rossi Espagnet M., Bassanelli E., Pietrafusa N., Figà-Talamanca L., De Palma L., Longo D., Napolitano A.

Comparison between BOLD-fMRI and Stereo-EEG in the pre-surgical evaluation of language dominance in children affected by pharmacoresistant epilepsy (SS 1811a), B-1406

Rosti C., Cellina M., Fetoni V., Pirovano M., Ciocca M., Oliva G.

Acute optic neuritis (ON): can magnetic resonance (MRI) in the acute setting help in determining the aetiology? (SS 311), B-0284

Rottoli F., De Mattia C., Sutto M., Colombo P.E., Rampoldi A., Torresin A.

Low-dose protocol in prostatic artery embolisation (PAE): dose assessment (SS 213), B-0128

Rousseau H.

TEVAR/EVAR: where we are and where we are going: A. TEVAR (E³ 526b), A-238

Rovira-Cañellas A.

Current guidelines and diagnostic criteria in multiple sclerosis (MS): Chairperson's introduction (SA 5b), A-208

Rovira-Cañellas A.

My three top tips for neuroimaging: Multiple sclerosis (SF 15c), A-763

Rowley H.A.

Gadolinium: image wisely: A. Intracranial gadolinium deposition: update and perspectives (PS 1227), A-591

Rozalli F.I., Fadzli F., Krisnan T., Rahmat K., Tan L.K., Shahrizaila N., Ramli N.

MRI assessment of the microstructural integrity of the peripheral nerves in Charcot-Marie-Tooth disease (SS 710a), B-0617

Rubbert C., Mathys C., Eickhoff S.B., Hoffstaedter F., Südmeyer M., Hartmann C.J., Turowski B., Schnitzler A., Caspers J.

Detection of Parkinson's disease based on resting-state inter-network functional connectivity using machine learning (SS 1511), B-1237

Rubin C.

Establishing competence in radiology: a UK perspective (Part 1) (PI 1), A-461

Rubtsov R., Kehler L., Giannakis A., Kreuter M., Eichinger M., Weinheimer O., Maier-Hein K., Kauczor H.-U., Heussel C.P.

Fully automated assessment of HRCT images for follow-up of IPF (MY 5), B-0402

Ruder T.

Why do I miss fractures in emergency?: C. Missed musculoskeletal injuries in whole-body MDCT examinations (RC 1617), A-839

Rudolph M., Baur A., Haas M., Mahjoub S., Cash H., Asbach P., Hamm B., Penzkofer T. Learning the language of PI-RADS version 2: correlation between prostate MRI lexicon terms and malignancy (SS 1807a), B-1357

Rueppel S., Lyschik S., Halfmann M.C., Benz S., Eichstädt J., Düber C., Kreitner K.-F., Emrich T., Hahn F.

T1 based myocardial tissue characterisation in healthy volunteers: reference values for novel parameters of tissue dispersion (SS 1003), B-0973

Runge V.

Gadolinium deposition: is it harmful?: Clinical recommendations in consideration of the EMA's pharmacovigilance and risk assessment committee recommendation for suspension of linear agents (SF 4), A-139

Runge V.

Clinical recommendations in context to current health authority regulations (SY 9)

Rusandu A., Ødegård A., Engh G.C., Olerud H.M.

80kV vs 100kV in the CT pulmonary angiography protocol: an evaluation of the impact on patient dose and image quality on two CT machines (MY 17), B-1297

Ruschi F.

Whole-body multidetector CT in polytrauma patients: incidence and clinical significance of missed diagnoses (SS 317), B-0298

Ryan A.G.

Pulmonary embolism: a joint challenge for diagnostic and interventional radiology!: Chairperson's introduction (RC 1209), A-587

Ryan J., Hollywood A., Stirling A., O' Hora L., Glynn M., Brady A., Dolan A., Lawler L., Bolster F.

Making the best of clinical radiology: a single-institution review of imaging referral appropriateness including cumulative monetary and dose estimates for inappropriate scans (SS 205), B-0176

Rychina I., Rienmüller T., Makarenko V., Berezitskiy V., Tikhonov A., Oreshkova J.A., Frank P., Bockeria L., Rienmüller R.

Investigation of a roll pump contrast media injector for individually adapted iodine concentrations (SS 1904a), B-1557

S

Sabet H.A.S., El Kady R.M., Omar N.N., Abbas A.M.

Diagnostic value of MR perfusion in characterisation of complex adnexal masses (SS 607), B-0473

Sabet S., Server S., Karalok I., Namal E.K., Inan N., Tokat Y.

Efficacy of intravoxel incoherent motion MRI in discrimination of metastatic vs non-metastatic abdominal lymph nodes in hepatobiliary malignancies: a correlation study with PET-CT (MY 3), B-0379

Sahan M.H., Inal M., Burulday V., Kultur T.

Evaluation of tendinopathy of the long head of the biceps tendon by strain and shear wave elastography (SS 1010), B-0954

Sala E.

The ten-minute abdominal MRI: make the dream come true!: Ovaries (SF 8c), A-352

Sala E.

Radiomics: what is it and how can we use it?: Radiomics: biological correlation (NH 12), A-575

Authors' Index

- Sala E.**
Update on functional genitourinary MRI: C. Uterus (E³ 1526b), A-751
- Sala E.**
Quantitative imaging in oncology: D. Imaging heterogeneity and genomic variability in ovarian cancer (E³ 1626b), A-865
- Salapura V.**
Highlighted Lectures: Routine cartilage evaluation and novel approaches (TF 1), A-689
- Salemi I., Ippolito D., Talei Franzesi C.R., Maino C., Cangioti C., Sironi S.**
Improved image quality of whole body low-dose CT study combined with iterative model reconstruction algorithms for follow-up of oncologic patients (SS 1016a), B-0897
- Salerno S., Tudisca C., Granata C., Origgi D., Moro L., Barbagallo M., Corsello G., Villani A.**
Radiation use in paediatric age: are paediatricians updates of the state of the art legislation? (MY 18), B-1495
- Salgado R.**
From diagnosis to prognosis: how does cardiac imaging affect patient outcome?: C. In coronary artery disease (RC 503), A-195
- Salgado R.**
Open and closed: the role of radiology in treatment of valvular heart disease: What to measure prior to transcatheter aortic valve implantation (TAVI) (E³ 24C), A-484
- Salgado R.**
Cardiac imaging: B. Imaging cardiac valves (E³ 1721), A-875
- Sali L., Ventura L., Borgheresi A., Delsanto S., Mantellini P., Mascacchi M., Zappa M., Grazzini G.**
Patient experience of screening CT colonography with reduced and full bowel preparation in a randomised trial (SS 601b), B-0521
- Saltybaeva N., Alkadhi H.**
Overranging dose reduction by dynamic collimators: evidence from clinical practice (SS 213), B-0123
- Saltybaeva N., Alkadhi H.**
Online platform for fast and accurate calculation of fetus dose in CT (SS 313), B-0310
- Saltybaeva N.**
Clinical diagnostic reference levels for x-ray medical imaging: The concept of local diagnostic reference levels (DRLs) (EU 3), A-506
- Samara E.**
Patient-specific dosimetry: Chairperson's introduction (RC 1713), A-923
- Samei E.**
Dose reduction and image quality implications of iterative image reconstruction in CT: C. Image quality assessment of iterative reconstruction: pitfalls and future directions (RC 1513), A-785
- Sampangi S., Shivalingappa S., Ashok Kumar M., Desai I., Kesari A., Basavalingu D., Verma A., Kallur K., Asokan P.**
Role of elastography in the characterisation of subcentimeter breast lesions (SS 302), B-0270
- Samreen N., Lee C., Adler K., Bhatt A., Hieken T., Zingula S., Glazebrook K.N.**
Utility of diffusion in evaluating chest wall invasion of breast tumours (SS 602), B-0504
- Sanchez J., de Bazelaire C.**
Interest of breast MRI surveillance in women with a personal history of breast invasive lobular carcinoma (SS 1902a), B-1610
- Sanchez-Salas R.**
Focal treatment of prostate cancer: Focal treatment of prostate cancer: opportunities, challenges and indications (SF 9a), A-396
- Sangma S., Gorski U., Yadav M., Yadav T., Khandelwal N.**
Treatment of varicose veins with endovenous laser ablation using low linear endogenous density (SS 1815), B-1334
- Santiago I.**
Imaging of benign liver lesions: still difficult?: A. Hepatic cysts: always simple? (RC 901), A-382
- Santos J.**
Balancing dose and image quality in CT: Keynote lecture (SS 314), K-07
- Santos J.**
EFRS meets Switzerland and Portugal: Introduction: Across Portugal (EM 4), A-495
- Santos J.M.M.M., Mourão de Abreu A., Garcia M.R.T., Franceschi L., Matos L.L., Silva C.J., Gebrim E.M.M., Gomes R.L.E.**
Oral cavity cancer staging by CT for the new TNM-8: using an extrapolated measurement to evaluate the depth of invasion (SS 1008), B-0902
- Santos R.A.M., Barreiro R.**
Abdominal and lumbar muscle evaluation by ultrasound (SS 1014), B-0966
- Santos R.A.M., Girão A.C., Figueiredo J.P.**
Relationship between body fat by DEXA and cardiovascular risk factors (MY 17), B-1313
- Santos R.A., Armada-da-Silva P.**
Vastus lateralis stiffness assessed by SSI elastography (SS 1014), B-0967
- Šaponjski D., Djuric Stefanovic A.**
Assessment of local vascular invasion in pancreatic carcinoma by MDCT using the angle measuring tool (SS 1901b), B-1527
- Sarabhai T., Stebner V., Wetter A., Kimmig R., Forsting M., Umutlu L., Grueneisen J.**
Simultaneous multiparametric PET/MRI for the assessment of therapeutic response to chemotherapy or concurrent radiochemotherapy of cervical cancer patients: preliminary results (SS 1816), B-1371
- Sardanelli F.**
MRI for early detection, staging and management of breast cancer: A. Preoperative staging with MRI: did the MIPA trial solve all issues? (RC 1202), A-554
- Sardanelli F.**
How to write a scientific paper and how to get it published: The study design and the structure of an original article (ESR Publication), A-931
- Sartoris R., Vilgrain V., Rautou P., Ronot M.**
CT-based liver surface nodularity quantification for the detection of clinically significant portal hypertension in cirrhotic patients (SS 601a), B-0427
- Sasiadek M.**
Dementia and movement disorders: A. MR contribution to diagnosis and differential diagnosis in dementia (E³ 821), A-302
- Sastoque G J.M., Lombardo S., Espejo Herrero J.J., Dominguez Paillacho I., Perez Montilla M., Zurera Tendero L.J.**
Performance and safety of pancreas biopsy: are there more complications made by routes of risk? (MY 9), B-0823
- Sato M., Ogura T., Yamanouchi S., Hayashi N., Watanabe H., Doi K.**
Development of a new image display system for angiography based on detection of electroencephalogram signals from operator's brain (SS 609), B-0451
- Sato Y., Tominaga J., Mori N., Matsuda Y., Okada Y., Takase K.**
CT evaluation of small pulmonary vessel area in patients with bronchiolitis obliterans syndrome after lung transplantation (SS 1904a), B-1550
- Sauer M., Pompe R., Tennstedt P., Budaues L., Salomon G., Adam G., Beyersdorff D.**
Correlation of short- and long-term urinary continence after radical prostatectomy with findings of preoperative multiparametric prostate MRI (SS 1907a), B-1569
- Saukko E., Grönroos J.M., Salminen P., Henner A., Nieminen M.T.**
Patient radiation dose and fluoroscopy time during ERCP: a single-centre retrospective study of influencing factors (SS 714), B-0744
- Saukko E., Wirtanen M., Kortelainen K.**
Does the post-processing annotation of images become a standard practice in digital radiography today? (SS 1814), B-1442
- Sauppe S., Kuhm J., Brehm M., Paysan P., Seghers D., Kachelrieß M.**
Sliding organ motion regularisation for motion-compensated cone-beam CT (CBCT) in image-guided radiation therapy (IGRT) (SS 1813), B-1432
- Sawicki L.M., Kirchner J., Grueneisen J., Ruhlmann V., Schaarschmidt B.M., Forsting M., Herrmann K., Antoch G., Umutlu L.**
Comparison of 18F-FDG PET/MRI and MRI alone for whole-body staging of 71 women with suspected recurrent pelvic cancer: a follow-up study (SS 707), B-0652
- Sbarra M., Miccò M., Gui B., Rodolfo E., Valentini A.L., Manfredi R.**
MRI predictive factors for vaginal stenosis in patients with cervical cancer after ChemoRadiation Therapy (CRT) (SS 607), B-0471
- Scaglione M.**
Mass casualties: Chairperson's introduction (PC 4), A-120
- Scaperrotta G.**
Changing the breast biopsy approach in a national cancer institute: impact on clinical routine (SY 10)
- Scarsbrook A.**
Merging the best: hybrid imaging: A. Hybrid imaging with SPECT/CT (RC 106), A-058
- Schaarschmidt B.M., Grueneisen J., Stebner V., Sawicki L.M., Buchbender C., Heusch P., Umutlu L., Antoch G., Poeppel T.**
Integrated ¹⁸F-FDG PET/MR for the initial detection of lymph node metastases in malignant melanoma: is sentinel lymph node biopsy still necessary? (SS 716), B-0706
- Schabel C., Vernuccio F., Ramirez Giraldo J., Nikolaou K., Marin D.**
Optimal energy level for renal lesion detection and characterisation on virtual monoenergetic images (SS 1007), B-0881
- Schabel C., Nikolaou K., Hurwitz L.**
Computed tomography CT: derived fractional flow reserve improves reader confidence for coronary CT angiography (SS 1803), B-1453

Authors' Index

Schaefer-Prokop C.M.

Patterns of pulmonary toxicity: A. Drug-induced lung disease (E³ 1526a), A-737

Schäfer F.M., Asbach P., Haas M., Hamm B., Baur A.

Prevalence and significance of incidental extraprostatic findings in patients undergoing magnetic resonance imaging of the prostate for detection of prostate cancer (SS 307), B-0251

Schäfer J.P.

No time to lose: aortic dissection – revisited: Endovascular treatment in aortic dissection (E³ 24A), A-078

Schawkat K., Sah B., Delso G., Ter Voert E., Schneider P., Reiner C.S., Huellner M., Veit-Haibach P.

Intravoxel incoherent motion diffusion-weighted MR imaging in gastro-esophageal cancer: correlation with ¹⁸F-FDG-PET and histopathology (SS 701b), B-0708

Schawkat K., Eshmuminov D., Lengggenhager D., Endhardt K., Vrugt B., Boss A., Petrowsky H., Clavien P.A., Reiner C.S.

Non-invasive preoperative quantification of pancreatic fibrosis and lipomatosis: correlation of magnetisation transfer imaging and multi-gradient echo MRI with histopathology (SS 1001a), B-0839

Scheffmann Olloni S., Villadsen N.

MRI of children aged 4-9 without anaesthesia using communication at the children's cognitive level (SS 614), B-0551

Schellhaas B., Hammon M., Strobel D., Görtz R., Cavallaro A., Janka R., Neurath M.F., Uder M., Seuss H.

Diagnostic accuracy and interobserver agreement: CEUS-LI-RADS vs MRI-LI-RADS (MY 15), B-1260

Schenk A., Chlebus G., Meine H., Thoduka S., Abolmaali N.

Deep learning for liver segmentation and volumetry in late phase MRI (SS 1805), B-1383

Schenk J.

Imaging of the brain in preterm infants: US screening in preterm infants: prognostic value from a clinical point of view (SF 12b), A-539

Scherr M.K.

Imaging of 'foreign bodies': C. Body packing: what to know about imaging and when should we suspect early complications? (RC 1317), A-647

Schiavone M.

Complementary diagnostic role of shear wave elastography (SWE) in assessment of thyroid nodules during ultrasound examination (SS 608), B-0489

Schima W.

My three top tips for abdominal imaging: Acute pancreatitis (SF 12a), A-526

Schima W.

New challenges of pancreatitis: A. Understanding the Atlanta 2012 classification of acute pancreatitis (E³ 1322), A-675

Schima W.

Case-Based Diagnosis Training - Part 2: Gastrointestinal (CB 2), A-977

Schimmöller L.

When to use hybrid imaging: Imaging prostate cancer: MRI or PSMA-PET/CT? (ESR/ESHI), A-201

Schindera S.T.

Single-dual-multi-energy CT: C. Clinical need of multi-energy CT (RC 113), A-036

Schindera S.T.

Strategies for dose reduction in computed tomography: from technical concepts to clinical practice: Dose reduction and image quality: when low is too low (EU 2), A-252

Schlemmer H.-P.

Imaging of the prostate: C. Imaging of PSA recurrence (RC 807), A-318

Schlemmer H.-P.

Do we need dynamic contrast enhancement (DCE) in prostate mpMRI?: Chairpersons' introduction (part 1) (PS 527), A-204

Schlemmer H.-P.

Focal treatment of prostate cancer: Chairperson's introduction (SF 9a), A-395

Schlemmer H.-P.

A multidisciplinary approach to prostate cancer: can we make a difference?: B. The radiologist: evidence-based use of multiparametric MRI (RC 1716), A-918

Schlett C.L.

The machines are coming: how will they change our future?: Big data for deep learning (NH 5), A-173

Schmaranzer F., Lerch T., Todorski I., Haefeli P., Hanke M., Werlen S., Siebenrock K., Tannast M.

Cartilage damage assessed with dGEMRIC occurs at the zone of 3D CT-based impingement simulation: a pilot study (SS 310), B-0303

Schmaranzer F., Haefeli P., Hanke M., Lerch T., Siebenrock K., Werlen S., Tannast M., Büchler L.

Comparing dGEMRIC and clinical outcome 6 years after FAI surgery with versus without microfracturing: a controlled pilot study (SS 610b), B-0539

Schmaranzer F., Degonda C., Lerch T., Todorski I., Siebenrock K., Cullmann J.L., Tannast M., Zheng G.

3D MR-based simulation of hip impingement is as accurate as 3D CT-based impingement simulation (SS 1410), B-1124

Schmidt Kobbe S., Daire J., Sciarra A., Leporq B., Van Beers B., Sempoux C., Pastor C.

Perfusion quantification and hepatic function with Gd-EOB-DTPA: hepatic fibrosis and hepatocellular transport (SS 201a), B-0010

Schneider G., Bucker A., Fenzl L.

Sampling errors in image-guided liver biopsies: depiction of the biopsy site on immediate post-interventional CE MRI (MY 9), B-0832

Schneider G., Bucker A., Massmann A.

High temporal resolution dynamic CE MRA in detection of reperfusion pulmonary arteriovenous malformations (PAVMs) in HHT-patients (SS 1815), B-1329

Schneider J., Raimann A., Boni-Mikats A., Krssak M., Klepochová R., Häusler G., Raum K., Patsch J.M.

Quantitative bone ultrasound: low sound wave propagation in cortical bone as a novel, non-invasive imaging biomarker in children and adolescents with hypophosphatemic rickets (SS 312), B-0345

Schöllnast H.

Functional imaging in oncology beyond morphology: where are we now?: B. CT perfusion techniques (RC 516), A-217

Schotten S., Meyer F., Mähringer-Kunz A., Weinmann A., Düber C., Kloeckner R.

Liver vein infiltration in patients with hepatocellular carcinoma: impact on survival (SS 301a), B-0196

Schoepf U.J.

CT imaging on the edge: kV adapted contrast administration (SY 15)

Schrading S.

Rethinking ductal carcinoma in situ (DCIS): B. Diagnosing DCIS (RC 1302), A-634

Schregel K., Tsogkas I., Behme D., Peter C., Maier I., Liman J., Knauth M., Psychogios M.

Collateral scores and perfusion parameters for outcome prediction in acute ischaemic stroke: how many scans are needed? (SS 1011a), B-0923

Schwaiger B.J., Gersing A., Hammel J., Mei K., Kopp F.K., Rummeny E.J., Wörtler K., Baum T., Noel P.B.

Three-material decomposition with dual-layer spectral detector CT compared to MRI for the detection of bone marrow oedema in patients with acute vertebral fractures (SS 610b), B-0529

Schwaiger B.J., Gersing A., Münzel D., Dangelmaier J., Prodinger P.M., Suren C., Rummeny E.J., Wörtler K.

MR imaging with metal artefact reduction for the differentiation between patients with and without infected total hip arthroplasty (SS 1410), B-1120

Sciuk A., Kidzinski R., Frankowska E.

Liver fibrosis vs cholangiocarcinoma MRI appearance and distinguishing features based on the DWI and ADC map (SS 701a), B-0604

Sconfienza L.M.

The radiological investigation of musculoskeletal tumours: A. Radiographs and ultrasound (RC 1610), A-841

Screaton N.J.

CT of vascular pulmonary diseases: A. CT imaging of pulmonary hypertension (E³ 218), A-068

Screaton N.J.

Pulmonary circulation and venous imaging: Keynote lecture (SS 1815), K-25

Seah J.C.Y., Tang J.S.N., Gaillard F.

Peering into the darkness: visualising what neural networks learn through generative deep learning (SS 1805), B-1385

Sebuodegård S., Moshina N., Waade G.G., Hofvind S.

The influence of breast compression on re-attendance in a population-based screening programme (SS 214), B-0134

Sebuodegård S., Hofvind S.

Interval breast cancer rates and histopathologic tumour characteristics after false-positive screening result in a population-based screening programme (SS 702), B-0677

Sechopoulos I.

Patient-specific dosimetry: A. Breast imaging dosimetry (RC 1713), A-924

Sedlacek O.L.

Lung cancer in the era of molecular oncology and immune therapy: C. PD-L1 positive lung tumours (E³ 118), A-057

Sefic-Pasic I., Dananovic A., Bukvic M., Terzic S., Agovic M., Vegar-Zubovic S.

Respiratory distress syndrome in neonates-comparison between lung ultrasound and chest x-ray (SS 1412), B-1163

Authors' Index

Sefidbakht S., Mina L., Ravanfar Haghighi R., Zeinali B., Saeedi-Moghadam M., Zarei F., Haseli S.

Implementing strategies for a better quality fetal MRI by technologist training and the effect on radiologist satisfaction (SS 1907b), B-1668

Sefidbakht S., Bagheri S., Etemadi Z., Zeinali B., Saeedi-Moghadam M., Asadi N., Vafaei H.

Added value of foetal MRI in evaluation of lung anomalies (SS 1907b), B-1669

Seidensticker M.

Percutaneous interventional procedures: a practical guide: C. Post-procedure follow-up and complication management (RC 809), A-367

Seker F., Pfaff J., Neuberger U., Nagel S., Ringleb P.A., Bendszus M., Möhlenbruch M.A.

Mechanical thrombectomy of M1 and M2 segment occlusions: a single-center experience with 546 patients (SS 611), B-0508

Seliverstova E., Seliverstov Y., Krotenkova M., Konovalev R., Sergeeva A.N., Illarionov S., Morozova S.

Structural and functional changes in resting brain activity in neurodegeneration according to VBM and rsfMRI comparison (SS 1411a), B-1035

Seo B.K., Park E.K., Kwon M., Ko C.S., Cha J., Cho K.R., Woo O.H.

Low-dose perfusion CT for quantification of tumour vascularity in breast cancer: correlation with prognostic biomarkers (SS 1802b), B-1415

Seo J.B.

The machines are coming: how will they change our future? Artificial intelligence applications in radiology (NH 5), A-172

Seo J.B.

Chronic obstructive pulmonary disease (COPD): B. Quantitative imaging biomarkers (RC 804), A-306

Seo M., Lee S., Choi J., Kim D.

Usefulness of spleen size and volume measured by computed tomography for predicting clinical outcome in chronic myeloid leukemia (SS 716), B-0707

Seow P., Ramli N., Hernowo A.T., Narayanan V., Wong J.H.

Lipid mapping for grading of gliomas (SS 211), B-0091

Seow P., Veeramuthu V., Narayanan V., Wong J.H., Hernowo A.T., Tan L., Ramli N., Fadzli F.

Neurometabolite alteration in the acute phase of mild traumatic brain injury (mTBI): an in vivo proton magnetic resonance spectroscopy (MRS) study (SS 1911a), B-1597

Serena E., Vedovo F., Bucci S., Trombetta C., Bertolotto M., Cova M.A.

Neoclititoris size and location: a preliminary pelvic MRI study (SS 1907b), B-1664

Sertorio F., Damasio M., Incarbono V., Wong M., Pistorio A., Mattioli G., Magnano G.

Non-contrast-enhanced MR angiography for detecting crossing renal vessels in infants and young children (< 6 years old): comparison with CE angiography and surgery (SS 612), B-0580

Seuri R.

Dose reduction: tips and tricks: B. Diagnostic reference levels in paediatric imaging: international recommendations (RC 912), A-390

Shahabpour M., De Maeseneer M.

Upper extremity: B. Wrist (E³ 919), A-445

Shaikh S.M.

To evaluate the role of 68Ga DOTA NOC receptor PET CT in detection of unknown primary neuroendocrine tumours (SS 1006), B-0984

Shaikh S.M.

To evaluate the role of 68Ga-PSMA PET-CT in patients with newly diagnosed high-risk prostate cancer (SS 1407), B-1070

Shao D.

Differentiation and diagnosis of benign and malignant testicular lesions using ¹⁸F-FDG PET/CT (MY 4), B-0399

Shao X., Xu W., Li C., Zhao X., Zhang W.

MRI findings of sacroiliac joint disorders in SAPHO syndrome (SS 1910), B-1617

Sharma J.P., Singh T., Singh K., Mohapatra I., Singh M.

Percentage signal recovery (PSR) calculated from dynamic susceptibility contrast perfusion MRI: accuracy in differentiating various enhancing intracranial mass lesions (SS 211), B-0095

Sharma N., Wallis M., Newcombe R.G., Puri S., Al-Attar M., Pascaline S., Hajaj M., Elsberger B., Goyal A.

Can documenting the number of abnormal nodes at axillary ultrasound accurately predict axillary nodal burden (SS 302), B-0275

Sharma N., Rajan S., Dall B.

Does breast MRI have a high negative predictive value for identifying residual axillary metastases in patients treated with neoadjuvant chemotherapy (SS 1802a), B-1397

Sheehan J.A., Durganau R., Tarmey T., O'Sullivan G.J., Sheppard D.

US-guided percutaneous renal biopsy: a 10 year retrospective analysis (MY 9), B-0828

Shehata M., Abou El-Ghar M.E., El-Diasty T., EL-Baz A.

An integrated CAD system of DWI MRI and laboratory biomarkers in the diagnosis of kidney transplant dysfunction (SS 1007), B-0887

Shelmerdine S.C.

Juvenile idiopathic arthritis (JIA): A. Conventional radiography, still a helpful method? (E³ 426), A-152

Shelmerdine S.C., Hickson M., Sebire N.J., Arthurs O.J.

Post-mortem magnetic resonance imaging appearances of foeticide in perinatal deaths (SS 1412), B-1169

Shelmerdine S.C., Mcdowell A., Carmichael D., Arthurs O.J.

High-resolution isotropic diffusion-weighted imaging in neonatal death investigation (SS 1412), B-1170

Shi R., Wu R., An D., Chen B., WU L., Xu J.

Global and segmental cardiac magnetic resonance tissue tracking of hypertrophic cardiomyopathy: how do hypertrophy and fibrosis contribute to myocardial deformation? (SS 1403), B-1158

Shin H., Minkler M., Jaeger L., Caliskan C., Dettmer S., Vogel-Claussen J., Wacker F., Prasse A.

Temporal subtraction of serial-computed tomography images for visualisation and quantification of disease progression in idiopathic pulmonary fibrosis (SS 304), B-0237

Shiner N.

The use of moulage to prepare first year diagnostic radiography students for the sight of open wounds: initial findings of a doctoral pilot study (SS 1414), B-1150

Shiri I., Geramifard P., Abdollahi H., Shayesteh S., Hajianfar G., Pouraliakbar H., Mohammadzadeh A., Bitarafan-Rajabi A.

Application of radiomics and artificial intelligence in survival prediction of lung cancer patients (SS 605), B-0477

Shiri I., Geramifard P., Abdollahi H., Bitarafan-Rajabi A., Mohammadzadeh A., Pouraliakbar H.

Multimodality radiomics signature analysis improves prediction power against Stand-Alone analysis of PET, CT and MRI images (SS 605), B-0478

Shiri I., Geramifard P., Bitarafan-Rajabi A., Mohammadzadeh A., Pouraliakbar H., Shayesteh S.P.

A deep learning-based radiomics model for classification of mammography mass lesions in breast cancer patient (SS 716), B-0700

Shiri I., Geramifard P., Bitarafan-Rajabi A., Mohammadzadeh A., Pouraliakbar H.

Deep convolutional neural network (D-CNN) for efficient and automatic lung cancer detection (SS 713), B-0734

Shiri I., Hajianfar G., Abdollahi H., Shayesteh S., Pouraliakbar H., Bitarafan-Rajabi A., Mohammadzadeh A., Geramifard P., Sanaat A.

MRI delta-radiomics feature robustness and reproducibility: the impact of image registration and day-to-day repeat-ability in GBM cancer patient (SS 713), B-0739

Shiri I., Hajianfar G., Abdollahi H., Abdollahi H., Pouraliakbar H.R., Bitarafan-Rajabi A., Mohammadzadeh A., Geramifard P., Sanaat A.

Wavelet-based radiomics texture features stability in MRI of GBM patients: a test-retest study (SS 713), B-0740

Shorikov M., Lapteva M., Polyakov P., Frantsev D., Sergeeva O.N., Dolgushin B.
Gd-BOPTA excretion MRI analysis in patients with compromised and non-compromised bile ducts (SS 601a), B-0423

Shorikov M., Tarachkova E., Panov V., Tyurin I.

Quantitative MRI analysis of cervical cancer parametrium invasion (SS 1816), B-1369

Shults E.

Primary diagnosis: when and why to use perfusion? (SY 18)

Shwaky N.O.

Transverse comparisons between ultrasound and radionuclide parameters in children with pelviureteric junction obstruction (MY 18), B-1501

Si-Mohamed S.A., Sigovan M., Normand G., Coulon P., Bar-Ness D., Bousset L., Douek P.

Multiphase urinary tract imaging with dual contrast using spectral photon-counting CT (SS 1807b), B-1467

Siauve N.

Placental imaging: how, when and why? Modern MRI of the placenta (SF 16), A-814

Sidhu P.S.

Update on the EFSUMB guidelines for the use of CEUS (SY 23)

Authors' Index

- Siedek F., Giese D., Weiss K., Ekdawi S., Brinkmann S., Schröder W., Bruns C., Maintz D., Haneder S.**
4D flow MRI for the analysis of celiac trunk and mesenteric artery stenoses (MY 7), B-0790
- Siegel E.L.**
Artificial intelligence: a strategic view: Keynote lecture (SF 6), A-980
- Siepmann S., Ziegeler K., Beck A., Diekhoff T., Bach A., Hamm B., Hermann K.**
Dose optimisation in digital radiography of the hands: evaluation of the GC85A low-dose technology (SS 310), B-0299
- Sigl B., Jockwitz C., Eickhoff S., Hofstaedter F., Rubbert C., Amunts K., Caspers S., Turowski B., Caspers J.**
Differential functional connectivity changes of subregions of the dorsal premotor cortex in healthy ageing (SS 1411a), B-1037
- Signore A.**
Non-oncological hybrid imaging: case-based: Hybrid imaging in inflammation: case-based (ESH), A-583
- Silva M., Jacobs C., Capretti G., Ciompi F., Van Ginneken B., Schaefer-Prokop C.M., Marchianò A., Pastorino U., Sverzellati N.**
Active surveillance of subsoil nodules detected by screening: safe strategy to reduce overtreatment (SS 1804), B-1349
- Silva M.**
Lung cancer in the era of molecular oncology and immune therapy: B. ALK-rearranged lung adenocarcinomas (E³ 118), A-056
- Silva R.**
Discovering Portuguese radiology: past, present, future: The soul of Portugal: Facts and sounds of the Portuguese guitar (part 3) (EM 2)
- Silva T.B., Mauad E.C., Sabino S.**
The customised training for radiographers and its importance for image quality improvement and an accurate diagnosis of breast cancer (SS 214), B-0138
- Silva V.**
EFRS meets Switzerland and Portugal: MRI, the image modality for the future: hybrid, diagnostic and therapeutic (EM 4), A-499
- Silva V.M.F., Ramos I., Marques M., Moreira J.**
Exposure to electromagnetic fields during a gradient echo sequence in a 3T MRI scanner along z-axis (MY 17), B-1314
- Simão D.M.B., Ribeiro L.P., Abrantes A.F., Pinheiro J.P., Almeida R.P., Brito A.Q., Rodrigues S.**
Effects of smoking on carotid artery structures and haemodynamics: role of the radiographer in ultrasound assessment (SS 1014), B-0965
- Simcock C.**
Successful paediatric imaging: A. Imaging the uncooperative child and children with disabilities (RC 514), A-225
- Simeonov G.**
Euratom Basic Safety Standards Directive: a comprehensive approach for radiation protection: Panel discussion: Is the Basic Safety Standards Directive a step forward for patients, clinical professionals and regulators? (part 6) (EU 1)
- Simeonov G.**
Euratom Basic Safety Standards Directive: a comprehensive approach for radiation protection: The European Commission's perspective and update on the transposition in the European Member States (EU 1), A-150
- Singhal A.A., Bajjal S.S., Sarin D., Arora S.K., Mithal A., Mishra S.**
Ectopic parathyroids: incidence, localisation trends and diagnostic evaluation: retrospective study from a single tertiary institute (SS 708), B-0673
- Singhal S., Saranga B.K., Balakrishnan D.**
Sarcopenic index as a predictor of post-transplant morbidity and mortality (SS 1901a), B-1516
- Singhal S., Prabhu N.K.**
The heart team: coronary imaging and treatment: Non-invasive cardiac imaging (MS 4), A-129
- Sinitsyn V.E.**
Abdominal emergencies: friends and enemies: Abdominal vascular emergencies: no time to lose (SF 17b), A-901
- Sinitsyn V.E.**
ESR and UEMS: a united European voice: The European Perspective (part 1): advocacy at the EU Level (part 1) (ESR/UEMS 1), A-182
- Sinn L.H.Y., Sitt J.C.M., Fong C.Y., Lui C.Y.**
Digital breast tomosynthesis (DBT) guided biopsy of thin breast patients: how tomosynthesis and special maneuvers contribute to the technical success (SS 1802a), B-1393
- Sirin Özcan A.N., Dirik E.B.**
Phase value assessment reveals iron accumulation in Parkinson disease (SS 1511), B-1234
- Sirlin C.B.**
Hepatocellular carcinoma: diagnosis, staging and current guidelines: Diagnosis of HCC, LI-RADS 2017: why we need it? (SF 1), A-018
- Skaane P.**
New mammography: tomosynthesis and future techniques: B. Clinical validation of tomosynthesis and results in the last 10 years: where do we stand? (RC 502), A-176
- Skaane P.**
Cancer screening: C. Breast cancer: to screen or not to screen (RC 1216), A-567
- Sklair-Levy M., Friedman E., Halshtok Neiman O., Shalmon A., Gotlieb M., Faermann R., Oaknin J., Izhaky D.**
Assessing the diagnostic accuracy of a 3D functional infrared imaging as adjunct screening for women at high risk for breast cancer (SS 1902a), B-1608
- Skornitzke S., Pahn G., Bahr A., Raddatz J., Kauczor H.-U., Stiller W.**
An automated alignment correction algorithm for CT imaging: evaluation based on a CT image quality phantom and application to sediment cores from cold-water coral mounds (SS 613), B-0544
- Skornitzke S., Kauczor H.-U., Stiller W.**
Evaluation of the effect of image noise on CT perfusion measurements using digital perfusion phantoms (SS 1413), B-1131
- Smiechowicz J., Rebollo Polo M., Gómez Chiari M., Muchart Lopez J., Fons Estupiña C.**
Systematic approach to the congenital abnormalities of the posterior fossa: a tertiary paediatric referral hospital experience in last five years (2012-2016) (SS 212), B-0160
- Smirnova A.V., Lukina O.V., Cherkashin M., Plakhotina N., Tkachev A., Anishkin M., Rukhlenko M.**
MR-perfusion characteristics and PET/CT comparison in patients with gliomas after radiotherapy (SS 1011b), B-1003
- Smit E.J., Meijer F.J., Prokop M.M.**
Virtual non-contrast CT derived from dynamic CTA in acute stroke (SS 711b), B-0695
- Smithuis F.**
Radiologic anatomy: lower extremities: Ankle (ESR/ESOR 1) A-255
- Smits M.**
My three top tips for neuroimaging: Non-enhancing brain tumours (SF 15c), A-764
- Smits M.**
Diffuse low-grade gliomas: new things you should know: B. Imaging patterns suggestive of different (molecular) subtypes of low-grade gliomas (RC 1711), A-910
- Snaith B., Harris M.A., Shinkins B., Jordaan M., Lewington A., Messenger M., Spencer N.**
Point of care creatinine testing: a feasibility study in an outpatient CT setting (SS 1014), B-0969
- Snene F., Hamard A., Greffier J., Viala P., Beregi J., Larbi A.**
Contribution of ultra-low dose CT in lumbar spine trauma (SS 610b), B-0531
- Snene F., Addala T., Greffier J., Viala P., Beregi J.P., Larbi A.**
Contribution of ultra-low-dose CT in extremities trauma (SS 1017), B-0949
- Snoeckx A., Broeckx B., Carpentier K., Corthouts R., Luyckx E., Nicolay S., Spinhoven M.J., Van Hoyweghen A., Cant J.**
Lesion detection on the "all-in-one" window: is it as good as on conventional window settings? A feasibility study (SS 1904a), B-1558
- Soares F.P., Aymon E., Burke A.M., Dijkstra S., Fossgaard J., Sanders S.N., Silva A.F.N., Sanderud A.**
Large-sized patient chest radiography: a relative visual grading analysis study (SS 714), B-0748
- Soares L., Ribeiro L.P., Abrantes A.F., Ribeiro A.M., Azevedo K.B., Almeida R.P., Lesyuk O., da Silva C.A.**
Patient perceptions of radiographer communication skills in general radiology (SS 1914), B-1638
- Sofia C., Tropea M., Di Grazia L., Spillare P., Boscolo Bariga N., Marino M., Tregnaighi A.**
The meconium sign in foetal MRI performed for the diagnosis of diaphragmatic hernia (SS 1412), B-1167
- Sokhi H.K., Patel S., Padhani A., Pope A.**
Audit of diagnostic yields of prostate cancer in biopsy naive patients at high risk of cancer on the London Cancer Alliance Best Practice Prostate Pathway (LCABPPP) (SS 1807a), B-1361
- Sokolowski F.C., Karius P., Lembcke A., Wagner P.M., Rodriguez Sánchez A., Dewey M.**
Extra-cardiac findings at cardiac MR imaging: a single-center retrospective study over 14 years (MY 7), B-0777
- Solanki R.K.N., Patel I.N.**
Assessment of mandibular involvement by oral cavity and oropharyngeal squamous cell carcinoma: CT scan and MRI evaluation (SS 1008), B-0904

Authors' Index

Song C., Jingliang C.

Application of dynamic contrast-enhanced MRI and diffusion-weighted imaging in differentiating nasopharyngeal carcinoma and nasopharyngeal lymphoma (SS 208), B-0074

Song L., Ma X., Zhao X., Zhao L., Fan Y., Wu B., Wang Z., Chen H.

Evaluation of dark blood LGE in assessing sub-endocardial MI and papillary muscle scar (MY 7), B-0781

Soo S., Rahmat K.

Overview of early clinical implementation of digital breast tomosynthesis: a single-centre experience (SS 202a), B-0084

Sorantin E.

Everything you need to know about 3D post-processing: Chairperson's introduction (RC 105), A-046

Sorochan O.

Ultrasound diagnostics of the respiratory distress syndrome in premature infants (MY 18), B-1499

Sosna J.

Big data: implications for medical imaging and the need for data protection and cyber security: Cyber security in radiology (PA 2), A-820

Sousa A.F.C., Santos J., Ferreira A.

Evaluation of occupational exposure from electromagnetic field radiation on mobile magnetic resonance imaging units (SS 614), B-0557

Souto S., Abrantes A.F., da Silva C.A., Ribeiro L.P.V., Almeida R.P., Azevedo K.B.

Job satisfaction of radiographers (SS 1914), B-1640

Spiliopoulos S.C.

Pulmonary embolism: a joint challenge for diagnostic and interventional radiology!: C. Updates on the endovascular treatment of massive and submassive pulmonary embolism (RC 1209), A-590

Spink C., John B., Schröder D., Krautschneider W., Fischbach R., Braunschweig M., Buhk J., Adam G., Koops A.

Non-invasive pressure monitoring after transjugular intrahepatic portosystemic shunt implantation with integrated sensors (SS 209), B-0035

Spirchez Z., Radu P., Al Hajjar N., Kacso G., Mocan T.

Prospective comparison US vs. CEUS guided percutaneous biopsy in the diagnosis of large intra- and retroperitoneal tumors (SS 609), B-0453

Sporea I., Bende F.B., Popescu A.S., Sirli R., Danila M., Nistorescu S., Fofiu R., Baldea V.

Performance of a 2D-SWE method for predicting different stages of liver fibrosis, using transient elastography as the reference method (SS 301b), B-0203

Springer E., Bogner W., Cardoso P., Nittka M., Pfeuffer J., Koerzdoerfer G., Kirsch R., Trattig S.

Evaluation of chronic MS lesions with T1 magnetic resonance fingerprinting (SS 311), B-0285

Srivastava D.N., Ha V., Monga A., Malhotra R.

Clinical outcome of rotational angiography in percutaneous laser disc decompression (SS 1809), B-1338

Stafrace S.

Imaging in abdominal emergencies: an (evidence-based) update: A. The acute abdomen in neonates (RC 512), A-190

Staglianò S., Tortora D., Severino M., Martinetti C., Garrè M., Rossi A., Morana G.

Paediatric astrocytic tumour grading: comparison between ASL and DSC MRI perfusion (SS 1811b), B-1478

Stajgis M.

The latest update in imaging of polytrauma patients: Chairperson's introduction: The role of proper imaging and management in patients after severe trauma (RC 1517), A-778

Stáreková J., Scherz B., Tahir E., Avanesov M., Patten M., Weinrich J.M., Müllerleile K., Adam G., Lund G.K.

Comparison of sports activity between ambitious triathletes with and without myocardial late gadolinium enhancement (MY 7), B-0780

Steinbach L.

Upper extremity sports injuries: A. Shoulder injuries in the throwing athlete (TC 1328), A-678

Steinbach L.

Upper extremity sports injuries: C. Interactive case discussion (part 1) (TC 1328), A-680

Steinfelder E.

Linking imaging biobanks to -omics: the role of BBMRI and ESR: Introduction to BBMRI biobanking and biomolecular resources research infrastructure (ESR/BBMRI-ERIC), A-612

Stenberg L.

Epilepsy: Keynote lecture (SS 1811a), K-29

Stern Padovan R.

Patient-doctor relationship and interdisciplinary communication in the radiology department: The radiologist as a patient (PA 1), A-698

Stief J.D., Lüdemann L., Denecke T., Hamm B., Geisel D.

Correlation between Gd-EOB-DTPA-enhanced MRI and T1rho in patients with and without liver cirrhosis (SS 201a), B-0009

Stiller W.

Strategies for dose reduction in computed tomography: from technical concepts to clinical practice: Chairperson's introduction (EU 2), A-247

Stocker D., Finkenstaed T., Kuehn B., Nanz D., Klarhöfer M., Kiefer B., Reiner C.S.

Performance of an automated vs manual MR scanner workflow of whole-body MRI (SS 1410), B-1125

Stöcklein S.

Psychoradiology: a blend of molecular, functional and structural imaging with a taste of psychology: Advanced imaging techniques: their role in neuropsychiatric disorders (MS 16), A-829

Storz C., Rosplecz S., Lorbeer R., Rathmann W., Reiser M.F., Hoffmann MD MPH U., Peters A., Schlett C.L., Bamberg F.

Phenotypic multi-component involvement of subclinical disease as quantified by MRI in subjects with prediabetes, diabetes and normal glucose tolerance (SS 303), B-0340

Storz C., Heber S.D., Rosplecz S., Machann J., Nikolaou K., Lorbeer R., Peters A., Schlett C.L., Bamberg F.

The role of visceral and subcutaneous adipose tissue measurements and their ratio by MRI in subjects with prediabetes, diabetes and healthy controls from a general population (SS 1001a), B-0838

Stosic-Opincal T.

Dementia and movement disorders: B. Imaging in Parkinsonism and other extrapyramidal disorders (E³ 821), A-303

Stoupis C.

Characterisation of focal liver lesions: Chairperson's introduction (E³ 620), A-260

Stoupis C.

Abdominal emergencies: friends and enemies: Expected and unexpected emergencies of abdominal viscera: radiology before surgery? (SF 17b), A-904

Sträter A.S., Huber A., Nadjiri J., Rasper M., Berndt M.T., Rummeny E.J., Rieber J.

Value of left ventricular fibrosis volume as a parameter for long-term survival after TAVI (SS 203), B-0149

Stratis A., Zhang G., Jacobs R., Bogaerts R., Bosmans H.

Task-based radiation dose assessment for paediatric dental CBCT imaging (SS 1813), B-1431

Streekstra G.J., de Roo M., Strackee S.D., Dobbe I.

The effect of motion blur and noise on the precision and accuracy of wrist joint kinematics detection from 4D-CT scans (SS 713), B-0732

Strickland N.H.

Daily use of mobile devices in radiology: B. Is it appropriate to read a study on a smartphone or a tablet? (RC 805), A-362

Struffert T.

Interventional: Chairperson's introduction (E³ 1923), A-970

Struik F., Fütterer J.J., van der Graaf M., Prokop M.M.

Performance of single-use syringe versus multi-use MR contrast injectors: a prospective comparative study (SS 614), B-0555

Studzinski J.

eHealth in radiology: policies, practices, pitfalls, potential: ESR-HIMSS Digital Imaging Adoption Model (ESR/EU), A-776

Su T., Jin L., Han Y.

Transverse and sigmoid sinus stenosis and pressure gradient in patients with pulsatile tinnitus (SS 608), B-0496

Sudarkina A., Dergilev A., Gorbunov N.

Quantitative analysis of diffusion weighted magnetic resonance imaging for characterization of mediastinal lymphadenopathy (SS 1904b), B-1576

Sudarski S., Henzler T., Haubenreisser H., Schönberg S.O., Gutzeit A.

Incidence of transient interruption of contrast (TIC): a retrospective single-centre analysis in 225 consecutive CT pulmonary angiography studies (SS 604), B-0459

Sudoř-Szopińska I.

MRI of articular cartilage and bone: areas of imaging confusion and practical solutions: C. Rheumatoid arthritis (RC 110), A-032

Suehiro E., Sekitani T., Tani W., Negi N., Fujii K., Yoshikawa T., Ohno Y.

Influence of reconstruction algorithms to chest CT examination in children: comparison of image quality among standard-, reduced- and ultra-low-dose CTs in chest phantom study (SS 712), B-0767

Suetens P.

Artificial intelligence: a strategic view: Image computing in radiology (SF 6), A-981

Sugawara H., Suzuki S., Katada Y., Ishikawa T., Fukui R., Yamamoto Y.

Accuracy of diameter measurement of vascular model: comparison of virtual monochromatic imaging in dual-energy CT with conventional 120-kVp scan (SS 1415), B-1048

Authors' Index

Sugiyama M., Takehara Y., Alley M., Unno N., Katahashi K., Wakayama T., Nozaki A., Naganawa S., Sakahara H.

4D flow analysis of abnormal haemodynamics within saccular aneurysm in contrast to fusiform aneurysm in abdominal aorta (SS 215), B-0028

Sulkowska K., Palczewski P., Furmanczyk-Zawiska A., Perkowski-Ptasinska A., Szeszkowski W., Durlik M., Golebiowski M.

Diffusion weighted magnetic resonance imaging in assessment of parenchymal damage in chronic kidney disease (SS 1007), B-0882

Sun K., Lu B.

The image quality of turbo high-pitch dual-source CT coronary angiography in patients with free-breathing, free heart rate and any BMI (MY 7), B-0774

Sun Y., Zhou Y., Wang Y., Han X., Ding W., Xu J.

Sex differences in resting-state cerebral activity alterations in internet gaming disorder (MY 8), B-0800

Suntharalingam S., Mikat C., Wetter A., Guberina N., Salem A., Heil P., Forsting M., Nassenstein K.

Feasibility of whole-body low-dose CT using spectral shaping for detection of osteolytic lesion in patients with multiple myeloma (SS 1413), B-1138

Suo X., Lei D., Gong Q.

Posttraumatic stress disorder-related alterations in modular characteristic and white matter connectivity of brain structural networks (SS 711a), B-0662

Sutter R.

Imaging the hip and thigh: A. Femoroacetabular impingement: what is it, how do I image it and does it matter? (RC 910), A-415

Svahn T., Sjöberg T., Shahgaldi K., Nordström J.

Performance and radiation dose comparison of the recently introduced ultralow-dose chest computed tomography (CT), standard-dose CT and digital chest radiography (SS 704), B-0640

Svensson A.

Optimising computed tomography: C. Optimising contrast delivery with MDCT (RC 1614), A-851

Svensson S.F., Heier-Baardson H., Nielsen B.E., Herud E.B., Holmen L.O., Andersen H.K., Martinsen A.C.T.

Optimisation of abdominal CT examinations across different scanners in one hospital using a new liver phantom (SS 1413), B-1137

Sverzellati N.

Thoracic manifestations of systemic disease: A. Systemic sclerosis (RC 1704), A-880

Swart L.E., Henneman M.M., Galema T.W., Bekkers J.A., Valkema R., Schurink C.A.M., Verkaik N.J., Roos-Hesselink J.W., Budde R.P.J.

The multidisciplinary "endocarditis team": results on imaging utilisation and diagnostic and therapeutic changes in the first 100 patients (SS 1903), B-1649

Syrgiamiotis V.

Successful paediatric imaging: Chairpersons' introduction: Paediatrics: more than just 'small adults' (part 1) (RC 514), A-223

Szabo A.G., Kozák L.R., Farkas K., Rudas G., Csukly G.

Impaired mixed emotion processing in the right ventrolateral cortex in schizophrenia (SS 711a), B-0659

Szabó L., Czibalmos C.L., Csécs I., Tóth A., Suhai F.I., Heltai K., Zima E., Gellér L., Becker D., Merkely B., Vágó H.

The role of cardiac magnetic resonance imaging (MRI) in the diagnostic work-up after aborted sudden cardiac death (SS 1903), B-1657

Szemplinska B., Maj E., Szeszkowski W., Prokopenko M., Cieszanowski A., Marchel A., Rowinski O.

The role of diffusion tensor imaging parameters in characterisation and differentiation of the spinal cord tumours (SS 1411b), B-1106

Szilveszter B., Oren D., Kolossvary M., Vecsey-Nagy M., Karady J., Suhai F., Apor A., Merkely B., Maurovich-Horvat P.

Left ventricular reverse remodeling after transcatheter aortic valve implantation as assessed by CT angiography (SS 203), B-0150

T

Tabone E., Doronzio V.M., Appendino E., Romano V., Pedalino S., Manfredi M., Mazzetti S., Regge D., Russo F.

Radiological Wheeler staging system: a valid tool to improve the local staging of organ-confined prostate cancer with mp-MRI (SS 1516), B-1244

Tack D.

Strategies for dose reduction in computed tomography: from technical concepts to clinical practice: Adapting protocols towards dose reduction in chest CT (EU 2), A-251

Tack D.

CT dose reduction: technique and applications in chest: Keynote lecture (SS 704), K-13

Tahmassebi A., Meyer-Baese A., Wengert G.J., Helbich T.H., Pinker-Domenig K.

Radiomics with MRI for early prediction of the response to neo-adjuvant chemotherapy in breast cancer patients (MY 16), B-1281

Takagi H., Kikuchi K., Tanaka R., Yoshioka K.

Noninvasive CT-derived FFR based on structural and fluid analysis with low radiation dose using a full iterative reconstruction (SS 1803), B-1457

Takehara S., Iwasawa T., Baba T., Ogura T., Oba M.S.

Comparison of ultra-low-dose computed tomography (ULDCT) and standard-dose computed tomography (SDCT) for the detection of interstitial lung disease (SS 704), B-0637

Talaat M., Abdel Razeq A., Elserougy L., Gaballa G.

Arterial spin labelling and diffusion tensor magnetic resonance imaging-derived metrics for differentiation of post-treatment brain tumour recurrence from tissue necrosis (SS 211), B-0092

Tali E.T.

Inflammatory and infectious CNS pathology: Chairperson's introduction (RC 1211), A-557

Talmaceanu D., Lenghel L.M., Baciut G., Baciut M., Rotar H., Bolog N., Buduru S., Daniil L., Dudea S.

The diagnostic value of ultrasonography in assessing temporomandibular joint disc position (SS 308), B-0255

Tanamala S., Ghosh R., Chilamkurthy S., Rao P., Biviji M.

Automatic detection of generalised cerebral atrophy using deep neural networks from head CT scans (SS 1805), B-1387

Tanenbaum L.

Advanced MR in the spine: a radiologist's view of the advanced techniques you need to know (SY 27)

Tang C., Zhou C., Schoepf U.J., Mastrodicasa D., Zhao Y., Lu L., Li X., Lu M., Zhang L.

Computer-assisted detection of acute pulmonary embolism in children and young adults: inter-observer effect (MY 18), B-1487

Tang S., Hu X., Gong Q., Huang X.

Phylloides tumours of resting-state functional connectivity of major depressive disorder in youth (SS 711a), B-0655

Tang W., Zhang Y., Cheng J.

Phylloides tumours of histogram analysis of the apparent diffusion coefficient for assessment of tumour grade (SS 1402a), B-1095

Tantawy W., Zarea A., Ibrahim A.S., Abdel Kawi M., Hussein Y., Nasr M., Barsoum M.

Value of the first day PET/CT in post thermal ablation of lung tumours (SS 616), B-0592

Tanturri De Horatio L.

Juvenile idiopathic arthritis (JIA): B. Ultrasound for detecting and grading of inflammation in JIA (E³ 426), A-153

Taoka T., Jost G., Naganawa S., Pietsch H.
Gd presence in the brain: impact of daytime and anaesthesia (SS 1011b), B-0995

Taori A.

Modified myocardial performance index for evaluation of foetal cardiac function in small for gestational age foetuses (SS 1503), B-1231

Taoussi R., Gechchar Z., Fehdi M., Mouhaoui M., Touil N., Kacimi O., Chikhaoui N., Lembarki G.

Simulation-based training for radiology professionals in the management of acute emergencies following contrast media reactions (SS 1017), B-0941

Tarmey T., McGreal P., McDermott A., Sheehan M., O'Connell A.

Radial scars detected at screening mammography: is surgical excision always indicated? (SS 1402a), B-1089

Taron J., Johannink J., Bitzer M., Nikolaou K., Notohamiprodjo M., Hoffmann R.

Added value of diffusion-weighted imaging in hepatic tumours and its impact on patient management (SS 701a), B-0601

Taroni P.

EIBIR Research Session: European imaging researchers united in diversity: Smart Optical and Ultrasound Diagnostics of Breast Cancer (SOLUS) Project: aims and objectives (EIBIR 1), A-322

Tavakoli A.A., Attenberger U., Budjan J., Schönberg S.O., Riffel P.

Improved DWI of the liver at 3T using respiratory triggering with simultaneous multi-slice acceleration (SS 701a), B-0606

Tavakoli Tabas S., Baran P., Lewis S., Heard R., Pacile S., Nesterets Y.I., Mayo S.C., Dullin C., Dreossi D., Arfelli F., Thompson D., McCormack M., Alakhra M., Brun F., Pinamonti M., Nickson C., Hall C., Zanconati F., Lockie D.J., Quiney H., Tromba G., Gureyev T.E., Brennan P.C.

A visual grading analysis of propagation-based phase-contrast CT mammography (SS 1802b), B-1416

Authors' Index

Taylor A.M.

Cardiac imaging: A. Grown-ups with congenital heart disease (E³ 1721), A-874

Taylor S.A.

Abdominal MRI: from standard to advanced protocols: B. Inflammatory bowel disease (RC 1701), A-878

Tazdait M., Bidault F., Ammari S.,

Balleyguier C.S., Planchard D., Soria J.,

Marabelle A., Besse B., Caramella C.

Patterns of responses in metastatic NSCLC during immunotherapy: comparison of RECIST 1.1, irRECIST and iRECIST criteria (MY 3), B-0368

Teh J.

Lower extremity: C. Chronic ankle pain (E³ 819), A-371

Teh J.

Acute trauma: patterns in the peripheral skeleton: Acute trauma: patterns in the peripheral skeleton (E³ 25D), A-720

Teh W.

How much is enough? Quantity vs quality: our initial experience with a new vacuum assisted breast biopsy device in the UK (SY 10)

Tejerina A.

A new biopsy technology combined with tomosynthesis guidance: our experience and initial results (SY 10)

ter Braak A., Plaisier P.W.,

Menke-Pluijmers M., Westenend P.J.

Selecting treatment options in patients with ductal carcinoma in situ (DCIS) using MRI (SS 1002), B-0913

Tesche C., Otani K., Albrecht M.,

De Cecco C.N., duguay T., Baumann S.,

Renker M., Varga-Szemes A., Schoepf U.J.

Effect of coronary calcium on the diagnostic performance of machine learning-based coronary CT angiography-derived fractional flow reserve: results from the machine registry (SS 1803), B-1454

Tessa C.

Novel ways to characterise myocardial tissue: T1 and T2 mapping: B. T2 mapping: technical considerations (RC 903), A-393

Testa F., Angarano N., Marchisio M.,

Olivero R., Fraire D., Verna V.

"How much radiation do my baby get sick?" Answering to worried moms about dental radiology in childhood (SS 308), B-0263

Tettero M.N.

Detection of colorectal cancer liver metastases with MRI: is diffusion-weighted imaging (DWI) solely as good as DWI + dynamic T1-weighted sequences after extracellular Gd? (SS 614), B-0558

Thakor K., Major V., Patel S., Bergman H.R.,

McGuire W., Lakhani A.

Comparing the detection rate of melanoma metastases on gadolinium-based contrast-enhanced MRI brain scan compared to a non-enhanced scan. (SS 614), B-0561

Tharwat Mohammed El-Sayed N.

Multiphase CT vs dynamic contrast-enhanced MRI in the characterisation of parotid gland tumours (MY 14), B-1196

Theilig D., Raabe P., Lüdemann L.,

Pratschke J., Hamm B., Denecke T., Geisel D.

GD-EOB-DTPA-enhanced MRI T1 relaxometry as an imaging-based liver function test compared with ¹³C-methacetin LiMAx test (SS 201a), B-0007

Thoeny H.C.

Radiology and Swiss chocolate: a sweet combination: Truffle No. 1: MR-diffusion of the urogenital tract: where it really helps (EM 1), A-451

Thoeny H.C.

Management of incidental findings in the genitourinary tract: B. Kidneys (RC 1307), A-626

Thoeny H.C.

Urogenital: C. Prostate imaging (E³ 1623), A-835

Thunberg S.J., Båvenäs H., Cederlund T.

A national web-based tool for optimisation of radiological protocols (SS 313), B-0312

Thurnher M.M.

Inflammatory and infectious CNS pathology: C. Inflammatory and infectious myelitis (RC 1211), A-560

Thurnher M.M.

My three top tips for neuroimaging: Ring-enhancing brain lesions (SF 15c), A-765

Tian J., Yang Y.

Dynamic evaluation of notch signaling-mediated angiogenesis in ischemic rat using magnetic resonance imaging (SS 711b), B-0689

Toepker M.

Case-Based Diagnosis Training - Part 1: Genitourinary (CB 1), A-966

Toghyan H., Al-Khatib A., Stenberg B.,

McQueen A.

The use of micro-flow imaging (MFI, Philips Medical Systems) in ultrasound guided tissue sampling of head and neck masses (SS 1508), B-1217

Tolan D.J.M.

Imaging of the complicated postoperative abdomen: C. Bowel (RC 401), A-098

Tolan D.J.M.

My three top tips for abdominal imaging: Chairperson's introduction (SF 12a), A-518

Tolan D.J.M.

My three top tips for abdominal imaging: Postoperative abdomen (SF 12a), A-519

Tolan D.J.M.

The anal canal: does MRI make it easy?: B. Fistulae-in-ano: detect, stage, classify (E³ 1522), A-795

Tolle S.

Radiology will survive, but will the radiologist still be there?: How to cope with the new IT developments: the developer's perspective (PI 2), A-509

Tononcelli E., Calabretta L., Ravanelli M.,

Lombardi D., Farina D., Maroldi R.

MRI profile of sinonasal mucosal melanoma: analysis of 46 cases (SS 308), B-0265

Torcitto A.G., Falsaperla D., Torrisi S.E.,

Mauro L.A., Pavone M., Russo G., Stefano A.,

Vancheri C., Palmucci S.

Assessment of survival in patients with idiopathic pulmonary fibrosis using Kurtosis and mean lung density HRCT indexes (MY 5), B-0420

Torheim T., Woitek R., Patterson A.J.,

Bedair R., Mendichovszky I.A., Caldas C.,

Markowetz F., Gilbert F.J.

Comparison of invasive lobular and invasive ductal carcinomas of the breast using 3T DCE-MRI (SS 202b), B-0104

Törnberg S

Chairperson's introduction: Screening for cancer: lessons learned and future challenges (RC 1216), A-564

Torresin A.

Single-dual-multi-energy CT: Chairperson's introduction (RC 113), A-033

Trattig S.

Linking imaging biobanks to -omics: the role of BBMRI and ESR: Radiomics: enhancing the value of images by standardised feature extraction (ESR/BBMRI-ERIC), A-615

Trebesci S., Drago S.G., Kurilova I.,

Lalezari F., Lambregts D.M., Smit E.,

Blank C.U., Aerts H.J., Beets-Tan R.G.H.

Radiomics as a predictive biomarker of metastatic response to immunotherapy (SS 316), B-0356

Trianni A.

Patient-specific dosimetry: C. Patient dose in fluoroscopy and interventional (RC 1713), A-926

Triantopoulou C.

Diffuse liver disease: Chairperson's introduction (E³ 320), A-087

Tripathi P., Rao S., Guo W., Rai B., Zeng M.

MRI-detected extramural vascular invasion is one of the strongest risk factors in predicting distant metastasis in rectal cancer (MY 15), B-1270

Triulzi F.M.

Imaging of the brain in preterm infants: The role of cerebral MRI: morphology and beyond (SF 12b), A-538

Triulzi F.M.

Understanding paediatric neuroradiology: C. Imaging in hypoxic-ischaemic injury and hypothermia: an update (RC 1712), A-891

Trofimenko I.

Evaluation after treatment: Q&A (SY 18)

Trojanowska A.

Post-treatment imaging of the head and neck: B. Normal findings after surgery (RC 1308), A-623

Trojanowska A.

Head and neck: A. Temporal bone and skull base (E³ 1423), A-700

Trojanowska A.

Josef Lissner Honorary Lecture: Human papilloma virus and head and neck cancer: the new face of malignancy (HL 3), A-714

Trümpler A.

Radiology and Swiss chocolate: a sweet combination: Interlude 1: From cocoa bean to chocolate creations (EM 1), A-452

Trümpler A.

Radiology and Swiss chocolate: a sweet combination: Interlude 2: From cocoa bean to chocolate creations (EM 1), A-454

Tsakok M., Little M., Millington R., Hynes G.,

Gleeson F., Anderson M.

Recurrence and survival following image-guided percutaneous microwave ablation in primary lung malignancy (MY 9), B-0831

Tsapaki V.

Dose management systems and repositories: part A: The benefits of dose management systems in view of the new Euratom Directive (EF 1), A-421

Tselikas L.

Musculoskeletal interventions: what every radiologist should know: C. Bone biopsy and pain treatment using cone-beam CT (CBCT) (RC 509), A-237

Tsetis D.K.

GI bleeding: how to solve the problem?: C. When is the interventional radiologist needed? (RC 101), A-006

Authors' Index

Tsili A., Ntorkou A., Astrakas L.G., Goussia A., Panopoulou E., Sofikitis N., Argyropoulou M.

Diffusion tensor imaging parameters in the identification of spermatogenesis in men with non-obstructive azoospermia (SS 1907b), B-1662

Tsuchiya M., Masui T., Katayama M., Sasaki M., Kawamura K., Hayashi Y., Yamada T., Sakahara H.

Factors related to bone marrow oedema of accessory navicular bone in the evaluation with MR imaging (SS 710b), B-0720

Tsurumaru D., Nishimuta Y., Muraki T., Asayama Y., Honda H.

Prediction of gastric cancer with synchronous hepatic metastasis by enhancement pattern of primary lesion using multiphasic contrast-enhanced computed tomography (SS 701b), B-0716

Tulay C., Aubry S., Podda A., Behr J.

Ultrasound of the posterior interosseous nerve in the arcade of Frohse (MY 13), B-1015

Tunlayadechanont P., Panyaping T., Cheecharoen P., Jindahra P.

Diagnostic value of contrast-enhanced 3D FLAIR sequence in acute optic neuritis (MY 14), B-1199

Türk S., Bayraktaroğlu S., Ramo E., Akagündüz Ö., Savaş R.

Correlation between apparent diffusion coefficient and standardised uptake values in head and neck carcinomas (SS 1508), B-1219

Tutar B., Esen G., Kara H., Guldogan N., Uras C.

Comparison of automated vs bilateral handheld whole-breast US in screening patients regarding efficacy and patient preference (MY 16), B-1293

Tyurin I.E.

Pneumonia: Chairperson's introduction (RC 1204), A-529

U

Uberoi R.

TEVAR/EVAR: where we are and where we are going: C. Post-EVG complication (E³ 526b), A-240

Uberoi R.

Pulmonary embolism: a joint challenge for diagnostic and interventional radiology!: B. What is new in the recently published guidelines for pulmonary embolism treatment? (RC 1209), A-589

Uhlig J., Lücke C., Vliegenthart R., Loewe C., Grothoff M., Jacquier A., Francone M., Lotz J., Gutberlet M.

Acute adverse events in cardiac MR imaging with gadolinium-based contrast agents: results from the European Society of Cardiovascular Radiology (ESCR) MRCT registry in 72,839 patients (SS 603), B-0563

Ullrich T., Schimmöller L., Quentin M., Schmaltz K.A., Rubbert C., Arsov C., Rabenalt R., Albers P., Antoch G.

Mp-MRI of the prostate: anti-peristaltic hyoscine butylbromide significantly decreases motion artefacts and allows better delineation of anatomic structures (SS 307), B-0252

Ullrich T., Schimmöller L., Quentin M., Laqua N., Blondin D., Arsov C., Rabenalt R., Albers P., Antoch G.

When does biopsy make sense in patients with an overall PI-RADS score of 3? (SS 1807a), B-1363

Ullrich T., Schimmöller L., Quentin M., Laqua N., Dietzel F., Arsov C., Rabenalt R., Albers P., Antoch G.

How to prevent patients with a false-positive overall score of PI-RADS 4 (SS 1807a), B-1364

Umutlu L., Nittka M., Kirsch R., Quick H., Herrmann K., Gratz M., Forsting M., Forsting M.

Multi-parametric 11C-methionine-MR/PET for brain tumour imaging utilising MR fingerprinting (MY 8), B-0796

Umutlu L.

Radiomics in breast imaging (SY 1a)

Uprimny C., Kroiss A., Decristoforo C., Fritz J., Nilica B., Horninger W., Virgolini I.

Additional value of early imaging of ⁶⁸Ga-PSMA-11 PET/CT in the assessment of local recurrence in prostate cancer patients with biochemical relapse (SS 1907a), B-1570

Us R., Matjačič A., Bizjak R., Hribar T., Malinova Z., Mekis N.

A tool for automated assessment of imaging system resolution (SS 1814), B-1448

Usanov M.S., Kulberg N.S., Petraikin A.V., Morozov S.P.

Newly developed curvelet-based noise reduction algorithm for volume CT data (SS 1905), B-1591

Usman A., Sadat U., Teng Z., Graves M., Boyle J., Gillard J.

Magnetic resonance imaging-based assessment of carotid atheroma: a comparative study of patients with and without coronary artery disease (SS 315), B-0219

V

Vaidya S.

Mass casualties: Mass casualty incidents: the London framework for planning (PC 4), A-121

Valdés Solís P.

Establishing competence in radiology: Obstacles to establishing competence in radiology (PI 1), A-464

Válek V.

Tips and tricks for abdominal ultrasound: Chairpersons' introduction (part 2) (WG 2), A-438

Valentini V.

New imaging approaches for radiotherapy: Chairpersons' introduction (part 1) (ESR/ESTRO), A-883

Valette P.-J.

Potential of micro-flow imaging in bowel application (SY 19)

Valle C., Bonaffini P., Invernizzi F., Barletta A., Casiraghi A., Pappini A., Sironi S.

Split-bolus vs single-bolus MDCT urography: comparison of urinary tract opacification, radiation dose exposure and diagnostic capability (SS 1807b), B-1468

van Assen M., De Cecco C.N., Vliegenthart R., Oudkerk M., Schoepf U.J.

Iodine quantification at rest and stress to differentiate ischaemic, infarcted and normal myocardium using dual-energy CT (SS 703), B-0757

van Assen M., van Dijk R., Kuijpers D., Vliegenthart R., Oudkerk M.

Cardiac magnetic resonance T1 reactivity in coronary artery disease (SS 1403), B-1152

van Assen M., Pelgrim G., Stijnen M., Van Tuijl S., Schoepf U.J., Vliegenthart R., Oudkerk M.

Intermodel agreement of myocardial blood flow quantification in dynamic myocardial perfusion CT (SS 1803), B-1458

van Beek E.J.R.

When and how to use perfusion imaging in pulmonary vascular and airway disease?: C. Nuclear medicine and hybrid imaging (RC 104), A-009

van Beek E.J.R.

MR imaging of the lungs: Chairperson's introduction (E³ 318), A-083

van Bommel R.M.G.

Incidence and tumour characteristics of bilateral and unilateral interval breast cancers at screening mammography (SS 702), B-0675

van Buchem M.

Altered mental state: Chairperson's introduction (RC 1311), A-636

van de Sande M.A.J.

New treatments for musculoskeletal tumours: New treatment paradigms in orthopaedic oncology (SF 17a), A-893

van den Hauwe L., Landen M., Vandereyken F., Vael R., Bracke P.

Who needs a CT scan? Incorporating S100B into existing guidelines in the management of mild traumatic brain injury (SS 317), B-0290

van den Hauwe L.

Cerebrovascular disease: B. Arterial dissection and vasculitis (RC 911), A-409

van der Eerden A.W., van den Heuvel T.L.A., Geurts B.H., Platel B., Vande Vyvere T., van den Hauwe L., Andriessen T.M.J.C., Góraj B.M., Manniesing R.

Automatic vs human detection of traumatic cerebral microbleeds on susceptibility-weighted imaging (SS 1911a), B-1594

Van Der Molen A.J., Reimer P., Dekkers I., Bongartz G., Thomsen H.S.

Updated evidence-based European Society of Urogenital Radiology (ESUR) Contrast Media Safety Committee (CMSC) Guidelines for prevention of post-contrast acute kidney injury (PC-AKI) (SS 1807b), B-1464

Van der Putten J., Zinger S., De With P.H.N., Prokop M.M., Hermans J.J.

Quantitative CT-based radiomics as predictor of local resectability of pancreatic ductal adenocarcinoma (SS 605), B-0480

van der Werf N., van Dijk E.J., Dickerscheid D., Kock M.C.

Radiation dose for digital breast tomosynthesis: influence of breast composition and breast thickness (SS 313), B-0311

van der Zijden T.

Stroke: emergent large vessel occlusion (ELVO): A. Selecting ELVO patients for endovascular therapy (E³ 1326b), A-666

van der Zijden T.

Interventional treatment of stroke: a game changer: Stroke, endovascular treatment: current approaches (SA 17), A-913

van Dijk R., van Assen M., Vliegenthart R., de Bock G., van der Harst P., Oudkerk M.

Semi-quantitative and quantitative magnetic resonance perfusion analysis: a meta-analysis (SS 1403), B-1155

Van Dyck P.

Knee: B. Chronic pain (E³ 1019), A-468

Authors' Index

van Ginneken B.

The machines are coming: how will they change our future?: Deep learning: current performance (NH 5), A-171

Van Goethem J.

The degenerative cervical spine:
A. Degenerative uncovertebral and facet disease (RC 111), A-020

Van Goethem J.

My three top tips for neuroimaging:
Chairperson's introduction (SF 15c), A-756

van Griethuysen J.J.M., Lambregts D.M., Trebeschi S., Maas M., Lahaye M.J., Beets G.L., Bakers F.C., Beets-Tan R.G.H., Aerts H.J.

Radiomics as a novel tool for primary nodal staging in rectal cancer (SS 316), B-0352

van Hamersvelt R.W., Zreik M., Voskuil M., Isgum I., Leiner T.

Deep learning-based analysis of the left ventricular myocardium in coronary CTA images improves specificity for detection of functionally significant coronary artery stenosis (SS 1803), B-1462

Van Hecke W.

Gadolinium: image wisely: B. Do we need gadolinium in imaging MS? Pros and cons (part 2) (PS 1227), A-593

van Hedent S., Tatsuoka C., Carr S., Eck B., Kessner R., Grosse Hokamp N., Ros P., Jordan D.W.

Impact of patient size and radiation dose on spectral accuracy in spectral detector CT: a phantom study (SS 213), B-0125

van Hedent S., Su K., Liang F., Kuo J., Jordan D.W., Eck B., Ros P.R., Muzic R.
Improving the sensitivity of bone mineral density assessment using spectral detector CT (MY 13), B-1017

van Nijnatten T., Lobbes M.B., Pinker K., Keating D.M., Sung J.S., Morrow M., Wildberger J.E., Smidt M., Jochelson M.S.
Is there a difference in the degree of enhancement in contrast-enhanced spectral mammography between invasive lobular carcinomas and invasive ductal carcinomas? (SS 1802b), B-1409

van Ommen F., Bennink E., Vlassenbroek A., Dankbaar J.W., schilham A., Viergever M.A., De Jong H.W.

Image quality of conventional images of dual-layer spectral CT: a phantom study (SS 1413), B-1130

Van Ongeval C.

Phenotype-genotype correlation and radiological screening for breast cancer in gene mutation carriers (SY 1a)

Van Ongeval C.

My three top tips for breast imaging: Treatment response and therapy monitoring (SF 8b), A-333

van Ooijen P.M.A.

Everything you need to know about 3D post-processing: B. Making better use of your 3D package: tips and tricks (RC 105), A-048

van Ooijen P.M.A.

Artificial intelligence (AI) applications: Data control in the era of AI: man or machine? (SF 10), A-993

van Rijn R.R.

Forensic imaging: Chairpersons' introduction (part 2) (RC 114), A-038

Van Rijn R.

Understanding paediatric neuroradiology:
B. Abusive head trauma: the role of CT and MRI (RC 1712), A-890

van Zwam W.

Interventional treatment of stroke: a game changer: Stroke, endovascular treatment: tandem lesions and acute phase stenting (SA 17), A-914

van't Sant-Jansen I., Engbersen M., Chandrasegaram-Shanmuganathan S., Lambregts D.M., Kok N.F., Beets G.L., Beets-Tan R.G.H., Aalbers A.G., Lahaye M.J.
Dedicated DW-MR imaging as an accurate selection tool for hyperthermic intraperitoneal chemotherapy (HIPEC) in patients with peritoneal carcinomatosis (PC) from colorectal origin (SS 1416), B-1085

van't Sant-Jansen I., Engbersen M., Lambregts D.M., Aalbers A.G., van Driel W., Beets-Tan R.G.H., Lahaye M.J.
Diagnostic value of imaging for the detection of peritoneal metastases: a meta-analysis (SS 1816), B-1376

Vancoillie L., Cockmartin L., Marshall N., Bosmans H.

Comparison of phantom target detectability for digital mammograms, tomosynthesis and synthetic mammograms (SS 702), B-0682

Vande Berg B.

MRI of articular cartilage and bone: areas of imaging confusion and practical solutions:
A. Bone oedema syndromes and avascular necrosis (RC 110), A-030

Vane M.L.G., van Nijnatten T., Nelemans P.J., Lobbes M.B., van Roozendaal L., Kooreman L., Keymeulen K., Smidt M., Schipper R.

Does breast cancer subtype affect the diagnostic performance of axillary ultrasound for nodal staging in breast cancer patients (SS 302), B-0274

Vanhoenacker F.M.H.M.

The radiological investigation of musculoskeletal tumours: Chairperson's introduction (RC 1610), A-840

Vanhoenacker F.M.H.M.

Infective/inflammatory disorders:
Infective/inflammatory disorders (E³ 25E), A-961

Vani V., Giannetto G., Pusceddu L., Morra L., Correale L., Del Santo S., Senore C., Regge D.

Patients' experience with, and factors for participation in flexible sigmoidoscopy and CT colonography screening insight from the Proteus Colon Trial (SS 601b), B-0520

Vaño E.

Clinical diagnostic reference levels for x-ray medical imaging: Panel discussion (part 3) (EU 3)

Vaño E.

Clinical diagnostic reference levels for x-ray medical imaging: The concept of diagnostic reference levels (DRLs) (EU 3), A-502

Varga-Szemes A., Duguay T., Todoran T., Fuller S., De Cecco C.N., Suranyi P., Edelman R.R., Koktzoğlu I., Schoepf U.J.
Combined assessment of peripheral artery disease by MRI-based vascular calcification visualisation and quiescent interval single-shot (QISS) MRA (SS 1415), B-1046

Varga-Szemes A., Duguay T., Todoran T., Penmetsa M., Fuller S., Suranyi P., De Cecco C.N., Mastrociccia D., Schoepf U.J.

Quiescent-interval single-shot (QISS) MRA for interventional procedure planning: a feasibility study in patients with peripheral artery disease (SS 1415), B-1047

Varoquaux D.

Head and neck emergencies: It is bleeding ... (SF 12c), A-543

Varotto A., Orsatti G., Crimi F., Cecchin D., Zucchetta P., Weber M., Stramare R., Giraud C.

Volumetric histogram-based analysis of SUV and ADC values for the assessment of paediatric sarcomas at staging: preliminary results of a PET/MR study (MY 18), B-1486

Vasco Aragão M.

Neurodegeneration/dementia: Keynote lecture (SS 1411a), K-19

Vassallo L., Tomasi Cont N., Doronzio V., Panzono R., Regge D., Martincich L.

Primary tumour location predicts the site of local relapse after nipple-areola complex (NAC)-sparing mastectomy (SS 202b), B-0107

Vassallo L., Doronzio V., Cappello G., Tabone E., Regge D., Martincich L.

Comparison of FOCUS (field-of-view optimised and constrained undistorted single-shot)-DWI with standard DWI-MRI and DCE-MRI in the qualitative assessment of breast lesions (SS 1402b), B-1114

Vassileva J.N.

Dose management systems and repositories: part A: Strategies for dose management for achieving optimised imaging (EF 1), A-420

Vassileva J.N.

Clinical diagnostic reference levels for x-ray medical imaging: Panel discussion (part 4) (EU 3)

Vázquez E.

State-of-the-art paediatric neuroradiology:
C. Imaging in paediatric neuro-oncology (RC 811), A-338

Veldhoen S., Behzadi C., Lenz A., Henes F., Rybczynski M., von Kodolitsch Y., Bley T.A., Adam G., Bannas P.

Non-contrast MR angiography for aortic monitoring in Marfan patients after aortic root surgery (SS 215), B-0022

Velthuis B.K.

Stroke: prediction of outcome: Keynote lecture (SS 1011a), K-17

Venancio J.

Prostate imaging reporting and data system (PI-RADS): Keynote lecture (SS 1807a), K-27

Venkatasamy A., Al Najdi A., Abu Eid M., Charpiot A., Debry C., Veillon F.

Imaging of facial neuritis using T2-weighted gradient-echo fast imaging employing steady-state acquisition after gadolinium injection (SS 208), B-0067

Venkatasamy A., Karol A., Huynh T., Charpiot A., Debry C., Veillon F.

Is gadolinium really necessary for intralabyrinthine schwannomas MRI examination? (SS 208), B-0069

Venkatasamy A., Al Ohraini Z., Charpiot A., Debry C., Veillon F.

Fast and accurate diagnosis of oval or round window perilymphatic fistula on CT and MRI without contrast injection on 101 patients with surgical confirmation (SS 308), B-0257

Authors' Index

Venkatesh S.K.

Tumour response assessment in abdominal imaging: A. Colorectal liver metastases (RC 1601), A-807

Venturini E., Panzeri M., Losio C., Rodighiero M., Tacchini S., Schiani E., Panizza P.

Digital breast tomosynthesis-guided vacuum-assisted biopsy (DBT-guided VAB): initial experience with patients positioned on a dedicated armchair (SS 1802a), B-1390

Verbist B.

Gadolinium: image wisely: C. Do we need gadolinium in imaging vestibular schwannomas? Pros and cons (part 1) (PS 1227), A-594

Verma M., Sood S., Singh B., Thakur M., Sharma S., Sharma S.

High diagnostic accuracy of k_{ep} on dynamic contrast-enhanced MRI perfusion in identifying vertebral malignancy (MY 13), B-1022

Vernooij M.W., Haller S., Frisoni G., Pizzini F., Yousry T.A., Bargallo Alabart N., Smits M., Schmidt R., Barkhof F.

Dementia imaging in Europe: results from the European Society for Neuroradiology (ESNR) Diagnostic Subcommittee Survey (SS 1411a), B-1039

Verschakelen J.A.

Patterns of pulmonary toxicity: C. Inhalation lung injury beyond smoking (E³ 1526a), A-739

Verstraete K.

Musculoskeletal: bones and soft tissues: Bone marrow diseases (BS 5), A-212

Verstraete K.

Bone, joint and soft tissue infection: A. Osteomyelitis (RC 410), A-133

Vietti Violi N., Hilbert T., Bastiaansen J., Ledoux J., Stemmer A., Stemmer A., Meuli R., Kober T., Schmidt Kobbe S.

Quantitative MRI of the pancreas: a feasibility study (SS 201b), B-0013

Vikestad K.G.

Closing the gap between education and clinical practice for radiographers: Chairpersons' introduction (part 1) (PC 13), A-657

Vilar J.

Errare humanum est: B. Errors in CT of the chest (E³ 1621), A-806

Vilela P.

Interventional treatment of stroke: a game changer: Chairperson's introduction (SA 17), A-912

Vilgrain V.

Hepatocellular carcinoma: diagnosis, staging and current guidelines: Screening for HCC, American, Asian and European guidelines: why are they different? (SF 1), A-017

Vilgrain V.

Characterisation of focal liver lesions: C. Fibrotic lesions (E³ 620), A-263

Vilgrain V.

Trends in quality education in radiology: Flipped classroom: paradigm shift with pathologists (ESOR), A-286

Vilgrain V.

My three top tips for abdominal imaging: Liver biopsy (SF 12a), A-523

Villa R., Paruccini N., Spadavecchia C., Baglivi A., Corso R., Crespi A.

Model observer techniques and an innovative statistical method for detectability evaluation in digital angiography: comparison with a 2AFC experiment (SS 213), B-0127

Villeirs G.M.

Do we need dynamic contrast enhancement (DCE) in prostate mpMRI?: A. Yes we do! (PS 527), A-206

Villeirs G.M.

Imaging of the prostate: B. MRI staging of prostate cancer (RC 807), A-317

Villeirs G.M.

Update on functional genitourinary MRI: B. Prostate (E³ 1526b), A-750

Vinke E.J., de Groot M., Venkatraghavan V., Klein S., Niessen W.J., Ikram M.A., Vernooij M.W.

Trajectories of imaging markers of the ageing brain: the Rotterdam study (MY 8), B-0794

Vinke E.J., Huizinga W., Bergthold M., Ikram M.A., Niessen W.J., Wenzel F., Vernooij M.W.

Comparing normative subcortical volume distributions across cohorts (SS 1911b), B-1678

Vinnicombe S.J.

The high-risk patient enigma: C. Can surgery be avoided? (E³ 1726a), A-908

Vitale D., Maccioni F., Buonocore V., Bencardino D., Lopez M., Iori A., Catalano C.

Accuracy of multi-parametric magnetic resonance imaging in the diagnosis and grading of intestinal acute Graft-versus-Host disease after allogeneic bone marrow transplantation (SS 1901c), B-1529

Vliegenthart R.

Cardiac and vascular: Chairperson's introduction (E³ 1323), A-640

Vliegenthart R.

Myocardial MRI: perfusion, tissue tracking and fibrosis: Keynote lecture (SS 1403), K-21

Vliegenthart R.

CT of the heart made easy: Cardiovascular risk estimation made easy: CA-scoring (E³ 24D), A-718

Vlychou M., Kyriakis I., Vassiou K., Tsougos I., Michalitsis S., Hantes M.

Diagnostic efficacy of a 3D sequence in the standard MR protocol among high risk patients for knee cartilage lesions (SS 310), B-0304

Vogel-Claussen J.

CT - patterns in chest radiology: back to basics and beyond: C. Ground glass opacities (GGO) and consolidation (RC 404), A-102

Vogl T.J., Graef K., Alizadeh L., Hammerstingl R., Nour Eldin N.

Parenchymal blood volume (PBV) measurement using C-arm-Dyna-CT as a prognostic marker for the response of HCC after repetitive transarterial chemoembolisation (TACE) (SS 209), B-0039

Vogl T.J., Reimann C., Puentes-Damm M., Hübner F., Bazrafshan B.

Feasibility study of microwave ablation system: localisation and eradication of tumorous lesions (SS 709), B-0622

Vogl T.J., Basten L., Naguib N.N.N., Nour-Eldin N.A.

Microwave ablation (MWA) of pulmonary neoplasms: clinical performance of MWA with spatial energy control vs conventional low-frequency MWA (SS 709), B-0623

Vogl T.J., Langenbach M.C., Hammerstingl R., Scholz J., Gruber-Rouh T.

Prospective randomised trial: tumour response of colorectal liver metastasis after transarterial chemoembolisation with two different protocols using MRI (SS 1409), B-1059

Vogl T.J., Alizadeh L., Albrecht M.H., Tischendorf P.

A comparative study of a new generation robotic angiography system based on patient dose and image quality during transarterial chemoembolisation (SS 1409), B-1062

Vogl T.J., Alizadeh L., Graef K., Nour-Eldin N.A.

Generation I vs new-generation cone-beam CT, digital subtraction angiography and digital fluoroscopy in patients undergoing TACE: comparison of radiation dose and image quality (SS 1409), B-1063

Vogl T.J., Zitsch M., Bechstein W., Trojan J.

Microwave ablation (MWA) in the treatment of colorectal liver metastases (CRLM): an eight-year follow-up study (SS 1509), B-1201

Voicu I.P., Napolitano A., Lattavo L., Carducci C., Rossi Espagnet M.C., Mastronuzzi A., Toma P., Colafati G.S.

Diffusion kurtosis imaging (DKI) can efficiently differentiate low- and high-grade gliomas in paediatric patients (SS 212), B-0153

Voicu I.P., Napolitano A., Lattavo L., Carducci C., Rossi Espagnet M.C., Mastronuzzi A., Toma P., Colafati G.

Grading of hemispheric gliomas in pediatric patients by using Diffusion Kurtosis MR imaging (SS 212), B-0159

Voicu I., Napolitano A., Lattavo L., Rossi Espagnet M., Carducci C., Mastronuzzi A., Toma P., Colafati G.

Diffusion kurtosis imaging (DKI) can help differentiate low- and high-grade brainstem gliomas in pediatric patients: a pilot study (SS 212), B-0157

Vollenbrock S.E., Voncken F.E., Lambregts D.M., Maas M., ter Beek L.C., Aleman B.M., Beets-Tan R.G.H., Bartels-Rutten A.

MRI for response assessment after neoadjuvant chemoradiotherapy in oesophageal cancer: added value of diffusion-weighted imaging (SS 701b), B-0717

Vollenbrock S.E., Voncken F.E.M., Lambregts D.M., Maas M., Vegt E., ter Beek L.C., Aleman B.M.P., Beets-Tan R.G.H., Bartels-Rutten A.

MRI vs FDG PET-CT for response assessment after neoadjuvant chemoradiotherapy in oesophageal cancer (MY 15), B-1274

von der Fehr T., Hjelte V., Erdal J.M., Helle T., Parker A.P.

CT hepatic contrast enhancement adjusted for body type versus lean body weight (SS 1014), B-0971

von Kalle T.

Paediatric musculoskeletal imaging: B. MRI of the temporomandibular joints: findings that can mimic arthritis (RC 112), A-011

von Spiczak J., Manka R., Gotschy A., Oebel S., Hamada S., Alkadhi H.

Fusion of coronary CT angiography and whole-heart 3D CMR myocardial perfusion: building a framework for comprehensive 3D cardiac imaging (SS 1503), B-1226

von Spiczak J., Mannil M., Alkadhi H., Manka R.

3D image fusion of whole-heart dynamic cardiac MR perfusion and late gadolinium enhancement: identifying areas for revascularisation (SS 1503), B-1227

Authors' Index

Vonder M., van der Aalst C.M., Vliegenthart R., Kaatee M., Gratama J., Kuijpers D., de Koning H., Oudkerk M.
Frequency and spectrum of incidental findings in cardiovascular disease CT screening trial (SS 603), B-0566

Vonder M., van der Aalst C.M., D'Archambeau O., Yperzele L., Vanacker P., Baar I., Muto M., Menovsky T., Parizel P.M.
Comparison of coronary calcium distribution in large population-based screening trials: Dutch (ROBINSICA) vs multi-ethnic (MESA) population (SS 603), B-0571

Voormolen M., Van der Zijden T., D'Archambeau O., Yperzele L., Vanacker P., Baar I., Muto M., Menovsky T., Parizel P.M.
Acute ischaemic stroke due to tandem occlusions of the internal carotid artery: results of endovascular recanalisation and clinical outcome (SS 1009), B-0858

Vucetic J., Ortega Millán M., Rivera Mata J., Palao Errando J., Barber Hueso C., Garcia Garcia R.
Do we diagnose it better? - new BI-RADS classification for microcalcifications (SS 202b), B-0101

Vucetic J., Palao Errando J., Barber Hueso C., Cárdenas Herrán J.S., Ortega Millán M., Garcia Garcia R.
Diagnosis and treatment of suspected high-grade lesions using ultrasound-guided vacuum-assisted breast biopsy (SS 1802a), B-1394

W

Waade G.G., Holen Á.S., Hanestad B., Sebuodegaard S., Moshina N., Pedersen K., Hofvind S.
Breast compression between women imaged using digital mammography and breast tomosynthesis in a population-based breast cancer screening programme (SS 214), B-0132

Wachabauer D., Röthlin F., Homolka P., Moshammer H.M., Ostermann H.
Evaluation of diagnostic reference levels for conventional radiography in Austria (SS 313), B-0317

Waldt S.
Shoulder: C. Postoperative (E³ 719), A-291

Walecki J.
Neurologic emergencies: Brain injury (BS 3), A-080

Wallis M.G.
Rethinking ductal carcinoma in situ (DCIS): C. Reducing overtreatment of DCIS (RC 1302), A-635

Walsh D.
Patient-doctor relationship and interdisciplinary communication in the radiology department: Patients' point of view (part 2) (PA 1), A-697

Walter S., Schneeweiß S., Maurer M., Lescan M., Bamberg F., Nikolaou K., Othman A.E.
Comparison of biphasic DE-CT with virtual unenhanced dual energy reconstruction and triphasic CT with true unenhanced images in patients with suspected acute bleeding (MY 7), B-0791

Walter S., Notohamiprodjo M., Keil M., Nikolaou K., Martirosian P., Gatidis S.
Comparison of local shim coils and slice-specific integrated shimming in EPI-based DWI of the head and neck region (SS 1008), B-0909

Waltrich N.K., Sawall S., Kachelrieß M.
Focal spot blur correction for cone-beam CT (CBCT) (SS 1813), B-1435

Wang C., Chen H., Lin W.
Core muscle composition and fat distribution in Parkinson's disease (SS 710a), B-0619

Wang D.
3D fast spin-echo T1 black-blood imaging for the preoperative detection of venous sinus invasion of meningioma: comparison with contrast-enhanced MRV (SS 1811b), B-1480

Wang F., Wu G., Chen W.
Investigation of intravoxel incoherent motion diffusion-weighted imaging for assessing bladder cancer invasiveness (SS 207), B-0063

Wang H., Guan J., Guo Y.
Female Skene's gland diseases: CT and MR imaging evaluation (SS 607), B-0472

Wang K.Y., Carlton J., Guffey D., Moron F.E.
Histogram analysis of ADC maps and FLAIR MR imaging can predict active demyelination in multiple sclerosis (SS 311), B-0277

Wang L., Tseng J., Lin Y.
Comparisons of imaging biomarkers on simultaneous choline PET and multiparametric MRI between TNM staging in high-risk prostate cancer patients (SS 1516), B-1250

Wang L., Wang D., Li X.
Radiomics signature from enhanced T1-weighted MR image helps to improve the differential diagnosis performance of sub-1cm breast mass (MY 16), B-1276

Wang L., Gong S.
A preliminary study of dual-energy CT spectral curve equation for the diagnosis of osteoporosis (SS 610a), B-0442

Wang L., Shenchu G., He B., Chen J.
Virtual bone mineral density imaging with third-generation dual-energy CT for diagnosis of osteoporosis: a preliminary study (MY 13), B-1018

Wang L., Zhang Y., Liu Z., Mao H.
Implications of 2-hydroxyglutarate in gliomas with IDH1/2 mutations (SS 1006), B-0986

Wang L., Zhang Y., Liu Z., Chen D., Liu L., Mao H.
Brain tumour-induced alterations in haemodynamic responses of BOLD fMRI (SS 1811b), B-1485

Wang M., Lu J., Dai Y., Xia Y.
Comparison of MRI and transvaginal ultrasonography in the diagnosis of retrocervical septum endometriosis (MY 4), B-0390

Wang M., Li W.
Subcortical nuclei in Alzheimer's disease: a volumetric and diffusion kurtosis imaging study (SS 1411a), B-1034

Wang M., Li W.
Subcortical nuclei and cognitive impairment in sub-acute mild traumatic brain injury: a diffusion kurtosis imaging and volumetric study (SS 1911a), B-1599

Wang R., Gao J., Zhou Y.
Automatic spectral chest CT assist protocol: can the improvement of the noise index setting further decrease the radiation dose and optimise the image quality? (SS 604), B-0463

Wang S., Tong T., Hu T., Peng W., Wang J., Huang L.
Utility of CT histogram parameters in discriminating between metastasis and non metastases among colorectal cancer patients with pulmonary lesions (SS 216), B-0171

Wang S., Li J.H.
Magnetic resonance imaging of hepatitis B virus-related hepatocellular carcinoma: correlations with imaging features and molecular marker glypican-3 (MY 15), B-1257

Wang W., Cheng J., Zhang Y.
Utility of histogram analysis of apparent diffusion coefficient maps obtained using 3.0T MRI for distinguishing uterine endometrial carcinoma from endometrial polyps (SS 607), B-0475

Wang W., Cheng J., Zhang Y.
Histogram analysis of apparent diffusion coefficients for monitoring early response in patients with breast cancer undergoing concurrent chemotherapy (SS 602), B-0497

Wang W., Cheng J., Zhang Y.
Histogram analysis of apparent diffusion coefficient maps for distinguishing lateral ventricle central neurocytoma from ependymoma (SS 1016b), B-0935

Wang W., Zhang Y., Cheng J., Zhang Z.
Differentiation of medulloblastoma and astrocytoma in children using histogram analysis of enhancement MRI (SS 1811b), B-1479

Wang W., Cheng J., Zhang Y.
Enhancement of MRI histogram in the identification of children with medulloblastoma and ependymoma (MY 18), B-1490

Wang W., Cheng J., Zhang Y.
Histogram analysis of apparent diffusion coefficients may predict molecular subgroups of medulloblastoma in children (MY 18), B-1496

Wang W.T., Zhu S., Ding Y., Yang L., Chen C., Ye Q., Zeng M., Rao S.
T₁ mapping on gadoxetic acid-enhanced MR imaging potentially predicts recurrence of HCC after hepatectomy (MY 15), B-1256

Wang W., Mao F., Cao J.Y., Fan P., Dong Y.
Application of contrast-enhanced ultrasound during microwave ablation for large benign thyroid nodules (SS 1509), B-1211

Wang X.
A glance of China through images: Application of artificial intelligence in prostate imaging (EM 3), A-950

Wang X., Sun C., Wang S., Cao J., Xu H., Gan S., Yin B., Bai G., Bai L.
Saliently alteration of hub profiles following acute mTBI (SS 1911a), B-1593

Wang X.
Logistic regression analysis and a risk prediction model of tumour spread through air spaces (STAS) in patients with stage I lung adenocarcinoma (MY 5), B-0404

Wang Y., Zhang W., Lui S.
Atypical functional connectivity between cerebral and cerebellar resting state networks in autism spectrum disorder (MY 17), B-1298

Wang Y., Ren K., Xie L., Zhang X.
Intravoxel incoherent motion and blood oxygen level-dependent of early iodinated contrast-induced acute kidney injury induced in a rabbit model (MY 4), B-0389

Wang Y., Lu J., Zhu L., Chen R., Jiang B., Jin Z.
Ovaries in patients with Mayer-Rokitansky-Küster-Hauser syndrome vs normal females: a retrospective cohort study with magnetic resonance imaging (SS 607), B-0467

Wang Z., Wang S., Sun C., Yin B., Bai G., Niu X., Sun Y., Zhang M., Bai L.
Atypical inter-hemispheric communication following subacute mild traumatic brain injury (SS 1911a), B-1596

Authors' Index

Wareing A.

Planning your career: Planning your professional development (BR 3), A-930

Washizuka F., Kitamura T., Hatakeyama T., Nakano H.

Reduction of contrast agent using virtual monochrome image in haemodynamics aortic phantom (SS 1014), B-0962

Wassef S., Stolpen A.

Evaluation of pelvic congestion syndrome with time-resolved MR angiography (SS 1815), B-1331

Watanabe A., Bradley W., Lim V.D., Chim C.Y.R.

Earlier detection of breast cancer using artificial intelligence (MY 16), B-1283

Wattjes M.P.

Current guidelines and diagnostic criteria in multiple sclerosis (MS): MRI for MS monitoring: the use of guidelines in clinical practice (SA 5b), A-210

Wawrzyniak P., Hebda A., Bobek-Billewicz B.

Three years of experience with magnetic resonance spectroscopy in spinal cord (SS 1411b), B-1107

Weber M.-A.

Lower extremity: B. Post-traumatic ankle (E³ 819), A-370

Weber M.-A.

Imaging the hip and thigh: C. Muscle injury of the hip and thigh (RC 910), A-417

Weber M.-A.

New treatments for musculoskeletal tumours: Multimodality imaging in treating and monitoring bone sarcoma (SF 17a), A-894

Weckbach S.

Whole-body MRI: ready for prime time?: Beyond oncology: rheumatology and more (SA 5a), A-200

Wegner F., Friedrich T., Panagiotopoulos N., Goltz J.P., Vogt F.M., Koch M.A., Buzug T.M., Barkhausen J., Haegele J.

Magnetic particle imaging: safe use of endovascular stents (MY 7), B-0793

Weidekamm C.

Postoperative imaging of sports injuries: B. ACL reconstruction and cartilage repair (TC 1628), A-871

Weidekamm C.

Postoperative imaging of sports injuries: C. Interactive case discussion (part 2) (TC 1628), A-873

Weidekamm C.

Advanced imaging techniques, algorithms and measurements: Keynote lecture (SS 1410), K-20

Weigel U.

EIBIR Research Session: European imaging researchers united in diversity: Laser and Ultrasound Co-analyser for Thyroid Nodules (LUCA) Project: latest results (EIBIR 1), A-320

Weikert T., Wyttenbach R., Nicolas G., Hendel R., Glessgen C., Bremerich J., Merkle E.M.

Automated translation of radiologic reports with deep learning-powered translation engines: a feasibility study (SS 605), B-0482

Weinheimer O., Galban C.J., Robinson T.E., Wielpütz M., Heussel C., Kauczor H.-U., Jobst B.

COPD phenotyping with parameter response maps based on paired inspiratory/expiratory low-dose computed tomography (SS 1905), B-1588

Weinrich J.M., Avanesov M., Henes F., Lenz A., Adam G., Bannas P.

Variability of MRI-derived aortic diameters in Marfan patients: comparison of inner vs outer vessel wall measurements (SS 215), B-0025

Weir A., Kelly B.S., Liew A., McCarthy P.

Metformin and intravenous contrast medium: a systematic review of international radiological societal guidelines (SS 205), B-0177

Weishaupt D.

Radiology and Swiss chocolate: a sweet combination: Introduction: What Swiss radiology and Swiss chocolate have in common (EM 1), A-450

Weishaupt D.

Abdominal MRI: from standard to advanced protocols: C. Pelvic floor disorder (RC 1701), A-879

Weiß J., Hoffmann R., Kessler E., Rempp H., Nikolaou K., Clasen S.

Feasibility, effectiveness and safety of percutaneous MR-guided ablation of small hepatic malignancies (SS 1509), B-1208

Weil L., Geier K.I., Kaul M., Späth L., Derlin T., Herrmann J., Adam G., Salamon J.

The role of diffusion weighted imaging for the differentiation of malignant and benign peripheral nerve sheath tumours (SS 1016b), B-0932

Wen J.

Differentiating primary CNS lymphomas from glioblastomas and inflammatory demyelinating pseudotumour using relative minimum apparent diffusion coefficients (SS 211), B-0094

Wen J.

Quantitative study of noninvasive prediction of glioma IDH1 gene status by APT combined with ASL imaging (MY 8), B-0799

Wen J.

A preliminary study on non-invasive prediction of IDH1 gene status in glioblastoma by intravoxel incoherent motion MR imaging (MY 8), B-0807

Weng Q., Zhang F., Xiong F., Jin Y., Song J., Chen M., Hui J., Ji J., Yang X.

Orthotopic lung cancer: molecular imaging-monitored intratumoural radiofrequency heat-enhanced HSV-TK gene therapy (SS 1406), B-1171

Weston M.

Placental imaging: how, when and why?: Chairperson's introduction (SF 16), A-813

Wibmer A.G., Robertson N.L., Ehdaie B., Stone S., Brawer M., Hricak H., Vargas H.

Cell cycle progression genomics and MRI features of prostate cancer: radiogenomic correlation and prognostic synergism (SS 307), B-0254

Wichmann J.L., Bucher A.M., Lenga L., Arendt C., Caruso D., D'Angelo T., Blandino A., Ascenti G., Vogl T.J.

Assessment of optimal window settings for display of traditional and noise-optimised virtual monoenergetic imaging in dual-energy CTPA (SS 604), B-0460

Widya R.L.

Obesity and type 2 diabetes: cardiovascular and cerebral aspects (SS 303), B-0330

Wielema M., Dorrius M., Dijkstra H., Langius E., De Bock G., Oudkerk M., Sijens P.

High reproducibility of breast lesion ADC values based on fixed size and shape region of interest in diffusion-weighted imaging (SS 1402b), B-1109

Wielpütz M.O.

When and how to use perfusion imaging in pulmonary vascular and airway disease?: B. MRI (RC 104), A-008

Wielpütz M.O.

Chest imaging of cystic fibrosis: from infants to adults: Chairperson's introduction (SF 13a), A-608

Wiesmüller M., Wüst W., May M.S., Uder M.

Staging of head and neck cancer by dual energy CT: comparison of dual and single source dual energy (SS 1008), B-0901

Wildberger J.E.

The heart between the lungs: Chairperson's introduction (E³ 618), A-256

Wildberger J.E.

The new horizon for radiology: Medical imaging and clinical laboratories: a fruitful liaison (NH 14), A-725

Willemink M.J., Maret E., Moneghetti K.J., Kim J.B., Haddad F., Kobayashi Y., Higashigaito K., Fearon W., Fleischmann D.

Aortomitral calcification is an independent predictor of mortality in TAVR patients (SS 215), B-0026

Williams M.

The heart between the lungs: B. Coronary artery disease (E³ 618), A-258

Wilman H.R., Bachitar V., Jacobs J., Newbould R., Gyngell M., Kelly C.J., Kelly M.D., Banerjee R.

Repeatability and reproducibility of multiparametric magnetic resonance imaging of the liver (SS 201a), B-0002

Wilson D.J.

Bone, joint and soft tissue infection: C. Pyomyositis and other soft tissue infections (RC 410), A-135

Winklhofer S., Burgstaller J., Held U., Finkenstaedt T., Del Grande F., Andreisek G., Steurer J., Bolog N.

Correlation of body mass index with paraspinal muscle fatty degeneration in non-diabetic patients with lumbar spinal canal stenosis: results from 685 patients (MY 13), B-1031

Wirth S.

GI bleeding: how to solve the problem?: Chairperson's introduction (RC 101), A-003

Wirth S.

Why do I miss fractures in emergency?: Chairperson's introduction (RC 1617), A-836

Wohlfahrt P., Richter C., Möhler C., Greilich S.

New imaging approaches for radiotherapy: Dual-energy CT: what are the benefits for radiotherapy? (ESR/ESTRO), A-885

Woisetschlager M., Spängeus A.

Model for improved correlation of BMD values between abdominal routine dual-energy CT data and DXA scans (SS 1905), B-1589

Wolf N.

State-of-the-art paediatric neuroradiology: A. Imaging myelin maturation disorders (RC 811), A-336

Wolters van der Weij E.

Closing the gap between education and clinical practice for radiographers: How can new teaching methods be implemented? (PC 13), A-660

Wong E., Chang T., Cho F., Lai M., Soong S., Law L., Yeung M., Tang K.

MRI findings of post-IGBT-treated cervical tumour (SS 1816), B-1370

Authors' Index

Wong Y., Wang L., Wu C.

Comparison of the inter-observer reliability of injury severity recording between unstructured and structured CT reports of blunt abdominal trauma (SS 317), B-0297

Woo S., Kim S., Cho J., Kim S.

Diagnostic performance of MRI for assessing parametrial invasion in cervical cancer: a head-to-head comparison between oblique and true axial T2-weighted images (SS 707), B-0649

Wörtler K.

Bone tumours: Bone tumours (E³ 25C), A-485

Woznitza N.H.

Making the most of social media: #MedRadJClub: a Twitter journal club (EFRS WS), A-788

Wressnegger A., Schestak C., Prosch H., Apfaltrer G., Ringl H., Apfaltrer P.

Individual and specific dose-level selection using dual-source computed tomography of the chest and its impact on image quality and radiation dose (SS 704), B-0633

Wright C.L., Binzel K., Zhang J., Maniawski P., Knopp M.V.

Higher definition head and neck imaging enabled with digital photon counting PET/CT: an intra-individual comparison with conventional photomultiplier PET/CT (SS 1508), B-1218

Wu F., Yang Q., Zhang C.

Characteristics of plaques and lenticulostriate arteries in stroke patients by whole-brain vessel wall (MY 8), B-0811

Wu F.Z.

Semiquantitative visual assessment of sub-solid pulmonary nodules ≤ 3 cm in differentiation of lung adenocarcinoma spectrum (SS 1804), B-1352

Wu H., Wu W.

Mammographic breast density analysis with automated volumetric breast density in a single centre of Taiwan women (SS 1902a), B-1607

Wu K., Gee M., Kaplan J.

Magnetic resonance enterography (MRE) surveillance of asymptomatic paediatric Crohn's disease patients (SS 612), B-0573

X

Xiao Y., Yan Z., Zhao Y., Tao B., Gong Q., Lui S.

Support vector machine-based classification of first-episode drug-naïve schizophrenia patients and healthy controls using structural MRI (SS 711a), B-0657

Xie L., Guo Y., Yang Z.

Assessment of the left ventricular myocardial strain in type 2 diabetes mellitus patients with hypertension using MR tissue tracking (SS 303), B-0339

Xie Q., Wu J., Ren Y., Pang H., Zhang H., Jin T., Wu Y., Yao Z., Feng X.

DCE-MRI in human gliomas: a surrogate for assessment of invasive hypoxia marker HIF-1 α based on MRI-neuronavigation stereotactic biopsies (SS 1811b), B-1483

Xie Q., Wang H., Guan J.

Hollowed adrenal gland sign in patients of septic shock: prevalence, CT appearance and consequence (SS 1007), B-0878

Xu H., Yang Z., Guo Y., Peng W., Peng W.

Impaired segmental myocardial microvascular dysfunction in chronic kidney diseases patients: assessed by cardiac magnetic resonance first-pass perfusion imaging (SS 1403), B-1154

Xu H., Gao Y.

Three-dimensional texture analysis technology in computed tomography: a new radiological marker in the pathology of liver cancer (SS 601a), B-0431

Xu H., Liu Y., Yuan H.

Effect of carotid endarterectomy on the distribution and value of cerebral blood flow: evaluation by territorial arterial spin labelling (SS 711b), B-0686

Xu J., Chen Y.Q.

A prospective study to compare the outcomes of MRF-TB and 12-core SB in different PSA groups (SS 1907a), B-1560

Xu K., Zhang Y.

The value of whole tumour volume-based T2 histogram analysis of differential diagnosis in paediatric posterior fossa tumours (SS 1811b), B-1475

Xu L., Li F., Du J.

Ultrasound molecular imaging of breast cancer in mcf-7 orthotopic mice model using a novel dual-targeted ultrasound contrast agent (SS 1406), B-1180

Xu R., Xu H., Yang Z., Guo Y.

Myocardial microvascular dysfunction in patients with end-stage renal disease: assessment with 3.0T cardiac magnetic resonance (SS 1403), B-1153

Xu W., Wen J., Li Y.

Using multiple linear regression to investigate IDH1 gene mutation in glioma by joint application of DCE-MRI and DSC-MRI (SS 1016b), B-0938

Xu X., Teng G.

Disrupted brain functional network architecture in long-term sensorineural hearing loss patients (MY 14), B-1185

Xue H.

A glance of China through images: Multimodality imaging for insulinoma detection (EM 3), A-948

Xue Y., Huang L.

Hybrid repair of aortic pathology involving aortic arch (SS 309), B-0223

Xuesong D., Zhang W.

Visually AcceSAbLe Rembrandt Image (VASARI) assessment features predict GBM recurrence patterns (SS 1016b), B-0937

Y

Yadav A., Bagarhatta M., Jaipal U.

PI-RADS version 2-based assessment of prostate in patients with borderline-elevated prostate-specific antigen levels: a prospective study (SS 1807a), B-1362

Yagami K., Miyoshi T., Shigeyama S., Okada H., Suzuki S., Foley S.J.

Effective dose calculations of trunk CT scans in single-energy CT (SECT) and fast kVp switching dual-energy CT (FKS-CT) (SS 314), B-0324

Yamada A., Nonaka T., Nakamura M., Suzuki T., Komatsu D., Fujita S., Fujinaga Y., Kadoya M.

Evaluation of T1 measurement methods of the liver in chronic liver disease (SS 1801), B-1315

Yamamura J., Aigner A., Schramm C., Zenouzi R., Adam G., Keller S.

Assessment of histological stage of fibrosis using relative liver enhancement in patients with primary sclerosing cholangitis (SS 1801), B-1317

Yamamura J., Sedlacik J., Schuler T., Buchert R., Kooijman-Kurfuerst H., Schramm C., Fiehler J., Adam G., Keller S.
The potential role of Gadoxetate disodium (Gd-EOB-DTPA) and diffusion-weighted magnetic resonance imaging in primary sclerosing cholangitis (SS 1801), B-1319

Yang F.

A glance of China through images: Multiparametric analysis in imaging liver disease (EM 3), A-947

Yang I., Wu B.

Locally advanced rectal cancer: the value of whole-tumour histogram-based texture analysis of baseline ADC map in predicting tumour response to neoadjuvant chemoradiotherapy (SS 1001b), B-0849

Yang L.

The concentration of iodine in perigastric adipose tissue: a novel index for assessment of serosal invasion in patients with gastric cancer after neoadjuvant chemotherapy (SS 701b), B-0709

Yang L., Zeng M., Rao S.

Assessing liver fibrosis with diffusion-weighted MRI: comparison between conventional and kurtosis models (SS 1801), B-1318

Yang L., Hou Y., Ma Y., Jia Z., Lu X.

Study on the optimum keV and different contrast agent concentration in coronary stent imaging using spectral CT: in vitro study (SS 703), B-0759

Yang Q., Yu T., Huang J., Su Y., Li J., Liang B.

Application of T1rho in evaluating liver fibrosis and correlation with liver function (SS 201a), B-0004

Yang S., Lu F., Zhan S.

USPIO-enhanced MRI study on electroacupuncture alleviating inflammatory response of permanent focal subacute-stage cerebral ischaemia in rats (SS 1011b), B-0999

Yang X., Miller E., Subramanian P., Williams T.M., Knopp M.V.

Multi-parametric MRI assessment of acute response to stereotactic body radiation therapy in patients with hepatocellular carcinoma or non-small cell lung cancer (SS 1416), B-1079

Yang Z., Jin H., Kim J.

A noise-robust and accurate measurement method for the wall thickness of small airways in low-dose CT scans (SS 713), B-0735

Yazicioglu Y., Pinker K., Tahmassebi A., Meyer-Baese A.

Determining leader nodes in dementia networks (SS 1411a), B-1036

Yilmaz P., Ikram M., Niessen W.J., Ikram M., Vernooij M.W.

Sum score of cerebral small vessel disease relates to risk of stroke, dementia and mortality in the Rotterdam study (MY 8), B-0797

Yim J., Kim Y.

Diagnostic efficacy of conventional gadolinium-enhanced MRI in the detection of recurrent hepatocellular carcinoma: intra-individual comparison with gadoxetic acid-enhanced MRI (SS 301a), B-0197

Yim Y., Kim J.Y., Jung S.C., Lee B.E., Kim S.J., Kim H.S., Lee D.H., Choi C.G., Park J.E.

Diagnostic performance of three-dimensional high resolution magnetic resonance imaging for intracranial aneurysms: comparison with digital subtraction angiography (SS 711b), B-0693

Authors' Index

Yin X., Gao F., Wang G.

Altered hippocampal GABA and glutamate levels and functional connectivity in multiple sclerosis (SS 311), B-0279

Ying T.M., Li Y., Wu W.C.V., Yuan C., Kwong L.W.D., Yip S.P., Law K.W.H., Lee W.Y.S.

Are there any differences in radiation-induced and non-radiation-induced carotid atherosclerosis? (SS 315), B-0217

Ying T.M., Cheng S., Ahuja A.

Computer-aided quantification of intranodal vascularity enhanced the accuracy of ultrasound in distinguishing metastatic and tuberculous cervical lymph nodes (SS 1508), B-1214

Yiqun S., Tong T.T., Gu Y.J.

Radiomic features from pretreatment MRI are associated with prognosis in rectal cancer patients: preliminary findings (SS 216), B-0163

Yoneda T., Iwata M., Indo H., Kurehana N., Yoshinaga S., Takeda M., Terasawa H.

ROI-based phase analysis for neuronal current MRI (SS 713), B-0738

Yoon D., Moon S.

Subtalar instability and lateral ankle instability: the difference with emphasis on subtalar ligaments using 3-D isotropic MRI (SS 710b), B-0724

Yoon J., Kim E., Okuaki T., Lee J.

Liver function estimation using gadoxetic acid-enhanced liver MRI (SS 1801), B-1321

Yoon S., Na D., Gwon H.

Diagnostic performance of US-based fine-needle aspiration criteria for thyroid malignancy: comparison of three international society thyroid imaging reporting and data systems (SS 708), B-0672

Yoshida M., Enokido K., Nishiyama T.

The diagnostic performance of automated breast ultrasound (ABUS) compared with handheld ultrasound (HHUS) (SS 202b), B-0106

Young L.K., Matthew S., Houston G.

Investigating potential gadolinium toxicity to gadoterate meglumine (Dotarem) in local renally insufficient adult and paediatric populations using bioinformatics data linkage (SS 1905), B-1585

Yousry T.A.

Radiologic anatomy: neuro: Cortical anatomy and primary functional areas (ESR/ESOR 3), A-561

Yousry T.A.

My three top tips for neuroimaging: Movement disorders (SF 15c), A-761

Yu Q., Quan X., Lu X.

Correlation analysis of quantitative CT parameters and pulmonary function in COPD patients (SS 304), B-0233

Yu Y., Ren Y., Pang H., Yao Z.

Quantitative T1rho-weighted magnetic resonance imaging in gliomas: a preliminary study of its biochemical mechanism (SS 1811b), B-1482

Yuan B., Zhang W., Lu X., Jia Z.

Evaluation of diagnostic value of iodine base material of dual-detector spectral CT for pulmonary aspergillosis invasion by ROC (SS 604), B-0456

Yuan Q.Q.

Study of image quality in chest CT using prospective ASIR-V (SS 704), B-0636

Yue Y., Lu X., Guo Q.

Oligaemia of tumour-involved lung displayed by Z-effect of dual-detector spectral CT (SS 604), B-0454

Yue Y., Lu X., Zhang W., Guo Q.

Segmental and sub-segmental pulmonary embolism displayed by dual-detector spectral CT (SS 604), B-0464

Yuekao L.

Early residual tumour differentiation from benign periabdominal thermal injury after radiofrequency ablation by spectral analysis with dual-energy computed tomography (MY 5), B-0418

Yun G., Kim Y., Lee Y.

Tumour heterogeneity of pancreas head cancer assessed by CT texture analysis: association with survival outcomes after curative resection (SS 201b), B-0020

Yun G., Yoon C., Seong N., Byeon J., Lee H., Kim Y.

Percutaneous treatment of postoperative benign hepaticojejunostomy strictures: temporary placement of covered metallic stents versus balloon dilation (SS 209), B-0032

Yun G., Kim Y., Choi S.

Sonographic features of medullary thyroid carcinoma: application of Thyroid Imaging Reporting and Data System (TIRADS) classification (SS 708), B-0664

Yusuf G.T.

A paediatric cost and safety analysis of contrast-enhanced ultrasound (SY 11)

Z

Zaccagna F., Riemer F., McLean M.A., Grist J.T., Schulte R., Watts C., Price S.J., Graves M.J., Gallagher F.A.

²³Na-MRI demonstrates a sodium gradient within gliomas as a biomarker of tumour heterogeneity (SS 1911b), B-1672

Zackrisson S.

New mammography: tomosynthesis and future techniques: A. Should we abandon 2D mammography? (RC 502), A-175

Zackrisson S.

Approaches to accelerating and standardising DBT reading in screening: what's new? Final results of the Malmö Breast Tomosynthesis Screening Trial (SY 1b)

Zackrisson S.

My three top tips for breast imaging: Screening with tomosynthesis (SF 8b), A-325

Zamboni G.

New challenges of pancreatitis: Chairperson's introduction (E³ 1322), A-674

Zamyshvskaya M., Zavadovskaia V., Zorkaltsev M., Udodov V., Grigoriev E.

Diabetic foot complicated by osteomyelitis: the role of multiparametric magnetic resonance tomography (SS 710b), B-0728

Zanardi S., Cappelli A., Mosconi C., Renzulli M., Modestino F., Golfieri R.

Percutaneous treatment of biliary lithiasis: personal experience (SS 209), B-0038

Zanetti M.

Bone, joint and soft tissue infection: B. Septic arthritis (RC 410), A-134

Zanetti M.

Small joints: Chairperson's introduction (E³ 1119), A-511

Zanirato Rambaldi G., Niro F., Galiè N., Zompatori M.

Diagnostic value of radiologic signs of pulmonary hypertension: pulmonary artery aortic ratio, pulmonary artery vertebral ratio and contrast regurgitation in hepatic veins (MY 5), B-0407

Zanirato Rambaldi G., Baldazzi M., Pierotti L., Carfagnini F., Zompatori M.

Simplified cystography protocol for dose exposure reduction in paediatric patients for the diagnosis of vesicoureteral reflux (SS 612), B-0579

Zannoni S., Pompili G., Tresoldi S., Di Leo G., Ravelli A., Primolevo A., Spadarella G., Carrafiello G.

Use of the previously proposed (2013) ultrasound total malignancy score (TMS) in the management of thyroid nodules (MY 14), B-1189

Zaottini F., Picasso R., Airdi S.

Ultrasound of the Thenar Motor branch in Carpal Tunnel Syndrome (SS 710a), B-0615

Zappa M., Doblas S., Cazals-Hatem D., Milliat F., Garteiser P., David M., Vilgrain V., Van Beers B., Ogier-Denis E.

7 T MR imaging for fibrosis evaluation in a radiation-induced murine model of colitis (SS 1901c), B-1528

Zarb F.

Maximising outputs from research: Chairpersons' introduction (part 1) (RC 414), A-140

Zawadzki R., Kubas B., Hładuński M., Zajkowska J., Zajkowska O., Jurgilewicz D., Garkowski A., Pancewicz S., Lebkowska U.

Proton magnetic resonance spectroscopy (¹H-MRS) of the brain in patients with tick-borne encephalitis (SS 311), B-0278

Zech C.J.

Imaging of the complicated postoperative abdomen: Chairperson's introduction (RC 401), A-095

Zeilinger M.

Radiographers in preclinical imaging research: Preclinical evaluation of PET tracers (SF 9b), A-425

Zerunian M., Bellini D.M., Caruso D., De Santis D., Biondi T., Laghi A.

Performance of texture analysis in predicting tumoural response to neoadjuvant chemoradiotherapy in rectal cancer patients studied with 3T MR (SS 216), B-0164

Zerunian M., Caruso D., Bellini D.M., De Santis D., Rivosecchi F., Laghi A.

MRI of rectal cancer response to therapy: comparison of T2, DWI and ADC between 3T and 1.5T (SS 216), B-0169

Zhang C., Chen N., Li K., Yang H.

Prefrontal lobe cortex-thalamus pathway impairment in intractable temporal lobe epilepsy with executive control function abnormal: evidence from structural and functional MRI study (SS 1811a), B-1403

Zhang D., Jin Z., Xue H., Yu S., Wu R.

Virtual monochromatic imaging improves the stent visualisation in lower extremity run-off CT angiography by dual-layer spectral detector CT (MY 7), B-0792

Zhang H., Tang Y.

Evaluation of pituitary micro-lesions using 3D space: the large sample analysis (SS 1911b), B-1670

Authors' Index

Zhang H., Tong T.T.

MR texture analysis: potential imaging biomarker for prediction of chemotherapy response in patients with colorectal liver metastases (MY 3), B-0367

Zhang J., Wu B., Zhou Y.

Analysis of the relationship between imaging patterns of calcification and response to chemotherapy in patients with colorectal metastases (SS 601a), B-0432

Zhang X., Li M., Mao L., Wang C., He S., Liu M.

Value of quantitative magnetic resonance imaging T1-relaxation time in predicting contrast-enhancement in breast cancer (SS 602), B-0502

Zhang Y.

In vivo tracing of superparamagnetic iron oxide-labelled bone marrow mesenchymal stem cells transplanted for traumatic brain injury by susceptibility weighted imaging in a rat model (SS 1006), B-0991

Zhang Z., Cheng J.

The value of readout-segmented diffusion-weighted imaging in the evaluation of parotid gland tumours (SS 208), B-0065

Zhang Z., Cheng J.

Metrics and textural features of MRI diffusion to improve classification of common parotid gland tumours (MY 14), B-1187

Zhao C.

Structural and functional brain abnormalities in schizophrenia: a cross-sectional study at different stages of the disease (SS 711a), B-0663

Zhao C.

Impacts of related risk factors on the efficacy of interventional treatment towards intractable postpartum haemorrhage (MY 9), B-0817

Zhao H.

The value of wide-detector helical CT combined with adaptive statistical iterative reconstruction-V in patients with high heart rate during coronary CT angiography (SS 703), B-0758

Zhao Q., Rong X., Yang Z., Diao K., Gao Y., Guo Y.

Semi-quantitative evaluation of coronary microvascular dysfunction in paediatric patients with leukaemia using magnetic resonance first-pass perfusion imaging (MY 7), B-0788

Zhao W.

Impact of tomosynthesis angular range on mass conspicuity in patients with dense breasts: experiences from a physicist's view (SY 1c)

Zheng L., Zhang C., Li K.

Feasibility of contrast-enhanced spectrum mammography in breast cancer diagnosis (SS 1802b), B-1412

Zheng X., Chen Y.Y., Xiao Y., Zheng D.

DKI can early differentiate radio-insensitive human nasopharyngeal carcinoma xenograft in nude mice (SS 208), B-0073

Zhou Y., Jing X., Ding J.

Risk factor-based prediction algorithm for liver function damage in patients with hepatocellular carcinoma after microwave ablation (SS 1509), B-1203

Zhou Y.

Meta-analysis of spectral CT image analysis tools and multi-phase CT enhancement in diagnostic accuracy of hepatic cell carcinoma (SS 1901a), B-1506

Zhou Y.

The influence of intelligent optimum tube voltage-combined low dose of contrast medium injection based on BMI on radiation dose and image quality of chest CT enhancement (SS 1904a), B-1559

Zhu L., Sun Z., Xue H., Qian T., Jin Z.

Compressed sensing accelerated 3D magnetic resonance cholangiopancreatography: application in pancreatic diseases (MY 3), B-0364

Zhu L., Li J., Sun Z., Xue H., Jin Z.

Dynamic-enhanced CT of multiple solid pancreatic lesions: prevalence and features of non-malignancies (MY 15), B-1259

Zhu L., Xue H., Sun Z., Nickel D., Qian T., Jin Z.

Evaluating autoimmune pancreatitis under corticosteroid treatment with T1 mapping (MY 15), B-1261

Zhu Y., Ma X., Zhao X.

Contrast-enhanced MR imaging 3D texture analysis as a potential tool for preoperative prediction of microvascular invasion in hepatocellular carcinoma (SS 1801), B-1325

Zhu Y., Li X., Wang F., Ye Z.

Intravoxel incoherent motion diffusion-weighted magnetic resonance imaging in characterisation of axillary lymph nodes: preliminary animal experience (MY 16), B-1280

Zhurbin E., Gayvoronskiy A., Zheleznyak I., Dekan V.

Diagnostic efficiency of ultrasonography in case of peripheral nerve traumatic injuries (SS 1411b), B-1101

Ziayee F., Ullrich T., Rabenalt R., Albers P., Antoch G., Schimmöller L.

Dynamic contrast-enhanced MRI (DCE) for prostate cancer detection: are qualitative and quantitative analyses the key to success? (SS 307), B-0248

Ziegeler K., Eshkal H., Schorr C., Sieper J., Diekhoff T., Makowski M.R., Hamm B., Hermann K.

Prevalence of fat metaplasia and other structural changes of sacroiliac joints in patients without axial spondyloarthritis: a cross-sectional MRI study (SS 310), B-0309

Zins M.

Spectral imaging: the future of CT? (SY 2)

Zins M.

Liver and bile duct pathologies: Chairperson's introduction (E⁹ 820), A-372

Zins M.

My three top tips for abdominal imaging: Bowel ischaemia (SF 12a), A-524

Zins M.

Tumour response assessment in abdominal imaging: C. Pancreatic adenocarcinoma (RC 1601), A-809

Zins M.

Abdominal emergencies: friends and enemies: Closed loop obstruction: a challenging diagnosis (SF 17b), A-903

Zlatareva D.

Radiologic anatomy: neuro: The basal ganglia of the brain revisited (ESR/ESOR 3), A-563

Zoet G.A., Benschop L., Budde R.P., de Groot C.J.M., Maas A.H.E.M., Roeters van Lenep J.E., van Rijn B.B., Velthuis B.K., Franx A.

Prevalence of subclinical coronary artery disease by coronary computed tomography among low risk women after preeclampsia (MY 7), B-0785

Zolda P.

EIBIR Research Session: European imaging researchers united in diversity: EIBIR's role in imaging research projects (EIBIR 1), A-323

Zopfs D., Lennartz S., Maintz D., Persigehl T.

Diagnostic value of virtual monoenergetic urographic phase images in the assessment of urothelial carcinoma (SS 1807b), B-1470

F

List of Authors & Co-Authors (F)

List of Authors & Co-Authors

A

- A. Aboueldahab N.: B-0034, B-1055
Aadnevik D.: A-389
Aalbers A.G.: B-1085, B-1376
Aandahl I.-J.: B-1309
Aase H.: B-1007
Abbas A.M.: B-0473
Abd El Bagi M.: B-0306
Abd Ellah M.M.H.: B-1423
Abdel Aal A.M.: B-0866
Abdel Aal A.M.K.: B-0034, B-1055
Abdel Aziz A.: B-1287
Abdel Hamid W.R.A.: B-0474, B-1113
Abdel Kawi M.: B-0592
Abdel M.: B-1252
Abdel Razek A.: B-0092
Abdel Razek N.M.: B-1389
Abdelhadi O.: B-0830
Abdel-Wahab R.: B-1544
Abdi R.: B-1466
Abdolell M.: B-0684, B-1606
Abdollahi H.: B-0477, B-0478, B-0739, B-0740
Abdolmohammadi J.: B-0287
Abdulla T.S.: B-0946
Abdullayev N.: B-0377, B-0511, B-0699, B-0927, B-1012, B-1023, B-1119
Abdullin I.I.: B-1561
Abelhafez E.M.: B-1502
Abeyakoon O.: B-0498, B-1094
Abidi Z.: B-0287
Abihanna M.: B-0245, B-1074
Abolmaali N.: B-1383
Abou El-Ghar M.E.: B-0887
Abou-Jaoude G.: B-1395
Abrantes A.F.: B-0329, B-0749, B-0965, B-1149, B-1445, B-1451, B-1637, B-1638, B-1640, B-1641, B-1642, B-1645
Abu Eid M.: B-0067
Achten E.: B-0540
Ackermans L.L.G.C.: B-0365
Acquafresca M.: B-0141
Adaletli I.: B-0582
Adam E.J.: A-148
Adam G.: B-0022, B-0025, B-0035, B-0780, B-0932, B-0990, B-1252, B-1319, B-1327, B-1569
Adam G.B.: B-1317
Adam G.G.A.: B-0692
Adams H.H.: B-1038
Adams L.: B-0061
Adams L.C.: B-0426
Addala T.: B-0949
Addeo G.: B-0056
Adelt S.: B-0894
Adler K.: B-0504
Adriaensen M.: A-179
Aerden D.: B-1044, B-1050
Aerts H.J.: B-0352, B-0356
Aertsen M.: B-1139
Afacan G.O.: B-0108
Agarwal A.: B-1507, B-1667
Agarwal S.: B-1667
Agati L.: B-0789
Ageev A.: B-1497
Aghaghazvini L.: B-1215
Aghahosseini F.: B-0500
Agildere A.M.: B-1004
Agirman M.: B-1422
Agostini S.: B-0056
Agovic M.: B-1163
Agri F.: B-1273
Agten C.A.: B-1123
Aguiar C.: B-0963
Aguiar P.: B-0992, B-1395
Aguilera del Hoyo F.: B-0175
Aguilera G.: B-0492, B-0667
Agulleiro D.: B-1223
Ahmad K.A.: B-1502
Ahmad M.: B-1207
Ahmed S.: B-0306
Ahn H.: B-1066
Ahn J.: B-1474
Ahuja A.T.: B-1214
Ahuja B.: A-544
Aigner A.: B-1317
Airdali S.: B-0615, B-0616
Aissa J.: B-0319, B-1235, B-1584
Aixut Lorenzo S.: B-0827
Akgündüz Ö.: B-1219
Akansel G.: B-0108
Akata D.: A-244, B-0322, B-1450
Akbas T.: B-0763
Akdulum I.: B-1505
Akgun A.S.: B-1422
Akhadov T.: B-0156, B-0806
Akhan O.: A-411
Akhmetzianov B.: B-1677
Akin I.: B-1354
Akin M.: B-1291
Akinci D.: A-365
Akinci D'Antonoli T.: B-0874
Akino N.: B-0428
Akita K.: B-1472
Akkaya Z.: B-0952, B-1618
Akkerhuis J.: B-1461
Aksakal M.: B-0205
Aksenova S.: B-1375
Al Dahery S.: B-0554
Al Hajjar N.: B-0453
Al Kamali A.: B-0346
Al Marakby A.: B-0950
Al Mohanna J.: B-0912, B-1289
Al Najdi A.: B-0067
Al Ohraini Z.: B-0257
Ala A.: B-1398
Alagic H.: B-1341
Alagic Z.: B-1341
Alagna G.: B-0266, B-0493, B-0668, B-1633
Alahmadi M.S.: B-1476
Alaia E.F.: B-0538
Alakhra M.: B-1416
Alam M.S.: B-0603
Alamo-Maestre L.: B-1491
Alatas I.: B-0581
Al-Attar M.: B-0275
Albaina Latorre L.: B-0992
Albano D.: B-0440, B-0719, B-0955, B-1616
Alberich-Bayarri A.: A-047, A-734, B-1380
Alberotanza V.: B-0144
Albers P.: B-0248, B-0252, B-1363, B-1364
Albiol A.: B-0121
Albiol F.: B-0121
Albisinni U.: B-0114
Albrecht M.: B-0752, B-0776, B-1232, B-1454
Albrecht M.H.: B-0258, B-0569, B-1049, B-1052, B-1062, B-1456, B-1515
Albuquerque M.L.L.: B-1285
Albuquerque T.C.V.: B-0879
Albweady A.A.: B-0982
Alcalá-Galiano A.: A-920
Aldossari K.: B-0982
Aldrighetti L.: B-0629, B-1205
Aleman B.M.: B-0717
Aleman B.M.P.: B-1274
Alfaleh H.: B-0306
Alfaqih M.: B-0951
Alfaro I.: B-1537
Alfayate Sáez E.: A-789
Alfonsi A.: B-0627, B-0820
Alharbi M.: B-0982, B-1476
Alhyari I.: B-1045
Ali M.: B-0786, B-1651
Ali R.M.K.M.: B-0135
Ali S.M.: B-0140
Ali T.F.T.: B-0247
Alimohammadpur R.: B-1466
Alison M.: A-648
Aliverti A.: B-0768
Alizadeh L.: B-0039, B-1062, B-1063
Alkadhhi H.: A-001, A-784, B-0047, B-0123, B-0310, B-0980, B-0981, B-1226, B-1227
Al-Khatib A.: B-1217
Allard P.-E.: B-1156
Allen C.: A-397
Alley M.: B-0028
Allimant C.: B-1053, B-1057
Almasi T.: B-0830
Almehmi A.: B-0866
Almeida C.M.: B-0326
Almeida R.P.P.: B-0329, B-0749, B-0965, B-1149, B-1445, B-1451, B-1637, B-1638, B-1640, B-1641, B-1642, B-1645
Al-Murshedi S.H.: B-1446
Al-Omari A.: B-1045
Alorfi F.: B-0306
Alqahtani F.: B-0158
Alqahtani S.J.M.: B-0746, B-0751
Alrowily M.: B-1446
Alsaad A.N.: B-1476
AlSaady R.: B-0946
Alsadiq M.R.: B-1659
Alsharif W.: B-1300
Alshahre O.: B-0306
Alster T.: B-0916
Altamash M.: B-0054
Altmirano J.: B-1116
Altay Ç.M.: B-0098
Althagafi M.S.J.: B-1476
Althoff C.E.: B-0001
Altman A.: A-035
Altabelli S.: B-0487, B-1623
Altomare C.: B-0627, B-0820
Altunkeser A.: B-1418
Alukic E.: B-0745
Álvares de Campos M.: B-0391
Alves E.D.: B-1233
Alves F.: B-0328
Alves Z.: B-0798
Amarnath C.: A-335
Amato F.: B-1292, B-1614, B-1630
Amato M.P.: B-0286
Amaxopoulou C.: B-1166
Ambrosetti M.C.: B-1519, B-1521
Amedro P.: B-1133
Amico V.: B-0958
Amin M.F.: B-0488, B-1399
Amini N.: B-0438
Amitai M.M.: B-0486
Ammari S.: B-0368, B-0737
Amodeo E.M.: B-0861, B-0898, B-0944
Amoretti N.: B-1025, B-1027
Amunts K.: B-1037
An C.: B-0192
An D.: B-1158
Anas M.: B-1411
Anastasia T.: B-1484
Andersen H.K.: B-1137
Andersen J.-G.: B-0140
Anderson M.: B-0831
Anderson N.: B-0731
Anderson S.E.: B-0537
Andersson B.T.: A-549, A-695
Andersson I.: B-1006, B-1628
Ando S.M.: B-0877
Ando T.: B-1391
Andrabi Y.: B-0951
Andrade S.: B-0694
Andrani F.: B-1541
André A.: B-0963
Andreani O.: B-1025, B-1027
Andreev G.: B-0406
Andreini D.: B-0031, B-0567, B-0755, B-1224, B-1459, B-1460, B-1658
Andreisek G.: A-514, B-1031
Andreu J.: B-1551
Andriessen T.M.J.C.: B-1594
Angaramo N.: B-0263
Angelakis A.: B-0430
Angelelli G.: B-0465
Angelidakis L.: B-1239
Angerer M.P.M.: B-1530
Anik Y.: B-0108

List of Authors & Co-Authors

Anishkin M.: B-1003
Annoni A.D.: B-0031, B-0755, B-1658
Antil N.: B-0401
Antoch G.: B-0248, B-0252, B-0319, B-0584,
B-0652, B-0706, B-1363, B-1364
Antonelli A.: B-0151, B-1493, B-1494
Antoniu A.: B-0468
Antunes S.: B-1365
Antunovic L.: B-1128
Anver A.B.: B-1476
Anzidei M.: A-359, B-0875
Aoyagi K.: B-0403, B-1581
Aparisi Gomez M.: B-0114, B-1625
Aparisi Gomez M.P.: B-1009
Apfaltrer G.: B-0633
Apfaltrer P.: B-0633
Apine I.: B-1530
Apor A.: B-0150
Appel E.: B-0319, B-1584
Appendino E.: B-0383, B-1064, B-1244, B-1246
Apperloo J.: B-0721
Aptel F.: B-0802
Aquino D.: B-0281
Aras F.: B-1291
Araujo Martins D.: B-0145
Araújo-Filho J.A.B.: B-0142, B-0977
Arboleda C.: B-1417
Arcidiacono P.G.: B-0816
Arcuri P.P.: B-0940
Ardali S.: B-1421
Arena C.: B-0168, B-0891, B-0892
Arendt C.: B-0460, B-0753
Arévalo A.: B-0925
Arfelli F.: B-1416
Argibay-Vazquez S.: B-0501
Argyropoulou M.I.: A-537, A-682, A-953, B-1662
Aringhieri G.: B-1242
Arkhipova I.: A-900
Armada-da-Silva P.: B-0967
Arman A.R.: B-0661
Arnolli M.: B-0825
Aronen H.: A-185
Arora A.: A-373
Arora S.K.: B-0673
Arpaci T.: B-0763
Arrigoni F.: B-0300, B-0612, B-0725, B-0729,
B-0829, B-0960, B-1344, B-1427, B-1542,
B-1543
Arrive L.: B-0301
Arslan A.S.: B-0108
Arslan M.F.: B-0098
Arslan S.: B-1418
Arsov C.: B-0252, B-1363, B-1364
Arteta C.: B-0868
Arthurs O.J.: B-1169, B-1170
Arun D.: B-1500
Anweiler-Harbeck D.: B-0259
Asadi H.: B-0856
Asadi N.: B-1669
Asayama Y.: B-0716
Asbach P.: A-899, B-0251, B-1357
Ascenti G.: B-0460, B-1536
Asghar M.: B-1509
Ashikhmin Y.: A-132
Ashok Kumar M.: B-0270
Ashraf N.: B-0306
Aslan A.: B-0433
Aslan H.: B-0661
Aslan S.: B-1082
Aslanidis I.: B-1249
Asokan P.: B-0270
Aspelin P.:
Assegnati G.: B-0532
Assenat E.: B-1053
Assuncao-Jr A.N.: B-0977
Astrakas L.G.: B-1662
Athanasiou A.: A-331, A-404, A-752
Attempati N.: B-0861, B-0898, B-0944
Attenberger U.: B-0606
Attye A.: B-0066, B-0802
Aubier M.: B-0414

Aubry S.: B-1015
Auclin E.: B-1575
Auer C.M.: A-774
Auer T.A.: B-0939
Aujero M.: B-1288
Aukland S.M.: A-889
Auricchio F.: B-1224
Auweter S.: B-0336
Avanesov M.: B-0025, B-0780
Avantsa R.: B-0260
Avenarius D.: A-010
Averlant L.: B-1654
Avesani G.: B-0250, B-0646
Aviram G.: A-449
Avni F.E.: A-649, B-1504
Awai K.: B-0428
Ayaz Ü.Y.: B-0305
Aydingoz U.: A-062, A-922, B-1421
Aymon E.: B-0748
Ayres V.J.: B-0269
Ayuso C.: A-096, A-243, B-0191, B-0610
Ayuso J.R.: B-1520
Azarine A.A.: A-618
Azevedo K.B.: B-1445, B-1638, B-1640, B-1641,
B-1645
Azrumelashvili T.: B-0037, B-0040, B-0041
Azulay N.: B-1043

B

Baar I.: B-0858
Baba T.: B-0637
Babel H.: B-1425
Babiloni C.: B-1033
Babiy A.: B-1078
Babkova A.: B-1200
Bacchini E.: B-0083
Bach A.: B-0299
Bacher K.: B-0540
Bachert P.: B-0363, B-0933
Bachitar V.: B-0002
Bacigalupo L.: B-0211
Baciu M.: B-1676
Baciu G.: B-0255
Baciu M.: B-0255
Badia S.: B-0060, B-0715
Badr S.: B-1122
Baduna M.: B-1530
Baek J.H.: B-1191
Baessler B.: B-0976, B-0979, B-1556
Baeyens J.P.: B-0721
Baffoni L.: B-0773
Bagarhatta M.: B-1362
Bagetakos I.: B-0499
Baggiano A.: B-0567, B-1459, B-1460
Bagheri S.: B-1669
Bagheri S.M.: B-0599
Baglioli A.: B-0127
Bagnardi V.: B-1377
Bahr A.: B-0544
Bai G.: B-1593, B-1596
Bai J.: B-0778
Bai L.: B-1593, B-1596
Bai W.: B-0583
Bai X.: B-0804
Baijal S.S.: B-0673
Baik J.: B-1212
Bailly S.: B-0052
Bajaj S.K.: B-0401
Bajic D.: B-1401
Bakdik S.: B-1418
Bakers F.C.: B-0352
Bakhshayeshkaram M.: B-0500
Bakic P.R.: B-1632
Balachandran V.: B-0374
Balaji R.: B-0701, B-0896, B-1254, B-1372
Balakrishnan D.: B-1516
Balbi M.: B-1469
Balcells A.: B-1251
Baldazzi M.: B-0579
Baldea V.: B-0203
Baldetti L.: B-0782
Baldo J.: B-0925
Balestriero G.: B-1650
Baleva D.: A-691
Bali M.A.: A-677, B-1083
Balleyguier C.S.: A-245, A-627, B-0368, B-1575,
B-1605
Balm A.J.M.: B-0068
Balodis A.: B-0814
Balster S.: B-0258
Baltzer P.A.T.: B-0079, B-0506, B-0507, B-0910,
B-0911, B-0912, B-1255, B-1289
Balvay D.: B-0476
Balzarini L.: B-1128
Balzer T.: SY 9
Bamberg F.: A-719, A-748, B-0334, B-0336,
B-0340, B-0791, B-0838, B-1356
Banaszek A.: B-1679
Bancroft L.W.: A-870, A-872
Banerjee R.: B-0002
Banfi C.: B-0567
Bankier A.A.: A-448
Bannas P.: B-0022, B-0025, B-1252
Baracco M.: B-1087
Barahona Z. D.: B-1251
Baran Aksakal F.N.: B-0205
Baran P.: B-1416
Baranzelli J.-P.: B-1309
Barbagallo M.: B-1165, B-1495
Barber Hueso C.: B-0101, B-1394
Barber I.: A-012
Barbera M.: B-0816, B-1134
Barbone G.E.: B-1041
Barbosa A.: B-0552
Barbosa Álvares M.C.: B-0391
Barbosa Jr. E.J.M.: B-0236
Barcsi G.: B-1655
Bargalló Alabart N.: B-1039
Bargellini I.: A-051
Barile A.: B-0300, B-0612, B-0725, B-0729,
B-0960, B-1344, B-1427
Barini M.: B-0410
Barker A.: B-0970
Barkhausen J.: B-0793, SY 1a
Barkhof F.: B-1033, B-1039
Barletta A.: B-1468
Barmettler F.: B-1612
Barnacle A.: A-045, A-107
Barnes P.: B-0684, B-1606
Bar-Ness D.: B-0543, B-0983, B-1467
Barnfield M.: B-0908, B-1192
Barnikol U.B.: B-0511
Baroncini M.: B-1040
Barone C.A.: B-1061
Barone D.: B-0589
Barone M.: B-0944
Barr R.G.: B-0267, SY 19
Barreiro R.: B-0966
Barroso E.: B-0187
Barry C.: B-0586
Barsi P.: B-1680
Barsoum M.: B-0592
Bartels-Rutten A.: B-0717, B-1274
Bartholmai B.: B-0045
Bartolini E.: B-0161
Bartolomé P.: B-0915
Bartolotta T.V.: B-1292, B-1614, B-1630, SY 6
Bartolucci M.: B-1183
Bartorelli A.: B-1460
Bartorelli A.L.: B-0755, B-1459
Bas H.: B-0952
Basavalingu D.: B-0270
Baselli G.: B-0029
Basile A.: A-235, B-0049, B-0873
Basile Fasolo C.: B-0890
Basilio R.: A-002, A-943
Ba-Ssalamah A.: A-384, A-866, B-0003, B-1077,
B-1255
Bassam L.: B-1287
Bassanelli E.: B-1404, B-1406
Bassi C.: B-1413

List of Authors & Co-Authors

- Bassi M.: *B-0588*
Basso L.: *B-0837*
Bastarrika G.: *A-812*
Bastati N.: *B-1077*
Bastati-Huber N.: *B-0003, B-1255*
Basten L.: *B-0623*
Bastiaansen J.: *B-0013*
Bastos-Leite A.J.: *A-638*
Batalov A.: *B-0086*
Batsak B.: *B-1229*
Battaglia E.: *B-1612*
Battaglia G.: *B-1041*
Battaglini M.: *B-0286*
Battista G.: *B-0114, B-1009, B-1625*
Battista R.: *B-1611*
Battistella G.: *B-1650*
Baudin G.: *B-1343*
Bauer S.: *B-0836*
Bäuerle T.: *A-843, B-1629*
Baum F.: *B-1609*
Baum T.: *B-0441, B-0529*
Baumann A.B.: *B-0541*
Baumann S.: *B-0776, B-1454, B-1456*
Baur A.: *A-916, B-0251, B-1357*
Baur-Melnyk A.: *B-0113*
Båvenäs H.: *B-0312*
Baxa J.: *B-0590*
Bayat S.: *B-0052*
Baykara Ulasan M.: *B-1206*
Bayou E.H.: *B-1605*
Bayraktaroglu S.: *A-881, B-1219*
Bayraktutan G.: *B-0712*
Bayramoglu Z.: *B-0582*
Bazhenova D.: *B-0928*
Bazrafshan B.: *B-0622*
Bazzocchi A.: *B-0114, B-1009, B-1625*
Beale T.: *A-169*
Beaumont C.M.J.: *B-0987*
Beaumont H.: *B-1343*
Beccaria K.: *B-0341*
Bechstein W.: *B-1201*
Bechter O.: *B-0362*
Beck A.: *B-0299*
Becker A.S.: *B-0273, B-0533, B-1627*
Becker C.D.: *A-215, A-510, A-607, A-819, B-0867*
Becker D.: *B-1657*
Becker F.: *B-0210*
Becker M.: *A-455, A-542, A-702, A-888, B-0499*
Becker N.: *B-0413*
Becker S.: *SY 27*
Beckmann J.: *B-0918*
Bedair R.: *B-0104*
Bedlington N.: *A-692, A-777, A-817*
Bednarova S.: *B-0630, B-1358, B-1547*
Beer A.: *B-0003*
Beer M.J.: *B-0178, B-0180, B-0294*
Beeres M.: *B-0528, B-1052*
Beets G.L.: *B-0352, B-1085, B-1204*
Beets-Tan R.G.H.: *A-066, B-0068, B-0172, B-0352, B-0356, B-0365, B-0717, B-0893, B-0917, B-1085, B-1204, B-1274, B-1376*
Behl N.: *B-0934*
Behme D.: *B-0923*
Behr J.: *B-1015*
Behzad Imsand S.: *B-0316, B-1135*
Behzadi C.: *B-0022, B-1327*
Beiderwellen K.J.: *B-1534*
Beigelman C.: *A-517*
Bekkers J.A.: *B-1649*
Beling M.: *B-0598*
Bell J.K.: *A-465*
Beller E.: *B-0541*
Belli C.: *B-0027*
Belli P.: *B-1419*
Bellini D.: *B-0060*
Bellini D.M.: *B-0164, B-0169, B-0357, B-0358, B-0715*
Bellomi M.: *B-1377*
Belluomini L.: *B-0588*
Belmonte E.: *B-0610*
Belousova E.: *B-1262*
Ben Cohen A.: *B-0486*
Ben Hassen W.: *B-1346*
Benac K.: *B-0476*
Bencardino D.: *B-1529*
Bendahan D.: *B-1024*
Bende F.B.: *B-0203*
Bender B.: *B-0090, B-0093, B-0808, B-1674*
Bendszus M.: *B-0264, B-0363, B-0508, B-0925*
Benea G.: *B-0588*
Benedetti G.: *B-0782, B-1134*
Benhalim M.M.: *B-1446*
Benhalim M.R.: *B-1303*
Benito Vicente C.: *B-0175*
Benjamin G.: *B-1595*
Benjamin R.: *B-1288*
Benjaminov O.: *A-262, A-340*
Benmerad M.: *B-0052*
Bennani S.: *B-1346*
Bennink E.: *B-1130*
Benschop L.: *B-0785*
Benz M.: *B-0835*
Benz S.: *B-0973, B-0974, B-1157, B-1159, B-1160, B-1653*
Beomonte Zobel B.: *B-0627, B-0820*
Beomonte Zobel B.B.: *B-0632, B-0994*
Bera G.: *B-0666*
Beregi J.P.: *B-0531, B-0949*
Berendsen A.: *B-1009*
Berenguer Haym M.: *B-0006*
Berezina N.: *B-1078, B-1548*
Bereznitskiy V.: *B-1557*
Berger A.: *B-0293*
Berger F.H.: *A-780*
Berger N.: *B-0273, B-1093, B-1627*
Bergin D.: *B-0670*
Bergman H.R.: *B-0561*
Bergsland N.: *B-0798*
Bergholdt M.: *B-1678*
Berindoague Neto R.: *B-0391*
Berliner C.: *B-1252*
Berlis A.: *B-0189*
Berlusconi M.: *B-1128*
Berman A.A.: *B-1497*
Bernúdez S.: *B-0694*
Bernard-Davila B.: *B-0507, B-1117*
Bernardi D.: *B-0077*
Bernardo S.: *B-0151, B-1493, B-1494*
Bernathova M.: *B-0079, B-0911*
Berndt M.T.: *B-0149*
Bernetti C.: *B-0627*
Bernier M.-O.: *B-0595*
Bernstein M.: *B-0546*
Bertalan Z.: *B-1013*
Bertelli E.: *B-0056*
Berti V.: *B-1183*
Bertolini M.: *B-0083*
Bertolotto M.: *A-106, B-1664, B-1665*
Bertrand A.-S.: *B-1343*
Bertucci C.: *B-0940*
Bertuzzo L.: *B-0018, B-0834, B-1522*
Besana F.: *B-1545*
Besse B.: *B-0368*
Bessems G.: *B-0118*
Bethge O.T.: *B-0319*
Bette S.: *B-0088*
Bevilacqua A.: *B-0589, B-0730*
Beyer L.P.: *B-0207*
Beyer T.: *A-653*
Beyersdorff D.: *B-1252, B-1569*
Bezzi M.: *A-412, B-0429*
Bhagwat K.A.: *B-1216*
Bhargava S.: *B-0681*
Bhargavi V.: *B-1058*
Bhat I.H.: *B-0585*
Bhatt A.: *B-0504*
Bialecka A.: *B-1009*
Bianchi A.: *B-0161, B-0719*
Bianchi M.: *B-0146*
Bianco F.: *B-0564*
Bican Y.: *B-1077*
Bick U.: *A-119*
Bidault F.: *B-0368*
Biddle D.J.: *B-0970*
Bienes G.H.A.A.: *B-1233*
Bier G.: *B-1674*
Bierma-Zeinstra S.M.: *B-0118*
Bignone R.: *B-1616*
Bignotti B.: *B-1613*
Bilbao J.I.: *A-414, A-972*
Bilhim T.: *A-686, B-0187*
Bilim G.O.: *B-0661*
Binst J.: *B-1139*
Binzel K.: *B-0888, B-0993, B-1218*
Biondi M.: *B-0853*
Biondi T.: *B-0164*
Bippus R.-D.: *B-1136*
Birch J.: *A-696*
Bisdas S.: *A-668*
Bisogno G.: *B-1492*
Bisschops B.: *B-1277*
Biswas A.: *B-1243*
Bitarafan-Rajabi A.: *B-0477, B-0478, B-0700, B-0734, B-0739, B-0740*
Bitencourt A.: *B-1285*
Bitzer M.: *B-0601*
Biviji M.: *B-0483, B-1386, B-1387*
Bizjak R.: *B-1448*
Bjelan M.: *B-1673*
Bjorkman B.: *B-1644*
Bjorndal H.: *B-0076, B-0676, B-1096*
Bjornstad A.: *A-659*
Blackham K.: *B-0516*
Bladowska J.: *B-1679*
Blanc R.: *B-0514, B-0518*
Blanco Pérez E.: *B-1465*
Blandino A.: *B-0460, B-1536*
Blank C.U.: *B-0356*
Blasenbrey T.: *B-0178, B-0180*
Blaszowsky L.: *B-0985*
Blazic I.: *B-0167*
Bley T.A.: *B-0022*
Bliddal H.: *B-1014*
Bliemsrieder E.: *B-0988*
Bloem J.L.: *A-214, A-892, B-0110*
Blondin D.: *B-1363*
Blumenstock G.: *B-0918*
Blystad I.: *B-0096*
Boateng E.Y.: *B-0742*
Boban J.: *B-1673*
Bobek-Billewicz B.: *B-1107*
Boccalini S.: *B-0143*
Bockeria L.: *B-1557*
Bockisch A.: *B-1621*
Boddaert N.: *B-0154, B-0341*
Bode P.K.: *B-1166*
Bodelle B.: *B-0346*
Boekestijn B.: *B-0011*
Boer D.D.: *B-0131*
Boers M.: *B-1008*
Boesen M.: *B-1014, SY 25*
Bogaert J.: *A-643, A-746*
Bogaerts R.: *B-1431*
Bogers A.: *B-0596*
Bogner K.: *B-1360*
Bogner W.: *B-0285, B-0620*
Bogue C.: *B-0574*
Bogveradze N.: *B-0014*
Bohndiek S.: *B-1094*
Boileau P.: *B-1025*
Boirie Y.: *B-0331*
Boita J.: *B-0550*
Böker S.M.: *B-0426*
Bokwa-Dabrowska K.: *B-0307*
Boll D.: *B-0835*
Bollineni V.R.: *B-1368*
Bollow M.: *B-1619*
Bolog N.: *B-0255, B-1031*
Bolstad K.N.: *A-782*
Bolster F.: *B-0176*
Bonaffini P.A.: *B-1468, B-1469*
Bonasera L.: *B-1183*

List of Authors & Co-Authors

Bonatti G.: B-0250, B-0646
Bonatti M.: B-0250, B-0646
Bongartz G.: B-1464
Bonilla S.: B-0116, B-0929
Boni-Mikats A.: B-0345
Böning G.: B-0292, B-0412, B-0446, B-0894,
B-0899, B-0961
Bonino F.: B-1420
Boninsegna E.: B-1065, B-1519, B-1523, B-1567
Bonito G.: B-1633
Bonne L.: B-0209
Bonnemaijer P.W.M.: B-0795
Bonneville F.: B-0692
Bonnici-Mallia M.: B-0214, B-0562
Bonomo L.: A-178, B-0185, B-0874
Bons L.R.: B-0143
Booij R.: A-850
Boomsma M.F.: B-0131
Boonen P.T.: B-1044, B-1050
Boos J.: B-0319, B-1584
Booz C.: B-0346, B-0439, B-1026, B-1515
Boraschi P.: B-1320
Borges A.: A-110
Borggrete J.: B-0377, B-0515, B-0699, B-0906,
B-0927, B-1012, B-1023, B-1119, B-1384,
B-1671
Borggrete M.: B-1354
Borgheresi A.: B-0521
Borghesi A.: B-0053
Boric I.: A-568
Borrego D.: B-0947
Borthne A.: B-1141
Bortolanza C.: B-1650
Bortsova G.: B-0485, B-0870, B-1038
Bortol M.: B-0678
Bos D.: B-0485, B-0512, B-0691
Bos P.: B-0068
Boschini A.: B-0773
Boscolo Bariga N.: B-1167
Bosmans H.: B-0682, B-1139, B-1431
Bosmans J.M.L.: B-0181
Boss A.: B-0273, B-0839, B-1627
Bossert M.: B-0597
Bossi Zanetti I.: B-0481
Boswijk E.: B-1051
Botelho N.:
Botsikas D.: B-0466, B-0499
Botta F.: B-0382
Böttcher J.: B-0349
Böttger S.: B-0346
Bottoni L.: B-0978
Bouaboula M.: B-1413
Bouchouicha A.: B-0476
Boudabbous S.: B-0112, B-0499
Boudghene F.: B-0386
Boudiaf N.: B-1676
Bouëté A.: B-0120
Bouëté J.-C.: B-0120
Bougias H.: B-1118
Boulay Coletta I.: B-0948
Boulin M.: B-1060
Bourcier R.: B-0688
Bourfiss M.: B-1656
Bourgioti C.: B-0468
Bourillon C.: B-0293
Bourrier P.: B-0422
Boussel L.: B-1467
Boutry N.: B-1504
Bouvier A.: B-1060
Boyer B.: B-1605
Boyer L.: B-0331
Boyle J.: B-0219
Bozzi A.: B-1623
Brabec J.: B-0868
Bracke P.: B-0290
Brader P.: A-027, A-342
Bradley W.: B-1283
Brady A.: A-852, A-990, B-0176
Brage K.: B-0953
Brambilla M.: A-228, A-456, B-0325
Brancatelli G.: A-016, A-242, A-339, B-0008

Brancato S.: B-1065, B-1567
Braren R.: B-0900, B-0988, SY 5
Brat H.: B-0314, B-0316, B-1135
Bratke G.: B-0727
Braun F.: B-0023
Braunschweig M.: B-0035
Bravin A.: B-1041
Brawer M.: B-0254
Breda S.: B-0118
Breen D.J.: B-0624
Brehm M.: B-1432
Brembilla G.: B-0230, B-0626, B-1365
Bremerich J.: A-394, B-0482
Brendle C.: B-0090, B-0093, B-0808
Brennan I.M.: B-0443
Brennan P.: B-0856, B-0857
Brennan P.C.: B-1416
Breznik S.: B-0864
Bricault I.: B-0186
Bridoux A.: B-1156
Briers E.: A-821
Briganti A.: B-1365
Briley-Saebø K.: B-0993
Brillet P.-Y.: B-0414
Brilli I.: B-1087
Brink J.A.: A-584, A-822
Brink M.: A-935, A-936, B-0238, B-0411
Brinkmann S.: B-0790
Brito A.Q.: B-0965
Brito J.: A-005
Brkic S.: B-1673
Brkljačić B.: A-283, A-406, A-664, A-775, B-0726
Broche L.M.: B-0547
Brockmann M.A.: B-0939
Broeckx B.: B-0181, B-1558
Broeders M.: B-0685
Broeders M.J.: B-0550
Broennimann C.: B-0549
Brookes A.L.: A-041
Brouhon L.: B-0318
Brountzos E.: A-239
Brown G.: A-282, B-0209
Brown J.: B-0142
Brown L.: B-0214, B-0562
Brown P.: B-0684, B-1606
Browne D.: B-1444
Brüggemann G.-P.: B-0727
Brugger P.: B-1168
Bruix J.: B-0191, B-0610
Brun F.: B-1416
Brunelli S.: B-0078, B-0082, B-1088
Bruners P.L.: B-0818
Brunetti A.: B-1616
Bruni S.: B-0947
Bruning T.: B-1461
Brunner S.: B-0207, B-0208
Bruno F.: B-0300, B-0436, B-0612, B-0725,
B-0729, B-0960, B-1427, B-1539
Bruno L.: B-0333
Bruns C.: B-0790
Bruzzi J.F.: B-0670, B-0671
Bruzzone M.G.: B-0281
Brzewski M.: B-0307
Bu X.: B-0653
Bucci S.: B-1664
Bucerius J.: B-1051
Buchbender C.: B-0706
Buchberger W.: B-1112
Bucher A.M.: B-0460, B-1052
Buchert R.: B-1319
Büchler L.: B-0539
Bücker A.: B-0832, B-1329
Buckle T.: B-0068
Buckley J.G.: B-0249
Budaeus L.: B-1569
Budde R.P.: B-0143, B-0337, B-0568, B-0785,
B-1461
Budde R.P.J.: B-0596, B-1649
Budjan J.: B-0606
Buduru S.: B-0255
Buhk J.-H.: B-0035

Bühler T.: B-0537
Buisink C.: A-422
Buisson A.: B-0117, B-0302
Bujila R.: B-1341
Bukvic M.: B-1163
Bulakbasi N.: A-911
Bulleri A.: B-0890, B-0891, B-0892
Bülrow R.: SY 1a
Buls N.: B-0721, B-1044, B-1050
Bulut T.: B-1429
Bulychkin P.: B-1248
Bumberger A.: B-0912
Bunck A.: B-0976, B-0983
Buonocore V.: B-1529
Bura V.: B-0190, B-0361
Bural I.: B-0258, B-1210
Burenchev D.V.: B-0182
Burgard C.A.: B-0242
Burgermeister S.: B-0112, B-0867
Burgstaller J.: B-1031
Burk K.S.: B-0016
Burke A.M.: B-0748
Burki S.: B-1509
Burns J.E.: B-1587
Burton N.C.: B-1176
Burulday V.: B-0954
Busato F.: B-1073
Buscarino V.: B-0382, B-1377
Busch J.: B-0061
Buschulte T.D.: B-0413
Busse H.: B-1564, B-1566
Butts Pauly K.: B-0821
Buzan M.T.A.: B-1222; B-0405
Buzug T.M.: B-0793
Buzzatti L.: B-0721
Byeon J.H.: B-0032

C

Cabanzo Campos L.B.: B-1551
Caccialupi C.: B-1032
Cáceres J.: A-805
Cademartiri F.: A-959, B-0333, B-0564, B-0565,
B-0779, B-0787
Cadório I.: B-0552
Cai H.: B-0524, B-1279
Cai X.: B-0884, B-1019
Caines J.: B-0684, B-1606
Çakir S.: B-1206
Calabrese M.: B-1613
Calabretta L.: B-0265
Calamai V.: B-1083
Calandrelli R.: B-0348
Calareso G.: B-0625
Caldarazzo lenco E.: B-1242
Caldas C.: B-0104
Calder A.D.: A-191
Caliskan C.: B-0237
Çaliskan E.: B-0582
Calkins H.: B-1656
Callegari L.: B-1016
Calli C.: A-081, A-941
Calliada F.: A-439
Calvo Imirizaldu M.: B-0915
Cambuí M.: B-1140
Camillieri F.: B-0097
Camlidag I.: B-0256, B-1082
Campa R.: B-0244, B-1068
Campagna R.: B-0117, B-0302
Campagnuolo T.: B-0487
Campanella R.: B-1000
Camparo P.: B-0448
Campbell N.M.: B-0167
Campeau N.: B-0546
Campoleoni M.: B-1165, B-1440
Camps Herrero J.: A-334, A-553
Canale S.: B-1605
Canaz H.: B-0581
Candanedo González F.: B-1092
Canellas R.: B-0016
Caneva A.: B-1088

List of Authors & Co-Authors

- Cangiotti C.: B-0024, B-0634, B-0897
Cankurtaran T.: B-1421
Cannao' P.M.: B-0786, B-1651
Cannata V.: B-1165
Cannataci C.: B-1090
Cannella A.: B-1336
Cannillo B.: B-0325
Cannizzaro E.: B-0300, B-0612, B-0725,
B-0829, B-0960, B-1427, B-1542, B-1543
Canossi B.: B-1611
Cant J.: B-1558
Cantisani V.: A-103, B-0221, B-0266, B-0493,
B-0668, B-1633, SY 6
Cao J.: B-1593
Cao J.Y.: B-1084, B-1211, B-1526
Cao L.: B-0199, B-1266
Cao M.: B-1173
Caparros Escudero C.: B-0145
Capitanio U.: B-0626
Cappelli A.: B-0038
Cappello G.: B-1114, B-1398, B-1592
Cappucci M.: B-0231
Capretti G.: B-1349
Capretti I.: B-0612, B-0729, B-0829, B-1427,
B-1542, B-1543
Capuani S.: B-0151
Cara Garcia M.: B-1275
Caramella C.: B-0368, B-1575
Caramella D.: B-0146, B-1320
Carbonaro L.A.: B-0503, B-1093
Carbone F.S.: B-0786
Carbone I.: B-0027, B-0789
Carbone M.: B-0144
Carbone S.F.: B-0853
Carchesio F.: B-0185, B-1061
Cárdenas Herrán J.S.: B-1394
Cardis E.: B-0595
Cardobi N.: B-0017
Cardone G.: B-0479
Cardoso A.F.V.: B-1637
Cardoso P.: B-0285
Carducci C.: B-0153, B-0157, B-0159
Carducci S.: B-1539
Carfagnini F.: B-0579
Carlino G.: B-1419
Carlsen J.: A-104
Carlton J.: B-0277
Carmichael D.: B-1170
Carmon E.: B-0268, B-0916
Carmona-Bozo J.C.: B-0498
Caroço R.: A-929
Carpentier K.: B-1558
Carr S.: B-0125
Carraco C.: B-0498
Carrafiello G.: B-0232, B-1189, B-1190
Carrasquinho R.: B-0329
Carrete Jr H.: B-1233
Carrié D.-G.: A-694
Carriero A.: B-0232, B-0410
Carrino J.: SY 25
Carroll A.: B-0070
Cartuan A.: B-0588
Caruana C.J.: B-1144
Caruso D.: B-0164, B-0169, B-0357, B-0358,
B-0460
Carvalho D.: B-0560
Carvalho de Siqueira E.: B-0391
Carvalho Silva Rabelo B.: B-0391
Casamassima E.: B-0227, B-0862
Casamassima N.: B-1016
Casarin A.: B-1562
Casella T.: B-0625
Caseiro Alves F.: A-293, A-684, A-688, A-876
Casella C.: B-1414
Cash H.: B-1357
Casiraghi A.: B-0851, B-1468, B-1518
Caspers J.: B-1037, B-1235, B-1237
Caspers S.: B-1037
Cassagnes L.: B-0331
Cassano E.: B-1090
Cassar-Pullicino V.N.: A-213
Cassinotto C.: B-1053, B-1057, B-1060
Castagna M.: B-1320
Castaldi B.: B-0773
Castaneda Vega S.: B-0090, B-0093, B-0808
Castañer E.: A-069, A-531
Castanho G.F.D.P.: B-0283
Castellano E.: A-250
Castellano I.: B-1398, B-1414
Castellote A.: B-0769
Castelo-Branco M.: B-0552, B-0559
Castera L.: B-0202
Castiglioni I.: B-0481
Castillejos Molina R.A.: B-0397
Castillo Balladarez E.H.: B-0272, B-1116
Castillo E.: B-0914
Castillo J.: B-1144
Castro German K.P.: B-1092
Castro L.H.M.: B-1400
Casula V.: B-1014
Catalano C.: B-0027, B-0151, B-0184, B-0221,
B-0244, B-0429, B-0493, B-0608, B-0611,
B-0630, B-0668, B-0789, B-0821, B-0843,
B-0875, B-1068, B-1337, B-1339, B-1342,
B-1493, B-1494, B-1529, B-1541, B-1547,
B-1633
Catalano M.: B-1128
Catalano O.A.: B-0985, B-1533
Catana C.: B-0985
Catania D.: A-628
Catania M.: B-1065, B-1567
Catellani M.: B-1071
Cattrysse E.: B-0721
Caturelli E.: B-0833
Caumo F.: B-0078, B-0082, B-1088
Caumon E.: B-1009
Cavallaro A.: B-1260
Cavallo A.U.: B-1623
Caviezel C.: B-1355
Cazals-Hatem D.: B-1528
Cecchi P.: B-1242
Cecchin D.: B-1486
Cederlund T.: B-0312
Celeng C.: B-1463
Celenk C.: B-0674
Celia A.: B-1562
Cellina M.: B-0284, B-0291, B-0683, B-1197,
B-1286, B-1612
Cenderello G.: B-0211
Cerntner F.S.: B-0243
Cereser L.: B-0046, B-0384
Cerimele F.: B-0890
Cerini P.: B-0232
Cerri F.: B-0891, B-0892
Cervelli R.: B-1320
Çetin N.: B-0495
Cetinoglu Y.K.: B-1429
Cevasco L.: B-0211
Ceyssens S.: B-0181
Cha J.: B-0241, B-0461, B-1132, B-1415
Chabrand P.: B-1024
Chalazonitis A.N.: B-1284
Chambers G.: B-0593
Chami L.: B-0666
Chammas M.C.: B-1186
Chamming's F.: B-1413
Champsaur P.: B-1024
Chandak S.: B-1667
Chandrasegaram-Shanmuganathan S.: B-1085
Chang D.-H.: B-1556
Chang H.M.: B-0195
Chang K.-J.: B-1590
Chang M.: B-0658
Chang M.-C.: B-0019
Chang T.Y.A.: B-1370
Chang W.: B-1194, B-1524
Chapa Iburguengoitia M.: B-1092
Chapiro J.: B-0446, B-1056
Charline Z.C.: B-0860, B-1228
Charpiot A.: B-0067, B-0069, B-0257
Chassagnon G.: B-1346, B-1353
Chatoupis K.: B-0468
Chatterjee P.: B-1675
Chatzinoff Y.: B-1126
Chau I.: B-0209
Chaudhari A.: B-1030
Chauveau C.: B-1122
Cheecharoen P.: B-1199
Chelaru R.L.: B-1069
Chelladurai A.: B-0347
Chellathurai A.: B-1500
Chen A.: B-1590
Chen A.-H.: B-0366
Chen B.: B-1158
Chen B.-B.: B-0019
Chen C.: B-1333
Chen C.-M.: B-0366
Chen C.-N.: B-1590
Chen C.-Z.: B-1256
Chen D.: B-1485
Chen E.: B-0947
Chen F.-P.: B-0534
Chen G.W.: B-0846
Chen H.: B-0781
Chen H.-L.: B-0619
Chen J.: B-0387, B-1018, B-1175, B-1178,
B-1587
Chen K.-Y.: B-1590
Chen M.: B-1171, B-1194
Chen N.: B-1403, B-1603
Chen Q.: B-1603
Chen R.: B-0467
Chen S.: B-0733
Chen W.: B-0063, B-1323
Chen X.: B-1603
Chen X.-L.: B-0394, B-0846
Chen Y.: B-0015, B-1181, B-1579, B-1636
Chen Y.Q.: B-1560
Chen Y.Y.: B-0073
Chen Z.: B-0884
Cheng A.K.C.: B-0193
Cheng J.: B-0065, B-0111, B-0475, B-0497,
B-0935, B-0936, B-1095, B-1187, B-1479,
B-1490, B-1496
Cheng M.-F.: B-0019
Cheng S.: B-1214
Cheng S.-H.: B-1264
Cheng X.: B-0936
Cherkashin M.: B-1003, B-1078, B-1145, B-1548
Chernova O.: B-1497
Chernovsky E.: B-0268
Cheung A.Y.-C.: B-0534
Cheung S.: B-0165
Chevalier M.: B-1628
Chevallier P.: B-1060
Chhabra A.: B-0071, B-1126
Chianca V.: B-0440, B-1616
Chilappetta M.: B-0874
Chiari C.: B-1428
Chien P.Y.C.: B-0193
Chikhaoui N.: B-0941
Chilamkurthy S.: B-0483, B-1386, B-1387
Chilvers G.: B-1359
Chim C.Y.R.: B-1283
Chin S.C.: B-0214, B-0562, B-1182
Chincarini M.: B-0166
Chipon E.: B-0186
Chiquet C.: B-0802
Chiramal J.A.: B-1379
Chirico G.: B-1165
Chiti A.: B-0452, B-1128
Chlebus G.: B-1383
Cho F.: B-1370
Cho J.Y.: B-0645, B-0649
Cho K.R.: B-1415
Cho S.B.: B-0854
Choi B.I.: B-1265
Choi C.G.: B-0693
Choi J.-I.: B-0707
Choi J.W.: B-0643, B-0801
Choi S.I.: B-0664
Choi Y.J.: B-0102, B-1191
Chong G.: B-1251

List of Authors & Co-Authors

Chong V.: A-013
Choo J.-Y.: B-0639
Choo K.S.: B-0575, B-0760
Chopra R.: B-1126
Chou I.C.: B-0194
Chow B.: B-0598
Chowdhury F.U.-H.: B-0593
Chowdhury V.: B-1507
Christeas N.: B-0188, B-0865
Christou A.: B-1086, B-1118
Chu F.: B-0193
Chu J.P.: B-1238
Chu L.: B-0253
Chu P.: B-1010
Chu Z.-Q.: B-0201
Chuan Y.: B-0989
Chun C.: B-0596
Chunchao X.: B-1267
Chung H.Y.: B-1620
Chung R.: B-1010
Chung S.R.: B-1191
Chung W.S.: B-0718
Chung W.-Y.: B-1099
Cianfoni A.: B-1001
Ciccarese F.: B-1073
Cicchetti G.: B-0874
Ciccotosto C.: B-1032
Cicero C.: B-1562
Cicero G.: B-1536
Cieszanowski A.: B-1106
Ciet P.: A-610, B-0768
Cina A.: B-0898, B-0944
Cindoruk M.: B-0205
Ciocca M.: B-0284
Ciompi F.: B-1349
Cioni R.: B-0185
Cipriani F.: B-1205
Cirigliano A.: B-0853
Ciritis A.: B-1627
Citone M.: B-0227, B-0862
Ciulla S.: B-1494
Clasen S.: B-1208
Claudon M.: A-437
Clauser P.: B-0079, B-0910, B-0911, B-0912, B-1289, SY 1c
Clavien P.-A.: B-0839
Clément O.: A-400, A-572, B-0293, SY 17
Clemente A.: B-0565
Clephas P.: B-0512
Clevert D.A.: A-441, A-663, B-0055, B-0057, SY 6, SY 23
Coan P.: B-1041
Coche E.: B-0424
Cockmartin L.: B-0682, B-1139
Coco S.: B-0027
Codari M.: B-0029, B-0332, B-0503
Coelho F.M.: B-0877
Coelho P.M.: B-1309
Coenen A.: B-0337, B-1456
Cognard C.: B-0692
Cohen J.: B-0050, B-0052
Coimbra E.: B-0187
Coindre J.-M.: B-0697
Colafati G.S.: B-0153, B-0157, B-0159
Çolakoglu M.K.: B-1324
Colarieti A.: B-1377
Collijn J.M.: B-0795
Collart J.: B-0424
Colletini F.: A-399, B-0381, B-1056
Collin A.: B-0514
Colombani S.: B-0921
Colombel M.: B-0245, B-1074
Colombo M.: B-0230, B-0626
Colombo P.E.: B-0128
Colosimo C.: B-0348
Coma A.: B-0769
Combs S.E.: B-0595
Como G.: B-0384, B-0425
Compagne K.: B-0512, B-1008
Conceição I.: B-1642
Condamine E.: B-0509

Conejero A.: B-0048
Conill C.: B-1520
Connor S.: K-24
Consiglio E.: B-1031
Constantino Rosa Santos S.: B-0595
Conte E.: B-0031, B-1459, B-1658
Contegiacomo A.: B-0861, B-0898, B-0944
Conti C.: B-0166
Conti M.: B-1224
Cook G.: A-203, A-741, B-0354, B-1080
Coolen J.: B-1574
Coppolino D.: B-0898
Corapcioglu F.: B-0108
Corazza A.: B-0440, B-0719
Corbi Bellot A.: B-0121
Corcioni B.: B-1073
Cornelissen S.A.: B-0021
Cornford E.J.: A-330
Corno L.: B-0948
Cornud F.: B-0448
Correale L.: B-0519, B-0520, B-0522
Coreas J.-M.: A-825, SY 13
Correia M.: B-0396
Correia M.T.: B-0187
Corrias G.: B-0216, B-0374, B-0840
Corsello G.: B-1495
Corso R.: B-0127, B-0444
Cortese F.: B-0532
Cortesi L.: B-1611
Cortet B.: B-1122
Corthouts R.: B-1558
Cosentino A.: B-0835, B-1225, B-1420
Cosottini M.: B-1242
Costa A.: B-1000
Costa A.R.: B-0326
Costa F.: B-1240
Costa G.: B-0146
Costa N.V.: B-0187
Costa N.V.V.P.: B-1077
Cotroneo A.R.R.: B-0564
Cotten A.: A-079, B-1122
Coudyzer W.: B-0021, B-1139
Coulon P.: B-0983, B-1467
Cousin S.: B-0698
Cova M.A.: A-897, B-0678, B-1439, B-1532, B-1664
Cova M.A.A.: B-1665
Cox K.: B-0602
Craddock A.: A-355
Crema M.D.: B-0301
Cremoneze A.: B-0283
Crespi A.: B-0127, B-1129
Crestani A.: B-0384, B-1358
Crijns A.P.G.: B-0595
Crimi F.: B-1486, B-1492
Cristel G.: B-1365
Crombag G.A.J.C.: B-0220, B-0222
Crombe A.: B-0697, B-0698
Cronin C.: B-0586
Cronin K.: B-1301
Crosby T.: B-0714
Crouzet S.: A-398, B-0245, B-1074
Csécs I.: B-1657
Csemez I.: B-0605
Csukly G.: B-0659
Cuatrecasas M.: B-1520
Cuccarini V.: B-0281
Cuenod C.A.A.: B-0293
Cueto Álvarez L.: B-0145
Cui L.: B-0421, B-0658, B-1572, B-1577
Cullmann J.L.: B-1124
Cuneo G.L.: B-1032
Cunha T.M.: A-769, B-0380, B-0396, B-0651
Cunningham D.: B-0209
Cuocolo R.: B-1616
Currò F.: B-0678
Cybulski A.J.: B-1065, B-1567
Cyran C.C.: A-344, B-1176
Czerny C.: A-014, A-701
Czimbalmos C.L.: B-1657

D

da Silva C.A.: B-1149, B-1637, B-1638, B-1640
Da Silva J.: B-1438
Dababou S.: B-0184, B-0630, B-0821, B-0875, B-1337, B-1339, B-1342, B-1541, B-1547
Dabizzi E.: B-0816
Dacquino G.M.: B-0789
Daemen M.J.: B-0222
Daghiri A.: B-1476
Dagna L.: B-1042
Dähner I.: B-1222
Dai Q.: B-1097, B-1098, B-1100, B-1103, B-1104
Dai Y.: B-0390
Dai Y.-L.: B-0409
Daire J.-L.: B-0010
Dalaker T.O.: B-0798
Dalen I.: B-0798
D'Alessio A.: B-1545
Dall B.: B-1397
Damascelli A.: B-1365
Damasio M.B.: B-0580
D'Ambrosio F.: B-0221, B-0266, B-0493, B-0668, B-1633
Damianou C.: B-1239
D'Amico N.C.: B-0479, B-0481
Damilakis J.: A-229, A-311, A-418, A-500, A-504, B-0771
Damodaran K.: B-0347
Dam-Vervloet L.A.: B-0131
Danaci M.: B-1082
D'Anastasi M.: B-0113
Dang H.: B-1181
Dangelmaier J.: B-1120, B-1121, B-1136
D'Angelo A.: B-1289, B-1419
D'Angelo P.: B-0046
D'Angelo T.: B-0460, B-1536
Dangouloff-Ros V.: B-0154
Daniel L.: B-0255
Daniele S.: B-0295
Danielli L.: B-1001
Danielsson M.: B-1438
Danila M.: B-0203
Dankbaar J.W.: B-1130, B-1463
D'Anna G.: B-0481
Danse E.: B-0424, SY 12
Dantas Jr R.N.: B-0977
Darabi M.: B-0599
D'Archambeau O.: B-0318, B-0858
Darnell A.: B-0191, B-0610, B-1520
Darrás C.: B-1116
Darrás Ismael C.: B-0914
Darwish H.S.: B-0400
Das M.: A-279
Dashti K.: B-0109
Dashyan V.: B-0690
Daugaard C.L.: B-1014
David M.: B-1528
Davies G.R.: B-0547
Davis M.: B-1300
Dazinger F.: B-0510
De Angelis C.: B-0332
De Backer J.: B-0236
De Backer W.: B-0236
de Bazelaire C.: B-1610
De Beaupaire I.: B-0154
de Beni S.: B-0452
De Bock G.: B-1109, B-1155
De Boer M.: B-1204
De Bondt T.: B-0318
de Bono J.S.: B-0393
De Brucker Y.: B-1044, B-1050
De Bruijine M.: A-735, A-982, B-0485, B-0768, B-0870, B-1038
de Campo J.: B-0765
de Campo M.: B-0765
de Caneda M.A.G.: B-0282
De Carli M.: B-0046
De Carlo M.: B-0146

List of Authors & Co-Authors

- De Cecco C.N.: B-0569, B-0752, B-0757,
B-0776, B-1046, B-1047, B-1049, B-1232,
B-1454, B-1455
- de Ceglie M.: B-0144
- De Cesari M.: B-0211
- De Cobelli F.: B-0230, B-0626, B-0629, B-0782,
B-0816, B-0847, B-1042, B-1134, B-1205,
B-1365
- De Cobelli O.: B-1071
- De concilio B.: B-1562
- De Coster B.: B-0224
- De Felice C.: B-1633
- De Francesco S.: B-0963
- De Geer J.: B-0337
- de Graaf R.: A-860
- de Groot C.: B-1009
- de Groot C.J.M.: B-0785
- de Groot M.: B-0794
- de Groot M.C.H.: B-0568
- de Haan D.: B-0907
- de Heer L.: B-0596
- de Heer P.: B-0883
- De Jong H.W.: B-1130
- de Jong K.P.: B-0825
- de Jong P.: B-1463
- de Jong P.A.: B-0568, B-0596, B-0691
- De Jonge M.C.: A-443
- de Kerviler E.: B-0120
- De Kerviler E.: B-0422
- De Keyzer F.: B-0362, B-1574
- De Koekkoek-Doll P.: B-1213
- de Koning H.J.: B-0566, B-0571
- de Korte C.L.: B-0957
- De la Barra C.: B-0492
- de la Cámara Egea M.A.: A-789
- De la Mora Malvárez M.: B-0397
- De Leo A.: B-1650
- De Leyn P.: B-1574
- de Ligt M.: B-1051
- De Luca S.: B-1336
- De Maeseneer M.: A-445
- de Mathelin M.: B-0119
- De Mattia C.: B-0128
- De Mey J.: B-0721, B-1044, B-1050
- de Miguel Criado J.: B-0175
- De Monte F.: B-0773
- de Mutsert R.: B-0204, B-0335
- De Nlsi M.: B-0077
- De Paepe K.N.: B-0209, B-0362, B-1202
- De Palma L.: B-1404, B-1406
- De Paoli A.: B-1225
- De Pascale L.: B-0525
- De Piano F.: B-0382
- De Robertis R.: B-0017
- de Roo M.: B-0732
- de Roos A.: B-0204
- De Rubeis G.: B-0789
- de Santis A.: B-0142
- De Santis D.: B-0164, B-0169, B-0357, B-0358,
B-0569, B-0715, B-0752, B-1049, B-1232
- de Sio I.: B-0833
- De Soccio V.: B-0221, B-0266, B-0493, B-0668,
B-1633
- De Stefano N.: B-0286
- De Tymowski C.: B-0422
- de Vecino M.C.A.: B-0282
- De Visschere P.: B-1067
- de Vito A.: B-0024, B-0634, B-0942, B-1328,
B-1514
- de Vries A.: B-0204
- de Vries A.P.J.: B-0883
- De Vries B.: B-1426
- De Vries B.A.: B-0118
- De Vuysere S.: B-1075
- De Wever W.: B-1574
- De With P.H.N.: B-0480
- Debray M.P.: B-0414
- Debry C.: B-0067, B-0069, B-0257
- Declerck J.: B-0868
- Decoster R.: A-551
- Decristoforo C.: B-1570
- Dedulle A.: B-0124
- Defebvre L.: B-1040
- Defilippi C.: B-0161
- Degonda C.: B-1124
- Dehairs M.: B-0126
- Deidier J.: B-0476
- Dekan V.: B-1101, B-1102
- Dekimpe C.: B-1025, B-1027
- Dekkers I.: B-0204, B-0883, B-1464
- Del Chiaro M.: A-222
- Del Grande F.: B-1031
- Del Maschio A.: B-0230, B-0626, B-0782,
B-0816, B-0847, B-1365
- Del Monte M.: B-1068
- del Rosario Perez M.:
Del Santo S.: B-0520, B-0522
- Del Sette B.: B-0232
- del Vecchio A.: B-1165, B-1440, B-1441
- Delalogue S.: B-1605
- Delattre B.: B-0466
- Delgado Alvarez I.: B-0769
- Delicque J.: B-1053, B-1057
- Della Seta M.: B-0381
- Delmaire C.: B-1040
- Delogu P.: B-1439
- Delorme S.: B-0413
- Delsanto S.: B-0519, B-0521
- Delso G.: B-0708
- Demaerel P.: A-558
- Demetter P.: A-221
- Demidova A.: B-1335
- Demircioglu A.: B-0355
- den Harder A.M.: B-0568, B-0596
- Denecke T.: A-967, B-0007, B-0009, B-0609,
B-0886
- Deng Y.: B-0417
- Denis de Senneville B.: B-0698
- Denjoy N.: A-151
- Dennler C.: B-1123
- Denysenkov V.: B-0030
- Derchi L.E.: A-625, A-818
- Dergilev A.: B-0641, B-1576
- Derlin T.: B-0932
- Derraz I.: B-0688
- Dervishi G.: B-1473
- Desai I.: B-0270
- Desai S.R.: A-738
- Desal H.: B-0688
- Desana B.: B-1392
- DeSilvestri A.: B-0267
- deSouza N.M.: A-545
- Dessouky R.A.K.: B-0071, B-1126
- Destito A.: B-0940
- Detante O.: B-0509
- Détraz L.: B-0688
- Detmer S.: B-0051, B-0235, B-0237
- Deutsch E.: B-0737
- Devappa V.: B-0770
- Devaraj A.: A-162
- Develter W.: A-124
- Devos H.: B-1044
- Dewey M.: A-273, B-0597, B-0598, B-0762,
B-0777
- Dhibar T.: B-1243
- Dhillon B.: B-0903
- Dhundass S.: B-0514
- Di Blasi A.: B-0532
- Di Chiara A.: B-0847
- Di Chio A.: B-1225, B-1420
- Di Egidio V.: B-0815
- Di Grazia L.: B-1167
- Di Leo G.: B-0503, B-1189
- Di Leo N.: B-0221, B-0266, B-0668
- Di Lorenzo C.: B-1336
- Di Luzio M.: B-0829, B-1539, B-1542, B-1543
- Di Maira T.: B-0006
- Di Martino M.: B-0429, B-0608, B-0611, B-0843
- Di Mento L.: B-1128
- Di Mizio V.: B-0815
- Di Paola V.: B-1567
- Di Pietro P.: B-1041
- Di Segni M.: B-0221, B-0266, B-0486, B-0493,
B-0668, B-1633
- Di Stasi C.: B-0861
- Di Trapani E.: B-1071
- Di Vittorio M.L.: B-1292, B-1614, B-1630
- Diacon T.: B-0343
- Diamant I.: B-0486
- Diana P.: B-0629, B-1205
- Diao K.: B-0788, B-1230
- Dias C.: B-0316
- Díaz Candamio M.J.: A-787
- Diciotti S.: B-0161
- Dick E.: A-645
- Dickerscheid D.: B-0311
- Dieckmeyer M.: B-0441
- Diederichs G.: B-0061
- Diefenbach M.: B-0441
- Diekhoff T.: B-0299, B-0308, B-0309, B-0530,
B-1029, B-1615, B-1619
- Dierckx R.A.J.O.: B-1345
- Dierickx D.: B-0362
- Dietrich U.: B-0259
- Dietzel F.: B-1364
- Dijkhoff R.A.P.: B-0850
- Dijkstra H.: B-1109
- Dijkstra S.: B-0748
- Dillenseger J.-P.: A-424
- Dilli A.: B-0305
- Dimai H.-P.: B-1013
- Dinevski D.: B-0864
- Ding H.: B-1193
- Ding J.: B-0387, B-1203
- Ding W.: B-0800
- Ding Y.: B-1256
- Dinkel J.: A-085, B-0405, B-0871
- Dinse B.: B-0925
- Dioguardi Burgio M.: A-341, B-0202
- Dionisi C.: B-0325
- Dippel D.W.: B-0512, B-1008
- Dirand A.-S.: B-0737
- Dirik E.B.: B-1234
- Dirim Mete B.: B-1429
- Distefano D.: B-1001
- Diwan K.: B-1108
- Dixit R.: B-1507
- Dixon A.K.: A-984
- Djurdjevic T.: B-0510
- Djuric Stefanovic A.: B-1527
- Dluzewski S.L.: B-0173
- Dobbe I.: B-0732
- Dobbin-Stacey R.: SY 25
- Doblas S.: B-1528
- Dobrynina L.: B-0215, B-1677
- Dodd J.D.: A-067
- Doellinger F.: A-611
- Dohmen C.: B-0511
- Doi K.: B-0451
- Dolan A.: B-0176
- Dolgun Barak A.: B-1421
- Dolgushin B.: B-0423, B-1248, B-1512
- Dominguez A.: A-040
- Dominguez Paillacho I.D.: B-0823
- Dominguez-Prado I.: B-0501
- Donatelli G.: B-1242
- Donati F.: B-1320
- Dong A.: B-0813
- Dong Y.: B-1084, B-1211, B-1526
- Dong Z.: B-0524
- Doni L.: B-1650
- Doniselli F.M.: B-1000
- D'Onofrio M.: A-440, A-824, B-0017, K-02,
SY 11
- Donoghue V.: A-952
- Donoso L.: A-585, A-721
- Donswijk M.: B-0893
- Dooms C.: B-1574
- Dorigo A.: B-1650
- Dorn F.: B-0122
- Dorn S.: B-0733
- Doronzio V.M.: B-0107, B-0378, B-1114,
B-1244, B-1592

List of Authors & Co-Authors

Dorrius M.: B-1109
Douek P.: B-0543, B-0983, B-1467
Dournes G.: A-086
Doweidar A.A.A.: B-0109
Dragean C.A.: B-1508
Drago A.: B-0144
Drago S.: B-0851, B-1328, B-1514, B-1518
Drago S.G.: B-0356
Drape J.L.: B-0117, B-0302
Dreger H.: B-0598
Dreher C.: B-0933
Dreossi D.: B-1416
Dresen R.: B-1075
Dreuil S.: B-0315
Dreval M.: B-0215
Drewes A.M.: B-0012
Dreyer K.J.: A-508, A-736
Drobní Z.: B-1655
Droguett E.: B-0914, B-1116
Droguett M.E.: B-0667
Dromain C.: A-386, A-755, A-867
Drzegza A.: A-582
Du J.: B-1180
Du R.: B-0075, B-0603
Duba I.: B-0772
Dubbeldam A.: B-1574
Düber C.: B-0036, B-0196, B-0210, B-0973,
B-0974, B-0975, B-1157, B-1159, B-1160,
B-1653
Dubost F.: B-0485, B-0870, B-1038
Duc N.M.: B-0449, B-1540
Duca P.: B-0008
Ducou Le Pointe H.: B-0120, B-0315
Ducroux C.: B-0518
Dudea S.: B-0255
Duerr H.R.: B-0113
Dufek D.: B-0868
Duffy P.: B-0574
Duguay T.: B-1454
Duguay T.M.: B-1046, B-1047, B-1456
Duijts L.: B-0768
Dullin C.: B-1416
Duman I.E.: B-0661
Dumic Cule I.: B-0726
Dumont J.: B-1040
Dumonteil S.: B-0680
Durando M.: B-1392, B-1398, B-1414, B-1613
Durganau R.: B-0828
Durlík M.: B-0882
Durmaz M.S.: B-1418
Duron L.: B-0514
Dürr M.: B-0001
Durukan G.: B-0433
Düsünceli Atman E.: B-0098
Dynder K.: B-0553
Džananović A.: B-1163

E

Ebdon-Jackson S.: A-145, A-149, A-857
Ebel S.: B-1222
Ebner R.: B-1471
Eck B.: B-0125, B-1017
Eckermann M.: B-1041
Eckersley R.: B-1659
Edelman E.R.: B-0142
Edelman R.R.: B-1046
Edyvean S.: A-925
Efremova M.: B-0369
Egan C.: B-1433, B-1436
Egenlauf B.: B-1549
Eggesbø H.B.: A-621
Ehara S.: B-0416
Ehdaie B.: B-0254
Eichinger M.: B-0402
Eichler K.: B-0289, B-0439, B-0824, B-1054
Eichstädt J.: B-0973, B-0974, B-0975, B-1157,
B-1159, B-1160, B-1653
Eickhoff S.: B-1037
Eickhoff S.B.: B-1235, B-1237
Eid K.: B-0537

Eid M.: B-0569, B-1232, B-1455
Eijgenraam S.: B-1030
Eilers C.: B-0975
Einspieler H.: B-0003
Einspieler I.: B-0900
Einstein A.: B-1010
Eisenblätter M.: A-862
Ekaeva I.: B-1249
Ekart R.: B-0864
Ekdawi S.: B-0790
Ekinci G.: B-0661
El Ameen N.F.: B-0488, B-1399
El Kady R.M.: B-0473
EL-Baz A.: B-0887
ElDeib N.A.E.: B-1411
El-Diasty T.: B-0887
Elentuck D.: B-0951
Elgendl A.: B-0863
Elgeti T.: B-0943
Elias Jr J.: B-0879
Eliezer M.: B-0066
Elizalde Pérez A.M.: B-0915
Elkiki H.A.: B-1503
Eller L.: B-0375
Eillmann S.: B-1629
Elmali M.: B-0256, B-0674
Elmas Z.N.: B-1538
Elmokadem A.: B-1544
El-Mossly D.M.: B-1502
ElRakhawy M.: B-1544
Elsayed S.B.: B-1666
Elsberger B.: B-0275
Elserougy L.: B-0092
ElShafey M.M.A.H.: B-0863
El-Zayadi A.A.: B-1544
Elzenbeck L.: B-0598
Emelianenko M.: B-1028
Eminian S.: B-0117
Emrich T.: B-0973, B-0974, B-0975, B-1157,
B-1159, B-1160, B-1653
Endhardt K.: B-0839
Engbersen M.: B-1085, B-1376
Engel G.: B-0061, B-0426
Engelhard K.: B-1360
Engelhard N.: B-0530, B-1029
Engelhorn T.: A-408, A-562
Engh G.C.: B-1297
England A.: B-0135, B-0741, B-1296, B-1303,
B-1444, B-1446
Enokido K.: B-0106
Entradas D.C.: B-0749
Enzinger C.: A-209
Eoli M.: B-0281
Erasmus H.-P.: B-0184, B-0630, B-1337,
B-1339, B-1342, B-1541, B-1547
Eraso A.: B-0595
Erben T.: B-0294
Erdal J.M.: B-0971
Erden A.: B-0842, B-1322
Erdogan N.: B-1429
Eren S.: B-0262, B-0712, B-1652
Ereno Ealo M.J.: A-234
Ergen F.B.F.: B-1421
Ergun O.: B-0495
Eriksen L.M.K.: B-1309
Ermolaeva V.: B-0576
Ernemann U.: B-0090, B-0093, B-0808, B-1674
Ertel N.: B-1055
Ertl-Wagner B.: A-337, A-757, A-827, B-1161
Eryilmaz M.A.: B-1418
Escal L.: B-1053
Escalard S.: B-0514
Eschbach R.S.: B-1176
Esen G.: A-332, B-1293
Esendagli Yilmaz G.: B-0205
Eser M.B.: B-0433
Eshkal H.: B-0309
Eshmuminov D.: B-0839
Eskreis-Winkler S.: B-0840
Espahbodi F.: B-1466
Espejo Herrero J.J.: B-0823

Espeland A.: B-0435
Esposito A.: B-0782, B-0816, B-0847, B-1365
Esposito F.: B-1414
Esser M.: B-0764, B-0766
Etemadi Z.: B-1669
Eustace S.J.: A-369, B-0972
Eva A.: B-0837
Ewencyk-Bitton I.: B-1605
Ewertson C.: A-442
Ezponda Casajús A.: B-0915
Ezziane M.: B-0386

F

Fabrizi C.: B-1009
Fabbro E.: B-0958
Fabian J.: B-0334
Fabiocchi F.: B-1460
Fabris C.: B-0166, B-1521, B-1523
Fabritius M.P.: B-0513, B-0517, B-0922
Facchinelli D.: B-1519
Faccinnetto A.: B-0202
Faccini R.: B-0162
Fadееva L.: B-1484
Fadzli F.: B-0617, B-1597
Faeghi F.: B-0287
Faermann R.: B-1608
Faggian A.: B-1090
Faggioni L.: B-0146
Fahed R.: B-0518
Fahlenkamp U.L.: B-0426
Fahrleitner-Pammer A.: B-1013
Faiella E.: B-0627, B-0632, B-0820
Fairweather-Tait S.: B-1009
Faivre J.-B.: B-0458, B-0462, B-1555
Falaschi F.: B-1320
Falcone G.: B-0227, B-0862
Falconi M.: B-1134
Faletti R.: B-1225, B-1420
Fallahian A.: B-0998
Fallenberg E.M.: A-174, A-329, A-754
Falsaperla D.: B-0049, B-0420, B-0873
Fan C.-M.: B-0534
Fan F.: B-0654
Fan G.: B-0658
Fan P.: B-1211, B-1526
Fan P.L.: B-1084
Fan S.: B-0170
Fan Y.: B-0781
Fancourt N.: B-0765
Fanelli F.: A-671, B-0227, B-0862
Fang Z.: B-1531, B-1535
Fantini C.: B-0462
Fantò C.: B-0077
Farah J.: B-0313
Farchione A.: B-0874
Fardin S.: B-0361
Farina D.: A-015, A-314, B-0265, B-0978
Fariz B.: B-0722
Farkas K.: B-0659
Farshad M.: B-1123
Faruch M.: A-945
Fasching P.A.: B-1629
Faschkami A.: B-0051
Favre J.: B-1425
Faymonville A.: B-1671
Fazzari F.: B-1460
Fearon W.: B-0026
Fedato C.: B-1087
Fedorenko E.: B-1561
Fedorov A.: B-1145
Feeley A.: B-0574
Feger S.: A-810, B-0597, B-0598, B-0762
Fehdi M.A.: B-0941
Fehrenbach U.: B-0292, B-0412, B-0894,
B-0899, B-0961
Fehrmann Efferoth A.: B-0976
Feida E.: B-1284
Feier D.S.: B-0003
Feiweiher T.: B-0620

List of Authors & Co-Authors

- Feldhaus F.: *B-0292, B-0412, B-0894, B-0899, B-0961*
Feldman E.: *B-0778*
Felloni P.: *B-0462*
Femia M.: *B-0382, B-1377*
Feng F.: *B-0810, B-1002*
Feng H.: *B-1347*
Feng S.-T.: *B-0524, B-1535*
Feng X.: *B-1483*
Feng Z.: *B-0654, B-1525*
Fenzl L.: *B-0832*
Ferda J.: *B-0590*
Fernandez Valverde F.: *B-0085*
Ferraioli G.: *SY 13*
Ferrari C.: *B-0787*
Ferrari M.D.: *B-1600*
Ferrari R.: *B-0162*
Ferraz H.B.: *B-1233*
Ferraz H.I.M.G.: *B-0964*
Ferreira A.: *B-0557*
Ferreira C.: *B-0552, B-0559*
Ferreira Marques E.: *B-1285*
Ferrer C.: *A-431*
Ferrer Puchol M.D.: *B-1465*
Ferrero G.: *B-0958*
Ferretti G.R.: *B-0050, B-0052*
Ferrone C.: *B-0985*
Fetita C.: *B-0414*
Fetoni V.: *B-0284*
Feuchtnr G.: *B-0148*
Fey N.P.: *B-1126*
Ficarra V.: *B-0384, B-1358*
Fichter A.: *B-0900*
Fiehler J.: *B-0189, B-1319*
Fielding P.A.: *B-0714*
Figà-Talamanca L.: *B-1406*
Figge C.: *SY 13*
Figiel J.: *B-1546*
Figueiredo D.: *B-0552*
Figueiredo J.P.: *B-1313*
Filipe J.P.: *B-1240*
Filippiadis D.: *A-109, A-236*
Fingerle A.A.: *B-0543, B-1121*
Fink G.R.: *B-0511, B-0927*
Finkenstaedt T.: *B-1125*
Finkenstaedt T.: *B-0533, B-1031*
Finocchiaro G.: *B-0281*
Fior D.: *B-0444*
Fiore A.: *B-1087*
Fiore S.: *B-1225, B-1420*
Fiorino C.: *B-1134*
Fischbach R.: *B-0035*
Fischer A.M.: *B-1354*
Fischer M.: *B-0533*
Fischer S.: *B-0030*
Fischer T.: *B-0001, B-0055, SY 3*
Fischer U.: *B-1609*
Fisher P.: *SY 1c*
Fiuzza M.: *B-0595*
Flacke S.: *B-0951*
Flaction L.: *B-1147, B-1643*
Fleischer S.: *B-0764*
Fleischmann D.: *B-0026*
Fleury E.F.C.: *B-0269*
Flohr T.: *B-0905, B-1026*
Floridi C.: *B-0291, B-1286, B-1612*
Floris R.: *B-0487, B-1623*
Fodero G.: *B-0940*
Fofiu R.: *B-0203*
Foley K.G.: *B-0714*
Foley S.J.: *A-629, B-0321, B-0324, B-1299, B-1301*
Follin A.: *B-0293*
Fomekong E.: *B-0438*
Fong C.Y.: *B-1393*
Fonio P.: *B-1225, B-1392, B-1398, B-1414, B-1420*
Fons Estupiña C.: *B-0160*
Forbrig R.: *B-0122*
Forghani R.: *B-1178*
Forman C.: *B-1156*
Forment Navarro M.: *B-1465*
Formenti A.: *B-0031, B-0755, B-1658*
Forner A.: *B-0191, B-0610*
Fornes V.: *B-0006*
Forrai G.: *A-906, K-03*
Forslin Y.: *B-0997*
Förster A.: *B-1582*
Förster K.: *B-1161*
Forsting M.: *B-0259, B-0355, B-0652, B-0796, B-1138, B-1367, B-1371, B-1621*
Forstner R.: *A-547*
Forte S.: *B-0919, B-1417*
Forte V.: *B-0221, B-0266, B-0493, B-0668*
Fos Guarinos B.: *B-1380*
Fosskaug J.: *B-0748*
Fotiadis N.: *B-0209, B-1202*
Fouque O.: *B-0414*
Fourcade M.: *B-1057*
Fouré A.: *B-1024*
Fourneau I.: *B-0224*
Fournier D.: *B-0314, B-0316, B-1135*
Fournier L.S.: *A-345, A-573, B-0476, B-1413*
Fraga Piñeiro C.: *B-0323*
Fraga Rivas P.: *B-0175*
Fragner R.M.: *B-0003*
Fragoso M.C.B.V.: *B-0877*
Fraire D.: *B-0263*
França M.M.: *A-089, A-685*
Francavilla M.: *B-0465*
Franceschelli G.: *B-1190*
Franceschi C.: *B-1009, B-1625*
Franceschi L.: *B-0902*
Francica G.: *B-0833*
Franco Monteiro Prado F.: *B-0391*
Francone M.: *A-193, A-598, B-0027, B-0563, B-0565, B-0789*
Frank P.: *B-1557*
Frankowska E.: *B-0604*
Frantsev D.: *B-0423, B-1512*
Franx A.: *B-0785*
Franz D.: *B-0441*
Frassoldati A.: *B-0588*
Frauenfelder G.: *B-0632, B-0994*
Frauenfelder T.: *A-049, A-100, B-0047, B-0273, B-1355*
Fredrikson S.: *B-0997*
Freeman S.: *B-0970*
Freiwald B.K.: *B-0919*
Freixo A.: *B-0552*
Frellesen C.: *B-0289, B-0528, B-1052*
Fremmelevholm L.: *B-0556*
French R.: *B-0951*
Frenzel T.: *B-1252*
Fressilli D.: *B-0221*
Frid M.: *B-0486*
Fridell K.: *B-1644*
Friedman E.: *B-1608*
Friedrich K.: *A-791*
Friedrich T.: *B-0793*
Frigerio A.: *A-633*
Frijia G.: *A-147, A-419, A-501, A-503, B-0595*
Frisoni G.B.: *B-1033, B-1039*
Fritz B.: *B-1430*
Fritz J.: *B-1570*
Froehlich J.: *B-0174*
Froelich M.F.: *B-0922, B-1076*
Froeling M.: *A-115*
Frøkjær J.B.: *B-0012*
Frood R.: *B-0908*
Frydrychowicz C.: *B-0359*
Fu G.: *B-0656*
Fu Y.: *B-0421, B-0490, B-1572*
Fuchentes S.: *B-1430*
Fuchs M.: *B-0530, B-1029*
Fuchsjäger M.H.: *A-324, A-407, A-693, A-884, B-1151*
Fuentes Corona R.E.: *B-1092*
Fuge J.: *B-0051*
Fujii K.: *B-0767, B-1391*
Fujinaga Y.: *B-1315*
Fujisawa Y.: *B-0043*
Fujita S.: *B-1315*
Fukui R.: *B-1048*
Fukuma E.: *B-1388*
Fuller F.: *B-0061*
Fuller S.: *B-1046, B-1047*
Furlin G.: *B-0282*
Furmanczyk-Zawiska A.: *B-0882*
Fusaro F.: *B-0232*
Fusaro M.: *B-1650*
Fusco G.: *B-0325*
Fusco R.: *B-1190*
Fusi I.: *B-0141*
Fütterer J.J.: *A-205, B-0555*
Fytousi N.: *B-0124*
-
- ## G
-
- Gaballa G.: *B-0092*
Gabata T.: *B-0198*
Gabbani G.: *B-0227, B-0862*
Gabbelloni M.: *B-0146*
Gadzhieva Z.: *B-1677*
Gaillard F.: *B-1385*
Galati G.: *B-0994*
Galban C.J.: *B-1588*
Galea N.: *B-0027, B-0789*
Galema T.W.: *B-1649*
Galeone C.: *B-0045*
Galia M.: *B-1616*
Galiè N.: *B-0407*
Gallagher F.A.: *A-060, B-1672, K-23*
Galle P.: *B-0036*
Galle P.R.: *B-0210*
Gallegos M.: *B-0272*
Galleguillos C.: *B-0914, B-1116*
Galleguillos M.C.: *B-0272*
Gallez B.: *B-0424*
Gallina S.: *B-0564*
Galmiche C.: *B-0059*
Galvano G.: *B-1336*
Gan S.: *B-1593*
Gandini G.: *B-1392, B-1398, B-1414*
Gangi A.: *A-413, B-0119, SY 3*
Ganych O.: *B-0370*
Ganzer R.: *B-1566*
Gao F.: *B-0279*
Gao J.: *B-0463*
Gao L.: *B-0455, B-1179*
Gao Y.: *B-0431, B-0638, B-0783, B-0788, B-1230*
Garattoni M.: *B-1073*
Garces Iñigo E.F.: *B-1162*
García Baizán A.: *B-0915*
García del Salto L.: *B-0175*
García Figueiras R.: *A-863*
García García R.: *B-0101, B-1394*
García M.: *B-0492*
García M.R.T.: *B-0902*
García Marcos R.: *A-366*
García-Aguilar J.: *B-0167*
García-Castro F.: *B-1380*
García-Criado Á.: *B-0191*
García-Peña M.P.: *A-882*
García-Perez F.: *B-0376, B-1253*
Gard C.: *B-1604*
Gardarsdottir M.: *K-04*
Gardelli G.: *B-1164*
Gårdling J.: *A-227*
Gareer S.: *B-1287*
Gariani J.: *B-0354*
Garkowski A.: *B-0278*
Garmpis D.: *B-1384*
Garolla M.: *B-1392*
Garrè M.L.: *B-1478*
Garrido C.S.: *B-0879*
Garteiser P.: *B-1528*
Garwood E.: *B-0538*
Garza Gangemi A.M.: *B-0397*
Gasbarrini A.: *B-1061*
Gaspar V.L.: *B-1149*
Gasperini C.: *B-0114*

List of Authors & Co-Authors

- Gatidis S.: B-0336, B-0766, B-0889, B-0909
Gatos I.: B-0430
Gatti M.: B-1225, B-1420
Gattoni M.: B-0886
Gaudio C.: B-1073
Gaudino S.: B-0348
Gautam A.A.: B-1595
Gautsch K.: B-1112
Gavazzi E.: B-0978
Gavelli G.: B-0589, B-0730
Gavrel M.: B-1575
Gawlitza J.: B-1566
Gawlitza J.F.M.: B-0234, B-1354
Gayef A.: B-0581
Gayvoronskiy A.: B-1101
Gazhonova V.E.: B-0369, B-1028
Geambastiani P.: B-1140
Gebauer B.: A-029, B-0446, B-1056
Gebrim E.M.M.: B-0902
Gee M.: B-0573
Geerlings M.I.: B-0691
Geers-van Gemeren S.: A-577
Gehweiler J.: B-0835
Geier K.I.: B-0932
Geiger J.: B-1166
Geisel D.: B-0007, B-0009, B-0609, B-0886, B-1056
Gellér L.: B-1657
Gelsomino F.: B-0855
Gempt J.: B-0088
Gendre P.: B-1025
Genesio L.: B-1562
Geng P.: B-1097, B-1098, B-1104
Gennari A.: B-1532
Gennaro G.: B-1628
Gennaro N.: B-0452
Gentilini M.A.: B-0077
Georg D.: A-919
George S.: B-0982
Geramifar P.: B-0477, B-0478, B-0700, B-0734, B-0739, B-0740
Gerardin E.: B-0066
Gerges M.: B-1288
Gerngross C.: B-0900
Gershan V.: A-308
Gersing A.S.: A-021, B-0529, B-1120, B-1121, B-1136
Gervais D.: B-0985, B-1533
Geske J.: B-0283
Geurts B.H.: B-1594
Gevenois P.A.: B-0642
Geyer B.: B-1340
Ghanouni P.: B-0821
Ghaye B.: A-084, A-588, B-0876
Ghelfi J.: B-0050
Ghiatas A.: B-1118
Ghimire P.: B-0119
Ghosh R.: B-0483, B-1386, B-1387
Ghoshhajra B.: B-1463
Giacobbe A.: B-0378, B-0383, B-1246
Giaconi C.: B-0168, B-0890, B-0891, B-0892
Giampalma E.: B-1164
Gianini A.C.C.: B-0269
Giannakis A.: B-0402, B-0871
Giannarini G.: B-0384
Giannazza E.: B-0567
Giannero C.: B-0300, B-0612, B-0725, B-0960, B-1344
Giannetto G.: B-0519, B-0520, B-0522
Giannini F.: B-0782
Giannini V.: B-0378, B-1246, B-1592
Giannotti E.: A-177, B-1636
Giannotti N.: B-1299
Gianolli L.: B-1042
Gibaud B.: A-457, A-616, A-991
Gibelli D.: B-1197
Gibson T.A.: B-0624
Giese D.: B-0790, B-0976
Giesel F.L.: B-0888
Giganti M.: B-0588
Gijbertse K.: B-0957
Gil R.: B-0380
Gilbert F.J.: A-116, B-0104, B-0498, B-1094
Gilkeson R.: B-1326
Gillard J.: B-0219
Gilles R.: B-1605
Gillespie C.D.: B-1554
Gillibert A.: B-0066
Gilligan P.: A-312, B-0972
Ginanni Corradini S.G.: B-0429, B-0608
Gioppo A.: B-0281
Giordana P.: B-1043
Giordano A.V.: B-0829, B-1539, B-1542, B-1543
Giordano J.: B-1552
Giorgi Rossi P.: B-0083
Giorgio A.: B-0286
Gioutlaki E.: B-1284
Giovanardi N.: B-0787
Girão A.C.: B-1313
Girardi V.: B-0487
Giraud C.: B-0620, B-1486, B-1492
Girometti R.: B-0046, B-0384, B-0425, B-1294, B-1358
Gitto S.: B-0625
Giudice D.: B-0136
Giudici F.: B-0678
Giuliani M.: B-1419
Giurazza F.: B-0994
Gizewski E.R.: B-0510
Gkali C.: SY 1b
Gkoumas S.: B-0549
Glazebrook K.N.: B-0504
Gleason A.: B-1126
Gleeson F.: B-0831
Glessgen C.: B-0482
Glodny B.: B-0510
Glück B.K.: B-0927
Glynn M.: B-0176
Gnannt R.: B-1166
Godazandeh F.: B-1466
Gödeny M.: B-0605
Godinho T.M.: B-0559
Goerg F.: B-0818
Goh V.J.: A-156, A-216, A-295, A-385, B-0354, B-1080
Gold G.: B-1030
Goldberg S.N.: A-388
Golding S.J.: A-025
Goldoni M.: B-0333, B-0787
Golebiowski M.: B-0882
Golfieri R.: B-0038, B-1073
Gollub M.J.: B-0167
Goloso B.: B-1439
Goltz J.P.: B-0793
Gomes F.V.: B-0187
Gomes I.: B-0326
Gomes L.G.: B-0877
Gomes R.L.E.: B-0902
Gómez Chiari M.: B-0160
Gonen M.: B-0167
Gong Q.: B-0655, B-0657, B-0662
Gong S.: B-0442, B-1193
Gong X.: B-0658
Gonzalez Balboa P.: B-1092
González de la Huebra Rodríguez I.: B-0915
Gonzalez P.: B-0272, B-0492
González Vázquez M.: B-0323
Goo J.M.: B-0044
Gooßen A.: SY 22
Góraj B.M.: B-1594
Göral K.A.: B-0155
Gorbach A.: B-0703
Gorbounov N.: B-0641
Gorbunov N.: B-1576
Gordillo Arnaud J.E.: B-0085
Gordon Boyd R.: B-0344
Gore R.M.: A-097
Gorsi U.: B-1334
Görtz R.S.: B-1260
Goselink R.: B-0957
Goshima S.: B-0607
Gossetti B.: B-0027
Gossye T.: B-0540
Gosvig K.K.: B-0747
Gottlieb M.: B-1608
Goto M.: B-1391
Gottschling S.: B-1222
Gotschy A.: B-1226
Gottlieb J.: B-0235
Gottschalk A.: B-0395
Gourtsoyianni S.: B-1519
Gourtsoyiannis N.: A-284
Goussia A.: B-1662
Gowda, G.: B-0260
Goyal A.: B-0275
Goyal L.: B-0985
Graef K.: B-0039, B-1063
Gräfe D.: B-1222
Grainger A.J.: A-444, A-571, A-708, A-710
Grams A.E.: B-0510
Graña L.: B-0501
Granados A.M.: B-1402
Granata C.: A-505, B-1165, B-1495
Granberg T.: B-0997
Grant D.: B-0344
Grant K.: B-0772, B-0905, B-1049
Granziera C.: A-114
Grassi A.: B-0853
Grassi R.: B-0525
Grasso R.F.: B-0627, B-0632, B-0820
Gratama J.W.C.: B-0566, B-0571
Gratz M.: B-0796
Graves M.: B-0219
Graves M.J.: B-0498, B-1672
Graziano L.: B-1285
Grazzini G.: B-0521
Grazzini I.: B-1032
Greco F.: B-0046, B-0384, B-1358
Greco G.: B-0625
Green C.: B-0361
Greenspan H.: B-0486
Greese J.: B-0308, B-1615, B-1619
Greffier J.: B-0531, B-0949
Grehten P.: B-1166
Greilich S.: A-885
Greiser A.: B-0978
Grenier N.: A-423, A-749, A-833, A-898
Grenier P.A.: A-122, A-305
Grevent D.: B-0154, B-0341
Grieten M.: B-0120
Griffon J.: B-0666
Grigoriev E.: B-0728
Grigorieva E.: B-0690
Grillo F.: B-0837
Grim C.: B-0621
Grimm J.: A-218
Grimm R.: B-0017
Grippos C.: B-1419
Grishchenkov A.: B-1102
Grist J.T.: B-1672
Grivas N.: B-1568
Grivegnée A.-R.: SY 1b
Grob D.: B-0238, B-0411
Grodan C.: B-1582
Gromov A.: B-0702, B-1247
Grönberg F.: B-1438
Grönroos J.M.: B-0744
Grosse Hokamp N.: B-0125, B-0377, B-0587, B-0699, B-0906, B-1012, B-1023, B-1119, B-1326, B-1473
Grossi E.: B-0479, B-0481
Grossi F.: B-0141
Grothoff M.: B-0563; B-1222
Grover H.: B-0505
Grover S.B.: B-0054, B-0271, B-0505, B-1373
Gruber G.M.: B-1168
Gruber-Rouh T.: B-0439, B-0528, B-0824, B-1052, B-1054, B-1059, B-1210
Gruenisen J.: B-0355, B-0652, B-0706, B-1367, B-1371
Grüneisen J.: B-0450
Grünig E.: B-1549
Gruszczynska K.: A-602

List of Authors & Co-Authors

- Gruszka E.: B-1679
Gu K.: B-0388, B-0650
Gu X.: B-1572
Gu Y.J.: B-0163
Guan J.: B-0472, B-0878, B-1663
Guaricci A.I.: B-0567, B-0779, B-1224, B-1460
Guarise A.: B-1562
Guarnaccia L.: B-1000
Guazzaroni M.: B-0487, B-1623
Guberina N.: B-0259, B-0836, B-1138, B-1621
Gubern-Mérida A.: B-1628
Gückel B.: B-0889
Gudbergsen H.: B-1014
Guedea F.: B-0595
Guenego A.: B-0518
Guenoern Z.: B-1077
Guenoun D.: B-1024
Guerini H.: A-348, B-0302
Guerra L.: B-0851
Guerreri M.: B-0151
Guerri S.: B-0114
Guffey D.: B-0277
Guggenberger R.: B-0533
Guglielmi G.: B-1009, B-1223, B-1625
Guglielmo M.: B-0031, B-0567, B-0755, B-0779, B-1224, B-1460, B-1658
Gui B.: B-0471
Guidarelli G.: B-1009, B-1625
Guidi E.: B-0168
Guimaraes L.S.: A-533
Guiney M.J.: B-0443
Guis S.: B-1024
Guiu B.: B-1053, B-1057, B-1060, SY 3
Gulati A.: B-1368
Gulati V.: SY 26
Gulcu A.: B-0226
Guldogan N.: B-1293
Güler E.: B-1538
Gulino P.: B-0161
Gullien R.: B-0140
Gunduz N.: B-0433
Güner N.B.: B-0226
Gunes Tatar I.: B-0495
Gunn A.: B-0034, B-1055
Günther R.W.: A-669, B-0446
Guo J.: B-0001
Guo Q.: B-0454, B-0464
Guo W.: B-1270
Guo W.-Y.: B-1099
Guo Y.: B-0339, B-0472, B-0788, B-1153, B-1154, B-1663
Guo Y.-K.: B-0338
Guo Y.-M.: B-0409
Gupta A.: B-1326
Gupta P.: B-1108
Gurcan N.I.: B-0581
Gurel S.: B-1330
Gureyev T.E.: B-1416
Gursoy M.: B-1429
Guseva E.: B-0182
Gusmini S.: B-0230, B-0629, B-0816, B-1205
Gutberlet M.: A-601, A-641, B-0563, B-0979, B-1222
Guthrie J.A.: A-521
Gutsalo J.: B-0406
Gutzeit A.: B-0174, B-0179, B-0459
Guven F.: B-0712
Guyomarç'h Delassale B.: B-0688
Guzzardi G.: B-0232, B-0410
Gwon H.Y.: B-0672
Gyebnár G.: B-1680
Gyngell M.: B-0002
-
- H**
-
- Ha H.I.: B-1269
Ha M.: B-0241, B-0461
Ha S.M.: B-1191
Ha V.: B-1338
Haage P.: A-356
Haakull A.E.: B-0140
- Haas M.: B-0251, B-1357
Habash Y.: B-0400
Haberal K.M.: B-1004
Habels M.-F.: B-1051
Habib Geryes B.: B-0313, B-0315
Habib N.: B-0037, B-0040, B-0041
Habl M.: B-0549
Habsah M.: B-0400
Hachulla A.-L.: B-1223
Hackl C.: B-0208
Haddad F.: B-0026
Hadebe N.S.: B-1309
Hadid-Beurrier L.: B-0313
Hadjidemetriou S.: B-1239
Hadlich T.: B-0023
Haefeli P.: B-0303, B-0539
Haegele J.: B-0793
Hagberg G.: A-846
Hagger J.: B-1381
Haghighi Z.: B-1221
Haghighikaboudkola M.: B-0287
Hagmann M.: B-0243
Hagverdiyeva G.: B-1248
Hahn A.: B-1434
Hahn F.: B-0973, B-0974
Hahn H.K.: A-864
Hahn S.: B-0044
Haitjema S.: B-0568
Hajaj M.: B-0275
Hajianfar G.: B-0477, B-0739, B-0740
Hajji M.: B-0422
Halaweish A.F.: B-0772, B-0905
Haldorsen I.S.: B-1368
Halfmann M.C.: B-0973, B-0974, B-1157, B-1159, B-1160, B-1653
Halilbasic E.: B-1255
Halimi P.: B-0293
Hall C.: B-1416
Halle M.: B-1368
Hallock F.: B-0001
Haller S.: A-762, B-1039
Halligan S.: A-566, A-793
Halpern C.: B-0821
Halpern E.J.: B-1423
Halshtok Neiman O.: B-1608
Hamada S.: B-1226
Hamard A.: B-0531
Hamed M.: B-1389
Hamed S.T.: B-1666
Hamm B.: A-722, B-0001, B-0007, B-0009, B-0061, B-0251, B-0299, B-0308, B-0309, B-0412, B-0426, B-0530, B-0548, B-0830, B-0886, B-0894, B-0899, B-0961, B-1029, B-1340, B-1357, B-1615, B-1619
Hammel J.: B-0529
Hammerstingl R.: B-0039, B-1059
Hammerstrøm L.: B-1312
Hammon M.: B-1260, B-1629
Hammond C.: A-816
Hamza H.: B-0470
Hamza H.M.: B-0950
Han F.: B-1179
Han J.: B-0643
Han N.Y.: B-0854
Han X.: B-0225, B-0800
Han Y.: B-0496
Han Y.E.: B-0854
Haneder S.: B-0790, B-1473
Hanestad B.: B-0132, B-1007
Hangaard S.: B-1014
Hanke M.: B-0303, B-0539
Hantes M.: B-0304
Harden S.: A-811
Hardy M.: A-548, B-1143, B-1308
Hare S.: B-0173
Hargreaves B.: B-1030
Harman M.: B-1538
Harris E.: A-886
Harris M.A.: B-0969, B-1143, B-1308
Hartenstein A.: B-0886
Hartmann C.J.: B-1237
- Hartmann I.: A-530
Harvey H.: SY 26
Hasanin A.: B-0950
Haseli S.: B-1668
Hashemi Beni R.: B-0500
Hashemi F.: B-1215
Hashizume K.: B-0350
Hassanein S.A.H.: B-0469
Hasson D.: B-1251
Hatakeyama T.: B-0962
Hatem A.: B-1045
Hatidakis A.A.A.: B-0771
Haubenreisser H.: B-0243, B-0459, B-0542, B-1354
Hauer R.N.W.: B-1656
Haug A.: B-0507
Hauge I.H.: B-1309
Hauke C.: B-0541
Häusler G.: B-0345
Hayashi N.: B-0451
Hayashi Y.: B-0720
Hazaimeh B.K.: B-1045
He B.: B-1018
He M.: B-1097, B-1195
He S.: B-0502
Healy D.: B-0586
Heard R.: B-1416
Hebda A.: B-1107
Heber S.D.: B-0336, B-0838
Heck O.: B-0509
Hedesiu M.: B-1184
Heeke B.: B-0034
Heeneman S.: B-0222
Heeren J.: B-0990
Heeringa J.: B-0118
Heerink W.J.: B-0825
Heffernan E.: B-0099
Hegde V.: B-0261
Hegele A.: B-1546
Heidenreich A.: B-1473
Heier-Baardson H.: B-1137
Heijmink S.: B-1565, B-1568
Heikkinen J.: B-1449
Heil A.: B-0264
Heil P.: B-0450, B-1138
Heiland S.: B-0264
Heine M.: B-0990
Heinemann V.: B-1076
Heinzler N.: B-1584
Heiß R.: B-0621
Hekimoglu B.: B-0305
Hekimsoy I.: B-1538
Helal M.H.: B-1287
Helbich T.H.: A-118, A-321, B-0079, B-0506, B-0507, B-0910, B-0911, B-0912, B-1117, B-1281, B-1289
Held U.: B-1031
Heldmann S.: B-0238
Hellbach K.: B-0541
Helle T.: B-0971
Helmberger T.K.: A-294, A-971
Heltai K.: B-1657
Hempel J.-M.: B-0090, B-0093, B-0808, B-1674
Hendel R.: B-0482
Henderson J.: B-0821
Henderson S.: B-1182
Hendrikse J.: B-0691
Henes F.O.: B-0022, B-0025
Henneman M.M.: B-1649
Henner A.: B-0130, B-0351, B-0744, B-1146, B-1310, B-1449, B-1452
Hennicaux J.: B-0458, B-0462, B-1555
Henzler T.: B-0234, B-0459, B-0542, B-1354, B-1582
Herholz K.: B-1033
Herlin C.: B-0435
Hermann K.-G.: B-0299, B-0308, B-0309, B-0530, B-1029, B-1615, B-1619
Hermans J.J.: B-0480
Hermans R.: A-622
Hernández Morales D.: B-0827

List of Authors & Co-Authors

Hernowo A.T.: B-0091, B-1597
Herranz M.: B-0501, B-0992, B-1395
Herrera I.: A-022
Herrmann J.: B-0932
Herrmann K.: B-0355, B-0584, B-0652, B-0796,
B-1367, B-1534, B-1621
Herrmann K.-G.: SY 14
Herth F.J.: B-0240
Herud E.B.: B-1137
Heskamp S.: A-426
Hess S.: B-0766
Hesse A.C.: B-0189
Hesse N.: B-0541
Heusch P.: B-0584, B-0706
Heussel C.P.: A-532, B-0240, B-0402, B-0405,
B-0871, B-1549, B-1588
Heussel P.D.C.P.: B-0240
Heuvelmans M.A.: A-447
Hickethier T.: B-0983, B-1556
Hickson M.: B-1169
Hieken T.: B-0504
Higaki T.: B-0428
Higashigaito K.: B-0026
Higgins R.: B-0970
Hilbert T.: B-0013, B-1488
Hilgendorff A.: B-1161
Hilgenfeld T.: B-0264
Hinterleitner C.: B-0704
Hinzpeter R.M.M.: A-127
Hiremath S.B.: B-1595
Hirner-Eppeneder H.: B-1176
Hirschmann A.: B-0538
Hirt P.: B-0050
Hizel K.: B-0205
Hjelle V.V.: B-0971
Hladuřnik M.: B-0278
Ho M.-C.: B-1590
Ho Y.C.: B-0193
Hoa P.N.: B-0449, B-1540
Hodel J.: A-211
Hoedl P.: B-1091
Hoefel C.: A-794
Höfer I.E.: B-0568
Hoffmann K.-T.: B-0359
Hoffmann MD MPH U.: B-0340
Hoffmann R.: B-0601, B-1208
Hoffmann U.: B-1463
Hofstaedter F.: B-1235, B-1237
Hofman P.A.: B-0220
Hofmann C.: B-0905
Hofmann F.O.: B-1076
Hofmann P.C.: B-1026
Hofmann V.: B-0835
Hofmeister J.: B-0112, B-0867
Hofstaedter F.: B-1037
Hofvind S.: B-0076, B-0132, B-0133, B-0134,
B-0676, B-0677, B-0681, B-1007, B-1096
Hogeweg L.: B-0870
Hogg P.H.: A-631, B-0135, B-0741, B-1296,
B-1303, B-1446
Hojreh A.: B-0155
Holch J.: B-1076
Holen Å.S.: B-0076, B-0132, B-0676, B-1007,
B-1096
Holla M.: A-938
Holly S.: B-0924
Hollywood A.: B-0176
Holmen L.O.: B-1137
Holmin S.: B-1438
Holst R.: B-1660
Holt J.: B-1288
Holter T.Ø.: B-1647
Holub P.: A-614
Holz J.: B-0699, B-1473
Hombreux A.: B-1043
Homolka P.: B-0317
Homsí R.: B-1350, B-1571
Honda H.: B-0716
Honegger J.: B-1674
Hong G.: B-1097, B-1098, B-1103, B-1104
Hong H.: B-0044

Hong Q.: B-1572
Hong S.H.: B-0239
Hong T.: B-0985
Hong W.: B-1269
Hoppe H.: A-665
Horger M.: B-0704
Hori M.: B-0607
Horion J.: B-0066
Hornbeck A.: B-0315
Horninger W.: B-1570
Hornung M.: B-0207, B-0208
Horoz S.: B-0322, B-1450
Horta M.: A-769, B-0380, B-0396, B-0651
Horvat J.V.: B-1117
Horvath E.: B-0272, B-0492, B-0494, B-0667,
B-0914, B-1116
Horvat-Maurovich P.: B-0596
Hosny S.: B-1666
Hosseini-Foucher C.: B-1552
Hota P.: B-1243
Hotfiel T.: B-0621
Ho-Thi P.: B-1566
Hotta M.: B-1081
Hou B.: B-0810, B-1181
Hou Y.: B-0455, B-0759
Houfflin-Debarge V.: B-1504
Houshyar R.: B-0361
Houssami N.: B-0077
Houston G.: B-0214, B-0562, B-1585
Houthoofd S.: B-0224
Hovda T.: B-0076, B-0676, B-1096
Howarth N.: A-160, B-0642
Howlett D.C.: A-853
Hribar T.: B-1448
Hricak H.: A-207, B-0254
Hsieh P.-L.: B-0194
Hu B.-Y.: B-0338
Hu S.: B-0491, B-0669, B-1188
Hu T.: B-0171, B-0360
Hu X.: B-0653, B-0655
Hu Y.-S.: B-1099
Hu Z.: B-1525
Huang D.: B-1659
Huang H.-C.: B-1021
Huang J.: B-0004
Huang K.: B-0200, B-0638
Huang L.: B-0171, B-0223
Huang M.: B-0524, B-0648, B-0852, B-1661
Huang S.: B-1531, B-1535
Huang X.: B-0653, B-0655
Huber A.M.: B-0149
Huber S.: A-927
Huber T.: B-0088
Hubert C.: B-0424
Hübner F.: B-0622
Huellner M.: B-0708
Hughes N.M.: B-0249
Hui J.: B-1171
Huicochea Castellanos S.: B-0374
Huijgen W.: B-0110
Huizinga W.: B-1678
Humphries P.D.: A-650
Hurwitz L.: B-1453
Hussain A.A.A.W.: B-0946
Hussein Y.: B-0592
Huston J.: B-0546
Hutt A.: B-0458, B-1555
Huy H.Q.: B-0449, B-1540
Huynh Anh M.: B-0426
Huynh T.T.: B-0069
Hwang J.-Y.: B-0575
Hwang S.I.: B-1066
Hye Mi G.: B-0102
Hyeyoon C.: B-0643
Hynes G.: B-0831
Hyodo T.: B-0607

Iacobellis F.: B-0295, B-0525
Iadevito I.: B-0295
Iafate F.: A-525
Iafate S.: B-0829, B-1542, B-1543
Iannelli M.: B-1665
Iannessi A.: B-1343
Ibe D.: B-1498
Ibes P.: B-0597
Ibraheem O.: B-0602
Ibrahim A.S.: B-0592
Ichikawa S.: B-1258
Ido M.: B-1391
Ienzi F.: B-1292, B-1630
Ienzi R.: B-1292, B-1614, B-1630
Ierace T.: B-0452
Iezzi R.: A-077, A-364, A-428, B-0185, B-1061
Igarashi T.: B-1388
Iida M.: B-0428
Ikram M.A.: B-0794, B-0795, B-0797, B-1038,
B-1678
Ikram M.K.: B-0795, B-0797
Iles S.E.: B-0684, B-1606
Iliadis K.: B-0343
Iliopoulos A.: B-0183
Illarioskin S.: B-0696, B-1035
Illing R.: B-0129, B-0183
Ilonca A.-D.: B-1053, B-1057
Ilves P.: B-0296
Imbault M.: B-0202
Imhof H.: A-024
Imran Al-Zubaer A.: B-1632
Imsand S.: B-0314
Inal M.: B-0954
Inan N.: B-0108, B-0379
Incarbone V.: B-0580, B-1016
Incerti E.: B-1042
Indestegee I.: B-1139
Indo H.: B-0738
Inecikli M.F.: B-0826
Invernizzi F.: B-1468, B-1469
Ioan I.: B-0917
Ioannidis G.: A-849
Iodice M.: B-1093
Iori A.P.: B-1529
Iotti V.: B-0083
Ippolito D.: B-0024, B-0444, B-0634, B-0851,
B-0897, B-0942, B-1129, B-1328, B-1513,
B-1514, B-1518, SY 12
Irión K.: A-304
Ironi G.: B-1042
Isgum I.: B-0568, B-1462
Ishiguchi T.: B-1391
Ishikawa T.: B-1048
Islak C.: B-0687
Islam S.: B-0822
Isoardi P.: B-1392
Italiano A.: B-0697, B-0698
Ito Y.: B-0428, B-1391
Ittermann T.: B-0447
Ittrich H.: B-0990
Ivanac G.: B-0726
Ivanoski S.P.: B-0535
Ivanovska T.: B-0768
Iwasawa T.: B-0637
Iwata M.: B-0738
Izhaky D.: B-1608, B-1609

J

Jaberg L.: B-1123
Jacków J.: B-0920
Jacob J.: K-15
Jacob S.: B-0595
Jacobs B.E.: B-1049, B-1456
Jacobs C.: B-1349
Jacobs J.: B-0002, B-0124
Jacobs R.: B-1431
Jacobson J.: A-798, A-800
Jacques T.: SY 25

List of Authors & Co-Authors

Jacquier A.: A-194, A-600, B-0563
Jacquiez C.: B-1040
Jaeger L.: B-0237
Jaermann Y.: A-496
Jafarinosar G.: B-0956
Jaffro M.: B-0860, B-1072
Jäger H.R.: A-410, SY 18
Jahnke P.: B-0548, B-0830
Jain P.: B-0505
Jain S.: B-1378, B-1379
Jain S.K.: B-0505
Jaipal U.: B-1362
Jäkel O.: A-887
Jalailah A.: B-1045
Jamali S.: B-1508
James J.: B-1636
James K.: B-0574
James S.L.J.: A-842
Jang A.: B-1509
Jang H.Y.: B-0718
Jang S.: B-0089
Jang S.K.: B-0577
Janka R.: B-1260, B-1629
Jankharia B.: B-0872
Jankowski A.: B-0052
Jannot A.-S.: B-1413
Jansen O.: A-667
Jantzen R.: B-0293
Janulcikas Ž.R.: B-0750
Jarczewski A.: B-0609
Jargiello T.: A-125, A-662
Jarrige V.: B-0315
Jaschke W.: B-0148, B-0572, B-1423
Jasperse B.: B-0068
Jayakumar M.: B-1601
Je B.-K.: B-0461
Jean C.: B-0802
Jean-Pierre A.: B-0313
Jehangir M.: B-1509
Jehs B.: B-0023
Jendeberg J.K.: B-1382
Jennings A.: B-1009
Jensen T.S.: B-0435
Jeon H.J.: B-0195
Jeon J.Y.: B-0434
Jeong H.-J.: B-0320
Jeong Y.-J.: B-0760
Jeong-Cheon A.: B-0461
Jesih P.A.: B-1443
Jesser J.: B-0925
Jeukens C.R.: B-1410
Ji J.: B-1171
Ji Q.: B-0201
Jia Y.: B-0524
Jia Z.: B-0455, B-0456, B-0759
Jiang B.: B-0467
Jiang J.: B-0421, B-1572
Jiang S.: B-0713
Jiang T.-A.: B-0206
Jiang Y.: B-1278, B-1290
Jiménez-Pastor A.: B-1380
Jin G.: B-1172
Jin H.: B-0735
Jin L.: B-0408, B-0496, B-0635, B-1351
Jin T.: B-1483
Jin Y.: B-1171, B-1179
Jin Z.: B-0467, B-0792, B-1181, B-1264, SY 15
Jin Z.Y.: A-946
Jin Z.-Y.: B-0364, B-1259, B-1261
Jindahra P.: B-1199
Jing W.: B-1295
Jing X.: B-1203
Jingliang C.: B-0074
Jobst B.J.: A-307, B-0413, B-1588
Jochelson M.S.: B-1409
Jockwitz C.: B-1037
Jofré H.: B-0048
Johannink J.: B-0601
Johansen S.: B-1147, B-1643
John B.: B-0035
Johnson D.: B-0822

Johnson G.: A-353
Johnson K.J.: A-731
Johnson K.S.: B-1006
Jolles B.: B-1425
Jonczyk M.: B-0446
Joo I.: B-1524
Jordaan M.: B-0969
Jordan D.W.: B-0125, B-1017
Jorge C.L.: B-1400
Jørgensen S.H.: B-0556
Joseph J.: B-1094
Jost G.: B-0995
Jost L.: B-1534
Joudiou N.: B-0424
Jouve de Guilbert P.-H.: B-0386
Jovicich J.: B-1033
JPND Working Group SRA-NED: B-1033
Juaneda M.: B-0992
Juárez-García M.S.: B-1551
Juhee K.: B-1052
Jukema J.W.: B-0335
Juluru K.: B-0705
Jung C.S.L.: B-0990
Jung E.-M.: B-0055, B-0207, B-0208
Jung S.C.: B-0693
Jung S.I.: B-0195
Jungmann P.M.: A-469
Jurgilewicz D.: B-0278
Juskanic D.: B-0924
Jussila A.-L.: B-0351
Jutte P.C.: B-1345

K

Kaatee M.: B-0566, B-0571
Kabaalioglu A.: B-0433
Kabbasch C.: B-0511, B-0515, B-0927
Kabin Y.: B-0702
Kachelrieß M.: A-654, B-0542, B-0733, B-0736, B-1432, B-1434, B-1435, B-1437
Kacimi O.: B-0941
Kacso G.: B-0453
Kadir T.: B-0868
Kadivar S.: B-1221
Kadoya M.: B-1315
Kaelin A.: B-1001
Kafrouni M.: B-1057
Kahl G.G.: B-1309
Kahn J.: B-0292, B-0412, B-0894, B-0899, B-0961, B-1056
Kahn J.-E.: B-1654
Kahn T.: B-1564, B-1566
Kaireit T.: B-0235
Kaiser C.: SY 1d
Kaissis G.: B-0900, B-0988
Kala P.: B-0260
Kalashnikova L.: B-0215
Kalcan S.: B-1324
Kaleci S.: B-0855
Kalender W.A.: A-146, A-230
Kalesnik A.: B-0406
Kalkan A.: B-0511
Kallemose T.: B-0747
Kallenbach K.: B-1105
Kallur K.: B-0270
Kalovidouri A.M.: B-0466, B-0499
Kaltenbach B.: B-0258, B-1054, B-1091
Kamalasanan A.: B-1182
Kamble A.: B-1282
Kamble A.N.: B-0100, B-1282
Kaminaga S.: B-0403, B-1581
Kamis M.F.A.K.: B-0105
Kamo M.: B-1472
Kamolov B.: B-1561
Kämpgen B.: B-1582, B-1583
Kanavaki A.: B-0430
Kandiloglu A.R.: B-1291
Kandolf R.: B-0979
Kang B.C.: B-0062
Kang E.-Y.: B-0241, B-0639, B-1132
Kang H.: B-0089

Kang S.: B-0415
Kang T.S.: B-0718
Kaniewska M.: B-0537
Kanki A.: B-0607
Kantarci M.: B-0262, B-0712, B-1652
Kapetas P.: A-327, B-0079, B-0506, B-0507, B-0911, B-0912, B-1289
Kaplan J.: B-0573
Kapustin V.: B-0702, B-1247, B-1561
Kara B.: B-0322, B-1450
Kara H.: B-1293
Karaban I.: B-1236
Karadayi A.: B-0722
Karady J.: B-0150, B-0596, B-0754, B-0761, B-1655
Karagun B.S.: B-0763
Karalok I.: B-0379, B-0581
Karampinos D.C.: B-0441, B-1122
Karanikas G.: B-0506
Karantanas A.H.: A-253, A-280, A-288
Karatopis A.: B-0129
Karadoprak S.: B-1505
Karavasilis E.: B-0129
Karcaaltincaba M.: A-167, A-535
Karcck M.: B-1105
Karius P.: B-0777
Karli Oguz K.: A-652
Karmazanovskiy G.: B-1262
Karnabatidis D.: B-0188, B-0865
Karol A.: B-0069
Karoussou-Schreiner A.: B-0120
Karppinen J.: B-0435
Karrasch S.: B-1356
Kartalis N.: A-220, A-351, A-704
Karwacki G.: B-0516
Karwoski R.: B-0045
Kashina E.: B-1677
Kasprian G.: B-0155, B-1168
Kassai Y.: B-1573
Kassas H.E.: B-1287
Kästel T.: B-0264
Katada Y.: B-1048
Katahashi K.: B-0028
Katayama M.: B-0720
Katramados I.: B-0870
Katsanos K.: A-432, A-673, B-0188, B-0865
Katsifarakis D.: A-630
Katulska K.: A-781
Katyan A.: B-0054, B-0271
Katz M.: B-0142
Kauczor H.-U.: A-170, A-565, B-0014, B-0240, B-0375, B-0402, B-0413, B-0437, B-0544, B-1105, B-1131, B-1278, B-1290, B-1356, B-1549, B-1588
Kauffman Ortega C.: B-0397
Kaul D.: B-0292, B-0381
Kaul M.: B-0932, B-0990
Kaup M.: B-0528
Kavanagh R.: B-0070, B-0574
Kavus M.: B-0661
Kawamura K.: B-0720
Kayano S.: B-1306
Kazemi-Shirazi L.: B-1255
Kazmierczak P.M.: B-1176
Keating D.M.: B-1409
Kecskemethy P.: SY 26
Keelson B.: B-0721
Keeser D.: A-831
Kehler L.: B-0402, B-0871
Keil M.: B-0909
Keil S.: B-0818
Keil V.C.: A-909
Keinrath G.: B-1176
Kelekis A.: K-26
Keller N.: B-1273
Keller S.: B-1317, B-1319
Kellermann M.: B-0621
Kelly A.: B-1301
Kelly B.E.: A-184, A-854
Kelly B.S.: B-0099, B-0177
Kelly C.J.: B-0002

List of Authors & Co-Authors

- Kelly E.: A-928
Kelly M.D.: B-0002
Kelly P.: B-0249, B-1299
Kelly-Morland C.: B-1080
Kelsch V.: B-0835
Kenchanahalli Rangaswamy V.: B-0770
Kenis S.F.: B-0218
Kennedy S.: B-0947
Kerleroux B.: B-1488
Kerlikowske K.: B-1604
Kesari A.R.: B-0270
Keserci B.: B-0449, B-1540
Kesim Ç.: B-1004
Kessler E.: B-1208
Kessner R.: B-0125, B-1326
Kettenbach J.: A-859
Keussen I.E.: A-052
Kevans D.: B-0443
Keymeulen K.: B-0274
Khaled W.: B-0117
Khalil A.M.-E.: B-0109
Khan F.: B-0214, B-0562
Khan S.: B-1675
Khandelwal N.: B-1334
Khanna G.: B-1373
Khatri G.: B-0401
Kheir H.: B-0470
Khong P.-L.: B-0075
Khoo S.G.: B-0070
Khouri Chalouhi C.: B-0008
Khung S.: B-1555
Kidikas H.: B-0814
Kidzinski R.: B-0604
Kiefer B.: B-1125
Kiefer L.S.: B-0334
Kies D.: B-1600
Kiessling F.M.A.: A-059
Kietselaer B.L.: B-1461
Kijowski R.: B-1424
Kikuchi K.: B-1457
Kilburn-Toppin F.: A-328
Kildal D.: B-0178, B-0180, B-0294
Kilic̆kesmez N.Ö.: B-1206
Killeen R.P.: B-0070
Kim C.: B-0241, B-0461, B-0639, B-1132
Kim C.K.: B-0388, B-0647, B-0650
Kim D.H.: B-0062
Kim D.J.: B-0639, B-1132
Kim D.K.: B-0058
Kim D.-S.: B-0320
Kim D.-W.: B-0707
Kim E.: B-1321
Kim H.: B-0044, B-0577, B-1132
Kim H.C.: B-0718
Kim H.J.: B-0577, B-0801
Kim H.S.: B-0087, B-0693
Kim J.: B-0718
Kim J.B.: B-0026
Kim J.H.: B-0735
Kim J.W.: B-0643
Kim J.Y.: B-0693
Kim K.A.: B-0643
Kim M.: B-0087, B-0575
Kim M.J.: B-0854, B-1269
Kim M.-J.: B-0192
Kim M.R.: B-0760
Kim N.: B-0239
Kim S.: B-0034
Kim S.H.: B-0645, B-0649, B-1474
Kim S.J.: B-0693, B-1474
Kim S.-K.: B-0461
Kim S.W.: B-0005
Kim S.Y.: B-0645, B-0649
Kim T.H.: B-0102, B-0415
Kim T.M.: B-0645
Kim T.Y.: B-1005
Kim W.: A-723, A-985, K-28
Kim Y.: B-0032
Kim Y.H.: B-0020
Kim Y.J.: B-0195
Kim Y.K.: B-0197, B-0664
- Kim Y.R.: B-0005
Kim Y.W.: B-0414
Kim Y.-W.: B-0575
Kimmig R.: B-1371
Kind M.: B-0697, B-0698
King A.: B-0624
King A.D.: A-434, A-624
King L.: B-0115
King S.: B-1304
Kinkel K.: A-767, SY 19
Kintzelé L.: B-0437
Kipp J.P.: B-0012
Kirchner J.: B-0584, B-0652
Kirienco A.: B-1128
Kirkbride T.E.: B-0731
Kirsch R.: B-0285, B-0796
Kirschke J.S.: B-0441, SY 5
Kirschning T.: B-0243
Kirubha Y.: B-1675
Kishida Y.: B-0043, B-0403, B-1348, B-1573, B-1578, B-1579, B-1581
Kita R.: B-0198
Kitagawa K.: B-0350
Kitamura T.: B-0962
Kitao A.: B-0198
Kitrou P.: B-0188, B-0865
Kitslaar P.: B-0754
Kiyon A.: B-1330
Kizilkilic̆ O.: B-0687
Kjaer A.: A-157
Kjaer P.: B-0435
Kjelle E.: B-1302, B-1311
Klang E.: B-0486
Klarhöfer M.: B-1125
Klauser A.: A-105, A-347, B-1423
Klausm M.: B-0014
Klaver C.C.W.: B-0795
Kleber F.X.: A-670
Klebermass-Schrehof K.: B-0155
Kleffel T.: B-0945
Klein S.: B-0794
Klepochová R.: B-0345
Kleven L.: B-1311
Klimenko A.: B-0710
Klingel K.: B-0979
Kloeckner R.: B-0196, B-0210
Klompenhouwer E.: B-1204
Klontzas M.: A-254
Klose U.: B-0090, B-0093, B-0808
Klosterkemper Y.: B-0319, B-1584
Klotz E.: B-0542
Klug G.: B-0148, B-0572
Klüter A.: B-1583
Klutmann S.: B-1252
Kmetjuk Y.: B-0703
Knapp K.: B-0746, B-0751
Knaup M.: B-0733, B-1434
Knauth M.: B-0189, B-0923
Knebel J.-F.: B-1273
Knezevic A.: B-0167
Knoflach M.: B-0510
Knopp M.I.: B-0888
Knopp M.V.: B-0888, B-0993, B-1079, B-1218
Ko C.S.: B-0241, B-1415
Ko Y.S.: B-0062
Kobayashi S.: B-0198
Kobayashi Y.: B-0026
Kober T.: B-0013, B-1488
Kocak B.: B-0687
Kocer N.: B-0687
Koch M.A.: B-0793
Kochalska K.: B-0553
Köcher M.: A-043
Kochura V.: B-0641
Kock M.C.: B-0311
Kockelkoren R.: B-0691
Koda W.: B-0198
Koenig A.: B-1546
Koerzdoerfer G.: B-0285
Kofflard M.: B-1461
Kofoid K.: B-0597
- Koh D.-M.: A-164, A-387, B-0209, B-0393, B-1083, B-1202
Köhler C.: B-0363
Kohler R.: A-112, A-540
Koivunen K.: B-1452
Kok H.K.: B-0856
Kok N.F.: B-1085
Koktzoglou I.: B-1046
Kolb A.: B-1428
Kolbitsch C.: A-656
Kolossvary M.: B-0150, B-0754, B-0761, B-1655
Komatsu D.: B-1315
Komljenovic D.: B-0545
Konen E.: B-0486
Konietzke P.: B-0240
Kononov R.: B-0696, B-1035
Kononov R.N.: B-0928
Koo A.: B-0844
Kooi M.E.: B-0220, B-0222
Kooijman-Kurfuerst H.: B-1319
Kool D.R.: A-940, K-18
Koops A.: B-0035
Kooreman L.: B-0274
Kopp C.W.: A-429
Kopp F.K.: B-0529, B-1136
Körber A.: B-1621
Kornienko V.: B-1484
Kortelainen K.: B-1442
Kortesiemi M.: A-310, A-783, SY 25
Koryukova K.: B-0429, B-0608, B-0611, B-0843
Köse T.: B-1538
Kossov F.: B-1248, B-1561
Kostash O.: B-0702
Köster F.: B-0900
Kott A.: B-0373
Kotter E.: A-361, SY 14
Kottlors J.: B-0515
Koulocheri D.: B-1086
Kousaka J.: B-1391
Koutoulidis V.: B-1086
Koutsouleris N.: A-830
Kouvelakis K.: B-1083
Kovacevic D.: B-0373, B-1069
Kozák L.R.: B-0659, B-1680
Kozaka K.: B-0198, B-0607
Kozic D.: B-1673
Kozlov V.: B-0703
Kozlova O.: B-0703
Kræima J.: B-1345
Krainik A.: A-639, B-0509, B-0802, B-1676
Krajina A.: A-053
Kraakstad C.: B-1368
Kramer J.: A-466
Kranewitter C.: B-0148
Kraus B.: A-550
Kraus M.S.: B-0764
Kräuter C.: B-1151
Krautschneider W.: B-0035
Krebs J.: B-0243
Krebs S.: B-0840
Kreitner K.-F.: A-289, A-570, B-0973, B-0974, B-0975, B-1157, B-1159, B-1160, B-1653
Kremneva E.I.: B-1407, B-1677
Kremser C.: B-0148, B-1423
Krenning B.: B-1461
Kress B.: B-0395
Krestin G.P.: A-319, B-0118, B-0143, B-1426
Kreuter M.: B-0402, B-0405, B-0871
Kreynina J.: B-1375
Kriachok I.: B-0703
Kribben A.: B-0450
Krisnan T.: B-0617
Kristoffersen Wiberg M.: B-0997
Kritter S.: B-0050
Krivosheeva N.: B-1335
Kroencke T.J.: B-0023, K-30
Kröger J.R.: B-1556
Krois W.: B-1168
Kroiss A.: B-1570
Krokidis M.: B-0231
Kroll J.: A-039

List of Authors & Co-Authors

- Krombach G.A.: A-869
Kromrey M.-L.: B-0447
Kröncke T.: B-0527, B-0945
Kröpil P.: B-0319, B-1584
Krotenkova M.: B-0215, B-0696, B-1035,
B-1407, B-1677
Krssak M.: B-0345
Kruit M.C.: B-1600
Kruk M.: B-0337
Krüll A.: B-1252
Krumina G.: B-1530
Krylov V.: B-0690
Kubas B.: B-0278
Kubasov A.: B-0406
Kubik-Huch R.A.: A-546, A-768, B-0537,
B-0919, B-1417
Kuchcinski G.: B-1040
Kuehn B.: B-1125
Kuhl C.K.: A-556, B-0818, K-16
Kuhm J.: B-1432
Kühn J.-P.: B-0447
Kuhn M.: B-1366
Kuhnigk J.-M.: B-0235
Kuijpers D.: B-0566, B-0571, B-1152
Kukkes T.: B-0130, B-1146
Kul M.: B-0842, B-1322
Kulberg N.S.: B-1591
Kultur T.: B-0954
Kumar A.: B-0054
Kumar S.: A-758
Kumari J.: B-1675
Kumari S.: B-1675
Kumari S.: B-1675
Kumlien E.: B-1401
Kunst J.: B-0868
Kunz W.G.: B-0088, B-0513, B-0517, B-0922
Kuo H.-T.: B-0194
Kuo J.-W.: B-1017
Kuo S.-F.: B-0534
Kuo Y.-T.: B-0194
Kupcs K.: B-0814
Küpeli A.: B-1324
Kuplevatskaya D.I.: B-1078, B-1220
Kuplevatsky V.: B-1548
Kuplevatsky V.I.: B-1078
Kupske A.: B-0282
Kural Rahatli F.: B-1004
Kurata A.: B-0337
Kurehana N.: B-0738
Kurilova I.: B-0356
Kurochkina N.: B-0696
Kuru Öz D.: B-0842, B-1322
Kurz K.D.: A-559
Kuznecova A.: B-1335
Kwon M.: B-1415
Kwon W.: B-1580
Kwon Y.W.: B-0801
Kwong D.L.: B-0075
Kwong L.W.D.: B-0217
Kyheng M.: B-0458
Kyotani K.: B-1573
Kyriakis I.: B-0304
- Łaguna P.: B-0307
Lahaye C.: B-0331
Lahaye M.J.: A-808, B-0172, B-0352, B-0893,
B-1085, B-1376
Lahdenperä A.: B-1452
Lai M.H.B.: B-1370
Laino M.E.: B-0216
Laitinen H.L.M.S.: B-1447
Lakhani A.: B-0561
Lalezari F.: B-0356
Lall C.: B-0190, B-0361
Lam G.T.: B-0499
Lamalle L.: B-0802
Lamb H.J.: A-619, B-0204, B-0335, B-0883
Lambregts D.M.: B-0352, B-0356, B-0365,
B-0717, B-0893, B-1085, B-1204, B-1274,
B-1376
Lanclus M.: B-0236
Landen M.: B-0290
Lang K.: B-1006, B-1417
Langenbach M.C.: B-0528, B-0824, B-1054,
B-1059
Langendijk J.A.: B-0595
Langer M.: B-0081
Langius E.: B-1109
Långkvist M.: B-1382
Laniado M.: A-064
Lansdorp B.: B-0825
Lansier A.: B-0293
Lao I.H.W.: B-0194
Lapegue F.: B-0302
Lapteva M.: B-0423, B-1512
Laqua N.: B-1363, B-1364
Lara Nuñez D.: B-1092
Larbi A.: B-0531, B-0949
Larici A.R.: A-446, A-603, B-0874
Larsen V.: B-0288
Larsson E.-M.B.: A-202, B-0096
Lashkhi K.: B-0014
Lassalle L.: B-0117, B-0302
Lassalle S.: B-1043
Lassche S.: B-0957
Latronico A.: B-1090
Lattanzi R.: B-0815
Lattavo L.: B-0153, B-0157, B-0159
Lau C.S.: B-1620
Lau W.H.V.: B-1620
Lauenstein T.C.: A-350, A-706
Laukamp K.R.: B-0906, B-1023, B-1671
Laulé M.: B-0597, B-0598
Laverman P.: A-354
Lavin P.: B-1277
Lavra F.: B-1455
Law K.W.H.: B-0217
Law L.Y.A.: B-1370
Lawler L.: B-0176
Lawrence H.: B-1646
Lawrence H.A.: B-1148
Laxmi V.: B-1507
Łazarczyk A.: B-0553
Le Blanc M.: B-0377, B-0587, B-1012, B-1023
Le Corroller T.: B-1024
Le Loarer F.: B-0697, B-0698
Le Roy J.: B-1133
Leander P.: A-507
Lebedev S.: B-1437
Lebkowska U.: B-0278
Leboeuf-Yde C.: B-0435
Lecler A.: B-0514, B-0802
Leclerc A.: B-0518
Leclerc X.: B-1040
Lecouvet F.E.: A-196, A-944
Lederlin M.: A-055
Ledikhova N.: B-0182
Ledoux J.-B.: B-0013
Lee B.E.: B-0693
Lee C.: B-0344, B-0504, B-0947
Lee C.-C.: B-1099
Lee C.H.: B-0643
Lee D.H.: B-0693, B-1269, B-1524
Lee E.S.: B-1265, B-1524
- Lee H.: B-0032, B-0192, B-1580
Lee H.J.: B-0718, B-1066
Lee J.: B-0388, B-0643, B-0650
Lee J.B.: B-1265
Lee J.C.: B-0236
Lee J.H.: B-1191
Lee J.J.: B-0947
Lee J.M.: A-019, B-1321, B-1524
Lee K.: B-1269
Lee K.H.: B-0193, B-1212, B-1620
Lee K.Y.: B-0461, B-0639, B-1132
Lee K.Y.Y.: B-0241
Lee S.: A-790, A-856, B-0190
Lee S.-E.: B-0707
Lee S.H.: B-0461
Lee S.-J.: B-0320, B-1474
Lee S.M.: B-0239, B-1269, B-1524
Lee T.K.: B-0361
Lee V.H.: B-0075, B-0603
Lee W.Y.S.: B-0217
Lee Y.: B-0461
Lee Y.H.: B-0005
Lee Y.J.: B-0020
Leen E.: A-823
Lefevre A.: B-0448
Lefevre G.: B-1654
Lefort M.: B-0666
Legostaeva L.: B-1407
Legrand M.: B-0422
Legroux-Gérot I.: B-1122
Lehmann K.S.: B-1340
Lei D.: B-0662
Leichter I.: B-0457
Leijenaar R.: A-574
Leiner T.: A-278, A-357, A-430, B-0568, B-0596,
B-1462, B-1463
Leiser P.: B-0243
Leite C.D.: B-1400
Leithner D.: B-0346, B-0439, B-0506, B-0507,
B-0753, B-1026, B-1091, B-1515
Lell M.: A-111, B-0733
Lemac D.: B-0726
Lembarki G.: B-0941
Lembcke A.: B-0777
Lemieux L.: B-1680
Lemos P.A.: B-0142
Lendak D.: B-1673
Lenga L.: B-0346, B-0439, B-0460, B-0753,
B-1515
Lenggenhager D.: B-0839
Lenghel L.M.: B-0255
Leni D.: B-0444
Lenkinski R.: SY 17
Lenkovicz J.: B-0874
Lennartz S.: B-0377, B-0587, B-0906, B-1012,
B-1023, B-1470
Lenz A.: B-0022, B-0025
Leonardi A.: B-0184, B-0875
Leone F.: B-0079, B-0683, B-1286, B-1612
Leoni S.: B-1042
Lepner U.: B-0296
Leporq B.: B-0010
Lerch T.: B-0303, B-0539, B-1124
Lerchbaumer M.H.: B-0055
Lerchenberger M.: B-0228
Lescan M.: B-0791
Lesyuk O.: B-0329, B-1149, B-1445, B-1451,
B-1638, B-1645
Lev Cohain N.: B-0457
Levent A.: B-0262, B-0712, B-1652
Levy R.: B-0154
Lewington A.: B-0969
Lewis S.: B-1416, B-1646
Li C.: B-0408, B-1617
Li F.: B-1180, B-1181
Li H.: B-0394, B-0653, B-0846
Li J.: B-0004, B-0848, B-1259, B-1271, B-1279,
B-1323
Li J.H.: B-1257
Li J.Y.: B-0201
Li K.: B-1110, B-1111, B-1403, B-1412, B-1603

L

- La Fougère C.: B-0889
La Grutta L.: B-0565
La Morte S.: B-0266
Labra Weitzler A.: B-1251
Lacampagne A.: B-1133
Lacelli F.: B-0958
Lacey S.: B-0765
Lacroix V.: B-0876
Ladd M.: B-0363, B-0933, B-0934
Laenen A.: B-0224
Lafourcade A.: B-0386
Lagalla R.: B-1616
Laganà D.: B-0232
Lagana' D.: B-0940
Laghi A.: B-0060, B-0162, B-0164, B-0169,
B-0357, B-0358, B-0715, B-1049

List of Authors & Co-Authors

- Li L.: B-1279
Li M.: B-0408, B-0502, B-0635
Li P.: B-1172
Li T.: B-0225, B-0756, B-1110, B-1111
Li W.: B-1034, B-1599
Li X.: B-0170, B-0417, B-0583, B-1276, B-1280, B-1487, B-1531, B-1535, B-1603
Li X.-G.: A-949
Li Y.: B-0111, B-0217, B-0409, B-0450, B-0654, B-0938, B-1172, B-1534
Li Y.L.: B-0193
Li Y.-M.: B-0989
Li Z.: B-0327, B-0594, B-1272, B-1531
Li Z.-L.: B-1267, B-1648
Li Z.P.: B-1535
Li Z.-P.: B-0524
Liang B.: B-0004
Liang F.: B-1017
Liang W.: B-0654, B-0992, B-1395
Licano M.: B-0397
Licano Zubiate M.: B-1092
Lidén M.: B-1382
Liebig T.: B-0511
Lievore E.: B-1562
Liew A.: B-0177
Lim V.D.: B-1283
Lima M.: B-0380, B-0651
Lima M.R.: B-0282
Liman J.: B-0189, B-0923
Lin A.-N.: B-0805
Lin C.-J.: B-1099
Lin D.-D.: B-0989
Lin J.: B-0804
Lin T.: B-0810, B-1002
Lin W.-C.: B-0619
Lin Y.-C.: B-0534, B-1250
Lin Y.-M.: B-0880
Linda A.: B-1294
Linder N.P.: B-1564, B-1566
Ling Ling P.: B-0501, B-0992
Lingor P.: B-1239
Lingsma H.: B-1008
Linova T.: B-1622
Linovs V.: B-1622
Little M.: B-0831
Little R.: B-0165
Liu F.: B-1424
Liu H.: B-0848, B-1174, B-1271, B-1323, B-1333
Liu J.: B-0656
Liu K.: B-0327
Liu K.-D.: B-1099
Liu L.: B-0570, B-1485
Liu M.: B-0502
Liu R.: B-0253
Liu X.: B-0338, B-0783, B-1019, B-1193
Liu Y.: A-403, B-0686
Liu Z.: A-951, B-0986, B-1193, B-1485
Ljuhar D.: B-1013
Ljuhar R.: B-1013
Lauger Rossello J.: B-0116
Llopis E.: A-512, A-569
Llorens R.: B-1162
Lo Mele M.: B-1087
Lo Re G.: A-123
Lobbess M.B.: B-0274, B-1409, B-1410
Lobbess M.B.I.: A-753
Loberg C.: B-0818
Lóbo C.F.T.: B-1400
Lockie D.J.: B-1416
Loewe C.: A-126, A-358, A-597, A-642, B-0563
Logager V.: A-379
Lohófer F.: B-0900, B-0988
Lollert A.: B-1157, B-1159, B-1160, B-1653
Lomas D.J.: A-166
Lombardi D.: B-0265
Lombardi S.: B-0851, B-0942, B-1513
Lombardo F.: B-0250, B-0646
Lombardo S.: B-0823
Lomp A.: B-0296
Londero V.: B-1294
Loney E.: A-541
Longere B.: B-1156, B-1654
Longo D.: B-1404, B-1406
Longo M.G.: B-0282
Longo R.: B-1439
Lonsdorf A.: B-0375
Loo C.: B-0917
Looby S.: B-0856, B-0857
Lopes do Rosario R.S.R.: B-0876
Lopes R.M.: B-0560
Lopez G.A.: B-1140
Lopez M.: B-1529
Lopez Rendon X.: B-0318
López-Meseguer M.: B-1551
Lorbeer R.: B-0334, B-0336, B-0340, B-0838, B-1356
Lord C.: B-0115
Lorenzin D.: B-0425
Lorenzon M.: B-1294
Lorenzoni V.: B-0779
Loria A.: B-1165, B-1440, B-1441
Lorusso F.: B-0465
Losio C.: B-1390
Lotte R.: B-0386
Lotz J.: A-620, B-0563
Louagé F.: B-0642
Lousada M.: B-0552
Loutfi A.: B-1382
Louvel G.: B-0737
Louw A.: B-1142
Loxley N.: B-1433, B-1436
Loy Rodas N.: B-0119
Lu B.: B-0774
Lu F.: B-0999
Lu J.: B-0390, B-0467
Lu L.: B-0653, B-1487
Lu M.J.: B-1487
Lu X.: B-0233, B-0454, B-0455, B-0456, B-0464, B-0713, B-0759, B-1333
Lu Z.: B-1333
Lualdi A.: B-1460
Lubbers M.M.: B-1461
Luboldt W.: B-0523
Luburich P.: B-0048
Luca A.: B-0033
Lucci C.: B-0691
Lucev J.: B-0864
Lucic M.A.: A-189
Lucidarme O.: B-0386, B-0666
Lücke C.: B-0563, B-0979, B-1222
Lücke S.: B-0375
Lüdemann L.: B-0007, B-0009
Lüdemann W.: B-0446, B-1056
Ludvik J.: B-0590
Lui C.Y.: B-1393
Lui S.: B-0656, B-0657, B-1298
Luiz V.R.: B-1641
Lukas C.: A-592
Lukas S.: B-0762
Lukina O.V.: B-1003
Lukyanchikov V.: B-0690
Lund G.K.: B-0780
Lundberg J.: B-1438
Lundberg P.: B-0096
Lundervold A.: B-0484
Lundervold A.S.: B-0484
Lunkiewicz M.: B-0919
Luo W.: B-0417
Lupescu I.G.: A-848
Lupo C.: B-1016, B-1292
Lurie D.J.: A-845, B-0547
Lurz P.: B-0979
Lutfi I.A.: B-0859
Luyckx E.: B-0181, B-1558
Luz J.H.M.: B-0187
Luz P.: B-0187
Luzzago S.: B-1071
Lv H.: B-1193
Lv Q.: B-0930, B-1477
Lv Y.: B-1002, B-1179
Lynn P.: B-0167
Lyra K.P.D.: B-1400
Lyschik S.: B-0973, B-0974
Lysdahl K.B.: B-1302
Lyu Y.: B-0810
Lyubinskij A.: B-0406

M

- Ma C.: B-1332
Ma X.: B-0781, B-1325
Ma Y.: B-0455, B-0759
Maas A.H.E.M.: B-0785
Maas M.: A-651, B-0352, B-0365, B-0717, B-0893, B-1204, B-1213, B-1274
Maccioni F.: A-796, B-1529
Machann J.: B-0334, B-0336, B-0838
Machida Y.: B-1388
Macho J.: A-915
Maciag E.: B-1551
Mack M.G.: A-315, A-699
Mackenzie A.: B-0550
MacMahon P.J.: B-1554
Madani G.: K-10
Mader K.S.: B-1381
Madoff R.: A-933
Madureira A.J.B.S.: A-606
Maeder J.P.: B-0996
Maeder R.: B-0030
Mæhle S.: B-1147, B-1643
Maffei E.: B-0333, B-0565, B-0779, B-0787
Magistrelli A.: B-1165
Magnano G.M.: B-0580
Magne N.: B-0066
Magri V.: B-1633
Maguire S.: B-0972
Mahajan H.: B-0351, SY 5
Mahemood S.A.: B-0946
Maher M.: B-0574
Maher S.: B-0470
Mahesh M.: A-459
Mahjoub S.: B-1357
Mahmood U.: B-0985, B-1533
Mahmoud K.: B-0034, B-1055
Mahnken A.: B-0371, B-1546
Mähringer-Kunz A.: B-0196
Maidment A.D.A.: B-1632
Maier A.: B-0733, B-1629
Maier I.: B-0923
Maier J.: B-0733, B-0736
Maier-Hein K.: B-0402, B-0871, B-1105
Maiettini D.: B-0959
Maillet B.: A-181, A-183
Maino C.: B-0024, B-0634, B-0897
Mainta I.: B-0499
Maintz D.: B-0377, B-0587, B-0699, B-0727, B-0790, B-0906, B-0976, B-0979, B-0983, B-1012, B-1023, B-1119, B-1470, B-1473, B-1556, SY 12
Maj E.: B-1106
Majer M.: B-0921
Majerus P.: B-0120
Majidi H.: B-1466
Majlis S.: B-0492, B-0494, B-0667
Majoie C.B.: B-0512, B-1008
Major V.: B-0561
Mak C.-W.: B-0194
Makarchuk M.: B-1236
Makarenko V.: B-1557
Maki H.: B-0350
Makowski M.R.: A-392, A-742, B-0061, B-0309, B-0426, B-1615
Maksimović R.: A-375
Malagoli E.: B-1128
Malakhanov V.: B-0841
Malamateniou C.: A-144
Malasevski A.: B-0479
Malavasi S.: B-0589, B-0730
Malchus N.: B-1094
Maleux G.: B-0021, B-0224
Malhotra R.: B-1338
Malich A.: B-0373, B-1069, B-1239
Malinauskaitė L.: B-0112

List of Authors & Co-Authors

- Malinova Z.: B-1448
Mallard S.: A-402
Mallet V.: B-0422
Malone D.E.: B-0070
Maly B.: B-0916
Maly Sundgren P.C.: A-463, A-536, A-683, A-766
Mamisich-Saupe N.: A-513
Manakova Y.: B-0641
Manavaki R.: B-1094
Mancini C.: B-0162
Mancini M.E.: B-0755, B-1459, B-1658
Mancuso G.: B-0027
Mandal A.K.: B-0054, B-0271, B-0505
Mandal S.: B-0545
Manesis E.: B-0430
Manfredi M.: B-1244
Manfredi R.: A-261, A-522, A-705, A-877, B-0185, B-0471, B-0861, B-0874, B-0898, B-0944, B-1061, B-1419
Mang T.: K-11
Manganaro L.: B-0151, B-1493, B-1494
Mangels N.: B-0990
Mangerud G.: B-0681
Mani C.: B-0271
Maniatis V.: A-605
Maniowski P.: B-0888, B-1218
Manka R.: B-0980, B-0981, B-1226, B-1227
Mann R.M.: A-326, A-907, B-1277, B-1628, SY 1d
Mannelli L.: B-0374, B-0840
Manniesing R.: B-1594
Mannil M.: B-0047, B-0533, B-0980, B-0981, B-1227
Manoharan T.: SY 1d
Mansour O.: B-0956
Mansour S.A.: B-1666
Mantellini P.: B-0521
Mantini C.: B-0564
Manzhurtsev A.: B-0156
Manzoni F.: B-0267
Mao F.: B-1084, B-1211, B-1526
Mao H.: B-0986, B-1485
Mao L.: B-0502
Mappa L.: B-0144
Maquet C.: B-0066
Marabelle A.: B-0368
Maravi P.: B-0385
Marcelin P.-J.: B-0697
Marcello R.: B-0532
Marchel A.: B-1106
Marchianò A.: B-1349
Marchianò A.V.: B-0165
Marchisio M.: B-0263
Marco Sanz A.G.: B-0175
Marcomini K.D.: B-0269
Marcon M.: B-0273, B-1627
Marconi S.: B-1224
Marcu M.: B-1184
Marcy P.-Y.: A-433
Mardanshahi Z.: B-0287
Marè V.: B-0162
Marek A.: B-0598
Maret E.: B-0026
Martia G.: B-1000
Mari A.: B-0056
Mariani D.: B-0683, B-1286
Mariani S.: B-0300, B-0612, B-0725, B-0729, B-0960, B-1344, B-1427
Mariano-Goulard D.: B-1057
Marie G.: B-0996
Marigliano C.: B-0060
Marin D.: B-0881
Marini F.: B-0939
Marini R.: B-1353
Marino M.A.: B-1167
Mariscotti G.: B-1392, B-1398, B-1414, B-1613
Mark E.B.: B-0012
Mark R.: B-0779
Markowitz F.: B-0104
Marochko N.: B-0576
Maroldi R.: A-023, A-436, B-0053, B-0265, B-0978
Maros M.E.: B-1582, B-1583
Marquering H.: B-1008
Marques A.: B-0963
Marques H.: A-687
Marques M.: B-1314
Marra P.: B-0230, B-0626, B-0629, B-1205
Marroccchio C.: B-0184, B-0630, B-0821, B-1337, B-1339, B-1342, B-1541, B-1547
Marrone G.: B-0033
Marsecano C.: B-0436
Marshall N.: B-0126, B-0682
Marsico S.: B-0487, B-1623
Marti-Bonmati L.: A-090, A-287, A-381, A-934, B-1162, B-1380
Marticorena Garcia S.R.: B-0001
Martin C.: B-1346, B-1353
Martin S.: A-061, B-0112, B-0867
Martin S.S.: B-0258, B-0346, B-0439, B-0753, B-0776, B-1026, B-1515
Martincich L.: B-0107, B-1114
Martinelli M.: B-0166
Martinelli N.: B-0719
Martinelli O.: B-0027
Martinello S.: B-1398
Martineti C.: B-1478
Martínez M.: B-0827
Martini K.: B-0047, B-1355
Martini Tinazzi P.: B-0017
Martinioli C.: A-346
Martins P.: B-0963
Martins P.M.: B-0552, B-0559
Martinsen A.C.: B-1647
Martinsen A.C.T.: B-1137
Martirosian P.: B-0909
Martola J.: B-0997
Martus P.: B-0597, B-0598, B-0889
Martynova N.: B-0406
Maruzzelli L.: B-0033
Mascagni L.: B-0231
Mascalchi M.: B-0161, B-0521
Mascaretti G.: B-0829, B-1542, B-1543
Mascaretti S.: B-0829, B-1542, B-1543
Masciocchi C.: B-0300, B-0436, B-0612, B-0725, B-0729, B-0829, B-0960, B-1344, B-1427, B-1539, B-1542, B-1543
Masha H.M.K.: B-0968
Massarelli C.: B-0144
Massaroni C.: B-0994
Masselli G.: A-380, A-815
Massimi L.: B-0348
Massmann A.: B-1329
Massoud M.: B-0034
Mastrodicasa D.: B-0564, B-0569, B-1047, B-1455, B-1487
Mastronuzzi A.: B-0153, B-0157, B-0159
Masui T.: B-0720
Masy M.: B-1552
Mateo Carballo F.: B-0145
Matheoud R.: B-0325
Mathalakath R.V.: B-1198
Mathys C.: B-1235, B-1237
Matinyan N.: B-1548
Matjašič A.: B-1448
Matos C.: A-219, A-374, A-968
Matos L.L.: B-0902
Matouskova T.: B-0590
Matsuda Y.: B-1550
Matsui O.: B-0198
Matthew S.: B-1585
Matthews J.: B-0972
Mattioli G.: B-0580
Mauad E.C.: B-0138
Maurel J.: B-1520
Maurer B.: B-0047
Maurer M.: B-0791
Maurer M.H.: B-0292, B-0412, B-0894, B-0899
Mauri G.: A-826, B-0452, B-1545
Mauro L.A.: B-0420
Maurovich-Horvat P.: B-0150, B-0598, B-0754, B-0761, B-1463, B-1655
Maus V.: B-0511, B-0515, B-0927, B-1012
May M.S.: B-0901
Mayer N.: B-0249
Mayer P.: B-0014
Mayerhöfer M.E.: A-159, A-199, A-740
Mayinger M.: B-0595
Mayo S.C.: B-1416
Mayr A.: B-0148, B-0572
Mayrhofer M.T.: A-613
Mazzei M.A.: A-099, A-690
Mazzetti S.: B-0378, B-0383, B-1064, B-1244, B-1246, B-1592
Mazziotti S.: B-1536
McCall J.: B-1202
McCarthy P.: B-0177
McCormack M.: B-1416
McCormick P.: B-0443
McDermott A.: B-0670, B-0671, B-1089
McDermott G.M.: B-1192
McDonald R.J.: A-137
Mcdowell A.: B-1170
McElroy S.: B-1080
McGee A.: B-0554, B-1300
McGill M.: B-0152
McGill N.: B-0624
McGinty G.: A-586
McGreal P.: B-1089
McGuire W.: B-0561
McKay C.: B-0972
McLean M.A.: B-1672
McLenachan S.L.: B-0097
McNally S.: B-0099
McNeill A.: SY 19
McNeill G.: B-0070
McNulty J.: A-037, A-401, A-493, A-786, B-1299
McQueen A.: B-1217
Mdletshe S.: B-1148
Meakin J.R.: B-0746, B-0751
Meaney J.F.M.: B-0443
Medici M.: B-0186
Medina-Omelas S.S.: B-0376, B-1253
Meeuwis C.: B-1277
Mehana S.M.: B-0885
Mehigan B.J.: B-0443
Mei K.: B-0529, B-1136
Meier-Schroers M.: B-1350, B-1571
Meijer F.J.A.: A-939, B-0695
Meine H.: B-1383
Meinel F.: B-0541
Mejdoubi M.: B-0921
Mekis N.: B-0745, B-1448
Melberg H.O.: B-1311
Melendez F.J.: B-0827
Meli A.: B-1016
Melnikov I.: B-0806
Melodelima C.: B-0245, B-1074
Meloni F.: B-0833
Melzig C.: B-1549
Mendichovszky I.A.: B-0104, B-1094
Menendez M.V.: B-0993
Menezes G.: B-1277
Menezes R.: B-0947
Meng-Na H.: B-0206
Menke-Pluijmers M.: B-0913
Menovsky T.: B-0858
Mensel B.: B-0447
Menschchikov P.E.: B-0156, B-0806
Mentzel H.-J.: B-0349
Menu Y.: A-285, A-528, A-932, B-0301
Mercan S.: B-1619
Mercatelli D.: B-0114, B-1009, B-1625
Mercer C.E.: B-0135
Mereu A.: B-0216
Merhemic Z.: A-082
Merkely B.: B-0150, B-0754, B-0761, B-1463, B-1655, B-1657
Merkle E.M.: B-0482
Mershin K.: A-131
Mershina E.: A-128

List of Authors & Co-Authors

- Merz K.: B-0412
Mess W.H.: B-0220, B-0222
Messalli G.: B-0564
Messenger M.: B-0969
Messerli M.: B-1105, B-1549
Messina C.: B-0440, B-0719, B-0955, B-1616
Messina F.: B-0158
Messiou C.: A-895
Metin Y.: B-1324
Metsälä E.: B-0130, B-1146
Mettivier G.: B-1439
Metzelder M.: B-1168
Metzler B.: B-0148, B-0572
Meuli R.: B-0013, B-0996
Meuli R.A.: B-1491
Meunier N.: B-1009
Mews J.: B-0530, B-1029
Meyer F.-I.: B-0196
Meyer H.-J.: B-0359
Meyer-Baese A.: B-1036, B-1281
Miccò M.: B-0471
Micelli M.V.: B-1539
Micelli M.V.M.: B-0436
Michaelis J.: B-1566
Michalitsis S.: B-0304
Michelis G.: B-0283
Michoux N.: B-0424, B-0876, B-1508
Midiri M.: B-0565
Miele V.: B-0056, B-0141, B-1183
Migaleddu G.: B-1242
Miglioretti D.: B-1010
Miglioretti D.L.: B-0685, B-1604
Mihnovits V.: B-0296
Mikat C.: B-1138
Mikhailov A.: B-0406, B-1220
Mikhalska L.: B-0703
Mikhaylova E.V.: B-0578
Milanese G.: B-0045, B-0047, B-0333, B-0787, B-1355
Milanesi O.: B-0773
Milani A.: B-0503
Milglane E.: B-0814
Milivojevic M.: B-1401
Miller E.: B-1079
Miller T.T.: A-707, A-709
Millet I.: B-0948
Milliat F.: B-1528
Millington R.: B-0831
Milosavljevic T.: B-1632
Milosevic Z.: B-0103, B-1115
Min L.A.: B-0365, B-0893
Mina L.: B-1668
Minami T.: B-0198
Minamimoto R.: B-1081
Minamoto N.: B-0416
Minasyan I.: B-1548
Minervini A.: B-0056
Minkler M.: B-0237
Miquel A.: B-0301
Mirafzal S.: B-0331
Miraglia R.: B-0033
Mirza M.A.H.A.: B-0688
Mishra A.: B-0946
Mishra S.: B-0673
Misra R.: B-0401
Mistretta F.A.: B-1071
Mitchell D.P.: B-1554
Mithal A.: B-0673
Mitreska N.: A-224
Mittal M.K.: B-0271
Mittal P.: B-0602, B-1373
Mittler J.: B-0210
Miitone A.: B-1041
Miyoshi T.: B-0324
Mizandari M.: B-0037, B-0040, B-0041
Mizzi A.: A-050, B-1144
Moawad S.: B-0034, B-1055
Mobark N.: B-1476
Mocan T.: B-0453
Mochalova E.: B-1407
Moche M.: B-1564
Moddemann M.: B-0036
Modest D.: B-1076
Modestino F.: B-0038
Moebus V.: B-1091
Moehrlen U.: B-1166
Moerup S.: B-0556
Mohammad S.A.: B-1502
Mohammad Zakir M.Z.: B-1675
Mohammadi S.: B-0680
Mohammadzadeh A.: B-0212, B-0477, B-0478, B-0700, B-0734, B-0739, B-0740, B-1221
Mohammadzadeh M.: B-0212, B-0998, B-1221
Mohammadzadeh V.: B-1221
Mohammed Ali A.H.: B-0741, B-1296
Mohammed N.-E.A.N.: B-1210
Mohapatra I.: B-0095
Möhlenbruch M.A.: B-0508
Möhler C.: A-885
Mohr B.: B-0238
Mokhtar O.: B-1287
Moldovan P.-C.: B-0245, B-1074
Mole' R.: B-0940
Molina M.: B-0048
Molinari F.: A-101, A-516
Møller H.: B-1660
Monaco C.G.: B-0165
Mondaini F.: B-0227, B-0862
Mondello S.: B-1536
Moneghetti K.J.: B-0026
Monga A.: B-1338
Montaldo L.: B-0425
Montandon S.: B-0314, B-0316, B-1135
Monteiro M.: B-0323
Montemezzi S.A.: B-1088
Montesinos Garcia P.: B-1465
Montet X.: B-0112, B-0466, B-0499, B-0867, SY 25
Monti C.B.: B-0786
Monti M.L.: B-1522
Montorsi F.: B-0626
Moon L.: B-0343
Moon S.G.: B-0724
Moon W.-J.: B-0801
Moorthy I.: B-0343
Morales P.H.D.M.: B-1186
Morana G.: A-676, B-1478, B-1650
Mordasini M.: A-494
Moreaud O.: B-1676
Moreau-Gaudry A.: B-0186
Moreira I.C.: B-0137
Moreira J.: B-1314
Morel B.: B-1488
Morgan D.: B-1654
Morgan P.S.: B-1144
Mori M.: B-1134
Mori N.: B-1550
Moriarty H.: B-1554
Morillo A.J.: B-0694
Morin P.: B-0331
Moritz A.: B-1455
Moro L.: B-1495
Moron F.E.: B-0277
Moroz A.: B-0696
Morozov S.: B-0182
Morozov S.P.: B-1591
Morozova S.: B-1035, B-1407, B-1677
Morra L.: B-0519, B-0520, B-0522
Morris E.A.: A-555, B-0506, B-0507, B-1117
Morrow M.: B-1409
Morscher S.: B-1094
Mortilla M.: B-0286
Morzenti S.: B-1129
Mosca S.: B-0959
Mosconi C.: B-0038
Moshhammer H.M.: B-0317
Moshina N.: B-0132, B-0133, B-0134
Mostbeck G.H.: A-004
Motosugi U.: B-0607, B-1258
Mottaghy F.: B-1051
Mottet N.: A-917
Motyer R.: B-0856, B-0857
Motyka S.: B-0620
Mouhaoui M.: B-0941
Mouloupoulos L.A.: B-0468
Mouloupoulos L.-A.: A-198
Mounier A.: B-0186
Mounir Y.: B-1287
Mourão de Abreu A.: B-0902
Mouri Y.: B-1391
Moussalli P.: B-0124
Mousseaux E.: B-0595
Mouthon L.: B-1353
Moya L.: B-0117
Moyle P.L.: B-1094
Moynihan B.: B-0857
Mozer P.: B-0386
Mpotsaris A.: B-0189, B-0511, B-0515, B-0927, B-1119
Muca M.: B-1665
Muccioli G.: B-0424
Muchart Lopez J.: B-0160
Mueller J.: B-1356
Mueller-Lisse U.G.: B-1366, B-1471
Mueller-Lisse U.L.: B-1366, B-1471
Mueller-Peltzer K.: B-0057
Muenzel D.: B-0543, B-1121
Muezzinoglu B.: B-0108
Mughetti M.: B-1164
Muglia R.: B-1209
Muglia V.F.: B-0879
Muhammad K.: B-0859
Muharemovic O.: B-0747
Mühlematter U.: B-0533, B-0980
Muin D.: B-1255
Mukhortova O.: B-1249
Mulder H.K.P.: B-1410
Mulert C.: B-1033
Mulholland K.: B-0765
Muller H.: B-1223
Muller J.S.: B-0282
Müllerleile K.: B-0780
Müller-Schimpfle M.P.: B-1091
Mulliez A.: B-0331
Münch B.: B-0359
Mungai F.: B-1183
Munnich A.: B-0154
Münzel D.: B-1120
Muraki T.: B-0716
Murer S.: B-1366
Murphy D.J.: A-257
Murphy M.: B-0586
Murphy P.: B-0574
Murphy S.: B-0857
Murphy S.F.: B-0443
Murraças A.C.C.: B-0559
Musacchia G.: B-1611
Muscogluri G.: B-0031, B-0779, B-1455
Mushtaq S.: B-0567, B-0755, B-0779, B-1459, B-1658
Musi G.: B-1071
Mussmann B.R.: A-226, B-0288
Muthayan P.: B-0347
Mutlu I.N.: B-1206
Mutlu U.: B-0795
Muto G.: B-0378, B-0383, B-1246
Muto M.: A-760, B-0858
Muzic R.: B-1017
Myklebust A.M.: B-1302

N

- Na B.: B-0320
Na D.G.: B-0672
Naas O.: B-1105
Nadjiri J.: B-0149
Nadriljanski M.: B-0103, B-1115
Naganawa S.: B-0028, B-0995
Nagasawa N.: B-0350
Nagel A.: B-0934
Nagel A.M.: B-0621
Nagel S.: B-0508, B-0943
Naggara O.: B-0688

List of Authors & Co-Authors

- Naghbi H.: B-0998
Naguib N.N.N.: B-0623, B-0824, B-1054, B-1210
Nahmani S.: B-0341
Nakai S.: B-0416
Nakamura M.: B-1315
Nakamura Y.: B-0428, B-0607
Nakano H.: B-0962
Nakano S.: B-1391
Nalbach T.: B-0572
Nam I.C.: B-1474
Namal E.K.: B-0379
Nance J.W.: B-0752, B-0776, B-1232
Nandwana S.: B-0602
Nanni C.: A-158
Nanz D.: B-1125
Napoli A.: B-0114, B-0184, B-0630, B-0821, B-0875, B-1337, B-1339, B-1342, B-1541, B-1547
Napolitano A.: B-0153, B-0157, B-0159, B-1042, B-1404, B-1406
Narasimha Krishna V.: B-0866
Narasingam A.: B-1500
Narayanan V.: B-0091, B-1597
Nardone V.: B-0853
Nasattii A.: B-1518
Nasr E.: B-1503
Nasr M.: B-0592
Nassenstein K.: B-1138
Natale L.: A-617
Natale R.: B-1343
Natella R.: B-0525
Nather J.C.: B-0879
Nattenmüller J.: B-0375
Navarra F.: B-0815
Navarro Aguilar V.: B-0006
Navin P.: B-0670, B-0671
Navone S.E.: B-1000
Nazarian S.: B-1656
Nazir R.: B-1509
Nederkoorn P.J.: B-0222
Negi N.: B-0767
Negrao de Figueiredo G.: B-1161
Negrao E.M.S.: B-1285
Negrelli R.: B-0834, B-1065, B-1521, B-1523, B-1567
Negro G.: B-1392
Nehrer S.: B-1013
Nel A.: B-1148
Nelemans P.J.: B-0274
Nelstrop H.L.: B-1192
Nensa F.: B-0355, B-1534
Nerad E.: B-0172
Neri E.: A-458, A-772, A-979, B-0168, B-0890, B-0891, B-0892
Nesterets Y.I.: B-1416
Neubauer C.: B-0081
Neubauer J.: B-0081
Neuberger U.: B-0508
Neuhaus V.: B-0699, B-1012, B-1023, B-1119
Neumaier C.E.: B-0837
Neurath M.F.: B-1260
Newbould R.: B-0002
Newby D.E.: B-0097
Newcombe R.G.: B-0275
Newton-Hughes A.: B-1639
Ngo C.: B-1413
Nguyen A.: B-0768
Nguyen H.: B-0190
Nguyen T.: B-1504
Nguyentat M.: B-0361
Nichelli L.: B-0286
Nicholson P.: B-0856
Nickel D.: B-1261
Nickson C.: B-1416
Nicolas G.: B-0482
Nicolau C.: A-896
Nicolay S.: B-1558
Nicolet L.: B-1420
Nicoletta D.: B-1469
Nicosia L.: B-1090
Nieboer K.: B-1044
Niedmann J.P.: B-0494
Niehues S.M.: B-1340
Nielsen B.E.: B-1137
Nieman K.: B-0337, B-1456, B-1461
Nieminen M.T.: B-0744, B-1014
Niesporek S.: B-0934
Niessen W.J.: A-733, B-0794, B-0795, B-0797, B-1038, B-1678
Niinimäki J.: B-0435
Niiniviita H.: B-0342, B-1447
Nijssen E.C.: B-1011
Nikolaïdou M.E.: B-0468
Nikolaou K.: A-155, A-596, B-0601, B-0704, B-0791, B-0838, B-0881, B-0889, B-0909, B-0918, B-1208, B-1453
Nikulina A.: B-0578
Nikupaavo U.: A-847
Nilica B.: B-1570
Nillesen M.: B-0957
Nimmada T.R.: B-0872, B-1378, B-1379
Ning G.: B-0583
Niro F.: B-0407
Nishie A.: B-0607
Nishimuta Y.: B-0716
Nishino R.: B-0416
Nishiyama T.: B-0106
Nistorescu S.: B-0203
Nitrosi A.: B-0083
Nittka M.: B-0285, B-0796
Niu X.: B-0246, B-0392, B-1596
Noble S.: B-1223
Nocivelli G.: B-0053
Noebauer-Huhmann I.-M.: K-09
Noël P.B.: A-249, B-0529, B-0543, B-1121, B-1136
Noeske J.: B-0439
Nomura C.H.: B-0142, B-0977
Nonaka T.: B-1315
Norajitra T.: B-0871, B-1105
Nordström J.: B-0640
Normand G.: B-1467
Norris D.G.: A-844
Notohamiprodjo M.: B-0601, B-0909
Nouh M.R.: B-0109
Nour Eldin N.-E.: B-0039, B-0824
Nour-Eldin N.-E.A.: B-0623, B-1063
Nous F.: B-0337, B-1461
Novikov M.: B-0703
Novotny P.: B-0868
Novovsad O.: B-0703
Nowakowska-Kotas M.: B-1679
Nowee M.E.: B-0365
Nozaki A.: B-0028
Nozaki T.: B-1472
Ntorkou A.: B-1662
Nudnov N.: B-1375
Numasaki H.: B-0416
Nunes K.R.S.B.: B-0282
Nuñez Peralta C.A.: B-0116
Nunninger M.: B-0830
Nural M.S.: B-1082
Nyapathi V.: B-0526
Nybing J.D.: B-1014
Nyborg T.: B-0140
-
- O**
-
- O' Hora L.: B-0176
Oaknin J.: B-1608, B-1609
Oba M.S.: B-0637
Obadia M.: B-0514
Oberaigner W.: B-1112
Obmann M.: B-0835
O'Brein F.M.: B-0249
O'Brien K.: B-0765
Ochoa Albiztegui R.E.: B-1117
O'Connell A.: B-1089
O'Connor J.: A-861, B-0165
O'Connor M.: B-0321
O'Connor M.: B-1309
O'Connor O.J.: B-0574
Ødegård A.: B-1297
Oebel S.: B-1226
Oei E.: B-0118, B-1030, B-1426
Oei E.H.G.: A-233
Offiah A.C.: A-837, B-0158
Ogier-Denis E.: B-1528
Ogul H.: B-0712
Ogura T.: B-0451, B-0637
Oguzkurt L.: A-858
Oh Y.-W.: B-0241, B-0639, B-1132
O'Hare A.: B-0856, B-0857
Ohno Y.: B-0043, B-0403, B-0767, B-1348, B-1573, B-1578, B-1579, B-1581
O'Hara L.R.: A-580
Ohyu S.: B-1578, B-1579
Oikarinen H.: B-0351
Oikonomou A.: A-163
Okada H.: B-0324
Okada Y.: B-1550
Okuaki T.: B-1321
Okuma H.: B-1388
Olaiya B.: B-0602
Olchowy C.: A-138
Oleaga Zufiria L.: A-186, A-460
Olerud H.M.M.: B-1141, B-1297, B-1302
Olesen S.S.: B-0012
Olimov B.: B-1561
Oliva G.: B-0284, B-0291, B-0683, B-1197, B-1286, B-1612
Oliveira A.: B-0963
Oliveira C.: B-0326
Oliveira D.: B-0963
Oliveira M.V.L.: B-1140
Olivero R.: B-0263
Olthof S.-C.: B-0889
Omar N.N.: B-0473
Omelchenko O.: B-1236
Omoumi P.: A-290, A-921, B-1425
Onal T.: B-0108
Öncü F.: B-1418
O'Neill C.: B-0249
Onishchenko M.: B-1028
Onishi H.: B-1258
Ono K.: B-1306
Onur M.R.: B-0322, B-1450
Onur O.: B-0927
Oostveen L.J.: B-0238, B-0411
Op De Beeck B.J.: A-292
Oppedal K.: B-0798
Ordás I.: B-1537
Ording Müller L.-S.: A-154
Ordu D.: B-0945
Ordu D.A.: B-0527
O'Regan K.: B-0249
O'Regan T.J.: B-1639
Orejuela J.F.: B-1402
Oren D.: B-0150
Oreshkova J.A.: B-1557
Orgera G.: B-0231
Örgüc I.S.S.: B-1291
Orhan Metin N.: B-1324
Origgio D.: B-0382, B-1495
Orlando A.: B-1292, B-1614, B-1630
Orlhac F.: B-0737
Orlov O.: B-1561
Orsatti G.: B-1486, B-1492
Orsi M.A.: B-0291, B-0683, B-1286, B-1612
Ortega Millán M.: B-0101, B-1394
Ørting S.N.: B-0870
Orvieto E.: B-1087
Osella Abate S.: B-1414
Oser R.: B-1055
Osiev A.: A-130
Osmani M.: B-0060
Osman N.: B-1502
Ospel J.M.: B-0516
Ostan R.: B-1009
Osterhoff G.: B-0533
Ostermann H.: B-0317
Osther P.J.S.: B-1660

List of Authors & Co-Authors

Ostojic J.: B-1673
O'Sullivan G.J.: B-0828
Ota H.: B-1306
Otaaduy M.C.G.: B-1400
Otani K.: B-0752, B-1049, B-1454
Othman A.E.: B-0791
Otto G.: B-0210
Oudard S.: B-0476
Oudkerk M.: B-0566, B-0571, B-0757, B-0825,
B-1109, B-1152, B-1155, B-1458
Overbosch J.: B-1345
Owczarczyk K.: B-1080
Owens C.: A-609, A-954
Oyar O.: B-1429
Oyen R.: B-0362
Oyen R.H.: A-832
Ozalp Ates F.S.: B-1618
Özbek S.S.: A-026
Ozcelik C.: B-0052
Özdemir H.O.: B-0769
Özdemir M.: B-0733
Ozdemir O.: B-1324
Özenirler S.: B-0205
Ozer T.: B-0722
Ozgen Mocan B.: A-168
Ozhan Oktar S.: B-0205
Özmen M.N.: A-834
Oztuna D.: B-0952
Ozturk M.: B-0674, B-1505
Ozturk M.H.: B-0305

P

Paalimäki-Paakki K.: B-1310, B-1452
Pacciardi F.: B-1320
Pacella C.M.: B-1545
Pacella G.: B-0627, B-0820
Pacifizi S.: B-0136
Pacile S.: B-1416
Padberg F.: A-828
Padhani A.R.: A-197, A-316, B-0244, B-1361,
SY 1b
Padoy N.: B-0119
Paech D.: B-0363, B-0933, B-0934
Pagan E.: B-1377
Paganelli G.A.: B-1545
Pages M.: B-1520
Pagniez J.: B-1654
Pagonidis K.: A-599
Pahn G.: B-0544, B-0983
Paiman E.H.M.: B-0335
Paiusco M.: B-0773
Paladini A.: B-0861
Palao Errando J.: B-0101, B-1394
Palczewski P.: B-0882
Palfrey R.M.: B-0746, B-0751
Palkhi E.Y.A.: B-0908
Palkó A.: A-241
Pallas R.J.: B-0714
Pallisa E.: B-1551
Palmer Sancho J.: B-0116
Palmisano A.: B-0782, B-0847
Palmucci S.: B-0045, B-0049, B-0420, B-0873
Palumbo P.: B-0300, B-0729, B-1344, B-1539
Pameijer F.A.: A-313
Pamminger M.: B-0572
Panagiotopoulos N.: B-0793
Pancewicz S.: B-0278
Panebianco V.: B-0244, B-1068, B-1547
Panes J.: B-1537
Panfilii M.: B-0348
Pang H.: B-1482, B-1483
Panizza P.: B-1390, B-1440, B-1441
Pankowska A.: B-0553
Panopoulou E.: B-1662
Panourgias E.: B-0468
Panov V.: B-1248, B-1369, B-1561
Pansini V.M.: B-1122
Panteleakou E.: B-0430
Panvini N.: B-0357, B-0358
Panyaping T.: B-1199

Panzeri M.M.: B-0230, B-0626, B-1134, B-1390
Panzone R.: B-0107
Papa S.: B-0479, B-0481
Papadimitos P.: B-0188, B-0865
Papadopoulos F.: SY 23
Papadopoulos P.: B-0161
Papageorgiou I.: B-0373, B-1069, B-1239
Papaioannou G.: B-0183
Papanikolaou N.: A-065, A-165, A-349, B-0129,
B-0183
Paparo F.: B-0211
Papassin J.: B-0509
Papp S.: B-1655
Pappini A.: B-1468, B-1469
Paragios N.: B-1353
Paramatti R.: B-0162
Parga Filho J.R.: B-0977
Parimalai A.N.: B-0347
Parizel P.M.: A-136, A-180, A-759, B-0181,
B-0318, B-0858
Park B.J.: B-0854
Park C.: B-0528, B-1091
Park C.H.: B-0102, B-0415
Park C.M.: B-0643
Park D.W.: B-1005
Park E.K.: B-1415
Park H.J.: B-1265
Park H.S.: B-0195
Park I.K.: B-0415
Park J.E.: B-0087, B-0693
Park J.J.: B-0647
Park K.J.: B-0064
Park M.: B-0801
Park S.B.: B-1265
Park S.-J.: B-0461
Park S.Y.: B-0058, B-1563
Park Y.: B-0643
Parker A.P.: A-161, A-467, B-0971
Parker G.: B-0165
Parlati A.: B-1518
Parretti F.: B-0056
Partelli S.: B-0629, B-1134
Partington K.: B-0344
Paruccini N.: B-0127, B-1129, B-1440
Parviz S.: B-1374
Pascaline S.: B-0275
Pascual Goni E.: B-0929
Pasha S.P.: B-1200
Pasquier H.: B-0314
Passarelli V.: B-1400
Passoni P.: B-0847
Pastor C.: B-0010
Pastorino U.: B-1349
Patel I.N.: B-0904
Patel M.J.: B-0016
Patel N.: B-0173, B-0624
Patel S.: B-0561, B-0946, B-1361
Patella F.: B-1190
Patelli G.: B-1545
Paterson A.: B-0152
Patino M.: B-0016
Patrão T.: B-0328
Patrunov Y.: B-0276
Patsch J.M.: B-0155, B-0345, B-1168
Pattacini P.: B-0083
Patten M.: B-0780
Patterson A.J.: B-0104, B-0498
Patzig M.: B-0122
Paulo G.: A-143, A-231, A-497, A-578, A-855
Paulo G.N.: B-0326
Pauly V.: B-1024
Pavan L.J.: B-1225, B-1398, B-1420
Pavone M.: B-0420
Pawaroo D.: B-0903
Payne J.L.: B-0684, B-1606
Paysan P.: A-655, B-1432
Pecchi A.: B-0855, B-1611
Pecoraro M.: B-0244, B-1068
Pecorelli A.: B-0942, B-1513
Pedalino S.: B-0378, B-0383, B-1064, B-1244
Pedersen K.: B-0132

Pedersen K.F.: B-0798
Pedersen M.R.V.: B-1660
Pedersen P.: B-0556
Pedicini V.: B-0452
Pediconi F.: A-405
Pedrazzani C.: B-0166
Pedrinolla B.: B-0646
Pedrosa Garriguet M.: B-1275
Peebles C.: A-745, A-960
Peetrons P.: A-797, A-799
Pekarovic D.: B-1443
Peker E.: B-0842, B-1618
Peleman M.: B-0540
Pelgrim G.J.: B-1458
Pelle M.: B-0410
Pellegriani M.: B-0077
Pellet-Barakat C.: B-0666
Penco S.: B-1090
Peng W.: B-0171, B-1154, B-1648
Peng Y.: B-1663
Peniaeva E.: B-0276
Penmetsa M.: B-1047
Pennati F.: B-0768
Pennings J.P.: B-0825
Pennisi G.: B-1225
Penzkofer T.: A-576, B-0886, B-1357
Peppi M.: B-0031, B-0567, B-0755, B-1224,
B-1459, B-1658
Pepin J.-L.: B-0052
Perez Lopez R.: B-0393
Perez Montilla M.E.: B-0823
Perez-Rovira A.: B-0768
Perier C.: B-0698
Perisinakis K.: A-034, B-0771
Perkowska-Ptasinska A.: B-0882
Perkuhn M.: B-1384, B-1671
Perrone N.: B-0958
Persigehl T.: B-0377, B-0587, B-1470
Persiva Morenza O.: B-1551
Perttu A.: B-1351
Perugin Bernardi S.: B-0211
Pesapane F.: B-1067
Pescarolo M.: B-0803
Pessis E.: B-0117
Peter C.: B-0923
Peters A.: B-0334, B-0336, B-0340, B-0838
Peters J.: A-937
Petersen T.-O.: B-1564
Petraikin A.V.: B-1591
Petralia G.: B-1071
Pettrash E.: B-0578
Petridis I.: B-0033
Petrillo M.: B-1190
Petrillo R.: B-0151, B-1493, B-1494
Petrone M.C.: B-0816
Petronio A.S.: B-0146
Petrovic D.J.: B-0213
Petrovicova A.: B-0924
Petrovsky H.: B-0839
Petrozza V.: B-0060
Petyt G.: B-1552
Peynircioglu B.: A-044
Pezzotti S.: B-0053
Pezzullo M.: A-644
Pfaff J.: B-0508
Pfahler V.: B-0113
Pfannenbergs C.: B-0889
Pfeiffer F.: B-0543
Pfeil A.: B-0349
Pfeuffer J.: B-0285
Pfirrmann C.W.A.: A-232, A-368, A-453, A-679,
A-681, B-1123, B-1430
Phan C.: B-0301
Phan T.V.: B-1489
Pianyk O.: B-1586
Picardi A.: B-0994
Picarra M.: B-0499
Picasso R.: B-0615, B-0616
Picchia S.: B-0060, B-0715
Picchio M.: B-1042
Piccini D.: B-1232

List of Authors & Co-Authors

Pichler F.: A-427
Piciucchi S.: B-0045
Pickup L.: B-0868
Pieper C.C.: B-0042
Pierotti L.: B-0579
Pierrat N.: B-0315
Pieterse T.: B-1646
Pietrafusa N.: B-1404, B-1406
Pietragalla M.: B-1183
Pietras J.: B-0509, B-1676
Pietruszka B.: B-1009
Pietsch H.: B-0995, SY 9
Pietura R.: B-0553
Pignataro P.: B-0465
Pignatelli M.: B-0231
Piha T.: A-773
Pijnappel R.M.: A-117, B-1277
Pijpers J.A.: B-1600
Pilius P.: B-0710
Pimenta A.S.: B-0326
Pina Insausti L.J.: A-246, B-0915, SY 1c
Pinamonti M.: B-1416
Pinheiro J.P.: B-0965, B-1445
Pinigin A.: B-0576
Pinker K.: B-0506, B-0507, B-0705, B-0911, B-1036, B-1091, B-1117, B-1409
Pinker-Domenig K.: A-743, B-1281
Pinochet M.A.: B-0272, B-0914, B-1116
Pinto A.: A-838
Pinto dos Santos D.: A-992
Pinto J.: B-0963
Pinto N.F.: B-1641
Pinto V.M.: B-0211
Piotin M.: B-0518
Pipan F.: B-0910, B-0912
Piradov M.: B-1407
Pires F.: B-0328
Pires Jorge J.: B-0130, B-1146, B-1643
Pires Jorge J.A.: B-1147
Pirimoglu B.: B-0262
Piron L.: B-1053, B-1057, B-1060
Pirovano M.: B-0284
Pirracchio R.: B-0476
Pirtoli L.: B-0853
Pisana F.: B-0542, B-0733
Pistorio A.: B-0580
Pithioux M.: B-1024
Pittari V.: B-1093
Pitton M.B.: B-0036, B-0210
Pizzini F.B.: A-595, B-1039
Pizzolon F.: B-0914
Pizzolon M.F.: B-0272
Plaisier P.W.: B-0913
Plakhotina N.: B-1003, B-1220
Planas L.: B-0048
Plancharde D.: B-0368
Platel B.: B-1594
Platt K.A.: B-0344
Platz Batista da Silva N.: B-0207, B-0208
Plonski L.: B-0268
Pluchino N.: B-0466
Poch F.: B-1340
Podda A.: B-1015
Poddubnyy D.: B-0308, B-1615
Podgórski P.: B-0920
Poeppel T.: B-0706
Poeppel T.D.: B-1621
Pogosbekyan E.: B-0086
Poillon G.: B-0066
Pokrajac D.: B-1632
Pokryszko-Dragan A.: B-1679
Polat A.V.: B-0674
Polat C.: B-0674
Poletti P.-A.: A-779
Polyn-Zaradna K.: B-0920
Polyakov P.: B-0423
Pompe R.: B-1569
Pompili G.: B-1189
Pompili M.: B-0833
Pomschar A.: B-1161, B-1356
Ponnatapura Satyanarayana J.: B-1405, B-1408

Pontana F.: A-259, B-1156, B-1654
Pontone G.: B-0031, B-0567, B-0755, B-0779, B-1224, B-1459, B-1460, B-1658
Poot D.: B-1426
Poot L.: B-0131
Pope A.: B-1361
Popescu A.S.: B-0203
Popli M.: B-0100, B-1108, B-1282
Porcu M.: B-0216
Poretti D.: B-0452
Portalez D.: B-1072
Portelli J.: A-579, A-632
Portugaller H.R.:
Posa A.: B-0185, B-1061
Pötter-Lang S.: B-1077, B-1255
Pouli S.: B-0771
Poupon C.: A-113
Pouraliakbar H.: B-0477, B-0478, B-0700, B-0734, B-0739
Pouraliakbar H.R.: B-0740
Power S.: B-0857
Pozdniakova V.: B-0174, B-0798
Požeg P.: B-0996
Pozzi Mucelli R.: A-703, B-0018, B-0166, B-0834, B-1065, B-1519, B-1521, B-1522, B-1523, B-1567
Prabhu N.K.: B-1517
Pradella S.: B-0141
Prampolini F.: B-0855
Prasse A.: B-0237
Prassopoulos P.K.: A-868
Pratschke J.: B-0007
Pravata E.: B-1001
Prayer D.: A-770, B-1168, K-22
Prayer F.: B-1168
Preibsch H.: B-0918
Preidler K.: B-1289
Premat K.: B-0518
Presazzi A.: B-0683, B-1286
Prestwich R.: B-0908, B-1192
Preuß D.: B-0597
Prevoo W.: B-1204
Preziosa G.C.: B-1469
Price S.J.: B-1672
Pricolo P.: B-1071
Primolevo A.: B-1189
Priovolos D.: B-1118
Prisner T.: B-0030
Privitera G.: B-0565
Prodi E.: B-1001
Prodinger P.M.: B-1120
Prokop M.: A-248, A-309
Prokop M.M.: B-0238, B-0411, B-0480, B-0555, B-0695
Prokopienko M.: B-1106
Pronin I.: B-0086, B-1484
Prono V.: B-0837
Prosch H.: A-054, A-942, B-0633
Provenzano E.: B-0498
Pruvo J.-P.: B-1040
Psychogios M.-N.: B-0189, B-0923, B-1239
Puentes-Damm M.: B-0622
Puglielli E.: B-0815
Pulli B.: B-1175, B-1178
Pumberger M.: B-0530, B-1029
Pungračar M.: B-1443
Purcell Y.M.: B-0070
Puri S.: B-0275
Pursanova D.: B-1249
Pusceddu C.: B-0628
Pusceddu L.: B-0519, B-0520, B-0522
Putha P.: B-1378, B-1379
Putz F.J.: B-0055
Putzier M.: B-0530, B-1029
Puylaert J.B.C.M.: A-520, A-646
Pyra K.K.: A-902

Q

Qanadli S.D.: A-070
Qechchar Z.: B-0941
Qi R.: B-0147
Qian T.-Y.: B-0364, B-1261
Qu J.: B-0353, B-0810
Quaia E.: B-1532
Quan X.: B-0233
Quarochioni S.: B-0300, B-0612, B-0725, B-0729, B-0960, B-1344, B-1427, B-1539
Quäschling U.: B-0359
Quentin M.: B-0252, B-1363, B-1364
Quere J.-B.: B-0301
Querques G.: B-1513
Quick H.H.: B-0796
Quilez A.: B-0915
Quiney H.: B-1416
Quinn E.: B-0344
Quiros-Gonzales I.: B-1094
Quitze A.: B-1327
Qureshi A.: B-1080

R

Ra J.C.: B-1265
Raabe P.: B-0007
Raafat T.: B-1503
Rabelink T.: B-0204
Rabenalt R.: B-0248, B-0252, B-1363, B-1364
Racine D.: B-1135
Raciti M.V.: B-1336
Radbruch A.: B-0363, B-0933, SY 9
Raddatz J.: B-0544
Radder A.: SY 5
Rademacher J.: B-0051
Radhakrishnan S.: B-1500
Radici V.: B-0549
Radovanovic Z.: B-1632
Radu P.: B-0453
Radzina M.: B-0814, B-1622
Rafaelsen S.R.: B-1660
Raffaelli C.-P.: B-1027, B-1043
Raftopoulos C.: B-0438
Ragab Y.: B-0470, B-0950
Ragot E.: B-0293
Rahmat K.: B-0084, B-0105, B-0617
Rai B.: B-1270
Raimann A.: B-0345
Raimondi E.: B-0209, B-0588, B-1083, B-1202
Raimondi S.: B-0382
Rainford L.: B-1148
Rainford L.A.: A-142, A-391, A-552, A-661, B-0554, B-1300, B-1646
Raininko R.: B-1401
Raissaki M.: A-141, A-192, A-658, B-0771
Raja A.Y.: B-0731
Raja S.: B-0982, B-1476
Rajan S.: B-1397
Rajani H.: B-1373
Rajgopalan N.: B-0261
Ralla B.: B-0061
Ramalho L.: B-0269
Ramirez Girlando J.C.: B-0881
Ramli Hamid M.T.: B-0105
Ramli N.: B-0091, B-0617, B-1597
Rammelsberg P.: B-0264
Ramo E.: B-1219
Ramos Botelho Antunes P.: B-0391
Ramos I.M.: B-0137, B-1314
Rampoldi A.: B-0128
Ramsden W.: A-462
Rana A.: B-1509
Rance B.: B-0476
Rancoita P.M.: B-0847
Rangari A.: B-1601
Ranieri A.: B-1545
Ranjan R.: B-1675
Ranschaert E.R.: A-363
Rao L.: B-1097, B-1098, B-1103, B-1104

List of Authors & Co-Authors

- Rao P.: B-0483, B-0872, B-1378, B-1386, B-1387
Rao S.: B-1270, B-1318
Rao S.-X.: B-1256
Rapisarda S.: B-0440, B-0719
Raspanti C.: B-0056, B-0227, B-0862
Rasper M.: B-0149, B-0900
Rasuli B.: B-1215
Rathmann W.: B-0340
Ratib O.: A-360, A-747
Ratti F.: B-0629, B-1205
Rau R.: B-1023
Rauch A.: B-1020
Rauch S.: B-0614, B-1423
Raum K.: B-0345
Rauscher G.: B-1604
Rausin L.: B-0120
Rautou P.E.: B-0202
Rautou P.-E.: B-0427
Ravaioli S.: B-0083
Ravanelli M.: B-0265, B-0978
Ravanfar Haghighi R.: B-1668
Ravelli A.: B-1189
Raya Povedano J.L.: B-0085, B-1275
Raymakers D.: B-0021
Raynaud J.-S.: SY 17
Re T.J.: B-0835
Rebollo Polo M.: B-0160
Rebonato A.: B-0959
Redheuil A.: A-483
Redi F.: B-1032
Reekers J.A.: A-042, A-672, A-973
Regent A.: B-1353
Regge D.: B-0107, B-0378, B-0383, B-0519, B-0520, B-0522, B-1064, B-1114, B-1244, B-1246, B-1592, K-01
Regier M.: B-1327
Reginelli A.: B-0525
Regini E.: B-1392
Regnard N.E.: B-0117, B-0302
Rehnitz C.: B-0437
Reidler P.: B-0228, B-0513, B-0517, B-0922
Reig O.: B-1520
Reijman M.: B-1030
Reijnierse M.: K-12
Reim M.: B-0296
Reimann C.: B-0622
Reimer P.: B-0371, B-1464
Reimer R.: B-0371
Reimers I.: B-0609
Reimold M.: B-0889
Reinboldt M.: B-0450
Reindl M.: B-0572
Reiner C.S.: B-0708, B-0839, B-1125
Reinert C.P.: B-0704
Reinert M.: B-1001
Reinstadler S.J.: B-0572
Reis C.: B-1240
Reis C.S.D.: B-1147, B-1643
Reis M.V.C.: B-0749, B-1451
Reiser M.F.: B-0340, B-1176, B-1366, B-1471
Reitan A.F.: B-1141
Reiter C.: B-1151
Reiter G.: B-1151
Reiter U.: B-1151
Rella R.: B-0525, B-1419
Remollo Friedemann S.: B-0827
Remond P.: B-0802
Rempp H.: B-1208
Remy J.: B-0458, B-0462, B-1552, B-1555
Rémy-Jardin M.: A-007, B-0458, B-0462, B-1552, B-1555
Ren C.: B-0111
Ren K.: B-0389
Ren Y.: B-0713, B-1482, B-1483
Renard Penna R.: B-0386
Rengier F.: B-1105, B-1549
Rengo M.: B-0060, B-0357, B-0358, B-0565, B-0715
Renker M.: B-1454, B-1456
Renovanz M.: B-0939
Rentsch M.: B-0228
Renz D.M.: B-0292, B-0349, B-0412, B-0894
Renz D.M.M.: B-0899
Renzulli M.: B-0038
Resaz R.: B-0837
Resende L.L.: B-1400
Resta D.: B-0465
Reutener M.: B-0306
Reuzé S.: B-0737
Revanna S.M.S.A.: B-0770
Revel M.-P.: A-604, B-1353
Revel-Dubois M.-P.: B-1346
Reymond E.: B-0050, B-0052
Rezayi A.: B-0599
Riaza Martin L.: B-0769
Anas M.: B-1411
Rezk M.: B-1411
Ribeiro L.P.: B-0329, B-0749, B-0965, B-1149, B-1445, B-1451, B-1637, B-1638, B-1642
Ribeiro L.P.V.: B-1640, B-1641, B-1645
Ribó Jacobí M.: B-0827
Ricart E.: B-1537
Riccardi L.: B-0773
Ricci F.: B-0564
Ricci P.: A-187, A-188
Riccitelli G.C.: B-1001
Richli Meystre N.: B-0130, B-1146
Richly H.: B-0836
Richter C.: A-885
Ricke J.: B-0113, B-1076, B-1176, B-1471
Rico Rodríguez O.C.: B-0397
Ridge C.A.: B-1554
Rieber J.: B-0149
Rieckmann N.: B-0598
Riederer I.: B-0543, B-1121
Riederer S.: B-0546
Riedl C.: B-0705
Rief M.: B-0597, B-0598, B-0762
Riemer F.: B-1672
Rienmüller R.: B-1557
Rienmüller T.: B-1557
Riera Soler L.: B-0769
Riethmueller J.: B-0764
Riffel P.: B-0606
Rigiroli F.: B-0481
Riibak M.-L.: A-905
Riklund K.: A-486, A-771
Rimola J.: A-281, A-527, B-0191, B-0610, B-1537
Rimondi E.: B-0114
Rinaldi P.: B-1289, B-1419
Ringelstein A.: B-0259
Ringl H.: A-534, B-0633
Ringleb P.A.: B-0508
Ringshausen F.: B-0051
Rio G.: B-0380, B-0651
Riondel F.: A-498
Rippel K.: B-0527, B-0945
Risaliti A.: B-0425
Rischpler C.: A-581
Rissi M.: B-0549
Ritter M.: B-1473
Riva L.: B-0024, B-0634, B-0942, B-1328, B-1514
Riva S.: B-0410
Rivas Loya R.: B-1345
Rivera A.: B-0145
Rivera Mata J.: B-0101
Rivers-Bowerman M.: B-0684, B-1606
Rivosecchi F.: B-0162, B-0169, B-0357, B-0358
Rizk B.: B-0314, B-0316, B-1135
Rizzati R.: B-0588
Rizzo A.: B-1087
Rizzo S.: A-028, B-0382, B-1377
Robben S.G.F.: A-955
Robb F.: SY 2
Robb F.: B-0737
Roberto L.: B-0525
Robertson N.L.: B-0254
Robinson L.: B-1639
Robinson L.: A-792
Robinson P.: A-416, A-515
Robinson T.E.: B-1588
Roccia S.: B-0940
Rocha N.: B-0139
Rocha T.O.: B-0879
Rockall A.G.: A-343, K-14
Rode A.: B-1060
Rodighiero M.G.: B-1390
Rodolfino E.: B-0471
Rodrigues dos Santos M.: B-0139, B-0743
Rodrigues P.P.: B-0137
Rodrigues S.: B-0749, B-0965, B-1445, B-1451, B-1637, B-1641
Rodrigues S.I.: B-1642
Rodríguez M.J.: B-1601
Rodríguez Ruiz A.: B-1628
Rodríguez S.: B-1520
Rodríguez Sánchez A.: B-0777
Roemer F.W.: A-031
Roeters van Lennep J.E.: B-0785
Rogalla P.: B-0947
Rohde S.: A-435
Rohrer L.: B-1491
Rohrmeier A.: B-0441
Roiaati S.: B-0815
Rollandi G.A.: B-0211
Rollandi L.-P.: B-0527, B-0945
Rollo C.: B-0627
Romanelli P.: B-1041
Romani M.: B-1419
Romano L.: B-0295
Romano S.: A-063
Romano V.: B-0378, B-0383, B-1244, B-1246
Romanov D.: B-1248
Romanucci G.: B-0078, B-0082, B-1088
Romero Martin S.: B-0085
Romero S.: B-1275
Rondenet C.: B-0948
Rong X.: B-0788
Ronot M.: A-088, B-0202, B-0427
Roos-Hesselink J.: B-0143
Roos-Hesselink J.W.: B-1649
Roques M.: B-0518
Ros P.R.: A-383, A-724, A-744, B-0125, B-1017
Rosa F.: B-0837
Rosati S.: B-0827
Rosen B.R.: B-0985, B-1533
Rosenberg Z.S.: B-0538
Rosendaal F.D.: B-0204
Rosendaal F.R.: B-0335
Rosendahl K.: A-732
Roshchin D.A.: B-1249
Roshchupkin G.V.: B-0795
Rosplecz S.: B-0334, B-0340, B-0838
Ross J.: B-0547
Rossi A.: B-1478
Rossi C.: B-1627
Rossi Espagnet M.C.: B-0153, B-0157, B-0159, B-1404, B-1406
Rossi F.: B-0286
Rossi M.: B-0231, B-0429, B-0608
Roszkopf A.B.: B-1123
Rosso A.: B-1006
Rosso R.: B-0049
Rostl C.: B-0284
Rostovtseva T.: B-0182
Rotar H.: B-0255
Rotenberg L.: B-1605
Röthlin F.: B-0317
Rötig A.: B-0154
Rotkopf L.: B-0088, B-0922
Rottoli F.: B-0128
Rouchy R.-C.: B-0186
Rousch M.: B-1410
Rousseau C.: B-1413
Rousseau H.: A-238
Roussel H.: B-1413
Rouviere O.: B-0245, B-1074
Rovira-Cañellas A.: A-208, A-763
Rowinski O.: B-1106
Rowley H.A.: A-591

List of Authors & Co-Authors

- Rozalli F.I.: B-0617
Rozhkova Z.: B-1236
Rubbert C.: B-0252, B-1037, B-1235, B-1237
Rübenthaler J.: B-0055, B-0057
Rubin C.: A-461
Rubini A.: B-0221, B-0668, B-1633
Rubins A.: B-1622
Rubins S.: B-1622
Rubtsov R.: B-0402
Rudas G.: B-0659, B-1680
Rudel A.: B-1025
Ruder T.: A-839
Rudolph M.: B-1357
Rudolph T.: B-0976
Rudolph V.: B-0976
Rueppel S.: B-0973, B-0974
Ruff C.: B-0764
Ruffion A.: B-0245, B-1074
Rühaak J.: B-0238
Ruhlmann V.: B-0652
Ruhnke H.: B-0023
Ruibal A.: B-0501, B-0992, B-1395
Ruiter S.J.S.: B-0825
Ruiz Salmeron R.: B-0145
Rukhlenko M.: B-1003
Rummeny E.J.: B-0149, B-0529, B-0543,
B-0900, B-0988, B-1120, B-1121, B-1136
Runge V.: A-139, SY 9
Ruprecht M.: B-0864
Rusandu A.: B-1297
Ruschi F.: B-0298
Ruschke S.: B-0441
Russo A.: B-1071
Russo F.: B-0378, B-0383, B-1064, B-1244,
B-1246, B-1592
Russo G.: B-0049, B-0295, B-0420, B-0873
Ryan A.G.: A-587
Ryan D.: B-0574
Ryan J.: B-0176
Rybczynski M.: B-0022
Rychina I.: B-1557
Rychkova I.: B-1335
Rymaszewska J.: B-0920
Ryu H.: B-0005, B-0575
-
- S**
-
- Sá dos Reis C.: B-0130, B-1146
Saal L.H.: B-1006
Saar S.: B-0296
Saba L.: B-0216, B-0374, B-0608, B-0611,
B-0840
Sabate Rotes A.: B-0769
Sabatino V.: B-0077
Sabet H.A.S.: B-0473
Sabet S.: B-0379, B-0581
Sabetrasekh P.: B-0212, B-0998
Sabino S.: B-0138
Sachs C.: B-1665
Sack I.: B-0001
Sadat U.: B-0219
Saddekní S.: B-0034, B-1055
Sade R.: B-0712
Sadik J.-C.: B-0514
Saeedi-Moghadam M.: B-1668, B-1669
Safa G.: B-1429
Safina M.: B-1292, B-1614, B-1630
Sah B.-R.: B-0708
Sahakyan D.: B-1548
Sahan M.H.: B-0954
Sahani D.V.: B-0016
Sahbee P.: B-0569
sahin G.: B-0952, B-1618
Sahm F.: B-0933
Saidon T.: B-0705
Sakahara H.: B-0028, B-0720
Sakai M.: B-0416
Sakuma H.: B-0350
Sala E.: A-352, A-575, A-751, A-865
Salamon J.: B-0932
Salapura V.: A-689
Salem A.: B-1138
Salem J.: B-1473
Salemi I.: B-0897
Salerno S.: B-1165, B-1495
Salgado R.: A-195, A-484, A-875
Sali L.: B-0521
Salman S.: B-1045
Salminen P.: B-0744
Salomon G.: B-1569
Salybaeva N.: A-506, B-0123, B-0310
Saltz L.: B-0167
Salvatore M.: B-1533
Salvesen Ø.: B-1368
Salvioni M.: B-0230, B-0629, B-1205
Salvioni R.: B-0625
Salvo V.: B-1068
Samara E.: A-923
Samei E.: A-785
Sammartano K.: B-1032
Sampangi S.: B-0270
Samreen N.: B-0504
Sanaat A.: B-0740
Sánchez Mateos D.: B-0006
Sanchez J.: B-1610
Sanchez Martinez A.L.: B-1551
Sánchez N.: B-0494
Sánchez Nava D.A.: B-0397
Sanchez S.: B-1520
Sanchez-Montanez Garcia-Carpintero A.:
B-0769
Sanchez-Salas R.: A-396
Sanders S.N.: B-0748
Sanderud A.: B-0742, B-0748
Sandford Z.: B-0868
Sanghavi P.S.: B-0872
Sangma S.: B-1334
Sani F.: B-0855
Sanje S.: B-1450
Sankaranarayanan S.: B-1500
Sansone M.: B-1190
Santalco A.: B-0024
Santiago I.: A-382
Santini V.: B-0821
Santoro A.: B-1009, B-1625
Santos A.L.: B-1275
Santos J.: A-495, B-0326, B-0328, B-0557, K-07
Santos J.M.M.M.: B-0902
Santos R.A.M.: B-0964, B-0966, B-0967, B-1313
Santucci D.: B-0627, B-0632, B-0820
Sanz-Rodrigo E.: B-1465
Sapena V.: B-0610
Şaponjski D.: B-1527
Sarabhai T.: B-1367, B-1371
Sarah P.: B-0856
Saranga B.K.: B-1516
Sardanelli F.: A-554, A-931, B-0029, B-0332,
B-0503, B-0786, B-1093, B-1651
Sarin D.: B-0673
Sartor H.: B-1006
Sartoris R.: B-0427
Sasaki M.: B-0720
Sasiadek M.: A-302, B-0920, B-1679
Sastoque.g. J.M.: B-0823
Sato M.: B-0451
Sato Y.: B-1550
Satta S.: B-1493, B-1494
Sauer M.: B-1569
Saukko E.: B-0342, B-0744, B-1442, B-1447
Saunavaara J.: B-0342
Sauter S.: B-1432, B-1434
Saut O.: B-0698
Sauter A.: B-1121, B-1136
Sauter A.W.: B-1381
Savaş R.: B-1219
Savatovsky J.: B-0514
Savlovskis J.: B-0814
Sawall S.: B-0733, B-0736, B-1435
Sawicki L.M.: B-0584, B-0652, B-0706
Sayit A.T.: B-0256
Sbarra M.: B-0471
Scaglione M.: A-120, B-0295
Scaperrotta G.: SY 10
Scarabello M.: B-0029, B-0332, B-1651
Scaramuzza D.: B-0165
Scardapane A.: B-0144, B-0465
Scarsbrook A.: A-058, B-0908, B-1192
Scavone A.: B-1336
Scavone G.: B-1336
Schaarschmidt B.M.: B-0584, B-0652, B-0706,
B-1367
Schabel C.: B-0881, B-1453
Schaefer-Prokop C.M.: A-737, B-0411, B-1349
Schäfer F.M.: B-0251
Schäfer J.F.: B-0764, B-0766
Schäfer J.P.: A-078
Schäfer S.: B-0447
Schaudinn A.: B-1564, B-1566
Schawkat K.: B-0708, B-0839
Scheel M.: B-0548, B-0830
Scheerlinck T.: B-0721
Scheffmann Olloni S.: B-0551
Scheidler J.: B-1366
Schelini M.: B-1186
Schellhaas B.: B-1260
Schena E.: B-0994
Schenk A.: B-1383
Schenk J.-P.: A-539
Schenkel M.: B-0537
Scherr M.: B-1366
Scherr M.K.: A-647
Scherz B.: B-0780
Schestak C.: B-0633
Scheulen M.: B-0836
Scheurig-Muenkler C.: B-0023, B-0527, B-0945
Schiari E.: B-1390
Schiappacasse G.: B-1251
Schiavone M.V.: B-0489
Schiestl T.: B-0510
Schild H.: B-0042, B-1350, B-1571
Schillham A.: B-1130
Schilling F.: B-0988
Schima W.: A-526, A-675
Schimmöller L.: A-201, B-0248, B-0252, B-1363,
B-1364
Schindera S.T.: A-036, A-252
Schindler A.: B-0541
Schinner R.: B-0541
Schiphof D.: B-0118
Schipper R.J.: B-0274
Schittenhelm J.: B-0090, B-0093, B-0808
Schlamp K.: B-0925
Schleich C.: B-0319
Schlemmer H.-P.: A-204, A-318, A-395, A-918,
B-0363, B-0375, B-0933, B-0934
Schlett C.L.: A-173, B-0334, B-0336, B-0340,
B-0838, B-1356
Schliitt H.J.: B-0207, B-0208
Schmaltz K.A.: B-0252
Schmaranzer F.: B-0303, B-0539, B-1124
Schmidt A.: B-1151
Schmidt B.: B-0542, B-0590, B-0772, B-0905,
B-1026
Schmidt K.-H.: B-0975
Schmidt M.: B-1156
Schmidt R.: B-1039
Schmidt S.: B-0180, B-1273
Schmidt S.A.: B-0178
Schmidt-Holtz J.: B-1327
Schmidt Kobbe S.: B-0010, B-0013
Schnapauff D.: B-1056
Schneeweiß S.: B-0791
Schneider F.: B-1360
Schneider G.: B-0832, B-1329
Schneider J.: B-0345
Schneider M.: B-1176
Schneider P.M.: B-0708
Schnitzler A.: B-1235, B-1237
Schob S.: B-0359
Schoder H.: B-0705

List of Authors & Co-Authors

- Schoepf U.J.: B-0337, B-0569, B-0752, B-0757, B-0776, B-1046, B-1047, B-1049, B-1232, B-1454, B-1455, B-1456, B-1458, B-1487, SY 15
- Schoeppe F.: B-0541
- Schoettler J.: B-0243
- Schöffski O.: B-0178, B-0180
- Schöllnast H.: A-217
- Scholtz J.-E.: B-1052
- Scholz J.: B-1059
- Scholz J.-E.: B-0528
- Schönberg S.O.: B-0243, B-0459, B-0606, B-1354, B-1582
- Schöppe F.: B-1161
- Schorr C.: B-0309
- Schotten S.: B-0036, B-0196, B-0210
- Schouten D.K.: B-0917
- Schradling S.: A-634
- Schramm C.: B-1317, B-1319
- Schramm P.: B-0189
- Schrauwen P.: B-1051
- Schregel K.: B-0923
- Schreuder F.H.: B-0220
- Schröder A.: B-0349
- Schröder D.: B-0035
- Schröder W.: B-0790
- Schuenke P.: B-0363
- Schuhmann M.: B-0240
- Schuler F.: B-0513, B-0922
- Schuler G.: B-0979
- Schuler T.: B-1319
- Schulte R.: B-1672
- Shults E.: SY 18
- Schulz H.: B-1356
- Schulz-Wendtland R.: B-1629
- Schurink C.A.M.: B-1649
- Schwaiger B.J.: B-0529, B-1120, B-1121, B-1136
- Schwaiger M.: B-0988
- Schwarz F.: B-0023, B-0527, B-0945
- Schwarz F.B.: B-0548, B-0830
- Schweinitz C.: B-0494
- Schwemmer C.: B-0776
- Schwenke C.: B-1615
- Schwindling F.S.: B-0264
- Sciarra A.: B-0010
- Scionti A.: B-0161
- Scioscia M.: B-0465
- Scipione R.: B-0184, B-0630, B-0875, B-1337, B-1339, B-1342, B-1541, B-1547
- Sciuk A.: B-0604
- Sconfienza L.M.: A-841, B-0440, B-0719, B-0955, B-1616
- Scott P.: B-1433, B-1436
- Scott V.: B-0680
- Scotti G.: B-0481
- Scotti V.: B-0267
- Screaton N.J.: A-068, K-25
- Scrimieri A.: B-0053
- Scuderi M.G.: B-0295
- Seah J.C.Y.: B-1385
- Sebire N.J.: B-1169
- Sebuodegaard S.: B-0132
- Sebuodegård S.: B-0076, B-0133, B-0134, B-0676, B-0677, B-1096
- Secchi F.: B-0029, B-0332, B-0786, B-1651
- Sechopoulos I.: A-924, B-0238, B-0411, B-0550, B-1628
- Secondini L.: B-0837
- Sedlacek O.L.: A-057
- Sedlacik J.: B-1319
- Sedlacek O.L.: B-0375
- Sedlmair M.: B-0590, B-1026
- Sefic-Pasic I.: B-1163
- Sefidbakht S.: B-1668, B-1669
- Seghers D.: B-1432
- Seidensticker M.: A-367
- Seifert S.: B-1471
- Seker F.: B-0508
- Seki S.: B-0043, B-0403, B-1348, B-1578, B-1579, B-1581
- Sekitani T.: B-0767
- Seletti V.: B-0045
- Seliverstov P.V.: B-0841
- Seliverstov Y.: B-1035
- Seliverstova E.: B-1035
- Sella T.: B-0268, B-0916
- Sellars M.: B-1659
- Sellner S.: B-0336
- Semenova N.: B-0156, B-0806
- Sempoux C.: B-0010
- Sencha A.: B-0276
- Sencha E.: B-0276
- Senore C.: B-0519, B-0520, B-0522
- Seo B.K.: B-1415
- Seo J.B.: A-172, A-306, B-0239
- Seo M.: B-0707
- Seong N.J.: B-0032
- Seow P.: B-0091, B-1597
- Sepponen P.: B-1449
- Serafini G.: B-0958
- Serena E.: B-1664
- Serfaty J.-M.: B-0688
- Sergeev D.: B-1407
- Sergeeva A.N.: B-1035, B-1677
- Sergeeva O.N.: B-0423, B-1512
- Serova N.S.: B-1200
- Serrado M.A.: B-0396
- Sertorio F.: B-0580
- Server S.: B-0379
- Seuri R.: A-390
- Seuss H.: B-1260
- Sever C.: B-0581
- Severino M.: B-1478
- Sevrjukov D.: B-0578
- Sforza C.: B-0029, B-1197
- Shahabpour M.: A-445
- Shahgeldi K.: B-0640
- Shahkarami V.: B-0212
- Shahrazaila N.: B-0617
- Shaikh S.M.: B-0984, B-1070
- Shakeel K.: B-1509
- Shakiba M.: B-0212, B-0998
- Shakirin G.: B-1384, B-1671
- Shalmon A.: B-1608
- Shamachar V.K.: B-0770
- Shams S.: B-0997
- Shao D.: B-0399
- Shao X.: B-1617
- Shariati H.K.: B-0742
- Sharifian H.: B-1215, B-1221
- Shariya M.: B-1200
- Sharma J.P.: B-0095
- Sharma N.: B-0275, B-1397
- Sharma R.K.: B-0742
- Sharma S.: B-1022, B-1667
- Shayesteh S.: B-0477, B-0739, B-0740
- Shayesteh S.P.: B-0700
- Sheehan J.A.: B-0828
- Sheehan M.: B-1089
- Sheehy N.: B-0443
- Shehata M.: B-0887
- Shelmerdine S.C.: A-152, B-1169, B-1170
- Shen B.: B-0524
- Shen C.: B-0353
- ShenChu G.: B-1018
- Sheppard D.: B-0670, B-0671, B-0828
- Sheu M.-J.: B-0194
- Shi K.: B-0338, B-1230
- Shi R.-Y.: B-1158
- Shigeyama S.: B-0324
- Shih T.-F.: B-0019
- Shimauchi A.: B-1388
- Shimizu T.: B-1258
- Shin C.: B-0241
- Shin H.-O.: B-0051, B-0235, B-0237
- Shin J.Y.: B-1191
- Shiner N.: B-1150
- Shinichiro S.: B-1573
- Shinkins B.: B-0969
- Shiri I.: B-0477, B-0478, B-0700, B-0734, B-0739, B-0740
- Shirokorad V.: B-1247
- Shirokorad V.I.: B-1249
- Shivalingappa S.S.: B-0270
- Shobeirian F.: B-0599
- Shorikov M.: B-0423, B-1369, B-1512
- Shorikov M.A.: B-1248
- Shrainer I.: B-0710
- Shwaky N.O.: B-1501
- Siauve N.: A-814
- Siciliano G.: B-1242
- Siddique M.M.: B-0354, B-1080
- Sidhu P.S.: B-1659, SY 23
- Siebenrock K.: B-0303, B-0539, B-1124
- Siedek F.: B-0790
- Siegel E.L.: A-980
- Siegel M.: B-0772
- Sieper J.: B-0308, B-0309, B-1615
- Siepmann S.: B-0299
- Siewert E.: B-0886
- Siğirci A.: B-1505
- Sigl B.: B-1037
- Signore A.: A-583, B-1533
- Signoriello M.: B-1129
- Signorotto P.: B-1440, B-1441
- Sigovan M.: B-0983, B-1467
- Sijens P.: B-1109
- Silva A.: B-0139, B-0559
- Silva A.F.N.: B-0748
- Silva B.: B-0552
- Silva C.: B-0272, B-0492, B-0494, B-0667, B-0914, B-1116
- Silva C.J.: B-0902
- Silva M.: A-056, B-0045, B-0333, B-0787, B-1349
- Silva R.: B-0138
- Silva T.B.: B-0138
- Silva V.: A-499
- Silva V.M.F.: B-1314
- Silvestri S.: B-0994
- Silvestri V.: B-1156, B-1654
- Sim K.C.: B-0854
- Simão D.M.B.: B-0965
- Simcock C.: A-225
- Simeonov G.: A-150
- Simioni M.: B-0250
- Si-mohamed S.A.: B-0543, B-0983, B-1467
- Simpson S.: B-1301
- Singer F.M.E.S.: B-1411
- Singer G.: B-0919
- Singh B.: B-1022
- Singh K.: B-0095
- Singh M.: B-0095
- Singh T.: B-0095
- Singhal A.A.: B-0673
- Singhal S.: B-1516, B-1517
- Sini C.: B-1134
- Sinitsyn D.: B-1407
- Sinitsyn V.E.: A-129, A-182, A-901, B-0710, B-0928
- Sinn L.H.Y.: B-1393
- Sioletic S.: B-1358
- Siracusano S.: B-1065, B-1567
- Siri G.: B-0211
- Sirin Özcan A.N.: B-1234
- Sirinelli D.: B-1488
- Sirli R.: B-0203
- Sirlin C.B.: A-018
- Sironi S.: B-0024, B-0444, B-0634, B-0851, B-0897, B-0942, B-1328, B-1468, B-1469, B-1513, B-1514, B-1518
- Sitt J.C.M.: B-1393
- Siva A.: B-0993
- Sjöberg T.: B-0640
- Sjölín M.: B-1438
- Skaane P.: A-176, A-567
- Skardelly M.: B-0090, B-0093, B-0808
- Sklair-Levy M.: B-1608
- Skoknic V.: B-0492
- Skoknic V.S.: B-0494, B-0667
- Skornitzke S.: B-0544, B-1131
- Skouen J.S.: B-0435

List of Authors & Co-Authors

- Škrk D.: B-0745
Skrypets T.: B-0703
Slater J.: B-0492, B-0667
Slowinski T.: B-0055
Smedby Ö.: B-0096
Smeets D.: B-1489
Smeets P.: B-0540
Smidt M.: B-0274, B-1409
Smiechowicz J.M.: B-0160
Smirnova A.V.: B-1003, B-1220
Smirnova E.: B-0406
Smit E.: B-0356
Smit E.J.: B-0695
Smit L.: B-1213
Smith A.: B-0602
Smith J.T.: B-0844
Smith R.A.: B-0685
Smith-Blindman R.: B-1010
Smithuis F.: A-255
Smits M.: A-764, A-910, B-1039
Smyth A.E.: B-0070
Snaith B.: B-0969
Snene F.: B-0531, B-0949
Snoeckx A.: B-0181, B-1558
Soares F.A.P.: B-0748
Soares L.: B-1638
Sobral D.M.: B-1645
Sofia C.: B-1167
Sofikitis N.: B-1662
Sohn J.S.: B-0718
Sokhi H.K.: B-1361
Sokolowski F.C.: B-0777
Solanki R.K.N.: B-0904
Solbiati L.: B-0452, B-1209
Solbiati M.: B-1209
Sollid B.: B-0140
Sommer G.: B-1381
Sommer W.H.: B-0088, B-0513, B-0517, B-0922, B-1076, B-1582, B-1583
Son E.J.: B-0102
Son Forget J.: B-0996
Son J.-Y.: B-1524
Sonck J.: B-1459
Song B.: B-0199, B-1266
Song C.: B-0074
Song D.E.: B-1191
Song J.: B-1171
Song L.: B-0781
Song Y.: B-1238, B-1279
Soni S.: B-0951
Soo S.W.: B-0084
Sood S.: B-1022
Soong S.I.: B-1370
Sorantin E.: A-046
Sorbo A.: B-0295
Sørensen J.S.: B-0435
Soria J.-C.: B-0368
Soricelli A.: B-1533
Sorochn O.: B-1499
Soroush H.: B-0998
Sosna J.: A-820, B-0457
Souchon R.: B-0245, B-1074
Soultatos A.: B-0430
Sousa A.F.C.: B-0557
Sousa Neto J.A.: B-0269
Sousa P.: B-1445
Souto S.: B-1640
Souza Guatelli C.: B-1285
Souza J.A.: B-1285
Soyer P.: B-0448
Spadarella G.: B-1189
Spadavecchia C.: B-0127, B-1129
Spallanzani A.: B-0855
Spanakis K.: B-0771
Spångeus A.: B-1589
Sparano A.: B-0295
Spatafora L.: B-1292, B-1630
Späth L.: B-0932
Specchio N.: B-1404
Spencer N.: B-0969
Spiliopoulos S.C.: A-590, B-0865
Spillare P.: B-1167
Spinhoven M.J.: B-1558
Spink C.: B-0035
Spirchez Z.A.: B-0453
Splendiani A.: B-0436
Spohrer K.: B-0234
Sporea I.: B-0203
Sprague B.: B-1604
Sprawka K.: B-0484
Spreafico C.: B-0625
Sprengers A.: B-0957
Springer E.: B-0285
Srinivasan R.: B-1021
Srivastava D.N.: B-1338
Stabile Ianora A.A.: B-0144, B-0465
Staebler A.: B-0918
Stafrace S.: A-190
Staglianò S.: B-1478
Stagni S.: B-0625
Stahl R.: B-0122
Stajgis M.: A-778
Stampanoni M.: B-1417
Stanca C.: B-0232
Standaert C.: B-1067
Stange R.: B-1564
Stangl K.: B-0598
Stáreková J.: B-0780
Starling N.: B-0209, B-1083
Staufner K.: B-1255
Stavrinou P.: B-1384
Stebner V.: B-0706, B-1371
Stefan R.: B-1122
Stefano A.: B-0049, B-0420, B-0873
Steffen I.: B-0943
Steinbach L.: A-678, A-680
Steinfelder E.: A-612
Stemmer A.: B-0013, B-0017, B-1346
Stenberg B.: B-1217
Stenberg L.: K-29
Stening T.: B-1583
Stensvoll M.L.: B-0140
Stephan F.: B-1091
Stern Padovan R.: A-698
Steurer J.: B-1031
Stief C.: B-1471
Stief J.D.: B-0009
Stieltjes B.: B-1381
Stierstorfer K.: B-1437
Stijnen M.: B-1458
Stiller W.: A-247, B-0544, B-1131
Stinson E.: B-0546
Stirling A.: B-0176
Stocker D.: B-1125
Stöcklein S.: A-829, B-1161
Stoekle E.: B-0697, B-0698
Stokanovic V.: B-1632
Stollberger R.: B-1151
Stolpen A.: B-1331
Stone S.: B-0254
Storz C.: B-0340, B-0838
Stosic-Opincal T.: A-303
Stöttinger A.: B-0912
Stoupis C.: A-260, A-904
Stöver T.: B-0258
Stowe J.G.: B-0321
Strackee S.D.: B-0732
Stramare R.: B-1486, B-1492
Sträter A.S.: B-0149
Stratis A.: B-1431
Streekstra G.J.: B-0732
Streitparth F.: B-0292, B-0349, B-0412, B-0446, B-0894, B-0899, B-0961
Strickland N.H.: A-362
Strobel D.: B-1260
Strobl S.: B-1423
Strøm B.: B-0130, B-1146
Stromillo M.L.: B-0286
Stroszczyński C.: B-0208
Strudwick R.: B-1639
Struffert T.: A-970
Struik F.: B-0555
Struthers A.D.: B-0214, B-0562
Studzinski J.: A-776
Stumpp P.: B-1564, B-1566
Sturm T.: B-0234
Su K.-H.: B-1017
Su T.: B-0496
Su Y.: B-0004
Su Y.-Y.: B-0194
Subbanna I.: B-1058
Subbotin Y.: B-1247
Subramanian P.: B-1079
Sudarkina A.: B-0641, B-1576
Sudarshan T.A.: B-1182
Sudarski S.: B-0459
Sudhakar K.: B-1675
Südmeyer M.: B-1235, B-1237
Sudol-Szopińska I.: A-032
Suehiro E.: B-0767
Suetens P.: A-981
Sugawara H.: B-1048
Sugihara N.: B-0043
Sugiyama M.: B-0028
Suhai F.I.: B-0150, B-1657
Suhling H.: B-0235
Sulkowska K.: B-0882
Sullivan C.J.: B-0443
Suman S.: B-0054
Summers P.: B-1000
Summers R.M.: B-1587
Summersgill J.: B-0214, B-0562
Sun C.: B-1593, B-1596
Sun C.C.: B-1535
Sun D.-P.: B-0194
Sun J.: B-0387
Sun K.: B-0774
Sun R.: B-0737
Sun Y.: B-0635, B-0800, B-1021, B-1596
Sun Z.-Y.: B-0364, B-1259, B-1261
Sung C.-M.: B-0534
Sung D.J.: B-0854
Sung J.S.: B-1409
Suntharalingam S.: B-0450, B-1138
Suo X.: B-0662
Suponeva N.: B-1407
Suranyi P.: B-1046, B-1047
Suren C.: B-1120
Surov A.: B-0359
Sutter R.: A-415, B-1430
Sutto M.: B-0128
Suutari H.: B-1452
Suzuki S.: B-0324, B-1048
Suzuki T.: B-1258, B-1315
Svahn T.M.: B-0640
Svedström E.: B-1447
Svensson A.: A-851
Svensson S.F.: B-1137
Sverzellati N.: A-880, B-0045, B-0333, B-0787, B-1349
Swami V.: B-0947
Swamy S.S.: B-1058
Swart L.E.: B-1649
Sweeney J.A.: B-0656
Swoboda B.: B-0621
Syrgiamiotis V.: A-223
Syväri J.: B-0441
Szabo A.G.: B-0659, B-1680
Szabó L.: B-1657
Szatmari P.: B-0129, B-0183
Szczepura K.: B-1303, B-1444
Szczerbo-Trojanowska M.: A-474
Szczesniak D.: B-0920
Szemplinska B.: B-1106
Szeszkowski W.: B-0882, B-1106
Szikora I.:
Szilveszter B.: B-0150, B-0754, B-0761, B-1655
Szuba A.: B-0920

List of Authors & Co-Authors

T

- Tabatabai G.: *B-0090, B-0093, B-0808*
Taberner Lopez E.: *B-1465*
Tabone E.: *B-0383, B-1064, B-1114, B-1244, B-1246*
Tacchini S.: *B-1390*
Tack D.: *A-251, B-0642, K-13*
Tadepalli M.: *B-1378, B-1379*
Tafari A.: *B-1065, B-1567*
Tagliafico A.: *B-0955, B-1613*
Tahir E.: *B-0780*
Tahmassebi A.: *B-1036, B-1281*
Tahon F.: *B-0509*
Tai H.-C.: *B-1590*
Taibbi A.: *B-1630*
Taibi A.: *B-1439*
Takagi H.: *B-1457*
Takahashi A.: *B-0416*
Takase K.: *B-1550*
Takashima S.: *B-0416*
Takeda M.: *B-0738*
Takehara S.: *B-0637*
Takehara Y.: *B-0028*
Takx R.A.: *B-1463*
Tala H.: *B-0494, B-0667*
Talaat M.: *B-0092*
Talaat S.M.M.T.: *B-1411*
Talarczyk P.: *B-0214, B-0562*
Talei Franzesi C.: *B-0024, B-0634, B-0851, B-0942, B-1518*
Talei Franzesi C.R.: *B-0897, B-1328, B-1513, B-1514*
Tali E.T.: *A-557*
Talmaceanu D.: *B-0255*
Talving P.: *B-0296*
Tamada T.: *B-0607*
Tamandl D.: *B-1255*
Tan L.K.: *B-0617, B-1597*
Tan S.: *B-0654*
Tanaka R.: *B-1457*
Tanamala S.: *B-1387*
Tandri H.: *B-1656*
Tanenbaum L.: *SY 27*
Tang C.X.: *B-1487*
Tang J.S.N.: *B-1385*
Tang K.K.: *B-1370*
Tang S.: *B-0653, B-0655*
Tang W.: *B-1095*
Tang X.: *B-1238*
Tang Y.: *B-0658, B-1670*
Tani W.: *B-0767*
Tannast M.: *B-0303, B-0539, B-1124*
Tantawy W.: *B-0592*
Tanter M.: *B-0202*
Tanturri De Horatio L.: *A-153*
Tanyildizi Y.: *B-0939*
Tao B.: *B-0657*
Taoka T.: *B-0995*
Taori A.: *B-1231*
Taourel P.: *B-0948*
Taoussi R.: *B-0941*
Tarachkova E.: *B-1248, B-1369*
Tarantini G.: *B-1320*
Tarasoutchi, F.: *B-0142*
Tarmey T.: *B-0670, B-0671, B-0828, B-1089*
Taron J.: *B-0601*
Taroni P.: *A-322*
Tartaglia C.: *B-0465*
Taschini S.: *B-0855*
Tassone E.: *B-0493*
Tateishi U.: *B-1472*
Tatsugami F.: *B-0428*
Tatsuoka C.: *B-0125*
Tatum S.: *B-1055*
Tavakol Olofsson P.: *B-1644*
Tavakoli A.A.: *B-0606*
Tavakoli Taba S.: *B-1416*
Tavares de Melo M.D.: *B-0977*
Tavolaro S.: *B-0386*
Tayebi M.: *B-1466*
Taylor A.M.: *A-874*
Taylor S.A.: *A-878*
Tazdait M.: *B-0368*
te Riele A.S.J.M.: *B-1656*
Teh J.: *A-371, A-720*
Teh W.: *SY 10*
Teichgräber U.K.: *B-0349, B-0373*
Teixeira B.C.: *B-0283*
Tejerina A.: *SY 10*
Teng G.: *B-1185*
Teng Z.: *B-0219*
Tennstedt P.: *B-1569*
ter Beek L.C.: *B-0068, B-0717, B-1274*
ter Braak A.: *B-0913*
Ter Voert E.: *B-0708*
Terasawa H.: *B-0738*
Terekhov M.: *B-0030*
Terracciano F.: *B-0833*
Terwindt G.M.: *B-1600*
Terzic S.: *B-1163*
Tesche C.: *B-1454, B-1456*
Tessa C.: *A-393*
Tessarini G.: *B-1650*
Testa F.: *B-0263*
Testoni S.: *B-0816*
Tettero M.N.: *B-0558*
Teufel M.: *B-0764, B-0766*
Thakar S.: *B-0261*
Thakor K.: *B-0561*
Thakur M.: *B-1022*
Thakur S.: *B-1117*
Thanabalasingam A.: *B-0980*
Tharwat Mohammed El-Sayed N.: *B-1196*
Theilig D.: *B-0007*
Theotokas I.: *B-0430*
Theysohn J.: *B-0450*
Thiele F.: *B-1384, B-1671*
Thiele H.: *B-0979*
Thierfelder K.: *B-0088, B-0513, B-0517*
Thierfelder K.M.: *B-0922*
Thilo C.: *B-0023*
Thoduka S.: *B-1383*
Thoeny H.C.: *A-451, A-626, A-835*
Thomas A.: *B-0306*
Thomas B.A.: *B-1049*
Thomas C.: *B-0319, B-1584*
Thomas D.: *B-1350, B-1571*
Thompson D.: *B-1416*
Thomsen H.S.: *B-1464*
Thomsen L.H.: *B-0870*
Thomsen M.G.: *B-0747*
Thong P.M.: *B-0449, B-1540*
Thornton J.: *B-0856, B-0857*
Thouly C.: *B-0316*
Thuring T.: *B-0549*
Thunberg P.: *B-1382*
Thunberg S.J.: *B-0312*
Thurnher M.M.: *A-560, A-765*
Thyss A.: *B-1343*
Tian J.: *B-0600, B-0689*
Tice J.: *B-1604*
Tiddens H.A.: *B-0768*
Tiderius C.J.: *B-1014*
Tien Y.-W.: *B-0019*
Tienken M.: *B-1252*
Tieulie N.: *B-1043*
Tigano G.: *B-1336*
Tikhonov A.: *B-1557*
Tilli M.: *B-0588*
Tillier C.: *B-1568*
Timmer M.: *B-1671*
Timmers J.: *B-0685*
Tincey S.R.: *B-0173*
Tinelli C.: *B-0267*
Tinôco Alvim de Souza F.: *B-0391*
Tipaldi M.A.: *B-0231*
Tirkos T.: *B-0190*
Tischendorf P.: *B-0289, B-1062*
Tisell A.: *B-0096*
Tkachev A.: *B-1003*
Tkachev S.: *B-1248*
Todoran T.: *B-1046, B-1047*
Todorski I.: *B-0303, B-1124*
Tofanelli L.: *B-0382*
Toghyan H.: *B-1217*
Toia P.: *B-0565*
Tokat Y.: *B-0379*
Toker A.: *B-0322, B-1450*
Tolan D.J.M.: *A-098, A-518, A-519, A-795*
Tolle S.: *A-509*
Toma P.: *B-0153, B-0157, B-0159*
Tomasello Weitz A.: *B-0827*
Tomas Cont N.: *B-0107*
Tombetti E.: *B-1042*
Tominaga J.: *B-1550*
Tomkova L.: *B-1294*
Tondo C.: *B-1224*
Tong T.: *B-0171, B-0360*
Tong T.T.: *B-0163, B-0367*
Tononcelli E.: *B-0265*
Tonutti M.: *B-0678, B-1439*
Tootell A.K.: *B-0135*
Topcuoglu O.M.: *B-1421*
Topping G.: *B-0988*
Torcitto A.G.: *B-0049, B-0420, B-0873*
Torheim T.: *B-0104, B-0498*
Törnberg S.: *A-564*
Torp S.: *B-1647*
Torre R.: *B-0959*
Torregrosa Andres A.: *B-0006*
Torresin A.: *A-033, B-0128*
Torrice P.: *B-0855, B-1611*
Torrissi S.E.: *B-0049, B-0420, B-0873*
Tortora D.: *B-1478*
Tortora G.: *B-0017*
Tosi E.: *B-1087*
Tosto S.: *B-1613*
Tóth A.: *B-1657*
Touil N.: *B-0941*
Toulgoat F.: *B-0688*
Toyohara J.: *B-1081*
Traply C.T.: *B-0288*
Trattign S.: *A-615, B-0285, B-0620, B-1117*
Traut S.: *B-0549*
Trauth M.: *B-0413*
Traylor K.S.: *B-1288*
Trebesch S.: *B-0352, B-0356, B-0365, B-1204*
Tregnaghi A.: *B-1167*
Tremper J.: *B-0413*
Trenti N.: *B-1128*
Tresoldi S.: *B-1189*
Treutlein M.: *B-0796*
Trianni A.: *A-926*
Triantopoulou C.: *A-087, B-1519*
Trifonova T.A.: *B-1249*
Trimboli R.M.: *B-0503, B-1093*
Trinkmann F.: *B-1354*
Trintignac A.: *B-0066*
Tripathi P.: *B-1270*
Triulzi F.M.: *A-538, A-891*
Troelsen A.: *B-0747*
Trofimenko I.: *B-0182, SY 18*
Trojan J.: *B-1201*
Trojanowska A.: *A-623, A-700, A-714*
Trolese F.: *B-1381*
Tromba G.: *B-1416, B-1439*
Trombetta C.: *B-1664*
Tropea M.: *B-1167*
Trovik J.: *B-1368*
Trueb P.: *B-0549*
Trumm C.G.: *B-0122, B-0228*
Trümpfer A.: *A-452, A-454*
Trzasko J.: *B-0546*
Tsakok M.: *B-0831*
Tsang H.H.L.: *B-1620*
Tsapaki V.: *A-421*
Tschischka A.F.: *B-0584*
Tscholl P.M.: *B-1430*
Tse M.L.D.: *B-0193*
Tselikas L.: *A-237*
Tseng J.-R.: *B-1250*
Tsetis D.K.: *A-006*

List of Authors & Co-Authors

Tsiflikas I.: B-0764, B-0766
Tsili A.C.: B-1662
Tsogkas I.: B-0923
Tsougos I.: B-0304
Tsuchiya M.: B-0720
Tsuruda K.: B-0684, B-1606
Tsurumaru D.: B-0716
Tucci Jr S.: B-0879
Tudisca C.: B-1495
Tulay C.: B-1015
Tunariu N.: B-0393
Tunlayadechanont P.: B-1199
Turan Bektas C.: B-1206
Türk S.: B-1219
Turnaoglu H.: B-1004
Turovski B.: B-1037, B-1235, B-1237
Tuscano B.: B-0008
Tutar B.: B-1293
Tyczynski B.: B-0450
Tysnes O.B.: B-0798
Tyurin I.E.: A-529, B-1369, B-1561
Tzedakis A.: B-0771
Tzimas C.: B-1284
Tzschätzsch H.: B-0001

U

Uberoi R.: A-240, A-589
Ublinskiy M.: B-0156, B-0806
Uchida M.: B-0272, B-1116
Uchigashima T.: B-0416
Uchio E.: B-0361
Uder M.: B-0621, B-0901, B-1260, B-1629
Udeshi U.: B-1359
Udodov V.: B-0728
Udwadia Z.: B-0872
Uhlig J.: B-0563
Ujlaki M.: B-0605
Ukkola L.: B-0351
Ulaner G.A.: B-0705
Ullich T.: B-0248, B-0252, B-1363, B-1364
Uluc M.E.: B-1429
Ulus S.: B-0763
Umatham R.: B-0934
Umutlu L.: B-0355, B-0584, B-0652, B-0706, B-0796, B-1367, B-1371, B-1534, B-1621, SY 1a
Ünal N.G.: B-1538
Unlu Y.: B-1418
Unno N.: B-0028
Upponi S.: B-0970
Uprimny C.: B-1570
Uras C.: B-1293
Urbani L.: B-1320
Us R.: B-1448
Usanov M.S.: B-1591
Useche N.: B-0694
Ushinsky A.: B-0361
Usman A.: B-0219
Usta E.B.: B-0661
Uzun C.: B-0098

V

Vacirca F.: B-0444
Vacondio R.: B-0083
Vael R.: B-0290
Vafaei H.: B-1669
Vafiadis I.: B-0430
Vágó H.: B-1657
Vahldiek J.L.: B-1340
Vaiani M.: B-0625
Vaidya S.: A-121
Vaidyanathan S.: B-0593, B-0908
Valbusa G.: B-0479, B-0481
Valdés Solís P.: A-464
Valdora F.: B-1613
Válek V.: A-438
Valenti M.: B-0410
Valentini A.L.L.: B-0471

Valentini B.B.: B-0282
Valentini M.: B-0077
Valentini V.: A-883, B-0874
Valerio M.C.: B-0244
Valerio R.M.F.: B-1400
Valette P.-J.: B-1060, SY 19
Valkema R.: B-1649
Valle C.: B-1468, B-1469
Vallee J.-P.: B-1223
Valverde Lavirgen S.: B-0116
van Alfen N.: B-0957
van Assen M.: B-0757, B-1152, B-1155, B-1455, B-1458
Van Beek E.J.: B-1532
van Beek E.J.R.: A-009, A-083
Van Beers B.: B-0010, B-0202, B-1528
van Berckel B.N.: B-1033
van Bommel R.M.G.: B-0675
van Buchem M.A.: A-636
van Dalen J.: B-0131
van de Sande M.A.J.: A-893
van de Vijver M.: B-1277
van den Bergh R.: B-1565
van den Bosch A.E.: B-0143
van den Brekel M.: B-1213
van den Brekel M.W.M.: B-0068
van den Hauwe L.: A-409, B-0290, B-1594
van den Heuvel T.L.A.: B-1594
van den Hoven A.T.: B-0143
van der Aalst C.M.: B-0566, B-0571
van der Eerden A.W.: B-1594
van der Geest R.J.: B-0220
van der Graaf M.: B-0555
van der Harst P.: B-1155
van der Hoorn A.: B-0907
van der Lugt A.: B-0485, B-0512, B-0691, B-1008
Van Der Molen A.J.: B-1464
van der Noordaa M.E.: B-0917
van der Poel H.: B-1565, B-1568
Van der Putten J.: B-0480
van der Roest R.: B-1568
van der Werf N.: B-0311
van der Zijden T.: A-666, A-913, B-0318, B-0858
van Dijk E.-J.: B-0311
van Dijk R.: B-1152, B-1155
van Driel W.: B-1376
Van Dyck P.: A-468
Van Engen R.: B-0550
van Es A.: B-0512, B-1008
van Ginneken B.: A-171, B-1349
Van Goethem J.: A-020, A-756
Van Gompel G.: B-0721, B-1044, B-1050
van Graan A.L.: B-1680
van Griethuysen J.J.: B-0365, B-1213
van Griethuysen J.J.M.: B-0352
van Hamersvelt R.W.: B-1462
Van Hecke W.: A-593
van Hedent S.: B-0125, B-1017
Van Holsbeke C.: B-0236
van Hoof R.: B-0220, B-0222
Van Hoyweghen A.: B-1558
van Leeuwen F.W.: B-0068
van Lunteren C.: B-0871
van Marken Lichtenbelt W.: B-1051
van Muilekom E.: B-1568
Van Muylem A.: B-0642
van Nijnatten T.: B-0274, B-1409
van Ommen F.: B-1130
Van Ongeval C.: A-333, SY 1a
Van Ooijen P.M.: B-1345
van Ooijen P.M.A.: A-048, A-993
van Oostenbrugge R.: B-0220, B-0222
Van Raemdonck D.: B-1574
van Rijn B.B.: B-0785
van Rijn R.R.: A-038, A-890
van Rijswijk C.S.: B-0110
van Roozendaal L.: B-0274
van Schagen S.J.: B-1309
van Staalduijn E.: B-0778
Van Tuij S.: B-1458

van Tulder G.: B-0485
van Urk J.: B-0917
van Zwam W.: A-914, B-0512, B-1008
Vanacker P.: B-0858
Vancheri A.: B-0873
Vancheri C.: B-0049, B-0420, B-0873
Vancoillie L.: B-0682
Vande Berg B.: A-030, B-0438
Vande Vyvere T.: B-1594
Vandecaveye V.: B-0362, B-1075
Vandemeulebroucke J.: B-1050
Vandereyken F.: B-0290
Vandermosten M.: B-1489
Vane M.L.G.: B-0274
Vanhoenacker F.M.H.M.: A-840, A-961
Vani V.: B-0519, B-0520, B-0522
Vaño E.: A-502
van't Sant-Jansen I.: B-1085, B-1376
Vanzulli A.: B-0008
Vardhanabhuti V.: B-0075, B-0603
Vargas H.A.: B-0254
Vargas M.I.: B-0466
Varga-Szemes A.: B-0569, B-0752, B-0776, B-1046, B-1047, B-1232, B-1454, B-1455
Varona Porres D.: B-1551
Varoquaux D.-A.: A-543
Varotto A.: B-1486, B-1492
Varrassi M.: B-1539
Vas D.: B-1537
Vasco Aragão M.D.F.: K-19
Vasilevska Nikodinovska V.: B-0535
Vassallo L.: B-0107, B-1114, B-1592
Vassileva J.N.: A-420
Vassiou K.: B-0304
Vaz Touret M.A.: B-0331
Vazhenin A.: B-1497
Vázquez Caruncho M.: B-0501
Vázquez E.: A-338
Vazquez Mendez E.: B-0769
Vecsey-Nagy M.: B-0150
Vedovo F.: B-1664
Vedsted P.: B-1660
Veeramuthu V.: B-1597
Vega de Andrea N.I.: A-789
Vegar-Zubovic S.: B-1163
Vegt E.: B-0893, B-1274
Veillon F.: B-0067, B-0069, B-0257
Veiss A.: B-0814
Veit-Haibach P.: B-0708
Velasco S.: B-0694
Veldhoen S.: B-0022
Veliou K.: B-1118
Velthuis B.K.: B-0785, B-1656, K-17
Veltman J.: B-1277
Veltri A.: B-0185
Venancio J.: K-27
Venkatasamy A.: B-0067, B-0069, B-0257
Venkatesh S.K.: A-807
Venkatraghavan V.: B-0794
Vento Torres M.: B-1162
Ventrella E.: B-0144
Ventura E.: B-1001
Ventura L.: B-0521
Ventura S.R.: B-0137
Venturini E.: B-1390, B-1440, B-1441
Venturini M.: B-0230, B-0626, B-0629, B-1205
Venugopal V.: B-0872
Verardo I.: B-0837
Verbeken E.: B-1574
Verbist B.: A-594
Verdonschot N.: B-0957
Vergesslich Rothschild K.A.: B-0155
Verhoef G.: B-0362
Verkaik N.J.: B-1649
Verma A.: B-0270
Verma M.: B-1022
Verma S.: B-0056
Verna V.: B-0263
Vernhet Kovacsik H.: B-1133
Vernooij M.W.: B-0118, B-0794, B-0795, B-0797, B-1038, B-1039, B-1678

List of Authors & Co-Authors

W

- Vernuccio F.: B-0008, B-0881
Verrusio M.: B-1611
Verschakelen J.A.: A-739, B-1574
Verschuere J.: B-1426
Verstraete K.: A-133, A-212
Vial Y.: B-1491
Viala J.: B-1605
Viala P.: B-0531, B-0949
Viana P.C.: B-0877
Vieira I.F.: B-0362
Vieira M.C.: B-0142
Viergever M.A.: B-1130
Vietti Violi N.: B-0013
Vigna L.: B-0325
Vignau J.: B-1122
Vignoli C.: B-0141
Vikestad K.G.: A-657
Vilana Puig R.: B-0191
Vilar J.: A-806
Vilela P.: A-912
Vilgrain V.: A-017, A-263, A-286, A-523, B-0202, B-0427, B-0730, B-1528
Villa R.: B-0127, B-1129, B-1440
Villadsen N.: B-0551
Villalon M.V.: B-0914
Villani A.: B-1495
Villeirs G.: B-1067
Villeirs G.M.: A-206, A-317, A-750
Vincenti M.: B-1133
Vinchon M.: B-1504
Vinci V.: B-0151, B-1493, B-1494
Vinke E.J.: B-0794, B-1678
Vinnicombe S.J.: A-908
Virella D.: B-0396
Virgolini I.: B-1570
Virshke E.: B-1512
Vissio E.: B-1414
Vitale D.: B-1529
Vitale S.: B-0532
Vitta L.: B-0343
Vlassenbroeck A.: B-0424
Vlassenbroek A.: B-1130
Vliegenhart R.: B-0595
Vliegenthart R.: A-640, A-718, B-0563, B-0566, B-0571, B-0757, B-0776, B-0825, B-1152, B-1155, B-1458, K-21
Vlychou M.: B-0304
Voena C.: B-0162
Vogel W.: B-0365, B-0893, B-1213
Vogel-Claussen J.: A-102, B-0051, B-0235, B-0237
Vogl T.J.: B-0030, B-0039, B-0258, B-0289, B-0346, B-0439, B-0460, B-0528, B-0622, B-0623, B-0752, B-0753, B-0776, B-0824, B-1026, B-1052, B-1054, B-1059, B-1062, B-1063, B-1091, B-1201, B-1210, B-1232, B-1515
Vogt F.M.: B-0793
Voicu I.P.: B-0153, B-0157, B-0159
Voisin B.: B-0670, B-0671
Vollenbrock S.E.: B-0717, B-1274
Volterrani L.: B-0853
von der Fehr T.: B-0971
von Eckardstein K.: B-1239
von Kalle T.: A-011
von Knebel Doeberitz P.: B-0569, B-0752
von Kodolitsch Y.: B-0022
von Krüchten R.: B-1356
von Spiczak J.: B-0980, B-0981, B-1226, B-1227
Voncken F.E.: B-0717
Voncken F.E.M.: B-1274
Vonder M.: B-0566, B-0571
Voormolen M.: B-0318, B-0858
Vorobyov N.: B-0406, B-1078, B-1220
Vos W.: B-0236
Voskuil M.: B-1462
Voyvoda N.: B-0722
Vrancken Peeters M.J.: B-0917
Vrugt B.: B-0839
Vucetic J.: B-0101, B-1394
Vuillemin V.: B-0302
Waade G.G.: B-0132, B-0133, B-0134
Wachabauer D.: B-0317
Wacker F.: B-0051, B-0235, B-0237
Wagner M.: B-0273, B-0426
Wagner P.M.: B-0777
Wagner R.: B-1222
Wagner W.: B-0240
Wakayama T.: B-0028
Waldt S.: A-291
Walecki J.: A-080
Walker C.: B-0970
Wallis M.G.: A-635, B-0275, B-1094
Walsh C.: B-0972
Walsh D.: A-697
Walter S.: B-0791, B-0909
Walter W.R.: B-0538
Walton L.A.: B-1303
Waltrich N.K.: B-1435
Wang C.: B-0502, B-1175, B-1178
Wang C.-K.: B-0619
Wang D.: B-0848, B-1271, B-1276, B-1323, B-1480
Wang F.: B-0063, B-0658, B-1280
Wang G.: B-0279
Wang H.: B-0472, B-0878, B-1663
Wang J.: B-0171
Wang K.: B-0600
Wang K.Y.: B-0277
Wang L.: B-0442, B-0889, B-0986, B-1018, B-1276, B-1485
Wang L.-J.: B-0297, B-1250
Wang M.: B-0390
Wang M.-L.: B-1034, B-1599
Wang R.: B-0463
Wang S.: B-0171, B-0360, B-1257, B-1593, B-1596
Wang W.: B-0475, B-0497, B-0935, B-1084, B-1211, B-1479, B-1490, B-1496, B-1526
Wang W.T.: B-1256
Wang X.: B-0404, B-1593
Wang X.-Y.: A-950
Wang Y.: B-0389, B-0467, B-0800, B-1010, B-1298, B-1323
Wang Z.: B-0781, B-0879, B-1193, B-1417, B-1596
Wareing A.: A-930
Warier P.: B-0872, B-1378, B-1379
Warking J.: B-1676
Wartjes J.B.: B-0096
Waryn M.-J.: B-0313
Washizuka F.: B-0962
Wassef S.: B-1331
Wasser M.: B-0011
Watanabe A.: B-1283
Watanabe H.: B-0451
Watson Y.: B-0165
Wattjes M.P.: A-210
Watts C.: B-1672
Wawrzyniak P.: B-1107
Weber M.: B-0079, B-0155, B-0506, B-0620, B-1168, B-1486
Weber M.-A.: A-370, A-417, A-894, B-0437
Weber T.F.: B-0014
Weber W.: B-0705
Weckbach S.: A-200
Weder W.: B-1355
Wegner F.: B-0793
Weidekamm C.: A-871, A-873, K-20
Weigel U.: A-320
Weikert T.: B-0482, B-1381
Weinheimer O.: B-0240, B-0402, B-0413, B-0871, B-1549, B-1588
Weinmann A.: B-0196
Weinrich J.M.: B-0025, B-0780
Weinstein S.: B-1632
Weir A.: B-0177, B-0670, B-0671
Weir-McCall J.: B-0214, B-0562
Weiser M.: B-0167
Weishaupt D.: A-450, A-879
Weiß C.: B-0243
Weiß J.: B-1208
Weiss K.: B-0727, B-0790, B-0976
Well L.: B-0932
Wells J.: B-1126
Welte T.: B-0051
Wen J.: B-0094, B-0799, B-0807, B-0938
Weng Q.: B-1171
Wengert G.J.: B-0506, B-0507, B-1281
Wenkel E.: B-1629
Wenz H.: B-1582
Wenzel F.: B-1678
Werlen S.: B-0303, B-0539
Werner Reyes M.F.: B-0827
Westbrook C.: B-1144
Westenend P.J.: B-0913
Westerlaan H.E.: B-0907
Weston M.: A-813
Westphalen A.C.: B-0879
Wetscherek A.: B-0405
Wetter A.: B-0450, B-0836, B-1138, B-1367, B-1371
Whitby E.H.: B-0987
Whittle C.: B-0494, B-0667
Wibmer A.G.: B-0254
Wichmann J.L.: B-0258, B-0289, B-0346, B-0439, B-0460, B-0753, B-1026, B-1052, B-1515
Wick M.C.: B-1341
Widya R.L.: B-0330, B-0335
Wiech D.: B-0373
Wielema M.: B-1109
Wielpütz M.O.: A-008, A-608, B-0240, B-0413, B-1588
Wieners G.: B-1056
Wiesinger B.: B-0918
Wiesmüller M.: B-0901
Wiestler B.: B-0088
Wietek B.: B-0918
Wiggermann P.: B-0207
Wildberger J.E.: A-256, A-725, B-0220, B-0222, B-1051, B-1409, B-1410
Wilkinson L.S.: B-0680
Wille M.M.W.: B-0870
Willemink M.J.: B-0026
Williams D.: B-0857
Williams M.: A-258, B-0097
Williams T.M.: B-1079
Willwacher S.: B-0727
Wilman H.R.: B-0002
Wilson D.J.: A-135
Windfuhr-Blum M.: B-0081
Windhager R.: B-1428
Windschuh J.: B-0933
Winfield J.: B-1080
Winkhofer S.: B-1031
Winter-Warnars G.: B-0917
Winzler S.: B-1069
Wirtanen M.: B-1442
Wirth S.: A-003, A-836
Wit E.: B-1565
Wohlfahrt P.: A-885
Woie K.: B-1368
Woisetschlager M.: B-1589
Woitek R.: B-0104, B-0498
Woitek R.A.: B-0079, B-1094
Wojtkiewicz G.R.: B-1175, B-1178
Wolf N.: A-336
Wolter P.: B-0362
Wolterink J.M.: B-0568
Wolters van der Weij E.: A-660
Won S.Y.: B-1563
Wong E.M.F.: B-1370
Wong H.Y.F.: B-0193
Wong J.H.D.: B-0091, B-1597
Wong M.C.Y.: B-0580
Wong Y.-C.: B-0297
Woo K.: B-1424
Woo O.H.: B-1415
Woo S.: B-0649
Wörtler K.: A-485, B-0529, B-1120

List of Authors & Co-Authors

Woznitza N.H.: A-788
Wressnegger A.: B-0633
Wright C.L.: B-0888, B-1218
Wu B.: B-0432, B-0781, B-0849
Wu C.-H.: B-0297
Wu F.: B-0811
Wu F.-Z.: B-1352
Wu G.: B-0063
Wu H.-K.: B-1607
Wu H.-M.: B-1099
Wu J.: B-1483
Wu K.: B-0573
Wu K.-H.: B-0534
WU L.: B-1158
Wu M.-H.: B-1590
Wu R.: B-0792, B-1158
Wu V.: B-1533
Wu W.C.V.: B-0217
Wu W.-P.: B-1607
Wu X.: B-0417
Wu Y.: B-1279, B-1483
Wurnig M.: B-0273
Wüst W.: B-0901
Wytenbach R.: B-0482

X

Xi Y.: B-0071, B-1126
Xia C.: B-1648
Xia Y.: B-0390
Xiao Y.: B-0073, B-0656, B-0657
Xie L.: B-0339, B-0389
Xie Q.: B-0878, B-1483
Xing W.: B-0387
Xing Z.: B-0989
Xiong F.: B-1171
Xiong Y.: B-1110, B-1111
Xu G.: B-0421, B-1572
Xu H.: B-0431, B-1153, B-1154, B-1593
Xu H.M.: B-0686
Xu H.-Y.: B-0338
Xu J.: B-0800
Xu J.-M.: B-1560
Xu J.-R.: B-1158
Xu K.: B-0658, B-1475
Xu L.: B-1180
Xu R.: B-1153
Xu W.: B-0938, B-1617
Xu X.-M.: B-1185
Xu X.R.: B-0989
Xue H.: B-0792, B-1181, B-1264
Xue H.-D.: A-948, B-0364, B-1259, B-1261
Xue Y.: B-0223
Xuesong D.: B-0937

Y

Yadav A.: B-1362
Yadav M.: B-1334
Yadav T.: B-1334
Yagami K.: B-0324
Yaguchi A.: B-0403
Yamada A.: B-1315
Yamada K.: B-1081
Yamada T.: B-0720
Yamaguchi T.: B-1306
Yamamoto Y.: B-1048
Yamamura J.: B-1317, B-1319
Yamanouchi S.: B-0451
Yamauchi F.I.: B-0877
Yamazaki A.: B-0350
Yan F.-H.: A-947
Yan H.: B-0713
Yan Z.: B-0657
Yang D.H.: B-0337
Yang F.: B-0654
Yang H.: B-1403
Yang H.-C.: B-1099
Yang H.K.: B-1524
Yang J.: B-0570

Yang L.: B-0709, B-0756, B-0759, B-0849,
B-1256, B-1318
Yang Q.: B-0004, B-0811
Yang S.: B-0999, B-1323
Yang X.: B-1079, B-1171, B-1172
Yang Y.: B-0689
Yang Z.: B-0339, B-0735, B-0783, B-0788,
B-1097, B-1098, B-1100, B-1103, B-1104,
B-1153, B-1154, B-1230
Yang Z.-G.: B-0338
Yankaskas B.: B-0685
Yao J.: B-1587
Yao L.: B-0656
Yao Z.: B-1482, B-1483
Yardimci A.H.: B-1206
Yazdani N.: B-1215
Yazicioglu Y.: B-1036
Ye Q.-H.: B-1256
Ye Z.: B-0170, B-1280
Yeh B.M.: B-1021
Yel I.: B-0258
Yeung M.W.R.: B-1370
Yildirim Donmez F.: B-1004
Yilmaz Ö.: B-1330
Yilmaz P.: B-0797
Yilmaz R.: B-0582
Yim J.-H.: B-0197
Yim Y.: B-0693
Yin B.: B-1593, B-1596
Yin X.: B-0279
Yin Z.: B-0658
Ying T.-C.M.: B-0217, B-1214
Yip S.P.: B-0217
Yiqun S.: B-0163
Yokoo P.: B-0283
Yokoyama K.: B-1081
Yoneda N.: B-0198
Yoneda T.: B-0738
Yoon C.J.: B-0032
Yoon D.Y.: B-0724
Yoon J.-H.: B-1321
Yoon K.-H.: B-0005
Yoon S.H.: B-0044
Yoon S.J.: B-0672
York H.: B-1147, B-1643
Yoshida K.: B-1472
Yoshida M.: B-0106
Yoshikawa T.: B-0043, B-0403, B-0767, B-1348,
B-1573, B-1578, B-1579, B-1581
Yoshinaga S.: B-0738
Yoshioka K.: B-1457
You H.: B-0810, B-1002
Young K.: B-1083
Young L.K.: B-1585
Younis A.: B-1503
Yousry T.A.: A-561, A-761, B-1039
Youssef A.: B-1503
Yperzeele L.: B-0858
Ytre-Hauge S.: B-1368
Yu M.H.: B-0195
Yu M.L.: B-0193
Yu Q.: B-0233
Yu S.: B-0792
Yu T.: B-0004
Yu Y.: B-1482
Yu Z.: B-0428
Yuan B.: B-0456
Yuan C.: B-0217
Yuan H.: B-0075, B-0686
Yuan Q.Q.: B-0636
Yücege M.: B-0495
Yucel C.: B-0205
Yue Y.: B-0454, B-0464
Yuekao L.: B-0418
Yui M.: B-1348, B-1573, B-1578, B-1579,
B-1581
Yun G.: B-0020, B-0032, B-0664
Yusuf G.T.: SY 11
Yveborg M.: B-1438

Z

Zabitova M.: B-1677
Zaccagna F.: B-1672
Zacharzewska-Gondek A.: B-1679
Zackrisson S.: A-175, A-325, B-1006, B-1628,
SY 1b
Zafeiropoulou K.: B-0468
Zagdanski A.M.: B-0422
Zahirifard S.: B-0500
Zaiss M.: B-0363, B-0933
Zajkowska J.: B-0278
Zajkowska O.: B-0278
Zakharova N.: B-0086
Zambon P.: B-0549
Zamboni G.: A-674, B-0018, B-0166, B-0834,
B-1065, B-1519, B-1521, B-1522, B-1523
Zamyshevskaya M.: B-0728
Zanardi S.: B-0038
Zanca F.: B-0314, B-0316, B-0318
Zanconati F.: B-0678, B-1416, B-1439
Zanelli E.: B-0046
Zanetti I.: B-1492
Zanetti M.: A-134, A-511
Zangos S.: B-0030
Zanirato M.: B-0017, B-0978
Zanirato Rambaldi G.: B-0407, B-0579
Zannoni S.: B-1189
Zanotel M.: B-1294
Zaottini F.: B-0615, B-0616
Zapf A.: B-0189
Zappa M.: B-0521, B-1528
Zarb F.: A-140
Zare Mehrjardi M.: B-0599
Zarea A.: B-0592
Zarei F.: B-1668
Zarqane H.: B-1133
Zatońska K.: B-0920
Zavadovskaia V.: B-0728
Zawadzki R.: B-0278
Zdesar U.: B-1443
Zech C.J.: A-095
Zeilinger M.: A-425, A-427
Zeinali B.: B-1668, B-1669
Zekry W.: B-1503
Zeltzer G.: B-0268
Zeng M.: B-1318
Zeng M.-S.: B-1256, B-1270
Zeng Q.: B-0417
Zenouzi R.: B-1317
Zerunian M.: B-0162, B-0164, B-0169
Zeynalova A.: B-0687
Zghaib T.: B-1656
Zhai X.: B-0638
Zhan S.: B-0999
Zhang C.: B-0811, B-0848, B-1271, B-1323,
B-1403, B-1412, B-1603
Zhang D.: B-0792
Zhang F.: B-1171, B-1172
Zhang G.: B-1431
Zhang H.: B-0367, B-1483, B-1670
Zhang J.: B-0286, B-0432, B-0888, B-0993,
B-1179, B-1218
Zhang L.: B-0638, B-0653, B-1126
Zhang L.J.: B-1487
Zhang M.: B-1596
Zhang W.: B-0456, B-0464, B-0656, B-0937,
B-1174, B-1298, B-1617
Zhang X.: B-0502
Zhang X.: B-0389, B-1295
Zhang X.M.: B-0015
Zhang Y.: B-0475, B-0497, B-0935, B-0986,
B-0991, B-1095, B-1475, B-1479, B-1485,
B-1490, B-1496, B-1580
Zhang Z.: B-0065, B-1187, B-1479, B-1535
Zhao C.: B-0663, B-0817
Zhao H.: B-0758
Zhao L.: B-0781, B-1172
Zhao P.: B-1193
Zhao Q.: B-0788
Zhao S.: B-1172

List of Authors & Co-Authors

Zhao W.: SY 1c
Zhao X.: B-0781, B-1325, B-1617
Zhao Y.: B-0657
Zhao Y.E.: B-1487
Zheleznyak I.: B-1101
Zheng D.: B-0073
Zheng G.: B-1124
Zheng J.: B-0840
Zheng L.: B-1412
Zheng W.: B-1603
Zheng X.: B-0073
Zhou C.S.: B-1487
Zhou H.: B-0600
Zhou J.: B-0428
Zhou P.: B-0394
Zhou Y.: B-0432, B-0463, B-0800, B-1172,
B-1203, B-1506, B-1559
Zhu L.: B-0364, B-0467, B-1259, B-1261,
B-1264
Zhu S.: B-1256
Zhu Y.: B-1280, B-1325
Zhurbin E.: B-1101, B-1102
Ziayee F.: B-0248
Ziegeler K.: B-0299, B-0309, B-1619
Ziegert M.: B-0548, B-0830
Zima E.: B-1657
Zimmer C.: B-0088
Zimmerman S.L.: B-1656
Zimmermann E.: B-0598, B-0762
Zimmermann S.: B-1430
Zimmermann T.: B-0036, B-0210
Zimny A.: B-0920
Zinger S.: B-0480
Zingg T.: B-1273
Zingula S.: B-0504
Zins M.: A-372, A-524, A-809, A-903, B-0948,
SY 2
Zitsch M.: B-1201
Zivadinov R.: B-0798
Zlatareva D.: A-563
Zoet G.A.: B-0785
Zografos G.: B-1086
Zografos K.: B-1086
Zolda P.: A-323
Zompatori M.: B-0407, B-0579, B-1164
Zopfs D.: B-0906, B-1470, B-1671
Zorkaltsev M.: B-0728
Zorzenon C.D.P.F.: B-1233
Zorzenon I.: B-1665
Zorzi M.: B-0078, B-0082, B-1087
Zou L.: B-1238
Zoumpoulis P.S.: B-0430
Zreik M.: B-1462
Zubareva E.A.: B-1335
Zucchetta P.: B-1486
Zugaro L.: B-0725, B-0729, B-0960, B-1344,
B-1427
Zuiani C.: B-0046, B-0384, B-0425, B-0910,
B-0912, B-1289, B-1294, B-1358
Zuniga J.R.: B-0071
Zuo Z.: B-0810
Zurera Tendero L.J.J.: B-0823



**List of Moderators
(G)**

List of Moderators

A

Abeyakoon O.: *SS 1416*
Abeyakoon O.: *SS 1802b*
Achten E.: *SS 1811a*
Adam E.J.: *IJQ*
Adda O.: *SY 2*
Agnello F.: *SS 1001a*
Agostini A.: *SS 301b*
Agrawal A.: *SS 317*
Ahuja B.: *SS 1907b*
Alberich-Bayarri A.: *SS 605*
Alexopoulou E.: *RC 412*
Antoch G.: *RC 106*
Aringhieri G.: *SS 1007*
Arkun R.: *SS 210*
Aukland S.M.: *SS 212*
Avni F.E.: *SS 1412*
Aydingoz U.: *ESR/ESOR 1*

B

Bader T.: *SS 701a*
Baltzer P.A.T.: *SS 1402b*
Bancroft L.W.: *TC 1328, TC 1428, TC 1528, TC 1628*
Bansal O.P.: *SS 1014*
Barile A.: *SS 610b*
Barr R.G.: *SY 19*
Barth B.K.: *SS 1807a*
Bartoloni A.: *SS 312*
Basta Nikolic M.: *SS 607*
Bastarrika G.: *SS 1503*
Bauer R.W.: *SS 604*
Baur A.: *SS 1907a*
Beardmore C.: *MY 17*
Beets-Tan R.G.H.: *ESR Publication*
Belfield J.: *SS 1007*
Bellin M.-F.: *RC 814*
Bérczi V.: *BS 6*
Beyer T.: *ESR/ESHI*
Biederer J.: *SS 704*
Bilbao J.I.: *SS 1409*
Binkert C.: *E³ 1626a, SS 1009*
Bisdas S.: *SS 1508*
Blazic I.: *SS 1516*
Bolstad K.N.: *SS 1813*
Bonaffini P.A.: *SS 1801*
Bongiovanni S.: *SS 1909*
Borges A.: *SS 708*
Bos D.: *SS 315*
Bosmans H.: *SS 313*
Bozzetti F.: *SS 1011a*
Brancatelli G.: *MY 3*
Brkljačić B.: *ESOR*
Broncano J.: *SS 1904b*

C

Caceres J.: *RTF Quiz*
Cademartiri F.: *SS 1903*
Cantisani V.: *SY 23*
Cappendijk V.: *SS 601b*
Carbonaro L.A.: *SS 1902a*
Carrino J.A.: *SY 25*
Cartes-Zumelzu F.: *RC 1711*
Casado Lopez A.M.: *SS 1811a*
Caseiro Alves F.: *EM 2*
Cassar-Pulicino V.N.: *E³ 25A, E³ 25B, E³ 25C, E³ 25D, E³ 25E*
Castillo J.: *SS 614*
Catalano C.: *SS 614*
Cavedon C.: *SS 713*
Chianca V.: *SS 1809*
Chidambaranathan N.: *BS 3, SS 608*
Chodorowska A.: *RC 1704*
Choi B.I.: *SS 1001a*
Cianfoni A.: *RC 111*

Claudon M.: *WG/EFSUMB 1, SY 19*
Clauser P.: *MY 16, SS 1402a*
Claussen C.D.: *SS 603*
Clément O.: *ESR Research, SY 17*
Clevart D.A.: *WG 1*
Colin C.: *SS 702*
Collettini F.: *SS 1509*
Cornud F.: *SS 1407*
Curvo-Semedo L.: *SS 1001b*

D

Damilakis J.: *ESR/EFOMP*
D'Anastasi M.: *SS 207*
de Lange C.E.: *RC 512*
de Rooij M.: *SS 1407*
de Roos A.: *SS 303*
Demaerel P.: *SS 1511*
Denecke T.: *SS 301a*
Denys A.: *SY 3*
Dewey M.: *CT 2, CT 6, CT 10, MY 15*
Dioguardi Burgio M.: *SS 1409*
D'Ippolito G.: *SS 301a*
Dixon A.K.: *MY 4*
Djilas-Ivanovic D.: *SS 1902a*
Dolic K.: *SS 1811b*
Donati O.F.: *IJQ*
Dondelinger R.F.: *MY 9*
Dosa E.: *SS 1415*
Drapé J.-L.: *SS 1010*
Dubourg B.: *SS 1903*
Dzaye O.: *C 14*

E

Ehman R.L.: *CT 2, CT 6, CT 10*
Elmas N.Z.: *SS 1801*
England A.: *SS 1014*
Epermane M.: *SS 610a*
Eriksen M.R.: *RC 108*
Erturk S.M.: *RC 1601*
Esen G.: *SS 302*
Esposito A.: *SS 1006*

F

Fanelli F.: *E³ 526b*
Farchione A.: *SS 316*
Fatehi M.: *SS 205*
Fernandez-Bayó J.: *SS 1805*
Fernandez Hernando M.: *SS 1810*
Filippone A.: *SS 2011a*
Fontaine L.: *SY 10*
Forrai G.: *SS 1002*
Fösleitner O.: *SS 1911b*
Franchi P.: *MY 5*
Francone M.: *SS 703*
Freeman S.: *SS 707*
Friedrich K.M.: *CB 1, CB 2*
Frigerio A.: *SS 202b*
Frija G.: *EU 1*
Froeling M.: *SS 1410*

G

Gallagher F.A.: *SS 1406*
Gangemi E.: *SS 1411a*
Gangi A.: *RC 509*
Garcia G.C.T.E.: *SS 208*
Gardarsdottir M.: *E³ 24C*
Gersing A.S.: *SS 1911a*
Gheonea I.-A.: *SS 602*
Giganti F.: *SS 1907b*
Golding S.J.: *MY 14*
Goldsher D.: *SS 1911a*
Gourtsoyianni S.: *ESR/ESOR 2, MY 3*
Gourtsoyiannis N.: *ESOR*

Grainger A.J.: *TC 1328, TC 1428, TC 1528, TC 1628*
Granata C.: *RC 912*
Grehan J.: *SS 1814*
Gremion I.: *EM 4*
Grenier P.A.: *SS 204*
Gruber H.: *SS 710a*
Gubskiy I.L.: *SS 701a*
Guerra A.: *SS 307*

H

Haliloglu M.: *MY 18*
Hamm B.: *EM 1, EM 2, EM 3*
Hanna S.: *SS 207*
Hausegger K.A.: *SS 1509*
Healy N.A.: *SS 702*
Helmberger T.K.: *SS 1416*
Henninger B.: *SS 210*
Hermoye L.: *SS 1016b*
Hernandez-Giron I.: *SS 1413*
Herold C.J.: *RC 104*
Herzog C.: *SS 203, SS 1415*
Hinzpeter R.M.M.: *SS 1017*
Hodler J.: *SS 1410*
Hrabak Paar M.: *RC 1603*
Husseiny Salama D.: *C 11*
Huyskens J.: *RC 408*

I

Ichikawa S.: *SS 201a*
Iliadis K.: *SS 612*
Ilic D.: *SS 709*
Inarejos E.: *SS 1910*
Ivanac G.: *SS 1802a*

J

Jacob J.: *SS 1004*
Jacobi-Postma L.: *SS 1016b*
Jäger H.R.: *SS 1011b*
Jin Z.Y.: *EM 3*
Johnson T.R.C.: *SS 604*
Jovanovic S.: *SS 1416*

K

Kaltenbach B.: *SS 601a*
Katsifarakis D.: *MY 17*
Kaya T.: *RC 410*
Kettenbach J.: *SS 1909*
Kilburn-Toppin F.: *E³ 1726a, SS 1002*
Kinner S.: *SS 1901c*
Kitrou P.M.: *MY 9, SS 215*
Kljucevsek D.: *SS 612*
Klompenhouwer E.G.: *SS 716*
Klontzas M.: *RC 910, S 3*
Knapp K.: *SS 1414*
Kondratyev E.: *SS 201b*
Kortesniemi M.: *SS 613*
Krokidis M.: *E³ 24A*
Kuhl C.K.: *SS 602*
Kurz K.D.: *SS 1011a*

L

Lamot U.: *SS 308*
Lawler L.P.: *RC 903*
Leander P.: *PI 2*
Lebovici A.: *SS 216*
Lee J.M.: *SS 601a*
Lehotska V.: *SS 1402a*
Leiner T.: *ESR/ESMRMB 1*
Lell M.: *SS 1008*
Ley-Zaporozhan J.: *SS 1804, SS 1904b*
Loewe C.: *E³ 24B, E³ 24D*

List of Moderators

Loizides A.: *SS 610a*
Loose R.W.R.: *EU 2*
Lotan E.: *SS 711a*
Lucic M.A.: *ESR/ESOR 3, S 4*
Lukas C.: *SS 1411b*

M

Mahesh M.: *EF 2*
Malagari K.: *BS 4*
Mann R.M.: *SY 1b*
Manoharan T.: *SY 1d*
Marincek B.: *BS 2*
Marino M.A.: *SS 302*
Markiet K.: *SS 608*
Marolt Music M.: *SS 214*
Massmann A.: *SS 309*
McGinty G.: *PI 3*
McNulty J.: *EM 4, PI 1*
Meder J.-F.: *RC 911*
Merhemic Z.: *MY 8*
Mildenberger P.: *C 12, PI 3*
Miletic D.: *SS 1414*
Mintert S.: *SY 22*
Mirón Mombiola R.: *SS 610b*
Moerup S.D.: *SS 314*
Mordasini M.: *EM 4*
Mordasini P.: *SS 611*
Morozov S.: *PI 2, SY 18*
Mostbeck G.: *SS 301b*
Mück F.: *SS 317*
Mueller-Lisse U.G.: *SS 1516*

N

Nair A.: *SS 704*
Neri E.: *SS 1905*
Niehues S.M.: *SS 316*
Nougaret S.: *MY 4*

O

Occhipinti M.: *SS 304*
O'Connor M.: *SS 714*
Offiah A.C.: *RC 112*
Oktay A.: *MY 16*
Oleaga Zufiria L.: *SS 208*
O'Leary D.: *SS 214*
Oyen R.H.: *RC 1307*
Ozgen Mocan B.: *SS 308*

P

Panebianco V.: *SS 1907a*
Papakonstantinou O.: *RC 110*
Parizel P.M.: *PS 1227*
Patkar D.P.: *BS 5*
Pavia M.: *E³ 1326b*
Penha D.: *SS 209*
Pereira P.L.: *WG 1*
Perez M.: *C 11*
Perez Rodrigo S.: *SS 1802a*
Pershina E.: *SS 303*
Pfammatter T.: *SS 1016a*
Pina Insausti L.J.: *SY 1c*
Piotrowska-Kownacka D.: *SS 1412*
Platzgummer H.: *SS 710a*
Plumb A.: *SS 1001b*
Pontana F.: *SS 1904a*
Popovic L.: *RC 814*
Posadzy M.S.: *MY 13*
Prokop M.: *SS 215*
Pronin I.N.: *SY 18*
Puech P.: *RC 807*
Puri S.K.: *RC 1301*
Pyatigorskaya N.: *SS 1905*

R

Radbruch A.: *SS 1011b*
Radeleff B.A.: *SS 1809*
Radzina M.: *SS 701b*
Ramos-Andrade D.: *SS 601b*
Rampado O.: *SS 1413*
Ratib O.: *ESHI*
Reijnierse M.: *RC 810*
Reiser M.F.: *E³ 526a, MY 13*
Reiter U.: *RC 503*
Revel M.-P.: *SS 304*
Riibak M.-L.: *SS 1816*
Riklund K.: *ESR/ESHI, ESHI*
Ringl H.: *SS 1901a*
Robinson S.: *RC 808, CB 1, CB 2*
Rockall A.G.: *SS 1816*
Romei C.: *SS 204*
Roos J.E.: *E³ 1526a*
Rosendahl K.: *E³ 426*
Rovira-Cañellas A.: *PS 1227, SS 311*
Roy C.: *SS 1807b*
Runge V.: *SY 9*

S

Samara E.: *SS 213*
Sánchez M.: *SS 616*
Santos J.: *EM 4*
Sappey-Marinier D.: *ESR/ESMRMB 1*
Sardanelli F.: *ESR Publication*
Savolainen S.: *SS 714*
Scapin E.: *SS 708*
Schlett C.L.: *SS 703*
Schmidt Kobbe S.: *SS 701b*
Schönberg S.O.: *SS 1914*
Screation N.J.: *SS 1815*
Secchi F.: *SS 1403*
Seidensticker M.: *SS 1016a*
Seimenis I.: *RC 1613*
Semple T.R.: *SS 712*
Shahabpour M.: *SS 1810*
Sidhu P.S.: *WG/EFSUMB 1, SY 6, SY 13*
Simic M.: *SS 616*
Sinitsyn V.E.: *SS 1803*
Smits M.: *SS 1811b*
Snoj Ž.: *TF 1*
Sommer G.: *SS 613*
Sommer W.H.: *SS 605, SS 1815*
Squarza S.A.C.: *SS 711b*
Steinfelder E.: *ESR/BBMRI-ERIC*
Stiller W.: *SS 213*
Struffert T.: *SS 611*
Studniarek M.: *E³ 1526b*
Stukalova O.: *SS 1003*
Sudot-Szopińska I.: *SS 1910*

T

Tack D.: *ESR/EFOMP*
Tacke J.: *SS 209*
Tamandl D.: *SS 201b*
Tan S.: *SY 26*
Tanner J.: *SS 202b*
Tardaguila de la Fuente G.: *SS 1901a*
Teneva T.G.: *TF 1*
Thomassin-Naggara I.: *SS 1402b*
Thurnher M.M.: *SS 211*
Toia P.: *SS 603*
Tolan D.J.M.: *SS 1017*
Tomà P.: *MY 18*
Tóth A.: *MY 7*
Traykova N.I.: *SS 1508*
Trianni A.: *EF 1, SS 205*
Tsitskari M.: *SS 609*
Tsougos I.: *SS 1911b*
Tyurin I.E.: *SY 18*
Tzalonikou M.: *RC 1710, SS 310*

U

Uberoi R.: *SS 609*

V

Valdés Solís P.: *PI 1*
van Beek E.J.R.: *SS 1403*
Van der Lugt A.: *ESR/BBMRI-ERIC*
Van der Molen A.J.: *SS 1807b*
Van Ongeval C.: *RC 1302, SY 1a*
Van Rijn R.R.: *SS 312*
van Zelst J.: *SS 1902b*
Vargas M.I.: *SS 1411b*
Vasco Aragão M.: *SS 1411a*
Vassallo E.: *SS 1008*
Vázquez E.: *RC 1712*
Verbist B.: *BS 1, MY 14*
Vernooij M.: *MY 8, SS 1511*
Vilanova J.C.: *SS 1807a*
Vilar J.: *MY 5, RTF Quiz*
Vilela P.: *SS 711b*
Villa R.: *SS 313*
Vinnicombe S.J.: *SS 1902b*
Vlahos J.: *SS 1904a*
Vlassenbroek A.: *SY 12*
Vock P.: *E³ 1226, S 1*
Vourtsis A.: *SS 1802b*

W

Weishaupt D.: *EM 1*
Wildberger J.E.: *SY 15*
Willemink M.J.: *SS 713*
Woitek R.: *SS 311*
Woznitza N.H.: *SS 1914*

Y

Yalynska T.A.: *E³ 24E, SS 1503*
Yousry T.A.: *SS 711a*
Yusuf G.T.: *SY 11*

Z

Zackrisson S.: *SS 202a*
Zanetti M.: *SS 710b*
Zech C.J.: *E³ 126*
Zins M.: *MY 7, MY 15*
Zlatareva D.: *S 2*